Presentation Number **ES 1**
Educational Session 1: Chemistry of Contrast Media - Basics - Probes and Suitable Imaging Modalities
September 5, 2012 / 07:45-08:15 / Room: Wicklow Hall 1

# Basics in Pharmacokinetics

***Twan Lammers**, , Aachen, Germany. Contact e-mail: tlammers@ukaachen.de*

Disclosure of author financial interest or relationships:
**T. Lammers**, None.

DOI: 10.1007/s11307-012-0598-3

Presentation Number **ES 10**
Educational Session 3: Post-processing & Cross Validation - Modeling and Quantification
September 5, 2012 / 08:45-09:45 / Room: Wicklow Hall 2

# Basic Principles of Tracer Kinetic Modeling

***Adriaan A. Lammertsma**, , Amsterdam, Netherlands. Contact e-mail: aa.lammertsma@vumc.nl*

Disclosure of author financial interest or relationships:
**A.A. Lammertsma**, Philips, Grant/research support; Hoffman - La Roche, Grant/research support .

Presentation Number **ES 11**
Educational Session 4: Biology & Pathology - Cardiovascular
September 5, 2012 / 07:45-08:15 / Room: The Auditorium

# Introduction to Biology and Treatments

***Michael V. McConnell**, , Stanford, CA, USA. Contact e-mail: mcconnell@stanford.edu*

Disclosure of author financial interest or relationships:
**M.V. McConnell**, GE Healthcare, Inc, Grant/research support .

Presentation Number **ES 12**
Educational Session 4: Biology & Pathology - Cardiovascular
September 5, 2012 / 08:15-08:45 / Room: The Auditorium

# Introduction to MR and PET Imaging

***Rene M. Botnar**, , London, United Kingdom. Contact e-mail: rene.botnar@kcl.ac.uk*

Disclosure of author financial interest or relationships:
**R.M. Botnar**, None.

Presentation Number **ES 13**
Educational Session 4: Biology & Pathology - Cardiovascular
September 5, 2012 / 08:45-09:15 / Room: The Auditorium

# Introduction to Molecular Contrast Agents and New Devices

***Klaas Nicolay**, , Eindhoven, Netherlands. Contact e-mail: k.nicolay@tue.nl*

Disclosure of author financial interest or relationships:
**K. Nicolay**, None.

Presentation Number **ES 14**
Educational Session 5: Chemistry of Contrast Media - Biologicals
September 5, 2012 / 08:45-09:15 / Room: Wicklow Hall 1

# Monoclonal Antibodies, Antibody Fragments, and Peptides

***Nick Devoogdt**, , Brussels, Belgium. Contact e-mail: ndevoogd@vub.ac.be*

Disclosure of author financial interest or relationships:
**N. Devoogdt**, Boehringer Ingelheim, Grant/research support; Ablynx, Grant/research support .

Presentation Number **ES 15**
Educational Session 5: Chemistry of Contrast Media - Biologicals
September 5, 2012 / 09:15-09:45 / Room: Wicklow Hall 1

# Protein and Oligo-nucleic Acid Scaffolds

***Vladimir Tolmachev**, , Uppsala, Sweden. Contact e-mail: vladimir.tolmachev@bms.uu.se*

Disclosure of author financial interest or relationships:
**V. Tolmachev**, Affibody AB, Consultant .

Presentation Number **ES 16**
Educational Session 5: Chemistry of Contrast Media - Biologicals
September 5, 2012 / 09:45-10:15 / Room: Wicklow Hall 1

# Reporter Gene Imaging

***Veerle Baekelandt***, *, Leuven, Belgium. Contact e-mail: Veerle.Baekelandt@med.kuleuven.be*

Disclosure of author financial interest or relationships:
**V. Baekelandt**, None.

Presentation Number **ES 17**
Educational Session 6: Biology & Pathology - Systems Biology and Its Link to MI
September 5, 2012 / 09:15-10:15 / Room: The Auditorium

# Systems Biology of Single Cells

***Hermann-Georg P. Holzhutter****, , Berlin, Germany. Contact e-mail: hergo@charite.de*

Disclosure of author financial interest or relationships:
**H.P. Holzhutter**, None.

Presentation Number **ES 18**
Educational Session 7: Chemistry of Contrast Media - Small Molecules
September 5, 2012 / 10:45-11:15 / Room: Wicklow Hall 1

# Hyper-polarized Probes

***Damian J. Tyler**, , Oxford, United Kingdom. Contact e-mail: damian.tyler@dpag.ox.ac.uk*

Disclosure of author financial interest or relationships:
**D.J. Tyler**, GE Healthcare, Grant/research support; Oxford Instruments, Grant/research support .

Presentation Number **ES 19**
Educational Session 7: Chemistry of Contrast Media - Small Molecules
September 5, 2012 / 11:15-11:45 / Room: Wicklow Hall 1

# Chelate Complexes for Imaging

***Dean Sherry**, , Dallas, TX, USA. Contact e-mail: Dean.Sherry@UTSouthwestern.edu*

Disclosure of author financial interest or relationships:
**D. Sherry**, None.

Presentation Number **ES 2**
Educational Session 1: Chemistry of Contrast Media - Basics - Probes and Suitable Imaging Modalities
September 5, 2012 / 08:15-08:45 / Room: Wicklow Hall 1

# Physical Limits: Sensitivity, Specificity, and Quantitation

***Bernd J. Pichler***[2]*, Fabian Kiessling*[1, 1]*, Aachen, Germany;* [2]*, Tübingen, Germany. Contact e-mail: Bernd.Pichler@med.uni-tuebingen.de*

Disclosure of author financial interest or relationships:
**B.J. Pichler**, Siemens, Grant/research support; AstraZeneca, Grant/research support; Bayer Healthcare, Grant/research support; Boehringer-Ingelheim, Grant/research support; Oncodesign, Grant/research support; Merck, Grant/research support; Bruker, Grant/research support; **F. Kiessling**, None.

Presentation Number **ES 20**
Educational Session 7: Chemistry of Contrast Media - Small Molecules
September 5, 2012 / 11:45-12:15 / Room: Wicklow Hall 1

# Labeling of (Bio)Molecules with Radiometals

***Danielle J. Vugts****, , Amsterdam, Netherlands. Contact e-mail: d.vugts@vumc.nl*

Disclosure of author financial interest or relationships:
**D.J. Vugts**, None.

Presentation Number **ES 21**
Educational Session 8: What Life Scientists Should Know About Imaging Modalities - MR Fundamentals for Life Scientists
September 5, 2012 / 10:45-11:15 / Room: Liffey Hall 2

# Introduction to MR Physics

***Andrew J. Fagan**, , Dublin, Ireland. Contact e-mail: FAGANAN@tcd.ie*

Disclosure of author financial interest or relationships:
**A.J. Fagan**, None.

Presentation Number **ES 22**
Educational Session 8: What Life Scientists Should Know About Imaging Modalities - MR Fundamentals for Life Scientists
September 5, 2012 / 11:15-11:45 / Room: Liffey Hall 2

# Introduction to MR Hardware

***Dominik von Elverfeldt***, *, Freiburg, Germany. Contact e-mail: dominik.elverfeldt@uniklinik-freiburg.de*

Disclosure of author financial interest or relationships:
**D. von Elverfeldt**, None.

Presentation Number **ES 23**
Educational Session 8: What Life Scientists Should Know About Imaging Modalities - MR Fundamentals for Life Scientists
September 5, 2012 / 11:45-12:15 / Room: Liffey Hall 2

# Contemporary MR: Pushing the Limits

***Joel R. Garbow**, , Bethesda, MD, USA. Contact e-mail: garbow@wustl.edu*

Disclosure of author financial interest or relationships:
**J.R. Garbow**, None.

Presentation Number **ES 24**
Educational Session 9: Post-processing & Cross Validation - Basics of Image Processing
September 5, 2012 / 10:45-12:15 / Room: Wicklow Hall 2

# Image Segmentation Methodology and Validation

***Wiro Niessen**, , Rotterdam, Netherlands. Contact e-mail: w.niessen@erasmusmc.nl*

Disclosure of author financial interest or relationships:
**W. Niessen**, Erasmus MC (Quantib), Stockholder .

Presentation Number **ES 25**
Educational Session 10: Biology & Pathology - Cancer
September 5, 2012 / 10:45-11:15 / Room: The Auditorium

# Image Analysis and Informatics

***Robert Gillies**, , Tampa, FL, USA. Contact e-mail: robert.gillies@moffitt.org*

Disclosure of author financial interest or relationships:
**R. Gillies**, Intezyne, Consultant .

Presentation Number **ES 26**
Educational Session 10: Biology & Pathology - Cancer
September 5, 2012 / 11:15-11:45 / Room: The Auditorium

# Biomarkers - Oncology and Inflammation

***Markus Rudin**, , Zurich, Switzerland. Contact e-mail: rudin@biomed.ee.ethz.ch*

Disclosure of author financial interest or relationships:
**M. Rudin**, Hoffmann-LaRoche Ltd, Basel, Switzerland, Grant/research support .

Presentation Number **ES 27**
Educational Session 10: Biology & Pathology - Cancer
September 5, 2012 / 11:45-12:15 / Room: The Auditorium

# Oncology and Inflammation

***Zaver M. Bhujwalla**, , Baltimore, MD, USA. Contact e-mail: zaver@mri.jhu.edu*

Disclosure of author financial interest or relationships:
**Z.M. Bhujwalla**, None.

Presentation Number **ES 28**
Educational Session 11: Chemistry of Contrast Media - Particles & Polymers
September 5, 2012 / 13:45-14:15 / Room: Wicklow Hall 1

# Basic Considerations on the Use of Particles and Polymers

***Hisataka Kobayashi**, , Bethesda, MD, USA. Contact e-mail: Kobayash@mail.nih.gov*

Disclosure of author financial interest or relationships:
**H. Kobayashi**, None.

Presentation Number **ES 29**
Educational Session 11: Chemistry of Contrast Media - Particles & Polymers
September 5, 2012 / 14:15-14:45 / Room: Wicklow Hall 1

# Established Particles and Polymers

***Willem J. Mulder***, , *New York, NY, USA. Contact e-mail: wjmmulder@gmail.com*

Disclosure of author financial interest or relationships:
**W.J. Mulder**, None.

Presentation Number **ES 3**
Educational Session 2: What Life Scientists Should Know About Imaging Modalities - Optical Imaging, Ultrasound, and Photo-acoustics
September 5, 2012 / 07:45-08:15 / Room: Liffey Hall 2

# Physics of Ultrasound Imaging

***Georg Schmitz**, Ruhr-University Bochum, Bochum, Germany. Contact e-mail: Georg.Schmitz@rub.de*

Disclosure of author financial interest or relationships:
**G. Schmitz**, None.

Presentation Number **ES 30**
Educational Session 11: Chemistry of Contrast Media - Particles & Polymers
September 5, 2012 / 14:45-15:15 / Room: Wicklow Hall 1

# Advances in Particles and Polymers

***Sanjiv S. Gambhir**, , Stanford, CA, USA. Contact e-mail: sgambhir@stanford.edu*

Disclosure of author financial interest or relationships:
**S.S. Gambhir**, General Electric, Grant/research support; Bayer-Schering, Grant/research support; Sanofi-Aventis, Grant/research support; CellSight, Stockholder; ImaginAB, Stockholder; Enlight, Stockholder; Endra, Stockholder; Bracco, Consultant; NinePoint Medical, Stockholder; Visualsonics, Consultant .

Presentation Number **ES 31**
Educational Session 12: What Life Scientists Should Know About Imaging Modalities - Nuclear Imaging
September 5, 2012 / 13:45-14:15 / Room: Liffey Hall 2

# Principle of PET and SPECT

***Steven Meikle**, , Sydney, NSW, Australia. Contact e-mail: steven.meikle@sydney.edu.au*

Disclosure of author financial interest or relationships:
**S. Meikle**, None.

Presentation Number **ES 32**
Educational Session 12: What Life Scientists Should Know About Imaging Modalities - Nuclear Imaging
September 5, 2012 / 14:15-14:45 / Room: Liffey Hall 2

# Detector Technologies

***Dennis R. Schaart**, , Delft, Netherlands. Contact e-mail: d.r.schaart@tudelft.nl*

Disclosure of author financial interest or relationships:
**D.R. Schaart**, Philips, Grant/research support .

Presentation Number **ES 33**
Educational Session 12: What Life Scientists Should Know About Imaging Modalities - Nuclear Imaging
September 5, 2012 / 14:45-15:15 / Room: Liffey Hall 2

# Hybrid Imaging Systems

***Roger Fulton**, , Sydney, NSW, Australia. Contact e-mail: r.fulton@physics.usyd.edu.au*

Disclosure of author financial interest or relationships:
**R. Fulton**, None.

Presentation Number **ES 34**
Educational Session 13: Post-processing & Cross Validation - New Imaging Tools: Cerenkov Luminescence Imaging
September 5, 2012 / 13:45-14:15 / Room: Wicklow Hall 2

# Faster Than the Speed of Light - Applications for Cerenkov Imaging

***Jan Grimm**, , New York, NY, USA. Contact e-mail: grimmj@mskcc.org*

Disclosure of author financial interest or relationships:
**J. Grimm**, None.

Presentation Number **ES 35**
Educational Session 13: Post-processing & Cross Validation - New Imaging Tools: Cerenkov Luminescence Imaging
September 5, 2012 / 14:15-14:45 / Room: Wicklow Hall 2

# Cerenkov Luminescence Endoscopy: Feasibility and Challenges

***Zhen Cheng**, , Stanford, CA, USA. Contact e-mail: zcheng@stanford.edu*

Disclosure of author financial interest or relationships:
**Z. Cheng**, None.

Presentation Number **ES 36**
Educational Session 13: Post-processing & Cross Validation - New Imaging Tools: Cerenkov Luminescence Imaging
September 5, 2012 / 14:45-15:15 / Room: Wicklow Hall 2

# Cerenkov Specific Contrast Agents

***Edward J. Delikatny**, , Philadelphia, PA, USA. Contact e-mail: delikatn@mail.med.upenn.edu*

Disclosure of author financial interest or relationships:
**E.J. Delikatny**, None.

Presentation Number **ES 37**
Educational Session 14: Biology & Pathology - CNS
September 5, 2012 / 13:45-14:15 / Room: The Auditorium

# Pathophysiology and Imaging of Neurodegenerative Diseases

***Karl Herholz**, , Manchester, United Kingdom. Contact e-mail: karl.herholz@manchester.ac.uk*

Disclosure of author financial interest or relationships:
**K. Herholz**, AVID/Eli-Lilly, Grant/research support; Elan, Consultant; GE Healthcare, Consultant .

Presentation Number **ES 38**
Educational Session 14: Biology & Pathology - CNS
September 5, 2012 / 14:15-14:45 / Room: The Auditorium

# Neuroplasticity

***Annemie van der Linden**, , Antwerp, Belgium. Contact e-mail: annemie.vanderlinden@ua.ac.be*

Disclosure of author financial interest or relationships:
**A. van der Linden**, None.

Presentation Number **ES 39**
Educational Session 14: Biology & Pathology - CNS
September 5, 2012 / 14:45-15:15 / Room: The Auditorium

# Pathophysiology and Imaging of Stroke

***Mathias Hoehn**, , Cologne, Germany. Contact e-mail: mathias@nf.mpg.de*

Disclosure of author financial interest or relationships:
**M. Hoehn**, None.

Presentation Number **ES 4**
Educational Session 2: What Life Scientists Should Know About Imaging Modalities - Optical Imaging, Ultrasound, and Photo-acoustics
September 5, 2012 / 08:15-09:00 / Room: Liffey Hall 2

# Advanced Microscopy Technologies

***Udo J. Birk**, , Heidelberg, Germany. Contact e-mail: u.birk@imb-mainz.de*

Disclosure of author financial interest or relationships:
**U.J. Birk**, None.

Presentation Number **ES 5**
Educational Session 2: What Life Scientists Should Know About Imaging Modalities - Optical Imaging, Ultrasound, and Photo-acoustics
September 5, 2012 / 09:00-09:45 / Room: Liffey Hall 2

# Optical Tomography

***Jorge Ripoll**, , Heraklion, Greece. Contact e-mail: jripoll@iesl.forth.gr*

Disclosure of author financial interest or relationships:
**J. Ripoll**, None.

Presentation Number **ES 6**
Educational Session 2: What Life Scientists Should Know About Imaging Modalities - Optical Imaging, Ultrasound, and Photo-acoustics
September 5, 2012 / 09:45-10:15 / Room: Liffey Hall 2

# Photo-acoustic Imaging

***Stanislav Y. Emelianov***, *, Austin, TX, USA. Contact e-mail: emelian@mail.utexas.edu*

Disclosure of author financial interest or relationships:
**S.Y. Emelianov**, None.

Presentation Number **ES 7**
Educational Session 3: Post-processing & Cross Validation - Modeling and Quantification
September 5, 2012 / 07:45-08:15 / Room: Wicklow Hall 2

# Basic Principles of Quantification Using PET

***Mark Lubberink**, , Uppsala, Sweden. Contact e-mail: mark.lubberink@radiol.uu.se*

Disclosure of author financial interest or relationships:
**M. Lubberink**, None.

Presentation Number **ES 8**
Educational Session 3: Post-processing & Cross Validation - Modeling and Quantification
September 5, 2012 / 08:15-08:15 / Room: Wicklow Hall 2

# Basic Principles of Quantification Using MR

***Markus Rudin**, University of Zurich, Zurich, Switzerland. Contact e-mail: rudin@biomed.ee.ethz.ch*

Disclosure of author financial interest or relationships:
**M. Rudin**, Hoffmann-LaRoche Ltd, Basel, Switzerland, Grant/research support .

Presentation Number **ES 9**
Educational Session 3: Post-processing & Cross Validation - Modeling and Quantification
September 5, 2012 / 08:15-08:45 / Room: Wicklow Hall 2

# Basic Principles of Quantification Using Optical Techniques

***Adrian Taruttis**, , Munich, Germany. Contact e-mail: adrian.taruttis@helmholtz-muenchen.de*

Disclosure of author financial interest or relationships:
**A. Taruttis**, None.

Presentation Number **P001**
Poster Session 1
September 5, 2012 / 18:00-18:00 / Room: The Liffey

# Longitudinal monitoring of stem cell fate in the myocardium by parametric R2 mapping

*Alessandro Ruggiero, Jamal Guenoun, Gabriela N. Doeswijk, Gabriel P. Krestin, Gyula Kotek,* ***Monique R. Bernsen****, Radiology, Erasmus MC - University Medical Center Rotterdam, Rotterdam, Netherlands. Contact e-mail: m.bernsen@erasmusmc.nl*

Background: In the last decade stem cells received a lot of interest because of their potential to regenerate tissue that has poor self renewal capacity upon damage. However, until now stem cell-based therapies have not been able to fulfill the expectations raised. In various application fields poor cell survival has been recognized as an important factor limiting therapeutic efficacy. Therefore non-invasive monitoring of cell fate is warranted for developing clinically effective stem cell therapy approaches. In this study we investigated the feasibility of the use of voxel-based R2 mapping as a tool to monitor the in vivo stem cell fate in myocardium when the cells are labeled with iron oxide particles. Method: Rat mesenchymal stem cells were double labeled with a bioluminescence reporter gene (luciferase) and ferumoxide particles (SPIO). Labeled cells (1.5x106) were injected in the myocardium (left ventricle) of healthy Wistar rats (n=9). For control purposes animals were also injected with dead, labeled cells (n=5) or saline (n=3). Cell fate was monitored over a period of 9 weeks by bioluminescence imaging following injection of D-Luciferine and quantitative magnetic resonance imaging, using a black blood FSE sequence with multiple echo times (between 4.4 and 26.4 ms). Results: In control animals, the signal in the myocardium was quite homogenous in the preferred regions for cell injection in these experiments such as the anterior and anterolateral segments with T2 values of 22.47+/-1.92 and 21.54+/-1.86 (prior to injection), respectively. In regions with higher cardiac motion such as the septal and the inferolateral segment R2 values showed more variations. However, this limitation did not interfere with the longitudinal assessment of the relaxivity of the injected cells. Overall, the difference in R2 and T2 values among the six different left ventricular segments was not statistically significant. In animals injected with viable double-labeled cells, bioluminescence imaging (BLI) revealed a significant increase in cell number during the first week with a steep decrease of cell numbers to undetectable levels during the second week. No BLI signal was obtained in animals injected with dead cells. MR imaging showed a sharp increase of T2 values at the injection site shortly after injection, followed by a very gradual decrease of T2 over a period of 9 weeks. No difference in appearance on T2-weighted images or in T2-values was observed between living and dead cells over the entire time period studied. Conclusions: Quantitative MR imaging by means of T2-mapping is not suitable for the in vivo assessment of stem cell fate in rat myocardium as validated by bioluminescence imaging. These results do not follow previous reports where it was proposed that based on the difference in r2 relaxivity between intra-cellular and extra-cellular SPIO, living cells may be distinguished from death cells based on their R2 profile.

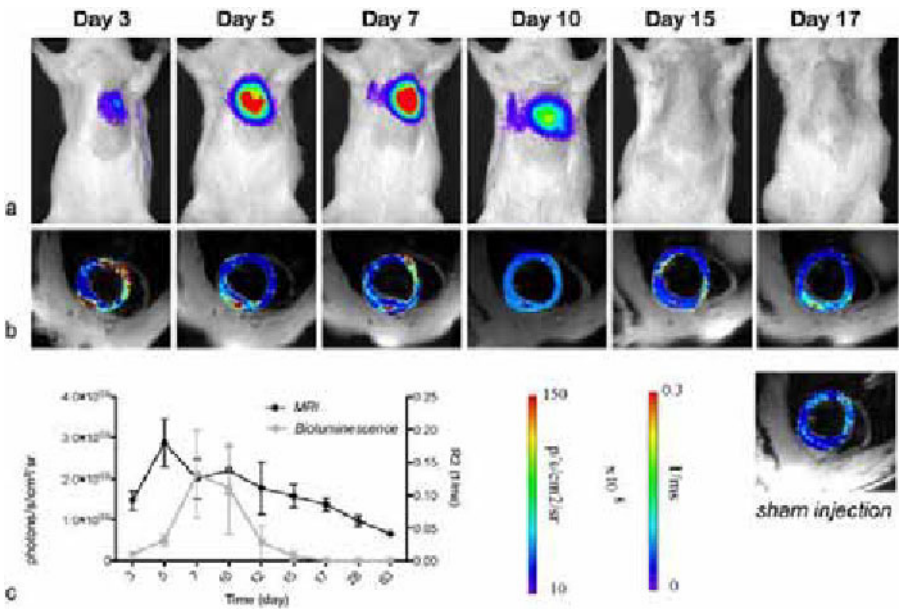


Longitudinal assessment of stem cell fate in the myocardium using BLI and parametric MRI.

Disclosure of author financial interest or relationships:
**A. Ruggiero**, None; **J. Guenoun**, None; **G.N. Doeswijk**, None; **G.P. Krestin**, GE Healthcare, Consultant; **G. Kotek**, None; **M.R. Bernsen**, None.

Presentation Number **P002**
Poster Session 1
September 5, 2012 / 18:00-18:00 / Room: The Liffey

# Molecular MRI of Atherosclerosis and Anti-Atherosclerotic Therapy Outcome by a Vascular Cell Adhesion Molecule-1 Targeted Contrast Agent

***Brigit denAdel***[1], *Carmen Burtea*[2], *Ernst Suidgeest*[3], *Sophie Laurent*[2], *Robert E. Poelmann*[1], *Robert N. Muller*[2], *Louise van der Weerd*[3,4], [1]*Anatomy and Embryology, Leiden University Medical Center, Leiden, Netherlands;* [2]*General, Organic and Biomedical Chemistry, University of Mons, Mons, Belgium;* [3]*Radiology, Leiden University Medical Center, Leiden, Netherlands;* [4]*Human Genetics, Leiden University Medical Center, Leiden, Netherlands. Contact e-mail: b.den_adel@lumc.nl*

Rationale Several MRI studies have shown that atherosclerosis can be detected in vivo. Non-targeted contrast agents (CA) can give good plaque enhancement albeit without discrimination of plaque components. Inflammation drives atherosclerotic plaque instability and acute thromboembolic events. Vascular Cell Adhesion Molecule-1 (VCAM-1) mediates rolling-type adhesion, is weakly expressed under baseline conditions but is rapidly induced in early plaque stages on activated vascular endothelium. In later plaque stages VCAM-1 is expressed on plaque vascular smooth muscle cells and macrophages. This study aims at characterizing atherosclerosis using VCAM-1 targeted USPIOs to detect inflamed lesions. Methods & Results A binding peptide for VCAM-1 was identified by phage displayed peptide library screening. Our peptide or a scrambled variant were covalently conjugated to an USPIO through their amino-terminal groups. The in vivo imaging potential of VCAM-1 targeted USPIOs was investigated both in aged ApoE-/- mice with and without atorvastatin treatment and young ApoE-/- mice exposed to a Western diet. In the latter mice, atherosclerosis was induced by placement of a constrictive collar around the left carotid artery to alter hemodynamic parameters locally. MRI of the aortic arch was performed on a 9.4 T vertical Bruker system, a 24 hours kinetics being obtained after intravenous injection of USPIO using a cine MRI FLASH sequence. High resolution MRI performed 1.5 hours after i.v. injection of VCAM-1 targeted USPIOs in aged ApoE-/- mice with plaques showed enhanced uptake of the CA on the vessel wall compared to the passive uptake of the scrambled variant. 6 hrs after injection, intraplaque binding of the CA was apparent. 24 Hours after injection, uptake was comparable in both groups. Uptake of VCAM-1 targeted USPIOs 1.5 h after injection was significantly increased in mice 3 weeks post collar placement whereas this binding was absent 6 hrs after injection. At later plaque stages this ratio between early and late imaging time points shifts to increased late enhancement, indicative of intra-plaque accumulation, while early enhancement due to endothelial targeting is reduced compared to early plaque stages. Thus the CNR ratio between early and late enhancement allows discrimination of plaque stages. Histology revealed colocalisation of VCAM-1 positive endothelial cells, smooth muscle cells and macrophages and iron deposits in the vessel wall corresponding to plaque stages. To test the potential of the CA to monitor not only plaque stage but also therapy response, aged ApoE-/-mice with advanced plaque were exposed to a western diet with or without added atorvastatin. After 6 weeks, mice were injected with VCAM-1 targeted CA. Mice on western diet had large and advanced plaques illustrated by a high CA uptake 6 hrs after injection. Mice treated with atorvastatin had both smaller plaques and less late CA uptake. Conclusion Our data indicate that VCAM-1 targeted USPIO holds great promise for diagnosis, monitoring treatment and staging of different stages of atherosclerosis.

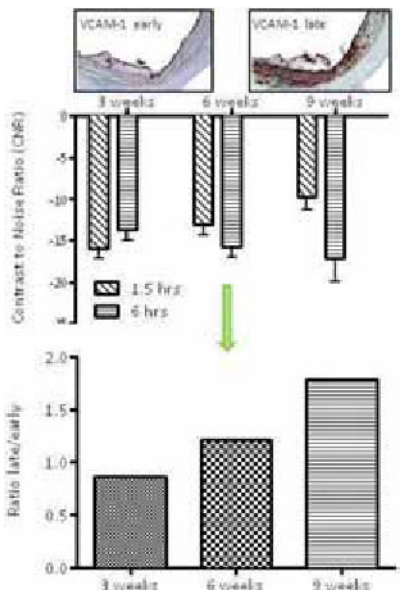


Disclosure of author financial interest or relationships:
**B. denAdel**, None; **C. Burtea**, None; **E. Suidgeest**, None; **S. Laurent**, None; **R.E. Poelmann**, None; **R.N. Muller**, None; **L. van der Weerd**, None.

Presentation Number **P003**
Poster Session 1
September 5, 2012 / 18:00-18:00 / Room: The Liffey

# Amyloid imaging agent 18F-flutemetamol is accumulated in atherosclerotic plaques

***Sanna Hellberg***[1], *Antti Saraste*[1,2], *Johanna M. Silvola*[1], *Olli Eskola*[1], *Heidi Liljenbäck*[1,3], *Jukka Laine*[4], *Pertti Lehikoinen*[5], *Pekka Saukko*[6], *Juhani Knuuti*[1], *Anne Roivainen*[1,3], [1]*Turku PET Centre, University of Turku, Åbo Akademi University and Turku University Hospital, Turku, Finland;* [2]*Department of Internal Medicine, Turku University Hospital, Turku, Finland;* [3]*Turku Center for Disease Modeling, University of Turku, Turku, Finland;* [4]*Department of Pathology, Turku University Hospital, Turku, Finland;* [5]*GE Healthcare Finland, Helsinki, Finland;* [6]*Department of Forensic Medicine, University of Turku, Turku, Finland. Contact e-mail: saelhe@utu.fi*

Introduction: Atherosclerosis is characterized by accumulation of oxidized lipids in the artery wall, triggering an inflammatory response. Since structure of oxidized low-density lipoprotein resembles that of amyloid protein, we hypothesized that amyloid-targeting tracer, $^{18}$F-flutemetamol, might show uptake in the atherosclerotic plaques in mice. Methods: Low-density lipoprotein receptor deficient mouse expressing only apolipoprotein B100 and overexpressing insulin-like growth factor II (IGF-II/LDLR$^{-/-}$ApoB$^{100/100}$) is a model of atherosclerosis and diabetes. Nine IGF-II/LDLR$^{-/-}$ApoB$^{100/100}$ mice on high-fat diet for 5 months and eight normally fed 10-month old C57BL/6N mice were studied. Biodistribution of $^{18}$F-flutemetamol in tissues at 30 minutes after intravenous injection (10.9±1.5 MBq) was examined ex vivo by gamma counter. In addition, uptake of $^{18}$F-flutemetamol was compared in the plaques and healthy vessel wall by digital autoradiography of aortic tissue sections. Results: The aortas of IGF-II/LDLR$^{-/-}$ApoB$^{100/100}$ mice showed large, inflamed atherosclerotic plaques. The autoradiography revealed 1.7-fold higher uptake in the plaques compared to healthy vessel wall (count densities 57.9±21.0 vs. 33.9±12.2, p=0.003) (Figure). The uptake of $^{18}$F-flutemetamol in the thoracic aortas of atherosclerotic and healthy mice didn't show statistical difference (percentage of injected radioactivity per gram of tissue 0.81±0.22 vs. 0.65±0.20, p=0.14). In atherosclerotic mice aorta-to-blood ratio was 0.76 (p=0.34), and aorta-to-myocardium ratio was 1.43 (p=0.07). Radioactivity was distributed especially to urine, kidney and liver, respectively. Conclusions: To our knowledge, this the first study demonstrating uptake of $^{18}$F-flutemetamol also in atherosclerotic plaques. The observed low uptake in the myocardium would facilitate the imaging of coronary arteries, but the high blood radioactivity might be a disadvantage. Further studies are warranted to clarify the mechanisms of uptake and the potential of the tracer for in vivo imaging of atherosclerosis.

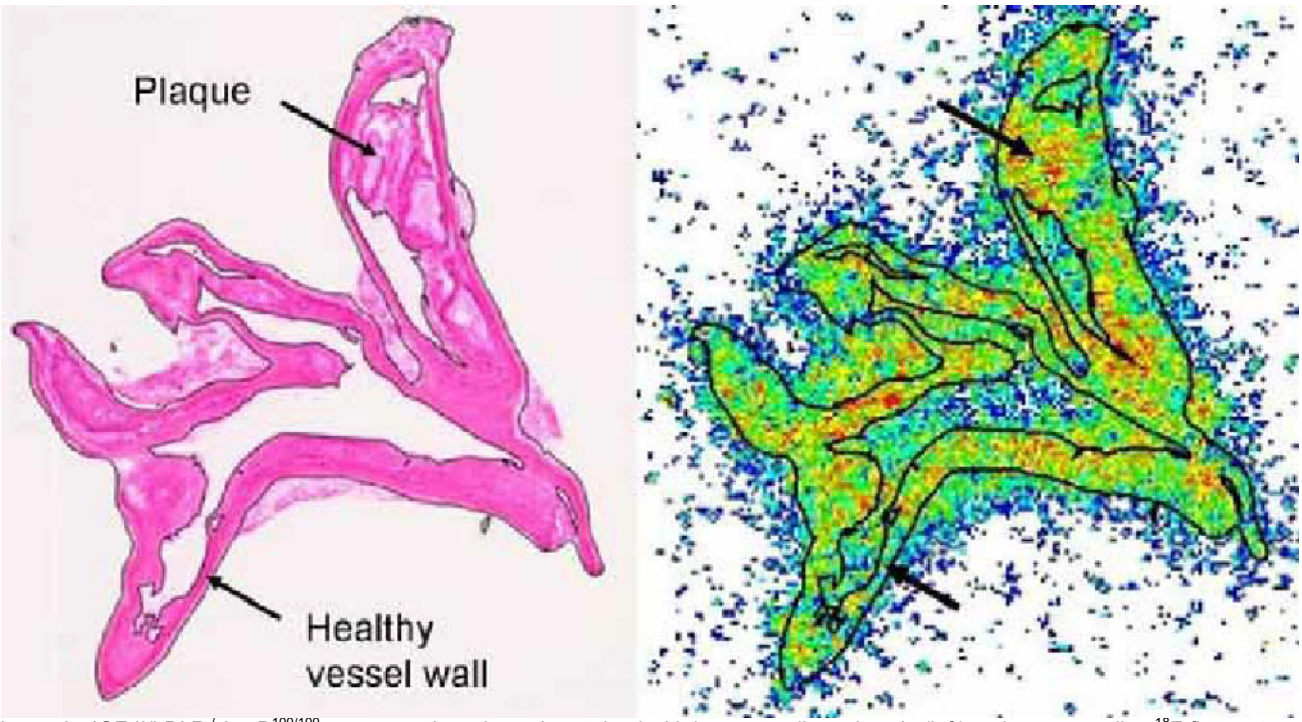


Figure: An IGF-II/LDLR$^{-/-}$ApoB$^{100/100}$ mouse aortic arch section stained with haematoxylin and eosin (left) and corresponding $^{18}$F-flutemetamol autoradiography image (right).

Disclosure of author financial interest or relationships:
**S. Hellberg**, None; **A. Saraste**, None; **J.M. Silvola**, None; **O. Eskola**, None; **H. Liljenbäck**, None; **J. Laine**, None; **P. Lehikoinen**, None; **P. Saukko**, None; **J. Knuuti**, Lantheus Inc, Consultant; Philips, Speakers bureau; **A. Roivainen**, None.

Presentation Number **P004**
Poster Session 1
September 5, 2012 / 18:00-18:00 / Room: The Liffey

# Evaluation of SPIO and Quantum Dot labelled high density lipoproteins for multimodal imaging of atherosclerotic plaques in ApoE-/- Mice

***Caroline Jung***[1], *Michael G. Kaul*[1], *Tanja Ducic*[2], *Oliver T. Bruns*[3], *Markus Heine*[5], *Barbara Freund*[4], *Harald Ittrich*[1], *Gerhard Adam*[1], [1]*University Hospital Hamburg Eppendorf, Hamburg, Germany;* [2]*Deutsches Elektronen Synchroton Desy, Research Centre of the Helmholtz Association, Hamburg, Germany;* [3]*Heinrich Pette for Experimental Virology and Immunology, University of Hamburg, Hamburg, Germany;* [4]*Biochemistry and Molecular Bilogy II, University Hospital of Hamburg Eppendorf, Hamburg, Germany;* [5]*Anatomy and Experimental Morphology, University Hospital of Hamburg Eppendorf, Hamburg, Germany. Contact e-mail: cjung@uke.de*

Purpose To evaluate Superparamagnetic iron oxide (SPIO) and Quantum Dot (QD) labelled high density lipoproteins (HDL) for imaging of atherosclerotic plaques with MR and several ex vivo imaging techniques in a clinically relevant mouse model. Material and Methods HDL nanosomes (HDL-NS) were synthesised in vitro by incorporation of QD and SPIO into the lipid core of HDL. HDL-NS were characterised by dynamic light scattering (DLS), size exclusion chromatography (FPLC) and by subsequent cholesterol and fluorescent measurements. For estimation of in vivo biodistribution, atherosclerotic plaque accumulation and blood clearance HDL-NS were applied intravenously (i.v.) and intraperitoneally (i.p.) into ApoE-/- mice followed by MR-imaging using a T2*w gradient echo sequence at 7T (Clinscan, Bruker). Additionally, 59Fe radioactive labelled HDL-NS were used for ex vivo biodistribution of different organs using a whole body y-counter (HAMCO). In vivo MR imaging was matched with ex vivo confocal fluorescence microscopy (CFM), ex-vivo MR imaging, x-ray fluorescence microscopy (X-ray FM) and histological analysis (Prussian Blue (PB) stains) of aortic specimens for visualization of HDL-NS uptake in atherosclerotic plaques. Results In vitro analyses (DLS, FPLC and fluorescence) confirmed equal size and function of HDL-NS compared to endogenous HDL. Radioactivity measurements at HAMCO showed a significant higher uptake of HDL-NS into atherosclerotic plaques after i.p. injection ($p<0.006$) in addition to a predominant accumulation in liver and spleen. Blood concentration time curves of both application approaches (i.v. and i.p.) showed a biphasic progress. Ex-vivo MRI, X-ray FM, CFM and PB stains of aortic specimens showed an uptake of HDL-NS into atherosclerotic lesions of ApoE-/- mice. Conclusion In vitro synthesis of HDL-NS with equal properties compared to native HDL was established. HDL-NS accumulation in atherosclerotic plaques can be visualized non-invasively by MRI after i.v. and i.p. injection proven by several ex-vivo imaging techniques.

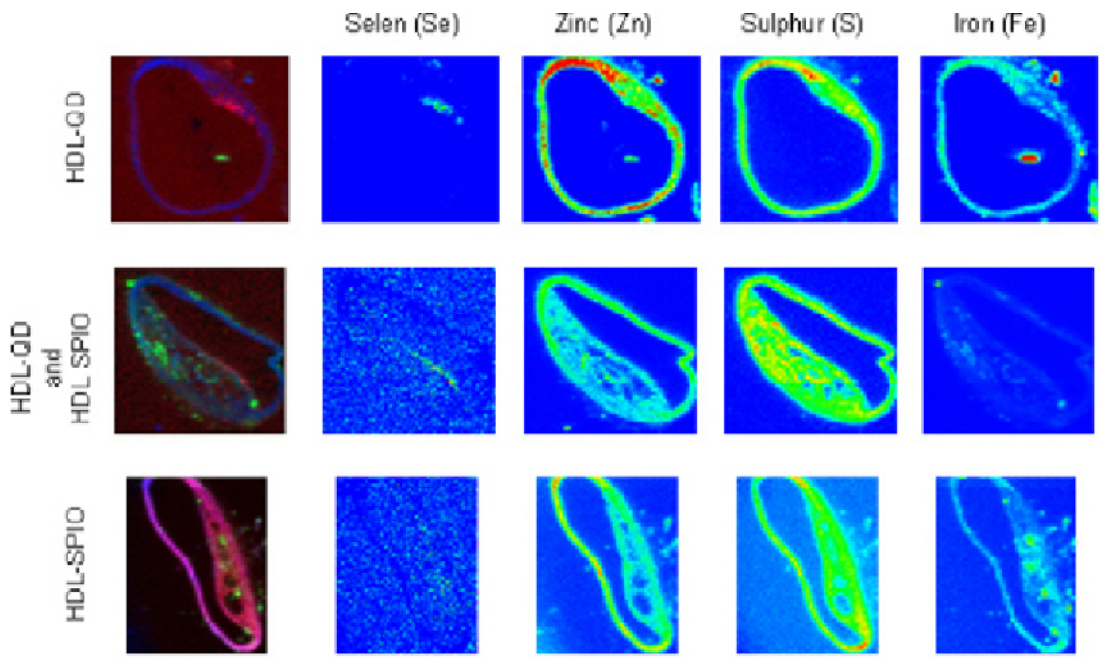


X-ray fluorescence microscopy at E=19.4keV: 2-D scanning image of 20 µm mice aorta cryo-cross-section after 20h in vivo treatment with HDL-QD, HDL-SPIO or both. Selen, which is part of the hydrophobe CdSe/CdS/ZnS core-shell-shell nanocrystal of QD was detectable within the plaque. The background signal for zinc, sulphur and iron was too high for discrimination between endogenous and injected elements.

Disclosure of author financial interest or relationships:
**C. Jung**, None; **M.G. Kaul**, None; **T. Ducic**, None; **O.T. Bruns**, None; **M. Heine**, None; **B. Freund**, None; **H. Ittrich**, None; **G. Adam**, None.

Presentation Number **P005**
Poster Session 1
September 5, 2012 / 18:00-18:00 / Room: The Liffey

# Statin therapy improves deep vein thrombosis (DVT) resolution while attenuating thrombus inflammation in vivo: assessment by multiplexed intravital fluorescence imaging

***Chase W. Kessinger***[1], *Jin Won Kim*[1], *Brian Thompson*[2], *Jason R. McCarthy*[2], *Peter K. Henke*[3], *Charles P. Lin*[2], *Farouc A. Jaffer*[1], [1]*Cardiology, Massachusetts General Hospital, Boston, MA, USA;* [2]*Center for Systems Biology, Massachusetts General Hospital, Boston, MA, USA;* [3]*Section of Vascular Surgery, University of Michigan, Ann Arbor, MI, USA. Contact e-mail: ckessinger@partners.org*

Introduction: Inflammation and fibrinolysis critically mediate deep vein thrombosis (DVT) resolution, with impaired DVT resolution leading to the burdensome and costly sequelae of the post-thrombotic syndrome. Here we tested the effects of a new clinically approved therapy, statins/HMG CoA reductase inhibitors, on murine DVT resolution and inflammation, using multispectral intravital fluorescence microscopy (IVFM). Methods: C57Bl/6J male mice (n=24) received topical ferric chloride to induce femoral venous thrombosis. Treatment with either atorvastatin (1.14 mg/kg, n=12) or PBS was initiated on day 1 and administered daily for 4 days by oral gavage. On day 3, mice were i.v. injected with macrophage-targeted nanoparticles (CLIO-AF555, ex/em 555/565nm) and an MMP activity sensor (MMPsense680, ex/em 680/700nm). On day 4, IVFM was performed. FITC-dextran (ex/em 490/520nm) injected prior to IVFM imaging provided venograms for measurement of thrombus length and thrombus area. The average whole thrombus, macrophage and MMP activity target-to-background ratios (TBR) were derived respectively from FITC, CLIO and MMPsense signals from mid-luminal z-stacks (40 μm thickness) through the thrombosed area. Imaging was followed by histopathology and fluorescence microscopy of cryosectioned tissue. Fluorescence molecular tomography/CT (FMT/CT) was performed in additional 12 mice using ferric chloride injury on the jugular vein with an injection of a near-infrared CLIO-VT680 (ex/em 670/688nm) 24 hours prior to day 4 imaging. Mice were orally treated with statin or PBS control starting on day 1. Results: High-dose acute statin therapy decreased inflammatory thrombus macrophages (macrophage TBR 3.1±0.3 vs. control 1.7±0.2, p=0.001) and MMP activity (TBR 1.8±0.2 vs. 1.3±0.1, p=0.021). Remarkably, statin therapy improved DVT resolution, as evidenced by reduced thrombus area (0.163±0.01 vs. control 0.195±0.03 $mm^2$, p<0.05) and reduced thrombus length (1.24±0.03 vs. control 1.36±0.05mm, p<0.05) compared to control. Non-invasive translational assessment of acute statin effects on DVT was performed using FMT/CT. Image datasets showed that thrombotic macrophage signal was significantly reduced in statin-treated compared to PBS control mice (macrophage TBR 1.8±0.1 vs. control 7.1±1.6, p=0.001). Correlative fluorescence microscopy and immunohistochemistry corroborated the in vivo imaging finding of reduced inflammation and also demonstrated reduced plasminogen activator inhibitor-1 (PAI-1) expression, consistent with a profibrinolytic effects of statin therapy. Conclusions: Statin therapy in acute DVT attenuates the thrombus inflammatory response and improves its resolution, as assessed by integrated molecular-structural in vivo imaging. These results support statins as clinically translatable therapy to improve DVT resolution and potentially limit the post thrombotic syndrome.

Disclosure of author financial interest or relationships:
**C.W. Kessinger**, None; **J. Kim**, None; **B. Thompson**, None; **J.R. McCarthy**, None; **P.K. Henke**, None; **C.P. Lin**, None; **F.A. Jaffer**, Boston Scientific, Merck, Siemens, Consultant; Abbott Vascular, Grant/research support .

Presentation Number **P006**
Poster Session 1
September 5, 2012 / 18:00-18:00 / Room: The Liffey

# Evaluation of dimeric (68)Ga-DOTA-RGD peptide for molecular imaging of α(v)β(3) integrin expression after myocardial infarction in rat

***Max Kiugel***[1], *Ingrid Dijkgraaf*[2], *Ville Kytö*[3], *Heidi Liljenbäck*[1], *Tiina Saanijoki*[1], *Pekka Saukko*[4], *Juhani Knuuti*[1], *Anne Roivainen*[1], *Antti Saraste*[1], [1]*Turku PET Centre, University of Turku, Turku, Finland;* [2]*Department of Nuclear Medicine, Radboud University Nijmegen Medical Centre, Nijmegen, Netherlands;* [3]*Department of Medicine, Turku University Hospital, Turku, Finland;* [4]*Forensic Medicine, University of Turku, Turku, Finland. Contact e-mail: max.kiugel@utu.fi*

Introduction: Radiolabelled RGD peptides have been extensively studied as α(v)β(3)- and α(v)β(5)-integrin targeting probes that could enable monitoring of angiogenesis and extracellular matrix remodelling following myocardial infarction. Multimeric RGD-peptides have been recently developed in order to improve their affinity and target-to-background ratio. The purpose of this study was to evaluate myocardial uptake of novel (68)Ga labelled dimeric RGD peptide DOTA-E-[c(RGDfK)]2 (Dijkgraaf I et al. EJNMMI 2011;38:128-37) targeting α(v)β(3) and α(v)β(5)-integrins after myocardial infarction (MI) in rats. Materials and methods: Male Sprague-Dawley rats (age 7.7 ± 1.4 weeks) underwent permanent surgical ligation of the left coronary artery to induce MI. Animals were studied 7 days (n=7) and 4 weeks (n=5) post-MI. Sham-operated rats were studied as controls (n=4 at 7 days and n=3 at 4 weeks). The rats were intravenously injected with 43.9 ± 6.3 MBq of (68)Ga-DOTA-E-[c(RGDfK)]2 (specific radioactivity 19.4 ± 4.2 MBq/nmol) via tail vein followed by 60-min dynamic PET acquisition. After PET, microCT imaging was performed using intravascular contrast agent to visualize blood pool. Immediately after PET/CT rats were killed, blood sample and the whole left ventricle were measured for (68)Ga-radioactivity using a gamma counter. The left ventricle was sliced into transverse cryosections at 1 mm intervals for analysis of histology and myocardial uptake of radioactivity as analysed by digital autoradiography. Results: Histology showed MI scar in all rats with coronary ligation, whereas sham operated rats had normal myocardium. Average MI size of the left ventricle circumference was 24.4 ± 16.1% at 7 days and 47.4 ± 20.4% at 4 weeks. Biodistribution showed higher (68)Ga-DOTA-E-[c(RGDfK)]2 uptake in the left ventricle myocardium than in blood in rats with MI ($p<0.001$). Average myocardium-to-blood ratio was 2.2 ± 0.9 after MI and 1.3 ± 0.3 after sham operation ($p=0.04$). Autoradiography showed low (68)Ga-DOTA-E-[c(RGDfK)]2 uptake in the myocardium of sham-operated rats and in the remote non-infarcted myocardium of rats with ligation. There was focally increased (68)Ga-DOTA-E-[c(RGDfK)]2 uptake colocalizing with the infarct scar and infarct border zones (Figure). Average uptake was 5.7 ± 0.8 folds higher in the infarcted area as compared with remote non-infarcted myocardium at 7 days post-MI and remained 4.8 ± 0.7 folds higher 4 weeks post-MI. In vivo images showed (68)Ga- DOTA-E-[c(RGDfK)]2 uptake colocalizing with infarcted area of the left ventricular myocardium as seen in PET/CT hybrid images. Conclusion: We found regionally increased uptake of (68)Ga-DOTA-E-[c(RGDfK)]2 in the infarcted rat myocardium at 7 days and 4 weeks after injury. This tracer could enable monitoring of α(v)β(3) and α(v)β(5)-integrin expression associated with myocardial repair after MI by PET.

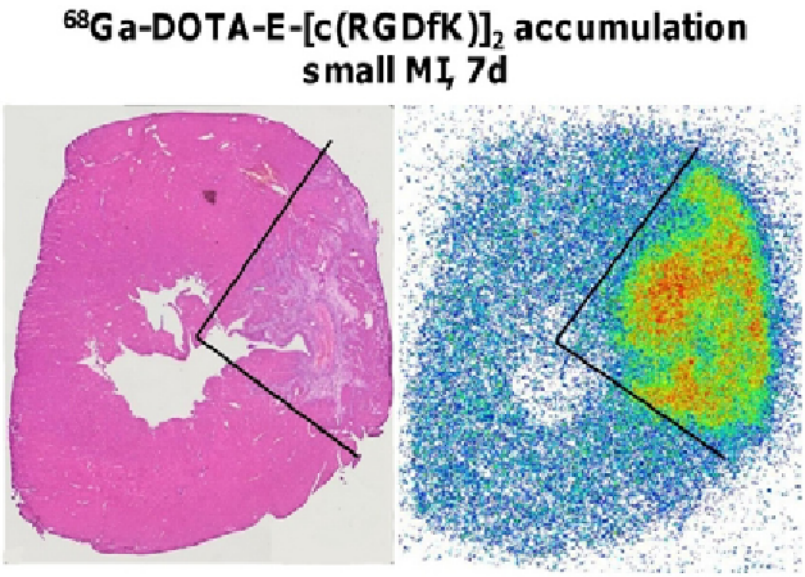


Disclosure of author financial interest or relationships:
**M. Kiugel**, None; **I. Dijkgraaf**, None; **V. Kytö**, None; **H. Liljenbäck**, None; **T. Saanijoki**, None; **P. Saukko**, None; **J. Knuuti**, Lantheus Inc, Consultant; Philips, Speakers bureau; **A. Roivainen**, None; **A. Saraste**, None.

Presentation Number **P007**
Poster Session 1
September 5, 2012 / 18:00-18:00 / Room: The Liffey

# In-vivo carotid ultrasound strain imaging for the quantification of liposomes vascular effect

***Kristen M. Meiburger***[1]*, Pierangela Giustetto*[2]*, Cinzia Boffa*[2]*, Enzo Terreno*[2]*, Mauro Castano*[3]*, Filippo Molinari*[1]*, [1]Department of Electronics and Telecommunications, Politecnico di Torino, Torino, Italy; [2]Molecular & Preclinical Imaging Center, Università degli Studi di Torino, Torino, Italy; [3]Bracco Research Center, Bracco Imaging SpA, Colleretto Giacosa (TO), Italy. Contact e-mail: kristen.meiburger@polito.it*

Motion of the artery wall can be associated with stresses due to blood pressure and blood flow, resulting in longitudinal and radial strain of the artery. This endothelial reaction is important for the diagnosis of cardiovascular diseases, giving insight on the mechanism of atherosclerosis, and for vascular therapy. Liposome nanoparticles are gaining increasing importance as targeting agents, molecular probes, and drug carriers. The aim of this study is to evaluate the vascular effect, in terms of longitudinal and radial displacements of the artery wall, of a liposomes bolus injected intravenously in mice with carotid ultrasound strain imaging. Six mice (C57, weight 22±4 gr) were tested. Three were i.v. administered a 180 µl bolus of stealth liposomes (DSPC/Peg 95/5); the other 3 were i.v. administered a 180 µl bolus of saline solution. The mean liposomes dimension was 120 nm (determined by dynamic light scattering method). The injected lipidic dose was 3.6 mg. Ultrasound high-resolution B-mode cineloops (frame rate: 33 fps) of the carotid artery were acquired with a 24 MHz probe (VEVO2100, VisualSonics, Toronto, Canada) before and 5 minutes after bolus injection. A speckle-tracking algorithm was used to study 5 cardiac cycles of each cineloop. The user selects different speckles for the distal and proximal wall of the carotid artery (Fig 1), then 2 matrices are defined for each speckle: a kernel and a search region. The kernel contains one or more speckles of the image; the search region defines the region used to search for the speckles in the successive frames. A normalized cross-correlation-based search algorithm is applied to determine the longitudinal and radial displacements (i.e., differences in position) occurring between 2 frames. The final displacements during one cardiac cycle are found by calculating the difference between the maximum and minimum displacement amplitudes. Before the liposomes bolus injection, the mean longitudinal and radial amplitude displacements were 0.020±0.003mm and 0.009±0.002mm for the distal wall, and 0.023±0.006mm and 0.051±0.008mm for the proximal wall. After bolus injection, the respective displacements were 0.028±0.007mm and 0.016±0.007mm (distal) and 0.023±0.005mm and 0.056±0.007mm (proximal), showing statistically different pre/post values for the distal wall (t-test $p<0.03$) but not for the proximal wall (t-test $p>0.5$). Before the saline bolus injection, the mean longitudinal and radial amplitude displacements were 0.017±0.005mm and 0.014±0.003mm for the distal wall, and 0.020±0.004mm and 0.058±0.010mm for the proximal wall (Table 1). After bolus injection, the respective displacements were 0.015±0.006mm and 0.012±0.005mm (distal) and 0.020±0.005mm and 0.051±0.009mm (proximal), showing no significant pre/post difference for either wall (t-test $p>0.5$ for all tests). The strain imaging revealed that significantly higher amplitude displacements were observable after the liposomes bolus injection in the distal wall, whereas this was not the case after the saline injection. This shows that liposomes produce a different endothelial effect than saline, and that they could be useful in vascular therapy.

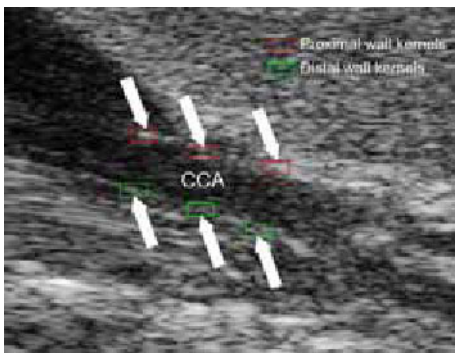


Initial user-selected kernels for the proximal wall (in red) and the distal wall (in green).

Overall results obtained

| Maximum displacements [mm] | Liposomes bolus | | Saline solution bolus | |
|---|---|---|---|---|
| | Pre | Post | Pre | Post |
| Longitudinal proximal wall | 0.023±0.006 | 0.023±0.005 | 0.020±0.004 | 0.020±0.003 |
| Radial proximal wall | 0.051±0.008 | 0.056±0.007 | 0.058±0.010 | 0.051±0.009 |
| Longitudinal distal wall | 0.020±0.003 | 0.028±0.007 | 0.017±0.005 | 0.015±0.006 |
| Radial distal wall | 0.009±0.002 | 0.016±0.007 | 0.014±0.003 | 0.012±0.005 |

Disclosure of author financial interest or relationships:
**K.M. Meiburger**, None; **P. Giustetto**, None; **C. Boffa**, None; **E. Terreno**, Bracco Imaging, Consultant; **M. Castano**, None; **F. Molinari**, None.

Presentation Number **P008**
Poster Session 1
September 5, 2012 / 18:00-18:00 / Room: The Liffey

# Hyperpolarized [1-13C] acetate for cardiac 3D MRI metabolic Imaging in middle size animal models

***Luca Menichetti***[1,2], *Francesca Frijia*[2], *Alessandra Flori*[3], *Vincenzo Lionetti*[3], *Giulio Giovannetti*[1], *Jan Henrik Ardenkjaer-Larsen*[4,5], *Simone L. Romano*[3], *Matteo Liserani*[2], *Giovanni Donato Aquaro*[2], *Vincenzo Positano*[2], *Fabio A. Recchia*[3], *Luigi Landini*[6,2], *M. F. Santarelli*[1,2], *Massimo Lombardi*[2], *[1]CNR Institute of Clinical Physiology, Pisa, Italy; [2]Fondazione CNR-Regione Toscana G.Monasterio, Pisa, Italy; [3]Scuola Sant'Anna, Sector of Medicine, Pisa, Italy; [4]GE Healthcare, Hillerod, Denmark; [5]Dept.Electronic Engineering, Technical University of Denmark, Copenhagen, Denmark; [6]Information Engeneering: EIT, Universisty of Pisa, Pisa, Italy. Contact e-mail: luca.m@ifc.cnr.it*

Dynamic nuclear polarization (DNP) with rapid dissolution together with Magnetic Resonance Chemical Shift Imaging (CSI) have been used for non-invasive real-time metabolic assessment in different experimental models. MRI with hyperpolarised 13C is a novel tool for in-vivo spectroscopy to estimate non-invasively the regional cardiac metabolism. Here, we report in vivo measurements of hyperpolarised acetate perfusion and metabolism, and we present a method based on a 3D Spiral CSI sequence for obtaining spatially and spectrally-resolved information on whole heart acetate cardiac metabolism. Experiments were performed in a pig model using intravenous injection of ~400 mg hyperpolarized TRIS-[1-13C]acetate mixture on a clinical 3T scanner. Material and Methods: Three healthy male farm pigs (38±2 kg) were studied in basal condition. Imaging experiments were performed on a 3T GE Signa HDx scanner (GE Healthcare) using a 13C quadrature birdcage coil (Rapid Biomedical). A volume corresponding to ~ 400mg of TRIS-[1-13C]acetate water/glycerol mixture (containing 330 nmoles Gd3+-complex and 5.5 µmoles of radical OX63) was polarized using an HyperSense DNP polariser (Oxford Instrument) for 1 hour. The volume after the fast dissolution was V=22 ml and the injected [1-13C]acetate dose was ~0.039 mmol/kg animal body weight. Anatomical reference images were acquired in the axial plane using a standard steady-state free precession (SSFP) sequence (body coil, FOV=30x30 cm2, FA=20°, TE/TR=3.8ms/7.52ms, matrix 224x160, slice thickness 5 mm, 20 slices). Metabolic information covering the whole heart was obtained using 3D IDEAL spiral CSI on the same region imaged by the anatomical reference scan (FOV= 30x30 cm2, slab thickness=100mm), starting 18 s after the beginning of the injection. Data were reconstructed using spectrally-preconditioned CS inversion followed by gridding reconstruction implemented in Matlab (The Mathworks). Image reslicing along cardiac short axis (SA) views and image fusion of 13C metabolite maps and anatomical 1H reference images were performed by PMOD software (PMOD Technologies Ltd). Results and Discussion: The Figure shows a representative map of hyperpolarised [1-13C]acetate in SA orientation through the heart. [1-13C]acetate is extracted in heart and clearly detected in the heart-chambers and myocardial wall. The feasibility study with hyperpolarized [1-13C]acetate has been performed, as far as we know, for the first time in pigs with this experimental approach. This is the first step towards the optimization of the tracer concentration and the sequence parameters in middle size animal model: this hopefully will ensure suitable MR signals in myocardial tissue, to study the conversion of [1-13C]acetate in Acetyl-CoA, catalyzed by acetyl-CoA synthetase, and [1-13C]acetyl-carnitine generated by acetyltransferase. [References: K. Golman, et al. Magn. Reson. Med. 59, 1005-1013; L. Menichetti, et al. Cont.Med.Mol.Imag. 7, 85-94; Bastiaansen J., et al. ISMRM Proceedings (2011); Jensen P.R. et al. J.Biol Chem, 284, 36077-36082].

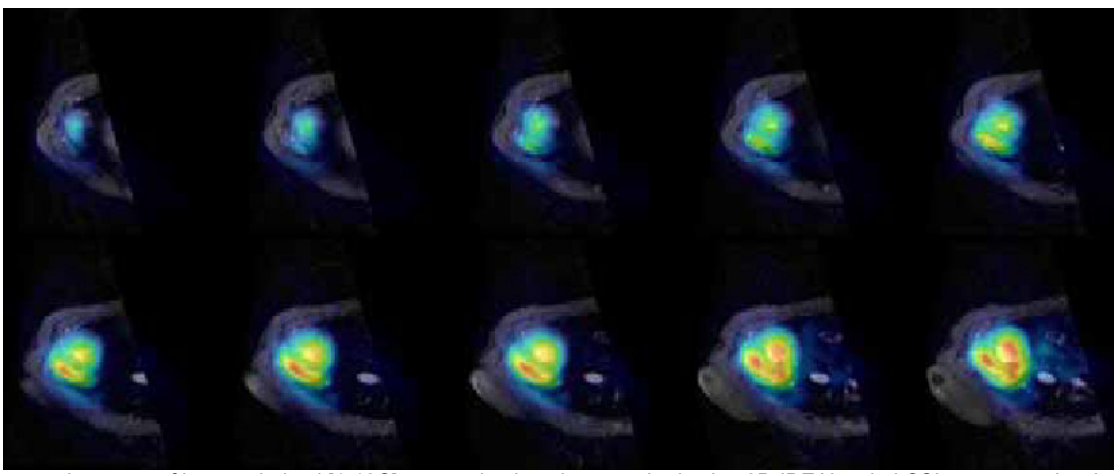

In vivo representative maps of hyperpolarised [1-13C] acetate in pigs: data acquired using 3D-IDEAL spiral CSI sequence showing the spatial distribution of [1-13C]acetate in SA views of the heart. Spectroscopic data were normalized to the maximum value of signal amplitude.

Disclosure of author financial interest or relationships:
**L. Menichetti**, None; **F. Frijia**, None; **A. Flori**, None; **V. Lionetti**, None; **G. Giovannetti**, None; **J. Ardenkjaer-Larsen**, None; **S.L. Romano**, None; **M. Liserani**, None; **G. Aquaro**, None; **V. Positano**, None; **F.A. Recchia**, None; **L. Landini**, None; **M.F. Santarelli**, None; **M. Lombardi**, None.

Presentation Number **P009**
Poster Session 1
September 5, 2012 / 18:00-18:00 / Room: The Liffey

# Targeting VEGFR Expression to Identify Accelerated Atherosclerosis

***Yared Tekabe***[1], *Maria Kollaros*[1], *Geping Zhang*[1], *Marina Backer*[2], *Joseph M. Backer*[2], *Lynne Johnson*[1], [1]*Columbia University, Yonkers, NY, USA;* [2]*SibTech, Brookfield, CT, USA. Contact e-mail: yt2166@columbia.edu*

The biology of the vulnerable plaque includes increased inflammation and rapid growth of vasa vasorum, processes that are characterized by vascular endothelial growth factor (VEGF) expression in response to hypoxia and inflammation and are accelerated in diabetes. We hypothesized that a novel radiolabeled probe (99mTc scVEGF-PEG-DOTA) targeting VEGFR1 and VEGFR2 can identify accelerated atherosclerosis in diabetes. Methods: At 6 wks of age, 5 apoE null mice were made diabetic with streptozotocin (DM) and 4 were not treated (NDM). At 25 wks of age all, mice were injected with 500 µCi 99mTc scVEGF-PEG-DOTA and 2-3 hr later (blood pool clearance) injected with eXIA CT contrast agent and underwent SPECT/CT imaging (Bioscan). At completion of imaging, mice were euthanized. The chest opened, aortic arch and great vessels dissected out and photographed in-situ and removed, paraffin embedded and sectioned and stained for VEGFR1, VEGFR2, macrophages (mac-3), and endothelial cells (factor VIII). Organs were harvested and counted in the well counter to determine biodistribution. ROIs were drawn around tracer localized to aortic root and arch from CT scan, tracer uptake was quantified as total and mean activity/voxel in µCi (InVivoScope software). ROIs were also placed in the pulmonary vein for mean activity/voxel background. Results: All 9 mice showed focal uptake of tracer localized by the CT contrast to the aortic root, arch, and neck vessels. Results were the following: Target to bknd was high for both DM and NDM (3.27±0.89 and 4.46±1.49) (P=0.18) while the total uptake (in µCi x 10-2) was significantly higher for DM than NDM (16.6±6.3 vs. 5.9±2.6) (P=0.02). Staining for VEGFR and macs as + cells/vascular section was higher in DM than in NDM (1844 vs. 697) and (2222 vs. 996) respectively. These results show good T/B uptake with more extensive uptake in DM compared to NDM. Staining for ECs showed staining confined to endovascular lining. Immunofluorescence studies show co-localization of VEGR1 predominantly with macrophages. Summary: 99mTc scVEGF-PEG-DOTA shows promise as a non-invasive approach to identify vulnerable plaque. In this model VEGFR expression was predominantly in macrophages and showed increased expression in diabetes.

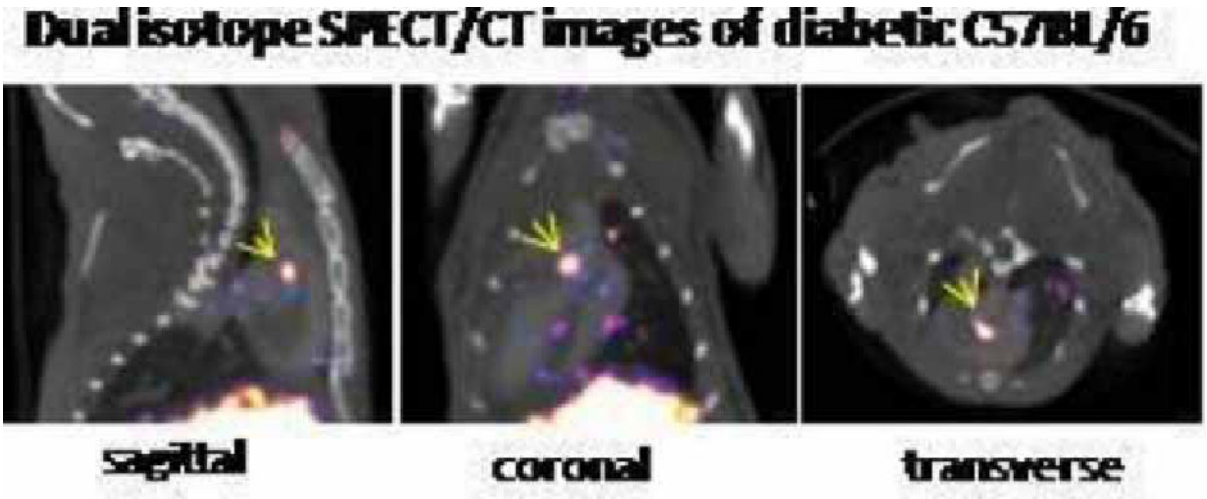


Disclosure of author financial interest or relationships:
**Y. Tekabe**, None; **M. Kollaros**, None; **G. Zhang**, None; **M. Backer**, None; **J.M. Backer**, SibTech, Inc., Stockholder; GlaxoSmishKline, Grant/research support; **L. Johnson**, None.

Presentation Number **P010**
Poster Session 1
September 5, 2012 / 18:00-18:00 / Room: The Liffey

# Micro PET/CT studies of carbon-11 labeled ammonium salts derivatives as myocardial perfusion PET imaging agents

***Darya Tsvirkun***, *Orit Jacobson Weiss, Galith Abourbeh, Eyal Mishani, Hadassah University Hospital, Jerusalem, Israel. Contact e-mail: daryatsv@gmail.com*

BACKGROUND: Coronary artery disease (CAD) is a blockage of the arteries that feed the heart muscle. The most common method for assessing CAD is myocardial perfusion scintigraphy. Although PET has several advantages over SPECT, due to the limited availability of suitable PET tracers, the majority of myocardial perfusion imaging (MPI) scans is performed using SPECT rather than PET. Recently, it has been shown that carbon-11 labeled ammonium salts have a great potential as PET MPI agents. AIMS: The aims of this study were (1) to develop 11C-labeled ammonium salt derivatives containing different functional groups including electron donating and electron withdrawing groups; (2) evaluate their structure-activity relationship (SAR) and (3) studying their biological potential as MPI agents by means of micro PET/CT screening. METHODS: Thus far, we developed and labeled three ammonium salt derivatives; Trimethyl-phenyl-ammonium (11C-TMA), (3-Methoxy-phenyl)-trimethyl-ammonium (11C-Meo-TMA) and Dimethyl-diphenyl-ammonium (11C-DMDPA). A rapid automated C-11 radiolabeling route was developed with no need of HPLC purification. To validate the lipophilicity of the tracers, LogP was calculated by the standard method using octanol:water. Dynamic Micro PET/CT imaging studies of all tracers were carried out in healthy rats. RESULTS & DISSCUSION: The compounds were labeled on the tertiary amine using either C-11-MeI or C-11-MeOTf to give the desired cationic salts - 11C-TMA, 11C-Meo-TMA and 11C-DMDPA with radiochemical yields of 15-20% decay corrected. After pH adjustments, we were able to capture the labeled products on cation exchange resins. The remainder of the unreacted precursor mass was washed using ethanol and water and the products were eluted with saline. The compounds were obtained in radiochemical purity of > 99% and specific activities of 771±300 calculated at end of synthesis. Micro PET/CT showed accumulation of all the compounds in the myocardium with peak SUV's of 4.2 for 11C-TMA and 11C-Meo-TMA at 10 min which decreased over time (Figure 1) and 6.8 for 11C-DMDPA (Figure 1) which reached a plateau. No uptake was seen in the lungs for all the compounds. 11C-TMA and 11C-Meo-TMA had lower uptake in the liver than 11C-DMDPA, however, since they had also lower uptake in the myocardium, the heart-to-liver ratio was similar for all the three compounds. This higher uptake of 11C-DMDPA in the liver can be explained by its higher hydrophobicity - LogP of -1.51 in comparison to 11C-TMA and 11C-Meo-TMA which had a LogP of -2.11 and -1.97, respectively. CONCLUSION: Both lipophilicity and charge density play a major role in cardiac accumulation of labeled ammonium salts. Preliminary SAR studies of 11C-labeled ammonium salts suggest that lipophilicity affects the initial uptake while the partial charge density dictates the retention of the tracer in the heart. Further studies of ammonium salts with a wide range of lipophilicity and charge density will broaden our understanding of the uptake mechanism and role for each parameter.

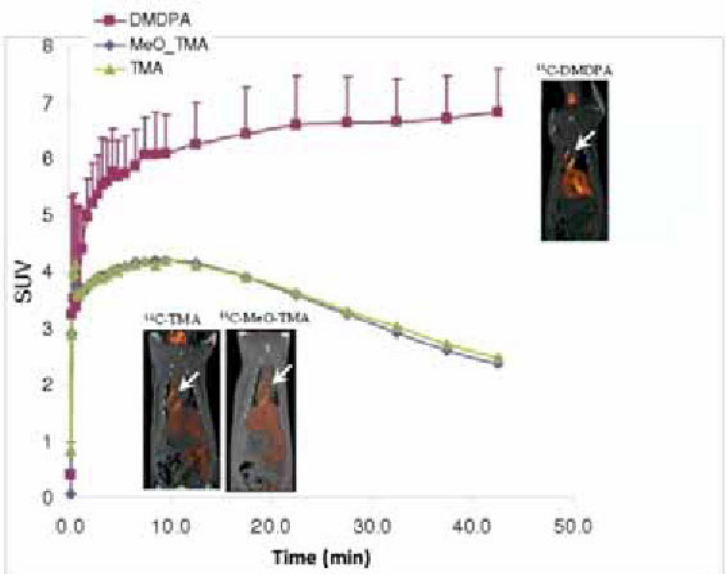


Figure 1. Time activity curve of heart activity uptake of 11C-DMDPA, 11C-TMA and 11C-Meo-TMA and representative fused micro PET/CT coronal images. The heart is marked with a white arrow.

Disclosure of author financial interest or relationships:
**D. Tsvirkun**, None; **O. Jacobson Weiss**, None; **G. Abourbeh**, None; **E. Mishani**, None.

Presentation Number **P011**
Poster Session 1
September 5, 2012 / 18:00-18:00 / Room: The Liffey

# Novel single-chain antibody-targeted microbubbles for diagnosis of thrombosis and monitoring of thrombolysis via non-invasive molecular ultrasound imaging

***Xiaowei Wang***[1]*, Christoph E. Hagemeyer*[1]*, Jan David Hohmann*[1]*, Ephraem Leitner*[1]*, Ingo Ahrens*[2]*, Karlheinz Peter*[1]*,*
*[1]Atherothrombosis & Vascular Biology, Baker IDI Heart and Diabetes Institute, Melbourne, VIC, Australia; [2]Department for Cardiology and Angiology, University Hospital Freiburg, Freiburg, Germany. Contact e-mail: xiaowei.wang@bakeridi.edu.au*

Background - Most acute cases of myocardial infraction and stroke are caused by atherothrombosis, when platelet adhesion, activation and aggregation, lead to thrombus formation and vessel occlusion. Glycoprotein (GP) IIb/IIIa complex, is the most abundant receptor expressed on the platelet surface1, responsible for adhesion and aggregation2. We have developed conformation-specific single-chain antibodies (scFv) that bind specifically to ligand-induced binding sites (LIBS) on activated GPIIb/IIIa2. We hypothesized that contrast enhanced ultrasound with microbubbles selectively targeted to activated platelets would offer real-time as well as high resolution molecular imaging of evolving and dissolving arterial thrombi. Methods and Results - Lipid-shell based air-filled microbubbles (MB) were conjugated to either a single-chain antibody (scFv) specific for activated GPIIb/IIIa (LIBS-MB), or a non-specific scFv (control-MB). Flow-chamber experiments demonstrated strong adhesion of LIBS-MB to immobilized activated platelets in comparison to the control-MB. Thrombi, induced in carotid arteries of C57Bl6-mice in vivo by ferric chloride injury, were assessed with ultrasound before and 20 minutes after microbubble injection, using greyscale area intensity measurement. Ultrasound imaging was performed on a longitudinal axis. Greyscale units converted to decibels demonstrated a significant increase after LIBS-MB but not after control-MB injection (9.55 ± 1.7 versus 1.46 ± 1.3 dB; $p<0.01$). After the administration of urokinase plasminogen activator (UPA), a reduction in thrombus size and/or thrombus dislodgement could be directly observed ($p<0.001$). Similar trends of results were obtained when comparing the thrombus area reduction to thrombus area grayscale intensity unit reduction. Time span of microbubbles injection and UPA administration was investigated. A second dose of LIBS-MB was required if UPA treatment was administrated later than 30 minutes post LIBS-MB injection. In addition to longitudinal section imaging cross section ultrasound imaging was also performed. The results in monitoring thrombolysis of cross section analysis are similar in the overall outcome to that of the longitudinal section analysis. Conclusions - We are able to demonstrate that our targeted microbubbles specifically bind to activated platelets in vitro and allow real-time molecular imaging of acute arterial thrombosis as well as monitoring of pharmacological thrombolysis in vivo. This non-invasive and cost effective imaging modality provides a unique opportunity to detect arterial (micro)thrombi with high resolution at an early stage allowing for early diagnosis and therapy and it allows to identify failure or success of thrombolytic therapy. References: 1. Peter K, Schwarz M, Nordt T, Bode C. Intrinsic activating properties of gp iib/iiia blockers. Thrombosis Research. 2001;103:S21-S27 2. Schwarz M, Meade G, Stoll P, Ylanne J, Bassler N, Chen Y, Hagemeyer C, Ahrens I, Moran N, Kenny D. Conformation-specific blockade of the integrin gpiib/iiia: A novel antiplatelet strategy that selectively targets activated platelets. Circulation research. 2006;99:25

Disclosure of author financial interest or relationships:
**X. Wang**, None; **C.E. Hagemeyer**, None; **J. Hohmann**, None; **E. Leitner**, None; **I. Ahrens**, None; **K. Peter**, None.

Presentation Number **P012**
Poster Session 1
September 5, 2012 / 18:00-18:00 / Room: The Liffey

# C-kit+ pluripotent bone marrow cells attenuate apoptosis in ischemic myocardium - in vivo assessment with hybrid FMT-XCT

***Moritz Wildgruber***[1], *Angelique Ale*[2], *Katja Kosanke*[1], *Reinhard Meier*[1], *Ernst J. Rummeny*[1], *Vasilis Ntziachristos*[2], [1]*Radiology, Technische Universität München, München, Germany;* [2]*Institute for Medical and Biological Imaging, Helmholtz Zentrum München, München, Germany. Contact e-mail: moritz.wildgruber@tum.de*

Purpose: To investigate the anti-apoptotic effect of therapeutically administered pluripotent c-kit+ bone marrow cells after murine myocardial infarction by hybrid Fluorescence Molecular Tomography - X-ray Computed Tomography targeting Annexin V (FMT-XCT). Materials and Methods: Myocardial ischemia (MI) was induced in kit+/+ mice, c-kit deficient KitW/W-v mice and bone marrow reconstituted KitW/W-v mice by 30 minutes ligation of the left anterior descending artery (LAD) with subsequent reperfusion. Mice were injected with the Annexin V targeted molecular imaging probe Annexin-Vivo750 4 hours prior to imaging. Additionally mice were injected with a long-circulating CT blood pool contrast agent (Exitron 12000) prior to imaging for better visualization of cardiac anatomy with subsequent facilitated organ segmentation. Hybrid FMT-XCT was performed 6 hours, 24 hours and 7 days after induction of ischemic injury. Molecular imaging signal for Annexin-Vivo750 was validated by ex-vivo cryoslicing, immunohistochemistry and flow cytometry. Results: Successful image acquisition of both FMT and CT angiography was achieved in all mice. In control kit+/+ mice the FMT signal for Annexin V peaked at 6 hours after myocardial infarction with subsequent decrease at 24 hours and 7 days after onset of ischemic injury. KitW/W-v mice revealed an increased and prolonged in-vivo apoptosis signal, which was associated with progressive decline in heart function. Bone marrow reconstitution was able to reduce cardiomyocyte apoptosis and rescue KitW/W-v mice from progressive heart failure. In-vivo apoptosis signal was verified after sacrifice by apoptosis staining using immunohistochemistry (TUNEL) and flow cytometry (Caspase-3). Hybrid acquisition of x-ray computed tomography allowed exact localization of the FMT signal to the left-ventricle and facilitated organ segmentation and attenuation correction. Conclusion: Hybrid FMT-XCT targeting Annexin V enables monitoring of the beneficial effects of c-kit stem cell treatment after myocardial ischemia in a murine ischemia-reperfusion model.

Disclosure of author financial interest or relationships:
**M. Wildgruber**, None; **A. Ale**, None; **K. Kosanke**, None; **R. Meier**, None; **E.J. Rummeny**, None; **V. Ntziachristos**, ERC, Grant/research support; Ithera Medical, Stockholder .

Presentation Number **P013**
Poster Session 1
September 5, 2012 / 18:00-18:00 / Room: The Liffey

# Assessing the effectiveness of $^{18}$F-FPBG and $^{123}$I-MIBG in small animal myocardial infarct imaging

***Sang-Keun Woo***[1], *Yong Jin Lee*[1], *Kyeong Min Kim*[1], *Un-Chol Shin*[1], *Jung Woo Yu*[1], *Kyo Chul Lee*[1], *Min Hwan Kim*[1], *Byung Seok Moon*[2], *Byung Chul Lee*[2], *Jae Ho Jung*[2], *Joo Hyun Kang*[1], *Sang Moo Lim*[1], *Gil Tae Hwang*[3], [1]*Molecular Imaging Research Center, KIRAMS, Seoul, Republic of Korea;* [2]*Department of Nuclear Medicine, Seoul National University Bundang Hospital, Seoul National University College of Medicine, Seongnam, Republic of Korea;* [3]*Department of Chemistry, Kyungpook National University, Daegu, Republic of Korea. Contact e-mail: skwoo@kcch.re.kr*

The aim of this study was to evaluate the rat myocardial infarct $^{18}$F-FPBG PET and $^{123}$I-MIBG SPECT image using small animal imaging system. Myocardial infarct (MI) model was prepared through permanently ligated left anterior descending artery of rat. PET/SPECT images were acquired using small animal PET/SPECT/CT scanner (InveonTM, Siemens) with physiological external monitoring system (BioVet, m2m Imag. Corp.). The meta-(3-[$^{18}$F]fluoropropyl) benzylguanidine ($^{18}$F-FPBG) PET imaging agent was an analogue of a norepinephrine such as $^{123}$I-MIBG. PET images were obtained by 70 min dynamic scan post injection of $^{18}$F-FPBG 37 MBq/0.2 mL via tail vein. SPECT images were acquired at 60 min post injection of $^{123}$I-MIBG 110 MBq/0.2 mL via tail vein with 143-175 energy window and 1.0 mm pinhole collimator. The CT images for anatomical information were acquired with 70 kVp, 400 uA, and 200 msec exposure time for each steps. The acquired PET list mode data was reconstructed by the Ordered Subset Expectation Maximization (OSEM) 2D with 4 iterations. The acquired SPECT list mode data was reconstructed by OSEM 3D with 4 subsets and 8 iterations. The normal rat bio-distribution of $^{18}$F-FPBG was evaluated at 5 min, 30 min, and 60 min in blood and heart wall region. The time activity curve of $^{18}$F-FPBG myocardium image was analyzed by the ASIPro software. The reconstructed image was converted to polar map after myocardium reorientation and contour setting by Cedars-Sinai method. To automatically make the myocardial contour and generate polar map, we used QPS software (Cedars-Sinai Medical Center). Rat myocardium was stained by hematoxylin and eosin (H&E) for reference value of MI size after the data obtained. The MI size in polar map was calculated as the percentage of lower threshold area in polar map from the total polar map area. The blood distribution of $^{18}$F-FPBG was 0.13 ± 0.01 %ID/g at 5 min, 0.12 ± 0.03 %ID/g at 30 min and 0.08 ± 0.01 %ID/g at 60 min. The heart wall distribution of $^{18}$F-FPBG was 2.77 ± 0.40 %ID/g at 5 min, 2.09 ± 0.34 %ID/g at 30 min and 1.22 ± 0.35 %ID/g at 60 min. $^{18}$F-FPBG was showed high contrast in the rat myocardium region. In the time activity curve of $^{18}$F-FPBG, the activity was increased from 10.23% at 2.5 sec until 100% at 85 sec, and then the activity was decreased continuously 41.79% at 70 min. $^{18}$F-FPBG image was showed high sensitivity in normal myocardium region, and it displayed high contrast compared to $^{123}$I-MIBG image in MI rat model. MI size of H&E staining was 2.37%. In the quantitative evaluation of infarct size by absolute threshold 60%, $^{123}$I-MIBG was evaluated to a larger MI size as 63.36% to compare with 3.44% of $^{18}$F-FPBG. We evaluated the small animal $^{18}$F-FPBG cardiac imaging using radiopharmaceuticals of small amounts by high sensitivity. $^{18}$F-FPBG is expected to be very useful as a PET imaging agent to substitute $^{123}$I-MIBG in the evaluation of cardiac disease.

Disclosure of author financial interest or relationships:
**S. Woo**, None; **Y. Lee**, None; **K. Kim**, None; **U. Shin**, None; **J. Yu**, None; **K. Lee**, None; **M. Kim**, None; **B. Moon**, None; **B. Lee**, None; **J. Jung**, None; **J. Kang**, None; **S. Lim**, None; **G. Hwang**, None.

Presentation Number **P014**
Poster Session 1
September 5, 2012 / 18:00-18:00 / Room: The Liffey

# Absence of T1 changes in the myocardium during transient oxygen challenge

***Marzena Wylezinska-Arridge***[1], *Jordi L. Tremoleda*[1], *Josef Habib*[2], *Daniel J. Stuckey*[2], *Willy Gsell*[1], [1]*Biological Imaging Centre, MRC Clinical Sciences Centre, Imperial College London, London, United Kingdom;* [2]*National Heart and Lung Institute, Imperial College London, London, United Kingdom. Contact e-mail: m.arridge@imperial.ac.uk*

Introduction: Changes in oxygen supply during gas anaesthesia can be used as a non-invasive method for assessing tissue oxygenation by studying BOLD signal changes with MRI. Since relaxation time T2* is affected by the HbO2/Hb ratio, tissue oxygenation could be evaluated with T2* contrast during oxygen challenge. This has been recently shown in the myocardium in rats [1,2]. However the signal changes may also be associated with variation in plasmatic oxygen concentration involving T1 changes due to paramagnetic properties of free O2. The aim of this study was to investigate T1 values during oxygen challenge. Methods: All animal studies were approved by the UK Home Office. MRI: Male Wistar rats (n=3; 8 weeks) were anesthetized with ~1.5% isoflurane, monitoring for HR, respiration and body temperature. MRI was done using a 4.7T DirectDrive Varian system with 40 G/cm gradients and a 72mm volume (quadrature) RF coil. For estimation of the longitudinal relaxation time T1 a Lock-Locker sequence [3] was used to acquire images with multi inversion recovery time (TI) following a double gated adiabatic inversion pulse. All TI frames were ECG gated; TI values were multiples of the RR period with additional delay between R wave and excitation pulse to shift images into end of systole. 20 frames were acquired resulting in TI ranging from 80ms to ~3000ms (shown in Fig 1A). Single slice in short axis view was acquired with the 1mm slice thickness , 51.2mmx51.2mm and 128 x128 pixel matrix TE=1.7 ms; TR=5000ms, flip angle=10. Imaging was done under breathing medical air (21%O2) or 100% O2. Acquisitions were performed allowing for a 5 min adaptation period after changing the O2 % in the breathing gas. T1 values were calculated using three parameter fit as described in [4] Blood sampling: The femoral artery was catheterized to withdraw of blood for systemic evaluation of O2 saturation, plasmatic O2 and CO2 levels in arterial blood during anesthesia in 21% and 100% O2. Results: Estimated T1 values averaged (n=3) from ROI selecting the myocardium were 1.023s ±0.136 and 1.010s ± 0.135 for 100% and 21% O2, respectively. At the same time there was a significant increase in arterial O2 Saturation (from 99.4± 0.2 at 100% O2 to 71.1±3.5 at 21% O2) and arterial free plasmatic oxygen, pO2 (280.9± 28 at 100% O2 to 38.8±3 at 21% O2). Fig 1B shows an example of T1 map. Discussion: We have previously shown that the increase in BOLD signal during oxygen challenge is accompanied by a remarkable change in T2*values (+14%;[1,2]). Our current study shows that T1 variations are not a significant source of signal changes observed in oxygen challenge. This support the hypothesis that contrast through changes in HbO2/Hb is the main source of signal changes observed during O2 challenge and reflects tissue oxygenation level and metabolism. References: 1.Wylezinska M et al. Proc. ISMRM 2011, 3384 2.Tremoleda et al. WMIC Meeting, P430 3.Price et al.J.of Cardiovasc. Magn.Reson.2011, 13,44 4.Karlsson M et al. Magn. Reson. Imag. 2000, 18,947-954

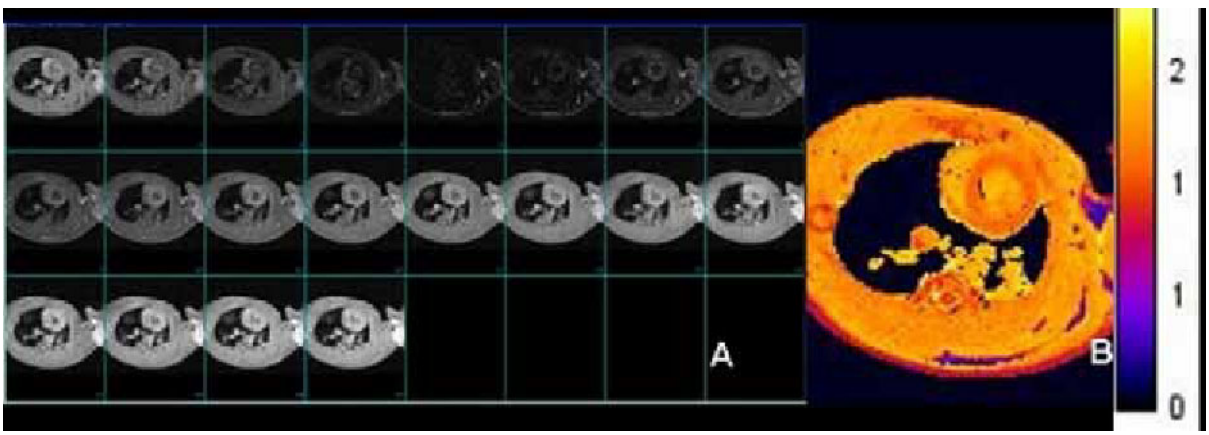


Fig. 1) A: Multi TI frames, B: Example of T1 map.

Disclosure of author financial interest or relationships:
**M. Wylezinska-Arridge**, None; **J.L. Tremoleda**, None; **J. Habib**, None; **D.J. Stuckey**, None; **W. Gsell**, None.

Presentation Number **P015**
Poster Session 1
September 5, 2012 / 18:00-18:00 / Room: The Liffey

# Imaging of infection: Evaluation of $^{68}$Ga-DOTA-Puromycin as potential in vivo imaging agent for bacterial infections

***Sebastian Eigner***[1]*, Thomas Ebenhan*[2]*, Denis R. Beckford Vera*[1]*, Katerina Eigner Henke*[1]*, [1]Department of Radiopharmaceuticals, Nuclear Physics Institute, Academy of Science of the Czech Republic, Husinec-Rez, Czech Republic; [2]Radiochemistry, NECSA, Pretoria, South Africa. Contact e-mail: eigner@ujf.cas.cz*

**Objectives:** Infectious diseases, such as tuberculosis, are responsible for significant numbers of newly infected patients and difficulties in diagnostics, especially in co-infection with e.g. HIV positive patients. Even with modern technologies it is still crucial to identify early stages of various infectious diseases before major organs are effected. Universal inhibition of protein synthesis by puromycin derivatives makes it a potential candidate to be modified as PET/SPECT tracer for differentiation of bacterial infection and unspecific inflammation. We recently proofed the suitability of $^{44}$Sc-DOTA-Puromycin to image increased protein synthesis in tumor cells. Therefore, the purpose of this study was to evaluate the potential of $^{68}$Ga-DOTA-Puromycin for the use as imaging agent of bacterial infection by determining protein synthesis of bacterial colonies infecting inner organs (lung, liver, brain, muscels). **Methods:** DOTA-Pur was purchased from Purimex, Germany and used without further purification. A $TiO_2$-based $^{68}$Ge/$^{68}$Ga generator was eluted fractionally to obtain $^{68}$Ga in 2 ml 0.6 M HCL. After adding 2 mL of HEPES 1M, ph=4, DOTA-Puromycin was added, incubated 20 min at 95° C and purified on Strata-X columns. Quality control was performed on TLC. Purity was determined by radio RP-HPLC. *In vivo* biodistribution of $^{68}$Ga-DOTA-Puromycin was studied by PET imaging and blood/urine sampling on rabbits carrying (1st group) non-bacterial inflammation (turpentine oil) and infections with Staphylococcus Aureus or (2nd group) tuberculosis infections in comparison to asthmatic diseases. **Results:** Labeling procedures were optimized, resulting in labeling yields of 65 ± 2,6 % and RCP of ≥ 98%. Preliminary *ex vivo* results showed total blood clearance within 45 min p.i. via-renal excretion. At 60 min p.i. no activity was found in potential target organs for infection, e.g. in lung, brain, liver or abdomen **Conclusions:** Due to the data obtained in *ex vivo* biodistribution of $^{68}$Ga-DOTA-Puromycin the compound seams to be a potential tracer for visualization of infectious diseases utilizing PETor PET/CT. Preclinical imaging studies to verify its *in vivo* behavior in rabbits bearing inflammation, bacterial and TB infection are currently conducted in the Department of Nuclear Medicine of the University of Pretoria.

Disclosure of author financial interest or relationships:
**S. Eigner**, None; **T. Ebenhan**, None; **D.R. Beckford Vera**, None; **K. Eigner Henke**, None.

Presentation Number **P016**
Poster Session 1
September 5, 2012 / 18:00-18:00 / Room: The Liffey

# Combining Bioluminescence and µCT Imaging to Study Bacterial Infections In a Murine Model of Osteomyelitis

***Jeffrey A. Meganck***[1], *Kevin P. Francis*[1], *Ed Lim*[1], *Ning Zhang*[1], *Brad Rice*[1], *Jonathan Pribaz*[3], *Jonathan H. Shahbazian*[3], *Jared Niska*[3], *Lloyd S. Miller*[2,3], [1]*PerkinElmer, Alameda, CA, USA;* [2]*Department of Orthopaedic Surgery, UCLA, Los Angeles, CA, USA;* [3]*Department of Medicine, UCLA, Los Angeles, CA, USA. Contact e-mail: jeff.meganck@perkinelmer.com*

The combination of optical and µCT imaging provides unique opportunities to monitor biological and molecular functions in an anatomical context. Previously, both modalities have been separately used to study bacterial infection in pre-clinical orthopaedic implant models. In clinical settings, osteomyelitis occurs with relatively low incidence. However, this disease represents a very challenging clinical problem that can sometimes require long hospitalization times and/or revision surgeries, and may be further complicated if multi-drug resistant bacteria are involved. Prior studies conducted by us and others have used bioluminescent strains of *S. aureus* for 2D optical imaging, usually with planar radiography or µCT imaging at a terminal timepoint. In this study, *in vivo* 2D and 3D bioluminescence and fluorescence imaging were combined with µCT imaging to track the the bacterial burden, neutrophil recruitment and bone damage in a mouse model of an orthopaedic implant infection longitudinally. Titanium Kirschner-wires (10 mm long, 0.8 mm diameter) were surgically placed in femurs of C57Bl/6 LysEGFP mice, which possess EGFP-fluorescent neutrophils. A bioluminescent *S. aureus* strain (Xen 29; 1000 CFUs) was inoculated onto the ends of the implants in the knee joints before closure. This resulted in a chronic implant infection with biofilm formation. *In vivo* bioluminescence, fluorescence and µCT imaging were performed on shaved mice at days 2, 5, 14, 19, 28, 33, and 48. To verify the biofilm location in 3D, a diffuse optical tomography reconstruction algorithm was used to generate 3D bioluminescence signals and co-registered with the µCT images. The bacterial bioluminescence signals initially increased, but then decreased to a steady-state level between days 14 and 48. Neutrophil EGFP-fluorescence decreased from days 2 to 19 and then remained below the level of detection. To quantify the anatomical bone changes on the µCT images, the volume of the distal femurs (25% of the total femoral length) was measured using a semi-automated contour based segmentation process. Image artifacts related to the titanium were excluded as much as possible to prevent bias on the volume measurements. Relative changes in bone volume were obtained by normalizing measurements from days 5, 14, 28 and 48 to day 2. The distal femur volume steadily increased through day 49, indicating that bone damage continued during this implant infection.

Disclosure of author financial interest or relationships:
**J.A. Meganck**, PerkinElmer, Employment; **K.P. Francis**, None; **E. Lim**, None; **N. Zhang**, PerkinElmer, Employment; **B. Rice**, None; **J. Pribaz**, None; **J.H. Shahbazian**, None; **J. Niska**, None; **L.S. Miller**, Stiefel/GlaxoSmithKline, Consultant; Allergan, Consultant; Pfizer, Grant/research support .

Presentation Number **P017**
Poster Session 1
September 5, 2012 / 18:00-18:00 / Room: The Liffey

# In vivo imaging and quantification of bacterial infection using a new red fluorescently labeled agent

*Sylvie Kossodo, Guojie Ho, Garry J. Cuneo, Jeff Morin, Jeannine Delaney, Wael Yared, Milind Rajopadhye,* ***Jeffrey D. Peterson****, LST, PerkinElmer, Boston, MA, USA. Contact e-mail: jeff.peterson@perkinelmer.com*

Bacterial infection is a serious and costly clinical issue, so there is significant need for preclinical tools for assessing infection and therapeutic intervention. Rapid and non-invasive imaging technologies and targeted imaging agents would prove invaluable in diagnosing and managing bacterial infections. To this end, we developed a unique type of fluorescent agent that can quickly target bacteria, providing a fluorescent method to quantify bacterial load during infection as early as one hour post-injection. A red cationic agent (BacteriSense645) targeting the negative charge at the surface of bacteria was developed (ex/em 635/656 nm). Specificity of binding to negative-charged molecules present on the bacterial membrane and cell envelope was tested using various glycolipids and lipopolysaccharide (LPS) bound to 96-well plates in the presence or absence of a competing positively-charged molecule. BacteriSense645 was able to effectively bind to negatively (phosphatidylserine, phosphatidylethanolamine, LPS and teichoic acid) but not to a neutral (phosphatidylethanolamine) charged surfaces, and a positively-charged competitor was able to significantly reduce binding. These results suggested that important negatively-charged components in both Gram-negative and Gram-positive bacteria were recognized. This was confirmed by in vitro binding of BacteriSense645 to Gram- Escherichia coli and Gram+ Staphylococcus epidermidis and assessment by fluorescence microscopy and flow cytometry. BacteriSense645 was found to bind to E.coli more efficiently than S. epidermidis (4 fold) and not to mouse skeletal muscle cells serving as a negative control. In vivo pharmacokinetic profiles in CD-1 mice showed a plasma half life of 15-45 min, depending on level of infectious burden, providing rapid clearance from circulation. Sensitivity of detection was assessed in SKH-1 E mice infected intramuscularly in the thigh with 100,000 - 100 million CFUs of E. coli and injected intravenously 24h later with 5 nmoles of BacteriSense645. Bacterial loads as low as 100,000 were detectable in mice imaged using the fluorescence tomography system (FMT2500), and this imaging agent was highly unique in its ability to provide optimal imaging just1 h following injection with a tissue half life of 3h and washout of the signal (blood and tissue) by 24 h, allowing daily repeat imaging in longitudinal infection models. Similar imaging results were obtained with S. epidermidis infected mice, supporting this agent's utility in Gram-positive bacterial infections as well. More importantly, BacteriSense645 was able to distinguish E. coli infection from LPS injected simultaneously in the contralateral thigh (106 +/- 31 vs 21 +/- 10 pmoles respectively by tomography, p=0.029; 0.051 +/- 0.005 vs 0.035+/-0.001 mean counts/energy by reflectance, p=0.0113). Taken together, these results highlight the value of BacteriSense645 in preclinical drug development studies.

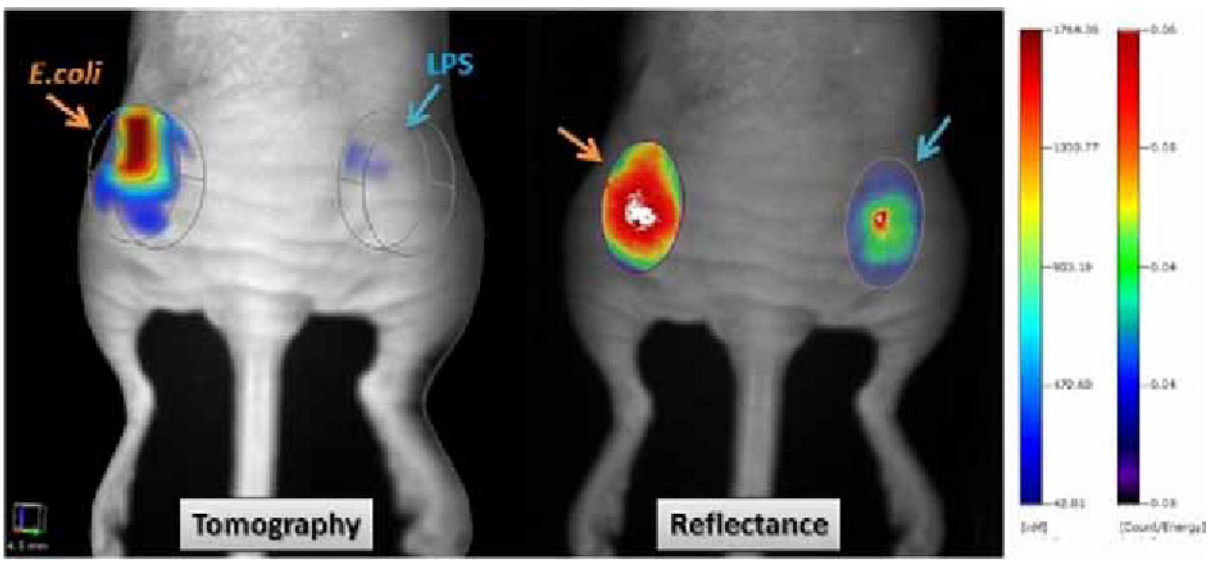


Disclosure of author financial interest or relationships:
**S. Kossodo**, PerkinElmer, Employment; **G. Ho**, None; **G.J. Cuneo**, PerkinElmer Life Sciences, Employment; **J. Morin**, Perkin Elmer, Employment; **J. Delaney**, PerkinElmer, Employment; **W. Yared**, Perkin Elmer, Employment; **M. Rajopadhye**, PerkinElmer, Inc., Employment; **J.D. Peterson**, PerkinElmer, Employment .

Presentation Number **P018**
Poster Session 1
September 5, 2012 / 18:00-18:00 / Room: The Liffey

# Validation of rabbit model of arthritis and skin inflammation with [$^{18}$F]FDG PET for preclinical evaluation of VAP-1 targeting imaging agents

***Anu Autio***[1], *Helena K. Ahtinen*[1], *Kimmo Jaakkola*[4], *Petteri Lankinen*[1], *Heidi Liljenbäck*[1], *Piritta Saipa*[1], *Petri J. Vainio*[2], *Sirpa Jalkanen*[3], *Anne Roivainen*[1,5], [1]*Turku PET Centre, Turku, Finland;* [2]*BioTie Therapies Corp., Turku, Finland;* [3]*MediCity Research Laboratory, Turku, Finland;* [4]*VTT Technical Research Centre of Finland, Turku, Finland;* [5]*Turku Centre for Disease Modelling, Turku, Finland. Contact e-mail: akauti@utu.fi*

**INTRODUCTION**: Vascular adhesion protein-1 (VAP-1) is an endothelial adhesion molecule that participates in leukocyte recruitment to inflamed tissues. For instance, dermal blood vessels in various inflammatory skin diseases (e.g. psoriasis), intestinal blood vessels in inflammatory bowel diseases and synovial blood vessels in inflamed joints (e.g. rheumatoid arthritis) express VAP-1 on their surface. VAP-1 is a promising target for in vivo imaging, since it is translocated to the endothelial cell surface upon inflammation. In this study, we set up a rabbit model of sterile skin inflammation and arthritis, and evaluated luminal expression of VAP-1 with specific antibody as well as metabolic activation at the sites of inflammation with 2-deoxy-2-[$^{18}$F]fluoroglucose [$^{18}$F]FDG PET. The anti-VAP-1 antibody, BTT-1023, is fully human and developed for the treatment of inflammatory diseases, such as rheumatoid arthritis. **MATERIALS AND METHODS**: Knee joint of male New Zealand white rabbits (n=7) were intra-articularly injected with phytohemagglutinin (PHA) (400 µg/ml) in 200 µl of RPMI to induce acute synovitis. Skin inflammation was induced to shaved area in the hind leg with 4 drops of 2,4-dinitrochlorobenzene (DNCB) dissolved in acetone. Progression of inflammation was evaluated by in vivo [$^{18}$F]FDG PET imaging at 8 h and 24 h after induction of inflammation. Anesthetized rabbits were intravenously administrated with 50 ± 1 MBq of [$^{18}$F]FDG and allowed to accumulate for 40 min. Animals were imaged with High Resolution Research Tomograph (HRRT) PET camera for 20 min. Regions of interest were defined to inflamed and control organs with Carimas 2.4 software. Immediately after PET scanning rabbits were intravenously injected with anti-VAP-1 antibody (BTT-1023, Biotie Therapies), killed and the inflamed and control tissues were collected and luminal expression of VAP-1 was evaluated by immunohistochemistry. **RESULTS**: Inflammation uptake of [$^{18}$F]FDG was comparable to the induction time as well as with the level of the luminal expression of VAP-1. The number of VAP-1 positive vessels was higher at 24 h than at 8 h after induction of inflammation. There were none or only few VAP-1 positive vessels in the healthy skin and synovial tissues. Both in knee and skin inflammation the uptake of [$^{18}$F]FDG was higher at 24 h than at 8 h after the induction and when compared to the uptake in the control tissue (Figure 1A). A representative PET image of the inflamed and control knee at 24 h post induction is shown in Figure 1B. **CONCLUSION**: The [$^{18}$F]FDG PET of rabbit synovitis and skin inflammation showed the progression of inflammation. These findings were comparable to the luminal expression of VAP-1. Our results revealed that the 24 h is optimal for both PHA and DNCB induced acute inflammation for preclinical evaluation of novel VAP-1 targeting imaging agents.

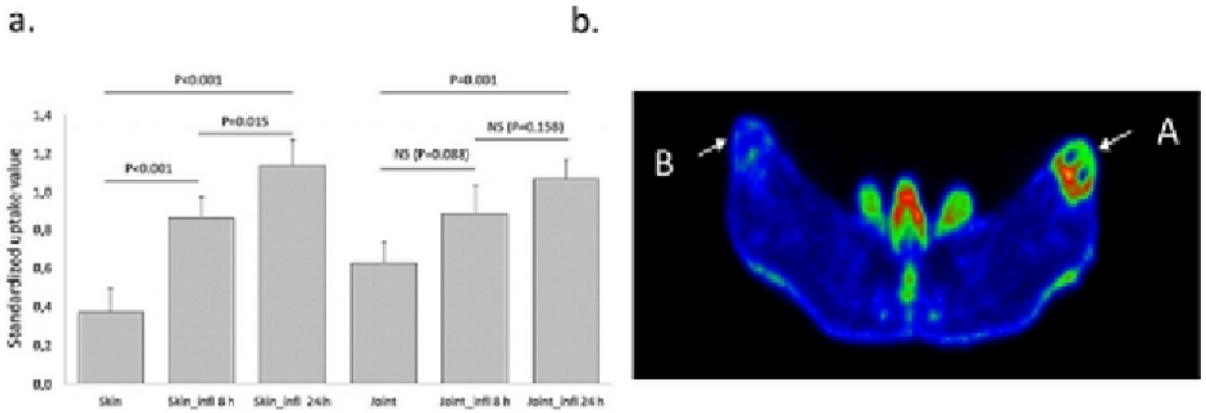


Figure 1a. The average standardized uptake values and the standard deviation of [$^{18}$F]FDG PET measurements for all inflamed and control organs.
Figure 1b. Transaxial view of inflamed rabbit knee joints as PET imaged with [$^{18}$F]FDG A=PHA induced joint inflammation and B=healthy control.

Disclosure of author financial interest or relationships:
**A. Autio**, None; **H.K. Ahtinen**, None; **K. Jaakkola**, None; **P. Lankinen**, None; **H. Liljenbäck**, None; **P. Saipa**, None; **P.J. Vainio**, Biotie Therapies, Employment; Biotie Therapies, Stockholder; **S. Jalkanen**, None; **A. Roivainen**, None.

Presentation Number **P019**
Poster Session 1
September 5, 2012 / 18:00-18:00 / Room: The Liffey

# PET In vivo imaging of 18kDa TSPO expression in a rat model of granuloma using [18F]DPA-714

***Raphael Boisgard***[1], *Benoit Jego*[1], *Benoit Theze*[1], *Géraldine Pottier*[1], *Bertrand Tavitian*[2], *Frederic Dolle*[2], [1]*CEA / DSV / I2BM / SHFJ / INSERM U1023, CEA, Orsay, France;* [2]*CEA / DSV / I2BM / SHFJ, CEA, Orsay, France. Contact e-mail: raphael.boisgard@cea.fr*

Inflammatory processes represent a key event for the organism in order to answer and defend itself against injury or infection by repairing tissues or eradicating infectious agents. These survival processes are also implicated in numerous human diseases, as causes or effects, in cases of deregulation or maladjusted answer to the injury. The in vivo quantification of inflammatory processes to understand mechanisms and also to quantify the level of the reaction represents an important challenge for molecular imaging. This objective is crucial for diseases of the central nervous system but also in the periphery for diseases with an inflammatory component such as autoimmune diseases. Here we chose to assess [18F]DPA-714, an 18 kDa TSPO PET-radioligand as a probe to report inflammation in a rat model of granuloma induced by turpentine oil administration in one thigh muscle. In vivo PET imaging, performed 24h post turpentine-administration, showed an increased uptake of [18F]DPA-714 within the inflamed muscle when compared to the control muscle, from already 2 minutes after injection of the radiotracer and up to 60 minutes. The calculated ratio at this last time point was 7.8±2.7, a significantly higher value than the one observed with another TSPO PET-radioligand, [11C]PK11195 (4.0 ± 0.7). This is a direct consequence of the higher level of [11C]PK11195 uptake in the control muscle, the uptake in the inflamed muscle being similar for the two radioligands (values of 0.40± 0.05 %ID/cc and 0.37± 0.06 %ID/cc for [18F]DPA-714 and [11C]PK11195, respectively). In vivo displacement studies with PK11195 and non-labeled DPA-714 showed a rapid and complete displacement of [18F]DPA-714 binding from the lesion. Immunohistochemistry analysis on slices obtained from the injected muscle shows a large increase of inflammatory cells and also an increased expression of the 18kDa TSPO. Ex vivo autoradiography demonstrated a high contrast in the lesion versus non injected muscle, which disappeared after adding an excess of PK11195 or non-labeled DPA-714. These results show that [18F]DPA-714 seems to be a promising radiotracer for imaging acute peripheral inflammation with PET, and this due to the lower background level observed in non-inflammatory tissue with this radiotracer in comparison to [11C]PK11195. Acknowledgement: The authors are grateful to Dr. M. Higuchi for providing the anti-TSPO antibody NP155.

Disclosure of author financial interest or relationships:
**R. Boisgard**, None; **B. Jego**, None; **B. Theze**, None; **G. Pottier**, None; **B. Tavitian**, None; **F. Dolle**, None.

Presentation Number **P020**
Poster Session 1
September 5, 2012 / 18:00-18:00 / Room: The Liffey

# Inflammation and macrophage imaging in the aging ApoE-/- mouse: the impact of exercise

*Erica N. Chirico[1,2], Fabien Chauveau[3], David Patsouris[1], Alain Geloen[1], Jennifer Rieusset[1], Vincent Pialoux[2], **Emmanuelle Canet-Souas**[1], [1]CarMeN (U1060 INSERM), University Claude Bernard Lyon 1, Oullins Cedex, France; [2]Center of Research and Innovation in Sports (EA647), University Claude Bernard Lyon 1, Villeurbanne, France; [3]CREATIS (CNRS UMR 5220), INSERM, University Claude Bernard Lyon 1, Lyon, France. Contact e-mail: emmanuelle.canet-soulas@univ-lyon1.fr*

Atherosclerosis is a chronic inflammatory disease that is overwhelmed by oxidative stress and inflammation, with macrophages being main actors in this process. Exercise training has been shown to reduce oxidative stress and inflammation, providing protection in many diseases. We hypothesize that exercise training could limit macrophage accumulation within the aortic arch and cerebral vessels as seen in MRI via a decrease in oxidative stress and inflammation. A 12-week exercise or sedentary program was enforced in young (8 weeks) and old (66 weeks) ApoE-/- mice on high fat/high cholesterol diet, followed by 2 MRI sessions. MRI of the aortic arch showed an increased vessel wall area in old untrained mice compared to old exercise trained mice. The old mice had a significantly increased vessels wall area compared to the young mice. In terms of T2* measurements, there was no difference in the delta between pre- and post-contrast. However, both young and old exercise trained mice had a higher pre- and post-T2* measurement. Exercise training was able to decrease systemic levels of oxidative stress and inflammation as old untrained mice had higher levels of AOPP, TNF, and IL-1b. This corresponded to oxidative stress and inflammation levels in the brain, as MDA, AOPP, TNF, and IL-1b were significantly increased in old untrained mice. This improvement in exercised trained mice was translated to MRI results of the brain. MRI showed an increase in macrophage accumulation in 83% the old untrained mice, while positive macrophage imaging was virtually absent in the old exercise trained mice (12%). In conclusion, these results suggest that the overall increase in systemic oxidative stress and inflammation common to atherosclerosis could increase plaque size and alter macrophage phenotype in the aorta, as well as increase macrophage accumulation within the brain. Exercise training was able to ameliorate these consequences by reducing systemic and local production of oxidative stress and inflammation.

Disclosure of author financial interest or relationships:
**E.N. Chirico**, None; **F. Chauveau**, None; **D. Patsouris**, None; **A. Geloen**, None; **J. Rieusset**, None; **V. Pialoux**, None; **E. Canet-Souas**, None.

Presentation Number **P021**
Poster Session 1
September 5, 2012 / 18:00-18:00 / Room: The Liffey

# Estimation of arthritis development and its suppression during glucocorticoid therapy by NIRF optical imaging

***Katja Dahlke***[1], *Frederic Dietzel*[1], *Michael K. Boettger*[2], *Mieczyslaw Gajda*[3], *Rolf Bräuer*[3], *Hans-Georg Schaible*[2], *Werner A. Kaiser*[1], *Ingrid Hilger*[1], [1]*Experimental Radiology, Institute of Diagnostic and Interventional Radiology Jena University Hospital, Jena, Germany;* [2]*Institute of Physiology University Hospital Jena, Jena, Germany;* [3]*Institute of Pathology University Hospital Jena, Jena, Germany.*
*Contact e-mail: Katja.Dahlke@med.uni-jena.de*

Purpose: Due to good accessibility to light and availability of near-infrared contrast agents, arthritic joints are ideal disease entities to be assessed via optical imaging to monitor early phases of arthritis development and of therapeutic efficacy. Nevertheless, very few data are available on the mechanisms governing signaling in perfusion-based approaches. Therefore, we investigated the local accumulation kinetics of two different optical probes in arthritic joints and their suppression during glucocorticoid therapy in the course of arthritis development. Materials and Methods: The antigen-induced-arthritis (AIA) model in rats was used. Animals were divided into 3 groups: arthritic, dexamethasone via Fortecortin® and immunized only. After adjoin intravenous injection of DY-752 (size: 800 Da) and DY-682-(rat) IgG (size: 150 kDa) probes into rats, acquired composite images were unmixed into the spectrum of the respective fluorophores. Fluorescence signaling was analyzed semi-quantitatively. Probe organ distribution was assessed. Additionally, joint swelling, blood cell counts, the capability of phagocytes for probe uptake, joint vessel density, histological scoring of arthritis was determined. Results: Analysis of NIRF fluorescence signals in joints revealed a rapid accumulation of the DY-752 probe and a steadily increased one for the DY-682-IgG probe. In the course of AIA, probe accumulation kinetics in arthritic joints were similar between each other with signals peaking as early as day one post AIA. Joint swelling and histological scoring were in accordance with signaling in the course of arthritis, together with white blood cell counts which revealed high numbers of maturated neutrophils and low ones of monocytes. Phagocytes were basically capable for probe uptake which was reduced in presence of dexamethasone. Particularly after 28 days post AIA, a high probe accumulation was found in arthritic animals, independently from the probe and organ. Conclusions: NIRF signaling in the course of AIA development closely reflects the pathophysiological events in arthritic joints. Only the short-term accumulation kinetics in arthritic joints showed a size-dependency of the probe, but not signaling in the course of AIA development. Repeated treatment of animals with dexamethasone distinctly suppressed probe accumulation in arthritic joints independently of their size and structure reflecting decreased arthritis severity.

Disclosure of author financial interest or relationships:
**K. Dahlke**, None; **F. Dietzel**, None; **M.K. Boettger**, None; **M. Gajda**, None; **R. Bräuer**, None; **H. Schaible**, None; **W.A. Kaiser**, None; **I. Hilger**, None.

Presentation Number **P022**
Poster Session 1
September 5, 2012 / 18:00-18:00 / Room: The Liffey

# Imaging Anti-Atherosclerotic Therapy Response and macrophage polarization in ApoE-/- Mice Using E-selectin Targeted USPIOs

***Brigit denAdel***[1], *Carmen Burtea*[2], *Sophie Laurent*[2], *Ernst Suidgeest*[3], *Robert E. Poelmann*[1], *Robert N. Muller*[2], *Louise van der Weerd*[3,4], [1]*Anatomy and Embryology, Leiden University Medical Center, Leiden, Netherlands;* [2]*General, Organic and Biomedical Chemistry, University of Mons, Mons, Belgium;* [3]*Radiology, Leiden University Medical Center, Leiden, Netherlands;* [4]*Human Genetics, Leiden University Medical Center, Leiden, Netherlands. Contact e-mail: b.den_adel@lumc.nl*

Introduction In atherosclerotic plaque development inflammatory processes play a key role. Imaging the inflammatory response using targeted contrast agents might allow identification of patients at risk of plaque rupture, and provide insight into the disease. E-selectin, a cell surface adhesion molecule, is induced on activated endothelium and mediates leukocyte adhesion. E-selectin recruits Ly6Chi monocytes to sites of endothelial dysfunction or inflammation. Ly6Chi monocytes adhere to activated endothelium, infiltrate lesions, and become lesional macrophages. Both M1 and M2 macrophages are present in atherosclerotic lesions; their balance is decisive in the path to plaque vulnerability where M2 cells predominate. Anti-atherosclerotic treatment results in either a reduction the macrophage pool, or influences macrophage differentiation. Statin treatment reduces the attraction of Ly6Chi cells and plaque progression and stimulates emigration of Ly6Chi cells out of the plaque. In contrast, fibrate treatment activates PPAR-α, priming resident Ly6Chi monocytes for M1 differentiation. We report the imaging potential of E-selectin targeted USPIOs to visualize atherosclerotic plaques and the ability to visualize the effect of statin or fibrate treatment on the macrophage pool in ApoE-/- mice. Methods A synthetic mimetic of sialyl Lewis X E-selectin ligand or a non-specific ligand were conjugated to USPIOs (Boutry,2006). In vivo imaging potential of E-selectin USPIOs was investigated firstly in aged ApoE-/- mice with and without atorvastatin or fenofibrate treatment(8 wks, supplemented in Western diet). Secondly, in young ApoE-/- mice atherosclerosis was induced by a constrictive collar around the left carotid artery allowing timed follow-up of plaque development. MRI of the aortic arch and carotids was performed on a 9.4 T vertical Bruker system at 1.5 and 24 hours after i.v. injection. Results & discussion Anti-atherosclerotic drug treatment decreased lesion size compared to untreated animals in all treatment groups, based on T1W MRI and histology. In statin treated animals E-selectin USPIO binding sign. decreased 1.5 h after USPIO injection, whereas this was not the case for fibrate treated mice. 24 hrs after injection, USPIO uptake in the plaque is dominated by passive uptake. Passive uptake was highest in the untreated animals; statin treatment affected the passive USPIO accumulation more than fibrate treatment. We conclude statin treatment results in a large reduction of the macrophage pool, whereas the fibrate treatment show less macrophage reduction. Extend of the macrophage pool was histologically validated using F4-80 and MoMa2. M1 and M2 cells were classified according to staining for MCP-1, and iNOS or CD206 and arginase-1 respectively. M1 cells predominated in fibrate treated mice, whereas the majority of macrophages is M2 in the statin group. Conclusion Combined imaging of E-selectin and the macrophage pool allows to monitor treatment outcome of antiatherosclerotic drugs. Our results show that statin treatment had a larger effect on plaque size and macrophage pool, as well as on E-selectin-USPIO uptake compared to fibrate treatment.

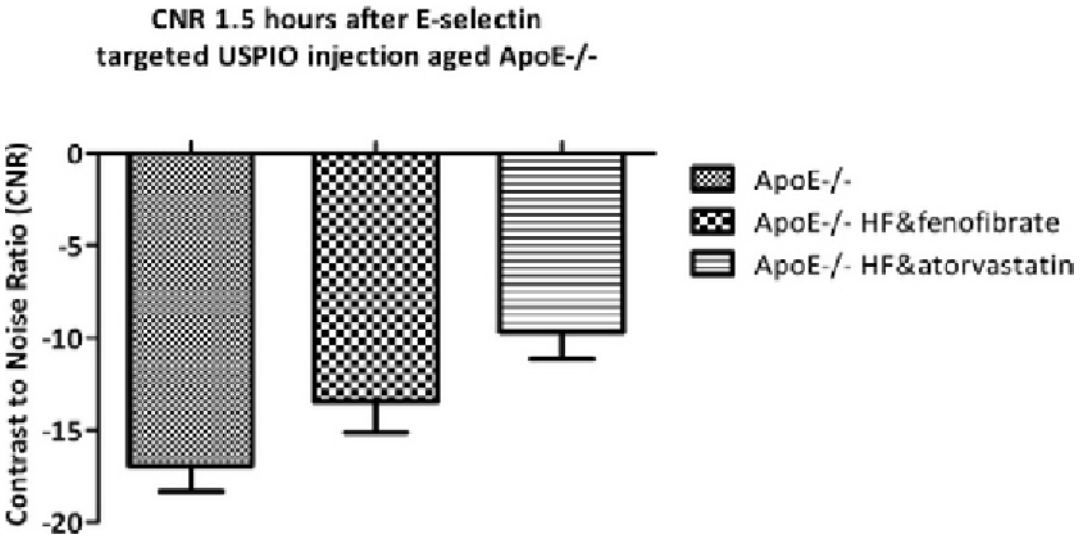


Disclosure of author financial interest or relationships:
**B. denAdel**, None; **C. Burtea**, None; **S. Laurent**, None; **E. Suidgeest**, None; **R.E. Poelmann**, None; **R.N. Muller**, None; **L. van der Weerd**, None.

Presentation Number **P023**
Poster Session 1
September 5, 2012 / 18:00-18:00 / Room: The Liffey

# Immunological analysis of targeted cancer therapy using light-emitting bacteria

***Van H. Dinh-Vu***[1,2], *Jung Eun Kim*[3], *Sin-Hyeog Im*[3], *Jung-Joon Min*[1,2], [1]*Laboratory of In Vivo Molecular Imaging, Gwangju, Republic of Korea;* [2]*Nuclear Medicine, Chonnam National University Hwasun Hospital, Gwangju, Republic of Korea;* [3]*Immune regulation and tolerance laboratory, Gwangju Institute of Science and Technology, Gwangju, Republic of Korea. Contact e-mail: dinhvan110887@yahoo.com.vn*

**Objectives:** Bacteria-mediated cancer therapy nowadays shows many promising advantages in cancer treatment compared to other conventional therapies. We have used two bioluminescent gram-negative bacterial strains *Salmonella typhimurium* defective in synthesis of ppGpp (StΔppGpp-lux) and *Escherichia coli* MG1655 (*E.coli*-lux) to treat ectopic CT26 colon cancer, interestingly, their therapeutic efficacy was different. After tail vein injection of those bacteria in tumor-bearing mice, initial tumor suppression was observed only with StΔppGpp-lux treated group, but not with *E.coli*-lux. We hypothesized that one of the reasons for tumor regression in StΔppGpp-lux treatment would be the strong immune-reaction between bacteria, tumor cells and immune cells inside tumor milieu, which couldn't be elicited by systemic injection of *E.coli*-lux. Immunological analysis was carried out by examining the modulatory cytokine profile as well as immune cell populations after StΔppGpp-lux and *E.coli*-lux infection. **Methods:** CT26 tumor-bearing mice were intravenously injected with StΔppGpp-lux or *E.coli*-lux and the tumor mass were removed at 5 dpi ('suppression stage') or when the tumor volume reach 1.500 $mm^3$ ('recurred stage') to access the relative mRNA cytokine expression in tumor mass utilizing the RT-PCR technique. Protein level of key cytokines in serum and tumor tissue in each group was examined during 'suppression stage'. Moreover, in order to identify the crucial immune cells in *Salmonella*-associated tumor regression, we analyzed the infiltrating immune cell subsets in tumor and tumor-draining lymph node by flow cytometry technique. The role of selected cytokines was further investigated by in vivo administration intravenously or intratumorally of appropriate antibody or recombinant cytokine, respectively. **Results:** Significant increase of local mRNA and protein level of IL-1β and TNF-α at 'suppression stage' was obtained only in StΔppGpp-lux-treated tumor, whereas in 'recurred stage', those levels returned to that before the treatment. Other cytokines such as IL-6, IL-10, IL-12, IFN-γ and TGF-β remained at basal level in both stages with either StΔppGpp-lux or *E.coli*-lux-infected tumors. In addition, systemic StΔppGpp-lux injection could trigger stronger immune reaction than *E.coli*-lux by increase of pro-inflammatory cytokine levels in serum and tumor mass as well as enhancement of immune cell subsets at both tumor site and lymph node. Impressively, administration of IL-1β antibody significantly diminished the effect of StΔppGpp-lux while tumor suppression was extended by local treatment of recombinant IL-1β. **Conclusions:** Taken together, these findings emphasize a crucial role of IL-1β and TNF-α in *Salmonella*-mediated therapy inducing tumor suppression as well as provide the bases for a novel combination therapy.

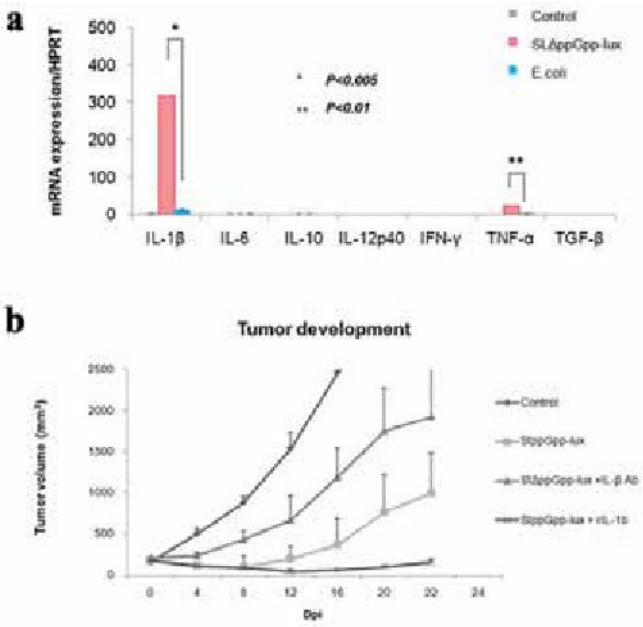


Disclosure of author financial interest or relationships:
**V.H. Dinh-Vu**, None; **J. Kim**, None; **S. Im**, None; **J. Min**, None.

Presentation Number **P024**
Poster Session 1
September 5, 2012 / 18:00-18:00 / Room: The Liffey

# Soft-matter meets condensed matter: synthesis and in vivo testing of long-circulating biocompatible stable gold nanoparticles

***Alexei A. Bogdanov***, *Gang Han[1], Suresh Gupta[1], Surong Zhang[1], [1]Radiology, University of Massachusetts Medical School, Worcester, MA, USA; [2]Biochemistry and Molecular Pharmacology, University of Massachusetts Medical School, Worcester, MA, USA. Contact e-mail: alexei.bogdanov@umassmed.edu*

Gold nanoparticles (GNPs) have been extensively tested as a platform for multiple diagnostic and imaging applications such as ultra-sensitive nucleic acid probes, radiosensitizers in radiation oncology and photoacoustic imaging. One of the major obstacles to a more widespread use of GNPs for in vivo applications is their limited biocompatibility and short half-life in circulation. We set forth to investigate whether previously developed long-circulating graft copolymer (PGC) [1,2], which is a typical example of biocompatible "soft matter", will enable the stabilization of GNPs (condensed matter) against aggregation. We synthesized and purified PGC with MPEG chains linked via stable and non-cleavable bonds to poly-L-lysine. We further used PGC for stabilizing GNPs during the synthesis using chloroauric acid in aqueous phase. Synthesis conditions were optimized using a high-throughput cross-titration PCR plate format with the parallel spectral plasmon peak analysis (Fig 1A). The stabilization of the resultant GNP with PGC was a consequence of stable coordination of surface gold atoms via free amino groups supplied by PGC which is analogous to the stabilization of GNPs with non-PEGylated polyamines [3]. The ultrafiltration-purified GNPs obtained under the optimized conditions had a gold core with a diameter of 9.3±2.6 nm (TEM, Fig. 1B), overall hydrodynamic diameter of 33.5±9.7 nm (LALLS), and zeta potential of -4.4±7.8 mV. The obtained GNPs were stable in the presence of various inorganic anions including phosphate. Trinitrobenzene sulfonic acid titration demonstrated the presence of amino groups on the surface, which were further covalently modified with various ligands and linkers including NHS-MAG3 for radiolabeling. In vivo studies in mice carrying LPS-induced inflammation lesions in femoral muscle showed that 99mTc labeled GNPs exhibited a biphasic behavior with a minor blood half-life component of approximately 4h with a stationary phase of 19.7±4.6 %ID/g blood observed at 22h after the I.V. administration (Fig. 1C). Due to their long circulation the GNPs accumulated in experimental inflammation over time as demonstrated using SPECT/CT(see Fig. 1C, arrow). Therefore, stable surface coating of GNPs with a protective layer of soft matter can yield small, stable and uniform functionalizable nanoparticles with long circulation times in the bloodstream. 1. Bogdanov A Jr. et al Radiology (1993) 187:701; 2. Bogdanov, A Jr. et al Theranostics 2012; doi:10.7150/thno.4070; 3. Song, W. et al. Small (2010) 6:239.

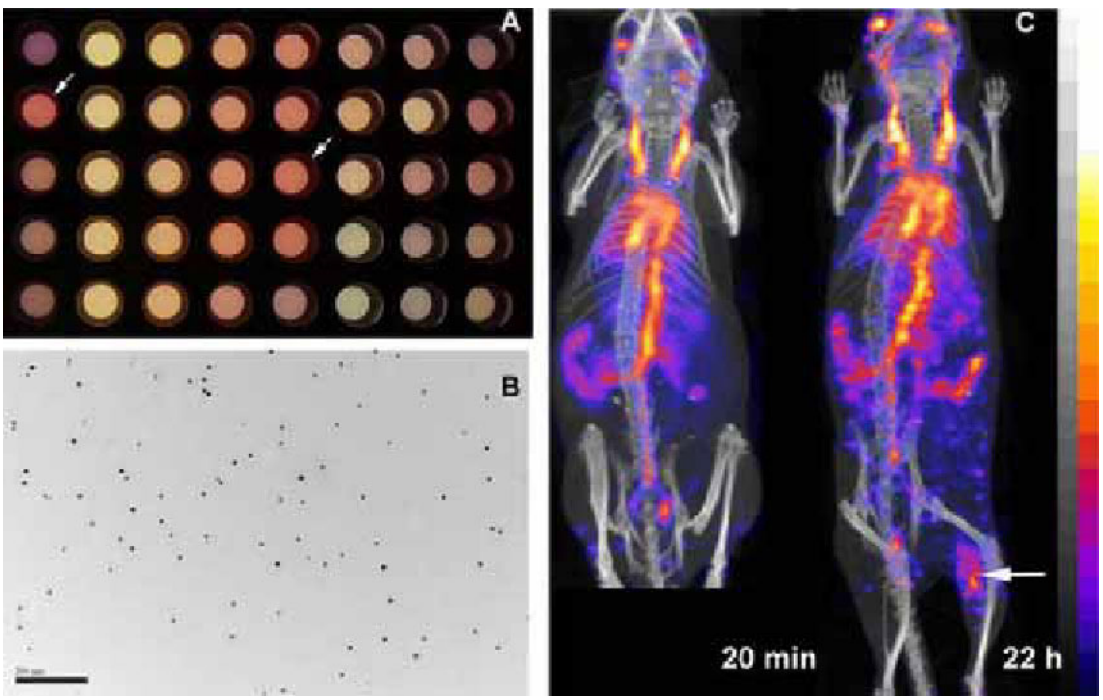


Fig.1. A- GNPs obtained at various PGC:Au ratios. GNPs with high intensity 535 nm plasmon peak are shown with arrows; B- TEM of GNP preparation shown in A with arrows. Bar= 200 nm; C- SPECT/CT of 99mTc labeled GNPs in mice at 20 min and 22 h post I.V. administration. The accumulation of GNPs in experimental LPS-induced inflammation is shown with an arrow.

Disclosure of author financial interest or relationships:
**A.A. Bogdanov**, None; **G. Han**, None; **S. Gupta**, None; **S. Zhang**, None.

Presentation Number **P025**
Poster Session 1
September 5, 2012 / 18:00-18:00 / Room: The Liffey

# Molecular Imaging of Radioiodine Labeled Eosinophil Cationic Protein: A Novel Diagnosis Tool in Allergic Inflammation Response

***Chia-Hung Hsieh**, Graduate Institute of Basic Medical Science, China Medical University, Taichung, Taiwan. Contact e-mail: chiahung2004@msn.com*

Asthma is a disorder of the conducting airways, which contract too much and too easily spontaneously and in response to a wide range of exogenous and endogenous stimuli. This airway hyperresponsiveness is accompanied by enhanced sensory irritability of the airways and increased mucus secretion. The different clinical expressions of asthma involve varying environmental factors that interact with the airways to cause acute and chronic inflammation, and the varying contributions of smooth muscle contraction, edema and remodeling of the formed elements of the airways. In recent years, clinical research has suggested an emerging clinical usefulness of eosinophil cationic protein (ECP) in the assessment and management of asthma. However, the biodistrubition and metabolism of circuiting ECP in living subjects is still unclear. The purpose of this study is to develop a novel noninvasive approach for assessing the process of asthma and the therapeutic effect for anti-allergic inflammation drugs in the living subjects. We synthesized the recombinant ECP and labeled it with I-123 by peptide radioiodination. The biodistribution and metabolism of radioiodine labeling ECP was observed in vivo by the MicroSPECT/CT imaging system. Furthermore, the microautoradiography was utilized to confirm the histological or cellular uptake of I-123- labeled ECP in the allergic inflammation. Our results demonstrated that the I-123- labeled ECP was accumulated in the intestinal mucosa and tracheal epithelium after i.v. injection into the normal mice. The metabolism and balance of circulating ECP within the body were controlled in the urinary and liver systems. Furthermore, the circuiting I-123-labeled CP has a specific targeting in the inflammation tissues in asthma mice. I-123-labeled ECP in the serum or other body fluids was uptaked and stored by the circulating neutrophils and monocytes and was accumulated in the site of allergic inflammation. Taken together, the radiolabelling ECP molecular imaging will be a good approach for overcoming the limitations of traditional approaches in assessing the severity and control of asthma because it provides noninvasive, repetitive and quantitative method to observe allergic inflammation in vivo.

Disclosure of author financial interest or relationships:
**C. Hsieh**, None.

Presentation Number **P026**
Poster Session 1
September 5, 2012 / 18:00-18:00 / Room: The Liffey

# Molecular Imaging of Macrophage Activation in Rheumatoid Arthritis-Bearing Mice

***Jeng-Jong Hwang***[1], *Chien-Hui Hsu*[1], *Wei-Hsun Wang*[1,2], *Ya-Fang Chang*[1], *Hui-Yen Chuang*[1], [1]*Biomedical Imaging and Radiological Sciences, National Yang-Ming University, Taipei, Taiwan;* [2]*Orthopedic Surgery, Changhua Christian Hospital, Changhua, Taiwan. Contact e-mail: jjhwang@ym.edu.tw*

Purpose Rheumatoid arthritis (RA) is one of autoimmune diseases, causing irreversible damage of joints, reducing quality of life and shortening the lifespan of the patients. Although the exact cause of this disease is still unclear, over-activated macrophages are reported to be highly associated with the progression of RA. 18F-FDG as the metabolic tracer seems to be ideal for imaging RA. In clinics, RA-related cytokines secreted from macrophages, such as TNF-alpha, IL-1, IL-6, are elevated in the synovial of the patients. Notably, the expression of granzyme B is often observed in the lining layers where the majority of cells are macrophages, and also in perivascular areas where macrophages and a small number of lymphocytes are mixed to form the diffuse cellular aggregates. Here, granzyme B combined with microPET/CT was also applied to detect the inflammation of RA. Methods RAW 264.7 mouse macrophage cell line constructed with a granzyme B promoter-driven luciferase reporter gene (pGBeLT) was used to examine the expression of granzyme B, and further confirmed with Western blotting and flow cytometry. We use lipopolysaccharide (LPS)-stimulated macrophage to mimic the joints of rheumatoid arthritis patients. Male DBA/1 mice, 10 wks old, were intradermal injected with bovine collagen type II. The clinical score, serum cytokines assayed with ELISA, 18F-FDG microPET/CT imaging, H&E staining and immunohistochemistry (IHC) were used to evaluate the symptom of RA. Results The expression of granzyme B in LPS-treated cells is closely correlated with the degree of the RA-related cytokines, TNF-alpha and IL-1 beta. The uptake of 18F-FDG in the joints, serum TNF-alpha and IL-1 beta were also significantly increased in mice with RA. Heavy bone erosion and macrophage accumulation in RA mice compared with those of the normal were demonstrated by H&E staining and IHC. Conclusion 18F-FDG microPET/CT may provide the longitudinal tracking of the immune reactions in RA-bearing small animal models, and facilitate the drug development for the autoimmune diseases. (This study was supported by a grant NSC 100-2321-B-010-013 from National Science Council, Taipei, Taiwan.)

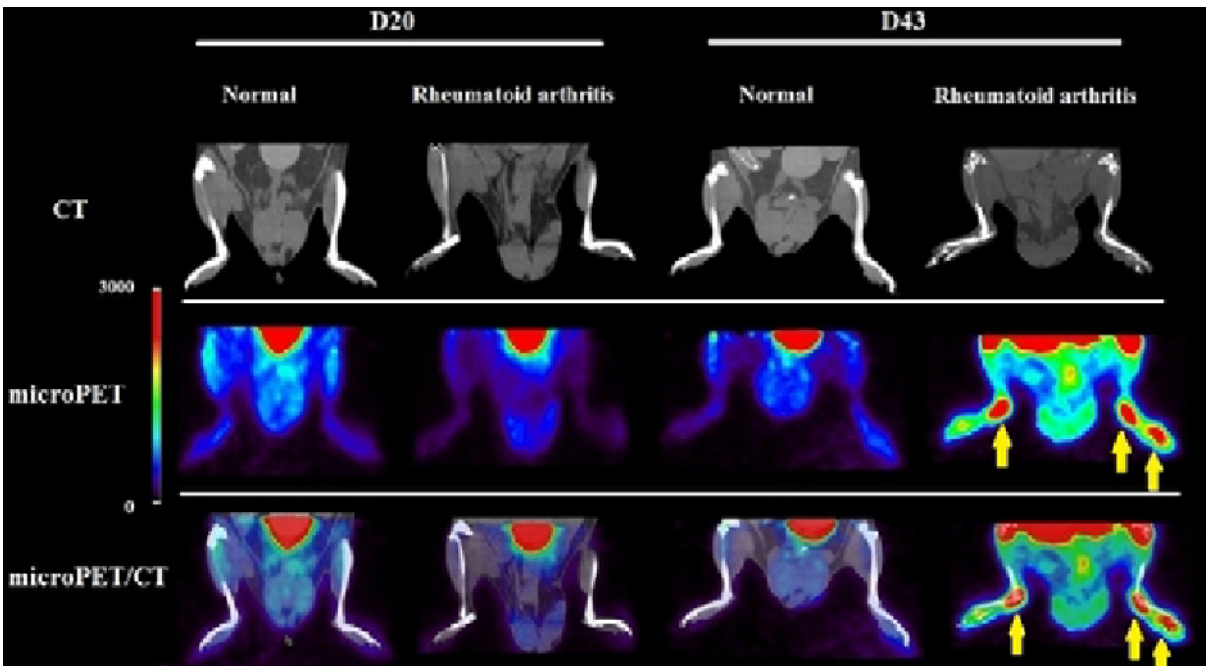


Fig. 1 [F-18]FDG PET/CT imaging of the normal and RA-bearing mice. Mice were i.v. injected with 18.5 MBq/100 ul [F-18]FDG, and imaged with microPET/CT 40 min post injection. No significant difference was found between the normal and RA mice on day 20 post first collagen induction, but severe RA could be observed (yellow arrows) on day 43.

Disclosure of author financial interest or relationships:
**J. Hwang**, None; **C. Hsu**, None; **W. Wang**, None; **Y. Chang**, None; **H. Chuang**, None.

Presentation Number **P027**
Poster Session 1
September 5, 2012 / 18:00-18:00 / Room: The Liffey

# Detection of single migrating dendritic cells in vivo by MRI

***Randall Lindquist**, Sebastian Papazoglou, Constantin Scharlach, Jörg Schnorr, Matthias Taupitz, Bernd Hamm, Eyk A. Schellenberger, Institut fuer Radiologie, Charite Universitaetsmedizin, Berlin, Germany. Contact e-mail: randall.lindquist@charite.de*

**Introduction** Dendritic cells initiate adaptive immune responses by presenting antigens to naive T cells in the T cell area of lymph nodes and the spleen. In certain cancer vaccines, autologous dendritic cells are used to to immunize patients against their own tumor cells, to generate therapeutic tumor immunity; tracking of these cells would be of great interest. Magnetic nanoparticles are often used as MR contrast agents; they provide strong T2* contrast, visible as hypointensities. Negative contrast is inherently problematic, as a relatively homogenous, strong background signal is required in order to visualize negative signal. When cells sufficiently labeled with magnetic nanoparticles are introduced into a magnetic field, their magnetic moment distorts the field into which they were introduced. The dimensions of this distortion markedly exceeds the dimensions of the cell, extending up to 400 µm, well over 20 cell diameters. We show here a novel method using MR phase images to visualize these distortions and identify individual dendritic cells *in vitro* and *in vivo*. **Methods and results** For phantom experiments, HeLa cells or primary mouse dendritic cells were labeled with iron nanoparticles and suspended in low-melting point agarose in NMR tubes; NMR tubes were placed in a falcon tube filled with agarose. All agarose was degassed by sonication and vacuum. The number of visualized spots varied linearly with the expected cell concentration, from 200 to 10,000 cells/mL. Post-processing of the MR images yields characteristic figures; cells are recognizable in the unprocessed images, but their visibility is dramatically enhanced by post-processing. An equal concentration of positively selected, unlabeled cells yielded no detectable signal. For *in vivo* experiments, dendritic cells were purified by immunomagnetic selection from mice, labeled with iron nanoparticles, and injected into the footpads of C57/Bl6 mice with LPS; contralateral footpads received LPS. Popliteal lymph nodes were imaged by MRI at time points from 4 to 48 hours post-injection. After MR imaging, mice were sacrificed and lymph nodes were analyzed histologically or by flow cytometry, to detect transferred cells and evaluate their iron content. Characteristic figures were observed in processed images, with no signal detected in uninjected or LPS-injected LNs. Subsequent FACS and histological analysis of imaged LNs revealed the presence of transferred, iron-loaded DCs only in DC-injected LNs, not in uninjected or LPS-injected LNs. MRI was performed on a 7T Bruker Pharmascan, using a volume coil for phantom experiments and a surface brain coil for in vivo experiments. **Conclusions** By imaging the magnetic field distortion induced by iron oxide nanoparticles, it is possible to detect single dendritic cells *in vitro* and *in vivo*, even though the cells themselves are markedly smaller than the individual voxels. These distortions are more specific for labeled cells than hypointensity-based negative contrast, as shown by subsequent histological and FACS analysis of imaged lymph nodes. **Acknowledgements** We would like to thank Susanne Mueller for technical assistance with MRI.

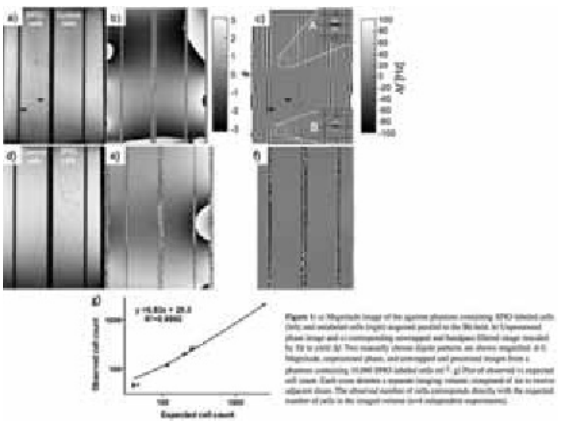

**Figure 1:** a) Magnitude image of the agarose phantom containing SPIO-labeled cells (left) and unlabeled cells (right) acquired parallel to the $B_0$ field. b) Unprocessed phase image and c) corresponding unwrapped and bandpass filtered image rescaled by TE to yield Δf. Two manually chosen dipole patterns are shown magnified. d-f) Magnitude, unprocessed phase, and unwrapped and processed images from a phantom containing 10,000 SPIO-labeled cells $ml^{-1}$. g) Plot of observed vs expected cell count. Each cross denotes a separate imaging volume, composed of six to twelve adjacent slices. The observed number of cells corresponds directly with the expected number of cells in the imaged volume (n=4 independent experiments).

Disclosure of author financial interest or relationships:
**R. Lindquist**, None; **S. Papazoglou**, None; **C. Scharlach**, None; **J. Schnorr**, None; **M. Taupitz**, None; **B. Hamm**, Deutsche Röntgengesellschaft European Congress of Radiology European Society of Euroradiology ESMRMB European School of Radiology Deutsche Forschungs-gemeinschaft, Other financial or material support; Bayer Schering Pharma Toshiba, Consultant; ESMRMB ESOR, Speakers bureau; Thieme Publishers Springer Publishers, Other financial or material support; All pharmaceutical and biochemical companies All medical technology companies All car companies, Stockholder; All pharmaceutical and biochemical companies All medical technology companies, Other financial or material support; **E.A. Schellenberger**, None.

Presentation Number **P028**
Poster Session 1
September 5, 2012 / 18:00-18:00 / Room: The Liffey

# Improved Assessment of Drug Response by Multi-modality Molecular Imaging in Collagen Antibody-induced RA

***Deanne Lister***, *Jeni Baranski, Tracey Woolliscroft, Meridith Baugher, Jeremy Castorena, Darren Shaw, Erin Trachet, Wilbur R. Leopold, Patrick McConville, Molecular Imaging, Inc., Ann Arbor, MI, USA. Contact e-mail: dlister@molecularimaging.com*

Objectives: Imaging biomarkers provide an opportunity to assess different mechanistic aspects of acute inflammation non-invasively and may aid decisions in drug discovery. The aim of this work was to test the ability for FDG PET (metabolism) and optical imaging biomarkers (cathepsin and MMP activity), via fluorescence molecular tomographic (FMT) imaging, to predict disease pathology and treatment response in mouse collagen antibody-induced rheumatoid arthritis (CAIA RA). Methods: CAIA RA was induced in female Balb/c mice by IV inj. of a monoclonal antibody cocktail on D0, followed by LPS inj. 6 days later. Footpad thickness (FT) and clinical score (CS) were used to assess disease progression. The study design incorporated untreated controls, and dexamethasone (DEX;3mpk;PO;QD) and methotrexate (MTX;3mpk;PO;QD) treated groups (n=10). PET scans of hind paws were acquired 1.5h after IV FDG inj. just before and just after the peak of swelling on D10 and on D14. Cathepsin (ProSense;PS) and MMP (MMPSense;MS) (PerkinElmer,MA) activatable fluorescent probes were injected IV 24 hours prior to fluorescence molecular tomography (imaging on D11 and D15). Histology was used to assess disease pathology with scoring for inflammation, panus, cartilage damage, bone resorption and periosteal/exostotic changes. Results: DEX produced near-full, and MTX a non-significant trend toward disease inhibition, compared to controls (VEH) based on traditional FT and CS measurements. Through FMT imaging, MS provided a more sensitive biomarker than PS due to greater disease-based activation. Hindpaw activation of MS and PS, and FDG SUV (see Fig) showed increase in untreated paws vs naïve paws, and vs DEX and MTX treated paws. The degree of modulation of all three imaging biomarkers was greater for DEX than MTX, compared with untreated controls. Histopathology scores showed significant disease inhibition for inflammation and cartilage damage (DEX and MTX) and for pannus, and bone resorption (DEX only), compared with untreated controls. Conclusions: FDG SUV and MS/PS activation provided sensitive and specific image biomarkers of acute inflammation and treatment-inhibition, in the mouse CAIA model. FDG PET imaging, and fluorescence molecular tomographic imaging of MMP and cathepsin activity via exogenous fluorescent probes all provided end points that were more predictive of disease pathology and treatment response than the traditional footpad swelling and clinical score measures in the CAIA model. These image-based biomarkers therefore provide more specific assessment of drug-based disease modification, than traditional measures, and can be used to improve decision making in RA drug discovery. FDG PET may additionally provide a translatable biomarker for use in clinical RA drug trials.

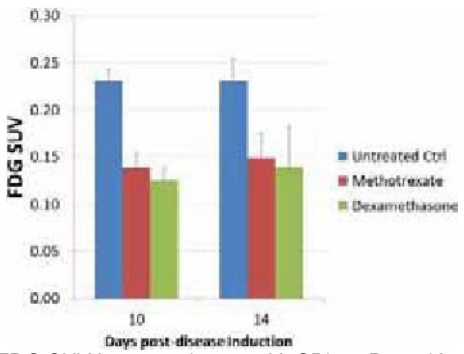


Mean FDG SUV by group (mean with SD) on Days 10 and 14.

End Points Summary (group mean values)

| Group | Max Footpad Thickness (mm) | Combined Histopath Score | FDG SUV (D10) | MMPSense Fluorescence Max (nM, D11) | ProSense Fluorescence Max (nM, D11) |
|---|---|---|---|---|---|
| Untreated Control | 8.3 | 11.4 | 0.23 | 736 | 250 |
| Methotrexate (3mg/kg; PO; QD) | 6.6 | 0.9* | 0.14* | 404* | 84* |
| Dexamethasone (3mg/kg; PO; QD) | 6.1* | 0.0* | 0.12* | 184* | 0* |

*P<0.05 vs Untreated Control

Disclosure of author financial interest or relationships:
**D. Lister**, Molecular Imaging, Inc., Employment; **J. Baranski**, Molecular Imaging, Inc., Employment; **T. Woolliscroft**, Molecular Imaging, Inc., Employment; **M. Baugher**, None; **J. Castorena**, None; **D. Shaw**, Molecular Imaging Inc., Employment; **E. Trachet**, None; **W.R. Leopold**, Molecular Imaging Inc., Employment; **P. McConville**, Molecular Imaging, Inc., Employment .

Presentation Number **P029**
Poster Session 1
September 5, 2012 / 18:00-18:00 / Room: The Liffey

# Radiolabeling optimization and targeting validation of a dual-domain cytokine ligand for inflammation imaging via TNF and IL-1 pathways

***Zhonglin Liu**, Christy Barber, Li Wan, James M. Woolfenden, Department of Medical Imaging, University of Arizona, Tucson, AZ, USA.*
*Contact e-mail: zliu@email.arizona.edu*

Tumor necrosis factor (TNF) and interleukin-1 (IL-1) are potent proinflammatory mediators in various inflammatory and autoimmune diseases. Their actions are regulated by soluble TNF receptors (TNFR1/TNFR2) and IL-1 receptor antagonist (IL-1ra). The aim of this study was to optimize radiolabeling approaches for a dual-domain fusion protein, TNFR2-Fc-IL-1ra, and validate its inflammation targeting capability via TNF and IL-1 pathways in a mouse ear edema model. **Methods**: We optimized a direct $^{99m}$Tc-labeling protocol using 2-iminothiolane (2-IT) thiolation to generate thiol binding sites. We investigated varying the molecular ratio of 2-IT to protein from 20 to 2000. Radiochemical purity (RCP) and stability were determined by high pressure liquid chromatography (HPLC). Subsequently, the optimized direct labeling approach was compared with indirect labeling via HYNIC conjugation. Radiopharmaceutical kinetics for both directly and indirectly $^{99m}$Tc-labeled TNFR2-Fc-IL-1ra was determined in healthy rats. $^{99m}$Tc-TNFR2-Fc-IL-1ra in vitro competitive binding assays were carried out using isolated rat polymorphonuclear leukocytes. The inflammation targeting capability of $^{99m}$Tc-TNFR2-Fc-IL-1ra was evaluated in a mouse model with right ear edema induced by 12-O-tetradecanoyl-phorbol-13-acetate (TPA) treatment (n=6). The left ear received vehicle only and served as a control. In vivo blocking studies were carried out by pre-injecting 500 μg unlabeled ligand (n=4). SPECT and autoradiograph images were acquired to validate tracer uptake in the inflamed ears. Inflammatory response and cytokine expression were evaluated by histological and immunohistological examination. **Results**: Radiolabeling yields increased with increasing amounts of 2-IT. When the 2-IT/protein ratio reached 1000, the radiolabeling yield was greater than 90% without significant colloid production. Stability tests showed no significant degradation of the product up to 6 hr in either saline at room temperature or serum at 37$^{o}$C. Radiolabeling yield with the HYNIC indirect approach was about 10% lower than that with direct labeling, and the product was less stable after 6 hr. In addition, HYNIC labeling resulted in significantly higher blood retention in rats compared to 2-IT thiolation. Binding of $^{99m}$Tc-TNFR2-Fc-IL-1ra to leukocytes gradually decreased with addition of increasing amounts of non-radiolabeled ligand. TPA-treated ears showed high tracer uptake, which was clearly detected by SPECT and autoradiograph imaging. Tracer activities (%ID/g) in the inflamed and control ears were 7.61±0.86 vs. 1.99±0.31 at 3 hr after injection ($P<0.05$). Blocking-study results indicated specificity of radioligand binding, with decrease in radioactive uptake in the inflamed ears to 3.61±0.35 ($P<0.05$). Western blotting showed high expression of IL-1β and TNF-α in the inflamed ears. **Conclusions**: Radiolabeling of TNFR2-Fc-IL-1ra with $^{99m}$Tc was successfully optimized. Direct labeling resulted in a more favorable kinetic profile than indirect labeling. This dual-domain ligand may provide an imaging tool for specific detection of inflammatory response in various human diseases.

Disclosure of author financial interest or relationships:
**Z. Liu**, None; **C. Barber**, None; **L. Wan**, None; **J.M. Woolfenden**, None.

Presentation Number **P030**
Poster Session 1
September 5, 2012 / 18:00-18:00 / Room: The Liffey

# Quantitative mass spectrometry imaging of elements for the characterization of animal models and distribution studies of metallo-drugs

***Andreas Matusch***[1], *Andreas Bauer*[1,2], *Johanna S. Becker*[3], [1]*Institute of Neuroscience and Medicine (INM-2), Forschungszentrum Jülich, 52425 Jülich, Germany;* [2]*Department of Neurology, Medical Faculty, Heinrich Heine University, 40225 Düsseldorf, Germany;* [3]*Central Division of Analytical Chemistry, Forschungszentrum Jülich, 52425 Jülich, Germany. Contact e-mail: a.matusch@fz-juelich.de*

Mass spectrometry imaging (MSI) allows a pixel-by-pixel chemical analysis of tissue sections and yields a set of intensity maps of ions of different mass to charge (m /z) ratios. Here we present a method where the material is ablated line by line by a focussed Nd-YAG laser and transported into the inductively coupled plasma ion source of a quadrupole mass spectrometer (LA-ICP-MSI). Sections of tissue homogenates spiked with multi-element standard suspensions serve as matrix adapted standards. The 13C signal averaged across the section serves as standard allowing the correction for different section thickness. Image reconstruction, calibration and analysis are performed using a work-up integrating software developed in house and the Pmod-package. ICP-MS is known as the MS technique with the highest concentration dynamical range spanning over nine decades for a quadrupol instrument. Typical parameters in routine applications of LA-ICP-MS are 100 µm spatial resolution, 5h analysis time for an area of 1cm2 and a precision of 11%, 13%, 10% and 16% (RSD) for the determination of Fe, Cu, Zn and Mn, respectively, in the cortex and striatum of 30 µm thick native cryosections of mouse brains. Amongst the various applications first a comprehensive overview of the distribution of Na, K, Ca, Mg, C, P, S, Fe, Cu, Zn, Mn in the healthy rat brain is presented. Next, findings in animal models of disease include constant Fe and increased Cu in the MPTP model of Parkinson's disease; increased Fe, Cu and Mn in the substantia nigra and decreased Fe and Cu in the striatum after 6-OHDA lesion of the medial forebrain bundle and a reversion of an increased Cu efflux by L-DOPA in these animals. In 1 year old APP swe single transgenic Alzheimer mice we detected a decrease of Cu. The distribution of platinum was mapped in mouse kidneys and in hair strands of a human subject treated with several cycles of cisplatiunum. The latter allowed a continuous drug monitoring over 105 days at intervals of 28.7 min allowing the determination of dose exposition, elimination half live and nadir of the outgrowth. In another animal study, we studied the distribution of 6Li after injection of a single dose of LiCl enriched in the stable isotope 6Li. Li was highly concentrated in the cortex, septal region and hypothalamus while basal ganglia and hippocampus showed lower concentrations. The quantitative study of Li-distributions in situ is an exclusive capacity of LA-ICP-MSI. Finally, element distributions in tissue sections of non-vertebrates are presented revealing fascinating functional details. In conclusion, quantitative elemental mass spectrometry imaging is a promising new method for the characterization of animal models and distribution studies of metallo-drugs.

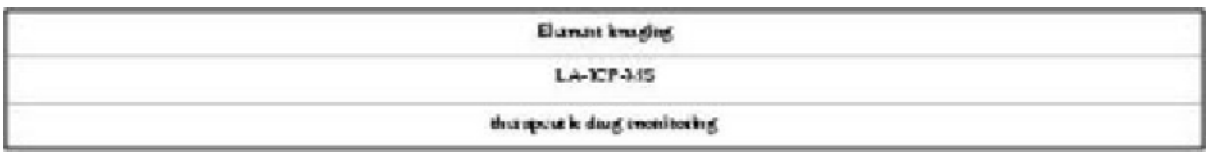


Disclosure of author financial interest or relationships:
**A. Matusch**, None; **A. Bauer**, None; **J.S. Becker**, None.

Presentation Number **P031**
Poster Session 1
September 5, 2012 / 18:00-18:00 / Room: The Liffey

# Leukocyte-Mimetic Microparticles of Iron Oxide for Noninvasive Molecular Imaging of Vascular Endothelial Inflammation

***Martina Mcateer***, *Kulveer Mankia, Neil Ruparelia, Andrew Jefferson, Leeanne Stork, Jurgen E. Schneider, Robin Choudhury, Cardiovascular Medicine, University of Oxford, Oxford, United Kingdom. Contact e-mail: martina@well.ox.ac.uk*

Background. Endothelial adhesion molecules are important mediators of monocyte recruitment to sites of vascular endothelial activation. We hypothesized that dual-ligand microparticles of iron oxide (1 μm diameter), targeted to P-selectin and vascular cell adhesion molecule-1 (VCAM-1) (PV-MPIO), would identify activated endothelial cells and enable in vivo mapping of vascular endothelial inflammation in mouse atherosclerosis using molecular magnetic resonance imaging (MRI). Methods and Results. Female apoE knockout (apoE-/-) mice, fed a standard chow diet for 8, 14, 20 or 30 weeks, underwent molecular MRI (9.4 Tesla) of the aortic root with PV-MPIO (n=6-7 per group) or control IgG-MPIO (n=2-3 per group). Dynamic non-invasive MRI showed rapid PV-MPIO binding to aortic roots in apolipoprotein E knockout (apoE-/-) mice, which was maximal 30 min post-MPIO injection (3.3 mg iron/kg) and maintained at 60 min. Minimal contrast effects were observed for control wild type C57/Bl6 mice (n=2) injected with PV-MPIO or for apoE-/- mice injected with control IgG-MPIO. Low MR signal areas, corresponding to PV-MPIO binding, were detected early during foam cell formation at 14 weeks, and increased by 1.8-fold at 20 weeks during fibrofatty lesion development (P<0.05) (Figure), but reduced 1.8-fold by 30 weeks (P<0.01). MR contrast effects were confined to regions of the root affected by atherosclerosis and not to lesion-free areas, as confirmed by histology. The number of bound PV-MPIO by histology correlated with low MR signal areas (R = 0.65; P<0.001) and lesion macrophage content (R = 0.53; P < 0.01). The contrast-to-noise ratios (CNR) of MPIO-positive lesion areas and adjacent blood pool increased by 87% (P<0.05), 100% (P<0.01) and 96% (P<0.01) at 14, 20 and 30 weeks respectively compared to equivalent pre-contrast aortic lesion areas. No difference in lesion CNR was observed between time-points. En face immunofluorescence and flow cytometry demonstrated selective binding of near-infrared fluorescently labeled PV-MPIO to activated endothelial cells (VCAM-1+ CD31+ CD11b-) in atherosclerosis-susceptible regions, with minimal association with other cell types, including macrophages or activated platelets. Conclusions. Leukocyte-mimetic MPIO bound with high affinity and specificity to activated endothelial cells. PV-MPIO rapidly achieved steady state accumulation at target, providing conspicuous MR contrast effects that can be objectively quantified. PV-MPIO binding also tracked quantitatively with lesion macrophage content across a range of lesion complexities. This approach offers a potential platform for quantitative non-invasive imaging of vascular inflammatory disease activity.

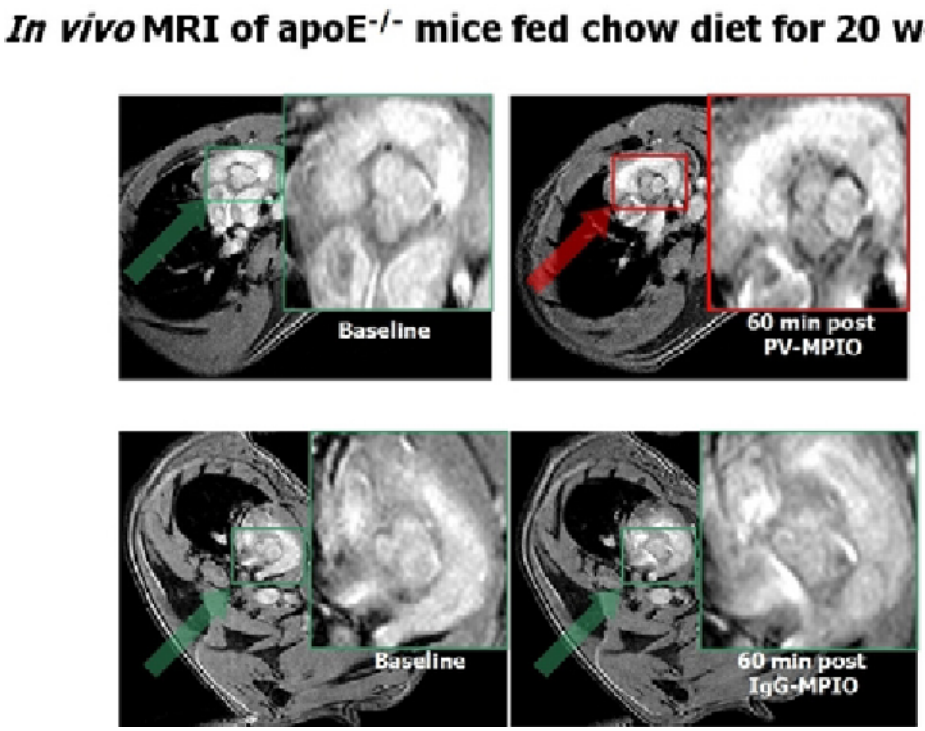


Disclosure of author financial interest or relationships:
**M. Mcateer**, None; **K. Mankia**, None; **N. Ruparelia**, None; **A. Jefferson**, None; **L. Stork**, None; **J.E. Schneider**, None; **R. Choudhury**, None.

Presentation Number **P032**
Poster Session 1
September 5, 2012 / 18:00-18:00 / Room: The Liffey

# Bimodal labeling of LPS for SPECT/CT and fluorescence dual imaging

*Vincent Duheron[1,2], **Mathieu Moreau**[1], Bertrand Collin[3], Wahib Sali[2], Claire Bernhard[1], Thomas Gautier[2], Francois Brunotte[3], Laurent Lagrost[2], Franck Denat[1], [1]Institut de Chimie Moléculaire de l'Université de Bourgogne, Dijon, France; [2]INSERM U866, Dijon, France; [3]Centre G.-F. Leclerc, Dijon, France. Contact e-mail: mathieu.moreau@u-bourgogne.fr*

Introduction: Lipopolysaccharides (LPS) or endotoxins are found inserted in the outer membrane of Gram-negative bacterias. Their appearance in blood stream triggers a massive secretion of pro-inflammatory cytokines in mammals. A controlled response allows the neutralization and elimination of LPS, whereas an excessive inflammatory response leads to severe circulatory and respiratory defects. It is the endotoxemic shock or septic shock that can leads to death [1]. Many approaches are used to study LPS, including labeling with radiochemicals (3H, 125I, 99mTc or 51Cr) or with fluorophores (FITC, Alexa488, Bodipy-FL). Bimodality is attracting more and more interest in the field of molecular imaging since the combination of two different techniques may provide complementary information, thus improving the accuracy of diagnosis. Combining nuclear modalities (PET or SPECT) with optical imaging is of particular interest, and the similar sensitivities of the two techniques allows to fuse the signaling moieties into a unique molecule, called monomolecular multimodality imaging agent (MOMIA), ensuring a same biodistribution of the two probes.[2] Method: A recently described bimodal probe, namely DOTA-Bodipy-NCS,[3] has been covalently attached to LPS. The integrity of the LPS after labeling procedure was checked by SDS-PAGE electrophoresis and β-hydroxymyristate titration (BHM). Pro-inflammatory activity of LPS was assessed by quantification of cytokines released by differentiated THP-1 cells. Results: LPS-DOTA-Bodipy was metallated with 111In to yield a high specific activity (600 MBq.mg-1), with a radiochemical purity >98 % after purification. Biodistribution of the radiolabeled compound was then evaluated in vivo in WT mice by SPECT-CT imaging. Radiolabeled LPS is rapidly eliminated from the bloodstream and accumulates in spleen and liver. Liver slices were then analyzed by confocal microscopy, and specific fluorescent signals in the cytoplasm of hepatocytes was detected, wich confirms the accumulation 111In-LPS-DOTA-Bodipy in the liver. Conclusion: These results demonstrate the efficiency of the conjugation process of our bimodal probe for biologics radiolabeling to assess biodistribution of LPS by in vivo non-invasive imaging and ex vivo fluorescence microscopy.This work proves the complementarity and the interest of combining radioisotopic and fluorescence imaging for the understanding of the elimination pathway of LPS. Acknowlegement: Support was provided by the CNRS, the University of Burgundy, the Conseil Regional de Bourgogne. References: [1] Cohen J., Glauser M. P. (1991) The Lancet, 338, 736-739, (1991). [2] Thorp-Greenwood F.L., Coogan M.P. (2010) Dalton Trans., 40, 6129-6143. [3] Bernhard, C., Goze, C., Rousselin, Y., Denat, F. (2010) Chem. Commun., 1359-7345.

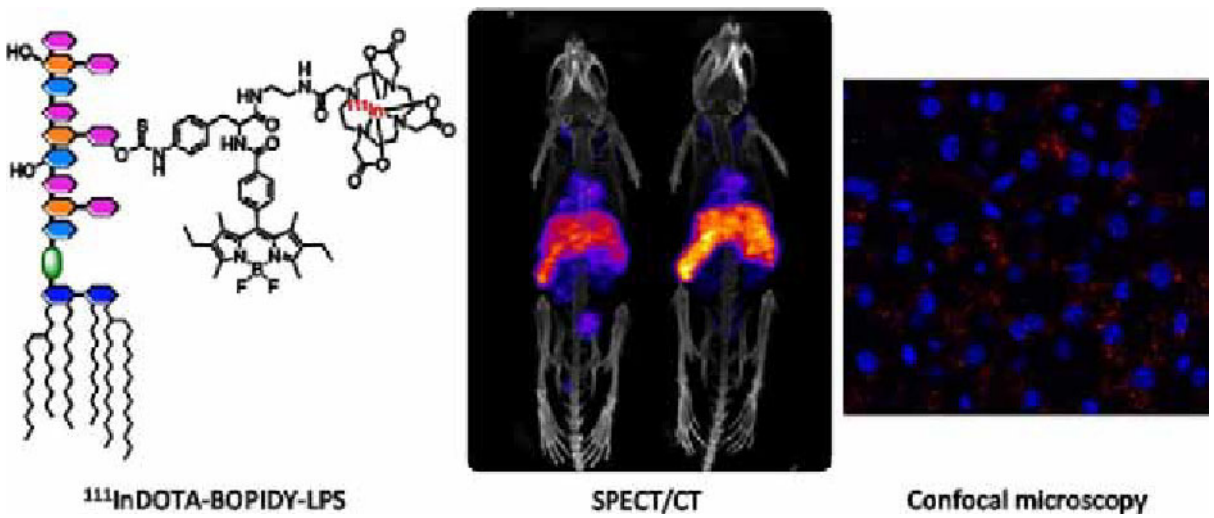


Disclosure of author financial interest or relationships:
**V. Duheron**, None; **M. Moreau**, None; **B. Collin**, None; **W. Sali**, None; **C. Bernhard**, None; **T. Gautier**, None; **F. Brunotte**, Bioscan, Grant/research support; **L. Lagrost**, None; **F. Denat**, None.

Presentation Number **P033**
Poster Session 1
September 5, 2012 / 18:00-18:00 / Room: The Liffey

# The Fate of Hyperpolarized [1-13C]Pyruvate in Livers is Determined by the Availability of Competing Substrates

***Karlos X. Moreno**, Dean Sherry, Craig Malloy, Matthew E. Merritt, Advanced Imaging Research Center, UT Southwestern Medical Center, Dallas, TX, USA. Contact e-mail: karlos.moreno@utsw.edu*

Magnetic resonance imaging of hyperpolarized (HP) 13C offers new opportunities in diagnostic imaging and for fundamental investigations of intermediary metabolism. Analysis of biochemical pathways in the liver is essential to understanding diseases such as diabetes or cirrhosis. In the liver, administration of HP [1-13C]pyruvate is followed by appearance of HP H13CO3- and 13CO2. These metabolites could be produced as a consequence of flux through one or more likely a combination of two different enzyme-catalyzed pathways; 1) the oxidative pathway representing flux through pyruvate dehydrogenase (PDH) or 2) the gluconeogenic pathway representing flux through pyruvate carboxylase (PC) followed by phosphoenolpyruvate carboxykinase (PEPCK). The latter pathway requires initial carboxylation of [1-13C]pyr. Although prior studies of livers perfused with HP [-13C]pyr indicated that HP H13CO3- and HP 13CO2 were derived largely as a result of flux through the gluconeogenic pathway but it is known that the relative contributions of these two competing pathways is sensitive to nutritional state. Here, we describe the influence of available substrates on the relative flux of HP [1-13C]pyr through PDH versus PEPCK in isolated livers. Livers from C57bl6 mice were perfused under standard conditions. Livers were perfused for 30 min using one of 3 different bolus conditions or a steady-state condition. All pyruvate and lactate containing solutions used [3-13C]pyr and [3-13C]lac. [1-13C]Pyruvate was hyperpolarized with an Oxford HyperSense DNP polarizer using the trityl radical. The HP [1-13C]pyr was injected at a 4 mM concentration over a period of 90 sec. The 13C NMR was carried out at 9.4 T using an Agilent VNMRS console. Conventional 13C NMR on tissue extracts were carried out at 14.1 T using an Agilent VNMRS console. A representative 13C NMR spectrum of a perfused liver after injection of HP [1-13C]pyr is shown in Figure 1a. As is typical in all HP experiments involving HP [1-13C]pyr, HP [1-13C]lac and [1-13C]ala were observed in all cases. The four-carbon tricarboxylic acid cycle intermediates, aspartate, fumarate and malate were also observed in all conditions studied. Although not commonly detected in liver tissue, HP 13CO2 and H13CO3- were detected for all perfusion conditions but clearly, the amounts of these products did depend upon the other substrates present in the perfusate (Figure 1b). A 3-fold increase in HP 13CO2 and H13CO3- was observed in livers perfused with lactate and pyruvate alone, and no octanoate was present. Previous results have established that most of the HP 13CO2 and H13CO3- observed would arise from PEPCK flux. To confirm the increased HP 13CO2 and H13CO3- appearance was from PEPCK flux, glutamate C4 resonances were analyzed from conventional 13C spectra of the liver tissue extracts (Figure 1c). Absent any octanoate, HP 13CO2 and H13CO3- appearance was the result of PDH flux. Thus, showing substrate availability can affect pyruvate oxidation significantly. The clinical significance of this result is that it may become possible to detect hepatic fatty acid oxidation deficiency in liver by increased bicarbonate production.

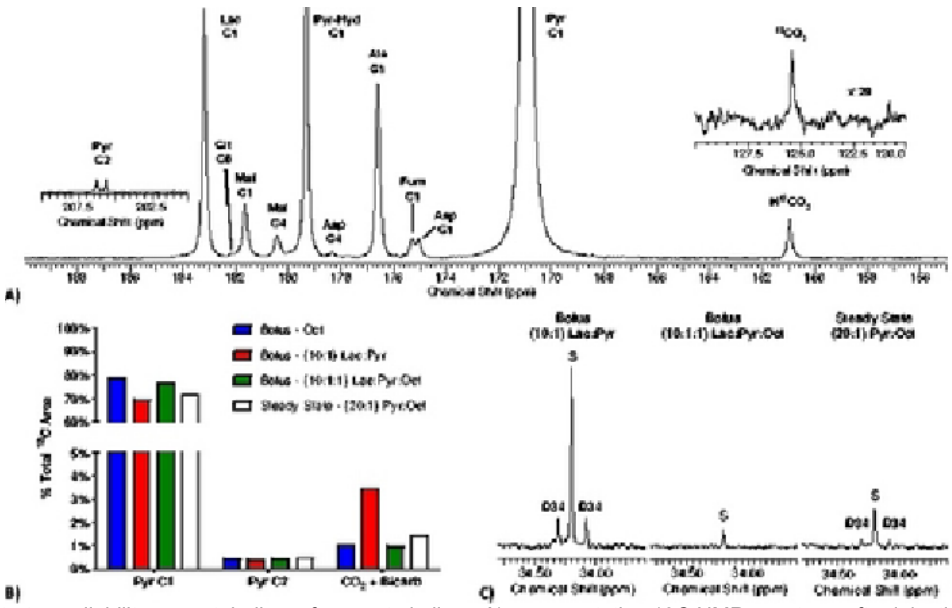


Figure 1. Effects of substrate availability on metabolism of pyruvate in liver. A) representative 13C NMR spectrum after injection of HP [1-13C]pyruvate (sum of 50 scans). B) variations in the amounts of HP H13CO3- and 13CO2 produced with differing substrate availability. C) glutamate C4 resonances of tissue extracts. (S = singlet, D34 = doublet due to C3-4 coupling).

Disclosure of author financial interest or relationships:
**K.X. Moreno**, None; **D. Sherry**, None; **C. Malloy**, None; **M.E. Merritt**, None.

Presentation Number **P034**
Poster Session 1
September 5, 2012 / 18:00-18:00 / Room: The Liffey

# Focal Muscle Vibration loading Induces Gut Inflammation

***Rao V. Papineni**, Douglas Vizard, Carestream Molecular Imaging, Carestream Health, Inc., Woodbridge, CT, USA. Contact e-mail: rao.papineni1@carestreamhealth.com*

Inflammatory diseases such as ulcerative colitis, inflammatory bowel disease, Arthritis and other diseases tend to recruit myeloid cells and result in inflammatory responses such as generation of reactive oxygen species (ROS). Development of non invasive luminescence imaging approaches is needed in evaluating and quantification of these inflammation responses. We have shown earlier that vibration loading targeted bone binding drugs to specific skeletal sites. Here we determined if the localized vibrations as any effect on the ROS production in the process. Vibration loading, was performed on athymic nude mice- subjecting them to vibration frequency of 70 Hz for 30 seconds each (3 times within a 5 minute time span) at the right thigh region. The early inflammation response ROS activity was monitored real-time in vivo using L-012 (8-amino-5-chloro-7-phenylpyridol [3,4-d]pyridazine-1,4(2H,3H)dione), a chemiluminescence reporter, using planar multimodal imaging system. 0.1 ml 1 mg/ml L-012 probe was injected (i.p.) in control and the experimental mice that were subjected to vibration loading. Significant enhancement in ROS activity was observed within 2 hrs of vibration loading predominantly in the gut region of the experimental set. The ROS activity detected as luminescence signals were more than 10-fold higher in gut region of mice subjected to localized muscle vibration loading as compared to that of the control mice. Further, the propagation of luminescence signal diminished faster in the experimental set of mice, compared to the control. This is likely due to the rapid consumption of the substrates- L-012 in mice subjected to localized vibration loading. Our results suggest abscopal molecular effects on gut physiological response due to the vibration muscle loading. Although cannot rule out completely the involvement of direct effects of vibration frequency on the gut resulting in the robust inflammatory response.

Disclosure of author financial interest or relationships:
**R.V. Papineni**, Carestream Health Inc, Employment; **D. Vizard**, Carestream Molecular Imaging, Employment .

Presentation Number **P035**
Poster Session 1
September 5, 2012 / 18:00-18:00 / Room: The Liffey

# Early diagnosis and progression visualization of rheumatoid arthritis using fluorogenic MMP-3 polymeric probes

***Ju Hee Ryu***[1], *Aeju Lee*[1], *Chang-Yong Ko*[2], *Han Sung Kim*[2], *Ick Chan Kwon*[1], *In-Chan Youn*[1], *Kwangmeyung Kim*[1], [1]*Biomedical Research Center, Korea Institute of Science and Technology, Seoul, Republic of Korea;* [2]*Department of Biomedical Engineering, Yonsei University, Wonju, Republic of Korea. Contact e-mail: jhryu@kist.re.kr*

Early start of treatment through an early diagnosis of rheumatoid arthritis (RA) could stop progression of the disease, but the early diagnosis is often associated with difficulties. Matrix metalloproteinase-3 (MMP-3) is thought to be notably important in the progression of RA. The MMP-3 polymeric probe was made by conjugating near infrared fluorescent dye, dark quencher, and MMP-3 substrate peptide, to chitosan nanoparticles. The use of fluorogenic MMP-3 polymeric probe injected intravenously, enabled a clear diagnosis of RA at two weeks after the first immunization and before any signals of anatomical or structural changes could be detected with the naked eye or micro-CT and histological analyses. Furthermore, MMP-3 polymeric probe enabled visualization progression of RA progression using near infrared fluorescent optical imaging system. The results of Western blotting and immunohistochemistry revealed the recovered fluorescence in in vivo imaging was attributed to the up-regulated MMP-3 activity in the arthritic joints. Therefore, this approach could be used for therapeutic monitoring and early diagnosis.

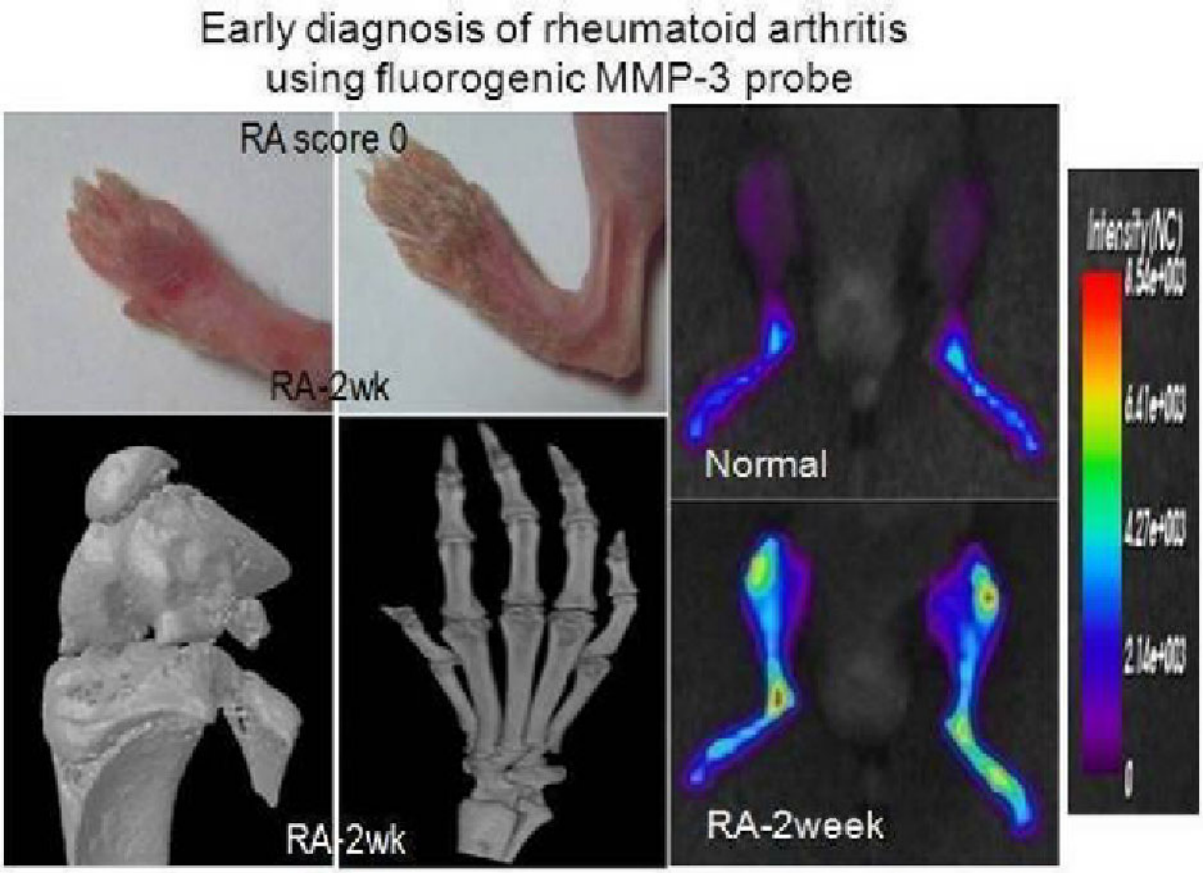


Disclosure of author financial interest or relationships:
**J. Ryu**, None; **A. Lee**, None; **C. Ko**, None; **H. Kim**, None; **I. Kwon**, None; **I. Youn**, None; **K. Kim**, None.

Presentation Number **P036**
Poster Session 1
September 5, 2012 / 18:00-18:00 / Room: The Liffey

# Near infrared fluorescent in vivo tracking of antigen presenting cells in non human primates

***Nina Salabert***[1,2], *Frédéric Martinon*[1,2], *Thierry Kortulewski*[3], *Antonio Cosma*[1,2], *Roger Le Grand*[1,2], *Catherine Chapon*[1,2], [1]*Division of Immuno-Virology, Institute for Emerging Diseases and Innovative Therapies (iMETI), CEA, Fontenay-aux-Roses, France;* [2]*UMR E1, Université Paris-Sud 11, Orsay, France;* [3]*Photonic microscopy platform, Institute of cellular and molecular radiation biology (IRCM), CEA, Fontenay-aux-Roses, France. Contact e-mail: nina.salabert@cea.fr*

Introduction: The skin is a very attractive organ for vaccination because of the high representation of the immune system, including several subsets of antigen presenting cells (APCs) which are able to migrate to the lymph nodes (LNs) and differentially stimulate T cells. Non invasive and longitudinal imaging approach is required to define the dynamics of migration of APCs located into the skin to the draining LNs after anti-HIV vaccination in order to study the mechanisms leading to induction of cellular and humoral immune responses. The objective of this study was to track APCs from the skin to the LNs using in vivo near infrared (FNIR) fluorescence imaging in a non human primate (NHP) model. Methods: A monoclonal anti-HLADR antibody, specific for APC, and its isotype control (IgG2a), labelled with a NIR fluorochrome (exc. 682nm; em. 710nm), were injected intradermally close to, respectively, the right and left inguinal draining LNs in a non infected NHP under anesthesia (n=3). In vivo imaging using a NIR fluorescent system (FluobeamTM, Fluoptics) was performed prior to and 5, 30 min, 2h, 4h, 6h, 24h, 30h and 48h post-injection. The fluorescent intensity was measured over time in both sites of injection (anti-HLADR-FNIR and IgG2a-FNIR) and in the lymph nodes using ImageJ software. Cells prepared from skin and LN biopsies were then analyzed using flow cytometry. In addition, confocal videomicroscopy was performed on whole skin biopsies to track APCs on both dermis and epidermis sides for up to 24 hours post-injection of labelled antibodies. Results: 4 hours post-injection of fluorescent labelled antibodies, 85±7% of the injected fluorescence was still measured on the injection site of the anti-HLADR-FNIR compared to 55±4% on the injection site of IgG2A-FNIR. A peak of fluorescence was observed in the draining LN 6 hours post-injection of anti-HLADR-FNIR whereas the fluorescent signal was lower and rapidly eliminated in the draining LN after IgG2a-FNIR injection. The flow cytometry analysis showed a higher number of immune cells specifically labelled with anti-HLADR-FNIR compared with the isotype control, 4 and 24 hours post-injection of labelled antibodies. These specifically labelled cells corresponded mainly to a phenotype of monocytes/macrophages (CD45+CD14+CD163+) cells. In the draining LN, 48h post-injection, cells stained by the anti-HLADR-FNIR fluorescent antibody were mainly myeloid dendritic cells (CD45+CD11c+) and B lymphocytes (CD45+CD20+). The confocal videomicroscopy confirmed that a higher number of cells were stained by anti-HLADR-FNIR compared to its isotype in the dermis and epidermis. Conclusion: In vivo NIR fluorescence imaging can be used to monitor APCs from the skin to the LNs in non human primate. This approach will permit the characterization of early cellular events in different experimental settings such as vaccination and immune therapeutic interventions.

Disclosure of author financial interest or relationships:
**N. Salabert**, None; **F. Martinon**, None; **T. Kortulewski**, None; **A. Cosma**, None; **R. Le Grand**, None; **C. Chapon**, None.

Presentation Number **P037**
Poster Session 1
September 5, 2012 / 18:00-18:00 / Room: The Liffey

# Whole animal, real-time detection of inflammation in mouse models with conjugated polymer nanoparticles responsive to reactive oxygen and nitrogen species

*Kanyi Pu, **Adam Shuhendler**, Jianghong Rao, Radiology, Stanford University, Stanford, CA, USA. Contact e-mail: adam18@stanford.edu*

Background: Reactive oxygen and nitrogen species (RONS) are important in acute (sterile or ischemic/reperfusion injury) and chronic inflammation (bacterial infection, tumor growth, cardiovascular disease, or arthritis). Local RONS generation precedes inflammatory cell arrival, providing imaging probes able to detect these pro-inflammatory chemicals the advantage of early inflammation detection. Previous probes have not been amenable to systemic administration. With the aim of whole animal imaging of inflammation, nanoparticle probes for RONS in the inflammatory microenvironment (NanoPRIME) have been designed as molecular beacons of this pathophysiological response to tissue injury. Methods: NanoPRIME were formed by nanoprecipitation of conjugated polymer and poly(ethylene glycol)-phospholipids, and the covalent surface modification with a dye (IR775-S) that allowed for both core quenching and a RONS-sensitive antenna shell. The stability and sensitivity of NanoPRIME were assessed in vitro against a variety of RONS species, as well as in cultured neutrophil-like cells and macrophages with and without stimulation by the pro-inflammatory lipopolysaccharide (LPS). The ability of NanoPRIME to identify inflammation in vivo was assessed in mouse models of LPS-induced peritonitis, spontaneous Corynebacterium bovis infection, and acute ear hole punch sterile injury. All animal fluorescence imaging was performed on a CRi Maestro hyperspectral imager with deconvolution of unactivated and activated NanoPRIME in vivo. Results: NanoPRIME were mono-dispersed with hydrodynamic diameters of less than 100 nm, and a core-shell architecture that allowed for efficient fluorescence resonance energy transfer from the excited conjugated polymer core to the quencher at the nanoparticle surface. In serum, NanoPRIME were stable over days, maintaining responsiveness to relevant levels of peroxynitrite, nitric oxide, hypochlorite and superoxide. Inflammatory cells induced by LPS activated NanoPRIME fluorescence, which was paralleled by activation in vivo by LPS-induced peritonitis. Due to their long-term stability and biocompatibility, NanoPRIME are the first RONS-sensitive fluorophore to be applied systemically and result in a long circulating probe capable of whole body detection of inflammation. Both acute (ear punch injury) and chronic inflammation (spontaneous C. bovis infection) were detected following intravenous injection of NanoPRIME without detectable activation in healthy tissues. NanoPRIME activation was observed 5 minutes following sterile injury, indicating that NanoPRIME activation precedes the arrival of cellular mediators of inflammation, and can occur in situ in direct response to RONS as chemical mediators of the early inflammatory cascade. In addition, NanoPRIME were not able to detect sites of injury following restitution, indicating the RNOS-specificity of activation. Conclusions: The sensitivity of the conjugated nanoparticle to inflammatory RONS allows NanoPRIME to identify both acute and chronic inflammatory microenvironments. NanoPRIME can clearly delineate the specific regions of pathophysiology that may require therapeutic intervention.

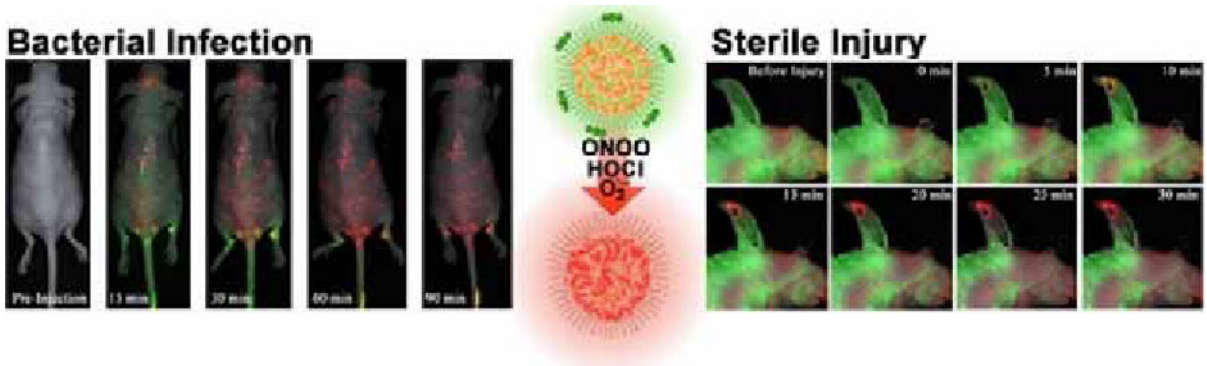


In the presence of peroxynitrite, hypochlorite, and superoxide, the FRET between the surface dye and the conjugated polymer core is abolished, activating NanoPRIME to signal inflammatory microenvironments. Left: After systemic administration, NanoPRIME accumulated (green) at the sites of spontaneous C. bovis infection in nude mice, and were then activated (red) in the inflammatory microenvironments of infection. Right: NanoPRIME were administered intravenously, followed by the induction of sterile injury to the ear. Within 5 min of injury, NanoPRIME signaled the presence of tissue injury and local inflammation, indicated by the transition from unactivated (green) to activated (red) probe.

Disclosure of author financial interest or relationships:
**K. Pu**, None; **A. Shuhendler**, None; **J. Rao**, None.

Presentation Number **P038**
Poster Session 1
September 5, 2012 / 18:00-18:00 / Room: The Liffey

# Monocyte/Macrophage Specific Fluorescent Probe Development for In Vivo Imaging of Inflammation

***Jung Sun Yoo***[1], *Sung-Chan Lee*[2], *Zhi Yen Jow*[1], *Raj Kumar Das*[1], *Pamela Yun Xiang Koh*[1], *Seong-Wook Yun*[2], *Young-Tae Chang*[1,2], [1]*Department of Chemistry, National University of Singapore, Singapore, Singapore;* [2]*Singapore Bioimaging Consortium, Agency for Science, Technology and Research (A*STAR), Singapore, Singapore. Contact e-mail: earedpotato@gmail.com*

Inflammation plays a central role in the development of numerous diseases such as arthritis, atherosclerosis, cancer and Alzheimer's disease. In recent years, imaging of inflammation has received particular attention as a tool to understand the pathophysiology during the progression of these diseases. Monocyte/Macrophage has been a major target for in vivo inflammation imaging, which reveals centers of inflammation in a patient and, thereby, contributes to diagnosis and therapeutic assessment. Labelling leukocytes with 99mTc-HMPAO has been widely used over the last 25 years as a "gold standard" for the imaging of inflammation. Because the cells labelled with 99mTc are re-injected into the patient, there are risks such as contamination of the blood cells and exposure of the operator to blood-borne pathogens. Therefore, the development of a new method to track infiltrating macrophages in inflamed areas by a direct administration of a tracer will provide significant impact in in vivo imaging and quantification of inflammation in various diseases. Our group has developed fluorescent compound libraries by combinatorial chemistry that possess significant skeletal and stereochemical diversity. Using this collection, we screened 1706 fluorescent compounds against different types of blood cells and discovered a series of probes to stain monocyte/macrophage specifically at different wavelength regions. One hit (BDNCA2-A8) from the BODIPY scaffold based library was validated in human peripheral leukocytes and adipose tissue derived cells to show high specificity for monocyte/macrophage depicting robustness as a tool for live cell imaging and fluorescence assisted cell sorting. The near-infrared fluorescent CyRCA-A4 probe was shown to target monocyte/macrophage in inflamed lesion in vivo utilizing the favourable optical properties of the NIR window, namely, relatively limited photon absorption by blood and reduced tissue autofluorescence. The localization of the NIR probe to the sites of inflammation was determined to be specific, and we validated this specific localization by successful in vivo visualization of inflammation in LPS injected mouse model as well as hind-limb ischemia model with a high target-to-background ratio. The monocyte/macrophage specific probes described above demonstrate the potential of our diversity-oriented fluorescence library approach for the development of highly selective inflammation imaging probes which will improve clinical staging of inflammation.

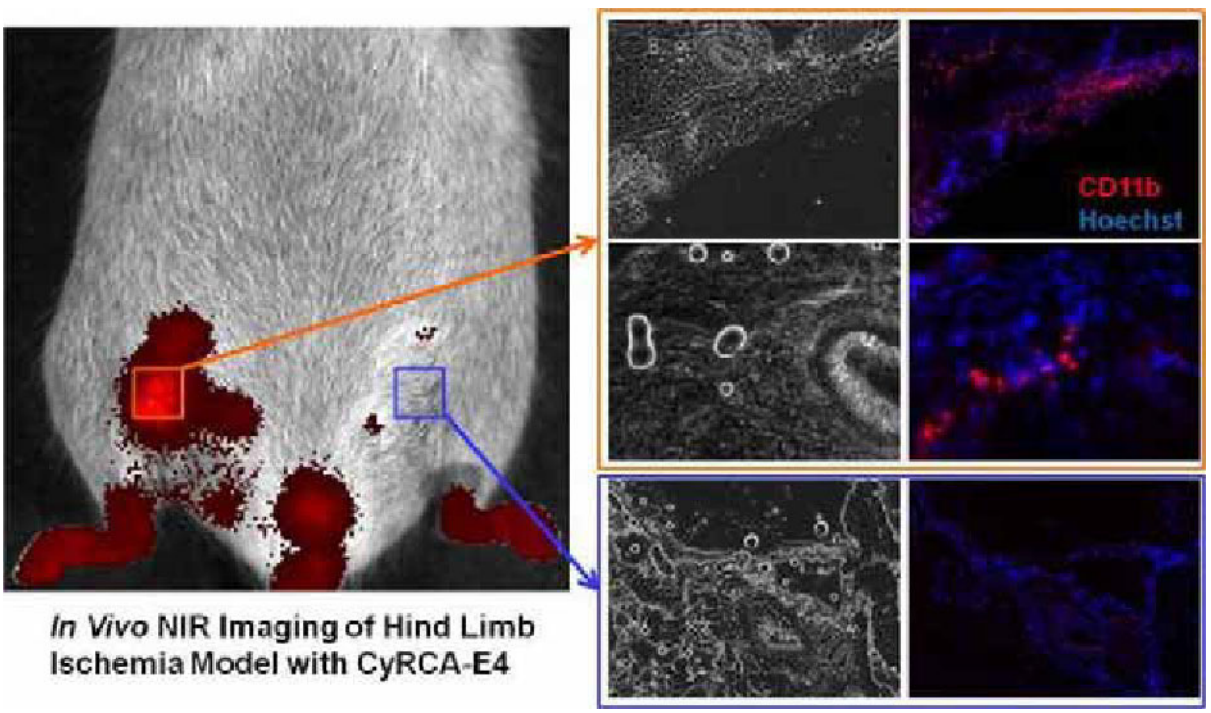


Disclosure of author financial interest or relationships:
**J. Yoo**, None; **S. Lee**, None; **Z. Jow**, None; **R. Das**, None; **P. Koh**, None; **S. Yun**, None; **Y. Chang**, None.

Presentation Number **P039**
Poster Session 1
September 5, 2012 / 18:00-18:00 / Room: The Liffey

# Brain perfusion SPECT in the mouse: physiologic pattern according to gender and age

***Ivayla Apostolova***[1], *Mathias Lukas*[1], *Jürgen Goldschmidt*[2], *Winfried Brenner*[1], *Ralph Buchert*[1], [1]*Nuclear Medicine, University Medicine Charite Berlin, Berlin, Germany;* [2]*Abteilung Akustik, Lernen, Sprache, Magdeburg, Leibniz Institute for Neurobiology, Magdeburg, Germany. Contact e-mail: ivaapost@hotmail.com*

Objective: Regional cerebral blood flow (rCBF) is a useful surrogate marker of neuronal activity and a parameter of primary interest in the diagnosis of a variety of diseases. Small animal SPECT with multi-pinhole collimators provides excellent spatial resolution at adequate sensitivity and, therefore, is a promising tool for mouse brain perfusion SPECT. The present study compared the kinetics of Tc-99m-HMPAO and -ECD in the brain of healthy mice by dynamic imaging. Further experiments investigated the regional pattern of HMPAO uptake, including lateral asymmetry, and the impact of potential covariates such as age and gender. Methods: The study included 28 healthy C57BL/6J mice. The kinetics of HMPAO and ECD in the brain was evaluated by fast dynamic planar imaging (5+5 mice, 10wk). In the remaining 18 mice (10 f, 8 m) two HMPAO SPECTs were performed, at juvenile age of 7.5±1.5wk and at young adult age of 19.1±4.0wk. Static SPECT of the brain was acquired with a nanoSPECT/CTplus (Bioscan/Mediso) equipped with general purpose mouse apertures (1.2kcps/MBq, FWHM=0.7mm). The 3-D MRI Digital Atlas Database of an Adult C57BL/6J Mouse Brain was used for ROI analysis. The SPECT images were stereotactically normalized into the atlas space using SPM8 and a custom made, left-right symmetric HMPAO template. Voxel intensities were scaled to the global HMPAO uptake. Voxel-by-voxel testing was performed in addition to ROI analysis (smoothing with an isotropic Gaussian kernel with 1.0mm FWHM, significance level p≤0.01 uncorrected, minimum cluster size of 1.0mm3). For testing of lateral asymmetry, each SPECT was left-right flipped prior to stereotactical normalization. Flipped and unflipped SPECTs were compared both on the basis of ROIs and voxel-by-voxel using paired tests. Results: Peak tracer uptake in the brain was similar for ECD and HMPAO: 1.8±0.2 and 2.1±0.6 %ID (p=0.357). However, washout from the brain after the peak was much faster for ECD than for HMPAO: 24±7 min versus 4.6±1.7 h (p=0.001). The general linear model for repeated measures with gender as intersubject factor revealed a significant increase of relative HMPAO uptake with age in the neocortex (p=0.018) and the hippocampus (p=0.012). A significant decrease was detected in the rest of midbrain (p=0.025) and the brainstem (p=0.004). A significant age*gender interaction was also found in the thalamus (p=0.050): females showed a decrease of relative HMPAO uptake (from 108.1±4.6 to 105.5 ±3.4; p=0.153) whereas there was an increase in males (from 104.0±3.2 to 106.0±4.3; p=0.182). There was a significant lateral asymmetry, with HMPAO uptake larger in the left hemisphere, primarily in the neocortex both at juvenile age (asymmetry index AI=2.7±1.7%, p=0.000) and at follow-up (AI=2.4±1.7%, p=0.000). Voxel-by-voxel testing confirmed the ROI-based findings (Fig. 1). Conclusion: High-resolution HMPAO SPECT is a promising technique for measurement of rCBF in preclinical research. It indicates age- and gender-related differences as well as lateral asymmetry of rCBF in the mouse brain during late maturation.

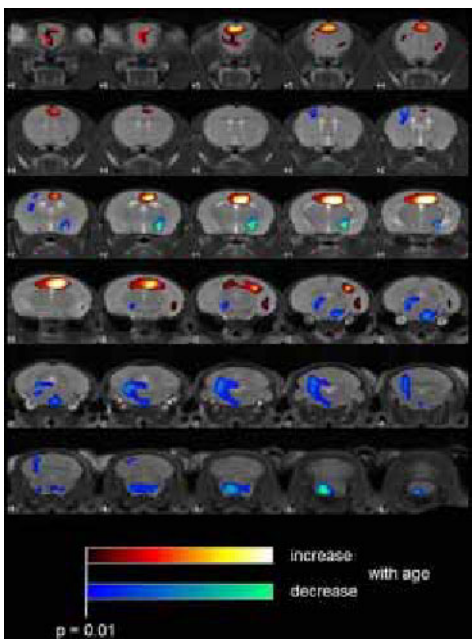


Disclosure of author financial interest or relationships:
**I. Apostolova**, None; **M. Lukas**, None; **J. Goldschmidt**, None; **W. Brenner**, nanoPET, Grant/research support; **R. Buchert**, None.

Presentation Number **P040**
Poster Session 1
September 5, 2012 / 18:00-18:00 / Room: The Liffey

# Diffusion kurtosis imaging reveals amyloidosis in the brain of APP/PS1 mice

***Christian Bigot***[1], *Greetje Vanhoutte*[1], *Sandra Pereson*[3], *Bob Asselbergh*[3], *Jelle Veraart*[2], *Jan Sijbers*[2], *Marleen Verhoye*[1], *Christine Van Broeckhoven*[3], *Annemie van der Linden*[1], [1]*Biomedical sciences, Bio-Imaging Lab, University of Antwerp, Antwerp, Belgium;* [2]*Physics, Vision Lab, University of Antwerp, Antwerp, Belgium;* [3]*Molecular genetics, VIB, University of Antwerp, Antwerp, Belgium.*
*Contact e-mail: christian.bigot@ua.ac.be*

Introduction and aim: The current study investigates the potential of diffusion kurtosis imaging (DKI) as a new magnetic resonance imaging (MRI) technique to assess amyloidosis in the brain of APP/PS1 mice. Conventional diffusion tensor imaging (DTI) assumes diffusion in an unrestricted environment(1). However, in biological tissues, there is always restriction that prohibits free water diffusion and hence we have to apply a higher b-value to probe such restricted diffusion. DKI has been proposed recently to probe such non-Gaussian diffusion property (2). Therefore, we investigated age related changes in DKI parameters of a group of APP/PS1 mice developing amyloid burden in the brain as compared to controls. Methods: DKI was conducted on a 9,4T MR system (Bruker Biospec, Ettlingen Germany) on a group of APP(swe)-PS1(L166p) and a control group WT mice at 2months (n=12/12) and was repeated at 4m (n=10/11) and 8m (n=6/6). Diffusion weighted images (DWIs) were acquired along 30 gradient directions with 7 different b-values (400, 800, 1200, 1600, 2000, 2400 and 2800s/mm2). The DWIs, together with 7 non-diffusion weighted (b0) images, were collected with a multi-slice SE 2-shot EPI sequence (TR/TE=7500/24ms, δ=5ms, Δ=12ms, acquisition matrix=96*64, zero filled to 128*64, spatial resolution:150*200*500µm3, NEX=4). Diffusion kurtosis tensor (KT) and diffusion tensor (DT) derived parametric maps were computed (Matlab), including mean kurtosis (MK), radial kurtosis (RK), axial kurtosis (AK) (figure 1A), mean diffusion (MD), axial and radial diffusion (AD, RD) parametric maps. Regions of interest were delineated in AMIRA (Mercury Computer systems, San Diego, USA) based on grey values of FA, MD and magnitude maps. Differences of diffusion parameters between WT and APP/PS1 mice were computed by means of multivariate ANOVA (Bonferroni Post-Hoc test) test in SPSS 20.0 (SPSS Inc. Chicago, USA). A subgroup of animals (n=4tg, n=4WT) was sacrificed for immunohistochemistry at 4 and 8 months. 4 sagittal slices per animal were rendered and stained for amyloid (4G8), astrocytes (GFAP) and microglia (IBA1) (figure 1D). These structures were quantified by ImageJ and expressed as percentage of the area covered. Results and discussion: Both DT and KT parameters of regions of which amyloid pathology is known (i.e. cortex, hippocampus) were analyzed and compared across ages and genotypes. In the cortex, KT parameters were significantly different across ages ($p<0.05$) within the APP/PS1 group and a significant genotype effect ($p<0.05$) was found at 8 months of age in both cortex and hippocampus (figure 1B). In contrast to KT parameters, no distinction could be made between APP/PS1 and control mice based on DT parameters, highlighting the contribution of DKI to neural tissue characterization. Immunohistochemical analyses revealed that significant differences in kurtosis parameters across genotypes and across age in the APP/PS1 group may be attributed to a higher amyloid burden and surrounding inflammatory response in APP/PS1 mice (figure 1c). Acknowledgments: This work was supported in part by EC-FP7 project NAD. References: 1. Jenssen et al., 2005 2. Wu et al., 2010

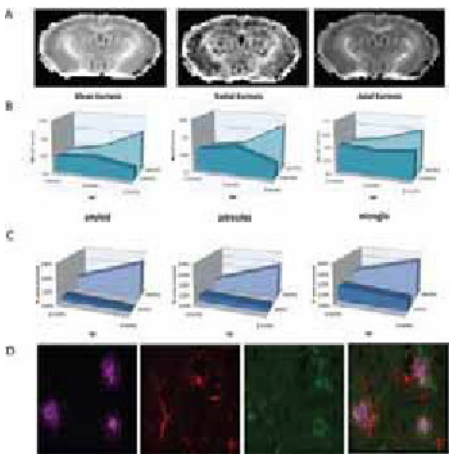

A. Parametric maps of mean kurtosis (left), radial kurtosis (middle) and axial kurtosis (right) B. Mean (left), radial (middle) and axial (right) kurtosis values of the cortex of APP/PS1 and control mice plotted across age. Note the significant genotype effect at 8 months and significant difference between 2 and 8 months within the APP/PS1 group. (0,006 < Standard error < 0,023) C. Percentage of the are covered by amyloid (left), astrocytes (middle) and microglia(right) of the cortex of APP/PS1 and control mice at 4 and 8 months of age. (standard error = 0,05 %) D. Fluorescence images of amyloid, astrocytes , microglia and overlay of mentioned structures. These are in respective order.

Disclosure of author financial interest or relationships:
**C. Bigot**, None; **G. Vanhoutte**, None; **S. Pereson**, None; **B. Asselbergh**, None; **J. Veraart**, None; **J. Sijbers**, None; **M. Verhoye**, None; **C. Van Broeckhoven**, None; **A. van der Linden**, None.

Presentation Number **P041**
Poster Session 1
September 5, 2012 / 18:00-18:00 / Room: The Liffey

# Characterization of a novel mouse model of spontaneous hemorrhagic stroke

***Salvador G. Castaneda**, Carsten Calaminus, Maren K. Koenig, Bernd J. Pichler, Department of Preclinical Imaging and Radiopharmacy, Eberhard Karls University of Tuebingen, Tuebingen, Germany. Contact e-mail: Salvador.castaneda@med.uni-tuebingen.de*

Background Hemorrhagic stroke (HS) occurs from the rupture of a vessel leading to deposition of blood on the surrounding tissue. It represents up to 13% of all strokes. HS research is limited because of its spontaneous nature. HS models usually require a surgically invasive procedure by which an autologous blood clot is injected onto the cerebral parenchyma in order to mimic the stroke. These models do not mimic accurately the pathological state of the subject previous to the acute condition. The necessity for this precondition led us to explore and initiate the characterization of a potential hemorrhagic stroke model using Magnetic Resonance Imaging (MRI), and Positron Emission Tomography (PET). Methods A multiparametric approach was made using in vivo MRI, PET, Electron Microscopy and Histology of the brain of the animals in order to determine the presence of lesions and their evolution in a 28 week longitudinal study. T1 weighted (T1w) images pre and post contrast agent injection and T2 weighted (T2w) images were acquired from the animals every two weeks (n=5). Furthermore, Apparent Diffusion Coefficient (ADC), Perfusion weighted images using Arterial Spin Labeling (ASL) and a static 10 min scan after 1 hour sleep uptake time of 18-FDG PET were also acquired. Regions of interest (ROIs) were drawn over the T2w lesions for retrospective analysis. Control animals were scanned as well. Results Hyper-intense lesions were observed from weeks 6 to 24 on post contrast T1w images with an increasing lesion volume both in striatal and cortical regions on the HS model animals. The volume of lesions peaked from week 12 to 24 with a maximum volume of 6mm3 and a minimal of 1mm3. No lesions were found on pre contrast images or in controls. Hypo-intense lesions in T2w images were observed from week 12 showing an increased volume until the end of the study. Maximum T2w lesion volume was 1mm3 and the minimum was 0.1mm3. Cortex lesions showed higher maximum lesion volume of 4.4mm3 in T2w images in comparison to striatum. The analysis of the T2w lesion ROIs corresponding to the ADC, ASL, and FDG maps suggest a specific pattern of development. ADC was notably increased on final lesion areas with suitably low perfusion. The FDG showed a constant increase that correlated positively with increased ADC but later lowered accompanied by decreased perfusion. Macroscopic observation, Electron microscopy and Histology showed disruption of capillaries and hemorrhage in the brain tissue. Conclusion Our results demonstrate this mouse model produces lesions on striatal and cortical regions of the brain measureable by MRI. The pattern of formation of these lesions studied longitudinally in vivo with MRI suggest a rupture of capillaries that lead to hemorrhage in the brain parenchyma which is represented by diffuse leakage lesions seen on the T1w post contrast images. These results show a potential HS model which could be useful for the study of preventive therapies and pathophysiology. Further studies of lesion formation, characterization, and their coincidence with behavioral abnormalities are currently underway to determine if the model is mimicking the human disease.

Disclosure of author financial interest or relationships:
**S.G. Castaneda**, None; **C. Calaminus**, None; **M.K. Koenig**, None; **B.J. Pichler**, Siemens, Grant/research support; AstraZeneca, Grant/research support; Bayer Healthcare, Grant/research support; Boehringer-Ingelheim, Grant/research support; Oncodesign, Grant/research support; Merck, Grant/research support; Bruker, Grant/research support .

Presentation Number **P042**
Poster Session 1
September 5, 2012 / 18:00-18:00 / Room: The Liffey

# Utilization of Bioluminescence Imaging to target and monitor radiation responses in an orthotopic glioma model - a pilot study

***Thomas Flannery***, *Shahnaz Al-Rashid, Stewart Church, Stephen McQuaid, Brian Herron, Kevin Prise, CCRCB, Queen's University Belfast, Belfast, United Kingdom. Contact e-mail: t.flannery@qub.ac.uk*

Introduction Malignant gliomas are the most common primary malignant brain tumour. In spite of radical surgical resection, radio/chemotherapy, tumour recurrence is inevitable resulting in the extremely poor patient outcomes observed. Various experimental models are in use to investigate the potential efficacy of novel more effective therapies for malignant glioma. In vitro assays provide an artificial environment for estimation of glioma tumorigenesis and do not reflect the complex interactions of the host-tumour microenvironment. The aim of this study was to investigate the potential for bioluminescence imaging (BLI) to study radiation responses using an orthotopic glioma model. Methods Following the necessary animal licensure approval, the human glioblastoma U87 cell line was stably transfected with luciferase reporter gene to monitor tumour growth and treatment response. Tumour cultures were propagated as neurospheres and subsequently injected into the basal ganglia of anaesthetised athymic nude mice using a stereotactic frame. Bioluminescence measurements were recorded over a 6-week period to document tumour growth, to target radiation exposure to the tumour (using a custom-made lead jig) and monitor response to radiation exposures (2Gy and 5Gy). Animals were monitored for signs of neurological/general deterioration and the brain removed from sacrificed animals for further evaluation. Results All animals tolerated radiation exposures well without apparent adverse effect. Irradiation of mouse brain using BLI-guidance and lead shielding was confirmed to increase markers of DNA damage following radiation exposure (confirmed on immunohistochemistry using anti-53BP and γ-H2AX antibodies). BLI measurements were also observed to decrease significantly following irradiation but to eventually recover and "catch up" on BLI measurements of non-irradiated control tumours. The progressive increase in BLI measurements correlated well with clinical deterioration in animals. Conclusion BLI can be used for both targeting radiation to orthotopic gliomas and for monitoring treatment response.

Disclosure of author financial interest or relationships:
**T. Flannery**, None; **S. Al-Rashid**, None; **S. Church**, None; **S. McQuaid**, None; **B. Herron**, None; **K. Prise**, None.

Presentation Number **P043**
Poster Session 1
September 5, 2012 / 18:00-18:00 / Room: The Liffey

# Assessing neurodegeneration, neuroinflammation and adult neural stem cell properties in a 6-OHDA Parkinson's disease mouse model using multimodal molecular imaging

***Inga B. Fricke***[1,2]*, Thomas Viel*[1]*, Alexis Vrachimis*[1,3]*, Maik Worlitzer*[2]*, Andreas Faust*[1]*, Lydia Wachsmuth*[4]*, Klaus Kopka*[3]*, Cornelius Faber*[4]*, Bertrand Tavitian*[5]*, Frederic Dolle*[5]*, Jens C. Schwamborn*[2,6]*, Andreas H. Jacobs*[1,6]*, [1]European Institute for Molecular Imaging (EIMI), University of Muenster, Muenster, Germany; [2]ZMBE, Institute of Cell Biology, Stem Cell Biology and Regeneration Group, University of Muenster, Muenster, Germany; [3]Department of Nuclear Medicine, University Hospital Muenster, Muenster, Germany; [4]Department of Clinical Radiology, University Hospital Muenster, Muenster, Germany; [5]CEA, I2BM, Service Hospitalier Frédéric Joliot, Orsay, France; [6]Interdisciplinary Centre for Clinical Research (IZKF), University of Muenster, Muenster, Germany. Contact e-mail: ifricke@uni-muenster.de*

**Introduction:** Parkinson's disease (PD) is the most common neurodegenerative disorder affecting motor function. It is caused by degeneration of dopaminergic neurons in the *substantia nigra* (SN). Currently only symptomatic treatment options exist. Therefore, regenerative approaches based on endogenous stem cell recruitment are appealing. The subventricular zone (SVZ) is a neurogenic niche in the adult brain, which provides neural stem cells migrating to the olfactory bulb as well as to lesion sites. However, degeneration of dopaminergic neurons is accompanied by neuroinflammation affecting neural stem cell properties. **Aim:** To non-invasively monitor neurodegeneration (ND), neuroinflammation (NI), and stem cell migration in a mouse model of PD by multi-modal molecular imaging employing micro single photon emission computed tomography (µSPECT), micro positron emission tomography (µPET), micro magnetic resonance imaging (µMRI) and *in vivo* bioluminescence imaging (BLI). **Methods:** Degeneration of the nigrostriatal system was induced by unilateral 6-Hydroxydopamine (6-OHDA) injection into the left SN of C57Bl6 mice. Controls were infused with vehicle. Three weeks after injection, integrity of the nigrostriatal system was assessed by [$^{123}$I]Ioflupane-µSPECT and microglia activation by [$^{18}$F]DPA-714-µPET. T2-weighted µMRI was performed in order to obtain anatomical information. Lentiviral-based reporter constructs carrying the firefly luciferase (fLuc) and mCherry genes under the control of different stem-cell specific and ubiquitous promoters are being constructed to analyze stem cell properties after injection into the SVZ using BLI and immunohistochemistry. **Results:** Three weeks after neurotoxin injection, µSPECT scans revealed a strong decrease in dopamine transporter ligand accumulation in the left striatum, compared to the normal right striatum. µPET with the TSPO ligand [$^{18}$F]-DPA-714 indicates an increase in tracer accumulation in the 6-OHDA-lesioned SN compared to the control region. These imaging results are currently being verified using immunohistochemistry. Experiments based on lentiviral vectors encoding fLucIRESmCherry under specific promoters to investigate neuroinflammation induced changes of stem cell properties are currently being performed. **Conclusions:** Combination of µSPECT, µPET and µMRI allows the assessment of neurodegeneration and neuroinflammation in the PD mouse model. Neural progenitor cell migration shall be followed using lentiviral-based reporter vectors and BLI. Stem cell differentiation-stage specific promoters will be used to visualize the influence of ND and NI on stem proliferation, migration and differentiation. **Acknowledgements:** The research leading to these results has received funding from the Interdisciplinary Center for Clinical Research (IZKF); Muenster; Germany (project SchwJ3/001/11) and the European Union's Seventh Framework Programme (FP7/2007-2013) under grant agreement n° 278850 (INMiND).

Disclosure of author financial interest or relationships:
**I.B. Fricke**, None; **T. Viel**, None; **A. Vrachimis**, None; **M. Worlitzer**, None; **A. Faust**, None; **L. Wachsmuth**, None; **K. Kopka**, None; **C. Faber**, None; **B. Tavitian**, None; **F. Dolle**, None; **J.C. Schwamborn**, None; **A.H. Jacobs**, Merck, Germany, Grant/research support .

Presentation Number **P044**
Poster Session 1
September 5, 2012 / 18:00-18:00 / Room: The Liffey

# Are subventricular zone endogenous neural stem cells responsible for the remyelination of the corpus callosum in the Cuprizone mouse model? An in-vivo bioluminescence and magnetic resonance imaging study

***Caroline Guglielmetti***[1,2], *Jelle Praet*[1,2], *Ruth Vreys*[1], *Janaki Raman Rangarajan*[3], *Frederik Maes*[3], *Marleen Verhoye*[1], *Peter Ponsaerts*[2], *Annemie van der Linden*[1], [1]*Department of Biomedical Sciences University of Antwerp, Bio Imaging Lab, Wilrijk, Belgium;* [2]*Department of Biomedical Sciences University of Antwerp, Laboratory of Experimental Hematology, Wilrijk, Belgium;* [3]*Medical Image Computing - ESAT/PSI, IBBT-KU Leuven Future Health Department, KU Leuven, Leuven, Belgium. Contact e-mail: caroline.guglielmetti@ua.ac.be*

Introduction: The Cuprizone (CPZ) mouse model is a valuable tool to study demyelination and remyelination processes[1]. We investigated if subventricular zone (SVZ) neural stem/progenitors cells (NSPC) migrate towards demyelinated areas and contribute to remyelination and for this purpose, NSPC were labelled with either micron-sized iron oxide particles (MPIO)[2] or with a lentiviral vector encoding the eGFP and Luciferase reporter proteins[3]. Magnetic resonance imaging (MRI) and bioluminescence imaging (BLI) were used to follow in vivo the migration of the labelled NSCP. Methods: Demyelination was induced by feeding eight weeks old mice a diet mixed with CPZ (0.2%) for a period of 4 weeks starting the day prior to SVZ NSPC labelling. MPIOs were injected intraventricular in twelve female C57BL/6 mice (n=6 CPZ treated mice; n=6 Controls, normal diet). MRI was performed on a 9.4T scanner in vivo at 4, 6 and 12 weeks post-injection (p.i.) and ex vivo at 12 weeks p.i. Quantification of MPIO load is based on the difference of the mean intensity values in the injected versus non injected olfactory bulb (OB) regions corrected by the standard error of the mean[4]. SVZ NSPC of C57BL/6J-Tyrc-2J/J (n=18 CPZ treated) were labelled following in situ transfection with an eGFP-T2A-Fluc lentivirus. BLI was performed weekly for a 12-week period. The ratio of the BLI signal in the OB to the total BLI signal measured was calculated to assess migration towards the OB. Immunofluorescent staining was performed for astrocytes, microglia, and neurons. Hypothesis: As CPZ-induced demyelination is associated with oligodendrocyte cell death in the splenium of the corpus callosum (CC), we expected MPIO and eGFP-T2A-Fluc labelled NSPC, or cells derived there-off, to end up in the splenium as observed with MRI, BLI and subsequent histological analysis. Results: MRI revealed hypointense voxels in OB for Controls and CPZ treated animals (A). However no significant differences between the two groups at 12 weeks p.i. could be detected ($p>0.05$, unpaired t-test). BLI showed a significant migration towards the OB over time starting from week 5 p.i. (repeated ANOVA, $p<0.05$) (B). No migration towards demyelinated areas could be detected with either of the two methods. Immunofluorescent analysis revealed that MPIO colocalized with neurons, astrocytes and microglia and that eGFP only colocalized with neurons (C). Conclusions: In situ labelling of endogenous NSPC showed no differences in SVZ NSPC-derived neuronal cell migration towards the OB between CPZ treated and Control mice and both MRI and BLI revealed no migration of labelled cells towards demyelinated areas, e.g. the splenium of the CC. Therefore our results, verified by histological analyses, suggest the involvement, either by nature or localisation, of different progenitor cells during remyelination. Acknowledgements: This work was supported in part by 7th FW INMiND GA N°278850. References: [1] Matsushima G K et al; Brain Pathology, 11: 107-116 (2001) [2] Vreys R et al; NeuroImage 49: 2094-2103 (2010) [3] Reumers V et al; Stem Cells 26: 2382-2390 (2008) [4] Vande Velde G et al; Neuroimage, minor revisions

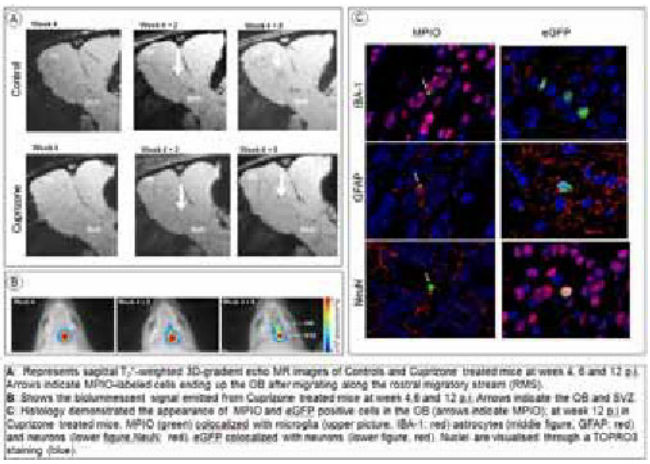


A: Represents sagittal $T_2$*-weighted 3D-gradient echo MR images of Controls and Cuprizone treated mice at week 4, 6 and 12 p.i. Arrows indicate MPIO-labeled cells exiting up the OB after migrating along the rostral migratory stream (RMS).
B: Shows the bioluminescent signal emitted from Cuprizone treated mice at week 4,6 and 12 p.i. Arrows indicate the OB and SVZ.
C: Histology demonstrated the appearance of MPIO and eGFP positive cells in the OB (arrows indicate MPIO); at week 12 p.i. in Cuprizone treated mice. MPIO (green) colocalized with microglia (upper picture, IBA-1: red) astrocytes (middle figure, GFAP: red) and neurons (lower figure,Neun: red). eGFP colocalized with neurons (lower figure, red). Nuclei are visualised through a TOPRO3 staining (blue).

Disclosure of author financial interest or relationships:
**C. Guglielmetti**, None; **J. Praet**, None; **R. Vreys**, None; **J. Rangarajan**, None; **F. Maes**, None; **M. Verhoye**, None; **P. Ponsaerts**, None; **A. van der Linden**, None.

Presentation Number **P045**
Poster Session 1
September 5, 2012 / 18:00-18:00 / Room: The Liffey

# in vivo imaging of dermal nerve-endings using SPECT/CT

***Catey L. Harwell***[1], *Mary Germino*[1], *Tamara L. Anderson*[2], *Kelly D. Orcutt*[1], *Jacob Hesterman*[1], *Monique Nysus*[2], *Jeffrey P. Norenberg*[2], *Jack Hoppin*[1], *Ajay Verma*[3], [1]*inviCRO, LLC, Boston, MA, USA;* [2]*College of Pharmacy, University of New Mexico, Albuquerque, NM, USA;* [3]*Biogen Idec, Cambridge, MA, USA. Contact e-mail: harwell@invicro.com*

Dermal nerve-endings are involved in many pain and sensory syndromes and currently require skin biopsies for their quantitation. Improved methods for quantifying dermal endings could be very useful for assessing disease progression and treatment response. In a previous study, researchers mapped catecholaminergic nerve ending distribution in rat skin using in vivo 125I-tyrosine labeling followed by ex vivo autoradiography. We used longitudinal in vivo SPECT/CT imaging with 125I-tyrosine to develop a novel imaging-based approach for qualitative and quantitative analysis of dermal nerve endings. Our methods can be adapted to the study of other types of dermal nerve fibers. Six male Sprague-Dawley rats were injected intravenously (IV) with ~1.25 mCi of 125I-tyrosine and imaged at 0, 4, and 24 hours post-injection (Fig. 1a, CT in gray, SPECT in orange/purple). For select animals, the skin was removed following the last image acquisition and ex vivo gamma counter measurements were performed. For each image, the CT was smoothed with a Gaussian filter and the animal's body contour was extracted via Otsu histogram-based thresholding. Hole-filling and pruning methods were applied to the body ROI to eliminate holes and narrow protrusions. The surface of the ROI was eroded and separately dilated; the result of the erosion was subtracted from that of the dilation to yield a 3.2mm-thick skin region-of-interest (ROI). Application of the skin ROIs to the SPECT reconstructions resulted in maps of skin SPECT uptake for each individual data set. Data were transformed to a common space by mapping segmented skin ROIs from each time point to a reference rat outline in 2D using a custom polar analysis routine. Further, a point-by-point registration algorithm was used to map each individual skin ROI to a 3D reference rat skin ROI. Individual 2D and 3D distributions were averaged to form temporal maps of the SPECT distribution of 125I-tyrosine as shown for individual time points in Figure 1b (2D) and Figure 1c (3D). Several zones, based on uptake patterns and physiological landmarks were identified in each set of images and used to build 3D (Fig. 1d) and 2D atlases of 125I-tyrosine distribution. Patterns of uptake were consistent with previously published ex vivo findings. Estimated in vivo percent injected dose per gram quantities correlated well with ex vivo estimates. The methods we have developed demonstrate in vivo 3D qualitative and quantitative evaluation of dermal nerve endings for the first time. Our methods can be applied to other probes that identify specific populations of dermal nerve endings in order to monitor progression of disease states such as diabetic neuropathy as well as response to treatment.

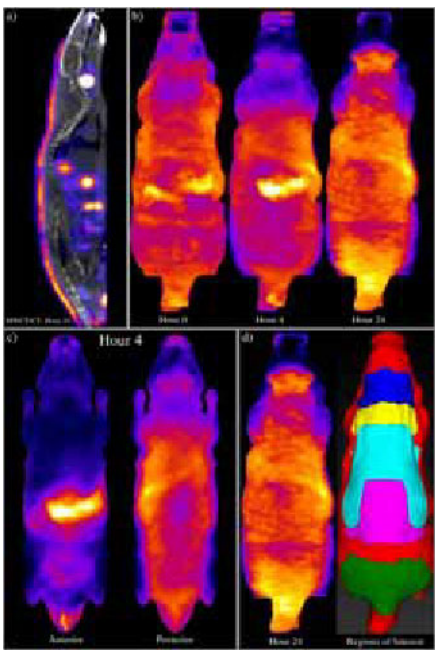


Disclosure of author financial interest or relationships:
**C.L. Harwell**, inviCRO, LLC, Employment; **M. Germino**, None; **T.L. Anderson**, None; **K.D. Orcutt**, inviCRO, Employment; **J. Hesterman**, inviCRO, Employment; **M. Nysus**, None; **J.P. Norenberg**, inviCRO, Grant/research support; Millennium Pharmaceuticals Inc, Consultant; Bracco Inc, Grant/research support; Hybridine Inc, Grant/research support; Positron Inc, Grant/research support; **J. Hoppin**, inviCRO, LLC, Employment; inviCRO, LLC, Stockholder; **A. Verma**, Biogen Idec, Employment .

Presentation Number **P046**
Poster Session 1
September 5, 2012 / 18:00-18:00 / Room: The Liffey

# [123I]Epidepride Neuroimaging of Dopamine D2D3 Receptor in Risperidone-treated Chronic MK-801 Rat Schizophrenia Model

***Yuan-Ruei Huang***, *Chieh Huang, Yu-Lung Wu, Kai-Hung Cheng, Jun-ming Shih, Kang-Wei Chang, Institute of Nuclear Energy Research, Longtan Township, Taiwan. Contact e-mail: yuanruei@iner.gov.tw*

Objectives The affinity of Iodine-123 form of epidepride is in picomolar range that makes it useful for microSPECT imaging of the D2/D3 receptors in brain, including the low density extrastriatal receptors. Our previous study indicated [123I]epidepride neuroimagings were available for tracing the alteration of striatal and extrastriatal dopamine system in chronic MK-801-induced rat schizophrenia model. Aim of present study is applied the [123I]epidepride neuroimaging platform to evaluate therapeutic effect of risperidone treatment on this animal model. Method(s) Rats received repeated injection of MK-801 (dissolved in saline, i.p., 0.3mg/kg per day) or saline for 5 weeks. Risperidone was injected intraperitoneally once a day for 4 weeks, beginning 1 week after the first administration of MK-801. After drugs treatment, total distance traveled (cm) and social interaction changes were tested. We obtained [123I]epidepride neuroimages from ex vivo autoradiography and microSPECT/CT and evaluated the changes of specific binding ratio. Result(s) Chronic MK-801 treatment for 5 weeks caused significantly increased local motor activity and induced an inhibition of social interaction. Moreover, repeated risperidone treatment could attenuate chronic MK-801-induced negative deficit but not the positive deficit. [123I]epidepride microSPECT/CT neuroimaging and ex vivo autoradiography were performed on striatum and midbrain. There were statistically significant decreases in specific binding ratio (SBR) in both striatum and midbrain between saline and MK-801 group. Meanwhile, in repeated risperidone treatment group, SBR of [123I]epidepride in striatum and midbrain were nearly identical to the SBR in saline group. . Conclusion We establish a rat schizophrenia model by chronic MK-801 administration for 5weeks. MicroSPECT imaging and ex vivo autoradiograph show that the MK-801-induced decrease in specific binding ratio of [123I]epidepride is prevented by risperidone treatment. Overall, the results indicate that [123I]epidepride imaging platform in our experiment is available for tracing the MK-801-induced changes in dopamine system. Most importantly, it could also be applied to the evaluation of the effects of antipsychotics.

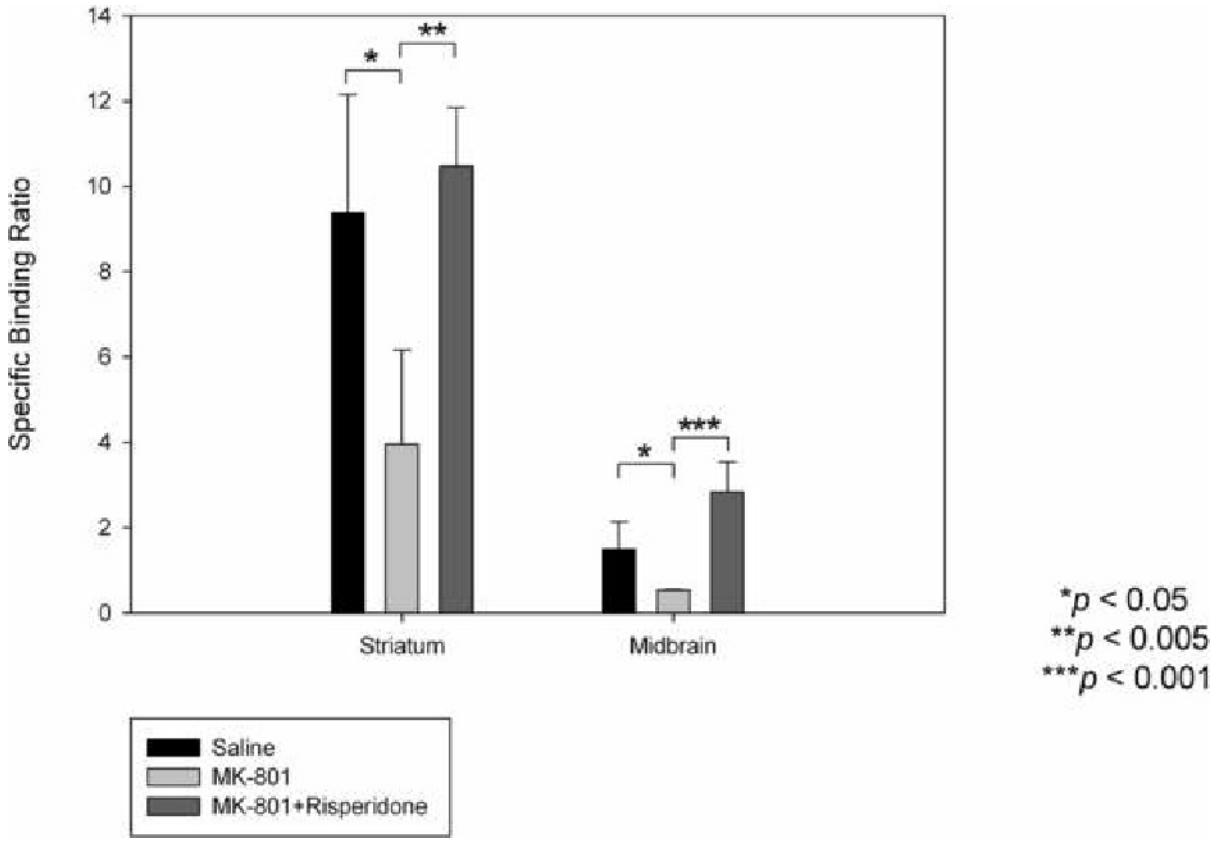


Disclosure of author financial interest or relationships:
**Y. Huang**, None; **C. Huang**, None; **Y. Wu**, None; **K. Cheng**, None; **J. Shih**, None; **K. Chang**, None.

Presentation Number **P047**
Poster Session 1
September 5, 2012 / 18:00-18:00 / Room: The Liffey

# Systemically Administered Long Term In Vitro Expanded Cord Blood Derived AC133+ Endothelial Progenitor Cells Home to Ischemic Brain and Induce Significant Decrease in Stroke Volume in MCAo Rat Model for Cerebral Ischemia

***Branislava Janic***[1], *Meser. M. Ali*[1], *Glauber Cabral*[2], *Robert A. Knight*[2], *Nadimpalli Ravi S Varma*[1], *Asm Iskander*[1], *Adarsh Shankar*[1], *James R. Ewing*[2], *Ali S. Arbab*[1], [1]*Radiology, Henry Ford Health System, Detroit, MI, USA;* [2]*Neurology, Henry Ford Hospital, Detroit, MI, USA. Contact e-mail: bjanic@rad.hfh.edu*

Background: Stem cells/progenitors are important for the development of cell therapies for vascular ischemic diseases. The crucial step in rescuing tissues from ischemia is improvement of vascularization that can be achieved by promoting neovascularization or growth of new blood vessels. Endothelial Progenitor Cells (EPCs) are the best candidates for developing such an approach due to their ability to self-renew, circulate and differentiate into mature endothelial cells (ECs). However, the successful clinical application of such therapy is limited by low quantities of EPCs that can be generated from patient and by the lack of adequate non-invasive imaging approach for in vivo monitoring bio-distribution of transplanted cells. Hypothesis: Long term expanded cord blood derived AC133+EPCs will selectively migrate to the ischemic brain parenchyma and exert their angiogenic effect and this process can be monitored by MRI due to the ability of these cells to create sufficient T2 and T2* shortening (MRI parameters) when magnetically labeled. Methods and Results: AC133+ cells were collected from CB using MidiMACS system. Cells were maintained in culture for 5 to 30 days at the cell concentration of 1x106/ml. At days 5-15 and 20-30 of the primary in vitro culture, cells were magnetically (FePro) and fluorescently (DiI) labeled and immediately IV injected into the rats with ischemic stroke. Rat stroke model was generated by transiently occluding middle cerebral artery for 2 hours. Twenty four hours later, animals underwent MRI to confirm and characterize stroke lesion and after the MRI scanning animals received IV injection of FePro labeled AC133+ EPCs. Seven and 14 days after injection, animals were again analyzed by MRI. Susceptibility weighted MR imaging (SWI) showed accumulation of FePro labeled cells in stroke affected hemispheres that was also detected by Prussian blue (PB) tissue section staining (detects iron in FePro labeled cells). Injected cells accumulated mainly within the ischemic boundary, within and around large thin blood vessels that are indicative of neoangiogenesis. Analysis of T2 maps constructed from T2WI images acquired with different echoes revealed that over the course of 15 days, stroke affected areas shrunk at the significantly higher rate in animals that received FePro labeled AC133+ EPCs as compared to the control animals. Conclusion: Data presented indicate that long term, in vitro expanded CB AC133+EPCs selectively migrated to the ischemic brain parenchyma, where they may have exerted therapeutic effect on development and extent of tissue damage, inflammation and time course of resolution following stroke onset.

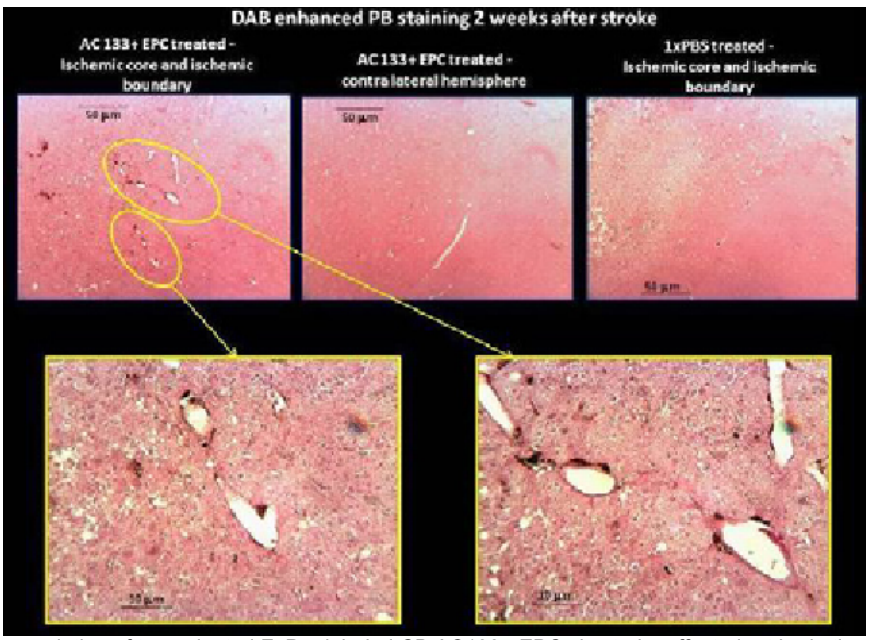


Accumulation of transplanted FePro labeled CB AC133+ EPCs in stroke affected rat brain tissue

Disclosure of author financial interest or relationships:
**B. Janic**, None; **M.M. Ali**, None; **G. Cabral**, None; **R.A. Knight**, None; **N. Varma**, None; **A. Iskander**, None; **A. Shankar**, None; **J.R. Ewing**, None; **A.S. Arbab**, None.

Presentation Number **P048**
Poster Session 1
September 5, 2012 / 18:00-18:00 / Room: The Liffey

# [18F]Altanserin PET in rats: Impact of P-glycoprotein inhibition

***Tina Kroll***[1], *David Elmenhorst*[1], *Andreas Matusch*[1], *Franziska Wedekind*[1,3], *Simone Beer*[1,2], *Angela Weisshaupt*[1], *Andreas Bauer*[1,3], [1]*Institute of Neurosciences and Medicine (INM 2), Jülich Research Center, Jülich, Germany;* [2]*Central Institute for Electronics (ZEL), Jülich Research Center, Jülich, Germany;* [3]*Department of Neurology, Medical Faculty, Heinrich-Heine-University Düsseldorf, Düsseldorf, Germany. Contact e-mail: t.kroll@fz-juelich.de*

The 5-HT2A antagonist [18F]altanserin is a positron-emission-tomography (PET) tracer which has been well-established in humans. It has also been applied as an in vivo method to assess serotonergic receptor availability in rats. However, brain uptake of [18F]altanserin is low and it is likely that the tracer is a substrate to the efflux transporter P-glycoprotein (PgP) in rodents. Therefore, the aim of this study is to investigate the in vivo brain uptake of [18F]altanserin with and without blockade of PgP by cyclosporine A (CsA), a well-known inhibitor of PgP. Small animal PET scans (Inveon dedicated PET, 180 min) in 18 male Sprague Dawley rats were performed with an i.v. injected bolus of [18F]altanserin (14-25 MBq); 8 of these animals received an additional bolus-infusion of CsA (47mg/kg). Arterial blood samples were obtained from a femoral artery in 3 control and 4 CsA-treated rats. Brain uptake of [18F]altanserin was determined (%ID/ml) and 5-HT2A receptor availability was subsequently estimated on the basis of time-activity curves (TACs), metabolite-corrected arterial input functions (2TCM and Logan graphical analysis) and reference tissue modeling (SRTM2, MRTM2, Logan non-invasive graphical analysis). Area-under-the-curve (AUC) analyses of the plots of regional brain uptake (%ID/ml) vs. time indicate that [18F]altanserin uptake is significantly increased after inhibition of PgP in all regions (Welch-test; all regions $p < 0.05$). This data indicates that the radiotracer [18F] altanserin is a substrate of PgP in rats. The increase of tracer uptake after PgP inhibition is region-dependent and ranges from 2.1 (cerebellum) to 2.8 fold (striatum) suggesting that PgP is not uniformly distributed in the rat brain. Compartmental and graphical pharmacokinetic models on the basis of arterial and reference input functions (cerebellum) proved to be suitable and highly consistent for estimating 5-HT2A receptor availability in untreated animals. Moreover, in vivo measurements of 5-HT2A receptor distribution are corresponding to in vitro data showing high receptor densities in cortical regions and lower binding in striatum and hippocampus. This specific distribution of 5-HT2A receptors remains unaltered after PgP inhibition with CsA. Comparison of arterial input functions and reference tissue models in CsA-treated animals revealed that outcome parameters of receptor densities differed significantly in subcortical (paired t-test: hippocampus $p = 0.03$ and striatum $p = 0.04$) but not in cortical regions, respectively. A possible reason for this finding is an unequal distribution of PgP throughout the brain. Lower PgP concentrations in the cerebellum will therefore affect pharmacokinetic models based on the cerebellum as reference region. In conclusion, the membrane efflux transporter PgP is a relevant factor for in vivo receptor studies with [18F]altanserin. Data on the anatomical distribution of PgP in the rodent brain are necessary to fully assess its influence on pharmacokinetic models.

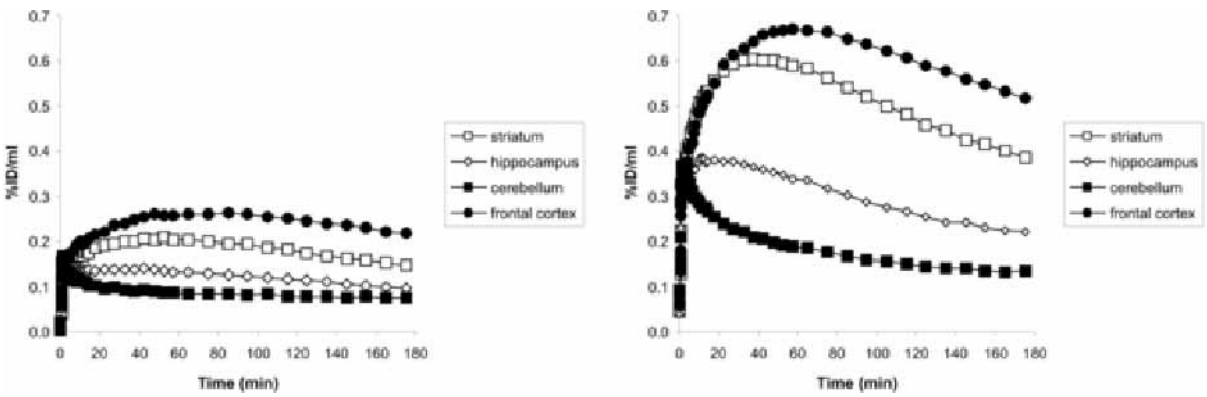


[18F]altanserin time-activity-curves normalized to injected dose obtained with small animal PET in a) untreated rats (n=10) and b) in rats treated with the P-glycoprotein inhibitor cyclosporin A (n=8)

Disclosure of author financial interest or relationships:
**T. Kroll**, None; **D. Elmenhorst**, None; **A. Matusch**, None; **F. Wedekind**, None; **S. Beer**, None; **A. Weisshaupt**, None; **A. Bauer**, None.

Presentation Number **P049**
Poster Session 1
September 5, 2012 / 18:00-18:00 / Room: The Liffey

# Surrogate HPLC fraction for small animal quantification of FAHA

***Jung-Wen Kuo***[1], *Kuan-Hao Su*[2], *Ren-Shyan Liu*[1,3], [1]*MAGIC/NRPGM, Nuclear Medicine, School of Medicine, National Yang-Ming University, Taipei, Taiwan;* [2]*Molecular Imaging Center, Chang-Gung Memorial Hospital, Linkou, Taiwan;* [3]*National PET/Cyclotron Center, Taipei Veterans General Hospital, Taipei, Taiwan. Contact e-mail: g880k13@ym.edu.tw*

Objectives: $^{18}$F-6-(fluoroacetamide)-1-hexanoicanilide ($^{18}$F-FAHA) is a potential probe for neurodegenerative disease, and its quantification could refer to the activities of histone deacetylases. In vivo, $^{18}$F-FAHA is rapidly metabolized not only in the tissues but in the periphery, and its metabolite $^{18}$F-FAC in the periphery would also flow into the brain. To indentify fractions of FAHA and FAC in the plasma is requisite for FAHA kinetic study. However, the fact that HPLC is impractical in small animals due to the invasive catheterization and the finite blood volume. Therefore, a substitute of the fractions might be needed for FAHA quantification. This study aims to evaluate the bias of FAHA kinetic analysis using the surrogate HPLC fractions for monitoring HDAC activity. Methods: A glioma-bearing rat was performed 60-min dynamic PET scan with $^{18}$F-FAHA and $^{18}$F-FAC, respectively. The HPLC fractions of the FAHA input function (IF) obtained from rats and monkeys were used to generate the variants of the fractions from those two curves shown in Fig 1. The $K_i$ of the FAC was calculated using Patlak analysis, and the FAC output function ($C_t$) from the periphery was estimated by $K_{iFAC}$ and the FAC fractions of the IF. Therefore, the bias of $K_i$ of FAHA calculated by the variant HPLC fraction could be evaluated by the above-mentioned indirect estimation method. Results: The $K_i$ of tumor with FAC was 0.0008 mlmin-1ml-1 calculated by Patlak analysis. The $C_t$ of FAHA contribution was obtained to deduce $C_t$ of the peripheral FAC from the total $C_t$ and the $K_i$ of FAHA was 0.0221 mlmin-1ml-1 computed using the rat HPLC fraction. The $K_i$ of FAHA decreases to 0.0166 mlmin-1ml-1 when replacing with the monkey HPLC fraction. The variant HPLC fractions were a mixture of the rat and monkey fractions and generated by interpolating the mixed fractions with these two curves. The mixing proportion of the HPLC fraction varied from the rat to the monkey resulted in reducing $K_i$ of FAHA estimated (Fig 2), and the evaluation of HDAC activity would have a bias of 30% underestimation using the monkey HPLC fraction. Conclusions: The results suggested that the bias was monotonic decreased when varying the proportional fraction of rat to that of monkey. Therefore, the surrogate HPLC monkey fraction could be a feasible choice for small animal quantification.

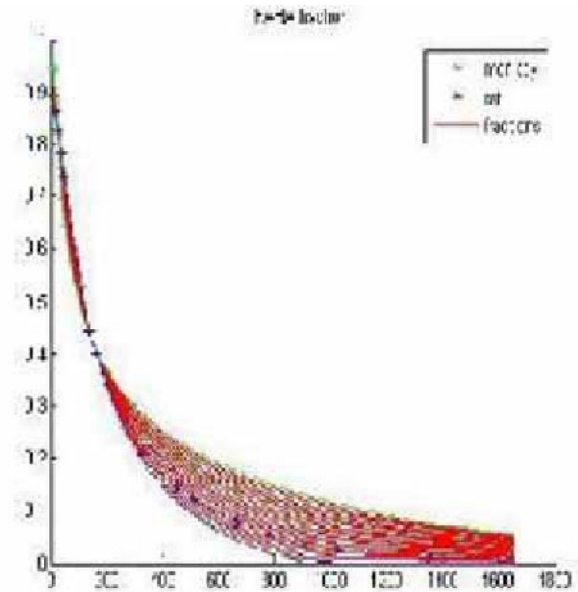

Fig1. The variant HPLC fractions were generated by interpolating the mixture of rat and monkey HPLC fractions.

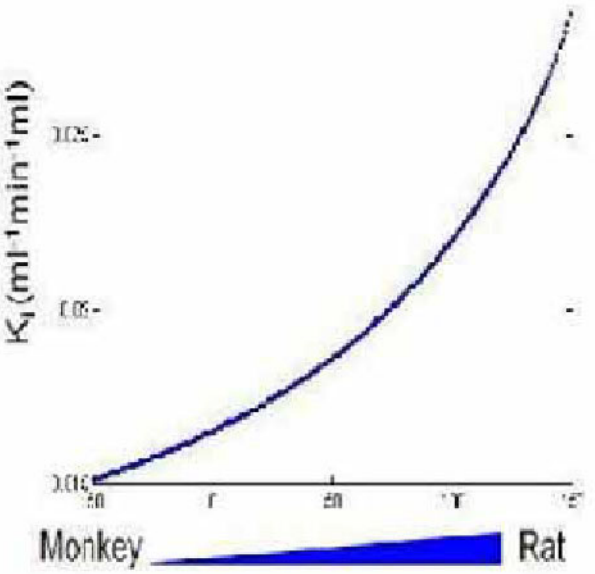


Fig2. The Ki of FAHA simulated by the varying the fractions from the monkey to the rat.

Disclosure of author financial interest or relationships:
**J. Kuo**, None; **K. Su**, None; **R. Liu**, None.

Presentation Number **P050**
Poster Session 1
September 5, 2012 / 18:00-18:00 / Room: The Liffey

# Functional [15O]H2O-PET enables the quantification of hemodynamic responses in the mouse brain induced by pharmacological stimulation

***Florian C. Maier***[1]*, Andreas Schmid*[1]*, Julia G. Mannheim*[1]*, Manfred Kneilling*[2]*, Bernd J. Pichler*[1]*,* [1]*Department of Preclinical Imaging and Radiopharmacy, Eberhard Karls University of Tuebingen, Tuebingen, Germany;* [2]*Department of Dermatology, Eberhard Karls University of Tuebingen, Tuebingen, Germany. Contact e-mail: florian.maier@med.uni-tuebingen.de*

Quantification of regional cerebral blood flow (rCBF) in small laboratory animals at baseline level as well as hemodynamic responses induced by various stimuli is of utmost interest for preclinical disease models of the neurovascular system, i.e. in vascular dementia. The rCBF in the brain of transgenic mice modelling vascular amyloidosis could be heavily altered. However, the absolute quantification of rCBF in mice remains difficult. Thus we first concentrated on the evaluation of [15O]H2O-PET rCBF quantification in mice determining variability and reliability (var and rel). Then we tested the validity of [15O]H2O-PET in a pharmacological stimulation study using bicuculline, a GABAA-receptor antagonist. 3 cohorts of C57BL/6 mice (cohort 1: 2.5 months old, weight: 24.5±0.7 g, n=5; cohorts 2 and 3: 19 months old, weight: 29.6±0.9 g, n=5 each) were injected with 26.2±3.4 MBq of [15O]H2O for the measurement of var/rel and hemodynamic responses in the cerebral cortex. For the var and rel scans, we measured mice as follows: cohort 1: 1st and 2nd scan were separated by 30 min; cohort 2: 1st and 2nd scan were separated by 8 days. For the pharmacological stimulation studies, mice were injected with 1.5 mg/kg bicuculline as follows: 1.0 mg/kg was infused in 2 min before [15O]H2O injection followed by an infusion of 0.5 mg/kg bicuculline in 10 min starting with [15O]H2O injection (cohort 3). Dynamic PET scans were performed for 10 min post injection (p.i.) and mice were anesthetized with 1.5% isoflurane evaporated in 100% oxygen. PET data were corrected for delay and dispersion and evaluated with a reversible single compartmental model. Additionally, 3D T2 weighted MR images were acquired for each mouse. Moreover, we analyzed blood gases pre and post [15O]H2O injection, ECG, breathing rates and body temperature were monitored throughout the entire study. Var and rel of rCBF measurements in cohort 1 were 4% and 98%, in cohort 2 4% and 81%, respectively with absolute rCBF values in the frontal part of the cerebral cortex of 314±32 ml/min/100g (test) and 317±23 ml/min/100g (retest) for cohort 1 and 176±24 ml/min/100g (test) and 168±25 ml/min/100g (retest) for cohort 2. Blood flow was significantly lower in older C57BL/6 mice (46% lower, p=1.8*10-05, n=5). In cohort 3, bicuculline challenges resulted in a significant 23±16% increase of rCBF in the frontal part of the cerebral cortex (baseline: 153±22 ml/min/100g; challenge: 187±27 ml/min/100g, n=5, p<0.05). Blood gases were partially affected by [15O]H2O-PET measurements: we detected differences of 10-25% in pO2, cK+ and ctHb while pH, pCO2, cNa+, cK+, cCa2+, cCl-, cGlu, ctHb and sO2 changes were below 10%. We could demonstrate the excellent var and rel of [15O]H2O-PET measurements in both young and aged C57BL/6 mice and thus the feasibility of quantitative mouse brain perfusion measurements with [15O]H2O. Furthermore, we were able to quantify changes in rCBF induced by a pharmacological stimulus (bicuculline). In ongoing experiments, we are including transgenic mice modelling Alzheimers Disease (APP23) and compare the stimulation pattern to [11C]flumazenil GABAA-binding.

Disclosure of author financial interest or relationships:
**F.C. Maier**, None; **A. Schmid**, None; **J.G. Mannheim**, None; **M. Kneilling**, None; **B.J. Pichler**, Siemens, Grant/research support; AstraZeneca, Grant/research support; Bayer Healthcare, Grant/research support; Boehringer-Ingelheim, Grant/research support; Oncodesign, Grant/research support; Merck, Grant/research support; Bruker, Grant/research support .

Presentation Number **P051**
Poster Session 1
September 5, 2012 / 18:00-18:00 / Room: The Liffey

# Role of Toll-like Receptor-4 in Neuroinflammation using Positron Emission Tomography after Cerebral Ischemia

***Abraham Martin***[1], *Ana Moraga*[2], *Boguslaw Szczupak*[1], *Eneko San Sebastián*[1], *Vanessa Gómez-Vallejo*[1,3], *Irati Markuerkiaga*[1], *Daniel Padró*[1], *Jordi Llop*[1,3], *Maria Angeles Moro*[2], *Ignacio Lizasoain*[2], [1]*Molecular Imaging Unit, CIC biomaGUNE, San Sebastián, Spain;* [2]*Unidad de Investigaciones Neurovasculares, Facultad de Medicina, Universidad Complutense, Madrid, Spain;* [3]*Radiochemistry, CIC biomaGUNE, San Sebastián, Spain. Contact e-mail: amartin@cicbiomagune.es*

Objectives: Toll-like receptors (TLRs) are considered to induce and mediate inflammatory reaction by production of inflammatory mediators [1], which are involved in the pathophysiological processes of cerebral ischemia injury. Among the family of TLRs, TLR4 has been the focus of particular interest since it is predominantly expressed in microglia and up-regulated following experimental stroke [2]. Inflammatory reaction involves a dramatic increase in the expression of the Translocator protein (TSPO) which is an attractive target for imaging cerebral inflammation [3]. Therefore, the aim of the present study is to image TSPO using [11C]PK11195 to elucidate the in vivo relationship between TLR4 and neuroinflammation after cerebral ischemia. Methods: Longitudinal PET imaging with [11C]PK11195 was performed to explore the changes in TSPO after 2, 7 and 14 days after permanent cerebral ischemia on TLR4-deficient mice and animals that express TLR4 normally. MRI imaging (T2W) was carried out to assess brain damage at 24 hours after reperfusion. In vivo imaging studies were conducted in parallel with immunohistochemistry (TSPO, GFAP and CD11b) of mice brains. Results: After 24 hours of cerebral ischemia, MRI showed a significant decrease (ca. 60%) of T2W volume on TLR4-deficient mice in relation to control animals. In mice that express TLR4 normally, [11C]PK11195 showed quasi-normal values at day 2, after what signals overshot to 50% of day 2 at day 7 followed by slight decrease at day 14. Interestingly, a similar time course was observed in the TLR4-deficient mice. Nevertheless, the absence of TLR4 demonstrated a reduction of [11C]PK11195 binding at days 7 and 14 after ischemia onset. As a result, the ratio of PET signals in the ischemic to contralateral areas varied from 1 at day 2 to 1.5 and 1.3 at day 7 in control and deficient to TLR4 mice, respectively. This suggests an involvement of TLR4 on TSPO expression after cerebral ischemia. Ex vivo immunohistochemical analysis confirmed the results obtained by in vivo PET imaging. A reduction of TSPO expression of ameboid cells (monocytic lineage) and reactive astrocytes was observed in the core of the infarction at day 14 after cerebral ischemia on deficient to TLR4 mice. Sham-operated animals did not show significant differences over time. Conclusions: Together, these findings provide the first evidence that [11C]PK11195 is capable to monitor the involvement of Toll-like receptor 4 in neuroinflammatory activity after cerebral ischemia. TLR4 may offer a promise as a novel therapeutic strategy for stroke neuroprotection. Therefore, TSPO radioligands may have the ability to monitor the effect of therapeutic approaches on secondary inflammation after cerebral ischemia. References: 1. Aderem et al., (2000) Toll-like receptors in the induction of the immune response. Nature 406:782-7 2. Tang et al., (2007) Pivotal role for neuronal Toll-like receptors in ischemic brain injury and functional deficits. PNAS 104:13798-803 3. Chen et al., (2004) Peripheral benzodiazepine receptor imaging in CNS demyelination: functional implications of anatomical and cellular localization. Brain 127:1379-92

Disclosure of author financial interest or relationships:
**A. Martin**, None; **A. Moraga**, None; **B. Szczupak**, None; **E. San Sebastián**, None; **V. Gómez-Vallejo**, None; **I. Markuerkiaga**, None; **D. Padró**, None; **J. Llop**, None; **M. Moro**, None; **I. Lizasoain**, None.

Presentation Number **P052**
Poster Session 1
September 5, 2012 / 18:00-18:00 / Room: The Liffey

# PET Imaging of Brain Metabolism, Perfusion and Dopamine D2 Receptor after Stroke

***Abraham Martin***[1], *Vanessa Gómez-Vallejo*[1,2], *Eneko San Sebastián*[1], *Daniel Padró*[1], *Irati Markuerkiaga*[1], *Irantzu Llarena*[3], *Jordi Llop*[1,2], [1]*Molecular Imaging Unit, CIC biomaGUNE, San Sebastián, Spain;* [2]*Radiochemistry, CIC biomaGUNE, San Sebastián, Spain;* [3]*Optical Spectroscopy, CIC biomaGUNE, San Sebastián, Spain. Contact e-mail: amartin@cicbiomagune.es*

Objectives: It is well-known that brain suffers pathophysiological changes after stroke, nevertheless, functional recovery processes in response to brain injury have not been fully elucidated to date. Neurotransmitter systems may play a key role in the recovery process of brain function and brain plasticity after experimental stroke. Therefore, the aim of the present study is to investigate the density of dopamine receptors and to elucidate their relationship with both pathophysiologic processes underlying ischemic disease and recovery of long-term brain function. Methods: Longitudinal PET imaging with [18F]FDG, [13N]ammonia and [11C]Raclopride were performed to explore the changes in brain glucose metabolism, perfusion and dopamine D2 receptor binding at 1, 3, 7, 14, 21 and 28 days after 2-hour transient middle cerebral artery occlusion (tMCAO) in rats. In vivo imaging studies were conducted in parallel using in vitro autoradiography with [3H]Raclopride and immunohistochemistry with tyrosine hiroxilase at different time points. Brain function recovery assessment was carried out using a simple neurological test for rats. Results: In the cerebral territory irrigated by the MCA, both PET [13N]ammonia and [18F]FDG demonstrated a significant decrease of the signal at 1 day after reperfusion. Brain perfusion with PET [13N]ammonia returned to quasi-normal values at day 3, after what signals overshot to 40% of control at day 7. Surprisingly, a similar time course was observed in the contralateral or non-ischemic area. The glucose metabolism of the brain evaluated by [18F]FDG showed a slight recovery around days 7-14 that did not reach control values in the ischemic territory. [11C]Raclopride binding showed similar control values around days 1-7, after what signals dropped to 70% of control at day 14 and onwards in the ischemic striatum. Interestingly, a slight increase of [11C]Raclopride binding was observed at days 1-3 and reaching the uppermost binding at day 7 in relation to control values in the contralateral to the lesion. This was followed by a reduction of the signals at days 14-28 to 40% of day 7. In vitro binding of [3H]Raclopride and immunohistochemical analysis of tirosin hidroxilase (TH) showed similar results to those obtained by in vivo PET imaging. Finally, the neurological test showed a dramatic loss of brain function during the first week after ischemia followed by a gradual recovery from day 7 to 28. Sham-operated and control animals did not show significant differences in both in vivo and in-vitro studies. Conclusions: Together, these findings evidenced a late compensatory increase of brain perfusion and glucose metabolism in both the ischemic and the contralateral territory. These changes are consistent with both dopamine receptor increase particularly in the contralateral hemisphere and to the brain functional recovery observed from seven days and onwards after cerebral ischemia. The results may provide information about the role of dopamine in the recovery of brain function after cerebral ischemia and may ultimately contribute to elucidate new mechanisms which may be involved in brain plasticity after experimental stroke.

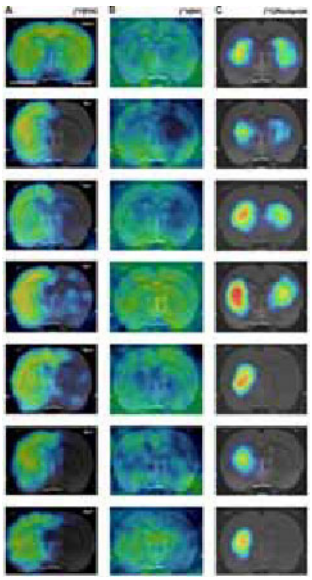

Serial images of [18F]FDG, [13N]ammonia and [11C]raclopride PET at control, day 1, day 7, day 14, day 21 and day 28 after MCAO. Normalized PET images of [18F]FDG (A), [13N]ammonia (B) and [11C]raclopride (C) signals after cerebral ischemia are co-registered with a MRI (T2W) rat template to localize anatomically the PET signal from left to right. Images correspond to the same representative animal for each time condition and radiotracer.

Disclosure of author financial interest or relationships:
**A. Martin**, None; **V. Gómez-Vallejo**, None; **E. San Sebastián**, None; **D. Padró**, None; **I. Markuerkiaga**, None; **I. Llarena**, None; **J. Llop**, None.

Presentation Number **P053**
Poster Session 1
September 5, 2012 / 18:00-18:00 / Room: The Liffey

# FDG-PET Brain Mapping of Neural Response of American Crows to Human Faces

***Robert Miyaoka***[1], *Donna Cross*[1], *Satoshi Minoshima*[1], *John Marzluff*[2], [1]*Radiology, University of Washington, Seattle, WA, USA;* [2]*Environmental and Forest Sciences, University of Washington, Seattle, WA, USA. Contact e-mail: rmiyaoka@u.washington.edu*

Crows can recognize and remember human faces. They can remember individuals as threatening or caring. In this work, FDG-PET brain mapping is used to investigate the different neural regions in the brain that are activated when crows are exposed to the individuals that captured them or the individuals that are caring for them. The goal of this investigation is to gain a deeper understanding of how wild crows integrate perception, memory and emotions. Methods: American crows (Corvus brachyrhynchos, =12) were captured by investigators wearing masks ("threatening"). After capture, the crows were housed for 4 weeks in individual cages and cared for by persons wearing a different mask ("caring"). Both masks were faces of people with neutral expressions so perception was conferred by behavior and not facial expressions. Before imaging each crow was blindfolded, removed from a covered cage, and administered ~1mCi of FDG via intraperitoneal injection. The crow was then placed back into its cage and soothing crow sounds were played for two minutes. After this rest period, the blanket covering the cage was lifted and the crow was exposed to the stimulus in 1 minute on/off blocks for 14 minutes. The stimuli were either: 1) face that captured it ("threatening"), 2) face that fed it ("caring"), or 3) empty room ("no face"). After the activation period, the crows were blindfolded; anesthetized with 3% isoflurane and imaged on a preclinical PET imaging system. The data corresponding to the 10 minute time frame from 27-37 minutes after FDG administration were reconstructed using 3D OSEM/MAP to a spatial resolution of 2.5 mm. FDG PET images were stereotaxically coregistered to a structural MRI and aligned to a jungle crow (Corvus macrorhynchos) atlas to better localize activation foci. Voxel-wise Z-mapping was used to evaluate group changes between different stimulation protocols. Results: Compared to "no face", the "threatening" face activated the acropallium (Z=4.4), brainstem (Z=4.2) and the nido/mesopallium (Z=41.). These areas of the brain are known to be associated with fear and startle responses. Compared to "no face", the "caring" face activated the septum (Z=4.0), medial striatum (Z=3.9) and the hippocampus (Z=3.9). These areas are involved in learning and memory. Finally the sight of a familiar face, either threatening or caring, activated the nidopallium (Z=4.2), lateral striatum (Z=4.0) and hippocampus (Z=3.8). Conclusions: In this first study using FDG-PET for wild crow brain mapping, we found activation patterns in crows similar to human fear response when exposed to a "threatening" face. In addition, we found that crows exposed to a known "caring" face activated neural regions associated with learning and memory. Future studies are planned to further investigate neural activation related to predator response (i.e., hawk), emotions (i.e., dead crow) and learning (i.e., new human holding dead crow).

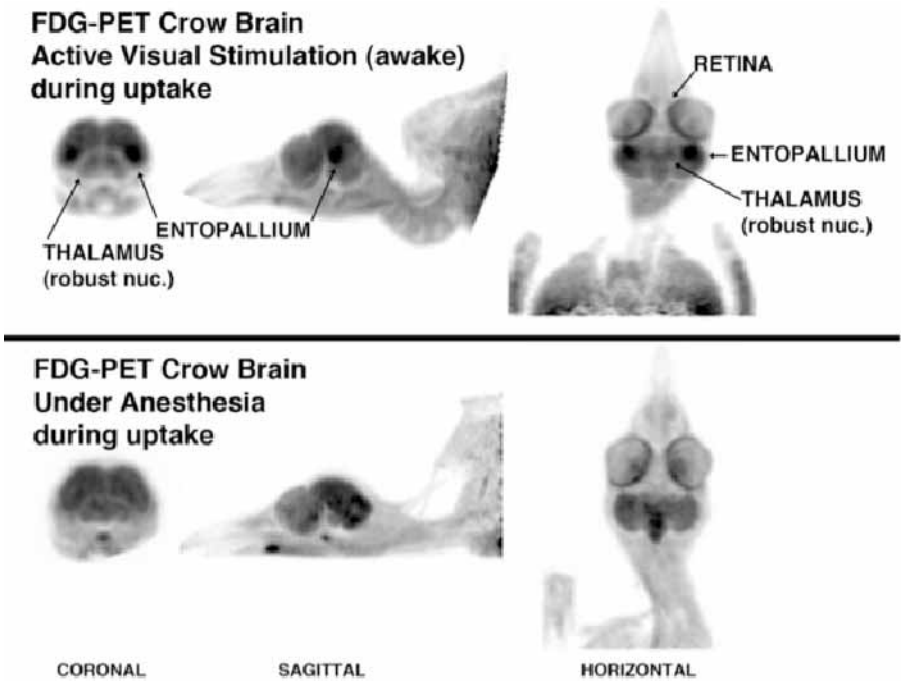


Disclosure of author financial interest or relationships:
**R. Miyaoka**, Philips Medical Systems, Grant/research support; Zecotek Medical Systems, Grant/research support; **D. Cross**, None; **S. Minoshima**, None; **J. Marzluff**, None.

Presentation Number **P054**
Poster Session 1
September 5, 2012 / 18:00-18:00 / Room: The Liffey

# IN VIVO IMAGING HEAT-SHOCK PROTEIN-70 INDUCTION AFTER BRAIN ISCHEMIA WITH A FAR-RED FLUORESCENT REPORTER MOUSE

*Xavier de la Rosa[1], Tomas Santalucia[1], Pierre-Yves Fortin[2], Jesus Purroy[1], Maria Calvo[3], Angelica M. Salas[1], Carles Justicia[1], Franck Couillaud[4], **Anna M. Planas**[1], [1]Brain Ischemia and Neurodegeneration, IIBB, CSIC, IDIBAPS, Barcelona, Spain; [2]BIO, UMR CNRS 3428, Université Bordeaux Segalen, Bordeaux, France; [3]Unitat de Microscòpia Òptica Avançada CCiTUB, School of Medicine, University of Barcelona, Barcelona, Spain; [4]RMSB, UMR CNRS 5536, Université Bordeaux Segalen, Bordeaux, France. Contact e-mail: ampfat@iibb.csic.es*

The inducible 72-kDa heat-shock protein (Hsp70) is not expressed in the adult mouse brain under physiological conditions but it is strongly induced following focal ischemia. This study was aimed to develop a fluorescent reporter mouse to image in vivo the expression of Hsp70 after brain ischemia. A 515-bp DNA fragment encompassing a proximal region upstream of the transcription initiation site plus the 5'UTR region was amplified by PCR from BALB/c mouse genomic DNA (Hspa1b promoter). This genomic sequence was ligated to the mplum cDNA (kindly provided by Dr. Roger Tsien, UCSD) and the SV40 polyA signal by using the Multisite Gateway kit from Invitrogen. A β-globin intron was subsequently inserted by restriction and ligation so the complete Hsp70-mPlum reporter vector was generated. The excitation and emission peaks of fluorescent mPlum protein are 590 and 649 nm, respectively. After testing the construct in cellular systems by transient transfection and induction of Hsp70, transgenic mice were generated at the Norsk Transgensenter (Norway) in a (C57BL/6J x CBA/J)F2 background and were backcrossed to C57BL6/J wild type mice for 7 generations. Wild type (WT) and transgenic littermates were differentiated by PCR amplification of the transgene in genomic DNA isolated from tail clips. Adult male wild type (WT) and mPlum transgenic mice were subjected to focal brain ischemia by 60-min intraluminal occlusion of the right middle cerebral artery (MCA), followed by reperfusion. Anesthetized living mice were observed in a fluorescence imaging system (Berthold Technologies). For intravital confocal microscopy, the day after induction of ischemia, mice were anesthetized with isofluorane and a cranial window sealed with a cover slip was opened in the skull of the ipsilateral hemisphere avoiding breaking the dura matter. Live observation of the cerebral cortex was carried out under high-speed confocal microscope (SP5Leica intravital) using an aqueous objective (25x) maintaining the mice under anesthesia (ketamine/xylazine). After in vivo imaging, the post-mortem brain was studied to detect the infracted zone and for immunohistochemistry against Hsp70 and mPlum. Cerebral ischemia induced strong mPlum fluorescence in the ipsilateral hemisphere as visualized at 30h with fluorescence reflectance imaging of the mice with intact skull. (Fig. 1) The fluorescent zone correspondend to the infarcted tissue plus the surrounding regions. Confocal microscopy allowed visualization of fluorescent neurons at the margin of infarction and endothelial cells within the ischemic core, as validated by immunohistochemical studies in the postmortem tissue. Collectively, we generated a Hsp70-mPlum reporter mouse that allows in vivo visualization of Hsp70 induction in the ischemic brain.

Figure 5

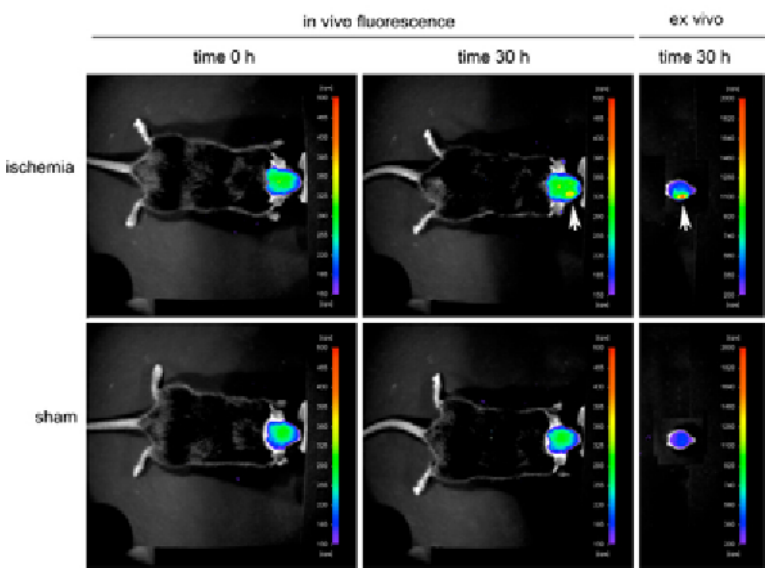


Disclosure of author financial interest or relationships:
**X. de la Rosa**, None; **T. Santalucia**, None; **P. Fortin**, None; **J. Purroy**, None; **M. Calvo**, None; **A.M. Salas**, None; **C. Justicia**, None; **F. Couillaud**, None; **A.M. Planas**, None.

Presentation Number **P055**
Poster Session 1
September 5, 2012 / 18:00-18:00 / Room: The Liffey

# Imaging Microglial Activation and Glucose Consumption in a Mouse Model of Alzheimer's Disease

***Sara Rapic***[1,3], *Heiko Backes*[3], *Thomas Viel*[1,3], *Markus P. Kummer*[4], *Parisa Monfared*[1,3], *Bernd Neumaier*[3], *Stefan Vollmar*[3], *Mathias Hoehn*[3], *Annemie van der Linden*[5], *Michael T. Heneka*[4], *Andreas H. Jacobs*[1,2], [1]*European Institute for Molecular Imaging (EIMI), Westfalian Wilhelms-University (WWU), Münster, Germany;* [2]*Interdisciplinary Centre for Clinical Research (IZKF), Westfalian Wilhelms-University (WWU), Münster, Germany;* [3]*Max Planck Institute for Neurological Research, Cologne, Germany;* [4]*Department of Neurology, Clinical Neurosciences, University of Bonn, Bonn, Germany;* [5]*Bio-Imaging Lab, University of Antwerp, Antwerp, Belgium. Contact e-mail: sara.rapic@nf.mpg.de*

**Introduction**. In Alzheimer's disease (AD), persistent microglial activation as sign of chronic neuroinflammation contributes to disease progression. Agonists that bind and activate the nuclear peroxisome proliferator-activated receptor gamma (PPAR-γ) suppress production of pro-inflammatory molecules at the transcriptional level. Our study aimed to *in vivo* visualize and quantify cerebral glucose metabolism and microglial activation and its therapy-induced modulation in 13 to 15 months old AD mice. **Methods**. Multi-tracer dynamic micro-positron emission tomography (μPET) imaging was performed in $APP_{Swe}/PS1_{\Delta E9}$ transgenic (Tg, *n* = 7) and C57BL/6J wild type mice (Wt, *n* = 8). Animals were imaged at baseline level and after treatment with pioglitazone, a PPAR-γ agonist (5 weeks treatment, 5 weeks wash-out). [$^{11C}$]-*(R)*-PK11195 and [$^{18}$F]fluoro-2-deoxy-2D-glucose ([$^{18}$F]FDG) were used to assess differences and changes in microglial activation and cerebral glucose consumption, respectively. [$^{18}$F]Fluoride imaging and magnetic resonance imaging (MRI) were performed to serve co-registration. Volumes of interest (VOIs) comprising various brain regions were mapped to quantify and calculate (i) percentage of injected dose per cubic centimetre (%ID/cc); (ii) standarized uptake value (SUV); (iii) [$^{11}$C]-*(R)*-PK11195 tracer distribution volume (DV); (iv) and [$^{18}$F]FDG Ki rate constants. Brains of representative Tg and Wt mice were stained before start of the experiments (12.5 months) and after the wash-out period (15 months) to determine the presence of microglia and amyloid-β (Aβ). **Results**. No statistically significant genotype- or treatment-dependent differences in [$^{11}$C]-*(R)*-PK11195 uptake and DV values could be observed in 13-14 months old animals, although immunohistochemistry verified substantial microglial activation in Tg mice at the age of 12.5 months. After the wash-out period (15 months), DV values in Tg mice were significantly higher compared to control mice, which was supported by immunohistochemistry data. [$^{18}$F]FDG Ki rate constants showed no genotype-, brain region- or treatment-dependent statistically significant differences. **Discussion**. Taken together, our data suggest that [$^{11}$C]-*(R)*-PK11195-μPET is able to assess microglial activation in AD mice only when a certain threshold of activation is reached. More specifically, we show significantly higher tracer DV in 15 months old Tg mice after discontinuation of pioglitazone, possibly indicating natural disease progression or rebound activation of microglia, but not at earlier disease stages. Therefore, with the given limitations of the radiopharmaceutical [$^{11}$C]-*(R)*-PK11195, subtle differences in microglial activation may be missed by this imaging method. Newly developed TSPO-targeted radiotracers with an improved target-to-background ratio may be able to detect activated microglia even at an earlier disease stage. **Acknowledgements**. This work was supported in part by 6th FW DiMI-NoE LSHB-CT-2005-512146, IZKF-SchwJ3/001/11 and 7th FW INMiND GA N°278850.

Disclosure of author financial interest or relationships:
**S. Rapic**, None; **H. Backes**, None; **T. Viel**, None; **M.P. Kummer**, None; **P. Monfared**, None; **B. Neumaier**, None; **S. Vollmar**, None; **M. Hoehn**, None; **A. van der Linden**, None; **M.T. Heneka**, None; **A.H. Jacobs**, Merck, Germany, Grant/research support .

Presentation Number **P056**
Poster Session 1
September 5, 2012 / 18:00-18:00 / Room: The Liffey

# PET-MRI in vivo imaging of nigro-striatal lesion in rats to assess drug effect

***Laura Ravasi**, Durieux Nicolas, Charlotte Laloux, Auger Florent, Maud Petrault, Régis Bordet, IMPRT, Lille, France. Contact e-mail: lauraravasi@gmail.com*

Background Animal models of Parkinson's disease are intended to better understand the evolution and treatment of such human disease. A unilateral lesion of nigrostriatal dopaminergic fibers is induced by a stereotaxic injection of 6-hydroxydopamine (6-OHDA) This study aims to assess whether Fluorinated fluorodeoxyglucose-Positron Emission Tomography ([18F]FDG-PET) is a way to in vivo characterize this lesion. Methods Ten male Wistar rats were enrolled. Over 4 weeks, Group A (n=5) was fed with a diet supplemented with 0.2% the neuroprotector fenofibrate, group B (n=5) was fed with a diet supplemented with vehicle. Stereotaxic administration of 4µg 6-OHDA in the left medial forebrain bundle was performed to all rats after 7 days; at day 21, apomorphine -induced turning behavior was tested to assess motor deficit. After this, imaging acquisitions on all rats of microPET (Inveon Siemens - 45 minutes after a 37 MBq [18F]FDG tail vein injection, 30-min static acquisition, at day 28) and Magnetic Resonance Imaging (scans on 7-Tesla Bruker Biospec, to obtain T2-weighted coronal views, at day 29) were performed. PET data analysis was performed on PET images fused with MRI T2 coronal images to draw striatal ROIs and enable quantification of regional cerebral metabolism through IRW. Immunochemistry was further performed for dopaminergic neuron counting purposes at day 30, when rats were sacrificed so that their brains could be removed from skull and embedded in paraffin. Brain slicing was performed within the nigrostriatal pathway. Results Behavioural deficit was confirmed by apomorphine-induced turning at day 21 in all rats. From an immunochemical point of view, 6-OHDA induced dopaminergic fiber lesions reached approximately 87% neuron loss in the left striatum compared to the right side. Interestingly, none of those 2 parameters was modified by fenofibrate administration. FDG-PET imaging did not show any differences in cerebral metabolism in right and left striatum. Comparison between groups showed no drug effect. Conclusion FDG radiotracer seems to not be sensitive enough to in vivo detect partial nigro striatal fiber degeneration. Histological results show that fenofibrate administered by supplemented diet at 0.2% for 4 weeks seems to not display any effect to prevent or cure nigro striatal fiber degeneration when provoked by 6-OHDA administration in rats. Our protocol is taking a new direction: [18F]-DOPA as tracer and an iron chelator (deferiprone) as treatment. Our pilot study with [18F]-DOPA-MicroPET/CT is promising since in vivo PET imaging is in agreement with histology results.

Disclosure of author financial interest or relationships:
**L. Ravasi**, None; **D. Nicolas**, None; **C. Laloux**, None; **A. Florent**, None; **M. Petrault**, None; **R. Bordet**, None.

Presentation Number **P057**
Poster Session 1
September 5, 2012 / 18:00-18:00 / Room: The Liffey

# The use of resting state functional MRI to assess functional connectivity in a mouse model of Alzheimer's disease

***Disha Shah***[1], *Elisabeth Jonckers*[1], *Christian Bigot*[1], *Greetje Vanhoutte*[1], *Marleen Verhoye*[1], *Bob Asselbergh*[2], *Sandra Pereson*[2], *Christine Van Broeckhoven*[2], *Annemie van der Linden*[1], [1]*Bio-Imaging Lab, UA, Wilrijk, Belgium;* [2]*Department of Molecular Genetics, UA, Wilrijk, Belgium. Contact e-mail: disha.shah@student.ua.ac.be*

Introduction: AD pathology is characterized mainly by the formation of amyloid plaques, tau-fibrils and neurodegeneration. Amyloid plaque deposition occurs at an early stage and is hypothesized to be the driving force behind AD. Resting state fMRI (rsfMRI) in human research has proven that subjects showing amyloid plaques but no other pathological hallmarks of AD exhibit altered functional connectivity in the brain (1). This suggests a possible relation between altered functional connectivity and amyloid plaque deposition. Human rsfMRI studies are limited in studying these correlations, as AD is a complex disease with many different pathological alterations. Using a mouse model mimicking only certain aspects of AD would facilitate the assessment of these correlations. The hypothesis of this study is that the functional connectivity alterations in AD are associated with the presence of amyloid plaques. Material and methods: 10 male APPPS1 mice (APP-KM670/671NL, PS1-L166P) bred on a C57BL6 background and 9 male control C57BL6 mice of (18.9 ±1.3) months old were imaged on a 7T Pharmascan (Bruker BioSpin, Germany). The APPPS1 mice show amyloid plaque deposition from 6 weeks onwards. The old age of the mice in this study ensures a heavy plaque load. Furthermore, these mice show no tau-pathology or neurodegeneration (2). Taken together, the APPPS1 mice are a model for amyloidosis, rendering them appropriate to study correlations involving amyloid plaques. The resting state data were acquired using a single shot gradient echo EPI sequence. For the analysis we opted for independent component analysis (ICA), which divides the brain into a number of components consisting of regions that are functionally connected. Results: The ICA analysis revealed differences in functional connectivity between both groups. The following components came out of the analysis: hippocampus, thalamus, hypothalamus, retrosplenial cortex, piriform cortex, entorhinal cortex, auditory cortex, visual cortex, somatosensory cortex and striatum. The regions that were affected were the hippocampus and cortical areas such as the piriform cortex. These results are in accordance with literature (2) and histological data that demonstrate heavy plaque load in the hippocampus and cortex. Conclusion: The fact that this mouse model shows only amyloid plaques and no other AD hallmarks and the observation of an altered functional connectivity suggest that amyloid plaque deposition and altered functional connectivity are related. Now that functional connectivity alterations are confirmed to occur in old mice with a heavy plaque burden, the next step would be to study young mice longitudinally to find out how exactly functional connectivity changes in relation to the progression of amyloid plaque deposition. Acknowledgements: The research leading to these results has received funding from the European Union's Seventh Framework Programme (FP7/2007-2013) under grant agreement n° 278850 (INMiND). References: 1) Sheline et al., (2010), Biol. psych. 67 (6): 584-587. 2) Radde et al., (2006), EMBO reports 7: 940-946.

Disclosure of author financial interest or relationships:
**D. Shah**, None; **E. Jonckers**, None; **C. Bigot**, None; **G. Vanhoutte**, None; **M. Verhoye**, None; **B. Asselbergh**, None; **S. Pereson**, None; **C. Van Broeckhoven**, None; **A. van der Linden**, None.

Presentation Number **P058**
Poster Session 1
September 5, 2012 / 18:00-18:00 / Room: The Liffey

# Small Animal PET Imaging of β-Amyloid Deposition in the Brain of APP23, Tg2576 and APPswe-PS1dE9 Mice with [$^{18}$F]flutemetamol

***Anniina Snellman***[1], *Francisco R. Lopez-Picon*[1], *Johanna Rokka*[2], *Olli Eskola*[2], *Ian Wilson*[7], *Gill Farrar*[7], *Mario Salmona*[6], *Gianluigi Forloni*[6], *Mika Scheinin*[4,5], *Olof Solin*[2,3], *Juha Rinne*[3], *Merja Haaparanta-Solin*[1], [1]*Turku PET Centre/ PET preclinical Laboratory, University of Turku, Turku, Finland;* [2]*Turku PET Centre/ Radiopharmaceutical Chemistry Laboratory, University of Turku, Turku, Finland;* [3]*Turku PET Centre, University of Turku, Turku, Finland;* [4]*Department of Pharmacology, Drug Development abd Therapeutics, University of Turku, Turku, Finland;* [5]*Unit of Clinical Pharmacology, TYKSLAB, Turku, Finland;* [6]*Mario Negri Institute for Pharmacological Research, Milan, Italy;* [7]*GE Healthcare Medical Diagnostics, Little Chalfont, Buckinghamshire, United Kingdom.*
*Contact e-mail: aepakk@utu.fi*

We evaluated [$^{18}$F]flutemetamol as a preclinical PET tracer for detecting β-amyloid (Aβ) deposition in APP23, Tg2576 and APPswe-PS1dE9 mouse models of Alzheimer's disease in vivo. [$^{18}$F]Flutemetamol was expected to show improved properties in preclinical PET imaging due to its high specific radioactivity. Methods: APP23 (n=3), Tg2576 (n=5), and APPswe-PS1dE9 (n=4) mice and their wild type littermates were investigated in a longitudinal PET imaging study. Mice were imaged repeatedly with an Inveon Multimodality PET/CT -scanner. Dynamic 60-minute PET scans were acquired at various ages of the mice, ranging from 7 to 22 months. The specific radioactivity of [$^{18}$F]flutemetamol at the end of synthesis was >1 TBq/μmol. [$^{18}$F]Flutemetamol retention in the brain was evaluated as bound-to-free ratios (B/F) from a late washout phase (50-60min), and as distribution volume ratios (DVR) using Logan graphical analysis with the cerebellar reference region input function. Mice from each strain were sacrificed at different time points to follow the Aβ deposition in the brain with Thioflavin S, and $Aβ_{1-40}$, $Aβ_{1-16}$ and $Aβ_{N3(pE)}$ immunohistochemistry. Results: In aged APP23 mice, increase in [$^{18}$F]flutemetamol retention was observed in the cortex of old transgenic mice. The DVRs for frontal cortex were 0.88 and 0.98 at 9 and 12 months respectively, increasing to 1.16 at 15 months, and 1.13 and 1.35 at 18 months. The B/F ratio for frontal cortex also increased from -0.19 and -0.06 at 9 and 12 months, to 0.14 at 15, and 0.15 and 0.35 at 18 months. APP23 mice showed slow deposition of large fibrillar Aβ deposits, with intense Thioflavin S staining and $Aβ_{N3(pE)}$ immunoreactivity seen at 15 months. For Tg2576 mice, the DVRs for frontal cortex were 0.90±0.15 at 12 months, 0.94±0.13 at 15 months, increasing slightly to 1.11 and 1.02 at 19 months, and to 1.11 and 1.24 at 22 months. However, the B/F ratios were <0 at all investigated time points. The Aβ deposition in the Tg2576 mice used in this study was surprisingly slow, and only a small number of immunohistochemically detectable Aβ deposits were present even at 22 months. In APPswe-PS1dE9 mice, no increase in Logan DVRs or B/F ratios was seen as the mice aged. DVRs were 0.93±0.02 at 12 months, and even decreased to 0.84 and 0.90 at 15 months, and 0.83 and 0.89 at 19 months. The B/F ratios were negative at all investigated time points, due to nonspecific binding to cerebellar white matter. In APPswe-PS1dE9 brain, Aβ deposition was fast, and an extensive amount of small, diffuse Aβ deposits were found already at 9 months. Conclusion: [$^{18}$F]flutemetamol shows potential for preclinical Aβ imaging studies, however, binding to murine Aβ deposits is highly dependent on the used mouse model, and the models should be validated individually. Using [$^{18}$F]flutemetamol, higher binding was seen in strains with slow Aβ deposition. The research leading to these results has received funding from the European Community's Seventh framework Programme (FP7/2007-2013) under grant agreement no.212043 and the clinical grants of Turku University Hospital (EVO) and the Academy of Finland.

Disclosure of author financial interest or relationships:
**A. Snellman**, None; **F.R. Lopez-Picon**, None; **J. Rokka**, None; **O. Eskola**, None; **I. Wilson**, GE Healthcare Medical Diagnostics, Employment; **G. Farrar**, None; **M. Salmona**, None; **G. Forloni**, None; **M. Scheinin**, None; **O. Solin**, None; **J. Rinne**, GE Healthcare, Finland, Consultant; **M. Haaparanta-Solin**, None.

Presentation Number **P059**
Poster Session 1
September 5, 2012 / 18:00-18:00 / Room: The Liffey

# Effects of morphine self-administration on glucose brain metabolism of adult rats that were exposed during their adolescence to the cannabinoid receptor agonist CP-55,940

***Maria L. Soto-Montenegro***[1,3], *Gonzalo L. Montoya*[4], *Veronica Garcia-Vazquez*[1,3], *Juan Jose Vaquero*[2], *Emilio Ambrosio*[4], *Manuel Desco*[1,2], [1]*Unidad de Medicina y Cirugia Experimental, Hospital General Universitario Gregorio Maranon, Madrid, Spain;* [2]*Departamento de Bioingenieria e Ingenieria Aeroespacial, Universidad Carlos III, Madrid, Spain;* [3]*CIBER de Salud Mental (CIBERSAM), Madrid, Spain;* [4]*Departamento de Psicobiologia, Universidad Nacional de Educacion a Distancia (UNED), Madrid, Spain. Contact e-mail: marisa@mce.hggm.es*

Introduction: Cannabinoid exposure during the periadolescent period has been proposed to promote the use of other more serious illicit drugs. However, how this cannabinoid history alters morphine-induced glucose brain metabolism remains unknown. The aim of this study is to check the effects of morphine self-administration on glucose brain metabolism of adult rats that were exposed during their adolescence to the cannabinoid receptor agonist CP-55,940. Methods: Male and female Wistar rats were administered with the cannabinoid agonist CP 55,940 (0.4 mg/2ml/kg i.p.) or its vehicle (VH) (ethanol:cremophor: saline; 1:1:18) once daily from postnatal day 28 to 38. When animals reached their 100 postnatal day they were trained for morphine self-administration (1 mg/Kg/injection) acquisition under a fixed ratio 1 (FR1) schedule of reinforcement for 15 days in daily sessions of 12 hours. After this phase, rats were submitted to daily 12 hours sessions for another 15 days with only saline. Eight groups of animals were studied according to the following factors: pre-treatment (CP or VH), treatment (morphine or saline) and gender (male or female) : VH-saline (M=10, F=8), VH-morphine (M=7, F=8), CP-saline (M=9, F=9) and CP-morphine (M=8, F=7). Imaging studies were performed at baseline time (day 100), 15 d (Acquisition) and 30 d (Extinction), to assess short-term effects, and 8 and 16 weeks to assess longer-term effects. Images were reconstructed using a 3D-OSEM algorithm (FIRST©). ROIs were drawn on coronal-sections: dorsal and ventral hippocampus, parietal, temporal and retrosplenial cortex, caudate-putamen, cerebellum, thalamus, brain stem, amygdale, thalamus, hypothalamus, nucleus accumbens and periaqueductal gray matter in both hemispheres, medial thalamus, background (BG) and whole brain (WB). To normalise FDG uptake, tissue activity was corrected by subtracting background and dividing by whole brain activity. Results are expressed as a percentage (%) ([FDG uptake=(study ROI-BG/WB)×100]. Results: The analysis of variance (ANOVA) of ROIs of three fixed factors with repeated measures on one of them, revealed significant effects on brain glucose metabolism of time ($p<0.001$, F3.244), sex ($p<0.001$, F=9.464), pre-treatment ( $p=0.006$, F=1.894) and treatment ($p<0.001$, F=2.404). A interaction between time and sex was found ($p=0.029$, F=1.294). Conclusions: The results demonstrate that chronic administration of CP-55,940 during adolescence modulates the brain metabolic responses to morphine self-administration in a sex-dependent manner. Supported by Ministerio de Sanidad y Consumo (FIS CP08/00017, FIS PI11/00616), CENIT-AMIT Ingenio 2010, Ministerio de Ciencia e Innovación (TEC2007-64731, TEC 2008-06715-C02-1, SAF2007-064890; PSI2010-20355 and RD06/001/0029 of Instituto de Salud Carlos III), ARTEMIS S2009/DPI-1802 and S-SAL/0261/2006; Consorcio I+D CANNAB-CM Program from Comunidad de Madrid; Fundación de Investigación Médica Mutua Madrileña; and Plan Nacional sobre Drogas 2008-2010.

Disclosure of author financial interest or relationships:
**M.L. Soto-Montenegro**, None; **G.L. Montoya**, None; **V. Garcia-Vazquez**, None; **J. Vaquero**, None; **E. Ambrosio**, None; **M. Desco**, None.

Presentation Number **P060**
Poster Session 1
September 5, 2012 / 18:00-18:00 / Room: The Liffey

# Effects on brain glucose metabolism of adult rats that were exposed during their adolescence to the cannabinoid receptor agonist CP-55,940

***Maria L. Soto-Montenegro***[1,3], *Gonzalo L. Montoya*[4], *Veronica Garcia-Vazquez*[1,3], *Juan Jose Vaquero*[2], *Emilio Ambrosio*[4], *Manuel Desco*[1,2], [1]*Unidad de Medicina y Cirugia Experimental, Hospital General Universitario Gregorio Maranon, Madrid, Spain;* [2]*Departamento de Bioingenieria e Ingenieria Aeroespacial, Universidad Carlos III, Madrid, Spain;* [3]*CIBER de Salud Mental (CIBERSAM), Madrid, Spain;* [4]*Departamento de Psicobiologia, Universidad Nacional de Educacion a Distancia (UNED), Madrid, Spain. Contact e-mail: marisa@mce.hggm.es*

Introduction: Cannabis is the most widely used illicit drug in the world. Their consumption during adolescence has been proposed to promote the use of other more serious illicit drugs. The aim of the present study is to check the possible changes on brain glucose metabolism of adult male and female rats that were exposed during their adolescence to the cannabinoid agonist CP-55,940. Materials and Methods: The cannabinoid agonist (0.4 mg/kg i.p) or its corresponding vehicle (VH) was administered i.p. once daily from day 28 to day 38 postnatal to male and female Wistar rats. Four groups of animals were studied at day postnatal 100: VH male (n=20); VH female (n=17); CP 55,940-exposed (CP) male (n=18) and CP-exposed female (n=18). Animals were anesthetized with isoflurane and [18F]fluoro-D-glucose (FDG) (1.02 ± 0.2 mCi for female and 1.06 ± 0.2 mCi for male) was injected by the tail vein. Following an uptake period of 35 min, animals were imaged during 60 min in an Argus small-animal PET/CT scanner (SEDECAL, Madrid, Spain). Images were reconstructed using a 3D-OSEM algorithm (FIRST©). ROIs were drawn on coronal-sections: dorsal hippocampus, ventral hippocampus, caudate-putamen, cerebellum, thalamus, brain stem, parietal cortex, temporal cortex, amygdale, thalamus, hypothalamus, nucleus accumbens, periaqueductal gray matter (PG) and retrosplenial cortex in both hemispheres, medial thalamus and whole brain. Standard uptake value (SUV) was determined for each ROI. [FDG uptake=(ROI/(Dosis/Weight)]. Results: Multivariate analysis of variance (MANOVA) of ROIs revealed significant effects on brain glucose metabolism related to sex ($p<0.001$, $F= 3.603$) but not treatment. In general, male brain uptake is slightly higher than that of females. Conclusions: Results demonstrate that chronic administration of CP-55,940 during adolescence resulted in no significant cerebral glucose metabolism changes in the adulthood. Another issue is to verify the extent to which cannabinoid agonist use may promote the use of other drugs of abuse. Supported by Ministerio de Sanidad y Consumo (FIS CP08/00017, FIS PI11/00616), CENIT-AMIT Ingenio 2010, Ministerio de Ciencia e Innovación (TEC2007-64731, TEC 2008-06715-C02-1, SAF2007-064890; PSI2010-20355 and RD06/001/0029 of Instituto de Salud Carlos III), ARTEMIS S2009/DPI-1802 and S-SAL/0261/2006; Consorcio I+D CANNAB-CM Program from Comunidad de Madrid; Fundación de Investigación Médica Mutua Madrileña; and Plan Nacional sobre Drogas 2008-2010.

Disclosure of author financial interest or relationships:
**M.L. Soto-Montenegro**, None; **G.L. Montoya**, None; **V. Garcia-Vazquez**, None; **J. Vaquero**, None; **E. Ambrosio**, None; **M. Desco**, None.

Presentation Number **P061**
Poster Session 1
September 5, 2012 / 18:00-18:00 / Room: The Liffey

# Molecular Imaging of a Murine Model for Aromatic L-Amino Acid Decarboxylase Deficiency

***Kai-Yuan Tzen***[1,2], *Ni-Chung Lee*[3], *Yih-Dar Shieh*[3], *Yin-Hsiu Chien*[3], *Pin-Wen Chen*[3], *Wuh-Liang Hwu*[3], [1]*Nuclear Medicine, National Taiwan University Hospital, Taipei, Taiwan;* [2]*Molecular Imaging Center, National Taiwan University, Taipei, Taiwan;* [3]*Medical Genetics and Pediatrics, National Taiwan University Hospital, Taipei, Taiwan. Contact e-mail: tzenky@ntuh.gov.tw*

**Background:** Aromatic L-amino acid decarboxylase (AADC) is responsible for the synthesis of dopamine and serotonin. Children with AADC deficiency show compromised development, particularly with regard to their motor functions. Currently, there is no effective treatment and also no animal model for AADC deficiency. **Methods & Materials:** We knocked in a common human mutation, IVS6+4A>T, into the mouse *Ddc* gene. Half of the homozygous mice ($Ddc^{IVS6/IVS6}$) were born alive, and in their brains the AADC mRNA lacked exon 6, resulting in no detectible AADC protein or activity and very low dopamine and 5-hydroxyindoleacetic acid (5-HIAA) levels. The $^{18}$F-DOPA and $^{18}$F-Fallypride PET scans were done in separate days. Both the $^{18}$F-DOPA and $^{18}$F-Fallypride PET scans were acquired for 60 min. at 30 min. after the i.v. injection of the PET imaging agents. The mice were anesthetized using isofluorane and scanned by small animal PET/CT scanner (eXplore Vista DR, GE Healthcare, USA). In $^{18}$F-Fallypride PET analysis, the binding potential ratios of [(mean striatal count-mean cerebellar count)/mean cerebellar count] were used to represent the radiopharmaceutical uptake by the striatum. **Results:** The $Ddc^{IVS6/IVS6}$ mice exhibited severe failure to thrive, dyskinesia, and clasping in their first 4 weeks of lives. Then, they had a catch-up growth, increase in dopamine level, and an improvement in motor function, though still had abnormal behaviors, altered autonomic control, and impaired maternal care. Brain expression array analysis revealed the up-regulation of a panel of neuropeptide genes in the 8-week-old mice. In the FDOPA PET study, none of the $Ddc^{IVS6/IVS6}$ mice, with ages 2-12 weeks, showed any signal over the caudate putamen (CP) regions. Analysis of CP tissues revealed zero AADC activity at 2, 4, and 8 weeks of age in comparison to the heterozygous ($Ddc^{+/IVS6}$) (5.56, 17.71 and 29.82 pmol/min/mg tissue at 2, 4, and 8 wks old) or wild-type ($Ddc^{+/+}$) mice (5.33, 35.31 and 51.95 pmol/min/mg tissue at 2, 4, and 8 wks old). Dopamine levels in CP tissue extracts were very low in young $Ddc^{IVS6/IVS6}$ mice, but the level increased gradually to more than 50% of the wild-type mice when they grew older. The Fallypride PET showed the dopamine receptor binding potential ratios of $Ddc^{IVS6/IVS6}$ mice were slightly lower than those of the wild-type mice (p=0.200). In **conclusion**, this is a new neurotransmitter deficiency animal model that does not need a rescue. The $Ddc^{IVS6/IVS6}$ mice exhibit many characteristics, both molecular and in PET imaging, similar to the human disease, and will be suitable for the developments of therapies for AADC deficiency. Brain adaptation to neurotransmitter deficiency is a complex and slow process. Findings from these mice suggest that regulation of neuropeptides is important for brain adaptation to chronic neurotransmitter deficiency.

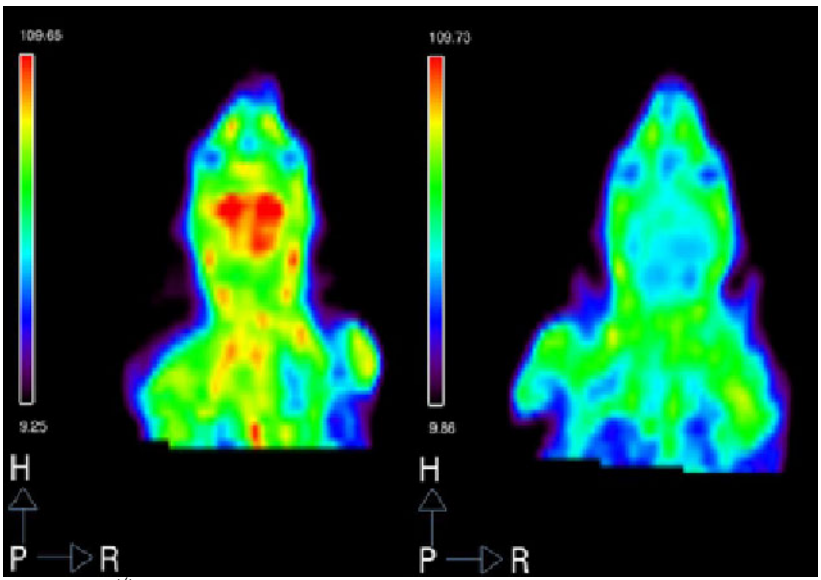


Lt: Striatal dopamine production in the $Ddc^{+/+}$ mouse can be demonstrated by FDOPA PET scan. Rt: FDOPA PET scan for a 12-week old $Ddc^{IVS6/IVS6}$ mouse showed no signal over the caudate putamen region.

Disclosure of author financial interest or relationships:
**K. Tzen**, None; **N. Lee**, None; **Y. Shieh**, None; **Y. Chien**, None; **P. Chen**, None; **W. Hwu**, None.

Presentation Number **P062**
Poster Session 1
September 5, 2012 / 18:00-18:00 / Room: The Liffey

# 5-$HT_{1A}$ Sex Differences of $B_{max}$ and $K_D$ in the Nonhuman Primate

***Dustin W. Wooten**, Ansel Hillmer, Jeffrey M. Moirano, Elizabeth O. Ahlers, Maxim S. Slesarev, Todd E. Barnhart, Mary L. Schneider, Bradley T. Christian, University of Wisconsin-Madison, Madison, WI, USA. Contact e-mail: dwooten@wisc.edu*

**Introduction:** Previous PET studies have shown sex-based differences in 5-$HT_{1A}$ binding with females having a higher binding potential ($BP_{ND}$) than males using [$^{11}$C]WAY100635 (Parsey et al., Jovanovic et al.). Because $BP_{ND}$ is a composite parameter representing receptor density ($B_{max}$), in vivo receptor ligand affinity ($1/K_{Dapp}$), and nonspecific binding ($f_{ND}$), it does not provide information to discriminate differences in $B_{max}$ and $K_{Dapp}$. Inherent to the $K_{Dapp}$ parameter are the effects of endogenous serotonin as a competitor to diminish specific binding. Thus a reduction in $BP_{ND}$ could be attributed to a decrease in receptor density or an increase in endogenous 5-HT binding. In this work, we use a multiple injection (MI) PET protocol with co-injections of radiolabeled and unlabeled 5-$HT_{1A}$ receptor antagonist, [$^{18}$F]mefway (MEF), to compare sex based differences of $K_{Dapp}$, $B_{max}$, and $BP_{ND}$ in a cohort of rhesus monkeys. **Methods:** PET MEF studies were performed on 17 (7m, 10f) rhesus monkeys using a 3-injection protocol which included partial saturation injections of MEF. The studies were optimized for precise measurement of $K_{Dapp}$ (via $k_{off}/k_{on}$) and $B_{max}$. Of the 17 studies, arterial plasma sampling of MEF was acquired on 11 subjects and a group input function (GIFs) for use on all subjects was derived for compartmental modeling. Male and female arterial input functions were examined separately to closely examine if sex differences were present in the plasma time course of MEF. Compartmental modeling was performed using a model to account for non-tracer doses of MEF for the estimation of $B_{max}$ and $K_{Dapp}$. $BP_{ND}$ estimates were also acquired using the MRTM and data from the first injection (high specific activity MEF, 90 minute duration) for comparison using the cerebellum (CB) as a reference region. Regions of interest were selected in high 5-$HT_{1A}$ binding regions of the hippocampus (HP), dorsal anterior cingulate cortex (dACC), raphe nuclei (RN), and amygdala (AM). Sex differences in parameters were considered significant for $p<0.05$. **Results:** Analysis of the male and female GIFs revealed similar shapes and slow clearance rates (based upon exponential decay of times >20 minutes) for male and female GIFs were within ~3%. Compartmental analysis of the parameters revealed no significant difference for $B_{max}$ in the HP, dACC, and AM, however, significance was observed in the RN. Significant differences in $K_{Dapp}$ were observed in HP, AM, and RN, but not in the dACC. Significant difference in $BP_{ND}$ was found in all areas except the dACC. Figure 1 shows bar plots of sex-based differences between males and females for $K_{Dapp}$, $B_{max}$, and $BP_{ND}$ in the various regions. **Conclusion:** These findings suggest that in the cortical regions of the brain, the sex-based differences in 5-$HT_{1A}$ binding of MEF are primarily due to $K_{Dapp}$, which could be attributed to lower endogenous 5-HT in females compared to males. In the raphe nucleus, consisting primarily of 5-$HT_{1A}$ autoreceptors, the differences are consistent with both a lower endogenous 5-HT and $B_{max}$ in females compared to males. **References:** Parsey R, et al. (2004) Brain Research; Jovanovic H, et al. (2008) NeuroImage

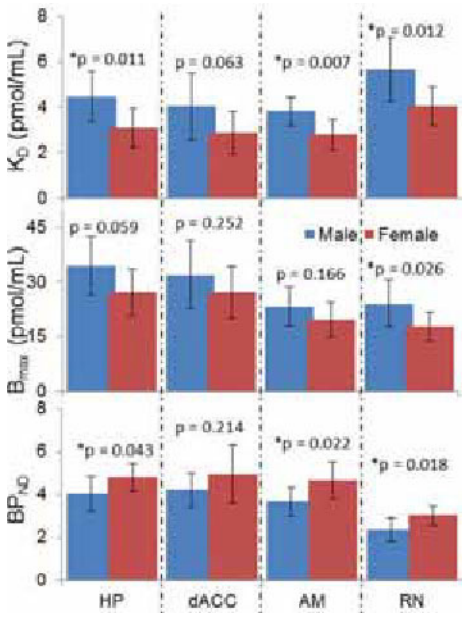


Figure 1: Sex based differences between males and females for $K_{Dapp}$, $B_{max}$, and $BP_{ND}$ in the various regions.

Disclosure of author financial interest or relationships:
**D.W. Wooten**, None; **A. Hillmer**, None; **J.M. Moirano**, None; **E.O. Ahlers**, None; **M.S. Slesarev**, None; **T.E. Barnhart**, None; **M.L. Schneider**, None; **B.T. Christian**, None.

Presentation Number **P063**
Poster Session 1
September 5, 2012 / 18:00-18:00 / Room: The Liffey

# Assessment of the metabolic profile in Type 2 diabetes mellitus with different blood-glucose control levels through proton MR spectroscopy

*Ping Zhang[1], Yu Rong[2], Zhiwei Shen[1], Yeyu Xiao[1], **Renhua Wu**[1], [1]Medical Imaging Department, The 2nd Affiliated Hospital of the Medical College of Shantou University, Shantou, China; [2]Neurology Department, The 2nd Affiliated Hospital of the Medical College of Shantou University, Shantou, China. Contact e-mail: rhwu@stu.edu.cn*

Objective: To investigate possible brain metabolic alterations in the left frontal cortex and left parietal white matter on multi-voxels proton magnetic resonance spectroscopy (1H MRS) in patients with type 2 diabetes mellitus (T2-DM) of different hemoglobin A1C (HbA1c) levels. Methods: Forty-two patients with T2-DM and thirty-four healty control subjects from 40-80 years were inclued in this study. All the subjects were dextromanual. For further evaluation the diabetic group was divided into three subgroups according to HbA1c levels (Subgroups 1: 15patients, HbA1c<6.5%; Subgroups 2: 14 patients, 6.5%≤HbA1c ≤7.5%; Subgroups 3 : 14 patients, HbA1c >7.5% ).They were collected by GE 1.5-T MR scallner and the multi-voxels were located over in the Semiovale center (TR/TE=1500ms/35ms). The data spectra in left frontal cortex and left parietal white matter were measured by the SAGE software. NAA)/ Cr, Cho/ Cr, MI/ Cr were calculated. Results: Cho/Cr ratios of patients with T2-DM were lower than the ratios of the control group both in the left frontal cortexand the left parietal white matter comparing with the control group (P=0.023, 0.000). Diabetic group and the control group did not differ significantly regarding their gender distributions. In the left frontal cortex ,Cho/Cr ratios were lower in the Sunbgroup 2 than in the Subgroup 1 (P=0.046) when MI/Cr ratios were higher in the Sunbgroup 3 than in the Subgroup 1 and Sunbgroup 1 (P=0.043 and 0.033). In the left parietal white matter , NAA/Cr ratios were lower in the Subgroup 1 than in the Sunbgroup 2 and Sunbgroup 2 (P=0.044,0.033), but MI/Cr ratios were higher in the Sunbgroup 3 than the ratios both in the Subgroup 1 and Sunbgroup 2 (P=0.031,0.034). The Cho/Cr ratios were lower both in the Subgroup 1 and Sunbgroup 2 than the ratios of control subjets (P=0.001 and 0.047) in the left frontal cortex . The Cho/Cr ratios were significantly lower in the three Subgroups than the ratios of control subjets (P=0.008,0.005 and 0.002) in the left parietal white matter .MI/Cr ratios were higher In the Sunbgroup 3 than the ratios of the control group both in the left frontal cortex and left parietal white matter (P=0.026,0.049). Conclusions : T2-DM can cause disordered the left frontal cortex and left parietal white matter metabolism.Their were different metabolic alterations in diferent parts of brain.The metabolic alterations were associated with the HbA1c levels that were inversely correlated with Cho/Cr ratios but positively correlated with MI/Cr ratios both in the left frontal cortical and parietal white matter.There were significant correlation between the HbA1c levels and glycemic control levels. The more poorly glycemic were controlled, the more significantly brain metabolites changed.

Disclosure of author financial interest or relationships:
**P. Zhang**, None; **Y. Rong**, None; **Z. Shen**, None; **Y. Xiao**, None; **R. Wu**, None.

Presentation Number **P064**
Poster Session 1
September 5, 2012 / 18:00-18:00 / Room: The Liffey

# Measurement of Receptor Occupancy of mGluR5 Negative Allosteric Modulator AFQ056 in Non Human Primate by [18F]FPEB PET

***Kenneth Zasadny**, Laigao Chen, Marc Skaddan, Kuo-Hsien Fan, Richard Coelho, Zhiyong Xie, Kyle Kuszpit, Gwen Currier, Anne M. Burkholder, Steven Kreuser, Marlo Volberg, Nancy Poy, Julie Cianfrogna, Patrick Trapa, Christopher Shaffer, Worldwide Research and Development, Pfizer, Groton, CT, USA. Contact e-mail: kenneth.zasadny@pfizer.com*

The mGluR5 negative allosteric modulator (NAM) AFQ056 has shown efficacy in MPTP-rendered Parkinsonian nonhuman primates (NHP) having L-DOPA-induced dyskinesias (LID) (Gregoire L, Parkinsonism Relat Disord 2011, 17:270). Since mGluR5 NAMs have shown sedation and cognitive disruption preclinically, we sought to define the exposure/receptor occupancy (RO) relationship of AFQ056 in NHP to help target clinical doses. PET imaging with [18F]FPEB may provide a translateable tool for measuring RO noninvasively (Wang J, Synapse 2007, 61:951). Though PET with [18F]FPEB may be possible using non-invasive reference-tissue methods in human, such methods may not be valid in NHP (Patel S, Nucl Med Biol 2007, 34:1009). We sought to establish the PET methodology of [18F]FPEB to measure RO in NHP using AFQ056 as a displacement drug. All animal study procedures conducted were approved by an institutional review committee (IACUC). Two male cynomolgus NHPs were utilized, in which an arterial access port was surgically implanted in the femoral artery for the purpose of providing a plasma input function curve. Each subject underwent 3 PET scans with [18F]FPEB: baseline and 2 drug doses of AFQ056 (0.074 and 0.34 mg/kg bolus IV). [18F]FPEB was synthesized to high specific activity using a Siemens Eclipse cyclotron and a GE FXn radiochemistry module. NHPs were maintained under isoflurane anesthesia during drug infusion and scanning while monitored for vital signs. Dynamic PET was conducted over 3hrs using a Siemens Focus220 PET scanner after infusion of 4.5 mCi [18F]FPEB, followed by serial arterial blood sampling for whole blood and plasma radioactivity and determination of percent parent tracer by HPLC. PET images were binned into 3D sinograms and reconstructed using iterative OSEM/MAP with attenuation and scatter correction. Brain volumes of interest were defined for NHPs on the baseline [18F]FPEB scan by deformable registration from a segmented brain atlas. Time-activity curves for multiple cortical, striatum and cerebellum regions were fit to a 2 tissue compartment model using PMOD software for determination of volume of distribution Vt. RO was determined by analysis of occupancy plots comparing the change in Vt relative to baseline Vt. [18F]FPEB PET data was well-fit by the 2 tissue compartment model. All quantified regions of interest resulted in reduced Vt with drug, with good fits to occupancy plots for all tissues. Cerebellum was determined to not be a suitable reference region for non-specific binding as a large change in Vt was observed at the highest AFQ056 dose in both subjects (59 and 71% reduction). Measured RO for AFQ056 was 73% at the 0.34 mg/kg dose and 51% at 0.074 mg/kg. Based on the drug exposure levels in a previous study to assess the ability of AFQ056 to decrease L-DOPA-induced dyskinesia in MPTP-rendered Parkinsonian NHPs (Shaffer C, Curr Neuropharm 2011, 9 suppl 1:59), the current data would predict that ≥80% RO is required for efficacy. This study shows that [18F]FPEB can be used to measure RO for mGluR5 NAMs, but requires arterial input function methodology, since a suitable reference tissue does not exist for cynomolgus NHP.

Disclosure of author financial interest or relationships:
**K. Zasadny**, Pfizer, Employment; **L. Chen**, Pfizer Inc., Employment; Pfizer Inc., Stockholder; **M. Skaddan**, Pfizer, Inc., Employment; **K. Fan**, Pfizer, Employment; **R. Coelho**, Pfizer Inc., Employment; **Z. Xie**, Pfizer, Employment; **K. Kuszpit**, Pfizer, Inc., Employment; **G. Currier**, Pfizer, Employment; **A.M. Burkholder**, Pfizer, Employment; **S. Kreuser**, None; **M. Volberg**, None; **N. Poy**, Pfizer, Employment; **J. Cianfrogna**, Pfizer, Employment; **P. Trapa**, None; **C. Shaffer**, Pfizer Inc, Employment; Pfizer Inc, Stockholder .

Presentation Number **P065**
Poster Session 1
September 5, 2012 / 18:00-18:00 / Room: The Liffey

# Regorafenib inhibits tumor growth, angiogenesis and metastasis formation in a murine model of colon cancer

***Lotfi Abou-Elkacem***[1], *Susanne Arns*[1], *Gunnar Brix*[2], *Dieter Zopf*[3], *Fabian Kiessling*[1], *Wiltrud Lederle*[1], [1]*RWTH Aachen University, Experimental Molecular Imaging, Aachen, Germany;* [2]*Division of Medical and Occupational Radiation Protection, Federal Office for Radiation Protection, Salzgitter, Germany;* [3]*Global Drug Discovery, Bayer Pharma AG, Berlin, Germany. Contact e-mail: labou-elkacem@ukaachen.de*

Introduction: Various studies have demonstrated that single blockade of VEGFR2 signaling is not efficient or can even lead to an evasive response with enhanced invasiveness and metastasis. Recently, Ang2 and its receptor Tie2 are discussed as mediators of tumor evasion and blockade of the Ang2/Tie2-axis prevented tumor angiogenesis, growth and metastasis1. Regorafenib (BAY 73-4506), a novel oral small molecule multikinase inhibitor, targeting VEGFR1,2,3, PDGFR-β, FGFR1, KIT, RET, B-RAF and Tie2 has recently been developed. We investigated the effects of regorafenib in a highly aggressive orthotopic mouse CT26 colorectal cancer model in comparison to DC101 an antibody inhibiting VEGFR2. Methods: CT26 tumor pieces were implanted orthotopically on the cecum of CD1 nude mice (n=18). Four days post-implantation (p.i.), the mice were divided randomly into three treatment groups: i) regorafenib 30mg/kg/d, ii) vehicle and iii) DC101 34mg/kg, i.p., every third day. Treatment was performed for 10 days and animal weight was controlled daily. Tumor growth and vascularization were assessed longitudinally at day 4, 7, 11 and 14 p.i. by T2w- and DCE-MRI with gadomer17 as contrast agent, respectively. Mice were sacrificed after the last MRI-measurements, tumors and organs suspicious of metastases were dissected and histological analyses were performed. Results: Regorafenib induced significant tumor growth inhibition (TGI), compared to vehicle treatment from day 7 p.i. ($p<0.01$) on resulting in tumor volume reductions of 75 to 85% by day 11 and 14 p.i. ($p<0.0001$), respectively. TGI was less pronounced in DC101 treated animals and occurred at a slower rate achieving significant reduction of tumor volumes only at day 14 p.i. ($p<0.0001$). A highly significant decrease in relative blood volume was observed in regorafenib-treated mice at day 11 ($p<0.01$) and day 14 p.i. ($p<0.0001$) vs vehicle. In DC101-treated animals, the decrease in the amplitude was lower, reaching significant difference vs vehicle only at day 14 p.i. ($p<0.01$). Immunohistochemical analysis demonstrated a stronger and significant reduction in microvessel density, angiogenic activity (VEGFR2) and a significantly increased apoptosis in regorafenib-treated tumors compared with DC101 at day 14 p.i.. No differences among groups were observed for vessel maturation and blood vessel permeability. No metastases were detected in livers of regorafenib-treated mice at day 14 p.i. in contrast to DC101- or vehicle-treated animals. Therapies with regorafenib and DC101 were well tolerated and no significant loss of animal weight occurred. Conclusion: Regorafenib efficiently inhibited tumor growth, vascularization and metastasis formation of a murine orthotopic model of colorectal cancer. Acknowledgment: This work was supported by Bayer Pharma AG. 1Mazzieri R. et al. Cancer Cell, 2011

Disclosure of author financial interest or relationships:
**L. Abou-Elkacem**, None; **S. Arns**, None; **G. Brix**, None; **D. Zopf**, Bayer Pharma AG, Employment; **F. Kiessling**, None; **W. Lederle**, None.

Presentation Number **P066**
Poster Session 1
September 5, 2012 / 18:00-18:00 / Room: The Liffey

# Near-Infrared Fluorescently Labeled Anti-HER2 Nanobody as Tracer for Optical Imaging of HER2 Expression

***Gezim Bala**, Sophie Hernot, Bram Roosens, Nick Devoogdt, Isabel Remory, Catarina Xavier, Steven Droogmans, Guy Van Camp, Vicky Caveliers, Tony Lahoutte, Bernard Cosyns, In Vivo Cellular and Molecular Imaging (ICMI), Vrije Universiteit Brussel (VUB), Brussels, Belgium. Contact e-mail: gezim.bala@vub.ac.be*

Background: Advances in optical imaging technologies have stimulated the development of near-infrared (NIR) fluorescently-labeled targeted probes for in vivo molecular imaging, such as intra-operative NIR fluorescence imaging. Hence, as complete resection of cancer lesions is one of the most important prognostic factors in cancer treatment, molecular navigation using NIRF-tracers should enable the surgeon to identify and completely remove even impalpable cancer lesions, while preserving healthy tissue during the intervention. In this regard, nanobody-based probes targeting the breast cancer marker Human Epidermal Growth Factor Receptor 2 (HER2) could be good candidates for NIR optical imaging due to their specific tumor targeting and fast blood clearance. Objectives: The aim of this study was to characterize the conjugation of the anti-HER2 nanobody 2Rs15d with the NIR fluorophore IRDye800CW, to evaluate its binding functionality in vitro and to test its application in vivo for the detection of HER2-positive tumors. Methods: IRDye800CW with N-hydroxysuccinimide ester as reactive group was conjugated to the 2Rs15d nanobody on lysines in the presence of a five-fold molar excess of dye to protein. The conjugated nanobody 2Rs15d-IRDye800CW was purified by size-exclusion chromatography. SDS-PAGE and mass-spectrometry were used to assess the purity and degree of conjugation of 2Rs15d-IRDye800CW. The absorbance spectrum of the sample was determined by spectrometry. Saturation binding studies on adherent cell cultures expressing HER2 were performed to determine the binding capacity of 2Rs15d-IRDye800CW. Finally, preliminary in vivo NIR optical imaging studies were carried out in mice bearing HER2-positive and HER2-negative (control) tumor xenografts. Results: The IRDye800CW was successfully conjugated to the 2Rs15d nanobody, with an average of 0.5 dyes per nanobody (composed as a mixture of 0, 1 and 2 dyes per nanobody). Cell binding studies showed that 2Rs15d-IRDye800CW had a KD of 13 nM and could distinguish between HER2-positive and -negative cells. Preliminary in vivo studies demonstrated the feasibility to detect HER2-positieve tumor xenografts 3 hours after injection of 2Rs15d-IRDye800CW, while no uptake was observed in HER2-negative tumors. Conclusion: Our results suggest that the conjugated anti-HER2 nanobody 2Rs15d-IRDye800CW can be used as a specific NIR probe for optical imaging of HER2 expression in vivo.

Disclosure of author financial interest or relationships:
**G. Bala**, None; **S. Hernot**, None; **B. Roosens**, None; **N. Devoogdt**, Boehringer Ingelheim, Grant/research support; Ablynx, Grant/research support; **I. Remory**, None; **C. Xavier**, None; **S. Droogmans**, None; **G. Van Camp**, None; **V. Caveliers**, None; **T. Lahoutte**, None; **B. Cosyns**, None.

Presentation Number **P067**
Poster Session 1
September 5, 2012 / 18:00-18:00 / Room: The Liffey

# Tumor Perfusion Correlates with Hyperpolarized Lactate in a Murine Model of Thyroid Cancer

***James A. Bankson***[1], *Vlad C. Sandulache*[2], *Yunyun Chen*[3], *Matthew E. Merritt*[4], *Stephen Y. Lai*[3], *John D. Hazle*[1], [1]*Imaging Physics, UT MD Anderson Cancer Center, Houston, TX, USA;* [2]*Bobby R. Alford Department of Otolaryngology - Head & Neck Surgery, Baylor College of Medicine, Houston, TX, USA;* [3]*Head and Neck Surgery, UT MD Anderson Cancer Center, Houston, TX, USA;* [4]*Advanced Imaging Research Center, UT Southwestern Medical Center, Dallas, TX, USA. Contact e-mail: jbankson@mdanderson.org*

Introduction: Anaplastic thyroid carcinoma (ATC) is a rare subtype with poor prognosis, accounting for more than half of deaths related to thyroid carcinoma. We recently demonstrated that inhibition of glucose catabolism using 2-deoxyglucose (2DG) potentiates cytotoxic effects of chemotherapy and radiation therapy, an effect shown in cells to correspond with a decrease in energy stores and intra-cellular reducing potential [1]. Dynamic magnetic resonance spectroscopy (MRS) of hyperpolarized (HP) [1-13C]-pyruvate [2] was also used to assess the activity of 2DG in vivo. Conversion of hyperpolarized pyruvate to lactate in tumor cells requires extravasation from blood vessels and transport across the cell membrane, and the latter has been shown as a potentially limiting factor [3]. We examined the role of vascular perfusion in HP signal dynamics by comparing dynamic contrast-enhanced (DCE-) MRI with dynamic HP-13C MRS in this orthotopic model system. Methods: Mice bearing ATC tumors (U-HTH83) were scanned by HP-13C MRS two hours after administration of 2DG (500 mg/kg IP) or sham therapy, then scanned again by DCE-MRI following a brief recovery period. Dynamic HP-13C MRS was acquired using a slice- and coil-localized pulse-acquire sequence repeated for three minutes beginning just prior to injection of 200 uL of 80mM HP-[1-13C]-pyruvate. Signal in resonances corresponding to the C1 label of pyruvate and lactate were integrated to generate time-intensity curves which were analyzed by NAUC and kinetic models accounting for exchange between physical and chemical compartments. DCE-MRI data was acquired using a fast spoiled gradient echo sequence repeated before, during and after injection of Gd-DTPA (0.2 mmol/kg). A constrained reconstruction algorithm [4] was used to estimate the arterial input function hightemporal resolution, and data was analyzed using a modified two-compartment model [5]. Results: The area under the lactate signal curve, normalized by the total 13C signal, was lower in tumors in animals given 2DG (N=3) compared to controls (N=4; $P = 0.0504$). Differences could specifically be attributed to the rate of conversion of HP pyruvate only in a model that accounts for both extravasation and transport ($P < 0.01$). Although no statistically significant differences in vascular parameters were observed between groups, correlation between KTrans and normalized lactate signal was high ($R2>0.9$) within groups. Conclusions: Vascular perfusion plays a significant role in the delivery of hyperpolarized tracers to their biological targets. Tracers that remain within vasculature can register significant signal with no apparent metabolites, regardless of the status of target tissue. Tumor perfusion changes as disease progresses and responds to therapy, necessitating that its influence be accounted for in the analysis of hyperpolarized tracer dynamics.
[1] Sandulache VC et al. Mol Cancer Ther (in press) [2] Ardenkjaer-Larsen JH et al. Proc Natl Acad Sci 100:10158-63, 2003 [3] Harris T et al. Proc Natl Acad Sci USA 106:18131-6, 2009 [4] Ragan D et al. NMR Biomed 24:373-84, 2011 [5] Tofts PS et al. J Magn REson Imaging 10:223-32, 1999

Disclosure of author financial interest or relationships:
**J.A. Bankson**, None; **V.C. Sandulache**, None; **Y. Chen**, None; **M.E. Merritt**, None; **S.Y. Lai**, None; **J.D. Hazle**, None.

Presentation Number **P068**
Poster Session 1
September 5, 2012 / 18:00-18:00 / Room: The Liffey

# Biodistribution of 68Ga-Labeled DOTA-Bisphosphonates

***Ralf K. Bergmann***[1], *Marian Meckel*[2], *Vojtech Kubicek*[3], *Frank Roesch*[2], [1]*Institute of Radiopharmacy, Helmholtz-Zentrum Dresden-Rossendorf, Dresden, Germany;* [2]*Nuclear Institute, Johannes Gutenberg University, Mainz, Germany;* [3]*Department of Inorganic Chemistry, Charles University Prague, Mainz, Germany. Contact e-mail: r.bergmann@hzdr.de*

Aim: Main indications of oncologic skeletal imaging are metastatic diseases in skeleton, bone pain in patients with known cancer, and primary bone tumors. Benign bone diseases like pediatric/adult back pain, bone viability and Paget's disease are also important indications of skeletal imaging. There are numerous studies with [18F]fluoride PET demonstrating the clinical utility. Similar characteristics show Tc-99m-labeled bisphosphonates. Combining the bone seeking properties, the advantages of PET, and the potential labeling with therapeutic radionuclides we studied DOTA-phosphonates radiolabeled with [68Ga]Ga3+. Methods: The following macrocyclic tetraaza based phosphonate chelators were used BPAMD ((4-{[(bis-phosphonomethyl) carbomoyl]methyl}-7,10-bis-(carboxymethyl)-1,4,7,10-tetraazacyclododec-1-yl)-acetic acid, BPAPD ((4-{[(bis-phosphonopropyl)carbomoyl]methyl}-7,10-bis-(carboxymethyl)-1,4,7,10-tetraazacyclododec-1-yl)-acetic acid and BPPED Tetraethyl 10-{[(2,2-bis-phosphonoethyl)hydroxyphosphoryl]methyl}-1,4,7,10-tetraazacyclododecane-1,4,7-triacetic acid. The DOTA based phosphonate ligands were labeled with [68Ga]GaCl3. The radiochemical purity of the labeled products was >95% determined with radio thin-layer chromatography. The biodistribution and biokinetics were compared with [18F]fluoride and [99mTc]Tc-MDP in Wistar rats using dissection, small animal PET and SPECT. All activity concentration data were calculated as SUV. Results: The compounds were labeled with high yields in ammonium acetate buffer with 68Ga, followed by a purification step using a cation exchange resin. High uptake values were detected for all 68Ga-phosphonates in the femura. The accumulation of [68Ga]BPPED in the bone was the highest and comparable with the uptake of [18F]Fluoride and [99mTc]Tc-MDP. The blood clearance of the [68Ga]BPPED was the fastest with a biexponential kinetics and half-life of 0.4 min and 6.9 min. The [68Ga]BPPED bone to blood ratio was also superior, however, not so large like of [18F]Fluoride and [99mTc]Tc-MDP. Conclusion: The [68Ga]BPPED showed in a preclinical setting excellent characteristics for skeletal imaging. It seems to be also a potential candidate for radionuclide therapy in oncology.

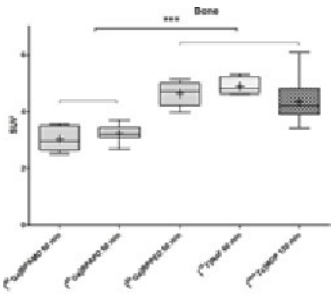


| Radiotracer | Bone | | | Blood | | |
|---|---|---|---|---|---|---|
| SUV | Mean | SD | n | Mean | SD | n |
| [68Ga]BPAMD 60 min | 3.02 | 0.43 | 5 | 0.58 | 0.11 | 5 |
| [68Ga]BPAPD 60 min | 3.31 | 0.31 | 5 | 0.56 | 0.13 | 5 |
| [68Ga]BPPED 60 min | 4.03 | 0.41 | 5 | 0.47 | 0.06 | 5 |
| [18F]fluoride 60 min | 4.87 | 0.32 | 4 | 0.03 | 0.01 | 4 |
| [99mTc]MDP 120 min | 4.76 | 0.66 | 21 | 0.08 | 0.04 | 13 |

SUV=(activity per gram / injected activity * body weight)

Disclosure of author financial interest or relationships:
**R.K. Bergmann**, None; **M. Meckel**, None; **V. Kubicek**, None; **F. Roesch**, None.

Presentation Number **P069**
Poster Session 1
September 5, 2012 / 18:00-18:00 / Room: The Liffey

# 166Holmium oxide sub-micronic nanoparticles as a brachytherapy agent in a peritoneal carcinosis

*Jacqueline Taleb[1], Pauline Bonazza[1], Laurence Marmuse[2], David Kryza[1,3], Marc Janier[1,3], Cedric Louis[2], Luca Maciocco[4], Pascal Perriat[5], Olivier Tillement[1], **Claire Billotey**[1,3], [1]Laboratoire de Physico-Chimie des Matériaux Luminescents, UMR 5620 CNRS, Universite Claude Bernard Lyon 1, Lyon, France; [2]NanoH, Saint-Quentin Fallavier, France; [3]Service de Médecine Nucléaire, Hôpital Edouard Herriot, Hospices Civils de Lyon, Lyon, France; [4]Advanced Accelerator Applications, Saint Genis Pouilly, France; [5]Laboratoire MATEIS, Matériaux Ingénierie et Science, UMR 5510 CNRS, INSA de Lyon, Lyon, France. Contact e-mail: claire.billotey@univ-lyon1.fr*

Background: Peritoneal carcinosis is a disease of poor prognosis (7 to 18 months of survival) with limited treatments. The most encouraging results are obtained with a treatment combining chemotherapy and hyperthermia (5 years survival in 40% to 45% of cases). The aim of this study was to evaluate the possibility to use 166Ho oxide sub-micronic particles (HOSMP) as a brachytherapy agent of peritoneal carcinosis via an intra-peritoneal injection (IP). Materials and methods: The peritoneal carcinosis was obtained by IP injecting 106 DHD K12 prob cells in BD IX rats. 20 days after induction of carcinosis CT scans were performed at 0, 2, 4, 6 and 24 h post IP injection of HOSMP to evaluate dispersion of HOSMP within the peritoneal cavity, in function of formulation of HOSMP solution and other experimental parameters (+/- peritoneal washing, 1 or 2 set of particles injection). Imaging results were compared to macroscopic examination. With selected particles injection parameters, a leaking test from peritoneal cavity was performed with low activated HOSMP at 72h and 11 days post-IP injection. A therapeutic test was performed in 20 rats after IP injection of 50 MBq of activated HOSMP, 10 days after carcinosis induction. The mean survival time of rats of this group was compared to a control (20 rats with carcinosis), and sham (20 rats injected with inactivated HOSMP) groups. The activations of the particles were performed through neutron irradiation in the high-flux reactor at the Institut Laue Langevin, Grenoble, France. Results: The solution was injectable and dispersible in the whole peritoneal cavity with a large predominance for the tumor area. The leakage from the peritoneal cavity after IP injection was less than 5 % even at 11 days. The mean survival time in rats treated with activated HOSMP was significantly longer (41 d) than in control (32 d-p< 0,0001) and SHAM (33.5 d - p=0,0237) groups. Conclusion: Brachytherapy of peritoneal carcinosis with 166Ho Oxide submicronic particles seem promising. New therapeutic tests should be performed by improving tumoral model (surgical ablation of tumor nodes before brachytherapy, as human management), and brachytherapy parameters (2 x 50 to 75 MBq administration in two times with few day interval) to obtain higher therapeutic efficacy.

Disclosure of author financial interest or relationships:
**J. Taleb**, None; **P. Bonazza**, None; **L. Marmuse**, None; **D. Kryza**, None; **M. Janier**, None; **C. Louis**, None; **L. Maciocco**, None; **P. Perriat**, None; **O. Tillement**, None; **C. Billotey**, None.

Presentation Number **P070**
Poster Session 1
September 5, 2012 / 18:00-18:00 / Room: The Liffey

# Synthesis, labelling and biodistribution studies of the new photosensitizer 2CPP

*Pedro M. Santos[1,2], Mafalda Laranjo[1,3], Ana M. Abrantes[1,3], Arménio Serra[5], Jorge Maia[4], António M. Rocha-Gonsalves[5], **Maria F. Botelho**[1,3], [1]Biophysics Unit, IBILI, CIMAGO, Faculty of Medicine, University of Coimbra, Coimbra, Portugal; [2]Faculty of Health Sciences, University of Beira Interior, Covilhã, Portugal; [3]CIMAGO, Faculty of Medicine, University of Coimbra, Coimbra, Portugal; [4]Faculty of Sciences, University of Beira Interior, Covilhã, Portugal; [5]Quimiotecnon, Chemistry Department, Faculty of Sciences and Technology, University of Coimbra, Coimbra, Portugal. Contact e-mail: filomena@ibili.uc.pt*

Introduction: Photodynamic therapy (PDT) is a promising new treatment modality for cancer. As photosensitizers (PS) exhibit great selectivity for tumour tissues, namely, porphyrin sensitizers, several attempts have been made to label these compounds with different radionuclides, assessing their potential use as tumour imaging agent. The radiolabelling of PS can be used to study its biodistribution in a non-invasive way, to identify target-organs, and to study pharmacokinetics and routes of excretion. This information can be of major importance to optimize the PDT protocols. The aim of this work was to label the water-soluble porphyrin, meso-bis[3,4-bis(carboxymethyleneoxy)phenyl]porphyrin (2CPP), with 99mTc in order to perform biodistribution studies and to evaluate its pharmacokinetics. Material and Methods: The synthesis of the 2CPP was achieved by condensation of the meso-free dypirromethane and the protected aldehyde. Then alcaline hydrolysis of the ester gives the porphyrin. In order to optimize labelling efficiency, several parameters were tested, namely, ligand and reducing agent (stannous chloride dihydrate) quantities, pH, radionuclide activity, temperature and incubation time. Radiochemical purity of the compound was characterized by ascending micro-chromatography. To evaluate radiopharmaceutical pharmacokinetics, the complex was injected in Balb/c mice. Immediately after administration of the 99mTc-2CPP, several images were obtained at different time periods. After image acquisitions, the animals were killed at different time intervals: 30, 120 and 240 minutes and samples were collected from organs and fluids. All organs were weighed and their radioactivities were measured using a well-counter. The percent of the injected activity per gram of organ was calculated. Results: Labelling procedure optimization lead to an efficiency superior to 80%. The complex remained stable for more than 4h. These efficiencies were obtained combining: 0.4mg 2CPP, pH=7, stannous chloride dihydrate 10 µg, 160 MBq 99mTc and incubation at room temperature (24±3 °C) for 20 minutes. Biodistribution studies showed that the complex was largely eliminated through the renal and hepatobiliary systems. Four hours after administration no significant activity was observed in any organs/tissue except the sites of excretion. Besides this a high lung activity was observed during 2 first hours after injection. Conclusion: The labelling of 2CPP with 99mTc was stable, as was proved by biodistribution, and was also reproducible. This complex has a quickly clearance, being eliminated by renal and hepaotobiliar system. Concerning the high lung uptake, futures studies will be conducted using animal models of lung cancer in order to explore this biodistribution profile.

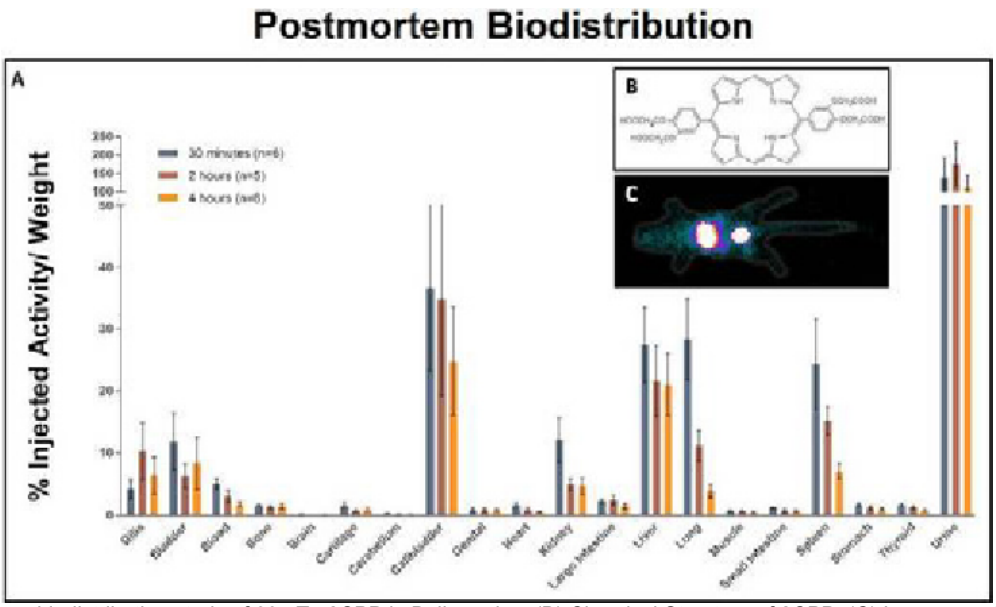


Figure: (A) Postmortem biodistribution study of 99mTc-2CPP in Balb-c mice. (B) Chemical Structure of 2CPP. (C) Image acquired at 120 minutes.

Disclosure of author financial interest or relationships:
**P.M. Santos**, None; **M. Laranjo**, None; **A.M. Abrantes**, None; **A. Serra**, None; **J. Maia**, None; **A.M. Rocha-Gonsalves**, None; **M.F. Botelho**, None.

Presentation Number **P071**
Poster Session 1
September 5, 2012 / 18:00-18:00 / Room: The Liffey

# A comparative study to analyse the potential of 99mTc-PEI-MP for diagnosis and 188Re-PEI-MP for therapy of bladder carcinoma and osteosarcoma

*Sara Ferreira[1,3], Mafalda Laranjo[1,2], Ana M. Abrantes[1,2], Ana F. Brito[1,2], Luís Metello[4], Jan Zeevart[5], Werner Louw[5], Irene Dormehl[6], **Maria F. Botelho**[1,2], [1]Biophysics Unit, IBILI, Faculty of Medicine, University of Coimbra, Coimbra, Portugal; [2]CIMAGO, Faculty of Medicine, University of Coimbra, Coimbra, Portugal; [3]School of Sciences, University of Minho, Braga, Portugal; [4]Nuclear Medicine Course, High Institute of Allied Health Technologies of Porto's Polytechnic Institute, Porto, Portugal; [5]Radiochemistry Department, NECSA, Pretoria, South Africa; [6]Department of Internal Medicine, University of Pretoria, Pretoria, South Africa. Contact e-mail: filomena@ibili.uc.pt*

Introduction: The water-soluble polymer PEI-MP (polyethyleneimine, functionalised with methylphosphonate groups) that might be labeled with 188Re (emits high energy β- particles) and 99mTc presents a strong potential for metabolic radiotherapy and diagnosis, respectively. The aim of this study was to evaluate in vivo the potential of 188Re-PEI-MP as therapeutic agent and 99mTc-PEI-MP as diagnostic agent for bladder carcinoma and osteosarcoma. Material and methods: Cytotoxicity of PEI-MP was investigated in bladder carcinoma cell line (CRL-1472) using the MTT test for different concentrations of PEI-MP (1 μM to 1000 μM) and incubation times (24h, 48h, 72h and 96h). Radiochemical purity of 99mTc-PEI-MP and 188Re-PEI-MP was achieved using ascending microchromatography. For the in vivo studies eight groups of Balb/c nu/nu mice were used: four normal groups injected with Na99mTcO4 (n=10), 99mTc-PEI-MP (n=10), Na188ReO4 (n=18) and 188Re-PEI-MP (n=17), respectively; two with bladder carcinoma xenotransplants injected with Na188ReO4 (n=8) and 188Re-PEI-MP (n=12), respectively; two with osteosarcoma xenotransplants injected with Na188ReO4 (n=17) and 188Re-PEI-MP (n=19) respectively. When the tumors reached the appropriate volume, radiopharmaceuticals were administered by an intravenous injection in the tail vein (22-37MBq), with the animal anesthetized and previously placed on the gamma camera detector. Immediately, a dynamic acquisition followed, with a 128x128 matrix for 10 min (20 frames, 30 seconds). Static images (2 min) were performed with a 256x256 matrix, where each of the six groups was divided into two groups, of which one was imaged at 120 minutes, and the other at 240 minutes. For biodistribution proposes, mice were euthanized 2 and 4 hours after injection and organ samples were weighted and counted in a well-counter to obtain percentage injected activity per gram of organ (%ID/g). Results and discussion: The MTT assay showed that PEI-MP is not cytotoxic. The radiochemical purity of 188Re-PEI-MP and 99mTc-PEI-MP was higher than 85%. Biodistribution results, with Na188ReO4 and Na99mTcO4, showed a higher uptake by the thyroid, bladder and stomach, following a normal biodistribution. The biodistribution with 188Re-PEI-MP and 99mTc-PEI-MP showed that the excretion of these complexes occurs primarily through the renal system, with a small fraction being eliminated by the hepatobiliary system. In mice with osteosarcoma tumor/muscle ratio was greater than 1.0, and for mice with bladder carcinoma the tumor/muscle ratio was greater than 1.5. Conclusions: The 188Re-PEI-MP seems to be promising in the treatment of both types of cancer, but with a greater potential for bladder cancer, given its biodistribution and tumor/muscle ratio. Following the same biodistribution as 188Re-PEI-MP, 99mTc-PEI-MP seems to be optimal for diagnosis and follow up of both types of cancer.

Disclosure of author financial interest or relationships:
**S. Ferreira**, None; **M. Laranjo**, None; **A.M. Abrantes**, None; **A.F. Brito**, None; **L. Metello**, None; **J. Zeevart**, None; **W. Louw**, None; **I. Dormehl**, None; **M.F. Botelho**, None.

Presentation Number **P072**
Poster Session 1
September 5, 2012 / 18:00-18:00 / Room: The Liffey

# Identification of Cancer Metastases using the Combination of PET and Viral Vectors

***Peter Brader***[1,3]*, Hedvig Hricak*[3]*, Thomas H. Helbich*[1]*, Gil Ziv*[2]*,* [1]*Radiology, Medical University Vienna, Vienna, Austria;* [2]*The Laboratory for Applied Cancer Research, Tel Aviv Sourasky Medical Center, Tel Aviv, Israel;* [3]*Radiology, Memorial Sloan Kettering Cancer Center, New York, NY, USA. Contact e-mail: peter.brader@meduniwien.ac.at*

Cancer is a prevalent disease worldwide and a primary cause of mortality in the western world. There are three main ways for dissemination of solid tumors: direct invasion, lymphatic spread and hematogenic spread. The presence of metastases is the most significant factor in predicting prognosis and therefore evidence of metastases will influence decision-making regarding treatment. The imaging modalities used in clinical practice for cancer staging include ultrasound, computed tomography (CT), magnetic resonance imaging (MRI), and positron emission tomography (PET) scanning. These imaging techniques are limited in the evaluation and localization of metastases due to their restricted ability to identify subcentimeter neoplastic disease. Hence, there is a need for an effective noninvasive modality that can accurately identify occult metastases in cancer patients. One such method is the combination of positron emission tomography with vectors designed for delivery of reporter genes into target cells. There are three main classes of reporter genes: receptors, transporters and enzymes. A membranous receptor, which is commonly used for imaging of endocrine cancers, is the somatostatin receptor (hSSTrs). In the transporter group, the human norepinephrine transporter (hNET) transgene carried by a recombinant vaccinia virus (GLV-1h99) resulted in specific uptake of the radiotracer [131I]-meta-iodobenzylguanidine (MIBG) in orthotopic mesothelioma and pancreatic ductal carcinoma tumor models. In the enzyme group, the herpes simplex virus-1 thymidine kinase (HSV1-tk) gene and its mutation were extensively studied as candidate reporter genes for imaging of cancer. Combination of HSV1-tk and PET imaging is based on the viruses of viral or nonviral vectors which can carry and selectively express the HSV1-tk reporter gene in a variety of cancer cells but not in normal cells. A radioactive tracer which is applied systemically is phosphorylated by the HSV1-tk enzyme, and as a consequence, the tracer accumulates in proportion to the level of HSV1-tk expression which can be imaged using PET (figure 1). In our studies we showed that the NV1023 herpes virus expressing the HSV-1-tk gene can track to draining lymph nodes following direct intratumoral injection and infect metastatic melanoma cells in the SLNs (sentinel lymph nodes). Nodal metastases can be then successfully identified by [18F]-2′-fluoro-2′-deoxy-1-β-D-β-arabinofur anosyl-5-ethyluracil ([18F]FEAU) PET imaging (figure 2). In another animal model we demonstrated that this combined imaging system could also be used to allow in vivo imaging and detection of cancerous neural invasion. Positron emission tomography with [18F]FEAU showed significantly higher uptake in neural invasion than in control animals. These diagnostic paradigms introduce an advantageous new concept in noninvasive molecular imaging with the potential benefits for improving patient care by providing guidance for therapy to patients with risk for metastases.

Disclosure of author financial interest or relationships:
**P. Brader**, None; **H. Hricak**, None; **T.H. Helbich**, Siemens, Grant/research support; Fond national bank austria, Grant/research support; **G. Ziv**, None.

Presentation Number **P073**
Poster Session 1
September 5, 2012 / 18:00-18:00 / Room: The Liffey

# Viral Nanoparticles as Novel Tumor Targeting Carriers to Image Brain Cancers

*Stephanie Chung[3], Amy M. Wen[2], Christine M. DeBaz[3], Sourav Dey[2], Nicole Steinmetz[2,3], **Ann-Marie Broome**[1], [1]Radiology & Radiological Science, Medical University of South Carolina, Charleston, SC, USA; [2]Biomedical Engineering, Case Western Reserve University, Cleveland, OH, USA; [3]Radiology, Case Western Reserve University, Cleveland, OH, USA. Contact e-mail: broomea@musc.edu*

Glioblastoma, a high-grade brain tumor that develops from astrocytes, is the most common adult malignant brain tumor and is particularly invasive. Treatment options for such malignant gliomas are multifaceted and may include surgery, radiation therapy, and chemotherapy. However, most of these brain tumors are incurable because the tumor cells infiltrate into the normal brain tissue, making surgical removal difficult and treatment complicated. Imaging modalities such as CT, the standard imaging modality used to detect the initial tumor mass, and MRI, used to assist in surgical resection, are limited in their ability to resolve the tumor cells invading the normal brain tissue. As a result, recurrences are frequent and the average survival time, according to the World Health Organization, is often less than 12 months after diagnosis. Ultimately, more patients with gliomas would benefit from the development of new, targeted detection agents and therapies. To develop imaging and therapeutic tools that take advantage of the diagnostic molecular signature, new technologies must employ a targeted-nanoparticle delivery design that can be noninvasively imaged and monitored in vivo, solubilize and systemically circulate a drug payload, provide an efficient and targeted release of drug into tumors, decrease release of the drug into surrounding tissues, and eventually clear from the tissue or body. To achieve this, we have utilized a plant viral nanoparticle, cowpea mosaic virus (CPMV), as the payload delivery vehicle (Fig. 1A). Based on the defined structure of CPMV, we precisely conjugated both a fluorophore for tracking uptake and accumulation into the cell and a biotin tag for extremely high affinity binding to streptavidin-labeled EGF, the targeting moiety. Using this strategy, we were able discriminate between glioblastoma cells that overexpress EGFR and glioblastoma cells that express no to minimal levels of EGFR in vitro (Fig. 1B). Further, we were able to image the uptake and accumulation of the EGFR-targeted CPMV into orthotopic brain tumors using in vivo fluorescence imaging (Fig. 1C). Current experiments are underway to deliver a therapeutic payload to the cancer.

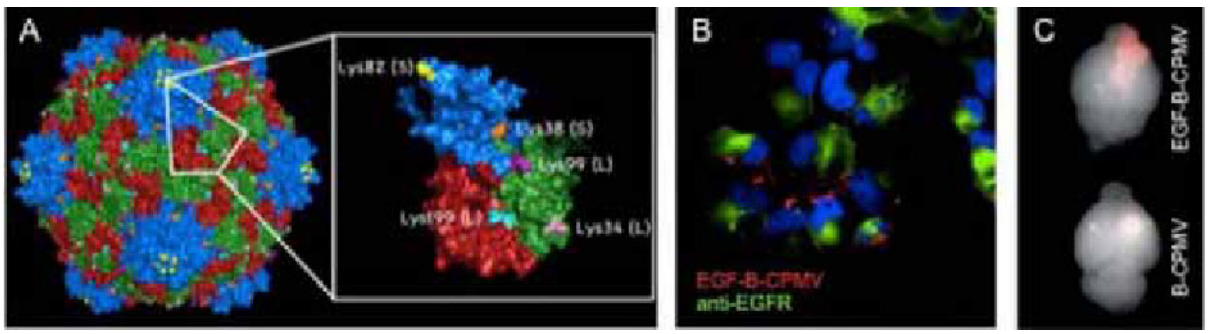


Disclosure of author financial interest or relationships:
**S. Chung**, None; **A.M. Wen**, None; **C.M. DeBaz**, None; **S. Dey**, None; **N. Steinmetz**, None; **A. Broome**, None.

Presentation Number **P074**
Poster Session 1
September 5, 2012 / 18:00-18:00 / Room: The Liffey

# Molecular Ultrasound with VEGFR2-Targeted Microbubbles (BR55) Reliably Depicts the High Angiogenic Activity in Very Early Breast Cancer

***Jessica Bzyl***[1], *Moritz Palmowski*[1,2], *Anne Rix*[1], *Susanne Arns*[1], *Jean-Marc Hyvelin*[3], *Sibylle Pochon*[3], *Josef Ehling*[1,4], *Simone Schrading*[5], *Fabian Kiessling*[1], *Wiltrud Lederle*[1], [1]*Experimental Molecular Imaging, RWTH Aachen University, Aachen, Germany;* [2]*Department of Nuclear Medicine, RWTH Aachen University, Aachen, Germany;* [3]*Bracco Suisse SA, , Geneva, Switzerland;* [4]*Institute of Pathology, RWTH Aachen University, Aachen, Germany;* [5]*Department of Diagnostic and Interventional Radiology, RWTH Aachen University, Aachen, Germany. Contact e-mail: jbzyl@ukaachen.de*

Objectives: Molecular ultrasound is well suited for the examination of tumor xenografts of well discernable sizes. In this study, we investigated whether the VEGFR-2 expression of very early and small breast carcinomas is high enough for reliable molecular ultrasound imaging with targeted microbubbles. Methods: MCF-7 breast cancer xenografts (n=23) ranging in sizes from 2 mm diameter up to 5 mm diameter were measured with automated 3D molecular ultrasound (25 MHz) using clinically translatable VEGFR2-targeted microbubbles (BR55). The relative tumor blood volume was assessed in parallel with non-targeted microbubbles (BR38). The in vivo ultrasound data were validated by quantitative immunohistochemistry of tumor sections. Results: The highest binding of VEGFR2-specific microbubbles was detected in very small lesions of 2 mm diameter. A significantly lower accumulation of BR55 was measured in larger tumors (p=0.023), but the binding of VEGFR2-targeted microbubbles was still high enough for imaging. The relative blood volume was comparable at all tumor sizes. Both findings were confirmed by immunohistochemistry. Additionally, a significant increase in the number of mature vessels with higher lumina was detected in larger tumors (p<0.01), explaining the decrease in VEGFR2 expression during tumor growth. Further, the vessel number decreased with increasing tumor size. Both, vessel maturation and the increase in vessel size provide explanation for the maintained blood volume despite the reduced vessel number. Conclusions: The angiogenic activity of very small breast lesions can very well be depicted by 3D molecular ultrasound using BR55, suggesting that molecular ultrasound has potential in detecting and characterizing very small lesions.

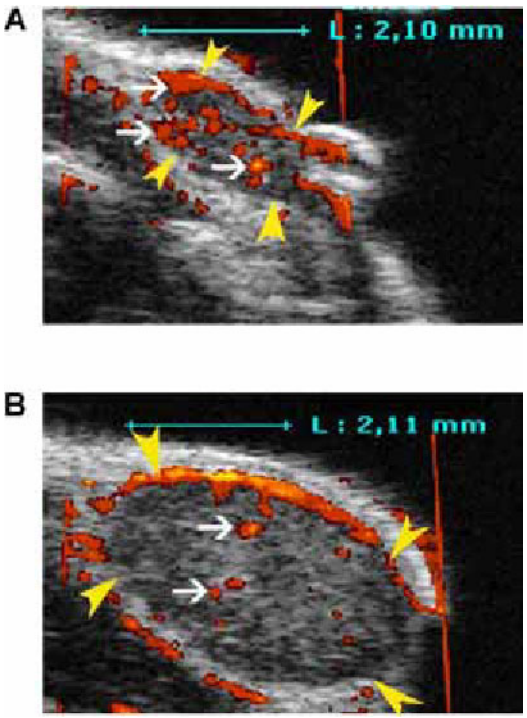


Images show binding of VEGFR2 targeted BR55 microbubbles in MCF-7 tumors (arrowheads). The signal of the microbubbles can be seen as a red overlay (arrows indicate representative signals). A) is a representative slice of the 3D acquisition of a tumor with 2 mm diameter and B) of a tumor with 4 mm diameter. In the tumors with 2 mm diameter significantly more BR55 microbubbles accumulated compared to all other tumor sizes.

Disclosure of author financial interest or relationships:
**J. Bzyl**, None; **M. Palmowski**, None; **A. Rix**, None; **S. Arns**, None; **J. Hyvelin**, Bracco Suisse SA, Employment; **S. Pochon**, Bracco Suisse SA, Employment; **J. Ehling**, None; **S. Schrading**, None; **F. Kiessling**, None; **W. Lederle**, None.

Presentation Number **P075**
Poster Session 1
September 5, 2012 / 18:00-18:00 / Room: The Liffey

# In Vivo Targeting and Imaging of Tumor Vasculature with Radiolabeled, Antibody-Conjugated Nano-Graphene

*Hao Hong[1], Kai Yang[2], Yin Zhang[1], Jonathan W. Engle[1], Liangzhu Feng[2], Charles P. Theuer[3], Todd E. Barnhart[1], Zhuang Liu[2], **Weibo Cai**[1], [1]University of Wisconsin - Madison, Madison, WI, USA; [2]Soochow University, Suzou, China; [3]TRACON Pharmaceuticals, Inc., San Diego, CA, USA. Contact e-mail: WCai@uwhealth.org*

**Objectives:** Our goal was to explore nano-graphene for in vivo tumor targeting and to quantitatively evaluate the pharmacokinetics and tumor targeting efficacy through positron emission tomography (PET) imaging, using $^{64}$Cu and $^{66}$Ga as the radiolabel. **Methods:** Nano-graphene oxide (GO) sheets, with amino group-terminated PEG chains (10 kDa) covalently attached, were conjugated to NOTA (1,4,7-triazacyclononane-1,4,7-triacetic acid, a suitable chelator for $^{64}$Cu and $^{66}$Ga) and TRC105 (a monoclonal antibody that binds to human and murine CD105, overexpressed on tumor neovasculature). FACS analyses, size measurements, and serum stability studies were performed to characterize the GO conjugates before in vivo investigation (PET, biodistribution, blocking studies, etc.) in 4T1 murine breast tumor-bearing mice. Findings from imaging studies were then validated by histology. **Results:** TRC105-conjugated GO, 20-30 nm in diameter, was specific for CD105 with little non-specific binding. Both $^{64}$Cu- and $^{66}$Ga-labled GO conjugates had excellent stability in mouse serum. Clearance of the GO conjugates in mice was via the hepatobiliary pathway. $^{64}$Cu/$^{66}$Ga-NOTA-GO-TRC105 accumulated rapidly in the 4T1 tumor and tumor uptake remained stable over time (3.8±0.4, 4.5±0.4, 5.8±0.3, and 4.5±0.4 %ID/g at 0.5, 3, 7, and 24 h p.i. for $^{66}$Ga; 5.8±0.6, 5.3±0.6, 4.0±0.4, and 3.4±0.1 %ID/g at 0.5, 3, 24, and 48 h p.i. for $^{64}$Cu; n = 4). Blocking studies confirmed CD105 specificity of $^{64}$Cu/$^{66}$Ga-NOTA-GO-TRC105, which was corroborated by biodistribution studies. Furthermore, microscopy examination of GO in light view mode and immunofluorescence staining revealed that targeting of NOTA-GO-TRC105 is tumor vasculature CD105 specific with little extravasation. **Conclusions:** For the first time, we demonstrated that GO can be specifically directed to the tumor neovasculature in vivo through targeting of CD105, a marker of tumor angiogenesis. The versatile chemistry of graphene-based nanomaterials makes them suitable nanoplatforms for future biomedical research, such as cancer theranostics.

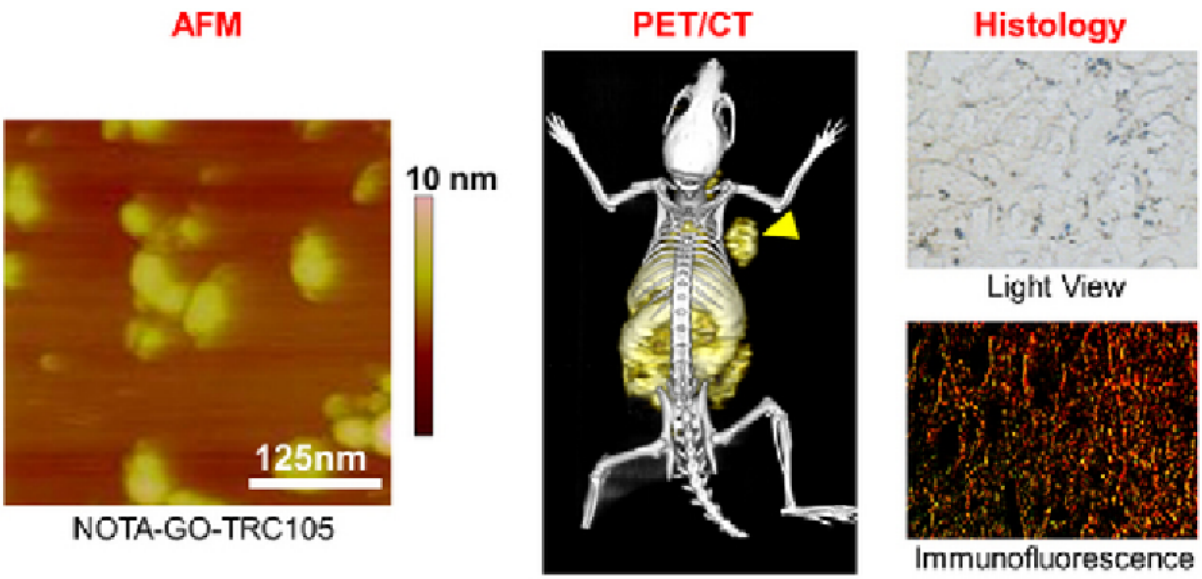


Disclosure of author financial interest or relationships:
**H. Hong**, None; **K. Yang**, None; **Y. Zhang**, None; **J.W. Engle**, None; **L. Feng**, None; **C.P. Theuer**, TRACON Pharmaceuticals, Inc., Stockholder; TRACON Pharmaceuticals, Inc., Employment; **T.E. Barnhart**, None; **Z. Liu**, None; **W. Cai**, None.

Presentation Number **P076**
Poster Session 1
September 5, 2012 / 18:00-18:00 / Room: The Liffey

# Biodistribution, MicroSPECT/CT Imaging and Therapeutic Efficacy of 188Re-liposome in a C26 Murine Colon Carcinoma Solid Tumor Model

***Ya-Jen Chang***[1], *Chin-Wei Hsu*[1], *Chih-Hsien Chang*[1], *Keng-Li Lan*[2], *Gann Ting*[1], *Te-Wei Lee*[1], [1]*Institute of Nuclear Energy Research, Taoyuan County, Taiwan;* [2]*Cancer Center, Taipei Veterans General Hospital, Taipei, Taiwan. Contact e-mail: yjchang@iner.gov.tw*

Liposomes are good drug delivery system which allow the encapsulation of drugs into vesicles for their delivery. In this study, the biodistribution and microSPECT/CT imaging of 188Re-liposomes administered by the i.v. route in murine C26-colon tumor-bearing mice were investigated. The anti-tumor effect of 188Re -liposome was assessed by tumor growth inhibition and survival ratio in a C26 murine colon carcinoma solid tumor model. For the biodistribution study, the highest uptake of liposome in tumors was 8.33%±0.25% at 24 h after 188Re-liposomes administration, and the tumor to muscle ratio of 188Re-liposomes was 18.75±2.77. With image analysis, the highest SUV in tumor was 2.81±0.26 at 24 h after injection of 188Re-liposomes. The Pearson correlation analysis showed a positive high correlation of tumor targeting or uptake of188Re-liposomes between biodistribution and microSPECT semi-quantification imaging analysis (r=0.992). In the study on therapeutic efficacy, tumor growth inhibition of mice treated with 188Re-liposome was obviously precisely controlled (Mean tumor size was 245.8 ± 150.23 mm3; Mean growth inhibition rate (MGI) was 0.135) and have longer median survival time (62 d) than those treated with anti-cancer drug 5-FU and untreated control mice (39 d and 30 d, respectively). Four (40 %) of the mice treated with radio-therapeutics 188Re-liposome were completely cured after 120 days. These results were pointed to the potential benefit of the radio-therapeutics 188Re-liposome for adjuvant cancer treatment on oncology applications.

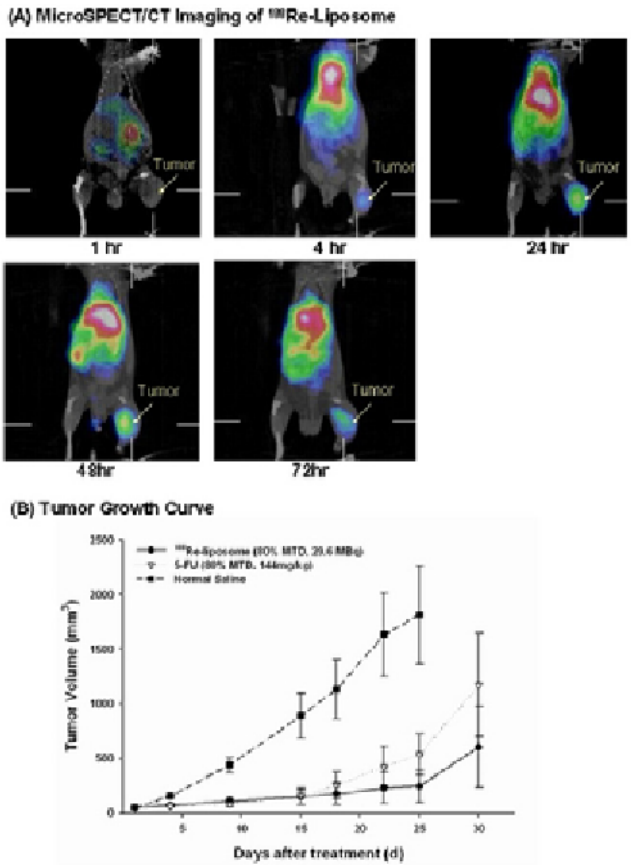


(A) The 188Re-liposome containing 0.5 mCi of 188Re was administered to each mouse by intravenous injection. The images were acquired at 1, 4, 24, 48 and 72 h after injection. (B)Tumor growth volume (mm3) versus time (days) curve for BALB/c mice implanted with C26 murine colon tumors after administering 188Re-liposome (22.2, 29.6 and 37 MBq) by single i.v. injection.

Disclosure of author financial interest or relationships:
**Y. Chang**, None; **C. Hsu**, None; **C. Chang**, None; **K. Lan**, None; **G. Ting**, None; **T. Lee**, None.

Presentation Number **P077**
Poster Session 1
September 5, 2012 / 18:00-18:00 / Room: The Liffey

# Combination of Rhenium-188-liposome and external beam radiotherapy against human esophageal cancer

***Yu-Jen Chen***[1,2], *Chih-Wen Chi*[1,5], *Chih-Hsien Chang*[3,4], *Yi-Jang Lee*[4], *Tien-Kuei Chang*[3], [1]*Department of Radiation Oncology, Mackay Memorial Hospital, Taipei, Taiwan;* [2]*Department of Medical Research, Mackay Memorial Hospital, Taipei, Taiwan;* [3]*Division of the Isotope Application, Institute of Nuclear Energy Research, Taoyuan, Taiwan;* [4]*Department of Biomedical Imaging and Radiological Sciences, National Yang-Ming University, Taipei, Taiwan;* [5]*Department of Biotechnology, Hungkuang University, Taichung, Taiwan. Contact e-mail: chenmdphd@gmail.com*

Purpose: The modes of radiotherapy (RT) for cancer treatment include external beam radiotherapy (EBRT) and internal beam radiotherapy (IBRT). EBRT delivering high-energy radiation beam can cover both gross tumor and potential microscopic tumor cells in tumor vicinity. IBRT emitting short-distance radiation can directly eradicate gross tumor inside torso. Esophageal cancer is one of the most treatment resistant malignancies with dismal prognosis. We proposed that combination of EBRT and IBRT may deliver radiation to simultaneously treat primary tumor, regional lymphatics and surrounding risky areas. Rhenium-188 (188Re)-liposome is a nanoparticle emitting gamma (for molecular imaging validation) and beta (for therapeutic RT) rays with biodistribution preferential to tumor. We established a experimental model of combinatory treatment and examined the effect of the EBRT and 188Re-liposome on human esophageal cancer xenograft . Materials and Methods: We prepared the 188Re-liposome with quality assurance according to previous work in clinical trial. Human esophageal cancer cell lines BE-3 (adenocarcinoma) and CE81T/VGH (squamous cell carcinoma) expressing luciferase gene for optical imaging were transplanted to nude mice for xenografts. The imaging modalities used included optical and nanoSPECT/CT imaging systems to examine the tumor uptake of 188Re-liposome and treatment result in xenograft models. Optimal dosing for EBRT and 188Re-liposome were assessed in a clinical practice-oriented way. Results: As for quality assurance, the labeling efficiency of 188Re-EMBDA (Rf =0) was 100%. The labeling efficiency and total activity of 188Re-liposome were 76.5% and 8731 μCi, respectively. For molecular imaging, nanoSPECT/CT scan results showed that esophageal cancer BE-3, but not CE81T/VGH, xenograft could uptake the 188Re-liposome 24 hours after injection. The EBRT alone inhibited the growth of BE-3 xenografts in a dose-dependent manner. The optimization of combinatory regimens revealed that EBRT with 3 Gy and 188Re-liposome with 310 μCi might be feasible for further preclinical study. Conclusion: Human esophageal adenocarcinoma BE-3 xenograft could uptake 188Re-liposome. The combination of EBRT with 188Re-liposome may be a potential treatment modality for esophageal cancer by providing molecular imaging, image-guided treatment and comprehensive radiation therapy coverage simultaneously.

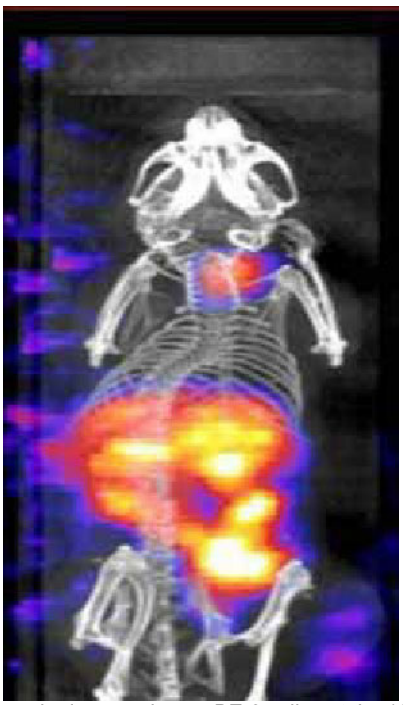

Human esophageal adenocarcinoma BE-3 cells uptake 188Re-liposome

Disclosure of author financial interest or relationships:
**Y. Chen**, None; **C. Chi**, None; **C. Chang**, None; **Y. Lee**, None; **T. Chang**, None.

Presentation Number **P078**
Poster Session 1
September 5, 2012 / 18:00-18:00 / Room: The Liffey

# Detection of glioblastoma response to temozolomide combined to Avastin® using MRI and PET imaging revealed [18F]-FLT as early predictive markers of treatment efficiency

***Aurélien Corroyer-Dulmont***[1], *Edwige Petit*[1], *Peres Elodie*[1], *Guillamo Jean-Sébastien*[2], *Varoqueaux Nathalie*[3], *Simon Roussel*[1], *Jerome Toutain*[1], *Divoux Didier*[1], *Ibazizene Méziane*[4], *Guillouet Stéphane*[4], *Lecocq Myriam*[1], *Andreas H. Jacobs*[5], *Barre Louisa*[4], *Myriam Bernaudin*[1], *Samuel Valable*[1], *[1]CNRS, CEA, Université de Caen Basse-Normandie, UMR ISTCT 6301, GIP CYCERON, CERVOxy, Caen, France; [2]CHU de Caen, Service de Neurologie, Caen, France; [3]Roche, Roche, Boulogne-Billancourt, France; [4]CEA, DSV/I2BM/LDM-TEP group, UMR ISTCT 6301, GIP CYCERON, LDM-TEP, Caen, France; [5]University of Münster, European Institute for Molecular Imaging - EIMI, D-48149, Münster, Germany. Contact e-mail: corroyer@cyceron.fr*

Objectives: The aim of this study was to identify imaging biomarkers based on PET and MRI predictive for the efficacy of chemotherapy with/without combined anti-angiogenic treatment in a preclinical model of glioma. Methods: Two models of glioma were used by orthotopic implantation of human U87 and human U251 gliomas in nude rats. Temozolomide (TMZ) and Bevacizumab (Avastin®) were administrated alone or in combination. MRI was performed to monitor changes in tumor volume at an early time after initiation of treatment (D+5) and at follow-up (D+12). The vasculature was characterized by MRI by measuring at D+5 (i) perfusion after a bolus injection of contrast agent (P904®, 200µmol/kg, Guerbet Research), (ii) Cerebral Blood Volume (CBV), (iii) vessel size, and (iv) vascular permeability after injection of Dotarem® (200µmol/kg, Guerbet SA). Glucose metabolism and cell proliferation were studied after injection of [18F]-FDG and [18F]-FLT at D+5 and D+6, respectively. Results: Five days after treatment, only the combined treatment with TMZ+Avastin® decreased the tumor volume for the U87 ($p<0.05$) and the U251 model ($p<0.01$), respectively. However, at D+12, TMZ alone reduced the tumor volume by 86% ($p<0.001$) and 93% ($p<0.001$) for the U87 and U251 models. Concerning the anti-angiogenic treatment, at D+12, there was a slight reduction in tumor volume (36% for U87 model and 31% for U251 model) and no synergistic effect was observed in the TMZ+Avastin® treatment group (volume reduction of 90% ($p<0.001$) and 95% ($p<0.001$) for U87 and U251 models). As expected, we showed that [18F]-FDG uptake was less important for animals treated with TMZ alone or combined with Avastin® for both glioma models. However, [18F]-FLT uptake was greatly reduced in TMZ alone or in TMZ+Avastin® group compared to control (rSUV U87: control = 10.8±3.5, TMZ = 5.2±0.7 and TMZ+Avastin® = 4.2±0.4 [$p<0.001$ and $p<0.001$]; rSUV U251: control = 6.7±0.7, TMZ = 3.0±0.9 and TMZ+Avastin® = 2.3±0.9 [$p<0.05$ and $p<0.01$]). Interestingly, [18F]-FLT uptake was correlated with overall survival ($r2=0.42$, $p=0.0007$ for U87 and $r2=0.57$, $p<0.0001$ for U251). MRI analysis revealed that relative blood volume (rBV) was significantly reduced in the presence of TMZ+Avastin® in the U87 tumor (control=2.2±0.3, TMZ+Avastin® = 1.5±0.3 ($p<0.01$)). In the U251 model, treatment with Avastin® leads to a decrease in rBV (0.99±0.1 versus 1.55±0.4 for the TMZ group, $p<0.01$). Changes in rBV were correlated with survival for U87 model but not for the U251 model. Conclusion: Our data indicate that [18F]-FLT as PET biomarker combined with rBV as MRI biomarker is an early predictor for response to treatment of experimental human gliomas in nude rats. These data also emphasize the interest to introduce, beyond [18F]-FDG, new PET tracer such as [18F]-FLT in cancer evaluation of treatment efficiency. This work was funded by: the INCA, the CNRS, the French Ministère de l'Enseignement Supérieur et de la Recherche, Roche, Guerbet, the Conseil Regional de Basse-Normandie, the European Union «Fonds Européen de Développement Régional pour le FEDER» and the TC2N «Trans Channel Neuroscience Network».

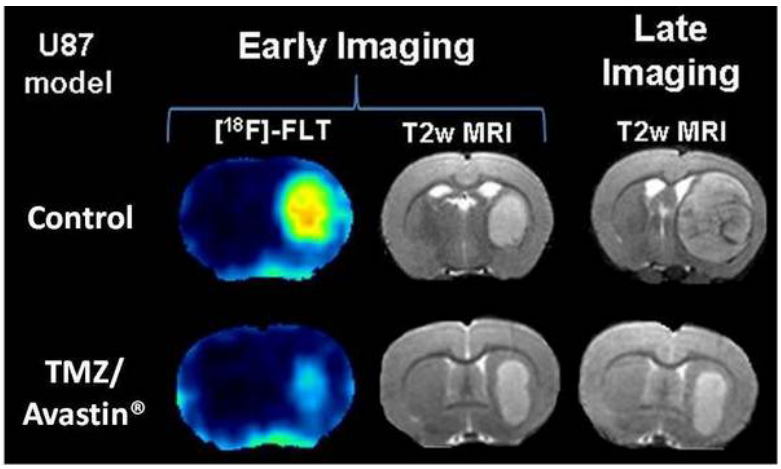


Disclosure of author financial interest or relationships:
**A. Corroyer-Dulmont**, None; **E. Petit**, None; **P. Elodie**, None; **G. Jean-Sébastien**, None; **V. Nathalie**, Roche, Employment; **S. Roussel**, None; **J. Toutain**, None; **D. Didier**, None; **I. Méziane**, None; **G. Stéphane**, None; **L. Myriam**, None; **A.H. Jacobs**, Merck, Germany, Grant/research support; **B. Louisa**, None; **M. Bernaudin**, None; **S. Valable**, None.

Presentation Number **P079**
Poster Session 1
September 5, 2012 / 18:00-18:00 / Room: The Liffey

# Synthesis and Evaluation of [$^{18}$F]-FEBNIM as a tracer for hypoxia

*Pierre Daumar, Sean Carlin, Megan Reese, Jason S. Lewis,* ***Nagavarakishore Pillarsetty****, Radiology, MSKCC, New York, NY, USA.*
*Contact e-mail: pillarsn@mskcc.org*

**Objectives:** Hypoxia is a common feature of most solid tumors and often leads to radioresistant phenotype, leading to poor outcomes in the patients. It is hypothesized that tumors may be treated more effectively by boosting the radiation dose delivered to the hypoxic regions, which contain radioresistant hypoxic cancer cells. Non-invasive imaging of hypoxic tumor regions would be an essential step for the implementation of image-guided radiotherapies. We have synthesized and evaluated the utility of a novel hypoxia tracer 2'-[$^{18}$F]-fluoroethyl-2-methyl-4-nitro-5-bromoimidazole ([$^{18}$F]-FEBNIM), which is a 4-nitroimidazole derivative, unlike the current hypoxia tracers such as [$^{18}$F]-FMISO, [$^{18}$F]-FAZA or [$^{124}$I]-IAZGP which are based on 2-nitroimidazole core. **Methods:** [$^{18}$F]-FEBNIM was synthesized by heating the precursor 2'-tosyloxyethyl-2-methyl-4-nitro-5-bromoimidazole 1 (Figure) with K[$^{18}$F]F/K2CO3/kryptofix in acetonitrile at 120 °C for 10 min and purified using HPLC. *In vitro* analysis was performed on HT29 cells by incubating in different oxygen concentrations (21% and 0.1 %) for 60 min and measuring uptake. Whole body biodistribution studies were performed in nude mice bearing HT29 xenografts at 30, 60 and 180 min post administration. **Results:** [$^{18}$F]-FEBNIM was synthesized in 8% yield (d.c.) with > 98% purity in 100 min. *In vitro* studies revealed that the relative tracer uptake in hypoxic vs normoxic conditions was 10 to 1, 60 min post incubation in HT29 cells. *In vivo* studies indicate that the compound has low accumulation in the tumor and rapidly clears from blood pool, via renal and hepatobiliary excretion pathways. The %ID/g values in tumor and muscle were 1.12 ± 0.25, 0.33 ± 0.16, 0.26 ± 0.27 and 0.68 ± 0.10, 0.11 ± 0.05, 0.51 ± 0.24 at 30, 60 and 180 min post administration respectively. **Conclusions:** We have successfully synthesized and evaluated a novel compound [$^{18}$F]-FEBNIM as a tracer for hypoxia. Our *in vitro* studies indicate that the compound shows preferential uptake in cells experiencing hypoxic conditions, successfully proving that 4-nitroimidazole derivatives have potential to be used as hypoxic tracers. However, due to rapid clearance from the blood pool the compound shows low uptake in the tumor and also exhibits low tumor to muscle and tumor to blood ratios, making it unsuitable for clinical applications.

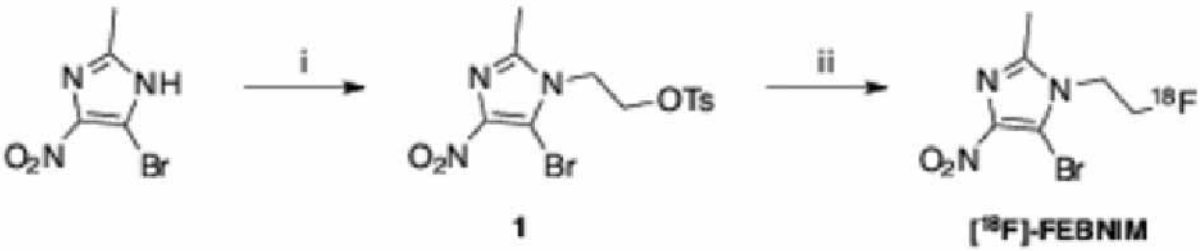


Reagents and conditions: i. Ethylene di(*p*-toluenesulfonate), $K_2CO_3$, DMF, 60 °C, 24 h ; ii. K[$^{18}$F]F, $K_{222}$, $K_2CO_3$, $CH_3CN$, 120 °C, 10 min.

**Figure.** Synthesis of precursor **1** and radiosynthesis of [$^{18}$F]-FEBNIM

Disclosure of author financial interest or relationships:
**P. Daumar**, None; **S. Carlin**, AstraZeneca, Grant/research support; **M. Reese**, None; **J.S. Lewis**, GEMS, Other financial or material support; **N. Pillarsetty**, None.

Presentation Number **P080**
Poster Session 1
September 5, 2012 / 18:00-18:00 / Room: The Liffey

# Efficient $^{18}$F-Labeling of pHLIP Peptide Analogues and their Biological Evaluation

*Pierre Daumar[1], Cindy A. Wanger-Baumann[1], **Nagavarakishore Pillarsetty**[1], Sean Carlin[1], Kuntalkumar Sevak[1], Oleg A. Andreev[2], Yana Reshetnyak[2], Jason S. Lewis[1], [1]Radiology, Memorial Sloan-Kettering Cancer Center, New York, NY, USA; [2]Physics, University of Rhode Island, Kingston, RI, USA. Contact e-mail: pillarsn@mskcc.org*

**Objectives:** Our laboratory is interested in developing universal tumor targeting agents by taking advantage of common features of cancer cells. Tumor acidity is one such common feature of solid tumors and also has potential as a prognostic indicator of tumor progression and metastasis. We have identified a 37 residue peptide named pH (Low) Insertion Peptide (pHLIP), which can be used as a platform to develop imaging agents that target acidic tissue. Our studies have demonstrated that $^{64}$Cu-labeled pHLIP derivative can target tumors in mice but had high background. Our objective was to develop $^{18}$F-labeling protocols for pHLIP derivatives with optimal biological properties and evaluate its ability to target tumors in vivo. **Methods:** pHLIP (D-WT-pHLIP **1**) and its shorter variants (D-short3E-pHLIP **3** and D-short3D-pHLIP **4**) and negative control (L-K-pHLIP **2**, designed to lack the pH-dependent behavior) were chosen as targeting vectors and modified with 6-azidohexanoic acid on the N-terminus to facilitate Huisgen "click" reaction. These peptides were labeled with [$^{18}$F] using click reaction with 6-[$^{18}$F]-fluoro-2-ethynyl pyridine as prosthetic labeling group ($H_2O$/EtOH/$CuSO_4$/Na ascorbate, 70 °C, 5 min) and purified using HPLC. This robust protocol allowed for the production of [$^{18}$F]-pHLIP derivatives and allowed their in vivo evaluation. Whole body biodistribution and PET imaging studies were performed in PC3 and LNCaP tumor bearing mice, at 2 and 4 hours after injection. Distribution of radioactivity was also investigated using digital autoradiography on tumor sections. **Results:** [$^{18}$F]-pHLIP derivatives were obtained in 5 - 15 % radiochemical yield (d.c.) with radiochemical purity > 98% in less than 90 min. In vivo PET imaging (Figure) and biodistribution studies performed on mice bearing tumors with [$^{18}$F]-**1**, [$^{18}$F]-**3** and [$^{18}$F]-**4**, indicated high uptake in LNCaP tumors and lower accumulation in PC3 tumors This is in line with previous findings from in vivo MR studies where the average volume pH in LNCaP tumors was shown to be lower than in PC3 tumors [1]. Control peptide [$^{18}$F]-**2** did not accumulate in the tumors. Biodistribution studies also showed high level of radioactivity in the liver and in the kidneys 4h p.i.. Autoradiography on LNCaP tumor sections 4h following [$^{18}$F]-**1** administration showed a clear pattern of higher radioactivity uptake in tumor regions lacking vascular perfusion which are usually acidic. Minimal defluorination was observed in vivo, suggesting the good stability of our prosthetic group. **Conclusions:** We have successfully developed an efficient and reliable $^{18}$F-labeling procedure for a large peptide pHLIP and its shorter variants via click chemistry using 6-[$^{18}$F]-fluoro-2-ethynyl pyridine as a prosthetic group. In vivo evaluation of $^{18}$F-labeled pHLIP derivatives revealed that tumor acidosis can be successfully targeted using these agents. Autoradiography studies clearly demonstrate that pHLIP derivatives accumulate in regions lacking vascular perfusion, which is consistent with the proposed mechanism of action of pHLIP. **References:** [1] Vavere, A. L. et al. (2009), Cancer Research, 69, 4510-4516 **Research support:** NIH R01 CA138468 (JSL)

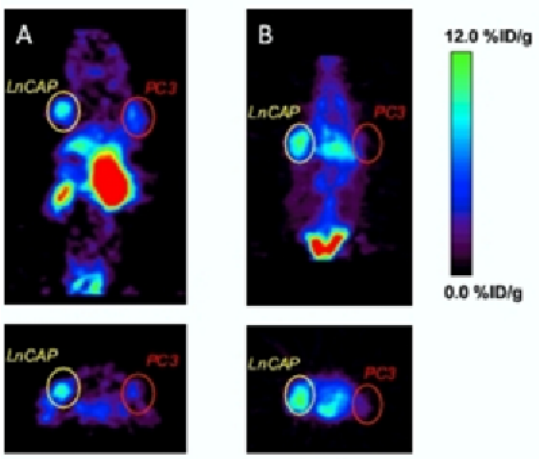


**Figure.** Representative PET images obtained with [$^{18}$F]-**3** (A) and [$^{18}$F]-**4** (B) in dual tumor bearing mice ; coronal and transverse planar images are shown.

Disclosure of author financial interest or relationships:
**P. Daumar**, None; **C.A. Wanger-Baumann**, None; **N. Pillarsetty**, None; **S. Carlin**, AstraZeneca, Grant/research support; **K. Sevak**, None; **O.A. Andreev**, General Electric Health Care, Consultant; **Y. Reshetnyak**, GE Healthcare, Grant/research support; GE Healthcare, Consultant; **J.S. Lewis**, GEMS, Other financial or material support .

Presentation Number **P081**
Poster Session 1
September 5, 2012 / 18:00-18:00 / Room: The Liffey

# New [$^{18}$F]-labelled Arylsulfone Inhibitors of Matrix Metalloproteinases as PET tracers

*Lorenza Fugazza[2], Francesca Casalini[1], **Giuseppe Digilio**[1], Lorenzo Tei[1], Armando Rossello[5], Elisa Nuti[5], Elisabetta Orlandini[5], Maria Azzurra Filannino[2], Valeria Muzio[2], Giovanna Esposito[3], Luca D'Angeli[3], Claudia Cabella[4], Alessandro Maiocchi[4], [1]Dipartimento di Scienze ed Innovazione Tecnologica, Università del Piemonte Orientale, Alessandria, Italy; [2]Research & Development, Advanced Accelerator Application, Colleretto Giacosa (TO), Italy; [3]Molecular Imaging Centre (CIM), University of Torino, Torino, Italy; [4]CRB, Bracco Imaging SpA, Colleretto Giacosa (TO), Italy; [5]Department of Medicinal ChemistryDepartment of Medicinal Chemistry, University of Pisa, Pisa, Italy. Contact e-mail: giuseppe.digilio@mfn.unipmn.it*

Matrix Metalloproteinases (MMPs) constitute a family of over 25 zinc- and calcium-dependent endopeptidases whose primary role is the degradation of specific components of the ECM. It is nowadays well-established that certain members of this family, most notably gelatinase A (MMP-2), can sustain all stages of tumor progression, including proliferation, migration, angiogenesis, invasion and metastasis [1]. In general, the relative level of each individual MMPs increases with increasing tumor stage and it is higher in malignant cancers than in normal or premalignant tissues, with maximum activity occurring at the tumor-stroma interface in areas of active invasion. Three new [$^{18}$F]-labelled MMP inhibitors (MMPi) as radiotracers for the molecular imaging of MMP-2/9 by Positron Emission Tomography (PET) have been synthesized (Figure 1). These inhibitors are based upon the arylsulfone scaffold [2], with carboxylate as the zinc binding group. The fluorinated MMPi showed a very good affinity against gelatinases ($IC_{50}$ in the nM range for MMP-2) and a fair selectivity for MMP-2/9 over MMP-1/3/14. Two of these compounds could be obtained in the [$^{18}$F]-radiolabelled form, with a RCY suitable for preclinical studies and very good purity (98%). The biodistribution in vivo of these radiotracers was largely dominated by the hydrophobicity of the compounds and by their high affinity for serum albumin (multiple binding site with $K_D$ in the order of 100 μM). Despite the non-optimal biodistribution,[$^{18}$F]-1a showed a fairly good uptake in a mouse tumor model (namely U-87 MG human glioblastoma subcutaneously grafted in athymic nude mice), with %ID/g levels reaching about 30% of that obtained with control [$^{18}$F]-FDG. The specificity of uptake was evaluated by comparing the accumulation of radioactivity in tumors in mice pretreated or not with ilomastat, a broad-spectrum MMP inhibitor, to saturate the target sites. We found that presaturation of MMPs by ilomastat decreased the uptake of the PET tracer by 20% with respect to untreated animals (Student's $p<0.05$). In conclusion, uptake of [$^{18}$F]]-1a in tumor results from a MMP-dependent (specific) contribution and a MMP-unrelated (aspecific) contribution, with the former accounting for about 20% of total uptake. Structural modification of the tracer aimed at decreasing the hydrophobicity of the molecule and affinity for binding to albumin has been designed to improve the specificity of tumor labelling and to allow for the unbiased assessment of MMP activity through [$^{18}$F]-PET imaging. Acknowledgments. This work is supported by the Regione Piemonte (Italy) as part of the Converging Technologies BIO_THER project and part of the PIIMDMT project. References [1] M Egeblad and Z Werb Nature Rev Cancer 2002, 2, 161-174. [2] E Nuti et al., J Med Chem 2009, 52, 6347-6361.

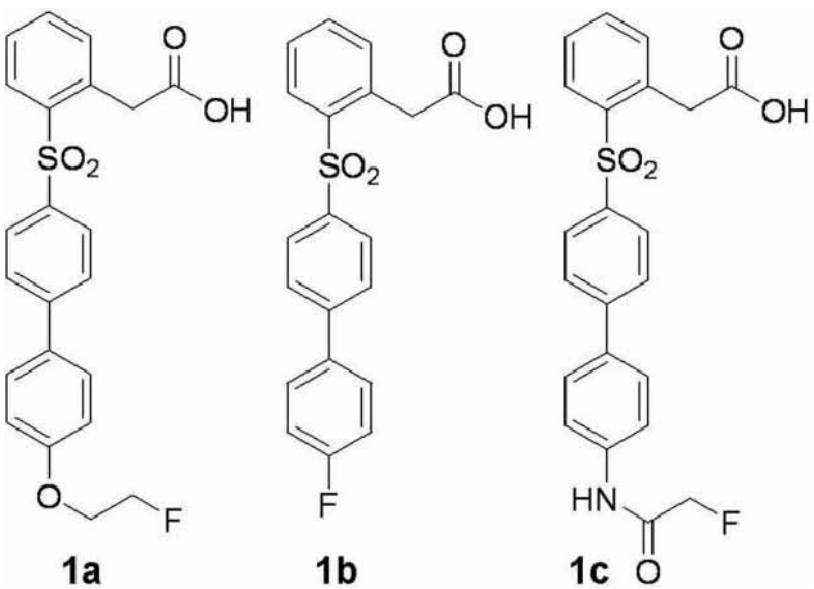


Disclosure of author financial interest or relationships:
**L. Fugazza**, None; **F. Casalini**, None; **G. Digilio**, None; **L. Tei**, None; **A. Rossello**, None; **E. Nuti**, None; **E. Orlandini**, None; **M. Filannino**, None; **V. Muzio**, None; **G. Esposito**, None; **L. D'Angeli**, None; **C. Cabella**, Bracco Imaging SpA, Employment; **A. Maiocchi**, Bracco Imaging, Employment .

Presentation Number **P082**
Poster Session 1
September 5, 2012 / 18:00-18:00 / Room: The Liffey

# A mathematical framework to evaluate the heterogeneity of tumor tissue

***Marco Dominietto**, Ruth Keist, Markus Rudin, Steffi Lehmann, Institute for Biomedical Engineering, ETH Zurich and University of Zurich, Zurich, Switzerland. Contact e-mail: dominietto@biomed.ee.ethz.ch*

Derivation of quantitative information descripting tissue morphology and physiology is critical for the evaluation of novel therapies. In oncology the situation is complicated by the well-known chaotic organization of the proliferative mass. This chaotic structure, which is reflected both by tissue morphology and the vascular architecture, is responsible for the heterogeneous behavior of tumors. The aim of this work is to present a mathematical framework that explicitly considers the spatial variability within imaging data sets. Such framework consists of two classes of geometrical estimators adapted for handling tumor images. The texture class allows estimating the fractal dimension (FD), which is a measure of the self-similarity at different length scales, and the lacunarity (L), which quantifies the relative distribution of substructures within the tissue. The shape class yields measures of the compactness, which describes the deviation of a mass from spherical symmetry, and the signature, which is a measure of the branching (or infiltration) of the tumor into the surrounded healthy tissue. We tested this analysis framework in an in-vivo study using a group of 12 mice injected s.c. with C51 tumor cells: 6 mice were treated with a proangiogenic drug (dimethyloxalylglycine, DMOG) and 6 with a placebo (saline). We analyzed some physiological parameters describing the tumor vasculature: permeability derived from DCE-MRI and perfusion (blood volume and flow) derived from DSC-MRI. This analysis was complemented by a detailed study of the vascular architecture using vessel size index (VSI) MRI and Synchrotron-micro-CT. We found significant differences in the FD and L values between treated and non-treated group either for both the permeability and perfusion maps (Table 1). The FD values increased significantly in response to treatment. A higher level of FD means smaller self-similarity and therefore more chaotic structure, which may reflect angiogenesis, i.e. an expansion of the chaotic capillary network. FD values did not change in response to treatment with the vehicle only. The L values remained unchanged in the DMOG group and significantly decreased in vehicle treated mice. Interestingly, no effect of drug treatment has been found comparing volume averaged values: this illustrates the superior sensitivity of the texture analysis in identifying morphological differences. The increase in FD values is corroborated by the structural analysis of the tumor vasculature: VSI showed a persistent predominance of capillaries during tumor growth, but no formation of bigger vessels indicating the absence of hierarchical organization. This is in line with the synchrotron-microCT results, which reveal a high number of highly tortuous capillaries in C51 (Fig. 2). In conclusion, the use of non-biased mathematical methods that account for the heterogeneity of tumor tissue enables the identification of changes that are masked when analyzing volume averaged data sets. The biological basis for the changes observed in FD and L remain to be analyzed. It is to be anticipated that such procedures will impact the evaluation of novel anti-cancer therapies.

Disclosure of author financial interest or relationships:
**M. Dominietto**, None; **R. Keist**, None; **M. Rudin**, Hoffmann-LaRoche Ltd, Basel, Switzerland, Grant/research support; **S. Lehmann**, None.

Presentation Number **P083**
Poster Session 1
September 5, 2012 / 18:00-18:00 / Room: The Liffey

# Development of targeted Gadolinium based nanoparticles as multimodal contrast agents in oncology

***Sandrine Dufort***[1], *Jessica Morlieras*[2], *Cedric Louis*[1], *François Lux*[2], *Véronique Josserand*[3,4], *Jean-Luc Coll*[3], *Olivier Tillement*[2], [1]*Nano H, Saint Quentin Fallavier, France;* [2]*LPCML, UMR CNRS 5620, Lyon, France;* [3]*INSERM U823, Grenoble, France;* [4]*OPTIMAL, Grenoble, France. Contact e-mail: sandrine.dufort@gmail.com*

Early and accurate detection of tumours, like the development of targeted treatments, is a major field of research in oncology. In this aim, nanoparticles emerged as promising candidates for the establishment of therapeutic protocols including targeting, diagnosis (with optical imaging) and cancer therapy. In this context, our lab has developed Gadolinium based Small Rigid Platforms (SRP) for multimodal imaging applications (MRI, X-ray tomography, scintigraphy and fluorescence imaging) and targeted therapies. The SRP are composed of gadolinium complexes covalently grafted to a polysiloxane matrix. These species present individually no toxicity and the DOTA(Gd) species have previously proven their efficiency as positive contrast agents for MRI. The SRP present a renal excretion due to their small size (around 5nm) and a passive accumulation in tumours according to the Enhanced Permeability and Retention (EPR) effect. This passive accumulation varies in function of the physiopathology of each tumours. In order to improve the accumulation in tumours with an active targeting, we have grafted cyclic RGD peptides (known for its affinity toward αvβ3 integrins) on the nanoparticles. In vitro fluorescence microscopy studies and flow cytometry analysis show a specific binding and internalization of cRGD-SRP compared to SRP or cRAD-SRP (SRP grafted with the negative control peptide) in cells expressing different levels of integrins. In vivo, the grafting of the cRGD or cRAD peptides on SRP doesn't modify their biodistribution. The presence of cRGD peptides increases the tumour accumulation of SRP whatever the route of administration. In conclusion, the combination of the enhanced properties of this agent with passive and active targeting will permit an important increase of the signal in the diseased zones in comparison with classical agents. This new type of platform is a promising tool for multimodal imaging in oncology.

Disclosure of author financial interest or relationships:
**S. Dufort**, None; **J. Morlieras**, None; **C. Louis**, None; **F. Lux**, None; **V. Josserand**, None; **J. Coll**, None; **O. Tillement**, None.

Presentation Number **P084**
Poster Session 1
September 5, 2012 / 18:00-18:00 / Room: The Liffey

# Volumetric Acoustic Radiation Force-Enhanced Ultrasonic Molecular Imaging

***Ryan C. Gessner**, Jason E. Streeter, Roshni Kothadia, Steven Feingold, Paul A. Dayton, Joint Department of Biomedical Engineering, University of North Carolina-North Carolina State, Chapel Hill, NC, USA. Contact e-mail: rgessner@email.unc.edu*

For over a decade, acoustic radiation force (ARF) has been proposed as a method to enhance targeted microbubble retention in Ultrasonic Molecular Imaging (USMI), since ARF can push microbubbles in contact with the vessel endothelium. However, almost all published data to date has been in-vitro. In this body of work, we demonstrate the application of ARF-enhanced USMI of angiogenesis in-vivo using volumetric imaging with a clinical US system. 3D ARF-enhanced USMI was performed on 5 rat fibrosarcoma tumors using size-selected microbubbles (Mean Diameter: ~ 2 μm) that were fitted with a cyclic RGD peptide, which is targeted to αvβ3. Nontargeted microbubbles were also evaluated to illustrate that non-specific adhesion is not enhanced with this technique. Three different very low-amplitude ARF pulse sequences, previously shown to produce non-destructive bubble translation in-vitro, (4.4, 13.4 and 20.6 kPa; Duty Cycle: 25%, Freq: 7MHz) were evaluated and compared to passive targeting studies in the same animal. The transducer was scanned 5 times at a constant speed of 1 mm/s across the tumor after microbubbles were administered via bolus injection. Volumetric acquisitions were obtained with a Siemens Sequoia in CPS mode with the same elevational scanning mechanism. The brightness of adherent MCAs was assumed to be correlated with the degree of biomarker expression, which is a common metric for this technique. 3D data was down-sampled offline at 800 μm intervals to yield independent imaging frames for analysis. Data in each frame was normalized to the mean pixel intensity of the passive targeting data. The maximum increase in targeting was achieved using the ARF-13.4 kPa setting. On average, ARF at 13.4 kPa yielded 80% greater targeting than with no ARF (13.4 kPa: 1.8 ± 1.1 vs No ARF: 1.0 ± 0.7; $p < 0.05$). Additionally, both the ARF-4.4 (1.4 ± 1.2) and ARF-20.6 (1.4 ± 1.1) settings produced statistically significant increases in targeting relative to the passive targeting case. It is hypothesized that the ARF-20.6 setting may have produced too much radiation force and dislodged bound bubbles, thus a reduction in targeting relative to the ARF-13.4 setting. ARF at 13.4 kPa with control microbubbles resulted in a slight decrease in non-specific microbubble adhesion relative to control microbubbles with no ARF (13.4 kPa: 0.7 ± 0.5 vs No ARF: 0.6 ± 0.3; $p > 0.05$). This in-vivo study demonstrates the enhancement of USMI with ARF, as assessed by 3D imaging with a clinical US system. Results show a significant improvement in sensitivity of 80% over traditional non-ARF-enhanced targeted imaging without a corresponding loss in specificity.

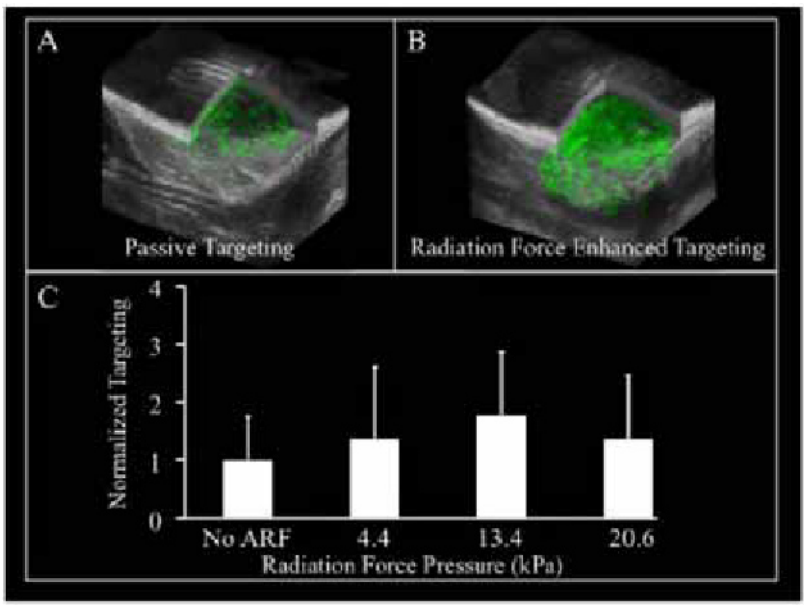


A and B) A side-by-side comparison of two volumetric datasets with corner cutaways. B-mode images (grayscale) are registered to the corresponding contrast specific images (green overlay). In both of these images, the same dose of targeted microbubbles was administered to the same animal. Radiation force was not applied in panel A, but was applied at 13.4 kPa in panel B. C) Normalized mean targeting as a function of acoustic radiation force pressure. The 4.4, 13.4 and 20.6 kPa settings each produced significantly ($p < 0.05$) better targeting than the no ARF case (passive targeting).

Disclosure of author financial interest or relationships:
**R.C. Gessner**, None; **J.E. Streeter**, None; **R. Kothadia**, None; **S. Feingold**, None; **P.A. Dayton**, Targeson, Inc., Consultant; National Institutes of Health, Grant/research support; Dept of Defense, Grant/research support; Siemens, Other financial or material support .

Presentation Number **P085**
Poster Session 1
September 5, 2012 / 18:00-18:00 / Room: The Liffey

# Evaluation Of Oncological PET tracers in Clinically Relevant Murine Inflammation Models

***Gayatri Gowrishankar***[1], *Aileen Hoehne*[1], *Andre Mueller*[2], *Norman Koglin*[2], *Ludger M. Dinkelborg*[3], *Sanjiv S. Gambhir*[1,4], [1]*Radiology, Stanford University, Stanford, CA, USA;* [2]*GDD TRG Oncology/ GT - Tumor Metabolism & Hypoxia, Bayer Pharma AG, Berlin, Germany;* [3]*Piramal Imaging, Berlin, Germany;* [4]*Bioengineering and Materials Sciences & Engineering, Stanford University, Stanford, CA, USA. Contact e-mail: gayatrig@stanford.edu*

Background: An essential criterion in the development of novel positron emission tomography (PET) tracers for oncology has always been the ability to distinguish tumors from inflammatory lesions. Thus far the standard practice has been to test new tracers in the turpentine oil induced sterile abscess model in rodents. Although some tracers showed no uptake in the turpentine induced lesions, clinical studies demonstrated their uptake in inflammatory lesions. We have therefore undertaken an effort to establish a series of clinically relevant inflammation models. Uptake of two tracers - [18F] fluorodeoxyglucose (FDG), which is known to be taken up in inflammation and (4S)-(3-[18F]fluoropropyl)-L-glutamate (FSPG/BAY 94-9392)- a promising novel Xc transport tracer for tumor imaging, was evaluated in these models. First longitudinal studies in the turpentine model were done and tracer uptake at early and late time points was evaluated. This was done to mimic acute and chronic inflammations, which involve different cellular subpopulations. The second model involved the induction of lung inflammation by intranasal administration of lipopolysaccharide (LPS). Inflammatory processes in the lung are known to lead to false positives in the clinics with FDG, which complicates diagnosis. Efforts to establish a murine sarcoidosis model as a third strategy are ongoing. Results: In the turpentine oil model, a high uptake of FDG was observed in the inflamed muscle at all the three time points (Table 1). The absolute uptake of FSPG in the inflamed muscle was much lower than FDG uptake (Table 1). The difference between inflamed muscle and contralateral muscle as calculated from ex-vivo biodistributions was similar for both tracers (6 fold at 1 week, $p < 0.0001$). In the LPS model, both FDG and FSPG were taken up in the inflamed lungs. While the difference in uptake between inflamed lungs and control lungs was similar for both tracers ( 2.5 fold, $p < 0.0001$), the absolute uptake of FSPG in the inflamed lungs was again lower than FDG (Table 1). However, since FSPG has a much lower background than FDG, its uptake in the inflamed lungs was visually detectable by PET as shown in Figure 1. For both models independent validation of inflammation by histopathology was done. Conclusion: FDG is strongly taken up in both inflammation models. The uptake of FSPG is less obvious in the turpentine oil model than in the LPS model. In both models, the absolute uptake of FSPG in inflammatory tissue was low and in the range of FDG uptake in the respective control tissues (Table 1). The uptake of these tracers in inflammatory lesions should also be viewed in the context of relative uptake in tumors as was shown in an earlier publication (Koglin N et al, Clin Canc Res 2011). In summary, observations from the turpentine oil model alone may be insufficient because for some tracers (eg.FSPG), the uptake in inflammation is close to background. Therefore oncological PET tracers aiming at increased specificity should be evaluated in more than one pre-clinical inflammation model.

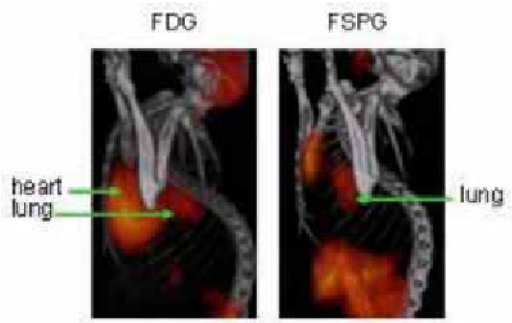


Fig 1: Micro PET/CT showing uptake of FDG and FSPGin the LPS inflammation model 24h after induction (both images on same scale)

| | | | | |
|---|---|---|---|---|
| | FDG | | FSPG | |
| | | | | |
| | | | | |
| | | | | |
| | | | | |
| | | | | |

Disclosure of author financial interest or relationships:
**G. Gowrishankar**, Bayer Schering Pharma, Grant/research support; **A. Hoehne**, None; **A. Mueller**, Bayer Healthcare, Employment; **N. Koglin**, Bayer, Employment; **L.M. Dinkelborg**, Piramal Imaging, Employment; **S.S. Gambhir**, General Electric, Grant/research support; Bayer-Schering, Grant/research support; Sanofi-Aventis, Grant/research support; CellSight, Stockholder; ImaginAB, Stockholder; Enlight, Stockholder; Endra, Stockholder; Bracco, Consultant; NinePoint Medical, Stockholder; Visualsonics, Consultant .

Presentation Number **P086**
Poster Session 1
September 5, 2012 / 18:00-18:00 / Room: The Liffey

# Visualization of Glucose Metabolism via a Near-infrared Fluorescent Probe in a Preclinical Xenograft Model

*Anatol Oleksijew, **Jonathan Hickson**, Abbott Laboratories, Abbott Park, IL, USA. Contact e-mail: jonathan.hickson@abbott.com*

For more than 20 years, elevated glucose uptake by malignant cells in comparison to normal tissue has allowed differentiation of cancer from benign tissue through the use of the PET radiotracer 18F-fluoro-2-deoxy-D-glucose (18F-FDG). In this study, we report the in vitro and in vivo characterization of a commercially available near infrared fluorescent analog of 18F-FDG, XenoLight RediJect 2-DG-750. A 3-6 fold increase in cellular uptake of 2-DG-750 was observed in vitro compared to free fluorescent control dye using Calu-6 human non-small cell lung cancer cells. Using naïve SCID-Beige animals, in vivo pharmacokinetics of the 2-DG-750 probe revealed a Cmax of 1.8 μM and was rapidly cleared from plasma (t1/2 ≤ 15 min); desirable characteristics for an imaging probe to achieve maximal tumor to background contrast. Fluorescent images of tumor targeting and retention of 2-DG-750 and control dye in subcutaneous Calu-6 xenografts were acquired using a Xenogen IVIS Spectrum imaging system. Fasted and non-fasted tumor bearing animals revealed significantly higher signal intensity above control dye (probe/control dye ratio, P/C = 122 and 53, respectively) at the site of the tumor 24 hours after injection, suggesting animal fasting may significantly increase probe uptake at the tumor site. Of note, the fluorescent signal was localized to the tumor for up to 14 days post injection. Together, these results suggest that 2-DG-750 may serve as a useful fluorescent probe for detecting and quantifying glucose uptake in preclinical animal models.

Disclosure of author financial interest or relationships:
**A. Oleksijew**, None; **J. Hickson**, None.

Presentation Number **P087**
Poster Session 1
September 5, 2012 / 18:00-18:00 / Room: The Liffey

# Intra-cellular behavior of αv-integrin GFP in osteosarcoma cells imaged in monolayer culture, 3D histoculture and in vivo

*Yasunori Tome[1,3], Naotoshi Sugimoto[4], Shuya Yano[1,2], Masashi Momiyama[1,2], Hiroki Maehara[3], Hiroyuki Tsuchiya[5], Katsuro Tomita[5], Fuminori Kanaya[3], Michael Bouvet[2], **Robert M. Hoffman**[1,2], [1]AntiCancer, Inc., San Diego, CA, USA; [2]Dept. of Surgery, University of California, San Diego, CA, USA; [3]Dept. of Orthopedic Surgery, Graduate School of Medicine, University of the Ryukyus, Okinawa, Japan; [4]Dept. of Physiology, Graduate School of Medical Sciences, Kanazawa University, Kanazawa, Japan; [5]Dept. of Orthopedic Surgery, Graduate School of Medical Sciences, Kanazawa University, Kanazawa, Japan. Contact e-mail: all@anticancer.com*

We describe here real-time imaging of αv integrin-GFP expression in osteosarcoma cells (143B) in vitro and in vivo. 143B cells were stably transfected with an αv integrin-GFP vector. Confocal microscopy demonstrated that αv integrin immunofluorescent staining colocalized with αv integrin-GFP fluorescence. In vitro, when αv integrin-GFP osteosarcoma cells were seeded on a dish coated with fibronectin, which bonds αv integrin. αv integrin adhesion plaques were observed by confocal microscopy using the Olympus FV1000. When αv integrin-GFP-expressing 143B cells (1×106) were transplanted in the tibia or injected subcutaneously in nude mice, the cells aligned along collagen orthotopic fibers. In the orthotopic model, osteosarcoma cells punctate expression of αv integrin-GFP was imaged in the osteosarcoma cells as they invaded muscular tissue. In the subcutaneous model, osteosarcoma cells, strongly expressing αv integrin-GFP, were observed around the blood vessels in the tumor. These results show that αv integrin-GFP allows the real-time imaging of the role of αv integrin during cancer cell invasion allowing the further understanding of its role in the process.

Disclosure of author financial interest or relationships:
**Y. Tome**, None; **N. Sugimoto**, None; **S. Yano**, None; **M. Momiyama**, None; **H. Maehara**, None; **H. Tsuchiya**, None; **K. Tomita**, None; **F. Kanaya**, None; **M. Bouvet**, None; **R.M. Hoffman**, None.

Presentation Number **P088**
Poster Session 1
September 5, 2012 / 18:00-18:00 / Room: The Liffey

# RFP-expressing glioma successfully resected in othotopic mouse models using fluorescence-guided surgery

*Masashi Momiyama[1,3], Yukihiko Hiroshima[1,2], Atsushi Suetsugu[1,2], Yasunori Tome[1], Sumiyuki Mii[1], Shuya Yano[1], Michael Bouvet[2], Takashi Chishima[3], Itaru Endo[3], **Robert M. Hoffman**[1,2], [1]AntiCancer, Inc., San Diego, CA, USA; [2]Dept. of Surgery, University of California, San Diego, CA, USA; [3]Dept. of Gastroenterological Surgery, Yokohama City University, Yokohama, Japan. Contact e-mail: all@anticancer.com*

Malignant glioma tumors are the most common primary central nervous system tumors and they are very difficult to completely resect due to their invasive margins. In this study, we compared fluorescence-guided and standard bright-light resection. U87-RFP human glioma cells (2 x 105) were injected stereotactically into the nude mouse brain through a craniotomy open window. Two weeks after tumor-cell inoculation, brain tumors were resected under fluorescence guidance or under bright light. U87-RFP tumors were clearly visualized under fluorescent microscopy with long working distance at the single cell level. Almost all cancer cells were removed using fluorescence-guided navigation without damage to the brain tissue. However, brain tumors were difficult to visualize under bright light and many residual cancer cells remained in the brain after surgery. These results suggest that fluorescence-guided surgery has significant potential for treatment of brain cancer.

Disclosure of author financial interest or relationships:
**M. Momiyama**, None; **Y. Hiroshima**, None; **A. Suetsugu**, None; **Y. Tome**, None; **S. Mii**, None; **S. Yano**, None; **M. Bouvet**, None; **T. Chishima**, None; **I. Endo**, None; **R.M. Hoffman**, None.

Presentation Number **P089**
Poster Session 1
September 5, 2012 / 18:00-18:00 / Room: The Liffey

# Enhancement of bacterial expression of renilla luciferase under PBAD promoter by disruption of ara operon in the Salmonella typhimurium

***Hyun Hong***[1,2], *Hyon E. Choy*[3], *Geun-Joong Kim*[4], *Dae Jin Lim*[3], *Misun Yun*[1,2], *Yoon Soon Moon*[1], *Jung-Joon Min*[1,2], [1]*Laboratory of in vivo Molecular Imaging, Chonnam National University Hwasoon Hospital, Gwangju, Republic of Korea;* [2]*Nuclear Medicine, Chonnam National University Hwasoon Hospital, Gwangju, Korea, Republic of., Republic of Korea;* [3]*Microbiology, Chonnam National University Medical School, Gwangju, Korea, Republic of., Republic of Korea;* [4]*Biological Sciences, College of Natural Sciences, Chonnam National University, Gwangju, Korea, Republic of., Republic of Korea. Contact e-mail: MedSciOri@gmail.com*

We have reported genetic engineering of attenuated Salmonella typhimurium defective in ppGpp synthesis (mSL) for tumor-specific targeting and treatment. The tumor-specific expression of cytotoxic drug (e.g. cytolysin A) could be achieved using inducible promoter such as PBAD, which is activated by inducer, L-arabinose. However, it is difficult to expect the controllability of gene expression because L-arabinose is the molecule that is metabolized into the D-xylulose-5-P by enzymes encoded in ara operon. Thus, the purpose of the study is to disrupt ara operon to increase the efficiency of L-arabinose for induction of reporter gene expression driven by PBAD. We performed linear DNA transformation by using λ red recombinase which exchanges ara operon with linear DNA including antibiotics resistance gene that are homologous to the regions adjacent to the ara operon. The generated ara operon-disrupted strains (mSLΔara) were transformed with the plasmid encoding renilla luciferase variant 8 (Rluc8) under the PBAD (mSLΔara-pBR8). mSLΔara-pBR8 or its mother strain (mSL-pBR8) was intravenously injected in the mice bearing CT26 cancer. The luminescence from each bacteria was compared to assess the promoter activity. The luciferase assay and Western blot analysis revealed 5-fold stronger expression of Rluc8 in mSLΔara than in mSL-pBR8 after induction by L-arabinose. After injection in the tumor bearing mice, mSLΔara-pBR8 and mSL-pBR8 revealed comparable numbers in tumor at each time point. In vivo bioluminescence imaging also showed stronger imaging signal (~ 5-fold) in tumor after injection of mSLΔara-pBR8 than after injection of mSL-pBR8. We could enhance the promoter activity in Salmonellae with disrupting the operon involved in the metabolic pathway of its inducer, L-arabinose. Our results can be employed to enhance the production of therapeutic molecules in tumor via bacteria.

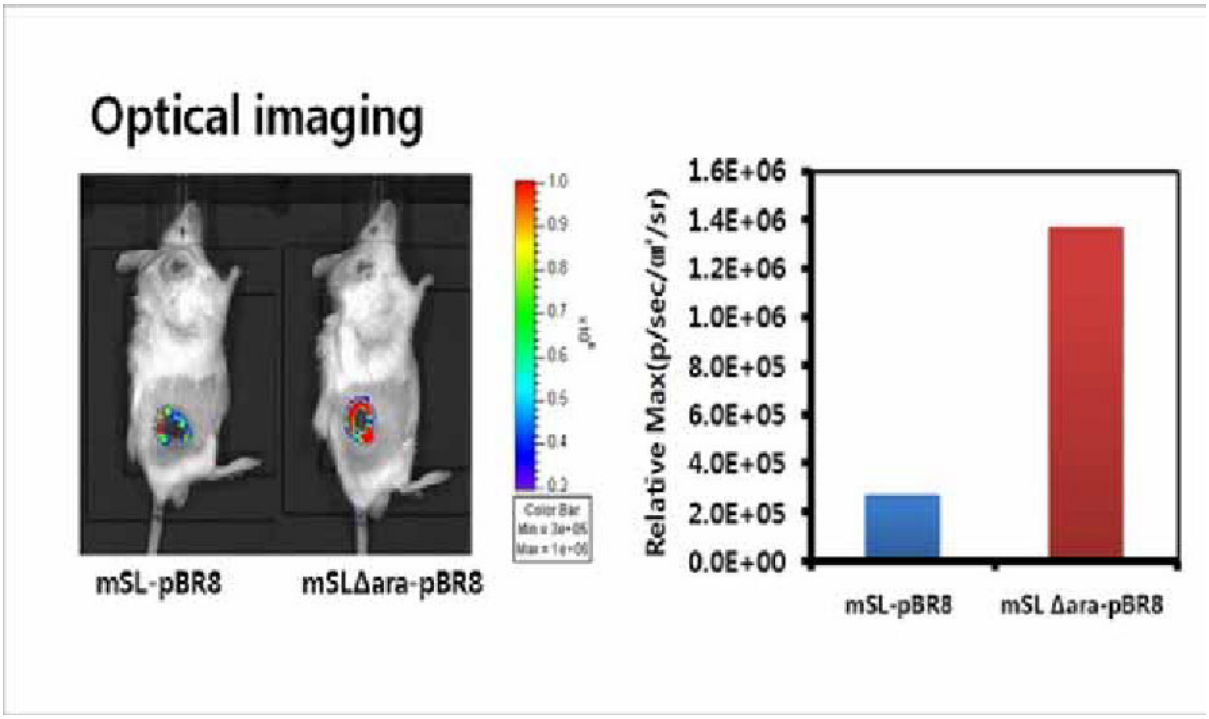


Disclosure of author financial interest or relationships:
**H. Hong**, None; **H. Choy**, None; **G. Kim**, None; **D. Lim**, None; **M. Yun**, None; **Y. Moon**, None; **J. Min**, None.

Presentation Number **P090**
Poster Session 1
September 5, 2012 / 18:00-18:00 / Room: The Liffey

# Early Therapy Response Assessment in Head and Neck Cancers Treated with EGFR-Specific Monoclonal Antibody

***Farzin Imani***[1], *Charles Laymon*[1], *Matthew Oborski*[1], *Robert Ferris*[2], *James M. Mountz*[1], [1]*Radiology, University of Pittsburgh Medical Center, Pittsburgh, PA, USA;* [2]*Otolaryngology, University of Pittsburgh Medical Center, Pittsburgh, PA, USA. Contact e-mail: imanif@upmc.edu*

Objectives : The utility of 2-deoxy-2-(18F)fluoro-D-glucose (FDG) PET for early prediction of head and neck squamous cell carcinoma (HNSCC) response to therapy was investigated. Methods : Four histologically proven HNSCC patients (4 m, 0 f, 31-51 y) enrolled in the study. The previously untreated patients were imaged during induction therapy using the EGFR-specific monoclonal antibody, cetuximab (ErbituxTM). FDG-PET studies were performed at baseline (T0), two weeks (T1) and four weeks (T2) after initiation of therapy. All patients had surgery a few days after the last PET scan to obtain molecular tissue markers. The maximal SUV of the lesions was acquired. Clinical follow-up (mean 5 mo, 4-8 mo) and multiple sequential imaging studies were used as the reference standard. T-test was performed to compare two groups. Results : Two cases showed significant improvement and two cases demonstrated progression on follow-up studies. Reduction of SUVmax of the lesions at T1 and T2 relative to the baseline (SUVR) properly correlated with the outcome. The patients who responded to therapy had significantly lower SUVR at T1 (mean: 0.41, sd: 0.064), and at T2 (mean: 0.28, sd: 0.017). There were no significant changes in SUVR in patients who did not respond to therapy (T1, mean: 0.97, sd: 0.065, T2, mean: 0.95, sd: 0.122). Statistical analysis showed significant difference between SUVR of two groups at T1 (p-value = 0.013) and at T2 (p-value = 0.017). Conclusions : This study shows FDG as a potential biomarker for early therapy response assessment for head and neck squamous cell carcinoma patients undergoing cetuximab therapy. Research Support: NIH grant 1U01CA140230 to Dr. Mountz and DE19727 to Dr Ferris.

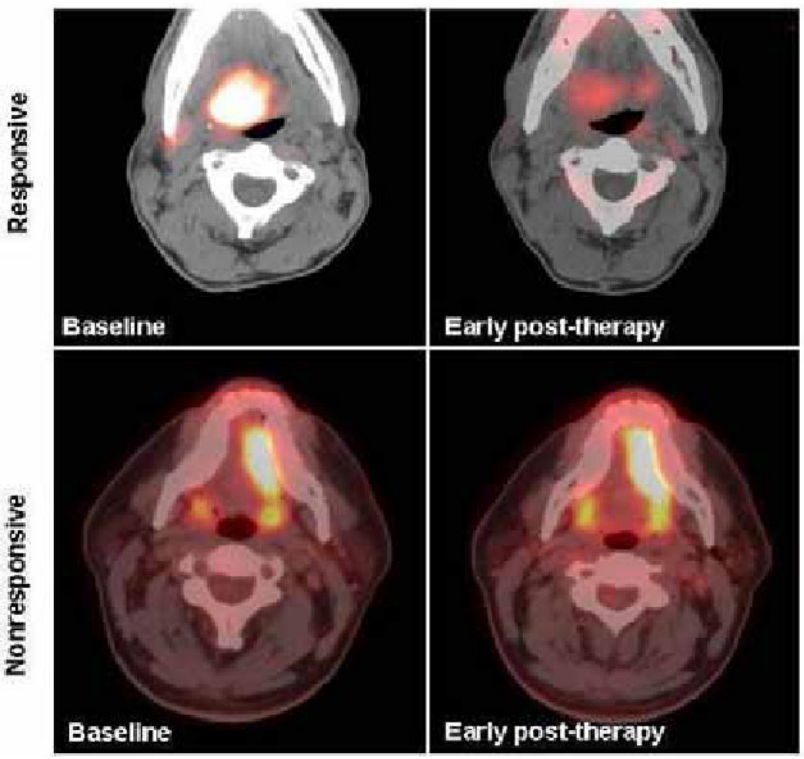


Supporting Figure: Example of 2 patients imaged at baseline (left) and at 2 weeks after initiation of induction therapy (right), Subject on top had a significant reduction of F-18 FDG uptake from baseline to therapy (Baseline SUV = 11.5 ,ETA SUV = 5.2 ) and a good outcome. Subject on bottom had no significant reduction of F-18 FDG uptake from baseline to therapy (Baseline SUV = 14.2, ETA SUV = 13.1 ) and a poor outcome.

Disclosure of author financial interest or relationships:
**F. Imani**, None; **C. Laymon**, None; **M. Oborski**, None; **R. Ferris**, None; **J.M. Mountz**, None.

Presentation Number **P091**
Poster Session 1
September 5, 2012 / 18:00-18:00 / Room: The Liffey

# Gadolinium based nanoparticles as radiosensitizing agents for radioresistant head and neck tumours

*Imen Miladi[1], Marie-Therese Aloy[3], Aurélie Berniard[1], Emma Armandy[3], Pierre Mowat[2], Mehdi Benchaib[5], Elisabeth Miot-Noirault[4], David Kryza[1], Claire Billotey[1], Pascal Perriat[2], François Lux[2], Olivier Tillement[2], Claire Rodriguez-Lafrasse[3], **Marc Janier**[1], [1]Hopital Edouard Herriot HCL, LPCML UMR 5620 UCBL1, Lyon, France; [2]Fennec Team La Doua, LPCML UMR 5620 UBL1, Lyon, France; [3]Centre Hospitalier Lyon Sud, EA3738 UCBL1, Lyon, France; [4]U990, Inserm, Clermont-ferrand, France; [5]Centre Hospitalier Lyon Sud, HCL, Lyon, France. Contact e-mail: marc.janier@univ-lyon1.fr*

Radiotherapy is one of the main therapies for cancer, but it remains limited when tumours are radioresistant such glioblastoma, head and neck tumours, osteo and chondrosarcomas for example. Several strategies aiming at radiosensitizing these resistant tumours are under development. One of those relies on the use of high density nanoparticles, which once delivered into the tumour should deliver secondary radiations amplifying the radiotherapy efficiency. A previous reported study from our consortium showed that Gadolinium Based Nanoparticles (GBN) were able to induce a clonogenic death of SQ20B cells in culture (human head and neck carcinoma cells). The present study aimed at the demonstration of the in-vivo radiosensitizing effect of these GBN on SQ20B xenograft tumour. Radiation Therapy (RT) was performed using a biological X-Ray Irradiator (X-RAD 320) (Byfleet, Surrey) with 320 KV X-rays. The field of irradiation was adapted according to tumor volume by using an adjustable collimator positioned 35 cm from the animals. The dose rate was of 2 Gy.min-1. Four/five weeks after tumor grafting, mice with tumor volume less than 400 mm3 were randomly selected for radiotherapy 5 minutes after intratumoral (IT) injection of either GBN or saline. Four groups of rats were compared: IT injection of saline only (Control) (n = 9), GBN IT injection only (GBN injection) (n = 9), IT injection of saline + 10 Gy radiation (IR 10Gy) (n = 13), and IT injection of GBN + 10 Gy (IR 10Gy + GBN) (n = 10). Compared to the progressive and massive increase in tumor volume observed in the control groups (control and GBN injection groups), 10 Gy radiation stabilized tumor evolution between the second and the third week after radiation. The tumors then started to develop again with a growth curve similar to that of the control group. In contrast, the combination of GBN with 10 Gy radiation limited spectacularly the SQ20B tumors growth. At the end of week 6, the mean reduction in tumor volume in the IR 10Gy + GBN group, was of 626 and 388% (P = 0,003) compared, respectively, to the control and only irradiated tumors. Moreover, in the end of our therapy study, tumors have disappeared in two mice given 10 Gy with GBN treatment. Combined with the in-vitro study, the reported results demonstrate a major radiosensitizing effect of Gadolinium Based Nanoparticles on radioresistant tumours such as Head and Neck carcinomas.

Disclosure of author financial interest or relationships:
**I. Miladi**, None; **M. Aloy**, None; **A. Berniard**, None; **E. Armandy**, None; **P. Mowat**, None; **M. Benchaib**, None; **E. Miot-Noirault**, None; **D. Kryza**, None; **C. Billotey**, None; **P. Perriat**, None; **F. Lux**, None; **O. Tillement**, None; **C. Rodriguez-Lafrasse**, None; **M. Janier**, None.

Presentation Number **P092**
Poster Session 1
September 5, 2012 / 18:00-18:00 / Room: The Liffey

# Biological evaluation of tricarbonyl Tc-99m/Re-188 labeled cRGD peptide for angiogenic theragnosis

***Jae Ho Jung**, Byung Seok Moon, Hong Jin Lee, Nam Hee Lim, Byung Chul Lee, Sang Eun Kim, Seoul National University Bundang Hospital, Seongnam, Republic of Korea. Contact e-mail: jaehoboa@paran.com*

Targeting of $\alpha_v\beta_3$ integrin with cRGD peptides are actively being pursued and affected as a specific tumor imaging and therapy method. Tc-99m and Re-188 represent an attractive pair of radionuclides for tumor diagnosis and therapy. In this study, we prepared novel radio-peptides with $^{99m}Tc(CO)_3$ or $^{188}Re(CO)_3$ core from same precursor and their biological evaluation were investigated in tumor xenograft models for tumor imaging and therapeutic effect. To develop highly selective and active radiolabeled cRGD peptide, we synthesized a novel technetium-99m labeled RGD peptide containing a negative charged pocket ($[^{99m}Tc(CO)_3L_3]$-, $L_3 = NO_2$) and also prepared rhenium-188 labeled cRGD peptide from same precursor. Cell binding assay was performed using human umbilical vein endothelial cells. Biodistribution studies of Tc-99m and Re-188 labeled cRGD peptide were done using Balb/c nude mice bearing U87-MG, respectively. SPECT/CT imaging for Tc-99m and antitumor effect for Re-188 labeled cRGD peptide were investigated in U87MG bearing mice including immunohistochemistry. The overall radiochemical yield of radiotracers after HPLC purification was 50-79% and the $IC_{50}$ values of this radiotracers were 0.4-0.5 nM, respectively. Biodistribution in Balb/c nude mice bearing U87-MG for Tc-99m labeled cRGD peptide showed low blood activity (0.16±0.02 %ID/g at 240 min), rapid hepatic clearance (3.10±0.58 %ID/g at 10 min vs 1.24±0.18 %ID/g at 240 min) and significantly high tumor accumulation (12.31±1.55 %ID/g at 60 min). Re-188 labeled cRGD peptide showed similar biodistribution pattern. In ROI quantification of animal SPECT/CT image of Tc-99m labeled cRGD peptide, AUC (%ID/g min)=2162, $C_{max}$ (%ID/g)=13.3, $T_{max}$ (min)= 5.0, $T_{1/2}$ (min)=75.66 and Cl (mL/min)=0.046 showed in mice bearing U87MG. Tumor therapeutic effect of Re-188 labeled cRGD peptide (11.1 MBq) treated mice significantly suppressed tumor growth by 69.39%. The anti-angiogenic effect was confirmed in immunohistochemistry (CD-31 and $\alpha_v\beta_3$ integrin expression levels). In summary, this study demonstrates that tricarbonyl Tc-99m labeled cRGD peptide exhibits specific $\alpha_v\beta_3$ integrin binding and potential *in vivo* biokinetic characteristics and Re-188 labeled cRGD peptide enhanced antiangiotherapeutic effects against solid tumor, which may make it a promising probe for specific tumor-induced angiogenesis imaging and angiogenic disease.

Disclosure of author financial interest or relationships:
**J. Jung**, None; **B. Moon**, None; **H. Lee**, None; **N. Lim**, None; **B. Lee**, None; **S. Kim**, None.

Presentation Number **P093**
Poster Session 1
September 5, 2012 / 18:00-18:00 / Room: The Liffey

# Cancer Specific Sentinel Lymph Node Mapping Using [Tc-99m]Tc-ICG-Folate Human Serum Albumin

***Se Hun Kang***, *Nam Suk Baek, Seo-il Kim, Seok-Ki Kim, Molecular Imaging and Therapy Branch, National Cancer Center, Goyang, Republic of Korea. Contact e-mail: neology7@ncc.re.kr*

A sentinel lymph node (SLN) mapping procedure requires many steps before/during surgical exploration, and each imaging step requires different characteristics from the SLN targeting agents. We developed a [Tc-99m]Tc-Indocyanine green-folate human serum albumin ([Tc-99m]Tc-ICG-FSA) kit as a cancer specific sentinel lymph node imaging agent. Folic acid was conjugated to the human serum albumin, and the reduced FSA was developed as a kit vial for [Tc-99m]Tc labeling. For near-infrared fluorescent (NIRF) imaging, ICG was bound to [Tc-99m]Tc-FSA as NIRF dye. Radiostability test of [Tc-99m]Tc-ICG-FSA was done in human serum at 37 °C for 24 h. To evaluate cancer specific uptake, in vitro uptake tests were also done using folic acid receptor over-expressing KB compared with MDAMB231, KPL4, MCF7 cancer cell lines. Animal SPECT and NIRF in vivo images were obtained using BALB/c nude mice. Consequently, [Tc-99m]Tc-ICG-FSA was successfully prepared. [Tc-99m]Tc labeling efficiency was > 99% in 10 min at r.t. and [Tc-99m]Tc-ICG-FSA showed high radiostability in human serum. In in vitro cancer specific cell uptake test, it showed high uptake in KB cancer cell, while the uptake ratio was decreased after adding free folic acid. Animal SPECT image showed the exact location of the SLN. Likewise, in vivo NIRF image showed the SLN without an invasive procedure. In conclusion, we developed a dual modal cancer specific SLN imaging agent, [Tc-99m]Tc-ICG-FSA. It is a very useful clinically and showed a very ideal nature for SLN mapping. It enabled a high signal-to-noise ratio on the SLNs and produced complementary dual modal signals with safety. It is an agent that promises to have positive clinical applications and may have great advantages to complement the conventional single modal methods. In addition, it could be applied as an imaging agent for folic acid receptor over-expressing cancer.

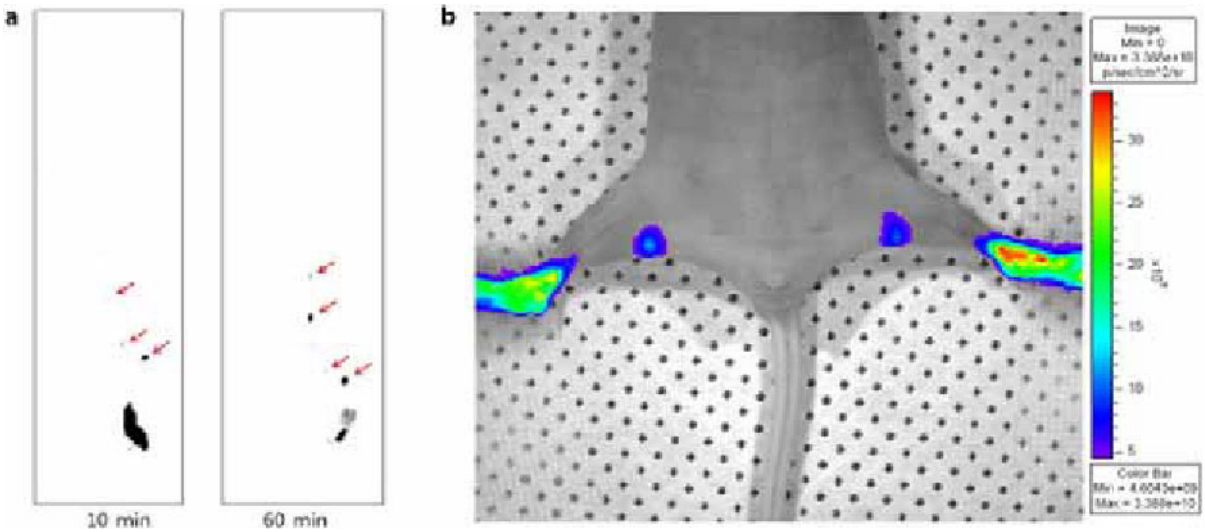


The Animal SPECT and NIRF in vivo images of [Tc-99m]Tc-ICG-FSA. a) Animal SPECT images at 10 & 60 min (100 μCi/50 μL inj. at the right hind foot pad). b) NIRF image at 60 min (100 μCi/50 μL inj. at the both hind foot pads).

Disclosure of author financial interest or relationships:
**S. Kang**, None; **N. Baek**, None; **S. Kim**, None; **S. Kim**, None.

Presentation Number **P094**
Poster Session 1
September 5, 2012 / 18:00-18:00 / Room: The Liffey

# Estimating the Contribution of Monocarboxylate Transporter to Kinetics of Hyperpolarized [1-$^{13}$C]Lactate MRS Signal

***Mikko I. Kettunen**, Brett W. Kennedy, De-En Hu, Kevin M. Brindle, Cancer Research UK Cambridge Research Institute & University of Cambridge, Cambridge, United Kingdom. Contact e-mail: mik21@cam.ac.uk*

Detection of lactate dehydrogenase (LDH) activity using hyperpolarized [1-$^{13}$C]pyruvate and $^{13}$C magnetic resonance spectroscopy (MRS) has proved to be a powerful approach for probing tissue metabolism *in vivo*. However, the potential problem with this experiment is that pyruvate must be administered at supra-physiological concentrations. This problem can be avoided by using hyperpolarized L-[1-$^{13}$C,U-$^{2}$H]lactate, which can be used at physiological concentrations, and measuring LDH-catalyzed hydrogen/deuterium exchange between endogenous protonated lactate and the injected deuterated lactate using a heteronuclear spin-echo experiment [1]. In this previous study an increase in the ratio of the echo signal to the FID signal observed immediately after the 10° pulse (echo/FID ratio) in the spin echo experiment was observed, which implied redistribution of lactate between the vascular and extravascular spaces. In the current study we investigated whether this change in echo/FID ratio could report on lactate transport into the tumor cells. **Methods** L-[1-$^{13}$C]lactate was prepared as described previously [1]. Female C57BL/6 mice bearing EL-4 lymphomas (n = 28, tumor size ~2 cm$^3$) were anesthetized with intra-peritoneal injections of Hypnorm/Hypnovel/dextrose-saline (4%:0.18%) in a 5:4:31 ratio (10 mL/kg body weight). Experiments were performed at 9.4 T using a $^{13}$C-surface coil (diameter 24 mm) placed directly over the tumor. Two hundred µl of 45-90 mM lactate was injected i.v. and data acquisition (repetition time 3.5 s, echo time 310 ms) was started 8 seconds after the beginning of injection. In some experiments, lactate transport into cells was challenged by injecting either a monocarboxylate transport (MCT) inhibitor (α-cyano-4-hydroxycinnamate, 4-CIN, 150 mg/kg i.p.) or non-labeled lactate (200 µl of 2M, i.p. or up to 10x the injected hyperpolarized concentration i.v.) prior to injection of the hyperpolarized L-[1-$^{13}$C]lactate. Peak integrals were calculated and the area under echo/FID ratio curve (AUC) up to the 40 s was estimated. **Results** AUC tended to increase with hyperpolarized lactate concentration, although this was not statistically significant. Similarly, only small changes were seen when cell transport of hyperpolarized lactate was challenged. Comparison of all control (n=17) and MCT-challenged (n=11) data showed a significant decrease in AUC (1.2±0.5 vs 0.7±0.4, $p<0.01$). The largest decrease in AUC was seen in animals in which hyperpolarized lactate uptake was challenged by high concentrations of unlabeled lactate injected i.v.. However, these animals developed cardiac arrhythmias, which is likely to affect the results. **Discussion** This study suggests that while lactate transport into the cells may play some part in the observed increase in echo/FID ratio, in this tumor model it seems likely that the movement of lactate between the vascular and interstitial pools has the biggest effect. **References** [1] Kennedy et al. JACS, 134(10):4969, 2012.

Disclosure of author financial interest or relationships:
**M.I. Kettunen**, GE Healthcare, Grant/research support; **B.W. Kennedy**, General Electric Healthcare, Grant/research support; **D. Hu**, None; **K.M. Brindle**, GE Healthcare, Grant/research support; GSK, Consultant .

Presentation Number **P095**
Poster Session 1
September 5, 2012 / 18:00-18:00 / Room: The Liffey

# Development of novel ultrasmall superparamagnetic iron oxide agent with monodisperse iron oxide core and multiple-interaction ligands for magnetic resonance imaging diagnosis of metastatic lymph nodes

***Eung-gyu Kim***[1], *Hye Rim Cho*[2], *Juyoung Park*[1], *Roh-Eul Yoo*[2], *Wan-Jae Myeong*[1], *Seung Hong Choi*[2], [1]*Research & Development Center, Hanwha Chemical Corp., Daejeon, Republic of Korea;* [2]*Radiology, Seoul National University Hospital, Seoul, Republic of Korea. Contact e-mail: kimeg@hanwha.co.kr*

Introduction: The accurate detection of lymph node metastases is crucial to successful tumor therapy. Recently, it was reported that ultrasmall superparamagnetic iron oxide (USPIO) enabled MR imaging of lymph node metastasis. For more effective diagnosis of metastatic lymph nodes, USPIO would be more uptaken in lymph nodes has a higher T2 relaxivity and be non-aggregated and stable in vivo. We developed a novel USPIO with monodisperse iron oxide core size of 14±1 nm and multiple-interaction ligands. This USPIO agent exhibited higher T2 contrast effect compared with current USPIO such as MION-47, although overall size is similar. The feasibility of detecting lymph node metastasis using the USPIO was evaluated using MR imaging in a rabbit model. Methods: USPIO with monodisperse iron oxide core and multiple-interaction ligands inspired by mussel adhesive protein was prepared according to previous report[1]. Core size, hydrodynamic diameter, T2 relaxivity were measured by TEM, DLS and MR scanner, respectively. To make metastatic lymph nodes, VX2 carcinomas were implanted into the thighs of 12 rabbits 3 or 4 weeks before MR imaging. In each rabbit, MR imaging was performed before and 24 hours after the injection of the USPIO (10.4mg Fe/kg). All rabbits were examined with 3.0 T MR scanner (Trio Trim, Siemens Healthcare, Erlangen, Germany) using 3D GRE sequence (FOV = 140x98 mm, FA = 12°, TR/TE = 51/22 msec, slice thickness = 2 mm, matrix = 256 x 180, NEX = 4, scan time = 12 min) was acquired. After MR imaging, all rabbits were sacrificed for the pathologic evaluation. MR images were compared with pathologic results. Results: The novel USPIO was very stable without aggregation in saline. The hydrodynamic diameter was 25~30nm and T2 relaxivity was 281 mM-1s-1 at 4.7T. Among all 12 rabbits, metastases were confirmed in 29 of 41 lymph nodes by pathology. In terms of sensitivity, the USPIO-enhanced MR imaging showed 100 % (29 of 29 metastatic lymph nodes), and the specificity was also 100 % (12 of 12 normal lymph nodes). USPIO-enhanced MR imaging clearly visualized the metastatic foci in each metastatic lymph node, which did not uptake our USPIO agent while normal lymphatic tissue accumulated the USPIO particles. Conclusion: We fabricated a novel USPIO MR imaging agent with monodisperse iron oxide core and multiple-interaction ligands for the detection of metastatic lymph nodes, which we believe is promising and challenging in the oncologic field. Reference: [1] Daishun Ling, Wooram Park, Yong Il Park, Nohyun Lee, Fangyuan Li, Changyeong Song, Su-Geun Yang, Seung Hong Choi, Kun Na, Taeghwan Hyeon

Disclosure of author financial interest or relationships:
**E. Kim**, None; **H. Cho**, None; **J. Park**, None; **R. Yoo**, None; **W. Myeong**, None; **S. Choi**, None.

Presentation Number **P096**
Poster Session 1
September 5, 2012 / 18:00-18:00 / Room: The Liffey

# Tissue Redox Activity as a Sensing Platform for Magnetic Resonance Imaging of Cancer: Diagnostic and Therapeutic Aspects

*Rumiana Bakalova[1], Zhivko Zhelev[1], **Daisuke Kokuryo**[1], Ichio Aoki[1], Veselina Gadjeva[2], Tsuneo Saga[1], [1]Diagnostic Imaging Program, Molecular Imaging Center, National Instituite of Radiological Sciences, Chiba, Japan; [2]Medical Faculty, Trakia University, Stara Zagora, Bulgaria. Contact e-mail: kokuryo@nirs.go.jp*

Background: Redox signalling is crucial for carcinogenesis and tissue redox activity has emerged as an important sensing platform for cancer diagnosis and planning of therapeutic strategy. The cells and tissues of healthy mammalian are characterized by low level of reactive oxygen species (ROS) and some constant (reference) level of reducing equivalents. Increasing of ROS above the critical level provokes genomic instability. Normal cells become malignant. The present study describes universal methodology for direct imaging of tissue redox activity in carcinogenesis, which allows a differentiation of cancer development from normal (healthy) condition. Methods: The experiments were conducted on: neuroblastoma-bearing, colon cancer-bearing and healthy mice (Balb/c nude). The tissue redox activity was visualized in vivo by nitroxide-enhanced MRI on anesthetized animals. The method is based on nitroxide redox cycle, coupled with appearance or disappearance of MRI signal. The half-life ($t_{1/2}$) of nitroxide-enhanced MRI signal in the respective tissue was used as a diagnostic marker. Results: The study provides direct evidence that healthy and cancer-bearing mammalian are characterized by different tissue redox activity - a basis for cancer diagnostic. The tissues (cancer and "normal") of cancer-bearing mammalian were characterized by long-lived MRI signal ($t_{1/2}$>14 min), indicating a high oxidative activity. The tissues of healthy organism were characterized by short-lived MRI signal ($t_{1/2}$=1~3 min), indicating a high reducing activity. The long-lived nitroxide-enhanced MRI signal in cancer-bearing mice is a result of excessive amounts of superoxide in their tissues (cancer and non-cancer). Conclusions: The high oxidative activity of cancer tissue is a fact despite of the widely accepted opinion that hypoxia develops in solid tumours. Presumably, it is due to abnormal generation of free superoxide instead of using oxygen to maintain normal homeostasis. The study shows that anti-cancer therapy should solve simultaneously two major problems: to stop proliferation and induce apoptosis in cancer cells, and to protect "normal" tissues of cancer-bearing organism from oxidative damage. There are two therapeutic targets and they are equally important for the success of therapy and survival of the organism. The proposed methodology is applicable in clinical laboratory practice on isolated biopsy specimens and blood samples for evaluation of the effectiveness of anti-cancer therapy, based on its effect on cellular/tissue redox activity.

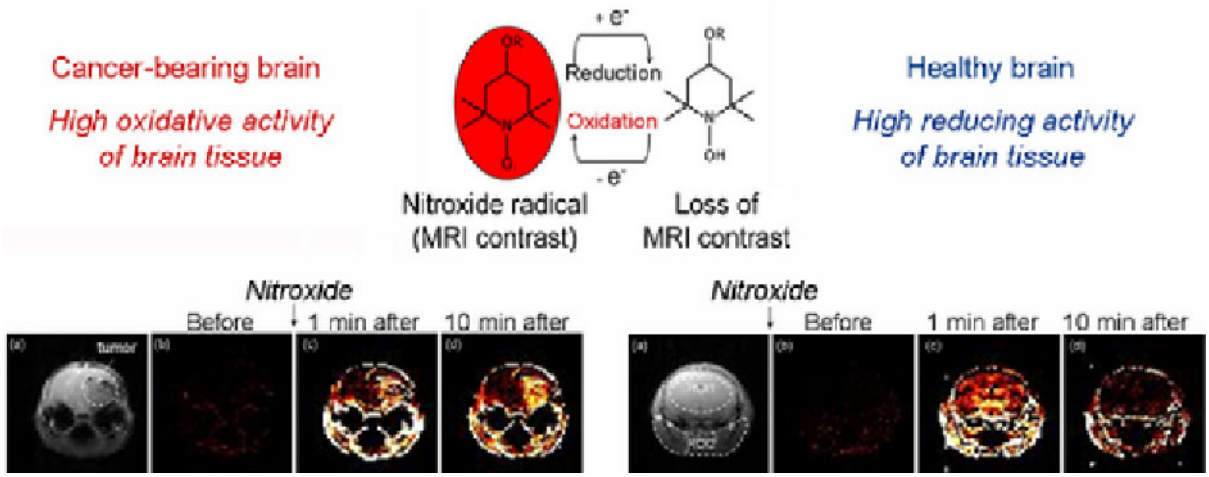


Disclosure of author financial interest or relationships:
**R. Bakalova**, None; **Z. Zhelev**, None; **D. Kokuryo**, None; **I. Aoki**, None; **V. Gadjeva**, None; **T. Saga**, None.

Presentation Number **P097**
Poster Session 1
September 5, 2012 / 18:00-18:00 / Room: The Liffey

# *N*-2-[$^{18}$F]Fluoroethyl-*N*-methyl-2-aminoethyl-tyrosine ([$^{18}$F]FEMAET) rapidly accumulates in PC-3 xenografts via amino acid transporters but is not further trapped by metabolism to an [$^{18}$F]Fcholine analog

*Aristeidis Chiotellis[1], Linjing Mu[1,2], Adrienne Müller[1], Claudia Keller[1], Karin Weyermann[1], Simon M. Ametamey[1], Roger Schibli[1,3],* ***Stefanie D. Krämer***[1], *[1]Center for Radiopharmaceutical Sciences ETH/USZ/PSI, ETH Zurich, Zurich, Switzerland; [2]Center for Radiopharmaceutical Sciences ETH/USZ/PSI, Dept. of Nuclear Medicine, University Hospital Zurich, Zurich, Switzerland; [3]Center for Radiopharmaceutical Sciences ETH/USZ/PSI, Paul Scherrer Institute, Villigen, Switzerland. Contact e-mail: stefanie.kraemer@pharma.ethz.ch*

Purpose: Several $^{18}$F- and $^{11}$C-labeled analogs of natural amino acids have proved to be useful for tumor imaging by PET. In contrast to other metabolic PET probes such as FDG and choline, amino acids are only exceptionally trapped by a metabolic step. An example is decarboxylation of [$^{18}$F]FDOPA in endocrine tumors. Tumor/background ratios are, therefore, often moderate. [$^{18}$F]Fcholine is a powerful PET probe for prostate cancer imaging in humans. After its uptake into metabolically active cells, it incorporates into membrane phospholipids, resulting in efficient trapping. Our goal was to combine the good uptake characteristics into tumor cells of tyrosine analogs with the trapping mechanisms of choline analogs (Figure). We hypothesized that increased cytochrome P450 activity of tumor cells will cleave the two moieties resulting in phospholipid incorporation of the $^{18}$F-carrying metabolite. Methods: The reference compound *N*-2-fluoroethyl-*N*-methyl-2-aminoethyl-tyrosine (FEMAET) and the chloride precursor for radio-labeling were synthesized by multi-step approaches. [$^{18}$F]FEMAET was prepared by a two step reaction sequence involving nucleophilic fluorination of the fully tert-butyl protected precursor and subsequent deprotection. Uptake of FEMAET into PC-3 prostate cancer cells was investigated *in vitro* in a competition assay with [$^{18}$F]FDOPA. The influence of neutral and cationic amino acids on [$^{18}$F]FEMAET cell uptake and efflux was tested to identify the involved transport systems. *In vivo* tumor uptake and whole body distribution of [$^{18}$F]FEMAET was studied by small animal PET with PC-3 xenograft-bearing mice. The metabolic fate of [$^{18}$F]FEMAET and potential incorporation of a radiometabolite into phospholipids was investigated with xenograft homogenates and blood plasma and urine samples by thin layer chromatography. Results: FEMAET was prepared in 17 % overall yield and > 95% purity. The decay corrected radiochemical yield of [$^{18}$F]FEMAET was about 8 % and the radiochemical purity was > 95 %. The identity of [$^{18}$F]FEMAET was confirmed chromatographically with the reference compound. Specific activity was in the range of 28 - 40 GBq/μmol at the end of synthesis. Addition of 100 μM FEMAET significantly reduced cell uptake of [$^{18}$F]FDOPA *in vitro*, suggesting competition for transport. Cell uptake and efflux experiments with [$^{18}$F]FEMAET indicated transport by large neutral amino acid (LAT) and cationic amino acid transport systems. The *in vivo* xenograft/background ratio reached 1.5 to 2 within 10 min after [$^{18}$F]FEMAET injection and stayed constant up to 150 min. Xenograft-to-liver and -kidney ratios were 1 to 1.5 from 60 min onwards (Figure). Xenografts, blood plasma and urine contained mainly [$^{18}$F]FEMAET 60 min after injection. No incorporation of radioactivity into phospholipids was detected. Conclusion: [$^{18}$F]FEMAET rapidly accumulates in PC-3 xenografts mediated by neutral and cationic amino acid transport systems. Metabolism is negligible and no metabolite is incorporated into phospholipids.

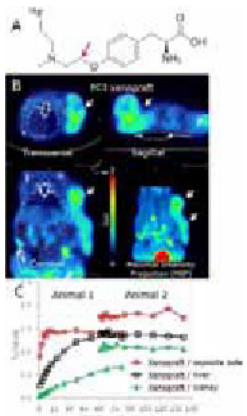

Figure: (A) Structure of [$^{18}$F]FEMAET, combining tyrosine with an $^{18}$F-labeled choline analog. Red arrow, expected oxydation and cleavage by metabolism. (B) PET images of a PC-3 xenograft-bearing NMRI nude mouse injected with 11 MBq [$^{18}$F]FEMAET. Averaged from 60 to 150 min after injection; arrows indicate xenograft. B) SUV ratios between xenograft and a corresponding region on the opposite shoulder, liver or kidney. Data from 2 mice.

Disclosure of author financial interest or relationships:
**A. Chiotellis**, None; **L. Mu**, None; **A. Müller**, None; **C. Keller**, None; **K. Weyermann**, None; **S.M. Ametamey**, None; **R. Schibli**, None; **S.D. Krämer**, None.

Presentation Number **P098**
Poster Session 1
September 5, 2012 / 18:00-18:00 / Room: The Liffey

# The Role of choline kinase and hypoxia in regulating breast cancer stem cell markers ABCG2, ALDH1A1 and CD44

***Balaji Krishnamachary***, *Marie-France Penet, Mayur Gadiya, Noriko Mori, Samata M. Kakkad, Yelena Mironchik, Kristine Glunde, Zaver M. Bhujwalla, Radiology, Johns Hopkins University, Baltimore, MD, USA. Contact e-mail: bkrishn1@jhmi.edu*

Introduction: Stem-like breast cancer cells (SBCCs) are drug resistant, invasive, and likely to lead to tumor recurrence and repopulation. High expression of the adhesion molecule CD44, of the drug transporter ABCG2, and of the enzyme ALDH1A1 are well-established markers associated with SBCCs-enriched tumor populations. Altered choline metabolism is one of the hallmarks of cancer. Cancers typically exhibit elevated phosphocholine (PC) mostly due to increased choline kinase (Chk) expression and activity, and this elevation is closely related to malignant transformation, invasion and metastasis. Similarly hypoxic tumor microenvironments are associated with increased aggressiveness. Moreover hypoxia can transcriptionally regulate Chk [1]. Here we examined the relationship between Chk and ABCG2, ALDH1A1 and CD44 in MDA-MB-231 tumors lentivirally transduced to express short hairpin RNA targeting choline kinase (shRNA-Chk), and investigated the association between hypoxia, CD44 and total choline (tCho) in these tumors. Method: In vivo studies were performed using MDA-MB-231 tumors or 231-hypoxia response element-red fluorescent protein (HRE-RFP) tumors derived from a sub line that stably expressed a red fluorescent marker, under control of HRE. Design, production, concentration and delivery of lentivirus expressing shRNA-Chk or empty vector (EV) were performed following our previously established protocol [2]. SBCCs marker expression in tumors was determined at mRNA levels by quantitative real-time PCR (q-RT-PCR) using specific primers. Protein expression was determined by immunoblot and immunohistochemistry on cells and tissue specimens using specific antibodies. 1H magnetic resonance spectroscopic images (MRSI) of tumors in mice were acquired with a 1 mm x 1 mm in-plane resolution from a 4 mm thick slice using a 4.7T Bruker Biospec spectrometer, and fluorescence images of fresh tumor slices were captured on a Nikon fluorescence microscope. Co-registration of images was performed using ImageJ software. Results: Lentiviral transduction of MDA-MB-231 tumors in vivo with Chk-shRNA resulted in a decrease of PC (Figure 1A) [2], of mRNA expression levels of Chk, ABCG2, and CD44 (Figure 1B), and of Chk, ABCG2, ALDH1A1 and CD44 proteins level (Figure 1C). Immunostaining of adjacent tumor sections for HIF-1α and CD44 support a close association between HIF-1α and CD44 expression, and confirm the expression of HIF-1α in and around red fluorescing tumor regions (Figure 1D). MR spectroscopic studies of 231-HRE-RFP tumors co-registered with fluorescence image showed association of elevated levels of tCho near or around the intense red fluorescing hypoxic regions of the tumor (Figure 1E), confirming earlier observations that Chk expression and PC increase with hypoxia. These data highlight the role of Chk and hypoxia in engendering a stem-like phenotype, and the potential importance of targeting Chk and hypoxia to minimize the burden of cells with stem-like characteristics in tumors. References: 1. Glunde et al., Cancer Res., 2008; 2. Krishnamachary, B et al., Cancer Research, 2009. Supported by NIH R01 CA136576 and P50 CA103175.

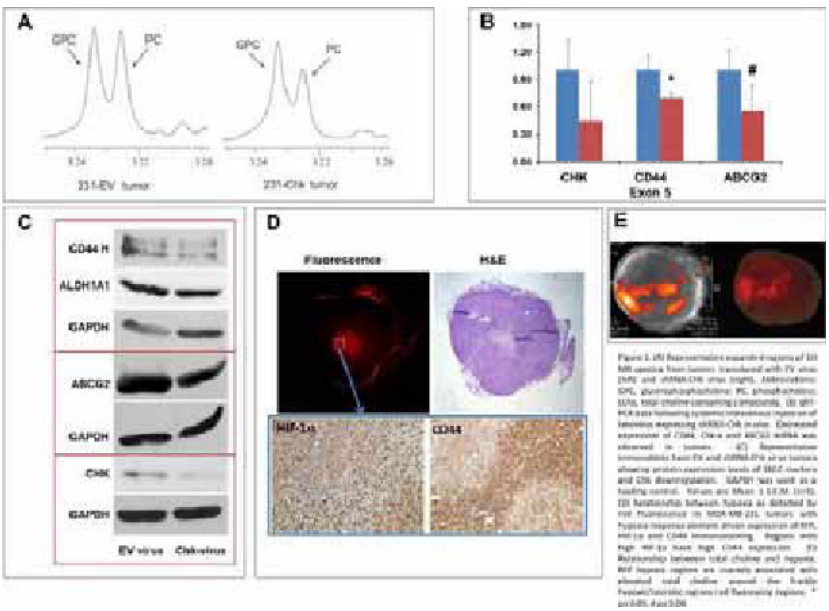


Disclosure of author financial interest or relationships:
**B. Krishnamachary**, None; **M. Penet**, None; **M. Gadiya**, None; **N. Mori**, None; **S.M. Kakkad**, None; **Y. Mironchik**, None; **K. Glunde**, None; **Z.M. Bhujwalla**, None.

Presentation Number **P099**
Poster Session 1
September 5, 2012 / 18:00-18:00 / Room: The Liffey

# Tumor-Targeted NIR Dyes for Fluorescence-Guided Surgery Philip S. Low, Sakkarapalayam M. Mahalingam, Lindsay E. Kelderhouse, Venkatesh Chelvam, Charity Wayua, Scott Poh, and Sumith Kularatne Department of Chemistry, Purdue University, West Lafayette, IN 47907 USA

***Philip S. Low***[1], *Sakkarapalayam M. Mahalingam*[1], *Lindsay E. Kelderhouse*[1], *Venkatesh Chelvam*[1], *Charity Wayua*[1], *Scott Poh*[1], *Sumith A. Kularatne*[2], [1]*Chemistry, Purdue University, West Lafayette, IN, USA;* [2]*OnTarget, West Lafayette, IN, USA. Contact e-mail: plow@purdue.edu*

Surgical resection of malignant disease is currently one of the most common and effective strategies for treating cancer. Unfortunately, quantitative tumor resection is currently limited by a surgeon's ability to distinguish malignant tissue from adjacent healthy tissue. Fluorescence guided surgery has emerged as a tool to aid surgeons in the identification and removal of diseased tissue. While non-targeted fluorescent dyes injected near the primary tumor mass have been shown to passively accumulate in tumors and lymph nodes, the resulting tumor to background ratios are often poor and boundaries between malignant and normal tissue can be difficult to define. To circumvent these problems, our lab has focused on the development of high affinity tumor-specific low molecular weight ligands that bind to receptors that are over-expressed on cancer cells, but either absent or expressed at low levels on healthy cells (1, 2). In this study, we link three different tumor-targeting ligands to near infrared (NIR) dyes and explore their use in murine models of fluorescence guided surgery. The three targeting ligands for which new data will be presented are: 1) DUPA, which selectively targets prostate specific membrane antigen (PSMA is over-expressed on prostate cancers and the neovasculature of essentially all solid tumors), 2) folate, which selectively targets the folate receptor (FR is over-expressed on cancers of the ovary, lungs, endometrium, kidney, breast, colon and myelogenous cells of the bone marrow), and 3) GASR2, which selectively targets the cholecystokinin 2 receptor (CCK2R is over-expressed on cancers of the colon, thyroid, lungs, brain, and gastrointestinal stromal tumors).(10-12) In vitro, all PSMA, FR, and CCK2R- targeted NIR dyes were found to have binding affinities in the low nanomolar range, and binding was shown to be quantitatively blocked with 100-fold excess of free ligand. Upon injection into mice with metastatic disease, the targeted NIR dyes allowed clear distinction of tumor tissue from adjacent healthy tissue. Moreover, the PK/PD properties of the low molecular weight targeted dyes as well as their fluorescence intensities in the tumor tissue were superior to tumor-targeted fluorescent antibodies raised against the same tumor-specific receptor. Within 1 hour following intravenous injection, the tumor-targeted NIR dyes allowed resection of cancer tissue that could be conducted until all fluorescent tissue was removed. Moreover, all resected fluorescent lesions were later confirmed by histology to be malignant. Collectively, these tumor-specific NIR dyes demonstrate significant potential for use in fluorescence-guided surgery by aiding in the complete resection of malignant tissue. 1. Optical Imaging of Metastatic Tumors Using a Folate-Targeted Fluorescent Probe. Kennedy, MD et al. J. Biomed. Optics 8:636-41 (2003). 2. Intraoperative Tumor-Specific Fluorescent Imaging in Ovarian Cancer by Folate Receptor-α Targeting: First In-Human Results. van Dam, GM et al. Nature Medicine 17: 1315-19 (2011).

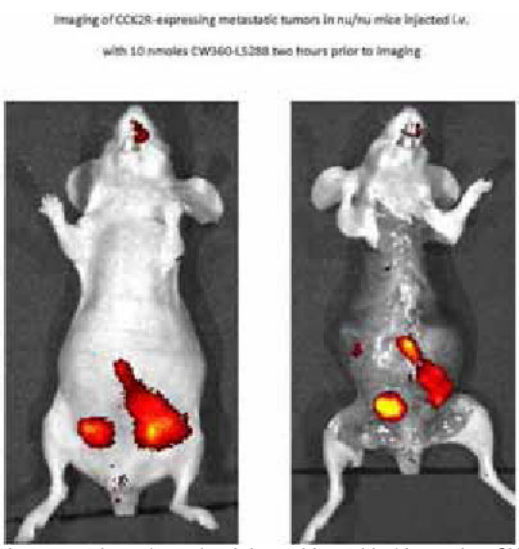


Imaging of CCK2R-expressing metastatic tumors in nu/nu mice injected i.v. with 10 nmoles CW360-LS288 two hours prior to imaging

Disclosure of author financial interest or relationships:
**P.S. Low**, OnTarget, Other financial or material support; Endocyte, Other financial or material support; **S.M. Mahalingam**, None; **L.E. Kelderhouse**, None; **V. Chelvam**, None; **C. Wayua**, None; **S. Poh**, None; **S.A. Kularatne**, None.

Presentation Number **P100**
Poster Session 1
September 5, 2012 / 18:00-18:00 / Room: The Liffey

# Molecular-Metabolic Imaging of Glutamine Catabolism in Murine Models of Hepatocellular Carcinoma (HCC) using MicroPET/CT

***Stephanie T. Murphy***[1], *Mariia Yuneva*[2], *Jinjin Feng*[1], *Youngho Seo*[1], [1]*Radiology and Biomedical Imaging, UCSF, San Francisco, CA, USA;* [2]*GW Hooper Foundation, UCSF, San Francisco, CA, USA. Contact e-mail: stephanie.taylor@ucsf.edu*

**Objectives**: The goal of this study was to correlate quantitative in vivo $^{18}$F-L-glutamine ($^{18}$F-Gln) metabolic kinetic parameters with activity levels of glutamine catabolism in different types of hepatocellular carcinoma. Using microPET/CT imaging techniques, our goal is to develop noninvasive and translational imaging techniques to investigate glutamine catabolism in vivo and metabolism-targeting therapeutics for HCC. **Methods**: For this study we used two transgenic mouse models of HCC induced by proto-oncogenes, MYC and MET. Biochemical data has shown that tumors induced by MYC have increased levels of glutamine catabolism compared to those induced by MET. The presence of tumors was confirmed in vivo with lipid-emulsion iodinated contrast-enhanced microCT. One hour dynamic PET data were acquired and reconstructed with CT-based attenuation correction for fasted MYC mice (n=3), fasted MET mice (n=2) and nonfasted MYC mice (n=3). The influx rate constants ($K_1$) for $^{18}$F-Gln uptake in tumor tissue (MYC tumors: n=11; MET tumors: n=4) using a one-tissue compartment model were derived from dynamic PET data using the left-ventricular blood pool time-activity curve as an input function. **Results**: Influx rate constants were significantly higher (P = 0.001) for MYC tumors ($K_1$ = 0.492 ± 0.135, n=5) than for MET tumors ($K_1$ = 0.140 ± 0.038, n=4) under fasting conditions. Rate constants were slightly higher for MYC tumors under fasting conditions ($K_1$ = 0.492 ± 0.135, n=5) than under nonfasting conditions ($K_1$ = 0.259 ± 0.186, n=6). **Conclusion**: Higher influx rate constants corresponded to elevated levels of glutamine catabolism as determined by biochemical assays. Fasting MYC mice resulted in slightly higher influx rate constants suggesting that fasting mice before scanning may increase $^{18}$F-Gln uptake. This initial study has demonstrated the use of $^{18}$F-Gln PET imaging as a tool to assess glutamine catabolism in HCC tumors in vivo.

Disclosure of author financial interest or relationships:
**S.T. Murphy**, None; **M. Yuneva**, None; **J. Feng**, None; **Y. Seo**, None.

Presentation Number **P101**
Poster Session 1
September 5, 2012 / 18:00-18:00 / Room: The Liffey

# Evaluation and optimization of EGFR-based ADEPT, using non-invasive time-domain near infrared fluorescence imaging

***Joanna Napp***[1,2], *Thomas Krüwel*[3], *Fernanda Ramos Gomes*[1], *Lutz F. Tietze*[4], *Walter Stühmer*[1], *Frauke Alves*[1,2], [1]*Molecular biology of Neuronal Signals, Max-Planck Institute for Experimental Medicine, Göttingen, Germany;* [2]*Hematology Oncology, Universitiy Medicine Göttingen, Göttingen, Germany;* [3]*Diagnostic Radiology, Universitiy Medicine Göttingen, Göttingen, Germany;* [4]*Organic and Biomolecular Chemistry, Universitiy Göttingen, Göttingen, Germany. Contact e-mail: jnowako1@gwdg.de*

The challenge facing cancer chemotherapy is the low selectivity to tumour cells versus normal cells. One possibility to overcome this problem is antibody-directed enzyme-prodrug therapy (ADEPT), in which a tumor specific antibody is used to carry a drug-activating enzyme to the tumor tissue. Site specific activation of prodrugs only within the tumor is a promising strategy to increase the specificity of treatment and to decrease toxicity in healthy tissues. Here we present the design, evaluation and optimization of a novel ADEPT concept, targeting EGFR (Epidermal Growth Factor Receptor) highly overexpressed in e.g. colorectal-, mammary- or squamous cell carcinoma. A clinically approved EGFR-targeting antibody, Cetuximab, was tested for its feasibility to deliver drug-activating enzyme, to the tumor. For this, Cetuximab was labeled with a near-infrared (NIR) fluorophore, Alexa 647 (Cetux-Alexa). Binding of Cetux-Alexa to highly EGFR-expressing- (MDA-MB-468), moderate EGFR-expressing- (MDA-MB-231) and EGFR-negative- (MCF-7) mammary carcinoma cells was analyzed in vitro, using fluorescence- and confocal microscopy. NIR fluorescence imaging was used to study the distribution and binding-kinetics of Cetux-Alexa in vivo in corresponding orthotopic mammary carcinoma models in nude mice. Fluorescence intensity, lifetime and location in vivo over time were measured with time-domain NIRF imager, OptixMX2 (ART, Canada). Distribution of the fluorescent probe in tumor sections was confirmed using LI-COR Odyssey imaging system as well as fluorescence microscopy. To study the feasibility of Cetuximab for ADEPT, the antibody was conjugated with Galactosidase (Cetux-Gal), and colorimetric cell-based assay was used to analyze the Galactosidase activity of the Cetux-Gal conjugate in vitro. Furthermore, the ability of Cetux-Gal conjugate to convert the nontoxic prodrug into a toxic drug was analyzed using in vitro cell-toxicity assays. Cetux-Alexa binds of EGFR-expressing cells in vitro, and stays bound to the membrane for at least 4 h. In vivo, Cetux-Alexa accumulates in EGFR-expressing tumors, leading in a very high tumor to background contrast for at least 2 weeks. No unspecific accumulation of the fluorescence conjugate in other organs (e.g. liver) could be observed, making the Cetuximab a very good candidate for ADEPT. Furthermore, Cetux-Gal was found to bind specifically to the EGFR-expressing cells in vitro, showing a high Galactosidase activity on highly-EGFR-expressing-, intermediate activity on moderate-EGFR-expressing- and no activity on EGFR-negative cells. In agreement, upon treatment of cells with Cetux-Gal in combination with prodrug, a strong cytotoxicity was obtained on highly EGFR-expressing, intermediate toxicity on moderate-EGFR-expressing and no toxicity on EGFR- Summarizing, the presented results will be used to design a novel ADEPT treatment, in which tumor-bearing mice will be treated with Cetux-Gal in combination with a highly potent prodrug. In future experiments, the efficacy of the therapy will be assessed by monitoring tumor growth/reduction with flat panel Volume Computed Tomography (fpVCT).

Disclosure of author financial interest or relationships:
**J. Napp**, None; **T. Krüwel**, None; **F. Ramos Gomes**, None; **L.F. Tietze**, None; **W. Stühmer**, None; **F. Alves**, None.

Presentation Number **P102**
Poster Session 1
September 5, 2012 / 18:00-18:00 / Room: The Liffey

# Intratumoral activity distribution of radiolabeled 177Lu-BR96 MAb at therapeutic absorbed doses over time evaluated in a syngeneic rat colon carcinoma model

***Anders Orbom***[1], *Erika Elgström*[2], *Sophie E. Eriksson*[2], *Rune Nilsson*[2], *Jan Tennvall*[2], *Sven-Erik Strand*[1], [1]*Medical Radiation Physics, Lund University, Lund, Sweden;* [2]*Oncology, Clinical Sciences, Lund University, Lund, Sweden. Contact e-mail: anders.orbom@med.lu.se*

INTRODUCTION The local therapeutic effects of radioimmunotherapy will affect tumor histology during the treatment. To study the intratumoral activity distribution during treatment we employed an existing experimental model of syngeneic rat colon carcinoma tumors expressing the Lewis Y antigen targeted by the mAb BR96. The aim of this study was to image the intratumoral distribution of therapeutic levels of 177Lu-labeled BR96 at different times post injection (p.i.) and to evaluate the activity distribution in relation to tissue histology. METHODS Brown Norway (BN) rats (n=21) were inoculated with BN7005-H1D2 cells and 2 weeks later injected i.v. with 400 MBq/kg body weight of 177Lu-DOTA-BR96. This activity resulted in complete remission after about 14 days in 5 of 6 animals in earlier studies (Eriksson et al. Cancer Biother Radiopharm 2012). While some animals did exhibit complete remission prior to scheduled sampling (n=1 at 6 d p.i. and n=3 at 8 d p.i.), the remainder were sacrificed and tumors excised at 1 d p.i. (n=3), 2 d p.i. (n=3), 3 d p.i. (n=3), 4 d p.i. (n=3), 6 d p.i. (n=2) and 8 d p.i. (n=3). Tumors were cryosectioned (10 μm) and imaged using a double sided silicon strip detector system for digital autoradiography. Adjacent sections were stained with hematoxylin and eosin for histology and, using immunohistochemistry, for antigen distribution (BR96), vasculature (RECA-1) and proliferating cells (anti-Ki67). RESULTS Preliminary analysis of imaged and stained sections indicate that for 2 of 3 tumors 1 d p.i. there is overlap between areas of high activity uptake and antigen-expressing cells. However, at later time points, high uptake routinely occurs in sparse areas not expressing the antigen and with prominent infiltration of stromal tissue. The overall density of viable tumor cells appears to decrease over time in tumors with a decreasing volume. For all tumors, areas with relatively high activity uptake did not stain positive for Ki-67, likely as an early effect of the high absorbed dose. CONCLUSION Although further quantitative analysis of the data is required, including absorbed dose estimations, the preliminary evaluation indicates a pattern with changing correlation between activity uptake and the density of viable, antigen expressing, cells over time.

Disclosure of author financial interest or relationships:
**A. Orbom**, None; **E. Elgström**, None; **S.E. Eriksson**, None; **R. Nilsson**, None; **J. Tennvall**, None; **S. Strand**, None.

Presentation Number **P103**
Poster Session 1
September 5, 2012 / 18:00-18:00 / Room: The Liffey

# Comparison of targeted antibody vs. small protein delivery within regions of orthotopic glioma tumors

***Kristian Sexton***, *Kimberley Samkoe, Jason Gunn, Brian W. Pogue, Dartmouth College, Hanover, NH, USA. Contact e-mail: Kristian.J.Sexton@Dartmouth.edu*

Fluorescence guided neuro surgery holds tremendous promise for improving prognosis in a number of different types of brain cancer. The blood brain barrier (BBB) prevents exogenously administered fluorescent dyes from leaking out of the vasculature into the normal brain. However, breakdown of the BBB in areas of tumor formation allows not only fluorophores to leak into tissue but also larger molecules including fluorophores conjugated to targeted proteins. Preferential accumulation in tumor areas due to this breakdown of the BBB as well as improved retention due to the targeting of surface receptors that are over expressed on cancer cells have the potential to allow significant specificity. However, BBB breakdown occurs gradually and as such only partial breakdown may occur in some areas of the tumor, particularly newly formed regions. The level of BBB breakdown may play a significant role in accessibility of different regions of the tumor to targeted probes of different sizes. Delivery of fluorescently labeled Cetuximab, a 152 kDa EGFR targeted antibody, was compared with delivery of fluorescently labeled anti-EGFR affibodies, 6.7 kDa targeted proteins, in a U251 GFP orthotopic glioma model. Tumor bearing mice were injected with a solution of 0.1 nmols of Cetuximab conjugated to IRDye 680RD and 0.1 nmols anti-EGFR targeted affibodies conjugated to IRDye 800CW. Control mice received no injections and allowed for tumor autofluorescence to be quantified. Injected mice were sacrificed at one hour post injection, brains were removed, flash frozen and sliced into 10 um sections. GFP allowed for positive identification of tumor areas using the GE Typhoon 9410 scanner. Tissue slices were further examined for protein distribution using the Odyssey scanner from Licor which allows for separation of the two signals. Analysis of the signal data revealed a significant increase in the ratio of affibody to Cetuximab on the outer edges of the tumors. This increase can be seen in the figure below which plots the ratio of Cetuxumab to affibody for the normal brain, tumor center, whole tumor and outer 25 um tumor edge. This is a significant finding for applications in fluorescence guided neuro surgery as identification of tumor margins is of critical importance. Any targeting agent that is better able to mark the edges and newly formed regions of the tumor may hold a significant advantage.

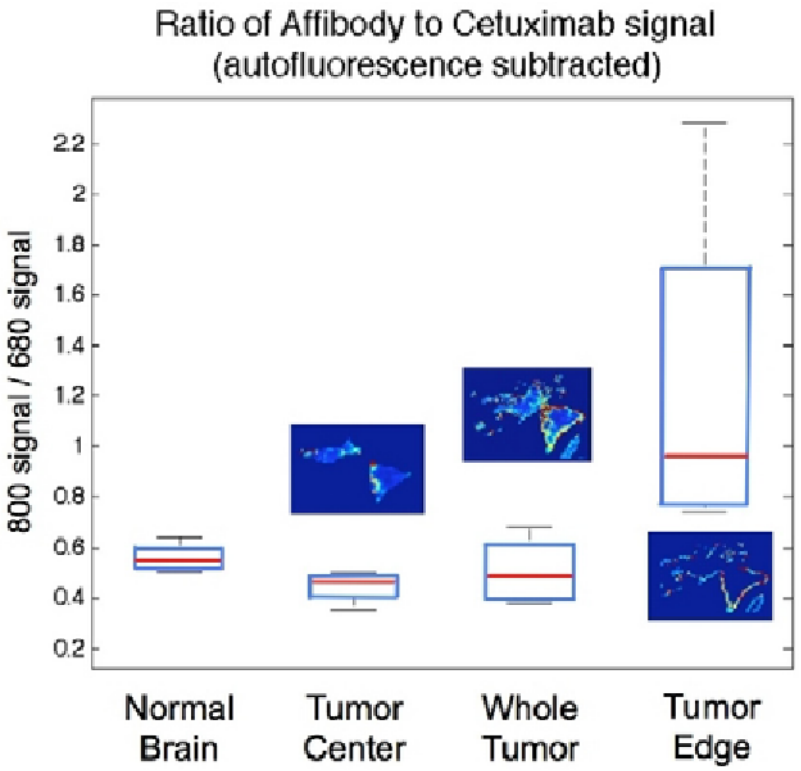


Disclosure of author financial interest or relationships:
**K. Sexton**, None; **K. Samkoe**, None; **J. Gunn**, None; **B.W. Pogue**, None.

Presentation Number **P104**
Poster Session 1
September 5, 2012 / 18:00-18:00 / Room: The Liffey

# Mucin related mRa96 antibody as a potential target for multimodality imaging of pancreatic ductal adenocarcinoma (PDAC)

*Janine Ring[1,3], **Travis Shaffer**[1,5], Anuja Ogirala[1,2], Lynda Cosgrave[1], Holger Kalthoff[4], Jan Grimm[1,2], [1]Molecular Pharmacology and Chemistry, Memorial Sloan Kettering Cancer Center, New York, NY, USA; [2]Department of Radiology, Memorial Sloan Kettering Cancer Center, New York, NY, USA; [3]Department of Clinical Radiology, University Hospital of Muenster, Muenster, Germany; [4]Division of Molecular Oncology, Institute for Experimental Cancer Research, Kiel, Germany; [5]Department of Chemistry, Hunter College of the City University of New York, New York, NY, USA. Contact e-mail: shaffert@mskcc.org*

Purpose: The purpose of our study was to characterize the mucin related mRa96 antibody and to test the ability of this probe to obtain antigen-specific multi-modality images of PDAC. Methods: The monoclonal antibody Ra96 (mAbRa96) was conjugated to HiLyte680 (HL680), USPIO-Cy5.5 and DFO-$^{89}$Zr for multimodality in vivo imaging. The in-vitro binding affinity of mAbRa96 -HL680, -USPIO-Cy5.5 and -DFO-$^{89}$Zr were evaluated on the pancreatic cancer cell line Capan-2 and HT1080 (fibrosarcoma) as a control by using flow cytometry, in cell western- and immunoreactivity assay. Multi-modality imaging was performed on Capan-2/HT1080 xenograft mice injected with mAbRa96-HL680, -USPIO-Cy5.5 or -DFO-$^{89}$Zr over serial time points (24h, 48h and 144h) by using FMT, PET and MRI. Furthermore, biodistribution was evaluated after 48h and 144h using both optical and radioactivity analysis. For immunohistochemistry, Capan-2 and HT1080 tumor sections were stained with mAbRa96 or Prussian blue for iron staining. Results: Flow cytometry revealed high binding affinity of mAbRa96-HL680 on Capan-2 cells and no specific binding on control HT1080 cells. These results were corroborated both with an immunoreactivity assay with $^{89}$Zr labeled and in cell western assay with USPIO-Cy5.5 mAbRa96. In-vivo imaging of Capan-2 tumors via FMT and PET demonstrated significantly higher uptake in pancreatic tumor, which was corroborated by biodistribution results. MRI revealed significant decrease in the T2 signal 24h after injection of iron oxide labeled mAbRa96. Immunohistochemistry investigations further validated the in-vivo optical imaging results. Conclusion: Our labeled mAbRa96 showed specific binding to the PDAC associated Ra-96 glycoprotein on Capan-2 in vitro and in vivo allowing multi-modality imaging of PDAC xenografted mice by FMT, PET, CT and MRI. With its high specificity for PDAC associated Ra-96 glycoprotein, mAbRa96 could ultimately be used to earlier diagnose PDAC with subsequent better clinical outcome.

Disclosure of author financial interest or relationships:
**J. Ring**, None; **T. Shaffer**, None; **A. Ogirala**, None; **L. Cosgrave**, None; **H. Kalthoff**, None; **J. Grimm**, None.

Presentation Number **P105**
Poster Session 1
September 5, 2012 / 18:00-18:00 / Room: The Liffey

# In-tumor self-assembly of a caspase-3-sensitive fluorescent probe provides cancer chemotherapy response monitoring

*Deju Ye, **Adam Shuhendler**, Sui Seng Tee, Lina Cui, Jianghong Rao, Radiology, Stanford University, Stanford, CA, USA. Contact e-mail: adam18@stanford.edu*

Purpose: Apoptosis, or programmed cell death, is vital for a number of physiological functions in multicellular organisms. The dyresgulation of apoptosis is reported to induce many diseases, including autoimmune and neurodegenerative diseases, heart failure, and cancer. Moreover, effective therapy of tumors requires the iatrogenic induction of tumor cell death through apoptosis. It is therefore important to provide noninvasive detection and monitoring of this process in patients undergoing treatment. Capsase-3 has been identified as a key mediator of apoptosis following tumor therapy, therefore, probes to specifically image caspsese-3 activity at early time points would be valuable for therapeutic response monitoring. A caspase-3 fluorescent probe that self-assembles into nanoparticles within tumor tissue has been designed and evaluated, providing a new approach for noninvasive imaging of chemotherapy-induced tumor apoptosis in vitro and in vivo. Methods: The probe (CaspRx) designed here is an iteration of our previous work on intracellular macrocyclization/self-assembly systems derived from the condensation of 2-cyano-6-hydroxyquinoline (CHQ) and free N-terminal cysteine. Upon cleavage of the Ac-DEVD (Ac-Asp-Glu-Val-Asp) linked to N-terminal of cysteine by caspase-3, which is then free to react with the CHQ, the intramolecular macrocyclization increases the hydrophobicity of CaspRx and promotes the self-assembly of likewise activated probes in situ into nanoparticles. The self-assembly of activated CaspRx was characterized with isolated caspase-3 enzyme, in cell culture models of chemotherapy, and in vivo in an animal model of cancer chemotherapy. CaspRx was conjugated to Cy5.5 for probe detection, and fluorescent microscopy and whole animal fluorescent hyperspectral imaging was performed using a CRi Nuance camera on an Olympus IX8 microscope and a CRi Maestro systems, respectively. Results: Upon incubation with caspase-3, CaspRx was activated and demonstrated to macrocyclize and self-assemble into nanoparticle with diameters of less than 100 nm. When incubated with staurosporine-treaed HeLa cells in vitro, CaspRx was found to be preferentially retained to a significantly greater extent in those cells positive for apoptosis relative to the untreated control, and this retention was abolished with the inhibition of caspase-3 prior to probe administration. Following the treatment of HeLa tumor xenografts with doxorubicin and the systemic administration of CaspRx, both the extent of probe accumulation and the retention of the probe were significantly greater in treated versus untreated tumors. Conclusion: The ability to monitor the response of tumors to chemotherapy at the sub-cellular level presents an opportunity to ensure the maintenance of effective therapies and to discontinue ineffective interventions at early time points, avoiding the development of drug resistance and enhancing treatment success rates. Through the molecular imaging results obtained, CaspRX holds great promise as a probe for the detection and monitoring of apoptosis following chemotherapy of cancer.

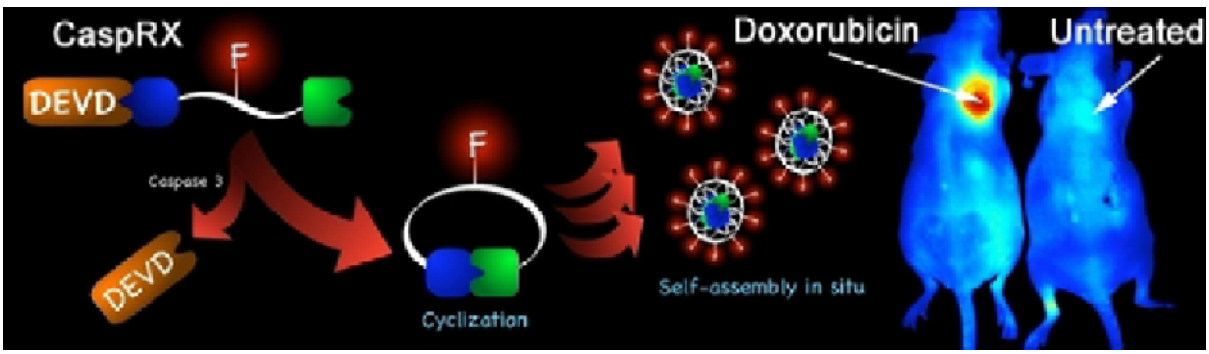


A novel probe, CaspRx, was synthesized with a caspase-3-cleavable moiety (DEVD) opposite to a moiety CHQ (left). Upon uptake and activation by caspase-3, DEVD is released, allowing intramolecular condensation to increase probe hydrophobicity, resulting in intracellular self-assembly into fluorescent nanoparticles. Both in vitro and in vivo, CaspRx is capable of indicating the positive response of a tumor to cancer chemotherapy (right).

Disclosure of author financial interest or relationships:
**D. Ye**, None; **A. Shuhendler**, None; **S. Tee**, None; **L. Cui**, None; **J. Rao**, None.

Presentation Number **P106**
Poster Session 1
September 5, 2012 / 18:00-18:00 / Room: The Liffey

# Quantitative Imaging of Targeted Ultrasound Contrast Agents

***Monica Siepmann***[1], *Jessica Bzyl*[2], *Stanley Fokong*[2], *Fabian Kiessling*[2], *Georg Schmitz*[1], [1]*Medical Engineering, Ruhr-University, Bochum, Germany;* [2]*Experimental Molecular Imaging, RWTH-Aachen University, Aachen, Germany. Contact e-mail: monica.siepmann@rub.de*

Ultrasound has gained interest in the field of molecular imaging in the last decade as it is cheap, widely available and offers real time imaging capability. A primary aim of ultrasound molecular imaging is the assessment of therapy response, which requires a quantification of the adherent contrast agent. Thus far the quantification of the agent was primarily based on the image intensity in different ultrasound imaging modalities. Intensity based quantification, however, requires well defined and constant imaging conditions, allowing only a relative quantification without calibration. The detection and quantification of single microbubbles (MB) presents a huge advance with regard to obtaining absolute quantitative results. The feasibility of absolute quantification by the detection of single MB destruction events is investigated in this work. Phantom and in vivo experiments demonstrate that individual MB can be detected in the ultrasound echoes and allow absolute counting of adherent MB. First, the absolute quantification of MB was tested in 3 gelatine phantoms containing MB in a concentration of 5000 MB/ml. The MB were dispersed in semifluid gelatine and refrigerated until the gelatine was solid. Two grams of silica gel per liter gelatine were added to provide background scattering. The phantoms were scanned with the Vevo2100 small animal imaging system using a 21 MHz transducer (Visualsonics). Scans were performed in the 3D Power Dop-pler mode, recording the digitized IQ-data. Single bubble destruction detection was achieved with a novel detection strategy recently proposed by our group, which is based on the analysis ofthe phase shift variance of the recorded In-phase/Quadrature-data. The detected destruction events were counted, yielding the MB number in the scanned 3D vol-ume and thus the absolute MB concentration. The method was then tested in vivo in animal models. In this context human epidermoid cancer xenografts were induced in the hind limb of three nude mice. The mice were sequentially in-jected a 10^7 MB bolus of two different MB types, experimental cyanoacrylate MB or the commercial agent Micro-marker (Bracco/Visualsonics), both targeted to VEGFR-2. Several minutes after injection, 3D Power Doppler scans were performed and evaluated as described for the phantom experiments above. The acoustic counts yielded an average concentration of 5113 MB/ml in the phantoms. Thus correct absolute quantification could be achieved. The single bubble destruction events were enhanced by up to 50 dB compared to background using the proposed detection method. The in vivo results demonstrate the detection of single targeted microbubbles in the tumor models for both agent types. Pre-contrast scans exhibited false detections of approximately 1 MB/mm^3 only. We conclude that counting of individual MB with the proposed method is feasible. It thus offers great potential in the evaluation of therapy response, which is subject to future investigation.

Disclosure of author financial interest or relationships:
**M. Siepmann**, None; **J. Bzyl**, None; **S. Fokong**, None; **F. Kiessling**, None; **G. Schmitz**, None.

Presentation Number **P107**
Poster Session 1
September 5, 2012 / 18:00-18:00 / Room: The Liffey

# Cyclooxygenase-2 increases the collagen content in the extracellular matrix of triple negative breast tumors and promotes higher vascular permeability

***Ioannis Stasinopoulos***, *Samata M. Kakkad, Marie-France Penet, Flonné B. Wildes, Arvind P. Pathak, Meiyappan Solaiyappan, Zaver M. Bhujwalla, The Russell H. Morgan Department of Radiology and Radiological Science, The Johns Hopkins University, Baltimore, MD, USA. Contact e-mail: istasin1@jhmi.edu*

Introduction: There is increasing evidence to suggest that high density of collagen I fibers in the extracellular matrix (ECM) is a predictor of increased metastasis. Cancer cells have been observed to migrate along these fibers during the metastatic journey. We previously observed that downregulating COX-2 significantly reduced metastasis, decreased expression of degradative enzymes such as matrix metalloproteinase 1, and altered the expression of ECM components such as hyaluronan and lumican that play a role in intra-fibrillar collagen spacing. Here, we have been investigating the role of COX-2 in altering structure and function of the ECM using MRI and second harmonic generation (SHG) microscopic imaging of tumors derived from triple negative breast cancer (TNBC) cells MDA-MB-231 and a derived clone stably expressing short hairpin RNA (shRNA) downregulating COX-2. Methods: Tumors derived from the TNBC cell line MDA-MB-231 and its clone (Clone 13) with lower basal and inducible COX-2 expression levels were imaged in vivo following orthotopic implantation in a mammary fat pad of female SCID mice. Tumors derived from these cells were used to investigate the relationship between COX-2 expression, interstitial fluid transport using MRI and collagen fiber density and volume using SHG microscopy. MRI was performed once tumor volumes were approximately 400-500 mm3. Interstitial transport parameters were measured from quantitative T1 maps obtained before and following intravenous administration of the contrast agent albumin-GdDTPA (500 mg/kg dose) on a 4.7 T Bruker spectrometer. Interstitial transport parameters calculated included number of draining and pooling voxels, draining and pooling rates, and volumes. SHG microscopy of tissue slices was performed using a 25× lens on a Zeiss 710 LSM NLO confocal microscope system equipped with a 680-1080 nm tunable Coherent Chameleon Vision II laser with automated pre-compensation and fast scanning at 40 nm/s. 3D image stacks were acquired from various fields of view. Collagen I fibers were imaged with incident laser light of 880 nm, detected at 410-470 nm. Collagen I fiber distribution was visualized and characterized using an in-house 3D analysis software developed to quantify fiber distance distributions and fiber volumes. Results and Discussion: Significant differences in the ECM structure (Figure 1 top panel), function and vasculature permeability (Figure 1, bottom panel), were evident between COX-2-high MDA-MB-231 tumors compared to COX-2-low Clone 13 tumors, which had less permeable vessels, reduced rates of pooling and draining of the contrast agent, and significantly reduced collagen I content. Here, for the first time, we have shown that downregulating COX-2 in TNBC cells profoundly impacts collagen 1 fiber density and volume and alters macromolecular transport. Understanding the role of COX-2 in TNBC and its impact on the ECM and macromolecular transport may provide new insights into preventing relapse and metastasis. This work supported by R01 CA82337 and P50 CA103175.

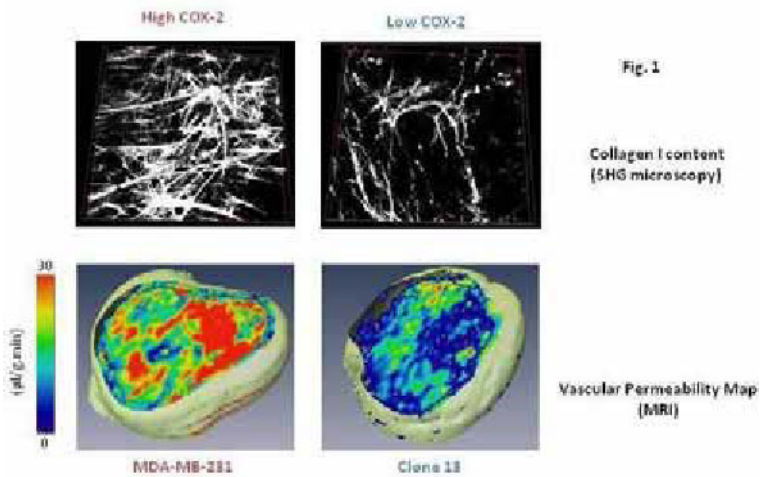


Fig. 1. COX-2 increases the collagen content of the ECM in triple negative breast cancer tumors (top) and promotes increased vascular permeability (bottom). 3D reconstructions of collagen content and vascular permeability maps of COX-2-high parental (left) and derivative COX-2-low (right) breast tumors are shown.

Disclosure of author financial interest or relationships:
**I. Stasinopoulos**, None; **S.M. Kakkad**, None; **M. Penet**, None; **F.B. Wildes**, None; **A.P. Pathak**, None; **M. Solaiyappan**, None; **Z.M. Bhujwalla**, None.

Presentation Number **P108**
Poster Session 1
September 5, 2012 / 18:00-18:00 / Room: The Liffey

# Bioluminescence Imaging and Cerenkov Luminescence Imaging in a Preliminary Investigation on the RETAAD Melanoma Tumor Model

***Jeffrey Steinberg***[1], *Prashant Chandrasekharan*[1], *Jean-Pierre Abastado*[2], *David W. Townsend*[3], [1]*Singapore Bioimaging Consortium, Agency for Science, Technology and Research, Singapore, Singapore;* [2]*Singapore Immunology Network, Agency for Science, Technology and Research, Singapore, Singapore;* [3]*Clinical Imaging Research Centre, Singapore, Singapore. Contact e-mail: jeffrey_steinberg@sbic.a-star.edu.sg*

Introduction In this study RETAAD mice that are transgenic for the human RET oncogene are used. This tumor model will develop spontaneous uveal melanomas which metastasize to various organs, including the skin and the lungs. Use of the RETAAD mice with implanted tumors can accurately model cancers that occur naturally in humans. The importance in using these mice is that while cancer is the leading cause of death in many countries, the mechanism of cause is still not clearly understood. For an appropriate treatment, the detection of the cancer has to be done at an early stage. By imaging the mice at various stages of cancer, the mechanics of the metastases can be modelled. The type of imaging used in this study is in vivo optical imaging, which is a well established tool in pre-clinical research for imaging various biochemical functions and identifying disease pathways. It is used to detect light emitted from bioluminescent materials in a technique known as bioluminescence imaging (BLI). A new technique known as Cerenkov luminescence imaging (CLI), which tracks PET radiotracers with optical imaging, was also used. Materials and Methods RETAAD mice with cutaneous tumors using a B16-luc cell line are used for the study. Each mouse is held for a period of 4 months to allow time for the spontaneous tumors to form. On the scan day, the mice are injected with D-luciferin substrate and held for 20-30 minutes before scanning. Then, it is placed inside the Caliper In Vivo Imaging System (IVIS) Spectrum. Several snapshots are taken in bioluminescence mode from various angles as well as a photograph with normal lighting for registration of the images. On a subsequent day, CLI was performed by imaging the mouse one hour after injection of 18-FDG. Results and Discussion Images demonstrating the metastases formed on the spontaneous tumor model are shown in the figure. As expected, the RETAAD mice spontaneously developed uveal melanomas which metastasized to various organs. Multiple cutaneous metastases are observed along the shoulder and flank. Also, visceral metastases occur in the abdominal region. Although not easily observed from the images, metastases also formed in the lungs. CLI was successful in correctly identifying the uveal and cutaneous metastases, and the results were comparable to BLI. Conclusion The RETAAD tumor model provides opportunities for researchers to observe metastatic growth of injected tumor cells. BLI is an appropriate imaging modality for measuring metastatic growth in this model due to metastases forming near the surface, such as in the eyes and skin. However, detection of visceral and lung metastases are less clear due to the depth of the source, but BLI is still sufficient for detection. CLI provides an alternative method to BLI for detecting metastases, but it is unclear whether the higher experimental cost of CLI is justified.

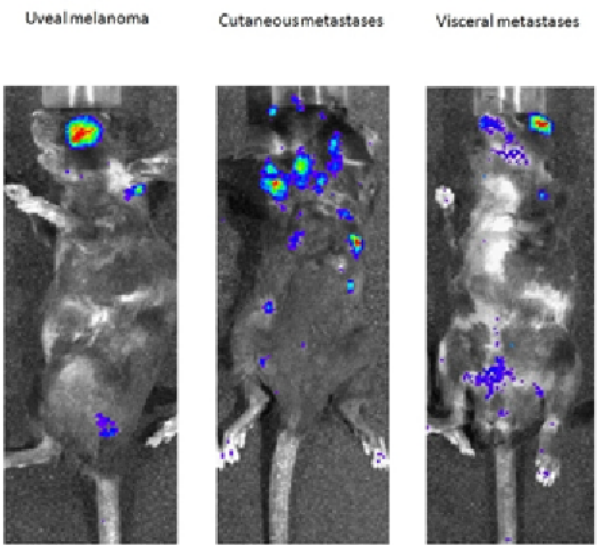


Disclosure of author financial interest or relationships:
**J. Steinberg**, None; **P. Chandrasekharan**, None; **J. Abastado**, None; **D.W. Townsend**, Siemens Healthcare, Other financial or material support .

Presentation Number **P109**
Poster Session 1
September 5, 2012 / 18:00-18:00 / Room: The Liffey

# Comparing Ultrasound Molecular Imaging, Perfusion Imaging, and Volume Measurements in Monitoring the Response to Therapy for Human Pancreatic Adenocarcinoma Tumorgrafts

***Jason E. Streeter***[1], *Silvia G. Herrera*[2], *Kennita A. Johnson*[1], *Joey Cao*[2], *Jen Jen Yeh*[2], *Paul A. Dayton*[1], [1]*Joint Dept of Biomedical Engineering, University of North Carolina-North Carolina State University, Chapel Hill, NC, USA;* [2]*Lineberger Cancer Center, University of North Carolina, Chapel Hill, NC, USA. Contact e-mail: jason.streeter@unc.edu*

Most pre-clinical drug trials use the change in tumor volume as the primary indicator for monitoring the response to therapy. However, tumor size measurements can be relatively inaccurate, and alone, may not reflect early changes in tumor physiology that occur as a response to treatment. Ultrasonic molecular imaging (USMI) and Dynamic Contrast Enhanced - Perfusion Imaging (DCE-PI) are two attractive alternatives to using tumor volume measurements. Since these techniques can provide information prior to the appearance of gross phenotypic changes, it has been proposed that USMI and DCE-PI could be used non-invasively to assess the response of a tumor to treatment at earlier time points than traditional methods. This study evaluated the efficacy of three different techniques, including tumor volume measurements, DEC-PI, and USMI, to predict the response to therapy in pre-clinical studies over a 14-day period. In this study, 10 nude mice with patient-derived tumorgrafts were used for both USMI and DCE-PI experiments. For each imaging technique, 5 animals received a dose of 30 mg/kg of MLN8237, an aurora kinase inhibitor, each day over a 14-day period while the remaining animals were treated with a control vehicle. Volumetric USMI was performed on day 1, day 3 and day 8 using size-selected microbubble contrast agents (MCAs) fitted with a cyclic RGD peptide, which targets the angiogenic integrin, αvβ3. Similarly, volumetric DCE-PI was performed on day 1, day 4, day 8 and day 14 using continuously infused non-targeted microbubbles. Volume measurements were assessed with ultrasound on day 1, day 4, day 8 and day 14. For USMI, Day 3 was the earliest point at which there was a statistical difference between the untreated and treated populations (Untreated: 0.92 ± 0.22 vs. Treated: 0.38 ± 0.23; $p < 0.05$). In contrast, statistically significant differences between the untreated and treated populations as monitored by DCE-PI were not detected until the Day 8 readpoint (Untreated: 1.07 ± 0.13 vs. Treated: 1.46 ± 0.57; $p = 0.05$). Finally, the volume measurements alone suggested that there were no statistical differences between treated and untreated populations at either day 3, 8, or 14. However, our data illustrates that volumetric tumor growth rates from treated animals typically begin to differ significantly after approximately two weeks. In conclusion, the USMI technique demonstrated that significant changes could be detected in the expression of angiogenic biomarkers in pancreatic adenocarcinoma patient-derived tumorgrafts in mice, in response to MLN8237 within 48 hours of treatment. In contrast, the DCE-PI technique showed significant changes after 7 days of treatment. Volume measurements showed no statistical differences between the treated and untreated populations at any readpoint over the 14-day period. Monitoring volumetric changes is the "gold standard" for evaluating treatment, however, our data suggests that USMI and DCE-PI may be viable alternatives to more traditional methods of measuring response to therapy.

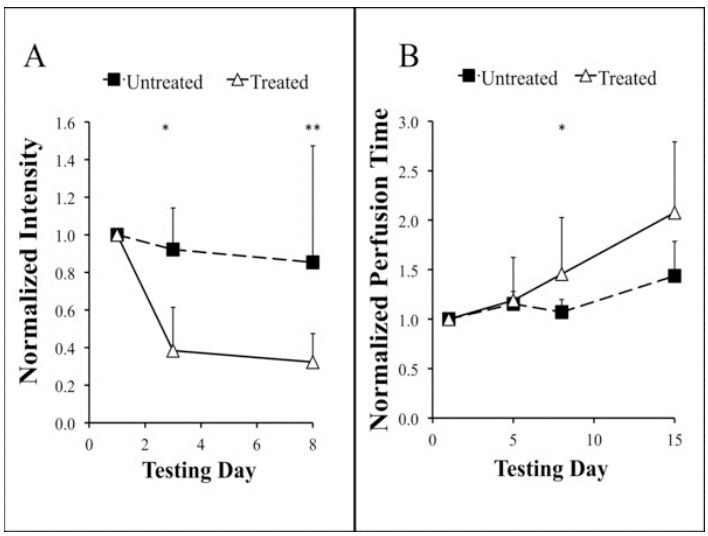


A) The percent change in volumetric targeted microbubble intensity for treated and untreated animals before and after therapy (N = 5). B) The average volumetric perfusion times before and after therapy for treated and untreated animals (N=5). * $p < 0.05$ and ** $p = 0.05$

Disclosure of author financial interest or relationships:
**J.E. Streeter**, None; **S.G. Herrera**, None; **K.A. Johnson**, None; **J. Cao**, None; **J. Yeh**, None; **P.A. Dayton**, Targeson, Inc., Consultant; National Institutes of Health, Grant/research support; Dept of Defense, Grant/research support; Siemens, Other financial or material support .

Presentation Number **P110**
Poster Session 1
September 5, 2012 / 18:00-18:00 / Room: The Liffey

# Development of a Near-infrared Fluorescent Melanocortin Receptor 1 Probe for Molecular Imaging of Melanoma

*Narges K. Tafreshi[1], Natalie M. Barkey[1], Timothy W. McCardle[2], Steven Enkemann[3], Veronica Estrella[1], Tingan Chen[4], Josef Vagner[5], Ariosto Silva[1], **David L. Morse**[1], [1]Cancer Imaging and Metabolism, Moffitt Cancer Center, Tampa, FL, USA; [2]Anatomic Pathology, Moffitt Cancer Center, Tampa, FL, USA; [3]Molecular Genomics, Moffitt Cancer Center, Tampa, FL, USA; [4]Analytic Microscopy Shared Resources, Moffitt Cancer Center, Tampa, FL, USA; [5]BIO5 Institute, University of Arizona, Tucson, AZ, USA. Contact e-mail: david.morse@moffitt.org*

Accurate determination of regional lymph node status is important for both prognostic evaluation and treatment planning in melanoma patients. The Melanocortin 1 receptor (MC1R) is overexpressed in most melanoma metastases, thus making it a promising target for imaging and therapy of melanomas. In this study, using DNA and tissue microarrays of normal tissues and patient samples of melanoma, the expression of MC1R in a large fraction of melanoma patients was confirmed. We have previously reported the development of a peptidomimetic ligand with high affinity for MC1R, and low affinity for MC4R and MC5R. Here, we have conjugated this ligand to a near-infrared fluorescent (FI) dye to generate a 2254 MW MC1R-specific optical probe (MC1R-800: 4-phenylbutyryl-His-(D)Phe-Arg-Trp-Gly-Lys(IRDye800CW-MPA)-NH2). Using A375 human melanoma cells engineered to overexpress MC1R and our in cyto binding assay, the binding affinity of MC1R-800 was determined to be high (0.4 ± 0.1 nM Ki). A375 cellular uptake of the probe was studied in vitro by FI microscopy. To study uptake of the probe into tumor cells in vivo, intravital confocal FI microscopy was performed using an A375/MC1R cell dorsal skin-fold window chamber tumor model. Probe extravasation, penetration into the tumor, and tumor cell binding and uptake was observed over a post-injection time-course. At 5 min to 2 hr after injection, most of the MC1R probe was observed on the surface of the tumor cells, while at 24 hr post-injection, the tumor cells had internalized the probe (Figure 1A). The in vivo tumor targeting of MC1R-800 was evaluated by i.v. injection of probe into nude mice bearing bilateral subcutaneous A375 tumors with low MC1R receptor number and engineered A375/MC1R cells. FI imaging showed that the agent had higher uptake values in tumors with high expression compared to low ($P<0.05$), demonstrating the effect of expression levels on signal intensity (Figure 1B, control). In addition, the tumor uptake was significantly blocked by co-injection with excess NDP-α-MSH peptide ($P<0.05$), indicating specificity of the probe in vivo (Figure 1B, blocking). The biodistribution of MC1R-800 was investigated in tumor bearing mice, showing high kidney uptake as early as 30 min post-injection. As kidney is known to express the MC5R, kidney uptake of the probe was reduced significantly ($P<0.05$) by co-injection of a ligand we previously determined to have higher MC5R affinity compared to MC1R. The pharmacokinetics of probe uptake and clearance was characterized using a three-compartment mathematical model, which includes tumor, kidney and mouse volumes, and assumes mass conservation of the ligand. This model was used to account for the interference of the tumor ligand release in the uptake and clearance dynamics of blood and kidneys. While this effect is negligible in humans, it is significant in mouse models. In conclusion, the imaging probe designed in this study demonstrates the potential for development of agents that can deliver imaging contrast and therapy to melanoma metastases that express MC1R.

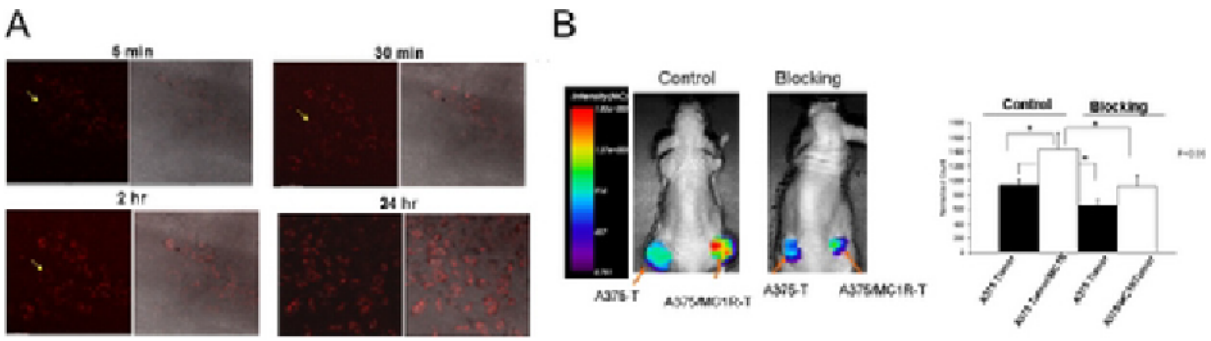


Figure 1. A) Intravital tumor cell uptake studies of the MC1R-800 probe using the dorsal skin-fold window chamber xenograft tumor model by confocal flouresence microscopy (left) with overlay of fluorescence signal on visible light images of cells (right). B) In vivo tumor targeting of MC1R-800. Representative image of normalized FI intensity maps of a mouse bearing xenograft tumors, 2 hr post i.v. injection of the probe (left mouse): A375 with low expression level of MC1R and A375/MC1R with high level of MC1R expression were used to form left and right flank tumors, respectively. A blocking experiment was performed using co-injection of 0.25 µg unlabeled NDP-α-MSH and 5 nmol/kg of the MC1R-800 probe to determine target specificity (right mouse). Inset shows the quantification of MC1R-800 normalized FI count of low and high expressing tumors in control and blocking animals. Data represent mean ± s.d. NC= Normalized Count

Disclosure of author financial interest or relationships:
**N.K. Tafreshi**, None; **N.M. Barkey**, Intezyne Technologies, Inc, Other financial or material support; **T.W. McCardle**, None; **S. Enkemann**, None; **V. Estrella**, None; **T. Chen**, None; **J. Vagner**, None; **A. Silva**, None; **D.L. Morse**, LiCor, Other financial or material support; Intezyne Technologies, Other financial or material support .

Presentation Number **P111**
Poster Session 1
September 5, 2012 / 18:00-18:00 / Room: The Liffey

# In Vtro and In Vivo Stability of 64Cu-labeled Trastuzumab in Blood in Mice

***Kazuhiro Takahashi****, Riyo Zochi, Koki Hasegawa, Shusaku Tazawa, Yoko Morimoto, Yasuyoshi Watanabe, CMIS, RIKEN, Kobe, Japan. Contact e-mail: kazu.takahashi@riken.jp*

Background: Targeting of HER2 with anti-HER2 antibody trastuzumab is a well-established strategy in the metastatic and adjuvant setting in HER2 positive breast cancer. For effective usage of antibodies, confirmation of the sufficient expression of HER2 in cancer tissue is required. Recently, the development of non-invasive molecular imaging method for defining the antigen expression is proceeding worldwide, alternative to invasive diagnostic biopsies. In previous studies, we established 64Cu-labeling method of HER2 and successfully obtained the PET images in which high activity was accumulated in target tumor. However, the clearance of radioactivity in blood is very slow. Therefore it is possible that uptakes in tissues depend on 64Cu released from DOTA chelate ,which is easily chelating with serum albumin. In order to estimate tissue uptakes of 64Cu- DOTA- trastuzumab, it is important whether the radioactivity in blood is 64Cu- DOTA- trastuzumab or not. Method: Anti-HER2 antibody trastuzumab were conjugated with chelating agent DOTA, and then reacted with 64CuCl2. After purification, 64Cu-DOTA- trastuzumab were obtained. At first, the produced 64Cu-DOTA- trastuzumab were incubated with mice blood for 6h, 12h and 24h.The second, the produced 64Cu-DOTA- trastuzumab was intravenously injected to BALB/c nu/nu mice. Blood samples were collected after 24h. The blood samples was centrifuged, and each plasma fraction and the original injected solution were treated to SDS page, and the gels were stained with CBB and performed on autoradiography with IP. Results: Each autoradiogram of gels from in vitro or in vivo study shows only single band of 148 kDa corresponds to trastuzumab, which was the same position of original 64Cu-DOTA- trastuzumab . And there is no band of 66 kDa corresponds to serum albumin. (Fig. 1)Conclusions: These results strongly suggests that most of 64Cu radioactivity in blood at 24 hours after injection is only 64Cu-labeled trastuzumab in living mice.

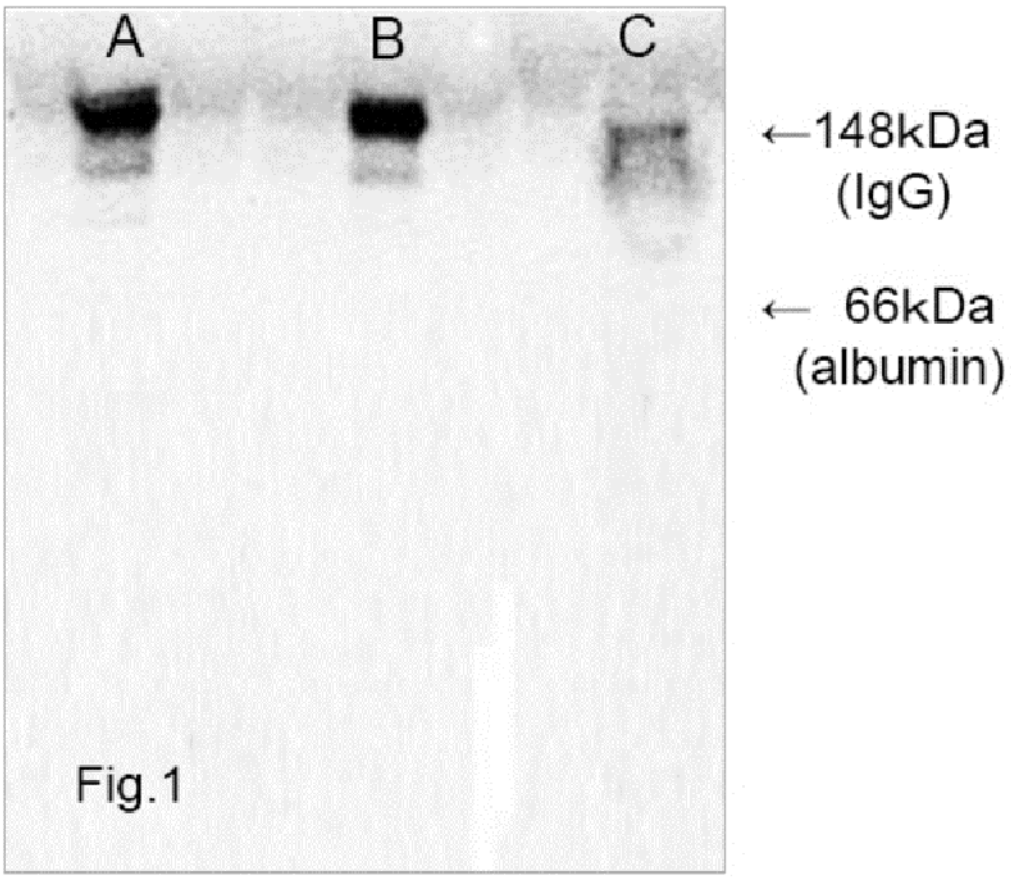


Fig.1. Autoradiogram from *in vivo* study. A: Original $^{64}$Cu-DOTA- trastuzumab. B: 5.6 MBq injection in mice. C: 5.6 kBq injection in mice.

Disclosure of author financial interest or relationships:
**K. Takahashi**, None; **R. Zochi**, None; **K. Hasegawa**, None; **S. Tazawa**, None; **Y. Morimoto**, None; **Y. Watanabe**, None.

Presentation Number **P112**
Poster Session 1
September 5, 2012 / 18:00-18:00 / Room: The Liffey

# Monitoring anti-angiogenic therapy with BR55, a VEGFR2 targeted ultrasound contrast agent

***Isabelle Tardy***, *Jean-Marc Hyvelin, Sibylle Pochon, Martine Theraulaz, Alexandre Helbert, Jeanneret Virginie, Lucille Valle, Mathew Von Wronski, Francois Tranquart, Bracco Suisse SA, Plan-les-Ouates, Switzerland. Contact e-mail: isabelle.tardy@brg.bracco.com*

Purpose: Ultrasound molecular imaging (USMI) allows assessment of both perfusion and molecular marker expression in tumors during longitudinal growth or during the monitoring of various treatments such as anti-angiogenic drugs. Tumoral vascular growth is triggered by different pro-angiogenic factors. Molecular imaging of these markers could predict the response to anti-angiogenic treatment at a very early stage possibly before any vascular changes. BR55, an ultrasound contrast agent designed for molecular imaging of human VEGFR2 (KDR), is functionalized with a heterodimer peptide that binds to KDR with high affinity. We tested the hypothesis that performing USMI with BR55 might be more predictive of anti-angiogenic treatment efficacy than changes in tumor volume. Methods and Materials: Spontaneous rat mammary tumor model (N-nitroso-N-methylurea treatment) and rat prostate tumor model (orthotopic implantation of G - Dunning R-3327 cells) were used. When tumor cross-sectional areas reached 0.4 cm2 (prostate tumor) or 1.5 cm2 (mammary tumor), animals received an anti-angiogenic treatment (sunitinib, LC-Laboratories, Woburn MA). Tumor response was monitored by USMI over a 10-day period. Contrast enhancement was quantified (from DICOM files) using a software package developed in-house. Time-intensity curves generated from linearized data were used to determine perfusion estimates during the initial wash-in phase. Targeted contrast enhancement due to bound BR55 microbubbles was assessed 10 minutes after BR55 injection. Perfusion parameters were measured in one scan plane across the largest section of the tumor, whereas BR55 binding was assessed for the whole tumor by moving the probe in 1mm steps from one tumor pole to the other one, 10 min after injection. Immunohistochemistry staining on both rat tumors was performed to assess the expression of VEGFR2. Results: Before treatment, tumors were highly perfused and VEGFR2 expression, assessed by BR55 binding, was well highlighted in the 3D volume of the tumor. Moreover, immunohistochemistry revealed a high expression of VEGFR2 in the tumor in agreement with a high binding of BR55 bubbles. Following treatment with sunitinib, parameters related to perfusion, BR55 binding and tumor size decreased in Dunning tumor model: the decrease of both perfusion parameter (30%) and BR55 binding (55%) appeared already one day after treatment and was more pronounced than morphological changes (10%). Furthermore, the decrease in BR55 binding was steeper and more consistent than perfusion changes throughout the treatment course. Similar results were obtained with NMU mammary tumor. Conclusion: These data suggest that ultrasound molecular imaging with BR55, a specific angiogenesis marker, is highly predictive of tumor response to anti-angiogenic treatment.

Disclosure of author financial interest or relationships:
**I. Tardy**, Bracco Suisse SA, Employment; **J. Hyvelin**, Bracco Suisse SA, Employment; **S. Pochon**, Bracco Suisse, Employment; **M. Theraulaz**, Bracco Suisse, Employment; **A. Helbert**, Bracco Suisse SA, Employment; **J. Virginie**, Bracco Suisse SA, Employment; **L. Valle**, None; **M. Von Wronski**, Bracco Suisse, Employment; **F. Tranquart**, Bracco Suisse SA, Employment .

Presentation Number **P113**
Poster Session 1
September 5, 2012 / 18:00-18:00 / Room: The Liffey

# Development of potent somatostatin antagonists for translational nuclear imaging of GRPr-positive tumor

***Xuejuan Wang***, *Peking University School of Oncology, Beijing Caner Hospital, Beijing, China. Contact e-mail: xuejuan_wang@hotmail.com*

Targeting of somatostatin receptor positive tumors with radiolabeled peptides is of interest for tumor localization, staging, therapy follow up and targeted radionuclide therapy. First clinical trial demonstrated the feasibility of imaging of neuroendocrine tumors (NETs) with somatostatin receptor (sstr) antagonist, and also revealed much higher imaging quality of sstr antagonist than that of agonist. The aim of this study is to continue developing more favourable sstr antagonists for somatostatin receptor-guided imaging and therapy. Methods: A potential sstr2-selective antagonists, JR6-8, were synthesized and coupled with the chelator (DOTA) for labeling with 111In. Binding affinity and tumor targeting were studied in HEK-sstr2 cell and tumors-bearing nude mice. Findings were compared with the published sstr2 antagonist 111In-DOTA-BASS. Results: All of antagonists in this study showed high and selective sstr2-binding affinities. Scatchard plots showed that all of four antagonists labeled many more sites than the sst2-selective agonist. In the sstr2-expressing tumors, similar specific accumulation of 111In-DOTA-JR6, 111In-DOTA-JR7 and 111In-DOTA-JR8 were observed, and the maximum tumor uptake was 28.21±3.94 %IA/g, 29.38±3.19 %IA/g, and 28.41±2.98 %IA/g at 4 h, comparing to 29.12 ± 3.90% IA/g of 111In-DOTA-BASS. However, tumor-to-kidney ratios of 111In-DOTA-JR6-8 were higher than that of 111In-DOTA-BASS. Conclusion: All of sstr2-selective antagonists in this study are as potent as 111In-DOTA-BASS, and will be another antagonist candidates for NETs targeting.

Disclosure of author financial interest or relationships:
**X. Wang**, None.

Presentation Number **P114**
Poster Session 1
September 5, 2012 / 18:00-18:00 / Room: The Liffey

# FDG-PET for Detection of Spontaneous Malignant Peripheral Nerve Sheath Tumors in a Transgenic Animal Model

***Jason Warram***[1], *Amber Martin*[1], *Amy Turk*[2], *Steven Carroll*[2], *Kurt R. Zinn*[1], [1]*Radiology, University of Alabama at Birmingham, Birmingham, AL, USA;* [2]*Neuropathology, University of Alabama at Birmingham, Birmingham, AL, USA. Contact e-mail: mojack@uab.edu*

Peripheral nerve sheath tumors are commonly detected by imaging using Magnetic Resonance (MR), Computed Tomography (CT), and plain film radiography. These imaging strategies lack sensitivity to distinguish benign from malignant tumors, important considering 90% of those diagnosed using tumor biopsy are shown to be benign. With the ability to sensitively detect and monitor metabolic activity in tumors, we hypothesize that Positron Emission Tomography (PET) following F-18-Fluorodeoxyglucose (FDG) could be used for the sensitive detection and pre-operative planning in patients with Malignant Peripheral Nerve Sheath Tumors (MPNST). To evaluate this hypothesis, a transgenic mouse model was generated overexpressing the NRG-1 isoform glial growth factor β3 (GGF β3) in myelinating Schwann cells on a heterozygous p53 absent background [protein zero (P0)- GGF β3: p53-/+ mice]. These mice develop hypertrophic neuropathy and MPNST in the trigeminal nerve ganglion (TNG) and dorsal root ganglion (DRG). Symptoms are first observed at 7 months of age and include resting tremors, gait abnormalities, decreased hind limb strength, and paralysis. FDG-PET imaging studies were performed to monitor the spontaneous development of MPNST in P0-GGFβ3:p53-/+ mice (N=11). Imaging was performed monthly beginning at 60 days of age. Mice were dosed with 200uCi FDG 60min pre-imaging and then imaged using a Flex Triumph PET/CT system. Image analysis was performed using Osirix 64-bit software. Mice were sacrificed at first sign of neuropathic symptoms (days 200-210) and tissues collected for histology. In the 11 mice serially imaged, FDG uptake was observed in the lumbar DRG in 5 mice as early as 81 days of age. Uptake was seen in the thoracic DRG in 4 mice as early as 103 days of age. FDG uptake in the TNG was also observed as early as 65 days of age in all mice. Histology was performed to confirm the presence of MPNST in these tissues. FDG-PET sensitively detected MPNST at an early stage in this transgenic model.

Disclosure of author financial interest or relationships:
**J. Warram**, None; **A. Martin**, None; **A. Turk**, None; **S. Carroll**, None; **K.R. Zinn**, None.

Presentation Number **P115**
Poster Session 1
September 5, 2012 / 18:00-18:00 / Room: The Liffey

# Tumor Invasion of Microglia/Macrophages and Astrocytes after ErPC3 Treatment in a Rat Glioma Model

*Ali R. Awde[1,3], Raphael Boisgard[1,3], Benoit Theze[1,3], Bertrand Tavitian[2], **Alexandra Winkeler**[1,3], [1]CEA/DSV/I2BM/SHFJ, Orsay, France; [2]CEA/DSV/I2BM, Orsay, France; [3]Inserm U1023, Université Paris Sud, Orsay, France. Contact e-mail: alexandra.winkeler@cea.fr*

Introduction: Glioblastoma multiforme (GMB) is the most malignant type of primary human brain tumor. Currently available GBM treatments are not particularly effective. Conventional treatment failure results from 1) the limitations of surgery, as tumor resection can only be performed if the patient's safety can be guaranteed, 2) the highly invasive nature of malignant glioma cells and 3) the strong resistance of gliomas to chemo- and/or radiotherapy. Gliomas are not exclusively composed of cancer cells but also of cells of the tumor microenvironment (TME), i.e. endothelial cells, immune cells and fibroblasts. Recently, it has become clear that the TME plays an important role in both disease progression and response to therapy. The alkylphosphocholine erufosine (ErPC3) has been shown to induce apoptosis in otherwise highly apoptosis-resistant glioma cell lines. Lately, we analyzed the effect of ErPC3 in a rat glioma model and demonstrated anti-neoplastic activity and apoptosis induction in 9L tumors in vitro and in vivo. Here, we investigated the effect of ErPC3 treatment on cells of the TME, in particular microglia/macrophages and astrocytes. Methods: 9L rat glioma cells were stereotactically implanted in the striatum of Fischer rats. ErPC3 treatment was started 11 days after tumor implantation and continued for 2 weeks with intraperitoneal injections of ErPC3 (40mg/kg body weight) every 48h. For immunohistochemical labeling, brains of glioma-bearing rats were frozen in isopentane and 20 µm-thick coronal brain sections were prepared on a cryostat. TUNEL staining to assess apoptotic cells was carried out in combination with immunostaining for the translocator protein 18kDa (TSPO), known to be over-expressed in GBM and activated glial cells. In order to investigate the presence of activated microglia/macrophages and astrocytes within the glioma, we performed multiple immunolabeling for TSPO, CD11b and glial fibrillary acidic protein (GFAP) as marker for TSPO positive cells, microglia/macrophages and astrocytes, respectively. Results: 9L glioma tumors grown in Fischer rats demonstrated strong expression of TSPO mostly restricted within the tumor in ErPC3 treated and mock-treated animals. However, ErPC3 medication yielded a decrease in TSPO signal that corresponded to TUNEL-positive areas. Furthermore, ErPC3 treatment showed an increase in CD11b-positive cells within the tumor core in comparison to mock-treated rats. A similar result was found for GFAP-positive cells, where numerous GFAP-positive cells were present within the tumor core of drug treated animals. In control injected rats CD11b and GFAP signal was mainly found at the tumor border. Conclusions: ErPC3 medication provokes increased apoptosis and a change in the TME with a strong infiltration of microglia/macrophages and astrocytes in 9L gliomas. Acknowledgement: This work has been supported by the Joint INCa / DAAD Translational Research Programme on Cancer. The authors are grateful to Dr. M. Higuchi for providing the anti-TSPO antibody NP155 and Genzyme for providing erufosine.

Disclosure of author financial interest or relationships:
**A.R. Awde**, None; **R. Boisgard**, None; **B. Theze**, None; **B. Tavitian**, None; **A. Winkeler**, None.

Presentation Number **P116**
Poster Session 1
September 5, 2012 / 18:00-18:00 / Room: The Liffey

# In vivo 1.5T 1H-MRS of human gallbladder bile: value exploration in hepatobiliary disease

*Xiaofeng Chen, Zhiwei Shen, Zhen Cao, Yan Lin, Miaomiao Zhang,* ***Renhua Wu****, Yeyu Xiao, Shantou University, Shantou, China.*
*Contact e-mail: rhwu@stu.edu.cn*

Objective To observe the manifestation and to explore the application value of the in vivo gallbladder bile 1H-MRS in the hepatobiliary desease especially in the malignant liver tumor according to the 1.5T 1H-MRS imaging study of humam gallbladder bile in the healthy volunteers and the patients with benign or malignant hepatobiliary desease. Objects and Methods Conventional T1WI and T2WI of liver and 1H-MRS of gallbladder bile were done on 11 healthy volunteers,8 patients with benign hepatobiliary diseases and 6 patients with malignant liver tumor. The conventional T1WI and T2WI of liver were read and analysed blinded by two experienced radiology doctors. The spectrum data was processed with the LCModel software,and then to read, calculate all the metabolite peak areas and metabolite peak area ratios. The experimental data was input and analyzed by SPSS17.0 statistics software. Results 1.Human gallbladder bile metabolites could be detected by using in vivo 1.5T 1H-MRS.The methyl peak of cholesterol and total bile acids(TBAs) at 0.9ppm, the methylene peak of lipids at 1.3ppm, the trimethylamine peak of phosphatidylcholine(PtC) at 3.2ppm and the water peak at 4.7ppm were observed in all of the spectrums. 2.In the control group,there were no statistical difference in different gender and different age about the 3 main metabolite peak areas:A(-CH3),A(-CH2-),A(-N(CH3)3) and 4 metabolite peak area ratios: A(-CH3)/A(Water),A(-CH2-)/A(Water),A(-N(CH3)3)/A(Water),A(-N(CH3)3)/A(-CH3)(all P>0.05). 3.There was statistical difference between the malignant group and the control group about A(-CH3)(P<0.05), it was lower in the malignant group than in the benign and the control group.And there were statistical differences between the malignant group and the control group also between the malignant group and the benign group about A(-CH3)/A(Water) and A(-N(CH3)3)/A(-CH3) (all P<0.05), A(-CH3)/A(Water) was lower but A(-N(CH3)3)/A(-CH3) was higher in the malignant group than in the other two groups. 4.The area under the ROC curve of the A(-CH3),A(-CH3)/A(Water) and A(-N(CH3)3)/A(-CH3) in diagnosis the malignant liver tumor were 0.812(P=0.038),0.859(P=0.017) and 0.929(P=0.004) respectively,all of them had certain diagnostic capability, and the diagnostic capability of A(-N(CH3)3)/A(-CH3) was highest,0.77 was the best critical point,its specificity were high(94.1%) but sensitivity slightly Low(80.0%). Conclusion 1. It was feasibile to detect human gallbladder bile metabolites by using in vivo 1.5T 1H-MRS,a number of metabolites peaks of gallbladder bile were detected. 2.In the control group,there were no obvious influence on the manifestation of in vivo 1H-MRS of gallbladder bile in different gender and different age. 3.The relative concentration of cholesterol,TBAs and PtC were descending in the malignant group,and the descending of cholesterol and TBAs were more apparent. 4.A(-CH3),A(-CH3)/A(Water) and A(-N(CH3)3)/A(-CH3) can be used as the diagnostic index of liver malignant tumor,and the diagnostic capability of A(-N(CH3)3)/A(-CH3) was highest.

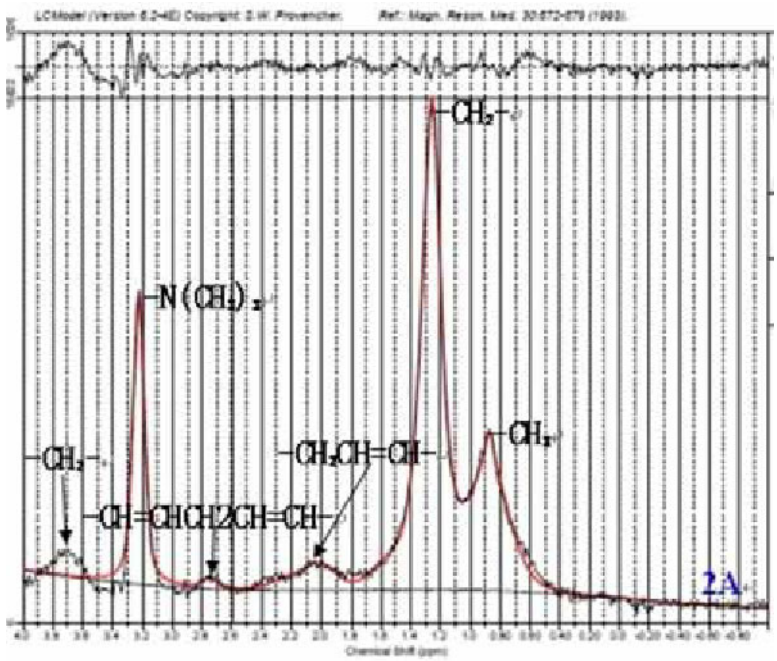


The in vivo 1H-MRS of gallbladder bile that use-suppressed of water

Disclosure of author financial interest or relationships:
**X. Chen**, None; **Z. Shen**, None; **Z. Cao**, None; **Y. Lin**, None; **M. Zhang**, None; **R. Wu**, None; **Y. Xiao**, None.

Presentation Number **P117**
Poster Session 1
September 5, 2012 / 18:00-18:00 / Room: The Liffey

# In vivo and in vitro evaluation of [$^{18}$F]F-GAZ, a novel hybrid radiotracer for imaging tumor hypoxia

***Melinda Wuest***, *Piyush Kumar, Monica Wang, Jennifer Yang, Hans-Soenke Jans, Leonard I. Wiebe, Dept. of Oncology, University of Alberta; Cross Cancer Institute, Edmonton, AB, Canada. Contact e-mail: mwuest@ualberta.ca*

**Aim:**To date all clinical PET radiotracers for imaging tumor hypoxia are only passively transported through the cell membrane leading to longer uptake, retention and imaging times based on slow background clearance. Specifically 2-nitroimidazoles (2-NIs) require more than 2h post injection in a patient until sufficient uptake levels in the target area together with optimal clearance from non-target tissues are reached. Several approaches have been attempted to overcome this problem, including conjugating 2-NIs to FDG, ATSM, tyrosine or peptides. The purpose of this study was to develop a novel azomycin-glucose conjugate (N-(2-[$^{18}$F]fluoro-3-(6-O-glucosyl)propyl-azomycin, [$^{18}$F]F-GAZ), and evaluate its uptake profile in vitro and in vivo. **Materials and Methods:** [$^{18}$F]F-GAZ was synthesized from its tetraacetyl nosylate precursor by nucleophilic radiofluorination. [$^{18}$F]F-GAZ was evaluated in vivo with EMT-6 tumor-bearing Balb/C mice utilizing both PET and biodistribution analysis. In vitro uptake of [$^{18}$F]FDG by EMT-6 cells was measured in the presence of unlabeled F-GAZ, 2-FDG and D-glucose. **Results:** In vivo, [$^{18}$F]F-GAZ was rapidly cleared from all tissues including the blood pool and kidneys, with ultimate accumulation in the urinary bladder. Uptake of tracer doses of [$^{18}$F]F-GAZ in EMT-6 tumors was fast, reaching a standardized uptake value (SUV) of 0.66 ± 0.05 within 5-6 min post injection that decreased to 0.24 ± 0.04 by 60 min post injection (n=6). A tumor-muscle ratio of 1.87 ± 0.18 was observed after 60 min. Total uptake of [$^{18}$F]F-GAZ in tumors (60 min) amounted to 1.25 ± 0.15 %ID/g versus 0.61 ± 0.14 %ID/g (n=4) in muscle. Similar biodistribution and excretion were observed using carrier-added (100 mg/kg) doses of F-GAZ. In vitro, D-glucose and unlabeled 2-FDG were two orders of magnitude more potent than F-GAZ as competitive inhibitors of [$^{18}$F]FDG uptake into EMT-6 cells: $IC_{50}$ 210 ± 20 μM for 2-FDG and 37 ± 4 mM for F-GAZ, respectively. **Conclusion:** Besides its interaction with glucose transporters, F-GAZ seems to be less transported in vivo in the presence of glucose. Interestingly, compared to FAZA less intracellular trapping of [$^{18}$F]F-GAZ was detected in tumor tissue. Its low in vivo toxicity and substantial retention in tumor tissue - as observed at high doses of F-GAZ - do provide rationale for further testing as a radiosensitizer for external beam radiation therapy of radioresistant hypoxic tumors.

Disclosure of author financial interest or relationships:
**M. Wuest**, None; **P. Kumar**, None; **M. Wang**, None; **J. Yang**, None; **H. Jans**, None; **L.I. Wiebe**, None.

Presentation Number **P118**
Poster Session 1
September 5, 2012 / 18:00-18:00 / Room: The Liffey

# Early therapy assessment of combined TRA-8 and carboplatin in triple-negative breast cancer mouse models using diffusion-weighted imaging and 1H MR spectroscopy

***Guihua Zhai***[1], *Hyunki Kim*[1,2], *David Sarver*[3], *Sharon Samuel*[1], *Lee Whitworth*[1], *Kurt R. Zinn*[1,2], [1]*Radiology, UAB, Birmingham, AL, USA;* [2]*Comprehensive Cancer Center, UAB, Birmingham, AL, USA;* [3]*Medicine, UAB, Birmingham, AL, USA. Contact e-mail: Guihua.Zhai@ccc.uab.edu*

Purpose: To measure the early therapy response of an anti-DR5 antibody, TRA-8, in combination with carboplatin using diffusion-weighted imaging (DWI) and single voxel 1H MR spectroscopy (MRS) in triple-negative breast-cancer mouse models. Methods: Eight groups (n=4-5 per group) of nude mice were used; groups 1-4 (or groups 5-8) were bearing subcutaneous 2LMP (or SUM159) tumor xenografts. Groups 1-4 (or groups 5-8) were injected with PBS (served as control), carboplatin (30mg/kg i.p.), TRA-8 (0.2mg, i.p.), and combination, respectively. TRA-8 was administrated on days 0 and 3, while carboplatin was administrated on day 1. DWI, MRS and anatomical MR imaging were performed on days 0, 3, and 7. Apparent-diffusion coefficient (ADC) of tumor regions, fat-water ratio in a voxel within the tumor, and tumor-volume measurements were made among groups 1-8 over 7 days, and statistically analyzed using one-way analysis of variance (ANOVA). Results: For groups 1-4, the ADC changes were -10.9±4.5% (mean±SE), -0.7±2.3%, 4.7±4.9%, and 7.1±5.8% on day 3, and -10.6±1.8%, 9.2±3.0%, 1.8±9.1%, and 4.0±4.0% on day 7, relative to day 0, respectively. The fat-water ratio changes were -35.6±19.2%, 16.5±36.0%, -25.0±18.6%, and 3.9±14.0% on day 3, and -22.8±41.8%, -16.1±23.0%, 15.7±16.4%, and 102.2±30.0% on day 7, respectively. The tumor-volume changes were 50.2±7.6%, 63.6±12.0%, 17.7±10.5%, and 1.4±4.7% on day 3, and 163.7±18.5%, 140.6±18.9%, 2.5±18.6%, and -24.4±7.4% on day 7. The ADC change of group 4 was significantly different from that of the control group on day 3 ($p=0.0156$), and the fat-water ratio change of group 4 was also significantly different from that of the control group on day 7 ($p=0.0088$). The tumor volume change of group 4 was significantly different from that of the control groups on days 3 and 7 ($p=0.0011$ and $p<0.0001$ respectively). For groups 5-8, the ADC changes were -1.3±4.3%, -6.4±6.9%, 9.9±11.3%, and 16.4±3.1% on day 3, and -3.0±1.0%, 9.9±9.5%, 17.9±15.4%, and 36.7±10.5% on day 7. The fat-water ratio changes were -32.9±17.0%, -19.0±17.0%, 108.0±45.6%, and 7.4±6.4% on day 3, and -32.6±21.7%, -19.2±28.0%, 41.3±47.0%, and 126.0±51.9% on day 7, respectively. The tumor-volume changes were 8.5±5.3%, 19.2±95.1%, -5.1±14.3%, and 13.0±3.8% on day 3, and 36.6±15.4%, 62.1±34.2%, -1.9±23.6%, and -12.1±13.2% on day 7. The ADC change of group 8 was significantly different ($p=0.0164$) from that of group 5 on day 7. The fat-water ratio change of group 7 was significantly different ($p=0.0015$) from that of group 5 on day 3, and the fat-water ratio change of group 8 was significantly different ($p=0.0115$) from that of the group 5 on day 7. Tumor size did not significantly differ among groups 5-8. Conclusion: Our results demonstrated the effective therapeutic response of TRA-8 in combination with carboplatin for two triple-negative breast cancer mouse models, suggesting both ADC values and fat-water ratio can be used as prognostic biomarkers to assess early therapeutic response.

Disclosure of author financial interest or relationships:
**G. Zhai**, None; **H. Kim**, None; **D. Sarver**, None; **S. Samuel**, None; **L. Whitworth**, None; **K.R. Zinn**, None.

Presentation Number **P119**
Poster Session 1
September 5, 2012 / 18:00-18:00 / Room: The Liffey

# Synthesis and a Critical Evaluation of a Peptide-NIR Fluorophere - Conjugate Biomarker for Molecular Imaging of Breast Cancer

*Changpo Chen[1], Kaijun Zhang[2,3], Bishnuhari Paudyal[2], Brian Gray[4], Koon Y. Pak[4], Eric Wickstrom[1,3], **Mathew L. Thakur**, [1]Biochemistry & Molecular Biology, Thomas Jefferson University, Philadelphia, PA, USA; [2]Radiology, Thomas Jefferson University, Philadelphia, PA, USA; [3]Kimmel Cancer Center, Thomas Jefferson University, Philadelphia, PA, USA; [4]MTTI, Molecular Targeting Technologies, Inc., West Chester, PA, USA. Contact e-mail: mathew.thakur@jefferson.edu*

Departments of Biochem. & Mol. Biol. 1, Radiology2, Kimmel Cancer Center3, Thomas Jefferson University, Philadelphia, PA and Molecular Targeting Technologies, Inc.4, West Chester, PA Objectives: The purpose is to design, synthesize and evaluate a receptor-specific peptide- fluorophore hybrid for optical imaging of breast cancer (BC). Method: VPAC1 receptors are densely expressed on all BC, but not on stroma or benign lesions. Our radiolabeled peptide TP3805 targeted VPAC1 specifically and distinguished malignant BC lesions from benign masses in transgenic mice that grow BC spontaneously. We have used TP3805 successfully for PET/PEM imaging of BC in humans. Optical imaging is a rapidly emerging imaging technology. TP3805 was synthesized with a C-terminal cysteine on NovaSyn® TG Sieber resin using the Fmoc protocol. Purified and characterized, TP3805 was incubated with a maleimide NIR dye CN-1016 (1.2:1) in PBS pH 6.5 and 10% DMF under argon to form a thioether bond. The reaction mixture was HPLC purified and analyzed by MS. Five µg (1 nmol) of the resultant hybrid fluorophore TP4303 were injected intravenously in 100 µl of sterile 0.9% NaCl into syngeneic mice bearing NAFA BC tumors derived from an MMTVneu transgenic mouse. Mice were imaged optically (FX-Pro, Carestream, CT) for up to 24 hrs (Ex - 730 nm, Em = 830 nm). ROI analysis was performed, tumor/muscle (T/M) and organ/muscle (O/M) ratios were calculated and evaluated statistically. Results: The molecular mass of TP4303 as determined by MS was 4305.5 (calculated 4306). All tumors were imaged distinctly. Tumor intensity was highest at 30 min. post injection (PI). T/M ratios were highest (4.3 ± 1.1) at 3 hr. PI. Intensity for muscle as well as for all other tissues declined as a function of time. Conclusion: A receptor-specific peptide-NIR fluorophore conjugate TP4303 can image BC in mice and is applicable in the future to image BC in humans. Support: NIH 1S10RR026678-01 (MLT).

Disclosure of author financial interest or relationships:
**C. Chen**, None; **K. Zhang**, None; **B. Paudyal**, None; **B. Gray**, Molecular Targeting Technologies, Inc., Employment; **K.Y. Pak**, Molecular Targeting Technologies, Inc., Stockholder; **E. Wickstrom**, None; **M.L. Thakur**, None.

Presentation Number **P120**
Poster Session 1
September 5, 2012 / 18:00-18:00 / Room: The Liffey

# MONOCYTE TRACKING AND EVALUATION OF THEIR PRO-ANGIOGENIC POTENTIAL WITH MR IMAGING IN A MURINE ISCHEMIC HIND LIMB MODEL

*Jelena Kolosnjaj-Tabi[1,2], Jose Vilar[3], Nathalie Luciani[2], Claire Wilhelm[2], Gwennhael Autret[1], Daniel Balvay[1], Jean Sebastien Silvestre[3], Florence Gazeau[2], **Olivier Clement**[1], [1]Laboratoire de Recherche en Imagerie, Inserm University Paris Descartes, Paris, France; [2]Laboratoire Matières et Systèmes Complexes, Paris-Diderot University CNRS UMR 7057, Paris, France; [3]PARCC, Inserm U 970, Paris, France. Contact e-mail: olivier.clement@inserm.fr*

Aim: Progress in molecular imaging has allowed approaches that enable single cell tracking in vivo that empower real time follow-up and assessment of the efficacy of treatment with transplanted cells. Among different approaches, high-resolution MRI (HR-MRI) appears promising for the survey of cell therapies, since it enables non-invasive visualization of single (labelled) cells and their therapeutic effect on surrounding tissues, provided that magnetic labelling does not alter cell function. In this experimental setting we evaluate the infiltration and effect of magnetically labelled monocytes (known for their pro-angiogenic action in our murine hind limb ischemia model) in vivo at different time points with a 4.7 T scanner provided with a cryogenic probe that allows a spatial resolution at micrometric scale. Methods: Murine bone marrow-derived monocytes were isolated and labelled with anionic ultra small iron oxide citrate-coated nanoparticles. Single-cell contrast agent internalization was evaluated by single cell magnetophoresis. Cell visualisation and quantification was optimized in vitro in agarose phantoms and in vivo in healthy mice. Subsequently, 5x105 murine monocytes were intravenously administered to mice with an ischemic hind limb (ischemia was induced by permanent femoral artery ligation). The distribution of labelled monocytes was evaluated by HR-MRI, performed with a cryogenic probe-equipped 4.7 T Scanner. A three-dimensional (3D) gradient echo sequence (TR/TE = 20/5 ms, flip angle=25°, resolution: 50 x 50 x 50 µm3) was used for cell detection. Angiogenesis was monitored in vivo by the MR scanner with the susceptibility-weighted imaging (TR/TE = 20/750 ms, flip angle=50°, resolution: 39 x 500 µm2) and post mortem with a high definition digital x-ray transducer. Results: When labelled monocytes are administered to mice, they migrate to the ischemic paw where they can be visualized by HR-MRI despite a relatively low iron uptake (approximately 2 pg of iron per cell, as determined by single cell magnetophoresis). Moreover, labelled cells have a statistically significant pro-angiogenic effect that is quantifiable and comparable to the effect of non-labelled monocytes, as confirmed by post mortem angiography. Conclusion: Our experimental conditions allow sufficient magnetic labelling of therapeutic cells that enables high-resolution MRI tracking in vivo and preserve the therapeutic action of administered cells.

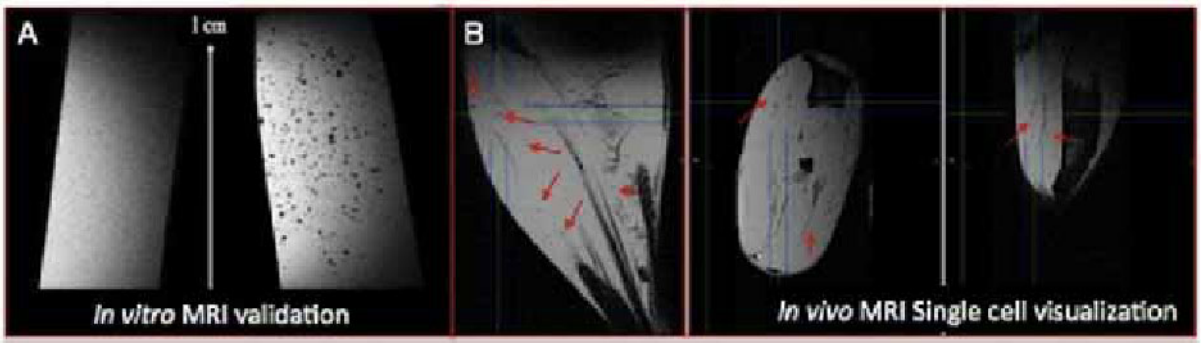


Visualization of labelled monocytes in A) agarose phantoms (left: control gel, right: gel spiked with labelled cells) and B) the ischemic limb of labelled monocyte treated mouse (red arrows), sagittal, axial and coronal view.

Disclosure of author financial interest or relationships:
**J. Kolosnjaj-Tabi**, None; **J. Vilar**, None; **N. Luciani**, None; **C. Wilhelm**, None; **G. Autret**, None; **D. Balvay**, None; **J. Silvestre**, None; **F. Gazeau**, None; **O. Clement**, None.

Presentation Number **P121**
Poster Session 1
September 5, 2012 / 18:00-18:00 / Room: The Liffey

# Gallium-68 labelled vascular adhesion protein 1 targeting peptide - the uptake in atherosclerotic plaques in mice

***Johanna M. Silvola***[1], *Iina Laitinen*[1], *Pauliina Luoto*[1], *Päivi M. Marjamäki*[1], *Seppo Ylä-Herttuala*[2], *Sirpa Jalkanen*[3], *Juhani Knuuti*[1], *Anne Roivainen*[1,4], [1]*Turku PET Centre, University of Turku and Turku University Hospital, Turku, Finland;* [2]*A. I. Virtanen Institute for Molecular Sciences, University of Eastern Finland, Kuopio, Finland;* [3]*MediCity Research Laboratory, University of Turku and National Institute of Health and Welfare, Turku, Finland;* [4]*Turku Center for Disease Modeling, University of Turku, Turku, Finland. Contact e-mail: johanna.silvola@utu.fi*

Object: The expression of vascular adhesion protein-1 (VAP-1) is induced at sites of inflammation where extravasation of lymphocytes from blood to the peripheral tissue occurs. VAP-1 is an adhesion molecule for leukocytes and it also possesses the monoamine oxidase enzyme activity. Inflammation has a prominent role in atherosclerosis, and therefore VAP-1 may be a potential target for imaging of inflammation associated with atherosclerotic plaques. The aim of this study was to investigate the uptake of 68Ga-labelled VAP-1 peptide targeting VAP-1 in atherosclerotic plaques in mice. Methods: Uptake of 68Ga-labelled VAP-1 peptide was investigated in atherosclerotic LDLR-/-ApoB100/100 mice at 20 minutes after injection. The uptake of 68Ga-labelled VAP-1 peptide in atherosclerotic plaques and healthy vessel wall was assessed by autoradiography of aortic cryosections. Results: The 68Ga-labelled VAP-1 peptide had reasonable good specific radioactivity (mean ratio ± SD 1.9 ± 0.4 GBq/μmol). After several months of a high fat diet, plaques in LDLR-/-ApoB100/100 mice were both inflamed and calcified. Autoradiography results showed significantly higher uptake of 68Ga-labelled VAP-1 peptide in the atherosclerotic plaques compared with healthy vessel wall (mean ratio ± SD 1.8 ± 0.3, p=0.01). Conclusion: We observed that 68Ga-labelled VAP-1 peptide is accumulated into the plaques of atherosclerotic mice. Further studies are warranted to assess the uptake of this tracer in younger animals and in earlier stages of plaque development.

Disclosure of author financial interest or relationships:
**J.M. Silvola**, None; **I. Laitinen**, None; **P. Luoto**, None; **P.M. Marjamäki**, None; **S. Ylä-Herttuala**, None; **S. Jalkanen**, None; **J. Knuuti**, Lantheus Inc, Consultant; Philips, Speakers bureau; **A. Roivainen**, None.

Presentation Number **P122**
Poster Session 1
September 5, 2012 / 18:00-18:00 / Room: The Liffey

# In vivo imaging T cells in the Rheumatoid arthritis with nano-sized iron oxide particles by MRI

***Chih-lung Chen***[1], *Cheng-Hung Chou*[2], *Chen-Hsuan Lin*[1], *Wen-Yuan Hsieh*[1], *Shian-Jy Wang*[1], *Chen Chang*[2], [1]*Biomedical Technology and Decive Research Labs, Industrial Technology Research Institute, Hsinchu, Taiwan;* [2]*Institute of Biomedical Sciences, Academia Sinica, Taipei, Taiwan. Contact e-mail: gregchen@itri.org.tw*

Introduction: Rheumatoid arthritis (RA) is a very common autoimmune disease. The activation of T-cells is believed to correlate with the pathogenesis of the condition. Understanding the initiation, migration, and distribution of the T-cells provides important perspectives regarding RA, and may also help the development of therapeutic interventions. An efficient MRI contrast agent and a successful technique to track non-phagocytic T-cells are needed. Materials and Methods: Synthesis and characterization of IOPC and IOPC-CD3 particles by DLS, flow cytometry and TEM. We detected the migration and accumulation of the T cells in the growth plate and femoral cartilage in a rat RA model with both in vivo and ex vivo MRI. Results and Discussion: We report a novel nano-sized MRI contrast agent, IOPC-CD3 particles, superparamagnetic iron-oxide particles coated with polyethylene glycol, with high transverse relaxivity (228 s-1mM-1), thus useful for MRI studies. IOPC-CD3 particles are the first reported magnetic particles that can label rat T-cells with over 90% efficiency. We detected the migration and accumulation of the T cells in the growth plate and femoral cartilage in a rat RA model with both in vivo and ex vivo MRI. Conclusion: Our results suggest that IOPC-CD3 particles are powerful and potential specific translational cellular imaging reagents that can be used to label non-phagocytic T-cells for in-vivo MRI cell trafficking studies, very useful to the field of regenerative medicine and inflammatory diseases.

Disclosure of author financial interest or relationships:
**C. Chen**, None; **C. Chou**, None; **C. Lin**, None; **W. Hsieh**, None; **S. Wang**, None; **C. Chang**, None.

Presentation Number **P123**
Poster Session 1
September 5, 2012 / 18:00-18:00 / Room: The Liffey

# Real time monitoring of apoptosis mediated by natural killer (NK) cells against cancer using a caspase 3 sensor in vitro

***Ho Won Lee***[1], *Yong Hyun Jeon*[1], *Sang-Woo Lee*[1], *Shin Young Jeong*[1], *Jeoung-Hee Ha*[2], *Alnawaz Rehemtulla*[3], *Byeong-Cheol Ahn*[1], *Jaetae Lee*[1], [1]*Nuclear Medicine, School of Medicine, Kyungpook National University, Daegu, Republic of Korea;* [2]*Pharmacology, School of Medicine, Kyungpook National University, Daegu, Republic of Korea;* [3]*Radiation Oncology, University of Michigan, Ann Arbor, MI, USA. Contact e-mail: howon1234@hanmail.net*

Objectives: Natural killer (NK) cells induce apoptosis through caspase 3-dependent pathway by combination of granzyme and perforin or TRAIL and FasL. Non-invasive imaging apoptosis sensor could allow rapid optimization of NK-mediated immunotherapy. Here, we attempted to real-time monitor apoptosis events (caspase 3 dependent cell death) mediated by NK cells in human breast cancer cells using split luciferae-based caspase 3 sensor. Methods: Previously, we reported caspase-3 sensor based on a split luciferase technology. Human breast cancer cell line (MDA-MB231/1833, as a target) expressing caspase 3 sensor was established (1833-Caspase 3 Sensor, briefly, 1833-C3S). NK92 cell line (as effector) was purchased from ATCC. To evaluate apoptosis induction by NK92 cells using an 1833-C3S, effector and target cell were co-cultured at E/T ratio of 5, 10, and15/1 for 9 h and then bioluminescence was measured. To (1) compare the level of apoptosis between non- /or stimulated NK92 cells (2) and monitor the level of apoptosis in target cells (1833-C3S) by NK92 according to time course, NK92 cells were incubated with PMA and ionomycin for 2 h and then simultaneously co-cultured with target cells at E/T ratio of 10:1. Sequential bioluminescence was measured every an hour for 6 h. Viability of target cell was determined using a CCK assay. Results: Bioluminescence in 1833-C3S cells was increased in a effectors-number dependent manner and a moderate correlation was observed between bioluminescence and E/T ratio (Fig. 1A, media, 5:1, 10:1 and 15:1, 351±27 RLU, 769±40 RLU, 930±22 RLU and 919±8 RLU, r2 = 0.79, respectively). CCK assay showed the decreased cell viability by number increase of NK92 cells (Fig. 1B, media, 5:1, 10:1 and 15:1 of E/T, 100±0%, 89±4%, 64±3%, 63±5%, respectively). Co-incubation of 1833-C3S with non-/or stimulated NK92 cells resulted in increase of fold induction of bioluminescence as time goes by. Interestingly, the high fold induction of bioluminescence of 1833-C3S cells by stimulated NK92 could be only detected in early time point (based on 3h, non-stimulated NK92 and stimulated NK92, 1.3 fold and 6.0 fold, $P<0.05$, respectively). Furthermore, fold induction of bioluminescence was still more increased in stimulated NK92 cells compared to non-stimulated NK92 cells at 6 h time point (Fig, 2A, non-stimulated NK92 and stimulated NK92, 3.8 fold and 14.2 fold, $P<0.05$, respectively). Cell viability assay resulted in 64±5% and 41±3% of non-stimulated and stimulated NK92 cells, respectively (Fig. 2B, $P<0.05$). Conclusions: We successfully established breast cancer cell line expressing caspase 3 sensor and monitored apoptosis mediated by NK92 cells in vitro. These results suggest that our caspase 3 sensors could be used as a useful tool to determine several important factors for optimization the NK-mediated immunotherapy such as selection of NK-stimulated cytokine cells, dose, frequency and route administration in vitro and in vivo.

Disclosure of author financial interest or relationships:
**H. Lee**, None; **Y. Jeon**, None; **S. Lee**, None; **S. Jeong**, None; **J. Ha**, None; **A. Rehemtulla**, None; **B. Ahn**, None; **J. Lee**, None.

Presentation Number **P124**
Poster Session 1
September 5, 2012 / 18:00-18:00 / Room: The Liffey

# Improvement of Fibered Fluorescence Microscopy for in vivo imaging of individual cells in mouse brain

***Jesus Pascual**, Veerle Reumers, Sarah-Ann Aelvoet, Chris Van den Haute, Veerle Baekelandt, Neurosciences, KU Leuven, Leuven, Belgium. Contact e-mail: jesus.pascualbrazo@med.kuleuven.be*

Fiber optic-based confocal fluorescent microscopy allows visualizing individual cells in deep brain regions of live animals with high temporal resolution, filling the gap between traditional neuroimaging techniques and 2-photon microscopy. The Cellvizio system uses a miniature fiber-optic probe to transport the emission light (488 nm) from the light source to the brain and from the brain to the detector. We employed state-of-the-art viral vectors to express fluorescent proteins and calcium sensitive dyes to visualize and record individual cells in live mice. However, fluorescent background was a limiting factor to distinguish individual cells. To overcome this limitation, we optimized viral vectors to increase the signal/noise ratio of eGFP fluorescent signal in anesthetized mice. Comparison of conventional and optimized viral vectors was carried out in different brain regions. The images were acquired with the same microscope settings, in order to compare the conditions that allow discriminating the individual cells from the background. In addition, we are exploring the possibility to monitor physiological parameters of the neurons in vivo, such as calcium signalling and redox state. We conclude that the combination of viral vector technology with this new in vivo optical imaging technique improves the quality of the images acquired in the brain of live mice.

Disclosure of author financial interest or relationships:
**J. Pascual**, Janssen Pharmaceutica, Grant/research support; **V. Reumers**, None; **S. Aelvoet**, None; **C. Van den Haute**, None; **V. Baekelandt**, None.

Presentation Number **P125**
Poster Session 1
September 5, 2012 / 18:00-18:00 / Room: The Liffey

# Intrinsic Feature Pose Measurement for Clinical Awake Subject Imaging

***James S. Goddard**, Image Signals and Machine Learning, Oak Ridge National Laboratory, Oak Ridge, TN, USA. Contact e-mail: goddard@ieee.org*

Intrinsic feature pose measurement for awake subject imaging has been further developed and implemented with testing in the clinical setting. This system tracks head motion during PET and SPECT scans. The intrinsic feature approach has been developed from previous work to provide reliable accurate pose measurements during scans. Previously, awake subject motion tracking for 3D imaging has been limited to measuring external targets or markers attached to the subject's head. While this approach has been shown to be useful, the use of external markers is undesirable for several reasons. An optical motion tracking system is described for acquiring real-time images, extracting and processing features to measure changes in 3D positions over time to calculate the pose changes by matching to a rigid body model. Mismatches and outliers are detected and omitted to improve accuracy. Validation results compared to known motion have been performed. Measurements with known phantom motion and live subject results from a PET scanner are presented to provide accuracy, performance, and repeatability.

Disclosure of author financial interest or relationships:
**J.S. Goddard**, None.

Presentation Number **P126**
Poster Session 1
September 5, 2012 / 18:00-18:00 / Room: The Liffey

# Usefulness of the segmental acquisition method in FDG PET/CT of rectal cancer patients

***Keisuke Tsuda***[1,2], *Kazuya Koyama*[2], *Yuto Iwabuchi*[2], *Takayuki Suzuki*[3], *Kazuhito Toya*[4], *Akira Hirayama*[5], *Hiroyuki Tsushima*[1], *Masahiro Fukushi*[6], *Noriyuki Moriyama*[2], *Hirofumi Fujii*[2], [1]*Ibaraki Prefectural University, Ami, Japan;* [2]*National Cancer Center, Kashiwa, Japan;* [3]*Toto Clinic, Tokyo, Japan;* [4]*Tokyo Medical Center, Tokyo, Japan;* [5]*GE Healthcare, Tokyo, Japan;* [6]*Tokyo Metropolitan University, Tokyo, Japan. Contact e-mail: ksk2da@gmail.com*

**Objectives:** FDG PET is now an essential tool for evaluating the activity of glucose metabolism in cancer. Since a long time is still required to obtain image data, body motions can easily deteriorate the quality of the PET images. We have reported that images of stationary objects obtained using the segmental acquisition method for FDG PET/CT were never worse than those obtained using the continuous acquisition method. We also demonstrated that, under some conditions, segmental images obtained by the superimposition of reconstructed images of each sinogram could provide better image quality than continuous images obtained using conventional continuous acquisition. Although we revealed that the segmental acquisition method improves image quality, the clinical benefits of this segmental acquisition in terms of diagnostic performance remain uncertain. In this study, we evaluated the usefulness of the segmental acquisition method over the continuous method in clinical FDG PET/CT for patients with rectal cancer. **Methods:** In phantom studies, an NEMA phantom comprising 6 spheres filled with FDG (sphere sizes: 6.23, 7.86, 10, 13, 17 and 37 mm) was evaluated, and a sphere of 37 mm was considered as a urinary bladder model. The radioactivity ratio for urinary bladder, spheres, and background was 36:8:1. The acquisition time was set to 3 minutes for the continuous method, and the acquisition time of 15 seconds was repeated 12 times for the segmental method. Acquired image data were reconstructed using FORE+OSEM algorithms. Segmental images were obtained by superimposing 12 reconstructed images. Furthermore, in clinical studies, 11 malignant lesions, 9 primary tumors and 2 lymph node metastases from 9 patients with rectal cancer were investigated. FDG PET assessments of these patients involved continuous imaging of the pelvic areas in both continuous and segmental acquisition modes. All obtained images were investigated visually and quantitatively, with quantitative assessments involving calculation of SUVmax and coefficient of variation (CV), after placing regions of interest (ROIs) on lesions. **Results:** In phantom studies, visual assessments revealed the segmental method as superior to the continuous method in terms of detectability of small spheres and image quality. SUVmax was similar for both acquisition methods. CV was 8% better with the segmental method than with the continuous method. In clinical studies, visual assessment revealed that the segmental method allowed better detection of lesions and evaluation of image quality than the continuous method. Quantitative assessment showed that CV was 43% higher with the segmental method than with the continuous method, while SUVmax was similar for both methods. **Conclusions:** According to our study, the segmental acquisition method allows better detection of lesions and image quality than the conventional continuous acquisition method in patients with rectal cancer. The segmental acquisition method appears likely to be useful for clinical FDG PET/CT.

Disclosure of author financial interest or relationships:
**K. Tsuda**, None; **K. Koyama**, None; **Y. Iwabuchi**, None; **T. Suzuki**, None; **K. Toya**, None; **A. Hirayama**, None; **H. Tsushima**, None; **M. Fukushi**, None; **N. Moriyama**, None; **H. Fujii**, None.

Presentation Number **P127**
Poster Session 1
September 5, 2012 / 18:00-18:00 / Room: The Liffey

# Pushing the limits of Clinical Time-of-Flight 18F-FDG PET/CT Faster and/or lower dose imaging

***Jun Zhang***[1,2], *Katherine M. Binzel*[1,2], *Nathan Hall*[1], *Xiaoli Liu*[1,2], *David Barker*[1], *Michael V. Knopp*[1,2], [1]*Radiology, Wexner Medical Center at The Ohio State University, Columbus, OH, USA;* [2]*Wright Center of Innovation in Biomedical Imaging, Wexner Medical Center at The Ohio State University, Columbus, OH, USA. Contact e-mail: zhang.538@osu.edu*

Objectives: State of the art Time-of-Flight PET/CT imaging appears to have more dynamic range then commonly appreciated which let to the goal to push the limits in reducing time and/or dose. To validate by qualitative and quantitative assessment an organ-adaptive acquisition approach with reduced dose how it is equivalent without impacting SUV, signal-noise ratio (SNR) and image quality. Methods: Phantom testing, patient data simulation, and subject validation were used. With a Gemini TF 64 PET/CT, hollow sphere phantoms with varying inner volumes and activities were scanned from 30s/bed-360s/bed. 35 clinical patients received 18FDG and were scanned with 180s/bed slab. Slab volumes were reconstructed from list-mode in 15s, 30s, 60s, 90s, 120s and 180s frame duration (FD) per bed position. Counts and count rate (CR) before and after scatter and attenuation corrections were determined. VOIs were placed on normal organs (cerebellum, heart, lung, liver, bone marrow (L5), kidney and bladder) and lesions; SUV and SNR were measured. Results were compared to local standard 90s/bed PET. Validation was based on PET/CTs of 5 subjects with <5mCi FDG under 90s/bed. Results: Target lesions showed consistent uptake from 15s/bed to 180s/bed with correlation to the 90s/bed standard (1.08, 0.99, 1.01, 1.00 and 0.98). All lesions visible on the standard 90s/bed PET were identified on all including the 15s/bed PET. CR was organ-specific and stable over all durations while total counts were proportional to time/bed and injected activity. No significant variance of CR, SUV and SNR were found in organs or lesions in regard to different frame durations ($p<0.01$). Compared to the 90s/bed, there were diverse and tissue-specific variances of SUV and SNR in regard to different FDs. The optimal organ-adaptive time/bed approach was determined which led to a 30-50% shorter acquisition time with a SUV and SNR variability of <6%. Validating that the approach can also be used to drastically reduce dose, the subjects with 3-5mCi FDG injected presented equivalent quality. Conclusion: This study demonstrated and confirmed that a reduction of acquisition time and/or tracer dose can be achieved without compromising visual and quantitative assessment using TOF PET/CT. The proposed organ-adaptive TOF acquisition approach enables a 40-50% time savings or radiation dose reduction or a combination benefit, without loss of diagnostic and quantitative quality.

Disclosure of author financial interest or relationships:
**J. Zhang**, None; **K.M. Binzel**, None; **N. Hall**, Enlyton,Ltd., Other financial or material support; **X. Liu**, None; **D. Barker**, Resurrection Health Care (PET/CT preceptorship conducted 1/2012), Honoraria; **M.V. Knopp**, None.

Presentation Number **P128**
Poster Session 1
September 5, 2012 / 18:00-18:00 / Room: The Liffey

# Anabolic and OVX-induced Changes in Bone Quality of the Proximal Mouse Tibia Vary with Skeletal Site as Assessed with Micro-CT and Image Registration Techniques

***Graeme M. Campbell***[1], *Friederike Grundmann*[2], *Nicolai Purcz*[3], *Markus Böttcher*[1], *Christian Schem*[2], *Sanjay Tiwari*[1], *Claus C. Glueer*[1], [1]*Diagnostic Radiology, University Hospital Schleswig-Holstein, Campus Kiel, Kiel, Germany;* [2]*Gynecology, University Hospital Schleswig-Holstein, Kiel Campus, Kiel, Germany;* [3]*Oral and Maxillofacial Surgery, University Hospital Schleswig-Holstein, Kiel Campus, Kiel, Germany. Contact e-mail: gcampbell73@gmail.com*

Introduction: Micro-computed tomography (micro-CT) enables highly accurate measurements of bone structure and mineral, and can be used in conjunction with molecular imaging in order to match molecular signals to specific skeletal sites. In studies of tumor progression substantial bone loss necessitates the definition of identical volumes of interest (VOIs) in baseline and follow-up scans in order to accurately quantify changes. We have developed and validated a method to transfer baseline VOIs onto follow-up images using image registration. In this study, we applied this technique to assess the changes in bone mass and structure in mice subjected to OVX-induced bone loss and anabolic bone apposition. Methods: Female CD1 mice were subjected to ovariectomy (OVX) at 10 weeks of age followed by parathyroid hormone injection at 6 months (hPTH(1-84), 40µg/kg s.c. 5dy/wk, N=6) or OVX only (N=5). The animals were micro-CT scanned (vivaCT 40, ScancoMedical, Switzerland) every week for four weeks in a full-body holder at a voxel size of 19µm, beginning at the time of PTH treatment in the first group and after OVX in the second. User-defined contours of baseline images isolated the trabecular regions of the epiphysis and metaphysis, and a "full proximal" region that included the trabecular bone of the epiphysis, metaphysis and growth plate. Cortical bone of the diaphysis was also isolated. Follow-up images were registered to baseline and the inverted transformation matrix was used to transform the baseline VOIs onto the follow-up images. Bone architecture and mineral parameters were quantified. Two-way repeated measures ANOVAs and paired t-tests determined time by group effects and baseline changes respectively. Significance was taken at $p < 0.05$. Results: Following PTH treatment, increases from baseline in BV/TV (+46.7%, p=0.004), BMD (+19.0%, p=0.002) and Tb.Th (+10.8%, p=0.002) were observed in the full proximal region at the end of the study. In the metaphyseal region, increases from baseline in BV/TV (+102.8%, p=0.012) and BMD (+30.0%, p=0.007) were detected. Increases in BV/TV (+58.8%, p=0.002) and BMD (+21.4%, p=0.002) were observed in the epiphysis while cortical thickness increased by 14.3% (p<0.001) after four weeks. OVX decreased BV/TV (-21.6%, p=0.004), BMD (-10.0%, p=0.003) and Tb.Th (-7.7%, p<0.001) in the full proximal region by the end of the study. No further changes were detected in the OVX group. Discussion: PTH treatment resulted in improved bone mineral and structure, while OVX reduced these over four weeks in the proximal tibia. Isolation of specific skeletal sites for analysis revealed larger changes in the metaphyseal region compared to the epiphysis or full trabecular regions. Although trends towards altered bone structure and mineral were observed in the epiphyseal and metaphyseal regions after OVX, significant changes were only detected in the full proximal region. Whether the lack of observed changes in these regions was genuine or due to limited resolution or sample size remains unclear. Future applications include studies of bone metastases in order to quantify bone loss in tumor models.

Disclosure of author financial interest or relationships:
**G.M. Campbell**, None; **F. Grundmann**, None; **N. Purcz**, None; **M. Böttcher**, None; **C. Schem**, None; **S. Tiwari**, None; **C.C. Glueer**, None.

Presentation Number **P129**
Poster Session 1
September 5, 2012 / 18:00-18:00 / Room: The Liffey

# Towards Standardized Dual Energy Processing for Preclinical microCT

***Willy Gsell***[2]*, Dustin Osborne*[1,3]*, [1]Graduate School of Medicine, University of Tennessee, Knoxville, TN, USA; [2]Biological Imaging Centre, Imperial College: MRC Clinical Sciences Center, London, United Kingdom; [3]Preclinical, Siemens Medical Solutions, Knoxville, TN, USA. Contact e-mail: willy.gsell@csc.mrc.ac.uk*

Introduction: Dual energy CT (DECT) has proved to be of real advantage in clinical studies allowing a refinement of the diagnosis by identification of the composition of hyperintense regions in contrast enhanced CT protocols without the need to acquire a pre-contrast volume. Such techniques could be used as an imaging method for preclinical models where localization and quantitative measurement of contrast agents are needed. The aim of this preliminary work was to assess the feasibility of DECT on current preclinical microCT by investigating photon flux at different energies, effect of beam hardening and noise characteristics of the images acquired at energies ranging from 40kVp to 120kVp. Methods: A 5-cylinder phantom was designed consisting of a central cylinder filled with water surrounded by four equally spaced cylinders with varying concentrations of iodinated contrast agent (1:37 mg/ml; 2:18.5 mg/ml) and CaCl2 (3:1M & 4:0.5M). Data were acquired at 40, 50, 110 and 120 kVp (0.5 mA). The data were acquired using 0.5 mm (40-50 kVp) and 1.5 mm Al filters (110-120 kVp). Adjusting the filter is needed to increase spectra separation. Because of severe effects in post-recon DECT, all data were corrected for beam hardening using a polynomial fit technique with correction coefficients calculated from the data. All data were calibrated to HUs. Data processing was performed in the Inveon Research Workplace (4.0) APEx Toolkit. Data were processed using a 2 basis material decomposition method and a linear fit method plotting the HU values versus material density at each energy to determine a proper image threshold. Results are illustrated in the attached figures. For all energies, XOP was used to model the X-ray spectra for conversion of the CT data to µ-maps. Data for bone/iodine suppression and blended images were calculated using each method. Results: The HUs for the different compartment are: water (12 ± 21; 16 ± 23; 26 ± 29 and 25 ± 29 for 40kVp, 50kVp, 110kVpand 120kVp respectively), Ultravist 370 dilution 1/10 (3651 ± 88, 4128 ± 88, 4500 ±84, 4420 ± 77), Ultravist 1/20 (1547 ± 36, 1735 ± 40, 1915 ± 46, 1887 ± 46), CaCl2 1M (1141 ± 23, 1054 ± 24, 665 ± 30, 630 ± 31) and CaCl2 0.5M (535 ± 20, 495 ± 21, 304 ± 29, 287 ± 29). The energy map between 120kVp and 50kVp shows a linear regression for Iodine (y = 1.07x) and Calcium (y = 0.59 x) with a bisecting line (y=0.83x) used to determine the image threshold. Virtual non-contrast images were created using both methods and are shown in the figure. Conclusions: This work illustrates the use of post-reconstruction dual energy methods with microCT. This is the first of a series of studies to work towards standardization of microCT methodology for acquiring dual energy data. microCT inherently has higher noise and more closely spaced X-ray spectrums than their clinical counterparts. This work indicates that material selective suppression/enhancement is possible on these systems using reconstructed image data. Future studies will include expanding this work to three basis materials and developing more robust acquisition and processing techniques.

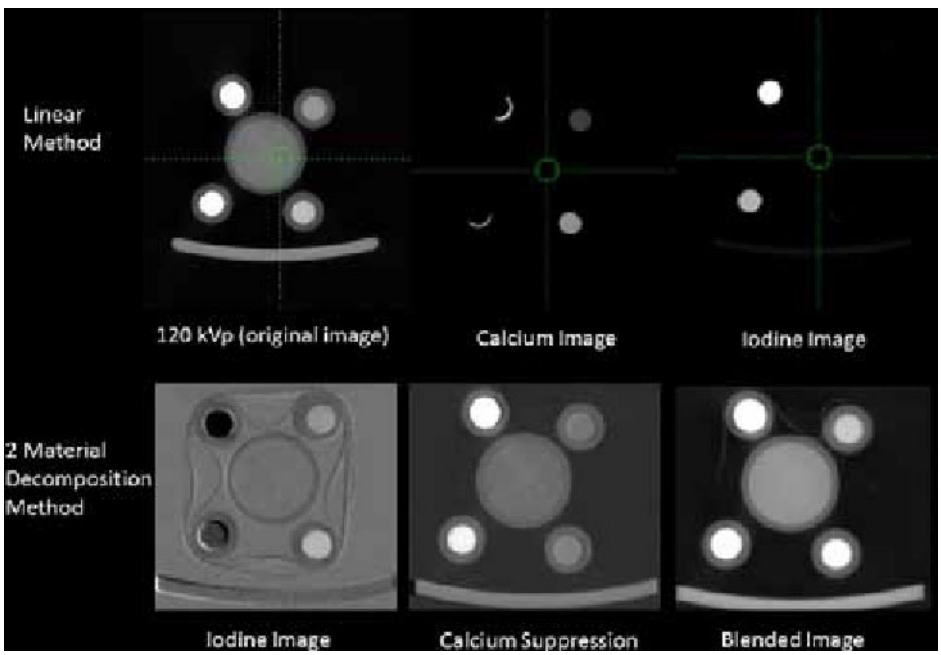


Disclosure of author financial interest or relationships:
**W. Gsell**, None; **D. Osborne**, University of Tennessee, Employment; Siemens Medical Solutions, Employment .

Presentation Number **P130**
Poster Session 1
September 5, 2012 / 18:00-18:00 / Room: The Liffey

# Development and Quantitative Assessment of a Beam Hardening Correction Model for Preclinical µCT

***Sucheta Mohapatra***[1], *John J. Sunderland*[2], *Susan A. Walsh*[2], *Michael Acevedo*[2], [1]*Biomedical Engineering, University of Iowa, Iowa City, IA, USA;* [2]*Radiology, University of Iowa, Iowa City, IA, USA. Contact e-mail: sucheta-mohapatra@uiowa.edu*

**OBJECTIVE**: The impact of x-ray beam hardening is significant in preclinical micro-CT imaging systems, adversely affecting both image quality and quantitation. In multimodality PET-CT imaging systems, uncorrected CT images lead to artifactual attenuation maps, resulting in quantitative errors in PET images. Although beam hardening corrections (BHC) are common, they are specific to the energy spectrum of the primary CT beam and must be tuned to combinations of peak voltage and tube filtration. The Inveon™ CT system uses a common linearization approach to BHC, but provides parameters for only a single kVp/filtration combination, resulting in non-quantitative and non-uniform CT images and attenuation maps for other acquisition settings. This study measures the beam hardening effect for 12 different kVp/filtration combinations on the Inveon™ system and generates specific BHC parameters for each setting. **MATERIALS AND METHODS**: Projection data was acquired on Inveon™ CT system, for uniform cylindrical water phantoms of two different diameters - 28 mm and 71 mm, selected to represent mouse and rat sizes respectively. Projections were acquired at four peak voltage settings - 40, 50, 60 and 80 kVp. At each voltage setting, the beam was filtered by additional tube filtration -0.5 mm, 1.0 mm and 1.5 mm Al (on top of 0.5 mm Al inherent tube filtration). For each kvp/filtration combination, the image of phantom was reconstructed without any BHC. Using the uncorrected image, we calculate the lengths of x-ray propagation through water and its associated attenuation for each ray in each view. The non-linear relationship between attenuation and path lengths is fitted to a 3rd order polynomial. The initial slope of this function is used to estimate the effective attenuation coefficient ($\mu_{eff}$) for water for the given energy spectrum. This estimated ($\mu_{eff}$) value and the calculated path lengths are used to generate the expected sum of attenuation coefficients along each x-ray path. Finally, a 3rd order polynomial, consistent with the Inveon™ beam-hardening model and software, is fit to transform the measured to the expected data. The coefficients of this trinomial are directly applied for beam-hardening correction during CT reconstruction. To demonstrate the correction model, each set of data is reconstructed thrice - without BHC, BHC by manufacturer's default coefficients and BHC with coefficients derived from proposed approach. **RESULTS**: Correction achieved with the proposed energy spectrum-specific BHC model effectively removes the characteristic cupping artifact, that is observed when the manufacturer's default BHC coefficients are applied during CT reconstruction. **CONCLUSION**: By incorporating a linearization based correction model, we generate twelve distinct sets of beam hardening correction parameters for the Inveon™ CT system, significantly expanding the quantitative performance of the CT system to a broad range of acquisition settings. The effectiveness of the approach has been validated through quantitative artifact-free CT reconstructions up to diameters of 71 mm.

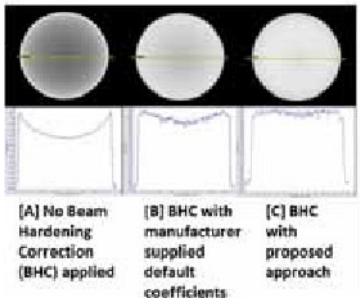

Figure 1- Axial profile diagrams of reconstructed images for 80 kVp, 0.5 mm added filtration.

[A] No Beam Hardening Correction (BHC) applied | [B] BHC with manufacturer supplied default coefficients | [C] BHC with proposed approach

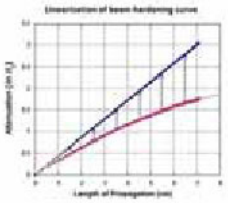

Figure 2 - Beam hardening curve (in red) fitted with a polynomial function The slope of the BH curve for thicknesses going to zero determines the effective attenuation coefficient (µeff) at a particular kVp-filtration setting. [Acquisition parameters: 80 kVp, 0.5 mm Al added filtration]

TABLE 1 Effective attenuation coefficient (µeff) estimated for water with corresponding estimate of effective energy for 12 combinations of kVp-filtration.

| Peak Anode Voltage (kVp) | Additional thickness of tube filtration (mm) Al | | |
|---|---|---|---|
| | 0.5 mm | 1.0 mm | 1.5 mm |
| 40 | 0.64/ 22.5 | 0.576/23.9 | 0.53/24.6 |
| 50 | 0.53/ 34.6 | 0.47/ 36.2 | 0.42e/38.0 |
| 60 | 0.48/ 30.0 | 0.41/ 28.2 | 0.38/29.1 |
| 80 | 0.42/29/ 28.0 | 0.37/34.0 | 0.33/34.0 |

Disclosure of author financial interest or relationships:
**S. Mohapatra**, None; **J.J. Sunderland**, Siemens Molecualr Imaging, Grant/research support; **S.A. Walsh**, None; **M. Acevedo**, None.

Presentation Number **P131**
Poster Session 1
September 5, 2012 / 18:00-18:00 / Room: The Liffey

# 3DBoneView : A 3D bone quantification and visualization software for micro-CT imaging

*Shouping Zhu[1], Xin Cao[1], Chunlin Chen[1], Tao Zhou[2], Xiaochao Qu[1], Duofang Chen[1], Jimin Liang[1], **Jie Tian**[1,3], [1]School of Life Sciences and Technology, Xidian University, Xi'an, China; [2]School of stomatology, Fourth Military Medical University, Xi'an, China; [3]Medical Image Processing Group, Institute of Automation,CAS, "Beijing,100190", China. Contact e-mail: tian@ieee.org*

Bones are among the most important components of human beings and animals, and many diseases developments and drug efficacy are related with the changes of bones. Micro-CT technology, with its high spatial resolution, low-cost, non-invasive characteristics, has become an important 3D imaging tools for small animals, and it is very suitable for bone imaging because of the relatively high density contrast between the bones and the surrounding soft tissues. In order to perform bone analysis by micro-CT, we not only need a high resolution micro-CT scanner, but also an easy-to-use bone analysis software. A 3D bone quantification and visualization software for CT imaging, 3DBoneView, has just been developed in our lab. The software is designed based on MITK (Medical Imaging ToolKit, http://www.mitk.net), and specifically for the micro-CT bone mineral density quantitative measurement and micro-structural analysis. The developed 3DBoneView software has been used to analysis two groups of bone samples, one group from normal mice, and the other from model mice (osteoporosis mice). Each group has three samples. The mean values of some typical bone parameters are shown in table 1. Compared with the normal group, the bone mineral density parameters and the bone trabecular parameters have an obvious difference in the model group. In the near future, we plan to improve the software performance and it will be freely available for research and education purpose.

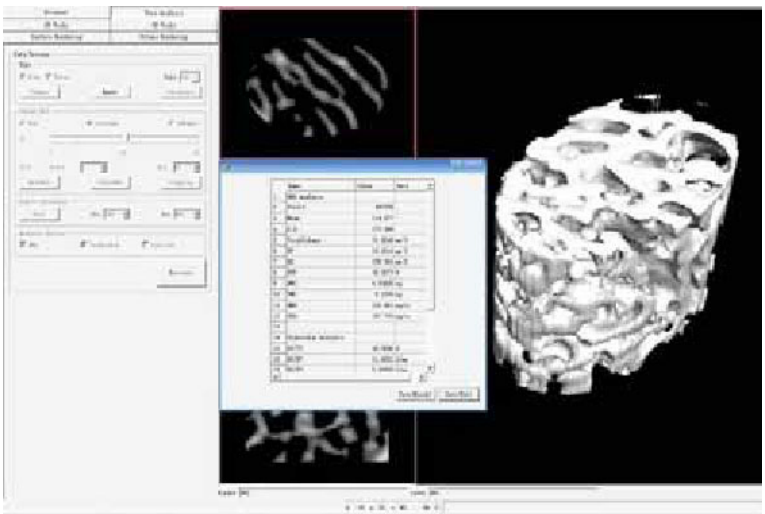

Table 1 Parameters of Bone Mineral Density Analysis and Bone Trabecular Analysis

| | Normal group | Model group |
|---|---|---|
| ROI volume (mm³) | 0.1855 | 0.1479 |
| Bone mineral content (BMC, mg) | 0.0951 | 0.0583 |
| Bone mineral density (BMD, mg/cc) | 344.5870 | 139.451.0 |
| Trabecular mineral content (TbMC, mg) | 0.0539 | 0.0139 |
| Trabecular mineral density (TbMD, mg/cc) | 385.9320 | 340.841.0 |
| Trabecular number (TbN, 1/mm) | 7.0876 | 3.2119 |
| Trabecular spacing (TbSp, mm) | 0.0804 | 0.1492 |
| Trabecular thickness (TbTh, mm) | 0.0611 | 0.0139 |
| Structure model index (SMI) | 0.2349 | 2.2400 |
| Degree of anisotropy (DA) | 0.9086 | 0.7088 |

Disclosure of author financial interest or relationships:
**S. Zhu**, None; **X. Cao**, None; **C. Chen**, None; **T. Zhou**, None; **X. Qu**, None; **D. Chen**, None; **J. Liang**, None; **J. Tian**, None.

Presentation Number **P132**
Poster Session 1
September 5, 2012 / 18:00-18:00 / Room: The Liffey

# Quantitative Estimation of Activity with an Artificial Neural Network for Multi-isotope SPECT Study

*Koichi Ogawa[1], **Shuko Abe**[1], Yusuke Koike[2], Izumi O. Umeda[2], Hirofumi Fujii[2], [1]Department of Informatics, Hosei Univ., Tokyo, Japan; [2]East Hospital, National Canser center, Kashiwa, Japan. Contact e-mail: shuko.abe.5c@stu.hosei.ac.jp*

**INTRODUCTION**: The aim of this study is to develop a method that measures the distributions of multiple isotopes in a body. If angiogenesis, hypoxia, and apoptotic changes could be successfully observed at a time, the obtained information would strongly contribute to the optimization of the therapeutic strategies and accurate evaluation of therapeutic effects. The simultaneous imaging of multiple radioisotopes would be applicable to the investigation of drug delivery systems. It is essential for the simultaneous acquisition of multiple radionuclides to set multiple energy windows to their photopeaks of each radionuclide. To accurately measure photon counts, we used a neural network method to remove the effects of crosstalk between the different photopeak energies and also remove scattered photons. **METHOD**: We assumed a study that used $^{99m}$Tc (photopeak energy: 141keV) and $^{111}$In (171 and 245 keV), and estimated the counts of primary photons, i.e., $^{99m}$Tc and $^{111}$In . The accuracy of estimation was compared with the following five methods with an artificial neural network (ANN). The neural network had three layers: one input layer with several units which is equal to the number of energy windows, one hidden layer with twice the number of units in the input layer and one output layer with three units. For values input into the units in the input layer, we used a predefined number of ratios of counts calculated with several energy windows, which are the ratios of the count $C_k$ acquired with the k-th narrow window to the sum of above counts $C_s$. That is, the value input into the k-th unit was the ratio $R_k$ to $C_s$. The outputs were three count ratios defined as follows: $R_{Tc}$ was the count ratio of primary photons for $^{99m}$Tc (141 keV), $R_{In1}$was the count ratio of primary photons for $^{111}$In (171 keV), and $R_{In2}$ was the count ratio of primary photons for $^{111}$In (245 keV). With these ratios we estimated each of the primary counts by multiplying $R_{Tc}$, $R_{In1}$, and $R_{In2}$ with $C_s$. **RESULTS**: In this simulation we used the Monte Carlo method to make original energy spectra of $^{99m}$Tc and $^{111}$In at each pixel position in a detector. We used the cylinder phantom filled with water, and accuracy was evaluated by the root mean square error in the reconstructed images. The number of projection views was 90 and the number of bins in each projection was 64. The pixel size was 0.5 cm. The numbers of emitted photons were 2 Giga for $^{99m}$Tc and 2 Giga for $^{111}$In . The ANN was trained with a back-propagation algorithm by using the generalized delta rule. The images were reconstructed by the ML-EM method. The results showed that the extra energy windows to measure scattered photons from different photopeaks improve the accuracy of estimating the primary photons of $^{99m}$Tc . On the other hand, these windows may decrease the accuracy of estimating the primary photons of $^{111}$In . **CONCLUSION**: We applied the ANN method to quantitatively measure the distribution of activities in the simultaneous data acquisition with a multiple isotope SPECT study, and the accuracy of the estimation was evaluated.

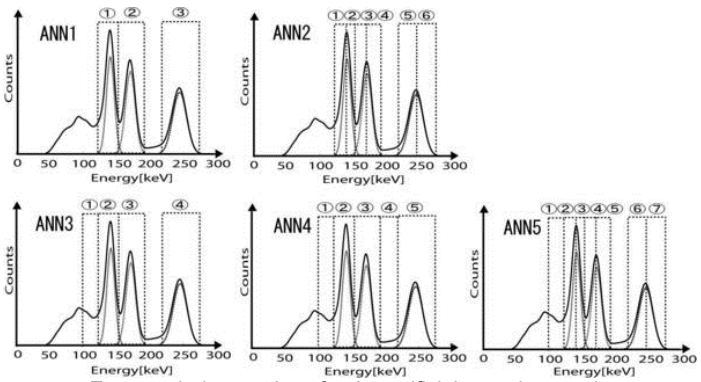


Energy window settings for the artificial neural network.

Normalized root mean square error in the reconstructed images.

| | | | | | |
|---|---|---|---|---|---|
| | | | | | |
| | | | | | |
| | | | | | |
| | | | | | |
| | | | | | |
| | | | | | |
| | | | | | |

The normalized root mean squared error of images corrected with the artificial neural network with an ideal reconstructed image acquired with a single radionuclide are calculated. The measurement was conducted in the ROI that was set to the small cylinders with a size of 300 pixels.

Disclosure of author financial interest or relationships:
**K. Ogawa**, None; **S. Abe**, None; **Y. Koike**, None; **I.O. Umeda**, None; **H. Fujii**, None.

Presentation Number **P133**
Poster Session 1
September 5, 2012 / 18:00-18:00 / Room: The Liffey

# Validation of a depth of interaction model for a small animal SPECT system

***Derek W. Austin***[1], *Bing Feng*[1], *Alan Stuckey*[2], *Dustin Osborne*[1,2], [1]*Preclinical Solutions, Siemens Healthcare, Knoxville, TN, USA;* [2]*Graduate School of Medicine, University of Tennessee, Knoxville, TN, USA. Contact e-mail: derek.w.austin@siemens.com*

Small animal SPECT systems can achieve high spatial resolution with the use of pinhole imaging techniques. However, pinhole SPECT systems are typically prone to parallax errors caused by the depth of interaction (DOI) of incident gamma rays that penetrate the detector at oblique angles. In addition to loss of resolution, this DOI effect can also introduce error in the magnification factor, and thus, the pixel size of the reconstructed object. To address this issue, we investigated the use of an energy-dependent DOI correction in our reconstruction software. First, we calibrated the geometry of our multi-pinhole SPECT system (5 pinholes per detector) by scanning a phantom containing multiple $^{57}$Co (122 keV) point sources. Proprietary software located the point sources in the projection images, followed the orbits of the point sources, and assigned them to pinholes. The system geometry was then derived from a maximum likelihood estimate of dot coordinates [1]. One of the calibration parameters included the effective focal length, which comprised the actual pinhole collimator focal length plus an average DOI. We then scanned a phantom injected with $^{125}$I and reconstructed the data without DOI correction; that is, the $^{125}$I data were reconstructed using the extracted system geometry from the $^{57}$Co calibration. When compared to its co-registered X-ray micro-CT image, the pixel size in the reconstructed SPECT image of the $^{125}$I phantom differed by roughly 2.5%. This difference was observable to the naked eye, suggesting the need for DOI correction. To apply DOI correction, our reconstruction software adjusted the effective focal length of the pinhole collimator as a function of the gamma energy. We calculated the mean DOI as a function of energy for the NaI crystal (thickness = 10 mm) in our SPECT detector using the NIST XCOM photon cross sections database [2]. To validate the calculated DOI values, we repeated the system calibration described above using point sources with the following isotopes: $^{125}$I (~30 keV), $^{99m}$Tc (140 keV), and $^{131}$I (364 keV). The mean DOI was extracted from each of these experiments and the results are shown below in Figure 1, together with the calculated values. Good agreement between calculated and measured DOI was obtained for energies below 150 keV. When our DOI correction was applied to the reconstruction of the $^{125}$I phantom, we obtained excellent co-registration with the respective X-ray micro-CT image. SPECT-CT images will be shown. Some discrepancy in the calculated and measured DOI for $^{131}$I (364 keV) is believed to be due to scatter, as scatter correction was not applied during the calibration experiments described above. Future work will include measurements with other isotopes such as $^{201}$Tl (70 keV) and $^{111}$In (171 and 245 keV) and incorporation of scatter correction to further improve our DOI model. **References:** [1] D. Beque, J. Nuyts, G. Bormans, P. Suetens, and P. Dupont, "Characterization of Pinhole SPECT Acquisition Geometry," *IEEE Trans. Med. Imaging*, vol. 22, pp. 599-612, 2003. [2] http://physics.nist.gov/PhysRefData/Xcom/html/xcom1.html.

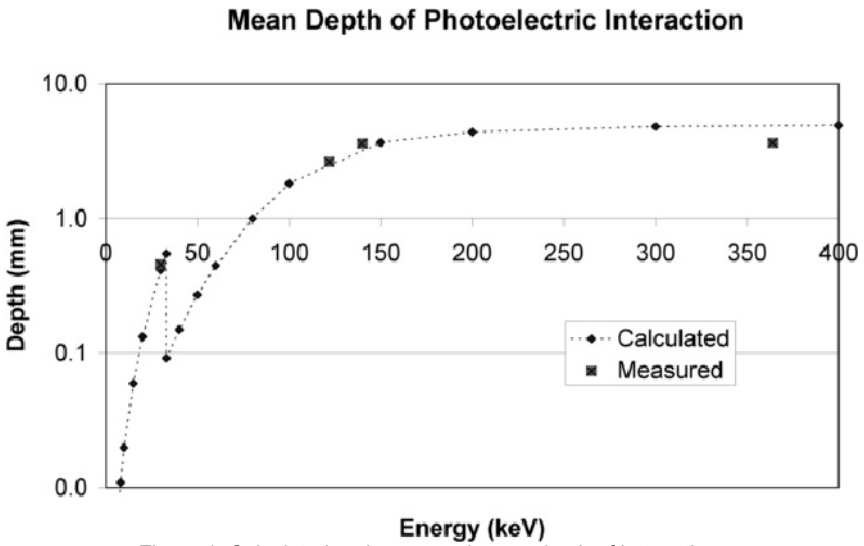


Figure 1. Calculated and measured mean depth of interaction.

Disclosure of author financial interest or relationships:
**D.W. Austin**, Siemens Healthcare, Employment; **B. Feng**, Siemens Medical Solutions, USA, Employment; **A. Stuckey**, Solex LLC, Stockholder; **D. Osborne**, University of Tennessee, Employment; Siemens Medical Solutions, Employment .

Presentation Number **P134**
Poster Session 1
September 5, 2012 / 18:00-18:00 / Room: The Liffey

# Small animal imaging with Human PET

***Mohamed-Ali Bahri***[1], *Sinan Tombuloglu*[1], *Geoff Warnock*[1], *Dounia Taleb*[1], *Florian Bretin*[1], *Christian Degueldre*[1], *Andre Luxen*[1], *Eric Salmon*[1], *Alain Plenevaux*[1], *Claude Comtat*[2], *Alain Seret*[1], [1]*Cyclotron Research Centre, University of Liège, Liege, Belgium;* [2]*Frédéric Joliot Hospital (SHSFJ), CEA, Orsay, France. Contact e-mail: M.Bahri@ulg.ac.be*

PET studies provide valuable information in the assessment of animal models for human diseases. MicroPET systems provide the high resolution needed to explore small organs but suffer from a reduced axial FOV. Multiple bed positions are then used to obtain whole body scans resulting in increased scan time and incomplete dynamic data. In contrast, human PET systems have larger axial FOV but a lower resolution. In this study, an image-based model of the scanner spatial response function combined with a 3D-OSEM reconstruction algorithm were used to improve spatial resolution of the Siemens ECAT EXACT HR+ PET scanner. A stationary double Gaussian model [1] of the ECAT EXACT HR+ point spread function was derived from 18F point source measurements performed at different radial and axial locations in the scanner FOV. This model was used in a 3D-OSEM reconstruction (3D-OSEM-RM). Sinograms were normalized and attenuation and scatter corrected using the Siemens ECAT tools before reconstruction. Both NEMA NU 2-1994 performance phantoms and NEMA NU4-2008 image quality phantom mimicking small animals were used to evaluate the accuracy of corrections for physical effects and the overall image quality. A 50 min dynamic FDG rat study was conducted on the ECAT HR+ and reconstructed with 3D-OSEM-RM. The images were used to compute the metabolic rate of glucose (MRglu) in multiple brain structures. These images were also visually compared to the static image obtained with a FOCUS 120 microPET immediately after the HR+ dynamic scan. The standard deviations of the two Gaussians used to model the transaxial (axial) resolution in a central FOV of 5 cm radius were $\sigma 1 = 1.6$ (2.75) mm and $\sigma 2 = 3.66$ (4.16) mm, and the ratio of the weights between the first and second Gaussians was $\rho = 0.2$ (0.7). Image uniformity and accuracy of scatter and attenuation corrections, evaluated following NEMA NU 2-1994, were found to be very similar between 3D-OSEM, 3D-OSEM-RM, 2D- and 3D-FBP reconstructed images. When using the NEMA NU4-2008 image quality phantom a significant increase of the hot rod recovery coefficient was observed. This effect was rod size dependent and amounted to 17-35% for the 3D-OSEM-RM compared to the 3D-OSEM and to 35-62% compared to the FBP reconstructions. Nevertheless the values obtained with 3D-OSEM-RM were around 20-35% lower than those obtained with the FOCUS 120 microPET scanner. Most of the small brain structures observed on microPET images were also visible on the images obtained with the HR+ scanner and 3D-OSEM-RM. Rat cerebral MRglu values calculated on 3D-OSEM-RM images were in the range of published values [2] (e.g. whole brain = 25.34 µmol/min/100g). Using an approximate model of the ECAT EXACT HR+ spatial response in 3D-OSEM resulted in sufficient image quality for dynamic whole body scans of small rodents, despite the large FOV, and resulted in improved contrast compared to images generated using the built-in software. This methodology will be applied for future small animal dosimetry and modeling studies in our laboratory. [1] Comtat et al. IEEE Nucl Sci Symp Conf Record. pp. 4120-4123 (2008) [2] Schiffer et al. J Nucl Med 48:277-287 (2007)

Disclosure of author financial interest or relationships:
**M. Bahri**, None; **S. Tombuloglu**, None; **G. Warnock**, UCB Pharma, Grant/research support; PMOD Technologies, Consultant; **D. Taleb**, None; **F. Bretin**, None; **C. Degueldre**, None; **A. Luxen**, GE Healthcare, Grant/research support; **E. Salmon**, None; **A. Plenevaux**, None; **C. Comtat**, None; **A. Seret**, None.

Presentation Number **P135**
Poster Session 1
September 5, 2012 / 18:00-18:00 / Room: The Liffey

# MicroPET Focus 120 scanner use at high-count rate

***Mohamed-Ali Bahri**, Geoff I. Warnock, Dounia Taleb, Florian Bretin, Andre Luxen, Eric Salmon, Alain Plenevaux, Alain Seret, Cyclotron Research Centre, University of Liège, Liege, Belgium. Contact e-mail: M.Bahri@ulg.ac.be*

Kinetic modeling of physiological processes using imaging techniques requires an accurate measurement of the time-activity curve of the tracer in plasma, known as the arterial input function (IF). The IF can be obtained by manual blood sampling, can be derived from PET images, or continuously measured by the use of small counting systems such as beta microprobes [1]. However, some beta microprobe systems can suffering from high background counts and low sensitivity compared to PET can obligate the use of activities higher than those typical for the imaging system. In the present study, the NEMA NU4-2008 image quality (IQ) phantom [2] was used to evaluate the image quality of the microPET Focus 120 at high activity values. Attenuation correction was obtained from transmission measurement using 57Co point source. Eight emission scans of 20 minutes were performed at decreasing activity starting from 109 MBq to 3.7 MBq (total activity in the field-of-view). To study the effect of normalization in high count rate studies, several normalization scans were performed using activities ranging between 18 and 212 MBq. Images were reconstructed with all corrections using Fourier rebinning and filtered backprojection. The mean activity and the coefficients of variation of the uniform slices were measured. All high activity reconstructed images showed a detector-block-patterned artifact with an overestimation of the counts when normalization activity is higher than that used in the IQ phantom and underestimation of the counts when normalization activity is below the activity used in the IQ phantom. Using the same high activity for acquisition and normalization considerably reduces the patterned-artifact but does not eliminate it entirely. The observed artifact is due to pulse pile-up in the detectors at high count-rates. A dedicated rejection of the pulse pile-up does not appear to have been implemented for the microPET Focus 120. An alternative would be to re-calibrate the detectors with higher activity values to prevent any pile-up effect or to create an attenuation volume into which phantoms or small animals could be inserted thus decreasing the artifact. This latter option is under development. References: [1] G. Warnock et al, European Journal of Nuclear Medicine and Molecular Imaging Research, 1-13 (2011) [2] NEMA Standards Publication NU4-2008. Rosslyn, VA: National Electrical Manufacturers Association; (2008).

Disclosure of author financial interest or relationships:
**M. Bahri**, None; **G.I. Warnock**, UCB Pharma, Grant/research support; PMOD Technologies, Consultant; **D. Taleb**, None; **F. Bretin**, None; **A. Luxen**, GE Healthcare, Grant/research support; **E. Salmon**, None; **A. Plenevaux**, None; **A. Seret**, None.

Presentation Number **P136**
Poster Session 1
September 5, 2012 / 18:00-18:00 / Room: The Liffey

# PIXSIC - Characterisation of a β+ intracerebral wireless probe for functional imaging coupled with behavioral studies performed on freely moving rats

*Julia Maerk[1], **Laure Balasse**[2], Didier Benoit[2], Mathieu Benoit[3], Jean-Claude Clemens[1], Sylvain Fieux[4], Denis Fougeron[1], Batiste Janvier[2], Michel Jevaud[1], Aurélie Genoux[2], Pascale Gisquet-Verrier[5], Françoise Lefebvre[2], Mohsine Menouni[1], Frederic Pain[2], Christian Tourvieille[4], Luc Zimmer[4], Christian Morel[1], Philippe Laniece[2], [1]CPPM - Centre de Physique des particules de Marseille, CNRS / IN2P3/ Université Aix-Marseille, Marseille, France; [2]IMNC - Imagerie et Modélisation en Neurobiolgie et Cancérologie, CNRS / IN2P3 / Univerité Paris7 et Paris 11, ORSAY, France; [3]PH-LCD, CERN, Geneva, Switzerland; [4]CERMEP, Groupement Hospitalier Est / Université Lyon 1, Lyon, France; [5]CNPS - Centre de Neuroscience de Paris-Sud, CNRS / Université Paris 11, Orsay, France. Contact e-mail: laure.balasse@u-psud.fr*

Advancing the understanding of neurophysiological mechanisms to decode the functional specificity of brain regions based on small animal in vivo studies requires the development of original and well-adjusted methods and instruments. In this field, an exciting challenge remains in the combination of brain imaging techniques and behavioral studies, which helps to associate molecular processes of neuronal communications to the related actions they initiate. However, recent approaches in this context - such as RATCAP and β-Microprobe - are still affected by important constraints considering the investigation of awake and freely moving animals. PIXSIC presents a novel strategy using a submillimetric telemetric pixellated probe for β+ radiotracer detection based on a reverse biased, high-resistivity silicon diode. The detector permits local time-activity measurements with high sensitivity and additional imaging features. The prototype of the sensor is 200 µm thick, 690 µm wide and 17 mm long and surrounded by 2 guard rings required to stabilize the probe edge with regard to leakage current. It comprises 10 pixels, with dimensions of 200 µm x 500 µm that are optimised in terms of beta+ sensitivity versus relative transparency to the gamma background. The probe, which can be stereotaxically implanted in the region of interest in rodent brain, is wire-bonded to a PCB fixed on the skull that supports the specific ASIC for the parallel signal processing of each pixel. The PCB is connected to a back-board carried by the animal in a backpack that incorporates the components required to drive the ASIC and to deliver a radio-frequency telemetric signal to the PC acquisition board. It also includes 2 micro-batteries for the power supply of all components. The assembly is sufficiently light and small to prevent any interference with the movements of the animal during the experiments. The RF module renders the setup fully autonomous and therefore limits stress induced in the animal during acquisition and enables behavioral studies. The physical characterisation of the complete system was performed with a beaker filled with a homogenous aqueous solution of $^{18}F$ and $^{11}C$ and confirmed the simulation results in terms of sensitivity with respect to the detection volume. Calculated pixel sensibilities were in the range of 70 cps/(MBq/ml) for $^{18}F$ and 140 cps/(MBq/ml) for $^{11}C$. Response uniformity of the 10 different pixels was evidenced. The theoretical beta-contribution to the signal was 60% and 80% for $^{18}F$ and $^{11}C$, respectively, with a residual noise mainly composed of non-specific gamma background. As a final result, we proved that parylene coating of the probe protects the sensors against humidity and that the detector sensitivity allows to perform accurate time activity curve measurements with a temporal resolution of less than 2 seconds.

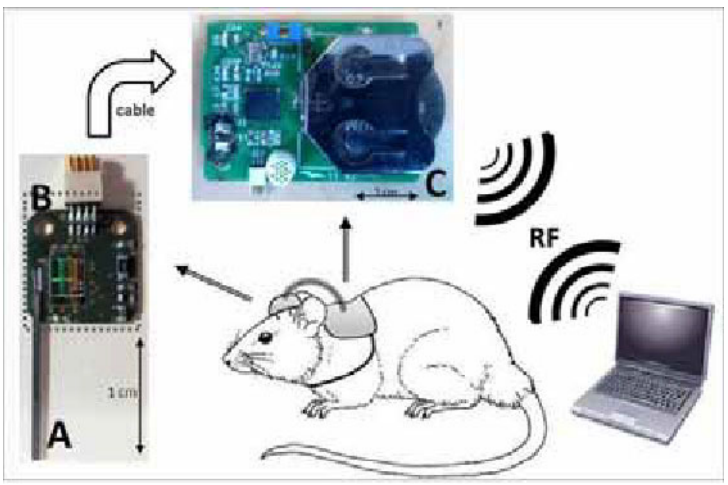


Figure 1 : Illustration of PIXSIC's main components for autonomous experimentation : Prototype of the PIXSIC detector with the silicon probe (A), the signal processing chip (B) and the backpack (C)

Disclosure of author financial interest or relationships:
**J. Maerk**, None; **L. Balasse**, None; **D. Benoit**, None; **M. Benoit**, None; **J. Clemens**, None; **S. Fieux**, None; **D. Fougeron**, None; **B. Janvier**, None; **M. Jevaud**, None; **A. Genoux**, None; **P. Gisquet-Verrier**, None; **F. Lefebvre**, None; **M. Menouni**, None; **F. Pain**, None; **C. Tourvieille**, None; **L. Zimmer**, None; **C. Morel**, None; **P. Laniece**, None.

Presentation Number **P137**
Poster Session 1
September 5, 2012 / 18:00-18:00 / Room: The Liffey

# Factors affecting the quantitative accuracy of the Inveon Small Animal PET scanner

***Simone Beer***[1,2], *Tina Kroll*[2], *David Elmenhorst*[2], *Stefan van Waasen*[1], *Andreas Bauer*[2,3], [1]*Central Institute for Electronics, Research Center Juelich, Juelich, Germany;* [2]*Institute of Neuroscience and Medicine (INM-2), Research Center Juelich, Juelich, Germany;* [3]*Department of Neurology, Medical Faculty, Heinrich-Heine-University Duesseldorf, Duesseldorf, Germany. Contact e-mail: si.beer@fz-juelich.de*

Small-animal PET is a valuable tool to study pharmacokinetics. For specific applications it is essential to calibrate the values of the reconstructed image voxels in units of radioactivity concentration with a high accuracy and to ensure the accuracy of the calibration over a period of time, particularly with regard to longitudinal studies. Quantitative accuracy might be affected by both correction methods like attenuation and scatter correction and the accuracy of calibration factors which are in turn affected by normalization and the estimation method of the calibration factors. The purpose of this work is to assess these factors and their specific contributions to quantitation accuracy and stability for the Inveon small-animal PET scanner [1]. **Material and methods** *Impact of normalization and calibration method* A 68Ge cylinder source of 6 cm diameter was used for normalization and calibration. Over a period of 326 days, 9 normalization scans of 10 hours each were performed. A quantification calibration scan (emission scan with 550x106 events, 30 min transmission scan) was performed 144 days after the first normalization scan with the same cylinder. Based on these normalizations, 9 images were reconstructed using FORE+FBP and attenuation correction. From one of the images, calibration factors were estimated following the procedure supposed by the supplier, with ROI diameters varying from 7.7 mm up to 54.3 mm. Additionally, calibration factors were estimated from all 9 images with a ROI diameter of 35 mm. *Impact of attenuation and scatter correction* Over a period of 49 days, a series of 73 PET scans of the same cylinder source was performed at a fixed position, with a 15 min transmission scan prior to each emission scan. Images were reconstructed using FORE and FBP with and without both attenuation and scatter correction, using the same normalization for all images, and corrected for the decay of 68Ge. ROIs of 41 mm diameter x 9.5 cm (~75% of the active diameter and axial FOV) were drawn and the average activity concentrations were estimated. **Results** The difference in calibration factors with varying ROI diameter was 4.3% for diameters from 7.7 to 46.5 mm, and 15% for diameters from 7.7 to 54 mm. Over the 9 normalizations and a ROI diameter of 35 mm, the %StdDev of the calibration factors was 0.4. %StdDev of the average activity concentrations were 0.29 for reconstruction with neither attenuation nor scatter correction, 1.06 with attenuation correction, and 0.91 with both attenuation and scatter correction. **Conclusion** The stability of the quantitation accuracy depends on several factors. The ROI size which is chosen during the calculation of calibration factors has the strongest impact on the stability of quantitation, followed by the attenuation correction of the emission data. Additional scatter correction improves the stability of quantitation. Thus, both a standardized calibration procedure with a fixed ROI diameter for the estimation of calibration factors and a dedicated cross-calibration accompanying each animal scan are advisable. **References** [1] Bao, Q., et al. J Nucl Med 50:401-408, 2009

Disclosure of author financial interest or relationships:
**S. Beer**, None; **T. Kroll**, None; **D. Elmenhorst**, None; **S. van Waasen**, None; **A. Bauer**, None.

Presentation Number **P138**
Poster Session 1
September 5, 2012 / 18:00-18:00 / Room: The Liffey

# Novel Readout Scheme for a Sub-Millimeter Resolution PET System

***Matthew Bieniosek***[1,4], *Peter D. Olcott*[3,4], *Craig S. Levin*[2,4], [1]*Electrical Engineering, Stanford University, Stanford, CA, USA;* [2]*Radiology, Stanford University, Stanford, CA, USA;* [3]*Bioengineering, Stanford University, Stanford, CA, USA;* [4]*Molecular Imaging Program at Stanford (MIPS), Stanford University, Stanford, CA, USA. Contact e-mail: mbieni@stanford.edu*

We are constructing a sub-millimeter resolution PET system to track and quantify smaller numbers of cells than currently possible. In this work we present results showing the identification of sub-millimeter LYSO scintillation crystals on a position sensitive solid state photomultiplier (PS-SSPM) using a novel pulse width modulation (PWM) technique for electronic readout. Position sensitive photo-detectors are often used in positron emission tomography (PET) scanners to readout light produced by scintillators. These detectors are made up of photo-diodes connected by a grid of resistors or a sheet resistance (see Fig. 1a). Each position sensitive photo-detector has 5 readout channels, one at each corner to determine the position of the signal and one channel for timing information. High resolution PET scanners have many small scintillation crystals, and therefore a large number of photo-detectors and readout channels. 3-D positioning PET detectors will further improve the performance of high resolution PET, but require many more readout channels. To make 3-D positioning detectors practical, PET readout electronics must be drastically simplified. In this work we present a time based readout system to simplify PET readout electronics by eliminating high numbers of analog-to-digital converters. PWM works by converting PET detector pulses into digital pulses with length proportional to pulse height. The digital pulses can then be highly multiplexed and read by a single time-to-digital converter. Our implementation of PWM uses a charge-to-time converter (CTC) to produce the digital pulse. The CTC consists of a charge sensitive pre-amp stage with a diode in parallel with the feedback capacitor and a discharge resistor from the pre-amp's input to ground (see Fig. 1c). When there is no signal the diode is on and conducts a current equal to the voltage on the pre-amp's input divided by the discharge resistor. Once a signal is presented to the pre-amp the output voltage drops causing the diode to turn off. The feedback capacitor integrates the charge of the pulse then linearly discharges through the resistor until the equilibrium voltage is restored and the diode turns back on. The signal from the pre-amp is sent to a comparator to create the digital pulse. A PWM circuit was constructed using ADA489 op-amps. Our circuit was tested with a 5mmx5mm position sensitive solid state photo multiplier (RMD) coupled to a 4x4 array of 0.9mm×0.9mm×15mm LYSO crystals irradiated by a Na-22 source. The signal from the CTC was sent to the scope to determine the signal's time over a scope threshold. Our experiments show that 511keV interactions can be identified from the sum of the position signals using PWM readout. The crystals can be identified in the flood map with a peak to valley ratio of 5.24. Our experiments show that a CTC PWM can be used to determine the energy and position of events of <1mm width scintillation crystals on position sensitive photo-detectors allowing for a highly compact PWM readout of 3-D positioning PET detectors designed for sub-mm resolution PET.

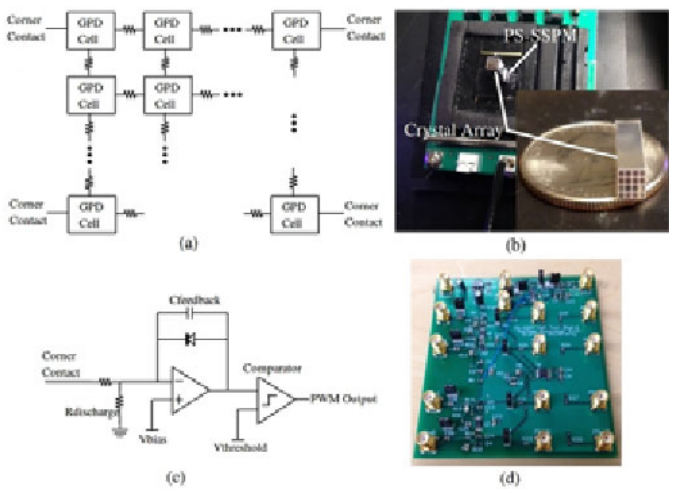


Figure 1: (a) The PS-SSPM architecture consisting of individual Geiger-mode photo-diodes (GPD) connected by a mesh of resistors. (b) The PS-SSPM and array of 0.9mmx0.9mmx15mm LYSO crystals used for our experiments. (c) Simplified PWM circuit diagram. Each corner contact is read by a PWM circuit which produces a digital pulse whose length is proportional to the input pulse height. (d) Our test PCB containing 4 PWM circuits as seen in (c), one for each corner channel.

Disclosure of author financial interest or relationships:
**M. Bieniosek**, None; **P.D. Olcott**, None; **C.S. Levin**, None.

Presentation Number **P139**
Poster Session 1
September 5, 2012 / 18:00-18:00 / Room: The Liffey

# Mouse imaging capabilities of the Inveon SPECT system using single and multi-pinhole collimators

***Frederic Boisson***[1], *David Zahra*[1], *Arvind Parmar*[1], *Marie-Claude Gregoire*[1], *Steven Meikle*[2], *Anthonin Reilhac*[1], [1]*LifeSciences, ANSTO, Kirrawee DC, NSW, Australia;* [2]*Brain and Mind Research Institute, THE UNIVERSITY OF SYDNEY, Sydney, NSW, Australia. Contact e-mail: fredericb@ansto.gov.au*

Among the modern nuclear imaging techniques, Single Photon Emission Computed Tomography (SPECT) has established itself in the field of small animal imaging and has given rise to many technological improvements in detector and collimation design as well as in image reconstruction techniques. The last decade has seen the advent of a large number of SPECT systems dedicated to small animal imaging, integrating various modes of operation. In the present study, we assessed the imaging capabilities of the Inveon SPECT system (Siemens Medical Solution, Knoxville, TN) using 3 different collimator plates dedicated for mouse imaging: a single pinhole with a 0.5mm aperture (MHR) and two 5-pinholes with 0.5mm (MBR) and 1mm (MWB) apertures respectively. We first measured the sensitivity and spatial resolution obtained with the three tested collimators at radii of rotation ranging from 25mm to 40mm and using line sources filled with $^{99m}$Tc. We then characterized the image quality obtained with the two available reconstruction algorithms (OSEM3D and MAP3D) and for the three tested collimators using the NU-4 Image Quality phantom and an ultra-micro Derenzo phantom. Multiple reconstructions were performed by varying the number of iterations and/or the prior strength in order to study the convergence properties of both algorithms but also to evaluate the effect of the parameters on the image quality and on the signal quantification. Two metrics were used to analyze the images obtained with the NU-4 Image Quality phantom: the recovery coefficient and the image noise (measured from the homogeneous region). The images obtained with the Derenzo phantom were used for visual assessment of image quality. Finally, an animal experiment was conducted to illustrate the system performance. 4 BALB/c mice were injected with a solution of $^{99m}$Tc-sestaMIBI and scanned immediately after injection for 3h in WB scanning-focus mode. Both multi-pinholes were used with the radius of rotation set to 30mm. The proposed method lied in the sequence of multiple tomographic acquisitions, each representing the different time frames needed to study the radiopharmaceutical kinetics. This method allowed first to determine the optimal time window of study but also to obtain the three-dimensional biodistribution of the compound with a resolution of 1mm. The measured spatial resolution ranged from 0.57 (MHR) to 1.0mm (MWB) while the system sensitivity was found to be between 29.3 (MHR) and 403.6cps/MBq (MWB). We found that 20 iterations (5 subsets) were sufficient to reach convergence with the Image Quality phantom scans using the single pinhole and with both algorithms. For the two multi-pinholes, the required numbers of iterations were found to be 35 and 100 (5 subsets) for the 0.5 and 1mm aperture respectively. Figure1 shows the recovery coefficients obtained at convergence for the three tested collimators. The reconstruction study also showed that MAP3D allowed better noise reduction without degrading the recovery coefficient compared to other regularization strategies, such as the premature termination of the OSEM3D reconstruction or OSEM3D followed by Gaussian filtering.

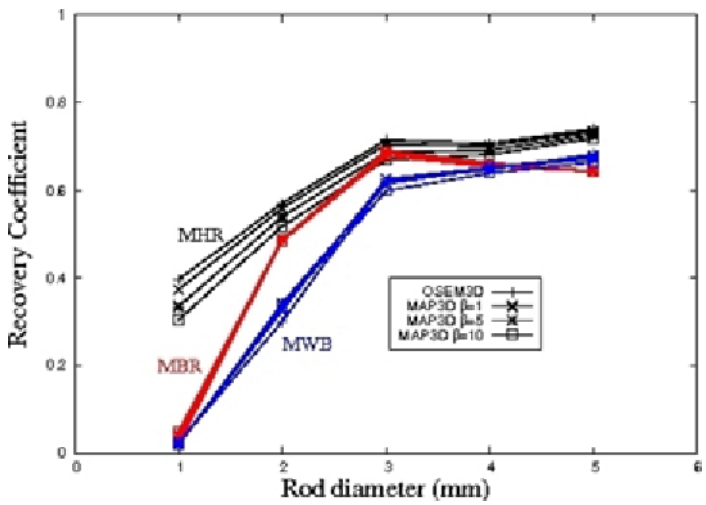


Recovery coefficients obtained for the three tested collimators and for the different reconstruction protocols.

Disclosure of author financial interest or relationships:
**F. Boisson**, None; **D. Zahra**, None; **A. Parmar**, None; **M. Gregoire**, None; **S. Meikle**, None; **A. Reilhac**, None.

Presentation Number **P140**
Poster Session 1
September 5, 2012 / 18:00-18:00 / Room: The Liffey

# Dosimetry for 6-[18F]Fluoro-L-DOPA in humans based on *in vivo* microPET scans and *ex vivo* tissue distribution in mice

***Florian Bretin**, Geoff I. Warnock, Mohamed-Ali Bahri, Lionel C. Libert, Christian Lemaire, Christophe Phillips, Alain Seret, Andre Luxen, Alain Plenevaux, Cyloctron Research Center, University of Liege, Liege, Belgium. Contact e-mail: Florian.Bretin@ulg.ac.be*

Radiation dosimetry of new radiopharmaceuticals generally starts with studies in small animals such as mice and rats. The traditional technique has long been *ex vivo* measurement of the biodistribution over time using harvested organs at different times post administration of the radiopharmaceutical. Since this approach requires a significant amount of animals, dynamic microPET studies, where the biodistribution of the tracer over time can be determined *in vivo* in a single scan, are an invaluable alternative. Due to known imaging artifacts and limitations, such as partial volume effect, a hybrid technique combining harvesting organs (post-scan) and dynamic imaging was introduced to achieve a cross-calibration to account for these limitations. Since 6-[18F]Fluoro-L-DOPA is a widely used PET tracer to study the dopaminergic system in neurology and oncology and there is no sound published dosimetry data, absorbed doses for major organs in humans were estimated using the traditional *ex vivo* technique and by dynamic microPET imaging in mice, allowing direct comparison of the results from the two techniques. The tissue distribution over time of 6-[18F]Fluoro-L-DOPA was determined by radioassay of harvested organs at 2, 5, 10, 30, 60, 120 minutes post administration (n=5 at each time point) in isoflurane-anaesthetized mice. Dynamic PET images were acquired with a FOCUS 120 microPET for 120 minutes after injection of 6-[18F]Fluoro-L-DOPA followed by radioassay of harvested organs (n=4). A bladder voiding scenario was used to simulate excretion every 2 h. The organ time-activity-curves (TACs) from both methods were extrapolated from a simulated 35 g standard mouse to a 70 kg standard male human using a technique based on organ to bodyweight ratios. The absorbed doses in major human organs were calculated with the commercially available human dosimetry software OLINDA/EXM (Version 1.1) using the extrapolated TACs. The extrapolated organ TACs obtained using the two methods showed a high correlation (average $r = 0.94 \pm 0.05$, $p < 0.001$). However, TACs from PET alone under- or overestimated the activity in individual organs in contrast to TACs obtained using the cross-calibration of the PET data with the activity in post-scan dissected organs. Those organs in the excretion pathways, comprising bladder wall, kidneys and liver, received the highest organ doses. The total body absorbed dose was 0.0118 mGy/MBq for both the imaging based and harvesting based methods. The effective dose was 0.0193 mSv/MBq for the hybrid imaging-harvesting technique and 0.0189 mSv/MBq for the pure harvesting technique. Scaling errors in the PET TACs are likely caused by quantification errors such as partial volume effects and image artifacts. The use of a hybrid imaging technique to cross-calibrate the TACs improved the accuracy of the imaging-based dosimetry estimates. Therefore the hybrid technique combining dynamic imaging and harvesting organs (post-scan) is a suitable alternative to the gold standard *ex vivo* radioassay method. It yields comparable results yet reduces significantly the amount of animals needed in the study and can accelerate data acquisition.

Disclosure of author financial interest or relationships:
**F. Bretin**, None; **G.I. Warnock**, UCB Pharma, Grant/research support; PMOD Technologies, Consultant; **M. Bahri**, None; **L.C. Libert**, None; **C. Lemaire**, None; **C. Phillips**, None; **A. Seret**, None; **A. Luxen**, GE Healthcare, Grant/research support; **A. Plenevaux**, None.

Presentation Number **P141**
Poster Session 1
September 5, 2012 / 18:00-18:00 / Room: The Liffey

# GPU accelerated realtime reconstruction of freehand SPECT examinations

***Aron Cserkaszky***[1,2], *Thomas Wendler*[2,1], *Stefan Wiesner*[2], [1]*Computer Aided Medical Procedures, TU Munchen, Munchen, Germany;* [2]*SurgicEye GmbH, Munchen, Germany. Contact e-mail: cserkaszky@yahoo.co.uk*

Purpose: Single Photon Emission Tomography (SPECT) examinations are gaining a foothold inside the operating room in techniques like the sentinel lymph node biopsy. This is mostly since the introduction of freehand SPECT, a modality which combines the standardly used gamma probes and novel SPECT reconstruction methods. The SurgicEye declipseSPECT is a system implementing freehand SPECT- It uses optical tracking of the gamma probe and enables the surgeon to get a 3-D view of the radioactive marker distribution by freehand scanning the area of interest. Here we show the feasibility of a realtime reconstruction algorithm, utilizing the massively parallel processing capabilities of modern Graphical Processing Units (GPU). This feature is more than just a speed increase of the computation; it opens new possibilities for the surgeon to achieve sufficient image quality with minimal amount of scanning time and full scan coverage of the areas containing radioactively marked structures. Methods: We modified a declipseSPECT system to implement image reconstruction on GPU. Our reconstruction algorithm uses the Maximum Likelihood Expectation Maximization (ML-EM) method to compute reconstructed images from the available measurements during the scanning. This is made possible by to the high speed of the GPU based solver, which can process 4 gigabyte of the system matrix entries per second in one iteration step. The reconstructions uses on-the-fly system matrix element generation, meaning that the matrix is not stored, rather recomputed when needed. Further, since freehand SPECT measurements are prone to noises from various causes, we created a realtime exposure analyzer algorithm that uses clustering, smoothing and speed filtering of the scanned measurements to precondition the system matrix and complement our reconstruction. Results: The raw speed increase of our GPU based reconstruction compared to CPU based methods is 15 fold. Our tests show effective artifact reduction of up to 53%. Conclusions: Realtime reconstruction of freehand SPECT data brings benefits in terms of speed and quality. Such implementation could bring significant improvements in the deployment of the system in the operating room.

Disclosure of author financial interest or relationships:
**A. Cserkaszky**, SurgicEye GmbH, Employment; **T. Wendler**, SurgicEye GmbH, Stockholder; **S. Wiesner**, SurgicEye GmbH, Employment .

Presentation Number **P142**
Poster Session 1
September 5, 2012 / 18:00-18:00 / Room: The Liffey

# Multi-mouse imaging on MicroPET-CT scanners - is seven too many?

***Timothy Doyle**, Pediatrics, Stanford University, Stanford, CA, USA. Contact e-mail: tim.doyle@stanford.edu*

The increasing use of molecular imaging techniques such as microPET has lead to the routine imaging of multiple mice simultaneously on scanners using "mouse hotels." Such rapid imaging of multiple animals allows increased throughput on limited instrument availability, permits increased use of radionuclide probe, as well as allowing more animals to be included in a study to increase statistical confidence. At the Stanford Small Animal Imaging Facility, four-mouse hotels are now used for most studies on both dedicated PET and PET-CT scanners. The field of view of the MicroPET-CT scanner has the capacity to include a seven-mouse hotel, and this study determines the qualitative and quantitative impact on imaging up to seven animals simultaneously. It has previously been shown that both sensitivity and resolution drop off significantly as a specimen is moved from the center to edge of the axial field of view of such scanners, although how this actually impacts animal studies has not been investigated. In this study, mice (FVB, female, c.30g) were injected with equal doses of F18-labelled sodium fluoride, and after one hour were sacrificed prior to starting imaging. Animals were sacrificed to ensure that no further excretion of probe occurred during subsequent imaging, and due to the extended imaging time required, to prevent the need for extended anesthesia. Mice were then placed in custom-made mouse hotel that could hold up to seven animals (in a 2-3-2 hexagonal layout), and CT followed by 15-minute static PET scans performed. Mice were then rearranged in the holder such that each animal was scanned in the middle position (optimal position for imaging). OSEM2D and OSEM3D/MAP reconstructions were performed on all datasets with CT attenuation correction. Further similar scans were performed with fewer animals, scanning 1, 3, 4 or 7 animals in the holder to determine the impact of animal number on image quality and quantification. In all cases, threshold-based regions of interest were created from the CT data for each animal, and these were used to determine the total radionuclide activity for each animal in each scan. This was compared to the total activity measured for one animal using a dose calibrator before each scan. For PET data reconstructed with OSEM2D protocols, less than 3% variance was observed when the animal position was altered from center to outer holders in the hotel, while less than 3.5% variance was observed when a OSEM3D/MAP reconstruction was applied to the same data. Similarly, less than a 5% difference was observed with OSEM3D/MAP reconstruction when 1, 3, 4 or 7 animals were scanned at one time, although larger variance (up to 12.5% variance) was observed with OSEM2D reconstructed data. Qualitatively, little significant difference could be observed whether the animal was scanned at a central or outer position in the hotel, or on whether there were multiple subjects in the field of view. This study suggests that the microPET-CT scanner can be used for routinely scanning up to 7 animals simultaneously.

Disclosure of author financial interest or relationships:
**T. Doyle**, None.

Presentation Number **P143**
Poster Session 1
September 5, 2012 / 18:00-18:00 / Room: The Liffey

# Positron Emission Tomography for Multiple Molecular Imaging

***Tomonori Fukuchi***[1], *Takahisa Hanada*[2], *Yilong Cui*[1], *Hiroshi Toyoda*[1], *Yasuyoshi Watanabe*[1], *Shuichi Enomoto*[1,2], [1]*Center for Molecular Imaging Science, RIKEN, Kobe, Japan;* [2]*Graduate School of Medicine, Dentistry and Pharmaceutical Sciences, Okayama University, Okayama, Japan. Contact e-mail: tfukuchi@riken.jp*

Positron Emission Tomography (PET) represents today essential role in nuclear medicine, due to its ability to provide quantitative bio-distribution of a molecular probe. However, PET works only for single probe simultaneously, because positron-electron annihilation always results in two 511-keV photons irrespective of nuclide. In order to overcome this limitation, we have been developing Polychrome-PET (P-PET) for multiple molecular simultaneous imaging. P-PET identifies different probes by detection of gamma-ray emitted successively after the positron. For the purpose of designing a practical P-PET, we carried out computer simulation using a Monte Carlo base simulator GATE (Geant4 Application for Tomographic Emission). In this simulation, semiconductor or scintillation gamma-ray detectors were added to the existing PET system. As the result, above 10% gamma-ray detection efficiencies were provided by additional gamma-ray detectors on outer ring geometry of the PET detectors. When P-PET measures multiple molecular probes, double- and triple-coincidence measurements will be performed in parallel. Therefore, in order to re-produce this situation in the simulator, we made a digital fantom by the superposition of two experimentally measured actual bio-distributions of different probes in small animals. In this digital fantom, two distributions corresponded to pure positron emitter and positron-gamma emitter, respectively. From measurement of this fantom by P-PET simulator, we calculated true double- and triple- coincidence rates under the condition of practical coincidence time window. To estimate imaging noise derived from the random coincidence of 3rd gamma-ray, we performed image reconstructions from two simulated data set separated by the condition of whether 3rd gamma-ray was coincident. As the results, we successfully produced 3D images of each probe distribution. We also considered useful radio-isotopes for P-PET and its applications based on nuclear decay database and this simulation results. Moreover, we also carried out experimental study of P-PET using a planer type PET system with additional Ge semiconductor gamma-ray detector. In this experiment, standard PET probe and a probe labeled by positron-gamma emitter were injected into a mouse. The collected data was distributed into two data sets whether Ge detector detected additional gamma-ray of not. These two data sets were used for image reconstruction independently. This experiment also supported the feasibility of P-PET.

Disclosure of author financial interest or relationships:
**T. Fukuchi**, None; **T. Hanada**, None; **Y. Cui**, None; **H. Toyoda**, None; **Y. Watanabe**, None; **S. Enomoto**, None.

Presentation Number **P144**
Poster Session 1
September 5, 2012 / 18:00-18:00 / Room: The Liffey

# A Large Field-of-View PET/CT Scanner for Simultaneous Imaging of Small Animals with Four-Layer Depth-of-Interaction Detectors

***Masafumi Furuta***[1], *Katsumi Sekikawa*[1], *Masanobu Sato*[1], *Yoshiyuki Yamakawa*[1], *Hiromichi Tonami*[1], *Junichi Ohi*[1], *Keishi Kitamura*[1], *Kimura Hiroyuki*[2], *Hideo Saji*[2], [1]*Technology Research Laboratory, Shimadzu Corp., Kyoto, Japan;* [2]*Graduate School of Pharmaceutical Sciences, Kyoto University, Kyoto, Japan. Contact e-mail: m_furuta@shimadzu.co.jp*

**Introduction** Small animal PET/CT has well established as an important imaging modality for preclinical application. Imaging multi-animals at the same time with a large field-of-view (FOV) PET/CT scanner is useful for reducing total time for data acquisition and the number of times to synthesize radiopharmaceuticals. Multi-animal imaging, in which each animal is positioned away from the center of the transaxial FOV, requires high spatial resolution throughout the FOV. This study aimed to develop and evaluate a large FOV PET/CT scanner with four-layer depth of interaction (DOI) detectors in order to achieve both high sensitivity and high spatial resolution. **System** The scanner consists of a PET scanner and a cone-beam CT. The PET detector ring consists of 36 detector modules arranged in a 3-ring configuration with a 183 mm diameter of the transaxial FOV and an axial FOV of 155.5 mm. The detector consists of four-layer of a 32 × 32 Lu1.8Gd0.2SiO5 (LGSO) crystal array and a 64ch position-sensitive photomultiplier tube (H8500). The cone-beam CT scanner consists of a micro-focus X-ray tube and a digital flat panel detector (FPD) with a 185mm diameter of the transaxial FOV and an axial FOV of 50mm. The CT has the larger FOV used for attenuation correction and image fusion. With multi-animal holders, four mice or two rats can be imaged at the same time. The reconstruction method is list-mode DRAMA (Dynamic Row-Action Maximum likelihood Algorithm). **Method** The scanner performance was evaluated with the NEMA NU-4 2008 standard. Some images of small animals were also obtained. In four-mouse imaging, each mouse was injected with about 1.3 MBq of FDG, and was set in order to a multi-animal holder. The acquisition time was 20 minutes. In two-rat imaging, each rat was injected with about 4.7 MBq of FDG, and the acquisition time was 15 minutes for each of two step positions. Both images were reconstructed without attenuation and scatter correction. **Result** and Discussion The radial spatial resolution (FWHM) ranged from 0.87 to 1.45mm, tangential FWHM from 0.88 to 1.33mm, and axial FWHM from 0.79 to 1.45mm as shown in Fig.1(a). The sensitivity at the center of the FOV was 11% as shown in Fig.1(b). The multi-animal images with high spatial resolution were also obtained with four mice and two rats, as shown in Fig.1(c) and (d), respectively. These results indicate that the large FOV scanner with the four-layer DOI detectors is a useful tool to realize simultaneous imaging of small animals and it could also be useful for imaging of medium animals such as rabbit.

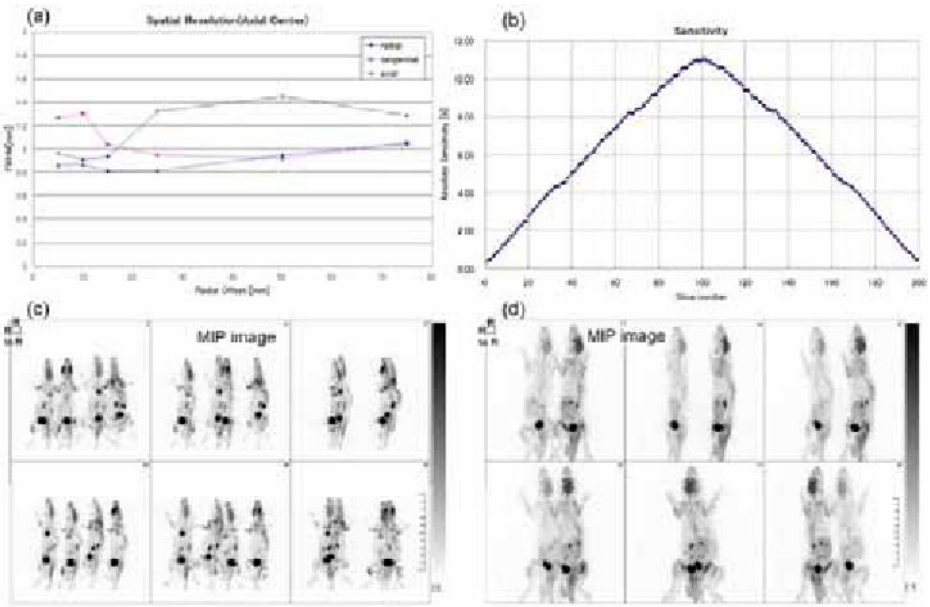


Fig.1 (a) Spatial resolution and (b) sensitivity of the PET scanner across the FOV. MIP (Maximum Intensity Projection) images of (c) four mice and (d) two rats.

Disclosure of author financial interest or relationships:
**M. Furuta**, Shimadzu Corp., Employment; **K. Sekikawa**, Shimadzu Corp., Employment; **M. Sato**, Shimadzu Corp., Employment; **Y. Yamakawa**, Shimadzu Corp., Employment; **H. Tonami**, Shimadzu Corp., Employment; **J. Ohi**, Shimadzu corp., Employment; **K. Kitamura**, Shimadzu Corporation, Employment; **K. Hiroyuki**, None; **H. Saji**, None.

Presentation Number **P145**
Poster Session 1
September 5, 2012 / 18:00-18:00 / Room: The Liffey

# Comparison of manual and automatic quantification of bone 99mTc-HDP SPECT/CT mouse scans

***Harald Groen***[1], *Artem Khmelinskii*[2], *Saskia Berndsen*[1], *Boudewijn Lelieveldt*[2,3], *Marion De Jong*[1,4], [1]*Nuclear Medicine, Erasmus MC, Rotterdam, Netherlands;* [2]*Image Processing & Radiology, LUMC, Leiden, Netherlands;* [3]*Mediamatics, Delft University of Technology, Delft, Netherlands;* [4]*Radiology, Erasmus MC, Rotterdam, Netherlands. Contact e-mail: h.c.groen@erasmusmc.nl*

Introduction In preclinical, translational research, dedicated animal-scanners are used more frequently. The big advantage of these scanners is that physiological processes can be studied inside living animals, the kinetic uptake of tracers can be measured and animal follow-up studies can be performed. As such, the total number of animals used for studies decreases while the amount of information per animal increases dramatically. However, a challenge is to objectively quantify the animal scans. One way to obtain quantifiable data is by using radioactive labeled compounds. In this study we investigate the relation between in-vivo and ex-vivo quantified data of whole-body bone scans obtained from mice, that are used e.g. in the field of arthritis studies, development of bone pain palliation agents and for bone metastases. Materials and Methods In total 3 mice were injected intravenously with 50 ± 6 MBq 99mTc-HDP and were scanned 4 hours post injection using the Bioscan NanoSPECT/CT. Whole-body scans were obtained during a 36 minute acquisition, followed by a whole-body CT scan. After the acquisition, the animal were euthanized, and selected tissue and bones were collected, i.e. part of the scull, vertebral, rib, humerus, ulna/radius, femur, tibia/fibula, knee joint, liver and muscle. The tissue and bones were collected in plastic tubes and scanned again with the NanoSPEC/CT. After acquisition, the tubes were counted in a gamma-counter, which is used as gold-standard for biodistributions. After reconstruction of the data, the bones were quantified using different methods using InVivoScope and an automatic CT-based method. For InVivoScope, three different methods were used; 1) each bone was summed into one 2D slice and a 30% contour was used to quantify the total activity, 2) a 3D threashold of more than 0.2 Bq/voxel of the bone was used to obtain a segmentation 3) based on the a CT treashold of 500 HU, a 3D mask, without gaps, was created and used as template for the tissue or bone. The later one was used as gold-standard. The automatic CT-based method was developed in Leiden and was based on the same approach as the gold-standard. Results Preliminary data show a linear relation (y=1.05x, R2=0.996) between the gamma-counter and total activity of each tube as determined by InVivoScope. As expected, the quantification of the actual tissue and bones was lower than the total activity inside the tube. With respect to the 3D-CT-based quantification, the 2D method showed the largest difference (8±21%), followed by the 3D threshold based method (7±12%) while the automatic method showed the lowest difference and standard deviation (4±5%). Conclusion In conclusion, in-vivo quantification with SPECT/CT imaging shows a perfect relation with the classically-used biodistribution and gamma-counter, although the method for segmentation can be of influence. The automatic developed quantification based on CT threshold shows to be a robust method and similar to manual segmentation.

Disclosure of author financial interest or relationships:
**H. Groen**, None; **A. Khmelinskii**, None; **S. Berndsen**, None; **B. Lelieveldt**, None; **M. De Jong**, None.

Presentation Number **P146**
Poster Session 1
September 5, 2012 / 18:00-18:00 / Room: The Liffey

# Segmentation of Whole-Body microSPECT Mouse Skeleton Images

***Harald Groen***[1], *Artem Khmelinskii*[2], *Marion De Jong*[1,3], *Boudewijn P. F. Lelieveldt*[2,4], [1]*Nuclear Medicine, Erasmus MC, Rotterdam, Netherlands;* [2]*Image Processing & Radiology, LUMC, Leiden, Netherlands;* [3]*Radiology, Erasmus MC, Rotterdam, Netherlands;* [4]*Mediamatics, Delft University of Technology, Delft, Netherlands. Contact e-mail: h.c.groen@erasmusmc.nl*

Introduction Whole-body SPECT/CT small animal imaging is widely used in pre-clinical research. Comparing and exploring whole-body datasets can be a difficult and time-consuming task due to the inherent heterogeneity of the data. The goal of this study is to provide a method to align and compare side-by-side multiple whole-body SPECT datasets in a common reference, eliminating any postural and positioning variability that exists between the subjects in cross-sectional and follow-up studies. Methods The first step of the proposed approach is to extract the skeleton from the SPECT data. Subsequently, the articulated MOBY mouse atlas is registered to the data following a hierarchical anatomical tree: first, the atlas is coarsely registered to the entire skeleton (see figure 1). Then, starting with the skull, each atlas bone is accurately registered to the correspondent bone in the data using the Iterative Closest Point approach. After the atlas is registered to the data, we apply the Articulated Planar Reformation algorithm to reformat the segmented data into segments corresponding to a mouse atlas and thus mapping the data to a standardized atlas space. The presented method is validated using 6 Balb/c mice, with both the 99mTc−MDP (n=3) and the 99mTc−HDP (n=3) bone-scan tracer. Results To validate the registration accuracy quantitatively and enable comparison with the registration error achieved in μCT data as reported in by Baiker et al. 2010, we used the same error metric to quantitatively evaluate the SPECT segmentation: the Euclidean point to surface distance. For each SPECT dataset, we calculated this distance between the registered atlas skeleton and the correspondent co-registered CT skeleton, before and after articulated registration. The obtained results indicate that after registration, the mean Euclidean distance decreased from 11.5 ± 12.1 to 2.6 ± 2.1 voxels and is of the same order as the previously published results for μCT, 1.8 ± 0.1 voxels. The entire articulated registration process was implemented in MATLAB R2008bTM and took approximately 2 minutes of runtime on a standard desktop PC. Applying the APR algorithm to multi-modal cross-sectional data proved to be useful to provide proper referencing and visualization for an intuitive exploration and comparison of μCT, SPECT data. Conclusions An articulated atlas-base skeleton segmentation method for SPECT whole-body small animal data was presented. The evaluation of the method demonstrated it to be accurate and robust for intuitive, side-by-side, whole-body, cross-sectional, longitudinal and multi-modal data exploration. When a tracer that doesn't concentrate in the bone is used and a complementary μCT is available the same approach holds true. In those cases, due to the robustness of the CT data, one can use the automatically segmented bones as masks for SPECT signal quantification. The approach presented here can be applied to other animals, provided an atlas.

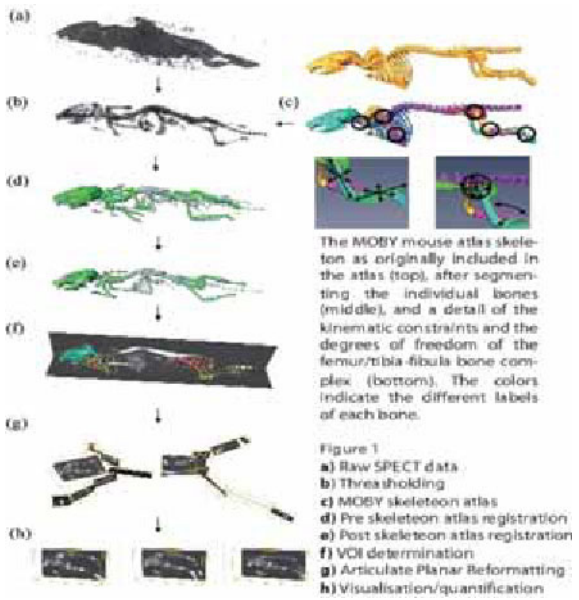

Segmentation of whole-body microSPECT mouse skeleton images

Disclosure of author financial interest or relationships:
**H. Groen**, None; **A. Khmelinskii**, None; **M. De Jong**, None; **B. Lelieveldt**, None.

Presentation Number **P147**
Poster Session 1
September 5, 2012 / 18:00-18:00 / Room: The Liffey

# Use of Dynamic Acquisition SPECT/CT to Evaluate Time Activity Relationships with Lymphoscintigraphy

***Nathan Hall***, *Nil Celebi Cherukuri, Matthew S. Zell, Jessica Campbell, Vicki Phillips, Bonnie Williams, Rick Layman, Michael V. Knopp, Radiology, The Ohio State University, Columbus, OH, USA. Contact e-mail: nathan.hall@osumc.edu*

PURPOSE: SPECT/CT data sets inherently provide the opportunity for quantification. Dynamic dataset acquisition with SPECT/CT is more difficult than with PET/CT due to the restriction of not obtaining data from all angles simultaneously. The purpose of this work was to demonstrate that dynamically acquired SPECT/CT data can produce quantitatively accurate time activity curves in a phantom and be applied to evaluate time-activity relationships with lymphoscintigraphy (LS). METHOD AND MATERIALS: Proof of concept was accomplished via phantom data acquisition acquired dynamically with a 16 slice SPECT/CT scanner in continuous mode for 6 cycles at 200 sec/cycle. Each dual head spin (6 total) was segmented into 32 (5.625°) angles and counts from both heads (total and geometric mean) were calculated and summed for the specified ROI (saline bag) to obtain a total activity for each of the 6 spins. 200 uCi Tc-99m pertechnetate in 10 ml saline was infused at a constant rate into a 50 cc saline bag containing 40 cc saline (agitated with $O_2$) suspended in a Jaszczak phantom filled with water during the dynamic scan acquisition. Attenuation corrected SPECT/CT data sets were then reconstructed and quantified. Using the same acquisition technique, dynamic SPECT/CT data was acquired immediately (2 patients), 15 minutes post-injection (2 patients), or 20 minutes post-injection (3 patients). Associated activities (counts) were measured (lymph nodes and injection site) using a 3D region of interest (ROI) tool with isocontour settings of 2% and 50% decay corrected to time of injection. The total activity per unit volume was plotted with respect each spin. Time-activity curves for each lymph node and injection site were calculated as percentage of the peak activity. RESULTS: For the phantom study, the total and geometric mean of counts for both camera heads summed for all 32 angles plotted for 6 sequential spins over 20 minutes generated an $R^2$ value of 0.9999 and 0.9997, respectively. Within each rotation there was variability in counts that was likely related in part to varying distance of the camera heads and attenuation from the table. Dynamic SPECT/CT LS images acquired immediately post-injection demonstrated uptake in the sentinel lymph within the first 10 minutes. With 15 and 20 minute post-injection start times the activity in the sentinel nodes had leveled off. Where appropriate, the plots were fitted to a line. A simultaneous injection and scan start time yields a linear relationship between time and lymph node activity as well as time and injection site activity similar to that observed in previous phantom experiments. CONCLUSION: Dynamic SPECT/CT data acquisition is capable of generating quantitatively accurate data sets that represent changes in activity in both phantom lesions and clinical LS studies binned in 3 minute intervals or less. Resultant data can be reconstructed into diagnostic quality SPECT/CT images and quantified using ROI techniques. This methodology may prove useful in assessing new radiopharmaceuticals as well as in adding dynamic and quantitative capabilities to standard nuclear medicine procedures.

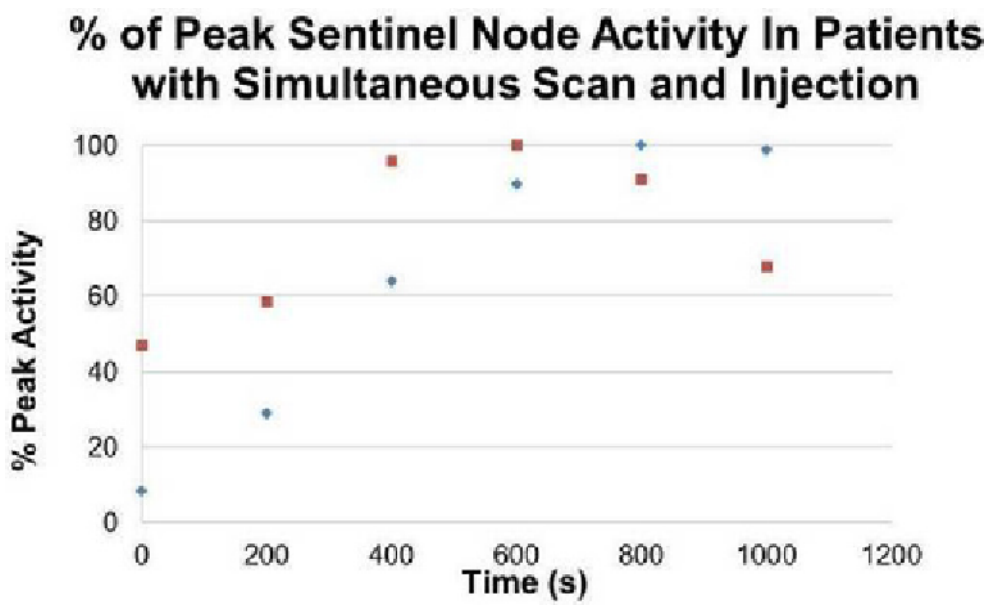


Disclosure of author financial interest or relationships:
**N. Hall**, Enlyton,Ltd., Other financial or material support; **N. Celebi Cherukuri**, None; **M.S. Zell**, None; **J. Campbell**, None; **V. Phillips**, None; **B. Williams**, None; **R. Layman**, None; **M.V. Knopp**, None.

Presentation Number **P148**
Poster Session 1
September 5, 2012 / 18:00-18:00 / Room: The Liffey

# Micro-liter Order Automated Blood Sampling System for Small Animal PET Functional Imaging

***Nobuya Hashizume***[1], *Yuichi Kimura*[2], *Takashi Yamada*[5,3], *Hiroshi Ikenuma*[3], *Takahiro Nishimoto*[1], *Kentaro Hatano*[3], *Hiroshi Toyama*[4], *Keishi Kitamura*[1], *Kengo Ito*[3], *[1]Technology Research Laboratory, Shimadzu Corp., Kyoto, Japan; [2]Molecular Imaging Center, National Institute of Radiological Sciences, Chiba, Japan; [3]Department of Clinical and Experimental Neuroimaging, National Center for Geriatrics and Gerontology, Aichi, Japan; [4]Department of Radiology, Fujita Health University, Aichi, Japan; [5]Department of Biological Chemistry, Chubu University, Aichi, Japan. Contact e-mail: hasizume@shimadzu.co.jp*

**Introduction** Quantitative molecular imaging using PET requires radioactivity concentrations in whole blood and plasma to estimate a behavior of an administered radiopharmaceutical in a target tissue. A small size of rodent restricts a volume of blood sample to a few micro-liters, and a rapid change in a time activity curve (TAC) requires a frequent sampling. Therefore, we had developed Microfluidic Mouse Plasma Counting System (μFmPC). However, the blood sampling was conducted manually, and it suffered from radiation exposure and some skill was requested to operators. Consequently, this study aimed to develop the automated blood sampling system. **System** μFmPC had following features: an acrylic disc (CD-Well) with channels for a blood sampling (1-4 μL, maximally 33 samplings), plasma separation with centrifugation, and radioactivity and the volume measurements for whole blood and plasma. CD-Well had 36 U-shaped channels with precise cross-section (0.1 $mm^2$) to measure volumes of whole blood and plasma accurately. The channels had hydrophilic inside wall with a tapered inlet that realized smooth and spontaneous entering of blood (Fig. 1(C)). Arterial blood was drawn from the femoral artery using a syringe pump at about 34 μL/sec (Carvo XCalibur, Tecan, Switzerland) (Fig. 1(A)) and was automatically dropped onto the inlet (Fig. 1 (B)). The syringe pump enabled reliable blood sampling regardless of varying blood pressure. The system was designed to have small dead volume, 15 μL, and it minimized the dispersion and bleeding. After the final blood sampling, CD-Well was centrifuged with 10,000 rpm for 5 min (Fig. 1(C)). CD-Well was then scanned by an ordinary flat bed scanner (GT-X970, Seiko EPSON Corp, Japan) with 600 dpi, and was exposed to an imaging plate (IP) for 20 min. The IP was scanned by a phosphor imaging plate scanner (BAS-5000, Fujifilm Corp, Japan) with 50 μm/pixel. The accurate volumes of whole blood and plasma were obtained from the scanner image. The radioactivity was derived from the IP image merged into the scanner image to identify radioactivity distributions of whole blood and plasma segments in the channel. **Method** An animal study was conducted using a rat. A rat was anesthetized with 2% isoflurane and a polyethylene catheter (PE-10) was inserted into the left femoral artery for blood sampling. 18F-FDG (20 MBq, 300 μL saline) was injected into the tail vain within 60 sec. The blood TAC was measured using μFmPC (ca. 2 μL/sample, 30 samples, minimum interval 20 sec for 60 min in total). **Result and Discussion** TAC in whole blood and plasma are shown in Fig. 1(D). All samplings for 60 min were succeeded. The peak was captured and the time history gradually decreased, that was reasonable shape. We conclude that the automated blood sampling system is a useful tool to realize μL-ordered blood sampling for fully quantitative molecular imaging for rodent using PET.

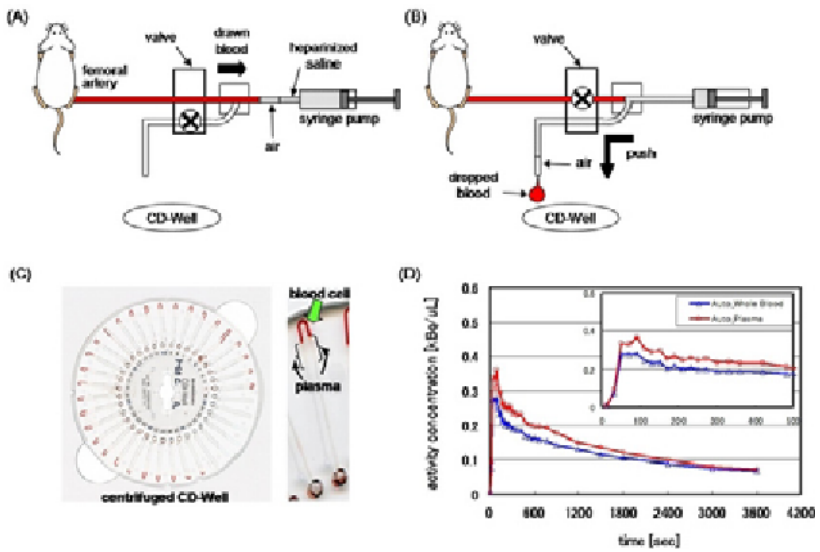


Fig. 1 (A), (B) The behavior of automated blood sampling system. (C) Plasma were separated by Centrifugation. (D) Radioactivity concentrations in whole blood and plasma using auto blood sampling system.

Disclosure of author financial interest or relationships:
**N. Hashizume**, Shimadzu Corporation, Employment; **Y. Kimura**, JSPS, Japan., Grant/research support; Shimadzu Corporation, Japan., Grant/research support; **T. Yamada**, None; **H. Ikenuma**, MICRON Inc., Employment; **T. Nishimoto**, Shimadzu Corporation, Employment; **K. Hatano**, None; **H. Toyama**, None; **K. Kitamura**, Shimadzu Corporation, Employment; **K. Ito**, None.

Presentation Number **P149**
Poster Session 1
September 5, 2012 / 18:00-18:00 / Room: The Liffey

# Performance Evaluation of a High Resolution PET/CT System for Use in Longitudinal Brain Imaging Studies

***Brad Kemp**, Val Lowe, Department of Radiology, Mayo Clinic, Rochester, MN, USA. Contact e-mail: kemp.brad@mayo.edu*

A bridging study was conducted to compare the performance of the Discovery RX and Discovery 690 ADC (DRX and D690 ADC, GE Healthcare) PET/CT systems in brain PET imaging. The DRX uses 4.2 x 6.3 x 30 mm lutetium-based crystals (LBC) arranged in a 9 x 6 block whereas the D690 ADC uses 3.8 x 3.8 x 25 mm LBC arranged in a 10 x 10 block of the same physical size. As such, the D690 ADC system has better resolution, especially in the axial direction. Therefore, an understanding of the relative imaging characteristics is vitally important as subjects are transitioned from the DRX to the D690 ADC in longitudinal brain studies. Resolution and brain phantom studies were conducted to characterize the systems and the results applied to clinical brain scans acquired on both systems. Methods: The spatial resolution of both systems was measured using a 0.3 mm Na-22 point source. The axial resolution was measured from an interleaved profile that was obtained by stepping the source in 0.25 mm increments. From this data the iterative reconstruction (IR) parameters that provide images of matched resolution were obtained. The Hoffman brain phantom was filled 17 MBq F-18, scanned in list mode and then rebinned such that the total prompts in the DRX and D690 ADC acquisitions were equal. The DRX data was reconstructed using standard IR; the D690 ADC reconstructions included those with resolution-matched (RM-IR) parameters. Regions of interest (ROIs) were drawn in grey matter, white matter and ventricular areas and mean uptake and contrast ratios were computed. Thirty patients undergoing a PET/CT brain study on the DRX were also scanned on the D690 ADC. A single F-18 FDG injection of 435 MBq mean activity was used. The PET data was acquired in list mode and then rebinned such that the total prompts in the two exams were equal. The DRX data was reconstructed using standard IR while the D690 ADC data was reconstructed with resolution-matched RM-IR. All images were spatially normalized to a template image and an atlas of ROIs was applied. The mean uptake in grey matter regions normalized to a reference region (pons) was computed. Results: The axial resolution of each system was matched at 5.4 mm full-width at half-maximum (FWHM); however the full-width at tenth-maximum (FWTM) was 9.4 mm for the D690 ADC and 11.5 mm for the DRX. The uptake in grey matter and white matter of the brain phantom was very similar for the RM-IR reconstructions with a < 5% bias in the mean uptake. Despite the RM-IR the images from the D690 ADC presented with 15% less uptake in the ventricles; this may be due to the improved axial FWTM resolution for the D690 ADC. The patient studies showed no significant difference in the normalized uptake in resolution-matched images. Similar to the brain phantom studies there is reduced uptake in ventricular areas for images acquired on the D690 ADC. Conclusions: This study has shown that the resolution-matched images from the D690 ADC can be used in a longitudinal brain imaging study.

Disclosure of author financial interest or relationships:
**B. Kemp**, None; **V. Lowe**, Bayer, Consultant; GE Health Care, Grant/research support; Siemens Molecular Imaging, Grant/research support; AVID Radiopharmaceuticals, Grant/research support .

Presentation Number **P150**
Poster Session 1
September 5, 2012 / 18:00-18:00 / Room: The Liffey

# Quantitative of CMRglc in Rat brain using a novel Microvolumetric Blood Counter System (CD-Well) and small animal PET

***Gen Kudo***[1,4], *Yuichi Kimura*[2], *Nobuya Hashizume*[3], *Hiroshi Toyama*[4], *Douglass C. Vines*[1], *David A. Jaffray*[1], [1]*STTARR, Princess Margaret Hospital, Toronto, ON, Canada;* [2]*Molecular Imaging Center, National Institute of Radiological Sciences, Chiba, Japan;* [3]*Technology Research Laboratory, SHIMADZU CORPORATION, Kyoto, Japan;* [4]*Radiology, Fujita Health University, Toyoake, Japan. Contact e-mail: gen.kudo@rmp.uhn.on.ca*

CD-Well is the novel apparatus for quantitative functional imaging using PET. It makes the time activity curve measurements in plasma and whole blood (pTAC,wTAC) practically feasible, and it enables a routine fully quantitative PET functional imaging using mice and rats. CD-Well is a specially designed apparatus to measure radioactivity concentration [Bq/μL] from a small drop of blood (less than 4μL).It is easy to conduct frequent blood sampling, for example every 10 [sec]. At this time, we tried both in vitro and in vivo Experiment using CD-Well and small animal PET (microPET Focus 220,SIEMENS ) validate of the accuracy of this system. First, we compared of the radioactivity concentration derived from CD-Well with that from an usual manual sampling. Second, we made an image of MRGlc using Patlak plot method. Needless to say, the measured time activity curve in arterial plasma using CD-Well is applied for the data analysis. As a result, we could measure both pTAC and wTAC and make a CMRglc image appropriate physiologically.

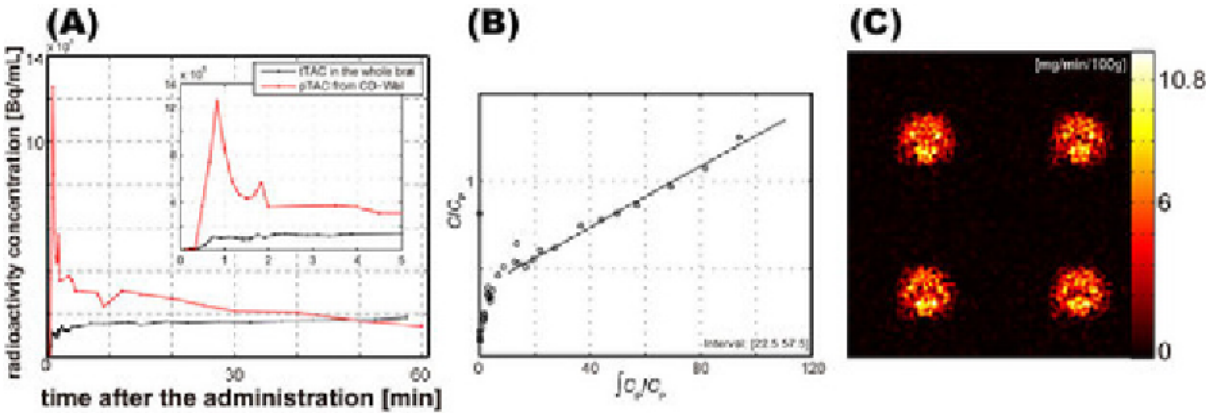


CMRglc image of rat brain using pTAC acquired with CD-Well.

Disclosure of author financial interest or relationships:
**G. Kudo**, None; **Y. Kimura**, JSPS, Japan., Grant/research support; Shimadzu Corporation, Japan., Grant/research support; **N. Hashizume**, Shimadzu Corporation, Employment; **H. Toyama**, None; **D.C. Vines**, None; **D.A. Jaffray**, Precision X-ray, Other financial or material support; Raysearch, Grant/research support; Philips, Grant/research support; Elekta, Grant/research support; General Electric, Grant/research support; IMRIS, Other financial or material support; Modus Medical, Grant/research support .

Presentation Number **P151**
Poster Session 1
September 5, 2012 / 18:00-18:00 / Room: The Liffey

# Optimization of Collimator and Reconstruction Parameters for SPECT Quantification

***Sarah J. McQuaid***[1,2], *Jonathan Gear*[3], *Stephen C. Moore*[2], [1]*Nuclear Medicine, Royal Surrey County Hospital, Guildford, United Kingdom;* [2]*Radiology, Brigham and Women's Hospital and Harvard Medical School, Boston, MA, USA;* [3]*Nuclear Medicine, Royal Marsden Hospital, Sutton, United Kingdom. Contact e-mail: sarah.mcquaid@nhs.net*

**Introduction:** Obtaining the best performance possible from a SPECT system requires simultaneous optimization of both the collimator parameters and the reconstruction parameters, since these parameters are coupled. The aim of this study was to perform a joint optimization of both of these aspects of SPECT imaging, using phantom acquisitions to determine the optimal collimation for estimating values of lesion-to-background activity ratio, as well as to investigate factors that influence the optimum collimation, such as lesion size and activity concentration. **Methods:** Projection data from the NEMA-IEC body phantom were acquired on a Philips Skylight SPECT system using the following parallel-hole collimators, each of which has a different geometric resolution: low-energy ultra-high resolution (LEUR), low-energy high-resolution (LEHR), low-energy general purpose (LEGP) and medium-energy general-purpose (MEGP). Tc-99m projections were obtained separately from the spheres (4 different sizes) and from the background so that they could be combined with different weightings prior to reconstruction, allowing the investigation of different lesion-to-background activity ratios. The LEHR data were then scaled to 10-million counts, while data from other collimators were scaled according to their sensitivities relative to LEHR. We then generated 100 realizations of Poisson noise from each essentially noise-free synthesized projection dataset. All noisy projections were reconstructed using OSEM (80 iterations, 10 subsets), and varying levels of Gaussian smoothing were applied to the reconstructed images. The lesion-to-background activity ratio, calculated for each sphere within every image, and the root-mean-squared-error (rMSE) of these estimates, were calculated over the noise realizations for each collimator. For each sphere size and activity ratio, the optimum collimator and reconstruction parameters were determined by fitting computed rMSE values to smooth polynomial functions to determine the global minimum rMSE. **Results:** The optimal collimator resolution for lesion quantification was found to depend on the size of the lesion, but was insensitive to the lesion-to-background activity ratio. For example, for a 6-to-1 activity ratio, the minimum rMSE of the estimated lesion-to-background activity ratio occurred with a system resolution of 14.8 mm at the center-of-rotation for a 37-mm-diameter sphere and 10.8 mm for a 17-mm-diameter sphere. These resolutions most closely match those produced by the LEGP and LEUR collimators respectively. These results indicate that the quantification of a large lesion benefits from the increased count levels obtainable with a poorer resolution collimator, whereas smaller lesions require a better resolution collimator to reach the optimum quantification performance. These findings can be used to assist in the selection of the most appropriate collimator in cases where lesion quantification is required. **Conclusions:** The optimum SPECT imaging parameters for estimating the activity ratio of a hot lesion in a warm background are dependent on the size of the lesion being imaged, but not the lesion-to-background activity ratio.

Disclosure of author financial interest or relationships:
**S.J. McQuaid**, None; **J. Gear**, None; **S.C. Moore**, None.

Presentation Number **P152**
Poster Session 1
September 5, 2012 / 18:00-18:00 / Room: The Liffey

# Experimental Validation of a Method for Fast Simulation of Yttrium-90 Bremsstrahlung

***Stephen C. Moore***[1,2], *Mi-Ae Park*[1,2], *Morgan Cervo*[1], *Stefan P. Müller*[3], [1]*Radiology, Brigham & Women's Hospital, Boston, MA, USA;* [2]*Radiology, Harvard Medical School, Boston, MA, USA;* [3]*Nuklearmedizin, Universitätsklinikum Essen, Essen, Germany. Contact e-mail: scmoore@bwh.harvard.edu*

**Introduction:** The beta emitter, Y-90, has been shown to have important applications in radioimmunotherapy and, more recently, in radioembolization of hepatic tumors by intra-arterial injection of radiolabeled microspheres. Unfortunately, it is challenging to obtain quantitatively accurate SPECT reconstructions of Y-90 because of its broad, continuous bremsstrahlung energy spectrum. The availability of an accurate forward projector is an essential requirement for iterative reconstruction algorithms. We have previously developed an approach for rapidly simulating bremsstrahlung photons arising from Y-90 beta particles emitted within soft tissue; this algorithm has been incorporated within a variance-reduced Monte Carlo (MC) forward projector and evaluated by comparing images and energy spectra acquired and simulated using the same Y-90 phantom and attenuator. **Methods:** Data were simulated and acquired from a 2.5-cm-diameter spherical source of Y-90 centered within a cylindrical water attenuator, 7.2-cm in diameter and 10.3 cm long. Energy spectra and projection images in 6 windows ranging from 59 to 563 keV were recorded for both a medium-energy low-penetration (MELP) and a high-energy general-purpose (HEGP) collimator on a Siemens Symbia SPECT-CT system. The sphere was approximately centered between the detectors, ~20 cm from each. For the simulation, the EGSnrc MC program was first run to generate list-mode files of all bremsstrahlung events arising from a Y-90 point source within a water attenuator. Conditional probability density functions derived from these data were used to obtain multi-dimensional tables of equally likely parameters for Y-90 bremsstrahlung production. Rapid simulation consisted of randomly selecting (1) a beta energy from a table of 100 equiprobable energies, (2) a radial distance to the location of bremsstrahlung production for the given beta energy, and (3) an equiprobable photon energy, given the chosen beta energy and range. Very low-abundance nuclear deexcitation and internal pair-production processes, yielding respectively 1.76-MeV and 511-keV annihilation photons, were also simulated. All photons were propagated further using our SPECT Monte Carlo simulator, which models all details of photon transport within an attenuator, a collimator, and a sodium-iodide gamma camera. To compare energy spectra and images, simulated data were scaled by the ratio of the total number of source decays acquired and simulated. **Results:** Simulation results were first corrected for the fact that bremsstrahlung photons of energy greater than 30 keV had originally been produced by EGSnrc in 2.5% of all Y-90 decays, instead of with the expected 3.3% abundance. The lead x-ray contribution to the simulated energy spectra was ~38% less than that acquired experimentally, likely due to additional lead shielding on the outside of the collimator and detector that were not modeled in the simulation. **Conclusion:** After correction for these effects, simulated and acquired energy spectra and images of the Y-90 sphere were in excellent agreement throughout the principal energy range of interest, for both for the MELP and HEGP collimators.

Disclosure of author financial interest or relationships:
**S.C. Moore**, None; **M. Park**, None; **M. Cervo**, None; **S.P. Müller**, None.

Presentation Number **P153**
Poster Session 1
September 5, 2012 / 18:00-18:00 / Room: The Liffey

# Breast Cancer detection with ClearPEM: Performance Studies with Gelatin Phantoms and First Results of the Clinical Trial

*Pedro Almeida[2], Miguel Castelo-Branco[3,4], Ricardo Bugalho[1], Ricardo J. Faustino[4], Claudia S. Ferreira[2,1], Nuno Ferreira[3,4], Nuno Matela[2], Jorge A. Neves[1], **Catarina Ortigão**[1], Joana E. Rio[4], Ana S. Rodrigues[1], Fabiana Rodrigues[4], Rui Silva[1], Joao Varela[1], [1]LIP - Lab. de Instrumentação e Física Experimental de Partículas, Lisbon, Portugal; [2]IBEB/FCUL - Inst. de Biofísica e Eng Biomédica, Lisboa, Portugal; [3]IBILI/FMUC - Inst. Biomédico de Investigação da Luz e Imagem, Coimbra, Portugal; [4]ICNAS - Inst. Ciências Nucleares Aplicadas à Saúde, Coimbra, Portugal. Contact e-mail: ortigao@lip.pt*

The ClearPEM detector is a dual planar Positron Emission Mammography (PEM) scanner that was developed by several Portuguese institutions within the framework of the international Crystal Clear Collaboration at CERN. The ClearPEM uses APD-based detector modules that are capable of measuring depth-of-interaction (DOI) with a resolution of 2 mm in LYSO:Ce crystals. The full system comprises 192 detector modules in a total of 6144 LYSO:Ce crystals and 384 32-pixel APD arrays readout by ASICs with 192 input channels, which represents an unprecedented level of integration in APD-based PET systems. The system includes Frontend and Data Acquisition electronics and a robotic gantry for detector placement and rotation. The software implements calibration (energy, time and DOI), normalization and image reconstruction algorithms. The scanner is installed at the Institute of Nuclear Sciences Applied to Health, in Coimbra, it was used for preclinical studies while the clinical protocol was being defined and approved and is now on the clinical trials phase. Detectability of breast cancer with the ClearPEM scanner was studied using gelatin phantoms. The methodology included the quantification of the homogeneity (BV) and statistical noise (COV) of the breast background images. Lesion detectability was evaluated using parameters such as lesion to background noise (LTBN) and lesion contrast recovery coefficient (CRC). Results indicate BV and COV of the order of 5-9% and 20-24%, respectively. ClearPEM images are globally homogeneous and detection of lesions is feasible down to 2 mm in diameter. Small LTB (Lesion to background ratio) and lesions of reduced dimensions showed less good contrast, but in most cases we report CRC values between 70% and 100%. A description of the method will be presented and results discussed. Clinical trial started on December 2011. A standard operation procedure was defined and followed in all exams. Several upgrades and debugs of image reconstruction softwares were performed. We will present results of the first exams on the conference.

Disclosure of author financial interest or relationships:
**P. Almeida**, None; **M. Castelo-Branco**, None; **R. Bugalho**, None; **R.J. Faustino**, None; **C.S. Ferreira**, None; **N. Ferreira**, None; **N. Matela**, None; **J.A. Neves**, None; **C. Ortigão**, None; **J.E. Rio**, None; **A.S. Rodrigues**, None; **F. Rodrigues**, None; **R. Silva**, None; **J. Varela**, None.

Presentation Number **P154**
Poster Session 1
September 5, 2012 / 18:00-18:00 / Room: The Liffey

# I-131 Rodent Imaging on the Inveon SPECT Platform Using a Novel Blended Collimator Acquisition Method

***Dustin Osborne***[1,2], *Alan Stuckey*[1], *Stephen J. Kennel*[1], *Tina A. Richey*[1], *Derek W. Austin*[2], *Bing Feng*[2], *Jonathan S. Wall*[1], [1]*Graduate School of Medicine, University of Tennessee, Knoxville, TN, USA;* [2]*Preclinical, Siemens Medical Solutions, Knoxville, TN, USA. Contact e-mail: dosborne@utk.edu*

Introduction Imaging of small animals with I-131 radiolabeled probes poses some challenges with regard to image acquisition and reconstruction. The high energy 364 keV emissions easily penetrate the collimators and pyramids of commercially available SPECT systems. This penetration results in increased noise and decreased contrast in the reconstructed images. This work addresses I-131 imaging on the Siemens Inveon SPECT system using a novel blended collimator acquisition. The protocol enables simultaneous use of both a high sensitivity and whole body collimator to acquire 2 different types of data in a single SPECT-CT acquisition. The result is a single scan containing information for both a large high resolution whole body FOV and high sensitivty with decreased collimator penetration. Methodology Three 25g mice with AA amyloid were injected with an I-131 labeled peptide (P5R) designed to target amyloid deposits, mainly in liver and spleen. A different multi-pinhole collimator was installed on each detector of the SPECT system. The first was a collimator designed for high sensitivity imaging with a single 2 mm pinhole. This collimator is thicker for decreased penetration of high energy photons but the resolution is ~2.4 mm. The second was designed for imaging a larger FOV with an outwardly focused 1mm multipinhole arrangement that resulted in a wider FOV but with increased photon penetration compared to the 2 mm single pinhole collimator. The protocol used for this acquisition was 60, 30 s projections acquired over 360 degrees. Both detectors were positioned at a 30 mm ROR with transaxial FOVs of 4.8 and 4.4 cm fpr the multi and single pinhole collimators respectively. All data were acquired helically with 90 mm of bed travel that acquired axial FOVs of 15.6 and 13.8 cm for the multi and single pinhole collimators. Data were reconstructed using an iterative MAP3D algorithm with 8 iterations and 6 subsets. Modeling of the detector point spread function was used to improve resolution and uniformity. Attenuation and scatter correction were applied to reduce noise and improve contrast. Results & Conclusions The data acquired show the potential for using a blended collimator acquisition in a routine manner. High quality images can be obtained using this type of acquisition method illustrating the time savings that can be realized using two different collimators to acquire data for two different imaging applications simultaneously. This work also shows that I-131 can be successfully imaged using the Inveon SPECT platform, although the system could benefit from additional shielding to minimize collimator penetration. The figure presented shows the whole body image with a larger FOV while the high sensitivity image shows decreased resolution, a smaller FOV and decreased penetration noise. The manufacturer reconstruction software was then used to create a single blended image from the two collimator acquisition. This image had the resolution of the 2 mm single pinhole collimator but used all of the count data collected with both collimators to create a single blended image to compliment the two images created from each collimator individually.

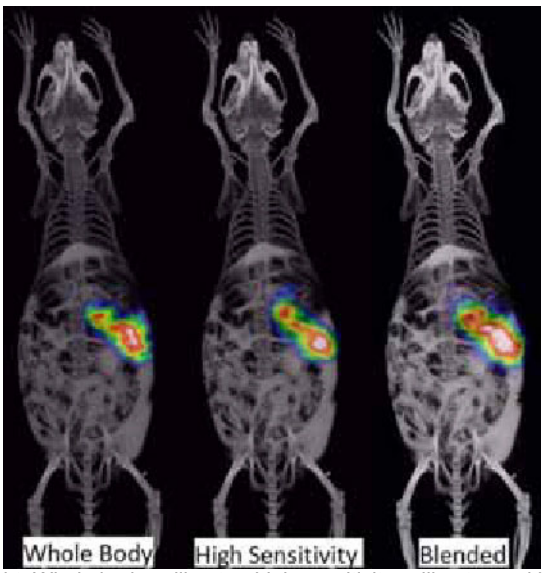

From left to right: Whole body collimator, high sensitivity collimator and blended image

Disclosure of author financial interest or relationships:
**D. Osborne**, University of Tennessee, Employment; Siemens Medical Solutions, Employment; **A. Stuckey**, Solex LLC, Stockholder; **S.J. Kennel**, solex, Stockholder; **T.A. Richey**, Solex, Stockholder; **D.W. Austin**, Siemens Healthcare, Employment; **B. Feng**, Siemens Medical Solutions, USA, Employment; **J.S. Wall**, Elan, Grant/research support; Solex LLC, Stockholder .

Presentation Number **P155**
Poster Session 1
September 5, 2012 / 18:00-18:00 / Room: The Liffey

# Model Based Image Extraction of the Tracer Arterial Input Function for Kinetic Analysis of Dynamic PET Data: A Statistical Approach

***Finbarr O'Sullivan***[1,2], *Jian Huang*[1], *Mark Muzi*[2], *David Mankoff*[2], [1]*Statistics, University College Cork, Cork, Ireland;* [2]*Radiology, University of Washington, Seattle, WA, USA. Contact e-mail: f.osullivan@ucc.ie*

In a dynamic Positron Emission Tomography (PET) imaging study, the local uptake of the tracer is a function of vascular delivery and retention. As a result, interpretation of the PET measured time-course information is best achieved when there is knowledge of the time-course of tracer in the arterial blood. But since direct sampling of blood as part of clinical or pre-clinical PET studies is increasingly impractical, there is now ongoing interest in image-based extraction of the blood time-course information. However the analysis of PET-measured blood pool signals is made difficult by the fact that such signals typically involve a combination of arterial, venous and tissue information. Thus a careful appreciation of these components is needed in order to isolate the arterial component. We have constructed a physiolocially based pharamokinetic (PBPK) model for representation of the circulation of the PET tracer atom in the body. The outputs of the model are time-course patterns of the activity of tracer atoms in regions such as the right and left venrticles of the heart, the lungs and venous blood prior to first pass contribution from the injection site. Significantly the model allows time steps to be matched to the heart rate of the subject under study. Data from historical populations of arterial and/or venous sampled blood curves are used to validate the representation of the model and construct an appropriate reference distribution for its parameters. The application of the PBPK model to time-course data from a region of interest measured by PET, allows the possibility to draw inferences about the PBPK model parameters for the subject under study. An algorithm has been implemented that statistically combines PBPK model parameter information from all voxels in the PET imaged tissue volume. An image based scaling procedure for the arterial time-course is also developed. The approach has been implemented for dynamic cerebral and thoracic PET studies with F-18 Flourodeoxyglucose and O-15 water in normal subjects and breast cancer subjects. Results obtained show that valid kinetic interpretation of PET time-course information can reliably be based on the image extracted PBPK model arterial input function. Extension of this approach to other tracers including F-18 Fluorothymidine and C-11 verapamil is also described. This work is supported in part by the Science Foundation Ireland (MI-2007) and the National Cancer Institute (CA-42045;AG031485) and the National Institute of Aging (031485) and the National Cancer Institute (P01-CA 42045;U01-CA148131;AGO31 485) and the National Institute of Aging (031485).

Disclosure of author financial interest or relationships:
**F. O'Sullivan**, None; **J. Huang**, None; **M. Muzi**, None; **D. Mankoff**, None.

Presentation Number **P156**
Poster Session 1
September 5, 2012 / 18:00-18:00 / Room: The Liffey

# Performance Evaluation of a Dual-ring Small Animal PET Scanner With Continuous LYSO Crystals

***Meg S. Pajak***[1], *Sally Pimlott*[2], *Jens Waldeck*[3], *Carlos Correcher Salvador*[4], *Antonio Soriano Asensi*[5], *David Volgyes*[6], *Clare McKeown*[7], *Kurt Anderson*[1], [1]*Beatson Institute for Cancer Research, Glasgow, United Kingdom;* [2]*University of Glasgow, Glasgow, United Kingdom;* [3]*Carestream Molecular Imaging, Woodbridge, CT, USA;* [4]*Oncovison, Valencia, Spain;* [5]*Institute for Instrumentation in Molecular Imaging, Valencia, Spain;* [6]*University of Oslo, Oslo, Norway;* [7]*NHS Scotland, Glasgow, United Kingdom. Contact e-mail: m.pajak@beatson.gla.ac.uk*

Small animal molecular imaging has become an invaluable tool in pre-clinical research for the investigation of cancer, infection, cardiac and neurological disorders and in drug development. The Albira imaging system (Carestream Molecular Imaging, USA) is one of very few commercially available multi-modal PET/SPECT/CT scanners. Its uniqueness lies mainly in the utilisation of continuous LYSO crystals and Position Sensitive Photomultiplier Tubes (PSPMT) in the PET scanner. This novel detector technology provides depth of interaction (DOI) information, which is used to correct the position of the lines of response and in turn enhances spatial resolution.[1] Each ring in the Albira's PET system consists of 8 detectors with continuous LYSO crystals that form octagonal geometry with the trans-axial field of view (FOV) of 80x80 mm. The double ring configuration used in this study has an axial FOV of 94 mm, which is sufficient to enable the imaging of the whole body of a mouse in one bed position. Although the continuous crystal design has advantages, this kind of geometry poses difficulties when reconstructing images using analytical algorithms due to the gaps in the sinograms coming from the angles in-between the detectors. We present the performance evaluation of the Albira PET module using the NEMA NU4-2008 standard procedure [2] and compare image reconstruction methodologies.[3] We assess spatial resolution, sensitivity, scatter fraction, noise equivalent counts (NEC) and image quality and compare the results from the one-ring Albira PET system.[1, 4] 1. Sanchez, F., et al. Medical Physics, 2012. 39(2): p. 643-653. 2. National Electrical Manufacturers Association, NEMA Standards Publication NU 4-2008, 2008 3. de Jong, H.W.A.M., et al. IEEE Transactions on Nuclear Science, 2003. 50(5): p. 1452-1456. 4. Balcerzyk, M., et al. 8th IEEE International Conference on BioInformatics and BioEngineering, BIBE 2008, 2008. p. 1-4.

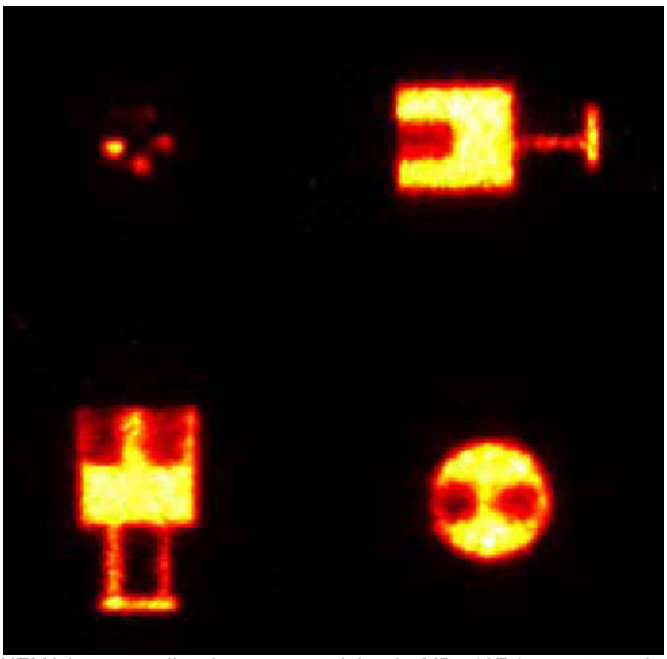

Images obtained from a NEMA image quality phantom containing 3.7MBq 18F (reconstructed with MLEM, 12 iterations)

Disclosure of author financial interest or relationships:
**M.S. Pajak**, Carestream Molecular Imagaing, Grant/research support; **S. Pimlott**, Carestream Healthcare Ltd, Grant/research support; **J. Waldeck**, Carestream, Employment; **C. Correcher Salvador**, Oncovision, Employment; **A. Soriano Asensi**, None; **D. Volgyes**, None; **C. McKeown**, None; **K. Anderson**, Carestream Molecular Imaging, Other financial or material support .

Presentation Number **P157**
Poster Session 1
September 5, 2012 / 18:00-18:00 / Room: The Liffey

# Internal light scattering in scintillation crystal as a method of LSF shape control in a high resolution detectors

***Vyacheslav Pedash**, ISMA NAS of Ukraine, Kharkov, Ukraine. Contact e-mail: pedash@gmail.com*

The ordinary scintillation detector for a gamma camera detection head where Anger logic is used for signal reconstruction consists of homogeneous scintillation crystal, light guide and position sensitive photo detector. Such a combination works well in the big whole body systems for relatively low energy isotope imaging. For the higher energy PET isotopes the thickness of the crystal must be increased. In the thick crystal scintillation light illuminates wider area on the output window which degrades spatial resolution. In the small gamma cameras for small animal imaging which are based on PS PMT the same problem arises even for low energy imaging. One of the well known approaches which is used to make light spread function more narrow is pixilated crystals. The series of gaps on the crystal surface filled with diffusive or specular reflector allows modulation of light spread function (LSF) and consequently improves intrinsic spatial resolution. The main disadvantage of this method is limitations on pixel size that arises from crystal properties and mechanical processing. The main objective of this work was to investigate by the means of mathematical simulation the alternative method of LSF form control. The method under study is based on the use of scintillation crystal with high internal scattering. Such a material could be thought as a step beyond the pixels. Two type of detectors were studied - large 400x600 mm detector viewed by PMT's for whole body imaging and 50x50 mm viewed by PS PMT for preclinical applications. The optimal scattering lengths for the crystals of different thickness were determined. It is shown, that decreasing of scattering length up to some limit doesn't affect total light collection coefficient. The further decreasing of scattering length degrades light collection severely but in the same time the width of LSF becomes more narrow which allows accurate position reconstruction. It is shown, that for each detector configuration the optimal scattering length could be determined on the base of tradeoff between total light collection and LSF shape.

Disclosure of author financial interest or relationships:
**V. Pedash**, None.

Presentation Number **P158**
Poster Session 1
September 5, 2012 / 18:00-18:00 / Room: The Liffey

# A low cost non-invasive SiPM PET calibration system

***Roger P. Rassool***[1], *Bryn Sobott*[1,3], *David J. Peake*[1,3], *Graeme J. O'Keefe*[2], [1]*School of Physics, The University of Melbourne, Melbourne, VIC, Australia;* [2]*Centre For PET, Austin Health, Heidelberg, VIC, Australia;* [3]*CRC for Biomedical Imaging, Melbourne, VIC, Australia. Contact e-mail: rogerpr@unimelb.edu.au*

This paper presents the design of a compact implementation of the NIAM (Non-Invasive Arterial Monitor) system aimed at quantitative measurement of the arterial input function for use in PET. A driving force behind the development of NIAM has been to facilitate clinical research trials quantified PET imaging and overcome the challenges imposed by reluctance to undertake trials which required invasive arterial sampling. Early NIAM systems were based on more traditional PMT technology and VME readout. As a consequence they were rather bulky and difficult to maneuver in patient settings and feedback gained during trials has motivated the development of a more compact device. The novel approach reported here exploits the attractive attributes of silicon photomultipliers (SiPM), including high gain and small size, which make them an ideal choice for next generation PET imaging systems. Furthermore, insensitivity to the adverse effects of magnetic fields will also drive their application in PET/MRI. Each NIAM detector module is based on an array of 144 x 3.4 mm wide and 20mm in depth LYSO crystals (Crystal Photonics) arranged in a square matrix and coupled to a SensL Matrix9 SiPM. Geant modelling of this arrangement has been used to ensure optimal light coupling and sharing. GATE simulations of NIAM also identified that a 6-block geometry was preferred for spatial uniformity and improved spatial resolution. A prototype NIAM3 system has now been built and consists of 6-NIAM SiPM detector modules, arranged in a hexagon with a bore of 80mm, which results in an active field of view of 50 mm^2. A customised readout strategy has been developed to allow real-time operation in list mode. Image reconstruction is performed using the iterative Maximum Likelihood Expectation Maximisation (MLEM) reconstruction algorithm. The software for this has been developed in-house. Investigations of count-rate linearity and efficiency, and spatial uniformity and resolution, together with overall spatial resolution are presented. The original design parameters of NIAM were specifically aimed at a practical cost-effective solution for patient wrist imaging. With the cost-effective availability of LYSO and SiPM technologies, NIAM's performance parameters now approaches that of pre-clinical imaging systems and will find application in many other areas, including targeted tumour and translational imaging programs. The expected performance of the system in these configurations is also discussed.

Disclosure of author financial interest or relationships:
**R.P. Rassool**, None; **B. Sobott**, None; **D.J. Peake**, None; **G.J. O'Keefe**, None.

Presentation Number **P159**
Poster Session 1
September 5, 2012 / 18:00-18:00 / Room: The Liffey

# Motion corrected SPECT awake animal imaging: A Fast Simulation Study

***Will Ryder**, Georgios I. Angelis, Andre Z. Kyme, Rezaul Bashar, Steven Meikle, Roger Fulton, Brain and Mind Research Institute, University of Sydney, Sydney, NSW, Australia. Contact e-mail: will.ryder@sydney.edu.au*

The possibility of correcting for motion in an awake animal imaging study, during image reconstruction, could allow greater range of studies that can be undertaken, as the animal will no longer need to be anesthetized. A SPECT acquisition was simulated, using fast Monte Carlo software, that incorporated experimentally measured motions of a rat's head from an optical motion tracking system; in total 17920 different animal poses were simulated. The total simulation time was 25 seconds on an Apple Macbook Pro laptop, with an I5 core (2.4Ghz). The single headed study comprised of 64 projections with 280 rigid phantom movements with 6 degrees of freedom during each projection and ~ 280k events per projection were detected; in this preliminary study attenuation modeling was not applied. The simulated acquisition was stored in a list-mode file format, so that each event could be correlated with motion and to use in the reconstruction of image. The reconstruction of the image was performed using a ML-EM list-mode iterative reconstruction method where the lines of response were corrected using the motion tracking data. In this study a comparison was made between motion-free, non-motion corrected and motion corrected images. It can be seen that the non-motion corrected images suffer from blurring that results in unusable images. Good agreement is observed between the motion corrected image and the motion-free image. Hence quantitative measurements could be possible for motion-corrupted data. It has been shown here that it is possible to simulate complex animal motions and reconstruct images with motion correction. The Monte Carlo software used in this work appears to be a useful and flexible tool for investigating motion effects and efficacy of motion correction methodologies in SPECT imaging.

Disclosure of author financial interest or relationships:
**W. Ryder**, None; **G.I. Angelis**, None; **A.Z. Kyme**, None; **R. Bashar**, None; **S. Meikle**, None; **R. Fulton**, None.

Presentation Number **P160**
Poster Session 1
September 5, 2012 / 18:00-18:00 / Room: The Liffey

# A Method for Improving Image Quality in Consecutive Single Photon and Positron Projection Imaging Studies in the Same Mouse

***Jürgen Seidel***[1,2], *Elaine Jagoda*[1], *Mark Williams*[1,2], *Michael Green*[1,2], *Peter Choyke*[1], [1]*Molecular Imaging Program, NCI, Bethesda, MD, USA;* [2]*Contractor, SAIC-Frederick, Inc., Frederick, MD, USA. Contact e-mail: jseidel1@mail.nih.gov*

Single photon imaging in small animals requires relatively large amounts of activity since collimator sensitivity is low. Positron imaging requires less activity but when bare positron detectors are exposed to high levels of single photon activity, image quality can suffer from pulse pile-up. Thus, positron imaging of an animal after single photon imaging to study one functional effect, followed by administration of a positron-emitting compound to study a second, can be problematic. Placing thin Pb sheets over the positron detector faces during imaging can potentially ameliorate this effect by preferentially absorbing typically low(er) energy single photons while allowing the higher energy annihilation gamma rays to pass through into the detectors. However, positron spatial resolution and sensitivity might be unacceptably compromised by this strategy so that comparison of these parameters with and without shielding is required. An F-18 capillary tube line source (1.2 mm ID x 70 mm long, 0.25 mCi) was imaged in projection with a pair of opposed planar, pixelated LYSO arrays (26 x 59, 1.5 mm square, 1.6 mm pitch) in time coincidence (10 ns window) separated by 21.8 cm with the line source midway between detectors. A Tc-99m syringe source (1.5 ml, 2.7 mCi) was then placed alongside the line source and this combination imaged. Finally, these same sources were imaged again but with 2-mm thick Pb sheets covering the full field-of-view of each detector. The results are summarized in the Table. The high singles rate on the detectors with Tc-99m in the FOV degrades both FWHM and, by nearly a factor of four, FWTM compared to F-18 alone. With the Pb sheets in place, image quality is restored albeit with a modest reduction in sensitivity (36% for this non-optimized Pb sheet thickness). Thus, this method may improve image quality in sequential single photon and positron projection imaging studies in the same mouse with acceptable reductions in positron imaging performance. A similar, optimized scheme might also improve image quality in consecutive SPECT/PET studies with PET scanners of cylindrical geometry where the Pb sheets would be replaced by a thin-walled Pb cylinder matched to the bore length and diameter.

| Image Type | Tc-99m/F-18 Activity Ratio | Singles Rate (cps) | FWHM (mm) | FWTM (mm) | F-18 Relative Sensitivity |
|---|---|---|---|---|---|
| F-18 Alone | 0.0 | 210,000 | 2.4 | 5.4 | 1.0 |
| F-18 + Tc-99m + Pb | 11.2 | 511,000 | 2.4 | 6.0 | 0.64 |
| F-18 + Tc-99m | 10.4 | 900,000 | 4.0 | 20.6 | - |

Disclosure of author financial interest or relationships:
**J. Seidel**, None; **E. Jagoda**, GE Heatlhcare, Grant/research support; **M. Williams**, None; **M. Green**, None; **P. Choyke**, GE Healtcare, Grant/research support; Philips Medical Systems, Grant/research support; Siemens Healthcare, Grant/research support .

Presentation Number **P161**
Poster Session 1
September 5, 2012 / 18:00-18:00 / Room: The Liffey

# Sub-millimeter I-131 SPECT with clustered pinholes

***Frans van der Have***[1,2]*, Marlies C. Goorden*[1]*, Rob Kreuger*[1]*, Ruud M. Ramakers*[1,2]*, Frederik J. Beekman*[1,2]*,* [1]*Radiation, Radionulides, and Reactors, Delft University of Technology, Delft, Netherlands;* [2]*MILabs, Utrecht, Netherlands. Contact e-mail: f.vanderhave@tudelft.nl*

A new pinhole collimator for imaging PET tracers was recently developed for the U-SPECT-II/CT system (MILabs, The Netherlands) to allow for simultaneous imaging of positron emitters and single photon emitters with sub-mm resolution. To this end a novel collimator was optimized for high-energy gamma photons by the use of clustered multi-pinholes (CMP). Small opening angles of each pinhole within a cluster strongly reduce resolution loss due to edge penetration. Here we test CMP for imaging with I-131 that emits high-energy photons (364 keV). A CMP collimator was placed in the triangular stationary detector set-up of the U-SPECT-II system. Images were obtained using pixel-based ordered subset reconstruction that uses a system matrix to correct for blurring due to pinhole size and detector resolution. The image resolution was determined with a Jaszczak hot capillary resolution phantom. The smallest rods that could be resolved in the reconstructed I-131 images have a diameter of 0.6 mm while 0.5 mm for Tc-99m and 0.8 mm for F-18 were obtained with the same collimator and 0.8 mm was obtained for I-131 in a SPECT collimator. Further improvements are expected with more refined modeling of photon transport during iterative reconstruction. The spectrum also shows a reduced scatter-to-primary ratio for imaging I-131 compared to SPECT collimators. We conclude that the collimator that was designed for imaging PET isotopes is also to be preferred for imaging high-energy SPECT isotopes such as I-131 in mice.

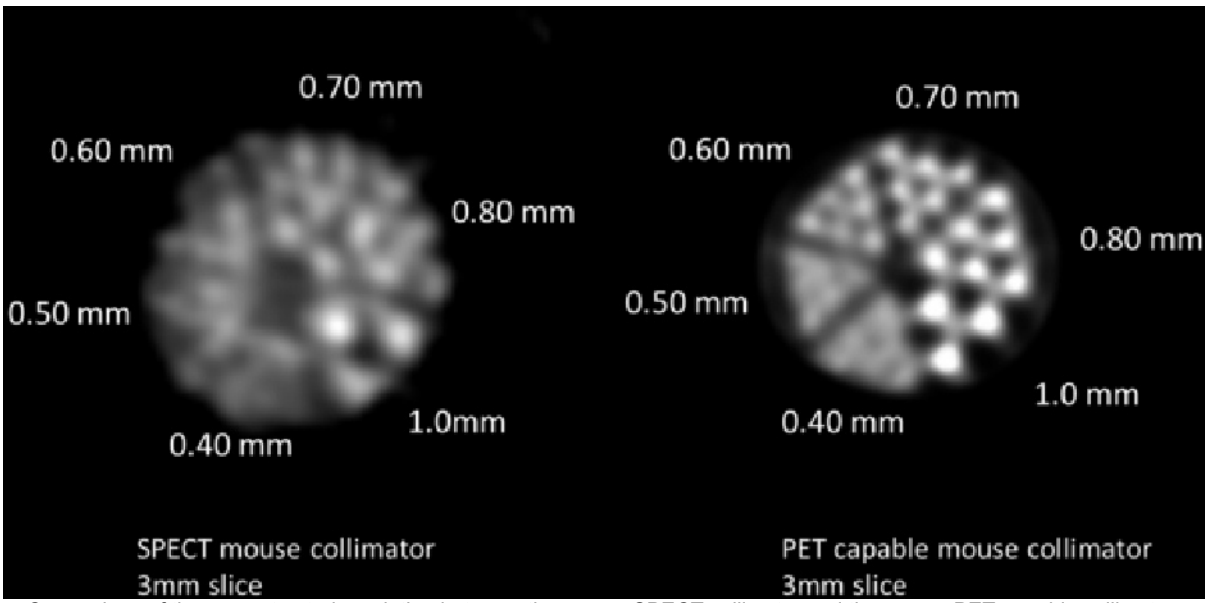


Comparison of the reconstructed resolution between the mouse SPECT collimator and the mouse PET-capable collimator.

Disclosure of author financial interest or relationships:
**F. van der Have**, MILabs, Employment; MILabs, Stockholder; **M.C. Goorden**, None; **R. Kreuger**, None; **R.M. Ramakers**, MILabs B.V., Employment; **F.J. Beekman**, MILabs, Stockholder; MIlabs, Honoraria; MILabs, Grant/research support .

Presentation Number **P162**
Poster Session 1
September 5, 2012 / 18:00-18:00 / Room: The Liffey

# Effects of Attenuation Map Inaccuracies on Quantitative Micro-SPECT

***Chao Wu***[1,2], *Peter Laverman*[3], *Otto C. Boerman*[3], *Frederik J. Beekman*[1,2], [1]*Section Radiation Detection and Medical Imaging, Delft University of Technology, Delft, Netherlands;* [2]*Rudolf Magnus Institute of Neuroscience, University Medical Center Utrecht, Utrecht, Netherlands;* [3]*Department of Nuclear Medicine, Radboud University Nijmegen Medical Centre, Nijmegen, Netherlands. Contact e-mail: c.wu@tudelft.nl*

**Objective:** Attenuation of photon flux on trajectories between the source and pinhole apertures affects the quantitative accuracy of reconstructed single-photon emission computed tomography (SPECT) images. Attenuation maps can be employed, e.g. from registered X-ray CT images, to correct for attenuation post-reconstruction, showing highly accurate quantification. Here we investigate effects of CT image inaccuracies (misregistration and errors in attenuation coefficients) to quantitative accuracy. **Methods:** A rat cadaver containing 12 small artificial Tc-99m sources with known activities was scanned in a U-SPECT-II/CT system. An attenuation map was derived from the CT image (as a gold standard), and then the map was shifted up to 3 mm or the attenuation coefficients in the maps were globally altered by 10%. A Chang-based first-order method was employed for post-reconstruction attenuation correction. Quantitative differences of the artificial sources in the SPECT images obtained after correction with accurate and inaccurate maps were calculated. The same procedure was performed for I-125, Tl-201 and In-111 with another three rat cadavers, respectively. **Results:** For Tc-99m, when the attenuation map was shifted by 3 mm in x, y and z directions, the quantitative differences (mean±std in %) of the artificial sources are 1.5±1.4%, 1.1±1.0% and 1.3±1.2%, respectively. By altering the attenuation coefficients to 0.9 or 1.1 times of the correct values, the results changes by 2.9±0.7%. For Tl-201 and In-111, we obtained similar results to Tc-99m. For I-125, the differences are larger: 4.0±3.2%, 4.9±3.6% and 2.3±1.9% for 3mm shifts in x, y and z directions, respectively; and 5.9±1.6% and 6.2±1.9% for increasing and decreasing the attenuation coefficients by 10%, respectively. **Conclusion:** We conclude that in micro-SPECT, inaccurate attenuation maps due to misregistration or inaccurate attenuation coefficients do not considerably affect quantitative accuracy. Generally, the differences introduced by inaccurate maps are less than 5% except for I-125. Due to its low photon energy, quantification of I-125 images are more sensitive to the accuracy of the maps, and the maximum differences can reach to about 10%.

Quantitative differences due to inaccurate attenuation map

| Diff (mean±std %) | 3mm shift in x direction | 3mm shift in y direction | 3mm shift in z direction | Increasing att. coef. by 10% | Decreasing att. coef. by 10% |
|---|---|---|---|---|---|
| I-123 | 4.0±3.2 | 4.9±3.6 | 2.3±1.9 | 5.9±1.6 | 6.2±1.9 |
| Tl-201 | 1.8±1.7 | 1.6±1.2 | 1.2±0.8 | 3.3±0.9 | 3.4±1.0 |
| Tc-99m | 1.5±1.4 | 1.1±1.0 | 1.3±1.2 | 2.9±0.7 | 2.9±0.7 |
| In-111 | 1.6±1.3 | 1.2±0.8 | 0.9±0.9 | 2.8±0.6 | 2.8±0.7 |

Disclosure of author financial interest or relationships:
**C. Wu**, None; **P. Laverman**, None; **O.C. Boerman**, None; **F.J. Beekman**, MILabs, Stockholder; MIlabs, Honoraria; MILabs, Grant/research support .

Presentation Number **P163**
Poster Session 1
September 5, 2012 / 18:00-18:00 / Room: The Liffey

# Estimating the spatial resolution limits for isotropic-3D PET detector "X'tal cube"

***Eiji Yoshida**, Hideaki Tashima, Fumihiko Nishikido, Yoshiyuki Hirano, Naoko Inadama, Hideo Murayama, Taiga Yamaya, Molecular Imaging Center, National Institute of Radiological Sciences, Chiba, Japan. Contact e-mail: rush@nirs.go.jp*

The detection of depth-of-interaction (DOI) is essential to achieve both high spatial resolution and high sensitivity for positron emission tomography (PET), since DOI information will reduce the parallax error due to the crystal penetration. In particular, performance of a small bore PET scanner is improved for dedicated human brain, human breast, and small animal imaging. We developed a novel, general purpose isotropic-3D PET detector X'tal cube by effective readout of scintillation photons from six sides of the crystal block. The X'tal cube is composed of the 3D crystal block with isotropic resolution and arrays of multi pixel photon counters (MPPCs). We have shown that the X'tal cube can achieve 1.9 mm uniform spatial resolution using the one pair prototype of the X'tal cubes with 3D grids of 2 mm pitch. Fig. 1 (a) shows the illustration of the X'tal cube with 3D grids of 2 mm pitch. In this work, we investigate spatial resolution of a PET scanner based on the X'tal cube using Monte Carlo simulations for predicting resolution performance in smaller 3D grid. The PET scanner of 15.6 cm in diameter was simulated. This PET scanner consisted of 24 X'tal cube detectors. For spatial resolution evaluation, a point source emitting 511 keV photons was simulated with all the physical processes involved during emission and interaction of positrons using the GATE. The interacted 3D grid is determined by finding the centroid which is weighted by each interaction intensity. These simulations were repeated, varying the radial offset of the point source to demonstrate the spatial resolution at different locations across the field-of-view (FOV). The simulated data were projected to the sinogram and reconstructed using the 2D filtered backprojection on each axial plane. Fig. 1 (b) shows average spatial resolutions for the X'tal cubes with 3D grids of several pitches. For all types of the X'tal cube, these detectors obtained uniform spatial resolution over the FOV. Also, as the 3D grid pitch was small, spatial resolution was improved adequately. The average spatial resolution of the X'tal cube with grids of 2 mm pitch was equal to the experimental data. Also, the average spatial resolution of the X'tal cube with 3D grids of 0.5 mm pitch was 0.7 mm. The X'tal cube along with excellent spatial resolution would lead to PET scanners with uniform spatial resolution across the FOV.

(a) X'tal cube

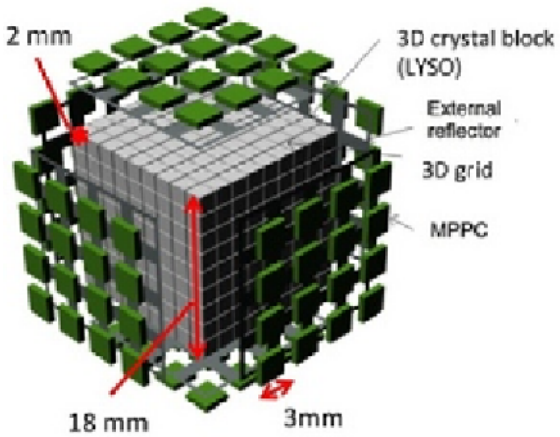


(b) Average spatial resolution

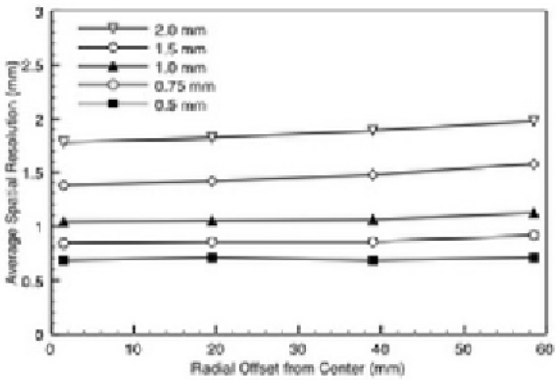


Disclosure of author financial interest or relationships:
**E. Yoshida**, None; **H. Tashima**, None; **F. Nishikido**, None; **Y. Hirano**, None; **N. Inadama**, None; **H. Murayama**, None; **T. Yamaya**, None.

Presentation Number **P164**
Poster Session 1
September 5, 2012 / 18:00-18:00 / Room: The Liffey

# Quantification of the Rat Heart Innervation Activity with Dynamic SPECT via Joint Estimation of Compartmental Model Parameters and Blood Input Function Directly from Projections

***Yunlong Zan***[1]*, Qiu Huang*[1]*, Rostyslav Boutchko*[2]*, Grant T. Gullberg*[2]*,* [1]*School of Biomedical Medical Engineering,, Shanghai Jiao Tong University, Shanghai, China;* [2]*Lawrence Berkeley National Laboratory, Berkeley, CA, USA. Contact e-mail: zanyunlong@gmail.com*

Objectives: The goal of this study is to develop an algorithm to quantify the innervation activity of the rat heart with 123I-MIBG using a slowly rotating clinical dual-head SPECT system mounted with two pinhole collimators. Methods: Sixty-six rotations of dynamic emission scans of spontaneously hypertensive rats were performed with a clinical SPECT scanner. Within each rotation 90 one-second projections were acquired. The initial time-activity curves (TACs) of every voxel were estimated from the raw data through a 4D reconstruction algorithm with B-spline functions. Then the reconstructed 4D results were segmented with an active contour based algorithm to obtain the blood pool region and the myocardium region. The initial TACs of all voxels in each region were averaged via a weighting function, which was 1 at the center of the region and decreased to 0 at the edge, to form a new TAC for each region. The new regional TACs were used as the initial guess in the iteration to estimate simultaneously the parameters of a one-compartment model and the coefficients of the B-spline functions through the least-square criterion. At every N-th iteration, the estimated coefficients of the B-spline functions were used to generate 4D emission maps, which were projected with the system matrix. The difference between these projections and the real measurements was introduced as a constraint to the least square estimation in order to ensure a proper convergence. Result: Digital phantom simulations and experimental data both showed good results in the 4D reconstruction of the B-spline coefficients. The presented approach of obtaining regional TACs outperformed the one extracting TACs from one voxel in each region or from the mean value of all the voxels in each region, in terms of the final estimation result. Simulation also showed that without the constraint introduced at every N-th iteration, the estimation could converge to a local minimum. Conclusions: We developed an algorithm to estimate simultaneously the blood input function and parameters of a one-compartment model directly from the 4D SPECT projections. The algorithm is promising in quantifying the norepinephrine washout and distribution volume in the rat heart and thus in evaluating changes in innervation activity of the rat heart.

Disclosure of author financial interest or relationships:
**Y. Zan**, None; **Q. Huang**, None; **R. Boutchko**, None; **G.T. Gullberg**, None.

Presentation Number **P165**
Poster Session 1
September 5, 2012 / 18:00-18:00 / Room: The Liffey

# Effect of Desflurane Anesthesia on the [18F]FDG Metabolism in Nude Mice

***Ralf K. Bergmann**, Institute of Radiopharmacy, Helmholtz-Zentrum Dresden-Rossendorf, Dresden, Germany. Contact e-mail: r.bergmann@hzdr.de*

Objectives: Dynamic small animal PET studies in mice require often anesthesia to reduce motion related artifacts. The volatile anesthetic with the most rapid onset and offset and with low metabolism is desflurane, which is used for human general anesthesia, however not common in animals. Therefore, we evaluated the [18F]FDG distribution in awake and desflurane anesthetized NCIH292 tumor bearing nude mice. Methods: Fed NCIH292 tumor bearing NMRI nu/nu mice were divided into control mice (CM), which were freely moving in a cage at 27°C, and non-moving anesthetized mice (AM), which were kept under 9% desflurane in 0.2 L/min O2, 0.3 L/min air at 36°C. After 1 h adaption to the experimental setup the CM and AM were injected with [18F]FDG (5 MBq, i.v. bolus). Blood glucose was measured before the experiment, at 0.5 h and at 1 h. Then all mice were anesthetized and PET was measured over 30 min, the activity concentration data were calculated as SUV median (25%, 75% percentile). Results: There was no difference of [18F]FDG brain uptake between CM 1.9 (1.6, 2.2) and AM 1.9 (1.6, 2.3). An unexpected [18F]FDG increase was observed in the tumors of AM 2.47 (1.67, 3.17), which was higher than in the CM 0.81 (0.66, 1.14). The [18F]FDG uptake in the heart was also larger in the AM. As expected was the muscle (gluteus supeficialis, biceps femoris) uptake higher in the CM and the resulting tumor to muscle ratio was therefore in the CM 0.32 (0.28, 0.48) less than in the AM 3.9 (2.5, 6.8). The blood glucose was elevated in the AM only at 30 min post anesthesia induction with 10.3 (7.33, 11.8) mmol/L vs. CM 6.2 (5.8, 7.4) mmol/L. Conclusions: Desflurane affects the [18F]FDG uptake in the NMRI nu/nu mouse tissues. This has to be considered for glucose metabolic explorations with mice under anesthesia. An adaption period of one hour for the mice under anesthesia normalizes the elevated blood glucose often occurring after anesthesia induction stress. Thus, in terms of comparability and correct interpretation of results obtained from PET experiments with mice under anesthesia is a standardized experimental setup mandatory.

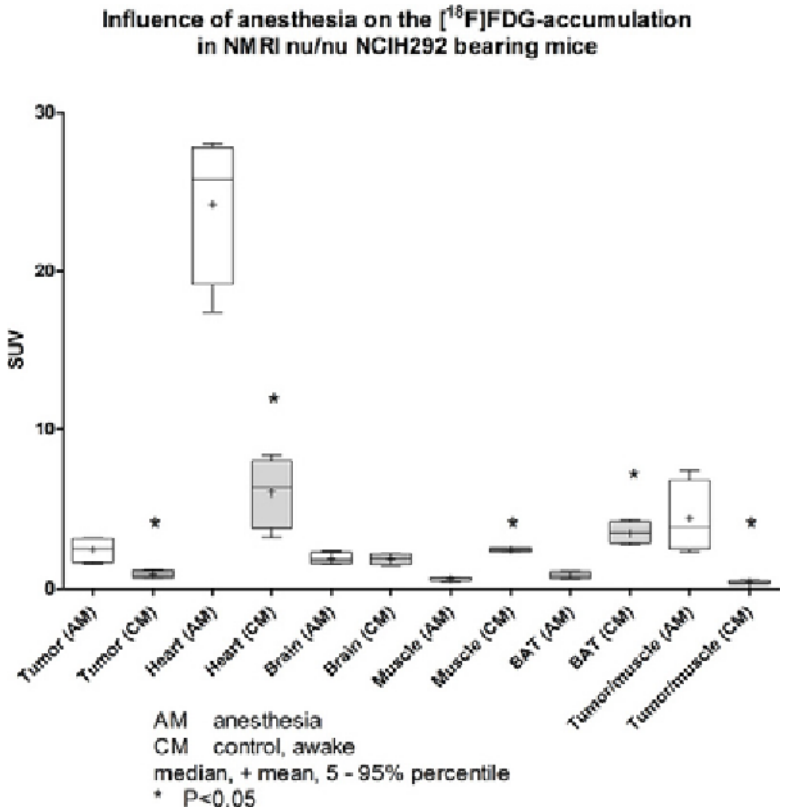


Disclosure of author financial interest or relationships:
**R.K. Bergmann**, None.

Presentation Number **P166**
Poster Session 1
September 5, 2012 / 18:00-18:00 / Room: The Liffey

# Transport Phenomena across the Blood-brain barrier: An Application to Phenylketonuria

*Uma S. Ranjan[1], Smruthy Sivakumar[2], Pooja Bhat[2], Sumana Srivatsa[2], **Alexander Fischer**[3], [1]Research Engineering Solutions, Philips Electronics India Ltd., Bangalore, India; [2]Biotechnology, PES Institute of Technology, Bangalore, India; [3]Molecular Imaging Group, Philips Research, Aachen, Germany. Contact e-mail: alexander.fischer@philips.com*

A common problem in characterizing blood-brain barrier is that the endothelial cell between the plasma and the brain compartment. Since sampling is not possible in the endothelial cell, pharmacokinetic modeling techniques usually combine the endothelial cell and the brain compartment into a single compartment. A disadvantage of this approach is that the transporters between the endothelial compartment and the brain compartment cannot be characterized. One such case is the transport of Phenylanine in patients suffering from Phenylketonuria (PKU). PKU is a metabolic disorder caused by the deficiency of phenylalanine hydroxylase that converts Phenylalanine to Tyrosine. This leads to a decreased catabolism of Phenylalanine which in turn has been observed to cause mental retardation due to accumulation of phenylanine in the brain. It has so far not been possible to quantitatively characterize this accumulation since it this necessitates the characterization of the Na+-LNAA transporter between the brain and endothelial cell. In the present work, we introduce the concept of "hidden compartment modeling" where a compartment which cannot be measured can still be characterized by transforming the system to a second order system (in time). A two compartment model consisting of the endothelial cell and the brain has been developed to describe the transport of phenlyalamine across the BBB, taking two transporters - L1 System and the Na+-LNAA System into consideration. The endothelial cell here is considered a hidden compartment, and two parameters, k1 and k2 are computed. k1 characterizes the rate of flow across the passive Na-independent L1 channel, and k2 characterizes the flow across the active Na-dependent Na+-LNAA transporter. High values of k2 have been found to correspond to low accumulation of phenylanine in the brain. The value of k2 can also be used to quantify efficacy of treatment. Time varying concentrations of phenylanine in the brain and plasma were obtained from graphical data published in a previous study [1]. For the 3 patients studied with confirmed phenylketonuria, it is seen that a patient subjected to 10 years of restricted diet shows a higher clearance compared to untreated patients. The conclusions from the study are 1. It is possible to accurately characterize transporters between the brain and the endothelial cell with hidden compartment models, which was hitherto not possible. 2. The clearance rate of phenylanine from the blood can be characterized quantitatively, which enables the detection of phenylketonuria at birth as opposed to first detection when symptoms of retardation are seen 3. It is possible to quantitatively characterize the efficacy of treatment to decide on treatment options. Currently, the only known treatment is diet control, and it is not possible to determine the extent and duration of the treatment. Parametric values derived from this compartmental model may be able to provide accurate follow-up and better options. References 1. H. E. Moller et al (1998), Blood brain barrier phenylanine Transport and Individual Vulnerability in Phenylketonuria, J. Cerebral Blood Flow and Metabolism, 1184-1191.

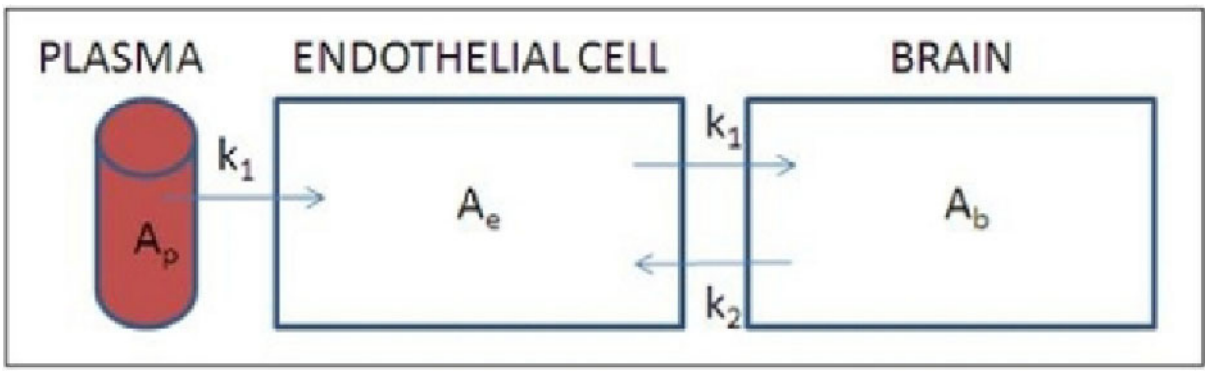


2-compartment model of blood-brain barrier

Disclosure of author financial interest or relationships:
**U.S. Ranjan**, None; **S. Sivakumar**, None; **P. Bhat**, None; **S. Srivatsa**, None; **A. Fischer**, None.

Presentation Number **P167**
Poster Session 1
September 5, 2012 / 18:00-18:00 / Room: The Liffey

# MRI and NMR study of engineered adipose tissues developed for reconstructive surgery

***Marc-Andre Fortin***[1,3], *Jean Lagueux*[3], *Maryse Proulx*[2,4], *Julie Fradette*[2,4], [1]*Génie des MInes, Métallurgie et Matériaux, Universite Laval, Quebec, QC, Canada;* [2]*Chirurgie, Université Laval, Quebec, QC, Canada;* [3]*Axe Métabolisme, Santé Vasculaire et Rénale, CHUQ, Quebec, QC, Canada;* [4]*LOEX, CHA-U.Laval, Quebec, QC, Canada. Contact e-mail: marc-andre.fortin@gmn.ulaval.ca*

INTRODUCTION: Adipose tissue substitutes are being developed as promising alternatives to autologous grafts, to answer the strong demand in reconstructive and plastic surgery (1) Trauma, tumour resection, congenital or acquired anomalies are the main causes justifying the need for such substitutes. Once developed in vitro, the adipose tissue grafts must be implanted in vivo, and their volume retention, vascularisation, as well as 1H spectroscopic properties, assessed by MR imaging. These are crucial for the development of future clinical implantation follow-up studies as well as for planning MRS studies. The characteristics of adipose grafts were studied in vitro with NMR, then in vivo in rodents at 1 Tesla MRI. METHODS: Reconstructed adipose grafts were developed with adipose-derived stem/stromal cells extracted from lipoaspirated subcutaneous tissue of a female donor (1). The endogenous production of extracellular matrix components was stimulated in vitro, leading to matrix deposition in the form of cell sheets which can be by lifted from culture plates with forceps and superimposed to create thicker tissues (~125mm3). Each one of these tissues was analysed in 1H-NMR (60 MHz) to quantify the water-to-lipid ratio, and also to measure T1 and T2 of each peak. The grafts were then subcutaneously implanted on the flanks of athymic mice. Native human and murine fat grafts were also implanted in animals, as well as reconstructed connective tissue grown without adipocytes. A 1T-MRI procedure was designed to scan animals (t = 0, 7, 14, 21 days) using T1-w. 2D SE (graft volume quantification), short-tau IR (fat signal nulling), as well as a rapid gradient IR sequence (for T1 maps). Finally, the blood volume in grafts was measured by DCE-MRI using a blood pool contrast agent (Gadomer). RESULTS : For reconstructed adipose tissues and for grafted native fat, NMR scans (Figure SI1) revealed the presence of two major proton populations (4.7 ppm: water; 0.9 - 2.24 ppm for 1H bound to lipids). For connective tissue, there was no major peak associated to lipids; strong indications of extracellular matrix were found (3.2 - 4.8: proteoglycans, hyaluronic acid, collagen), correlating with the weak signal in T1-w. MRI (Figure 1). A strong correlation was found between the fat content (0.9 - 2.24 NMR peak), and the brightness of T1-w. imaged tissues (Figure 1). The grafts were successfully visualised at 1 T MRI over a period of 21 days, and the delineation of the grafts allowed for the precise measurement of volumes over time. Short-Tau IR images (TI : 115 ms) were used to allow the delineation of adipose grafts from the host native fat (Figure SI2). DCE MRI indicated the vascularisation of adipose tissues at day 14 and 21 post-implantation. CONCLUSION: Adipose tissues were successfully implanted in athymic mice, and the volume retention and remodeling over time, measured. IR procedures could be used to differentiate reconstructed tissues from the native fat. The tissues were vascularised by day 14, which is essential to achieve viable grafts. Finally, NMR data confirmed the strong potential of these grafts for MRS. REF.: 1) Vermette et al., Biomaterials 2007.

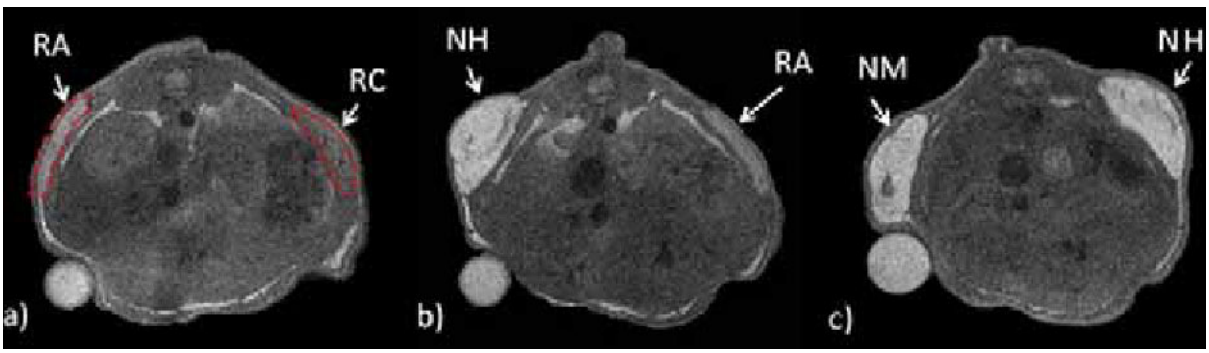


Figure 1. T1-w. spin-echo images (1 T) at the day of implantation : a) reconstructed adipose tissue (RA) and reconstructed connective tissue (RC); b) native human fat (NH) and reconstructed adipose tissue (RA); c) native murine fat (NM) and native human fat (NH).

Disclosure of author financial interest or relationships:
**M. Fortin**, None; **J. Lagueux**, None; **M. Proulx**, None; **J. Fradette**, None.

Presentation Number **P168**
Poster Session 1
September 5, 2012 / 18:00-18:00 / Room: The Liffey

# Normal whole-body anatomy of mouse based on preclinical 1.5T MRI and micro-CT acquisitions

*Jean-Philippe Dillenseger[1], **Christian Goetz**[1,2], Amira Sayeh[1], André Constantinesco[1], Philippe Choquet[1,2], [1]UF6237 Preclinical imaging, HUS, Strasbourg, France; [2]Institut de Mécanique des Fluides et des Solides, CNRS, Strasbourg, France. Contact e-mail: christian.goetz@chru-strasbourg.fr*

Introduction Merging different modalities is the current paradigm in clinical and preclinical imaging field. It is argued that adding morphology to molecular or functional information improves image analysis and diagnosis accuracy. Indeed, the combination of PET (alternatively SPECT) and MRI is currently the object of intense research activity, both for human and small animal applications. However the latter species does not benefit of a large number of anatomy references and especially there is a lack of description of anatomy in plane that could be correlated with tomographic imaging modalities. Many anatomical books focus on one organ (brain for instance) or on development stages. This is the reason why we began to work on a mouse in plane anatomy atlas, with the limited goal of providing a practical tool and not an exhaustive anatomical description. Material and methods The preclinical MRI is working at a field value of 1.5T (OPTImouse, RS2D, Bischwiller, France). A 40mm internal diameter RF coil (RapidBiomedical, Würzburg, Germany) is used for whole body imaging of mice. Common acquisition sequences (SpinEcho, GradientEcho and Fast SpinEcho) proton density, T1 and T2 weighted, with or without Gd based contrast agents (administered intra-venously or sub-cutaneously) are applied to provide multiple MR images of the same individual. The CT component of a microSPECT-CT (eXplore speCZT 120 Vision, GE, Waukesha, USA) is the source of the µCT images. In vivo acquisition protocols, with a reconstructed voxel of 100x100x100µm3 are used, with or without iodine based contrast agents (administered intra-venously or intra-peritonealy). All acquisitions are done ungated. Mice are kept anesthetized (Isoflurane + air) and warmed in imaging chambers (Minerve, Esternay, France) including landmarks, which fit in both imaging instruments. MRI and µCT were located near each other so that multimodality imaging of the same individual is achieved by moving the cell from one system to the other. Results Transverse, sagittal and coronal MR and µCT images were annotated, with the help of common mouse anatomical books (1,2,3,4). Conclusion We showed the very first illustrations of a future reference document, able to provide an help to mouse imaging practitionners. At this stage, we have only worked on images obtained on live animals, acquired with standard protocols, and so including all artefacts linked to physiological movements, in order to match daily use of such instruments. The next steps will consist in correlation on euthanasied animals, fixed with standard compounds, of MR and CT images and anatomy in plane as well as in vivo correlation with functional modalities. References 1 Cook MJ. Anatomy of the Laboratory Mouse Academic Press, 1965 http://www.informatics.jax.org/cookbook/ 2 Popesko P et al. A Colour Atlas of the Anatomy of Small Laboratory Animals: Rat, Mouse, Golden Hamster. Mosby, 1992 3 Iwaki T. A Color Atlas of Sectional Anatomy of the Mouse. Braintree Scientific, 2001 4 Bab I et al. Micro-Tomographic Atlas of the Mouse Skeleton Springer, 2007

Disclosure of author financial interest or relationships:
**J. Dillenseger**, None; **C. Goetz**, None; **A. Sayeh**, None; **A. Constantinesco**, None; **P. Choquet**, RS2D, Grant/research support .

Presentation Number **P169**
Poster Session 1
September 5, 2012 / 18:00-18:00 / Room: The Liffey

# In vivo accumulation and toxicity of silica nanoparticles in immunocompetent mice

***Young-Hwa Kim***[1,2], *Hyewon Youn*[1], *Mi Jeong Kim*[1], *Dong Soo Lee*[1], *June-Key Chung*[1,2], *Keon Wook Kang*[1], [1]*Department of Nuclear Medicine, Seoul National University College of Medicine, Seoul, Republic of Korea;* [2]*Department of Biomedical Sciences, Seoul National University College of Medicine, Seoul, Republic of Korea. Contact e-mail: cine82@snu.ac.kr*

Purpose: Recently nanoparticles have a potential for various biomedical applications including molecular imaging and drug delivery. Clearance of circulating nanoparticles is critical for in vivo application. The aim of this study was to evaluate the accumulation and toxicity of silica nanoparticles by different administration routes in mice. Methods: We used 50 nm core-sized PEGylated silica nanoparticles with far red fluorescent dye (BODIPY) and cobalt ferrite core (MNP-SiO2). Cytotoxicity test was performed using MTT assay for 72 hrs. MNP-SiO2 nanopaticles were administrated to mice either subcutaneously (s.c.) or intravenously (i.v.) (100 μg/mouse). Mice were monitored for 6 months using optical imaging system (CRi MaestroTM), and the tissue sections from the various mouse organs were observed by transmission electron microscopy (TEM) and hematoxylin and eosin (H&E) staining. For quantitative analysis, the amount of cobalt from silica nanoparticles in the extracted mouse organs were measured by inductively coupled plasma mass spectrometer (ICP-MS). Results: According to Dynamic Light Scattering (DLS) analysis, the hydrodynamic size of MNP-SiO2 was 69.2 ± 1.5 nm. The viability of WI-38 and HeLa cells were observed in more than 80% with 0.2 ~ 0.8 mg/ml MNP-SiO2 treatments. In vivo optical imaging showed that MNP-SiO2-fluorescent signals were significantly decreased over time, which was accumulated in spleen and liver. The signals were not detected at 3 months after injection. The amount of cobalt from silica nanoparticles in the extracted mouse organs was also significantly decreased, which were not detected in lymph nodes at 30 days after injection. In addition, MNP-SiO2 did not induce any systemic toxicity determined by H&E stained tissue sections and had no significant weight loss. Conclusion: We monitored the accumulation, clearance and toxicity of MNP-SiO2 in different administrated manner. These findings provide useful information to understand the factors affecting nanoparticle biodistribution in in vivo.

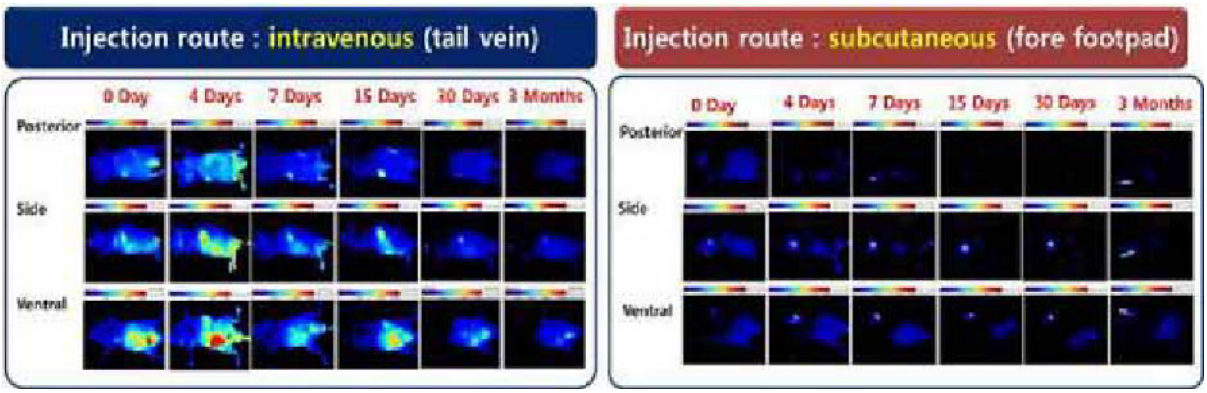


Disclosure of author financial interest or relationships:
**Y. Kim**, None; **H. Youn**, None; **M. Kim**, None; **D. Lee**, None; **J. Chung**, None; **K. Kang**, None.

Presentation Number **P170**
Poster Session 1
September 5, 2012 / 18:00-18:00 / Room: The Liffey

# A Multivariate Approach to Hypothesis Testing and Power Analysis in Pre-clinical Imaging

***Edward J. Soares***[1], *Jack Hoppin*[2], *Jacob Hesterman*[2], [1]*Mathematics and Computer Science, College of the Holy Cross, Worcester, MA, USA;* [2]*inviCRO LLC, Boston, MA, USA. Contact e-mail: esoares@holycross.edu*

In this work, we provide a framework for conducting a multivariate hypothesis test and power analysis with application to pre-clinical imaging studies. Specifically, we derive curves relating the sample size required to identify a statistically significant result to the difference in population mean vectors (effect size) between treatment and control groups, for a fixed significance level and power. We focus our attention on the two-sample case using a one-way multivariate analysis of variance (MANOVA) with homogeneity of covariance matrices. The analysis pertains to the measurement of an arbitrary number of features, however we specifically examine the cases where each measurement vector is composed of either one or two features. The results generally show that as the effect size decreases, the sample size required for identifying a statistically significant difference increases. When the population standard deviations of the two features are equal, then the more negatively correlated the features, the smaller the sample size that is required to detect a statistically significant difference, for a fixed effect size. When the population standard deviations of the two features are unequal, then the correlation between the features and the proportionality constant between the standard deviations both influence the relationship between effect size and sample size.

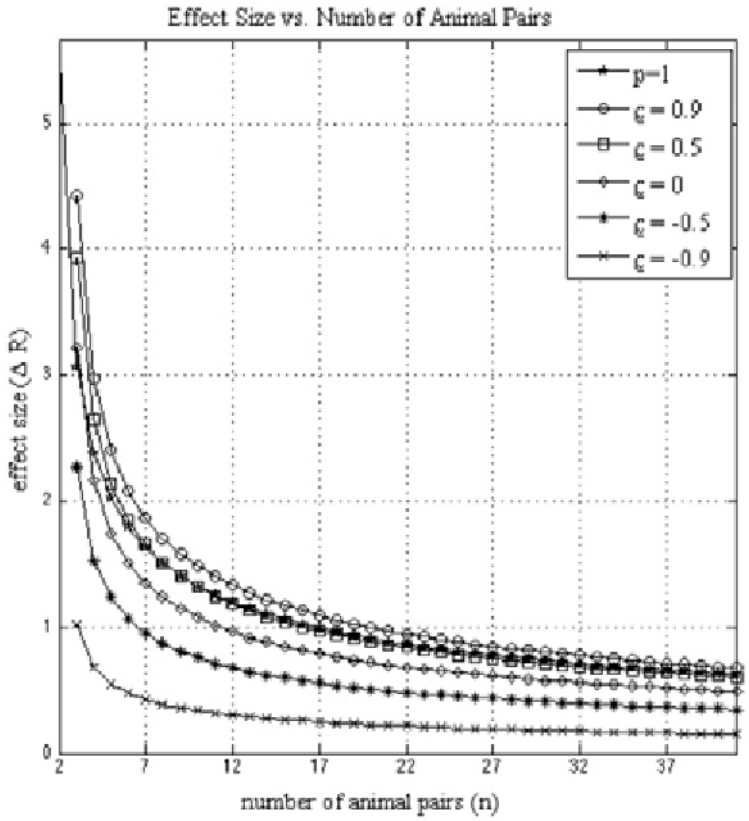


A plot of effect size ΔR vs number of animal pairs (n) for one (p = 1) and two (p = 2) measured features plotted over the range 2 - 41.

Disclosure of author financial interest or relationships:
**E.J. Soares**, None; **J. Hoppin**, inviCRO, LLC, Employment; inviCRO, LLC, Stockholder; **J. Hesterman**, inviCRO, Employment .

Presentation Number **P171**
Poster Session 1
September 5, 2012 / 18:00-18:00 / Room: The Liffey

# Potential Protective Effect of Acetyl-L-Carnitine in Prolonged Anesthetic Exposure-induced Neural Damage in the Developing Monkey Brain

***Cheng Wang***[1], *Xuan Zhang*[1], *Glenn D. Newport*[1], *Shuliang Liu*[1], *Fang Liu*[1], *Ralph Callicott*[1], *Marc Berridge*[2], *Scott M. Apana*[2], *Joseph P. Hanig*[3], *William Slikker*[1], *Merle G. Paule*[1], [1]*NCTR/FDA, Jefferson, AR, USA;* [2]*3D Imaging LLC, Little Rock, AR, USA;* [3]*CDER/OPS/Office of Testing & Research, FDA, Silver Spring, MD, USA. Contact e-mail: Cheng.Wang@fda.hhs.gov*

The inhalation anesthetics nitrous oxide (N2O) and isoflurane (ISO) are commonly used for surgical procedures in human infants. Combined exposures to N20 and ISO are known to cause neurotoxicity (abnormal apoptotic cell death) in pediatric animal models. L-carnitine, an anti-oxidant dietary supplement, has been reported to minimize neuronal damage in some models of neurotoxicity. MicroPET/CT imaging is capable of detecting and localizing changes in cellular markers of brain damage associated with developmental exposures to general anesthetics. By monitoring changes in the uptake of the specific radiotracer [18F]-FEPPA--thought to highlight glial activation associated with neurotoxicity—it should be possible to determine the severity, duration and location of neuronal damage associated with exposure to general anesthetics. On postnatal day (PND) 5, rhesus monkeys (4/group) were exposed to a mixture of 70% N2O. 29% oxygen plus 1% ISO, or this anesthetic mixture plus acetyl-L-carnitine (aLc) (100mg/kg) for 8 hours; control monkeys were exposed to room air only. [18F]-FEPPA (FEPPA), a peripheral benzodiazepine receptor marker thought to highlight glial activation was injected intravenously and microPET/CT images were obtained one day and one and three weeks after anesthetic exposure. One day after anesthetic exposure the uptake of FEPPA was significantly increased only in the temporal lobe and one week after exposure uptake was significantly increased in only the frontal lobe. No significant differences in uptake were seen in any area after 3 weeks. Co-administration of aLc effectively blocked the increase in FEPPA uptake in both the temporal and frontal lobes. These findings suggest that microPET/CT imaging of FEPPA uptake may be useful for monitoring the time-course and location of adverse neural events that are associated with developmental exposures to general anesthetics. In addition, aLc appears to be a compound capable of protecting against at least some of the adverse effects associated with such exposures. This work was supported by E-7285-NCTR/FDA and CDER/FDA.

Disclosure of author financial interest or relationships:
**C. Wang**, None; **X. Zhang**, None; **G.D. Newport**, None; **S. Liu**, None; **F. Liu**, None; **R. Callicott**, None; **M. Berridge**, Janssen RD, Grant/research support; FDA, Grant/research support; **S.M. Apana**, None; **J.P. Hanig**, None; **W. Slikker**, None; **M.G. Paule**, None.

Presentation Number **P172**
Poster Session 1
September 5, 2012 / 18:00-18:00 / Room: The Liffey

# PET in conscious rodents - quantification of stress during the training process

***Geoff I. Warnock**, Mohamed-Ali Bahri, Florian Bretin, Alain Seret, Andre Luxen, Alain Plenevaux, Cyclotron Research Center, University of Liege, Liege, Belgium. Contact e-mail: gwarnock@ulg.ac.be*

Recently several methods for performing PET studies in conscious rodents have been developed [1-3]. These methods have the potential to greatly improve the translational nature of PET studies in rodents. One of the most easily implemented methods is the training of a rat to tolerate head fixation in a restraining device. Training consists of intervals of restraint over several days. However, the stress induced by this training procedure has not been quantified in detail. Limited changes in plasma corticosterone have been reported, but this data may be confounded by sample timing and baseline levels. An implantable telemetry system (Telemetry Research) was used to remotely measure blood pressure, heart rate and core temperature during training. Transmitters were implanted in the abdominal cavity under isoflurane anesthesia, with the blood pressure sensor fixed in the abdominal aorta. Training was started after a recovery period of at least 1 week. Training consisted of a 5 min period of acclimatization in the cage containing the restraining device, followed by increasing durations of restraint in the device on subsequent training days (15, 30, 45, 60, 90 min). Telemetry data was acquired from 5 min prior to acclimatization to 60 minutes post-training. In this initial pilot study, a single rat was trained, without head fixation, for 4 consecutive days and again on day 7. All reported values are mean ± SEM across the five training days. In the home cage, prior to acclimatization, baseline heart rate (HR) was 294 ± 15 bpm. During the acclimatization period, HR was elevated to 411 ± 7 bpm. Immediately after starting training, HR was 419 ± 16 bpm. During the training period HR showed a tendency to decrease, with raised periods at undefined intervals. After return to the home cage, HR remained elevated for 15-20 min before returning to a value (313 ± 9 bpm) close to baseline. A similar pattern was seen in blood pressure (mean; BP). Baseline BP was 76 ± 7 mmHg, increasing to 94 ± 9 mmHg during acclimatization. After commencing training, a peak in BP was reached at 102 ± 8 mmHg. After the 15-20 min recovery interval, BP returned to a baseline of 77 ± 9 mmHg. The HR and BP responses to acclimatization and to the training protocol persisted throughout all training days, with the main noticeable difference being the number of bouts of increased HR, which increased with training duration. Core body temperature (baseline: 37.45 ± 0.21 °C) increased during restraint training, with a subsequent post-training peak (38.21 ± 0.03 °C). Measurement of core temp is complicated during longer training sessions by the need to charge the transmitter. This early data indicates that stress induced by the training procedure for conscious PET persists after several days of training. In subsequent studies the head will be fixed and the effect of the training on plasma corticosterone and central glucose metabolism (using [18F]FDG) will be examined. [1] Momosaki et al. (2004) Synapse 54:207-213 [2] Wyss et al. (2009) NeuroImage 48:339-347 [3] Itoh et al. (2009) J Nucl Med 50:749-756

Disclosure of author financial interest or relationships:
**G.I. Warnock**, UCB Pharma, Grant/research support; PMOD Technologies, Consultant; **M. Bahri**, None; **F. Bretin**, None; **A. Seret**, None; **A. Luxen**, GE Healthcare, Grant/research support; **A. Plenevaux**, None.

Presentation Number **P173**
Poster Session 1
September 5, 2012 / 18:00-18:00 / Room: The Liffey

# Quantitative Assessment of [18F]-FEPPA Uptake as a Biomarker of Anesthetic-Induced Neurotoxicity

***Xuan Zhang***[1], *Merle G. Paule*[1], *Glenn D. Newport*[1], *Marc Berridge*[2], *Scott M. Apana*[2], *William Slikker*[1], *Cheng Wang*[1], [1]*NCTR/FDA, Jefferson, AR, USA;* [2]*3D Imaging, LLC, Little Rock, AR, USA. Contact e-mail: xuan.zhang@fda.hhs.gov*

Ketamine is a dissociative anesthetic that is primarily used for the induction and maintenance of general anesthesia. It has been reported that blockade of NMDA receptors by ketamine may cause neurotoxicity in neonatal rats when given over a 12 hour period during the brain growth spurt. Noninvasive and quantitative imaging of neuronal activity in the brains of rodents may detect possible metabolic alterations induced by ketamine. Since it is known that the levels of peripheral benzodiazepine receptors (PBRs) increase in areas of neuronal injury following exposure to neurotoxicants, PBRs are widely recognized as important targets for imaging using positron emission tomography (PET). On PND 7, rat pups in the experimental group were exposed to 6 injections of ketamine (20 mg/kg at 2 h intervals) and control rat pups received 6 injections of saline. On PNDs 14, 21 and 28, [18F]-FEPPA (18.5 MBq) was injected i.p. and thirty minutes later microPET images were obtained over 90 minutes. Radiolabeled tracer accumulation in regions of interest (ROIs) in the frontal cortex was converted into Standard Uptake Values (SUVs). On PND 14, the uptake of [18F]- FEPPA was significantly increased in ketamine-treated rats. On PND 21, PND 28 and PND 35, however, no significant difference was found in radiotracer uptake in the frontal cortex, compared with controls. This preliminary study demonstrates that microPET imaging is capable of distinguishing differences in retention of [18F] -FEPPA in the brains of rodents and suggests that this approach may provide a minimally invasive biomarker of pathogenic process associated with neurotoxicity induced by ketamine. (Supported by CDER and NCTR)

Disclosure of author financial interest or relationships:
**X. Zhang**, None; **M.G. Paule**, None; **G.D. Newport**, None; **M. Berridge**, Janssen RD, Grant/research support; FDA, Grant/research support; **S.M. Apana**, None; **W. Slikker**, None; **C. Wang**, None.

Presentation Number **P174**
Poster Session 1
September 5, 2012 / 18:00-18:00 / Room: The Liffey

# Realtime three dimensional optoacoustic imaging of perfusion

***Andreas Buehler**, X. Luís Deán-Ben, Jing Claussen, Vasilis Ntziachristos, Daniel Razansky, Institute for Biological and Medical imaging, Helmholtz Zentrum München, German Research Center for Enviromental Health, Neuherberg, Germany. Contact e-mail: andreas.buehler@helmholtz-muenchen.de*

Small animal imaging plays an important role in basic research, drug discovery and clinical translation due to the widespread use of animal models of human disease in understanding systemic responses. A powerful imaging modality is multispectral optoacoustic tomography (MSOT), a hybrid imaging approach that can resolve optical contrast through several centimeters of tissue with the temporal and spatial resolution achieved by ultrasound imaging. Hence, it has the capacity to simultaneously visualize structural, functional and molecular information non-invasively. As consequence various optoacoustic imaging systems have been developed with different illumination configurations and detection geometries. Frequently, focused detectors are utlilized for cross-sectional image formation in real-time. Yet, optoacoustic imaging has the potential to provide three dimensional imaging. Herein, we report on a novel optoacoustic tomography system for 3D imaging at video-rate with high spatial resolution upto 200µm. We showcase the real-time 3D imaging performance of the system by monitoring perfusion in phantoms and living mice following injection of Indocyaninegreen. Multi-spectral capabilities are also showcased by resolving externally administered contrast agent based on its unique spectral signature without using background measurements made prior to the probe's administration. The system paves the way for high resolution in-vivo visualization of fast dynamic phenomena in three dimensions including whole-body longitudinal molecular imaging studies.

Disclosure of author financial interest or relationships:
**A. Buehler**, None; **X. Deán-Ben**, None; **J. Claussen**, iThera Medical, Employment; **V. Ntziachristos**, ERC, Grant/research support; Ithera Medical, Stockholder; **D. Razansky**, iThera Medical GmbH, Stockholder .

Presentation Number **P175**
Poster Session 1
September 5, 2012 / 18:00-18:00 / Room: The Liffey

# High resolution imaging of phosphatidylserine-exposing cells within live tumor allograft by means of multispectral optoacoustic tomography (MSOT)

***Andreas Buehler***[1], *Eva Herzog*[1], *Angelique B. Ale*[1], *Bradley D. Smith*[2], *Vasilis Ntziachristos*[1], *Daniel Razansky*[1], [1]*Institute for Biological and Medical imaging, Helmholtz Zentrum München, German Research Center for Enviromental Health, Neuherberg, Germany;* [2]*University of Notre Dame, Notre Dame Integrated Imaging Facility, Notre Dame, IN, USA. Contact e-mail: andreas.buehler@helmholtz-muenchen.de*

Tumor targeting is of high clinical and biological relevance, and major efforts have been made to develop molecular imaging technologies for visualization of the disease markers in tissue. Of particular interest is apoptosis which has a profound role within tumor development and has significant effect on cancer malignancy. Herein, we report on targeting of phosphatidylserine-exposing cells within live tumor allograft models using a synthetic near infrared zinc(II)-dipicolylamine probe. Visualization of the probe biodistribution is performed with whole body multispectral optoacoustic tomography (MSOT) system and subsequently compared to results attained by planar and tomographic fluorescence imaging systems. Compared to whole body optical visualization methods, MSOT attains remarkably better imaging capacity by delivering high-resolution scans of both disease morphology and molecular function in real time. Enhanced resolution of MSOT clearly showed that the probe mainly localizes in the vessels surrounding the tumor, suggesting that its tumor selectivity is gained by targeting the phosphatidylserine exposed on the surface of tumor vessels. The current study demonstrates the high potential of MSOT to broadly impact the fields of tumor diagnostics and preclinical drug development.

Disclosure of author financial interest or relationships:
**A. Buehler**, None; **E. Herzog**, None; **A.B. Ale**, None; **B.D. Smith**, None; **V. Ntziachristos**, ERC, Grant/research support; Ithera Medical, Stockholder; **D. Razansky**, iThera Medical GmbH, Stockholder .

Presentation Number **P176**
Poster Session 1
September 5, 2012 / 18:00-18:00 / Room: The Liffey

# Quantifying Tumor Interstitial Fluid Pressure in mice xenografts via non-invasive Scanning Acoustic Microscopy

***Ralph Pflanzer***[1], *Amit Shelke*[2], *Robert Sader*[3], *Matthias Hofmann*[1], *Jürgen Bereiter-Hahn*, [1]*Clinic of Dermatology, Venerology and Allergology, Goethe University Frankfurt am Main, Frankfurt am Main, Germany;* [2]*Institute for Cell Biology and Neurosciences Kinematic Cell Research Group, Goethe University Frankfurt am Main, Frankfurt am Main, Germany;* [3]*Dept. of Oral, Craniomaxillofacial and Facial Plastic Surgery, Medical Center of the Goethe-Universityrt am Main, Frankfurt am Main, Germany. Contact e-mail: ralphpflanzer@gmail.com*

Tumor tissue as an abnormally growing tissue is characterized by an impaired lymph drainage and a chaotically organized vessel network in its peripheral regions. The resulting fluid accumulation inside the tumor contributes to an often observed elevated tumor interstitial fluid pressure (TIFP). This outwardly directed pressure gradient prevents an efficient uptake of larger, macromolecular anti-cancer drugs - such as monoclonal antibodies (mAB) - in therapy of these types of cancers. High TIFP could also be shown to induce mechanical strain in the tumor cortex providing a trigger factor to cell proliferation. On subcutaneously implanted, vulva-carcinoma derived A431 tumor xenografts in nude mice, pressure values of up to 15 mm Hg could be measured. Two invasive techniques, the wick-in-needle technique and the micropuncture method, are commonly available for these investigations. With scanning acoustic microscopy (SAM) at various frequencies in the range of 5-30 MHz, a novel approach is proposed to overcome the drawbacks of invasive pressure assessment methods. Analysis of amplitude and time-of-flight acoustic signals provide the potential to quantify TIFP. Furthermore, biomechanical properties such as tissue attenuation, elasticity and inhomogeneity are more readily accessible. Invasive and non-invasive techniques have been used to assess and calibrate pressure under different treatment regimens on A431 tumors, such as angiogenesis-inducing vascular endothelial growth factor (VEGF-A and VEGF-C) and anti-cancer drugs like Cetuximab-class of antibodies. In addition, making tumor vessel network structures visible via mouse heart perfusion and a maceration preparation process of mouse tumor tissue could provide a helpful tool to support various imaging techniques on tumor microenvironment. Further investigations are undertaken to enhance understanding of tumor architecture and to make non-invasive ultrasound methods available for possible in-situ applications in small animals or small, sub-surface areas like subdermal tissues.

Disclosure of author financial interest or relationships:
**R. Pflanzer**, None; **A. Shelke**, None; **R. Sader**, None; **M. Hofmann**, None; **J. Bereiter-Hahn**, None.

Presentation Number **P177**
Poster Session 1
September 5, 2012 / 18:00-18:00 / Room: The Liffey

# Photoacoustic Imaging of Phantom Samples: Experiment and Reconstruction

*Xueyan Liu[1], **Jie Tian**[1,2], Dong Peng[4], Wei Guo[3], Xibo Ma[2], Chenghu Qin[2], [1]Sino-Dutch Biomedical and Information Engineering School, Northeastern University, "Shenyang,110004", China; [2]Medical Image Processing Group, Institute of Automation,CAS, "Beijing,100190", China; [3]The College of Electronic Information & Control Engineering, Beijing University of Technology, "Beijing,100124", China; [4]Life Sciences Research Center, School of Life Sciences and Technology, Xidian University, "Xi'an,710071", China. Contact e-mail: tian@ieee.org*

The experimental setup for the PA imaging system is described below. Pulses from a Q-switched Nd: YAG Laser operating at a wavelength of 532 nm with pulse duration of 7 ns, and a repetition rate of 10 Hz, were employed as the light source to generate a distribution of photoacoustic sources in a sample. The incident energy density of the laser beam was controlled below 20 mJ/cm2 and a piece of ground glass was used to homogenize the laser beam. The hydrophone (Precision Acoustics Ltd) with a diameter of 1 mm was used to detect the source around the imaging cross section perpendicular to the axis of the laser irradiation. A personal computer is used to control the steps. The transducer rotationally scanned the sample from 0 to 360 degrees with a step size of 1.8 degrees, At each angle, the PA signals is first amplified through a pulse amplifier, then recorded and averaged 256 times by an oscilloscope (MSO4000B, Tektronix), and finally transferred to a personal computer for imaging. An iterative reconstruction integrating simultaneous algebraic reconstruction technique (SART) and filtered back-projection (FBP) approach was applied to our photoacoustic imaging of the optical absorption in phantoms. We measured the PA pressure from an absorber fabricated by embedding a thin pencil core disc, 0.5 mm in diameter and 1 mm in height(figure 1(a)), and two absorber source in figure 1(c), within a cylindrical turbid phantom made of a mixture (water = 200 ml, and gelatin = 30 g) at a depth of 5 mm. The laser beam with homogeneous intensity distribution was projected normally to the disc surface. The reconstructed image of the pencil core disc phantom is shown in figure 1(b) and (d), with the cross section of the phantom shown in and (c). The reconstructed image is in excellent agreement with the original phantoms.

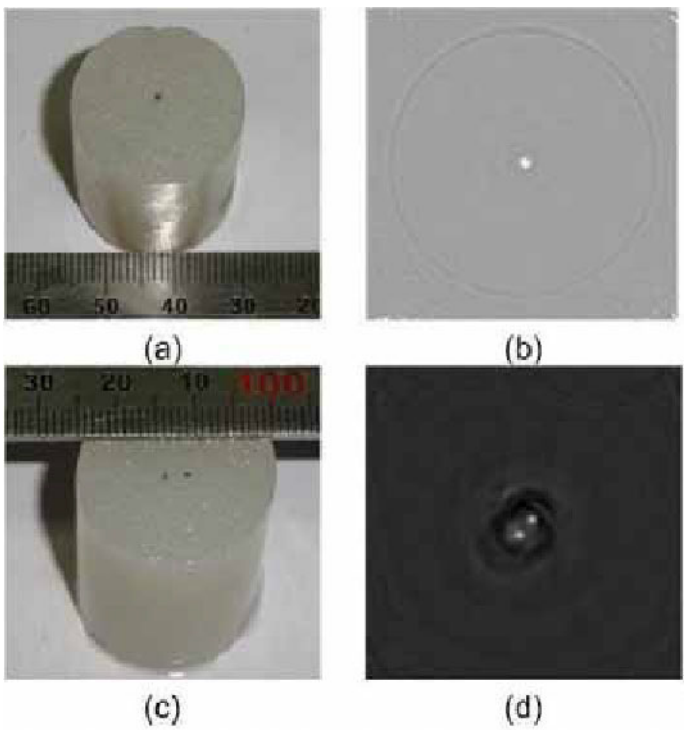


Figure 1. Photoacoustic imaging of a slice of imitative sample that was buried 0.5 cm deep in the phantom. (a), (c) are pictures of the imaged cross-section of the sample; (b), (d) are reconstructed images by SART-FBP algorithm.

Disclosure of author financial interest or relationships:
**X. Liu**, None; **J. Tian**, None; **D. Peng**, None; **W. Guo**, None; **X. Ma**, None; **C. Qin**, None.

Presentation Number **P178**
Poster Session 1
September 5, 2012 / 18:00-18:00 / Room: The Liffey

# Improving Photoacoustic Tomography Image Reconstruction by Accounting for Changes in Water Temperature

***Dominique Van de Sompel**, Laura S. Sasportas, Sarah Bohndiek, Anca Dragulescu-Andrasi, Sanjiv S. Gambhir, Radiology, Stanford University, Stanford, CA, USA. Contact e-mail: dominiqu@stanford.edu*

Photoacoustic tomography (PAT) combines the high spatial resolution of ultrasound with the high optical contrast of diffuse optical imaging. Recent years have seen a rapid proliferation of PAT scanner designs. Many of these designs use water as a coupling medium between the subject and the ultrasound transducers. To enable small animal imaging, the water is commonly heated to body temperature by a pumping system. However, pumping systems often generate small air bubbles in the water, which may collect on the subject's surfaces and destroy the ultrasound signal. Hence the heating pump is usually switched off during the scan, causing a small, gradual drop in temperature. This drop is often ignored in image reconstruction algorithms, which instead assume a constant temperature throughout the scan. While the speed of sound (SOS) is well known to change with water temperature, relatively little attention has been paid to characterizing the image artifacts that result from ignoring intra-scan temperature changes in PAT scans. Furthermore, no study has reported on the efficacy of intra-scan SOS corrections to improve reconstructions. The work presented here addresses this gap. We scanned several subjects using a commercial PAT system, namely two physical phantoms, a perfused and excised mouse brain, and a subcutaneous living mouse tumor model. During each scan, the heating system was switched off and the water temperature was continuously monitored. The subjects were then reconstructed using filtered backprojection, both with and without variable SOS corrections. For the latter, we assumed a constant initial, mean, or final water temperature. We demonstrated that ignoring gradual and seemingly small drops in temperature (1-5°C, starting from 37-38°C) can lead to substantial image artifacts. These can be difficult to distinguish from true structures, particularly in complex scenes. On the other hand, the intra-scan SOS corrections yielded substantial image quality improvements. We validated the improvements in two ways. First, we compared the physical phantom reconstructions with and without SOS corrections to the phantoms' known ground truths. Second, for all subjects, we compared reconstructions with variable SOS corrections to reconstructions from scans where the pumping system was left on, and for which a constant SOS could be used. For the latter, extra care was taken to remove bubbles from the subjects' surfaces. Both validation strategies yielded good agreements between the variable SOS reconstructions and the ground truth or truly constant SOS reconstructions. In summary, we dramatically improved image quality by monitoring the water temperature and subsequently applying variable SOS corrections. We did so for physical phantoms, ex vivo tissue, and in vivo mouse imaging. Hence our results carry a wide applicability to any systems where the water temperature may change during a scan. In other words, temperature monitoring and variable SOS correction are an important and effective solution for any PAT systems where controlling the water temperature is impractical, or where the use of a heating pump increases the risk of air bubble formation.

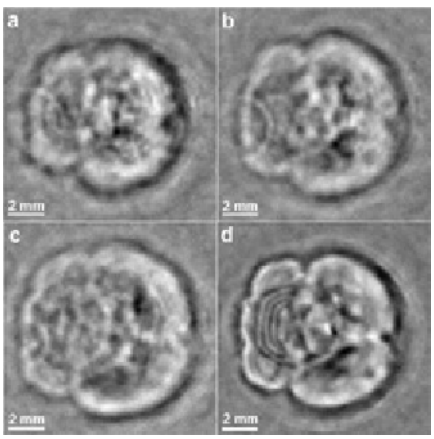


Fig. 1. Efficacy of accounting for gradual changes in the speed of sound. Filtered backprojection reconstructions of a perfused and excised mouse brain assuming the temperature to be (a) constant at the initial measured value, (b) constant at the mean measured value, (c) constant at the final measured value, and (d) gradually changing in accordance with the measured temperature history. The scan was performed using a commercial PAT scanner with 128 transducers arranged in a spiral pattern within a hemispherical bowl. The bowl was rotated through 360 degrees in 180 increments over the course of a 45 minute scan. During this time, the water temperature dropped from 38.0°C to 33.3°C.

Disclosure of author financial interest or relationships:
**D. Van de Sompel**, None; **L.S. Sasportas**, None; **S. Bohndiek**, None; **A. Dragulescu-Andrasi**, None; **S.S. Gambhir**, General Electric, Grant/research support; Bayer-Schering, Grant/research support; Sanofi-Aventis, Grant/research support; CellSight, Stockholder; ImaginAB, Stockholder; Enlight, Stockholder; Endra, Stockholder; Bracco, Consultant; NinePoint Medical, Stockholder; Visualsonics, Consultant .

Presentation Number **P179**
Poster Session 1
September 5, 2012 / 18:00-18:00 / Room: The Liffey

# Comparison of Deconvolution Filters for Photoacoustic Tomography

***Dominique Van de Sompel**, Laura S. Sasportas, Jesse V. Jokerst, Sanjiv S. Gambhir, Radiology, Stanford University, Stanford, CA, USA. Contact e-mail: dominiqu@stanford.edu*

Photoacoustic tomography (PAT) combines the high spatial resolution of ultrasound with the high optical contrast of diffuse optical imaging. The literature on PAT has seen the rapid development of scanner designs and reconstruction methodologies. The main reconstruction paradigms are one-step analytical backprojection, time reversal, and model-based iterative reconstruction algorithms. While time reversal and iterative methods offer superior image and system modeling capabilities, one-step analytical backprojection methods have been popular because of their speed and relative ease of implementation. A key step in analytical backprojection algorithms is to deconvolve the recorded pressure signals by the transducers' impulse response prior to backprojection. Deconvolution is notoriously ill-defined, and differences in its implementation can have a large impact on the reconstructed image quality. Its optimization is therefore of critical importance. Yet to the best of our knowledge, no direct comparisons of deconvolution filters have been published for PAT. In this work, we address this key gap and compare the merits of three well-known deconvolution methods when used in a filtered backprojection algorithm. The methods tested are the standard Fourier division technique, the Wiener deconvolution filter, and a Tikhonov L-2 norm regularized matrix inversion approach. Our experiments used subjects of various appearances, namely two man-made phantoms, a perfused and excised mouse brain, and a subcutaneous tumor living mouse model. Validation was performed by comparing the phantom reconstructions to their known ground truths, and the mouse brain reconstructions to physical sections obtained after the scans. The pressure data was acquired using a PAT scanner with a rotatable hemispherical bowl, into which 128 ultrasound transducer elements were embedded in a spiral pattern. Image quality was assessed qualitatively and quantitatively, the latter using the full width at half maximum (FWHM) and contrast-to-noise ratio (CNR) of selected image features. This was evaluated as a function of data sampling density, which was varied by changing the number of rotation angles of the bowl. For all objects, we found that the Wiener filter achieves the highest image resolution (see Fig.1). However, the image quality of the Wiener filter tended to degrade more rapidly with decreasing data sampling density than that of the Fourier and Tikhonov methods. In conclusion, we recommend using the Wiener filter when the sampling density of the available pressure data is high. In cases where the sampling density is restricted, for example by geometric or time constraints, the Fourier and Tikhonov L-2 norm approaches provide greater robustness in terms of the CNR of image features. More generally, our results showed that the reconstructed image quality is highly sensitive to the particular deconvolution method used. The implications of our work are therefore that any groups implementing PAT reconstruction algorithms should carefully optimize the data deconvolution operation. This result is likely to hold for any reconstruction methods relying on pressure data deconvolution.

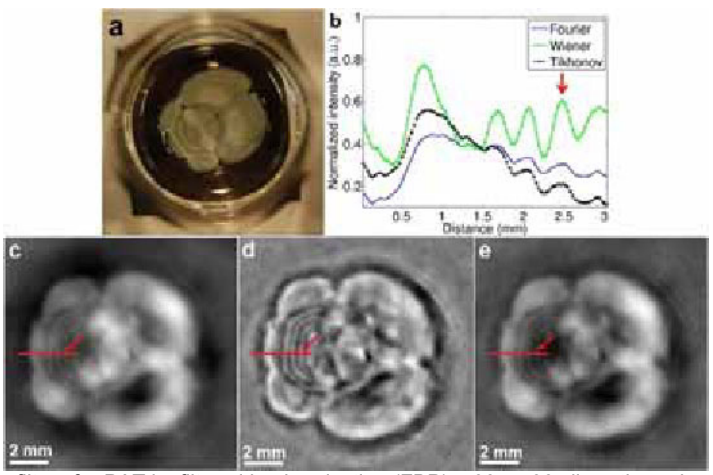


Fig. 1. Comparison of deconvolution filters for PAT by filtered backprojection (FBP). 400 x 400 slices through 400 x 400 x 200 reconstructions of a perfused and excised mouse brain. (a) Section of the same brain showing the main anatomical structures present in the reconstructed images. (b) Intensity profiles through the reconstructed slices. (c) FBP reconstruction with Fourier deconvolution, (d) FBP reconstruction with Wiener deconvolution, (e) FBP reconstruction with Tikhonov deconvolution. All reconstructions used data from 180 bowl positions of the scanner. The red arrows indicate a linear feature of interest, in the reconstructed slices as well as the intensity profiles. The red lines show the locations of the intensity profiles shown in (b).

Disclosure of author financial interest or relationships:
**D. Van de Sompel**, None; **L.S. Sasportas**, None; **J.V. Jokerst**, None; **S.S. Gambhir**, General Electric, Grant/research support; Bayer-Schering, Grant/research support; Sanofi-Aventis, Grant/research support; CellSight, Stockholder; ImaginAB, Stockholder; Enlight, Stockholder; Endra, Stockholder; Bracco, Consultant; NinePoint Medical, Stockholder; Visualsonics, Consultant .

Presentation Number **P180**
Poster Session 1
September 5, 2012 / 18:00-18:00 / Room: The Liffey

# Iterative Photoacoustic Tomography Strategy for Faster 3D Small Animal Imaging

***Dominique Van de Sompel***, *Jesse V. Jokerst, Sarah Bohndiek, Sanjiv S. Gambhir, Radiology, Stanford University, Stanford, CA, USA. Contact e-mail: dominiqu@stanford.edu*

Photoacoustic tomography (PAT) is an emerging modality offering high-resolution imaging of optical contrast deep within living tissue. To date, most studies have reconstructed images using analytical methods such as filtered backprojection (FBP), popular for their speed and ease of implementation. Unfortunately, these are only exact when the pressure data is densely sampled over a detection surface that encloses the object. To minimize image artifacts such as streaking, most practical 3D scanners move arrays of limited numbers of transducers through a range of positions to increase the sampling density, leading to scan times of several to tens of minutes. In this work, we explore a strategy to lower the required sampling density using a 3D model-based iterative least squares algorithm (ILS). It outperforms FBP under incomplete sampling conditions by explicitly minimizing the difference between the measured and forward simulated pressure signals. This study presents a demonstration of the practical feasibility of 3D model-based reconstruction, improving over previous work which has been largely restricted to 2D reconstructions due to the high computational burden of model-based methods. We acquired data by scanning physical phantoms (N=3) and subcutaneous mouse tumor models (N=5) with a 128-transducer PAT system, optimized for 3D small animal imaging. The system's ultrasound transducers are arranged in a spiral pattern within a hemispherical bowl, which can be rotated to increase the sampling density (SD). Scans were acquired at 2, 4, 8, 16, 32, 64 and 120 bowl positions (uniformly spaced over 360 degrees) and reconstructed using FBP and ILS. To circumvent memory issues, ILS's system matrix values were computed on the fly with a GPU. Reconstructions converged after ~15 iterations of conjugate gradient descent. We validated ILS by comparing its reconstructions to a reference image. For the phantoms, the reference image was the known ground truth; for the tumor models, it was a high SD (120 bowls) FBP reconstruction. To compare FBP and ILS at any given SD, we used both visual assessment and quantitative metrics, namely contrast-to-noise ratio (CNR) and the root-mean-square error from the reference image (RMSE). Fig.1 and S1 show a number of representative results. Fig.1 confirms that the improvement by ILS over FBP is greatest at low SDs. In qualitative terms, ILS yielded two noticeable improvements. First, it reduced streak artifacts (green arrows). Second, it made visible some of the structures not visible in FBP reconstructions, particularly the smaller vessels (red arrows). In the case of the in vivo tumors, the improved structures were mostly deeper-lying blood vessels (Fig. S1). In quantitative terms, ILS produced better CNRs and RMSEs than FBP, again at lower SDs. The improved CNR and RMSE at a given SD are significant because they enable more precise ROI selection and improved quantitation, respectively. In summary, the value of ILS is that it allows lower SDs, hence reducing scan times in time-sensitive applications such as dynamic PAT (higher 3D frame rates) and 3D multi-wavelength PAT (more wavelengths within a given time).

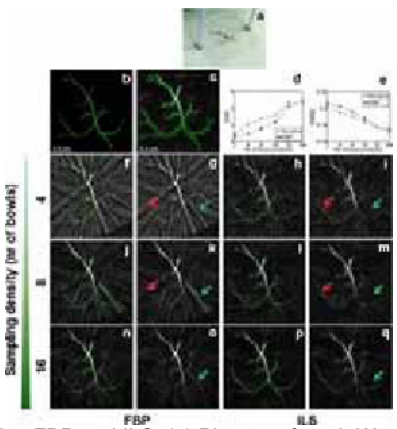


Fig. 1. Reconstructions of a known vessel phantom using FBP and ILS. (a) Phantom from k-Wave toolbox printed on overhead projector film. (b) digital ground truth of the phantom. (c) mask (green overlay) used for CNR computations. (d,e) CNR and RMSE as a function of sampling density (number of bowl positions). The reconstructions were scaled to give the minimum possible RMSE from the reference image. At higher sampling densities, ILS began to yield grainier reconstructions than FBP, resulting in a cross-over of the CNR and RMSE curves above 16 bowl positions. This may be alleviated in future work using image regularization priors such as minimal total variation. (f-q) Maximum Intensity Projections (MIPs) of various reconstructions. Column 1 (f,j,n): FBP with ground truth overlay in green. Column 2 (g,k,o): FBP. Column 3 (h,l,p): ILS with ground truth overlay in green. Column 4 (i,m,q): ILS. Lastly, green arrows indicate streak artifacts. Red arrows indicate smaller features rendered by ILS but not FBP.

Disclosure of author financial interest or relationships:
**D. Van de Sompel**, None; **J.V. Jokerst**, None; **S. Bohndiek**, None; **S.S. Gambhir**, General Electric, Grant/research support; Bayer-Schering, Grant/research support; Sanofi-Aventis, Grant/research support; CellSight, Stockholder; ImaginAB, Stockholder; Enlight, Stockholder; Endra, Stockholder; Bracco, Consultant; NinePoint Medical, Stockholder; Visualsonics, Consultant .

Presentation Number **P181**
Poster Session 1
September 5, 2012 / 18:00-18:00 / Room: The Liffey

# Quantification software in Nuclear Cardiology: can we all agree on values?

***Sergey V. Nesterov***[1], *John O. Prior*[2], *Roberto Sciagrà*[3], *Chunlei Han*[1], *Juhani Knuuti*[1], [1]*Turku PET Centre, University of Turku, Turku, Finland;* [2]*Nuclear Medicine, Lausanne University Hospital, Lausanne, Switzerland;* [3]*Nuclear Medicine Unit, University of Florence, Florence, Italy. Contact e-mail: sergey.nesterov@tyks.fi*

Introduction. Quantification of myocardial perfusion (MP) or oxidative metabolism (OM) is possible using dedicated software (SW). The number of SW packages and models available is substantial and grows. Although they all are validated against something, the question remains how precise are their agreements on values they provide. It is of utmost important to ensure that any user receives the similar results. The aim of our effort is to cross-compare various models and SW for quantification of cardiac PET data; our team has gradually grown to a multi-lab worldwide endeavor. The first project (Nesterov et al., 2009) is already published; it focused on intra- and interobserver reproducibility of Carimas SW. In that study four different observers analysed 20 15O-water studies twice; global ICC was 0.99 in the expert and 0.89 in the novice. Methods. The observers analyse various series of dynamic PET images from characterized patient populations with existing SW packages. The dedicated linear mixed model for the repeated measures is applied to the data; where appropriate we also use linear regression and Bland-Altman plots. The intra- and interobserver reproducibility are assessed on global, regional and segmental levels with intraclass correlation coefficients (ICC) serving the main agreement metric. ICC values over 0.81 represent a very good agreement; in between 0.61 and 0.80 - a substantial one. All reasonable differences between SW are calculated. The current project focused on 48 13N-ammonia studies analysed in three different labs by three observers with established SW solutions - Carimas, PMOD and FlowQuant. In all the three packages 1TC model described by DeGrado et al. (1996) is utilized, the first two also implemented a 2TC model (Hutchins et al. 1990). Results. With 13N-ammonia all SW implementing 1TC are in very good agreement at the global level: Carimas vs PMOD - 0.831, Carimas vs. FlowQuant - 0.846, PMOD vs. FlowQuant - 0.828 (ICC). Carimas and PMOD had also a substantial agreement on a 2TC model: 0.745. The only statistically significant ($p<0.05$) difference at the global level was 0.16±0.12 mL/min/g between PMOD and FlowQuant; differences between PMOD and Carimas, 0.08±0.10 mL/min/g and between Carimas and FlowQuant - 0.08±0.08 mL/min/g were not significant. The difference between PMOD and Carimas in 2TC was not significant - 0.17±0.20 mL/min/g. Conclusions. The ongoing software validation programme is aiming to create a more predictable analysis environment in Nuclear Cardiology. The 1TC models in three different SW packages are in good agreement but less good with 2TC models. The project with nine different SW packages and 100 82Rb studies has started, and will be finished in 2012. Next steps also include finding the best models and creating a worldwide database of healthy hearts for different radiotracers.

Disclosure of author financial interest or relationships:
**S.V. Nesterov**, None; **J.O. Prior**, None; **R. Sciagrà**, None; **C. Han**, None; **J. Knuuti**, Lantheus Inc, Consultant; Philips, Speakers bureau .

Presentation Number **P182**
Poster Session 1
September 5, 2012 / 18:00-18:00 / Room: The Liffey

# Clinical, Histopathological and Molecular Characterisation of Asinine Pulmonary Fibrosis

***Amy Miele***[1,3], *Nicole Du Toit*[2], *Sionagh Smith*[3], *William A. Wallace*[4], *Tobias Schwarz*[3], *John Murchison*[5], *Mark Bradley*[6], *Haslett Chris*[1], *Bruce McGorum*[3], *Kevin Dhaliwal*[1], [1]*Centre for Inflammation Research, University of Edinburgh, Edinburgh, United Kingdom;* [2]*Veterinary Laboratory, The Donkey Sanctuary, Sidmouth, United Kingdom;* [3]*Royal (Dick) School of Veterinary Studies, University of Edinburgh, Edinburgh, United Kingdom;* [4]*Department of Pathology, New Royal Infirmary, Edinburgh, United Kingdom;* [5]*Department of Radiology, New Royal Infirmary, Edinburgh, United Kingdom;* [6]*School of Chemistry, University of Edinburgh, Edinburgh, United Kingdom. Contact e-mail: a.c.miele@sms.ed.ac.uk*

The donkey sanctuary in Devon reports a 35% prevalence of Asinine Pulmonary Fibrosis (APF) at routine necropsy. We propose that APF is a spontaneous model with important translational relevance to human fibroproliferative conditions. Detailed multidisciplinary characterisation (macroscopic, mesoscopic, microscopic and molecular) of APF will facilitate the validation of this hypothesis. Evaluation of CT images and corresponding histopathological sections has identified two distinct patterns of fibrosis within APF affected tissue. The ‘bronchocentric' pattern shares many pathological features with chronic hypersensitivity pneumonitis, while the ‘peripheral pattern' encompasses features of other human fibrotic lung diseases. Molecular characterisation of APF affected tissue utilising immunohistochemistry and western blot demonstrated increased expression of key molecular markers of fibrosis: MMP9, α-SMA, Tenascin, lysyl oxidase (LOX) and lysyl oxidase-like molecule 2 (LOXL2). A similar expression was shown in human lung biopsies, indicating the cross-species conservation of pro-fibrotic pathways but also a process of active fibrogenesis within APF tissue. In order to begin to evaluate the dynamic expression of key molecular markers *in vivo*, we have utilised the cutting edge imaging modality: probe based confocal laser endomicroscopy (pCLE). So far we have established that pCLE allows visualisation of disrupted alveolar architecture within areas of fibrosis in *ex vivo* APF affected tissue. This is similar to the pattern observed in human patients suffering from pulmonary fibrosis. Our ultimate goal is to utilise pCLE in combination with specifically synthesised contrast agents or ‘smartprobes' to detect critical molecular targets *in vivo*. This will allow minimally invasive, real time molecular imaging at a cellular level. Such a tool could provide new possibilities in the diagnosis and monitoring of fibroproliferative diseases across species and has the potential to drive the development of upcoming anti-fibrotic therapies.

Disclosure of author financial interest or relationships:
**A. Miele**, None; **N. Du Toit**, None; **S. Smith**, None; **W.A. Wallace**, None; **T. Schwarz**, None; **J. Murchison**, None; **M. Bradley**, None; **H. Chris**, None; **B. McGorum**, None; **K. Dhaliwal**, None.

Presentation Number **P183**
Poster Session 1
September 5, 2012 / 18:00-18:00 / Room: The Liffey

# 18F-FDG PET/CT in diagnosis and monitoring of IgG4-related systemic disease

***Jingjing Zhang**, Zhaohui Zhu, Fang Li, Dept. Of Nuclear Medicine, Peking Union Medical College Hospital, Beijing, China. Contact e-mail: zhangjingjingtag@163.com*

IgG4-related systemic disease (IgG4-RSD) is a clinical entity being increasingly recognized in recent years. The disease usually involves various organs, including pancreas (also known as autoimmune pancreatitis), parotid glands, lacrimal glands, salivary glands, lymph nodes, lungs, biliary tract, aorta, kidneys, prostate, etc. It is generally considered as an autoimmume disease but easy to be confused with malignant tumors. The diagnosis is sometimes challenging and a good understanding of the disease is essential to reach a correct diagnosis. Most importantly, the disease has a good response to steroids and immunosuppressants, with a prognosis quite different from those of malignancies. A few case studies have indicated the value of 18F-FDG PET/CT in IgG4-RSD. This study was prospectively designed to investigate the role of PET/CT in diagnosis, assessing involvement, guiding biopsy, and monitoring the treatments in a relatively large group of IgG4-RSD patients. Methods: A total of 23 patients (M14, F9, aged 61.6±8.3) diagnosed as IgG4-RSD according to clinical symptoms, abnormally elevated serum IgG4 levels, images, biopsy and/or clinical follow-ups underwent 18F-FDG PET/CT. Fifteen of the patients also accepted PET/CT follow-ups 2 weeks to 2 months after steroid therapy. One hour after intravenous injection of 3.7-5.5 MBq/Kg 18F-FDG, whole body PET/CT scans were routinely performed using a Siemens Biograph64 TrueV system. Results: All 23 patients were found with intense 18F-FDG uptake lesion(s) in the body, and 16 patients (70%) showed abnormal uptakes in more than two organs. In the 23 patients, 11 had pancreas involement, 10 with lymph nodes, 6 with salivary glands, 4 with lungs, 4 with the abdominal aorta walls, 3 with liver, and 3 with kidney involvement, et al. The standardized uptake values (SUV) of the lesions ranged from 1.0 to 6.3 (3.1±1.5). The morphology of the lesions were variant from diffuse to nodular forms, however, the disease could be indicated in most cases if the typical manifestations and involement had been in good understanding in advance. In the 15 cases with PET/CT follow-ups, the 18F-FDG uptake was remarkably decreased after steroid therapy of 60 mg prednisone per day typically, even with only 2 week of treament. Conclusions: 18F-FDG PET/CT may play an important role in guiding diagnosis, assessing involvement, and monitoring early response to treatments of IgG4-RSD. A good understanding of the disease is very important to make a correct dicision-making for further diagnosis and proper management.

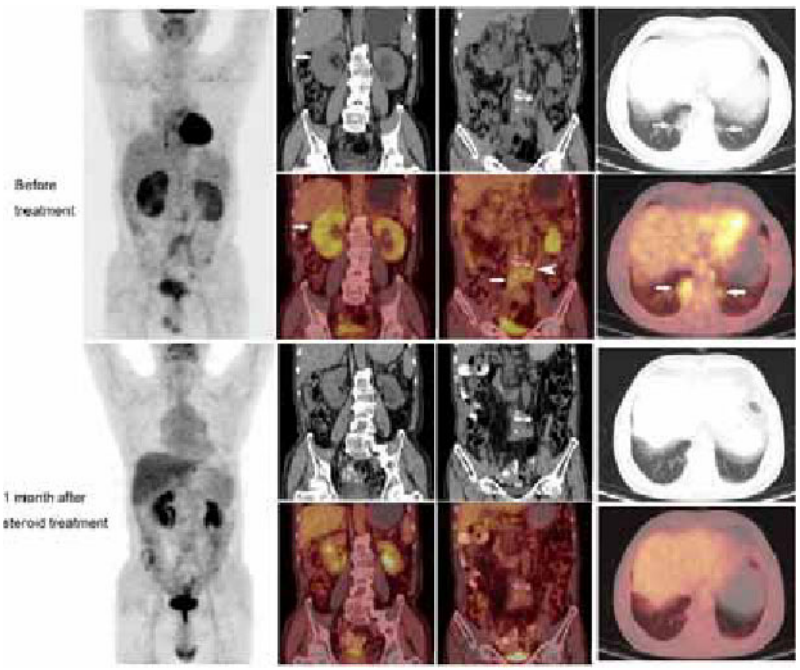


Figure Comparison of PET/CT images before and 1 month after steroid treatment in a patient with IgG4-related system disease. Moderate to intense 18F-FDG uptake was found in the lungs, kidneys, aorta wall (arrow), and left middle ureter (arrow head).

Disclosure of author financial interest or relationships:
**J. Zhang**, None; **Z. Zhu**, None; **F. Li**, None.

Presentation Number **P184**
Poster Session 1
September 5, 2012 / 18:00-18:00 / Room: The Liffey

# The central cortical responses of 18F-FDG uptake in a rat model of central auditory pathway with rat voice stimulation by high resolution small animal positron emission tomography

*Wei-Chung Hsu[1,3], **Kai-Yuan Tzen**[2,3], Te-Huei Yeh[1,3], Patrice Tran Ba Huy[4], Michele Duet[5], [1]Otolaryngology, Head and Neck Surgery, National Taiwan University Hospital, Taipei, Taiwan; [2]Nuclear Medicine, National Taiwan University Hospital, Taipei, Taiwan; [3]Molecular Image Center, National Taiwan University, Taipei, Taiwan; [4]Otolaryngology, Head and Neck Surgery, Hopital Lariboisiere, Paris, France; [5]Nuclear Medicine, Hopital Lariboisiere, Paris, France. Contact e-mail: tzenky@ntuh.gov.tw*

Background: We have previously set up an animal model of central auditory pathway in rats by high resolution small animal positron emission tomography (PET), which demonstrated increased glucose metabolism by 18F-FDG uptake in inferior colliculus (IC) and auditory cortex (AC). However, conventional image processing achieved by 3D ordered subsets-expectation maximization (OSEM) reconstruction algorithm and region of interest (ROI) analysis were not satisfied for objective localization and quantitatively analysis for cerebral cortex. Therefore, we further apply 3D voxel-based analysis for PET images with the recorded rat voice stimulation to optimize the functional information of brain plasticity. Methods: Fluorine-18-labeled fluorodeoxyglucose (18F-FDG) was use in an animal model of central auditory pathway imaging in the rat brain by PET. Unilateral cochlear ablation by micro-surgery was applied to normal hearing female adult rats. 18F-FDG PET scans were done 2 weeks to 24 weeks after operation. Group A was stimulated by white noise as usual protocol and group B was stimulated by pre-recorded rat voice with an ultra-high frequency, ranged from 300-600 kHz. The18F-FDG PET scans were acquired for 50 min. at 45 min. after the i.v. injection of FDG. The rats were anesthetized using isofluorane and scanned by small animal PET/CT scanner (eXplore Vista DR, GE Healthcare, USA). After image acquisition, the analysis was performed by statistical parametric map (SPM) program. Results: In group A, the radioactivity of contralateral IC was statistically significant higher than pre-surgery control images prominently. However, the cortical responses were vague and only showed minimal uptakes in auditory cortex. In group B, the rat brains not only demonstrated prominent IC responses but also diffuse, bilateral cortical radioactivities beyond auditory cortex. Conclusions: Our study demonstrated that SPM program could be utilized in voxel-based brain analysis of small animal model. By white noise stimulation, the rat brains could demonstrate prominent IC response and minimal auditory cortex responses. However, by rat voice stimulation, the rat brains not only demonstrated prominent IC response but also auditory cortical responses. Besides, some upgrade and downgrade responses were also noted in the other cortical areas and midbrain/or brainstem regions, which still needs further confirmation and interpretations. The methodology might facilitate the accuracy of the spatial preprocessing procedures and the statistical significance of the comparison between control and experimental groups. Figure legends: Upper raw: Control-Group A rats with white noise stimulation, it revealed ipsilateral higher uptakes in IC (right) and only minimal uptakes in AC (left). Lower raw: Control-Group B rats with rat voice stimulation; it showed both higher uptakes in AC (left) and IC (right).

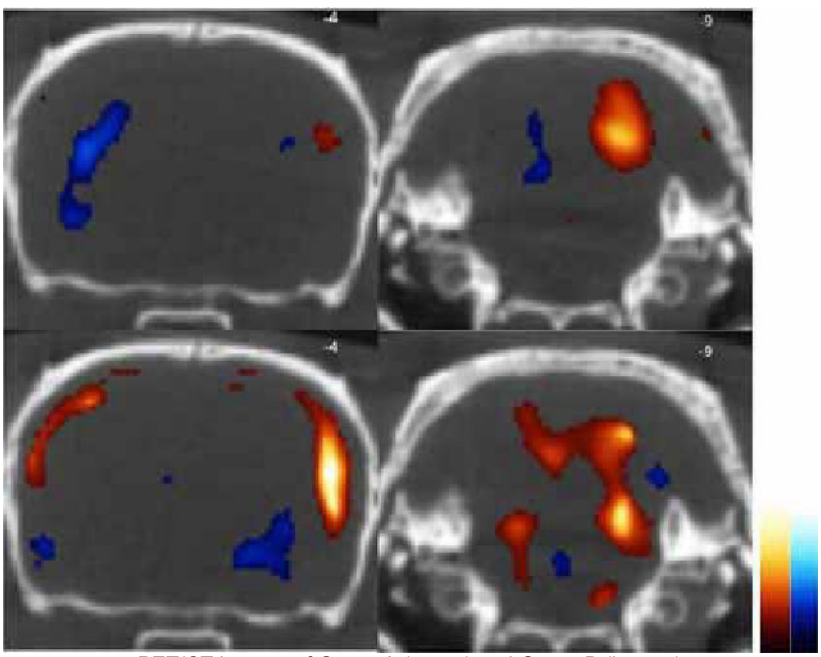

PET/CT images of Group A (upper) and Group B (lowere)

Disclosure of author financial interest or relationships:
**W. Hsu**, None; **K. Tzen**, None; **T. Yeh**, None; **P. Tran Ba Huy**, None; **M. Duet**, None.

Presentation Number **P185**
Poster Session 1
September 5, 2012 / 18:00-18:00 / Room: The Liffey

# Evaluation of Callosal Motor Fiber Location in the Human Brain: A Diffusion Tensor Tractography and Functional MRI study

***Dong Hoon Lee***[1]*, Cheol Pyo Hong*[1]*, Sung Ho Jang*[2]*, Bong Soo Han*[1]*,* [1]*Radiological Science, Yonsei University, Wonju, Republic of Korea;* [2]*Physical Medicine and Rehabilitation, Yeungnam University, Daegu, Republic of Korea. Contact e-mail: ldhdaum@yonsei.ac.kr*

The corpus callosum (CC) is the largest fiber bundle in the human brain interconnection the two cerebral hemispheres. Recently, many neuroscientists have been studied CC using diffusion tensor tractography (DTT) technique. Especially, assessment of callosal motor fiber (CMF) in the CC is known that cross primarily through the anterior midbody of the CC in the previous study. However, Wahl et al. found that CMFs cross through the posterior body and isthmus. In this study, we assessed the CMF which related foot fibers in the CC and measured anatomical location using DTT combined fMRI. We also measured fractional anisotropy (FA) and apparent diffusion coefficients (ADC) values to confirm the normal range. Fourteen healthy subjects participated in this study. DTI data were obtained Philips 1.5T Gyroscan intera MR scanner. The data were acquired with following parameters: matrix=128×128, FOV=221mm, TR/TE=10726/76ms, b-value=1000s/mm2, slice thickness=2.3mm and 32 diffusion-sensitizing gradients direction. The eddy currents and motion effects were corrected by registering all diffusion-weighted images to non-diffusion weighted image using twelve-parameter affine registration. The data were analyzed using the DtiStudio 3.0.2 with the termination criteria for fiber tracking: FA<0.2, angle change>70°. FMRI data were obtained following these parameters: matrix=64×64, FOV=210mm, TR/TE=2000/60ms, slice thickness = 5mm and using a block paradigm (foot grasp-release movements at 1Hz frequency). These data were analyzed using SPM2 with p<0.05. The ROIs were drawn in the fMRI activation area and CC in the color-coded FA map. After CMF was reconstructed, we overlaid fiber tract on the each subject b=0 image. The anatomical location of CMF was measured as followed: 1) The CC distance which is between most anterior point and posterior point of each subject is measured. 2) The distance between innermost point of fiber and the most posterior point of CC is also measured. 3) The relative distance was represented ratio of 1) and 2). The FA and ADC values were also measured based on the extracted fibers. The mean±standard deviation of each subject distance ratio for CMF which related foot movement was represented 29.08±3.42. The values are on within the isthmus distance range of CC. The distance ratio of isthmus was located in 20~33% in the posterior of CC, generally by Jancke et al. Our results represented that CMF are located on the posterior part of isthmus, strictly. In the isthmus, our results are located in 40~90% backward considered to our results distributions. The values for FA and ADC are 0.54±0.02 and 8.03×10-4±1.16×10-4, respectively. In this study, we evaluated the CMF related foot fiber relative location in the CC. Our results well matched previous researches indication that are CMFs located in the posterior body and isthmus. We also confirmed that the foot fibers CMF are located in the posterior part of isthmus, relatively. Although our results have some limitation such as considering only CMF related foot fibers and tracking algorithms, we believe that our results seem to be a good preliminary data for detailed anatomical location of CMF in the CC.

Disclosure of author financial interest or relationships:
**D. Lee**, None; **C. Hong**, None; **S. Jang**, None; **B. Han**, None.

Presentation Number **P186**
Poster Session 1
September 5, 2012 / 18:00-18:00 / Room: The Liffey

# Quantification of FDG PET images by population-based input function demonstrates reduced CMRglc in reference regions of dementia patients

***Joseph Lewis***[1], *Stephen F. Carter*[2,1], *Marie-Claude Asselin*[1], *Karl Herholz*[1], *Rainer Hinz*[1], [1]*Wolfson Molecular Imaging Centre, University of Manchester, Manchester, United Kingdom;* [2]*Division of Alzheimer Neurobiology, Karolinska Institutet, Stockholm, Sweden. Contact e-mail: joseph.lewis-2@postgrad.manchester.ac.uk*

**Introduction:** Investigations into the progression of dementia using [18F]-fluorodeoxyglucose (FDG) Positron Emission Tomography (PET) are carried out using the non-invasive ratio to reference region method, which assumes that the reference region is unaffected in disease states. We compared the cerebral metabolic rates of glucose (CMRglc) in commonly used reference regions between a cohort of control subjects and a group of dementia patients to assess the changes in the reference regions. **Methods:** Seven controls (age 68.1 ± 6.2 years, MMSE 29.7 ± 0.5, mean ± SD) and 8 patients of which 5 with mild cognitive impairment (MCI, age 75.2 ± 7.7 years, MMSE 28.4 ± 1.8) and 3 with mild Alzheimer's disease (AD, age 76.7 ± 4.7 years, MMSE 26 ± 1.7) underwent volumetric structural T1-weighted MRI (3T, Philips) and high resolution PET imaging (HRRT, Siemens) for 60 min after injection of 370MBq FDG. Dynamic PET images were reconstructed using ordered-subsets expectation maximisation with resolution modelling and frame-by-frame motion correction. Anatomical regions were defined using a probabilistic brain atlas [Hammers et al, 2003]. CMRglc maps were obtained via Patlak analysis with a population-based input function [Takikawa et al, 1993] individually scaled using 3 venous blood radioactivity measurements taken at 40, 50 and 60 min post injection along with blood glucose measurements. The cerebellum and precentral gyrus were investigated as reference regions and the parahippocampal gyrus as a target region of early detection of metabolic changes in AD. Target to reference ratios were calculated using 25-60 minute images. Statistical comparisons between groups were performed using Mann Whitney U-tests. **Results:** Differences between diseased groups and controls are presented in Figure 1. CMRglc decrease in the target region (Fig. 1A) was 32% (p=.002) and 23% (p=.011) on the left and right sides, respectively. CMRglc was also decreased by 22% (p=.105, Fig. 1A) and 24% (p=.049, Fig. 1A) in the cerebellum and precentral gyrus, respectively. When using ratios of target to reference region, smaller decreases in FDG uptake were found: 11% (p=.064) and 5% (p=.487) with the cerebellum (Fig. 1B), and 14% (p=.004) and 8% (p=.049) with the precentral gyrus (Fig. 1B). **Conclusion:** Using minimally invasive measurements for CMRglc estimation instead of calculating FDG uptake ratios enhanced differences between patients and controls, implying a greater sensitivity to detect disease and monitor progression. The method used in this study could feasibly be implemented clinically with potentially significant impact on study outcome. Larger group sizes will be presented to confirm these findings. **References:** Hammers et al. Hum Brain Mapp 2003; 19: 224-47 Takikawa et al. Radiology 1993; 188: 131-136

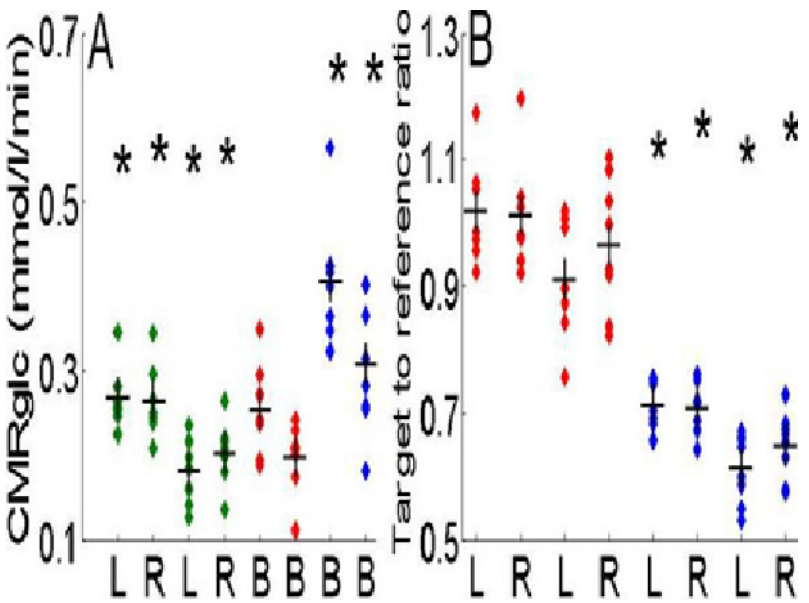


**Figure 1:** Data from each group (diamonds) along with group mean (black crosses). A shows CMRglc for the left (L) and right (R) parahippocampal gyrus in controls and disease respectively (green) and bilaterally (x axis, B) for the cerebellum (red) and precentral gyrus (blue). B shows parahippocampal gyrus in units of target to cerebellum ratio (red) and target to precentral gyrus ratio (blue). Asterisk indicate p-values <.05 from independent samples Mann Whitney U test.

Disclosure of author financial interest or relationships:
**J. Lewis**, None; **S.F. Carter**, None; **M. Asselin**, None; **K. Herholz**, AVID/Eli-Lilly, Grant/research support; Elan, Consultant; GE Healthcare, Consultant; **R. Hinz**, None.

Presentation Number **P187**
Poster Session 1
September 5, 2012 / 18:00-18:00 / Room: The Liffey

# FDG PET/CT IN TRAUMATIC BRAIN INJURY

***Jyotsna Rao**, Kavitha Nallapareddy, Alka A. Chengapa, Apollo Gleneagles PET CT Ctr, Hyderabad, India. Contact e-mail: jyotsnael@gmail.com*

Traumatic brain injury (TBI) forms a major part of neurological practice and is often causes diagnostic and ethical dilemma. About 25% of these patients may die and about 40% will have permanent deficits. CT and MRI are indicated in the acute setting, particularly CT due to cost and convenience. PET not usually performed in the acute setting may be useful in long term management by aiding in prognostication. We present our experience in evaluating these patients with FDG PET/CT. Aim: To evaluate the role of FDG PET/CT in the management of traumatic brain injury. Material and methods: A retrospective analysis of reports of five patients with traumatic brain injury with subacute and chronic history scanned between March 2008 and November 2011 was done. Pediatric and adults scans were included in the study. Patients were scanned 4 hours after intravenous injection of 18F FDG. Reporting of scans was done by a radiologist and PET physician. Follow up was obtained where possible. Results: There was sparing of right frontal, parietal and both occipital lobes in the first patient with severe hypometabolism in the rest of the brain and no significant CT abnormality. Bilateral symmetric mild hypometabolism was seen the second patient (CT showed mild cortical atrophy). The third patient showed severe left cerebral hemisphere hypometabolism with right cerebellar diaschisis. Severe hypometabolism was noted in the left cerebral hemisphere and moderate in the right temporal, occipital lobes and thalamus with a left subdural hematoma. The fifth patient showed bilateral temporal, occipital, left frontal bilateral thalamic and cerebellar hypometabolism. Only mild hypometabolism was noted in the parietal lobes, CT showing a left fronto parietal depressed fracture. Conclusion: In the small number of patients with TBI, FDG PET showed different patterns and degrees of hypometabolism which likely helped in prognostication. It may be considered in the work up of such patients although; larger studies are required for more definitive data. The use of PET/MRI may prove more useful in certain patients.

Disclosure of author financial interest or relationships:
**J. Rao**, None; **K. Nallapareddy**, None; **A.A. Chengapa**, None.

Presentation Number **P188**
Poster Session 1
September 5, 2012 / 18:00-18:00 / Room: The Liffey

# Magnetic Resonance Spectroscopy (MRS) On Brain Tumours. Clinical Experience

***Silvia Tomas Hernandez**, Latha Senthil, Nigel P. Davies, Neuroradiology, University Hospitals Birmingham NHS Fundation Trust, Birmingham, United Kingdom. Contact e-mail: stomas@hotmail.co.uk*

Purpose: Magnetic Resonance Imaging (MRI) has been key in the diagnosis and follow up of brain tumours. New advanced MRI techniques offer the opportunity of further characterisation of lesions non invasively. MRS is a powerful non-invasive molecular imaging technique that gives information about chemical components of tissue. It has been shown to help with differentiating neoplastic and non-neoplastic lesions as well as primary brain tumours from metastases and with grading of tumours. MRS is used in our centre when standard Computed Tomography (CT) and standard MR sequences have not been diagnostic, particularly when biopsy of the lesion carries high risk. We review our experience over a two year period on the accuracy of and value added by MRS for characterisation of brain lesions. Materials and Methods: 75 MR brain spectroscopy scans were identified using Clinical Radiology Integrated System (CRIS) database that were carried out between 1st January 2009 and 31st December 2010. The reason for requesting MRS to be performed was identified on requests or radiology reports. Results of MRS were obtained from the reports and compared with the gold standard. As gold standard we used final diagnosis from biopsy/histology or clinical follow up. The MRS reports were divided into non diagnostic due to poor technical quality of scan, conclusive (definite report provided) or inconclusive. Results: Of the 75 scans, 54 were to clarify the presence of primary brain tumour against other pathologies (group 1), 14 for assessing possible recurrence versus radio necrosis (group 2) and 7 for grading of primary brain tumours (group 3). In group 1, 2 scans were of poor technical quality, 40 scans were conclusive, 12 were non conclusive. Of the 40 conclusive scans: sensitivity 100%, specificity 71%, negative predictive value 100% and positive predictive value 85%. In group 2, 14 were conclusive and consistent with tumour recurrence confirmed on follow up. In group 3, 7 were conclusive with sensitivity 50%, specificity 67%, negative predictive value 50% and positive predictive value 67%. Conclusion: Only a small number of cases were non diagnostic due to poor technical quality which shows this technique to be very robust in routine clinical practice. In our practice, MRS has proven very useful when differentiating primary brain tumours from other pathologies greatly improving the accuracy of diagnosis non-invasively. We had a small number of patients referred for assessment of recurrence or grading of primary brain tumours which makes interpretation of the data difficult. Further studies in our centre are planned.

Caracterisation of brain lesions results

| | | | |
|---|---|---|---|
| TP | 22 | FP | 4 |
| TN | 10 | FN | 0 |
| Not clear yet | 4 | | |

Disclosure of author financial interest or relationships:
**S. Tomas Hernandez**, None; **L. Senthil**, None; **N.P. Davies**, None.

Presentation Number **P189**
Poster Session 2
September 6, 2012 / 15:15-15:15 / Room: The Liffey

# A Ratiometric (r2/r1) Method to Measure pH by a Dendrimer-based pH-Responsive MRI Contrast Agent

***Meser. M. Ali**, Mohammed P. Bhuiyan, Nadimpalli Ravi S Varma, Branislava Janic, James R. Ewing, Ali S. Arbab, Radiology, Henry Ford Hospital, Detrit, MI, USA. Contact e-mail: mesera@rad.hfh.edu*

Introduction: The tumor microenvironment is frequently characterized by an acidic extracellular pHe and a neutral to alkaline intracellular pH. A similar pH gradient is not observed in normal tissues. This unique pH environment in tumor tissue impacts tumor pathology and treatment. Low extracellular pH combined with higher intracellular pH is also important in chemotherapy since weak acid drugs which are protonated at high pH can become trapped inside of tumor cells, conversely weak base drugs are trapped outside. Therefore a method to assess pHe throughout the tumor tissue would provide a useful tool to: 1) detect metastatic vs. benign tumors before metastasis has occurred; 2) evaluate the effect of pH-altering chemotherapies; and 3) predict efficacy before chemotherapy is applied. Since the tumor environment can be heterogeneous, ideally a method for measuring pH should have high spatial resolution. Methods: We have proposed a novel method based on a ratiometric approach that consists of measuring the ratio between the transverse and the longitudinal paramagnetic contribution to the water proton relaxation rate, i.e. r2/r1. The liquid phantoms were scanned by 3T and 7T scanners. For measurements of T1 relaxation times, axial spin echo (SE) sequences were obtained with multiple TR (50, 100, 200, 300, 500, 750, 1000, 1500, 2000, 3000 and 5500 ms) and TE (8.4 ms) values. All sequences were acquired with field of view (FOV) = 24 mm2, matrix size = 128X64, one slice, thickness = 1 mm, and NEX = 1. MR images were transferred to an off-line server and reconstructed using home-written software. T1 maps of the samples were calculated by fitting the appropriate relaxation equation to the image data, assuming monoexponential signal decay (for T1) on a pixel-by-pixel basis. . For T1 maps, all echoes were summed for each TR and then fitted using the equation Mz(t) = M0 (1 -exp(TR/T1)). T2 maps were generated by summing data across all TRs, and then fitting the summed values using the equation Mxy(t) = M0 (exp(-TE/T2). The longitudinal and transverse relaxation times of the Gd-G5 in solution were then measured in ROIs selected in the calculated sample maps. Result and Discussion: The transverse and longitudinal relaxation times in water of (Gd-DOTA-4AmP)-G5, a G5-PAMAM dendrimer-based MRI contrast agent were measured at 3T and 7T as a function of solution pH. At 3T, the longitudinal relaxivity (r1) of (Gd-DOTA-4AmP)-G5 increased from 7.65 to 9.63 mM-1s-1 (on a per Gd3+ basis) when changing pH from 8.81 to 6.35, while transverse relaxivity (r2) decreased from 37.85 to 33.4 mM-1s-1. At 7t, the same trends were demonstrated, but r2 and r1 both lower than at 3T. Thus, both transverse and longitudinal relaxivities of Gd-G5 exhibited a strong and reversible pH dependency. The r2/r1 ratio showed a linear relationship in a pH-responsive manner, and this pH response was independent from their absolute concentration. Importantly, the nanoprobe (Gd-G5) shows pH response in the range of 6.35 to 8.81, the pH range commonly found in most of solid tumors, microenvironment; this r2/r1 ratio is responsive to as little as 0.2 pH units of change.

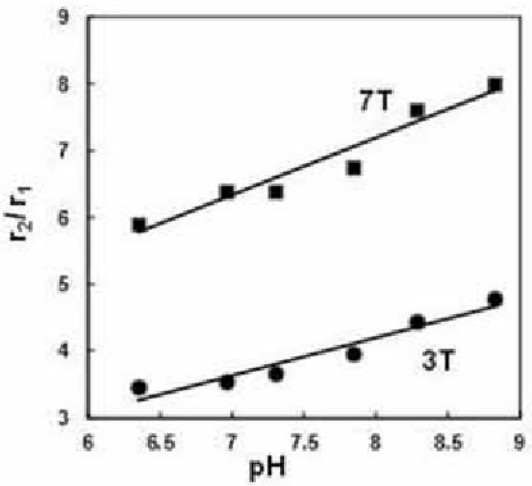


**Figure**: $r_2/r_1$ ratio of Gd-G5 shows pH response at both 3T and 7T,respectively.

Disclosure of author financial interest or relationships:
**M.M. Ali**, None; **M.P. Bhuiyan**, None; **N. Varma**, None; **B. Janic**, None; **J.R. Ewing**, None; **A.S. Arbab**, None.

Presentation Number **P190**
Poster Session 2
September 6, 2012 / 15:15-15:15 / Room: The Liffey

# New Gd-containing non lamellar lipid-superstructures: relaxometric, structural characterizations and bimodal imaging of human ovarian carcinoma cells

***Francesca Arena***[1], *Antonella Accardo*[2], *Diego Tesauro*[2], *Giancarlo Morelli*[2], *Eliana Gianolio*[1], [1]*Chemistry, University of Torino, Torino, Italy;* [2]*Biological Sciences, University of Naples "Federico II", Naples, Italy. Contact e-mail: francesca.arena@unito.it*

During the course of the last decades an increasing interest as been devoted to the study of nano-particles able to vehicle imaging probes as well as for drug delivery. A newsworthy alternative to the more classical lamellar phase matherials such as micelles and liposomes is represented by non lamellar nanoparticles, formed by self-assembling of lipid mesophases. Their peculiar internal structure, in which intercrossing water channels are partitioned by lipid bilayers, featuring both hydrophilic and hydrophobic domains, allows for the incapsulation of high payload of imaging and therapeutic molecules. 1 Very few systems loaded with chelated metal ions included in the internal phase framework have been reported.2 In particular, to our knowledge, this is the first Gd-containing "cubosome like" system, with potential applications as MRI probe, in which the Gd(III) metal ion is included in a thermodynamically highly stable complex. Here we report the synthesis, the structural and the relaxometric characterization of liquid-crystalline lipid nanoparticles (NPs) constituted by glycerol mono-oleate (MO) or di-oleate (DO) lipids, a Gd-DTPA like complex functionalized with two C18 lipophilic chains (1÷20% wt), and the fluorescent Rhodamine-PEG2000-PE (0.1%). NPs were stabilized by the nonionic block copolymer Pluronic F127 and, for cellular uptake experiments, functionalized with an amphiphilic folic acid containing molecule (3%wt). Systems where characterized using relaxometric measurements, DLS and Cryo-TEM analysis for particle size and morphology. The relaxivity values of MO- and DO-based NPs containing different amounts (1÷20% wt) of (C18)2 DTPA(Gd) were measured at 20 MHz and 298K . The paramagnetic systems were also characterized through the registration of NMRD profiles. MO- and DONPs relaxivities are quite similar for the different loading values, with a slight increase when the percentage of Gd-complex is brought to 20%. These particles are characterized by diameters ranging from 110nm to 200 nm and a negative surface charge. To determine the specificity and the efficacy of the delivery, the GdNPs were evaluated in IGROV-1 and Hela, FR-positive cells lines and in FR-negative B16F10and K562 cells. A preferential uptake efficiency of DONPs-FA in IGROV-1 cells with respect to DONPs without folic acid, expecially at low concentrations of nanoparticles or at short incubation times, was observed. By comparing the uptake efficacy of DONPs-FA and DONPs in other cell types with lower or absent expression of folate receptors (B16F10, K562 and HeLa) we observed a drastic drop in Gd(III) and Rhod-PE content. References: 1. A. Yaghmur, O. Glatter, Advances in Colloid and Interface Science 2009, 147-148, 333-342 2. M.J. Moghadda et al, Soft Matter, 2011, 7, 10994-11005.

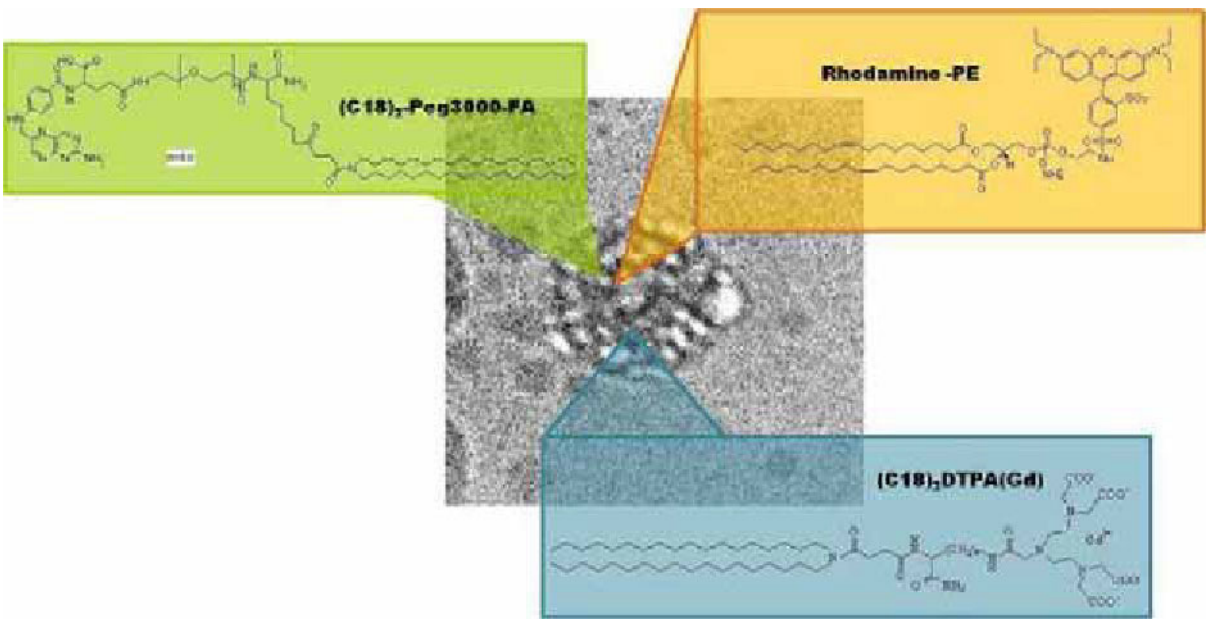


Disclosure of author financial interest or relationships:
**F. Arena**, None; **A. Accardo**, None; **D. Tesauro**, None; **G. Morelli**, None; **E. Gianolio**, None.

Presentation Number **P191**
Poster Session 2
September 6, 2012 / 15:15-15:15 / Room: The Liffey

# Functionalization of USPIO with Fucoidan for MRI Molecular Imaging of Activated Platelet-rich Thrombus

***Laure Bachelet-Violette***[1,2], *Christine Ménager*[3], *Michimasa Suzuki*[1], *Jean-Michel Serfaty*[1], *Jean-Baptiste Michel*[1], *Frédéric Chaubet*[1,2], *Didier Letourneur*[1,2], [1]*Hemostasis, Bioengineering and Cardiovascular Remodelling, INSERM U698, Paris, France;* [2]*Cardiovascular Bioengineering, Université Paris 13 - Institut Galilée, Villetaneuse, France;* [3]*Laboratoire Physicochimie des Electrolytes, Colloïdes et Sciences Analytiques - PECSA, UMR 7195-UPMC-CNRS-ESPCI, Paris, France. Contact e-mail: laure.bachelet@gmail.com*

Introduction: P-selectin, a cell adhesion molecule expressed on activated platelets and endothelial cells, plays an important role by mediating leucocytes/platelets or endothelium interactions and is largely described as a candidate for the diagnosis of vascular diseases such as atherothrombosis. P-selectin is also known to strongly interact with polysaccharides like fucoidan, a natural sulfated poly-L-fucose. Fucoidan exhibits a high affinity (KD=1 nM) for P-selectin (Bachelet L., Biochim Biophys Acta 2009), and is able to bind to activated platelets and endothelium in vivo in rat models of atherothrombotic diseases (Rouzet F., J Nucl Med 2011). The present study describes the functionalization of USPIO with fucoidan for the in vivo MRI detection of rich-platelets thrombi. Methods: Fucoidan was aminated to its reducing end. Ultra-small superparamagnetic iron oxide nanoparticles prepared from ferrofluid (Roger J., Eur. Phys. J. App. Phys. 1999) were first coated with carboxymethyldextran (CMD). Then, coupling agents were used to graft USPIO-CMD with aminated fucoidan. The interaction between these functionalized USPIO and activated platelets in human whole blood was studied in vitro by flow cytometry. USPIO-CMD-fucoidan and USPIO-CMD (used as control) were injected in rats with aneurysmal atrial trombi, an experimental model associated with platelets activation. Results: The USPIO-CMD and USPIO-CMD-fucoidan present respectively an average diameter around 30 nm and 50 nm, a zeta potentiel of -10.3 mV and -14.3 mV, a high relaxivities (r1=15 mM-1.s-1; r2=119 mM-1.s-1 and r1=15 mM-1.s-1; r2=137 mM-1.s-1 at 60 MHz) and are stable in 0.15 M NaCl. USPIO-CMD-fucoidan was able to inhibit in vitro the binding of an anti-P-selectin antibody to activated platelets in human whole blood. By 4.7T MRI using T2*-weighted sequences, we found that USPIO-CMD-fucoidan detected in vivo activated platelets in aneurismal thrombi (Figure). Conclusion: USPIO-fucoidan is a new P-selectin-targeted imaging agent for the detection by MRI of platelet-rich thrombi.

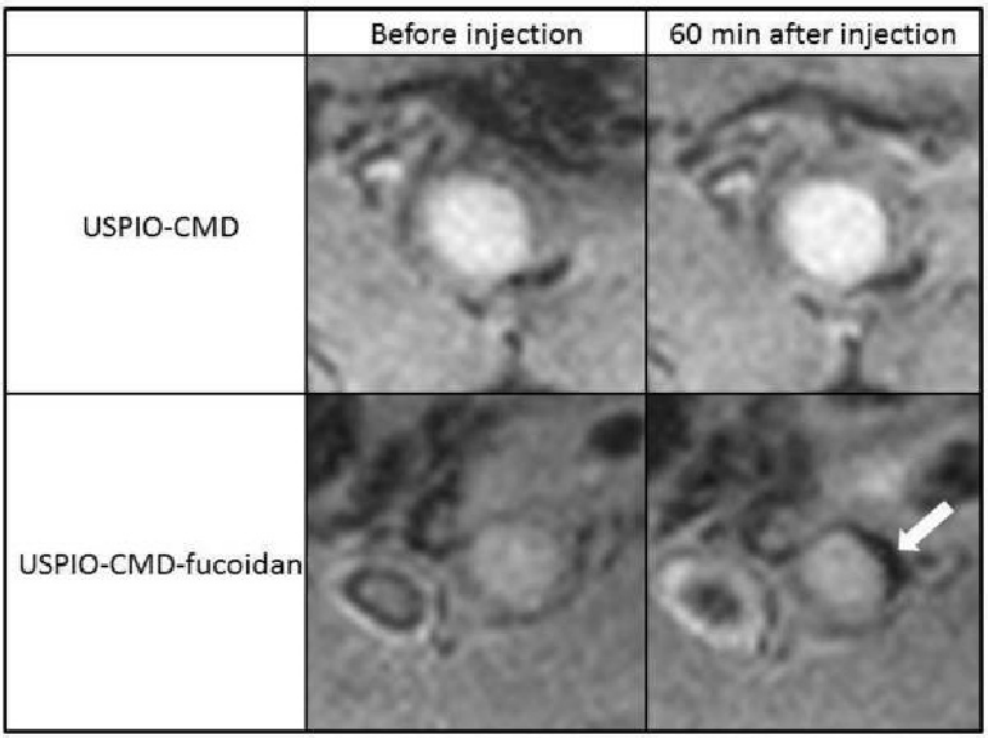


Disclosure of author financial interest or relationships:
**L. Bachelet-Violette**, None; **C. Ménager**, None; **M. Suzuki**, None; **J. Serfaty**, None; **J. Michel**, None; **F. Chaubet**, None; **D. Letourneur**, None.

Presentation Number **P192**
Poster Session 2
September 6, 2012 / 15:15-15:15 / Room: The Liffey

# Redox-sensitive dendrimeric β-CD/Gd(III) chelates supramolecular adducts

***Mauro Botta**, Jonathan Martinelli, Kalaivani Thangavel, Lorenzo Tei, Dipartimento di Scienze e Innovazione Tecnologica, Universita` del Piemonte Orientale ‘‘Amedeo Avogadro", Alessandria, Italy. Contact e-mail: mauro.botta@mfn.unipmn.it*

The design of responsive ("smart") probes represents one of the most exciting research areas in the development of MRI contrast agents. Their performance can be modulated by changes in the physiological environment such as pH, partial oxygen pressure, metal ion concentration or enzyme activity. We have prepared a new macromolecular architecture consisting of eight β-cyclodextrin (CD) units attached to a PAMAM-G1 dendrimer through a disulfide bond that can be cleaved under reducing conditions like those where specific enzymes or high radical concentrations are associated with a disease state (e.g. tumors or strokes). Each CD cavity can host a hydrophobic moiety from a suitably functionalized Gd-complex, with the binding affinity depending on the nature of the pendant moiety. The activation of the agent is signaled by a large decrease of the relaxivity associated with a pronounced decrease of the rotational dynamics on passing from the supramolecular system to the free complexes. As MRI probe, we have synthesized a novel dimeric chelate (Figure 1) based on the AAZTA platform and bearing a pendant adamantyl moiety obtained through the formation of a thiourea between the isothiocyanate group of the starting dimeric bifunctional chelate and the amino group of (1-adamantyl)methylamine. The relaxivity of the Gd(III) complex ($r_1$ = 16.7 $mM^{-1}$ $s^{-1}$; 20 MHz, 298 K) is about 135% higher than for the parent GdAAZTA complex. This functionalized ditopic Gd complex shows excellent properties for the possible use as MRI probe of high efficiency: i) two bound water molecules in fast exchange with the bulk; ii) high stability over a wide range of pH; iii) high thermodynamic stability and kinetic inertness towards transmetallation reactions. The formation of the inclusion compounds has been followed via proton NMR relaxometric titrations. The ditopic complex shows a very high affinity (~$10^6$ $M^{-1}$) for the CD units of the dendrimer and the $r_1$ value is sensibly enhanced (up to +70%) upon binding. The fast release of the Gd-complex and of the CD units under reducing conditions has been measured at 310 K by relaxometry. A ca. 25% decrease of $r_1$ was measured at 1 T. NMRD profiles were measured (298 and 310 K) before and after cleavage of the supramolecular assembly. Finally, investigations on the competition between the paramagnetic dendrimer and human serum albumin were carried out by relaxometric techniques. Interestingly, the paramagnetic probes are not displaced by HSA from the dendrimeric structure, thus being potentially suitable for in vivo applications. Furthermore, the non-covalent nature of the interaction between the substrate and the Gd-based probe ensures this latter can be cleared from the body faster than other macromolecular systems, thus reducing their potential toxicity in vivo. Finally, the versatility of β-cyclodextrins as supramolecular host makes this system of potential high interest for dual imaging or theranostic purposes.

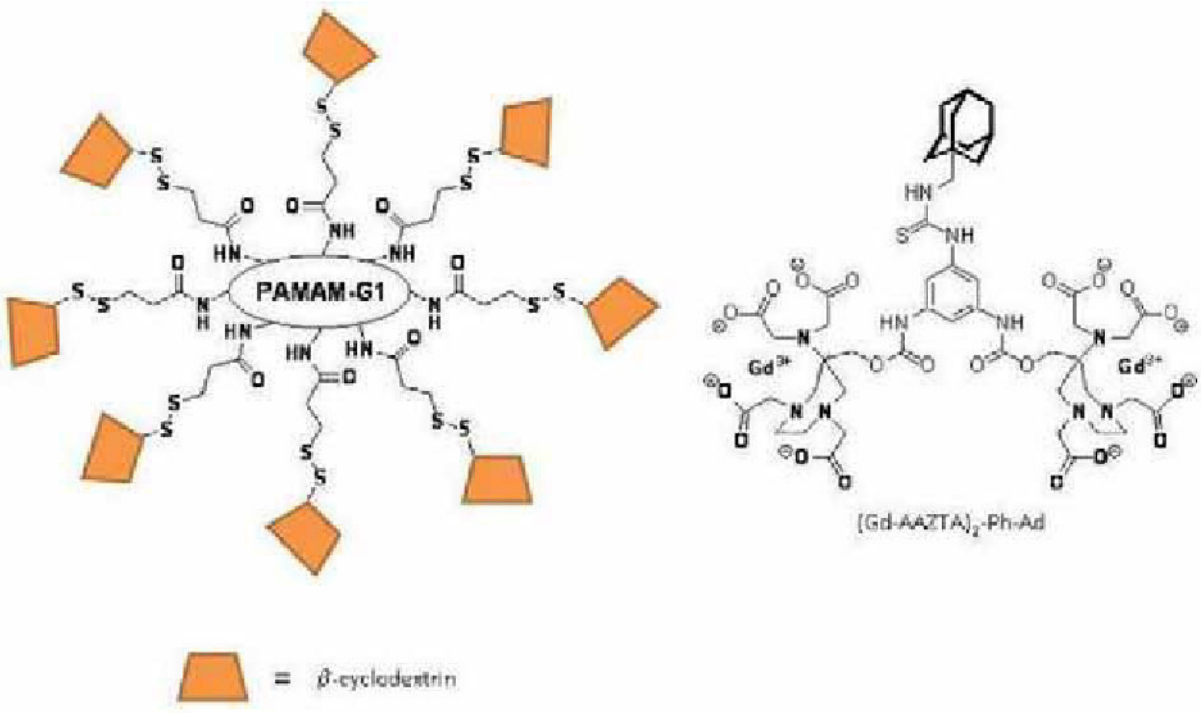


Structures of PAMAM-$CD_8$ (left), and $(Gd\text{-}AAZTA)_2$-Ph-Ad

Disclosure of author financial interest or relationships:
**M. Botta**, None; **J. Martinelli**, None; **K. Thangavel**, None; **L. Tei**, None.

Presentation Number **P193**
Poster Session 2
September 6, 2012 / 15:15-15:15 / Room: The Liffey

# Hyperpolarized $^{13}$C N-acetyl-aspartylglutamate: A novel MR probe for characterization of prostate cancer

***Albert P. Chen***[1], *Charles H. Cunningham*[2,3], *Yi-ping Gu*[2], *[1]GE Healthcare, Toronto, ON, Canada; [2]Imaging Research, Sunnybrook Health Sciences Centre, Toronto, ON, Canada; [3]Biophysics, University of Toronto, Toronto, ON, Canada. Contact e-mail: Albert.Chen@ge.com*

**Introduction:** Glutamate carboxypeptidase II (GCPII), also known as prostate specific membrane antigen (PSMA) is a transmembrane folate hydrolase and expressed in the tissues of CNS, kidneys and prostate. The enzyme catalyzes the hydrolysis of N-acetyl-aspartylglutamate (NAAG) to glutamate and N-acetylaspartate (NAA). PSMA has been used as a target for imaging and therapeutic agents for prostate cancer since elevated expression of PSMA is correlated with pathological stage and disease recurrence (Rena G. Lapidus et al. The Prostate. 2000;45:350-354). In111 capromab pendetide (ProstaScint®; Cytogen Corp.) is an FDA approved radiolabeled antibody of PSMA for use as a SPECT agent in prostate cancer patients. But ProstaScint® exam suffers from low specificity and issues inherent of SPECT technique and large molecular weight agents. Alternative to the antibody approach, targeted imaging of PSMA may be performed by utilizing it's enzymatic activity. With the development of DNP-dissolution method that enables real time MR metabolic imaging with hyperpolarized $^{13}$C substrates, it may be feasible to use pre-polarized $^{13}$C enriched NAAG to probe PSMA activity in prostate cancer. **Methods:** Sample preparation: N-acetyl-aspartyl-[1-$^{13}$C]glutamate (Isotec) was dissolved in pyruvic acid (not enriched, Isotec) to ~1M concentration and doped with 15mM OX63 (Oxford Instruments) then polarized and dissolved using a Hypersense DNP polarizer (Oxford Instruments). NMR: Experiments were performed using a GE MR750 3T scanner (GE Healthcare). Spectra from ~3ml of the hyperpolarized solution were acquired using a pulse-acquire sequence (10° tip angle, TR=3s). Data were also acquired at thermal equilibrium (24µl of Omniscan was added, 90° tip angle, TR=5s, 512 scans) to estimate the polarization achieved by DNP. **Results and Discussions:** In DNP-dissolution studies, because the pre-polarized magnetization is unrecoverable and decays with $T_1$ relaxation, the site of $^{13}$C enrichment is typically the one that gives the substrate the longest $T_1$. The C1 glutamate carbon of NAAG was chosen because the carboxylic acid $^{13}$C atoms have longer $T_1$ than the amide $^{13}$C atoms. The acetyl carbon was not considered because the chemical shift between the substrate and the metabolic product ($^{13}$C-acetyl-aspartate) is likely to be very small (Wilson et al. PNAS. 2009;106:5503-5507). MR spectra of hyperpolarized N-acetyl-aspartyl-[1-$^{13}$C]glutamate are shown in Fig 1. Natural abundant $^{13}$C pyruvate from the solvent was also detected. The NAAG resonance at 178 ppm is ~3 ppm downfield from the expected metabolite [$^{13}$C]glutamate resonance. This large chemical shift difference could allow potential *in vivo* detection of PSMA metabolism. The $T_1$ of N-acetyl-aspartyl-[1-$^{13}$C]glutamate was 18s and the polarization in solution was ~4% (~16,000 fold enhancement) measured at ~15s post dissolution. **Conclusion:** The potential of using hyperpolarized $^{13}$C N-acetyl-Aspartyl-glutamate as a MR probe for characterization of prostate cancer is presented. Detection of PSMA metabolic activity in real time with this probe will be investigated in prostate cancer models in future studies.

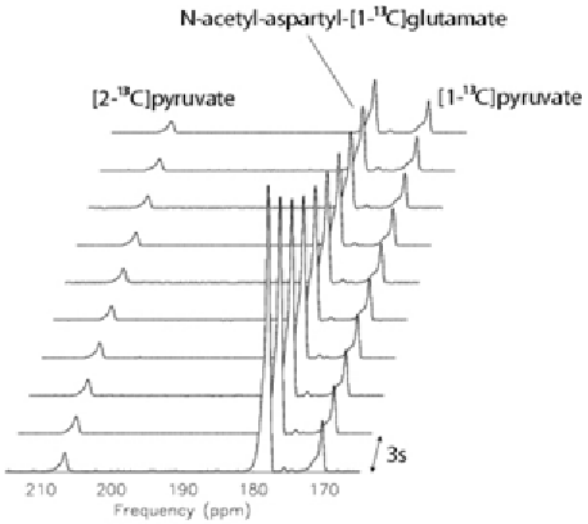


**Fig 1.** MR spectra of hyperpolarized N-acetyl-aspartyl-[1-$^{13}$C]glutamate.

Disclosure of author financial interest or relationships:
**A.P. Chen**, GE Healthcare, Employment; **C.H. Cunningham**, GE Healthcare, Grant/research support; **Y. Gu**, None.

Presentation Number **P194**
Poster Session 2
September 6, 2012 / 15:15-15:15 / Room: The Liffey

# Magnetic Resonance Investigation of Alkyl-PEI2k/SPIO labeled Endothelial Progenitor Cells in a Lung Carcinoma Xenograft Model

***Cong Chen***[1], *Hong Yu*[1], *Rui Xia*[2], *Hua Ai*[3], *Xiangsheng Xiao*[1], *Fabao Gao*[2], [1]*Radiology, Changzheng Hospital,Second Military Medical University, Shanghai, China;* [2]*Radiology, West China Hospital,Sichuan University, Chengdu, China;* [3]*National Engineering Research Center For Biomaterials, Sichuan University, Chengdu, China. Contact e-mail: congchen99@163.com*

Purpose: To assess the feasibility of labeling endothelial progenitor cells (EPCs) with N-Alkyl-polyethylenimine 2 kDa-stabilized superparamagnetic iron oxide (Alkyl-PEI2k/SPIO), thereby enabling noninvasive investigation of EPCs with magnetic resonance imaging in a lung carcinoma xenograft model. Materials and Methods: Protocols for sampling human peripheral blood were approved by Institute's Ethics Review Committee and animal experiments were approved by Institute's Animal Care and Use Committee. EPCs were derived from human peripheral blood and labeled with Alkyl-PEI2k/SPIO. EPCs viability and activity after labeling were evaluated in vitro. Alkyl-PEI2k/SPIO labeled EPCs were injected intravenously 7 days after inoculation of A549 lung cancer cells subcutaneously (group A) or co-injected subcutaneously with A549 cells (group B) while A549 cells were inoculated subcutaneously without EPCs as control (group C). A four-week follow-up was performed by MR imaging with TurboRARE-T2 and MGE-T2*. Statistical analyses were performed with Student's t-test. Results: Labeling efficacy of EPCs was almost 100%, and no significant effects on EPCs viability were found after labeling. In MRI study in vivo, schistic or linear hypointense regions were observed at tumor margins at day 7 or 8 after EPCs administration and gradually extended into the inner of tumor in group A while low signal intensity regions dispersed inside the tumor with its growth in group B. The results were confirmed by Prussian blue staining and immunofluorescence. Conclusion: The strategy of labeling EPCs with Alkyl-PEI2k/SPIO allows noninvasive magnetic resonance investigation of EPCs involvement in tumor neovasculature.

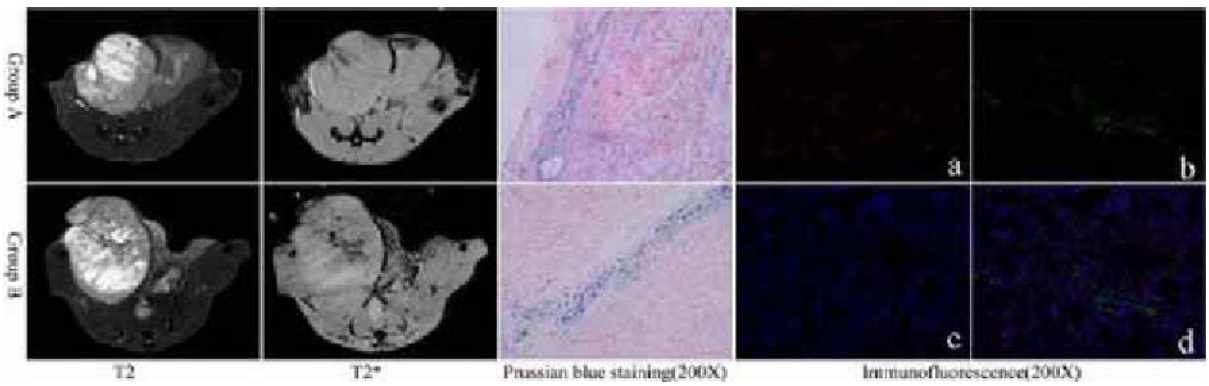


In vivo MRI at day 28 and Prussian blue staining(200×) in Group A and Group B. Schistic and linear hypointense regions were observed at tumor margins and extended into the inner of tumor in group A while low signal intensity regions dispersed inside the tumor in group B, and prussian blue positive cells at sites corresponding to MRI. Both anti-human CD31 positive cells (green fluorescence) and anti-mouse CD31 positive cells (red fluorescence) were showed by immunofluorescence (200×).

Disclosure of author financial interest or relationships:
**C. Chen**, None; **H. Yu**, None; **R. Xia**, None; **H. Ai**, None; **X. Xiao**, None; **F. Gao**, None.

Presentation Number **P195**
Poster Session 2
September 6, 2012 / 15:15-15:15 / Room: The Liffey

# Exploring the fate of cell-internalized MRI Gd-based contrast agents

***Enza Di Gregorio**, Eliana Gianolio, Stefania Rachele, Silvio Aime, Chemistry & Molecular Imaging Center, University of Turin, Torino, Italy. Contact e-mail: enza.digregorio@unito.it*

Introduction: In vivo MRI tracking of labelled cells is still a topic of huge interest. Most often the cells are labelled with Iron Oxide nanoparticles. However, Gd-chelates have also been proposed. The threshold for the MRI visualization of a cell is in the order of 107-109 Gd-chelates per cell.1 Such a high payload of stable Gd(III)-chelates seems to be well tolerated by the cellular machinery as low cytotoxicity has been reported for several cell types. Cell viability tests are usually carried out at short times after incubation, no study of the "fate" of cell internalized Gd-complexes at longer time has been reported. The knowledge of the "in cellulo" behavior of Gd-complexes may also provide some new insight into the understanding of the etiology of pathologies related to the release of Gd3+ ions such as NSF (Nephrogenic Systemic Fibrosis). Methods: J774(murine macrophages) and NIH-3T3(murine fibroblasts) cells were incubated with two commercial contrast agents (Gd-DTPA and Gd-HPDO3A), washed extensively and reincubated for 1-4 days. The total amount of internalized Gd(III) was determined through a relaxometric method and the amount of intact Gd-complex was determined by mass spectrometry using a calibration curve obtained with an appropriate internal standard (Tm-DTPA or Tm-HPDO3A). Results: Up to 4 days no sign of transformation for both complexes internalizated in NIH-3T3 fibroblasts was detected. Vice versa, a net difference in the behavior of Gd-DTPA and Gd-HPDO3A has been observed when the Gd-complexes are internalized into J774 macrophages. Whereas Gd-HPDO3A appears to maintain its integrity also after four days into macrophages, only ca. half of the Gd(III) present in these cells is under the form of intact complex when the internalized complex is Gd-DTPA. Insight on the intracellular transformation of Gd-DTPA have been acquired through the registration of NMRD profiles of macrophages treated with Gd-DTPA and reincubated for a long time. The obtained NMRD profiles have a peculiar shape well different from that of Gd-DTPA. Analogous profiles have been obtained upon internalizing other less stable polyamminocarboxylate Gd(III) complexes. The herein reported data clearly reflects the ability of macrophages to transform Gd-DTPA in respect to fibroblasts which appears to reflect the specific ability of macrophage enzymatic armoury to attack xenobiotics. These exogenous molecules are able to iper-activate NF-kB pathway that promotes the expression of a high levels of pro-inflammatory cytokines and various metallo-enzymes such as Mn-SOD and NADPH oxidase. Conclusion: The observed behaviour can be accounted in terms of the different stability and rigidity of the two investigated systems being the Gd-HPDO3A more robust and stable. The degradation of Gd-DTPA in J774 macrophages calls for more attention in the cell labeling and cell-targeting procedures with Gd(III) complexes. References 1) Aime S., Cabella C. , Colombatto S., Geninatti Crich S., Gianolio E., Maggioni F. J. Magn. Reson Imag. 2002, 16, 394-406. 2) De Galdo F, Wermuth J. P, Addya S, Fortina P, Jimenez S.A, Ann Rheum Dis 2010, 69:2024-2033.

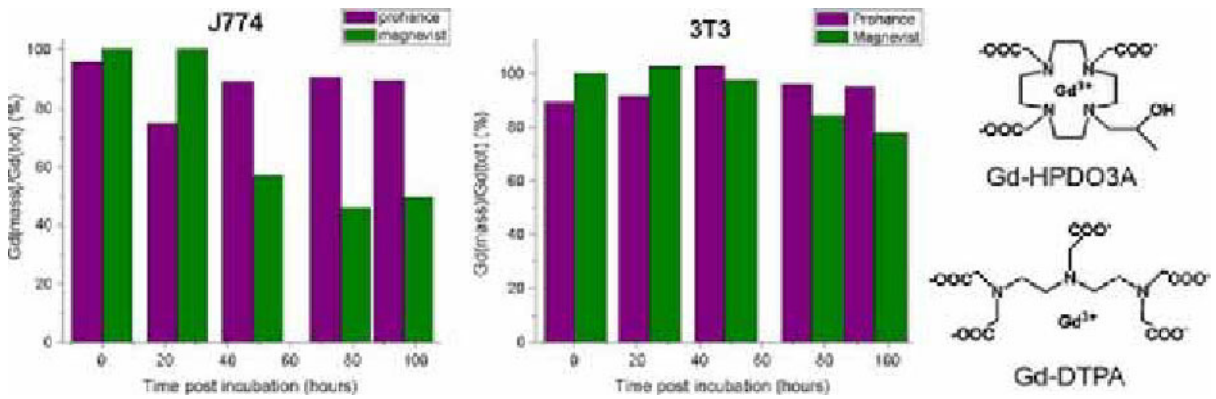


Disclosure of author financial interest or relationships:
**E. Di Gregorio**, None; **E. Gianolio**, None; **S. Rachele**, None; **S. Aime**, Bracco Imaging, Consultant; Bruker, Grant/research support .

Presentation Number **P196**
Poster Session 2
September 6, 2012 / 15:15-15:15 / Room: The Liffey

# Direct coupling of Annexin A5 to VSOP yields ultrasmall, highly covered Probes for MR Imaging of Apoptosis

***Lena Figge**, Jörg Schnorr, Matthias Taupitz, Bernd Hamm, Eyk A. Schellenberger, Experimental Radiology, Charité - University Medicine Berlin, Berlin, Germany. Contact e-mail: lena.schoenzart@charite.de*

Introduction Apoptosis (or programmed cell death) is a well-regulated process, which is critical for development and tissue homeostasis of multicellular organisms. It is often deregulated in diseases such as atherosclerosis, multiple sclerosis, or cancer, making it an attractive target for molecular imaging. The process of apoptosis includes the externalization of phosphatidylserines, which can be targeted with Annexin A5 (Anx). Here we present very small iron oxide particles (VSOP) that are coated with Anx resulting in Anx-VSOP with a hydrodynamic diameter of only 17 nm, that specifically bind to apoptotic cells leading to signal loss in T2*-weighted MR measurements. Methods The synthesis of Anx-VSOP and M1234-VSOP (M1234: inactive Anx variant) was done in two steps: (1) activation of the citrate surface of the VSOP using EDC and Sulfo-NHS (2) covalent attachment of Anx and M1234 to the activated citrate surface via lysine groups of Anx and M1234 The synthesized particles were purified and then analyzed using native PAGE. The amount of VSOP was calculated by iron measurements (≈6500 Fe/VSOP based on TEM measurements). The approximate number of Anx per VSOP was calculated after measuring the protein concentration via BCA assay. To determine the stability, size measurements in water and CaCl2-containing buffer and relaxivity measurements in water and serum were performed. To analyze the specific binding of Anx-VSOP to apoptotic cells, Jurkat T cells were treated with Camptothecin to induce apoptosis. Treated and untreated cells were incubated with Anx-VSOP and M1234-VSOP. The cells were washed and the resulting cell pellets were imaged on a clinical 1.5 T MR scanner. Results Anx-VSOP and M1234-VSOP have a hydrodynamic diameter of 17 nm and 14 nm, respectively, and a R2 of 60 mM-1s-1. Approximately 10 Anx are bound to the VSOP surface. The incubation of Camptothecin-treated Jurkat cells with Anx-VSOP leads to a strong signal reduction on T2*-weighted MR imaging. The T2*-weighted MR image and calculated T2*-times are shown in Figure 1. Conclusions The synthesis of Anx-VSOP is very straightforward and highly reproducible. Anx and M1234 were successfully attached to the citrate surface of the VSOP via a covalent linkage. The synthesized particles are stable in serum for at least 24 h, which makes them applicable for in vivo measurements. Incubation of apoptotic cells with Anx-VSOP leads to a stronger signal loss in T2*-weighted MR imaging in comparison to untreated cells and the nonbinding control probe M1234-VSOP, due to specific binding of the Anx-VSOP to phosphatidylserines exposed by apoptotic cells. References Schellenberger E, Schnorr J, Reutelingsperger C, Ungethüm L, Meyer W, Taupitz M, Hamm B, (2008) Linking Proteins with Anionic Nanoparticles via Protamine: Ultrasmall Protein-Coupled Probes for Magnetic Resonance Imaging of Apoptosis. Small, 4(2), 225-230

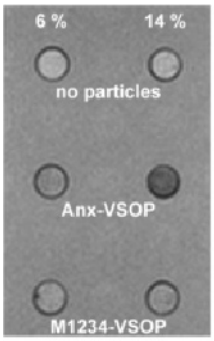


| | untreated (6 % apoptotic cells) T2* | Camptothecin-treated (14 % apoptotic cells) T2* |
|---|---|---|
| **Anx-VSOP** | 16 ms | 7 ms |
| **M1234-VSOP** | 24 ms | 19 ms |

**Figure 1:** T2*-weighted MR image (left) and calculated T2*-times (right) of untreated and Camptothecin-treated Jurkat cells incubated with Anx-VSOP and M1234-VSOP: specific binding of Anx-VSOP to phosphatidylserines of apoptotic cells leads to strong signal reduction in T2*-weighted MR imaging. Relaxation times were calculated from ROIs in T2*-weighted MR images generated with varying echo times.

Disclosure of author financial interest or relationships:
**L. Figge**, None; **J. Schnorr**, None; **M. Taupitz**, None; **B. Hamm**, Deutsche Röntgengesellschaft European Congress of Radiology European Society of Euroradiology ESMRMB European School of Radiology Deutsche Forschungs-gemeinschaft, Other financial or material support; Bayer Schering Pharma Toshiba, Consultant; ESMRMB ESOR, Speakers bureau; Thieme Publishers Springer Publishers, Other financial or material support; All pharmaceutical and biochemical companies All medical technology companies All car companies, Stockholder; All pharmaceutical and biochemical companies All medical technology companies, Other financial or material support; **E.A. Schellenberger**, None.

Presentation Number **P197**
Poster Session 2
September 6, 2012 / 15:15-15:15 / Room: The Liffey

# Calix[4]resorcinarenes based "theranostic" MRI agents

***Simonetta Geninatti- Crich***[1], *Diego Alberti*[1], *Diana E. Burghelea*[1], *Paolo Minazzi*[2,3], *Camilla Cavallotti*[3], *Giovanni B. Giovenzana*[2,3], *Silvio Aime*[1], [1]*Department of Chemistry, Center for Molecular Imaging, University of Torino, Torino, Italy;* [2]*Scienze del Farmaco, Università degli Studi del Piemonte Orientale "Amedeo Avogadro", Novara, Italy;* [3]*Cage Chemicals S.r.l., Novara, Italy. Contact e-mail: simonetta.geninatti@unito.it*

Much attention is currently devoted to the development of agents for procedures in which disease diagnosis and therapy are combined. These "theranostics" agents contain both drugs and imaging reporters within a single formulation. Usually, theranostics are made up by nanoparticles that, as a consequence of their size and versatile composition, can deliver a high number of diagnostic and therapeutic molecules in the same particle. Drawbacks associated to their nano-size are the long extravasation time (also in the presence of EPR effect) and low diffusion at the pathological target site. For these reasons, the use of nanosized carriers may reduce the omogeneous distribution of the drug and the imaging agent in the tumor region. In this work an alternative low molecular weight Gd based "theranostic" agent has been synthesized and tested on cellular systems. The agent contains up to 8 Gd-AAZTA-(CH2)9-COOH complexes linked to a calix[4]resorcinarenes moiety through a short PEG chain (figure). The good performance as MRI probe is provided by the presence of the contrast units with q=2 endowed with high relaxivity (r1p=14.7 mM-1s-1 at 0.5T per Gd). Calix[n]arenes and calixresorcinarenes, together with crown ethers and cyclodextrins are one of the major classes of macrocyclic organic "host" compounds in supramolecular chemistry.1 Calix[4]arenes form stable complexes with different classes of drugs and molecules of biological interest. For example "host-guest" complexes between fluorescent dyes and calixarenes have been studied as specific sensors of biological substances2, particularly neurotransmitters of the acetylcholine and the carnitine type, steroids (cortisone, prednisone) as well as other organic analytes. The fluorescent dye (such us rhodamine B or LCG, N,N'-dimethyl-9,9'-biacridinium dinitrate) shows a large change in fluorescence, ideally a strong quenching or enhancement, upon binding to the host. Moreover, it has been reported that calyx[4]arenes are taken-up by cells by non yet understood processes and localize in acidic vescicles.3 On the basis of these considerations in the first part of this study, the interaction between calix[4]resorcinarenes based imaging probes and fluorescent probes (rhodamine and LCG) or steroidic drugs (prednisone) have been tested in vitro. Then the ability of these theranostic agents to deliver inside target cells the fluorescent dye or the drug has been tested on target tumor cells. In order to increase the specific uptake in particular by ovarian cancer and breast cancer cells, a new agent has been synthesized. In respect to the parent one in which two Gd-AAZTA units have been substituted with two folic acid moieties. The calix[4]resorcinarenes moiety maintains the binding capabilities towards hydrophobic drugs/dyes and the improved targeting ability has been tested on different tumor cell lines. .

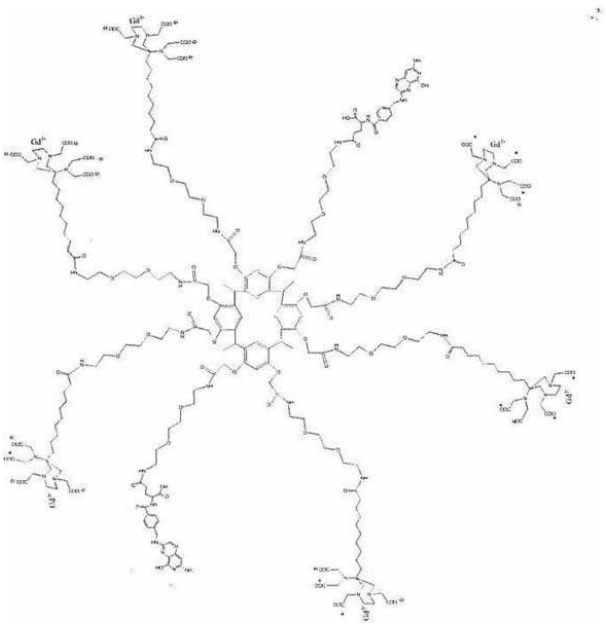

Disclosure of author financial interest or relationships:
**S. Geninatti- Crich**, None; **D. Alberti**, None; **D.E. Burghelea**, None; **P. Minazzi**, Cage Chemicals s.r.l., Other financial or material support; Aspect Imaging, Consultant; **C. Cavallotti**, CAGE Chemicals Srl, Other financial or material support; ASPECT IMAGING, Consultant; **G.B. Giovenzana**, CAGE Chemicals srl, Grant/research support; **S. Aime**, Bracco Imaging, Consultant; Bruker, Grant/research support .

Presentation Number **P198**
Poster Session 2
September 6, 2012 / 15:15-15:15 / Room: The Liffey

# A novel approach towards Ca2+-responsive MRI probes

***Karolina Jankowska***[1], *Martin E. Maier*[2], *Nikos K. Logothetis*[1,3], *Goran Angelovski*[1], [1]*Physiology of Cognitive Processes, Max Planck Insitute for Biological Cybernetics, Tuebingen, Germany;* [2]*Faculty of Science, Department of Chemistry, Insitute of Organic chemistry, Eberhard Karls University, Tuebingen, Germany;* [3]*Division of Imaging Science and Biomedical Engineering, University of Manchester, Manchester, United Kingdom. Contact e-mail: karolina.jankowska@tuebingen.mpg.de*

Calcium, present in high concentrations in the brain, plays an important role in neuronal signalling, e.g. through the transfer of charges between synapses, or triggering the release of neurotransmitters. It has been previously demonstrated that the concentration of Ca2+ changes significantly during neural activity.[1] However, used techniques are highly invasive and can only cover a small area of the brain at any moment with limited tissue penetration. Magnetic Resonance Imaging (MRI) on the other hand is non-invasive and allows the mapping of the whole brain at unlimited depths. To measure neural activity through changes in Ca2+ concentration using MRI, responsive contrast agents have been designed.[2] Recent reports of a system based on 3,2-hydroxypyridinone (3,2-HOPO) have demonstrated its attractive features as a contrast agent enabling this system to supersede current probes.[3] It exhibits high relaxivity values and a thermodynamic stability comparable with commercial agents. Moreover, it also has negligible interactions with interfering endogenous ions, despite the high number of coordinated water molecules. To the best of our knowledge there are currently no responsive probes based on this system. Therefore, we focused on the fusion of a 3,2-HOPO MR probe with a Ca2+ chelator. We show for the first time a facile synthesis to obtain a new HOPO-based MR-reporter without specialized equipment[3] and the introduction of a Ca2+ responsive moiety. We present the performance of this novel Ca2+ responsive probe from in vitro to more biologically realistic conditions. 1. Nicholson, C., et al., Calcium and potassium changes in extracellular micro-environment of cat cerebellar cortex. Journal of Neurophysiology, 1978. 41(4): p. 1026-1039. 2. Que, E.L. and C.J. Chang, Responsive magnetic resonance imaging contrast agents as chemical sensors for metals in biology and medicine. Chemical Society Reviews, 2010. 39(1): p. 51-60. 3. Werner, E.J., et al., High-Relaxivity MRI Contrast Agents: Where Coordination Chemistry Meets Medical Imaging. Angewandte Chemie-International Edition, 2008. 47(45): p. 8568-8580.

Disclosure of author financial interest or relationships:
**K. Jankowska**, None; **M.E. Maier**, None; **N.K. Logothetis**, None; **G. Angelovski**, None.

Presentation Number **P199**
Poster Session 2
September 6, 2012 / 15:15-15:15 / Room: The Liffey

# Dual $^{1}H/^{19}F$ MR imaging approach for detection of enzyme activity

***Aneta Keliris***[1], *Ilgar Mamedov*[3], *Gisela E. Hagberg*[3], *Nikos K. Logothetis*[3,4], *Klaus Scheffler*[1,2], *Joern Engelmann*[1], [1]*Department of High-Field Magnetic Resonance, Max-Planck-Institute for Biological Cybernetics, Tuebingen, Germany;* [2]*Department of Neuroimaging and MR-Physics, University of Tuebingen, Tuebingen, Germany;* [3]*Department of Physiology of Cognitive Processes, Max-Planck-Institute for Biological Cybernetics, Tuebingen, Germany;* [4]*Department of Imaging Science and Biomedical Engineering, University of Manchester, Manchester, United Kingdom. Contact e-mail: aneta.keliris@tuebingen.mpg.de*

Numerous processes taking place in living organism demand the action of enzymes. These catalysts serve as indicators of diseases and are used as markers of gene expression. Hence, a development of imaging probes allowing noninvasive *in vivo* mapping of enzyme activity by means of Magnetic Resonance Imaging (MRI) would provide a powerful means for assaying the efficacy of gene therapies and diseases diagnostics. Several mono-modal enzyme-responsive MRI probes have been reported over the years. Nevertheless, dual-modality imaging has recently attracted much attention as the way to facilitate visualization of enzyme activity *in vivo* by combining the benefits of different imaging techniques. In this line, we now demonstrate a smart dual-modal $^{1}H/^{19}F$ MRI probe, Gd-DOMF-Gal, sensing the activity of beta-galactosidase (marker enzyme used for revealing gene expression) as a prototype of a novel class of probes for specific detection of enzymes. In its molecular design we explored the use of a self-immolative linker that was inserted between the imaging reporters ($Gd^{3+}$-chelate and a fluorine-bearing unit) and an enzyme recognizable moiety. The enzymatic activation of the probe resulted in a decomposition of the self-immolative spacer with release of imaging moieties leading to alternations in $^{1}H/^{19}F$ MRI signal intensities. Accordingly, as shown in the representative images (Fig.1, left) of phantoms filled with solutions of Gd-DOMF-Gal and samples treated with beta-galactosidase in phosphate buffer (PBS), no $^{19}F$ MRI signal was detected for intact probe (intramolecular relaxation enhancement of fluorine relaxation times by paramagnetic gadolinium), whereas a $^{19}F$ MRI signal of increasing intensity was observed after enzymatic conversion [1]. The corresponding proton $T_1$ map (Fig.1, right) acquired during the same imaging session on a 7T scanner (~25°C) prior to $^{19}F$ measurements displayed a significantly longer $T_1$ in the samples pre-incubated with beta-galactosidase. The longitudinal relaxivity ($r_1$) of Gd-DOMF-Gal in PBS was found to be 6.7±0.6 $mM^{-1}s^{-1}$ and 5.1±0.5 $mM^{-1}s^{-1}$ for the cleaved complex (300 MHz,~25°C), whereas at 123 MHz the $r_1$ values were found to be 9.6±0.1 $mM^{-1}s^{-1}$1 and 7.0±0.1 $mM^{-1}1s^{-1}$, respectively. To explore the effect of buffer composition on relaxivity we also determined the $r_1$ values at 123 MHz (~25°C) in HEPES buffer (does not coordinate to gadolinium center) where the relative change in relaxivity $\Delta r_1$ of 46% between Gd-DOMF-Gal and cleaved complex was higher than $\Delta r_1$ obtained in PBS buffer (27%) [1]. In order to increase probe sensitivity, we have now introduced structural modifications and synthesized derivatives of Gd-DOMF-Gal with an increased number of fluorine per molecule. Here, we will present the rationale for our molecular design and MR evaluation of the enzymatic conversion of $^{1}H/^{19}F$ probes under *in vitro* conditions and in a cellular model. With this approach that explores the use of self-immolative spacers we will also extend in the future the application of the proposed model for the detection of other enzymes. [1] Keliris et al., Contrast Media Mol. Imaging (2012), in press.

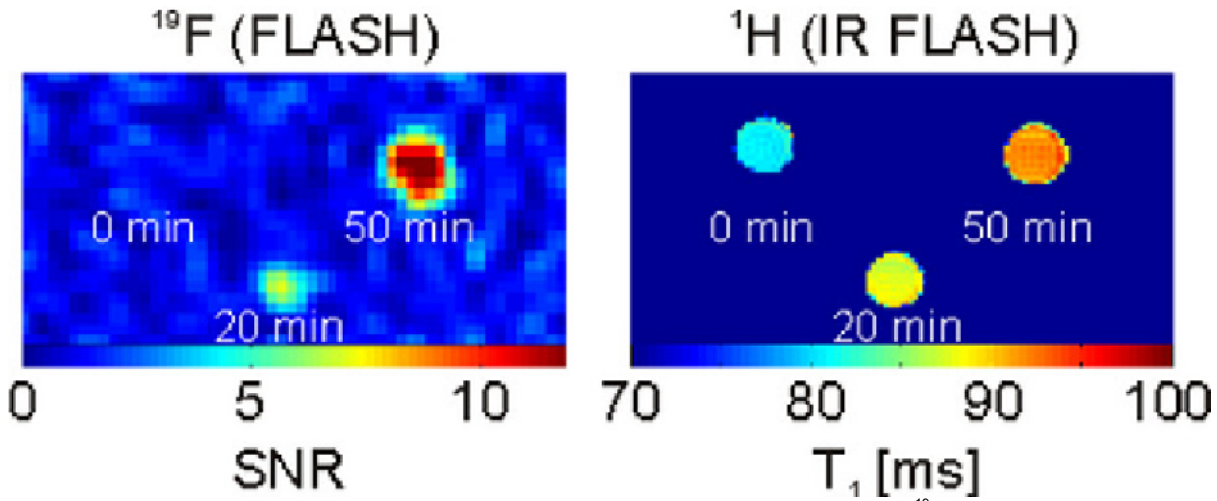


Fig 1.Conversion of Gd-DOMF-Gal in vitro by beta-galactosidase after incubation for indicated time periods. $^{19}F$ MR images (left) and the corresponding proton $T_1$ map (right image) acquired at 7T (~25°C) [Keliris et al., Contrast Media Mol. Imaging (2012), in press].

Disclosure of author financial interest or relationships:
**A. Keliris**, None; **I. Mamedov**, None; **G.E. Hagberg**, None; **N.K. Logothetis**, None; **K. Scheffler**, None; **J. Engelmann**, None.

Presentation Number **P200**
Poster Session 2
September 6, 2012 / 15:15-15:15 / Room: The Liffey

# Hollow Manganese Oxide Nanoparticle as a T1 Shortening Contrast Agent for Target-Specific Magnetic Resonance Imaging

***In Su Lee***[1], *Tae Lin Ha*[2], *Geun Ho Im*[3], *Jung Hee Lee*[3], [1]*Department of Chemistry, POSTECH, Pohang, Republic of Korea;* [2]*Deaprtment of Chemistry, Kyung Hee University, Yongin, Republic of Korea;* [3]*Department of Radiology, Samsung Medical Center, Sungkyunkwan University School of Medicine, Seoul, Republic of Korea. Contact e-mail: insulee97@postech.ac.kr*

The further development of nanoparticulate MRI contrast agents will require materials that have much more enhanced relaxivity and can operate at much lower concentrations of potentially toxic metal ions. In this context, hollow nanoparticles with interior void spaces are attractive candidates for advanced MRI contrast agents owing to their large water-accessible surface area, which is able to carry high payloads of MR-active magnetic centers, and the ability of the interior void space to take up large amounts of drug molecules. We will present our recent researches with hollow Mn3O4 nanoparticles (HMON) which show the greatly enhanced relaxivities and drug loading capacity, comparing with those having solid interior. We will also discuss the development of a platform protocol for fabricating target-specific multimodality imaging probes based on T1 MRI contrast HMON. Their well-directed characteristics as a target specific imaging agent, including a successful in-vivo T1 contrast MRI diagnosis of cancer tissue, will be demonstrated.

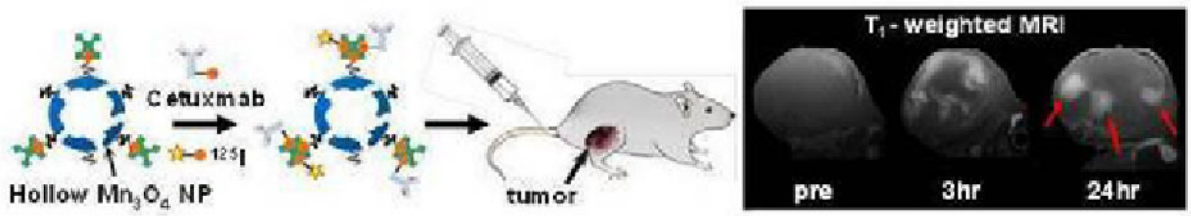


Disclosure of author financial interest or relationships:
**I. Lee**, None; **T. Ha**, None; **G. Im**, None; **J. Lee**, None.

Presentation Number **P201**
Poster Session 2
September 6, 2012 / 15:15-15:15 / Room: The Liffey

# Gadolinium Complexes of Monophosphinic Acid DOTA Derivative Conjugated to Cyclodextrin Scaffolds: Efficient MRI Contrast Agents for Higher Magnetic Fields

*Zuzana Kotkova[1], Jan Kotek[1], Lothar Helm[2], **Ivan Lukes**[1], [1]Inorganic Chemistry, Universita Karlova, Faculty of Science, Prague 2, Czech Republic; [2]Bâtiment de chimie UNIL, EPFL SB ISIC LCIB, CH-1015 Lausanne, Switzerland. Contact e-mail: Ivan.Lukes@natur.cuni.cz*

Middle-molecular-weight MRI contrast agents based on conjugates of phosphinic acid DOTA analogue, 1,4,7,10-tetraazacyclododecane-4,7,10-triacetic-1-{methyl[(4-aminophenyl)methyl]phosphinic acid} (DO3APABn), with amino-substituted cyclodextrins were prepared and studied by a variety of physico-chemical methods. The conjugates were formed by reaction of the corresponding isothiocyanate with per-6-amino-α/β-cyclodextrin and were complexed with LnIII ion to get the final complexes, (LnL)6-α-CD and (LnL)7-β-CD. Solution structure of the complexes was estimated by investigation of the EuIII complexes. The GdIII conjugate complexes are endowed with a short water residence time (τM ~10-15 ns) and a high abundance of the twisted-square antiprismatic diastereoisomer. They show a high 1H relaxivity at high fields due to a convenient combination of the fast water exchange rate and slow rate of the molecular tumbling given by their macromolecular nature. The 1H relaxivities per molecule of contrast agent (CA) are very high reaching up to ~140 s-1 mM-1 and ~100 s-1 mM-1 at 25 oC and magnetic fields 1.5 T and 3 T, respectively, which is the highest reported longitudinal relaxivity for kinetically stable contrast agents of an intermediate molecular mass (<10 kDa) with one water molecule in the first coordination sphere.

Disclosure of author financial interest or relationships:
**Z. Kotkova**, None; **J. Kotek**, None; **L. Helm**, None; **I. Lukes**, None.

Presentation Number **P202**
Poster Session 2
September 6, 2012 / 15:15-15:15 / Room: The Liffey

# Overcoming Biological MT Effects by use of ParaCEST MRI Contrast Agents Possessing Highly Shifted Amide Proton Signals

***Mark Milne***[1], *Todd K. Stevens*[2], *Adam A. Elmehriki*[1], *Mojmir Suchy*[1,2], *Robert Bartha*[2], *Robert H. E. Hudson*[1], [1]*Chemistry, Universtiy of Western Ontario, London, ON, Canada;* [2]*Centre for Functional and Metabolic Mapping, Robarts Research Institute, London, ON, Canada. Contact e-mail: mmilne9@uwo.ca*

Over one-half of all magnetic resonance (MR) images use some form of exogenous contrast agent. Currently all clinically available MRI contrast agents are based on chelated gadolinium ion ($Gd^{3+}$) and function as T1 relaxation agents. Recently, new agents have been described that rely on paramagnetic chemical exchange saturation transfer (ParaCEST) phenomena to produce contrast.[1] The benefit of this new class of agent is the increase in environmental sensitivity, which current agents are lacking.[2] The ability to monitor small changes in both pH and temperature may permit more ready identification of cancerous tissues which possess lower pH and higher temperatures compared to normal tissue.[3] Ligands possessing proximal amide protons in a 1,4,7,10-tetraazacyclododecane- 1,4,7,10-tetraacetamide (DOTAM) structure have shown to be sensitive to temperature and pH within the physiological range. Substitution on the amide[4a-c] can fine tune the sensitivity of the observable signal to environmental conditions, such as temperature, pH or enzymatic activity.[5] The ParaCEST technique requires a pre-saturation pulse to excite the frequency of interest (|δ| >> 0 ppm) which through chemical exchange generates contrast by causing attenuation of the bulk water signal (δ = 0 ppm). The drawback of using a pre-saturation pulse is the magnetisation transfer (MT) that can arise from saturation of endogenous biological molecules which ultimately can diminish the observable signal, jeopardising the value of the agent when used for biological imaging. To deal with inherent MT effects present in ParaCEST scans in vivo, we have discovered an agent that possesses signals outside the range of biological MT. $Tm^{3+}$ t-Butyl shows a signal at -102 ppm, compared to bulk water at physiological conditions (37 °C, pH 7), which is outside any background effects (Figure 1), giving rise to an improved signal to noise ratio. These signals are in stark contrast to other $Tm^{3+}$ agents whose amide signals are usually between -40 and -50 ppm (Table 1). Ultimately this could lead to more sensitive agents that will support the use of lower agent concentrations. **References** 1. K. M. Ward, A. H. Aletras, R. S. Balaban, J. Magn. Reson. **2000**, 143, 79-87. 2. M. Woods, E. W. C. Donald, A. D. Sherry, Chem. Soc. Rev. **2006**, 35, 500-511. 3. R. A. Gatenby, R. J. Gillies, Nat. Rev. Cancer. **2004**, 4, 891-899. 4. a) A. C. L. Opina, Y. Wu, P. Zhao, G. Kiefer, A. D. Sherry, Contrast Media Mol. I. **2011**, 6, 459-464. b) M. Suchy, A. X. Li, R. Bartha, R. H. E. Hudson, Bioorg. Med. Chem. **2008**, 16, 6156-6166. c) M. M. Ali, G. S. Liu, T. Shah, C. A. Flask, M. D. Pagel, Accounts Chem. Res. **2009**, 42, 915-924. 5) B. Yoo, M. D. Pagel, J. Am. Chem. Soc. **2006**, 128, 14032-14033.

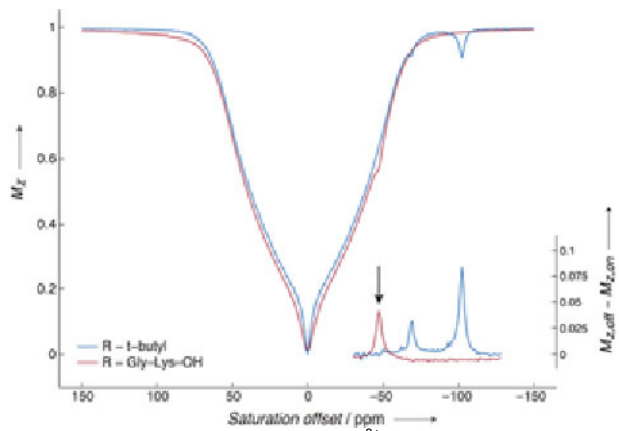


Figure 1. CEST spectrum of $Tm^{3+}$ t-Butyl (10 mM, -68 ppm, -102 ppm) and $Tm^{3+}$ Gly-Lys-OH (10 mM, -45 ppm) in 6% agar to mimic biological MT effects. Pre saturation for 2 s at 20 μT.

Table 1. Comparison of $Tm^{3+}$ DOTAM Amide Signals

| Agent (4a,b) | Amide Shift (ppm, 37 °C) |
|---|---|
| $Tm^{3+}$ DOTAM-Gly-OH (4a) | -31 |
| $Tm^{3+}$ DOTAM-$CH_2PO_3Et_2$ (4a) | -40 |
| $Tm^{3+}$ DOTAM-Gly-Lys-OH (4b) | -45 |
| $Tm^{3+}$ DOTAM-Gly-Phe-OH (4b) | -45 |
| $Tm^{3+}$ DOTAM-t-Butyl | -68, -102 |

Disclosure of author financial interest or relationships:
**M. Milne**, None; **T.K. Stevens**, None; **A.A. Elmehriki**, None; **M. Suchy**, None; **R. Bartha**, BioScape Imaging Solutions Inc, Stockholder; BioScape Imaging Solutions Inc, Employment; **R.E. Hudson**, None.

Presentation Number **P203**
Poster Session 2
September 6, 2012 / 15:15-15:15 / Room: The Liffey

# Development of Hyaluronic acid & PEG conjugated iron oxide nanoparticle for cancer diagnosis with MRI

***Myeong Ju Moon***[1,2], *Seon U Heo*[1], *In-Kyu Park*[2], *Yong Yeon Jeong*[1], [1]*Department of Radiology, Chonnam National University Medical School, Gwangju, Republic of Korea;* [2]*Biomedical Sciences, Chonnam National University Medical School, Gwangju, Republic of Korea. Contact e-mail: mjmoon2398@gmail.com*

Recently lot of Superparamagnetic Iron Oxide Nanoparticles(SPIONs) has been prepared for diagnostic enhancement studies. But the successful in vivo application for diagnosis has been hindered due to various problems which physical(size, shape), chemical(surface properties), and biological(targeting efficiency). This work has been designed to overcome the drawbacks for SPIONs in vivo diagnostic applications. In this study, SPIONs were coated with dopamine which provides amine functionality, making the situation amicable for further functionalization or conjugation with polymers or targeting agents. Hyaluronic acid coated SPIONs(HA-SPIONs) was prepared to target CD44 expressed cancer and the carrier was conjugated to PEG for longer circulation in blood and also for the biocompatibility(PEG-HA-SPIONs, HA-SPIONs-PEG). All midway products and final products(PEG-HA-SPIONs, HA-SPIONs-PEG) were characterized with TEM(shape), DLS(size), ELS(surface charge), TGA(content of polymer) and MRI(T2-relaxationtime). The tests of cellular level were progressed using CT26 and NIH3T3 cell line for confirming cell viability, cell specific uptake and phantom tube MRI image. And final products were injected to xenograft mice bearing CT26 cell line for MRI cancer diagnosis. At the result, Hydrodynamic particle size of SPIONs-embedded supra-assembly was found to range between 100 and 170nm, and its surface charge was slightly negative confirmed by ELS measurement. And polymer content of all SPIONs surface was increased according to continue to the next step. As a result of scanning MR, signal drop was confirmed at HA-SPION treated cells. After HA-SIPONs intravenous injection to tumor bearing mice, signal drop was confirmed at tumor regions. And HA-SPIONs were dropped signal more than PEG-SPIONs. Furthermore, PEGylated HA-SPIONs were dropped signal more than HA-SPIONs at tumor regions. In conclusion, HA-SPIONs were targeted specifically to the CD44, MR signal drop of PEGylated HA-SPIONs was better than HA-SPIONs and PEG-SPION in vivo.

Disclosure of author financial interest or relationships:
**M. Moon**, None; **S. Heo**, None; **I. Park**, None; **Y. Jeong**, None.

Presentation Number **P204**
Poster Session 2
September 6, 2012 / 15:15-15:15 / Room: The Liffey

# A Simultaneously Theranostic Imaging for EGFR Mutant (L858R) Non-Small Cell Lung Cancer

***Chia-Hsin Pan***[1], *Chia-Hao Su*[2], *Jyh-Horng Chen*[1,3], [1]*Interdisciplinary MRI/MRS Lab, Department of Electrical Engineering and Molecular Imaging Center, National Taiwan University, Taipei, Taiwan;* [2]*Center for Translational Research in Biomedical Sciences, Kaohsiung Chang Gung Memorial Hospital, Kaohsiung, Taiwan;* [3]*Graduate Institute of Biomedical Electronics and Bioinformatics, National Taiwan University, Taipei, Taiwan. Contact e-mail: yolanda1019@hotmail.com*

Molecular bio-imaging is to visualize *in vivo* the alternations of histological and cellular architecture underlying healthy or patho-physiological condition in a noninvasive manner. The goal of this study is to develop a theranostic contrast agent used in magnetic resonance image (MRI) to achieve the simultaneous imaging and therapy on xenograft non-small cell lung cancer (NSCLC) murine model. The gefitinib is the targeting drug that is specifically efficient to NSCLC patient with EGFR mutation (L858R), and it functionalized to inhibit the tyrosine kinase of EGFR for blocking the signal transduction pathway. In this study, the small molecules of modified gefitinib were conjugated on aqueous $Fe_3O_4$ nanoparticles, through the blood system delivered it to the tumor site since the abundant blood vessels and leaky epithelium of tumors. The bi-functional nanocontrast agent $Fe_3O_4$@gefitinib possessed the ability to achieve imaging and therapy simultaneously. To verify the drug efficacy of $Fe_3O_4$@gefitinib, MTT assay was performed. As the results, we found that the PC9 cell was responded to $Fe_3O_4$@gefitinib, and the IC 50 (the half inhibitory concentration) was 2 μM. In contrast, the A549 cells were resistant to the $Fe_3O_4$@gefitinib even the dose was increased to 100 μM. For cell targeting assay, we could observe the iron oxide nanoparticles accumulated at cytoplasm with the Perls' blue iron stain. As incubation time increased, the more nanoparticles were internalized into the intracellular part. Furthermore, the $Fe_3O_4$@gefitinib NPs were injected to tumor bearing mice by tail vein. Comparing pre-injection and post-injection, $T_2$-weighted images showed signal intensity of tumor decreased after $Fe_3O_4$@gefitinib injection. Further, we tested the feasibility and evaluation of therapeutic response with diffusion MR imaging and ADC mapping of tumor region. The ADC values of treated mouse were slightly increasing in treatment course while the control model was decreasing. Herein, we produced the theranostic nanocontrast agent $Fe_3O_4$@gefitinib to achieve imaging and therapy simultaneously. The *in vitro* assays showed $Fe_3O_4$@gefitinib efficiently inhibited the cell viability. In the *in vivo* imaging, the $T_2$-weighted images showed the tumor was negative enhanced and signal intensity decreased 15% at 4~9 hours and after 24 hours it dropped 23%. As the result, it demonstrated that the $Fe_3O_4$@gefitinib could target to tumor through the blood circulation system. We also performed some preliminary study to verify the feasibility of MR technique applied in treatment response evaluation.

Disclosure of author financial interest or relationships:
**C. Pan**, None; **C. Su**, None; **J. Chen**, None.

Presentation Number **P205**
Poster Session 2
September 6, 2012 / 15:15-15:15 / Room: The Liffey

# Synthesis of Mannose-PEG-Superaramagnetic Iron Oxide Nanoparticles as Magnetic Resonance Contrast Agent for Lymph Node Imaging

***In-Kyu Park***[1,4], *Hieu Vu-Quang*[1,4], *Chong-Su Cho*[2], *Joon Haeng Rhee*[4], *Yong Yeon Jeong*[3], [1]*Biomedical Sciences, Chonnam National University Medical School, Gwangju, Republic of Korea;* [2]*Research Institute for Agriculture and Life Sciences, Seoul National University, Seoul, Republic of Korea;* [3]*Department of Radiology, Chonnam National University Hwasun Hospital, Hwasun, Republic of Korea;* [4]*Clinical Vaccine R&D Center, Chonnam National University, Gwangju, Republic of Korea. Contact e-mail: pik96@chonnam.ac.kr*

The aim of the study is to detect metastatic lymph nodes which are hard to distinguish from normal nodes, because of their same size and shape, by Magnetic Resonance Imaging (MRI). Many contrast agents have been developed to target to Antigen-Presenting Cells (APCs) which migrate to the lymph node and can be detected by MRI. In this study, we synthesized super paramagnetic iron oxide nanoparticles (SPIONs) carrying immobilized mannose sugar on the surface for targeting to APCs through the specific interactions of mannose on the SPIONs with mannose receptor on these cells. The surface of SPIONs were conjugated with 3-aminopropylltriethoxysilane (APTES) and then Mannose-PEG was immobilized onto APTES-modified SPIONs by conventional method using EDC/NHS coupling agents to produce mannose-PEG-coupled SPIONs. We have supposed that hydrophilic PEG corona layer in mannose-PEG-SPIONs can serve to be prevented from aggregation during the systemic circulation and that mannose ligands present on mannose-PEG-SPIONs be targeted effectively to APCs which are then accumulated in lymph nodes. The accumulations of the SPIONs in the lymph nodes lead to decrease signal intensities in MR images. The Mannose-PEG-SPIONs were characterized by TEM, ELS, XRD, SQUID, and uptake of mannose-PEG-SPIONs by macrophage cells was confirmed by FACS analysis and fluorescent microscopy. For in vivo study, rats were intravenously injected with Mannose-PEG-SPIONs and PEG-SPIONs as a control and then scanned by MRI after 1h, 2h, 3h and 24h. MRI studies demonstrated that the accumulation in the lymph nodes of Mannose-PEG-SPIONs was significantly more intense than PEG-SPIONs that is , non-target to macrophage and also lymph nodes, which were also confirmed by Prussian blue staining of lymph nodes. Based on these results, Mannose-PEG-SPIONs have a great potential for lymph node imaging in order to detect metastatic lymph nodes at the early stage. Currently, some studies are under ways to test the delectability of the metastatic lymph nodes in tumor bearing mouse model by mannose-PEG-SPIONs.

Disclosure of author financial interest or relationships:
**I. Park**, None; **H. Vu-Quang**, None; **C. Cho**, None; **J. Rhee**, None; **Y. Jeong**, None.

Presentation Number **P206**
Poster Session 2
September 6, 2012 / 15:15-15:15 / Room: The Liffey

# Environment and mobility influence relaxivity of nanoparticles

*Codi A. Gharagouzloo[2], **Ravi T. Seethamraju**[1], Mukesh G. Harisinghani[3], Srinivas Sridhar[2], [1]MR R&D, Siemens Medical Solutions, USA Inc., Boston, MA, USA; [2]Nanomedicine, Northeastern University, Boston, MA, USA; [3]Radiology, Massachusetts General Hospital, Boston, MA, USA. Contact e-mail: ravi.seethamraju@siemens.com*

Aim: To investigate the influence of media and environment on the measurement of nanoparticle relaxivity Background: In clinical studies involving USPIOs, considerable scatter is observed in the measured relaxivity across studies even when the dosage and body habitus are identical. The measured reaxivities are more consistent only when measured longitudinally in the same subject and not across subjects. Here we explore the reason behind this phenomenon through phantom experiments. Methods: Vials (22.6 mm diameter) consisting of different amounts of Feraheme ((AMAG Pharmaceuticals, Inc, Lexington, MA) were diluted in Water, 1% Agar and 2% Agar solutions to yield concentrations of 0, 1, 5, 10, 50, 100, 500 µg/ml. The vials from the same dilution base were then closely bundled in a hexagonal fashion around the vial void of Feraheme. These bundles where then placed in a wrist coil and imaged on a 1.5T clinical scanner with a multi echo spin echo sequence (TE=11.6-58ms, TR=2000ms) and a multi echo UTE sequence (TE= 0.05- 12.2ms, TR=57, 1000ms). Also in a different experiment only the undoped vials were placed wide apart and imaged with the same sequences. Results: As seen from fig 1a isolating the vials had considerable influence on the measured T2 from the spin echo experiment in the case of water undiluted vials. This is also seen in the case of the vials with Feraheme bundles, however in both cases the measured T2 reduces considerably with the addition of Agar and with higher concentration of Feraheme. In the case of UTE experiments the separation is evident in the case of lower concentrations of Feraheme (Fig 1c and 1d). Conclusions: It is necessary to consider relative relaxivity instead of absolute relaxivity for comparing studies; hence it would be ideal to acquire a pre contrast dataset to obtain the relative relaxivity.

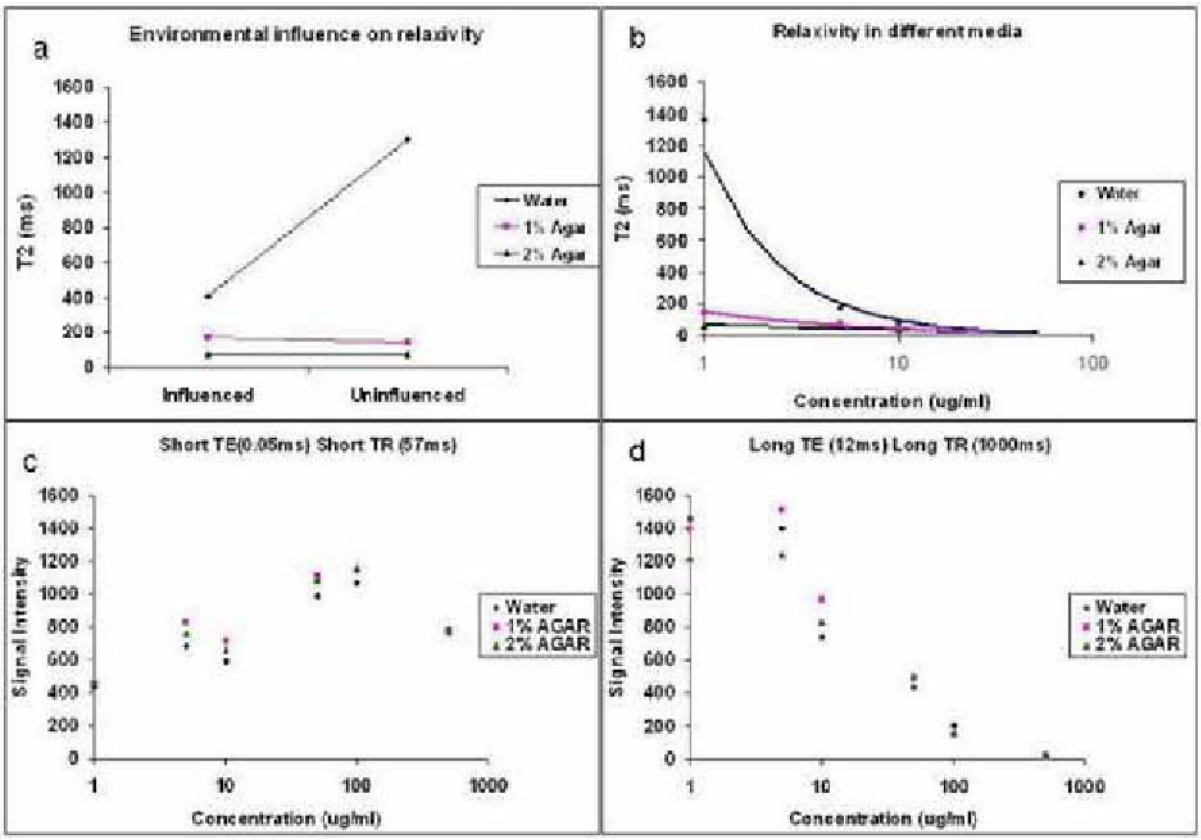


Disclosure of author financial interest or relationships:
**C.A. Gharagouzloo**, None; **R.T. Seethamraju**, Siemens Medical Solutions, USA Inc., Employment; **M.G. Harisinghani**, None; **S. Sridhar**, None.

Presentation Number **P207**
Poster Session 2
September 6, 2012 / 15:15-15:15 / Room: The Liffey

# T1 modulation of the PARACEST effect in nitroxyl Eu(DOTA-tetraamide)

*S James Ratnakar, Subha Viswanathan, Matthew E. Merritt, Chein-yuan Lin, Lloyd L. Lumata,* ***Dean Sherry****, Zoltan Kovacs, Advanced Imaging Research Center, UT Southwestern Medical Center, Dallas, TX, USA. Contact e-mail: Dean.Sherry@UTSouthwestern.edu*

Modulation of water exchange rates in Eu(DOTA-tetraamide) complexes by steric and the electronic factors has been one approach our lab has taken in the design of responsive ("smart") PARACEST agents. The 1H T1 and T2 relaxation times of the exchanging pools also influence the efficiency of chemical exchange saturation transfer between pools of protons. Here, we report the first rationally designed PARACEST agent in which the CEST efficiency is modulated by the longitudinal relaxation time, T1, of bulk water protons. The design includes an Eu3+ complex with two covalently appended TEMPO (2,2,6,6-(tetramethylpiperidin-1-yl)oxyl) units on the pendant arms of a DOTA-tetraamide scaffold (1). As anticipated an aqueous sample containing this complex as the paramagnetic biradical form shortens the T1 of solvent protons substantially and this, in turn, quenches the CEST signal from the exchanging Eu3+-bound water molecule. As predicted, the CEST signal of the same Eu3+ complex is "turned on" by addition of a free radical scavenger (L-ascorbic acid) to reduce the paramagnetic nitroxide centers. This activation effect has been shown to be entirely due to lengthening of the T1 of bulk water protons. The CEST images of phantoms containing either 11 mM Eu3+(1) or 11 mM Eu3+(1) plus L-ascorbic acid (2), both at pH 7, show a dramatic difference in contrast (Figure 1). Since nitroxyl radicals can be deactivated under certain biological conditions, this preliminary work suggests that EuDOTA-tetraamide nitroxyl derivatives may be used as redox sensitive PARACEST probes.

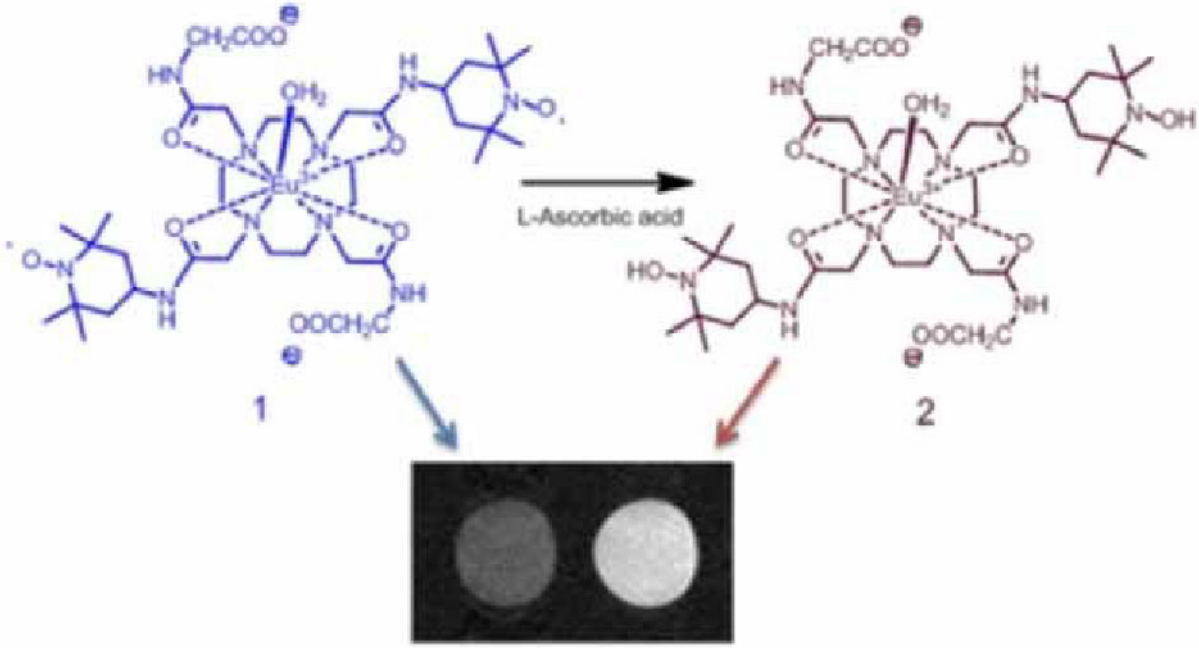


Figure 1. CEST images (9.4T) of the two compounds shown were acquired using a fast spin echo seqence (TR/TE=5100/10ms), 128 x 128 matrix, and a 5 sec, 10 μT presaturation pulse set at 50 ppm.

Disclosure of author financial interest or relationships:
**S. Ratnakar**, None; **S. Viswanathan**, None; **M.E. Merritt**, None; **C. Lin**, None; **L.L. Lumata**, None; **D. Sherry**, None; **Z. Kovacs**, None.

Presentation Number **P208**
Poster Session 2
September 6, 2012 / 15:15-15:15 / Room: The Liffey

# A Europium(III)-based PARACEST Agent as an Efficient Singlet Oxygen Probe

***Bo Song***[1], *A Dean Sherry*[1,2], [1]*Chemistry, University of Texas at Dallas, Richardson, TX, USA;* [2]*Advanced Imaging Center, UT Southwestern Medical Center, Dallas, TX, USA. Contact e-mail: bo.song@utdallas.edu*

Singlet oxygen, 1O2, the lowest excited electronic state of molecular oxygen, has aroused much interest as a chemical and biological oxidant for environmental and biological systems. However, some results are still controversial, mainly because of the lack of a reliable in vivo detection method for 1O2. A new type of MRI agent based on Chemical Exchange Saturation Transfer (CEST) offers considerable advantage over conventional T1 agents which make them attractive for developing biologically responsive sensors. Here, a europium(III) complex (EuL1) was developed as a PARACEST agent for selective sensing of 1O2. It can specifically react with 1O2 to form an endoperoxide (EP-EuL1) which is accompanied by 3 ppm downshift in the water exchange CEST peak and an increase in CEST intensity (Figure 1). The ratio of CEST intensities after activation of EuL1 at 54 versus 47 ppm was found to be linearly dependent on the concentration of 1O2. The applicability of the probe was demonstrated by detection of 1O2 generated from a MoO42-/H2O2 system and a photosensitization system of 5,10,15,20-tetrakis(1-methyl-4-pyridinio)-porphyrin tetra( p-toluenesulfonate) (TMPyP). These results suggest that EuL1 may prove useful as efficient 1O2 PARACEST probe in vivo.

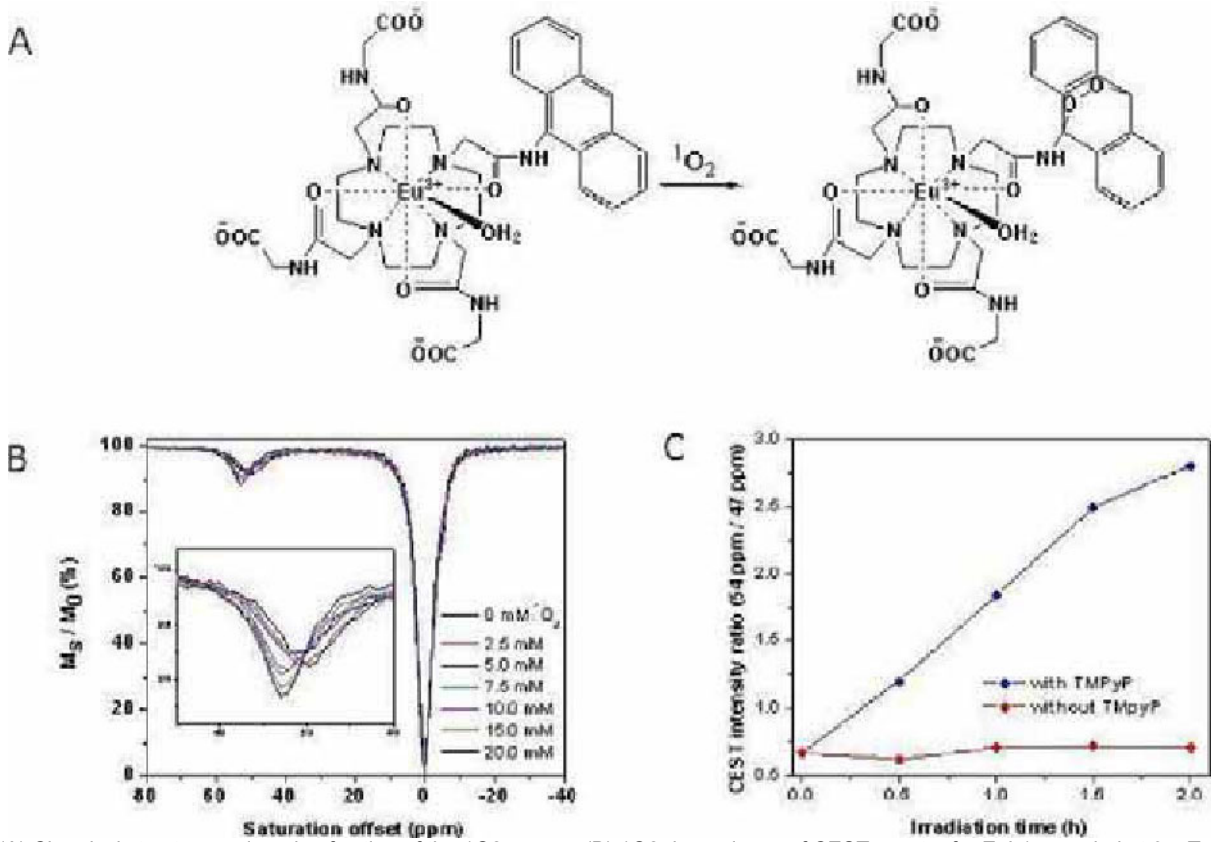


Figure 1. (A) Chemical structure and mode of action of the 1O2 sensor. (B) 1O2 dependence of CEST spectra for EuL1 recorded at 9.4 T and 298 K. Insert: expanded view of the water exchange peak as a function of 1O2 concentration. (C) Reaction of EuL1 with 1O2 generated by photosensitization of TMPyP.

Disclosure of author financial interest or relationships:
**B. Song**, None; **A. Sherry**, None.

Presentation Number **P209**
Poster Session 2
September 6, 2012 / 15:15-15:15 / Room: The Liffey

# Small sized liposomes and discoidal micelles by incorporation of amphiphilic Mn(II) complexes

***Lorenzo Tei***[1], *Gabriele A. Rolla*[1], *Mauro Botta*[1], *Giovanni B. Giovenzana*[3], *Valeria De Biasio*[3], *Enzo Terreno*[2], *Gilberto Mulas*[2,5], *Lucas W. Starmans*[4], [1]*Scienze ed Innovazione Tecnologica, Università del Piemonte Orientale "Amedeo Avogadro", Alessandria, Italy;* [2]*Chemistry, University of Torino, Torino, Italy;* [3]*Scienze del Farmaco, Università del Piemonte Orientale "Amedeo Avogadro", Novara, Italy;* [4]*Biomedical Engineering, Eindhoven University of Technology, Eindhoven, Netherlands;* [5]*Porto Conte Ricerche Srl, Tramariglio, Alghero (SS), Italy. Contact e-mail: lorenzo.tei@mfn.unipmn.it*

Introduction. $Mn^{2+}$ ion has five unpaired d-electrons, long electronic relaxation time and labile coordinated water molecule(s) which make it a valid alternative to $Gd^{3+}$ in the design of contrast agents for medical Magnetic Resonance Imaging. In order to ensure in vivo safety and high contrast agent efficiency, it is advisable to use ligands that form thermodynamically and kinetically stable Mn(II) complexes leaving enough space in the inner coordination sphere for at least one water molecule. In this work, EDTA and 1,4-DO2A (1,4,7,10-tetraazacyclododecane-1,4-diacetic acid) were chosen as core ligands for the preparation of amphiphilic Mn(II) complexes bearing one or two aliphatic chains of different length (C12 or C16). The two hydrophobic chains attached in different points of the ligand structure (Figure) serve to rigidify the chelate in the lipid bilayer of liposomes and thus to optimize the motional coupling between the paramagnetic unit and the nanoparticle. Liposomes are the most clinically established nanosized systems and the possibility to tune their size is very important to modulate and improve their pharmacodynamic properties. Methods. The ligands reported in the Figure were synthesized in good yield and the resulting Mn(II) complexes were studied by $^1$H NMR relaxometry by recording the variation of the longitudinal relaxivity with magnetic field and temperature. In water, all complexes formed aggregated structures of variable shape even at very low concentration (< 0.2 mM). Also liposomes were prepared by hydration of a thin lipidic film consisting of DPPC, DSPE-PEG2000 and the amphiphilic Mn(II) complex (or the corresponding diamagnetic Zn(II) complex) in molar ratio 85:5:10 or 75:5:20. Both aggregates and vesicles were characterized by dynamic light scattering in order to assess the mean hydrodynamic diameter and the polydispersity of the system. Cryo-transmission electron microscopy was also employed to characterize size and shape of the aggregated structures. Results. Small unilamellar vesicles of about 30 nm were formed by incorporation of 10% Mn(**1**) in the lipid bilayer while by incorporation of larger amount of chelate (20%), micellar aggregates of about 15 nm were obtained. The relaxivity ($r_1$) of both particles were determined as 9.2 and 11.0 $mM^{-1}s^{-1}$ (20 MHz, 310 K), respectively. Interestingly, the two adjacent C12 chains seems to force the vesicle to assume this curvature as, using Mn(**2**), the corresponding liposomes have size of about 110 nm. In case of Mn(**4**) and Mn(**5**), liposomes of 109 and 124 nm and with $r_1$ of 12.3 and 13.0 $mM^{-1}s^{-1}$ (20 MHZ, 310 K) were obtained, respectively. Analogous vesicles were formed by incorporating the corresponding Zn(II) chelates in the membrane and ProHance® in the aqueous compartment in order to estimate the rate of water diffusion through the membrane which resulted to be faster for liposomes containing chelates with shorter chains. With all chelates, also the formation of micellar aggregates in water was followed by DLS and relaxometry with the aim to characterize fully these kind of lipidic new systems.

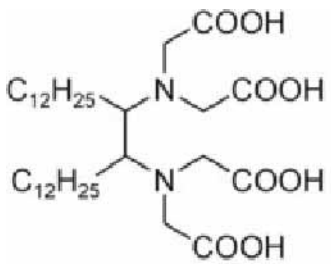


**1**

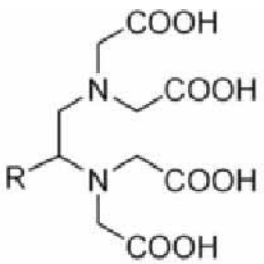


R = $C_{12}H_{25}$ (**2**)
R = $C_{16}H_{33}$ (**3**)

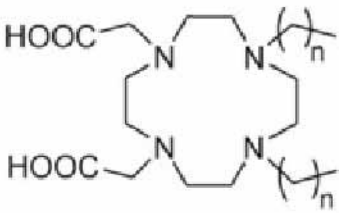


n = 11 (**4**)
n = 15 (**5**)

Disclosure of author financial interest or relationships:
**L. Tei**, None; **G.A. Rolla**, None; **M. Botta**, None; **G.B. Giovenzana**, CAGE Chemicals srl, Grant/research support; **V. De Biasio**, None; **E. Terreno**, Bracco Imaging, Consultant; **G. Mulas**, None; **L.W. Starmans**, None.

Presentation Number **P210**
Poster Session 2
September 6, 2012 / 15:15-15:15 / Room: The Liffey

# Novel probes for 19F-MRI using Perfluorinated Bisphosphonates

*Gavin D. Kenny, Karen Shaw, Saranja Sivachelvam,* ***Rafael Torres Martin de Rosales****, Division of Imagign Sciences & Biomedical Engineering, King's College London, London, United Kingdom. Contact e-mail: rafael.torres@kcl.ac.uk*

19F-MRI remains underused in clinical practice despite clear advantages such as ease of quantification and lack of interference from body tissues. One of its major disadvantages, however, is low sensitivity [1]. As a consequence most 19F-MRI probes designed to date need perfluorinated groups in order to provide enough signal. However, the number of fluorine atoms that a molecule can carry is limited for several reasons. First is solubility, as the fluorine content increases, the water solubility decreases, limiting their applications as molecular imaging agents. Furthermore, in order to maximise signal and avoid imaging artifacts 19F-MRI contrast agents should have one single 19F resonance, and hence the fluorine atoms must be in the same chemical and magnetic environment. We believe that by using a combination of nanoparticle (to increase fluorine content) and relaxation rate enhancement approaches (to increase sensitivity) we can address these problems. We have shown that bisphosphonates (BPs) bind very strongly and with high in vivo stability to several inorganic materials [2]. These include metal oxides of lanthanides that are known to enhance the relaxation rate of 19F spins [3]. We have synthesised and characterised perfluorinated bisphosphonates (19F-BPs, See X-ray structure in figure) with a single and narrow resonance in the 19F-NMR spectrum that can be attached to these nanomaterials and positions the perfluorinated group at a suitable distance from the lanthanide ions for relaxation rate enhancement. When bound, 19F-BPs fluorine atoms are protected from the environment by other BP conjugates, (e.g. BP-PEGs), hence avoiding the solubility problem of perfluorinated compounds in vivo. Thus, by combining high numbers of magnetically equivalent 19F spins with the relaxation rate enhancement properties of lanthanides our aim is to develop sensitive and stable agents for 19F-MRI. The results including relaxation rate measurements as well as 19F-MRI studies will be presented. References [1] E. Terreno, D. Delli Castelli, A. Viale and S Aime, Chem. Rev., 2010, 110, 3019-3042 [2] a) R. T. M. de Rosales, R. Tavaré, Rowena L. Paul, Maite Jauregui-Osoro, A. Protti, G. Varma, I. Szanda and P. J. Blower, Angew. Chem. Int. Ed., 2011, 50, 5509-5513. b) R. T. M. de Rosales, R. Tavaré, A. Glaria, G. Varma, A. Protti and P. J. Blower, Bioconjugate Chem., 2011, 22, 455-465. [3] a) K. H. Chalmers, A. M. Kenwright, D. Parker, and A. M. Blamire, Magn. Reson. Med., 2011, 66, 931-936; b) K. H. Chalmers, E. De Luca, N. H. M. Hogg, A. M. Kenwright, I. Kuprov, D. Parker, M.Botta, J. I. Wilson and A. M. Blamire, Chem. Eur. J., 2010, 16, 134-148

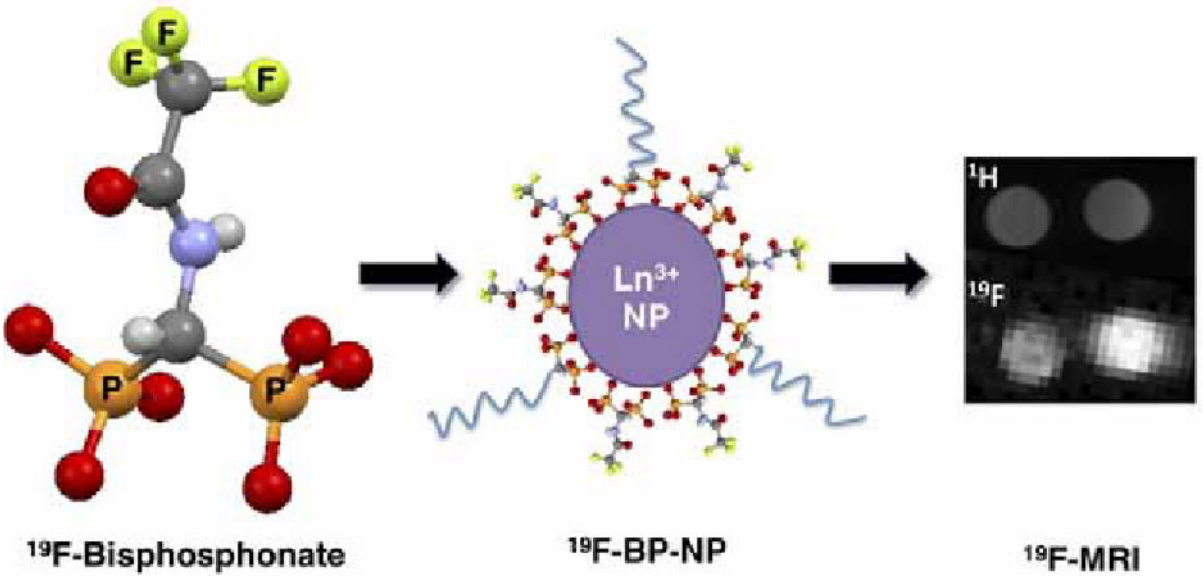


Disclosure of author financial interest or relationships:
**G.D. Kenny**, None; **K. Shaw**, None; **S. Sivachelvam**, None; **R. Torres Martin de Rosales**, None.

Presentation Number **P211**
Poster Session 2
September 6, 2012 / 15:15-15:15 / Room: The Liffey

# Gadolinium Chelate as Intravascular MRI Contrast Agent

***Chang-Tong Yang**, Prashant Chandrasekharan, Zihan Poh, Edward G. Robins, Kai-Hsiang Chuang, Singapore Bioimaging Consortium, A*STAR, Singapore, Singapore. Contact e-mail: yang_changtong@sbic.a-star.edu.sg*

Gadolinium-based contrast agents are widely used in MRI to enhance the image quality, but small molecule gadolinium chelates are currently characterized by rapid excretion and transient contrast retention.[1-2] We developed new gadolinium chelate GdDO3A conjugated with lysine derivative (CA2) (Fig. A), possessing higher r1 relaxivity and longer blood half life. CA2 was synthesized, characterized by ESI-MS and purified by HPLC. Three cell lines, namely HEK293, HeLa and A549 were used to assess the cell viability of CA2 at various concentrations after 24 hours incubation at 37 oC respectively (Fig. B). It can be concluded from the figure that the cytotoxicity is insignificant for CA2 at low Gd concentrations up to 0.2 mM, which is considerably higher than the concentration that would be employed in imaging (about 0.012 mM). The IC50 values are 1.27, 1.15 and 1.25 in HEK293, HeLa and A549 cell lines respectively. Relaxivity measurements were conducted on a Varian 9.4T and a Siemens 3.0T systems, T1 was measured by inversion recovery spin echo in aqueous phantoms with concentrations 0.4, 0.2 0.1, 0.05, 0.025, 0.0125 and 0.00625 mM Gd. The r1 relaxitivity of CA2 (5.4 mM-1s-1 at 9.4 T (Fig. C) and 5.0 mM-1s-1 at 3T (Fig. D) respectively) in H2O at 25 oC are both higher than that of the clinically used Dotarem and Magnevist. In vivo study was conducted on Wistar rats (male, weight 330 ± 10 g) under 2% isoflurane anesthesia. CA2 were injected (dosage: 0.04 mmol Gd/kg body weight) through tail vein. T1-weighted images were acquired every 6.4 s for 48 min with T1-weighted gradient echo sequence (TR/TE=50/3 ms, flip-angle = 20 degree, resolution=230 µm, thickness=2 mm). In vivo imaging studies of CA2 conducted on a Varian 9.4T in rats demonstrated that contrast enhancement in the brain artery immediately after tail vein injection (Fig. E & F). Time course of MRI signal intensity (up to 48 min post injection) in the brain artery showed considerable signal enhancement (about 50%). Compared with Dotarem (Guerbet, France), which showed similar peak enhancement as CA2, the enhancement by CA2 remained high (about 30%) even at 48 mins post-injection. This indicates CA2 has much longer blood half-life and could potentially advantageous for angiography and tissue targeting. Long circulation property of CA2 enables angiography of HT1080 xenograft tumor (with high levels of expression of VPF/VEGF) even after 30 mins post injection acquired using a time-of-flight sequence (TR/TE=20 ms/4.36 ms, 0.3 mm slices, flip angle=55o) (Fig G). Such contrast agent could be beneficial for tumor detection and to assess response to chemotherapy by contrast enhanced perfusion imaging of tumors [1] Fu, et al, Biomacromolecules, 2007, 8, 1519-1529. [2] Tóth, et al, Chem.Eur. J. 1999, 5, 1202-1211.

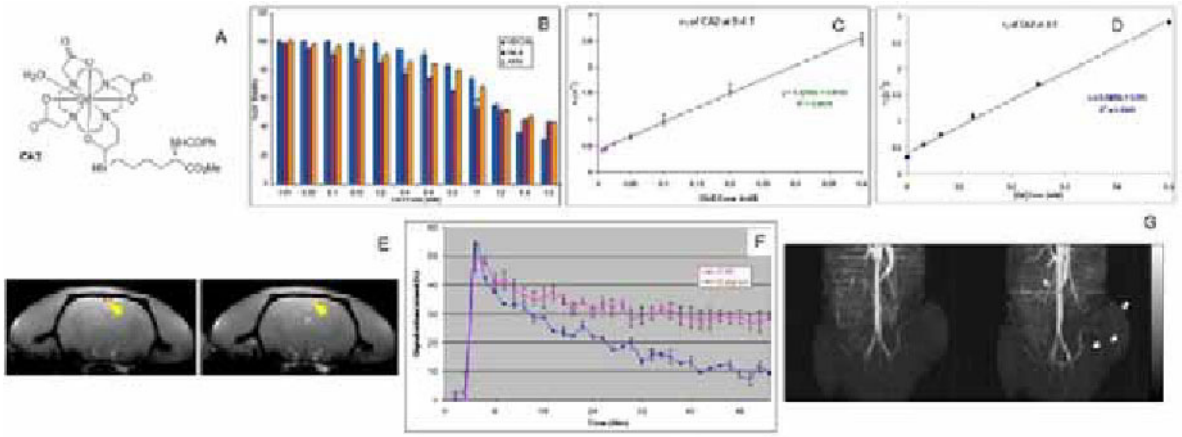


**A)** Structure of **CA2**. **B)** Cell viability of **CA2** in HEK293, HeLa and A549 cell lines. **C)** T1 relaxivity (r1) of **CA2** at 9.4 T. **D)** T1 relaxivity (r1) of **CA2** at 3 T. **E)** MR images of the brain artery in Wistar male rat (left) pre and (right) post (2 mins) injection of **CA2** (0.04 mmol Gd kg$^{-1}$ BW) injection. **F)** Time course of MRI signal intensity in the brain artery with **CA2** and Dotarem. **G)** Pre- and post-contrast Time-of-Flight images taken 30 mins after i.v. injection of **CA2**.

Disclosure of author financial interest or relationships:
**C. Yang**, None; **P. Chandrasekharan**, None; **Z. Poh**, None; **E.G. Robins**, None; **K. Chuang**, None.

Presentation Number **P212**
Poster Session 2
September 6, 2012 / 15:15-15:15 / Room: The Liffey

# Single-step stereospecific fluorination at the 2′-arabino-position of pyrimidine nucleosides: Synthesis of 18F-FMAU

*Nashaat Turkman, Vincenzo Paolillo, Juri G. Gelovani, **Mian M. Alauddin**, Experimental Diagnostic Imaging, UT MD Anderson Cancer Center, Houston, TX, USA. Contact e-mail: alauddin@mdanderson.org*

Introduction: Direct fluorination at the 2′-arabino-position of a pyrimidine nucleoside has been a long-standing problem because of the neighboring-group participation of the C2-carbonyl oxygen to from an intermediate anhydro compound. Recently, we reported for the first time on stereospecific fluorination at the 2′-arabino-position of a pyrimidne nucleoside exemplified via radiosynthesis of 2′-deoxy-2′-fluoro-5-methy-1-β-D-arabinofuranosyluracil (18F-FMAU), albeit in low yields. Now we report results of an investigation on a single-step stereospecific fluorination of a variety of precursors for synthesis of 18F-FMAU. Methods: Scheme 1 represents radiofluorination of precursor compounds for synthesis of 18F-FMAU. Seven nucleoside precursor compounds were synthesized in multiple steps through protection of the appropriate functional groups followed by conversion of the 2′-hydroxyl group into two different leaving groups, mesylate and nosylate, for fluorination and radiofluorination reactions. Direct fluorination at the 2′-arabino position was performed using K18F/kryptofix at different temperatures. A solution of the precursor in dry MeCN was heated at temperatures between 80-90oC for 20 min. The crude reaction mixture was passed through a silica gel solid phase extraction cartridge, eluted with EtOAc, and the crude product was hydrolyzed by reaction with a strong base. Finally, the desired product was isolated by purification using high-performance liquid chromatography (HPLC). Results: All the precursor compounds were obtained in moderate to high yields in multiple steps. Radiofluornation reaction of these precursors produced the desired arabino-nucleoside analogue 18F-FMAU in low and variable yields (0.1-2.0 %, d. c., Table 1). Conclusion: A novel single-step method for stereospecific fluorination of the intact pyrimidine nucleoside at the 2′-arabino position has been investigated. All seven precursors produced the desired product (18F-FMAU) in low yields. This method is applicable for radiosynthesis of the 2′-deoxy-2′-fluoro-5-substituted-1-β-D-arabinofuranosyluracil analogues, including 18F-FEAU, 18FFIAU, 18F-FFAU, 18F-FCAU, and 18F-FBAU using the appropriate precursors for PET imaging. However, further studies are needed to improve the yield.

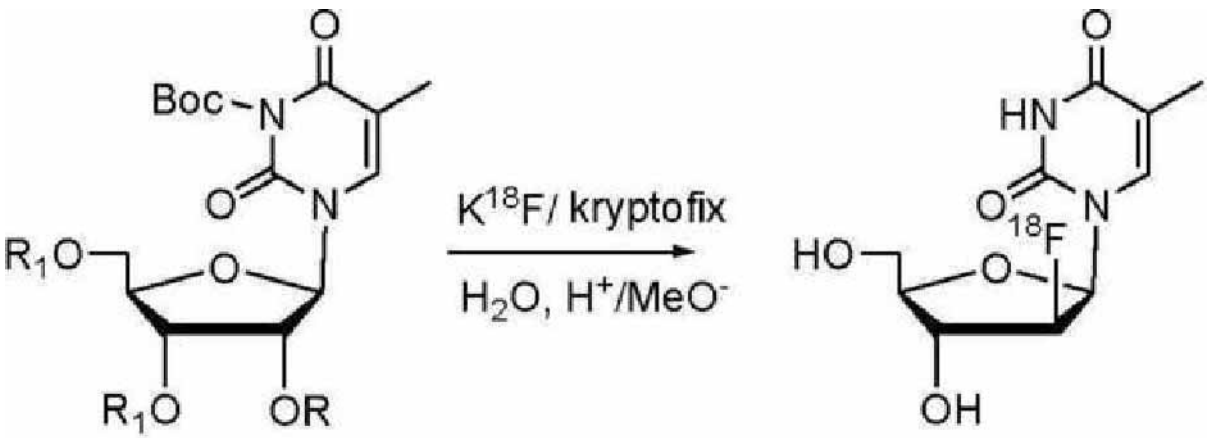


Synthetic Scheme 1
Radiofluorination of precursor compounds

| Comp. # | solvent | Temp | yield |
|---|---|---|---|
| 8a | MeCN | 90oC | 1.00 |
| 8b | MeCN | 90oC | 0.50 |
| 8c | MeCN | 90oC | 0.10 |
| 8d | MeCN | 90oC | 0.06 |
| 8e | MeCN | 90oC | 0.70 |
| 8f | MeCN | 90oC | 1.00 |
| 8g | MeCN | 90oC | 1.00 |

Disclosure of author financial interest or relationships:
**N. Turkman**, None; **V. Paolillo**, None; **J.G. Gelovani**, Macrocyclics, Consultant; SibTech, Consultant; **M.M. Alauddin**, None.

Presentation Number **P213**
Poster Session 2
September 6, 2012 / 15:15-15:15 / Room: The Liffey

# Molecular Imaging Agents for Parkinson's Disease

*Naomi Shakerdge, Krista Neal, Pamela McLean, **Brian Bacskai**, Neurology, Harvard Medical School, Charlestown, MA, USA. Contact e-mail: bbacskai@partners.org*

Parkinson's disease (PD) is a debilitating neurodegenerative disease that is diagnosed primarily with a neurological exam; there is no blood test or brain scan to diagnose PD. Post-mortem confirmation of the diagnosis is performed by the identification of Lewy bodies and Lewy neurites containing aggregated alpha-synuclein, the hallmark pathology of PD. If this pathology could be detected quantitatively early in the disease, it would greatly benefit patient diagnosis, disease treatments, and clinical research. In addition, an imaging marker specific to PD pathology could be used to distinguish clinically similar neurodegenerative disease such as Alzheimer's (AD), dementia with Lewy bodies (DLB), Parkinson's with dementia (PDD), and other Parkinsonian diseases. Our goal is to develop a contrast agent that can enter the brain, selectively bind PD pathology, and be detectable with one or more imaging modalities. Analogous to Pittsburgh compound B (PiB) an amyloid binding compound which is used in Alzheimer's disease diagnosis and research, a successful contrast agent could be radiolabeled for PET or SPECT imaging. In this study, we screened a library of small molecule fluorescent compounds to assess their potential as imaging agents for PD. The compounds in this library are all low molecular weight, fluorescent, and untested in their ability to bind alpha-synuclein aggregates. The initial screening process included immunohistochemistry-based validation of Lewy pathology in human tissue sections followed by staining with the fluorescent compounds to identify any which showed some specificity for PD pathology. We also evaluated binding in Alzheimer's tissue to assess the specificity for PD vs AD aggregates, and found some compounds with preferential binding characteristics. A second procedure utilized two cell culture models of alpha-synuclein aggregation to enable high throughput screening, however, these assays were not predictive of binding to Lewy bodies. We evaluated the ability of our lead compounds to cross the blood-brain-barrier using real time in vivo imaging of mouse brain, and determined that some of the compounds could enter brain. Several compounds were identified that show promise as contrast agents for imaging PD with selectivity over Alzheimer pathology and good brain entry, but require additional characterization. Ultimately, these fluorescent compounds will be radiolabeled and evaluated as PET ligands for non-invasive imaging.

Disclosure of author financial interest or relationships:
**N. Shakerdge**, None; **K. Neal**, None; **P. McLean**, None; **B. Bacskai**, None.

Presentation Number **P214**
Poster Session 2
September 6, 2012 / 15:15-15:15 / Room: The Liffey

# Radiolabeled γ-AApeptides: A New Class of PET Tracers

*Hao Hong[1], Youhong Niu[2], Yunan Yang[1], Haifan Wu[2], Yin Zhang[1], Jonathan W. Engle[1], Todd E. Barnhart[1], Jianfeng Cai[2], **Weibo Cai**[1], [1]University of Wisconsin - Madison, Madison, WI, USA; [2]University of South Florida, Tampa, FL, USA. Contact e-mail: WCai@uwhealth.org*

**Objectives:** The goal of this study was to design, synthesize, and characterize $^{64}$Cu-labeled γ-AApeptides, a new class of peptidomimetics with superb stability, for positron emission tomography (PET) imaging applications. **Methods:** A γ-AApeptide that mimics the tripeptide sequence RGD (i.e. arginine-glycine-aspartic acid, potent integrin αvβ3 antagonist) is termed "γ-AA1", which was conjugated to DOTA (1,4,7,10-tetraazacyclododecane-1,4,7,10-tetraacetic acid) via a linker and termed "γ-AA2". Flow cytometry studies were performed in U87MG cancer cells (integrin αvβ3-positive) to evaluate the binding affinity of the γ-AApeptide-based conjugates for integrin αvβ3. γ-AA2 was labeled with $^{64}$Cu and the enzymatic stability of $^{64}$Cu-γ-AA2 was measured by radioHPLC. PET imaging, biodistribution, and blocking studies were performed on U87MG tumor-bearing mice to evaluate the in vivo tumor targeting efficacy of $^{64}$Cu-γ-AA2. **Results:** γ-AA1 and γ-AA2 had similar binding affinity to integrin αvβ3 as the c(RGDyK) peptide (a commonly used integrin αvβ3 antagonist). However, the enzymatic stability was much higher: 8% degradation of $^{64}$Cu-γ-AA2 and 100% degradation of $^{64}$Cu-labeled c(RGDyK) respectively after incubation with 0.1 mg/mL pronase at 37 °C for 2 h. Uptake of $^{64}$Cu-γ-AA2 in the U87MG tumor was clearly visible as early as 0.5 h p.i., which remained persistent over time (0.9±0.3, 1.0±0.2, 1.1±0.2, and 0.7±0.2 %ID/g at 0.5, 2, 4, and 24 h p.i.; n = 3). $^{64}$Cu-γ-AA2 clears rapidly from the circulation and excellent tumor contrast was observed, with tumor/muscle ratio of 3.8±0.9, 4.8±1.8, 5.8±1.4, and 8.3±3.9 at 0.5 h, 2 h ,4 h, and 24 h p.i. respectively. Administering a blocking dose of the c(RGDyK) peptide significantly reduced the U87MG tumor uptake, thereby confirming in vivo target specificity of $^{64}$Cu-γ-AA2. **Conclusions:** We report PET imaging of integrin αvβ3 with a $^{64}$Cu-labled γ-AApeptide-based RGD mimetic, which exhibited comparable integrin αvβ3 binding affinity as the c(RGDyK) peptide but significantly higher resistance to enzymatic degradation and better in vivo stability, despite its shorter sequence and linear nature. This study establishes γ-AApeptides as a novel class of enzymatically stable targeting ligands for molecular imaging applications.

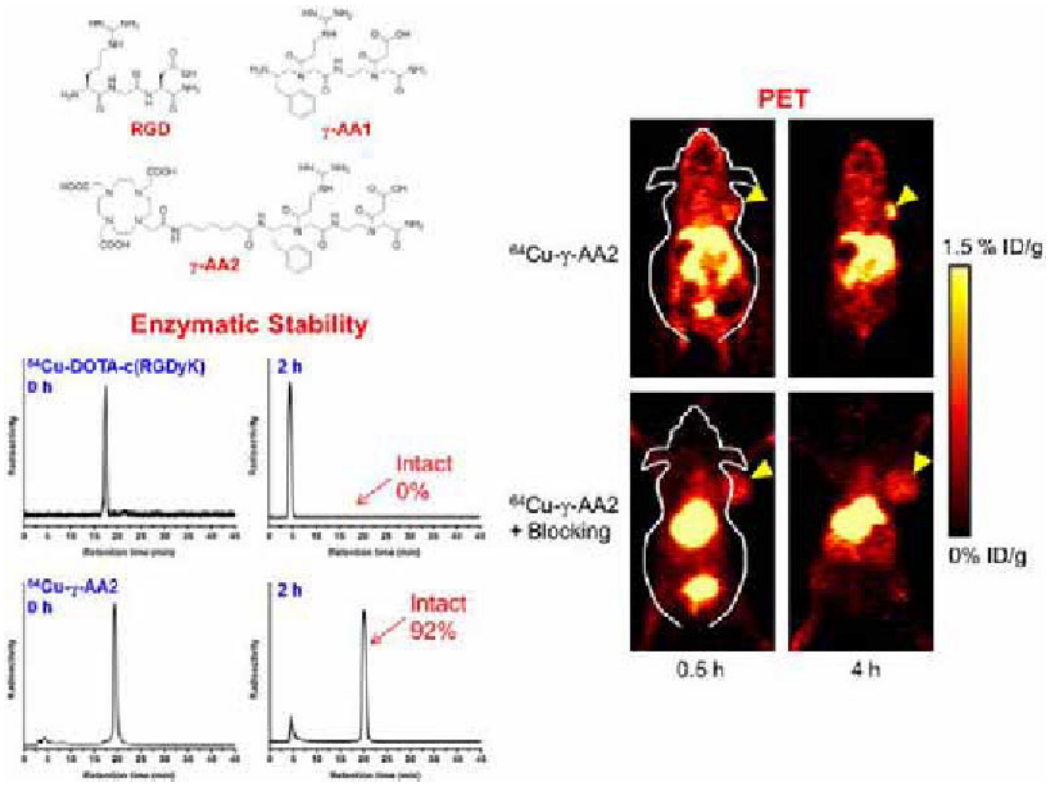


Disclosure of author financial interest or relationships:
**H. Hong**, None; **Y. Niu**, None; **Y. Yang**, None; **H. Wu**, None; **Y. Zhang**, None; **J.W. Engle**, None; **T.E. Barnhart**, None; **J. Cai**, None; **W. Cai**, None.

Presentation Number **P215**
Poster Session 2
September 6, 2012 / 15:15-15:15 / Room: The Liffey

# Comparison among the 18F-FMAU, 18F-FDG and 18F-FLT as PET probe in colorectal cancer

***Yi-Chun Chien***[1,2], *Hueisch-Jy Ding*[2], *Chih-Hao K. Kao*[3,4], *Jeng-Jong Hwang*[1], [1]*Department of biomedical image and radiological sciences, National yang-ming university, Taiwan, ROC., Taipei, Taiwan;* [2]*Department of Medical Imaging and Radiological Sciences, I-Shou University, Kaohsiung, Taiwan;* [3]*Department of Radiopharmaceutical Production, Buddhist Tzu Chi General Hospital, Hualien, Taiwan;* [4]*Department of Radiological Technology, Tzu Chi College of Technology, Hualien, Taiwan. Contact e-mail: chienyc@isu.edu.tw*

Objective: The aim is to compare the efficiency among 18FDG, 18FLT and 18FMAU in colorectal cancer diagnosis. Methods: 18F-FMAU and 18F-FLT can be prepared via a two and one step synthesis. The cellular uptakes of CT26 cells were used with 18F-FLT, 18F-FMAU and 18F-FLT. The cellular uptakes of CT26 were dividing into control group, H2O2 tread and irradiation group. Uptake time is 30, 60 and 120 min. Before practiced, these CT26 cells were treated with and without 0.34 uM BVDU. And then remove the medium at 30, 60 and 120 min. Conclusion: We found the 18FDG and 18FLT were not distinguished whether the CT26 cells irradiate with 2Gy or not. However, the uptake values of 18FMAU were decrease from 8 (% Dose / 106 cells) to 3 (irradiation group) or 2 (H2O2 tread group).

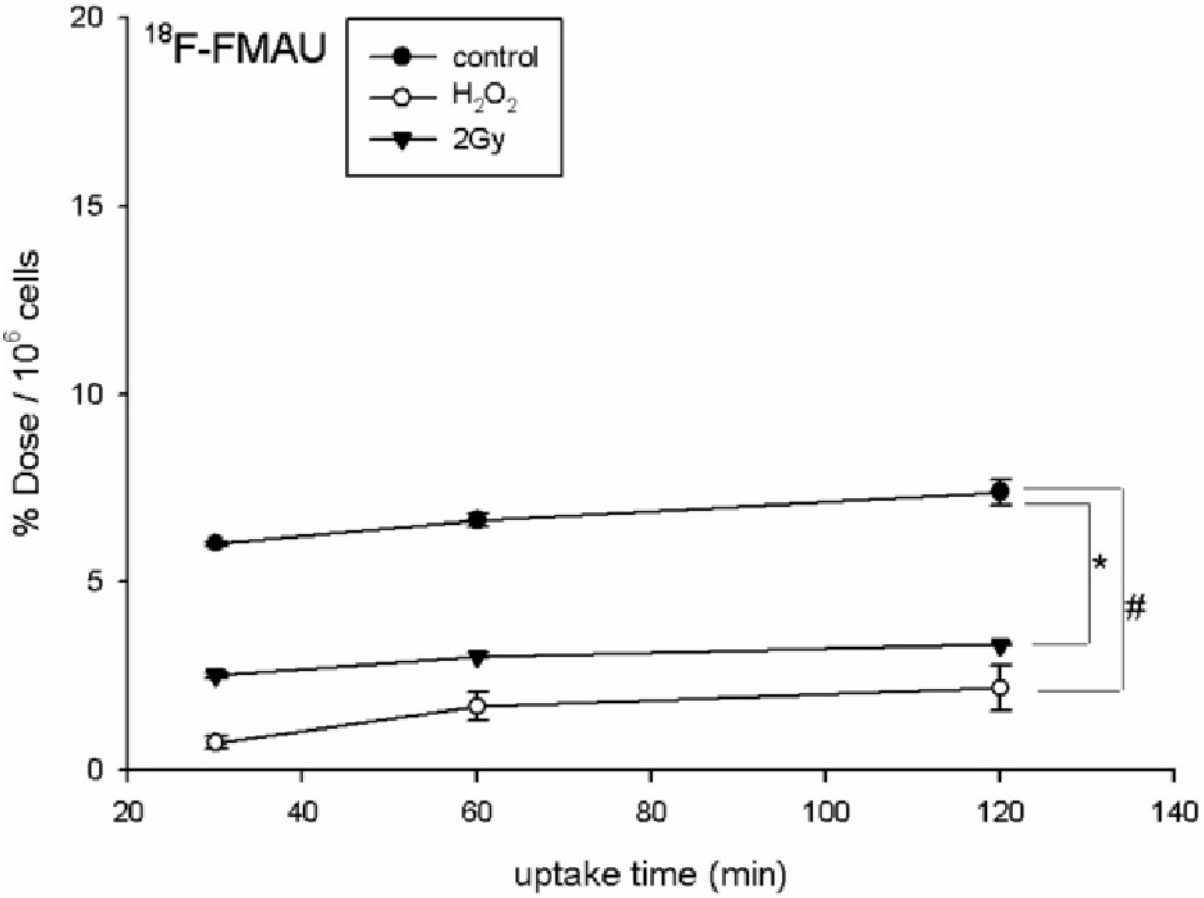


Disclosure of author financial interest or relationships:
**Y. Chien**, None; **H. Ding**, None; **C.K. Kao**, None; **J. Hwang**, None.

Presentation Number **P216**
Poster Session 2
September 6, 2012 / 15:15-15:15 / Room: The Liffey

# Utilization of Probes for In Vivo Imaging of Tumor Senescence by Positron Emission Tomography(PET) or Optical Imaging (OI)

***Jonathan Cotton**, Kerstin Fuchs, Anna Teske, Christian Kesenheimer, Bernd J. Pichler, Department of Preclinical Imaging and Radiopharmacy, Eberhard Karls University Tuebingen, Tuebingen, Germany. Contact e-mail: joncotton@gmail.com*

Cell senescence is broadly defined as the general biological program by which growth is ceased and is accompanied by distinct changes in metabolic pathways. Recently, senescence is recognized to play an important role in cancer treatment and therapy resistance. Treatment-associated senescence can be a measure of chemotherapeutic success and the detection of senescent cells might also offer diagnostic opportunities for detecting of preneoplastic lesions. One of the most widely used markers for senescent cells is the senescence-associated (SA)-β-galactosidase (β-gal). Several SA-β-gal substrates have been developed and are currently used ex vivo and in vitro to show β-gal expression. However, it has recently come to light, that α-fucosidase (α-fuc) shows much higher specificity for senescence. Glycosidases are situated in the lysosomes, which in senescent cells are often noticeably enlarged. No attempts to use molecular probes to test for in vivo senescence have been reported in the literature so far. We aim to utilize SA-β-gal and α-fuc substrates as radiolabel PET-probes for non-invasive in vivo imaging of senescence and enlarged lysosomes. Our senescence models have been verified with in vitro experiments in HCT116 and MCF7 cells. Cells were treated with 250nM Doxorubicin (Dox), a chemotherapeutical, to induce senescence, stained with either a β-gal staining kit or LysoTracker®. We propose novel glycosidase substrates 1(A-C) and 2(A-C) to probe glycosidase activity and to image senescence, while 3(A-C) serve as a control (to date, there is no reported evidence of increased glucosidase activity in senescence). The structures we synthesized are confirmed with mass-spectroscopy and nuclear magnetic resonence spectroscopy and characterization is aided by thin layer chromatography and also gas- and liquid-chromatography. Structures from family B and C contain basic nitrogen(s) and are therefore intended to be pH-trapped in the acidic lysosomes, providing an enhanced signal. To date, we successfully synthesized the chemical precursors for structures 1(A+B), 2(A) and their cold standards. C-11 labeling experiments have also been successfully conducted on structurally similar precursors. Analysis of the two cell lines showed, that Dox-treated cells, not only became positive for β-gal staining, but also presented with greatly enlarged lysosoms. For the LysoTracker® staining, ~90% of HCT116 and ~60% of the MCF7 cells treated with Dox, stained positive compared to untreated HCT116 (~10%) and MCF7 (~15%) cells, which showed only slight positive results. Currently, we performed fluorescence-activated-cell-sorting experiments with a nilred-labeled α-L-Fucoside-Inhibitor 2D (JC106) and could show that labeled with Dox-treated MCF7 cells showed higher accumulation of JC106 compared to untreated MCF7 cells. Thus, in vitro measurements of senescence in cell culture experiments using JC106 also seems to be a promising tool to detect senescence in vivo, in experimental tumor animal models. The next steps will include in vitro cell tests using our radiolabled molecules to detect senescence, before we go into first animal studies.

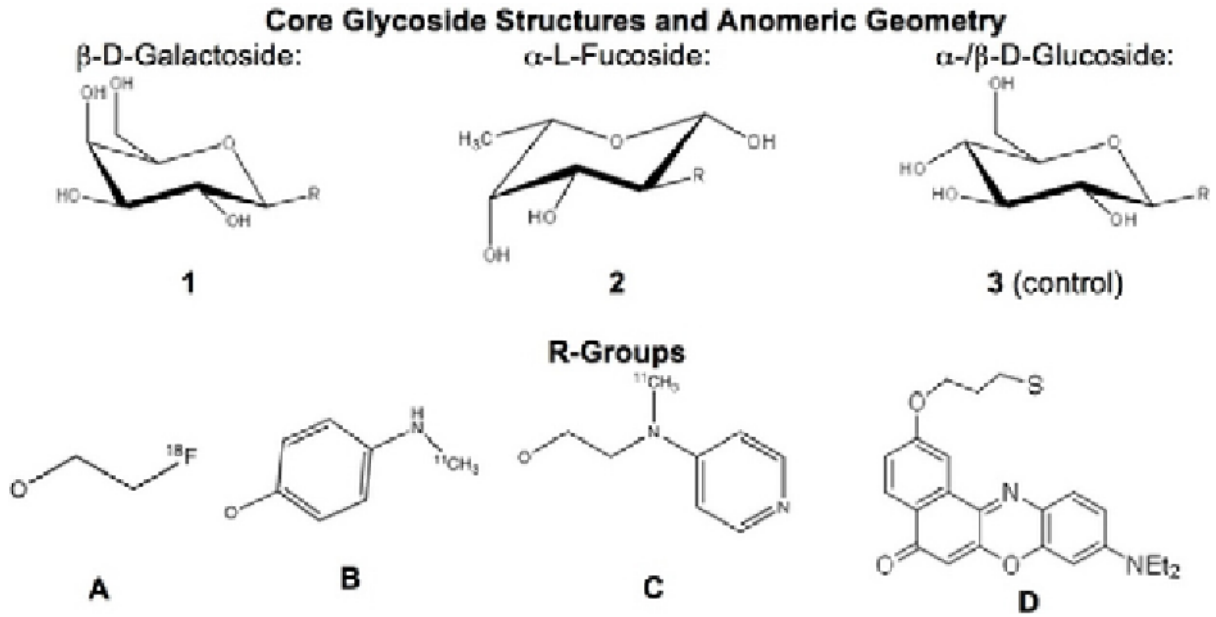


Disclosure of author financial interest or relationships:
**J. Cotton**, None; **K. Fuchs**, None; **A. Teske**, None; **C. Kesenheimer**, None; **B.J. Pichler**, Siemens, Grant/research support; AstraZeneca, Grant/research support; Bayer Healthcare, Grant/research support; Boehringer-Ingelheim, Grant/research support; Oncodesign, Grant/research support; Merck, Grant/research support; Bruker, Grant/research support .

Presentation Number **P217**
Poster Session 2
September 6, 2012 / 15:15-15:15 / Room: The Liffey

# PET imaging of pulmonary embolism with 18F-Fluorogas and 64Cu-MAA

***Veronique Dumulon-Perreault***[1], *Etienne Croteau*[2], *Samia Ait-Mohand*[1], *Rene Ouellet*[1], *Jacques A. Rousseau*[1], *Jean-François Beaudoin*[1], *Roger Lecomte*[1], *Eric E. Turcotte*[1], *Brigitte Guerin*[1], [1]*Universite de Sherbrooke, CIMS, Sherbrooke, QC, Canada;* [2]*National Cardiac PET Centre, University of Ottawa Heart Institute, Ottawa, ON, Canada. Contact e-mail: Veronique.Dumulon-Perreault@USherbrooke.ca*

Objectives : Two different tracers are required for lung embolism evaluation by ventilation and perfusion. The ventilation study is usually accomplished with an aerosol (99mTc-Technegas), while the accompanying perfusion assay is done with 99mTc-labeled albumin macroaggregates (99mTc-MAA). The goal of this study is to evaluate the potential of two other isotopes for microPET imaging in rats. The new preparations require F-18 and Cu-64 to yield 18F-Fluorogas and 64Cu-MAA. Methods: Prior to the PET imaging sequence, autologous cloths were injected to the rat via the jugular vein to produce embolism. 18F-Fluorogas (37-50MBq/0.1 mL) was generated using [18F]-NaF and a commercially available generator (Technegas generator; Cyclomedica, Sydney, Australia). The animal breathes for 5 min and then is placed in a LabPET scanner. A dynamic image is acquired for 30 min. 64Cu-MAA were prepared by direct addition of [64Cu]-Cu(OAc)2 to MAA particles (4-8 millions, from a commercial Draximage MAA kit), followed by a 15 min incubation at 75 °C in saline. A 45 min dynamic image is acquired directly after the injection of around 20MBq of 64Cu-MAA via the tail vein. Results: Almost no deposit in the respiratory tract was observed and the 18F-Fluorogas particles reached the periphery of the lung. The distribution of 18F is uniform in the lungs for both healthy and embolized rats. The biological half-life for this tracer is around 10-15 min. The distribution of 64Cu-MAA was relatively uniform in lungs of healthy rats, whereas a perfusion defect was apparent in the upper posterior segment lobe of the embolized rat. Conclusions: 18F-Fluorogas and 64Cu-MAA in healthy and embolized rats confirmed the potential of these tracers for the detection of pulmonary embolism by PET imaging.

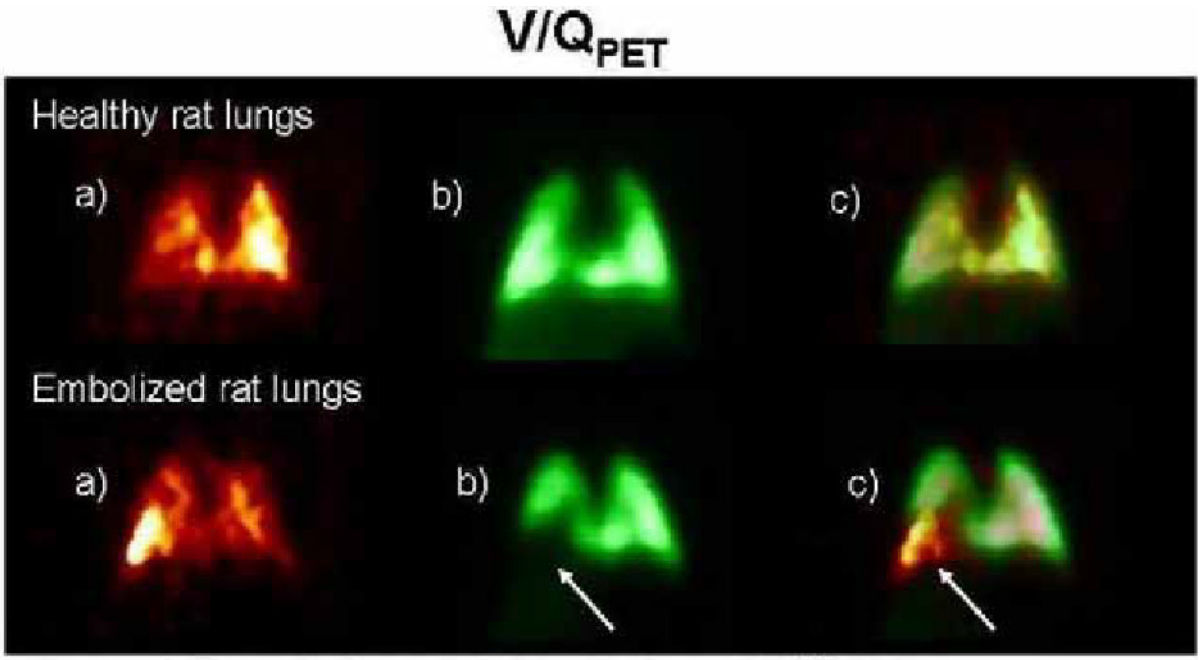


Coronal filtered view of a) Ventilation with $^{18}$F-Fluorogas, b) Perfusion with $^{64}$Cu-MAA, c) Fusion images; white arrows: lobar embolism.

Disclosure of author financial interest or relationships:
**V. Dumulon-Perreault**, None; **E. Croteau**, None; **S. Ait-Mohand**, None; **R. Ouellet**, None; **J.A. Rousseau**, None; **J. Beaudoin**, None; **R. Lecomte**, Gamma Medica, Stockholder; Gamma Medica, Consultant; **E.E. Turcotte**, None; **B. Guerin**, None.

Presentation Number **P218**
Poster Session 2
September 6, 2012 / 15:15-15:15 / Room: The Liffey

# Evaluation of CardioPET, a potential PET tracer for myocardial fatty acid metabolism, in rats treated with a nutritional supplement

***David R. Elmaleh***[1], *Timothy M. Shoup*[1], *Whitney Michalek*[2], *Angela Ferris*[2], *Ali A. Bonab*[2], *Alan J. Fischman*[2], [1]*Radiology, Massachusetts General Hospital, Boston, MA, USA;* [2]*Shriners Hospitals for Children, Boston, MA, USA. Contact e-mail: DELMALEH@PARTNERS.ORG*

Objectives: CardioPET (trans-9-[18F]fluoro-3,4-methyleneheptadecanoic acid), a modified fatty acid closely resembling naturally-occurring free fatty acids, undergoes metabolic trapping in heart tissue. As with other tracers of mitochondrial fatty acid oxidation in the heart, competing liver uptake is a problem. Our earlier study indicated that heart-to-liver ratios in fed and fasted mice were 3.27 and 0.28, respectively. In this study, the pharmacokinetic behavior of CardioPET was evaluated in rats treated with the nutritional supplement Ensure. Methods: Biodistribution of CardioPET was determined in non-fasted rats at 5, 30, 60min (n = 5). Overnight fasted rats were given Ensure (250 microliter) via a tube placed in the stomach 10 minutes prior to injection of CardioPET and were sacrificed at 50 minutes. Untreated fasted rats served as a control. The animals were euthanized by C02 overdose and subjected to complete necroscopy. Tissues were weighed and counted using a Wizard gamma-counter and results were expressed as %dose/gram tissue mean +/- SEM. Results: In the non-fasted rats, heart-to-liver ratios at 5, 30 and 60 min were 1.16, 2.46 and 2.30, respectively. The heart-to-liver ratio in the overnight fasted animals was 0.34 and was only slightly increased in overnight fasted animals fed Ensure 10 minutes prior to CardioPET administration. Conclusion: The feeding state is an important factor in heart imaging. Non-fasting rats in our studies resulted in a heart/liver ratio >1. The slight improvement observed in heart-to-liver ratio indicates that fasting has by far the strongest effect. Therefore, fasting, amount of intra lipid in the supplemental nutrient and time of its administration prior to tracer introduction affect liver uptake. Standardized fasting, intra lipid diet, and time of nutrition introduction should improve heart. Other diet and fasting pharmacokinetic will be reported.

Disclosure of author financial interest or relationships:
**D.R. Elmaleh**, None; **T.M. Shoup**, None; **W. Michalek**, None; **A. Ferris**, None; **A.A. Bonab**, None; **A.J. Fischman**, None.

Presentation Number **P219**
Poster Session 2
September 6, 2012 / 15:15-15:15 / Room: The Liffey

# Molecular imaging of the mitochondrial function during apoptosis using 18F-labelled phosphonium cations

***Anna Haslop***[1,3], *Lisa A. Wells*[2], *Philip Murphy*[3], *Antony Gee*[4], *Nicholas J. Long*[1], *Christophe Plisson*[2], [1]*Chemistry, Imperial College London, London, United Kingdom;* [2]*Imanova Ltd, London, United Kingdom;* [3]*GSK, London, United Kingdom;* [4]*Division of Imaging Sciences, King's College London, London, United Kingdom. Contact e-mail: ah505@ic.ac.uk*

Introduction: The discovery that mitochondria are involved in the early stages of apoptosis has opened a whole new area for researchers to target.[1] The depletion of the mitochondrial inner membrane potential is found to be an initial step and a point of no return for apoptosis. Compounds such as lipophilic cations that are selectively taken-up into the mitochondria owing to this potential lend themselves to biomolecular imaging. Previous literature reports state that phosphonium salts have shown this dependency but are limited due to poor radiochemical yields or complex multi-steps syntheses.[2] The aim of this work was to efficiently synthesise a library of radiolabelled phosphonium cations via 'Click' chemistry and analyse their suitability to act as imaging probes for apoptosis by measuring their selective and membrane potential dependent uptake into the mitochondria. Methods: Phosphonium salts bearing a fluorine-labelled 1,2,3-triazole moiety were prepared via the 'Click' reaction between [18F] fluoroethyl azide and phosphonium salts bearing terminal alkynes. The 18F labelled azide was prepared on an Advion MinuteMan microfluidic platform and purified by distillation prior to coupling with the alkyne precursors. The chain length between the phosphorus centre and the triazole, and the functional groups on the phenyl rings were varied in order to investigate the effect on the reaction rates, the lipophilicity of the compound and the ability to be selectively taken up into the mitochondria. Results: The compounds shown in figure 1 were successfully synthesised with both 18F and 19F isotopes. The two-step radiosynthesis allowed rapid synthesis times (less than 1 hour), high radiochemical purities and suitable radiochemical yields for future clinical application. The functionalised tracer was obtained in yields ranging from 0.6-1.5 GBq (corresponding to 14-50% of fluoroethyl azide incorporation) and the formulated product was obtained in activities between 131.5 to 334.0 MBq/ml. Varying the chain length and the addition of functional groups has allowed the lipophilicity to be a tuneable characteristic. Initial cell assays have shown that compound 1 failed to enter the cell, but with functional group modification cellular uptake was observed. The uptake into the cells could also be reduced by the treatment of the anti-cancer drug, cisplatin. Conclusions: A radiolabelling method has been successful in preparing 18F-labelled phosphonium cations in good radiochemical purities and radiochemical yields relevant for clinical imaging. Further studies are underway to test if cell and tissue uptake of the labelled phosphonium salt is selective and dependent on mitochondrial membrane potential. Research Support: BBSRC and GSK References: [1] V. Rostovtsev, K. Sharpless, L. Green, V. Fokin, (2002), Angewandte Chemie-International Edition, 41, 2596-2599. [2] V. Ravert and I Madar, (2004), Journal of Labelled Compounds and Radiopharmaceuticals, 47, 469-476

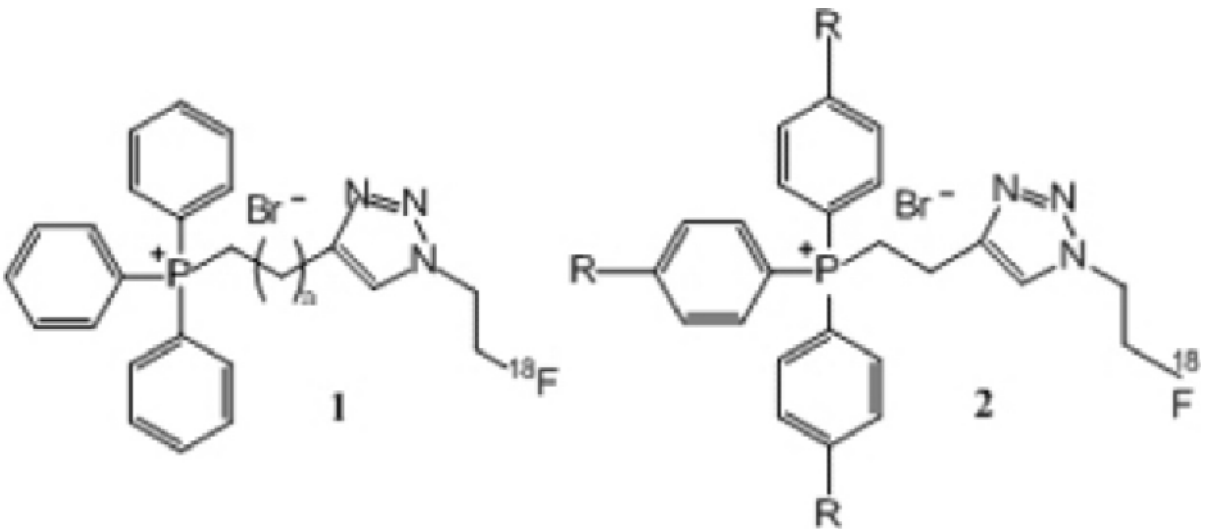


Figure 1. Structures of 18F labelled phosphonium cations

Disclosure of author financial interest or relationships:
**A. Haslop**, None; **L.A. Wells**, None; **P. Murphy**, GlaxoSmithKline, Employment; **A. Gee**, None; **N.J. Long**, None; **C. Plisson**, None.

Presentation Number **P220**
Poster Session 2
September 6, 2012 / 15:15-15:15 / Room: The Liffey

# Synthesis, 99mTc-Tricarbonyl labeling and biological evaluation of pyridyltriazol derivative of Methoxy phenyl piperazine as a potential 5HT1A receptor imaging agent

***Leila Hassanzadeh***[1], *Mostafa Erfani*[2], *Seyed Esmaeil Sadat Ebrahimi*[1], [1]*Radiopharmacy, Faculty of Pharmacy, Tehran University of Medical Sciences, Tehran, Iran., Tehran, Islamic Republic of Iran;* [2]*Nuclear Science Research School, Nuclear Science & Technology Research Institute (NSTRI), Atomic Energy Organization of Iran (AEOI), P.O. Box:11365-3486, end of Kargar Ave., Tehran, Iran., Tehran, Islamic Republic of Iran. Contact e-mail: l_analytic@yahoo.com*

Introduction: Serotonin and its various receptors has been tightly implicated in the pathogenesis of depression, anxiety, schizophrenia, epilepsy and eating disorders. Specific radioligands and single-photon emission computer tomography (SPECT) or positron emission tomography (PET) allow for a quantitative imaging of brain 5-HT1A receptor distribution in living animals and humans.1-(2-methoxyphenyl) piperazine pharmacophore, a fragment of the true 5HT1A antagonist WAY100635, is being found in numerous selective 5HT1A imaging agents. The successful development of 99mTc-TRODAT as a radioligand for the dopamine transporter has shown the feasibility of imaging specific transporters in the brain with radiotracers based on 99mTc. In this study, a new arilpiperazine derivative was synthesized and radiolabeled by 99mTc-carbonyl precursor. Method: A phenyl piperazine triazole derivative was prepared and desired structure was confirmed by NMR and Mass spectrometries. The ligand was radiolabelled with the precursor [99mTc] [(H2O)3(CO)3]+ and characterized by HPLC. The labeling conditions were optimized in the aspect of PH, reaction temperature, time and amount of ligand. The radiochemical purity of the intermediate and final complex were evaluated by HPLC methods. Stability in human serum, Octanol/water partition coefficient, in vivo biodistribution of labeled compound were carried out in Wistar rat. Result: The synthesis of Triazole complex was carried out in over 90% yield and respectively labeled with 99mTc-Tricabonyl core in over 95% radiochemical purity that was determined by HPLC. Biodistribution studies have shown brain uptake of 0.95±0.07 %ID/g at 2min post injection. Radioligand had about over 6 hours, in vivo stability in human serum albumin. Receptor binding assays indicated specific binding of radioligand to 5HT1A receptors. The partition coefficient (log P) was calculated as 1.35±0.08. The labeled compound was stable even up to 24 hours in room temperature. Conclusion: The results indicates that the way of synthesis is reliable and reproducible and has high yield steps. Radiolabeling of compound is high yield and has high radio chemical purity. The radio labeled compound is more than 24 hr stable. It has more lypophilicity, higher brain uptake and binding to receptor than propargyl ligand in our previous studies. Regional brain distribution study showed a clear correlation between distribution of radioactivity and distribution of 5HT1A receptors in the brain.

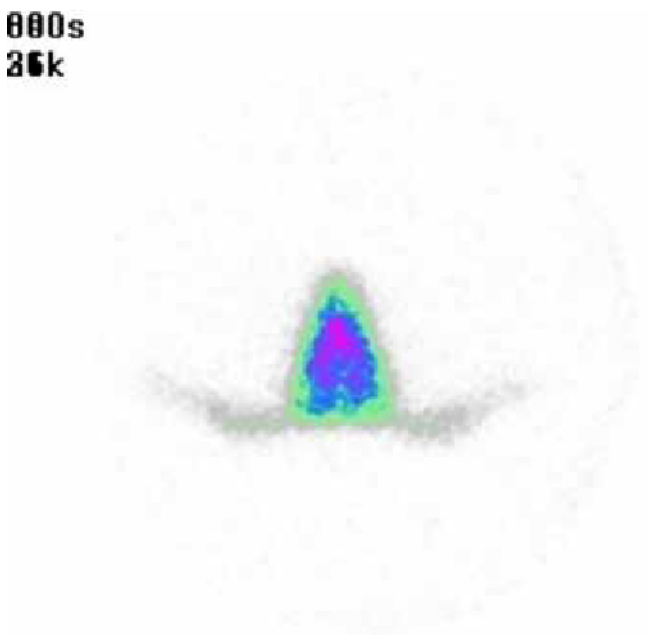


Disclosure of author financial interest or relationships:
**L. Hassanzadeh**, None; **M. Erfani**, None; **S. Sadat Ebrahimi**, None.

Presentation Number **P221**
Poster Session 2
September 6, 2012 / 15:15-15:15 / Room: The Liffey

# Optimization of Generator Technology Capability: Compare with elute efficiency by different purify conditions for Ga-68 PET radiopharmaceutical labelling

***Min-Lung Hsieh**, Hsin-Han Hsieh, Ming-Hsin Li, Institute of Nuclear Energy Research, Taoyuan, Taiwan. Contact e-mail: MinLung@iner.gov.tw*

Objectives: PET scintigraphy with 68Ga-labelled peptides is becoming the major subject in Nuclear Medicine and used all over the world. In tradition, the PET studies are performed with F-18 radiopharmaceuticals requiring an onsite cyclotron and cost expensive, it will replaced by Ga-68 radiopharmaceuticals nowadays. Ga-68 radionuclides can produced by 68Ge/68Ga generator which is easier availability and more flexibility in use. In order to optimize the elute efficiency, different parameters of 68Ge/68Ga generator were tested, such as different type of solid column materials, different weights of solid column material, different preconditions of solid column material, different lengths of column, different radius of column, different species of elute solution, different concentrations of elute solution, different rates of elution and so on. Through above variables to find the best condition of 68Ge/68Ga generator. 68Ge/68Ga generator (long-lived) supply an excellent source of positron-emitting 68Ga (short-lived). In our purpose, we want to develop a purify condition for generator, which not only has high affinity for germanium but also has low affinity for gallium. Successfully used in routine application and might contribute to a experiment for the clinical PET in the future. Methods: The radionuclides 68Ge were obtained from a 69Ga/Ag alloy target, electrodeposited on silver substrate. For pre-purification, the enriched-69Ga sample was carried out by S-910 absorption column. The pH of the sample was adjusted with 2 M NaOH, dissolved in a certain volume of 10 N HNO3 solutions after it is added to an amount of distilled water. Subsequently, add a pre-weighed stable isotope gallium ion source.TiO2 powder was selected as adsorbent and conditioned by heating process. The powder was dipped in 1.0M HCl over 24h, and then rinsed with distilled water until the pH value fall between 5~6, as well as the precipitates were baked in the oven at a particular temperature .A total of 3g of pre-treatment TiO2 was filled into a Borosilicate Glass Column. The washing step have been performed in column that contained 3g TiO2, and the column washed with about 50mL of 0.001M HCl followed by 50 mL of 0.1M.finally,the column was eluted with 0.1M HCl at a flow of 3 mL per minute. Results Our work shows that the activities of the eluant of 68Ge via de-sorption and washing process comprises excess 95 % of 68Ga could be eluted. The mean percentages and standard deviation (SD) of the activity by Multi-channel analyzer were 75.6 and 1.43(n=8) at a flow of 2 mL /min, the 68Ga breakthroughs were 0.002005 and 0.0002947 respectively. Conclusions: To develop a purify schedule and find a great elute condition, which efficient and stable system for processing 68Ge/68Ga generator-produced 68Ga enough for different clinical application.

Disclosure of author financial interest or relationships:
**M. Hsieh**, None; **H. Hsieh**, None; **M. Li**, None.

Presentation Number **P222**
Poster Session 2
September 6, 2012 / 15:15-15:15 / Room: The Liffey

# Synthesis of [$^{11}$C]dehydropravastatin designed as a PET probe for *in vivo* study on the functions of OATP1B1 and MRP2 transporters in the liver

***Ryosuke Ijuin***[1], *Tadayuki Takashima*[1], *Yasuyoshi Watanabe*[1], *Yuichi Sugiyama*[2], *Masaaki Suzuki*[1], [1]*Center for Molecular Imaging Science, RIKEN, Kobe, Japan;* [2]*Graduate School of Pharmaceutical Sciences, The University of Tokyo, Bunkyo-ku, Japan. Contact e-mail: ryoijuin@riken.jp*

**Objectives:** Drug transporters mediate the uptake and excretion of drugs in various organs. Therefore, the knowledge of transporter functions in the body would be valuable not only for diagnosis but also the evaluation of the drug efficacy. In this context, we intended to synthesize [$^{11}$C]dehydropravastatin, a newly designed PET probe, for evaluation of the functions of the OATP1B1 and MRP2 transporters in the liver. **Methods:** The synthesis of [$^{11}$C]2′,3′-dehydropravastatin (**5**) has been planned by the rapid cross-coupling (*C*-[$^{11}$C]methylation reaction) between $sp^2_{(vinyl)}$-$sp^3$ carbons using [$^{11}$C]methyl iodide and an organoboron precursor **4** in the $^{11}$C-labeling step [1], and subsequent deprotection and hydrolysis. **Results and Discussion:** The synthesis of radioactive [$^{11}$C]dehydropravastatin (**5**) was accomplished via the deesterification of pravastatin (**1**) and reconstruction of a whole skeleton of **5** with new ester moiety. Thus boronated ester **4** was synthesized by esterification of alcoholic intermediate **2** and boronated acid **3** using diethyl chlorophosphate. The synthesis of **5** was conducted by one-pot manner as follows. Thus, the reaction of [$^{11}$C]methyl iodide and **4** was conducted in the presence of $Pd_2(dba)_3$, P(*o*-toly)$_3$, and $K_2CO_3$ (in 1:3:4 molar ratio) at 65 °C for 5 min. Successive treatments of the resulting mixture with a solution of TBAF, and then with an aqueous NaOH solution, giving the desired [$^{11}$C]dehydropravastatin (**5**) with (i) total radioactivity, 1.2 GBq; (ii) radio purity, >99%; chemical purity, 98%; (iii) radio chemical yield, 64%; decay correct yield, 19.7%; specific radioactivity, 79 GBq/μmol. The total synthesis time was 34±2 min. PET studies using rats (22±1 MBq/body) indicated that the radioactivity was identifiable in the liver and kidneys within 2 min after the radiotracer administration and then in intestine and urinary bladder furing 5-10 min as shown in Figure 1. Such image flows were regulated by rifampicin (typical OATPs inhibitor) and the use of Mrp2-deficient rats, concluding that **5** would be a PET probe useful for OATP1B1 and MRP2 transporters in the liver. **Reference:** 1) H. Doi, M. Suzuki et. al., *Chem. Eur. J.*, **2009**, *15*, 4165-4171

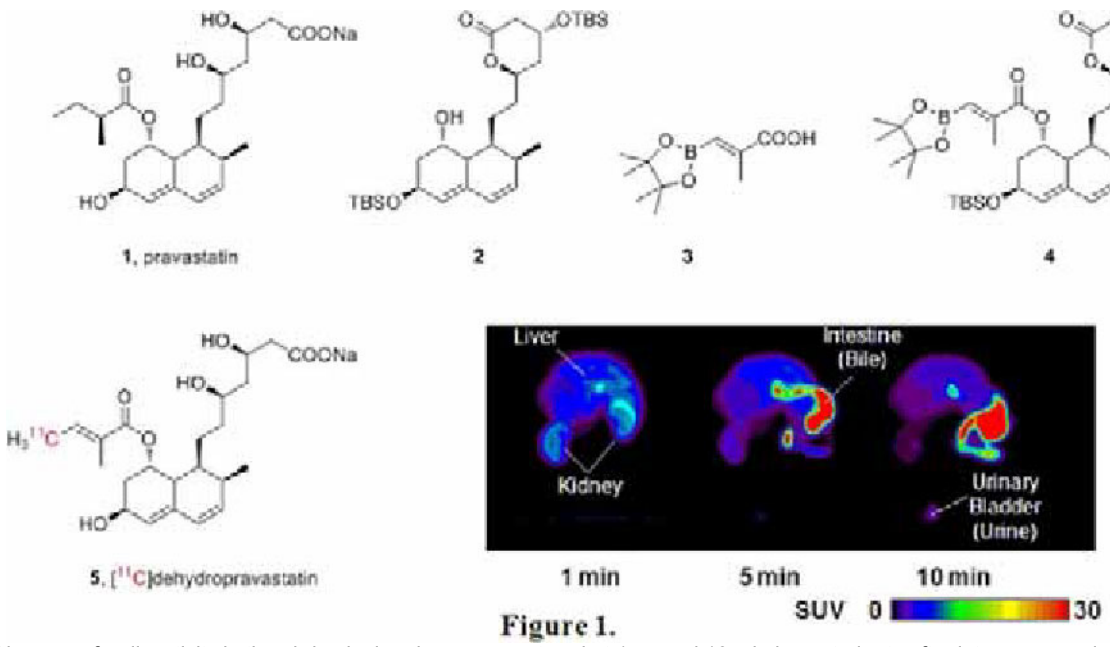


Figure 1.
PET images of radioactivity in the abdominal region were captured at 1, 5, and 10 min in control rats after intravenous administration of **5**.

Disclosure of author financial interest or relationships:
**R. Ijuin**, None; **T. Takashima**, None; **Y. Watanabe**, None; **Y. Sugiyama**, None; **M. Suzuki**, None.

Presentation Number **P223**
Poster Session 2
September 6, 2012 / 15:15-15:15 / Room: The Liffey

# Microfluidic Polymer Monoliths for [18F]Fluoride Concentration, Activation and Solid Phase Radiofluorination

***Rehana Ismail***[1,2], *Ariella Machness*[1,2], *R. Michael van Dam*[1,2], *Pei Yuin Keng*[1,2], [1]*Crump Institute of Molecular Imaging, University of California, Los angeles, Los Angeles, CA, USA;* [2]*Department of Molecular & Medical Pharmacology, David Geffen School of Medicine, Los Angeles, CA, USA. Contact e-mail: rismail@mednet.ucla.edu*

To date, the major obstacle in clinical advancement of PET imaging for cancer research is the limited accessibility of diverse arrays of PET probes due to the need for highly trained radiochemists, dedicated automated synthesizer modules, specialized instrumentation and the expensive infrastructure for radiation shielding. Microfluidic systems are emerging as a promising radiosynthesis technology to reduce the reaction time, precursor consumption, space, and the cost of radiation shielding. Our group is developing functional porous polymer supports with high permeability and high surface areas for [18F]fluoride trapping, activation and radiolabeling reactions on a continuous-flow glass microfluidic chip. Here, we report a proof-of-concept demonstration of an integrated flow-through microfluidic system capable of performing [18F]fluoride pre-concentration, activation and solid phase radiofluorination reaction. A polymer monolith containing imidazolium cation was synthesized by in situ co-polymerization of 4-vinylbenzyl chloride and divinylbenzene (DVB) within the vinylized microchannels of a glass microfluidic chip (FC_R150.696; Micronit). The monolith was washed thoroughly with THF to remove excess starting materials. The reactive benzyl chloride moieties were then functionalized with N-methyl imidazole (1mM) at 90oC with a flow rate of 17uL/min. On a separate microchip, we have also prepared a polymer monolith functionalized with a fluoride ion reactive 3-phenylpropyl 4-vinylbenzenesulfonate moieties for on-chip solid phase radiofluorination reaction. In our preliminary study, the [18F]fluoride ion in [18O]H2O (50µL) was diluted with 450 µL of THF, and then flowed through the microchip containing the imidazolium monolith at 33 µL/min. The residual water was removed by flushing the monolith with 100µL of CH3CN. The trapped [18F]fluoride was subsequently released from the microchip with 200 µL of K2CO3/Kryptofix in a mixture of CH3CN/H2O (99:1 v/v) and 100uL of CH3CN. The trapping and releasing efficiency was found to be 100% and 69%± 7% respectively over three experiments. The reactivity of the released [18F]KF/K2.2.2 complex was investigated by performing a standard microdroplet radiofluorination of mannose triflate on a Teflon-coated glass substrate at 110oC. We achieved comparable radiofluorination efficiency (84% ± 7% (n=3)) of mannose triflate (Radio-TLC in Fig. 1A) using the activated [18F]KF/K2.2.2 complex released from the microchip, without performing additional azeotropic distillation. This result showed that the microfluidic anion exchange platform could efficiently perform solvent exchanges and [18F]fluoride ion activation processes, which are the major limitations in current flow-through microfluidic radiosynthesizers. Independently, we have demonstrated the solid phase radiofluorination of the 3-phenylpropyl 4-vinylbenzenesulfonate polymer monolith on the flow-through microfluidic chip with 75% fluorination efficiency. We will be integrating the [18F]fluoride activation flow-through microchip and the sulfonate ester microchip towards the development of a rapid, simple, and efficient PET probe synthesizer.

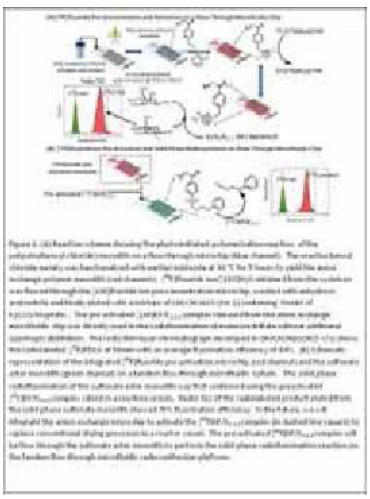

Disclosure of author financial interest or relationships:
**R. Ismail**, None; **A. Machness**, None; **R. van Dam**, Sofie Biosciences, Inc., Consultant; Sofie Biosciences, Inc., Stockholder; **P. Keng**, None.

Presentation Number **P224**
Poster Session 2
September 6, 2012 / 15:15-15:15 / Room: The Liffey

# Carbon-11 labeled benzimidazole inhibitor of TIE-2 and VEGFR-2 receptor tyrosine kinases as a molecular imaging agent for angiogenesis

*Samar Dissoki, Galith Abourbeh, Eyal Mishani,* ***Orit Jacobson Weiss****, Hadassah University Hospital, Jerusalem, Israel. Contact e-mail: oritjacobson@yahoo.com*

Angiogenesis is one of the hallmarks of tumor growth and metastasis. The angiogenic factors, including members of the vascular endothelial growth factor (VEGF) and the angiopoietin (Ang) families are released by the tumor during angiogenesis to activate endothelial cells in established blood vessels via binding to the Tie2 and VEGR-2 receptors and induce endothelial proliferation and migration. Development of dual VEGFR2 and Tie-2 PET biomarkers may have an important role in molecular imaging of angiogenic processes. Aims: Development of C-11 labeled angiogenesis biomarker which target the VEGR-2/TIE2 receptors. Methods: ATV-1, a potent and selective VEGFR-2/TIE-2 antagonist, was labeled with C-11 via methylation on the secondary amine using 11C-CH3I. Blood stability tests as well as biodistribution and PET imaging were carried out. Results & Discussion: ATV-1 was synthesized and labeled with C-11 with an overall radiochemical yield of 12±2% based on 11CO2 activity and a specific activity of 15,430 Ci/mmol (n = 4). ATV-1 selectivity to VEGR-2/Tie2 was determined against other protein kinases including EGF-R wt, ERBB2, KIT wt, PDGFR-α and PDGFR-β. ATV-1 was found to possess a high selectivity and inhibitory activity against TIE-2 and VEGFR-2 (IC50 = 21 nM and 11 nM, respectively). The stability of 11C-ATV-1 was tested in human blood, with 60% intact biomarker recovered at time 0 and 50% after 1h incubation. No metabolites were found to form over time. The distribution of 11C-ATV-1 was tested in a healthy rat using micro PET/CT and a gamma-counter. 11C-ATV-1 accumulated predominantly in the liver, which might be explained by its hydrophobicity. Almost no uptake was seen in the kidneys. Conclusion: The ability of 11C-ATV-1 to image angiogenesis processes involving up-regulation of TIE2 and VEGFR-2 receptors need to be further evaluated in-vivo. High uptake of 11C-ATV-1 in the liver would restrict its usefulness as an imaging agent in close proximity to the liver.

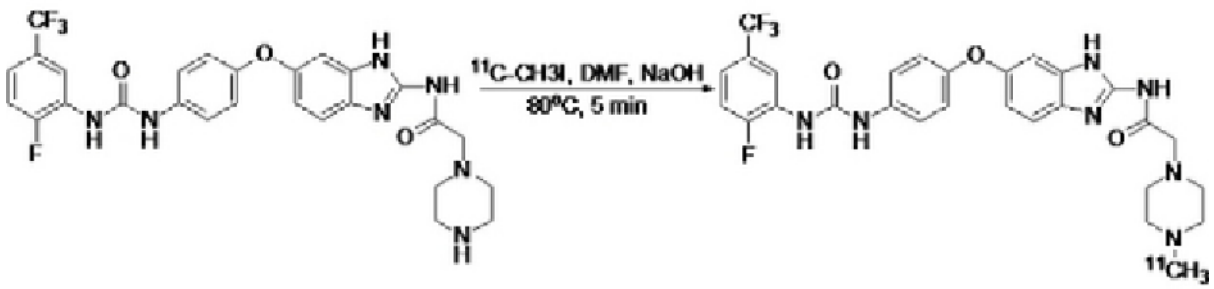


Radiosynthesis of 11C-ATV-1

Disclosure of author financial interest or relationships:
**S. Dissoki**, None; **G. Abourbeh**, None; **E. Mishani**, None; **O. Jacobson Weiss**, None.

Presentation Number **P225**
Poster Session 2
September 6, 2012 / 15:15-15:15 / Room: The Liffey

# In vivo evaluations and microPET studies of $^{18}$F-labeled phosphonium cations for developing novel myocardial imaging agents

***Dong-Yeon Kim***[1,2], *Hyeon Sik Kim*[1], *Hee-Seung Bom*[1], *Ho-Chun Song*[1], *Jung-Joon Min*[1], [1]*Nuclear Medicine, Chonnam National University Medical School, Gwangju, Republic of Korea;* [2]*Chemistry, Dongguk University-seoul, Seoul, Republic of Korea. Contact e-mail: blueburr@gmail.com*

Objectives: Despite substantial advances in the diagnosis and treatment of cardiovascular diseases, there are a few radiopharmaceuticals for diagnosis of ischemic heart diseases (IHD) using PET. Thus, four kinds of $^{18}$F-labeled tetraphenylphosphonium cation derivatives ($^{18}$F-TPPs) were synthesized with different carbon chain lengths and functional groups that accumulated in cardiomyocytes depending on mitochondrial membrane potential. Here, we evaluated the performance of each $^{18}$F-TPPs as novel myocardial imaging agents. Methods: $^{18}$F-(5-Fluoropentyl)triphenylphosphonium cation ($^{18}$F-FPTP), $^{18}$F-(6-fluorohexyl)triphenylphosphonium cation ($^{18}$F-FHTP), $^{18}$F-(2-(2-fluoroethoxy)ethyl)triphenylphosphonium cation ($^{18}$F-FETP), $^{18}$F-(2-(2-fluoroethoxy)ethyl)tris(4-methoxyphenyl)phosphonium cation ($^{18}$F-FETMP) were synthesized via two-step nucleophilic substitution reactions. To confirm the activity of $^{18}$F-TPPs in vivo, biodistribution was assessed in BALB/c mice at 10, 30, 60, and 120 min after i.v. injection of 7.4 MBq of each radiotracer. A dedicated microPET/CT scanner was used for in vivo imaging of radiotracer kinetics. Results: The heart-to-blood ratio of $^{18}$F-FPTP, $^{18}$F-FHTP, $^{18}$F-FETP, $^{18}$F-FETMP was approximately 50, 30, 55 and 34 at 10 min respectively, indicating rapid clearance of each compound from the blood. The heart-to-lung, heart-to-liver ratios of $^{18}$F-FPTP, $^{18}$F-FHTP, $^{18}$F-FETP, $^{18}$F-FETMP were > 4, > 3, > 4, > 2 and > 3, > 4, > 11, > 2 respectively at 10 min after radiotracer injection indicating that $^{18}$F-TPPs are optimal as a cardiac imaging agents. Conclusions: $^{18}$F-TPPs showed stable uptake in the myocardium and rapid clearance from other organs, and enabled an excellent image quality. $^{18}$F-TPP derivatives might have a potential to be utilized as a novel myocardial agent for PET and be useful for clinical cardiac PET/CT applications.

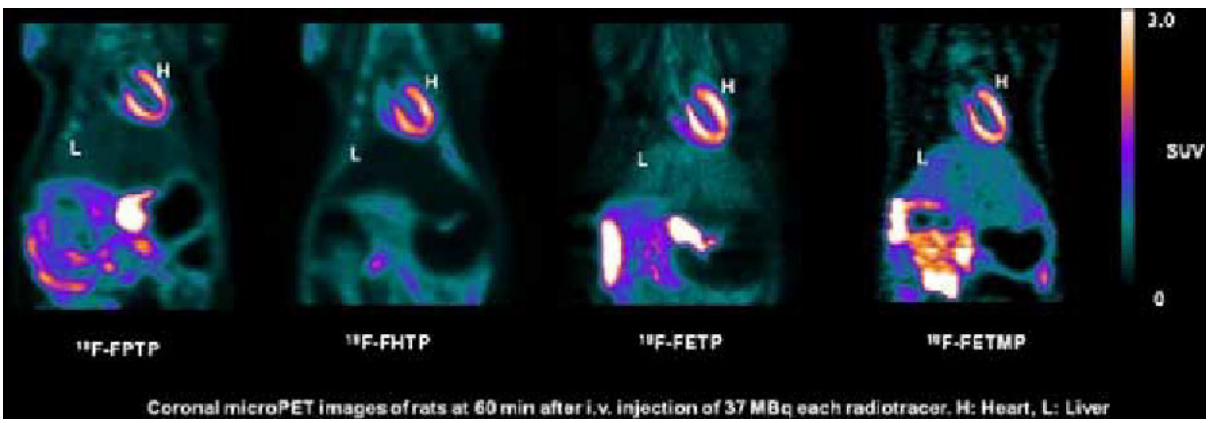

Coronal microPET images of rats at 60 min after i.v. injection of 37 MBq each radiotracer. H: Heart, L: Liver

Disclosure of author financial interest or relationships:
**D. Kim**, None; **H. Kim**, None; **H. Bom**, None; **H. Song**, None; **J. Min**, None.

Presentation Number **P226**
Poster Session 2
September 6, 2012 / 15:15-15:15 / Room: The Liffey

# Comparison of PET myocardial imaging between[F-18]FPTP and [N-13]NH3

***Hyeon Sik Kim**, Dong-Yeon Kim, Park Hyeong Ju, Byeong-il Lee, Misun Yun, Yoon Soon Moon, Hee-Seung Bom, Jung-Joon Min, nuclear medicine, Chonnam National University Hwasun Hospital, Hwasun, Jeonnam, Republic of Korea. Contact e-mail: knkc1120@nate.com*

Introduction:Positron emission tomography(PET) has several technical advantages over SPECT. However, the short half-life of currently used PETcardiac tracers limit the widespread clinical use of PET due to the needfor a nearby cyclotron or generator. [18F]-labeled tracers would avoid this limitation and facilitateclinical protocols. To address this need, we developed [18F]-labeled phosphoniumcation, 5-([F-18]fluoropentyl)triphenylphosphonium salt ([F-18]FPTP) and compared the characteristics of microPET images with that using [13N]-ammonia in rat myocardial infarction model. Methods: We estimated time-activity curve and contrast-ratio (myocardium/blood, myocardium/liver and myocardium/lung) of [N -13]NH3 and [F-18]FPTP images in normal rats (n = 3). AmmoniaPET study was performed after injection of [N-13]NH3(37MBq) 3 days after generation of MI in rats. [F-18]FPTP PET study was performed using the same animal next day. MicroPET images were acquired for 30 min after injection of radiotracer. We estimated the correlation ofmyocardial perfusion imaging between [N-13]NH3 and [F-18]FPTPin 17 segments of polar map. Result: [F-18]FPTPrevealed excellent retention in myocardium and rapid washout from the liver and lung, while[N-13]NH3revealed relatively lower accumulation in the heart and slow washout from the liver. In rat MI models, both tracers showed well-delineated perfusion defect in the anterolateral wall of the left ventricle. The location and size of perfusion defect of both tracers showed high correlation ($r = 0.86$, $P < 0.0001$). The average image contrast of [F-18]FPTP revealed higher than that of [N-13]NH3(0.60 vs. 0.35 ). Conclusion: [F-18]FPTPcardiac microPET imaging provides excellent image quality and uptake properties than [N-13]NH3in rats. The long half-life of [F-18] renders this tracer useful for clinicalPET/CT applications in the workup of patients with suspected or proven coronary artery disease.

Disclosure of author financial interest or relationships:
**H. Kim**, None; **D. Kim**, None; **P. Hyeong Ju**, None; **B. Lee**, None; **M. Yun**, None; **Y. Moon**, None; **H. Bom**, None; **J. Min**, None.

Presentation Number **P227**
Poster Session 2
September 6, 2012 / 15:15-15:15 / Room: The Liffey

# Synthesis and radiopharmacological evaluation of an 18F-labelled norbornene derivative for rapid copper-free click chemistry reactions

***James C. Knight**, Melinda Wuest, Jenilee Way, Frank Wuest, Oncology, University of Alberta, Edmonton, AB, Canada. Contact e-mail: jknight@ualberta.ca*

**Aim:** Click chemistry reactions are characterized by their speed, reliability, high yields and selectivity. Due to these characteristics, bioorthogonal click chemistry reactions which proceed without the presence of a copper catalyst could feasibly be applied *in vivo* to facilitate a pretargeting approach for imaging tumours by PET. In pursuit of this goal, we have developed a rapid, high-yielding, and reliable synthetic procedure towards a novel 18F-labelled compound (**[18F]NFB**). This compound contains a ring-strained norbornene species which undergoes an inverse electron demand Diels-Alder click reaction with tetrazines. To assess its suitability as a diagnostic probe we have evaluated its behaviour in non-tumour-bearing mice. Furthermore, we have also assessed the ability of **[18F]NFB** to undergo rapid click chemistry reactions with a tetrazine species in biological media. **Materials and Methods:** 2-[(1S,2S,4S)-Bicyclo[2.2.1]hept-5-en-2-yl]ethanamine was reacted with N-succinimidyl-4-[18F]fluorobenzoate (**[18F]SFB**) in acetonitrile for 20 min at room temperature to give **[18F]NFB**. This radiotracer was then evaluated in terms of its biodistribution (mean ± SD), blood clearance kinetics, and metabolic stability in non-tumour-bearing BALB/C mice. The ability of **[18F]NFB** to undergo copper-free click reactions with a tetrazine species was assessed via radio-TLC in acetonitrile, phosphate buffered saline, fetal bovine serum and blood. The reaction kinetics were also evaluated by measuring the characteristic tetrazine absorption over the course of the reaction. **Results:** We have determined that **[18F]NFB** exhibits high metabolic stability with ~90% remaining intact up to 30 minutes following administration. This compound also exhibits rapid blood clearance ($t_{1/2}$ = 69s). Furthermore, we have determined that **[18F]NFB** undergoes rapid and high-yielding click chemistry reactions with a tetrazine derivative in biological media. **Conclusion:** The present study showed that the 18F-labelled compound **[18F]NFB** is suitable for molecular imaging and is capable of undergoing rapid and selective copper-free click chemistry reactions in biological media. These properties indicate that **[18F]NFB** could potentially be used to facilitate a pretargeting approach for imaging tumours by PET.

Disclosure of author financial interest or relationships:
**J.C. Knight**, None; **M. Wuest**, None; **J. Way**, None; **F. Wuest**, None.

Presentation Number **P228**
Poster Session 2
September 6, 2012 / 15:15-15:15 / Room: The Liffey

# Introduction of a New N2S2-type Galactopyranoside Derivative OCTAM-ah-GalNAc for Liver Imaging

***Tsai-Yueh Luo***[1,2], *Show-Wen Liu*[1], *Bor-Ching Cheng*[1], *Lie-Hang Shen*[1], [1]*Institute of nuclear energy research, Taoyuan, Taiwan;* [2]*Central Taiwan University of Science and Technology, Taichung, Taiwan. Contact e-mail: tylo@iner.gov.tw*

Introduction. The asialoglycoprotein receptor (ASGPR) located on the hepatocyte cell surface is specific for galactose-terminated ligands and correlated with liver damage. In this study, a new galactopyranoside derivative, 6-[3',6'-Diaza-5'-oxo-3'- (2''-triphenylmethyl thioethyl)-8'- triphenylmethylthio]octanamidohexyl β-N-acetylgalactosamine (OCTAM-ah-GalNAc), was synthesized and evaluated for its potential use in nuclear medicine. Methods. The synthetic procedure of OCTAM-ah-GalNAc was divided into three parts: (A) synthesis of the N2S2 moiety, (B) synthesis of ah-GalNAc4 and (C) synthesis of OCTAM-ah-GalNAc. The affinity of OCTAM-ah-GalNAc for ASGPR in liver cells was assessed by competitive binding analysis. In vivo experiments in a rat model bearing N1S1 liver cancer were performed to evaluate the efficacy of 188Re-OCTAM-ah-GalNAc for liver functional tests. Results. OCTAM-ah-GalNAc has three important characteristics: (1) high affinity for ASGPR via GalNAc; (2) suitability for 99m Tc or 188Re binding via the N2S2 core; and (3) chemical stability via its bifunctional ligand with thiol-protective CPh3 group . OCTAM-ah-GalNAc had a greater inhibitory effect on anti-ASGPR antibody binding (84.39 ± 11.56%) than the other two galactose derivatives, 4-aminophenyl beta-D-Galactopyranoside and lactobionic acid. The radiochemical purity of 188Re-OCTAM-ah-GalNAc was greater than 90 %. Uptake of 188Re-OCTAM-ah-GalNAc by the liver of normal rats was greater than that of N1S1 hepatoma rats. Conclusions. OCTAM-ah-GalNAc has favorable steric binding affinity to ASGPR. Our data indicate that labeling of OCTAM-ah-GalNAc with isotopes may have potential as a functional imaging agent for liver cells.

Disclosure of author financial interest or relationships:
**T. Luo**, None; **S. Liu**, None; **B. Cheng**, None; **L. Shen**, None.

Presentation Number **P229**
Poster Session 2
September 6, 2012 / 15:15-15:15 / Room: The Liffey

# Microreactor with Phase-change Microvalves for High-pressure Batch Synthesis of Radiotracers

***Xiaoxiao Ma***[1,2], *Wei-Yu Tseng*[1,2], *Mark Eddings*[1,2], *R. Michael van Dam*[1,2], [1]*Crump Institute for Molecular Imaging, UCLA, Los Angeles, CA, USA;* [2]*Molecular and Medical Pharmacology, UCLA, Los Angeles, CA, USA. Contact e-mail: helenxxma@gmail.com*

OBJECTIVE: Batch microfluidic devices offer many advantages for PET radiotracer synthesis. While a number of different platforms have been reported mainly using 2-[18F]fluoro-2-deoxy-D-glucose ([18F]FDG) as a model compound, most have inherent limitations in material or structure that would preclude the use of high temperature and pressure that would be required for syntheses of some other radiotracers such as [1-(2'-deoxy-2'-[18F]fluoroarabinofuranosyl)cytosine ([18F]FAC)[1]. While flow reactors are capable of sustaining high pressures, performing radiosyntheses in the smaller volumes that can be achieved with microscale batch reactors has important benefits such as conserving expensive/scarce reagents and improving specific activity [2]. METHODS: We report here a tubing microreactor with phase-change valves that can perform batch synthesis (several μL) under more demanding reaction conditions. Phase-change valves3 are the only practical type of microvalve reported to sustain the anticipated high pressures needed to synthesize [18F]FAC. Valves are closed by solidifying a phase-change material (e.g. water or molten wax) that obstructs the channel. Here we adapt this approach using dimethyl sulfoxide (DMSO) as the phase-change material due to its high freezing point (19°C) and compatibility with radiochemistry. We mounted a tubing reactor (1m long 0.012"ID) on a custom-built fixture that cools (using a Peltier device) liquid in the two ends of the tubing to act as valves and heats the liquid in the remainder of the tubing (Fig.1A). The tubing is coiled such that most of its length is in contact with the heater. In this setup, valves were found to close within 3s and withstand >140 psig pressure. As a proof-of-concept, we performed the fluorination step of [18F]FAC synthesis which is typically performed in acetonitrile (MeCN) at 165°C, generating 121 psig vapor pressure (Fig.1B). The premixed solution of precursor and dried [18F]fluoride in MeCN was loaded into the tubing reactor flanked by plugs of DMSO using a syringe pump. The cooler was activated to freeze the DMSO, followed by heating of the rest of the tubing to perform the fluorination at 165°C for 15 min. After cooling, the DMSO plugs were melted, and the DMSO and fluorination product were pumped out by the syringe pump and collected in separate tubes for analysis. RESULTS: Radio-TLC analysis of the crude product showed the conversion efficiency in this non-optimized study to be 67±3% (n=3) (Fig.1C). Because some volume in the tubing near the cooler is unheated, we estimate the conversion efficiency in the heated portion is slightly higher, close to what is routinely obtained with a conventional radiosynthesizer. CONCLUSIONS: We have demonstrated that radiochemical reactions at high temperatures and pressures can be performed inside a tubing batch microreactor with phase-change valves. Future efforts will focus on optimization of the microreactor design and reaction conditions. Because phase-change valves can be implemented in a variety of geometries and materials, it may be possible to develop a disposable microfluidic chip/kit for radiotracer synthesis based on this approach.

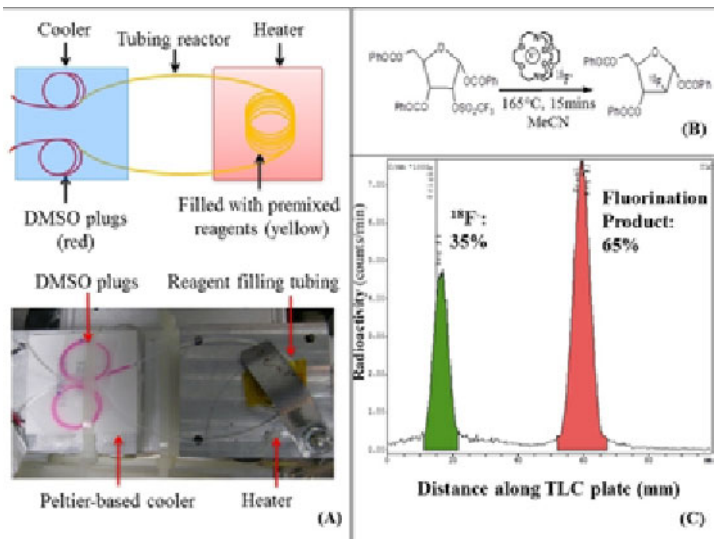


Fig. 1: (A) Schematic (top) and photograph (bottom) of tubing reactor. (B) Scheme for fluorination reaction of [18F]FAC synthesis. (C) Radio-TLC chromatogram of fluorination product from tubing microreactor.

Disclosure of author financial interest or relationships:
**X. Ma**, None; **W. Tseng**, None; **M. Eddings**, None; **R. van Dam**, Sofie Biosciences, Inc., Consultant; Sofie Biosciences, Inc., Stockholder .

Presentation Number **P230**
Poster Session 2
September 6, 2012 / 15:15-15:15 / Room: The Liffey

# High potential of 99mTc-NTP 15-5 as a SPECT radiotracer for cartilage pathologies in human

***Elisabeth Miot-Noirault***[1], *Florent Cachin*[1,3], *Aurélien Vidal*[1], *François Gouin*[2], *Stéphane Boisgard*[1,4], *Philippe Auzeloux*[1], *Marc Filaire*[3], *Caroline Peyrode*[1], *Dominique Heymann*[2], *Françoise Redini*[2], *Jean-Michel Chezal*[1], [1]*UMR 990 INSERM, Clermont-Ferrand, France;* [2]*UMR S 957, Nantes, France;* [3]*Jean Perrin Center, Clermont Ferrand, France;* [4]*Gabriel Montpied Hospital, Clermont Ferrand, France. Contact e-mail: elisabeth.noirault@inserm.fr*

Background: Our group develops 99mTc-N-(triethylammonium)-3- propyl-[15]ane-N5 (99mTc-NTP 15-5), which binds to proteoglycans (PG) in cartilage. Potential clinical applications include the assessment of degenerative, and malignant cartilage diseases. Methods: We have assessed 99mTc-NTP 15-5 radiotracer in: (i) healthy animals, (ii) animals developing osteoarthritis, and (iii) animals with primary and recurrent grade II orthotopic chondrosarcoma. Considering pathological models, 99mTc-NTP 15-5 imaging was performed at regular intervals after pathology induction and tracer uptake followed as a function of time. The potential of the radiotracer to bind to human articular cartilage was also evaluated after ex vivo incubation with osteoarthritic knee parts and large knee specimens, and compared to. results obtained with 99mTc-HMDP bone radiotracer. Results: In healthy animals, a high and specific accumulation of 99mTc-NTP 15-5 was observed in cartilage (about 5.5 +/- 1.7 % of ID/g of tissue at 15 min after iv injection), with a highly contrasted joint imaging. In the meniscectomized guinea pig model of osteoarthritis, 99mTc-NTP 15-5 imaging allowed in vivo the assessment of PG changes associated to both the hypertrophic and decompensation responses of degenerative cartilage. In the orthotopic swarm rat chondrosarcoma models (both the primary growth and recurrent models) a significant uptake of the tracer was evidenced at the tumoural site at very early stage, and strongly correlated with tumoural growth. It should be mentionned that 99mTc-HMDP imaging was negative during the whole study, even at the later stage of tumoural development or recurrence. Ex vivo incubation with human specimens evidenced cartilage to cortical bone uptake ratios about 3.90± 2.35 and 0.76±0.24, respectively, for 99mTc-NTP 15-5 and 99mTc-HMDP. Visual analysis of fused SPECT/ CT slices confirmed selective, intense 99mTc-NTP 15-5 accumulation in articular cartilage, whereas 99mTc-HMDP binding was low. Furthermore cartilage defect visualized on CT was clearly associated with focal decreased uptake of 99mTc-NTP 15-5. Conclusions: 99mTc-NTP 15-5 has the potential to be the first and only radiopharmaceutical able to provide in vivo a specific diagnosis and staging of cartilage diseases in human and prompt us to initiate clinical transfert. Grants: Ligue Contre Le Cancer ; Fondation pour la recherche Medicale ; Regional Innovation fund OSEO This work was conducted in close collaboration with Cyclopharma Laboratoires (Pr S. Askienazy)

Disclosure of author financial interest or relationships:
**E. Miot-Noirault**, None; **F. Cachin**, None; **A. Vidal**, None; **F. Gouin**, None; **S. Boisgard**, None; **P. Auzeloux**, None; **M. Filaire**, None; **C. Peyrode**, None; **D. Heymann**, None; **F. Redini**, None; **J. Chezal**, None.

Presentation Number **P231**
Poster Session 2
September 6, 2012 / 15:15-15:15 / Room: The Liffey

# A Fully Automated one Pot Synthesis of 2‘-Deoxy-2‘-[$^{18}$F]fluoro-9-β-D-Arabino-furanosylguanine [$^{18}$F]F-AraG: A Novel PET Imaging T Cell Activation Agent

***Mohammad Namavari**, Sanjiv S. Gambhir, Radiology, Stanford University, Stanford, CA, USA. Contact e-mail: namavari@stanford.edu*

**Purpose:** 9-(β-D-Arabinofuranosyl)guanine (AraG) is a guanosine analog that has been used in the treatment of T cell lymphoblastic disease. It is able to target the intracellular enzyme dCK and dGK. We have been developing strategies to radiolabel AraG with $^{18}$F for PET imaging of T cell activation. A fully automated one-pot synthesis of a radiofluorinated AraG, 2‘-deoxy-2‘-[$^{18}$F]fluoro-9-β-D-arabinofuranosylguanine ([$^{18}$F]F-AraG) as an imaging agent has now been developed and is detailed here. **Procedure:** The one-pot radiosynthesis involves a direct radiofluorination of 2-N-acetyl-6-O-((4-nitrophenyl)ethyl)-9-(3‘,5‘-di-O-trityl-2‘-O-trifyl-β-D-ribofuranosyl)guanine (**1**) with [$^{18}$F]fluoride to form 2-N-acetyl-6-O-((4-nitrophenyl)ethyl)-9-(3‘,5‘-di-O-trityl-2‘-[$^{18}$F]fluoro-β-D-arabino-furanosyl)guanine (**2**). Hydrolysis of the protecting groups in **2** first with 0.5N $NaOCH_3$ and then with 1N HCl, yielded [$^{18}$F]F-AraG. A complete automated one-pot synthesis of [$^{18}$F]F-AraG was performed in the GE TRACER lab FX-FN synthesis module . **Results:** A reliable and automated synthesis of [$^{18}$F]F-AraG has been accomplished. The radiochemical yield was 3-5 % (decay corrected) with a specific activity of 1.5-1.8 Ci/μmol. Our cell uptake studies indicated that T cells activated with 50 nM PMA and 1 ug/mL ionomycine took up 4.7-fold more (p=0.003) [$^{18}$F]F-AraG than control cells. **Conclusion:** Clinically grade [$^{18}$F]F-AraG has been successfully synthesized by a direct fluorination of an appropriate precursor of a guanosine nucleoside in an automated synthesis module. This tracer also shows promising uptake in activated T cells as compared to control cells. Further PET imaging studies in small animals are planed.

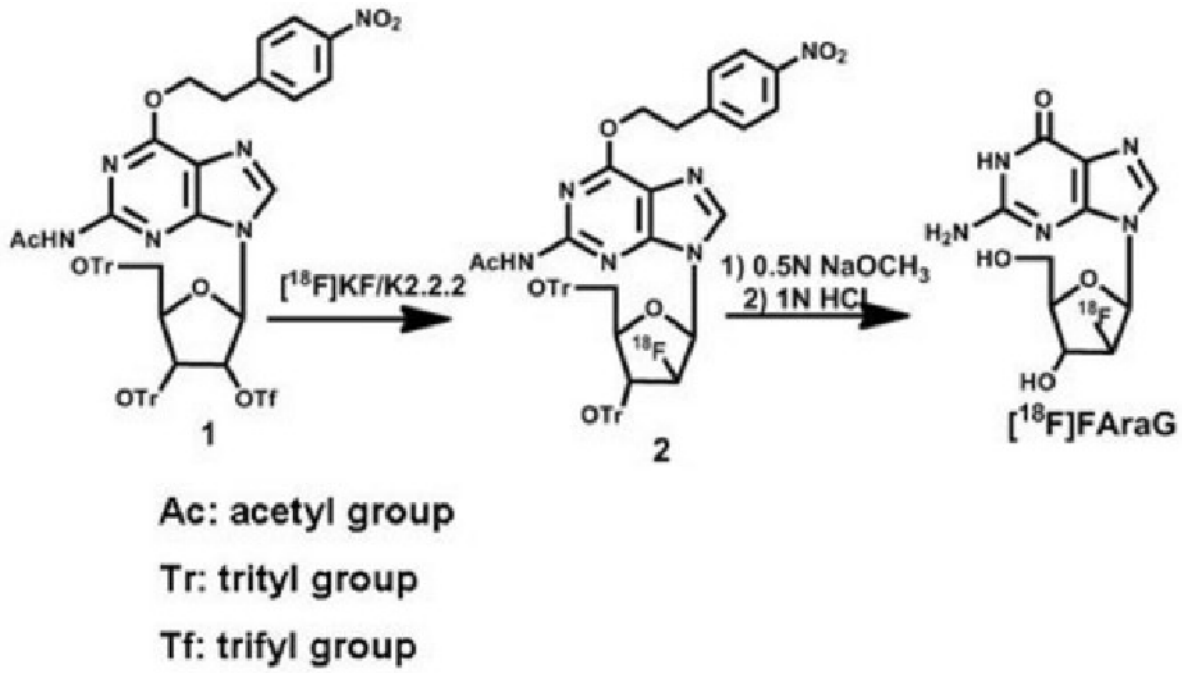


Schematic synthesis of [$^{18}$F]FAraG

Disclosure of author financial interest or relationships:
**M. Namavari**, None; **S.S. Gambhir**, General Electric, Grant/research support; Bayer-Schering, Grant/research support; Sanofi-Aventis, Grant/research support; CellSight, Stockholder; ImaginAB, Stockholder; Enlight, Stockholder; Endra, Stockholder; Bracco, Consultant; NinePoint Medical, Stockholder; Visualsonics, Consultant .

Presentation Number **P232**
Poster Session 2
September 6, 2012 / 15:15-15:15 / Room: The Liffey

# *In Vivo* Imaging of Blood-brain Barrier Permeability with 2-Amino-[3-$^{11}$C]isobutyric Acid by Positron Emission Tomography

***Maki Okada***[1], *Atsushi B. Tsuji*[1], *Tatsuya Kikuchi*[1], *Hidekatsu Wakizaka*[1], *Toshimitsu Okamura*[1], *Ming-Rong Zhang*[1], *Toshimitsu Fukumura*[1], *Koichi Kato*[1,2], [1]*Molecular Probe Program, National Institute of Ragiological Science, Chiba, Japan;* [2]*Department of Integrative Brain Imaging, National Center of Neurology and Psychiatry, Kodaira, Japan. Contact e-mail: mokada@nirs.go.jp*

The blood-brain barrier (BBB) prevents the various substances from entering into brain. This robust protecting system restricts the passage of cerebral therapeutic agents. Thus the operation of BBB system is widely being developed to achieve the effective delivery of the various agents. Furthermore, the abnormalities of the BBB function associated with neurological disorders are well-known. The *in vivo* imaging of individual BBB permeability by positron emission tomography (PET) is desired for monitoring the operation of BBB system and for understanding the relationships between BBB function and neurological disorders. 2-Aminoisobutyric acid (AIB) is an unnatural amino acid which is carried mainly by the system-A amino acid transporter. Since this transporter does not exist in the luminal membrane of the BBB, AIB hardly penetrates BBB. Once AIB passes through the BBB, it is rapidly taken into brain cells. These biological characters suggest the AIB labeled with $^{11}$C will be a suitable probe for evaluating BBB permeability. In this study, we verified the feasibility of 2-amino-[3-$^{11}$C]isobutyric acid ([3-$^{11}$C]AIB) as a probe for imaging the BBB permeability with small animal PET. The rats were injected the BBB disruption agent (lipopolysaccharide and others) in the right striatum and PBS was injected in the left striatum as a control. The small animal PET was conducted for 60 min. To confirm the accordance of the [3-$^{11}$C]AIB accumulated region and the BBB leakage region, the accumulated region of [3-$^{11}$C]AIB was compared to that of the traditional BBB leakage markers, [$^{14}$C]sucrose and Evans blue. For the rigorous evaluation, [3-$^{11}$C]AIB, [$^{14}$C]sucrose and Evans blue were simultaneously injected to a same rat, and the accumulation of each compound was measured with the *ex vivo* double tracer autoradiography (for [3-$^{11}$C]AIB and [$^{14}$C]sucrose) and fluorescence detection (for Evans blue) in the same brain slice. The *in vivo* metabolic stability of [3-$^{11}$C]AIB was assessed by the analysis of radiolabeled substances in the rat plasma and brain with a HPLC equipped with a radio detector. In the PET study, [3-$^{11}$C]AIB clearly visualized the BBB lesion site, and the [3-$^{11}$C]AIB accumulation gradually increased with time in both lesion and control sides. However [3-$^{11}$C]AIB uptake in the BBB lesion side was significantly higher than in the control side, and this difference was detected in the earlier phase (from 5 min after injection of [3-$^{11}$C]AIB). *Ex vivo* brain slice study showed [3-$^{11}$C]AIB well co-localized with [$^{14}$C]sucrose and Evans blue, indicating that [3-$^{11}$C]AIB accumulated in the BBB leakage region. However, the signal to noise ratio of [$^{14}$C]sucrose was lesser than that of [3-$^{11}$C]AIB and the Evans blue method had poor-reproducibility. Any metabolites were not detected in the rat plasma and brain up to 60 min after administration, indicating that [3-$^{11}$C]AIB was highly stable *in vivo*. In conclusion, these results suggest that [3-$^{11}$C]AIB PET is a promising sensitive *in vivo* imaging method for assessing BBB permeability. This method could be usable for monitoring the operation of BBB system, resulting in the improvement of the strategy of cerebral drug delivery.

Disclosure of author financial interest or relationships:
**M. Okada**, None; **A.B. Tsuji**, None; **T. Kikuchi**, None; **H. Wakizaka**, None; **T. Okamura**, None; **M. Zhang**, None; **T. Fukumura**, None; **K. Kato**, None.

Presentation Number **P233**
Poster Session 2
September 6, 2012 / 15:15-15:15 / Room: The Liffey

# Radiosynthesizer software applied to mobile devices for the rapid communication of PET probe synthesis outcomes

***Kevin Quinn***[1], *Shane Claggett*[1], *Mark Lazari*[1,2], *Jeff Esterby*[3], *Melissa Esterby*[3], *R. Michael van Dam*[1,2], [1]*Crump Institute for Molecular Imaging, Department of Molecular & Medical Pharmacology, UCLA, Los Angeles, CA, USA;* [2]*Biomedical Engineering Interdepartmental Program, UCLA, Los Angeles, CA, USA;* [3]*Sofie Biosciences, Culver City, CA, USA. Contact e-mail: KQuinn@mednet.ucla.edu*

**Objective:** PET imaging is dependent upon the timely production of short-lived (e.g. [18F]fluoride ~110min half-life) radioactive probes. The isotope is first produced in a cyclotron, then delivered to a radiochemistry facility where it is incorporated into a chemical synthesis before undergoing quality control and transport to the site of use for administration. Depending on the length of the synthesis, this process can take anywhere from ~2hrs ([18F]Fluorodeoxyglucose, [18F]FDG) to a half-day (1-(2′-deoxy-2′-[18F]fluoroarabinofuranosyl)cytosine, [18F]FAC). Rapid communication between the radiochemist and the users in the lab or clinic are essential for the uninterrupted operation of imaging centers, where patient retention, especially for clinical trials, can be difficult when unplanned complications in probe production occur. Most radiopharmacies rely on informal correspondence via email or phone to alert synthesis completion times, yields, and delays. This can introduce time lags, which can have substantial effects on imaging studies. Previously, we developed ELIXYS, a cassette-based radiosynthesizer with a flexible and intuitive interface for PET probe development, optimization, and routine production. Here, we present an enhancement of the client-server software to show the status of the synthesis from any location, allowing researchers and physicians automatic, real-time updates about key events that may affect scheduling. **Method:** We created a downloadable application (app) for iPhone and Android smartphones that enables radiochemists, researchers, and clinicians to view the current details of the synthesis from any location. The app, which requires a security login, allows for multiple levels of reporting from high-level synthesis times and yields to a more detailed look on a unit-operation basis. For routine production with minimal intervention, radiochemists can utilize the app to monitor synthesis progress away from the hot cell, while clinicians and researchers can track problems and yields to appropriately queue animals and patients. Additionally, the ELIXYS server can be configured to send email and text messages to the users to alert them of key events such as completion, failures, and yields. **Results:** The app was successfully implemented on the system at our UCLA test site, simplifying the radiochemistry reporting process to downstream researchers. **Conclusion:** The addition of a smartphone application and customizable messaging to the ELIXYS platform provides freedom and streamlining to the synthesis of PET probes.

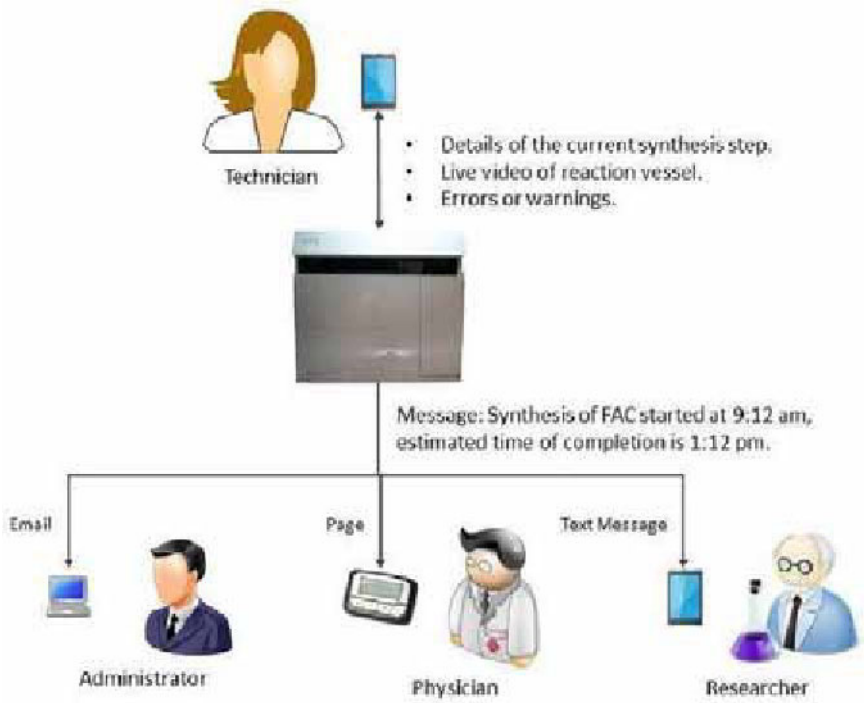


Disclosure of author financial interest or relationships:
**K. Quinn**, Sofie Biosciences, Consultant; **S. Claggett**, Sofie Biosciences, Consultant; **M. Lazari**, None; **J. Esterby**, Sofie Biosciences, Consultant; **M. Esterby**, Sofie Biosciences, Inc., Employment; Sofie Biosciences, Inc., Stockholder; **R. van Dam**, Sofie Biosciences, Inc., Consultant; Sofie Biosciences, Inc., Stockholder .

Presentation Number **P234**
Poster Session 2
September 6, 2012 / 15:15-15:15 / Room: The Liffey

# Synthesis and evaluation of oleanolic acid conjugated lactoferrin for plaque imaging

*Sung-Min Kim, Il-ha Jeong, Min Su Lim, Chulhyun Lee,* ***Eun Kyoung Ryu****, Korea Basic Science Institute, Chungbuk, Republic of Korea. Contact e-mail: ekryu@kbsi.re.kr*

Alzheimer's disease (AD) is a neurodegenerative disorder and leading dementia. Aβ-amyloid is one of the pathological hallmarks for early detection of AD. Oleanolic acid (OA), a pentacyclic triterperioid found in a variety of plant species, has been recently reported that it has therapeutic effect in preventing the progression of AD. For desirable drugs or diagnosis agents for AD, they need to penetrate the brain-blood barrier (BBB). Lactoferrin (Lf) receptor has been demonstrated existing on the BBB in various species and involved in Lf transport across the BBB in vitro and in vivo. Therefore, in this study we synthesized and evaluated a novel radioligand with conjugated OA and Lf for diagnosis of AD. OA conjugated lactoferrin (OA-Lf) was prepared from two steps; In order to conjugate OA and Lf, we used ethylenamine linkage between OA and Lf. The radiolabeled OA-Lf was prepared from iodogen method with 123I. In vitro study, the conjugated compound was disaggregated to Aβ(1-42) aggregates for 24 h incubation. Initial brain uptake of 123I-OA-lactoferrin within 2 min was %ID/g and showed higher brain uptake than that of 123I-lactoferrin. Therefore, this data suggest that OA-Lf effectively block aggregation and fibril formation in vitro, and radiolabeled OA-Lf appears as a potential radioligand for Aβ-amyloid imaging.

Disclosure of author financial interest or relationships:
**S. Kim**, None; **I. Jeong**, None; **M. Lim**, None; **C. Lee**, None; **E. Ryu**, None.

Presentation Number **P235**
Poster Session 2
September 6, 2012 / 15:15-15:15 / Room: The Liffey

# Reusable electrochemical cell for rapid microfluidic human dose synthesis of 18F-labeled radiotracers

***Saman Sadeghi***[1], *Vincent Liang*[1], *Suh Y. Woo*[1], *Curtis Wu*[1], *R. Michael van Dam*[1,2], [1]*MOLECULAR AND MEDICAL PHARMACOLOGY, UCLA, LOS ANGELES, CA, USA;* [2]*Biomedical Engineering Interdepartmental Program, UCLA, Los Angeles, CA, USA. Contact e-mail: samsadeghi@mednet.ucla.edu*

Chemical reactions such as radiofluorination and deprotection have been observed to proceed with remarkable speed within flow-through microfluidic devices, promising ultra-fast production of short-lived tracers for positron emission tomography (PET). Flow-through systems capable of nearly every process in multi-step syntheses have been reported and even reached the commercial marketplace, but conventional vial-based modules are still used to remove water from [18F]fluoride and perform other solvent-exchange processes. The combination of conventional and microfluidic elements often makes the overall systems more complex than their conventional counterparts. An alternative drying method based on solvent-exchange within an electrochemical cell with glassy carbon anode electrode has reported [1]. We had previously described an improvement in reliability and reusability by changing to a metal anode and had used a simple platform to synthesize low doses of Tetraacetylated [18F]Fluoro-glucose ([18F]FTAG), an intermediate of 2-Deoxy-2-[18F]Fluoro-d-glucose ([18F]FDG) [2]. Further electrode characterization and integration with a flow-through synthesizer, as reported here, enabled fully automated synthesis (using electrical feedback information from the cell to control timing of each step) of up to 50mCi of [18F]FDG. XPS studies revealed that the performance of the device depends strongly on the particular choice of anode material, and is hypothesized to be related to surface oxides, depth of intercalation and the nature of chemical bonds formed on the surface during the electrochemical process. Surface characterization results were used to gain a better understanding of the adsorption process and aid the selection of highest efficiency electrode material. The highest trapping efficiency was observed on a brass electrode at room temperature with 20V DC potential, where at 93±2% (n=41) of the [18F]fluoride was separated on the anode in less than 30 seconds from 1mL of water. The same flow cell was used in multiple experiments, and [18F]FDG was synthesized from the resulting anhydrous [18F]fluoride with decay corrected radiochemical yield > 40% for multi-human doses [10-50mCi] in under 15 minutes overall synthesis time. Linking the microfluidic cell and the flow-through synthesizer eliminated the process of moving dried [18F]fluoride from one compartment to another, which can cause noticeable radioactivity losses during transit between the solvent exchange and reaction vessel, especially when very small volumes are involved. Reliable trapping and release of [18F]fluoride in an electrochemical micro flow cell consisting of a brass anode and platinum plated cathode, and integration with the synthesizer described here, can potentially be extended to produce a wide variety of radiotracers in sufficient quantities to meet clinical demands. The flow-through design can also lend itself to easy integration with existing quality control methods for a complete bench-top clinical radiotracer synthesis platform. References: [1] H. Saiki, et. al., Appl Radiat Isot, vol. 68, pp. 1703-1708, 2010 [2] S. Sadeghi, et. al., J Nucl Med. 2011; 52 (Supplement 1):286

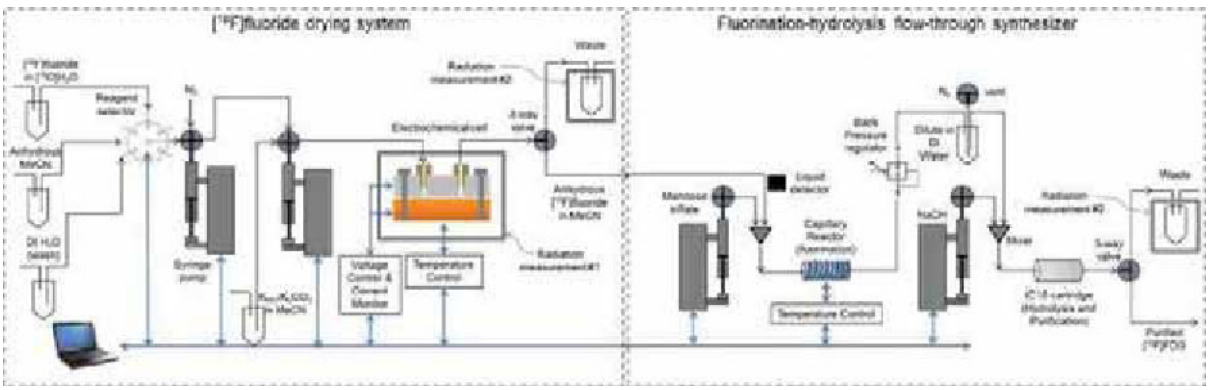

Schematic of control and measurement system for electrochemical flow cell (left) and flow-through radiosynthesizer (right).

Disclosure of author financial interest or relationships:
**S. Sadeghi**, None; **V. Liang**, None; **S.Y. Woo**, None; **C. Wu**, None; **R. van Dam**, Sofie Biosciences, Inc., Consultant; Sofie Biosciences, Inc., Stockholder .

Presentation Number **P236**
Poster Session 2
September 6, 2012 / 15:15-15:15 / Room: The Liffey

# L-Oligonucleotides as versatile complementary radionuclide transporters for molecular imaging of pretargeted tumour tissue

***Maik Schubert***[1], *Christian Förster*[1], *Ralf K. Bergmann*[1], *Stefan Vonhoff*[2], *Sven Klussmann*[2], *Martin Walther*[1], *Jens Pietzsch*[1], *Hans-Jürgen Pietzsch*[1], *Joerg Steinbach*[1], [1]*Helmholtz-Zentrum Dresden-Rossendorf, Dresden, Germany;* [2]*NOXXON Pharma AG, Berlin, Germany. Contact e-mail: maik.schubert@hzdr.de*

Objectives: In contrast to natural occurring D-oligonucleotides mirror-image L-configured oligonucleotides (L ONs) are characterized by high metabolic stability, very low immunogenicity and bio-orthogonality neglecting endogenous hybridization targets. Biodistribution studies of radiolabeled L-ONs demonstrated their favourable suitability as complementary system for specific delivery and accumulation of radionuclides in pretargeted tumor tissues. The main focus of this work was to achieve optimized radiopharmacokinetics in terms of high blood availability (AUC) for high rates of tumor accumulation combined with low unspecific accumulations especially in the highly radiosensitive kidneys. Our strategy was based on the PEGylation of our 17mer-L-ON lead sequence with different molecular weights of PEG entities. Secondly, by the introduction of NOTA and DOTA as radionuclide chelating units and subsequent labeling with 68Ga and 64Cu the influence of the resulting radiochelates on biodistribution behaviour was also investigated. Methods: Our L-ON lead structure was conjugated at 3'-position with different PEG units. Reductive cleavage of the disulfide bond at 5' position generated a sulfhydryl group which was used for binding of our newly developed NOTA-maleimide derivatives as well as a commercially available DOTA-maleimide (see structures in figure below). The resulting NOTA- and DOTA-L-ON-PEG conjugates were labeling with 64Cu and 68Ga and intravenously administrated into healthy Wistar rats. Biodistribution data by organ and tissue sampling 5 min and 60 min p. i. were determined. By the help of dynamic PET studies the half lifes of blood circulation were calculated. Results: By the increase of PEGylation grade a significantly decrease in kidney uptake 60 min p. i. from (56.3±4.1)%ID to (6.5±0.4)%ID for 64Cu-derivatives and from (52.4±6.1)%ID to (6.9±0.6)%ID for 68Ga-derivatives (see diagram in figure below) were achieved. Up to 10 kDa PEG, no significant increase of the very low unspecific liver accumulation from ~2%ID to ~4%ID was measured. These substances were almost exclusively excreted by the kidneys into the urine. The activity concentrations in all other organs, except the blood, were negligible (< 0.5%ID/g). The half-lifes of blood circulation were 10 min (2 and 5 kDa PEG), 28 min (10 kDa PEG), and 39 min (20 kDa PEG). The biodistribution behavior was nearly independent in terms of radionuclides (68Ga/64Cu) and chelators (NOTA/DOTA). Based on gel-electrophoresis, no PEG-induced inhibition of hybridization was found; in vitro hybridizations of complementary L-ON strands were completed in <30 s, whereas the optimal stoichiometry was between 1:1 (2-5 kDa) and 1:1,25 (10-20 kDa). Conclusion: PEGylation of our L ON led to strongly reduced kidney uptake, favorable blood circulation half-lifes, and very low unspecific tissue accumulations. Best results in terms of low kidney and low liver accumulations, almost exclusively renal excretion and high blood availabilities were found for the 10 kDa PEG derivatives. Proof-of-concept experiments in animal tumor models showed the ability of specific radionuclide transport to pretargeted tumor tissue.

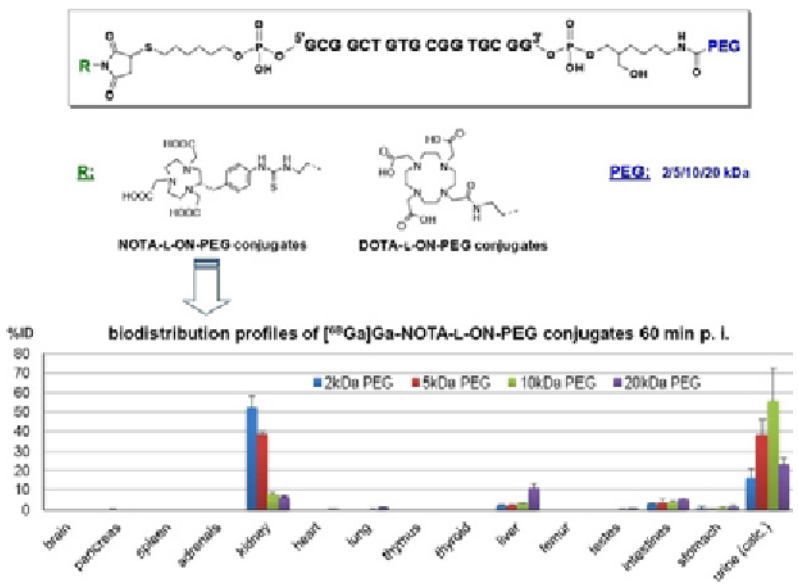


Structure and biodistribution profile of [68Ga]Ga-NOTA-L-ON-2-20kDa-PEG derivatives

Disclosure of author financial interest or relationships:
**M. Schubert**, None; **C. Förster**, None; **R.K. Bergmann**, None; **S. Vonhoff**, None; **S. Klussmann**, NOXXON Pharma AG, Stockholder; NOXXON Pharma AG, Employment; **M. Walther**, None; **J. Pietzsch**, None; **H. Pietzsch**, None; **J. Steinbach**, None.

Presentation Number **P237**
Poster Session 2
September 6, 2012 / 15:15-15:15 / Room: The Liffey

# Synthesis and Pharmacological Evaluation of $^{11}$C-Labeled Piperazine Derivative as a PET Probe for Sigma Receptor Imaging

***Svetlana V. Selivanova***[1], *Annamaria Toscano*[2], *Carmen Abate*[2], *Francesco Berardi*[2], *Adrienne Müller*[1], *Stefanie D. Krämer*[1], *Roger Schibli*[1], *Simon M. Ametamey*[1], [1]*Center for Radiopharmaceutical Sciences, ETH Zurich, Zurich, Switzerland;* [2]*Dipartimento Farmacochimico, Università degli Studi di Bari Aldo Moro, Bari, Italy. Contact e-mail: svetlana.selivanova@pharma.ethz.ch*

Both subtypes of sigma (σ) receptors, $\sigma_1$ and $\sigma_2$, are overexpressed in many cancers with $\sigma_2$ proposed as a biomarker of tumor proliferation. σ Receptors are also abundant and are involved in various pathological processes in central nervous system. We are interested in developing a high affinity selective $\sigma_2$ radioligand, in particular for *in vivo* monitoring of proliferative status of solid tumors and response to anti-cancer therapies. 1-Cyclohexyl-4-[3-(5-methoxy-1,2,3,4-tetrahydronaphthalen-1-yl)propyl]piperazine (PB28) represents one of the lead candidates in the development of σ receptor ligands for therapeutic and diagnostic applications. However, its utility is limited due to relatively high lipophilicity. We synthesized a more hydrophilic analogue **1** (Figure 1, log$D_{7.4}$ = 2.38). Binding affinity ($K_i$) of its S-enantiomer, (-)-(*S*)-**1**, to $\sigma_2$ was 5.92 ± 0.52 nM with ~15-fold selectivity over $\sigma_1$ ($K_i$ = 94.6 ± 12.6 nM). (-)-(*S*)-**1** was radiolabeled with $^{11}$C via standard *O*-alkylation of desmethyl precursor **2** with $^{11}$C-methyliodide in an automated module. $^{11}$C-(-)-(*S*)-**1** was produced in 53 ± 7 % isolated decay-corrected yield with radiochemical and chemical purity over 99% and specific activity greater than 100 GBq/μmol. Average synthesis time including semi-preparative HPLC purification was 30 min. PET imaging was performed in mice bearing EMT6, C6 or PC-3 tumors after i.v. injection of $^{11}$C-(-)-(*S*)-**1**. For C6 xenografts low target-to-nontarget ratio did not allow clear tumor visualization. No accumulation was visible in EMT6 tumor, which is commonly used to evaluate $\sigma_2$ ligands, or PC-3 tumor with SUV 0 indicating poorly perfused tissue. Brain uptake was low and homogeneous (SUV 0.9-1.3). High accumulation of radioactivity was observed in liver and intestine suggesting hepatobiliary clearance. *In vitro* autoradiography with $^{11}$C-(-)-(*S*)-**1** using rat brain slices resulted in a heterogeneous binding of the tracer with the highest accumulation in olfactory bulb, cerebellum, and cortex. This binding was successfully blocked by 10 μM of either, haloperidol, (+)-(*R*)-**1**, or PB28. In conclusion, despite excellent *in vitro* properties, $^{11}$C-(-)-(*S*)-**1** was not superior in imaging $\sigma_2$ receptors *in vivo*. Other derivatives are currently being evaluated.

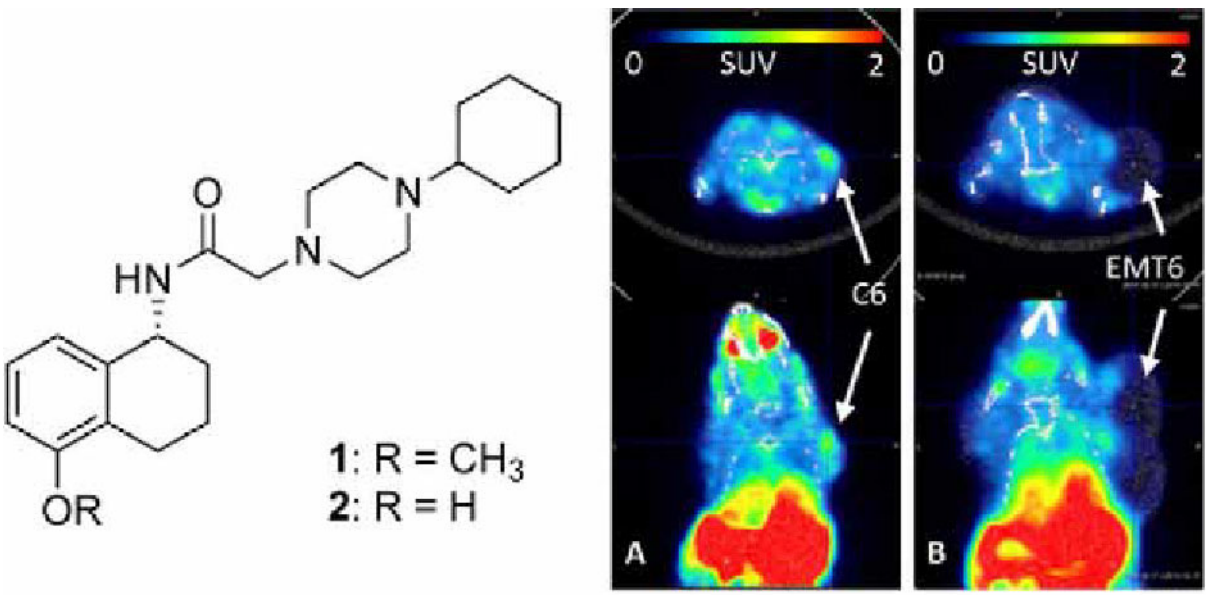


Figure 1. Chemical structure of the σ receptor ligand. PET image of C6 (**A**) and EMT6 (**B**) xenografts with $^{11}$C-(-)-(*S*)-**1**, averaged 10-60 min.

Disclosure of author financial interest or relationships:
**S.V. Selivanova**, None; **A. Toscano**, None; **C. Abate**, None; **F. Berardi**, None; **A. Müller**, None; **S.D. Krämer**, None; **R. Schibli**, None; **S.M. Ametamey**, None.

Presentation Number **P238**
Poster Session 2
September 6, 2012 / 15:15-15:15 / Room: The Liffey

# Efficient synthesis of [$^{11}$C]Am80, a PET probe for a retinoic acid receptor, via a novel rapid Pd$^{0}$-mediated methoxy[$^{11}$C]carbonylation using boronic acid ester and [$^{11}$C]carbon monoxide in MeOH-DMF under atmospheric pressure

***Misato Takashima***[1,2], *Hideki Ishii*[1], *Masaaki Suzuki*[1], [1]*Center for Molecular Imaging Science, RIKEN, Kobe, Japan;* [2]*Medical Photonics Research Center, Hamamatsu University, School of Medicine, Hamamatsu, Japan. Contact e-mail: misatot@hama-med.ac.jp*

**Objectives:** Retinoic acids are the biologically active metabolites of vitamin A and play important roles in cell differentiation, proliferation, and apoptosis. We have recently reported the synthesis of [$^{11}$C]ATRA by Pd$^{0}$-mediated rapid C-[$^{11}$C]methylation as natural type PET probe for in vivo imaging of retinoic acid receptors (RARs).[1] Am80 (tamibaroten), synthetic selective agonist for RAR α/β, was developed to improve therapeutic potency and reduce adverse effects of ATRA.[2] Our aim here is to $^{11}$C-radiolabel carbonyl group of acid moiety in this compound for in vivo imaging of RAR. **Methods:** We explored to realize the rapid Pd$^{0}$-mediated methoxy[$^{11}$C]carbonylation using [$^{11}$C]O and arylboronic acid neopentyl glycol esters under mild conditions by screening previous alkoxycarbonylation reactions. **Results & Discussion:** We found that reaction manipulated from Yamamoto's method[3] at ambient temperature under atmospheric pressure! in MeOH-DMF for 5 min afforded $^{11}$C-labeled esters in radiochemical yields of 17~46% (decay-corrected, based on [$^{11}$C]O). The yield was increased up to 72% by trapping [$^{11}$C]O at -15 °C then at ambient temperature for 5 min using of two-fold excess amounts of solvents and reagents. The reaction conditions were well applied to the synthesis of [$^{11}$C]Am80. Thus one-pot reaction of methoxy[$^{11}$C]carbonylation and the following hydrolysis by KOH at 80 °C for 2 min gave [$^{11}$C]Am80 in 38% radiochemical yield (decay-corrected, based on [$^{11}$C]O) and >99% radiochemical purity. The isolated radioactivity was 1.4 GBq with 44 GBq/μmol specific radioactivity after a 40 min synthesis time. **Conclusion:** The rapid Pd$^{0}$-mediated methoxy[$^{11}$C]carbonylation of boronic acid esters was established under mild conditions and applied to the synthesis of [$^{11}$C]Am80. This simple, clear-cut methodology could also be applicable to alternative synthesis of [$^{11}$C]Am80 through amide bond linkage using the corresponding amine nucleophile. **References:** [1] Suzuki, M., et al., *J. Labelled Compd. Radiopharm.* **2011**, *54*, S92.; Suzuki, M., et al., *Positron Emission Tomography - Current Clinical and Research Aspect*; InTech, **2012**. [2] Kagechika, H., et al., *J. Med. Chem.*, **1988**, *31*, 2182-2192. [3] Yamamoto, Y. *Adv. Synth. & Catal.* **2010**, *352*, 478-492.

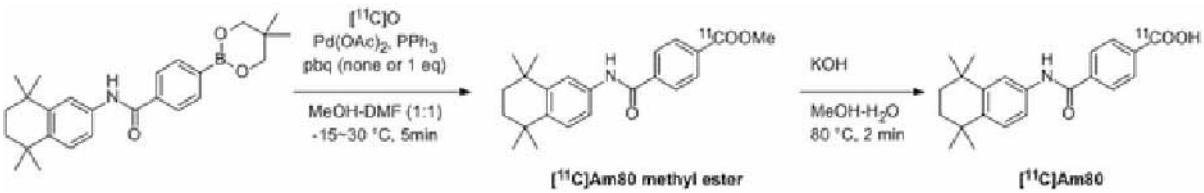


Disclosure of author financial interest or relationships:
**M. Takashima**, None; **H. Ishii**, None; **M. Suzuki**, None.

Presentation Number **P239**
Poster Session 2
September 6, 2012 / 15:15-15:15 / Room: The Liffey

# Synthesis and Evaluation of [123I]Iodooctyl Fenbufen Amide as A SPECT Tracer for Studying Cox Enzymes

***Shu-Fan Tien**, Chung-Shan Yu, Department of Biomedical Engineering and Environmental Sciences, National Tsing Hua University, ROC, Hsinchu, Taiwan. Contact e-mail: u9612048@oz.nthu.edu.tw*

[123I]Iodooctyl fenbufen amide ([123I]IOFA) was prepared from the precursor N-octyl-4-oxo-4-(4'-(trimethylstannyl)biphenyl-4-yl)butanamide with a radiochemical yield of 15%, a specific activity of 10 GBq/μmol and radiochemical purity of 95%. Analysis of binding of [123I]IOFA to Cox-1 and Cox-2 using HPLC with gel filtration column showed a selectivity ratio of 1:1.3. The inhibition assay showed that IOFA 2 exhibited a comparable IC50 value as that of fenbufen and far less ettective than that of cox-1 and cox-2 specific inhibitors. Single Photon Emission Computer Tomography (SPECT) imaging of [123I]IOFA 2 in a normal rat showed that a lower uptake and homogeneous pattern of radioactivity was distributed in the liver. By contrast, SPECT images of [123I]IOFA 2 in a rat with thioacetamide-induced cholangiocarcinoma displayed a higher uptake and heterogeneous pattern of radioactive accumulation with hot spots in tumor lesions. Immuno histological staining against cox-1 and cox-2 enzymes showed elevated expression of both cox enzymes are found in tumor rat and weak activities in the case of normal rat. The present study of [123I]IOFA demonstrated a positive correlation of inflammation to tumor lesion.

Disclosure of author financial interest or relationships:
**S. Tien**, None; **C. Yu**, None.

Presentation Number **P240**
Poster Session 2
September 6, 2012 / 15:15-15:15 / Room: The Liffey

# Small-Animal PET evaluation of the putative P-glycoprotein modulator HM30181

***Thomas Wanek***[1], *Florian Bauer*[2], *Severin Mairinger*[1], *Johann Stanek*[1], *Claudia Kuntner*[1], *Markus Mueller*[3], *Thomas Erker*[2], *Oliver Langer*[1,3], [1]*Health & Environment Department, AIT Austrian Institute of Technology GmbH, Seibersdorf, Austria;* [2]*Department of Medicinal Chemistry, University of Vienna, Vienna, Austria;* [3]*Department of Clinical Pharmacology, Medical University of Vienna, Vienna, Austria. Contact e-mail: thomas.wanek@ait.ac.at*

The adenosine triphosphate-binding cassette (ABC) transporter P-glycoprotein (Pgp, ABCB1) restricts brain uptake of several drugs by active ATP-driven efflux transport. The anthranilic acid derivative HM30181 is a novel, highly selective and potent inhibitor of Pgp which does not inhibit ATPase activity of other drug efflux transporters, such as MRP1 (ABCC1), MRP2 (ABCC2) and MRP3 (ABCC3) and partially inhibits BCRP (ABCG2) only at very high concentrations. Oral co-administration of HM30181 (10 mg/kg body weight) with the chemotherapeutic drug paclitaxel, which is a known substrate of Pgp, increased the oral bioavailability of paclitaxel approximately 12-fold in rats. Aim of this study was to develop carbon-11-labelled HM30181 as PET tracer for the visualization of Pgp density at the murine blood-brain barrier (BBB). **METHODS:** [$^{11}$C]HM30181 was synthesized by *O*-[$^{11}$C]methylation of *O*-desmethyl HM30181, which was prepared in a 5-step synthesis, using [$^{11}$C]methyl triflate. Groups of female FVB wild-type mice (n=4 per group) underwent PET scans with the Pgp substrate radiotracer (*R*)-[$^{11}$C]verapamil following i.v. pre-treatment with either unlabelled HM30181 or vehicle solution. Unlabelled HM30181 was administered at 2 different doses (10 or 21 mg/kg body weight) and time points (60 or 10 min before radiotracer injection). In a second set of experiments, female FVB wild-type, Mdr1a/b$^{(-/-)}$, Bcrp1$^{(-/-)}$ and Mdr1a/b$^{(-/-)}$Bcrp1$^{(-/-)}$ mice underwent [$^{11}$C]HM30181 PET scans (n=4 per group). Brain uptake of (*R*)-[$^{11}$C]verapamil and [$^{11}$C]HM30181 was expressed as the brain-to-blood radioactivity concentration ratio $K_{b,brain}$ at 60 min after radiotracer injection. **RESULTS:** Brain uptake of (*R*)-[$^{11}$C]verapamil was not increased in HM30181 pre-treated wild-type mice compared to vehicle-treated mice, irrespective of the time point of HM30181 pre-administration or administered dose. Treatment with 21 mg/kg HM30181 caused immediate death in 2 out of 4 studied animals and this dose group was therefore discontinued. Brain uptake of [$^{11}$C]HM30181 in wild-type, Mdr1a/b$^{(-/-)}$ and Bcrp1$^{(-/-)}$ mice was low and not statistically different ($K_{b,brain}$: wild-type: 1.9±0.2; Mdr1a/b$^{(-/-)}$: 2.8±0.7; Bcrp1$^{(-/-)}$: 2.6±0.4). However, $K_{b,brain}$ of [$^{11}$C]HM30181 was significantly, i.e. 4.7-fold higher in Mdr1a/b$^{(-/-)}$Bcrp1$^{(-/-)}$ compared to wild-type mice ($P<0.01$). **CONCLUSION:** Our data suggest that HM30181 does not inhibit Pgp at the murine BBB because pre-treatment of wild-type mice with unlabelled HM30181 had no effect on the brain uptake of (*R*)-[$^{11}$C]verapamil. At tracer concentrations as used in PET experiments [$^{11}$C]HM30181 seemed to be a dual substrate of Pgp and Bcrp as brain uptake of [$^{11}$C]HM30181 was several times higher in animals lacking both efflux transporters than in wild-type or single transporter knockout mice. Due to its low brain uptake [$^{11}$C]HM30181 does not appear to be suitable as a PET tracer for visualization of Pgp expression levels at the BBB.

Disclosure of author financial interest or relationships:
**T. Wanek**, None; **F. Bauer**, None; **S. Mairinger**, None; **J. Stanek**, None; **C. Kuntner**, None; **M. Mueller**, None; **T. Erker**, None; **O. Langer**, None.

Presentation Number **P241**
Poster Session 2
September 6, 2012 / 15:15-15:15 / Room: The Liffey

# A Glass Vial Instability is Revealed in Translational GMP Development of a Novel Tc-99m Nano-sized Colloid for Clinical Trials

***Pamela L. Zabel**, Christina S. Keller, Nuclear Medicine, London Health Sciences Centre, London, ON, Canada. Contact e-mail: pzabel@uwo.ca*

Translation of a molecular imaging tracer from bench to bedside requires many steps to make it clinically available for patients. We developed/patented a Tc-99m labeled Cysteine Rhenium Colloid for sentinel node studies in cancer patients. It is a reformulation of Tc-99m Sulfur Colloid optimized to <0.1 micron using cysteine, higher ratios of perrhenate:thiosulfate and a more neutral pH. The smaller size circumvents the need for a filtration step that otherwise wastes 70-90% radioactivity. Preclinical rabbit lymphoscintigraphy studies revealed excellent trapping of CRC compared to 3 other colloids in primary nodes. Sterile hospital productions passed all quality control tests over 2 year evaluation periods. Translation for Clinical Trials required 3 binders of regulatory submissions to Health Canada, contract manufacturing at a licensed GMP manufacturer and revalidation of long term stability of the 3 vial kit. METHODS: Contract manufacturing involved transfer of the preparation technology and included confirmation that the vials met all USP specifications for Type I Borosilicate Glass. 3 productions were evaluated for all quality control tests (sterility, endotoxins, pH, clarity, radiochemical purity and filtration particle sizing to 24 hours) and stored for repeated stability tests up to 2 years. Filtration particle sizing is determined with radioactive filter retention on 0.1µm, 0.22µm and 0.45µm filters. RESULTS: Initially, the 3 GMP production lots met all quality control specifications. Long term stability testing started to fall outside of specifications for particle sizing at 7 months. Particulates eventually became visible within the vial containing phosphate buffer. No vials were released for clinical trial use. Contracted analysis by scanning electronic microscopy and energy dispersive spectroscopy revealed glass delamination and flake- like crystals containing C, O, Na, Si, Al and P at the vial surface. DISCUSSION: Certificates of Analysis indicated glass was USP Type I-compliant. Accurate information on production processes that stabilize vial surfaces from leaching and delamination may not be readily available, especially if vials are obtained from third party distributors. Better initial 2-year stability results for our colloid formulation may have been due to an acidic ammonium sulfate treatment post vial production that provides more resistance to delamination and leaching. Quality control testing of final product particle size provided early detection of the glass vial instability. CONCLUSION: A glass vial instability prevented the start of a clinical trial on a promising novel Tc-99m colloid probe for sentinel node studies. Distributors of pharmaceutical glass vials may often change their source supplier so that processes applied in production may not be evident despite certificates showing USP compliance. An alternative GMP manufacturer with treated vials is sought for production of stable Tc-99m Cysteine Rhenium Colloid for completion of our clinical trials authorized by Health Canada (4 indications). RESEARCH SUPPORT of Canadian Institute for Health Research is gratefully acknowledged.

Disclosure of author financial interest or relationships:
**P.L. Zabel**, None; **C.S. Keller**, None.

Presentation Number **P242**
Poster Session 2
September 6, 2012 / 15:15-15:15 / Room: The Liffey

# A Preliminary Report on HER1-targeted PEGylated PLGA Immunonanobubbles as an Intratumor-specific targeted Ultrasound Contrast Agent

***Arifudin Achmad**, Aiko Yamaguchi, Masaya Miyazaki, Eri Horisoko, Ayako Taketomi-Takahashi, Tetsuya Higuchi, Yoshito Tsushima, Diagnostic Radiology and Nuclear Medicine, Gunma University Graduate School of Medicine, Maebashi, Japan. Contact e-mail: deanzification@yahoo.com*

**Purpose:** Microbubbles (MB) as ultrasound (US) contrast agents are prevented from reaching the tumor cell surface by their relatively large size and their non-targeted and non-stealth properties. Stable nanobubbles (NB) with molecular targeting properties might be able to pass the immature tumor vascular wall and target tumor cells directly. We have developed Cetuximab-labeled PEG-PLGA immunonanobubbles (immunoNB) as an HER1-targeted contrast agent for US molecular imaging of HER1-expressing breast cancer xenografts. **Materials and Methods:** NB were formulated from PLGA-PEG polymers by an emulsion-solvent evaporation technique. Biotinylated Cetuximab was coupled to the NB by biotin-avidin bridging chemistry to form immunoNB. Characterization was performed using dynamic light scattering & scanning electron microscopy. US images were obtained using 5-13 MHz linear array probe with 0.05-1.3 mechanical index (MI) in high definition tissue harmonic imaging mode, *in vitro* in an echogenic gel (clinical perfluorobutane US contrast MB was used as a positive control) and *in vivo* on nude mice implanted subcutaneously with HER1-positive human breast cancer MDA-MB-231 cells. ImmunoNB (200µl, 10mg/mL) were injected i.v. and intratumorally. **Results:** Mean size and zeta potentials of NB and immunoNB were 328nm and 3.77mV and 540nm and 0.707mV. *In vitro* study showed enhancement from accumulation of injected immunoNB as did the positive control with MI from 0.05 to 0.5, began to break with 0.75 MI, and almost disappeared on 1.0 MI. *In vivo* study with i.v. injection (0.2 MI) showed a slight and short (less than 30 sec.) enhancement of tumor mass and accumulation of immunoNB in the liver. After intratumoral injection, bright enhancement of the whole tumor was clearly visible, even up to an MI of 0.9. Enhancement immediately disappeared after the flash mode was operated. **Conclusion:** We have developed HER1-targeted PEGylated PLGA immunoNB for US contrast imaging. This immunoNB was as well visualized and as strong as the positive control. Enhancement was visible on early phase after i.v. injection and more significant enhancement was visible after intra tumoral injection.

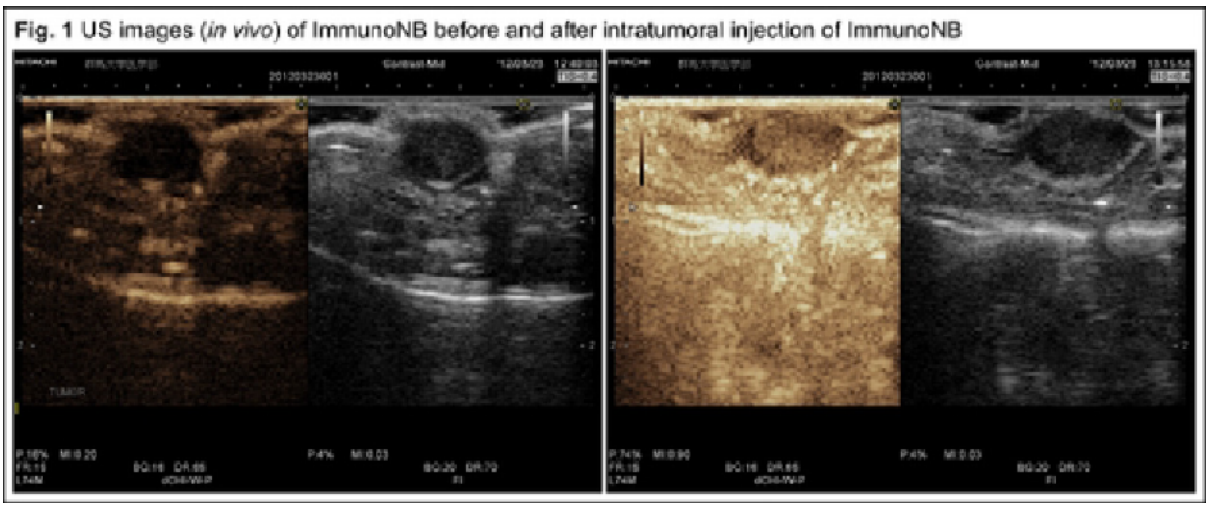

**Fig. 1** US images (*in vivo*) of ImmunoNB before and after intratumoral injection of ImmunoNB

Disclosure of author financial interest or relationships:
**A. Achmad**, None; **A. Yamaguchi**, None; **M. Miyazaki**, None; **E. Horisoko**, None; **A. Taketomi-Takahashi**, None; **T. Higuchi**, None; **Y. Tsushima**, None.

Presentation Number **P243**
Poster Session 2
September 6, 2012 / 15:15-15:15 / Room: The Liffey

# Metabolic and antiproliferative effects of proteasome inhibition in rat hepatoma

***Annette Altmann***[1,2], *Annette Markert*[1,2], *Michael Eisenhut*[3], *Tilman Schoening*[4], *Vasileos Askoxylakis*[5], *Uwe Haberkorn*[1,2], [1]*Nuclear Medicine, University of Heidelberg, Heidelberg, Germany;* [2]*Nuclear Medicine, DKFZ, Heidelberg, Germany;* [3]*Dept. of Radiopharmaceutical Chemistry, DKFZ, Heidelberg, Germany;* [4]*Dept. of Pharmacy, University Hospital, Heidelberg, Germany;* [5]*Dept, of Radiooncology, University Hospital, Heidelberg, Germany. Contact e-mail: a.altmann@dkfz.de*

Aim: Proteasome inhibitors are known to influence the key steps of tumor cell regulation which may lead to an inhibition of proliferation and tumor cell death both in vitro and in vivo. These strong antiproliferative effects of the proteasome inhibitor Bortezomib have been found in a variety of hematological and solid cancer cells. Furthermore, the compound has marked clinical activity even in the setting of relapsed refractory multiple myeloma (MM). In this study we examined the effects of Bortezomib on rat Morris hepatoma (MH3924A) cells in vitro and in tumor bearing animals. Methods: MH3924A cells were exposed to different concentrations of Bortezomib (1nM-1µM) for 12, 24 or 48 hours. The effect on proliferation and metabolism was measured in uptake experiments using 3H-thymidine (TdR), 3H-FDG, 14C-aminoisobutyric acid (AIB) and 3-O-Methyl-D-(3H)glucose. We also assessed p21CIP/WAF1 transcription using real time PCR. Apoptosis measurement and the cell cycle analysis were performed by the Annexin V/Propidium Iodide Assay and FACS analysis. For the determination of in vivo effects the FDG metabolism was measured in a small animal PET system in tumor bearing ACI rats prior and 1 day after Bortezomib therapy. Results: Bortezomib induced a dose-dependent reduction of proliferation in MH3924A cells and an increase of the apoptotic cell fraction. Furthermore, hepatoma cells treated with 100nM Bortezomib for 12h and 24h showed an arrest in the G2/M phase. The cell cycle arrest was associated with an increased p21CIP/WAF1 expression. Furthermore significant and dose-dependent decrease of the AIB uptake was seen after Bortezomib treatment for 48h. In contrast, the FDG uptake increased up to 1.8fold, and the 3-O-methyl-D-glucose uptake up to 2.6fold. In tumor bearing rats a dose-dependent decrease of FDG uptake was observed at 1 day after treatment. Conclusions: Proteasome inhibition leads to induction of apoptosis, cell cycle arrest and changes in metabolism which can be measured by PET and, therefore, presents a promising approach for clinical application.

Disclosure of author financial interest or relationships:
**A. Altmann**, None; **A. Markert**, None; **M. Eisenhut**, Bayer Pharma, Consultant; **T. Schoening**, None; **V. Askoxylakis**, None; **U. Haberkorn**, None.

Presentation Number **P244**
Poster Session 2
September 6, 2012 / 15:15-15:15 / Room: The Liffey

# Bortezomib induces differentiation effects and changes in metabolism in anaplastic thyroid carcinoma

***Annette Altmann***[1,2], *Annette Markert*[2], *Michael Eisenhut*[3], *Tilman Schoening*[4], *Vasileos Askoxylakis*[5], *Uwe Haberkorn*[1,2], [1]*Nuclear Medicine, University of Heidelberg, Heidelberg, Germany;* [2]*Nuclear Medicine, DKFZ, Heidelberg, Germany;* [3]*Radiopharmaceutical Chemistry, DKFZ, Heidelberg, Germany;* [4]*Radiooncology, University of Heidelberg, Heidelberg, Germany;* [5]*Pharmacy, University of Heidelberg, Heidelberg, Germany. Contact e-mail: a.altmann@dkfz.de*

The proteasome activity has been used as a molecular target for cancer therapy. In this study, we studied the effects of the proteasome inhibitor Bortezomib on anaplastic thyroid (ATC) carcinoma cells which are usually resistant to many therapeutic approaches. Methods: The ATC cell lines C643 and SW1736 were treated with Bortezomib (1 nM - 1 μM) for 12h to 72 h. Therapy induced growth inhibition was analyzed by the measurement of thymidine uptake and of the viable cell number. Apoptosis and cell cycle analysis were done using the Caspase-Glo 3/7 assay and FACS analysis. Furthermore, changes at the transcriptional level were assessed by gene chip analysis and real-time quantitative PCR (qPCR). In addition, the activity of the nuclear factor (NF)-κB and p53 signal transduction pathways was monitored with an luciferase assay using the reporter constructs pNF-κB-TA-Luc and pp53-TA-Luc. Metabolic changes and iodide symporter (NIS) activity were determined by uptake studies with fluorodeoxyglucose (FDG), aminoisobutyric acid (AIB) and Na125Iodide. In vivo effects on glucose metabolism were measured in a small animal PET with FDG in C643 or SW1736 tumor-bearing nude mice 1 d or 2 d after treatment. Results: Bortezomib exposure led to growth inhibition, apoptosis and G2-M cell cycle arrest associated with upregulation of p21CIP1/WAF1expression in both cell lines. Glucose metabolism and AIB uptake significantly decreased in vitro whereas in tumor bearing animals only SW1736 tumors showed a decrease in FDG uptake at 2 d after therapy. The transcriptional profile revealed an increased expression of genes involved in stress response, apoptosis, regulation of the cell cycle and differentiation. qPCR showed an upregulation of the tumor necrosis factor (TNF)-related apoptosis-inducing ligand (TRAIL) and of the thyroid-specific transcription factors Pax8 and TTF-1 leading to expression of the thyroid-specific target genes thyroglobulin (Tg), sodium iodide symporter (NIS), thyreoperoxidase (TPO) and thyroid stimulating hormone receptor (TSHr) and to a moderate accumulation of iodide in SW1736 and C643 cells. Conclusion: Bortezomib is a promising antineoplastic agent for the treatment of ATC. To improve the clinical outcome further investigation into the potential of Bortezomib therapy of thyroid cancer as mono- as well as combination therapy is needed.

Disclosure of author financial interest or relationships:
**A. Altmann**, None; **A. Markert**, None; **M. Eisenhut**, Bayer Pharma, Consultant; **T. Schoening**, None; **V. Askoxylakis**, None; **U. Haberkorn**, None.

Presentation Number **P245**
Poster Session 2
September 6, 2012 / 15:15-15:15 / Room: The Liffey

# Development of Novel Activatable Theranostic Nanoparticles for combined Cancer MR Imaging and Therapy

***Celina Ansari***[1,2], *Grigory A. Tikhomirov*[2], *Su Hyun Hong*[1,2], *Lisa M. Coussens*[3], *Jianghong Rao*[2], *Heike E. Daldrup-Link*[1,2], [1]*Radiology, Stanford University, Stanford, CA, USA;* [2]*Molecular Imaging Program at Stanford, Stanford University, Stanford, CA, USA;* [3]*Department of Cell & Developmental Biology, Oregon Health and Science University, Portland, OR, USA. Contact e-mail: cansari@stanford.edu*

Purpose: To develop novel, multifunctional "theranostic" nanoparticles (TNPs) that provide specific tumor delivery, tumor enzyme-specific activation and in vivo imaging capability. Methods: TNPs were synthetized by linking FDA-approved ferumoxytol nanoparticles to a peptide-conjugated prodrug of acedemethylcolchicin (ICT3104), which can be activated by matrix metalloproteinases (MMP-14). Physicochemical characteristics and MMP14-activation of TNPs were determined in vitro. Then, mice with MMTV PymT tumors underwent MR imaging before and after IV injection of ferumoxytol, ferumoxytol-ICT3104, ICT3104, or served as untreated controls. MR signal enhancement, nanoparticle accumulation, MMP-expression and extent of necrosis in tumors and normal organs were compared between different groups using an analysis of variance (ANOVA). Results: In vitro studies confirmed MMP-14 activation of TNPs and significant apoptosis induction of TNP-treated MMP-14 expressing MMTV PyMT tumor cells. In vivo studies demonstrated significant MR signal enhancement of MMTV PyMT tumors after injection of TNPs, which correlated with TNP-tumor accumulation on histopathology. Significant MMP-14 expression and necrosis was only found in TNP-treated tumors, but not normal organs. Conclusion: MMP-14 activatable TNPs are retained in and selectively treat MMP-14 expressing malignant tumors. The TNP tumor accumulation can be monitored with MR imaging. Activatable TNPs hold the potential to improve targeted cancer therapies, and ultimately, enable personalized therapy regimen. Acknowledgement: The authors acknowledge support from NIH/NCI R21CA156124 and a pilot grant from the Stanford Center for Cancer Nanotechnology Excellence and Translation (CCNE-T; NIH/NCI U54 CA151459). We thank Dr. J. Gill and co-workers from the University of Bradford, UK, for providing ICT3104 for this project.

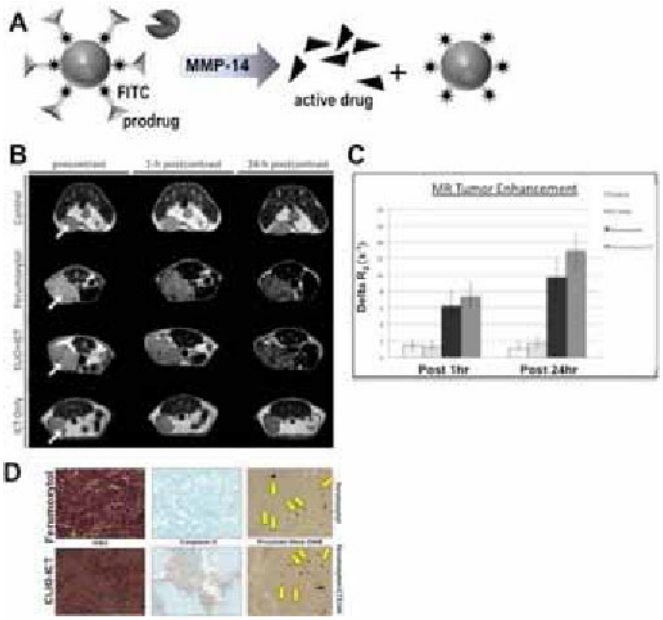


A) SCHEMATIC REPRESENTATION OF MECHANISM OF ACTION OF THERANOSTIC NANOPARTICLE VIA ACTIVATION OF MMP-14. B) AXIAL T2-WEIGHTED MR IMAGES (TR 2500 MS, TE 80 MS) OF MMTV PYMT MAMMARY TUMORS BEFORE AND AFTER INTRAVENOUS INJECTION OF DIAGNOSTIC AND THERAPEUTIC NPS. CONTRAST AGENT ACCUMULATION IS NOTED AS A NEGATIVE (DARK) SIGNAL ENHANCEMENT OF THE TUMORS. C) . MR SIGNAL ENHANCEMENT DATA IN TUMORS CORRESPONDING TO FIGURE 4 QUANTIFIED AS ΔR2 = (R2PRE - R2POST). DATA ARE DISPLAYED AS MEAN DATA OF N=6 TUMORS IN EACH GROUP FOR 1H AND 24H TIME POINTS. D) HISTOLOGI CORRELATIONS OF NP TREATED TUMORS CONFIRM TUMOR ACCUMULATION OF DIAGNOSTIC AND THERANOSTIC AND THERANOSTIC NPs AS WELL AS INDUCTION OF TUMOR NECROSIS BY THERANOSTIC NPs.

Disclosure of author financial interest or relationships:
**C. Ansari**, None; **G.A. Tikhomirov**, None; **S. Hong**, None; **L.M. Coussens**, None; **J. Rao**, None; **H.E. Daldrup-Link**, GE Global Research, Grant/research support .

Presentation Number **P246**
Poster Session 2
September 6, 2012 / 15:15-15:15 / Room: The Liffey

# MicroPET/CT imaging of orthotopic pancreatic tumor-bearing mice using the integrin tracer $^{64}$Cu-labeled cyclam-RAFT-c(-RGDfK-)$_4$ peptide

***Winn Aung***[1], *Zhao-Hui Jin*[1], *Takako Furukawa*[1], *Michael Claron*[2], *Didier Boturyn*[2], *Chizuru Sogawa*[1], *Atsushi B. Tsuji*[1], *Hidekatsu Wakizaka*[1], *Toshimitsu Fukumura*[1], *Jean-Luc Coll*[3], *Yasuhisa Fujibayashi*[1], *Pascal Dumy*[2], *Tsuneo Saga*[1], [1]*Molecular Imaging Center, Diagnostic Imaging Program, National Institute of Radiological Sciences, Chiba, Japan;* [2]*Département de Chimie Moléculaire, UMR5250, CNRS, Université Joseph Fourier, Grenoble, France;* [3]*INSERM U823, Institut Albert Bonniot, Université Joseph Fourier, Grenoble, France. Contact e-mail: winn@nirs.go.jp*

**Background:** Adenocarcinoma of the pancreas has the worst prognosis among solid tumors. Early diagnosis and efficient therapeutic measure remain as the major challenges. A suitable animal model that mimics the clinical situation as closely as possible is essential for developing and comparing new diagnostic and therapeutic strategies. A new PET imaging probe,$^{64}$Cu-labeled cyclam-RAFT-c(-RGDfK-)$_4$ ($^{64}$Cu-RAFTRGD) peptide has been examined for visualization and quantification of $\alpha_V\beta_3$ integrin expression in a variety of animal tumor models by our group. **Aim:** The purpose of this study is twofold: (1) to develop a clinically adapted orthotopic xenotransplantation model of pancreatic cancer that reflects the clinical situation, (2) to perform systematic preclinical evaluation of $^{64}$Cu-RAFTRGD probe, allowed in this model. **Materials and Methods:** Expression of $\alpha_V\beta_3$ integrin in several human pancreatic cancer cell lines was examined with western blotting and fluorescence-activated cell sorting (FACS). The representative cell line BxPc-3 which was stably transfected with red fluorescence reporter protein (RFP) that could be detected with optical imaging system, was used for surgical orthotopic implantation (SOI). *In vivo* probe biodistribution and receptor blocking study, preclinical PET imaging co-registered with contrast enhanced computed tomography (CECT), post imaging *ex vivo* autoradiography and histochemical studies were done. **Results:** Most of pancreatic cancer cell lines showed integrin $\alpha_V\beta_3$ expression. With appropriate surgical approach, orthotopic xenograft was established in pancreas of recipient nude mice by implantation of a piece of subcutaneous tumor developed in donor mice. *In vivo* biodistribution with blocking study confirmed that the efficient binding of probe to tumor is highly $\alpha_V\beta_3$ integrin specific. $^{64}$Cu-RAFTRGD PET imaging combined with CECT that provided anatomical delineation of tumor, encouraged for precise and easy detection of pancreatic cancer lesion. In addition, post imaging autoradiography and histochemical examination validated the accumulation of $^{64}$Cu-labeled probe in tumor versus non-tumor tissues. **Conclusion:** Our results suggest that $^{64}$Cu-RAFTRGD PET imaging can be potentially applicable for the diagnosis of $\alpha_V\beta_3$ expressing pancreatic cancer.

Disclosure of author financial interest or relationships:
**W. Aung**, None; **Z. Jin**, None; **T. Furukawa**, None; **M. Claron**, None; **D. Boturyn**, None; **C. Sogawa**, None; **A.B. Tsuji**, None; **H. Wakizaka**, None; **T. Fukumura**, None; **J. Coll**, None; **Y. Fujibayashi**, None; **P. Dumy**, None; **T. Saga**, None.

Presentation Number **P247**
Poster Session 2
September 6, 2012 / 15:15-15:15 / Room: The Liffey

# Sunitinb Induces Vascular Regression Without Killing Endothelial Cells

*Yoshinori Kato[1], Wenlian Zhu[1], Dmitri Artemov[1], Susanta K. Sarkar[2], Marina Backer[3], **Joseph M. Backer**[3], [1]In vivo Cellular Molecular Imaging Center Program, The Johns Hopkins University School of Medicine, Baltimore, MD, USA; [2]Translational and Experimental Medicine, Sanofi Oncology Division, Cambridge, MA, USA; [3]SibTech, Inc., Brookfield, CT, USA. Contact e-mail: jbacker@sibtech.com*

Vascular endothelial growth factor (VEGF) acting via corresponding receptors (VEGFR) promotes and supports tumor angiogenesis. VEGF/VEGFR signaling is the major target for current approved and experimental anti-angiogenic drugs. As reported in preclinical and several clinical studies, at the beginning of the treatment these drugs induce rapid transient vascular regression. This effect is detectable by various imaging methodologies and is confirmed by a significant decrease in microvascular density by immunochemical analysis (1, 2). The underlying mechanisms of drug-induced transient vascular regression are not established. One possibility would be an actual loss of endothelial cells, either by drug-induced death or by sheddinginto the circulation. Alternatively, it is possible that these drugs induce retraction of immature capillaries with their cells being "re-cycled' by re-incorporating into more stable parental blood vessels. To test these alternatives, we employed sunitinib therapy (80 mg/kg per day for 4 days, orally) for orthotopic human breast carcinoma MDA231luc (a luciferase-expressing derivative of MDA-MB-231 cells) grown in immunodeficient mice. Immediately before sunitinib therapy, tumor-bearing mice were injected with a near-infrared fluorescent tracer scVEGF/Cy, a monomericprotein combining two receptor-binding 3-112aa fragments of VEGF site-specifically derivatized with Cy5.5 fluorescent dyevia an N-terminal cysteine-containing tag (3). In this tumor model, scVEGF/Cy accumulates predominantly in tumor endothelial cells via VEGFR-mediated endocytosis and allows for in vivo near-infrared fluorescent imaging of the tumor vasculature. In the course of sunitinib therapy, mice were daily imaged, and intensities of the signal in the areas of interest in individual mice were determined for each time point. As a result of sunitinib therapy, the signal intensity in all control and all but one treated mice declined approximately 3-fold. The kinetics of the signal decline were approximated as exponential and half-life of Cy5.5 in tumors were calculated for individual mice. There was no difference between control and treated mice, suggesting that the clearance of Cy5.5 from the vasculature of control and sunitinib-treated mice is determined by similar mechanism(s), and that there is no additional sunitinib-induced mechanism(s), such as physical loss of endothelial cells. In vivo imaging data are in sharp contrast with immunohistochemical analysis of tumor tissue obtained from those same mice: a dramatic decline in the prevalence of pan-endothelial marker CD31 and VEGFR-2 in treated miceindicates significant sunitinib-induced vascular regression. Comparing imaging and immunohistochemical data, it is tempting to suggest that sunitinib-induced vascular regression is dueto the retraction of immature capillaries, rather than to a physical loss of endothelial cells, however further research is necessary to establish molecular mechanisms of the process. References 1. Blankenberg et al., Transl. Oncol. 3(1):56-64, 2010. 2. Levashova et al., J. Nucl. Med. 51(6):959-66, 2010. 3. Backer et al. Nature Med. 13(4):504-9, 2007.

Disclosure of author financial interest or relationships:
**Y. Kato**, None; **W. Zhu**, None; **D. Artemov**, None; **S.K. Sarkar**, Sanofi, Employment; **M. Backer**, None; **J.M. Backer**, SibTech, Inc., Stockholder; GlaxoSmishKline, Grant/research support .

Presentation Number **P248**
Poster Session 2
September 6, 2012 / 15:15-15:15 / Room: The Liffey

# Immuno-SPECT Imaging of EGFR expressing Tumors using 177Lu-nimotuzumab

***Denis R. Beckford Vera***[1], *Lajos Balogh*[2], *Zita Postenyi*[2], *Domokos Mathe*[3], *Sebastian Eigner*[1], *Katerina Eigner Henke*[1], *Rene Leyva Montana*[4], *Frantisek Melichar*[1], [1]*Nuclear Physics Institute AS CR, Husinec-Rez, Czech Republic;* [2]*National F.J.C Research Institute for Radiobiology and Radiohygiene, Budapest, Hungary;* [3]*CROMED Translational Research Center Ltd, Budapest, Hungary;* [4]*Center of Isotopes, Ciudad de La Habana, Cuba. Contact e-mail: beckford@ujf.cas.cz*

Objectives: Immuno SPECT imaging is a powerful tool to guide monoclonal antibodies based therapy. Nimotuzumab radiolabeled with 99mTc and 188Re have been successfully used for imaging and therapy of EGFR overexpressing tumors in clinical trials. 177Lu is being strongly considered for radioimmunotherapy due to its excellent nuclear properties. In addition, its gamma-ray emissions are suitable for imaging and dosimetry determination. Therefore, the goal of this work was to evaluate whether 177Lu-nimotuzumab is suitable for immuno-SPECT imaging of epidermal growth factor receptor (EGFR) expressing tumors. Methods: Nimotuzumab was modified with p-SCN-Bn-DOTA and later radiolabeled with n.c.a. 177Lu. The radioimmunoconjugate was characterized by size exclusion radio-HPLC. Specificity and affinity were tested using radioimmunoassays in a cell line overexpressing EGFR. NanoSPECT/CT image study was performed in Male Wistar rats bearing subcutaneous human C6 glioma xenografts. Rats were intravenously injected with 20 MBq of 177Lu-nimotuzumab. After 30 hours post injection whole body NanoSPECT/CT images where acquired for 60 min. 0.6 mL of iododixanol was administered during the CT acquisition. Image analysis was performed using VivoQuant software. Data were quantitatively extracted, decay corrected and percentages of the organs and tumor uptake were determined in relationship to whole body. Dogs with thyroid carcinoma and oral melanoma where also investigated. SPECT/CT image of dogs were acquired 2 hours post injection. Results: Radiochemical yield and specific activity of 177Lu-Nimotuzumab were higher than 95% and 1.3 GBq/mg, respectively. The binding of 177Lu-nimotuzumab to A431 cells showed to be EGFR specific. C6 glioma tumors in rats were clearly visualized 1 day after injection. Tumor uptake was 7.68 % ID/cm3. Relevant uptake of 177Lu-Nimotuzumab was also observed in rat's liver and kidneys. Dogs: 177Lu-nimotuzumab showed clear uptake in thyroid carcinoma (150x90x85 mm) and its lung metastases (3 - 8 mm in diameter) 2 hours post injection. The uptake of 177Lu-nimotuzumab in the primary thyroid carcinoma and its metastases was 4.5 % ID/cm3. The uptake in the small lung metastases was homogeneous unlikely in the huge primary tumor. No appreciable tumor uptake of 177Lu-nimotuzumab was observed in the dog with oral melanoma. Conclusions: This study demonstrated the potential of 177Lu-nimotuzumab for quantitative noninvasive SPECT imaging of EGFR expressing tumors.

Disclosure of author financial interest or relationships:
**D.R. Beckford Vera**, None; **L. Balogh**, None; **Z. Postenyi**, None; **D. Mathe**, CROmed Ltd, Stockholder; Mediso Ltd., Consultant; CROmed Ltd, Employment; **S. Eigner**, None; **K. Eigner Henke**, None; **R. Leyva Montana**, None; **F. Melichar**, None.

Presentation Number **P249**
Poster Session 2
September 6, 2012 / 15:15-15:15 / Room: The Liffey

# Multifunctional Unimolecular Micelles for Image-Guided Drug Delivery in Cancer

*Hao Hong, Yuling Xiao, Yin Zhang, Alireza Javadi, Jonathan W. Engle, Wenjin Xu, Yunan Yang, Todd E. Barnhart, Shaoqin Gong,* ***Weibo Cai****, University of Wisconsin - Madison, Madison, WI, USA. Contact e-mail: WCai@uwhealth.org*

**Objectives:** To design, synthesize, and characterize multifunctional unimolecular micelles, made of hyperbranched amphiphilic block copolymers, for cancer-targeted drug delivery and non-invasive positron emission tomography (PET) imaging in tumor-bearing mice. **Methods:** The hyperbranched amphiphilic block copolymer, Boltorn® H40-poly(L-glutamate-hydrazonedoxorubicin)-b-poly(ethylene glycol), was conjugated with cyclic RGD peptides (cRGD, for integrin αvβ3 targeting) and macrocyclic chelators (NOTA, for $^{64}$Cu-labeling). The final conjugate was named as "H40-DOX-cRGD", where DOX (i.e. doxorubicin) was covalently linked via a pH-labile hydrazone linkage to enable pH-controlled drug release. H40-DOX (without cRGD) was also synthesized as a control. Flow cytometry, confocal microscopy, and MTT assay were carried out to measure the integrin αvβ3 targeting characteristics of H40-DOX-cRGD in vitro. After $^{64}$Cu-labeling, PET imaging, biodistribution and blocking studies were performed to evaluate the tumor targeting efficacy of H40-DOX-cRGD in vivo, which was further validated by ex vivo experiments. **Results:** The unimolecular micelles exhibited a uniform size distribution (36±3 nm) and pH-sensitive drug release behavior.H40-DOX-cRGD had much higher cellular uptake in U87MG cancer cells (due to integrin αvβ3-mediated endocytosis) than H40-DOX, which led to higher cytotoxicity. In U87MG tumor-bearing mice, $^{64}$Cu-labeled H40-DOX-cRGD also exhibited significantly higher tumor uptake (4.1±0.5, 5.7±1.2, 3.7±0.8, and 3.1±0.2 %ID/g at 0.5, 4, 16, and 24 h p.i. respectively) than H40-DOX-$^{64}$Cu, which was confirmed by biodistribution studies. Furthermore, ex vivo optical imaging of DOX fluorescence confirmed that DOX was indeed delivered to the tumor at a much higher level by H40-DOX-cRGD (i.e. active targeting) than H40-DOX (i.e. passive targeting). **Conclusions:** These unimolecular micelles that synergistically integrated passive and active tumortargeting abilities, pH-controlled drug release, PET imaging capabilities, and suitable size range, are promising drug nanocarriers for cancer theranostics.

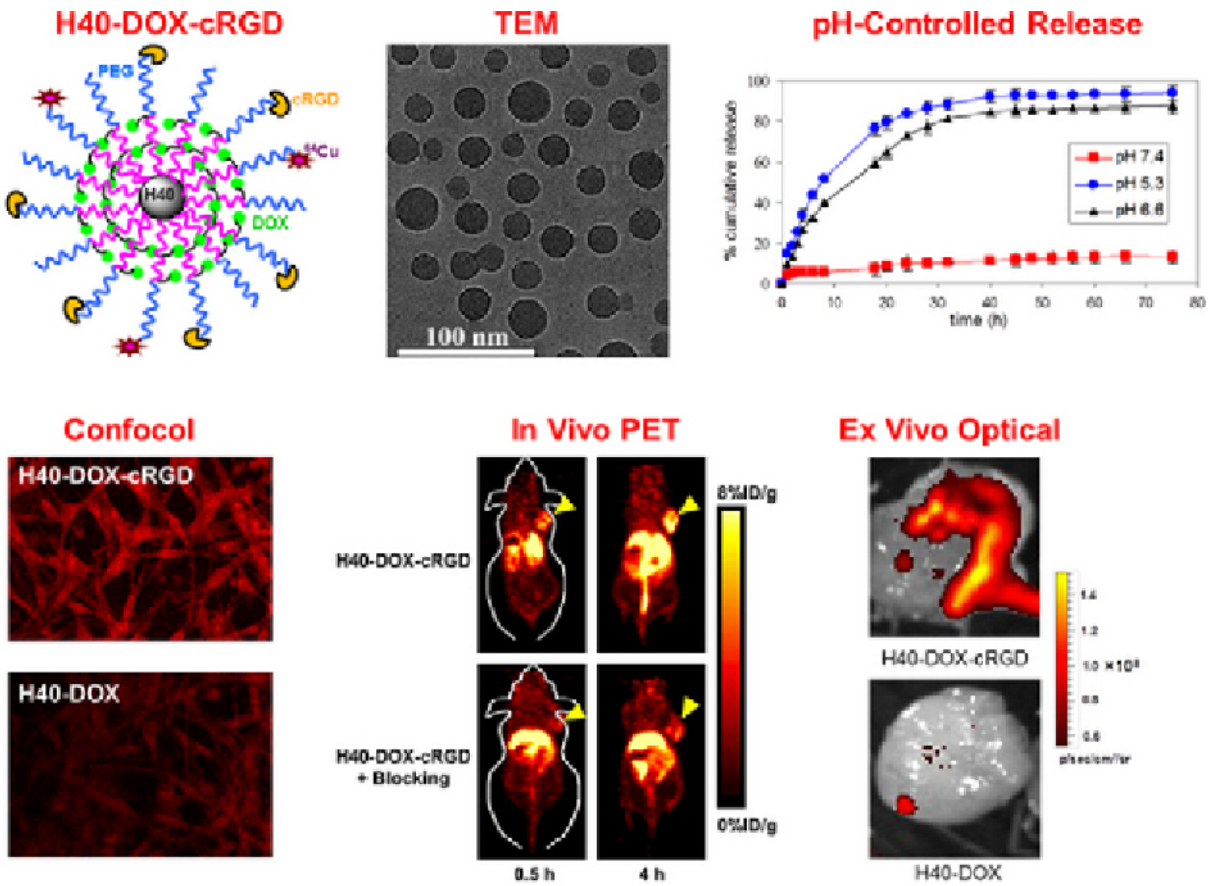


Disclosure of author financial interest or relationships:
**H. Hong**, None; **Y. Xiao**, None; **Y. Zhang**, None; **A. Javadi**, None; **J.W. Engle**, None; **W. Xu**, None; **Y. Yang**, None; **T.E. Barnhart**, None; **S. Gong**, None; **W. Cai**, None.

Presentation Number **P250**
Poster Session 2
September 6, 2012 / 15:15-15:15 / Room: The Liffey

# [18F]-FLT Positron Emission Tomography can be used to image the response of sensitive tumours to PI3-Kinase inhibition with the novel agent GDC-0941

***Chris Cawthorne***[1], *Ian Wilson*[2], *Natalie Burrows*[3], *Roben Gieling*[3], *Jamil Gregory*[1], *Alison M. Smigova*[1], *Muhammad Babur*[1,3], *Kaye Williams*[1,3], [1]*Preclinical Laboratory, Wolfson Molecular Imaging Centre, Manchester, United Kingdom;* [2]*Medical Diagnostics Discovery, The Grove Centre, Amersham, United Kingdom;* [3]*Hypoxia and Therapeutics Group, The University of Manchester, Manchester, United Kingdom. Contact e-mail: christopher.cawthorne@manchester.ac.uk*

Abstract The Phosphatidylinositide 3-kinase (PI3-K) pathway is deregulated in a range of cancers, and several inhibitors of this enzyme are entering the clinic. A current problem for such targeted therapeutics in drug discovery pipelines is the lack of biomarkers for use in clinical trials, to allow the assessment of early therapeutic response and thus better patient management. Here, we assessed uptake of the PET tracer [18F]-Fluorodeoxythymidine (FLT) in response to reduction of PI3-K signalling mediated by the novel PI-3K inhibitor GDC-0941 in both ectopic and orthotopic xenograft models. Methods Nude mice bearing U87 and HCT116 xenografts were imaged for 105 minutes dynamically with [18F]-FLT at baseline (when tumours were~200mm3) and after acute (18h) or chronic (186h) treatment with 50mg/kg GDC-0941 or vehicle twice daily by gavage. An orthotopic model consisting of HCT116 liver metastases obtained after primary inoculation of cells into the spleen was also imaged at baseline and after acute/chronic GDC-0941 therapy. Regions of Interest (ROIs) were drawn manually over tumours/metastases and maximum standard uptake value (SUV)s for tumour uptake were calculated, as was uptake normalised to mean activity in blood pool as estimated by an ROI drawn on the heart contents (NUV). Tumour tissue was analysed at sacrifice for expression of TK1, cleaved PARP and phospho-AKT. Results Growth of U87 xenografts was significantly inhibited by GDC-0941 treatment throughout the course of the study (average growth rate of treated = -1.0±9.3 mm3, control = 69.2±22.1mm3 per day, $p<0.05$). Growth of HCT116 xenografts was not significantly different between groups (average growth rate of treated = 37.3±8.4 mm3, control =46.2±11.9 mm3 per day); however growth of HCT116 liver metastases was significantly reduced (Liver:bodyweight ratio of 0.11±0.01 vs 0.06±0.01, $p<0.01$). Uptake of [18F]-FLT was reduced in GDC-0941 treated animals bearing U87 xenografts or HCT116 liver metastases at the acute timepoint compared to baseline (NUVmax of 2.17±0.38 vs 1.59±0.29, $p<0.01$; 2.42±0.19,1.8±0.12 $p<0.05$ respectively), but was unchanged in unresponsive HCT116 xenografts. Conclusion [18F]-FLT is a strong candidate for the non-invasive measurement of GDC-0941 action. In addition to FLT, we are assessing the performance of a range of other imaging agents, including proprietary tracers, that can potentially bring value in monitoring of PI3-kinase targeting therapies.

Disclosure of author financial interest or relationships:
**C. Cawthorne**, GE Healthcare, Grant/research support; **I. Wilson**, GE Healthcare Medical Diagnostics, Employment; **N. Burrows**, None; **R. Gieling**, None; **J. Gregory**, None; **A.M. Smigova**, None; **M. Babur**, None; **K. Williams**, GE, Grant/research support .

Presentation Number **P251**
Poster Session 2
September 6, 2012 / 15:15-15:15 / Room: The Liffey

# Fluorescence surgical navigation system using in breast cancer lymph node mapping surgery

***Chongwei Chi***[1], *Jinzuo Ye*[1], *Guojun Zhang*[2], *Chenghu Qin*[1], *Jie Tian*[1], [1]*Medical Image Processing Group, Institute of Automation,CAS, "Beijing,100190", China;* [2]*The Cancer Hospital, Shantou University Medical College, Shantou, China. Contact e-mail: chichongwei@fingerpass.net.cn*

In clinical surgery, we hope that more and more sophisticated medical equipment to guide the surgery. Intraoperative real-time image is not only convenient for the operation of the surgeon, but also available to doctors some additional physiological information. This real-time intraoperative image information cannot be achieved, in terms of the traditional medical imaging equipment. This article, we developed a dual camera surgical navigation system basing on the fluorescence characteristics of ICG dye. The system is mainly used to guide the surgeon to find female axillary lymph nodes. We mainly did three things: 1. Designed the optical path according to the lens flange distance; 2. Writing software visualization and image mosaic function; 3. did some ICG pre-experiment with our dual camera system. The system has two CCD cameras, one used to collect near-infrared fluorescence images (ProEM 1024B EMCCD, Princeton Instrument, USA) and the other one used to collect the visible images (Pilot piA1400-17gc, Basler, Germany). The two cameras receive the two beams of light separated by the prism (NT49-683, Edmund Optics, USA) and work in video mode. We place the fluorescence filter (wavelength 810nm-870nm) in front of EMCCD camera and visible light filter (Wavelength 400nm-650nm) in front of color CCD camera. Because the distance between the CCD chip to the lens end is 55mm. We choose Nikon lens (Nikon Nikkor 70-300mm, f/4.5-5.6G). The F-mount flange distance is 46.5mm. The optical path increases to 55.15mm when the light gets through the prism. The distance is suitable for our use. We use LED (Near-infrared light source, Center wavelength 760nm) and halogen (DCRIII, SCHOTT, Germany) to provide light source. The software consists of two parts, control part and the image processing part. The main function of control part is to set some of the basic parameters of the camera, including exposure time, gray color selection, EM gains, etc. There are two main functions of imaging processing part. One is to obtain the camera data and display in video mode. The other is to flatten the fluorescence images and color images. We have done some experiments on the ICG imaging to verify the feasibility of the system. Judging from the experimental results, when the lens focal length is 70mm and the object distance is 46cm, the imaging area would be 7.9cm * 7.9cm. The imaging area changes to 12.5cm * 12.5cm when the object distance increases to 67cm. We have also done the IGG fluorescence experiments in mice and rabbits. ICG dye was injected through the tail vein of mice, and we can see the fluorescence clearly. We mainly did 10 experiments on rabbits, and the sentinel lymph node was cut down. We hope that more meaningful experiments can take advantage of the dual-camera imaging system. Ultimately, we expect that the system can be used in clinical, to solve the existing problems.

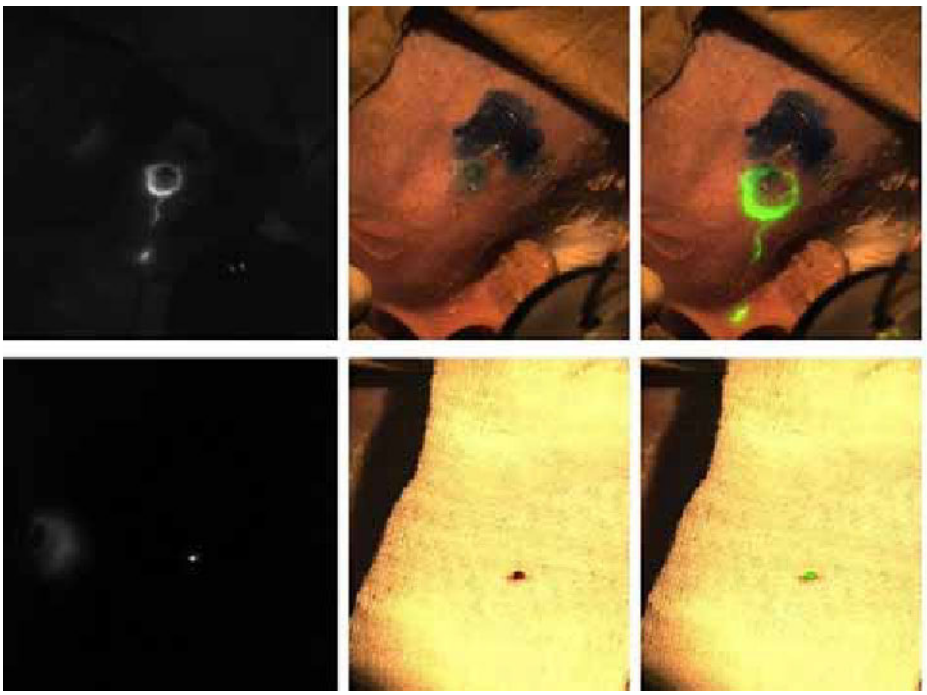

Disclosure of author financial interest or relationships:
**C. Chi**, None; **J. Ye**, None; **G. Zhang**, None; **C. Qin**, None; **J. Tian**, None.

Presentation Number **P252**
Poster Session 2
September 6, 2012 / 15:15-15:15 / Room: The Liffey

# Assessment of Treatment Response of Concurrent Pulsed Radiotherapy (PRT) and Temozolomide by MicroPET/CT in a Murine Orthotopic Model of Glioblastoma Multiforme

*David Lee[1], **John L. Chunta**[1,2], Jiayi Huang[1], Sean S. Park[1,3], Sarah A. Krueger[1], Dianne Schoenherr[1], Inga Grills[1], George D. Wilson[1], Brian Marples[1], [1]Radiation Oncology, Beaumont Health System, Royal Oak, MI, USA; [2]Molecular Imaging, Inc., Ann Arbor, MI, USA; [3]Radiation Oncology, Mayo Clinic, Rochester, MN, USA. Contact e-mail: jchunta@molecularimaging.com*

Purpose/Objective: Glioblastomas (GBM) are aggressive brain tumors that are highly resistant to therapy. While conventional radiation therapy (RT) with temozolomide (TMZ) has improved median survival from 12.1 to 14.6 months, the majority of patients succumb to this disease due to local failure. To overcome this resistance, we evaluated the efficacy of pulsed low-dose radiotherapy (PRT) combined with TMZ as a novel treatment strategy, and evaluated efficacy using 18F-FDG μPET/CT imaging and immunohistochemistry. Materials/Methods: Intracranial tumors were established by injecting U87 GBM cells in Nu-Foxn1nu mice using a stereotactic device. Tumor burden was determined by contrast-enhanced μCT and these volumes were applied to 18F-FDG μPET data to evaluate tumor metabolic activity (SUVmax). Six treatment groups were evaluated; 1) control 2) TMZ alone 3) RT alone 4) PRT alone 5) RT+TMZ 6) PRT+TMZ. Tumors were irradiated 7-10 days post-implantation to a total dose of 14 Gy over 7 consecutive days. Radiation was delivered using either a single 2 Gy dose/day (RT) or 10 pulses of 0.2 Gy with an inter-pulse interval of 3 minutes (PRT), to the same total daily dose of 2 Gy. TMZ (10mg/kg) was administered by oral gavage 1 hr prior to daily RT or PRT treatment. At sacrifice, tumors were harvested for immunohistochemistry. Results: TMZ (10mg/kg) produced a modest growth delay of 2 weeks compared with controls ($p<0.05$). Compared to TMZ alone, combining TMZ with RT or PRT resulted in an additional 3−4 week growth delay ($p<0.01$). PRT+TMZ also resulted in a larger decline in SUVmax after treatment than RT+TMZ ($p=0.01$), but the SUVmax rebounded for each group during regrowth. Less normal brain damage, as assessed by Nissl staining, was seen after PRT+TMZ as compared with RT+TMZ ($p<0.01$). Levels of tumor apoptosis (TUNEL), proliferation (Ki67) and recruitment of CD45+/F4/80+ macrophages to the invasive tumor margins were similar for both the RT+TMZ and the PRT+TMZ treated groups. Significantly, CD45+/CD133+ bone marrow-derived cells were only seen in the hypoxic regions of tumors treated with TMZ alone or RT+/-TMZ, and not in tumors that that received PRT+/-TMZ. Conclusions: PRT+TMZ proved to be the most efficacious treatment, with diminished normal tissue side effects, as compared to the other treatment groups. Although the overall rate of tumor regrowth was similar after PRT+TMZ and RT+TMZ, PRT+TMZ produced a more effective initial response as determined by tumor volume and SUVmax. Interestingly, while normal tissue sparing with PRT was expected, the recruitment of the CD45+/CD133+ subpopulation of bone marrow-derived monocytic lineage cells to the hypoxic regions of other groups was unanticipated. These CD45+/CD133+ cells may ultimately be responsible for a microenvironment that causes faster regrowth. However, since the PRT-TMZ treated tumors regrew without CD45+/CD133+ cell recruitment, this suggests that there is an alternative pathway, and/or associated cell types, that are responsible for post-treatment tumor progression. This pathway may present an additional novel target for inhibition in multimodal treatment strategies for GBM.

Disclosure of author financial interest or relationships:
**D. Lee**, None; **J.L. Chunta**, Molecular Imaging, Inc., Employment; **J. Huang**, None; **S.S. Park**, None; **S.A. Krueger**, None; **D. Schoenherr**, None; **I. Grills**, None; **G.D. Wilson**, None; **B. Marples**, None.

Presentation Number **P253**
Poster Session 2
September 6, 2012 / 15:15-15:15 / Room: The Liffey

# Maximizing dendritic cell migration after vaccination therapy

***I.Jolanda.M. de Vries***[1], *Mangala Srinivas*[1], *Erik H.J.G. Aarntzen*[1], *Carl G. Figdor*[1], *Arend Heerschap*[2], [1]*Tumor Immunology, NCMLS, Radboud University Nijmegen Medical Centre, Nijmegen, Netherlands;* [2]*Radiology, Radboud university Nijmegen Medical Centre, Nijmegen, Netherlands. Contact e-mail: j.devries@ncmls.ru.nl*

Cellular therapy is key component of the recent paradigm shift in medicine, where a patient's own resources are harnessed towards a cure. For example, autologous antigen-presenting cells, principally dendritic cells (DCs), from a cancer patient are used to stimulate their immune system against the disease. Although about 20 clinical trials involving intradermally delivered DCs have been carried out, no more than 4% of the cells have reproducibility reached the target lymph nodes. However, the few cells reaching the lymph nodes are able to interact with and activate lymphocytes. Optimization of this migration has proved difficult, in large part because there was no suitable in vitro assay to accommodate the large cell numbers typically used in such trials (millions of cells). We have recently developed such an assay, based on scale migration of DCs in a collagen scaffold using 19F imaging to measure cell migration. The 3D scaffold mimics biological tissue. The assay can handle opaque tissue samples, which is a major strength compared to traditional microscopy-based migration assessments. Here we validate the assay results with clinical DC migration data. In particular, we find that bolus injections of over 1 million cells result in extensive cell death and therefore reduced migration. Our 19F labeling has previously been shown to be well-tolerated by DCs. Migration occurred only with lower cell numbers, and always only in the migration layer. An example of data with 5 million cells in a tissue sample is shown (B). Migration did not occur in the control regions, for all cell numbers (C; red bars indicate cells in the migration and blue in the control regions respectively). The in vitro migration data show a strong correlation between the total cell number and their migration (F). We found that decreasing the number of cells in the cell layer resulted in a higher percentage of migration. Moreover, we found no difference in migration rates whether we used tissue samples or the gel scaffold. When 111In-labeled DCs were injected intradermally in melanoma patients and subsequently imaged using scintigraphy, we found that between 1-4% of the total cells reached the draining lymph nodes (D,E). Furthermore, the number of migratory cells increased as the total number of cells dropped from 5 to 0.1 million. This is in line with our assay results (F). However, the discrepancy at the lowest cell number is due to the low sensitivity of clinical scintigraphy, which was not able to detect the small numbers of migratory cells when only 0.5 million cells were transferred to the patient. This low sensitivity of clinical imaging techniques is one key reason why an in vitro assay is necessary to optimize cell migration. Furthermore, this also greatly reduces costs and logistic issues. Previous migration assays suffered from being restricted by cell numbers, often only up to 10e5 cells per assay, and/or required transparent samples. Our assay allows us to use the large cell numbers used in the clinic, together with opaque samples, including tissue. Thus, these assays could be carried out using human cells in human tissue.

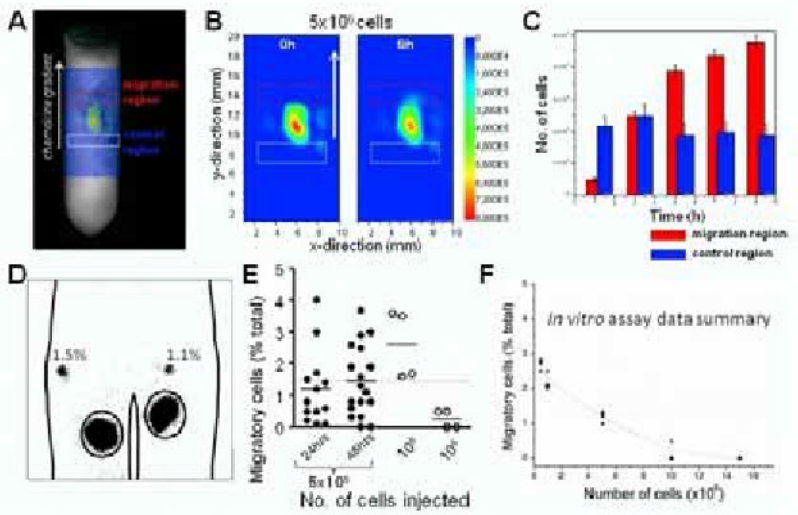


Disclosure of author financial interest or relationships:
**I. de Vries**, None; **M. Srinivas**, None; **E. Aarntzen**, None; **C.G. Figdor**, None; **A. Heerschap**, None.

Presentation Number **P254**
Poster Session 2
September 6, 2012 / 15:15-15:15 / Room: The Liffey

# Quantifying Radiation Neuroprotection by MRI

***Joel R. Garbow***[1], *Xiaoyu Jiang*[1], *Jeremy Cates*[2], *John A. Engelbach*[1], *Dinesh Thotala*[2], *Robert E. Drzymala*[2], *Dennis E. Hallahan*[2], *Joseph J. Ackerman*[1], [1]*Department of Radiology, Washington Univ--EPS, Saint Louis, MO, USA;* [2]*Department of Radiation Oncology, Washington University, Saint Louis, MO, USA. Contact e-mail: garbow@wustl.edu*

Radiation necrosis is a severe, but late occurring, type of injury to normal tissue, within and surrounding a radiation treatment field. It has been suggested that late time-to-onset radiation necrosis results from acute vascular (endothelial) apoptosis caused by the radiation. Direct over-expression of wild-type GSK-3β, a serine/threonine kinase responsible for both cell death and cell survival, is known to induce apoptosis in various cell types in culture. Specific inhibitors of GSK-3β ameliorate this apoptotic process. We have employed MRI to quantify the ability of SB415286, an inhibitor of GSK-3β, to slow the development of radiation necrosis in mouse brain following high-dose radiation treatment. Two cohorts of mice (n=3) were irradiated with the Leksell Gamma Knife Perfexion, a state-of-the-art unit used for stereotactic irradiation of patients with benign and malignant brain tumors. Mice in these cohorts were irradiated with a single 45-Gy dose (50% isodose) of Gamma Knife radiation. In this mouse model, radiation necrosis following 45 Gy of irradiation routinely begins to develop 10-12 weeks post irradiation. Mouse cohort #1 was an irradiated, but untreated, control; cohort #2 received GSK-3β inhibitor SB415286 (1 mg/kg) 24 hours, 12 hours, and 30 minutes prior to irradiation. Mice were imaged every 3 weeks, beginning 7 weeks post irradiation, using an Agilent/Varian DirectDrive 4.7-T small-animal MR scanner. All the mice were sacrificed following the last imaging session at 22 weeks post irradiation. Slices from representative contrast-enhanced, T1-weighted spin-echo images, collected 12 and 16 weeks post-irradiation, are shown in Figure 1(A) for untreated control (top) and SB415286-treated (bottom) mice. At 16 weeks post irradiation, regions of hyperintensity associated with radiation necrosis are much larger in the control mouse than in the inhibitor-treated mouse. For each mouse in each cohort, regions of interest were drawn around the entire brain in 10 contiguous image slices, chosen to include the irradiated region, and histograms of image-pixel intensity were constructed. Figure 1(B) shows representative histograms for a cohort of untreated control mice and a cohort (n=3) of non-irradiated mice. For non-irradiated subjects, the intensity distribution histogram is symmetric, with the majority of the pixels being distributed in the intensity range 0.6 - 1.4 about a normalized mean of 1.0. An intensity threshold of 1.4 (Figure 1(B), arrow) was chosen as the cutoff for normal brain tissue. For images of irradiated mice, the number of pixels exceeding this threshold served to measure the volume of radiation necrosis. The average numbers of hyperintense pixels for cohorts of control and SB-415286-treated mice are plotted as a function of time post irradiation in Figure 1(C). (Prior to 13 weeks post-irradiation, no hyperintense pixels were observed in any mice.) The neuroprotective effects of SB-415286 are clearly seen in the reduced volume of the hyperintense, necrotic region in the treated mice. MRI offers a powerful, promising tool for preclinical assessment of neuroprotective agents, one readily translated to the clinic.

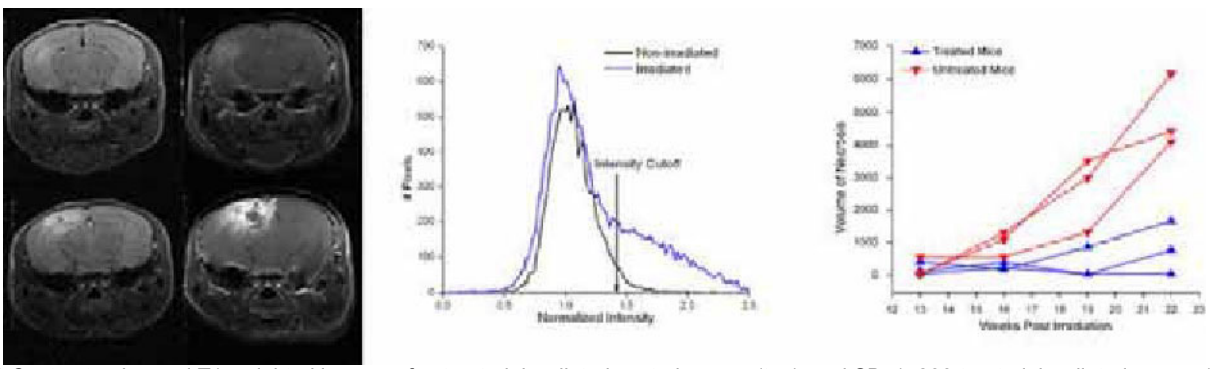


Figure: (left) Contrast-enhanced T1-weighted images of untreated, irradiated control mouse (top), and SB415286-treated, irradiated mouse (bottom), 16 (left) and 22 (right) weeks after Gamma Knife irradiation. (middle) Image-pixel intensity histogram for non-irradiated (black) and untreated irradiated (blue) mice; the intensity cutoff used to define hyperintense pixels, corresponding to necrotic tissue, is indicated by the arrow. (right) Average, MRI-defined volumes of radiation necrosis vs. time post-irradiation for cohorts (n=3) of untreated, irradiated control mice and SB415286-treated, irradiated mice.

Disclosure of author financial interest or relationships:
**J.R. Garbow**, None; **X. Jiang**, None; **J. Cates**, None; **J.A. Engelbach**, None; **D. Thotala**, None; **R.E. Drzymala**, None; **D.E. Hallahan**, None; **J.J. Ackerman**, None.

Presentation Number **P255**
Poster Session 2
September 6, 2012 / 15:15-15:15 / Room: The Liffey

# Reconstruction of absorption improves accuracy of in-vivo biodistribution determination using whole body FMT scans

***Felix Gremse**, Sijumon Kunjachan, Benjamin Theek, Wiltrud Lederle, Twan Lammers, Fabian Kiessling, ExMI, RWTH-Aachen, Aachen, Germany. Contact e-mail: fgremse@ukaachen.de*

**Introduction** FMT and CT are well-suited for combining anatomical and molecular imaging capabilities. Data sets can be fused, enabling association of the FMT signal to appropriate organs or lesions. Using whole body CT-FMT scans of mice at several time points, the organ kinetics of molecular probes can be determined in-vivo. However, fusion revealed deficiencies in the FMT reconstruction such as dislocated signal in the air or in other places where it cannot be explained. These problems can be attributed to assumptions in the FMT reconstruction such as simplified mouse shape or homogeneous tissue properties. Therefore, we determine the the shape of the mouse from the CT data for an improved FMT reconstruction. Furthermore, organs can be segmented and, together with organ-specific absorption coefficients, provide a better model for the fluorescence reconstruction. However, this requires automated or manual segmentation, which is difficult for native CT scans. To overcome this, we determine the 3D absorption map numerically and show the effect on reconstruction accuracy using phantoms and whole body scans of mice after injection of a probe with strong liver and tumor accumulation. **Methods** A software system was implemented for marker detection in CT and FMT data sets enabling automated fusion. The outer shape of the object is automatically segmented. The pixels are projected onto the surface of the object to serve as boundary values in a finite difference model. Using the excitation pass of FMT, a 3D absorption map of the object is computed using nonlinear optimization and automated differentiation of the inverse diffusion problem. Subsequently, the 3D fluorescence image is reconstructed using the normalized Born ratio. Phantoms containing different concentrations of absorptive dye but constant fluorescence concentration were imaged. 6 nude mice were imaged at 5 time points up to 72 hours after injection of an unspecific contrast agent with large molecular weight(fluorochrome bound to a polymer). Absorption and fluorescence of organs was quantified in-vivo using manual segmentation based on the CT data and, for the last time point, compared to values determined from excised organs. **Results** Automated fusion and shape extraction succeeded in all scans. Phantom experiments revealed that presence of absorption causes underestimation of fluorescence using the incorrect assumption of homogeneous absorption. This was corrected by using the reconstructed absorption maps. Determination of absorption in-vivo resulted in significantly ($P<0.001$) higher absorption for heart, liver, stomach and intestine compared to the whole body average, which was validated by ex-vivo measurements. Furthermore, correlation of reconstructed fluorescence with data from excised organs was significantly increased ($P<0.05$). **Conclusions** Usage of shape and absorption information improves accuracy of fluorescence reconstruction. Reconstruction of absorption from the optical raw data together with automated shape segmentation and marker detection alleviates the need for manual segmentation before reconstruction of fluorescence.

Reconstructed absorption is elevated in heart, liver, stomach and intestine.

Disclosure of author financial interest or relationships:
**F. Gremse**, Philips, Grant/research support; **S. Kunjachan**, None; **B. Theek**, None; **W. Lederle**, None; **T. Lammers**, None; **F. Kiessling**, None.

Presentation Number **P256**
Poster Session 2
September 6, 2012 / 15:15-15:15 / Room: The Liffey

# MR imaging and hyperthermic ablation using ferromagnetic nanoparticles

***Vít Herynek***[1], *Pavla Jendelova*[2], *Emil Pollert*[3], *Daniel Jirak*[1], *Karolina Turnovcova*[2], *Miroslav Veverka*[3], *Pavel Veverka*[3], *Milan Hajek*[1], *Eva Sykova*[2], [1]*MR Unit, Department of Diagnostic and Interventional Radiology, Institute for Clinical and Experimental Medicine, Prague, Czech Republic;* [2]*Department of Neuroscience, Institute of Experimental Medicine ASCR, Prague, Czech Republic;* [3]*Department of Magnetics and Superconductors, Institute of Physics ASCR, Prague, Czech Republic. Contact e-mail: vit.herynek@medicon.cz*

**Introduction** Ferromagnetic nanoparticles may serve for both diagnostic and therapeutic purposes. They represent a suitable contrast agent for magnetic resonance imaging (MRI) in vivo and they can also be used for guided temperature-controlled thermoablation. The aim of our study was to test encapsulated perovskite ferromagnetic particles as a contrast agent for MRI, a cellular label, and an agent for thermal ablation. **Materials** Manganese perovskite nanoparticles ($La_{1-x}Sr_xMnO_3$), varying in size over a range of 18 - 21 nm and with different La/Sr ratios, were synthesized and subsequently coated by $Si0_2$ to minimize their toxicity; the coating thickness was 20 nm. Toxicity test: The particles were added to culture medium with rat mesenchymal stem cells and incubated for 48 hours, then the nanoparticles were washed out and cell viability was evaluated using trypan blue. Cell proliferation was evaluated using the Xcellingence System. In vivo MRI: Nanoparticles (2.5µg in 5µl susp.) were injected into the brain of a rat and scanning with a Bruker Biospec imager 4.7 T using a T2-weighted image sequence, 1 and 7 days post-injection. In vivo thermal ablation: The rat was exposed to high frequency magnetic field (480 kHz, 12 mT) for 60 minutes 1 day after injection of the nanoparticles. The lesion was assessed by histology (NeuN + DAPI, cresyl violet and Hematoxylin-Eozin staining). **Results** The viability of cells incubated with the nanoparticles was in the range of 72 - 85%, whereas a control sample reached 92%. Although the coating substantially improved cell viability, the nanoparticles were still slightly toxic. This also resulted in the lower adhesion of a small part of the labeled cells after 48 hours of incubation. Proliferation was slowed down at the time the nanoparticles were added to the media; however, overall proliferation was not changed. The injection of the nanoparticles into the rat brain provided superior MR contrast. Histology staining confirmed damage to the tissue around the injection site after exposition to the high frequency magnetic field. **Conclusion** Coating of perovskite nanoparticles substantially reduces toxicity and may be further improved by surface functionalization. After their injection, the nanoparticles can be easily tracked by MRI in vivo. Due to their ferromagnetic properties, they can be locally heated by an external high frequency magnetic field which leads to tissue ablation in their vicinity. **Acknowledgement** The study was supported by a grant project No. FR-TI3/521 (Ministry of Industry and Trade, Czech Republic), and by a project MZ0IKEM2005 (Ministry of Health, Czech Republic).

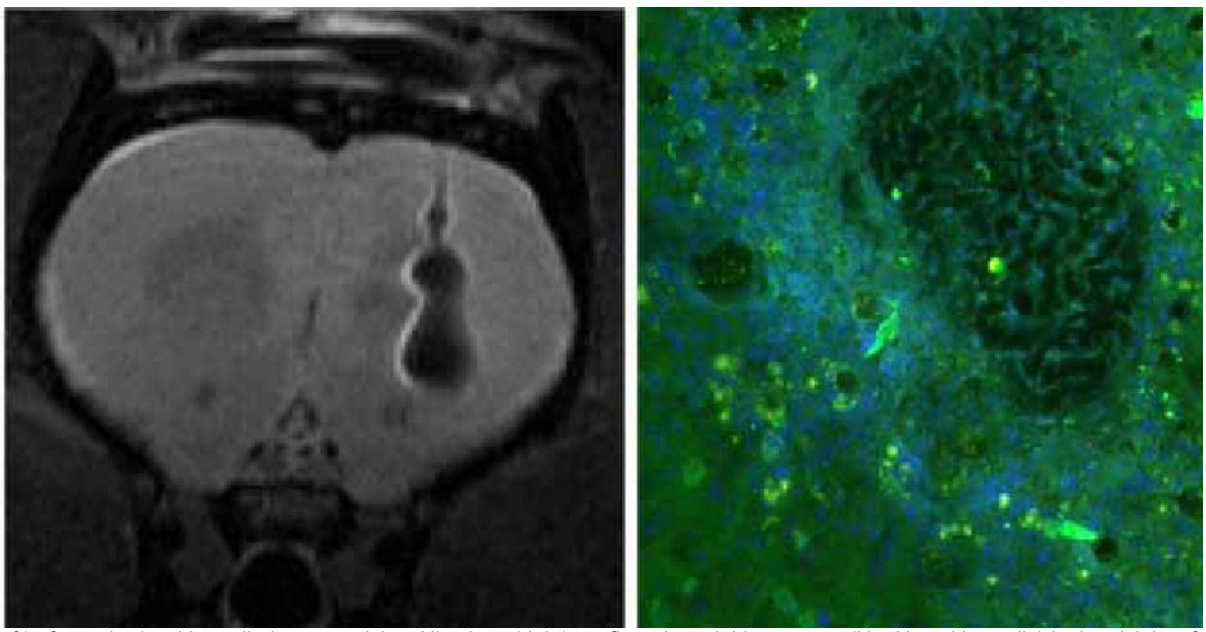

MR image (left) of a rat brain with applied nanoparticles. Histology (right) confirmed no viable neurons (NeuN positive cells) in the vicinity of the injection site.

Disclosure of author financial interest or relationships:
**V. Herynek**, None; **P. Jendelova**, None; **E. Pollert**, None; **D. Jirak**, None; **K. Turnovcova**, None; **M. Veverka**, None; **P. Veverka**, None; **M. Hajek**, None; **E. Sykova**, None.

Presentation Number **P257**
Poster Session 2
September 6, 2012 / 15:15-15:15 / Room: The Liffey

# Fluorescence-guided surgery in RFP-expressing pancreatic cancer in nude mouse models greatly improves outcome compared to bright-light surgery

*Cristina A. Metildi[2], Sharmeela Kaushal[2], Chanae Hardamon[2], Cynthia S. Snyder[2], Michael Bouvet[2], **Robert M. Hoffman**[1,2], [1]AntiCancer, Inc., San Diego, CA, USA; [2]Dept. of Surgery, University of California, San Diego, CA, USA. Contact e-mail: all@anticancer.com*

Orthotopic mouse models of human pancreatic cancer were established using the BxPC-3 RFP-expressing pancreatic cancer cell line in nude mice. Two weeks after implantation, the mice were randomized to undergo bright light surgery (BLS) or fluorescence-guided surgery (FGS). Pre- and postoperative images were obtained with the Olympus OV-100 Small Animal Imaging System to assess completeness of surgical resection. Whole body imaging of the mice was performed weekly in the postoperative period to assess for recurrence and follow tumor progression. Additionally, half of the mice were randomly selected to undergo 4 weeks of postoperative gemcitabine treatment. At six weeks postoperatively, or when premorbid, the mice were sacrificed and primary pancreatic tumor burden was measured using ImageJ v1.440. A more complete resection of pancreatic cancer was achieved using FGS compared to BLS: 98.9% vs 77.1%, p=0.005. Sixty-three percent of the mice undergoing BLS had evidence of gross residual disease, whereas 20% of mice undergoing FGS received a complete resection and an additional 75% of the mice were left with minimal residual disease (p=0.0001). At six weeks, the primary pancreatic tumor burden was significantly less with FGS compared to BLS: 19.341±5.26 mm2 vs. 6.194±3.61 mm2, p=0.048. In a pilot survival study, FGS alone was associated with a decreased risk of tumor recurrence (HR=0.093, 95% CI 0.013-0.645), and mean overall survival was lengthened from 18.5 weeks to 28.2 weeks. The addition of adjuvant gemcitabine (GEM) to FGS further lengthened mean overall survival to 42.75 weeks (p=0.019). Three of the four mice in the FGS with adjuvant GEM group were alive at 12 months postoperatively and all of the mice (n=4) were free of tumor at time of sacrifice. This novel approach has potential to improve outcomes in the surgical treatment of pancreatic cancer.

Disclosure of author financial interest or relationships:
**C.A. Metildi**, None; **S. Kaushal**, None; **C. Hardamon**, None; **C.S. Snyder**, None; **M. Bouvet**, None; **R.M. Hoffman**, None.

Presentation Number **P258**
Poster Session 2
September 6, 2012 / 15:15-15:15 / Room: The Liffey

# Cancer cell-synchronized chemotherapy enabled by methioninase treatment and cell-cycle specific imaging with fluorescent proteins

*Shuya Yano[1,2], Shukuan Li[1], Qinghong Han[1], Yuying Tan[1], Toshiyoshi Fujiwara[3], **Robert M. Hoffman**[1,2], [1]AntiCancer, Inc., San Diego, CA, USA; [2]Dept. of Surgery, University of California, San Diego, CA, USA; [3]Div. of Surgical Oncology, Dept. of Surgery, Okayama University Graduate School of Medicine, Dentristry and Pharmaceutical Sciences, Okayama, Japan. Contact e-mail: all@anticancer.com*

Cancer cells of all types have a generally elevated requirement for methionine compared to normal cells. This phenomenon is termed methionine-dependence and may be due to excessive methylation reactions in cancer cells, since methionine is the global source of cellular methyl groups. Deprivation of methionine α,γ lyase (methioninase or METase) selectively arrests cancer cells during late S-phase, where they are highly sensitive to chemotherapy drugs which damage DNA. Cancer cells, transformed to express different color fluorescent reporters during specific phases of the cell cycle (fluorescent ubiquitination-based cell cycle indicator [FUCCI] ), were used to monitor the onset of the S-phase block due to methionine deprivation effected by METase. The S-phase-blocked cancer cells fluoresced yellow or green, in contrast to cancer cells in G1 which fluoresced red. Cancer cells, synchronously blocked in S-phase by METase and identified by their yellow-green fluorescence, were administered chemotherapy drugs which interact with DNA or block DNA synthesis such as doxorubicin, cisplatin or 5-fluorouracil. We have termed this strategy color-coded chemotherapy. The procedure was highly effective against the cancer cells. In contrast, treatment of cancer cells with drugs only, and without methioninase-effected S-phase synchrony, led to the majority of the cancer cell population being blocked in G phase (red fluorescent) where they were resistant to the drugs. The selective anticancer strategy and technology described in this report, whereby cancer cells are selectively and synchronously blocked in S-phase in the most drug-sensitive phase of the cell cycle where they are identified by fluorescent reporters and then treated with S-phase- specific-drugs, should be a general approach to the treatment of cancer.

Disclosure of author financial interest or relationships:
**S. Yano**, None; **S. Li**, None; **Q. Han**, None; **Y. Tan**, None; **T. Fujiwara**, None; **R.M. Hoffman**, None.

Presentation Number **P259**
Poster Session 2
September 6, 2012 / 15:15-15:15 / Room: The Liffey

# Strategy for modulating the Phagocytosis by pretreating PEGylated Liposomal doxorubicin

***Wei-Hsin Hsu***, *Ya-Jen Chang, Si-Yen Liu, Chih-Hsien Chang, Te-Wei Lee, Institute of Nuclear Energy Research, Taoyuan County, Taiwan. Contact e-mail: casio_300m@hotmail.com*

Nanoparticle have been applied to drug delivery for almost 30 years that are designed as multifunction for delivery, controlled release and long circulation time. Furthermore, nanocarriers can selectively target cancer sites through enhanced permeability and retention (EPR) effects. However, it was found that nano-liposome usually accumulated in liver and spleen in vivo biodistribution. In this study, we tried to reduce the liver and spleen uptake of 188Re-liposome by injection of PEGylated liposomal doxorubicin, in vivo. Colon carcinoma C26 murine tumor-bearing mice were intravenously injected with PEGylated liposomal doxorubicin (LipoDox) before treating the radio-therapeutic nanodrug, 188Re-liposome. And then, the mice were subjected to perform bio-distribution examination and nano-SPECT/CT imaging. The imaging was quantified by InvivoScope (Bioscan). Based on bio-distribution data, the optimal dose of LipoDox was 2.5mg/kg (10% maximum tolerated dose, MTD). In contrast to control group, pretreating LipoDox group showed higher uptake in the tumor tissue (9.7% ± 1.0%) and lower liver uptake (4.1% ± 0.4%) at 24 hours after intravenous administration. The toxicities are assessed by biochemistry analysis for liver and kidney function in mice after intravenous injection. In addition, nanoSPECT/CT imaging showed that pretreated LipoDox group was more accumulation of activity in the tumor and longer circulation time in vivo than without pretreating. That was also confirmed by the ex-vivo biodistribution data. In conclusion, pretreatment of PEGylated liposomal doxorubicin can improve the tumor uptake of 188Re-liposome and reduce the liver and spleen accumulation that were prolonged the circulation time, in vivo. We have demonstrated that decoy strategy could enhance therapeutic efficacy in the C26 murine solid tumor-bearing mice.

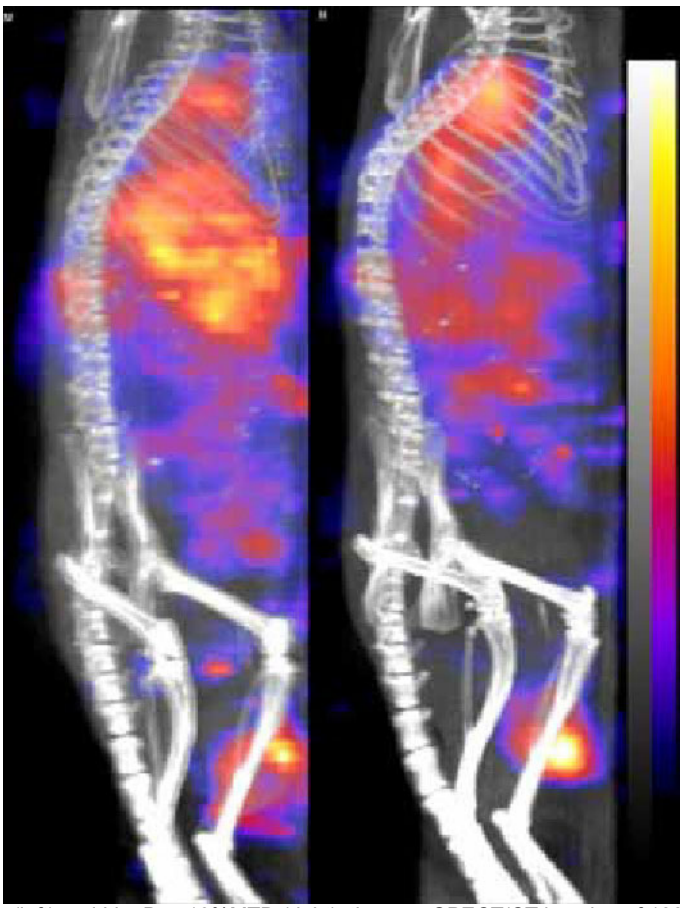

Fig. 1 After treating the normal saline (left) and LipoDox 10%MTD (right), the nanoSPECT/CT imaging of 188Re-liposome targeted C26 tumors in BALB/c mice.

Disclosure of author financial interest or relationships:
**W. Hsu**, None; **Y. Chang**, None; **S. Liu**, None; **C. Chang**, None; **T. Lee**, None.

Presentation Number **P260**
Poster Session 2
September 6, 2012 / 15:15-15:15 / Room: The Liffey

# MRI of Brain Metastasis in a Breast Cancer Mouse Model: Comparison between the Uptake of Gd-DTPA and USPIO

***Lilia Ileva***[1], *Pavan P. Adiseshaiah*[2], *Diana C. Haines*[3], *Joseph Kalen*[1], *Scott McNeil*[2], *Patricia S. Steeg*[5], *Marcelino Bernardo*[4,6], [1]*Small Animal Imaging Program, Frederick National Laboratory for Cancer Research, SAIC-Frederick, Inc, Frederick, MD, USA;* [2]*Nanotechnology Characterization Laboratory, Frederick National Laboratory for Cancer Research, SAIC-Frederick, Inc, Frederick, MD, USA;* [3]*Pathology/Histopathology, Frederick National Laboratory for Cancer Research, SAIC-Frederick, Inc, Frederick, MD, USA;* [4]*Imaging Physics, Frederick National Laboratory for Cancer Research, SAIC-Frederick, Inc, Frederick, MD, USA;* [5]*Laboratory of Molecular Pharmacology, National Cancer Institute, NIH, Bethesda, MD, USA;* [6]*Molecular Imaging Program, National Cancer Institute, NIH, Bethesda, MD, USA. Contact e-mail: ileval@mail.nih.gov*

**Introduction:** Conducting preclinical drug efficacy studies require the use of well characterized animal models, standardized imaging techniques and consistent animal handling techniques. We investigated the potential of a brain metastatic tumor model [1] to evaluate novel nanoformulations for MR imaging and therapy. DCE-MRI of Gadolinium (Gd) based small molecule contrast agent (GBCA) Gd-DTPA followed by multiple time points T2* weighted MRI of ultrasmall superparamagnetic iron oxide (USPIO) Ferumoxytol were performed to evaluate tumor uptake and wash-out characteristics. **Objectives:** The primary objectives of this study are: (1) Detection of small brain metastasis in a breast cancer mouse model with a clinical 3T MRI using a multiple mouse coil array; (2) Correlation between MRI images and Histopathology; and (3) Comparison of GBCA and USPIO uptake in a brain metastasis animal model. **Materials and Methods:** Six (6) Female athymic nude mice are injected into the left ventricle of the heart with 1.75 x $10^5$ MDA-MB 231 BR EGFP cells/100 µL HBSS. Two mice without cell injection are used as controls. At 23 days post-injection, animals are imaged with DCE-MRI during which 0.2 mmol Gd/kg Magnevistis is administrated intravenously. At 25 days post-cell injection the animals are injected with 5 mg Fe/kg Ferumoxytol and imaged with a T2*-weighted four echoes MRI sequence at pre-contrast and at 30 min, 2, 4, 6, 8, and 24 hours post-contrast. Multislice T2-weighted turbo spin echo (T2W-TSE) was applied in both cases before the contrast administration. A 4-mouse multiple coil array for simultaneous imaging was utilized in the study for high throughput [2]. Mice were sent for histopathology 28-31 days post cell injection depending of their moribund status. **Data Analysis:** Regions of interest (ROI) were drawn on the facial artery for the blood signal versus time curve and on every slice of the brain to obtain the brain tissue signal versus time. Elimination half-life (T1/2) of the contrast agents (CAs), the max concentration of Gdmax and ΔR2*max (R2*=1/T2*) for USPIO were calculated. The ratio (λ) of the brain tissue concentration to arterial whole blood concentration was also calculated. The contrast uptake and the percent contrast uptake were compared in the metastatic to the control brains for each CA. **Results and Discussions:** Metastases (diameter >0.2mm) are identifiable 23 days after the cell implantation. Edema, which appears hyperintense in the T2*-weighted images improves the visualization of the metastatic lesions. A good correlation was observed between the metastasis in the MR images with the histopathology. Mice brains with metastatic lesions demonstrated a 31% higher uptake of Gd contrast compared to the control mice and only a 5% higher uptake than controls for the USPIO. Therefore, the smaller GBCA demonstrates a higher permeable flow through the Blood Brain Barrier (BBB) than the larger USPIO blood pool agent particles.

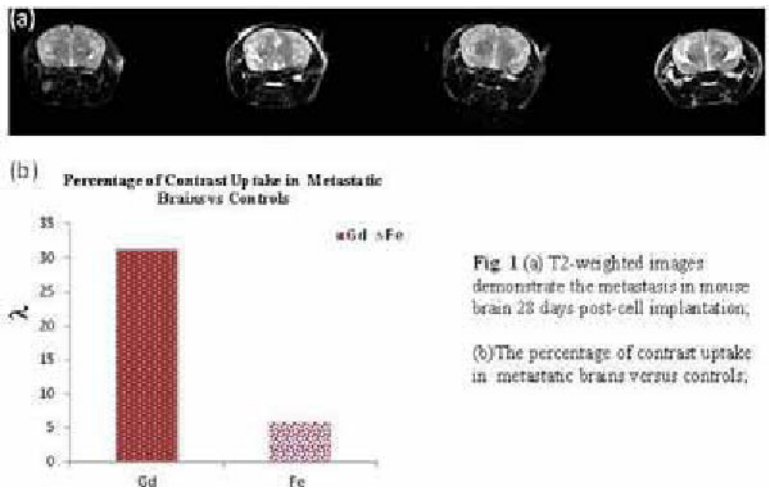


**Fig. 1** (a) T2-weighted images demonstrate the metastasis in mouse brain 28 days post-cell implantation; (b)The percentage of contrast uptake in metastatic brains versus controls;

Disclosure of author financial interest or relationships:
**L. Ileva**, None; **P.P. Adiseshaiah**, None; **D.C. Haines**, None; **J. Kalen**, None; **S. McNeil**, None; **P.S. Steeg**, None; **M. Bernardo**, None.

Presentation Number **P261**
Poster Session 2
September 6, 2012 / 15:15-15:15 / Room: The Liffey

# Initial Studies with the microIGRT: An Orthovoltage Image Guided Micro Irradiator for Preclinical Translational Radiobiology

*Sammantha G. Price, **Enrique W. Izaguirre**, Radiation Oncology, Washington University ihn Saint Louis, Saint Louis, MO, USA.*
*Contact e-mail: eizaguirre@radonc.wustl.edu*

Purpose: The goal of this study was to characterize our small animal image guided micro irradiator, the microIGRT, for preclinical translational radiobiological research and to present the initial studies of healthy tissue response and tumor control experiments. The microIGRT has a dual gantry architecture with a microCT subsystem gantry for low dose high resolution anatomical imaging and treatment planning and a second coaxial micro irradiation subsystem (microRT) gantry for conformal image guided orthovoltage irradiation. We present a comparative analysis between clinical radiation therapy and the microIGRT preclinical data to establish a link between clinical treatment protocols and small animal conformal irradiation. Methods: The microCT image resolution, contrast, and dose were evaluated with specialized phantoms and animal models. The microRT subsystem percent depth dose, beam profile, multibeam irradiation precision and conformality, animal repositioning accuracy, mechanical resolution, and dosimetric accuracy were measured using specialized phantoms equipped with radiochromic film. For each measurement, results were compared with standards adapted from external beam linac and patient quality assurance protocols scaled to animal dimensions and orthovoltage energies. We performed fractionated treatments, multibeam irradiations, modulated beams, image guided treatment verification, and therapeutic irradiation doses in two treatment sites, brain and lung. Instrument dosimetric data acquired irradiating phantoms that mimic these two anatomical sites was used to establish comparisons between clinical and preclinical radiotherapy treatments at both anatomical sites. Results: The microCT imaging dose is 4.15 cGy/scan for 800 um imaging resolution and up to 33.2 cGy/scan for 100 um imaging resolution. The 300 kVp radiotherapy beam has 265 um penumbra, 7% homogeneity, and 9% symmetry. Anatomical positioning is within 500 um for fractionated treatments and multibeam isocentric irradiation central axis uncertainty is within a 150 um radius for multibeam treatments. Three and five beam irradiations were delivered to a small animal body and head phantom with radiochromic film to simulate lung and brain treatment. A three beam irradiation to the lung yielded a 625 um penumbra. Compare this value with a human treatment penumbra of 1 cm and penumbra scales as the ratio between body sizes. The homogeneity of our system is similar to the 10% typically used in clinical treatment planning. Conclusion: The microIGRT instrument developed by our group provides imaging and treatment capabilities that satisfy requirements established by scaling clinical imaging and radiotherapy protocols to animal models to perform clinically relevant translational radiobiological experiments. By comparing preclinical and clinical treatment metrics, the extent of translation can be determined and improved, leading to better understanding of preclinical results and improved correlation with clinical procedures.

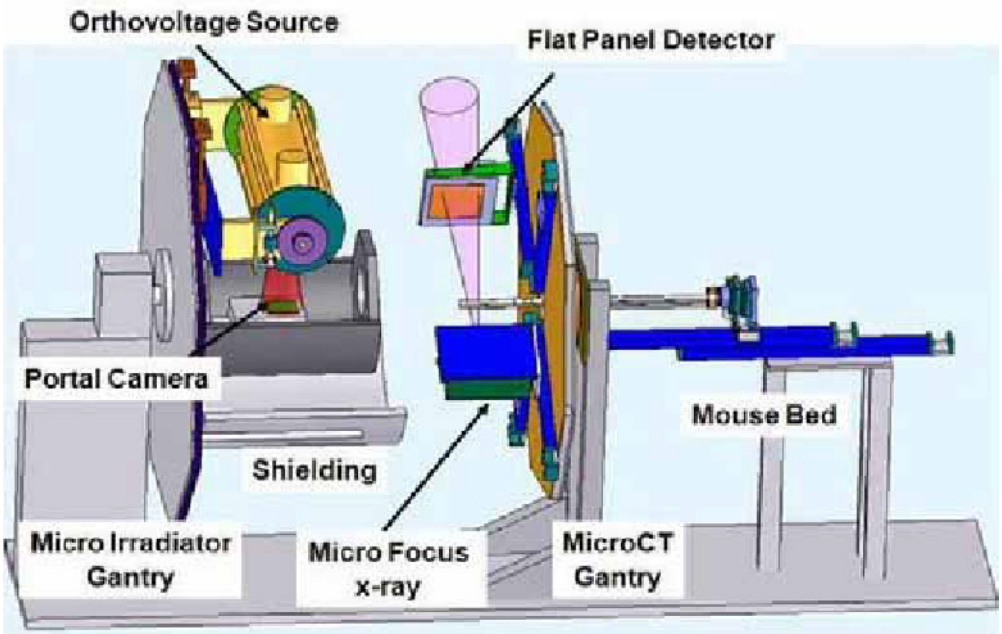


3D rendering of the microIGRT

Disclosure of author financial interest or relationships:
**S.G. Price**, None; **E.W. Izaguirre**, None.

Presentation Number **P262**
Poster Session 2
September 6, 2012 / 15:15-15:15 / Room: The Liffey

# Optical Imaging using a Cy5** labeled peptide targeting the Met receptor (Met) to evaluate the efficacy of a Met tyrosine kinase inhibitor (TKI) in human gastric carcinoma (MKN-45) mouse xenografts

***Elaine Jagoda***[1], *Sibaprasad Bhattacharyya*[2], *Stephanie Histed*[1], *Avrum Leeder*[3], *Lisa Riffle*[3], *Joseph Kalen*[3], *Fabiola Cecchi*[4], *Donald P. Bottaro*[4], *Peter Choyke*[1], [1]*Molecular Imaging Program, NCI, Bethesda, MD, USA;* [2]*CSP, SAIC, Frederick, MD, USA;* [3]*SAIP, SAIC, Frederick, MD, USA;* [4]*UOB, NCI, Bethesda, MD, USA. Contact e-mail: ejagoda@mail.nih.gov*

**Objectives**:The overexpression of hepatocyte growth factor receptor protein (Met) in a variety of cancers has been linked to increased proliferation and progression to metastatic disease. Met-directed TKIs have shown therapeutic potential so an endoscopic imaging agent targeting Met could aid in patient selection and monitor responses to Met-targeted therapies. In previous studies a Met specific peptide (~ 3 kDa) labeled with [$^{99m}$Tc], (AH113018) showed in vitro high affinity (nM) binding to Met using MKN-45 cells (MKN; high Met expression) and exhibited in vivo tumor uptakes in MKN xenografts sufficient for visualization with SPECT. Using this Met specific peptide labeled with Cy5** (Cy5Met, AH112543), optical imaging was used to assess changes in Met status in either vehicle or Met TKI treated MKN xenografts and compared to changes in tumor volumes. **Methods**: MKN xenografts were treated with the Met TKI, PHA 665752 (TX), or vehicle (Vh) and imaged using a fluorescent imaging system (Maestro) before treatment (Day 0) and then at Day 4, 11 and 18 following treatment; tumor volumes (caliper) were measured at the same times. Mice were injected with Cy5Met (1 nmole, Peak emission:675nM) and imaged after 1 h from which tumor uptakes (signal intensity (SI), scaled counts/sec) were determined. Day 18 tumor samples were taken to determine Met content and necrosis. **Results**: In optical images of MKN xenografts, Cy5Met accumulated in tumors (ranging from 2 to 5 fold above non-target tissue) and kidneys as the only other visible organ (Fig 1). Significant decreases (~55%) in Cy5Met tumor uptakes were observed in the TX vs Vh groups at Day 11 and 18 (Table 1). Similar significant decreases at Day 11 and 18 were observed for the tumor volumes in TX vs Vh of 44% and 62%, respectively. At Day 4 Cy5Met tumor uptakes and tumor volumes although decreased 13% and 5%, respectively, were not significant. Total Met content per tumor of Day 18 tumor samples was significantly decreased (~40%) in TX vs Vh,which was reflective of tumor volume decreases as significant decreases in Met content (ng) per mg of tumor protein were not observed. Substantial necrosis was also observed in these Day 18 tumor samples from both groups. Cy5Met tumor uptakes correlated to tumor volumes in which tumors <600 mm$^3$ exhibited ~3 fold greater slopes compared to larger tumors indicating the larger tumors had reduced uptake in relation to their volume. For these Day 18 tumor samples 90% of the tumors were >500 mm$^3$. This necrosis as well as optical detection limitations associated with the larger tumor sizes, could in part explain the significant decrease of Cy5Met uptakes in TX vs Vh tumors at Day 18. **Conclusions**: While Cy5Met was able to detect efficacy of a Met TKI in MKN tumors, the decreased tumor uptakes in TX xenografts maybe more reflective of decreased tumor volumes and necrosis rather than actual changes in Met expression. These data suggest that Cy5Met may have diagnostic utility for endoscopic imaging for detecting Met expressing tumors and monitoring volume changes during Met TKI therapy.

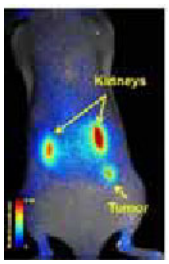


Fig.1 Optical image obtained 1 h after IV injection of Cy5.5labeled Met specific peptide in MKN-45 mouse xenograft (tumor volume ~ 70 mm$^3$ )

Cy5Met MKN tumor uptakes (SI) and volumes (mm$^3$)

| mean value(SD)[1] | | | | | | | | |
|---|---|---|---|---|---|---|---|---|
| Days post treatment | 0 | | 4 | | 11 | | 18 | |
| | SI | mm$^3$ | SI | mm$^3$ | SI | mm$^3$ | SI | mm$^3$ |
| Vehicle | | | | | | | | |
| | | | | | | | | |
| | | | | | | | | |

[1] n= 7 or 8
[2] P< 0.05

Disclosure of author financial interest or relationships:
**E. Jagoda**, GE Heatlhcare, Grant/research support; **S. Bhattacharyya**, None; **S. Histed**, None; **A. Leeder**, None; **L. Riffle**, None; **J. Kalen**, None; **F. Cecchi**, None; **D.P. Bottaro**, None; **P. Choyke**, GE Healtcare, Grant/research support; Philips Medical Systems, Grant/research support; Siemens Healthcare, Grant/research support .

Presentation Number **P263**
Poster Session 2
September 6, 2012 / 15:15-15:15 / Room: The Liffey

# Depiction of inflammatory processes in tumors using non-invasive NIR optical imaging in vivo

***Katharina Jannasch***[1]*, Christian Dullin*[2]*, Pia Welker*[3]*, Kai Licha*[3]*, Frauke Alves*[1]*,* [1]*Hematology and Oncology, University Medicine Goettingen, Goettingen, Germany;* [2]*Diagnostic Radiology, University Medicine Goettingen, Goettingen, Germany;* [3]*mivenion GmbH, Berlin, Germany. Contact e-mail: kjannasch@med.uni-goettingen.de*

Inflammatory processes can be detected in the microenvironment of all tumors even in early stages of tumor development. Aim of this study was to establish, validate and optimize the depiction of inflammatory processes in different in vivo tumor mouse models over time using Near Infrared Fluorescence (NIRF) optical imaging. Hence, the optical imaging system Optix MX2 (ART, Montreal, Canada) in combination with the NIR fluorescent probe MN2012 (Mivenion, Berlin, Germany) has been used for serial investigations of tumor composition. This new approach uses synthetic dendritic polyglycerol sulfates which bind to P-Selectin, L-Selectin, HGF and TGF-beta with high affinity. These unique macromolecules have been described to show anti-inflammatory effects in vivo (Dernedde et al 2010). We compared the applicability of MN2012 to two commercially available activatable probes: MMPSense which is activated by MMP cleavage and ProSense activated by cathepsins (both Perkin Elmer, Waltham, USA). In order to understand the differences in tumor-related inflammation in different origination of the tumors three different mammary tumor models were applied: State of the art mammary carcinoma model applying cells from transgenic Her2/neu-mice by orthotopical transplantation in the mammary gland of syngenic FVB/N-mice, Her2/neu-transgenic mice developing mammary tumors at the age of about 12 months and a mammary tumor model that was chemically induced by 7,12-dimethylbenz[α]anthracene (DMBA) in combination with hormone stimulation by medroxyprogesterone-acetate (MPA) in FVB/N mice. Mice of all three groups were investigated at two time points, first after developing small (0.05 $cm^3$) and second after developing tumors of medium (0.5 $cm^3$) size. We were able to show, that in DMBA-treated mice tumors were distinguishable using all three probes, whereas tumors of Her2/neu-transgenic mice lacked signals when using MN2012 but not MMPSense or ProSense. This was observed independently of the tumor size. Dependent on the model, either MMPSense or ProSense resulted in the most intensive fluorescence whereas MN2012 gave weaker signals. However, calculation of tumor-to-background-ratios resulted in higher values for MN2012 accounting for better identifiability of specific contrast using this probe. In contrast to MMPSense or ProSense, MN2012 lacks interfering liver signals from degradation of the probe. Our results demonstrate that MN2012 is a promising new probe that can be used specifically for the depiction of inflammatory processes in tumors in vivo. It shows an excellent tumor-to-background-ratio leading to better visibility of the tumor. Moreover, MN2012 lacks interfering liver signals from degradation of the probe. Dernedde J, Rausch A, Weinhard M, Enders S, Tauber R, Licha K, Schirner M, Zügel U, von Bonin A, Haag R. Dendritic polyglycerol sulfates as multivalent inhibitors of inflammation. Proc Natl Acad Sci U S A 2010, 107:19679-84.

Disclosure of author financial interest or relationships:
**K. Jannasch**, None; **C. Dullin**, None; **P. Welker**, mivenion GmbH, Employment; **K. Licha**, mivenion GmbH, Germany, Employment; mivenion GmbH, Germany, Stockholder; **F. Alves**, None.

Presentation Number **P264**
Poster Session 2
September 6, 2012 / 15:15-15:15 / Room: The Liffey

# In vivo imaging of intracellular proteins, hTERT and HIF-1α, using TAT peptide conjugated antibody with fluorescence dye

***Kyung Oh Jung**, Hyewon Youn, Mi Jeong Kim, Dong Soo Lee, June-Key Chung, Department of Nuclear Medicine, Seoul National University College of Medicine, Seoul, Republic of Korea. Contact e-mail: blpg86@korea.ac.kr*

Objectives: Traditional antibody targeted imaging and therapy have been focused on membrane proteins. Targeting intracellular proteins in vivo has been of great challenge. Human telomerase reverse transcriptase (hTERT) and hypoxia inducible factor-1α (HIF-1α) can be excellent intracellular targets because of their high expression in most cancers. We developed the antibody-based fluorescent probes with cell penetrating TAT peptide for imaging intracellular proteins, hTERT and HIF-1 α. Methods: hTERT and HIF-1α antibodies conjugated with the TAT peptide were labeled a fluorescence dye (FPR-648). Hep3B and U2OS were used as hTERT positive and negative cells, respectively. HeLa cells were used to visualize HIF-1α. The mRNA and protein expressions of hTERT and HIF-1α were measured by RT-PCR and Western blot, respectively. Intracellular localization of the probes was evaluated by confocal microscopy and Tissue-FAXS. Live cell imaging was performed by fluorescent microscopy. In nude mice having xenograft, tumors were visualized using optical imaging device, MaestroTM. Results: hTERT was detected in Hep3B but not in U2OS, and HIF-1α was only detected in hypoxia condition. Cells with hTERT positive signals were 9.65% in U2OS and 78.54% in Hep3B cells. In HeLa cells, the HIF-1α positive cells were 0.47% in normoxia and 56.07% in hypoxic condition. In mice model, Hep3B tumors were visualized clearly. The fluorescence signals of HeLa tumors in hypoxic condition were higher than in normoxic condition. Conclusion: We developed new probes for imaging intracellular proteins, hTERT and HIF-1α, using the TAT conjugated antibodies. This TAT conjugated antibody system can be useful for targeting intracellular proteins, showing big impact on imaging and therapy of cancers.

Disclosure of author financial interest or relationships:
**K. Jung**, None; **H. Youn**, None; **M. Kim**, None; **D. Lee**, None; **J. Chung**, None.

Presentation Number **P265**
Poster Session 2
September 6, 2012 / 15:15-15:15 / Room: The Liffey

# Multimodal Liposomal Imaging Agents for SPECT/MRI with Modified Polyethylene Glycol for Assessing *In Vivo* Biodistribution and Enhanced Tumour Uptake

***Tammy L. Kalber***[1,2], *Nick Mitchell*[3], *Katherine Ordidge*[1,2], *Adam Badar*[1], *Samantha L. Chalker*[3], *Sam M. Janes*[2], *Mark Lythgoe*[1], *Helen C. Hailes*[3], *Alethea B. Tabor*[3], [1]*Centre for Advanced Biomedical Imaging, University College London, London, United Kingdom;* [2]*Centre for Respiratory Research, University College London, London, United Kingdom;* [3]*Department of Chemistry, University College London, London, United Kingdom. Contact e-mail: t.kalber@ucl.ac.uk*

Liposomes are versatile tools that enable a host of applications ranging from drug and gene delivery to tumours as well as bimodal imaging agents[1]. *In vivo* liposomes preparations have previously utilized PEG2000 to reduce their clearance, and increase their half-life, resulting in significant uptake within subcutaneous tumours over 24 hours[2]. However, PEG2000 liposomes are shown not to be taken up *in vitro*, reducing their efficiency[3]. To combat this, the liposomes in this study have been formulated with a modified PEG coating to generate liposomes that are both multifunctional for a range of imaging platforms (SPECT/MRI and Fluorescence) but also optimal passive delivery agents for tumour delivery. Liposomes were formulated with a high degree of short n-ethylene glycol (n-EG) lipid conjugate DODEG4 to give a uniform distribution of shielding (50%)[4]. To generate multifunctional liposomes for imaging, a fluorescent FITC conjugated lipid (1%) as well as a DOTA conjugated lipid (30%) for the incorporation of $^{111}$In (SPECT), or $Gd^{3+}$ (MRI) were used. To avoid potential interaction of the short n-EG lipid DODEG4 may interact with imaging moieties, three DOTA lipids were synthesized with different n-EG spacer units between the DOTA and the lipid, known as DEG1SL, DEG3SL and DEG6SL. The respective qualities of the DODEG4 liposomes as imaging tracers for both SPECT (NanopSPECT/CT, Mediso) and MRI (Agilent 9.4T), their uptake in a range of tumour cell lines *in vitro* (fluorescence microscopy and FACS analysis), and finally their *in vivo* biodistribution (SPECT) was evaluated and compared to a DEG3SL PEG2000 liposome as a control (7% PEG2000). All liposomes formulations showed comparable T1 relaxivities to Gd.DOTA (Dotarem®) with DEG1SL exhibiting increased relaxivity due to rigidity in the structure reducing tumbling rates, and DEG6SL exhibiting the lowest. DEG3SL chelated $^{111}$In most efficiently, although all liposomes showed a high labeling efficiency (>77%). All DODEG4 liposomes showed a high degree of uptake and internalization in a range of tumour cell lines *in vitro*. However, the DEG3SL PEG2000 liposome was shown to have some electrostatic interaction with the cell surface but no internalization consistent with previous studies (Fig 2A)[3]. The biodistribution showed that the DEG3SL formulation had the shortest half-life with uptake within the liver and spleen at 3 hours whereas both the DEG6SL and DEG3SL PEG2000 liposomes were very similar (Fig 1B) including uptake in MDA-MB-231 subcutaneous tumours (Fig 1C). In conclusion the results of our study show that these multimodal liposomes can be utilized as functional SPECT and MR agents. As the DODEG4 liposomes were capable of cellular internalization and showed similar biodistributions and tumour uptake to PEG2000, these liposomes have the potential to deliver drugs more efficiently, bringing this technology one step closer to the clinic. Refs: 1) Kamaly N et al. Bioconjugate Chemistry. 2008;19;118. 2) Maruyama, K. Adv. Drug Deliv. Rev. 2011;63:161. 3) Hatakeyama, H et al. Adv. Drug Deliv. Rev. 2011;63:152. 4) Hurley CA. et al. Org Biomol Chem. 2008;6:2554.

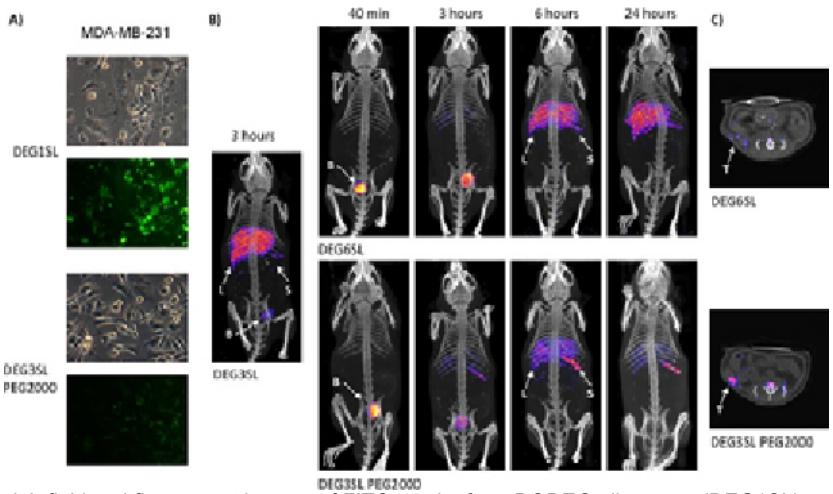


Figure 1: A) Corresponding brightfield and fluorescent images of FITC uptake for a DODEG4 liposome (DEG1SL) compared to PEG2000. B) $^{111}$In SPECT images of liposome distributions for DODEG4 liposomes DEG3SL and DEG6SL compared to PEG2000 (B- bladder, L-liver, and S- spleen). C) $^{111}$In SPECT transverse images of liposome uptake in a MDA-MB-231 subcutaneous tumour for a DODEG4 liposome (DEG6SL) compared to PEG2000 (T - tumour).

Disclosure of author financial interest or relationships:
**T.L. Kalber**, None; **N. Mitchell**, None; **K. Ordidge**, None; **A. Badar**, None; **S.L. Chalker**, None; **S.M. Janes**, None; **M. Lythgoe**, None; **H.C. Hailes**, None; **A.B. Tabor**, None.

Presentation Number **P266**
Poster Session 2
September 6, 2012 / 15:15-15:15 / Room: The Liffey

# Evaluation of specific accumulation of $^{64}$Cu-labeled Cetuximab and Trastuzumab in tumor-bearing mice

***Yousuke Kanayama***[1], *Chinuyo Sumita*[1], *Shusaku Tazawa*[1], *Riyo Zochi*[1], *Yoko Morimoto*[1], *Koki Hasegawa*[1], *Emi Hayashinaka*[1], *Sachi Sugita*[2,1], *Yosky Kataoka*[1], *Yasuhiro Wada*[1], *Kazuhiro Takahashi*[1], *Yasuyoshi Watanabe*[1], [1]*RIKEN Center for Molecular Imaging Science, Kobe, Japan;* [2]*MICRON Inc., Kobe, Japan. Contact e-mail: ykana@riken.jp*

Since the first therapeutic antibody Rituximab was approved by US FDA in 1997, monoclonal antibodies become a major strategy of targeted therapy especially for cancer. For effective usage of antibodies, confirmation of the sufficient expression of target molecule in cancerous tissue is required. Recently, the development of non-invasive molecular imaging method for defining the antigen expression is proceeding worldwide, alternative to invasive diagnostic biopsies. In previous studies, we established $^{64}$Cu-labeling method of antibodies and successfully obtained PET images in which high activity was accumulated in target tumor. However, those accumulations couldn't directly indicate the antigen expression, because that might include the non-specific accumulation caused by various factors such as dissociated $^{64}$Cu. Therefore, to confirm the target expression, specific accumulation of the antibody probe must be clarified. In this study, we investigated the specificity of $^{64}$Cu-labeled Cetuximab and Trastuzumab, which are widely used therapeutic antibodies, with PET imaging, *ex vivo* autoradiography (ARG), immunofluorescent staining, and micro ARG methods in tumor-bearing mice. Anti-EGFR antibody Cetuximab and anti-HER2 antibody Trastuzumab were conjugated with chelating agent DOTA, and then reacted with $^{64}CuCl_2$ respectively. After purification, $^{64}$Cu-DOTA-Cetuximab and $^{64}$Cu-DOTA-Trastuzumab were obtained. To prepare the tumor-bearing mice, human epidermoid carcinoma cells A431 and rat glioma cells C6 were inoculated to BALB/c nude mice. Each probe was intravenously injected to the mice 2 days before PET imaging. After 30 min of data acquisition, mice were sacrificed and tumor regions were dissected. Then the tumor tissues were embedded and frozen with O.C.T. compound. Frozen tissues were sliced to 20 μm thickness sections and subjected to *ex vivo* ARG and immunofluorescent staining. For the micro ARG, mice were perfused with paraformaldehyde for fixation before dissecting the tumor regions. On the other hand, another group of tumor-bearing mice were used for blocking study, in which approximately 650 fold non-labeled Cetuximab or Trastuzumab were injected 3 hour before $^{64}$Cu-labeled probe injection. As a result, high accumulations of $^{64}$Cu-labeled Cetuximab and Trastuzumab in the A431 tumor region were determined by PET imaging, *ex vivo* ARG, and micro ARG. Moreover, the accumulations decreased in blocking study. Furthermore, in immunofluorescent staining, similar localization was observed between target molecule expression and non-labeled antibody distribution. These results strongly indicate the specific accumulations of $^{64}$Cu-labeled Cetuximab and Trastuzumab in PET imaging.

Disclosure of author financial interest or relationships:
**Y. Kanayama**, None; **C. Sumita**, None; **S. Tazawa**, None; **R. Zochi**, None; **Y. Morimoto**, None; **K. Hasegawa**, None; **E. Hayashinaka**, None; **S. Sugita**, None; **Y. Kataoka**, None; **Y. Wada**, None; **K. Takahashi**, None; **Y. Watanabe**, None.

Presentation Number **P267**
Poster Session 2
September 6, 2012 / 15:15-15:15 / Room: The Liffey

# Targeted imaging of brain tumor using genetically engineered *Salmonella typhimurium*

***Sae-Ryung Kang***, *Sheng Nan Jiang, Ari Chong, Misun Yun, Yoon Soon Moon, Jung-Joon Min, Laboratory of In Vivo Molecular Imaging, Department of Nuclear Medicine, Chonnam National University Hwasun Hospital & Medical School, Hwasun, Republic of Korea. Contact e-mail: campanella9@naver.com*

OBJECT: It has been reported that salmonella can colonize hypoxic and necrotic tumor regions after intravenous injection into tumor-bearing mice. In this study, we proposed a novel strategy for brain tumor targeting with engineered *S. typhimurium*. MATERIALS and METHODS: 9L or Lewis lung cancer cell (LLC) both stably transfected with firefly luciferase (Fluc) were implanted into nude mice or BALB/c mice by stereotaxic injection into the striatum. Brain tumor formation was monitored by bioluminescence optical imaging study after D-luciferin injection. After brain tumor formation, attenuated *S. typhimurium* defective in the synthesis of ppGpp (ΔppGpp SL) transformed with bacterial luciferase (Lux) operon-encoding plasmid, pLux (ΔppGpp SL-Lux) were injected into tail veil. Bacterial migration could be monitored without injection of substrate because Lux operon encodes both bacterial luciferase and its substrate-forming enzymes. Bioluminescence signals from tumor cells or bacteria were monitored by cooled CCD camera (IVIS 100, Caliper) to show the tumor location or to trace the migration of the salmonellae. Immunofluorescence staining also performed in frozen section of mouse brain tissue. RESULTS: Optical signal from brain tumor was detected 10 days and became prominent 15 days after tumor cell inoculation. After bacterial injection, ΔppGpp SL-Lux exclusively localized in the brain tumor region as well as in the liver and spleen of 9L and LLC bearing mice. Immunofluorescence staining also demonstrated that salmonella accumulated in the brain tumor. CONCLUSION: Our data indicate that attenuated *S. typhimurium* can target brain tumor as well as other systemic cancer, and provide potential of imageable therapeutic probe for brain tumor when the bacteria would be engineered to deliver therapeutic drugs.

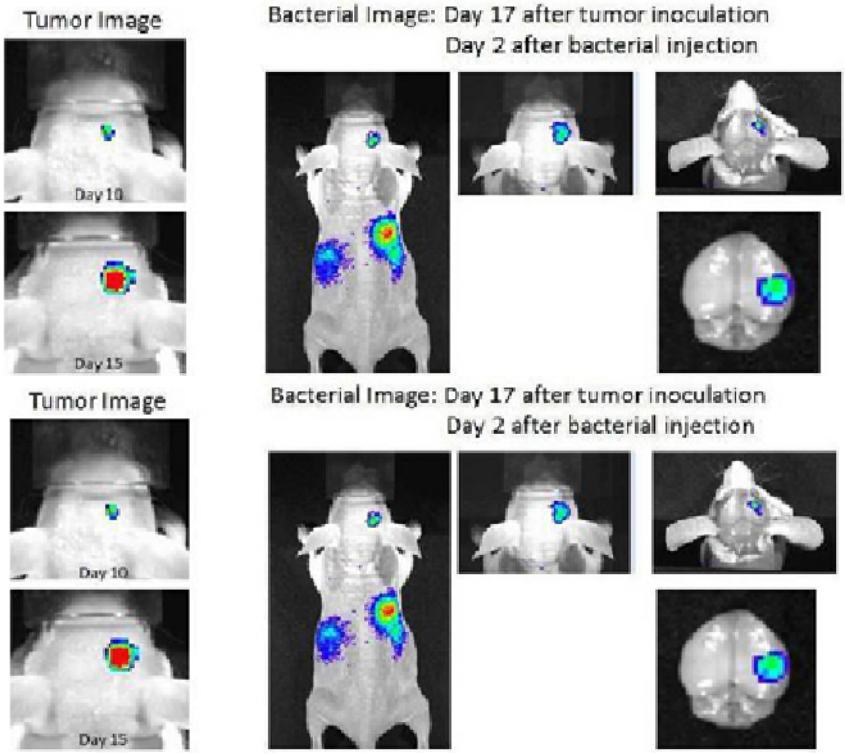


Disclosure of author financial interest or relationships:
**S. Kang**, None; **S. Jiang**, None; **A. Chong**, None; **M. Yun**, None; **Y. Moon**, None; **J. Min**, None.

Presentation Number **P268**
Poster Session 2
September 6, 2012 / 15:15-15:15 / Room: The Liffey

# Early Treatment Response Monitoring using $^{18}$F-PET imaging during Fractionated Radiotherapy of Head and Neck Cancer Xenografts

***Sarah A. Krueger***[1], *Jiayi Huang*[1], *John Torma*[1], *John L. Chunta*[4], *Mitual Amin*[2], *Inga Grills*[1], *Alvaro A. Martinez*[5], *Ching-yee O. Wong*[3], *Brian Marples*[1], *Di Yan*[1], *George D. Wilson*[1], [1]*Radiation Oncology, William Beaumont Hospital, Royal Oak, MI, USA;* [2]*Pathology, William Beaumont Hospital, Royal Oak, MI, USA;* [3]*Nuclear Medicine, William Beaumont Hospital, Royal Oak, MI, USA;* [4]*Molecular Imaging, Inc, Ann Arbor, MI, USA;* [5]*21st Century Oncology, Farmington Hills, MI, MI, USA. Contact e-mail: sarah.krueger@beaumont.edu*

**Objective/Purpose(s):** Positron emission tomography (PET) using $^{18}$F-fluorodeoxyglucose (FDG) is an attractive imaging method given its ability to provide metabolic and possible biological information. Previous work in our group showed a direct correlation between FDG-PET imaging and biomarker histology in a series of head and neck small cell carcinoma (HNSCC) xenografts treated with a single dose of subcurative RT. Based upon these initial findings, we subsequently examined the predictive ability of FDG-PET after fractionated RT using a more clinically applicable treatment regime. **Materials/Methods:** Xenografts were established on the flanks of athymic female NIH III HO mice using a low passage HNSCC cell line, UT14. Tumors were allowed to grow to approximately 500 -1000 mm$^3$ before radiation therapy (RT) and then treated for 5 weeks of conventionally fractionated (2 Gy/day) RT to a total dose of 50 Gy. FDG-PET and CT scans were dynamically acquired for 70 minutes using a FLEX Triumph™ trimodality microPET/SPECT/CT system. Dynamic FDG-PET data were analyzed to generate tumor time activity curves (SUV, RI, SF, and Ki) with the aid of contrast-enhanced CT-derived volumes. Tumors were collected at the completion of the study and stained with hematoxylin and eosin for histological confirmation by a board-certified pathologist. All animal experiments were conducted with the approval and oversight of institutional animal care and use committee. **Results:** Of the ten xenografts, 4 showed local failure (LF) and 6 demonstrated local control. A total of 104 PET scans were performed, and 80 scans from week 0-7 were analyzed for the study. RI and SF at week 1 (after 10 Gy) appeared to be the optimal predictors for LF (AUC = 0.92 for both) and were significantly higher for the LF group (p = 0.03 for both). In contrast, SUV and Ki during RT were not significant predictors for LF. RI > 0 after the first week of RT predicted for 100% LF at 4 months after RT as compared to 0% if RI < 0 (p = 0.003), although one xenograft with RI < 0 at week 1 had a late failure after 4.4 months. **Conclusions:** Although this pilot study was limited to 10 animals, acute changes in FDG metabolism were measured. RI and SF of PET images obtained after the first week of fractionated RT appear to provide an accurate prediction of treatment response. Additional translational studies are ongoing to examine other HNSCC xenografts and other radiotracers, such as $^{18}$F-3'-fluoro-3'-deoxy-L-thymidine (FLT) and $^{18}$F-fluoromisonidazole (FMISO).

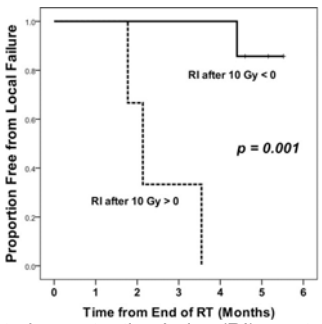


**Figure 1:** ***Retention Index predicts local failure*** In this study, a retention Index (RI) greater than 0 after the first 10 Gy of fractionated radiotherapy is highly predictive of local failure. The solid line represents tumors with RI < 0 after 10 Gy; the dashed line represents tumors with RI > 0 after 10 Gy.

Accuracy of PET parameters at different time points during or after fractionated radiation therapy (RT) in predicting local failure

| Week* | Volume† AUC‡ | Volume† p-value‡ | SUV† AUC‡ | SUV† p-value‡ | RI† AUC‡ | RI† p-value‡ | SF† AUC‡ | SF† p-value‡ | Ki† AUC‡ | Ki† p-value‡ |
|---|---|---|---|---|---|---|---|---|---|---|
| 0 | 0.54 | NS | 0.86 | NS | 0.71 | NS | 0.71 | NS | 0.65 | NS |
| 1 | 0.64 | NS | 0.86 | NS | 0.92 | 0.03 | 0.92 | 0.03 | 0.86 | NS |
| 2 | 0.71 | NS | 0.71 | NS | 0.92 | 0.03 | 0.93 | 0.03 | 0.79 | NS |
| 3 | 0.71 | NS | 0.71 | NS | 0.97 | NS | 0.97 | NS | 0.86 | NS |
| 4 | 0.79 | NS | 0.86 | NS | 0.79 | NS | 1.00 | 0.01 | 0.79 | NS |
| 5 | 0.86 | 0.06 | 0.79 | NS | 0.64 | NS | 0.79 | NS | 0.79 | NS |
| 6 | 0.93 | 0.03 | 0.71 | NS | 0.71 | NS | 0.71 | NS | 0.71 | NS |
| 7 | 0.92 | 0.03 | 0.86 | 0.03 | 0.93 | NS | 0.97 | NS | 0.93 | 0.03 |

*Week = time from the start of radiotherapy (which lasted 5 weeks), Volume = tumor volume as determined from the CT scan, SUV = standard uptake value, RI = retention index, SF = sensitivity factor, Ki = kinetic index.

†AUC = area under the receive operating characteristic (ROC) curve. An AUC of 1 denotes perfect predictive accuracy, an AUC of 0.5 denotes complete lack of predictive accuracy, and an AUC of less than 0.5 denotes that the prediction is opposite from the initial hypothesis.

‡p-value = assessed using the Wilcoxon test, NS = not significant.

Disclosure of author financial interest or relationships:
**S.A. Krueger**, None; **J. Huang**, None; **J. Torma**, None; **J.L. Chunta**, None; **M. Amin**, None; **I. Grills**, None; **A.A. Martinez**, None; **C.O. Wong**, None; **B. Marples**, None; **D. Yan**, None; **G.D. Wilson**, None.

Presentation Number **P269**
Poster Session 2
September 6, 2012 / 15:15-15:15 / Room: The Liffey

# Fusion protein-based BRET probes for highly specific in vivo imaging of HIF-active tumor cells

***Takahiro Kuchimaru**, Keisuke Hirota, Tomoya Suka, Tetsuya Kadonosono, Shinae Kizaka-Kondoh, Graduate School of Bioscience and Biotechnology, Tokyo Institute of Technology, Yokohama, Japan. Contact e-mail: tkuchimr@bio.titech.ac.jp*

In solid tumors, hypoxic microenvironment is often generated by uncontrolled tumor growth and immature blood vessels during angiogenesis. Under hypoxic conditions, hypoxia inducible factors (HIFs) are activated, inducing a vast array of gene products that control energy metabolism, neovasucularizaion, survival and cell migration. Many of them promote both tumor progression and resistance to therapies (Oncogene, 2009, 29, 625). Recent studies have also shown that HIF-1 is associated with the promotion and maintenance of stem cell-like cancer cells (Cell Stem Cell, 2011, 8. 399). Therefore, the HIF-active tumor cell is a promising target for establishing novel strategies for cancer therapy and diagnosis (Adv Drug Deliv Rev, 2009, 61, 623). We have been developing imaging probes for detecting HIF-active cells in vivo. Recently we developed POH-NIRF, a near-infrared fluorescence (NIRF)-labeled recombinant protein consisting of a protein transduction domain (PTD), an oxygen-dependent degradation domain (ODD) and a Halotag domain through which a NIRF-ligand can be covalently bound. POH-NIRF can efficiently penetrate a cell membrane and is delivered to whole body through PTD function. POH is then degraded in ubiquitin-proteasome system via the ODD function in cells without HIF activity and its fragments with NIRF are excreted from cells, whereas POH-NIRF remains stable and accumulated in HIF-active cells (PLoS One, 5, e15736, 2010). POH-NIRF efficiently detects HIF-active cells in xenograft tumor models. However, to obtain HIF-specific images, we have to wait for 15 - 24 h after intravenous injection of the probe because NIRF dyes of the degraded probe become a source of non-specific fluorescence signals in the entire body, particularly in excretory organs. To shorten the period detecting HIF-active cells and reduce non-specific fluorescence signals, we have developed a novel probe POR-NIRF that consists of PTD, ODD and renilla luciferase (Rluc) labeled with a NIRF dye. POR-NIRF was designed to generate bioluminescence resonance energy transfer (BRET) in the presence of coelenterazine, a substrate of Rluc. We expected that when a coelenterazine was injected, BRET would occur in POR-NIRF and emit fluorescence in cells with HIF activity. While, in cells without HIF activity, Rluc would be degraded quickly and thus no BRET would be generated, decreasing non-specific fluorescence signals in the entire body. In vitro experiments, the BRET signal was successfully detected in the presence of coelenterazine, resulting in approximately 100-fold increase of integrated fluorescence intensity in the wavelength range 650 - 750 nm. Then we attempted to detect HIF-active cell by BRET imaging in xenograft tumor models. As expected, nonspecific fluorescence signals in the excretory organs were markedly reduced and HIF-active cells were successfully visualized in tumors 6 h after intravenous administration. Overall results suggest that POR-NIRF will become a powerful tool to spatiotemporally analyze HIF-active cells in vivo.

Disclosure of author financial interest or relationships:
**T. Kuchimaru**, None; **K. Hirota**, None; **T. Suka**, None; **T. Kadonosono**, None; **S. Kizaka-Kondoh**, None.

Presentation Number **P270**
Poster Session 2
September 6, 2012 / 15:15-15:15 / Room: The Liffey

# Non-invasive CT-FMT imaging of the biodistribution and tumor accumulation of vascular-targeted polymeric nanomedicines

***Sijumon Kunjachan***[1], *Felix Gremse*[1], *Fabian Kiessling*[1], *Twan Lammers*[1,2], [1]*Department of Experimental Molecular Imaging, University Hospital, RWTH - Aachen University, Aachen, Germany;* [2]*Department of Targeted Therapeutics, University of Twente, Enschede, Netherlands. Contact e-mail: skunjachan@ukaachen.de*

We investigated the biodistribution and tumor targeting potential of passively and actively targeted polymeric nanomedicines using optical imaging. To this end, tumor vascular targeting peptides NGR-, RGD- and DRG- (control peptide) containing HPMA copolymers were labeled with Dy680, and their target site accumulation was compared to that of Dy750-labeled peptide-free control copolymers. A novel hybrid 3D CT-FMT based imaging protocol was used to visualize and quantify the (kinetics of) tumor accumulation, and to assess probe localization in healthy organs. The polymer-peptide constructs pHPMA-Dy680-NGR, pHPMA-Dy680-RGD, and pHPMA-Dy680-DRG were administered intravenously to subcutaneous CT26 tumor bearing mice (n=3 per peptide), at a dose of 2.5 nmol equivalent dye. To minimize inter-individual variability, similarly sized (~67 kDa) passively targeted control copolymer (pHPMA-Dy750) was co-injected. The biodistribution of both polymers was monitored in parallel at early (15 min, 30 min and 1 h) and late time points (4, 24, 48 and 72 h) using a combination of micro-computed tomography (Imaging GmbH, Erlangen, Germany), organ segmentation (Imalytics Research Workstation) and 3D fluorescence molecular tomography (FMT 2500, PerkinElmer). After 72 h, the animals were sacrificed, tumors and organs were excised, and probe accumulation was quantified ex vivo. Early time point studies using fluorescence reflectance imaging (FRI) nicely showed that the polymeric nanomedicines traversed through the heart and tumor immediately after injection (Fig 1A). In line with the principles of Enhanced Permeability and Retention- mediated passive tumor targeting, the control copolymer pHPMA-Dy750 slowly but steadily accumulated in the tumor over time, reaching a plateau of around 7 % of the injected dose/ normalized tumor volume at 24 h. The RGD- and NGR-targeted probes, on the other hand, accumulated in tumors much more rapidly, with already at 1 and 4 h post i.v. and a relatively strong signal was detectable in tumors (Fig 1B). As expected, pHPMA-Dy680-DRG (control) displayed similar tumor accumulation patterns to those of pHPMA-Dy750. The biodistribution of probes were quantified using 3D FMT, based on fusion with the (organ) pre-segmented CT images (Fig 1C). This innovative approach demonstrated significant differences in active versus passive targeted nanocarriers in tumor and healthy organs. Active targeting resulted in effective early binding to the tumor vasculature and consequently significant amount in liver and kidney, whereas passively- targeted nano-formulations accumulated quite substantially in the tumor over time (Fig 1D). Ex vivo organ accumulation studies convincingly confirmed these findings (Fig 1E), both qualitatively and quantitatively. A novel CT-FMT based hybrid-imaging protocol to non-invasively visualize and analyze probe accumulation in tumors and healthy organs was developed, and its suitability for quantitative biodistribution monitoring was demonstrated using passively and actively targeted polymeric nanomedicines.

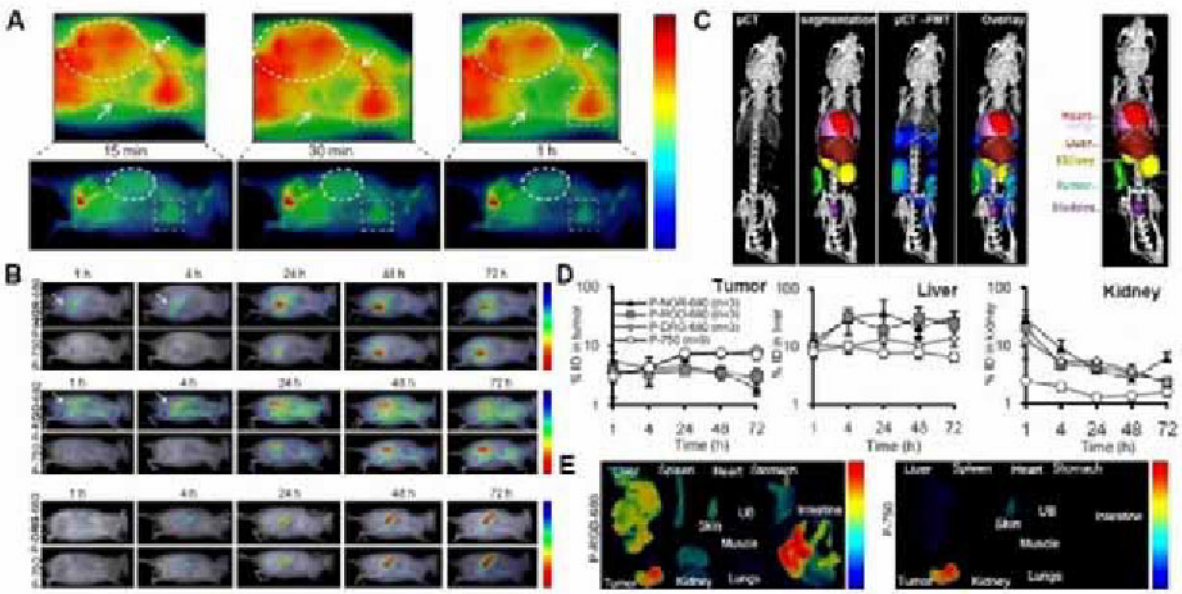


Disclosure of author financial interest or relationships:
**S. Kunjachan**, None; **F. Gremse**, Philips, Grant/research support; **F. Kiessling**, None; **T. Lammers**, None.

Presentation Number **P271**
Poster Session 2
September 6, 2012 / 15:15-15:15 / Room: The Liffey

# Non-invasive probing of orthotopic human acute myeloid leukemia development in mouse bone marrow thanks to near-infrared-2-Deoxyglucose (NIR-2DG): specificity, efficiency and exploitability

*Carolien Woolthuis[1], Linda Ariza-McNaughton[1], Dominique Bonnet[1], **Francois LASSAILLY**[2], [1]Haematopoietic Stem Cell Laboratory, London Research Institute - Cancer Research UK, London, United Kingdom; [2]In Vivo Imaging Facility, London Research Institute - Cancer Research UK, London, United Kingdom. Contact e-mail: francois.lassailly@cancer.org.uk*

Introduction: Human acute myeloid leukemia (hAML) originates from a rare population of leukemia stem cells (LSCs) (Bonnet & Dick 1996, Nature). Orthotopic xenotransplantation of LSCs in highly immunocompromised mice allows to faithfully recapitulate many features of the human disease, therefore allowing to analyze its physiopathology and assess new therapeutic strategies in a clinically relevant setting. Unfortunately, longitudinal monitoring of AML development and response to treatment remains a challenging task involving invasive bone marrow (BM) punctures. Because gene transfer into LSCs impedes on their capability to engraft, bioluminescence (BLI) tracking cannot be implemented routinely for primary AML. We previously showed that near-infrared (NIR) staining of leukemic cells with lipophilic dyes was not a satisfying option for this application neither (Lassailly F et al, Blood 2010). Since glucose transporter expression and / or metabolism rate are frequently increased in various cancers, including leukemia, we wondered whether NIR-2-Deoxyglucose (NIR-2DG) could be a reliable tool for longitudinal quantification of human leukemia development and response to treatment. Methods As a starting point to assess NIR-2DG, we generated 2 mouse models based on orthotopic transplantation of hAML cell lines lentivirally transduced with luciferase. After administration of NIR-2DG, mice were imaged using NIR imaging (reflectance imaging, spectral unmixing and fluorescence tomography). Bioluminescence imaging (planar and diffuse luminescent tomography), was used as a positive control to locate leukemia cells and analyze the co-localization with NIR signals. Healthy animals injected with the same amounts of probe were used as stringent negative controls. Results: Starting with mice at an advanced stage of leukemia development, we observed a clear AML related increase of NIR signal as compared to healthy controls, associated with a good co-localization of BLI and NIR signals. After detailed flow cytometry analysis of different bones, we demonstrate that the frontoparietal bones of the skull, called calvaria, are a good BM compartment to analyze leukemia development. These, and other superficial sites of the skeleton therefore offer a convenient window to analyze the bone marrow. We exploited these anatomical sites to determine if evolution of NIR signal intensity over time would be useful for monitoring AML progression / response to treatment. Only the terminal stages of the disease induced a significant NIR signal increase. Conclusions: We conclude that NIR-2DG provides good enough data to make a convincing proof of principle. However, considering the dynamic range of quantification, it is unlikely that this strategy can be exploited to monitor the development of AML and / or its response to treatment. More importantly, these results underline the importance to include exploitability studies in order to demonstrate, beside extreme cases, how useful is the technology to assess biological questions.

Disclosure of author financial interest or relationships:
**C. Woolthuis**, None; **L. Ariza-McNaughton**, None; **D. Bonnet**, None; **F. LASSAILLY**, None.

Presentation Number **P272**
Poster Session 2
September 6, 2012 / 15:15-15:15 / Room: The Liffey

# The multi-kinase inhibitor R1530 reduces tumor glucose uptake in the H460a human NSCLC xenograft model in vivo

*Mark Dvorozniak, Kenneth Kolinsky, Brian Higgins, Kathryn Packman, Pamela Carroll,* ***Edmund C. Lee****, Discovery Oncology, Hoffmann-La Roche Inc., Nutley, NJ, USA. Contact e-mail: Edmund.Lee@Roche.com*

Introduction: The glucose analog, 2-deoxy-2-[18F]fluoro-D-glucose (18F-FDG), is widely used in positron emission tomography (PET) to monitor cellular glucose uptake of tumor tissue in oncology. Other glucose analog probes such as 2-deoxy-glucosone-750 (2DG-750; Caliper Life Sciences, Hopkinton, MA) and 2-deoxy-glucose-IRDye800CW (2DG-IR800; Li-Cor) are also gaining importance in small animal fluorescence imaging (FLI) to access tumor glucose uptake and disease burden in preclinical studies in vivo. R1530 is a pyrazolobenzodiazepine, which has been shown to inhibit multiple kinases that regulate various biological pathways involved in tumor cell cycle regulation and angiogenesis. We have previously demonstrated that R1530 has in vivo anti-tumor activity in a broad spectrum of human tumor xenograft models including H460a, A549, MDA-MB-435, 22RV1, LoVo and HCT116. Here, we applied in vivo FLI and demonstrated that R1530 reduces tumor uptake of 2DG-750 in the H460a human NSCLC xenograft model. Methods and Materials: H460a tumor-bearing mice were treated orally (po) with vehicle or R1530 at 25mg/kg twice daily (BID) for 4 consecutive days. Before each FLI session, mice were fasted or remain fed for 12 hr before receiving 10 nmoles of 2DG-750 (XenoLight Rediject 2DG-750; Caliper) via intravenous injections. Two hours after 2DG-750 injections, mice were imaged using IVIS® Spectrum system and data were collected and analyzed with Living Image 4.2 software (Caliper). Total photon fluxes within each fixed region of interest (ROI) covering either whole tumor or non-tumored region (background) of individual mice were determined. Results: Consistent with previously reported for 18F-FDG PET, fasting significantly enhanced tumor 2DG-750 uptakes compare to the non-tumor background region in the tumor-bearing mice. Importantly, when dosed at 25mg/kg po BID, R1530 significantly reduced tumor uptake of 2DG-750 compare to the vehicle-treated controls in the H460a xenograft model. Conclusion: Our data demonstrated that R1530 reduces tumor glucose uptake, which translated into antitumor activity in the H460a human NSCLC xenograft model. R1530 is currently in clinical testing.

Disclosure of author financial interest or relationships:
**M. Dvorozniak**, None; **K. Kolinsky**, None; **B. Higgins**, Roche, Employment; Roche, Stockholder; **K. Packman**, Hoffmann-La Roche, Inc., Employment; **P. Carroll**, Hoffman-LaRoche, Employment; **E.C. Lee**, Hoffmann-La Roche Inc., Employment .

Presentation Number **P273**
Poster Session 2
September 6, 2012 / 15:15-15:15 / Room: The Liffey

# Ionizing-radiation switch for transcriptional targeting of cancer genetic therapy

*Luen Hwu[1], Ai-Leen Huang[1], **Ren-Shyan Liu**[1,2], [1]MAGIC/NRPGM, Nuclear Medicine, Faculty of Medicine, National Yang-Ming University, Taipei, Taiwan; [2]National PET/Cyclotron Center, Taipei Veterans General Hospital, Taipei, Taiwan. Contact e-mail: rsliu@vghtpe.gov.tw*

Objectives: IR-inducible promoter is the pre-determined factor for successful radiogene therapy. E4- or E9ns2-pCMV$_{basal}$ has been used as the IR-inducible promoter. However, these chimeric promoters may result in ubiquitous transgene expression without IR irradiation due to strong pCMV$_{basal}$ activity. In this study, we developed a 9 copies tandem repeated CArG element (E9) as IR-inducible promoter and compared with E4-pCMV$_{basal}$ in vitro and in vivo by using two-step transcriptional amplification (TSTA) system and bioluminescent imaging techniques. Methods: We established a stable H1299 clone harbored pSTOP-FLuc (H1299/pSTOP-FLuc). The transcriptional pausing signals (STOP) were flanked by two loxP sites and were placed at the junction of pCMV and firefly luciferase (fluc). To demonstrate the tightly IR-inducible E9 promoter activity, we constructed two NLScre expression plasmids in which the Cre recombinase was tagged with the sequence of Nuclear Localization Signal from the SV40 T antigen, and the Cre expression was controled by E4-pCMV$_{basal}$ and E9, respectively. We also performed the same TSTA experiment on the mouse xenografted tumor model. The IR-inducible fluc expression was quantified by illuminator and in vivo bioluminescence imaging. Results: With or without IR triggering, strong FLuc activity constitutively expressed from the E4-pCMV$_{basal}$ -NLSCre construct when transfected into H1299/pSTOP-FLuc cells. In the absence of Cre recombinase, the minimal FLuc activity was retained. In contrast, the maximal FLuc activity was activated when the exogenous Cre was expressed from the IR-inducible promoter due to excision of loxP-flanked STOP by Cre. In contrast, the E9- NLSCre activity maintained almost inert state in the absence of IR triggering. Prominent FLuc activity was activated by E9 in vitro and in vivo at six hours post-2 Gy IR. Conclusions: The E9 promoter, possesses tightly-regulated IR-inducible activity in vitro and in vivo. This promoter is suitable for spatial and temporal control of transgene expression in transcriptional targeting for gene therapy.

Disclosure of author financial interest or relationships:
**L. Hwu**, None; **A. Huang**, None; **R. Liu**, None.

Presentation Number **P274**
Poster Session 2
September 6, 2012 / 15:15-15:15 / Room: The Liffey

# Evaluation iron pool in cancer cells and tissues and its validation as inflammation biomarker of early stage of cancer by Ferric-desferoxamin MR imaging

*Nathupakorn Dechsupa, Anan Udom-uttaracheewa, Chatchanok Udomtanakunchai, Dutsadee Suttho, Kriengsak Khattiya,* ***Samlee Mankhetkorn****, Laboratory of Physical Cjhemistry, Molecular and Cellular Biology; Center of Excellence for Molecular Imaging, Department of Radiologic Technology, Faculty of Associated Medical Sciences, Chiang Mai University, Maung, Thailand. Contact e-mail: samlee@cemithai.com*

The study aimed to investigate the differential iron pool of cancer cells/tissues and normal cells/tissues by using MRI and histological techniques. Comparison with normal PBSCs, the ferric ion was hyperpermeable across plasma membrane in small cell lung carcinoma GLC4 cells. Prussian Blue staining indicative of Fe(III) ion was prominent in storage in erythromyelogenous leukemic K562 and small cell lung carcinoma GLC4 cells compared with PBSCs. In addition, both K562 and GLC4 cells were overexpressed of vascular permeability factor/vascular endothelial growth factor which in turn might stimulate the hyperpermeable to ferric ion. With respect to normal animals, in Wistar rat staining for iron was almost absent in the liver and scarce in the red pulp of the spleen. By contrast, in Wistar rat implanted with GLC4 cells iron was abundant in stromal and tumor cells in the invasion, angiogenic, necrotic and hemorrhagic regions. The differential accumulation of iron cancer cells/tissues and normal cells/tissues can be clearly shown by T2W images of ferric-desferoxamin MRI in both cell phantom and in Wistar rat implanted with GLC4 cells. The particular observation was that the ferric-desferoxamin MR imaging can reveal the accumulation of iron in inflammatory stage which is an early stage of cancer. The results suggest that the tumor subverts iron recycling to its own advantage that can be used as a sensitive biomarker for early stage of cancer imaging.

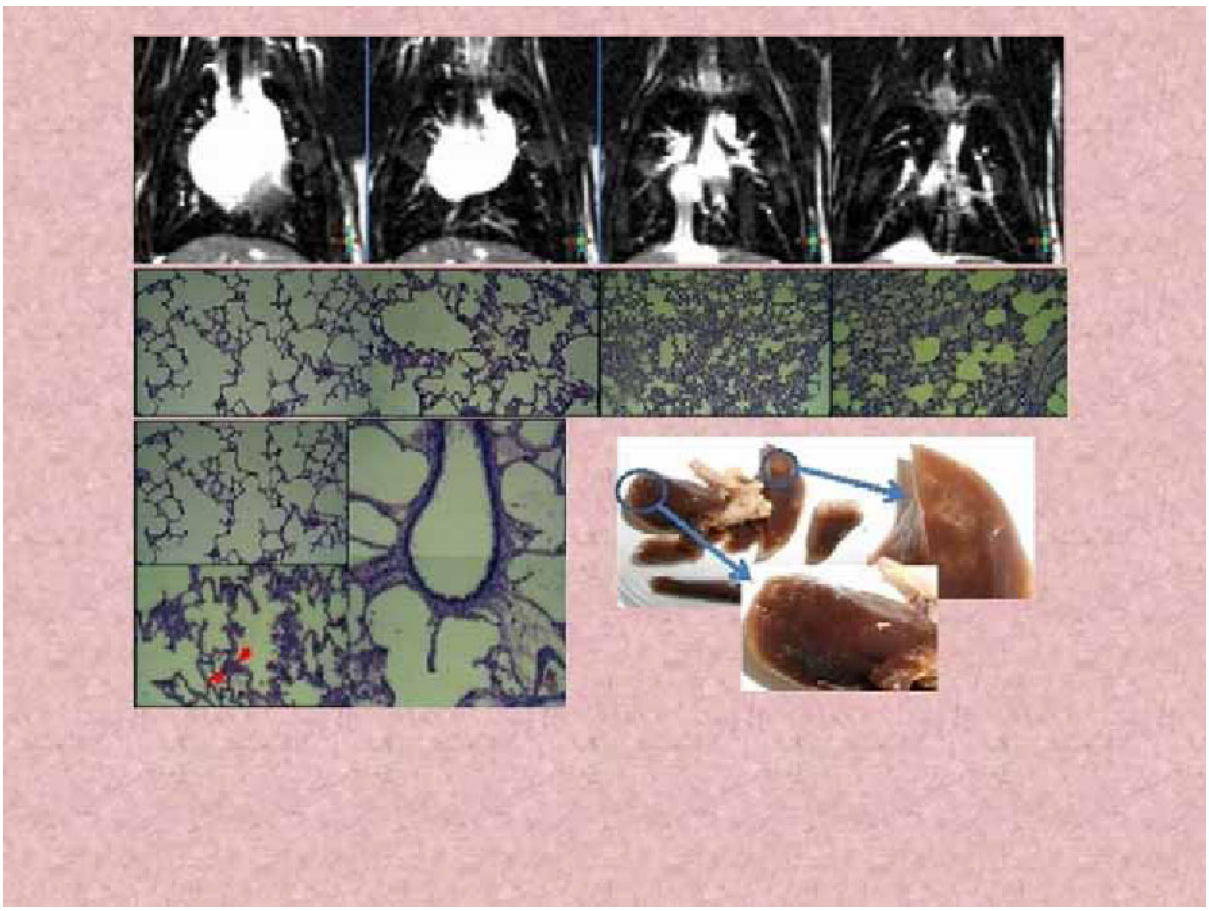

Figure 1. T2-weighted images, photomicrographs of lung tissue section and lung of human small lung carcinoma cell xenografted rats

Disclosure of author financial interest or relationships:
**N. Dechsupa**, None; **A. Udom-uttaracheewa**, None; **C. Udomtanakunchai**, None; **D. Suttho**, None; **K. Khattiya**, None; **S. Mankhetkorn**, None.

Presentation Number **P275**
Poster Session 2
September 6, 2012 / 15:15-15:15 / Room: The Liffey

# In vivo parametrisation of liver lesions using mouse SPECT/CT

***Domokos Mathe***[1], *Ildiko Futo*[2], *Ildiko Horvath*[2], *Daniel Veres*[3], *Krisztian Szigeti*[2], [1]*CROmed Ltd, Budapest, Hungary;* [2]*Biophysics and Radiation Biology, Semmelweis University, Budapest, Hungary;* [3]*Nanobiotechnology and In Vivo Imaging Centre, Semmelweis University, Budapest, Hungary. Contact e-mail: domokos.mathe@cromedresearch.com*

Objectives. The role of Kupffer-cells in liver steatosis, liver fibrosis and liver metastasis is subject to active research. According to previous in vitro studies published, the number and grade of liver tumors is inversely correlated with the mean number of liver Kupffer cells. Therefore our group has been researching appropriate, quantitative SPECT/CT in vivo imaging methods and image analytics to measure tumor grade, stage or liver lesion extent based on Kupffer cell imaging. Methods. We examined healthy control BALB/c mice (n=3) and MATN2 transgenic knock-out hepatocellular carcinoma mouse models (n=9). We used 99mTc-Nanocolloidal human serum albumine (mean diameter 80 nm) as radiopharmaceutical (90 MBq/animal iv., 2h post injection) for helical liver SPECT imaging with a voxel size of 0.2 mm.(NanoSPECT/CT Plus, Mediso, Hungary). Reconstructed volumes were used to segment the liver radioactivity volume using Otsu-thresholding with VivoQuant (inviCRO, US). Thus a liver radioactivity 3D map was generated. Standardized uptake values per animal were obtained from quantitated SPECT data. In the liver volume, an activity histogram was also defined for all animals. Skewness and kurtosis of the SPECT histogram was calculated for each animal.In all animals after imaging autopsy was performed the next day to provide control measurement of net liver volume and mass. Liver radioactivity volume was plotted against SUV from data as a means of validation for SUV calculations. Ex vivo liver tumor mass was used as objective disease grade. Results. An uptake with cold spots as tumors was observed in all diseased animals in SPECT/CT scans. SUV of livers correlated significantly ($p<0.05$) with segmented net radioactivity volumes in liver. A very strong ($p<0.001$) significant correlation was found between ex vivo liver tumor mass and both skewness and kurtosis of the 3D radioactivity map histogram in each animal. Conclusion. We have validated a simple and very effective means to quantitatively characterize liver cold spot lesions resulting from Kupffer cell disfunctions as a consequence of tumor burden. This SPECT/CT method is ready to measure liver damage in vivo, longitudinally and in a quantitative way.

Disclosure of author financial interest or relationships:
**D. Mathe**, CROmed Ltd, Stockholder; Mediso Ltd., Consultant; CROmed Ltd, Employment; **I. Futo**, None; **I. Horvath**, None; **D. Veres**, None; **K. Szigeti**, None.

Presentation Number **P276**
Poster Session 2
September 6, 2012 / 15:15-15:15 / Room: The Liffey

# Secreted Gaussia Luciferase as a Biomarker for Monitoring Tumor Colonization of Bacteria

***Vu H. Nguyen***[1,2], *Thuy X. Phan*[1,2], *Misun Yun*[1,2], *Yoon Soon Moon*[1,2], *Hyon E. Choy*[3], *Jung-Joon Min*[1,2], [1]*Laboratory of In Vivo Molecular Imaging, Gwangju, Republic of Korea;* [2]*Nuclear Medicine, Chonnam National University, Gwangju, Republic of Korea;* [3]*Microbiology, Chonnam National University, Gwangju, Republic of Korea. Contact e-mail: nghongvu13@gmail.com*

Optical imaging with luminescent markers has been exploited as common tools to visualize migration or proliferation of bacteria in living subjects. However, to monitor the distributions as well as the proliferation of bacteria in vivo, luminescence imaging has a limitation in small animals because of poor penetration through deep tissue. Therefore, our goal is to create a novel biomarker which could enable quantitation of injected bacteria in vivo longitudinally regardless of bacterial location. In our study, we employed Gaussia luciferase (Gluc) which has been well known as a secreted protein in mammalian system but not in prokaryotic one. To enable Gluc be secreted out of bacteria, a leader signal which responsible for the secretion of Gluc in eukaryotic cells was replaced by a strong prokaryotic secretory sequence. The novel recombinant Gluc protein shows significant enhancement of secretion in DH5a (~40%) and wild type E. coli (~10%). To apply for in vivo monitoring, the secretion system was constructed under control of a constitutive expressing promoter. The bacteria expressing Gluc were injected intravenously into normal as well as CT26 tumor-bearing mice. The serum was collected according to the indicated time points and subjected to luminescent assay using a luminometer or a cooled CCD camera (IVIS 100). The result showed the good correlation of bacteria number and the secreted Gluc activity detected in the blood of normal mice ($R^2$~0.9) as well as in tumor bearing mice ($R^2$~0.8). This is the first study of monitoring bacterial proliferation in living animals using Gluc expressing bacteria. This system could extend the application of optical imaging technique in monitoring bacteria-mediated cancer therapy.

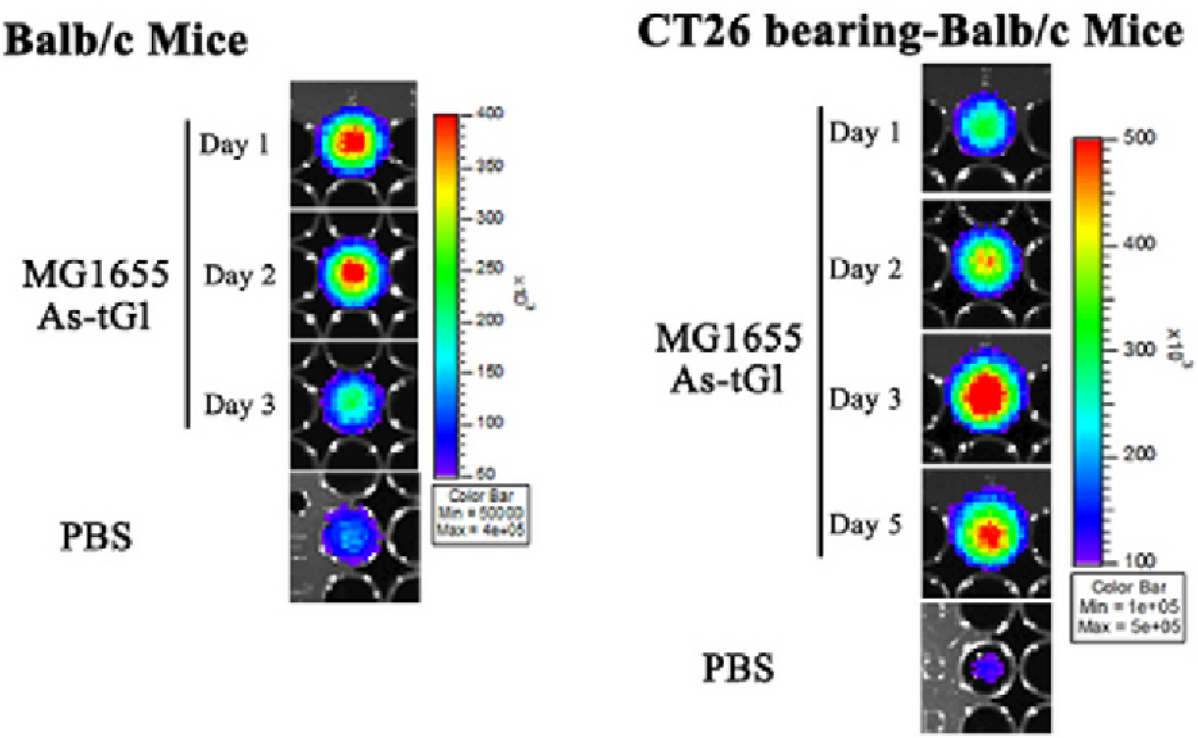


Figure 1. The signal from secreted Gaussia luciferase was detected in blood after bacterial injection with indicated time points.

Disclosure of author financial interest or relationships:
**V.H. Nguyen**, None; **T.X. Phan**, None; **M. Yun**, None; **Y. Moon**, None; **H. Choy**, None; **J. Min**, None.

Presentation Number **P277**
Poster Session 2
September 6, 2012 / 15:15-15:15 / Room: The Liffey

# Early detection of lung tumor using ultrashort echo time (UTE) and RARE $T_2$-weighted MRI on Lewis lung carcinoma (LLC-LM) pulmonary metastasis model

***Chia-Hsin Pan***[1], *Chia-Hao Su*[2], *Chia-Hsien Cheng*[3], *Jyh-Horng Chen*[1,4], [1]*Interdisciplinary MRI/MRS Lab, Department of Electrical Engineering and Molecular Imaging Center, National Taiwan University, Taipei, Taiwan;* [2]*Center for Translational Research in Biomedical Sciences, Kaohsiung Chang Gung Memorial Hospital, Kaohsiung, Taiwan;* [3]*Division of Radiation Oncology, Department of Oncology, National Taiwan University Hospital, Taipei, Taiwan;* [4]*Graduate Institute of Biomedical Electronics and Bioinformatics, National Taiwan University, Taipei, Taiwan. Contact e-mail: yolanda1019@hotmail.com*

Lung cancer is the leading cause of cancer-related death in worldwide, and CT is the standard imaging technique for acquiring lung anatomy in current. As to MRI of lung, it was challenging because of low proton density, high air susceptibility and spontaneous motion, especially on small animals with rapid heart rate and respiratory rate. With advance in MR technique, the ultrashort echo time dramatically reduced aforementioned problems.However, our study showed that it's hard to detect tumor simply depend on acquiring UTE images alone, because both of tumor and vessels exhibited hyperintensity thus unable to differentiate. Although motion artifact still existed in RARE $T_2$-weighted images with respiratory trigger module, it exhibited significant contrast between lung vessels and tumor. Furthermore, with SPIO injection, the contrast became more clearly for detecting tumors. In this study, the radiation-induced lung metastasis model is used. The male C57BL/6 mice (5-6 weeks age) were injected subcutaneously with 1 x $10^6$ LLC-LM cells at right hind limbs. At 8 days after implantation, a cobalt-60 unit was used to irradiate the limb tumor with 50Gy (five 10-Gy daily fractions). Using a 7-Tesla MRI system (BioSpec 70/30 USR, Bruker) with a 12 cm inner bore diameter gradient (BGA12-S, Bruker), and a 35 mm inner-diameter volume coil for RF transmission and reception. The TurboRARE $T_2$ pulse sequence and and UTE pulse sequence were used for *in vivo* animal MR imaging. In Figure 1a, the UTE image showed the motion artifact was totally avoided, but it's hard to differentiate the hyperintensity of vessels and tumor. Although the RARE $T_2$-weighted image with blurring induced by motion, the tumor exhibited significant contrast difference with vessels. The tumor size in this case is 3 mm in diameter. Another case showed in Figure 1b, a 6-mm tumor mass was detected. After SPIO injection, the tumor region was delineated more clearly and the signal intensity of vessels were reduced, therefore the tumor could be distinguished easily. As our results, MR imaging is potential to acquire lung anatomy. It's suggested to use both of UTE sequence and Rare $T_2$-weighted sequence to acquire lung images. The SPIOs is prominent to enhance the contrast between lung parenchyma and tumors for early detection of lung cancer. In future, we will try to diminish the limitation of the detected tumor size.

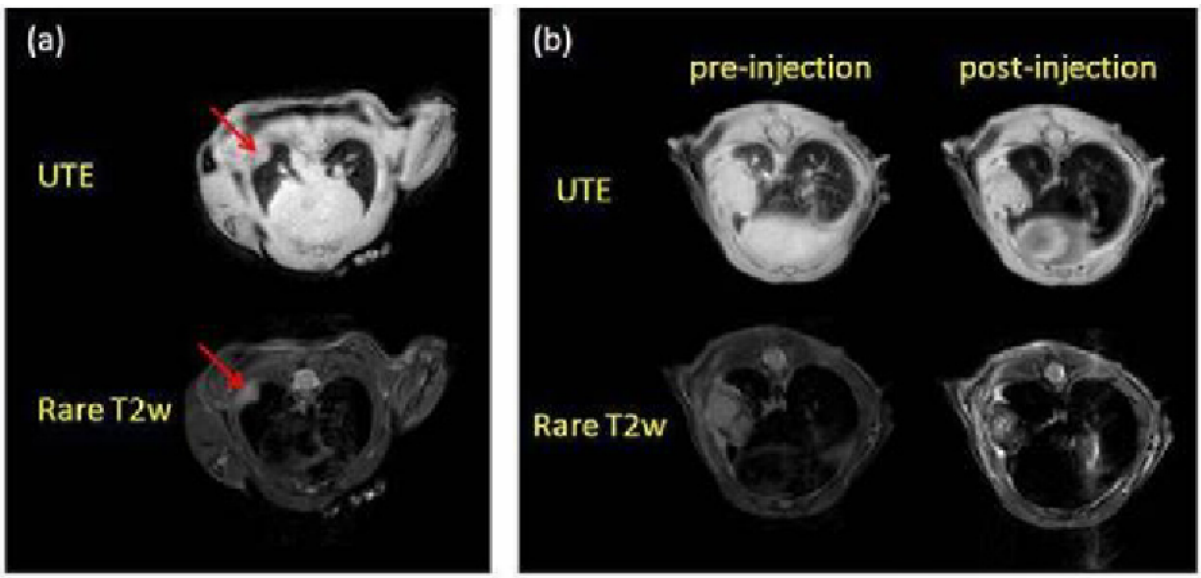


Fig. 1. (a) The lung tumor beside the chest wall was in 3 mm diameter. (b) A 6-mm tumor mass was detected. After SPIO injection, the hyperintensity of lung vessels were reduced and the tumor was clearly delineated.

Disclosure of author financial interest or relationships:
**C. Pan**, None; **C. Su**, None; **C. Cheng**, None; **J. Chen**, None.

Presentation Number **P278**
Poster Session 2
September 6, 2012 / 15:15-15:15 / Room: The Liffey

# Imaging Altered Drug Clearance in Colon Cancer Xenograft Model using (99m)Tc-Sestamibi

***Arvind Parmar***[1], *John Allen*[2], *Frederic Boisson*[1], *Marie-Claude Gregoire*[1], *Stephen Clarke*[2], *Andrew Katsifis*[1], *Graham R. Robertson*[2], [1]*Lifesceinces, Australian Nuclear Science and Technology Organisation, Lucas Heights, NSW, Australia;* [2]*Cancer Pharmacology Unit, ANZAC Research Institute, University of Sydney, Concord, Sydney, NSW, Australia. Contact e-mail: arvind.parmar@ansto.gov.au*

BACKGROUND: Multidrug resistance (MDR) and drug toxicity are two major hurtles to the success of anticancer therapy. In addition, evidence of altered drug clearance has also been reported in cancer patients. (99m)Tc-sestamibi(MIBI) is a widely used radiopharmaceutical for myocardial and oncologic imaging. Because of its unique role as a P-glycoprotein (P-gp)-specific substrate, this compound can be used to examine drug clearance by studying P-gp functional activity in vivo under pathologic conditions. Level of P-gp in tissues is reflected in the effective concentration of drugs in the blood and other organs. The main objective of this study is to use MIBI as a tool to investigate P-gp activity in various organs in tumoured mice for the predicting drug clearance and tissue toxicity. METHOD: Colon26 xenograft implanted subcutaneously in Balb/c x DBA mice were used for this study. Mice were divided in three groups i) control, ii) colon26 tumour-day12 and iii) colon26 tumour-day14, n=3 in each group. On the day of imaging mice were administered 20- 40 MBq of MIBI intravenously and a tomographic SPECT scan was performed for 0-3hrs using multipinhole mouse collimators on a Siemens preclinical Inveon SPECT/CT scanner. After imaging session mice were sacrificed and tissues were collected for biodistribution using gamma-counter. Inveon IRW software was used for reconstructing the images, data analysis and to obtain kinetic curves for heart, liver, kidneys, heart, brain, tumour, intestine, gallbladder and urinary bladder. RESULTS: The SPECT imaging and biodistribution data for MIBI was investigated and compared with the normal and the tumour mice. The Kinetic curves from SPECT imaging data revealed that the tumour mice showed slower rate of clearance in kidneys, intestines, gall bladder and liver compare to the control mice. This has been also supported by biodistribution data where low uptake was seen in intestines, liver, urine and bile fluid in the tumour groups compare to the control group.(please see the table given below) CONCLUSION: This study demonstrated significant altered drug clearance in tumoured mice. SPECT imaging using 99mTc-sestamibi may be a useful tool for predicting drug clearance and toxicity.

. Biodisribution data of 99m Tc-sestamibi at 3hr post administration.

| Tissues | Groups | | |
|---|---|---|---|
| | Control | Tumour Day12 | Tumour Day14 |
| Liver | 8.1±2.4 | 6.2±2.0 | 5.0±1.9 |
| Intestine Small | 43.42±3.1 | 24.2±6.8 | 19.7±7.8 |
| Intestine large | 12.4±3.6 | 5.9±0.3 | 10.4±6.8 |
| Urine | 60.0±14.0 | 23.3±15 | 19.0±9.1 |
| Bile fluid | 15.0±3.1 | 8.3±2.1 | 5.8±2.1 |

Table 1. The data expressed in Mean %ID/g±SEM (n=3).

Disclosure of author financial interest or relationships:
**A. Parmar**, None; **J. Allen**, None; **F. Boisson**, None; **M. Gregoire**, None; **S. Clarke**, None; **A. Katsifis**, None; **G.R. Robertson**, None.

Presentation Number **P279**
Poster Session 2
September 6, 2012 / 15:15-15:15 / Room: The Liffey

# A Novel Near Infrared Optical Imaging Probe for Detecting Prostate-Specific Membrane Antigen (PSMA) Expression Non-Invasively

*Sunetra Ray[1], Derek W. Bartlett[2], Lola Rahib[2], Anna M. Wu[3], Christian P. Behrenbruch[2], **Rajendra Singh**[1], [1]Caliper LifeSciences, a PerkinElmer Company, Alameda, CA, USA; [2]ImaginAb Inc, Los Angeles, CA, USA; [3]Molecular and Medical Pharmacology, UCLA, Los Angeles, CA, USA. Contact e-mail: rajendra.singh@perkinelmer.com*

Prostate-specific membrane antigen (PSMA) is a type II, transmembrane glycoprotein that is overexpressed on the surface of prostate tumor cells and in the neovasculature of many solid tumors. This unique expression of PSMA makes it a useful biomarker as well as an important extracellular target for imaging agents. The aim of this study was to develop a novel near infrared (NIR) fluorescently labeled imaging agent to non-invasively image and quantify tumor-associated PSMA expression in vivo. To achieve this, we used a human PSMA-targeted, bivalent engineered antibody fragment called a cys-diabody (Cys-Db), which is formed by two cross-paired scFv homodimers with terminal cysteines for site-specific conjugation. The PSMA-Cys-Db molecules were conjugated with a stable, thiol-reactive near infrared (NIR) VivoTag 680-XL dye for in vivo optical imaging applications. Fluorescence microscopy confirmed membrane localization of the NIR-labeled PSMA-Cys-Db conjugate in PSMA-expressing human prostate adenocarcinoma cell lines. Concentration-dependent binding of the probe to the PSMA+ cells was also demonstrated by flow cytometry. The in vivo plasma pharmacokinetic profile was assessed in mice by measuring plasma fluorescence at different times after intravenous injection with the agent (2.5 mg/kg), and tissue biodistribution was determined by imaging on the IVIS Spectrum. The probe showed rapid clearance with a plasma half-life of 4 hours, and in vivo and ex vivo biodistribution assessment showed significantly higher signal within the PSMA+ tumors. Tumor signal peaked at 3-5 hours following intravenous injection of PSMA-Cys-Db, decreasing gradually thereafter. In vivo quantification of tumor signal in nude mice showed significantly higher tumor signal in PSMA+ 22Rv.1 tumors than in PSMA- PC3M tumors (3.3 +/- 0.7x109 versus 1.9 +/- 0.3 x109 average radiant efficiency, respectively at 5 h imaging time, p=0.018; 2.8 +/- 0.6x109 versus 1.8 +/- 0.3 x109, respectively at 24 h imaging time, p=0.03). In conclusion, the new NIR-labeled PSMA-targeted cys-diabody targets PSMA receptors with high specificity, thereby allowing rapid detection (within 5 h) and quantification of PSMA expression in vivo.

Disclosure of author financial interest or relationships:
**S. Ray**, PerkinElmer, Employment; **D.W. Bartlett**, ImaginAb, Inc., Employment; **L. Rahib**, ImaginAb, Employment; **A.M. Wu**, ImaginAb, Inc., Consultant; ImaginAb, Inc., Stockholder; **C.P. Behrenbruch**, ImaginAb, Inc., Stockholder; **R. Singh**, PerkinElmer, Employment .

Presentation Number **P280**
Poster Session 2
September 6, 2012 / 15:15-15:15 / Room: The Liffey

# Clinically translatable VEGFR2 targeted microbubbles (BR55) enable assessment of early liver dysplasia

***Anne Rix***[1], *Christoph Grouls*[1,2], *Maximilian Hatting*[3], *Sibylle Pochon*[4], *Wiltrud Lederle*[1], *Isabelle Tardy*[4], *Christiane K. Kuhl*[2], *Christian Trautwein*[3], *Fabian Kiessling*[1], *Moritz Palmowski*[1,5], [1]*Department of Experimental Molecular Imaging, RWTH-Aachen University, Aachen, Germany;* [2]*Department of Diagnostic and Interventional Radiology, RWTH-Aachen University, Aachen, Germany;* [3]*Department of Internal Medicine III, RWTH-Aachen University, Aachen, Germany;* [4]*Bracco Suisse SA, Geneva Research Center, Geneva, Switzerland;* [5]*Department of Nuclear Medicine, RWTH-Aachen University, Aachen, Germany. Contact e-mail: arix@ukaachen.de*

Purpose: Analyzing the potential of assessing liver dysplasia using a clinically translatable ultrasound contrast agent targeted to VEGFR2 (BR55). Materials and Methods: Liver imaging was performed using a clinical ultrasound system equipped with the contrast-specific software. Nemo-P knockout mice with liver dysplasia and wild-type mice were examined. Two different types of contrast agents were applied: (i) non-targeted, commercially available, second-generation microbubbles (SonoVue®) and (ii) clinically translatable VEGFR2-targeted microbubbles (BR55). Contrast agent kinetics were assessed over 4 minutes; 5 min after injection the amount of microbubble retention was quantified using replenishment analysis. In-vivo binding-specificity of BR55 was tested in knockout mice. In-vivo ultrasound signal was correlated to immunohistochemistry. Results: The peak enhancement of both contrast agents was at a comparable level in healthy and dysplastic livers (SonoVue®: p=0.4606; BR55: p=0.4318). This was confirmed by immunohistochemistry, where an equal vessel density was found in both groups. Using SonoVue®, the signal in healthy and dysplastic livers decreased similarly over 4 min. BR55 provided a significantly higher signal 2, 3 and 4 min after injection in dysplastic livers compared to healthy liver tissue (p=0.0303, 0.0480, 0.0480, respectively). The amount of stationary BR55 5 min after injection was significantly higher in dysplastic than in healthy livers (p=0.0097). Immunohistochemistry also confirmed a significantly higher level of VEGFR2 in dysplastic livers (p= 0.0231). Binding specifity of BR55 to VEGFR2 was proven by in-vivo competition in dysplastic livers (p=0.0262). Conclusion: VEGFR2-targeted microbubbles (BR55) enable to distinguish early stages of liver dysplasia from normal liver before changes in vascularisation can be depicted with nontargeted contrast agents.

Disclosure of author financial interest or relationships:
**A. Rix**, None; **C. Grouls**, None; **M. Hatting**, None; **S. Pochon**, Bracco Suisse SA, Employment; **W. Lederle**, None; **I. Tardy**, Bracco Suisse SA, Employment; **C.K. Kuhl**, None; **C. Trautwein**, None; **F. Kiessling**, None; **M. Palmowski**, None.

Presentation Number **P281**
Poster Session 2
September 6, 2012 / 15:15-15:15 / Room: The Liffey

# In vivo MRI visualization of drug release induced by non focused Ultrasound in an experimental tumor model

***Silvia Rizzitelli**, Pierangela Giustetto, Cinzia Boffa, Marta Ruzza, Juan C. Cutrin, Daniela Delli Castelli, Silvio Aime, Enzo Terreno, Molecular & Preclinical Imaging Center, University of Torino, Torino, Italy. Contact e-mail: silvia.rizzitelli@unito.it*

Liposomes loaded with the antracycline Doxorubicin are clinically used as anticancer chemotherapy drug indicated to treat many solid tumors . The incapsulation of the cytotoxic drug into well-tolerated liposomes significantly reduces the severe side effects of the drug, driving the accumulation of the therapeutic to the tumor. However, several approaches aimed at controlling and optimizing the local release of the drug in the lesion are under scrutiny. Among them, the use of Ultrasound as external triggering factor has received attention and it has been demonstrated useful on experimental tumor model on mice. Recently, we demonstrated that low frequency non focused US can induce a mechanical release of the liposomal payload (both in vitro and in vivo) using MRI as visualization modality to provide an excellent spatio-temporal control of the release process. To this purpose, stealth liposomes with a Doxyl-like formulation, but encapsulating the clinically approved MRI agent Gadoteridol instead of the drug, was prepared to have a clinically-safe MRI probe acting as a release imaging reporter. In this contribution, a nanoconstruct consisting of the MRI probe and the drug was prepared and tested in vivo on an experimental murine model of breast cancer. First, the sonosensitivity of the theranostic nanosystem was checked in vitro with the aim of finding the experimental conditions for which the release of doxorubicin could be mimicked by Gadoteridol. Interestingly the release of Gadoteridol and Doxorubicin from the same nanocarrier was very similar (see the Figure). For in vivo experiments, the amount of the injected compounds has to be carefully tuned to reach the threshold of the MRI visualization for the Gadoteridol release without changing the clinical dose of the drug. For this reason, the release efficiency was also measured in systems containing two liposome populations (with the same lipid components) each one encapsulating the respective chemical (Doxorubicin or Gadoteridol). Again, the results obtained supported the view that Gadoteridol is a good imaging reporter for the release of the anticancer drug. As in vivo proof-of-concept, the theranostic liposomes were injected in the tail vein of mice grafted with a syngeneic breast cancer model. The subcutaneous tumor was exposed to a single shot of pulsed non focused US (duty-cycle 50 %, insonation 2 min) just after the liposome injection to maximize the local release of the drug and its diffusion in the tumor mass. Mice received a single dose of chemoterapeutic (5 mg/kg bw) per week for three weeks and the ‘US group' was insonated after each injection. Mice were monitored by MRI over the three weeks and T1 and T2 contrast was measured in tumor, liver, spleen and kidneys. Furthermore, MRI was also used to monitor the tumor growth (see the figure). A more rapid tumor shrinkage was observed for mice exposed to US. Organs were explanted at different timepoints and subjected to conventional histology as well as to confocal fluorescence microscopy and MALDI imaging, to assess the tumor distribution of the liposomes payload and evaluate the differences between ‘US-exposed' and control groups.

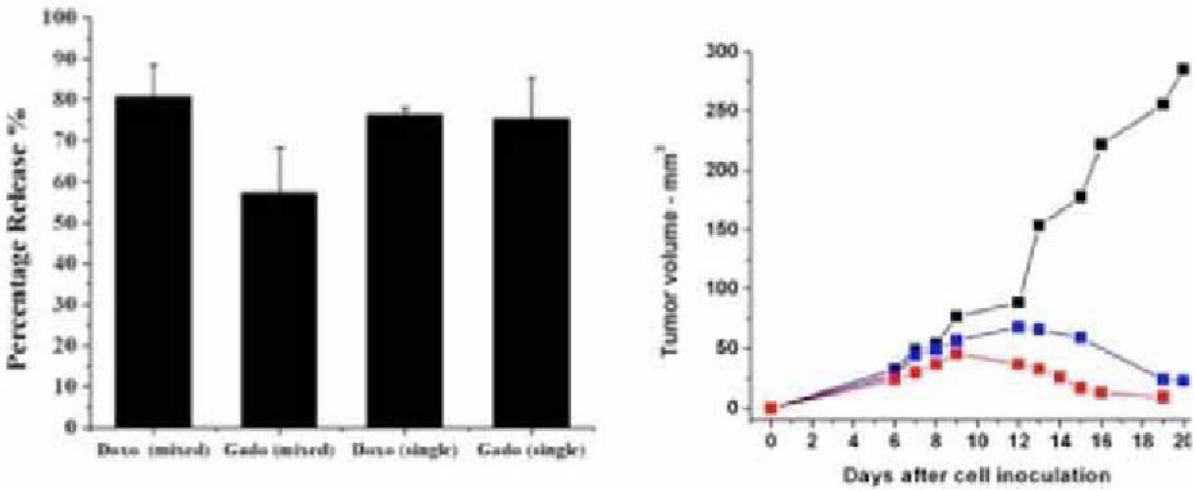


Left: Percentage release of Doxorubicin (Doxo) and Gadoteridol (Gado) from a single liposome or a mixture of two liposomes each one loaded with the drug and the MRI agent. The release was evaluated from fluorescence (Doxorubicin) or relaxometric (Gadoteridol) mesurements. US frequency 0.7 MHz, total insonation time 2 min, duty-cycle 50% (tON 1 sec). Right:Tumor growth assessed by T2-weighted MR images of mice treated with Doxyl-like liposomes containing Doxorubicin and Gadoteridol with (red) and without (blue) local insonation at the tumor. In black the tumor growth wihout chemoterapeutic treatment. Doxorubcin-loaded liposomes were injected i.v. at day 7 and at day 14. Non focused US (0.7 MHz, total time 2 min, duty-cycle 50 %) were applied just after each drug administration.

Disclosure of author financial interest or relationships:
**S. Rizzitelli**, None; **P. Giustetto**, None; **C. Boffa**, None; **M. Ruzza**, None; **J.C. Cutrin**, None; **D. Delli Castelli**, None; **S. Aime**, Bracco Imaging, Consultant; Bruker, Grant/research support; **E. Terreno**, Bracco Imaging, Consultant .

Presentation Number **P282**
Poster Session 2
September 6, 2012 / 15:15-15:15 / Room: The Liffey

# Noninvasive Molecular Imaging of Tumor-tropic Cells containing Raman Nanospheres in the murine brain

***Laura S. Sasportas***[1], *Cristina Zavaleta*[1], *Paul J. Kempen*[2], *Sanjiv S. Gambhir*[1], [1]*Radiology, Stanford University, Stanford, CA, USA;* [2]*Material Science and Engineering, Stanford University, Stanford, CA, USA. Contact e-mail: lss@stanford.edu*

One of the most challenging steps in brain tumor therapy is to accurately delineate tumor margins for optimal surgical resection, significantly impacting patient outcomes. Several groups have been studying the delivery of nanoparticles and/or nanoparticles-loaded cells into brain tumors. There is a need for (1) enhancing the glioma targeting efficacy of nanoparticles while (2) lowering the dose of nanoparticles in the reticulo-endothelial system (RES). To achieve this goal, we propose to use tumor-tropic cells as a delivery vehicle for delivering surface enhanced Raman spectroscopy (SERS) gold nanoparticles into brain tumors. We chose two carrier cell types known to be tumor-tropic: (1) Macrophages which can be harvested from the patient's blood and are typically recruited by gliomas as "tumor-associated macrophages" and (2) Mesenchymal Stem Cells (hMSCs) harvested from the bone marrow which harbor high tropism for human glioma. In order to explore the potential of these cells to be loaded with nanoparticles, we incubated RAW264.7 human macrophages with SERS nanoparticles at various concentrations (0.05 nM - 0.4 nM) during 10-24 hours. The 120 nm-diameter SERS consists of a Raman active layer adsorbed onto a 60-nm diameter gold core coated with silica (Fig. 1A), which emits a unique Raman spectrum upon excitation with a 785-nm laser (Fig. 1D). Raman imaging demonstrated high signal in the macrophages (Fig. 1C), which mirrored the reference spectrum of pure SERS (Fig. 1D). To confirm intracellular location, we performed Scanning Electron Microscopy (SEM) imaging of Secondary electrons (SE) and Backscattered electrons (BSE) which demonstrated SERS both on the surface and within phagocytic vesicles of the RAW264.7 cells (Fig.1E-F). Furthermore, we quantified the effect of SERS incubation concentration on the average Raman signal per RAW264.7 (Fig.1L). When we performed SERS uptake studies on hMSCs, they did not passively or actively (using transfection reagents) take up SERS. However, we achieved an effective loading of hMSCs with SERS using electroporation (Fig. 1 G-I), as confirmed by SEM images (Fig.1 J-K). In order to quantitatively assess the detection of SERS-loaded cells in the brain, we stereotactically injected a low number (1x10^4) of SERS-loaded RAW264.7 cells intracranially in a live mouse. *In vivo* non-invasive Raman imaging by raster scanning over the living mouse skull revealed a high Raman signal in the injection area (Fig. 1N-O). Furthermore, *ex vivo* Raman imaging of excised brain sections showed a well-delineated area of high Raman signal (Fig. 1P) correlating with the reference spectrum of SERS (Fig. 1Q). Here we demonstrated the capability of both macrophages and hMSCs to be loaded with SERS in cell culture. We have also shown the potential for macrophage cells to deliver SERS to the brain, which can be imaged by non-invasive *in vivo* Raman imaging. We are currently investigating the potential of those SERS-loaded cells to delineate tumor margins *in vivo* in a human glioma model. These results may eventually lead to novel strategies for surgical planning, intraoperative image guided surgery, and treatment of glioblastomas.

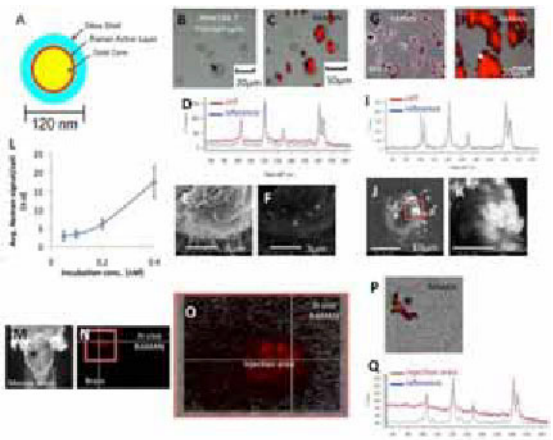


Figure 1. (A) Schematic of a SERS Raman nanoparticle (B) Brightfield, (C) Raman images of RAW264.7 macrophages incubated with SERS nanoparticles. (D) Raman spectrum of cell (arrow in (C)) as compared with the reference spectrum of pure SERS. (E)Secondary electrons (SE), (F) Backscattered electrons (BSE) SEM images of RAW264.7 cell showing localization of SERS-nanoparticles. (G-I) Same as above and (J-K) Mixed SE-BSE SEM images, for human mesenchymal stem cells electroporated with SERS. (L) Average Raman signal per RAW264.7 cell incubated with various concentrations of SERS. (M) Schematic, (N-P) in vivo Raman images of mouse brain after intracranial injection (location indicated by*) of SERS-loaded RAW264.7cells. (P) Ex vivo Raman imaging of brain section and (Q) corresponding Raman spectrum of the injection area (crosshair in (P)).

Disclosure of author financial interest or relationships:
**L.S. Sasportas**, None; **C. Zavaleta**, None; **P.J. Kempen**, None; **S.S. Gambhir**, General Electric, Grant/research support; Bayer-Schering, Grant/research support; Sanofi-Aventis, Grant/research support; CellSight, Stockholder; ImaginAB, Stockholder; Enlight, Stockholder; Endra, Stockholder; Bracco, Consultant; NinePoint Medical, Stockholder; Visualsonics, Consultant .

Presentation Number **P283**
Poster Session 2
September 6, 2012 / 15:15-15:15 / Room: The Liffey

# Comparing gold nanospheres and gold nanorods as Raman molecular imaging agents for assessing tumor margins in orthotopic gliomas

***Laura S. Sasportas***, *Jesse V. Jokerst, Cristina Zavaleta, Paul J. Kempen, Sanjiv S. Gambhir, Bioengineering, Radiology, Stanford University, Stanford, CA, USA. Contact e-mail: lss@stanford.edu*

One of the most challenging steps in brain tumor therapy is to accurately delineate tumor margins for optimal surgical resection. Several groups have been studying the delivery of nanoparticles to brain tumors, via targeting molecules or the Enhanced Permeability and Retention (EPR) effect. These nanoparticles could guide preoperative and intraoperative tumor margins imaging, significantly improving patient outcomes. Here we compare two types of Raman imaging gold nanoparticles and evaluate their potential as multimodality molecular imaging agents for orthotopic human gliomas. For this purpose, we chose two gold-based nanoparticles, because of the high Surface-Enhanced Raman Scattering (SERS) effect provided by gold. The first particle, a 120 nm-total diameter gold nanosphere, consists of a Raman active molecular layer (trans-1,2-bis(4-pyridyl)-ethylene) adsorbed onto a 60-nm diameter gold core coated with silica (Fig. 1A-B). We further modified the particles with DOTA-Gd3+ via a maleimide linkage, resulting in a triple modality gold nanosphere (GNS) that can be imaged using MRI, Photoacoustics (PA), and Raman imaging. The second particle that we synthesized is a 45 nm long, 20 nm thick gold nanorod (GNR) coated with a Raman molecular tag (IR792) and a PEG layer (Fig.1C-D). This particle can be imaged using Raman and PA imaging. The GNS has a negative zeta potential (-22mV) and its optical absorbance peaked in the visible range, at 540 nm (Fig.1E), with a very high absorbance coefficient of 2.75 x 1010 cm^-1M^-1. The GNR have a zeta potential of +10mV, an absorption peak at 661nm in the near infrared range (Fig.1G), and an absorbance coefficient of 3.11 x 109 cm^-1M^-1. Upon excitation with a 785-nm laser, each particle emits a unique and easily distinguishable Raman spectrum (Fig.1F, H). We performed intravenous injections (n=3 mice) of GNS (170μL at 16nM) or GNR (100μL at 4nM) in mice bearing orthotopic U87 human glioma xenografts. *In vivo* non-invasive Raman imaging by raster scanning over the living mouse head revealed a high Raman signal in the glioma area at 3h and 48h following GNS injection. In both cases, following perfusion and fixation, Raman imaging of the excised 300μm thick brain sections showed a well-delineated area of high Raman signal (Fig. 1I, K). For both the GNR and GNS injections, high signal co-localized within the glioma tissue, and correlated with the reference spectrum of the nanoparticles (Figs. 1I-K), We quantified the uptake of both gold nanoparticles by the glioma and concluded that both particles exhibit a similar tumor to background ratio of 3.1 per pmole of particle injected (Fig.1J, n=3 slices/brain). Here we demonstrated the capability of both GNS and GNR to accumulate equally within orthotopic human glioma xenografts, owing to the EPR effect. We are currently investigating the *in vivo* non-invasive PA imaging properties of both gold nanoparticles for deep tissue imaging. These results could significantly accelerate the translation of novel gold nanoparticle based agents from bench to operating room for intraoperative multimodality brain imaging, and help select the ideal particles for this application.

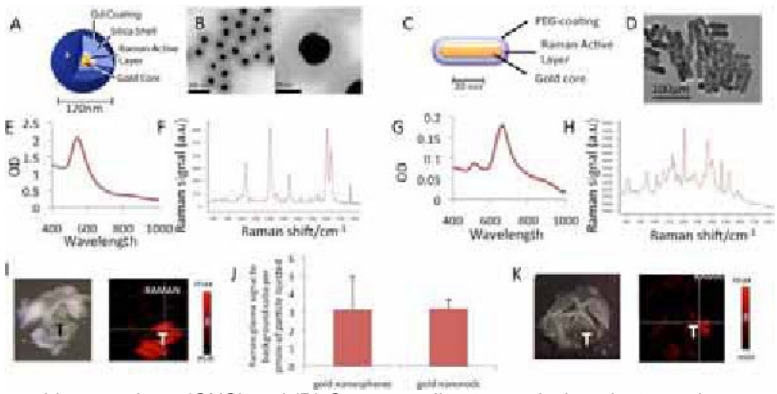


Figure 1. (A) Schematic of a Raman gold nanosphere (GNS) and (B) Corresponding transmission electron microscopy (TEM) image. (C) Schematic of a gold nanorod (GNR) and (D) corresponding TEM image. (E) UV-Vis absorption spectrum of GNS and (F) Raman spectrum of GNS upon excitation by a 785nm laser. (G) UV-Vis absorption spectrum of GNR and (H) Raman spectrum of GNR upon excitation by a 785nm laser. (I) Photograph and Raman image of an excised 300μm thick brain section of a mouse bearing an established U87 glioma, 48h after receiving an intravenous injection of GNS. (J) Quantification and comparison of Raman glioma to brain background signal ratio for animals injected with GNS and GNR, normalized by the amount (pmoles) of nanoparticles injected. (K) Photograph and Raman image of an excised 300μm thick brain section of a mouse bearing an established U87 glioma, 24h after receiving an intravenous injection of GNR.

Disclosure of author financial interest or relationships:
**L.S. Sasportas**, None; **J.V. Jokerst**, None; **C. Zavaleta**, None; **P.J. Kempen**, None; **S.S. Gambhir**, General Electric, Grant/research support; Bayer-Schering, Grant/research support; Sanofi-Aventis, Grant/research support; CellSight, Stockholder; ImaginAB, Stockholder; Enlight, Stockholder; Endra, Stockholder; Bracco, Consultant; NinePoint Medical, Stockholder; Visualsonics, Consultant .

Presentation Number **P284**
Poster Session 2
September 6, 2012 / 15:15-15:15 / Room: The Liffey

# Comparative analysis of FDG and FLT uptake in different lung carcinoma cell lines

***Sonja Schäfers***[1], *Lydia Wachsmuth*[2], *Stefan Wagner*[3], *Sven Hermann*[1,5], *Thomas Viel*[1], *Carsten Müller-Tidow*[4], *Klaus Kopka*[3], *Michael Schäfers*[1,5], *Cornelius Faber*[2,5], *Andreas H. Jacobs*[1,5], [1]*European Institute for Molecular Imaging (EIMI), University Hospital of Münster, Münster, Germany;* [2]*Clinical Radiology, University Hospital of Münster, Münster, Germany;* [3]*Nuclear Medicine, University Hospital of Münster, Münster, Germany;* [4]*Molecular Hematology and Oncology, University Hospital of Münster, Münster, Germany;* [5]*Interdisciplinary Centre of Clinical Research (IZKF), University of Münster, Münster, Germany. Contact e-mail: s.schaefers@uni-muenster.de*

**Introduction:** Lung cancer is the most common cause of cancer-related death worldwide. For defining treatment strategies non-invasive longitudinal assessment of tumor progression is important. This may be performed by employing molecular imaging techniques, such as positron emission tomography (PET) and magnetic resonance imaging (MRI). **Aim:** To evaluate glucose metabolism and tumor proliferation by 2-deoxy-2-[$^{18}$F]fluoro-D-glucose (FDG) and 3'-deoxy-3'-[$^{18}$F]fluoro-L-thymidine (FLT) µPET in conjunction with µMRI in various lung cancer cell lines grown *in vivo* with respect to tumor type- and size-dependent differences of radiotracer uptake. **Methods:** Five lung cancer cell lines (A549, HTB56, EBC1, H1975, NCI H82) were implanted subcutaneously in NMRI nude mice (n=3 tumors per mouse, n=4 mice per cell line). Tumor growth was followed by caliper measurements. Two and four weeks after implantation FDG- and FLT-PET were performed employing a high-resolution HIDAC µPET camera (spatial resolution 0.7 mm FWHM). Radiotracer uptake was quantified in % ID/ml. In some animals (n=9) T2 weighted morphological MRI was performed at 9.4 T (Bruker Biospec, in plane resolution 137 µm, slice thickness 1 mm) and the apparent diffusion coefficient (ADC) was determined by diffusion weighted (DWI) MRI. Histology was performed to correlate µPET findings with tumor proliferation (Ki67), human equilibrative nucleoside transporter-1 (hENT1) and thymidine kinase 1 (TK-1) expression. **Results:** All tumors showed similar growth *in vivo*. The uptake of FLT differed significantly between cell lines, with H1975 and A549 demonstrating the highest radiotracer uptake of 12.2 ± 1.1 % IDmax/ml for H1975 and 8.6 ± 0.6 % IDmax/ml for A549. All other cell lines showed lower uptake (HTB56: 4.7 ± 0.1 % IDmax/ml; EBC1: 4.6 ± 0.3 % IDmax/ml; NCI H82: 4.5 ± 0.6 % IDmax/ml). In H1975 and A549 tumors FDG uptake was significantly lower and therewith comparable to the other investigated cell lines (H1975: 6.0 ± 0.9 % IDmax/ml; A549: 3.6 ± 0.3 % ID/ml; HTB56: 5.8 ± 0.3 % IDmax/ml; EBC1: 4.4 ± 0.3 % IDmax/ml; NCI H82: 6.1 ± 0.9 % IDmax/ml). The investigated cell lines differed with respect to intratumoral homogeneity, clearly visible on µMR as well as on µPET images. This finding could be confirmed by immunohistochemistry. Quantitative evaluation of MRI data and immunohistochemistry (Ki67, hENT1, TK-1) and a detailed comparison to µPET images is still ongoing. **Conclusion:** Tumor tissue heterogeneity varies considerably between different lung cancer cell lines. Furthermore, these cell lines differ in their *in vivo* uptake of the proliferation marker FLT. These data suggest that inter-individual differences in FLT uptake have to be taken into account when employing FLT-PET for treatment planning in clinical situations. **Funding:** Supported in part by EU FP7 IMI project QuIC-ConCePT; grant agreement N° 115151

Disclosure of author financial interest or relationships:
**S. Schäfers**, None; **L. Wachsmuth**, None; **S. Wagner**, None; **S. Hermann**, None; **T. Viel**, None; **C. Müller-Tidow**, None; **K. Kopka**, None; **M. Schäfers**, Siemens Medical Solutions, Grant/research support; **C. Faber**, None; **A.H. Jacobs**, Merck, Germany, Grant/research support .

Presentation Number **P285**
Poster Session 2
September 6, 2012 / 15:15-15:15 / Room: The Liffey

# Monitoring targeted radionuclide therapy of [131I]m-iodobenzylguanidine (mIBG) in murine models of neuroblastoma using 124I-mIBG PET and bioluminescence imaging

*Stephanie T. Murphy[1], Shorouk F. Dannoon[1], Henry F. VanBrocklin[1], jW. ,Clay Gustafson[2], Erin A. Nekritz[2], Willam Weiss[3], Katherine K. Matthay[2], **Youngho Seo**[1], [1]Radiology and Biomedical Imaging, University of California, San Francisco, San Francisco, CA, USA; [2]Pediatrics, University of California, San Francisco, CA, USA; [3]Neurology, University of California, San Francisco, CA, USA. Contact e-mail: youngho.seo@ucsf.edu*

**Objectives:** 131I-mIBG is used as a targeted radionuclide therapy agent for neuroblastoma, the most common extracranial cancer in children. Using murine xenograft models of neuroblastoma, we evaluated 124I-mIBG PET/CT dosimetry and bioluminescence imaging (BLI) methods to follow the 131I -mIBG treatment. **Methods:** NB1691-luc, a human neuroblastoma cell line (NB1691) transfected with luciferase, was implanted in the left renal capsule of 5 athymic mice. Baseline 124I-mIBG PET imaging and dosimetry and D-luciferin (100 µL at 30 mg/ml) BLI were performed for all animals. 7-23 MBq of 131I-mIBG were administered intravenously to three animals that were alive after a 5-day session of 124I-mIBG PET pretherapy scans. BLI was performed to follow the 131I-mIBG treatment at 3-4 day intervals until mortality. Maximum radiance values from three different views of BLI were quantified to show the tumor response. **Results:** Prior to 131I-mIBG therapy, all animals showed clear 124I-mIBG PET uptake or BLI signals from renal capsule tumors. After the 131I-mIBG treatment, the decrease in BLI signals was observed within 10 days in the three surviving animals. The BLI signal reduction reached a level that was comparable or even lower to the baseline BLI signals in all three treated animals. **Conclusion:** Bioluminescence imaging showed utility in assessing 131I-mIBG therapy of neuroblastoma renal capsule xenograft tumors in murine models. Processing of 124I-mIBG PET/CT data for tumor dosimetry of 131I-mIBG therapy is underway. We are also extending our therapy monitoring strategy to evaluate the combination therapy of 131I-mIBG with chemotherapeutic drugs.

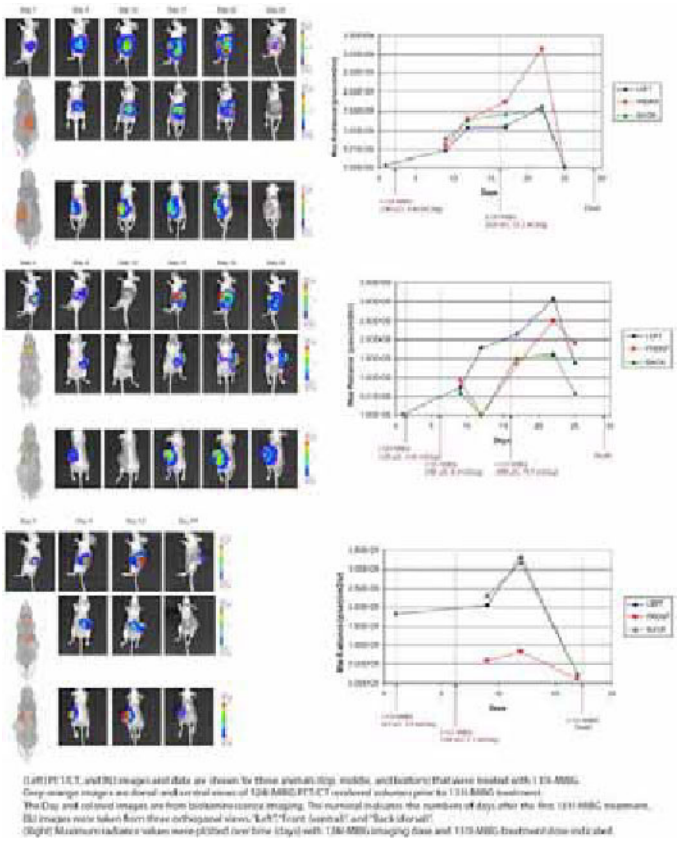

Disclosure of author financial interest or relationships:
**S.T. Murphy**, None; **S.F. Dannoon**, None; **H.F. VanBrocklin**, Cancer Targeted Technologies, LLC, Grant/research support; iTi Health, Inc., Grant/research support; Varian Biosynergy, Grant/research support; **J. Gustafson**, None; **E.A. Nekritz**, None; **W. Weiss**, None; **K.K. Matthay**, None; **Y. Seo**, None.

Presentation Number **P286**
Poster Session 2
September 6, 2012 / 15:15-15:15 / Room: The Liffey

# Synthesis and Preclinical Evaluation of Al$^{18}$F Labeled Gastrin-Releasing Peptide Receptor Antagonists for Tumor Imaging

***Svetlana V. Selivanova***[1], *Adrienne Müller*[1], *Stefanie D. Krämer*[1], *Roger Schibli*[1], *Simon M. Ametamey*[1], *Keith Graham*[2], *Sandra Borkowski*[2], *Timo Stellfeld*[2], *Ludger M. Dinkelborg*[2], [1]*Center for Radiopharmaceutical Sciences, ETH Zurich, Zurich, Switzerland;* [2]*Global Drug Discovery, Bayer HealthCare, Berlin, Germany. Contact e-mail: svetlana.selivanova@pharma.ethz.ch*

Radiolabeled bombesin analogues may serve as useful radiopharmaceuticals for imaging gastrin-releasing peptide receptor (GRPR) positive tumors. Previously described bombesin antagonist labeled with $^{68}$Ga showed high tumor uptake and favorable pharmacokinetics.[1] $^{18}$F radioisotope has better physical properties in terms of spatial resolution and dosimetry. We aimed at developing and evaluating $^{18}$F labeled antagonist and comparing it to earlier reported $^{68}$Ga-analogue. Six Al$^{18}$F-NOTA labeled antagonists were synthesized using simple kit-like AlF method, comparable in efficiency to metal coordination chemistry. No usual drying step was needed since reaction occurs in aqueous buffer. Solid-phase extraction was sufficient to purify the radiolabeled products. Total synthesis time was under 30 minutes, including purification and quality control. All analogues displayed high binding affinities to GRPR ($K_i$ ~1 nM) as determined by competitive binding assay. Lipophilicity was estimated by HPLC method giving values log$D_{7.4}$ = -0.3 - -3.0. *In vivo* PET imaging was performed in nude mice bearing PC-3 xenografts. All radiolabeled compounds showed high tumor uptake and low background radioactivity. The main difference in radiotracer distribution was observed in non-target organs and tissues (namely in liver and intestines). Radioactivity accumulation in tumor was successfully blocked by pre-injection with 50 µg bombesin. One compound, Al$^{18}$F-NOTA-4-amino-1-carboxymethyl-piperidine-D-Phe-Gln-Trp-Ala-Val-Gly-His-Sta-Leu-$NH_2$ (**1**) ($K_i$ = 0.68 ± 0.06 nM, log$D_{7.4}$ = -1.7), was selected for further investigation. *Ex vivo* biodistribution indicated 4.5 ± 0.8 %ID/g tumor uptake compared to 1.6 ± 0.4 %ID/g under blocking conditions. High tumor to blood ratio (58) and tumor to muscle ratio (57) were calculated. *In vivo* metabolism of this radiotracer was studied in normal mice by analyzing blood and urine samples using UPLC and TLC. At 15 min after injection the amount of parent compound in blood was 75%, while two unidentified more hydrophilic radiometabolites were observed. Urine contained these two hydrophilic radiometabolites mostly (25% and 69% respectively) with <5% parent radiotracer. In conclusion, the Al$^{18}$F-NOTA labeled antagonist **1** is a good candidate for imaging GRPR-positive tumors and merits further translation towards investigation in humans. [1] Mansi R. et al. Eur. J. Nucl. Med. Mol. Imaging, 38: 97-107, 2011.

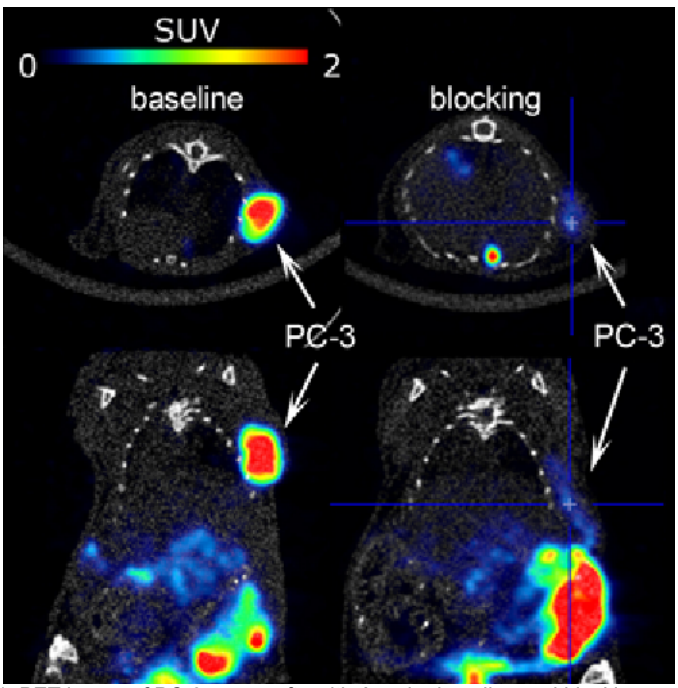


Figure 1. PET image of PC-3 xenografts with **1** under baseline and blocking conditions.

Disclosure of author financial interest or relationships:
**S.V. Selivanova**, None; **A. Müller**, None; **S.D. Krämer**, None; **R. Schibli**, None; **S.M. Ametamey**, None; **K. Graham**, Bayer Healthcare, Employment; **S. Borkowski**, Bayer AG, Employment; **T. Stellfeld**, Bayer Pharma AG, Employment; **L.M. Dinkelborg**, Piramal Imaging, Employment .

Presentation Number **P287**
Poster Session 2
September 6, 2012 / 15:15-15:15 / Room: The Liffey

# Reproducibility study of 13C magnetic resonance spectroscopy using hyperpolarized [1-13C] pyruvate

***Eva Serrao***[1,2], *Tiago B. Rodrigues*[1,2], *Mikko I. Kettunen*[1,2], *Ferdia Gallagher*[1,2], *Brett W. Kennedy*[1,2], *De en Hu*[1,2], *Joan Boren*[1,2], *Helen Sladen*[1,2], *Kevin M. Brindle*[1,2], [1]*Cambridge Research Institute, Cambridge, United Kingdom;* [2]*Department of Biochemistry, University of Cambridge, Cambridge, United Kingdom. Contact e-mail: eva.serrao@cancer.org.uk*

Background: [1-13C]pyruvate is a well established substrate in the field of dynamic nuclear polarization/MRI. This emerging technique has the potential to offer novel biological and physiological insights into cancer. Preclinical studies have reported [1-13C]pyruvate to be a good imaging marker for early response to therapy. Although the first clinical trial is already being undertaken in prostate cancer, the reproducibility of serial scans has never been determined. The aim of this study is to determine the reproducibility of [1-13C]pyruvate as a 13C-labelled magnetic resonance spectroscopy (13C-MRS) probe, in an implanted murine lymphoma model. Methods: C57BL/6 mice were implanted subcutaneously in the flank with EL-4 cells (a murine lymphoma) and divided into two cohorts. In one of the cohorts, mice were fasted for 18 hours (n=8) while in the other they had no dietary restriction (n=5). All mice were anaesthetized with isoflurane, taped to a holder and placed in a heated probe to maintain a constant core body temperature of ~37C. Respiratory rate and body temperature were monitored throughout the entire experiment by a Biotrig physiological monitor (Small Animal Instruments, Stony Brook, NY). A 20-mm surface coil (Rapid Biomedical GmbH, Rimpar, Germany) was placed over the tumors and 13C-MR spectra were acquired from a 6 mm slice immediately after i.v. injection of 0.2 ml of pyruvate, using a 7 T horizontal bore magnet (Varian, Palo Alto, CA). The hyperpolarized solutions of [1-13C]pyruvate were prepared using a polarizer (Hypersense, Oxford Instruments, Oxford, UK). Each mouse was submitted to the same imaging protocol twice, with a 4 hour interval between scans. All mice were recovered from anaesthesia after the first scan and the fasted cohort was kept fasted between scans. 13C spectroscopic data were fitted to the modified Bloch equations to calculate the rate constant for conversion of pyruvate to lactate (kP) using Matlab (Mathworks). Coefficients of variation (CV) and differences in kP values between studies in the same individual were calculated to determine the reproducibility. Results: The CV for the mean kP between animals in which [1-13C]pyruvate was injected was 13.270 ± 9.987% for the fasted mice and 47.873±22.086% for the non-fasted mice. The mean percentage change in the kP value observed between the first and the second scan was 117% in the non-fasted mice, and 15% in the fasted animals. There was a significant difference of the kP mean of the first scan between the fasted and non-fasted cohort, as well as between the first and the second scan of the non-fasted mice. Time of injection, tumor size, and body weight did not appear to contribute to the variability of the scans. Conclusions: [1-13C]pyruvate is reproducible as a probe with relatively low variability, when performed in fasted mice. Animal fasting is a crucial requirement for serial assessment.

Disclosure of author financial interest or relationships:
**E. Serrao**, General Electric Company, Grant/research support; **T.B. Rodrigues**, GE, Grant/research support; **M.I. Kettunen**, GE Healthcare, Grant/research support; **F. Gallagher**, GE Healthcare, Grant/research support; **B.W. Kennedy**, General Electric Healthcare, Grant/research support; **D. Hu**, None; **J. Boren**, None; **H. Sladen**, GE Healthcare, Grant/research support; **K.M. Brindle**, GE Healthcare, Grant/research support; GSK, Consultant .

Presentation Number **P288**
Poster Session 2
September 6, 2012 / 15:15-15:15 / Room: The Liffey

# Radionulclide-carrying liposomes with excellent clearance from reticuloendothelial system for diagnostic tumor imaging and radionuclide therapy

***Izumi O. Umeda***[1], *Yusuke Koike*[1,2], *Sadaaki Kimura*[1], *Kenjirou Higashi*[2], *Kunikazu Moribe*[2], *Keiji Yamamoto*[2], *Hirofumi Fujii*[1], [1]*Functional Imaging Division, National Cancer Center, Kashiwa, Japan;* [2]*Graduate School of Pharmaceutical Sciences, Chiba University, Chiba, Japan. Contact e-mail: izumi.umeda@gmail.com*

**Objectives:** Radionuclide-carrying liposomes are promising radiopharmaceuticals for diagnostic tumor imaging and radionuclide therapy because of their high specific affinity to tumors. But, conventional liposomes also accumulate in reticuloendothelial systems (RES), such as liver and spleen, even though they are PEGylated. This has hindered their clinical application. The aim of this study is to produce novel radionuclide-carrying liposomes that are expected to bring about rapid clearance of radionuclide from RES. For this purpose, we designed unique nuclide-ligand complexes rapidly cleared from cells after RES trapping. **Methods:** Liposomes were composed of DSPC and cholesterol. $^{99m}$Tc-ethylenedicysteine (EC) or $^{111}$In-EC was encapsulated in liposomes by the active loading method. Biodistribution of obtained liposomes were studied in sarcoma-180-bearing ddY mice, comparing to conventional liposomes encapsulating $^{111}$In-nitrilotriacetic acid (NTA). The chemical structure of excreted radionuclide-ligand complexes were analyzed using HPLC with an ODS column. *In vivo* images were acquired using a small animal SPECT/CT scanner (Bioscan). **Results and Discussion:** $^{99m}$Tc-EC/$^{111}$In-EC liposomes showed similar biodistribution to $^{111}$In-NTA liposomes until 6-12 hrs after the intravenous injection. After that, $^{99m}$Tc-EC/$^{111}$In-EC were, however, rapidly washed out from liver (2.8 % /3.6% injected dose/g at 24hrs) and spleen (13.1 %/12.9 %/g) while keeping good retention in the tumor (4.8%/5.1%/g). On the contrary, $^{111}$In-NTA was retained in the liver (12.3%/g) and spleen (33.5%/g) as well as tumor (11.5%/g). There was little difference in the biodistribution between $^{99m}$Tc-EC liposomes and $^{111}$In-EC liposomes. $^{99m}$Tc-EC liposomes and $^{111}$In-EC liposomes were rapidly excreted into the urine; 48%/41% of injected dose were excreted by 24 hrs. On the other hand, $^{111}$In-NTA liposomes were excreted in the urine only less than 6%. HPLC analysis confirmed that $^{99m}$Tc-EC and $^{111}$In-EC were excreted keeping their original complex formation. *In vivo* SPECT imaging at 24hrs after the injection successfully visualized these different biodistribution patterns: $^{99m}$Tc-EC/$^{111}$In-EC liposomes well depicted tumors with low uptake of liver and spleen while $^{111}$In-NTA liposomes failed to selectively image tumors due to high uptake of liver and spleen. Excellent RES clearance of our novel liposomes should be attributed to the behavior of $^{99m}$Tc-EC/$^{111}$In-EC after the release from liposomes in the RES, that is, they were able to come out of the RES and be excreted via the blood circulation. **Conclusions:** $^{99m}$Tc-EC/$^{111}$In-EC carrying liposomes could be excellent tumor imaging agents because they selectively accumulate in tumors with low RES uptake. Radionuclide therapy using $^{186/188}$Re-EC liposomes and $^{90}$Y-EC liposomes would be also promising.

Disclosure of author financial interest or relationships:
**I.O. Umeda**, None; **Y. Koike**, None; **S. Kimura**, None; **K. Higashi**, None; **K. Moribe**, None; **K. Yamamoto**, None; **H. Fujii**, None.

Presentation Number **P289**
Poster Session 2
September 6, 2012 / 15:15-15:15 / Room: The Liffey

# Improvement of temozolomide chemotherapy for experimental gliomas using lentiviral vector-based anti-MGMT shRNA technology

***Thomas Viel***[1], *Parisa Monfared*[1], *Sonja Schäfers*[1], *Katrin Büther*[1], *Inga B. Fricke*[1], *Bastian Zinnhardt*[1], *Yannic Waerzeggers*[1], *Michael Schäfers*[1,2], *Andreas H. Jacobs*[1,3], [1]*European Institute for Molecular Imaging (EIMI), Westfälische Wilhelms-Universität (WWU) Muenster, Muenster, Germany;* [2]*Department of Nuclear Medicine of the University Medical Center, Westfälische Wilhelms-Universität (WWU) Muenster, Muenster, Germany;* [3]*Interdisciplinary Centre of Clinical Research (IZKF), Westfälische Wilhelms-Universität (WWU) Muenster, Muenster, Germany. Contact e-mail: vielt@uni-muenster.de*

Introduction: Despite treatments combining surgery, radiation-, and chemo-therapy, most patients affected by glioblastoma (GBM) have a poor prognosis. Addition of temozolomide (TMZ) to radiation therapy is now the standard therapy in clinical application, but effectiveness of TMZ is limited by tumor over-expression of the DNA repair protein O6-methylguanine-DNA methyltransferase (MGMT). Aim: To use high specific and efficient RNA interference technology to modulate MGMT expression in order to increase TMZ efficiency in resistant GBM. Methods: 2 anti-MGMT and 1 control shRNA sequences were cloned into a lentivirus backbone (pLKO). Lentiviruses were used to infect human GBM cell lines with high MGMT expression (LN18, T98 and VU28). MGMT depletion was assessed using western blot. Growth and clonogenic assays were used to correlate inhibition of MGMT and sensitivity toward TMZ. Nude mice subcutaneously (s.c.) xenografted with cells depleted or not in MGMT were treated with daily injections of TMZ (50 mg/kg). Tumour sizes were measured using caliper before, after 7 and after 12 days of treatment. Nude mice were also s.c. xenografted with wild type GBM cells expressing high MGMT. Lentiviruses expressing the shRNA sequences together with the luciferase reporter gene were injected directly into the tumours 2 days before treatment with TMZ. Bioluminescence imaging (BLI) was used to follow the virus infection, and tumour size evolution was evaluated using caliper measurement. Results: A specific inhibition of MGMT expression was observed at the protein level using the two anti-MGMT shRNA sequences in the 3 GBM cell lines. Reduction of TMZ LD50 was observed after down-regulation of the MGMT protein in culture using both clonogenic and growth assays. Tumour growth inhibition was observed following TMZ treatment for the xenografts with low MGMT expression in contrast to xenografts with high MGMT expression. BLI measurement showed that lentiviruses were able to transduce GBM xenografts efficiently in vivo. Most importantly, the treatment combining injection of a lentivirus expressing an anti-MGMT shRNA and TMZ induced a reduction of the size of the tumours, in contrast to treatments combining lentivirus expressing the shRNA control and TMZ. Conclusions: Inhibition of MGMT expression could be obtained through the use of virally delivered shRNA, leading to improvement of the TMZ treatment effect in culture and in vivo. Anti-MGMT shRNA gene therapy could be used in combination with TMZ chemotherapy in order to improve the treatment of resistant GBM. Acknowledgement: supported by Joint Translational Research Programme on Cancer (DAAD-INCa, PKZ: D/0811485), the BMBF funding MoBiMed (01EZ0811), and CLINIGENE NoE (LSHB-CT-2006-018933)

Disclosure of author financial interest or relationships:
**T. Viel**, None; **P. Monfared**, None; **S. Schäfers**, None; **K. Büther**, None; **I.B. Fricke**, None; **B. Zinnhardt**, None; **Y. Waerzeggers**, None; **M. Schäfers**, Siemens Medical Solutions, Grant/research support; **A.H. Jacobs**, Merck, Germany, Grant/research support .

Presentation Number **P290**
Poster Session 2
September 6, 2012 / 15:15-15:15 / Room: The Liffey

# Preclinical characterization of a dual-labeled trastuzumab-based imaging agent for diagnosing advance gastric cancer

***Xuejuan Wang**, Peking University School of Oncology, Beijing Caner Hospital, Beijing, China. Contact e-mail: xuejuan_wang@hotmail.com*

Purpose: On the basis of the results of the ToGA trial, HER2 status is included in the diagnostic workup of patients presenting with advanced gastric cancer. Trastuzumab, a humanized monoclonal antibody against HER2, is found to improve response rate and survival of those patients. Our aim was to synthesize and optimize a dual-labeled trastuzumab-based PET imaging agent to provide unique opportunities for noninvasive nuclear imaging with subsequent fluorescence image-guided resection and pathology. Methods: Trastuzumab was conjugated with both a radiometal chelating group (DOTA) and a fluorescent dye (IRDye 800CW), and radiolabeled with 64Cu. Purity, stability, immunoreactivity, internalization, and biodistribution were evaluated in HER2+ cells and tumors. Results: 64Cu-DOTA-trastuzumab-IRDye 800 demonstrated high purity by both chemical and fluorometric determinations. Both flow cytometry and the Lindmo assay demonstrated a high binding affinity of 64Cu-DOTA-trastuzumab-IRDye 800 to HER2-overexpressing cells. The dual-labeled conjugate was stable in PBS, but not in serum after 24h at 37° C. Larger molecules (>150KD) were seen after a 24h incubation in human serum. Biodistribution studies revealed tumor-specific accumulation of 64Cu-DOTA-trastuzumab-IRDye 800 in NCI-N87 tumors, and tumor uptakes at 24h and 48h were 10.23±1.11% and 14.62±13.23%, respectively following intravenous administration. The tumor-to-muscle ratio was 7.00 at 24h, and increased to 16.32 at 48h. Liver and kidney showed marked uptake of the dual-labeled imaging agent. Conclusion: 64Cu-DOTA-trastuzumab-IRDye 800 is an effective diagnostic biomarker that can be used to validate dual-labeled, molecularly targeted imaging agents and can allow these agents to be translated into clinical practice for identifying HER2+ lesions of gastric cancer.

Disclosure of author financial interest or relationships:
**X. Wang**, None.

Presentation Number **P291**
Poster Session 2
September 6, 2012 / 15:15-15:15 / Room: The Liffey

# Benign and malignant pleural effusion diagnosis with 1 H-MRS:a preliminary research

***Renhua Wu**, Yan Ding, Haiyang Dai, Shantou University, Shantou, China. Contact e-mail: rhwu@stu.edu.cn*

Objective To find the difference of the metabolite profiles between benign and malignant pleural effusion using clinic 1.5T 1H Magnetic resonance spectroscopy, and evaluate the feasibility and accuracy of MRS in distinguishing benign and malignant pleural effusion compared with clinic proofs. Methods Pleural effusion samples were collected from 32 clinical diagnosed lung cancer, tuberculosis and pneumonia patients. 50 ml fresh pleural effusion each patient was collected in a round plastic ball and tested using 1.5T clinic GE signa MR device. Parameters were: standard 8 channel head coil, voxel size was 20×20×20mm, TR=1500ms, TE=30ms. Shimming was performed automatic and water suppression was more than 99%. Record the chemical shifts of all major metabolic peaks and the area under the peaks in the spectral lines. Statistical analysis was performed on SPSS 17.0 software and $p < 0.05$ was considered with statistically significance. Results The main metabolites in the pleural effusion include valine (val), isoleucine (Iso), lysine (lys), lactic acid (Lac), choline (Cho) and inositol (MI). Comparing benign with malignant pleural effusion, we found that for benign pleural effusion samples, the peaks and metabolite areas of val, Iso and Lac are higher than pleural effusion from lung cancer patients with statistical significance ($p < 0.05$). For pleural effusion from lung cancer samples, the peaks and metabolite areas of Cr and MI are higher than benign samples collected from patients with tuberculosis and pneumonia with statistical significance ($p < 0.05$). The metabolic peaks and metabolite areas between inflammatory pleural effusion and tuberculosis pleural effusion have no statistical significance. Conclusion MRS has potential values in distinguishing the benign pleural effusion from the malignant ones. The high peak and concentration of Cho and MI may indicate malignant pleural effusion.

Disclosure of author financial interest or relationships:
**R. Wu**, None; **Y. Ding**, None; **H. Dai**, None.

Presentation Number **P292**
Poster Session 2
September 6, 2012 / 15:15-15:15 / Room: The Liffey

# Development of a ribosome-display identified knottin-like scaffold for molecular imaging of cancer

***Frederic Zoller***[1,2], *Annette Markert*[1], *Annette Altmann*[1,2], *Walter Mier*[2], *Uwe Haberkorn*[1,2], [1]*Clinical Cooperation Unit Nuclear Medicine, DKFZ, Heidelberg, Germany;* [2]*Department of Nuclear Medicine, University Hospital Heidelberg, Heidelberg, Germany. Contact e-mail: frederic.zoller@med.uni-heidelberg.de*

Objective: Ribosome display is a perspective screening technology for the identification of novel affinity binders. In this study, we performed a high-throughput screening of a miniprotein library based on the scaffold Min-23 to evolve a new molecular entity against the Notch-ligand delta-like ligand 4 (DLL4). DLL4 is strongly overexpressed in tumor endothelia and discussed as relevant target for diagnostic imaging and therapy of angiogenesis. Due to the remarkable stability and the tolerance to sequence mutagenesis, the two-disulfide-stabilized miniprotein Min-23 is an appropriate scaffold structure for new ligand design and especially for molecular imaging. Methods: Ribosome display screening using a customized Min-23 library against the recombinant extracellular domain of Dll4 was performed to generate a DLL4-binding motif. Surface plasmon resonance (SPR) experiments, cell binding assays, biodistribution studies and PET imaging with tumor-bearing small animal models were carried out to characterize the miniprotein in vitro and in vivo. Results: A high proteolytic stability (half-life in human serum > 30 hours) and target specificity (KD = 44 nM) and cell binding capability against HUVEC (16±2% binding/10^6 cells) was determined. These characteristics enabled clear visualization of AR42J-tumor in rats already 20 min after administration of the iodine-124 labelled tracer using PET. Ex vivo biodistribution studies (3.9±0.9% ID/g, tumor/muscle-ratio 9.7±1.2) confirmed the tumor targeting properties of the anti-DLL4 miniprotein. Thereby, depending on the disulfide configuration the Min-23 derivatives demonstrated a different in vitro and in vivo binding behavior. Structural analysis verified that only the native-like folded regioisomer allows for tumor imaging. Moreover, the tumor accumulation of the radiotracer could be blocked with unlabelled compound. Conclusion: The ribosome display-evolved Min-23 derivative represents a novel, non-immunoglobulin affinity agents targeting DLL4. The findings reported accentuate the potential of this high-throughput screening technology for the generation of new molecular imaging probes for cancer research. Therefore, further investigations on this miniprotein are warranted to evaluate this novel anti-Dll4 candidate for clinical application.

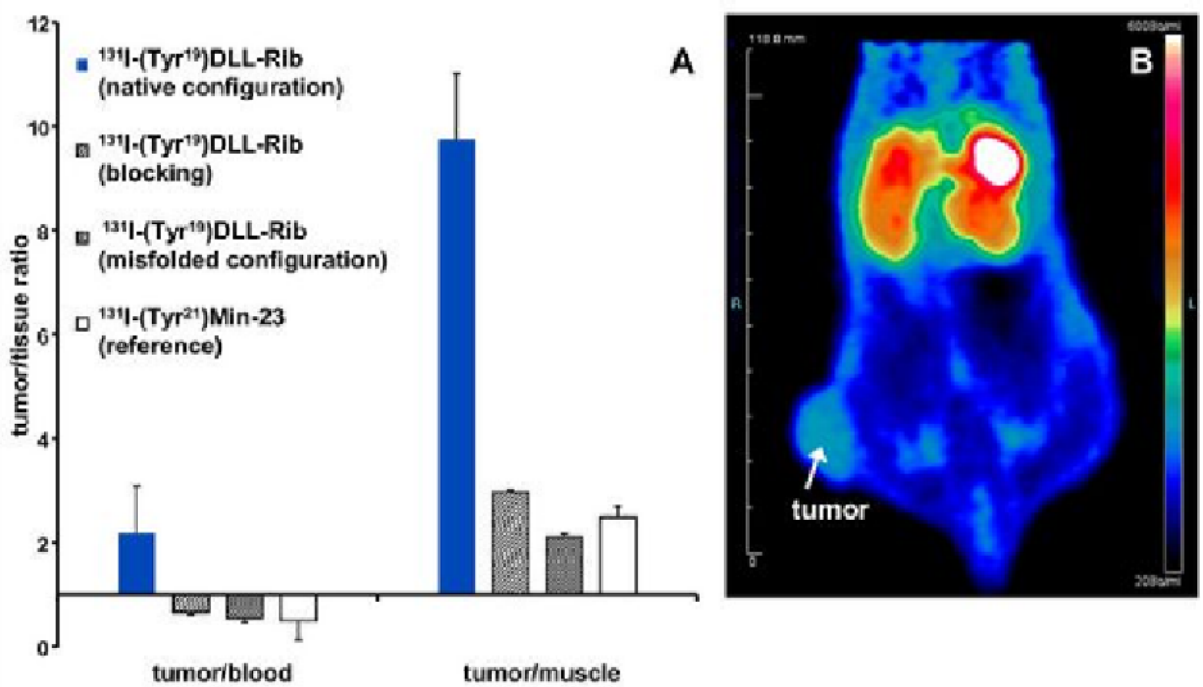


Ex vivo biodistribution studies (A) and PET-imaging with iodine-124 labelled miniprotein (B) demonstrate tumor targeting properties.

Disclosure of author financial interest or relationships:
**F. Zoller**, None; **A. Markert**, None; **A. Altmann**, None; **W. Mier**, None; **U. Haberkorn**, None.

Presentation Number **P293**
Poster Session 2
September 6, 2012 / 15:15-15:15 / Room: The Liffey

# Luciferase evaluation for sensitive dual color imaging of stem cell grafts in the mouse brain

***Markus Aswendt***[1], *Laura Mezzanotte*[2], *Rob C. Hoeben*[3], *Clemens Lowik*[2], *Mathias Hoehn*[1], [1]*In-Vivo-NMR Laboratory, Max-Planck-Institute for Neurological Research, Cologne, Germany;* [2]*Department of Endocrinology and Metabolic Diseases, Leiden University Medical Center, Leiden, Netherlands;* [3]*Department of Molecular Cell Biology, Leiden University Medical Center, Leiden, Netherlands. Contact e-mail: markus.aswendt@nf.mpg.de*

Objectives: Bioluminescence imaging (BLI) has become the method of choice for optical tracking of cells in vivo. Novel cell-based therapies benefit from the high bioluminescence sensitivity combined with a high signal-to-noise ratio and the quantitative correlation of emitted photons to number of cells. However, up to now the use of luciferases has not been optimized for sensitive neuroimaging. We compared 4 different luciferases expressed by tumor cells and neural stem cells (NSCs) in vitro and in vivo. Furthermore, we explored the possibility to discriminate luciferase signals based on different substrates and by applying a spectral unmixing algorithm. Methods: The full length cDNA of the luciferin-dependent CBG99 (click beetle, λmax 540 nm), Luc2 (firefly, λmax 615 nm), PpYRE9 (firefly, 630 nm) and the coelenterazine-dependent hRLuc (sea pansy, λmax 480 nm) were cloned into the vector pCDH-EF1-MCS-T2A-copGFP (Biocat, Heidelberg, Germany). HEK 293 cells and NSCs were transduced and FACS sorted for a homogenous copGFP signal. The sensitivity limit in vitro was determined with a dilution series from 5 to 5000 live cells after addition of 1 mM D-Luciferin (Synchem, Felsberg, Germany) or 60 µM coelenterazine-h (CTZ-h) using the IVIS Spectrum (Caliper, Mainz, Germany). For in vivo experiments, different cell amounts were stereotactically implanted into the striatum of nude mice and for comparison also under the skin of the back. Images were acquired with the same set-up after i.p. injection of 150 mg/kg D-Luciferin or 1 mg/kg Rediject CTZ-h (Caliper). Results: We systematically determined minimal detectable cell numbers with 4 different luciferases in tumor cells and NSCs (Fig. 1). In vitro 5-50 Luc2, hRLuc and CBG99 cells were detectable and 500 PpYRE9 cells. By applying a spectral unmixing algorithm, CBG99 signal could be precisely separated from PpyRE9 signal and less precisely from the signal of the Luc2 cells. All luciferin dependent luciferase signals were separated from the CTZ-h dependent hRLuc. The minimal detectable cell number for subcutaneous implants was 500 cells (Luc2, CBG99) and for intracerebral implants ~6x10^4 (Luc2, CBG99 and hRLuc). Conclusion: In summary CBG99 and PpYRE9 are the best couple for dual color imaging due to good spectral resolution. Nevertheless Luc2 and hRluc luciferases provide dual color imaging using two different substrates with higher sensitivity. This comparison and optimization of luciferases for in vivo neuroimaging permits protocols for visualization of distinct cell populations in vivo. Acknowledgements: This work was financially supported by grants from the Volkswagen Foundation (I/83 443) and the EU-FP7 program ENCITE (HEALTH-F5-2008-201842) and TargetBraIn (HEALTH-F2-2012-279017).

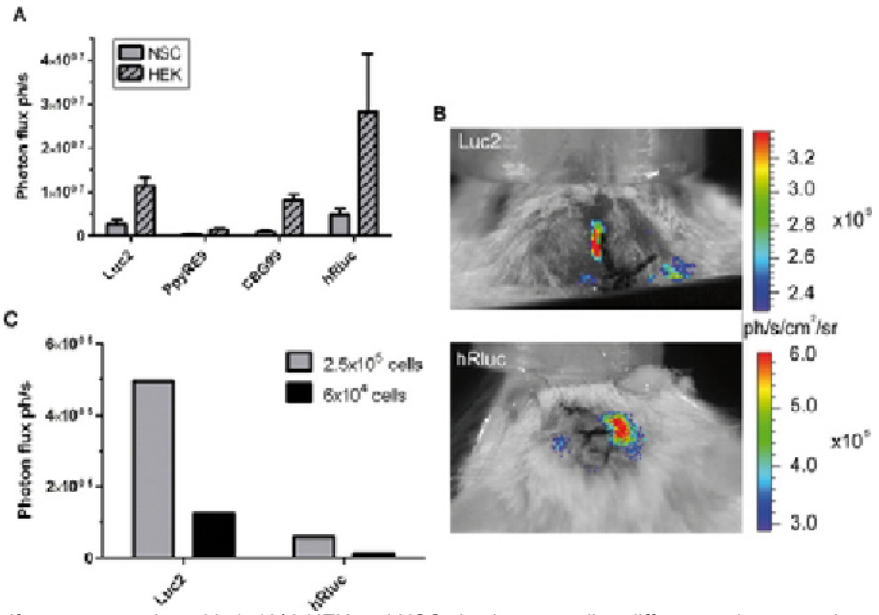


Fig. 1: A) Comparison of luciferase expression with 1x10^3 HEK and NSCs in vitro, revealing differences in expression strength and photon flux. B) Representative in vivo image of the mouse head, with signal from Luc2 and hRluc cells implanted into the mouse brain. C) Quantitative evaluation revealed approx. 8x higher sensitivity for Luc2 expressing cells in vivo.

Disclosure of author financial interest or relationships:
**M. Aswendt**, None; **L. Mezzanotte**, None; **R.C. Hoeben**, None; **C. Lowik**, None; **M. Hoehn**, None.

Presentation Number **P294**
Poster Session 2
September 6, 2012 / 15:15-15:15 / Room: The Liffey

# Neurodevelopmental Effects of High Magnetic Fields in the Development of an Intact Living Organism: Ceanorhabditis elegans

***Ricardo J. Faustino***[1,2], *Antero J. Abrunhosa*[1,2], *Miguel Castelo-Branco*[1,2], [1]*Institute of Nuclear Sciences Applied to Health (ICNAS), Coimbra, Portugal;* [2]*Institute of Biomedical Research on Light and Image (IBILI), Coimbra, Portugal. Contact e-mail: ricardofaustino@uc.pt*

The aim of our research is to observe possible changes on the nervous system of an intact living organism, C. elegans, continuously exposed to high magnetic fields during its full biological development. Our working hypothesis is that high magnetic fields (up to 14 Tesla) could induce physical and biochemical changes on living organisms, more specifically in nervous cells, through a mechanism known as mechanotransduction. We are specially focused on the development process because it is believed that it is when rapidly divinding cells are more exposed to this kind of effects. C. elegans was chosen as a model because it is a very well studied model in molecular biology. A special, transgenic, strain of C. elegans (OH441 like UNC-119) that expresses Green Fluorescent Protein (GFP) was used to obtain detailed fluorescent microscopic images of the nervous system after the exposures. The biometric image analysis of critical components of the nervous system and other biological data was performed using dedicated image processing software. Results obtained so far during a full development cycle of C. elegans failed to show any statistically significant variation in the cell biology and developmental parameters of the living organism. Present studies are expected to contribute to elucidate the role of high magnetic fields on the nervous system of C. elegans and contribute for the assessment of the safety and lack of bioeffects of high magnetic fields increasingly being used in biomedical imaging systems.

Disclosure of author financial interest or relationships:
**R.J. Faustino**, None; **A.J. Abrunhosa**, None; **M. Castelo-Branco**, None.

Presentation Number **P295**
Poster Session 2
September 6, 2012 / 15:15-15:15 / Room: The Liffey

# Using NF-κB Molecular Imaging to Evaluate the Therapeutic Effect of Sorafenib in Hepatocellular Carcinoma

***Fei-Ting Hsu***[1], *I-Tsang Chiang*[1], *Yu-Chang Liu*[1], *Hsin-Ell Wang*[1], *Ren-Shyan Liu*[1], *Wuu-Jyh Lin*[2], *Jeng-Jong Hwang*[1], [1]*Dept. of Biomedical Imaging and Radiological Sciences, National Yang-Ming University, Taipei, Taiwan;* [2]*Division of Radioisotope, Institute of Nuclear Energy Research, Taoyuan, Taiwan. Contact e-mail: sakiro920@hotmail.com*

Purpose: Liver cancer, comprised mainly of hepatocellular carcinoma (HCC), is the fourth leading cause of cancer death worldwide. Sorafenib (Nexavar, BAY 43-9006), a multikinase inhibitor, has been proposed to suppress HCC cell growth and inhibition of tumor angiogenesis. NF-κB is an inducible transcriptional factor for the expression of multiple genes involved in tumorigenesis, Here, we demonstrate the effect of sorafenib on NF-κB activity by using multimodalities of molecular imaging in human HCC cell lines and HCC-bearing animal model. Methods: We constructed a Huh7 stable cell clone with NF-κB responsive element to drive dual reporter genes, tk and luc2, and co-transfected with a third rfp reporter gene, renamed as Huh7/NF-κB-tk-luc2/rfp cells. The effects of sorafenib on HCC cells in vitro were assayed with MTT and mitochondria membrane potential (MMP) for cytotoxicity, EMSA for NF-κB/DNA binding activity, Western blotting for NF-κB regulated downstream proteins. Huh7/NF-κB-tk-luc2/rfp tumor-bearing mice were divided into two groups: vehicle (0.1% DMSO) and sorafenib alone (20 mg/kg/d for 30 days by gavage). The effects of sorafenib on dynamic change of NF-κB activation in tumor were evaluated with BLI and micro-SPECT/CT. Tumor growth inhibition was evaluated with digital caliper and BLI. Mice were sacrificed at the end of experiment for Western blot, H&E stain and whole-body autoradiography. Results: The expressions of NF-κB and its effector proteins (VEGF, MMP-9, XIAP, Bcl-2, and Cyclin D1) were inhibited by sorafenib. Moreover, Sorafenib significantly increased the percentage of unstained cells (the degree of MMP loss) in a time-dependent manner. In addition, sorafenib effectively suppresses constitutively activated NF-κB expression, and suppresses tumor growth in Huh7/NF-κB-tk-luc2/rfp tumor-bearing mice. Conclusions: Human HCC could be suppressed by sorafenib via NF-κB and its effector proteins in Huh7/NF-κB-tk-luc2/rfp tumor bearing mice evaluated with multimodalities of molecular imaging. (This study was supported by a grant NSC 101-2623-E-010-005-NU from National Science Council, Taipei, Taiwan.)

Disclosure of author financial interest or relationships:
**F. Hsu**, None; **I. Chiang**, None; **Y. Liu**, None; **H. Wang**, None; **R. Liu**, None; **W. Lin**, None; **J. Hwang**, None.

Presentation Number **P296**
Poster Session 2
September 6, 2012 / 15:15-15:15 / Room: The Liffey

# Photoacoustic imaging of gene expression in tumours: high resolution deep tissue imaging of tyrosinase labelled cells in the mouse

***Amit P. Jathoul***[1], *Jan Laufer*[4], *Peter Johnson*[1], *Olumide Ogunlade*[2], *Edward Zhang*[2], *Mark Lythgoe*[3], *R. Barbara Pedley*[1,3], *Paul Beard*[2], *Martin A. Pule*[1], [1]*Haematology, UCL Cancer Institute, London, United Kingdom;* [2]*Medical Physics and Bioengineering, UCL, London, United Kingdom;* [3]*Centre for Advanced Biomedical Imaging, UCL, London, United Kingdom;* [4]*Julius Wolff Institut, Charité, Berlin, Germany. Contact e-mail: a.jathoul@cancer.ucl.ac.uk*

Introduction: Photoacoustic imaging (PAI) is an emerging preclinical in vivo imaging modality thus far generally limited to imaging vasculature or vascularised tumours due to contrast afforded by endogenous haemoglobin (Hb). Cells and tissues remain invisible unless exogenous agents are injected to selectively enhance their contrast. Recently, genetic labels have been described and are under development, but none have so far been capable of longitudinally imaging cellular growth in vivo without the need for administration of a contrast agent. Methods: We stably retrovirally transfered a cassette of genes encoding human tyrosinase co-expressed with a functionally informative truncated human CD34 cell membrane marker that invoked the biosynthesis of eumelanin into different cell types. This system provided sensitive contrast for PAI using a Fabry-Perot detector-based photoacoustic system, as well as the detection of cells by flow cytometry and quick sorting of positively expressing cells using clinical-grade magnetic selection columns. Results: Using three-dimensional visualisation, we readily observed expressing cells injected subcutaneously into mice, along with their development and growth into tumours, and their association with surrounding vasculature, for a period of a month. Histological staining confirmed the presence of melanin pigment localised to the tumours. The excellent photoacoustic contrast achieved allowed high resolution images to be acquired at depth (8 mm) using wavelengths extending into the infrared (IR). Further, by multispectral imaging, vasculature and tumour could be acquired together or individually allowing co-localisation or independent feature analysis. Conclusion: This work illustrates the potential for using genetic labelling with tyrosinase for high-resolution preclinical in vivo imaging.

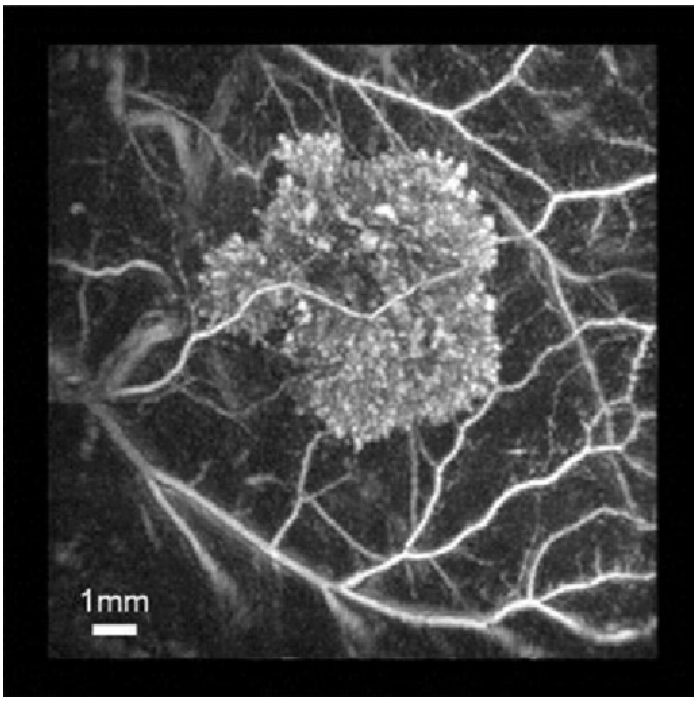


Subcutaneously injected cells imaged in vivo by photoacoustic imaging. x-y maximum intensity projections of 3D photoacoustic images acquired of 5 x 106 tyrosinase expressing K562 cells subcutaneously injected into a nude mouse (excitation wavelength=600nm). The cells produced eumelanin, which is a source of cellular contrast in the images.

Disclosure of author financial interest or relationships:
**A.P. Jathoul**, None; **J. Laufer**, None; **P. Johnson**, None; **O. Ogunlade**, None; **E. Zhang**, None; **M. Lythgoe**, None; **R. Pedley**, None; **P. Beard**, None; **M.A. Pule**, None.

Presentation Number **P297**
Poster Session 2
September 6, 2012 / 15:15-15:15 / Room: The Liffey

# Characterisation of a bright and stable rainbow of firefly luciferases: enhanced tools for in vivo bioluminescence imaging

***Amit P. Jathoul***[1], *Simon Thomas*[2], *Brian Philip*[1], *Martin A. Pule*[1], [1]*Haematology, UCL Cancer Institute, London, United Kingdom;* [2]*Academic Haematology, Royal Free Hospital, Room 2/296, Rowland Hill Street, London, United Kingdom. Contact e-mail: a.jathoul@cancer.ucl.ac.uk*

Firefly luciferase (Fluc) is an invaluable genetic label for molecular or cellular in vivo imaging. However, problems still impact on its optimal use, such as attenuation of wild-type (WT) Fluc emission (wavelength max ca.560nm) by haemoglobin, the xenogenic nature of the transgene, susceptibility to thermal inactivation and scatter inherent as photons pass through tissues. For example, labelling and tracking of human T-cells by bioluminescence has proven difficult. We addressed these problems by producing a number of thermostable Photinus pyralis (Ppy)-based Fluc mutants of a variety of colours, codon optimised for mammalian cell expression. Mutant genes were incorporated into useful retroviral constructs fused to membrane bound Gaussia luciferase (Gluc) bearing a Myc tag via a Foot and Mouth Disease (FMD) 2A self-cleavage sequence that allowed 1:1 co-expression of products. This allowed FACS analysis, cell sorting and also signal normalisation. The Fluc mutants were superior to WT in terms of expression in primary human T-cells, brightness at 37oC in T-cell lines and resistance to bathochromic shift. Thermostabilisation improved light yield in vitro and in vivo and two levels of stability mutants were created, with one set more stable to temperature than WT and much brighter, and one set much more stable to temperature and pH at the expense of some light yield, though still brighter or comparable to WT. Lastly, a red stable Fluc, x11 red, displayed a peak emission wavelength of ca.620nm, among the furthest red Ppy Flucs known. These Flucs represent enhanced tools for in vivo bioluminescence imaging.

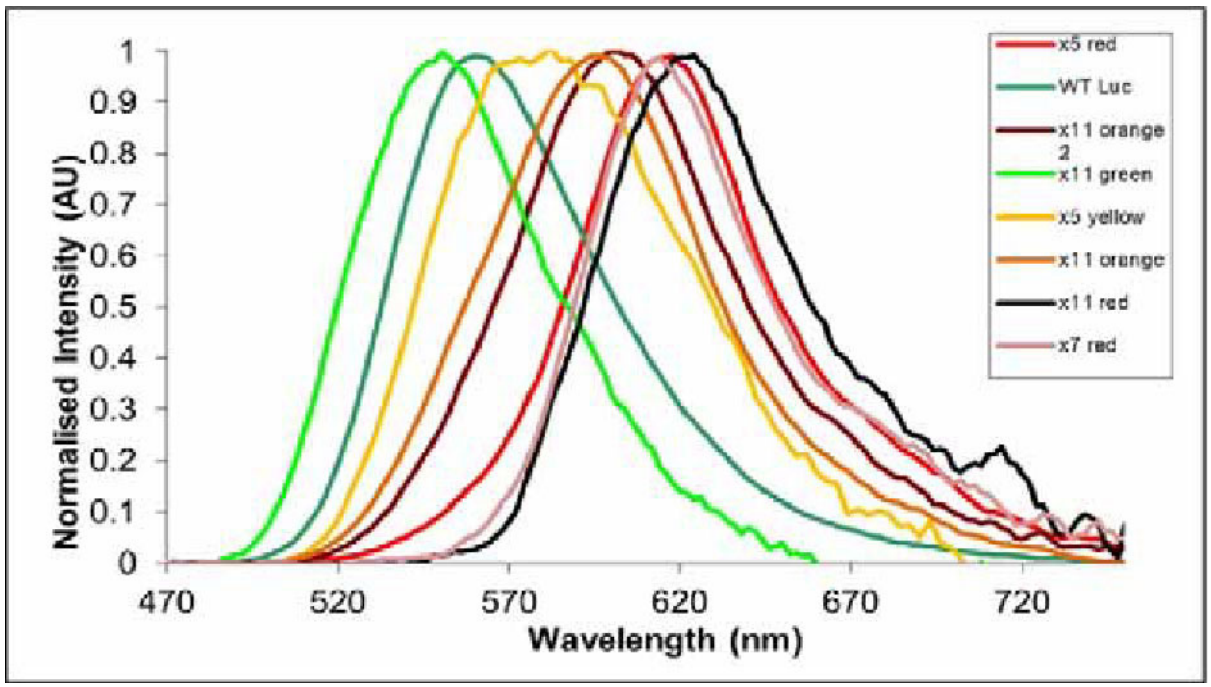


Bioluminescence spectra of Flucs in Jurkat T-cells at 37oC. Jurkat T-cells were retrovirally transduced with a different coloured Fluc mutants and light emission was recorded in a Thermo Lab Systems spectrofluorometer set at 37oC after addition of 20ul 500uM luciferin substrate.

Disclosure of author financial interest or relationships:
**A.P. Jathoul**, None; **S. Thomas**, None; **B. Philip**, None; **M.A. Pule**, None.

Presentation Number **P298**
Poster Session 2
September 6, 2012 / 15:15-15:15 / Room: The Liffey

# Monitor Androgen Deprivation and Androgen Receptor Blockade Therapy with a Functional Dual Reporter System

***Ziyue Karen Jiang***, *Lily Wu, Molecular Medical Pharmacology, University of California, Los Angeles, Los Angeles, CA, USA. Contact e-mail: jiangpkp@gmail.com*

Hormonal manipulation remains the first line systemic treatment for advanced prostate cancer. It includes surgical and medical means of androgen deprivation and androgen receptor (AR) blockade therapies. However, the majority of patients will develop castration resistant prostate cancer, often with metastasis to the skeleton bone that accounts for the lethality of this disease. Therefore, a reliable imaging modality capable of active surveillance of tumor recurrence as well as new emergence of metastasis would greatly benefit the timing and decision-making in adopting second line therapies. To this end, we recently constructed a prostate specific yet androgen independent promoter system, namely PSES-TSTA (Prostate Specific Enhancer Sequence coupled with Two-Step Transcriptional Amplification). We used this transcriptional enhancer system to drive PET and optical imaging reporters and successfully visualized subcutaneous tumor and intra-tibial metastasis in castrated mice. The androgen independency of PSES-TSTA secured viability of this imaging approach when only castrated level of androgen is available, and is attributed to the composition of the chimeric PSES sequence - an androgen inducible element derived from the prostate specific antigen (PSA) gene promoter and an androgen suppressible element from the prostate specific membrane antigen gene enhancer (PSME). Another challenge faced by patients after hormonal ablation therapy is the urgent need for effective second-line therapies. Interestingly, a growing body of evidence points out that even at the stage of castration resistant prostate cancer, AR remains active and most prostate cancer still rely on the androgen - AR axis for proliferation and survival. Accordingly, much effort has been devoted to the development of second generation anti-androgen agents such as MDV3100 and abiraterone. Therefore, it would be greatly beneficial to establish a practical and reliable reporting system that reflects the functional activation/inhibition status of this androgen-AR axis so that the efficacy of such new drugs can be monitored at the molecular level. Inspired by previous results, we separated the two components of PSES and generated two imaging reporters: PSA-driven Firefly Luciferase (PSA-FL) and PSME-driven Renilla Luciferase (PSME-RL). Based on their respective response to androgen signaling, we anticipated that this dual reporter system will exhibit a decrease in the PSA-FL signal with a simultaneous increase of the PSME-RL signal in the face of an effective anti-androgen therapy. Indeed, we observed such pattern of reporter gene expression in multiple prostate cancer cell lines. Importantly, this system is able to differentiate the potency and efficacy between the first generation and the more potent second generation AR antagonists. Moreover, the simultaneous application of the PSME- and PSA-driven reporter system is advantageous over the single PSA promoter-based reporter in that it rules out the effect of tumor mass reduction on the readout because both up- and down-regulation of gene expression are being assessed and imaged.

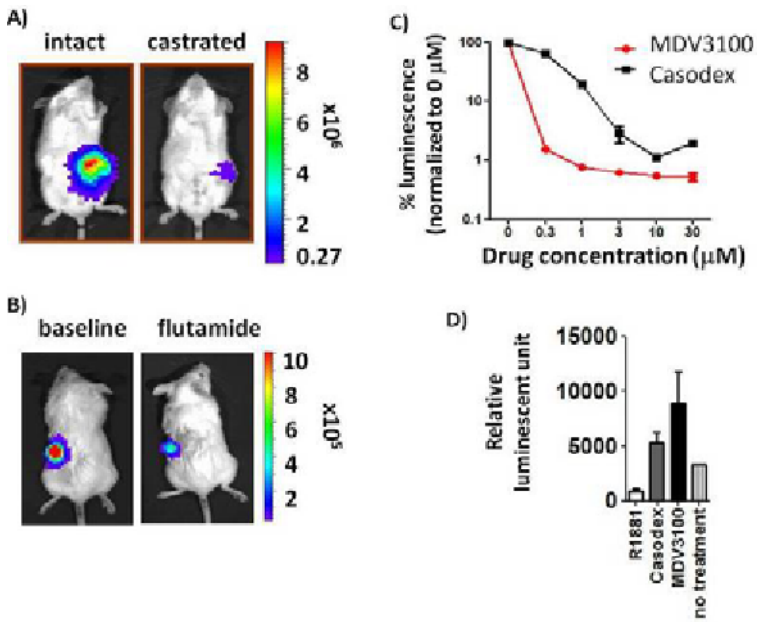


In the dual reporter system, PSA-FL signal was turned off by surgical castration (A), androgen receptor (AR) blockade by flutamide (B), and escalating dose of AR antagonists Casodex and MDV3100 (C). The PSME-RL reporter is suppressed by synthetic androgen R1881 but elevated by Casoedex and MDV3100 (D). In (A) and (B), same animals were monitored over time; (C) and (D) were in vitro culture experiments.

Disclosure of author financial interest or relationships:
**Z. Jiang**, None; **L. Wu**, None.

Presentation Number **P299**
Poster Session 2
September 6, 2012 / 15:15-15:15 / Room: The Liffey

# In vivo magnetic resonance imaging of transgenic mice expressing human ferritin

***Hoe Suk Kim***[1], *Hyun Jung Joo*[1], *Jisu Woo*[1], *YoonSeok Choi*[1], *Seung Hong Choi*[1], *Hyeonjin Kim*[1,2], *Woo Kyung Moon*[1,2], [1]*Radiology, Institute of Radiation Medicine Medical Research Center, Seoul National University, Seoul, Republic of Korea;* [2]*Seoul National University, Seoul, Republic of Korea. Contact e-mail: hoeskim@gmail.com*

Purpose: This study aims to produce the transgenic mice (TG) engineered for MRI studies based on the ubiquitous expression of ferritin MRI reporter gene in diverse tissues. Methods: Transgenic mice (TG) expressing myc-tagged human heavy chain ferritin (myc-hFTH) under the control of a ubiquitous CAG promoter were produced. The expression of myc-hFTH in diverse tissues of the myc-hFTH TG was assessed by RT-PCR, Western blotting and immunohistochemistry. The iron accumulation and the deposition of ferritin aggregates in tissues of myc-hFTH TG and WT were analyzed by Prussian blue staining and transmission electron microscopy. The myc-hFTH TG (n=9) and wild type mice (WT) (n=4) were subjected to MRI on 9.4T MR scanner. An 8-point T2* mapping was performed using a multiple gradient echo sequence T2*was estimated pixel by pixel by using a routine least-squares fitting algorithm. Results: We generated the myc-hFTH TG expressing myc-hFTH in brain, heart, liver, lung, spleen, pancreas, kidney and intestine. The myc-hFTH TG showed no apparent pathological symptoms and no histological changes compared to WT. The expression of myc-hFTH in the brain and liver tissues of myc-hFTH TG led to a significant decrease in T2* values, as shown by noninvasive MRI, compared to WT ($P < 0.05$, TG vs. WT). Conclusions: This study demonstrates that the novel myc-hFTH TG, which expresses an MRI reporter in many tissues, would be a valuable animal model of FTH-based molecular imaging in which to study potential therapies for cell and tissue grafting using an MRI technique. These mice could also serve to study disease related with iron metabolism Acknowledgement: This work was supported by the National Research Foundation of Korea (NRF) grant funded by the Korean government (MEST) (2011-0003657, 2011-0004322, 2011-0000174, 2011-0005381) and by a grant from the Innovative Research Institute for Cell Therapy, Republic of Korea (A062260). YS Choi is the recipient of a fellowship from the Brain Korea 21 (BK21) program.

Disclosure of author financial interest or relationships:
**H. Kim**, None; **H. Joo**, None; **J. Woo**, None; **Y. Choi**, None; **S. Choi**, None; **H. Kim**, None; **W. Moon**, None.

Presentation Number **P300**
Poster Session 2
September 6, 2012 / 15:15-15:15 / Room: The Liffey

# Preclinical Biodistribution Studies of 68Ga-labeled Anti-miR15b Molecules

***Jussi A. Mäkilä***[1], *Anu Kiviniemi*[2], *Heidi Liljenbäck*[3,4], *Joonas Mäkelä*[2], *Tiina Saanijoki*[3], *Pasi Virta*[2], *Harri Lönnberg*[2], *Tiina Laitala-Leinonen*[1], *Anne Roivainen*[3,4], [1]*Cell Biology and Anatomy, University of Turku, Turku, Finland;* [2]*Department of Chemistry, University of Turku, Turku, Finland;* [3]*Turku PET Centre, Turku University Hospital, Turku, Finland;* [4]*Turku Center for Disease Modeling, University of Turku, Turku, Finland. Contact e-mail: jussma@utu.fi*

Introduction: MicroRNAs (miRNAs) are endogenous, small non-coding RNA molecules that bind to the 3' untranslated region of mRNAs and induce translational repression or mRNA degradation. Chemically synthesized miRNAs have been shown to regulate gene expression and cell physiology in vitro. We studied the whole-body distribution and kinetics of intravenously administered 68Ga-labeled anti-miR15b molecules in adult male rats. Materials and methods: Four 22-mer RNA molecules containing either seven galactoses and NOTA chelator (68Ga-NOTA-RNA-GAL), an unmodified (68Ga-NOTA-RNA), modified NOTA chelator (68Ga-NOTA(mod)-RNA) or DOTA chelator (68Ga-DOTA-RNA) were used in this study. For comparison, 68Ga-labeled NOTA-chelated oligonucleotide with six thymine residues (68Ga-NOTA-T6), the chelator (68Ga-NOTA), and the 68Ga-labeling reaction mixture alone were used. Each rat was given 10-20 MBq of 68Ga-labeled RNA, NOTA or 68Ga. Biodistribution was evaluated by performing a 60-min dynamic PET imaging with HRRT-camera (High Resolution Research Tomography). After PET imaging, the rats were euthanized, tissue samples were excised, weighed and measured for radioactivity using a gamma counter. Results: 68Ga-NOTA-RNA-GAL induced 14-fold radioactivity in liver as compared to 68Ga-NOTA-RNA. Both 68Ga-NOTA-RNA and 68Ga-NOTA(mod)-RNA induced multifold radioactivity in kidneys (20-30 fold), bone (4-13 fold) and bone marrow (7-23 fold), as compared with 68Ga-NOTA-T6 and 68Ga-NOTA. 68Ga-DOTA-RNA was almost identical to 68Ga-NOTA-RNA. The 68Ga-NOTA-T6 excreted into urine, and also accumulated in small intestine and white adipose tissue. The 68Ga-NOTA accumulated in kidneys and also excreted into urine. The radioactivity derived from 68Ga reaction mixture alone had a strong tendency to accumulate in liver, spleen, lungs and bones, but did not accumulate in kidneys or excrete into urine. Conclusion: The tendency of 68Ga-NOTA-RNA to accumulate in kidneys, bone and bone marrow can not be explained by the properties of NOTA chelator. To increase uptake of 68Ga-NOTA-RNA into bone, bisphosphonates are introduced to the molecules. Further studies with bisphosphonate conjugated RNA molecules are in progress.

Disclosure of author financial interest or relationships:
**J.A. Mäkilä**, None; **A. Kiviniemi**, None; **H. Liljenbäck**, None; **J. Mäkelä**, None; **T. Saanijoki**, None; **P. Virta**, None; **H. Lönnberg**, None; **T. Laitala-Leinonen**, None; **A. Roivainen**, None.

Presentation Number **P301**
Poster Session 2
September 6, 2012 / 15:15-15:15 / Room: The Liffey

# Follow up tracking of D2R+ human mesenchymal stem cells with $^{18}$F-Fallypride microPET in rats

***Erik Mille***[1], *Franz J. Gildehaus*[1], *Veronika Schönitzer*[2], *Florian Haasters*[2], *Stefanie Käsbauer*[2], *Janette M. Carlsen*[1], *Guido Boening*[1], *Wolfgang Böcker*[2], *Peter Bartenstein*[1], *Matthias Schieker*[2], [1]*Dept. of Nuclear Medicine, Ludwig-Maximilians-University, Munich, Germany;* [2]*Dept. of Surgery, Ludwig-Maximilians-University, Munich, Germany. Contact e-mail: erik.mille@med.uni-muenchen.de*

Preclinical in vivo studies have shown a generally positive effect of infusing undifferentiated stem cells on the regeneration of various tissues, such as bone, cartilage and myocardium. One important issue is to survey the location and survival of mesenchymal stem cells (MSCs). Detecting these cells by means of histology and with immunochemistry is often difficult and does not allow for follow-up studies in vivo. In the current study we used $^{18}$F-Fallypride (FP) to track hTert immortalized human MSCs transduced with the D2R80A by lentiviral gene transfer. The RT-PCR provided proof that the D2-receptor is expressed and immunofluorescence analysis confirmed the expression on the cell surface. The functionality of the receptor was shown by cell binding assays using $^{18}$F-FP and a fluorescence labelled D2R antagonist. Further in vitro experiments showed that the proliferative capacity was reduced compared to control MSCs, whereas the migration capacity was not impaired. The stem cell character of the cells, however, persisted as it was shown through adipogenic and osteogenic differentiation. Cell suspension of 2x10$^7$ MSCs expressing the $D_2$-receptor (SCP1-D2R80A) in 80 µl 1xPBS were injected into a muscular pouch in the thigh of athymic rats (n=4). To check for unspecific effects from treatment, receptor-negative MSCs (SCP1-mock) were applied to the contralateral side. On day 0, 1 and 7 post transplatation, PET scans after i. v. injection of the tracer (app. 20 MBq of $^{18}$F-FP) were acquired on a small animal scanner (Siemens DPET) for 90 min and dynamically reconstructed. In three animals the cells could be detected at day 0 and 1, in one animal they were observed even at day 7 after cell transplantation. The receptor positive cells were visible whereas the receptor negative ones could not be delineated. VOI-based time-activity curves (TACs) indicate that there is specific binding and there were median binding ratios at day 0 of approx. 2.1 : 1 and 4.8 : 1 at day 1 for the receptor-positive cells compared to the contralateral muscle as control region (on day 7 the binding ratio was 2.0 : 1). We suppose that the absence of specific uptake at day 7 in the majority of the animals is probably due to the use of human MSCs in not completely immunodeficient rats. Our experiments proof the concept of using transduced cells for the long-term measurement of transplanted cells in vivo. The in vitro and in vivo results show that the reporter system D2R80A / $^{18}$F-FP is feasible as a construct for detecting MSCs in new cell-based therapeutic approaches.

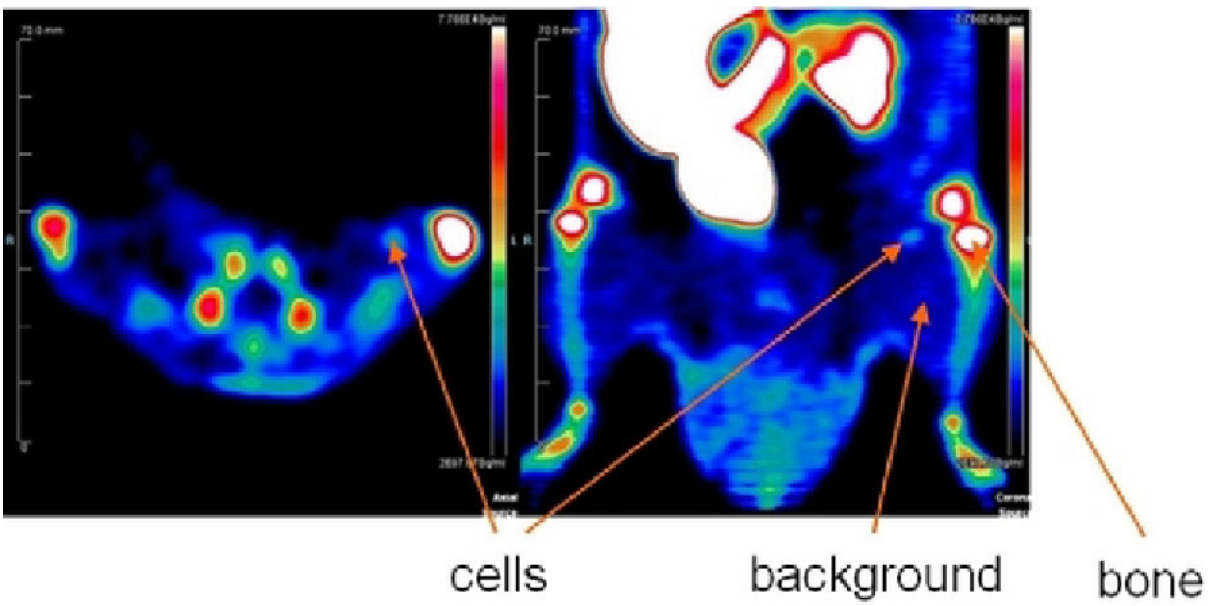


PET scan showing D2-receptor-positive cells at day 7 after transplantation.

Disclosure of author financial interest or relationships:
**E. Mille**, None; **F.J. Gildehaus**, None; **V. Schönitzer**, None; **F. Haasters**, None; **S. Käsbauer**, None; **J.M. Carlsen**, None; **G. Boening**, None; **W. Böcker**, None; **P. Bartenstein**, Siemens, Grant/research support; **M. Schieker**, None.

Presentation Number **P302**
Poster Session 2
September 6, 2012 / 15:15-15:15 / Room: The Liffey

# Tracking hMSC's in a Rat Model of Female Stress Urinary Incontinence Using Bioluminescence and Cryo Fluorescent Imaging

***Joseph Molter***[1], *Zhina Sadeghi*[2], *Zhenghong Lee*[1,3], *Michael Kavran*[2], *Adonis Hijaz*[2], *Chris Flask*[1,3], [1]*Radiology, Case Western Reserve University, Cleveland, OH, USA;* [2]*Urology, University Hospitals of Cleveland, Cleveland, OH, USA;* [3]*Biomedical Engineering, Case Western Reserve University, Cleveland, OH, USA. Contact e-mail: jpm57@case.edu*

Introduction: Stress Urinary Incontinence (SUI) is caused by damage to the connective tissue in the vagina during birth. This results in progressive weakening in the ligaments in the pelvis and potentially incontinence. The goal of this study was to use in vivo Bioluminescent Imaging (BLI) and in situ high resolution cryo-fluorescence imaging to track bone marrow-derived human mesenchymal stem cells (hMSCs) as a potential therapy for SUI. Methods: For in vivo BLI imaging, 5 female Sprague-Dawley rats (age = 7-9 weeks) underwent an established vaginal distention (VD) procedure to simulate the injury associated with vaginal delivery (Lin et al. 2008). To initiate the VD injury a series of catheters of increasing size were inserted into the vagina. A balloon catheter was inflated in the vagina for 4 hours. Incontinence was measured by leak point pressure from an implanted suprapubic tube. Following the (VD) procedure, each rat was injected periurethrally with 1 million hMSCs. The hMSCs were transfected with a reporter gene containing luciferase for BLI. An additional 3 rats (controls) were injected with hMSCs but with no (VD). BLI was performed 1 hour after hMSC injection and then at 1,2,3,4,7 days post-therapy in all 8 rats. The region of Interest (ROI) was defined centered on the BLI signal, and mean value was calculated. For in situ cryo-fluorescence imaging, 2 rats were periurethrally injected with 3 million hMSCs . These hMSCs were labeled with LavaCell®, a cell membrane marker that produces an orange fluorescent signal. One of these two rats had undergone the (VD) procedure as above. Animals were euthanized 1 hour post injection of the hMSCs and immediately frozen with a cryostat compound in liquid nitrogen. Animals were than imaged on the CryoViz imaging system to obtain high resolution (17um) 3D images of each rat's pelvis. Results: All 8 of the rats produced a BLI signal on Days 0-4 following hMSC injection. A two-way ANOVA was performed with ROI mean of the longitudinal BLI data. The results demonstrated that there was a difference in signal from injected MSCs between those with VD and without ($p = 0.024$, and $F > Fcrit$). Signals were undetectable after 7 days. The systemically-injected rat showed a strong BLI signal in the lung typical of intravenous injections, the BLI signal was undetectably after 1 day. In Situ cryo-fluorescent imaging of the rat with local hMSC injection and VD showed a focal signal from the LavaCell® agent in the vaginal connective tissue suggestive of hMSC homing. Cryo-fluorescent imaging of the rat with similar a hMSC injection but no VD showed Lavacell© signal in needle tracks of the injection sites but no focal homing. Conclusion: BLI allows monitoring of the stem cell activity and viability over time in a rat model of SUI. In Situ cryo-fluorescence imaging shows the exact location of the stem cells and a verification of their homing in the target region. Given that previous studies have demonstrated the effectiveness of hMSCs therapy for reducing incontinence in this rat model. These imaging techniques provide the opportunity to effectively assess hMSC location and viability.

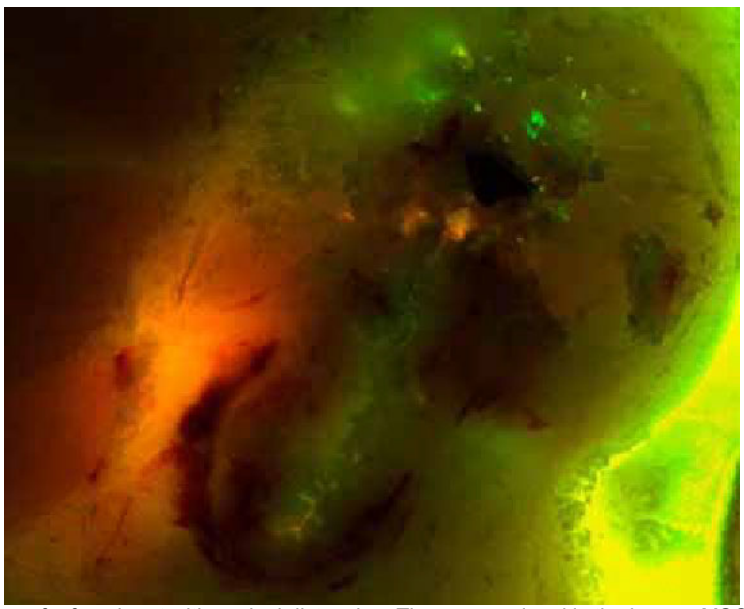

Cryo-fluorescent image of a female rat with vaginal distension. The orange signal is the human MSCs in the vaginal wall.

Disclosure of author financial interest or relationships:
**J. Molter**, None; **Z. Sadeghi**, None; **Z. Lee**, None; **M. Kavran**, None; **A. Hijaz**, None; **C. Flask**, None.

Presentation Number **P303**
Poster Session 2
September 6, 2012 / 15:15-15:15 / Room: The Liffey

# Modified Cypridina luciferase - a new bioluminescence reporter for in vivo molecular imaging applications

***Maxim A. Moroz**, Juan Zurita, Larissa Shenker, Vladimir Ponomarev, MSKCC, New York, NY, USA. Contact e-mail: morozm@mskcc.org*

Introduction and Objective: Bioluminescence imaging (BLI) has been revered by the scientific community as an extremely versatile tool allowing for ultrasensitive non-invasive detection of transduced cell populations in vivo in different biomedical applications. Following the discovery of a luciferin-based Firefly luciferase (Fluc), this technique has evolved and a range of new bioluminescence genetic reporter systems have been developed including new luciferin-based Italian firefly (Iluc), Click beetle (CBluc), as well as coelenterazine-based Renilla (Rluc) and Gaussia (Gluc) luciferases. We have explored the feasibility of in vivo imaging of a new class of BLI reporters - cypridin-based luciferases. Cypridina luciferase (Cluc) is a secreted bioluminescent protein cloned from the ostracod, Cypridina Noctiluca, which catalyzes the oxidation of its substrate cypridin to produce light, with a maximum wavelength emission at 465 nm. We aimed to develop a modified Cluc reporter with limited secretion and significant light output for in vivo imaging applications. Methods: A series of Cluc-based mutants with truncated N-terminal secretory signal and/or fused with transmembrane domains from different membrane receptors (membrane-anchored mutants) were developed. Green fluorescent protein (GFP) was used as an independent marker of normalized reporter gene expression. Transduced and non-transduced C6 rat glioma cells were used in all studies. Luciferase-transduced xenografts were established in nude mice and assessed using IVIS 200 BLI system. For comparative experiments, cells and tumors expressing Click Beetle Red (CBRLuc), Fluc, RLuc and Gluc luciferases were used. Results: Several constructs bearing native and modified Cypridina luciferases and GFP were successfully cloned and confirmed by sequencing analysis. In vitro BLI assessment showed extremely high light output from the native Cluc-transduced C6 rodent glioma cells (1.12 x 109 + 0.23 x 108 photons/sec/105 cells), that was ~ 2 fold higher than CBRluc or Fluc and more than 5 fold higher than both the Rluc and Gluc signals. While 90% of the native Cluc enzyme was secreted into the culture medium, the signal from a membrane-anchored (ma)-Cluc mutant cells was ~80% of the total flux. The in vivo assessment showed a strong focal BLI signal coming from ma-Cluc-expressing tumors, while a diffuse whole-animal bioluminescence was observed in mice bearing native Cluc xenografts. In addition we were able to show the feasibility of concurrent BLI of ma-Cluc expression along with the luciferin- and coelenterazine-based luciferases; this triple-substrate imaging approach allowed for non-invasive visualization of up to three tumors/cell populations within the same animal. Conclusion: We developed and tested a new BLI reporter gene based on Cypridina luciferase that showed limited secretion and high light output. Our experiments allowed us to adopt this new and potent reporter gene for further in vivo imaging applications as an individual BLI reporter as well as in combination with other luciferases.

Disclosure of author financial interest or relationships:
**M.A. Moroz**, None; **J. Zurita**, None; **L. Shenker**, None; **V. Ponomarev**, None.

Presentation Number **P304**
Poster Session 2
September 6, 2012 / 15:15-15:15 / Room: The Liffey

# Radio-sensitizing effect of chromatin remodeling factor Brahma-related Gene 1 bromodomain was visualized using bioluminescent images

***Juri Na***[1,2], *Hyewon Youn*[1,4], *Mi Jeong Kim*[1,3], *Eui-Chong Kim*[5], *Dong Soo Lee*[1,6], *Jongbum Kwon*[7], *June-Key Chung*[1,2], [1]*Department of Nuclear Medicine, Seoul national univ., Seoul, Republic of Korea;* [2]*Biomedical Sciences, College of Medicine, Seoul national univ., Seoul, Republic of Korea;* [3]*Laboratory of Molecular Imaging and Therapy, Cancer Research Institute, Seoul national univ., Seoul, Republic of Korea;* [4]*Cancer Imaging Center, Seoul National University Cancer Hospital, Seoul national univ. Hospital, Seoul, Republic of Korea;* [5]*Department of Laboratory Medicine, Seoul national univ. Hospital, Seoul, Republic of Korea;* [6]*Molecular Medicine and Biopharmaceutical Sciences, WCU Graduate School of Convergence Science and Technology, Seoul national univ., Seoul, Republic of Korea;* [7]*Department of Life science, Ewha Womans Univ., Seoul, Republic of Korea. Contact e-mail: najul@snu.ac.kr*

Objectives: Brahma-related gene 1 (BRG1) is a core protein of SWI/SNF chromatin-remodeling complex. BRG1 bromodomain (BRD) as an inhibitor for DNA double strand breaks (DSB) repair inactivates the SWI/SNF complexes, resulting inefficient DSB repair and inducing radiosensitivity. In this study, we visualized the radio-sensitizing effect of BRG1-BRD using a bioluminescent imaging system. Methods: HT29-CMV-luciferase (HT29-luc) cells were established through retro-viral system and pMX-BRG1-BRD retro-viral vector was used for BRG1-BRD overexpression. The vectors including BRG1-BRD dimer and tetramer were also cloned for evaluating multimeric effect. 137Cs irradiator (IBL 437C) was used to deliver ionizing radiation around cells. Radio-sensitizing effect was investigated by luciferase activity and apoptosis analysis. BRG1-BRD overexpressed HT29-luc cells were subcutaneously injected in nude mice and these mice were irradiated using a Linear Accelerator (LINAC). The luciferase signals were monitored using IVIS 100 for 41 days. Results: BRG1-BRD monomer, dimer and tetramer overexpressed cells were less proliferative (33.3 %, 70.3 % and 52.6 %) than control cells at the 2 days after irradiation treated. Apoptotic cells of BRG1-BRD monomer and dimer groups were increased 10 %, 15 % more than those of control cells at 72 hrs after radiation. In ex vivo study, the luciferase signals of BRG1-BRD dimer overexpressed HT29-luc cells were 21% lower than control cells at the day 27 after Cs-137 γ-ray irradiated. In in vivo study, the luciferase signals of BRG1-BRD monomer overexpressed HT29-luc cells were 6.9% lower compared to those of control cells at the day 38 after high energy X-ray radiation. Conclusion: We demonstrated radiation-sensitizing effect of BRG1-BRD over-expression using bioluminescent imaging system. Less irradiation can be applied for tumor therapy by elevating the amount of BRG1-BRD in the tumor cells.

Disclosure of author financial interest or relationships:
**J. Na**, None; **H. Youn**, None; **M. Kim**, None; **E. Kim**, None; **D. Lee**, None; **J. Kwon**, None; **J. Chung**, None.

Presentation Number **P305**
Poster Session 2
September 6, 2012 / 15:15-15:15 / Room: The Liffey

# Optical imaging of thermo-induced gene silencing in tumors

***Karine Pinel***[1]*, Christelle Debeissat*[2]*, Coralie Genevois*[3]*, Franck Couillaud*[1]*,* [1]*UMR 5536 - CNRS, Centre de Résonance Magnétique des Systèmes Biologiques, Bordeaux, France;* [2]*UMR 5231 - CNRS, Imagerie Moléculaire et Fonctionnelle, Bordeaux, France;* [3]*UMS 3428 - CNRS, Unité Mixte de Service, Bordeaux, France. Contact e-mail: karine.pinel@rmsb.u-bordeaux2.fr*

Abnormal regulation of gene expression is the hallmark of cancer, and hence a therapeutic target. The recent discovery of RNA interference (RNAi) mechanisms provides a way to reduce or inhibit virtually any overexpressed gene. It's however crucial to ascertain both spatial and temporal control of gene inhibition. In the present project, RNAi was driven by a microRNA placed under transcriptional control of the thermo-inducible heat shock 70B promoter. Spatially resolved, non-invasive physical methods provide a way to activate the Hsp70B promoter and thus, to control gene silencing by local hyperthermia. The feasibility of such an approach was studied by targeting firefly luciferase (LucF) expression with a specific microRNA (miRLuc), both in vitro cell lines and in vivo xenograft subcutaneous tumors in mice using bioluminescence imaging (BLI). Plasmids encoding for constitutive expression of LucF and constitutive expression of miRLuc were co-transfected in U87 human glioblastoma cells. LucF activity was inhibited by the miRLuc expression. Both, the number of miRLuc copies encoded by the plasmid and the number of miRLuc targets were shown to be important parameters for maximal inhibition (up to 90% inhibition) of LucF enzymatic activity. By placing miRLuc under transcriptional control of Hsp70B promoter, inhibition was induced by hyperthermia (45°C, 8 min) and became transient with maximum inhibition occurring 46 hours after heating. In vivo experiments were performed using a U87 cell line stably transformed for constitutive expression of LucF and thermo-inducible expression of 4 copies of miRLuc. A U87 cell line expressing LucF and a thermo-inducible unrelated microRNA was used as control. LucF-targeted and control cell lines were used to generate subcutaneous xenograft tumors on immunodeficient mice on left and right legs, respectively. Tumor growth was monitored by a calipers square measures and BLI to follow expression of a bioluminescent gene. MiRluc expression was induced by hyperthermia by putting both legs in a water-bath (45°C, 8 min). A second bioluminescent gene, the Renilla Luciferase (LucR), was placed under the control of the Hsp70B promoter, this reporter gene allowed to control the heat shock activation. Tumors expressing the thermo-inducible miRLuc exhibited a significant decrease in the BLI signal as compared to the contra-lateral control tumors starting two days later and lasted for two weeks. Our data show the in vivo feasibility of thermo-inducible control of miRNA expression and specific gene inhibition within a tumor. This strategy could be used to target a therapeutic-relevant gene and open the way for clinical perspectives using currently available methods such as focused ultrasound, radiofrequency and laser for local control of hyperthermia.

Disclosure of author financial interest or relationships:
**K. Pinel**, None; **C. Debeissat**, None; **C. Genevois**, None; **F. Couillaud**, None.

Presentation Number **P306**
Poster Session 2
September 6, 2012 / 15:15-15:15 / Room: The Liffey

# Electroacupuncture attenuates ΔFosB Expression and hyperactivities after Chronic Exposure to Amphetamine in Mice

***J. Ren***[1], *Yan Jaing*[1], *Jian Kong*[1], *Charng-ming Liu*[1], *Philip K. Liu*[1], *Christina Liu*[1,2], [1]*Radiology, Mass General Hospital, Charlestown, MA, USA;* [2]*NIBIB, NIH, Bethesda, MD, USA. Contact e-mail: jqren@partners.prg*

PROPOSE Changes in gene expression by alternative splicing have been proposed to be an integral part of behavioral adaptation in humans exposed to drug of addiction. We have shown that chronic exposure to amphetamine (AMPH) results in behavioral sensitization and enhanced alternative splicing of immediate early genes such as FosB to ΔFosB mRNA in the reward pathway of living mouse brains. Acupuncture is being used to treat drug addiction in human with some success. This study aims to investigate whether or not electroacupuncture (EA) can reduce ΔFosB expression at mRNA and protein levels in the amphetamine sensitized mice using in vivo gene transcript-targeted MRI (GT-tMRI) and immunohistochemistry (ICH). METOHD AND MATERALS A total of n = 16 mice received D-AMPH (4 mg/kg, sc) every other day for a total seven doses (sensitization), then half of the mice received EA or mock EA treatment during the period of withdrawal. EA was applied bilaterally on 36S points located in the upper hind legs for 20 min (2Hz/1mA) every other day for two weeks, while the other half of the animals received puncture but no electric stimulation (mock EA). On the day of the MRI, we delivered SPION-sODN (a MRI T2 constrast agent targeting ΔfosB mRNA) via intracerebroventricular (icv) infusion; all animals received the same dose of AMPH (i.p.) four hours later. We acquired a series of T2*W MRI with incremental TEs three hours later which allowed R2* map calculation (R2* =1/T2*X1000, 1/sec). We preformed region of interest analysis comparing the mean R2* values in selected brain regions of the reward pathway as indicators of ΔFosB mRNA expression. In a parallel study, we obtained brain tissue samples of these two groups of animals to compare ΔFosB protein expression by ICH. Power analysis ($p = 80\%$, $\alpha = 0.05$) determined the numbers of mice to be treated in each group; we performed Student t test to determine the significance at $p < 0.05$. RESULTS Based on ΔFosB mRNA targeting MRI, we found that EA treatment significantly attenuated AMPH-induced hyper-activity and ΔFosB mRNA level in the medial prefrontal cortex (mPFC) and nucleus accumbens (NAc). ICH also confirmed the reduction in ΔFosB protein in the NAc of sensitized mice that underwent EA treatment. CONCLUTION We observed that EA can suppress alternative splicing and ΔFosB expression both at the gene transcript and protein levels in animal model of drug abuse. Such finding indicates that ΔFosB mRNA can be a potential biomarker for drug addiction treatment.

Disclosure of author financial interest or relationships:
**J. Ren**, None; **Y. Jaing**, None; **J. Kong**, None; **C. Liu**, None; **P.K. Liu**, None; **C. Liu**, None.

Presentation Number **P307**
Poster Session 2
September 6, 2012 / 15:15-15:15 / Room: The Liffey

# Multimodality Imaging of Breast Cancer Bone Metastasis

***Pedro Sanches***[1], *Eric Kaijzel*[2], *Ivo Que*[2], *Rob C. Hoeben*[3], *Clemens Lowik*[2], *Holger Gruell*[1,4], [1]*Dept. Biomedical Engineering, Eindhoven University of Technology, Eindhoven, Netherlands;* [2]*Dept. Endocrinology, Leiden University Medical Centre, Leiden, Netherlands;* [3]*Dept. Molecular Cell Biology, Leiden Univeristy Medical Centre, Leiden, Netherlands;* [4]*Biomolecular Engineering, Philips Research, Eindhoven, Netherlands. Contact e-mail: p.sanches@tue.nl*

**Introduction** Bone is one of the most common metastatic target sites in breast cancer [1], with more than 200 thousand new cases of invasive cancer diagnosed in the US alone, in 2011[2]. We set out to establish a multimodality imaging platform for bone metastasis in small animals as a tool to non-invasively quantify metastasis growth, the ensuing bone lesions and possible response to treatment. The use of a tumor cell line expressing reporter genes is an ideal study model, as we can use tracers to specifically pinpoint the location of tumor cells *in vivo*. In particular, the intracellular accumulation of the radiolabeled tracer $^{123}$I-FIAU promoted by the reporter gene herpes simplex virus-1 thymidine kinase (HSVTK-1) can be imaged and quantified *in vivo* by the highly sensitive nuclear imaging technique of SPECT with sub-millimeter resolution. In this study, a mouse model of osteolytic metastatic bone tumors (expressing HSVTK-1) was characterized with SPECT/CT, MRI and µCT over time. To our knowledge this is one of the few reports where the combination of soft tissue information from MRI and reporter gene imaging by SPECT is used to follow metastatic bone lesions. **Methods** A bone-metastasis forming human adenocarcinoma cell line, MDA-MB-231, was genetically modified to stably express HSVTK-1. Intracardiac injection in 4-5 week old female nude mice yields bone metastasis detectable after ca. 20 days. Metastases growth was imaged weekly by SPECT/CT (50 MBq of $^{123}$I-FIAU, imaging 12 h p.i.) and T2-weighted MRI over 40 days. The areas with metastases were harvested and imaged by µCT and further analyzed by histology. **Results** The animals developed multiple bone metastases in diverse sites, namely: femur, tibia, iliac crest, skull and shoulder blade (Fig. 1-A and C). The first detectable activity spots, around day 20, were typically smaller than 5 mm$^3$ and not yet clearly visible by MRI but would increase in volume and in amount of %ID over the weeks. The SPECT/MRI overlays show the activity is homogenously spread in the metastases (Fig. 1-C). Increasing values of activity were correlated to increased volumes by a linear relationship ($R^2$ = 0.97). Osteolytic bone lesions were visible by CT and µCT (Fig. 1-B). **Conclusions** A new multimodality imaging platform has been established that non-invasively combines images of active tumor areas ($^{123}$I-FIAU SPECT), the complete tumor masses (MRI) and the corresponding bone lesions (CT and µCT). There is a linear relationship between the volume of the metastasis and the activity signal from SPECT which can be used for therapeutic follow-up. Next, we intend to use this platform in a preclinical efficacy study to follow tumor progression and regression. **References** [1] Yoneda *et al.* 2005 Biochem Biophys Res Commun [2] DeSantis *et al.* 2011 CA Cancer J Clin **Acknowledgements** This project is funded by the EU FP7 project Sonodrugs (NMP-4-LA-2008-213706)

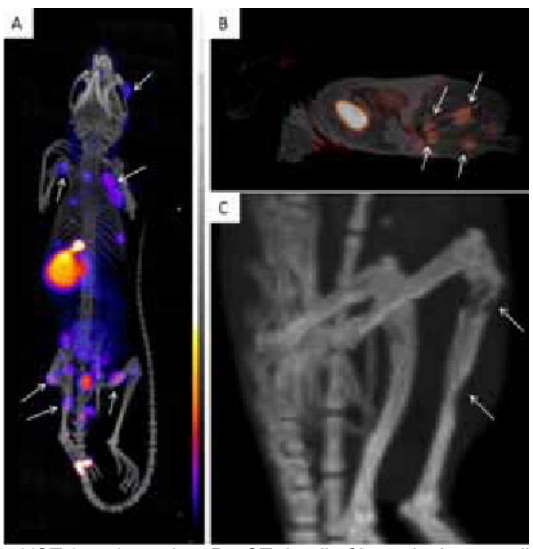


**Figure 1. Bone metastases.** A - SPECT (color)/CT (grey) overlay. B - CT detail of bone lesions on tibia. C- SPECT (color)/MRI (grey) overlay with tumor masses in white. White arrows point to metastases.

Disclosure of author financial interest or relationships:
**P. Sanches**, None; **E. Kaijzel**, None; **I. Que**, None; **R.C. Hoeben**, None; **C. Lowik**, None; **H. Gruell**, Philips, Employment .

Presentation Number **P308**
Poster Session 2
September 6, 2012 / 15:15-15:15 / Room: The Liffey

# Study of miRNA let-7i in regulating cell invasiveness and tumor recurrence of HNSCC by using multimodality molecular imaging

***Cheng-Han Tsai***[1], *Liang-Ting Lin*[1], *Muh-Hwa Yang*[2,3], *Ren-Shyan Liu*[3,4], *Yi-Jang Lee*[1], [1]*Department of Biomedical Imaging and Radiological Sciences, National Yang-Ming University, Medical school, Taipei, Taiwan;* [2]*Clinical Medicine, National Yang-Ming University, Medical school, Taipei, Taiwan;* [3]*Medicine, National Yang-Ming University, Medical school, Taipei, Taiwan;* [4]*Molecular and Genetic Imaging Core, National Yang-Ming University, Medical school, Taipei, Taiwan. Contact e-mail: g39620021@ym.edu.tw*

Head and neck squamous cancer cells (HNSCCs) are the sixth most common malignancy worldwide. HNSCCs usually expressed high local invasiveness in upper aerodigestive tract. It has been reported that the local invasive ability of HNSCCs is caused by the Epithelial-mesenchymal transition (EMT) regulated through the coordination of Twist and Bmi1, which further suppresses let-7i miRNA to promote metastasis. However, whether the Twist1-let-7i also controls the distal and lymph node metastasis of HNSCCs in vivo remains elusive. Here, we investigated the effects of Twist1-let7i signaling pathway on the progression of human HNSCCs in nude mice using the reporter gene imaging system. We established stable cell lines by transfecting pmR-mcherry-sponge-let-7i and pmR-mcherry-let-7i into two HNSCC cell lines FaDu and OECM-1 that express high and low level of let-7i, respectively. Subsequently, these cell lines were transduced with a co-expressed multi-reporter gene system including EGFP, fluc and HSV1-tk using the lentivirus. The resultant cell lines were named FaDu-spg-let-7i-3R cells and OECM1-let-7i-3R cells. These clones were separately implanted in the tongue tips of nude mice and monitored using the in vivo imaging system (IVIS) and uSPECT/CT periodically. Compared to the parental cells, the tumor formation was enhanced in FaDu-spg-let-7i-3R cells, but was suppressed in OECM1-let-7i-3R cells via the results of animal imaging. Additionally, the role of let-7i on the intrinsic metastatic ability of both cell lines was determined using tail vein injection. Consistently, the lung accumulations of FaDu-spg-let-7i-3R cells were stronger than that of OECM1-let-7i-3R cells. This observation was opposed to the parental cell types. We expect to use this system as preclinical model to predict the favor location invaded by HNSCC during tumor development. Moreover, whether the tumor recurrence or distal metastasis is related to let-7i would be explored as well.

Disclosure of author financial interest or relationships:
**C. Tsai**, None; **L. Lin**, None; **M. Yang**, None; **R. Liu**, None; **Y. Lee**, None.

Presentation Number **P309**
Poster Session 2
September 6, 2012 / 15:15-15:15 / Room: The Liffey

# In vivo determination of the fraction of reporter gene expressing cells from a mixed tumor population, using multi-exponential relaxometric MRI

***Moriel Vandsburger**, Marina Radoul, Yoseph Addadi, Michal Neeman, Biological Regulation, Weizmann Institute of Science, Rehovot, Israel. Contact e-mail: moriel.vandsburger@gmail.com*

**Introduction** MRI reporter genes have been used for in vivo imaging of cell survival and proliferation, however sparse cell densities have limited imaging of cell migration to a single study. We used ferritin as an MRI reporter gene, and R2 mapping with bi-exponential analysis for quantitative in vivo tracking of fibroblast recruitment to a solid tumor. **Methods** Human ovarian carcinoma cells (MLS) and CV-1 fibroblasts over-expressing either HA-tagged human ferritin heavy chain (CV1-FHC) or the red fluorescent protein tomato (CV1-T) were used. MRI was performed on a horizontal bore 9.4T scanner (Bruker, Germany). Prior to injection, CV1-FHC cells were grown in medium supplemented with 1mM ferric citrate for 48 hours. Hind limb tumors were generated via subcutaneous injection of $4x10^6$ MLS-eGFP cells in CD1-nude female mice. In co-injection (CoI) studies, MLS cells were mixed with either $1x10^6$ CV1-T (Control, n=5), or $1x10^6$ CV1-FHC and $1x10^6$ CV1-T cells (Ferritin, n=5). For recruitment studies, either $2x10^6$ CV1-FHC and $2x10^6$ CV1-DiR (Ferritin, n=5), or just $2x10^6$ CV1-DiR (Control, n=5) cells were delivered via intraperitoneal (IP) injection 4 days after tumor initiation. Multi-slice multi-spin echo (MSME) MRI (TE=7.7ms*30echos, TR=3s, FOV= 2.8x2.8cm, Matrix=256x256, AV=3, slices=5-8) was performed at days 3, 5, and 10 in CoI studies, and days 0, 2, 4, 7, and 9 following fibroblast injection in recruitment studies. R2 was quantified by fitting signal decay curves from MSME images to the equation $I=I_0e^{-R2*TE}+C$. The R2 of CV1-FHC ($R2_{fhc}$) was quantified with MSME imaging of pure CV1-FHC cell phantoms. Bi-exponential analysis was performed by fitting signal decay curves from each pixel to the equation $I=I_0(Ae^{-TE*R2fhc}+Be^{-TE*R2c})+C$, where R2c is the mean R2 of all control tumors, and A and B represent the relative contribution of each component. The high R2 fraction, representing the fractional contribution of CV1-FHC cells to the signal decay, was calculated as A/(A+B)*100. Whole body in vivo fluorescence imaging was performed on days 0, 3, and 10 in CoI, and days 7 and 9 post injection in recruitment studies. **Results** CoI studies illustrated a core-to-rim migration of CV1-FHC cells in both R2 (Figure S2) and high R2 fraction measurements between days 3 and 10. Fluorescence imaging revealed a parallel decrease in the ratio of tomato:eGFP radiance. In recruitment studies (Figure), mean tumor R2 values increased rapidly after IP injection of CV1-FHC, stabilizing after 4 days. Measurement of the high R2 fraction revealed continuous accumulation of CV1-FHC cells at the tumor rim between 2-7 days post injection. Fluorescence imaging confirmed the co-localization of CV1-DiR and MLS-eGFP signals. **Conclusions** Use of ferritin over-expression enabled in vivo imaging of fibroblast migration within and recruitment to a solid tumor. While mono-exponential R2 mapping revealed low densities of CV1-FHC cells, bi-exponential analysis quantified the contribution of CV1-FHC cells to the signal decay. Compared to existing methods that report only the total of labeled cells, this method reports the fraction of ferritin over-expressing cells within a mixed population.

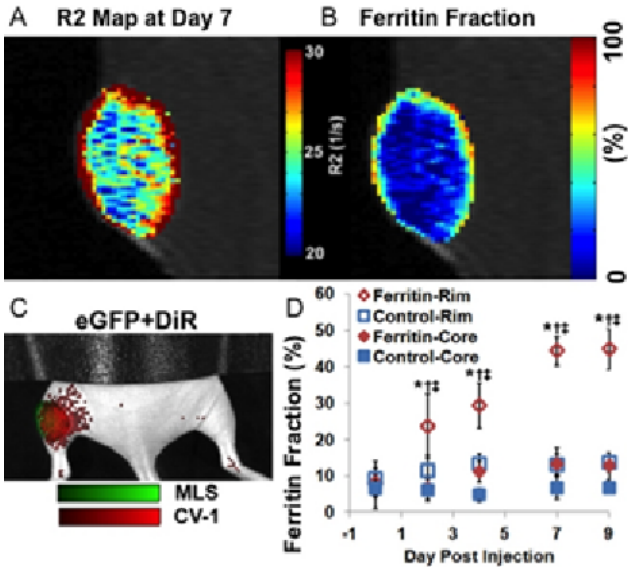


Figure. (A) R2 mapping of tumors revealed recruitment of ferritin over-expressing fibroblasts to the tumor rim. (B) Bi-exponential modeling quantifies the fractional contribution of ferritin over-expressing fibroblasts to tumor relaxation. (C) In vivo fluorescence imaging confirmed the recruitment of DiR labeled fibroblasts to eGFP expressing tumors. (D) The fractional contribution of ferritin over-expressing fibroblasts to tumor relaxation revealed continued recruitment to the rim up to 7 days after remote injection. (*P<0.05 vs. Control, †P<0.05 vs. Core, ‡P<0.05 vs. Day 0).

Disclosure of author financial interest or relationships:
**M. Vandsburger**, None; **M. Radoul**, None; **Y. Addadi**, None; **M. Neeman**, None.

Presentation Number **P310**
Poster Session 2
September 6, 2012 / 15:15-15:15 / Room: The Liffey

# Development of Mouse Model to in vivo Track the Migration of Bone Marrow Progenitor Cells

***Nadimpalli Ravi S Varma***[1], *Asm Iskander*[1], *Branislava Janic*[1], *Adarsh Shankar*[1], *Meser. M. Ali*[1], *Ali S. Arbab*[1,2], [1]*Cellular and Molecular Imaging Laboratory, Henry Ford Hospital, Detroit, MI, USA;* [2]*Radiology, Wayne State University School of Medicine, Detroit, MI, USA. Contact e-mail: ravin@rad.hfh.edu*

Involvement of exogenously administered bone marrow or peripheral blood derived or endogenous bone marrow derived EPCs in tumor neovascularization has been determined mostly by invasive or ex vivo methods such as immunohistochemistry from biopsy materials or by fluorescent microscope following the administration of genetically altered EPCs. Alternatively investigators have used transgenic animal model (usually carrying reporter protein, such as GFP or RFP to determine the involvement of endogenous cells in tumor neovascularization. Making of animal model that will allow in vivo tracking the involvement of endogenous bone marrow cells to tumor development and neovascularization is challenging. The following criteria should be present to make an ideal model; 1) the animal should have reporter only in bone marrow cells if the target is to determine the effect of bone marrow cells, 2) all other tissues of the body except bone marrow cells should not have any reporter positive cells, 3) if vasculogenesis/angiogenesis is the target, then reporter gene should be expressed under the guidance of specific promoter, (such as Tie2 or ICAM), 4) tumors or lesion should be produced with cells that should not have similar reporter gene or protein. However, to be able to track the migration of reporter positive endogenous bone marrow cells by in vivo imaging, the number of promoter driven reporter positive cells should be sufficient enough or all migrated bone marrow cells should be positive for the reporter. The purpose of this study was to establish a chimeric athymic mouse model to determine the involvement of bone marrow progenitor cells (BMPC) by in vivo optical imaging in the development of implanted tumors. Transgenic mice universally expressing GFP under the human UBC promoter was used as donors. Athymic mice were sub-lethally irradiated and 24 hours after irradiation recipient mice received bone marrow cells intravenously that are collected from donor transgenic mice. Engraftment efficiency following IV or IP administration of donor bone marrow cells was determined by flowcytometer using peripheral blood. Following acceptable engraftment (>50% engraftment) tumors were implanted and the migration of GFP+ cells was determined by in vivo optical imaging. Presence of GFP+ cells, expression of different markers and factors were also validated by fluorescent microscopy and immunohistochemistry. IV administration was important to establish successful engraftment of donor bone marrow cells. More than 50% engraftment efficiency was achieved by 28 days. Accumulation of GFP+ cells in implanted tumors was detected as early as 3 days following tumor implantation. Accumulation of GFP+ cells were confirmed by both fluorescent imaging and fluorescent microscopy, indicating the involvement of BMPCs during the development of tumor. There were higher level of expression of PDFG, VEGF and SDF-1α observed at the site of accumulation of GFP+ cells. We were able to establish an effective chimeric mouse model. By utilizing chimeric mouse model we'll be able to show the involvement of BMPCs in the development of tumor and resistance to antiangiogenic treatment.

Disclosure of author financial interest or relationships:
**N. Varma**, None; **A. Iskander**, None; **B. Janic**, None; **A. Shankar**, None; **M.M. Ali**, None; **A.S. Arbab**, None.

Presentation Number **P311**
Poster Session 2
September 6, 2012 / 15:15-15:15 / Room: The Liffey

# Activity and Expression of Histone Deacetylase in Transgenic Huntington Mice: Comparison of Positron Emission Tomography and Immunohistochemistry

***Hsin-Hsien Yeh***[1,2], *Leo G. Flores*[1], *Daniel Young*[1], *Uday Mukhopadhyay*[1], *Patrick J. Gillespie*[1], *Asutosh Pal*[1], *Hwan Jeong*[3], *Nobuyoshi Fukumitsu*[4], *Kazuma Ogawa*[5], *William Tong*[1], *Mian M. Alauddin*[1], *C. Allen Chang*[2], *Ren-Shyan Liu*[2,7], *Karl Herholz*[6], *Juri G. Gelovani*[1], [1]*Department of Experimental Diagnostic Imaging, The University of Texas MD Anderson Cancer Center, Houston, TX, USA;* [2]*Department of Biomedical Imaging and Radiological Sciences, National Yang-Ming University, Taipei, Taiwan;* [3]*Jeonbuk Regional Cyclotron Research Center and Biotracer Imaging Lab, Chonbuk National University Medical School and Hospital, Jeonju, Republic of Korea;* [4]*Proton Medical Research Center, University of Tsukuba, Tsukuba, Japan;* [5]*Graduate School of Natural Science and Technology, Kanazawa University, Kanazawa, Japan;* [6]*Wolfson Molecular Imaging Centre, University of Manchester, Manchester, United Kingdom;* [7]*Schoolt of Medicine, National Yang-Ming University, Taipei, Taiwan. Contact e-mail: skyeyeh@live.com*

Introduction: Histone deacetylase (HDAC) inhibitors are currently undergoing clinical trials for treatment of various neurodegenerative diseases, including Huntington disease (HD). Development of disease modifying epigenetic therapies could delay or prevent the progression of clinical symptoms in patients diagnosed with HD. Molecular imaging of epigenetic regulation by HDACs may elucidate their involvement in the pathogenesis of HD. Non-invasive imaging of HDAC activity in the brain can be used as pharmacodynamic biomarker of HDAC inhibition. Previously, we developed 6-(fluoroacetamido)-1-hexanoicanilide ([18F]FAHA), which is a substrate radiotracer for PET imaging of pan-HDAC activity in the brain. In this study we aimed to assess activity and expression of HDACs in transgenic mice with HD. Materials and Methods: Hemizygous R6/2 transgenic (tg) mice were bred and reared in our colony; littermates without CAG repeat expansion were used as wild-type (wt) control. The weight and motor performance of the animals were monitored up to 12 or 13 weeks of age. Dynamic imaging was acquired weekly or bi-weekly in 2D mode for 30 min with microPET/CT system INVEON after injection of [18F]FAHA (11.1 MBq/150 µl). After the last imaging session, the mice were sacrificed and their brains analyzed using immunohistochemistry (IHC) to assess the localization and magnitude of expression of different HDAC subtypes. Results: Both, the weight and motor performance in tg mice progressively decreased over time and were significantly decreased at 12 weeks post natal, as compared to wt mice. A gradual increase of brain [18F]FAHA accumulation with age was observed in tg (Fig.1) and wt mice. Up to week 8, [18F]FAHA accumulation tended to be higher in tg mice than in controls, but this difference disappeared thereafter (Suppl.1). Histochemically expression of HDAC 6 was increased in the substantia nigra. Expression of HDACs 4 and 7 was decreased in some cerebellar structures, while the level of acetylation of histone H3 was increased. Conclusions: Histochemical changes of HDAC expression in tg mice were restricted to few subtypes and brain regions. These changes were probably too subtle to be detectable by [18F]FAHA PET, which showed generally preserved [18F]FAHA accumulation in tg mice. Longitudinal intervention studies using a radiotracer with improved specificity and less intense systemic metabolism would be required to investigate the effects of HDAC inhibition in tg mice.

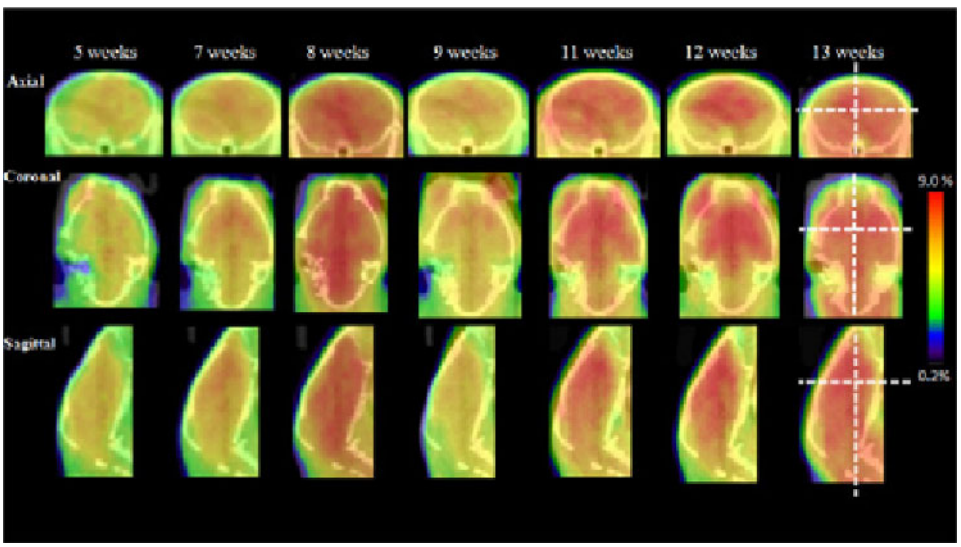


Disclosure of author financial interest or relationships:
**H. Yeh**, None; **L.G. Flores**, None; **D. Young**, None; **U. Mukhopadhyay**, None; **P.J. Gillespie**, None; **A. Pal**, None; **H. Jeong**, None; **N. Fukumitsu**, None; **K. Ogawa**, None; **W. Tong**, None; **M.M. Alauddin**, None; **C. Chang**, None; **R. Liu**, None; **K. Herholz**, AVID/Eli-Lilly, Grant/research support; Elan, Consultant; GE Healthcare, Consultant; **J.G. Gelovani**, Macrocyclics, Consultant; SibTech, Consultant .

Presentation Number **P312**
Poster Session 2
September 6, 2012 / 15:15-15:15 / Room: The Liffey

# Increased resistance to chemotherapy in hypoxia: how prostate cancer is affected?

*Liliana Pedrosa[1,4], Ana C. Mamede[1,3], **Ana M. Abrantes**[1,2], Ana S. Pires[1,4], Maria F. Botelho[1,2], [1]Biophysics Unit, IBILI, Faculty of Medicine, University of Coimbra, Coimbra, Portugal; [2]CIMAGO, Faculty of Medicine, University of Coimbra, Coimbra, Portugal; [3]CICS-UBI, Health Sciences Research Center, University of Beira Interior, Covilhã, Portugal; [4]Faculty of Sciences and Technology, University of Coimbra, Coimbra, Portugal. Contact e-mail: mabrantes@ibili.uc.pt*

Introduction: Hypoxia can be defined as a loss of oxygen in tissues, which is a characteristic of solid tumors. Genetic instability, high rate of glycolysis, cell cycle arrest and loss of apoptosis control are some of the mechanisms by which cancer cells try to adapt to hypoxia. Cancer cells in hypoxic environment usually have a clinically aggressive phenotype, resulting in a poor prognosis. Hypoxia normally provides an increased resistance to chemotherapy and radiotherapy, leading to an increased risk of recurrence and progression of the disease, making it more difficult to treat. The increase of hypoxia may be critical in the development, progression and metastasis of prostate cancer (PC). Material and methods: All studies were performed in two PC cell lines obtained in ATCC: LNCaP (which expresses androgen and estrogen receptors) and PC3 (that doesn't express these hormonal receptors). Dose-response curves of cisplatin, doxorubicin and epirubicin in both cell lines and in normoxia and hypoxia were determined. For that, plated cells were incubated with different concentrations of cisplatin, doxorubicin and epirubicin for different periods of time and cell proliferation was evaluated through MTT assay. After, cells were incubated with IC50 (half maximal inhibitory concentration) of these drugs in normoxia (20% oxygen) and hypoxia (2% oxygen) in order to evaluate the effect of hypoxia in cell proliferation after chemotherapy treatment. To assess cell proliferation, MTT assay was performed. For this, drugs were added to plated cells and after 48 hours, MTT was added and the results are obtained in an ELISA spectrophotometer. Results and discussion: Through the dose-response curves, we can see that doxorubicin and epirubicin (compared with cisplatin), has a more powerful anti-proliferative effect in both cell lines under study, being the epirrubicin somewhat more effective than its chemical analog, doxorubicin. For the same drug, the inhibition of cell proliferation is higher in LNCaP than in PC3 cell line (table 1). In order to analyze the cell resistance to chemotherapy, and after the incubation of cells with IC50 of the drugs in normoxia and hypoxia, our results show that epirubicin in LNCaP cell line is the drug less effective in hypoxia being the ratio found for cell proliferation between hypoxia and normoxia (H/N) equal to 1.964±0.478 (MED±SD). On the other hand, doxorubicin appears to be the most effective drug in hypoxia, being the H/N equal to 1.253±0.238 (MED±SD). In cancer cell line PC3, the less effective drug in hypoxia was the epirubicin (H/N=1.883±0.262 (MED±SD) and the more effective was cisplatin (H/N=1.551±0.259 (MED±SD)). Conclusions: Through this work it can be concluded that under hypoxic conditions the cell lines increases their resistance to chemotherapy. Interestingly, despite the obtained dose-response curves of doxorubicin and epirubicin are very similar in each cell line this does not apply under conditions of hypoxia. In fact, hypoxic cell lines under study have an H/N different for these two drugs, suggesting a high resistance to epirrubicin under conditions of hypoxia.

| Cytostatic drug | Cell line | Time (h) | $IC_{50}$ (μM) | $R^2$ |
|---|---|---|---|---|
| Cisplatin | PC3 | 24 | 126,03 | 0,85 |
| | | 48 | 29,71 | 0,96 |
| | | 72 | 16,03 | 0,99 |
| | | 96 | 12,94 | 0,96 |
| | LNCaP | 24 | 100,10 | 0,94 |
| | | 48 | 27,15 | 0,99 |
| | | 72 | 15,03 | 0,98 |
| | | 96 | 2,07 | 0,92 |
| Doxorubicin | PC3 | 24 | 10,20 | 0,94 |
| | | 48 | 1,45 | 0,96 |
| | | 72 | 0,43 | 0,96 |
| | | 96 | 0,99 | 0,98 |
| | LNCaP | 24 | 0,52 | 0,93 |
| | | 48 | 0,06 | 0,99 |
| | | 72 | 0,03 | 0,99 |
| | | 96 | 0,02 | 0,99 |
| Epirubicin | PC3 | 24 | 9,26 | 0,95 |
| | | 48 | 1,29 | 0,98 |
| | | 72 | 0,56 | 0,97 |
| | | 96 | 0,74 | 0,98 |
| | LNCaP | 24 | 0,23 | 0,94 |
| | | 48 | 0,05 | 0,99 |
| | | 72 | 0,03 | 0,99 |
| | | 96 | 0,03 | 0,99 |

Fig. 1 - Half maximal inhibitory concentration of cisplatin, doxorubicin and epirubicin in LNCaP and PC3 prostate cancer cell lines after 24, 48, 72 and 96hours of incubation in normoxia. R2 represents the coefficient of determination for the dose-response curves adjusted to growth sigmoidal function.

Disclosure of author financial interest or relationships:
**L. Pedrosa**, None; **A.C. Mamede**, None; **A.M. Abrantes**, None; **A.S. Pires**, None; **M.F. Botelho**, None.

Presentation Number **P313**
Poster Session 2
September 6, 2012 / 15:15-15:15 / Room: The Liffey

# Can Nuclear Medicine help to discover potential relationships between intracellular uptake of glucose, androgen receptor and Her2/neu expression in prostate cancer?

*Liliana Pedrosa[1,4], Ana C. Mamede[1,3], **Ana M. Abrantes**[1,2], Ricardo Teixo[1,4], João E. Casalta-Lopes[1], Ana S. Pires[1,4], Ana Gonçalves[5,2], Ana B. Sarmento-Ribeiro[5,2], Maria F. Botelho[1,2], [1]Biophysics Unit, IBILI, Faculty of Medicine, University of Coimbra, Coimbra, Portugal; [2]CIMAGO, Faculty of Medicine, University of Coimbra, Coimbra, Portugal; [3]CICS-UBI, Health Sciences Research Center, University of Beira Interior, Covilhã, Portugal; [4]Faculty of Sciences and Technology, University of Coimbra, Coimbra, Portugal; [5]Applied Molecular Biology and Hematology Group, Faculty of Medicine, University of Coimbra, Coimbra, Portugal. Contact e-mail: mabrantes@ibili.uc.pt*

Introduction: Prostate cancer (PC) is one of the most common cancers around the world and several molecular mechanisms that characterize this disease are still unrevealed. The androgen receptor (AR) activates the expression of genes involved in growth, differentiation and maintenance of prostatic epithelium. Her2/neu is a protein whose signals are correlated with AR. Her2/neu it is known to be a prognostic factor and is already used as a therapeutic target in breast cancer. Overexpression of this protein promotes the activation of AR and enhances the binding of promoters of genes regulated by androgens. This overexpression also causes the activation of PI3K/Akt pathway and promotes cell proliferation and survival. Since a richer medium in glucose is likely to increase proliferation and survival of PC cancer cells, this study intend to investigate the correlation between the glucose uptake and the expression of AR and Her2/neu through influx studies using the glucose analog 18F-Fluorodeoxyglucose (18F-FDG) and the technique of flow cytometry. Material and methods: Studies were performed in a PC cell line that expresses androgen and estrogen receptors, LNCaP (ATCC). To perform influx studies, cell suspensions were incubated with 18F-FDG (25μCi/ml) and studies were conducted under conditions of high (4.5g/L - HG) and low (1g/L - LG) glucose content. Experiments were also conducted in a RPMI culture medium HG but without phenol red (estrogen analog). The AR protein expression was assessed by flow cytometry, as well as the Her2/neu expression. Results: We observed significant differences ($p<0.05$) in the 18F-FDG uptake over time, being verified an increase in uptake over time in the three different culture medium compositions (figure 1). Moreover, we observed significant differences in 18F-FDG uptake in all three medium studied ($p<0.05$). The greater uptake of 18F-FDG occurs when cells are under LG conditions and uptake in the HG medium but without phenol red is higher than when there is phenol red in the medium. We verified significant differences ($p<0.05$) in each time in the three medium studied. AR expression was higher in the cells cultured in HG medium than in the other media. The cells cultured in LG registered the lower expression of this receptor. Comparing the expression of AR in LNCaP cells cultured in the three different media compared two by two, we observed significant differences for all cases ($p<0.05$).There was a very high expression of Her2 in the HG medium, approximately 2.5 fold higher than the Her2 expression in the LG medium and 2 fold higher than the expression verified in the phenol free medium. Compared two by two, the expression of Her2 in the three media studied in LNCaP cells shown significant differences ($p<0.05$) in all cases. Conclusions: In this study, we can conclude that 18F-FDG uptake is performed in a different rate according to availability of glucose in the medium, as well as the presence of phenol. The results obtained related to Her2/neu expression suggest a relationship between its expression, AR expression and the level of glucose in culture medium.

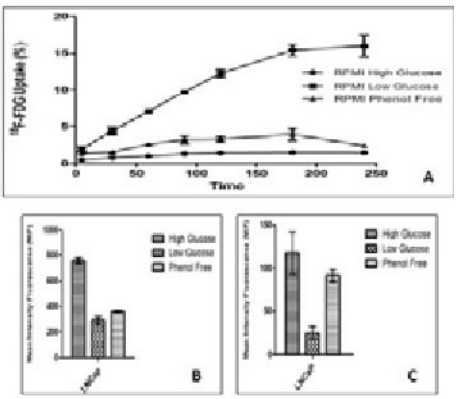


Fig 1 - A) 18F-FDG uptake (%) (n=4), B) expression of AR receptor (n=3) and C) expression of Her2/neu (n=3) in LNCaP prostate cancer cell line in RPMI medium high glucose, low glucose and high glucose phenol free.

Disclosure of author financial interest or relationships:
**L. Pedrosa**, None; **A.C. Mamede**, None; **A.M. Abrantes**, None; **R. Teixo**, None; **J.E. Casalta-Lopes**, None; **A.S. Pires**, None; **A. Gonçalves**, None; **A.B. Sarmento-Ribeiro**, None; **M.F. Botelho**, None.

Presentation Number **P314**
Poster Session 2
September 6, 2012 / 15:15-15:15 / Room: The Liffey

# Computed Tomography Imaging and Radiation Therapy Using Gold Polymeric Micelles

***Ajlan Al Zaki**, Daniel Joh, Zhiliang Cheng, Gary Kao, Jay F. Dorsey, Andrew Tsourkas, University of Pennsylvania, Philadelphia, PA, USA. Contact e-mail: ajlan@seas.upenn.edu*

Recently, gold nanoparticles (AuNPs) have generated much interest as both diagnostic imaging and therapeutic ("theranostic") agents. AuNPs are attractive for imaging applications as they are nontoxic, provide almost three times greater X-ray attenuation per unit weight than iodine, and generally exhibit significantly longer circulation times than tri-iodobenzene adducts. Additionally, previous animal and cell studies have shown that AuNPs can sensitize tumor cells to ionizing radiation (IR). Our objective is to develop tumor-targeted gold-loaded polymeric micelles (GPMs) as theranostic nanoplatforms for greater accuracy and effectiveness in early cancer detection and treatment. Using a microemulsion synthesis method, we have prepared GPMs, with hydrodynamic diameters ranging from 63 to 125 nm, by incorporating 1.9 nm AuNPs into the self-assembled micelles from the biocompatible and biodegradable amphiphilic diblock co-polymer polyethylene glycol-b-polycaprolactone (PEG-b-PCL). It has been found that the CT number in Hounsfield units (HU) increased linearly as the concentration of GPMs increased. Compared to current iodine based X-ray contrast agents, the measured HU values from GPMs were significantly higher. Pharmacokinetic data revealed that GPMs exhibit a longer circulation half-life (t1/2 > 6 hr) than conventional iodinated agents. CT imaging of GPMs, administered in mice intravenously, shows an enhancement of blood vessels post-injection followed by a gradual decrease over 24 hours. In addition, it was found that radiation induced dsDNA breaks are enhanced in the presence of GPMs. HT 1080 cells irradiated (4 Gy) in the presence of GPMs (100ug/ml) exhibit roughly 2.1 times higher density of DNA double strand breaks (i.e. gh2ax foci) compared to cells treated with radiation alone. Extension of these capabilities to human cancer patients could allow for effective accumulation and visualization of GPMs within tumors via CT and enhance the efficacy of radiation therapy.

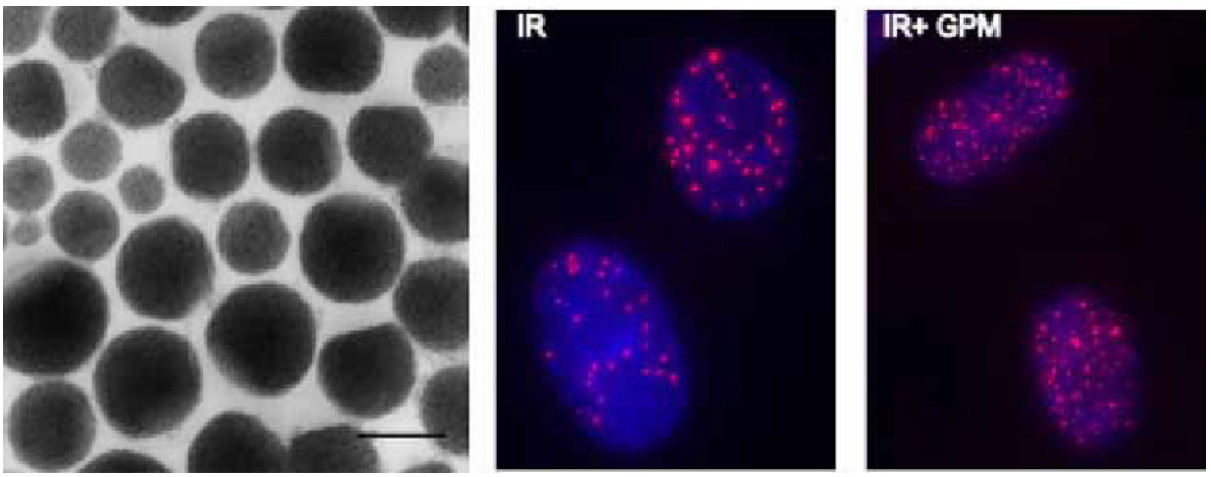


Figure 1. (Left) TEM image of GPM with 1.9nm AuNPs encapsulated within micellar core (scale bar = 100nm). (Right) Immunofluorescence imaging of gh2ax, which is a marker for unrepaired dsDNA breaks, on HT1080 cells with and without GPMs.

Disclosure of author financial interest or relationships:
**A. Al Zaki**, None; **D. Joh**, None; **Z. Cheng**, None; **G. Kao**, None; **J.F. Dorsey**, None; **A. Tsourkas**, None.

Presentation Number **P315**
Poster Session 2
September 6, 2012 / 15:15-15:15 / Room: The Liffey

# Choline kinase protein but not phosphocholine is necessary for cancer cell survival

*Noriko Mori[1], Flonné B. Wildes[1], **Zaver M. Bhujwalla**[1,2], [1]JHU ICMIC Program, The Russell H. Morgan Department of Radiology and Radiological Science, The Johns Hopkins University School of Medicine, Baltimore, MD, USA; [2]The Sidney Kimmel Comprehensive Cancer Center, The Johns Hopkins University School of Medicine, Baltimore, MD, USA. Contact e-mail: zaver@mri.jhu.edu*

Introduction: Choline kinase (Chk) is the enzyme that catalyzes the first step in phosphatidylcholine biosynthesis, and high Chk expression and increased phosphocholine (PC) levels are frequently observed in aggressive cancers. Activated choline metabolism, termed the 'cholinic phenotype', is common in cancer and can be detected by magnetic resonance spectroscopy (MRS) or positron emission tomography (PET) imaging of labeled choline. Unraveling the role of Chk and PC could provide new insight into the malignant phenotype and lead to the development of novel treatment strategies. We have previously shown that downregulation of mRNA and protein levels of Chk significantly reduced proliferation in breast cancer cells and tumors. Here we investigated the effect of the Chk inhibitor, V-11-0711 (Vertex Pharmaceuticals (Europe) Ltd), which reduces the function of Chk by binding to the active site. We examined Chk protein expression levels, cell proliferation, and PC, glycerophosphocholine (GPC), and total choline (PC+GP+choline) levels in MDA-MB-231 human breast cancer cells following treatment with this inhibitor. We also investigated the effect of Chk protein levels on cell proliferation by using siRNA against Chk (siRNA-chk) in the presence or absence of V-11-0711. Methods: MDA-MB-231 cells were grown in RPMI-1640 medium supplemented with 10% FBS. Fully relaxed 1H MRS of the water-soluble phase was performed on a Bruker Avance 500 spectrometer. Immunoblot analysis was performed with 50 µg protein from cell lysates at 48 h post-treatment using a polyclonal Chk-α antibody (custom made) and a monoclonal GAPDH antibody (Sigma) as loading control. The CCK-8 assay (Dojindo Molecular Technologies, Inc. MD) was performed to measure proliferation 3 days after the medium was changed to culture medium at 48 h post-treatment. Results and Discussion: Treatment with 1µM V-11-0711 did not significantly reduce cell proliferation under the conditions used here (in previous testing 10µM V-11-0711 showed 15% reduction in cell proliferation), although levels of PC and tCho did decrease significantly in a dose dependent manner. GPC levels did not change significantly. siRNA-chk reduced Chk protein to an undetectable level, and proliferation was significantly reduced whether V-11-0711 was present or not. Our results demonstrate that under these conditions reduction of PC has little affect on the proliferation of breast cancer cells as long as Chk protein levels are not reduced. These data are consistent with results obtained by Miyake et al., [1] on the potential role of Chk as a chaperone protein, and suggest that the Chk protein may be essential in cancer cell proliferation. The data support the development of strategies that destabilize or downregulate Chk protein. [1] Miyake T et al., Oncogene (2011).

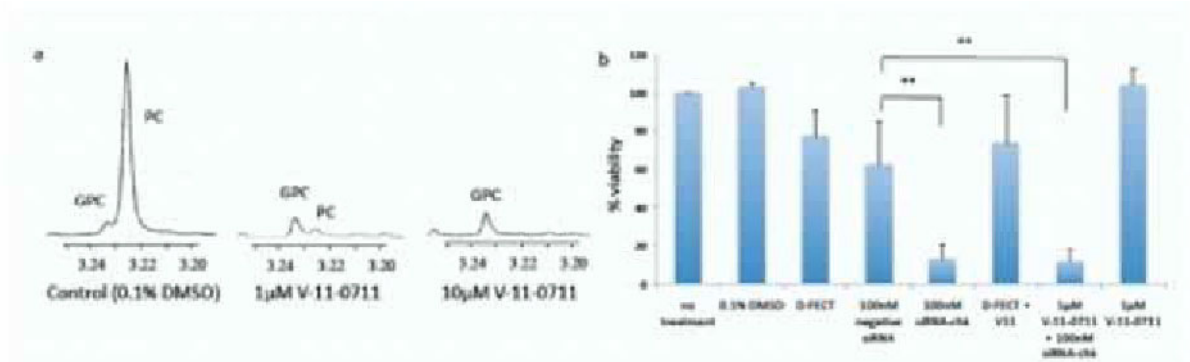


Figure 1: a) Representative $^1$H NMR spectra expanded to show the 3.20-3.25 ppm region of MDA-MB-231 cells treated with V-11-0711. b) Cell viability/proliferation as determined by the CCK-8 assay in MDA-MB-231 cells treated with 0.1% DMSO (vehicle control), D-FECT (DharmaFECT: transfection reagent), 100nM siRNA-chk and/or 1 µM V-11-0711 for 48 hours. Assays were done at 3 days after medium was changed to culture medium at 48 h post-treatment. The viability of no treatment is considered as 100%. Values are mean ± st andard deviation. ** represents $P < 0.01$ vs negative siRNA.

Disclosure of author financial interest or relationships:
**N. Mori**, None; **F.B. Wildes**, None; **Z.M. Bhujwalla**, None.

Presentation Number **P316**
Poster Session 2
September 6, 2012 / 15:15-15:15 / Room: The Liffey

# Cholangiocarcinoma diagnosis: the role of 18F-FDG and 18F-choline

*Ana F. Brito[1,2], Ana M. Abrantes[1,2], Mónica Mendes[1,3], Fábio Veríssimo[1,4], Francisco Castro-Sousa[5,2], José Tralhão[5,1], **Maria F. Botelho**[1,2], [1]Biophysics Unit, IBILI, Faculty of Medicine, University of Coimbra, Coimbra, Portugal; [2]CIMAGO, Faculty of Medicine, University of Coimbra, Coimbra, Portugal; [3]Faculty of Sciences and Technology, University of Coimbra, Coimbra, Portugal; [4]Coimbra College of Agriculture, Coimbra, Portugal; [5]Surgical Department, Surgery A, HUC, Coimbra, Portugal. Contact e-mail: filomena@ibili.uc.pt*

Introduction: Cholangiocarcinoma (CC) is the second most common primary liver tumor. The incidence of CC is increasing worldwide. This disease often presents with advanced non-specific symptoms. Local invasion, regional extension and distant metastases preclude resection in the majority of patients, and neither radiation nor conventional chemotherapy significantly improves survival. The use of PET with 18F-FDG has been widely used in the detection of various solid tumors. More recently, another radiopharmaceutical, 18F-choline, has emerged as a promising weapon in tumor detection. Thus, this study aims to evaluate 18F-FDG and 18F-choline uptake in a cholangiocarcinoma cell line and compare them, in order to verify which is the best tracer for tumor detection. Methods: The cell line used is TFK-1 (DSMZ). 18F-FDG and 18F-choline were incubated in a cell suspension with 2×106 cells/ml (25μCi/ml). Samples of 200μl were collected to eppendorf tubes for tracer uptake calculation. Eppendorfs were then centrifuged and radioactivity of cell pellets and supernatants was measured with a well-type gamma counter. Results: We observed a higher 18F-choline than 18F-FDG uptake. After 120 minutes incubation with radiopharmaceuticals, the 18F-FDG uptake is about 3% and 18F-choline uptake is about 30%, i.e., about 10 times more. Conclusions: These results show that the cell line under study has a 18F-choline uptake about 10 times higher than 18F-FDG. In clinical practice, 18F-choline may be a better option for cholangiocarcinoma diagnosis than 18F-FDG.

Disclosure of author financial interest or relationships:
**A.F. Brito**, None; **A.M. Abrantes**, None; **M. Mendes**, None; **F. Veríssimo**, None; **F. Castro-Sousa**, None; **J. Tralhão**, None; **M.F. Botelho**, None.

Presentation Number **P317**
Poster Session 2
September 6, 2012 / 15:15-15:15 / Room: The Liffey

# The role of gossypol, quercetin and cytochalasin-B in hepatocellular carcinoma therapy

*Ana F. Brito[1,2], Fábio Veríssimo[3,1], Marina Ribeiro[1,4], Ana M. Abrantes[1,2], Francisco Castro-Sousa[5,2], José Tralhão[5,1], **Maria F. Botelho**[1,2], [1]Biophysics Unit, IBILI, Faculty of Medicine, University of Coimbra, Coimbra, Portugal; [2]CIMAGO, Faculty of Medicine, University of Coimbra, Coimbra, Portugal; [3]Coimbra College of Agriculture, Coimbra, Portugal; [4]Faculty of Sciences and Technology, University of Coimbra, Coimbra, Portugal; [5]Surgical Department, Surgery A, HUC, Coimbra, Portugal. Contact e-mail: filomena@ibili.uc.pt*

Introduction: Hepatocellular Carcinoma (HCC) is the most common primary liver malignancy with a rising incidence worldwide. Therapies are very often palliative and have little effect on patient survival. Glucose transporter 1(GLUT-1) is overexpressed in HCC and promotes tumorigenesis. Conversely, suppression of GLUT-1 significantly impaired growth and invasiveness of HCC cell lines. Consequently it was proposed that GLUT-1 could be an innovative therapeutic target for HCC. Some compounds as gossypol, flavonoids and cytochalasin-B have shown potencial as GLUT-1 function inhibition and it can be useful therapeutical weapons against HCC. A Positron Emission Tomography (PET) using the radiolabeled glucose analogue 18F-FDG (2-[18F]fluorodeoxyglucose) enables the detection of increased glycolysis events in cancer cells. 18F-FDG is transported into the cell mainly through the GLUT-1 and 3. The aim of this study is to evaluate the potential anticancer effect of gossypol, quercetin (a flavonoid) and cytochalasin-B on two HCC cell lines which differ on p53 expression, HePG2(wp53) and HuH7(mp53), as well as check the effect of these compounds on 18F-FDG uptake in these cell lines. Materials and methods: The cell lines were propagated in the presence of gossypol, quercetin and cytochalasin-B in several concentrations. Cell proliferation was evaluated by the MTT test.18F-FDG was incubated in a cell suspension with 2×106 cells/ml (25μCi/ml) in cells pre-incubated with gossypol, quercetin and cytochalasin-B and control cells. Samples were collected to eppendorf tubes for tracer uptake calculation. Eppendorfs were then centrifuged and radioactivity of cell pellets and supernatants was measured with a well-type gamma counter. Results: All compounds induced a decrease in cell proliferation on both cell lines, and was shown that their effect depends on the time, having gossypol the more expressive results. For example, the IC50 with gossypol incubation after 24 hours was 5.97μM to HepG2 and 7,17μM to HuH7. For quercetin, the value of IC50 after 24 hours was respectively 47,64μM and 182,5μM, and for cytochalasin-B, the values was respectively 80,89μM and 28,01μM. In addition, for the cell lines studied, gossypol, quercetin and cytochalasin-B was able to decrease the percentage of 18F-FDG uptake. Conclusion: These results shown that gossypol, quercetin and cytochalasin-B have anti-proliferative effect on HCC cell lines studied. These compounds also have shown ability to decrease the uptake of 18F-FDG. More studies must be done to clarify the role of p53 in the anti-proliferative effect of these compounds in HCC as well as the effect in the uptake of the 18F-FDG.

Disclosure of author financial interest or relationships:
**A.F. Brito**, None; **F. Veríssimo**, None; **M. Ribeiro**, None; **A.M. Abrantes**, None; **F. Castro-Sousa**, None; **J. Tralhão**, None; **M.F. Botelho**, None.

Presentation Number **P318**
Poster Session 2
September 6, 2012 / 15:15-15:15 / Room: The Liffey

# Characterization and therapeutic trials in MIA PaCa-2 pancreas cancer cell line

*Rui V. Gradiz[3,2], Ana M. Abrantes[1,2], Ana C. Mamede[1,4], Lina Carvalho[5,2], Henriqueta C. Silva[6,2], Ana Alarcão[5], Luís Mesquita[6], Rui Nobre[7], Anabela Mota-Pinto[3,2], **Maria F. Botelho**[1,2], [1]Biophysics Unit, IBILI, Faculty of Medicine, University of Coimbra, Coimbra, Portugal; [2]CIMAGO, Faculty of Medicine, University of Coimbra, Coimbra, Portugal; [3]General Pathology Service, Faculty of Medicine, University of Coimbra, Coimbra, Portugal; [4]CICS-UBI, Health Sciences Research Center, University of Beira Interior, Coimbra, Portugal; [5]Anatomic Pathology Service, Faculty of Medicine, University of Coimbra, Coimbra, Portugal; [6]Medical Genetics Unit, Faculty of Medicine, University of Coimbra, Coimbra, Portugal; [7]Center for Neuroscience and Cell biology, University of Coimbra, Coimbra, Portugal. Contact e-mail: filomena@ibili.uc.pt*

Introduction: Pancreatic cancer is the fourth leading cause of cancer worldwide. MIA PaCa-2 is a human pancreatic duct adenocarcinoma cell line, a cancer that represents about 90% of all pancreatic tumors. To use this cell line as a model of pancreatic cancer it is important to verify if it represents a neuroendocrine tumor, if it expresses somatostatin 2 and neurotensin 1 receptors, thus allowing target diagnostic and therapeutic approaches experiments, and what are the major genetic abnormalities involved in carcinogenic transformation. It is also important to assess the response of this cell line to major cytostatic agents. Materials and methods: MIA PaCA-2 cell line was acquired from ATCC. Immunohistochemical staining technique was used to identify epithelial (CK-19 and MNF-116), mesenchymal (vimentin) and endocrine (chromogranin A, CD56 and synaptophysin) markers. Western blotting technique allowed the detection of somatostatin 2 and neurotensin 1 receptors. Mutational analysis was carried out by PCR (CDKN2A, exons 1alpha, 2 and 3), sequencing (KRAS codons 12, 13 and 61, TP53 exons 4, 5, 6 7 and 8) and multiplex PCR followed by capillary electrophoresis for microsatellite instability analysis (BAT25, BAT 26, NR21, NR22 and NR24 mononucleotide repeats). To obtain uptake curves, 2x106 cells/mL were incubated with growing activities of [99mTc]-TOC and [177Lu]-DOTA-TATE. Duplicated samples of pellet and supernatant were taken and the activity was measured in a well counter at 5, 30, 60, 90 and 120 minutes. The percentage of uptake was calculated by the ratio between the pellet and the supernatant. The IC50 for cytostatics (5-FU and everolimus) was achieved by MTT technique. Results: MIA PaCa-2 cells express CK-19, MNF-116, vimentin, chromogranin A, somatostatin 2 and neurotensin 1 receptors. Genotyping revealed a homozygous deletion of CDKN2A involving both P16 and P14, homozygous mutations in codon 12 of KRAS and in exon 7 of P53 (p.R248W) and no microsatellite instability. [99mTc]-TOC uptake increased over time and with the growing activities, reaching 1.98% with 200µCi at 120 minutes. [177Lu]-DOTA-TATE uptake maintained stable over time at different activities and reached 0.42% with 25µCi at 30 minutes. It was not possible to calculate IC50 for 5-FU at 24 and 48 hours, but at 72 hours it was 49.83µM (r2=0.93) and at 96h 8.32µM (r2=0.93). Everolimus IC50 was 27.88µM at 24h (r2=0.93) and 20.09µM (r2=0.94) at 48h. Conclusions: MIA PaCa-2 cells are EMT (epithelial-mesenchymal transition) cells of pancreas adenocarcinoma with neuroendocrine-like differentiation and somatostatin 2 and neurotensin 1 receptors. They harbor genetic mutations promoting proliferation and anti-apoptotic pathways involving KRAS, CDKN2A and P53. Also, they are capable of uptake of radiolabeled somatostatin analogs. Uptake of [99mTc]-TOC is time and dose depending. 177Lu-DOTATATE has a lower captation than 99mTc and its control. 5-FU and everolimus inhibit MIA PaCa-2 cell proliferation.

Disclosure of author financial interest or relationships:
**R.V. Gradiz**, None; **A.M. Abrantes**, None; **A.C. Mamede**, None; **L. Carvalho**, None; **H.C. Silva**, None; **A. Alarcão**, None; **L. Mesquita**, None; **R. Nobre**, None; **A. Mota-Pinto**, None; **M.F. Botelho**, None.

Presentation Number **P319**
Poster Session 2
September 6, 2012 / 15:15-15:15 / Room: The Liffey

# Multidrug resistance in hepatocellular carcinoma: studies with 18F-FDG and 99mTc-MIBI

*Mónica Mendes[1,3], Ana F. Brito[1,2], Ana M. Abrantes[1,2], Fábio Veríssimo[4,1], Ana Gonçalves[6,2], Ana B. Sarmento-Ribeiro[6,2], Francisco Castro-Sousa[5,2], José Tralhão[5,1], **Maria F. Botelho**[1,2], [1]Biophysics Unit, IBILI, Faculty of Medicine, University of Coimbra, Coimbra, Portugal; [2]CIMAGO, Faculty of Medicine, University of Coimbra, Coimbra, Portugal; [3]Faculty of Sciences and Technology, University of Coimbra, Coimbra, Portugal; [4]Coimbra College of Agriculture, Coimbra, Portugal; [5]Surgical Department, Surgery A, HUC, Coimbra, Portugal; [6]Applied Molecular Biology and Hematology Group, Faculty of Medicine, University of Coimbra, Coimbra, Portugal. Contact e-mail: filomena@ibili.uc.pt*

Introduction and aim: Hepatocellular Carcinoma (HCC) is known to be highly resistant to chemotherapy, which is due in part to overexpression of multidrug resistance proteins (MDR). A common method to measure the function of these proteins involves the study of radiolabeled substrate 99mTc-MIBI uptake. Recent studies have demonstrated that 18F-FDG uptake is associated with tumor differentiation and the expression of these proteins in HCC. This study aims to evaluate and compare the uptake and retention of 18F-FDG and 99mTc-MIBI in two human HCC cell lines with different expression levels of p53 and to correlate with the expression of three MDR proteins (Pgp, MRP1 and LRP). Materials and methods: The human HCC cell lines used were HepG2 (wp53) and HuH7 (mp53). Cell suspensions were incubated with 2x106cells/ml with 18F-FDG and 99mTc-MIBI (25µCi/ml). Samples of 200µl were collected at different periods of time which were centrifuged separating the supernatant from the pellet. Activity was measured in a well counter. The retention of 18F-FDG and 99mTc-MIBI was obtained by incubating the cell suspension with radioisotope during 60 minutes. Thereafter, the cells were centrifuged and medium renewed. The following procedure was similar to the uptake studies. The proteins levels of Pgp, MRP1 and LRP were determined by flow cytometry. Results: It was found that HuH7cell line which expresses a mutated form of p53 is one that has higher levels of uptake and retention of 99mTc-MIBI and also 18F-FDG. The HepG2 cell line has a lower uptake and retention and a higher expression of MRP1. The levels of Pgp and LRP expression are similar for both cell lines. Conclusions: It is clear that there is an inverse relationship between MRP1 expressions and uptake and retention of 99mTc-MIBI and 18F-FDG. The uptake and retention profiles for the two radiopharmaceuticals are similar, showing that the 18F-FDG can be used to study the action of MDR proteins in hepatocellular carcinoma cells, presented as an alternative to 99mTc-MIBI.

Disclosure of author financial interest or relationships:
**M. Mendes**, None; **A.F. Brito**, None; **A.M. Abrantes**, None; **F. Veríssimo**, None; **A. Gonçalves**, None; **A.B. Sarmento-Ribeiro**, None; **F. Castro-Sousa**, None; **J. Tralhão**, None; **M.F. Botelho**, None.

Presentation Number **P320**
Poster Session 2
September 6, 2012 / 15:15-15:15 / Room: The Liffey

# Targeted-split Enzyme Complementation to Interrogate the Cancer Signature Using Molecular Imaging

***Ann-Marie Broome***[1,2]*, Gopalakrishnan Ramamurthy*[2]*, Kari Lavik*[2]*, Michael Pinter*[1]*, Ian Kinstlinger*[2]*, James Basilion*[1,2]*,* [1]*Biomedical Engineering, Case Western Reserve University, Cleveland, OH, USA;* [2]*Radiology, Case Western Reserve University, Cleveland, OH, USA. Contact e-mail: broomea@musc.edu*

Noninvasive detection of any disease is a crucial step in the prevention, treatment and reduction of the mortality rate. Further, tailoring clinical diagnostics and therapeutics to specific forms of cancer and even to the precise aberrant biological events underlying cancer development in a particular patient has focused significant research on molecular signatures. For instance, cell surface receptors important in tumorigenesis are expressed at different levels during the multistage process and are routinely used to guide treatment regimes. Moreover, mutational events that drive a normal cell to become a cancer cell require the coordinated overexpression of not just one receptor at a time, but rather multiple biomarkers. Many cancers, including gliomas, are characterized by an abnormal increase in the activity of epidermal growth factor receptors (EGFR) and transferrin receptors (TfR). Our data of representative human cancer cell lines demonstrate unique, observable expression patterns for the two receptors. Current diagnostic techniques such as medical imaging, tissue biopsy, and bioanalytical assay of body fluids are relatively insensitive and lack the specificity to detect these physiologic changes simultaneously. To develop imaging tools that take advantage of the molecular signature, new technologies must employ an activity-based imaging agent conjugated to a targeting element. By linking a reporter enzyme, such as β-gal, to a targeting moiety, either ligand or a short peptide, signal-amplification at the molecular level is achieved. We divided β-gal into unique, independent polypeptides that reassemble and complement enzymatic activity in bacteria and in mammalian cells. We created two sets of complementing pairs that individually have no enzymatic activity. However, when brought into close proximity, complementing pairs associate, resulting in detectable enzymatic activity. We then constructed a targeting complex composed of reporter fragment, linker, and targeting moiety. Our studies demonstrate a time course- and dose-dependent uptake in vitro. Further, we were able to simultaneously visualize the two cell surface receptors implicated in gliomas, EGFR and TfR, using complementing pairs of the targeted reporter fragment complex. In addition, we were able to image orthotopic brain tumor accumulation and localization of the targeted-enzyme when a fluorescence reporter was added to the complex, as well as immunohistochemical staining of the β-gal reporter complex ex vivo. After fluorescence imaging localized the β-gal complexes to the brain tumor, we topically applied a bioluminescent β-gal substrate to serial sections of the brain to evaluate the delivery and integrity of enzyme. Robust bioluminescence was captured within the tumor after 3 min, indicating that β-gal maintained its activity. Current experiments are underway to image the enzyme complementation noninvasively in vivo.

Disclosure of author financial interest or relationships:
**A. Broome**, None; **G. Ramamurthy**, None; **K. Lavik**, None; **M. Pinter**, None; **I. Kinstlinger**, None; **J. Basilion**, Akrotome Imaging Inc, Stockholder .

Presentation Number **P321**
Poster Session 2
September 6, 2012 / 15:15-15:15 / Room: The Liffey

# A PSMA-targeted Theranostic Nanoplex Combining TRAIL Gene cDNA and Prodrug Enzyme Delivery For Prostate Cancer Treatment

***Zhihang Chen***[1], *Balaji Krishnamachary*[1], *Cong Li*[2], *Sangeeta Ray*[1], *Paul T. Winnard*[1], *Martin Pomper*[1], *Zaver M. Bhujwalla*[1], [1]*JHU ICMIC Program, Russell H. Morgan Department of Radiology and Radiological Science, Johns Hopkins University School of Medicine, Baltimore, MD, USA;* [2]*School of Pharmacy, Fudan University, Shanghai, China. Contact e-mail: zchen19@jhu.edu*

We have been developing a prostrate specific membrane antigen (PSMA)-based platform to deliver a prodrug enzyme and small interfering RNA (siRNA) for theranostic imaging. PSMA is a type II integral membrane protein with abundant expression on the surface of prostate carcinomas. Here we have extended the platform for gene delivery of tumor necrosis factor-related apoptosis-inducing ligand (TRAIL) cDNA. The PSMA-targeted nanoplex delivered TRAIL cDNA and a prodrug enzyme, bacterial cytosine deaminase (bCD), for theranostic imaging of metastatic prostate cancer. TRAIL has been reported to specifically kill malignant cells but to be relatively nontoxic to normal cells. The prodrug enzyme bCD converts the non-toxic prodrug 5-fluorocytosine (5-FC) to the active cytotoxic drug 5-fluorouracil (5-FU). Our prototype nanoplex was synthesized by conjugating: (i) a low molecular weight urea-based PSMA targeting moiety (2-(3-[1-carboxy-5-[7-(2,5-dioxo-pyrrolidin-1-yloxycarbonyl)-heptanoylamino]-pentyl]-ureido)-pentanedioic acid, (ii) the prodrug-activating enzyme bCD that converts nontoxic 5-FC to cytotoxic 5-FU, (iii) the near-infrared fluorescent probe Cy5.5 labeled linker poly-L-lysine (PLL), and (iv) the GFP-TRAIL pDNA delivery vector: PEI (polyethyleneimine)-PEG (polythethyeneglycol) co-grafted-polymer. The nanoplex was tested in PSMA-expressing PC-3 PIP and low-PSMA expressing PC-3 FLU human prostate cancer cells. As shown in Figure 1, exposure of cells to the nanoplex for 6 h resulted in the PSMA targeting moiety providing higher specificity of uptake in cells with high PSMA expression as evident from the increased GFP expression and decreased cell viability in MTT assays. While 5-FC was not added to the cells here, its availability will further reduce cell viability for cancer cell-specific treatment.

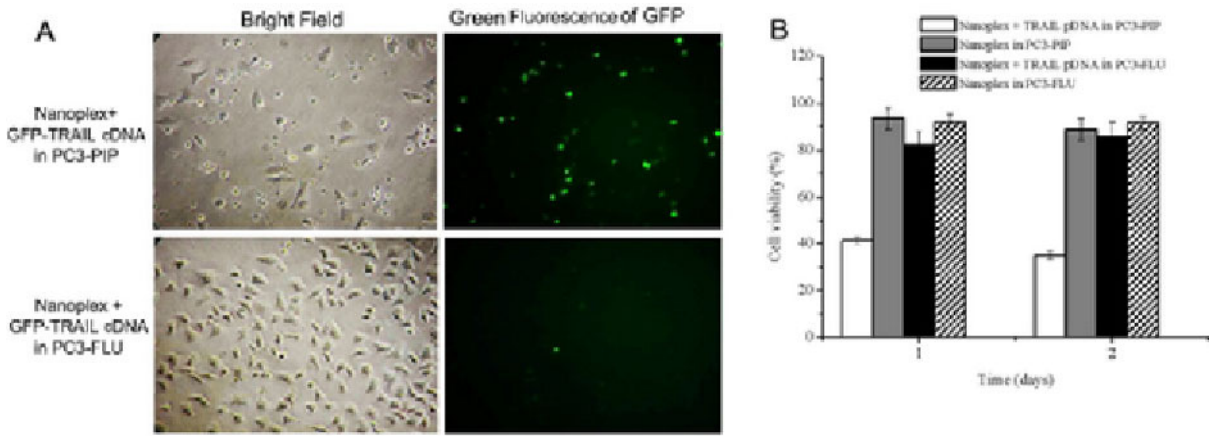


Figure 1: (A) Fluorescence microscope imaging of PC3-PIP (PSMA+) and PC3-FLU (PSMA-) cells. Cells were treated with GFP-TRAIL pDNA/nanoplex for 24 h (concentration of pDNA: 2 μg/ml; N/P ratio: 50). (B) Cell viability studies of PC3-PIP and PC3-FLU cells with different treatments. Cells were treated with GFP-TRAIL pDNA/nanoplex for 24 and 48 h (concentration of pDNA: 2 μg/ml; N/P ratio: 50). Values are generated from two separate experiments with three wells per experiment per condition.

Disclosure of author financial interest or relationships:
**Z. Chen**, None; **B. Krishnamachary**, None; **C. Li**, None; **S. Ray**, None; **P.T. Winnard**, None; **M. Pomper**, None; **Z.M. Bhujwalla**, None.

Presentation Number **P322**
Poster Session 2
September 6, 2012 / 15:15-15:15 / Room: The Liffey

# Dox-loaded Microbubbles Combined with Ultrasound to Drug-Sensitive and MDR Cells for Reversal of Multidrug Resistance

***Zhiting Deng***, *Fei Yan, Qiaofeng Jin, Hairong Zheng, Paul Lauterbur Center for Biomedical imaging, Institute of Biomedical and Health Engineering, Shenzhen Institutes of Advanced Technology, Chinese Academy of Sciences, Shenzhen, China. Contact e-mail: zt.deng@siat.ac.cn*

Multidrug resistance (MDR) remains one of the major obstacles for successful cancer chemotherapy. Early studies suggested that overexpression of P-glycoprotein (Pgp) protein was one of the major mechanisms for multiple drug resistance (MDR) in cancer cells. A new effective approach to overcome MDR is to use ultrasound and microbubble mediated drug delivery to increase drug accumulation in drug resistant cancer cells. In this work, the experimental results showed that with treatment of ultrasound and doxorubicin ( DOX ) loaded microbubbles, there were more than one-fold increase in intracellular DOX for drug-sensitive cell line (MCF-7) and respective P-glycoprotein expressing cell line (MCF-7/ADR) compared with treatment of ultrasound and DOX-liposomes. And significant decreases in drug efflux rates were observed at 30, 90 and 120 mins for both drug-sensitive and drug-resistant cell lines receiving ultrasound and microbubbles. The enhanced accumulation and retention of DOX by ultrasound and microbubbles resulted in greater cytotoxicity in both MCF-7 and MCF-7/MDR cell lines, as indicated by the MTT assay. These data suggest that ultrasound and microbubbles may facilitate the uptake of intact DOX-loaded microbubbles into cells, allowing greater retention of DOX in both Pgp and non-Pgp expressing cells. Given the narrow therapeutic window for doxorubicin, this increase in tumor accumulation could significantly improve the anti-tumor efficacy and reduce the toxic side effect.

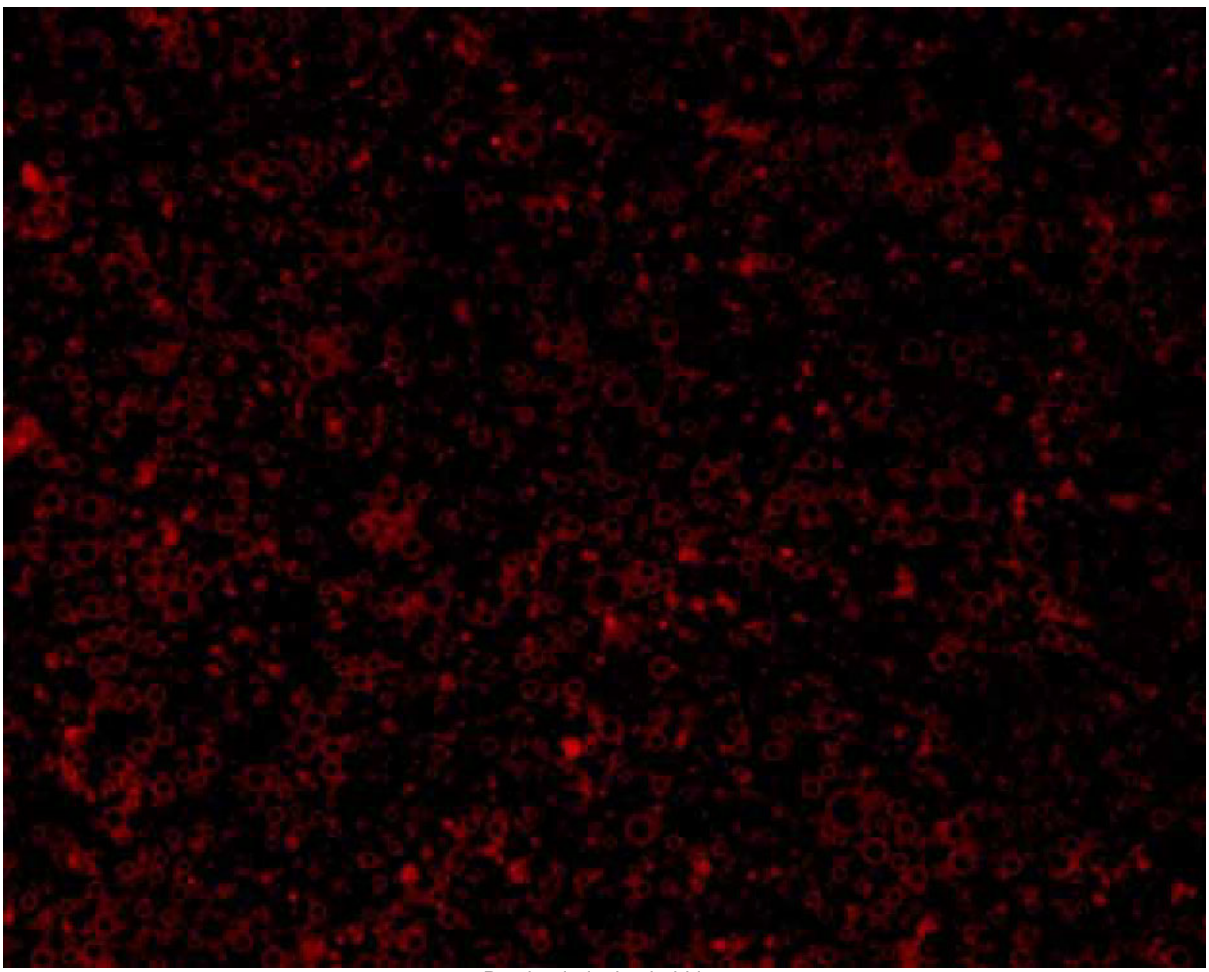

Dox loaded microbubbles

Disclosure of author financial interest or relationships:
**Z. Deng**, None; **F. Yan**, None; **Q. Jin**, None; **H. Zheng**, None.

Presentation Number **P323**
Poster Session 2
September 6, 2012 / 15:15-15:15 / Room: The Liffey

# Three-dimensional visualization of tumor vessel architecture and antibody penetration using multispectral fluorescence ultramicroscopy

***Michael Dobosz***[1,2], *Steffen Strobel*[1], *Vasilis Ntziachristos*[2], *Werner Scheuer*[1], [1]*Pharma Research & Early Development (pRED), Roche Diagnostics GmbH, Penzberg, Germany;* [2]*Institute for Biological and Medical Imaging, Technical University of Munich, Munich, Germany. Contact e-mail: Michael.Dobosz@roche.com*

Detailed analysis of vessel structure in tumor xenografts is an integral part of testing new anti-angiogenic compounds in preclinical cancer models. Different in vivo and ex vivo technologies are applied to evaluate the therapeutic efficacy of such drugs. An established read-out is micro vessel density which is conventionally performed by staining formalin fixed paraffin embedded tissue (FFPT) slides of explanted tumor tissue with antibodies targeting antigens expressed on vessels. This procedure has different disadvantages. Formalin fixation crosslinks antigens which may modify epitopes and thus, retrieval methods for demasking epitopes have to be performed. Secondly, the analysis of a restricted number of slides may not be representative for the whole tumor section. In addition, analysis of slides in a 2-dimensional fashion is of only restricted use for the detailed description of the complexity of three-dimensional elements. We, for the first time, describe a new method which circumvents these problems. The application of 3D multispectral fluorescence ultramicroscopy allows the quantitative analysis of the vessel architecture and - simultaneously - the penetration behaviour of an antibody targeting a tumor cell surface antigen. This can be accomplished by the i.v. injection of Lectin (labeled with Alexa647) and an anti-Her2 antibody (labeled with Alexa750) into a tumor xenograft. Thereafter, tumors are explanted, specimens are cleared to prevent scattering and optical sectioning is applied to examine the whole tumor sections in a three dimensional way. In order to analyze the reconstructed 3D datasets, we have created a software algorithm which possesses excellent performance in segmentation and quantification of different vessel parameters (e.g. diameter, length, volume, number of segments and branchpoints) and antibody distribution (e.g. uniformity, location, total signal). Results of such measurements provide relevant information regarding different vessel features after an anti-angiogenic therapy and the effect of such treatments regarding changes in penetration of therapeutic antibodies. This new approach facilitates the quantitative analysis of different vessel parameters and tumor penetration kinetics of antibodies. Compared to established methods 3D multispectral fluorescence ultramicroscopy is less laborious and less error-prone and thus is able to improve the drug development process.

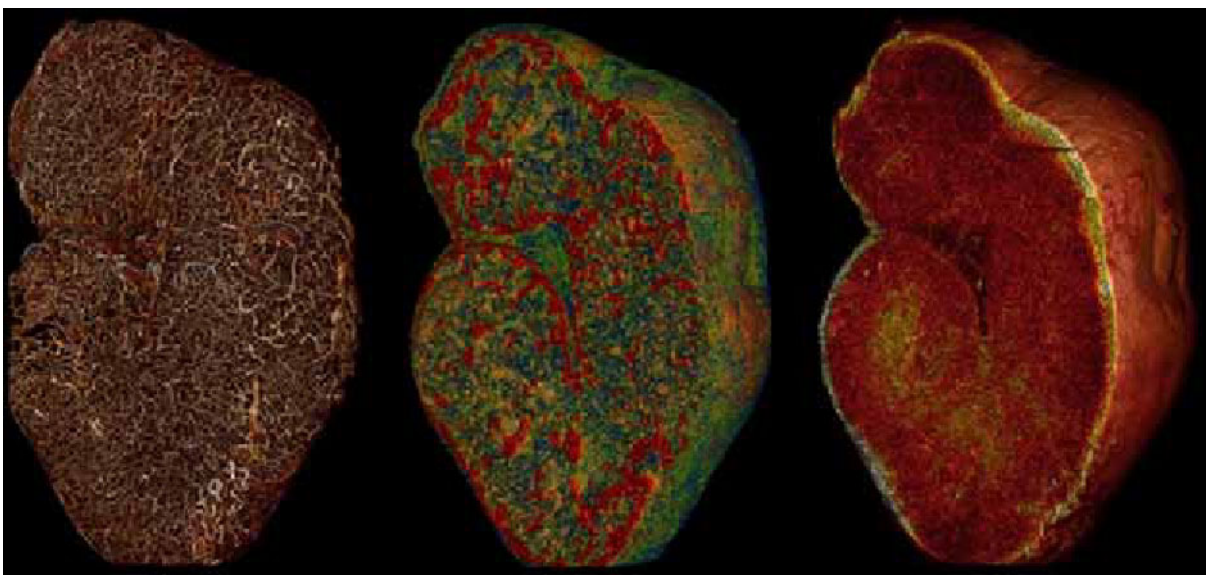

3D volume rendering of tumor vessel, antibody penetration and tumor morphology. (a) Tumor vessels are labeled with lectin-Alexa647. (b) Tumor penetration of Alexa750 labeled anti-Her2 antibody. (c) Tumor morphology is visualized from tissue autofluorescence. Data are illustrated as pseudo color image.

Disclosure of author financial interest or relationships:
**M. Dobosz**, Roche Diagnostics GmbH, Employment; **S. Strobel**, Roche Diagnostics GmbH, Consultant; **V. Ntziachristos**, ERC, Grant/research support; Ithera Medical, Stockholder; **W. Scheuer**, Roche Diagnostics GmbH, Employment .

Presentation Number **P324**
Poster Session 2
September 6, 2012 / 15:15-15:15 / Room: The Liffey

# TARGETED LIPOSOME-LOADED MICROBUBBLES FOR SELECTIVE ULTRASOUND ASSISTED CIRCULATING TUMOR CELL THERAPY

***Bart Geers***[1]*, Olivier De Wever*[2]*, Marc Bracke*[2]*, Stefaan De Smedt*[1]*, Ine Lentacker*[1]*,* [1]*Lab of general biochemistry and physical pharmacy, Ghent University, Gent, Belgium;* [2]*Laboratory of experimental oncology, Ghent University, Gent, Belgium. Contact e-mail: bart.geers@ugent.be*

One of the main problems in cancer treatment is disease-relapse through metastatic colonization due to circulating tumor cells, which is the cause of most cancer deaths. To the best of our knowledge there is no device that is able to detect these cells and specifically destroy them before they can do any harm. Hence we took the challenge to design such a device based on liposome-loaded microbubbles. Liposome-loaded microbubbles have a known potential for ultrasound induced drug-delivery to cancer cells . The basic idea is to design a liposome-loaded microbubble that is able to sensitively and specifically detect circulating tumor cells that express an antigen specific for a circulating metastasis cell (e.g. N-cadherin). Microbubbles are loaded with liposome-antibody conjugates that are covalently-linked to the surface of the microbubbles via thiol-maleimide bonds. These microbubbles can selectively bind N-cadherin expressing tumor cells and subsequent insonation would allow us to selectively deliver therapeutic molecules into these cells. In this study we wanted to answer the following scientific questions: a) can we design a targeted liposome-loaded microbubble; b) is this microbubble able to bind to N-cadherin expressing HMB2-cells; c) can we specifically detect these HMB2-cells in a more complex mixture (i.e.: HMB2 cells mixed with another cell type not expressing the N-cadherin protein); and d) are we able to selectively deliver small molecules after ultrasound treatment with this system. Microbubble design feasibility was shown by loading Bodipy-labeled targeted liposomes on the surface of the bubble. Antibody labeling was shown by staining the bubbles with a secondary anti-mouse antibody. Confocal microscopy showed clear co-localization of the green- and red-fluorescent dyes, the maximum antibody-loading was afterwards determined with flow cytometry. The interaction of the microbubbles with the N-cadherin expressing HMB2-cells was analyzed with flow cytometry. For this purpose the cells were labeled with the aspecific green-fluorescent dye Cell Tracker® and the microbubbles were loaded with red-fluorescent DiD-labeled targeted or non-targeted liposomes. Results clearly indicate an increase in events positive for both green- and red-fluorescence upon targeting to N-cadherin. The same protocol was used to quantitatively show this interaction in a medium mixed with non-labeled epithelial cells (not-expressing the N-cadherin protein). Results indicate a significant increase in green fluorescence of the event population positive for DiD. To confirm selective targeting in this complex medium we performed confocal microscopy as well, also showing selective targeting to the N-cadherin expressing cells. Finally specific delivery of small molecules upon ultrasound was shown with Propidium Iodide-filled targeted and non-targeted liposomes loaded on the bubbles. Flow cytometry analysis shows an increased delivery of Propidium Iodide to N-cadherin expressing cells upon ultrasound, there where off-target delivery remained minimal. Hence we can conclude that delivery to specific cell types using drug-loaded microbubbles is feasible.

Disclosure of author financial interest or relationships:
**B. Geers**, None; **O. De Wever**, None; **M. Bracke**, None; **S. De Smedt**, None; **I. Lentacker**, None.

Presentation Number **P325**
Poster Session 2
September 6, 2012 / 15:15-15:15 / Room: The Liffey

# CD133-expressing thyroid cancer cells are in an undifferentiated state, radioresistant and survive radioiodide therapy

***Chien-Chih Ke***[1,2], *Ren-Shyan Liu*[2,4], *Chen-Hsen Lee*[3,4], *An-Hang Yang*[4], *Ling-ming Tseng*[1,4], *Yi-Fang Tsai*[1,4], *Chin-Wen Chi*[1,4], *Oscar K. Lee*[1,4], *[1]Institute of Clinical Medicine, School of Medicine, National Yang-Ming University, Taipei, Taiwan; [2]Nuclear Medicine, School of Medicine, National Yang-Ming University, Taipei, Taiwan; [3]Surgery, National Yang-Ming University, Taipei, Taiwan; [4]Taipei Veterans General Hospital, Taipei, Taiwan. Contact e-mail: s2289.tw@yahoo.com.tw*

Introduction: Thyroid cancer is the most common endocrine-related cancer. Due to the cancer cells' ability of taking up iodide, radioactive I-131 therapy is effective and regularly used as a part of thyroid cancer management. Despite an overall relatively good prognosis compared to other cancers, patients with recurrent or metastatic thyroid cancer are not rare. Cancer stem cell theory describes a cell population capable of self-renewal and differentiation within the tumor. CD133-expressing cells have been shown to mark thyroid cancer stem cells that possess the characteristics of stem cells and have the ability to initiate tumors. However, no reports have addressed as yet the role of CD133-expressing cells in thyroid cancer radiotherapy. The aim of this study is to investigate whether CD133+ cells contribute to the radioresistance of thyroid cancer and thus potentiate future recurrence and metastasis. Methods: Radiosensitivity of CD133 positive and negative thyroid cancer cell lines was assessed. The gene expression profiles of isolated CD133+ and CD133- populations derived from cell lines and primarily cultured papillary thyroid cancer (PTC) cells were analyzed using quantitative real-time PCR. Mice bearing ectopic thyroid tumors were subjected to I-131 therapy followed by gene expression analysis for the tumor cells. Results: The anaplastic thyroid cancer cell line ARO showed a higher CD133+ population and higher radioresistance. These CD133+ cells, which exhibited higher radioresistance, also showed higher expression of the Oct4, Nanog and Glut1 genes compared to the CD133- cells from the same cell line. The CD133+ population was found to be enriched after the cells were γ-irradiated due to the higher apoptotic rate of CD133- cells. In vivo I-131 therapy of ARO-hNIS tumors, which stably expressed human sodium iodide symporter, resulted in an elevated expression of CD133, Oct4, Nanog, Lin28 and Glut1. The CD133+ population in primarily cultured papillary thyroid cancer cells also showed higher expression of Oct4, Nanog, Sox2 and Lin28, and lower expression of various thyroid specific genes, namely NIS, Tg, TPO, TSHR, TTF1 and Pax8. CD133 expression was also detected in parafilm-embedded thyroid cancers. Conclusion: This study demonstrates the existence of CD133-expressing cells in thyroid cancers. These cells showed a higher radioresistance and were in a more primitive and undifferentiated status. In addition, in vitro γ-irradiation and in vivo I-131 therapy enriched the CD133+ population and elevated CD133 expression in the surviving cells. Taken together, CD133+ thyroid cancer cells possess a greater potential to survive radiotherapy and to contribute to the future recurrence of thyroid cancer. Future therapeutic development for thyroid cancer may focus on the selective killing of these cells.

Disclosure of author financial interest or relationships:
**C. Ke**, None; **R. Liu**, None; **C. Lee**, None; **A. Yang**, None; **L. Tseng**, None; **Y. Tsai**, None; **C. Chi**, None; **O.K. Lee**, None.

Presentation Number **P326**
Poster Session 2
September 6, 2012 / 15:15-15:15 / Room: The Liffey

# Induced differentiation of anaplastic thyroid cancer by histone deacetylase inhibitor treatment is correlated with CD133+ population

***Chien-Chih Ke***[1,2], *Ren-Shyan Liu*[1,3], *Oscar K. Lee*[2,4], *Chin-Wen Chi*[2,4], *Chen-Hsen Lee*[2,4], [1]*MGAIC/NRPGM, School of Medicine, National Yang-Ming University, Taipei, Taiwan;* [2]*Clinical Medicine, Pharmacology, National Yang-Ming University, Taipei, Taiwan;* [3]*Dept of Nuclear Medicine, Faculty of Medicine, National Yang-Ming University, Taipei, Taiwan;* [4]*Emergency Medicine and Surgery, Taipei Veterans General Hospital, Taipei, Taiwan. Contact e-mail: s2289.tw@yahoo.com.tw*

Objectives: It was reported that with treatment of histone deacetylase inhibitor (HDACi) trichostatin A (TSA), anaplastic thyroid cancer cells re-expressed sodium iodide symporter, thyroperoxidase and thyroglobulin, and the iodide uptake and retention were restored. Also TSA induced differentiation of several types of cancer, including thyroid cancer. CD133, expressed by hematopoietic stem cells, was recently reported to mark the ARO anaplastic thyroid cancer stem cells. In this study, we aimed to evaluate the cancer differentiation effect by TSA monitored by CD133 expression. Methods: Upon treatment of different doses of TSA for various time periods, the CD133+ population was monitored by flow cytometry analysis. These TSA treated ARO cells were evaluated for the of thyroid transcription factor (TTF1) gene expression by quantitative real time PCR. After treatment of TSA, these cells were subjected to γ-irradiation with various doses to check the radiosensitivity. Results: CD133+ cells in whole population decreased to 43% and 33% after treated with 100 and 250 ng/ml TSA for 2 days, respectively, compared to 59% of non-treated group. This decrease of CD133+ population was reversibly recovered after withdrawal of TSA in the culture. With continuous treatment of TSA, cells showed a stable, 25~30% in population which expressed CD133. After irradiation, these TSA-treated cells showed radiosensitivity. The expression of TTF1 was increased in ARO cells treated with TSA. Conclusions: We have proved the differentiation effect of TSA on ARO cells. TSA decreased the CD133+ population, increased the TTF1 gene expression and radiosensitivity of ARO cells. This phenomenon may be applied on the combined radioiodide and HDACi treatment on poorly differentiated thyroid cancer.

Disclosure of author financial interest or relationships:
**C. Ke**, None; **R. Liu**, None; **O.K. Lee**, None; **C. Chi**, None; **C. Lee**, None.

Presentation Number **P327**
Poster Session 2
September 6, 2012 / 15:15-15:15 / Room: The Liffey

# Development of NIR fluorescent anti-HER2 VHHs for breast cancer imaging

***Marta M. Kijanka***[1]*, Sabrina Oliveira*[2]*, Mohamed El Khattabi*[3]*, Paul van Bergen en Henegouwen*[1]*, [1]Department of Biology, Utrecht University, Utrecht, Netherlands; [2]Department of Pathology, University Medical Center Utrecht, Utrecht, Netherlands; [3]QVQ BV, Utrecht, Netherlands. Contact e-mail: m.m.mania@uu.nl*

The membrane protein HER2 is expressed in tumor cells from 18-25% of all cases of breast cancer. Since expression of HER2 is completely absent in normal breast cells, HER2 is an ideal tumor marker that can be used for the early diagnosis of breast cancer. The goal of our study is to develop new technologies for the optical imaging of breast cancer. In our approach we make use of antibody fragments form Llama glama, indicated as VHHs. The VHHs are the Variable domain of the Heavy chain of naturally occurring Heavy-chain only antibodies (HcAb) which have a molecular weight of 15 kDa: 10 times smaller than conventional monoclonal antibodies. Despite their small size, they are able to bind specifically and with high affinities to their targets. VHHs have excellent properties for rapid optical imaging (such as tumor penetration and fast clearance from blood). Here we present the generation of novel anti-HER2 VHHs specifically aimed for optical breast cancer imaging. To obtain this goal phage display libraries were developed for selections of specific anti-HER2 VHHs. These newly developed VHHs were then conjugated to a near infrared (NIR) fluorophore and tested in vitro for their potential as probes for optical molecular imaging.

Disclosure of author financial interest or relationships:
**M.M. Kijanka**, None; **S. Oliveira**, None; **M. El Khattabi**, QVQ BV, Employment; **P. van Bergen en Henegouwen**, None.

Presentation Number **P328**
Poster Session 2
September 6, 2012 / 15:15-15:15 / Room: The Liffey

# Taking a closer look: Validating in vivo results with multispectral microscopy

*Kenneth Wong, James R. Mansfield,* ***Jae Beom Kim****, PerkinElmer, Alameda, CA, USA. Contact e-mail: jaebeom.kim@perkinelmer.com*

In vivo optical imaging is a valuable tool for monitoring the distribution of proteins and biomarkers in living animals non-invasively. However, a critical and sometimes overlooked component of the method development of these experiments is the validation of the results obtained in vivo through complementary methods. Of the two major small animal optical imaging modalities, bioluminescence and fluorescence, only the latter offers the capability to easily validate in vivo results through ex vivo or in situ microscopic imaging. Near-Infrared-labeled antibodies are widely imaged in vivo to determine the biodistribution of a protein or as a means of quantitating tumor size non-invasively. However, as these probes sometimes bind to necrotic regions in tumors or get trapped in interstitial spaces, it is important to confirm their biodistribution and quantitation of concentration with high resolution imaging. For that, advances in multispectral fluorescence microscopy and automated image analysis can add significant information on the physiology of diseases. Here, we present a few different models to validate the biomarkers from animal tissues or cultured cells using multispectral imaging. First, we used 4T1-GFP tumor cells and implanted the cells into the flank regions of athymic nude mice. Whole animal GFP imaging was done using a cooled CCD camera. Tumor masses were dissected and processed to make paraffin sections. These were de-paraffinized and mounted with DAPI-containing mounting media without any further incubation with GFP antibody. Tissue sections were imaged using a CCD camera that is equipped with liquid crystal tunable filters for both DAPI and GFP. Images were processed for spectral unmixing for DAPI and GFP as well as tissue autofluorescence. In addition, to compare the unmixed GFP signals with that of immunohistochemistry, we stained the tissue sections with GFP antibody. Our results showed that unmixed GFP signals from raw tissues correlate with the signals obtained from GFP immunohistochemistry. In the second model, we detected some biomarkers in a newly derived tumor cell line. For this study, we implanted luciferase labeled MDA-MB-231 cells (MDA-MB-231-luc2) into mammary fat pads of female athymic nude mice. Bioluminescent images confirmed the secondary tumors in axillary lymph nodes and their growth was monitored using whole animal imaging. The secondary tumors were dissected and a new cell line was generated (MDA-MB-231-luc2-LN). To examine the expression of biomarkers for tumorigenesis, cells were grown on coverslips overnight and incubated with an antibody cocktail containing antibodies against phospho-p44/42 (Erk1/2), phospho-Akt, and phospho-S6 ribosomal proteins. These antigens were detected with different fluorophores. After staining, multispectral imaging was performed followed by spectral unmixing for each dye. The results showed different subcellular localization of each marker. In sum, Multispectral imaging and spectral unmixing analyses can give in depth information for both in vivo and in vitro with enhanced sensitivity.

Disclosure of author financial interest or relationships:
**K. Wong**, None; **J.R. Mansfield**, PerkinElmer, Inc, Employment; **J. Kim**, PerkinElmer, Employment .

Presentation Number **P329**
Poster Session 2
September 6, 2012 / 15:15-15:15 / Room: The Liffey

# 131I labeled ApoPep-1 imaging for monitoring tumor apoptosis and therapy effect induced anti-cancer drugs

***Jung Eun Kim***[1], *Byeong-Cheol Ahn*[1], *Ho Won Lee*[1], *Mi-hye Hwang*[1], *Sang-Woo Lee*[1], *Byung-Heon Lee*[2], *Jaetae Lee*[1], [1]*Nuclear Medicine, Kyungpook National University School of Medicine/Hospital, Daegu, Republic of Korea;* [2]*Biochemistry and Cell Biology, Kyungpook National University School of Medicine, Daegu, Republic of Korea. Contact e-mail: gene7302@hotmail.com*

Background: The purpose of this study is to investigate 131I-labeled apopep imaging of the anticancer effects of cisplatin, 5-FU and cetuximab therapy on gastric cancer cells (SNU cells). Methods: SNU-effluc cell line was established by transfected with retrovirus expressing effluc into SNU cells. The effluc expressed cells were analyzed by FACS and sorted with CD 90.1 microbead The expression of effluc gene was verified by luciferase assay. Cell proliferation assay was performed for cell characterization between parent SUN and SNU-effluc cells. We treated for 48hrs cisplatin, 5-FU and cetuximab to induce apoptosis of SNU-effluc cells. Tumor cells treated after anti-cancer drugs were incubated with 131I labeled ApoPep-1. We assayed using bioluminescence imaging device (IVIS) and γ-camera. Results: Bioluminescent signals were found to correlate with cell numbers in SNU -effluc cells but not in SNU cells. CCK assay data showed that there was no significant difference of cell proliferation rate between SNU and SNU-effluc cells. In in vitro bioluminescence imaging data, bioluminescence signal of all therapy groups showed lower than no-treat group. The BLI signal of the cisplatin treated group showed the lowest among treated group. Whereas uptake of 131I of all therapy groups showed higher than no-treat group. The uptake of 131I of the cisplatin treated group showed the highest among treated group. Conclusions: 131I labeled ApoPep-1 imaging can provide as a high sensitivity of nuclear imaging tool for monitoring tumor apoptosis and therapy effect induced anti-cancer drugs.

Disclosure of author financial interest or relationships:
**J. Kim**, None; **B. Ahn**, None; **H. Lee**, None; **M. Hwang**, None; **S. Lee**, None; **B. Lee**, None; **J. Lee**, None.

Presentation Number **P330**
Poster Session 2
September 6, 2012 / 15:15-15:15 / Room: The Liffey

# Direct Identification of Cancer Stem Cells by In vivo Molecular Imaging and Aldefluor Assay

***Wei-Ying Kuo***[1], *Luen Hwu*[1], *Ren-Shyan Liu*[1,2], [1]*MAGIC/NRPGM, Nuclear Medicine, School of Medicine, National Yang-Ming University, Taipei, Taiwan;* [2]*National PET/Cyclotron Center, Taipei Veterans General Hospital, Taipei, Taiwan. Contact e-mail: kiki0502@gmail.com*

Objectives: Plenty of evidences indicate that solid tumors contain cancer-initiating cells (CICs) that are capable to regenerate a tumor which has been surgically removed, treated with chemotherapy or radiation therapy. Furthermore, CICs are also the key player in tumor metastasis. Recently, cell surface markers, such as CD133 or CD44, are used to identify CICs in vitro. However, these markers are limited in determining and tracking CICs in vivo. Aldehyde dehydrogenase class 1A1 (ALDH1A1) has been identified as highly expressed in normal and cancer stem cells. The Aldefluor assay allows the identification and isolation of viable cells with high expression of ALDH. In this study, we used reporter gene-based in vivo imaging and Aldefluor assay to track CICs from solid tumors and analyzed the gene expression profiles of CICs. Methods: To label and identify cells in vivo and in vitro, we established stable clones stably expressed a triple fused reporter construct (DsRedm-Fluc-tTKsr39) driven by CMV promoter in H1299 non-small cell lung cancer (NSCLC) cells. Using the Aldefluor assay, we further isolated CICs from xenografted tumors which co-express the reporter gene and ALDH activity. The differences of gene expression were compared by microarray analysis. Results: Although published data showed that CICs can be enriched by culturing tumor cells under serum-free medium with EGF (epidermal growth factor) and bFGF (Basic Fibroblast Growth Factor), but the environment for the in vitro spheroid culture system is still far from the in vivo tumor microenvironment. Thus, in this study, the gene expression profiles of CICs we isolated from xenografted tumors guided by the molecular imaging is more feasible. Our results clearly showed the CICs labeled by reporter genes and expressing ALDH activity as well (Fig1 and 2). Conclusions: Using the in vivo reporter gene imaging and Aldefluor assay, we may identify CICs directly in the xenografted tumor. This technology might provide an useful tool for better understanding of the molecular mechanism of CSCs.

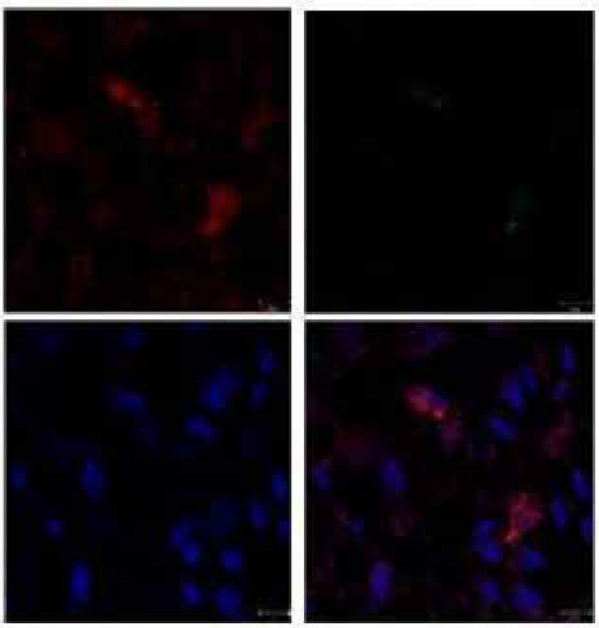

Fig. 1. Immuno-fluorescence of H1299-CMV-3H cells(DsRedm) with a specific antibody for ALDH1A1 was performed. Only ALDHbr cells showed specific fluorescence (green, nucleus in blue), Bar 10 μm.

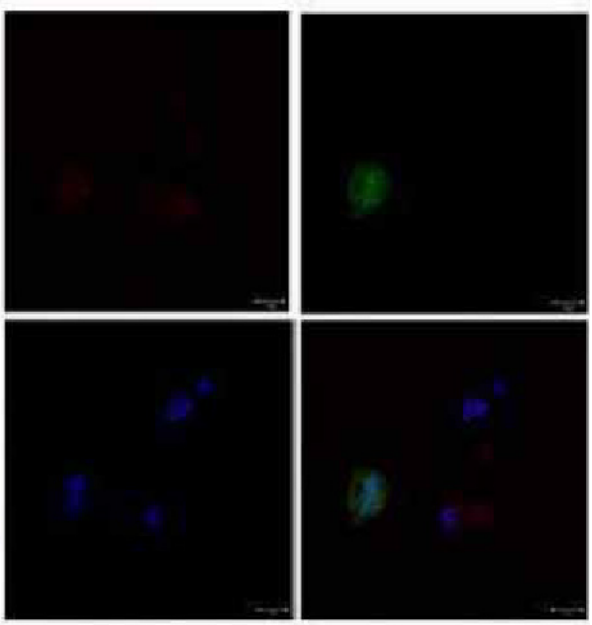

Fig. 2. ALDH protein expression analysis of aldefluor+ tumor cells by Aldefluor assay, Bar 10 μm.

Disclosure of author financial interest or relationships:
**W. Kuo**, None; **L. Hwu**, None; **R. Liu**, None.

Presentation Number **P331**
Poster Session 2
September 6, 2012 / 15:15-15:15 / Room: The Liffey

# From microscopic to macroscopic imaging of the hypoxia induced plasticity of cancer cell invasion

***Steffi Lehmann***[1,2]*, Veronika A. te Boekhorst*[3]*, Sjoerd V. Helvert*[2]*, Markus Rudin*[1]*, Peter Friedl*[2,3]*,* [1]*Institute of Biomedical Engineering, University and ETH Zurich, Zurich, Switzerland;* [2]*Nijmegen Center for Molecular Life Sciences, Radboud University Nijmegen Medical Centre, Nijmegen, Netherlands;* [3]*Genitourinary Medical Oncology, MD Anderson Cancer Center, Houston, TX, USA. Contact e-mail: lehmann@biomed.ee.ethz.ch*

Tumor hypoxia, a clinically established microenvironmental parameter, strongly contributes to overall cancer progression including increased metastasis and resistance to therapy. On the cellular level, hypoxia triggers the stabilization of oxygen-sensitive transcription factors, hypoxia inducible factors (HIFs), which initiate an adaptive program promoting angiogenesis, anaerobic metabolism, cell survival and migration. Consequently, *in vitro* studies using cells grown in monolayers, link hypoxia and HIF activation to the induction of epithelial-to-mesenchymal transition (EMT), including increased motility and invasiveness. However, the relevance of these findings in more complex environments and *in vivo* remains largely undefined. Using spheroid models of collective breast and squamous cancer cell invasion into 3D collagen lattices, we therefore assessed the impact of low oxygen concentrations on invasion mode and efficiency by live cell imaging and confocal microscopy. Within 72-96 hours, hypoxia (0.2 % $O_2$) led to a drastic EMT-like switch from collective to single cell dissemination, with down-regulation of E-cadherin as well as up-regulation of Snail and Oct-4. Hypoxia-induced single cell migration comprised both mesenchymal, protease-dependent and amoeboid, protease-independent migration modes with cells displaying spindle-shaped and rounded morphologies, and varying degrees of pericellular collagen degradation and proteolytic trail formation. This hypoxia induced plasticity of cancer cell invasion was prevented by stable knock-down of HIF-1α implicating this factor as major upstream regulator of the transition in migration style. Ongoing experiments address the metastatic seeding potential of hypoxia-conditioned cells *in vivo* by whole-body bioluminescence imaging and *ex vivo* histological analysis. Specifically, mouse 4t1 breast cancer cells stably expressing firefly luciferase, pre-cultured under normoxic and hypoxic conditions, are tail-vein injected into syngenic mice to assess potential differences in metastasis formation. In conclusion, hypoxia mediates fast and pronounced plasticity of cancer cell invasion and dissemination via HIF-1α, with implications for an altered metastatic potential.

Disclosure of author financial interest or relationships:
**S. Lehmann**, None; **V.A. te Boekhorst**, None; **S.V. Helvert**, None; **M. Rudin**, Hoffmann-LaRoche Ltd, Basel, Switzerland, Grant/research support; **P. Friedl**, None.

Presentation Number **P332**
Poster Session 2
September 6, 2012 / 15:15-15:15 / Room: The Liffey

# Synthesis and biological characterization of an EGFR targeting liposomal drug in a tumor-bearing animal model

*Keng-Li Lan[3], **Jia-Je Li**[1], Chao-Cheng Chen[1], Wen-Chun Tsai[1], Ren-Shyan Liu[2], C.Allen Chang[1], Hsin-Ell Wang[1], [1]Department of Biomedical Imaging and Radiological Sciences, National Yang-Ming University, Taipei, Taiwan; [2]Department of Nuclear Medicine and National PET/Cyclotron Center, Taipei Veterans General Hospital, Taipei, Taiwan; [3]Cancer Therapy Center, Taipei Veterans General Hospital, Taipei, Taiwan. Contact e-mail: uvpxyz@gmail.com*

Objectives: EGF dependent signal transduction pathways have been demonstrated as important targets for anticancer treatment. This study developed an EGFR-targeting liposomal drug and performed its biological characterization in a tumor-bearing mouse model. Methods: Hexa-histidine tagged recombinant human EGF was expressed in yeast, purified, and characterized. The recombinant EGF was conjugated to LipoDox® to give an EGFR-targeting liposome (EGF-LipoDox, 4.9~9.9 μg EGF/ μmole lipid). Both LipoDox® and EGF-LipoDox were labeled with $^{111}$In to afford their radioactive surrogates. The specific binding, internalization and cytotoxicity ($IC_{50}$) of EGF-LipoDox in high EGFR-expression breast cancer cell line (MDA-MB468) were investigated and compared with those of LipoDox®. The biodistribution and pharmacokinetics of radioactive counterparts in MDA-MB468 tumor-bearing animals were studied. Result: Significantly higher uptake of EGF-LipoDox compared with LipoDox® was observed in MDA-MB468 cells. The dramatically reduced cellular uptake after blocking with an excess of Cetuximab (C225), an anti-EGFR antibody, indicated the specificity of EGF-LipoDox to EGFR. EGF-LipoDox was 10-fold more cytotoxic than LipoDox® ($IC_{50}$ = 0.1 and 1 μM, respectively). The distribution of $^{111}$In-EGF-LipoDox after i.v. injection into tumor-bearing mice revealed a faster pharmacokinetic profile than that of $^{111}$In-LipoDox. The liver and spleen uptake at 4 h p.i. was 43.85±4.24 and 70.56±18.31 %ID/g for EGF-LipoDox, and was 17.03±1.63 and 17.68±1.42 %ID/g for LipoDox®. The blood clearance was 1.69 mL/h for EGF-LipoDox, while was only 0.01 mL/h for LipoDox®. At 48 h post-injection of $^{111}$In-labeled liposomal drugs, the tumor uptake and tumor-to-muscle ratio for EGF-modified liposome (1.18±0.53 %ID/g; 6.18) were less than those for commercial LipoDox® (7.80±2.70 %ID/g; 16.45). Conclusion: The results of this study suggested that, though EGF conjugation to liposomal drugs may promote the in vitro specific cellular uptake and cytotoxicity in high EGF receptor-expressed cells, it may also enhance the excretion by organs with reticuloendothelial system and thus hinder the ability of PEG to prolong systemic circulation of liposome.

Disclosure of author financial interest or relationships:
**K. Lan**, None; **J. Li**, None; **C. Chen**, None; **W. Tsai**, None; **R. Liu**, None; **C. Chang**, None; **H. Wang**, None.

Presentation Number **P333**
Poster Session 2
September 6, 2012 / 15:15-15:15 / Room: The Liffey

# Screening and identification of a peptide specifically targeted to the PG-like-region of human carbonic anhydrase IX from a Phage Display library

***Shoaib Rana***[1,2], *Felix Nissen*[3], *Annette Altmann*[2,3], *Uwe Haberkorn*[2,3], *Vasileios Askoxylakis*[1], [1]*Radiation Oncology, University Hospital Heidelberg, Heidelberg, Germany;* [2]*Clinical Cooperation Unit Nuclear Medicine, German Cancer Research Center, Heidelberg, Germany;* [3]*Nuclear Medicine, University Hospital Heidelberg, Heidelberg, Germany. Contact e-mail: shoaib.rana@dkfz.de*

Introduction Carbonic anhydrase IX (CA IX) is a hypoxia-regulated transmembrane protein, which is overepressed in many types of human cancer. [1-4] In contrast to the nearly ubiquitous family of different carbonic anhydrase enzymes, CA IX exhibits an extra proteoglycan-like region (PGLR). Aim of the present study is to identify new peptide ligands with specificity and affinity for the PG-like region of CA IX. Such peptides might be used for specific targeting and imaging of human carbonic anhydrase IX and visualization of tumor hypoxia. Material & Methods In order to identify such a binder, the PGLR domain (75aa) was synthesized by solid phase peptide synthesis. Phage display was performed by biopanning against synthetic PGLR employing a 12 amino acid library. The identified peptide PGLR-P1 was chemically synthesized, labeled with 125I and characterized for binding and metabolic stability. For in vitro characterization kinetic, competition and internalization studies were carried out on the CA IX positive renal cell carcinoma cell line SKRC 52. The CA IX negative pancreatic carcinoma cell line BxPC-3 was used as negative control. Serum stability of PGLR-P1 was investigated in human serum. Organ distribution studies were carried out in Balb/c mice, carrying SKRC 52 tumors transplanted subcutaneously into the trunk. Results / Conclusion In vitro binding experiments of 125I-labeled-PGLR-P1 revealed an increased uptake in CA IX positive cells over time. Radioligand binding was inhibited up to 97% by the unlabeled peptide. Internalization studies showed no increased uptake of the radioligand, which indicates binding of the peptide solely to the cell membrane. Experiments using the negative control cell line BxPC3 as target revealed a reduced activity to the background level. Organ distribution studies revealed a higher accumulation in SKRC 52 tumors than in most of the organs. These data indicate that PGLR-P1 is a promising lead structure for the development of a new ligand targeting the PGLR region of human carbonic anhydrase IX.

Disclosure of author financial interest or relationships:
**S. Rana**, None; **F. Nissen**, None; **A. Altmann**, None; **U. Haberkorn**, None; **V. Askoxylakis**, None.

Presentation Number **P334**
Poster Session 2
September 6, 2012 / 15:15-15:15 / Room: The Liffey

# The Utility of Cerenkov Luminescence Imaging for In Vitro Drug Discovery.R Robertson, M Borland, D Cvet, A McDonald, D Bradley. The Biomedical Imaging Group and Molecular Pathology Group, Millennium: The Takeda Oncology Company, Cambridge MA USA

***Robbie Robertson**, Millennium Pharmaceuticals, Inc., Somerville, MA, USA. Contact e-mail: shovelt700@yahoo.com*

Introduction:Cerenkov Luminescence Imaging (CLI) is a new, exciting, and constantly evolving nuclear imaging modality. In an effort to further show the utility of CLI for drug discovery purposes our lab has undertaken an in vitro experiment to test a newly developed in vitro assay for radiotracer uptake experiments. In this model we used CLI to image 2-deoxy-2-(18F)fluoro-D-glucose (FDG) uptake using a novel 3D tumor culture system. The resulting cellular 3D model provides a means by which a researcher may closely mimic and monitor the hypoxic and nutrient deficient environment typically encountered in the in vivo setting of tumor growth. Due to the versatility of this assay it is possible to monitor ongoing molecular events (i.e. glucose uptake, receptor targeting) from such a model system over consecutive days of imaging and drug treatment.Methods:Six cell lines were used to generate spheroids. Briefly, spheroid cultures were engineered with 2x105 cells which were harvested from normal cell specific culture conditions. Multicellular spheroids were collected and fasted for 1 hr prior to FDG addition in a low glucose media. Fifty µCi/well of 18F-FDG was added to spheroids and allowed to distribute for a period of one hour in a CO2 incubator. Imaging was accomplished on the Xenogen Spectrum system with a 5 min acquisition time, open filter set, stage position was set to C for viewing. ROI analysis of images was done using the IVIS Living Image 4.0 software package provided with the Xenogen system. Western and histology analysis were done to investigate morphology, GLUT1 levels and FDG signal in this system. Results:Average radiance was measured from the spheroid cultures. Ranking of the cultures based on FDG uptake was possible allowing a highest to lowest rating. Spheroids were monitored over an eight day period for FDG uptake. A grow trend across all groups was evident from this longitudinal imaging data. The new spheroid culturing technique had a decrease in cell viability for the first six days with a recovery and upward trend for FDG uptake. Histology stains of spheroids (H&E) showed in vitro morphology consistent with disease diagnosis. Conclusion:It is a well known phenomenon that cells growing in a 3D culture environment are characteristically more drug resistant then those identical cells grown in a 2D environment. The ability to monitor this type of resistant phenotype in vitro could provide valuable information for future drug design. We investigated a new 3D cell culture system as a potential way to investigate this phenomenon for future drug studies.The radiotracer 18F-FDG was used for investigating the viability of this model. We created spheroids from multiple cell lines and monitored FDG uptake in an in vitro environment. The ability to monitor FDG uptake in vitro by this quick a repeatable assay expands on the utility of CLI from the in vivo setting. We predict that've CLI utilized with this new 3D cell system has tremendous potential for transforming the way radioactive tracers are monitored in a cell culture setting.

Disclosure of author financial interest or relationships:
**R. Robertson**, Millennium Pharmaceuticals, Inc., Employment .

Presentation Number **P335**
Poster Session 2
September 6, 2012 / 15:15-15:15 / Room: The Liffey

# HIF-1α silencing is not sufficient to inhibit invasion and degradation of the extracellular matrix by MDA-MB-231 human breast cancer cells

***Tariq Shah**, Balaji Krishnamachary, Flonné B. Wildes, Yelena Mironchik, Zaver M. Bhujwalla, JHU ICMIC Program, Johns Hopkins University, Baltimore, MD, USA. Contact e-mail: tariq196@yahoo.com*

**Introduction:** The hypoxia inducible factor (HIF) is a master regulator of hypoxia inducible genes several of which facilitate invasion and metastasis. The MDA-MB-231 human breast cancer cell line is an aggressive triple negative cell line that is highly metastatic. Here we genetically engineered MDA-MB-231 cells to silence the expression of either HIF-1α (HIF-1α silenced) or both α isoforms of HIF, subsequently called doubly silenced cells. We investigated the ability of MDA-MB-231 breast cancer cells perfused under normoxic and hypoxic conditions to degrade extracellular matrix (ECM) and determined the associated changes in metabolism using our MR compatible cell perfusion assay. **Methods:** Experiments were performed under normoxic or hypoxic conditions at oxygen tensions of 20% and 1% respectively. MR data were acquired every 12 h over a period of 2 days. Degradation of ECM by cancer cells was determined at the 24h time point relative to the initial time point from the proton ($^1$H) images by drawing a region of interest (ROI) around the ECM region. The degradation index was defined as $(ROI_{0h}-ROI_{24h})/ROI_{0h}$. One dimensional $^1$H MR profiles of intracellular water acquired along the length (z-axis) of the sample by diffusion-weighted (DW) MRI were used to derive an invasion index by quantifying the number of cells invading into the ECM. Intracellular metabolite levels were derived from unlocalized DW $^1$H MR spectra. **Results and Discussion:** Figure 1 shows T1-weighted $^1$H MR images demonstrating degradation of ECM by parental MDA-MB-231 cells and their HIF silenced counterparts under normoxia and hypoxia. Under hypoxic conditions, MDA-MB-231 cells completely degraded ECM within 24 instead of 48 h. This enhanced degradation of ECM under hypoxia may be driven by the upregulation of a number of proteolytic enzymes involved in ECM degradation. HIF-1α silenced cells showed similar degradation as parental cells under normoxia and hypoxia. On the other hand doubly silenced cells showed significantly reduced ($p<0.01$) degradation of ECM compared to parental cells under normoxia or hypoxia. These cells also showed significantly decreased invasion even under normoxic conditions compared to parental cells. The absence of any significant difference in ECM degradation between HIF-1α silenced and parental cells, but a significant difference observed in the doubly silenced cells indicates the role of HIF-2α in these cells, and is currently under investigation. Quantitative analyses of metabolites demonstrated significantly decreased total choline ($p<0.07$) and phosphocholine ($p<0.05$) in HIF-1α silenced and doubly silenced cells compared to parental cells. These results suggest that in vivo, cells in or near hypoxic regions are likely to be more invasive and degrade the ECM, which can influence metastasis as well as drug delivery. These data also indicate that targeting HIF-1α alone is not sufficient to attenuate the invasiveness of these triple negative breast cancer cells under hypoxia, and both HIF-1α and HIF-2α downregulation is required to attenuate or inhibit invasion and metastasis in these cells. Supported by NIH P50CA103175

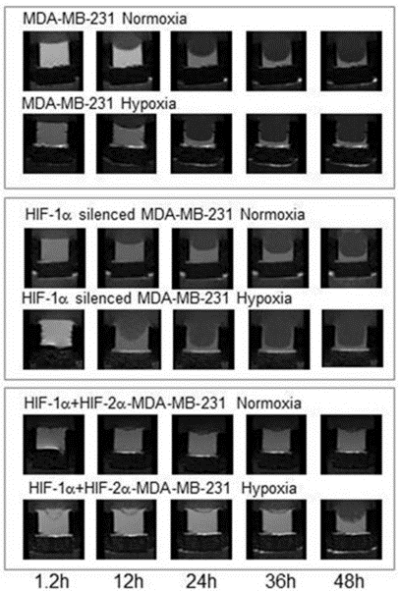


Figure 1 Representative T1-weighted images of the ECM chamber region acquired at various times showing ECM degradation by MDA-MB-231 cells and their HIF counterparts under normoxia or hypoxia

Disclosure of author financial interest or relationships:
**T. Shah**, None; **B. Krishnamachary**, None; **F.B. Wildes**, None; **Y. Mironchik**, None; **Z.M. Bhujwalla**, None.

Presentation Number **P336**
Poster Session 2
September 6, 2012 / 15:15-15:15 / Room: The Liffey

# Mechano-molecular imaging of the role of COX-2 in cell traction force

*A Rum Yoon[2], **Ioannis Stasinopoulos**[1], Steven An[2], Zaver M. Bhujwalla[1], [1]The Russell H. Morgan Department of Radiology and Radiological Science, The Johns Hopkins University, Baltimore, MD, USA; [2]Bloomberg School of Public Health, The Johns Hopkins University, Baltimore, MD, USA. Contact e-mail: istasin1@jhmi.edu*

The cytoplasmic enzyme cyclooxygenase (COX)-2 is a critical determinant of human breast cancer invasion and metastasis. Poorly differentiated MDA-MB-231 human breast cancer cells stably expressing COX-2 shRNA have lost their ability to secrete secondary lipid mediator products of the COX reaction, as well as to invade and degrade reconstituted extracellular matrix in vitro. COX-2-silenced cells inoculated in vivo show significant reduction of tumor growth and extrapulmonary colonization than their parental counterpart. Based on compelling evidence for the positive correlation between cancer invasion and cell motility, we interrogated and imaged the cell traction force of highly metastatic MDA-MB-231 cells and COX-2 silenced cells to understand the role for COX-2 in mediating this force. We plated individual COX-2-high parental MDA-MB-231 and derivative COX-2-silenced cells on an elastic gel block coated with type I collagen, and measured the distribution of contractile stresses arising at the interface between each adherent cell and its substrate. For each adherent breast cancer cell (Fig. 1a, phase contrast), images of fluorescent microbeads embedded near the gel apical surface (Fig. 1b) were taken before and after cell detachment with trypsin. The displacement field between a pair of images was then obtained by identifying the coordinates of the peak of the cross-correlation function. From the displacement field (Fig.1c) and known elastic properties of the gel (Young's modulus of ~1,300 Pascal (Pa) and a Poisson's ratio of 0.48), the traction field was calculated using Fourier transform traction cytometry. Fig.1d shows a representative traction map of MDA-MB-231 parental cell: The cell boundary is shown by the white line, colors show the magnitude of the traction in Pa, and arrows show the direction and relative magnitude of the tractions. We found that COX-2-silenced cells were smaller (2908+331 μm2 parental vs 2028+196 μm2 COX-2-silenced, $P<0.05$) and exercised lower cell traction force upon their surrounding. The net contractile moment, which is a scalar measure of the cell's contractile strength, was approximately 60% lower (t-test, $P<0.005$) in COX-2-silenced cells compared to their parental counterpart (Fig.1e). Consistent with these physical attributes, COX-2-silenced cells expressed a 4.6-fold reduction of the transcript coding for RhoJ, a member of the family of Rho GTPases that regulate actin contractions during lamellipodia formation. In addition, COX-2-silenced cells displayed a reduced rate of cytoskeleton (CSK) remodeling as assessed by spontaneous nanoscale movements of an individual RGD-coated microbead tightly anchored to the living CSK. To our knowledge this is the first report linking the expression of COX-2 with increased cell traction force and CSK remodeling in a highly metastatic human breast cancer. Taken together, our findings identify a novel mechanism by which a major mediator of inflammation facilitates cancer cell motility, invasiveness and metastasis. Supported by NIH P50 CA103175 and R01 CA 82337. First two authors share equal first authorship; Last two authors share equal senior authorship.

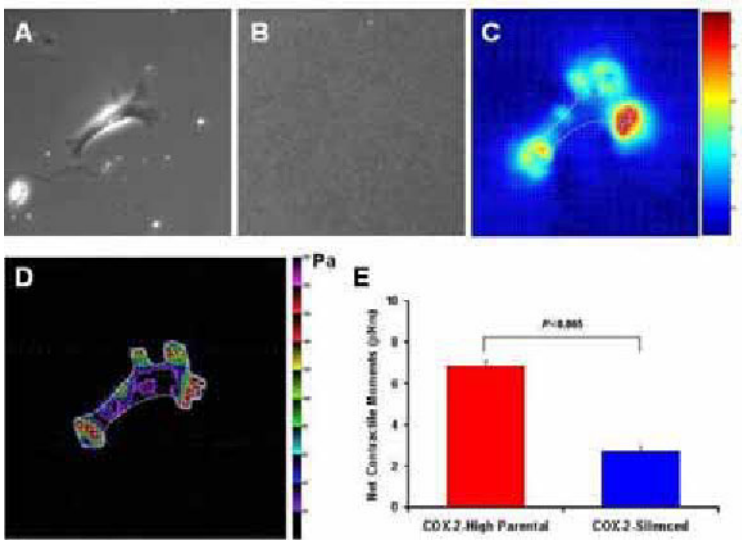


Disclosure of author financial interest or relationships:
**A. Yoon**, None; **I. Stasinopoulos**, None; **S. An**, None; **Z.M. Bhujwalla**, None.

Presentation Number **P337**
Poster Session 2
September 6, 2012 / 15:15-15:15 / Room: The Liffey

# Smart probes for optical imaging of cancer

***Christiane H. Wenk***[2,3]*, Véronique Josserand*[1,2]*, Pascal Dumy*[2,3]*, Didier Boturyn*[2,3]*, Jean-Luc Coll*[1,2]*,* [1]*Cibles diagnostiques ou thérapeutiques et vectorisation de drogues dans les cellules tumorales, CRI-INSERM U823, Grenoble, France;* [2]*Université Joseph Fourier, Grenoble, France;* [3]*CNRS, UMR-5250, Grenoble, France. Contact e-mail: Christiane.Wenk@ujf-grenoble.fr*

We made the chemical design of an innovative "smart" fluorescent molecule for the diagnosis and the therapy of cancer. This molecule is based on the RAFT-c(RGD)4, targeting the integrin alpha v beta 3 onto which we introduced a peptidic cleavable cassette that can be digested by metallo-proteases overexpressed in tumors. Its cutting site is surrounded by a couple of fluorescent molecules that can work as a FRET pair. The principle is that the fluorescence of the molecular complex is quenched as long as the molecule is intact and it becomes fluorescent as soon as the peptide bond of the cassette is cut by the enzyme. This should increase the tumor specificity because the molecule will bind to 2 different tumor associated proteins, but should also provide direct information of the enzymatic activity present in the tumor mass. This is thus a powerful diagnostic tool, but can also be further developed as a specific drug delivery system.

Disclosure of author financial interest or relationships:
**C.H. Wenk**, None; **V. Josserand**, None; **P. Dumy**, None; **D. Boturyn**, None; **J. Coll**, None.

Presentation Number **P338**
Poster Session 2
September 6, 2012 / 15:15-15:15 / Room: The Liffey

# The discovery of Oct4 pseudogenes in non-small cell lung cancer

***Hsiang-Lin Yu***[1,4], *Luen Hwu*[1], *Ya-Ju Hsieh*[2], *Ren-Shyan Liu*[1,3], *C.Allen Chang*[4], [1]*MAGIC/NRPGM, Nuclear Medicine, Faculty of Medicine, National Yang-Ming University, Taipei, Taiwan;* [2]*Medical Imaging and Radiological Sciences, Kaohsiung Medical University, Kaohsiung, Taiwan;* [3]*Nuclear Medicine, Taipei Veterans General Hospital, Taipei, Taiwan;* [4]*Biomedical Imaging and Radiological Sciences, National Yang-Ming University, Taipei, Taiwan. Contact e-mail: kevin_0510@hotmail.com*

Purpose: Oct4, the transcription factor, known as a significant regulatory gene in the pluripotency and self-renewal of embryonic stem cells, is specifically expressed in the undifferentiated cells such as stem cells but also detected in some cancer cells. Recently, investigation of Oct4 expressed stem-like cells in cancer is an important issue in cancer research. However there are six Oct4 pseudogenes in human genome which have high sequence homogeneity with Oct4 gene, and is possible to cause false-positive results due to the existence of these pseudogenes while detecting Oct4. To data, Oct4 pseudogenes have been disclosed in head and neck cancer, glioma and breast cancer. This research takes the advantages of RT-PCR. DNA sequencing and reporter gene to detect the pseudogenes and Oct4 in human non-small cell lung cancer , in order to prove whether it is appropriate to use Oct4 as a marker of cancer stem cells in cancer diagnosis. Materials and methods: We used RT-PCR and DNA sequencing to detect the Oct4 expression level in non-small cell lung cancer cell line -H1299 and embryonic carcinoma cell line-NCCIT. In addition, we also transfected Oct4 promoter driven reporter gene into these cells in order to demonstrate whether there is Oct4 transcripted activity in these two cell lines. Result: The sequencing results showed that the RT-PCR product from NCCIT has 100% similarity with the Oct4 sequence on the NCBI (National Center of Biotechnology Information), however the RT-PCR product of H1299 has 98% similarity with Oct4 pseudogene 1(Oct4-pg1) but only 96% similarity with the parental Oct4. Furthermore, 48 hours after the transfection of the Oct4 promoter driven reporter gene into the cells, the reporter gene can only be detected in NCCIT. Conclusions: The results show that the Oct4 pseudogene exists in H1299 cell line. If Oct4 is used as a marker of H1299 cancer stem cells, coexistence of Oct4 and its pseudogenes may cause high possibility of false positive results. Our results also reveal that Oct4 pseudogene does not have the function of transcription factor.

Disclosure of author financial interest or relationships:
**H. Yu**, None; **L. Hwu**, None; **Y. Hsieh**, None; **R. Liu**, None; **C. Chang**, None.

Presentation Number **P339**
Poster Session 2
September 6, 2012 / 15:15-15:15 / Room: The Liffey

# Curcumin Inhibits Radiation-induced Radioresistance via Suppression of NF-κB Pathway in Human Hepatocellular Carcinoma Cells

***I-Tsang Chiang***[1], *Fei-Ting Hsu*[1], *Yu-Chang Liu*[1], *Hsin-Ell Wang*[1], *Ren-Shyan Liu*[1], *Wuu-Jyh Lin*[2], *Jeng-Jong Hwang*[1], [1]*National Yang Ming University, Taipei, Taiwan;* [2]*Division of Radioisotope, Institute of Nuclear Energy Research, Taoyuan, Taiwan. Contact e-mail: john740604@yahoo.com.tw*

Purpose: Resistance of human hepatocellular carcinoma to radiotherapy is a major challenge to current treatment. The NF-κB signaling pathway plays an important role in tumor development and progression, and results in unsatisfactory treatment outcome. Inhibition of the NF-κB signaling cascade may sensitize the resistant cancer cells to chemotherapy and/or radiotherapy. Since curcumin, a component of turmeric Curcuma longa, has been shown to inhibit NF-κB activation, whether it can sensitize the human hepatocelluar carcinoma to radiation was investigated in this study. Methods: The established Huh7/NF-κB-tk-luc2 stable clone was used in this study. Cells were treated with vehicle, curcumin, radiation, and combination of curcumin with radiation, respectively. The effects of curcumin on radiation-induced cell cytotoxicity and cell apoptosis were evaluated with MTT assay, DNA fragmentation, and flow cytometry. The NF-κB activation was assayed with electrophoretic mobility shift assay (EMSA) and NF-κB reporter gene assay. The NF-κB regulated downstream gene products in proliferation, angiogenesis, and invasion were determined with Western blotting. Results: Curcumin significantly enhanced radiation-induced cell cytotoxicity and depletion of mitochondrial membrane potential. Notably, radiation-induced NF-κB activity was significantly inhibited by curcumin. Curcumin also decreased NF-κB regulated downstream gene products, cyclin-D1, Bcl-2, matrixmetalloproteinase-9 (MMP-9), and vascular endothelial growth factor (VEGF), which were induced by radiation and mediate the radioresistance. Conclusion: Curcumin may sensitize the human hepatocelluar carcinoma cells to radiation via the suppression NF-κB activity and NF-κB regulated downstream gene products. (This study was supported by a grant NSC 101-2623-E-010-005-NU from National Science Council, Taipei, Taiwan.)

Disclosure of author financial interest or relationships:
**I. Chiang**, None; **F. Hsu**, None; **Y. Liu**, None; **H. Wang**, None; **R. Liu**, None; **W. Lin**, None; **J. Hwang**, None.

Presentation Number **P340**
Poster Session 2
September 6, 2012 / 15:15-15:15 / Room: The Liffey

# Histone methylation sensing reporter for development of in vitro high throughput screening and in vivo pharmacodynamic imaging

***Yun-Chen Chiang**, Brian Rabinovich, Juri G. Gelovani, Department of Experimental Diagnostic Imaging, Univeristy of Texas MD Anderson Cancer Center, Houston, TX, USA. Contact e-mail: ychiang@mdanderson.org*

Introduction: Recent studies demonstrated that carcinogenesis may result not only from genetic alterations, but also several epigenetic mechanisms, such as DNA methylation and histone modifications. These molecular alterations may lead to gene expression changes that contribute to carcinogenesis, including abnormal proliferation or the ability to evade apoptosis. In particular, methylation of K9 and K27 residues in histone H3 is causes transcriptional repression of several critical tumor suppressor genes and promotes carcinogenesis. However, only few approaches have been developed to date for imaging histone methylation in living cells in vitro or in tumors in vivo. Methods and Results: We developed a real-time histone methylation sensing reporter system with nuclear localization using a split firefly luciferase complementation approach. To develop this reporter system, different length N-terminal fragments of histone H3 containing methylated lysine residues K9 and K27 were examined for binding to the HP1 or Pc adaptor proteins and the most tightly binding methylated H3 fragment was identified. We identified the most suitable linker peptide, without losing selectivity to the N-terminal of either HP1 or Pc adaptor proteins were cis-linked with 8 amino acids (GGGSGGGS). The entire resulting "sensor" element was then sandwiched between the N- and C-terminal halves of firefly luciferase. Nuclear localization signal (NLS) sequences were added to the C-terminal of corresponding firefly luciferase halves to achieve nuclear localization of the reporter. When the K9 and K27 lysine residues of the histone H3 fragment are methylated, this fragment binds to the HP1 or Pc domain, which brings the two halves of split firefly luciferase together and reconstitutes enzymatic activity (Fig. 1A). However, mutations of K9 to L9 or K27 to L27 prevented the reconstitution of luciferase activity. These reporter cassettes were inserted into lentiviral vectors (Fig. 1B), that were used to stably transduce PC3 prostate carcinoma cells. The functionality and selectivity of these PC3/H3K9-HP1/FLuc and PC3/H3K27-Pc/FLuc reporter cell lines and their mutant pair were assessed in vitro using activators and inhibitors of histone methyl transferases (HMT). Conclusions: We developed and optimized a real-time histone methylation sensing reporter system with nuclear localization. This new reporter assay system can be used for in vitro high throughput screening and optimization of novel activators and inhibitors of HMTs and should be applicable for in vivo imaging of pharmacodynamics of selected drug candidates in mice.

Disclosure of author financial interest or relationships:
**Y. Chiang**, None; **B. Rabinovich**, None; **J.G. Gelovani**, Macrocyclics, Consultant; SibTech, Consultant .

Presentation Number **P341**
Poster Session 2
September 6, 2012 / 15:15-15:15 / Room: The Liffey

# Delivery of siRNA to several tumor cell lines using a small molecule as an effective transfection system

***David R. Elmaleh***[1], *Timothy M. Shoup*[1], *Michael R. Hamblin*[2], *Masayoshi Kawakubo*[2], *Alan J. Fischman*[3], *Kazue Takahashi*[4], [1]*Nuclear Medicine and Molecular Imaging, Massachusetts General Hospital, Boston, MA, USA;* [2]*Dermatology, Wellman Center for Photomedicine, Massachusetts General Hospital, Boston, MA, USA;* [3]*Shriners Hospitals for Children, Boston, MA, USA;* [4]*Pediatrics Medical Services, Massachusetts General Hospital, Boston, MA, USA. Contact e-mail: DELMALEH@PARTNERS.ORG*

Objective: We tested the hypothesis that biotin can be used as a delivery probe of siRNA into tumor cells. In this study, siRNA compositions containing biotin and a fluorescent dye were evaluated for their transfection to different tumor cell lines. Methods: Three biotinilated siRNA probes targeting the fire fly (FF, bioluminescence) sequence in A549luc tumor cells were designed. Dy547 was also incorporated into the siRNA probes in order to examine siRNA uptake by cells. Molecular arrangements of these siRNA probes are: Oligo #1, biotin 5' - sense FF - 3' Dy547/antisense FF; Oligo #3, Dy547 5'- sense FF - 3' biotin/antisense FF; and Oligo #4, sense FF/biotin 5'-antisense FF - 3' Dy547. These compositions were incubated with lung A549, small squamous CAL, breast MDA, prostate PC3 and peritoneal (control) cells. The oligos were added at 50 nM and cultured for 4 hours then 20 ul of FBS was added to continue culture for 40 hrs. Wells were washed with PBS and incubated with Hoechest (1 ug/ml) as a nuclei counter-staining. Images of Dy547 (red), Hoechst (blue) and phase contrast were captured using a fluorescent microscope controlled by the Openlab imaging software, which merged three images. Bioluminescence was assayed for the two best siRNA oligos from the fluorescent study. A549Luc cells were plated at 5,000 cells per well of 96 well plate. The siRNA's were incubated at 5, 50 and 250 nM in serum free media (50 ul /well) for 4 hours then regular culture media (10% FBS in D'MEM) was added to 200 ul and cultured for 2 days. Cells were washed with fresh media and Luciferine was added at 0.5 mg/ml. Luminescence was read using an M5 plate reader (Molecular Devices). Assays were in triplicate and mean values plotted. Results: Microscopic analysis show siRNA probes are delivered to the nuclei of tumor cells with the best delivery by Oligo #3 followed by the Oligo #1 and the Oligo #4. Although some fluorescent was observed by normal cells it was not delivered into the nuclei. Surprisingly, positioning of the biotin on the 3' or 5' of the sense or antisense strands did not dramatically affect delivery efficiency. The bioluminescence study showed that Oligo #3 significantly reduced the bioluminescent signal. Conclusions: Biotinylated siRNAs are taken up by tumor cells in the absence of a delivery reagent to functionally silence gene expression. Biotinylation of siRNA allows for effective intracellular delivery of the siRNA molecule. Such compositions are useful in the delivery or targeting of therapeutic or diagnostic agents, i.e. delivery or targeting of iRNA agents to tumor cells where a nucleic acid based therapeutic agent is conjugated. Four biotin moieties conjugated to the 3' and 5' ends of the sense and antisense strands may provide siRNA delivery of other double stranded nucleic acid treatment and diagnostics.

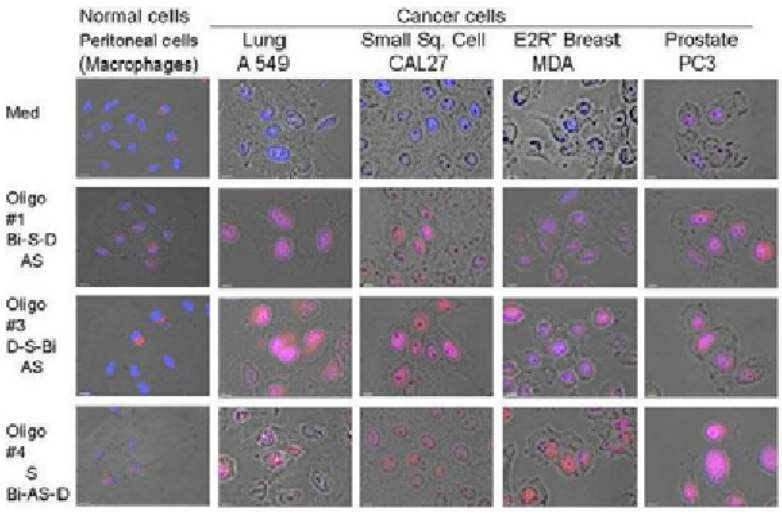


siRNA Data Images

Disclosure of author financial interest or relationships:
**D.R. Elmaleh**, None; **T.M. Shoup**, None; **M.R. Hamblin**, None; **M. Kawakubo**, None; **A.J. Fischman**, None; **K. Takahashi**, None.

Presentation Number **P342**
Poster Session 2
September 6, 2012 / 15:15-15:15 / Room: The Liffey

# An improved approach to Ultrasound cell sonoporation mediated by the use of nanosystems

***Giuseppe Ferrauto***[1], *Pierangela Giustetto*[1], *Daniela Delli Castelli*[1], *Marta Ruzza*[1], *Silvio Aime*[1], *Enzo Terreno*[2], [1]*Chemistry, Molecular Imaging Center- University of Turin, Torino, Italy;* [2]*Chemistry, Molecular and Preclinical Imaging Centers, Torino, Italy. Contact e-mail: giuseppe.ferrauto@unito.it*

Developing methods to improve the efficiency of cell labeling is still an important topic. So far, different route for the internalization of drugs and macromolecules (proteins or DNA) into cells have been investigated including pinocytosis, receptor/transported mediated-endocytosis, and electroporation. The first two strategies cause the entrapment of the molecule into intracellular endocytic vesicles, thus avoiding the diffusion of the agent into the cytosol. Coneversely, electroporation is able to locate molecules directly in the cytosol, but this procedure suffers for an intrinsic toxicity both in vitro and in vivo. Recently, the diffusion of Ultrasound (US) diagnostic method suggests the possibility to investigate new US-guided internalization procedure. Initially, US stimulation was used to simply increase the permeabilization of cell membranes, thus allowing the passage of molecules from the external solution to the cytosol. Later, new procedures were developed including the use of microbubbles that, upon US stimulation, are able to oscillate and create cavitation events that induce the formation of transient or permanent pores into cell membranes. For these reasons there is a lot of interest to optimize insonation parameters and experimental set-up and to evaluate the possible synergic role of micro/nano systems to increase the internalization and the cell viability by sonoporation. This study was aimed at optimizing the US parameters and assess the role played by liposomes and microbubbles on the internalization promoted by US. Murine breast cancer cells (TSA) were placed into a PBS solution containing Prohance (Gadoteridol), a commercial MRI contrast agents and sonoporated with the addition of microbubbles or liposomes. The sonoporation was carried by using a non focused 1 MHz transducer with acoustic intensity of 1.3±0.2 W/cm2, varying the different parameters (duty cycle, insonation time, intensity) and emphasis was given to assess the amount of probe internalization (by relaxometric mesurements) and cell viability (tripan blue exclusion assays). Moreover a new sterile set-up was realized in order to verify if cells could maintain their viability and functionality after sonoporation. Cells were able to attach to the plate and to duplicate without any morphological change after US exposure. Sonoporated U937 (human pro-monocytic) cells were able to differentiate and duplicate into macrophages after incubation with TPA (2-O-tetradecanoylphorbol-13-acetate). The results showed a good reproducibility and the role played by liposome size, membrane composition and encapsulated material has been evaluated. In conclusion the optimization of the insonation parameters and the presence of lipidic nanosystems along with the cells can substantially improve the overall efficiency of the sonoporation method. .

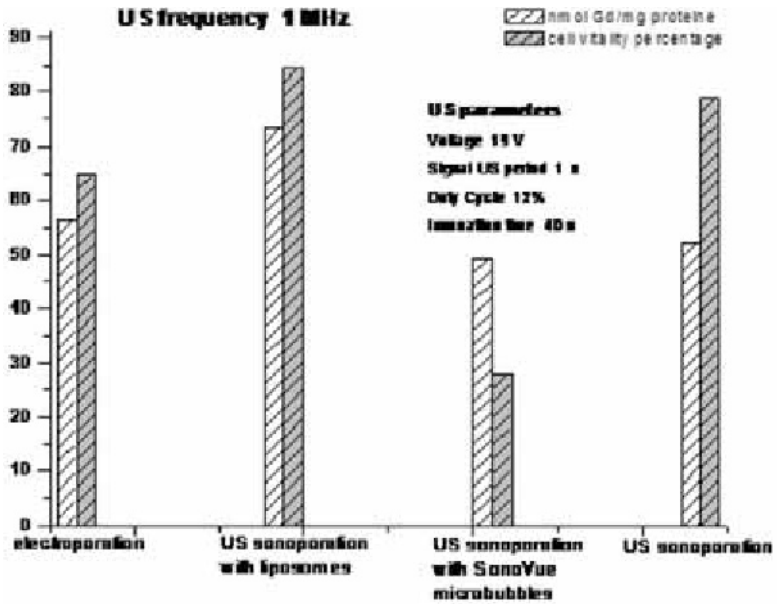


Disclosure of author financial interest or relationships:
**G. Ferrauto**, None; **P. Giustetto**, None; **D. Delli Castelli**, None; **M. Ruzza**, None; **S. Aime**, Bracco Imaging, Consultant; Bruker, Grant/research support; **E. Terreno**, Bracco Imaging, Consultant .

Presentation Number **P343**
Poster Session 2
September 6, 2012 / 15:15-15:15 / Room: The Liffey

# The adipogenic, chondrogenic, osteogenic and neurogenic differentiation of human mesencymal stem cells overexpressing MR reporter

***Hoe Suk Kim**, Jisu Woo, YoonSeok Choi, Woo Kyung Moon, Radiology, he Institute of Radiation Medicine, Medical Research Center, Seoul National University, Seoul, Republic of Korea. Contact e-mail: hoeskim@gmail.com*

Purpose: This study is to investigate the differentiation ability of the human mesenchymal stem cells (hMSCs) overexpressing MR reporter, ferritin into adipogenic, chondrogenic, osteogenic, and neurogenic lineage. Methods: The hMSCs were transduced with lentivirus carrying myc-tagged human heavy chain ferritin (myc-hFTH) and green fluorescence protein (GFP). The overexpressions of myc-hFTH and GFP in myc-hFTH_hMSC were detected by Western blot and fluorescence microscope. The mesencymal stem cell surface markers and the pluripotency marker were analyzed by flow cytometry and RT-PCR. Cell viability, migration ability, and released cytokine were investigated by MTT assay, transwell assay and ELISA, respectively. The adipogenic, chondrogenic, osteogenic, and neurogenic differentiations of hMSCs and myc-hFTH_hMSCs were investigated in special differentiation media. Total cellular iron contents was measured by total iron reagent kit. in vitro MRI study of cell phantom was performed on clinical 3T MR scanner. Result : myc-FTH_hMSCs stably expressing ferritin and GFP were established. The overexpression of myc-hFTH in hMSCs incubated with feric amonium citrate (FAC) led to an increase in cellular total iron amount and a significant decrease in T2* values, as shown by non-invasive MRI, compared to control hMSCs. The overexpression of ferritin and GFP by lentiviurs did not influence the cell viability and proliferation of hMSCs. The significant alterations of the phenotype (CD29+/CD105+/CD34-/CD45-), the pluripotency marker (OCT-4 and Sox-2) and the released cytokines (IL-5, IL-10, IL-12p70, TNF-alpha) were not observed in myc-FTH_hMSCs as compared with hMSCs. After treatment with bFGF, the migration ability of myc-FTH_hMSCs was no changed. myc-FTH_hMSCs exhibited the differentiation of adipogenic, chondrogenic, osteogenic and neurogenic lineage. Conclusions: myc-hFTH_MSCs would be valuable stem cell source to evaluate the potential cell therapies for diverse disease using MRI. Acknowledgement: This work was supported by the National Research Foundation of Korea (NRF) grant funded by the Korean government (MEST) (2011-0003657, 2011-0004322, 2011-0000174, 2011-0005381) and by a grant from the Innovative Research Institute for Cell Therapy, Republic of Korea (A062260).YS Choi is the recipient of a fellowship from the Brain Korea 21 (BK21) program.

Disclosure of author financial interest or relationships:
**H. Kim**, None; **J. Woo**, None; **Y. Choi**, None; **W. Moon**, None.

Presentation Number **P344**
Poster Session 2
September 6, 2012 / 15:15-15:15 / Room: The Liffey

# Polymer-based hybrid biomaterials for gene delivery and imaging

*Ran Namgung[1], Hyunwoo Kim[1], Mi-Kyeong Jang[2], Jae-Woon Nah[2], In-Kyu Park[3], **Won Jong Kim**[1], [1]Chemistry, POSTECH, Pohang, Republic of Korea; [2]Nano Polymer Science and Engineering, Sunchon National University, Suncheon, Republic of Korea; [3]Biomedical Sciences, Chonnam National University Medical School, Gwangju, Republic of Korea. Contact e-mail: wjkim@postech.ac.kr*

Ran Namgung1, Hyunwoo Kim1, Mi-Kyeong Jang2, Jae-Woon Nah2, In-Kyu Park3, Won Jong Kim1,* 1Department of Chemistry, Pohang University of Science and Technology, Pohang 790-784, Korea. 2Department of Nano Polymer Science and Engineering, Sunchon National University, 315 Maegok-dong, Suncheon, Jeonnam, 540-742, Korea 3 Department of Biomedical Sciences, Chonnam National University Medical School, Gwangju 501-746, Korea During the last decades, the advancement in nanotechnology has lead to various developments of nanoparticles. Depending on their composition, size, and structures, nanoparticles have intrinsic unique physical and optical properties so that those attract great research interests in biomedical fields. Specially biocompatible polymers have been utilized in biomedical fields, especially in drug/gene delivery area, due to their diversity of composition, structure and easy functionalization. To develop more sophisticated nanoconstruct, many researchers are endeavoring to construct more intelligent nanostructures by hybridizing organic materials such as polymer and inorganic nanoparticles. This hybrid nanostuctures bring out not only its own characteristics but also synergistic effects. In this study we designed three polymer-inorganic nanostructures as smart gene delivery agents. First, we developed magnetic-guided gene carrier by conjugating cationic polymers with a superparamagnetic iron oxide nanoparticle (BPEI-SPION). Under the magnetic field, BPEI-SPION has shown enhanced gene transfection efficiency compared to BPEI25K, a gold standard in non-viral gene delivery. Second, we prepared a dual purposed nanostructure which is potential of both gene delivery and MR imaging (BPEI-SNT). By using tube-shaped silica nanoparticle, we introduced cationic polymer and inorganic imaging agents (quantum dots and iron oxide nanoparticles) individually in one particle without any interfering effects. Graphene Oxide (GO) is very useful for modification as it contains many hydroxyl, carboxylic acid and other reactive groups available to ligand conjugation and other modification. Also, GO has a good biocompatibility due to its many hydrophilic groups. GO has been used as a drug delivery vehicle because sp2 carbon network of GO can interact with hydrophobic drug, single nucleotide etc. However, to be an efficient gene delivery vector, GO should be modified with cationic polymeric gene carrier. Polyethylenimine(PEI) has been widely used as a non-viral gene delivery vector. Therefore, we developed GO-conjugated PEI as an excellent transfecting agent. It was revealed that GO-conjugated PEI showed high gene transfection efficiency and low cytotoxicity. Furthermoere, this conjugate exhibited remarkable photoluminescence highlighting its potential as bioimaging agent. These researches of novel organic-inorganic nanostructures will become the foundation on the developments of multipurpose therapeutic biomaterials

Disclosure of author financial interest or relationships:
**R. Namgung**, None; **H. Kim**, None; **M. Jang**, None; **J. Nah**, None; **I. Park**, None; **W. Kim**, None.

Presentation Number **P345**
Poster Session 2
September 6, 2012 / 15:15-15:15 / Room: The Liffey

# Transverse and Longitudinal MRI Relaxation Rates in MagA-expressing Human Cancer Cells

*Anindita Sengupta[1,2], Roja Rohani[1], R. Terry Thompson[1,2], **Frank S. Prato**[1,2], Donna E. Goldhawk[1,2], Neil Gelman[1,2], [1]Imaging, Lawson Health Research Institute, London, ON, Canada; [2]Medical Biophysics, Western University, London, ON, Canada. Contact e-mail: prato@lawsonimaging.ca*

**INTRODUCTION** Iron labeling of cells for MRI detection has been accomplished using genetic engineering to overexpress proteins involved in iron transport and storage. Gene-based iron labeling has the potential for long-term cell tracking and holds promise for developing reporter genes to monitor cellular changes. Our work involves MagA, a putative iron transport protein involved in magnetosome formation in magnetotactic bacteria. MagA has been overexpressed in mammalian cells, leading to observable changes in MRI signals (1,2). Measurements of MRI relaxation rates of MagA-expressing cells are important for optimizing cell detection and specificity, and for developing quantification methods. Previously R2 (1/T2) relaxation rates were measured in MagA-expressing cells (2). We present measurements of the total transverse relaxation rate (R2*), its irreversible and reversible components (R2 and R2′, respectively) and the longitudinal relaxation rate (R1) from human tumor cells. **METHODS** Cultures of MDA-MB-435 cells consisted of the untransfected parental line and those expressing MagA. Cells were grown to confluency in the presence or absence of iron-supplementation (250 μM ferric nitrate). Thirty million cells were placed in 1% gelatin/phosphate buffered saline pH 7.4 (PBS) and centrifuged at 400xg in wells from a 96-well break-apart plate. Samples were embedded in a 9cm spherical phantom filled with gelatin/PBS and imaged on a 1.5T MR scanner. Measurements of R2 were acquired using nine spin-echo images each with a different echo time (13-300 ms). For R1, spin-echo images with six inversion times (22-3800 ms) were acquired. For R2*, a multi-echo spoiled gradient echo sequence using 12 echo times (5-80 ms) was applied. Voxel dimensions were 1.5x0.6x0.6mm for R2 and R2* acquisitions and 1.5x0.9x0.9mm for R1 acquisitions. R2*, R2 and R1 were determined by curve fitting of mean region of interest signals (most voxels in each well) using standard equations. R2′ was obtained by subtraction (R2*-R2). **RESULTS AND DISCUSSION** Measured values of the relaxation rates (including standard errors from curve fitting) are shown in the figure. All relaxation rates are higher for iron-supplemented, MagA-expressing cells compared to parental controls; however, R2* provided the strongest absolute difference and R2′ showed the strongest relative difference. This is consistent with the notion that R2′ may be a more specific indicator of iron-based contrast than R2 as observed in brain tissue (3). The iron-related contribution to transverse relaxation increases with field strength (3), thus, differences between MagA-expressing and parental cells should be greater at higher fields. **CONCLUSION** MagA expression leads to increased relaxation rates in MDA-MB-435 cells, with the strongest relative effect occurring for R2′.

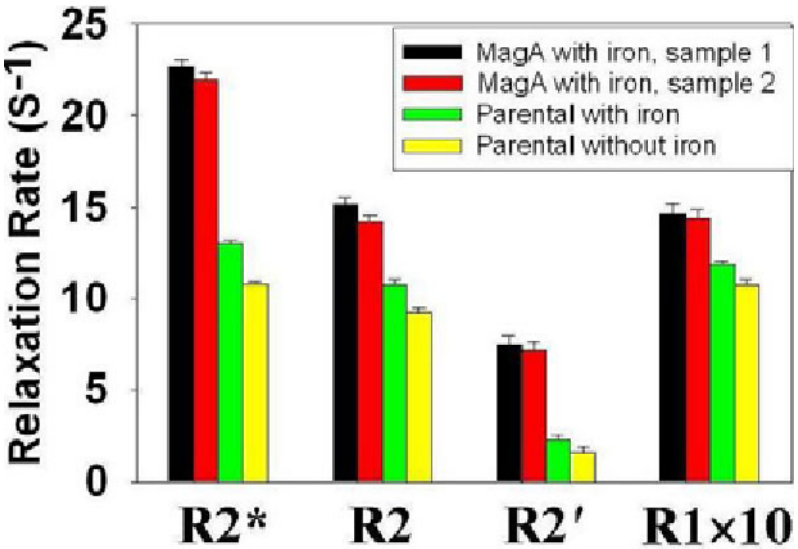


Relaxation rates of MagA-expressing cells and their parental controls. Duplicate measurements were obtained for MagA-expressing cancer cells cultured in iron-supplemented medium (black and red). These data are compared to untransfected controls grown with (green) or without (yellow) iron supplementation.

Disclosure of author financial interest or relationships:
**A. Sengupta**, None; **R. Rohani**, None; **R. Thompson**, None; **F.S. Prato**, None; **D.E. Goldhawk**, None; **N. Gelman**, None.

Presentation Number **P346**
Poster Session 2
September 6, 2012 / 15:15-15:15 / Room: The Liffey

# Functional multiplex reporter assay using tagged Gaussia luciferase

***Sjoerd van Rijn***[1], *Jonas Nilsson*[2,1], *David Noske*[1], *Peter W. Vandertop*[1], *Bakhos A. Tannous*[3], *Thomas Wurdinger*[1,3], [1]*Neurosurgery, VU University Medical Center, Amsterdam, Netherlands;* [2]*Radiation Sciences, Umeå University, Umeå, Sweden;* [3]*Neurology, Massachusetts General Hospital, Boston, MA, USA. Contact e-mail: s.vanrijn@vumc.nl*

We have developed a multiplex bioluminescence assay that allows monitoring of many variables in real-time within the same biological system. This assay is based on Gluc since this reporter is highly sensitive, naturally secreted, and can be detected in the conditioned medium of cells in culture as well as in the blood of animals ex vivo, allowing real-time monitoring of cellular variables. We constructed a library of lentiviral vectors consisting of the Gluc cDNA fused to ten different epitope tags at its C-terminus, under the constitutively active cytomegalovirus (CMV) promoter resulting in GlucFlag, GlucHis, GlucHA, GlucAcV5, GlucV5, GlucGlu, GlucMyc, GlucKt3, GlucAu1, GlucE2. We employed U87 cells for validation of the Gluctag multiplex system. These cells were transduced with each of the lentiviral vectors to produce ten different cell lines, each stably expressing a different Gluctag In order to demonstrate the use of the Gluctag system for multiplex applications, we mixed equal numbers of the ten different U87 Gluctag cells and plated them in a single well. Over time, we measured the total Gluc level in aliquots of the conditioned medium. The levels of the individual Gluctag reporters in the mixed culture medium were analyzed by immunobinding with the different tag specific antibodies. We were able to monitor in real-time the growth of the individual U87 Gluctag cell populations in the mixed culture. Immunostaining confirmed the expression of each tag in the corresponding cells in the mixed culture. To demonstrate the use of the Gluctag system for multiplex applications in vivo, we mixed equal numbers of U87 cells expressing the ten different Gluctag and implanted the heterogeneous cell pool subcutaneously in nude mice. We monitored tumor growth by Fluc bioluminescence imaging and total Gluc blood assay. Importantly, we were able to efficiently monitor the growth of the individual subpopulation of the U87 cells expressing the different Gluctag reporters in the same tumor over time. We confirmed the expression of all tags in the same tumor by immunostaining. To determine the applicability of the Gluctag multiplex system in deep tissues, the mixture of the ten different U87-FM-Gluctag-CFP cells were implanted orthotopically in the brain of nude mice. We monitored tumor growth by Fluc bioluminescence imaging and total Gluc blood assay. Again, we were able to monitor the intracranial growth of the individual subpopulations of U87 cells expressing the Gluctag reporters within the same brain tumor in real-time, by blood sampling and the application of our Gluctag multiplex reporter system. We have developed a multiplex reporter system to monitor multiple biological variables in real-time. The secreted Gaussia luciferase was fused to ten different epitope tags (Gluctag), each expressed in different tumor cells. By immunobinding of the tags followed by Gluctag detection, this system allowed the independent and real-time monitoring of mixed cell cultures in vitro and of mixed subcutaneous and intracranial tumor subpopulations in vivo.

Disclosure of author financial interest or relationships:
**S. van Rijn**, None; **J. Nilsson**, None; **D. Noske**, None; **P.W. Vandertop**, None; **B.A. Tannous**, None; **T. Wurdinger**, None.

Presentation Number **P347**
Poster Session 2
September 6, 2012 / 15:15-15:15 / Room: The Liffey

# Mean Lung Attenuation Coefficient Estimation using Maximum Likelihood Reconstruction of Attenuation and Activity for MRI-Segmentation-based Attenuation Correction in PET/MR

***Yannick Berker***[1,2], *André Salomon*[2,3], *Fabian Kiessling*[1], *Volkmar Schulz*[1,2], [1]*Department of Experimental Molecular Imaging, RWTH Aachen University Hospital, Aachen, Germany;* [2]*Molecular Imaging Systems, Philips Technologie GmbH Innovative Technologies, Research Laboratories, Aachen, Germany;* [3]*Division of Imaging Sciences and Biomedical Engineering, King's College London, St. Thomas Hospital, London, United Kingdom. Contact e-mail: yberker@ukaachen.de*

In clinical PET, photon attenuation is a major source of potential image artifacts. Routinely solved in PET/CT using CT-based attenuation correction (AC), it is still largely unsolved in PET/MR. In approaches based on MR image segmentation, image voxels are assigned predefined attenuation coefficients (μ) to yield an attenuation (μ-)map. However, mean lung attenuation coefficients (LAC) vary by up to a factor of 2, depending on patient (e.g., disease state) and acquisition (inspiration state, patient positioning) [1]. Consequently, the choice of inappropriate LAC in segmentation-based AC can have significant impact on PET quantification [2]. Maximum Likelihood reconstruction of Attenuation and Activity (MLAA) without tissue classification has already been used in MR-AC, but yielded errors in mean LAC of up to 20% in the lungs when exploiting a segmentation of the lung from CT data [3]. **Methods** In this work, we used CT datasets of 3 patients to simulate PET acquisitions in the GATE particle simulation toolkit. Subsequently, the lungs were segmented from CT and reference LAC values were determined (S0). 5 MLAA studies were carried out using different initial μ-maps. S1: original CT-based μ-map. S2/S3: The lung was assigned a homogeneous initial μ of ~0 cm^-1/0.05 cm^-1, respectively. S4: To imitate MR data segmented into 5 tissue classes, the out-of-lung body portion of the S2 μ-map was segmented into 4 tissue classes by nearest-neighbor classification: air, μ=0 cm^-1; fat, μ=0.09 cm^-1; soft tissue, μ=0.1 cm^-1; and bone, μ=0.13 cm^-1. MLAA was applied using original (S1) and modified (S2-4) attenuation maps. The segmentation was included in the MLAA algorithm by only updating the mean LAC, thus keeping μ of the rest of the body fixed in all iterations. In study S5, the S4 μ-map was used with a lung segmentation split into coronal slices to be updated separately. We investigated the evolution of LAC as a function of MLAA iteration number and compared the values after 10 MLAA iterations with the reference values from CT. **Results** Reference mean LAC values are between 0.015 cm^-1 and 0.027 cm^-1 (S0, see table). MLAA convergence was always reached after 6 iterations (patient P1, see figure) and 3 iterations (P2&3). Constrained MLAA was able to recover the original mean LAC with an error between +6% and +9% compared to reference values (S1). The results are mostly independent of the initial LAC with a maximum error difference of less than -10% (S2&3). The use of segmented attenuation maps yielded comparable results (+2% to +6%, S4). Slightly better results were obtained with a lung segmentation sliced in coronal direction to represent vertical LAC gradients (+1% to +5%, S5). **Conclusion** MLAA constrained by lung segmentation is a promising approach to yield reliable mean LAC for patient-individual attenuation maps for PET/MR, with no accuracy impairment by a 5-class body segmentation. This work was supported by the EC 7 FP project SUBLIMA. [1] Verschakelen et al. Computed Tomography of the Lung: A Pattern Approach. Berlin: Springer-Verlag, 2007 [2] Keereman et al. Med Phys. 2011;38:6010-9 [3] Salomon et al. IEEE Trans Med Imaging. 2011;30:804-13

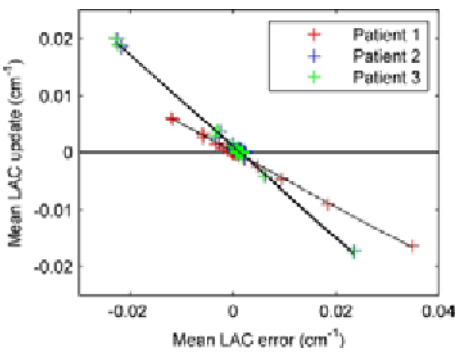


Scatter plot of mean LAC error vs. mean LAC update by patient for all studies (S1-5). The evolution of mean LAC over iterations is exponential, as confirmed by the linear dependence of the LAC update on the LAC error.

Mean LAC: CT reference values (S0) and errors in reconstruction studies (S1-5)

| Patient \ Study | S0 (cm^-1) | S1 error (%) | S2 error (%) | S3 error (%) | S4 error (%) | S5 error (%) |
|---|---|---|---|---|---|---|
| P1 | 0.0155 | -8.5 | -2.9 | -1.4 | +2.0 | +6.3 |
| P2 | 0.0269 | -7.3 | -8.2 | +3.7 | +5.8 | +9.5 |
| P3 | 0.0271 | -5.1 | -6.9 | +2.2 | +5.1 | +4.6 |

Disclosure of author financial interest or relationships:
**Y. Berker**, None; **A. Salomon**, None; **F. Kiessling**, None; **V. Schulz**, Philips Research, Employment .

Presentation Number **P348**
Poster Session 2
September 6, 2012 / 15:15-15:15 / Room: The Liffey

# Monte Carlo PET Simulation of Effect on Image Quality of Various MR-Compatible Animal Bed Materials

***Geron Bindseil***[1], *William B. Handler*[1], *Blaine A. Chronik*[1,2], [1]*Department of Physics and Astronomy, Western University, London, ON, Canada;* [2]*Robarts Research Institute, Western University, London, ON, Canada. Contact e-mail: gbindsei@uwo.ca*

**Introduction** A single animal imaging bed suitable for both PET and MRI is a requirement for simultaneous techniques and is desirable for sequential methods in order to eliminate animal positioning differences between modalities. It is important to investigate the effects of different MR-compatible bed materials on PET image quality. A suitable material for the animal holder should have low scattering and absorption of photons. Carbon fiber, typically used with PET, is expensive. It is also electrically conductive and thus in some circumstances unsuitable for PET-MRI due to RF heating. A comprehensive Monte Carlo simulation has been developed that uses the actual histogramming and image reconstruction software of the commercial PET system. This process was used to investigate how different MR-compatible bed materials affect PET image quality. **Methods** Simulated PET data were generated with the GEANT4 Application for Tomographic Emission (GATE) package [1]. The Siemens Inveon small-animal PET scanner was modeled. The coincidence timing and energy windows were 3.43 ns and 350-650 keV with a 14.6% energy blurring. Simulated emission data were first converted to the list-mode data format of the scanner and then all histogramming and reconstruction were performed in the scanner's software. Attenuation correction sinograms were generated within GATE by a custom algorithm which calculates the mean free path between each crystal pair. OSEM3D-MAP reconstruction was performed with default settings (16 subsets and 4 iterations) and scatter correction. The NEMA small animal image quality phantom with an initial activity of F-18 at 3.7 MBq was simulated for 20 minutes. The decay of F-18 and positron annihilation were simulated. The phantom was located on slightly larger animal bed consisting of a 6.35-mm-thick half-tube with six small lengthwise internal channels for heating water. The bed also contained two delrin tubes for anaesthetic gas. The four different bed materials tested were: PMMA, PVC, G10, and FR4. For comparison, the phantom was also simulated with the standard carbon fiber pallet included with the scanner. Each image was scaled by a single calibration factor such that the mean voxel value was 1 in the uniform region of the carbon fiber case. Recovery coefficients for activity-filled rods of various diameters, and the spill over ratios (SORs) for the water- and air-filled cold regions were computed. **Results** The normalized mean activities in the uniform region, percent standard deviations, SORs and scatter fractions are summarized in Table 1 for various bed materials. Recovery coefficients for various rod diameters are shown in Figure 1. PMMA tended to have slightly better performance measures; however the difference between materials was not very large. **Conclusion** The results suggest that none of the MR-compatible bed materials tested have a significant impact on PET image quality when compared with the standard carbon fiber pallet. This result suggests that a wider range of materials could be considered when developing a MR/PET bed system. [1] Jan, S. et al 2004 Phys. Med. Biol. 49 4543.

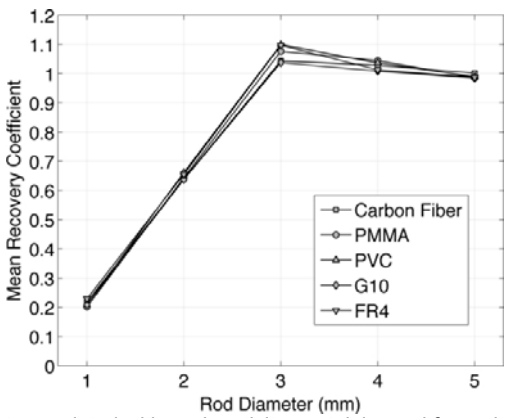


Mean recovery coefficient associated with each activity-containing rod for various animal bed materials.

Simulated PET Performance Measures for Various Bed Construction Materials

| Bed Material | Mean in Uniform Region (Normalized to Carbon Fiber) | Percent Standard Deviation (%) | Spill Over Ratio for Water Cavity (%) | Spill Over Ratio for Air Cavity (%) | Total Coincidences (prompts) (x10$^6$) | Fraction of Coincidences Scattered (%) |
|---|---|---|---|---|---|---|
| Carbon Fiber Pallet | 1.00000 | 0.54 | 8.04 | 3.89 | 2.1988 | 16.6 |
| PMMA | 0.99826 | 3.91 | 6.68 | 3.91 | 2.1709 | 17.7 |
| PVC | 1.00014 | 3.97 | 7.25 | 4.35 | 2.1706 | 17.4 |
| G10 | 1.00078 | 4.01 | 7.39 | 4.14 | 2.1402 | 18.3 |
| FR4 | 1.00136 | 4.73 | 7.71 | 4.11 | 2.1403 | 18.3 |

Disclosure of author financial interest or relationships:
**G. Bindseil**, None; **W.B. Handler**, None; **B.A. Chronik**, None.

Presentation Number **P349**
Poster Session 2
September 6, 2012 / 15:15-15:15 / Room: The Liffey

# A simple way for accurate coregistration of datasets from a microSPECT-CT and a preclinical 1.5T MRI

*Jean-Philippe Dillenseger[1], Christian Goetz[1,2], Amira Sayeh[1], André Constantinesco[1], **Philippe Choquet**[1,2], [1]UF6237 Preclinical imaging, HUS, Strasbourg, France; [2]Institut de Mecanique des Fluides et des Solides, CNRS, Strasbourg, France. Contact e-mail: pchoquet@unistra.fr*

Introduction Combined multimodality instruments have already demonstrated their interest, both in clinical and preclinical fields. Due to the richness in soft tissues contrast, it was stated that coupling scintigraphic modalities with MRI will overcome the advantages of CT. However, it is more challlenging and costly to combine any instrument with MRI due to magnetism. While the current setup of PET-CT is aligned machines, there are 3 described possibilities for coupling scintigraphy and MRI: together in line, an insert placed into a standard MR system and a completely new system. As not all applications require the necessity of applying imaging protocols at the same time on both modalities, using different apparatus remains a solution for multimodality with MRI, especially for small animal imaging. We propose a simple tool, to facilitate coregistration between images acquired on a preclinical MRI and microSPECT-CT data, when the animal is moved between systems. Material and methods MRI system (OPTImouse, RS2D, Bischwiller, France) uses a 1.5T cryogen-free superconducting magnet. It takes up a floor area of 1.20m x 2m while the 5G line is at 80cm away from the center of the magnet in the worst case. For mice whole body imaging, a RF coil (RapidBiomedical, Würzburg, Germany) of 40mm in diameter is used, which remains inside the magnet. The microSPECT-CT (eXplore speCZT Vision 120, GE, Waukesha, USA) is installed 2 to 3m away from the MRI, thanks to the short extension of the magnet fringe field. Imaging chambers (Minerve, Esternay, France) share common support on each imaging instrument, allowing for quick and efficient docking. The tool for coregistration consists in a catheter fixed on a flexible plastic sheet, placed around the animal, and filled with a solution containing iodine, copper sulfate and radioisotope. Mice are kept anesthetised and warmed in the imaging chambers during acquisitions. Multimodality imaging is achieved sequentially by moving the chamber from one system to the other, which takes approximately 20s. Amide (http://amide.sourceforge.net/) is used for coregistration of acquired data. Results Acquisitions on phantom demonstrated the resolution accuracy of the coregistration process. Relative to the radiopharmaceutical used, bone, muscular perfusion and tumor imaging were performed and coregistered on 3D high resolution T1 and T2 weighted whole body images of the same mice acquired sequentially, as well on CT whole body images when meaningful. Conclusion We have demonstrated that a simple, cheap tool, easy to fill, could efficiently help for coregistration of preclinical images, acquired on separate imaging apparatus. The simplicity of the concept allows for an easy and quick setup, without wasting time. Results on phantoms show that the coregistration is adequate, showing in small animals that merging scintigraphic data with MRI could be done even without a combined acquisition system.

Disclosure of author financial interest or relationships:
**J. Dillenseger**, None; **C. Goetz**, None; **A. Sayeh**, None; **A. Constantinesco**, None; **P. Choquet**, RS2D, Grant/research support .

Presentation Number **P350**
Poster Session 2
September 6, 2012 / 15:15-15:15 / Room: The Liffey

# Quantitative imaging of the distribution of probes by normalizing unmixed multispectral optoacoustic images

***X. Luís Deán-Ben**, Vasilis Ntziachristos, Daniel Razansky, Helmholtz Zentrum Muenchen, Neuherberg, Germany. Contact e-mail: xl.deanben@helmholtz-muenchen.de*

Multispectral optoacoustic tomography (MSOT) is emerging as a promising new tool for molecular imaging applications in small animals commonly used in biological research. As diffuse light can reach several millimetres to centimetres in biological tissues, optoacoustic tomography provides rich optical contrast in deep tissues with a much higher resolution as compared to diffuse optical techniques. Furthermore, any light absorbing molecule can yield specific contrast if imaged at several optical wavelengths, so that high versatility in molecular imaging can be achieved with MSOT. A two-step procedure is usually followed in order to image distribution of the optical reporter agent of interest. First, image reconstruction is performed for each optical wavelength from the corresponding optoacoustic signals acquired at several locations around the imaging sample. Subsequently, an unmixing algorithm is applied to the set of tomographic reconstructions, which allows identifying the specific spectral variations in the absorption due to each of the absorbing substances present. Ideally, the unmixed image corresponding to the injected probe should represent its actual concentration, which is proportional to the optical absorption coefficient. However, tomographic optoacoustic reconstructions correspond to the optical absorbed energy, which is affected by light attenuation, so that regions with a high light fluence may appear bright in the images even if concentration of the absorbing substances is low. Acoustic attenuation further reduces the amplitude of the optoacoustic signals as they propagate through the tissue. Thereby, absorbers located deeper would generally appear weaker in the images as compared to shallow absorbers having similar concentration. In this work, we introduce a procedure to correct for the attenuation effects in the unmixed images. For this, the original optoacoustic images are processed in order to estimate the smooth spatial variations caused by attenuation. For convenience, oxygenated and deoxygenated haemoglobin are considered to have the same extinction coefficients in optoacoustic image at 800nm used for normalization, so that absorption is not affected by oxygenation distribution. Finally, the processed image is used to normalize the images retrieved with the unmixing algorithm in order to improve quantification. Performance of the method is showcased in tissue mimicking phantoms and in a post-mortem mouse containing insertions with an optical probe at different depths.

Disclosure of author financial interest or relationships:
**X. Deán-Ben**, None; **V. Ntziachristos**, ERC, Grant/research support; Ithera Medical, Stockholder; **D. Razansky**, iThera Medical GmbH, Stockholder .

Presentation Number **P351**
Poster Session 2
September 6, 2012 / 15:15-15:15 / Room: The Liffey

# Experimental performance of blind unmixing methods in multispectral optoacoustic imaging

***X. Luís Deán-Ben**, Nikolaos C. Deliolanis, Vasilis Ntziachristos, Daniel Razansky, Helmholtz Zentrum Muenchen, Neuherberg, Germany. Contact e-mail: xl.deanben@helmholtz-muenchen.de*

Optoacoustic imaging has experienced vast development in the last decade and a growing number of applications are emerging due to the important advantages it can provide, in particular its rich optical contrast and good ultrasonic resolution at depths beyond the optical diffusion limit in vivo. Furthermore, by imaging at several optical wavelengths, multispectral optoacoustic tomography (MSOT) provides high versatility in molecular imaging applications due to ability to differentiate between intrinsic biomarkers and other spectrally distinct light absorbing contrast agents. Molecular imaging with optoacoustics implies distinguishing light absorption due to an injected optical probe from the background absorption, which is present in the images. For this, the specific absorption spectrum of the probe is identified in a sequence of images at several wavelengths with a procedure termed multispectral unmixing. If the absorbing substances in the sample are known, the unmixing can be done with e.g. least-square fitting to the corresponding spectra. As light absorption in biological tissues in the near infrared is mainly due to blood, the images can be fitted to three absorbing components, namely the probe of interest and oxygenated and deoxygenated haemoglobin. A different approach, termed blind unmixing, consists in estimating both the spectra of the absorbing substances and their spatial distribution without considering any a priori information. In this work, we compare the experimental performance of the basic spectral fitting method and two blind unmixing approaches in terms of their sensitivity to the detection of low probe concentrations. The blind unmixing algorithms considered are the combination of principal component analysis and independent component analysis (PCA-ICA) as well as the vertex component analysis (VCA). It is subsequently shown that overall blind unmixing methods attain significantly higher sensitivity with the main factor being distortion of the spectral variations in the images due to wavelength-dependent light attenuation, nonuniform illumination patterns, and wavelength instability of the laser excitation.

Disclosure of author financial interest or relationships:
**X. Deán-Ben**, None; **N.C. Deliolanis**, None; **V. Ntziachristos**, ERC, Grant/research support; Ithera Medical, Stockholder; **D. Razansky**, iThera Medical GmbH, Stockholder .

Presentation Number **P352**
Poster Session 2
September 6, 2012 / 15:15-15:15 / Room: The Liffey

# Ultra-low Dose CT and MR Dual Attenuation Correction for Positron Emission Tomography

***Gaspar Delso***[1,2], *Patrick Veit-Haibach*[1], *Cäcilia E. Mader*[1], [1]*Nuklearmedizin, UniversitatsSpital Zurich, Zurich, Switzerland;* [2]*Applied Science Lab, GE Healthcare, Waukesha, WI, USA. Contact e-mail: gaspar.delso@ge.com*

Positron Emission Tomography (PET) requires attenuation correction in order to yield quantitative images. The current gold standard for attenuation correction is Computed Tomography (CT) data. Combining PET with Magnetic Resonance (MR) scanners has, among other, the advantage of eliminating the radiation dose of CT. MR-based attenuation correction is, however, not as accurate as that achieved with CT. Tri-modality PET/CT-MR systems, on the other hand, could be switched between CT-based and MR-based attenuation correction depending on the clinical indication. We describe here a method to combine an ultra-low dose (ULD) CT scan with MR data to achieve the dose reduction of MR-based attenuation correction, while avoiding two of its main pitfalls: field-of-view truncation and lack of bone attenuation. Methods The proposed method relies on the acquisition of a set of two-point Dixon MR sequences in order to construct whole-body datasets of the patient water and fat distribution. These volumes can be used to create an attenuation map representing the fatty and soft tissue, as described in [Martinez-Möller2009]. These sequences can be effectively integrated in a clinical MR protocol for oncology, as discussed in [Eiber2011] In a second step, the patient is moved to the PET/CT subsystem, where the standard CT acquisition for attenuation correction (approx. 140 KV, 17 mAs) is replaced by an ULD CT (e.g. 100 KV 10 mAs). Lower settings are possible, but conditional to the performance degradation of the X-ray tube at low currents. Note that the impact of this change to standard clinical workflow is negligible. The ULD-CT is then processed with a regularized segmentation procedure [Chan&Vese2001] to extract the body contour. A two-pass thresholding is used to obtain the cortical bone. These are then incorporated to the MR-based attenuation map and reconstructed. Results The described method was tested on a set of PET/CT-MR clinical data. The ULD scan was measured to deliver a dose of approximately 0.3 mGy (CTDIvol), as opposed to the 4.5 mGy of a standard attenuation correction CT. The segmentation algorithm was capable of extracting the patient profile in all cases, introducing some errors only in cases where important streak artifacts were present (e.g. in the presence of prosthetic implants). However, the impact of these artifacts can be limited by incorporating some a-priori knowledge of the MR field-of-view. The cortical bone was obtained robustly for the head, hip and limbs. Ongoing work is aimed at improving the segmentation of the spine and ribcage. The incorporation of this information into the attenuation map is very robust, as it is only applied in regions without MR signal. Conclusion Our results show that CT images acquired with practically the lowest settings that the system can achieve are sufficient to provide the two key pieces of information missing in MR data: The bones and the patient contour. A system could therefore operate in a low-dose mode and achieve almost "gold standard" PET accuracy, without the need for additional ultra-short echo time MR scans or time-consuming iterative truncation correction.

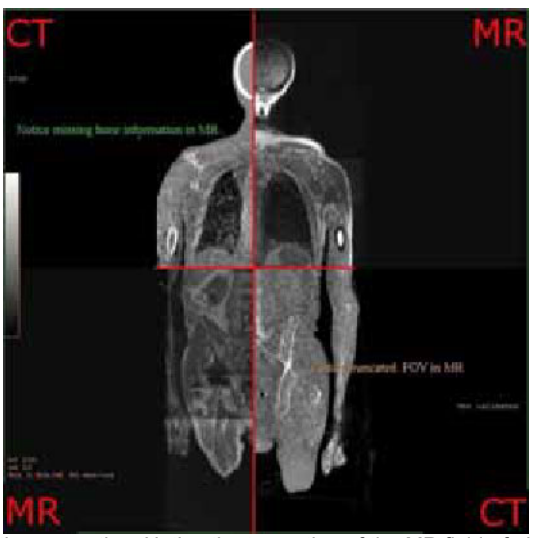


Tiled view of CT and MR data for attenuation correction. Notice the truncation of the MR field-of-view and missing cortical bone information.

Disclosure of author financial interest or relationships:
**G. Delso**, GE Healthcare, Employment; **P. Veit-Haibach**, Siemens, Grant/research support; Bayer Healthcare, Grant/research support; **C.E. Mader**, None.

Presentation Number **P353**
Poster Session 2
September 6, 2012 / 15:15-15:15 / Room: The Liffey

# TOPEM: a PET TOF endorectal probe, compatible with MRI for diagnosis and follow up of prostate cancer

***Franco Garibaldi***[1], *Stefano Colilli*[7], *Luigi Cosentino*[2], *Francesco Cusanno*[8], *Paolo Finocchiaro*[2], *Federico Giove*[10], *Fausto Giuliani*[7], *Flavio Loddo*[3], *Maurizio Lucentini*[7], *Franco Meddi*[10], *Bruno Maraviglia*[10], *Emilio Monno*[6], *Roberto Perrino*[3], *Antonio Ranieri*[3], *Fabio Santavenere*[7], *Paolo Musico*[4], *Raffaele De Leo*[9], *Roberto Perrino*[5], *Massimo Gricia*[7], [1]*INFN Rome, Rome, Italy;* [2]*INFN LNS, Catania, Italy;* [3]*INFN Bari, Bari, Italy;* [4]*INFN Genova, Genova, Italy;* [5]*INFN Lecce, Lecce, Italy;* [6]*Agency ENEA, Rotondella, Italy;* [7]*ISS, Rome, Italy;* [8]*TUM, Menchen, Germany;* [9]*Physics, University of Bari, Bari, Italy;* [10]*University of Rome La Sapienza, Rome, Italy. Contact e-mail: franco.garibaldi@iss.infn.it*

Prostate cancer (PCa) is the leading cancer and the second leading cause of cancer death in men. The inhability to predict which patiens have indolent or aggressive disease, complicates the choice of the therapy. Treatment decisions are based on making a best guess at the biology of the tumor from as much indirect information as possible, PSA, digital rectal examination and biopsy that is blind. MRI lack sensitivity and specificity. For this reason PCa tends to undergo definitive treatment despite the side effects of bowel, bladder and/or sexual dysfunction. Current imaging techniques provide limited information for disease staging but cannot detect early disease. Accurate staging would facilitate treatment decisions. New anatomic, functional imaging techniques are needed. Small lesions should be detected, i.e., recurrent tumors in the surgical bed, local lymph node invasion and other subtle manifestations of the disease in men with an elevated PSA but no other symptoms. A key goal of PCa imaging is to be able to detect minimal disease. It is important to know whether the tumor has spread beyond the prostate capsule. It would be possible to guide treatment decisions and avoid unnecessary surgeries. Imaging techniques can help surgery detecting limph nodes and tumor margins. TOPEM project proposes a multimodality imaging detector that can play a crucial role by merging anatomical and functional details from simultaneous PET and MRI scans. MRI is the ideal complement to radionuclide imaging techniques for soft tissues. The internal probe will be used in coincidence with external dedicated detectors and/or a standard PET ring. Performance is dominated by the endorectal probe. The electronics must measure coincidences with a precision of 300 ps or less. Exploiting the TOF capability allows an increase in the SNR/NECR. For compactness, MRI compatibility and timing resolution, Silicon Photomultipliers (SiPM) have to be used. Dual imaging agents PET optical will be available soon, allowing surgery in detecting limph nodes and tumor margins. An endorectal PET detector working in coincidence with an external detector has several advantages: attenuation reduced, good spatial resolution insensitive to the intrinsic performance of the external detector, high efficiency. Measurements have been performed with finger counters, 1.5x1.5x15 mm3 (LYSO) coupled to two SiPM to study the optimization of timing resolution and Depth Of Interaction (DOI) resolution.We obtained, for the first time, a very good timing (~ 200 ps) and DOI (1mm) resolution at the same time. The final detector will be built with 128 of such finger scintillator coupled one to one to two SiPM in order to optimize the light collection. The electronic system incorporates a dedicated ASIC. A sophisticated cooling and a control systems for feedback on the power supply are needed. The system will have to cool the electronics down to ~ 22 deg and heat the external part in contact with the patient body (32-40 C). The compatibility of the PET system with MRI is not a problem provided the components of the PET are insensitive to the magnetic field

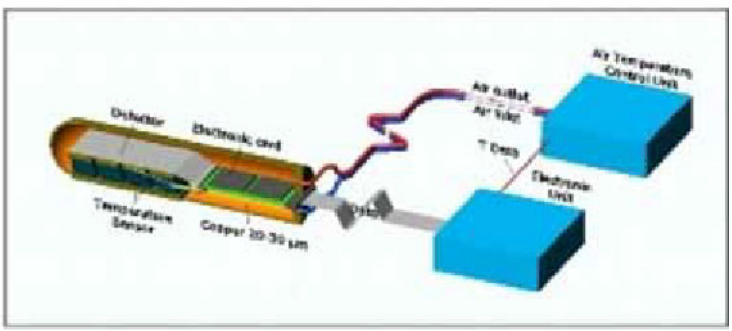


Layout of the PET edorectal prostate probe

Probe expected perfomance

| Dimension | Spatial resolution | DOI resolution | Efficiency | Electronic channels |
|---|---|---|---|---|
| 25 x 30 x 15 mm³ | 1 mm | 1 mm | ~ 2.5 times a standard PET | 256 |

Disclosure of author financial interest or relationships:
**F. Garibaldi**, None; **S. Colilli**, None; **L. Cosentino**, None; **F. Cusanno**, None; **P. Finocchiaro**, None; **F. Giove**, None; **F. Giuliani**, None; **F. Loddo**, None; **M. Lucentini**, None; **F. Meddi**, None; **B. Maraviglia**, None; **E. Monno**, None; **R. Perrino**, None; **A. Ranieri**, None; **F. Santavenere**, None; **P. Musico**, None; **R. De Leo**, None; **R. Perrino**, None; **M. Gricia**, None.

Presentation Number **P354**
Poster Session 2
September 6, 2012 / 15:15-15:15 / Room: The Liffey

# Dual-Tracer CT-Guided Fluorescence Tomography Can Remove Non-Specific Uptake Effects of a Targeted Tracer

***Robert Holt***[1], *Kenneth M. Tichauer*[2], *Fadi El-Ghussein*[2], *Frederic Leblond*[2], *Brian W. Pogue*[2,1], [1]*Department of Physics and Astronomy, Dartmouth College, Hanover, NH, USA;* [2]*Thayer School of Engineering, Dartmouth College, Hanover, NH, USA. Contact e-mail: robert.w.holt@dartmouth.edu*

Fluorescence tomography (FT) can be used to image molecular expression with targeted fluorescence tracers in preclinical small animal applications. FT suffers from lower spatial resolution and high background signals, yet it has high sensitivity and the ability to simultaneously image multiple tracers. In this study, a new approach is proposed that capitalizes on this second property to improve targeted fluorescence image contrast, by employing a second untargeted tracer which provides a stable way to suppress non-specific background. The approach involves the normalized subtraction of the untargeted fluorescence projection data from the targeted fluorescence data prior to image reconstruction to remove contrast from non-receptor mediated uptake of the targeted tracer, for instance in organs of filtration like the liver or kidneys. This method includes an effective estimation of the subject's optical properties and a specialized scaling method to accommodate possible magnitude mismatch in the optical projection data sets. The basic concept of this dual-tracer difference approach is explored here in phantom experiments and simulations. A demonstration of the approach in a mouse brain tumor model is shown. The simulation study was performed using NIRFAST (www.nirfast.org), an open source tool developed to model light transport in tissue. For the simulation (domain shown in figure 1a), both inclusions in the targeted reconstruction (figure 1b) had an 8:1 inclusion to background ratio (IBR) to mimic the distribution of a targeted tracer, whereas in the untargeted reconstruction (figure 1c) the top inclusion had 8:1 IBR and the right hand inclusion had 4:1 IBR to simulate the effect of an targeted tracer. The reconstruction based on the difference of the data from these simulations (figure 1d) resulted in a nearly infinite contrast ratio for the right hand inclusion, as expected, meaning that this method has merit mathematically. An experiment was performed using a cylindrical phantom (figure 1e) with the same geometry and fluorescence contrast ratios as the simulation. The fluorophores used were IRDye 800CW (LICOR Biosciences) and AlexaFluor 647 (Life Technologies). It was imaged using a custom non-contact microCT-guided FT system, using lasers at 635nm (figure 1f) and 755nm (figure 1g) to excite the dyes separately, and differencing was performed. The results show that in the difference image (figure 1h), the recovered contrast in the inclusions with different dye concentration was much higher than anywhere else, indicating that effect of non-specific uptake can be removed from FT images using this dual-tracer difference approach. The method was also applied in a case study of a mouse model with orthotopic glioma tumor (figure 1i). Imaging was performed using the same techniques as the phantom study at 4 h after the injections of 2 nmoles of untargeted Alexa Fluor 647 and epidermal growth factor receptor targeted IRDye 800CW-EGF. The difference image reconstruction was successful (figure 1j), showing that this method works for in vivo data. The details of implementation and the limits on non-specific background suppression are outlined.

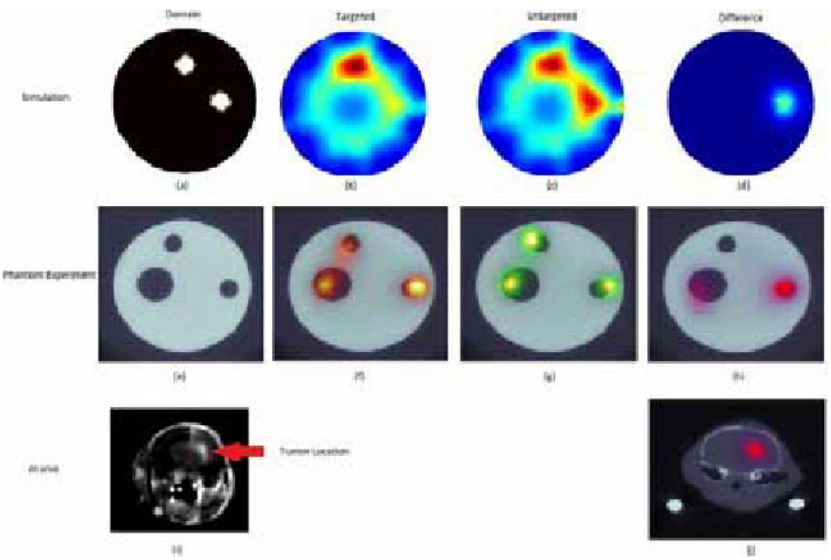

Figure 1. (a-d) Simulated results showing advantage of optical projection differencing. (e-h) Experimental phantom results showing optical differencing. (i-j) Results of application in mouse model.

Disclosure of author financial interest or relationships:
**R. Holt**, None; **K.M. Tichauer**, None; **F. El-Ghussein**, None; **F. Leblond**, None; **B.W. Pogue**, None.

Presentation Number **P355**
Poster Session 2
September 6, 2012 / 15:15-15:15 / Room: The Liffey

# The effects of number of segments in segmentation-based whole-body PET/MR attenuation correction: evaluation with PET/CT data of liver and spine cancer patients

***Joong Hyun Kim***[1], *Jae Sung Lee*[1], *In Chan Song*[2], *Dong Soo Lee*[1], [1]*Department of Nuclear Medicine, Seoul National University, Seoul, Republic of Korea;* [2]*Department of Radiology, Seoul National University, Seoul, Republic of Korea. Contact e-mail: jhkim419@gmail.com*

For the attenuation correction (AC) in PET/MRI system, segmentation-based methods which categorize tissue groups based on MRI intensities are mostly used. By using DIXON sequence, more accurate quantification is possible because the fat segments can be separated from soft-tissue. However, the standard uptake value (SUV) of the lesions in the liver and spine, which have higher attenuation coefficients than other organs, can be under-estimated and this can lead to misinterpretation of clinical cases. In this study, the possible bias in the SUV estimation was evaluated using segmentation-based AC with and without DIXON sequence using PET/CT data of liver and spine cancer patients. Forty patients who had liver or spine lesions and underwent $^{18}$F-FDG PET/CT scan were participated (F:M=18:22, liver:spine=20:20, 60.5±11.4 y, and 57.7±10.4 kg). Only the body regions were extracted from CT images and categorized into 4 tissue groups (4T AC; air-pocket, lungs, fat, and soft-tissue; DIXON) using Hounsfield unit (HU) thresholds which were determined on CT histogram. The fat segment was comprised in soft-tissue group for 3T AC (air-pocket, lungs, and soft-tissue; non DIXON) map. Mean attenuation coefficient for each group was calculated from 40 CT images and assigned to the attenuation maps. PET sinograms were reconstructed using CT, 3S, and 4S AC maps, and mean SUVs in the lesion were compared. Mean attenuation coefficients for air-pocket, lungs, fat, and soft-tissue were 0.0056, 0.0338, 0.0895, and 0.0989 cm-1, respectively. Using 3T AC, the SUVs were under-estimated by 11.1±2.6% and 16.4±8.5% for liver and spine lesion relatively to the CT AC, respectively. Using 4T AC, the SUVs were under-estimated by 6.82±3.78% and 14.74±7.47% for liver and spine lesion relatively to the CT AC, respectively. In 3T AC, the SUVs of liver and spine lesion were considerably under-estimated, however in 4S AC, under-estimation of liver SUV was decreased. The fat segmentation was helpful for liver SUV quantification. In spine lesions, the segmentation-based AC yielded ~15% negative bias in SUV regardless of the inclusion of fat segment, due to the much higher density of bone than other soft-tissue organs. For more accurate quantification of bone segments, bone segmentation technique such as ultra-short time echo sequence or template-based AC should be applied to whole-body AC. The results of this study will be useful for understanding the organ-dependent bias in SUV between PET/CT and PET/MRI.

Disclosure of author financial interest or relationships:
**J. Kim**, None; **J. Lee**, Samsung Electronics, Grant/research support; **I. Song**, None; **D. Lee**, None.

Presentation Number **P356**
Poster Session 2
September 6, 2012 / 15:15-15:15 / Room: The Liffey

# A scientific based method of optimizing the adjustments of the Taylor Spatial Frame (TSF) based upon functional and anatomical data from 18F PET /CT: preliminary results

***Ann Larkin***[1], *Gerald Q. Maguire*[2], *Marilyn E. Noz*[3], [1]*Medical Physicist, Dublin, Ireland;* [2]*School of Information and Communication Technology, KTH Royal Institute of Technology, Stockholm, Sweden;* [3]*Department of Radiology, New York University School of Medicine, NY, NY, USA. Contact e-mail: ann.m.larkin@gmail.com*

OBJECTIVE: In this study we explore the possibility of accurately monitoring tibial alignment induced by Taylor Spatial Frames (TSFs), using cross-sectional functional data obtained from PET and structural data obtained by CT examinations. MATERIALS AND METHODS: The TSF is an external fixator used to correct complex fractures and bone deformities. It consists of two rings connected to each other by six telescoping linkage rods. By altering the length of the rods, bone fragments attached to the rings can be moved through space to simultaneously correct displacements of angulation, translation and rotation. Once the TSF is attached to the bone, planar radiographs are obtained which allows the fracture alignment to be modeled. Parameters from the patient specific model are entered into a software program which produces a "prescription" of the required strut adjustments. The struts are adjusted daily by the patient until the correct alignment is achieved. Over time this results in the fracture or deformity healing with anatomic or near-anatomic alignment. The adjustment process can take several weeks, after which time the frame remains in place for several months to permit adequate bone healing. The TSF is removed when planar radiographs of the bone confirm complete healing. Sodium fluoride 18F is a diagnostic molecular imaging agent used for identification of new bone formation and the detection of skeletal abnormalities. 18F uptake in the skeleton is dependent on regional blood flow and new bone (osteoid) formation.18F is substituted for hydroxyl groups in hydroxyapatite and becomes covalently bound to the surface of new bone. Uptake is higher in osteoid bone because of the higher availability of binding sites. The purpose of this study is to determine if PET/CT imaging can be used to provide the clinician with accurate information to model the fracture or deformity and monitor the bone healing process. RESULTS: Several aspects of the PET/CT examination will be presented. Optimal scan parameters will be determined to minimize the radiation burden to the patient. The effective dose to the patient will be quantified and the associated risks discussed. Image processing techniques will be analyzed to determine the optimal reconstruction parameters such as the number of iterations and subset filters. The most appropriate software to reconstruct the images will be identified. The degree of scatter induced by the presence of the TSF will be quantified and methods to reduce / eliminate the scatter will be discussed. The feasibility of identifying and quantifying new bone growth using SUV analysis will be investigated. CONCLUSION: This study will present the benefits and limitations of using cross-sectional functional data obtained from PET and structural data obtained by CT examinations to monitor tibial alignment induced by TSFs.

Disclosure of author financial interest or relationships:
**A. Larkin**, None; **G.Q. Maguire**, None; **M.E. Noz**, None.

Presentation Number **P357**
Poster Session 2
September 6, 2012 / 15:15-15:15 / Room: The Liffey

# The PET Performance Measurements of A Next Generation Dedicated Small Animal PET/MR Scanner

***Chih-Chieh Liu***[1], *Mosaddek Hossain*[1], *Ilja Bezrukov*[1,3], *Hans F. Wehrl*[1], *Armin Kolb*[1], *Martin S. Judenhofer*[2], *Bernd J. Pichler*[1], [1]*Department of Preclinical Imaging and Radiopharmacy, Eberhard-Kals-University Tuebingen, Tuebingen, Germany;* [2]*Biomedical Engineering, University of California, Davis, CA, USA;* [3]*Intelligent Systems, Max-Planck-Institute, Tuebingen, Germany. Contact e-mail: Chih-Chieh.Liu@med.uni-tuebingen.de*

The combination of PET/MR allows to perform multi-parametric studies yielding a powerful tool to cross-validate and correlate molecular PET and functional MR data. To obtain accurate quantification results, the evaluation of performance variation of the MR compatible PET scanner under the influence of MRI is the primary goal of this work. The NEMA protocol is adopted to evaluate the performance of our in-house developed dedicated small animal PET-insert outside and inside the 7T small animal MRI scanner. The PET-insert is built with total of 48 LSO detector blocks in a diameter of 120 mm. There are 3 detector blocks in axial direction (70mm axial FOV) allowing to image rats including brain and heart. The individual scintillation crystal dimension is 1.5x1.5x10mm$^3$. Before acquiring the NEMA measurements, normalization measurements over 16 h were performed using a 68Ge cylindrical phantom with a diameter of 65mm and length of 110mm. In addition, the background count rate was measured for 9 h. The spatial resolution of the PET-insert was measured with fixed counts for each position by a FDG filled capillary with a diameter of 0.63mm. The sensitivity was measured with a 22Na point source located in central axis and moved by 1mm steps in axial direction. The in-house EM reconstruction algorithm was implemented to account for the unique geometric factor of the PET-insert and it is able to integrate corrections. MR-based attenuation correction was developed and successfully applied to one rat PET data. The attenuation map is created by segmenting a 3D fast low angle shot (FLASH) sequence. The spatial resolution, represented by FWHM and FWTM, degrades as the radial distance increases. Outside the MRI, the ranges of spatial resolution are 1.4mm~2.5mm (FWHM) and 3.0mm~5.0mm (FWTM) from center to 30mm radial distance. Inside the MRI, the ranges of FWHM and FWTM are 2.0mm ~3.0mm and 4.0mm~5.4mm, respectively. This degradation is caused by a low frequency noise introduced by the MR system, which affects predominately the FWTM. This noise will be removed by an additional filter at the MR cabin. First versions of this filter have been successfully tested. The max sensitivity is 2.9% when measured outside the MRI and 2.6% inside MRI. The decreasing is also caused by the low frequency noise resulting from a high dead time of the entire system. The FWHM, measured outside the MRI of 1.4mm, is consistent with the theoretical value of 1.36mm. The next steps include the test of the RF filter to remove the low frequency noise to maintain the PET spatial resolution and sensitivity performance inside the MRI. The attenuation correction is evaluated by a cylindrical phantom and the results of a rat brain data show a 25% underestimation in quantities if no attenuation correction is applied. Further, we are finishing the remaining measurements based on the NEMA protocol, including the scatter fraction, count losses, the count rate of randoms, and the image quality evaluation and accuracy of corrections.

Disclosure of author financial interest or relationships:
**C. Liu**, None; **M. Hossain**, None; **I. Bezrukov**, None; **H.F. Wehrl**, None; **A. Kolb**, None; **M.S. Judenhofer**, None; **B.J. Pichler**, Siemens, Grant/research support; AstraZeneca, Grant/research support; Bayer Healthcare, Grant/research support; Boehringer-Ingelheim, Grant/research support; Oncodesign, Grant/research support; Merck, Grant/research support; Bruker, Grant/research support .

Presentation Number **P358**
Poster Session 2
September 6, 2012 / 15:15-15:15 / Room: The Liffey

# Multimodal tomography for localization of BMP2 transduced cells for spine fusion

***Yujie Lu***[1], *LaShan Simpson*[2], *ZaWaunyka Lazard*[3], *Elizabeth Olmstead-Davis*[3], *Alan Davis*[3], *Jennifer West*[2], *I-Chih Tan*[1], *Chinmay D. Darne*[1], *Mary A. Hall*[1], *Holly Robinson*[1], *Eva Sevick*[1], [1]*Institute of Molecular Medicine, University of Texas Health Science Center at Houston, Houston, TX, USA;* [2]*Department of Bioengineering, Rice University, Houston, TX, USA;* [3]*Center for Cell and Gene Therapy, Baylor College of Medicine, Houston, TX, USA. Contact e-mail: yujie.lu@uth.tmc.edu*

Bone morphogenetic proteins (BMPs) are well known for their osteoinductive potential, yet effective clinical utilization for bone repair using recombinant BMP2 protein suffers from a short-lived bolus effect. Recently, Davis and coworkers (Tissue Engineering Part A, 16, 3727-3736, 2010)developed a cell-based gene therapy approach that utilizes virally transduced fibroblasts encapsulated in poly(ethylene glycol) diacrylate (PEGDA) hydrogel microspheres to enable sustained BMP2 delivery, protection from host immune response, and localized placement for bone fusion. However, assessment of implantation position and longitudinal evaluation of BMP2 expression and therapeutic response in vivo requires three-dimensional tomography. Recently, we developed a tri-modality (NIRF(Near-infrared Fluorescence)/PET/CT) tomography system by integrating time-dependent, optical components and a miniaturized NIR intensified camera into a Siemens Inveon scanner to perform NIRF imaging (785/830 nm) of BMP2 transduced fibroblasts encapsulated in AlexaFluor790-labeled PEGDA hydrogel microspheres after injection in the right paraspinous muscle of a mouse. NIRF/CT imaging was performed at day 15 post-injection. CT imaging was performed using high spatial resolution mode to acquire the imaging information of new bone due to its low contrast compared to surrounding tissues. Subsequent standard CT scanning and NIRF tomography were performed to obtain the entire mouse surface information and image the fluorescence photon distribution on the mouse surface at four different projections ($0^{\circ}$, $45^{\circ}$, $180^{\circ}$, $315^{\circ}$; Figs.1a-1d). The fluorescent photon distribution was mapped onto the CT-derived surface using a pinhole camera model. The volumetric mesh consisting of about 13,000 discretized points was generated using the CT volume for NIRF tomography. A linear reconstruction algorithm with a high-order simplified spherical harmonics approximation was developed to realize NIRF tomography. Figs.1e-1h show the comparison between CT images in high spatial resolution mode and NIRF tomography. New bone formation observed in CT images was also visualized in NIRF tomography, and consistent with the therapeutic response to the implant. These results demonstrate the potential of multimodality NIRF tomography in a biologically pertinent animal model system. This work is supported by NIH R01CA135673 (EMS-M), DOD W81XWH-07-1-0215 (EO-D and ARD), W81XWH-07-1-0281(EO-D and ARD), DARPA W911NF-09-1-0040 (EO-D and ARD), and a training fellowship (YL) from the Keck Center Computational Cancer Biology Training Program of the Gulf Coast Consortia (CPRIT Grant No. RP101489).

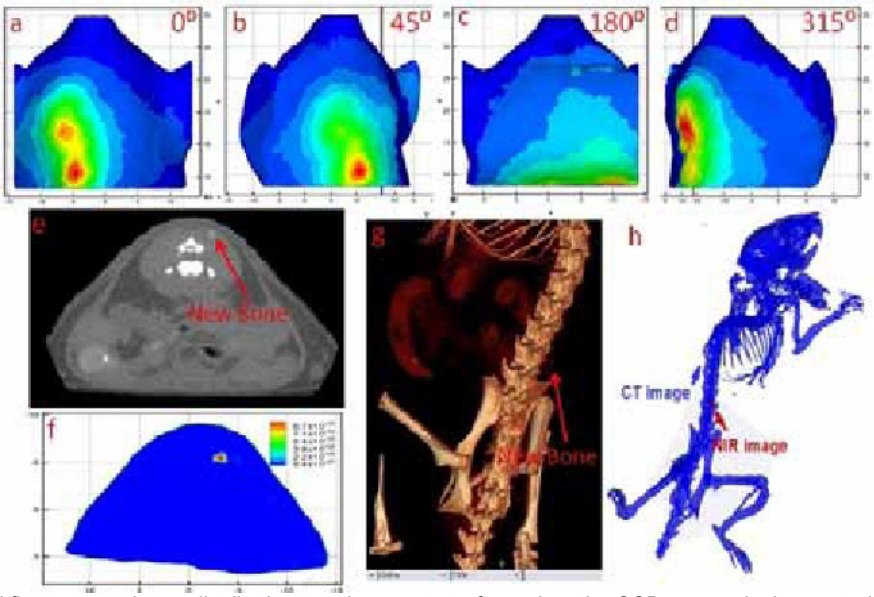


Figures 1a-1d are the mapped fluorescent photon distributions on the mouse surface when the CCD camera in the gantry is at different positions; figures 1e and 1f are the cross-sections of the CT and NIRF reconstructions, respectively; and figures 1g and 1h are the 3-D CT and NIRF/CT multimodal 3-D images (In figures 1e and 1g, CT images were acquired using high spatial resolution mode and new bone has low CT contrast. In figure 1h, the CT domain shows original bone information and the top 90% reconstructed volumes are shown in NIRF tomography. )

Disclosure of author financial interest or relationships:
**Y. Lu**, None; **L. Simpson**, None; **Z. Lazard**, None; **E. Olmstead-Davis**, None; **A. Davis**, None; **J. West**, None; **I. Tan**, None; **C.D. Darne**, None; **M.A. Hall**, None; **H. Robinson**, None; **E. Sevick**, Tactile, Inc, Grant/research support; Siemens Preclinical Solutions, Other financial or material support .

Presentation Number **P359**
Poster Session 2
September 6, 2012 / 15:15-15:15 / Room: The Liffey

# Presentation of test measurements with a dynamic list-mode sequential pre-clinical SPECT/MRI system using non-multiplexing multi-pinhole apertures

***Domokos Mathe***[1], *Gabor Nemeth*[2], *István Bagaméry*[2], [1]*CROmed Ltd, Budapest, Hungary;* [2]*Mediso Medical Imaging Systems Ltd., Budapest, Hungary. Contact e-mail: domokos.mathe@cromedresearch.com*

Objectives: As the resolution of SPECT is without theoretical limits and longer lived isotopes can provide valuable biokinetic data on both therapeutic radiopharmaceuticals and protein/peptide molecules, it is of high importance to integrate a magnetic resonance and a SPECT tomography imaging system. Methods: We show some preliminary results for a new, compact, sequential pre-clinical SPECT/MR scanner with list-mode SPECT acquisition and non-multiplexing multipinhole apertures. In the system, in a distance less than 10 cm modalities are organized sequentially. The SPECT/MR system was constructed on the basis of NaI(Tl) crystal SPECT technology using full digital Non-Anger electronics and a permanent magnet 1 T MR . The Mediso nanoScan® SPECT/MR imaging system has 4 gamma detectors (27x27 cm each) organized in a square form. A special 3D EM SPECT reconstruction (Tera-Tomo 3D) has been developed. Physical corrections for attenuation and scatter are based on a real time Monte-Carlo simulation on a high-performance Graphics Processing Unit. Count data are acquired in list mode on each detector. The SPECT is aligned axially in front of the MR component with 90 mm diameter and 60 mm high barrel FOV, specified with 100 micron areal pixel resolution (Aspect, Israel). The subject is sent from the SPECT area to the MR subsystem bore in the animal bed. Center of the SPECT FOV is close to the MR magnet bore opening (distance: 8 cm). We have measured the SPECT performance with working MR system using a specially designed new general purpose non-multiplexing multi-pinhole aperture set for mouse whole body studies. Images of a Jaszczak phantom filled with 99mTc-pertechnetate were acquired to this end. SPECT image reconstruction from binned list mode data was performed using the Tera-Tomo 3D SPECT reconstruction. We also present signal/noise ratio (S/N) of the MR subsystem before and after integration using a 35 mm diameter coil. Results: Using the multi-pinhole (12) general purpose apertures with a diameter of 1 mm and 30x15 mm FOV, the Jaszczak phantom's smallest resolved hot rod was 0.6 mm in diameter. Magnification factor of the aperture proved to be over 5. Using the proprietary 3D reconstruction algorithm in helical scans, it was possible to quantitate radioactivity from an activity-filled (10 MBq) cylinder 30 mm long, 15 mm in diameter with an error less than 6%. Volumetric sensitivity of the same measurement was 1206 cps/MBq. MR subsystem S/N ratio was 784/mm3 before the integration. With working SPECT electronics within the combined system this ratio was 732/mm3. Conclusions: The nanoScan® imaging system fulfils the aim of increased sensitivity and soft tissue contrast for truely dynamic SPECT/MR imaging. There is practically no cross-talk of modalities. The sequential Mediso nanoScan® SPECT/MR system presented here is a novel solution with high SPECT resolution, increased sensitivity and molecular MR imaging in the same animal. General purpose mouse whole-body images can be acquired with less artifacts more dynamic quantitation, and a valuable increase in internal radiation dosimetry from MR volumetric data. Research support: Mediso Ltd.

Disclosure of author financial interest or relationships:
**D. Mathe**, CROmed Ltd, Stockholder; Mediso Ltd., Consultant; CROmed Ltd, Employment; **G. Nemeth**, Mediso Ltd., Employment; **I. Bagaméry**, Mediso Ltd, Stockholder .

Presentation Number **P360**
Poster Session 2
September 6, 2012 / 15:15-15:15 / Room: The Liffey

# Physical and User Evaluation of a Small Animal PET/MR System

***Kalman L. Nagy***[1], *Jenny Häggkvist*[1], *Miklós Tóth*[1], *Péter Major*[2], *Gergely Patay*[2], *Domokos Mathe*[3], *Judit Lantos*[2], *Christer Halldin*[1], *Balázs Gulyás*[1], [1]*Dept. Clinical Neuroscience, Karolinska Institutet, Stockholm, Sweden;* [2]*Mediso Ltd, Budapest, Hungary;* [3]*CROmed ltd., Budapest, Hungary. Contact e-mail: kalmanagy@gmail.com*

Objectives: PET/MRI has numerous advantages for preclinical imaging over PET/CT, including the high soft tissue contrast in brain imaging and the absence of radiation dose in longitudinal and cancer studies. On the other hand, MRI scans usually take longer time than CT scans and they may require special equipment and procedures. Hence the practical utility of a PET/MR system is important to assess. We tested the first Mediso nanoScan® PET/MRI a compact sequential PET/MRI system, evaluating both standardized image parameters and practical workflow. Methods: The PET detector utilizes pixelated LYSO crystal matrices and position sensitive photomultiplier tubes. The PET field of view (FOV) is 94.75 mm axially and 120 mm in the trans-axial direction while the MR FOV is 100 mm axially and 35 or 60 mm in diameter depending on the RF coil used. The MRI component is based on a 1 tesla vertical field permanent magnet (Aspect Imaging, M2). Very low fringe field of the magnet allowed for tight integration of the PET and the MRI subunits. Distance between the center of the PET and the MRI FOV is only 31.4 cm. PET performance of the scanner was assessed using the NEMA NU-4 standard. Results were compared to performance tests reported in the literature for pre-clinical PET scanners. The NEMA tests for MRI do not form such a well established benchmark as those for PET thus MR performance is presented through animal scans. The system was used in several brain imaging studies in rodents and a total of over 100 PET/MRI scans were performed to date including both dynamic and static acquisitions. Observations about practical usage of the scanner are summarized. Results: Peak absolute sensitivity of the PET is 8.4%, the second highest on the market. Spatial resolution measured according to the standard is unequalled and 0.8 mm rods in a micro Derenzo phantom scan were clearly resolved using 3D MLEM reconstruction. Peak noise equivalent count rates are 406 and 120 kcps for mouse and rat like phantoms, respectively. Magnet homogeneity is better than +/- 1 ppm in 25 mm diameter spherical volume (DSV) and better than +/- 3.3 ppm in 50 mm DSV. Stability of the magnet allowed for acquisitions exceeding 20 minutes without interleaved calibrations. A 3D MRI scout image of a 6 cm axial region, suitable for basic attenuation correction, together with shimming and all pre-scan calibrations was acquired in 4.5 minutes. High resolution T2 weighted 3D fast spin echo scans of the rat brain were obtained in 20 minutes and T1 weighted steady state scan of the same region and resolution was completed in 10 minutes. Monitoring body temperature and respiration assisted in maintaining safe anesthesia and successful longitudinal animal studies. Conclusions: We found sequential PET/MRI a feasible and very attractive alternative to PET/CT with special regard to brain studies. PET image quality of the nanoScan® PET/MR excels among preclinical PET scanners. Thanks to the low fringe field and the internal RF shielding of the instrument its operation requires no special tools or precautions. Usability and workflow efficiency of the system are comparable to that of a combined PET/CT system.

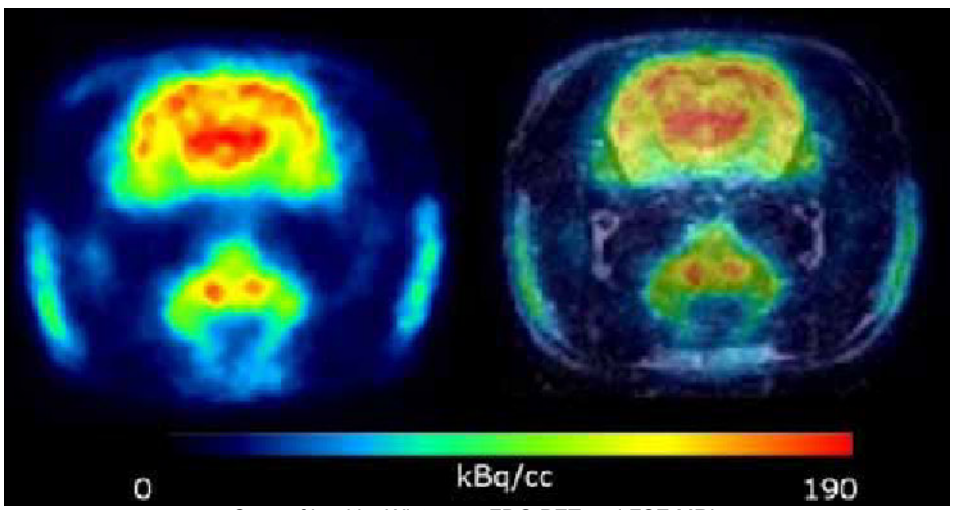

Scan of healthy Wistar rat: FDG PET and FSE MRI.

Disclosure of author financial interest or relationships:
**K.L. Nagy**, Mediso Medical Imaging, Consultant; **J. Häggkvist**, None; **M. Tóth**, None; **P. Major**, Mediso Ltd., Employment; **G. Patay**, Mediso Ltd., Employment; **D. Mathe**, CROmed Ltd, Stockholder; Mediso Ltd., Consultant; CROmed Ltd, Employment; **J. Lantos**, Mediso Ltd., Employment; **C. Halldin**, None; **B. Gulyás**, None.

Presentation Number **P361**
Poster Session 2
September 6, 2012 / 15:15-15:15 / Room: The Liffey

# Whole Body Murine Organ Segmentation Using microCT and Advanced 3D Level Set Algorithms

***Dustin Osborne***[1,2], *Deniz Aykac*[3], *Shaun Gleason*[3], *Ryan Kerekes*[3], *Jonathan S. Wall*[1], *Jens Gregor*[4], *Vincent Paquit*[3], [1]*Graduate School of Medicine, University of Tennessee, Knoxville, TN, USA;* [2]*Preclinical, Siemens Medical Solutions, Knoxville, TN, USA;* [3]*Imaging, Signals, and Machine Learning group, Oak Ridge National Labs, Oak Ridge, TN, USA;* [4]*Computer Science, University of Tennessee, Knoxville, TN, USA. Contact e-mail: dosborne@utk.edu*

Introduction: Whole body segmentation of murine models using CT data is critical for accurate analysis of organ volumes and for accurate segmentation of regions of interest that can be passed to PET or SPECT data for use in comparing imaging results with biodistribution data. Previous work in this field examined a 2D segmentation routine with a level set implmentation using the "active contours without eges" method. This work focused on segmentation of the spleen and worked by segmenting the data slice by slice to create a 3D region of interest from the 2D segments. This work examines the development of an original 3D implementation of a level set algorithm for use in segmentation of critical organs in rodents that can be used in biodistribution comparisons. The organs segmented for this preliminary work were the heart, lung and kidneys. Methodology: CT data were acquired using wild type mice and standard CT protocols of 80 kVp and 0.5 mA. For each dataset, 220-360 projections were acquired over 220-360 degrees with each dataset sampled at 1 projection per degree of rotation. Each of the animals were injected with contrast either peritoneally with Iohexol or via tail vein injection with Fenestra VC. All scans for this preliminary study were performed post-mortem with the mice sacrificed after sufficient distribution of the tracer. Organ segmentation was performed using an original semi-automated 3D level sets implementation, characterized by 3D formulations of finite difference scheme, grayscale statistical weighting, and proximity weighting. Starting from seed points manually selected in the middle of the organ (to improve speed and accuracy) our level sets segmentation algorithm iteratively clusters voxels together until a stable contour corresponding to the organ envelop is found. The attached figure shows the initial segmentation results for heart (red), left lung (yellow), left kidney (blue) and right kidney (green). Region of interest statistics were then calculated for the segmented volumes. Results & Conclusions The initial results show that this algorithm is robust enough to handle a wide variety of imaging conditions and organs within a rodent subject. The segmentation results shown in the image show clear segmentaiton of the selected organs and provide the initial confirmation needed to continue development on this algorithm for increasing segmentation quality and accuracy. Region of interest statistics for the segmented volumes are indicated in the included table.

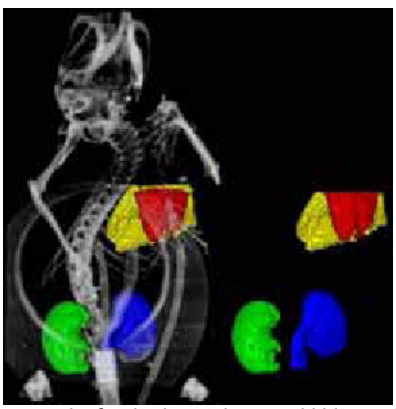

The attached figure shows the preliminary segmentation results for the heart, lung and kidneys. The image on the left shows the regions overlayed on the CT data with the right hand side showing only the segmented regions of interest.

Region of Interest Statistics

| | X-Dim (mm) | Y-Dim (mm) | Z-Dim (mm) | Volume (cc) |
|---|---|---|---|---|
| lung | 9.350 | 12.404 | 9.057 | 0.210 |
| Heart | 7.656 | 7.705 | 6.544 | 0.105 |
| Left Kidney | 5.195 | 7.271 | 10.391 | 0.131 |
| Right Kidney | 5.297 | 6.348 | 9.350 | 0.148 |

Disclosure of author financial interest or relationships:
**D. Osborne**, University of Tennessee, Employment; Siemens Medical Solutions, Employment; **D. Aykac**, None; **S. Gleason**, None; **R. Kerekes**, None; **J.S. Wall**, Elan, Grant/research support; Solex LLC, Stockholder; **J. Gregor**, None; **V. Paquit**, None.

Presentation Number **P362**
Poster Session 2
September 6, 2012 / 15:15-15:15 / Room: The Liffey

# Quantitative, simultaneous PET/MRI for intra-tumoral imaging using MR-compatible PET scanner

*Thomas S. Ng[1], James Bading[2], Ryan Park[3], Hargun S. Grewal[1], **Daniele Procissi**[1,4], David Colcher[2], Peter S. Conti[3], Simon R. Cherry[5], Andrew Raubitschek[2], Russell Jacobs[1], [1]Beckman Institute, Caltech, Pasadena, CA, USA; [2]Cancer Immunotherapeutics& Tumor Immunology, Beckman Research Institute at City of Hope, Duarte, CA, USA; [3]Molecular Imaging Center, USC Keck School of Medicine, Los Angeles, CA, USA; [4]Radiology, Northwestern University, Chicago, IL, USA; [5]Biomedical Engineering, UC Davis, Davis, CA, USA. Contact e-mail: d-procissi@northwestern.edu*

INTRODUCTION : Hybrid PET/MRI technology is progressively being developed for small-animal and clinical use and has the advantage of providing MR images that are spatially and temporally coincident with the simultaneously acquired PET images. The potential to monitor subtle changes in tumor microenvironment using combined functional MRI and PET lies in the ability to quantitatively characterize intra-tissue heterogeneity using multiple parameters. While several efforts have been devoted to developing and validating the new technology only a few have focused on the issue of quantitative and spatial fidelity of simultaneous PET/MRI images. Here, we systematically evaluated the ability of a small-animal MR-compatible PET scanner to accurately depict heterogeneous patterns of radiotracer uptake in tumors using complementary techniques including a commercial microPET scanner. METHODS : Quantitative imaging characteristics of the MR-compatible PET ("PET/MRI") scanner were evaluated with phantoms using calibration coefficients derived from a mouse-sized linearity phantom. PET imaging performance was compared to a commercial small-animal PET system (microPET R4) and autoradiography in tumor-bearing mice. Pixel and structure-based similarity metrics were used to evaluate image concordance among modalities. Feasibility of simultaneous PET/MRI functional imaging of tumors was explored by following 64Cu-labeled antibody uptake in relation to diffusion-MRI using co-occurrence matrix analysis. RESULTS : The PET/MRI scanner showed stable and linear response. Activity concentration recovery values (measured/true activity concentration) calculated for 4 mm diameter rods within linearity and uniform activity rod phantoms were near unity ((0.97±0.06) and (1.03±0.03) respectively). Intra-tumoral uptake patterns for both 18F-FDG and a 64Cu-antibody acquired using the PET/MRI scanner and microPET were highly correlated with autoradiography ($r > 0.99$) and with each other ($r = 0.97±0.01$) (Figure 1). Based on this, we performed a preliminary study comparing diffusion-MRI and radiolabeled antibody uptake patterns over time and visualized movement of antibodies from the vascular space into the tumor mass. CONCLUSIONS : The MR-compatible PET scanner provided tumor images that were quantitatively accurate and spatially concordant with autoradiography and the microPET R4. Co-occurrence matrix approaches enabled effective analysis of multimodal image sets. These observations confirm the ability of the current simultaneous PET/MRI system to provide accurate observations of intra-tumoral function and serve as a benchmark for future evaluations of hybrid instrumentation.

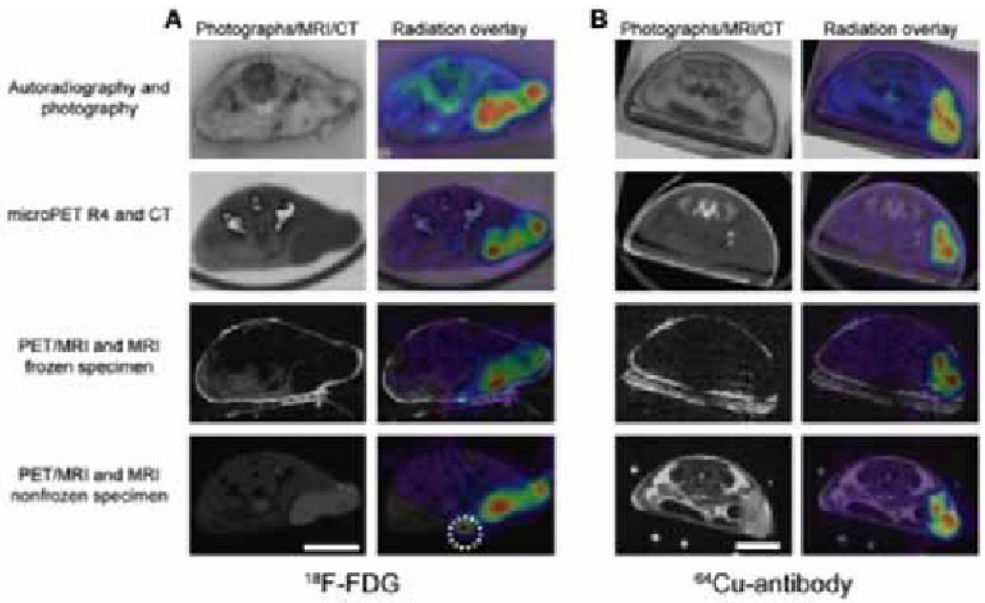


Figure 1: Image pattern comparison between different modalities of the same tissue show congruence of radioactive patterns.

Disclosure of author financial interest or relationships:
**T.S. Ng**, None; **J. Bading**, None; **R. Park**, None; **H.S. Grewal**, None; **D. Procissi**, None; **D. Colcher**, ImaginAb, Grant/research support; UCLA, Grant/research support; **P.S. Conti**, None; **S.R. Cherry**, GE Healthcare, Grant/research support; Radiation Monitoring Devices Inc., Grant/research support; Siemens Molecular Imaging, Honoraria; **A. Raubitschek**, None; **R. Jacobs**, None.

Presentation Number **P363**
Poster Session 2
September 6, 2012 / 15:15-15:15 / Room: The Liffey

# Simultaneous Breast MR-PET - Practical considerations and initial in-vivo human results

*Spencer L. Bowen[2], **Ravi T. Seethamraju**[1], HImanshu Bhat[1], Alexander R. Guimaraes[2], Ciprian Catana[2], [1]MR R&D, Siemens Medical Solutions, USA Inc., Boston, MA, USA; [2]Radiology, Massachusetts General Hospital, Charlestown, MA, USA. Contact e-mail: ravi.seethamraju@siemens.com*

Aim: To conduct a feasibility study for simultaneous Breast MR-PET imaging on an integrated whole body MR-PET scanner in a routine clinical setting. Background: Current studies [1,2] suggest that combining information from PET or PEM with MR has higher diagnostic specificity for breast cancer over MR alone. The advent of whole body integrated MR-PET scanners has opened up the possibility of combining Breast MR with PET imaging for tumor evaluation in a single scan setting. MR provides good soft tissue contrast, morphology and contrast kinetics when compared to CT and with the current concerns with CT radiation, MR is a better alternative. Methods: Healthy IRB approved female subjects were injected with FDG and scanned in a Biograph mMR MR-PET scanner (Siemens healthcare) in a prone position with the breasts hanging freely in a 4 channel open breast array MR coil (Invivo). PET was acquired at a single bed position (12 minute acquisition) simultaneously with MR. For this initial study no MR contrast was administered and the following routine MR sequences were obtained bilaterally: Axial T2 2D TSE, Axial T1 2D FLASH and 3D VIBE. For attenuation correction of the subject an additional VIBE DIXON scan was obtained [3] with the FOV adjusted to fully cover both the breasts and torso. The attenuation map of the breast coil was estimated from a CT scan via a bilinear mapping of Hounsfield units to linear attenuation coefficients at 511 keV followed by an affine registration to the PET frame of reference. PET images were reconstructed with an OP-OSEM algorithm [4] with corrections applied for scatter, randoms, dead-time, tracer decay and attenuation due to the breast coil and the subject. Results and conclusion: The initial results with this configuration have provided clinically relevant breast MR images with qualitatively accurate registration between the modalities (fig 1.). Additional studies with patients with known pathology are envisaged to establish or improve the current configuration. 1. Linda Moy, et.al., J Nucl Med 2007; 48:528-537 2. Andrei Iagaru, et.al., Annals of Nuclear Medicine Vol. 21, No. 1, 33-38, 2007 3. Matthias Eiber, et.al., Eur J Nucl Med Mol Imaging (2011) 38:1691-1701 4. Andrea Varrone, et.al. Eur J Nucl Med Mol Imaging (2009) 36:1639-1650

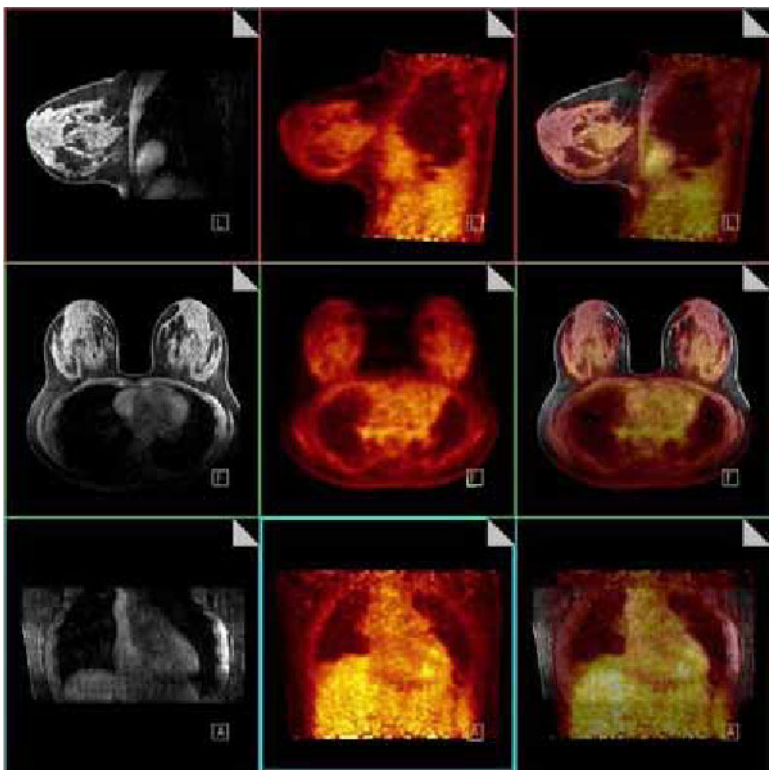

Co-registered MR-PET images from the whole body MR-PET scanner. Left column MR, middle column PET and fused images on the right

Disclosure of author financial interest or relationships:
**S.L. Bowen**, None; **R.T. Seethamraju**, Siemens Medical Solutions, USA Inc., Employment; **H. Bhat**, Siemens Medical Solutions USA Inc, Employment; **A.R. Guimaraes**, None; **C. Catana**, None.

Presentation Number **P364**
Poster Session 2
September 6, 2012 / 15:15-15:15 / Room: The Liffey

# Preclinical Imaging Certification Program

***David Stout**, M&M Pharmacology, UCLA Crump Institute, Los Angeles, CA, USA. Contact e-mail: dstout@mednet.ucla.edu*

Introduction: Over that past decade there has been astounding growth of preclinical imaging methods and equipment suitable for in vivo investigation of metabolism; however expertise and personnel to operate these systems has not kept pace. As systems become easier to use and more automated, users of these systems has shifted from physicists and engineers to biologists and animal care specialists. Training has historically come from labs and companies that developed the technology, or from training programs such as the UC Davis Preclinical Imaging Workshop that was supported by the now cancelled NIH Small Animal Imaging Resource Program (SAIRP). The Society of Nuclear Medicine (SNM) has stepped up to help support this training program, however it is insufficient to train only 20-25 people once per year. Other programs, such as the University of Tubingen in Germany, have seen an overwhelming demand for this labor and time intensive training. There exists a worldwide demand for training, coupled with the need for consistent education regarding imaging and physiological experimental issues. Companies and academic labs also could benefit from an educated labor pool from which to hire educated personnel. Challenges: Holding a workshop is time and labor intensive and is confined to a single location. The increasing range of imaging modalities and few sites that have most of these systems is also a limitation. The crucial hands-on work with animals, radiation and often biosafety agents (tumors) is also a challenge. Proposal: We propose to use the materials presented at the UC Davis and Tubingen workshops as a model for education, consisting of both lectures and hands-on modules. The lectures can be taught in association with conferences where in vivo imaging techniques are presented, including WMIC, SNM, AALAS and IEEE-MIC. This provides a mobile setting enabling people around the world to more easily access training. Knowledgeable people to teach these modules are already likely to be attending these conferences and might be more willing to participate without additional travel demands. Hands-on training using animals must be a separate component, which would be offered at multiple sites that would only need to train based their specific modalities and expertise. For example, a PET-centric site would teach PET, whereas a site focusing on optical might focus on their expertise. After lecture education about imaging modalities and experimental design considerations, the hands-on training would focus on the practical necessities of the process, reducing the time and training requirements. Sites would be encouraged to set up training programs for a fee and offer them a few times per year, based on demand. People taking the program would be certified for the various modules and for the specific modalities which they choose. Contribution: A curriculum meeting is planned for Wednesday June 13 immediately following the preclinical education session at the SNM meeting. If you would like to be a part of this meeting or offer advice on the program, please contact the author or members of the SNM Best Practices in Prelcinical Imaging Task Force.

Disclosure of author financial interest or relationships:
**D. Stout**, Sofie Biosciences, Stockholder .

Presentation Number **P365**
Poster Session 2
September 6, 2012 / 15:15-15:15 / Room: The Liffey

# World's first preclinical 3T PET/MR insert with fully digital silicon photomultiplier technology

***Bjoern Weissler***[1], *Peter Michael Dueppenbecker*[1], *Pierre Gebhardt*[2], *André Salomon*[2], *Benjamin Goldschmidt*[3], *Paul Marsden*[2], *Fabian Kiessling*[3], *Volkmar Schulz*[1,3], [1]*Philips Research, Aachen, Germany;* [2]*King's College, London, United Kingdom;* [3]*RWTH-University, Aachen, Germany. Contact e-mail: bjoern.weissler@philips.com*

**Introduction:** The development of a highly integrated and MRI-compatible PET detector remains as one of the main challenges towards a truly simultaneous PET/MR scanner. Here we present the world's first PET/MR scanner design with fully digital silicon photomultiplier technology (dSiPMs). It is based on the previous insert with analog SiPMs demonstrated by Schulz et al. in [1] and [2]. The new architecture promises outstanding PET performance and increased MRI compatibility as well as improvements in workflow. **Scanner description:** The PET ring is realized by 10 high resolution PET detector modules - each equipped with up to 2x3 digital detector stacks. Every stack scintillates the gammas using 12mm long crystals arranged in a 30x30 array with a 1mm pitch. Through a light guide the crystals are coupled to 4x4 quad dSiPMs placed on detector electronics especially designed for MRI compatibility. The digital detectors offer superior PET performance, which will result in higher spatial resolution and in increased sensitivity (also at higher count rates), while on the other side offer less temperature dependence and lower power consumption with respect to the previously used analog SiPM/ASIC combination [3] [4]. The PET camera covers a cylindrical volume of 216mm x 96mm (transverse diameter x axial dimension) surrounding a PET compatible, easily exchangeable MRI RF-coil. Currently a 46mm PET compatible mouse-Tx/Rx-coil is being developed as the first implementation. In order to enable the full advantage of 4D-simultaneaous PET/MR multiple possibilities to synchronize the two modalities up to direct connection to the MR scanner hardware were implemented. The insert is prepared to interface different animal environment systems. **PET/MR compatibility:** Main challenge of the project is still, that the MR components inside the PET detector have to be transparent for the gammas, while the PET system itself with its 71 FPGAs and its 3840 purely digital dSIPM detectors should not influence the MRI scanner. To accomplish this, a lot of new measures were taken: B0 distortion of almost all system-components will be very low as specially manufactured components are used. Data transfer and synchronization of the PET detector modules will be done only by specially engineered optical transceivers. Eddy currents in the RF-screen of the PET detector will be reduced by new carbon fiber housings. Furthermore important is the power supply concept that allowed the usage of only one EN60601 approved power supply for the insert. **Results:** The novel fully digital PET/MR scanner design will be presented in detail and initial results with a sparsely equipped insert regarding MR-compatibility and PET performance will be shown on the conference. **References:** [1]: Schulz et al. WMIC-2011, T119 [2]: Schulz et al. NSS-MIC-2011, J2-5 [3]: Dueppenbecker et al. NSS-MIC-2011, J1-3 [4]: Degenhardt et al. NSS-MIC-2009, J04-1

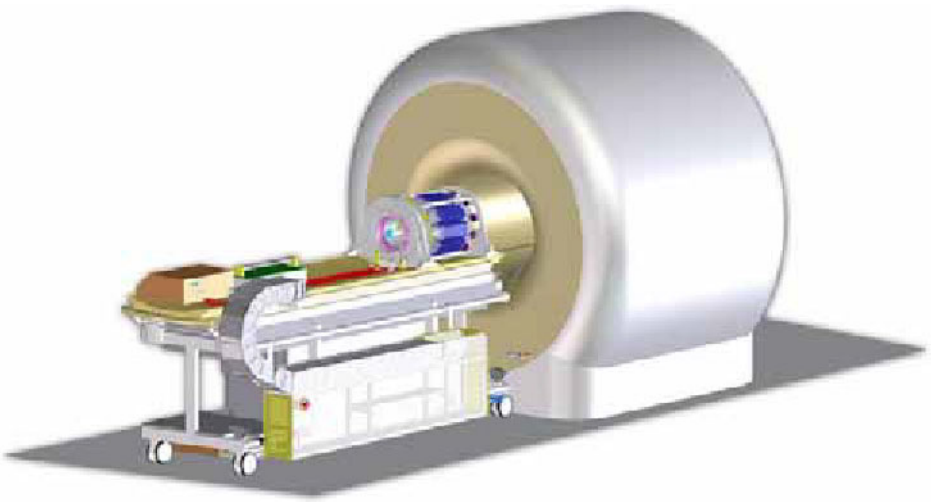

Workflow improvement: The insert is mounted on a trolley and can be rolled in front of the Philips 3T Achieva MRI scanner, where the patient table picks it up. Only one power cord, cooling and a single cable for data transport - coming from a 19" cabinet permanently installed in the technical room - have to be connected.

Disclosure of author financial interest or relationships:
**B. Weissler**, Philips Technologie GmbH Innovative Technologies, Employment; **P. Dueppenbecker**, Philips Research, Employment; **P. Gebhardt**, None; **A. Salomon**, None; **B. Goldschmidt**, None; **P. Marsden**, None; **F. Kiessling**, None; **V. Schulz**, Philips Research, Employment .

Presentation Number **P366**
Poster Session 2
September 6, 2012 / 15:15-15:15 / Room: The Liffey

# Multimodal image registration with normalized mutual information based on Kullback-Leiber distance

***Jung Woo Yu***[1,2], *Sang-Keun Woo*[1], *Nam Gyu Kwon*[1], *Yong hyun Chung*[2], *Jong Guk Kim*[1], *Ji-Ae Park*[1], *Joo Hyun Kang*[1], *Byung Il Kim*[1], *Sang Moo Lim*[1], *Kyeong Min Kim*[1], [1]*Molecular Imaging Research Center, KIRAMS, Seoul, Republic of Korea;* [2]*Department of Radiological Science, Yonsei University, Wonju, Republic of Korea. Contact e-mail: silvermare@yonsei.ac.kr*

Registration of small animal multimodal image is necessary to accurately evaluate diagnostic and therapeutic effect in preclinical phases. The aim of this study was to improve registration efficiency through normalized mutual information (NMI) based on assessment of Kullback-Leiber distance (KLD) between small animal PET and CT/MRI image. The PET/CT imaging studies were performed with a dedicated small animal PET/CT scanner (Inveon). PET imaging was started 60 min post injection of $^{18}$F-FDG via tail vein. List mode data was reconstructed using OSEM 2D algorithm after converting sinogram using FORE. The CT images were acquired with following settings: X-ray Voltage=70 kVp, Anode Current=400 μA, Exposure Time=200 ms. The MRI images were obtained with the diagnostic 3T-MRI (MAGNETOM) followed by T1-weighted VIBE sequence: Repetition Time=11.6 ms, Echo Time=3.1 ms, Flip Angle=10 degree. Registration was executed by NMI algorithm with calculation of KLD between PET and CT/MRI image. NMI was carried out by trilinear interpolation with 42 separations. KLD was calculated iteratively between pixel to pixel by analyzing and sampling at the ideal distribution using following formula: $D(P \parallel Q) = \Sigma P(x) \ln P(x) / Q(x)$. Registration efficiency was compared by the $R^2$ (correlation coefficient) and KLD between images evaluated with regression analysis before and after warping. Dimension of PET image was 128×128×164 and voxel size was 0.78×0.78×0.78 mm. Dimension of CT image was 352×352×564 and voxel size was 0.23×0.23×0.23 mm. Dimension of MR image was 682×694×679 and voxel size was 0.31×0.31×0.31 mm. The KLD between PET and CT was $9.45\times10^4$ and between PET and MRI was $4.66\times10^6$ before registration. After registration between PET and CT without warping, $R^2$ was 0.233 and KLD was 564.55. After registration between PET and CT with warping, $R^2$ was 0.233 and KLD was $1.57\times10^6$. After registration between PET and MRI without warping, $R^2$ was 0.236 and KLD was 124.45. After registration between PET and MRI with warping, $R^2$ was 0.272 and KLD was 127.52. We confirmed that correlation coefficient was improved in registration with warping between PET and CT/MRI. Multimodal image registration method should be adapted the algorithm considering the image characteristic.

Disclosure of author financial interest or relationships:
**J. Yu**, None; **S. Woo**, None; **N. Kwon**, None; **Y. Chung**, None; **J. Kim**, None; **J. Park**, None; **J. Kang**, None; **B. Kim**, None; **S. Lim**, None; **K. Kim**, None.

Presentation Number **P367**
Poster Session 2
September 6, 2012 / 15:15-15:15 / Room: The Liffey

# Cryo-imaging as a quantitative pre-clinical method to determine the amount and spatial distribution of drugs in lung tissue: A feasibility study

*Friedrich Prade[1], Nikolaos C. Deliolanis[3], Katie Dextraze[1], **Nirav Barapatre**[1], Vasilis Ntziachristos[3], Oliver Eickelberg[1,2], Otmar Schmid[1], [1]Comprehensive Pneumology Center, Institute of Lung Biology and Disease, Helmholtz Zentrum München, Neuherberg, Germany; [2]Comprehensive Pneumology Center, Institute of Experimental Pneumology, Klinikum der Universität München, Munich, Germany; [3]Institute of Biological and Medical Imaging, Helmholtz Zentrum München, Neuherberg, Germany. Contact e-mail: nirav.barapatre@helmholtz-muenchen.de*

One of the key therapeutic approaches in the lung diseases is the delivery of drugs directly to lungs through its airways. The efficacy of drugs will depend on the amount of the drug and the location of its deposition. Hence, the quantification of drug amount and its spatial distribution in lungs are indispensable factors in the validation of any drug in pre-clinical research. Optical microscopy is, in general, the method of choice for determining drug dose and distribution in biological experiments, because in vivo experiments can be performed with it. However, the biological tissue interacts strongly with the visible light. Due to absorption and scattering of the light, the quantification and mapping of the drug dose becomes increasingly difficult. We, therefore, use Cryo-Imaging (Steyer et al, 2009) as the experimental method for determining the factors like, attenuation coefficient of the lung tissue and as a validation tool for the drug dose and distribution. Cryo-Imaging involves imaging and slicing of the specimen in an alternate manner. It requires a conventional cryomicrotome to be fitted with an imaging unit capable of recording bioluminescent or fluorescent signal at multiple wavelengths. The specimen block is first imaged then sliced by a defined thickness. This procedure is repeated until the whole specimen is recorded (Sarantopoulos et al, 2011). Since each block face image also contains the fluorescent signal from the bulk of the specimen due to scattering effects, the net fluorescence per slice is derived by mathematically correcting for the bulk effects. The corrected individual slices are stacked together to reconstruct a 3D distribution of the fluorophore. The sum of the net fluorescence from all the slices gives the total amount of fluorophore present in the specimen. The advantage of this method lies in its ability to obtain images with high spatial resolution and high sensitivity for the fluorescent signal. A known amount of fluorescent polystyrene particles (ø450nm, excitation @ 680nm; emission @ 710nm) was instilled intratracheally to the lungs of a mouse. It was sacrificed immediately after the application of the fluorescent particles. The lungs were removed, fixed in an OCT solution and snap frozen. The frozen block was then cryo-imaged with a slice thickness of 100 µm. A 3D distribution of the fluorophore in the lungs was reconstructed programmatically in MATLAB. Figure 1 shows a single slice of the reconstructed volume. Steyer, G. J., Roy, D., Salvado, O., Stone, M. E. and Wilson, D. L. (2009) Ann. Biomed. Eng. 37, 1613-1628. Sarantopoulos, A., Themelis, G. and Ntziachristos, V. (2011) Mol. Imaging Biol. 13, 874-885.

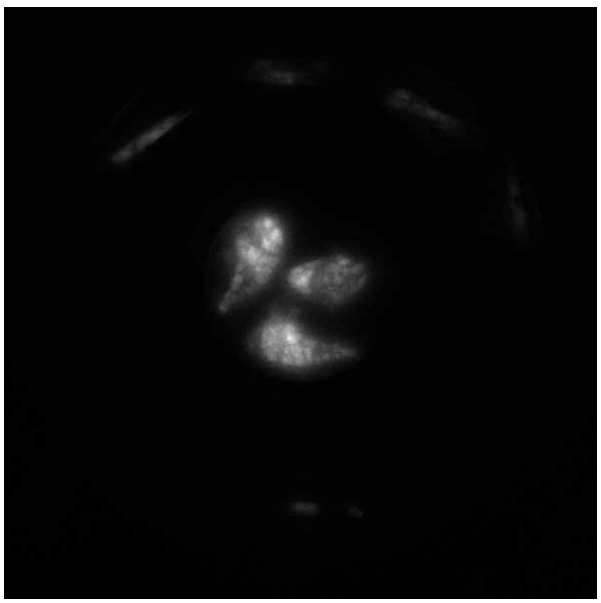

Figure 1. A fluorescent image of lungs taken with the Cryo-Imaging setup. Three lobes of the right lung can be seen distinctly.

Disclosure of author financial interest or relationships:
**F. Prade**, None; **N.C. Deliolanis**, None; **K. Dextraze**, None; **N. Barapatre**, None; **V. Ntziachristos**, ERC, Grant/research support; Ithera Medical, Stockholder; **O. Eickelberg**, None; **O. Schmid**, None.

Presentation Number **P368**
Poster Session 2
September 6, 2012 / 15:15-15:15 / Room: The Liffey

# Receptor-mediated uptake of near infrared-labeled transferrin using FRET tomographic imaging

*Ken Abe[1], Lingling Zhao[2], Xavier Intes[2], **Margarida Barroso**[1], [1]Cardiovasculaar Sciences, Albany Medical College, Albany, NY, USA; [2]Biomedical Engineering, Rensselaer Polytechnic Institute, Troy, NY, USA. Contact e-mail: barrosm@mail.amc.edu*

Transferrin (Tfn) is a well known iron-binding protein, which is responsible for carrying iron into the cells via its binding to the transferrin receptor (TFR). Moreover, Tfn has been widely used as carrier for anti-cancer drug delivery systems since the TFR is upregulated in tumors. Targeted delivery is an important and promising approach for the development of effective therapy in cancer applications. Here, we report on the use of near-infrared (NIR) FRET tomographic imaging to visualize the receptor-mediated Tfn cellular uptake. We have combined a multispectral time-resolved fluorescence molecular tomography (FMT) imaging with NIR FRET probes to assess quantitatively the receptor-mediated uptake of NIR-iron bound Tfn by monitoring in vivo FRET between NIR-donor-Tfn and NIR-acceptor-Tfn bound to TFR homodimers (Figure 1A). Thus, the reduction in donor lifetime associated with FRET is used as a marker of cellular internalization. To validate NIR FRET FMT imaging of transferrin uptake, we have developed a unique optical imaging platform to perform NIR FRET FMT in cancer cell suspensions and animals pre-injected with a matrigel plug containing cancer cells. As a proof of principle, we have internalized AF700-iron bound Tfn (donor) and AF790-iron bound Tfn into human breast cancer cells that overexpress TFR (T47D). Cell suspensions were imaged using a time-resolved wide-field illumination strategy that allows the acquisition of functional and fluorescence tomographic data sets at high-spatial and high-spectral density (690-1000nm spectral range). The system acquires data in the transmittance geometry, at the excitation and emission wavelengths consecutively thanks to the Liquid Crystal Tunable Filter (LCTF). The time-gated ICCD acquires time-resolved data with a 200ps time gate width and a 20ps time delay to obtain time point spread function (TPSF) over a 3ns time window (150 gates). The system has been thoroughly tested (supplementary information). In this intermolecular NIR FRET assay, the level of donor lifetime reduction can be extended by increasing the relative concentration of quenched vs. non-quenched donors. Higher acceptor:donor (A:D) ratios will result in a higher amount of acceptors available to quench the donor molecules, increasing the potential for FRET events to occur. An example of the % of NIR donor Tfn molecules undergoing FRET (fd) versus A:D ratios, as estimated by our imaging platform, is provided in Figure 1B. We have established that the estimated percentage of donor Tfn molecules undergoing FRET using lifetime measurements retains linearity over the 2:1 to 4:1 A:D ratio range (Figure 1B). These results establish the feasibility of performing NIR FRET FMT to measure Tfn uptake in cancer cells. Our long term goal is to use the NIR FRET FMT imaging modality to measure FRET between NIR-labeled donor and acceptor Tfn-TFR complexes in vivo in live animals bearing breast cancer tumors. FRET-FMT will provide localization and bio-distribution of receptor-mediated uptake of NIR-Tfn for the quantitative detection of the Tfn-based targeted delivery systems for diagnostic and therapeutic use.

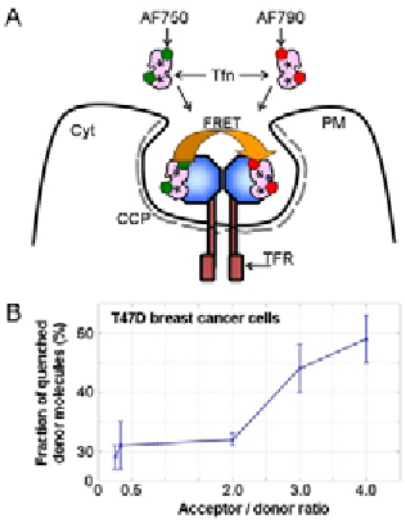


Figure 1. NIR-Tfn FRET system. (A) Two molecules of NIR-labeled Tfn (iron-bound) bind one TFR homodimer at the plasma membrane (PM). TFR-Tfn complexes are internalized into cells via clathrin-coated pits (CCP). Energy transfer (FRET) occurs between AlexaFluor 750-Tfn (AF700-Tfn; donor) and AF790-Tfn (acceptor) upon their binding to the TFR homodimer at the PM. (B) T47D human breast cancer cell suspensions (400,000 cells/well) pre-internalized with different acceptor/donor ratios of AF750-Tfn and AF790-Tfn were imaged using NIR FRET FMT. The estimated fraction of quenched donors (FRETing donors) is shown for different acceptor/donor ratios.

Disclosure of author financial interest or relationships:
**K. Abe**, None; **L. Zhao**, None; **X. Intes**, None; **M. Barroso**, None.

Presentation Number **P369**
Poster Session 2
September 6, 2012 / 15:15-15:15 / Room: The Liffey

# Imaging Rotating Specimens in Optical Projection Tomography

***Udo J. Birk***[1,2], *Jorge Ripoll*[3], [1]*Superresolution Microscopy, Institute of Molecular Biology, Mainz, Germany;* [2]*Kirchhoff Institute for Physics, University Heidelberg, Heidelberg, Germany;* [3]*Institute of Electronic Structure and Laser, Foundation for Research and Technology - Hellas, Iraklio, Greece. Contact e-mail: u.birk@imb-mainz.de*

Optical Projection Tomography (OPT) allows imaging of live samples with sizes from about 1cm down to the microscopic range with scalable resolution. Previous work has shown that correction of specimen movement is crucial for imaging in OPT. So far, correction has been restricted to translational movement and to correct for inaccurate rotation of the specimens during the acquisition, i.e. the object rotation is aligned with the rotation axis used for tomographic imaging (z-axis). However, in order to proceed towards true 3D imaging of live samples, all 6 degrees of freedom (3 translational and 3 rotational) need to be considered in order to facilitate in vivo imaging, of which only 4 have been addressed previously. Here, we present additional means to estimate object rotation perpendicular to the z-axis of the OPT device. This task requires interpolation of the rotation in both x- and y-direction, as a typical OPT data stack consists of projection images missing the depth information which is present in other 3D scanning microscopy approaches. We present a discussion of the requirements under which these interpolation methods can be applied, and show first reconstructed images of samples rotating along both x- and y-axis. The correction methods presented are a major step in imaging of life animals which can be computationally separated into several rigid objects (head, upper torso, legs,…). These rigid bodies can be reconstructed independently, and can then be joined to produce the final 3D image.

Disclosure of author financial interest or relationships:
**U.J. Birk**, None; **J. Ripoll**, None.

Presentation Number **P370**
Poster Session 2
September 6, 2012 / 15:15-15:15 / Room: The Liffey

# Design and characterization of a dedicated small animal Raman imaging instrument

***Sarah Bohndiek***[1], *Ashwin Wagadarikar*[2], *Dominique Van de Sompel*[1], *Ellis Garai*[3], *Cristina Zavaleta*[1], *Siavash Yazdanfar*[2], *Sanjiv S. Gambhir*[1], [1]*Molecular Imaging Program at Stanford, Stanford University, Stanford, CA, USA;* [2]*Applied Optics Lab, GE Global Research, Niskayuna, NY, USA;* [3]*Mechanical Engineering, Stanford University, Stanford, CA, USA. Contact e-mail: bohndiek@stanford.edu*

Introduction: Raman spectroscopy is a powerful analytical tool based on inelastic light scattering. In vivo applications have been limited by the relatively weak Raman effect (~1 per 10 million elastic scatter events) and poor depth of penetration (<1mm). Recently, Surface Enhanced Raman Scattering (SERS) has been shown to overcome these limitations, enabling the use of Raman spectroscopy as a molecular imaging technique. Advantages include high sensitivity, the optical stability of SERS nanoparticles and the ability to multiplex signals. Expansion of this technique is limited by the lack of a dedicated small animal Raman imaging instrument. Existing methods for Raman mapping typically generate images by raster scanning the sample under a laser spot needing long scan times (hours) to image small areas of interest. The solution demonstrated here is a line-scanning system, which uses galvo mirrors to scan the laser line over the animal. This allows a wide field of view (31mm x 25mm) to be imaged in under 30 minutes, without sacrificing sensitivity. Aim: To develop a dedicated small animal Raman instrument for high speed, wide area imaging. Materials and Methods: The system consists of an optical assembly for laser excitation and Raman signal collection (Fig. 1a, b). The 785nm laser (MiniLite, BaySpec) was coupled to external optics using a 105µm multimode fiber. The Raman signal collection was performed with a Czerny-Turner spectrometer (Shamrock 303i, Andor) coupled with an electron-multiplying CCD (Luca 604 EMCCD, Andor). The spectrometer was operated with a wavenumber range of 665 - 1771cm-1. All measurements were performed using a laser power of 290mW. SERS active nanoparticles (S440, Cabot Inc.) consisted of a 60nm diameter gold core covered with a layer of Raman active material and a silica coating. Procedures performed on animals were approved by the University's Institutional Animal Care and Use Committee. Quantitative Raman spectral umixing was performed offline using a modified direct classical least-squares (DCLS) algorithm. Results and Discussion: The spatial resolution of the system (Fig. 1c) was limited by the laser line width and CCD pixel size (250 µm perpendicular, 8 µm parallel to the line). The location and depth of the focal plane was determined by scanning a 5µl aliquot of S440 nanoparticles (100pM) through "z" (Fig. 1d). The spectral resolution was 25cm-1. The maximum imaging depth for SERS nanoparticles was found to be 4mm using a tissue mimicking phantom (Fig. 1e). The four principal components of the signal from a uniform phantom containing 24pM S440 SERS nanoparticles are shown in Fig. 1f. The measured spectral contribution from S440 declined towards the outer edges of the imaging area where the free space signal dominated; the S440 contribution was uniform (within 10%) in an area of 18 mm x 21mm. The limit of detection was found to be 3.1pM. Detection of SERS signal in a living subject was demonstrated by imaging the liver at 1 h after tail-vein injection of S440 nanoparticles (Fig. 1g). In summary, we have built and characterized the first dedicated small animal instrument capable of fast, wide-area Raman imaging.

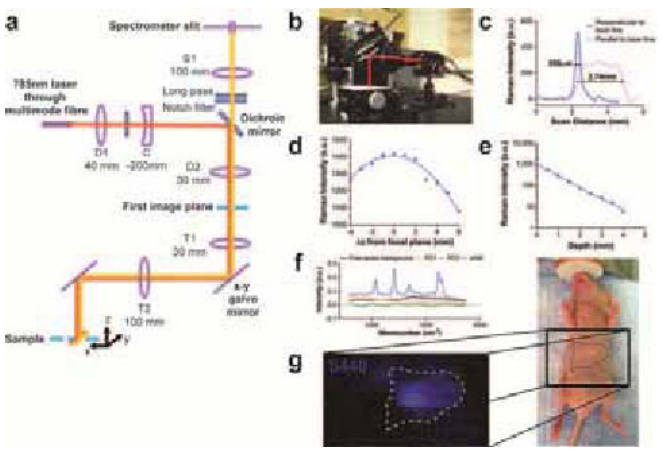


Figure 1: (a) Layout of the optical system. (b) Photograph of the system with light path overlaid in red. (c) Line spread function and associated full width at half maximum parallel (2.74mm) and perpendicular (0.25mm) to laser line (d) Raman scatter intensity from SERS nanoparticles as a function of vertical displacement from the focal plane and (e) depth below tissue equivalent material (f) The four principal components of the Raman scatter intensity from a uniform phantom containing SERS S440 nanoparticles dispersed in agar; spectra offset for clarity. (g) Imaging of the mouse torso at 1 h after tail-vein injection of 0.8nM S440 SERS nanoparticles.

Disclosure of author financial interest or relationships:
**S. Bohndiek**, None; **A. Wagadarikar**, None; **D. Van de Sompel**, None; **E. Garai**, None; **C. Zavaleta**, None; **S. Yazdanfar**, General Electric Company, Employment; General Electric Company, Stockholder; **S.S. Gambhir**, General Electric, Grant/research support; Bayer-Schering, Grant/research support; Sanofi-Aventis, Grant/research support; CellSight, Stockholder; ImaginAB, Stockholder; Enlight, Stockholder; Endra, Stockholder; Bracco, Consultant; NinePoint Medical, Stockholder; Visualsonics, Consultant .

Presentation Number **P371**
Poster Session 2
September 6, 2012 / 15:15-15:15 / Room: The Liffey

# Establishment of dicentric chromosome assay by digital microscopic imaging

***Tsui-Jung Chang***[1], *Ching-Yan Tsai*[1], *Ping-Hung Yu*[1], *Kuei-Fang Lee*[2], *Ingrid Y Liu*[2], *Chih-Hsien Chang*[1], [1]*Isotope Application Division, Institute of Nuclear Energy Research, Taoyuan, Taiwan;* [2]*Molecular Biology and Human Genomics, Tzu Chi University, Hualien, Taiwan. Contact e-mail: tjchang@iner.gov.tw*

Dose estimation is considered to be an important first step in the medical treatment of persons exposed to radiation. Many countries around the world have been making great efforts to develop better capabilities for emergency preparedness nuclear accidents. Dose estimation is considered to be an important first step in the medical treatment of persons exposed to radiation. Methods: Radiation dosimetry was first performed using alanine/EPR dosimetry with US National Institute for Standards and Technology (NIST) standard pellet. The average dose rate to water in the target zone on the day of field mapping was 0.633 Gy/min. The blood samples were irradiated with 0, 0.5, 1, 2, 3, 4 and 5 Gy 60Co gamma rays at room temperature. Dosimetry was further validated with a thermoluminescence dosimeter (TLD). Giemsa staining was used for staining of dicentric chromosome. Dicentric chromosome assay (DCA) was established by automated digital microscopic molecular imaging as a golden standard for biodosimery estimation. Results: DCA was established by microscopic imaging. The data of Alanine/EPR dosimetry showed a high agreement with those by thermoluminescence dosimeter (R2=0.998). The calibration curve for dose-dicentric chromosome frequency effect by 60Co gamma rays was established. Interlaboratory Comparison was also confirmed the results. Conclusions: This study clearly demonstrates the ability of an automated digital microscopic imaging for analysis of chromosome aberration; it enhances the analytic speed and accuracy. It would be very important for emergency preparedness nuclear accidents.

Disclosure of author financial interest or relationships:
**T. Chang**, None; **C. Tsai**, None; **P. Yu**, None; **K. Lee**, None; **I. Liu**, None; **C. Chang**, None.

Presentation Number **P372**
Poster Session 2
September 6, 2012 / 15:15-15:15 / Room: The Liffey

# A miniaturized fluorescence imaging probe for maxillofacial surgery

***Jean-Guillaume Coutard***[1], *Christian A. Righini*[2,3], *Michel Berger*[1], *Sylvain Gioux*[1], *Véronique Josserand*[2], *Michelle Kéramidas*[2], *Jean-Marc Dinten*[1], *Jean-Luc Coll*[2], [1]*DTBS, CEA, Grenoble, France;* [2]*Institut Albert Bonniot, INSERM-UJF, Grenoble, France;* [3]*CHU de Grenoble, Grenoble, France. Contact e-mail: jean-guillaume.coutard@cea.fr*

In recent years near-infrared (NIR) fluorescence imaging has witnessed a very rapid growth particularly in the context of preclinical and clinical surgical guidance. Based on the capability to excite and to collect the fluorescence of a tracer that targets a tissue of interest, it requires both the development of fluorescent contrast agents and intraoperative imaging systems to guide the surgeon. Of particular challenge is the design of a clinically compatible instrument that performs optimally fluorescence imaging while integrating within the clinical workflow. A few parameters of paramount importance are the choice of the proper excitation light for the fluorophore, filtered white light for scene visualization, adequate field of view, optimal light filtration and collection, and ergonomic design. While such instruments are becoming available, their size (usually > 70 mm in diameter), precludes their use during many surgeries. We present here the design of a new imaging system dedicated to maxillofacial surgery. With a diameter of only 22 mm, it does not to obstruct the surgeon's view in addition to be hand held- friendly, while not compromising on fluorescence imaging quality. A novel approach based on the projection of both white light and NIR excitation light through a multimode fiber bundle ensures optimal and efficient illumination. This solution allows the production of a uniform circular spot, overlapping both homogeneous white light and monochromatic light excitation. The use of multiple illumination fibers arranged in a ring permits the delivery of a high power density of NIR laser light while being safe (class 1 laser). Thanks to an excitation at 740 nm and a broad emission collection, this imaging system can work optimally with a wide range of 800 nm fluorophores. Finally all illumination components have been integrated in together with a 17 mm circular consumer-grade monochrome CCD camera and a cylindrical housing for a diameter less than 1 inch.We evaluated the performance of our imaging system during pre-clinical experiments on mice with peritoneal carcinomatosis injected with 10 nmol of Angiostamp® (Fluoptics). The results showed that the probe can detect fluorescence in cancerous tissue with efficiency similar to existing larger size systems while dramatically reducing size, complexity and cost. Overall, the system has a 80 microns resolution, a 40 x 30 mm2 field-of-view, and is capable of a shining 100 µW/mm2 of NIR light and 1000 lux of white light. This preclinical evaluation opens the gate to the translation of this new imaging device to clinics.

Disclosure of author financial interest or relationships:
**J. Coutard**, None; **C.A. Righini**, None; **M. Berger**, None; **S. Gioux**, None; **V. Josserand**, None; **M. Kéramidas**, None; **J. Dinten**, None; **J. Coll**, None.

Presentation Number **P373**
Poster Session 2
September 6, 2012 / 15:15-15:15 / Room: The Liffey

# Multiple view fluorescence optical tomography with virtual structured light

*Nicolas Ducros[1], Andrea Bassi[1], Gianluca Valentini[1], Martin Schweiger[2], Simon Arridge[2], **Cosimo D'Andrea**[1], [1]Dept.Physics, Politecnico di Milano, Milano, Italy; [2]Centre for Medical Image Computing, University College London, London, United Kingdom. Contact e-mail: cosimo.dandrea@polimi.it*

Fluorescence Mediated Tomography (FMT) is an emerging 3D optical imaging technique that aims at localizing and quantifying in vivo molecular specimens targeted by selective fluorescent markers. Generally, FMT consists of raster scanning a point source on the sample surface and acquiring (e.g by a CCD) the fluorescence light exiting the sample for each position of the illumination spot. Moreover, multiple views of the sample are acquired to improve the spatial resolution. By applying inverse algorithms on the whole data set, the fluorochome distribution inside the sample can be reconstructed. In order to obtain a good reconstruction quality, the acquisition of a large data set is necessary, which leads to long acquisition and reconstruction times. Both aspects set significant limitations for the in vivo application of FMT. Recently, a huge effort has been devoted to the reduction of the data set, while preserving the reconstruction quality. This leads, to a strong shrinkage of the amount of data that must be acquired and input in the reconstruction algorithm needed to solve the inverse problem. This full compression approach is achieved by acting on both the illumination and detection side. In the first case, only few well chosen patterns of structured light, are retained, which reduces both acquisition and reconstruction times. Concerning the detection side, data compression of the fluorescence images is performed by selecting few spatial components (e.g. in Fourier or Wavelets basis). Here the advantage is limited to the reduction of the computational time because the CCD is intrinsically parallel in detection. It is worth noting that in both cases the data set reduction originates from the fundamental observation that biological tissue behaves as a low pass filter in the spatial domain. Recently, we have experimentally demonstrated the effectiveness of a multiple-view full compression tomographic approach on cylindrical phantoms mimicking biological tissues with fluorescent inclusions[1]. In the reconstruction procedure, the propagation of the optical field in turbid media was modelled by the TOAST package. In the present work, we further exploit this new tomographic approach to more complex geometries. This represents a fundamental step towards its application to animal models. The whole tomographic procedure (experimental and reconstruction) will be described. In particular, we will discuss the choice of the source patterns and the effect of compression on the acquisition/reconstruction times. Different types of source patterns will be compared. A novel method, namely the virtual source patterns, will be introduced to consider any kind of patterns, e.g., patterns with negative and complex amplitude, in order to alleviate the problem of the intrinsic positivity of light beams. Moreover, we will describe the experimental procedure to make a wide field structured light pattern compatible with a non symmetric rotating object. Preliminary reconstructions on animal model will be also shown. References 1. N. Ducros, A. Bassi, G. Valentini, M. Schweiger, S. Arridge, and C. D'Andrea, Opt. Lett., 36(8):1377-1379 (2011)

Disclosure of author financial interest or relationships:
**N. Ducros**, None; **A. Bassi**, None; **G. Valentini**, None; **M. Schweiger**, None; **S. Arridge**, None; **C. D'Andrea**, None.

Presentation Number **P374**
Poster Session 2
September 6, 2012 / 15:15-15:15 / Room: The Liffey

# An automated rotational center location method for Optical Projection Tomography

***Di Dong***[1], *Shouping Zhu*[2], *Chenghu Qin*[1], *Varsha Kumar*[3], *Jens Stein*[3], *Stefan Oehler*[4], *Charalambos Savakis*[4], *Jie Tian*[1], *Jorge Ripoll*[5], [1]*Medical Image Processing Group, Institute of Automation,CAS, "Beijing,100190", China;* [2]*School of Life Science and Technology, Xidian University, Xian, China;* [3]*Theodor Kocher Institute, University of Bern, Bern, Switzerland;* [4]*B.S.R.C. Alexander Fleming, Varkiza, Greece;* [5]*Institute of Electronic Structure and Laser, Foundation for Research and Technology-Hellas (FORTH), Heraklion, Greece. Contact e-mail: dongdi@fingerpass.net.cn*

Abstract: Rotational center location is important for highly precise optical projection tomography (OPT). In an OPT setup developed at FORTH, frequent changes of center of rotation (COR) often happen since the experimental geometry changes regularly. However, current methods are not convenient in frequent centering experiments because these methods require either prior scanning of other phantom, or special structures existing in the specimen, or direct participation during the centering. The variance method for example, consists of searching for the center position by reconstructing the same slice several times with different offset values, and then choosing the optimum offset value using the variance of the reconstructed slice. However, this method needs a manual selection of COR search region which is inconvenient. A center-of-mass based method has been introduced in Computed Tomography (CT) applications, which can automatically find the rotational center with good accuracy. Unfortunately the out-of-focus problems, scattering, and noise in OPT make the center-of-mass method invalid. To solve these problems, a coarse-fine centering method is proposed, which includes two steps shown in Fig. 1: a preliminary location based on projection of the center-of-mass and then a detailed center search based on variances of a set of reconstructed images. Through the two steps our method can automatically locate the COR without prior scanning. Experimental results show that our COR location is effective both for in vivo and ex vivo OPT data with a displaced COR.

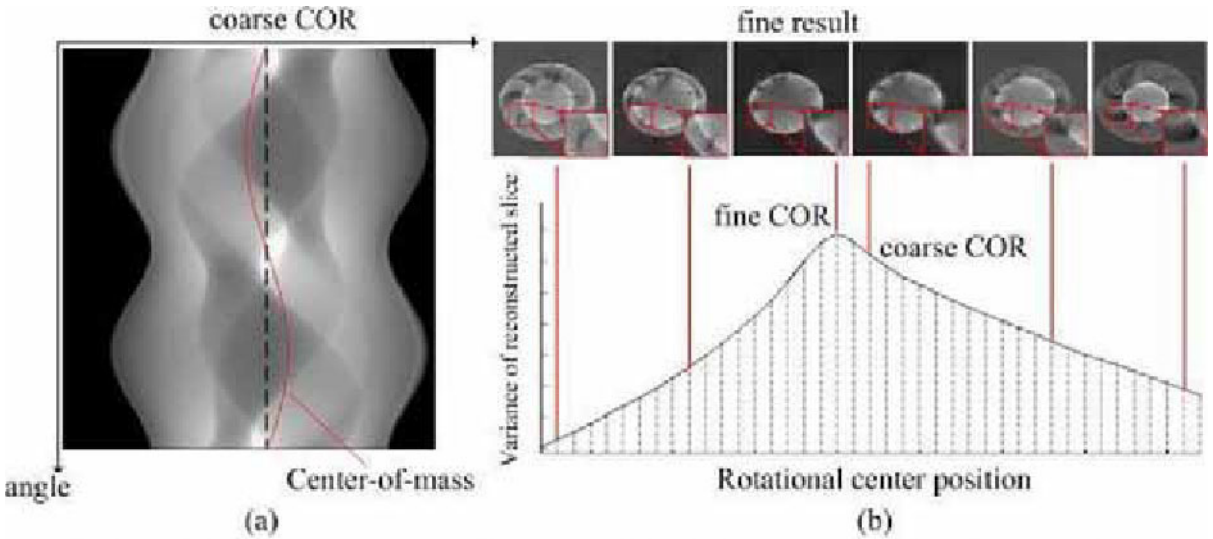


Fig. 1. Scheme of coarse-fine COR location. (a) coarse search with center-of-mass method. (b) fine search around coarse result with variance method.

Disclosure of author financial interest or relationships:
**D. Dong**, None; **S. Zhu**, None; **C. Qin**, None; **V. Kumar**, None; **J. Stein**, None; **S. Oehler**, None; **C. Savakis**, None; **J. Tian**, None; **J. Ripoll**, None.

Presentation Number **P375**
Poster Session 2
September 6, 2012 / 15:15-15:15 / Room: The Liffey

# Development of Intensity Spatial Distribution Based on the Green's function In New Fluorescence Molecular Tomography Imaging System

*Toktam Jahanfar[1,2], **Marjaneh Hejazi**[1,2], Amir Homaun Jafari[1,2], Sima Saleh[1,2], Hanieh Mohammadreza[1,2], [1]Medical Physics and Bioengineering, , Tehran, Islamic Republic of Iran; [2]Medical Physics And Bioengineering, Tehran University of Medical sciences, Tehran, Islamic Republic of Iran. Contact e-mail: mhejazi@sina.tums.ac.ir*

Fluorescence molecular tomography (FMT) is an emerging functional imaging modality and it widely used in biological research, drug discovery, and clinical practice. In this modality an analytic and computable model of the propagation of radiation in tissue is essential for meaningful interpretation of the biological processes. The analytic method includes a forward and a reconstruction algorithm. The forward problem for a given 3D source distribution, seeks to determine the photon density on the surface of a sample which is based on the diffusion approximation. The precise solution of the forward problem is essential for applying a fast image reconstruction in a specific geometrical coordinates. A new FMT imaging system has been designed in a cylindrical geometry. Therefore the aim of this article is to develop a fast forward algorithm using a Green's function for the FMT imaging system. The algorithm is based on diffusion approximation and evaluated by numerical method. The results showed the significant correlation coefficients (R >0.92) with numerical method. We have presented an approximate algorithm based on the Born approximation, that solve the 3D diffusion equation in homogeneous turbid media. The algorithm can be used as part of the reconstruction program using FMT.

Disclosure of author financial interest or relationships:
**T. Jahanfar**, None; **M. Hejazi**, None; **A. Jafari**, None; **S. Saleh**, None; **H. Mohammadreza**, None.

Presentation Number **P376**
Poster Session 2
September 6, 2012 / 15:15-15:15 / Room: The Liffey

# Characterization of Multivalent Targeted Molecular Imaging Probes

***Yolaine Jeune-Smith***[1], *Jatinder S. Josan*[2], *Craig S. Weber*[3], *Ariosto Silva*[1], *Ronald M. Lynch*[3], *Josef Vagner*[4], *Victor J. Hruby*[4], *Robert Gillies*[1], *David L. Morse*[1], [1]*Cancer Imaging and Metabolism, H. Lee Moffitt Cancer Center & Research Institute, Tampa, FL, USA;* [2]*Chemistry and Biochemistry, University of Arizona, Tucson, AZ, USA;* [3]*Physiology, University of Arizona, Tucson, AZ, USA;* [4]*BIO5 Institute, University of Arizona, Tucson, AZ, USA. Contact e-mail: yolaine.smith@moffitt.org*

An emerging theme in the biochemistry of cancer targeting is the use of multiple copies of binding moieties (multivalency) to provide enhanced binding avidity and cooperativity. We have used novel cyclene scaffolds to construct and characterize mono-, bi- and tri-valent targeted fluorescent imaging probes using a high-affinity ligand antagonist of the delta opioid receptor (δOR). The constructs were conjugated to a near infrared fluorescent dye, Cy5. The number and length of the scaffold linker arms were altered to test the effect of these variables. The multivalent constructs were evaluated for binding, tumor selectivity, pharmacokinetics (PK) and biodistribution using in vitro and in vivo models of cancer. The compounds, Figure 1A, were synthesized at the University of Arizona. HCT-116 colorectal cancer cells engineered to overexpress the δOR and parental cells were used as positive and negative tumor lines, respectively. Binding avidities ($K_i$) were determined by competitive binding assays using a labeled δOR agonist with a known affinity ($K_d$) as the competing ligand. Subcutaneous xenograft tumors were grown bilaterally in the left and right flanks of nude mice. Following tail vein injection of probe, in vivo fluorescence images were acquired using the IVIS 200 optical scanner (PerkinElmer). Biodistribution and PK of tumor and organ uptake and clearance were evaluated through a time-course of in vivo and ex vivo image acquisitions. A significant increase in binding avidity was observed as the number of binding moieties per construct increased, Figure 1B. Increased linker arm length did not significantly alter the binding avidities. The targeted probes were all selectively retained in the δOR expressing tumors relative to the negative tumors ($p<0.05$), Figure 1C. The monovalent constructs were cleared from the entire animal and negative tumors by ~8 hours, while being retained in the positive tumors for over 100 hours. In contrast, the multivalent probes were retained in the kidneys up to 150+ hours. Binding avidity increased with multimericity and all targeted probes were selectively retained in δOR positive tumors. All multivalent constructs were retained in the kidneys. The pharmacokinetics of probe uptake and clearance were characterized using a three-compartment mathematical model, which includes tumor, kidney and mouse volumes, and assumes mass conservation of probe. This model was used to account for probe release from tumor in the uptake and clearance dynamics of blood and kidneys. While this effect is negligible in humans, it is significant in mouse models.

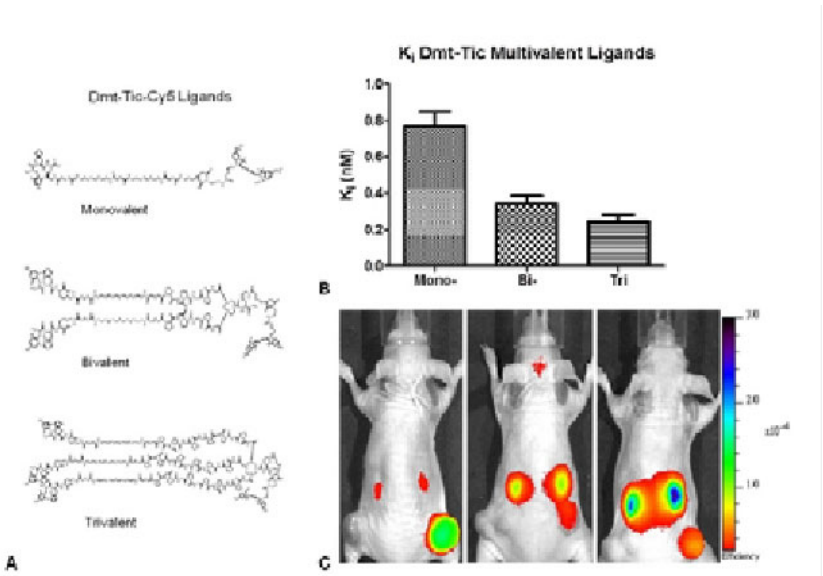


Figure 1. (A) Structure of the Dmt-Tic-Cy5 compounds. (B) $K_i$ values of the multivalent ligands. Mean $K_i$ values are significantly different, $p=0.0004$. (C) Fluorescence images of nude mice 5 hours postinjection of the monovalent, bivalent and trivalent ligands, left to right.

Disclosure of author financial interest or relationships:
**Y. Jeune-Smith**, None; **J.S. Josan**, None; **C.S. Weber**, None; **A. Silva**, None; **R.M. Lynch**, None; **J. Vagner**, None; **V.J. Hruby**, None; **R. Gillies**, Intezyne, Consultant; **D.L. Morse**, LiCor, Other financial or material support; Intezyne Technologies, Other financial or material support .

Presentation Number **P377**
Poster Session 2
September 6, 2012 / 15:15-15:15 / Room: The Liffey

# A Novel Molecular Imaging Approach of Fluorescence Lifetime Imaging Microscopy (FLIM) Based On Nonnegative Matrix Factorization Methods

*Paritosh Pande, **Javier A. Jo**, Biomedical Engineering, Texas A&M University, College Station, TX, USA. Contact e-mail: javierjo@tamu.edu*

Fluorescence lifetime imaging microscopy (FLIM) represents a relatively novel and powerful tool for fluorescence based functional and molecular imaging. In the general approach, it is assumed that the target fluorophores have mono-exponential decay dynamics with known lifetimes, and consequently the mixture fluorescence dynamics is modeled as multi-exponential decay wherein each exponential component corresponds to a specific fluorophore. The sample fluorescence decay at each pixel is thus fitted to the corresponding multi-exponential model, and the estimated pre-exponential weights are used as surrogates for the fluorophore contributions. When the lifetime values of the fluorophores are not known a priori, the global analysis approach is applied. These methods, however, suffer from several limitations. First, the assumption of mono-exponential fluorescence decays for each fluorophore is quite often inaccurate. Second, most of these methods are restricted to two-component models; thus, they can handle at most two fluorescent species. Third, an accurate fitting of fluorescence decay data to a multi-exponential model requires signal-to-noise levels that are in many cases impractical. Fourth, unless extremely short excitation light pulses are used, time deconvolution of the instrument response from the fluorescence decay data is required prior to lifetime estimation, which results in an additional computational burden. Lastly, all these methods have been applied to single spectral channel FLIM data and are thus unable to exploit the spectral information contained in multispectral FLIM data. In this study we present the application of nonnegative matrix factorization (NMF) to multispectral FLIM data. NMF is a multivariate data analysis technique that is aimed at extracting nonnegative signatures of pure components and their nonnegative abundances from an additive mixture of those components. In the context of FLIM data analysis, unmixing amounts to expressing the bulk fluorescence signal obtained from a sample as a weighted sum of fluorescence signals of the constituent fluorophores present in that sample, where the weights correspond to the relative contributions of the constituent fluorophores' signal to the bulk fluorescence signal. Unlike other approaches mentioned earlier, which make assumptions about the functional form of the constituent fluorophore decay profiles and are mainly restricted to two component models, NMF is able to handle more than two fluorescence species showing complex decay dynamics (i.e. non-exponential decay) and can be directly applied to raw multispectral FLIM data obviating the need to perform time deconvolution, resulting in lesser computational time and relaxed SNR requirements. Finally, the new set of FLIM features obtained through NMF of multispectral FLIM data are not only more intuitive and easy to interpret than the standard intensity and lifetime values, but they also allow for tissue characterization, as demonstrated here by their ability to discriminate different types of atherosclerotic plaques based on its application to multispectral FLIM data of fresh postmortem human coronary arteries.

Disclosure of author financial interest or relationships:
**P. Pande**, None; **J.A. Jo**, None.

Presentation Number **P378**
Poster Session 2
September 6, 2012 / 15:15-15:15 / Room: The Liffey

# Endoscopic Imaging of Cerenkov Luminescence

***Sri Rajasekhar Kothapalli***[1], *Hongguang Liu*[1], *Joseph C. Liao*[2,3], *Zhen Cheng*[1], *Sanjiv S. Gambhir*[1,4], [1]*Molecular Imaging Program at Stanford, Department of Radiology and Bio-X Program, Stanford University, Palo Alto, CA, USA;* [2]*Urology, Stanford University, Palo Alto, CA, USA;* [3]*Urology, Veterans Affairs Palo Alto Health Care System, Palo Alto, CA, USA;* [4]*Bioengineering and Materials Science & Engineering, Stanford University, Palo Alto, CA, USA. Contact e-mail: ksraj@stanford.edu*

We demonstrate feasibility of endoscopic imaging of Cerenkov light originated when charged nuclear particles, emitted from radionuclides, travel through a biological tissue of living subjects at superluminal velocity. The endoscopy imaging system consists of conventional optical fiber bundle/ clinical endoscopes, an optical imaging lens system, and a sensitive low-noise charge coupled device (CCD) camera. Figures A and B show that coupling and transmission efficiency increases with an increase in the etendue (product of fiber core area and solid angle) of the endoscope/optical fiber. Systematic studies using phantom samples (0.2 ml PCR tube) show that Cerenkov light from as low as 1 µCi of radioactivity emitted from 18F-Fluorodeoxyglucose [18F-FDG] can be coupled and transmitted through conventional optical fibers and endoscopes. We quantified the contribution of gamma scintillation, when high energy gamma radiation from a 18F-FDG radioactive solution is irradiating the 6 mm optical fiber optic bundle, to the total Cerenkov light detected. Our experimental results show that the contribution of gamma scintillation when the radioactive sample is within the field of view of the imaging system and when not in the field of view of the imaging system is about 9.5% and 3% respectively. We then studied spectral characteristics and transmission efficiency of Cerenkov light, emitted from 10µCi of 18F-FDG in 10µL solution, transmitted through the 6 mm fiber optic bundle. These results show that background (gamma scintillation) corrected Cerenkov light coupling efficiency (from the source to the output end of the fiber bundle) is about 50% in the visible region and about 40% in the near infrared region (720 nm to 840nm). For in vivo experiments, mice (n=4) bearing subcutaneous C6 glioma were administered with 34.78-35.89 MBq (940-970 µCi) 18F-FDG via tail vein injection and imaged 90 minutes post-injection using the fiber bundle. The distal end of the fiber bundle is placed (outside the body) close to several tissues of interest. T¬¬he proximal end that transmits Cerenkov light originating from the respective tissue (due to the 18F-FDG uptake) was imaged by the CCD camera of the imaging system. Fig. C shows Cerenkov luminescence imaging results from a 6 mm fiber bundle overlaid on a bright-field image of the mouse for anatomical reference. Relatively high signals from the subcutaneous tumor and brain indicate high tracer uptake in these organs. We further validated our in-vivo results with respective ex-vivo imaging of different organs, as shown in Fig. D. Our promising results support future investigations of endoscopic molecular imaging based on Cerenkov luminescence.

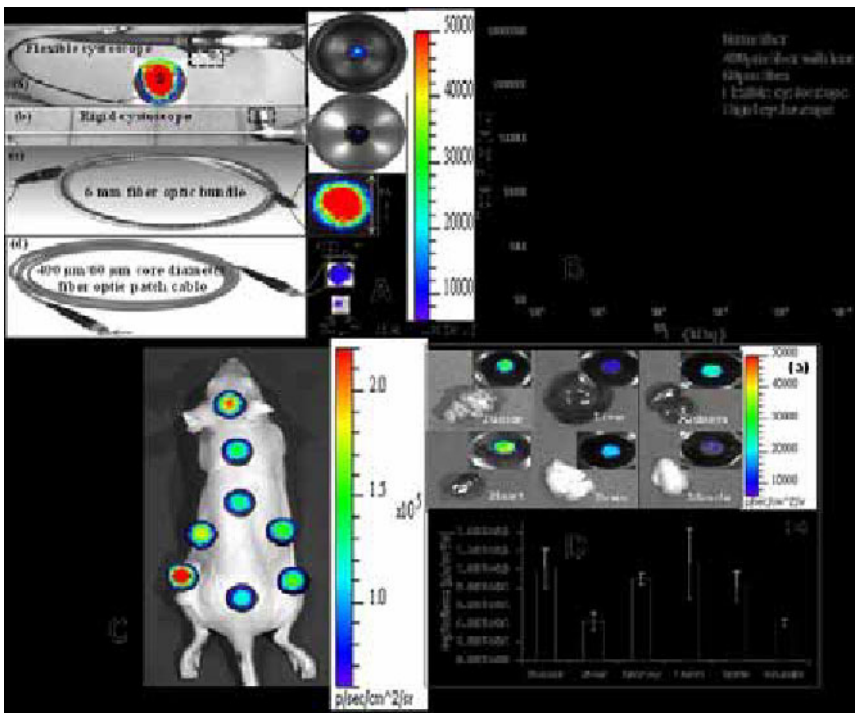


Disclosure of author financial interest or relationships:
**S. Kothapalli**, None; **H. Liu**, None; **J.C. Liao**, None; **Z. Cheng**, None; **S.S. Gambhir**, General Electric, Grant/research support; Bayer-Schering, Grant/research support; Sanofi-Aventis, Grant/research support; CellSight, Stockholder; ImaginAB, Stockholder; Enlight, Stockholder; Endra, Stockholder; Bracco, Consultant; NinePoint Medical, Stockholder; Visualsonics, Consultant .

Presentation Number **P379**
Poster Session 2
September 6, 2012 / 15:15-15:15 / Room: The Liffey

# Whole body fluorescent lifetime imaging of protease activatable probes

***Anand T. Kumar***[1], *Craig J. Goergen*[1], *William L. Rice*[1], *David E. Sosnovik*[1], *Alexei A. Bogdanov*[2], [1]*Athinoula A Martinos Center for Biomedical Imaging, Radiology, Harvard Medical School and Massachusetts General Hospital, Charlestown, MA, USA;* [2]*Radiology, University of Massachusetts Medical School, Worcester, MA, USA. Contact e-mail: ankumar@nmr.mgh.harvard.edu*

We investigated applications of fluorescence lifetime (FL) imaging for the detection of activatable probes (AP) in whole animal mouse models of cardiac disease and cancer. Previous applications of AP's have primarily focused on continuous wave (CW) excitation and detection, which is intensity based and therefore insensitive to FL. FL is a useful photophysical property that is independent of probe concentration and excitation power. FL is of special importance in the context of APs since the quenching mechanism often involves non-radiative transfer, which alters the FL. Moreover, FL is directly related to quantum yield, which in turn affects the CW intensity. Thus, FL characterization is critical for accurate quantification of in vivo imaging with APs. Activatable probes, originally developed for cancer imaging, are composed of a long-circulating copolymer backbone with self-quenched fluorophores in the inactive state. Fluorescence is generated once the backbone is cleaved by cathepsins and/or metalloproteases. We have characterized the in vitro and in vivo FLT of two cathepsin-activatable near-infrared probes (PGC-800CW and ProSense-750) using a time domain fluorescence imaging system. The in vivo studies were performed in mouse models of post myocardial infarction (MI). The central observation is that while FL increases for PGC-800CW from 0.29 ns in vitro to 0.47 ns in vitro after trypsin activation, and to 0.7 ns in vivo in MI mice, ProSense-750 shows no significant lifetime change in vitro upon trypsin activation (0.6 ns), and a small but significant shift in vivo (0.75 ns). Also, both probes show a significant lifetime shift between the liver and the heart, which offers a practical advantage by allowing the separation of the large background signal from the liver, a major confounding factor in CW imaging (Supplemental Data). Despite previous works using APs, the mechanisms behind the quenching of APs are not well understood. We hypothesize that multiple factors are involved in the distinct observations with PGC and ProSense, including multiple quenching mechanisms (static and dynamic quenching) and the influence of tissue environment. While static quenching (due to ground state complex formation, for example) alters the absorbance of AP-linked dyes, the FL is unchanged. However, dynamic quenching affects FL but does not alter the steady state absorbance spectra. Preliminary time course measurements of PGC-800CW after trypsin activation indicate a rapid (< 3 min) rise of FL from the quenched (0.29 ns) to the activated (0.47 ns) state but a much slower (> 30 min) rise of the CW intensity (Supplemental Data). This suggests that both static and dynamic quenching could simultaneously be involved; we are exploring the possibility that the rapid lifetime change corresponds to a release of dynamic quenching due to enzymatic cleavage, while the slow intensity change corresponds to a release of H-aggregates that cause static quenching. Ongoing work is focused on further delineating the specific mechanisms behind quenching and probe activation in PGC and ProSense, with the ultimate goal of quantitative imaging of protease activity in vivo.

Disclosure of author financial interest or relationships:
**A.T. Kumar**, None; **C.J. Goergen**, None; **W.L. Rice**, None; **D.E. Sosnovik**, Siemens Medical, Grant/research support; **A.A. Bogdanov**, None.

Presentation Number **P380**
Poster Session 2
September 6, 2012 / 15:15-15:15 / Room: The Liffey

# Radionuclide quantification with multi-spectral Čerenkov Tomography for a small animal imaging system

***Chaincy Kuo***[1], *Ruby K. Gill*[2], *Gregory S. Mitchell*[2], *Brad Rice*[1], *Simon R. Cherry*[2], [1]*In Vivo Imaging R&D, Caliper, a PerkinElmer Company, Alameda, CA, USA;* [2]*Biomedical Engineering, University of California, Davis, CA, USA. Contact e-mail: chaincy.kuo@perkinelmer.com*

The detection of Čerenkov radiation emitted by charged radionuclide decay products is a promising method to track radionuclide distribution in vivo, particularly for beta-minus emitting nuclides used for radiotherapeutics, which cannot be imaged accurately by other methods. In this work, we present a method for three dimensional localization and quantification of radionuclide distribution derived from multispectral Čerenkov tomography combined with in vitro calibration. Nuclides undergoing beta-minus decay will produce Čerenkov light while emitted electrons travel faster than the speed of light in tissue. The Čerenkov emission spectrum is broad and inversely proportional to the square of the photon wavelength. The propagation of Čerenkov photons in tissue follow a diffusion model and therefore diffuse tomography techniques previously developed for bioluminescence imaging can be applied. By imaging Čerenkov at multiple wavelengths, then applying the diffuse tomography methods, the source distribution of radionuclides can be determined with resolution of 1-3 mm. 10 µCi of 90Y was pipetted into a 3µL well located at the tip of a 3 mm diameter tissue phantom rod and then capped. The rod was imaged at different depths in a mouse-shaped tissue phantom designed to match the optical properties of mouse muscle. Čerenkov photons produced by the beta-minus emission from 90Y were imaged through a series of 20 nm bandwidth emission filters with central wavelengths spanning 560-640 nm in a highly sensitive optical imaging instrument with a CCD cooled to -90 °C. The instrument is calibrated in physical units allowing spectral images to be photon radiance units. A structured-light projector is used to determine the surface topography of the subject. In vitro concentrations of 90Y were imaged in a microtiter plate and measured for Cerenkov photon output. These measurements were verified against Monte Carlo simulations to within 15% difference. In vitro values for Čerenkov photon output per decay were used to calculate the activity level in the rod tips. The reconstruction method utilizes a non-negative least squares algorithm to solve for the localization and quantification. Reconstruction center of mass for the two rod depths in the tissue phantom cases were localized within a few tenths of a millimeter, validated with CT co-registration. The quantification error in the rod tip activity was at most 41%, when considering the experimentally derived Čerenkov photon output for 90Y. These results show encouraging possibilities for quantitative radiotherapeutic in vivo imaging in preclinical research using multispectral Čerenkov luminescence tomography.

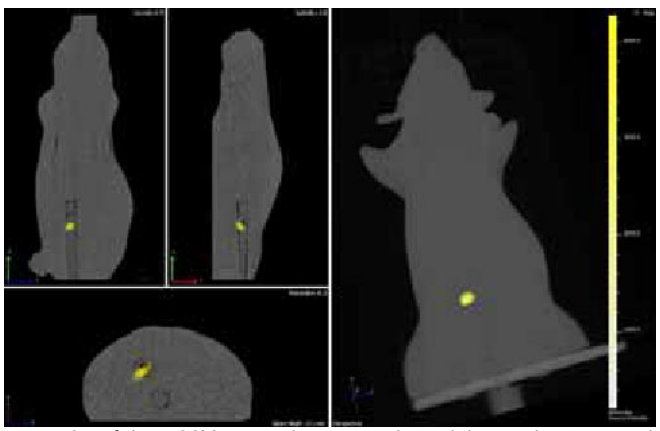

Quantitative Cerenkov Tomography of deep 90Y source in mouse-shaped tissue phantom, registered to CT for validation.

Cerenkov Tomography Quantification and Localization

| | | Activity [µCi] | Depth [mm] |
|---|---|---|---|
| Deep Rod | Experimental | 10 | 7.4 |
| | Cerenkov Tomography | 7.2 | 7.2 |
| Shallow Rod | Experimental | 10 | 3.5 |
| | Cerenkov Tomography | 10 | 3.2 |

Disclosure of author financial interest or relationships:
**C. Kuo**, Caliper, a PerkinElmer Company, Employment; **R.K. Gill**, None; **G.S. Mitchell**, None; **B. Rice**, None; **S.R. Cherry**, GE Healthcare, Grant/research support; Radiation Monitoring Devices Inc., Grant/research support; Siemens Molecular Imaging, Honoraria.

Presentation Number **P381**
Poster Session 2
September 6, 2012 / 15:15-15:15 / Room: The Liffey

# A new method for imaging motility non-invasively in animals

***Sunkuk Kwon**, Cynthia Davies-Venn, Eva Sevick, Institute of Molecular Medicine, University of Texas Health Science Center - Houston, Houston, TX, USA. Contact e-mail: sunkuk.kwon@uth.tmc.edu*

Objective: Depending upon the excitation wavelength, tissue autofluorescence is produced by endogenous chromophores, such as elastin and collagen. It has also been shown that chlorophyll from the alfalfa in commonly used laboratory murine diets fluoresces between 650 to 750 nm. Thus, when mice are excited by 660 nm excitation light, strong background autofluorescence resulting from ingested food along the gastrointestinal (GI) tract in the abdominal region is detected. While the autofluorescence signal in the GI tract limits in vivo fluorescence molecular imaging, it may provide an opportunity to image dynamic intestinal motions. The GI tract has various controlled motions, such as peristaltic and segmental motions, to mix and propel its contents during digestion and absorption. Recently, we demonstrated for the first time, non-invasive near-infrared fluorescence (NIRF) imaging with sufficient temporal resolution and sensitivity to image dynamic contractile motion of the murine intestines following injection of an exogenous NIR fluorophore, indocyanine green (ICG). Upon injection, ICG is secreted into bile from the liver via the biliary tracts, enabling fluorescent delineation of the intestine. Since ingested food travels through the GI tract, we also hypothesize that autofluorescence imaging can be used to non-invasively assess intestinal motions in mice. In this study, we non-invasively and quantitatively imaged for the first time, intestinal contractile activity in mice using autofluorescence induced by standard murine diet containing chlorophyll without administration of exogenous imaging agents. Methods: Mice were dynamically imaged for 5 mins immediately after and up to 24 hrs after injection of ICG. The mice were illuminated first with 785 nm light and then 660 nm light for acquisition of the NIR fluorescent signal at 830 nm and the autofluorescence signal at 710 nm, respectively. NIRF and autofluorescence imaging data were analyzed to generate three dimensional spatio-temporal maps to quantify intestinal motions. Thus, the propagation velocity and the frequency of intestinal contractility were assessed. Results: The secretion of ICG-laden fluorescent bile into the duodenum was observed in vivo. In addition, mice showed different digestive status at each imaging time point as indicated by autofluorescence imaging. Different patterns of the intestinal motility, such as peristaltic and segmental motions, were dynamically imaged in vivo using diet-induced autofluorescence and ICG fluorescence imaging. Dynamic autofluorescence imaging showed the frequency of peristalsis and propagation velocity were 28.6 cycles/min and 1.82 ± 0.56 cm/s, respectively, which is agreement with our data using NIRF imaging with injection of ICG, indicating there is no effect of administration of ICG on intestinal motions. Conclusions: Dynamic autofluorescence as well as ICG fluorescence imaging techniques can provide a tool to monitor intestinal disorders or dysfunction and response to therapeutic agents with high spatial and temporal resolution and minimal invasiveness in a truly physiological setting.

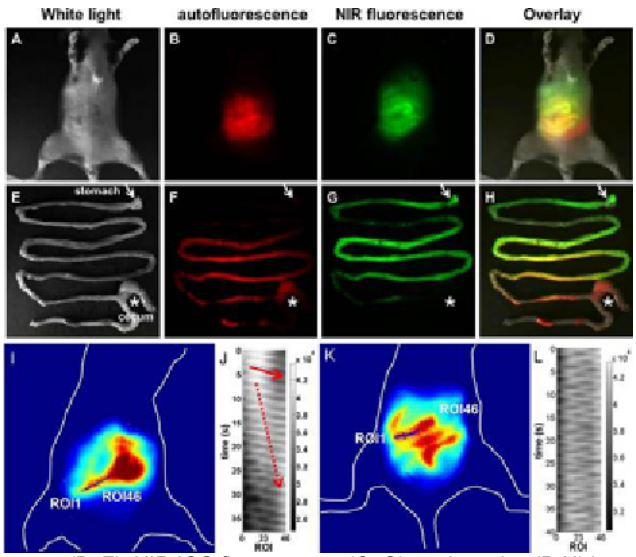


White light (A, E), endogenous red-fluorescence (B, F), NIR ICG fluorescence (C, G), and overlay (D,H) images in mice (A,B,C,D) and isolated GI tract (E,F,G,H) from the body 2 hr after i.v. injection of ICG, showing different distribution of fluorescence along the GI tract. Fluorescent images (I, K) in the ventral view of a mouse after selection of 46 ROIs along the fluorescent small intestine. Three-dimensional spatio-temporal maps of fluorescent intensity as a function of time and ROI demonstrate the propagation of the contractile waves (J) indicated by a red arrow and segmental motion (L). The patterns illustrated in Figure J are similar to those during the migrating motor complexes (MMC), due to slow movement of fluorescent intraluminal contents (red broken arrow).

Disclosure of author financial interest or relationships:
**S. Kwon**, None; **C. Davies-Venn**, None; **E. Sevick**, Tactile, Inc, Grant/research support; Siemens Preclinical Solutions, Other financial or material support .

Presentation Number **P382**
Poster Session 2
September 6, 2012 / 15:15-15:15 / Room: The Liffey

# In vivo haemoglobin imaging in animals and humans is going 4D

***Martin J. Leahy***, *[1]Physics, NUI Galway, Galway, Ireland; [2]NBIP Ireland, Royal College of Surgeons, Dublin, Ireland. Contact e-mail: martin.leahy@nuigalway.ie*

Haemoglobin is a molecule of extraordinary importance for living tissues, since it transports the nutritional oxygen to the cells. Our hospitals are dominated by the use of non-light microscopy for imaging of tissues and the macrocirculation. In general these technologies serve a small % of the world's seven billion inhabitants very well, but it is now clear that, even in well developed countries, this approach to medical imaging cannot serve the future needs of society (cost, safety, resolution…). Meanwhile, living longer has exacerbated the challenges of diabetes and cancer, which have their origins and clinical manifestation in the microcirculation. Photonics promises to bring healthcare to the next level, as it is the only means to see cells and molecules in small, accessible, low cost and safe imaging systems. Recently high resolution label-free imaging of the haemoglobin in the microcirculation at clinically relevant depths and has become available in research labs. Uptake in the clinic requires the ability to address a need and important physiological events often happen over periods of seconds; heartbeat, breathing, endothelial dependent and other forms of vasomotion. These new imaging systems based e.g. on optical coherence tomography and photoacoustic microscopy take some hours to process 3D images of the microcirculation and often the images require significant ‘touch-up'. Several groups are pushing these technologies to clinically relevant speeds and depths. We have developed 1D (laser Doppler), 2D (tissue viability imaging -'TiVi') and 3D (correllation mapping Optical Coherence Tomography (OCT)) methods for imaging the microcirculation in vivo in animals and humans. This paper will describe our latest results in demonstracting tomographic microcirculation imaging in humans using easily accessible commercial OCT systems.

Disclosure of author financial interest or relationships:
**M.J. Leahy**, None.

Presentation Number **P383**
Poster Session 2
September 6, 2012 / 15:15-15:15 / Room: The Liffey

# Differentiating a target of interest from tissue autofluorescence in vivo by fluorescence lifetime imaging

***Guobin Ma***[1], *Ivo Que*[2], *Alan Chan*[2,3], *Clemens Lowik*[2], [1]*ART Advanced Research Technologies Inc., Montreal, QC, Canada;* [2]*Molecular Imaging Laboratories, Leiden University Medical Center, Leiden, Netherlands;* [3]*Percuros B.V., Enschede, Netherlands. Contact e-mail: gma@art.ca*

The ability to differentiate a fluorescent target of interest from background or other non-relevant targets is of importance to researchers during in vivo experiments in order to obtain pathophysiological information. There are a wide variety of molecules present in living tissue that can act as biochemical sources of autofluorescence. Examples include tryptophan, NADH, pyridoxine, collagen, elastin, flavins, porphyrins, as well as chlorophyll present in animal food. If the emission band of a fluorescent reporter overlaps with tissue autofluorescence or non-targets, the fluorescent signal of interest will be mixed with signals from all the fluorescent sources in the spectral band. Thus to differentiate a fluorescence signal produced by a target of interest from other sources, the current method of choice is spectral unmixing. We present here an alternative approach to separate a signal of interest by using fluorescence lifetime, which is an intrinsic characteristic of a fluorescent reporter. It adds another parameter to distinguish different fluorescent reporters as well as tissue autofluorescence, even when the emission bands are highly overlapped where spectral unmixing is not effective. In our experiment, the mammary fat pad of a Balb/c nude mouse was injected with HEK 293T cells (one thousand cells in a 10 µl injection volume) transfected with a Katushka-expressing plasmid near infrared fluorescence protein. At 5 minutes post injection, the mouse was whole body scanned by Optix MX3, a time domain in vivo small animal imager with fluorescence lifetime feature. The acquired images are shown in Figure 1. From the intensity image (a), it is hard to identify the cell injection region, as indicated by the oval. Fortunately, with fluorescence lifetime image (b) we can easily identify the region where Katushka labeled cells were injected although the fluorescence signals from other regions are even higher than this region. On the other hand, the measured in vivo fluorescence signal is a combination of many components. In the cell injection region, the signal is dominated by Katushka, so a single exponential decay model is good enough to fit the measured fluorescence signal. As a result, the fitting goodness χ^2 is close to one. In other regions, all kinds of tissue autofluorescnce in the spectral band contribute. As a result, a single lifetime model is not proper to fit all the lifetimes. Therefore the χ^2 is far away from one. In light of this, the image of lifetime fitting goodness (c) provides another indication of the cell injection region. This is very interesting and useful. Here the sample is open labeled. The lifetime and fitting goodness dually confirm the differentiation of target of interest from tissue autofluorescence. If a fluorescent reporter is injected by tail vein and we want to track its distribution by in vivo imaging, the intensity-only result may be misleading. However, with fluorescence lifetime information, we can easily identify the fluorescence signal of interest and exclude all other noises including tissue autofluorescence.

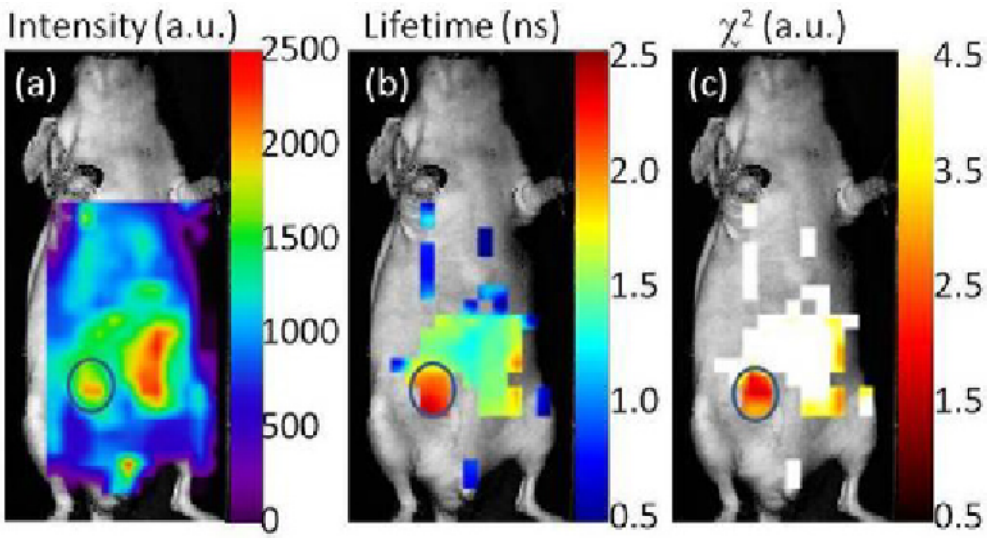


Fluorescence intensity (a), lifetime (b), and goodness of lifetime fitting (c) images of a mouse injected with cells labeled by Katushka near infrared fluorescent protein obtained by an Optix MX3 imaging system. Lifetime information helps us to easily differentiate the signal from the injected cells labeled by Katushka, as indicated by the oval region.

Disclosure of author financial interest or relationships:
**G. Ma**, None; **I. Que**, None; **A. Chan**, Softscan Healthcare Group, Consultant; **C. Lowik**, None.

Presentation Number **P384**
Poster Session 2
September 6, 2012 / 15:15-15:15 / Room: The Liffey

# Microscope system for localization in tissues of a contrast agent using time-gated fluorescence of lanthanides

***Nghia T. Nguyen***[1], *Jean-Michel Tualle*[1], *Eric Tinet*[1], *Frédéric Chaubet*[2], *Graciela Pavon-Djavid*[2], [1]*Laboratoire de Physique des Lasers, CNRS UMR7538, Université Paris 13, Villetaneuse, France;* [2]*Bio-ingénierie des Polymères Cardiovasculaires, INSERM U698, Université Paris 13, Villetaneuse, France. Contact e-mail: ntnghia3n3@yahoo.com*

We developed in our laboratories a fluorescence imaging microscope system intended for the measurements of the localization and the concentration within tissues of a macromolecular Gd-based MR contrast agent for the visualization of atherosclerotic lesions. The contrast agent is partially fitted with Tb ions whose long fluorescence emission time constant enables us to have a suitable signal to noise ratio, despite a low intensity, using time gated imaging after the other sources of fluorescence have decayed. The excitation source, on top of the inverted microscope, is a laser diode emitting at 371nm. The fluorescence signal is imaged on an ICCD camera. A microcontroller synchronizes electrical gating of the ICCD after the laser pulse and generally controls automatically all parts of the measurement process. For tissue identification, we acquire a "white" color image using the standard halogen lamp of the microscope. This image is synthesized by the use of the combination of three successive images with three fundamental colors filters: red, green and blue. Then our software assembles the color and fluorescence images. First images of rat arteries show that the contrast agent is indeed localized on specific regions of the tissues.

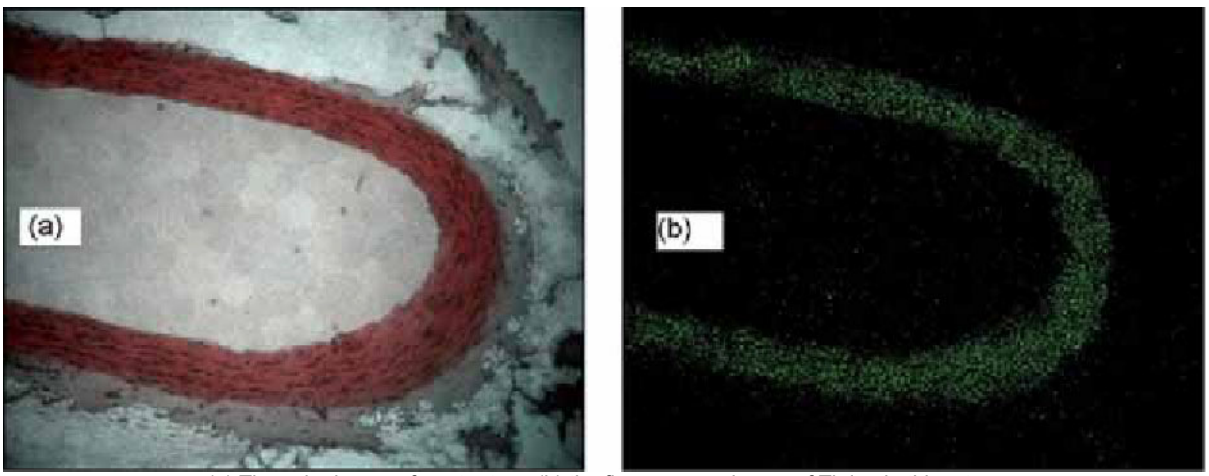

(a) The color image of a rat artery; (b) the fluorescence image of Tb ion in this artery

Disclosure of author financial interest or relationships:
**N.T. Nguyen**, None; **J. Tualle**, None; **E. Tinet**, None; **F. Chaubet**, None; **G. Pavon-Djavid**, None.

Presentation Number **P385**
Poster Session 2
September 6, 2012 / 15:15-15:15 / Room: The Liffey

# Bioluminescent imaging of hepatic caspase-3 activity in mice

***Michitaka Ozaki***[1], *Sanae Haga*[2,3], *Takeaki Ozawa*[4], [1]*Dept of Health Sciences, Hokkaido Univ SOM, Sapporo, Japan;* [2]*Dept of Dermatology, Hokkaido Univ SOM, Sapporo, Japan;* [3]*The Japan Society for the Promotion of Science, Tokyo, Japan;* [4]*Dept of Chemistry, School of Science, The University of Tokyo, Tokyo, Japan. Contact e-mail: ozaki-m@med.hokudai.ac.jp*

Apoptosis-mediated damage of cells and organs is a serious concern in various pathological situations. Therefore, the *in vivo* visualization of capase-3 activity may lead to better understandings of damage mechanisms. Here, we demonstrate caspase-3 activity by the luciferase-based optical probe of live liver cells challenged by various stimuli, and also *in vivo* imaging of caspase-3 activity of the post-ischemic liver. METHODS: We developed a novel probe (pcFluc-DEVD) of cyclic luciferase reflecting caspase-3 activity. Two fragments of DnaE inteins are fused to neighboring N- and C-terminal ends of firefly luciferase (Fluc) connected with a substrate sequence of caspase-3 (DEVD). After translation into a single polypeptide, the N- and C-terminal ends of luciferase are ligated by protein splicing, which produces a closed circular polypeptide chain. The structure of the cyclic luciferase is distorted. Therefore, the luciferase loses its bioluminescence activity (inactive form). Once caspase-3 is activated in cells (DEVD is cleaved), Fluc changes into an active form if the substrate sequence is digested using the protease, restoring luminescence activity. By transfecting an adenovirus cording for pcFluc-DEVD (Ad*pcFluc-DEVD*), we investigated whether this probe monitors apoptosis in live AML12 liver cells by staurosporine (STS), Fas-ligand (FasL) or hypoxia/reoxygenation (H/R), and in the post-ischemic liver in mice. RESULTS: STS and FasL activate caspase-3 in caspase-8-independent and dependent manner, respectively. First, we measured caspase-3 activity in STS- or FasL (Jo2 antibody)-treated AML12 cells transiently transfected with Ad*pcFluc-DEVD*. In live AML12 cells, the signals from the probe started to increase immediately and peaked at 2 - 4 hr after 1 μM STS and 2 μg/ml Jo2 administration, respectively. In both stimuli, caspase-3 activity was paralleled with apoptotic cell death. Next, we measured caspase-3 activity in post-hypoxic AML12 cells by this probe. During hypoxia, caspase-3 activity dropped to the bottom level. However, it rapidly recovered to the pre-hypoxic level after reoxygenation and started to rise until 4 - 6 hr post-H/R. Then, we tried to evaluate *in vivo* apoptosis by measuring caspase-3 activity in mouse hepatic ischemia/reperfusion (I/R). 60min of hepatic ischemia caused great increase of capase-3 activity at 6 - 9 hr post-I/R, whereas 30 min of liver ischemia caused small increase at 2 hr post-I/R (Figure). Prolonged ischemia (90 min), however, showed minimal increase of caspase-3 activity, reflecting extended necrotic cell death rather than apoptotic cell death. CONCLUSIONS: The caspase-3 probe successfully illustrated apoptotic damage *in vitro* and *in vivo* . Visualizing apoptotic damage of cells/organs may provide important insights into various physio-pathological conditions.

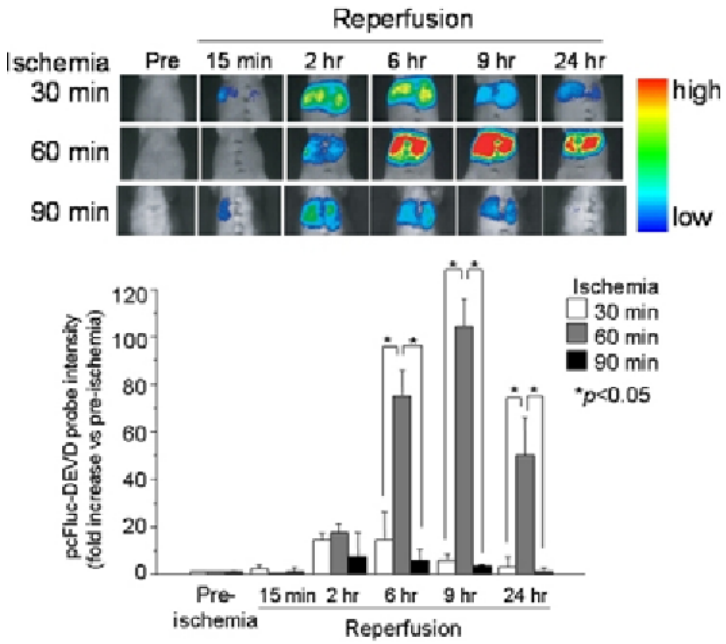


Figure: In vivo bioluminescent imaging of caspase-3 activity of mouse liver during reperfusion.

Disclosure of author financial interest or relationships:
**M. Ozaki**, None; **S. Haga**, None; **T. Ozawa**, None.

Presentation Number **P386**
Poster Session 2
September 6, 2012 / 15:15-15:15 / Room: The Liffey

# in vivo Imaging of Mechanical Injury Induced Changes in Plant Leaf's Delayed Luminescence and Wound Signaling

***Rao V. Papineni****, William E. McLaughlin, Robert Brandau, Carestream Molecular Imaging, Carestream Health, Inc., Woodbridge, CT, USA. Contact e-mail: rao.papineni1@carestreamhealth.com*

Insect herbivory or mechanical injury to leaf alters photosynthesis process, and in turn affects the plant yield. Delayed fluorescence of plants also known as delayed luminescence is emitted by the chlorophyll a molecules in PS2 antennae and has similar spectral properties as of chlorophyll a fluorescence. The delayed luminescence prevails for several minutes even after the illumination is stopped, while emission of chlorophyll a fluorescence ends immediately as the illumination stops. We used planar optical imaging techniques to determine changes in delayed luminescence of whole leaf subjected to mechanical injury simulating insect damage. The generation of reactive oxygen species (ROS), an early response in the wound signaling process at the leaf injury site(s) was captured using luminol based chemiluminescence approach. Here, we show that mechanical injury to detached whole leaf results in irreversible effects on the delayed luminescence. Further, infiltration of the luminol through the stalk of the leaves resulted in significant increase in chemiluminescence signals at the injury sites indicating the rapid production of reactive oxygen species (ROS) in response to injury. The signal detection at the wound sites were up to 10-fold higher compared to the surrounding areas of the leaf. Herbicides mostly inhibit photosynthesis acting directly on the chlorophyll functions. The imaging technologies described here can potentially be used for screening new herbicides, in evaluation of pesticides capable of inducing plant defense mechanisms.

Disclosure of author financial interest or relationships:
**R.V. Papineni**, Carestream Health Inc, Employment; **W.E. McLaughlin**, Carestream Molecular Imaging, Employment; **R. Brandau**, Carestream Health Inc, Employment .

Presentation Number **P387**
Poster Session 2
September 6, 2012 / 15:15-15:15 / Room: The Liffey

# Development of a Multispectral 3D Cerenkov Luminescence Tomography System for dedicated Small Animal Imaging in Drug Development

***Thomas Poeschinger***[1], *Werner Scheuer*[1], *Alexander D. Klose*[2], [1]*pRED, DTA Oncology, Roche Diagnostics GmbH, Penzberg, Germany;* [2]*Radiology, Columbia University, New York, NY, USA. Contact e-mail: thomas.poeschinger@roche.com*

*In vivo* imaging of specific molecular events that are associated with disease emerges as valuable tool in modern biomedical research and drug development. Cerenkov luminescence tomography (CLT) refers to a novel noninvasive optical molecular imaging strategy, which aims at the quantitative determination of the 3D biodistribution of radiopharmaceuticals in living small animals. Unlike in conventional nuclear imaging, CLT exploits the Cerenkov effect where optical photons are released during the decay of radiotracers in tissue. CLT calculates spatial maps of the tracer distribution from surface measurements using appropriate light propagation models. Here, we propose the concept of a dedicated small animal Cerenkov tomography system, which shall improve on currently available optical imaging technology by combining multispectral and multi-view data acquisition with an optimized reconstruction algorithm that considers both the spectral properties of tissue and the geometry of the animal. The system is optimized for imaging in the visible range between 500 nm and 700 nm, and takes the $\lambda^2$-depencende of the Cerenkov radiation into account. For light detection a highly sensitive CCD camera is used. The camera is coupled to an automated filter wheel, which captures Cerenkov light images at five different wavelengths. A two-mirror deflection unit provides simultaneous detection of the ventral and dorsal side of the animal. In addition, transillumination measurements are utilized for the calculation of optical tissue absorption, which enables quantitative reconstruction of the *in vivo* 3D tracer distribution. For tomographic reconstruction, we are using a light propagation model based on the simplified spherical harmonics ($SP_N$) approximation of the radiative transfer equation. The $SP_N$ equations are solved with a finite-difference technique for a curved geometry of the animal surface. In a concluding example, we will demonstrate multispectral Cerenkov tomography to spatially resolve the 3D biodistribution of the radiotracer 18F-FDG in a preclinical small animal cancer model. Using radiopharmaceuticals for preclinical *in vivo* imaging is advantageous, since many of the tracers are already clinically approved and routinely employed in clinical nuclear imaging studies. Hence, molecular imaging using CLT in small animals may serve as a useful predictor of the outcome of clinical drug efficacy trials and could help to reduce attrition rates as well as costs in the late phase of the drug development process.

Disclosure of author financial interest or relationships:
**T. Poeschinger**, Roche Diagnostics GmbH, Employment; **W. Scheuer**, Roche Diagnostics GmbH, Employment; **A.D. Klose**, None.

Presentation Number **P388**
Poster Session 2
September 6, 2012 / 15:15-15:15 / Room: The Liffey

# Cherenkov emission spectroscopy of cancer during external beam radiation therapy

***Brian W. Pogue**, Scott C. Davis, Rongxiao Zhang, Adam Glaser, David Gladstone, Thayer School of Engineering, Dartmouth College, Hanover, NH, USA. Contact e-mail: brian.w.pogue@dartmouth.edu*

External beam radiation from linear accelerators is routinely used as the workhorse for radiotherapy of cancer, and this delivery produces large amounts of broadband Cherenkov light in the tissue where dose is deposited. The emission can be sampled with gated acquisition, to reveal optical images, and spectral signatures that are altered by the molecules within the tissue. The signal is dominated by the blue end of the spectrum, which is heavily attenuated by blood, but the red and infrared wavelengths can be shown to penetrate through several centimeters of tissue, and be detected to sample the tissue features. Monitoring of hemoglobin oxygen saturation is possible, as the absorptive attenuation of blood is well characterized, and with spectral fitting this can be estimated absolutely. Additionally, monitoring of luminescent species in the tissue is possible, especially if they emit in the red or infrared bands. Cellular mitochondria assay with protoporphyrin IX fluorescence is feasible, and the detection peaks at 640-700nm are readily tracked in the spectrum. The tissue oxygen partial pressure can be tracked with administration of an oxygen sensitive phosphor, and it is shown that this can be sampled through up to 2cm of tissue with reasonable accuracy in estimation of pO2 via the luminescence lifetime. Monte Carlo modeling of the incident radiation and the resulting Cherenkov and luminescence can be done with GEANT4 simulations, and the data shows the sampling depth can vary from just a few millimeters up to two centimeters, based upon the wavelength chosen and the beam to fiber geometry chosen. Near infrared wavelengths penetrate the best in the 700-900nm range, and detection with a gated spectrometer CCD provides sufficient detection to monitor this signal. The utility of this signal is still unknown, however this presents the first attempt to document the signal in vivo, and its availability in all patients undergoing radiation therapy is as yet unexploited.

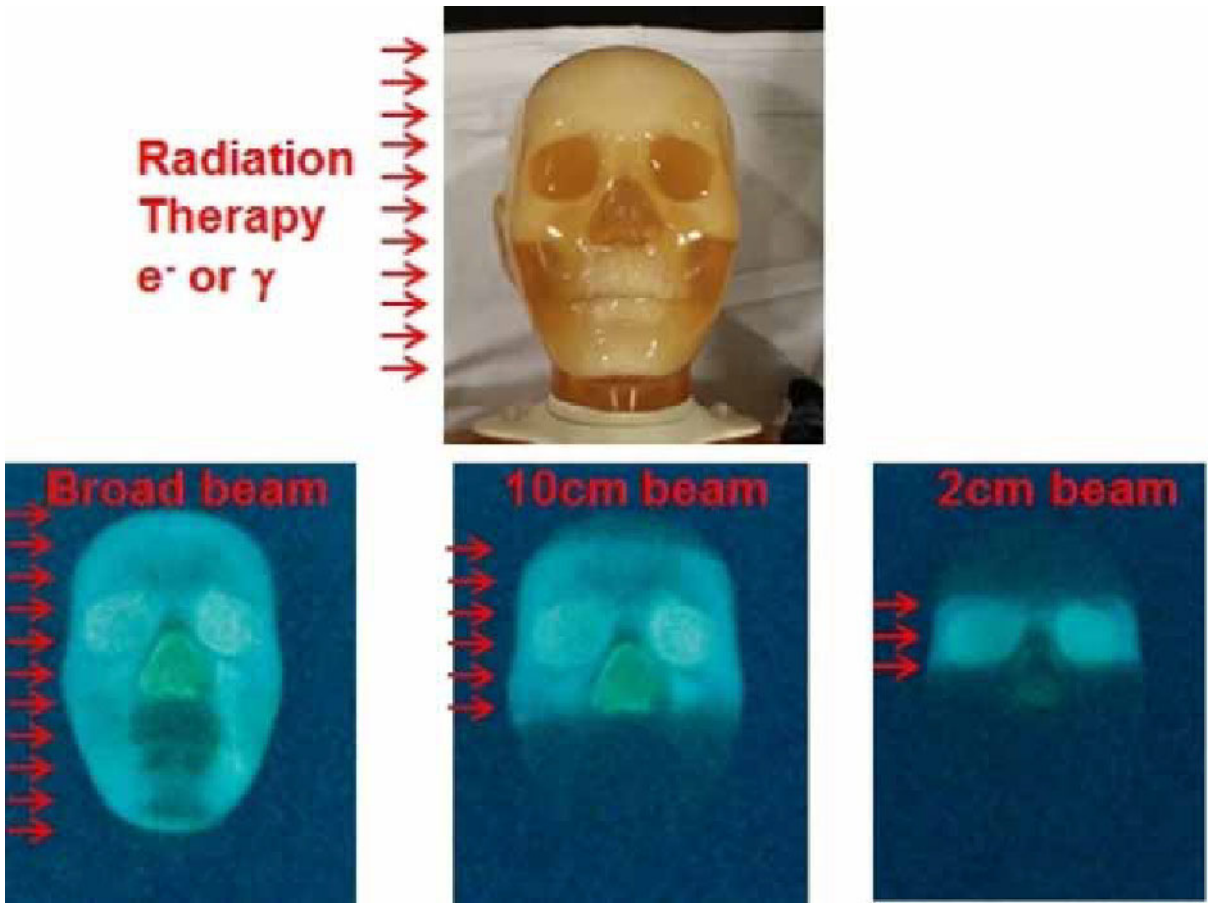


Radiation therapy of a head phantom shows images of the blue-dominated Cherenkov emission, from a wide beam (whole head), a 10 cm beam, and a 2 cm beam.

Disclosure of author financial interest or relationships:
**B.W. Pogue**, None; **S.C. Davis**, None; **R. Zhang**, None; **A. Glaser**, None; **D. Gladstone**, None.

Presentation Number **P389**
Poster Session 2
September 6, 2012 / 15:15-15:15 / Room: The Liffey

# Develop a fast forward algorithm using a finite element method for the Fluorescent Molecular Tomography system

***Sima Saleh**, Marjaneh Hejazi, Amir Homaun Jafari, Hanieh Mohammadreza, Research Center of Technology and Science in Medicine/Tehran University of Medical sciences, Tehran, Iran, Tehran univesity of medical sience, Tehran, Islamic Republic of Iran. Contact e-mail: s_saleh@razi.tums.ac.ir*

Introduction: Fluorescent Molecular Tomography (FMT) is a non-invasive method for imaging the biological tissue at cellular level. The cell function can be shown by using nanoparticles (such as Quantum Dots) and suitable wavelength of optical radiation. In this modality an numerical and computable model of the propagation of radiation in tissue is essential for meaningful interpretation of the biological processes. The numerical method includes a forward and a reconstruction algorithm.The Finite element method is a fast and flexible numerical technique which is used to solve diffusion equations. Therefore the aim of this article is to develop a fast forward algorithm using a finite element method for the FMT imaging system Materials and Methods:In this study, FMT system was implemented in tomography method. The algorithm was then written based on the Born approximation for a homogenous infinite turbid medium. The results were validated with experimental studies using a fluorescent source embedded in a homogeneous tissue-like phantom. Result: The results showed the significant correlational coefficients (R >0.9) which demonstrated the high accuracy of the algorithm. Keywords— Fluorescence Molecular Tomography, Forward problem, Finite element method,

Disclosure of author financial interest or relationships:
**S. Saleh**, None; **M. Hejazi**, None; **A. Jafari**, None; **H. Mohammadreza**, None.

Presentation Number **P390**
Poster Session 2
September 6, 2012 / 15:15-15:15 / Room: The Liffey

# Dynamic Fluorescence Mediated Tomography

***Metasebya Solomon***[1], *Walter J. Akers*[2], *Ralph Nothdurft*[2], *Samuel Achilefu*[2,1], *Joseph P. Culver*[2,1], [1]*Biomedical Engineering, Washington University in Saint Louis, Saint Louis, MO, USA;* [2]*Radiology, Washington University School of Medicine, St. Louis, MO, Saint Louis, MO, USA. Contact e-mail: solomonm@mir.wustl.edu*

Dynamic fluorescence imaging is an emerging technology that can provide enhanced non-invasive functional and molecular level detail. While dynamic imaging via fluorescence reflectance imaging (FRI) recently allowed segmentation of various internal organs (based on their different kinetic behaviors (Hillman et al. 2007 Nat. Photonics), FRI sensitivity declines quickly with depth and a 2D geometry precludes co-registration with 3D modalities such as MRI, CT, PET or SPECT. Three-dimensional fluorescence mediated tomography (FMT) provides considerably improved deep-tissue sensitivity, volumetric localization and increased quantitative accuracy. However, FMT typically images on the time scales of minutes to hours, too slow to monitor the uptake dynamics of a vascular injection. In this work, we overcome this limitation and demonstrate dynamic tomography of fluorescent diagnostic imaging agents in tumor bearing mice. We demonstrate that video-rate FMT is fast enough to enable imaging of cardiac, respiratory and pharmacokinetic induced dynamic fluorescent signals and from these measurements the real-time uptake of injected agents can be deduced. Anatomically guided dynamic fluorescence molecular tomography was made possible by combining our recently published fiber based, video-rate (30 Hz) FMT system with a preclinical NanoSPECT/CT (Bioscan) (Solomon et al. JBOE 2011). Fluorescent dye (LS301, cypate (dye) conjugated to a peptide targeted to tumor margin integrin receptors) was administered by a bolus tail vein injection. The dynamics of the injection were monitored for 10 minutes continuously, followed by CT without moving the animal. To delineate the different internal organs based on differences in the kinetics of injected contrast agents, we used a seed-based correlation analysis. First, a global signal, an average of the time traces for all voxels, was linearly regressed to remove correlation associated with systemic circulation. Secondly, time courses were extracted from the dynamic imaging series for target regions guided by organ locations in the corresponding anatomical X-ray CT images. For each region of interest (heart, lung, liver, kidney, tumor), a 1 mm3 volume seed region was chosen for correlation analysis. Then a Pearson correlation coefficient was calculated between each seed region and every other voxel's throughout the imaging volume (Fig1). For each seed, the images show high correlation with the surrounding voxels and the expected shapes of the heart, lung, liver, kidney and tumor are retrieved. Note that the seed region for the kidney on the left, accurately identifies the kidney on the right and vice versa (i.e. there is high correlation between the left and right kidney). The anatomical co-registration in this dataset also serves to validate the performance of the dynamic FMT imaging and the accuracy of the seed-based analysis in delineating the shapes of the different internal organs. In summary, this technique provides a powerful pharmacokinetic analysis of optical agents which has potential for reporting the disease state of the internal organs and to monitor their response to therapeutic agents.

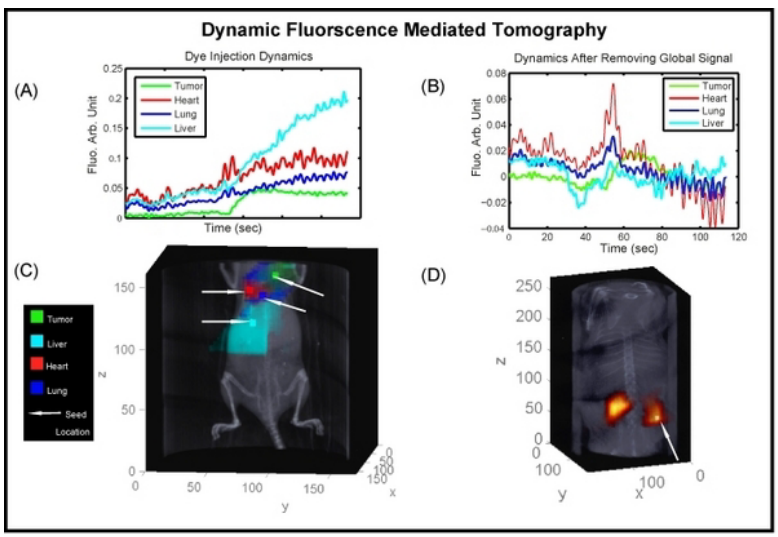


Figure 1: (A) Time traces from seed regions in different organs are used for correlation analysis. Small arrows represent seed locations. (B) Time courses after removal of a global signal associated with systemic circulation. (C) Correlation map color coded and co-registered to an anatomical X-ray CT. Each seed shows high correlation with the surrounding voxels and demarcates the expected shapes of the heart, lung, liver, and tumor.(D) Correlation map for a dorsal view, co-registered to its corresponding CT, using a seed region in the right kidney. The correlation map shows high values in the functionally related left kidney.

Disclosure of author financial interest or relationships:
**M. Solomon**, None; **W.J. Akers**, None; **R. Nothdurft**, None; **S. Achilefu**, None; **J.P. Culver**, None.

Presentation Number **P391**
Poster Session 2
September 6, 2012 / 15:15-15:15 / Room: The Liffey

# Real-time Intravital Multiphoton Fluorescence Microscopy of Nanoparticle Trafficking and Sub-Hepatic Metabolism

***Jeffrey S. Souris***[1], *Shih-Hsun Cheng*[4,3], *Feng Chieh Li*[2], *Chin-Tu Chen*[1], *Leu-Wei Lo*[3], [1]*Department of Radiology, The University of Chicago, Chicago, IL, USA;* [2]*Department of Physics, National Taiwan University, Taipei, Taiwan;* [3]*Division of Medical Engineering Research, National Health Research Institutes, Zhunan, Taiwan;* [4]*Institute of NanoEngineering and MicroSystems, National Tsing Hua University, Hsinchu, Taiwan. Contact e-mail: sourisj@uchicago.edu*

Nanoparticles that do not undergo renal excretion or *in vivo* degradation generally accumulate in the liver, often with undesirable consequences. However, little is known of the dynamics of nanoparticle uptake or fate in this environment. In the current work, we demonstrate the use of *in vivo* multiphoton fluorescence microscopy to track, with sub-cellular resolution, the hepatic uptake and metabolism of nanoparticles in real-time. To accomplish this task we synthesized ~100 nm diameter mesoporous silica nanoparticles (MSNs) by conventional sol-gel chemistry, incorporating fluorescein isothiocyanate (FITC) within the MSN's silica framework during co-condensation. Such topology considerably protects the 2-photon excitable fluorophore from photobleaching and $O_2$ quenching. To assess the significance of nanoparticle charge in hepatic sequestering, MSN surface charge modifications were made by post-synthesis exposure of the nanoparticles to 3 different concentrations of 3-aminopropyl-trimethoxysilane (APTMS) to yield FITC-MSN (unmodified), FITC-MSN-1X (modified with 1 equivalent concentration of APTMS), and FITC-MSN-3X (modified with 3 equivalent concentration of APTMS). Morphologies of these resulting moieties were then characterized by transmission electron microscopy, dynamic light scattering, $N_2$ adsorption-desorption isotherm analysis, and zeta potential measurement. Real-time intravital multiphoton microscopy was accomplished by using a 780 nm titanium-sapphire laser excitation source in conjunction with a galvanometer-driven x-y raster scanning mirror and an optically-modified conventional inverted microscope. Fluorescence and second harmonic generation signals were collected in epi-illuminated / back-scattered geometries and processed using dichroic mirrors and band-pass filters into four simultaneous detection channels: 390±10, 460±25, 525±25, and 590±40 nm. Direct visualization of anatomy was achieved by the surgical implantation of glass/metal hepatic imaging chambers in C57BL/6 mice - held in registration via a window-mating adapter plate on the microscope's specimen stage. With the fenestrated animal affixed to the microscope's specimen stage, FITC-MSNs were administered through an indwelling jugular vein catheter. Approximately 7 minutes post-injection, negatively charged FITC-MSNs (Figure1a, left) began to aggregate in hepatic sinusoids. After ~26 minutes, significant aggregation of negatively charged FITC-MSNs became evident within the hepatic vasculature (Figure 1a, right). No aggregation of positively charged FITC-MSN-3X nanoparticles in hepatic blood vessels was observed (Figure 1b, all). However, substantial hepatic endosomal accumulation of FITC-MSN-3X nanoparticles was observed 30 minutes following their injection, perhaps reflecting apolipoprotein E and IgA -binding enhanced uptake. Ongoing studies are aimed at substantiating our postulation that the aggregation of negatively charged FITC-MSNs in hepatic vasculature arises first from binding of serum proteins to nanoparticles, followed by their opsonin-mediated uptake by macrophages lining the walls of sinusoids.

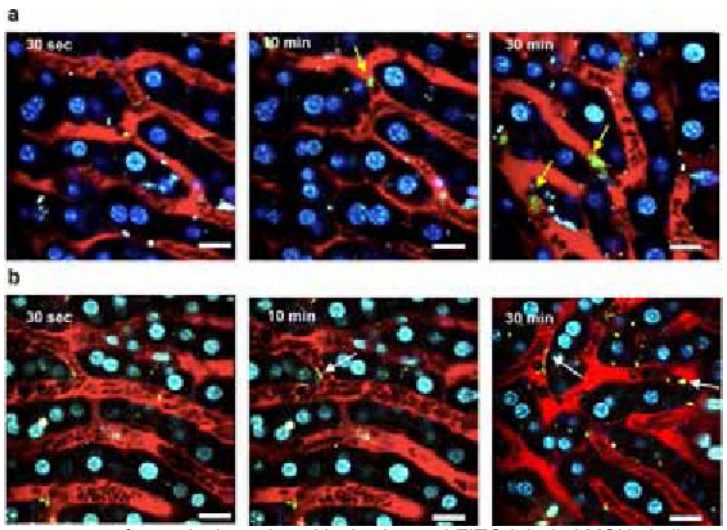


**Figure 1**. Real-time multiphoton frame captures of negatively and positively charged FITC-labeled MSNs in liver, acquired approximately 30 µm below the capsule. Times indicate period post-injection of (a) FITC-MSN (yellow arrows) and (b) FITC-MSN-3X (white arrows). Images, with 50 µm scale bars, were merged from three channels - Red: rhodamine-dextran R6G staining of sinusoids, Green: fluorescence of FITC-MSNs, and Blue: hepatocyte nuclei labeled with Hoechst 33342.

Disclosure of author financial interest or relationships:
**J.S. Souris**, None; **S. Cheng**, None; **F. Li**, None; **C. Chen**, BioMed Global, Consultant; RefleXion, Consultant; **L. Lo**, None.

Presentation Number **P392**
Poster Session 2
September 6, 2012 / 15:15-15:15 / Room: The Liffey

# Light transport in turbid media based on simplified spherical harmonics coupled with radiosity theory

*Defu Yang[1], Xueli Chen[1], Xiaochao Qu[1], Jimin Liang[1], **Jie Tian**[1,2], [1]School of Life Sciences and Technology, Xidian University, Xi'an, China; [2]Medical Image Processing Group, Institute of Automation,CAS, "Beijing,100190", China. Contact e-mail: tian@ieee.org*

Cavity cancer, such as gastric cancer, bladder cancer and cervical cancer, still remain difficlut to detect in the early stage with the existing techniques. In the existing techniques, bad reconstructed images would be obtained without the special disposal of the cavity region (non-scattering region). Several solutions have been proposed to handle with the light propagation in the non-scattering region, such as the hybrid radiosity-diffusion model (HRDM). The HRDM that applied for the interested region that scattering dominated over the absorption limits the application for whole body imaging. So we proposed the hybrid simplified spherical harmonics approximation coupled with radiosity theory (SPN-radiosity) method (HSPM) to model the light propagation in turbid media. In the HSPM, the SPN equation used to describe the light propagtion in scattering region while the radiostiy theory model the light transport in cavity. The SPN approximation and the radiosity theory were coupled by a special boundary condition to model the light transport in turbid media. Here, the simulation platform of the digital mouse was used to verify the accuracy of the HSPM. The torso section of the digital mouse atlas was extracted from CT and cryosection data and main organs were selected to simulate the tissue's heterogeneity. In this simulation stomach was regard as the nonscattering region. To simulation the source, a solid sphere of 1mm radius was located around the center of the body. The resulte caculated by HSRM and the one caculated by HRDM were both compared with the simulated results obtained by MOSE which based on Monte Carlo method. Compared results were respectively chosen at the height of z=26.5mm, z=30.5mm and z=34.5mm. The compared results demonstrated that the SPN-radiosity method performed better than diffusion-radiosity method, as shown in Fig.1(b). Concluded our compared results suggested that the HSRM could be used to model light propagation in turbid medium and has a more extensive applicability than HRDM.

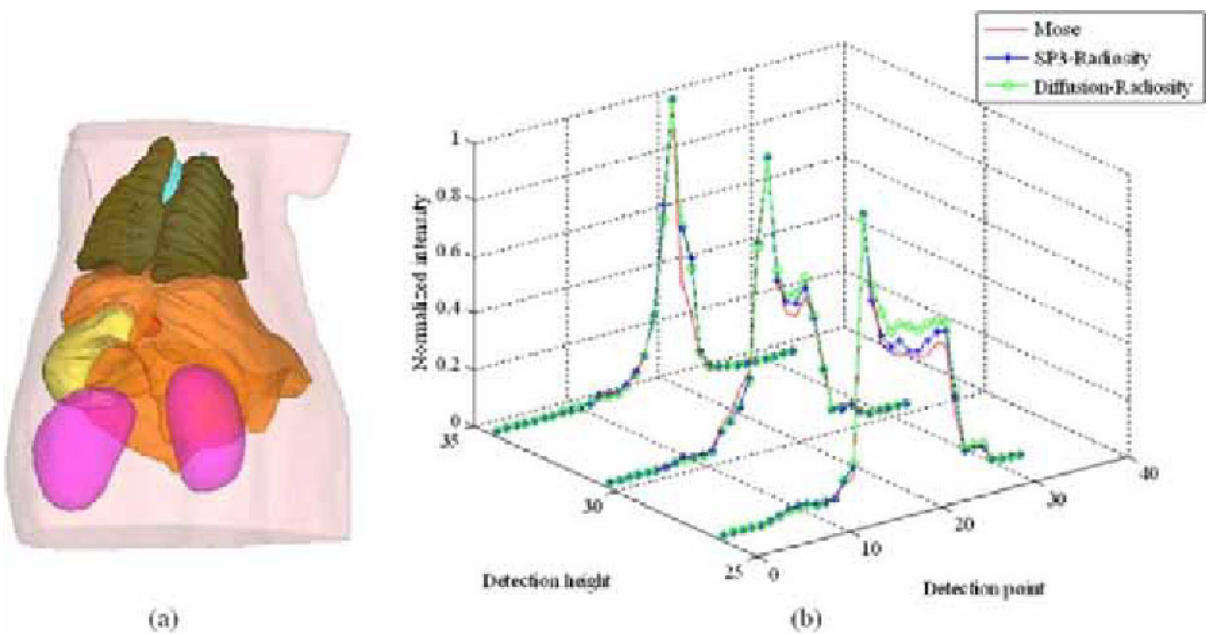


Fig.1 (a) the digital mouse atlas in which contains the main organs: muscle,heart,stomach,liver,lung, kidney. The red solid sphere is the light source which radius is 1mm. (b) the compared results among the SPN-radiosity obtained, the diffusion-radiosity method and the simulation platform MOSE based Monte Carlo method acquired.

Disclosure of author financial interest or relationships:
**D. Yang**, None; **X. Chen**, None; **X. Qu**, None; **J. Liang**, None; **J. Tian**, None.

Presentation Number **P393**
Poster Session 2
September 6, 2012 / 15:15-15:15 / Room: The Liffey

# A Monte Carlo method based endoscopic optical imaging study using Molecular Optical Simulation Environment

*Shenghan Ren[1], Xueli Chen[1], Xiaochao Qu[1], Jimin Liang[1], **Jie Tian**[1,2], [1]School of Life Sciences and Technology, Xidian University, Xi'an, China; [2]Medical Image Processing Group, Institute of Automation,CAS, "Beijing,100190", China. Contact e-mail: tian@ieee.org*

The optical imaging is a non-invasive technique that has become a valuable tool for the noninvasive detection because of its significant advantages in detection sensitivity, image quality, and system simplicity. However, the optical imaging is not appropriate for the detection of internal organs that are deep inside the large animal or human body. These mesurements are either inaccurate or immeasurable due to the severe attenuation of light. Endoscopic optical imaging (EOI) overcomes this limitation and improves this inaccuracy or immeasurability by taking the detector closer to the region of interest with a minimally invasive approach. In order to model EOI, establishing a realistic endoscopic geometry and developing an accurate forward model are needed. The forward model is difficult to solve with deterministic techniques especially in complex tissue. However, Monte Carlo (MC) method is a statistical method can solve the problem by sampling a mass of random variables relevant to the physical processes. MC method has been generally considered as the gold standard of modeling light propagation in heterogeneous tissues and used to validate the results obtained by other models. Molecular Optical Simulation Environment (MOSE) which was developed by our team is a simulation platform for light propagation in biological tissue. We added the function of EOI simulation in its new version. The Monte Carlo method based EOI was studied by using MOSE. As shown in fig.1, a three-dimensional heterogeneous numerical phantom including the endoscopic geometry was designed and used to study the light propagation of EOI. The endoscopic geometry was a cylinder coupled with a region of cavity (tissue T5) where the cylinder denotes the CCD detector. The detailed geometrical parameters and relevant optical properties are listed in table 1. The simulation result is shown in fig. 1. In general, the light propagation in EOI is studied with Monte Carlo method. The result has a good agreement with that of deterministic method and real experiment.

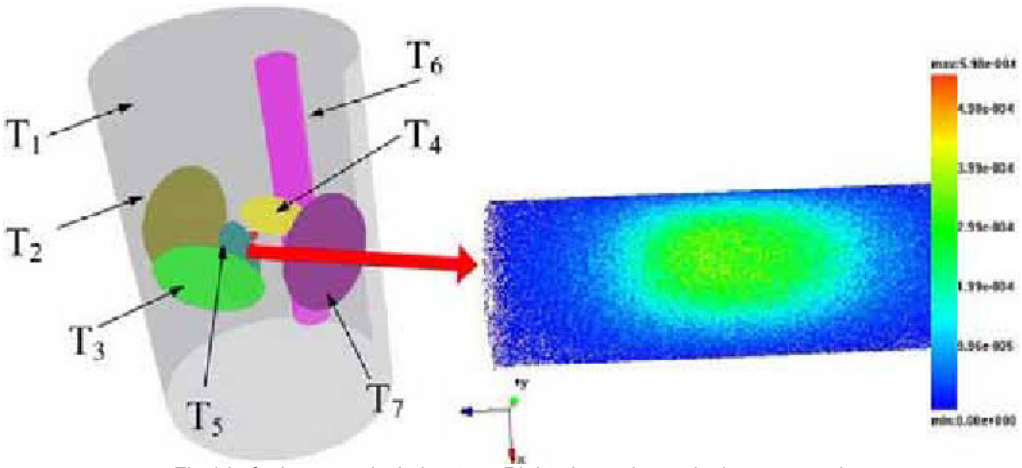


Fig.1 Left: the numerical phantom; Right: the endoscopic detector result

Table 1 geometrical parameters and relevant optical properties of the phantom. In unit of mm

| Tissue | shape | center | size | absorption coefficient | Reduced Scattering Coefficient |
|---|---|---|---|---|---|
| T1 | cylinder | (0, 0, 0) | (120, 120, 300) | 0.0010 | 12.273 |
| T2 | ellipsoid | (-80, 0, 0) | (70, 60, 60) | 0.3670 | 22.091 |
| T3 | ellipsoid | (0, -80, 0) | (60, 30, 30) | 0.0884 | 2.3383 |
| T4 | ellipsoid | (0, 30, 0) | (50, 30, 30) | 0.0786 | 10.066 |
| T5 | ellipsoid | (0, -40, 0) | (70, 20, 20) | 0 | 0 |
| T6 | cylinder | (0, 80, 0) | (20, 30, 160) | 0.1021 | 24.144 |
| T7 | ellipsoid | (80, 0, 0) | (70, 60, 60) | 0.3670 | 22.091 |

Disclosure of author financial interest or relationships:
**S. Ren**, None; **X. Chen**, None; **X. Qu**, None; **J. Liang**, None; **J. Tian**, None.

Presentation Number **P394**
Poster Session 2
September 6, 2012 / 15:15-15:15 / Room: The Liffey

# Optimal selection of imaging wavelengths for spectral unmixing

***Martijn Van de Giessen***[1,2], *Laura Mezzanotte*[3], *Jouke Dijkstra*[1], *Boudewijn Lelieveldt*[1,2], [1]*Division of Image Processing, Leiden University Medical Center, Leiden, Netherlands;* [2]*Department of Intelligent Systems, Delft University of Technology, Delft, Netherlands;* [3]*Department of Endocrinology, Leiden University Medical Center, Leiden, Netherlands. Contact e-mail: m.vandegiessen@lumc.nl*

Introduction Real-time multispectral intra-operative imaging of fluorescent probes imposes constraints on the imaging hardware that are not present in pre-clinical imaging. First, all spectral bands must be imaged simultaneously. This constraint, together with the small form factor of the camera limits the number of imaged wavelengths. The absolute minimum number of acquired spectral bands is the number of probes (and tissue auto-fluorescence) that need to be separated. For probes with peaks that are far apart, one can select imaging bands centered on the peak wavelengths. However, for peaks close together or for probes with broad spectra measurements at other wavelengths may give better unmixing results. In this work a method is proposed to determine the optimal measurement wavelengths based on measured spectra. Methods Assuming a linear mixing model, the measured light intensity in a single spectral band to a mix of probes can be described by a row in a mixing matrix. Similar rows (i.e. measurements) add little information about the ratio between imaged probes, contrary to very different rows. Mathematically, in the latter case, rows are linearly independent, while in the former case they are (almost) linear dependent. The condition number of a matrix [1] is small for spectra that are linearly independent (the desired situation). Therefore we propose to select wavelengths such that the condition number is minimal. Unmixing results using 'optimal' wavelengths are compared to unmixing using 'peak' wavelengths of the probes for simulated multispectral images with increasing noise levels. Probe spectra are measured with the Maestro system between 630nm and 850nm (interval 20nm). The experiment is repeated for all combinations of 2 to 5 probes: AF680, QD700, AF750, QD800 and skin auto-fluorescence. For in-vitro multi-spectral luminescence data from the IVIS Spectrum system, the unmixing results using optimized and peak wavelengths are compared to unmixing based on all acquired wavelengths (500nm to 700nm, interval 20nm) in in-vitro experiments with wells of two mixed probes: CBG99 (540nm) and PpYRE8 (620nm). Results In simulations the 'peak' unmixing errors were on average 2.86 times larger than the 'optimal' unmixing errors. This number varied from comparable errors for peaks far apart (e.g. AF680 and AF750) to a 9.01 times larger error for peaks close together (AF680 and QD700). Selecting the optimal wavelengths was especially beneficial for 3 or more probes. The IVIS in-vitro measurements showed that unmixing with the 'optimal' wavelengths was 8.9% more precise than using the 'peak' wavelengths. A qualitative example is given in the figure. Conclusions The results clearly showed that selecting the optimal wavelengths as proposed gives almost 3 times more accurate estimates than measuring at the spectral peaks of the imaged probes, both in simulations as in real measurements. Acknowledgement This research was supported by the Center for Translational Molecular Medicine (MUSiS). [1] Silvan-Cardenas and Wang, Fully Constrained Linear Spectral Unmixing: Analytic Solution Using Fuzzy Sets, IEEE Trans. Geoscience and Remote Sensing, 2010

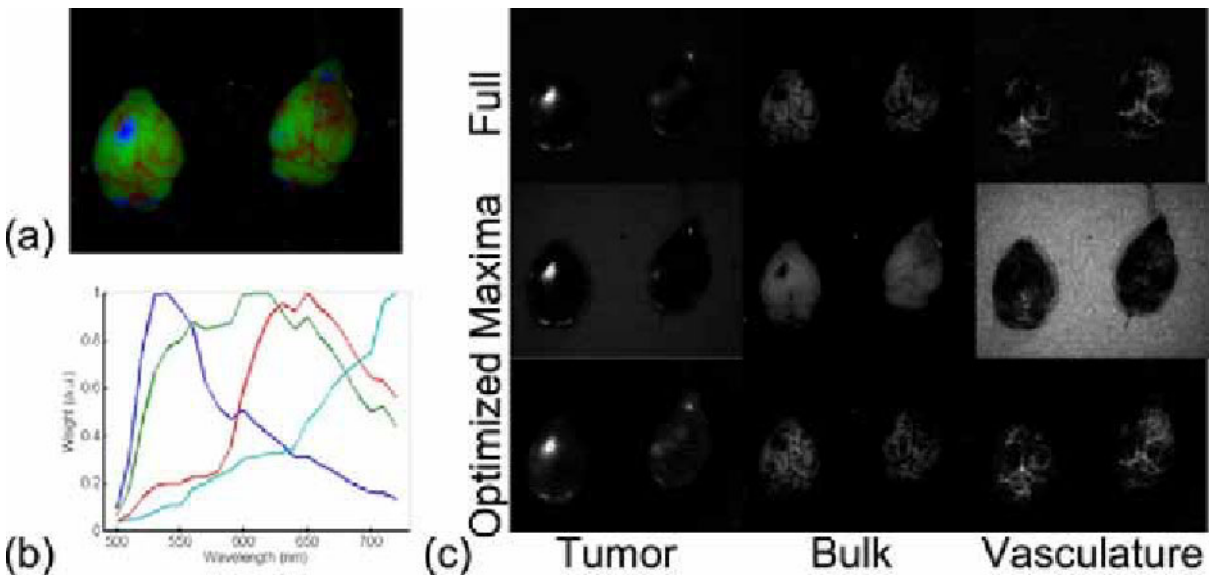


(a) False color image of mice brains with tumor (blue) and bulk (green) and vasculature (red). (b) Spectra corresponding to the brain structures in (a) with additionally the background (cyan). (c) Unmixing results using the full spectrum (21 wavelengths), using 4 wavelengths at the maxima of the spectra and using 4 optimized wavelengths. Especially in the vasculature the difference between unmixing using maxima and optimized wavelengths can be appreciated.

Disclosure of author financial interest or relationships:
**M. Van de Giessen**, None; **L. Mezzanotte**, None; **J. Dijkstra**, None; **B. Lelieveldt**, None.

Presentation Number **P395**
Poster Session 2
September 6, 2012 / 15:15-15:15 / Room: The Liffey

# A new Mathematical Strategy for Raman Spectral Imaging Analysis

***Dominique Van de Sompel**, Ellis Garai, Cristina Zavaleta, Sanjiv S. Gambhir, Radiology, Stanford University, Stanford, CA, USA.*
*Contact e-mail: dominiqu@stanford.edu*

Raman spectroscopy is a powerful technique to quantify compounds present in a sample using the compound-specific spectra generated by inelastic scattering of laser light. Among its many promising areas of application, Raman spectroscopy has gained growing interest from the biomedical research community, where it promises to enable sensitive and multiplexed imaging of nanoparticles for both diagnostic and therapeutic applications. Raman spectra require analysis by an appropriate computer algorithm. The most commonly used algorithm is the least squares (LS) method. However, LS is sensitive to variations in the background signal when the analyte (compound of interest) signal is weak. We propose a novel method to improve the robustness of concentration estimates to natural variability in both the analyte and background spectra. The method is an extension of the standard LS method, and takes the form of a hybrid least squares and principal component analysis algorithm (HLP). The improved performance of HLP is achieved by allowing the declared reference spectra to vary in accordance with their principal components, as observed in previously acquired training sets. The amount of variation allowed is constrained by the eigenvalues of the principal component analysis of the training spectra. We demonstrate improved robustness compared to LS with a polynomial background model as well as the hybrid linear analysis (HLA) technique. HLA is a state-of-the art method designed to improve robustness to background variability when the analyte spectrum is known. Our analyte is a solution of Raman-enhanced gold-silica nanoparticles. These particles have garnered significant interest because of their multiplexing capabilities, high sensitivity, and ability to be targeted to particular biomarkers in vivo. We demonstrate the superior performance of HLP compared to LS and HLA on both simulated and experimental data. For our simulated data, we digitally combined nanoparticle and paraffin spectra in several dynamic ratios. For our experimental data, we placed serial dilutions of nanoparticles on both an artificial, variable background phantom and an excised pig colon. All experiments showed an improvement by HLP over LS and HLA in the closeness of fit as well as the accuracy of concentration estimates. The closeness of fit was measured by the Durbin-Watson statistic, which quantifies positive serial correlation in the error residuals. The average reductions in positive serial correlation by HLP over LS and HLA were 59% and 15%, respectively. The improvement in concentration estimates was greatest for lower nanoparticle concentrations, where the reductions in concentration error compared to LS and HLA were on average 30% and 5%, respectively. The experimental data also showed a two-fold improvement in the lowest concentration detectable. Lastly, our method was shown to increase sensitivity and reduce cross-talk in multiplexing applications. The results of this work are significant because improved sensitivity and multiplexing capabilities push the limits of important Raman applications such as early colon cancer detection and intra-operative tumor margin detection.

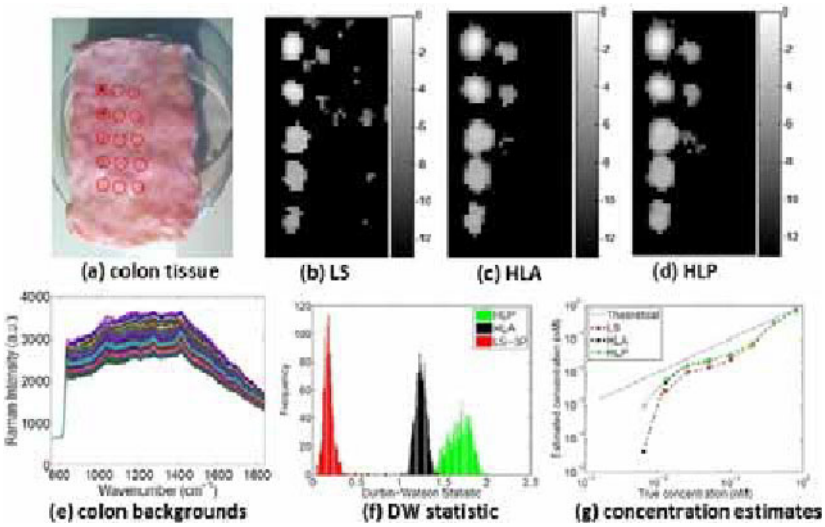


Figure 1: (a) Excised pig colon tissue with nanoparticle drops (red circles). (b-d) Log2 of nanoparticle concentration estimates (nM) by LS, HLA and HLP. (e) Natural variability in pig colon background spectra. (f) Histogram of the Durbin-Watson statistic for the error residuals at all pixels in the raster scan of the pig colon sample with nanoparticle drops. A value of two indicates no positive serial correlation in the error residuals, which indicates a better fit and is therefore desired. Values towards zero signify increasing degrees of positive serial correlation. (g) Concentration estimates by LS, HLA and HLP.

Disclosure of author financial interest or relationships:
**D. Van de Sompel**, None; **E. Garai**, None; **C. Zavaleta**, None; **S.S. Gambhir**, General Electric, Grant/research support; Bayer-Schering, Grant/research support; Sanofi-Aventis, Grant/research support; CellSight, Stockholder; ImaginAB, Stockholder; Enlight, Stockholder; Endra, Stockholder; Bracco, Consultant; NinePoint Medical, Stockholder; Visualsonics, Consultant .

Presentation Number **P396**
Poster Session 2
September 6, 2012 / 15:15-15:15 / Room: The Liffey

# Successful intraoperative identification of ureters using near-infrared fluorescence and low-dose Methylene Blue

***Floris Verbeek***[1], *Joost van der Vorst*[1], *Boudewijn Schaafsma*[1], *Rutger-Jan Swijnenburg*[1], *Baptist Trimbos*[2], *Henk W. Elzevier*[3], *Clemens Lowik*[4], *Cornelis J. van de Velde*[1], *John V. Frangioni*[5], *Alexander Vahrmeijer*[1], [1]*Surgery, Leiden University Medical Centre, Leiden, Netherlands;* [2]*Gynecology, Leiden University Medical Centre, Leiden, Netherlands;* [3]*Urology, Leiden University Medical Centre, Leiden, Netherlands;* [4]*Endocrinology, Leiden University Medical Centre, Leiden, Netherlands;* [5]*Deparment of Medicine, Beth Israell Deaconess Medical Center, Harvard Medical School, Boston, MA, USA. Contact e-mail: f.p.r.verbeek@lumc.nl*

Background: Iatrogenous ureteral damage is a rare, but serious complication during lower abdominal surgery. Since ureteral damage is often missed, it can lead to severe morbidity such as genitourinary fistula formation or major renal complications. Near-infrared (NIR) fluorescence imaging is a promising technique that offers intraoperative, real-time, visual information during surgery. Methylene blue (MB) becomes a moderate-strength fluorophore emitting at ≈ 700 nm when diluted to levels that are almost undetectable to the human eye. Since MB is cleared renally, we hypothesized that low-dose MB can be used as a NIR fluorescent tracer for intraoperative identification of the ureters. Methods: At present, eleven of the intended 12 patients that underwent lower abdominal surgery were included in this feasibility and dose finding study. To determine optimal timing and dose, we intravenously injected MB, at doses of 0.25, 0.5 or 1 mg/kg, after exposure of the ureters. Subsequently intraoperative NIR fluorescence imaging was performed using the Mini-FLARE imaging system for up to 60 min following MB injection. Results: In all patients the ureter was clearly visualized using NIR fluorescence in a time window from 5 to 60 min. Maximal contrast was obtained at 45 minutes post injection. The mean signal-to-background ratio of the ureter versus surrounding tissue was 2.48 ± 0.72 (N = 4), 6.49 ± 5.95 (N = 4) and 10.01 ± 8.80 (N = 3) for the 0.25, 0.5 and 1 mg/kg groups, respectively. No significant differences between dose groups were found (P = 0.28) Conclusions: This study demonstrates the first successful use of NIR fluorescence using low-dose MB for the identification of the ureters during lower abdominal surgery.

Disclosure of author financial interest or relationships:
**F. Verbeek**, None; **J. van der Vorst**, None; **B. Schaafsma**, None; **R. Swijnenburg**, None; **B. Trimbos**, None; **H.W. Elzevier**, None; **C. Lowik**, None; **C.J. van de Velde**, None; **J.V. Frangioni**, None; **A. Vahrmeijer**, None.

Presentation Number **P397**
Poster Session 2
September 6, 2012 / 15:15-15:15 / Room: The Liffey

# Polarization sensitive optical computed tomography

***Giannis Zacharakis***[1], *Vadim Y. Soloviev*[2], *Teresa Correia*[2], *Athanasios Kokolakis*[3], *Rosy Favicchio*[2], *Androniki Toska*[3], *Simon Arridge*[2], *Jorge Ripoll*[1], [1]*Institute of Electronic Structure and Laser (IESL), Foundation for Research and Technology - Hellas (FORTH), Heraklion, Greece;* [2]*Computer Science, Univercity College London, London, United Kingdom;* [3]*Department of Dermatology, University Hospital of Heraklion, Heraklion Crete, Greece. Contact e-mail: zahari@iesl.forth.gr*

Optical computed tomography has been applied in a variety of applications covering a wide range of scales from microscopy to mesoscopy and macroscopy 1. It can be considered the optical equivalent of X-ray-CT and it is applied to structures where light absorption is the dominant process. Applications range from imaging in developmental biology, gene expression, disease monitoring, cancer treatment etc. It has however, been shown to produce very valuable results both qualitatively and quantitatively in applications where the samples exhibit significant scattering, even if simple photon back-projection algorithms are used. Such applications include Optical dosimetry in cancer treatment plans 2 and Optical Projection Tomography 3. This can be greatly aided if small apertures are used for the detection reducing the contribution of diffused light. Here we present a new system that exploits polarization sensitive measurements to improve on current imaging limits, when detecting light transmitted through scattering samples. In Polarization Optical computed Tomography (POT) the two states of polarization are used to distinguish between light that travels through and around the samples and hence between light that has been scattered or attenuated. In this study phantoms and tissue biopsies from skin cancer lesions have been used. The experimental setup is depicted schematically in Figure 1, together with characteristic reconstructions from a phantom with varying diffusion. The light source was a white light lamp consisting of 80 LEDs. A diffuser was placed between the light source and the optical components enabling homogeneous illumination and the light was then guided to a linear polarizer. The sample was positioned on a rotational stage covering 360 degrees with adjustable rotation step. Light signals were detected by a sensitive CCD camera equipped with a 50mm f/2.8 objective lens. A second polarizer was attached to the input of the lens and its axis was adjusted either parallel or perpendicular to the polarization of the illumination light. The whole experimental procedure was controlled with in-house developed software and images were stored on a PC. The reconstructions correspond to 3D attenuation maps of the samples, which can then be used for identifying the lesion, calculating its depth and characterizing its state (malignant or benign). A large number (n=20) of biopsy sample were measured, including atypical navi and malignant melamomas and the results are in excellent agreements with those provided by histology, demonstrating the potential of the technique. References 1. V. Ntziachristos, Going deeper than microscopy: the optical imaging frontier in biology, Nat. Methods, 7, 603 - 614 (2010) 2. A. E. Papadakis, G. Zacharakis, T.G. Maris, J. Ripoll, J. Damilakis, A New Optical-CT Apparatus for 3-D Radiotherapy Dosimetry: Is Free Space Scanning Feasible?, IEEE Trans. Med. Imaging, 29, 1204 - 1212 (2010) 3. H. Meyer, A. Darrell, A. Metaxakis, C. Savakis and J. Ripoll, Optical Projection Tomography for In-Vivo Imaging of Drosophila melanogaster, Microscopy and Analysis, 22, 19 - 22, (2008)

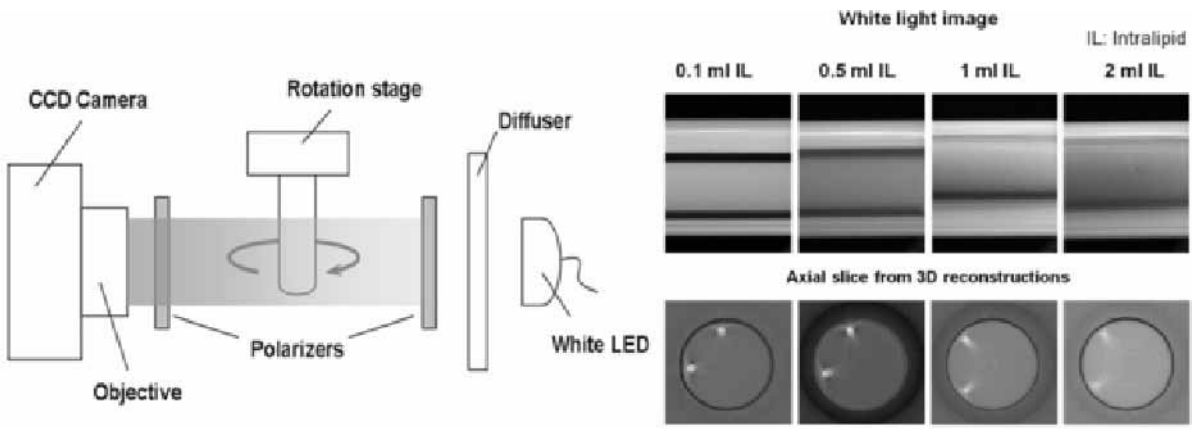


Experimental setup for polarization sensitive optical computed tomography and image reconstructions of a phantom with varying scattering properties.

Disclosure of author financial interest or relationships:
**G. Zacharakis**, None; **V.Y. Soloviev**, None; **T. Correia**, None; **A. Kokolakis**, None; **R. Favicchio**, None; **A. Toska**, None; **S. Arridge**, None; **J. Ripoll**, None.

Presentation Number **P398**
Poster Session 2
September 6, 2012 / 15:15-15:15 / Room: The Liffey

# Fast reconstruction techniques for 360 degrees in-vivo tumour imaging, using datasets from a hybrid Fluorescence Molecular Tomography - X Ray Computed Tomography system to incorporate prior information

***Athanasios Zacharopoulos***[1,2], *Jorge Ripoll*[1], *Simon Arridge*[2], [1]*Inst. of Electronic Structure & Laser, FORTH-IESL, Heraklion, Crete, Greece;* [2]*CMIC, UCL, London, United Kingdom. Contact e-mail: azacharo@iesl.forth.gr*

Recent developments in Fluorescence Molecular Tomography (FMT) include the introduction of X-ray Computed tomography (XCT) to a hybrid system that allows for 360 degrees projections viewing for both modalities. Using the XCT derived structural information as prior information to the FMT reconstruction and the 360 degrees system to increase the number of viewing angles enables the full tomographic reconstruction, improves imaging resolution, and enhances visualization of the results. The additional structural information from the XCT is utilised to build an accurate geometrical model for the finite elements solution of the FMT reconstruction. In addition atlas based and extracted from the segmented XCT image, anatomical information procures optical parameters distributions (absorption and scattering) used as priors for the forward calculations employed. In non-contact Fluorescence Molecular Tomography, the large number of measurements poses a challenge since the reconstruction methods used rely on the inversion of a derivative operator and the explicit formulation and storage of this operator in a matrix is generally not feasible. We adopted a matrix-free method that addresses the problems of large data sets and reduces the computational cost and memory requirements for the reconstructions. Using experimental data from the Helmholtz Zentrum Muenchen we tested the fast algorithm using the pre-segmented XCT image to reconstruct for a Tumour in the neck area with reconstruction times faster than 2 minutes for 1046017 data points on the surface of the mouse. The tumour was recovered successfully as it can be seen in the three dimensional display of the reconstructed tumour with the XCT image, providing a fast and useful visualisation tool.

Disclosure of author financial interest or relationships:
**A. Zacharopoulos**, None; **J. Ripoll**, None; **S. Arridge**, None.

Presentation Number **P399**
Poster Session 3
September 7, 2012 / 15:15-15:15 / Room: The Liffey

# Non-linear ultrasound imaging detects liposomes diffusion and accumulation in tumors

***Pierangela Giustetto***[1], *Kristen M. Meiburger*[2], *Mauro Castano*[3], *Cinzia Boffa*[1], *Enzo Terreno*[1], *Filippo Molinari*[2], [1]*Molecular Imaging Center, University of Torino, Torino, Italy;* [2]*Biolab Dept. of Electronics and Telecommunications, Politecnico of Torino, Torino, Italy;* [3]*Bracco Research Center, Bracco Imaging SpA, Colleretto Giacosa, Torino, Italy. Contact e-mail: pierangela.giustetto@unito.it*

Molecular ultrasound imaging (MUI) has emerged as a promising new non-invasive imaging strategy to study biological processes at a molecular level. Ultrasounds have advantages such as: high spatial and temporal resolution, real time imaging, no dangerous radiations, non-invasiveness, repeatability of clinical examination and relatively low costs. Molecular ultrasound contrast agents (MUCA) are nano- or micro-size particles. They can either be microbubbles (with or without specific targets) or gas-filled liposomes. The aim of this work is to study the dynamic nonlinear behavior of water-filled nano-liposomes and their accumulation in tumor during in-vivo experiments. A VEVO 2100 system (VisualSonics Inc.) equipped with an 18 MHz (MS-250) probe with frame rate of 18 fps was used. Power output was set at 4% and contrast gain at 26 dB for all images acquisitions. We studied six C57 mice that were grafted subcutaneous melanoma B16 tumor cells. First, 200 µl of stealth liposomes (DSPC encapsulated with a 300 mM solution of clinically approved MRI agent Gd-HPDO3A), with diameter of 157 nm and Gd3+ concentration of [11.7 mM], were injected in the tail vein of mice. We collected MUCA images and then, after a few hours, we repeated the experiment on the same animal by injecting untargeted microbubbles (Vevo MicroMarker, VisualSonics) with a diameter ranging from 2.3 to 2.9 micrometer. All MUCA monitoring lasted 15 minutes after injection. The pre-processing consisted of two steps: 1) manual selection of the tumor ROIs, which were kept constant for all the images of the series; and 2) motion correction for video data spatially realigned. The ROIs were drawn on the first image after injection, where contrast was maximized. We measured the two different echo-power (EP) values from nonlinear scattering signals of liposomes and microbubbles. EP values were calculated with the VEVO 2100 software package and average pixel signal intensities (SI) with the MicroDicom software. SI was expressed as Contrast to Noise Ratio (CNR) percentage. CNR results were compared using Student's t-test. Results showed significant values of the liposomes echo-power signal, even though they were lower than those of the microbubbles (fig. 1-a,b). Additionally, when low average B-mode SI values were observed (usually decreasing enhancement identifies a poor vascularization of tissue), the liposomes EP signal increased and persisted for a longer time (Table 1). These preliminary results suggest that the liposomes nanosystem commonly employed in MRI can be detected with nonlinear contrast micro-ultrasound modality. The combination of ultrasound high frequency systems and multi-functional nanoprobes might be useful to improve molecular minimally invasive imaging strategies and to increase the effect of therapeutic agents encapsulated in nanoprobes.

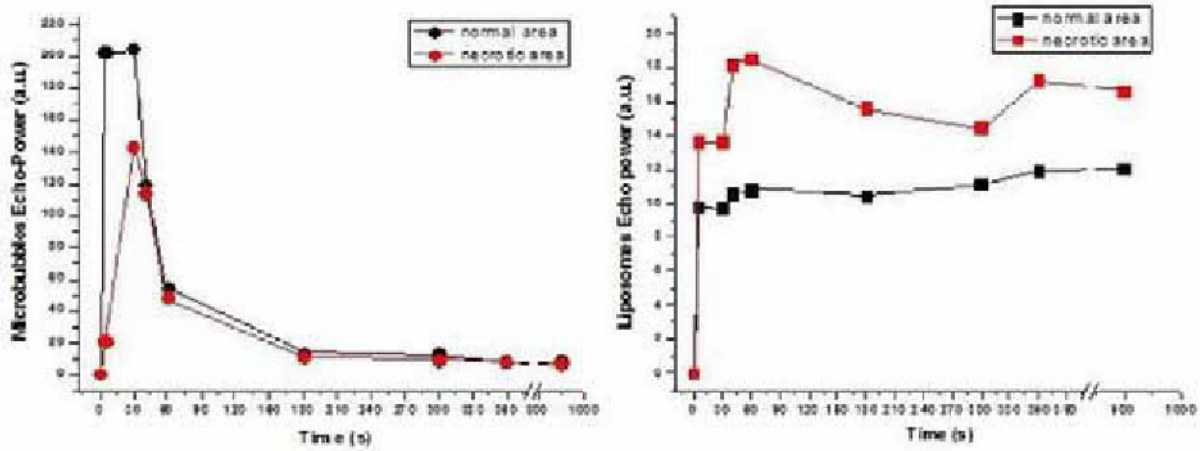


Tumor Roi area and CNR percentage values

| | ROI AREA | CNR % |
|---|---|---|
| ROI 1 | 408 | 18973 |
| ROI 2 | 230 | 10377 |
| ROI 3 | 773 | 14039 |

Disclosure of author financial interest or relationships:
**P. Giustetto**, None; **K.M. Meiburger**, None; **M. Castano**, None; **C. Boffa**, None; **E. Terreno**, Bracco Imaging, Consultant; **F. Molinari**, None.

Presentation Number **P400**
Poster Session 3
September 7, 2012 / 15:15-15:15 / Room: The Liffey

# Possible toxicological side effects after i.v. administration of iodine CT contrast agents

***Julia G. Mannheim**, Thomas Schlichthärle, Bernd J. Pichler, Department of Preclinical Imaging and Radiopharmacy, Eberhard Karls University of Tuebingen, Tuebingen, Germany. Contact e-mail: julia.mannheim@med.uni-tuebingen.de*

Small animal computed tomography (CT) imaging suffers from poor soft tissue contrast. Therefore for most imaging applications injections of contrast agents (CAs) are necessary. Previous studies already showed that six commercially available CT CAs (ExiTron nano 12000 & 6000, Exia160 & 160XL, Fenestra VC & LC), all iodine based, have different specific organ uptake. Regarding to the specific study, CAs and uptake time must be chosen carefully. However, some of those CAs could be detected up to 120 h and beyond after injection. Hence toxicological side effects can result. Aim of this study is to evaluate those six CAs regarding possible side effects after CA injection. We injected intravenously 100 µl/25 g body weight (bw) CA in C57BL/6 mice (5 mice per group, 3 mice as control) at day 1, 2 & 7. On day 2 & 7 blood samples were taken to determine blood counts. On day 2 thyroxine values (T4) were determined. On day 7 liver enzymes (ALT & AST) were additionally determined. Then mice were sacrificed and organs were harvested for further ex vivo analyses, including RT-PCR and histological staining. A decrease in bw was detected for all CA groups on day 2. For the control group no change in bw was detected over time. Bw of the CA groups was normalized after day 5 to the same level as the control group. A highly significant decrease ($p < 0.01$) of T4 values was detected for both ExiTron nano groups on day 2. For both Exia groups a significant decrease ($p < 0.05$) was detected. However, for both Fenestra groups a highly significant increase of T4 values was detected compared to the control group. We detected an increase in liver enzymes ALT & AST for both ExiTron nano groups on day 7. For both Fenestra groups an increase in ALT values was found. For hematokrit and hemoglobin values we found significantly higher values on day 2 for the Exia 160XL and Fenestra VC group. The ExiTron nano 12000 group showed a significant increase in hemoglobin. On day 7 a significant increase in hematokrit was found for the ExiTron nano 12000 and Fenestra LC group. For hemoglobin an increase for both Exia groups was detected. Thrombocyte values were highly significant decreased for both ExiTron groups and the Fenestra VC group on day 2. On day 7 a decrease was detected for both ExiTron nano groups. However, an increase was seen for both Exia groups and the Fenestra LC group. An increase in red blood cells was determined on day 2 for the Exia 160 XL, Fenestra VC and the ExiTron nano 12000 group. On day 7 an increase in red blood cells was detected for the ExiTron nano 12000 and the Fenestra LC group. No change in white blood cells was seen on day 2. On day 7 a significant increase was detected for the Exia 160 group. To conclude it was shown that the tested iodine based CAs have an influence on the physiological parameters, which was especially seen after day 1 of CA injection. Those influences shall be taken into account for CT studies as they can bias the results and might change the animal model being studied. This is specifically the case for longitudinal studies. Further histological staining and RT-PCR will prove if inflammation processes are present.

Disclosure of author financial interest or relationships:
**J.G. Mannheim**, None; **T. Schlichthärle**, None; **B.J. Pichler**, Siemens, Grant/research support; AstraZeneca, Grant/research support; Bayer Healthcare, Grant/research support; Boehringer-Ingelheim, Grant/research support; Oncodesign, Grant/research support; Merck, Grant/research support; Bruker, Grant/research support .

Presentation Number **P401**
Poster Session 3
September 7, 2012 / 15:15-15:15 / Room: The Liffey

# Ultrasound Imaging using Gas-Generating Polymeric Particles

***Hyun Su Min***[1,2], *Heebeom Koo*[1], *Kwangmeyung Kim*[1], *In-San Kim*[4], *Kuiwon Choi*[1], *Kinam Park*[5], *Yongseok Choi*[2], *Ick Chan Kwon*[1], *Moon Hee Han*[3], *Jae Young Lee*[3], [1]*Center for Theragnosis, Biomedical Research Institute, Korea Institute of Science and Technology, Seoul, Republic of Korea;* [2]*School of Life Science and Biotechnology, Korea University, Seoul, Republic of Korea;* [3]*Department of Radiology, Seoul National University Hospital, Seoul, Republic of Korea;* [4]*Department of Biochemistry and Cell Biology, Cell & Matrix Research Institute, Kyungpook National University, Daegu, Republic of Korea;* [5]*Department of Pharmacy, Purdue University, West Lafayette, IN, USA. Contact e-mail: hs-min@kist.re.kr*

Ultrasound is widely available imaging method in public due to its convenience of assessment and noninvasive way. Many kinds of microbubble type ultrasound contrast agents have been developed for improved ultrasound imaging. However, microbubble agents have short half-life in acoustic field during ultrasound imaging for its low stability. Herein, we developed gas-generating polymeric particles that may produce microbubble for ultrasound imaging instead of gas encapsulated microbubble agents. At first we prepared gas generating microsphere, continuous ultrasound imaging property was characterized with time and concentration in vitro study. For vivo, left ventricle of heart was imaged after intravenous injection of microsphere into rats. We also prepared nanoparticle using gas-generating polymer coated with Pluronic (F68). The stable F68 shell of nanoparticles enabled the rationally controlled hydrolysis after their accumulation in tumor site. Over time, nanoparticles can generate CO2, combine each other, and change into microbubbles for ultrasound imaging. In this study, we showed the ultrasound contrast increase in vitro and also imaged tumor site after tail vein injection of gas-generating nanoparticle into mice.

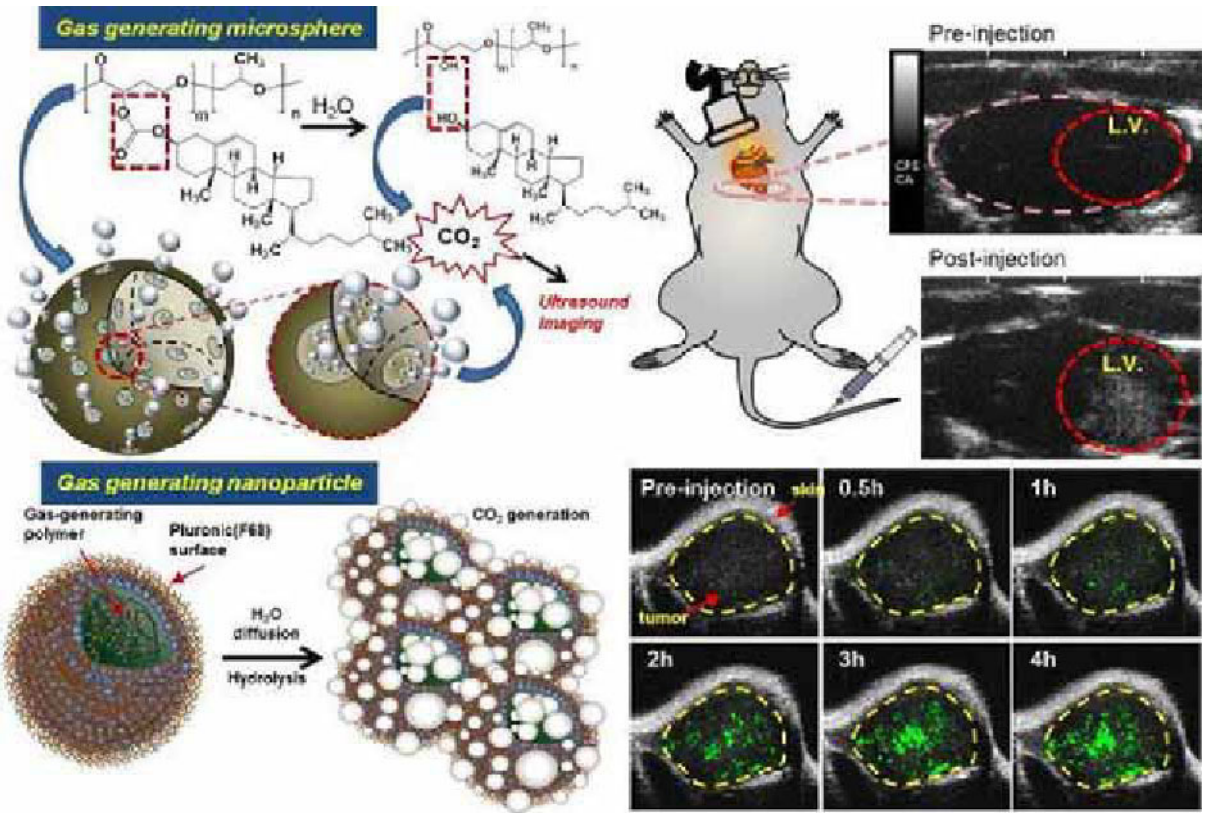


Disclosure of author financial interest or relationships:
**H. Min**, None; **H. Koo**, None; **K. Kim**, None; **I. Kim**, None; **K. Choi**, None; **K. Park**, None; **Y. Choi**, None; **I. Kwon**, None; **M. Han**, None; **J. Lee**, None.

Presentation Number **P402**
Poster Session 3
September 7, 2012 / 15:15-15:15 / Room: The Liffey

# Novel ultrasound contrast agents with a liquid core for imaging and therapy

*Ksenia Astafyeva[1], Romain P. Berti[1], Christine Contino-Pépin[4], Nicolas Tsapis[3], Wladimir Urbach[2,1], **Nicolas Taulier**[1], [1](Laboratoire d'Imagerie Paramétrique (UMR 7623), CNRS - UPMC, Paris, France; [2]Laboratoire de Physique Statistique (UMR CNRS 8550), Ecole Normale Supérieure, Paris, France; [3]Faculty of Pharmacy (UMR CNRS 8612), Université Paris Sud - CNRS, Paris, France; [4]Institut des Biomolécules Max Mousseron (UMR 5247), Université d'Avignon et des Pays de Vaucluse, Avignon, France. Contact e-mail: nicolas.taulier@upmc.fr*

The field of ultrasound contrast agents (UCA) is now expanding beyond pure ultrasonography to combine diagnostic imaging with subsequent localised drug or gene delivery. We developed new biocompatible nanosized ultrasound contrast agents (nUCA) to encapsulate hydrophobic drugs and capable to rupture under control of a focused ultrasound field. They consist of a liquid perfluorocarbon core, in which drugs can be inserted, and a shell made of either polymers or fluorinated surfactants. Because of a liquid core, our nUCA are highly stable and last several weeks in solution. Changing the perfluorocarbon core and/or the chemical structure of the shell can alter physical properties such as capsule radius, shell thickness, density and adiabatic compressibility. The relationship between these physical characteristics and their ultrasonic properties has also been investigated. Ultrasound attenuation and speed of sound measurements were carried out from 3 to 90 MHz and a model describing attenuation and speed of sound of the nUCA emulsions was proposed. Both experiments and theory showed that the thickness of the capsules shell has a great influence on the nUCA acoustic behaviour: the thinner the shell the stronger the echogenic enhancement. Ultrasound backscatter measurements at a typical medical frequency of 5 MHz showed that the echogenicity of thin capsules is comparable to that of commercial contrast agents. Finally using a commercial echography we have checked that in mice our agents induce a significant enhancement in the backscattered signal (30 dB at 14MHz). Thus our nUCA successfully exhibit simultaneous functions of both an imaging agent and a drug carrier.

Disclosure of author financial interest or relationships:
**K. Astafyeva**, None; **R.P. Berti**, None; **C. Contino-Pépin**, None; **N. Tsapis**, Guerbet, Grant/research support; **W. Urbach**, None; **N. Taulier**, None.

Presentation Number **P403**
Poster Session 3
September 7, 2012 / 15:15-15:15 / Room: The Liffey

# Developing multivalent sulphonylurea probes for beta cell imaging

***Andrej Babic***[1], *Smaragda Lamprianou*[2], *Heiner Glombik*[3], *Hans-Paul Juretschke*[3], *Paolo Meda*[2], *Norbert Lange*[1], [1]*School of Pharmaceutical Sciences, Universities of Geneva and Lausanne, Geneva, Switzerland;* [2]*Department of Cell Physiology and Metabolism, University of Geneva, Geneva, Switzerland;* [3]*Sanofi Germany, Frankfurt, Germany. Contact e-mail: andrej.babic@unige.ch*

The development of probes that would specifically bind to the insulin-producing beta cells of pancreas is a prerequisite for the development of an efficient method to non invasively image the natural history of diabetes, and to evaluate candidate therapeutic approaches. As yet, this development awaits the identification of both a suitable beta cell-specific target, and of a probe that could selectively bind to it. We posited that the simultaneous targeting of a couple of beta cell receptors with multiple copies of partially selective ligands, would improve the cell specificity and binding affinity of a probe, as well as its internalization, all changes expected to be beneficial for beta cell imaging. To test this hypothesis, we targeted the sulphonylurea receptor SUR-1 with conjugates containing various numbers of glibenclamide molecules, attached to the 5th generation of rhodamineX-labelled PAMAM-G5 dendrimers (Ø ~5.4 nm). Most of the modifications of the glibenclamide structure significantly reduced the binding affinity of the monovalent derivatives, as evidenced by increased IC50 values for the displacement of [3H]-glibenclamide in monolayer cultures of MIN6 (the IC50 value of the native form of the sulphonylurea was 60 nM). However, the IC50 of the dendrimers carrying 2-4 copies of the same glibenclamide derivatives improved by more than 10 fold, indicating an increased avidity of the multivalent probes. Thus, multivalency favors the binding of a partially selective ligand to insulin-producing cells. Several probes were synthesized, which differed by either the glibenclamide loading or the modifications of this sulphonylurea. Those probes featuring good avidity were tested for specificity of the fluorescence labelling they induce in cultures of transformed insulin-producing MIN6 cells, and unrelated cell types (HeLa and Panc-1 cells). Several multivalent probes were found to specifically label MIN6 cells, which express SUR-1, but neither HeLa nor Panc1 cells, which lack this receptor. When the experiments were run at 4 degrees C, most of the fluorescence signal was at the membrane of MIN6 cells, whereas, when the experiments were run at 37 degrees C, a sizable portion of this labelling also appeared within the cytoplasm, indicating a rapid internalization of the probe. Candidate probes were further shown to label primary mouse and human beta cells in the same pattern observed in transformed cell lines. Thus multivalent glibenclamide probes provide for the specific labelling of insulin-producing beta cells. The study provides the proof of principle that multivalent probes promote the labelling of beta cells by ligands that are not per se ideal when used in isolation. The data open the possibility that multivalent dendrimers may be versatile tools for the non invasive imaging of beta cells, by a variety of imaging modalities.

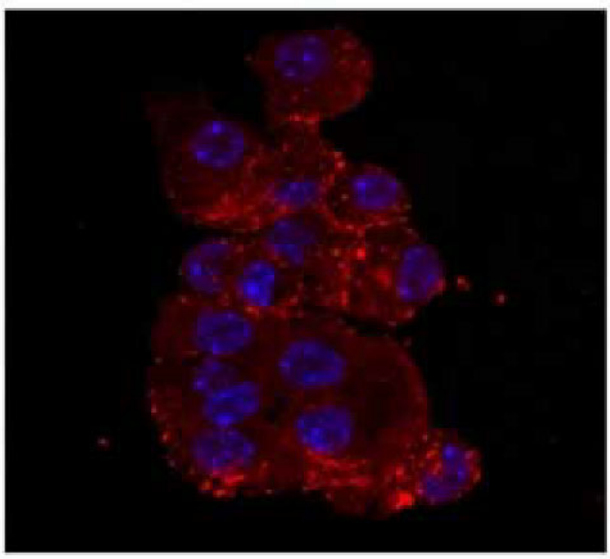

Disclosure of author financial interest or relationships:
**A. Babic**, None; **S. Lamprianou**, None; **H. Glombik**, Sanofi, Employment; **H. Juretschke**, Sanofi-Aventis D GmbH, Employment; **P. Meda**, Sanofi, Grant/research support; Servier, Grant/research support; Novo Nordisk, Grant/research support; **N. Lange**, Swiss Science Foundation, Grant/research support .

Presentation Number **P404**
Poster Session 3
September 7, 2012 / 15:15-15:15 / Room: The Liffey

# An Annulus Fibrosus Targeted Bimodal Magnetic Resonance and Fluorescence Imaging Probe for Early Diagnosis of Intervertebral Disc Degeneration

***Mingfeng Bai***[1,2], *Hye-Yeong Kim*[1], *Michael Mcclincy*[3], *Nam Vo*[3], *Gwendolyn A. Sowa*[3], *James Kang*[3], [1]*Radiology, University of Pittsburgh, Pittsburgh, PA, USA;* [2]*University of Pittsburgh Cancer Institute, University of Pittsburgh, Pittsburgh, PA, USA;* [3]*Orthopaedic Surgery, University of Pittsburgh, Pittsburgh, PA, USA. Contact e-mail: baim@upmc.edu*

Throughout the life span, nearly everyone suffers from low back pain (LBP). Despite the recent advances of LBP research, this prevalent neurological ailment remains difficult to be diagnosed and treated. The most common causes of LBP are musculoligamentous injuries (muscle strains and lumbar sprains) and intervertebral disc degeneration (IDD). Although most musculoligamentously-injured patients recover within days or weeks, disc degeneration usually causes chronic back pain. Nonsurgical treatments for LBP caused by disc degeneration often fail, whereas surgical techniques including lumbar fusion and disc replacement have limitations. Typically non-surgical treatment of IDD is most effective when it is detected early. For this reason, establishing reliable imaging method for early diagnosis of disc degeneration is critical. Unfortunately, no reliable imaging methods for early IDD detection have been established. Therefore, there is urgent need to develop imaging techniques that can characterize disc degeneration at the molecular and cellular level to provide insights into the function status of the tissue for early diagnosis of LBP. The aim of this project is to develop the first imaging probe that allows annulus fibrosus (AF) targeted MRI/optical imaging. For this purpose, we developed a functional and fluorescent AF targeting molecule (HYK-FM) and conjugated it to polyethylene glycol (PEG) to prevent plasma protein binding and absorption. The resulting PEG-HYK-FM was then attached to the surface of carboxymethyl dextran-coated iron oxide (DSPIO) to allow AF targeted MRI/optical imaging. Upon the synthesis of the HYK-FM-PEG-DSPIO probe, cytotoxicity and ex vivo imaging was investigated. HYK-FM-PEG-DSPIO and HYK-FM showed cell viability, which was comparable to clinically approved Gd-DTPA (Magnevist). Significant fluorescence signal was observed in ex vivo intervertebral disc samples treated with HYK-FM-PEG-DSPIO and HYK-FM. This indicates that our AF targeted bimodal MRI/optical imaging contrast agent has the potential to diagnose disc degeneration at early stage.

Disclosure of author financial interest or relationships:
**M. Bai**, None; **H. Kim**, None; **M. Mcclincy**, None; **N. Vo**, None; **G.A. Sowa**, None; **J. Kang**, Stryker Spine, Grant/research support .

Presentation Number **P405**
Poster Session 3
September 7, 2012 / 15:15-15:15 / Room: The Liffey

# Functionalized titanate nanotubes as a new versatile platform for theranostic applications

***Julien Boudon***[1], *Renée Mayap Talom*[1], *Jérémy Paris*[1], *Anne-Laure Papa*[1], *Claire Bernhard*[2], *Yann Bernhard*[2], *Richard A. Decréau*[2], *Franck Denat*[2], *David Vandroux*[3], *Paul Walker*[4], *Céline Mirjolet*[5], *Alexandra Oudot*[5], *Bertrand Collin*[5], *Nadine Millot*[5], [1]*Laboratoire Interdisciplinaire Carnot de Bourgogne, UMR 6303 CNRS/Université de Bourgogne, DIJON, France;* [2]*Institut de Chimie Moléculaire de l'Université de Bourgogne, UMR 6302 CNRS/Université de Bourgogne, DIJON, France;* [3]*NVH Medicinal, Centre Hospitalier Universitaire, DIJON, France;* [4]*Service de Spectroscopie par Résonance Magnétique, Centre Hospitalier Universitaire, DIJON, France;* [5]*Centre Georges François Leclerc, DIJON, France. Contact e-mail: julien.boudon@u-bourgogne.fr*

Titanate nanotubes (TiONts) have received more and more attention[1] since their pioneering discovery.[2] Recently, they have been considered for biomedical applications[3] but not yet as a carrier of therapeutic molecules. Previously, our group reported the synthesis of TiONts with a controlled morphology[4] and demonstrated that TiONts were internalized by cells without inducing cytotoxicity.[5, 6] Nevertheless, prior to their use as carriers, it was necessary to determine TiONts biodistribution which has not been reported till date. Our study lies on two biomedical imaging techniques for non-invasive and real-time in vivo evaluation of nanovectors:[7, 8] a) SPECT (particularly suitable for these studies[9]) and b) MRI with an emphasis on Ultrasmall SuperParamagnetic Iron Oxide (USPIO) particles (widely investigated as T2-MR contrast agent).[10] Herein we present the development of a novel carrier based on functionalized TiONts for their use as MRI, SPECT and Optical Imaging (OI) agents. The following pathway was investigated: (i) a direct conjugation was realized to prepare TiONts with functional groups at their surface; (ii) a macrocyclic compound chelating agent was covalently attached to the latter functional groups: either 1,4,7,10-tetraazacyclododecane-1,4,7,10-tetraacetic acid (DOTA), for 111Indium labelling (gamma-emitting radionuclide half-life t1/2 ≈ 3 days) or phthalocyanines for optical imaging; (iii) a covalent coupling of functionalized PEGs was performed on TiONts conjugates to increase TiONt dispersion, stealth and biocompatibility; (iv) USPIO-coated TiONts were also developed to combine both the magnetic detection (MRI) and the delivery of drugs for theranostic applications.[11] The grafting of the organic molecules (DOTA, PEG, phthalocyanine) and of the USPIO was proven by different analyses and among them zeta potential, XPS, elemental analysis and thermogravimetric analysis. For the first time, a systematic TiONt-based study is carried out to evaluate the impact of TiONt-conjugates on physiological properties such as blood circulation time and biodistribution in a mouse model. [1] T. Sekino, in Inorganic and Metallic Nanotubular Materials: Recent Technologies and Applications, Springer-Verlag, Berlin, 2010, Vol. 117, pp 17-32. [2] T. Kasuga, M. Hiramatsu et al., Langmuir 1998, 14 (12), 3160-3163. 10.1021/la9713816 [3] L. Niu, M. Shao et al., J. Mater. Sci. 2008, 43 (5), 1510-1514. 10.1007/s10853-007-2374-3 [4] A.-L. Papa, N. Millot et al., J. Phys. Chem. C 2009, 113 (29), 12682-12689. 10.1021/jp903195h [5] C. Mirjolet, A.-L. Papa et al., Radiother. Oncol. submitted. [6] A.-L. Papa et al., Nanotoxicology submitted. [7] R. Saito, J. R. Bringas et al., Cancer Res. 2004, 64 (7), 2572-2579. 10.1158/0008-5472.can-03-3631 [8] C. Tassa, S. Y. Shaw et al., Acc. Chem. Res. 2011, 44 (10), 842-852. 10.1021/ar200084x [9] D. Kryza, J. Taleb et al., Bioconjugate Chem. 2011, 22 (6), 1145-52. 10.1021/bc1005976 [10] K. M. Krishnan, Ieee Transactions on Magnetics 2010, 46 (7), 2523-2558. 10.1109/tmag.2010.2046907 [11] A.-L. Papa, L. Maurizi et al., J. Phys. Chem. C 2011, 115 (39), 19012-19017. 10.1021/jp2056893

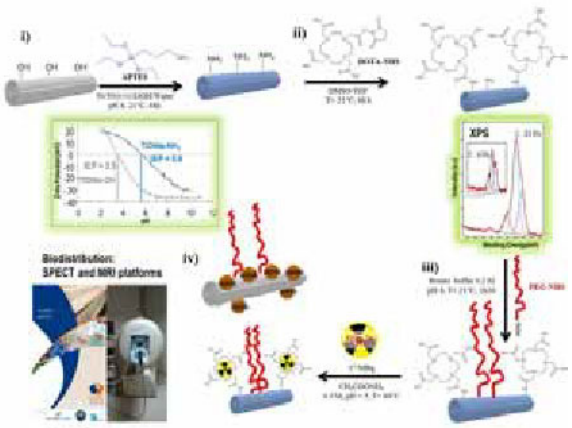


Disclosure of author financial interest or relationships:
**J. Boudon**, None; **R. Mayap Talom**, None; **J. Paris**, None; **A. Papa**, None; **C. Bernhard**, None; **Y. Bernhard**, None; **R.A. Decréau**, None; **F. Denat**, None; **D. Vandroux**, None; **P. Walker**, None; **C. Mirjolet**, None; **A. Oudot**, None; **B. Collin**, None; **N. Millot**, None.

Presentation Number **P406**
Poster Session 3
September 7, 2012 / 15:15-15:15 / Room: The Liffey

# Albumin based targeted bionanoparticles formed via non-covalent self-assembly

***Anton Bunschoten***[1], *Tessa Buckle*[1], *Joeri Kuil*[1], *Omgo E. Nieweg*[2], *Fijs van Leeuwen*[1], [1]*Radiology, Leiden University Medical Center, Leiden, Netherlands;* [2]*Surgical Oncology, the Netherlands Cancer Institute, Amsterdam, Netherlands. Contact e-mail: a.bunschoten@lumc.nl*

Human serum albumin (HSA) is a biological nanocarrier that forms non-covalent complexes with e.g. bilirubin, steroids and long chain fatty acids. It is present in high concentrations in human plasma where it maintains the osmotic pressure, functions as a buffer and binds lypophilic endo- and exogenous compounds. HSA has multiple clinical applications of which HSA nanoparticles (NanoColl) are an example. These albumin nanoparticles, when labeled both with fluorescence (ICG) and radioactivity (99mTc), have been shown to improve clinical sentinel lymph node procedures.[1-3] To study the possibility of expanding this dye based non-covalent functionalisation to a targeted approach, we explored the ability of HSA to form non-covalent self-assembled complexes with targeting peptides conjugated to NIR cyanine dyes. The interaction of NIR cyanine dyes and NIR-labeled peptides with HSA were studied by FRET quenching interactions between covalently attached Cy5 and non-covalently bound ICG, IR783-CO2H and three IR783-labeled targeting peptides. Binding of NIR-dyes to HSA resulted in a decrease in Cy5-fluorescence, which allowed us to monitor complex assembly and disassembly. Both IR783-CO2H and ICG bind to HAS to form non-covalent complexes. The IR783-labeled targeting peptides were also able to bind to albumin. The non-covalent host-guest interactions between HSA and several IR783-labeled peptides allowed for the formation of (bio)nanoparticles that target integrins, the chemokine receptor 4 (CXCR4), and the somatostatin receptor. The value of such non-covalent nanoparticles is confirmed in vitro and in vivo; the CXCR4 targeted derivative was capable of binding to CXCR4-expressing cells and yielded an improved retention of the hybrid compound in the first draining lymph nodes compared to HSA alone. By binding NIR-dye labeled peptides to an already clinically approved HSA-scaffold, we have readily formed targeted bionanoparticles that might find their way into the clinic more easily compared to fully synthetic (in)organic nanoparticles. The same interaction of NIR-dye labeled targeting peptides with HSA can also have a large influence on the biodistribution and retention of NIR-labeled imaging agents in vivo. Cyclic RGD, which targets αvβ3-integrins, labeled with a NIR-dye demonstrated a 10-fold increase in retention due to its interaction with albumin in vivo.[4] 1. Buckle T, van Leeuwen AC, Chin PT et al. Nanotechnology 2010; 21: 355101. 2. van der Poel HG, Buckle T, Brouwer OR, Valdes Olmos RA, van Leeuwen FWB. Eur. Urol. 2011; 60: 826-833. 3. Brouwer OR, Klop WMC, Buckle T et al. Ann. Surg. Oncol. 2012, DOI 10.1245/s10434-011-2180-7. 4. Bunschoten A, Buckle T, Visser N et al. ChemBioChem 2012, accepted for publication.

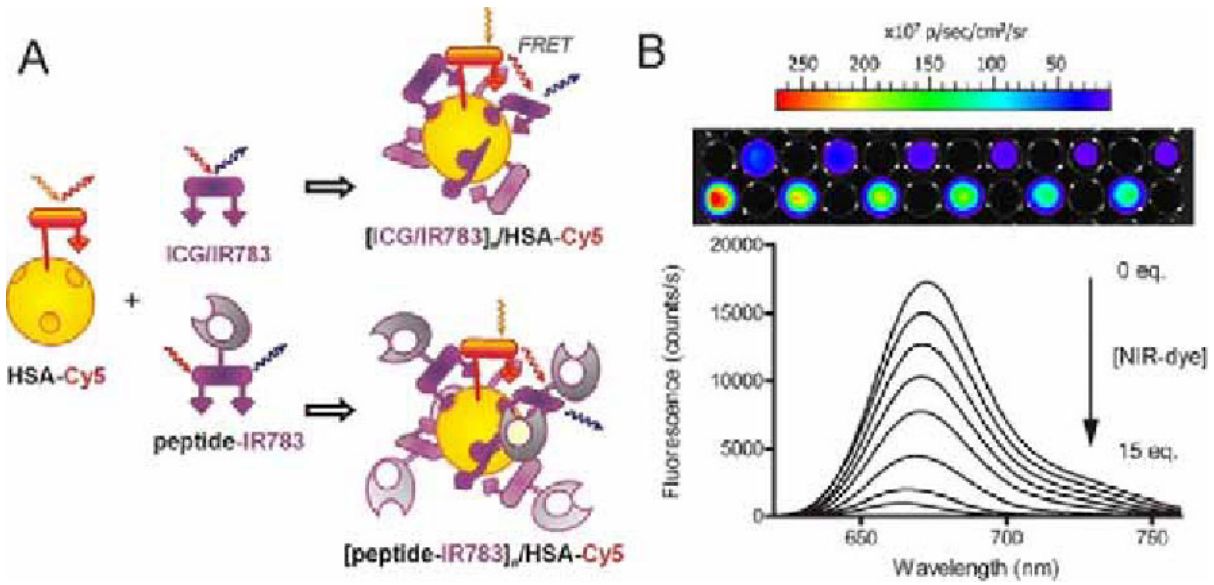


A) Assembly of the non-covalent complexes. B) quenching of the cy5 fluorescence on HSA upon binding of NIR-dyes.

Disclosure of author financial interest or relationships:
**A. Bunschoten**, None; **T. Buckle**, None; **J. Kuil**, None; **O.E. Nieweg**, None; **F. van Leeuwen**, None.

Presentation Number **P407**
Poster Session 3
September 7, 2012 / 15:15-15:15 / Room: The Liffey

# Multimodal Gold-Coated Iron Oxide Glyconanoparticles for MRI, CT and US

***Monica Carril***[1], *Eneko San Sebastián*[1], *Itziar Fernández*[3], *Irati Markuerkiaga*[1], *Isabel García*[1,2], *Juan Rodríguez*[3], *Soledad Penadés*[1,2], [1]*CIC biomaGUNE, San Sebastian, Spain;* [2]*CIBER-BBN, San Sebastián, Spain;* [3]*CIC bioGUNE, Derio, Spain. Contact e-mail: mcarril@cicbiomagune.es*

Non-invasive imaging techniques are key tools in medicine for early detection of severe pathologies. Magnetic resonance imaging (MRI), X-ray computed tomography (CT), positron emission tomography (PET) and ultrasound (US) are examples of frequently employed techniques in clinical use, which offer anatomical and functional information from inside the body. Nevertheless, the nature and quality of information gathered from each technique varies with their different spatial resolution and sensitivity. The use of contrast agents is a frequent strategy to enhance the image contrast and to provide additional functional information. In this context, there is a growing interest in the design of contrast agents which could be simultaneously visualised by different imaging techniques and obtain complementary information in a more efficient manner.[1] We present herein the application of superparamagnetic gold-coated iron oxide glyconanoparticles of 6 nm as contrast agents for X-ray CT, ultrasound (US) and T2-weighed magnetic resonance imaging (MRI). The gold-coated iron oxide nanoparticles employed for this purpose were prepared through thermal decomposition of iron and gold salts in a two-step process. The so-obtained nanoparticles were further functionalised with thiol ending ligands bearing both sugars and a carboxylic acid moiety in a 1:1 ratio (Figure 1). Such glyconanoparticles have been further functionalized and successfully tested as targeted probes in MRI.[2] In the pursuit of novel multimodal contrast agents, we foresaw that the gold coating could increase the contrast of these nanoparticles when irradiated with X-rays. Additionally, we postulated that, despite their nanometric size, their metallic core could enhance contrast in ultrasound scanning. Furthermore, their magnetite content is a source of negative contrast in MRI. To prove these hypotheses, phantoms of water solutions of such nanoparticles at increasing concentrations were measured employing all three non-invasive imaging techniques. The resulting images showed that these kinds of glyconanoparticles can effectively be used as contrast agents in MRI, CT and US and could be useful for future applications as multimodal-targeted contrast agents for targeted imaging. [1] Louie, A. Chem. Rev. 2010, 110, 3146. [2] a) García, I.; Gallo, J.; Genicio, N.; Padró, D.; Penadés, S. Bioconjugate Chem. 2011, 22, 264; b) Gallo, J.; García, I; Genicio, N.; Padró, D.; Penadés, S. Biomaterials 2011, 32, 9818.

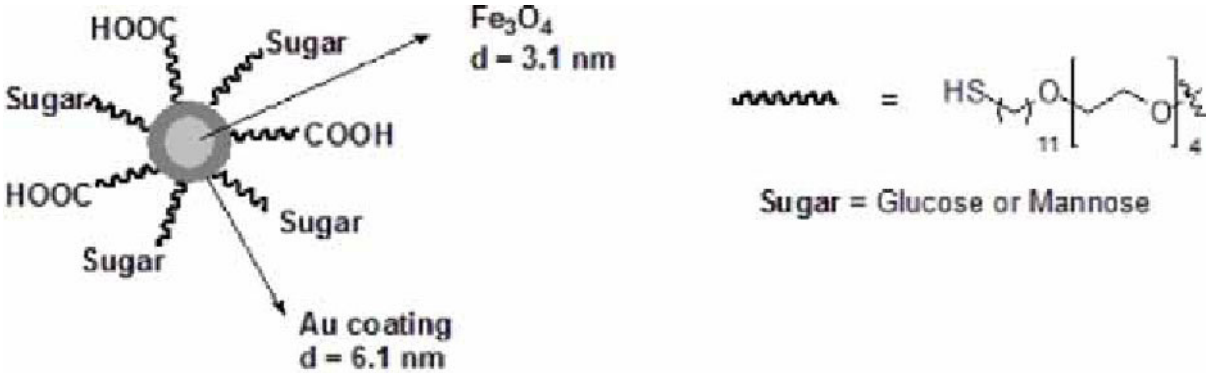


Figure 1. Structure of Fe3O4@Au glyconanoparticles employed for multimodal imaging.

Disclosure of author financial interest or relationships:
**M. Carril**, None; **E. San Sebastián**, None; **I. Fernández**, None; **I. Markuerkiaga**, None; **I. García**, None; **J. Rodríguez**, None; **S. Penadés**, None.

Presentation Number **P408**
Poster Session 3
September 7, 2012 / 15:15-15:15 / Room: The Liffey

# Multifunctional glycol chitosan nanobubbles for multimodal theranostic applications

*Roberta Cavalli[1], Monica Argenziano[1], Agnese Bisazza[1], Elena Torres[2], Pierangela Giustetto[2], Alessandro Maiocchi[3], **Enzo Terreno**[2], [1]Dipartimento di Scienza e tecnologia del Farmaco, Università degli Studi di Torino, Torino, Italy; [2]Dipartimento di Chimica IFM and Molecular and Preclinical Imaging Centers, Università degli Studi di Torino, Torino, Italy; [3]Bracco Imaging Spa, Colleretto Giacosa (Torino), Italy. Contact e-mail: enzo.terreno@unito.it*

Microbubbles, core-shell structures containing a gas, are clinically used as injectable contrast agents for Ultrasound (US) imaging. Recently, smaller bubbles termed nanobubbles (sub-micron diameter) have attracted attention as new strategy for cancer diagnosis and therapy. Particularly, polymeric nanobubbles have been proposed to increase blood lifetime and improve tumor accumulation by passive targeting after in vivo administration. The aim of this work was to design novel formulations of nanobubbles using glycol chitosan as shell component to improve water solubility and biocompatibility of the bubbles. Stability was further increased by adding Pluronic F127 in the formulation. The so-formulated nanobubbles showed a mean diameter of about 450 nm and a polydispersity index of 0.18, with a surface charge of about + 15 mV. The stability of the formulation was proved stored at 4°C, room temperature and after plasma incubation at 37 °C. The nanobubbles showed no haemolytic activity on red blood cells and no cytotoxicity on Vero cell lines. In vitro ecographic experiments with nanobubbles (performed on Visualsonics VEVO 2100) allowed to detect an echo-acoustic signal using non-linear contrast modality. The ability of such system to act as drug delivery system has been investigated selecting a systemic corticosteroid, prednisolone phosphate (PLP), used for the treatment of various inflammatory and immune diseases including arthritis, lupus and asthma. To develop an imaging probe that could act as reporter of delivery and release of PLP from the nanobubbles, several paramagnetic Gd(III)-complexes structurally reminiscent of the drug (i.e. containing a steroidic moieties) have been co-loaded with the drug on the nanobubbles. Proton relaxivity mesurements confirmed the incorporation of the metal complexes and allowed to study the release process using MRI due to the different relaxivity displayed by the bubble-bound complex compared with the free, released, probe. The in vitro release kinetics of PLP from nanobubbles was evalueted using the "dyalisis bag technique" in the absence and in the presence of US (at a frequence of 2MHz). In vitro release experiments showed that, in the presence of US a 76 % of PLP is released from nanobubbles after 24 h with a prolonged release kinetics. On the contrary, in the absence of US the percentage of PLP released reached only 30 % after 24 h (Figure 1). Research funded by INTA project.

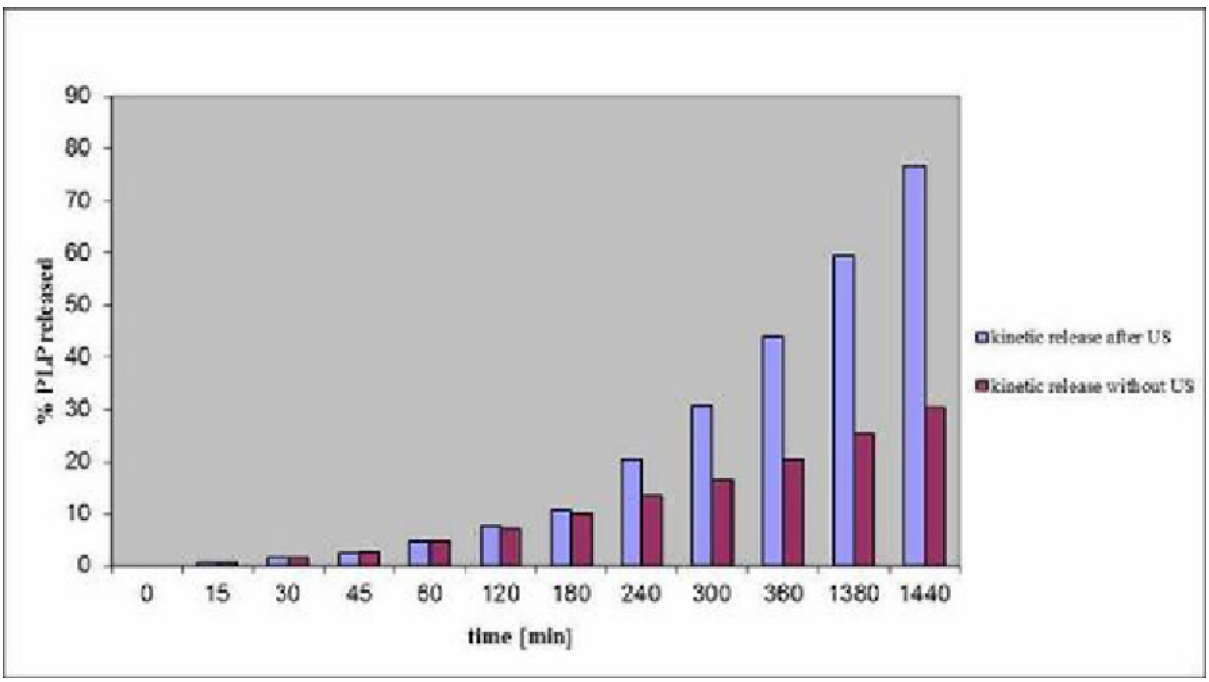


Figure 1: In vitro release kinetics of PLP from glycol chitosan nanobubbles in the presence and in the absence of US (2MHz).

Disclosure of author financial interest or relationships:
**R. Cavalli**, None; **M. Argenziano**, None; **A. Bisazza**, None; **E. Torres**, None; **P. Giustetto**, None; **A. Maiocchi**, Bracco Imaging, Employment; **E. Terreno**, Bracco Imaging, Consultant .

Presentation Number **P409**
Poster Session 3
September 7, 2012 / 15:15-15:15 / Room: The Liffey

# Development of cationic gelatin nanocarrier as multi-functional theranostic nanoprobe

***Ming Ju Chou***[1], *Yen Rong Chen*[2], *Yi You Huang*[1], [1]*Institute of Biomedical Engineering, National Taiwan University, Taipei City, Taiwan;* [2]*Department of Biomedical Science and Technology, Collage of Life Science, National Taiwan University, Taipei City, Taiwan. Contact e-mail: f95548060@ntu.edu.tw*

Nanotechnology plays an important role in cancer diagnosis and therapy. In development of imaging contrast agent, the nanoparticles (NPs) as the imaging probe can label the sub-cellular molecular to enhance spectral resolution. For the research of cancer therapeutic drug, NPs as a drug carrier have advantages of superior drug protection, high drug loading efficiency, and good tumor permeability, which makes drug delivered selectively to increase uptake of tumor and decrease damage of normal tissue. The aim of this study is to develop a nano-delivery system with multi-functional diagnostic agent of medical imaging combined with encapsulation of protein drug as a theranostic nanoprobe. NPs made by biodegradable material have been demonstrated as potential candidate for non-toxic and biocompatible drug carrier. Through surface modification of cationic molecules, NPs can possess high positive charge which is high affinity to cell membrane to enhance cellular uptake. Magnetic Resonance Imaging (MRI) contrast agent and fluorescence imaging agent conjugated with cationic nanoparticles can be applied as a nanoprobe which provide the multimodality of medical imaging. Cationic nanoparticles were prepared by biodegradable polymer- gelatin with surface modification of low-molecular-weight branch polyethylenimine(PEI). The fluorescent agent (RITC) and MRI contrast agent (Gadolinium, Gd) were loaded into the carriers as a diagnostic nanoprobe. The cationic surface of NPs can be used to adsorb plasmid as a gene carrier and used to adsorb protein to be a theranostic agent, which has dual-function including molecular imaging and therapeutic drug. In this study, the optimal component of the NPs was performed by modifying particle size, surface charge and the loading ratio of contrast agent. By verifying condition of synthetic process of gelatin nanoparticles(GNPs), the particle size was provided with the size near 100 nm. GNPs cross-linked with PEI (MW=1800) performed a stable composition with high positive zeta potential (~55 mV) and buffering effect. Cell viability assay (MTT assay) showed that gelatin-PEI nanoparticles(G-PEI NPs) were low cytotoxicity similar to GNPs. For protein drug carrier purpose, green fluorescent protein (GFP) was used to be the protein drug model. The experimental data of SDSPAGE showed that GFP was adsorbed in G-PEI NPs well, and cellular uptake test demonstrated that G-PEI NPs were delivered to cytoplasm efficiently compared with GNPs. In multi-modality of medical imaging use, NPs labeled RITC may provide a specific signal of fluorescence at emission wavelength of 570nm, which could avoid the noise from autofluorescence of tissue. G-PEI NPs conjugated with DTPA as Gd3+ chelator could be the MRI T1 weight contrast agent. In conclusion, the study presents that G-PEI NPs possess the function of medical imaging multi-modalities. High encapsulating efficiency of protein may overcome the limitation in delivery of protein drug in vivo. The cationic multi-functional nanoparticles as the theranostic agent may provide a potential formulation for cancer early detection and therapeutics in the future.

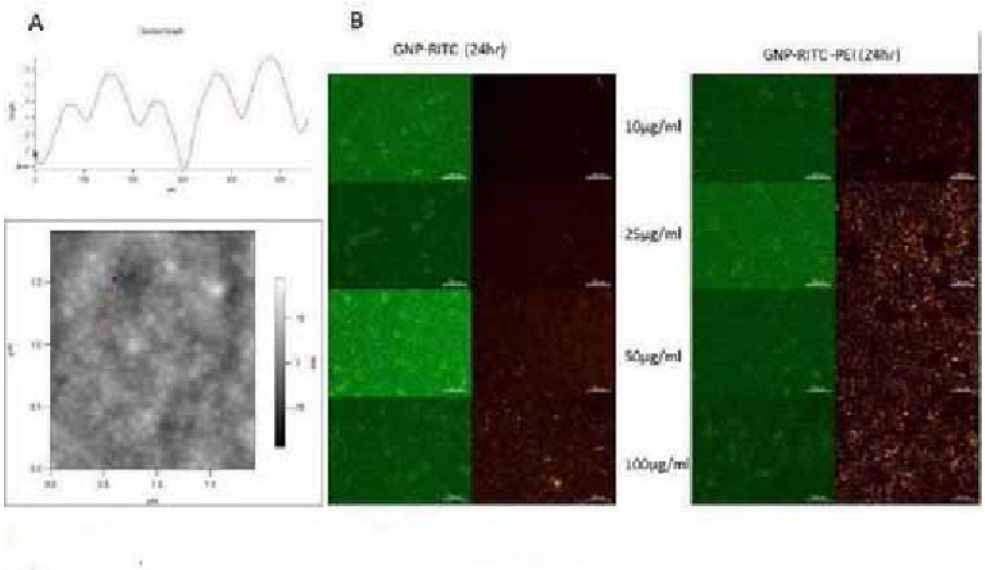


Figure A: AFM photograph of G-PEI NPs morphology. Figure B: Cellular uptake of GNP-RITC and GNP-RITC-PEI

Disclosure of author financial interest or relationships:
**M. Chou**, None; **Y. Chen**, None; **Y. Huang**, None.

Presentation Number **P410**
Poster Session 3
September 7, 2012 / 15:15-15:15 / Room: The Liffey

# MOLECULAR IMAGING TO ASSESS TUMOR-ASSOCIATED MACROPHAGES WITH TARGETED NANOPARTICLES

***Lynda Cosgrave***[1], *Anuja Ogirala*[1], *Janine Ring*[3], *Ralph Weissleder*[2], *Jason S. Lewis*[1], *Jan Grimm*[1], [1]*Radiology, MSKCC, NYC, NY, USA;* [2]*Broad Institute, Harvard Medical School / MGH, Boston, MA, USA;* [3]*Radiology, University of Muenster, Muenster, Germany. Contact e-mail: cosgravl@mskcc.org*

Introduction Poor tumor prognosis has been shown to correlate negatively with the accumulation and increased infiltration of macrophages (tumor associated macrophages - TAM) into tumor tissues. These cells and their sub-populations are indicated in various tumor-promoting processes e.g. tumor angiogenesis, tumor cell migration etc. [2, 3] It would be of significant clinical value to be able to quantify TAM in patients non-invasively to further refine the prognosis. Method This project aims to target these TAM both in vivo and in vitro using modified non-toxic cross-linked iron oxide nanoparticles (CLIO). The use of these particles will allow TAM investigation to occur over several modalities including fluorescence imaging, FACS (after conjugation to fluorophores), and PET (after conjugation to 89Zr). Results Currently, CLIO nanoparticles have been successfully conjugated to a variety of fluorophores using standard bioconjugation chemistry. The absorption and emission characteristics of the fluorophores, post-conjugation was confirmed. FACS analysis of TAM from xenografted tumors in mouse models has been successful with a library of relevant antibodies. Additionally the fluorophore-conjugated nanoparticles have been applied both to macrophages in culture and directly in vivo via tail vein injection in mice. Analysis by FACS and iron staining of the tumor section was performed 24hrs post injection and successful targeting of TAM by the nanoparticles is apparent. CLIO nanoparticles were labelled successfully with desferrioxamine (DFO) which allowed for 89Zr chelation. The resulting radioactive nanoparticle formulation is currently being applied in vivo to CT26 xenografted mice and PET images and radioactive biodistributions are being analysed at several stages. Conclusions A multimodal nanoparticle based agent has been successfully synthesised and shown to be appropriate for TAM analysis both in vitro and ex vivo. In vivo imaging is presently underway and is allowing for further quantification of TAM within the tumor tissues. References 1. Ruhrberg C. et al, Nature Medicine 16, 861-862 (2010). 2. Qian B.Z. et al, Cell 141 39-51 (2010) 3. Mantovani A. et al Curr. Opin. Immunol. 22, 231-237 (2010).

Disclosure of author financial interest or relationships:
**L. Cosgrave**, None; **A. Ogirala**, None; **J. Ring**, None; **R. Weissleder**, None; **J.S. Lewis**, GEMS, Other financial or material support; **J. Grimm**, None.

Presentation Number **P411**
Poster Session 3
September 7, 2012 / 15:15-15:15 / Room: The Liffey

# Synthesis of CoFe2O4@NaYF4 (Yb, Er) Hybrid Nanoparticles for Use as a Multi-mode Molecular Imaging Contrast Agent

***Xianjin Cui***[1], *Rafael Torres Martin de Rosales*[1], *Maite Jauregui-osoro*[1], *Mark Green*[1,2], *Phil Blower*[1], [1]*Imaging Science, King's College London, London, United Kingdom;* [2]*Physics, King's College London, London, United Kingdom. Contact e-mail: xianjin.cui@kcl.ac.uk*

CoFe2O4@NaYF4(Yb, Er) hybrid nanoparticles were obtained by thermal decomposition. The magnetic core can function as MRI T2 contrast, and meanwhile the doped NaYF4 shell exhibits a high affinity to 18F-fluoride for PET imaging, with a labelling efficiency of 92.7%. CoFe2O4@NaYF4 could be a good candidate for fluorescent imaging as NaYF4 nanoparticles doped with Yb and Er were reported as up conversion phosphor with a strong emission at 800 nm near infrared region under excitation of 980 nm. Transmission Electron Microscope (TEM) images showed a very narrow particle size distribution and a mean diameter of 15 around nm. Dynamic Light Scattering (DLS) results suggested that these nanoparticles can be stabilized against aggregation by derivatising with the small ligand Mercaptosuccinic acid (MSA) or functional polymer bis phosphonate PEG, with a hydrodynamic size of ca 140 nm.

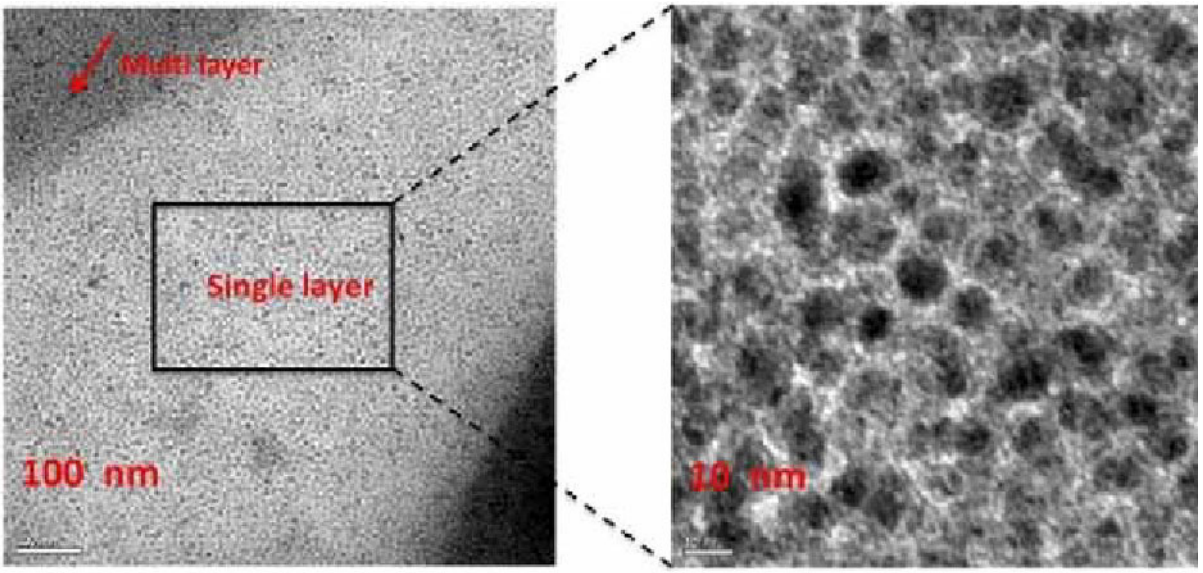


TEM images of CoFe2O4@ NaYF4 nanoparticles.

Disclosure of author financial interest or relationships:
**X. Cui**, None; **R. Torres Martin de Rosales**, None; **M. Jauregui-osoro**, None; **M. Green**, None; **P. Blower**, None.

Presentation Number **P412**
Poster Session 3
September 7, 2012 / 15:15-15:15 / Room: The Liffey

# New imaging agents for targeting chemokine receptor CXCR4

***Pauline Désogère***[1], *Sophie Poty*[1], *Melpomeni Fani*[3], *Helmut R. Maecke*[3], *Frederic Boschetti*[2], *Christine Goze*[1], *Franck Denat*[1], [1]*ICMUB, dijon, France;* [2]*Chematech, dijon, France;* [3]*Universitätsklinikum, freiburg, Germany. Contact e-mail: pauline.desogere@u-bourgogne.fr*

The chemokine receptor 4 (CXCR4) is overexpressed in several cancers and as such presents an enticing target for molecular imaging of metastases and metastatic potential of the primary tumor. CXCR4-based imaging agents could also be useful for diagnosis and therapeutic monitoring. CXCR4 inhibitors, both peptide-based and small molecules, such as AMD 3100 and AMD 3465, have been developed as potential therapeutics.[1][2] To image CXCR4 expression in tumor models, macromolecular agents such as 111In- and 18F-labeled peptides and 125I-labeled monoclonal antibodies have been investigated using either SPECT (Single Positron Emission Computed Tomography) or PET (Positron Emission Tomography).[3][4] Very recently, AMD 3100 and AMD 3465 were metallated with radionuclides, such as 99mTc and 64Cu, but these complexes have a low in-vivo stability leading to the decomplexation of the metal.[5][6][7] The objective of this work is to investigate the synthesis of new AMD 3100 and AMD 3465 analogues: the AMD-like moiety will serve as a carrier for specific delivery of the radionuclide (64Cu, 68Ga, 111In, 18F) to cancer tissues. To this aim, we will consider the introduction on the spacer of a chelator selective of the targeted metal or of a group allowing 18F substitution. This route also offers the possibility of attaching a fluorescent tag for optical imaging or a bimodal system for both radio-(PET/SPECT) and fluorescence imaging. [1] A. P. Vicari, C. Caux, Cytokine Growth Factor Rev., 2002, 13, 143, [2] E. D. Clercq, Pharmacol. Ther., 2010, 128, 509, [3] S. Nimmagadda, M. Pullambhatla, M. G. Pomper, J. Nucl. Med., 2009, 50,1124, [4] S. Nimmagadda, M. Pullambhatla, K. Stone, G. Green, Z. M. Bhujwalla, M. G. Pomper, Cancer Res. 2010, 70, 3935, [5] O. Jacobson, I. D. Weiss, L. Szajek, J. M. Farber, D. O. Kiesewetter, Bioorg. Med. Chem., 2009, 17, 1486, [6] J. M. Zhang, J. H. Tian, T. R. Li, H. Y. Guo, L. Shen, Chin. Chem. Lett., 2010, 21, 461, [7] R. A. De Silva, K. Peyre, M. Pullambhatla, J. J. Fox, M. G. Pomper, S. Nimmagadda, J. Nucl. Med. 2011, 52, 986.

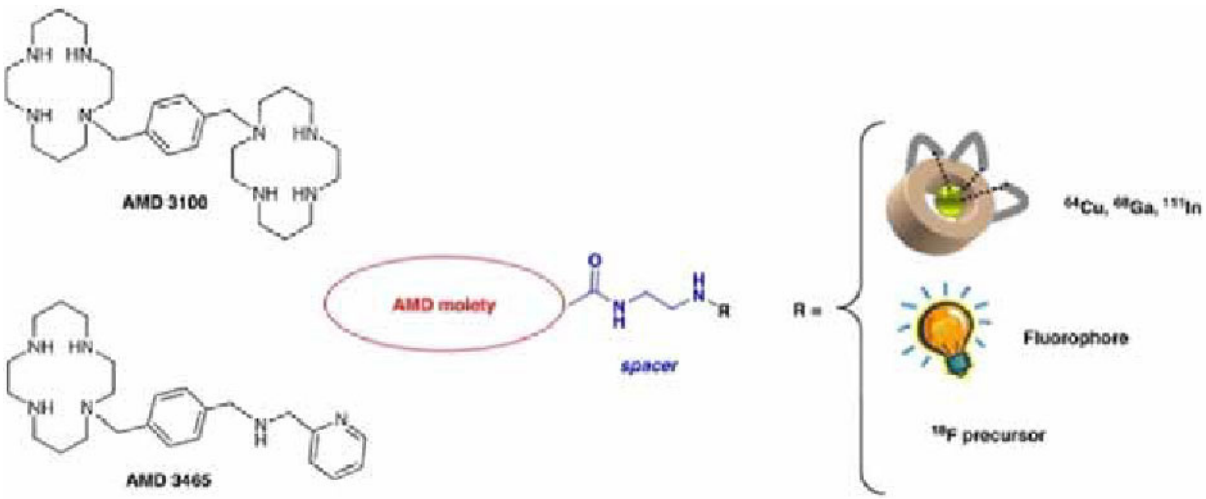


Disclosure of author financial interest or relationships:
**P. Désogère**, None; **S. Poty**, None; **M. Fani**, None; **H.R. Maecke**, None; **F. Boschetti**, None; **C. Goze**, None; **F. Denat**, None.

Presentation Number **P413**
Poster Session 3
September 7, 2012 / 15:15-15:15 / Room: The Liffey

# Development of a multifunctional surface-switchable platform for combined imaging and therapy

***Anita Gianella***[1], *Aneta J. Mieszawska*[1], *Freek J. Hoeben*[2], *Henk M. Janssen*[2], *Peter A. Jarzyna*[1], *David P. Cormode*[1], *Omid C. Farokhzad*[3], *Robert Langer*[4], *Zahi A. Fayad*[1], *Willem J. Mulder*[1], [1]*Translational and Molecular Imaging Institute, Mount Sinai School of Medicine, New York, NY, USA;* [2]*SyMO-Chem B.V., TU/e Helix, Eindhoven, Netherlands;* [3]*Laboratory of Nanomedicine and Biomaterials and Department of Anesthesiology, Brigham and Women's Hospital, Harvard Medical School, Boston, MA, USA;* [4]*Department of Chemical Engineering, Massachusetts Institute of Technology, Cambridge, MA, USA. Contact e-mail: anita.gianella@gmail.com*

Introduction One of the main aspects that influences pharmacokinetics and targeting of intravenously administrated nanoparticles is the nanoparticle's coating. Polymers, such as polyethylene glycol (PEG), reduce recognition by the mononuclear phagocyte system (MPS). To enhance specific uptake, the nanoparticle can be functionalized with targeting ligands. However, their presence can cause augmented recognition by the MPS and endothelial or circulating cells. In the current study we have developed a multifunctional platform with a surface-switchable coating that has targeting moieties shielded by a metalloproteinase-2 (MMP2) cleavable PEG coating. Upon MMP2 exposure, which is expressed in several pathological tissues, the targeting moieties become available for targeting. Methods and Results The surface-switchable platform is based on nanoemulsions with a soybean core and a PEG-lipid coating (Fig. 1A). To allow surface-switching we synthesized a PEG350 phospholipid to which PEG2000 is conjugated via an MMP2 cleavable peptide unit (mPEG-MMP2p-DSPE) (Fig. 1B). The final product was characterized by 1H-NMR, LC-MS, MALDI-TOF and HPLC and the purity was estimated to be ≥ 91%. The nanoemulsions were synthesized by lipid film hydration and subsequent emulsification. The lipid coating was comprised of cholesterol, mPEG350-DSPE, mPEG3000-DSPE to provide shielding and biotin-PEG1000-DSPE as a model for targeting. By varying the phospholipids ratios it was possible to control avidin-induced aggregation and binding to an avidin coated surface. These data supported our hypothesis that shielding of targeting moieties decreased interactions with proteins. Based on these results, we selected a formulation with 10% PEG shielding, 2.5% biotin lipid and replaced the mPEG3000-DSPE by mPEG-MMP2p-DSPE. After MMP2 incubation PEG chains are cleaved (Fig. 1C). We observed that mPEG-MMP2p-DSPE nanoemulsions that were pre-incubated with MMP2 aggregated upon incubation with avidin and the relative particle diameter increased by a factor 2 to 3, similar to the control with the freely exposed biotin-PEG1000-DSPE. Conversely, mPEG-MMP2p-DSPE nanoemulsions not pre-incubated with MMP2 did not aggregate. The cleavage by MMP-2 was also confirmed by binding experiments and mass spectroscopy. To demonstrate the versatility of the platform we included oleic acid coated iron oxide (IO) or oleyl mercaptan coated gold (Au) nanocrystals as well as the lipophilic drug simvastatin to render so-called theranostic nanoparticles, exhibiting both therapeutic and diagnostic properties. In Fig. 1D and E we present size, polydispersity measurements as well as transmission electron microscopy (TEM) images of theranostic nanoemulsions. CT and MRI data of Au and IO nanoemulsions demonstrated the diagnostic properties (Fig. 1D, F). Conclusion In the current study we have synthesized a new MMP2 cleavable PEG-lipid and included it in the corona of a multifunctional nanoemulsion platform. Upon incubation with MMP2 the targeting ligands become available for binding. Future studies will be aimed at evaluating this multifunctional platform for specific targeting of extravascular cell types.

Disclosure of author financial interest or relationships:
**A. Gianella**, None; **A.J. Mieszawska**, None; **F.J. Hoeben**, None; **H.M. Janssen**, None; **P.A. Jarzyna**, None; **D.P. Cormode**, Philips, Consultant; **O.C. Farokhzad**, BIND Biosciences, Consultant; Selecta Biosciences, Consultant; **R. Langer**, None; **Z.A. Fayad**, None; **W.J. Mulder**, None.

Presentation Number **P414**
Poster Session 3
September 7, 2012 / 15:15-15:15 / Room: The Liffey

# New BODIPY-macrocycle derivatives for bimodal imaging

*Damien Lhenry, **Christine Goze**, Claire Bernhard, Franck Denat, ICMUB, University of Burgundy, Dijon, France. Contact e-mail: christine.goze@u-bourgogne.fr*

The interest for multimodal agents increased significantly in the last decades. Multimodal imaging agents can provide complementary information improving the accuracy of disease, diagnosis and enhancing patient management.1 Each imaging modality (SPECT, PET, Optical Imaging, MRI) has its own strengths and weaknesses, and thus, combining different and complementary systems can overcome inherent limitations associated with any one individual technique. The objective of this work was to develop new bimodal agents for SPECT/PET and optical imaging, based on borodipyrromethene (BODIPY) and tetraazamacrocycle (DOTA, DOTAGA, NOTA, NODAGA). These new bimodal systems benefit on one hand, from the excellent luminescent properties of the BODIPY fluorophore and on the other hand, from the optimized coordination properties of the macrocyclic ligands.2 The BODIPY unit can be modulated in order to displace the emission wavelength of the different systems to the near infrared for in vivo imaging. Complexation with cold isotopes of metals of interest for nuclear imaging (Ga(III), In(III), Cu(II), Zr(IV)) was investigated, and the photophysical properties of the resulting systems were studied. 1 (a) A. Louie, Chem. Rev. 2010, 110, 3146-3195. (b) J. Kuil, A. H. Velders, F. W. B. ven Leeuwen, Bioconjugate Chem. 2010, 21, 1709-1719. (c) L. E. Jennings, N. L. Long, Chem. Commun. 2009, 28 (24), 3511-3524. 2 (a) C. Bernhard, C. Goze, Y. Rousselin, F. Denat, Chem. Commun. 2010, 46, 8267-8269. (b) C. Bernhard, M. Moreau, D. Lhenry, C. Goze, F. Boschetti, Y. Rousselin, F. Brunotte, F. Denat, Chem. Eur. J. 2012, DOI:10.1002/chem. 201200132.

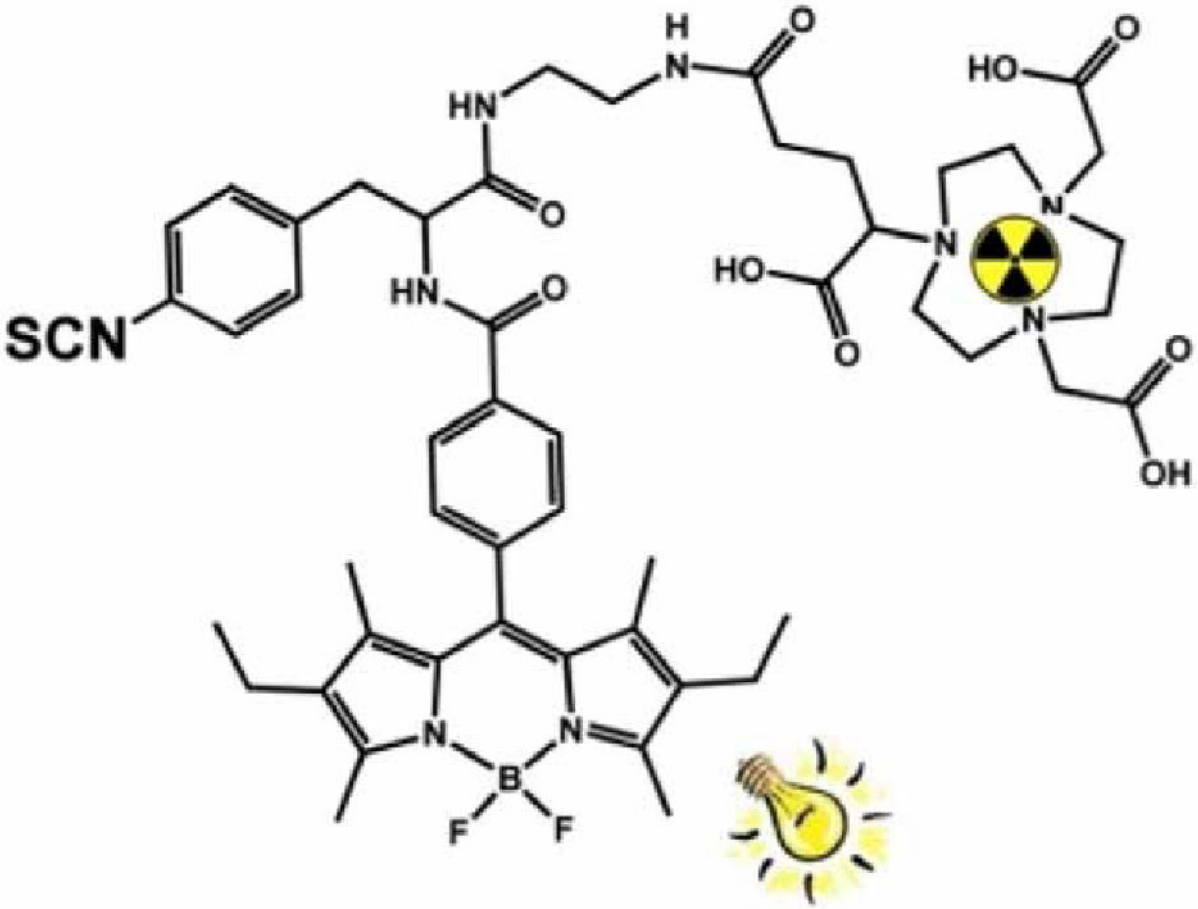


Disclosure of author financial interest or relationships:
**D. Lhenry**, None; **C. Goze**, None; **C. Bernhard**, None; **F. Denat**, None.

Presentation Number **P415**
Poster Session 3
September 7, 2012 / 15:15-15:15 / Room: The Liffey

# Development of a brain targeting RVG peptide linked with SS-PEI to deliver neuron specific microRNAs to the brain

***Jaeho Jang***[1], *Do Won Hwang*[2,3], *Duhwan Lee*[4], *Hyewon Youn*[2,5], *Won Jong Kim*[4], *Dong Soo Lee*[1,2], [1]*Molecular Medicine and Biopharmaceutical Science WCU Graduate school of Convergence science and Technology, Seoul National University, Seoul, Republic of Korea;* [2]*Nuclear Medicine, Seoul National University College of Medicine, Seoul, Republic of Korea;* [3]*Institute of Radiation Medicine, Medical Research Center, Seoul, Republic of Korea;* [4]*Chemistry, Pohang University of Science and Technology, Pohang, Republic of Korea;* [5]*Cancer Imaging Center, Seoul National University Cancer Hospital, Seoul, Republic of Korea. Contact e-mail: asakura14@hotmail.com*

Purpose: Cationic polyethyleneimine (PEI) polymer has been widely used as a best intracellular gene carrier for efficient gene therapy. However, its cytotoxicity due to the non-biodegradable characteristics interrupts the clinical application of PEI to the drug delivery research. In this study, we modified PEI molecule with disulfide (-S-S-) linkage in the branched PEI and examined the targeting effect of microRNA (miRNA) using rabies virus glycoprotein (RVG)-labeled disulfide PEI to the brain for efficient brain delivery in vivo. Methods: PEI molecule was modified with disulfide (-S-S-) bonds in its backbone and the polymer was conjugated with RVG peptide containing SH moieties using MAL-PEG-NHS linker. Mouse neuroblastoma Neuro2a which is an acetylcholine receptor positive cell line and HeLa cells for negative control were used to confirm the specific delivery of miRNA. The cytotoxicity test was conducted using Cell counting kit-8 (CCK-8). The polymer and miRNA complex size was analyzed by Zetasizer Nano S (Malvern Instrument). For in vivo experiments, cy5.5-labeled miRNAs were incubated with RVG-SSPEI for 15 minutes at room temperature and intravenously injected to ICR mice. After 4 hours, organs including a brain were collected and fluorescence signals were detected using a Maestro imaging device (CRi). Result: Cytotoxicity assay results show less toxicity in RVG-SSPEI group, compared with non-modified PEI group. The complexation of RVG-SSPEI and miRNA was confirmed by Zeta potential and gel retardation analysis. Through the receptor mediated endocytosis, 3 fold higher uptake rate of cy5.5-labeled miR-124a was shown in Neuro2a cells compared to HeLa cells using RVG-SSPEI. After intravenous injection of cy5.5-miR-124a and PEI complexes, higher fluorescent signal was detected from the mouse brains in RVG-SSPEI group compared to SSPEI group. Conclusion: We developed brain specific miRNA delivery system using RVG peptide in vivo. These results demonstrate that RVG-SSPEI mediated neuron specific miRNA delivery to the brain could be used to in vivo oligomer delivery system for oligomer-based therapy.

Disclosure of author financial interest or relationships:
**J. Jang**, None; **D. Hwang**, None; **D. Lee**, None; **H. Youn**, None; **W. Kim**, None; **D. Lee**, None.

Presentation Number **P416**
Poster Session 3
September 7, 2012 / 15:15-15:15 / Room: The Liffey

# Drug Delivery System using Carboxylation Chitosan Conjugated Doxorubicin

***Mi-Kyeong Jang***[1], *Jae-Woon Nah*[2], [1]*Polymer Science & Engineering, Sunchon National University, Suncheon, Republic of Korea;* [2]*Polymer Science & Engineering, Sunchon National University, Suncheon, Republic of Korea. Contact e-mail: jmk8856@sunchon.ac.kr*

Chitosan has been reported to enhance drug transportation across the nasal or mucosal layer without tissue damage. Furthermore, the cationic properties of chitosan offer valuable properties for drug delivery systems, gene delivery systems, and tissue engineering and imaging materials. Since carboxymethylation gives anionic properties to chitosan, carboxymethyl chitosan is useful to the drug delivery system. Thanou et al. have reported that N-carboxymethyl chitosan is useful for enhancing intestinal absorption of low-molecular weight heparin. In this study, used to carboxymethyl group modified Chitosan and methoxy poly(ethylene glycol) for doxorubicin (DOX) delivery carrier. DOX is an anthraquinone anticancer drug that is commonly used for treatment of human malignancies. However its clinical usage, carries substantial risk of cardiomyopathy and life-threatening heart failure. Accordingly, many studies have been conducted using adjunctive therapy to counteract the adverse effects of DOX. A drug delivery system based on micelles or nanoparticles has received attention due to the potential for drug targeting, long drug circulation times, prevention of unwanted effects and various biomedical applications. The aim of the present study was to investigate the effects of DOX in cancer cells in order to clarify if a time/concentration range for optimal DOX-induced apoptosis exists. The chemical structure of the conjugate was determined by FT-IR (Fourier transform infrared) and 1H-NMR (1Proton Nuclear Magnetic Resonance). The Carboxymethyl chitosan-graft-poly(ethylene glycol)/DOX conjugate nanoparticles were formed through the aggregation of hydrophobic DOX. The size and morphology of prepared nanoparticles were characterized using DSC (dynamic light scattering) and TEM (transmission electron microscope). The results showed that the nanoparticles were spherical and their size was less than 100 nm. The in vitro cytotoxicity of PEG modified Carboxylation Chitosan/DOX conjugate nanoparticles was tested by the MTT assay. This study was supported by Ministry of Knowledge Economic (MKE).

Disclosure of author financial interest or relationships:
**M. Jang**, None; **J. Nah**, None.

Presentation Number **P417**
Poster Session 3
September 7, 2012 / 15:15-15:15 / Room: The Liffey

# New glycogen-based nanoprobes for multimodal imaging

***Daniel Jirak***[1], *Martin Hruby*[2], *Sergey K. Filippov*[2], *Ondrej Sedlacek*[2], *Miroslav Vetrik*[2], *Jan Kovar*[1], [1]*Department of Diagnostic and Interventional Radiology, Institute for Clinical and Experimental Medicine, Prague, Czech Republic;* [2]*Institute of Macromolecular Chemistry, Academy of Sciences of the Czech Republic, Prague, Czech Republic. Contact e-mail: daji@ikem.cz*

Glycogen (GG) is the main animal D-glucose storage polysaccharide., presented mostly in liver and muscles. GG is hyperbranched poly(D-glucose) with D-glucose units connected with each other. This poly(D-glucose) is a natural high-molecular-weight fully biodegradable dendrimer structurally related to dextrin, but much more branched. Therefore GG is relatively inert to amylases (which are omnipresent in bloodstream), but is intracelularly degraded by glycogen debranching enzyme. This means that it should be relative stable after intravenous administration in bloodstream (its molecular weight is well-above renal threshold, so it cannot be directly eliminated by kidneys without previous biodegradation), but should be rapidly degraded after internalization into cells into D-glucose. This would be an advantageous behavior for a carrier for numerous magnetic resonance imaging (MRI) or drug delivery applications. No such system is described in literature yet. We report of new glycogen-based biodegradable nanoprobes that have been successfully exploited for multimodal imaging in-vivo. GG from oyster was directed towards functionalization with gadolinium(III) complex (DOTA-Gd, a MRI contrast agent) and Dyomics 615, a fluorescent label. The GG from oyster has narrow size distribution in aqueous solution with hydrodynamic radius RH = 27 nm. This size is suitable for the EPR-based solid tumor targeting. The GG was reacted with allyl bromide to introduce double bonds yielding product containing 0.131 allyl groups per D-glucose unit. The double bond was quantitatively converted to primary amino group by photochemical addition of cysteamine hydrochloride and further reacted with Dyomics 615 hydroxysuccinimide ester and DOTA hydroxysuccinimide ester. The product was finally converted by chelation of gadolinium(III) chloride in ammonium acetate buffer to a conjugate having DH = 89 nm, $\zeta$ = 45 mV containing 0.33 wt. % Dyomics 615 and 3.19 wt. % gadolinium. The fate of the conjugate was followed in healthy mice after intravenous application by magnetic resonance imaging (MRI) for six hours. The mouse was examined at a 4.7-T Bruker Biospec MR scanner equipped with a small resonator coil using T2* weighted gradient echo sequences for anatomy and T1 weighted gradient echo sequences for the dynamic contrast-enhanced magnetic resonance.imaging (DCE-MRI) to assess distribution of contrast agent before (as a reference) and after contrast agent administration (60µl). There was no significat accumulation of the contrast agent in reticuloendothelial system and also no significant accumulation was found in kidneys (which may cause nephrotoxic effects especially in the case of anticancer delivery systems). There was clearly seen gradual accumulation of degradation fragments in urine bladder. The study was supported by a grant projects: # P207/10/P054, # P108/10/1560, P108/12/0640 and P304/12/0950 (GACR) and by a project MZ0IKEM2005 (Ministry of Health, Czech Republic).

Disclosure of author financial interest or relationships:
**D. Jirak**, None; **M. Hruby**, None; **S.K. Filippov**, None; **O. Sedlacek**, None; **M. Vetrik**, None; **J. Kovar**, None.

Presentation Number **P418**
Poster Session 3
September 7, 2012 / 15:15-15:15 / Room: The Liffey

# Synthesis and Application of AOI-Derivatives for in-vivo Imaging of Aβ-Plaques in APP23 Alzheimer Mice with Near Infrared Optical Imaging and MRI

***Christian Kesenheimer**, Ramona Stumm, Florian C. Maier, Bernd J. Pichler, Department of Preclinical Imaging and Radiopharmacy, Eberhard Karls University Tuebingen, Tuebingen, Germany. Contact e-mail: christian.kesenheimer@med.uni-tuebingen.de*

In an aging society, the study and treatment of neurodegenerative diseases such as Alzheimer's and Parkinson's Disease (AD and PD) have become increasingly important. AD accounts for approximately 70% of the neurodegenerative disease cases. However, current biomarkers such as [11C]-PIB are only poorly evaluated and to date no reliable amyloid tracer has been developed for in-vivo applications in small animals. Aim: We thus are interested in developing a multi-modality probe to image and validate the Aβ-plaque load in AD, utilizing near-infrared optical and magnetic resonance imaging. Based on the structure of AOI-987 (1), published from Hintersteiner et al. [Nature Biotech. 2005, 23, 5, 577-583], we have synthesized structural derivatives (2-5) from the lead structure (1), with varying lipophilicity, binding behaviour and resonance properties for MRI (Figure 1). Methods: In a preliminary study, we performed in-vivo OI and MR scans with transgenic APP23 mice and respective littermate controls (24 months old). Mice were scanned with a high resolution T1 weighted gradient echo sequence in the MR (gre3DT1, resolution: 125x125x110 µm^3). Additionally, mice were also scanned in an OI system. Isoflurane anesthesia was maintained at 1.5% with oxygen as carrier gas and animals were scanned for 90 min. Throughout the entire study, the body temperature was maintained at 37±0.1°C. For MR scans, the frontal cortex served as target region, while the cerebellum was considered as the reference region. Animals were sacrificed at the end of the respective study and ex-vivo correlations (histology and ex-vivo OI scans) were performed. Results: With compounds (2) and (4) (F-19 labelled), we have started to perform in-vivo experiments with APP23 mice. Both compounds readily penetrate the blood-brain barrier and enrich in the frontal cortex of APP23 mice. The injected doses were the same as described in the publication of Hintersteiner et al. and have been 2.5 µg per mouse (Age of mice: 24 months, 50 µL of a 50µg/mL solution of the dye in 0.9% NaCl). The lead substance (1) was tested on APP23 mice at different age where the OI signal correlated with the plaque load and showed a strong in-vivo signal. Besides optical imaging we also applied in-vivo MRI (Sequence: gre3DT1) to see if we can oberserve a signal changes in the frontal cortex through the uptake of the compounds. We could see a significant increase of signal intensity with the F-19-labelled compound (4). Conclusion: The synthesized AOI-derivatives are promising candidates to extend their applicability from pure near-infrared optical imaging to magnetic resonance imaging. As near-infrared imaging has only limited spatial resolution, while MR lacks sensitivity, a combination could be important for correlations of in-vivo findings from both modalities. With the successful synthesis of the 19F-bearing AOI-compound (4), an equivalent 18F-derivative would be of great interest for the application in PET-studies and is the goal of our current efforts.

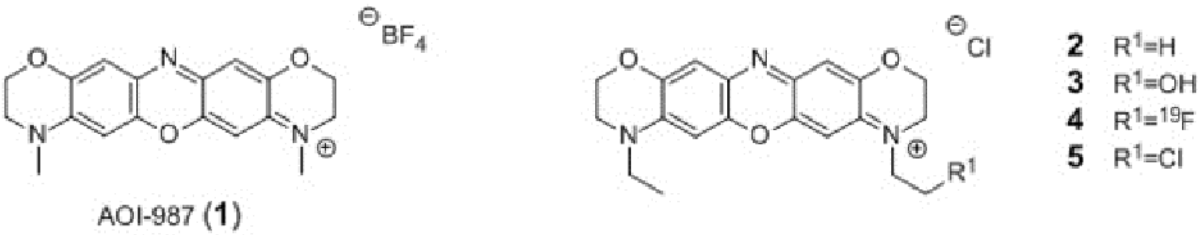


Figure 1: Lead structure AOI-987 (1) and structural derivatives (2-5)

Disclosure of author financial interest or relationships:
**C. Kesenheimer**, None; **R. Stumm**, None; **F.C. Maier**, None; **B.J. Pichler**, Siemens, Grant/research support; AstraZeneca, Grant/research support; Bayer Healthcare, Grant/research support; Boehringer-Ingelheim, Grant/research support; Oncodesign, Grant/research support; Merck, Grant/research support; Bruker, Grant/research support .

Presentation Number **P419**
Poster Session 3
September 7, 2012 / 15:15-15:15 / Room: The Liffey

# Synthesis and Functional Evaluation of Size-controlled $Gd_2O_3$ Nanoparticles for Dual Photoacoustic and Magnetic Resonance Imaging

***Yu Kimura***[1], *Ryota Kamisugi*[1], *Yasuhiko Tabata*[2], *Tetsuya Matsuda*[3], *Michiko Narazaki*[3], *Teruyuki Kondo*[1], [1]*Advanced Biomedical Engineering Research Unit, Kyoto University, Kyoto, Japan;* [2]*Institute for Frontier Medical Sciences, Kyoto University, Kyoto, Japan;* [3]*Graduate School of Informatics, Kyoto University, Kyoto, Japan. Contact e-mail: ykimura@scl.kyoto-u.ac.jp*

Recently, we have succeeded in design and synthesis of a series of novel chiral dendrimer-amine-coordinated gadolinium (Gd) complexes as highly sensitive MRI contrast agents.[1] Here, we report our further study on the synthesis and functional evaluation of novel size-controlled $Gd_2O_3$ nanoparticles (NPs), which are expected as a new dual molecular probe for photoacoustic (PA) and magnetic resonance (MR) imaging. $Gd(NO_3)_3{\cdot}6H_2O$ was dissolved in diethylene glycol (DEG) at 100 $^{o}$C, and the mixture was sequentially heated with stirring and a small amount of NaOH and water. The reaction mixture was slowly added to acetone, which enables the precipitation and isolation of pure $Gd_2O_3$ NPs covered with DEG. Then, the obtained $Gd_2O_3$-DEG NPs were dispersed into water, and the treatment of $Gd_2O_3$-DEG NPs with gelatin (Mw: 2,000) in water, followed by lyophilization gave novel $Gd_2O_3$-DEG NPs modified by gelatin ($Gd_2O_3$-DEG-gelatin NPs). Although $Gd_2O_3$-DEG NPs were gradually aggregated and precipitated after 30 h (particle diameter: over 300 nm), no aggregation of novel $Gd_2O_3$-DEG-gelatin NPs were observed in water with keeping the particle diameter constant (*ca.* 100 nm). TEM observation revealed that the nanoparticles have a hydrodynamic diameter of 100 nm, where the thickness of the outer layer is 10-30 nm, and small dots (5 nm) are observed. It is conceivable that the outer layer of the NPs consists of gelatin, and the inner small dots are unconjugated $Gd_2O_3$ because of their high electron density. The remaining space in the NPs is filled by DEG. The TG-DTA results demonstrated that there was still massive DEG inside $Gd_2O_3$-DEG-gelatin NPs. Functional evaluations of novel $Gd_2O_3$-DEG NPs were performed as follows. Photoacoustic (PA) images of mice at 710 nm before and after the subcutaneous injection clearly showed the intense signal at the injected area. No PA signals for DEG or gelatin were observed at all. While the relaxivity (r1) of the contrast agent, Magnevist®, for clinical use is 4.89 L/mmol·sec, the relaxivity of the present NPs is 9.51 L/mmol·sec, and they have an approximately two times higher T1 attenuating capability. MR images of a whole mouse after the intravenous injection clarified that the present nanoparticles freely circulate in the blood vessels without undesirable accumulation in the lungs. At least, we consider that these NPs could be useful as contrast agents for angiography. In addition, signals in the liver were diminished, while signals in the colon were observed on MR imaging 24 h after injection. This result indicates that the injected NPs could be eliminated through the bile duct. In conclusion, we have succeeded in synthesis and functional evaluation of novel size-controlled $Gd_2O_3$-DEG NPs modified by gelatin, which are highly promising as a dual molecular probe for PA and MR imaging. (1) Kondo, T. et al. PCT Int. Appl. WO2009069833 (2009).

Disclosure of author financial interest or relationships:
**Y. Kimura**, None; **R. Kamisugi**, None; **Y. Tabata**, None; **T. Matsuda**, None; **M. Narazaki**, None; **T. Kondo**, None.

Presentation Number **P420**
Poster Session 3
September 7, 2012 / 15:15-15:15 / Room: The Liffey

# MR Imaging of Sentinal Lymph Nodes using different sized superparamagnetic iron oxide nanoparticles

***Pontus Kjellman***[1,3], *Rene in 't Zandt*[2,3], *Fredrik Olsson*[3], *Sarah Fredriksson*[3], *Sven-Erik Strand*[1], [1]*Medical Radiation Physics, Lund University, Lund, Sweden;* [2]*Lund University BioImaging Center, Lund University, Lund, Sweden;* [3]*Genovis AB, Lund, Sweden. Contact e-mail: pontus.kjellman@genovis.com*

Background: The metastatic spread, in breast cancer and malignant melanoma, mostly occurs through the lymphatic system. Histological examination of the first lymph node draining the tumor (the sentinel lymph node, SLN) reveals if the tumor has metastasized [1]. The vision of this project is to be able to target and image the SLN of patients with breast cancer or malignant melanoma in order to facilitate the surgical procedure. Multimodal nanoparticles will be used that by design have a retention time in the SLN over 24 hours allowing for diagnostic imaging prior to surgery. When designing nanoparticles for this purpose it is important to consider choice of material, surface charge, size, colloidal stability and biological compatibility. Superparamagnetic iron oxide nanoparticles (SPIONs) of various sizes and similar charge labeled with fluorescent dye was used to target and image the SLN in rats using MRI. In this preclinical model, the SLN is the popliteal node while the iliac node can be considered to be the 2nd lymph node in the lymphatic system downstream from the hind paw. Materials and Methods: Two different sized SPIONs (27 and 67 nm) were constructed by coating 11 nm iron oxide cores with polyethylene glycol of varying molecular weight. The SPIONs were labeled with a fluorescent dye, DY-647, to enable detection in histology sections. The dynamics of the SPIONs were evaluated in vivo by a subcutaneous injection in the right hind paws of rats. The retention of the particles in the lymphatic system was then visualized in vivo, 24 hours post injection, for the popliteal and the iliac lymph nodes. These lymph nodes were visualized by the acquisition of a 3D volume using MR imaging operating at 2.4T (Bruker Avance II system, 3D gradient echo, TE 6 ms, TR 27 ms). It is anticipated that higher levels of SPIONs will lead to larger susceptibility effects (higher T2-relaxivity) and as such to more signal loss in the MR images. For optimal detection of the lymph nodes, a 3D volume with and one 3D volume without lipid suppression were acquired. Animals were sacrificed after the MRI measurement and the popliteal and iliac lymph nodes were removed for histological analysis. Results: The T2-relaxivity of both particles showed to be similar dissolved in water. The MRI results showed apparent differences in the build-up of the various SPIONs in the SLN 24 hours post injection (figure 1). Also a clear difference in the amount of particles was observed when comparing the lymph nodes downstream of the SLN. When examining tissue sections, of the lymph nodes, using fluorescence microscopy the particles were located in endosomes inside the cells whereas the distribution of the particles reflected a similar distribution as has been observed in the MR images. Conclusion: Particle size plays an important role in the retention in the SLN. This facilitates the design of SPIONs that are optimized to target the sentinel lymph node (SLN) in patients with breast cancer or malignant melanoma. More detailed studies will focus on the dynamics of SPION transport from the hind paw into the SLN.

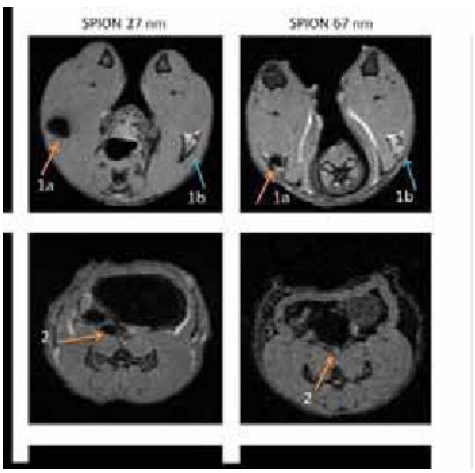


Figure 1: In vivo MR images of the popliteal nodes (1) which are the sentinel nodes after injection in the paw. At the control side (1b) no SPIONs are detected while at the injected side (1a) the presence of SPIONs leads to clear signal void in the MR images. Interestingly, the 27 nm particles seem to be present at a higher level than the 67 nm particles despite a higher relaxivity value for the large particles (data not shown). The 27 nm particles are clearly detected in the iliac node (2) while no particles can be seen in the iliac node after MR imaging when 67 nm particles were injected.

Disclosure of author financial interest or relationships:
**P. Kjellman**, Genovis AB, Employment; **R. in 't Zandt**, Genovis AB, Employment; Genovis AB, Stockholder; **F. Olsson**, Genovis AB, Employment; **S. Fredriksson**, Genovis AB, Employment; **S. Strand**, None.

Presentation Number **P421**
Poster Session 3
September 7, 2012 / 15:15-15:15 / Room: The Liffey

# SPIO-containing unilamellar polyion complex vesicles (PICsome) for in vivo tumor detection using MRI

***Daisuke Kokuryo***[1], *Yasutaka Anraku*[2], *Akihiro Kishimura*[2], *Sayaka Tanaka*[3], *Mitsunobu R. Kano*[3], *Tsuneo Saga*[1], *Kazunori Kataoka*[2,3], *Ichio Aoki*[1], [1]*Diagnostic Imaging Program, Molecular Imaging Center, National Instituite of Radiological Sciences, Chiba, Japan;* [2]*Graduate School of Engineering, University of Tokyo, Tokyo, Japan;* [3]*Graduate School of Medicine, University of Tokyo, Tokyo, Japan. Contact e-mail: kokuryo@nirs.go.jp*

Introduction: Size-tunable unilamellar polyion complex vesicles (PICsome) has been developed as a novel nano-vesicle for therapeutics and diagnosis (Anraku Y, et al; J Am Chem Soc., 2010). The accumulation of Cy5-labeled PICsomes in tumor has recently been demonstrated using a fluorescence imaging technique (Anraku Y, et al: Chem Comm., 2011). It was found that the half-life of the PICsomes in the bloodstream can be extended over 24 hours by adjusting the size of PICsomes, providing ample time for the vesicles to accumulate in the target tissue. For the present study, PICsomes containing super paramagnetic iron oxide nanoparticle (SPIO, ferucarbotran) were developed and in vivo accumulation in mouse tumor was evaluated with MR imaging. Methods: Female Balb/c nude mice were used for in vivo MR imaging experiments. A subcutaneous tumor model was created by injecting Colon26 cancer cells ($1.0 \times 10^6$ cells / 50 μl) into the rump of the animals and allowing them to grow for 7 to 8 days. SPIO (Resovist®), which contains ferucarbotran as a major component, was encapsulated in the Cy5-labeled PICsomes. The diameter of the PICsomes was about 100 nm. The PICsomes were administered to the model mice via the tail vein in a 0.45 mg/kg dose of iron. As a control group, SPIO alone was injected via the tail vein of tumor model mice. All MR image acquisitions were performed on a 7.0 Tesla animal MRI (Magnet: Kobelco and JASTEC, Japan, Console: Bruker-Biospin, Germany) with a 35 mm inner-diameter transmit/receive volume coil (Rapid Biomedical, Germany). $T_1$-weighted and $T_2$-weighted MR images were acquired before, immediately after, at 3, 6 and 24 hours after the drug administration. Imaging parameters were as follows: TR/TE/NEX = 400 ms / 9.57 ms / 4 ($T_1$-weighted image), 3000 ms / 30 ms / 1 ($T_2$-weighted image); FOV = 38.4 mm × 19.2 mm; and Matrix = 256 × 128. After MR image acquisition was completed for the PICsome group, fluorescence images were acquired using a fluorescence imager (Maestro Ex, Caliper LifeScience, USA) to confirm the accumulation of PICsomes at the tumor region. Results & Discussion: For 3-24 hours after PICsome administration, the $T_2$-weighted signal intensity in the tumor region significantly decreased from the intensity before administration. After 24 hours the area in tumor showing decreased $T_2$-weighted signal expanded, and it was also possible to detect decreased signal intensity in the $T_1$-weighted images. At the same time, the fluorescence signal also increased in the tumor region in comparison to the signal before administration. On the other hand, there were no signal changes in the subcutaneous tumor using SPIO alone, probably because the drug was predominantly captured by the Kupffer cells in the liver (Kato N, et al: Invest Radiol., 1999). These results indicate that the SPIO-containing PICsome passively accumulated due to EPR (Enhanced Permeability and Retention) effect and altered the MR signal in the tumor region specifically.

Disclosure of author financial interest or relationships:
**D. Kokuryo**, None; **Y. Anraku**, None; **A. Kishimura**, None; **S. Tanaka**, None; **M.R. Kano**, None; **T. Saga**, None; **K. Kataoka**, None; **I. Aoki**, None.

Presentation Number **P422**
Poster Session 3
September 7, 2012 / 15:15-15:15 / Room: The Liffey

# Development of Novel Imaging Tracers for Molecular Profiling of Tumors

*Nashaat Turkman, Galina Mikheeva, Juri G. Gelovani,* ***Victor Krasnykh****, Experimental Diagnostic Imaging, UT MD Anderson Cancer Center, Houston, TX, USA. Contact e-mail: vkrasnykh@mdanderson.org*

The use of tumor-targeted therapeutics suitable for systemic delivery is a promising approach to treat late metastatic cancer. The efficacy of this approach critically depends on the levels of expression of drug-targeted molecular signatures of tumors. Therefore, molecular profiling methods that are accurate and sensitive are urgently needed to improve the outcomes of cancer treatments. Such novel methods can be developed using molecular imaging of tumors. The ultimate goal of our research is to improve the sensitivity and specificity of molecular profiling of tumors by positron emission tomography (PET) by developing a new generation of targeted PET radiotracers. To this end, we take advantage of unique biological properties of Designed Ankyrin Repeat Proteins (DARPins)—small, rationally designed proteins, which have high affinity and specificity for their targets, are easy to produce and purify, and are stable in circulation. The specific objective of this study was to demonstrate the feasibility of site-specific labeling of a DARPin with a radioisotope suitable for PET. In particular, we wished to label the DARPin G5, which was designed to bind human epidermal growth factor receptor type 2 (Her2) with high affinity (KD of 90 pM), with Gallium-68 (Ga-68) using DOTA (1,4,7,10-tetraazacyclododecane-1,4,7,10-tetraacetic acid) chelator. To achieve site-specific conjugation of DOTA to DARPin, we modified the carboxy terminus of G5 genetically to contain a unique cysteine residue. The resultant protein, G5C, was produced in E.coli and purified by chromatography to homogeneity with yields of ~50 mg per liter of a suspension culture. Next, we confirmed the reactivity of this cysteine's thiol group by conjugating G5C with AlexaFluor488-maleimide, which was nearly 100%-efficient. By using flow cytometry with isogenic cell lines differing only by their Her2 expression phenotypes, we showed that this conjugation does not compromise the Her2-binding ability of the DARPin. Having established the thiol group reactivity, we used maleimide-mediated conjugation to produce DOTA-derivatized DARPin, G5C-DOTA. Next, G5C-DOTA was radiolabeled with Ga-68 using physiological conditions that resulted in efficient (more than 60%) incorporation of radionuclide. In summary, this proof-of-concept study demonstrated that derivatives of DARPins that are suitable for site-specific conjugation can be easily produced and labeled with fluorophores and PET-enabling radioisotopes under conditions preserving their target-binding ability.

Disclosure of author financial interest or relationships:
**N. Turkman**, None; **G. Mikheeva**, None; **J.G. Gelovani**, Macrocyclics, Consultant; SibTech, Consultant; **V. Krasnykh**, None.

Presentation Number **P423**
Poster Session 3
September 7, 2012 / 15:15-15:15 / Room: The Liffey

# Molecular imaging of CXCR4-expressing tumors using multimodal peptide multimers

***Joeri Kuil***[1], *Tessa Buckle*[1], *Hushan Yuan*[2], *Lee Josephson*[2], *Fijs van Leeuwen*[1], [1]*Radiology, Leiden University Medical Center, Leiden, Netherlands;* [2]*Center for Translational Nuclear Medicine and Molecular Imaging, Massachusetts General Hospital and Harvard Medical School, Charlestown, MA, USA. Contact e-mail: J.Kuil@lumc.nl*

The interaction between the chemokine receptor 4 (CXCR4) and stromal cell-derived factor-1 (SDF-1) is a natural regulatory process in the human body. CXCR4 is also over-expressed in 23 types of cancer were it plays a role in, among others, the metastatic spread [1]. Therefore, it is an emerging biomarker in the field of tumor imaging. CXCR4 is also used as a target for cancer therapy and chemosensitization. Several peptide antagonists for CXCR4 have been developed, including the potent 14 amino acid-containing disulfide-bridged Ac-TZ14011 cyclic peptide. To allow for integrated in vitro fluorescence imaging and in vivo SPECT/CT imaging and fluorescence guided surgery we have developed a multimodal (hybrid) label, consisting of a Cy5.5-like fluorophore and a DTPA chelate for indium labeling. This multimodal label has been conjugated to a monomeric, dimeric and tetrameric Ac-TZ14011 derivative. Confocal microscopy revealed that all three multimodal multimers were membrane bound at 4 degrees Celsius, consistent with CXCR4 binding in vitro. The unlabeled dimer and tetramer had a somewhat lower affinity for CXCR4 than the unlabeled monomer. However, when labeled with the multimodal label the CXCR4 affinity of the dimer and tetramer (Kd = 93.1 nM and 80.5 nM, respectively) was considerably higher compared to the labeled monomer (Kd = 186.9 nM). SPECT/CT tumor visualization in mice was possible with all three compounds and the fluorescence guided surgery was done with the monomer. On top of that, biodistribution studies revealed that the additional peptides in the dimer and tetramer reduced nonspecific muscle uptake compared to the monomer, resulting in tumor-to-muscle ratios of 7.41 for the dimer and 5.47 for the tetramer. In conclusion, multimerization improved the efficacy of multimodal labeled peptide [2,3]. References [1] Furusato, B., Mohamed, A., Uhlen, M., Rhim, J.S., CXCR4 and cancer. Pathol. Int., 2010, 60 (7), 497-505. [2] Kuil, J., Velders, A.H., Van Leeuwen, F.W.B., Multimodal tumor-targeting peptides functionalized with both a radio-and a fluorescent-label. Bioconjugate Chem., 2010, 21 (10), 1709-1719. [3] Kuil, J., Buckle, T., Oldenburg, J., Yuan, H., Borowsky, A.D., Josephson, L., van Leeuwen, F.W.B., Hybrid peptide dendrimers for imaging of chemokine receptor 4 (CXCR4) expression. Mol. Pharm., 2011, 8 (6), 2444-2453.

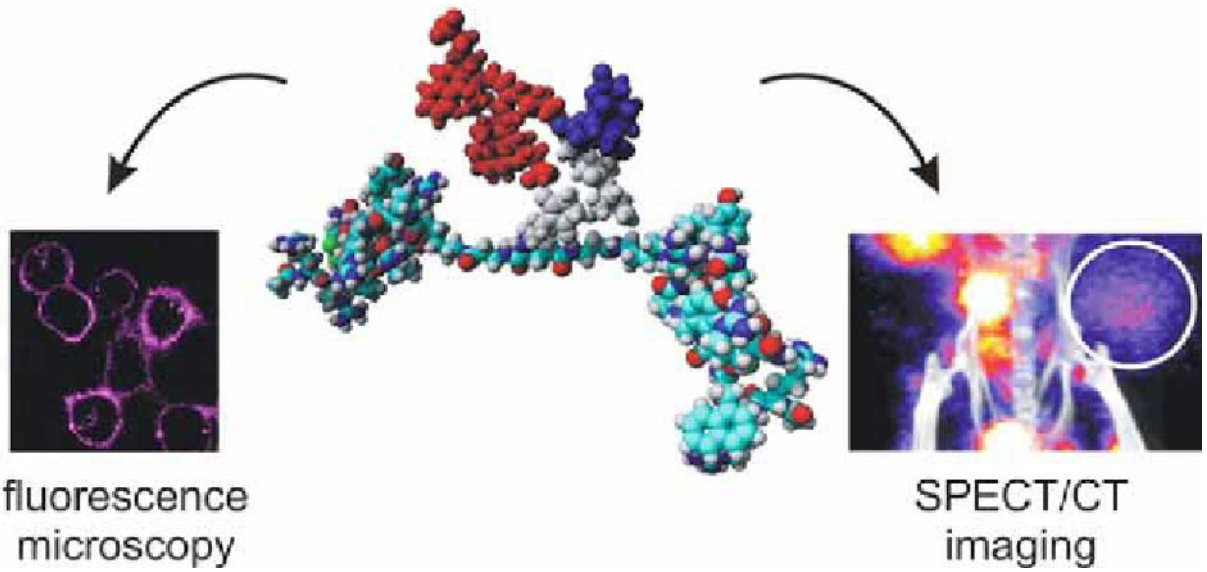


Disclosure of author financial interest or relationships:
**J. Kuil**, None; **T. Buckle**, None; **H. Yuan**, None; **L. Josephson**, None; **F. van Leeuwen**, None.

Presentation Number **P424**
Poster Session 3
September 7, 2012 / 15:15-15:15 / Room: The Liffey

# Tumor Targeted PET and MR Imaging with I-124 labeled Anti-TAG-72 Humanized Antibody Conjugated Iron Oxide Magnetic Nanoparticle

***Tae Sup Lee***[1], *In Ho Song*[1], *Hyo Jung Hong*[2], *Rita Song*[3], *Kwang Il Kim*[1], *Yong Jin Lee*[1], *Joo Hyun Kang*[1], [1]*Molecular Imaging Research Center, KIRAMS, Seoul, Republic of Korea;* [2]*Department of Systems Immunology, College of Biomedical Scinece, Kangwon National University, ChunCheon, Republic of Korea;* [3]*Nano/Bio Chemistry Laboratory, Institut Pasteur Korea (IP-K), Seongnam-si, Republic of Korea. Contact e-mail: nobelcow@kirams.re.kr*

Dual-modal nanoparticles with PET and MR imaging moiety could be useful for non-invasive and highly sensitive imaging of various biological events, including cancer diagnosis. We prepared anti-TAG-72 specific humanized antibody (3E8) conjugated iron oxide magnetic nanoparticles (IOMNPs) and subsequently radiolabeled with I-124. IOMNPs were conjugated with 3E8 antibody and radiolabeled with I-124 by Iodogen method. I-124-3E8-IOMNPs were purified by ultrafiltration and radiolabeling yield and purity were checked by ITLC. 3E8-IOMNPs or I-124-3E8-IOMNPs incubated with TAG-72 expressing LS174T cells and TAG-72 non-expressing MCF7 cells for Prussian blue staining or in vitro cell binding assay, respectively. T2 weighted MR imaging performed in LS174T tumor model using 3E8-IOMNPs for optimizing maximum T2 signal reduction in tumor. MR images of I-124-3E8-IOMNPs were obtained at pre-contrast and 1h , 4 h post-injection. PET images of I-124-3E8-IOMNPs were acquired at 5 h post injection. Localization of dual-modal nanoparticle was verified by digital wholebody autoradiography (DWBA). Two molecule of 3E8 antibody conjugated to one IOMNP analyzed by BCA protein assay. Radiolabeling yield of 3E8-IOMNPs with I-124 was >90% and radiochemical purity was above 98%. In prussian blue staining, 3E8-IOMNPs showed specific binding to TAG-72 expressing LS174T cells, but not bound to TAG-72 non-expressing MCF7 cells. In cell binding assay, I-124-3E8-IOMNPs showed 4 times higher uptake in LS174T cells than that in MCF7 cells. After 3E8-IONMPs was intravenously injected in LS174T bearing mice, T2 weighted MR images obtained. MR signal intensity at 4 h post injection in LS174T tumor was markedly decreased to 60% of signal intensity in pre-contrast MR image. I-124-3E8-IOMNPs were localized in LS174T tumor at T2 weighted MR and PET images, However, reticuloendothelial system also showed high uptake of I-124-3E8-IOMNPs. The location of I-124-3E8-IOMNPs within tumor in T2 weighted MR image was verified by digital wholebody autoradiography. PET/MR dual modality imaging nanoparticle with anti-TAG-72 specific human antibody was specifically bound to TAG-72 expressing tumor and it could be used as a theranostic platform for imaging and therapy to cancer specific target by further modification including drug or therapeutic radioisotope.

Disclosure of author financial interest or relationships:
**T. Lee**, None; **I. Song**, None; **H. Hong**, None; **R. Song**, None; **K. Kim**, None; **Y. Lee**, None; **J. Kang**, None.

Presentation Number **P425**
Poster Session 3
September 7, 2012 / 15:15-15:15 / Room: The Liffey

# Size-controllable Magnetic Polymeric Nanobubbles as Dual-modal Contrast Agents for Ultrasound and MR Imaging

***Zhe Liu**, Fabian Kiessling, Jessica Gätjens, Department of Experimental Molecular Imaging, Helmholtz Institute of Biomedical Engineering, Aachen, Germany. Contact e-mail: zhliu@ukaachen.de*

Introduction: Magnetic resonance (MR) and ultrasound (US) imaging are widely-used diagnostic modalities for experimental and clinical applications. In this research, size-controllable polymeric nanobubbles were designed as dual-modal contrast agents for US and MR imaging. Methods: These nano-sized imaging probes were prepared via a one-step polymerization to form PBCA nanobubbles. The magnetic nanobubbles were generated incorporation with iron oxide nanoparticles encapsulation in the shell. They showed a varied size distribution (300 nm to 2.2 μm) with changing agitation speed from 1000 to 10000 rpm. Results: The hybrid nano-sized imaging agents exhibited strong contrast in US (comparable to microbubble counterparts), and an increased transversal relaxation rate in MR was also observed. Moreover, they displayed a good persistence to US-induced bubble destruction, which demonstrated their utility as functional carriers for US-triggerable theranostic applications (same to microbubbles). Conclusion: In conclusion, these magnetic nano-sized hybrid materials are highly interesting systems for bimodal MR-US imaging, and their potential applications as vehicles for MR-guided US-mediated drug and gene delivery can be outlooked.

Disclosure of author financial interest or relationships:
**Z. Liu**, None; **F. Kiessling**, None; **J. Gätjens**, None.

Presentation Number **P426**
Poster Session 3
September 7, 2012 / 15:15-15:15 / Room: The Liffey

# Ultrasmall Rigid Platforms : from multimodal imaging to theranostic applications

***François Lux***[1], *Lucie Sancey*[1], *Sandrine Dufort*[2,4], *Géraldine Le Duc*[3], *Jean-Luc Coll*[4], *Stephane Roux*[5], *Pascal Perriat*[6], *Olivier Tillement*[1], [1]*Laboratoire de Physico-Chimie des Matériaux Luminescents, Villeurbanne, France;* [2]*Nano-H S.A.S, Saint-Quentin Fallavier, France;* [3]*ESRF, Biomedical beamline, Grenoble, France;* [4]*Institut Albert Bonniot, Grenoble, France;* [5]*Institut UTINAM, Besançon, France;* [6]*MATEIS, Lyon, France. Contact e-mail: francois.lux@univ-lyon1.fr*

UltraSmall Rigid Platforms (USRP) are nanoparticles with a size lesser than 5 nanometers composed of polysiloxane and gadolinium complexes covalently grafted to the inorganic matrix. These nanoparticles combine nano-objects advantages (multimodality, passive concentration in tumour by Enhanced Permeability and Retention (EPR) Effect, longer circulation in blood) and molecular advantages (renal excretion, no captation by macrophages…). They can be used as contrast agents for 4 different types of imaging: Magnetic Resonance Imaging, Scintigraphy, Fluorescence Imaging and X-Ray tomography. The in-vivo biodistribution on healthy rats and mice indicate that they freely circulate in the blood vessels without undesirable accumulation in the lungs, spleen and liver; the USRP are eliminated exclusively by renal excretion. The combination of the different imaging modality is important to benefit from the advantage of each (resolution for MRI imaging and sensitivity for scintigraphy). The injection of the USRPs in tumour bearing (9L, U87, etc) animals reveals their concentration in the tumour by EPR effect. Active targeting can be used to increase this accumulation in the tumour. The USRP have also therapeutic properties, in vitro and in vivo results indicate that they possess a great potential for radiosensitization (i.e. enhancement of the therapeutic properties of the radiotherapy by the use of an agent). For this type of treatment, the following of the particles by imaging techniques after the injection is a key point in order to determine the opportune moment to "launch" radiotherapy. The USRPs have to be activated when there are still particles in the tumour but no more in the surrounding healthy tissues. This activation leads to a huge increase of the lifespan of gliosarcoma (9L) bearing rats when they were treated by radiotherapy after intravenous injection of USRPs. To conclude, USRPs exhibit an interesting potential for image-guided radiotherapy which should permit to adapt the therapy to each patient.

Disclosure of author financial interest or relationships:
**F. Lux**, None; **L. Sancey**, None; **S. Dufort**, None; **G. Le Duc**, None; **J. Coll**, None; **S. Roux**, None; **P. Perriat**, None; **O. Tillement**, None.

Presentation Number **P427**
Poster Session 3
September 7, 2012 / 15:15-15:15 / Room: The Liffey

# Effect of poly(lactic acid) stereochemistry on tumor imaging with using nanocarrier "Lactosome"

***Akira Makino***[1], *Ayaka Tomoike*[1], *Isao Hara*[2], *Eiichi Ozeki*[2], *Shunsaku Kimura*[3], *Masahiro Ono*[1], *Hideo Saji*[1], [1]*Department of Patho-bioanalysis, Graduate School of Pharmceutical Sciences, Kyoto University, Kyoto, Japan;* [2]*Technology Research Laboratory, Shimadzu Corporation, Kyoto, Japan;* [3]*Department of Materials Chemistry, Graduate School of Engineering, Kyoto University, Kyoto, Japan. Contact e-mail: makino@pharm.kyoto-u.ac.jp*

<Introduction> AB- and $A_3B$-Lactosome are core-shell type polymeric micelles, which are composed of AB and $A_3B$ type amphiphilic polydepsipeptides, respectively. The A unit represents a hydrophilic block of poly(sarcosine), which is natural polypeptide, and shows high solubility in aqueous solution in similarity with poly(ethylene glycol) (PEG). The B unit is a hydrophobic block and composed of poly(L-lactic acid). On these Lactosome surfaces, poly(sarcosine) chains are densely aligned as a state of polymer brush. Owing to the poly(sarcosine) polymer brush structure, Lactosomes are hardly recognized by reticulo-endothelial systems (RES). Therefore, Lactosome with diameter of 30 nm has been shown to accumulate passively at solid tumor regions by the enhanced permeation and retention (EPR) effect. Further, Lactosome can encapsulate hydrophobic compounds in its core region in the similar manner to other core-shell type polymeric micelles. By encapsulating signal compounds (SCs) such as radioisotopes and near-infrared fluorescein compounds to the Lactosome core region, Lactosome can be used successfully for tumor imaging. In order to encapsulate SCs stably in Lactosome, it is useful to modify SCs with attaching a hydrophobic poly(lactic acid) chain. Furthermore, we expect that the stability of SCs in Lactosome can be controlled by combination of stereochemistry of poly(lactic acid) between the compoment of Lactosome and the attached one to SCs. Therefore, in this study, the effect of stereochemistry of SC-attached poly(lactic acid) (SC-PLA) on tumor imaging with using AB and $A_3B$ type Lactosomes is examined together with evaluation of the stability of these Lactosomes in blood circulation. <Method> Three types of SC-PLAs of SC-attached poly(L-lactic acid), poly(D-lactic acid), and poly(D,L-lactic acid) (SC-PLLA, SC-PDLA, and SC-PDLLA) were synthesized. The imaging probes of possible combinations between three kinds of the SC-PLAs and two kinds of amphiphilic polydepsipeptides were abbreviated as AB-Lactosome(L), AB-Lactosome (D), AB-Lactosome(DL), $A_3B$-Lactosome(L), $A_3B$-Lactosome (D), and $A_3B$-Lactosome(DL). To the tumor bearing mice, these SC-attached Lactosomes were intravenously administrated, and their biodistribution was evaluated. Additionally, amphiphilic polydepsipeptide is directly modified with radioistopes, and used for evaluation of the Lactosome stability in blood pool during circulation. <Conclusion> From the circular dichlorism (CD) measurements, it was revealed that hydrophobic PLLA region in both AB- and $A_3B$ type amphiphilic polydepsipeptides forms left-handed helical structure. Further, SC-PLLA and SC-PDLA forms left- and right-handed helical structure, respectively. On the other hand, SC-PDLLA takes random structure. Biodistribution of prepared six types Lactosomes, which is determined by signal detection from SC-PLA, is changed by SC-PLA stereochemistry. In this presentation, the possible control of half-life time of Lactosome in blood circulation with using SC-PLA stereochemistry and consequent signal-to-bakground contrast on tumor imaging are discussed.

Disclosure of author financial interest or relationships:
**A. Makino**, None; **A. Tomoike**, None; **I. Hara**, None; **E. Ozeki**, None; **S. Kimura**, None; **M. Ono**, None; **H. Saji**, None.

Presentation Number **P428**
Poster Session 3
September 7, 2012 / 15:15-15:15 / Room: The Liffey

# Site-specific labeling of Nanobody-based imaging probes

***Sam Massa***[1,2], *Catarina Xavier*[1], *Matthias D'huyvetter*[1], *Vicky Caveliers*[1,4], *Tony Lahoutte*[1,4], *Serge Muyldermans*[2,3], *Nick Devoogdt*[1], [1]*In Vivo Cellular and Molecular Imaging Laboratory, Vrije Universiteit Brussel, Brussels, Belgium;* [2]*Laboratory of Cellular and Molecular Immunology, Vrije Universiteit Brussel, Brussels, Belgium;* [3]*Department of Structural Biology, Vlaams Instituut voor Biotechnologie, Brussels, Belgium;* [4]*Nuclear Medicine Department, UZ Brussel, Brussels, Belgium. Contact e-mail: sam.massa@vub.ac.be*

Introduction - The development of a homogeneous tracer population for non-invasive molecular imaging is of great importance for obtaining consistent biodistribution data and a successful clinical translation. A commonly used strategy for labeling antibody-derived imaging probes is to use the primary amines of the surface exposed lysine residues. This labeling technique results however in a heterogeneous mixture of tracers with different amount of labels at different positions, with possible negative effect on the biodistribution behavior of the tracer. Nanobodies (Nbs), the isolated antigen binding domain of heavy chain antibodies, already have proven to be proficient tools for non-invasive molecular imaging: they are small (ca. 15 kDa), stable, soluble and show a high binding specificity and affinity for their target. Aim - To safeguard their intrinsically high binding specificity and affinity, and to increase the tracer's specific activity and homogeneity, the ability of Nbs to be site-specifically conjugated to a label via a thio-ether bond was investigated. Results - In order to achieve this, an unpaired cysteine was introduced at the surface of a Nb. Initially, positions with conserved amino acids were chosen for mutation: on the C-terminal end of the Nb (following the poly-histidine tail) or in a conserved cavity of the surface (to avoid dimerization). These constructs were still functional, but the introduction of the cysteine caused expression problems and resulted in a low yield. Introducing a 14 amino acids-long linker between the Nb and the cysteine offered a solution. This new construct was produced in the same amount as the original Nb and was capable of binding recombinant target antigen with equal affinity. However, because of the availability of the unpaired cysteine the Nbs dimerized spontaneously. Consequently a reduction step is necessary in order to be able to label the Nb site-specifically. This reduction step is however critical when working with antibody-derived domains, since they contain a disulfide bridge that is crucial for the domain's stability. The dimerized constructs were successfully reduced through the use of the mild reducing agent 2-mercaptoethylamine, with conservation of the Nb's functionality. After site-specific coupling with DTPA-maleimide and labeling with 111In, a radiochemical stable complex was formed. The labeled Nb was still capable of binding in vitro specifically to the recombinant antigen and to cells expressing the antigen. Moreover, the site-specific labeled Nbs were able to accumulate significantly in the tumor of xenografted mice in vivo and manifested a high contrast at an early time point after injection (1 h - 1,5 h). Conclusion - These results provide a versatile strategy for the site-specific labeling of Nbs with either radionuclides for PET (68Ga, 64Cu), SPECT (111In) and therapy (177Lu), or with fluorescent dyes. This is not only preserving the intrinsically high binding specificity and affinity of the probe, but also results in the production of a homogeneous group of tracers for use in clinical molecular imaging.

Disclosure of author financial interest or relationships:
**S. Massa**, None; **C. Xavier**, None; **M. D'huyvetter**, None; **V. Caveliers**, None; **T. Lahoutte**, None; **S. Muyldermans**, None; **N. Devoogdt**, Boehringer Ingelheim, Grant/research support; Ablynx, Grant/research support .

Presentation Number **P429**
Poster Session 3
September 7, 2012 / 15:15-15:15 / Room: The Liffey

# $^{64}$Cu@Gadonanotubes: A Novel MRI/PET Multimodal Imaging Agent of Carbon Nanotube Design

***Michael Matson***[1,2], *Brandon Cisneros*[3], *Ali Azhdarinia*[4], *Eva Sevick*[4], *Lon J. Wilson*[2], *[1]Department of Natural Sciences, University of Houston-Downtown, Houston, TX, USA; [2]Department of Chemistry, Rice University, Houston, TX, USA; [3]Department of Surgical Oncology, MD Anderson Cancer Center, Houston, TX, USA; [4]Center for Molecular Imaging, The University of Texas Health Science Center, Houston, TX, USA. Contact e-mail: matsonm@uhd.edu*

**Objective:** Herein, we report a multimodal PET/MRI imaging probe that combines the picogram sensitivity of $^{64}$Cu PET imaging with the Gadonanotubes (GNTs), an MRI contrast agent that enhances both $T_1$- and $T_2$-weighted MR imaging. **Methods:** Synthesized from commercially-available, single-walled carbon nanotubes (SWNTs, Carbon Solutions, Inc), ultra-short SWNTs (US-tubes, 20-80 nm long) were produced following HCl purification, treatment with fluorine gas, and subsequent pyrolysis. The US-tubes were then individualized using $Na^0$ in tetrahydrofuran. The US-tubes were bath sonicated in a solution of high-specific-activity $^{64}CuCl_2$ (Washington University, St. Louis, MO) diluted in 5 mM acidic $GdCl_3$ for 30 min and allowed to stabilize for an additional 30 min. The stability of the agent was assessed by subjecting the $^{64}$Cu@GNT complex to simulated in vivo challenges with PBS (25°C) and mouse serum (40°C), followed by microcentrifugation to monitor leaking of $^{64}$Cu from the agent. MicroPET/CT images were acquired in mice (both tumor-bearing and non-tumor bearing) following intravenous injection of free $^{64}$Cu and $^{64}$Cu@GNT. **Results:** The loading efficiency of $^{64}$Cu into the GNT was over 98%. The multimodal agent demosntarted excellent stability as no leaking of $^{64}$Cu was observed upon in vitro challenge with PBS or mouse serum. Following an initial wash with serum, all subsequent washes showed less than 5% $^{64}$Cu leakage, with less than 1% in all cases by the third serum wash. The imaging studies showed different distribution patterns for free $^{64}$Cu compared to $^{64}$Cu@GNT, indicating stable retention of the radionuclide in the agent. **Conclusions:** The unique stability of the $Gd^{3+}$-ion clusters within the GNTs appear to have successfully aided the encapsulation of $^{64}Cu^{2+}$ ions within GNTs to produce a stable, multimodal PET/MRI imaging probe that successfully sequesters toxic $Gd^{3+}$ ions while simultaneously trapping $^{64}Cu^{2+}$ ions. This conclusion suggests that carbon nanotube capsules can be exploited to encapsulate various combinations of imaging probes (PET, MRI, CT, SPECT, etc.) tailored for personalized medicine.

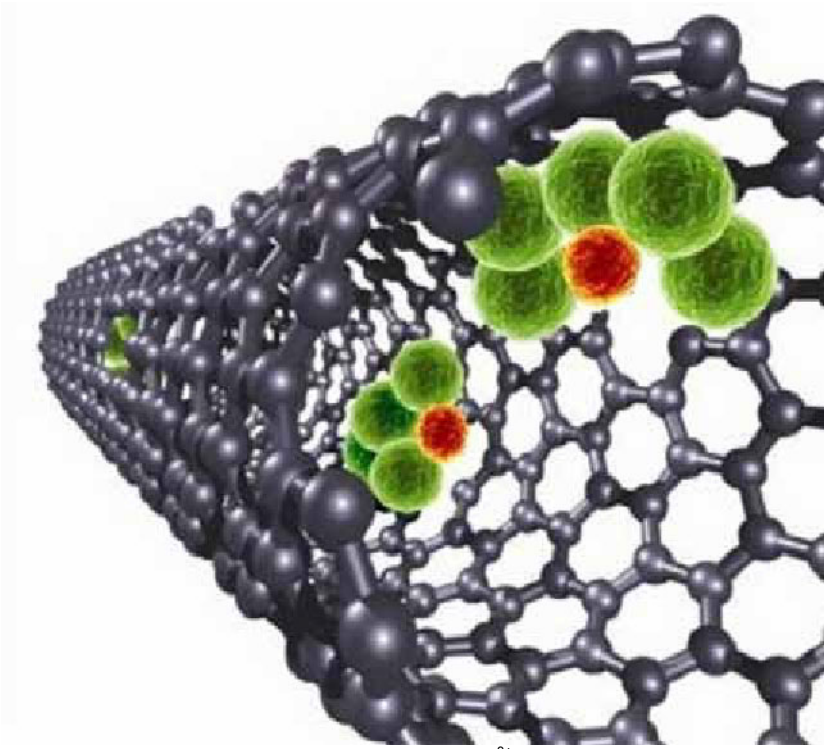

Artistic depiction of $^{64}$Cu@GNT, drawn to scale, with green spheres representing $Gd^{3+}$ ions, orange spheres representing $Cu^{2+}$ ions, and black spheres representing the carbon atoms of the nanotube.

Disclosure of author financial interest or relationships:
**M. Matson**, None; **B. Cisneros**, None; **A. Azhdarinia**, None; **E. Sevick**, Tactile, Inc, Grant/research support; Siemens Preclinical Solutions, Other financial or material support; **L.J. Wilson**, None.

Presentation Number **P430**
Poster Session 3
September 7, 2012 / 15:15-15:15 / Room: The Liffey

# Multi-functional Aptamer-Conjugated Hollow Nanoshells for Image-Guided Photothermal Ablation of Head and Neck Cancer

***Marites P. Melancon***[2,1], *Min Zhou*[1], *Chiyi Xiong*[1], *Qian Huang*[1], *Rui Zhang*[1], *Peter B. Allen*[4], *Andrew D. Ellington*[4], *Jeffrey N. Myers*[3], *R. Jason Stafford*[2], *Chun Li*[1], *Chun Li*[1], [1]*Experimental Diagnostic Imaging, UT-MD Anderson Cancer Center, Houston, TX, USA;* [2]*Imaging Physics, UT-MD Anderson Cancer Center, Houston, TX, USA;* [3]*Head and Neck Surgery, UT-MD Anderson Cancer Center, Houston, TX, USA;* [4]*Institute of Cellular and Molecular Biology, UT-Austin, Austin, TX, USA. Contact e-mail: mmelancon@di.mdacc.tmc.edu*

Introduction: Antibodies, aptamers and peptides have all been used for targeting of tumor cells with high binding affinity and good specificity. In this study, we compared the binding affinity and selective targeting of aptamer versus antibody targeted to epidemeral growth factor receptors (EGFR) which are overexpressed in 90% of oral cancer. Methods: Aptamers was conjugated to hollow nanoshell (apt-HAuNS) by attaching an SH-terminated ss-DNA to the HAuNS first and then adding the RNA targeted to EGFR having 22 complementary bases to the ss-DNA. Apt-HAuNS was characterized in terms of size, surface charge, absorption and number of aptamer per particle. The in vivo pharmacokinetics and in vivo biodistribution of 111In-labeled apt-HAuNS was also evaluated in nude mice bearing OSC19 tumors in the tongue. Controls such as PEG-HAuNS and cetuximab-conjugated HAuNS (C225-HAuNS) were used (n=3/group). SPECT-CT imaging was done to show selective targeting and imaging capability of the agent, while histology was used to confirm the presence of nanoshell in the tumor tissues. Results: Attachment aptamer to the HAuNS does not alter the absorbance profile or the size of the bare HAuNS (λmax = 800 nm, diameter = 55 nm). Surface charge becomes more negative upon conjugation of the aptamer (-51.42 vs -19.00 for PEG-HAuNS). The number of aptamer/particle was calculated to be ~250. In vitro cell binding and in vivo biodistribution showed selective binding of the aptamer-HAuNS (Figure A). SPECT-CT imaging also showed that there is more uptake with aptamer-HAuNS compared with C225- and PEG-conjugated HAuNS (Figure B). Dark-field microscopy of the tumor tissues confirmed the presence of nanoshell in the tumor. Conclusion: Aptamer is a promising ligand for image-guided therapy of tumors and cancer cells overexpressing EGFR.

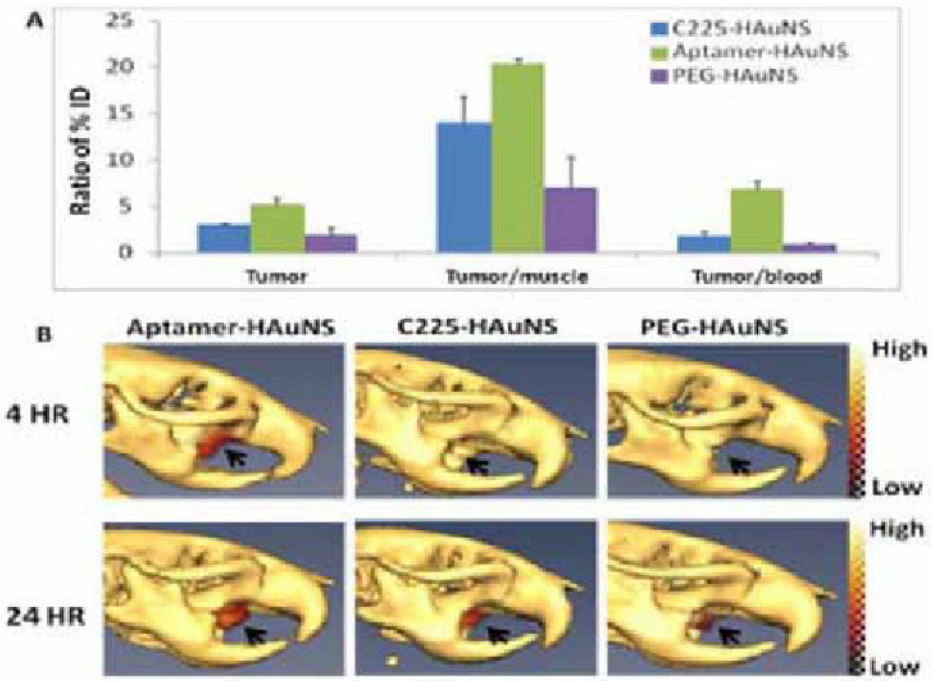


**Figure 1.** (A). In vivo biodistribution of mice bearing OSC19 in the tongue. (B) SPECT-CT images of the same mice after intravenous injection of 111In-labeled agents.

Disclosure of author financial interest or relationships:
**M.P. Melancon**, None; **M. Zhou**, None; **C. Xiong**, None; **Q. Huang**, None; **R. Zhang**, None; **P.B. Allen**, None; **A.D. Ellington**, None; **J.N. Myers**, None; **R. Stafford**, None; **C. Li**, None; **C. Li**, None.

Presentation Number **P431**
Poster Session 3
September 7, 2012 / 15:15-15:15 / Room: The Liffey

# In vivo Imaging with Biologics: Novel Site-Specifically Labeled Antibody-Like Scaffolds with Improved Stability, Avidity and Pharmacokinetics

***Sina Meyer***[1], *Nicole Berntsen*[1], *Regina Link*[2], *Susan Cellitti*[3], *Bernhard H. Geierstanger*[3], *Mauro Zurini*[2], *Hilmar Ebersbach*[2], *Rainer Kneuer*[1], [1]*Global Imaging Group, Novartis Institutes for BioMedical Research (NIBR), Basel, Switzerland;* [2]*Novartis Biologics Center, Novartis Institutes for BioMedical Research (NIBR), Basel, Switzerland;* [3]*Protein Engineering, Genomics Institute of the Novartis Research Foundation (GNF), San Diego, CA, USA. Contact e-mail: brit_sina.meyer@novartis.com*

Monoclonal antibodies (mAb) exceed low molecular weight molecule drugs in respect to high target specificity and affinity, lower toxicity and increased half-life in vivo. However, employing mAb as molecular imaging agents results in low target/background ratios, due to their long half-lives in plasma. Single chain variable fragments (scFv) have been previously used for molecular imaging, since they successfully penetrate solid tumors in vivo and are cleared from the blood pool quickly. Unfortunately, their relatively small size (25 kDa) results in renal uptake and therefore fast overall clearance impairing further accumulation at the target. Employing antibody-like scaffolds as highly improved biologics imaging agents, three independent hypotheses are being tested: First, a comparative study of smaller formats such as single domain (sd), scFv, and diabody vs. full size IgG will yield the most suitable imaging agent depending on stability, binding kinetics, cellular internalization and pharmakokinetics. Second, random vs. site-specific labeling through hexa-histidine purification tags, cysteine or pyrroline-carboxy-lysine residues is being investigated to prove advantages of consistently labeled imaging agents such as constant binding affinity, high fluorescent signal intensity, and efficacy of labeling. Third, multivalent polymers will be introduced to the imaging agents to optimize pharmacokinetics and avidity. The results from these studies will yield a preferred imaging agent that can be used as a template for other targets on demand. Moreover, this toolbox could be used to explore in vitro expression, intracellular fate, or native substrates of a chosen target, as well as expression and biodistribution in vivo.

Disclosure of author financial interest or relationships:
**S. Meyer**, Novartis, Grant/research support; **N. Berntsen**, None; **R. Link**, Novartis, Employment; **S. Cellitti**, GNF/Novartis, Employment; **B.H. Geierstanger**, Novartis, Employment; **M. Zurini**, None; **H. Ebersbach**, None; **R. Kneuer**, Novartis Pharma, Employment .

Presentation Number **P432**
Poster Session 3
September 7, 2012 / 15:15-15:15 / Room: The Liffey

# Dual-Mode Probe, Copper-64 Conjugated SPIO Nanoparticles, Is An Effective Approach to Monitor Bio-distribution of Implanted Stem Cells

***Shadreck Mzengeza***[1], *Esmat Elhami*[3], *Bo Xiang*[2], *Arnold Kell*[5], *Andrew L. Goertzen*[1], *Darren H. Freed*[4], *Rakesh C. Arora*[4], *Ganghong Tian*[2], [1]*Radiology, University of Manitoba, Winnipeg, MB, Canada;* [2]*Cardiac Studies Group, Institute for Biodiagnostics, National Research Council Canada, Winnipeg, MB, Canada;* [3]*Department of Physics, University of Winnipeg, Winnipeg, MB, Canada;* [4]*Cardiac Science Program, St Boniface General Hospital, Winnipeg, MB, Canada;* [5]*Steacie Institute for Molecular Sciences, National Research Council Canada, Ottawa, ON, Canada. Contact e-mail: smzengeza@hsc.mb.ca*

Introduction: Magnetic resonance imaging (MRI) is currently used for tracking of implanted stem cells. Due to insufficient sensitivity, however, bio-distribution of implanted stem cells could not be reliably determined. To improve cell tracking, we have developed a radioactive tracer conjugated superparamagnetic iron oxide nanoparticles. Efficacy of the new nanoparticles for monitoring of cell distribution was assessed in a rodent model of heart infarction. Objective: This present study was to: 1) determine a dual-mode nanoparticle; 2) assess systemic distribution of stem cells labeled with the nanoparticle. Methods: Superparamagnetic iron oxide (SPIO) nanoparticles were prepared via hydrolysis of the chelated iron alkoxide complexe at elevated temperature. The hydrolyzed complex was then dissolved in chelating diethylene glycol. In order to make the SPIO nanoparticles water-soluble and biocompatible a dispersion of the nanoparticles in hexane was treated separately with a solution of 3,4-dihydroxyphenylalanine (DOPA) and (3-carboxypropyl)trimethylammonium chloride in a mixture of buffer and ethanol. After dialysis against water, the SPIO nanoparticles were conjugated to an N-hydroxysuccinimide (NHS) derivative of 1,4,7,10-tetraazacyclododecane-1,4,7,10-tetraacetic acid (DOTA) in dimethylformamide A suspension of the nanoparticles in ammonium acetate buffer pH 7 was incubated at 43C with a solution of 64Cu-copper acetate in ammonium acetate to conjugate the 64Cu to the nanoparticle. To assess bio-distribution of the dual-mode nanoparticle, 650 µCi of 64Cu-nanoparticles was injected into rats via tail. To assess efficacy of the dual-mode nanoparticle for cell tracking, adipose-derived stem cells labeled with the nanoparticle were injected into a tail vein of rats. Whole-body PET and MRI images were acquired using the Siemens P4 camera and a 7 Tesla MR scanner, respectively. Results: PET images showed that the dual-mode nanoparticles distributed non-selectively throughout body when it was delivered into a tail vein. In contrast, the majority of the nanoparticle-labeled stem cells were found in the lungs when the cells were injected intravenously. Both PET and MRI showed a similar bio-distribution of the nanoparticle and nanoparticle-labeled cells. Furthermore, tissue sections of the vital organs (lungs, heart, liver, and kidneys) showed a positive SPIO staining. In particular, the SPIO staining correlated well with PET and MRI results. Conclusion: Dual-mode nanoparticles are a useful approach for quantitative characterization of the bio-distribution of implanted stem cells.

Disclosure of author financial interest or relationships:
**S. Mzengeza**, None; **E. Elhami**, None; **B. Xiang**, None; **A. Kell**, None; **A.L. Goertzen**, None; **D.H. Freed**, None; **R.C. Arora**, None; **G. Tian**, None.

Presentation Number **P433**
Poster Session 3
September 7, 2012 / 15:15-15:15 / Room: The Liffey

# OCMCh-PEI introduced homing peptide for targeting angiogenic blood vessel

***Jae-Woon Nah**, Mi-Kyeong Jang, Polymer Science & Engineering, Sunchon National University, Suncheon, Republic of Korea.*
*Contact e-mail: jwnah@sunchon.ac.kr*

New biological system for cancer therapy has been investigated using anti-angiogenic gene delivery system. Anti-angiogenic therapy is used to inhibit tumor growth and metastasis by destroying neighboring blood vessels that supply tumor cells with oxygen and nutrients and also provide an exit route for tumors to enter the bloodstream (Kim, 2005). Especially, the αvβ3/ αvβ5 integrin which is expressed on endothelial cells during angiogenesis has high binding affinity in RGD peptide. Except it, there are many homing peptides (HPs) to target specific tissue as penetrate the specific tumor cell membrane. Chitosan has been reported to enhance drug transportation across the nasal or mucosal layer without tissue damage.5 Furthermore, the cationic properties of chitosan offer valuable properties for drug delivery systems, gene delivery systems, and tissue engineering and imaging materials. Among various chitosan, low molecular weight water-soluble chitosan(LMWSC) is useful to the drug delivery system for introducing these HPs since LMWSC gives high reactivity which is good for conjugation various functional group due to amine group. In this study, LMWSC-PEG-parclitaxel(LMPXPEG) nanoparticle introduced HPs for targeting angiogenic blood. First, the physicochemical properties of LMPXPEG nanoparticle introduced HPs (LMPXPEG-HPs nanoparticle) were investigated by using 1H-NMR, dynamic light scattering (DLS) and Transmission Electron Microscope (TEM). The LMPXPEG-HPs nanoparticle was investigated potential as carrier of anticancer agent. In the FT-IR spectra of the LMPXPEG, a peak appeared at 1730 cm-1 corresponding to carbonyl group (C=O) and the characteristic peak corresponding. At 1H-NMR spectra, specific peaks (phenyl group 7.5~8.0ppm) by pacalitaxel appeared at DMSO. The LMPXPEG-HPs nanoparticle formed around 1570 nm sized unimodal nanoparticles with fairly narrow distributions. Mophologies of complexes by TEM were well-formed spherical shape, and the average diameter measured by DLS was 100 ~ 200 nm and formed 174~300 nm sized unimodal nanoparticles with fairly narrow distributions. This research was supported by Ministry of Knowledge Economic (MKE) and Basic Science Reaseach Program through the National Reseach Foundation of Korea (NRF) funded by the Ministry of Education, Science and Technology (2011-0012039)

Disclosure of author financial interest or relationships:
**J. Nah**, None; **M. Jang**, None.

Presentation Number **P434**
Poster Session 3
September 7, 2012 / 15:15-15:15 / Room: The Liffey

# A Novel Tumor-targeting Small Molecule PET/Fluorescence Dual Imaging Probe

***Dongfeng Pan***[1], *Li Xiao*[1], *Yi Zhang*[1], *Wei Yue*[2], *Ji-ping Wang*[2], [1]*Radiology, Univ of VA-Environmental Scies, Charlottesville, VA, USA;* [2]*Endocrinology, University of Virginia, Charlottesville, VA, USA. Contact e-mail: dp3r@virginia.edu*

Objective: To synthesize and develop a novel tumor-targeting small molecule PET/fluorescence dual imaging probe Methods: Tumor-specific heptamine-cyanine dye was conjugated with DOTA and radiolabeled with Cu-64 for dual-modality imaging. Detailed spectroscopic properties of the probe PC 1001 were obtained. In vitro cellular uptake studies were performed in tumor (MCF-7) and non-tumor (MCF-10A) cells to establish tumor-specific selectivity. Inhibition studies for tumor-specific uptake were performed to offer plausible mechanism of action. In vivo fluorescence and PET imaging of breast tumor xenograft in mice at various time points were carried out and analyzed. Blood clearance (half-life in blood), biodistribution, tumor-specific uptake and plasma binding were demonstrated in quantitative manner. Ex vivo histology (H/E staining) and confocal fluorescence imaging were examined at microscopic level. Results: The conjugation of DOTA-Cu moiety to heptamethine cyanine dye remained similar fluorescence properties E=82,880 cm-1M-1, Ex/Em=750/820 nm as that of the original dye indicating no significant effect on optical properties upon PET probe attachment. Time-dependent cellular accumulation suggested significantly higher probe uptake (>2-fold) in MCF-7 tumor cells than in control MCF-10A epithelial cells. Inhibition studies revealed the possible mechanism to be organic anion transport polypeptide (OATP) mediated uptake. Dual-modality PET/fluorescence imaging by the probe demonstrated desirable accumulation in tumor sites. SUV analysis of tumor verses muscle (control) suggested a factor of 5.8±0.2 fold increase in uptake over 48 h post probe injection. Blood clearance half-life of the probe was observed to be 257±13 min. Microscopic fluorescence imaging of ex vivo harvested tissue indicated that the probe was mainly associated with viable tumor but not with necrotic tissue. Conclusion: A highly effective dual-modality (PET/fluorescence) imaging probe is obtained, and its feasibility for tumor-specific imaging is demonstrated. The results indicate that the probe is well-suited to advance into pre-clinical evaluation.

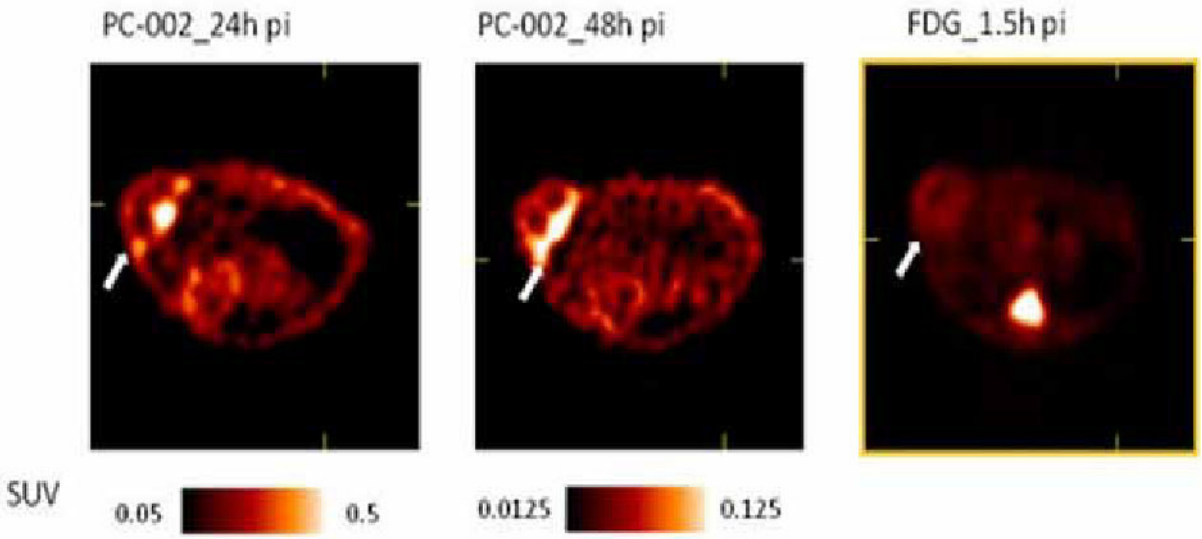


PET images of nude mice with MCF-7 tumor

Disclosure of author financial interest or relationships:
**D. Pan**, None; **L. Xiao**, None; **Y. Zhang**, None; **W. Yue**, None; **J. Wang**, None.

Presentation Number **P435**
Poster Session 3
September 7, 2012 / 15:15-15:15 / Room: The Liffey

# Development of PET/MR/NIR trimodal imaging probe based on polyelectrolyte nanogels

*Yong Taik Lim, **Hye Sun Park**, Graduate School and Department of Analytical Science and Technology, Chungnam National University, Daejeon, Republic of Korea. Contact e-mail: hyesun-1981@hanmail.net*

Challenges in diagnostic imaging have led to an explosion of interest in combining modalities to more accurately interpret disease and abnormalities in vivo. By combining dual- and triple imaging modalities, many shortcomings that are present for single-modality imaging methods can be overcome. We have designed and synthesized positron emission tomography (PET)/magnetic resonance (MR)/near-infrared (NIR) trimodal imaging nanoprobe in a facile synthesis process based on the ionic gelation of biocompatible polyelectrolytes. Synthesized MnFe2O4 nanoparticles in organic solvents were encapsulated in the ionic nanocomplex in aqueous solutions by ligand exchange on the particle surface prior to gelation process. Amine functionalized ionic nanocomposite surfaces were used to modify for labeling imaging agents for PET and NIR imaging. The macrocyclic chelator, 2-(p-isothiocyanatobenzyl)-1,4,7-triazacyclononane-N,N',N''-triacetic acid ((p-SCN-Bn)-NOTA) and NIR fluorescent dyes, IRDye800® were sequentially conjugated on the particle surfaces. NOTA modified nanopartigles allowed chelation of gallium-68 for PET imaging. We quantitatively evaluated and controlled tri-functional properties of the particles. This facile method for the preparation of multimodality imaging probes based on polyelectrolyte composites and their surface modifications has a promising potential for application in many other biomedical and clinical research fields such as cell trafficking, and in vivo imaging fields.

Disclosure of author financial interest or relationships:
**Y. Lim**, None; **H. Park**, None.

Presentation Number **P436**
Poster Session 3
September 7, 2012 / 15:15-15:15 / Room: The Liffey

# Development of $^{125}$I/I-RGD-DOTA-Gd as a Dual-Modality Imaging Agents for Tumor-Targeting

***Ji-Ae Park***[1], *Jung Young Kim*[1], *Yong Jin Lee*[1], *Yin Ohk Ko*[1], *Sang-Keun Woo*[1], *Jong Guk Kim*[1], *Sang Moo Lim*[2], *Kyeong Min Kim Kim*[1], [1]*Molecular Imaging Research Center, Korea Institute of Radiological & Medical Science, Seoul, Republic of Korea;* [2]*Department of Nuclear Medicine, Korea Institute of Radiological & Medical Science, Seoul, Republic of Korea. Contact e-mail: jpark@kirams.re.kr*

Development of a dual modality imaging agent for SPECT and MRI could significantly contribute to improve the accuracy of tumor targeting and diagnosis. Dual modality imaging agents based on small-molecule have the potential to enable the control of the amount of probes and clinical applications. In this study, we introduce a cRGD-DOTA-Gd labeled with iodide isotopes (radioactive $^{125}$I and non-radioactive $^{127}$I) for dual SPECT/MR image probe. Methods: Synthesis of c(iodoYKRGD) was based on standard Fmoc protocols. The $^{125}$I labeling was using the chloramin-T method. Both non-radioactive(I-RGD-DOTA-Gd) and radioactive($^{125}$I-RGD-DOTA-Gd) were identified and purified by semi-preparative HPLC. In vitro properties of relaxivity, cytotoxicity and serum stability were tested and analyzed. Biodistribution experiment and small-animal imaging using SPECT and MRI were performed in nude mice bearing subcutaneous U87MG glioblastoma xenografts. The imaging of SPECT and MRI were obtained with sequential injection of these complexes, respectively Results: The formation of I-RGD-DOTA-Gd was confirmed by analytical and spectroscopic techniques. $^{125}$I-RGD-DOTA-Gd was obtained with high radio chemical purity and characterized by comparing its HPLC profile with that of corresponding I-RGD-DOTA-Gd. Co-injection of a mixture of$^{125}$I-RGD-DOTA-Gd would give peaks at the same retention time, with showing their chemical and structural equivalence. The results of stability assay showed that $^{125}$I-RGD-DOTA-Gd remains stable enough in mouse serum for as long as 3 days. In vivo imaging of SPECT and MRI showed significant enhancement in the region of tumor. Conclusion: This hybrid imaging probe using cRGD was successfully synthesized and applicable to tumor targeting imaging by both SPECT and MRI. The combination of I-RGD-DOTA-Gd and $^{125}$I-RGD-DOTA-Gd enables to overcome the sensitivity difference problem by regulating the ratio, becomes applicable to tumor imaging of dual modality imaging agents by the method of sequential injection.

Disclosure of author financial interest or relationships:
**J. Park**, None; **J. Kim**, None; **Y. Lee**, None; **Y. Ko**, None; **S. Woo**, None; **J. Kim**, None; **S. Lim**, None; **K. Kim**, None.

Presentation Number **P437**
Poster Session 3
September 7, 2012 / 15:15-15:15 / Room: The Liffey

# Bimodal Imaging of Inflammation with SPECT and MRI using 125I-labelled VCAM-1 Antibody-Nanoparticle Conjugates

***Niral Patel***[1,2], *Ben Duffy*[1], *Adam Badar*[1], *Mark Lythgoe*[1], *Erik Arstad*[2], [1]*UCL Centre for Advanced Biomedical Imaging, Division of Medicine and Institute of Child Health, University College London, London, United Kingdom;* [2]*Department of Chemistry and Institute of Nuclear Medicine, University College London, London, United Kingdom. Contact e-mail: zccac71@ucl.ac.uk*

Introduction: Vascular Cell Adhesion Molecule (VCAM-1) plays a key role in leukocyte recruitment to regions of inflammation, and as such may provide a biomarker for early diagnosis of numerous diseases. We and others have shown VCAM-1 targeting iron oxide can identify regions of acute inflammation on MRI (K. Kelly, et al. 2005). However, quantification of MRI hypointensities is problematic, and the sensitivity of the technique is low. Several attempts have been made to image VCAM-1 expression with radiolabelled antibodies; however low signal-to-noise ratios have been achieved (R. Burns, et al. 2001). Accordingly, there is a need to further develop methods for imaging inflammation. In this work, micron sized iron oxide particles were conjugated to 125I-radiolabelled antibodies with the purpose of imaging VCAM-1 expression using SPECT and MRI in a rat model of cerebral inflammation. Methods: Anti-rat, CD106 antibody was conjugated to 1 micron-sized tosyl-activated, iron oxide particles using methods described previously (M. McAteer, et al. 2007). This complex was used in two experiments: Experiment 1: Tumour Necrosis Factor-α (TNF-α) was intra-cerebrally administered into the left hemisphere of an adult rat followed by intravenous injection of the VCAM targeting contrast agent. This was followed by ex-vivo MRI in order to determine localisation of the contrast agent. Experiment 2: The contrast agent was labelled with I125 and intravenously administered after TNF-α injection into the right hemisphere of an adult rat. This was followed by investigations into: Blood clearance of the administered tracer; Ex vivo SPECT/CT and MRI brain imaging using a nanoSPECT system and a 9.4T MR system and; Biodistribution of the radio-labelled agent in a healthy control. Results: Following the injection of TNF-α, significantly more hypointensities were observed in the injected (left) hemisphere (fig.1A), demonstrating high-affinity for the VCAM-1 receptor. Multimodal imaging of the radiolabelled nanoparticle demonstrated good co-localisation between the MRI and SPECT (Fig. 1C), although the MRI (Fig. 1B) displayed a reduced amount of hypointensities compared to the non-radiolabelled compound. The fused SPECT/MRI image illustrates increased signal in the affected cerebral hemisphere (right side). The clearance study indicated rapid blood clearance of the radiolabelled contrast agent (Fig. 1D): only 0.60 %ID/g of the complex remained at 2 mins following administration. Biodistribution in a healthy rat at 10 min post-injection revealed a moderate uptake of the radio-complex in the lungs (%ID/g = 3.93 ± 0.67), spleen (%ID/g = 2.47 ± 0.87) and liver (%ID/g = 1.71 ± 0.64), whilst minimal uptake was found in the brain (%ID/g = 0.016 ± 0.007), indicating extremely low background signal in a healthy control. Conclusion: Combining the high sensitivity of SPECT with the high resolution of MRI, our 125I-labelled antibody/nanoparticle complex has the ability to image VCAM-1 expression and demonstrates favourable pharmacokinetics. Our preliminary results warrant further investigation towards developing a dual modality diagnostic tool for imaging inflammation.

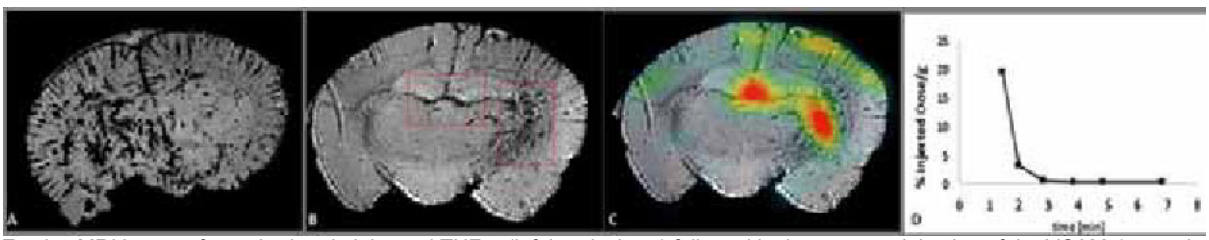


Fig. 1: A; Ex-vivo MRI image of a rat brain administered TNF-α (left hemisphere) followed by intravenous injection of the VCAM-1 targeting contrast agent, (Experiment 1). B; Ex-vivo MRI image of a rat brain administered TNF-α (right hemisphere) followed by intravenous injection of the 125I-radiolabelled complex, (Experiment 2). C; Fused SPECT/MRI, ex-vivo image of a rat brain administered TNF-α (right hemisphere) followed by intravenous injection of the 125I-radiolabelled complex, (Experiment 2). The SPECT signal is localised in the same region as the MRI hypointensity signals highlighted in Fig. 1B. D; Blood clearance graph of the 125I-radiolabelled complex administered into the same rat model of cerebral inflammation (Experiment 2). Slices were selected according to the site of injection

Disclosure of author financial interest or relationships:
**N. Patel**, None; **B. Duffy**, None; **A. Badar**, None; **M. Lythgoe**, None; **E. Arstad**, None.

Presentation Number **P438**
Poster Session 3
September 7, 2012 / 15:15-15:15 / Room: The Liffey

# Curcumin analogues attenuate copper-induced crosslinking of amyloid beta

*Xueli Zhang[1,2], Anna Moore[1], **Chongzhao Ran**[1], [1]Martinos Center for Biomedical Imaging, Massachusetts General Hospital/Harvard Medical School, Charlestown, MA, USA; [2]Center fro Drug Discovery, China Pharmaceutical University, Nanjing, China. Contact e-mail: cran@nmr.mgh.harvard.edu*

Amyloidosis in Alzheimer's disease (AD) starts with gradual aggregation of amyloid β (Aβ) species into neurotoxic soluble dimers and oligomers, and insoluble fibrils and plaques. The aggregation process could be divided into two categories: reversible aggregation due to physical hydrophobic stacking, and irreversible aggregation due to covalent crosslinking. Many compounds have been shown to attenuate the aggregation process or to accelerate the aggregation into fibrils. However, few compounds have been able to inhibit covalent crosslinking of Aβ. In our previous reports, we have demonstrated that curcumin derivatives could be used as Near Infrared (NIR) and PET imaging probes for both soluble and insoluble Aβ species in vitro and in vivo. We also showed that curcumin derivatives had different fluorescence responses towards Aβ with various amino acid substitutions. Both fluorescence data and 1H NMR spectra indicated that one of the derivatives, CRANAD-3, could specifically interact with the core fragment of Aβ. In addition, our data suggested that CRANAD-3 certainly interacted with H13 (histidine13), whose imidazole moiety is an essential binding site for copper, which plays a critical role in covalent crosslinking of Aβ, and has been considered as an important triggering factor for AD. In the current study, we designed and synthesized curcumin derivative CRANAD-17, in which imidazole rings were incorporated to compete with Histidine13 of Aβ for copper binding. SDS-PAGE and western blot results showed that CRANAD-17 was capable of inhibiting Aβ42 crosslinking induced by copper, indicating the possibility of using this compound for AD therapy. Since CRANAD-17 is also a fluorescent probe and could be easily adapted into a PET probe, it could potentially be used as a theranostic probe.

Disclosure of author financial interest or relationships:
**X. Zhang**, None; **A. Moore**, Fluoropharma, Grant/research support; **C. Ran**, None.

Presentation Number **P439**
Poster Session 3
September 7, 2012 / 15:15-15:15 / Room: The Liffey

# Specific Binding and Uptake of mVCAM-1 Targeting Magneto-Optical Nanoparticle Probe in Murine Endothelial Cells

***Gabriella Rimkus***[1], *Cordula Gruettner*[2], *Sibylle Bremer-Streck*[3], *Hartmut Oehring*[4], *Martin Foerster*[5], *Karl-Heinz Herrmann*[6], *Ines Krumbein*[6], *Juergen R. Reichenbach*[6], *Werner A. Kaiser*[1,6], *Ingrid Hilger*[1], [1]*Dept. of Experimental Radiology, IDIR I, Jena University Hospital - Friedrich Schiller University Jena, Jena, Germany;* [2]*micromod Partikeltechnologie GmbH, Rostock-Warnemuende, Germany;* [3]*Dept. of Clinical Chemistry and Laboratory Diagnostics, Jena University Hospital - Friedrich Schiller University Jena, Jena, Germany;* [4]*Institute of Anatomy II, Jena University Hospital - Friedrich Schiller University Jena, Jena, Germany;* [5]*Clinic of Internal Medicine I, Pneumology, Jena University Hospital - Friedrich Schiller University Jena, Jena, Germany;* [6]*Medical Physics Group, IDIR I, Jena University Hospital - Friedrich Schiller University Jena, Jena, Germany. Contact e-mail: Gabriella.Rimkus@med.uni-jena.de*

Introduction: Multimodal imaging is a viable tool to detect inflammatory processes or increased expression of cell surface molecules (e.g. mVCAM-1 on endothelial cells) as response to inflammatory stimuli on a molecular-cellular level before pathophysiological changes occur. Here, we propose a magneto-optical mVCAM-1 addressing probe for the multimodal detection of inflammatory processes. Methods: We designed a nanoparticle based mVCAM-1 magneto-optical probe by covalently conjugating near infrared fluorescent DY-649/VCAM-1 antibodies to cross-linked dextran coated iron oxide nanoparticles. For determination of the binding specificity of the probe a control probe with isotype control antibody as vectorization module was also coupled to the magnetic nanoparticle. Physicochemical characteristics like hydrodynamic diameter, amounts of conjugated antibody / dye and agglomeration behaviour of the nanoparticle probe were determined. Specificity of binding of the magneto-optical probe to and uptake into murine endothelial cells was tested using flow cytometry, optical imaging, MRI and TEM. Inflammation was modeled by stimulation of the endothelial cells with TNF-α, which resulted in upregulation of mVCAM-1 expression on the cell surface. Results: Conjugation of anti-VCAM-1 antibody/DY-649 or isotype control/DY-649 constructs to the magnetic nanoparticles resulted in comparable amounts of conjugated antibody/DY-649 on the nanoparticle surface (2.5-3.1 nmol antibody/mg Fe and 2.8-4.6 nmol DY-649/mg Fe) and slightly increased hydrodynamic diameters. Nanoparticle vectorization with antibody/dye constructs only altered the relaxivities r2 and r2*, but not in r1. Using flow cytometry and a whole body NIRF optical imaging device, we demonstrated binding of the VCAM-1 targeted magneto-optical probe to murine endothelial cells and revealed specificity by reduced fluorescence signals after blocking with a sixfold excess of unlabelled anti-mVCAM antibody. Upregulation of mVCAM-1 expression by stimulation of the endothelial cells with TNF-α increased the fluorescence signals considerably. Corresponding results were shown in MRI measurements. Here, the stimulation of endothelial cells with TNF-α resulted in a decrease of the r2* value after, whereas block experiments with excess of unlabelled anti-mVCAM-1 antibody did not alter this relaxivity. TEM images showed a distinct deposition of the nanoparticle probe in endosomes and secondary lysosomes which indicate internalization of our mVCAM-1 targeting probe via receptor-mediated endocytosis. All results demonstrate the specific binding properties and internalization of the designed VCAM-1 specific magneto-optical nanoparticle based probe. Conclusion: We showed that our magneto-optical nanoparticle based probe selectively binds to mVCAM-1 on endothelial cells and internalizes via receptor-mediated endocytosis. Our probe shows good capabilities to be used as a contrast agent for multimodal imaging for detection of diseases with increased mVCAM-1-expression (e.g. inflammation) with MRI and optical imaging in murine animal models.

Disclosure of author financial interest or relationships:
**G. Rimkus**, None; **C. Gruettner**, None; **S. Bremer-Streck**, None; **H. Oehring**, None; **M. Foerster**, None; **K. Herrmann**, None; **I. Krumbein**, None; **J.R. Reichenbach**, None; **W.A. Kaiser**, None; **I. Hilger**, None.

Presentation Number **P440**
Poster Session 3
September 7, 2012 / 15:15-15:15 / Room: The Liffey

# A dual modality marker for optical and SPECT cell tracking

*Yuzhen Wang[1], Miles P. Smith[1], Brian Gray[2], Xinrong Liu[1], Koon Y. Pak[2], **Mary Rusckowski**[1], [1]Radiology, University of Massachusetts Medical School, Worcester, MA, USA; [2]Molecular Targeting Technologies, West Chester, PA, USA. Contact e-mail: Mary.Rusckowski@umassmed.edu*

We are investigating a DOTA conjugated lipophilic DiD analog (fluorescence emission 670 nm) named MTTI-157 as a dual labeled membrane marker for tracking stem cells. MTTI-157 was labeled with $^{111}$In and evaluated in LS-174T cancer cells as a model for stem cells. The incorporation and retention over time of both fluorescence and nuclear label was evaluated in vitro and in normal mice. Radiochemical specific activity of 74 uCi/ug could be reached with greater than 90% radiochemical purity by HPLC. Maximum relative fluorescence without loss of cell viability was attained with a dye concentration of 20 x $10^{-6}$ M and $10^7$ cells in 1 ml. Incorporation of $^{111}$In-MTTI-157 into cells afforded about 1 uCi per $10^6$ cells (about 1% of activity added). The dual labeled cells exhibited normal viability and proliferation with retention of both labels as confirmed by both fluorescence microscopy and $^{111}$In counting. SPECT/CT scans of mice receiving $^{111}$In-MTTI-157 labeled cells (about 12-15 uCi) by tail vein showed radioactivity restricted to the lungs in the earliest scans on day 0 that redistributed within hours to include the liver and spleen thereafter. SPECT scans through day 5 showed distribution unchanged with only lungs, liver and spleen still apparent. No indication of $^{111}$In instability was observed as evidenced by the absence of activity in kidneys and bladder on any day. Parallel whole body activity measurements (decay corrected) confirmed $^{111}$In retention out to day 7; beyond that time activity was too near background for accurate determination. Corresponding whole body optical images showed fluorescence in the lungs, liver, and spleen, but now out through day 21 that was confirmed in optical scans of the excised organs as well. Fluorescence microscopy of tissue frozen sections showed cell associated MTTI-157 signal at all time points. This dual labeled cell marker, $^{111}$In-MTTI-157, has provided a means to monitor the in vivo fate of cells out through 21 days in vivo with no evidence of label instability. This cell marker will be evaluated further for tracking the fate of stem cells in vivo for potential use in cell based therapies.

Disclosure of author financial interest or relationships:
**Y. Wang**, None; **M.P. Smith**, None; **B. Gray**, Molecular Targeting Technologies, Inc., Employment; **X. Liu**, None; **K.Y. Pak**, Molecular Targeting Technologies, Inc., Stockholder; **M. Rusckowski**, None.

Presentation Number **P441**
Poster Session 3
September 7, 2012 / 15:15-15:15 / Room: The Liffey

# Theranostic Ultrasmall Rigid Platforms: biological characterisation from sub-cellular to organ level

***Lucie Sancey***[1], *Jessica Morlieras*[1], *Wael Rima*[2], *Anna Mignot*[1], *G. Braga-Alcantara*[2], *Sandrine Dufort*[3], *Pierre Mowat*[1], *Stephane Roux*[4], *Pascal Perriat*[2], *François Lux*[1], *Olivier Tillement*[1], [1]*Equipe FENNEC, UMR CNRS 5620 - Univ. Lyon1 LPCML, Villeurbanne, France;* [2]*Laboratoire MATEIS, UMR CNRS 5510, Lyon, France;* [3]*Nano-H SAS, , Saint-Quentin Fallavier, France;* [4]*Institut UTINAM, UMR 6213 CNRS - Univ. Franche-Comté, Besançon, France. Contact e-mail: lucie.sancey@univ-lyon1.fr*

UltraSmall Rigid Platforms (USRPs) are hybrid nanoparticles made of polysiloxane and gadolinium complexes, contrast agent for MRI and X-ray tomography, covalently grafted to the inorganic matrix. USRPs can be labeled with either fluorescent and/or nuclear probes. The overall size of these nanoparticles is < 5-nm to ≈ 7-nm depending on the labeling, thus favouring renal excretion in small animals. USRPs combine nano-objects advantages, i.e. multimodality, passive accumulation in tumour by Enhanced Permeability and Retention (EPR) effect, long blood circulation, and molecular advantages such as renal excretion, no macrophages uptake and ligand-grafting possibilities to increase specific tumour uptake. In addition to their multi-imaging properties, USRPs possess a great potential for radiosensitisation due to the presence of gadolinium. To better understand and increase USRPs therapeutic efficiency and limit side-effects during radiotherapy, different chemical compositions have been prepared and characterised chemically and biologically using various modalities. The hydrodynamic radii or aggregation of USRPs have been dose-dependently studied by FCS (fluorescence correlation spectroscopy) in the presence of cells. Cellular internalisation of the untargeted and targeted-USRPs has been observed by confocal studies on relevant cell types. Freshly obtained and aged USRPs were characterised by ICP-AES (inductively coupled plasma atomic emission spectroscopy) after biodistribution in mice; specific attention being paid to tumours and excretion organs ex-vivo. To conclude, USRPs possess an interesting potential for image-guided radiotherapy that should allow a personalised-therapy. Understanding their cellular internalisation and trafficking as well as their in vivo biodistribution may improve their efficiency.

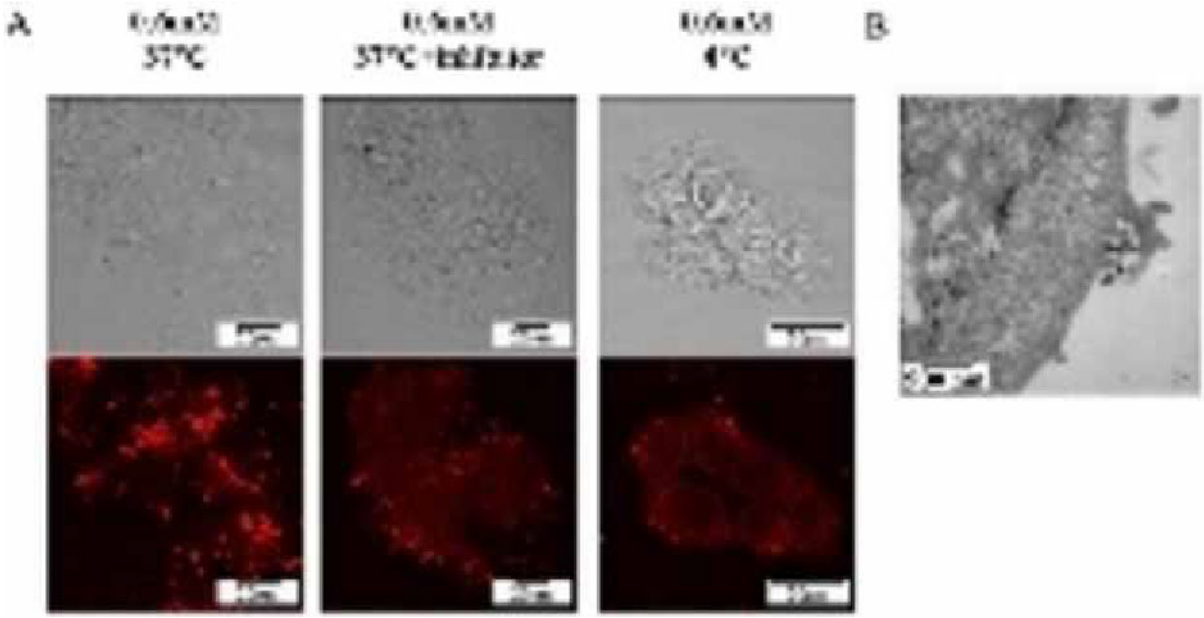


Example of internalisation study: A- Cells were incubated with fluorescent-USRPs at 37°C, in medium alone or containing macropinocytosis inhibitor amiloride. In medium at 37°C, USRPs were highly internalised in vesicles. In the presence of amiloride, USRPs were weakly internalised by passive diffusion; the incubation at 4°C confirmed these results. B- TEM cliché of cells incubated with USRPs at 37°C indicating macropinocytosis internalisation of the nanoparticles.

Disclosure of author financial interest or relationships:
**L. Sancey**, None; **J. Morlieras**, None; **W. Rima**, None; **A. Mignot**, None; **G. Braga-Alcantara**, None; **S. Dufort**, None; **P. Mowat**, None; **S. Roux**, None; **P. Perriat**, None; **F. Lux**, None; **O. Tillement**, None.

Presentation Number **P442**
Poster Session 3
September 7, 2012 / 15:15-15:15 / Room: The Liffey

# Annexin A5 fusion protein with extended blood half-life for improved bioavailability

*Akvile Häckel, Lena Figge, Franziska Appler, Jörg Schnorr, Bernd Hamm,* ***Eyk A. Schellenberger****, Experimental Radiology, Charité University Medicine Berlin, Berlin, Germany. Contact e-mail: eyk.schellenberger@charite.de*

Annexin A5 is a human protein (35 kDa) that has been extensively used to detect phosphatidylserine (PS) exposing cells. One especially attractive target is apoptosis (or programmed cell death), which is altered in numerous diseases. PS appears on the outer cell surface within a few hours after initiating stimuli of apoptosis and represents a highly accessible target for Annexin A5 with strong binding affinity. Many variants of human recombinant Annexin A5 have been already well-analyzed as imaging probes, particularly with radioactive labeling for cancer diagnostics. However, there are still limitations for certain in vivo targets, partially due to the very short blood half-life. Here we present an Annexin A5 fusion protein, expressed in E.coli and purified using anionic exchange columns, which can be labeled with thiol-reactive fluorescent dyes as well as with radioactive labels. This construct has an increased blood half-life for improved bioavailability as well as almost no immunogenicity in comparison with PEGylated (coupled with polyethylene glycol, PEG) probes. The circulation time can be modified by changing the length of the fusion partner of Annexin A5. The presented method allows the expression and production of high amounts of long circulating Annexin A5 without the necessity of PEGylation, thereby avoiding potential toxic affects of PEG. It is readily applicable to other recombinant protein or peptide-based imaging probes.

Disclosure of author financial interest or relationships:
**A. Häckel**, None; **L. Figge**, None; **F. Appler**, None; **J. Schnorr**, None; **B. Hamm**, Deutsche Röntgengesellschaft European Congress of Radiology European Society of Euroradiology ESMRMB European School of Radiology Deutsche Forschungs-gemeinschaft, Other financial or material support; Bayer Schering Pharma Toshiba, Consultant; ESMRMB ESOR, Speakers bureau; Thieme Publishers Springer Publishers, Other financial or material support; All pharmaceutical and biochemical companies All medical technology companies All car companies, Stockholder; All pharmaceutical and biochemical companies All medical technology companies, Other financial or material support; **E.A. Schellenberger**, None.

Presentation Number **P443**
Poster Session 3
September 7, 2012 / 15:15-15:15 / Room: The Liffey

# Tumor-targeting gold particles for CT/optical dual cancer imaging

***In-Cheol Sun***[1], *Heebeom Koo*[1], *Ye Sun Han*[2], *In-San Kim*[3], *Sang Yoon Kim*[4], *Beom Suk Lee*[4], *Ick Chan Kwon*[1], *Kwangmeyung Kim*[1], *Cheol-Hee Ahn*[5], [1]*Center for Theragnosis, Korea Institute of Science and Technology, Seoul, Republic of Korea;* [2]*Department of Advanced Technology Fusion, Konkuk University, Seoul, Republic of Korea;* [3]*Kyungpook National University, Daegu, Republic of Korea;* [4]*Asan Medical Center, University of Ulsan College of Medicine, Seoul, Republic of Korea;* [5]*Department of Materials Science and Engineering, Seoul National University, Seoul, Republic of Korea. Contact e-mail: pfesun@kist.re.kr*

We developed a matrix metalloproteinase (MMP)-sensitive, tumor-targeting imaging probe with gold nanoparticles (AuNPs) for fluorescence optical imaging and computed tomography (CT). Glycol chitosan (GC) was used as a reducing agent and stabilizer of AuNPs to improve the stability and tumor-targeting properties. Cy5.5 fluorescent dye and black hole quencher were conjugated to MMP substrate peptide and the other end of peptide was chemically linked to GC coated AuNPs (BCMG-AuNP). Those particles showed excellent stability in the physiological condition and this enabled BCMG-AuNP to absorb X-ray more intensively. The tumor tissues were imaged with the probe through CT and optical imaging. We were able to obtain the anatomical in vivo imaging of tumor through CT due to the selective accumulation of probes in tumor tissues. In addition, The near infrared fluorescence (NIRF) of BCMG-AuNPs was effectively quenched by the combinational quenching system and the quenched fluorescence was recovered by MMP enzymes, which makes it possible to detect tumors as well as nanomolar amounts of protease, both in vitro and in vivo. Therefore, this BCMG-AuNP probe was expected to provide the platform of multimodal imaging probe for cancer detection and various applications such as drug screening or monitoring for therapeutic efficacy in vivo.

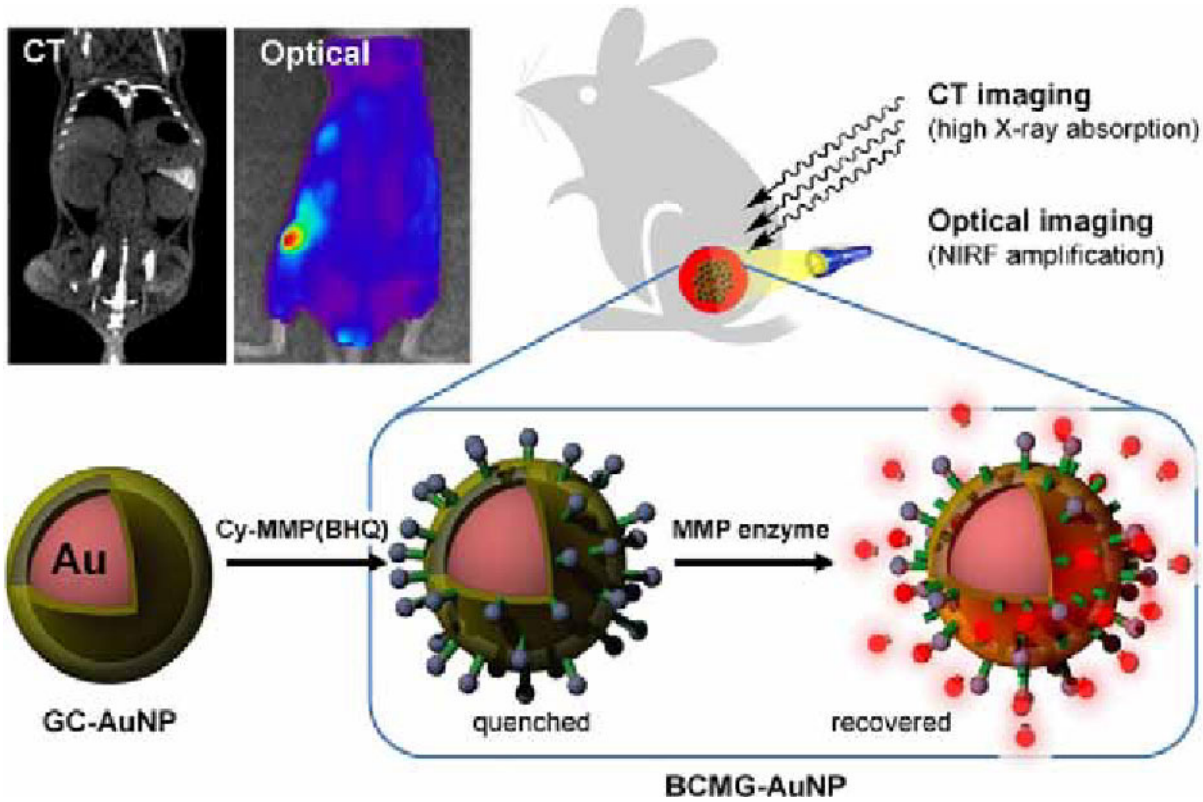


Disclosure of author financial interest or relationships:
**I. Sun**, None; **H. Koo**, None; **Y. Han**, None; **I. Kim**, None; **S. Kim**, None; **B. Lee**, None; **I. Kwon**, None; **K. Kim**, None; **C. Ahn**, None.

Presentation Number **P444**
Poster Session 3
September 7, 2012 / 15:15-15:15 / Room: The Liffey

# Glycodendron Clearing Agents for Pretargeting Radioimmunotherapy

***Barney Yoo***[1], *Sarah M. Cheal*[2], *Geralda Torchon*[1], *Guangbin Yang*[1], *Anna Dilhas*[1], *Jun Pu*[1], *Peter Smith-Jones*[2], *Steven M. Larson*[2], *Ouathek Ouerfelli*[1], [1]*Organic Synthesis Core Facility, Molecular Pharmacology and Chemistry Program, Memorial Sloan-Kettering Cancer Center, New York, NY, USA;* [2]*Department of Radiology, Memorial Sloan-Kettering Cancer Center, New York, NY, USA.*
*Contact e-mail: yoob@mskcc.org*

Pretargeting radioimmunotherapy (PRIT) is a strategy to address limitations of conventional radioimmunotherapy. In PRIT the radionuclide is administered separately from the tumor targeting monoclonal antibody (mAb), enabling the use of clearing agents to further reduce levels of non-tumor associated mAb. Here we describe the development of a specific class of glycodendron for use as a preclinical and clinical PRIT clearing agent. These molecules contain a single, terminal amine linked to an aliphatic dendron core bearing multiple thio-N-acetylgalactosamine (α-SGalNAc) end groups. The terminal amine can be modified to accommodate desired functionality such as a biotin or DOTA group. These glycodendrons are designed to capture unbound mAb constructs and target the complex to the asialylglycoprotein (ASGP) receptor in the liver for degradation. The α-SGalNAc units on the glycodendrons are designed to mimic the polyvalent interactions between the ASGP receptor and its natural ligands. Antibody capture can be achieved by incorporating binding pairs, such as biotin/streptavidin, or hapten/bispecific antibodies. Previous assessments of glycodendrons as clearing agents had shown promise, however the difficulty in obtaining these compounds hampered further development. To obtain these glycodendrons, we devised a straightforward linear strategy, where each generation was introduced in a stepwise manner and then linked with pre-functionalized α-SGalNAc end groups. The α- form of the thio-sugar was obtained from the development of a selective synthetic route. Dendron precursors and final products were characterized by HPLC, mass spectrometry, and NMR. The chemistry proved to be highly robust, resulting in the desired molecules with excellent monodispersity, purity and structural integrity. We sought to evaluate the clearing capacity in vivo for these glycodendrons and to examine the effects of carbohydrate valency or size - such insights might help to guide the design of less complex molecules. To address this question, a series of biotin linked glycodendrons displaying four, eight, sixteen or thirty-two α-SGalNAc units were prepared, then evaluated for their capacity to remove a 131I labeled single chain variable fragment antibody-streptavidin (131I-scFv-SAv) construct from the blood and tissue of mice. The data show that the glycodendron agents all facilitate removal of the 131I-scFv-SAv construct from blood, and enhance liver targeting/uptake of the 131I-scFv-SAv construct. It also suggests that the lower molecular weight glycodendron may require larger molar amounts to obtain clearance comparable to the higher generation compounds. In this work we describe glycodendron clearing agents which can be obtained with excellent monodispersity and purity. While we demonstrate the clearing capacity for these molecules using a biotin/mAb-streptavidin system, the glycodendrons are synthetically highly versatile, and can be readily made to accommodate other binding systems, such as a hapten/bispecific antibody combination. Currently we are undertaking studies to incorporate these clearing agents in various multistep targeting approaches.

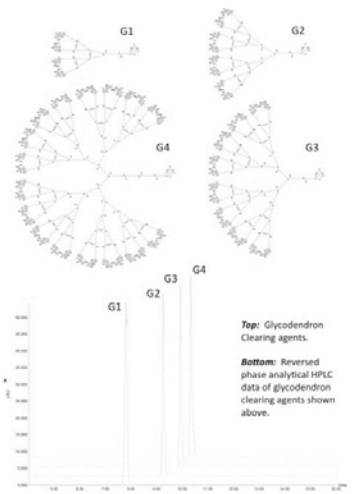


Disclosure of author financial interest or relationships:
**B. Yoo**, None; **S.M. Cheal**, None; **G. Torchon**, None; **G. Yang**, None; **A. Dilhas**, None; **J. Pu**, None; **P. Smith-Jones**, None; **S.M. Larson**, None; **O. Ouerfelli**, None.

Presentation Number **P445**
Poster Session 3
September 7, 2012 / 15:15-15:15 / Room: The Liffey

# Preclinical evaluation of [$^{11}$C]-methyl-methyl-diphenyl-ammonium as candidate agent for imaging and quantification of myocardial blood flow using PET

***Galith Abourbeh**, Orit Jacobson Weiss, Darya Tsvirkun, Eyal Mishani, Cyclotron Unit, Hadassah Hebrew University Hospital, Jerusalem, Israel. Contact e-mail: abourbehg@hadassah.org.il*

**Introduction** Myocardial perfusion imaging (MPI) is clinically employed to evaluate ischemia non-invasively in patients with suspected coronary artery disease (CAD). Positron emission tomography (PET)-MPI could provide quantitative data about myocardial blood flow, and is a powerful tool for diagnosing obstructive CAD. Of the currently investigated radiopharmaceuticals for PET-MPI [1-4], the potential of ammonium-salt derivatives, particularly that of [$^{11}$C]-methyl-methyl-diphenylammonium ([$^{11}$C]DMDPA), has been reported. [5, 6] **Aim** To investigate the potential use of [$^{11}$C]DMDPA for PET-MPI. **Methods** The radiosynthesis of [$^{11}$C]DMDPA has been published. [5] The stability of [$^{11}$C]DMDPA *in vivo* was examined in healthy rats (n=6). At different time points after injection rats were sacrificed; radioactivity was extracted from the blood, liver and urine, measured and analyzed for radioactive metabolites. Cardiac uptake and distribution kinetics of [$^{11}$C]DMDPA and [$^{13}$N]$NH_3$ were compared in healthy rats (n=4 and n=3, respectively) by small animal-dedicated PET/CT (μPET/CT). The feasibility of detecting ischemic/ non-perfused myocard regions using [$^{11}$C]DMDPA was evaluated by PET/CT scans carried out in pigs (n=3) in rest and under adenosine stress (500 μg/kg/min, 6 min), using a new swine model of permanent partial coronary artery occlusion. [5] **Results** *In vivo* stability was examined in rats after injection of [$^{11}$C]DMDPA. Specifically, radioactivity was extracted from blood, liver and urine, measured and analyzed for radioactive metabolites. Results indicated high levels (>80%) of radioactivity extraction from plasma, liver and urine, with no apparent radioactive metabolites. Distribution kinetics of [$^{11}$C]DMDPA and [$^{13}$N]$NH_3$ in rats were compared using μPET/CT. Time activity curves of [$^{11}$C]DMDPA indicated rapid, high and sustained cardiac accumulation, with a mean standardized uptake value (SUV) of 5.9 at 10 min after injection. At the same time, a mean cardiac SUV of 2.2 was obtained for [$^{13}$N]$NH_3$. As indicated in Table 1, [$^{11}$C]DMDPA presented higher heart/ tissue radioactivity uptake ratios compared to [$^{13}$N]$NH_3$. Thus, both absolute cardiac accumulation and heart/ tissue ratios of [$^{11}$C]DMDPA were superior to those of [$^{13}$N]$NH_3$. Using a swine model of impaired coronary artery perfusion, injection of [$^{11}$C]DMDPA under pharmacological stress in two pigs clearly detected a severe defect in the left ventricular wall, which did not fill under rest conditions, and was consistent with a myocardial infarction imaging pattern. Adenosine stress-images following [$^{11}$C]DMDPA injection to the third pig showed a severe inferolateral defect that filled-in at rest (Fig.1), compatible with the clinical pattern of "reversible ischemia". **Conclusions** Current data indicate that [$^{11}$C]DMDPA is highly stable *in vivo*, has rapid, high and sustained cardiac uptake, and provides better quality images than [$^{13}$N]$NH_3$, sustaining further research into its potential use in PET-MPI. **1.** *Curr Cardiol Reports* 2011; 13:145 **2.** *Circulation* 2009; 2:77 **3.** *Mol Imaging Bio*l 2011; 13:511 **4.** *Semin Nucl Med* 2011; 41:305 **5.** Ilovich O, *Mol Imaging Biol* 2012 **6.** *Mol Imaging Biol* 2011; 13:128

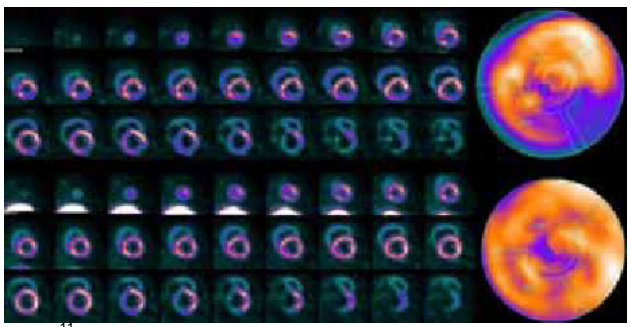

Short-axis representations and polar maps of [$^{11}$C]DMDPA at stress (top) and rest (bottom) obtained between 5 and 20 min in the third pig. Injected doses were 173.9, and 188.0 MBq, respectively. Scales are normalized to the highest activity levels in the myocardium.

Heart/ tissue radioactivity uptake ratios at 10 min after i.v. injection of [$^{11}$C]DMDPA and [$^{13}$N]$NH_3$ into rats

| Tissue | [$^{11}$C]DMDPA | [$^{13}$N]$NH_3$ |
|---|---|---|
| Blood pool | 3.0 | 1.6 |
| Lungs | 8.4 | 2.1 |
| Liver | 1.3 | 0.6 |
| Kidneys | 3.5 | 0.6 |

Disclosure of author financial interest or relationships:
**G. Abourbeh**, None; **O. Jacobson Weiss**, None; **D. Tsvirkun**, None; **E. Mishani**, None.

Presentation Number **P446**
Poster Session 3
September 7, 2012 / 15:15-15:15 / Room: The Liffey

# Noninvasive Quantification of Muscarinic Acetylcholine Receptor and Subtype M3 Receptor in vivo with Positron Emission Tomography in Ischemic Myocardical Injuries

***Lihong Bu**, Renfei Li, Xiaofei Wen, Baozhong Shen, the 4th hospital of Harbin Medical University, Heilongjiang, China. Contact e-mail: bulihong@gmail.com*

Purpose: The objective of this study was to produce the muscarinic receptors targeted probe 11C-MQNB and to characterize the muscarinic receptor and subtype M3 receptor in vivo on acute myocardial-infracted dogs. Materials and Methods: The Experiments were performed on dogs with acute myocardial infarction which induced by interventional techniques. The distribution, density and affinity constants of myocardial muscarinic receptors were studied noninvasively by PET/CT with 11C-MQNB. The M2-to-M3 receptor ratio was evaluated by competition experiments with displacement of 11C-MQNB by methoctramine and 4-DAMP in 4 myocardial-infracted dogs respectively and compared with the values in the same 4 dogs before they were induced to infarct. Western Blot Analysis was performed to determine the density of the M2 and M3 receptor in vitro, too. Results: The synthesis of 11C-MQNB is successful and Labeled material had a specific radioactivity ranging from 12 to 80 GBq/μmol at the time of the first injection. The mean muscarinic receptor concentration was significantly higher in myocardial infarct dogs than in control subjects which was confirmed by both PET (B'max, 56.33±3.015 tissue versus 75.49±4.178 pmol/mL tissue, P<.005) with slightly decreased affinity constants (Kd, 0.078±0.004 versus 0.065±0.005 pmol/mL,P<0.05). Competition experiments with 11C-MQNB indicate that the proportion of muscarinic M2 and M3-receptors is 64.3/12.5 versus 51.431/24.371 respectively before and after infarction. Western Blot proved that M3 receptor increased significantly in ischemic myocardial injuries (infarction/normal ratio is 1.176/1 for M2 receptor and 1.504/1 for M3 receptor.) Conclusions: Acute myocardial infraction results in an up regulation of myocardial muscarinic receptors, especially subtype M3 receptor, but a slight down regulation of the affinity constant for M receptor. PET/CT molecular imaging and competition experiment with 11C-MQNB can be used to quantify the M and M3 receptor, which will be a new method for the research of M receptor and its subtype in vivo. Key Words: PET/CT; muscarinic M3 receptor; acute myocardial infarction; molecular imaging; [11C]- methyl-quinuclidinyl-benzilate

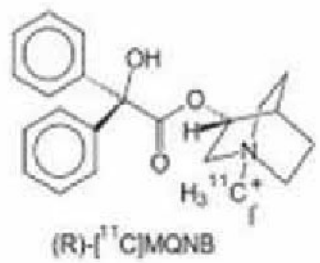


Figure 1 Chemical structure of $^{11}$C-MQNB

Figure 2 Biodistribution of $^{11}$C-MQNB in normal dogs

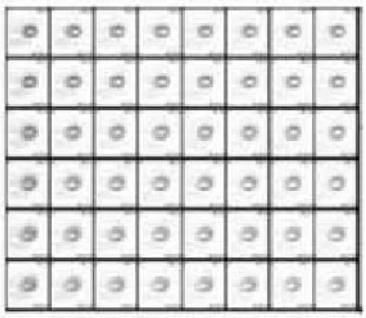

Figure 3 $^{11}$C-MQNB imaging of normal dog's heart

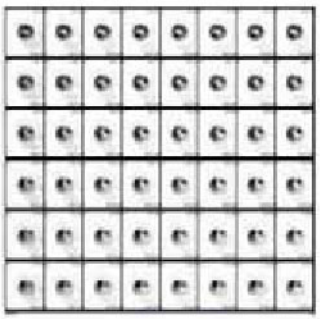

Figure 4 $^{11}$C-MQNB imaging of acute myocardium infarction in dogs

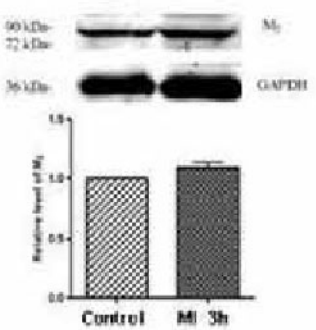


Figure 5 western Blot of M2 receptor 3h after myocardial infarction

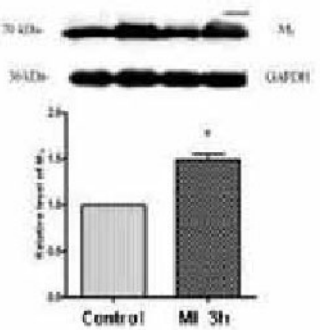


Figure 6 western Blot of M3 receptor 3h after myocardial infarction

Disclosure of author financial interest or relationships:
**L. Bu**, None; **R. Li**, None; **X. Wen**, None; **B. Shen**, None.

Presentation Number **P447**
Poster Session 3
September 7, 2012 / 15:15-15:15 / Room: The Liffey

# $^{18}$F-FPP-(RGD)$_2$ uptake tracks effect of drugs on murine ischemic infarcts

***Edwin Chang***[2,1], *Evgenios Neofytou*[3,1], *Keren Ziv*[1,2], *Xi Wang*[3,1], *Xiaoyuan (Shawn) Chen*[4,1], *Sanjiv S. Gambhir*[1,2], *Ramin E. Beygui*[3,1], *Zhen Cheng*[1,2], [1]*Radiology, MIPS, Stanford University, Stanford, CA, USA;* [2]*Radiology, Canary, MIPS, Stanford University, Palo Alto, CA, USA;* [3]*Medicine, Falk Cardiovascular Research Center, Stanford University, Stanford, CA, USA;* [4]*NIBIB, NIH, Bethesda, MD, USA. Contact e-mail: echangcv@stanford.edu*

**Introduction:** Our myocardial infarction (MI) is produced by ligating the left anterior descending (LAD) portion of the heart's coronary artery thereby producing an ischemic infarction downstream from the ligature. This leads to collateral neovascularization which entails stabilization of hypoxia inducible factor (HIF-1α) followed by expression of endothelial $\alpha_v\beta_3$ integrins. We hypothesized that the $\alpha_v\beta_3$ integrin tracer, $^{18}$F-FPP-(RGD)$_2$, tracks ischemic wound healing as its uptake is associated with tissue integrin expression which in turn is related to the dynamic hypoxic status of the recovering infarct. Drugs that stabilize HIF-1α (deferoxamine or DFO) should accelerate ischemia-driven wound healing that in turn is reflected in augmented $^{18}$F-FPP-(RGD)$_2$uptake. **Methods:** Female FVB mice (14-18 week, N=7 per experiment) were used for MI models with 4-7 for SHAM treatment. Additional mice (n=5 MI, n=5 MI+DFO, n=5 SHAM, FvB females, 14-18 weeks) were recruited to assess effect of DFO on infarct size. Infarcted areas were confirmed with triphenyl tetrazolium chloride (TTC). $^{18}$F-FPP-(RGD)$_2$tracer uptake into infarcted cardiac tissue was measured via small animal positron emission tomography (PET). Computed Tomography (CT) scans were done in tandem to PET scans in order to identify regions of tracer uptake. Area (range: 85-620 mm3) and intensity of uptake (range of %IDmean/g: 0.15 to 1.67) were assessed for up to 3 weeks post-operation. Blood ejection fraction through the left ventricle was determined via Bright Blood Magnetic Resonance Imaging (MRI). **Results:** As assessed via PET/CT, regions of ischemic infarction corresponded to regions of $^{18}$F-FPP-(RGD)$_2$ uptake. Areas of tracer uptake appeared 1 day post-operation and persisted for 3 weeks. Total area of uptake peaked at around 9 days (~600 mm3) post-operation followed by progressive shrinkage. Even though the uptake area declined, the %IDmean/g and %IDmax/g of $^{18}$F-FPP-(RGD)$_2$ still persisted (0.15 and 0.9 respectively) 18 days post-infarction. Intraperitoneal injections (every two days, 40mg/kg) of deferoxamine (DFO) accelerated the decline in infarcted area (N=7 per cohort, P<0.02). However, those same regions presented significantly augmented %IDmean/g values when compared to saline-injected controls (N=7 per cohort, P<0.05, %IDmean/g: 0.35+/-0.03 vs 0.65+/-0.05, Control Saline vs. DFO-treated). In our MRI studies, all mice subjected to experimental myocardial infarction alone displayed a left ventricle that had an eccentric contraction with inefficient clearance of blood from the chamber. DFO treatment restored a symmetrical, spheroidal pattern of left ventricular contraction with enhanced ejection fraction. **Conclusions:** These studies show the feasibility in using $^{18}$F-FPP-(RGD)$_2$ as a PET tracer that tracks myocardial infarction, as well as the efficacy of drugs designed to modulate MI.

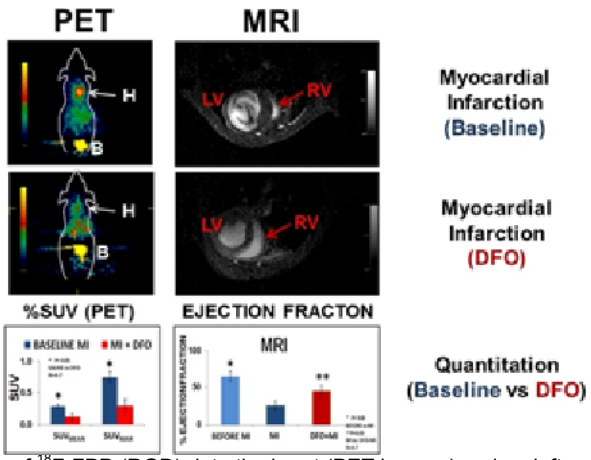


The effect of deferoximine (DFO) on uptake of $^{18}$F-FPP-(RGD)$_2$ into the heart (PET images) and on left ventricular contraction (MRI images) for mice subjected to experimentally-induced myocardial infarction (MI). Daily administration of DFO (40mg/kg/day) significantly (P<0.05, n=4-7 mice per experimental group) reduced area of $^{18}$F-FPP-(RGD)$_2$ uptake compared to baseline mice that were induced with vehicle (i.e. saline). This is reflected in reduction of %SUV for DFO-treated mice compared to vehicle controls (PET column). DFO restores cardiac ejection volumes to 69% of levels found in un-infracted mice (lower right hand graph; MRI column). For PET, H-heart, B-bladder. For MRI, LV-left ventricle, RV-right ventricle.

Disclosure of author financial interest or relationships:
**E. Chang**, Bayer-Healthcare Inc., Grant/research support; GE-Healthcare Inc., Grant/research support; **E. Neofytou**, None; **K. Ziv**, I'm LSRF fellow, my fellowship is supported by Pfizer Fellowship, Other financial or material support; **X. Wang**, None; **X. Chen**, None; **S.S. Gambhir**, General Electric, Grant/research support; Bayer-Schering, Grant/research support; Sanofi-Aventis, Grant/research support; CellSight, Stockholder; ImaginAB, Stockholder; Enlight, Stockholder; Endra, Stockholder; Bracco, Consultant; NinePoint Medical, Stockholder; Visualsonics, Consultant; **R.E. Beygui**, None; **Z. Cheng**, None.

Presentation Number **P448**
Poster Session 3
September 7, 2012 / 15:15-15:15 / Room: The Liffey

# LOX-1 targeting Nanobodies for SPECT Imaging of Atherosclerosis

***Jens De Vos***[1,3], *Alexis Broisat*[4], *Jakub Toczek*[4], *Catherine Ghezzi*[4], *Tony Lahoutte*[3], *Serge Muyldermans*[1,2], *Nick Devoogdt*[3], [1]*Laboratory of Cellular and Molecular Immunology (CMIM), Vrije Universiteit Brussel, Brussels, Belgium;* [2]*Department of Structural Biology, VIB, Brussels, Belgium;* [3]*Laboratory of In Vivo Cellular and Molecular Imaging (ICMI), Vrije Universiteit Brussel, Brussels, Belgium;* [4]*Radiopharmaceutiques Biocliniques, INSERM, Grenoble, France. Contact e-mail: Jens.De.Vos@vub.ac.be*

OBJECTIVES. Lectinlike Oxidized LDL Receptor-1 (LOX-1) is a receptor for oxidized LDL and a potential marker of the human atherosclerotic plaque (1). Li et al. used LOX-1 as a target for in vivo imaging of atherosclerotic plaques in mice. Due to the blood clearance of the probe, imaging was performed 24h p.i. (2). We recently used nanobodies targeting VCAM1 as molecular imaging probes to detect atherosclerotic plaques by non-invasive in vivo imaging 3h p.i. (3). Nanobodies are the smallest antigen binding fragments of heavy-chain antibodies from Camelidae and are particularly suited as probes for in vivo imaging (4). The objective of this study is to develop nanobodies targeting LOX-1 for the detection of atherosclerotic lesions in preclinical animal models of atherosclerosis. METHODS. A dromedary was immunized with both mouse LOX-1 (mLOX-1) and human (hLOX-1) recombinant proteins. An immune nanobody library was generated, phage-displayed and biopannings were performed on recombinant mLOX-1 and hLOX-1. The affinities of the nanobodies for mouse and/or human recombinant LOX-1 and the targeted epitope were evaluated in vitro. The nanobodies targeting mLOX-1 were labeled with 99m-technetium (Tc) and injected in APOE-/- mice and in control C57Bl/6 mice to evaluate their plaque targeting using SPECT/CT imaging. After euthanasia, organs and tissues were counted in a gamma counter to determine the biodistribution ex vivo. RESULTS. Nanobodies binding different epitopes on either mouse or human recombinant LOX-1 with nanomolar affinity were generated. After 99m-Tc labeling the nanobodies still bound mLOX-1. The anti-mLOX-1 nanobody with the best affinity showed only moderate uptake in atherosclerotic lesions in the aortic arch of ApoE-/- mice using SPECT/CT imaging 3h p.i. The uptake determined by ex vivo counting was higher in aortas of the ApoE-/- mice than in aortas of the C57Bl/6 control mice. CONCLUSIONS. Nanobodies binding recombinant mouse and human LOX-1 with nanomolar affinity were generated. One nanobody targeting mLOX-1 showed a relatively low in vivo uptake in aortic atherosclerotic lesions. We conclude that the nanobodies selected for strong binding to recombinant LOX-1 protein are not optimal for in vivo detection of LOX-1 expression, possibly due to structural differences between LOX-1 recombinant protein and LOX-1 expressed in atherosclerotic lesions. In future experiments nanobodies could be selected on cells expressing mouse or human LOX-1. REFERENCES. (1) Kataoka, H. et al. Expression of Lectinlike Oxidized Low-Density Lipoprotein Receptor-1 in Human Atherosclerotic Lesions. Circulation 99, 3110-3117 (1999). (2) Li, D. et al. Molecular imaging of atherosclerotic plaques targeted to oxidized LDL receptor LOX-1 by SPECT/CT and magnetic resonance. Circ Cardiovasc Imaging 3, 464-472 (2010). (3) Broisat, A. et al. Nanobodies Targeting Mouse/Human VCAM1 for the Nuclear Imaging of Atherosclerotic Lesions. Circulation Research 110, 927-937 (2012). (4) Vaneycken, I. et al. Immuno-imaging using nanobodies. Current Opinion in Biotechnology 22, 877-881 (2011).

Disclosure of author financial interest or relationships:
**J. De Vos**, None; **A. Broisat**, None; **J. Toczek**, Advanced Accelerator Applications, Grant/research support; **C. Ghezzi**, None; **T. Lahoutte**, None; **S. Muyldermans**, None; **N. Devoogdt**, Boehringer Ingelheim, Grant/research support; Ablynx, Grant/research support .

Presentation Number **P449**
Poster Session 3
September 7, 2012 / 15:15-15:15 / Room: The Liffey

# PET imaging of glucagon-like peptide receptor upregulation after myocardial ischemia/reperfusion injury

***Haokao Gao***[1,2], *Dale O. Kiesewetter*[1], *Xiaoxiang Zhang*[1], *Ning Guo*[1], *Gang Niu*[1], *Xiaoyuan Chen*[1], [1]*Laboratory of Molecular Imaging and Nanomedicine (LOMIN), National Institute of Biomedical Imaging and Bioengineering (NIBIB), National Institutes of Health (NIH), Bethesda, MD, USA;* [2]*Department of Cardiology, Xijing Hospital, The Fourth Military Medical University, Xi'an, China. Contact e-mail: haokao.gao@gmail.com*

Objectives : Glucagon-like peptide (GLP-1) and its receptor (GLP-1R) exhibit cardioprotective effects after myocardial ischemia/reperfusion (MI/R) in both animal studies and human clinical trials. The purpose of this study is to monitor the presence and time course of regional myocardial GLP-1R expression after MI/R with non-invasive positron emission tomography (PET). Methods : Male SD rats underwent 45 min transient left coronary artery occlusion followed by reperfusion. In vivo PET imaging was performed to determine myocardial uptake of 18F-FBEM-Cys40-exendin-4 at different time points following reperfusion. The localization of uptake of 18F-FBEM-Cys40-exendin-4 was determined by imaging co-registration with 18F-FDG PET and CT scan. Ex vivo autoradiography, GLP-1R immunohistochemical staining and western blot analysis were performed to confirm the PET results. Results : Myocardial origin and infarcted/ischemic area localization of 18F-FBEM-Cys40-exendin-4 accumulation was confirmed by image co-registration with microCT and 18F-FDG. At 8 h after MI/R, tracer uptake in the infarcted/ischemic region is 0.37 ± 0.05 %ID/g, significantly higher than that in the control group ($p < 0.01$). The localized tracer uptake decreased along with time. The specificity of tracer uptake into ischemic myocardium was supported by decreased tracer uptake after pretreating the rats with excess amount of unlabeled exendin-4. Immunohistochemical staining and western blotting of GLP-1R protein of excised cardiac sections confirmed that the change in uptake observed by PET corresponded to a change in GLP-1R expression. Conclusions : Non-invasive PET imaging using 18F-FBEM-Cys40-exendin-4 revealed a dynamic pattern of GLP-1R upregulation in the infarcted/ischemic area after MI/R. The imaging results will provide guidance for optimization of the time frame of therapeutic intervention.

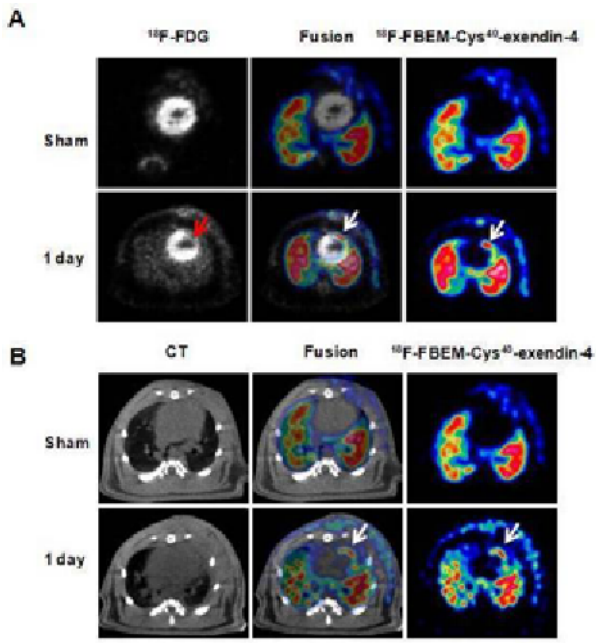


FIGURE 1. (A) Co-registration of 18F-FBEM-cys40-exendin-4 PET imaging with 18F-FDG PET imaging. (B) Representative transaxial PET images using 18F-FBEM-cys40-exendin-4 at different times after MI/R. The high 18F-FBEM-cys40-exendin-4 uptake region from the infarcted/ischemic myocardium is indicated by white arrows, and the triangle indicates 18F-FBEM-cys40-exendin-4 signal from the surgical wound, which is present in both sham operated and MI/R animals.

Disclosure of author financial interest or relationships:
**H. Gao**, None; **D.O. Kiesewetter**, None; **X. Zhang**, None; **N. Guo**, None; **G. Niu**, None; **X. Chen**, None.

Presentation Number **P450**
Poster Session 3
September 7, 2012 / 15:15-15:15 / Room: The Liffey

# In-vivo molecular imaging of silent cardiac ischemia with a new ultrasound contrast agent binding to both E- and P-selectin in rat

***Jean-Marc Hyvelin**, Isabelle Tardy, Patricia Emmel, Maria Costa, Delphine Colevret, Philippe Bussat, Mathew A. von Wronski, Thierry Bettinger, Francois Tranquart, Bracco Suisse SA, Plan-Les-Ouates, Geneva, Switzerland. Contact e-mail: jean-marc.hyvelin@bracco.com*

Objectives: Evaluation of chest pain suggestive of myocardial ischemia remains challenging more particularly in the absence of ECG abnormalities and with normal cardiac biomarkers. A hallmark of ischemia/reperfusion (I/R) relies on the rapid activation of endothelial cells, which is characterized by the production of inflammatory adhesion molecules, such as P- and E-selectin. Ultrasound molecular imaging (USMI) can provide evidence at the molecular level for cardiovascular diseases. We developed a new ultrasound contrast agent functionalized with a recombinant P-selectin glycoprotein ligand-1 analog (rPSGL-Ig). These microbubbles (MB), so called MBrPSGL-Ig are capable of recognizing both E- and P-selectin. We hypothesized that MBrPSGL-Ig could detect the "molecular footprint" of the recent cardiac ischemic event. Material and Methods: Myocardial I/R sequence was performed in rat heart by ligaturing the left anterior descending (LAD) coronary artery during 20 min followed by reperfusion. USMI (Siemens Sequoia, 15L8 probe, CPS mode, MI 0.25) were performed 2h (n=32), 5h (n=16) and 24h (n=10) after reperfusion. Late phase enhanced contrast ultrasound signal, measured in ischemic and in control myocardium in the same animal, was linearized using software package developed in house. Localisation of ischemic area was determined by the absence of contrast enhanced signal during ischemia, using BR38 a non-targeted contrast agent. The derived ratio ischemic/control myocardium obtained with MBrPSGL-Ig was then compared to that of MB functionalized with antibody specific for E- or P-selectin (MBE and MBP, respectively) and to that of BR38. E- or P-selectin expressions in myocardium were determined by immunohistochemistry. Results: We ensured that in our model of transient cardiac I/R, necrosis was not a major component as demonstrated by negative tetrazolium chloride staining as well as no impairment of the left ventricle function. Ischemic area was nicely delineated by the absence of BR38 accumulation during ligature of the LAD. In rat reperfused for 2h, 5h and 24h, late phase signal of MBrPSGL-Ig was higher in ischemic area compared to control area in the left myocardium, and spatial accumulation of MBrPSGL-Ig matched with ischemic area (Figure 1). Calculated ratio (ischemic/control myocardium) decreased with the duration of reperfusion (4.8±1.6, 3.7±0.9 after 2h, 5h reperfusion, respectively) and still remained high after 24h (2.4±1.0). In contrast there was no accumulation of BR38 in the ischemic area. Comparison of late phase signal in response to MBrPSGL-Ig to those obtained with MBE and MBP, suggested that both E- and P-selectin were expressed after 2h and 5h reperfusion. However, after 24h reperfusion MBP binding was barely detectable unlike MBE. These later results were in agreement with immunohistochemistry data showing concomitant expression of extracellular E- and P-selectin at 2h and 5h, whereas after 24h extracellular P-selectin was barely detectable. Conclusion: These results suggest that USMI of E- and P-selectin using MBrPSGL-Ig provides reliable evidence of a recent myocardial ischemic event even in the late phase of reperfusion.

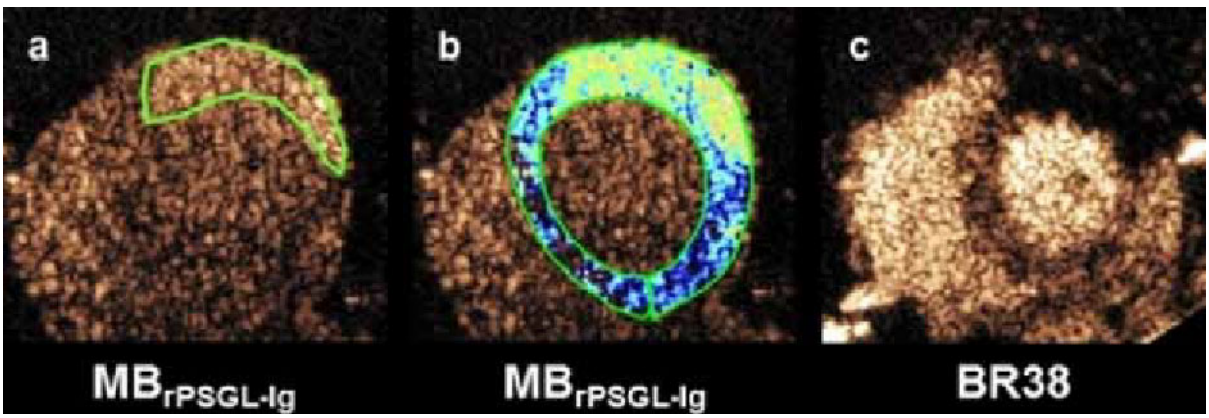


Figure 1: Ultrasound molecular imaging of selectins in rat myocardium after 20min ischemia followed by 2h reperfusion. a, b show late phase enhanced signal in response to MBrPSGL-Ig. In b, colorized image of MBrPSGL-Ig accumulation in the myocardium. c, localisation of the ischemic area after injection of BR38 during ischemia

Disclosure of author financial interest or relationships:
**J. Hyvelin**, Bracco Suisse SA, Employment; **I. Tardy**, Bracco Suisse SA, Employment; **P. Emmel**, Bracco Suisse SA, Employment; **M. Costa**, Bracco Suisse SA, Employment; **D. Colevret**, Bracco Suisse SA, Employment; **P. Bussat**, Bracco Suisse SA, Employment; **M.A. von Wronski**, Bracco Suisse, Employment; **T. Bettinger**, Bracco Suisse SA, Employment; **F. Tranquart**, Bracco Suisse SA, Employment .

Presentation Number **P451**
Poster Session 3
September 7, 2012 / 15:15-15:15 / Room: The Liffey

# Diagnosis and monitoring of atherosclerosis in ApoE-/- mice by using Gadospin F

***Caroline Jung***[1], *Harald Ittrich*[1], *Michael G. Kaul*[1], *Markus Heine*[1], *Tanja Ducic*[2], *Gerhard Adam*[1], [1]*Diagnostic and Interventional Radiology, University Hospital Hamburg Eppendorf, Hamburg, Germany;* [2]*Deutsches Elektronen Synchotron DESY, Research Centre of Helmholtz Association, Hamburg, Germany. Contact e-mail: cjung@uke.de*

Purpose The aim of this study was to investigate the feasibility of noninvasive detection and monitoring of plaque burden in Apo E KO mice by using Gadospin F (GDF). Materials and Methods To monitor the progression of atherosclerosis ApoE-/- (n=5) and wildtype mice (n=2) fed with Western diet for 15, 20, 25 and 30 weeks were imaged before and two hours after i.v. injection of GDF (dosis 100 µmol/kg). MRI examinations were performed at 7T (Clinscan, Bruker). A 3D Inversion Recovery Gradient echo sequence was planned transversal covering the aorta starting from the aortic root. Parameters were: FOV=35mm; matrix 196, 64 slices with thickness 180µm; TR=650ms TE=2.0ms TI=250ms; FA=20°; NSA=6, resulting in a measuring time 9min and a resolution of 180x180x180 µm3. In addition, dynamic scans were acquired to determine the blood clearance. To evaluate the enhancement of aortic wall, for each slice, the percent enhancement (% ENH), relative to the muscle was calculated according to the following equation: %ENH = (Vpost/Vpre-1) x 100, with value V = SIwall/ SImuscle. After MRI, aortas were excised to analyse the GDF uptake by X-ray fluorescence microscopy (X-ray FM). Results Dynamic MRI scans showed the best signal enhancement in the vessel lesions two hours after application of GDF. At that timepoint no more contrast agent was detectable in the blood. Two days after injection the signal enhancement of the plaque vanished completely. We observed a gradual and considerable increase in plaque CNR and size on MR images for the different disease stages. The X-ray FM proved the localisation of GDF within the plaque. Conclusions We established the detection of atherosclerotic lesions by using GDF and defined the best measuring time. In addition we could assess changes of plaque sizes at various stages of atherosclerosis through signal intensity measurements.

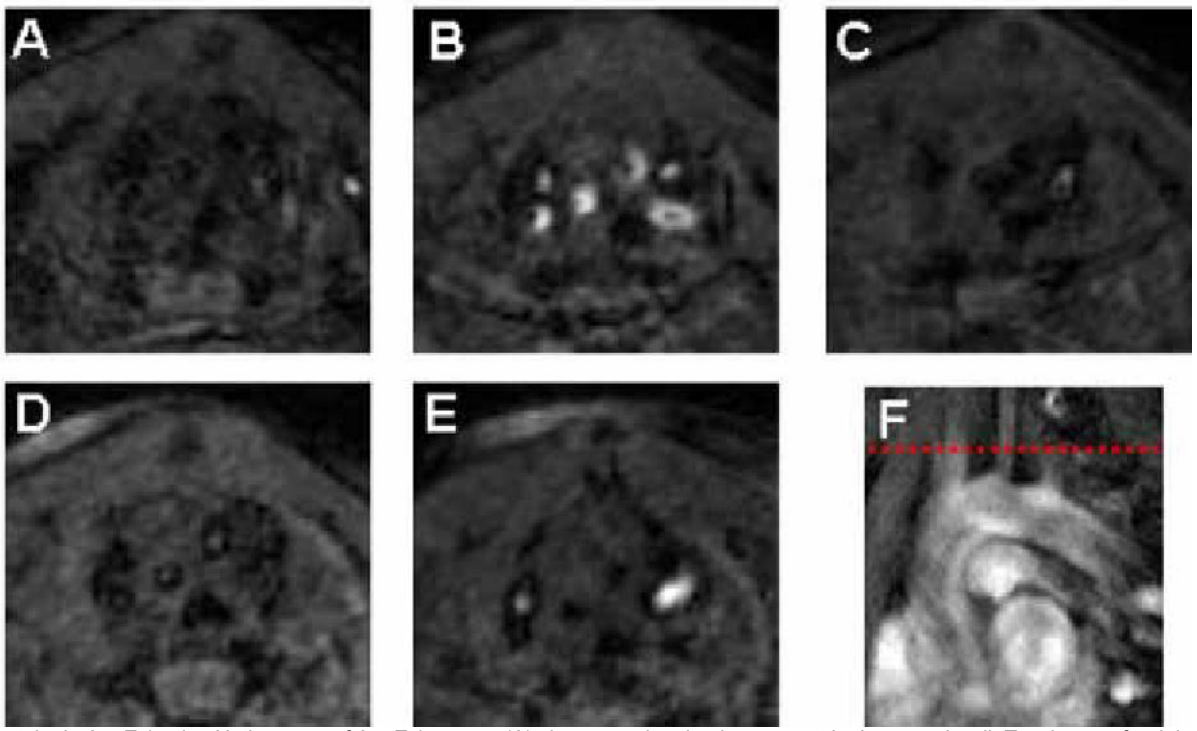


Gadospin F uptake in ApoE-/- mice Native scan of ApoE-/- mouse (A) shows no signal enhancement in the vessel wall. Two hours after injection of 100 µmol/kg Gadospin F a signal enhancement is detectable in the ApoE-/- mouse (B) which is vanished completely two days after injection (C). Wildtype mouse as negative control shows no difference between pre- and post contrast (D,E). (Scan orientation is shown in (F).)

Disclosure of author financial interest or relationships:
**C. Jung**, None; **H. Ittrich**, None; **M.G. Kaul**, None; **M. Heine**, None; **T. Ducic**, None; **G. Adam**, None.

Presentation Number **P452**
Poster Session 3
September 7, 2012 / 15:15-15:15 / Room: The Liffey

# Serial intravital fluorescence imaging of inflammatory thrombus macrophages and proteinase activity predicts experimental deep venous thrombosis resolution in vivo

***Chase W. Kessinger***[1], *Jason R. McCarthy*[2], *Charles P. Lin*[2], *Peter K. Henke*[3], *Farouc A. Jaffer*[1], [1]*Cardiology, Massachusetts General Hospital, Boston, MA, USA;* [2]*Center for Systems Biology, Massachusetts General Hospital, Boston, MA, USA;* [3]*Section of Vascular Surgery, University of Michigan, Ann Arbor, MI, USA. Contact e-mail: ckessinger@partners.org*

Introduction: Inflammation following deep venous thrombosis (DVT) critically modulates thrombus resolution. However, it is unknown whether the degree of in vivo thrombus inflammation predicts the magnitude of acute thrombus resolution. In this study, we utilize serial, two timepoint multispectral intravital microscopy (IVM) at day 4 and 6 post-thrombosis to spatially delineate and quantify macrophage infiltration in the thrombus, and then to determine the degree of thrombus resolution in vivo. Methods: C57Bl/6J male mice (n=6) underwent topical ferric chloride application to the femoral vein to induce thrombosis. On day 3, mice were i.v. injected with macrophage-targeted dextranated nanoparticles (CLIO-AF555, ex/em 555/565nm) and an MMP activity sensor (MMPsense680, ex/em 680/700nm). On day 4, survival IVM of resident thrombus macrophages and MMP activity was performed. In addition, FITC-dextran based venography was concomitantly performed to analyze DVT area and length. On day 6, a second IVM venography IVM study was performed to evaluate thrombus resolution. Mid-luminal IVM z-stacks (40 μm thickness) of the thrombosed area were analyzed using ImageJ. Thrombus ROIs were outlined using FITC-dextran generated angiograms, and used in calculating macrophage target-to-background ratios (TBR) and thrombus area and length. Contralateral sham femoral veins were imaged as controls to show thrombus specification accumulation of macrophages. Imaging was followed by histopathology and fluorescence microscopy of cryosectioned thrombosed femoral vein tissue. Results: At day 4, the baseline femoral DVT area and length were 0.22±0.08mm2 and 1.29±0.16mm (mean±sd), respectively. Day 4 thrombus macrophages were readily visualized. The macrophage distribution was heterogeneous with peripheral infiltration of the thrombus, with occasional penetration into the thrombus interior. At day 6, the thrombus area and length were reduced compared to day 4 ($p<0.005$ for both). Of note, the day 4 thrombus macrophage TBR significantly predicted the degree of thrombus reduction in area and length (Pearson correlation of initial macrophage TBR and (1)Δthrombus area, $r=0.97$, $p=0.001$; (2)Δthrombus length, $r= 0.92$, $p=0.01$). MMP activity TBR also significantly correlated with thrombus length reduction from day 4 to 6 ($r=0.92$, $p=0.01$). Conclusion: This serial in vivo assessment of murine DVT resolution provides new quantitative data that the degree of macrophage infiltration and MMP activity at day 4 predicts the magnitude of thrombus resolution at day 6. Molecular imaging of DVT inflammation in vivo could provide new insights into DVT resolution and the development of the post-thrombotic syndrome, and also in evaluating inflammation-modulating therapies for improved DVT resolution.

Disclosure of author financial interest or relationships:
**C.W. Kessinger**, None; **J.R. McCarthy**, None; **C.P. Lin**, None; **P.K. Henke**, None; **F.A. Jaffer**, Boston Scientific, Merck, Siemens, Consultant; Abbott Vascular, Grant/research support .

Presentation Number **P453**
Poster Session 3
September 7, 2012 / 15:15-15:15 / Room: The Liffey

# Impact of Testosterone Depletion on Myocardial Perfusion in Rats by using [$^{13}$N]$NH_3$-PET Imaging

***Yun Lin**, Damaris Kukuk, Anke Stahlschmidt, Gerald Reischl, Bernd J. Pichler, Department of Preclinical Imaging and Radiopharmacy, Eberhard Karls University Tuebingen, Tuebingen, Germany. Contact e-mail: yun.lin@med.uni-tuebingen.de*

Introduction: Testosterone deficiency is a common issue in elderly men and advanced prostate cancer patients receiving androgen deprivation therapy. Male with lower testosterone level have been reported for higher cardiovascular risks [1]. The aim of this study is to investigate the effects of testosterone depletion through surgical castration on the myocardial perfusion in rats by using animal PET imaging with the perfusion marker [$^{13}$N]$NH_3$. A further point is to study the impact of stress on myocardial perfusion by using dobutamine under testosterone depletion. Materials and Methods: Adult male Wistar rats were separated into castration (bilateral surgical castration, n=13) and control (sham, n=7) groups at the age of 15 weeks. The rest/stress phases [$^{13}$N]$NH_3$-PET were performed 8 weeks post castration (*p.c.*). Ten minutes list mode data with intravenous tail vein injection (*i.v.*) of ~2 mCi [$^{13}$N]$NH_3$ were acquired for each phase. There was about 10 min waiting time between the two PET scans to allow for $^{13}$N decay without moving the rats. Dobutamine stimulating myocardial perfusion was administrated after the rest phase with stepwise increasing infusion rate (5 µg/kg/min *2 min, 10 µg/kg/min *2 min, 20 µg/kg/min *9 min) where the stress phase started during the final infusion rate. The dynamic data was sorted into 22 frames and reconstructed by OSEM 2D algorithm. The regions of interest were placed at center 6 consecutive planes of short axial myocardium and left ventricle blood pool. A two-tissue compartment model was applied for evaluating the myocardial blood flow (MBF). The image analysis was performed with the software PMOD. Results: MBF at rest phase didn't differentiate between the castration (3.26±0.57 ml/min/g) and control (3.12±0.88 ml/min/g) groups. However, the MBF at stress phase stimulated by dobutamine was significantly lower ($P<0.01$) in the castration group (8.15±1.08 ml/min/g) than the control group (9.64±1.69 ml/min/g). The coronary vasodilatation reserve ($CVR=MBF_{stress}/MBF_{rest}$) of the castration group (2.54±0.35) decreased significantly ($P<0.05$) compared with the control group (3.18±0.81). Conclusion: The data showed the castrated rats remained normal MBF at rest phase comparable to control rats, but were unable to reach the same MBF level after stress stimulation. Our [$^{13}$N]$NH_3$-PET imaging results could indicate the risks of low testosterone level on cardiovascular disease because of lower MBF under stress phase. The future study will evaluate the importance of testosterone level on MBF by applying testosterone replacement on the castrated rats.

1. Liu PY, Death AK and Handelsman DJ, *Androgens and cardiovascular disease*. Endocr Rev. 2003 Jun;24(3):313-40.

Disclosure of author financial interest or relationships:
**Y. Lin**, None; **D. Kukuk**, None; **A. Stahlschmidt**, None; **G. Reischl**, None; **B.J. Pichler**, Siemens, Grant/research support; AstraZeneca, Grant/research support; Bayer Healthcare, Grant/research support; Boehringer-Ingelheim, Grant/research support; Oncodesign, Grant/research support; Merck, Grant/research support; Bruker, Grant/research support .

Presentation Number **P454**
Poster Session 3
September 7, 2012 / 15:15-15:15 / Room: The Liffey

# A cardiac MRI study using hyperpolarized [1-13C]pyruvate after coronary occlusion and reperfusion in pigs

*Giovanni Donato Aquaro[1], Francesca Frijia[1], **Luca Menichetti**[2,1], M. F. Santarelli[2,1], Vincenzo Positano[1,2], Alessandra Flori[3], Vincenzo Lionetti[3], Rolf F. Schulte[6], Florian Wiesinger[6], Jan Henrik Ardenkjaer-Larsen[4,5], Simone L. Romano[3], Giulio Giovannetti[2], Fabio A. Recchia[3], Luigi Landini[7,1], Massimo Lombardi[1], [1]Fondazione CNR-Regione Toscana G.Monasterio, Pisa, Italy; [2]CNR Institute of Clinical Physiology, Pisa, Italy; [3]Scuola Sant'Anna, Sector of Medicine, Pisa, Italy; [4]GE Healthcare, Hillerod, Denmark; [5]Department of Electrical Engineering, The Technical University of Denmark, Kgs Lyngby, Denmark; [6]GE Global Research, Munich, Germany; [7]Department of Information Engineering: EIT, University of Pisa, Pisa, Italy. Contact e-mail: luca.m@ifc.cnr.it*

Introduction. Hyperpolarized 13C-pyruvate cardiac magnetic resonance (MRI) is a promising new technique for the assessment of myocardial energy substrate metabolism in vivo. We tested the effectiveness of this technique to quantify myocardial pyruvate uptake and the formation of its metabolites lactate and bicarbonate in a pig model of acute ischemia and reperfusion. Materials & Methods. Imaging experiments were performed on a 3T GE Excite HDx scanner (GEHC, Milwaukee, USA) using a 13C quadrature birdcage coil. Seven pigs were equipped with a pneumatic occluder placed around the left anterior descending coronary artery. After post-surgical recovery, the pigs were subjected to 13C-MRI after injection of [1-13C]pyruvate, hyperpolarised with a DNP polarizer (Hypersense, Oxford Inst, UK). The injected [1-13C]pyruvate dose was 0.13 mmol/kg body weight. Anatomical reference images were acquired in the axial plane using a standard steady-state free precession sequence. Metabolic information covering the whole heart was obtained using 3D IDEAL spiral CSI prescribed on the same region imaged by the anatomical reference scan (FOV= 30x30 cm2, slab thickness=100 mm), starting 20s after the beginning of the injection. The IDEAL spiral CSI was set up with 11 echo times, a constant relative echo time spacing of 0.9 ms and constant flip angle of 7°. Data were reconstructed using spectrally-preconditioned CS inversion followed by gridding reconstruction implemented in Matlab. 3D axial volumes were reconstructed for pyruvate, lactate, and bicarbonate. Short axis (SA) cardiac views were reformatted by PMOD software by using the anatomical images as reference. Quantitative analysis was performed on SA views by custom (HIPPO-C13) software. Myocardial contours were manually defined in anatomical SA views. A reference point corresponding to superior insertion of the right ventricular wall was defined. Slices were classified as basal, middle, or apical by the operator. The myocardium was divided in six (basal and medium slices) or four (apical slices) equiangular segments and the corresponding polar maps were extracted. Values were averaged leading to a 16-segments model of metabolite distribution, following AHA guidelines. Results. During occlusion, we found a decrease of 13C-lactate (-21±26% vs 3±16%, P<0.0001) and 13C-bicarbonate (-29±34% vs 33±52%, P<0.0001) in the myocardial segments at risk as compared with remote segments. In the same segments, the 13C-lactate signal increased during reperfusion (20±42% vs -7±22%, P=0.0007), consistent with the enhanced pyruvate reduction in the post-ischemic phase, while 13C-bicarbonate was found persistently reduced (-38±27% vs 36±51%, p<0.0001) consistent with the expected presence of post-ischemic depression of the oxidative metabolism. Conclusions. 13C-pyruvate MRI is sufficiently sensitive to detect transient changes in regional myocardial metabolism in an in vivo model of ischemia-reperfusion.

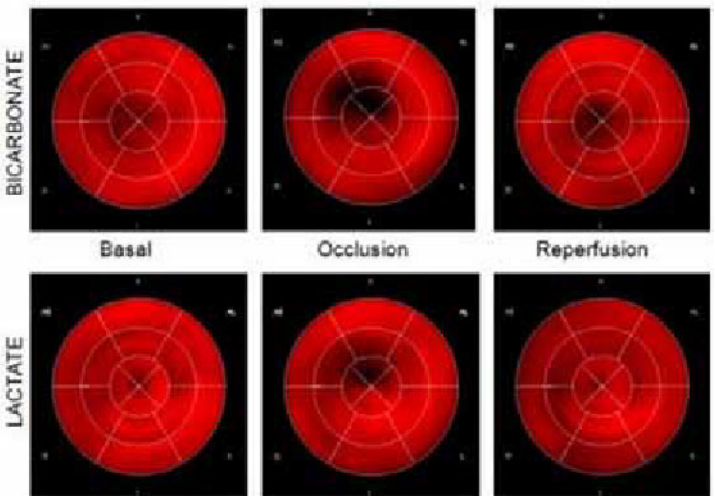


16-segments model representation of bicarbonate (upper) and lactate (lower) metabolites distribution, in basal condition(left), during occlusion (middle) and reperfusion (right).

Disclosure of author financial interest or relationships:
**G. Aquaro**, None; **F. Frijia**, None; **L. Menichetti**, None; **M.F. Santarelli**, None; **V. Positano**, None; **A. Flori**, None; **V. Lionetti**, None; **R.F. Schulte**, None; **F. Wiesinger**, None; **J. Ardenkjaer-Larsen**, None; **S.L. Romano**, None; **G. Giovannetti**, None; **F.A. Recchia**, None; **L. Landini**, None; **M. Lombardi**, None.

Presentation Number **P455**
Poster Session 3
September 7, 2012 / 15:15-15:15 / Room: The Liffey

# Comparison between magnetic nanoparticle-combined cardiac MRI and conventional cardiac MRI for detection of myocardial inflammation, and visualization of inflammatory evolution in experimental autoimmune myocarditis rat model

***Hyeyoung Moon***[1,2], *Hyo Eun Park*[3], *Jongeun Kang*[1], *Kiyuk Chang*[3], *Kwan Soo Hong*[1,2], *[1]Divison of MR research, Korea Science Institute, ChungcheongBuk-Do, Republic of Korea; [2]Bio-Analytical Science, University of Science and Technology, Daejeon, Republic of Korea; [3]Department of Internal Medicine, Catholic University, Seoul, Republic of Korea. Contact e-mail: hymoon@kbsi.re.kr*

Clinically, cardiac MRI (CMR) has emerged as a leading imaging tool in the diagnosis of myocarditis. However, myocardial inflammation, a critical pathogenic factor in myocarditis, cannot be directly visualized by conventional CMR. In our study, we investigated whether PEGylated fluorescent magnetic nanoparticles (MNP) could detect the inflammatory areas in experimentally induced autoimmune myocarditis (EAM) rats, and compared the detectability of focal inflammation area in the myocardium between MNP-enhanced CMR and conventional CMR as diagnosis of myocarditis. MNP-CMR was also employed to noninvasively track the evolution of inflammation in myocarditis. We performed in vivo CMR in EAM and control rats using a 4.7 T MRI system. At first, T2W, and pre-MNP MRI were performed, and then early gadolinium enhancement (EGE) and late gadolinium enhancement (LGE) MRI were performed after tail vein injection of Gd-DTPA (Magnevist®, 0.1 mmol/kg). Then, after 24 hrs of tail vein injection of home-made MNPs (10 mg Fe/kg), post-MNP MRI was performed. To observe the inflammatory evolution, we acquired the pre-MNP CMR images at 15D post-immunization (PI), and then 5 mg Fe/kg of MNP-FITC was intravenously injected. Post-MNP CMR was acquired at 16D and 20D PI. After acquiring post-MNP CMR at 20D PI, same dose of MNP-RITC was injected in the same rats. Then, post-MNP CMR imaging was performed at 21D PI. Relatively large areas of myocardial inflammation in EAM rats were detected by conventional T2W-, EGE-, LGE-MRI, while small-sized inflammation regions consistently failed to be detected. The superiority of MNP-CMR to conventional MRI was clearly shown for focal inflammation (Fig. 1), including visualization of the inflammatory evolution. MNP-CMR could effectively visualize myocardial inflammatory cellular infiltrates, and monitor the dynamic evolution of myocardial inflammation in a preclinical model of EAM. We showed that MNP-CMR could be a highly efficient tool for visualizing myocardial inflammation in the early phase of the EAM with a potential for quantifying the response to specific therapies for myocarditis. Furthermore, this MRI method along with histopathological analysis of the MRI-guided biopsies will assist in the diagnosis of the focal manifestations of myocarditis.

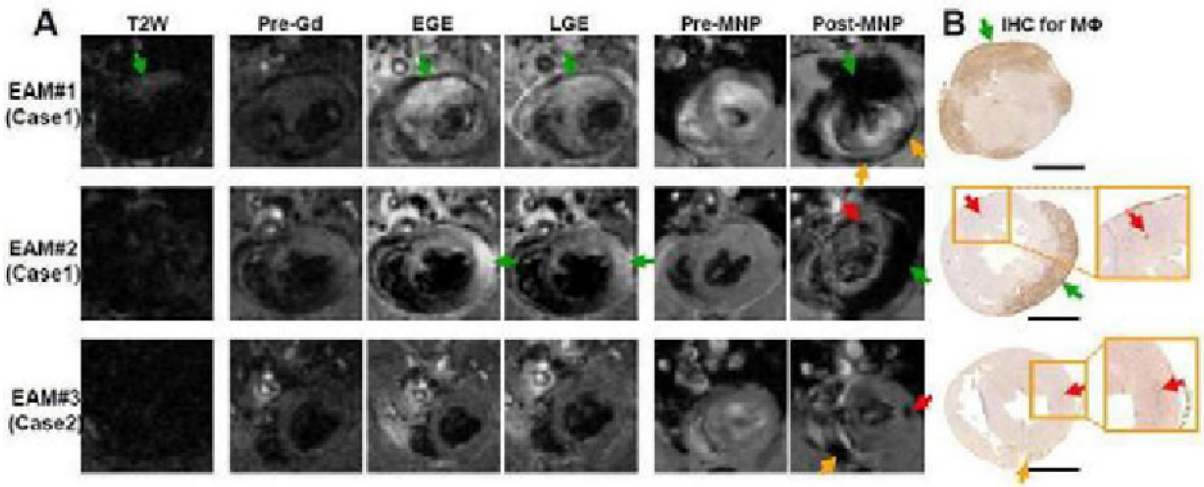


Figure 1. Head-to-head performance comparison between MNP-CMR and conventional (T2W-, EGE-, and LGE-) CMR. Three Representative T2W-, EGE-, LGE-, and MNP-CMR (Post-MNP) images sequentially obtained in the same EAM rats are shown with corresponding IHC-stained images (IHC). Large inflammation areas (green arrows) were detected by conventional and MNP-CMR, while focal and/or less severe inflammation areas (yellow and red arrows) could be detected only by MNP-CMR (red arrows; note that the diameter of macrophage cluster in IHC image (red arrow of EAM#2) was ~200 μm). Scale bars: 5mm

Disclosure of author financial interest or relationships:
**H. Moon**, None; **H. Park**, None; **J. Kang**, None; **K. Chang**, None; **K. Hong**, None.

Presentation Number **P456**
Poster Session 3
September 7, 2012 / 15:15-15:15 / Room: The Liffey

# Therapeutic Efficacy of Different Nanoparticle Formulations of Glucocorticoids as a Treatment for Atherosclerosis Assessed by Multimodal Imaging

***Maarten J. Otten***[1], *Mark E. Lobatto*[1,2], *Claudia Calcagno*[1], *Gert Storm*[3], *Erik S. Stroes*[2], *Zahi A. Fayad*[1], *Willem J. Mulder*[1], [1]*Mount Sinai School of Medicine, Translational and Molecular Imaging Institute, New York, NY, USA;* [2]*Academic Medical Center, Amsterdam, Netherlands;* [3]*Utrecht University, Utrecht, Netherlands. Contact e-mail: motten@hotmail.com*

Objectives: We previously established that liposomal nanoparticle formulations of prednisolone phosphate can non-specifically target atherosclerotic plaques and exert profound local anti-inflammatory activity. With the purpose of finding a lead formulation for future human clinical trials, in this study we aimed to evaluate the therapeutic efficacy of different nanoparticle formulations of glucocorticoids at a lower dose (prednisolone phosphate 10mg/kg, dexamethasone phosphate 10mg/kg, and budesonide phosphate 1 mg/kg) in a rabbit model by noninvasive clinical multimodal imaging. In addition, we assessed pharmacokinetics, biodistribution and toxicity of the compounds. Methods: 2 New Zealand white rabbits received a high-fat diet in combination with a double balloon injury of the abdominal aorta to induce atherosclerotic lesions. After six months of diet animals underwent a baseline 18F-FDG PET-CT scan, T1-weighted MRI and a DCE-MRI to assess inflammation, plaque size, permeability and neovascularization, respectively. The rabbits were randomized into four different groups (the different glucocorticoid formulations and a saline control group) and were administered a single intravenous dose of nanoparticle treatment. To evaluate therapeutic efficacy, the rabbits were imaged 2 days and 7 days after initiating therapy and were sacrificed for histological assessment afterwards. In addition, 18 healthy New Zealand white rabbits were divided into 6 groups (n=3/group) and were injected with the different nanoparticle formulations or free circulating glucocorticoids. Blood was withdrawn at different time points for clinical chemistry and to establish pharmacokinetics. Rabbits were sacrificed at set endpoints to assess organ biodistribution by HPLC. Results: Nanoparticulate prednisolone phosphate significantly reduced 18F-FDG PET-CT signal two and seven days post-injection (16% and 20%, $p<0.05$). DCE-MRI showed a significant reduction in plaque permeability in the liposomal prednisolone phosphate group by an observed decrease in the functional parameters Area Under the Curve (AUC), by 24% and 28%, and K-trans by 25% and 28% (all $p<0.05$) after two and seven days. Liposomal budesonide caused a reduction of AUC and K-trans by 20% 2 days post-injection ($p<0.05$). The clinical chemistry in healthy rabbits showed no changes in liver or kidney markers in all groups. Injections of nanoparticle formulations of glucocorticoids caused a significantly smaller increase in neutrophil and decrease in lymphocyte counts compared to free circulating glucorticoids. Conclusion: A single intravenous injection of nanoparticulate glucocorticoids in a rabbit atherosclerosis model significantly decreased inflammatory activity and plaque permeability in atherosclerotic plaques, as established by non-invasive multimodal imaging. In addition, clinical chemistry showed no systemic immunosuppression. This nanotherapy may provide a rapid anti-inflammatory response in patients that can benefit from short-term therapy after an acute atherothrombotic event, by modulating inflammation and permeability of atherosclerotic plaques, possibly for the prevention of future events.

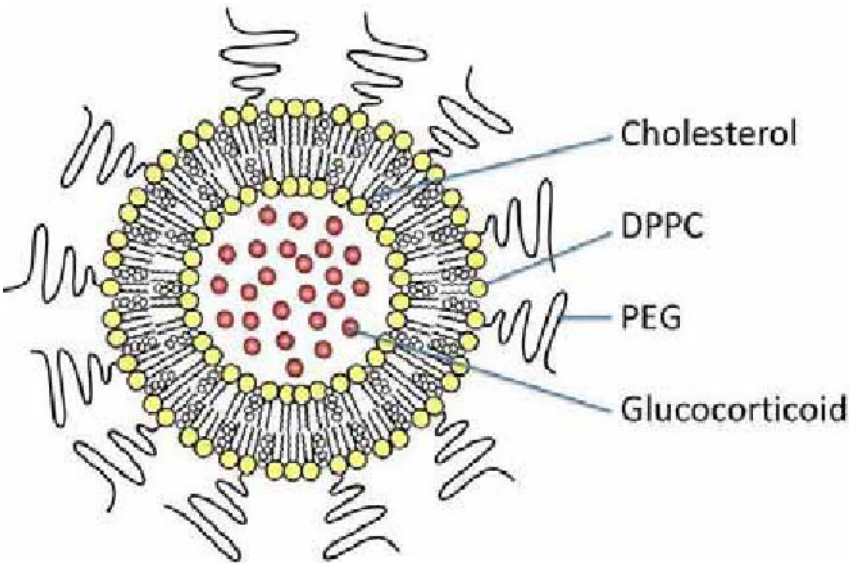


Schematic of a liposomal nanoparticle loaded with glucocorticoids.

Disclosure of author financial interest or relationships:
**M.J. Otten**, None; **M.E. Lobatto**, None; **C. Calcagno**, None; **G. Storm**, None; **E.S. Stroes**, None; **Z.A. Fayad**, None; **W.J. Mulder**, None.

Presentation Number **P457**
Poster Session 3
September 7, 2012 / 15:15-15:15 / Room: The Liffey

# Spontaneous myocardial infarctions are associated with coronary atherosclerosis and thrombosis: new imaging-guided findings in SR-B1-/-/ ApoE-R61hypo mice

***Andrea Starsichova***[1], *Sven Hermann*[1], *Michael T. Kuhlmann*[1], *Bodo Levkau*[2], *Michael Schäfers*[1], [1]*European Institute for Molecular Imaging, University of Muenster, Muenster, Germany;* [2]*Institute for Pathophysiology, University of Duisburg-Essen, Essen, Germany. Contact e-mail: starsich@uni-muenster.de*

Atherosclerosis is the most common pathologic process that leads to serious cardiovascular events such as myocardial infarction or stroke. One of the biggest challenges for translational imaging research - from basic science to clinical applications - is to find relevant animal models of atherosclerosis, which are associated with clinical features of disease. A promising model might be a transgenic mouse deficient for Scavenger Receptor class B type 1 (SR-B1-/-) and expressing reduced levels of a point mutant form of Apolipoprotein E (ApoE-R61hypo). Our previous data (see WMIC 2011 abstract #P428) confirmed that all these mice die within four weeks after onset of a high fat / high cholesterol diet (HFC), probably due to acute myocardial infarctions. However, if these events result from unstable atherosclerotic lesions in the coronary arteries remained unclear. To investigate this issue we applied serial F-18-FDG-PET imaging in 19 mice under HFC diet. Once we observed newly occuring transmural myocardial defects of glucose consumption, hearts were explanted and subsequently processed for systematic histological analysis by serial cutting from apex to base. Accordingly, hearts from 11 mice under normal chow diet were analyzed. We found atherosclerotic plaques in coronary arteries in all hearts of mice under HFC diet and in a majority of hearts of mice under normal chow diet. The lesions ranged from mild non-stenotic to stenotic phenotypes. However, the most striking difference between the groups was the finding of thrombi only in the HFC diet group, mainly located in arteries supplying the inferoseptal regions of the left ventricle. Thus, in SR-B1-/-/ ApoE-R61hypo mice the HFC diet seems to trigger the development of unstable plaque phenotypes. In summary, we propose that occlusive coronary atherosclerosis and/or thrombi formation, most likely due to plaque rupture or erosion are the cause of myocardial defects (found by FDG-PET) in SR-B1-/- ApoE-R-61 hypo mice under HFC diet. To our knowledge this is the first proof of coronary atherosclerosis associated with spontaneous thrombus formation and clinical infarction events in a mouse model of atherosclerosis. This model could evolve as a unique opportunity to test new imaging approaches for visualization of unstable plaques.

Disclosure of author financial interest or relationships:
**A. Starsichova**, None; **S. Hermann**, None; **M.T. Kuhlmann**, None; **B. Levkau**, None; **M. Schäfers**, Siemens Medical Solutions, Grant/research support .

Presentation Number **P458**
Poster Session 3
September 7, 2012 / 15:15-15:15 / Room: The Liffey

# Imaging RAGE expression in limb ischemia

***Yared Tekabe**, Maria Kollaros, Lynne Johnson, Columbia University, Yonkers, NY, USA. Contact e-mail: yt2166@columbia.edu*

Background and hypothesis: The prevalence of peripheral artery disease (PAD) in the general population is 12-14%, affecting 20% of those > 70 years and contributes to significant morbidity. Limb ischemia in diabetics takes a particularly malignant course. Receptor for advanced glycation endproducts (RAGE) expression contributes to the impaired angiogenic response to limb ischemia in diabetes. We hypothesized that we could document and quantify on in-vivo SPECT imaging increased RAGE expression in diabetes with 99mTc anti-RAGE F(ab')2 monoclonal antibody. Methods: Male wild-type (WT) C57BL/6 mice were either made diabetic or left as control. Mice were treated with 5 consecutive daily doses of STZ dissolved in citrate buffer (55 mg/kg pH 4.5) via the intraperitoneal route. Two months later, 5 diabetic and 5 non-diabetic mice underwent femoral artery ligation. On the left side, the vascular bundle was isolated from below the inguinal ligament proximally to the bifurcation distally and the femoral artery was dissected free and tied with non absorbable sutures. The right leg served as control. Five days later mice were injected with 300 uCi 99mTc anti-RAGE F(ab')2 and 4 hours later (blood pool clearance) underwent SPECT/CT imaging on nanoSPECT/CT (Bioscan, Washington DC). At completion of imaging, the mice were euthanized, the hind limbs counted in a gamma well counter. Because of small tissue sizes, histology was performed on limbs from separate experiments. The scans were reconstructed and processed using InVivoScope software (Invicro, Boston, MA). Images were cropped to remove bladder activity and serial 5 voxel thick transverse sections were selected from level of hip joints to distal hind limb. Regions of interest were drawn and activity in mCi summed for each limb and subsequently divided by the injected dose (ID). Results: Data expressed as %ID x 10-3 are summarized in the Table. There was a good correlation between %ID from the scans and %ID/g from the ex-vivo well counting: R=0.601; P=0.01. Immunohistological staining showed greatest RAGE staining in ischemic limbs of diabetic mice localized primarily to muscle cells. Summary: Imaging and quantifying RAGE expression in limb ischemia in diabetes may serve as a useful tool to evaluate the effect of therapy to block RAGE expression and thereby promote the angiogenic response to ischemia in peripheral vascular disease.

Data expressed as %ID x 10-3

| | Left leg | Right leg | Ratio |
|---|---|---|---|
| Diabetic | 1.40±0.30 | 0.97±0.24 | 1.31±0.31 |
| Non-diabetic | 0.72±0.27 | 0.48±0.14 | 1.56±0.60 |
| P value | 0.008 | 0.004 | NS |

Disclosure of author financial interest or relationships:
**Y. Tekabe**, None; **M. Kollaros**, None; **L. Johnson**, None.

Presentation Number **P459**
Poster Session 3
September 7, 2012 / 15:15-15:15 / Room: The Liffey

# Evaluation of FDG uptake in apolipoprotein E-deficient mice atherosclerotic lesions by *in vivo* PET/CT imaging and *ex vivo* autoradiography

***Jakub Toczek**, Alexis Broisat, Laurent M. Riou, Daniel Fagret, Catherine Ghezzi, Radiopharmaceutiques Biocliniques, INSERM U1039 & Université Joseph Fourier (Grenoble I), La Tronche, France. Contact e-mail: jakub.toczek@gmail.com*

**Background:** The early detection of vulnerable coronary atherosclerotic plaques is a challenge in the field of nuclear cardiology. One of the hallmarks of vulnerable lesions is a high degree of inflammation. [18F]-fluorodeoxyglucose (FDG) is a widely used positron emission tomography (PET) tracer. Its potential to detect vulnerable atherosclerotic plaques in human, through a high uptake by inflammatory cells with a high metabolic activity is currently evaluated in several clinical trials. However, few preclinical studies were conducted and led to contradictory results. The objective of the present study was to investigate the *in vivo* and *ex vivo* FDG uptake in the widely used apolipoprotein E-deficient mice (apoE$^{-/-}$) model of atherosclerosis using a state-of-the-art small-animal dedicated PET/CT camera and autoradiography, respectively. **Methods and Results:** Thirteen (13) apoE$^{-/-}$ mice aged 36 ± 2 weeks were used. The animals fed a high-fat western type chow for 25 ± 6 weeks were fasten for 13 hrs before the imaging protocol. Animals were injected with 12 ± 2 MBq of FDG. In order to minimize background activity in muscles and brown fat tissues, a group of animals was anesthetized 60 min prior to the injection of FDG and kept at 37°C (AT group, n = 7). A second group of animals was injected conscious and kept awaken throughout the accumulation period at room temperature (24°C) (CS group, n = 6). A PET acquisition was performed from 150 to 180 min post-injection (p.i.) in both groups. AT animals also underwent serial PET/CT acquisitions at earlier time points (30, 60 and 120 min p.i.). Animals were euthanized at 3 hr p.i. and an *ex vivo* analysis including autoradiography of aortic arch sections was performed. No focal uptake of FDG corresponding to atherosclerotic lesion uptake could be identified on PET/CT images in either group. *Ex vivo* analysis (see Figure) showed a significantly higher uptake in atherosclerotic lesions than in the lesion-free aortic wall (AT group, 5.1 ± 2.3 & 2.4 ± 1.0 %ID/g, respectively; CS group, 5.1 ± 2.7 & 1.7 ± 0.6 %ID/g respectively; $p < 0.05$ for both) as well as significantly higher activity in atherosclerotic lesions than in the blood (AT group: 1.3 ± 0.5 %ID/g & CS group: 0.6 ± 0.2 %ID/g; $p < 0.01$ vs. lesion for both groups). A similar uptake was observed in atherosclerotic lesions and the periaortic brown adipose tissue for the AT group (5.9 ± 4.0 %ID/g, p = NS vs. lesion), whereas accumulation at room temperature in CS animals resulted in higher uptake in periaortic brown tissue (15.0 ± 9.1 %ID/g, $p < 0.05$ vs. lesion). **Conclusion:** *In vivo* high resolution, small animal-dedicated PET/CT imaging failed to identify aortic atherosclerotic lesions in anesthetized and conscious apoE$^{-/-}$ mice following FDG injection despite elevated lesion-to-blood and lesion-to-lesion-free aortic wall ratios as assessed by *ex vivo* analysis. In addition, brown adipose tissue located in the vicinity of the thoracic aorta displayed high FDG uptake thereby preventing good contrast between lesions and the surrounding non-vascular tissue and potentially jeopardizing the use of FDG for atherosclerotic lesion imaging in apoE$^{-/-}$ mice.

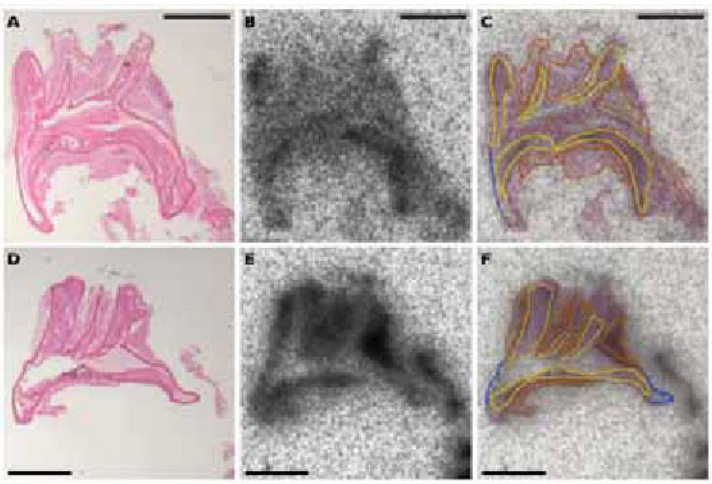


**Figure.** Autoradiographic analysis of FDG uptake in aortic arch of anesthetized (A, B, C) and conscious (D, E, F) apoE$^{-/-}$ mice. Histological coloration (A, D), autoradiography (B, E) and fusion image (C, F) with regions of interest: atherosclerotic lesions (yellow), lesion-free aortic wall (blue) and periaortic brown adipose tissue (brown). Scale bar: 1mm.

Disclosure of author financial interest or relationships:
**J. Toczek**, Advanced Accelerator Applications, Grant/research support; **A. Broisat**, None; **L.M. Riou**, None; **D. Fagret**, None; **C. Ghezzi**, None.

Presentation Number **P460**
Poster Session 3
September 7, 2012 / 15:15-15:15 / Room: The Liffey

# Optimization of Contrast Enhanced Micro-Computed Tomography for imaging the vascular network in laboratory rodents

***Jordi L. Tremoleda**, Willy Gsell, Biological Imaging Centre / MRC Clinical Sciences Centre, Imperial College London, London, United Kingdom. Contact e-mail: jordi.lopez-tremoleda@csc.mrc.ac.uk*

Introduction: Microscopic computed tomography (micro-CT) has proven a very efficacious imaging technique for high density structures such as bone, providing excellent spatial resolution through rapid acquisition times allowing for high put-through preclinical screenings. However, its application for imaging low density organs and body fluids is limited by their poor contrast. To improve their visualization, exogenous contrast agents have been successfully applied in clinical practice but their implementation in preclinical models has proven challenging due to the rapid clearance of the contrast agents along with the limitations of preclinical CT systems for carrying ultrafast acquisition. Herein we present a methodology for visualizing the vascular network in mice Methodology: Healthy C57Bl/6 mice were used in this study (n=6). By using a long acting blood-pool metal-based nanoparticle contrast agent specifically formulated for preclinical CT imaging, ExiTron™ nano 12000, we optimized image acquisition parameters and volume-rendering technique obtaining good visualization of the blood vessels. Animals were anaesthetized with isoflurane (1-1.5%) in 1L/min O2 lying in supine position on a heated pad to regulate body temperature. ECG electrodes and a respiratory cuff were placed for monitoring heart and respiratory rate, respectively. Tail vein was cannulated for administration of contrast agent (70-100ul to an equivalent does of 1200mg iodine/kg BW within 1 min administration time). A combined PET/SPECT/CT preclinical scanner was used (Inveon, Siemens Preclinical Solutions, Inc.).The CT acquisition was performed with the x-ray source set to 80Kvp and 500uAmp, with 330 projection of 5 frames exposure of 40 ms, with an overall exposure time of 220ms with cardiac and respiratory gating. An initial CT acquisition was acquired before contrast administration to create a mask for post-processing subtraction from the contrast enhanced acquired imaged. A second acquisition was performed 5-10 min after injection of the contrast agent to allow for physiological stabilization. Analysis was performed in IRW 3.0 (Siemens Preclinical Solutions, Inc.). Results: The combination of the contrast agent ExiTron™ nano 12000 with an optimized image protocol for the gated CT acquisition allowed us to obtain a good contrast enhancement of the blood providing a good visualization of the blood vessels structure and anatomical identification of the heart down to a resolution of 35um (Fig1). All animals recovered well after contrast injection and image acquisitions. Discussion: Optimized contrast enhanced micro-CT represents an important refined method for imaging soft the vascular network in laboratory rodents, increasing the versatility of the CT modality. It also allows for co-registration of anatomical and metabolic data in multimodality PET/SPECT and CT imaging units providing a unique tool for further cardiovascular and angiogenesis preclinical studies.

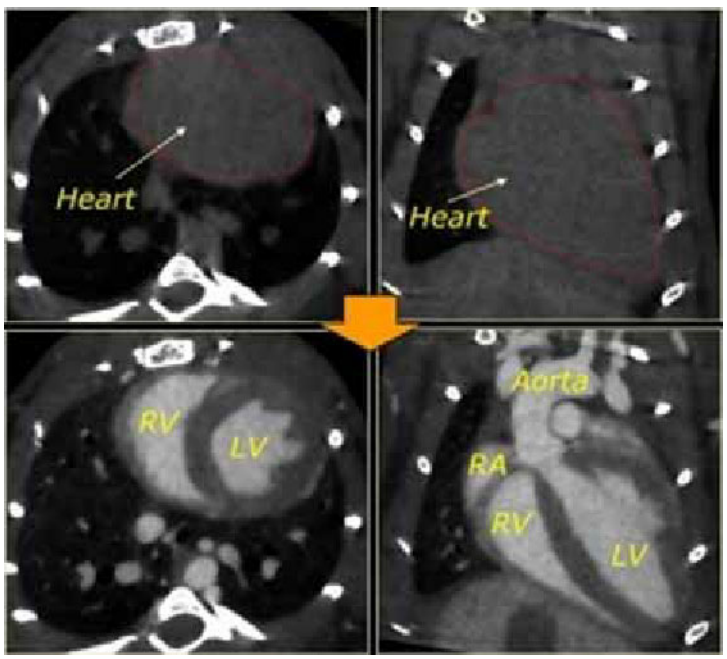


Figure 1: Transaxial and coronal images of mouse heart before and after injection with a single dose of Exitron™nano 12000.

Disclosure of author financial interest or relationships:
**J.L. Tremoleda**, None; **W. Gsell**, None.

Presentation Number **P461**
Poster Session 3
September 7, 2012 / 15:15-15:15 / Room: The Liffey

# Regional Estimates of Myocardial Work and Metabolic Rate of FDG Using Simultaneous PET/MRI

***Alexander Veress***[1,2], *Andrew Hernandez*[3], *Hans F. Wehrl*[4], *Bernd J. Pichler*[4], *Grant T. Gullberg*[3,5], [1]*Mechanical Engineering, University of Washington, Seattle, WA, USA;* [2]*Bioengineering, University of Washington, Seattle, WA, USA;* [3]*Department of Radiotracer Development & Imaging Technology, Lawrence Berkeley National Laboratory, Berkeley, CA, USA;* [4]*Department of Radiology, Laboratory for Preclinical Imaging and Imaging Technology of the Werner Siemens-Foundation, University of Tübingen, Tübingen, Germany;* [5]*Department of Radiology, University of California San Francisco,, San Francisco, CA, USA. Contact e-mail: averess@u.washington.edu*

Background: Dual modality PET/MRI offers potentially the only modality that is able to simultaneously measure regional cardiac work and metabolic energetics. PET/MRI scanners provide high resolution functional information by way of DENSE or tagged MRI as well as metabolic information from PET imaging. The goal of this project was to determine regional myocardial work and compare this information with metabolic information provided by the PET image data to determine if there a direct relationship between local work and metabolism. Methods: Three normotensive lewis rats were imaged using an MRI imaging system with a PET insert. The PET insert, consisting of 16 LSO-APD block detector modules having a 72 mm axial FOV, was placed in a 7T small animal MRI scanner. The rats were injected with 1-2 mCi of 18FDG and simultaneous PET and tagged MRI imaging were performed. The myocardial external minute work (MEMW) was determined by first obtaining an estimate of the myocardial end-systolic stress through the analysis of a subject-specific finite element model. The passive material properties and active contractile properties were determined through optimization of the deformations at end-systole and end-diastole respectively. The end-systolic regional strain values were determined using HARP analysis of the tagged MRI data. These results were then used to obtain an estimate of the MEMW. The PET images were reconstructed as a dynamic sequence of 3D images to obtain time activity curves for blood input sampled from the left ventricular blood pool (~40 mm3) and for the left ventricular myocardial (~250 mm3). The time activity curves were fit to a two-compartment irreversible model to obtain the metabolic rate Ki for FDG. Regional Ki values were correlated with regional MEMW. Results: Comparison of the mid-ventricular values of MEMW and the Ki values for each of the three rats showed positive correlations. The three rats had r2 values of 0.71, 0.43, and 0.67, respectively. Conclusion: These results suggest that simultaneous PET/MRI imaging is able to measure the relationship between cardiac work and metabolic rate of glucose. This is a preliminary result in the goal to use PET/MRI to simultaneously calculate cardiac oxygen utilization and cardiac work (ratio=cardiac efficiency) and to relate cardiac efficiency to the metabolism of energetic substrates.

Disclosure of author financial interest or relationships:
**A. Veress**, None; **A. Hernandez**, None; **H.F. Wehrl**, None; **B.J. Pichler**, Siemens, Grant/research support; AstraZeneca, Grant/research support; Bayer Healthcare, Grant/research support; Boehringer-Ingelheim, Grant/research support; Oncodesign, Grant/research support; Merck, Grant/research support; Bruker, Grant/research support; **G.T. Gullberg**, None.

Presentation Number **P462**
Poster Session 3
September 7, 2012 / 15:15-15:15 / Room: The Liffey

# 99mTc-Tetrofosmin versus 99mTc-sestamibi: Systematic evaluation in small animal multipinhole-SPECT/CT to study murine myocardial perfusion

***Alexis Vrachimis***[1,2], *Sven Hermann*[1], *Otmar Schober*[2], *Michael Schäfers*[2], [1]*European Institute for Molecular Imagiong, University of Muenster, Muenster, Germany;* [2]*Department of nuclear medicine, University Hospital Muenster, Muenster, Germany. Contact e-mail: vrachal@uni-muenster.de*

Background: "Man to mouse" translation of clinical protocols to measure myocardial perfusion in mouse models of human disease is important for basic biomedical research. As to SPECT approaches, different 99mTc-labelled perfusion tracers are predominantly used for clinical myocardial perfusion imaging, however, studies evaluating and adjusting protocols for these tracers in high-resolution pinhole SPECT in mice are lacking. Aim of this study is to evaluate two clinically available 99mTc-labelled myocardial perfusion tracers (MIBI vs. Tetrofosmin; TETRO) in mice using four different imaging protocols. Methods: Adult C57BL/6 male mice were injected with MIBI or TETRO (4 MBq/g body weight) either intravenously through the tail vein (n=5) or retroorbitally (n=5) or intraperitoneally (i.p.) under anesthesia (n=3) or i.p. in an awake state (n=3) at rest. Directly after injection, a multi-frame SPECT/CT acquisition was started with six subsequent time frames of 10 min each. The reconstructed images of the different protocols were assessed visually by three experts in consensus reading. Furthermore time-activity-curves were generated from regions-of-interest (ROIs) for various organs (normalized uptake index). Results: In the visual analysis, the best image quality was found for MIBI for both intravenous injection protocols. TETRO had equivalent image quality only in the case of retroorbital injections. These results were confirmed by quantitative analysis where left ventricular uptake of TETRO after tail vein injections was found to be significantly lower for all time points accompanied with a significantly higher washout of 33% for TETRO vs. 16% for MIBI (p=0.009) from 10 to 60 min p.i.. Remarkably, LV washout from 10 to 60 min p.i. was significantly higher for TETRO when applied by tail vein injections when compared to retroorbital injections (22%, p=0.008). Liver uptake was significant and comparable for both tracers at all time points. Pulmonary uptake was for both tracers minor for all time points. Conclusion: MIBI injected either through the tail vein or the retroorbital plexus results in the best image quality for purposes of myocardial perfusion of the murine heart by pinhole SPECT/CT. On the other hand, TETRO has a similar image quality only for the retroorbital injection route.

Disclosure of author financial interest or relationships:
**A. Vrachimis**, None; **S. Hermann**, None; **O. Schober**, None; **M. Schäfers**, Siemens Medical Solutions, Grant/research support .

Presentation Number **P463**
Poster Session 3
September 7, 2012 / 15:15-15:15 / Room: The Liffey

# Serial monitoring of vascular inflammation in a mouse model of shear-stress induced atherosclerosis with small animal F-18-FDG PET/CT

***Christian Wenning***[1,2], *Christopher Kloth*[1], *Sven Hermann*[1], *Michael T. Kuhlmann*[1], *Otmar Schober*[2], *Andreas H. Jacobs*[1], *Michael Schäfers*[1], [1]*European Institute for Molecular Imaging -EIMI-, University of Münster, Münster, Germany;* [2]*Department of Nuclear Medicine, University Hospital Münster, Münster, Germany. Contact e-mail: cwenning@uni-muenster.de*

Introduction: Detection of inflamed, potentially rupture-prone atherosclerotic plaques is of crucial importance. An animal model seeming suitable for exploration of rupture-prone plaques is a carotid artery cuff-model (surgical placement of a predefined cuff around the common carotid artery) in ApoE-/- mice under a cholesterol-rich diet, which leads to accelerated shear-stress-induced atherosclerosis with characteristics of inflamed, instable plaques upstream and more stable plaques downstream the cuff [1]. This project analyses the inflammatory status of carotid artery plaques with serial F-18-FDG PET/CT in the left and right common carotid artery. Methods: ApoE-/- mice (n=27, age 4 weeks) were fed with a cholesterol-rich diet. After 4 weeks on diet a cuff of predefined size was placed around the left (n=16) or right (n=11) common carotid artery, leading to a defined conical vessel stenosis. This, in turn, modulates local endothelial shear stress, which induces the development of plaques with different patterns of atherosclerosis as described [1]. 4, 6 and 8 weeks after surgery F-18-FDG PET/CT (quadHIDAC-PET, Oxford Positron Systems Ltd, UK, fused with Inveon-CT, Siemens Medical Solutions, USA) was performed. Local F-18-FDG uptake was quantified by volumes of interest (VOIs) which were CT-based placed upstream (US) und downstream (DS) of the cuff as well as on the contralateral carotid artery. Regional F-18-FDG uptake was divided by the contralateral carotid artery uptake subsequently. 8 weeks after surgery the carotid arteries were explanted and processed for histological analysis (HE and Mac-3 staining). Results: 4 and 6 weeks after surgery the regions US and DS of the cuff showed no or only a mildly increased F-18-FDG uptake in comparison to the contralateral carotid artery (cuff on left side 4 weeks: US=1.13±0.14 vs. DS=1.05±0.19, 6 weeks: US=1.16±0.23 vs. DS=1.03±0.26 and cuff on right side 4 weeks: US=1.25±0.27 vs. DS=1.21±0.27, 6 weeks: US=1.00±0.26 vs. DS=1.02±0.19; all p=ns). Interestingly, there was a distinctly increased uptake in the US-plaques of the right carotid artery but only a mildly increased uptake in the US-plaques of the left carotid artery. DS-plaques did not show an increased uptake regardless of the side of cuff implantation (left side: US=1.10±0.26 vs. DS=1.05±0.32, p=ns; right side: US=1.30±0.36 vs. DS=1.01±0.19, p=0.03). Overall, there was a correlation between F-18-FDG uptake and the presence of macrophages in the plaques. Conclusions: High-resolution F-18-FDG-PET/CT is able to identify inflamed atherosclerotic plaques and distinguish them from non-inflamed plaques in the carotid artery cuff-model. Nevertheless, there seem to be differences in the extent of plaque inflammation subject to the cuff placement side (left vs. right carotid artery). This might reflect different pathophysiological characteristics of plaque development possibly due to different patterns of blood flow. References: 1. Cheng et al. Atherosclerotic lesion size and vulnerability are determined by patterns of fluid shear stress. Circulation. 2006;113:2744-2753

Disclosure of author financial interest or relationships:
**C. Wenning**, None; **C. Kloth**, None; **S. Hermann**, None; **M.T. Kuhlmann**, None; **O. Schober**, None; **A.H. Jacobs**, Merck, Germany, Grant/research support; **M. Schäfers**, Siemens Medical Solutions, Grant/research support .

Presentation Number **P464**
Poster Session 3
September 7, 2012 / 15:15-15:15 / Room: The Liffey

# Novel F-18 Ammonium Salt Derivative as a Biomarker for PET Imaging of Myocardial Perfusion

***Shimon Yitshak***, *Orit Jacobson Weiss, Galith Abourbeh, Eyal Mishani, Hadassah University Hospital, Jerusalem, Israel. Contact e-mail: shimi777@gmail.com*

Coronary artery disease (CAD) is one of the most common causes of death in the Western world. During the last two decades, Positron Emission Tomography (PET) imaging has become more accessible for assessment of ischemia, even in early stages. However, due to lack of a suitable PET tracer, most myocardial perfusion imaging (MPI) scans are performed with Single Photon Emission Computed tomography (SPECT) tracers, which have lower imaging properties. Previously, our group developed several C-11 ammonium salt tracers for MPI. The structure activity relationship suggests that both lipophilicity and charge density affect the performance of these compounds as MPI probes. The lead compound, Dimethyl-diphenyl-ammonium (DMDPA) had relatively high uptake in the myocardium. However, the short half-life of C-11 might limit its clinical use in the future. Aims: This study aims to develop a stable F-18 labeled MPI agent, based on DMDPA, which will enable clear visualization of the myocardium at longer time points and be more available for future clinical use. Methods: Fluoro-Butyl-diphenylamine (FBMDPA) was successfully synthesized and labeled with F-18. The precursor for the labeling consists of the diphenylamine group and a butyl chain which contains Iodine as a leaving group (IBDPA). 18F-FBMDPA was labeled in two steps: a nucleophilic displacement of the aliphatic Iodine group followed by methylation of the tertiary amine using methyl triflate and purification by reversed-phase HPLC. This synthesis was converted into a fully automated module. Stability and blood stability tests along with dynamic micro PET/CT imaging studies of 18F-FBMDPA were carried out. Results & Discussion: FBMDPA was labeled with fluoride-18 with an overall radiochemical yield (decay corrected) of 5±1% based on 18F activity at start of synthesis. Nucleophilic displacement of iodine was achieved in 60% yield, however, methylation to form the quaternary amine was challenging due a steric interference of the molecule. Yet, the methylation was successful with methyl triflate. 18F-BMDPA was obtained in a radiochemical purity of >99% and a specific activity of 3600±1200 Ci/mmol. PET imaging showed that 18F-BMDPA had a steady retention in the myocardium during a 60 min scan (SUV of 2.53±0.2, n=3, Figure 1). Defluorination was not detected in-vitro and in-vivo. 18F-BMDPA was also accumulating in metabolic organs such as liver, intestine and kidneys. Conclusions: We successfully labeled the MPI agent18F-BMDPA. 18F-BMDPA proved to be stable and accumulated in the myocardium, however, its relative high uptake in the liver due to mitochondrial uptake or metabolic processing, would restrict its utility. More hydrophilic imaging agents can be developed and may improve the image quality.

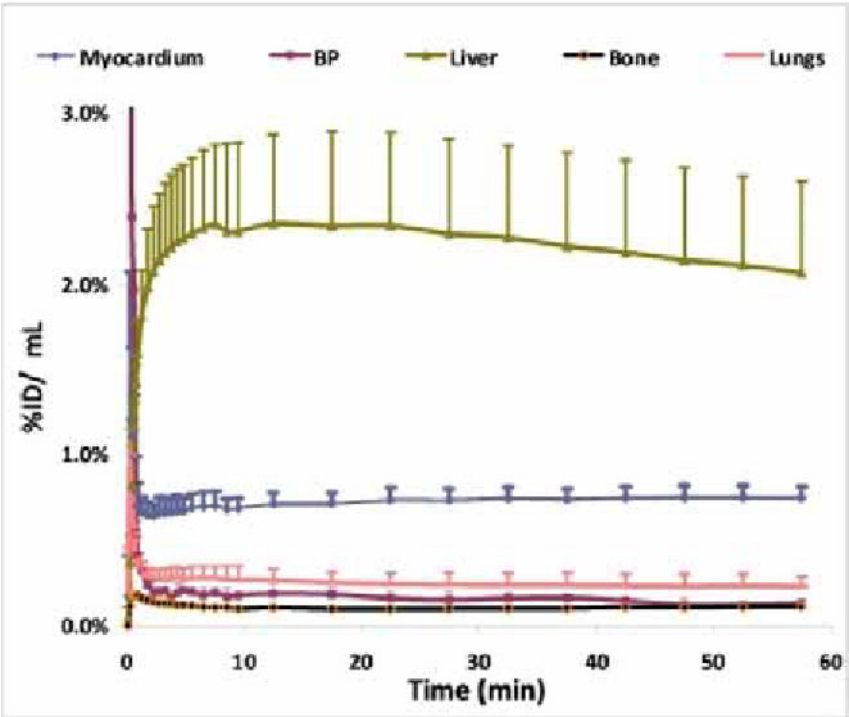


Figure 1. Time activity curve of 18F-FBMDPA.

Disclosure of author financial interest or relationships:
**S. Yitshak**, None; **O. Jacobson Weiss**, None; **G. Abourbeh**, None; **E. Mishani**, None.

Presentation Number **P465**
Poster Session 3
September 7, 2012 / 15:15-15:15 / Room: The Liffey

# Manganese-enhanced MRI tracks declining pancreatic insulin content and beta cell mass in a mouse model of type 1 diabetes

***Patrick Antkowiak***[1], *Brian K. Stevens*[2], *Marcia McDuffie*[2], *Frederick Epstein*[1,3], [1]*Biomedical Engineering, University of Virginia, Charlottesville, VA, USA;* [2]*Microbiology, University of Virginia, Charlottesville, VA, USA;* [3]*Radiology, University of Virginia, Charlottesville, VA, USA. Contact e-mail: pfa7p@virginia.edu*

Introduction: Type 1 diabetes (T1D) is characterized by an inability to maintain blood glucose homeostasis, and it occurs due to the autoimmune destruction of the insulin-producing pancreatic β cells. There is no current gold standard method for noninvasively detecting changes in functional β cell mass (BCM). Mn2+-enhanced MRI (MEMRI) may represent an attractive solution, as Mn2+ has been shown to enter β cells through glucose-stimulated voltage-gated calcium channels, and Mn2+ increases the nuclear magnetic resonance longitudinal relaxation rate R1. We have previously used MEMRI to detect a gross loss of BCM in mice but have not determined the ability to detect the small gradations in functional BCM that occur during T1D progression. Purpose: Our purpose was to test the hypothesis that measurements of the Mn2+-enhanced pancreatic relaxation rate R1 would reflect decreases in functional BCM, with pancreatic insulin as a gold standard measure of BCM. We applied Mn2+-enhanced R1 mapping of the pancreas to cytoxan (Cy)-accelerated BDC2.5 T-cell receptor transgenic mice on a non-obese diabetic (NOD) background, a T1D model that predictably progresses toward T1D within 8 days after Cy injection. Methods: We performed MEMRI in n=26 Cy-accelerated NOD-BDC2.5 transgenic mice (Tg+) and in n=24 of their transgene-negative (Tg-) littermates who do not develop T1D during this time. To initiate T1D progression, 200 mg/kg Cy was injected i.p. Imaging was performed before Cy injection (day 0) and on days 3-7 after Cy injection on a 7T Bruker Clinscan MRI system. Mice were injected with glucose to stimulate β-cell Ca2+ channels and MnCl2 to label β cells. R1 mapping MRI was performed 1 hour after glucose+MnCl2 injection to quantify pancreatic R1. After MRI, mice were sacrificed for pancreatic insulin content measurement via insulin ELISA. Results: Mn2+-enhanced pancreatic R1 is shown in Figure A for mice on days 0 and 3-7. Pancreatic R1 remained constant in Tg- mice after Cy injection and decreased progressively in Tg+ mice, mirroring their T1D progression and loss of BCM confirmed by pancreatic insulin (Figure B). Differences were observed in same-day Tg+ mice vs. Tg- mice for all days except day 0 (*p < .01). Pancreatic R1 and insulin in day 0 Tg+ mice were different from Tg+ mice on all other experimental days (#p <.05), and R1 in day 3 Tg+ mice was significantly different from day 7 Tg+ mice (&p < .05). Mn2+-enhanced pancreatic R1 correlated well with pancreatic insulin, with R2=0.76 (Figure C). Discussion: The constant pancreatic R1 in Tg- mice after Cy injection was indicative of their retained functional BCM, while the incrementally decreasing pancreatic R1 in Tg+ mice reflected their declining BCM during that time. Mn2+-enhanced R1 reflected pancreatic insulin content. These results support the hypothesis that Mn2+-enhanced pancreatic R1 mapping MRI can detect decreases in functional BCM that occur during the progression of T1D. Future work will investigate the use of approved Mn2+-based contrast agents for potential human translation Funding: American Diabetes Association Basic Science Award 7-09-BS-52.

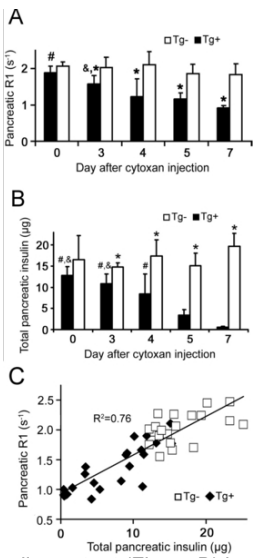


Mn2+-enhanced pancreatic R1 (Figure A) and pancreatic insulin content (Figure B) in cytoxan-acclerated NOD-BDC2.5 mice. Figure C: correlation between Mn2+-enhanced pancreatic R1 and pancreatic insulin content.

Disclosure of author financial interest or relationships:
**P. Antkowiak**, None; **B.K. Stevens**, None; **M. McDuffie**, None; **F. Epstein**, Siemens, Grant/research support .

Presentation Number **P466**
Poster Session 3
September 7, 2012 / 15:15-15:15 / Room: The Liffey

# Longitudinal MR imaging of pancreatic islets using magentoliposomes

***Ashwini Atre***[1], *Ting Yin*[1], *Karim Louchami*[2], *Sonu Sharma*[1], *Michel Hodenius*[3], *Willy Malaisse*[2], *Uwe Himmelreich*[1], [1]*Department of Diagnostic and Pathology, KU Leuven, Leuven, Belgium;* [2]*Laboratoire d'Hormonologie Expérimentale, CP 626, Université Libre de Bruxelles, Bruxelles, Belgium;* [3]*Lab of BioNano Colloids, KU Leuven, Kortrijk, Belgium. Contact e-mail: ashwini.atre@med.kuleuven.be*

Introduction: Diabetes Mellitus (DM) is one the endocrine metabolic diseases resulting from decline in the insulin secretion or β cell function. Pancreatic Islets (PIs) have been transplanted in the liver and the fate of PIs was monitored using magnetic resonance imaging (MRI); wherein, islets were labeled with commercially available contrast agents [1]. Studies so far indicate that longer incubation durations were needed to achieve adequate PI labeling for in vivo imaging [1, 2]. It is necessary to find suitable particles which are bio-compatible and are more rapid for efficient PI labeling to avoid adverse effects on PI function. It was shown for stem cell labeling that cationic magnetoliposomes (MLs) are taken up without any toxic long term effects [2]. In the first part of this study, we have established a labeling protocol for an insulinoma cell line and freshly isolated PIs using cationic MLs. Based on the labeling concentration, islet transplantations were done in order validate long-time MRI detectability in vivo. Materials and Methods: INS -1 cells: Insulinoma (INS-1) cells were labeled with Resovist, Endorem (+/- PLL) and cationic MLs at different concentration (50, 100, 200µg Fe/ml for 4, 24,). MLs were synthesized as described in [2]. Pancreatic Islets: Pancreatic islets were isolated from female, Sprague Dawley rats (175 -299 gm). Collagenase induced digestion was done and islets were handpicked and counted. In both cell types, labeled samples were collected for high resolution MR scanning, viability testing, electron microscopy and prussian blue staining and ICP-MS for iron quantification. Functional assays like insulin secretion and response to glucose were performed. In vivo experiments: In order to check if the in vitro optimized labeling conditions result in sufficient in vivo MRI detectability, healthy rats received freshly isolated islets, labeled with magnetoliposomes. Labeled islets were transplanted in the kidney capsule and followed with MRI longitudinally. Results INS-1 labeled with different labeling conditions showed varying uptake with different particles. INS-1 resulted in a 100% labeling efficiency after a 24hrs exposure. Resovist labeled at 200µg Fe/ml, Endorem +PLL at 50 µg Fe/ml and Cationic MLs at 100µg Fe/ml resulted in efficient labling after 4hrs. No particle showed detectable toxic effects post labeling. In contrast, efficient labeling (> 90%) for freshly isolated PIs, was only achieved after 72 hrs of co-incubation with most of the tested particles. Only cationic MLs showed very good uptake after 24hrs with low iron concentrations of 50 µg Fe/ml. PI function was not affected under those conditions. Longitudinal detection of ML labeled cells and PIs was possible in vivo in rats with high resolution 3D T2* w MRI. Conclusion: Cationic MLs are safe contrast agents for longitudinal and reproducible in vivo visualization of engrafted pancreatic islets in rodent models. Reference: 1) Kriz J., et. al. Tranplantation, 2005; 2)Kim H. et.al. NMR in Biomedicine 2009; 3) Soenen S., et.al. ChemBioChem 2009

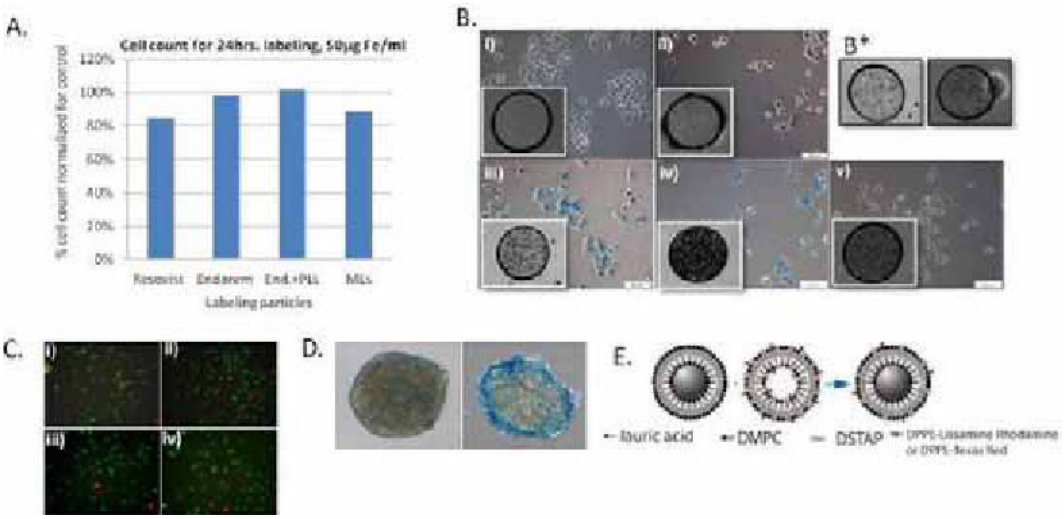


(A). INS-1 cells were labeled with different NPs. And counted post labeling. (B). Prussian Blue staining for different conditions, inset showing respective 3D T2* w images, i) Non labeled cells , ii) Resovist 200µg Fe/ml, iii) Endorem +PLL, 4hrs, iv) Endorem, 24hrs. , v) Cationic MLs, 50µg Fe/ml, 4hrs.; B*) label dilution after2nd passage for Endorem +PLL and MLs (C). Qualitative viability staining (Green: viable cells; red: Dead Cells); labeled for 24hrs., for 50µg Fe/ml i) Endorem, ii) Endorem +PLL, iii) MLs, iv) Resovist (D). Islets labeled for different labeling conditions ; i) Resovist, 48hrs. ii) Cationic MLs, 24hrs. (E) layout of Cationic MLs

Disclosure of author financial interest or relationships:
**A. Atre**, None; **T. Yin**, None; **K. Louchami**, None; **S. Sharma**, None; **M. Hodenius**, None; **W. Malaisse**, None; **U. Himmelreich**, None.

Presentation Number **P467**
Poster Session 3
September 7, 2012 / 15:15-15:15 / Room: The Liffey

# Evaluation of 18F-FDG uptake in the brain in the fasting and glucose stimulated state in a rat model of obesity and its lean counterpart

***Antonietta Bartoli***[1], *Maria Angela Guzzardi*[1], *Letizia Guiducci*[1], *Silvia Burchielli*[2], *Piero A. Salvadori*[1], *Patricia Iozzo*[1], [1]*Institute of Clinical Physiology, National Research Council (CNR), Pisa, Italy;* [2]*Fondazione Toscana Gabriele Monasterio, Pisa, Italy. Contact e-mail: bartoli@df.unipi.it*

Background and aim Obesity plays a central role in the insulin resistance syndrome, which includes hyperinsulinemia, hypertension, hyperlipidemia, type 2 diabetes mellitus, and an increased risk of atherosclerotic cardiovascular disease [Steinberger et al, Circulation 2003]. Obesity and its complications are associated with an increased prevalence of neurodegenerative diseases. The aim of this study is to investigate the correlation between obesity and cerebral 18F-FDG uptake under fasting conditions and in response to hyperglycemia in adult obese and lean rats. Materials and Methods Twenty genetically obese Zucker rats (fa/fa) and their lean counterpart (fa/+) were studied (10-13 weeks old). Each group was subdivided in two subgroups (n=10): the fasting (F) and the hyperglycemic (H) one. The animals of the F group were fasted for 12 h, while in the H group an acute hyperglycemia status was induced by an i.p. injection of glucose (2g/kg). All the animals underwent PET scan with a dedicated small animal scanner, YAP-(S)PET II developed by the Dept. of Physics of the Pisa University. On the day of the study, the animals were anaesthetized with i.p. injection of Zoletil (40 mg/kg) and Xylazine (10 mg/kg), venous catheters were placed in the femoral vein and anaesthesia maintained by isofluorane at 2%. Approximately 37 MBq of 18F-FDG were injected via the femoral vein and a static PET scan of 20 min was performed after 45 min of uptake. The images were reconstructed with an EM algorithm with 20 iterations. Blood glucose levels were measured prior to tracer administration and every 5 minutes during the uptake time by blood sampling from tail vein. Regions of Interest were manually drawn on the transaxial section of the rats brain and the standard uptake value (SUV) was used to evaluate the 18F-FDG accumulation. To estimate glucose uptake, thus discounting for the competitive effect of hyperglycemia on 18F-FDG uptake, SUVs were normalized to a standard glucose concentration as proposed by the EANM procedure guidelines: SUVnorm= SUV * glucoseplasma (mmol/L)/5(mmol/L). Normalized SUVs of obese and lean rats were compared in both fasting and acute hyperglycemia conditions using ANOVA. Results Lean fasted rats had an average plasma glucose level of 6.5 mmol/l, while in the lean H group the plasma glucose level was threefold. In obese animals, the plasma glucose level in fasting conditions was close to the value of the lean H group (around 17.4 mmol/l) and about 1.5 times higher in hyperglycemic subgroup. SUV values were greater in the lean F animals than in the other groups. After correcting for the competitive action of hyperglycemia, a progressive increase in normalized SUVs was observed with lowest values in the lean F group, followed by the lean H ($p=0.07$ vs F), the obese F ($p<0.005$ vs lean F), and the obese H subgroup ($p<0.0001$ vs lean F, $p=0.0008$ vs lean H, and $p<0.04$ vs obese F). Conclusions The brain glucose uptake of obese rats is higher than that of lean ones, even in the fasting state. This indicates a constant brain exposure to an higher load of endogenous glucose. Nevertheless, in obese animals a response to glucose load is still present.

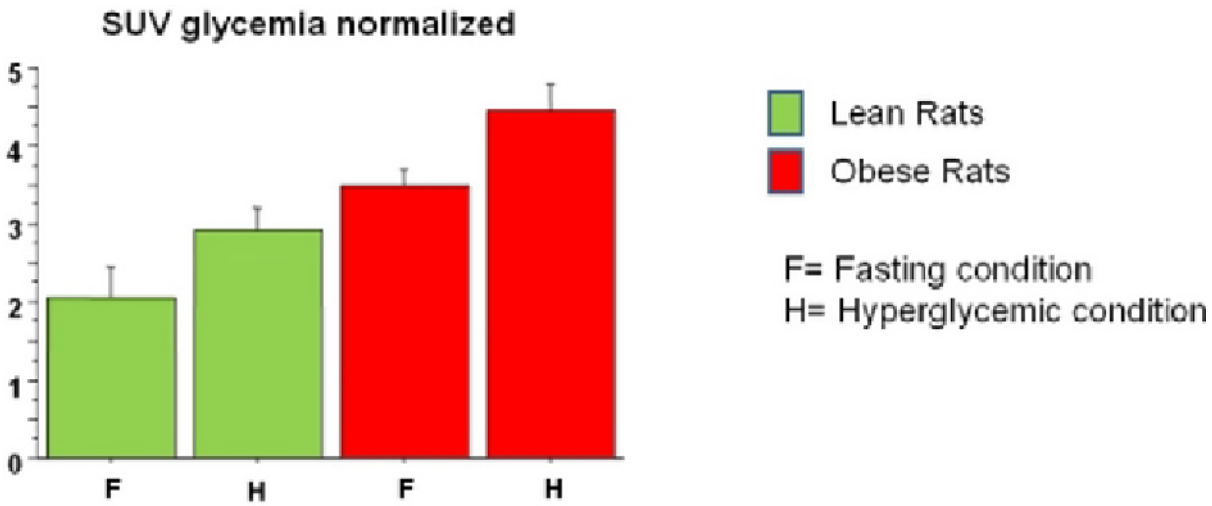


Mean normalized SUVs of obese and lean rats in both fasting and acute hyperglycemia conditions.

Disclosure of author financial interest or relationships:
**A. Bartoli**, None; **M. Guzzardi**, None; **L. Guiducci**, None; **S. Burchielli**, None; **P.A. Salvadori**, None; **P. Iozzo**, None.

Presentation Number **P468**
Poster Session 3
September 7, 2012 / 15:15-15:15 / Room: The Liffey

# Multimodality noninvasive imaging of the functional beta-cell mass using various formats of the beta-cell surface specific monoclonal autoantibody IC2

***Carl-Henrik Brogren***[1,5], *Ida D. Pedersen*[1], *Kathrine L. Jensen*[1], *Arnaud Briat*[2], *Laurence Renaut*[3], *Philippe Mondon*[3], *Wilma Petersen*[4], *Srirang Manohar*[4], *Karsten Buschard*[1], *Daniel Christiaen*[2], [1]*The Bartholin Institute, Copenhagen Biocenter, Copenhagen, Denmark;* [2]*Animascope, Grenoble-Geneve, France;* [3]*Millegen, Labege, France;* [4]*Institute for Biomedical Technology, University of Twente, Enschede, Netherlands;* [5]*Dept Biomedical Sciences, University of Copenhagen, Copenhagen N, Denmark. Contact e-mail: henrik@brogren.dk*

Background and aims: For more than a decade multiple tracers have been investigated for quantitative and specific in vivo imaging of beta-cell mass (BCM). However, each of these approaches has been limited, with the possible exception of the monoclonal autoantibody IC2 which has shown sufficient specificity and affinity ofr beta cell mass and function . This rat monoclonal IgM antibody was raised in a newly diabetic BB-rat and has been shown to have a unique specificity for the surface of insulin secreting pancreatic β-cells. As an IgM, this tracer molecule has a long circulation time resulting in poor signal to noise ratios in imaging studies, so attempts have been made to use the pepsin fragments F(ab')2 and Fab, or recombinant and chimeric forms of the antibody. These smaller fragments, ranging from 50-150 kDa, should have improved in vivo clearance kinetics for imaging. The pancreas is high vascularized, and the vasculature of the inflamed pancreas is leaky, enabling delivery of a wide variety of tracers to target islets. Materials and methods: First fully noninvasive imaging trials were done on rats with a 2-head SPECT and 111In-labelled IC2 as tracer., which were followed by biodistribution studies in both rats and mice using 125I Iodogen-labeled IC2-IgM, F(ab')2, and Fab. The control monoclonal antibodies included K14D10, A2B5, and a rat isotype IgM control. Gaussia luciferase-IC2-diabody conjugates have been previously been reported for use as bioluminescence imaging agent in mice. The third modality in progress applies gold nanorods labeled with IC2 in animal photoacoustic imaging, and the fourth modality is near-infrared fluorescence-mediated tomography using Vivotag-680 and VivoTag-750 labeled pepsin fragments of F(ab')2 and Fab plus a newly engineered recombinant chimeric rIC2-hIgG1 format applied in mice BCM imaging. Results: The pancreatic targeting and beta cell specificity was further demonstrated in biodistribution studies in rats and mice using radioiodinated IC2, F(ab')2 and Fab fragments. We have recently developed NIR dye labeled versions of IC2 for noninvasive imaging. Fluorescence-mediated tomography (FMT-NIR) of these IC2-derived agents confirmed unique specificity for functional beta-cells. We will further verify this in preclinical trials using a 4-head NanoSPECT-CT and will continue to explore our new chimeric rIC2-hIgG1 and diabody formats. Conclusion: IC2 fragments or chimeric engineered derivatives offer the appropriate size and retension of beta cell specificity such that they may have utility in clinical noninvasive imaging of functional BCM. The ultimate goal is a clinical method for early diagnosis and use as an outcome measure to follow the effects of beta-cell growth promoting drugs, stem-cell therapy and islet transplantation. Supported by: JDRF International, EU-Fasilis Program, The Danish Diabetes Society, BioCampus Research Priority Area - Univ. Copenhagen, and ImmunoSigns ApS.

Disclosure of author financial interest or relationships:
**C. Brogren**, None; **I.D. Pedersen**, None; **K.L. Jensen**, None; **A. Briat**, None; **L. Renaut**, None; **P. Mondon**, Millegen SA, Employment; **W. Petersen**, None; **S. Manohar**, PA Imaging BV, Stockholder; **K. Buschard**, None; **D. Christiaen**, None.

Presentation Number **P469**
Poster Session 3
September 7, 2012 / 15:15-15:15 / Room: The Liffey

# Measuring Glucose Metabolism in Rodent Skeletal Muscles by [18F]-FDG PET/CT Imaging as a Translational Biomarker for Type II Diabetes Research

***Laigao Chen**, Kyle Kuszpit, Aijun Zhu, Kenneth Zasadny, Declan Flynn, Thomas Bocan, Worldwide Research & Development, Pfizer Inc., Groton, CT, USA. Contact e-mail: laigao.chen@pfizer.com*

INTRODUCTION Type II diabetes is characterized by insulin resistance in target tissues such as skeletal muscle and adipocytes which means that insulin mediated glucose uptake into these tissues is compromised. The ability to measure changes in glucose uptake in a longitudinal manner in rat models would provide a translational biomarker to validate the mechanism of action for regulating skeletal muscle glucose uptake for multiple research programs including AMP-activated protein kinase (AMPK). In this study, we aim to test the feasibility by applying [18F]-FDG PET/CT imaging to measure the effect of insulin (1 unit/kg, I.P.) and AICAR (5-aminoimidazole-4carboxamide ribonucleoside, 300 mg/kg, S.C.) on glucose uptake in skeletal muscles in rats. AICAR is a cell permeable analog of AMP, thus making it a useful tool to probe for AMPK activation in muscle beds, while insulin serves as a positive control. METHODS This study used twelve male SD rats (12 weeks) that were evenly segregated into three treatment groups: vehicle, AICAR and insulin. Rats were fasted overnight to achieve consistent baseline plasma glucose level. Fifteen minutes post compound dosing, rats were anesthetized with isoflurane and injected i.v. with [18F]-FDG (~1.5 mCi/rat). Rats were then allowed to wake in their home cages during a 60 minute tracer uptake phase. They were anesthetized again with isoflurane and scanned at the hind limb region using a Focus 220 PET scanner for 10 minutes and then transferred to an eXplore Locus MicroCT scanner for a 10 minute CT scan. Rats were then sacrificed using CO2 and tissue samples (blood, liver, heart and multiple skeletal muscle beds) were collected and counted for radioactivity using a gamma counter. To quantify the [18F]-FDG uptake on images, the PET image of each rat was coregistered onto its own CT image and regions of interest (ROIs) around multiple skeletal muscles were manually drawn on PET/CT fused images. The mean Standard Uptake Values (SUV) within the ROI of each muscle was calculated. RESULTS Both AICAR and insulin increased glucose uptake within various skeletal muscle beds in the lower limb in rats. Rats treated with AICAR had statistically significant increases in [18F]-FDG uptake in tibialis anterior , gastrocnemius, extensor digitorum longus (EDL) , soleus muscles when compared to the vehicle group. Rats treated with insulin had statistically significant increases in [18F]-FDG uptake in tibialis anterior, quadriceps, EDL, soleus and flexor digitorum superficialis (FDS) muscles when compared to the vehicle group. The largest elevation of [18F]-FDG uptake was seen at EDL for both AICAR and insulin (4-5 fold increase). Insulin had a stronger effect than AICAR on elevating [18F]-FDG uptake at tibialis anterior, soleus and FDS. Insulin had no effect on gastrocnemius while AICAR did show an increase. Insulin markedly increased cardiac glucose uptake while AICAR did not have significant effect in the heart. CONCLUSION We conclude that [18F]-FDG PET/CT imaging is a viable translational biomarker for glucose uptake in skeletal muscles for developing type II diabetes drug treatments that address insulin resistance.

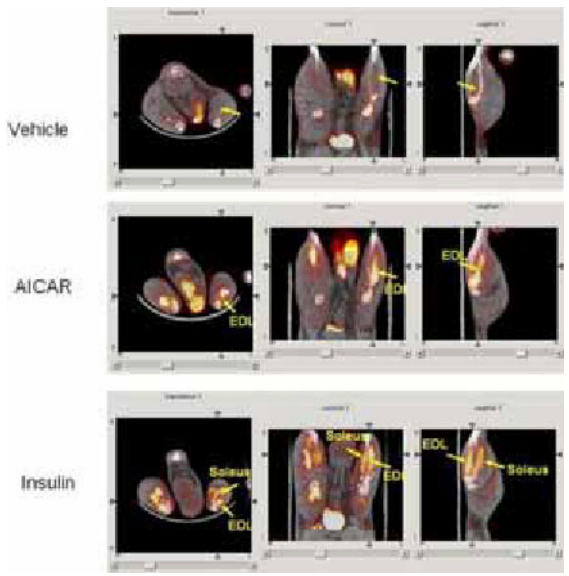


[18F]-FDG uptake in rat skeletal muscles by the three treatment groups on representative PET/CT fused images.

Disclosure of author financial interest or relationships:
**L. Chen**, Pfizer Inc., Employment; Pfizer Inc., Stockholder; **K. Kuszpit**, Pfizer, Inc., Employment; **A. Zhu**, Pfizer Inc., Employment; **K. Zasadny**, Pfizer, Employment; **D. Flynn**, Pfizer, Employment; **T. Bocan**, Pfizer, Employment; Pfizer, Stockholder .

Presentation Number **P470**
Poster Session 3
September 7, 2012 / 15:15-15:15 / Room: The Liffey

# A MicroPET Study of Brown Adipose Tissue Uptake of 18F-FDG in Obesity and diabetic Mouse Models with sodiumlevothyroxine interference

***Wuying Cheng***, *Chenxi Wu, Zhaohui Zhu, Yonghong Dang, Yi Sun, Fang Li, PET center,Peking Union Medical College Hospital, Beijing, China. Contact e-mail: cwypumch@126.com*

Objective: Obesity and diabetes threaten human being's health severely. Recent study has revealed that brown adipose tissue(BAT)may be a promising solution for treating obesity and diabetes by burning energy for thermogenesis. This study aimed to investigate the 18F-FDG uptake in BAT of obesity and diabetic mouse models with Euthyrox(sodiumlevothyroxine) interference. Methods: Thirty-four "Inprinting Control Region" (ICR) mice (4 weeks old) were randomly divided into 6 groups: Group A(n=5) and B(n=6) were bred with the normal food, and group C(n=5),D(n=6),E(n=6),F(n=6) were all bred with special high-fat food. Group E and F were additionally treated with intraperitoneal injection of streptozocin (70mg/kg,) for 3 days in the 3rd week to develop diabetes model. Since the 10th week.Group B,D,F were treated with Euthyrox(33μg/kg) via gastrogavage daily since the 10th week. A microPET scan was underwent 60 minutes after intraperitoneal injection of 3.7 MBq 18F-FDG using a Siemens Inveon system. The standardized uptake value (SUV) of BAT at the shoulder region was measured, and the ratio to SUV of liver (L) of each mouse was used to comapare the BAT uptake among different groups. Weight and blood glucose level in all groups were measure at the end of 11st week. Results: 1.The weight of group C and D were significantly higher than that of the control group ($P<0.05$), while the ratio of BAT uptake of FDG to that of liver in group C decreased dramatically compared with group A(2.24±0.80 vs 4.78±1.64,$P<0.05$). Euthyrox could effectively improve the BAT uptake of FDG in obesity mice( group D=4.18±1.37)compared with group C($P<0.05$).There was no significant difference of BAT uptake among group A,B, and D. 2.The blood glucose level of group E was much higher than that of group A($P<0.05$),while the BAT uptake of FDG in group E was significant lower that that of group A(1.40±0.37 vs 4.78±1.64,$P<0.05$).However, neither BAT uptake of FDG nor blood glucose level was improved after Euthyrox interference in group F. Conclusion: BAT uptake of FDG was dramatically decreased in both obesity and diabetic mice. Euthyrox helps to activate BAT in obesity mice.However, it seems that Euthyrox has no effect for BAT uptake and blood glucose in diabetic mice.

Disclosure of author financial interest or relationships:
**W. Cheng**, None; **C. Wu**, None; **Z. Zhu**, None; **Y. Dang**, None; **Y. Sun**, None; **F. Li**, None.

Presentation Number **P471**
Poster Session 3
September 7, 2012 / 15:15-15:15 / Room: The Liffey

# Designing GLP-1-based Peptides for SPECT, PET and Fluorescence Imaging of Beta Cell Mass in the Intact Pancreas

***Savita Dhanvantari***[1,3], *Babak Behnam Azad*[2], *Vanessa A. Rota*[3], *Rebecca M. McGirr*[1], *Ting-Yim Lee*[1,3], *Leonard G. Luyt*[2,4], [1]*Lawson Health Research Institute, London, ON, Canada;* [2]*Chemistry, Western University, London, ON, Canada;* [3]*Medical Biophysics, Western University, London, ON, Canada;* [4]*London Regional Cancer Program, London, ON, Canada. Contact e-mail: sdhanvan@lawsonimaging.ca*

The glucagon-like peptide-1 receptor (GLP-1R) is expressed on pancreatic beta cells, and mediates glucose-dependent insulin secretion by GLP-1. Our group has generated 111In- and 68Ga-labelled serum-stable analogs of GLP-1 to image changes in beta cell mass during the development of Type 1 diabetes. We have previously shown that the native structure of GLP-1 (7-37) can be modified in several ways to generate a clinically useful beta cell SPECT imaging probe by: 1) improving serum stability to a half-life of 13h by substituting L-Ala8 to D-Ala8; 2) derivatization of Gly22 for DOTA side-chain conjugation via a short PEG linker; and 3) derivatization of Gly37 for DOTA conjugation with or without the PEG linker (Behnam Azad et al, Bioorg Med Chem 2010). Biodistribution and ex vivo gamma camera imaging showed significant and specific uptake of [111In]Lys37-DOTA-GLP-1 in the pancreas (1.3±0.1% ID/g tissue, reduced to 0% in the presence of unlabelled GLP-1, $p<0.01$). However, SPECT imaging showed uptake only in the kidneys with no signal visible from the pancreas. We then investigated the use of [68Ga]Lys37-DOTA-GLP-1 for PET imaging, as PET is more sensitive and quantitative than SPECT. The 68Ga-labelled probe also showed specific uptake in the pancreas of C57BL/6 mice, as indicated by biodistribution analysis 4h after injection (2±0.5% ID/g tissue vs 0.5±0.2% when blocked by excess exendin-4, $p<0.05$), and showed significant accumulation in vivo in INS-1 cell tumors in Balb/c nu/nu mice. Again, however, the intact pancreas could not be detected in vivo due to signal accumulation in the kidneys. In order to investigate GLP-1R distribution in the mouse pancreas, we generated and characterized Lys37-fluorescein-GLP-1. The fluorescent GLP-1 analog bound GLP-1R with good affinity (IC50=92 nM) and bound in an exendin-4-displaceable manner to GLP-1-positive cells in sections of pancreatic tissue. Immunohistochemical analyses with Lys37-fluorescein-GLP-1 showed high levels of GLP-1R expression in both beta and alpha cells of the islet, as well as ductal cells, and low levels of expression in the exocrine pancreas. These results indicate that GLP-1R expression is not restricted to beta cells, and PET imaging may potentially overestimate beta cell mass. To reduce the renal accumulation of [68Ga]Lys37-DOTA-GLP-1, we reduced its overall positive charge through acetylation of Lys26 and Lys34 and replacement of Arg36 with Gly36. Dynamic PET scanning after injection into C57BL/6 mice revealed reduced renal accumulation of the probe, but the pancreas again could not be visualized. Attempts to separate the tissues using the 2-compartment Logan analysis method did not result in detection of a pancreatic PET signal. We conclude that developing GLP-1-based SPECT or PET probes for imaging intact beta cell mass is not feasible, given the high renal accumulation of radiolabelled analogs, the low abundance of beta cells in the pancreas, and the expression of GLP-1R in both beta and non-beta cells of the pancreas. Such probes, however, may be useful for the in vivo imaging of GLP-1R-positive insulinomas, or perhaps islet transplants.

Disclosure of author financial interest or relationships:
**S. Dhanvantari**, None; **B. Behnam Azad**, None; **V.A. Rota**, None; **R.M. McGirr**, None; **T. Lee**, GE Healthcare, Grant/research support; GE Healthcare, Other financial or material support; **L.G. Luyt**, None.

Presentation Number **P472**
Poster Session 3
September 7, 2012 / 15:15-15:15 / Room: The Liffey

# On the use of L-DOPA as an imaging biomarker for transplanted islet mass

***Olof Eriksson***[1], *Akiva Mintz*[2], *Ali Naji*[2], *Abass Alavi*[2], [1]*Preclinical PET Platform , dept of Medicinal Chemistry, Uppsala University, Uppsala, Sweden;* [2]*Perelman School of Medicine, University of Pennsylvania, Philadelphia, PA, USA. Contact e-mail: olof.eriksson@pet.medchem.uu.se*

Background: Non-invasive methodologies for monitoring the islet graft would greatly enhance the possibilities of developing islet transplantation as a permanent cure for T1D. The endocrine pancreas share many properties with the central nervous system, especially the monoamine signaling pathways. Therefore, clinically established PET tracers such as [18F]L-DOPA are prime candidates for imaging of transplanted islet mass. Method: Sections of subcutaneous human islet grafts explanted from mice and isolated human islets were stained for insulin and DDC to demonstrate expression of the L-DOPA decarboxylation mechanism in islets. Freshly isolated human islets and an insulinoma cell line (βCT3) was incubated with [18F]L-DOPA alone or in the presence of DDC or COMT inhibitors to investigate if the cellular uptake was mediated by enzymes involved in dopamine metabolism. SCID mice, transplanted with long-term subcutaneous human islet graft, were administered [18F]L-DOPA and examined by μPET. Results: Confocal microscopy confirmed co-localisation of DDC and insulin in human islets. DDC-positivity was confirmed in transplanted human islets by IHC. Uptake of [18F]L-DOPA in islet or insulinoma cells were decreased by >80% by co-incubation of DDC inhibitor carbidopa, and increased 2-fold by inhibition of COMT, one of the main cathecholamine routes for degradation. Viability and function of subcutaneously transplanted islet cells in SCID mice was confirmed by curing STZ-induced T1D and explantation of the graft induced recurrence of hyperglycemia. Whole body [18F]L-DOPA images of euglycemic mice demonstrated irregular distribution of radiotracer uptake at the site of the grafted islet cells in the abdominal wall. Conclusion: Based on the in vitro and in vivo evidence presented here, we are proposing to further validate FDOPA-PET as a sensitive imaging modality for imaging extrahepatically transplanted islets.

Disclosure of author financial interest or relationships:
**O. Eriksson**, None; **A. Mintz**, None; **A. Naji**, None; **A. Alavi**, None.

Presentation Number **P473**
Poster Session 3
September 7, 2012 / 15:15-15:15 / Room: The Liffey

# Characterization by Magnetic Resonance Imaging of in vivo body fatness in risperidone-treatedC57B6 /J female mice

***Auger Florent**, Laura Ravasi, Durieux Nicolas, Plate-forme imagerie du vivant, IMPRT, Lille, France. Contact e-mail: florent.auger@univ-lille2.fr*

Introduction Antipsychotic drugs are known to induce metabolic disorders in human and rodents: weight gain, hyperglycemia, glucose intolerance, insulin resistance, dyslipidemia.This study aims to characterize the in vivo effects of risperidone treatment with or without curcumin supplemented-diet on lipid distribution in C57B6/J female mice through a 7-Tesla Bruker Biospec Magnetic Resonance imaging system (MRI). Material and Methods Twelve female mice (7 week-old) were divided into two groups of 6 animals. One group was treated weekly over 24 weeks with intraperitoneal injection of 12.5 mgkg-1 of risperdal (long-acting risperidone) prior to sacrifice. The other group received intraperitoneal injections of the vehicle of risperdal. Mice were housed six to a cage and maintained on a 12-h light, 12-h dark cycle with ad libitum access to food and water. In vivo imaging Fat accumulation and liver volume were in vivo quantified on T1-weighted axial and coronal slices, and lipid hepatic accumulation was measured via Magnetic Resonance Spectroscopy (MRS). Histological staining and liver lipid assay Following MR examinations, mice were sacrificed. Inguinal adipose tissues and livers were weighted. Livers were then fixed in 4% paraformaldehyde for Oil Red O staining. ORO-stained sections (7 µm thick) of frozen liver were performed to assess the degree of steatosis. Livers lipids droplets were quantified using image J software (1.43, Wayne Rasband, NIH, USA). Liver lipid assay was also performed to quantify triglycerides by chemical dosage technique. Results A long treatment with risperidone in female mice induces an increase of body weight, hepatic lipid and inguinal adipose tissue accumulation. These two last results were retrieved with MR techniques. MRS allows quantifying hepatic lipids while the 3D reconstruction of T1 weighted images give an accurate volume of adipose tissue. We obtain, on the one hand, a strong correlation between autopsy data and MRI volumetric analysis and on the other hand a strong correlation between MRS, chemical assay and histological staining. Conclusions This pilot study shows that a non-invasive technique such as MRI allows the in vivo characterization of body fatness distribution. Authors Florent Auger 1, Laura Ravasi 1, Nicolas Durieux 1, Regis Bordet1 1. IMPRT Plate-forme imagerie du vivant. Pôle recherche. Lille. France

Disclosure of author financial interest or relationships:
**A. Florent**, None; **L. Ravasi**, None; **D. Nicolas**, None.

Presentation Number **P474**
Poster Session 3
September 7, 2012 / 15:15-15:15 / Room: The Liffey

# In-vivo real time MR imaging of lipid metabolism in brown adipose tissue with triglyceride-rich lipoprotein-USPIO nanosomes

***Harald Ittrich***[1], *Alexander Bartelt*[2], *Oliver T. Bruns*[3], *Kersten Peldschus*[1], *Michael G. Kaul*[1], *Ulrich Tromsdorf*[4], *Gerhard Adam*[1], *Jörg Heeren*[2], [1]*Department of Diagnostic and Interventional Radiology, University Medical Center Hamburg Eppendorf, Hamburg, Germany;* [2]*Institute of Biochemistry and Molecular Biology II: Molecular Cell Biology, University Medical Center Hamburg Eppendorf, Hamburg, Germany;* [3]*Section Electron Microscopy, Heinrich-Pette-Institute for Experimental Virology and Immunology, Hamburg, Germany;* [4]*Institute of Physical Chemistry, University of Hamburg, Hamburg, Germany. Contact e-mail: ittrich@uke.uni-hamburg.de*

Purpose: The aim of the study was to develop dynamic MRI methods for a non-invasive in-vivo imaging of uptake of triglyceride rich lipoprotein SPIO nanosomes (SPIO-TRL) in brown adipose tissue (BAT, metabolic body heat generator) and measurement of lipase activity and in BAT in cold exposed and warm mice. Material and Methods: A new class of particles was designed in vitro with a highly monodispers magnetic iron oxide core (USPIO) embedded in a TRL nanosome complex (SPIO-TRL). In vivo MRI was performed using a static T2*w 2D gradient echo (GRE) sequence (TR/TE 254/6.9 ms, FoV 40×30 mm, eff. voxel volume 0.15×0.15×1 mm) before and after and dynamic T2*w GRE (TR/TE 85/6.9 ms, FoV 34×34 mm, eff. voxel volume 0.21×0.21×1.3 mm) during the i.v. application of SPIO-TRL in cold-exposed (4°C, BAT activated) and warm (22°C, control, BAT inactive) FVB mice using a 3T scanner (Philips Intera) with a custom made small animal solenoid coil. Relaxometric R2* measurements were performed before and after SPIO-TRL application using a fat-saturated 3D multi-echo gradient echo sequence (TR 65 ms, inter echo time 2.8ms, FoV 50×50mm, eff. voxel volume 0.39×0.42×2mm). SNR in inferior vena cava (VCI), aorta, liver, and BAT as well as R2* of liver and BAT were measured for estimation of SPIO-TRL blood clearance resp. SPIO-TRL uptake in BAT. Uptake kinetics and R2* of both animal groups were tested for statistical significance (t-test, $p<0.05$) and matched with histology (H&E, Prussian blue) and electron microscopy. Results: In vivo MRI showed a rapid SNR decrease with an exponentional recovery in VCI and aorta and a two-phase exponential SNR drop after SPIO-TRL in liver and BAT. Liver SNR decrease was similar in both, cold and warm mice ($p>0.05$). Cold mice showed a significantly accelerated and forced SNR decline in BAT ($p<0.05$). Correlating the R2* (in sec-1) cold showed a significantly higher increase compared to warm mice ($p<0.05$). Corresponding to MR imaging histology and electron microscopy showed an accelerated accumulation of SPIO-TRL in BAT and Kupffer cells of the liver. Conclusions: SPIO-TRL uptake in and lipase activity of BAT can be monitored by real time in vivo MRI. Different enzyme activity levels (cold-exposed vs. warm) in BAT can be detected non-invasively by MRI.

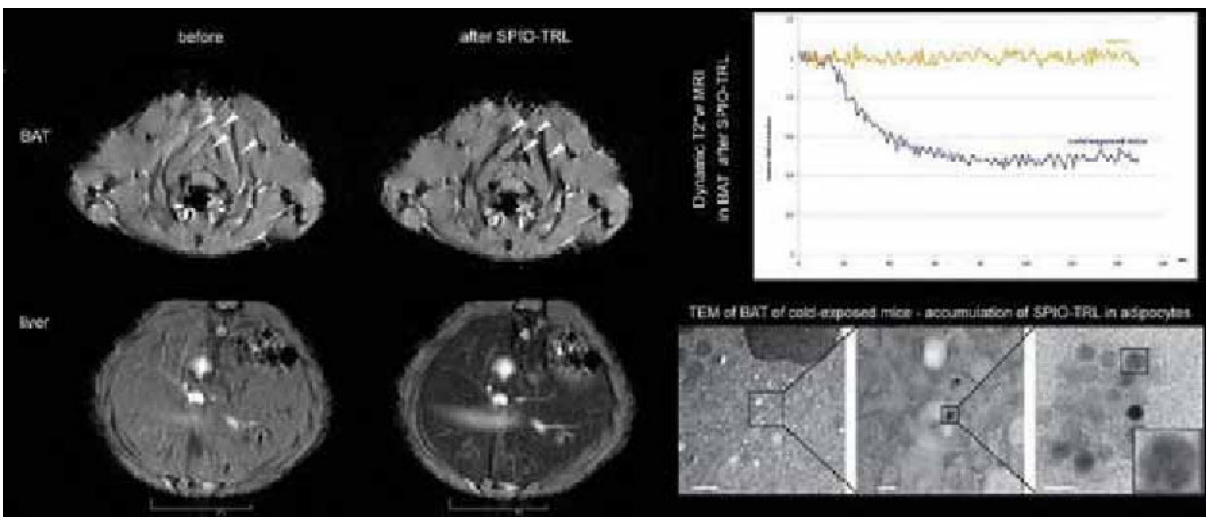


Disclosure of author financial interest or relationships:
**H. Ittrich**, None; **A. Bartelt**, None; **O.T. Bruns**, None; **K. Peldschus**, None; **M.G. Kaul**, None; **U. Tromsdorf**, None; **G. Adam**, None; **J. Heeren**, None.

Presentation Number **P475**
Poster Session 3
September 7, 2012 / 15:15-15:15 / Room: The Liffey

# In-vivo MR quantitation of liver steatosis after partial hepatectomy in an animal model at 3T

***Harald Ittrich***[1], *Jörg Heeren*[2], *Johannes Herkel*[3], *Kersten Peldschus*[1], *Peter Bannas*[1], *Andreas Koops*[1], *Gerhard Adam*[1], [1]*Department of Diagnostic and Interventional Radiology, University Medical Center Hamburg Eppendorf, Hamburg, Germany;* [2]*Institute of Biochemistry and Molecular Biology II: Molecular Cell Biology, University Medical Center Hamburg Eppendorf, Hamburg, Germany;* [3]*I. Department of Internal Medicine, University Medical Center Hamburg Eppendorf, Hamburg, Germany. Contact e-mail: ittrich@uke.uni-hamburg.de*

Purpose The aim of the study was to compare different MR fat imaging sequences for a non-invasive in-vivo measurement of liver steatosis after partial hepatectomy in different mice models. Material and Methods In-vivo MRI was performed before, 6h, and 24h after partial hepatectomy (PH) in apolipoprotein E (ApoE) deficient and wildtype mice (WT, control) using a clinical 3T scanner (Philips Intera) with a custom made small animal solenoid coil. 4 different T1-weighted T1w sequences were estimated: TSE, fat-saturated (fat-sat) TSE, water-saturated (wat-sat) TSE, and an in/opposed-phase (iop) FFE. SNR was measured in liver at all time points by placing ROIs in the corresponding regions corrected by standardized external control tubes filled with water and oil using ImageJ (NIH). Liver lipid concentrations (LLC, µg/mg protein) were measured at each time point after liver removal by laboratory methods. Differences in liver fat content after PH between both animal groups were tested for statistical significance (t-test, $p<0.05$). Pearson's correlation coefficient (r) between SNR and fat concentrations was calculated for all sequences. Results In-vivo measurements showed time dependent SNR changes in both groups correlating to the LLC changes after PH. Laboratory measured LLC showed accelerated increase in ApoE mice of 123.2±8.8% after 6h and 240.0±25,8% after 24h in comparison to WT mice (6h: 39.0±17,1%, 24h: 166.2±16.8%). R between SNR and LLC showed the best correlation for T1w wat-sat TSE (r=0.98), followed by iop FFE (r=-0.95), fat-sat TSE (r=0.84), and normal T1w TSE (r=0.75). Conclusions Liver lipid concentrations in small animal models after partial hepatectomy can be measured non-invasively by MRI at a clinical 3T MR System. Defects in liver lipid metabolism (e.g. apolipoprotein E) can be detected non-invasively by MRI.

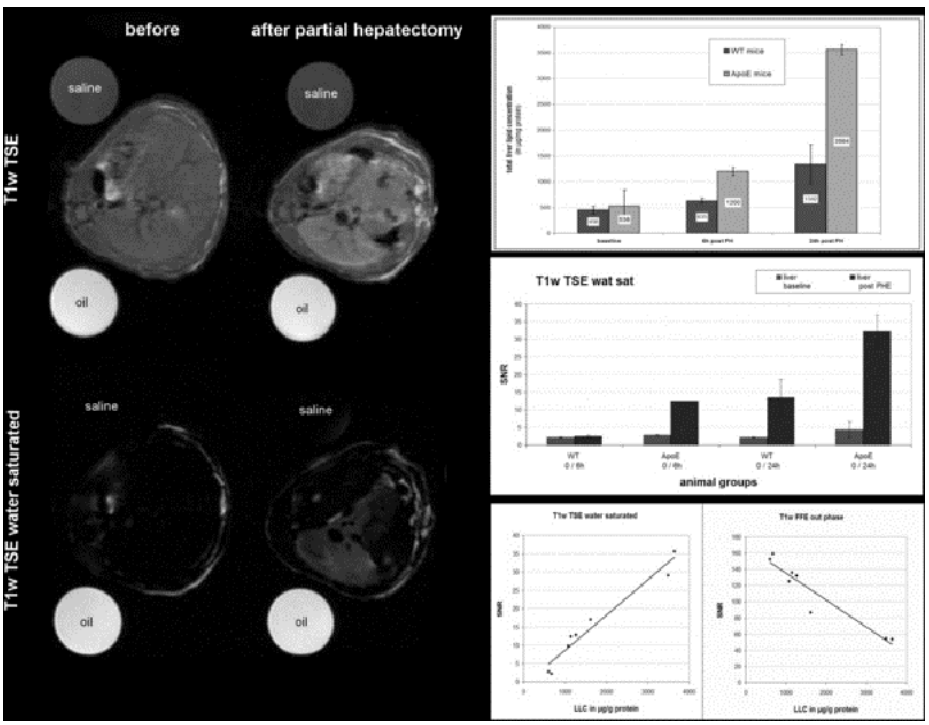


Disclosure of author financial interest or relationships:
**H. Ittrich**, None; **J. Heeren**, None; **J. Herkel**, None; **K. Peldschus**, None; **P. Bannas**, None; **A. Koops**, None; **G. Adam**, None.

Presentation Number **P476**
Poster Session 3
September 7, 2012 / 15:15-15:15 / Room: The Liffey

# Effects of isoflurane anesthesia on hyperpolarized $^{13}C$ metabolic measurements in rat brain

***Sonal Josan***[1,2], *Kelvin Billingsley*[2], *Lasitha Senadheera*[5], *Jae Mo Park*[2], *Yi-Fen Yen*[2], *Ralph E. Hurd*[3], *Adolf Pfefferbaum*[1,4], *Daniel M. Spielman*[2], *Dirk Mayer*[1,2], [1]*Neuroscience Program, SRI International, Menlo Park, CA, USA;* [2]*Radiology, Stanford University, Stanford, CA, USA;* [3]*GE Healthcare Applied Science Lab, Menlo Park, CA, USA;* [4]*Department of Psychiatry and Behavioral Sciences, Stanford University, Stanford, CA, USA;* [5]*Radiation Oncology, Stanford University, Stanford, CA, USA. Contact e-mail: sjosan@stanford.edu*

Anesthetic agents like isoflurane (Iso) are potent cerebral vasodilators, with reported dose-dependent increase in cerebral blood flow and cerebral blood volume (CBV) [1-4]. Despite its ubiquitous use in hyperpolarized $^{13}C$ MRI pre-clinical research studies, a quantitative assessment of its effect on metabolic measurements is limited. This work aims to investigate the effect of Iso dose on hyperpolarized $^{13}C$ MR measurements of metabolite ratios and apparent conversion rate constants. Setup, substrate and polarization were same as [5]. Healthy male Wistar rats were anesthetized with Iso in oxygen (1.5 L/min). Respiration, temperature, heart rate and oxygen saturation were monitored throughout the experiment. Three rats received 4 injections of hyperpolarized [1-$^{13}C$]pyruvate (Pyr) each, alternately at low or high Iso doses. The low dose was approximately 0.75-1.5%, targeting a respiration rate of about 80-85 bpm and the high dose was 2-3.25% targeting a respiration rate of about 50-55 bpm. After each injection, Iso was slowly ramped to the next target dose, and maintained at the target for at least 10 min before the Pyr injection. Three control rats received 3 Pyr injections each while maintaining constant Iso and respiration rate, to assess variability among injections. Dynamic 2D spiral chemical shift imaging [5] was used to acquire 16 time-points starting 3s after start of Pyr injection. The time-averaged metabolite maps and time-courses from a brain ROI (red box) show greatly elevated Pyr at high Iso, consistent with the vasodilation effect, while lactate (Lac) was unchanged. Hence, the Lac/Pyr ratios vary significantly with Iso dose (solid lines in graph, high=0.56±0.04, low=0.34±0.04, P=0.03). In contrast, the Lac/Pyr ratios of the control rats (dashed lines) were similar for the 3 injections. The apparent rate constants estimated from the time-courses also differ considerably ($K_{pl}$=0.025±0.003 $s^{-1}$ vs. 0.016±0.002 $s^{-1}$, P=0.03). Higher Pyr signal was observed in both brain and vasculature (black box) regions. The brain Pyr signal arises largely from CBV as the metabolic conversion is fast compared to blood-brain transport [6]. The ratios of products, bicarbonate (Bic)/Lac avoid the vasodilation effect on the substrate and did not vary with Iso dose. A similar variation was also observed with hyperpolarized [1-$^{13}C$]ketoisocaproate and its conversion to leucine in the brain, indicating that the effect is not specific to Pyr. Thus, cerebral metabolite-to-substrate ratios and apparent rate constants can depend markedly on isoflurane anesthesia dose in rats. The data also suggest that ratios of products, e.g. Bic/Lac are largely insensitive to isoflurane levels. This study highlights the importance of careful attention to selection of anesthetic agent and consistency of dose when comparing data. [1] Hansen et al. Anesthesiology 1988; 69:p332 [2] Lenz et al. Anesthesiology 1998; 89:p1480 [3] Todd et al. J. Neurosurgical Anesthesiology 1996; 8:p296 [4] Hendrich et al. Magn Reson Med 2001; 46;p202 [5] Mayer et al. Magn Reson Med 2011; 65:p1228 [6] Hurd et al. J. Cerebral blood flow & metabolism 2010; 30:p1734

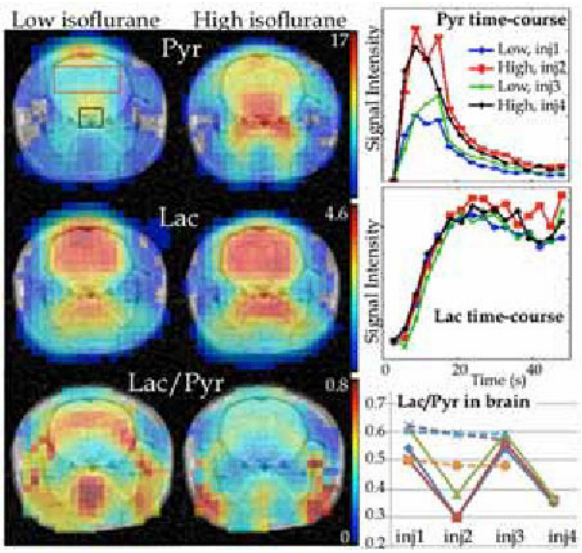


Disclosure of author financial interest or relationships:
**S. Josan**, None; **K. Billingsley**, None; **L. Senadheera**, None; **J. Park**, None; **Y. Yen**, None; **R.E. Hurd**, GE Healthcare, Employment; **A. Pfefferbaum**, None; **D.M. Spielman**, None; **D. Mayer**, None.

Presentation Number **P477**
Poster Session 3
September 7, 2012 / 15:15-15:15 / Room: The Liffey

# In vivo imaging of bone repair under the influence of recombinant human BMP-2 in critical sized long bone defects reveals a transient dose response

***Kenneth M. Kozloff***[1], *Joseph S. Tramer*[1], *Ed Berryman*[2], *Joseph E. Perosky*[1], *Eric Vanderploeg*[2], *Steven A. Goldstein*[1], *Cedo M. Bagi*[2], [1]*Orthopaedic Surgery, University of Michigan, Ann Arbor, MI, USA;* [2]*Pfizer, Inc., Groton, CT, USA. Contact e-mail: kenkoz@umich.edu*

Recombinant human BMP2 (rhBMP2) is a potent anabolic agent that induces bone repair. However, supraphysiologic doses required may limit application safety. The purpose of this study was to monitor rhBMP2 dose response in a critical long bone defect through longitudinal imaging and functional gait testing to determine minimal effective dosing over 8 weeks of bone repair. Adult male Sprague-Dawley rats were grouped as follows: sham-operated control; absorbable collagen sponge (ACS)+PBS control; ACS+low rhBMP2 (0.75 µg), ACS+high rhBMP2 (3.75 µg). A unilateral 5mm mid-diaphyseal femoral defect was stabilized with a custom PEEK fixation plate and ACS constructs were implanted. Sham rats received incision with no fixator. Rats returned to normal cage activity for 4 or 8 week recovery. All changes are $p<0.05$ unless noted, n=8/group. Dynamic weight bearing tests observed a decrease in percent body mass placed on operated limbs 2 days post-surgery compared to baseline in empty (-16%) and low BMP (-13%) rats with a corresponding shift to the contralateral limb in rats with empty defects (+13%). By 3 weeks, hindlimb gait patterns did not differ from baseline, although a gradual transition in mass distribution from hind to forelimbs was observed in sham and empty groups. In vivo µCT quantified regenerate bone mineral content (BMC) during healing. At 2 weeks, high BMP induced 232% increase in BMC over ACS alone, while low BMP showed a modest (73%) but not significant increase. By 4 weeks, BMP induced a dose dependent increase in BMC (163% low, 315% high), and this response continued through 6 weeks (242% low; 342% high). Ex vivo µCT at 4 weeks confirmed a dose response with significant increase in BMC (194%, 482%), bone volume (252%, 730%) , and bone volume fraction (193%, 436%) in low and high BMP respectively compared to ACS alone. Between 4 and 8 weeks, low BMP induced increases in BMC from 19 mg to 34 mg to reach high BMP levels which remained unchanged over the same time period (38mg vs. 39 mg). Qualitative observation of ex vivo µCT images suggests reorganization of bone between 4 and 8 weeks at both BMP doses from a woven to lamellar appearance. Empty sites remained unhealed at 8 weeks. In summary, rhBMP2 induced an early dose dependent response that equilibrated by 8 weeks in a critical sized rat femoral defect. These data suggest that similar regenerate bone volumes can be accomplished with smaller doses of rhBMP2 in the long-term healing environment.

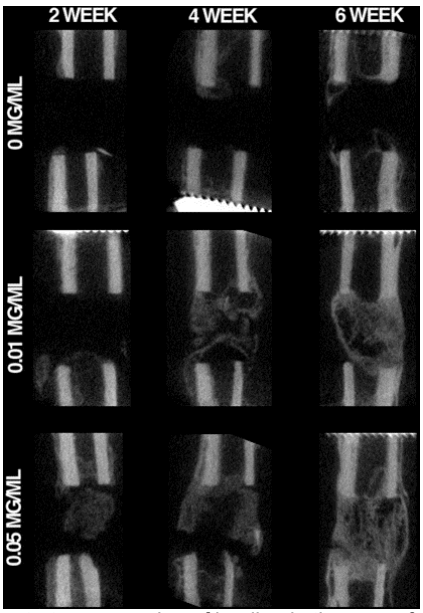


Representative in vivo microCT cross sections demonstrate progression of healing in the 5 mm fracture callus across 6 weeks of longitudinal microCT imaging. Animals receiving collagen sponge alone (0 mg/mL) demonstrate small amounts of bone formation at the original cortical bone boundaries. Animals receiving 0.01 mg/mL and 0.05 mg/mL BMP2 appear to differ in the initial rate of bone formation within the fracture site. 0.05 mg/mL BMP2 induces a rapid early bone formation response visible by 2 weeks following injury, while a similar response is evident at 4 weeks in the 0.01 mg/mL treatment group. By 6 weeks, cortical bone bridging is observed in both low and high BMP2 treatment groups, with minimal difference evident between groups.

Disclosure of author financial interest or relationships:
**K.M. Kozloff**, None; **J.S. Tramer**, None; **E. Berryman**, None; **J.E. Perosky**, None; **E. Vanderploeg**, Pfizer, Employment; **S.A. Goldstein**, None; **C.M. Bagi**, Pfizer, Inc., Employment; Pfizer, Inc., Stockholder .

Presentation Number **P478**
Poster Session 3
September 7, 2012 / 15:15-15:15 / Room: The Liffey

# Evaluation of efficient transplant of mesenchymal stem cells in diabetic mouse model using in vivo bioluminescence imaging

***Song Lee***[1,2], *Mi Jeong Kim*[1,3], *Do Won Hwang*[1], *Hyewon Youn*[1,4], *Dong Soo Lee*[1,5], [1]*Nuclear Medicine, Seoul National University College of Medicine, Seoul, Republic of Korea;* [2]*Radiation Medicine, Seoul, Republic of Korea;* [3]*Laboratory of Molecular Imaging and Therapy, Cancer Research, Seoul, Republic of Korea;* [4]*Cancer Imaging Center, Seoul, Republic of Korea;* [5]*Molecular Medicine and Biopharmaceutical Science, WCU Graduate school of Convergence science and Technology, Seoul National University, Seoul, Republic of Korea. Contact e-mail: ssong277@hanmail.net*

Objectives: The non-invasive in vivo cell tracking after transplant is one of important experiment for examining the fate characteristics in vivo. It is essential to determination of efficient injection route for high therapeutic effect. In this study, we monitored the localization and distribution of transplanted mesenchymal stem cells with comparison of systemic and local injection using bioluminescence imaging in mouse models of diabetes. Methods: Bone marrow-derived mensenchymal stem cells isolated from BALB/c mouse were infected with luciferase gene (mMSC-luc). Diabetes in mice was induced by streptozotocin (STZ) in multiple low doses. mMSCs-luc were locally injected to the pancreas area or systemically injected through pancreatic duct of diabetic BALB/c nude mice. After transplant, the distribution and fate of mMSC-luc was in vivo monitored using the IVIS optical imaging device. Potential therapeutic effect of transplanted mMSC-luc in diabetic mice was evaluated by daily fasting glucose level, intraperitoneal glucose tolerance test (IPGTT) and immunohistochemistry. Results: The luciferase activity of mMSC-luc was significantly increased dependent on cell number. The in vivo luciferase signals in both local and systemic transplantation group were elevated during 7 days, however, the distribution pattern was different. The luciferase signals transplanted locally were strongly observed at the transplanted site, whereas those transplanted systemically were widely distributed within whole pancreas. In all mice implanted with mMSCs-luc, fasting glucose levels and tolerance were maintained in high glucose levels until 7 days after trnaplant. However, pancreatic regenerating area was detected in nearby mMSC-luc transplanted area. Conclusions: We visualized the in vivo distribution of mesenchymal stem cells transplanted to local or systemic routes using bioluminescence imaging. These results suggest that stem cells therapy transplanted via various injection routes could be easily monitored using in vivo bioluminescence imaging techniques.

Disclosure of author financial interest or relationships:
**S. Lee**, None; **M. Kim**, None; **D. Hwang**, None; **H. Youn**, None; **D. Lee**, None.

Presentation Number **P479**
Poster Session 3
September 7, 2012 / 15:15-15:15 / Room: The Liffey

# Volumetric Functional MR Imaging of Pancreatic Activation

***Lara Leoni***[1], *Anita H. Dhyani*[1], *Muhammad E. Haque*[1], *Philip A. Vargas*[1], *Xiaobing Fan*[1], *Qingfei Luo*[2], *Jia-Hong Gao*[1], *Patrick J. La Riviere*[1], *Brian B. Roman*[1], [1]*Radiology, University of Chicago, Chicago, IL, USA;* [2]*Radiology, Stanford University, Palo Alto, CA, USA. Contact e-mail: leoni@uchicago.edu*

Although the endocrine pancreas and its function are well documented, beta-cell mass and the minimum concentration of islets necessary for maintaining glucose homeostasis under a variety of conditions has been elusive. Development of non-invasive techniques that can link beta-cell mass and its function are of great interest, since it is the loss of cell mass that results in an insulin insufficiency characteristic of Type I diabetes. But, the endocrine tissue comprises just 2% of the pancreas and is dispersed throughout the pancreatic head, body, and tail, making it a challenging region to target and image. Recently, there has been growing interest in the use of manganese-enhanced MRI (MEMRI) for probing beta cell mass and function since Mn accumulates intracellularly via open ligand gated calcium channels. Previous in vivo studies have only focused on the splenic region of the pancreas and usually a small image ‘slice' of approximately 5mm thick. To improve the impact of this technique, we investigated a large region of the pancreas by standard ROI analysis of multiple regions and slices following the onset of diabetes. Five normal and six diabetic rats were imaged. Initially, hot spots reminiscent of pancreatic islets were identified across the whole pancreas. An average volume of 336.71±219.12 mm3 for the control group and 94.12±63.74 mm3 for the diabetic animals was analyzed ($p < 0.05$). Although both groups showed a significant increase in normalized signal enhancement (SE) following MnCl2 (4.95±1.63 and 4.24±2.16 respectively) no significant increase was measured following an IP glucose challenge. The same images were then analyzed encompassing the entire pancreatic regions. On average, 1350.56±840.05 mm3 were considered. The change in normalized SE following Mn uptake was 5.31±1.52 in the control group and 2.59±1.10 in the diabetic one ($p<0.05$). Glucose challenge induced a further significant increase in normalized SE (0.91±0.45) in healthy animals while no further increase was measured in the diabetics (0.15±0.41). As this analysis is operator dependent, we also examined the implementation of a fMRI approach to detect pancreatic areas of activation. Although normally conducted in the brain and with a large bank of voluteers, Mn induced MRI changes in response to glucose in the pancreas can be large and therefore possible to detect via smaller sample size. This approach is fairly operator neutral. An equal set of images were acquired at baseline, during Mn administration, and during the glucose challenge. A Gaussian filter was used to smooth the images and T-maps were created using a completely automated method where the mean images for the three conditions (baseline, Mn, glucose) were compared. Three slices per subject were analyzed (n=2) and on average, a 50% increase in normalized SE was found following Mn, and an additional 40% increase was measured after glucose challenge. Despite the limited sample size, this method is very promising and has high potential for clinical translation thanks to its automation and lack of operator bias.

Disclosure of author financial interest or relationships:
**L. Leoni**, None; **A.H. Dhyani**, None; **M.E. Haque**, None; **P.A. Vargas**, None; **X. Fan**, None; **Q. Luo**, None; **J. Gao**, None; **P.J. La Riviere**, None; **B.B. Roman**, None.

Presentation Number **P480**
Poster Session 3
September 7, 2012 / 15:15-15:15 / Room: The Liffey

# Functional evaluation of normothermic ischemia/reperfusion injury in mice kidney combining CEST-pH mapping and BOLD MRI

***Dario L. Longo***[1,3], *Juan C. Cutrin*[2,4], *Filippo Michelotti*[1], *Stefania Lanzardo*[2], *Silvio Aime*[1,3], [1]*Department of Chemistry, University of Turin, Turin, Italy;* [2]*Department of Clinical and Biological Sciences, University of Turin, Turin, Italy;* [3]*Molecular Imaging Center, University of Turin, Turin, Italy;* [4]*Lab. of Hypoxia and Inflammation, Ininca - Conicet, Buenos Aires, Argentina. Contact e-mail: dario.longo@unito.it*

Renal damage after ischemic/reperfusion (I/R) injury may results in acute renal failure (ARF), evolving to loss of renal function due to cellular injury and death. Non-invasive imaging techniques are required to allow the visualization and evaluation of function of different renal compartments in a longitudinal manner. Among the different physiological parameters that is possible to image in vivo, pH is one of the most important, being directly related to the primary kidney function of extracting protons from blood. We recently have shown that it was possible to monitor a marked alteration of pH values in a glycerol-induced rhabdomyolisis mouse model [1]. In the present study we investigated the feasibility of using a pH-sensitive CEST-MRI contrast agent, combined with blood-oxygenation level dependent (BOLD) MRI for the evaluation and monitoring of the alteration in renal function following normothermic I/R injury in mouse kidney in vivo. BALB/c mice were anesthetized i.p. and kept under a heating lamp to maintain constant their body temperature. Flank incision was made to expose the left renal pedicle to induce 20 (n=5), 30 (n=5) and 40 min (n=5) of ischemia which was followed by reperfusion for 24 and 48 hours. Color changes of kidneys were monitored to indicates sufficient renal ischemia and reperfusion. MR images were acquired with a Bruker MRI scanner operating at 7.0 Tesla before, and 24h and 48h after the I/R injury. A clinical dose of Iopamidol (0.75 g Iodine / kg b.w.) was injected via a catheter into the tail vein to acquire CEST images to calculate pH values. BOLD images were acquired with a multiple recalled gradient echo sequence (TE 3-39 ms). Axial sections from both kidney were sectioned at 5 µm with paraffin and stained with hematoxylin-eosin and examined by light microscopy. Quantification of tubular injury score was assessed by counting the percentage of tubular necrosis and proteinaceous casts in the outer stripe of the outer medulla (OSOM) in ten fields using a scale from 0 to 5. In both kidneys we observed, 15 min after Iopamidol injection, and before the I/R injury, a mean pH value of 6.7. After 24 h the I/R injury, we observed a slight pH increase in the left kidney correlated to the time of injury (mean pH values of 6.9, 7.15 and 7.1 for 20, 30 and 40 min of ischemia, respectively). At 48 h pH values were higher for both the injured and the control kidney. Mean R2* BOLD measurement increased from baseline during ischemia damage in both the cortex and outer medulla (Fig. 1). Renal architecture from the non-ischemic kidney was normal in the three groups of ischemia injury. Less than 10 % of tubular necrosis as well as casts formation were observed in mice submitted to 20 min of ischemia. Prolonging ischemia time resulted in extensive proximal tubular necrosis with altered tubular architecture in the OSOM with necrotic cell debris, hyaline casts of the tubules and severe congestion after 40 min of ischemia. MR-CEST pH mapping and BOLD imaging are useful in identifying renal dysfunction following I/R injury, enabling differentiation of damage severity. [1] Longo D. Proc. Intl. Soc. Mag. Reson. Med. 2011; 19:T230

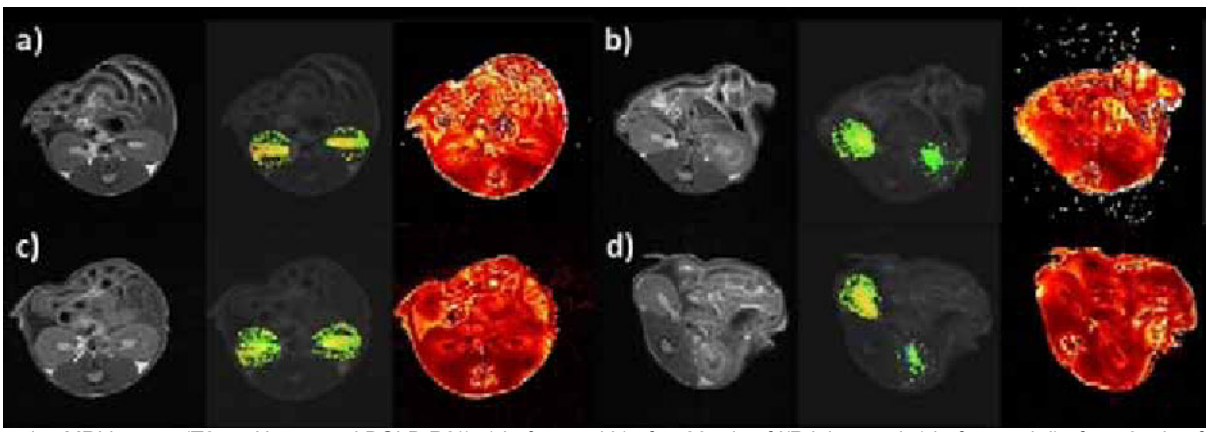


Representative MRI images (T2w, pH map and BOLD R2*) a) before and b) after 20 min of I/R injury and c) before and d) after 40 min of I/R injury

Disclosure of author financial interest or relationships:
**D.L. Longo**, None; **J.C. Cutrin**, None; **F. Michelotti**, None; **S. Lanzardo**, None; **S. Aime**, Bracco Imaging, Consultant; Bruker, Grant/research support .

Presentation Number **P481**
Poster Session 3
September 7, 2012 / 15:15-15:15 / Room: The Liffey

# *Ex vivo* identification and *in vivo* validation of a novel visceral amyloid imaging peptide

***Emily B. Martin***[2], *Stephen J. Kennel*[2,1], *Tina A. Richey*[2], *Alan Stuckey*[1], *Angela Williams*[2], *Dustin Osborne*[1], *Keiichi Higuchi*[3], *Jonathan S. Wall*[2,1], [1]*Radiology, University of Tennessee Graduate School of Medicine, Knoxville, TN, USA;* [2]*Medicine, University of Tennessee Graduate School of Medicine, Knoxville, TN, USA;* [3]*Aging Biology, Shinshu University Graduate School of Medicine, Matsumoto, Japan. Contact e-mail: emarti15@utk.edu*

Visceral amyloid is a complex pathology comprising protein fibrils and numerous accessory molecules. It is associated with a myriad of diseases including type 2 diabetes, chronic inflammation and myeloma, but the US currently offers no method to effectively image this pathology in patients. To this end, we have developed a peptide, p5 that was shown to bind amyloid *in vivo* using a mouse model of reactive (AA) amyloidosis. We now extend these studies with $^{125}$I-p5 to include a murine model of apolipoprotein AII (ApoA2c) amyloidosis. Micro-autoradiography was used to show weak retention of the peptide in intestinal, hepatic, and pulmonary deposits, but surprisingly, there was no uptake of radiotracer in the splenic amyloid *in vivo*. Therefore, the aim of this study was to assess the reactivity of peptide p5 (+8 net charge) with ApoA2c amyloid *in vitro* and to evaluate a variant of this polybasic motif, peptide p5R+14 (+12 net charge), for imaging this amyloid *in vivo*. Peptide p5R+14 was radiolabeled with $^{125}$I and purified using size exclusion chromatography with Sephadex G25. For *ex vivo* amyloid binding assays, amyloid-laden tissues were homogenized in buffer containing non-ionic detergent and a mixture of protease inhibitors. The insoluble fraction containing the bulk of amyloid was collected by centrifugation and resuspended for use in a binding assay. $^{125}$I-labeled p5 and p5R+14 peptides (~200,000 cpm) were added to 50 µL of homogenized tissue suspension from wild type or amyloid-laden ApoA2c mice. After 1 h incubation, the pellet was isolated and the bound peptide measured by gamma counting. For *in vivo* imaging, peptides were radiolabeled as above and the radiopurity assessed by using SDS-PAGE and phosphor imaging. Approximately 300 µCi was injected iv in the lateral tail vein of ApoA2c mice (*n*=3). SPECT/CT images were acquired using the Inveon System at 4 h pi. Organs were harvested and biodistribution of radiotracer was determined and recorded as % injected dose/gram. In parallel, tissues were fixed in formalin, paraffin embedded, sectioned and exposed to photographic emulsion for 4 days. Both peptide p5 and p5R+14 bound ApoA2c amyloid-laden tissues in the ex vivo assay; notably, reactivity with the splenic homogenate was ~25% and ~70%, respectively. Peptide p5R+14 bound in greater amounts to all tissue samples as compared to p5. *In vivo* biodistribution studies confirmed that p5R+14 bound splenic (7.5 ± 2.8 %ID/g) and cardiac (4.5 ± 0.8 %ID/g) tissue amyloid as well as deposits in the lung, intestines and liver. Micro-autoradiography studies established that $^{125}$I-p5R+14 co-localized with amyloid deposits in positive organs. Although $^{125}$I-p5 was not detected in splenic ApoA2c amyloid *in vivo*, binding was observed using homogenized tissue suggesting the presence of inaccessible binding sites in the tissue amyloid. The $^{125}$I-p5R+14 peptide successfully imaged cardiac amyloid in the preclinical model of visceral amyloidosis which was predicted by data from the *ex vivo* assay. These data suggest that p5R+14 may prove to be a valuable tool for amyloid imaging in patients with these devastating diseases.

Disclosure of author financial interest or relationships:
**E.B. Martin**, Solex LLC, Stockholder; **S.J. Kennel**, solex, Stockholder; **T.A. Richey**, Solex, Stockholder; **A. Stuckey**, Solex LLC, Stockholder; **A. Williams**, None; **D. Osborne**, University of Tennessee, Employment; Siemens Medical Solutions, Employment; **K. Higuchi**, None; **J.S. Wall**, Elan, Grant/research support; Solex LLC, Stockholder .

Presentation Number **P482**
Poster Session 3
September 7, 2012 / 15:15-15:15 / Room: The Liffey

# Probing In Vivo Liver Metabolism with Hyperpolarized Pyruvate

***Matthew E. Merritt***[1], *Karlos X. Moreno*[1], *Crystal Harrison*[1], *Craig Malloy*[1,3], *Dean Sherry*[1,2], [1]*UTSW Medical Center, Dallas, TX, USA;* [2]*Chemistry, University of Texas at Dallas, Richardson, TX, USA;* [3]*Cardiology, North Texas VA Healthcare System, Dallas, TX, USA. Contact e-mail: matthew.merritt@utsouthwestern.edu*

INTRODUCTION. Hepatic metabolism is intimately connected to whole body glucose homeostasis as well as a gamut of other physiological parameters. Any real time method that could image hepatic energetics would be a boon for diagnosing a variety of hepatic metabolic pathophysiologies. It has been shown that hyperpolarized [1- $^{13}$ C]pyruvate can be used to image the rat liver in vivo, and recent studies with the perfused liver showed that fasting can cause significant changes in the $^{13}$C NMR spectrum following infusion of the same imaging agent. The initial results in the perfused liver seemed to indicate that the appearance of [$^{13}$C]bicarbonate following the infusion of [1-$^{13}$C]pyruvate arises from flux through phosphoenolpyruvate carboxykinase (PEPCK), a remarkable observation since this pathway would require a minimum of 6 steps to generate CO2. Other possible sources include flux through pyruvate dehydrogenase (PDH), or decarboxylation during a forward turn of the tricarboxylic acid (TCA) cycle. A possible complication for observing forward turnover of the cycle using hyperpolarized [1-$^{13}$C]pyruvate is the degenerate chemical shifts of [6-$^{13}$C]citrate and [1-$^{13}$C]malate. This issue can be overcome by using [2-$^{13}$C]pyruvate as the imaging agent, the metabolites of which produce distinct chemical shifts. Here we compare and contrast measurement of real time hepatic metabolism using a variety of pyruvate $^{13}$C labeled isotopomers in the perfused liver and in vivo. METHODS. Livers were excised from the C57bl6 mouse, cannulated through the portal vein and perfused in a custom rig at 8 ml/min. Various isotopomers of pyruvate were hyperpolarized with an Oxford HyperSense DNP polarizer using the trityl radical. $^{13}$C NMR was carried out at 9.4 T using an Agilent VNMRS console. Gated proton decoupling was used during the data acquisition period. In vivo results were obtained with a homebuilt polarizer paired with an Agilent VNMRS 4.7 T horizontal bore imaging system. RESULTS. Figure 1 illustrates the data that can be acquired in a perfused liver following an injection of hyperpolarized [2-$^{13}$C]pyruvate. The excellent chemical shift resolution allows a variety of metabolites of pyruvate to be monitored including malate, aspartate, and citrate. In agreement with our earlier results with [1-$^{13}$C]pyruvate, the signal associated with [3-$^{13}$C]citrate is much smaller than that of [2-$^{13}$C]malate, indicating that exchange between oxaloacetate and malate is much faster than the condensation of oxaloacetate with acetyl-CoA to for citrate. Previous in vivo experiments had failed to monitor any of the 4-carbon TCA cycle intermediates obtained in the perfusion experiment. Figure 1 (right) shows the data obtained in vivo in the C57bl6 animal using [1-$^{13}$C]pyruvate. The data was obtained via slice localized spectroscopy, and the enhanced sensitivity gained from capturing the majority of the liver shows that the 4-carbon intermediates are present in the mouse liver given the right conditions. In conclusion, the in vivo results validate the previously published results using the perfused liver model.

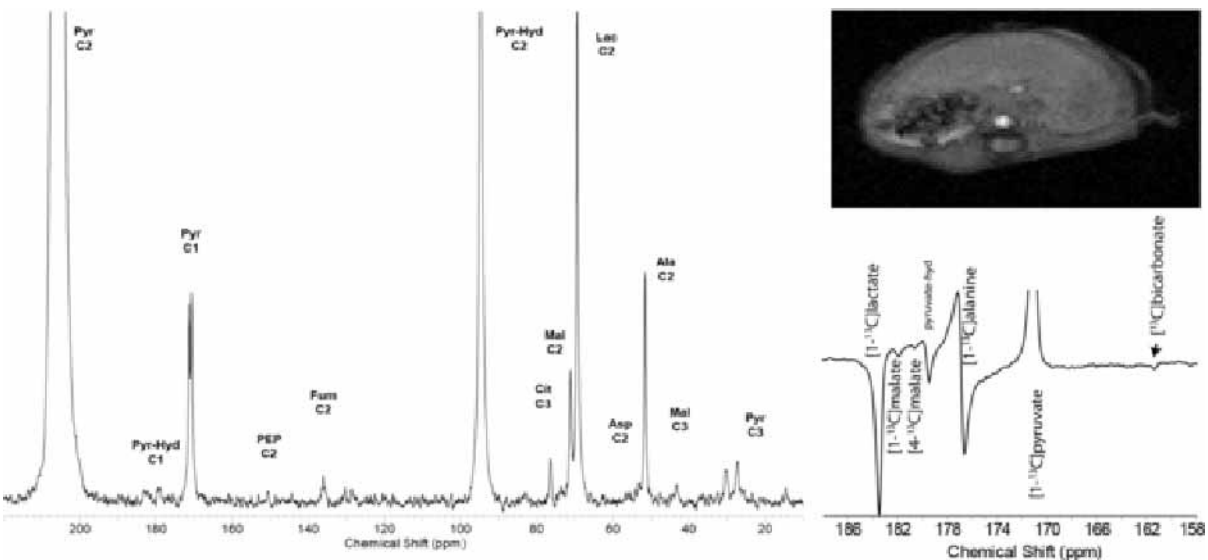


Figure 1. (left) The $^{13}$C NMR spectrum of a perfused liver following injection of [2-$^{13}$C]pyruvate. (right,top) Gradient echo proton image used for planning the slice selective $^{13}$C spectra shown in the bottom panel. Note the presence of 4-carbon intermediates that develop followin ghte injection of [1-$^{13}$C]pyruvate.

Disclosure of author financial interest or relationships:
**M.E. Merritt**, None; **K.X. Moreno**, None; **C. Harrison**, None; **C. Malloy**, None; **D. Sherry**, None.

Presentation Number **P483**
Poster Session 3
September 7, 2012 / 15:15-15:15 / Room: The Liffey

# [$^{64}$Cu]- and [$^{68}$Ga]NODAGA-exendin-4 as pancreatic beta cell specific imaging agents

***Kirsi Mikkola***[1], *Cheng-Bin Yim*[1], *Veronica Fagerholm*[1], *Tamiko Ishizu*[1], *Viki-Veikko Elomaa*[1], *Johan Rajander*[2], *Jori Jurttila*[1], *Tiina Saanijoki*[1], *Tuula Tolvanen*[1], *Martin Behe*[4], *Martin Gotthardt*[3], *Anne Roivainen*[1], *Olof Solin*[1], *Pirjo Nuutila*[1], [1]*Turku PET Centre, University of Turku, Turku, Finland;* [2]*Accelerator Laboratory, Åbo Akademi University, Turku, Finland;* [3]*Department of Nuclear Medicine, Radboud University Nijmegen Medical Centre, Nijmegen, Netherlands;* [4]*Center for Radiopharmaceutical Sciences ETH-PSI-USZ, Paul Scherrer Institute, CH-5232 Villigen-PSI, Switzerland. Contact e-mail: kkmikk@utu.fi*

**Aims:** In diabetes mellitus, pancreatic islet beta cells are destroyed resulting in loss of insulin production. Quantitative non-invasive positron emission tomography (PET) imaging of pancreatic beta cells would serve as a valuable diagnostic tool, and provide means to monitor therapeutic interventions. The glucagon-like peptide 1 receptor (GLP-1R) is abundantly expressed in pancreatic beta cells and is considered a promising molecular target for imaging intact pancreatic beta cells, transplanted islets or insulinomas. The aim of this study was to compare the suitability of the GLP-1R PET tracers [$^{64}$Cu]NODAGA-exendin-4 ([$^{64}$Cu]Ex) and [$^{68}$Ga]NODAGA-exendin-4 ([$^{68}$Ga]Ex) as pancreatic beta cell imaging agents. **Materials & Methods:** To evaluate the biodistribution of the tracers *ex vivo*, rats weighing 292 ± 31 g were injected with 91 ± 26 MBq/kg [$^{64}$Cu]Ex (injected mass 1.5 ± 1.3 nmol/kg) or with 119 ± 15 MBq/kg [$^{68}$Ga]Ex (injected mass 9.6 ± 2.6 nmol/kg). After 5 min, 1 h, 18 h or 40 h for [$^{64}$Cu]Ex and at 1 h for [$^{68}$Ga]Ex (n=3-6 per group) selected organs were excised. The organ-specific radioactivity was reported as a percentage of the injected radioactivity dose per gram of tissue (% ID/g). The GLP-1R specificity was assessed by co-injecting an excess of unlabelled exendin-3 (7 mg/kg) with the tracers. Pancreatic cryosections, 20 µm, were cut and the distribution of radioactivity was assessed with autoradiography. Uptake ratios of islets to exocrine pancreas were analysed at all time points by selecting the ten most prominent islets in each tissue section; three sections per animal. Islet labelling was verified by insulin immunohistochemistry. [$^{64}$Cu]Ex radiation doses for humans were extrapolated from the rat biodistribution results using the OLINDA/EXM version 1.0 software. **Results:** Most of the injected radioactivity was distributed to the kidneys (30 ± 3 % ID/g for [$^{64}$Cu]Ex and 28 ± 7 % ID/g for[$^{68}$Ga]Ex at 1 h post-injection, p.i.). Lower levels were found in lungs and stomach wall. Uptake of radioactivity in the pancreas was low for both tracers (0.09 ± 0.02 % ID/g for [$^{64}$Cu]Ex and (0.04 ± 0.007 % ID/g for [$^{68}$Ga]Ex at 1 h p.i.). The islet to exocrine pancreas uptake ratio was higher for [$^{64}$Cu]Ex (67 ± 9, n=6) compared to [$^{68}$Ga]Ex (23 ± 3, n=6), P<0.001 at 60 min p.i. (Figure 1). The [$^{64}$Cu]Ex uptake in islets, lungs and stomach wall but not in the kidneys, was blocked by the injection of unlabelled exendin-3, indicating that the radiotracer uptake was GLP-1R specific. The estimated effective radiation dose of [$^{64}$Cu]Ex for a 70-kg human adult was 0.053 mSv/MBq, which means 26.5 mSv for a clinical dose of 500 MBq. For the kidney, the absorbed dose was 0.49 mSv/MBq. **Conclusion:** Based on the autoradiography results, [$^{64}$Cu]Ex is a better tracer than [$^{68}$Ga]Ex for beta cell imaging. The long physical half-life ($t_{1/2}$ = 12.7 h) of copper-64 facilitates long study protocols and makes it suitable for preclinical investigations. However, the high radiation burden for the kidneys limits the use of [$^{64}$Cu]Ex as a clinical tracer.

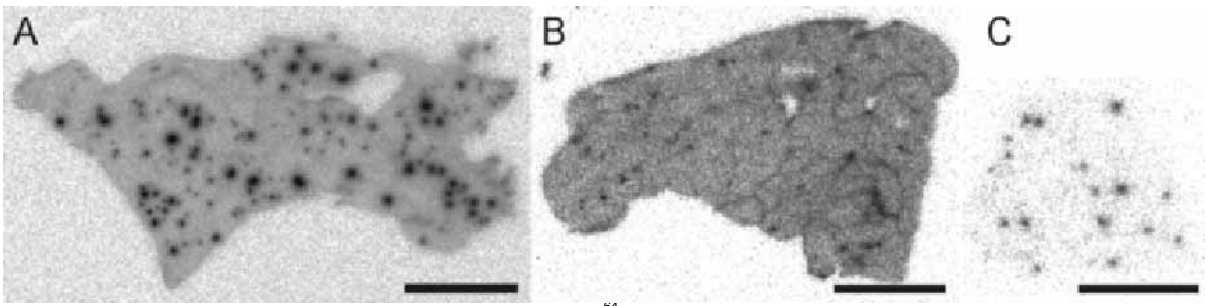


**Figure 1. Representative autoradiographs of rat pancreatic sections.** [$^{64}$Cu]NODAGA-exendin-4 (A) labelled pancreatic islets with higher contrast than [$^{68}$Ga]NODAGA-exendin-4 (C), as shown at 60 min post tracer injection. Co-injection of unlabelled exendin-3 with [$^{64}$Cu]NODAGA-exendin-4 (B) or [$^{68}$Ga]NODAGA-exendin-4 (not shown) significantly reduced islet uptake. Scale bar is 5 mm.

Disclosure of author financial interest or relationships:
**K. Mikkola**, None; **C. Yim**, None; **V. Fagerholm**, None; **T. Ishizu**, None; **V. Elomaa**, None; **J. Rajander**, None; **J. Jurttila**, None; **T. Saanijoki**, None; **T. Tolvanen**, None; **M. Behe**, None; **M. Gotthardt**, Sanofi Aventis, Grant/research support; **A. Roivainen**, None; **O. Solin**, None; **P. Nuutila**, None.

Presentation Number **P484**
Poster Session 3
September 7, 2012 / 15:15-15:15 / Room: The Liffey

# Analyzing the skeletal phenotype of DDR2-/- mice with high resolution CT

***Jeannine Missbach-Guentner***[1,2], *Christian Dullin*[1], *Frauke Alves*[2,3], [1]*Diagnostic Radiology, University Medicine, Goettingen, Germany;* [2]*Hematology/Oncology, University Medicine, Goettingen, Germany;* [3]*Biology of neuronal Signals, MPI for Experimental Medicine, Goettingen, Germany. Contact e-mail: j.missbach@med.uni-goettingen.de*

Introduction: Loss of tyrosine kinase DDR2, a collagen receptor, leads to skeletal malformations and dwarfism in a murine knock out model. Since the rare human syndrome of "Spondylo-meta-epiphyseal dysplasia (SMED)" has been recently identified as a missense mutation of DDR2, the understanding of pathological mechanisms and effects of DDR2 loss is of increasing interest. The aim of this study was to functionally analyze the skeleton of DDR2 knock out mice as an ideal model for SMED, using high resolution computed tomography. Methods: 6 to 7 weeks old DDR2-/- C57/BL6 mice and wild type controls were anesthetized and scanned using flat panel detector based cone beam volume computed tomography (fpVCT; GE Global Research Niskayuna, NY, USA) every 2 weeks for a period for four month. Thereafter they were scanned monthly for a period of 12 month. Axial images, multiplanar reconstruction and volume rendering images were obtained and analyzed with voxtools 3.0.64 Advantage Workstation 4.2 (GE Healthcare, Buckinghamshire, UK) as well as with a proprietary software, which was developed by our group based on the algorithm "skeleton". Ex vivo scans of selected bones from mature mice were performed with the GE Locus SP micro-CT (GE Healthcare and ART, Montreal Canada) achieving an isotropic resolution of 8 µm. Data sets were analyzed with MicroViewTM (GE Healthcare). Results: Besides the recently characterized features of SMED, such as short limbs and rib abnormalities, we found a changed geometry of the pelves in female DDR2-/- mice during ontogenesis, hallmarked by a narrow pelvic cavity, which explains the inability of these mice to deliver offspring. The typical broadening of enchondral ossificated bones like the sternum, ribs and vertebrae in DDR2-/- mice was systematically quantified over time by performing a modified 3D skeletonization to calculate medial axes and the corresponding thicknesses. Relative bone mineral density was determined over time within the right femur and sternum and suggested a notable decrease of bone mineral density especially in the epiphysis of long bones in mature DDR2-/- animals of both sexes. High resolution micro-CT data sets of the lumbar column revealed a distinctive platyspondyly with multiple exostoses in DDR2-/- mice in comparison to wildtype controls. We also show data to assess the porosity and bifurcation indices of the trabecular meshwork within the lumbar vertebrae. Conclusions: Non-invasive imaging by various CT-techniques shows an excellent sensitivity and accuracy in visualizing skeletal malformations in a murine DDR2 knock out model. Moreover, the high resolution data sets allow a detailed assessment of functional parameters of the bone, like relative bone mass density and its changes over time in a longitudinal study. CT analysis is therefore a helpful tool to evaluate effects of DDR2 loss.

Disclosure of author financial interest or relationships:
**J. Missbach-Guentner**, None; **C. Dullin**, None; **F. Alves**, None.

Presentation Number **P485**
Poster Session 3
September 7, 2012 / 15:15-15:15 / Room: The Liffey

# Multi-Tissue Metabolic Imaging of Glucose and Fatty Acid Metabolism in an Animal Model of Type-2 Diabetes Mellitus

*Sudheer D. Rani, Samuel T. Nemanich, Nicole Fettig, **Kooresh I. Shoghi**, Department of Radiology, Washington University in St. Louis, St. Louis, MO, USA. Contact e-mail: shoghik@wustl.edu*

Objective: Type-2 Diabetes Mellitus (T2DM) is a result of systemic disturbances in metabolism and insulin signaling in peripheral tissues. Pre-clinical positron emission tomography (PET) imaging affords the opportunity to interrogate multiple tissues in parallel to characterize disease mechanisms and efficacy of therapies. To that end, the objective of this study was to non-invasively characterize metabolic disturbances in liver, heart, muscle, and brown adipose tissue (BAT) in an animal model of T2DM using pre-clinical PET following therapy. Methods: The study comprised of 3 groups with 4-6 rats per group all under fasting conditions: 1) Lean rats; 2) Zucker Fatty Diabetic (ZDF) rats; 3) ZDF treated with the PPARg agonist rosiglizatine (RSG) for 5 weeks (ZDF+RSG). Rats were imaged at age of 19 weeks with [11C]Acetate, [11C]Palmitate and 18FDG in series to estimate myocardial blood flow (as published previously), glucose metabolism, and fatty acid (FA) metabolism, respectively. Overall, imaging session lasted 2-3 hours. Where applicable, therapy was initiated 5 weeks before imaging. The arterial input function was estimated using the hybrid image-blood sampling algorithm with C-11 metabolite correction. To estimate the dual-input from the hepatic artery (HA) and portal vein (PV) to the liver, the PVs of 8 rats were cannulated to characterize the kinetics of [11C]Palmitate and 18FDG in the PV. A sum of two-exponentials transfer-function (TF) was optimized to estimate PV kinetics by convolution with arterial input function. Average TF parameter estimates were used to derive PV kinetics for each study. Subsequently, the liver dual input was reconstructed using a weighted sum of HA and PV. A 2-tissue compartment 3 to 4 parameter model (depending on tissue) was used to estimate FDG kinetics. The kinetics of [11C]Palmitate was estimated using a 3-tissue compartments 5 to 6 parameter model depending on tissue. Both micro-parameters of metabolism and lumped-parameters of glucose utilization and FA oxidation and utilization were estimated. Differences in measures were evaluated by student t-test or two-way ANOVA where appropriate. A P value of $P< 0.05$ was considered statistically significant. Results: Fractional glucose uptake in the liver was lower in ZDF rats compared with Lean. RSG resulted in increased FDG uptake in the liver. No significant differences in FDG uptake were observed in muscle, potentially due to differences in GLUT in fasting conditions. In contrast, in both heart and BAT, FDG uptake was lower in ZDF rats and increased significantly following therapy with RSG. FA transport and oxidation was significantly lower in BAT of ZDF rats, which increased significantly to levels seen in lean rats following RSG. Overall FA utilization was significantly higher in muscle and heart of ZDF rats compared to lean, which reduced significantly following RSG. Conclusion: Pre-clinical PET imaging was employed to quantify substrate metabolism in liver, heart, muscle and BAT with implications in characterizing progression of metabolic diseases and efficacy of therapies.

Disclosure of author financial interest or relationships:
**S.D. Rani**, None; **S.T. Nemanich**, None; **N. Fettig**, None; **K.I. Shoghi**, None.

Presentation Number **P486**
Poster Session 3
September 7, 2012 / 15:15-15:15 / Room: The Liffey

# Curcumin derivatives as imaging probes for interscapulae brown adipose tissue

***Chongzhao Ran***[1], *Xueli Zhang*[1,3], *Hongbin Zhang*[2], *Yu-Hua Tseng*[2], *Anna-Liisa Brownell*[1], *Anna Moore*[1], [1]*Martinos Center for Biomedical Imaging, Massachusetts General Hospital/Harvard Medical School, Charlestown, MA, USA;* [2]*Joslin Diabetes Center, Harvard Medical School, Boston, MA, USA;* [3]*Center for Drug Discovery, China Pharmaceutical University, Nanjing, China. Contact e-mail: cran@nmr.mgh.harvard.edu*

Brown adipose tissue (BAT), known widely as a 'good fat', has recently re-emerged as a target for research in a variety of diseases. BAT levels inversely correlate with body-mass index, particularly in the aged population, suggesting its potential role in obesity and diabetes of adults. PET imaging with 18F-FDG is currently the most commonly used method for visualizing BAT. However, stimulation of BAT by cold exposure or drug pretreatment is needed to obtain reproducible PET images. Through screening of a small library of fluorescent probes, we found that BAT can be imaged with curcumin derivatives using near infrared (NIR) optical imaging. One of the probes, CRANAD-2, clearly labeled the interscapular BATs in mice at 60 min after injection. By introducing an 18F and a minor structural modification, CRANAD-2 was then adapted into a PET probe. Both optical and PET images indicated that CRANAD-2 and its 18F analogue had high specificity towards BAT in mice. We also showed that spectral unmixing could be used to dissect fluorescence signals from BAT, WAT (white adipose tissue) and skin. In addition, we demonstrated that the selected probe could be used for monitoring the activation of BAT by norepinephrine treatment. The advantage of our probe is that no stimulation/pretreatment is needed. We believe our probe will be a very useful tool for imaging BAT.

Disclosure of author financial interest or relationships:
**C. Ran**, None; **X. Zhang**, None; **H. Zhang**, None; **Y. Tseng**, None; **A. Brownell**, None; **A. Moore**, Fluoropharma, Grant/research support .

Presentation Number **P487**
Poster Session 3
September 7, 2012 / 15:15-15:15 / Room: The Liffey

# CT Perfusion Monitoring of Pancreatic Blood Flow in Streptozotocin-induced Diabetic Rats

***Joo Ho Tai***[1,2], *Jennifer Hadway*[1], *Ian Welch*[3], *Ting-Yim Lee*[1,2], [1]*Lawson Health Research Institute, St. Joseph's Healthcare, London, ON, Canada;* [2]*Imaging Research Laboratories, Robarts Research Institute, Western University, London, ON, Canada;* [3]*Animal Care and Veterinary Services, Western University, London, ON, Canada. Contact e-mail: jtai@imaging.robarts.ca*

Introduction; Type 1 Diabetes (T1D) is an autoimmune-mediated disease destroying β-cells in the islets of Langerhans throughout the pancreas. A common feature of immune-mediated diseases is the build-up of an inflammatory infiltration in the target organ. The subsequent inflammatory response dilates the blood vessels around the site of inflammation, allowing increased blood flow to the area. Inflammation in pancreatic islets is the initial pathological consequences of T1D, leading to the early and progressive loss of β-cell mass prior to the onset of diabetes. It develops a chronic pancreatic insulitis persisting for 5-15 years without overt clinical symptoms such as high blood glucose or HbA1c. We have developed a high-resolution dynamic contrast enhanced-CT (DCE-CT) technique to quantitatively and precisely assess blood flow (BF) in microvessels in an organ or tissue of interest. In the current study, we measured DCE-CT derived BF in the pancreas of streptozotocin (STZ)-induced diabetic rats to investigate how BF correlated with change of blood glucose and whether it could be used as a surrogate imaging marker for the inflammatory responses involved in the development of diabetes of the rat. Methods; The male Wistar rats were given a single injection of 55 mg/kg, i.p. of STZ (n = 3) or a control injection with vehicle only (n = 3). Before scanning, each rat was weighed and maintained under inhalational anesthesia with a mixture of O2 and 0.75~1.5% isoflurane during scanning. Fasting blood glucose (FBG) was measured from the tail vein using hand-held glucometer. Intravenous bolus injection of ketamine/xylazine was followed to facilitate intubation. To suppress spontaneous respiration, pancuronium was given i.v. and during the 1st phase of scanning, artificial ventilator was turned off. Physiological parameters including pCO2, pO2, heart rate, and body temperature were maintained within normal range. Each rat was scanned using a clinical CT scanner (GE Healthcare) with infusion of iodinated contrast agent (Omnipaque 300, GE Healthcare) at day 0 (D0; baseline, before STZ or vehicle treatment) and D3, 6, 9 & 18 (after the treatment). After scanning, quantitative maps of average (AVG) and BF were calculated from the acquired images with the CT Perfusion software (GE Healthcare). The contrast-enhanced AVG maps highlighting the pancreas and the spleen were calculated by averaging dynamic CT images within peak artery density window (AVG*hi*, Figure) and used to contour the rat pancreas to measure the pancreatic BF parameter values. Results; Both FBG and DCE-CT derived pancreatic BF were significantly increased at D3 in STZ-treated rats, compared to those in control rats (Figure). Even though the transient increase in BF of the diabetic rat arised from the acute toxicity of STZ on the insulin-secreting β-cells, prior histopathological studies showed that the toxicity elicited only a mild inflammatory response in the pancreas at D3. Conclusion; These results suggest the potential feasibility of using DCE-CT to monitor for early and ongoing autoimmune-mediated inflammatory reaction in the pancreas of an appropriate T1D animal model.

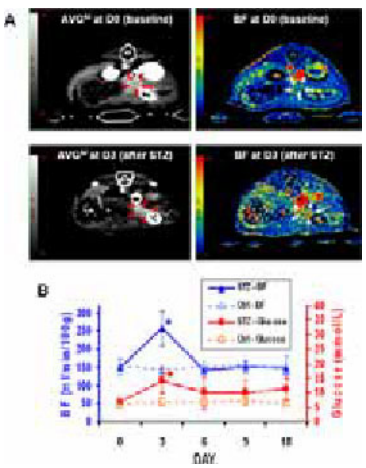


Figure A. Representative transaxial AVG*hi* and BF maps at D0 (baseline) and D3 (after STZ treatment) indicating the region of pancreas highlighted in the AVG*hi* maps (red arrows; white arrows in corresponding BF maps). B. Changes in fasting blood glucose (red lines, right axis) and DCE-CT derived BF (blue lines, left axis) in the pancreas of STZ-induced diabetic rats (n = 3) and control rats (Ctrl, dotted lines, n = 3) before (baseline, D0) and after STZ treatment (upto D18) (mean ± SD, *; $p \leq 0.05$ *vs.* corresponding control group, Mann-Whitney *U* test).

Disclosure of author financial interest or relationships:
**J. Tai**, None; **J. Hadway**, None; **I. Welch**, None; **T. Lee**, GE Healthcare, Grant/research support; GE Healthcare, Other financial or material support .

Presentation Number **P488**
Poster Session 3
September 7, 2012 / 15:15-15:15 / Room: The Liffey

# An ovarectomized mouse model of bone loss reveal reduced uptake of a fluorescent bisphosphonate but no quantitative differences in binding are observed in a parathyroid hormone induced bone gain mouse model

***Sanjay Tiwari***[1], *Graeme M. Campbell*[1], *Friederike Grundmann*[2], *Nicolai Purcz*[3], *Markus Böttcher*[1], *Olga Gavrilova*[1], *Marc Müller*[1], *Robert Tower*[1], *Christian Schem*[2], *Claus C. Glueer*[1], [1]*Diagnostic Radiology, UK-SH, Kiel, Germany;* [2]*Gynecology, UK-SH, Kiel, Germany;* [3]*Oral and Maxillofacial Surgery, UK-SH, Kiel, Germany. Contact e-mail: stiwari@email.uni-kiel.de*

Introduction: We tested the utility of the fluorescent pamidronate, Osteosense 750 (Perkin Elmer) as a reliable marker of bone remodeling. We hypothesized that bone formation activity would be detected by increased binding of Osteosense750 to mineralized areas as well as greater retention of the bound probe. Conversely, bone loss activity would be detected by decreased binding due to less mineralized areas as well as an increased rate of removal of the fluorescent probe. Such an imaging tool would be useful for monitoring effectiveness of anti-resorptive therapy. Method: One group of mice were ovarectomized (OVX) at 16 weeks to induce osteoporosis (n=8). A second group of mice were treated with parathyroid hormone (PTH) intermittently (40 µg/kg, n=8), which has been reported to result in an anabolic effect with an increase in bone mass. A third group consisted of sham operated mice which were used as controls. The three groups of mice were injected with Osteosense 750 every two weeks and fluorescent signal was quantified at the distal femur/proximal tibia knee region of the hind legs as well as the spine, using a Fluorescent Molecular Tomography unit (FMT2500, Perkin Elmer). Bone density measurements were obtained by performing parallel micro-CT scans (vivaCT40, Scanco Medical). Weekly FMT and micro-CT scans were performed for a period of 4 weeks. Results: Micro-CT measurements confirmed that upon intermittent PTH administration, bone density of the knee region increased significantly over the 4 week period. Measurement of Osteosense750 fluoresence revealed no significant increase in signal and no difference in retention of signal compared to control mice ($p < 0{,}001$). Biochemical markers showed increased serum Osteocalcin (Osteoblast activity) and TRAcP (osteoclast activity) levels. Micro-CT measurement in ovarectomized mice revealed a significant decrease in bone density within two weeks. Osteosense750 fluoresence revealed a significant decrease in signal in the ovarectomized mice but no significant difference in the retention of the signal was observed. Conclusion: In ovarectomized mice follow up administration of Osteosense750 revealed decreased binding, possibly reflecting decreased bone surface area. In mice treated with Parathyroid Hormone, increase in bone deposition activity giving rise to increased bone density is not detected quantitatively by Osteosense 750 binding.

Disclosure of author financial interest or relationships:
**S. Tiwari**, None; **G.M. Campbell**, None; **F. Grundmann**, None; **N. Purcz**, None; **M. Böttcher**, None; **O. Gavrilova**, None; **M. Müller**, None; **R. Tower**, None; **C. Schem**, None; **C.C. Glueer**, None.

Presentation Number **P489**
Poster Session 3
September 7, 2012 / 15:15-15:15 / Room: The Liffey

# In Vivo Imaging of Free Radicals with MRI in Diabetes

***Rheal Towner***[1], *Nataliya Smith*[1], *Debra Saunders*[1], *Florea Lupu*[2], *Dario C. Ramirez*[3], *Sandra E. Gomez-Mejiba*[3], *Marcelo G. Bonini*[4], *Marilyn Ehrenshaft*[5], *Ronald P. Mason*[5], [1]*Advanced Magnetic Resonance Center, Oklahoma Medical Research Foundation, Oklahoma City, OK, USA;* [2]*Cardiovascular Research, Oklahoma Medical Research Foundation, Oklahoma City, OK, USA;* [3]*Experimental Therapeutics, Oklahoma Medical Research Foundation, Oklahoma City, OK, USA;* [4]*Pharmacology, University of Illinois, Chicago, IL, USA;* [5]*Laboratory of Pharmacology & Chemistry, NIEHS, Research Triangle Park, NC, USA. Contact e-mail: Rheal-Towner@omrf.org*

Introduction: Oxidative stress plays a crucial role in many disease processes, including diabetes. In this study we report on the in vivo imaging of protein/lipid radicals for the first time. A novel approach involves the use of molecular MRI and immuno-spin trapping to monitor levels of reactive free radicals in oxidative stress-related diseases. In this study, mMRI assessments focused on the liver, kidney and lung regions, which are all organs that undergo diabetes-associated pathologies. Methods: To recognize the DMPO-protein/lipid radicals, a mouse monoclonal anti-DMPO antibody was used (Fig. 1). The macromolecular contrast material, biotin-BSA-Gd-DTPA, was prepared as previously described [1]. C57BL/6J mice (n=20; 6-8 weeks) were treated with STZ (100 mg/kg i.p./day for 2 days), and between 4-6 weeks mice were assessed for glucose levels. DMPO (25 µl in 100 µl saline) was administered i.p. 3 x daily (every 6 hours) for 5 days (i.e. 0.42 µl DMPO/µl saline/day). Mice were initiated administration of DMPO 7 weeks following STZ administration, prior to injection of the anti-DMPO probe. MR experiments were carried out under general anaesthesia (1 2% Isoflurane, 0.8-1.0 L/min O2). MR equipment that was used included a Bruker Biospec 7.0 Tesla/30 cm horizontal-bore imaging spectrometer. Anaesthetised (2% Isoflurane) restrained mice were placed in an MR probe, and their tissues/organs (liver/kidneys/heart) were localised by MRI. Mice were imaged at 8 weeks following STZ administration. T1-weighted images were obtained using a FISP (Fast Imaging with Steady state Precession) sequence (TR 3.6 ms, TE 1.8 ms, 4 steps per acquisition, 3x3 cm2 FOV, 1 mm slice thickness, 8 segments, scan repetition time 10 s). Statistical differences between the probe administered and control groups, were analyzed with an unpaired, two-tailed Student t test by using commercially available software (InStat; GraphPad Software, San Diego, CA). A p value of less than 0.05 was considered to indicate a statistically significant difference. Results: MR signal intensities, which increase in the presence of a Gd-based molecular probe, were significantly higher within livers, kidneys and lungs of diabetic animals administered the anti-DMPO probe, compared to controls. Fluorescence images validated the location of the anti-DMPO probe in excised tissues via conjugation of streptavidin-Cy3 which targeted the probe biotin moiety, and immunohistochemistry was used to validate the presence of DMPO-adducts in diabetic mouse livers. Conclusions: This is the first report of imaging in vivo membrane-bound (e.g. protein and lipids) radicals. Although the application presented was in a diabetes model, this method could be invaluable in assessing the involvement of free radical damage to proteins and membrane-bound lipids in multiple tissue/organ pathologies associated with various oxidative stress-related diseases. mMRI provides the advantage of image resolution, as well as the assessment of the spatial location of in vivo oxidative stress events, coupled with immuno-spin trapping, in heterogeneous tissues or organs.

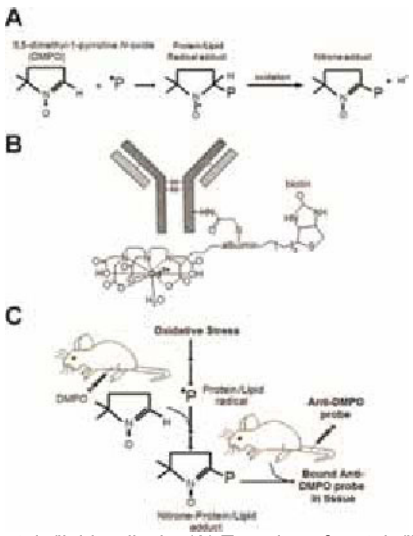


Figure 1: Schematic description of in vivo imaging of protein/lipid radicals. (A) Trapping of protein/lipid radicals with DMPO. Protein/Lipid Radical adducts can be assessed by immuno-trapping. (B) Illustration of the anti-DMPO mMRI probe. (C) Immuno-trapping of protein/lipid radicals with anti-DMPO mMRI probe. DMPO is injected i.p. to trap protein/lipid radicals. Anti-DMPO is injected i.v. to target Nitrone-Protein/Lipid adducts, which can be visualized in vivo ny mMRI.

Disclosure of author financial interest or relationships:
**R. Towner**, None; **N. Smith**, None; **D. Saunders**, None; **F. Lupu**, None; **D.C. Ramirez**, None; **S.E. Gomez-Mejiba**, None; **M.G. Bonini**, None; **M. Ehrenshaft**, None; **R.P. Mason**, None.

Presentation Number **P490**
Poster Session 3
September 7, 2012 / 15:15-15:15 / Room: The Liffey

# A partial loss of insulin-producing beta cells is detected by non-invasive bioluminescence imaging, and manganese-enhanced MRI in female RIP-DTr mice

***Laurent Vinet***[1], *John M. Virostko*[2], *Pedro L. Herrera*[1], *Xavier Montet*[3], *Alvin C. Powers*[4], *Paolo Meda*[1], [1]*Cell Physiology and Metabolism, University of Geneva, Geneva, Switzerland;* [2]*Institute of Imaging Science, Vanderbilt University, Nashville, TN, USA;* [3]*Department of Radiology, Geneva University Hospital, Geneva, Switzerland;* [4]*Division of Diabetes, Endocrinology, and Metabolism, Vanderbilt University, Nashville, TN, USA. Contact e-mail: laurent.vinet@unige.ch*

Non-invasive imaging of the insulin-producing beta cells is expected to provide novel information about the natural history of their loss in diabetes, and about their potential recovery after targeted therapy. However, it remains to be shown whether imaging methods can detect the 30-50% loss of beta cells, which is anticipated in patients with type 2 diabetes, the largest target of the imaging methods, specifically under clinically relevant conditions. Also questioned is the ability of imaging methods to identify the possible recovery of some of these cells. To address these questions, we have investigated transgenic mice whose beta cells express firefly luciferase (Luc) and the receptor for diphtheria toxin (DTR), under control of the insulin promoter (Ins or RIP). In this line, injection of luciferin induces the production of light from beta cells, whereas injection of diphtheria toxin induces the loss of about 99% and 50% beta cells in males and females, respectively. Ins-Luc-DTR mice received an ip injection of 150 mg/Kg bw luciferin to be imaged by bioluminescence (BLI) using a IVIS 200 apparatus, prior and after 3 injections of 5 µg /Kg bw diphtheria toxin, on days 0, 3 and 4. Thereafter, groups of 3-5 mice were repeatedly monitored for various periods of time, and up to one year. The pancreatic signal, reporting on beta cell mass, decreased sharply in all animals after the diphtheria toxin injections. However, this decrease was about 95% in male mice, and 50% in female mice, consistent with the residual levels of pancreatic insulin, which were about 0.5% and 50% the control value during the first 2 months after the diphtheria toxin injection. The pancreatic BLI signal and the insulin content of males did not change with time. In contrast, both the bioluminescence signal and the insulin content of pancreas progressively increased with time in several, but not all female mice, returning to control levels 8-12 months after the diphtheria toxin injections. Thus, BLI allows for the quantitative evaluation of graded beta cell loss, and for monitoring its recovery. Other RIP-DTR mice were imaged by manganese-enhanced MRI (MEMRI), using a 1.5T Philips Achieva apparatus and a surface coil adapted for mice, after the i.p. injection of 7.9 mg/Kg bw MnCl2 and 2 g/Kg bw glucose,T1-weighted images were obtained using a multi-slice gradient echo sequence before and one week after the diphtheria toxin injections mentioned above. The pancreatic signal, reporting on beta cell mass, decreased in all animals after the diphtheria toxin injections. However, this decrease was about 66% in male mice and 31% in female mice, paralleling the difference in the insulin content of males and females, one week after the diphtheria toxin injection. Thus, a clinically translatable MEMRI approach can discriminate mice with different beta cell and insulin contents. The data provide the proof of principle that alterations in beta cell mass expected in patient with type 2 diabetes can be quantified, as a function of time, in individual mice, using methods that do not involve isotopic labelling. Some of these methods could conceivably be translated into the clinical arena.

Disclosure of author financial interest or relationships:
**L. Vinet**, None; **J.M. Virostko**, None; **P.L. Herrera**, None; **X. Montet**, None; **A.C. Powers**, Lilly, Inc, Grant/research support; National Institutes of Health, Grant/research support; Juvenile Diabetes Research Foundation, Grant/research support; VA Research Service, Grant/research support; **P. Meda**, Sanofi, Grant/research support; Servier, Grant/research support; Novo Nordisk, Grant/research support .

Presentation Number **P491**
Poster Session 3
September 7, 2012 / 15:15-15:15 / Room: The Liffey

# Bioluminescence Imaging Reveals Dynamics of Beta Cell Loss in the Non-obese Diabetic (NOD) Mouse Model

***John M. Virostko***[1], *Armandla Radhika*[2], *Alvin C. Powers*[2], [1]*Institute of Imaging Science, Vanderbilt University, Nashville, TN, USA;* [2]*Division of Diabetes, Endocrinology, and Metabolism, Department of Medicine, Vanderbilt University, Nashville, TN, USA. Contact e-mail: jack.virostko@vanderbilt.edu*

The ability to image pancreatic beta cell mass in a model of type 1 diabetes mellitus would provide insight into the dynamics of autoimmune diabetes and serve as a useful tool for evaluating therapeutics. The non-obese diabetic (NOD) mouse has long served as a model of type 1 diabetes and has proven useful in revealing the fundamental immune process resulting in beta cell destruction. To determine the dynamics of beta cell mass in the NOD mouse, we developed a transgenic mouse line that expresses the luciferase (Luc) optical reporter under control of the insulin promoter on the NOD background. Bioluminescence imaging (BLI) of this NOD-Luc mouse model reveals light emission solely from the beta cell that can be imaged noninvasively using a CCD camera to monitor beta cell mass. Consistent with previous studies of the NOD model, NOD-Luc mice exhibited insulitis and progression towards hyperglycemia with increasing age. Bioluminescence also decreased with increasing age and correlated with morphometric measurements of beta cell mass, serum insulin measurements, and pancreatic insulin content, indicating that BLI provides a noninvasive metric of beta cell mass in this model. Diabetes incidence was 67% in female mice and 57% in male mice, with an earlier incidence in female mice. In mice that became diabetic, a steady decline in bioluminescence measurements preceded the onset of hyperglycemia by several weeks, with hyperglycemia ensuing after a loss of BLI of approximately 90%. Statistical modeling revealed that BLI could be used as a predictive tool to presage the onset of hyperglycemia. Mice that did not become hyperglycemic also displayed a decrease in bioluminescence with increasing age, suggesting that these mice also exhibited beta cell destruction. However, the magnitude of bioluminescence decrease was not as great in mice that did not become hyperglycemic and BLI stabilized in these mice at approximately 40% of the initial bioluminescence. The preclinical monitoring of beta cell mass developed in this model should increase our understanding of autoimmune diabetes, provide an early biomarker of beta cell loss to help identify important therapeutic windows, and permit standardization of therapeutic dosage and timing to the status of beta cell loss.

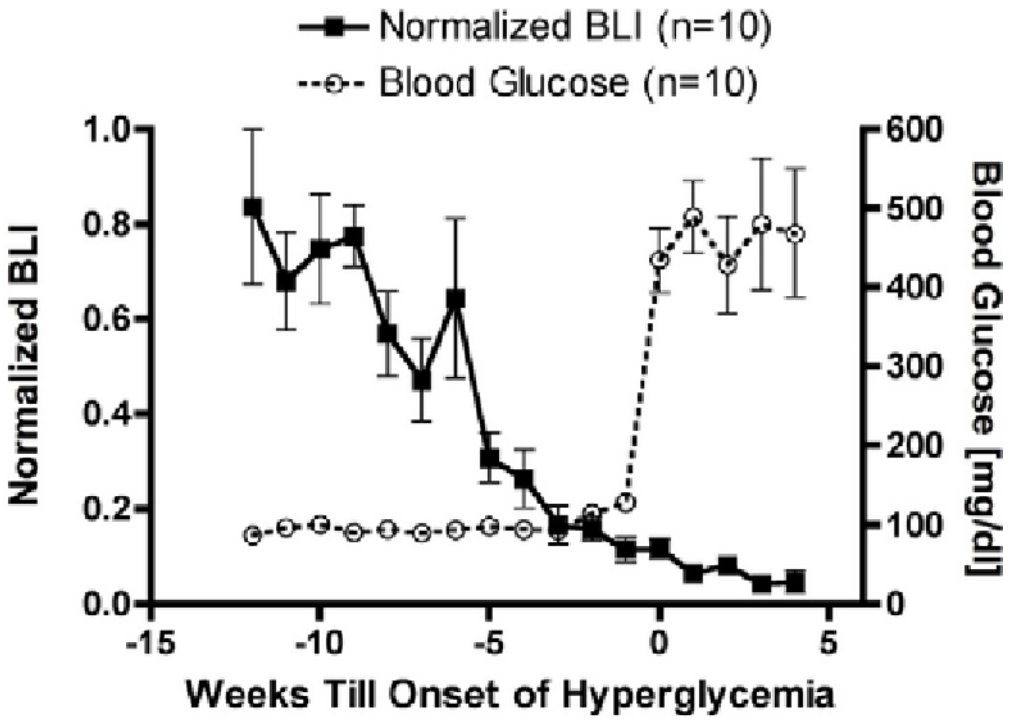


Female NOD-Luc mice that become diabetic display a gradual reduction in BLI with increasing age that precedes hyperglycemia by several weeks.

Disclosure of author financial interest or relationships:
**J.M. Virostko**, None; **A. Radhika**, None; **A.C. Powers**, Lilly, Inc, Grant/research support; National Institutes of Health, Grant/research support; Juvenile Diabetes Research Foundation, Grant/research support; VA Research Service, Grant/research support .

Presentation Number **P492**
Poster Session 3
September 7, 2012 / 15:15-15:15 / Room: The Liffey

# Heparin-binding peptides bFGF and p5R bind to different targets in amyloid-laden mice and controls

***Jonathan S. Wall***[2,1]*, Robert Donnell*[3]*, Tina A. Richey*[2]*, Alan Stuckey*[1]*, Keiichi Higuchi*[4]*, Emily B. Martin*[2]*, Stephen J. Kennel*[2,1]*,*
*[1]Radiology, University of Tennessee Graduate School of Medicine, Knoxville, TN, USA; [2]Medicine, University of Tennessee Graduate School of Medicine, Knoxville, TN, USA; [3]Pathobiology, University of Tennessee College of Veterinary Medicine, Knoxville, TN, USA; [4]Aging Biology, Shinshu University Graduate School of Medicine, Matsumoto, Japan. Contact e-mail: jwall@utmck.edu*

The peptide p5R is one of a panel of polybasic, heparin-binding peptides that we have shown capable of preferentially binding amyloid deposits *in vivo* and in tissue sections. Basic fibroblast growth factor (bFGF) also binds heparin-like heparan sulfate proteoglycans (HSPG) and in one study was shown to bind to Aβ amyloid deposits in the brains of transgenic mice when administered intranasally (Shi J, *et al.* (2002) **J Nucl Med.**, Aug;**43**(8):1044-51). The aim of this study was to compare the biodistribution of radioiodinated bFGF and peptide p5R in 2 murine models of visceral amyloidosis as well as in wild type mice by using SPECT imaging, tissue biodistribution measurements and micro-autoradiography. Both proteins were radiolabeled with $^{125}$I and purified by size exclusion chromatography using a Sephadex G25 solid phase. Radiopurity was assessed by SDS-PAGE and phosphor imaging. Mice (n = 3 per group) were injected with 44 ± 10 µCi of $^{125}$I-bFGF or 121 ± 5 µCi of $^{125}$I-p5R (Mean ± SD) iv in the lateral tail vein. At 2 h pi the mice were euthanized and SPECT/CT images acquired using an Inveon trimodality platform. Tissues were then harvested at necropsy and the biodistribution of radiotracer calculated and expressed as % injected dose per gram tissue (%ID/g). Finally, tissue samples were fixed in formalin, paraffin embedded, sectioned and exposed to photographic emulsion for 4 d (p5R) or 8 d (bFGF). Even though both bFGF and peptide p5R bind heparin and amyloid, their biodistribution was remarkably different in all 3 mouse models. Both bound AA amyloid in the liver spleen, kidneys, pancreas and other sites of deposition. However, $^{125}$I-bFGF was also observed in normal tissue at sites of "expected" HSPG synthesis including the hepatic and splenic sinusoids, and renal glomerulae. In mice with advanced ApoA2c amyloidosis $^{125}$I-bFGF was observed in micro-autoradiographs bound to splenic, pulmonary and hepatic amyloid deposits; however there was also considerable binding of this radiotracer in non-amyloid laden regions of these organs which complicated interpretation of specific binding. In contrast, $^{125}$I-p5R peptide bound preferentially to amyloid in the liver and lung and not the surrounding healthy tissue. Of note, the p5R peptide did not bind significantly to splenic ApoA2c amyloid, and observation that is under further investigation. These data indicate that even though bFGF and p5R react with both heparin and amyloid the distribution of the p5R target *in vivo* is greatly restricted as compared to the ligands bound by bFGF. The data suggest that the 2 proteins have distinct but overlapping reactivity profiles and further that p5R, because of its lack of binding to HSPG in healthy organs could be used for the radiodetection of visceral amyloid with minimal contribution of binding to healthy tissues.

Disclosure of author financial interest or relationships:
**J.S. Wall**, Elan, Grant/research support; Solex LLC, Stockholder; **R. Donnell**, None; **T.A. Richey**, Solex, Stockholder; **A. Stuckey**, Solex LLC, Stockholder; **K. Higuchi**, None; **E.B. Martin**, Solex LLC, Stockholder; **S.J. Kennel**, solex, Stockholder .

Presentation Number **P493**
Poster Session 3
September 7, 2012 / 15:15-15:15 / Room: The Liffey

# Arginine-rich peptide p5R provides enhanced binding to visceral amyloid deposits *in vitro* and *in vivo*

***Jonathan S. Wall***[2,1]*, Tina A. Richey*[2]*, Alan Stuckey*[1]*, Angela Williams*[2]*, Ying Huang*[1]*, Emily B. Martin*[2]*, Dustin Osborne*[1]*, Sallie D. Macy*[2]*, Stephen J. Kennel*[2,1]*, [1]Radiology, University of Tennessee Graduate School of Medicine, Knoxville, TN, USA; [2]Medicine, University of Tennessee Graduate School of Medicine, Knoxville, TN, USA. Contact e-mail: jwall@utmck.edu*

Although recent advances have been made in the translation of novel tracers for imaging Aβ amyloid in patients with mild cognitive impairment and Alzheimer's disease, routine methods for imaging the whole body distribution of visceral amyloidosis are unavailable in the US. Patients in the US with diseases such as light chain (AL) or reactive (AA) amyloidosis, as well as those with transthyretin (ATTR) are forced to travel to London, England to seek whole body amyloid imaging studies for monitoring response to therapy and prognostication In attempts to develop synthetic peptides for peripheral amyloid imaging, we identified a heparin-binding peptide, p5 that preferentially bound amyloid *in vivo* and did not associate significantly with heparan sulfate glycosaminoglycans expressed by healthy tissues. The next generation of amyloid-reactive peptides was synthesized with varied sequences, tested in battery of assays and the arginine-substituted peptide, p5R, was selected for further evaluation as a specific amyloid-reactive reagent *in vitro* and *in vivo*. The p5R peptide was radiolabeled and the reactivity of p5R with heparin and $^{125}$I-p5R with synthetic amyloid fibrils assessed and compared to peptide p5. The kinetic biodistribution of $^{124}$I-p5R and $^{124}$I-p5 was compared in wild type mice by using dynamic PET imaging. The long term reactivity of $^{125}$I-p5R and $^{125}$I-p5 in amyloid *in vivo* was compared in individual mice using serial SPECT imaging up to 72 hrs pi. Preferential binding of $^{125}$I-p5R with amyloid *in vivo* was confirmed by micro-autoradiography. Peptide p5R bound to heparin and synthetic amyloid fibrils with greater affinity than p5 based on the salt concentration required for release of each peptide. In healthy mice, the $^{124}$I-p5R was rapidly cleared from the circulation by the kidneys where it was catabolized and dehalogenated. In contrast, in mice with AA amyloidosis, $^{125}$I-p5R accumulated in amyloid-laden tissues within 2 h post-injection and remained visible in SPECT images as late as 72 h pi providing tissue-to-muscle ratios of 80:1 and 143:1 in the liver and spleen, respectively. Both biotinylated and $^{125}$I-labeled p5R peptide could be used to accurately detect human AL, AA and ATTR amyloid in formalin-fixed, paraffin-embedded tissue sections. Based on these findings, we suggest that p5R may be an effective agent for detecting amyloid deposits *in vivo* and *ex vivo*. Due to its faster clearance from the kidney and enhanced binding to amyloid, relative to p5, p5R is optimized for use as a radiotracer for the non-invasive molecular imaging of visceral amyloid deposits in patients.

Disclosure of author financial interest or relationships:
**J.S. Wall**, Elan, Grant/research support; Solex LLC, Stockholder; **T.A. Richey**, Solex, Stockholder; **A. Stuckey**, Solex LLC, Stockholder; **A. Williams**, None; **Y. Huang**, None; **E.B. Martin**, Solex LLC, Stockholder; **D. Osborne**, University of Tennessee, Employment; Siemens Medical Solutions, Employment; **S.D. Macy**, None; **S.J. Kennel**, solex, Stockholder .

Presentation Number **P494**
Poster Session 3
September 7, 2012 / 15:15-15:15 / Room: The Liffey

# CT and $^{19}$F MR Imaging for Quantitative Tracking of Encapsulated Mesenchymal Stem Cells in a Peripheral Arterial Disease Model

***Guan Wang***[1,2], *Yingli Fu*[1,3], *Steven M. Shea*[4], *Judith A. Cook*[1], *Dara Kraitchman*[1,3], [1]*Radiology and Radiological Science, Johns Hopkins University, Baltimore, MD, USA;* [2]*Electrical and Computer Engineering, Johns Hopkins University, Baltimore, MD, USA;* [3]*School of Medicine, Johns Hopkins University, Baltimore, MD, USA;* [4]*Center for Applied Medical Imaging, Siemens Corporation, Corporate Research and Technology, Baltimore, MD, USA. Contact e-mail: wangg62@gmail.com*

**Introduction**: Nearly 12% of the Americans suffer from peripheral arterial disease (PAD) and, due to the extent of their disease, some are not eligible for conventional angioplasty or surgical bypass. Microencapsulated stem cell (SC) therapy offers a novel means to transplant allogeneic SCs to avoid immunorejection and enable tracking using conventional imaging modalities. However, quantitative evaluation of cell fate has been elusive. In this study, we explore c-arm CT and $^{19}$F-MRI for serial evaluation of dual X-ray/MR-visible SC microcapsules (XMRCaps) in a rabbit PAD model using clinical imaging systems. **Methods**: XMRCaps were produced using a modified alginate-poly-L-lysine-alginate microencapsulation method impregnating 12% v/v perfluorooctyl bromine (PFOB) and human SCs. In vitro validation studies were performed in an agarose phantom consisting of four layers of 50, 100, and 200 XMRCaps. C-arm CT images (dynaCT, Siemens Artis Zee, 240° scan angle; 0.5° increment; 0.36 μGy dose per pulse; 48 cm field of view) were acquired and reconstructed at 0.37 mm$^3$ voxel size. $^{19}$F MRI was acquired with a 4-channel Tx/Rx $^{19}$F coil using a steady-state free precession pulse sequence (TrueFISP, Siemens Tim Trio, 4.1 ms repetition time; 2.0 ms echo time; 32 averages; 250x250mm field of view with 192x192 image matrix, 1002 Hz/pixel bandwidth, 1.3x1.3x1.25 mm voxel size). Reference $^1$H MRI was acquired with the system single channel body coil or the system body matrix coil (6 channel phased-array) using a gradient echo sequence (15 ms repetition time; 5.45 ms echo time 186x230 mm field of view, 0.45x0.45x1.5mm voxel size). Segmentation of CT and MRIs was performed using a region-growing algorithm. Relative fluorine concentration was determined by integrating $^{19}$F signal intensity over the segmented volume. In vivo studies were performed in two rabbits receiving 4-6 XMRCap injections in the medial thigh. CT and MRI volumes were acquired at one and two weeks after XMRCap administration. **Results**: Calculated XMRCap volumes in CT and MRIs were highly concordant in vitro (y=0.8x+3.0, R=0.95). In the in vivo studies, the XMRCap injection sites were visible at both time points. In addition, XMRCap volume decreased 27.6±9.6% over a week, whereas the $^{19}$F concentration decreased 50.6±6.8%. **Conclusions**: MRI provides accurate assessment of XMRCap volumes that are slightly larger than CT perhaps due to partial volume effects with MRI. In vivo, degradation of XMRCaps in the ischemic environment of the PAD rabbit could be quantified on MRI and CT. However, only MRI was able to demonstrate the more profound changes in density of the XMRCap injections as decreasing fluorine concentrations. Thus, MRI provides a method to quantify the changes in microcapsules and, thereby stem cell engraftment, more precisely without ionizing radiation.

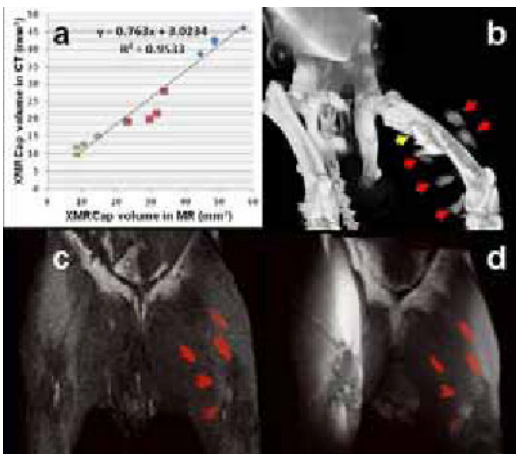


Fig1 (a) Linear regression analysis of the volumes of 200(blue), 100(red) and 50(green) XMRCaps in MR vs. CT. (b) DynaCT image of a rabbit model of PAD acquired one week after XMRCap injection. Arrows denote the platinum coil (yellow) and the injection sites (red). (c) $^{19}$F MR image (red) of the same rabbit fused with gray scale proton MR image acquired shortly after DynaCT imaging. The volumes and the locations of the injections are highly consistent with those in the CT image. (d) $^{19}$F MR image (red) of the same rabbit fused with gray scale MR proton image acquired two weeks after injection. Both the volume and fluorine concentration of the injections significantly decreased.

Disclosure of author financial interest or relationships:
**G. Wang**, None; **Y. Fu**, None; **S.M. Shea**, Siemens Corporation, Corporate Research & Technology, Employment; **J.A. Cook**, None; **D. Kraitchman**, SIemens Healthcare, Grant/research support; Boston Scientific Corporation, Grant/research support; Surefire Medical, Inc., Grant/research support; MRI Interventions, Other financial or material support .

Presentation Number **P495**
Poster Session 3
September 7, 2012 / 15:15-15:15 / Room: The Liffey

# Click chemistry for 18F-labelling of exendin-4

***Cheng-Bin Yim***[1], *Kirsi Mikkola*[1], *Johanna Rokka*[1], *Veronica Fagerholm*[1], *Johan Rajander*[2], *Viki-Veikko Elomaa*[1], *Tuula Tolvanen*[1], *Vesa Oikonen*[1], *Tamiko Ishizu*[1], *Pirjo Nuutila*[1], *Olof Solin*[2,1], [1]*Turku PET Centre, University of Turku, Turku, Finland;* [2]*Accelerator Laboratory, Åbo Akademi University, Turku, Finland. Contact e-mail: chbiyi@utu.fi*

Quantitative non-invasive imaging of intact or transplanted pancreatic beta-cells would provide a valuable tool for diagnosing diabetes and for monitoring the effects of therapeutic interventions. Exendin-4 is a stable analogue of glucagon-like peptide 1 (GLP-1), which targets the GLP-1 receptor (GLP-1R). The GLP-1R is abundantly expressed in pancreatic beta-cells and is considered a promising molecular target for beta-cell imaging [1]. 18F-labelled target-specific peptides are becoming widely used as in vivo imaging agents, because 18F is readily available from most small medical cyclotrons, has a half-life (110 min) that matches the pharmacokinetics of most peptides, and because 18F decays with almost 100% positron efficiency while its low positron energy (635 keV) results in high imaging resolution (<2 mm) [2]. Methods based on the Cu(I)-catalyzed alkyne/azide cycloaddition (click chemistry) were explored for the fluorination of peptides [3]. This reaction is chemoselective and fast, which can be performed in high yields under mild reaction conditions, and the 1,2,3-triazole formed has similar polarity and size with an amide bond [4]. We have designed a 18F-labelled exendin-4, using the cycloaddition between an azide-functionalized exendin-4 and [18F]fluoro-propargyl-triethylene glycol (Figure 1). In short, alkyne tosylate 1 and the 18F-fluoride-Kryptofix complex are allowed to react in DMSO (100 °C). Subsequently, peptidyl azide 3 is added to the reaction mixture and allowed to react in the presence of CuSO4 (1.2 equiv) and sodium ascorbate (1.5 equiv). Radiochemical yield of precursor 2 and 18F-exendin-4 (4) are determined by TLC and HPLC, respectively. Currently, the scope of this reaction is being explored and its labelling conditions optimized. Preclinical studies with 18F-exendin will include in vivo stability, dosimetry, and distribution kinetics in healthy and diabetic rat models, and results will be compared to a reference (64Cu-NODAGA-exendin). [1] M. Gotthardt, M. Fischer, I. Naeher, J. B. Holz, H. Jungclas, H.-W. Fritsch, M. Béhé, B.Göke, K. Joseph, T. M. Behr, Eur. J. Nucl. Med. Mol. Imaging. 2002, 29, 597-606. [2] W. Wadsak, M. Mitterhauser, Eur. J. Radiol. 2010, 73, 461-9. [3] Z.-B. Li, Z. Wu, K. Chen, F. T. Chin, X. Chen, Bioconjugate Chem. 2007, 18, 1987-94. [4] V. D. Bock, H. Hiemstra, J. H. van Maarseveen, Eur. J. Org. Chem. 2006, 51-68.

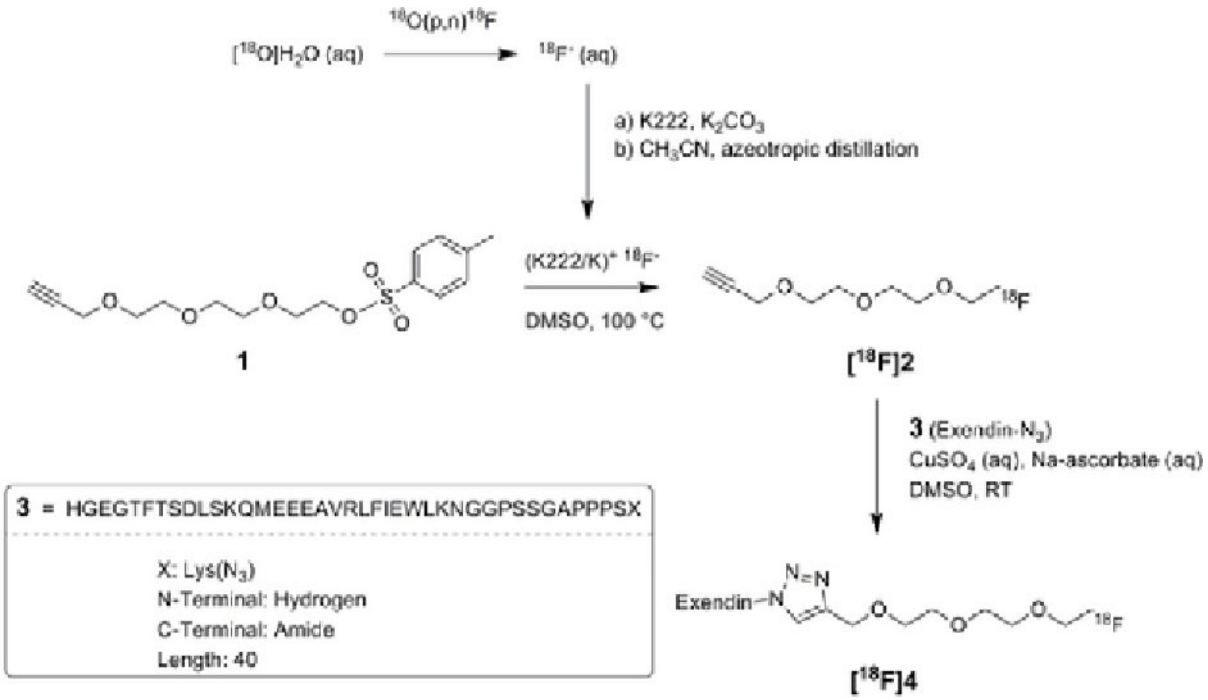


Production of 18F-fluoride, nucleophilic 18F-labeling and synthesis of exendin-4 via click chemistry.

Disclosure of author financial interest or relationships:
**C. Yim**, None; **K. Mikkola**, None; **J. Rokka**, None; **V. Fagerholm**, None; **J. Rajander**, None; **V. Elomaa**, None; **T. Tolvanen**, None; **V. Oikonen**, None; **T. Ishizu**, None; **P. Nuutila**, None; **O. Solin**, None.

Presentation Number **P496**
Poster Session 3
September 7, 2012 / 15:15-15:15 / Room: The Liffey

# In Vivo [18F]FDG PET Imaging as A Biomarker to Assess Mechanism of Glucokinase Activator (GKA) in SD/JVC Healthy Male Rats

***Aijun Zhu**, Laigao Chen, Kenneth Zasadny, Kyle Kuszpit, Gwen Currier, Richard Coelho, Marc Skaddan, Thomas Bocan, Preclinical BioImaging Center, PharmaTherapeutics Precision Medicine, Pfizer Inc, Groton, CT, USA. Contact e-mail: aijun.zhu@pfizer.com*

Introduction The novel glucokinase (GK) activators augment both glucose-induced insulin secretion in β-cells and hepatic glucose metabolism, and as a result lead to improved clearance of glucose from the blood stream. The glucokinase activators (GKAs), as a new class of therapeutic agents, might be applicable in the treatment of diabetes. PET imaging of liver metabolism by [18F]FDG has been employed clinically in diabetic patients and normal subjects and a relationship between fasting plasma glucose and FDG influx was observed. In this research project, we explored the feasibility to assess the mechanism of the glucokinase activator drug PSN-GK1 (J. Med. Chem. 2008, 51, 4340-45; PF-04670586) in SD (Sprague-Dawley)-JVC (jugular vein cannulated) healthy male rats by in vivo [18F]FDG PET imaging of the liver as a potential biomarker, since the GKA increases glucose utilization in primary hepatocytes, GKA drugs augment hepatic glucose metabolism. Experiments and Methods 16 healthy male Sprague-Dawley (Charles River) JVC rats (315.6±2.6 g) were used, and all PET imaging experiments were performed over three days. All rats were fasted overnight prior to imaging to obtain baseline glucose levels. Animals were separated into four groups (4 rats/group): The first group was treated with vehicle (0.5% methylcellulose); the other three groups were treated with the GKA drug PF-04670586 of 5mg/Kg, 30mg/Kg and 100mg/Kg respectively. The GKA drug was diluted so that it was dosed by 5.0ml/Kg. After the weights of rats were measured, dosing was administered by oral gavage (PO) 60 minutes prior to FDG tracer injection and dynamic PET imaging. Blood samples were drawn during 60 min of PET imaging at 2, 5, 10, 20, 30, 45 and 60 min post FDG injection for input functions of Patlak equation application which shows blood influx rate of liver (Ki, ml/g/min; J Cereb Blood Flow Metab. 1983, 3, 1-7). Results Ki values for each group were calculated and showed an increasing trend due to increases of the PF-drug dose levels: Ki were from 0.002359 to 0.008557 ml/g/min. There was no quantitatively different insulin or C-peptide response between the vehicle group and drug-treated. Conclusion [18F]FDG PET imaging is able to measure influx constants (Ki values) of glucose metabolism to assess GKA drug effects with a high drug dose (ex. 100 mg/Kg). There exists a good correlation between the Ki values by [18F]FDG PET imaging and glucose levels. Acknowledges Thanks a lot to Patricia Bourassa, Karen Atkinson, and Jeffrey Pfefferkorn for help and discussion.

Disclosure of author financial interest or relationships:
**A. Zhu**, Pfizer Inc, Employment; **L. Chen**, Pfizer Inc., Employment; Pfizer Inc., Stockholder; **K. Zasadny**, Pfizer, Employment; **K. Kuszpit**, Pfizer, Inc., Employment; **G. Currier**, Pfizer, Employment; **R. Coelho**, Pfizer Inc., Employment; **M. Skaddan**, Pfizer, Inc., Employment; **T. Bocan**, Pfizer, Employment; Pfizer, Stockholder .

Presentation Number **P497**
Poster Session 3
September 7, 2012 / 15:15-15:15 / Room: The Liffey

# BRAIN METABOLIC DECREASE AND 5HT1A RECEPTOR BINDING POTENTIAL ENHANCEMENT AFTER ELECTRICAL KINDLING IN RATS

***Pablo Bascuñana***[1], *Mercedes Delgado*[1], *Julian Javela*[1], *Ruben F de la Rosa*[1], *Luis G. García*[1], *James Kelly*[2], *Miguel A. Pozo*[1,2], [1]*Cartografía Cerebral, UCM, Madrid, Spain;* [2]*Instituto Tecnológico PET, Madrid, Spain. Contact e-mail: p.bascunana@pluri.ucm.es*

The aim of this study was to evaluate metabolic and neuroreceptors changes during epileptogenesis induced by electrical kindling in the rat brain. All experiments were made with male Sprague Dawley rats (300 ± 33 g), which were implanted electrodes in ventral hippocampus according to stereotaxic atlas (Paxinos and Watson, 1986). Electrode correct placement was checked by a high resolution CT. Rats were kindled through daily stimulation in ventral hippocampus with a 60 Hz-1 second train of 50 μA over its afterdischarge threshold. Seizures behavior was evaluated, as follows: stage 1, behavioral arrest or mouth/facial movements; stage 2, head nodding; stage 3, forelimb clonus; stage 4, rearing; stage 5, falling according to Racine (1972). Completion of kindling was considered when stage 5 seizures were observed for 3 consecutive experimental days. The 100% of the animals reached kindling in 25 stimulations (5 weeks). To study eventual brain changes along electrical kindling we have compared metabolism and 5HT1A receptor binding potential (BP) in rat brain before and after kindling progression using a dedicated small-animal PET-CT hybrid scanner (Albira Ars, Oncovision, Spain). To measure the brain metabolism, FDG (18.5MBq) was injected and a static PET scanner was performed. MPPF (14.8MBq) was administered and a dynamic PET was done in order to quantify the 5HT1A BP. ROIs for quantification of metabolic activity and 5-HT1A BP were drawn over the MR brain image of each animal. To obtain a better resolution of the distribution of the FDG uptake from the different brain structures, 3D ex vivo autoradiography was performed. To achieve this, when kindling was finished, rats were decapitated after the i.v. injection of FDG (55.5MBq) and the brain was immediately cut in 40μm slices and exposed to autoradiographic film. After developing the films, slices were used for in vitro MPPF autoradiography. Our results show that electrical kindling produces hypometabolism located in striatum and contralateral cortex, especially in entorhinal cortex. Also, we have found hypometabolism trend in dorsal hippocampus situated contralaterally to the electrode. In parallel, we find an increased 18F-MPPF binding potential in kindled rats, being statistically significant in septum and contralateral entorhinal cortex. Taken all this data together, our data provide a further evidence of functional changes in brain metabolism and in the serotonergic system in epileptogenesis.

Disclosure of author financial interest or relationships:
**P. Bascuñana**, None; **M. Delgado**, None; **J. Javela**, None; **R. F de la Rosa**, None; **L.G. García**, None; **J. Kelly**, Instituto Tecnológico PET, Employment; **M.A. Pozo**, None.

Presentation Number **P498**
Poster Session 3
September 7, 2012 / 15:15-15:15 / Room: The Liffey

# F-18 Labeled Blood Clots for Measurement of Therapeutic Efficacy in a Rabbit Embolic Stroke Model

***Marc Berridge***[1,2], *Jeff O. Hatton*[1], *Scott M. Apana*[2], *Christina L. Carpenter*[2], *John D. Lowery*[1], *Terri L. Alpe*[1], *Michael J. Borrelli*[1], *Aliza T. Brown*[1], *William C. Culp*[1], [1]*University of Arkansas for Medical Sciences, Little Rock, AR, USA;* [2]*3D Imaging, Little Rock, AR, USA. Contact e-mail: mberridge@3dimagingllc.com*

Purpose: In a rabbit model of embolic stroke, blood taken from a rabbit is allowed to clot in tubing to form 4 x 0.6 mm clots, single clots are then injected angiographically via the internal carotid artery and allowed to flow naturally to occlude a portion of the cerebral circulation. The location of the clots was also determined angiographically. Outcome following experimental treatment has previously been determined by TCC staining post-mortem. A real time in vivo method was desired to localize and quantify the clots to determine treatment efficacy in real time. Method: MicroPET imaging was used to localize the clots and quantify their response to treatment. Three day old autologous clots were rinsed with saline solution, radiolabeled by reaction with [F-18]succinimidyl-4-fluorobenzoate (SFB) in saline at 37C for two hours and then rinsed with saline. Validation experiments showed clot interior and exterior were uniformly labeled. 30 min after clot injection, PET scanning of the rabbit brain was begun. Dynamic scanning was carried out for 15 min before treatment , during 60 min of treatment (TPA, and/or microbubbles + ultrasound), and during a 15 min post-treatment period. An FDG scan after completion of the clot scan was sometimes used to provide anatomic detail. Results: Clots behaved differently. Many fragmented during administration, with fragments detected in additional locations to the expected sites. Most clots and their fragments were unchanged during the pre-treatment period. During treatment clots dissolved at different rates. Many dissolved completely, some were unchanged. Breakup of clots was also observed, and movement of clots to new locations in the circulatory system during treatment. Quantitative curves showed clot dissolution over time, while 3D time-lapse display gave clear perception of clot reaction to treatment. Conclusion: The number of animals studied to date is insufficient for conclusions about treatment efficacy. However, the technique clearly affords a detailed method to directly observe the effects of stroke treatments on a natural clot model in vivo. Immediate effects such as clot fragmentation and motion were easily observed and quantified. The technique will be useful to explore the many potential variables affecting treatment efficacy as well as treatment options.

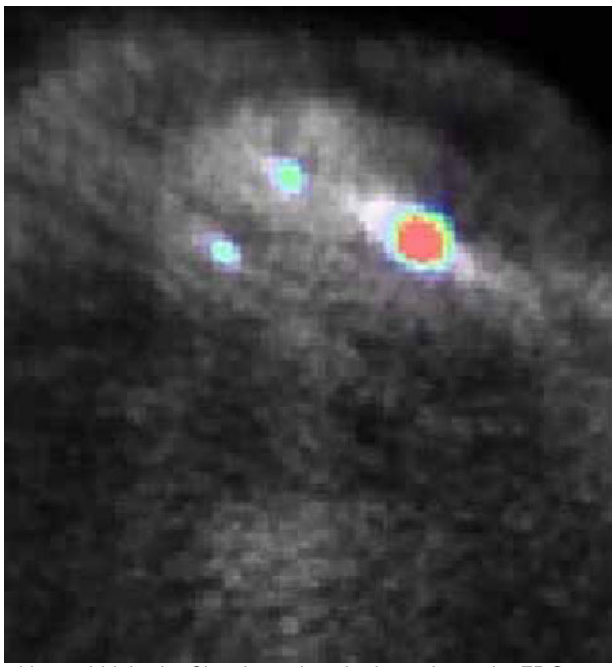

Transaxial projection image of clots observed in a rabbit brain. Clot shown in color intensity scale, FDG anatomic reference image shown in gray scale.

Disclosure of author financial interest or relationships:
**M. Berridge**, Janssen RD, Grant/research support; FDA, Grant/research support; **J.O. Hatton**, None; **S.M. Apana**, None; **C.L. Carpenter**, None; **J.D. Lowery**, None; **T.L. Alpe**, None; **M.J. Borrelli**, None; **A.T. Brown**, None; **W.C. Culp**, None.

Presentation Number **P499**
Poster Session 3
September 7, 2012 / 15:15-15:15 / Room: The Liffey

# [18F]GE180, a new TSPO radiotracer, performs better than [11C]PK11195: direct comparison in experimental stroke in rats

***Herve Boutin***[1], *Gavin D. Brown*[1], *Renaud Maroy*[2], *Karl Herholz*[1], *Muhammad Babur*[1], *Alison M. Smigova*[1], *Paul A. Jones*[3], *William Trigg*[3], [1]*Faculty of Medicine and Human Sciences - Wolfson Molecular Imaging Centre, University of Manchester, Manchester, United Kingdom;* [2]*SHFJ, CEA, Orsay, France;* [3]*GE Healthcare Limited, Amersham, United Kingdom. Contact e-mail: herve.boutin@manchester.ac.uk*

Background: [11C]PK11195 is still the most used translocator protein 18kDa (TSPO) radiotracer used to assess microglial activation in clinical PET imaging but a troublesome radiochemistry and high non-specific binding has led to extensive effort over the past decade to find a better alternative. Over this period, several compounds have been identified and tested in preclinical models[1]. However, it is now clear that thorough validation of each new tracer is required. We are presenting here the first preclinical evaluation of a new radiotracer [18F]GE180[2] by direct comparison with [11C]PK11195 in the same animals following experimental stroke. Methods: Wistar rats (357±44g) were used and middle cerebral artery occlusion (MCAO) was performed for 60min as described elsewhere[3]. [11C]PK11195 and [18F]GE180 were synthetized as previously described[2,4,5]. During all procedures, animals were kept under isoflurane anaesthesia and body temperature and respiration rate were monitored. All procedures were carried out in accordance with the Animals (Scientific Procedures) Act 1986. One day post-MCAO, a MRI T2-weighted scan was performed to assess brain damage. Six animal were scanned at day 5-6 post-MCAO with [11C]PK11195 and [18F]GE180 within 24h. For the in vivo displacement study, four animals were scanned with [18F]GE180 +PK11195 or +GE180 (1mg/kg) injected 20min after [18F]GE180. Images were segmented using the Local Means Analysis (LMA) method and the organ mean Time Activity Curves were corrected for Partial Volume Effect[6]. Both methods were applied using the BrainVisa/Anatomist framework (http://brainvisa.info/). PET-CT images were also co-registered with the MRI. Results: Image analysis revealed that [18F]GE180 uptake was significantly higher in the core of ischemic lesion (+24%) and lower in the healthy contralateral tissue (-18%) than [11C]PK11195 with ROIs determined by automatic PET segmentation (Fig.1A). Analysis using MRI-based ROIs gave similar results. Consequently, direct comparison of the ratio between the lesion and the contralateral healthy tissue for [11C]PK11195 and [18F]GE180 showed that [18F]GE180 gave a significantly better (+52%) contrast between the lesion and the healthy tissue (Fig.1B). The displacement study showed that full displacement of [18F]GE180 was obtained within 5-10min post-injection of the cold ligands (Fig.1C) Conclusions: [18F]GE180 displayed significantly better in vivo binding and pharmacokinetic than [11C]PK11195 in this preclinical model of neuroinflammation. References: [1]. Chauveau F. et al. (2008) Eur.J.Nucl.Med.Mol.Imaging. 35:2304-2319. [2]. Wadsworth H. et al. (2012) Bioorg.Med.Chem.Lett. 22:1308-1313. [3]. Longa E.Z. et al. (1989) Stroke 20:84-91. [4]. Camsonne R. et al. (1984) J.Labelled Comp.Radiopharm. 21:985-991. [5]. Cremer J.E. et al. (1992) Int.J.Rad.Appl.Instrum.B. 19:159-166. [6]. Maroy R. et al. (2010) Med Phys. 37:1507-1517.

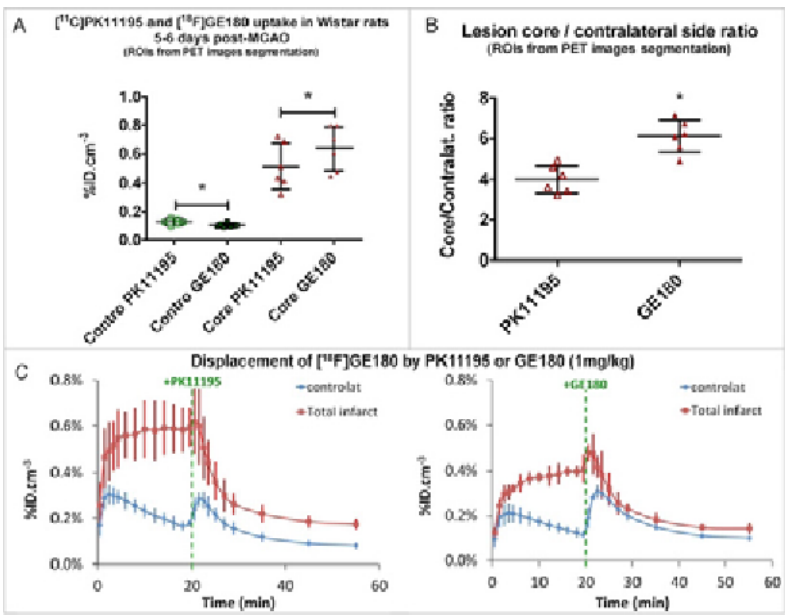


Disclosure of author financial interest or relationships:
**H. Boutin**, General Electric, Other financial or material support; **G.D. Brown**, None; **R. Maroy**, PMOD, Other financial or material support; **K. Herholz**, AVID/Eli-Lilly, Grant/research support; Elan, Consultant; GE Healthcare, Consultant; **M. Babur**, None; **A.M. Smigova**, None; **P.A. Jones**, GE Healthcare, Employment; **W. Trigg**, GE Healthcare, Employment .

Presentation Number **P500**
Poster Session 3
September 7, 2012 / 15:15-15:15 / Room: The Liffey

# A conceptually new [$^{18}$F] PET tracer with diagnostic potential in Alzheimer's Disease: design, synthesis, radiochemistry and preclinical PET imaging experiments

***Elisa Calamai***[1], *Sergio Dall'Angelo*[1], *Juozas Domarkas*[3], *David Koss*[1], *Timothy J. McCarthy*[2], *Marco Mingarelli*[3], *Gernot Riedel*[1], *Lutz F. Schweiger*[3], *Andrew Welch*[3], *Bettina Platt*[1], *Matteo Zanda*[1], [1]*Institute of Medical Sciences, School of Medical Sciences, University of Aberdeen, Aberdeen, United Kingdom;* [2]*Precision Medicine, Pfizer WRD, Groton, CT, USA;* [3]*John Mallard Scottish PET Centre, School of Medicine and Dentistry, University of Aberdeen, Aberdeen, United Kingdom. Contact e-mail: e.calamai@abdn.ac.uk*

Barbiturates are central nervous system (CNS) depressants.[1] To our knowledge they have never been used as tracers for PET imaging of the brain. We hypothesised that radiofluorinated barbiturates might be useful PET tracers for the imaging of CNS disorders, such as Alzheimer's disease (AD) for several reasons. Firstly, barbiturates have an excellent ability to cross the blood-brain-barrier (BBB). Secondly, they are known to be chelators[2] of metal cations, such as Zn(II) and Cu(II), which are found in many neurodegenerative disorders, including AD.[3] Furthermore, it is known that barbiturates have a remarkable capacity to form stable supra-molecular structures with polar molecules.[4] This might lead to the formation of aggregates of barbiturates with amyloid peptides and tau protein aggregates, key hallmarks of AD. We have synthesised a new $^{18}$F-labelled barbiturate with high radiochemical purity (≥99%). To determine his potential in pre-clinical model of AD, dynamic PET/CT brain scans were performed on wild type (WT) and transgenic mice (APP/PS1 and Tau mice PLB2). PET/CT scans confirmed good brain uptake in all cases (peak activity ca. 7 min post injection). It is noteworthy that WT and APP/PS1 showed significantly different clearance modes (Figure 1). In order to investigate the nature of the target(s), *in-vitro* tests with amyloid and Thioflavin T were carried out. These confirmed the interaction of the barbiturate with artificial amyloid aggregates. Finally, a fluorescent version of barbiturate was synthesised and submitted to tissue labelling and immunocytochemistry assays on brain of aged transgenic mice, confirming the affinity of barbiturate for amyloid plaques formed within the brain of transgenic Alzheimer's mice. References: [1] J. A. Richter, J. R. Holtman. *Prog. Neurobiol.* **1982**, *18*, 275-319. [2] (a) A. Tochowicz, K. Maskos, R. Huber, V. D. Oltenfreiter, A. Yiotakis, M. Zanda, W. Bode, P. Goettig, *J. Mol. Biol.* **2007**, *371*, 989-1006 and references therein; (b) M. S. Masoud, S. S. Haggag, E. A. Khalil, *Nucleos. Nucleot. Nucl.* **2006**, *25*, 73-87 (c) Y. Xiong, C. He, T.-C. An, C.-H. Cha, X.-H. Zhu, *Transit. Metal Chem.* **2003**, *28*, 69-73. [3] (a) S. A. James, I. Volitakis, P. A. Adlard, J. A. Duce, C. L. Masters, R. A. Cherny, A. I. Bush *Free Radic. Biol. Med.* **2012**, *52*, 298-302 (b) B. Platt, *J. Alzheimers Dis.* **2006**, *10*, 203-213 (c) L. M. Sayre, G. Perry, P. L. R. Harris, Y. Liu, K. A. Schubert, M. A. Smith *J. Neurochem.* **2000**, *74*, 270-278 (d) C. L. Masters; R. Cappai; K. J. Barnham, V. L. Villemagne *J. Neurochem.* **2006**, *97*, 1700-1725 (e) A. Rauk, *Chem. Soc. Rev.* **2009**, *38*, 2698-2715 (f) M. P. Cuajungco, K. Y. Fagét *Brain Res. Rev.* **2003**, *41*, 44-56 (g) D. Beauchemin, R. Kisilevsky *Anal. Chem.* **1998**, *70*, 1026-1029. [4] S. J. Yagai *Photochem. Photobiol.C* **2006**, *7*, 164-182.

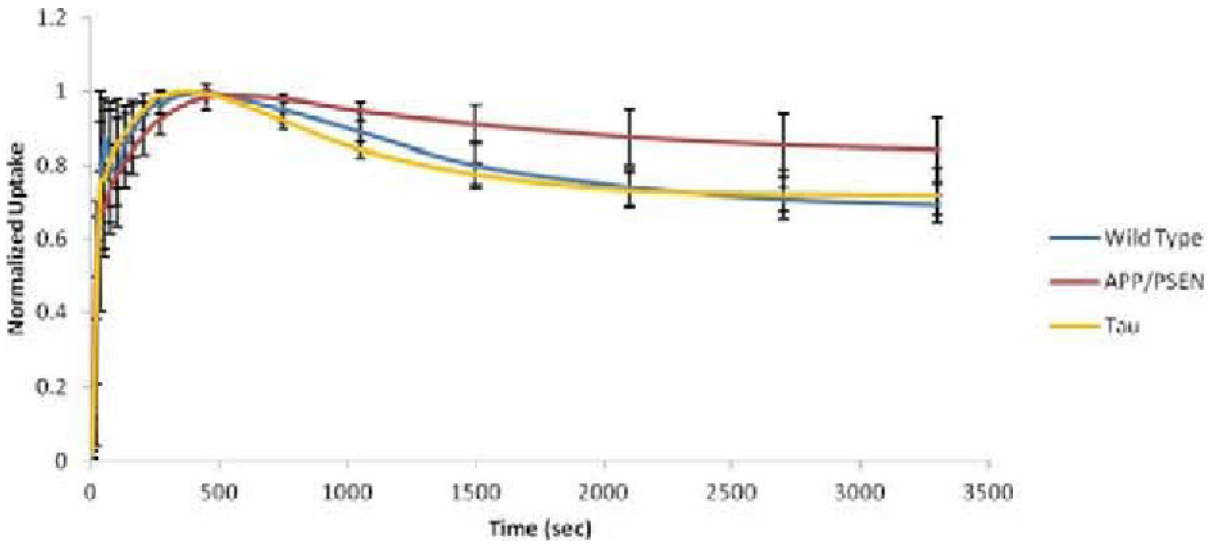


Figure 1. Time-course of activity, normalized to peak values, in wild type (WT, n=4), and transgenic Alzheimer mice [APP/PS1 (n=5) and PLB2-Tau (n=4)].

Disclosure of author financial interest or relationships:
**E. Calamai**, None; **S. Dall'Angelo**, None; **J. Domarkas**, None; **D. Koss**, None; **T.J. McCarthy**, Pfizer, Inc, Employment; **M. Mingarelli**, None; **G. Riedel**, None; **L.F. Schweiger**, None; **A. Welch**, None; **B. Platt**, None; **M. Zanda**, None.

Presentation Number **P501**
Poster Session 3
September 7, 2012 / 15:15-15:15 / Room: The Liffey

# Analysis of 123I-Albumin administered via intrathecal injection in rats and squirrel monkeys

***William Cupelo***[1], *Jacob Hesterman*[1], *Kelly D. Orcutt*[1], *Catey L. Harwell*[1], *Rob Callan*[1], *Dustin Kentala*[2], *Mark R. Lane*[2], *Jack Hoppin*[1], *Ajay Verma*[3], [1]*inviCRO, Boston, MA, USA;* [2]*MPI Research, Mattawan, MI, USA;* [3]*Biogen Idec, Cambridge, MA, USA. Contact e-mail: cupelo@invicro.com*

Drug delivery to the brain via intrathecal injection is attractive due to the circumvention of the blood-brain barrier. Some previous studies have sought to evaluate intrathecal pharmacokinetics using blood and/or CSF samples, but little is known of the overall distribution of injected compounds throughout the intrathecal space and into the ventricles. The purpose of this work was to develop a novel method for assessing the kinetics of intrathecally administered radiopharmaceuticals in the cerebrospinal fluid of rats and squirrel monkeys using high-resolution microSPECT/CT. Techniques have been developed that enable direct injection into the lumbar intrathecal space in rats and squirrel monkeys. Because of the small size and inconsistent flow characteristics of the CSF, this study focused on the longitudinal distribution of different volumes of intrathecally-injected 123I-Albumin, a well-characterized radiotracer. Volumes of 10, 50, and 100 uL were injected into 2, 4, and 2 rats, respectively, while volumes of 30 and 100 uL were injected into individual squirrel monkeys. Imaging was also performed following intravenous injection of 100uL for both species. Whole-body SPECT/CT data were acquired for the first hour post-injection and again at 2 (rats only) and 6 hours post-injection. Following reconstruction, SPECT and x-ray CT 3D tomograms were co-registered for ROI analysis. Figures below shows a maximum-intensity projection image of 123I-Albumin at 6 hours following a 50µL intrathecal injection in a rat (Figure 1a) and 100µL injection in a squirrel monkey (Figure 1c whole-body, Figure 1d focused brain). Appropriate species-specific brain atlases were fit to the skull in the x-ray CT image at each time point enabling an estimate of uptake and concentration in the primary regions of the brain as a function of time. For analysis of the kinetics of the relevant radiopharmaceutical in the spinal column of the rat, the vertebrae were segmented using a connected thresholding algorithm (shown in red in Figure 1b) and the spinal column was classified by defining a cylindrical ROI within the vertebrae (shown in green in Figure 1b). Data corresponding to the atlas from each rat data set were registered to one another to form an average distribution of tracer in the brain. Brain voxels were classified as either ventricle (shown in cyan in Figure 1b) or tissue, based on the activity distribution. Brain tissue distribution was successfully verified against ex vivo gamma counter measurements. A novel approach for assessing the kinetics of intrathecally administered radiopharmaceuticals within the cerebrospinal fluid of rats and squirrel monkeys has been developed. This effort lays the foundation for studying the kinetics of any radiolabeled molecule within the CSF space and the development of brain atlases incorporating species-specific ventricle regions.

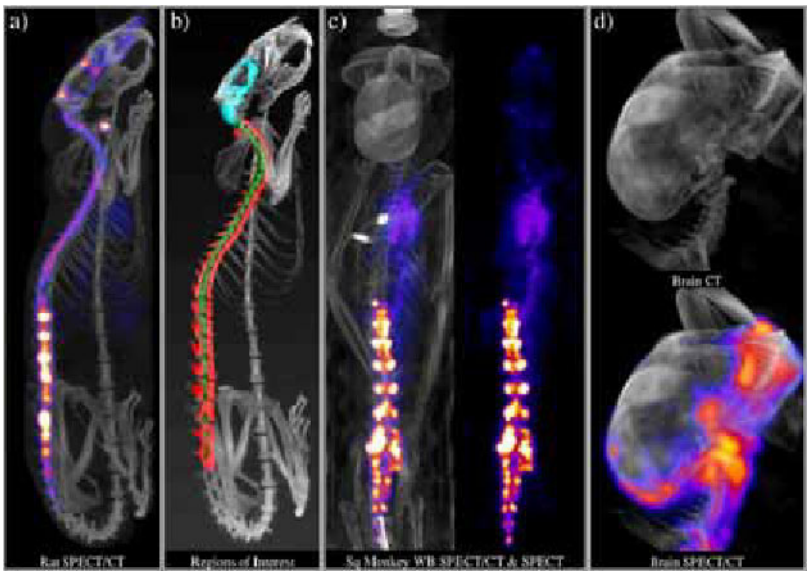


Disclosure of author financial interest or relationships:
**W. Cupelo**, inviCRO, LLC, Employment; **J. Hesterman**, inviCRO, Employment; **K.D. Orcutt**, inviCRO, Employment; **C.L. Harwell**, inviCRO, LLC, Employment; **R. Callan**, inviCRO, Employment; **D. Kentala**, MPI Research, Employment; **M.R. Lane**, None; **J. Hoppin**, inviCRO, LLC, Employment; inviCRO, LLC, Stockholder; **A. Verma**, Biogen Idec, Employment .

Presentation Number **P502**
Poster Session 3
September 7, 2012 / 15:15-15:15 / Room: The Liffey

# Why Use DKI and not DTI to Detect Microstructural Differences in the Hippocampus of Rats Exposed to Chronic Mild Stress?

***Rafael Delgado y Palacios**, Johan Van Audekerke, Annemie van der Linden, Marleen Verhoye, Bio-Imaging Lab, University of Antwerp, Antwerp, Belgium. Contact e-mail: rafael.delgadoypalacios@ua.ac.be*

**Introduction:** Diffusion kurtosis imaging (DKI) has recently been established as a sensitive method to examine the microstructure of neural tissue. However, because the acquisition and processing of DKI data is more time-consuming and more demanding for the hardware than conventional diffusion tensor imaging (DTI), the use of DKI is limited, despite its advantages. Therefore, this study examines the use of conventional DTI to assess the diffusion properties in the hippocampus of chronic mild stress (CMS) exposed rats, since CMS has been found to induce subtle regional microstructural changes, which could be detected by DKI[1]. **Material & Methods:** Data of 21 Wistar rats were used in this study. Seven rats were not exposed to CMS. The remaining rats were exposed to CMS and can be classified in two groups, i.e. an 'anhedonic' group, which shows anhedonic-like behavior and the 'resilient' group, which lacks the anhedonic-like behavior after CMS exposure. Diffusion weighted images (DWIs) were acquired along 30 gradient directions with 7 different b-values ($b_1$=400, $b_2$=800, $b_3$=1200, $b_4$=1600, $b_5$=2000, $b_6$=2400 and $b_7$=2800 s/mm$^2$), together with 7 non-diffusion weighted ($b_0$) images, using a multi-slice spin echo 2-shot EPI sequence with following parameters: TR/TE=3000/25ms, δ=5ms, Δ=12ms, acquisition matrix=128*64, FOV=35*17.5mm$^2$, slice thickness=1mm, NEX=4. For every animal, the DWIs were co-registered to the first $b_0$ image with rotation of the b-matrix. Subsequently, all DWIs were fitted to the non-monoexponentional DKI model to estimate the second-order diffusion tensor ($DT_{DKI}$) and fourth-order kurtosis tensor (KT). To mimic conventional DT estimation, DT($b_{all}$) and DT($b_i$) were obtained by fitting the $b_0$ images and all DWIs and a data subset -comprising DWIs acquired with a certain $b_i$- to the monoexponentional DTI model, respectively. KT-derived, i.e. mean (MK), axial (AK) and radial (RK) kurtosis parametric maps, and DT-derived -mean (MD), axial (AD) and radial (RD) diffusivity and fractional anisotropy (FA)- parametric maps were computed. The hippocampus of each subject was manually segmented using AMIRA software (Amira, Visage Imaging Inc., CA, USA). **Results:** The conventional estimation of the diffusion parametric maps by fitting the $b_0$ images and the DW images with a certain diffusion weighting ($b_1$-$b_7$) resulted in a strong b-value dependency of the directional diffusivities and FA. However, comparing the DT($b_i$)-derived parameters among the three groups with ANOVA tests showed no significant differences ($p > 0.05$). Furthermore, the diffusion parametric maps, derived from the DT($b_{all}$), did not show any difference among the three groups ($p > 0.05$). On the other hand, MK and RK are significantly decreased in both CMS exposed groups as compared with the control group ($p < 0.05$)[1]. **Conclusion:** In order to detect changes in the diffusion pattern of water molecules in the hippocampus, as a result of the microstructural alterations caused by CMS exposure, DKI shows promising results, whereas conventional DTI processing is not able to pick up these subtle changes.
**Reference:** [1]Delgado y Palacios et al. (2011) Biol. Psychiatry 70(5):449-57.

Disclosure of author financial interest or relationships:
**R. Delgado y Palacios**, None; **J. Van Audekerke**, None; **A. van der Linden**, None; **M. Verhoye**, None.

Presentation Number **P503**
Poster Session 3
September 7, 2012 / 15:15-15:15 / Room: The Liffey

# A1 adenosine receptors in the rat brain: Kinetic and equilibrium modeling of [18F]CPFPX PET imaging is validated by displacement and autoradiographic experiments

***David Elmenhorst***[1], *Tina Kroll*[1], *Franziska Wedekind*[1,3], *Simone Beer*[2,1], *Angela Weisshaupt*[1], *Andreas Matusch*[1], *Andreas Bauer*[1,3], [1]*Institute of Neurosciences and Medicine, INM-2, Forschungszentrum Jülich, Jülich, Germany;* [2]*Central Institute for Electronics, Forschungszentrum Jülich, Jülich, Germany;* [3]*Neurological Department, Heinrich-Heine-University Düsseldorf, Düsseldorf, Germany. Contact e-mail: d.elmenhorst@fz-juelich.de*

Adenosine is an important net-inhibitory neuromodulator which is coupled to the neuronal energy metabolism. Primary objective was to verify the suitability of quantification methods for the A1 adenosine receptor (A1AR) in the rat brain with [18F]CPFPX with special emphasize on the possibility to perform non-invasive longitudinal investigations in the same animal. In-vivo ([18F]CPFPX PET) and in-vitro ([3H]DPCPX autoradiography) measurements of binding were acquired in the same rats. Compartmental and graphical pharmacokinetic models based on an arterial and a reference region input function were evaluated and compared. 15 rats underwent 120 min [18F]CPFPX PET investigations in a dedicated small animal scanner. In all animals arterial blood samples were drawn and corrected for metabolites. In 5 animals the ligand was injected as bolus, in 10 animals as bolus plus constant infusion of which 5 animals received the selective antagonist DPCPX during the steady state phase of ligand delivery. Afterwards, saturation binding autoradiography was performed (n = 9). Dynamic binding of [18F]CPFPX is well described by a two compartment model, graphical and multilinear methods which reveal highly correlated parameters. The region with the lowest distribution volume (VT) was the olfactory bulb with a 3 to 4 times lower VT in contrast to the thalamus. Bolus plus constant infusion application lead to steady state conditions from 40 to 50 min onwards. The tissue plasma ratio during steady state was highly correlated to the kinetic VT estimates with a bias of less than 5% in the high binding regions. Binding potentials (BPND) related to the olfactory bulb were calculated with the simplified and multilinear reference tissue models and compared to BPND based on VT values. Blood based (VT) and reference region based (BPND) PET quantification showed a significant linear relationship to the corresponding autoradiographic determinations. A dose of 1 mg DPCPX per kg bodyweight administered after 70 min lead to a rapid reduction of specific binding in all regions. The occupancy of A1ARs by this dose of DPCPX determined with the Lassen plot was on average 93%. The results show that [18F]CPFPX PET can be used for quantitative measurements of A1ARs in the rat brain.

Disclosure of author financial interest or relationships:
**D. Elmenhorst**, None; **T. Kroll**, None; **F. Wedekind**, None; **S. Beer**, None; **A. Weisshaupt**, None; **A. Matusch**, None; **A. Bauer**, None.

Presentation Number **P504**
Poster Session 3
September 7, 2012 / 15:15-15:15 / Room: The Liffey

# Diffusion Tensor Imaging and 1H HR-MAS spectroscopy in a mouse model of ALS: a longitudinal study

*Zineb Saghi[1], **Pedro M. Enriquez-Navas**[1], Marta Cejudo-guillén[2], Diana Caballero-Hernández[2], Maria Luisa Garcia-Martin[1], David Pozo[1,2], [1]Nanodiagnostic, Andalusian Centre for Nanomedicine and Biotechnology (BIONAND), Campanillas, Spain; [2]CELLULAR THERAPY AND REGENERATIVE MEDICINE, Andalusian Molecular Biology and Regenerative Medicine Centre (CABIMER), Sevilla, Spain. Contact e-mail: pmenriquez@bionand.es*

Amyotrophic lateral sclerosis (ALS) is a human neurodegenerative disease that affects to the upper and lower motoneurons. Their effects result in a progressive muscle weakness and atrophy. In addition, it is almost invariably fatal 3 to 6 years after the beginning of the symptoms. Although there is non-effective treatment, some drugs help to modify ALS symptoms. Besides the lack of efficient therapeutic alternatives, there is an urgent need for early diagnosis in order to battle ALS. We present herein a longitudinal study in the SOD-1G93A mouse model for ALS. The water diffusion properties, particularly the fractional anisotropy, and the metabolomic profile of the brain, brainstem and the spinal cord were characterized at 8, 12 and 16 weeks. For that purposes, we used in vivo diffusion tensor magnetic resonance imaging (DT-MRI) and high-resolution magic angle spinning (HR-MAS) spectroscopy of intact biopsies. This is the first study that address by MRI/HR-MAS in a comprehensive way the natural course of the ALS disease.

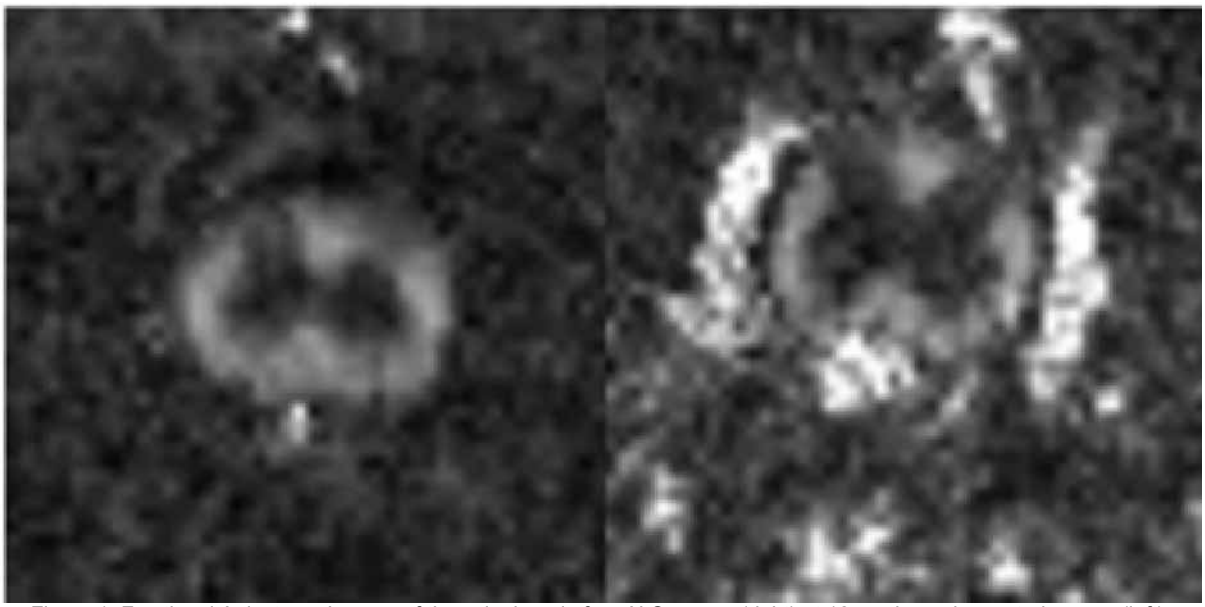

Figure 1: Fractional Anisotropy Images of the spinal cord of an ALS mouse (right) at 12 weeks and a control mouse (left).

Disclosure of author financial interest or relationships:
**Z. Saghi**, None; **P.M. Enriquez-Navas**, None; **M. Cejudo-guillén**, None; **D. Caballero-Hernández**, None; **M. Garcia-Martin**, None; **D. Pozo**, None.

Presentation Number **P505**
Poster Session 3
September 7, 2012 / 15:15-15:15 / Room: The Liffey

# EFFECTS OF P-CHLOROAMPHETAMINE ON THE METABOLIC PET IMAGING IN A MODEL OF EPILEPTOGENESIS INDUCED BY REPEATED ADMINISTRATION OF PENTYLENETETRAZOLE

***Luis G. García***[1,2], *Mercedes Delgado*[1], *Pablo Bascuñana*[1], *Ruben F de la Rosa*[1], *Paloma Bermejo-Bescos*[1,2], *Sagrario Martín-Aragon*[1,2], *Karim Jiménez-Aliaga*[1,2], *James Kelly*[3], *Miguel A. Pozo*[1,3], [1]*Cartografía Cerebral, UCM, Madrid, Spain;* [2]*Farmacología, UCM, Madrid, Spain;* [3]*Instituto Tecnológico PET, Madrid, Spain. Contact e-mail: lgarciag@farm.ucm.es*

Pentylenetetrazole (PTZ) is a GABAergic blocker which when administered repeatedly at sub-convulsive doses induces the appearance of spontaneous seizures (kindling). Little is known about the role of serotonin in this pathology. Furthermore, the hippocampal neurons are vulnerable to epilepsy-induced pathologic changes and often manifests as neuronal death. The objective of this study was to determine the role of serotonergic input in PTZ-induced epileptogenesis. To this aim, the effects of PTZ on glucose consumption, modulation of neurotransmitters receptors (glutamatergic, GABAergic and serotonergic) and the brain intracellular events that predispose for developing to neurons for apoptosis signalling were evaluated. Male Sprague-Dawley rats weighing aprox. 250g were used. The epileptogenesis was induced by repeated administration of PTZ (35 mg/kg; 6 sessions in a period of 2 weeks). Previously to the induction of epileptogenesis, an acute dose of the serotonergic neurotoxin p-chloroamphetamine (PCA) was administered in order to provoke a partial (2.5 mg/kg) or a full lesion (10 mg/kg) of the serotonergic axon terminals. The brain metabolism was evaluated by using a small animal PET device (Albira ARS, Oncovision, Spain) before and after the kindling protocol using 18F-FDG as radiotracer. The expression of receptors were determined by autoradiographic techniques using specific radioactive-labelled ligands and the expression of the apoptosis markers p53, Bcl-2, bcl-XL, Bax and PARP was analysed by Western blotting. Furthermore the activation of caspases -3, -6, -8 and -9 was also evaluated by the assay of enzymatic activity using fluorogenic substrates. After 3 days of PCA administration, a reduction of the 18F-FDG uptake in several brain areas studied in a dose-related pattern was observed. Furthermore, this effect seems to be time-dependent, as after three weeks from the neurotoxin administration, the metabolism was reduced even more as measured by SUV. In this context, PCA 2.5 mg/kg generated a reduction of 7.36 % in hippocampus after 3 days and this reduction reached 19.95 % after 3 weeks, compared with the basal metabolic activity. After six sessions of PTZ, the rats showed an increased epileptogenic behaviour which correlates with a significant reduction of the FDG uptake in epilepsy related areas such as neocortex (SUV=3.58 before vs 2.87 after 6 PTZ sessions) and hippocampus (SUV=4.17 vs 3.36). We did not find that PCA altered significantly the glucose metabolism in this model of epileptogenesis. In conclusion, these results show that repeated exposition to PTZ is accompanied with a gradual reduction of brain metabolism, which is also found in epileptic patients. This reduction was not affected by previous PCA injection. By other hand, the serotonergic lesion induced by systemic administration of PCA reduced the brain metabolism in different brain areas. With the data we have at this moment, it is not clear if such as metabolic effect is due to neural death or by reduction of serotonergic cerebral activity.

Disclosure of author financial interest or relationships:
**L.G. García**, None; **M. Delgado**, None; **P. Bascuñana**, None; **R. F de la Rosa**, None; **P. Bermejo-Bescos**, None; **S. Martín-Aragon**, None; **K. Jiménez-Aliaga**, None; **J. Kelly**, Instituto Tecnológico PET, Employment; **M.A. Pozo**, None.

Presentation Number **P506**
Poster Session 3
September 7, 2012 / 15:15-15:15 / Room: The Liffey

# Brain activation mapping using double bolus FDG acquisition scheme in rats

***Willy Gsell***[1], *Ann-Marie Waldron*[1], *Anouk Schrantee*[1], *Josef Habib*[3], *Jordi L. Tremoleda*[1], *Alice Egerton*[2], *Oliver Howes*[2], [1]*Biological Imaging Centre, MRC Clinical Sciences Centre/Imperial College London, London, United Kingdom;* [2]*Psychiatric Imaging, MRC Clinical Sciences Centre/Imperial College London, London, United Kingdom;* [3]*National Heart and Lung Institute, Imperial College London, London, United Kingdom. Contact e-mail: willy.gsell@csc.mrc.ac.uk*

fMRI has become the brain activation mapping method of choice, yet it only provides indirect measurements of neural activity, as it depends on local adaptations in blood flow. In contrast FDG PET is a good indicator of brain metabolism as the brain relies almost exclusively on glucose as an energy substrate, and its uptake is closely associated with neuronal activity (Sokoloff 2008). However it too has drawbacks as examining changes in physiological states may require repeated tests. To overcome these limitations, we propose an alternative FDG PET technique employing a double-bolus method that allows for brain activation mapping in different physiological states in one session. While the feasibility of this technique has been demonstrated in clinical studies, the aim of this work was to develop this technique for preclinical use, validating it with a well-known pharmacological challenge (amphetamine). Methods: Male Sprague-Dawleys (300-350g) were fasted overnight. Anaesthesia was induced by inhalation of isofluorane (5% for induction, and 2% for maintenance during preparation and scanning). The femoral artery and vein were cannulated for blood sampling and injection of FDG and/or pharmacological challenge respectively. Throughout the procedure respiration rate, plasmatic glucose level and blood gas were measured. Experiments were acquired on a small animal PET/CT scanner (Inveon, Siemens Medical Solutions). An i.v bolus of 35-40MBq FDG was administered and the scan started simultaneously. At 50 mins, an i.v amphetamine (1mg/kg) or saline challenge was given followed by a second bolus of 35-40MBq at 60 mins. Arterial blood samples were taken every 6 seconds for the first minute after each bolus, and then at gradually increasing time points. Data were then rebinned into 68 frames following the same scheme as the invasive arterial sampling and reconstructed using OP-MAP algorithm . A matrix of 256 x 256 and a zoom of 1.8 were applied to all data during reconstruction. Arterial input function was derived from the images by drawing a region of interest in the cardiac left ventricle cavity (IRW 4.0). Data were then modeled using a graphical Patlak methods to generate the ki map for the first and the second 20-45 mins following the respective FDG bolus injection. Both ki maps were then subtracted to generate the brain activation map. Results: The time activity curves showed as predicted considerable increases in activity after amphetamine challenge vs. saline. Amphetamine induced a strong increase of FDG uptake with patterns of activation in the insular cortex and caudate putamen similar to already published activation maps using phMRI (Schwarz et al., 2007). The ki differences for amphetamine and saline were (0.0326) and (-0.002) respectively. Conclusion: We demonstrated here the feasibility of the use of double bolus FDG in rodents to investigate brain activation induced by a pharmacological challenge. To our knowledge, this is the first time that such technique is used in rodents. References Gsell W,et al. (2000) J Chem Neuroanat.Dec;20(3-4):215-24. Sokoloff L. (2008). Cogn Neurodyn. Mar;2(1):1-5.

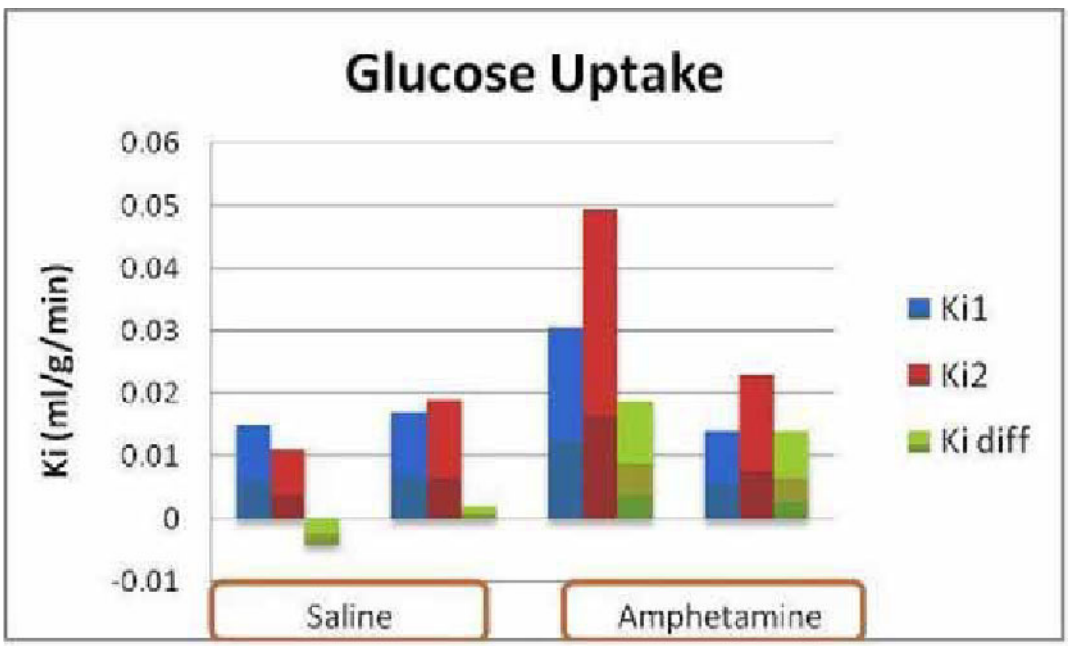


Disclosure of author financial interest or relationships:
**W. Gsell**, None; **A. Waldron**, None; **A. Schrantee**, None; **J. Habib**, None; **J.L. Tremoleda**, None; **A. Egerton**, None; **O. Howes**, None.

Presentation Number **P507**
Poster Session 3
September 7, 2012 / 15:15-15:15 / Room: The Liffey

# Validation of [11C]PBR28 as a TSPO radioligand in rat using the nanoScan® PET/MRI small animal scanner

*Janine Doorduin[1,2], Miklós Tóth[1], Jenny Häggkvist[1], Kalman L. Nagy[1], Andrea Varrone[1], Domokos Mathe[3], Christer Halldin[1], **Balázs Gulyás**[1], [1]Clinical Neuroscience, Karolinska Institute, Stockholm, Sweden; [2]Department of Nuclear Medicine and Molecular Imaging, University Medical Center Groningen, Groningen, Netherlands; [3]CROmed Ltd., , Budapest, Hungary. Contact e-mail: balazs.gulyas@ki.se*

Dedicated small animal PET scanners provide us with an opportunity to study microglia activation in small animal disease models longitudinally, using PET radioligands binding to the translocator protein (TSPO). [11C]PBR28 is a recently developed TSPO radioligand with the help of which microglia activation can be studied in the human, non-human primate and rodent brain. There are however methodological challenges for quantification of this receptor and, consequently, microglia activation. There is no suitable reference region and the use of plasma-derived input is not an option for longitudinal studies. The aim of the present study was therefore to evaluate the use of the semi-quantitative standardized uptake value (SUV) as an outcome measure in small animal PET studies on microglia activation for the TSPO ligand [11C]PBR28. In addition, the test-retest variability of the SUV was determined. Healthy male Wistar rats (n=8, 363±57 grams) were divided in two groups. The first group (n=4) was used to determine the correlation between the distribution volume (VT) obtained by Logan graphical analysis and the SUV (t=57-63 min after injection). In the second group (n=4) the test-retest variability of the SUV (t=57-63 min) was determined, with a 7-day interval between scans. Dynamic PET scans of 63 minutes were acquired after injection of 23±5 MBq [11C]PBR28, with the nanoScan® PET/MRI (Mediso Ltd, Budapest, Hungary). A MRI scan was made for anatomical reference. For the first group arterial blood samples (n=16) were taken during the scan for radioactivity measurements in blood and plasma, as well as radiometabolite analysis (n=3). The brain uptake of [11C]PBR28 was highest at 1 minute after injection and reached a steady state at 45 minutes. [11C]PBR28 in blood and plasma peaked at 10-15 seconds after injection. Radiometabolite analysis showed that at 4 minutes after injection 43±10% of the total radioactivity in plasma was [11C]PBR28, which was reduced to 4±3% at 60 minutes.The time-activity curves of 9 different regions were fitted with Logan graphical analysis, using radiometabolite corrected plasma input. The whole brain VT was 43.1±1.2. The highest VT was found in the cerebellum (54.0±1.9), whereas the thalamus had the lowest VT (34.2±2.7). A statistical significant correlation ($r^2=0.95$; $p<0.0001$) was found between the VT and the SUV (0.63±0.05 for whole brain). The whole brain uptake of [11C]PBR28 in the test-retest study (average SUV 0.49±0.07) showed an intersubject variability of 14.3% and a retest variability of 13.6%. The interclass correlation coefficient (ICC) was 0.59, showing that the variability is higher between than within rats. Similar or higher ICC values (0.58-0.88) were found for the other brain areas, with exception of the cortex (0.33). The SUV of [11C]PBR28 showed a high correlation with the VT as obtained by Logan graphical analysis, as well as a good test-retest variability. For future longitudinal small animal PET studies the SUV can thus be used to describe [11C]PBR28 uptake in healthy brain tissue.

Disclosure of author financial interest or relationships:
**J. Doorduin**, None; **M. Tóth**, None; **J. Häggkvist**, None; **K.L. Nagy**, Mediso Medical Imaging, Consultant; **A. Varrone**, None; **D. Mathe**, CROmed Ltd, Stockholder; Mediso Ltd., Consultant; CROmed Ltd, Employment; **C. Halldin**, None; **B. Gulyás**, None.

Presentation Number **P508**
Poster Session 3
September 7, 2012 / 15:15-15:15 / Room: The Liffey

# Diffusion of conventional and calcium sensitive MRI contrast agents in the rat cerebral cortex

***Gisela E. Hagberg***[1], *Ilgar Mamedov*[1], *Anthony Power*[1], *Michael Beyerlein*[1], *Hellmut Merkle*[3], *Kirti Dhingra*[1], *Vojtech Kubicek*[2], *Nikos K. Logothetis*[1], [1]*MPI Biological Cybernetics, Tübingen, Germany;* [2]*Depatment of Inorganic Chemistry Charles University in Prague, Faculty of Science, Prague, Czech Republic;* [3]*LFMI-NINDS, National Institutes of Health, Bethesda, MD, USA. Contact e-mail: gisela.hagberg@tuebingen.mpg.de*

Calcium sensitive MRI contrast agents can only yield quantitative results if the agent concentration in the tissue is known. The agent concentration could be determined by diffusion modeling, if relevant parameters were available. We have established an in vivo MRI based method capable of determining diffusion properties of conventional and calcium sensitive agents. Simulations and experiment demonstrate that the method is applicable both for conventional contrast agents with a fixed relaxivity value, and for calcium sensitive contrast agents. Sprague-Dawley rats (N=19, 220-300g) were used as approved by the local authorities in compliance with guidelines EUVD 86/609/EEC. Physiological signs were monitored throughout the experiment and remained within physiological limits. Surgery was performed after anesthesia (2.0%isoflurane, Forene, urethane (1.5 g/kg, i.p.) and xylocain (locally)). A burr hole was made above the primary sensory cortex (S1) and a guiding cannula was implanted and fixed prior to positioning in a stereotaxic holder and insertion of a glass capillary (tip: OD: 21-30µm, ID: 6-10µm) in the center of S1. The glass capillary was connected to an injection pump via 6.5m long fused silica tubes and the rat positioned in the center of a 7T Bruker Biospec 70/30 scanner (BGA-9S, Helmholtz RF volume transmission coil, 2cm single loop receiving surface coil). Biodistribution and diffusion of the contrast agents were imaged continuously before, during and after a 1.1±0.3µl slow bolus infusion, with a rate of 32±9nl/min by a T1-weighted RARE sequence (TE/TR 9/290ms) and by quantitative mapping of T1 times by a Look-Locker inversion recovery sequence with a single-shot EPI read out (11.5/8000ms; TI1=35ms, TIdelay=250ms, total of 18 LL images). Data analysis consisted of estimation of the Gadolinium concentration from the images and non-linear fitting of the diffusion equation (Figure). The D* values observed for conventional and responsive contrast agents[1-3] in vivo by MRI were in agreement with model predictions for extra-cellular diffusion and previous findings using other measurement techniques[4], the only exception being Dextran10k (Table 1). This compound has been used both as an extra-cellular tracer for diffusion measurements, and as a neuroanatomical connectivity tracer. The MRI method described is based on long observation times (up to 20h) and assessed both extra-cellular diffusion and intra-cellular transport across extended brain regions of Dextran10k. The apparent diffusion coefficient determined for the calcium sensitive contrast agents may be used to determine local tissue concentrations and to design infusion protocols that maintain the agent concentration at a steady-state, hereby enabling quantitative sensing of the local calcium concentration. 1. Dhingra K et al., Chem Commun (2008) 29:3444-6; 2. Mamedov I. et al., ACS Chemical Neuroscience (2010) 1:819-828; 3. Kubìček V et al., CMMI(2010) 5(5):294-296; 4. Sykova E, Nicholson C Physiol Rev (2008) 88:1277-1340; 5. Thorne RG, Nicholson C. Proc Natl Acad Sci U S A (2006) 103(14):5567-72

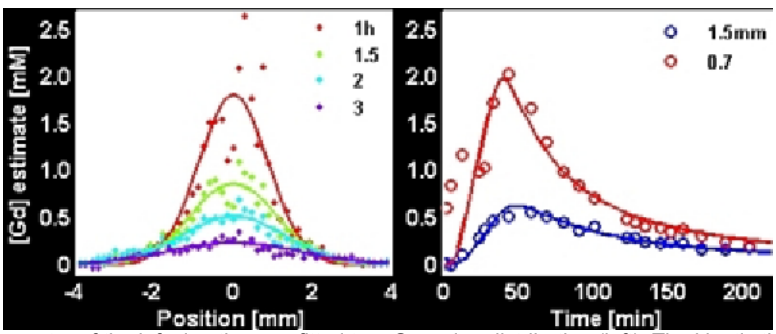


Biodistribution profiles through the center of the infusion tip were fitted to a Gaussian distribution (left). The kinetic time course at two different voxels, located at 0.7 and 1.5mm from the infusion tip, were fitted by the diffusion equation (right).

Predicted and observed apparent diffusion coefficient, D* in rat primary sensory cortex

| Acronym | Compound | d H [nm] | Expected D* [$10^{-4}$ $mm^2/s$] | Observed D* [$10^{-4}$ $mm^2/s$] |
|---|---|---|---|---|
| Gd-L1 | Gadonic acid (Dotarem) | 0.8-1 | 2.11-2.66a | 2.46+/-0.52 |
| Gd-L2 | DOTA-Dextran 10kDa | 4.5 | 0.78b | 1.35+/-0.78 |
| Gd-L3 | DOTA-cyclic PERA based [1] | - | - | 2.11+/-0.71 |
| Gd-L4 | DOTA-hexyl amido-bis(methyl triphosphonate) [2] | 1.58 | 1.39b | 1.30+/-0.70 |
| Gd-L5 | DOTA-bisphosphonate [3] | - | - | 1.22+/-0.04 |

Expected D*: a From experimental observations; b Based on the hydrodynamic diameter, $d_H$, and the Thorne and Nicholson model for predicting tortuosity [5]

Disclosure of author financial interest or relationships:
**G.E. Hagberg**, None; **I. Mamedov**, None; **A. Power**, None; **M. Beyerlein**, None; **H. Merkle**, None; **K. Dhingra**, None; **V. Kubicek**, None; **N.K. Logothetis**, None.

Presentation Number **P509**
Poster Session 3
September 7, 2012 / 15:15-15:15 / Room: The Liffey

# Adequate kinetic model for 15O-labeled oxygen in quantitative assessment of CMRO2 using PET - A clearance measurement of 15O-radioactivity following the intra-carotid bolus injection of labeled oxyhemoglobin in experimental animals

***Hidehiro Iida***[1], *Nobuyuki Kudomi*[2], *Satoshi Iguchi*[1], *Tetsuaki Moriguchi*[1], *Kazuhiro Koshino*[1], *Tsutomu Zeniya*[1], *Akihide Yamamoto*[1], *Yuki Hori*[1], *Junichiro Enmi*[1], *Hidekazu Kawashima*[1], [1]*National Cerebral Cardiovascular Center, Suita City, Japan;* [2]*kagawa University Schoold of Medicine, Takamatsu, Japan. Contact e-mail: iida@ri.ncvc.go.jp*

Backgrounds Regional cerebral metabolic rate of oxygen (CMRO2) and oxygen extraction fraction (OEF) have been quantitatively assessed using 15O-labeled oxygen (15O2) and PET both in experimental animals and in human. A number of mathematical formulations have been proposed for various PET scanning protocols. There has been a common assumption, in which the extracted 15O2 from the capillary bed to the brain tissue is metabolised immediately to become labeled water (H215O), so that backflux of 15O2 from the brain is negligibly small. Encouraging results were shown in early 70's (Ter-Pogossian MM et al., JCI 1970) but was limited with a large level of background, attributed to a single photon detector design. Seki et al (JCBFM, 2003) recently observed that the clearance after bolus administration of 15O2-labeled Oxy-hemoglobin (15O2-Hb) into the carotid artery of rats differs from that after the bolus injection of H215O, suggesting the presence the backflux or the limitation in the compartment model in 15O2 PET, unless technical errors are included due to the difficulty in small animal experiments. Purpose This study was aimed at evaluating whether or not the clearance of 15O2 from brain is identical to that for H215O. Adequacy of the assumption of instantaneous metabolism of 15O2 to become H215O was then investigated. Methods Three independent PET experiments were carried out on 2 monkeys of body weight 7.0-7.5 kg. Blood samples with 15O2-Hb, and with C15O-hemoglobin (C15O-Hb), as well as H215O-saline of approximately 20 MBq in 0.4 mL were injected into the carotid artery by slow bolus, immediately after the initiation of PET scanning using an ECAT HR scanner in listmode. The 15O2-Hb and C15O-Hb were prepared using the previously presented artificial lung (Magata et al., JCBFM 2003; Temma et al. Brain Res, 2008; Temma et al., EJNMMI 2010), by circulation the venous blood with the introduction of 15O2 and C15O gases. Dynamic images were reconstructed using FBP for 30x1 sec, 15x2 sec, 12x5 sec, and 18x10 sec, in total 5min. Five ROIs were defined on reconstructed images in the middle-carotid artery territory of the injected hemisphere on different slice levels. Time-activity curves were fitted to a single exponential function, and then the clearance slopes were compared between 15O2-Hb and H215O. Results Typical coincidence counting rate of the whole PET gantry was approximately 35 kcps, 60 kcps and 30 kcps at peak, corresponding to the 15O2-Hb, H215O and C15O-Hb, respectively. Deadtime loss was <5% at all scans. The clearance slopes were close to each other between 15O2-Hb and H215O (see Table), while much faster for C15O-Hb. Conclusion The clearance of 15O radioactivity for 15O2-Hb was identical to that for H215O, suggesting that negligible amount of back diffusion of non-metabolized 15O2 is a good approximation. Sophisticated mathematical approaches are thus verified to further improve the accuracy in the quantitative assessment of CMRO2 in vivo.

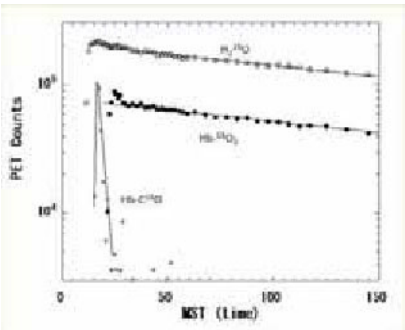


Results of the clearance slope values

| | | | |
|---|---|---|---|
| | | | |
| | | | |
| | | | |
| | | | |
| | | | |
| | | | |

Disclosure of author financial interest or relationships:
**H. Iida**, None; **N. Kudomi**, None; **S. Iguchi**, None; **T. Moriguchi**, None; **K. Koshino**, None; **T. Zeniya**, None; **A. Yamamoto**, None; **Y. Hori**, None; **J. Enmi**, None; **H. Kawashima**, None.

Presentation Number **P510**
Poster Session 3
September 7, 2012 / 15:15-15:15 / Room: The Liffey

# Development a useful I-123-Epidepride small animal imaging platform for pre-clinical drug study about schizophrenia

***Shih-Ying Lee**, Kang-Wei Chang, Yuan-Ruei Huang, Yu-Lung Wu, Jun-ming Shih, Chieh Huang, Chia-Chieh Chen, INSTITUTE OF NUCLEAR ENERGY RESEARCH, Taoyuan County, Taiwan. Contact e-mail: shihying@iner.gov.tw*

Background The recently reporters indicated that significantly lower D2/D3 values were observed in the midbrain of patients with schizophrenia compared to controls, and no statistically significant difference in the thalamus. The dopamine D2 receptor density in extrastriatal areas was 10-100 times lower than that in the basal ganglia. I-123-epidepride had high affinity for dopamine D2/D3 receptor, which enable measurements in low-density receptor regions such as the thalamus and the temporal cortex. I-123-Epidepride had been used to measure receptor occupancy of neuroleptics in schizophrenic patients. Our aim was to provide a potential probe for extrastriatal dopamine D2/D3 receptors, combine with microSPECT and development a useful small animal imaging platform for pre-clinical drug study about schizophrenia. We continue provide a novel integrated imaging in CNS drug evaluation and provide new opportunities in drug development. Method(s) The Radiochemical purity of I-123-Epidepride was >95% determined by HPLC equipped with a radiodetector. Sprague-Dawley rats (250-300 grams) were used in this study and each rat were injected 5mCi I-123-Epidepride via tail vein. For ex vivo autoradiography, rats were sacrificed after 30min and 180 min distribution. Then, the brains were sliced into 20 μm transverse sections. Images were acquired at 30min after radiol-tracer injection. A commercial microSPECT/CT (X-SPECT scanner, Gamma Medica Inc.) with high-resolution multi-pinhole collimator was applied for tomographic scan. For schizophrenia drug study, rats were oral administration of Amisulpride for 14 days. The SPECT/CT fused images were displayed on Reveal MVS to draw regions of interest (ROIs) in the striatum, thalamus and midbrain for semi-quantitative analysis. Result(s) Ex vivo autoradiography show that I-123-Epidepride accumulated in the striatum at 180 min, and the specific binding ratio (16.3) was higher than 30 min (4.74). Extrastriatal region included thalamus and midbrain. The specific binding ratio in thalamus at 30 min (1.95) was higher than 180min (0.83). The result was similar in midbrain. We compared with the microSPECT/CT images after rats administrated with I-123-Epidepride or I-123-IBZM. I-123-IBZM radioactivity accumulated only in striatum at 30 min of the rat brain. But, I-123-Epidepride radioactivity accumulated in striatum and extrastriatal regions. We used I-123-Epidepride to evaluate Amisulpride drug effect on dopamine D2/D3 receptors. For an amisulpride dose of 12mg/kg/day, the D2/D3 receptor occupancy rate was 29.7% in the striatum, 64.7% in the thalamus, and 58.8% in the midbrain. Higher occupancy in extrastriatal than striatal regions is evident in this study. Conclusion Our image results demonstrated that I-123-Epidepride is a good tracer and had higher binding affinity of dopamine D2/D3 receptor in extrastriatal regions than I-123-IBZM. We establish a useful small animal imaging platform for pre-clinical drug study about schizophrenia, and hope this tool can help reduce the significant cost of bringing new drugs from discovery to the marketplace.

Disclosure of author financial interest or relationships:
**S. Lee**, None; **K. Chang**, None; **Y. Huang**, None; **Y. Wu**, None; **J. Shih**, None; **C. Huang**, None; **C. Chen**, None.

Presentation Number **P511**
Poster Session 3
September 7, 2012 / 15:15-15:15 / Room: The Liffey

# Survival of Neural Stem Cells can be Improved by Co-Transplantation of bFGF-Producing Helper Cells Under Control of Doxycycline

***Yajie Liang***, *Louise Ågren, Agatha Lyczek, Piotr Walczak, Jeff W. Bulte, Dept. of Radiology, Johns Hopkins University School of Medicine, Baltimore, MD, USA. Contact e-mail: agetliang@gmail.com*

Cell-based therapy of neurological disorders may be hindered by poor survival of the graft. Since survival of neural progenitor cells (NPCs) is highly dependent on the presence of growth factors, studies have been performed on constitutive expression of growth factors by NPCs in order to improve their survival. Associated risks include the use of a lenti- or retrovirus and the risk of tumorigenesis after random insertion of genes. Another potential pitfall may be the lack of control of expression of growth factors, with high levels being potentially toxic to both the graft and host. We aimed at enhancing survival of grafted NPCs by the use of helper cells expressing growth factors under the control of doxycycline (Dox). A tetracycline inducible expression system (TetON) consisting of M2rtTA and target genes (growth factors, GFs, and fluorescent proteins, FPs) driven by a TRE promoter was cloned into lentivectors for transduction of helper cells (Fig. 1A). Mouse C17.2 helper cells were transduced with lentiviral vectors encoding basic fibrobast growth factors (bFGF), fluorescent reporter (mCherry) and TetON system elements. The expression level of the target genes bFGF and mCherry could be induced by presence of Dox in a dose-dependent manner (Fig 1b). The efficacy of our strategy was then evaluated in vitro using human NPCs (ReNcells). ReNcells were plated onto uncoated culture plates with or without helper cells. The addition of Dox significantly improved the survival of ReNcells in co-culture with engineered C17.2 helper cells (C17.2-Eg), but not for cells co-cultured with wildtype (WT) cells. A mixture of 1E5 ReNcells and 1E5 C17.2 helper cells was then transplanted into Rag2-/- immunodeficient mice. The survival of ReNcells was significantly improved in the Dox-treated (100 mg/kg/day s.c.) C17.2-Eg helper cell group. (*p<0.05, Fig. 1c,d). Importantly, in the absence of Dox, the pro-survival effect was obviated These results suggest that co-engraftment of helper cells is beneficial, and the flexibility inherent to this strategy (choice of growth factors, timing of switch on-expression) opens up a window of opportunities for refining cell-based therapies.

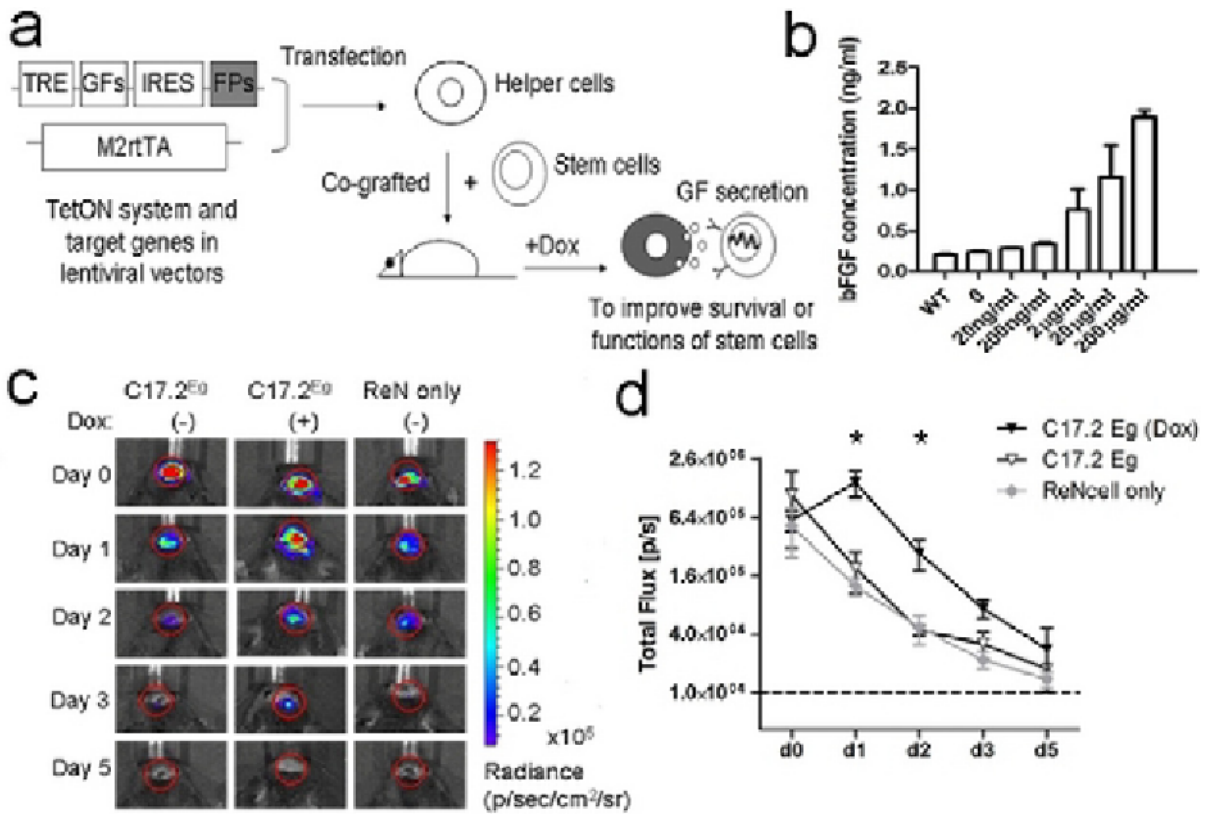


Disclosure of author financial interest or relationships:
**Y. Liang**, None; **L. Ågren**, None; **A. Lyczek**, None; **P. Walczak**, None; **J.W. Bulte**, Philips, Grant/research support; Q Therapeutics, Grant/research support .

Presentation Number **P512**
Poster Session 3
September 7, 2012 / 15:15-15:15 / Room: The Liffey

# Positron Emission Tomograghy with [13N]ammonia Evidences Long-term Cerebral Hyperperfusion after 2h-Transient Focal Ischemia

***Abraham Martin***[1], *Eneko San Sebastián*[1], *Vanessa Gómez-Vallejo*[1,2], *Jordi Llop*[1,2], [1]*Molecular Imaging Unit, CIC biomaGUNE, San Sebastián, Spain;* [2]*Radiochemistry, CIC biomaGUNE, San Sebastián, Spain. Contact e-mail: amartin@cicbiomagune.es*

Objectives: It is well known that after cerebral ischemia, brain suffers blood flow changes over time that have been correlated with inflammation, angiogenesis and functional recovery processes. Nevertheless, post-ischemic spatiotemporal changes of brain perfusion have not been fully investigated to date. The purpose of the present study was to elucidate long-term cerebral hyperperfusion in specific brain regions within the infarcted territory, in the homologous contralateral hemisphere as well as in neighboring regions to the ischemic lesion using PET [13N]ammonia. Methods: Longitudinal in vivo PET imaging with [13N]ammonia was performed to explore brain perfusion changes at 1, 3, 7, 14, 21 and 28 days after 2-hour transient middle cerebral artery occlusion. PET images were analyzed to quantify the evolution of brain perfusion (i) in both the entire ischemic and contralateral territories and (ii) in specific brain regions such as orbitofrontal, motor, somatosensory and insular cortices, caudate putamen, amygdala, hippocampus, thalamus and cerebellum. Results: In the cerebral territory irrigated by the MCA, [13N]ammonia PET demonstrated a non-significant decrease (ca. 40%) of the signal 1 day after reperfusion with respect to signals in the control cerebral tissue. This decrease was followed by a return to quasi-normal values at 3 days after reperfusion and an increase thereafter with an overshoot at day 7 after reperfusion. After day 14, the PET signal decreased to reach control signal values at day 28 after ischemia. Interestingly, a similar time course was observed in the contralateral area. As a result, the ratio of PET [13N]ammonia varied from .8 at day 1 to 1.1 at day 14 after reperfusion. Different brain regions showed a specific involvement in blood perfusion after ischemia. Perfusion in cortical areas (orbitofrontal, motor, somatosensory and insular) decreased at day 1 after reperfusion followed by an increase thereafter at day 7. Caudate putamen showed a dramatic perfusion decrease at day 1 after ischemia in relation to control. This was followed by a return to quasi-normal control values at day 7 and by a subsequent slight decline thereafter. Amygdala showed a similar perfusion profile to that presented in the cortex and caudate. Hippocampus (a remote region to the middle cerebral artery irrigation) also showed, surprisingly, a significant increase at day 7, evidencing the role of neighboring regions in the perfusion changes after cerebral ischemia. On the other hand, thalamus presented a non-significant increase of perfusion ratio signal from 7 to 21 days, while cerebellum did not show any significant post-ischemic perfusion change over time. Conclusions: [13N]ammonia shows hemodynamic changes after stroke involving hyperperfusion that might be related to angiogenesis and functional recovery. Long term blood hyperperfusion is found both in ischemic and remote areas to infarction. The results reported here may have significant practical importance as they could contribute to a better understanding of the cerebral lesions following ischemia, their reversibility and the adequate time windows for potential therapeutic intervention.

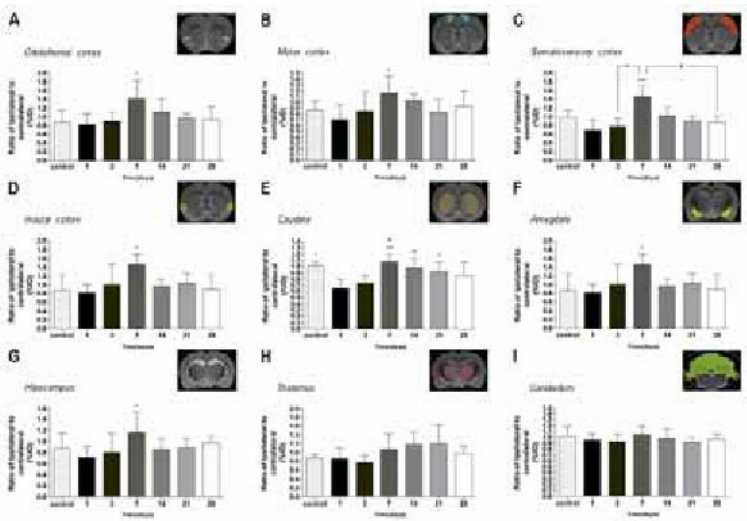


Time course of the ipsi-to-contralateral [13N]ammonia PET signal ratios after ischemia in different brain regions. The percentage of injected dose (%ID/g, mean±s.d.) (A-I) were quantified in nine ROIs defined for each animal over the entire ipsilateral and contralateral orbitofrontal cortex (A), motor cortex (B), somatosensory cortex (C), insular cortex (D), Caudate (E), Amygdala (F), Hippocampus (G), Thalamus (H) and Cerebellum (I). The upper right panels of each figure show the selected brain regions of interest (ROIs) for the quantification defined over a MRI (T2W) template.

Disclosure of author financial interest or relationships:
**A. Martin**, None; **E. San Sebastián**, None; **V. Gómez-Vallejo**, None; **J. Llop**, None.

Presentation Number **P513**
Poster Session 3
September 7, 2012 / 15:15-15:15 / Room: The Liffey

# ULTRA-SENSITIVE MOLECULAR MAGNETIC RESONANCE IMAGING OF CEREBROVASCULAR CELL ACTIVATION

***Axel Montagne**, Maxime Gauberti, Eric Maubert, Denis Vivien, INSERM UMR-S 919, Caen, France. Contact e-mail: amontagne@cyceron.fr*

Background: Following injury to the central nervous system (CNS), endothelial cells from the cerebrovasculature become activated and express inflammatory biomarkers. To overcome the limitation of plasmatic biomarkers to detect CNS suffering, in situ detection of disease-related proteins by molecular imaging have been proposed and successfully used in several neurological pathologies using positron emission tomography (PET). However, limited availability and low spatial resolution impairs the use of PET in routine clinical practice. In this study, our aim was to reveal CNS suffering by unmasking cerebrovascular cells activation using a highly sensitive strategy of molecular magnetic resonance imaging (MRI). Material and Methods: Using both in vitro and in vivo experiments, we optimized contrast carrying particles, targeting moieties and MRI protocols to allow ultra-sensitive imaging of cerebrovascular inflammation. After selection of the best contrast agent candidate (an optimized microsized particle of iron oxide, MPIO), we performed in vivo molecular MRI on a set of pre-clinical models for vascular dementia, ischemic/hemorrhagic stroke, Alzheimer's disease and multiple sclerosis. Results and conclusion: Remarkably, contrast-enhanced MRI using our optimized probe revealed hypoperfusion-triggered CNS suffering in vascular dementia, predicted ischemic lesion evolution following stroke, unmasked amyloid-induced cerebrovascular activation in Alzheimer disease and allowed monitoring of disease activity during experimental autoimmune encephalomyelitis. Hence, microsized ultra-sensitive endothelium-targeted particles of iron oxide are promising for early diagnosis and monitoring of CNS suffering.

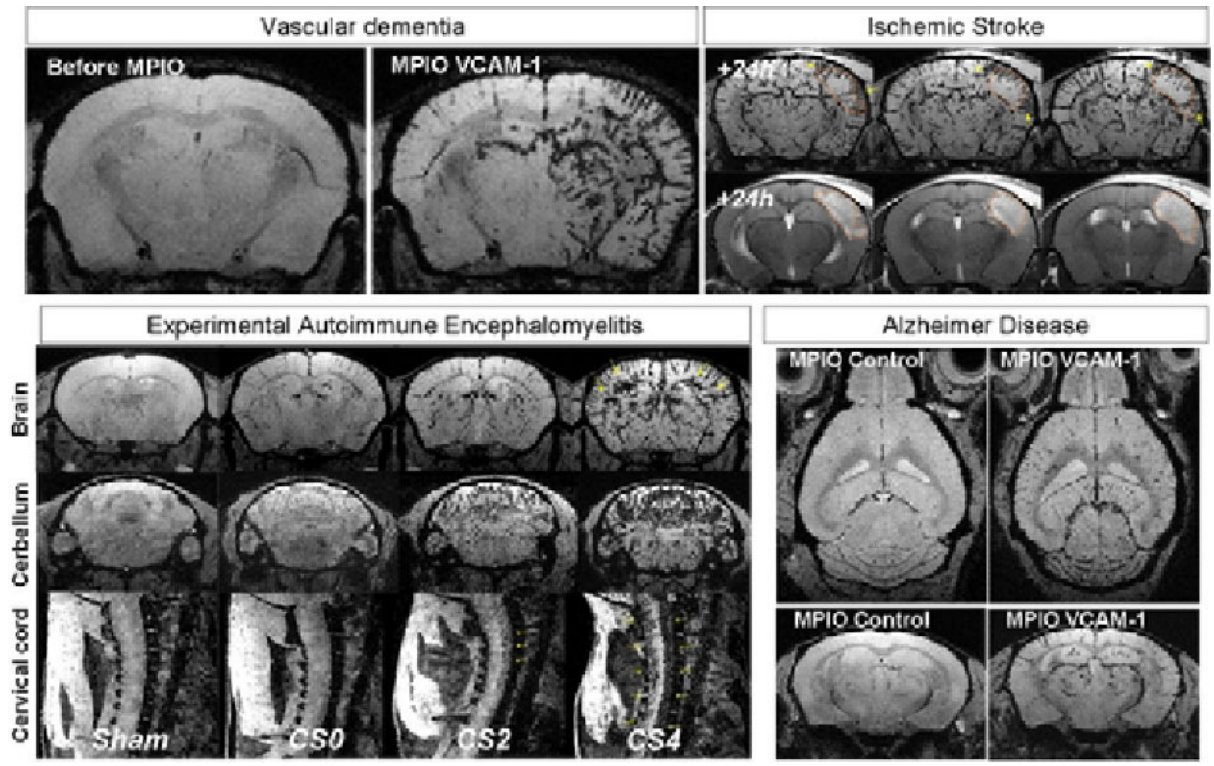


Optimized MPIOs targeting VCAM-1 reveal CNS suffering with high sensitivity. Vascular dementia: representative images of a mouse during the pre-symptomatic stage of a vascular dementia model (permanent ligation of the right common carotid artery) before and after MPIOs-VCAM-1 administration, revealing pre-symptomatic CNS suffering. Ischemic stroke: 24 hours after ischemic stroke, MPIOs-VCAM-1 reveal a viable perilesional area which will be recruited by the ischemic core in the subacute stage of lesion evolution. EAE: In this mouse model for multiple sclerosis, MPIOs-VCAM-1 reveal CNS inflammation in the forebrain, the cerebellum and the spinal cord, predominantly in the white matter. Higher is the activity of the disease (Clinical Score, CS), larger are the areas of MPIO binding. Alzheimer Disease: In transgenic mice (APP/PS1) which spontaneously form Aβ aggregates, MPIOs-VCAM-1 reveal cerebrovascular cells activation and CNS suffering.

Disclosure of author financial interest or relationships:
**A. Montagne**, None; **M. Gauberti**, None; **E. Maubert**, None; **D. Vivien**, None.

Presentation Number **P514**
Poster Session 3
September 7, 2012 / 15:15-15:15 / Room: The Liffey

# Development of Novel Cannabinoid type 2 Receptor Tracers for PET Imaging

***Linjing Mu***[1], *Daniel Bieri*[2], *Roger Slavik*[2], *Konstantin Drandarov*[2], *Adrienne Müller*[2], *Stefanie D. Krämer*[2], *Roger Schibli*[2,1], *Simon M. Ametamey*[2], [1]*Nuclear Medicine, Universitätsspital Zürich, Zürich, Switzerland;* [2]*Department of Chemistry and Applied Biosciences, ETH, Zürich, Switzerland. Contact e-mail: linjing.mu@usz.ch*

The cannabinoid receptor type 2 (CB2) has very low expression levels in brain tissue under normal conditions, however, it is up-regulated in cerebellum, cortex and brainstem in pathological conditions such as neuroinflammation and neurodegenerative diseases including Parkinson's and Alzheimer`s disease. As part of our program to develop a brain PET tracer towards CB2, we selected a promising lead structure, designated KD-2, from the literature [1] and evaluated its potential as an imaging agent for the CB2. The radiosynthesis of [11C]-KD-2 was successfully accomplished in a one-step reaction sequence starting from a phenolic precursor and [11C]-methyl iodide. The final product was obtained in 99% radiochemical purity after semi-HPLC purification and specific activity was high and ranged from 80 to 320 GBq/µmol. In vitro competitive binding assays were performed with membranes containing human CB2 and CB1 using [3H]-CP-55940. Achieved affinities were comparable to literature. Permeation of KD-2 across P-glycoprotein transfected MDCK epithelial cells was moderate, but in the range of blood-brain barrier permeating compounds. No efflux of KD-2 by P-glycoprotein was detected. In vitro plasma binding was very high with a free fraction of 0.1%. The distribution coefficient (LogD) of [11C]-KD-2 in octanol/buffer at pH 7.4 was 3.29 ± 0.04 (n = 6). In vitro autoradiography of rat and mouse spleen slices demonstrated that [11C]-KD-2 exhibits high specific binding to CB2, which was blocked by 5 uM WIN 55212-2 (Fig. 1). Preliminary PET studies with rats showed that radiolabeled [11C]-KD-2 accumulated in liver, spleen and intestine. Radioactivity in the brain was significantly lower than in the periphery. Uptake in pons and cerebellum was higher than in hippocampus and caudate/putamen, which is in agreement with the expression pattern of CB2 in the rat brain. The accumulation in spleen was displaced by 1.5 mg/kg GW405833, indicating specific binding. Furthermore, eight new derivatives of KD-2 were designed and synthesized in our laboratory. Their binding affinities towards human CB2 and CB1 were determined and the Ki values for the CB2 receptor ranged from 0.7 - 1220 nM, with a selectivity hCB2 over hCB1 from 10 to >10'000. The most promising candidates will be radiolabeled with 11C or 18F for further in vitro and in vivo evaluation.
[1]: Pasquini et al., J. Med. Chem., 54 (15), 5444-53 (2011).


Figure 1: In vitro autoradiography of rat spleen (A1) and mouse spleen slices (B1) with 0.6 nM [11C]-KD2 in the presence of 5 µM blocking agent WIN-55212-2 (A2 and B2).

Disclosure of author financial interest or relationships:
**L. Mu**, None; **D. Bieri**, None; **R. Slavik**, None; **K. Drandarov**, None; **A. Müller**, None; **S.D. Krämer**, None; **R. Schibli**, None; **S.M. Ametamey**, None.

Presentation Number **P515**
Poster Session 3
September 7, 2012 / 15:15-15:15 / Room: The Liffey

# 18F-Fluorodeoxyglucose associated with Positron Emission Tomography and Computerized Tomography reveals cytokine-induced changes in tissue metabolism

***Laura Ravasi***[1]*, Auger Florent*[1]*, Durieux Nicolas*[1]*, Patrick Losey*[1]*, Nicola R. Sibson*[2]*, Daniel C. Anthony*[2]*, Régis Bordet*[1]*,*
*[1]Pharmacology, IMPRT, Lille, France; [2]Pharmacology, University of Oxford, Oxford, United Kingdom. Contact e-mail: lauraravasi@gmail.com*

Background Tumor Necrosis Factor (TNF) expression is elevated in a variety of neuropathologies, including multiple sclerosis, cerebral malaria, HIV encephalitis. However, the consequences of such high cerebral TNF expression remain unresolved. Using magnetic resonance imaging we demonstrate that a focal intrastriatal injection of TNF causes a significant, acute reduction (15-30%) in cerebral blood volume, which is dependent on TNF-receptor type 2 activation. This is followed by a significant reduction in tissue water diffusion (ADC) at 24h, which may indicate compromise of tissue energy metabolism. The aim of the current study was to clarify the changes in cerebral metabolism induced by cytokine injection. Material and methods Wistar rats underwent microsurgery to stereotaxic inject a 10µL solution containing TNF-α (1,5 µg), or InterLeukin1-β (10ng) or saline. PET/CT scans were performed on a MicroPET (INVEON, Siemens Preclinical Medical Solutions). After a fasting of 6 hours, the rats were tail vein injected with ~ 37 MBq of [18F]FDG. At 30 minutes after injection, they underwent a CT scan, for attenuation correction purposes, followed by a 30-min static PET acquisition starting at 45 min after radiotracer injection. Rats underwent MicroPET acquisition at 1h, 4h and 24 h after microsurgery. To assess relative regional cerebral metabolism, ROIs were drawn on left and right striatum, whole brain and cerebellum by use of IRW software version 3.0. Regional metabolism was compared between ipsi and contralateral striatum at all time points. We compared n=3 rats per type of injected solution and per time point. Results As expected, no change in [18F]FDG distribution was observed in the saline injected rats. In the group of rats injected with TNF-α, we were surprised to observe no changes in radiotraceur uptake at 1h and 4h, i.e. in the early, low flow time points as opposed to the significant increase (>20%) of metabolism in the injected striatum at 24 hours, when ADC is reduced. For the rats that were administered with InterLeukin-1β, no metabolic changes were observed at early and late time points, despite ADC changes observed through MRI imaging. Conclusion These findings suggest that the observed ADC changes following TNF injections are unlikely to be associated with metabolic insufficiency. However, the findings also demonstrate that FDG PET can be used to reveal the presence of TNF-induced inflammation in the Central Nervous System.

Disclosure of author financial interest or relationships:
**L. Ravasi**, None; **A. Florent**, None; **D. Nicolas**, None; **P. Losey**, None; **N.R. Sibson**, None; **D.C. Anthony**, None; **R. Bordet**, None.

Presentation Number **P516**
Poster Session 3
September 7, 2012 / 15:15-15:15 / Room: The Liffey

# Neurography: Imaging Neural Transport with a Molecular Imaging Agent

*Lucia LeRoux, Sebastian Bredow,* ***Dawid Schellingerhout****, Departments of Radiology and Experimental Diagnostic Imaging, University of Texas M.D. Anderson Cancer Center, University of Texas M D Anderson Cancer Center, Houston, TX, USA. Contact e-mail: Dawid.Schellingerhout@mdanderson.org*

Purpose: To develop an agent for imaging retrograde axonal transport in nerve tissues based on the optical labeling of a non-toxic fragment of tetanus toxin. Materials and Methods: A His-tagged recombinant tetanus toxin fragment (TTc) was produced in E.coli, purified, and labeled with a variety of Alexa fluorophors for optical imaging studies. Gel electrophoresis (SDS-PAGE) and quantitative immunodetection studies were performed. Cell uptake studies were performed to assess in vitro efficacy. Labeled TTc was injected into the soleus muscle of C57bl and Balb/C mice, and Wistar rats, and imaging performed with the IVIS 200 (Xenogen). In situ validation was performed with laser scanning confocal microscope FV 1000 (Olympus) utilizing intact glycerol mounted samples, and cryo-sections. Results: Gel electrophoresis and quantitative immunodetection indicated that the integrity and immune reactivity of the protein was preserved after labeling. Cell uptake assays indicated robust uptake in differentiated PC12 cells. In vivo optical imaging demonstrated the uptake of TTc-Alexa in the sciatic nerve and spinal cord. Progressive uptake and transport of the agent could be seen along the course of the sciatic nerve and spinal cord. Confocal microscopy studies on intact excised nerve segments and cryosections confirmed the compound uptake in nerve fascicles of the sciatic nerve. Axonal nerve uptake and superficial lymphatic uptake were clearly distinguishable, and transport was shown to be nerve-specific. Immunohistochemistry on cord sections demonstrated the presence of the agent in spinal cord neurons. Conclusion: Fluorescently labeled TTc is taken up into motor nerve endings after intramuscular injection, and is retrogradely transported in nerve axons. This process can be demonstrated with non-invasive in vivo imaging, and allows nerve anatomy and function to be studied.

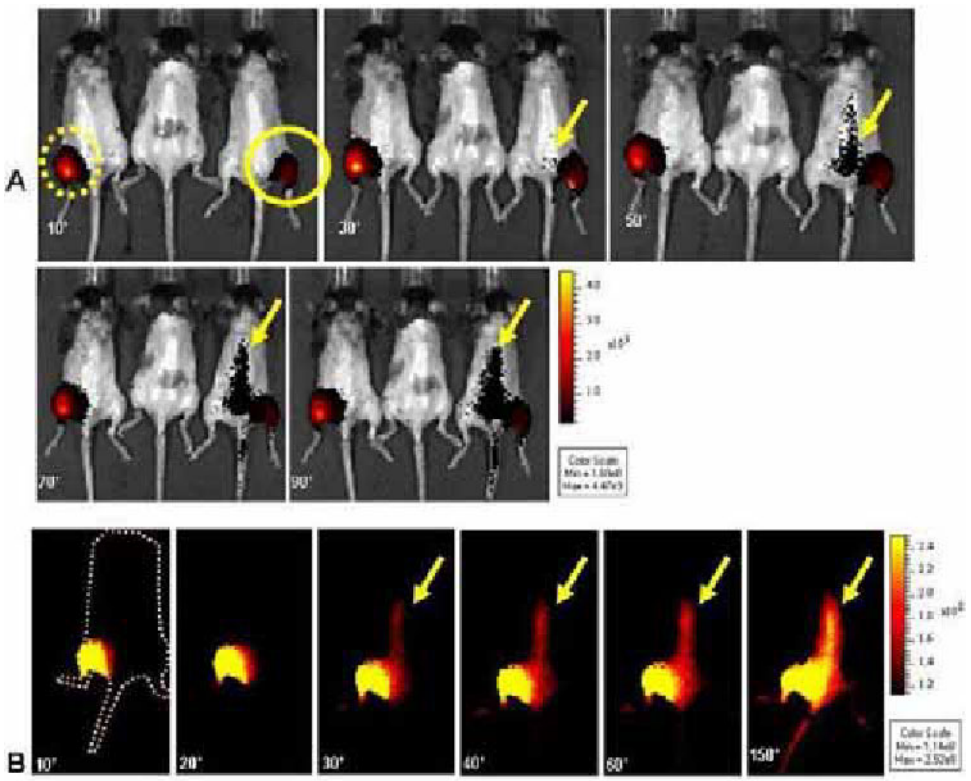


Figure 2

Disclosure of author financial interest or relationships:
**L. LeRoux**, None; **S. Bredow**, None; **D. Schellingerhout**, None.

Presentation Number **P517**
Poster Session 3
September 7, 2012 / 15:15-15:15 / Room: The Liffey

# Long-term studies of glucose metabolism by using 18F-FDG PET in transient focal cerebral ischemia in rats

***Jun-ming Shih**, Yuan-Ruei Huang, Yu-Lung Wu, Shih-Ying Lee, Kang-Wei Chang, Chia-Chieh Chen, Institute of Nuclear Energy Research, Taoyuan County, Taiwan. Contact e-mail: jmshih@iner.gov.tw*

Objectives : Some evidences showed small animal PET with 18F-FDG is sensitive to metabolic changes that occur after ischemic brain injury. This study used 18F-FDG PET to evaluate the long-term metabolic change in transient ishchemic rat animal model. Methods: SD rats were used in this study. Transient focal ischemia was induced by occlusion of the right middle cerebral artery (MCA). A small craniectomy was made above the rhinal fissure, and over the trunk of the right (MCA) ,the artery was ligated with a 10-0 suture.Then, both common carotid arteries (CCA) were also occluded for 90 min. At 1, 7, 14, 21, 35 days after MCAO respectively, brain imaging were acquired by a high-resolution PET. The rats were administered 2mCi 18F-FDG via tail vein. The images were acquired in the microPET within 10 min after the 30-min period. Result: No significant of 18F-FDG uptake changes in both right and left brain of control rat. The ROIs corresponding to the ischemic area showed a obvious reduction in 18F-FDG uptake when compared with contralateral hemisphere. At 1, 7, 14, 21, 35 days after MCAO , the ratio of infarcted and non-infarcted hemisphere of 18F-FDG radioactivity is 0.63, 0.74, 0.77, 0.84, 0.86 respectively, indicted that increased over reperfusion time, the slowly recovery appeared but still can not return to normal level. Conclusion: We successfully demonstrated a longterm study on transient ischemic stroke rat for glucose metabolism by 18F-FDG PET .Our results showed that infarcted area will progressively recover the metabolic activity by increasing reperfusion time This study was supported by grant awarded by the department of industrial technology, Ministry of Economic Affairs, R.O.C

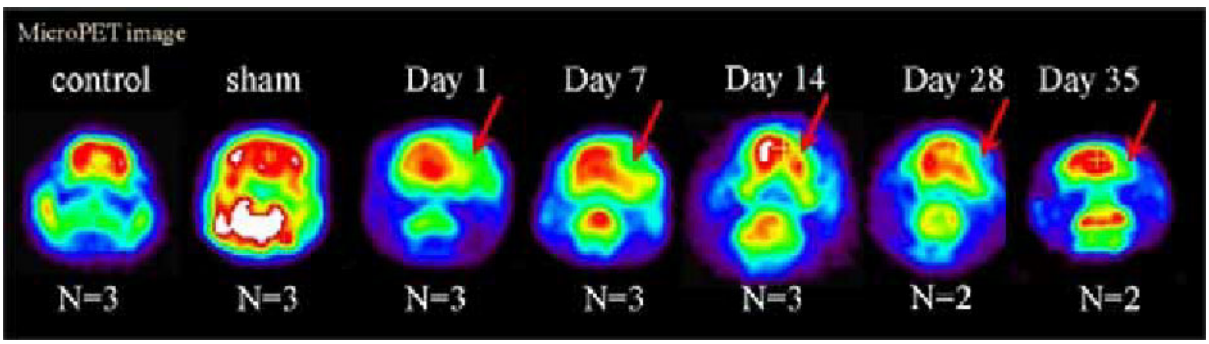


Disclosure of author financial interest or relationships:
**J. Shih**, None; **Y. Huang**, None; **Y. Wu**, None; **S. Lee**, None; **K. Chang**, None; **C. Chen**, None.

Presentation Number **P518**
Poster Session 3
September 7, 2012 / 15:15-15:15 / Room: The Liffey

# Using FDG-PET to test amphetamine-induced neurotoxic effects in the Pleiotrophin Knockout mouse model

***Maria L. Soto-Montenegro***[1,3], *Esther Gramage*[4], *Gonzalo Herradon*[4], *Manuel Desco*[1,2], [1]*Unidad de Medicina y Cirugia Experimental, Hospital General Universitario Gregorio Maranon, Madrid, Spain;* [2]*Departamento de Bioingenieria e Ingenieria Aeroespacial, Universidad Carlos III, Madrid, Spain;* [3]*CIBER de Salud Mental (CIBERSAM), Madrid, Spain;* [4]*Laboratorio de Farmacologia, Departamento de Ciencias Farmaceuticas y de la Alimentacion, Universidad CEU San Pablo, Madrid, Spain. Contact e-mail: marisa@mce.hggm.es*

Introduction: Pleiotrophin (PTN) is a cytokine necessary for survival and differentiation of dopaminergic neurons. Pleiotrophin is upregulated in different brain areas after amphetamine administration suggesting a neuroprotective role of PTN against amphetamine-induced neurotoxicity. In immunochemistry studies, our group recently compared the effects of amphetamine administration in PTN genetically deficient (PTN -/-) and wild type (PTN +/+) mice, uncovering that amphetamine causes an ~70% decrease in the protein levels of tyrosine hydroxylase (TH) in the striatum of PTN -/- mice while only ~35% TH loss was observed in wild type mice, suggesting the PTN knockout mouse as a new animal model to study amphetamine-induced neurodegeneration of dopaminergic terminals in the striatum. The aim of the study is to use the PTN-/- mouse model to test the possibility of using Possitron Emission Tomography (PET) to assay glucose uptake as an in vivo marker of amphetamine-induced neurotoxicity in the striatum. Methods: 6 PTN-/- mice were included in this study. These animals received 4 consecutive injections i.p. of amphetamine (10 mg / kg) (N=3) or saline (10mg/kg) (N=3) with an interval of 2 hours between administrations. Imaging studies were performed after four days of the end of the protocol of drug administration with an Argus small-animal PET/CT scanner (SEDECAL, Madrid, Spain). [18F]fluoro-D-glucose (FDG) (0.5 mCi aprox.) was injected by the tail vein and after an uptake period of 35 min, animals were imaged during 60 minutes. Images were reconstructed using a 3D-OSEM algorithm (FIRST©). Regions of interest (ROIs) were drawn on coronal-sections: caudate-putamen, background (BG) and whole brain (WB). To normalize FDG uptake, tissue activity was corrected by subtracting background and dividing by whole brain activity. Results are expressed as a percentage (%) ([FDG uptake=(study ROI-BG/WB)×100]. Results: In confirmation of the above mentioned studies of our group, we found a significant amphetamine-induced depletion of TH levels in immunohistochemical studies and of dopamine transporter (DAT) levels in Western blots carried out in the striatum of amphetamine-treated PTN-/- mice compared to saline-treated mice. The FDG uptake in amphetamine-treated animals was significantly lower compared with saline animals ($p = 0.03$). Discussion: Using the PTN-/- mouse model, the data demonstrate the correlation between amphetamine-induced dopaminergic denervation and reduction of FDG uptake in the striatum. The data support the use of PET to test FDG uptake in order to efficiently assay amphetamine neurotoxic effects in the striatum in vivo. Acknowledgements: This work has been supported by Ministerio de Sanidad y Consumo (FIS CP08/00017, FIS PI11/00616), CENIT-AMIT Ingenio 2010, Ministerio de Ciencia e Innovación (SAF2009-08136), TEC2007-64731, TEC 2008-06715-C02-1, ARTEMIS S2009/DPI-1802 program from Comunidad de Madrid and Fundación de Investigación Médica Mutua Madrileña.

Disclosure of author financial interest or relationships:
**M.L. Soto-Montenegro**, None; **E. Gramage**, None; **G. Herradon**, None; **M. Desco**, None.

Presentation Number **P519**
Poster Session 3
September 7, 2012 / 15:15-15:15 / Room: The Liffey

# Measuring Glucose Concentrations in the Rat Brain Using TE-Averaged PRESS at 7T

***Jeffrey Steinberg***, *S. Sendhil Velan, Singapore Bioimaging Consortium, Agency for Science, Technology and Research, Singapore, Singapore. Contact e-mail: jeffrey_steinberg@sbic.a-star.edu.sg*

Introduction: Glucose in the brain is an important molecule in the brain for assessing a range of diseases, including dementia, schizophrenia, and cancer. Positron emission tomography (PET) using FDG is the most commonly used method for measuring glucose consumption in the brain, but it is limited in that it can only measure uptake, not the actual glucose concentration. In order to measure the concentration in vivo, magnetic resonance spectroscopy (MRS) needs to be used. However, it is difficult to quantify the concentration due to water suppression affecting the 4.6 ppm and 5.2 ppm peaks as well as the other metabolite and macromolecular peaks overlapping with the other glucose signals. By using a technique called TE-averaging, multiple in phase resonance glucose signals at different TE values can be summed constructively to reveal a relatively unobstructed glucose signal. Materials and Methods: The brains of nine rats were scanned on a Bruker ClinScan 7T MRI before and after fasting. The scans consisted of a standard 13 ms TE PRESS scan and a TE-averaged scan, which takes an equal number of averages for eight separate TE values ranging from 60 to 95 ms in increments of 5 ms. This range was carefully chosen to minimize the signal from glutamate and glutamine while maximizing the signal from glucose. The signal of interest is at 3.85 ppm, which is a combination of signals from the α-glucose 5CH, α-glucose 6CH, and β-glucose 6CH protons. The result is a negative signal in the real frequency spectrum, whereas signals from nearby metabolites are positive. The reduction in glucose signal relative to creatine at longer TE values was corrected by using a brain phantom with a high concentration of brain metabolites to estimate the reduction. The basis files for fitting also corrected for the T2/T2* loss in signal for each TE value used in the average. Using these corrections, the TE-13 and TE-averaged spectra were fitted in LCModel using the basis files created using Versatile Simulation, Pulses and Analysis (VeSPA). Results and Discussion: The estimated brain glucose in all rats increased after feeding with a noticeably larger glucose signal as well as fasted and fed glucose-to-creatine ratios of 0.30 ± 0.14 and 0.46 ± 0.19 respectively. Short TE data at 13 ms had measured ratios of 0.46 ± 0.46 and 0.26 ± 0.21 for the fasted and fed rats respectively. Using Student's t-test (one-tailed, 95% confidence interval), it was found that the increase in glucose concentration was significant with a p-value of 0.002 for the TE-averaged data and insignificant with a p-value of 0.14 for the TE13 data. Also, the figure demonstrates the noticeable increase in glucose concentration after feeding from the increase in signal at the identified 3.85 ppm peak. Conclusion: TE-averaging can be used to minimize the influence of macromolecular signals and other metabolite signals to give more accurate, consistent estimates of glucose concentrations in the brain.

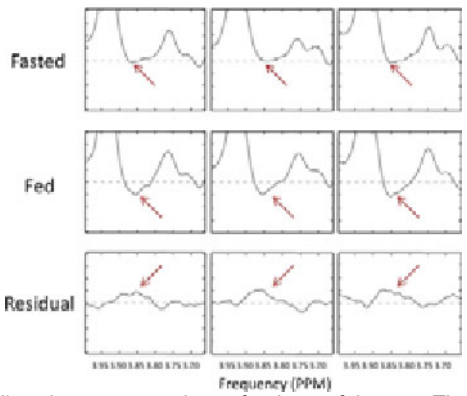


The fasted, fed, and the residual (fasted minus fed) real spectra are shown for three of the rats. The glucose signal at 3.85 ppm becomes significantly more negative for the fasted rats after they have been fed, indicating an increase in glucose concentration.

Fasted vs Fed Glucose-to-Creatine Levels

| | | | | |
|---|---|---|---|---|
| | | | | |
| | | | | |
| | | | | |
| | | | | |
| | | | | |
| | | | | |
| | | | | |
| | | | | |
| | | | | |

Measured glucose-to-creatine levels in the rat brain before and after feeding using the TE-averaged (TEavg) and 13 ms TE (TE13) PRESS sequences.

Disclosure of author financial interest or relationships:
**J. Steinberg**, None; **S. Velan**, None.

Presentation Number **P520**
Poster Session 3
September 7, 2012 / 15:15-15:15 / Room: The Liffey

# MicroPET imaging of regional metabolic activity in rats with temporary middle cerebral artery occlusion

***Hsu-Yin Tseng***, *Wen Yuan Chang, Jyh-Cheng Chen, Dept. of Biomedical Imaging and Radiological Sciences, National Yang-Ming University, Taipei, Taiwan. Contact e-mail: vicky210025@hotmail.com*

Purpose- Middle cerebral artery occlusion (MCAO) in rodents is an experimental model of cerebral ischemia that is essential to in vivo pathophysiological processes and is widely used for the evaluation of treatment efficacy after brain injury. In this study, the MCAO in rodents were applied to analyze 18F-FDG kinetics with micro positron emission tomography (microPET) when the middle cerebral artery was reopened. Methods- Sprague-Dawley rats were anaesthetized with chloral hydrate and subjected to 60 min of intraluminal middle cerebral artery occlusion with subsequent reperfusion, in three groups: control group , observed immediately after MCA reopening group and observed 24hrs after MCAO group. For all groups, microPET imaging with 18F-FDG was used to evaluate brain glucose metabolism. Results- The imaging data acquired from microPET were displayed, analyzed and coregistered with built-in MRI template by PMOD 3.2. 18F-FDG metabolism was evaluated by drawing ROIs in the bilateral cortex for each slice . After 4 hrs MCAO,the ipsilateral cortex region of 18F-FDG uptake is higher than contralateral cortex region by 12%. However, the ipsilateral cortex region of 18F-FDG uptake was lower than contralateral cortex region by 18% after 24hrs MCAO, in which pharmacokinetic parameter K1 in ipsilateral cortex region is 0.07ml/cm3/min, and the contralateral cortex region is 0.1 ml/cm3/min. Conclusions- In this study, using 18F-FDG with microPET scan is effective in durative detection of metabolic changes and calculating pharmacokinetic parameter of 18F-FDG. In the future, using medications or instrument involved could use this study as a reference to design the treatment protocol to reduce the affected region.

Disclosure of author financial interest or relationships:
**H. Tseng**, None; **W. Chang**, None; **J. Chen**, None.

Presentation Number **P521**
Poster Session 3
September 7, 2012 / 15:15-15:15 / Room: The Liffey

# Characterization of a novel radiotracer targeting synaptic vesicle protein 2A (SV2A)

***Geoff I. Warnock***[1], *Joel Aerts*[1], *Mohamed-Ali Bahri*[1], *Florian Bretin*[1], *Tim Buchanan*[2], *Henrik Klitgaard*[2], *Nathalie Mestdagh*[2], *Anne Valade*[2], *Alain Seret*[1], *Andre Luxen*[1], *Eric Salmon*[1], *Alain Plenevaux*[1], [1]*Cyclotron Research Center, University of Liege, Liege, Belgium;* [2]*UCB Pharma S.A., Brussels, Belgium. Contact e-mail: gwarnock@ulg.ac.be*

Synaptic vesicle protein 2A (SV2A) has been identified as the binding site of the antiepileptic levetiracetam (Keppra) [1]. SV2 proteins are critical for proper nervous system function and have been demonstrated to be involved in vesicle trafficking. Their implication in epilepsy makes them an interesting therapeutic target, and the widespread distribution of SV2A in particular may provide an opportunity to develop a PET-based measure of neuronal function in brain diseases. [18F]UCB-H is a fluorine-18 radiolabelled PET imaging agent with a nanomolar affinity for the human SV2A protein. Preclinical PET studies in rodents were carried out using male SD rats, imaged under isoflurane anaesthesia in a Siemens Concorde Focus 120 microPET scanner. Arterial input function was measured using an arteriovenous shunt method and beta microprobe system. [18F]UCB-H was injected IV (3.8 ± 0.54 mCi bolus, specific activity 8.5 ± 0.86 Ci/μmol immediately after synthesis) and dynamic PET data acquired in list mode for 90 min. Images were reconstructed using filtered back projection with correction for all physical effects except scatter. These scans revealed high uptake of [18F]UCB-H in brain and spinal cord, matching the expected homogeneous distribution of SV2A in the rodent brain [2]. Notably, the kinetics of [18F]UCB-H uptake in the brain were fast, peaking at up to 30 % ID/$cm^3$ before a rapid decline. Metabolism of [18F]UCB-H in vivo followed a typical pattern of rapid initial metabolism followed by a reducing rate of metabolism over time, with less than 20% of the activity in plasma attributable to the parent compound after 30 minutes, and was highly reproducible between subjects. One major metabolite was identified. The uptake of [18F]UCB-H in the brain over time was well fitted by a classical 1-tissue compartment model. Mean parameter estimates (mean ± SD, n=7, whole brain VOI) were $K_1$: 3.58 ± 0.65 ml/$cm^3$/min, $k_2$: 0.21 ± 0.03 $min^{-1}$, $V_t$: 17.21 ± 2.52 ml/$cm^3$. Uptake of [18F]UCB-H was blocked by pretreatment with brivaracetam (21 mg/kg IV, 10 min prior to [18F]UCB-H), a recently described high affinity SV2A ligand with a 20-fold higher affinity for SV2A than levetiracetam [3]. In contrast, pretreatment with ucb-100230-1, a diastereoisomer of brivaracetam with 3200-fold lower affinity for SV2A [3], had no clear effect of the brain uptake of [18F]UCB-H. Our results indicate that [18F]UCB-H is a suitable radiotracer for the quantification of SV2A proteins in vivo and for estimating target occupancy of drugs targeting SV2A. This is the first PET tracer for in vivo quantification of SV2A. The necessary steps for implementation of [18F]UCB-H production under GMP conditions have been completed and first in human studies are planned. References [1] Lynch, B.A. et al. (2004) PNAS 101(26):9861-6. [2] Janz, R. & Sudhof, T.C. (1999) Neuroscience 94(4):1279-1290. [3] Gillard, M. et al. (2011) Eur J Pharmacol 664:36-44.

Disclosure of author financial interest or relationships:
**G.I. Warnock**, UCB Pharma, Grant/research support; PMOD Technologies, Consultant; **J. Aerts**, None; **M. Bahri**, None; **F. Bretin**, None; **T. Buchanan**, UCB, Employment; **H. Klitgaard**, None; **N. Mestdagh**, None; **A. Valade**, None; **A. Seret**, None; **A. Luxen**, GE Healthcare, Grant/research support; **E. Salmon**, None; **A. Plenevaux**, None.

Presentation Number **P522**
Poster Session 3
September 7, 2012 / 15:15-15:15 / Room: The Liffey

# The fMRI signal intensity changes of cervical spinal cord with electrical stimulation

*Zhiwei Shen, Yeyu Xiao, **Renhua Wu**, Shantou University, Shantou, China. Contact e-mail: rhwu@stu.edu.cn*

Object: To investigate the signal intensity changes in functional magnetic resonance imaging (fMRI) activity in the cervical spinal cord with electrical stimulation. Method: The cervical spinal cord fMRI, using electrical simulation (5-10 mA, 5Hz) at the right palm of the hand, were acquired form 8 healthy volunteer at 1.5 T with a single-shot fast spin-echo imaging sequence. The fMRI data was analyzed with SPM2 and the signal intensity changes were performed with Marsbar. Results: All subjects had activation localized at C5-C7 vertebral level. Signal increases were measured in all subjects; however 0ne subject was ejected for the extreme high signal gain. The rest of average fractional signal change was 4.34±0.28% at C5 (n=2), 10.33±5.81% at C5/C6 (n=3), 1.51±3.01% at C6 (n=6), 5.85 at C6/C7 and 9.92±4.77% at C7 (n=4). Conclusion: The results of this study indicate that fMRI can be used to assess activity in the cervical spinal cord and have the potential clinical value to evaluate electrical stimulation treatment effect, although the accuracy this method and the repeatability of the results would be further improved.

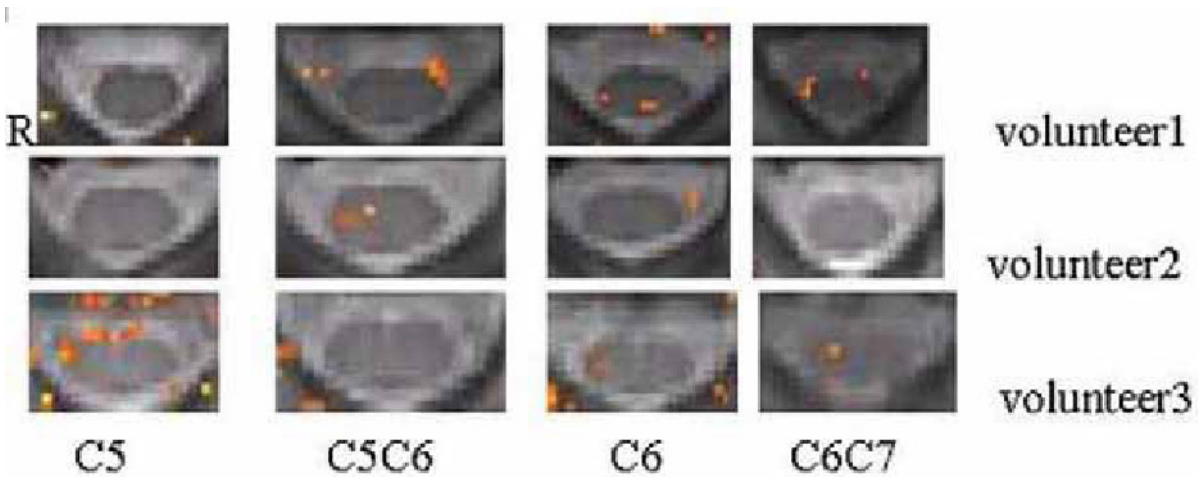


fMRI in the cervical spinal cord with electrical stimulation

Disclosure of author financial interest or relationships:
**Z. Shen**, None; **Y. Xiao**, None; **R. Wu**, None.

Presentation Number **P523**
Poster Session 3
September 7, 2012 / 15:15-15:15 / Room: The Liffey

# In vivo I-123-Epidepride MicroSPECT imaging of dopamine D2/D3 receptor occupancy with Amisulpride

***Yu-Lung Wu**, Jun-ming Shih, Yung-Ruei Huang, Kang-Wei Chang, Shih-Ying Lee, Chia-Chieh Chen, Institute of Nuclear Energy Research, Taoyuan County, Taiwan. Contact e-mail: ylwu@iner.gov.tw*

Objective: Atypical antipsychotic drug is effective and has lower side effect than typical antipsychotic drug. Atypical antipsychotic can combine with mesolimbic dopamine D2 receptor with lower striatal D2 receptor occupancy. Amisulpride is an atypical antipsychotic drug and has affinity for D2/D3 dopamine receptors. In this report, we studied dopamine D2/D3 receptor occupancy with amisulpride in vivo by I-123- Epidepride MicroSPECT imaging. Method: We fed amisulpride to SD rats and divided into three groups of high dose (11.42mg/kg/ day), low dose (5.71 mg/kg/day) and control. After feeding 14 days, the MicroSPECT imaging acquired after injection of I-123-epidepride into amisulpride-treat rats. We quantitated the absorption values of I-123-epidepride and computed the occupancy rate data. Results: For all amisulpride-treat dose, the mean D2/D3 receptor occupancy rate was 40.8 % in the striatum,60.1% in the thalamus and 59.5 % in the midbrain. In our study amisulpride-treated rats had higher D2/D3 receptor occupancy in the thalamus and midbrain than in the striatum. This result is similar to other atypical antipsychotic drug that lower striatal D2 receptor occupancy and higher occupancy of mesolimbic cortical dopamine D2/D3 receptors. Conclusion: In our in vivo study amisulpride can occupy mesolimbic dopamine D2/D3 receptor with lower striatal D2 receptor occupancy. This result is similar to other atypical antipsychotic.

Disclosure of author financial interest or relationships:
**Y. Wu**, None; **J. Shih**, None; **Y. Huang**, None; **K. Chang**, None; **S. Lee**, None; **C. Chen**, None.

Presentation Number **P524**
Poster Session 3
September 7, 2012 / 15:15-15:15 / Room: The Liffey

# Preclinical SPECT imaging of VEGF Receptors in Tumor Vasculature in the Course of Treatment with Pazopanib

*Mary Rusckowski[1], Dengfeng Cheng[1], Yuzhen Wang[1], Miles P. Smith[1], Susanta K. Sarkar[2], Charles B. Davis[3], Jeanelle McSurdy-Freed[3], Marina Backer[4], **Joseph M. Backer**[4], [1]Division of Nuclear Medicine, University of Massachusetts Medical School, Worcester, MA, USA; [2]Translational and Experimental Medicine, Sanofi-Aventis Oncology Division, Cambridge, MA, USA; [3]Oncology R&D, GlaxoSmithKline, Collegeville, PA, USA; [4]SibTech, Inc., Brookfield, CT, USA. Contact e-mail: jbacker@sibtech.com*

Signaling via receptors for vascular endothelial growth factor (VEGFR) promotes and supports tumor angiogenesis, and therefore these receptors are the targets for several approved and experimental anti-angiogenic drugs. However, these drugs typically help only a small and unpredictable number of patients. Pre-clinical and clinical evidence indicates that VEGFR inhibitors induce initial vascular regression and/or normalization of tumor vasculature that leads to tumor growth delay and/or shrinkage and, hence, improved progression-free survival. However, initial vascular regression is followed by the rebound of tumor vasculature. This rebound vasculature is resistant to VEGFR inhibitors despite abundant VEGFR presence. These complexities and, particularly, the opposing processes of vascular regression and rebound, bring a critical need for imaging-based guidance for optimization and management of anti-angiogenic therapy. To image the target of these inhibitors, we have recently developed a molecular imaging tracer, scVEGF/99mTc, engineered single chain (sc) form of VEGF site-specifically radiolabeled with 99mTc for SPECT imaging. The tracer binds to and is internalized by VEGF receptors overexpressed in angiogenic vasculature in tumor and inflammatory diseases and was used for monitoring changes in VEGFR prevalence in response to FDA-approved VEGFR inhibitors sunitinib and pazopanib in two tumor models with rather dramatic vascular regression (1, 2). To further validate VEGFR imaging we explored effects of pazopanib on the relatively slow growing subcutaneous renal cell carcinoma Caci-2 in female CB17/SCID mice. In this model, pazopanib accumulated in tumor as judged by mass-spec analyses of harvested tumors and induced a modest inhibition of tumor growth with correspondingly modest changes in vascular density as judged by immunostaining for VEGFR-2 and pan-endothelial marker CD31. There was a small but statistically significant difference in tracer tumor uptake between control and treated mice when cohorts of mice were analyzed by both biodistribution and imaging. These findings indicate that VEGFR imaging correctly reflects the magnitude of changes in VEGFR prevalence in response to anti-angiogenic treatment. Experiments are in progress to establish how to use VEGFR imaging for optimization of treatment regimens combining VEGFR inhibitors and chemotherapeutic drugs. Reference 1. Blankenberg et al., Transl. Oncol. 3(1):56-64, 2010 2. Levashova et al., J. Nucl. Med. 51(6):959-66, 2010

Disclosure of author financial interest or relationships:
**M. Rusckowski**, None; **D. Cheng**, None; **Y. Wang**, None; **M.P. Smith**, None; **S.K. Sarkar**, Sanofi, Employment; **C.B. Davis**, GlaxoSmithKline, Employment; **J. McSurdy-Freed**, GlaxoSmithKline, Employment; **M. Backer**, None; **J.M. Backer**, SibTech, Inc., Stockholder; GlaxoSmishKline, Grant/research support .

Presentation Number **P525**
Poster Session 3
September 7, 2012 / 15:15-15:15 / Room: The Liffey

# in vivo imaging of soluble T cell receptors using single photon emission computed tomography

***Arnaud Briat***[1], *Rebecca Ashfield*[2], [1]*ANIMASCOPE, Archamps, France;* [2]*IMMUNOCORE, Oxford, United Kingdom. Contact e-mail: a.briat@animascope.eu*

Introduction. Cancer treatment is undergoing a paradigm shift with the inclusion of molecular targeted therapies into standard regimens. As therapies become more personal, there is an increasing need for biomarkers and diagnostics that can be used to determine whether or not an individual patient is likely to respond to a targeted drug. Soluble T cell Receptors (TCRs) are an entirely novel class of targeting agent since they target antigens not accessible to monoclonal antibodies by recognizing disease-associated peptide epitopes presented on the cell surface by Class I HLA molecules. TCRs can therefore virtually target any epitopes including those originated from intracellular proteins. In the current study, we report the first proof of concept for the use of TCRs as nuclear imaging agents for cancer diagnosis. Materials and methods. Engineered J82 Minigene cells expressing the cancer antigen Melan-A26-25 (presented by HLA-A2) were implanted subcutaneously into the right flank of NMRI nude mice (n = 6). Soluble T cell receptors targeting the antigen Melan-A26-25 were conjugated with DTPA and subsequently labeled with indium 111 by incubating 100 micrograms of protein with 148 MBq of [111In] in presence of acetate (radiolabeling efficiency of 96,8 % as controlled by thin layer chromatography) and purified by size exclusion chromatography. Specific activity was 1,49 MBq per micrograms of protein. J82 tumor-beating mice received an intravenous injection of 13 to 15 MBq of [111In]-DTPA-TCR and pinhole-SPECT/CT images acquisition was performed at 24, 48 and 72 hours post-injection (9 pinholes, 24 projections of 75 seconds each). Results. SPECT images demonstrated tumor accumulation of radiolabeled TCRs in all tumor-bearing animals from day 1. Tumor-to-background ratios ranged from 2.64 ± 0.29 at 24 hours post TCRs injection to 2.80 ± 0.13 at 72 hours (Mean ± SEM). Tracer radioactivity was also observed in the liver and kidneys. High kidneys activity of radiolabeled peptides is commonly observed and additional treatment may help to prevent or reduce this phenomenon by increasing renal clearance. Current experiments are aimed at consolidating these data by increasing specific activity and in vivo stability of the tracer coupling and by testing the binding of TCRs to cancer cells expressing natural levels of cancer epitope in vitro and in vivo. Conclusion. These results demonstrate the feasibility of non-invasively monitoring the expression of cancer antigens in vivo using radiolabeled T cell receptors, opening the way to a wide range of applications and previously inaccessible disease targets. In parallel to these cancer studies, we are applying this technology to image beta cell mass as a mean to monitor diabetes progression.

Disclosure of author financial interest or relationships:
**A. Briat**, None; **R. Ashfield**, Immunocore Ltd, Employment .

Presentation Number **P526**
Poster Session 3
September 7, 2012 / 15:15-15:15 / Room: The Liffey

# Multimodality imaging of experimental gliomas in a cranial window model

***Katrin Büther***[1], *Raghu Erapaneedi*[2], *Thomas Viel*[1], *Stefan Wagner*[3], *Klaus Kopka*[3], *Sven Hermann*[1], *Michael Schäfers*[1,4], *Friedemann Kiefer*[2], *Andreas H. Jacobs*[1,4], [1]*European Institute for Molecular Imaging EIMI, University of Münster, Münster, Germany;* [2]*Mammalian Cell Signaling Laboratory, Max Planck Institute for Molecular Biomedicine, Münster, Germany;* [3]*Department of Nuclear Medicine, University Hospital Münster, Münster, Germany;* [4]*Department of Nuclear Medicine and Interdisciplinary Centre for Clinical Research (IZKF), University Hospital Münster, Münster, Germany. Contact e-mail: butherk@uni-muenster.de*

**Introduction:** Glioblastomas are the most malignant type of primary human brain tumors. They are highly vascularized and have the tendency to infiltrate. In many cases glioma growth also leads to the breakdown of the blood-brain barrier (BBB) in the vicinity of the tumor. Because of the poor prognosis for patients with high-grade gliomas it is important to decipher and understand the disease progress and the response to therapy. Non-invasive imaging modalities allow the characterization of disease specific changes. **Aim:** To investigate the dynamics of glioma tumor growth and related angiogenesis in a cranial window model by 2-photon microscopy, optical imaging and µPET. **Methods:** An orthotopic glioma mouse model was established in a cranial window. Human Gli36dEGFR mCherry cells ($2x10^5$ cells) were stereotactically implanted into the brain of SCID mice (n=20). Glioma growth and the generation of tumor associated blood vessels were monitored daily using 2-photon microscopy. Imaging of the intracranial growing gliomas was also performed employing fluorescence resonance imaging (FRI) and micro positron emission tomography (µPET). Molecular targets of interest for imaging included expression levels of mCherry, activity of matrix metalloproteinases (MMP) and amino acid transport (*O*-(2-$^{18}$F-fluoroethyl)-L-tyrosine, $^{18}$F-FET). BBB permeability was assessed by i.v. injection of Evans Blue dye. For image validation, brains were analyzed by immunohistochemistry and immunofluorescence. **Results:** Five days after implantation, gliomas could be observed by 2-photon microscopy. Using FITC-dextran we were able to monitor vascular changes at the site of the tumor. Within 7 days (5-12 days after transplantation) pre-existing vessels remodeled and new vessels were recruited. Injection of Evans Blue indicated that the blood-brain barrier was compromised due to glioma growth. In optical imaging the fluorescence signal of the implanted glioma cells could be observed after 8 days and showed exponential growth. The identity of the tumor could also be confirmed by $^{18}$F-FET µPET and immunohistochemistry. Co-registration of 2-photon-microscopy with µPET and immunohistochemical data is currently being established. **Conclusion:** Investigation of tumor growth and its related angiogenesis in a cranial window model of glioma is feasible using different molecular imaging modalities. Future work concentrates on the kinetics of morphological and functional vascular changes and tumor growth during the course of anti-angiogenetic therapy and/or chemotherapy. **Acknowledgement:** This work is supported by BMBF grant MoBiMed (01EZ0811) and the Max Planck Society.

Disclosure of author financial interest or relationships:
**K. Büther**, None; **R. Erapaneedi**, None; **T. Viel**, None; **S. Wagner**, None; **K. Kopka**, None; **S. Hermann**, None; **M. Schäfers**, Siemens Medical Solutions, Grant/research support; **F. Kiefer**, None; **A.H. Jacobs**, Merck, Germany, Grant/research support .

Presentation Number **P527**
Poster Session 3
September 7, 2012 / 15:15-15:15 / Room: The Liffey

# Tumour targeting of the anti-EphA3 antibody, chIIIA4, reduces tumour burden and effects vasculature of human prostate cancer tumour xenografts

***Glenn Cartwright***[1], *Mary E. Vail*[2], *April Tan*[2], *Catherine To*[2], *Carmel Murone*[1], *F. T. Lee*[1], *Angela Rigopoulos*[1], *Diana D. Cao*[1], *Andrew M. Scott*[1], *M. Baer*[3], *Christopher Bebbington*[3], *V. Palath*[3], *Geoffrey T. Yarranton*[3], *Martin Lackmann*[2], [1]*Ludwig Institute for Cancer Research, Heidelberg, VIC, Australia;* [2]*Department of Biochemistry and Molecular Biology, Monash University, Clayton, VIC, Australia;* [3]*KaloBios Pharmaceuticals, Palo Alto, CA, USA. Contact e-mail: glenn.cartwright@ludwig.edu.au*

Eph receptor tyrosine kinases (Ephs) and their membrane bound ephrin ligands (ephrins) control cell positioning and tissue organisation. Their de-regulated re-emergence in adults contributes to tumour invasion, metastasis and neo-angiogenesis. Due to over-expression in a wide variety of human tumours there is increasing interest in Ephs and ephrins as targets for anti-cancer therapies. In particular, large-scale screens for frequent somatic mutations in tumour patients emphasise EphA3 as a candidate cancer gene and our analysis of a variety of human tumour sections by immunohistochemistry reveals EphA3 expression, not only in the tumour cells but in the stroma as well, both in the mesenchymal cells and in some cases the vasculature. We have previously shown that the mIIIA4 monoclonal antibody, specific for native EphA3, efficiently targets EphA3 positive human tumour xenografts. We now demonstrate that the human/mouse chimeric agonistic anti-EphA3 antibody, chIIIA4, inhibits tumour growth by disrupting tumour stroma and neo-vasculature. Furthermore, we have utilized intravital multiphoton microscopy to monitor quantum dot-labelled chIIIA4 targeting in vivo, thereby allowing us to directly visualise expression of EphA3 on tumour vasculature as well as monitoring disruption of the tumour vasculature and dispersion of the stromal tumour capsule in chIIIA4-treated tumours. The high-affinity recombinant humaneered™ version, KB004, is now in Phase 1 clinical trials in hematological malignancies .

Disclosure of author financial interest or relationships:
**G. Cartwright**, None; **M.E. Vail**, None; **A. Tan**, None; **C. To**, None; **C. Murone**, None; **F.T. Lee**, None; **A. Rigopoulos**, None; **D.D. Cao**, None; **A.M. Scott**, None; **M. Baer**, None; **C. Bebbington**, KaloBios Pharmaceuticals, Employment; **V. Palath**, None; **G.T. Yarranton**, KaloBios Pharmaceuticals, Employment; **M. Lackmann**, None.

Presentation Number **P528**
Poster Session 3
September 7, 2012 / 15:15-15:15 / Room: The Liffey

# DEVELOPMENT OF AN OPTICAL ASSAY TO STUDY THE EFFECT OF UPSTREAM PSEUDOHYPOXIC MOLECULAR FACTORS ON HIF1α

***Manoj N. Desai***[1,2], *Divya Vats*[1,2], *Steffi Lehmann*[1], *Ruth Keist*[1,2], *Markus Rudin*[1,2], [1]*Institute of Biomedical Engineering, Zurich, Switzerland;* [2]*Institute of Pharmacology and Toxicology, Zurich, Switzerland. Contact e-mail: desai@biomed.ee.ethz.ch*

Introduction: Rapid tumor cell growth creates intracellular hypoxia. The key factor that responds to such change in cellular oxygen level is known as hypoxia-inducible factor (HIF). In previous studies from this lab, Lehmann et al. developed a multimodal tool to target the downstream HIF signaling pathway (Lehmann et al. 2009). Today, it is well established that HIF activity is not only regulated by tissue levels of molecular oxygen. One factor associated to the HIF pathway is the mammalian target of rapamycin (mTOR). Yet the molecular mechanism and biological relevance of oxygen-independent HIF1α activation by mTOR are poorly understood. Objective: In an effort to develop in vivo assays for studying different molecular events involved upstream of HIF-pathway and cancer progression, we employed both in vitro and in vivo fluorescence imaging of NIRF fusion proteins with key downstream effectors in the HIF-pathway and tumor angiogenesis. Methods: Murine colon cancer carcinoma cell line, C51, was stably transfected with CMV and HRE (hypoxia responsive element) driven mCherry reporter construct. To elucidate the HIF regulation by mTOR, rapamycin treatment was carried out under hypoxia (using a hypoxic chamber) and normoxia (using the prolyl hydroxylase inhibitor dimethyloxalylgylcine, DMOG) by Western blot. This was further investigated under in vivo conditions by generating subcutaneous tumors from the stably transfected C51 cells expressing HRE-mCherry and treating them with either vehicle, rapamycin and a HIF inhibitor. Ex vivo studies were performed with excised tumors by immunofluorescence assessing the regulation of HIF1α, mTOR, CD31 and CA9. Results: In DMOG treated cells, down regulation of HIF1α upon treatment with rapamycin confirms that inhibition of mTOR reduces the level of endogenous HIF1α. In in vivo studies in mice we observed that treatment with rapamycin (2mg/kg/day) led to reduced levels of HIF1α and a significant decrease in tumor growth, whereas treatment with a HIF inhibitor did not show a significant decrease in HIF activity for the duration of the treatment period. Immunofluorescence revealed that both CD31 and CA9 stains reflected the efficacy of the treatment. Yet, we did not observe a significant correlation between HIF1α and mTOR levels. Outlook: During hypoxia, mTOR appears not to be able to maintain the cellular homeostasis. The lack of correlation between HIF signaling and mTOR levels indicates the the presence of positive and/or negative feedback loops. The understanding ow which appears essential for understanding the interplay of HIF and mTOR regulation on tumor angiogenesis and growth progression. Lehmann S. et al (2009), Longitudinal and multimodal in vivo imaging of tumor hypoxia and its downstream molecular events. PNAS, 106 (33), p 14004-9. Pencreach E. et al (2009), Marked Activity of Irinotecan and Rapamycin Combination toward Colon Cancer Cells In vivo and In vitro Is Mediated through CooperativeModulation of theMammalianTarget of Rapamycin/Hypoxia-Inducible Factor-1α Axis. Clinical Cancer Research, 15 (4), p 1297-1307.

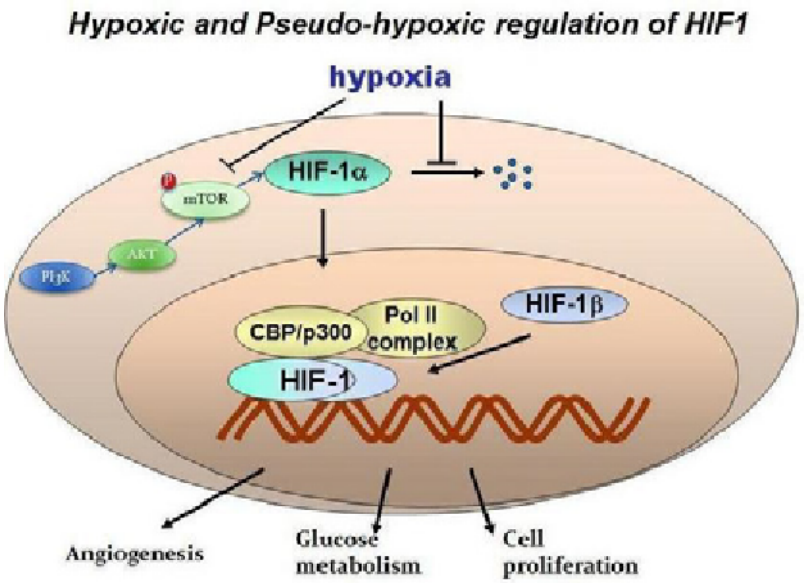


Disclosure of author financial interest or relationships:
**M.N. Desai**, None; **D. Vats**, None; **S. Lehmann**, None; **R. Keist**, None; **M. Rudin**, Hoffmann-LaRoche Ltd, Basel, Switzerland, Grant/research support .

Presentation Number **P529**
Poster Session 3
September 7, 2012 / 15:15-15:15 / Room: The Liffey

# Evaluation of bivalent antiHER2 Nanobody constructs for improved cellular retention and in vivo tumor targeting

***Matthias D'huyvetter***[1,2], *Marek Pruszynski*[3], *Eftychia Koumarianou*[3], *Vicky Caveliers*[1], *Catarina Xavier*[1], *Nick Devoogdt*[1], *Ganesan Vaidyanathan*[3], *Tony Lahoutte*[1], *Michael R. Zalutsky*[3], [1]*In Vivo Cellular and Molecular Imaging Lab (ICMI), Vrije Universiteit Brussel, Brussels, Belgium;* [2]*Molecular and Cellular Biology Expert Group, Radiobiology Unit, Belgian Nuclear Research Center, SCKCEN, Mol, Belgium;* [3]*Department of Radiology, Duke University Medical Center, Durham, NC, USA. Contact e-mail: mdhuyvet@vub.ac.be*

Introduction: Nanobodies are small (15 kDa) antibody fragments with beneficial pharmacokinetic properties, and those targeted to HER2 can be used for the molecular imaging of HER2 overexpressing breast cancer. Labelled with a therapeutic radionuclide, these Nanobodies may be used for the treatment of HER2 overexpressing cancer. However, long term tumour exposure is limited, which makes them suboptimal for therapeutic applications. Binding kinetics of Nanobodies can be improved by developing bivalent constructs, which may enhance cellular retention. In this study, the monovalent nanobodies 2Rb17c (targets the epitope responsible for receptor-mediated endocytosis) and 2Rs15d (binding does not induce endocytosis) were selected to develop the bivalent constructs 2Rb17c-2Rb17c, 2Rs15d-2Rb17c and 2Rb17c-2Rs15d. Materials and Methods: The Nanobody constructs were designed and produced according to a previously established protocol. They were labeled with radioiodine using the residualizing prosthetic group N-succinimidyl 4-guanidinomethyl-3-iodobenzoate ([*I]SGMIB). Improved cellular retention and in vivo behavior have been demonstrated when antibodies and their fragments were radioiodinated using [*I]SGMIB. Affinities of the radiolabeled Nanobody constructs were obtained on HER2+ BT474/M1 cells. Internalization assays were performed in a pair-label format at 37°C over 0, 1, 2, 4, 6, 24h, using Nanobodies labeled with either [125I]SGMIB or [131I]SGMIB. The constructs, labeled with AlexaFluor488, were analyzed in parallel for internalization at incubation time points (37°C) 0-2-6-24h with a Zeiss Axio Observer widefield fluorescence microscope, through a 63x oil immersion objective lens. Results: KD values of 0.17 ± 0.02, 0.58 ± 0.15 and 1.05 ± 0.1 nM were obtained for radiolabeled 2Rb17c-2Rb17c, 2Rb17c-2Rs15d and 2Rs15d-2Rb17c compared to 4.73 ± 0.4 and 1.7 ± 0.2 nM for 2Rs15d and 2Rb17c, respectively. The internalization assays revealed a significant higher degree of cellular retention (membrane bound + internalized fraction) for all three radiolabeled bivalent constructs at all time points compared to their monovalent subparts, with values after 24h incubation of about 60% of the added activity for the bivalent Nanobody constructs versus about 25% for the monovalent Nanobodies. Total cell retention was the highest at all time points for the bivalent 2Rb17c-2Rb17c Nanobody construct, with values of 92.35%, 90.92%, 88.19, 87.63% and 62.63% of the added activity after 1, 2, 4, 6, and 24h incubation. The fluorescent images confirmed the higher cellular retention of the bivalent Nanobody constructs. Conclusion: Significant higher cellular retention was observed for all three bivalent Nanobody constructs compared to their monovalent subparts. The best KD values and highest amount of cellular retention were observed for the 2Rb17c-2Rb17c Nanobody construct. A planned in vivo analysis in HER2+ tumor bearing mice will generate additional data to select the optimal Nanobody construct. Research support: Matthias D'huyvetter is funded by a SCKCEN/VUB grant, together with a 2011-2012 Belgian American Education Foundation (BAEF) Fellowship.

Disclosure of author financial interest or relationships:
**M. D'huyvetter**, None; **M. Pruszynski**, None; **E. Koumarianou**, None; **V. Caveliers**, None; **C. Xavier**, None; **N. Devoogdt**, Boehringer Ingelheim, Grant/research support; Ablynx, Grant/research support; **G. Vaidyanathan**, None; **T. Lahoutte**, None; **M.R. Zalutsky**, None.

Presentation Number **P530**
Poster Session 3
September 7, 2012 / 15:15-15:15 / Room: The Liffey

# New Gd(III)-based probes for the molecular imaging of MMPs by MRI

***Giuseppe Digilio***[1], *Valeria Catanzaro*[2], *Valeria Menchise*[3], *Sergio Padovan*[3], *Concetta Gringeri*[1], *Linda Chaabane*[4], *Silvio Aime*[2], [1]*Dipartimento di Scienze ed Innovazione Tecnologica, Università del Piemonte Orientale, Alessandria, Italy;* [2]*Department of Chemisty IFM & Center for Molecular Imaging, University of Turin, Torino, Italy;* [3]*Institute for Biostructures and Bioimages c/o University of Turin, Consiglio Nazionale delle Ricerche, Torino, Italy;* [4]*INSPE-Division Neuroscience, San Raffaele Scientific Institute, Milano, Italy. Contact e-mail: giuseppe.digilio@mfn.unipmn.it*

Novel Gd-based contrast agents (CAs) for the molecular imaging of matrix metalloproteinases (MMPs) through MRI were synthetized and characterized in vitro and in vivo. These probes were based either on the PLG*LWAR peptide sequence, known to be hydrolyzed between gly and leu by a panel of MMPs or the NIPVS*LYA sequence, which is more specific to MMP-2. A Gd-DOTA chelate was conjugated to the N-terminal position through an amide bond, either directly to proline or through a hydrophilic spacer. Both CA were made strongly amphiphilic by conjugating an alkyl chain at the C-terminus of the peptide sequence. Upon MMP-dependent cleavage, the CAs lose the C-terminal tetrapeptide and the alkyl chain, thus undergoing to an amphiphilic-to-hydrophilic transformation that alters tissue pharmacokinetics. These probes were systemically administered to mice bearing a subcutaneous B16.F10 melanoma, either pre-treated or not with the broad spectrum MMP inhibitor GM6001 (Ilomastat). The washout of Gd-contrast enhancement in DCE-MR images was significantly faster for untreated subjects (displaying MMP activity) with respect to treated ones (MMP activity inhibited). Ultimately, the washout kinetics of Gd-contrast enhancement from the tumor microenvironment gave a qualitative picture of tissue MMP activity. To get a more quantitative description of MMP-activity, the measurement of the molar ratio of intact versus cleaved probe within the ROI is needed, in a manner which is independent from the absolute concentration of gadolinium within the tissue. To this purpose, the Gd-probes were inserted into stealth liposomes to obtain systems amenable to the evaluation of the uncleaved vs cleaved probe through the ratiometric approach, which consists into the measurement of the $R_{2p}/R_{1p}$ ratio (S. Aime et al., J. Am. Chem. Soc. 2006, 128, 11326-11327). Preliminary results about the application of the ratiometric approach showed that the optimal imaging field for our liposome-carried probe is in the range 3-7 T, and that total concentration of Gd within the ROI for accurate measurement should not be less than 250 μM. Acknowledgments: This work is supported by the Regione Piemonte (Italy) as part of the PIIMDMT project, EC-FP6-project MEDITRANS (Targeted Delivery of Nanomedicine: NMP4-CT-2006-026668) and carried out under the frame of ESF COST Action D38.

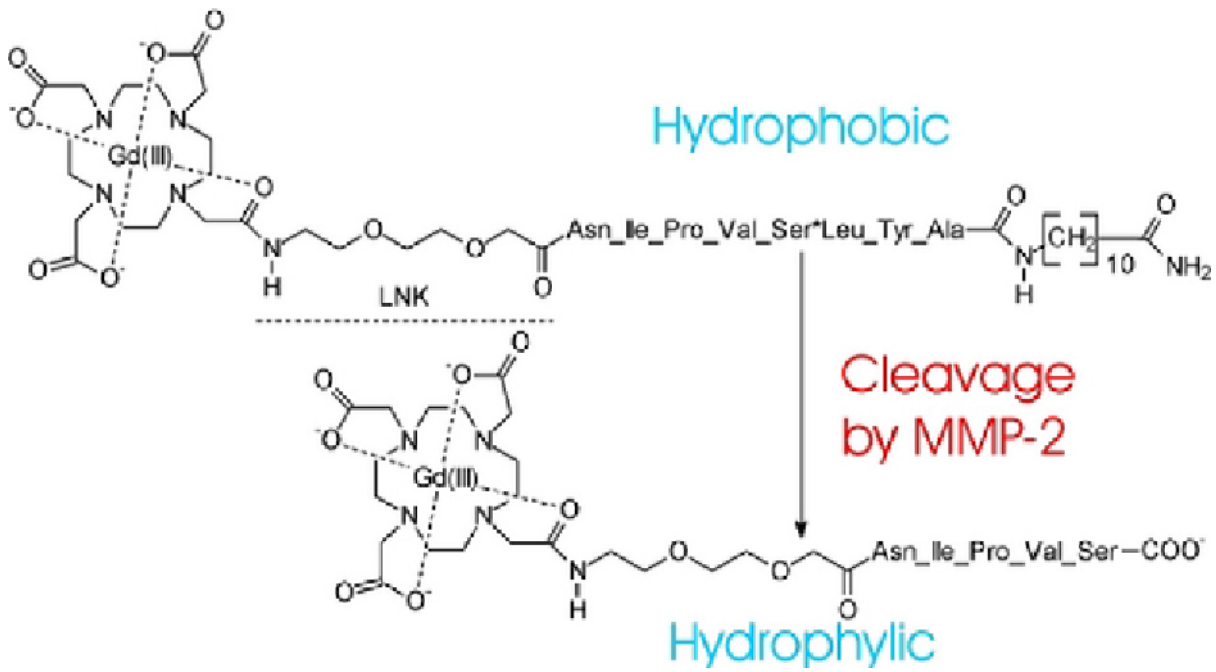


Disclosure of author financial interest or relationships:
**G. Digilio**, None; **V. Catanzaro**, None; **V. Menchise**, None; **S. Padovan**, None; **C. Gringeri**, None; **L. Chaabane**, None; **S. Aime**, Bracco Imaging, Consultant; Bruker, Grant/research support .

Presentation Number **P531**
Poster Session 3
September 7, 2012 / 15:15-15:15 / Room: The Liffey

# Noninvasive measurement of PI3K pathway signaling in renal cell carcinoma with 89Zr-G250, a radiotracer targeting Carbonic Anhydrase IX

***Michael Doran***[1], *Michael J. Evans*[2], *Sarah M. Cheal*[1], *Blesida Punzalan*[1], *Steven M. Larson*[1], *Charles L. Sawyers*[2,3], *Jason S. Lewis*[1], [1]*Department of Radiology, Memorial Sloan Kettering Cancer Center, New York, NY, USA;* [2]*Human Oncology and Pathogenesis Program, Memorial Sloan Kettering Cancer Center, New York, NY, USA;* [3]*Howard Hughes Medical Institute, Memorial Sloan Kettering Cancer Center, New York, NY, USA. Contact e-mail: doranm1@mskcc.org*

A noninvasive technology that quantitatively measures the activity of oncogenic signaling pathways could broadly impact cancer diagnosis and treatment monitoring. Although inhibitors of PI3K pathway signaling (e.g. rapamycin) confer a survival benefit in metastatic renal cell carcinoma (RCC), responses are variable and short-lived. Consequently, there is an urgent need to develop new biomarkers reflective of pathway activation to document which patients respond to treatment. In the context of loss of the tumor suppressor VHL, inhibitors of PI3K pathway signaling have been shown to confer therapeutic benefit by suppressing HIF1-α transcriptional activity, raising the possibility that a HIF1-α target gene could serve as a noninvasive biomarker of effective therapeutic intervention in patients. To this end, we have developed 89Zr-labeled G250, a positron-emitting monoclonal antibody directed to Carbonic Anhydrase IX, a thoroughly validated HIF1-α target gene. 89Zr-G250 shows high affinity for CAIX in multiple preclinical models of VHL-null RCC in vitro and in vivo. Moreover, 89Zr-G250 PET resulted in improved tumor contrast compared to 124I-G250, a radiolabeled construct currently under evaluation in man. Finally, 89Zr-G250 effectively measures treatment induced changes in CAIX expression with BEZ235—a dual PI3K/mTOR inhibitor—at concentrations sufficient to inhibit tumor proliferation. Collectively, these results suggest that relative changes in CAIX expression can serve as a biomarker of pathological activation of PI3K pathway signaling in RCC, and promote the use of 89Zr-G250 PET to monitor tumor response to this class of therapies.

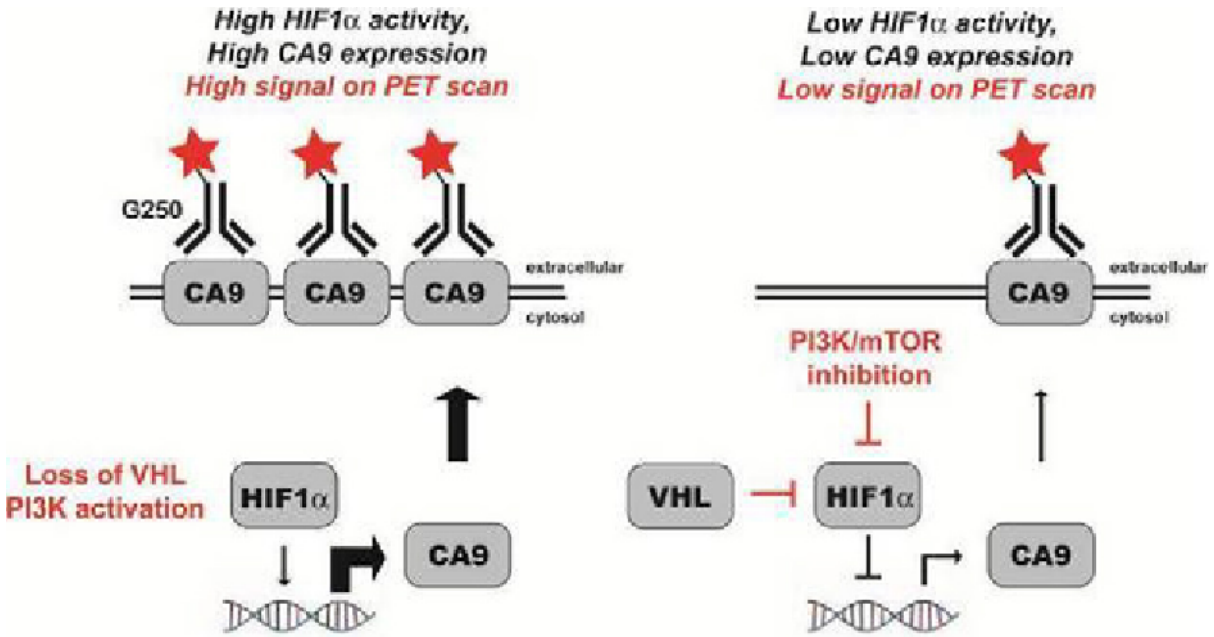


Representation of loss of PET signal due to down regulation of Carbonic Anhydrase IX expression following PI3K inhibition.

Disclosure of author financial interest or relationships:
**M. Doran**, None; **M.J. Evans**, None; **S.M. Cheal**, None; **B. Punzalan**, None; **S.M. Larson**, None; **C.L. Sawyers**, None; **J.S. Lewis**, GEMS, Other financial or material support .

Presentation Number **P532**
Poster Session 3
September 7, 2012 / 15:15-15:15 / Room: The Liffey

# Longitudinal Non-invasive Tracking of Tumor Growth Using Multispectral Optoacoustic Tomography (MSOT)

***Wouter H. Driessen***[1,2], *Neal Burton*[1,2], *Jing Claussen*[1,2], *Stefan Morscher*[1,2], *Daniel Razansky*[2,3], *Vasilis Ntziachristos*[2,3], [1]*iThera Medical, GmbH, Neuherberg, Germany;* [2]*The Institute for Biological and Medical Imaging, Helmholtz Center Munich, Neuherberg, Germany;* [3]*Technische Universität München, München, Germany. Contact e-mail: wouter.driessen@ithera-medical.com*

In order to develop novel therapeutic strategies for malignancies, it is crucial to have an understanding of tumor growth characteristics. Non-invasive, preclinical (molecular) imaging modalities can provide the essential link between in vitro experiments and the successful translation of novel treatments to the clinic. Here, we describe multispectral optoacoustic tomography (MSOT) as an imaging modality that simultaneously visualizes anatomical, functional and molecular contrast for the characterization of tumor growth in two orthotopic tumor models (U87MG brain tumor xenografts and syngeneic 4T1 breast tumors). MSOT is a powerful novel imaging modality that decomposes the spectral response of tissue chromophores in vivo, with high resolution and at depths of up to several centimeters. It provides the possibility to separate endogenous chromophores of interest such as oxy-/deoxy-hemoglobin as well as extrinsically administered photo-absorbing agents including nanoparticles and fluorescent dyes or proteins. Here, we used this technology to non-invasively track tumor growth characteristics of orthotopic breast and brain tumors using three methods. Firstly, we followed tumors longitudinally by determining total hemoglobin levels and oxy- and deoxy-hemoglobin ratios. As tumors grow, an increase in vascularization is necessary for the tumor to survive. This increased tumor-perfusion leads to increasing total hemoglobin-content over time. In later stages, as increased vascularization can no longer keep up with the growing tumor, a relative increase in deoxygenated hemoglobin can be observed, especially in the core of larger tumors. This process can be visualized and quantified through the intact skin and skull of adult mice, allowing long term tracking of tumors such as glioblastomas. Secondly, we determined the time-dependence of alpha(v)beta(3)-integrin expression during tumor-growth as a surrogate marker for tumor vascularization. Receptor-expression was determined by systemically administering a NIR-labeled RGD-peptidomimitic after which MSOT-imaging was performed and photoacoustic signal quantified. Thirdly, tumor growth can be tracked by transducing tumor cell-lines with a NIR fluorescent protein (iRFP). Due to very low background signals, this protein can be visualized by MSOT with great accuracy and sensitivity. Breast tumor growth curves were determined and compared to caliper measurements. At various points in time, MSOT findings were validated using histology. These studies show that MSOT can yield the simultaneous visualization of anatomical, functional and molecular contrast with a spatial and temporal resolution typical for ultrasound imaging and can become an invaluable tool for longitudinal tumor tracking studies. Future studies will include the assessment of treatment response by MSOT.

Disclosure of author financial interest or relationships:
**W.H. Driessen**, iThera Medical, Employment; **N. Burton**, iThera Medical, Employment; **J. Claussen**, iThera Medical, Employment; **S. Morscher**, iThera Medical GmbH, Employment; **D. Razansky**, iThera Medical GmbH, Stockholder; **V. Ntziachristos**, ERC, Grant/research support; Ithera Medical, Stockholder .

Presentation Number **P533**
Poster Session 3
September 7, 2012 / 15:15-15:15 / Room: The Liffey

# Intravital Imaging of Tumor Cell Uptake In Vivo using Targeted Fluorescent Probes

***Veronica Estrella***[1], *Tingan Chen*[2], *Narges K. Tafreshi*[1], *Allison S. Cohen*[1], *Natalie M. Barkey*[1], *Ariosto Silva*[1], *Mark C. Lloyd*[2], *David L. Morse*[1], [1]*Cancer Imaging and Metabolism, H Lee Moffitt Cancer Center, Tampa, FL, USA;* [2]*Analytic Microscopy Core Facilty, H Lee Moffitt Cancer Center, Tampa, FL, USA. Contact e-mail: Veronica.Estrella@moffitt.org*

The development of tumor-targeted and fluorescent molecular imaging agents has potential for clinical use in cancer staging by detection of regional lymph node involvement and for image guided surgery. Since fluorescent dyes are inherently more stable than radionuclides with short half-lives, fluorescence is also useful in the pre-clinical evaluation of binding moieties for tumor biomarkers that could be used for the development of targeted nuclear imaging probes and therapeutics. An important question in the development of these targeted probes is the determination of cellular uptake. Cell uptake can increase the magnitude and duration of agent build-up and retention in the tumor. Probes can be evaluated in vitro using an incubation chamber on a fluorescence microscope to determine the route and timing of cellular uptake (Figure 1A). However, these systems do not model delivery of agent through the vasculature, penetration into the tumor, and cell binding and uptake in the context of the tumor microenvironment. We have developed a number of high-affinity (low nM Ki) tumor-targeted and fluorescently-labeled molecular imaging probes in a range of sizes, from relatively small (~1400-2700 MW) peptidomimetic ligand-dye conjugates (e.g. Dmt-Tic-Lys(Cy5)-OH, 4-phenylbutyryl-His-(D)Phe-Arg-Trp-Gly-Lys(IRDye800CW-MPA)-NH2, and IRDye800CW-MPA-PEGO-dihydroxycysteine(palmitoyl)2-Gly-Ser-Ac-PEGO-NH2) larger (~150 kDa) monoclonal antibody-based fluorescent probes (e.g. MamAb-680, CA9Ab-680, and CA12Ab-680), and much larger multivalent targeted polymer micelle nanoagents (~80 nm diameter) which can specifically target marker expressing tumors relative to non-expressing tumors as determined by in vivo fluorescence imaging. We have developed both peptide-agonist and -antagonist based probes. Based on the range of sizes represented in this set of targeted molecular imaging probes, we anticipate differences in vascular circulation time, and in the in the rates of extravasation, tumor penetration and cellular uptake (e.g. receptor mediated uptake in the case of agonist versus pinocytotic membrane recycling in the case of a high affinity antagonist with a very low off rate). To characterize the pharmacokinetics of these processes for our set of diverse targeted fluorescent probes, we have developed an intravital fluorescence microscopy method to study the early time points following intravenous injection of probe. Using the mouse dorsal skin-fold window chamber tumor xenograft model (Figure 1B), where a chamber is mounted on the animal, a layer of skin removed and a collagen construct containing tumor cells (target-expressing or non-expressing controls) and a GFP rat microvascular network is implanted in the wound of the chamber under the coverslip. After tumor growth and establishment of patent vasculature, the targeted probe is intravenously injected and a series of confocal fluorescence imaging acquisitions offers a window into the kinetics of extravasation and tumor cell internalization of the probe in real time (Figure 1C & D). A three-compartment mathematical model was used to characterize the probe uptake and clearance from the tumor and tumor cells.

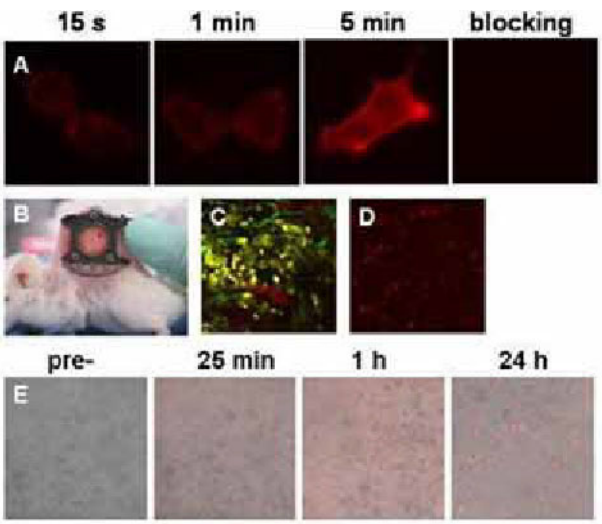


Figure 1. A) In vitro fluorescence uptake study of Cy5 labeled peptide conjugate. B) Dorsal skin-fold window chamber. C) Intravital confocal fluorescence image of patent GFP vessels (green) and tumor cells (yellow) after injection of Cy5 peptide conjugate (red). D) Overlay of intravital fluorescence image of tumor cells with internalized Cy5-labeled peptide antagonist with the corresponding visible light image, 24 h post injection.

Disclosure of author financial interest or relationships:
**V. Estrella**, None; **T. Chen**, None; **N.K. Tafreshi**, None; **A.S. Cohen**, None; **N.M. Barkey**, Intezyne Technologies, Inc, Other financial or material support; **A. Silva**, None; **M.C. Lloyd**, None; **D.L. Morse**, LiCor, Other financial or material support; Intezyne Technologies, Other financial or material support .

Presentation Number **P534**
Poster Session 3
September 7, 2012 / 15:15-15:15 / Room: The Liffey

# Studies with an inactive form of a targeted cell death detection agent to better understand the contribution of the enhanced permeability and retention (EPR) effect to non-specific agent uptake in tumors

***Sarah L. Fawcett****, Andre Neves, Tiago B. Rodrigues, Kevin M. Brindle, Brindle Laboratory 140, Cambridge Research Institute, Cambridge, United Kingdom. Contact e-mail: slf43@cam.ac.uk*

While the EPR effect in tumors, which is caused by disordered neo-angiogenesis and defective endothelial fenestrations, is useful for therapy, from a targeted imaging perspective such a phenomenon serves only to mask specific contrast by promoting non-specific probe retention. The C2A domain of synaptotagmin I, which binds the phosphatidylserine (PS) exposed by dead and dying cells, has been used as a targeted imaging agent for detecting cell death (Krishnan, Neves et al. 2008). Introduction of a single cysteine residue into this protein by site-directed mutagenesis, at a site that is distant from the PS-binding site (Alam, Neves et al. 2010), has allowed selective modification of the agent (termed C2Am) with fluorescent, radionuclide or MR-detectable labels. In order to distinguish specific probe binding from non-specific, EPR-dependent, probe retention we compared C2Am with a second site-directed mutant, which had been rendered unable to bind PS by introducing a second mutation at the PS-binding site (D108N; iC2Am). Both the active and inactive forms of C2Am were modified with Alexafluor™-750 (Invitrogen). C2Am and iC2Am were administered in vivo to tumor-bearing Eμ-myc mice, which are a genetically engineered lymphoma tumor model. Some animals received cyclophosphamide treatment 24 hours prior to imaging and necropsy. The LI-COR® Pearl™ Impulse near-infrared and Xenogen IVIS®-200 imaging systems were used to image Alexafluor™-750-labeled C2Am and iC2Am in vivo and also in excised tissues prior to fixation for histological examination. High resolution scans of formalin fixed tissue sections were performed using the LI-COR® Odyssey® near infra-red imaging system. These images were correlated with H&E, terminal deoxynucleotidyl transferase dUTP nick end labeling (TUNEL) and cleaved caspase-3 (CC3) staining of parallel histological sections. C2Am showed significantly increased labeling of treated tumours in vivo with respect to untreated tumors, whereas for the inactive probe (iC2Am) there was only a small increase in labeling of treated tumors and the absolute levels of fluorescence were very low. Analysis of tumor sections ex vivo showed a 9-fold increase in C2Am probe fluorescence in sections from treated as compared with untreated tumors, whereas with iC2Am there was no significant difference in the levels of fluorescence. These experiments have confirmed that C2Am detects cell death specifically in vivo and the experiments with the inactive mutant (iC2Am) have enabled us to determine the contribution of the EPR effect to the signal observed. Alam, I. S., A. A. Neves, et al. (2010). "Comparison of the C2A domain of synaptotagmin-I and annexin-V as probes for detecting cell death." Bioconjug Chem 21(5): 884-891. Krishnan, A., A. Neves, et al. (2008). "Detection of cell death in tumors by using MR imaging and a gadolinium-based targeted contrast agent." Radiology 246(3): 854-862.

Disclosure of author financial interest or relationships:
**S.L. Fawcett**, Cambridge Bimomedical Research Centre, Grant/research support; GlaxoSmithKline, Grant/research support; Licor, Other financial or material support; Cancer Research UK, Other financial or material support; **A. Neves**, None; **T.B. Rodrigues**, GE, Grant/research support; **K.M. Brindle**, GE Healthcare, Grant/research support; GSK, Consultant .

Presentation Number **P535**
Poster Session 3
September 7, 2012 / 15:15-15:15 / Room: The Liffey

# A comparison of radionuclide- and fluorescence-labeled Annexin V and Synaptotagmin I for detecting tumor cell death in murine lymphoma models

***Sarah L. Fawcett****, Andre Neves, Kevin M. Brindle, David Y. Lewis, Brindle Laboratory 140, Cambridge Research Institute, Cambridge, United Kingdom. Contact e-mail: slf43@cam.ac.uk*

Both Annexin V and the C2A domain of synaptotagmin I bind exposed phosphatidylserine (PS) in dead and dying cells. Annexin V has long been used as a probe for detecting cell death in vitro and in vivo and has been the subject of clinical trials. A site-directed mutant of the C2A domain of synaptotagmin I (C2Am) has recently been demonstrated to show more specific binding than Annexin V to apoptotic and necrotic cells in vitro (Alam, Neves et al. 2010). Using clinical grade Annexin V-HYNIC (supplied by the NIH bio-repository) and C2Am-HYNIC, radiolabelling with 99mTc was performed. In vitro cell binding assays were carried out using EL4 murine lymphoma cells, with and without etoposide treatment. In vivo bio-distribution studies were also performed in EL4-bearing C57/Bl6 mice with both agents. The activity of treated EL4 cell pellets was significantly greater (2 to 3-fold) than untreated cells when labeled with C2Am, whereas no difference could be detected with Annexin. There was significant labeling of the untreated cells by Annexin, with ~40% of total activity retained as compared with less than 10% for C2Am. Similarly, when considering C2Am-HYNIC-99mTc in vivo, a significant difference was demonstrated in the %ID/g between etoposide-treated and untreated EL4 tumours at 2, 6 and 24 hours after probe administration. No significant difference was observed for Annexin-V-HYNIC99mTc. Retention in the liver at 24 hours was less than 5%ID/g for C2Am as compared with up 40%ID/g for Annexin. There was also a 2-fold increased %ID/g in the kidneys with Annexin as compared to C2Am. Annexin Vivo 750™ (PerkinElmer) and C2Am conjugated to Alexafluor™-750 (Invitrogen) were administered to tumor-bearing Eμ-myc (genetically engineered lymphoma model ) that had been treated with cyclophosphamide. Twenty four hours after probe injection, tissues were removed and formalin fixed for histological examination. High resolution scans of ex vivo tissue sections were performed using the LI-COR® Odyssey® near infra-red imaging system. These images were correlated with H&E, Terminal deoxynucleotidyl transferase dUTP nick end labeling (TUNEL) and cleaved caspase-3 (CC3) staining of parallel histological sections. For Annexin V, there was ~6-fold increase in fluorescence of tumour sections from treated as compared with untreated animals. C2Am showed a ~9-fold increase. When comparing histologically proven areas of cell death within a tumour section with histologically viable areas, there was up to a 50-fold increase in fluorescence for tumors labeled with C2Am. At 24 hours after Annexin or C2Am administration there was a 25-fold increased fluorescence in the renal cortex, and a 10-fold increase in the skeletal muscle of animals receiving Annexin relative as compared to those receiving C2Am. In these lymphoma models, using both SPECT and NIR-labeled agents, C2Am appears to be superior to Annexin-V, both in terms of bio-distribution profile and the ability to differentiate treated from untreated tumours. Alam, I. S et al. (2010). "Comparison of the C2A domain of synaptotagmin-I and annexin-V as probes for detecting cell death." Bioconjug Chem 21(5): 884-891.

Disclosure of author financial interest or relationships:
**S.L. Fawcett**, Cambridge Bimomedical Research Centre, Grant/research support; GlaxoSmithKline, Grant/research support; Licor, Other financial or material support; Cancer Research UK, Other financial or material support; **A. Neves**, None; **K.M. Brindle**, GE Healthcare, Grant/research support; GSK, Consultant; **D.Y. Lewis**, None.

Presentation Number **P536**
Poster Session 3
September 7, 2012 / 15:15-15:15 / Room: The Liffey

# Application of MR and Bioluminescence Dual Reporter Gene Imaging for in vivo Monitoring Tumor Growth

*Yifan Wang, **Fabao Gao**, Department of Radiology, Molecular Imaging Library, Chengdu, China. Contact e-mail: gaofabao@yahoo.com*

PURPOSE To enrich our understanding on the mechanism of colorectal cancer occurrence and development, we applied MR and bioluminescence dual reporter gene imaging to monitor tumor growth and development. METHOD AND MATERIALS Recombinant adenovirus vector carrying a novel double-promotor reporter gene that consists of human transferrin receptor and firefly luciferase was constructed. Human colorectal cancer LOVO cells were infected with Ad-TFRC-Luciferase adenovirus. Quantitative real-time PCR (Q-PCR) and Western blot analysis were performed to evaluate expression of transferrin receptor in LOVO cells. LOVO colorectal tumor model was established by subcutaneously injecting 1×107 double-labeled LOVO cells in the groin area of BALB/C nu/nu mice. After inoculation, 7T MR and optical imaging were performed to monitor serially tumor growth and development for 2 weeks. After imaging, tumor tissues were collected and subjected to Prussian blue staining and immunohistochemical staining. RESULTS Ad-TFRC-Luciferase adenovirus vector has been successfully constructed,and the virus titer was 1.6×1010 pfu/ml. Adenovirus transfection efficiency was 90% at a multiplicity of infection (MOI) of 50. Dual reporter gene expression had no adverse effects on cell proliferation or viability compared with control group. The Western blot and Q-PCR data indicated that transferrin receptor was significantly excessively expressed in LOVO cells transfected by Ad-TFRC-Luciferase. MR T2-weighted and T2*-weighted images showed that the hypointense regions where tumor cells were located were enlarged dramatically over time and the anatomical information of tumor local extension was observed. However the anatomical information was unable to be visualized by bioluminescence imaging due to scattering of the photons from tumor. Optical signal could be detected in 2 weeks. Histology finding confirmed the imaging results and showed that there were angiogenesis and lymphangiogenesis in the border zone of the tumor. CONCLUSION MR and bioluminescence dual reporter gene imaging system provides a powerful tool for monitoring tumor growth and development.

Disclosure of author financial interest or relationships:
**Y. Wang**, None; **F. Gao**, None.

Presentation Number **P537**
Poster Session 3
September 7, 2012 / 15:15-15:15 / Room: The Liffey

# Tumor imaging using [18F]FDG PET fused with fluorescence optiical tomography

***Anikitos Garofalakis***[1,2], *Albertine Dubois*[1,2], *Benoit Theze*[1,2], *Bertrand Czarny*[4], *Bertrand Tavitian*[1,3], *Frederic Duconge*[1,2], [1]*Service Hospitalier Frédéric Joliot, CEA, Insitut de l'imagerie Biomédicale, Orsay Cedex, France;* [2]*INSERM Unité 1023, , Orsay Cedex, France;* [3]*Université Paris Sud, , Orsay Cedex, France;* [4]*Service d'Ingénierie Moléculaire de Protéines, CEA, Institut de Biologie et de Technologies de Saclay, Gif/Yvette Cedex, France. Contact e-mail: anikitos.garofalakis@cea.fr*

The fusion of small animal PET imaging with fluorescence diffuse optical tomography (fDOT) has been recently proposed as a promising multimodal approach for small animal studies. This method has been already used to demonstrate the quantification capacity of fDOT using PET1,2. The applications of this type of multimodal imaging can be particularly useful in oncology. Novel optical probes can be evaluated when they are compared to the PET scans of tumor metabolism when using the 2-deoxy-2-[18F]fluoro-D-glucose ([18F]FDG) tracer. Also synergic information from the monitor of several molecular pathways inside the same subject can be provided. Here, we study the additional benefits provided by PET/fDOT imaging comparing the biodistribution of [18F]FDG in tumors with three different fluorescent probes: a fluorescent glucose analog, a protease activatable optical probe and a fluorescent ligand of αvβ3 integrin. Methods: Sequential fDOT/PET/CT imaging of mice was performed with a custom multimodal mouse supporting system that allows the subject to be transfered between a fDOT instruments and a small animal PET/CT scanner. Experiments were performed in xenografted tumor models derived from the human breast cancer line MDA-MB 231 and compared to ex vivo analysis. We tested the following optical probes: a fluorescent glucose analog IRDye 800CW 2-DG (Licor, Lincoln), the cathepsin - sensitive probe Prosense680(Perkin Elmer) and the Arg-Gly-Asp(RGD)-based fluorescent probe AngioStamp (Fluoptics, Grenoble, France) for the labeling of avβ3 integrins. Results: The three dimensional (3D) reconstructed signals showed that the fluorescent glucose analog does not co-localized with [18F]FDG. Histologic analysis showed that the optical probe co-localizes with the GLUT-1 receptor distribution (Figure). Fusion of [18F]FDG with the other fluorescent probes demonstrated that tumor at early stage show exhibit a distribution of optical signal in the borders of the tumor and partially overlapping with the FDG signal while for bigger tumors there is an optical signal distribution inside the tumor volume as given by PET. Conclusions: The added value of hybrid PET/fDOT over the two modalities acquired separately has been validated both for cross-validation of probes and for better characterization of tumor models. For the case of the fluorescent glucose analog we showd that it cannot be used as a surrogate probe the PET tracer. For the case of the cathepsin activated probe and the RGD-ligand the multimodal approach demonstrated the variability of both the protease activity and the αvβ3 integrin expression during tumor growth. 1. Garofalakis A, Dubois A, Kuhnast B, et al. In vivo validation of free-space fluorescence tomography using nuclear imaging. Opt Lett. 2010;35(18):3024-3026. 2. Nahrendorf M, Keliher E, Marinelli B, et al. Hybrid PET-optical imaging using targeted probes. Proc. Natl. Acad. Sci. U.S.A. 2010;107(17):7910-7915.

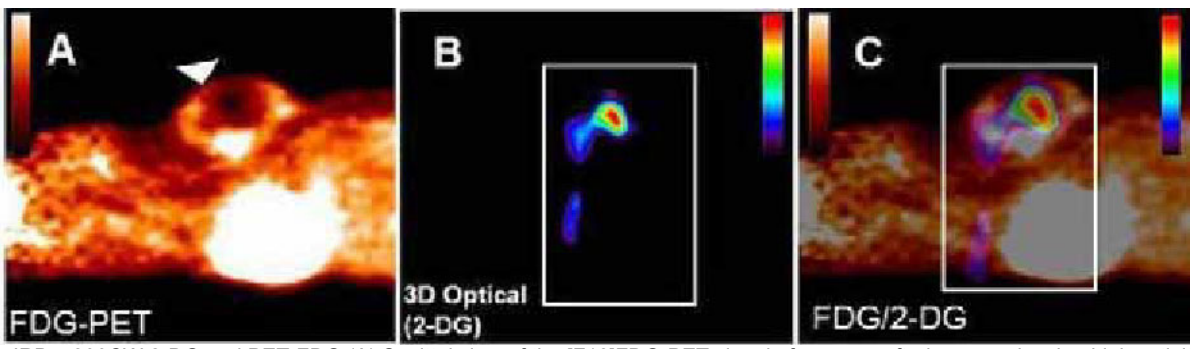


Imaging using IRDye800CW 2-DG and PET-FDG (A) Sagittal view of the [F18]FDG-PET signal of a xenografted mouse showing high activity at the site of the xenografted tumor. The arrow pinpoints the position of the tumor as identified by [F18]FDG. (B) The fDOT IRDye800CW 2-DG signal at the corresponding sagittal plane. The fused PET/fDOT sagittal image(C) shows that the optical signal occupies the low [F18]FDG-PET region.

Disclosure of author financial interest or relationships:
**A. Garofalakis**, None; **A. Dubois**, None; **B. Theze**, None; **B. Czarny**, None; **B. Tavitian**, None; **F. Duconge**, None.

Presentation Number **P538**
Poster Session 3
September 7, 2012 / 15:15-15:15 / Room: The Liffey

# Targeted imaging of breast tumor progression and therapeutic response in a human uMUC-1 expressing transgenic mouse model

***Subrata K. Ghosh***[1], *Masashi Uchida*[1], *Byunghee Yoo*[1], *Alana W. Ross*[1], *Sandra J. Gendler*[2], *Anna Moore*[1], *Zdravka Medarova*[1], [1]*Radiology, Molecular Imaging Laboratory, MGH/HST Athinoula A. Martinos Center for Biomedical Imaging, Massachusetts General Hospital/Harvard Medical School, Charlestown, MA, USA;* [2]*Biochemistry and Molecular Biology, Mayo Clinic, Scottsdale, AZ, USA. Contact e-mail: subrata@nmr.mgh.harvard.edu*

Early tumor detection and effective treatment of breast cancer are urgently needed to control the disease. Detection of the disease at the pre-malignant stage would be highly advantageous providing that targeted contrast agents are developed. The goal of the present study was 1) to investigate whether monitoring disease progression from pre-malignancy to full-blown cancer is feasible using a tumor-specific MR contrast agent and 2) to utilize this agent for monitoring therapeutic response in breast cancer. To achieve our goals we used a previously developed by us contrast agent (MN-EPPT), which consists of cross linked superparamagnetic iron oxide nanoparticles (MN) for MR imaging, modified with Cy5.5 dye (for near infrared optical fluorescence imaging (NIRF)), and conjugated to peptides (EPPT), specifically targeting the underglycosylated mucin-1 tumor antigen (uMUC-1) expressed in over 90% of breast cancers. As an animal model we used transgenic MMT mice expressing polyoma virus middle T (PyMT) and human MUC-1 double transgenes that develop spontaneous mammary carcinoma (4-9 weeks: hyperplasia and 10-16 weeks: visible tumor). uMUC-1 transgenic mice that express human uMUC-1 but do not develop tumors were used as controls. After i.v. injections of the contrast agent in tumor bearing animals, MN-EPPT co-localized with expressed uMUC-1 reflecting target specific binding as shown by fluorescence microscopy of tumor sections. In vivo imaging of MMT mice and control MUC-1 transgenic mice demonstrated accumulation of the MN-EPPT probe in the mammary fat pad/tumor that generated detectable contrast on T2-weighted MR images (Figure A, outlined) and on in vivo near-infrared optical images. There was a significant shortening ($n = 3$, $p < 0.05$) of the average T2 relaxation times of the mammary fat pad in MMT mice that developed cancer (15 wks of age) compared to MMT mice with pre-malignancy (8 weeks of age). More importantly, compared to baseline T2 relaxation times detected in the MUC-1 control mice, the T2 relaxation times of 8-wk old MMT mice were also shorter ($p < 0.05$) (Figure B). This indicated that our method could distinguish between the pre-malignant state and normal tissue. These results were confirmed by near infrared optical imaging. Next, we examined whether the MN-EPPT probe could be used for monitoring therapeutic response to doxorubicin. We treated MMT mice with doxorubicin (7 mg/kg, once a week for two weeks) and observed significant changes in tumor size as measured by both MRI and optical imaging. Furthermore, tumor delta-T2s were significantly reduced by treatment with doxorubicin indicating lower accumulation of MN-EPPT. This correlated with a lower level of uMUC1 expression in the doxorubicin-treated tumors, as confirmed by immunoblotting. Our study could provide a very sensitive molecular approach for monitoring tumor progression and therapeutic response. It can also be instrumental in diagnosing pre-malignancy in breast cancer.

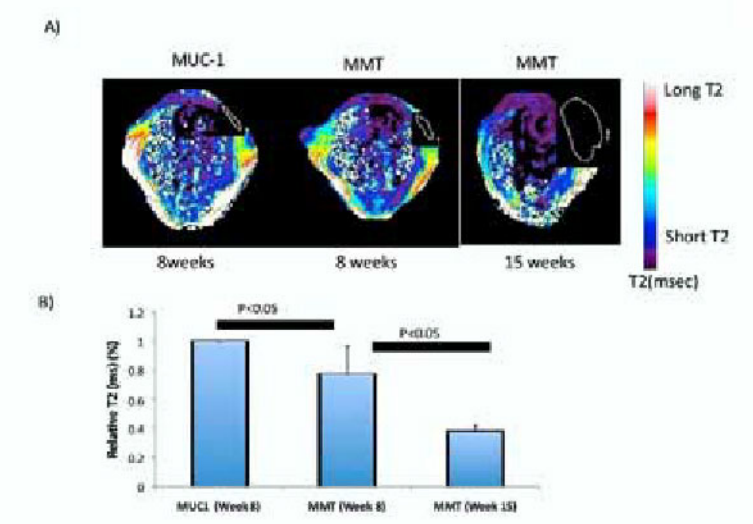


Disclosure of author financial interest or relationships:
**S.K. Ghosh**, None; **M. Uchida**, None; **B. Yoo**, None; **A.W. Ross**, None; **S.J. Gendler**, None; **A. Moore**, Fluoropharma, Grant/research support; **Z. Medarova**, None.

Presentation Number **P539**
Poster Session 3
September 7, 2012 / 15:15-15:15 / Room: The Liffey

# Time Resolved Imaging of Contrast Kinetics (TRICKS) used in rats to evaluate tumor response to Peptide Receptor Radionuclide Therapy (PRRT)

***Joost Haeck***[1,2], *Karin Bol*[3,1], *Marion De Jong*[2,1], *Jifke Veenland*[3,1], *Monique R. Bernsen*[1,2], [1]*Radiology, Erasmus Medical Centre, Rotterdam, Netherlands;* [2]*Nuclear Medicine, Erasmus Medical Centre, Rotterdam, Netherlands;* [3]*Biomedical Informatics Group Rotterdam, Erasmus Medical Centre, Rotterdam, Netherlands. Contact e-mail: j.haeck@erasmusmc.nl*

**Introduction:** Dynamic contrast-enhanced (DCE) MRI has become an important tool to stage tumor malignancy and therapy response. Peptide Receptor Radionuclide Therapy (PRRT) using [177Lu-DOTA0, Tyr3]Octreotate targets somatostatin-receptor bearing cells. Efficiency of such a treatment approach can be studied in the CA20948 rat pancreatic tumor model that over expresses the somatostatin receptor. Peptide delivery to the tumor is a factor which may play an important role in the therapeutic efficacy of PRRT; well perfused tumors allow more peptide to reach the tumor. The challenge we face is measuring perfusion in small laboratory animals as both high spatial and high temporal resolution imaging is required. Acquiring high spatial resolution images increases scan-time, but at the same time the fast physiological processes, like a 350 bpm heart rate, requires high temporal resolution imaging. The purpose of this study was to evaluate the use of a keyhole acquisition technique(TRICKS), used in clinical settings for angiography, for acquiring high spatial and high temporal resolution DCE-MRI and to validate the technique in a treatment setting in the rat tumor model following PRRT. **Methods:** Lewis rats (n=10) bearing subcutaneous CA20948 tumors were imaged in an animal 7T scanner (Agilent, Oxford, UK). 5 control animals received no treatment and 5 animals received 177Lu-octreotate (370MBq/7nmol). Animals were imaged 2 days before treatment followed by scans every 4 days after treatment. A spin echo T1 map and TRICKS (TR/TE 10/2ms, FA 12°, FOV 5cm, 116x116 matrix, Tres 4.3s) were acquired and quantitative parameters (Hayton *et al*, Med Image Anal, 1997) were calculated using Matlab. **Results:** Using TRICKS it was possible to acquire images with a spatial resolution of 0.2x0.2x0.7 mm at a temporal resolution of 4.3 seconds. The high temporal resolution allows accurate pharmacokinetic modeling of the perfusion data to calculate quantitative parameters, and the high spatial resolution allows us to delineate small volumes. Hayton a shows stable perfusion parameters in the control group, in contrast to the therapy group where large changes take place. **Conclusion:** Using TRICKS it is possible to acquire dynamic perfusion data with a $0.03mm^3$ voxel size at 4.3 seconds per volume. Quantitative analysis of the DCE-MRI data reveals that there are large changes in perfusion properties following PRRT which are not present in the non-treated group. Further studies are needed to establish whether changes perfusion parameters correlate to response to the treatment.

Disclosure of author financial interest or relationships:
**J. Haeck**, None; **K. Bol**, None; **M. De Jong**, None; **J. Veenland**, None; **M.R. Bernsen**, None.

Presentation Number **P540**
Poster Session 3
September 7, 2012 / 15:15-15:15 / Room: The Liffey

# Humanized anti-EGFR antibody fragment/dual enzyme system assists in MR imaging of the receptor deletion variant expression in vivo

***Alexei A. Bogdanov**, Mohammed S. Shazeeb, Suresh Gupta, Radiology, University of Massachusetts Medical School, Worcester, MA, USA. Contact e-mail: alexei.bogdanov@umassmed.edu*

The constitutively active EGFRvIII deletion mutant receptor is a major determinant of tumor growth and poor prognosis in glioblastoma multiforme [1]. Humanized mAb EMD72000 differentiates between cells that express wild-type vs. EGFRvIII due to a better exposure of the epitope on EFGFR domain III. We performed targeted imaging of EGFRvIII by tracking peroxidase-generated products of diTyr-DTPAGd (a paramagnetic peroxidase substrate) in U87ΔEGFR and Gli36ΔEGFR orthotopic human glioma xenografts as well as the wild-type tumor models. F(ab')2 fragments of EMD72000 mAb were covalently linked to a pair of deglycosylated horseradish peroxidase (HRP) and glucose oxidase (GOX). This dual enzymatic system is self-complementing and can be used as a signal amplification system [2] for targeted imaging of receptors in vivo. We expected a prolonged MR signal enhancement at the sites of receptor binding due to the formation of polymerized products of diTyr-DTPAGd oxidation by mAb conjugates [2]. F(ab')2 fragments of mAb were conjugated to enzymes using bisaromatic hydrazone bonds and purified by HPLC. The conjugates were characterized in U87ΔEGFR cell culture and optimal ratios of HRP and GOX conjugates were determined to provide the maximum signal with low cytotoxicity. F(ab')2-GOX and F(ab')2-HRP were also modified with NHS-MAG3 for radiolabeling. Ten days after stereotaxic cell implantation, each animal was imaged using T1-weighted spin-echo 3T MRI (TR/TE=700ms/8.2ms): 1) on Day 1 - images were acquired after IV injection of 0.1 mmol/kg diTyr-DTPAGd over a 1.5h period; 2) on Day 2 - anti-EGFRvIII conjugates (100 μg mAb/animal) were injected IV, and then 4h later 0.1 mmol/kg diTyr-DTPAGd was administered followed by MRI at 2h. Both 99mTc-labeled conjugates showed specific binding to U87ΔEGFR cells in vitro and in vivo (Fig.1 A,B). MR T1-weighted images showed significantly higher enhancement and longer retention of the MR signal on Day 2 in rats pre-injected with conjugates compared to Day 1 over the same time period due to the conjugate co-localization at the EGFRvIII target sites (Fig. 1C). The washout of the contrast agent was best modeled using a biexponential decay as compared to Gli36ΔEGFR-bearing rats. U87ΔEGFR tumors showed biexponential MR signal decay on both days. Administration of EGFRvIII-targeted mAb conjugates resulted in specific binding to U87ΔEGFR cells of which at least ~20% remained on the surface enabling the reaction with the contrast agent. The biexponential decay constants on Day 2 for both Gli36ΔEGFR and U87ΔEGFR animals were not significantly different indicating a similarity of conjugate accumulation in both tumor models, which resulted in a similar bimodal washout of the contrast agent. References: [1] Hu J et al. (2011) PNAS 108:15984; [2] Bogdanov A, et al. (2007) Bioconjug Chem 18: 1123; [3] Shazeeb MS, et al. (2011) Cancer Res 71: 2230.

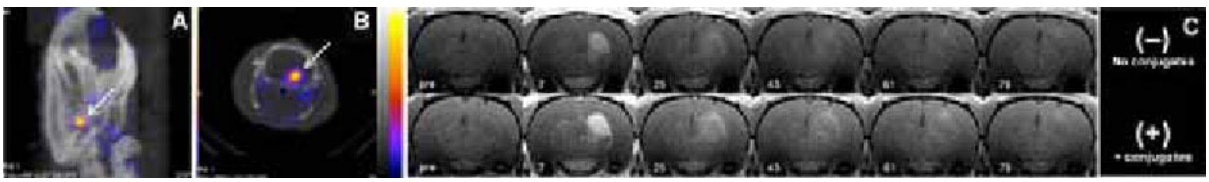


Fig. 1. A- sagittal and B- axial SPECT/CT images of rat brain showing 99mTc-labeled mAb conjugates in U87ΔEGFR tumors (arrows); C - T1-weighted sequential rat brain images of U87ΔEGFR xenografts after the injection of diTyr-GdDTPA; (-) diTyr-GdDTPA with no conjugate pre-injection; (+) f diTyr-GdDTPA following IV injection with anti-EGFRvIII conjugates in the same animal in matched slices (time in minutes).

Disclosure of author financial interest or relationships:
**A.A. Bogdanov**, None; **M.S. Shazeeb**, None; **S. Gupta**, None.

Presentation Number **P541**
Poster Session 3
September 7, 2012 / 15:15-15:15 / Room: The Liffey

# Three-Dimensional Bioluminescence Reconstruction using Compact 1 Tesla MRI

***Jacob Hesterman***[1], *Tonya Coulthard*[2], *Balázs Viszoczki*[1], *Alexander D. Klose*[3], *Karl Schmidt*[1], *Jinzi Zheng*[4], *Cheng Jin*[4], *Jack Hoppin*[1], [1]*inviCRO, Boston, MA, USA;* [2]*Aspect Imaging, Toronto, ON, Canada;* [3]*Neurological Institute, Columbia University, New York, NY, USA;* [4]*STTARR, Toronto, ON, Canada. Contact e-mail: hesterman@invicro.com*

Bioluminescence imaging is the most prevalent in vivo pre-clinical imaging modality largely due to high-sensitivity for classifying cell proliferation, low cost and high-throughput. While "single-cell" sensitivities are reported, fundamental limitations of the optical signal (absorption and scatter) often limit quantitative assessment. In an attempt to improve quantitation of bioluminescence signal, we present first efforts at incorporating 3D anatomical information collected with a high-throughput, compact MR imaging system into a 3D bioluminescence reconstruction platform. A prototype multi-modality imaging cassette comprised of plexi-glass plates with an inner surface-to-surface distance of 15mm was prepared in which the mouse was stabilized for transportation under anesthesia between the two imaging modalities. Optical images were collected on an IVIS Spectrum (Perkin Elmer, Inc.) in an orthotopic prostate model (PC3-luc6, Fig. 1a). Luminescence images were collected in both the prone and supine position for 120s at 580, 600, 620, 640 and 660nm at 10 minutes post IP injection of 60mg/kg of D-luciferin. MR imaging was performed using a 1T compact MRI system (M2, Aspect Imaging). A T2-weighted image highlights the location of the tumor in Figure 1b. Three-dimensional (3D) spatial maps of the light emission density [photons cm-3 s-1] are obtained by employing a light source reconstruction algorithm for scattering and strongly absorbing media. This algorithm consists of a light propagation model based on a set of high-order simplified spherical harmonics (SPN) equations and a linear solver based on Kaczmarz method. The SPN equations predict the light intensity distribution [photons cm-2 s-1] on the tissue surface for a given light source distribution and spectral band. The linear solver utilizes the multispectral predictions and calculates the unknown light emission density inside tissue for given bioluminescence images taken at the tissue surface. The co-registered MR images are utilized by the light source reconstruction algorithm in two different ways: the MR data set provides the small-animal tissue surface geometry required by the light propagation model; the major organs are segmented and yield accurate absorption property maps based on the blood oxygenation level as a function of wavelength. Results of the effort are shown in Figure 1c. in which the bioluminescence reconstruction (prism color scale) is super-imposed with the MR image (gray scale). A surface rendering of the tumor (red) is provided in Figure 1d. Anatomical information provided by MRI enabled the successful 3D reconstruction and localization of the bioluminescence signal within the animal as well as improved accuracy of estimating the light emission density from deep-seated sources.

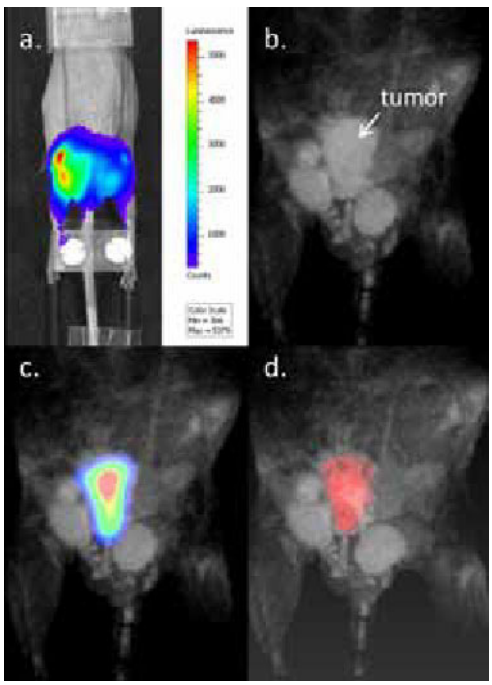


Disclosure of author financial interest or relationships:
**J. Hesterman**, inviCRO, Employment; **T. Coulthard**, Aspect Imaging, Employment; **B. Viszoczki**, inviCRO LLC, Employment; **A.D. Klose**, None; **K. Schmidt**, inviCRO LLC, Consultant; **J. Zheng**, None; **C. Jin**, None; **J. Hoppin**, inviCRO, LLC, Employment; inviCRO, LLC, Stockholder .

Presentation Number **P542**
Poster Session 3
September 7, 2012 / 15:15-15:15 / Room: The Liffey

# Design and Synthesis of a novel fluorescent Photoprobe targeted to Aminopeptidase N (APN/CD13)

*Anke Hahnenkamp[1], Michael Schäfers[3], Christoph Bremer[2], **Carsten Hoeltke**[1], [1]Dept. of Clinical Radiology, University Hospital Muenster, Muenster, Germany; [2]Clinic for Radiology, St. Franziskus Hospital Muenster, Muenster, Germany; [3]European Institute for Molecular Imaging, University of Muenster, Muenster, Germany. Contact e-mail: carsten.hoeltke@uni-muenster.de*

Aminopeptidase N (APN/CD13) is a zinc-dependent ectoenzyme located in the outer cell membranes of various cell types. APN has been identified as an important mediator of tumor angiogenesis promoting progression, metastasis and tumor cell survival. While mainly absent on normal vasculature APN is highly expressed on newly developing tumor vessels, where it is located on both the endothelial surface and in the pericyte/smooth muscle layers of tumor vessels. Peptides that contain the amino acid sequence Asn-Gly-Arg (NGR) bind to APN in tumor vasculature [Pasqualini R et al., Canc Res. 2000,60;722-727]. Optical imaging of APN-expressing target tissue is possible with NGR-based probes as has been shown earlier [von Wallbrunn A et al., J Biomed Opt. 2008,13(1);011007]. Here we present the design and synthesis of a non-peptide fluorescent probe based on a recently developed small molecule APN inhibitor [Zhang X et al., Curr Med Chem. 2008,15;2850-2865]. Based on the non-peptide lead structure we de novo synthesized modified derivatives of this small molecule APN inhibitor. Starting from 4-hydroxyproline and two different aromatic building blocks we synthesized three modified derivatives with PEG spacers carrying an amino group for dye labeling (Fig.1A). Labeling of promising precursor compounds was performed with Cy 5.5 NHS-ester and the resulting probes tested in cell binding assays. Therefore, different cell lines were tested for the expression of APN. FACS analysis and immunocytometry reveal a high amount of APN on e.g. breast cancer cell line BT549, while MDA-MB 231 cells show no expression of the target. Accordingly, BT549 cells show a high signal intensity in fluorescence microscopy, while MDA-MB 231 cells show only a week signal (Fig.1B/C). Interestingly, the probes behave differently concerning the site of modification. While tracers modified on the "left" side of the structure (Fig.1A top) show specific binding behavior, a modification on the "right" side of the molecule does not yield the expected specificity. In conclusion, we successfully synthesized novel APN/CD13 targeted fluorescent photoprobes. In vitro, the imaging of target expressing cells could be shown. Future experiments will show the performance of the probes in vivo.

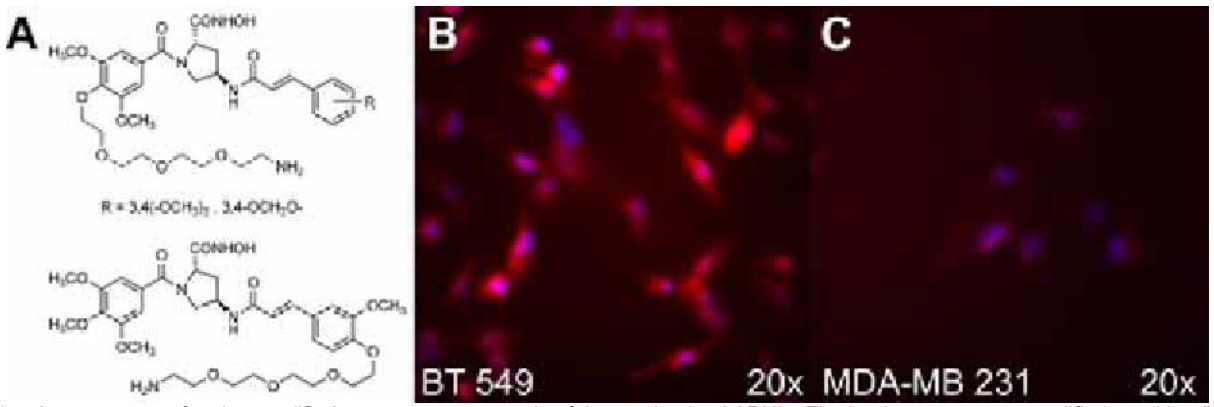


Fig.1A. Molecular structures of amino modified precursor compounds of the synthesized APNIs. The lead structure was modified on either "side" of the molecule with a short PEG chain carrying an amino group. B and C: Fluorescence microskopy images of cell binding assays on BT 549 and MDA-MB 231 cells showing the specificity of the developed tracer (Cy 5.5 and DAPI channel overlay).

Disclosure of author financial interest or relationships:
**A. Hahnenkamp**, None; **M. Schäfers**, Siemens Medical Solutions, Grant/research support; **C. Bremer**, None; **C. Hoeltke**, None.

Presentation Number **P543**
Poster Session 3
September 7, 2012 / 15:15-15:15 / Room: The Liffey

# Intracellular αv integrin-GFP behavior imaged in lung metastasis formation in nude mouse models

*Yasunori Tome[1,3], Naotoshi Sugimoto[4], Shuya Yano[1,2], Masashi Momiyama[1,2], Hiroki Maehara[3], Hiroyuki Tsuchiya[5], Katsuro Tomita[5], Fuminori Kanaya[3], Michael Bouvet[2], **Robert M. Hoffman**[1,2], [1]AntiCancer, Inc., San Diego, CA, USA; [2]Dept. of Surgery, University of California, San Diego, CA, USA; [3]Dept. of Orthopedic Surgery, Graduate School of Medicine, University of the Ryukyus, Okinawa, Japan; [4]Dept. of Physiology, Graduate School of Medical Science, Kanazawa University, Kanazawa, Japan; [5]Dept. of Orthopedic Surgery, Graduate School of Medical Science, Kanazawa University, Kanazawa, Japan. Contact e-mail: all@anticancer.com*

We report here imaging the behavior of αv integrin linked to GFP in osteosarcoma cells which are colonizing the lung of nude mice. 143B osteosarcoma cells expressing αv integrin-GFP were generated by transfection of an αv integrin-GFP vector. Confocal microscopy with the FV1000 (Olympus Corp., Tokyo, Japan) demonstrated that αv integrin immunofluorescence staining colocalized with αv integrin-GFP fluorescence. To generate pulmonary colonies, osteosarcoma cells, stably expressing αv integrin-GFP, were injected intravenously (1×106) via the tail vein of nude mice. Eight weeks after injection, both lungs were harvested and observed by confocal microscopy within 1 hour after harvesting. Scattered-expression of αv integrin-GFP was observed in the pulmonary osteosarcoma colonies. In contrast, osteosarcoma cells strongly expressed αv integrin-GFP when aligned along the edge of colonies and around blood vessels. Expression of αv integrin-GFP can be imaged in lung metastasis which will allow further understanding of its role in this process.

Disclosure of author financial interest or relationships:
**Y. Tome**, None; **N. Sugimoto**, None; **S. Yano**, None; **M. Momiyama**, None; **H. Maehara**, None; **H. Tsuchiya**, None; **K. Tomita**, None; **F. Kanaya**, None; **M. Bouvet**, None; **R.M. Hoffman**, None.

Presentation Number **P544**
Poster Session 3
September 7, 2012 / 15:15-15:15 / Room: The Liffey

# Non-invasive imaging of orthotopic patient pancreatic tumors in nude mice using fluorescent proteins

*Atsushi Suetsugu[1,3], Matthew H. Katz[4], Jason B. Fleming[4], Mark Truty[4], Ryan M. Thomas[4], Mohamed K. Hassanein[1], Hisataka Moriwaki[3], Michael Bouvet[2], Shigetoyo Saji[5], **Robert M. Hoffman**[1,2], [1]AntiCancer, Inc., San Diego, CA, USA; [2]Dept. of Surgery, University of California, San Diego, CA, USA; [3]Dept. of Gastroenterology, Gifu University Graduate School of Medicine, Gifu, Japan; [4]Dept. of Surgical Oncology, MD Anderson Cancer Center, Houston, TX, USA; [5]Dept. of Surgical Oncology, Gifu University Graduate School of Medicine, Gifu, Japan. Contact e-mail: all@anticancer.com*

In order to help develop more effective treatment for pancreatic cancer, we developed a multicolor imageable orthotopic mouse model for individual human pancreatic-cancer patients. Pancreatic cancer patient tumor specimens were initially established in SCID-NOD mice. The tumors were then passaged orthotopically into transgenic nude mice expressing GFP in almost every tissue. Both the primary tumors and resultant metastasis acquired GFP stroma and could be imaged by GFP fluorescence. GFP stroma included cancer-associated fibroblasts (CAFs). Further passage to nude mice expressing RFP in almost all tissues resulted in tumors and metastasis acquiring RFP stroma in addition to their GFP stroma, including CAFs. Further passage to transgenic nude mice expressing CFP in almost all tissues resulted in tumors and metastasis acquiring CFP stroma in addition to RFP and GFP stroma including CAFs. The model can be used to image primary and metastatic progression of patient pancreatic tumors, study acquisition of stroma and to test both standard and novel cancer- and stroma-targeting agents. The imageable tumor-graft model should prove valuable for treatment evaluation of individual cancer patients, as well as for evaluation of experimental therapeutics targets in the tumor or the tumor microenvironment such as cancer-associated fibroblasts (CAFs).

Disclosure of author financial interest or relationships:
**A. Suetsugu**, None; **M.H. Katz**, None; **J.B. Fleming**, None; **M. Truty**, None; **R.M. Thomas**, None; **M.K. Hassanein**, None; **H. Moriwaki**, None; **M. Bouvet**, None; **S. Saji**, None; **R.M. Hoffman**, None.

Presentation Number **P545**
Poster Session 3
September 7, 2012 / 15:15-15:15 / Room: The Liffey

# Detection of Cell Death with GE152 in a Small Animal Model: A Tool for Early Assessment of Tumour Therapy Response

***Susan Hoppmann***[1], *Ella Hirani*[1], *Graeme McRobbie*[1], *Roger M. Bjerke*[2], *Bente E. Arbo*[2], *Chris Cawthorne*[3], *Kaye Williams*[3], *Kathryn L. Simpson*[4], *Caroline Dive*[4], *Aileen Hoehne*[5], *Sanjiv S. Gambhir*[5], *Duncan R. Hiscock*[1], [1]*Medical Diagnostics, The Grove Centre, GE Healthcare, Amersham, United Kingdom;* [2]*Medical Diagnostics, GE Healthcare, Oslo, Norway;* [3]*Preclinical Laboratory, Wolfson Molecular Imaging Centre, The University of Manchester, Manchester, United Kingdom;* [4]*Clinical and Experimental Pharmacology, Paterson Institute for Cancer Research, Manchester Academic Health Science Centre, Christie Hospital, The University of Manchester, Manchester, United Kingdom;* [5]*Molecular Imaging Program at Stanford (MIPS), Department of Radiology, Stanford University School of Medicine, Stanford, CA, USA. Contact e-mail: susan.hoppmann@ge.com*

Early assessment of drug treatment response is a major challenge in anti-cancer therapy. Apoptosis is a key biological response and marks the beginning of tumour mass reduction following therapy. One of the earliest events in apoptosis is the externalization of the phospholipid phosphatidylethanolamine (PE) which is normally restricted to the inner leaflet of the lipid bilayer, making PE an attractive target for cell death imaging. GE152 comprises a group of 99mTc radiolabelled peptides with nanomolar affinity for PE. Here, we investigate the efficacy of GE152 in preclinical apoptosis animal models and subsequently optimise our lead compounds by introducing a PEG-linker in order to improve pharmacokinetics (PK) for radionuclide imaging. GE152 radiolabelling precursors were prepared by conjugating pre-activated cPn216-glut-OH or cPn216-glut-PEG12-OH to cinnamycin. PE-affinity studies for GE152 peptides were performed using a Biacore 3000 with immobilized PE-containing liposomes on an activated L1 chip. In vivo biodistribution (n=3 for each group and time point) of 99mTc-radiolabelled GE152 was assessed in a) a murine lymphoma (EL4) tumour therapy model treated with either saline/DMSO (control) or a mixture of etoposide/cyclophosphamide (therapy) and b) a murine inducible HT29 colorectal cancer cell death switch model where xenografts inducibly express either a constitutively active form of caspase-3 or an inactive point mutant. Caspase-3 activity of tumour homogenates was assessed using Caspase-Glo® assay (Promega). Naïve rat biodistributions with PEG12-modified GE152 were performed to determine if a PEG12 linker would improve PK. Cellular binding of PEG12-modified GE152 to late apoptotic EL4, late and early apoptotic Jurkat cells and non-induced cells was assessed at 30, 60 and 90min after adding the compound. Biodistribution of GE152 in the EL4 mouse model showed increased tumour retention following chemotherapy, with positive tumour:muscle and tumour:blood ratios. GE152 tumour uptake (7.5±0.9%ID/g in treated and 4.9±0.1%ID/g in control tumours, 90min p.i., $p<0.05$) positively correlated with tumour caspase-3 activity. In the death switch model, GE152 demonstrated greater uptake in tumours undergoing apoptosis than in controls (3.6±0.1%ID/g and 1.2±0.2%ID/g, 90 min p.i., $p<0.01$). These data are in line with caspase activity levels determined both enzymatically and by IHC. PEG12-modified GE152 showed comparable affinity to non-PEGylated GE152 for PE (Kd 32 nM and Kd 20 nM, respectively) as determined by Biacore studies. Biodistribution studies in naïve rats demonstrated that the introduction of the PEG linker successfully reduced liver retention (1.1±0.05%ID/g to 0.26±0.03%ID/g, 60min p.i., $p<0.01$) showing improved imaging PK. PEGylated GE152 showed good differentiation between apoptotic and non-apoptotic cells in vitro (5.2±1.1-fold uptake by late apoptotic EL4 and 3.8±0.5-fold uptake by late apoptotic Jurkat after 30min incubation, 2.1±0.3-fold uptake by early apoptotic Jurkat after 90min compared to control cells). The data suggests that GE152 imaging agents have promising diagnostic value for early detection of apoptosis.

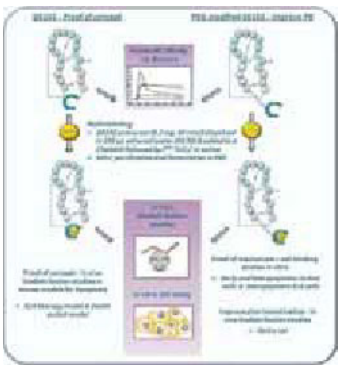

Disclosure of author financial interest or relationships:
**S. Hoppmann**, GE Healthcare, Employment; **E. Hirani**, None; **G. McRobbie**, GE Healthcare, Employment; **R.M. Bjerke**, None; **B.E. Arbo**, None; **C. Cawthorne**, GE Healthcare, Grant/research support; **K. Williams**, GE, Grant/research support; **K.L. Simpson**, None; **C. Dive**, None; **A. Hoehne**, None; **S.S. Gambhir**, General Electric, Grant/research support; Bayer-Schering, Grant/research support; Sanofi-Aventis, Grant/research support; CellSight, Stockholder; ImaginAB, Stockholder; Enlight, Stockholder; Endra, Stockholder; Bracco, Consultant; NinePoint Medical, Stockholder; Visualsonics, Consultant; **D.R. Hiscock**, GE Healthcare, Employment .

Presentation Number **P546**
Poster Session 3
September 7, 2012 / 15:15-15:15 / Room: The Liffey

# 3-Dimensional Texture Analysis of Collagen Fibers for Functional Characterization of the Tumor Extracellular Matrix

***Samata M. Kakkad***[1,2], *Alireza Akhbardeh*[1], *Meiyappan Solaiyappan*[1], *Marie-France Penet*[1], *Dieter Leibfritz*[2], *Kristine Glunde*[1], *Zaver M. Bhujwalla*[1], [1]*Radiology and Radiological Science, The Johns Hopkins University School of Medicine, Baltimore, MD, USA;* [2]*Chemistry and Biology, University of Bremen, Bremen, Germany. Contact e-mail: skakkad1@jhmi.edu*

Introduction: Collagen I (Col1) forms an integral part of the tumor extracellular matrix (ECM) and plays an important role in cancer cell dissemination and macromolecular transport. Col1 fiber orientation and alignment are predictors for survival in patients[1]. Second harmonic generation (SHG) microscopy can be used to detect the intrinsic signal of Col1 fibers. The major challenges of processing the Col1 fiber image data to understand their role in the tumor ECM are the size of the 3D data, the complexity of fiber patterns, and their distribution across tissue sections. Here we have developed, for the first time, automated quantification of Col1 fiber distribution and orientation using Haralick texture features analysis and applied it to understand the effects of 5-fluorouracil (5-FU) treatment in a human breast cancer xenograft model. Methods: Female severe combined immunodeficient mice were inoculated in the mammary fat pad with MDA-MB-231 cells. Once tumor volumes were approximately 300-400 mm3, mice were treated with 160 mg/kg dose of 5-FU. SHG microscopy was performed on fresh excised tumor central slices using a Zeiss 710 multiphoton microscope as previously described[2]. Tile scans were used to image the entire tumor slice in 3D using a 25x lens. Analysis was done in MATLAB (Mathworks Inc.). Two major structural characteristics of the Col1 fiber network in the ECM can be computed using image processing techniques: 1) spatial characteristics using Euclidean distance maps to collectively represent the sparseness and density of the distribution [2]; 2) textural characteristics of the fiber patterns that vary across the tissue from straight/aligned fibers to curly/crisscross fibers for which texture analysis method using co-occurrence matrix approaches proposed by Haralick et al can be applied[3]. The Haralick's co-occurrence matrix extracts fibers and finds spatial inter-relations of the fibers. Features extracted include energy, entropy, variance, maximum probability, and inverse variance. We segmented and clustered these 5 Haralick's texture features, and color-coded the 3D projected image to represent the 3D fiber orientation in 2D. Results and Conclusion: Haralick texture feature extraction distinguished fiber distribution of curly and overlapping fibers from straight and sparsely distributed fiber. Figure 1 displays structural characterization of the Col1 fiber orientation in 3D visualized in a 2D image. The dark red color represents curly fibers and the light blue color represents straight and more sparely distributed fibers. Preliminary studies identified differences in entropy between control and treated tumors - supplementary data. High-resolution microscopic images of Col1 fiber distribution can be quantified for orientation in 3D and will advance characterization of the ECM. The analysis can be applied to understand cancer and identify and improve cancer treatment response and outcome. References: [1]Keely et al., Am J Pathol. 2011; [2]Kakkad et al., Neoplasia, 2010; [3]Haralick et al., IEEE Transactions on systems, man and cybernetics, 1973;Acknowledgement: Supported by P50 CA103175 and P30 CA006973.

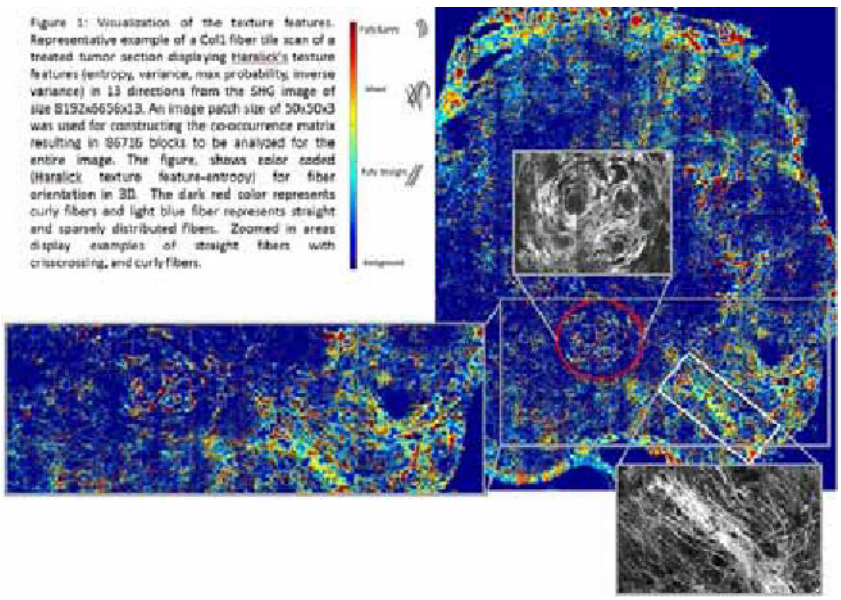


Disclosure of author financial interest or relationships:
**S.M. Kakkad**, None; **A. Akhbardeh**, None; **M. Solaiyappan**, None; **M. Penet**, None; **D. Leibfritz**, None; **K. Glunde**, None; **Z.M. Bhujwalla**, None.

Presentation Number **P547**
Poster Session 3
September 7, 2012 / 15:15-15:15 / Room: The Liffey

# Influence of ferric-desferoxamin complex on enhancement of T1 and T2 relaxation of proton in tissue equivalent phantoms and its biodistribution in rats

***Poladate Kantakam**, Apijit Chaichana, Nutthapong Moonkum, Chutimon Sanjai, Suchart Kothan, Nathupakorn Dechsupa, Chatchanok Udomtanakunchai, Samlee Mankhetkorn, Anan Udom-uttaracheewa, Radiologic Technology, Laboratory of Physical Chemistry, Molecular and Cellular Biology; Center of Excellence for Molecular Imaging,Faculty of Associated Medical Sciences, Chiang Mai University, Chiang Mai, Thailand. Contact e-mail: hanjing_10@hotmail.com*

The potential applications of macrocyclic molecules as drugs and imaging products are emerging fields of research.Therefore, this study was proposed to characterize a paramagnetic ferric-desferroxaminemesylate complex. The complexefficiently enhanced both the T1 and T2 image contrast of phantoms by increasing in the protons of water molecules relaxing the so-called "relaxivity" of the complex. The T1-relaxivity determined inthree conditions such as 3.7% agarose gel, RPMI 1640 culture medium and distilled water was almost the same, being equal to 10.5 ± 0.004 $mM^{-1}.s^{-1}$. While the T2-relaxivity was 1.17± 0.2 $nM^{-1}.s^{-1}$ in 3.7% agarose gel, 1.34 ± 0.2 $nM^{-1}.s^{-1}$ in RPMI 1640 culture medium and 1.45± 0.2 $nM^{-1}.s^{-1}$ in water.The biodistribution of the complex was studied by T1-wieght and T2-wieght imaging compared with Gd-DOTA and Gd-DTPA complex.Among these complexes, ferric-desferoxamin was found to penetrate into the soft tissues by which allow clearly visualizing soft tissues and organs. The ferric-desferoxamin complex could be considered (a) as a tissue MR-contrast agent for the study of the urinary system, brain and hearts, (b) as a suitable probe for bioconjugation with biomolecules for specific targeted contrast agents and (c) as a probe for directed labeling of stem cells for stem cell homing, engrafting and function in vivo. drug response during cancer treatments and stem cell labeling.

Disclosure of author financial interest or relationships:
**P. Kantakam**, None; **A. Chaichana**, None; **N. Moonkum**, None; **C. Sanjai**, None; **S. Kothan**, None; **N. Dechsupa**, None; **C. Udomtanakunchai**, None; **S. Mankhetkorn**, None; **A. Udom-uttaracheewa**, None.

Presentation Number **P548**
Poster Session 3
September 7, 2012 / 15:15-15:15 / Room: The Liffey

# Evaluation of preclinical, multimodal therapy monitoring including multiparametric MR using a hNIS- expressing tumour xenograft mouse model

***Eva J. Koziolek***[1], *Randi Pose*[2], *Agnieszka Tarkowska*[2], *Ivayla Apostolova*[3], *Winfried Brenner*[3], *Udo Schumacher*[2], *Gerhard Adam*[1], *Michael G. Kaul*[1], [1]*Diagnostic and Interventional Radiology, University Hospital Hamburg Eppendorf, Hamburg, Germany;* [2]*Anatomy, University Hospital Hamburg Eppendorf, Hamburg, Germany;* [3]*Nuclear Medicine/Small Animal Imaging Centre, Charité - Universitätsmedizin Berlin, Berlin, Germany. Contact e-mail: ekoziole@uke.de*

Purpose: The human sodium iodine symporter (hNIS), a basolateral membrane protein, actively accumulates iodide inside cells and so forth has been successfully exploited in diagnosis and treatment of thyroid disease. By gene transfer hNIS expression could be used to treat nonthyroid malignant disease. The purpose of our study was to establish a tumour xenograft mouse model allowing multimodal tumour imaging and monitoring of hNIS gene transfected tumours. Materials and Methods: Tumour cells of human origin (colon,breast) were stably transfected with the hNIS gene. Mouse tumour xenograft models were established by inoculating ~1x106 cells over the right scapula subcutaneously. To establish the oestrogen-positive breast cancer model, an oestrogen pellet (90 day-release) was implanted subcutaneously. MRI Imaging was performed on a dedicated preclinical small animal 7T MR (ClinScan, Bruker) and SPECT imaging using a preclinical small animal SPECT/CT (NanoSPECT, Mediso). To monitor tumour growth by MRI, tumour size was measured using a T2-weighted sequence. Additionally, diffusion weighted imaging (DWI) and dynamic contrast enhanced (DCE) MRI (0.15 Mmol/kg Gd-DTPA) were performed. To visualize tracer accumulation and measure tracer retention time, SPECT imaging was performed using Tc99m (100 MBq). Results: hNIS- expression in both tumour entities was visualized by a strong Tc99m-uptake via SPECT-imaging when compared to tumour xenografts bearing untransfected tumour cells. MR imaging allowed a precise delineation of tumour mass and estimation of tumour volume. Signal enhancement measured by DCE was predominantly found in the tumour periphery, whilst homogenous tumour tissue showed a more uniform contrast agent distribution. Increased apparent diffusion coefficient (ADC) in the tumour center gave the indication of necrotic tissue. Conclusions: The NIS-transfected tumour xenograft model seems to be a promising tool for tumour imaging and monitoring. Further validation can be performed by pharmacokinetic modelling of tumour-specific tracer uptake and analyzed MR parameters such as diffusion, perfusion and permeability of the tumour tissue in order to predict therapy response.

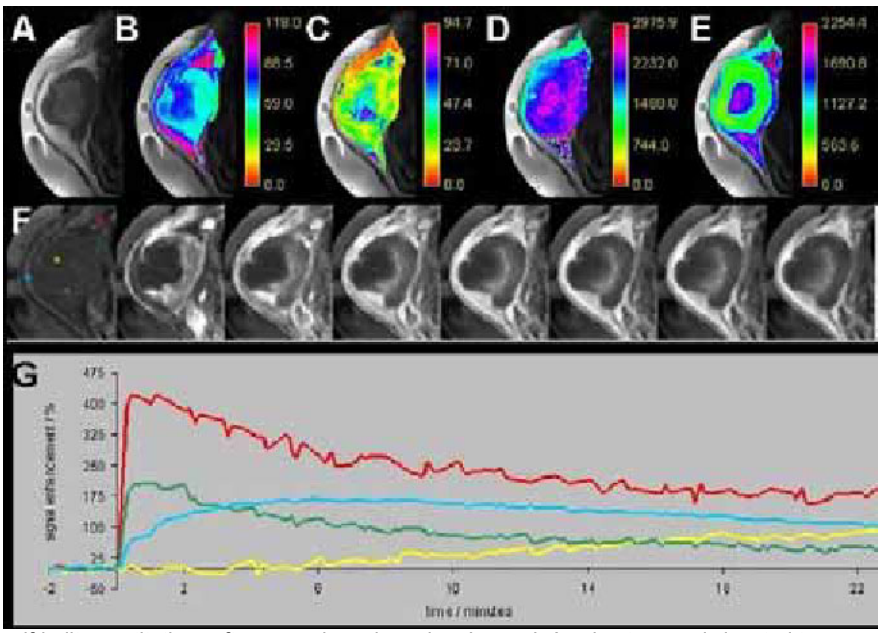


Multi-parametric MRI using a self-built quantitative software package based on ImageJ: A subcutaneously located tumour embedded in ultrasound-gel is shown. T2-weighted MRI (A), with partly fused quantitative maps of T2 [ms] (B), T2* [ms] (C), T1 [ms] (D), and apparent diffusion coefficient [µm2/s] (E). The heterogeneity of the tumour tissue is well demonstrated by dynamic contrast enhanced MRI after the contrast agent bolus is applied (F). The dynamic response in the signal enhancement (G) from four regions corresponding to the coloured dots (F) is plotted showing various wash-in/wash-out patterns.

Disclosure of author financial interest or relationships:
**E.J. Koziolek**, None; **R. Pose**, None; **A. Tarkowska**, None; **I. Apostolova**, None; **W. Brenner**, nanoPET, Grant/research support; **U. Schumacher**, None; **G. Adam**, None; **M.G. Kaul**, None.

Presentation Number **P549**
Poster Session 3
September 7, 2012 / 15:15-15:15 / Room: The Liffey

# Fluorescence Imaging Reveals Differential Drug Delivery to the Mandible Regardless of Bone Turnover Status

***Kenneth M. Kozloff***[1,2], *Joseph E. Perosky*[1], *Adrienne F. Alimasa*[1,2], *Laurie K. McCauley*[3], [1]*Orthopaedic Surgery, University of Michigan, Ann Arbor, MI, USA;* [2]*Biomedical Engineering, University of Michigan, Ann Arbor, MI, USA;* [3]*Periodontics and Oral Medicine, University of Michigan, Ann Arbor, MI, USA. Contact e-mail: kenkoz@umich.edu*

Osteonecrosis of the jaw (ONJ) is a detrimental condition of exposed bone in the oral cavity that has been found in patients treated with bisphosphonates for multiple myeloma and metastatic bone disease [1]. While associated with bisphosphonate (BP) use, it is unknown what role BPs play in the etiology of ONJ. If local BP concentration is responsible for the occurrence of ONJ, then understanding factors that regulate BP localization is of high importance. The purpose of this study was to investigate the role of bone turnover in the local accumulation of BPs at skeletal sites (mandible, femur, and tibia). Recently we have demonstrated the use of far-red fluorescent pamidronate (FRFP) as an imaging strategy to visualize and quantify local bisphosphonate concentration in the skeleton [2]. In the current study, high and low bone turnover states were induced by parathyroid hormone (PTH) and BP treatment, and compared to a control group (PBS) using fluorescent-labeled BPs to assess local drug concentration. Fourteen week male Balb/c mice were treated with rhPTH[1-34] (80µg/kg daily), pamidronate (PAM, 1.07 mg/kg daily), or PBS injection for 1 week (n=14-16/group), after which mice were injected with a single dose of a FRFP (Osteosense 750, 100 nmol/kg). Twenty-four hours after injection, mice were euthanized and femora, tibiae, and mandibles were excised and imaged under fluorescence illumination to quantify average FRFP signal at anatomic sites of interest. Statistical changes were at the level $p<0.05$ unless otherwise noted. Serum collected at euthanasia from a subset of mice revealed the bone turnover markers, osteocalcin and TRACP5b, increased and decreased after 1 week of PTH or PAM respectively. However significant changes in bone mass or surface area by µCT were not observed at any site. FRFP signal was normalized by bone surface area (FRFP/BS) measured by µCT to compare BP delivery at multiple sites. For all treatment groups, FRFP/BS in the mandible was higher than both femur (PTH=26%, PBS=69%, PAM=39%) and tibia (PTH=99%, PBS=187%, PAM=120%). For femora and tibiae, FRFP delivery in the context of PTH-induced high bone turnover increased compared to PBS (Femur=37%, Tibia=43%) and increased marginally, but not significantly vs. PAM low turnover groups (Femur=26%, Tibia=29%). Interestingly, mandibles were less sensitive to treatment effects, as FRFP/BS was equivalent across treatment groups. Dynamic histomorphometry revealed FRFP spatially followed calcein and alizarin labels administered 6 and 1 day prior to FRFP. These findings suggest that, at the femur and tibia, local bone turnover regulates local BP delivery, however the mandible may be particularly susceptible to high levels of BP delivery regardless of bone turnover condition. References: 1. Khosla et al 2007 J Bone Miner Res 22:1479; 2. Kozloff et al 2010 J Bone Miner Res 25:1748

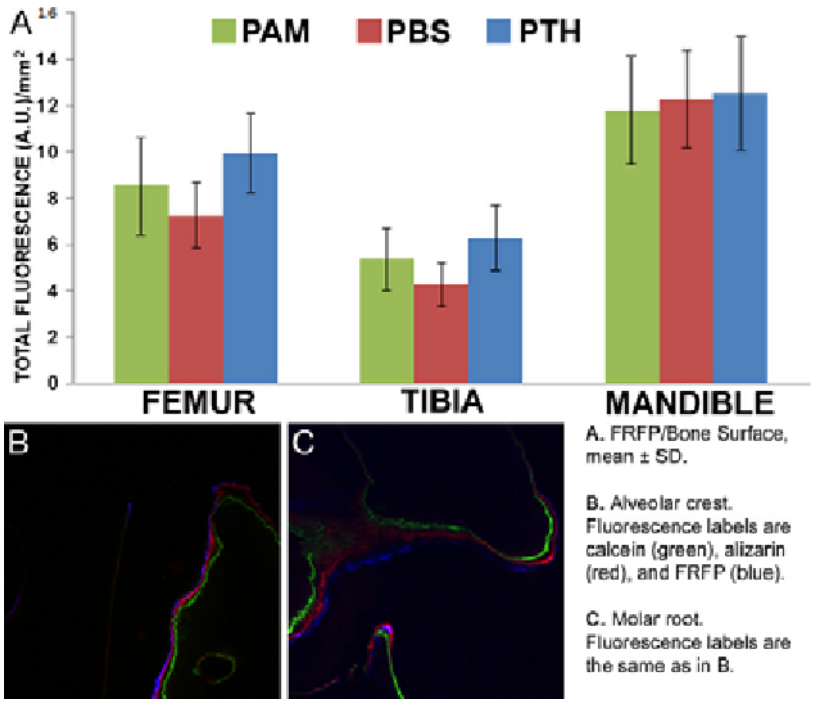


A. FRFP/Bone Surface, mean ± SD.

B. Alveolar crest. Fluorescence labels are calcein (green), alizarin (red), and FRFP (blue).

C. Molar root. Fluorescence labels are the same as in B.

Disclosure of author financial interest or relationships:
**K.M. Kozloff**, None; **J.E. Perosky**, None; **A.F. Alimasa**, None; **L.K. McCauley**, None.

Presentation Number **P550**
Poster Session 3
September 7, 2012 / 15:15-15:15 / Room: The Liffey

# Comparison of nanobodies and conventional monoclonal antibodies for in vivo fluorescence imaging of lymphomas

***Alexander Lenz***[1,2], *Valentin Kunick*[1,2], *Lennart Well*[1,2], *Welbeck Danquah*[2], *Friedrich Haag*[2], *Martin Trepel*[3], *Gerhard Adam*[1], *Harald Ittrich*[1], *Friedrich Koch-Nolte*[2], *Peter Bannas*[1], [1]*Diagnostic and Interventional Radiology, University Medical Center Hamburg-Eppendorf, Hamburg, Germany;* [2]*Institute of Immunology, University Medical Center Hamburg-Eppendorf, Hamburg, Germany;* [3]*Department of Oncology and Hematology, University Medical Center Hamburg-Eppendorf, Hamburg, Germany. Contact e-mail: a.lenz@uke.de*

Purpose: Noninvasive imaging of cell surface proteins using specific antibodies yields a great potential for the detection and characterization of tumors in vivo. However, the focus has shifted from monoclonal antibody-based probes to smaller probes, which offer superior tissue penetration and reduced serum half-life. Here we compared different formats of llama-derived nanobodies as alternatives to monoclonal antibodies for specific in vivo fluorescence imaging of lymphomas in a mouse model. Materials and Methods: We used the ecto-enzyme ART2 on lymphoma cells as a model target and compared three different formats of ART2-specific nanobodies with a conventional rat antibody (Nika102, 150 kD): A monovalent llama nanobody s+16a (15 kD), a bivalent diabody derived from s+16a (s16-s16, 30kD), and a bivalent fusion protein of s+16a with the Fc domain of murine IgG1 (s+16-mFc, 80 kD). All constructs were labeled with the near-infrared fluorochrome AF680. Athymic nude mice, bearing ART2-positive and ART2-negative tumors, were injected i.v. with the AF680-conjugates. Circulating and excreted conjugates were monitored in plasma and urine and in vivo near-infrared fluorescence imaging was performed over 24h. Differences in tissue penetration and target binding were further analyzed by FACS and fluorescence microscopy of dissected tumors. Results: In vivo imaging revealed specific labeling of ART2-positive tumors but not of ART2-negative tumors with all AF680-conjugates. The smallest constructs s+16a and s16-s16 revealed rapid renal elimination with highest signal-to-background ratio of ART2-positive tumors. The larger constructs s+16mFc and Nika102 revealed long circulation times in plasma, resulting in interfering unspecific background signals. Immunohistochemistry of tumors revealed deep penetration and homogenous labeling of tumor tissue with the smallest constructs s+16a and s16-s16, which was confirmed by FACS analyses. Conclusion: Our results highlight the advantages of nanobody-based probes as diagnostic tools for the specific detection of lymphomas in vivo. Renally excreted small nanobody-formats (< 60 kD) can be used for specific in vivo imaging of lymphomas with a significantly higher signal-to-background ratio than larger antibody-constructs (> 60kD) that are retained in circulation. Therefore, single domain and bivalent nanobodies seem particularly suited for short-term diagnostic imaging, whereas reformatted nanobody-Fc fusion proteins appear particularly suited for long-term applications

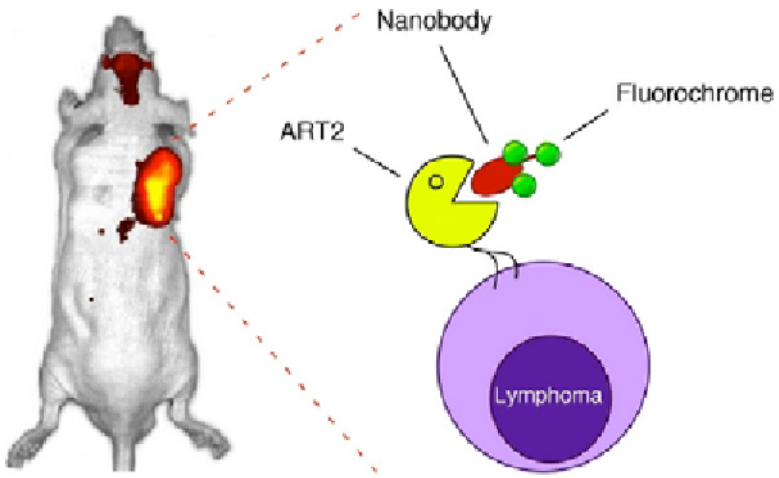


**Fig. 1:** NIRF-image of a mouse carrying an ART2-positive tumor on the right side and an ART2-negative tumor on the left side (fluorescent image on photograph overlay). Images were acquired 2h after injection of the AF680-conjugated nanobody *s+16a*, which specifically binds to ART2 on the cell surface of lymphoma cells (schematic drawing).

Disclosure of author financial interest or relationships:
**A. Lenz**, None; **V. Kunick**, None; **L. Well**, None; **W. Danquah**, None; **F. Haag**, Analytical Services North, Honoraria; **M. Trepel**, None; **G. Adam**, None; **H. Ittrich**, None; **F. Koch-Nolte**, Ablynx, Grant/research support; **P. Bannas**, None.

Presentation Number **P551**
Poster Session 3
September 7, 2012 / 15:15-15:15 / Room: The Liffey

# Use of multimodality molecular imaging in study of 188Re liposomal drugs on lung cancer bearing mice model

*Liang-Ting Lin[1], Chih-Hsien Chang[2], Te-Wei Lee[2], Chia-Che Tsai[2], Ren-Shyan Liu[3], Hsin-Ell Wang[1], **Yi-Jang Lee**[1], [1]Department of Biomedical Imaging and radiological Sciences, National Yang-Ming University, Taipei, Taiwan; [2]Institute of Nuclear Energy Research, Taoyuan, Taiwan; [3]School of Medicine, National Yang-Ming University, Taipei, Taiwan. Contact e-mail: yjlee2@ym.edu.tw*

According to the World Health Organization (WHO) world cancer reports, lung cancer is the most common cause of cancer death worldwide. Survival from lung cancer is poor and no effective screening is available. Clinically, more than 60% of the lung cancer-bearing patients are treated with chemotherapy. However, use of chemotherapy is usually accompanied by severe side effects because of low specificity and complications. Liposome embedded drugs have been developed for a long-term and specific accumulation in tumor. The enhanced permeability and retention (EPR) effect is a special condition caused by the immature blood vessel networks established by the tumor tissues. Drugs embedded in liposomes would pass through the immature vasculatures, and specifically accumulate inside the lesions. Here, we embedded doxorubicin in nanopegylated liposome, and conjugated with theragnostic radioisotope, rhenium-188, to test the treatment efficacy of human lung cancer in the preclinical model. Additionally, we have successfully established a platform for non-invasive imaging and tracking of human lung cancer in small animal by LT-3R, a lentiviral-based multicistronic reporter system containing green fluorescent protein (GFP), firefly luciferase (fLuc), and Herpes simplex virus 1-thymidine kinase (HSV1-tk). These reporter genes were used to demonstrate the relationship between the imaging results and tumor growth. Both orthotopic and xenograft model were established and monitored with bioluminescent signals by IVIS system. 123I-FIAU SPECT/CT imaging confirmed the anatomic localization of implanted tumors. Bio-distribution and pharmacokinetic results characterized the properties of liposomal drugs. The retention of 188Re activity in blood, spleen, and liver was observed. Tumor-to-muscle ratio was confirmed both in bio-distribution and SPECT/CT imaging, suggesting the nanopegylated liposome is dominant in uptaking of human lung cancer. In the near future, we will complete the whole study with therapeutic efficacy analysis on lung cancer animal model. These findings would be important for clinical trial in the future. In conclusion, this work is a study of using multiple reporter system as a preclinical platform for monitoring liposomal drug therapy.

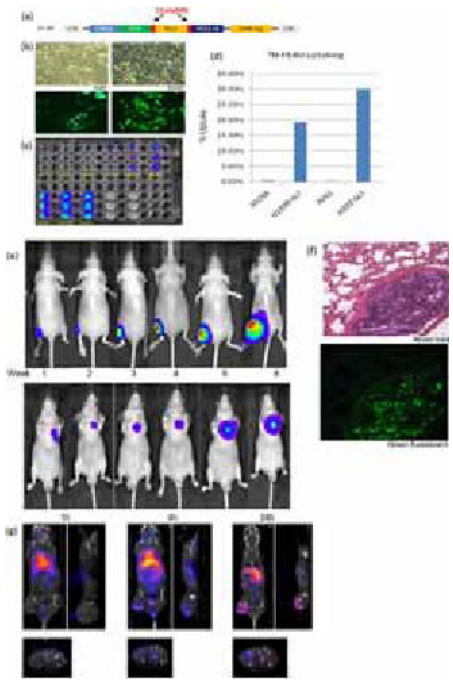

Disclosure of author financial interest or relationships:
**L. Lin**, None; **C. Chang**, None; **T. Lee**, None; **C. Tsai**, None; **R. Liu**, None; **H. Wang**, None; **Y. Lee**, None.

Presentation Number **P552**
Poster Session 3
September 7, 2012 / 15:15-15:15 / Room: The Liffey

# Multimodal hypoxia imaging in a preclinical glioma model

***Alessia Lo Dico***[1,2], *Sara Belloli*[3], *Cristina Martelli*[1], *Anna Degrassi*[4], *Micaela Russo*[4], *Silvia Valtorta*[3], *Umberto Gianelli*[5], *Delfina Tosi*[5], *Sergio Todde*[3], *Cristina Monterisi*[3], *Giovanni Lucignani*[1], *Rosa Maria Moresco*[3], *Luisa Ottobrini*[1,6], *[1]Dept of Biomedical Sciences and Technologies, Centre of Molecular and Cellular imaging-IMAGO, University of Milan, Milan, Italy; [2]Supported by a fellowship from the Doctorate School of Molecular Medicine, University of Milan, Milan, Italy; [3]IBFM-CNR, Technomed Found. and Dept. of Surgical Sciences, University of Milan Bicocca, Nuclear Medicine Dept. San Raffaele Scientific Institute, Milan, Italy; [4]Nerviano Medical Sciences, Nerviano (MI), Italy; [5]Dept. of Medicine Surgery and Dentistry, University of Milan, Milan, Italy; [6]Institute for Molecular Bioimaging and Physiology (IBFM), National Council of Researches (CNR), , Milan, Italy. Contact e-mail: alessia.lodico@unimi.it*

Introduction: Molecular imaging techniques allow early characterization of tumors and quantification of biological processes in vivo. The aim of our study is to analyze the relationship between tumor growth and tumor hypoxia in an orthotopic glioma murine model by using a multimodal procedure, and to compare the features of the different imaging techniques in revealing hypoxia induction. Materials and methods: Engineered U251 cells were gently provided by Dr. Giovanni Melillo, National Cancer Institute, Frederick (MD). These cells express the luciferase reporter gene under control of a constitutive promoter (U251-LUC) or under control of three copies of a Hypoxic Responsive Element (U251-HRE). Cells has been analyzed by means of three different approaches: 1) In vitro evaluation of transcriptional activation of HIF-1α at different times after deferoxamine (DFX) treatment by immunocytochemistry (ICC). 2) In vivo analysis of tumoral progression in orthotopic murine models obtained by stereotaxic injection of 105 glioma cells; animals were monitored weekly with BLI (CCD camera), PET ([18F]FDG,[18F]FAZA,[18F]FLT) and MRI to evaluate tumoral progression and hypoxia activation. 3) Ex vivo analysis by H&E staining and hypoxia markers (HIF-1α and CAIX) were performed. Results: In vitro studies showed no differences among the two cell lines as regards to HIF-1α activation kinetic with a peak of activation between 3 and 6h and a decrease at 20h. In vivo, U251-HRE model showed a detectable and progressive luciferase activity induction starting at 18 days from injection demonstrating that luminescence expression is dependent on HRE-mediated activation. On the other hand, in U251-LUC model luciferase activity was detectable immediately after injection and remained proportional to tumor growth. Lesions were highly proliferative ( [18F]FLT) but hypo-metabolic ([18F]FDG). In partial agreement with the results of U251-HRE, a hypoxia dependent [18F]FAZA uptake was observed at later times (30 days). MRI provided morphological characterization and diffusion studies showed hypoxic necrotic areas only at later days. Ex vivo H&E staining demonstrates that tumors were characterized by nuclear atypia, brisk mitotic activity, microvascular proliferation and necrosis. HIF-1α and CAIX were clearly expressed in hypoxic areas, especially in the inner part of the tumor. Conclusions: This study demonstrates that the U251-HRE orthotopic murine model may be proposed as a predictive and reliable tool to evaluate hypoxia dependent processes of human glioma in preclinical studies by BLI. Differences among the three imaging techniques may be related to methods sensitivity. Further ex vivo post mortem measurements of HIF-1α and CAIX at earlier times will be performed. Additional studies will be conducted to understand the clinical meaning of early or delayed hypoxia identification in terms of response to treatment. References: SEMENZA GL. Curr Opin Cell Biol 13(2):167-71, 2001. Review. RAPISARDA A. Cancer Research 62, 4316-4324, 2002

Disclosure of author financial interest or relationships:
**A. Lo Dico**, None; **S. Belloli**, None; **C. Martelli**, None; **A. Degrassi**, None; **M. Russo**, None; **S. Valtorta**, None; **U. Gianelli**, None; **D. Tosi**, None; **S. Todde**, None; **C. Monterisi**, None; **G. Lucignani**, None; **R. Moresco**, None; **L. Ottobrini**, None.

Presentation Number **P553**
Poster Session 3
September 7, 2012 / 15:15-15:15 / Room: The Liffey

# Ultrasound-Guided Photoacoustic Sentinel Lymph Node Mapping using Silica-Coated Gold Nanoplates

***Geoffrey Luke***[1], *Ashvin Bashyam*[2], *Kimberly A. Homan*[2], *Stanislav Y. Emelianov*[1,2], [1]*Electrical and Computer Engineering, University of Texas at Austin, Austin, TX, USA;* [2]*Biomedical Engineering, University of Texas at Austin, Austin, TX, USA. Contact e-mail: geoffluke@utexas.edu*

Many types of cancer, including breast, oral, and skin cancers, metastasize through the lymphatic system. Identifying the metastatic state for the sentinel lymph node (SLN) is critical for staging and treatment planning. Current methods require an invasive biopsy and often include the use of radioactive colloids. Photoacoustic (PA) imaging can be used to guide and minimize the invasiveness of the procedure by providing high resolution images of the SLN. We have developed a new PA imaging contrast agent, silica-coated gold nanoplates (Si-Au NPs), for use in PA image-guided SLN biopsy. These particles exhibit a five-fold increase in optical absorption over gold nanorods and can be easily tuned to absorb optical wavelengths of 1064 nm, where light penetration in tissue is greatest and inexpensive lasers are widely available. Furthermore, the silica coating adds stability and enhances the PA signal. Gold nanoplates were synthesized using a seed-mediated growth method. The nanoplates were isolated from nanospheres via selective precipitation. Next, the nanoplates were coated with polyethylene glycol and a thin silica layer was added via a modified Stöber method. Transmission electron microscopy and ultraviolet-visible spectrophotometry were used to characterize the Si-Au NPs, showing an average edge length of 100 nm, an average thickness of 7 nm (panel a), and an absorption peak near 1064 nm. The Si-Au NPs were sterilized via ultraviolet irradiation and 40 µL were injected submucosally into the tongue of Nu/Nu immunodeficient mice. The particles drained through the lymphatics to the mandibular lymph nodes. High frequency ultrasound and PA imaging were performed in the region surrounding the SLN before and at various time points after Si-Au NP injection. Representative images are shown in panels b and c. The low background signal from endogenous chromophores at 1064 nm demonstrates that AuNPs are the primary source of PA signal. Results show the Si-Au NPs drained to the SLN within the first 5 minutes, then diffused throughout the SLN over the course of the next 3 - 4 hours. The Si-Au NPs exhibited a strong signal at up to 48 hours after the injection, suggesting slow clearance. In addition, the Si-Au NPs remained stable after 5 hours of cumulative imaging. These results suggest that Si-Au NPs, when coupled with PA imaging, could be used as a noninvasive alternative to biopsies to locate and evaluate the SLN for cancer staging. These particles could also be used as localized heating agents for PA image-guided photothermal therapy for noninvasive ablation of the lymph node, thus removing the necessity for surgery.

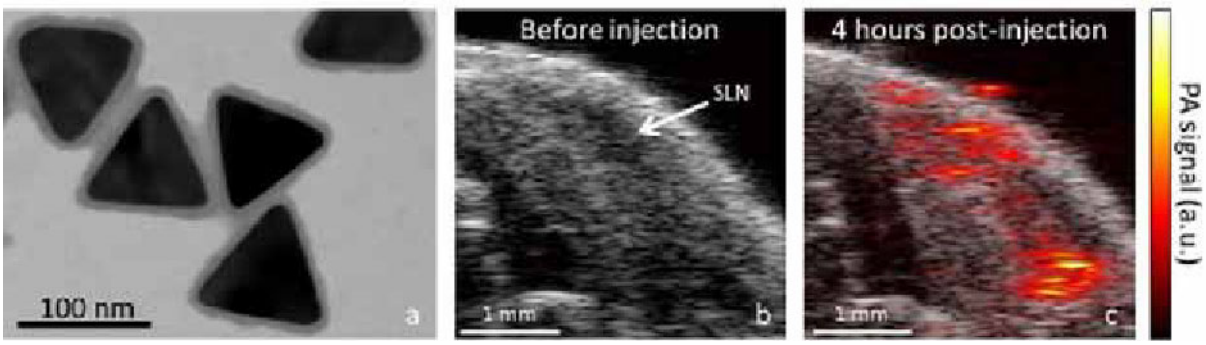


Disclosure of author financial interest or relationships:
**G. Luke**, None; **A. Bashyam**, None; **K.A. Homan**, None; **S.Y. Emelianov**, None.

Presentation Number **P554**
Poster Session 3
September 7, 2012 / 15:15-15:15 / Room: The Liffey

# Different anesthetics impact tumor hypoxia and muscle oxygenation

***Moritz Mahling***[1], *Kerstin Fuchs*[1], *Florian C. Maier*[1], *Bernd J. Pichler*[1], *Manfred Kneilling*[1,2], [1]*Department for Preclinical Imaging and Radiopharmacy, University of Tuebingen, Tuebingen, Germany;* [2]*Department of Dermatology, University of Tuebingen, Tuebingen, Germany. Contact e-mail: moritz.mahling@med.uni-tuebingen.de*

Tumor hypoxia is an indicator for tumor progression and poor prognosis. Techniques to detect tumor hypoxia include 18F-fluoro-azomycine arabinoside (18F-FAZA), a positron emission tomography (PET) biomarker for non-invasive in vivo detection of hypoxic tumor regions and oxygen probe systems for invasive in vivo hypoxia measurements. In recent studies we showed significant differences in physiologic parameters and 18F-FAZA uptake between mice breathing room air (21% O2) or pure oxygen. The aim of this study was to investigate the impact of different anesthetics on 18F-FAZA uptake and fluorescence based pO2 probe measurements in muscle tissue and carcinomas of room air or 100% O2-breathing mice. We inoculated CT26 colon carcinomas subcutaneously at the upper flank of female BALB/c mice and performed in vivo studies 12-15 days afterwards. In experiments mice spontaneously breathed room air (21% oxygen) or 100% O2 starting 30 minutes before and during isoflurane (I, 1.5%) or ketamine/xylazine (K/X, 100 and 5 mg/kg) anesthesia. In littermates of one experimental group we placed a pO2 probe (OxyLite, Oxford Optronix, Oxford, UK) in the center of the CT26 colon carcinoma and a second probe in the gastrocnemius muscle. After a 10 minute calibration period we recorded pO2 values for 60 minutes. A second experimental group of CT26 colon carcinoma bearing mice was investigated by 10 min static PET scans 1h, 2h and 3h after 18F-FAZA injection. Tumor to muscle ratios (t/m) were calculated by drawing spheres (r = 2.0 mm) around the hottest tumor voxel and in the contralateral muscle tissue using PMOD software. Invasive pO2 probe measurements in air breathing mice showed a significant lower mean tumor pO2 (1.0 ± 0.11 mmHg) and mean muscle pO2 (33.8 ± 3.06 mmHg) during ketamine/xylazine compared to isoflurane anesthesia (isoflurane: tumor: 2.4 ± 1.98 mmHg, p = 0.0136; muscle: 57.4 ± 2.72 mmHg, p = 0.0009, n = 8). Analysis of oxygen breathing mice revealed an equivalent tendency towards a reduced pO2 in tumor (11.4 ± 3.33 mmHg) and muscle tissue (85.5 ± 7.44 mmHg) of ketamine/xylazine anesthetized mice (isoflurane: tumor: 17.4 ± 7.89 mmHg, muscle: 102.1 ± 10.02 mmHg, n = 8 - 9). PET measurements 3h after 18F-FAZA injection displayed significant increased tumor/muscle ratios in ketamine/xylazine anesthetized mice compared to isoflurane anaesthetized room air or 100% oxygen breathing mice (air: 7.0 ± 0.99 (K/X) vs. 2.0 ± 0.33 (I), p < 0.0001, n = 8-12; oxygen: 4.3 ± 0.43 (K/X) vs. 1.7 ± 0.23 (I), p = 0.02, n = 8-9). Ketamine/Xylazine anaesthesia caused reduced tumor and muscle pO2 levels (invasive probe measurements) and an increased t/m ratio (non-invasive PET studies) compared to isoflurane anaesthesia. Our studies demonstrate the strong impact of different anesthetics and breathing regimes on in vivo hypoxia measurements. Consecutive studies have to be conducted to investigate the spatial and temporal correlation of these different techniques in order to establish a gold standard for hypoxia imaging.

Disclosure of author financial interest or relationships:
**M. Mahling**, None; **K. Fuchs**, None; **F.C. Maier**, None; **B.J. Pichler**, Siemens, Grant/research support; AstraZeneca, Grant/research support; Bayer Healthcare, Grant/research support; Boehringer-Ingelheim, Grant/research support; Oncodesign, Grant/research support; Merck, Grant/research support; Bruker, Grant/research support; **M. Kneilling**, None.

Presentation Number **P555**
Poster Session 3
September 7, 2012 / 15:15-15:15 / Room: The Liffey

# Bioluminescence and fluorescence imaging in the detection of response to near infrared photoimmunotherapy: Immediate effects in an orthotopic breast cancer model

***Makoto Mitsunaga***[1], *Takahito Nakajima*[1], *Kohei Sano*[1], *Gabriela Kramer-Marek*[2], *Peter Choyke*[1], *Hisataka Kobayashi*[1], [1]*Molecular Imaging Program, NCI/NIH, Bethesda, MD, USA;* [2]*Radiation Oncology Branch, NCI/NIH, Bethesda, MD, USA. Contact e-mail: mit@jikei.ac.jp*

Targeted cancer therapies offer the promise of more effective tumor control with fewer side effects than conventional cancer therapies. We recently reported a new type of monoclonal antibody (mAb)-based immunotherapy (photoimmunotherapy; PIT) that utilizes a mAb conjugated with a near infrared (NIR) phthalocyanine dye, IRDye700DX (IR700). IR700 is not only phototoxic, but also fluorescent, and thus can be used as a theranostic imaging agent. *In vitro* molecular target-specific cell death occurs during NIR light exposure in cells previously incubated with mAb-IR700 conjugates. However, documenting rapid cell death *in vivo* is difficult because there are no immediate changes in tumor size. The aim of this study was to monitor the effect of mAb-IR700 mediated PIT with bioluminescence and fluorescence imaging. Luciferase-transfected breast cancer cells (MDAMB-468luc, epidermal growth factor receptor, EGFR/HER1, positive) were used for both *in vitro* and *in vivo* experiments. After validation of target-specific phototoxicity with NIR light exposure up to 8 J/cm$^2$ *in vitro*, we employed a bilateral orthotopic breast cancer model using MDA-MB-468luc tumors in female athymic mice. Mice received intravenous EGFR-targeting panitumumab-IR700 conjugate. One side was shielded from NIR light, while the other was treated with NIR light ranging from 50 to 150 J/cm$^2$. Bioluminescence imaging (BLI) and fluorescence imaging (FLI) were performed before and after NIR light exposure. NIR light dose-dependent cell killing was successfully monitored by the BLI signal *in vitro*. Although tumor sizes were unchanged, BLI signals decreased by >95% immediately after PIT *in vivo* when NIR light intensity was high (>100 J/cm$^2$), however, in mice receiving lower intensity (50 J/cm$^2$), tumors recurred with gradually increasing BLI signal. *In vivo* FLI showed decreased intensity in the treated tumor and showed a halo of increased intensity around the tumor indicating the release of IR700 from necrotic cells. Thus, PIT can be shown to induce massive cell death immediately after exposure of NIR light as demonstrated with *in vivo* BLI and FLI.

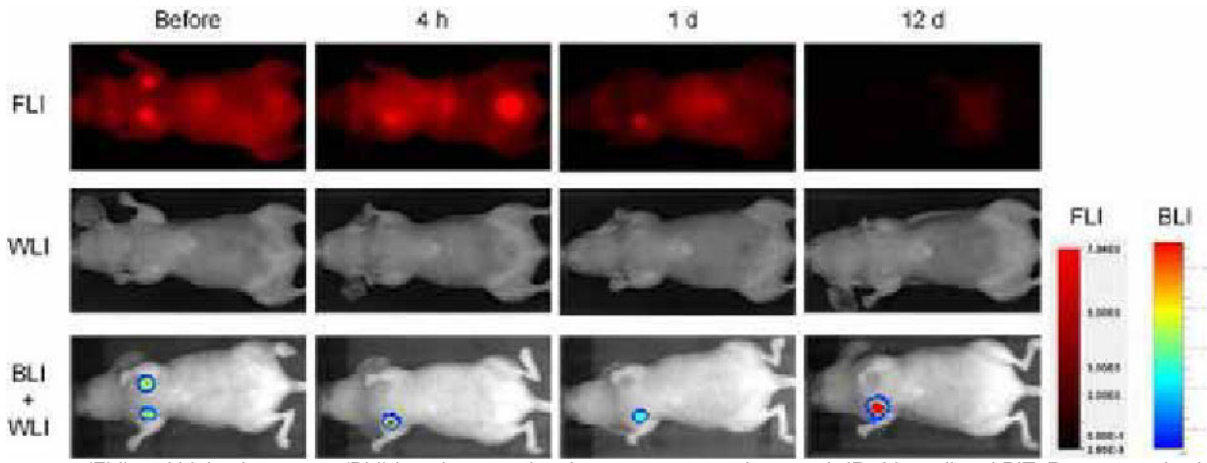


IR700 fluorescence (FLI) and bioluminescence (BLI) imaging over time in response to panitumumab-IR700 mediated PIT. Representative images were shown. Before: just before NIR light treatment.

Disclosure of author financial interest or relationships:
**M. Mitsunaga**, None; **T. Nakajima**, None; **K. Sano**, None; **G. Kramer-Marek**, None; **P. Choyke**, GE Healtcare, Grant/research support; Philips Medical Systems, Grant/research support; Siemens Healthcare, Grant/research support; **H. Kobayashi**, None.

Presentation Number **P556**
Poster Session 3
September 7, 2012 / 15:15-15:15 / Room: The Liffey

# Quantitative imaging of tumor vascularization by 3D ultrasound contrast-enhanced imaging: role of liposomes and microbubbles

***Filippo Molinari***[1], *Kristen M. Meiburger*[1], *Pierangela Giustetto*[2], *Cinzia Boffa*[2], *Enzo Terreno*[2], *Mauro Castano*[3], [1]*Department of Electronics and Telecommunications, Politecnico di Torino, Torino, Italy;* [2]*Molecular & Preclinical Imaging Center, University of Torino, Torino, Italy;* [3]*Bracco Research Center, Colleretto Giacosa (TO), Italy. Contact e-mail: filippo.molinari@polito.it*

Contrast-enhanced ultrasound imaging (CEUS) has proven effective in assessing the vascularization of tumors in-vivo. Unlike perfusion studies, which are mainly focused on blood flow changes in time, 3D CEUS allows an accurate reconstruction of tumor vascular pattern. Traditional contrast agents consist of gas-filled microbubbles, which do not extravasate but have limited duration. The aim of this study was to compare tumor vascular patterns as assessed by 3D CEUS when using traditional microbubbles and water-filled liposomes. We tested 7 C57Bl6 mice (10 weeks old, weight 23±4 gr). Syngeneic tumor cells (melanoma B16) were subcutaneously grafted in the rear thigh. Using a VisualSonics VEVO2100 equipped with a 24-MHz probe, traditional high-resolution (HR) US images were acquired, along with 3D CEUS images of the tumor. First we acquired a basal 3D image of the lesion (without any contrast). Then we injected a 50 µl bolus of non-targeted Vevo MicroMarker (Bracco, Geneve) optimized for use on the Visualsonics HR Micro-Ultrasound System. The bolus of contrast agent was followed by the injection of 40 µl of saline solution. We waited for the complete destruction of the microbubbles (about 30 minutes) and then injected a 200 µl bolus of stealth liposomes (DSPC encapsulated with a 300 mM solution of the clinically approved MRI agent Gd-HPDO3A). The mean liposomes diameter was 157 nm and the Gd3+ concentration was 12.7 mM. The 3D CEUS images were intensity normalized and then the bright microbubbles were segmented by using Otsu's thresholding. The obtained mask was reduced by a combination of distance transform and morphological skeletons. This operation reduced the blooming due to the contrast agent interaction with ultrasounds while maintaining the correctness of the spatial distribution of the vascular tree. Once skeletonized, the resulting 3D representation was analyzed in order to extract 7 descriptors of the vascular pattern: the number of vascular trees, number of branches, vessel radius, vascular density, 2D tortuosity, 3D tortuosity, number of vascular flexes. Fig 1 shows the 3 sets of images we acquired during a single experiment. The left column is relative to the pre-contrast CEUS images, the middle to the liposome CEUS, and the right to the microbubbles CEUS. The top row depicts the raw CEUS image (one slice of the volume), the middle the corresponding skeleton slice, and the bottom the volume rendering of the skeleton. Table 1 reports the 7 parameters we measured on the skeletons. Although contrast is much higher with microbubbles than liposomes (Fig 1), some the skeleton parameters calculated from the liposome CEUS images are consistent with those calculated using microbubbles. The number of vascular trees and all the tortuosity measurements do not vary when using liposomes or microbubbles. The asterisks in Table 1 show the parameters that were not statistically different between liposomes and microbubbles CEUS skeletons (Students' paired t-test, 95% confidence level). Since liposomes are used for cancer therapy and drug delivery, we believe that they could also be used for a quantification of the tumor vascularization changes.

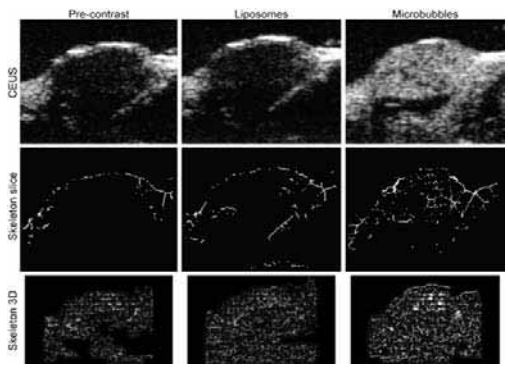


CEUS image (first row), corresponding skeleton (second row), and 3D reconstructed vascular skeleton (bottom row) of the same tumor in three conditions: pre-contrast (first column), after liposomes bolus (second column), and after microbubbles bolus (third column).

Skeleton vascular parameters

| | | | | | | | |
|---|---|---|---|---|---|---|---|
| Pre-contrast | 19±2 | 0.002±0.001 | 98±10 | 2.75±1.00px | 102±31.12* | 4.30±0.90 | 3.67±1.14* |
| Liposomes | 22±1 | 0.012±0.010 | 175±1.10 | 3.67±1.10 | 15.50±1.23 | 6.90±0.83 | 6.33±2.33 |
| Microbubbles | 23±2 | 0.014±0.010 | 206±5 | 5.74±1.43px | 15.7±1.43 | 7.01±0.76 | 6.66±2.45* |

Disclosure of author financial interest or relationships:
**F. Molinari**, None; **K.M. Meiburger**, None; **P. Giustetto**, None; **C. Boffa**, None; **E. Terreno**, Bracco Imaging, Consultant; **M. Castano**, None.

Presentation Number **P557**
Poster Session 3
September 7, 2012 / 15:15-15:15 / Room: The Liffey

# FLT can early reflect response of tumor proliferation to multikinase inhibitor (sorafenib) treatment in a human renal cell carcinoma xenograft: comparison with Ki-67

*Masahiro Murakami, Songji Zhao, Yan Zhao, Nusrat Fatema Chowdhury, Wenwen Yu, Ken-ichi Nishijima, Mitsuyoshi Takiguchi, Nagara Tamaki,* ***Yuji Kuge****, Hokkaido University, Sapporo, Japan. Contact e-mail: kuge@ric.hokudai.ac.jp*

Introduction: Sorafenib, a small molecule multikinase inhibitor, has been approved for treating renal cell carcinomas (RCCs). The action mechanisms are considered to be mediated through its effects on angiogenesis including VEGFR and PDGFR and tumor proliferation including Raf/MEK/ERK. However, response of tumor proliferation after sorafenib treatment has yet to be clarified. 18F-fluorothymidine (FLT) PET which reflects thymidine kinase-1 activity is one of the tumor proliferation markers, and may play an important role to assess early response of tumor proliferation after cancer therapy. Ki-67 labeling index is another proliferation marker which is a reliable tumor prognostic marker with biopsy samples or excised tumor tissues. The early identification of therapeutic response to sorafenib is indispensable for selecting optimal individual treatment strategy, but no reliable predictors are clinically available yet. Thus, we assessed whether FLT can early evaluate tumor proliferation status after sorafenib treatment in a human RCC xenograft, and compared the results with Ki-67 labeling index. Materials & methods: Human RCC xenograft (A498) was established in nude mice, and evaluation of 3H-FLT uptake, the tumor growth curve, and histochemical staining of Ki-67 were performed. Mice were assigned to control and sorafenib treatment groups. Mice in the treatment groups were treated with sorafenib (80 mg/kg, p.o.). On day 1, 2, 3, and 7 after sorafenib treatment, mice were sacrificed 2 hours after 3H-FLT injection. Tumor volumes were measured every day from start of the treatment. Results: 3H-FLT uptakes (%ID/g/kg) in the tumor were significantly increased by 6.6-, 5.4-, 3.3- and 3.2-fold on day 1, 2, 3 and 7 after treatment with sorafenib respectively, compared with control groups (0.014±0.004 and 0.093±0.024 on day 1 ($P < 0.01$), 0.019±0.006 and 0.103±0.031 on day 2 ($P < 0.01$), 0.030±0.012 and 0.100±0.021 on day 3 ($P < 0.01$), and 0.023±0.006 and 0.073±0.019 on day 7 ($P < 0.05$) in the control and the treatment groups, respectively). Ki-67 labeling indexes in the tumor were significantly increased by 1.2-fold on day 2 and 3 after treatment with sorafenib, respectively, compared with control groups. No significant change in tumor sizes was observed between pre- and post-treatment with sorafenib. Discussion: Surprisingly, both proliferation marker (3H-FLT uptake & Ki-67 index) increased after sorafenib treatment in RCC xenograft, although tumor size did not change. Unfortunately, the details of the mechanism were unknown. Grepin et al. also showed activation of tumor proliferation with increased pEGFR after antiangiogenic therapy by bevacizumab in RCC xenograft. The antiangiogenic therapy including sorafenib may increase tumor proliferation in RCC xenograft, although further investigation on the mechanism is required. Conclusion: 3H-FLT uptake in the tumor was dramatically increased after 1-day treatment of sorafenib in RCC xenograft. Ki-67 index was also slightly increased. These results indicate that FLT can sensitively reflect early response of tumor proliferation to multikinase inhibitor treatment with sorafenib in a human RCC xenograft.

Disclosure of author financial interest or relationships:
**M. Murakami**, None; **S. Zhao**, None; **Y. Zhao**, None; **N. Chowdhury**, None; **W. Yu**, None; **K. Nishijima**, None; **M. Takiguchi**, None; **N. Tamaki**, None; **Y. Kuge**, None.

Presentation Number **P558**
Poster Session 3
September 7, 2012 / 15:15-15:15 / Room: The Liffey

# Mathematical Modeling of the Sequence of and Interactions Between Cellular Programs in Response to Oncogene Inactivation Measured by Bioluminescence Imaging

***Chinyere I. Nwabugwu***[1,2], *Dean W. Felsher*[3], *David Paik*[1], [1]*Radiology, Stanford University, Stanford, CA, USA;* [2]*Electrical Engineering, Stanford University, Stanford, CA, USA;* [3]*Medicine, Stanford University, Stanford, CA, USA. Contact e-mail: chinyere@stanford.edu*

Purpose: In some tumors, the inactivation of MYC alone is adequate to induce sustained tumor regression, a phenomenon known as oncogene addiction. The response in different tumor types (T-cell acute lymphoblastic leukemia, osteosarcoma, and hepatocellular adenocarcinoma) involves different combinations of cellular programs such as proliferative arrest, apoptosis, senescence and the inhibition of angiogenesis. Some of the programs are cell intrinsic while others are modulated through the host immune system. We have created a mathematical model that captures the tumor growth kinetics as a function of these different cellular programs. Materials and Methods: We created a new mathematical model of tumor growth/regression kinetics incorporating cell intrinsic mechanisms (apoptosis, proliferative arrest, differentiation/dormancy) and immune-mediated cell extrinsic mechanisms (senescence and anti-angiogenesis). The stochastic model consists of 10 cellular states (MYC on, MYC off, undergoing apoptosis, proliferating, differentiated, senescent, etc.) with probabilistic transitions and the ability to control the expression of transgenic MYC using the tetracycline system. We have performed simulations of the three tumor types under varying conditions (immunosuppression, varying relapse rates, etc). We compiled data from a number of published studies on these three tumor types consisting primarily of in vivo bioluminescence imaging. Results: After running simulations, our model recapitulates features such as the different rates and delays in the tumor kinetics measured from in vivo experimental data from mouse models. Several emergent behaviors of the model have come to light. Empirically, proliferation immediately follows oncogene inactivation but there is a 4-5 day delay in apoptosis. A chain of sub-states from commitment to apoptosis to actual cell death exhibits this behavior. Furthermore, the per-cell rate of tumor relapse had almost no bearing on the time to relapse. The rate governing mutations leading to the transition from MYC off to escaped had little effect on deterministic simulations but a significant effect on our stochastic model. Empirically, the regression kinetics had little variability while the relapse growth kinetics showed greater variability. Our stochastic model exhibited this same behavior. Conclusion: The initial results from our new model are helping to uncover the sequence of and interaction between cellular mechanisms involved in tumor response to oncogene inactivation such as might be encountered using targeted therapeutics, which will eventually help to optimize treatment. Our model is simple, consisting of only time-homogeneous transitions of cells that are statistically independent, and yet is able to recapitulate the complex response of tumors to oncogene inactivation.

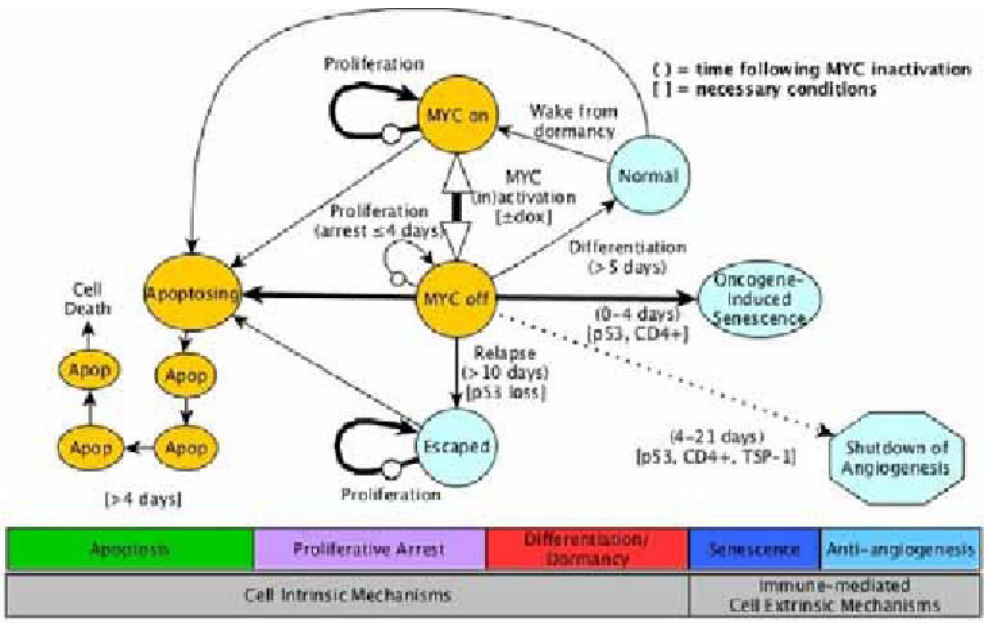


Stochastic Model of Tumor Response to Oncogene Inactivation

Disclosure of author financial interest or relationships:
**C.I. Nwabugwu**, None; **D.W. Felsher**, None; **D. Paik**, None.

Presentation Number **P559**
Poster Session 3
September 7, 2012 / 15:15-15:15 / Room: The Liffey

# A novel method to quantify IRDye800CW-fluorescent probes in tissue distribution studies

***Sabrina Oliveira***[1,2], *Ruth Cohen*[3], *Marijke Stigter van Walsum*[3], *Guus A. van Dongen*[3], *Sjoerd G. Elias*[4,5], *Paul J. van Diest*[2], *Willem Mali*[4], *Paul van Bergen en Henegouwen*[1], [1]*Department of Biology, Utrecht University, Utrecht, Netherlands;* [2]*Department of Pathology, University Medical Center Utrecht, Utrecht, Netherlands;* [3]*Departments of Otolaryngology/Head and Neck Surgery and Nuclear Medicine and PET Research, VU University Medical Center, Amsterdam, Netherlands;* [4]*Department of Radiology, University Medical Center Utrecht, Utrecht, Netherlands;* [5]*Julius Center for Health Sciences and Primary Care, University Medical Center Utrecht, Utrecht, Netherlands. Contact e-mail: s.oliveira@uu.nl*

Recent advances in near-infrared imaging technologies have enabled further developments of probes for optical molecular imaging1-3. In view of new developments of probes for screening of patients or improved diagnosis of cancer, new assays are currently needed at the preclinical level. Namely, a lack of accurate quantification of fluorescent probes in tissues for biodistribution studies is still a matter of concern. This fact is due to the possibility of quenching of the fluorescence when fluorophores are closely located and the scattering of photons by tissue components. Studies thus far only present a relative appreciation of fluorescence accumulated at the organs, by imaging whole organs with the same imaging systems used for living mice4,5. These are far from ideal and the information obtained cannot be expressed as percentage of injected dose per gram of tissue (% ID/g). Alternatively, one could employ radiolabeling to enable biodistribution studies, but this could alter the probe and is not the ideal route to take during development of probes for optical imaging6. Here we describe a new method for quantification of IRDye800CW-fluorescent probes in tissues and we compare this new method with the generally used method that employs a gamma counter for quantification of PET tracers. This new method circumvents the issues abovementioned through homogenization of the organs and dilution of the lysates, in order to infer in the linearity range of fluorescence. To this end, the monoclonal antibody cetuximab was conjugated to both the near-infrared fluorophore IRDye800CW and the PET tracer zirconium (89Zr). This dual-labeled probe was injected in nude mice bearing A431 human tumor xenografts and 24 h post injection, organs and tumors were collected. For direct comparison of the two methods, each of these organs and tumors was halved in order to apply both methods to the same organ. Importantly, tumor uptake determined by IR-quantification resulted in 15.1 ± 3.7 % ID/g, while gamma ray-quantification resulted in 13.9 ± 2.6 % ID/g. These results show that, although small variations were observed, the quantification of IR-fluorescence yields comparable results to the ones obtained based on gamma rays quantification. In conclusion, the novel method for quantification of IRDye800CW is here compared to the traditional gamma quantification of zirconium, giving similar results in % ID/g. This new method is considered very useful in the context of the development of IR-fluorescent probes for optical molecular imaging, giving the possibility to accurately quantify fluorescent probes in tissues7. Acknowledgements This research was supported by the Center for Translational Molecular Medicine (MAMMOTH) References (1)Hillman, E. M. et al. Philos Transact A Math Phys Eng Sci 2011, 369, 4620-43; (2)Ntziachristos, V. Philos Transact A Math Phys Eng Sci 2011, 369, 4666-78; (3)Keereweer, S. et al. Curr Pharm Biotechnol 2012, 13, 498-503; (4)Gong, H. et al. Neoplasia 2010, 12, 139-49; (5)Hou, Y. et al J Nanobiotechnology 2010, 8; (6)Cohen, R. et al. EJNMMI 2011, 1, 31; (7)Oliveira, S. et al. Mol Imaging 2012, 11, 33-46.

Disclosure of author financial interest or relationships:
**S. Oliveira**, None; **R. Cohen**, None; **M. Stigter van Walsum**, None; **G.A. van Dongen**, None; **S.G. Elias**, None; **P.J. van Diest**, None; **W. Mali**, None; **P. van Bergen en Henegouwen**, None.

Presentation Number **P560**
Poster Session 3
September 7, 2012 / 15:15-15:15 / Room: The Liffey

# The optical imaging of enhanced tumor targeting by surface engineered Salmonella typhimurium

***Seung-Hwan Park***[1,2], *Deok-Mi Kim*[1,2], *Hee-Seung Bom*[2], *Hyon E. Choy*[3], *Jung-Joon Min*[1,2], [1]*In Vivo Molecular Imaging, Chonnam National University, Gwangju, Republic of Korea;* [2]*Nuclear medicine, Chonnam National University, Gwangju, Republic of Korea;* [3]*Microbiology, Chonnam National University, Gwangju, Republic of Korea. Contact e-mail: biocell75@gmail.com*

We previously reported that certain strains of bacteria could target and proliferate in tumor. The bacteria have been applied for specific delivery of protein drugs to tumor. However, targeting efficiency showed variable depending on tumor types. Thus, we employed bacterial surface engineering to enhance targeting efficiency. In this study, we displayed specific peptide sequence (ACDCRGDCFCG; cyclic RGD sequence) in the external loop of outer membrane protein A (OmpA) of attenuated Salmonella typhimurium (mSL) to explore the changes of bacterial tropism for tumor cells. We constructed expression vector encoding fusion protein with OmpA and specific (cyclic RGD-ompA) or scrambled peptides (as a control) that are controlled by inducible promoter (pBAD) to transform mSL (mSL-rgd). The Western blot analysis showed successful expression of cyclic RGD-ompA in mSL-rgd. Under the microscopic analysis, mSL-rgd had significantly higher activity accumulation in integrin-positive cancer cells (U87MG and MDA-MB-435) but not in integrin-negative tumors (MCF-7 cells) compared with mSL-aaa and also co-localized on the surface of U87MG and MDA-MB-435 cells. Tumor accumulation of mSL-rgd could be effectively blocked by synthetic cyclic RGD peptide in αvβ3-positive cells, suggesting αvβ3 specificity of mSL-rgd in vitro. In order to monitor in vivo distribution of the bacteria, the bacteria strain was further transduced with bacterial luciferase (Lux) operon using p22 bacteriophage (mSL-rgd-lux). In vivo bioluminescence imaging showed strong targeting efficiency of mSL-rgd-lux in U87MG-bearing nude mice and MDA-MB-435-bearing nude mice as compared to mSL-lux and mSL-aaa-lux. In the tumor tissue, photon flux from mSL-rgd-lux was found to be approximately one thousand-fold higher than that from mSL-lux. Bacterial viable counting also revealed significant improvement of tumor accumulation of mSL-rgd-lux (10,000 fold) than mSL-lux. The mSL-rgd-lux remained in tumor over 20 days as is confirmed by optical imaging and histological analysis. Therapies with mSL-rgd-lux resulted in significant tumor shrinkage and even complete disappearance in mice with MDA-MB-435 breast cancer. We successfully engineered tumor-targeting bacterial strain that showed higher targeting accumulation by using surface display of RGD in OmpA. The surface engineered bacteria have a potential to deliver higher amount of protein drugs and to target tumor more efficiently.

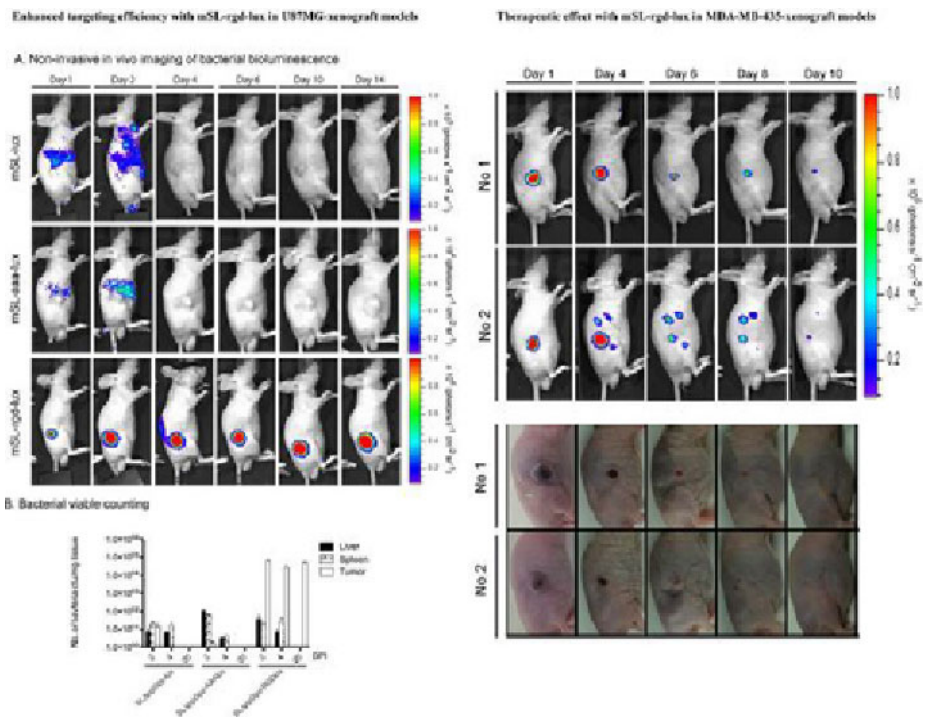


Disclosure of author financial interest or relationships:
**S. Park**, None; **D. Kim**, None; **H. Bom**, None; **H. Choy**, None; **J. Min**, None.

Presentation Number **P561**
Poster Session 3
September 7, 2012 / 15:15-15:15 / Room: The Liffey

# In-vivo imaging of Cancer using targeted Nanoparticles

***Apurva Patel***[1], *Ed Lim*[3], *Ning Zhang*[3], *Kevin Francis*[2], *Rajendra Singh*[2,3], *Mandip Sachdeva*[1], [1]*Pharmaceutical Sciences, Florida A & M University, Tallahassee, FL, USA;* [2]*Preclinical Imaging, Caliper- a PerkinElmer Company, Alameda, CA, USA;* [3]*In Vivo Imaging R&D, Caliper- a PerkinElmer Company, Alameda, CA, USA. Contact e-mail: apurvapatel85@gmail.com*

Purpose: Cancer is one of the leading causes of deaths (7.6 million deaths annually) worldwide. One approach in the treatment of cancer that has generated interest in recent years is the use of novel drugs that selectively inhibit tumor blood supply, thus controlling cancer cell survival, proliferation and/or metastasis, used in combination with conventional anticancer or antiangiogenic drugs. The objectives of this study are: 1) to formulate tumor homing pegylated CREKA peptide coated nanoparticles of DIM-P (PCNCs-D), in conjunction with versions that contain D-luciferin (PCNCs-Dl), XenolightDiR (PCNCs-Di), or both reagents in combination (PCNCs-Dc), 2) In-vivo imaging of tumor progression / tumor vasculature and tracking of the nanoparticle delivery system. Methods: Nanoparticles were prepared with DIM-P (NCs-D)/ D-luciferin (NCs-Dl)/XenolightDiR(NCs-Di), Compritol, Miglyol, DOGS-NTA-Ni and sodium taurocholate, using a high pressure homogenizer (Nano-DeBEE). PCNCs-D and PCNCs-Dl/PCNCs-Di/PCNCs-Dc were prepared by conjugating NCs-D and NCs-Dl/ NCs-Di with 6His-PEG2K-CREKA peptide, and then characterized for physical properties and binding efficiency. Pharmacokinetic parameters of formulations were evaluated in BALB/c mice. In-vivo imaging of tumors and tracking of nanoparticles was carried out with an IVIS® Spectrum CT (Caliper life Sciences), using bioluminescence (luciferin) and fluorescence (Xenolight DIR), following I.V. / I.P. delivery of nanocarriers. Results: Particle size of PCNCs-D was 190-200 nm. The PCNCs-D formulation showed an initial burst release followed by a slow release up to 72 hr (90%) of DIM-P. PCNCs-D showed ($p<0.001$) 8 fold higher binding to the clotted plasma proteins compared to NCs-D. Pharmacokinetic parameters showed that nanoparticle increased luciferin accumulation in tumors with half-life of 4.64 ± 0.39 hr. PCNC-Dc allowed us to track and visualize migration in tumors of these nanoparticles by use of IVIS system. In-vivo imaging following exposure of PCNCs-Dl/PCNCs-Di revealed the tumor environment and tumor vasculature, where the PCNCs-Di were found to migrate more in newly formed vasculature and Total Radiant Efficiency [p/s] / [$\mu W/cm^2$] was $2.1*10^{12} \pm 0.5*10^{12}$ over the period of 0.5 hr to 3hr while NCs-Di didn't show any specific migration and Total Radiant Efficiency [p/s] / [$\mu W/cm^2$] was $0.6*10^{11} \pm 0.18*10^{11}$. Conclusion: The results emanating from these studies demonstrate the potential of nanoparticles for increasing the duration of substrate activated luminescence and the role of PCNCs as effective tumor homing imaging/drug delivery systems for cancer treatment.

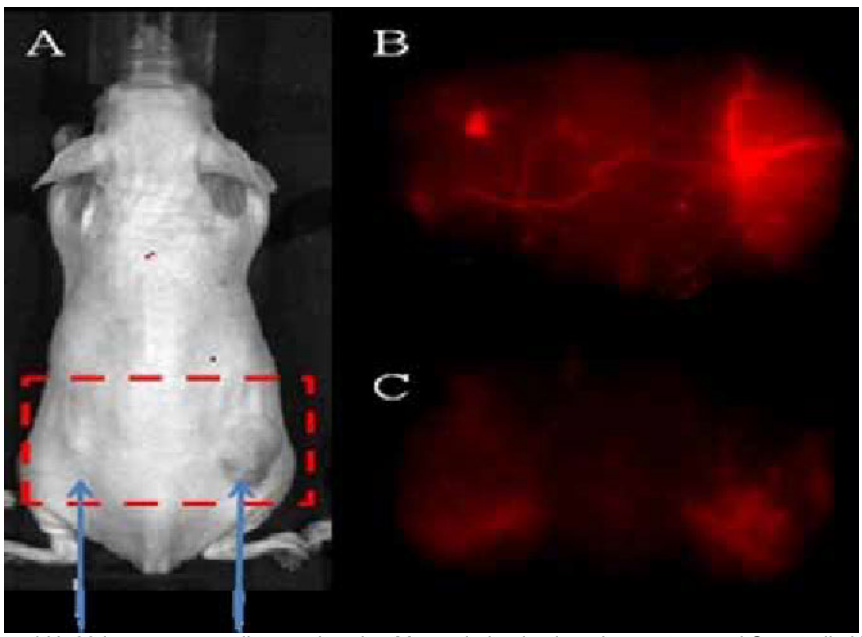


Fig. In-Vivo Imaging; A) A549 and H460 lung cancer cell tumor bearing Mouse in in-vivo imaging system and Spectrally Unmixed Image of Vasculature with B) PCNCs-Di and C) NCs-Di

Disclosure of author financial interest or relationships:
**A. Patel**, None; **E. Lim**, None; **N. Zhang**, PerkinElmer, Employment; **K. Francis**, None; **R. Singh**, PerkinElmer, Employment; **M. Sachdeva**, None.

Presentation Number **P562**
Poster Session 3
September 7, 2012 / 15:15-15:15 / Room: The Liffey

# Targeted in vivo imaging of tumor vasculature using a near infra-red labeled tomato lectin agent

*Jeff Morin, Jeannine Delaney, Guojie Ho, Garry J. Cuneo, Milind Rajopadhye, Wael Yared,* ***Jeffrey D. Peterson****, Sylvie Kossodo, LST, PerkinElmer, Boston, MA, USA. Contact e-mail: jeff.peterson@perkinelmer.com*

Tumor neo-vasculature, characterized by the development of abnormal, leaky and tortuous blood vessels, represents a key target for cancer imaging and therapy. Among the various recognized tools for measuring microvessel density is tomato (Lycopersicon esculentum) lectin, a single polypeptide glycoprotein that binds to sugar-containing proteins present on the endothelium. The aim of this study was to develop a near infra-red tomato lectin imaging agent to non-invasively assess tumor vasculature in vivo. Conjugation of the near infra-red fluorophore VivoTag 680 XL (epsilon=210,000 M/cm; abs/em max 665/688 nm) to tomato lectin was carried out by addition of the fluorophore in a DMSO solution to lectin in aqueous sodium bicarbonate. Yields of greater than 95% were achieved, based on absorbance, with a typical loading of 2 dyes per lectin. The resulting imaging agent, tLectin 680, preferentially labeled primary human umbilical vein endothelial cells. Specificity of the binding was validated by control experiments using free dye and competitive blockade with excess unlabeled tomato lectin. In vivo, non-invasive, real-time imaging and quantification of tumor neo-vasculature was performed in two models: matrigel plugs containing bFGF, VEGF and heparin injected into the flank of SKH-1 mice and nude mice bearing Lewis Lung Carcinoma tumors. Using Fluorescence Molecular Tomography (FMT) 6 hours after tLectin 680 (4 nmoles) intravenous injection, tumor endothelium-associated fluorescence was detected in matrigel plugs and this signal corresponded to labeling of neo-vessels present in the plugs as assessed by fluorescence microscopy. In vivo quantification of tumor fluorescence showed significantly higher signal in flank tumors versus control (non-tumor) contra-lateral flanks (total fluorescence: 50.96 +/-12 versus 2.32 +/- 1 pmol, p=0.005; mean fluorescence concentration: 126.74 +/- 17.44 versus 44.22 +/- 3.58 nM, p=0.002). Fluorescence microscopy of frozen tumor sections showed the specific localization of the agent to tumor vessels and this observation was further validated by co-labeling with FITC-labeled CD31. Vessels in other organs such as liver and kidney were also readily detectable. Importantly, tumor fluorescent signal, as quantified by FMT, correlated (R2= 0.90) with vascularization, as assessed by vessel counts using fluorescence microscopy: Lewis Lung Carcinomas 177.6 +/- 15 nM, 27.7 average vessels/field, HT-29 118.1 +/- 6 nM, 13.4 vessels/field, and matrigel plugs 73.6 +/- 9 nM, 5.5 vessels/field. There was also an excellent correlation (R2= 0.99) between CD-31 and tLectin 680 signals: Lewis Lung Carcinomas, 27.7 vessels/field with tLectin vs. 32 vessels/field with CD-31; HT-29, 13.4 vessels/field vs. 15.4 vessels/field, and matrigel plugs 5.5 vessels/field vs. 7 vessels/field. These results highlight the value of tLectin 680 combined with FMT imaging in assessing vascularity in vivo and in real time, without termination of mice, excision and processing of the tissue, thus improving the efficacy, early detection and monitoring of anti-angiogenic therapies.

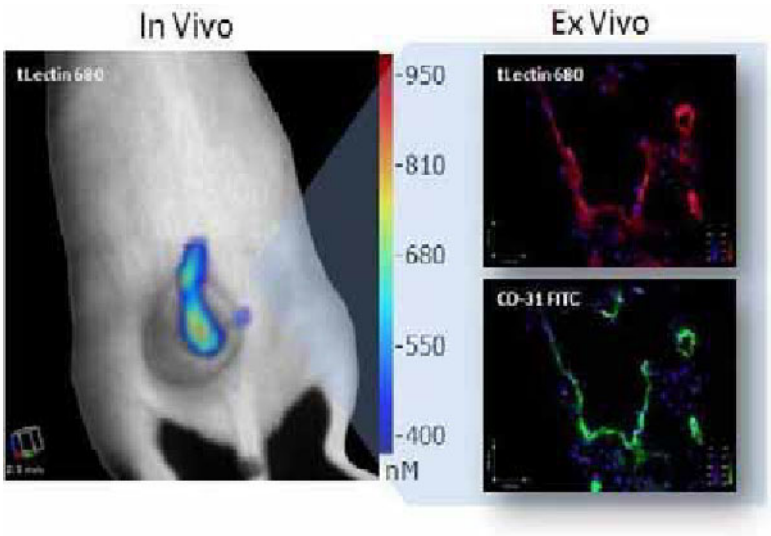


Disclosure of author financial interest or relationships:
**J. Morin**, Perkin Elmer, Employment; **J. Delaney**, PerkinElmer, Employment; **G. Ho**, None; **G.J. Cuneo**, PerkinElmer Life Sciences, Employment; **M. Rajopadhye**, PerkinElmer, Inc., Employment; **W. Yared**, Perkin Elmer, Employment; **J.D. Peterson**, PerkinElmer, Employment; **S. Kossodo**, PerkinElmer, Employment .

Presentation Number **P563**
Poster Session 3
September 7, 2012 / 15:15-15:15 / Room: The Liffey

# Quantitative assessment of folate receptor expression by FMT imaging of mouse tumor xenografts with a near-infrared fluorescent folate agent

*Kevin Groves, Bagna Bao, Jun Zhang, Garry J. Cuneo, Wael Yared, Milind Rajopadhye,* ***Jeffrey D. Peterson****, Life Sciences and Technology, PerkinElmer, Boston, MA, USA. Contact e-mail: jeff.peterson@perkinelmer.com*

Folic acid (vitamin B9) is an essential nutrient required by eukaryotic cells for survival that is acquired and internalized via folate receptors (FR) on the cell surface. In particular, it is the highly metabolic cells that upregulate FR, and many different human tumor cells, including ovarian, breast, cervical, renal, colorectal and nasopharyngeal cancer cells show significant upregulation as compared to normal tissues. As such, folic acid has been successfully exploited as a cancer specific targeting moiety for the efficient delivery of chemotherapeutic agents, drug carriers, photosensitizers and diagnostic reporters. Critical to the success of such agents is the determination of the level of FR expression for a given tumor, since weak FR-expressing cancers will not respond well to folate-targeted therapies. There is therefore a need for specific and quantitative imaging agents and methods for the determination of FR expression in vivo. Optical imaging in the near-infrared (NIR) range allows efficient penetration of photons through living tissue and minimizes interference from tissue autofluorescence. Combined with quantitative fluorescence molecular tomography (FMT), NIR fluorescent agents have emerged as invaluable tools for quantitative, deep tissue imaging across a range of important areas of disease research including oncology. We have developed a new, near-infrared fluorescent folate targeted imaging agent and used it to noninvasively quantify FR expression in vivo by FMT of mouse tumor xenografts. Three different cell types, KB, HeLa and HT-29, with varying degrees of FR expression were employed in the present studies. In vitro, the binding of the folate agent to each cell type was visualized by fluorescence microscopy and compared with FITC-labeled anti-FR antibody and the binding was quantified by flow cytometry which indicated a Kd of approximately 5 nM. Specificity of the agent was demonstrated by blocking of the signal by addition of an excess of unlabeled folic acid. In vivo quantification was performed by injection of 2 nmol of the agent into nude mice bearing KB, HeLa or HT-29 tumor xenografts and imaging by FMT at 4 to 24 h post injection. KB tumors showed a high level of FR expression in the tumors (300-400 pmol, as quantified by FMT), with little fluorescence in other tissues except the kidneys at 4 h post injection biodistribution study. Consistent with the in vitro profile, HeLa and HT-29 tumors had less tumor fluorescence. Both tumor cell lines showed significant (70-80%) knockdown of signal by co-injection of the mice with unlabeled folic acid and ex vivo colocalization with FR antibody on tumor slices, confirming the in vivo specificity of the agent. Thus, we have demonstrated the ability of this new agent to quantify FR expression both in vitro and in vivo and, combined with FMT, to noninvasively distinguish between high and lower FR expressing tumors.

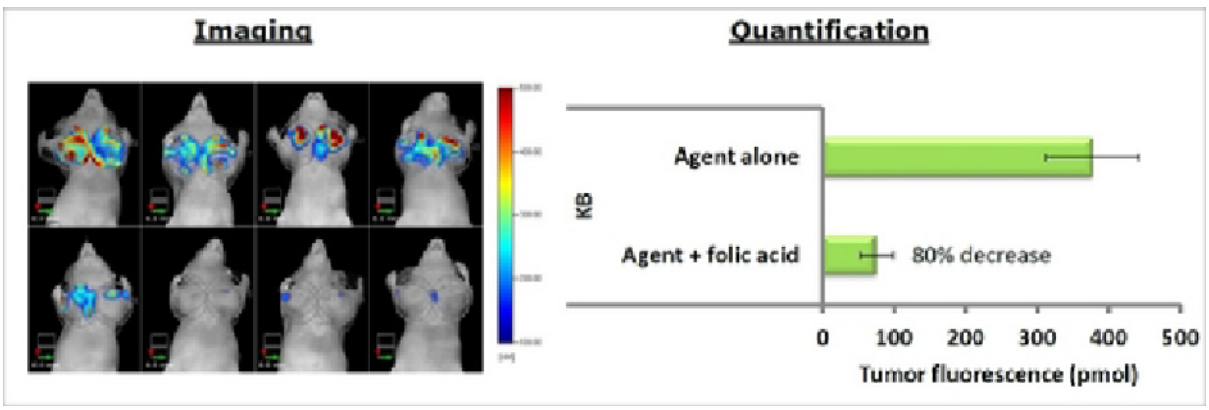


Disclosure of author financial interest or relationships:
**K. Groves**, PerkinElmer, Employment; **B. Bao**, None; **J. Zhang**, PerkinElmer, Employment; **G.J. Cuneo**, PerkinElmer Life Sciences, Employment; **W. Yared**, Perkin Elmer, Employment; **M. Rajopadhye**, PerkinElmer, Inc., Employment; **J.D. Peterson**, PerkinElmer, Employment .

Presentation Number **P564**
Poster Session 3
September 7, 2012 / 15:15-15:15 / Room: The Liffey

# Serial Diffusion MRI to monitor and predict outcome of targeted nanotherapy CRLX101

*Thomas S. Ng[1], David Wert[2], Hargun S. Grewal[1], **Daniele Procissi**[1,3], David Colcher[4], Andrew Raubitschek[4], Russell Jacobs[1], [1]Beckman Institute, Caltech, Pasadena, CA, USA; [2]Pathology and Microbiology, University of Nebraska, Omaha, NE, USA; [3]Radiology, Northwestern University, Chicago, IL, USA; [4]Cancer Immunotherapeutics & Tumor Immunology, Beckman Research Institute at City of Hope, Duarte, CA, USA. Contact e-mail: d-procissi@northwestern.edu*

PURPOSE: Targeted cancer treatments using therapeutic nanoparticles are being developed to reduce systemic toxic effects of traditional chemotherapies and to enhance tumor response. The nanoparticle CRLX101 is a cyclodextrin-based polymer conjugate of camptothecin (CPT) which has been shown to be effective in animal lymphoma models. Here, we evaluate the efficacy of diffusion-weighted magnetic resonance imaging (diffusion MRI) to monitor early response of CRLX101 in a preclinical model of lymphoma but also to evaluate its potential as a long term therapeutic response predictor using a simplified logistic model of tumor growth. EXPERIMENTAL DESIGN: Diffusion MRI was serially (7 days post-treatment) performed following CRLX101 administration, in a murine Burkitt's lymphoma model. Animals treated with conventional non targeted therapy inrinotecan (CPT-11) and saline were also imaged as comparison and as a negative control, respectively. Tumor Apparent diffusion coefficient (ADC) values were generated from the MR images. By assuming a linear relationship between ADC and tumor cellular density the MR data was plugged into a mathematical model of tumor growth (N.C. Atuegwu et al, Magn Resonance in Medicine 66:1689-1696 (2011)) and was used to obtain an estimate of cell proliferation rates for the three different cohoorts. Histological analysis using cleaved-caspase 3, TUNEL, Ki-67 and H&E were conducted on tumor samples for correlation with imaging results. RESULTS & DISCUSSION: CRLX101 treatment resulted in a reduction of tumor volume compared to CPT-11 and controls confirming its therapeutic effect. The mean ADC change for CRLX101 treated tumors at day 2, 4 and 7 post-treatment were 16 ± 9%, 24 ± 10% and 49 ± 17% respectively. These changes were statistically greater than the controls ($p \leq 0.02$) and noticeably greater than CPT-11 treated tumors (5 ± 5%, 14 ± 7% and 18 ± 6%) (Figure 1 A, B). By plugging in the early time points (day1,4) ADC values into the cell proliferation model it was possible to reliably predict long term differences between the proliferation rates of untreated and CRLX101 and CPT-11 treated cohorts Fig 1(C,D, E). Interestingly when considering CPT-11 ADC and tumor volume growth data alone through day 7 one would expect that the tumor may be responding to treatment, albeit less than the nanoparticle treatment. However, analysis of the model generated proliferation data indicated that between day 4 and 7 CPT-11 tumors showed a trend towards positive proliferation rates (increase in cell proliferation), suggesting treatment failure. The latter analysis is consistent with the histology results conducted on the same cohoorts. This study demonstrates that ADC parameter obtained with diffusion MRI can not only visualize early response following CRLX101 targeted nanotherapy but also provide image-derived modeling of cell proliferation rates, thus providing a tool for long term treatment outcome.

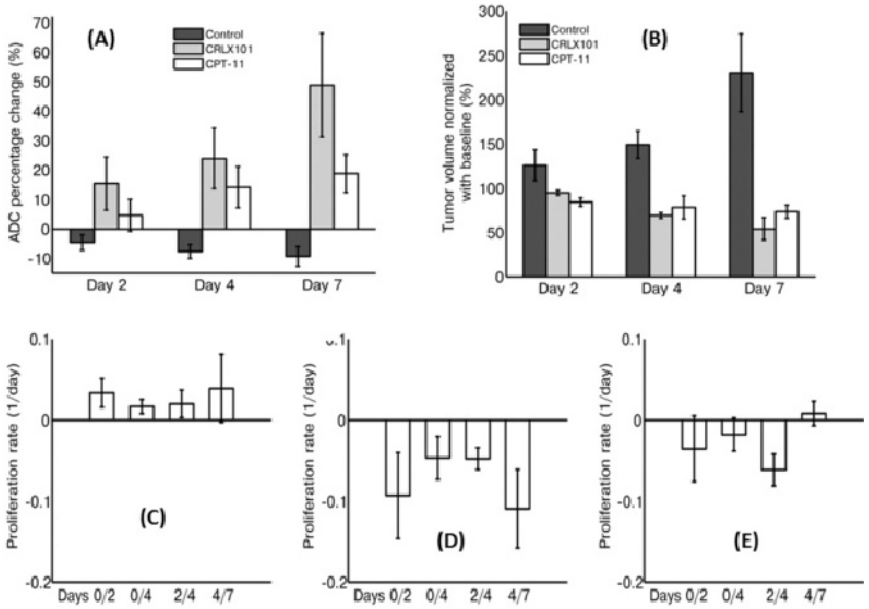


Fig 1 (A) Tumor ADC and (B) tumor volume Day 1,4 and 7. Model generated Proliferation Rates for (C) control, (D) CRLX101 and (E) CPT-11 between day 0/2, day 0/4, day 2/4, and day 4/7.

Disclosure of author financial interest or relationships:
**T.S. Ng**, None; **D. Wert**, None; **H.S. Grewal**, None; **D. Procissi**, None; **D. Colcher**, ImaginAb, Grant/research support; UCLA, Grant/research support; **A. Raubitschek**, None; **R. Jacobs**, None.

Presentation Number **P565**
Poster Session 3
September 7, 2012 / 15:15-15:15 / Room: The Liffey

# Multimodal *in vivo* imaging of prostate cancer xenografts in mice by anti-[$^{18}$F]FACBC PET and fluorescence based optical imaging

*Helena K. Ahtinen[1], Heidi Liljenbäck[1,2], Saija Savolainen[2,3], Olli Eskola[1], Paul A. Jones[4], Sari Mäkelä[2,5], Matti Poutanen[2,3],* ***Anne Roivainen***[1,2]*, [1]Turku PET Centre, University of Turku, Turku, Finland; [2]Turku Center for Disease modeling, University of Turku, Turku, Finland; [3]Department of Physiology, University of Turku, Turku, Finland; [4]GE Healthcare, Medical Diagnostics, London, United Kingdom; [5]Functional Foods Forum, University of Turku, Turku, Finland. Contact e-mail: anne.roivainen@utu.fi*

**Introduction:** Prostate cancer (PCa) is the most common cancer type in men in Western countries. One of the main challenges in drug development is to find methods to assess anti-cancer therapies over the course of treatment *in vivo*. Positron emission tomography (PET) tracer, anti-1-amino-3-[$^{18}$F]-fluorocyclobutane-1-carboxylic acid (anti-[$^{18}$F]FACBC) is a synthetic L-leucine analog and has shown high uptake in PCa. It is hypothesized that anti-[$^{18}$F]FACBC is transported into the cell by L-type amino acids transporter. Major advantage of anti-[$^{18}$F]FACBC with regards to prostate imaging, is the low accumulation in urinary bladder. Purpose of this study was to evaluate if anti-[$^{18}$F]FACBC PET would be suitable for non-invasive monitoring of tumour growth in mouse xenograft model. **Methods:** Androgen-independent human PCa cells expressing red fluorescent protein (PC-3-RFP, Anticancer) were implanted subcutaneously (s.c.) or orthotopically (o.t.) in immunodeficient mice. Tumour growth was evaluated once a week for 5 weeks after cell inoculation by 1) external caliper, 2) fluorescence based optical *in vivo* imaging and 3) anti-[$^{18}$F]FACBC PET. After the last 30-min dynamic PET imaging, mice were sacrificed and *ex vivo* biodistribution of $^{18}$F-radioactivity was evaluated by measuring excised tissues with a gamma counter. **Results:** Optical imaging signal correlated well with s.c. tumour volume (correlation coefficient 0.94). Both s.c. and o.t. tumours were clearly detectable by RFP fluorescence based optical imaging and anti-[$^{18}$F]FACBC PET (Figure 1). The tumour radioactivity reached a plateau approximately at 20 min after intravenous bolus injection of anti-[$^{18}$F]FACBC. According to *ex vivo* measurements the tumour-to-muscle ratios varied markedly, and were as high as 8.3 (range 0.97-8.3) at 5 weeks of tumour growth. However, the anti-[$^{18}$F]FACBC radioactivity did not correlate with tumour volume. **Conclusion:** In this study, fluorescence based optical *in vivo* imaging was superior for monitoring growth of PCa xenografts in mice. Anti-[$^{18}$F]FACBC PET delineated also o.t. PCa xenografts in mice and further studies are warranted to clarify its value to assess the efficacy of novel anti-cancer therapies.

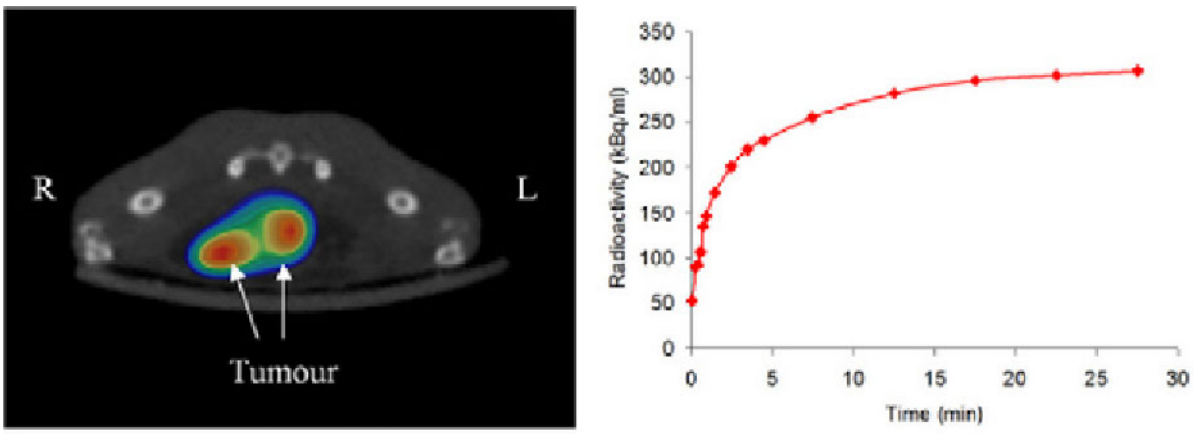


Figure 1. Representative anti-[$^{18}$F]FACBC PET image (left) and time-radioactivity curve (right) of PC3-RFP o.t. tumour in immunodeficient mouse.

Disclosure of author financial interest or relationships:
**H.K. Ahtinen**, None; **H. Liljenbäck**, None; **S. Savolainen**, None; **O. Eskola**, None; **P.A. Jones**, GE Healthcare, Employment; **S. Mäkelä**, None; **M. Poutanen**, None; **A. Roivainen**, None.

Presentation Number **P566**
Poster Session 3
September 7, 2012 / 15:15-15:15 / Room: The Liffey

# Optimization of pharmacokinetic profile for theranostic temperature sensitive multimodal liposomes using optical imaging

***Elena V. Rosca***[1], *Michael J. Wright*[1], *Andrew D. Miller*[1], *Wladyslaw Gedroyc*[2], *Maya Thanou*[1], [1]*Institute of Pharmaceutical Science, King's College London, London, United Kingdom;* [2]*Department of Experimental Medicine, Imperial College, London, United Kingdom. Contact e-mail: elena.rosca@kcl.ac.uk*

Imaging techniques are being increasingly used as diagnosis tools but also in the delivery of therapies. For instance tissue ablation using Magnetic Resonance Imaging guided High Intensity Focused Ultrasound (MRIgFUS) is a novel technique that has taken centre stage as a treatment method for several diseases. Recently there has been increased interest in applying this technique in the treatment of cancer. The release from thermosensitive drug loaded liposome by MRIgFUS will be a highly localized, specific treatment and it should result in a reduction of side effects. Tumours present an increased Enhanced Permeability Retention (EPR) effect due to their leaky vasculature and thus nanoparticles tent to accumulate resulting to an increased drug concentration. For instance doxorubicin, a common chemotherapeutic agent, with serious side effects and cardiac toxicity has been encapsulated in liposomal particles demonstrating an improved therapeutic effect. A drawback of this approach is that the release of the drug is slow and thus cancerous cells get exposed to small quantities of drug for a longer period of time leading to the development of resistance. We developed image guided thermosensitive liposomes whose release can be triggered at a temperature of 42°C, thus exposing the tumour cells to a high concentration of drug in a short time. The heating can be accomplished using MRIgFUS as our particles contain a Gadolinium labelled lipid which facilitates their MRI imaging. However, this approach requires knowledge of the time at which the treatment should commence. Thus optimal tumour accumulation is paramount to this approach. We have developed a unique Near Infrared (NIR) labelled lipid which when incorporated into the particles allows monitoring of the kinetics and tumour accumulation over time using optical imaging, as preclinical model. We have demonstrated that the labelled particles have very good short term stability at 37°C in high serum concentration (<10% release in 80% serum after 1 hour incubation) and good long term stability (<45% release in 20% serum after 24 hours). We demonstrated in vitro cell toxicity of the heat activated particles and compared it with the toxicity of liposomal doxorubicin. Cells incubated with heated particles showed 60.5% cell death at 10 μM Doxorubicin concentration after 24 hour incubation post heating, while the liposomal doxorubicin at the same concentration and incubation time resulted in 13.5% cell death. In vivo imaging of subcutaneous xenografts with the same cells indicates maximum tumour accumulation at 8 hours post injection. Most studies investigate tumour accumulation at 24 hours post injection when we actually observed a reduction in signal at that time point, indicating that if the MRIgFUS treatment would occur at this point the delivered dose would be suboptimal. Using this imaging tool we can study the effect of different parameters such as nanoparticle size, PEGylation, targeting moieties and tumour types on the pharmacokinetic profile of particles to maintain optimal drug delivery upon activation by FUS.

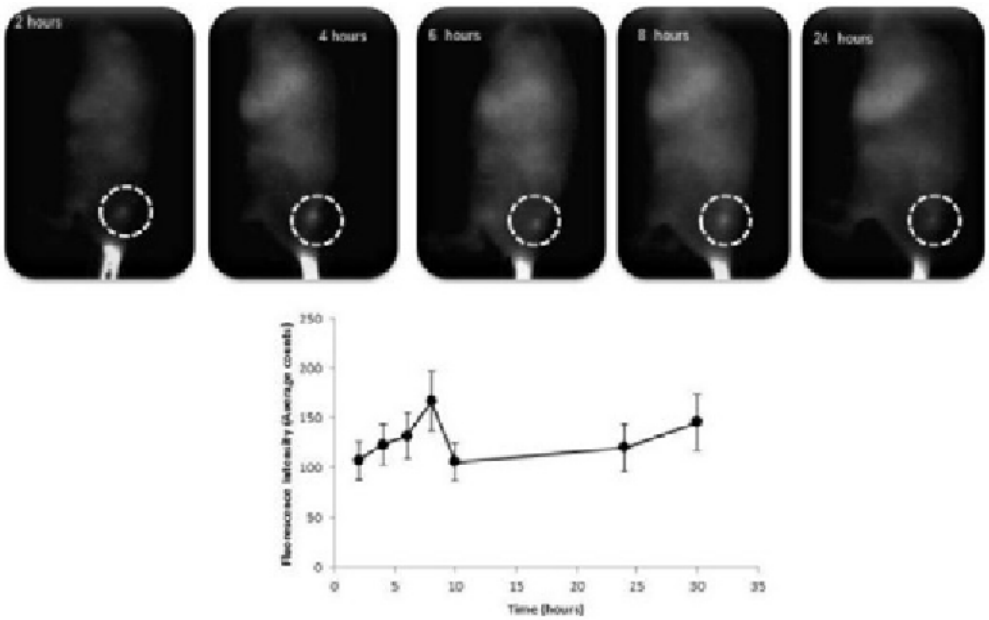


Disclosure of author financial interest or relationships:
**E.V. Rosca**, None; **M.J. Wright**, None; **A.D. Miller**, None; **W. Gedroyc**, Insightec Israel, Consultant; **M. Thanou**, None.

Presentation Number **P567**
Poster Session 3
September 7, 2012 / 15:15-15:15 / Room: The Liffey

# Heteronuclear Proton MRI: A new MR-Technique for Cell Tracking

***Rebecca Schmidt***[1], *Klaus Strobel*[1], *Olga Reifschneider*[2], *Daniela Delli Castelli*[4], *Silvio Aime*[4], *Christoph Bremer*[3], *Cornelius Faber*[1], [1]*University Hospital of Muenster, Department of Clinical Radiology, Muenster, Germany;* [2]*University of Muenster, Institute of Inorganic and Analytical Chemistry, Muenster, Germany;* [3]*St. Franziskus Hospital, Clinic for Radiology, Muenster, Germany;* [4]*University of Turin, Department of Inorganic and Physical Chemistry and Materials Research, Torino, Italy. Contact e-mail: rebeccaschmidt@uni-muenster.de*

*In-vitro*-labeling of cells for their *in-vivo*-detection by Magnetic Resonance Imaging (MRI) is a common method for following and understanding biological processes as well as for monitoring therapies. Traditionally, for cell tagging Gd- or Fe-based contrast agents are used which alter the MR relaxation in their vicinity and thus induce either a positive or a negative contrast *(Rogers et al. 2006)*. However, the unambiguous identification of the labeled cells is often hampered by background signal. A contrast agent that can be detected independently from the water signal to avoid disturbing background noise would be desirable. For this, Thulium-1,4,7,10-tetramethyl-1,4,7,10-tetraazacyclododecane-1,4,7,10-tetraacetate (Tm-DOTMA, Macrocyclics, USA) which has already been used for MR thermometry and PARACEST-imaging, is a convenient agent. It has 12 equivalent methyl protons with a chemical shift of ~100 ppm **(Fig. 1suppl.)** *(Hekmatyar et al. 2005, Delli Castelli et al. 2010)*. This highly shifted signal can be detected independently from the water signal by ultra-short echo time imaging (UTE) *(Strobel et al. 2012)*. The aim of our study was to explore the feasibility of imaging Tm-DOTMA labeled cells *in vivo*. HT-1080 cells (human fibrosarcoma) were labeled with 10 µmol Tm-DOTMA / $1x10^6$ cells using electroporation. Trypan blue exclusion test showed no significant toxicity. Due to the self-fluorescence of Tm-DOTMA (extinction 253 nm / emission 460 nm), the inclusion of this complex could be visualized by a fluorescence microscope (Nikon Instruments Europe, UK). No comparable fluorescence was detected in non-labeled cells **(Fig. 2suppl.)**. Non-localized spectroscopy on phantoms filled with labeled cells showed an average of about $5x10^9$ Tm-DOTMA molecules per cell. Two nude mice received a subcutaneous injection of $4x10^6$ Tm-DOTMA labeled cells into their right flank. MR images were obtained on a BioSpec 94/20 (Bruker, Germany) equipped with a 1T/m gradient system and a 35mm birdcage coil over a period of 8 days. Animals were investigated using a 3D-UTE sequence with radial acquisition and a 365 µs gaussian pulse excitation. Anatomical reference images were acquired using FLASH- and RARE sequences. Tm-DOTMA labeled cells were observed within 2 h scan time with signal-to-noise-ratio values up to 33 (day 0) showing the negligible water background **(Fig. 1)**. Detection of the Tm-DOTMA signal was possible during the 8 days of examination with an average half-value-period of 27.7 h. For validation of the MR data, tumors were explanted and Tm distribution was determined by laser ablation inductively-coupled plasma mass spectrometry (LA-ICP-MS, LSX213 Cetac iCAP Q, ThermoScientific, USA) showing Tm only in the tumor, but not in the surrounding fatty tissue **(Fig. 3suppl.)**. These results show the feasibility of obtaining virtually background-free signal of HT-1080 cells labeled with Tm-DOTMA using 3D UTE. This approach of heteronuclear proton MRI may provide a versatile tool to follow labeled cells *in vivo* and thus facilitate the application of molecular MRI without the need for extra MR-equipment.

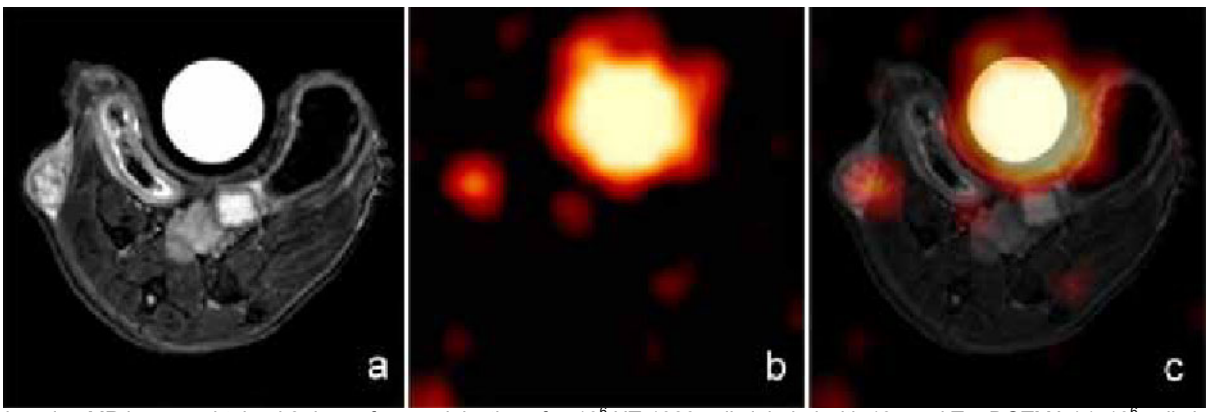


**Fig. 1:** axial murine MR images obtained 8 days after s.c. injection of $4x10^6$ HT-1080 cells labeled with 10 µmol Tm-DOTMA / $1x10^6$ cells into the right flank. A control tube containing an aqueous solution of 0.25 mM TM-DOTMA was placed under the mouse. a: axial anatomical RARE-image. The grown tumor is a sign of the good biocompatibility of Tm-DOTMA. b: 3D UTE, 2.5mm-slice of the same position as a). The methyl proton signal of Tm-DOTMA is clearly detectable. c: Image fusion of a) and b).

Disclosure of author financial interest or relationships:
**R. Schmidt**, None; **K. Strobel**, None; **O. Reifschneider**, None; **D. Delli Castelli**, None; **S. Aime**, Bracco Imaging, Consultant; Bruker, Grant/research support; **C. Bremer**, None; **C. Faber**, None.

Presentation Number **P568**
Poster Session 3
September 7, 2012 / 15:15-15:15 / Room: The Liffey

# Multimodal Imaging of Early Passage Cervix Cancer Xenografts

***Shawn Stapleton***[1,4], *Naz Chaudary*[2], *Michael Milosevic*[3,4], *Anthony Fyles*[3,4], *Melania Pintilie*[5], *Warren Foltz*[4], *David E. Green*[4], *Douglass C. Vines*[4], *David A. Jaffray*[1,4], *Richard P. Hill*[1,2], [1]*Medical Biophysics, University of Toronto, Toronto, ON, Canada;* [2]*Ontario Cancer Instititue, Princess Margaret Hospital, Toronto, ON, Canada;* [3]*Radiation Oncology, University of Toronto, Toronto, ON, Canada;* [4]*Radiation Medicine Program, Princess Margaret Hospital, Toronto, ON, Canada;* [5]*Biostatistics, Princess Margaret Hospital, Toronto, ON, Canada. Contact e-mail: shawn.stapleton@rmp.uhn.on.ca*

Introduction: Multimodal imaging provides a valuable tool to probe the phenotypic features of the tumour microenvironment. Used individually, modalities such as: positron emission tomography (PET) can be used to probe metabolic (e.g. 18FDG) and hypoxic (e.g. 18FAZA, 18F-MISO) features of tumours; while computed tomography (CT) and magnetic resonance imaging (MRI) can be used to probe angiogenic and metastatic features. Used in combination, imaging can probe the potential interplay between the aforementioned phenotypes. The primary aim of our study was to establish a multimodal imaging approach using dynamic contrast enhanced (DCE)-MRI, DCE-CT and 18FDG to characterise the tumour microenvironment. Imaging was performed on a novel early passage xenograft model of cervix cancer. The tissue used for xenograft implantation was obtained from patients who are also undergoing multimodal imaging. A future aim of this study is to determine to what extent primary xenografts recapitulate the human tumours from which they were derived using multimodal imaging. Methods: Cervix cancer biopsies from 3 patients were used to generate 9 orthotopic cervix xenografts in mice. DCE-CT, DCE-MRI and 18FDG-PET were performed. Co-registration was facilitated using the Minerve System (Bioscan, USA) to immobilise the mice for the duration of imaging. A software package was developed to facilitate simultaneous analysis of each data set. The data was analysed on 3 spatial scales: whole tumour, voxel and clustered. Voxels were clustered into three types (hyper, normally, and hypo- perfused) based on their enhancement compared to muscle. The semi-quantitative parameter %ID per g was used for PET and the parameters Ktrans, Ve and Vp were derived from the DCE-CT and DCE-MRI data using the modified Tofts model. Results/Discussion: Acquired data sets showed good co-registration between all imaging modalities. Qualitatively, the spatial enhancement patterns observed on DCE-CT and DCE-MRI scans agreed. On the whole tumour level, there was a significantly elevated 18FDG-PET uptake compared muscle. The voxel scale analysis gave information about the spatial relationship between perfusion and 18FDG uptake (Figure 1). Clustered voxel analysis showed that >70% of each tumours volume was normally or hyper-perfused. There was no significant difference in the %ID per g between the hyper-, normally, and hypo-perfused regions. Overall, there was no correlation between DCE-MRI or DCE-CT and 18FDG-PET on all three scales. The lack of correlation may be reflective of the underlying tumour biology and current effort is underway to validate using histology. Additionally, work is underway to compare multimodal imaging of human tumours with their xenograft counterparts. In conclusion, this work demonstrates the ability to perform pre-clinical multimodal imaging in a novel early passage cervix xenograft model.

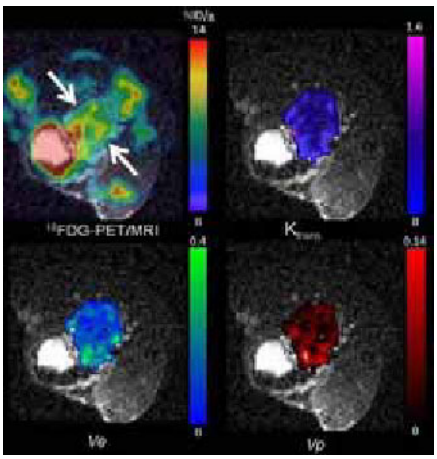


Figure 1. An example data set highlighting 18FDG-PET-MRI analysis performed on a voxel by voxel basis. The top right image shows the %ID\g of 18FDG-PET overlaid on a T1-weighted MRI image. The tumour is located adjacent to the bladder and is identified by the arrows. The remaining three images depict DCE-MRI derived kinetic parameters Ktrans, Ve and Vp. There was no correlation between %ID\g and Ktrans, Ve or Vp on a voxel by voxel basis in any of the mice.

Disclosure of author financial interest or relationships:
**S. Stapleton**, None; **N. Chaudary**, None; **M. Milosevic**, None; **A. Fyles**, None; **M. Pintilie**, None; **W. Foltz**, None; **D.E. Green**, None; **D.C. Vines**, None; **D.A. Jaffray**, Precision X-ray, Other financial or material support; Raysearch, Grant/research support; Philips, Grant/research support; Elekta, Grant/research support; General Electric, Grant/research support; IMRIS, Other financial or material support; Modus Medical, Grant/research support; **R.P. Hill**, None.

Presentation Number **P569**
Poster Session 3
September 7, 2012 / 15:15-15:15 / Room: The Liffey

# Monitoring of Metastatic Breast Cancer Using Bioluminescence Tomography for Quantitative Assessment of Radiation Treatment Effects

*Ji-Yeon Park[1,2], **Tae-Suk Suh**[1,3], Tobi Schmidt[4,6], Edward Grave[5,6], Jeong-Woo Lee[7,8], Christopher Contag[4,6], [1]Biomedical Engineering, The Catholic University of Korea, Seoul, Republic of Korea; [2]Research Institution of Biomedical Engineering, The Catholic University of Korea, Seoul, Republic of Korea; [3]Advanced Research Center for Medical Physics, The Catholic University of Korea, Seoul, Republic of Korea; [4]Pediatrics, Stanford University, Palo Alto, CA, USA; [5]Radiation Oncology, Stanford University, Palo Alto, CA, USA; [6]Molecular Imaging Program at Stanford, Stanford University, Palo Alto, CA, USA; [7]Research Institution of Health Science, Korea University, Seoul, Republic of Korea; [8]Radiation Oncology, Konkuk University Medical Center, Seoul, Republic of Korea. Contact e-mail: suhsanta@catholic.ac.kr*

To evaluate radiation treatment effects on mammary carcinoma cells, quantitative photon radiance were monitored to track light-emitting cancer cells and metastasis using in vivo bioluminescence imaging. Eight female BALB/c mice aged 8 weeks were orthotopically injected with $5\times10^4$/cc 4T1 tumor cells into the abdominal mammary gland. The firefly luciferase-based bioluminescence images were acquired every 2-3 days for 1 month. Bioluminescent intensity was analyzed in average surface radiance (photons/sec/cm$^2$/sr) taken in 3-dimensional bioluminescence tomography (BLT). After 1 week, single-radiation dose of 20 Gy was delivered by orthovoltage X-rays. Variation of detected bioluminescence signals emitted from molecular cancer cells was depicted on BLT images. To delineate tumor volumes according to bioluminescence intensity on anatomical images for radiation therapy, BLT images were registered with the micro computed tomography (CT) images using surface-constrained warping. Multispectral BLT images elaborated on early detection of cancer cells and characteristics of tumor growth and metastasis for more accurate determination of internal bioluminescent sources. The radiation-treated mice having only primary tumor volumes showed 67% decrease in bioluminescent signals, while the mice with metastatic cancer cells suggested 88% reduction, as compared to the control group. Registration of BLT with CT images guided molecular cancer cells on anatomical coordinates. The BLT imaging was a useful tool to localize cancer cells and to quantify radiation response. Application of BLT led to more accurate definition of tumor volumes including molecular probe-based microscopic cancer cells. Monitoring of bioluminescence signals enables to diagnose real-time metastatic behavior of cancer cells and determine optimal radiation treatment strategies adapted to tumor characteristics.

Disclosure of author financial interest or relationships:
**J. Park**, None; **T. Suh**, None; **T. Schmidt**, None; **E. Grave**, None; **J. Lee**, None; **C. Contag**, ConcentRx Corp, Other financial or material support; Origin Therapeutics, Stockholder; Olympus, Other financial or material support; Tansderm Inc., Other financial or material support; Cygnet Biofuels, Other financial or material support .

Presentation Number **P570**
Poster Session 3
September 7, 2012 / 15:15-15:15 / Room: The Liffey

# MRI tracking of nanoparticle-labeled melanoma cells improves the predictive power of an experimental brain metastasis model

***Terje Sundstrøm***[1,2], *Ingvild Wendelbo*[1], *Erlend Hodneland*[1], *Arvid Lundervold*[1], *Inderjit Daphu*[1], *Kai Ove Skaftnesmo*[1], *Heike Immervoll*[3], *Eva Sykova*[4], *Morten Lund-Johansen*[2,5], *Rolf Bjerkvig*[1], *Frits Thorsen*[1], [1]*Department of Biomedicine, University of Bergen, Bergen, Norway;* [2]*Department of Neurosurgery, Haukeland University Hospital, Bergen, Norway;* [3]*Department of Pathology, Haukeland University Hospital, Bergen, Norway;* [4]*Department of Neuroscience, Institute of Experimental Medicine, Academy of Sciences of the Czech Republic, Prague, Czech Republic;* [5]*Department of Surgical Sciences, University of Bergen, Bergen, Norway. Contact e-mail: terje.sundstrom@gmail.com*

Introduction: Melanoma death rates continue to rise, in part due to its aggressive, and not yet understood, targeting of the brain. Melanoma brain metastasis carries a dismal prognosis. Most promising drugs against metastatic melanoma are never licensed as they fail to show patient benefit in expensive clinical trials. These are clear indications of the poor predictivity of experimental metastasis models. Translation of ever increasing, large-scale pharmacogenomic data further highlights the need for more stringent preclinical model systems. We have addressed these issues by developing a robust model of melanoma brain metastasis. Materials and methods: Several melanoma cell lines were derived in our laboratory from an integrated human biobank (Wang et al 2011). These cell lines were labeled with poly-L-lysine coated maghemite nanoparticles (SPIONs) (Babic et al 2008) and injected into the left cardiac ventricle of immunodeficient mice. Tumor cell load to the brain was visualized by magnetic resonance imaging (MRI) T2* weighted MGE sequences (TR/TE/ST 1500 ms/7.2 ms/1.0 mm; scan time 6 min 24 sec). Automated quantification thereof was based on adaptive thresholding in conjunction with a trained neural network. Automated signal detection was compared to manual/visual signal registration. Bioluminescence imaging (BLI) and MRI was used to follow tumor development. Results: SPION exposure did not affect viability, growth or migration in multiple melanoma cell lines across several in vitro monolayer and spheroid assays. Cells were efficiently labeled with 10 µg/mL of SPIONs for 24 hours. Numerous labeled cell lines displayed similar features on brain MRI (Fig. 1A). Brain tumor development recapitulated the widespread nature seen in humans, and histology and immunohistochemistry was unchanged for cell lines exposed to nanoparticles (Fig. 1B). There was a strong subjective (Fig. 1C) and objective ($R^2$ = 0.921, $p < 0.001$) concordance between automated and manual signal detection. Automated quantification of labeled cells in the brain and brain metastasis showed a sigmoid association with increasing doses of inoculated cells ($10^4$, $10^5$, 5 x $10^5$, and $10^6$) (Fig. 1D, left and middle). MRI was superior to BLI in discriminating all degrees of injection success; several animals judged as "hits" by BLI could be classified as "misses" by MRI, e.g. the two outliers in the $10^6$ group (Fig. 1D, left). Brain metastasis was strongly correlated with the automated signal detection ($R^2$ = 0.708, $p < 0.001$) (Fig. 1D, right), and was unaffected by labeling (labeled vs unlabeled groups; tumor count p = 0.686 and survival p = 0.547) (Fig. 1B and 1D, middle). Conclusion: Melanoma cells were unaffected by nanoparticle labeling. Automated quantification analysis of labeled cells in the brain was robust and correlated significantly with brain metastasis. By implementing the model developed here, the predictive power of preclinical studies on the biology and/or treatment of melanoma brain metastasis will improve, ultimately reducing the number of clinical trials that fail to show patient benefit.

Disclosure of author financial interest or relationships:
**T. Sundstrøm**, None; **I. Wendelbo**, None; **E. Hodneland**, None; **A. Lundervold**, None; **I. Daphu**, None; **K. Skaftnesmo**, None; **H. Immervoll**, None; **E. Sykova**, None; **M. Lund-Johansen**, None; **R. Bjerkvig**, None; **F. Thorsen**, None.

Presentation Number **P571**
Poster Session 3
September 7, 2012 / 15:15-15:15 / Room: The Liffey

# An efficient reconstruction method for bioluminescence tomography

*Wei Guo[1], Kebin Jia[1], Xin Yang[2], Xueyan Liu[3], Jinchao Feng[1], Chenghu Qin[2], Xibo Ma[2], **Jie Tian**[2], [1]The College of Electronic Information & Control Engineering, Beijing University of Technology, Beijing, China; [2]Medical Image Processing Group, Institute of Automation,CAS, "Beijing,100190", China; [3]Sino-Dutch Biomedical and Information Engineering School, Northeastern University, Shenyang, China. Contact e-mail: tian@ieee.org*

Optical molecular imaging in small animals has been attracting much interest in recent years as a noninvasive method of monitoring physiological and pathological activities at the molecular level. Bioluminescence tomography (BLT) can three-dimensionally reconstruct the actual internal bioluminescent probe in small animals with a sensitive charge-coupled device (CCD) camera capturing the surface light signals. BLT is an ill-posed problem. Fortunately, it has been theoretically proven that the solution uniqueness can be established under practical constraints using a priori knowledge. In general practical applications, the volumes of the bioluminescent probes are very small compared with the whole reconstruction domain in BLT practical applications. Therefore, a priori information about the source sparse distribution can be used for constraining the problem and improving the reconstruction. Spares regularization method can efficiently employ the sparsity of source distribution and is much suitable for solving the inverse problem in BLT. In this study, we propose an efficient sparse regularization for BLT based on Variable splitting. According to several characters such as huge dimensionality and nonsmoothness, the objective function of sparse regularization is converted into the constrained problem and the regularizer is minimized under the constraint by variable splitting. Then, the constrained problem can be exactly and fast solved by iteratively solving a sequence of unconstrained subproblems. To validate the effectiveness of the proposed method in turbid mouse geometry, experiments with a heterogeneous 3D mouse atlas are conducted.

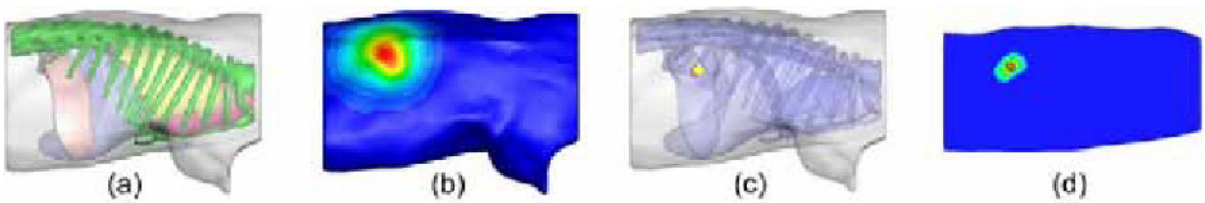


simulation experiments with a heterogeneous 3D mouse atlas. (a) The torso of the mouse atlas model with six tissues, (b) the simulated photondistribution on the surface, (c) the iso -surface views of the results, where the small sphere denotes the actual source, (d) the corr-esponding TransVerse view, where the small black circle denotes the actual source.

Disclosure of author financial interest or relationships:
**W. Guo**, None; **K. Jia**, None; **X. Yang**, None; **X. Liu**, None; **J. Feng**, None; **C. Qin**, None; **X. Ma**, None; **J. Tian**, None.

Presentation Number **P572**
Poster Session 3
September 7, 2012 / 15:15-15:15 / Room: The Liffey

# The inhibition effect of ApoG2 on gastric cancer and its efficacy evaluation by bioluminescence imaging in vivo

*Yonghua Zhan[1], Jing Xin[1], Jimin Liang[1], Yongzhan Nie[2], **Jie Tian**[1,3], [1]School of Life Sciences and Technology, Xidian University, Xi'an, China; [2]Department of Gastroenterology and State Key Laboratory of Cancer Biology, Xijing Hospital, Fourth Military Medical University, Xi'an, China; [3]Medical Image Processing Group, Institute of Automation,CAS, "Beijing,100190", China. Contact e-mail: tian@ieee.org*

Aims: Apogossypolone (ApoG2) as attractive non-peptidic small molecular inhibitors is a novel derivate of gossypol. Up to now, it has been found that ApoG2 has the significant anticancer effect on several cancers with little toxicity. However, whether or not it can inhibit the growth of gastric cancer cells has not been demonstrated. Therefore, this study was aimed to investigate the anti-growth effect of ApoG2 and its basic mechanism on SGC-7901 gastric cancer cell line in vitro, and meanwhile the anti-cancer effect on SGC-7901-luc xenograft animal models was evaluated by noninvasive bioluminescence imaging in vivo. Methods: The anti-growth effect of ApoG2 and gossypol was measured by MTT assay and the colony formation assay. Then the ability of inducing apoptosis by ApoG2 and gossypol was evaluated by flow cytometry. Besides, the nuclei changes caused by ApoG2- and gossypol-induced apoptosis were visualized by Hoechst 33258. To determine the changes of protein levels by ApoG2, western blotting was conducted. In vivo bioluminescence imaging was performed to evaluate the anti-cancer effect of ApoG2. Results: MTT assay and the colony formation assay was investigated the anti-growth effect of ApoG2 and gossypol on SGC-7901 cell line. The MTT assay results showed that ApoG2 has the significant anti-growth effect on SGC-7901 cell line in a dose- and time-dependent manner (Fig. A a). The 50% inhibition concentration of gossypol and ApoG2 is 5.6μM and 18.7μM at 72h, respectively (Fig. A b). The colony formation assay revealed that ApoG2 has a fascinating inhibition effect for a long time (Fig. B). Flow cytometry analysis and Hoechst 33258 stain results showed that ApoG2 and gossypol can induce apoptosis evidently (Fig. C). Western blotting results revealed that ApoG2-induced apoptosis is via the mitochondrial signal pathway. In vivo bioluminescence imaging was obtained after treatment with ApoG2 at 100mg/kg once per three days and the fluorescence intensity showed that ApoG2 has the significant anticancer effect on SGC-7901-luc xenograft animal models (Fig. D). Conclusions: ApoG2 has the significant anti-growth effect in vitro by inducing apoptosis with little cell toxicity and the significant anti-cancer effect in vivo. ApoG2 may be a potential chemotherapeutic agent as non-peptidic small molecular inhibitors of Bcl-2 family proteins for the treatment of gastric cancer.

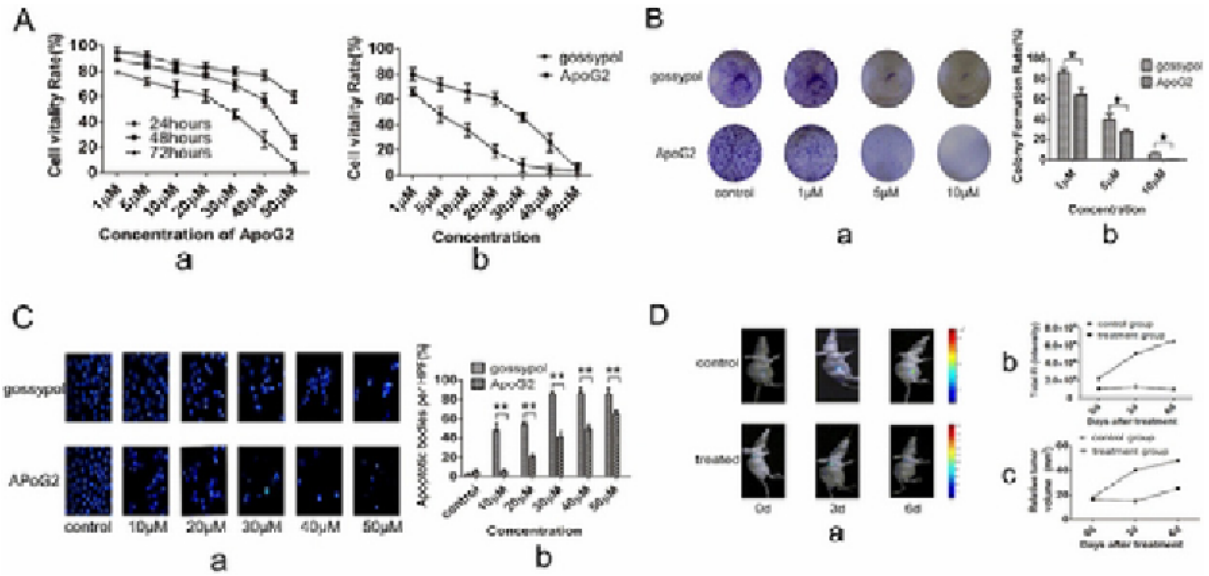


Fig. 1 MTT assay (A): the anti-growth effect of ApoG2 in a time-and dose-dependent manner on SGC-7901 cells (a) and the anti-growth effect of gossypol is evident compared to ApoG2 at 72h (b); colony formation assay (B): inhibition of colony formation of SGC-7901 by ApoG2 or gossypol at 14 days (a) and analysis statistically (b)*, P<0.05, statistically difference in the percentage of colony formation between ApoG2 and gossypol; Apoptosis detection (C): staining with Hoechst 33258,the apoptotic bodies was visualized in SGC-7901 induced by ApoG2 and gossypol at 48h (a) and analysis statistically of the number of apoptotic bodies (b)**, P<0.01, statistically significant difference in the number of apoptotic bodies between ApoG2 and gossypol; In vivo anticancer effect on SGC-7901-luc-bearing nude mice model (D): bioluminescence imaging (a), fluorescence intensity from tumors (b) and tradition tumor volume measurement (c) after treatment with ApoG2 at 100mg/kg once per three days.

Disclosure of author financial interest or relationships:
**Y. Zhan**, None; **J. Xin**, None; **J. Liang**, None; **Y. Nie**, None; **J. Tian**, None.

Presentation Number **P573**
Poster Session 3
September 7, 2012 / 15:15-15:15 / Room: The Liffey

# OKN-007 Nitrone-Induced Glioma Growth Regression in a F98 Rat Model

***Rheal Towner***[1], *David L. Gillespie*[2], *Debra Saunders*[1], *Osama Abdulla*[3], *Edward Hsu*[3], *Andrea L. Schwager*[4], *Randy L. Jensen*[2], [1]*Advanced Magnetic Resonance Center, Oklahoma Medical Research Foundation, Oklahoma City, OK, USA;* [2]*Huntsman Cancer Institute, University of Utah Health Sciences Center, Salt Lake City, UT, USA;* [3]*Bioengineering, University of Utah, Salt Lake City, UT, USA;* [4]*Interdepartmental Program in Neuroscience, University of Utah, Salt Lake City, UT, USA. Contact e-mail: Rheal-Towner@omrf.org*

Introduction: Glioblastoma multiforme has a poor prognosis in humans despite current treatment options. Grading and identification criteria that can be used to provide information regarding tumor behavior include cell proliferation, nuclear atypia, neovascularization and the presence of necrosis and/or apoptotic regions. Many of these grading and identification criteria can be measured with the use of magnetic resonance imaging (MRI) and MR spectroscopy (MRS) methods. Methods: F98 cells were infected with a modified pMMP retrovirus fused with the coding sequences for luciferase and hygromycin (pMMP-LucHygro), and implanted. OKN007 was administered in drinking water (0.018%; ~10 mg/kg body weight/day), starting from 15 days after F98 glioma cell implantations. Rats were anesthetized (isoflurane) and injected i.p. with 50 mg/kg firefly D-Luciferin and photographed 5 min after injection with an IVIS 100 imaging system. Images were quantified using LivingImage software (Xenogen). MRI was done on a 7.0 Tesla/30 cm imaging system (Bruker). Anesthetized animals were placed in a 72 mm quadrature volume coil (transmission), and a surface coil (reception). Rat imaging was done using T2-weighted RARE with a TR of 3000 ms, a TE of 63 ms, 20 transverse 1 mm-thick slices, a FOV of 3.5×3.5 cm2. MR spectroscopy was done using STEAM with a TE of 4.4 ms, a TM (mixing time) of 10 ms, a TR of 3000 ms, and 256 averages. VAPOR water suppression was used. Immunohistochemistry (IHC) was used to observe levels of hypoxia inducible factor 1alpha (HIF-1alpha), vascular endothelial growth factor (VEGF), carbonic anhydrase IX (CA-IX), glucose transporter 1 (Glut-1), MIB-1 (proliferation index), microvessel density (MVD), and apoptosis (cleaved caspase 3). Results: From MR and bioluminescence image detection of F98 gliomas, OKN-007 was found to decrease tumor growth. MR spectroscopy analysis (Fig. 1), indicated F98 glioma-induced alterations in tumor metabolites (tCho (total choline), tCr, NAA (N-acetyl aspartate), Lip1.3 (methylene hydrogens in lipid acyl groups), Lip5.3 (olefinic hydrogens in unsaturated lipid acyl groups)), were found to revert back to normal levels following OKN-007 treatment. IHC was used to assess levels of angiogenic (VEGF, HIF-1α, MVD), cell differentiation (CAIX), cell proliferation (Glut-1, MIB-1), and apoptosis (cleaved caspase 3), markers. OKN-007 resulted in significant decreases in angiogenesis (HIF-1α ($p<0.05$) and MVD ($p<0.05$), but not VEGF) and cell proliferation (Glut-1 ($p<0.05$) and MIB-1 ($p<0.01$)), and a significant increase in apoptosis (cleaved caspase 3 ($p<0.001$)), compared to untreated animals. Conclusions: MRI and MRS methods were successfully used to monitor the anti-glioma therapeutic effect of OKN-007. Due to its multiple targets (cell proliferation, angiogenesis (although not necessarily through the VEGF pathway), and apoptosis), OKN-007 may be an ideal therapeutic alternative, or may compliment current therapeutic protocols for gliomas. References:

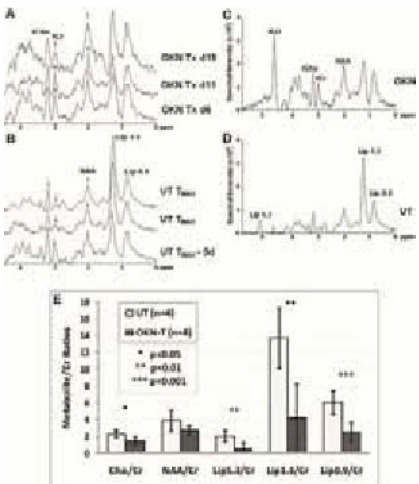

Figure 1: Representative STEAM-localized MR spectra obtained from (A,C) OKN-007-treated, or (B,D) untreated, F98 glioma-bearing rats. (E) Average metabolite/Cr ratios. Peak assignments: N-acetyl aspartate (NAA), total creatine (tCr), total choline (tCho), methylene acyl lipid hydrogens (Lip1.3), methyl acyl lipid hydrogens (Lip0.9), and olefinyl hydrogens (Lip5.3). Significant decreases in Cho/Cr (*$p<0.01$), Lip1.3/Cr and Lip5.3/Cr (**$p<0.01$), and Lip0.9/Cr (***$p<0.001$) were seen in OKN-007-treated rats (n=8) compared to untreated animals (n=4).

Disclosure of author financial interest or relationships:
**R. Towner**, None; **D.L. Gillespie**, None; **D. Saunders**, None; **O. Abdulla**, None; **E. Hsu**, None; **A.L. Schwager**, None; **R.L. Jensen**, Medtronic, Consultant; Pharmoco Kinesis, Consultant .

Presentation Number **P574**
Poster Session 3
September 7, 2012 / 15:15-15:15 / Room: The Liffey

# Multiple PET Imaging Using $^{18}$F-FDG, $^{18}$F-FDOPA and $^{18}$F-FLT in a Genetically Engineered Mouse Model for neuroblastoma

***Kai-Yuan Tzen***[1,4], *Yen-Lin Liu*[5], *Meng-Yao Lu*[2], *I-Shing Yu*[6], *Chiung-Nien Chen*[3], *Wen-Ming Hsu*[3], [1]*Department of Nuclear Medicine, National Taiwan University Hospital, Taipei, Taiwan;* [2]*Department of Pediatrics, National Taiwan University Hospital, Taipei, Taiwan;* [3]*Department of Surgery, National Taiwan University Hospital, Taipei, Taiwan;* [4]*Molecular Imaging Center, National Taiwan University, Taipei, Taiwan;* [5]*Department of Pediatrics, Buddhist Tzu Chi General Hospital, Taipei Branch, New Taipei, Taiwan;* [6]*Transgenic Mouse Models Core, National Core Facility Program for Biotechnology, Taipei, Taiwan. Contact e-mail: tzenky@ntuh.gov.tw*

**Background:** Neuroblastoma (NB) is a childhood cancer that originates from the sympathetic nervous system. Despite modern multimodality therapy, NB with amplification of *MYCN* oncogene represents a special genetic subtype with multiple metastases at diagnosis and a very poor treatment outcome. This study aims to explore the role of positron emission tomography/computed tomography (PET/CT) scans in characterizing the *TH-MYCN* transgenic mice, which is a preclinical model system that recapitulates most major genetic, phenotypic and clinical aspects of the human *MYCN*-amplified NB. **Materials and Methods:** The 129/SvJ-Tg (*TH-MYCN*) mouse strain was provided by Chiba Cancer Center Research Institute, Chiba, Japan and maintained at Transgenic Mouse Models Core, Taipei, Taiwan. After weaning and genotyping, female hemizygous *TH-MYCN* mice were screened with high-frequency ultrasound (US) on a weekly basis. Mice with US-identified abdominal mass were further studied with PET/CT using $^{18}$F-fluorodeoxyglucose ($^{18}$F-FDG), $^{18}$F-fluoro-dihydroxyphenylalanine ($^{18}$F-FDOPA), and $^{18}$F-L-thymidine ($^{18}$F-FLT). The $^{18}$F-FDG, $^{18}$F-DOPA and $^{18}$F-FLT PET scans were done in separate days. All the PET scans were acquired for 60 min. at 30 min. after the i.v. injection of the imaging agents. The mice were anesthetized using isofluorane and scanned by small animal PET/CT scanner (eXplore Vista DR, GE Healthcare, USA). Necropsy was undertaken after the mice died naturally or after they were sacrificed due to humanity consideration. **Results:** Fifteen mice were screened with US at age 66.4±17.6 days. Seven (47%) were identified with tumors with moderate echogenicity located at the pre-aortic area between kidneys and liver. The size of tumors first detected by US was 0.65±0.66 cm$^3$. The plain CT could not discern the tumors from adjacent organs. Calcification was found by CT in 5/7 (71%) tumors. Fifteen PET/CT scans were performed in these 7 mice at age 74.3±11.3 days. $^{18}$F-FDG (n=5; tumor-to-liver uptake ratio (T/L): 4.25±1.25) and $^{18}$F-FDOPA PET (n=4; T/L: 5.37±1.49) successfully visualized the abdominal tumors. While $^{18}$F-FLT PET showed poor uptake of the agent by the tumors (n=6; T/L: 0.92±0.07), in contrast to FDG (P=0.0001) and FDOPA (P=0.0001). In older mice, tumors showed a trend of higher FDG uptake (P=0.13, $R^2$=0.5907) and lower FDOPA uptake (P=0.06, $R^2$=0.8894), while the FLT uptake remained low (P=0.0240, $R^2$=0.7582). On necropsy (mean time from the last PET scan to necropsy, 3.0±2.3 days), the tumors usually encapsulated major blood vessels and showed tight adhesion to the kidneys. **In conclusion:** (1)There is no distant metastasis detected in such an early stage by PET scans; (2)High FDOPA uptake in younger mice NBs suggested high content of AADC(aromatic L-amino acid decarboxylase); (3)High FDG uptake in older mice NBs suggested poor prognostic molecular imaging phenotype; (4)Low uptake of FLT in all NBs suggested low thymidine kinase content in the NBs and FLT may not be sensitive enough to detect the proliferation activity. (5)FDG and FDOPA PET scans are feasible in characterizing the molecular nature of NBs in the *TH-MYCN* mice model. The mechanism needs further confirmation.

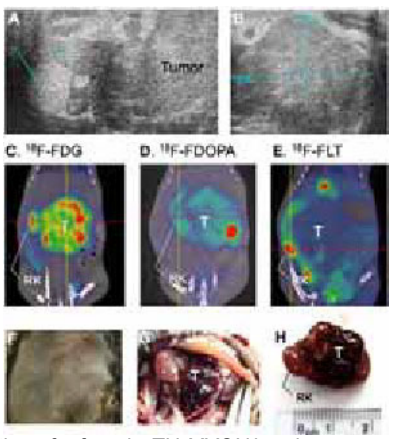


The ultrasound images, PET scans and gross examination of a female *TH-MYCN* hemizygous mouse with NB tumor. (A-B) Ultrasound screening at age 87 days showed a mass with heterogeneous echogenicity adjacent to the right kidney (RK). (C-E) PET scans using three PET probes showing an FDG-high, FDOPA-low, FLT-negative phenotype (FDG/FDOPA/FLT, at age 89/95/94 days, T/L ratios 6.621/3.169/0.794 respectively). (F-H) Necropsy at age 97 days showed abdominal distention, ecchymosis, and a dark reddish tumor encapsulating bilateral kidneys. (Abbreviations: T, tumor; RK, right kidney)

Disclosure of author financial interest or relationships:
**K. Tzen**, None; **Y. Liu**, None; **M. Lu**, None; **I. Yu**, None; **C. Chen**, None; **W. Hsu**, None.

Presentation Number **P575**
Poster Session 3
September 7, 2012 / 15:15-15:15 / Room: The Liffey

# Early assessment of temozolomide treatment efficacy in experimental gliomas using [18F]FLT microPET

***Thomas Viel***[1], *Stefan Wagner*[2], *Lydia Wachsmuth*[3], *Sonja Schäfers*[1], *Michael T. Kuhlmann*[1], *Cornelius Faber*[3], *Klaus Kopka*[2], *Michael Schäfers*[1,2], *Andreas H. Jacobs*[1,4], [1]*European Institute for Molecular Imaging (EIMI), Westfälische Wilhelms-Universität (WWU) Muenster, Muenster, Germany;* [2]*Department of Nuclear Medicine, University Hospital Muenster, Westfälische Wilhelms-Universität (WWU) Muenster, Muenster, Germany;* [3]*Department of Clinical Radiology, University Hospital Muenster, Westfälische Wilhelms-Universität (WWU) Muenster, Muenster, Germany;* [4]*Interdisciplinary Centre of Clinical Research (IZKF), Westfälische Wilhelms-Universität (WWU) Muenster, Muenster, Germany. Contact e-mail: vielt@uni-muenster.de*

Introduction: Addition of temozolomide (TMZ) chemotherapy to radiation therapy is now the standard clinical protocol for treatment of patients with glioblastoma (GBM). However, there is considerable uncertainty with regards to the effectiveness of TMZ. Assessment of treatment efficacy is performed using magnetic resonance imaging (MRI) after 3 months of treatment. Due to the rapid evolution of the disease, methods to assess TMZ efficacy early during treatment is needed. Positron Emission Tomography (PET) after injection of 3'-Deoxy-3'-[18F]fluoro-L-thymidine (FLT) is used to assess cell proliferation in vivo and could be used for an early evaluation of TMZ efficacy during GBM treatment. Aim: To monitor the anti-proliferative effect of TMZ in a mouse model of GBM using of FLT microPET. Methods: A glioma cell line displaying a low resistance to TMZ (Gli36dEGFR) was treated with low dose of TMZ (50 µM) in order to obtain a stable cell line displaying a higher resistance to TMZ, as measured using growth and clonogenic assays. Resistant and sensitive GBM cells were sub-cutaneously (s.c.) or intra-cranially (i.c.) xenografted into nude mice. Mice were treated during 7d with daily injections of 25 or 50 mg/kg of TMZ. Efficacy of TMZ treatment was measured using FLT microPET before treatment, and after 2 and 7d of treatment. MicroPET was performed 70 min after i.v. injection of 12.0 MBq FLT in a 20 min acquisition using a high-resolution HIDAC microPET camera. Computed Tomography (CT) or MRI were used to measure the size of the tumor. Results: FLT-PET performed in mice bearing sensitive and resistant Gli36dEGFR s.c. xenografts before and 7d after treatment with 25 or 50 mg/kg of TMZ showed that variation of FLT accumulation at day 7 is correlated with the variation of tumour size at day 7. FLT-PET quantifications allowed a discrimination between resistant and sensitive tumours ($p<0.01$). FLT-PET performed on mice bearing sensitive and resistant Gli36dEGFR s.c. xenografts before and 2 d after treatment with 25 mg/kg of TMZ showed that variation of FLT accumulation at day 2 is correlated with the variation of tumour size at day 7. This result was confirmed in mice bearing i.c. sensitive Gli36dEGFR xenografts. The variation of FLT accumulation between d0 and d2 was higher in resistant xenografts compared to the sensitive ones but the difference between the two groups was not significant. Conclusions: Our results indicate that FLT-PET could be appropriate for an early evaluation of the response of GBM to TMZ chemotherapy. Acknowledgement: supported by Joint Translational Research Program on Cancer DAAD-INCa (PKZ: D/0811485), the BMBF funding MoBiMed (01EZ0811), and CLINIGENE NoE (LSHB-CT-2006-018933)

Disclosure of author financial interest or relationships:
**T. Viel**, None; **S. Wagner**, None; **L. Wachsmuth**, None; **S. Schäfers**, None; **M.T. Kuhlmann**, None; **C. Faber**, None; **K. Kopka**, None; **M. Schäfers**, Siemens Medical Solutions, Grant/research support; **A.H. Jacobs**, Merck, Germany, Grant/research support .

Presentation Number **P576**
Poster Session 3
September 7, 2012 / 15:15-15:15 / Room: The Liffey

# 18F-FAZA PET-CT Mouse Imaging Reproducibility in Primary Orthotopic Cervix Tumours

***Douglass C. Vines***[1,2], *Trevor D. McKee*[2,3], *Shawn Stapleton*[1,2], *Naz Chaudary*[3], *David Green*[2], *Harald Keller*[1,2], [1]*University of Toronto, Toronto, ON, Canada;* [2]*Princess Margaret Hospital, Toronto, ON, Canada;* [3]*Ontario Cancer Institute, Toronto, ON, Canada. Contact e-mail: doug.vines@rmp.uhn.on.ca*

Introduction: Imaging of tumour hypoxia in mouse models of human cancer using small animal PET-CT with 18F-FAZA have been performed. However, the reproducibility of imaging mice with primary orthotopic cervix tumours has not been determined. Orthotopic cervix tumours are more clinically relevant then sub-cutaneous tumors because orthotopic placement models the tumor microenvironment (vascular development, flow resistance, necrosis, pressure) better than xenografts grown at subcutaneous or intramuscular sites. The purpose of this pilot study was to evaluate reproducibility of PET uptake of 18F-FAZA in mice with orthotopic cervix tumours after 2 scans within 24 hours. Methods: Human cervix cancer cells were implanted into the cervix of mice to generate orthotopic cervix xenografts. Mice (n=7) were injected awake via tail vein with 18F-FAZA (12-20 MBq), kept awake for the uptake period then anesthetized (1.5% isoflurane in medical air) for a 20 min PET scan using a Siemens Focus 220 scanner. CT scans were acquired immediately after PET. After CT mice were allowed to recover and all imaging was repeated between 23-24 h later. Acquisition parameters of net injected 18F-FAZA, awake uptake time, and scan start time post-injection were recorded for each scan. There were no changes or interventions to the mice from day 1-2 except possible tumour growth. Images were quantitatively assessed by manually placing 3D regions-of-interest (ROI) over the entire tumour and right quadriceps muscle on fused PET-CT scans. Mean and maximum percent injected dose of 18F-FAZA per gram of mouse weight (%ID/g) were determined. Since orthotopic cervix tumours are adjacent to both bladder and bowel and 18F-FAZA is cleared into both from the GU and GI systems, this presents a challenge as some spill-over of 18F-FAZA uptake due to partial-volume effects appears in the gross tumour volume (GTV) drawn on the fused CT, thus falsely elevating both mean and maximum %ID/g. Consequently, two different ROI methods were used to avoid this spill-over. In the first method a 2 mm erosion of the surface of the original GTV was created. The second method also started with the original GTV and empirically used a 5 %ID/g as an upper threshold to exclude high-uptake voxels. The average changes (day 2-day 1) for mean and maximum %ID/g were calculated for muscle, erosion, and threshold ROIs. The erosion and threshold methods mean %ID/g were also compared to each other and an r value determined. Results: Acquisition parameters of net injected 18F-FAZA, awake uptake time, and scan start time post-injection from day 1-2 had average absolute differences of 3 MBq, and 2.6, and 1.6 min respectively. Overall mean and maximum %ID/g, and the average change (day 2-day 1) mean and maximum %ID/g are listed in the table. Comparison of the erosion and threshold ROIs using the mean %ID/g yielded r = 0.91. Conclusions: This study demonstrated that the changes in acquisition parameters from day 1-2 were small and this did not seem to affect the uptake of 18F-FAZA in muscle or tumour. The variation in uptake of 18F-FAZA from day 1-2 for muscle and tumour is small indicating that our method is reproducible.

18F-FAZA Uptake

| | %ID/g | | | |
|---|---|---|---|---|
| | Mean ± SD | Avg change | Max ± SD | Avg change |
| Muscle | 0.9 ± 0.1 | 0.04 | 1.9 ± 0.2 | 0.1 |
| Tumour (erosion ROI) | 1.1 ± 0.2 | 0.2 | 5.8 ± 1.2 | 1.3 |
| Tumour (threshold ROI) | 1.8 ± 0.2 | 0.1 | | |

Disclosure of author financial interest or relationships:
**D.C. Vines**, None; **T.D. McKee**, Pfizer, Grant/research support; Molecular Insight Pharmaceuticals, Grant/research support; **S. Stapleton**, None; **N. Chaudary**, None; **D. Green**, None; **H. Keller**, None.

Presentation Number **P577**
Poster Session 3
September 7, 2012 / 15:15-15:15 / Room: The Liffey

# Detection of Metastasis in Xenograft Models of Malignant Peripheral Nerve Sheath Tumors using F18-FDG and Bioluminescence Imaging

***Jason Warram***[1], *Amber Martin*[1], *Amy Turk*[2], *Steven Carroll*[2], *Kurt R. Zinn*[1], [1]*Radiology, University of Alabama at Birmingham, Birmingham, AL, USA;* [2]*Neuropathology, University of Alabama at Birmingham, Birmingham, AL, USA. Contact e-mail: mojack@uab.edu*

The metastasis of Malignant Peripheral Nerve Sheath Tumors (MPNST) is most commonly associated with hereditary neurofibromatosis type 1 (NF1) which occurs in 15% of NF1+ MPNST patients. Distant metastasis typically occurs in bone, brain, and organs of the intra-abdominal and intra-thoracic cavities. A typical 5-year survival for nonmetastatic patients with MPNST is 54% while the 5-year survival for metastatic patients is 33%. To explore the characteristics of NF1 associated MPNST metastasis, three commonly used MPNST cells lines were intravenously implanted into NOD.Cg-Prkdcscid Il2rgtm1Wjl/SzJ mice (N=5, 1x106/0.1ml/mouse). Human NF1+ MPNST cell lines, ST88-14 and T265-2C, were used in addition to a non-NF1 associated MPNST cell line, STS-26T. All cell lines used were Luciferase positive. After injection, the mice were imaged at several time points over 22 days using Fluorodeoxyglucose (FDG) Positron Emission Tomography (PET) imaging to monitor metastasis based on metabolic activity and also Bioluminescence Imaging (BLI) to monitor metastatic development based on Luciferase expression (CMV-driven). Histology was performed to confirm the presence of established metastatic tumors in all mice. On day 8 post IV implant, the mean whole body BLI counts, or total tumor burden, for the ST88-14, T265-2C, and STS-26T were 1.59x106 (+/-7.23x105), 4.29x104 (+/-1.85x103), and 1.51x105 (+/-5.31x104), respectively. By day 22 however the mean whole body BLI counts for the ST88-14, T265-2C, and STS-26T were 5.53x108 (+/-4.03x108), 3.92x104 (+/-4.00x103), and 8.04x106 (+/-5.52x106), respectively. The difference between day 8 and day 22, which represents total metastatic tumor growth, was 5.51x108 counts for the ST88-14 and 7.89x106 counts for the STS-26T. However for the T265-2C cell line, there was an 8.6% decrease in counts. For the ST88-14 and STS-26T cell line groups, BLI revealed metastasis in the lung, lumbar spine, intestine, and femur. By day 22, there was no bioluminescent signal detected in any tissues for the T265-2C group. DICOM analysis of mean pixel intensity using 64-bit Osirix software revealed a 2-fold higher whole body uptake of FDG in the ST88-14 cell group over the T265-2C cell group at day 8 PET imaging. The FDG uptake was 3-fold higher for the STS-26T cell group over the T265-2C cell group. This trend was maintained at day 22 PET imaging with a 2.4-fold higher FDG uptake in the ST88-14 cell group and 1.6-fold higher uptake in the STS-26T over the T265-2C cell group. For the ST88-14 and STS-26T cell groups, the FDG tissue uptake correlated with luciferase signal in the lumbar spine, thoracic spine, and intestine. In conclusion, the ST88-14 cell line outperformed the STS-26T and T265-2C in establishing a metastatic model of MPNST as determined by BLI and FDG-PET imaging. The poor metastatic performance of the T265-2C cell line suggests that inducible models of metastatic MPNST used for preclinical research may be NF1 independent.

Disclosure of author financial interest or relationships:
**J. Warram**, None; **A. Martin**, None; **A. Turk**, None; **S. Carroll**, None; **K.R. Zinn**, None.

Presentation Number **P578**
Poster Session 3
September 7, 2012 / 15:15-15:15 / Room: The Liffey

# Early development of LO1, a novel IgG monoclonal natural antibody, for the imaging of oxidised LDL in atherosclerotic plaque

***Ramzi Y. Khamis***[1], *Shang-HUng Chang*[1], *Joseph J. Boyle*[1], *Niall Burke*[1], *Colin Bicknell*[2], *Michael Johns*[1], *Dorian O. Haskard*[1], [1]*Vascular Sciences Section. National Heart and Lung Institute, Imperial College London, London, United Kingdom;* [2]*Department of Surgery and Cancer, Imperial College London, London, United Kingdom. Contact e-mail: r.khamis@imperial.ac.uk*

The identification of vulnerable atherosclerotic plaque is a major priority in the field of translational cardiovascular medicine. Targeting oxidised LDL (oxLDL) epitopes for imaging presents a promising opportunity to determine plaque vulnerability based on plaque ‘inflammation'. This new paradigm for identifying vulnerable plaque is further augmented by the development new imaging technologies such as Near Infra Red Fluorescence (NIRF). We isolated a novel IgG3κ natural antibody against oxLDL (designated mAb LO1) from an LDL receptor deficient hypercholesterolaemic mouse. LO1 reacts with copper-oxidised LDL, but minimally with native LDL in vitro. Characterisation of mAb LO1 revealed specificity to malondialdehyde-conjugated LDL (MDA-LDL), an epitope expressed in heavily oxidised LDL and which is known to reflect culpability in human atherosclerotic lesions. LO1 was successfully biotinylated with retention of function. Immunohistochemical staining showed mAb LO1 colocalisation to mouse atherosclerotic lesions and to necrotic core within culprit human carotid atherosclerotic plaque. By screening a phage library expressing single chain variable region antibodies (scFv), we selected an anti-idiotype scFv (designated H3) that neutralises mAb LO1 binding to MDA-LDL. Comparison of amino acids in H3 with apoB, the major LDL protein, showed homologous sequences, suggesting H3 has structural similarities to the mAb LO1 binding site on MDA-LDL Amino acid substitutions between H3 and an irrelevant control scFv C12 showed that residues in the H3 CDRH2, CDRH3 and CDRL2 are all critical for mAb LO1 binding, consistent with a conformational epitope on H3 involving both heavy and light chains. We utilised the anti-idotype H3 to purify LO1 and sequence LO1 with mass spectrometry. LO1 was deactivated followed attempted labelling utilising amine chemistry but remained active followed labelling the SH groups. LO1 was subsequently successfully labelled with a Near Infra Red Fluorescence (NIRF) agent for in vivo imaging studies. We are also molecularly expressing various sized constructs of LO1 for utility in multimodality cardiovascular imaging, including PET.

Disclosure of author financial interest or relationships:
**R.Y. Khamis**, GSK, Grant/research support; **S. Chang**, None; **J.J. Boyle**, None; **N. Burke**, None; **C. Bicknell**, None; **M. Johns**, None; **D.O. Haskard**, None.

Presentation Number **P579**
Poster Session 3
September 7, 2012 / 15:15-15:15 / Room: The Liffey

# VEGF enhance the permeability of the blood-brain barrier

***Shize Jiang**, Rui Xia, Lei Wang, Fabao Gao, department of radiology, molecular imaging library, Chengdu, China. Contact e-mail: jiangshize1990@163.com*

Background: The blood-brain barrier (BBB) is a tightly regulated barrier that strictly controls the exchanges between the blood and brain components, which could also impede drugs from entering into brain when in morbid condition. The vascular endothelial growth factor (VEGF) is one of the most important growth factors in the process of angiogenesis and vasculogenesis. Purpose: We aim to: (1) find an effective way to increase the permeability of BBB with the help of vascular endothelial growth factor (VEGF) so as to benefit the central nervous system (CNS) drug delivery; (2) find an effective method for the measurement of the extent of the BBB permeability by MRI in vivo. Materials and Methods: 24 KM mice were randomly divided into 3 groups. There are two treatment groups which treated with different dosage of Hu-VEGF165 and one control group treated with saline. The mice were examined by MRI before and 5min, 10min, 15min after the injection of Gd-DTPA, respectively and 7T MRI was performed 8 hours after treatment for the mice. MRI sequences included MSME-T1, RARE-T2 and DWI. The mice received Evans Blue by venous injection after MRI examination. They were sacrificed 0.5h after the injection of Evans Blue and perfused with saline and paraformaldehyde sequentially. The brain specimens were removed and fixed for histological study. Results: MRI examination showed the group treated with higher dosage had a significantly higher signal intensity of brain parenchyma than the control ($P<0.001$), and the group treated with lower dosage had a slightly higher signal intensity, the difference was not obvious. The extravasation of Gd-DTPA observed within the brain indicated an impairment of the BBB integrity. Evans blue perfusion revealed the fluorescence intensity of the brain parenchyma was higher in VEGF-treated animals compared with control. An increase in brain parenchyma perfusion correlated with an increase in VEGF administration. The results are concordant well with MRI examination. Minimal edema among these three groups was also investigated both by DWI and H-E staining; however, no significant difference was found. Conclusion: The permeability of BBB was higher in VEGF-treated animals compared with controls and exogenous application of VEGF can modulate the permeability of BBB. This may be a new direction to deliver drugs to the CNS. MRI examination correlated well with histological study in the measurement of BBB permeability, providing an ideal method for BBB study in vivo.

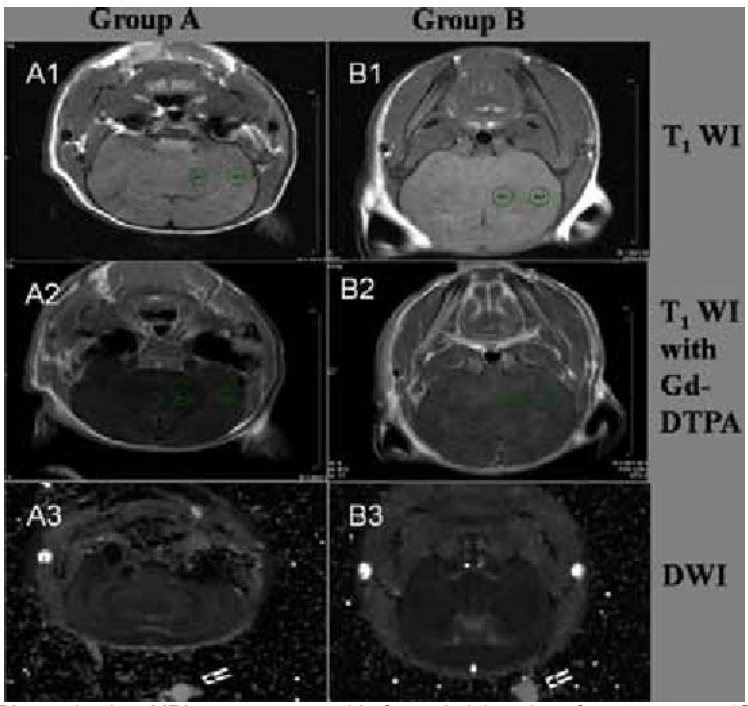


Permeability of blood vessels by MRI examination. MRI scans generated before administration of contrast agent (Gd-DTPA) in two groups of mice (A1 and B1) and the others scanned immediately after the injection of Gd-DTPA (A2 and B2). Group A was pretreated with 200ul saline. Group B was pretreated with 200ul VEGF (0.015mg/ml) for 8hours. ROI (region of interest) is for the measurement of signal intensity. ROI1 stands for the region of basal ganglia and ROI2 stands for the region of cerebral cortex. DWIs (A3 and B3) of these two groups show no significant difference. Arrowheads indicate water tube.

Disclosure of author financial interest or relationships:
**S. Jiang**, None; **R. Xia**, None; **L. Wang**, None; **F. Gao**, None.

Presentation Number **P580**
Poster Session 3
September 7, 2012 / 15:15-15:15 / Room: The Liffey

# Identification of neurogenic microRNAs involved in activating neuronal differentiation induced by neurogenin 1 (ngn 1) via microarray analysis

***Hyun Jeong Oh***[1], *Do Won Hwang*[1,2], *Hyewon Youn*[1,3], *Dong Soo Lee*[1,2], [1]*Department of Nuclear Medicine, Seoul National University College of Medicine, Seoul, Republic of Korea;* [2]*Institute of Radiation Medicine, Medical Research Center, seoul, Republic of Korea;* [3]*Laboratory of Molecular Imaging and Therapy, Cancer Research Institute, seoul, Republic of Korea. Contact e-mail: holyhiphop@lycos.co.kr*

Purpose: MicroRNAs (miRNAs) are known to act as post-transcriptional modulators of gene expression. It has been reported that miRNA could affect neuronal differentiation by binding it to target mRNA. Neurogenin1 (Ngn1) which is known as a basic helix loop helix transcription factor has been used as an activator of neuronal differentiation. The aim of this study is to investigate the novel neurogenic miRNA expressed in neuronal precursor cells differentiated into neuronal lineage induced by ngn1 via miRNA microarray. Methods: pcDNA3.1His/Ngn1 was used for induction of neuronal differentiation in neuronal precursor cells. Neuroblastoma and dorsal root ganglia hybrid F11 cell line was maintained in general culture medium on gelatin coated dish. F11 cells transfected with ngn1 were incubated in DMEM supplemented with 0.5% FBS for 1 day. MiRNA microarray analysis was performed from isolated total RNA using agilent microarray scanner. Functional annotation for target genes of miRNAs was searched by the Database for Annotation, Visualization and Integrated Discovery (DAVID) v6.7. Results: Ngn1 gene was detected in ngn1-overproduced F11 cells by RT-PCR, compared to mock-transfected F11 cells. Based on the signal intensity levels and fold changes between mock-transfected and ngn1-transfected F11 cells, 240 upregulated miRNAs including miR-132, exhibiting greater than two fold changes and 5 fold signal intensity levels were considered as neurogenic miRNAs. The identified microRNAs were further analyzed in terms of gene ontology (GO), based on their target mRNAs. Target genes of identified miRNAs were associated with neurogenesis, axon guidance and several cell proliferation pathways. Conclusions: In this study, we examined the miRNA expression profiling in ngn1-overproduced neuronal precursor F11 cells, via miRNA microarray. This study represents that the identified neurogenic microRNAs could be used as new inducer for neuronal differentiation in terms of stem cell-based therapy.

Disclosure of author financial interest or relationships:
**H. Oh**, None; **D. Hwang**, None; **H. Youn**, None; **D. Lee**, None.

Presentation Number **P581**
Poster Session 3
September 7, 2012 / 15:15-15:15 / Room: The Liffey

# The Spatial Distribution of Glycine in Rat Glioma Revealed by in vivo Chemical Shift Imaging

***Feng-Mao Chiu***[1,2], *Nai-Wei Yao*[2], *Jaya Seema*[2], *Chiao-Chi V. Chen*[2], *Chen Chang*[2], *Jyh-Horng Chen*[1,2], [1]*Graduate Institute of Biomedical Electronics and Bioinformatics, National Taiwan University, Taipei, Taiwan;* [2]*Institude of Biomedical sciences, Academia Sinica, Taipei, Taiwan. Contact e-mail: layzack121@gmail.com*

Introduction: Glycine was increasingly recognized as a tumor biomarker by magnetic resonance spectroscopy (MRS)[1,2]. But it is unknown how the distribution of glycine is correlated with the spatial heterogeneity of tumors. Chemical shift imaging (CSI) appears as an ideal tool to investigate the issue due to its acquisition of spatial information of metabolites. Another focus of this study is to understand the relationship among tumor biomarkers including glycine, choline, and lactate with respect to the different areas of tumors. Materials and methods: A rat glioma model formed from C6 cells was used. 6×105 C6 cells were injected into the right striatum in a volume of 0.6 μL in a 9-week-old Sprague-Dawley rat on the stereotaxic apparatus using a 30-gauge needle and a micro-infusion pump. CSI MR experiments were performed on the 4.7T Biospec 47/40 spectrometer. For the CSI reference image, the T2 weighted images (T2WI) were acquired by fast spin echo sequence. The CSI was acquired with field of view (FOV) =3.2 cm, slice thickness=2.5 mm, 1 slices, TR=2500 msec, TE=136 msec, number of excitations (NEX)=10, matrix size=16×16. The rats were scanned in the third week after the induction of C6 glioma. The acquired spectras were processed by MATLAB. The metabolic images were reconstructed by 3D Interactive Chemical Shift Imaging V1.9.1.0 - 3DiCSI which directly read the original raw data, and the image size were zero-filled to 64×64. Results and discussion: The tumor implanted in the right striatum of the rat brain was detected on T2WI. The spectras of CSI show decreased NAA, decreased Cr, increased Choline, increased Lactate, and increased Glycine on the tumor side as compared with the contralateral side. The metabolic images reconstructed from CSI demonstrate the spatial distribution of the various metabolites. NAA signals were absent in the tumor area. Cho levels were elevated in the tumor hemisphere, especially surrounding the peripheral area of the tumor. The signal levels of Lac and Gly were enhanced in the tumor with an increasing gradient towards the core. The results indicate that the three tumor markers, Cho, Lac, and Gly exhibit unique distributional patterns with respect to the tumor region. The findings suggest that the neuron loss in the glioma led to decreased NAA. The tumor periphery is characterized with rapid growth of the tumor cells due to sufficient blood supply. The proliferation of tumor cells may heighten the levels of the cellular lipid membrane, and thus caused the distribution pattern of Cho around the tumor borders. The tumor core is normally hypoxic. This could be responsible for elevations in Glycine and Lactate, two metabolites associated with hypoxic stress[3]. The unique distribution patterns of the three tumor markers reveal the different metabolic characteristics in relation to the spatial heterogeneity of tumors. The use of CSI to detect the metabolic changes of multiple tumor markers can be very useful for monitoring the stages of tumors. Reference: [1] Shah T, et al. NMR Biomed. 2011 [2] Bobek-Billewicz B, et al. Folia Neuropathol. 2010 [3] Furuya S, et al. PNAS. 2000

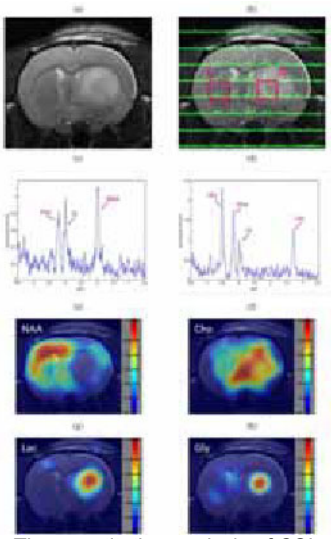

The quantitative analysis of CSI

| | NAA/Cr | Cho/Cr | Lac/Cr | Gly/Cr |
|---|---|---|---|---|
| Tumor side | 0.50±0.18 | 1.20±0.13 | 0.91±0.20 | 1.20±0.28 |
| Contralateral side | 1.20±0.15 | 0.68±0.18 | 0.15±0.05 | 0.24±0.01 |

Disclosure of author financial interest or relationships:
**F. Chiu**, None; **N. Yao**, None; **J. Seema**, None; **C.V. Chen**, None; **C. Chang**, None; **J. Chen**, None.

Presentation Number **P582**
Poster Session 3
September 7, 2012 / 15:15-15:15 / Room: The Liffey

# Applications of Novel ΔR2-mMRA Technology and MR Spectroscopy to Observe the Morphology of Blood Vessel in Alzheimer's Disease Animal Model

***Ming-Shiuan Chiueh***[1,2], *Feng-Mao Chiu*[1], *Jyh-Horng Chen*[1], *Chungming Chen*[2], [1]*Interdisciplinary MRI/MRS Lab, Department of Electrical Engineering and Molecular Imaging Center, National Taiwan University, Taipei, Taiwan;* [2]*Graduate Institute of Biomedical Engineering, National Taiwan University, Taipei, Taiwan. Contact e-mail: dwsonor@yahoo.com.tw*

Most studies of the Alzheimer's disease are on the associated nerve system nowadays. However, the recession on the brain capillaries circulation also play an important role in AD. In this paper, we use the ΔR2-mMRA to estimate the changes of the brain neurotransmitters by MR image of the brain capillaries and the related CBF (cerebral blood flow) in the AD's animal model (by MRS) to show the effectiveness of our new method in the animal model. Early detection by observing and comparing the change in the AD disease using ΔR2-mMRA may be promising in the future AD's patients gradually lose their memory, causing the barrier in the language and emotion socialization. It has been shown that beta-amyloid plaques and neurofibrillary tangles in the brain lead to symptoms of the AD's patients. In this study, we focus on the degeneration or apoptosis on the brain capillaries in the beta-amyloid plaques and neurofibrillary tangles area. 3DΔR2-mMRA technologies, visualizing the morphology difference of small blood vessel in the AD'sl rats and MRS are performed to detect the molecular changes of metabolites in the brain. In our MRS results, we used the ratio of N-acetylaspartate (NAA) and creatine (Cr) to define NAA concentration. In normal rat, NAA/Cr= 1.13, which is higher than that in Alzheimer disease rat, NAA/Cr= 0.87; While the Cho/Cr ratio are about the same in both rats, around 0.63. (shown in Fig. 1A). Furthermore, ΔR2-mMRA technology provides the angiography of the small blood vessels at the same time (Fig.1B). The small blood vessels numbers are reduced in the brain of Alzheimer induced rat, especially in cortex and hippocampus (the white arrow in Fig. 1B) compared to our control data. It might indicate that that blood vessels Atrophied was in progress in the Alzheimer-induced rat. In addition to that, CBF studies similar decreased values in the basal forebrain and hippocampus of Alzheimer's animal model (Fig.1C). These results suggest that abnormal microcirculation contribute to the pathogenesis of Alzheimer's disease and precedes the onset of anatomy image. In summary, we use the novel ΔR2-mMRA angiograph, MR spectroscopy and CBF to the early detection of Alzheimer's animal model. By observing the dynamic change behavior of the degeneration of brain small blood vessels and metabolites concentration of brain, MR imaging may provide a new method for early diagnosis of Alzheimer's disease in the near future.

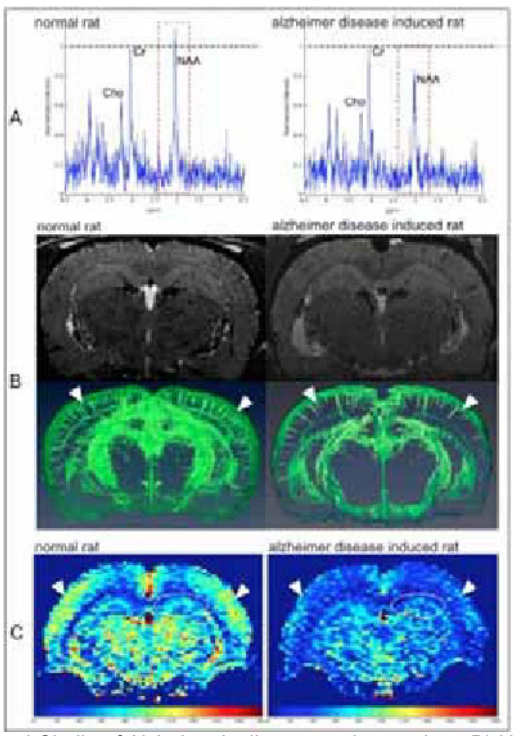


Fig.1 A) The MR spectrum of NAA, Creatine, and Cholin of Alzheimer's disease and normal rat. B) Using novel 3DΔR2-mMRA of brain small blood vessel angiography, compared by Alzheimer's disease and normal rat. C) The brain CBF color mapping of Alzheimer's disease and normal rat.

Disclosure of author financial interest or relationships:
**M. Chiueh**, None; **F. Chiu**, None; **J. Chen**, None; **C. Chen**, None.

Presentation Number **P583**
Poster Session 3
September 7, 2012 / 15:15-15:15 / Room: The Liffey

# Improved magnetic particle spectrometer providing high field amplitudes for investigation of hysteresis effect in superparamagnetic nanoparticle tracers

***Marlitt Erbe**, Timo F. Sattel, Thorsten M. Buzug, University of Luebeck, Luebeck, Germany. Contact e-mail: erbe@imt.uni-luebeck.de*

The novel and very promising tomographic method magnetic particle imaging (MPI) is capable of detecting the spatial and temporal distribution of a superparamagnetic iron-oxide (SPIO) nanoparticle tracer within a patient in 3D and in real-time. Oscillating magnetic excitation fields are applied imposing a magnetization change on the tracer material, which can be detected in receive coils due to the reciprocity principle. Gradient fields featuring a field free point (FFP) as well as a linearily increasing field strength originating from the FFP are superimposed to the excitation fields. Thus, only the tracer material located at the FFP contributes to the detected signal, since everywhere else the high field strength forces the SPIO particles into saturation. By moving the FFP through the region of interest spatial encoding is achieved. The physical behaviour of the tracer material is one of the crucial aspects regarding the performance of MPI with respect to sensitivity and spatial resolution. The best results were up till now achieved in measurements using the former magnetic resonance imaging (MRI) liver contrast agent Resovist® (Bayer Schering Pharma) as MPI tracer. However, providing tracer particles optimized for MPI will considerably enhance the sensitivity of this method. To analyze the MPI performance of a certain SPIO tracer a magnetic particle spectrometer (MPS) is used. The MPS uses the same physical principles as MPI, but without applying spatial encoding. It is hence possible to analyze the suitability of a SPIO tracer for use in MPI. Since the physical behaviour of Resovist® and comparable tracer particles is not yet fully understood, it is of great importance for the tracer development to provide information about the particle behaviour for a broad range of parameters. Formerly introduced MPS studies allowed for an excitation field strength of not more than 30 mT/$\mu_0$. Since hysteresis effects do preponderate especially at higher excitation field strengths, stronger magnetic fields are needed to detect and visualize these effects. An optimized MPS was therefore designed and is presented in this work, which allows for excitation field strengths up to 40 mT/$\mu_0$. At these high field strengths hysteresis effects in the particles' magnetization behaviour lead to a phase shift in the detected MPS signal. This is visible in the formation of waves in the particle spectrum. This effect increases with increasing excitation field strength as visible in the measurements presented in Figure 1. These measurements were performed with 10 µl undiluted Resovist®. Analyzing these measurements and the corresponding hysteresis effects will allow for a more detailed characterization and a deeper understanding of the anisotropy properties of SPIO particles. The presented optimized MPS hence provides essential information advancing the MPI tracer development and therefore also the MPI performance. In addition, information about hysteresis effects will be useful for hyperthermia applications as well.

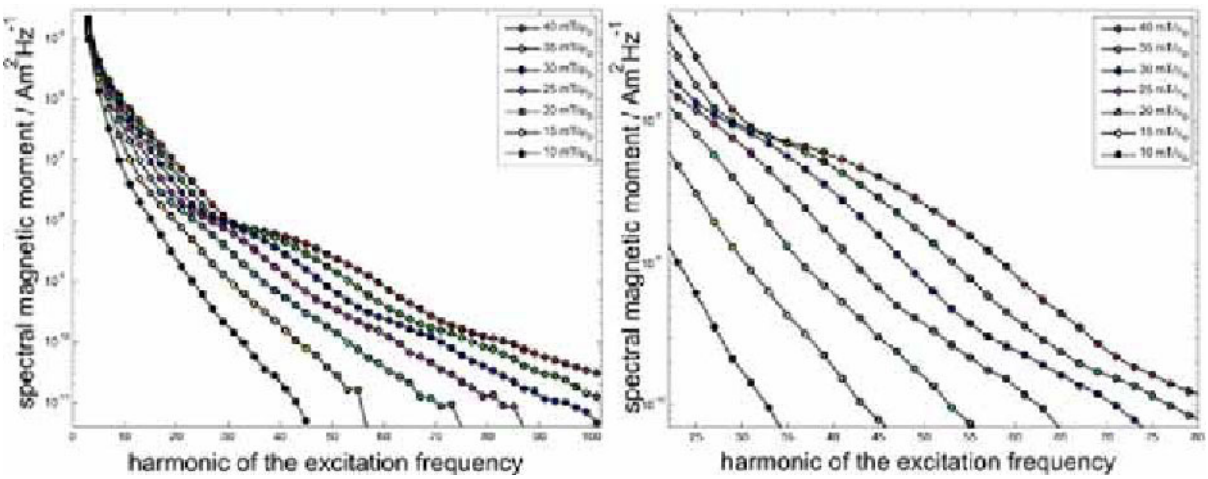


Figure 1. Odd harmonics of the magnetic moment from an MPS measurement of a sample of 10 µl undiluted Resovist® and an excitation frequency of 25 kHz. The excitation field strength is varied between 10 and 40 mT/$\mu_0$. The plot on the right shows a zoom of the region in which the wave effects in the spectrum are clearly detectable.

Disclosure of author financial interest or relationships:
**M. Erbe**, None; **T.F. Sattel**, None; **T.M. Buzug**, None.

Presentation Number **P584**
Poster Session 3
September 7, 2012 / 15:15-15:15 / Room: The Liffey

# Non-invasive quantification of cells using magnetic particles and Electron Paramagnetic Resonance

*Jesse Trekker[1,3], Peter Vaes[2], Sonu Sharma[3], Ashwini Atre[3], Stephanie Teughels[2], **Uwe Himmelreich**[3], [1]imec, Leuven, Belgium; [2]PEPRIC nv, Leuven, Belgium; [3]Department of Radiology and Pathology, KU Leuven, Leuven, Belgium. Contact e-mail: Uwe.Himmelreich@med.kuleuven.be*

Intro: The use of superparamagnetic iron oxide nanoparticles (SPIO) within magnetic resonance imaging (MRI) has over the years gained lots of interest. Labeling of cells with SPIOs has become a routine to detect and track cells with high resolution in vivo (1). Recent advances turn to quantitative MRI and focus on determining the amount of cells based on the contrast generated by the SPIOs in the MR images (2). A number of special pulse sequences has been recommended but due to complex adjustment methods none of them is currently used routinely. In this report, the performance of several commercial and in house SPIOs was investigated towards a highly sensitive, direct, and quantitative SPIO detection technique based on electron paramagnetic resonance (EPR). Methods: SPIO characterization: Endorem, Resovist were used as described previously (1). Small core SPIOs (7 nm - mPEGSi-7) and large core SPIOs (13 - mPEGSi-13) were synthesized by the thermal decomposition method and were functionalized with a PEGylated silane. Magnetoliposomes (MLs) were prepared by co precipitation and enwrapped by a liposome. 150 µl of different concentrations of SPIOs were placed in a PEPRIC particle spectrometer (PPS) (Pepric NV, Leuven BE) and the signal was measured at ~100 Gauss. The excitation frequency was set to ~300 MHz. A background reference measurement was taken for correction. Cell labeling: MSCs and Cl2slow cells were labeled with different concentrations of SPIOs. After SPIO internalization the cells were harvested and suspended in 150 µl of PBS. Different amounts of cells were placed in the PPS and the signal was measured in the same matter as previous stated. For comparison, intracellular iron amounts were measured by ICP-OES. Results: The sensitivity of five SPIOs were tested. Endorem had a sensitivity of 1.43 mV/µmol Fe. Different concentrations of Endorem were tested and a linear behavior of concentration versus EPR signal was found. Resovist had a similar sensitivity to Endorem of 1.43 mV/µmol Fe. A higher sensitivity was detected for ML with a value of 2.5 mV/µmol Fe. Different liposome coatings were tested (cationic, anionic), but no effect was found. To study the effect of the core size, two in house prepared SPIOs with similar coatings were measured. The mPEGSi-7 had a sensitivity of 0.85 mV/µmol of Fe. A ten-fold increase in sensitivity was measured for the mPEGSi-13 SPIO to ~9 mV/µmol Fe, indicating that a larger core produces higher EPR signals. After labeling of cells (1, 3), the EPR signal was measured. Although measured signals were lower than for suspended SPIOs, we were still able to detect less than 50000 cells labeled with mPEGSi-13 SPIOs. Conclusion: The EPR approach is an easy to use, completely non-invasive method to determine the intracellular iron concentrations. In addition it is non destructive, so that the cells can be used after the EPR measurement. In the future the PPS will be used to detect SPIOs in more complex samples such as tissue. Ref: 1. A. Crabbe, et al. Cell Transpl. 19: 919 2010 2. W. Liu, et al. EJRAD, 70: 258 2009 3. S. Soenen, et al. WIREs Nanomed. Nanobiotech. 3: 197 2011

| Sample | mV/µmol Fe |
|---|---|
| Resovist | 1.43 |
| Endorem | 1.43 |
| ML | 2.50 |
| mPEGSi-7 | 0.85 |
| mPEGSi-13 | 8.93 |

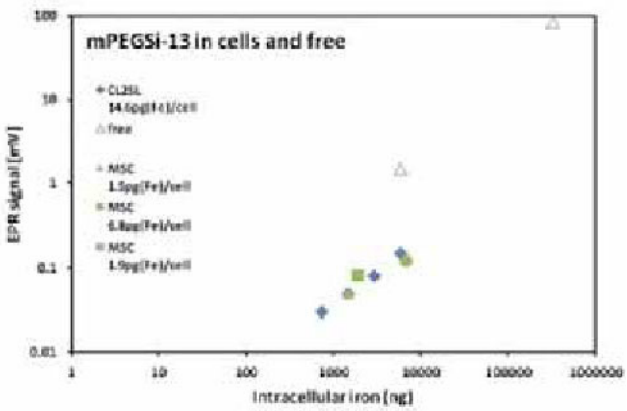


Left: Table of the EPR sensitivity of different SPIOs. Right: Graph of the EPR signal (mV) versus the total amount of internalized iron (ng). Cl2slow and MSCs were measured with different intracellular iron concentrations.

Disclosure of author financial interest or relationships:
**J. Trekker**, None; **P. Vaes**, Pepric, Employment; **S. Sharma**, None; **A. Atre**, None; **S. Teughels**, Pepric nv, Employment; Pepric nv, Stockholder; **U. Himmelreich**, None.

Presentation Number **P585**
Poster Session 3
September 7, 2012 / 15:15-15:15 / Room: The Liffey

# Effect of coating material on biodistribution and relaxometric properties at 7T MRI - comparison of self-synthesized monodisperse, polymer coated SPIO and dextran coated FeraSpin S®

***Nina Raabe***[1], *Sunhild C. Salmen*[5], *Barbara Freund*[2], *Markus Heine*[4], *Thomas Ernst*[1], *Michael G. Kaul*[1], *Rudolph Reimer*[3], *Gerhard Adam*[1], *Harald Ittrich*[1], [1]*Department of Diagnostic and Interventional Radiology, University Medical Center Hamburg-Eppendorf, Hamburg, Germany;* [2]*Department of Biochemistry and Molecular Biology II, University Medical Center Hamburg-Eppendorf, Hamburg, Germany;* [3]*Heinrich-Pette-Institute for Experimental Virology and Immunology, Hamburg, Germany;* [4]*Department of Anatomy II: Experimental Morphology, University Medical Center Hamburg-Eppendorf, Hamburg, Germany;* [5]*Institute of Physical Chemistry, University of Hamburg, Hamburg, Germany. Contact e-mail: ninaraabe@alice-dsl.net*

Superparamagnetic iron oxide nanoparticles (SPIO) are widely investigated for their use as contrast agents in magnetic resonance imaging. Thereby the fundemental knowledge of coating dependent in vivo distribution and relaxometric properties of SPIO is essential for an optimal particle choice regarding the diverse approaches at clinical and preclinical studies at MRI. Therfore the purpose of this study was to evaluate the influence of two different coating materials of superparamagnetic iron oxide nanoparticles on their in vivo distribution and relaxometric MR properties. For this purpose self-synthesized polymer-coated, monodisperse SPIO(PNP) were compared to the commercially produced, preclinical carboxydextran-coated SPIO FeraSpin S® (Milteny Biotec GmbH, Germany). Both particles had equal hydrodynamic diameters (20-30nm) and were i.v. injected at iron concentrations of 25 and 50µg (n = 3 per SPIO and dosage). DSC-MRI (30min) and T2* relaxometry were performed on a 7T small animal MR scanner(ClinScan®, Bruker, Germany) and evaluation was done for liver, spleen, muscle and kidney. MR findings were matched with histology (Prussian Blue) and transmission electron microscopy of tissue samples. Both SPIOs showed an organ specific and dose dependent distribution with the highest uptake in the liver, followed by the spleen. DSC of PNP showed an initial fast signal decrease in the liver followed by a stable phase after ~ 300s, while FeraSpins S® showed an almost linear signal change in the liver. Similar signal changes were found in the spleen, but to a lower extent than in the liver. The absolute signal change instead was dependent on the iron concentration for both SPIO. There was no significant signal change in muscle or kidney for both SPIO. ΔR2* in the liver was higher for FeraSpins S® than for PNP at concentrations of 25 µg, while T2* shortening was too high for reliable measurements in the liver at a concentrations of 50 µg as well as for PNP in the spleen at 25 and 50 µg. The cellular uptake was proven by ultra structural analysis. Taking this together we were able to show that the coating of SPIO may have an important impact on the in vivo distribution and MR imaging properties of SPIO. Our study shows that the evaluated carboxydextran-coated SPIO seem to circulate longer than the polymer-coated SPIO, with a concomitend diverse saturation of signal change in liver and spleen. This may be due to a coating dependent agglomeration of PNP in vivo, which matched findings of additional in vitro studies regarding the particle agglomeration of SPIO in dependency on the surrounding biofluid.

Disclosure of author financial interest or relationships:
**N. Raabe**, None; **S.C. Salmen**, None; **B. Freund**, None; **M. Heine**, None; **T. Ernst**, None; **M.G. Kaul**, None; **R. Reimer**, None; **G. Adam**, None; **H. Ittrich**, None.

Presentation Number **P586**
Poster Session 3
September 7, 2012 / 15:15-15:15 / Room: The Liffey

# Automated breast density measurement with MRI at 3T using the DIXON sequence: comparison with mammographic breast density estimation

***Katja Pinker-Domenig**, Georg J. Wengert, Wolf-Dieter Vogl, Wolfgang Bogner, Heinrich F. Magometschnigg, Thomas H. Helbich, Department of Radiology, Division of Molecular and Gender Imaging, Medical University of Vienna, Vienna, Austria. Contact e-mail: katja.pinker@meduniwien.ac.at*

PURPOSE To develop a fully automated quantitative volumetric MRI breast density measurement system using the Dixon sequence and to correlate it with standard mammographic density estimation using the user-assisted thresholding method (Cumulus). METHOD AND MATERIAL 35 healthy women (age range of 21-68; mean 38 years) were included in this prospective IRB-approved study. Breast density was calculated from digitized mammograms using Cumulus, a user-assisted interactive thresholding technique and with radiation- and compression-free MRI using the Dixon sequence (TR/TE 6ms/ 2.45ms/2.67ms, 192 slices, matrix 352 x 352, 1mm isotropic, TA 3:38 min). All MRI-measurements were performed on a 3T scanner with a 4-channel dedicated breast coil. The Dixon sequence acquires two separate datasets in one sequence, one representing the fatty components and one the fibroglandular components of the breast. The MRI breast density measurement system uses a fully automated segmentation of the anatomic region of the breast and calculates the total volume of the breast (cm3), the percentage of fatty tissue (%) and the percentage of fibroglandular tissue (%). Mean values were compared using student's t-test. Additionally, one of the four standard BI-RADS® density categories was allocated to each of the mammograms. Descriptive statistics using the 25-75 % percentile were used to define the typical range of MRI density readings corresponding to the 4 BI-RADS® categories of breast density. RESULTS Percentage MRI breast density correlated with percentage mammographic breast density as estimated with Cumulus ($r = 0.83$; $P < 0.0001$). MRI breast density measurements ranged from 1.70% to 61.9% (mean 29.05%). Mammographic breast density results ranged from 5.42% to 74.33% (mean 40.23%). Compared with the BIRADS categories, 25-75% percentile assessment demonstrated an interquartile range of MRI percentage breast density of 2.4-9.4% for BIRADS-1, 7.25-26.88% for BIRADS-2, 26.1-48.43% for BIRADS-3 and 39.7-53.9% for BIRADS-4. Quantitative MRI breast density readings were consistently lower than qualitative BI-RADS® assessment CONCLUSION Fully automated quantitative volumetric MRI breast density measurement using the Dixon sequence correlates well with mammography-based quantitative breast density readings. In contrast to the semi-automated thresholding approach, it is fast, user-independent and radiation- and compression-free.

Disclosure of author financial interest or relationships:
**K. Pinker-Domenig**, None; **G.J. Wengert**, None; **W. Vogl**, None; **W. Bogner**, None; **H.F. Magometschnigg**, None; **T.H. Helbich**, Siemens, Grant/research support; Fond national bank austria, Grant/research support .

Presentation Number **P587**
Poster Session 3
September 7, 2012 / 15:15-15:15 / Room: The Liffey

# Automated breast density measurement with MRI at 3T using the DIXON sequence: proof of concept

***Georg J. Wengert****, Katja Pinker-Domenig, Wolf-Dieter Vogl, Hubert Bickel, Benedikt Brück, Thomas Helbich, Department of Radiology, Division of Molecular and Gender Imaging, Medical University of Vienna, Vienna, Austria. Contact e-mail: georg.wengert@meduniwien.ac.at*

PURPOSE Breast density is one of the strongest predictors of breast cancer risk. To-date breast density measurement is performed qualitatively using mammography with radiation and compression. The aim of this study is to introduce a novel radiation-free, fully automatic quantitative volumetric breast density measurement with MRI using the Dixon sequence and to quantify the variations in breast tissue and volume measurements due to patient positioning. METHOD AND MATERIALS 33 healthy volunteers without any history of breast disease (age range of 21-68; mean 38 years) were included in this prospective IRB-approved study. In all healthy volunteers breast density was measured with radiation- and compression-free MRI using the Dixon sequence (TR/TE 6ms/ 2.45ms/2.67ms, 192 slices, matrix 352 x 352, 1mm isotropic, TA 3:38 min). All measurements were performed on a 3T Scanner with a 4-channel dedicated breast coil. The Dixon sequence acquires two separate datasets in one sequence, one representing the fatty components and one the fibroglandular components of the breast. Our MRI breast density measurement system uses a fully automated segmentation of the anatomic region of the breast and generates a combined histogram resulting in two discriminable clusters of fatty and fibroglandular breast tissue. The system automatically calculates the total volume of the breast (cm3), the percentage of fatty tissue (%) and the percentage of fibroglandular tissue (%). Each volunteer was scanned twice with a delay of approximately 30 min in between the two examinations. Both breast density measurements were correlated. REULTS Quantitative volumetric breast density measurement with MRI using the Dixon sequence was successfully performed in all healthy volunteers. In both examinations, density values ranged from 1.6% to 61.9% (mean 29.05%). There was excellent correlation of percentage breast density, total breast volume and total volume of fibroglandular tissue in all healthy volunteers for both measurements ($r = 0.97$; $P < 0{,}0001$). CONCLUSION Fully automated quantitative volumetric measurement of breast density with MRI using the Dixon sequence is a robust method, which allows a reliable and reproducible assessment of breast density, a strong predictor of breast cancer risk.

Disclosure of author financial interest or relationships:
**G.J. Wengert**, None; **K. Pinker-Domenig**, None; **W. Vogl**, None; **H. Bickel**, None; **B. Brück**, None; **T. Helbich**, None.

Presentation Number **P588**
Poster Session 3
September 7, 2012 / 15:15-15:15 / Room: The Liffey

# Hypoxia and vasculature in models of lung cancer: location, location, location

***Marta Vilalta***[1], *Nicholas P. Hughes*[1], *Sarah J. Moore*[3], *Leanne Sayles*[2], *Alejandro Sweet-Cordero*[2], *Jennifer R. Cochran*[3], *Amato Giaccia*[1], *Edward E. Graves*[1], [1]*Division of Radiation Oncology, Stanford University, School of Medicine, Stanford, CA, USA;* [2]*Department of Pediatrics, Satnford University, Stanford, CA, USA;* [3]*Department of Bioengineering, Satnford University, Stanford, CA, USA. Contact e-mail: mvilalta@stanford.edu*

Hypoxia is a well-established mediator of radiation sensitivity. Recently, studies have shown that it is also involved in tumor aggressiveness and metastasis. However, much of our knowledge of hypoxia is based on preclinical studies using xenograft tumors implanted subcutaneously in mice. It is known that these models exhibit important differences in behavior from human tumors. Previously, we have shown that subcutaneously implanted lung tumors in mice exhibit significant hypoxia while both orthotopic and spontaneous tumors are much better oxygenated. Furthermore, when we treated these tumor models with PR-104, a chemotherapeutic agent that selectively kills hypoxic cells, only subcutaneously tumors exhibited DNA damage response. We hypothesize that these differences in hypoxia are due to differences in vascularity and perfusion between these tumor systems. Thus, the aim of this study was to compare vessel presence and functionality in these preclinical models of lung cancer. We employed spontaneous lung tumors initiated by tissue-specific activation of K-ras, as well as subcutaneous and orthotopic implanted mouse lung cancer cells derived from the spontaneous models. Dynamic contrast enhanced magnetic resonance (DCE-MRI) was performed on all tumor models in order to measure vascular perfusion. Just prior to animal sacrifice, the animals were injected with Hoechst 33324. After sacrifice, the tumors were harvested and analyzed postmortem by Immunohistochemistry (IHC) to evaluate the distribution of Hoechst 33324, representing perfused areas, as well as a vascular marker, Meca 32, in order to compare at a microscopic level the presence and functionality of the vasculature across these different preclinical models. Both orthotopic implanted and spontaneous lung tumor models showed elevated contrast agent uptake (gadolinium) injected during DCE-MRI imaging process, demonstrating the leakiness and, therefore, the functionality of the vasculature within these tumors. However, little gadolinium uptake was observed within the bulk of the subcutaneous implanted tumors, showing the dysfunction of the vessels in this tumor model. These results were corroborated at the microscopic level by analyzing staining of the cells surrounding the vessels by Hoechst 33342. While the subcutaneous tumors showed only some positive staining at the rim of the tumors, staining was detected throughout the spontaneous tumors. Furthermore, positive Meca-32 staining was seen at the edge as well as in the internal part of the subcutaneous tumors. However in the case of the spontaneous tumors, the vessels were much bigger and well formed compared to the subcutaneous implanted ones. These results show the influence that a specific preclinical tumor model can play in the physiologic behavior of the tumor system. From this study we can also conclude that the discrepancy in the hypoxia level in these different tumor models could be a consequence of the variation in both vessel formation and functionality. Thus, judicious selection of preclinical lung tumor models is essential for the study of both, hypoxia and angiogenesis as well as therapies targeting these phenomena.

Disclosure of author financial interest or relationships:
**M. Vilalta**, None; **N.P. Hughes**, None; **S.J. Moore**, None; **L. Sayles**, None; **A. Sweet-Cordero**, None; **J.R. Cochran**, None; **A. Giaccia**, None; **E.E. Graves**, None.

Presentation Number **P589**
Poster Session 3
September 7, 2012 / 15:15-15:15 / Room: The Liffey

# A New Strategy for Chemical Exchange-dependent Saturation Transfer Imaging

*Zhuozhi Dai[1], Gang Xiao[2], Zhiwei Shen[1], Lvhao Wang[1], Phillip Zhe Sun[3], **Renhua Wu**[1], [1]medical imaging, Shantou University Medical College, Shantou, China; [2]Math and Information Technology, Hanshan Normal University, Chaozhou, China; [3]Radiology, Harvard Medical School, Charlestown, MA, USA. Contact e-mail: rhwu@stu.edu.cn*

Introduction: Chemical exchange-dependent saturation transfer (CEST) imaging, a novel molecular imaging technology, which can be applied to detect both the physical and physiological situations in vivo noninvasively, such as tissue pH, amide proton transfer, glycogen, glycosaminoglycan, lipid, enzymes and even the gene. The currently using CEST imaging sequences need a long pre-saturation to maintain the steady state, which have the shortcomings in temporal resolution and specific absorption rate. We proposed a new scanning strategy based on gradient echo sequence and the magnetization transfer technology here to realize the CEST imaging which has very good temporal resolution. Methods: The CEST phantoms were prepared with 3% agar-gel and 50mmol/L creatine. The pH was 6.6 at room temperature. The gradient echo sequence with magnetization transfer was used at Agilent 7T/160 animal scanner with a volume RF coil. The pulse pre-saturation offsets were set array from-4ppm to 4ppm with interval 0.1ppm. The pre-saturation time was 10ms, RF power was 0.98μT. Other imaging parameters were set as follows: Flip Angle=20°, TR=17.18ms, TE=2.6ms, Slice thickness=2mm, single slice, field of view=60×60mm, Matrix=128×128, number of average=1 and acquisition bandwidth=50kHz. Total scan time for one imaging was about 1.9s. 81 images were got and processed to obtain the Z-spectrum using intrinsic VnmrJ 3.1A workstation. Results: From the Z-spectrum, we can see a good CEST effect at 1.87ppm, which is the exact resonance point for the creatine. The CEST effect was abort 20 percent. In addition, the spatial resolution of the CEST imaging is excellent. Conclusion: Our CEST phantoms proved that we can detect the CEST effect using our new sequence. This finding may provide a complement for traditional CEST imaging sequence, and has its potential advantages in temporal resolution. This technology can be easily translated to obtain CEST imaging in most clinic MR machines.

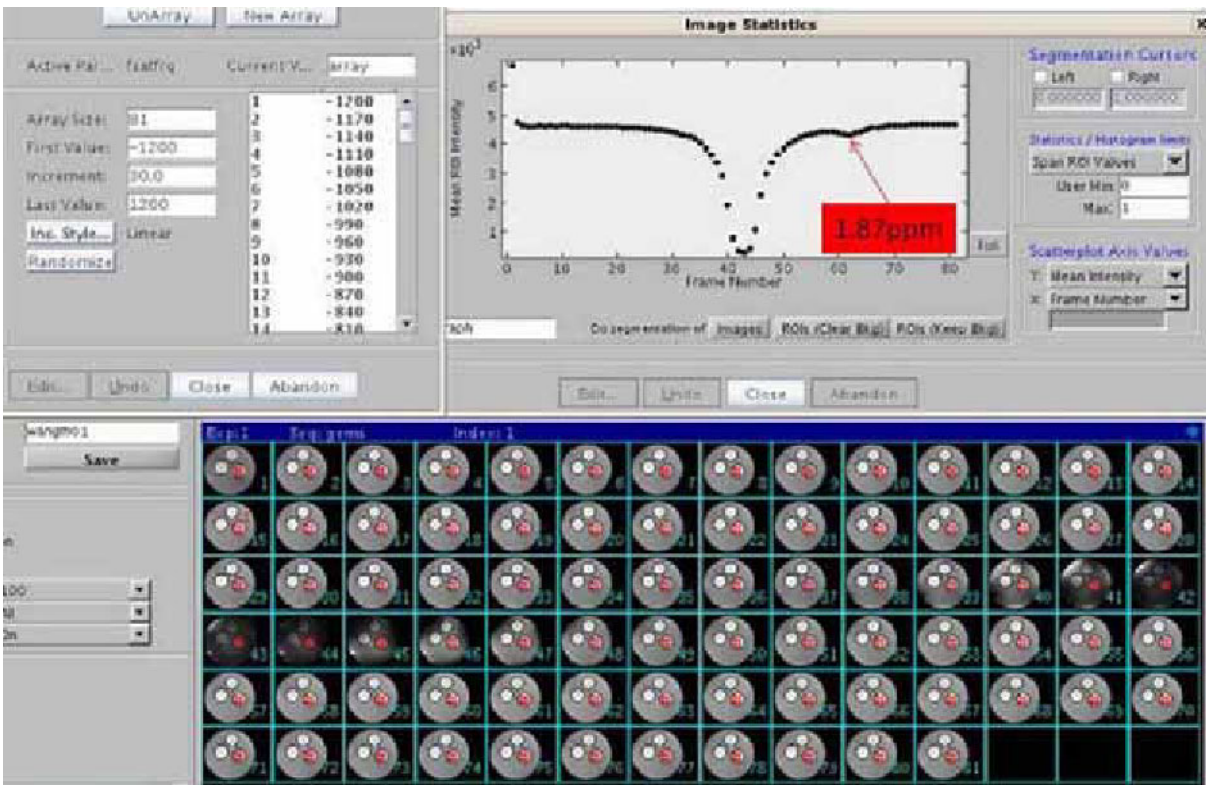


Z-spectrum

Disclosure of author financial interest or relationships:
**Z. Dai**, None; **G. Xiao**, None; **Z. Shen**, None; **L. Wang**, None; **P. Sun**, None; **R. Wu**, None.

Presentation Number **P590**
Poster Session 3
September 7, 2012 / 15:15-15:15 / Room: The Liffey

# Concentration-Sensitive Chemical Exchange Saturation Transfer Imaging Using Magnetization Transfer Prepared Gradient Echo Sequence at 1.5 T Clinical Scanner

***Gang Xiao***[1], *Zhuozhi Dai*[2], *Phillip Zhe Sun*[3,4], *Renhua Wu*[2], [1]*Department of Mathematics and Technology, Hanshan Normal University, Chaozhou, China;* [2]*Department of Radiology, 2nd Affiliated Hospital of Shantou University Medical College, Shantou, China;* [3]*Athinoula A. Martinos Center for Biomedical Imaging, Department of Radiology, Massachusetts General Hospital and Harvard Medical School, Charlestown MA 02129, MA, USA;* [4]*Neuroprotection Research Laboratory, Department of Radiology and Neurology, Massachusetts General Hospital and Harvard Medical School, Charlestown MA 02129, MA, USA. Contact e-mail: xiao.math@yahoo.com.cn*

Introduction: Chemical exchange saturation transfer (CEST) labeling is similar to magnetization transfer preparation in which a RF pre-pulse is applied so that dilute exchangeable proton groups can be detected via the abundant solvent signal. In this work, iopamidol solution was imaged via CEST imaging using magnetization transfer prepared gradient echo sequence on a 1.5 T Clinical Scanner. Methods: The iopamidol solution were prepared with 13 ,26, 52 and 104 mmol/L and imaged using a GE Signa HDX 1.5T Scanner with radiofrequency selective magnetization transfer prepared single-slice gradient echo sequence. The offset of magnetization transfer pre-saturation pulse was set at -275Hz, 275Hz, respectively. Other imaging parameters were: TR=40ms, TE=3.3ms, slice thickness=5mm, field of view=16×16mm, NEX=10 and acquisition bandwidth=31.25 kHz. The total scan time was about 2.5 min. The images were processed using Matlab. Results: CEST imaging contrast increase with iopamidol solution concentration, and the difference of the CEST imaging between 13 and 104 mmol/L is approximately 25%. Conclusion: Our data show that magnetization transfer-prepared gradient echo MRI is capable of capturing CEST contrast from iopamidol solution at 1.5 T, which remains promising for clinical translation.

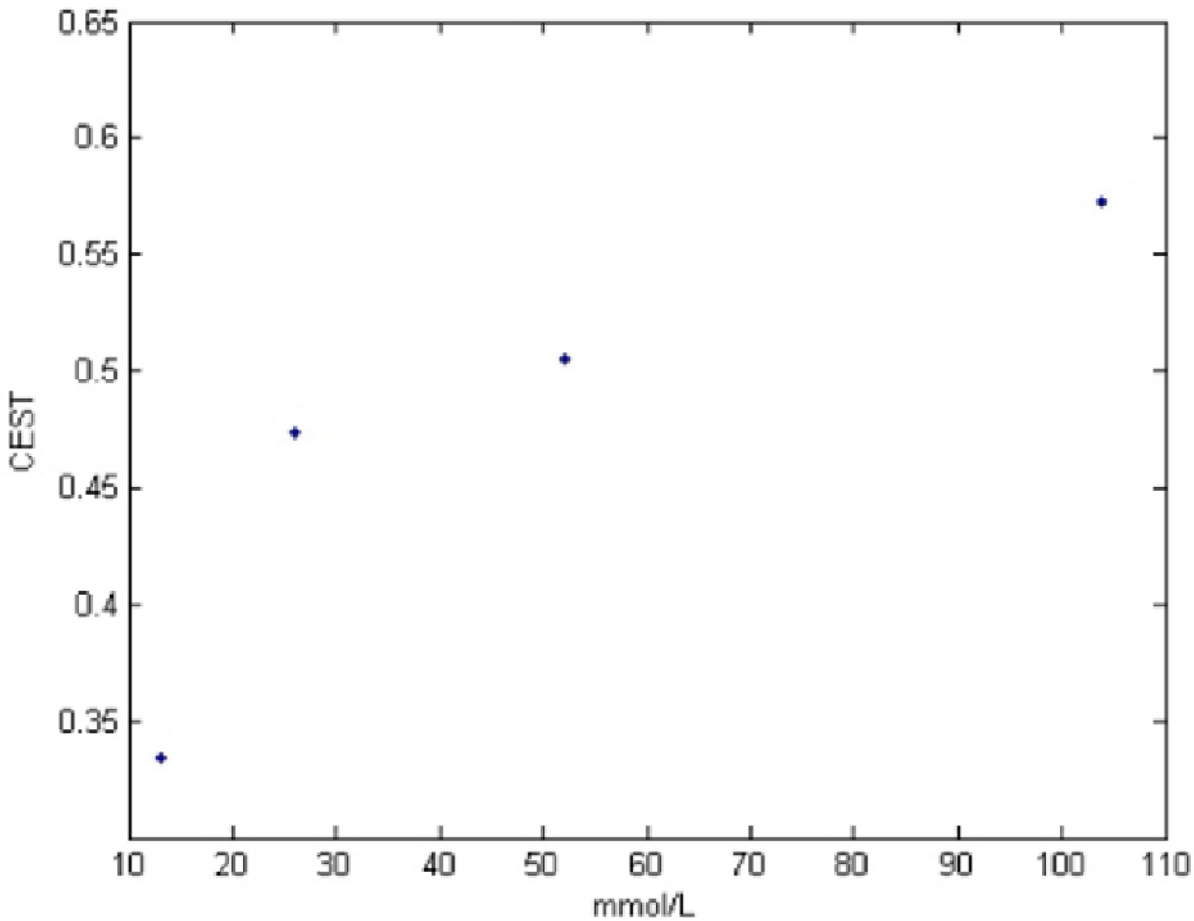


The different concentration of iopamidol solution and the intensity of CEST imaging using the magnetization transfer prepared gradient echo sequence.

Disclosure of author financial interest or relationships:
**G. Xiao**, None; **Z. Dai**, None; **P. Sun**, None; **R. Wu**, None.

Presentation Number **P591**
Poster Session 3
September 7, 2012 / 15:15-15:15 / Room: The Liffey

# Intraoperative Near-Infrared Fluorescence Imaging of Parathyroid Adenomas using Low-Dose Methylene Blue

***Joost van der Vorst***[1], *Boudewijn Schaafsma*[1], *Floris Verbeek*[1], *Rutger-Jan Swijnenburg*[1], *Merlijn Hutteman*[1], *Job Kievit*[1], *Jaap Hamming*[1], *John V. Frangioni*[2], *Cornelis J. van de Velde*[1], *Alexander Vahrmeijer*[1], [1]*Department of Surgery, Leiden University Medical Center, Leiden, Netherlands;* [2]*Division of Hematology/Oncology, department of Medicine, Beth Israell Deaconess Medical Center, Boston, MA, USA. Contact e-mail: j.r.van_der_vorst@lumc.nl*

Background: Intraoperative detection of parathyroid adenomas can be challenging. Near-infrared (NIR) fluorescence imaging is a promising technique that offers intraoperative, real-time, visual information during surgery. We hypothesized that low-doses of the 700-nm NIR fluorophore methylene blue (MB) could be used to provide intraoperative identification of parathyroid adenomas. Methods: MB was injected at a dose of 0.5 mg/kg as a slow bolus into 9 consecutive patients who underwent parathyroid surgery for primary hyperparathyroidism (N = 8) or parathyromatosis (N = 1). MB was administered after exploration of the neck region or thoracotomy. Intraoperative NIR fluorescence imaging was performed using the Mini-FLARE™ imaging system. Results: In 6 of 9 patients, a total of 6 parathyroid adenomas could be clearly visualized using NIR fluorescence. Five of these 6 patients had a positive preoperative 99mTc-sestamibi SPECT scan. In 1 of 6 patients with a positive 99mTc-sestamibi SPECT scan, NIR fluorescence was negative intraoperatively, but the nodule was found to be a parathyroid carcinoma by histopathology. Conclusion: This is the first study to show that low-dose MB can be used as a NIR fluorescence tracer for intraoperative identification of parathyroid adenomas and suggests a high correlation with preoperative 99mTc-sestamibi SPECT scanning.

Disclosure of author financial interest or relationships:
**J. van der Vorst**, None; **B. Schaafsma**, None; **F. Verbeek**, None; **R. Swijnenburg**, None; **M. Hutteman**, None; **J. Kievit**, None; **J. Hamming**, None; **J.V. Frangioni**, None; **C.J. van de Velde**, None; **A. Vahrmeijer**, None.

Presentation Number **P592**
Poster Session 3
September 7, 2012 / 15:15-15:15 / Room: The Liffey

# Manganese-enhanced MRI distinguishes normoglycemic and type 2 diabetic patients

***Laurent Vinet***[1]*, Diomidis Botsikas*[2]*, Sylvain Terraz*[2]*, Paolo Meda*[1]*, Xavier Montet*[2]*,* [1]*Cell Physiology and Metabolism, University of Geneva, Geneva, Switzerland;* [2]*Department of Radiology, Geneva University Hospital, Geneva, Switzerland. Contact e-mail: laurent.vinet@unige.ch*

A non-invasive method to image the mass and/or function of human pancreatic islets is needed to monitor the progression of diabetes, and the effect of therapeutic interventions. As yet, no method is available for this purpose, which could be applied to in situ human islets. Specifically, no method has yet be shown to allow for detection of the 30-50% change in beta cell mass that is anticipated in most persons with type 2 diabetes. Animal and in vitro studies have documented that infusion of manganese, a cation which mimics the behaviour of calcium, enhances the MRI of the endocrine pancreas. Here, we have tested whether a similar approach could discriminate diabetic and non-diabetic patients. To address this question, we first evaluated the manganese uptake by islets isolated from normoglycemic and type 2 diabetic individuals. We then compared by manganese-enhanced MRI (MEMRI) the enhancement of the signal of pancreas and liver in normoglycemic and type 2 diabetic patients. Human islets isolated from 3 normoglycemic multi-organ donors and one person with type 2 diabetes were imaged in a 1.5T MR system (Philips Achieva), using a T1-weighted gradient echo sequence, without any previous treatment or after a 30 min exposure to 12.5 μM manganese chloride. The signal to noise ratio of all islet samples was increased after the exposure to manganese, and this increased was larger in the islets isolated from the normoglycemic individuals than in those isolated from the type 2 diabetic. The data show that human pancreatic islets rapidly incorporate sufficient levels of manganese, to enhance the MRI contrast. Whole body MEMRI examinations were performed in 230 normoglycemic patients and 41 type 2 diabetic patients using a 1.5T MR system (PhilipsAchieva or Siemens Magnetom Espree), Most sessions involved a T1-weighted gradient echo sequence acquired both before any infusion, and 20 min after a 0.5 ml/kg b.w. infusion of manganese dipyridoxal diphosphate, at a rate of 2-3 ml/min. Analysis showed that manganese enhanced the pancreas signal in both normoglycemic and type 2 diabetic patients. However, this enhancement was 30% lower in the latter than in the former group of patients, consistent with the changes in beta cell mass that are anticipated from pathology studies in the European population. In contrast, the liver signal, which was also enhanced by manganese infusion, was similar in the very same 2 groups of patients. The data show that manganese can discriminate the MRI pancreas signal of normoglycemic and type 2 diabetic patients. Therefore, further developments of MEMRI, in order to specifically tailor MRI to the endocrine pancreas conditions, are expected to provide valuable tools for the non-invasive monitoring of alterations in both beta cell mass and function in the clinical arena.

Disclosure of author financial interest or relationships:
**L. Vinet**, None; **D. Botsikas**, None; **S. Terraz**, None; **P. Meda**, Sanofi, Grant/research support; Servier, Grant/research support; Novo Nordisk, Grant/research support; **X. Montet**, None.

Presentation Number **P593**
Poster Session 3
September 7, 2012 / 15:15-15:15 / Room: The Liffey

# In vivo [F-18]FDDNP PET demonstration of brain tau deposits in chronic traumatic encephalopathy

***Vladimir Kepe**, (Henry) Sung-Cheng Huang, Gary W. Small, Jorge Barrio, David Geffen School of Medicine, University of California at Los Angeles, Los Angeles, CA, USA. Contact e-mail: vkepe@mednet.ucla.edu*

Long term effects of traumatic brain injuries and repetitive sub-traumatic concussions are known to lead to neurodegenerative changes including tau neurofibrillary pathology in frontal lobe and subcortical areas [1,2]. We have applied [F-18]FDDNP PET imaging to demonstrate the presence of tau pathological protein deposits in vivo in the brains of subjects with chronic traumatic encephalopathy (CTE). Methods: Three subjects with CTE received [F-18]FDDNP PET. [F-18]FDDNP distribution volume ratios (DVRs), in reference to cerebellar gray matter, were determined for several cortical and subcortical areas. Comparisons were made with results obtained from five control subjects. Findings: We have observed increased [F-18]FDDNP binding in several subcortical areas in all three CTE subjects compared to controls. Cortical involvement was variable but all three subjects had signal in structures of medial temporal lobe above the levels observed in control subjects. Interpretation: [F-18]FDDNP PET is a sensitive in vivo method for demonstrating tau pathological deposition in the brains of subjects with CTE. In addition to subcortical regions, our results point to the presence of tau pathological deposits in the medial temporal lobe and to variability of signal in other cortical regions. [F-18]FDDNP PET is useful for detection of tau pathological changes in CTE and potentially can be used for monitoring of therapeutic interventions. These results show for the first time the feasibility of in vivo tau imaging with [F-18]FDDNP in CTE. [1] DeKosky ST, Ikonomovic MD, Gandy S. Traumatic Brain Injury - Football, Warfare, and Long-Term Effects. N Engl J Med 2010;363:1293-1296. [2] Omalu B, Hammers JL, Bailes J, Hamilton RL, Kamboh I, Webster G, Fitzsimmons RP. Chronic traumatic encephalopathy in an Iraqi war veteran with posttraumatic stress disorder who committed suicide. Neurosurg Focus 2011;31:E3.

Disclosure of author financial interest or relationships:
**V. Kepe**, None; **(. Huang**, None; **G.W. Small**, POM Wonderful, Grant/research support; Lilly, Consultant; Novartis, Speakers bureau; Co-inventor of FDDNP, Other financial or material support; Novartis, Consultant; Forest, Speakers bureau; **J. Barrio**, None.

Presentation Number **P594**
Poster Session 3
September 7, 2012 / 15:15-15:15 / Room: The Liffey

# C-11 PiB retention in the deep and superficial white matter of dementia patients with various etiology

*Sun Young Chae[1], Jungsu Oh[1], Jae Hong Lee[2], Seung Jun Oh[1], Duk L. Na[3], Sang Won Seo[3], **Jae Seung Kim**[1], [1]Nuclear Medicine, Asan Medical Center, Seoul, Republic of Korea; [2]Neurology, Asan Medical Center, Seoul, Republic of Korea; [3]Neurology, Samsung Medical Center, Seoul, Republic of Korea. Contact e-mail: jaeskim@amc.seoul.kr*

Purpose: C-11 Pittsburgh Compound B (PiB) PET has shown significantly higher PiB reterntion in the gray matter (GM) of Alzheimer disease (AD) patients than normal controls (NCs) and also higher retention within the white matter (WM) than GM in NCs. Although PiB retention in WM may be attributable to nonspecific binding with slow kinetics, the nature of PiB retention in WM remains unclear in dementia patients. We evaluated the regional differences of PiB retention in superficial and deep WM between NCs and patients with AD, subcortical vascular dementia (SVaD) or Lewy body dementia (LBD) to characterize the PiB retention in WM. Methods: We studied 9 NCs (male:female = 2:7, 68.3 y), 10 AD (male:female = 6:4, 70.2 y), 28 SVaD (male:female = 14:14, 74.2 y) and 28 LBD (male:female = 16:12, 70.6 y) patients. All subjects underwent C-11 PiB PET 1hr after injection of C-11 PIB (370-555 MBq) and volumetric T-1 MRI. To achieve the accurate quantification of PiB retention, partial volume correction was performed using 25 tissue model by the FreeSurfer software. We calculated the mean PIB uptake ratio (UR) of lobar-parcellated 13 GMs, 10 superficial WMs, and 1 deep WM, by dividing the cerebellar cortical uptake as the reference. We compared URs of lobar-parcellated GM, superficial WMs and deep WM among four groups. Results: PiB URs in cortical GM were increased in all (100%) of AD, 7(25%) SVaD and 11 (39%) LBD patients compared to those of NCs. PiB URs in deep WM were significantly lower in SVaD than those in NCs ($p<0.05$) and not different between PiB-positive (PiB+) and PiB-negative (PiB-) SVaD groups. PiB- group of dementia, except SVaD, showed lower PiB URs in superficial WM than in deep WM, but PiB+ group showed reverse pattern ($p<0.05$) and PiB URs were higher in frontal and parietal superficial WMs beneath GMs showing highest PiB URs. There was no significant difference of PiB UR in brain stem and cerebellar WM among 4 groups. Conclusion: Our findings suggest that PiB retention of deep WM is nonspecific and can be influenced by ischemia, whereas PiB retention of superficial WM changed with A-beta deposits in dementia patients.

Disclosure of author financial interest or relationships:
**S. Chae**, None; **J. Oh**, None; **J. Lee**, None; **S. Oh**, None; **D.L. Na**, None; **S. Seo**, None; **J. Kim**, None.

Presentation Number **P595**
Poster Session 3
September 7, 2012 / 15:15-15:15 / Room: The Liffey

# Imaging brain aromatase in human with [$^{11}$C]cetrozole

***Kayo Takahashi***[1], *Takamitsu Hosoya*[2], *Tadayuki Takashima*[1], *Masaaki Tanaka*[3], *Akira Ishii*[3], *Yasuhito Nakatomi*[3], *Shusaku Tazawa*[1], *Kazuhiro Takahashi*[1], *Hisashi Doi*[1], *Yumiko Watanabe*[1], *Yasuhiro Wada*[1], *Masaaki Suzuki*[1], *Hirotaka Onoe*[1], *Yasuyoshi Watanabe*[1], [1]*Center for Molecular Imaging Science, RIKEN, Kobe, Japan;* [2]*Institute of Biomarerials and Bioengineering, Tokyo Medical and Dental University, Tokyo, Japan;* [3]*Dept. of Physiology, Graduate School of Medicine, Osaka City University, Osaka, Japan. Contact e-mail: kayo.takahashi@riken.jp*

Aromatase is an enzyme converting androgens to estrogens. It plays a crucial role in hormone-dependent breast cancer, since breast cancer cells highly express aromatase and local synthesis of estrogen stimulates proliferation of cancer cells. Besides the breast cancer, the enzyme aromatase is distributed throughout the body including brain. In brain, high amount of the enzyme is located in the amygdala and hypothalamus. Brain aromatase is reported to be involved in the synaptic plasticity, neurogenesis, and neuroprotection, pathophysiology of Alzheimer's disease and autism, and also regulation of sexual and emotional behaviors. To develop a new diagnosis method for breast cancer and also to investigate the functional activity of aromatase in the brain, we developed an original PET probe, $^{11}$C-labeled cetrozole. PET studies performed in rats and rhesus monkeys, demonstrated that this novel PET probe is superior to early-developed $^{11}$C-labeled vorozole in terms of specificity and metabolic stability. After safety examination and approval by the ethics committee, we proceeded to human PET studies. During PET scans for 60 min, arterial blood samples were collected from 5 male volunteers, and venous blood samples from the rest. Collected blood samples were used as an input function in quantitative analysis of the PET data, to analyze metabolites, and to measure sex steroids, etc. The distribution pattern of [$^{11}$C]cetrozole was unique in human as well as that of [$^{11}$C]vorozole which highly accumulated in the thalamus. Our data indicate that there might be a positive correlation between aromatase level in the brain and cooperativeness as a character.

Disclosure of author financial interest or relationships:
**K. Takahashi**, None; **T. Hosoya**, None; **T. Takashima**, None; **M. Tanaka**, None; **A. Ishii**, None; **Y. Nakatomi**, None; **S. Tazawa**, None; **K. Takahashi**, None; **H. Doi**, None; **Y. Watanabe**, None; **Y. Wada**, None; **M. Suzuki**, None; **H. Onoe**, None; **Y. Watanabe**, None.

Presentation Number **P596**
Poster Session 3
September 7, 2012 / 15:15-15:15 / Room: The Liffey

# Using pH-weighted MRI to detect the ischemic penumbra at 1.5 Tesla

***Renhua Wu**, Wenbin Yang, Miaomiao Zhang, Phillip Zhe Sun, Shantou University, Shantou, China. Contact e-mail: rhwu@stu.edu.cn*

The classic definition of the ischemic penumbra is a hypoperfused region in which metabolism is impaired, but still sufficient to maintain cellular polarization. Diffusion-weighted MRI (DWI) can identify regions of cellular depolarization. Anaerobic metabolism and the formation of lactate lead to a decrease in pH in acute ischemic stroke. Such a pH decrease should be visible before cellular depolarization occurs and we hypothesized that pH-weighted imaging (pHWI) may predict the outer edges of the ischemic penumbra. pH-weighted MRI was obtained by probing the pH-dependent amide proton transfer between endogenous mobile proteins/peptides and tissue water. Ischemic acidosis can be imaged via an endogenous pH-weighted MRI technique. Twenty human who suffered from stroke were studied using multiparametric MRI. In the acute phase, areas of reduced pH were always larger than or equal to DWI deficits. Our studies demonstrated that pH MRI deficit detects not only tissue that's abnormal on DWI, but also additional hypoperfused tissue with altered oxygen metabolism, suggesting that it may serve as a novel metabolic imaging marker for the ischemic penumbra that does not require injection of an exogenous contrast agent. These observations highlight the potential value of performing pH imaging in acute stroke patients. Additional study is needed to compare this approach with established measures based on perfusion-weighted MRI (PWI), blood volume, and mean transit times measures will have to be performed to further confirm whether this approach will be suitable as an addition to current multimodality acute stroke protocols and their parametric evaluation.

Disclosure of author financial interest or relationships:
**R. Wu**, None; **W. Yang**, None; **M. Zhang**, None; **P. Sun**, None.

Presentation Number **P597**
Poster Session 3
September 7, 2012 / 15:15-15:15 / Room: The Liffey

# Patient selection for breast cancer molecular imaging trials - Can HER-2/neu overexpression status of primary invasive breast cancer be predicted before diagnostic biopsy with mammography and breast ultrasound features?

***Arthur Adams***[1], *Kenneth Gilhuijs*[1,2], *Kenneth E. Pengel*[2], *Claudette Loo*[2], *Willem Mali*[1], *Sjoerd G. Elias*[1,3], [1]*Department of Radiology, University Medical Center Utrecht, Utrecht, Netherlands;* [2]*Department of Radiology, Netherlands Cancer Institute - Antoni van Leeuwenhoek Hospital, Amsterdam, Netherlands;* [3]*Julius Center of Health Sciences and Primary Care, University Medical Center Utrecht, Utrecht, Netherlands. Contact e-mail: a.adams@umcutrecht.nl*

Background The HER-2/neu receptor is an important prognostic and predictive marker and a feasible target for molecular imaging of breast cancer. Efficient selection of patients with HER-2/neu overexpressing cancer for early phase molecular imaging trials aiming at imaging the primary cancer (for screening or diagnostic applications) is required, as prevalence of overexpression of HER-2/neu is only 15-20%. However, selection should not depend on the result of a diagnostic biopsy, as this could affect the molecular imaging result. Mammography and breast ultrasound features have potential to predict HER-2/neu overexpression, as imaging phenotype is likely to be influenced by molecular expression patterns. Also, these features are readily available as part of the diagnostic workup and can be obtained before any interventional procedure. The aim of this study was to investigate to what extent mammography and ultrasound imaging features could be used to predict overexpression status of the HER-2/neu receptor. Methods Mammography and ultrasound imaging features of 606 early invasive breast cancers were scored according to the BI-RADS lexicon. HER-2/neu status was determined on surgical specimens. Cancers with a score of 3+, or 2+ and a HER-2 to chromosome 17 centromere ratio >2.0 on FISH, were considered overexpressing HER-2/neu. Multivariable logistic regression was applied to identify imaging features predicting HER-2/neu overexpressing cancer. Model predictive performance measures were corrected for over-optimism with bootstrapping. Results HER-2/neu overexpression occurred in 80 cancers (13%). On multivariable analysis, presence of microcalcifications (OR 3.4, 95%-CI 2.1-5.8, p<0.001) on mammography, and posterior attenuation of a mass (OR 0.5, 95%-CI 0.3-0.9, p=0.014) on ultrasound, were statistically significant independent predictors. Non-significant predictors were breast density ACR category 3/4 (OR 0.9, 95%-CI 0.5-1.6) and mass presence (OR 0.8, 95%-CI 0.4-1.4) on mammography, and circumscribed mass-margin (OR 0.8, 95%-CI 0.3-2.1) and irregular mass-shape (OR 1.3, 95%-CI 0.8-2.1) on ultrasound. The area under the ROC curve (AUC) was 0.69 (95%-CI 0.63-0.75, p<0.001). After adjustment for over-optimism, post-test probabilities of HER-2/neu overexpression were 23-37% for cancers with microcalcifications, without posterior attenuation, and 5-10% for cancers without microcalcifications, with posterior attenuation (adjusted AUC: 0.67). Discussion Microcalcifications on mammography, and posterior acoustic attenuation of masses on ultrasound were predictors of HER-2/neu overexpression, indicating that imaging characteristics reflect molecular expression patterns in breast cancer. The discriminative power of the investigated imaging features was however modest and likely insufficient for efficient pre-biopsy HER-2/neu overexpressing cancer selection by themselves. Addition of DCE-MRI or FDG-PET features could be considered, in a stepwise approach to contain costs. Competitive strategies may be measurement of free circulating extracellular domain of HER-2 in blood, as well as sampling of suspicious axillary lymph nodes for HER-2/neu assessment.

Disclosure of author financial interest or relationships:
**A. Adams**, None; **K. Gilhuijs**, None; **K.E. Pengel**, None; **C. Loo**, None; **W. Mali**, None; **S.G. Elias**, None.

Presentation Number **P598**
Poster Session 3
September 7, 2012 / 15:15-15:15 / Room: The Liffey

# A simple visual score of heterogeneity of FDG uptake as prognostic marker in sarcoma patients

***Ivayla Apostolova***[1], *Ingo G. Steffen*[1], *Anja Schräpler*[1], *Frank Hofheinz*[2], *Ralph Buchert*[1], *Winfried Brenner*[1], [1]*Nuclear Medicine, University Medicine Charite Berlin, Berlin, Germany;* [2]*Helmhotz-Zentrum Dresden Rossendorf, Dresden, Germany. Contact e-mail: ivaapost@hotmail.com*

Objectives Spatial heterogeneity of FDG uptake in the tumor is a promising predictor of patient outcome in various tumor entities. Different definitions have been proposed for spatial heterogeneity of tracer uptake and mathematical approaches range from simple to very sophisticated algorithms. Here we propose a simple score for visual assessment of both heterogeneity (VSHETER) and shape irregularity (VSIRREG) of FDG uptake in the primary tumor. The prognostic value of these new scores was evaluated in sarcoma patients with F18-FDG-PET for initial staging. Methods In total 56 sarcoma patients (30 m, median age 15 y, range 2-61 y) were included retrospectively. Histological subtypes were 22 Ewing sarcomas (EWS), 17 osteosarcomas (OS) and 17 sarcomas with various subtypes (VS). Primary tumors were visually analyzed for maximum tracer uptake relative to the liver uptake (5-score), size (3-score), heterogeneity of FDG uptake (3-score), irregularity of the shape of FDG uptake (3-score) and central necrosis (yes/no). The presence or absence of metastases was also taken into account (yes/no). The metabolic tumor volume (MTV) was measured using the semi-automatic ROVER 3D segmentation tool which is based on thresholding at the volume-reproducible intensity threshold after subtraction of the local background. Cox proportional hazards models and corresponding hazard ratios (HR) were used to analyze the predictive value of the visual scores as well as SUVmax and MTV for overall survival (OAS) and progression free survival (PFS). Results 40 patients (17 EWS, 15 OS, 8 VS) survived till the end of the follow-up ranging from 9.1 to 97.8 months (median 46.5 months). Overall survival of non-survivors ranged from 2.7 to 49.6 months (median 17.1 months). A significant association with sarcoma subtype was observed for SUVmax ($p<0.01$), VSHETER ($p=0.05$) and central necrosis ($p<0.01$). Multivariate cox proportional hazard analysis revealed VSHETER (HR=2.4, $p=0.01$) and tumor subtype (VS vs EWS, HR=4.9, $p<0.01$) as significant predictors of PFS whereas there was no significant association of PFS with VSIRREG, central necrosis, presence of metastatses, SUVmax or MTV. OAS was associated with the presence of metastases (HR=5.1, $p=0.01$), VSHETER (HR=2.6, $p=0.04$) and tumor subtype (VS vs EWS, HR=3.2, $p=0.05$). Conclusion A simple visual 3-score for heterogeneity of FDG uptake in the primary tumor provides additional power for the prognosis of sarcoma patients based on F18-FDG-PET. Simple visual scores are easily implemented in the routine clinical workflow.

Disclosure of author financial interest or relationships:
**I. Apostolova**, None; **I.G. Steffen**, None; **A. Schräpler**, None; **F. Hofheinz**, None; **R. Buchert**, None; **W. Brenner**, nanoPET, Grant/research support .

Presentation Number **P599**
Poster Session 3
September 7, 2012 / 15:15-15:15 / Room: The Liffey

# Grading of malignant breast tumors using quantitative diffusion weighted imaging at 3T

***Hubert Bickel**, Katja Pinker-Domenig, Wolfgang Bogner, Georg J. Wengert, Thomas H. Helbich, Dpt. of Radiology, Medical University of Vienna, Vienna, Austria. Contact e-mail: hubert.bickel@meduniwien.ac.at*

Purpose: Diffusion weighted imaging (DWI) is a non-invasive method to estimate the diffusivity of certain tissues. Restricted diffusivity has been proved to be associated with malignancy in breast tumors. The purpose of this study is to evaluate, if quantitative diffusion weighted imaging (DWI) using apparent diffusion coefficient (ADC) maps at 3T allows a differentiation of different pathological grades in malignant breast tumors. Materials and methods: 181 patients with suspicious breast lesions detected in routine breast screening (BI-RADS® 3-5) were included in this IRB-approved study. All examinations were performed before any intervention and histopathological verification was reached in all patients after the magnetic resonance imaging (MRI) measurements. A 3T Scanner with a dedicated 4-channel breast coil and a standardized measurement protocol was used for the examinations. The protocol contained a T2-weighted, a dynamic contrast enhanced (DCE) T1- and a diffusion weighted sequence using b-values of 50 and 850. Apparent diffusion coefficient (ADC) maps were calculated and 2-dimensional regions of interest were drawn in the area with the lowest ADC-values. Mean ADC-values were compared using one way ANOVA and Games Howell post hoc test. Results: Histopathology identified 23 grade 1 tumors, 74 grade 2 tumors and 84 grade 3 tumors. The overall mean ADC-value was 0.96×10-3mm$^2$/s. The ADC-values for the different grades were 1.05×10-3mm$^2$/s for grade 1 (n=23), 0.95×10-3mm$^2$/s for grade 2 (n=74) and 0.94×10-3mm$^2$/s for grade 3 lesions (n= 84). No difference could be found between grade 2 and 3 tumors (p=.96), the differences between grade 1 and 2 (p=.14) and 1 and 3 (p=.07) were not significant. The mean ADC-value of the combined high grade (grade 2 and 3) tumors (n=158) was 0.95×10-3mm$^2$/s, being significantly lower than the one of the low grade tumors (p=.026). Conclusion: While not being able to reliably discriminate between the single different grades of malignant breast tumors, quantitative diffusion weighted imaging using ADC-maps at 3T may be used to discriminate between high and low grade breast malignancies.

Disclosure of author financial interest or relationships:
**H. Bickel**, None; **K. Pinker-Domenig**, None; **W. Bogner**, None; **G.J. Wengert**, None; **T.H. Helbich**, Siemens, Grant/research support; Fond national bank austria, Grant/research support .

Presentation Number **P600**
Poster Session 3
September 7, 2012 / 15:15-15:15 / Room: The Liffey

# Near-Infrared Fluorescence Sentinel Lymph Node Mapping of the Oral Cavity in Head and Neck Cancer Patients

***Martin C. Boonstra***[1], *Joost van der Vorst*[1], *Boudewijn Schaafsma*[1], *Floris Verbeek*[1], *Stijn Keereweer*[4], *Jeroen Jansen*[2], *Lilly-Ann van der Velden*[2], *Antonius Langeveld*[2], *Merlijn Hutteman*[1], *Clemens Lowik*[3], *Cornelis J. van de Velde*[1], *John V. Frangioni*[5,6], *Alexander Vahrmeijer*[1], [1]*Surgery, Leiden university medical center, Leiden, Netherlands;* [2]*Otorhinolaryngology Head and Neck surgery, Leiden university medical center, Leiden, Netherlands;* [3]*Endocrinology, Leiden university medical center, Leiden, Netherlands;* [4]*Otorhinolaryngology Head and Neck surgery, Erasmus medical Center, Rotterdam, Netherlands;* [5]*Radiology, Beth Israel Deaconess Medical Center, Boston, MA, USA;* [6]*Hematology/Oncology, Beth Israel Deaconess Medical Center, Boston, MA, USA. Contact e-mail: m.c.boonstra@lumc.nl*

Objectives: Elective neck dissection is frequently performed during surgery in head and neck cancer patients. The sentinel lymph node (SLN) procedure can prevent the morbidity of a neck dissection and improve lymph node staging by fine pathology. Near-infrared (NIR) fluorescence imaging is a promising technique to identify the sentinel lymph node (SLN) intraoperatively. This feasibility study explored the use of indocyanine green adsorbed to human serum albumin (ICG:HSA) for SLN mapping in head and neck cancer patients. Materials and Methods: A total of 10 consecutive patients with oral cavity or oropharyngeal cancer and a clinical N0 neck were included. After exposure of the neck, 1.6 mL of ICG:HSA (500 μM) was injected at 4 quadrants around the tumor. During the neck dissection, levels I, II, III and IV were measured for fluorescence using the Mini-FLARE imaging system. Results: In all 10 patients, NIR fluorescence imaging enabled visualization of one or more SLNs. A total of 17 SLNs were identified. The mean contrast between the fluorescent signal of the lymph nodes and of the surrounding tissue was 8.7 ± 6.4. In 3 patients, of which 1 was false-negative, lymph node metastases were found. After administration of ICG:HSA, the average number of fluorescent lymph nodes significantly increased over time ($P < 0{,}001$). Conclusion: This study demonstrated feasibility to detect draining lymph nodes in head and neck cancer patients using NIR fluorescence imaging. However, the fluorescent tracer quickly migrated beyond the SLN to higher tier nodes.

Disclosure of author financial interest or relationships:
**M. Boonstra**, None; **J. van der Vorst**, None; **B. Schaafsma**, None; **F. Verbeek**, None; **S. Keereweer**, None; **J. Jansen**, None; **L. van der Velden**, None; **A. Langeveld**, None; **M. Hutteman**, None; **C. Lowik**, None; **C.J. van de Velde**, None; **J.V. Frangioni**, None; **A. Vahrmeijer**, None.

Presentation Number **P601**
Poster Session 3
September 7, 2012 / 15:15-15:15 / Room: The Liffey

# Acute invivo FDG-PET changes associated with chronic antitumour activity after treatment with investigational proteasome inhibitor MLN9708

***Daniel P. Bradley***[1,2], *Robbie Robertson*[1,2], *Nibedita Chattopadhyay*[2], *Allison Berger*[2], *Melissa S. Germanos*[1], [1]*Biomedical Imaging Group, Millennium, Cambridge, MA, USA;* [2]*Cancer Pharmacology, Millennium, Cambridge, MA, USA. Contact e-mail: daniel.bradley@mpi.com*

Introduction Clinical FDG PET data is emerging as an early PD biomarker for sensitivity to specific targeted therapies. Early clinical studies, e.g. imatinib mesylate in GIST, showed FDG-PET metabolic responses beforehand and sometimes without equivalent RECIST response but correlated with PFS and OS {van den Abeele et al., ASCO 2002}. More recent studies have begun to explore FDG-PET with other targeted therapies, e.g. pre and d15 post vemurafenib in melanoma and pre and d2 post gefitinib in NSCLC FDG PET responses were observed {McCarthur et al, JCO 2012 & Sunaga et al., Lung Cancer 2008} In the current study the utility of FDG-PET to resolve early responses in two primary human tumour explants models with differing sensitivity to the investigational proteasome inhibitor MLN9708, currently in Phase 2 clinical development, will be presented. Methods PHTX192Lu and 132Lu primary human lung adenocarcinoma explants were grafted s.c. in SCID mice and grown to 200-300mm^3, randomized and selected for imaging. MLN9708 (11mg/kg, s.c.) was dosed after the baseline scan; animals were scanned 6, 24 and 48 hrs. Animals were fasted ~6 hrs prior to imaging and received FDG administration 1 hour prior to imaging session. A 10 min static image (followed by an 8 minute attenuation correction scan) was acquired using a Siemens microPET R4 (Siemens Medical, Knoxville, TN, USA). PET data was reconstructed using a 2D ordered-subset expectation maximization (OSEM) method, resulting in whole body images 128 x 128 x 63 voxels, using AsiPro (Siemens). Results Earlier studies demonstrated the chronic 21d antitumour activity of MLN9708 in PHTX192Lu and 132Lu primary human tumor explants, with moderate/low and high efficacy respectively (t/c average tumor treated÷average tumor control at d21 0.8 'vs.' 0.29). FDG SUVmx from the PHTX132Lu demonstrated a significant 48hr ~35% decrease (See fig). The FDG SUVmx response at 48hr will be presented from the MLN9708 insensitive model, PHTX192Lu Figure. FDG SUVmx (mean±SEM) and PET images illustrate a statistcally significant ~35% decrease at 48hrs ($P<0.05$, paired student t-test) and a global decrease in FDG PET signal across the whole tumor. Conclusion In the current study, 1/ MLN9708 produced chronic anti tumor activity as determined by conventional caliper tumor volume measurements and 2/ a single dose of MLN9708 produced a profound decrease in FDG signal. The use of FDG-PET as an early and non-invasive marker to measure anti tumor activity during treatment with the proteasome inhibitor MLN9708 continues to be investigated preclinically.

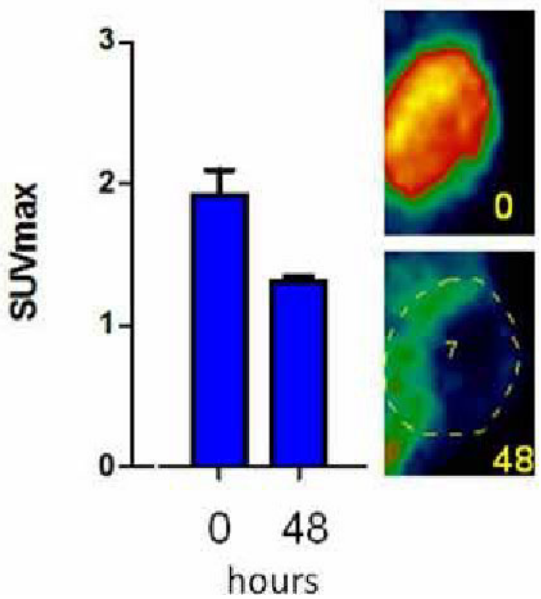


Disclosure of author financial interest or relationships:
**D.P. Bradley**, Millennium, Employment; **R. Robertson**, Millennium: The Takeda Oncology Company, Employment; **N. Chattopadhyay**, Millennium Pharmaceuticals, Employment; **A. Berger**, Millennium Pharmaceuticals Inc, Employment; **M.S. Germanos**, Millennium: The Takeda Oncology Company, Employment .

Presentation Number **P602**
Poster Session 3
September 7, 2012 / 15:15-15:15 / Room: The Liffey

# A hybrid radioactive and fluorescent tracer for sentinel node biopsy in penile carcinoma as a potential replacement for blue dye?

***Oscar R. Brouwer***[1,3], *Nynke S. van den Berg*[3,1], *Henk G. van der Poel*[2], *Bas W. van Rhijn*[2], *Axel Bex*[2], *Wim Meinhardt*[2], *Simon Horenblas*[2], *Fijs van Leeuwen*[3,1], *Renato A. Valdés Olmos*[1], [1]*Nuclear Medicine, Netherlands Cancer Institute, Amsterdam, Netherlands;* [2]*Urology, Netherlands Cancer Institute - Antoni van Leeuwenhoek hospital, Amsterdam, Netherlands;* [3]*Radiology, Leiden University Medical Center, Leiden, Netherlands. Contact e-mail: o.brouwer@nki.nl*

Introduction Sentinel node biopsy is typically performed using lymphatic mapping with blue dye and a radiocolloid. Fluorescence based surgical guidance may facilitate the intraoperative detection of a sentinel node and its afferent lymphatic duct. However, due to its limited tissue penetration, radioguidance remains indispensable. To combine the beneficial properties of both modalities, we recently introduced a hybrid radioactive and fluorescent tracer (ICG-99mTc-nanocolloid). The purpose of this study was to examine the added value of sentinel node biopsy in penile carcinoma using ICG-99mTc-nanocolloid. Material and methods 48 patients with penile squamous cell carcinoma staged with cN0 groins were prospectively included. After intradermal injection of ICG-99mTc-nanocolloid in 3 depots (0.4 ml) proximally around the tumor, lymphoscintigraphy and SPECT/CT were performed to preoperatively identify the sentinel nodes. Patients were operated between 4-27 hours after injection. Immediately before the operation, a mean volume of 1.0 ml of patent blue dye was also injected. Intraoperatively, sentinel nodes were acoustically localized with a gamma ray detection probe and visualized using patent blue dye and/or fluorescence-based tracing with a near-infrared light camera. A portable gamma camera was used before and after sentinel node excision to confirm excision of all sentinel nodes. Results Injection of ICG-99mTc-nanocolloid resulted in preoperative sentinel node visualization in all patients, with a total of 138 identified sentinel nodes. All sentinel nodes could be intraoperatively identified using a combination of radio- and fluorescence guidance. In total, 98% of the sentinel nodes could be visualized using the fluorescence camera, while 53% was stained by the blue dye. Post-excision imaging with the portable gamma-camera revealed additional sentinel nodes in 9 patients. Ex vivo, all radioactive lymph nodes were fluorescent and vice versa indicating the stability of the hybrid tracer. A sentinel node was tumor positive in 10 patients. Conclusion ICG-99mTc-nanocolloid allows for preoperative sentinel node visualization and concomitant intraoperative radio- and fluorescence guidance to the sentinel nodes in penile carcinoma patients. The hybrid approach seems to improve optical sentinel node identification compared to blue dye. This data suggests that by using this hybrid approach, the standardly used blue dye can be omitted.

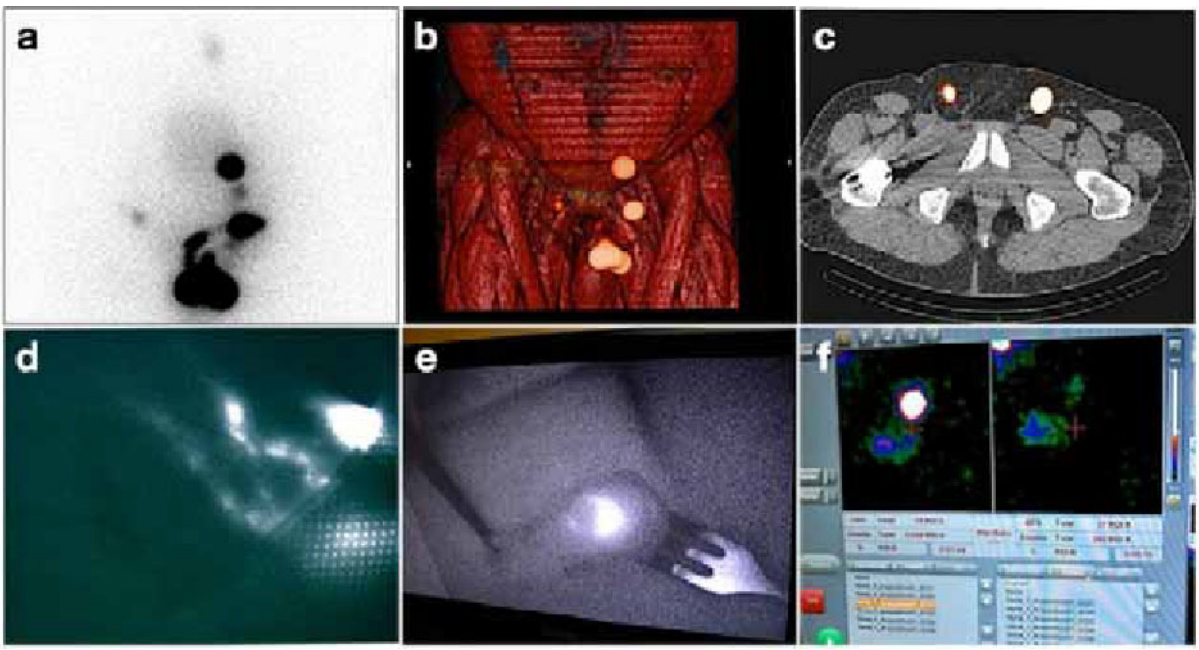


Disclosure of author financial interest or relationships:
**O.R. Brouwer**, None; **N.S. van den Berg**, None; **H.G. van der Poel**, None; **B.W. van Rhijn**, None; **A. Bex**, None; **W. Meinhardt**, None; **S. Horenblas**, None; **F. van Leeuwen**, None; **R.A. Valdés Olmos**, None.

Presentation Number **P603**
Poster Session 3
September 7, 2012 / 15:15-15:15 / Room: The Liffey

# Intraoperative hybrid navigation based on SPECT/CT as a means to expand the boundaries of fluorescence guided surgery

***Oscar R. Brouwer***[1,2], *Tessa Buckle*[2,1], *Anton Bunschoten*[2], *Joeri Kuil*[2], *Alexander Vahrmeijer*[3], *Thomas Wendler*[4], *Henk G. van der Poel*[5], *Renato A. Valdés Olmos*[1], *Fijs van Leeuwen*[2,1], [1]*Nuclear Medicine, Netherlands Cancer Institute, Amsterdam, Netherlands;* [2]*Radiology, Leiden University Medical Center, Leiden, Netherlands;* [3]*Surgery, Leiden University Medical Center, Leiden, Netherlands;* [4]*Computer-Aided Medical Procedures, Technische Universtität München, Munich, Germany;* [5]*Urology, Netherlands Cancer Institute - Antoni van Leeuwenhoek hospital, Amsterdam, Netherlands. Contact e-mail: o.brouwer@nki.nl*

Background: Hybrid tracers that are both radioactive and fluorescent help extend the use of fluorescence guided surgery to deeper structures. Such hybrid tracers facilitate preoperative surgical planning using (3D) scintigraphic images and enable synchronous intraoperative radio- and fluorescence guidance. Nevertheless, we previously found that improved orientation during laparoscopic surgery remains desirable. This study aims to provide a proof of concept of how intraoperative navigation based on preoperative SPECT/CT images may help improve hybrid radio- and fluorescence guided surgery. Methods : A hybrid navigation approach based on optical tracking of a fluorescence endoscope was applied in a validation study in 5 patients undergoing an inguinal sentinel lymph node biopsy, followed by a phantom study and one clinical pilot case in a laparoscopic setting. After placing/injection of a hybrid radioactive and fluorescent tracer consisting of 99mTc-nanocolloid and the fluorescent dye indocyanine green, preoperative SPECT/CT images are acquired with a fixed reference target placed on a rigid structure on the phantom/patient. By also attaching a reference target to the fluorescence endoscope/gamma probe, the preoperative SPECT/CT can be processed by the navigation system to a virtual view of the SPECT/CT images from the perspective of the endoscope. Results : After feeding the SPECT/CT images to the navigation system, optical tracking could be used to position the tip of the fluorescence endoscope/gamma probe relative to the preoperative 3D imaging data. This hybrid navigation approach allowed us to localize the preoperatively defined lesions with an error <1cm in the inguinal sentinel node biopsy patients. Furthermore, the laparoscopic set-up enabled accurate localization of marker seeds in a phantom set-up. In addition, the approach was used to navigate towards the prostate in a patient undergoing robot assisted prostatectomy. Navigation of the tracked fluorescence endoscope towards the target identified on SPECT/CT resulted in real- time gradual visualization of the fluorescent signal in the prostate, thus providing an intraoperative confirmation of the navigation accuracy. Conclusions : Image navigation in hybrid surgical guidance procedures appears to be technically feasible, and may be a next step to fine-tune the hybrid surgical guidance process.

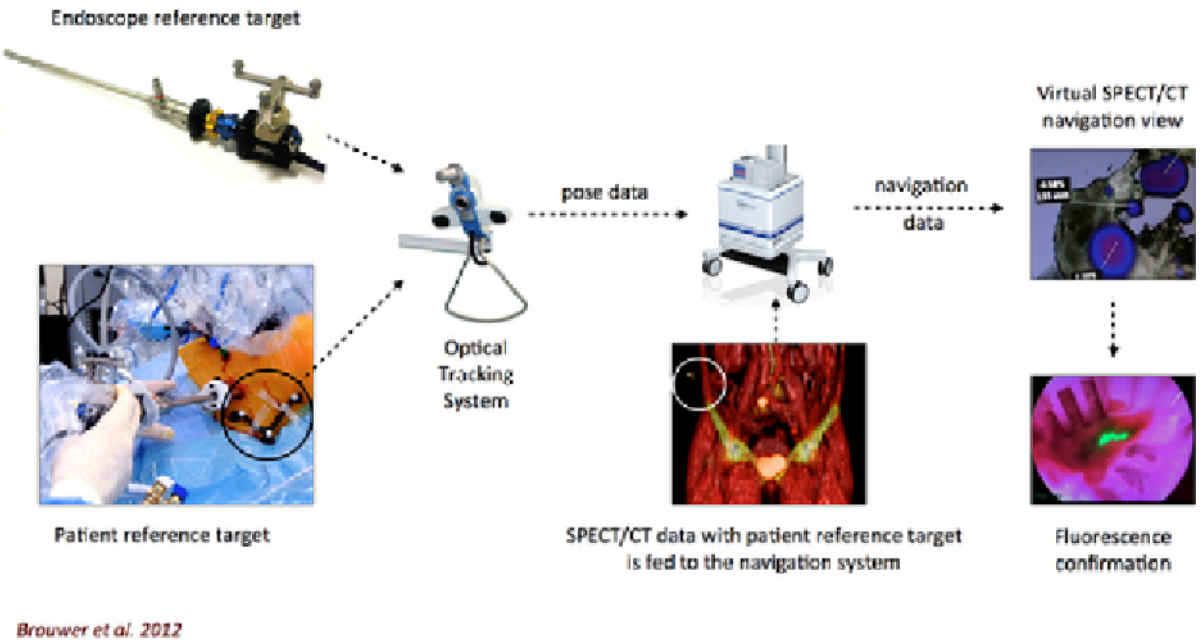


Disclosure of author financial interest or relationships:
**O.R. Brouwer**, None; **T. Buckle**, None; **A. Bunschoten**, None; **J. Kuil**, None; **A. Vahrmeijer**, None; **T. Wendler**, SurgicEye GmbH, Stockholder; **H.G. van der Poel**, None; **R.A. Valdés Olmos**, None; **F. van Leeuwen**, None.

Presentation Number **P604**
Poster Session 3
September 7, 2012 / 15:15-15:15 / Room: The Liffey

# A hybrid tracer for pre-, intra- and post-operative imaging: an example for SLN biopsy of prostate cancer

***Tessa Buckle***[1,2], *Nynke S. van den Berg*[1,2], *Oscar R. Brouwer*[3], *Renato A. Valdés Olmos*[3], *Henk G. van der Poel*[4], *Fijs van Leeuwen*[1,2], [1]*Radiology, Interventional Molecular Imaging, LUMC, Leiden, Netherlands;* [2]*Radiology and Nuclear Medicine, NKI-AvL, Amsterdam, Netherlands;* [3]*Nuclear Medicine, NKI-AvL, Amsterdam, Netherlands;* [4]*Urology, NKI-AvL, Amsterdam, Netherlands. Contact e-mail: t.buckle@lumc.nl*

INTRODUCTION Integration of molecular imaging and in particular intraoperative image guidance is expected to improve the surgical accuracy of, for instance, laparoscopic lymph node dissection. The hybrid tracer ICG-99mTc-nanocolloid, which is both radioactive and fluorescent, was used to combine preoperative sentinel lymph node (SLN) identification and intraoperative visualization of the SLN in patients with prostate cancer. Additionally, the influence of the location of the tracer deposits on the drainage profile was evaluated by relating the fluorescent signal present in embedded tissue specimens to the preoperatively detected SLNs. METHODS 35 patients with prostate carcinoma, scheduled for robot assisted laparoscopic prostatectomy (RALP) and lymph node dissection were included. Before surgery, ICG-99mTc-nanocolloid was injected into the prostate under ultrasound guidance. Subsequent lymphoscintigraphy and single-photon emission computed tomography/ computed tomography (SPECT/CT) imaging of pelvic nodes was performed to preoperatively determine the location of the SLNs. During the surgical procedure, a fluorescence laparoscope, optimized for detection in the near infrared range, was used to visualize the nodes identified on SPECT/CT. Radioactive and fluorescent signals in the excised SLNs were measured and the correlation between the two was studied. Placement of the fluorescent tracer deposits in paraffin-embedded prostate samples was correlated to the number and location of the SLNs as seen on preoperative lymphoscintigraphy and SPECT/CT. RESULTS The hybrid nature of the imaging agent enabled preoperative identification of the SLNs via the radioactive component and intraoperative detection via fluorescence imaging. Stability of the imaging agent was shown by a strong correlation between the radioactive and fluorescent signals measured in the excised tissue samples. Fluorescence particularly improved surgical guidance in area's with a high radioactive background such as the injection site but is limited by severe tissue attenuation of the signal. Therefore, radio guidance to the area's of interest is still desirable. Initial fluorescent based tissue evaluation revealed a large variation in the location of the intraprostatic tracer deposits ex vivo. Tracer deposits situated in the peripheral zone could be correlated to a higher amount of visualized LNs compared to deposits in the central zone (4.7 vs 2.4 lymph nodes per patient). Furthermore, tracer depostis located on either the left or right side of the prostate predominantly resulted in unilateral drainage. When tracer deposits were equally distributed, bilateral drainage was observed. CONCLUSION ICG-99mTc-nanocolloid can be used for combined preoperative and intraoperative visualization of the SLN in prostate cancer patients. The correlation between the location of the tracer deposits within the prostate and the number and location of the preoperatively visualized SLNs suggests that placement of tracer deposits is of influence on the lymphatic drainage pattern.

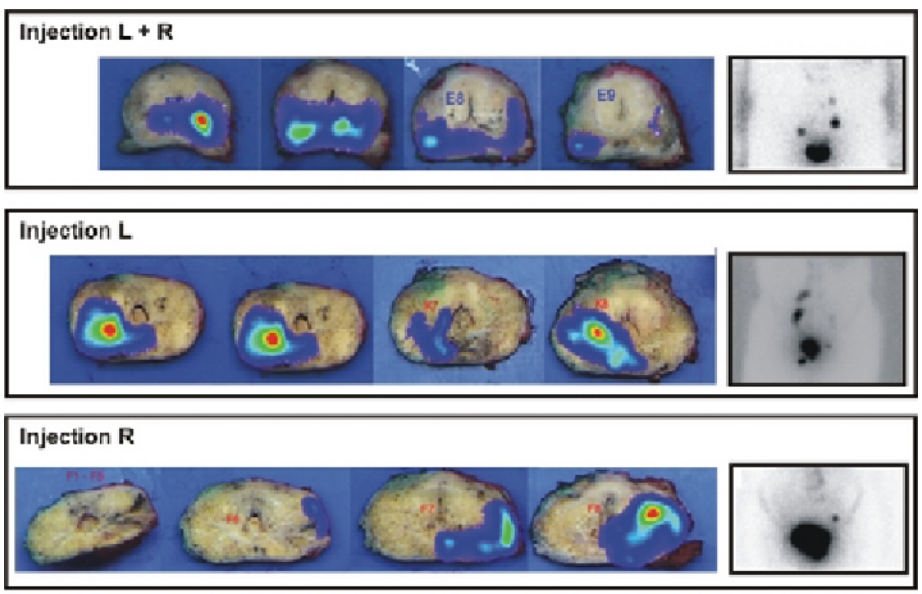


Disclosure of author financial interest or relationships:
**T. Buckle**, None; **N.S. van den Berg**, None; **O.R. Brouwer**, None; **R.A. Valdés Olmos**, None; **H.G. van der Poel**, None; **F. van Leeuwen**, None.

Presentation Number **P605**
Poster Session 3
September 7, 2012 / 15:15-15:15 / Room: The Liffey

# Discovery of Cell-Surface Markers for Molecular Imaging of Lung Cancer

***Allison S. Cohen***[1], *Farah K. Khalil*[2], *Eric A. Welsh*[3], *Steven Enkemann*[4], *Noel Clark*[5], *David L. Morse*[1], [1]*Department of Cancer Imaging and Metabolism, H. Lee Moffitt Cancer Center and Research Institute, Tampa, FL, USA;* [2]*Department of Anatomic Pathology, H. Lee Moffitt Cancer Center and Research Institute, Tampa, FL, USA;* [3]*Biomedical Informatics Shared Resource, H. Lee Moffitt Cancer Center and Research Institute, Tampa, FL, USA;* [4]*Molecular Genomics Shared Resource, H. Lee Moffitt Cancer Center and Research Institute, Tampa, FL, USA;* [5]*Tissue Core Shared Resource, H. Lee Moffitt Cancer Center and Research Institute, Tampa, FL, USA. Contact e-mail: Allison.Cohen@moffitt.org*

The discovery of bona fide cell-surface markers for lung cancer is a key initial step in the development of lung cancer specific molecular imaging probes. Once determined, such markers may be useful targets for the development of nuclear imaging probes for the detection of metastasis, regional lymph node involvement, and to follow therapy response. Additionally, fluorescently labeled targeted probes can be developed for real-time surgical guidance through the use of endoscopic instruments with fluorescence capability. In cases where lung-conservation is imperative, real-time fluorescence imaging using tumor-specific molecular imaging probes could enable the detection and removal of residual disease during surgery and could profoundly affect the course of treatment by reducing the number of patients with incomplete resections. For this study, gene expression profiling was performed using DNA microarray data from patient samples of lung cancer and normal tissues. Available data sets were compiled and filtered for cell-surface, secreted, extracellular matrix, and plasma membrane genes. The resulting list of genes were ranked by their intensity and breadth of expression among the lung cancer samples relative to their differentially low expression in normal/unaffected lung samples and in other tissues of concern, e.g. liver, kidney, heart, etc. From this ranked list, twelve markers (CA9, CA12, CTAG2, CXorf61, DSG3, FAT2, KISS1R, GPR87, LYPD3, OPRD1, SLC7A11 and TMPRSS4) were selected for confirmation of protein expression by immunohistochemistry (IHC). Seven of these markers were selected based solely on their high and broad expression among the lung cancer samples relative to normal lung. Figure 1A shows the expression profile of the most promising of these genes, TMPRSS4. The additional five markers were selected based on their profile and that there are currently available molecular imaging probes for these markers (CA9, CA12, OPRD1 and SLC7A11), or a known high affinity ligand and structure activity relationships for the development of a probe (KISS1R). Figure 1B shows the expression profile of KISS1R. We are in the process of evaluating these markers by IHC pathology of a lung cancer tissue microarray. We have recently developed monoclonal antibody probes against both CA9 and CA12 and there is a commercially available near-infrared (NIR) fluorescent carbonic anhydrase inhibitor-based probe (Hypoxysense, PerkinElmer). We have also developed a high-affinity fluorescent probe specific for the delta-opioid receptor (OPRD1) based on the peptidomimetic antagonist Dmt-Tic-Lys(Cy5)-OH which has high tumor specificity and favorable pharmacokinetics and biodistribution profiles in small animal models of cancer. An $^{18}$F-glutamate derivative PET agent has also been developed that targets the $x_C^-$ transporter (SLC7A11). High-affinity peptidomimetic ligands are known for the KiSS-1 receptor (KISS1R) that could be used to develop a novel targeted imaging probe. When protein expression is confirmed in patient samples, these newly identified markers should be useful for the development and clinical use of targeted molecular imaging probes for lung cancer.

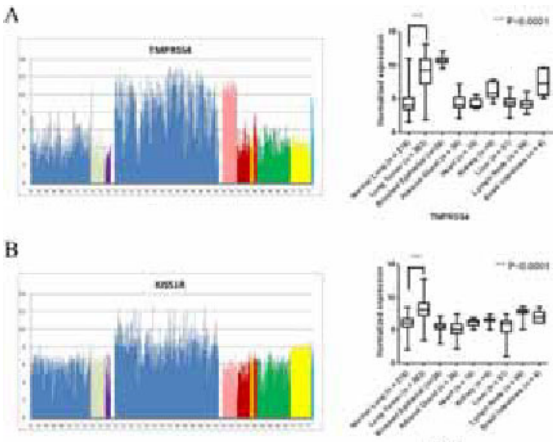


DNA microarray expression profiles for TMPRSS4 and KISS1R in normal lung, lung tumors, and various other normal samples. Left blue = Adjacent normal, Gray = Commercial vendor, outlier samples, Light green = Lung transplants, Purple = Pleura, Center blue = Tumor, Pink = Brushed airway epithelial cells, Dark Red = Adrenal gland, Dark Yellow = Heart, Red = Kidney, Green = Liver, Yellow = Lymph node, Turquoise = Small Intestines. Data are represented as mean ± sd. Asterisks indicate a significant difference between lung tumor and normal lung.

Disclosure of author financial interest or relationships:
**A.S. Cohen**, None; **F.K. Khalil**, None; **E.A. Welsh**, None; **S. Enkemann**, None; **N. Clark**, None; **D.L. Morse**, LiCor, Other financial or material support; Intezyne Technologies, Other financial or material support .

Presentation Number **P606**
Poster Session 3
September 7, 2012 / 15:15-15:15 / Room: The Liffey

# Relative Biodistribution and Tumor Uptake of 124I-NM404 in Humans with Non-small Cell Lung Cancer

***Yamil Fourzali***[1], *Lance T. Hall*[1], *Hilary Hernan*[2], *Jamey Weichert*[1,3], *Anne M. Traynor*[2], [1]*Radiology, University of Wisconsin, Madison, WI, USA;* [2]*Medical Oncology, University of Wisconsin, Madison, WI, USA;* [3]*Novelos Therapeutics, Inc, Boston, MA, USA. Contact e-mail: yfourzali@uwhealth.org*

NM404 is a refined, second-generation diapeutic phospholipid ether analogue that is characterized by preferential tumor uptake and prolonged tumor retention in 50/52 xenograft, spontaneous and transgenic preclinical tumor models. Isosteric iodine substitution in NM404 affords either a diagnostic agent (e.g. using 124I for cancer-selective PET imaging) or a molecular radiotherapeutic agent (e.g. using 131I for cancer-selective cytotoxicity), both of which are in clinical development. NM404 and related alkylphospholipids enter malignant cells via membrane lipid rafts which are overexpressed in cancer cells. Our lab is developing radioiodinated NM404 as a diagnostic and therapeutic ("diapeutic") agent for the detection and treatment of multiple solid tumors, including non-small cell lung cancer (NSCLC). The aim of this study is to demonstrate the relative biodistribution and tumor uptake of 124I-NM404 in humans with NSCLC evaluated with PET/CT. Methods: 3 patients with metastatic NSCLC were injected with 185 MBq of 124 I-NM404. Whole body PET/CT scans were obtained at 5 time points over 6 days after injection. 18F-FDG PET scans were obtained 24 hours prior to 124 I-NM404 injection. Qualitative (visual) and quantitative (SUV) analysis of major organs and malignant tumors was performed. Results/Analysis: In the first 24 hours, initial uptake of NM404 was highest in the blood pool compared to other organs, but blood pool also decreases most rapidly during the first 24 hours. This is likely due to high initial albumin binding. Liver uptake in 2 of the 3 subjects demonstrated the second highest uptake with mild clearance in the first 24 hours. From 1 to 6 days, uptake becomes relatively stable. The spleen in these 2 subjects demonstrated similar SUVmax and SUVavg as well as a similar trend of radiotracer clearance. Mice data demonstrates a similar pattern of clearance. One subject had higher uptake in the liver that did not change significantly over 6 days. The etiology of this finding is not known. There was normal hepatic FDG uptake and no anatomical abnormalities were seen on CT. Incidentally, this patient had a previous splenectomy and thus this may have an effect on relative hepatobiliary uptake and/or retention. Uptake and excretion in the major organs and blood pool of all 3 patients was very conistent (except for liver in 1 patient above). The most constant uptake was seen in the kidneys. NM404 does not crosses the blood brain barrier and no uptake was seen in normal brain (stable SUVmax and SUVav < 1). Two subjects demonstrated both FDG and NM404 avid malignant lung lesions. One patient did not have evidence of malignancy on either FDG or NM404. Multiple FDG avid lung lesions were positive on NM404 PET 1 or 2 days post injection. A <1 cm FDG avid pulmonary lesion was not avid with NM404. There were 3 intensely NM404 avid brain metastases, only one was detectable with FDG. All of the NM404 avid malignant lesions increased uptake with time. In conclusion, the relative normal organ biodistribution of 124I-NM404 is reproducible and malignant tumor uptake has prolonged retention with increasing tumor to background over time.

Fused 124I-NM404 PET/CT of a patient with metastatic non-small cell lung cancer 6 days after injection with 185 MBq of 124I-NM404.

Tumor SUVmax compared to Organ SUVav

| | | | | | |
|---|---|---|---|---|---|
| | | | | | |
| | | | | | |
| | | | | | |
| | | | | | |
| | | | | | |
| | | | | | |
| | | | | | |

Average tumor SUVmax and organ SUVav. Blood pool and liver uptake decrease through time. Kidney uptake is stable. Minimal uptake in lung and femur is stable and no significant uptake is seen in the normal brain. Tumor uptake increases through time.

Disclosure of author financial interest or relationships:
**Y. Fourzali**, None; **L.T. Hall**, None; **H. Hernan**, None; **J. Weichert**, Novelos, Stockholder; **A.M. Traynor**, None.

Presentation Number **P607**
Poster Session 3
September 7, 2012 / 15:15-15:15 / Room: The Liffey

# Relative Biodistribution and Tumor Uptake of 131I-NM404 in a Human Subject with Advanced Colon Cancer

***Lance T. Hall***[1], *Yamil Fourzali*[1], *Jamey Weichert*[1,3], *Glenn Liu*[2], [1]*Radiology, University of Wisconsin, Madison, WI, USA;* [2]*Medical Oncology, University of Wisconsin, Madison, WI, USA;* [3]*Novelos Therapeutics, Inc, Boston, MA, USA. Contact e-mail: LHall@uwhealth.org*

NM404 is a refined, second-generation diapeutic phospholipid ether analogue that is characterized by preferential tumor uptake and prolonged tumor retention in 50/52 xenograft, spontaneous and transgenic preclinical tumor models. Isosteric iodine substitution in NM404 affords either a diagnostic agent (e.g. using 124I for cancer-selective PET imaging) or a molecular radiotherapeutic agent (e.g. using 131I for cancer-selective cytotoxicity), both of which are in clinical development. NM404 and related alkylphospholipids enter malignant cells via membrane lipid rafts which are overexpressed in cancer cells. Results from a Phase 1a dosimetry trial with 10 mCi of 131I-NM404 in 8 human patients with advanced solid cancers (breast, prostate, ovarian, colon) indicated intense tumor uptake, low coefficient of variance for patient blood and urinary elimination, as well as acceptable normal organ dosimetry. This study reports the preliminary biodistribution and tumor uptake of 131I-NM404 from the first patient in a Phase 1b maximum tolerable dose (MTD) study in humans with advanced cancer. Methods: The first patient enrolled is a 48-year-old male with metastatic colon cancer status post muliple previous surgeries, chemo- and radio-therapies. The patient was injected with 185 MBq I-131 NM404 (pre-therapy dosimetry scan). Whole body planar images were obtained at 6 time points over 6 days. Two weeks after normal biodistribution of the dosimetry phase, the patient was injected with approximately 1 GBq of I-131 NM404. Whole body planar and SPECT images of the thorax and upper abdomen were obtained at 6 time points over 6 days. Additional SPECT/CT images were also obtained at 14 and 21 days. Results: Pretherapy study: Blood pool uptake slowly decreased over time. Uptake was identified within the liver and to lesser degree in the spleen. Faint uptake was seen early in the kidneys, decreasing throughout the study. No significant uptake was seen in the bladder, thyroid or bone marrow. Mild bowel uptake was noted. Treatment study: Treatment dose biodistribution was similar to the pretherapy study. NM404 uptake was noted within multiple lung and hepatic metastases, which correlated with metastatic lesions seen on CT. These started as a mild-moderate uptake seen 72 hours after radiotracer injection. Progressively, uptake increased, with most intensity seen by the end of day 21, significantly above normal background uptake. Most intense NM404 avid lesions were noted in the right lower lung. These metastases were not clearly seen in the pretherapy scan. Smaller pulmonary metastases (1.3-1.8 cm) demonstrated mild to moderate uptake at the end of the study. Less than 1 cm lung nodules did not demonstrate significant NM404 uptake. This is of unclear etiology but may be attributed to small lesions below the spatial resolution of the SPECT camera. Conclusion: The first patient with metastatic colon cancer evaluated for maximum tolerable dose with 131I-NM404 demonstrates in the pre and post-therapy scans the expected biodistribution in normal organs as well as the expected progressive uptake in metastases.

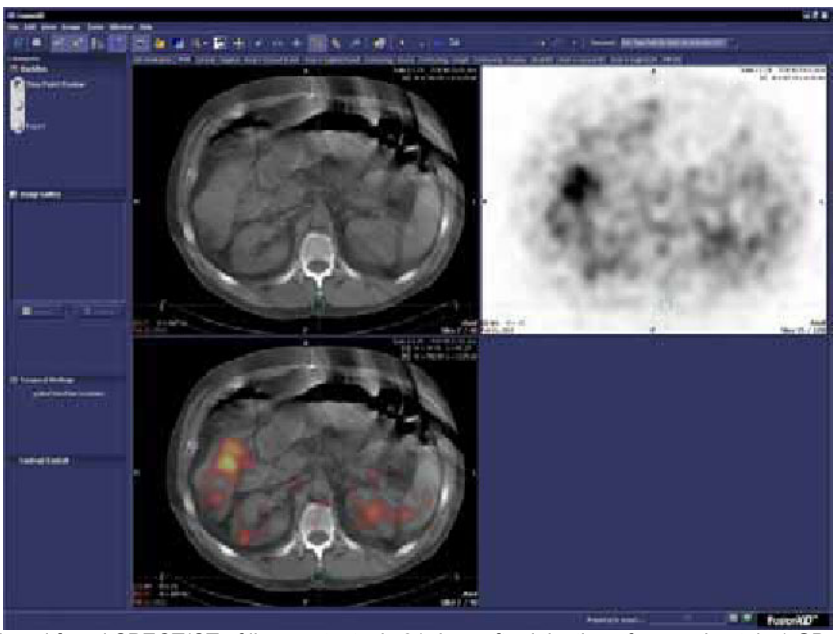

Axial CT,SPECT, and fused SPECT/CT of liver metastasis 21 days after injection of approximately 1 GBq of 131I-NM404.

Disclosure of author financial interest or relationships:
**L.T. Hall**, None; **Y. Fourzali**, None; **J. Weichert**, Novelos, Stockholder; **G. Liu**, None.

Presentation Number **P608**
Poster Session 3
September 7, 2012 / 15:15-15:15 / Room: The Liffey

# First in Human Use of 124I-NM404 PET/CT in Primary and Metastatic Brain Tumors

***Lance T. Hall***[1], *Yamil Fourzali*[1], *Hilary Hernan*[2], *Jamey Weichert*[1,3], *Anne M. Traynor*[2], [1]*Radiology, University of Wisconsin, Madison, WI, USA;* [2]*Medical Oncology, University of Wisconsin, Madison, WI, USA;* [3]*Novelos Therapeutics, Inc, Boston, MA, USA. Contact e-mail: LHall@uwhealth.org*

NM404 is a refined, second-generation diapeutic phospholipid ether analogue that is characterized by preferential tumor uptake and prolonged tumor retention in 50/52 xenograft, spontaneous and transgenic preclinical tumor models, including gliomas. Isosteric iodine substitution in NM404 affords either a diagnostic/imaging agent (e.g. using 124I for cancer-selective PET imaging) or a molecular radiotherapeutic agent (e.g. using 131I for cancer-selective cytotoxicity), both of which are in clinical development. NM404 and related alkylphospholipids enter malignant cells via membrane lipid rafts which are overexpressed in cancer cells. Our lab is developing radioiodinated NM404 as a diagnostic and therapeutic ("diapeutic") agent for the detection and treatment of multiple solid tumors, including primary and metastatic brain tumors. The purpose of this study is to demonstrate the first successful use of 124I NM404 PET/CT in humans with gliomas and brain metastases. Methods: One patient with multiple brain metastases from lung cancer was injected with 185 MBq of 124I-NM404 and imaged with PET/CT at 5 time points over 6 days. One patient with glioblastoma multiforme was injected with 185 MBq of 124I-NM404 and imaged with brain PET/CT at 3 time points over 3 days. Quantitative and qualitative analysis of the PET images were performed and compared to MRI. Tumor to background ratios (T:B) were calculated by placing regions of interest (ROI's) around tumors and comparing to ROI's placed in the contralateral normal brain. Results/Analysis: In both brain metastases and glioma patients, feint uptake of 124I-NM404 was noted within 6 hours after injection and significantly intensified at later time points. There was no significant background uptake in normal brain, though blood pool uptake was present. MRI images of multiple brain metastases in the same patient ranged in size from 0.8 - 2.7 cm in greatest dimension, showed peripheral contrast enhancement, and correlated very well with 124I-NM404 PET/CT images. Normal brain background SUVavg was very consistent at 0.2 - 0.3 at all time points. SUVmax and (T:B ratios) for the 3 largest tumors ranged from 1.2 - 1.5 (T:B 4 - 5) at 6 hours, 2.2 - 2.9 (T:B 7.3 - 9.7) at 24 hours, 2.9 - 4.2 (T:B 14.5 - 21) at 48 hours, and 4.2 - 5.7 (T:B 21 - 28.5) at 144 hours. MRI images of the glioblastoma multiforme tumor measured 3.7 x 4.1 cm in greatest axial dimensions and demonstrated heterogeneous T1 contrast enhancement and T2 signal. PET/CT images also demonstrated heterogeneous areas of 124I-NM404 uptake, including areas of intense uptake and areas of mild uptake. There were areas of discordant contrast enhancement and mild or absent NM404 uptake. Normal brain background SUVavg was very consistent at 0.3 at all time points. SUVmax and T:B ratios were 1.1 and 3.7 at 6 hours, 2.0 and 6.7 at 24 hours, 2.5 and 8.3 at 48 hours, respectively. In conclusion, 124I-NM404 PET/CT successfully images brain metastases and gliomas in humans and demonstrates significant tumor to background uptake and prolonged retention. These attributes make this novel agent a promising "diapeutic" candidate for brain tumors.

Axial PET of glioblastoma multiforme tumor imaged 48 hours after injection with 185 MBq of 124I-NM404. Note heterogenous uptake within the tumor. Uptake in the midline and along the scalp is blood pool activity.

Tumor SUVmax Compared to Normal Brain SUVav

| | 4-6hrs | 24 hrs | 48hrs | 144 hrs |
|---|---|---|---|---|
| GBM | 1.1 | 2.0 | 2.5 | 3.3 |
| Met 1 | 1.2 | 2.2 | 2.9 | 4.2 |
| Met 2 | 1.5 | 2.5 | 4.2 | 4.9 |
| Met 3 | 1.5 | 2.9 | 3.9 | 5.7 |
| Normal brain background | 0.3 | 0.3 | 0.3 | 0.3 |

SUVmax in the GBM and brain metastases increases with time, while the uptake of 124I-NM404 in normal brain is very low and stable through time.

Disclosure of author financial interest or relationships:
**L.T. Hall**, None; **Y. Fourzali**, None; **H. Hernan**, None; **J. Weichert**, Novelos, Stockholder; **A.M. Traynor**, None.

Presentation Number **P609**
Poster Session 3
September 7, 2012 / 15:15-15:15 / Room: The Liffey

# Real-Time Intraoperative Imaging with $^{99m}$Tc Sestamibi can Reduce Time in the Operating Room during Parathyroidectomy

***Nathan Hall***[1], *Natalie B. Jones*[2], *Amit Agrawal*[3], *Amanda Hayes*[1], *Alicia K. McGough*[1], *Michael V. Knopp*[1], *John Phay*[2], *[1]Radiology, The Ohio State University, Columbus, OH, USA; [2]Surgical Oncology, The Ohio State University, Columbus, OH, USA; [3]Otolaryngology, The Ohio State University, Columbus, OH, USA. Contact e-mail: nathan.hall@osumc.edu*

Background: Minimally invasive parathyroidectomy for primary hyperparathyroidism relies on pre-operative localization of a parathyroid adenoma and intraoperative confirmation removal. Intraoperative confirmation of resection can be accomplished with intraoperative PTH monitoring with or without localization assistance utilizing using accomplished utilizing $^{99m}$Tc Sestamibi (MIBI) with a handheld gamma probe. Both techniques have limitations. PTH monitoring can add significant time to the procedure and gamma probe localization requires uptake of MIBI by the adenoma. We investigated the novel technique of using intraoperative MIBI images of the neck region to localize and confirm complete removal of hyperfunctioning parathyroid tissue. Methods: Preoperative diagnostic MIBI scans were performed on 10 patients for hypercalcemia/hyperparathyroidism evaluation. On the day of surgery, MIBI (8.3 ± 0.2 mCi) was administered prior to the scheduled operative procedure. A portable, large field-of-view gamma camera (Ergo$^{TM}$ LFOV General Purpose Imager (Digirad)) was utilized intraoperatively these cases performed by two surgeons. Intraoperative images were acquired of the patient's necks pre- and post-resection of suspected parathyroid tissue. Imaging of all resected tissue was also acquired immediately post resection. Intraoperative PTH monitoring and pathologic evaluation was performed as standard of care for verifying resection of the parathyroid adenomas. Results: In all 10 cases, MIBI parathyroid glands were visible on preoperative diagnostic imaging as well as intraoperative imaging just prior to incision. Post-resection images were acquired for 3-5 minutes. Corresponding radioactivity in the neck was absent in 8/10 cases immediately following the removal of suspected parathyroid adenoma tissue, which indicated successful removal, as verified by subsequent intraoperative PTH monitoring. In 2/10 cases, either residual radioactivity was noted in the thyroid bed or lack of radioactivity noted on specimen imaging led the surgeon to excise additional tissue. Subsequent patient images demonstrated removal of the residual radioactivity. The mean preoperative and post resection PTH levels were 110 ± 26 and 21 ± 12 pg/ml, respectively. Intraoperative specimen imaging successfully verified resection of hyperfunctioning parathyroid tissue in all 10 patients and the results were available 35 ± 12 and 25 ± 10 minutes earlier than postop PTH and pathology results, respectively. Conclusion: In this pilot study, we demonstrate the utility of intraoperative nuclear imaging to localize and confirm complete removal of hyperactive parathyroid glands. The approximate time savings in the operating room using this technique was found to be approximately 30 minutes for these 10 patients. This technique could provide a cost effective, accurate method to assist surgeons performing parathyroidectomies.

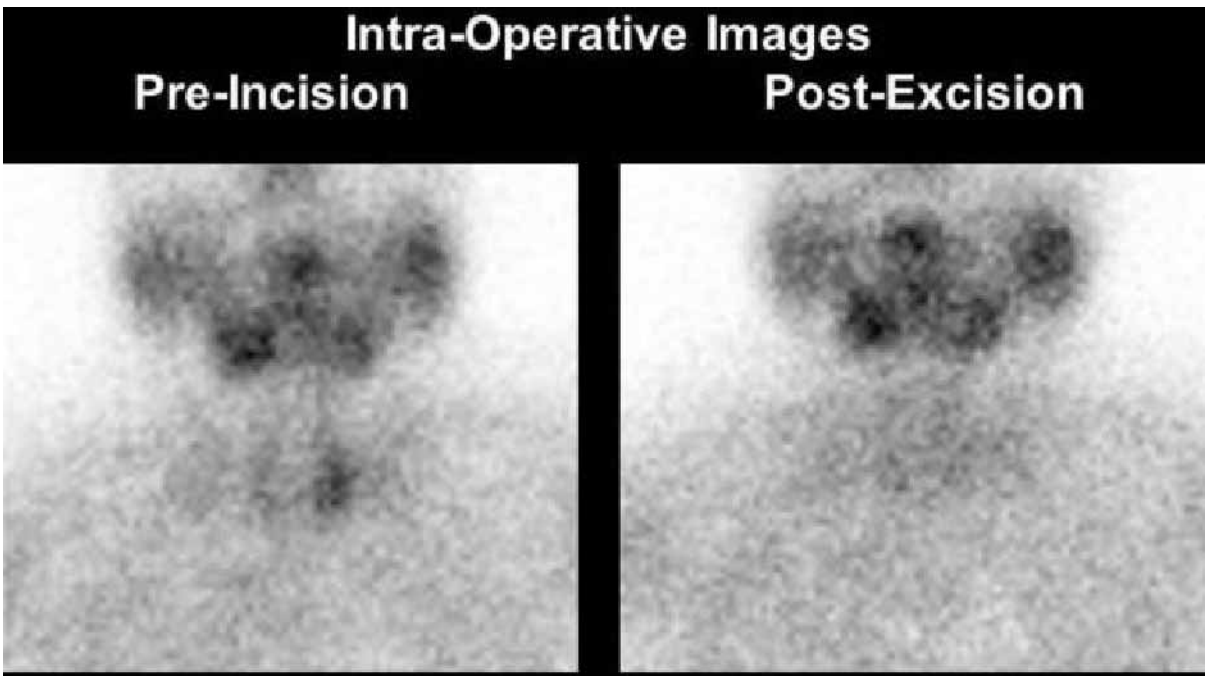


Disclosure of author financial interest or relationships:
**N. Hall**, Enlyton,Ltd., Other financial or material support; **N.B. Jones**, None; **A. Agrawal**, None; **A. Hayes**, Digirad, Grant/research support; **A.K. McGough**, Digirad, Grant/research support; **M.V. Knopp**, None; **J. Phay**, None.

Presentation Number **P610**
Poster Session 3
September 7, 2012 / 15:15-15:15 / Room: The Liffey

# Evaluation of $^{18}$FDG PET/CT Image Quality with Prolonged Injection-to-Scan Times

***Nathan Hall***[1], *Douglas A. Murrey*[1], *Stephen Povoski*[2], *David Barker*[1], *Jun Zhang*[1], *Eamonn Bahnson*[1], *Andrew Chow*[1], *Edward W. Martin*[2], *Michael V. Knopp*[1], [1]*Radiology, The Ohio State University, Columbus, OH, USA;* [2]*Surgical Oncology, The Ohio State University, Columbus, OH, USA. Contact e-mail: nathan.hall@osumc.edu*

Background: PET radiotracers are widely used for cancer staging, monitoring of therapy, and restaging. However, the use of PET/CT has been limited with respect to injection-to-scan time (IST) due to radiotracers with short half-lives. The aim of this study was to evaluate prolonged IST $^{18}$FDG PET/CT image quality using a single dose of $^{18}$FDG. Methods: As part of perioperative imaging clinical trials, 72 patients from 2005 to 2011 were injected with $^{18}$FDG prior to surgical exploration, biopsy, and possible resection of known/suspected malignancy. Each patient underwent postoperative $^{18}$FDG PET/CT of the surgical field utilizing the same preoperative $^{18}$FDG dose. Two nuclear medicine physicians evaluated postoperative PET/CT image quality independently on a 1-3 scale (1=good image quality, 2=adequate image quality, and 3=poor image quality), blinded to all clinical data and scanning parameters. Results: Mean $^{18}$FDG injected dose, IST, and patient weight (Wt) were 16.0 (±2.9, 9.1-26.1) mCi, 525 (±137, 178-853) minutes and183 (±41, 113-300) lbs, respectively. Wt and IST were significant predictors of image quality (p>0.001). Good, adequate and poor image quality groups had mean IST of 390 (±108, 178-579), 557 (±97, 336-753), and 679 (±87, 547-853) minutes that were all significantly different from each other (P<0.001). The mean Wt of the good image quality group (157, (±24, 113-207) differed significantly from both the adequate (187 (±40, 118-300)) (P=0.006) and poor groups (216 (±39, 134-260)) (P<0.001). There was good agreement between readers (Cohen's Kappa = 0.61). Conclusion: Good to adequate $^{18}$FDG PET/CT image quality can be reliably obtained for prolonged IST intervals up to 5 half-lives utilizing a single dose of $^{18}$FDG. These results demonstrate the feasibility of prolonged IST $^{18}$FDG PET/CT imaging. This opens the door for the utilization of PET/CT imaging for novel applications that may necessitate prolonged IST.

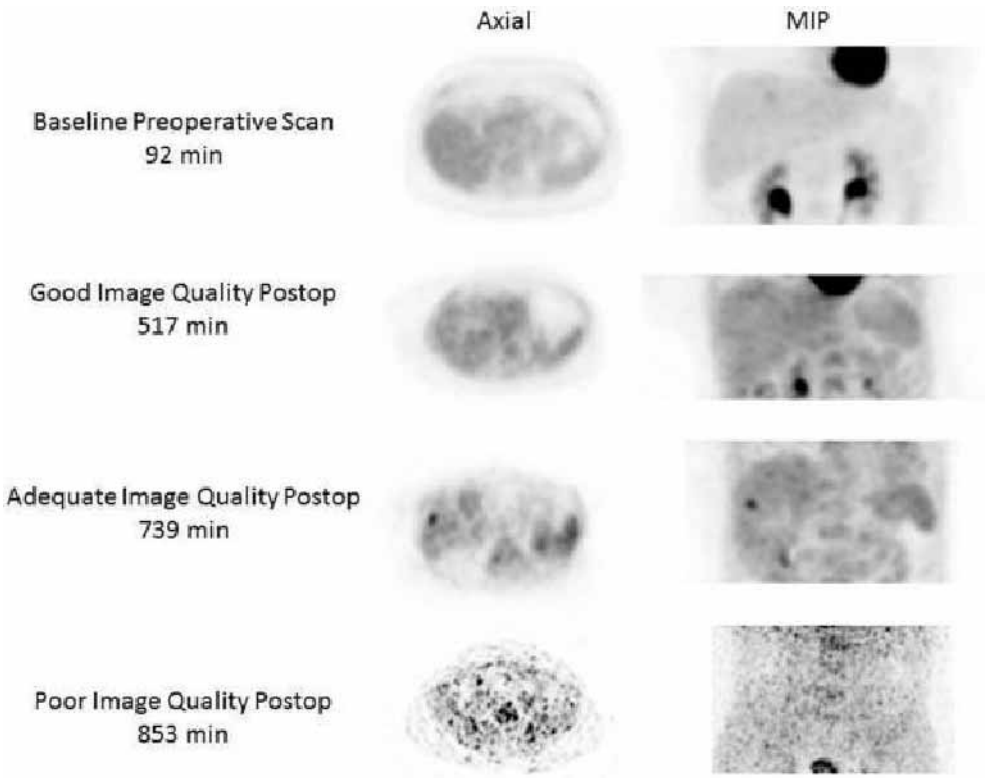


Disclosure of author financial interest or relationships:
**N. Hall**, Enlyton,Ltd., Other financial or material support; **D.A. Murrey**, None; **S. Povoski**, Enlyton,Ltd., Other financial or material support; **D. Barker**, Resurrection Health Care (PET/CT preceptorship conducted 1/2012), Honoraria; **J. Zhang**, None; **E. Bahnson**, None; **A. Chow**, None; **E.W. Martin**, None; **M.V. Knopp**, None.

Presentation Number **P611**
Poster Session 3
September 7, 2012 / 15:15-15:15 / Room: The Liffey

# Mechanistic background of indocyanine green-fluorescent imaging for intraoperative identification of hepatocellular carcinoma

***Takeaki Ishizawa***[1], *Yasuteru Urano*[2], *Masayo Sakabe*[2], *Nobuhiro Harada*[1], *Yoichi Miyata*[1], *Yoshikuni Kawaguchi*[1], *Koichi Masuda*[1], *Junichi Kaneko*[1], *Yasuhiko Sugawara*[1], *Kiyoshi Hasegawa*[1], *Norihiro Kokudo*[1], [1]*Hepatobiliary and Pancreatic Surgery Division, Department of Surgery, Graduate School of Medicine, University of Tokyo, Tokyo, Japan;* [2]*Bioimaging and Biomagnetics Division, Department of Biomedical Engineering, Graduate School of Medicine, University of Tokyo, Tokyo, Japan. Contact e-mail: tish-tky@umin.ac.jp*

Objective: Although fluorescent imaging using preoperative intravenous injection of indocyanine green (ICG) has been clinically applied to the real-time identification of liver cancers during hepatectomy, it remains unclear why ICG accumulates in cancerous tissues of hepatocellular carcinoma (HCC) at the time of surgery. Methods: ICG (0.5 mg/kg) was intravenously injected for a routine liver function test in 170 patients with HCC. Resected specimens were sliced and all cut surfaces were intraoperatively examined using the fluorescent imaging system. Any fluorescing lesions (≥ 5 mm) were marked for subsequent microscopic examination. Gene expression profiles were compared between cancerous tissues and background non-cancerous liver parenchyma with microarray analysis and immunohistochemical staining in 19 patients (19 HCCs). Results: ICG-fluorescent imaging identified 277 out of the 280 (99%) microscopically-confirmed HCCs. Their fluorescent patterns were classifiable into a total fluorescent type (the cancer tissues showed a uniform fluorescence, n = 130), a partial fluorescent type (n = 114), and a rim fluorescent type (only the surrounding liver parenchyma showed fluorescence, n = 33). 58 out of the 68 well-differentiated HCCs (85%) was classified into the total fluorescent type, while 18 out of the 23 poorly differentiated HCCs (78%) appeared as rim-fluorescent-type lesions. Among 280 HCCs, 21 nodules (8%) were grossly unidentifiable and detected only by fluorescent imaging on the resected specimen. Microarray analysis revealed that the ratio of gene expression in cancerous tissue to non-cancerous liver tissue tended to be higher in 13 HCCs with tumorous fluorescence of ICG (the total fluorescent type or the partial fluorescent type) than in 6 rim-fluorescent-type HCCs as for Na(+)-dependent taurocholate co-transporting polypeptide (NTCP; median [range], 0.93 [<0.01 - 1.75] vs. 0.12 [0.01-0.47], P = 0.018) and OATP8 (0.54 [0.01-1.89] vs. 0.06 [<0.01-0.89], P = 0.161), which are associated with portal uptake of ICG by hepatocyte, while no difference between the groups was observed in MRP2, which is associated with biliary excretion of ICG (1.02 [0.74-1.83] vs. 0.59 [0.25-1.92], P = 0.188). Such differences in gene expression profiles in OATP8 and NTCP according to the types of ICG-fluorescence were also supported by the results of immunohistochemical staining. Conclusion: In differentiated HCC tissues, portal uptake function is preserved but there exists disordered biliary excretion of ICG probably because of morphologic changes rather than functional changes associated with cancer progression, which enables visualization of HCC by ICG-fluorescent imaging. Such findings obtained by ICG-fluorescent imaging may also be useful for prediction of effect of chemotherapy and development of novel anticancer drugs.

Disclosure of author financial interest or relationships:
**T. Ishizawa**, None; **Y. Urano**, None; **M. Sakabe**, None; **N. Harada**, None; **Y. Miyata**, None; **Y. Kawaguchi**, None; **K. Masuda**, None; **J. Kaneko**, None; **Y. Sugawara**, None; **K. Hasegawa**, None; **N. Kokudo**, None.

Presentation Number **P612**
Poster Session 3
September 7, 2012 / 15:15-15:15 / Room: The Liffey

# Dynamic molecular imaging of HSV-1 oncolysis in liver metastases by PET-CT

***Darshini Kuruppu***[1,2], *Anna-Liisa Brownell*[2], *Kimmo Jokivarsi*[2], *Umar Mahmood*[2], *McIntosh Bryan*[2], *Jacob Hooker*[2], *Kenneth K. Tanabe*[1], [1]*Surgery, Massachusetts General Hospital, Boston, MA, USA;* [2]*Radiology, Massachusetts General Hospital, Boston, MA, USA. Contact e-mail: dkuruppu@partners.org*

Background: Viral oncolysis by conditionally replicating Herpes simplex virus 1 (HSV-1) is a promising therapeutic option for cancers that are not responsive to current therapies, especially liver metastases. These viruses replicate in mitotically active cancer cells compared to quiescent cells. The resulting waves of virus replication following initial infection of a cell generate a maximal viral dose that is greater than the input dose. As such viral oncolysis therapy needs to be stringently monitored for the magnitude and sites of viral replication. At present this is achieved by tissue sampling (e.g. biopsy), a technique that is invasive and cumbersome for repetitive monitoring of virus in human subjects. A non-invasive molecular imaging technique such as PET can be manipulated to allow for localization of virus repetitively and quantitatively in real time. We present dynamic miroPET-CT imaging of HSV-1 mutant (HSV-Luc) in liver metastases following its administration via the portal circulation in a murine model using [18F]FHBG. Methods: Focal liver metastases were created in balb/C mice by subcapsular insertion of tumor cells in matrigel. Virus (HSV-Luc at 1x107 pfu) was administered into the spleen one week later when the tumors were approximately 10mm3. The conditionally replicating mutant HSV-Luc has the ribonucleotide reductase gene responsible for its replication inactivated by insertion of the β-galactosidase gene. HSV-Luc also expresses the firefly luciferase gene that allows for bioluminescence imaging with luciferin. HSV-1 expresses viral thymidine kinase, which allows for PET imaging with use of FHBG. The guanine derivative FHBG is phosphorylated by viral thymidine kinase which has a large substrate range compared to its mammalian counterpart, and phosphorylated [18F]FHBG is trapped intracellularly. Virus was imaged with PET at 3 and 5 days post virus administration using [18F]FHBG (100μCi). The tumors were subsequently resected to identify virus by LacZ staining. Results: Bioluminescence detection of the virus with luciferin confirmed the expression of virus in the liver and tumors. PET-CT imaging at day 3 and 5 demonstrated virus in the focal liver metastases with PET two hours after [18F]FHBG injection by which time the radioligand is washed out from the liver. Time Activity Curves from the dynamic images confirmed the virus washout from the liver and accumulation in the tumor. Virus localized in the focal liver metastasis was clearly visible by PET imaging at both time points by 3D rendering. Virus in the tumor was visualized by in vitro staining for LacZ expression. Conclusion: Virus expressed in focal liver metastases following its delivery into the portal circulation can be imaged non-invasively with PET using [18F]FHBG. This imaging capability allow for direct translation in to the clinics for determining sites and magnitude of viral replication in ongoing and future clinical trials of HSV-1 oncolysis for liver metastases.

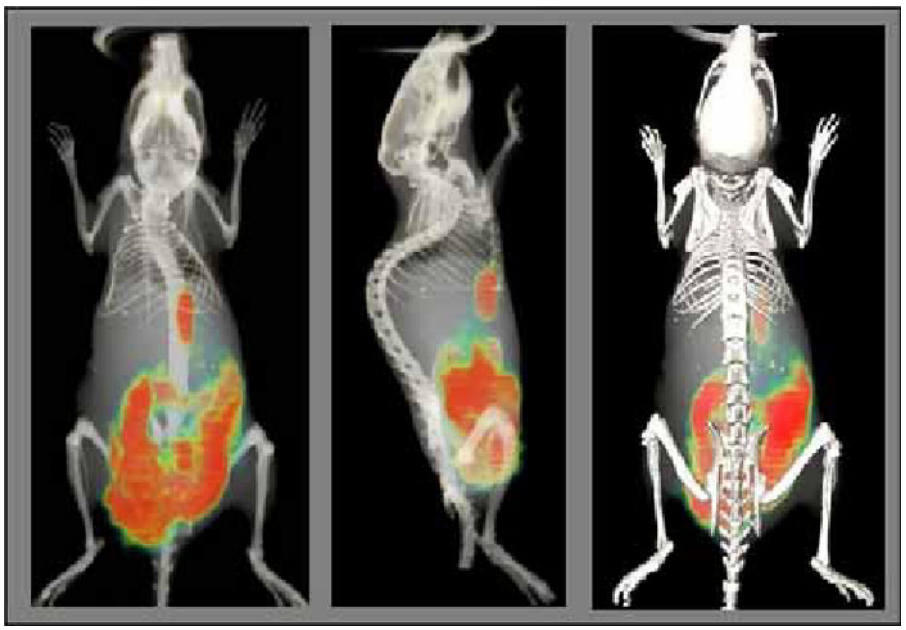

microPET-CT imaging of HSV-1 in focal liver metastases with [18F] FHBG 3 days after virus administration.

Disclosure of author financial interest or relationships:
**D. Kuruppu**, None; **A. Brownell**, None; **K. Jokivarsi**, None; **U. Mahmood**, None; **M. Bryan**, Gamma Medica Inc., Employment; **J. Hooker**, None; **K.K. Tanabe**, None.

Presentation Number **P613**
Poster Session 3
September 7, 2012 / 15:15-15:15 / Room: The Liffey

# Metabolic imaging of breast tumors with dedicated breast 18F-FDG PET-CT: comparison with MRI

***Heinrich F. Magometschnigg***, *Katja Pinker-Domenig, Hubert Bickel, Benedikt Brück, Georg J. Wengert, Thomas H. Helbich, Medical University Vienna, Vienna, Austria. Contact e-mail: h.magometschnigg@gmail.com*

Introduction To assess metabolic imaging of breast tumors with dedicated breast 18F-FDG PET-CT and compare it with contrast-enhanced high temporal and spatial resolution 3T MRI (3T CE-MRI). Material and Methods 159 breast lesions classified by mammography or ultrasound as BI-RADS® 4 or 5 were included in this IRB approved prospective study. All patients were examined with 18F-FDG PET-CT and 3T CE-MRI of the breast. Examinations were scheduled no longer than 3 days apart. The MRI protocol consisted of a T2-w and a contrast-enhanced high resolution 3D-T1-w sequence before and after application of a standard dose Gd-DOTA. All patients were subjected to 18F-FDG PET-CT scanning using a combined PET-CT in-line system (Biograph, Siemens, Erlangen, Germany). A prone PET dataset over the same region was acquired allowing the same patient geometry as with MRI. Patients were injected with approximately 300 MBq 18F-FDG based on the patients weight. Scanning was started 45 min after injection. CT data was used for attenuation correction. Dedicated breast PET-CT was assessed for 18F-FDG-avidity of lesions. Tumors were classified as positive when 18F-FDG-uptake was greater than blood-pool activity. Lesions within tissues demonstrating moderate/high physiologic background activity were considered positive if the activity was greater than the adjacent physiologic activity. 3T CE-MRI was assessed for lesion morphology and enhancement kinetics and classified according to BI-RADS®. All lesions were histopathologically verified. Results PET-CT had a good sensitivity of 96%, a specificity of 76% and a diagnostic accuracy of 90%. Positive predictive value (PPV) was 0.91 (CI 0.84-0.95) and negative predictive value (NPV) was 0.88 (CI 0.74-0.95). 3T CE-MRI had an excellent sensitivity of 100%, a specificity of 80% and a diagnostic accuracy of 94%. PPV was 0.93 (CI 0.87-0.96) and NPV was 1 (0.91-1). There were 46 benign and 113 malignant lesions. Mean histopathological size was 26.03mm (range 5-90mm). The 5 false negative lesions in PET-CT were small lesions (mean 11.2mm), had a very low SUV (mean SUVmax 1.59) or were adjacent to tissue with high physiologic activity or low grade IDCs. Conclusion Although 3T CE-MRI of the breast is superior, metabolic imaging with dedicated breast 18F-FDG PET-CT allows detection and assessment of breast tumors with a good sensitivity and specificity. False negative results seem to be influenced by tumor size (<12 mm) and low SUV associated with high physiologic background activity. Clinical Relevance 3T CE-MRI is superior to PET-CT for assessment of breast lesions, but dedicated breast PET-CT is a valid alternative in patients, who are unsuitable for MRI.

Disclosure of author financial interest or relationships:
**H.F. Magometschnigg**, None; **K. Pinker-Domenig**, None; **H. Bickel**, None; **B. Brück**, None; **G.J. Wengert**, None; **T.H. Helbich**, Siemens, Grant/research support; Fond national bank austria, Grant/research support .

Presentation Number **P614**
Poster Session 3
September 7, 2012 / 15:15-15:15 / Room: The Liffey

# Human Deoxyguanosine Kinase - a promising non-immunogenic reporter gene for nuclear imaging in humans

***Maxim A. Moroz***[1], *Nagavarakishore Pillarsetty*[2], *Yury Likar*[1], *Juan Zurita*[1], *Larissa Shenker*[1], *Sean Carlin*[1], *Megan Reese*[1], *Maria Spassova*[3], *Ouathek Ouerfelli*[3], *Vladimir Ponomarev*[1], [1]*Radiology, MSKCC, New York, NY, USA;* [2]*Radiochemistry, MSKCC, New York, NY, USA;* [3]*SKI, MSKCC, New York, NY, USA. Contact e-mail: morozm@mskcc.org*

Introduction and objective: Nuclear imaging utilizes imaging technologies such as PET, gamma camera and autoradiography. A panel of reporter genes available for these modalities has greatly expanded over the past decade; however there is a great demand in new non-immunogenic reporters suitable for human applications. In this abstract we discuss testing the Human Deoxyguanosine Kinase (hdGK) as a new nuclear reporter gene. This endogenous enzyme catalyzes the phosphorylation of purine deoxynucleosides and their analogs, using nucleoside triphosphate as a phosphate donor. Isolated natural and/or transgene expression and the availability of the newly developed radiotracer [18F]-labeled fluoro-adeno-guanosine ([18F]-FLAG) make hdGK a promising candidate to be utilized as a new reporter agent for PET imaging in humans. Methods: Novel human deoxyguanosine-based reporter gene construct was developed and transduced into U87 (human glioma) and C6 (rat glioma) cells lines. Non-transduced cells were used as reference for all further in vitro and in vivo studies. Green fluorescent protein (GFP) was used as an independent marked of reporter gene expression. Pure cell populations were acquired using FACS sorting. The in vitro 2-hour radiotracer uptake assay was performed with [3H]-AraG, [14C]-TdR and [18F]-FLAG. In vivo 18F-FLAG accumulation was assessed in mice and rats using PET, followed by tissue sampling. Results: A new reporter construct bearing human deoxyguanosine kinase and GFP was successfully cloned and confirmed by sequencing analysis. Human and rodent glioma cells were transduced with the gene-reporter construct and purified to 100% pure population. In vitro uptake analysis showed high levels of [3H]-AraG and [18F]-FLAG accumulation in hdGK transduced cells (42+3 cells/media ratio and 81+9 cells/media ratio for C6 and U87 cells respectively) in comparison to low accumulation in wild type C6 (6+2 c/m ratio) and U87 (7+2 c/m ratio) cells. In vivo 18F-FLAG PET imaging and bio-distribution analysis in mice and rats showed substantial levels of radiotracer accumulation in the heart, liver and intestine. There was a modest increase in [18F]-FLAG accumulation in hdGK-expressing xenografts in a rat tumor model. Conclusion: We developed and tested a new human-derived reporter gene based on hdGK that showed specificity and high phosphorylation activity with purine nucleoside analogs in vitro. In vivo, in an animal model we have observed [18F]-FLAG accumulation in tissues with natural and transgene expression of hdGK.

In vivo accumulation of 18F-FLAG in mice and rats.

| Organ | Accumulation/mouse (%ID/g) | Accumulation/rat (%ID/g) |
|---|---|---|
| Lung | 0.019 +- 0.024 | 0.0017 +- 0.00023 |
| Heart | 0.0102 +- 0.012 | 0.026 +- 0.0102 |
| Stomach | 0.11 +- 0.016 | 0.019 +- 0.0036 |
| Intestine | 0.13 +- 0.034 | 0.010 +- 0.0049 |
| Liver | 0.39 +- 0.11 | 0.076 +- 0.017 |
| Spleen | 0.083 +- 0.021 | 0.0076 +- 0.0032 |
| Blood | 0.034 +- 0.011 | 0.0012 +- 0.00034 |
| Muscle | 0.0054 +- 0.012 | 0.0013 +- 0.00033 |

Disclosure of author financial interest or relationships:
**M.A. Moroz**, None; **N. Pillarsetty**, None; **Y. Likar**, None; **J. Zurita**, None; **L. Shenker**, None; **S. Carlin**, AstraZeneca, Grant/research support; **M. Reese**, None; **M. Spassova**, None; **O. Ouerfelli**, None; **V. Ponomarev**, None.

Presentation Number **P615**
Poster Session 3
September 7, 2012 / 15:15-15:15 / Room: The Liffey

# A Smart Sensor Probe to Detect Enzymatic Activity of Prostate Specific Membrane Antigen

***Anuja Ogirala**, Lynda Cosgrave, Nilesh Shah, Ouathek Ouerfelli, Jan Grimm, Memorial Sloan-Kettering Cancer Center, New York, NY, USA. Contact e-mail: ogiralaa@mskcc.org*

INTRODUCTION Prostate Specific Membrane Antigen (PSMA) has been shown to be a more accurate indicator of prostate cancer aggressiveness than the widely accepted Prostate Specific Antigen (PSA). PSMA is expressed in 94.3% to 100% of primary and 57.7% - 100% of metastatic prostate carcinomas (Nonaka 2010). It is highly expressed on prostate cancer cells, approximately 100-fold higher than on normal prostate epithelium (Su 1995). The use of PSA screening for the disease is now controversial due to a significant number of false positives and false negatives. In addition, PSMA has been shown to be expressed strongly in prostate carcinomas with little or no PSA present (Chuang 2007). Importantly, PSMA has carboxypeptidase activity, which we employed here to indicate the level of PSMA. Herein, we utilize the luciferin-luciferase system to report on PSMA activity via a modified luciferin probe, D-Luciferin-L-Glutamate (Glu-LUC). MATERIALS AND METHODS In solution, Glu-LUC shows no emission due to our modification, but the strong bioluminescence of luciferin is observed upon activation by PSMA either in vitro or in vivo. In this study, we have successfully characterized the enzymatic activity of PSMA utilizing recombinant proteins, prostate cancer cells in vitro and in vivo imaging of subcutaneous prostate cancers in mice. In addition, we acquired EPS Urine from patients, which was obtained post-DRE massage and was then assayed for PSMA activity in a buffer containing ATP, Mg 2+, and Glu-LUC. Bioluminescence was measured using the IVIS 200 and PSMA activity was the quantified against a profile of known PSMA standards to determine the concentration of PSMA in each patient sample. RESULTS Our assays exhibited an excellent high signal to noise ratio with an approximate 50 fold signal-to-noise ratio in vitro and a 30 fold signal to noise ratio, in vivo. We additionally validated our results through the use of a PSMA specific inhibitor, which resulted in immediate loss of signal. We have furthermore tested the clinical translatability of this agent in testing patient urine samples and prostatic secretions. We have detected the presence and specific amounts of PSMA in both urine and prostatic secretions via quantitative Western and then confirmed the activity of PSMA in these samples via Glu-LUC activation. Glu-LUC activation by PSMA containing clinical samples, interestingly revealed an increase in bioluminescence, which correlated to general aggressiveness of the tumors. Glu-LUC thus serves as a PSMA sensor, detecting the presence of PSMA via its enzymatic activity, which may lead to a fast and sensitive assay to detect and even characterize prostate cancer.

Disclosure of author financial interest or relationships:
**A. Ogirala**, None; **L. Cosgrave**, None; **N. Shah**, None; **O. Ouerfelli**, None; **J. Grimm**, None.

Presentation Number **P616**
Poster Session 3
September 7, 2012 / 15:15-15:15 / Room: The Liffey

# Predictability of treatment effects with Cu-ATSM PET in head-and-neck cancers: Comparison with FDG-PET

***Hidehiko Okazawa***[1], *Yoshitaka Sato*[1], *Yuichi Kimura*[2], *Myungmi Oh*[2], *Tetsuya Mori*[1], *Yasushi Kiyono*[1], *Shigeharu Fujieda*[2], [1]*Biomedical Imaging Research Center, University of Fukui, Eiheiji-cho, Japan;* [2]*Department of Otorhinolaryngology, Faculty of Medical Sciences, University of Fukui, Eiheiji-cho, Japan. Contact e-mail: okazawa@u-fukui.ac.jp*

Distribution of [Cu-62]-diacetyl-bis(N4-methlythiosemicarbazone) (Cu-ATSM) has been reported to reflect the resistant hypoxic tissue in malignant tumors especially in squamous cell carcinomas. The tracer distributions were compared between [F-18]-fluorodeoxyglucose (FDG) and Cu-ATSM, and evaluated the predictability of effectiveness of tumor treatment. METHODS: Forty-two patients with head-and-neck cancer (mean age: 67 ± 12 y.o.) underwent Cu-ATSM- and FDG-PET within a week interval. Six of them were followed up after treatment using Cu-ATSM PET. Dynamic Cu-ATSM PET images were acquired for 20 min after the injection of 600-800 MBq tracer. After co-registration of Cu-ATSM and FDG PET images using CT or MRI, multiple small ROIs were drawn on tumor mass using anatomical images and applied to the PET images to evaluate standardized uptake values (SUV). SUV values were obtained for each ROI (SUVroi) and the slopes of regression line between Cu-ATSM and FDG were determined for each tumor. Mean and maximum SUV values of tumors for each PET tracer were obtained and effects of treatment were compared with SUV values of the two tracers. In cases of residual tumors after treatment, location of the residual tumor and tracer accumulation before the treatment were compared to evaluate relationship between tracer accumulation and the tumor resistance to the treatment. RESULTS: Thirty-nine patients had squamous cell carcinoma and three were adenocarcinoma. Although adenocarcinoma showed similar and spatially homogenous tumor accumulation for both tracers, squamous cell carcinoma showed high peripheral Cu-ATSM accumulation and relatively homogeneous FDG uptake in the tumor mass. The means of regression slopes were -0.13 ± 0.08 (negative correlation) for SCC and 0.27 ± 0.12 (positive correlation) for adenocarcinoma. In 6 cases of advanced squamous cell carcinoma, tumors were treated by chemoradiation, and three of them who showed high Cu-ATSM accumulation in the periphery of the tumor had residual tumor tissue in the same region after the treatment, which was considered to reflect resistant tissue of the tumor. CONCLUSION: In patients with head-and-neck cancer, intratumoral distribution of Cu-ATSM and FDG showed negative correlation in squamous cell carcinoma although adenocarcinoma showed positive correlation; the tendency was similar to lung cancers in our previous study. The results from the follow-up study indicated that the regions of high Cu-ATSM accumulation in squamous cell carcinoma may predict resistant tissue after the cancer therapy.

Disclosure of author financial interest or relationships:
**H. Okazawa**, None; **Y. Sato**, None; **Y. Kimura**, None; **M. Oh**, None; **T. Mori**, None; **Y. Kiyono**, None; **S. Fujieda**, None.

Presentation Number **P617**
Poster Session 3
September 7, 2012 / 15:15-15:15 / Room: The Liffey

# Recurrent Cancer Involving the Peripheral Nervous System Identified by FDG PET/CT

***Patrick Peller**, Andrew Crush, Robert Murphy, Department of Radiology, Mayo Clinic, Rochester, MN, USA. Contact e-mail: ppeller@pol.net*

Purpose: Identifying the etiology of peripheral neuropathies in patients with malignancies is challenging from both a clinical and an imaging perspective. We evaluated the ability of PET/CT to detect malignant involvement of the peripheral nervous system (PNS) in patients with a prior history of cancer. Methods: A retrospective analysis of a prospective database of patients presenting with neuropathy and a prior history who underwent a FDG PET/CT scan from 9/01/05 to 9/01/09 was undertaken. Patients were included if the neurologic examination documented a regional pain syndrome, motor abnormalities or sensory deficits and PET/CT was ordered within 1 month of presentation. Peripheral nerve involvement was confirmed by biopsy and/or resolved with cancer treatment. The location of PNS involvement and other sites of disease identified on PET/CT were correlated to the pathologic results and clinical outcome. Results: A peripheral neuropathy led to PT/CT evaluation in 216 patients with subsequently biopsy or clinical follow-up. Of the 216 patients, 89 had lymphoma, 81 breast cancer, 31 lung cancer, 8 head and neck, 6 melanoma and 1 colon cancer (122 female, 94 male; mean age 64.4±10.6). FDG uptake indicative of recurrent malignancy was identified in the PNS on PET/CT scans of 132 patients (61.1%). When B-cell NHL was the dominant histology, PET /CT scans identified multiple nerve involvement in 58% (36/62) with synchronous CNS involvement in 25%. The sciatic nerve was the single most commonly affected nerve with NHL. Breast cancer involved the brachial plexus preferentially, identified in 66 patients (81.5%). PNS involvement in the remaining cancer patients was uncommon in only 19.6% (9/46). FDG PET/CT was able to differentiate an active tumor from post-treatment changes. Conclusions: PET/CT led to detection of malignancy in cancer patients presenting for neuropathy. In patients with known treated malignancy and neuropathy FDG PET/CT has the advantage of high sensitivity for identifying malignant involvement of the peripheral nervous system.

Disclosure of author financial interest or relationships:
**P. Peller**, None; **A. Crush**, None; **R. Murphy**, None.

Presentation Number **P618**
Poster Session 3
September 7, 2012 / 15:15-15:15 / Room: The Liffey

# Can metabolic imaging with 3D multivoxel proton MR spectroscopy at 3 Tesla improve the positive predictive value for breast cancer diagnosis?

***Katja Pinker-Domenig****, Benedikt Brück, Stephan Gruber, Wolfgang Bogner, Hubert Bickel, Thomas H. Helbich, Dept. of Radiology, Division of Molecular and Gender Imaging, Medical University of Vienna, Vienna, Austria. Contact e-mail: katja.pinker@meduniwien.ac.at*

Purpose To prospectively evaluate the diagnostic performance of high field (3T) three-dimensional (3D) multivoxel proton (1H) magnetic resonance (MR) spectroscopy in patients with breast tumors using histopathologic findings as the standard of reference. Material and Methods In this IRB approved study 141 patients with a suspicious breast lesions detected by mammography or breast ultrasound were examined at 3T. MR sequence protocol consisted of a 3D-1H-MRSI (10 x 10 x 10 mm; TA 11min), which was performed before application of contrast agent to avoid contamination of spectra, a T2-weighted and a high resolution T1-weighted sequence before and after application of a standard dose Gd-DOTA. 22 Patients had to be excluded due to insufficient data quality due to motion artefacts. Lesion morphology and EH-kinetics were assessed and classified according to BI-RADS®. 3D-1H-MRSI findings were defined as positive if the signal-to-noise ratio (SNR) of the choline resonance peak was greater than or equal to 2.55 and as negative in all other cases. 3D-1H-MRSI findings were correlated with histopathologic findings. Results A total of 119 patients (age range, 24-86 years) were finally included. The median lesion size at MR imaging was 2,5 cm (range, 0,5-9,8 cm). Histopathology proved 74 (62%) of 119 lesions to be malignant, and 45 (38%) to be benign. A choline peak was present in 85 of 119 lesions. There was a choline peak in 70 of the 74 cancers and in 15 of 45 benign lesions. 3D-1H-MRSI had a sensitivity of 93% and a specificity of 91%. The use of 3D-1H-MRSI as an adjunct to MR imaging would have significantly increased the positive predictive value (ppv) of biopsy from 85% to 95% (p=0.047). If biopsy had been performed only in the lesions with a choline peak at 3D-1H-MRSI, biopsy may have been spared in 30 (67%) of the 45 benign lesions. Conclusion 3D-1H-MRSI was successfully incorporated into a routine breast MR imaging protocol at 3T. 3D-1H-MRSI significantly increased the ppv of breast biopsy as compared to MRI alone. Clinical Relevance 3D-1H-MRSI at 3T has the potential to reduce the number of lesions detected at CE-MRI of the breast that require biopsy.

Disclosure of author financial interest or relationships:
**K. Pinker-Domenig**, None; **B. Brück**, None; **S. Gruber**, None; **W. Bogner**, None; **H. Bickel**, None; **T.H. Helbich**, Siemens, Grant/research support; Fond national bank austria, Grant/research support .

Presentation Number **P619**
Poster Session 3
September 7, 2012 / 15:15-15:15 / Room: The Liffey

# Near-Infrared Fluorescence Lymphatic Imaging of Lymphangiogenesis in Metastatic Melanoma and Post-Surgical Recovery

***John C. Rasmussen***[1], *I-Chih Tan*[1], *Eva Sevick*[1], *Janice N. Cormier*[2], [1]*Institute of Molecular Medicine, University of Texas Health Science Center Houston, Houston, TX, USA;* [2]*Department of Surgical Oncology, The University of Texas M.D. Anderson Cancer Center, Houston, TX, USA. Contact e-mail: johnras@hotmail.com*

An increasing body of histologic evidence highlights the role lymphangiogenesis plays in metastatic disease even before metastasis occurs. However, clinical imaging modalities with the spatial and temporal resolutions required to image these lymphatic changes in vivo have not been available. The evaluation and treatment of melanoma patients includes the pathologic assessment of regional lymph nodes using the techniques of sentinel lymph node biopsy (SLNB) and immunohistochemical evaluation. When the sentinel node is cancer positive, standard-of-care includes complete lymph node dissection (CLND) from which up to 60% of patients develop lymphedema, a poorly understood chronic progressive lymphatic disease characterized by debilitating swelling of the affected limb. We recently developed near-infrared fluorescence (NIRF) imaging techniques to non-invasively image human lymphatics following intradermal administration of microdose amounts of contrast agent. Distinct architectural and functional differences were observed between healthy and diseased lymphatics. In this ongoing, two part FDA approved feasibility study, we seek to use NIRF imaging of abnormal lymphatics as prognostic/diagnostic indicators of metastatic disease and acquired lymphedema. In part one of this study, 18 melanoma subjects undergoing wide local excision and SLNB, receive intradermal injections of 25 μg indocyanine green (ICG) near the tumor and in the limb draining to the same nodal basin. Additional injections are administered in the corresponding contralateral sites and serve as controls. The total dose of ICG is ≤ 400 μg. A custom, NIRF imaging system illuminates the injection sites with 785 nm excitation light and acquires dynamic images of fluorescent lymphatics using an intensified, charge coupled device camera. In the second part of the study, subjects with tumor positive sentinel lymph nodes are longitudinally imaged three additional times, once just prior to CLND and twice more at four month intervals. Lymphatic images are assessed and correlated to metastatic disease and to post-surgical lymphatic recovery. Of the 10 SLNB subjects imaged to date, the tumor-draining lymphatics were tortuous in two, dilated in two others, and normal in six. Five subjects had abnormal, tortuous lymphatic capillaries radiating from the tumoral injection sites, but only the two subjects with the dilated tumor-draining lymphatics had positive sentinel lymph nodes and were enrolled in the longitudinal study. The first of these had normal limb lymphatics throughout the all the imaging sessions with no evidence of lymphedema. The second had fluorescent lymphatic capillaries distal the tumor prior to SLNB and subsequently developed fluorescent dermal backflow as shown below and as commonly seen in subjects with lymphedema. Whether the dermal backflow resolves or portends onset of lymphedema remains to be seen during the follow up sessions. These studies indicate that abnormal lymphatic architecture, as assessed by NIRF imaging, may provide prognostic/diagnostic indication of metastatic disease and lymphedema. Supported by the National Institutes of Health (R01 CA128919 and U54 CA1356404).

Disclosure of author financial interest or relationships:
**J.C. Rasmussen**, None; **I. Tan**, None; **E. Sevick**, Tactile, Inc, Grant/research support; Siemens Preclinical Solutions, Other financial or material support; **J.N. Cormier**, None.

Presentation Number **P620**
Poster Session 3
September 7, 2012 / 15:15-15:15 / Room: The Liffey

# Molecular imaging as a predictive diagnostic method for the therapeutic efficacy of radiotherapy in xenograft model of human colorectal cancer

*Young Eun Cho[1], **Miyeoun Song**[1], Eun-Ju Do[1], Haeyon Jeon[1], Soo Jung Park[1], Byung-Heon Lee[3], In-San Kim[3], Dae Hyuk Moon[2], Byong Duk Ye[2], Seung-Jae Myung[2], [1]Asan Institue for Life Sciences, Asan Medical Center, Seoul, Republic of Korea; [2]Department of Gastroenterology and Nuclear Medicine, Asan Medical Center, Seoul, Republic of Korea; [3]Department of Biochemistry and Cell Biology, Kyungpook National University, Daegu, Republic of Korea. Contact e-mail: drsong@chol.com*

Aim It was reported that molecular imaging using phosphatidylseine-recognizing peptide (PSP), a synthetic near-infrared (NIR) fluorescent probe, indicated apoptotic cells. This study was to evaluate an ability of this molecular imaging technique as a rapid predictive diagnostic method of therapeutic efficacy for radiotherapy in human colorectal cancer model. Materials and Methods Percentage of radiation (10Gy)-induced apoptotic cells between HCT116 and HT29 was determined at post-0, 4, 24 and 48 hours by FACS using Annexin V and PSP staining. Human colorectal cancer cells (5 ×106 cells; HCT116 or HT29) were intramuscularly xenografted on both legs of Balb/c nude mouse. At 10 days after implantation, left side tumor (LT) was irradiated with 10Gy while right side tumor (RT) served as an individualized control, and PSP combined with Cy5.5 was immediately injected via tail vein. Molecular serial images were achieved both 1 day (1D) and 8 days (8D) after radiation using IVIS, Xenogen system (Caliper). Tumor size of both legs was serially measured using Vernier caliper (Mitutoyo) and ultrasound system before radiation, on 1D and 8D. The mice were sacrificed on 1D and 8D, respectively. TUNEL and caspase-3 staining was performed to detect apoptotic cells of irradiated and control tumor. Results In vitro irradiated-HCT116 cells had significant increased apoptotic cells compared to irradiated-HT29 cells. The results were consistent at 4, 24 and 48 hours after radiation ($p<0.005$). On 1D, the fluorescent intensity of images increased approximately two times (LT; 2.9E+09 vs. RT; 1.6E+09) in HCT116 tumor model, however, HT29 tumor model showed no signal difference between irradiated tumor and control. At 1D, no changes in tumor sizes were observed in both HCT116- (LT; 1.2±0.9cm3 vs. RT; 1.2±0.1cm3) and HT29-xenograft model (LT; 1.5±0.1cm3 vs. RT; 1.6±0.1cm3). At 8D HCT116 tumor model had a significant reduction (LT; 0.6±0.2cm3 vs. RT; 1.4±0.3cm3 , $p<0.05$) in tumor size relative to its control, whereas the size of HT29-induced tumor was slightly reduced (LT; 1.0±0.2cm3 vs. RT; 1.7±0.5cm3, $p=0.2$). TUNEL-positive cells were observed to be higher in irradiated-HCT116 tumor than irradiated-HT29 tumor at 1D. Conclusion Our results show that fluorescent uptake at 1 day post radiation predicts therapeutic response of cancer radiation. The molecular imaging using synthetic NIR PS-specific peptide probe is a useful tool for rapid predictive diagnosis of therapeutic efficacy of radiotherapy. Grant: The National Research Foundation of Korea (No. 2011-0019632) These authors (Y.C., M.S.) contributed equally to this work. Corresponding author (S.-J. M.)

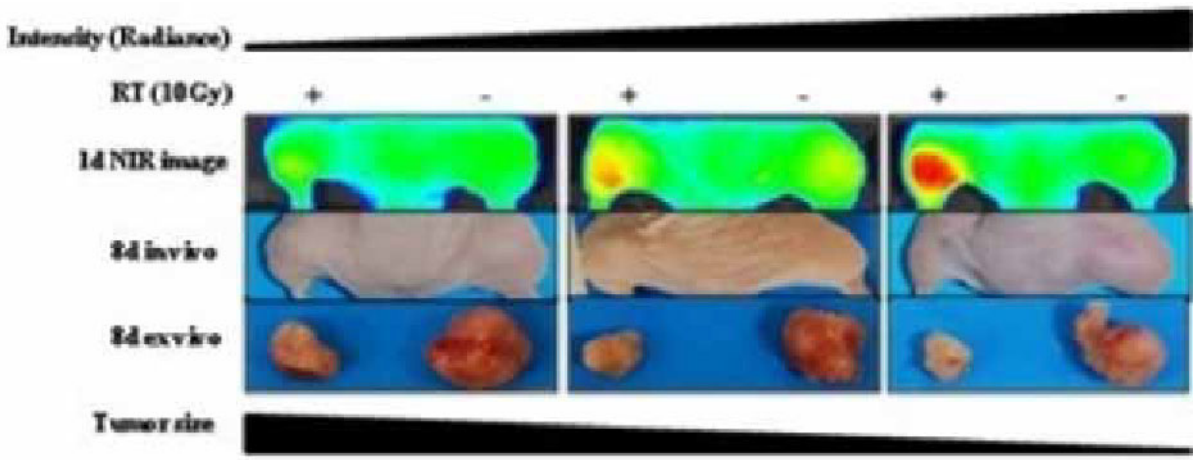


Disclosure of author financial interest or relationships:
**Y. Cho**, asan medical center, Grant/research support; **M. Song**, None; **E. Do**, None; **H. Jeon**, None; **S. Park**, None; **B. Lee**, None; **I. Kim**, None; **D. Moon**, None; **B. Ye**, None; **S. Myung**, None.

Presentation Number **P621**
Poster Session 3
September 7, 2012 / 15:15-15:15 / Room: The Liffey

# Automated breast density measurement with MRI at 3T confirms higher breast density in breast cancer patients

***Georg J. Wengert***, *Katja Pinker-Domenig, Hubert Bickel, Heinrich F. Magometschnigg, Michael R. Curda, Thomas H. Helbich, Department of Radiology, Division of Molecular and Gender Imaging, Medical University of Vienna, Vienna, Austria. Contact e-mail: georg.wengert@meduniwien.ac.at*

PURPOSE Breast density is one of the strongest predictors of breast cancer risk. To-date breast density measurement is performed qualitatively using mammography neccessitating radiation and compression. The aim of this to measure and compare breast density in breast cancer patients and age-matched healthy controls with radiation- and compression-free MRI using the Dixon sequence. MATERIAL AND METHODS 19 histopathologically verified breast cancer cases and 19 healthy controls (age range of 34 to 68; mean 50 years) were included in this IRB approved prospective study. Each cancer case was matched to a control case by date of birth and age at examination. Density was measured separately in all participants with radiation- and compression free 3T MRI using the Dixon sequence (TR/TE 6ms/ 2.45ms/2.67ms, 192 slices, matrix 352 x 352, 1mm isotropic, TA 3:38 min) with a 4-channel dedicated breast coil. The Dixon sequence acquires two separate datasets in one sequence, one representing the fatty components and one the fibroglandular components of the breast. Our breast density measurement system works fully automated and calculated the total volume of the breast (cm3), the percentage of fatty tissue (%) and the percentage of fibroglandular tissue (%). In each group normal distribution (Kolmogorov-Smirnov-Test; P = 0.12) and variance homogeneity (Levenes Test; P = 0.69) was determined to accomplish independent t-test (P = 0.316). RESULTS Quantitative volumetric breast density measurements with MRI using the Dixon sequence were successfully performed in both groups. Breast density ranged from 1.7 % to 58.4 %, mean density for all women was 21.24 %. Mean percentage density was higher in breast cancer patients as compared with healthy controls with an average of 24% (SD 16.9%) vs. 18.4% (16.6). Breast density decreased gradually with age in both cancer patients (r2=0.237) and healthy controls (r2=0.259). CONCLUSION Breast cancer patients have higher breast density as compared to healthy women. Although not statistically significant due to the small sample size, these results are entirely consistent with the fact that breast density is a strong risk factor for breast cancer.

Disclosure of author financial interest or relationships:
**G.J. Wengert**, None; **K. Pinker-Domenig**, None; **H. Bickel**, None; **H.F. Magometschnigg**, None; **M.R. Curda**, None; **T.H. Helbich**, Siemens, Grant/research support; Fond national bank austria, Grant/research support .

Presentation Number **P622**
Poster Session 3
September 7, 2012 / 15:15-15:15 / Room: The Liffey

# Optical-guided surgery of fibrosarcoma on cat patients. A veterinary clinical study

***Christiane H. Wenk***[1,2]*, Véronique Josserand*[1,2]*, Stéphanie Guillermet*[4]*, Corinne Tenaud*[1,2]*, Dorothée M. Waterlot-Virieux*[3]*, Claude Carozzo*[3]*, Frédérique Ponce*[3]*, Jean-Luc Coll*[1,2]*, [1]Cibles diagnostiques ou thérapeutiques et vectorisation de drogues dans les cellules tumorales, CRI-INSERM U823, Grenoble, France; [2]Université Joseph Fourier, Grenoble, France; [3]VetAgro Sup, Lyon, France; [4]Fluoptics®, Grenoble, France. Contact e-mail: Christiane.Wenk@ujf-grenoble.fr*

INTRODUCTION: In most cancers, tumor resection is the first therapeutic indication before chemotherapy or radiotherapy assuming that the tumor is removable. Since the patient survival strongly depends on the exhaustiveness of the tumor resection, innovative methods improving the quality of cancer surgery are needed to lower the risks of postoperative local recurrence. In a previous preclinical study on mice bearing peritoneal carcinomatosis we compared the quality of tumor removal, performed under conventional light, versus near-infrared (NIR) image guided surgery using a tumor targeting probe (RAFT(c[-RGDfK-])4-Alexa Fluor®700) and a portable clinical imaging device (FluobeamTM). The results showed that optical guidance greatly improved the quality of the surgery by doubling the number of detected nodules and reducing significantly the duration of the surgery. As an evaluation regarding clinical surgery in humans we transferred this technology, consisting of the RAFT-RGD-probe (AngioStampTM) and the Fluobeam™, into a clinical veterinary phase, that is to say the clinical surgery of spontaneous tumors in cats. METHODS: Twelve fibrosarcoma bearing cats addressed by veterinary practitioners were included in the study after owner's consent. Diagnosis was based on clinical and morphological data (aspirations and biopsies) and primary tumor spreading was evaluated by x-rays scanner. 16, 24 or 36 hours before the surgery, cats received a single dose of AngioStampTM (0.15 to 0.6 mg/kg) intravenously and tumor resection was performed conventionally by the surgeon. Fluorescence imaging was made at several steps of the surgery as well as on the surgical specimens (tumor tissue, tumor margins and surrounding healthy tissues). Histological analyses were carried out and the samples' tumor infiltration as well as the αvβ3 integrin expression levels (immunohistochemistry), were compared to the fluorescent signals of the samples. Cats were then submitted to a long term clinical follow up. RESULTS: All cats displayed a fluorescent signal in the tumor indicating the good tumor targeting of the fluorescent tracer. For the first experimental condition (AngioStampTM 0.6 mg/kg 16 hours before surgery) the tumor/healthy tissue ratio was 4 ±1, then the tracer dose was decreased and the delay before surgery was augmented leading to a tumor/healthy tissue ratio of 14±1 when cats were injected with AngioStampTM 0.3 mg/kg 36 hours before surgery. Regarding the anatomopathological analyses, no false negative were found and the percentage of tumor cells per sample was linearly correlated with the intensity of the fluorescent signal. All cats recovered well from the surgery and imaging and are submitted to a long term clinical follow up which is still ongoing one year after the beginning of the study.

Disclosure of author financial interest or relationships:
**C.H. Wenk**, None; **V. Josserand**, None; **S. Guillermet**, Fluoptics, Employment; **C. Tenaud**, None; **D.M. Waterlot-Virieux**, None; **C. Carozzo**, None; **F. Ponce**, None; **J. Coll**, None.

Presentation Number **P623**
Poster Session 3
September 7, 2012 / 15:15-15:15 / Room: The Liffey

# Tumor Visualization in the OR and Pathology

***Michelle M. Williams***[1,2], *Douglas A. Murrey*[1], *Andrew Chow*[1], *Deborah A. Hurley*[1], *Edward W. Martin*[1], *Stephen Povoski*[1], *Nathan Hall*[1], *Michael V. Knopp*[1,2], [1]*Radiology, OSUWMC, Columbus, OH, USA;* [2]*Imaging Science, Wright Center for Innovation, Columbus, OH, USA. Contact e-mail: Michelle.Williams@osumc.edu*

Advanced imaging techniques that push the cutting edge of clinical research are largely misunderstood or underappreciated. This is especially relevant to surgical procedures where high-resolution imaging can make significant differences in patient outcomes. The Ohio State Wexner Medical Center and The James Comprehensive Cancer Center have used the Inveon, a multi-modal scanning system from Siemens Preclinical that allows for many advanced imaging techniques, to facilitate in-vivo translational imaging of small animals. The experience gained from the small animal research is now being used to examine human tissue samples in parallel with traditional methods. The Inveon system as used at the OSUWMC has a trans-axial bore size of 10cm for microPET and 12 cm microCT. Since the system functions as a cohesive unit, PET and CT data can be precisely registered for multi-modal analysis. The microPET subsystem has a spatial resolution of 0.79 mm and will image positron-emitting radio nuclides such as 18F, 124I, 68Ga, and 67Cu. The acquisition time for the microCT ranges between 7 and 14 minutes per bed position. The microCT subsystem has a spatial resolution of 10 microns and an acquisition time of 3-12 minutes. This results in a combined PET/CT scan with 10 times the resolution of conventional scanning systems while still maintaining a typical capture time under 15 minutes. This enables high-resolution imaging of a patient specimen in roughly the same time required to perform a low-resolution scan of the patient in a full-body scanner. The speed and size of the Inveon system opens the possibility of in-theatre scanning of patient tissues to assess margins in near-real-time. This would result in reduced trauma to the patient, reduced patient transit times, and potentially reduce the need for the patient to be operated on a second time if post-op scanning reveals tissue was missed in the initial surgery. Beyond minimizing risk and maximizing patient outcomes, these advanced imaging techniques provide a dramatic increase in information to the surgical team and pathology. Mineralization and density data enables localization of surgically placed markers of staples as well as characteristics of the anatomy of interest. The increased data facilitates the identification of targets marked for further scrutiny. Palpable lumps marked in surgery can reveal multiple, clustered nodes on the high-resolution CT imagery when traditional imaging techniques show only undifferentiated masses. The increased resolution identifies smaller hypoxic and necrotic regions, resulting in increased detail in pathological directions and greater speed when compared to using traditional sutures and beads alone. The reduction in pathology response times and improvement of reporting is a significant asset to patient care. The imaging techniques developed at OSUWMC with the Inveon scanners will streamline patient care, improve operating procedures, and provide new tools to improve clinical outcomes. By adding new imaging products to the traditional tools used today, OSUWMC is pushing the boundaries of patient care and medical science.

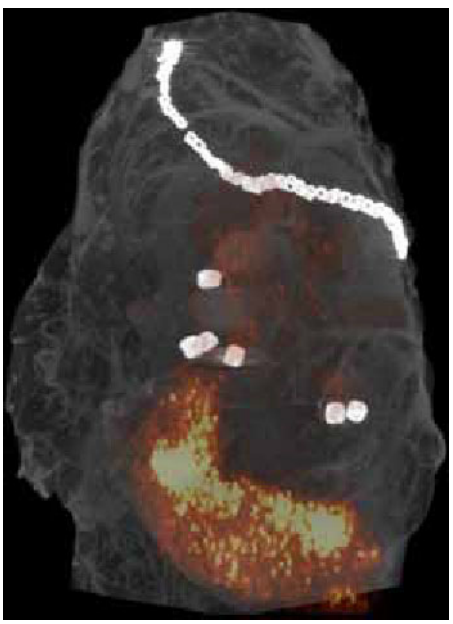

Portion of colon metastasis fused to omentum, imaged with 18-FDG

Disclosure of author financial interest or relationships:
**M.M. Williams**, None; **D.A. Murrey**, None; **A. Chow**, None; **D.A. Hurley**, None; **E.W. Martin**, None; **S. Povoski**, Enlyton,Ltd., Other financial or material support; **N. Hall**, Enlyton,Ltd., Other financial or material support; **M.V. Knopp**, None.

Presentation Number **P624**
Poster Session 3
September 7, 2012 / 15:15-15:15 / Room: The Liffey

# Biodistribution and Radiation Dosimetry of Apoptosis Imaging Agent 18F-CP-18 Measured in Healthy Volunteers*

*Mohan Doss[1], R. Katherine Alpaugh[2], **Jian Q. Yu**[1], [1]Diagnostic Imaging, Fox Chase Cancer Center, Philadelphia, PA, USA; [2]Protocol Support Lab, Fox Chase Cancer Center, Philadelphia, PA, USA. Contact e-mail: Michael.Yu@fccc.edu*

Objectives: Human safety, biodistribution, dosimetry, and imaging characteristics of the apoptosis imaging agent 18F-CP-18 or (18S,21S,24S,27S,30S)-27-(2-carboxyethyl)-21-(carboxymethyl)-30-((2S,3R,4R,5R,6S)- 6-((2-(4-(3-[F18]fluoropropyl)-1H-1,2,3-triazol-1-yl)acetamido)methyl)-3,4,5- trihydroxytetrahydro-2H-pyran-2-carboxamido)-24-isopropyl-18-methyl-17,20,23,26,29-pentaoxo-4,7,10,13-tetraoxa-16,19,22,25,28-pentaazadotriacontane-1,32-dioic acid) were evaluated in a Phase 0 clinical trial (ClinicalTrials.gov Identifier:NCT01362712). 18F-CP-18 is a novel PET imaging agent that targets cells with high caspase 3 levels enabling the assessment of apoptotic activity. Identifying such patients through PET imaging could aide in evaluating the effectiveness of cancer treatments. Methods: Seven healthy volunteers (5 females, 2 males) aged 31-55 were administered 500-700 MBq of 18F-CP-18 intravenously and imaged with a PET/CT scanner. Five sequential whole body PET/CT scans with ultra-low dose CT (CT parameters: 140 kV, 20 mA, 0.6 sec rotation, Helical) from top of skull to mid-thigh were performed over 2.8 hours following the injection. In addition, a PET/CT scan covering mid-thigh to toes was performed following the first whole body PET/CT scan. Vital signs and EKG were monitored prior to, periodically during, and immediately following the final imaging. All subjects also had a 24 hour follow-up visit. The PET images were analyzed to determine the integrated activity in the visualized organs including brain, breasts (for females), heart, kidneys, liver, spleen, testes (for males), and urinary bladder. The residence times were determined from multi-exponential regression of organ uptake data normalized by injected dose. Radiation dose was estimated using OLINDA/EXM software for standard male and female phantoms using bladder voiding model with 4.8 hr and 1 hr voiding intervals. Results: No adverse events were noted during the 24 hour post-injection monitoring period. Kidneys and bladder showed significantly enhanced uptake in comparison to background activity with rapid renal clearance of the activity from the blood and minimal retention in other organs. For the female phantom, urinary bladder had the highest dose at 750±90 μGy/MBq in the 4.8 hr bladder voiding model and 200±20 μGy/MBq in the 1 hr model. The effective dose was 50±5 μSv/MBq for the 4.8 hr model, reducing to 18±1 μSv/MBq in the 1 hr model. For a typical injected dose of 555 MBq, the effective dose would be approximately 28 mSv for the 4.8 hr model and 10 mSv for the 1 hr model. The doses for the male phantom model were lower. Conclusions: 18F-CP-18 was found to have a diffuse uptake in most organs except for urinary bladder and the kidneys, potentially reducing lesion visibility in these organs. The effective dose of ~28 mSv for a typical injected dose for female phantom using the 4.8 hr bladder voiding model is below the FDA guidelines for a research subject. The effective dose and the bladder dose can be reduced by more frequent voiding. 18F-CP-18 can be used safely for assessing apoptotic activity. *This work was supported by Siemens Molecular Imaging - Biomarker Research.

Disclosure of author financial interest or relationships:
**M. Doss**, None; **R. Alpaugh**, None; **J.Q. Yu**, Siemens Molecular Imaging, Grant/research support .

Presentation Number **P625**
Poster Session 3
September 7, 2012 / 15:15-15:15 / Room: The Liffey

# Novel Tc-99m Colloid shows Excellent Trapping and Blue Dye Concordance in Sentinel Nodes from a Comparative Retrospective Study in Breast Cancer Patients

***Pamela L. Zabel***[1], *Frances C. Wright*[2], *Muriel Brackstone*[3], [1]*Nuclear Medicine, London Health Sciences Centre, London, ON, Canada;* [2]*Surgical Oncology, Sunnybrook Medical Centre, Toronto, ON, Canada;* [3]*Surgical Oncology, London Health Sciences Centre, London, ON, Canada. Contact e-mail: pzabel@uwo.ca*

The most powerful prognostic factor of survival of breast cancer is regional lymph node status. Thus, it is important to identify patients with nodal involvement in order to guide the most appropriate therapy. The sentinel lymph node(s) (SLN) is the lymph node(s), in a given lymphatic basin, which first receives lymphatic flow from a primary tumor. The status of the SLN is indicative of the spread of cancer. A radioactive tracer that is efficiently trapped in the first 1-3 SLN allows for less invasive surgery/fewer complications compared to total axillary node dissection (11-20 nodes). SLN detection is listed as a clinical priority for use of the isotope technetium-99m (Tc-99m) when isotope shortages occur. The current Tc-99m Sulfur Colloid used for SLN imaging and detection is not of optimal size and often requires a filtration, wasting 70-90% radioactivity. We have developed/patented Tc-99m Cysteine Rhenium Colloid (CRC), which is optimally sized for lymph node detection without filtration. Excellent trapping of CRC compared to other colloids was demonstrated in SLN of a rabbit lymphoscintigraphy model . A retrospective chart review was designed to analyze the lymph node identification rate of Tc-99m CRC compared to Tc-99m sulfur colloid (SC) in breast cancer patients at two Canadian hospitals in Ontario. METHODS:Data from 1205 patients undergoing surgery for early clinically node negative breast cancer was retrospectively collected by chart review between 2002 and 2010 from two separate Ontario hospitals, 602-603 at each site. One site used unfiltered Tc-99m CRC injected intradermally while the other used unfiltered Tc-99m SC injected subdermally. Both sites used peri-tumoral injection of blue dye 5 minutes preoperatively. Sentinel node identification rates were compared (Chi Square analysis), as were the mean number of nodes identified (student's T-test). Concordance with blue dye uptake was evaluated and data were compared to the surgical pathology of identified SLNs. RESULTS: Successful axillary sentinel lymph node identification rates were not statistically different, at 99.5% (CRC) and 99.17% (SC), p=0.51. Greater leakage past 1-2 SLN occurred for SC so that the mean number of nodes identified was statistically higher for SC, 2.71 vs 2.01 for CRC, p=0.008. More trapping occurred in initial nodes for CRC. Concordance with blue dye for first, second and third node respectively was excellent for CRC (93%, 83%, 79%) compared to SC (90%,80%,75%). No adverse reports were indicated for CRC or SC. CONCLUSIONS :Tc-99m CRC was able to successfully identify sentinel lymph nodes in breast cancer patients as well as the standard Tc-99m SC. Trapping of CRC in the sentinel nodes was excellent with less migration onto further nodes. CRC is a good alternative to traditional SC, particularly in times of critical isotope shortages from aging nuclear reactors since wastage from filtration is unnecessary. Health Canada has approved further evaluation in a prospective open safety registry clinical trial (4 indications). RESEARCH SUPPORT of Canadian Institute for Health Research is gratefully acknowledged.

Disclosure of author financial interest or relationships:
**P.L. Zabel**, None; **F.C. Wright**, None; **M. Brackstone**, None.

Presentation Number **P626**
Poster Session 3
September 7, 2012 / 15:15-15:15 / Room: The Liffey

# Combined Imaging with 18F-FLT PET/CT and 99m-Tc-Hynic-Annexin V SPECT to Guide Therapy with EGFR Antagonists and Bcl-xL Inhibitors in Non-Small Cell Lung Cancer

***Antonella Zannetti***[1], *Francesca Iommelli*[1], *Viviana De Rosa*[1], *Anna Nardelli*[1], *Giovanni Ortosecco*[1], *Silvana Del Vecchio*[2], [1]*Institute of Biostructures and Bioimages, National Research Council, Naples, Italy;* [2]*Department of Biomorphological and Functional Sciences, University of Naples "Federico II", Naples, Italy. Contact e-mail: antonella.zannetti@cnr.it*

EGFR mutational status, activation of downstream signaling and effective apoptotic cascade are all factors that may affect tumor response to EGFR antagonists in non-small cell lung cancer (NSCLC). Our aim was to test whether combined imaging with 18F-Fluorothymidine (18F-FLT) PET/CT and 99m-Tc-Hynic-annexin V SPECT can provide clues for selection of patients with NSCLC candidate to treatment with reversible and irreversible EGFR tyrosine kinase inhibitors (TKI) or combined treatment with Bcl-xL inhibitors. NSCLC cells bearing activating or secondary mutations of EGFR (HCC827, H1975, and H1650) were subcutaneously injected into flanks of individual female BALB/c (nu/nu) mice. Tumor bearing animals (at least 4 for each cell line and for each treatment) were treated for 3 days by oral gavage with 50 and 150 mg/kg/d erlotinib, 50 mg/kg/d CL-387,785, an irreversible EGFR TKI, 25 and 50 mg/kg/d WZ4002, an irreversible EGFR TKI with a higher affinity for T790M mutant EGFR than for wild-type EGFR, 6.25 mg/Kg/d ABT-263, a Bcl-xL inhibitor, and a combination of erlotinib (50 mg/kg/d) and ABT-263 (6.25 mg/Kg/d). Imaging studies were performed by injecting 7.4 MBq 18F-FLT through tail vein and 1h post-injection animals were subjected to microPET/CT scan. Quantitative analysis was performed on reconstructed images by drawing three-dimensional regions of interest around tumors to determine SUVmax in the baseline and post-treatment microPET/CT studies. The percentage change of 18F-FLT uptake was determined in each animal. Furthermore, animals bearing tumors that were resistant due to dysregulation of Bcl-2 family members (H1650), were subjected to small animal SPECT with 99mTc-Hynic-annexin V before and after combined treatment with erlotinib and ABT-263 or single agent alone. After imaging studies, animals were sacrificed, tumors were removed and tested for Ki-67 immunostaining and percentage of apoptotic cells (Tunel). Sensitive tumors (HCC827) showed mean decreases in 18F-FLT uptake of 45% and 28% with high and low dose regimens of erlotinib, respectively. Resistant NSCLC cells bearing T790M mutation (H1975) showed mean increases in 18F-FLT uptake of 27% and 33% with high and low doses of erlotinib, respectively. Treatment with CL-387,785, low-dose WZ4002, and high-dose WZ4002 caused mean decreases in tracer uptake of 21%, 26% and 36%, respectively. NSCLC cells that were resistant because of dysregulation of Bcl-2 family members (H1650) showed mean reductions in 18F-FLT uptake of 49% and 23% with high and low doses of erlotinib, respectively, whereas the addition of ABT-263 did not affect 18F-FLT uptake. Conversely, the combined treatment with erlotinib and ABT-263 caused an increase of 99mTc-Hynic-annexin V uptake in H1650 tumors whereas no change of tracer uptake occurred after single agent treatment. In excised tumors Ki-67 immunostaining and Tunel assay confirmed imaging findings. In conclusion, 18F-FLT PET/CT and 99mTc-Hynic-annexin V SPECT may contribute to the selection of patients that may benefit from treatment with reversible and irreversible EGFR TKIs or combined treatment with Bcl-xL/Bcl-2 inhibitors.

Disclosure of author financial interest or relationships:
**A. Zannetti**, None; **F. Iommelli**, None; **V. De Rosa**, None; **A. Nardelli**, None; **G. Ortosecco**, None; **S. Del Vecchio**, None.

Presentation Number **P627**
Poster Session 4
September 8, 2012 / 14:45-14:45 / Room: The Liffey

# Characterization of a Calcium-responsive MR-Agent in Cellular Model Systems

***Goran Angelovski***[1], *Sven Gottschalk*[2], *Milena Milosevic*[3], *Pavle Andjus*[3], *Nikos K. Logothetis*[1,4], [1]*Physiology of Cognitive Processes, Max Planck Institute for Biological Cybernetics, Tuebingen, Germany;* [2]*High-Field Magnetic Resonance Center, Max Planck Institute for Biological Cybernetics, Tuebingen, Germany;* [3]*Institute for Physiology and Biochemistry, Faculty of Biology, University of Belgrade, Belgrade, Serbia;* [4]*Division of Imaging Science and Biomedical Engineering, University of Manchester, Manchester, United Kingdom. Contact e-mail: goran.angelovski@tuebingen.mpg.de*

Introduction Calcium is an essential metal ion for life. In the brain, essential intracellular signaling processes are known to depend on Ca2+ influx from the extracellular space. Any substantial fluctuation in extracellular Ca2+ concentrations is likely to have important functional effects. Hence, the ability to non-invasively observe these changes in Ca2+ concentrations using MRI would be of paramount importance for biological research. Our recently developed smart contrast agent (SCA) showed remarkable longitudinal relaxivity changes upon interaction with Ca2+ in buffer and biologically relevant solutions, such as a model of an extracellular matrix[1]. Presently, our goal is to study the potential MR-response of our SCA in cellular model systems, as well as to characterize its physiological effects on cells and intracellular Ca2+. Methods We have designed a model system that mimics living tissues in regards to density and partially occupied (extracellular) volume by using monodisperse polystyrene microspheres. Furthermore, growing fibroblast cells (3T3) as 3D culture embedded in an extracellular matrix gel (Matrigel) were used. Microspheres were mixed or cells were perfused with a cell culture medium containing SCA. Next, we manipulated the extracellular Ca2+ concentration and determined ΔT1 with inversion recovery experiments in an NMR spectrometer at physiological temperature. Furthermore, we monitored changes in intracellular Ca2+ and ATP-induced Ca2+ transients upon the addition of SCA to primary glial cells (conventional 2D culture of astrocytes) and checked for concentration dependence in experimental perfusion chambers. For these experiments, we used laser scanning confocal microscopy imaging using Ca2+ sensitive fluorescent probes. Results and conclusions Inversion recovery experiments revealed a change in T1 of a few milliseconds upon the alteration of Ca2+ concentrations that were comparable to changes induced during neural activity. Physiological experiments using confocal fluorescence microscopy showed that SCA reduces intracellular Ca2+ concentration upon its addition and influences ATP-induced Ca2+ transients in astrocytes. However, the response to ATP recovers after waiting for 10 minutes. Moreover, SCA is not toxic at the applied concentrations (up to 1.8 mM) and its presence does not interfere significantly with intracellular Ca2+ signaling. Overall, the 3D cellular model demonstrates that the T1-response of our SCA to extracellular Ca2+ fluctuations would be sufficient to allow the development of an entirely new in vivo fMRI method that is not based on the BOLD signal. References 1. Angelovski G, Fouskova P, Mamedov I, Canals S, Toth E and Logothetis NK, ChemBioChem 2008, 9, 1729-1734.

Disclosure of author financial interest or relationships:
**G. Angelovski**, None; **S. Gottschalk**, None; **M. Milosevic**, None; **P. Andjus**, None; **N.K. Logothetis**, None.

Presentation Number **P628**
Poster Session 4
September 8, 2012 / 14:45-14:45 / Room: The Liffey

# Folic acid-adsorbed nano-probes of poly (lactide)-co-d-alpha-tocopheryl poly (ethylene glycol) succinate [PLA-TPGS] copolymer for iron oxide formulation for targeted MRI

***Prashant Chandrasekharan***[1,2], *Chang-Tong Yang*[1], *Kai-Hsiang Chuang*[1], *Si-Shen Feng*[2,3], [1]*Singapore Bioimaging Consortium, Singapore, Singapore;* [2]*Department of Chemical and Biomolecular Engineering, National University of Singapore, Singapore, Singapore;* [3]*Nanoscience and Nanoengineering Initiative, National University of Singapore, Singapore, Singapore. Contact e-mail: prashant@sbic.a-star.edu.sg*

**Introduction**: The folate receptors (FR-alpha) are greatly expressed on the surface of certain cancer cells compared to the normal cells [1]. Targeted delivery of small molecules is achieved by tagging folic acid to these molecules. Folic acid and its conjugate are taken up by FR-alpha receptor over expressing cells by means of receptor mediated endocytosis. Here a proof-of-concept work was done to show folic acid adsorbed on the surface of polymer nano-probes of PLA-TPGS encapsulating iron oxide nanoparticles that can be used to detect tumor. **Methods and Results**: Polymer nano-probes of PLA-TPGS encapsulating iron oxide nanoparticles (SPIOs-PNP) were formulated by a nanoprecipitation method [2]. The SPIOs-PNP were functionalized by adsorbing folic acid on to the surface (IOs-PNP-FOL) by physically mixing the SPIOs-PNP in a saturated solution of folic acid followed by dialysis to remove unadsorbed folic acid. The adsorption was confirmed by transmission electron microscopy (TEM) and X-ray photoelectron spectroscopy (XPS). The nano-probes were monodisperse and had a hydrodynamic diameter of 283 nm. The particles were tested for cell viability by MTT using MCF-7 breast cancer cells with FR-alpha receptor over expression. Cell viability showed 15-20% reduction in cell viability for IOs-PNP-FOL at high nano-probe concentrations equivalent of 100 and 200 µg Fe per well. Cells were viable at lower concentrations of SPIOs-PNP-FOL. Cell uptake experiment performed using ICP-MS showed that SPIO-PNP-FOL were taken up 1.48, 1.88 and 4 folds greater than the SPIOs-PNP at equivalent concentrations of 50, 25 and 12.5 µg Fe. Further targeting effect was confirmed using Prussian blue staining. Relaxivity of the nano-probe were measured using a multiple echo T2 sequence using a 9.4T Varian MRI scanner. The T2 relaxivity (r2) was found to be similar to that of the SPIOs-PNP (164 mM-1s-1). MRI images acquired at a 7T Bruker ClinScan (TR/TE= 1500/36 ms, resolution=100 µm, thickness=1 mm) using SCID mice with MCF-7 xenograft, showed a 1.5 fold and 2 fold increased accumulation of SPIOs-PNP-FOL in kidney and tumor respectively when compared with that of SPIOs-PNP. It is well known that the kidneys have an increased expression of FR-alpha receptor apart from tumor [3]. The increase in contrast in kidney and tumor using SPIOs-PNP-FOL when compared to SPIOs-PNP, demonstrates the targeting efficiency of the formulated polymer nano-probe. **References**[1] Meiser R, Henning TD, Sophie B et al, Radiology, 255 (2010), 527-535. [2] Prashant C, Dipak M, Chang YT et al, Biomaterials, 31 (2010), 5588-5597,[3] Hilgenbrink AR, Low PS, J.Pham. Sci, 94 (2005), 2135-2146.

Disclosure of author financial interest or relationships:
**P. Chandrasekharan**, None; **C. Yang**, None; **K. Chuang**, None; **S. Feng**, None.

Presentation Number **P629**
Poster Session 4
September 8, 2012 / 14:45-14:45 / Room: The Liffey

# Enhancement kinetic of a blood pool contrast agent (gadofosveset) in mouse at 1.5T: comparison of IV and SC administration routes

*Christian Goetz[1,2], Jean-Philippe Dillenseger[1], Amira Sayeh[1], André Constantinesco[1], **Philippe Choquet**[1,2], [1]UF6237 Preclinical imaging, HUS, Strasbourg, France; [2]Institut de Mecanique des Fluides et des Solides, CNRS, Strasbourg, France. Contact e-mail: pchoquet@unistra.fr*

Introduction Small animal multimodality imaging often requires multiple administration of compounds: radiopharmaceuticals and contrast agents for instance. These procedures are not safe for mice due to the low blood volume (about 1.5ml for a 25g individual). Even if it is not lethal for the animal, increase in blood volume had many consequences. In this case, considering that the experiment was done in homeostasis conditions could be questionable. It renders other administration routes desirable when possible. Classic Gd based MR contrast agents are quickly eliminated from blood, which could also be a difficulty for the setup of MRI experiments, implying the use of fast acquisitions schemes. Gadofosveset (Ablavar®, Lantheus Medical Imaging, N. Billerica, MA, USA) is a blood pool contrast agent and so it presents a potential for small animal imaging, especially at 1.5T due to relaxivity properties of Gd based contrast agents. We report here the comparison between intra-venous and sub-cutaneous administration of gadofosveset to normal mice. Methods MRI system (OPTImouse, RS2D, Bischwiller, France) uses a 1.5T cryogen-free superconducting magnet. For mice whole body imaging, a RF coil (RapidBiomedical, Würzburg, Germany) of 40mm in diameter is used, which remains inside the magnet. Mice are kept anesthetised (isoflurane + air) and warmed in an imaging chamber (Minerve, Esternay, France) that fit inside the coil. Ten C57Bl6 (weight between 20-30g) mice were included. On each individual, two sets of acquisitions at one week interval were done. First an image before administration of gadofosveset followed by a time series after SC administration one week and after IV administration the other. Injection was done via a catheter put either in caudal vein or sc. T1 weighted gradient echo sequences were used designed to allow for a time point every 2min. Using ImageJ (http://rsbweb.nih.gov/ij/) ROIs were drawn around organs of interest (heart wall, liver, large vessels, muscles) and S/N ratio calculated taking standard deviation of signal measured in a ROI outside the mouse body as noise. Results Time courses of SNR show that the compound allows for 20min on the average of enhancement, with a delay for the SC route. Conclusion We have showed that it is possible to do MR angiography using a blood pool contrast agent administered either IV or SC. The latter is desirable when doing multimodality, while the former is essential pour DCE-MRI. The potential of this contrast agent remains to be evaluated in pathological models.

Disclosure of author financial interest or relationships:
**C. Goetz**, None; **J. Dillenseger**, None; **A. Sayeh**, None; **A. Constantinesco**, None; **P. Choquet**, RS2D, Grant/research support .

Presentation Number **P630**
Poster Session 4
September 8, 2012 / 14:45-14:45 / Room: The Liffey

# Yb-HPDO3A, an outstanding MRI-CEST agent for in vivo pH mapping

***Daniela Delli Castelli***[1,2], *Giuseppe Ferrauto*[1], *Juan C. Cutrin*[1], *Enzo Terreno*[1], *Silvio Aime*[1], [1]*University of Turin, Bibiana, Italy;* [2]*Chimica, University, Turin, Italy. Contact e-mail: daniela.dellicastelli@unito.it*

Mapping pH at the high spatial resolution of MR images is a task of considerable interest as pH appears to be an important biomarker in the diagnostic assessment of diseases such as stroke or cancer. Several agents whose contrast enhancing abilities are responsive to pH, have been proposed. To be translatable to in vivo applications the proposed imaging procedure for pH assessment has to be independent from the knowledge of the local concentration of the MRI contrast agent. CEST agents represent a relatively new class of MRI contrast enhancers that act through the transfer of saturated magnetization to the "bulk" water signal. As the exchange of mobile protons is modulated by pH, CEST agents are good candidates for pH mapping. However to be effective, also for CEST agents, a proper strategy that makes the pH assessment independent from the local concentration is necessary. The title complex, Yb-HPDO3A, is present in solution as two main isomers, characterized by having the exchangeable -OH proton resonance at 99ppm and 71ppm, respectively. The two -OH resonances display a slightly different saturation transfer (ST) profile vs. pH. Thus a ratiometric method based on the ratio of the observed ST values at different pH values can be set up in order to get rid of the knowledge of the actual concentration of the MRI agent. After validation of the proposed ratiometric method on buffered aqueous solutions, Yb-HPDO3A has been applied to assess in vivo the extracellular pH of a murine melanoma. This tumor is known to be highly aggressive and tumor cells proliferate very fast. The uncontrolled growth is responsible for causing regions characterized by hypoxic conditions and the resulting anaerobic glycolysis processes are the primary cause of extracellular pH lowering. Mice bearing melanoma corresponding to a different grade of tumor growth were tested. The in vivo pH maps have been compared with ex vivo histology of the same regions and correlations between pH values and histological characteristics have been drawn. Following an i.v. injection of 1.2 mmol/Kg of YbHPDO3A, a ST% of about 20% has been measured in a tumor mass at the beginning of its development (mean diameter size about 2mm); at this stage, the measured extracellular pH has more or less a physiological value (ca. 7.4). As the tumor grows, an i.v. injection of YbHPDO3A at the same administered dose, produces a lower ST effect, probably because of a lower perfusion of the tissue, and the measured extracellular pH becomes more and more acidic. Moreover, the pH values are heterogeneously distributed across the mass ranging from 6.2 to 7.0. Histology performed on excised tumor tissues displays a high number of cells expressing HIF (hypoxia inducible factor) for tumor at a late development stage. Conversely, at a very early stage of the tumor progression histology doesn't provide evidence for HIF expression.

Disclosure of author financial interest or relationships:
**D. Delli Castelli**, None; **G. Ferrauto**, None; **J.C. Cutrin**, None; **E. Terreno**, Bracco Imaging, Consultant; **S. Aime**, Bracco Imaging, Consultant; Bruker, Grant/research support .

Presentation Number **P631**
Poster Session 4
September 8, 2012 / 14:45-14:45 / Room: The Liffey

# Thiol-reactive liposomes to label cells with Gd(III) for MRI applications

*Cinzia Boffa[1], **Giuseppe Digilio**[2], Valeria Menchise[3], Eliana Gianolio[1], Franco Fedeli[1], Silvio Aime[1], [1]Department of Chemisty IFM & Center for Molecular Imaging, University of Turin, Torino, Italy; [2]Dipartimento di Scienze ed Innovazione Tecnologica, Università del Piemonte Orientale, Alessandria, Italy; [3]Institute for Biostructures and Bioimages c/o university of Turin, Consiglio Nazionale delle Ricerche (CNR), Torino, Italy. Contact e-mail: giuseppe.digilio@mfn.unipmn.it*

Mammalian cells display a large number (about 3-18 x 10^9 SH groups per cell) of reactive protein thiols on the extracellular side of the plasma membrane (Exofacial Protein Thiols, EPTs). These EPTs, which originate from protein cysteine residues, are quite reactive and can be chemically labeled by suitably designed MRI contrast agents. We have recently shown that compound Gd-DO3A-PDP, a Gd-DO3A-like complex functionalized with the 2-pyridinedithio chemical function for the recognition of EPTs, can be used to label cultured cells through the formation of disulfide bridges with the cell's EPTs.[1] The Gd(III) chelate anchored on the cell surface is transported into the cytoplasm, By this route, up to 1.2x10^10 Gd atoms per single cell could be internalized by either human myeloid leukemia K562 cells or mouse melanoma B16 cells. The amount of internalized Gd is dependent upon the availability of EPTs, whose levels are influenced by the extracellular redox microenvironment. Therefore, the level of EPTs in tissue can be thought of as a marker of the redox microenvironment. In normoxic microenvironment EPTs are in equilibrium with oxidized forms, mostly represented by disulfides, S-thiolated, S-nitroso or sulphenic species. In reducing microenvironments, such as those encountered in tumor hypoxia, EPTs are thought to reach maximum levels. Accordingly, the thiol-reactive probe injected into B16 tumor xenografts showed to be taken up and retained in the tumor for a longer time with respect to control (non thiol-reactive) Gd-DO3A.[2] We have synthesized liposomes functionalized at the surface with thiol-reactive groups (DSPE-PEG-PDP) and filled within the inner aqueous cavity with Gd-HPDO3A to increase the payload of paramagnetic centers that can be delivered to cells. A further advantage in the use of Gd-loaded liposomes to label cells is that they offer potential for theranostics applications or image-guided drug delivery. In vitro experiments have shown that i) liposomes functionalized with DSPE-PEG-PDP can be internalized more efficiently by B16 cells than liposomes lacking the thiol-reactive function and ii) internalization is dependent on the levels of EPTs displayed by cells. Furthermore, if cells are cultured in a simulated reducing environment (e.g. high GSH/GSSG ratio) uptake of thiol-reactive liposomes further increases. These results outline a potential role of thiol-reactive liposomes as probes responsive to the extracellular redox microenviroment. [1] G. Digilio, V. Menchise, E. Gianolio, V. Catanzaro, C. Carrera, R. Napolitano, F. Fedeli and Silvio Aime Exofacial Protein Thiols as a Route for the Internalization of Gd(III)-Based Complexes for Magnetic Resonance Imaging Cell Labeling J. Med. Chem. (2010) 53, 4877-4890 DOI: 10.1021/jm901876r. [2] V. Menchise, G. Digilio, E. Gianolio, E. Cittadino, V. Catanzaro, C.Carrera, S. Aime. In Vivo Labeling of B16 Melanoma Tumor Xenograft with a Thiol-Reactive Gadolinium Based MRI Contrast Agent Molecular Pharmaceutics (2011) 1750-1756 DOI: 10.1021/mp2001044.

Disclosure of author financial interest or relationships:
**C. Boffa**, None; **G. Digilio**, None; **V. Menchise**, None; **E. Gianolio**, None; **F. Fedeli**, Bracco Imaging spa, Consultant; **S. Aime**, Bracco Imaging, Consultant; Bruker, Grant/research support .

Presentation Number **P632**
Poster Session 4
September 8, 2012 / 14:45-14:45 / Room: The Liffey

# Magnetic glyconanoparticles for labelling stem cells: in Vivo Tracking of Endogenous Neural Progenitors

***Isabel García***[1,2], *Gema Elvira*[3], *Marina Benito*[4], *Juan Gallo*[1], *Manuel Desco*[4,5], *Jose A. García-Sanz*[3], *Augusto Silva*[3], *Soledad Penadés*[1,2], [1]*Biofunctional Nanomaterials Unit, CICbiomaGUNE, San Sebastian, Spain;* [2]*CIBER-BBN, San Sebastián, Spain;* [3]*Department of Cellular and Molecular Medi, Centro de Investigaciones Biológicas (CIB-CSIC), Madrid, Spain;* [4]*Medicina y Cirugía Experimental, Hospital General Universitario Gregorio Marañón, Madrid, Spain;* [5]*Department of Bioengineering and Aerospatial Engineering, Universidad Carlos III, Madrid, Spain. Contact e-mail: igarcia@cicbiomagune.es*

The use of stem cells to correct and regenerate some cell populations is being explored in order to develop efficient clinical stem cell therapies. The cell localization and distribution must be determined in a non-invasive manner. In fact, in vivo tracking and localization of stem cells is one of the main challenges in imaging. The use of superparamagnetic iron oxide or metal-doped iron oxides allows a non-invasive detection to identify and follow the cell fate by magnetic resonance imaging (MRI). Superparamagnetic nanoparticles are the preferred magnetic label for MRI due to its biocompatibility and strong effects into transverse relaxation. Our laboratory has experience in preparing gold nanoclusters functionalized with different types of carbohydrates (glyconanoparticles) for biomedical applications. We have recently prepared biofunctional high quality magnetic core-shell Fe3O4@Au glyconanoparticles (mGNPs) functionalized with antibodies for specific cell labelling. , We present herein the application of the magnetic glyconanoparticles (mGNPs) to in vivo tracking of neural cell subpopulation migrating towards a brain damage site. mGNPs was coupled to the monoclonal antibody Nilo2 that recognizes alive neuroblast cells. The Nilo2-mGNP conjugates were suitable for magnetic resonance imaging detection and were used to analyze in vivo specifically labeled endogenous neuroblasts of the subventricular region (SVZ) and their migration from their niche towards an induced astrocytoma lesion site (Figure 1).

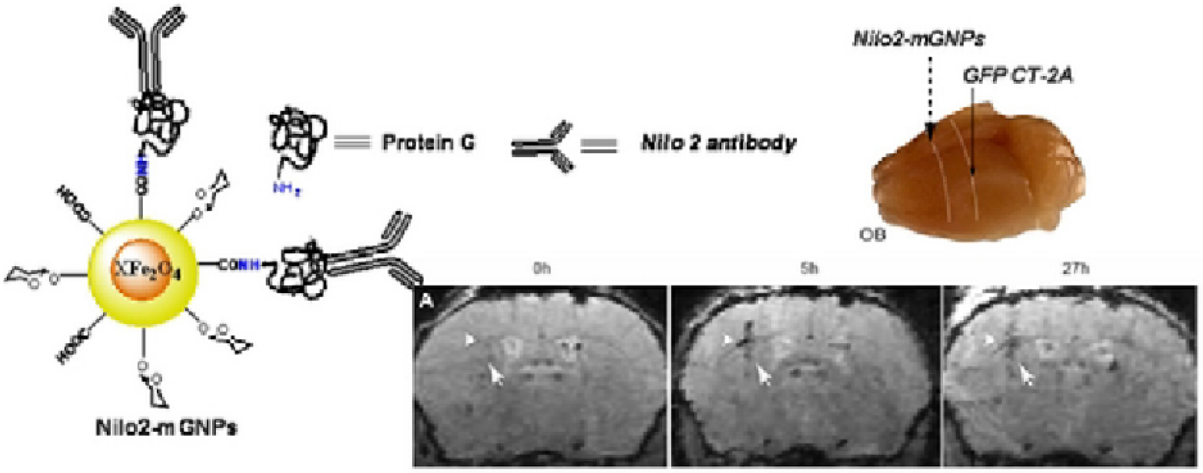


Figure 1. Schematic representation of Nilo2-mGNPs conjugate and analysis, using MRI, of Nilo2+ cell migration before (0h), 5 h and 27 h after CT-2A tumor cells injection in a pre-injected Nilo2-mGNP brain.

Disclosure of author financial interest or relationships:
**I. García**, None; **G. Elvira**, None; **M. Benito**, None; **J. Gallo**, None; **M. Desco**, None; **J. García-Sanz**, None; **A. Silva**, None; **S. Penadés**, None.

Presentation Number **P633**
Poster Session 4
September 8, 2012 / 14:45-14:45 / Room: The Liffey

# Comparative studies of antagonist-based metabotropic glutamate-receptor targeted MRI contrast agents

***Sven Gottschalk***[1]*, Anurag Mishra*[2]*, Neil Sim*[2]*, David Parker*[2]*, Joern Engelmann*[1]*, [1]High-Field Magnetic Resonance, Max Planck Institute for Biological Cybernetics, Tuebingen, Germany; [2]Department of Chemistry, Durham Unibersity, Durham, United Kingdom. Contact e-mail: sven.gottschalk@tuebingen.mpg.de*

Targeting receptors is a widely used concept for competitive binding in brain imaging techniques such as positron emission tomography and optical imaging and an ongoing debate exists whether antagonist- or agonist-based approaches are more beneficial. So far, applying competitive binding for brain functional magnetic resonance imaging (fMRI) has not been demonstrated. Our intention is to develop antagonist-based glutamate (Glu) "responsive" MRI contrast agents (CAs) that would allow imaging of Glu fluctuations in specific brain regions associated with neural activity. We have therefore chosen CAs that bind to the metabotropic Glu-receptor subtype 5 (mGluR5).[1] Such molecules will bind both to neuronal postsynaptic receptors as well as to those expressed on astrocytes. Hence, these CAs can act both as "markers" of receptor density and as indicator of neuronal activation. Ideally, for the latter, after Glu binding to the receptor (i.e. upon Glu release at the synapse) the CA will be released, in turn leading to a reduction in image contrast, followed by a restoration of equilibrium and re-binding of the CA to the receptor. These events are believed to occur over a period of a few seconds allowing data acquisition using modern fast MR-techniques.[2] We have synthesized different prospective CAs derived from potent mGluR5-antagonists (alkynes (e.g. MPEP or MTEP) and dipyridyl/heterobiaryl amides [1]) coupled to DOTA-derived gadolinium chelates. These CAs were evaluated for cellular labeling, cytotoxicity, antagonistic activity, and receptor binding: (A) Binding affinity studies in cultured primary rat astrocytes (expressing mGluR5 as shown by immunofluorescence) showed that three of the compounds increased the cellular relaxation rate R1,cell up to 135% of control (200μM, 45 min., 37°C). These studies were also done at 0°C (to prevent endocytosis). Under these conditions R1,cell was increased only to ~110% of control. MRI-measurements were done with a 3T human whole body scanner. (B) None of the CAs had cytotoxic effects at the concentrations used (24h incubation). (C) Antagonistic activity of the CAs was calculated as changes in EC50 of Glu using a calcium fluorescence assay on primary rat astrocytes. Two of the compounds with increased R1,cell also retained significant antagonistic activity, one in each structural class.[1] (D) Receptor binding and reversibility was demonstrated for one of the dipyridyl derivatives (which have an inherent fluorescence that changes upon binding) on commercially available receptor preparations containing recombinant human mGluR5.[1] By using primary rat astrocytes as cellular model to investigate our newly developed mGluR5-targeted MRI contrast agents, we were able to identify two promising candidates. The CAs are based on the structures of antagonists to mGluR5 and our studies demonstrate that it might be possible to use these targeted CAs to image receptor density in the brain using MRI. Furthermore, our results point towards the possibility of using MRI for brain functional measurements employing competitive binding approaches.[1]Mishra, Gottschalk, Chem Sci 3(2012)131; [2]Logothetis, Nature 453(2008)869

Disclosure of author financial interest or relationships:
**S. Gottschalk**, None; **A. Mishra**, None; **N. Sim**, None; **D. Parker**, None; **J. Engelmann**, None.

Presentation Number **P634**
Poster Session 4
September 8, 2012 / 14:45-14:45 / Room: The Liffey

# Role of exofacial protein thiols in the cytosolic delivery of the cysteine-rich cell penetrating peptide CyLoP-1

***Sven Gottschalk**, Rajendra Joshi, Joern Engelmann, High-Field Magnetic Resonance, Max Planck Institute for Biological Cybernetics, Tuebingen, Germany. Contact e-mail: sven.gottschalk@tuebingen.mpg.de*

**INTRODUCTION:** Recently, exploiting cell-surface thiols (also known as exofacial protein thiols (EPTs)) to obtain better cellular delivery when using thiolated biomolecules such as cell penetrating peptides (CPPs), has gained increasing attention as promising new mechanism. Still, plenty questions remain to be answered. For disulfide-containing CPPs a correlation between EPTs and uptake efficiency was discussed [1]. Our cysteine-rich CPP CyLoP-1 (Cytosol Localizing Peptide-1) has been shown to be more efficient in cytosolic targeting than other established CPPs [2]. Aim of the present study was to evaluate if modification of available EPTs influences the cytosolic delivery of CyLoP-1. Furthermore, the question was asked how the uptake of the reduced and oxidized version of CyLoP-1 (CyloP-1 [RED.]/[OX.]) is influenced by this EPT-modification. **METHODS:** To test our hypothesis, B16.F10 cancer cells, that are known to have a high number of EPTs [3] were subjected to tris(2-carboxethyl)phosphine (TCEP) or N-ethylmaleimide (NEM) to increase or reduce the number of available EPTs, respectively [3]. Internalization of CyLoP-1 [RED.] or [OX.] (both covalently bound to lysine-FITC) was evaluated according to [2] (both 2.5µM, after 3 and 18 hours). **RESULTS:** Pre-treatment of B16.F10 cells with TCEP (i.e. higher number of available EPTs) increased the intracellular delivery of CyLoP-1 [RED.] and CyLoP-1 [OX.] after 3h of incubation (Fig. 1A). While no significant effect with NEM-treatment was seen for CyLoP-1 [OX.], pre-treatment with 20µM NEM significantly decreased delivery of CyLoP-1 [RED.] (Fig. 1A). In contrast to [3] (who used up to 200µM NEM) in our cell model, higher concentrations of NEM lead to pronounced cell death already after 15min (data not shown). Similar effects as seen after 3h of incubation with CPPs were also observed for 18h incubation with both CyLoP-1 [RED.]/[OX.] (Fig. 1B). In these experiments, even lower NEM-concentrations had to be used, due to otherwise massive cell death. **CONCLUSION:** Using a cell line which is known for its high amount of EPTs in combination with EPT-modifications we were able to demonstrate, that intracellular delivery of the cysteine-rich CPP CyLoP-1 is highly dependent on the number of available EPTs (i.e. reduced surface thiols). By this, we further strengthen the notion of an important role for EPTs when using thiolated compounds for cell delivery. **REFERENCES:** [1] Torres, Gait, Trends Biotechnol 30(2012)185; [2] Jha, Bioconjug Chem 22(2011)319; [3] Menchise, Mol Pharm 8(2011)1750

**Figure 1A**

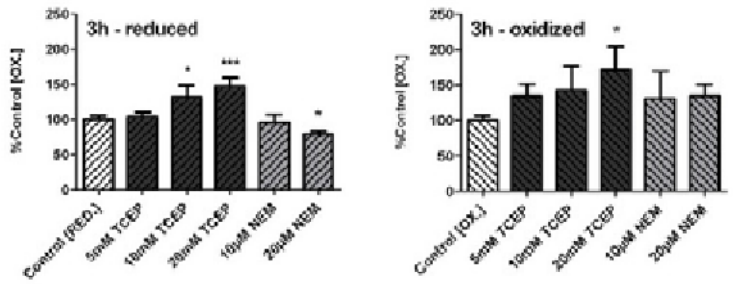


**Figure 1B**

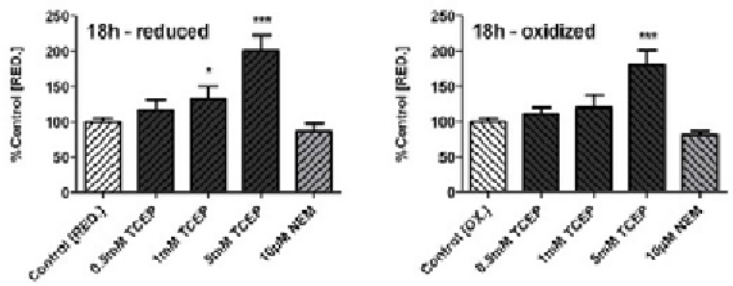


**Intracellular delivery of reduced [RED.]/oxidized [OX.] CyLoP-1. A) 3h after incubation with 2.5µM of each CPP and pre-treatment with TCEP or NEM. B) after 18h incubation with CPPs and pre-treatment with TCEP or NEM. (*P<0.05; ***P<0.001 vs. Control).**

Disclosure of author financial interest or relationships:
**S. Gottschalk**, None; **R. Joshi**, None; **J. Engelmann**, None.

Presentation Number **P635**
Poster Session 4
September 8, 2012 / 14:45-14:45 / Room: The Liffey

# Self-Assembled Amphiphilic Block Copolymers Yield High Relaxivity Nanoparticles for Molecular MRI

***Michael E. Hahn***[1,2], *Lyndsay M. Randolph*[2], *Nathan C. Gianneschi*[2], [1]*Radiology, University of California San Diego, San Diego, CA, USA;* [2]*Chemistry and Biochemistry, University of California San Diego, Sand Diego, CA, USA. Contact e-mail: michaelhahn828@gmail.com*

A central goal of molecular MRI research is the design and synthesis of high relaxivity contrast agents that can be targeted to diseased tissues. We sought to develop an organic nanoparticle platform for the display of $Gd^{3+}$ ions in a unique arrangement. The nanoparticle platform was selected for two purposes: 1) it may lead to an increased reorientational correlation time and thereby an enhanced *r*1 as compared to current clinically available MRI contrast agents, and 2) to serve as a scaffold for further multivalent derivitization with targeting moieties. An amphiphilic block copolymer was synthesized using a robust and functional group tolerant living polymerization method. $Gd^{3+}$ ions are present in the hydrophilic block of the polymer. Upon self-assembly in water, the block copolymers form micellar nanoparticles, as demonstrated by transmission electron microscopy and dynamic light scattering. Importantly, nuclear magnetic resonance spectroscopy demonstrated that the *r*1 per $Gd^{3+}$ ion within the nanoparticle was approximately 20 $s^{-1}mM^{-1}$, corresponding to an *r*1 per particle of approximately 30,000 $s^{-1}mM^{-1}$. Given the inherently lower sensitivity of MRI as compared to other modalities for molecular imaging, it is critically important to develop MRI contrast agents that maximize *r*1 per $Gd^{3+}$ ion. This is especially important when imaging of molecular biomarkers that are present at low target concentration *in vivo* is desired. Toward this goal, we have designed and synthesized high relaxivity nanoparticle contrast agents that display significantly enhanced *r*1 per $Gd^{3+}$ ion compared to the current clinically available contrast agents. These nanoparticles, together with molecular targeting strategies being developed in our laboratory, may lead to highly sensitive MR-based molecular imaging contrast agents.

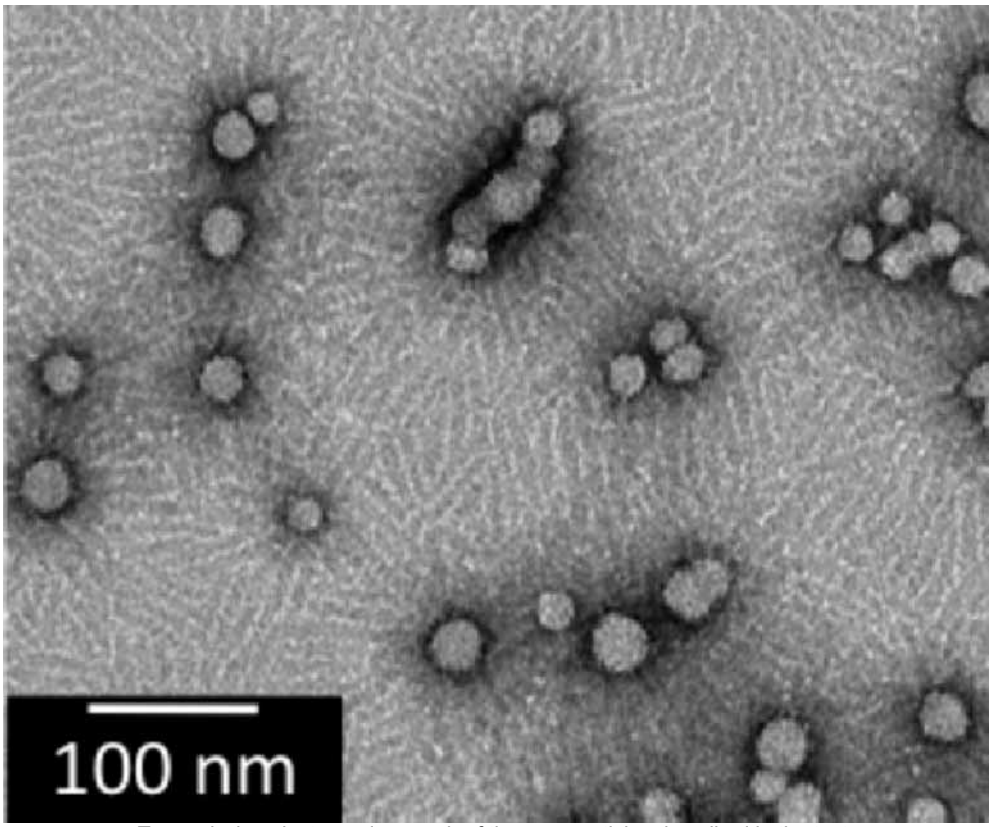


Transmission electron micrograph of the nanoparticles described in the text.

Disclosure of author financial interest or relationships:
**M.E. Hahn**, None; **L.M. Randolph**, None; **N.C. Gianneschi**, None.

Presentation Number **P636**
Poster Session 4
September 8, 2012 / 14:45-14:45 / Room: The Liffey

# Visualization of therapeutic angiogenesis with a polymer-based magnetic resonance imaging contrast agent

***Jun-ichiro Jo***[1,2], *Xue Lin*[2], *Teppei Nakahara*[1], *Ichio Aoki*[1], *Tsuneo Saga*[1], *Yasuhiko Tabata*[2], [1]*Molecular Imaging Center, National Institute of Radiological Sciences, Chiba, Japan;* [2]*Department of Biomaterials, Institute for Frontier Medical Sciences, Kyoto University, Kyoto, Japan. Contact e-mail: junjo@nirs.go.jp*

INTRODUCTION: With the recent progress of tissue engineering technology, the effects of regeneration-induction therapy of various tissues have been experimentally demonstrated in animal models. Furthermore, some clinical trials have also been successfully performed. Under these circumstances, it is strongly required to develop a non-invasive imaging method that can accurately evaluate the process of tissue regeneration and healing. Among various imaging modalities, magnetic resonance imaging (MRI), having a high spatial resolution and tissue contrast, is expected to be an optimal modality for this purpose. For the application of MRI for the monitoring of tissue regeneration, effective delivery of MRI contrast agents to the region being regenerated or repaired is essential. In this study, a new polymer-based MRI contrast agent has been designed to evaluate the therapeutic angiogenesis. METHODS: Gadolinium ions (Gd) and cyclic peptides containing an arginine-glycine-aspartic acid (RGD) sequence (cRGD) with an inherent affinity for the αvβ3 integrin expressed on activated endothelial cells during angiogenesis were chemically introduced to dextran (cRGD-dextran-Gd). The amount of Gd and cRGD to dextran and the longitudinal relaxivity of cRGD-dextran-Gd were evaluated. To examine the interaction between the cyclic RGD and the αvβ3 integrin, the fluorescein-labeled dextrans with or without the cRGD were cultured with human umbilical vein endothelial cells (HUVEC) expressing the αvβ3 integrin. Right femoral, external iliac, and deep femoral and circumflex arteries and veins were surgically ligated to prepare a mouse model of hindlimb ischemia. A laser Doppler analysis and histological evaluation revealed that the hindlimb ischemia was naturally healed accompanied with angiogenesis in the ischemic region without any treatments. In this study, mice 7 days after the vascular ligation were used as an angiogenesis model. MRI (T1-weighted image (T1WI)) was performed after intravenous injection of cRGD-dextran-Gd into the mice. RESULTS AND DISCUSSION: The amount of Gd and cRGD introduced was calculated to be 25 and 3.7 molecules for one dextran molecule, respectively. The longitudinal relaxivity of cRGD-dextran-Gd was calculated to be 5.3 sec-1mM-1, which is higher than that of Magnevist® (4.7 sec-1mM-1). The fluorescein-labeled cRGD-dextran was internalized into HUVEC to a greater extent than dextran-Gd. It is likely that the affinity of cRGD for the αvβ3 integrin on the HUVEC surface enabled the fluorescein-labeled cRGD-dextran to strongly interact with the cells, resulting in the enhanced internalization by a receptor-mediated fashion. The ischemic-angiogenic region was clearly enhanced in T1WI after the intravenous injection of cRGD-dextran-Gd. It was also found that the fluorescein-labeled cRGD-dextran was co-localized in the integrin αvβ3-positive region in the ischemic-angiogenic region after the intravenous injection. Therefore, it is clearly demonstrated that the affinity of cRGD for the integrin αvβ3 enabled the cRGD-dextran conjugates to be selectively delivered to the ischemic-angiogenic region of mice with hindlimb ischemia.

Disclosure of author financial interest or relationships:
**J. Jo**, None; **X. Lin**, None; **T. Nakahara**, None; **I. Aoki**, None; **T. Saga**, None; **Y. Tabata**, None.

Presentation Number **P637**
Poster Session 4
September 8, 2012 / 14:45-14:45 / Room: The Liffey

# Synthesis and Functional Evaluation of Chiral Dendrimer-amine-coordinated Gd Complexes as Highly Sensitive MRI Contrast Agents

***Yu Kimura***[1], *Yuka Miyake*[1], *Syungo Ishikawa*[1], *Hiroki Kijitori*[1], *Yasuhiko Tabata*[2], *Tetsuya Matsuda*[3], *Michiko Narazaki*[3], *Tetsuya Yano*[4], *Teruyuki Kondo*[1], [1]*Advanced Biomedical Engineering Research Unit, Kyoto University, Kyoto, Japan;* [2]*Institute for Frontier Medical Sciences, Kyoto University, Kyoto, Japan;* [3]*Graduate School of Informatics, Kyoto University, Kyoto, Japan;* [4]*Canon Incorporated, Tokyo, Japan. Contact e-mail: ykimura@scl.kyoto-u.ac.jp*

Gd-MRI contrast agents (CAs) can enhance the contrast of MR images by reducing the longitudinal relaxation time (T1) of water.[1] However, since clinically-used Gd-MRI CAs have only low sensitivity, and need high dosage (*ca.* 0.5 M). The reason of low sensitivity is: among the 9 coordination sites of Gd, up to 8 are solidly occupied with ionic chelating ligands, such as DTPA and DOTA, and thus only 1 remains for coordination with free water, which is observed by MRI. Thus, there is a strong need for the development of highly sensitive MRI CAs based on a new principle. Here, we report synthesis and functional evaluation of novel chiral dendrimer-amine-coordinated Gd complexes as highly sensitive MRI CAs. First, chiral diols as building blocks, were prepared by using Os-catalyzed asymmetric dihydroxylation, and as a result of repeated binding of chiral diols, $2^{nd}$-generation dendrons were obtained in high yield.[2] Then, the reaction of these dendrons with 1,4,7-triazacyclononane gave new $2^{nd}$-generation chiral dendrimer-amine ligands. Hydrolysis of the acetal protecting groups, and the subsequent complexation with $GdCl_3$ gave new and highly sensitive chiral Gd-MRI CAs, $2^{nd}$-(*R*) and $2^{nd}$-(S).[3] As mentioned above, the established low-molecular-weight Gd CAs such as Gd-DTPA and Gd-DOTA have ionic chelating ligands that strongly suppress 8 coordination sites of Gd. On the other hand, the novel Gd complexes have a triamine ligand and three chloride ligands, which stably occupy 6 coordination sites of Gd. Accordingly, 3 coordination sites remain for water molecules, and the present Gd complexes show longitudinal relaxivity that is 3 times higher than that of Gd-DTPA. In addition, the central Gd is considered to be covered through weak coordination by OH groups at the dendrimer end, and they may dissociate only when a small, but highly polar, water molecule approaches. Quantitatively, the r1 values of $2^{nd}$-(*R*) and $2^{nd}$-(*S*) were 11.4 and 11.1 $mM^{-1}s^{-1}$, respectively, which are approximately 3 times higher than that of Gd-DTPA (r1 = 4.6 $mM^{-1}s^{-1}$). (7T MRI, 24 $^{o}$C). In contrast to amine-terminated dendrimer Gd-MRI CAs, such as Gd-functionalized PAMAM and PPI dendrimers, neither cytotoxic effect through L929 cell viability assay nor *in vivo* toxicity in mice was observed for either $2^{nd}$-(*R*) or $2^{nd}$-(*S*). Since most of the *in vivo*-injected Gd-DTPA was excreted through the kidney, and accumulated in the bladder within 30 min, little contrast enhancement was observed except for the kidney. In contrast, no accumulation *in vivo* of $2^{nd}$-(*R*) or $2^{nd}$-(*S*) in specific organs, such as the liver and kidney, was observed with high and prolonged contrast enhancement throughout the entire bodies of mice. They also showed improved vascular retention and a moderate renal excretion rate (completely excreted after 24 h). The present results may make it possible to greatly reduce the dose of MRI CAs, and enhance the quality of life of patients. [1] Caravan,P.; Ellison, J.J.; McMurry,T.J.; Lauffer,R.B. Chem.Rev. 1999,99,2293-2352. [2] Chang,H.-T.; Chen,C.-T.; Kondo,T.; Siuzdak,G.;Sharpless,K.B. Angew.Chem.,Int.Ed.Engl. 1996,35,182-186. [3] Kondo,T. et al. PCT Int.Appl. WO2009069833(2009).

Disclosure of author financial interest or relationships:
**Y. Kimura**, None; **Y. Miyake**, None; **S. Ishikawa**, None; **H. Kijitori**, None; **Y. Tabata**, None; **T. Matsuda**, None; **M. Narazaki**, None; **T. Yano**, None; **T. Kondo**, None.

Presentation Number **P638**
Poster Session 4
September 8, 2012 / 14:45-14:45 / Room: The Liffey

# Evaluation of liposomal contrast agent gadolisome for mouse MR imaging: comparison with gadofluorine M

***Shigeru Kiryu***[1], *Yusuke Inoue*[2], *Kouhei Shimomura*[3], *Kohki Yoshikawa*[3], *Kuni Ohtomo*[4], [1]*Radiology, Institute of Medical Science, The University of Tokyo, Tokyo, Japan;* [2]*Diagnostic Radiology, Kitasato University School of Medicine, Sagamihara, Japan;* [3]*Radiotechnical Sciences, Komazawa University, Tokyo, Japan;* [4]*Radiology, University of Tokyo, Tokyo, Japan. Contact e-mail: kiryu-tky@umin.ac.jp*

Liposomal contrast media, gadolisome, is equipped with gadolinium-labeled dendrons in the surface and acts as a positive MR contrast agent. Due to its large particle size, gadolisome also serve as a blood-pool agent. We investigated the kinetics of gadolisome in mice in comparison with a lipophilic micellar contrast agent, gadofluorine M, which enhanced the blood vessels for a long time. Mice were imaged under isoflurane anesthesia using a T1-weighted, three-dimensional fast low-angle shot sequence after intravenous injection of gadolisome or gadofluorine M, and the time course of the contrast effect of vessels and organs was examined. The visualization of vessels on maximum intensity projection (MIP) images was also assessed. A marked enhancement in the blood vessels was observed soon after injection of gadolisome, and decreased gradually. The spleen was also enhanced evidently after injection of gadolisome. The enhancement peaked 1 h after injection of gadolisome and decreased gradually. A slight enhancement was observed in the liver and kidneys. The liver enhancement was relatively constant over 6 h, and decreased slowly but was still evident at 3 weeks. The enhancement of kidneys was almost disappeared at 24 h. In comparison with gadolisome, contrast enhancement in the liver, kidney, and spleen was generally higher for gadofluorine M. The enhancement in the intestinal wall, and axially and inguinal lymph nodes was evident only after gadofluorine M injection. The degree and time course of blood enhancement after injection of gadofluorine M were similar to those after injection of gadolisome. On MIP images, the blood vessels were visualized soon after injection of gadolisome or gadofluorine M. The visualization of blood vessels on MIP images was evident still 6 h after injection of gadolisome, however it became obscure after 1 h after injection of gadofluorine M with the increasing the enhancement of the background organs. The enhancement of the organs was generally lower after injection of gadolisome in comparison with gadofluorine M. The enhancement of blood vessels was evident both with gadolisome and gadofluorine M, however the visualization of blood vessels on MIP images was prolonged longer after injection of gadolisome, due to lower enhancement of the background organs.

Disclosure of author financial interest or relationships:
**S. Kiryu**, Bayer Schering Pharma AG, Berlin, Germany, Other financial or material support; DS Pharma Biomedical, Japan, Other financial or material support; **Y. Inoue**, None; **K. Shimomura**, None; **K. Yoshikawa**, None; **K. Ohtomo**, None.

Presentation Number **P639**
Poster Session 4
September 8, 2012 / 14:45-14:45 / Room: The Liffey

# Europium(III) and Ytterbium(III) Complexes with DO3A Derivative Containing Aminic Coordinating Group as Chemical Exchange Saturation Transfer Agents

***Tereza Krchova***[1], *Jan Kotek*[1], *Daniel Jirak*[2], *Jana Havlickova*[1], *Ivana Cisarova*[1], *Ivan Lukes*[1], [1]*Department of Inorganic Chemistry, Faculty of Science, Charles University in Prague, Prague, Czech Republic;* [2]*Department of Radiodiagnostic and Interventional Radiology, Institute for Clinical and Experimental Medicine, Prague, Czech Republic. Contact e-mail: tereza.krchova@natur.cuni.cz*

New class of contrast agent based on Chemical Exchange Saturation Transfer (CEST) mechanism was relatively recently introduced and shows a high potential for the development of novel applications in Magnetic Resonance Imaging (MRI). Especially, PARACEST agents employing extension of the NMR shift scale using a presence of paramagnetic metal ion (bound in suitable complexes) are nowadays of the main interest. In this respect, we prepared DO3A derivatives (DO3A-AE, DO3A-AEMe and DO3A-AEMe2) containing (dimethyl/methyl)aminoethyl semi-labile coordinating pendant arm and studied its physico-chemical properties. Protonation constants of DO3A-AE as well as thermodynamic stability constants of complexes with selected metal ions were determined by potentiometry. Determining the dissociation constant pKA = 5.83 of protonated primary amine function in Gd-DO3A-AE was useful for further CEST experiments. We explored the CEST effect of the lanthanide(III) complexes with DO3A-AE and DO3A-AEMe. From the pH-dependent Z-spectra it was found that Yb(III) and Eu(III) complexes possessed two pools of exchangeable protons; the protons are these of aminic pendant arm, which is upon deprotonation coordinated and therefore, the protons are distinguished as axial/equatorial ones. Upon heating, the CEST effect increases and two CEST signals found in the Z-spectra coalesce at ~60 °C due to increasing rate of the chemical exchange, as evidenced by temperature-dependence of the Z-spectra. The synthesis and characterization of title ligands as well as studies of their lanthanide complexes as potential CEST contrast agents will be presented in more detail.

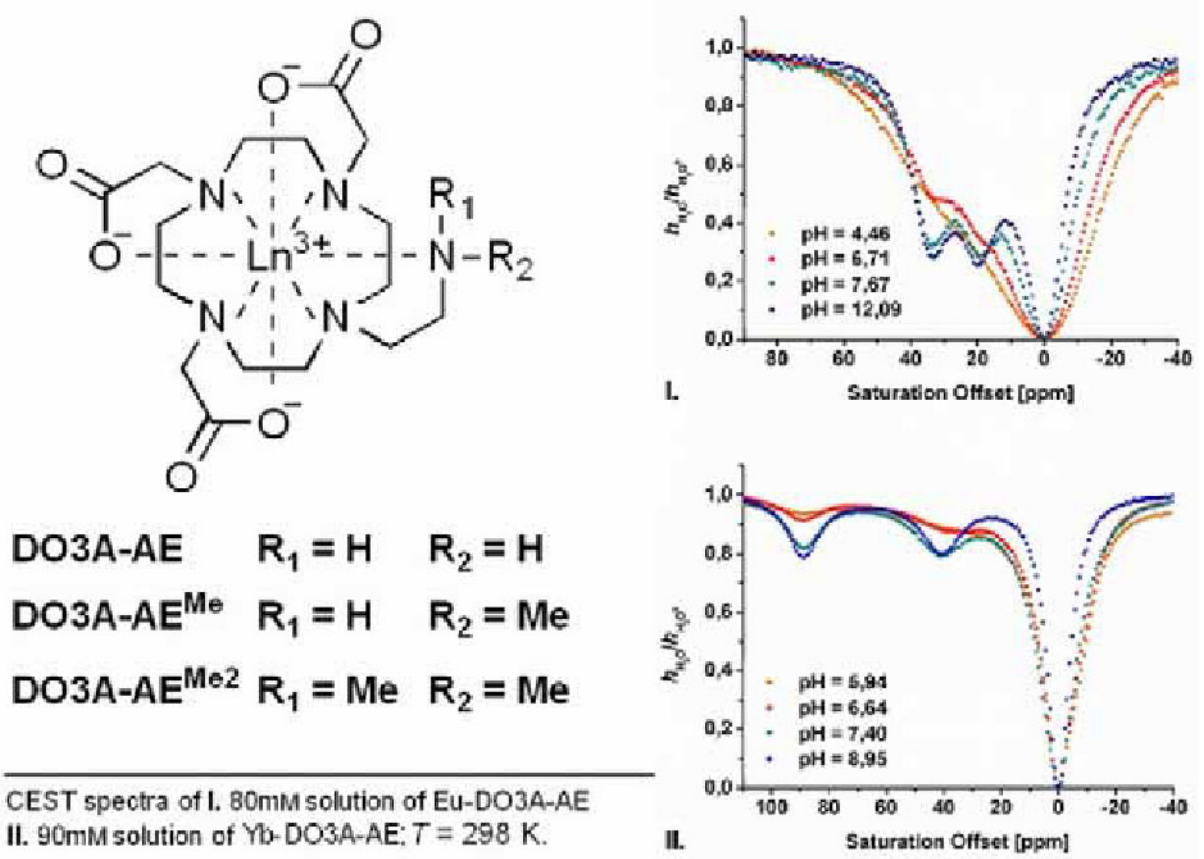


CEST spectra of **I.** 80mM solution of Eu-DO3A-AE
**II.** 90mM solution of Yb-DO3A-AE; *T* = 298 K.

Disclosure of author financial interest or relationships:
**T. Krchova**, None; **J. Kotek**, None; **D. Jirak**, None; **J. Havlickova**, None; **I. Cisarova**, None; **I. Lukes**, None.

Presentation Number **P640**
Poster Session 4
September 8, 2012 / 14:45-14:45 / Room: The Liffey

# Image-Guided Sentinel Lymph Node Mapping Using Zwitterion-Stabilized MR/Optical Imaging Nanoprobe

*Dongkyu Kim, Il-ha Jeong, Min Kyung Chae, Jee-Hyun Cho,* ***Chulhyun Lee****, Korea Basic Science Institute, Chungbuk, Republic of Korea. Contact e-mail: chulhyun@kbsi.re.kr*

Current biomedical imaging modalities such as magnetic resonance imaging (MRI), computed tomography (CT) and positron emission tomography (PET) have become an essential tool in the diagnosis of various diseases. However, single imaging modality tends to be inadequate for comprehensive imaging. Therefore, nanoparticle probes with multimodalities are becoming important tools to overcome the shortcomings of single imaging modalities. Here, we report a zwitterions stabilized superparamagnetic iron oxide nanoparticle based MR/optical probe and its application for sentinel lymph node mapping as dual imaging agent. First, we developed a simple method for synthesizing superparamagnetic nanoparticles (SPIONs) as small, stable contrast agents for magnetic resonance imaging (MRI) based on sulfobetaine zwitterionic ligands. SPIONs synthesized by thermal decomposition were coated with zwitterions to impart water dispersibility and high in vivo stability through the nanoemulsion method. Zwitterion surfactant coating layers are formed easily on oleic acid stabilized SPIONs via hydrophobic and van der Waals interactions. Our zwitterion coated SPIONs (ZSPIONs) had ultra-thin (~5 nm) coating layers with mean sizes of 12.0 ± 2.5 nm, measured by dynamic light scattering (DLS). Upon incubation in 1 M NaCl and 10% FBS, the ZSPIONs showed high colloidal stabilities without precipitating, as monitored by DLS. The T2 relaxivity coefficient of the ZSPIONs, obtained by measuring the relaxation rate based on the iron concentration was 261 mM-1s-1. This value was much higher than that of the commercial T2 contrast agent due to ultra-thin coating layer. Furthermore, we confirmed that ZSPIONs can be used as MR contrast agents for in vivo applications such as tumor imaging and lymph node mapping. Next, ZSPION with surface amine groups were synthesized. The reaction between amine modified ZSPION and Cy 5.5-NHS yielded hybrid nanoparticle for MR/optical dual imaging agent. Future research will be focused on in vivo application of MR/optical dual imaging agent in diagnosis of metastasis.

Disclosure of author financial interest or relationships:
**D. Kim**, None; **I. Jeong**, None; **M. Chae**, None; **J. Cho**, None; **C. Lee**, None.

Presentation Number **P641**
Poster Session 4
September 8, 2012 / 14:45-14:45 / Room: The Liffey

# Development of responsive imaging probes for metabotropic glutamate receptors

***Anurag Mishra***[1], *Sven Gottschalk*[2], *Neil Sim*[1], *Joern Engelmann*[2], *David Parker*[1], [1]*Chemistry Department, Durham University, Durham, United Kingdom;* [2]*High Field MR Centre, Max Planck Institute for Biological Cybernetics, Tuebingen, Germany. Contact e-mail: anurag.mishra@durham.ac.uk*

In spite of decades of work by neuroscientists, understanding how our brain functions is still a milestone question. A range of techniques, such as electrical measurements with single or multiple electrodes, pharmacological testing, non-invasive computational methods and BOLD fMRI is being used to address this fundamental issue. None of these techniques provides complete understanding. To achieve a better appreciation of brain function and dysfunction, a multimodal approach is required that can combine the advantages of each technique. We propose the development of a new measurement technique. Our objective is to develop glutamate (Glu) responsive contrast agents (RCAs) to image changes in different parts of the brain upon neural activation. Glutamate is abundantly present in the mammalian central nervous system, and plays a critical role in mediating excitatory signals through both G-protein-coupled metabotropic receptors and ligand-gated ionotropic receptors present on postsynaptic neuronal cells. The metabotropic Glu receptor subtype 5 (mGluR5) is known to be actively involved in transducing excitatory signals via G-protein coupled secondary messengers between neurons through Glu. In this work, we have developed two series of Glu-RCAs containing various specific mGluR5 antagonists (based on aromatic alkyne and dipyridyl/heterobiaryl amide)[1] to exploit their potential application as responsive MR imaging probes. 1) The first set of molecules is derived from GdDOTA where antagonists were integrated into these structures in a modular fashion. 2) The second set of molecules is derived from trans 1,3-N,N-DO2A where 2nd-N of macrocycle was appended with a lumophore to allow visualization using luminescence methods and 4th-N was incorporated with antagonists to target the receptors. The biocompatibility of these Glu-RCAs was evaluated on mGluR5 expressing primary astrocytes. In vitro MR relaxivity measurements showed a significant (~40%) increase in relaxation rate in the presence of high abundance of mGluR5 in cortical primary astrocytes cell suspensions[2]. The reversibility of probe binding to the receptor sites, induced by added Glu, was demonstrated using optical emission, and the antagonistic activity of complexes was defined by calcium binding assays. The lumophore coupled RCAs are being evaluated using in cellulo luminescence measurements assays under appropriate physiological conditions. References. [1] C. G. Rousseaux, J. Toxicol Pathol, 2008, 21, 25. [2] A. Mishra, S. Gottschalk, J. Engelmann, D. Parker, Chem. Sci., 2012, 3(1), 131.

Disclosure of author financial interest or relationships:
**A. Mishra**, None; **S. Gottschalk**, None; **N. Sim**, None; **J. Engelmann**, None; **D. Parker**, None.

Presentation Number **P642**
Poster Session 4
September 8, 2012 / 14:45-14:45 / Room: The Liffey

# Different coating impacts on cell uptake: using Gd based nanomagnetic particles

***Nader Riyahi Alam***[1], *Gholamreza Azizian*[1], *Soheila Haghgoo*[2], *Reza Zohdiaghdam*[1], *Mohammad reza Moghimi*[3], [1]*Medical Physics & Biomedical Engineering, Tehran university of medical sciences(TUMS), Tehran, Islamic Republic of Iran;* [2]*Pharmaceutical Department, Food & Drug Laboratory Research Center, Ministry of Health, Tehran, Islamic Republic of Iran;* [3]*School of Pharmacy, Shaheed Beheshti University of Medical Sciences, Tehran, Islamic Republic of Iran. Contact e-mail: riahinad@sina.tums.ac.ir*

Introduction: For reduce toxicity, increasing biocompatibility and half-life, and preventing the nanoparticles aggregations, contrast agents in MRI should be coated with various chelates. We present here the comparison of the magnetic properties, relaxometry and cell-uptake of three gadolinium-based nanoparticles(NPs) with diethyleneglycol(DEG) and methoxy-polyethylene-glycol-silane(MW=550&2000) as Gd2O3-DEG, SPGO-mPEG-silane550&SPGO-mPEG-silane2000 coatings in RPMI and SK-MEL3 cell-line. Materials and Methods: DEG coating was performed using the a new supervised polyol method. Filtration (0.2µm) and dialysis (1000 and 12000Da) were carried out for Gd2O3-DEG. Small particulate gadolinium oxide (SPGO<40nm) and mPEG-silane550&2000Da were used to prepare nanoparticles using PEG coating method and size of nanoparticles were obtained by DLS.The maximum signal intensity and relaxivities measurement were prepared using 1.5T MRI scanner. Nanoparticles tubes were prepared by certain concentrations (0.3, 0.6, 0.9 and 1.2 mM) in water and RPMI. SK-MEL3 cell were incubated in different concentrations of Gd2O3 for 2 h at 37°C in 5% CO2 atmosphere. After incubation cells were washed and prepared for MRI measurements. Relaxation rates of R1(1/T1) and R2(1/ T2) were calculated by exponential curve fitting of the signal intensity vs. time(TRorTE). After relaxation rates determination for different concentration, the R1 or R2 vs. concentration curve were plotted and thereby, the molar relaxivities (r1 and r2) as the curve slope could be calculated. Results and Discussion: Nanoparticles sizes of Gd2O3-DEG, SPGO-mPEG-silane550 and SPGO-mPEG-silane2000 by the synthesis route could be reached to 5.9, 51.3, 194.2 nm; respectively. Whereas, both r1 and r2 for three nanoparticles in cell culture medium (RPMI) and cell line relative to water have been decreased but ratios of r2/r1 had different behavior. As for Gd2O3, r2/r1 ratio increases from 0.89 in water to 1.27 in RPMI and to 0.92 in cell line. That increase was due to the effect of cell uptake of Gd2O3-DEG served as T1-based contrast agent that could be seen from incremental relationship of signal intensities vs different concentrations. However, it is clearly shown in table 1 that the r2/r1 ratios for pegylated NPs were substantially decreased when measured in RPMI and cell line compared to water served them as negative T2-based contrast agent. Despite the large size of pegylated NPs, especially SPGO-mPEG-silane2000, changes of r2/r1 in cell line were considerable that showed their cell uptake effect. Despite their negative signal part of changes should be due to their uptake increase as well as to their biocompatibility. Conclusion: Size and relaxometry of NPs with three different coatings in their MRI studies showed that Gd2O3-DEG NPs are efficient in cell uptake and could potentially act as positive contrast agents candidates, while, particle size and nature of pegylation NPs seem to play important roles in their magnetic properties served them as negative contrast agents in MR molecular imaging.

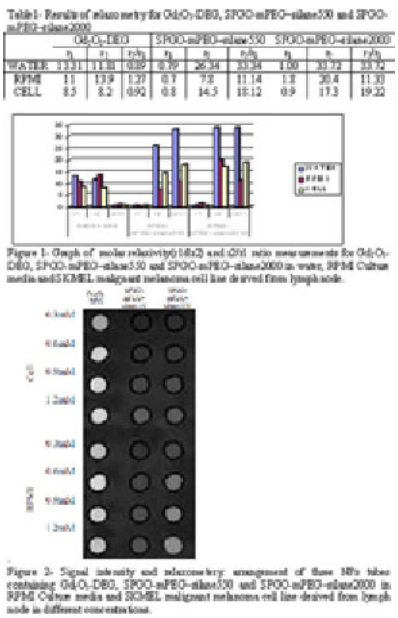

Disclosure of author financial interest or relationships:
**N. Riyahi Alam**, None; **G. Azizian**, None; **S. Haghgoo**, None; **R. Zohdiaghdam**, None; **M. Moghimi**, None.

Presentation Number **P643**
Poster Session 4
September 8, 2012 / 14:45-14:45 / Room: The Liffey

# Development of Nucleic Acids Based-Probes for the 19F MRI/MRS of Biomolecules

***Takashi Sakamoto***[1], *Hikaru Hayakawa*[1], *Jyun Sasaki*[1], *Satomi Kishi*[1], *Kenzo Fujimoto*[1,2], [1]*School of Materials Science, Japan Advanced Institute of Science and Technology, Nomi, Ishikawa, Japan;* [2]*Research Center for Bio-Architecture, Japan Advanced Institute of Science and Technology, Nomi, Ishikawa, Japan. Contact e-mail: tsakamo@jaist.ac.jp*

19F MRI/MRS is promising technology because of its relatively high sensitivity and low background in biological specimen. Various molecular probes for 19F MRI/MRS have been reported, however, in most case, the targets of these probes were limited to protein. Probes that can detect specifically other biomolecules, such as nucleic acids, lipid, sugar, ions and other small biomolecules, has been scarcely reported. In this study, we adopt synthetic oligonucleotide that can recognize various biomolecules as a recognition site of molecular probe for 19F MRI/MRS. Phosphoramidite derivatives containing bis(trifluoromethyl)benzene (BTB) moiety for labeling of oligonucleotide were developed and introduced to oligonucleotide sequences by general cyanoethyl phosphramidite chemistry. For nucleic acid detection and potassium detection, molecular beacon typed oligonucleotide and thrombin aptamer were adopted, respectively. Firstly, we designed and synthesized a molecular beacon typed probe having a fluorine and Gd(III) chelate at the 5' and 3' termini, respectively (19F-MB, Figure. 1a). In the absence of target nucleic acid, it is expected that the distance dependent paramagnetic relaxation enhancement (PRE) effect of the paramagnetic Gd(III) at the 3' termini quenches the 19F MR signal of the fluorine compound at the 5' termini. The addition of target nucleic acid causes change in the distance between 5' and 3' termini, and then the PRE effect is reduced. Thus the 19F MR signal is expected to be turned on. To confirm this signal turn-on manner of the probe, 19F NMR spectra were measured in the presence or absence of the target oligonucleotide. As shown in Figure 1a, the 19F MR signal of the 19F-MB appeared by the addition of oligonucleotide having a complementary sequence for the 19F-MB. The addition of uncomplimentary sequence (Figure S2) did not affect the 19F MR signal indicating that the 19F-MB could discriminate the sequence of nucleic acids. Next, we designed and synthesized a thrombin aptamer (TBA)-based probe having a BTB at the 5' termini of the TBA (19F-TBA, Figure 1b). As the structure of the thrombin aptamer is changed by potassium cation dependent intramolecular G-quadruplex formation, it is expected that the environment around the BTB at the 5' termini of the probe could be detected as chemical shift change in the 19F MR signal. As shown in Figure 1b, the chemical shift of the 19F MR signal of the 19F-TBA was clearly shifted toward low magnetic field by the addition of KCl. The UV melting profile and CD spectrum of the 19F-TBA with KCl showed characteristic behavior of the G-quadruplex structure (Figure S3), suggesting that the change in chemical shift was caused by the environmental change around the BTB moiety at the 5' termini with the potassium cation-dependent G-quadruplex formation. In conclusion, we demonstrated that the target dependent conformational change of oligonucleotide is useful to control 19F MR signal, and successfully developed molecular probes that can detect nucleic acids and potassium cation.

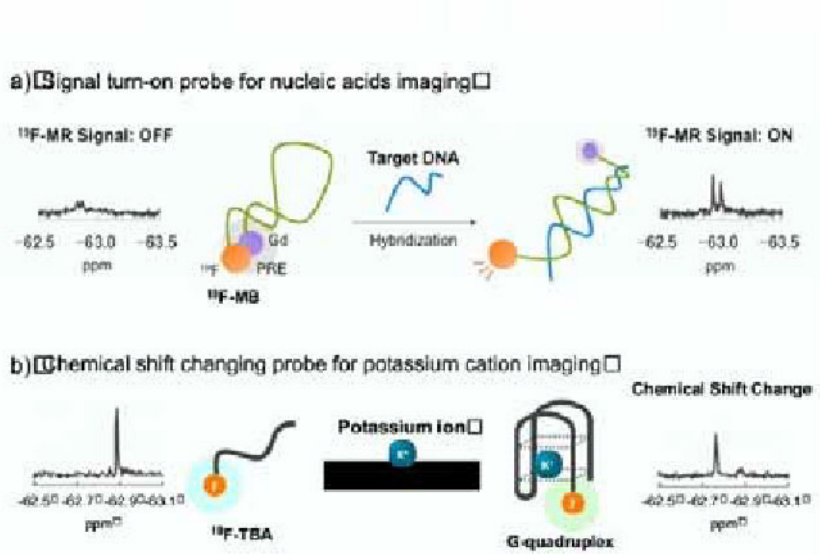


Figure 1 Schematic drawings of nucleic acid based molecular probes for 19F MRI/MRS of nucleic acids (a) and potassium cation (b).

Disclosure of author financial interest or relationships:
**T. Sakamoto**, None; **H. Hayakawa**, None; **J. Sasaki**, None; **S. Kishi**, None; **K. Fujimoto**, None.

Presentation Number **P644**
Poster Session 4
September 8, 2012 / 14:45-14:45 / Room: The Liffey

# PEG-related nanocarriers, potential as diagnostic agent and its immune response

***Kouichi Shiraishi***[1], *Mikiko Hamano*[2], *Kumi Kawano*[2], *Yoshie Maitani*[2], *Taiki Aoshi*[3], *Ken J. Ishii*[3], *Masayuki Yokoyama*[1], [1]*Research Center for Medical Science, Jikei University School of Medicine, Minato, Japan;* [2]*Institute of Medicinal Chemistry, Hoshi University, Shinagawa, Japan;* [3]*Laboratory of Adjuvant Innovation, National Institute of Biomedical Innovation, Ibaraki, Japan. Contact e-mail: kshiraishi@jikei.ac.jp*

Poly(ethylene glycol) (PEG) is a water soluble, bio-inert, and non-toxic polymer that is widely used in the field of pharmaceutics. PEGylation is commonly used method to improve and control pharmacokinetics. Nowadays, most of nanoparticles for drug targeting therapy as well as for diagnosis are used PEGylation for surface coating to avoid interaction with plasma proteins and reduce uptake from reticuloendothelial system. However, in recent papers, PEG related immune response after 1st dose of PEG-liposome was reported. Second dose of PEG-liposome rapidly cleared from blood and accumulated extensively in liver. This phenomenon is known as accelerated blood clearance (ABC) phenomenon. Mechanism of ABC phenomenon is not completely clear yet, however, existence of anti PEG-IgM antibody (PEG-IgM) is suggested after 1st dose of PEG-liposomes. PEG is believed to be non or less immunogenic material, however, this PEG related immunoresponse, a production of PEG-IgM, was found in ABC phenomenon. The IgM production by the first dose of PEG-related nanocarriers will become serious issue. Because PEG related diagnostic agents will lose the ability by the IgM. This includes repeated injection of such PEG related diagnostic agents lose reliability of the diagnosis in such immunnoactive state. This indicates only one chance to use the nanoparticles for diagnosis, as well as for therapy. This ABC phenomenon must be evaded for diagnostic purpose. We have prepared a polymeric micelle MRI contrast agent from PEG-poly(L-lysine) block copolymer for tumor imaging. This block copolymer formed polymeric micelle with hydrophilic interaction of poly(L-lysine) blocks inner core and outer PEG shell. We examined effect of our PEG block copolymer micelle MRI contrast agent and PEG-liposomes on PEG related immune response of ABC phenomenon. PEG related nanocarriers, such as PEG-liposome, hydrophobic core of polymeric micelles (PEG-PBLA micelle and PEG-PLA micelle) and polymeric micelle MRI contrast agent were injected as first dose, and ABC phenomenon was detected by second dose of PEG-liposome. At seven days from the first dose, plasmas were obtained and subjected to ELISA assay to observe IgM and IgG production. No IgM and IgG production was found in polymeric micelle MRI contrast agent, whereas PEG-liposome and hydrophobic core of polymeric micelles produced IgM. Interestingly, the polymeric micelle MRI contrast agent did not change plasma concentration when we injected into PEG-liposome-injected ABC(+) mice. So far, no relation between the IgM and the polymeric micelle MRI contrast agent was found even the polymeric micelle has PEG outer shell. This MRI contrast can use repeatedly without PEG-liposome related immune response.

Disclosure of author financial interest or relationships:
**K. Shiraishi**, None; **M. Hamano**, None; **K. Kawano**, None; **Y. Maitani**, None; **T. Aoshi**, None; **K.J. Ishii**, None; **M. Yokoyama**, None.

Presentation Number **P645**
Poster Session 4
September 8, 2012 / 14:45-14:45 / Room: The Liffey

# Molecular imaging of atherosclerotic plaque via profilin-1 antibody labeled quaternized chitosan encapsulated magnetic nanoparticles

***Yabin Wang***[1], *Hongbing Deng*[2], *Tao Su*[1], *Feng Cao*[1], [1]*Dept. of Cardiology, Xijing Hospital Fourth Military Medical University, Xian, China;* [2]*College of Food Science & Technology of Huazhong Agriculture University, wuhan, China. Contact e-mail: scottss0415@gmail.com*

Abstract Background Atherosclerosis and its complications are the major cause of mortality all over the world. It is reported recently that profilin-1, an intracellular actin-binding protein, plays a pivotal role on progression of atherosclerotic lesions. The rationale of our study was to use a novel molecular imaging probe to assess atherosclerotic plaque invasively by magnetic resonance imaging (MRI). This probe was constructed through conjugating profilin-1 antibody with quaternized chitosan encapsulated magnetic nanoparticles (QC-MNPs). Methods QC-MNPs were characterized by transmission electron microscopy (TEM), the mean particle size and size distribution were measured by laser light scattering technique. Profilin-1 antibody was conjugated to QC-MNPs via carboxyl and amine condensation. The probe was purified by high speed centrifugate. Zeta potential and absorption band of probe were detected by zeta potential analysis and UV (ultraviolet)-Vis absorption spectroscopy respectively to testify whether profilin-1 antibody was successfully conjugated to nanoparticles. Twenty New Zealand white rabbits were fed western diet for 16 weeks after balloon injury. 3.0T MRI was performed to visualize atherosclerotic lesions of abdominal aorta on both T1- and T2- weighted spin-echo images before and after the probe was injected into ear veins of rabbits respectively. B-mode ultrasound imaging and histological analysis were applied to evaluate the effectiveness of the probe on assessment of atherosclerotic plaque. Results The results revealed that the mean size of QC-MNPs was 35.7 nm, and the distribution of particles size ranged from 20 nm to 70 nm. Compared with unlabeled QC-MNPs, the mean zeta potential of probe changed from -47.1 mv to -2.17 mv. UV (ultraviolet)-Vis absorption spectroscopy showed that the absorption band of probe was between 250-300 nm, while unlabeled QC-MNPs had no absorption band. In vivo 3.0T MRI revealed that after probe injection, the area of atherosclerotic plaque in abdominal aorta exhibited lower T2 signal intensity compared with the signal before probe injection. The result of MRI was confirmed by ex vivo histological analysis and in vitro B-mode ultrasound imaging. Conclusions Profilin-1 antibody labeled QC-MNP, a novel molecular imaging probe, provides potential for noninvasive assessment of atherosclerotic plaque by MRI.

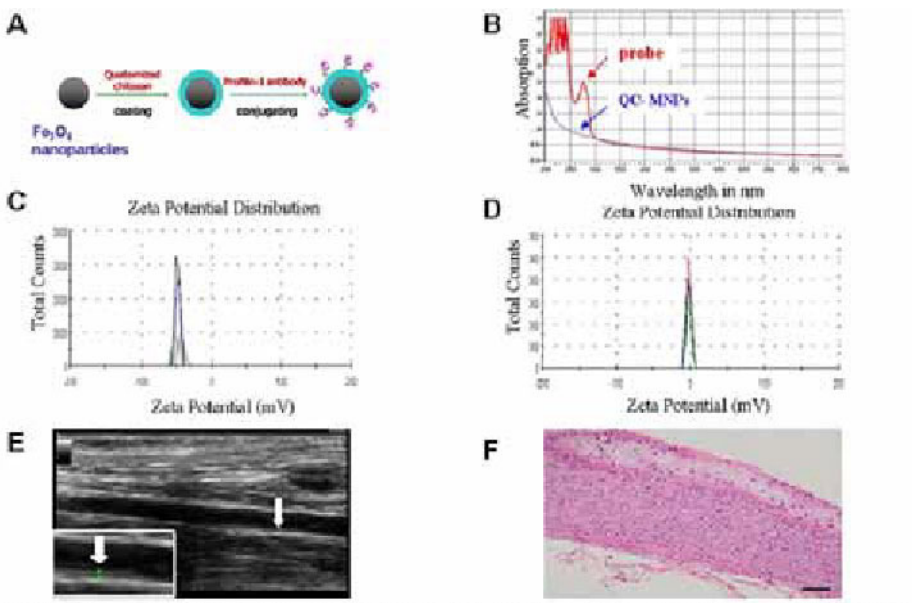


**Figure 1. characterization of probe, ultrasound imaging and histological analysis of atherosclerotic plaque in abdominal aorta.**
A. Synthesis illustration of probe . B. Ultraviolet absorption band of probe and QC- MNPs (quaternized chitosan encapsulated magnetic nanoparticles). C. Zeta potential distribution of QC- MNPs . D. Zeta potential distribution of probe. E. B-mode ultrasound imaging showed atherosclerotic plaque in abdominal aorta. F. Hematoxylin-eosin staining revealed the morphology of atherosclerotic plaque. Scar bar: 100 u m.

Disclosure of author financial interest or relationships:
**Y. Wang**, None; **H. Deng**, None; **T. Su**, None; **F. Cao**, None.

Presentation Number **P646**
Poster Session 4
September 8, 2012 / 14:45-14:45 / Room: The Liffey

# Mitochondrial Targeting Cationic Gd(III) Chelate as Tumor-Selective MRI Contrast Agent

***Chang-Tong Yang***, *Prashant Chandrasekharan, Kai-Hsiang Chuang, Edward G. Robins, Lab of Molecular Imaging, Singapore Bioimaging Consortium, A*STAR, Singapore, Singapore. Contact e-mail: yang_changtong@sbic.a-star.edu.sg*

Introduction: A new class of organic cations, such as triphenylphosphonium (TPP), 2-(diphenylphosphoryl)-ethyldiphenyl-phosphonium (TPEP), represents novel molecular probes for imaging tumor due to the positive charge and the lipophilic property. The mitochondrial transmembrane potential in carcinoma cells is significantly higher than that in normal epithelial cells ($\Psi\Delta m$ = 60 mV).[1-2] Cationic molecules can therefore be driven electrophoretically through membranes by the negative mitochondrial transmembrane potential and accumulate inside the energized mitochondria of tumor cells. Background: Cationic PET radiotracers such as 64Cu-labeled triphenylphosphonium have been shown to preferentially accumulate in tumors in athymic nude mice bearing U87MG human glioma xenograft.[3] Based on the experiences in PET studies, here we developed a new cationic Gd(III) chelate -- GdDO3A-2-(diphenylphosphoryl)-ethyldiphenyl-phosphonium (Fig. A) -- as a potential tumor-selective MRI contrast agent. Methods and Results: Gd(DO3A-xy-TPEP)+ was synthesized and characterized by ESI-MS. The compound was purified by HPLC. Five different cell lines, namely HEK 293, HeLa and A498, HT1080 and HK2 were used for in vitro cytotoxicity evaluation using CCK-8 Kit. In vitro cell viability in five different cell lines showed insignificant cytotoxicity at low [Gd] concentrations up to 0.2 mM for all cell lines. The IC50 values are 0.92, 0.92, 0.79, 0.49 and 0.45 mM for HEK 293, HeLa, A498, HT1080 and HK2 cell lines, respectively (Fig.B). Cell uptake assessed by ICP-MS for the Gd(DO3A-xy-TPEP)+ displays considerable uptake by HT1080 fibrosarcoma cells and A498 kidney cancer cells, of about six to seven times, compared with uptake by normal human kidney cells at Gd cell loading concentrations of 1 mM and 0.5 mM (Fig. C). T1 relaxivity measurements and in vivo study were conducted on a Bruker 7T Clinscan MRI system. T1 was measured by inversion recovery spin echo in aqueous phantoms with concentrations 0.4, 0.2 0.1, 0.05, 0.025, 0.0125 and 0.00625 mM Gd (Fig. D). The T1 relaxivity r1 (5.9 mM-1s-1) in H2O at 25 oC is higher than that of the clinically used ones (3.9 and 4.1 mM-1s-1 for Gd-DOTA and Gd-DTPA, respectively). Gd(DO3A-xy-TPEP)+ was injected (dosage: 0.01 mmol Gd/kg body weight) through tail veins of female SCID mice (weight 20 ± 2 g) bearing A498 xenograft under 1% isoflurane anesthesia. In vivo imaging study demonstrated significant signal enhancement at the site of the tumors (Fig E & F). It could be expressed that Gd(DO3A-xy-TPEP)+ has advantages of tumor targeting for diagnostic imaging. Study on mitochondrial targeting of Gd(DO3A-xy-TPEP)+ on A498 tumor cells is in progress. [1] Madar, et al, J. Nucl. Med. 1999, 40, 1180. [2] Johnson, et al, Proc. Natl. Acad. Sci. U.S.A.1980, 77, 990. [3] Yang, et al, Bioconjugate Chem. 2008, 2008.

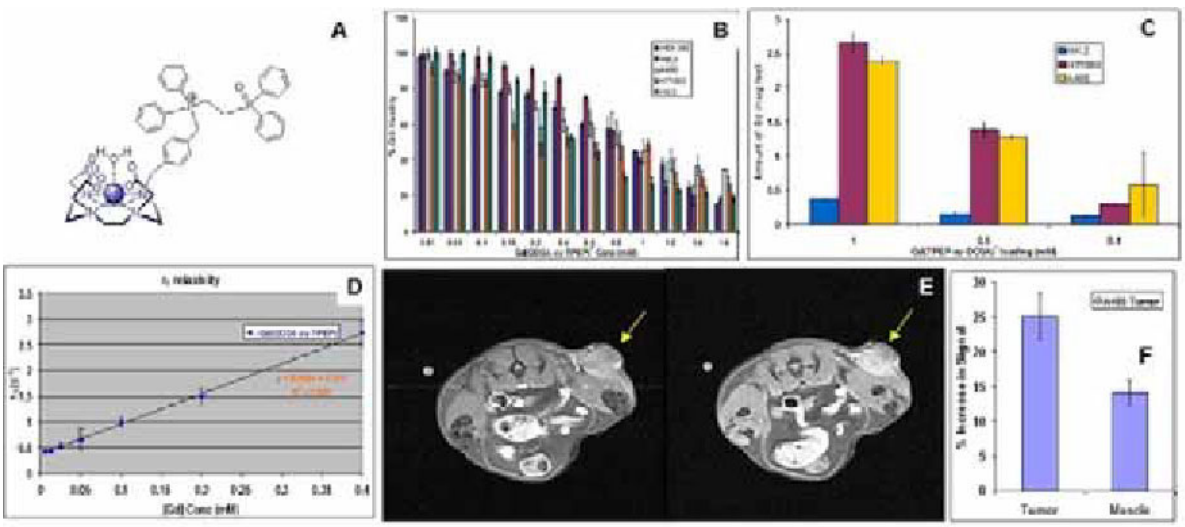


A) Structure of Gd(DO3A-xy-TPEP)+ B) Cell viability of Gd(DO3A-xy-TPEP)+ in HEK293, HeLa, A498, HT 1080 and HK2 cell lines C) Cell uptake of Gd(DO3A-xy-TPEP)+ on HK2, HT1080 and A498 cell lines D) T1 relaxivity (r1) of Gd(DO3A-xy-TPEP)+ E )Representative axial T1 images (arrow showing the xenograft tumor) at pre-injection (left) and 20 minutes post-injection (right) of Gd(DO3A-xy-TPEP)+ at a dose of 0.01 mmol/kg of body weight. F) Change in signal from tumor in comparison to the muscle 20 minutes Post-injection.

Disclosure of author financial interest or relationships:
**C. Yang**, None; **P. Chandrasekharan**, None; **K. Chuang**, None; **E.G. Robins**, None.

Presentation Number **P647**
Poster Session 4
September 8, 2012 / 14:45-14:45 / Room: The Liffey

# Development of RGD-liposomes for MR imaging of pancreatic tumor

***Mitsuyoshi Yoshimoto***[1,2], *Takuya Hayakawa*[1], *Masayuki Yamaguchi*[1], *Sadaaki Kimura*[1], *Izumi O. Umeda*[1], *Hirofumi Fujii*[1], [1]*Functional Imaging Division, National Cancer Center Hospital East, Kashiwa, Japan;* [2]*Division of Cancer Development System, National Cancer Center Research Institute, Tokyo, Japan. Contact e-mail: miyoshim@ncc.go.jp*

Introduction: Pancreatic cancers highly express αvβ3 integrin. We previously demonstrated that SPECT with $^{111}$In-DOTA-c(RGDfK) successfully detected pancreatic cancers in a hamster carcinogenesis model. MRI can provide more excellent anatomical details in vivo than SPECT and it also offers a high contrast between target tissues and the surrounding ones using contrast agents. We synthesized RGD-liposomes loaded with ferrioxamine B (Fe-deferoxamine) as MR contrast agents and estimated their usefulness in pancreatic tumor imaging. Methods: Liposomes (DSPC : cholesterol : mPEG-DSPE = 1.1 : 1: 0.15) were prepared by thin film hydration method. The amount of RGD modification was optimized by changing ratios of maleimide-mPEG-DSPE to total amount of mPEG-DSPE between 1.0 and 50.0 %. RGD-liposomes were prepared by coupling c(RGDfk)-SH with maleimide-mPEG-DSPE. Particle size of the liposomes and content of ferrioxamine B in the liposomes were measured . Binding affinities of RGD-liposomes to αvβ3 integrine were assessed as 50% inhibitory concentrations ($IC_{50}$s) for $^{125}$I-echistatin binding to PANC-1 human pancreatic cancer cells. Biodistribution of $^{111}$In-loaded RGD-liposomes were investigated in PANC-1 bearing mice. From the results of biodistribution studies, RGD(5.0%)-liposome was used for in vivo MR imaging. PANC-1 bearing mice were scanned in a 9.4T MRI system using an 8-channel mouse body coil before and 4 and 24 h after injection of RGD(5.0 %)-liposome loaded with ferrioxamine B (22 - 24 μmol as phospholipids). T1-weighted images were acquired using a fast spin echo sequence with fat suppression (TR = 476 ms, TE = 8.7 ms, flip angle = 90°, voxel resolution = 0.156 × 0.156 × 1 mm). Results: Particle size of RGD-liposomes was 103.7 ± 3.9 nm and ferrioxamine B content in liposome were 15.2 ± 1.2 μg/μmol phospholipids. RGD-liposomes dose-dependently inhibited the binding of $^{125}$I-echistatin to PANC-1. The $IC_{50}$ values were 5-67 μM as phospholipids. RKG-liposome and bare liposome did not inhibit the binding. In biodistribution study using $^{111}$In-loaded liposomes, RGD(50%)-liposome showed rapid clearance from blood (0.41 %ID/g at 4 h). Significant accumulation in spleen was found in proportion to the amount of RGD modification (170.4 - 403.9 %ID/g at 24 h). Bare liposome showed the highest tumor uptake (2.80 %ID/g) at 24 h, whereas RGD-liposomes showed the lower tumor uptake (1.47 - 2.25 %ID/g). However, tumor to blood (T/B) and muscle (T/M) ratios of RGD(5.0%)-liposome was highest among the liposomes used in this study (3.7 and 8.0, respectively). MR studies revealed that RGD(5.0%)-liposome loaded with ferrioxamine B enhanced T/M signal ratio on T1 images by 40 % compared with RKG-liposome as control. Conclusion: Ferrioxamine B was successfully loaded into RGD-liposomes that showed high affinity to αvβ3 integrin. MR imaging suggested that RGD-liposomes might be possible candidates for MR imaging of pancreatic cancer.

Disclosure of author financial interest or relationships:
**M. Yoshimoto**, None; **T. Hayakawa**, None; **M. Yamaguchi**, None; **S. Kimura**, None; **I.O. Umeda**, None; **H. Fujii**, None.

Presentation Number **P648**
Poster Session 4
September 8, 2012 / 14:45-14:45 / Room: The Liffey

# A peptide-targeted MRI contrast agent, CREKA-Tris-Gd(DOTA)3, for breast cancer molecular imaging

***Zhuxian Zhou***, *Zhen Ye, Xueming Wu, Xiaoyue Shi, Zheng-Rong Lu, Biomedical Engineering, Case Western Reserve University, Cleveland, OH, USA. Contact e-mail: zxz166@case.edu*

Rational design and develop of targeted contrast agents binding to cancer-related proteins is critical for more accurate cancer diagnosis and prognosis by magnetic resonance (MR) imaging. CREKA is a tumor-homing pentapeptide (Cys-Arg-Glu-Lys-Ala) specifically homes to tumors by binding to fibrin-associated clotted plasma proteins in tumor. In this study, we synthesized and evaluated a CREKA peptide targeted Gd-DOTA monoamide conjugate [CREKA-Tris-Gd(DOTA)3] for MR molecular imaging of breast tumors. CREKA and three Gd-DOTA monoamide chelates were attached to a maleimide-functional trialkyne scaffold via thiol-maleimide and azide-alkyne click chemistry, respectively. CREKA-Tris-Gd(DOTA)3 has a excretable small molecular structure with a molecular weight of 2914 Da. The T1 relaxivity of CREKA-Tris-Gd(DOTA)3 is 8.06 mM-1s-1 per Gd (24.18 mM-1s-1 per molecule) at room temperature and 1.5 T. Fluorescence imaging showed high binding specificity of CREKA to a 4T1 breast tumor model in mice and no binding for the scrambled peptide CERAK. The CREKA peptide-targeted contrast agent resulted in greater contrast enhancement than the corresponding CERAK agent and the commercialized contrast agent ProhanceTM in tumor at a dose of 0.1 mmol Gd/kg in female athymic mice bearing 4T1 breast carcinoma xenograft. This small molecular contrast agent was easily excreted from body after the imaging study. The targeted MRI contrast agent has a potential for specific cancer molecular imaging with MRI.

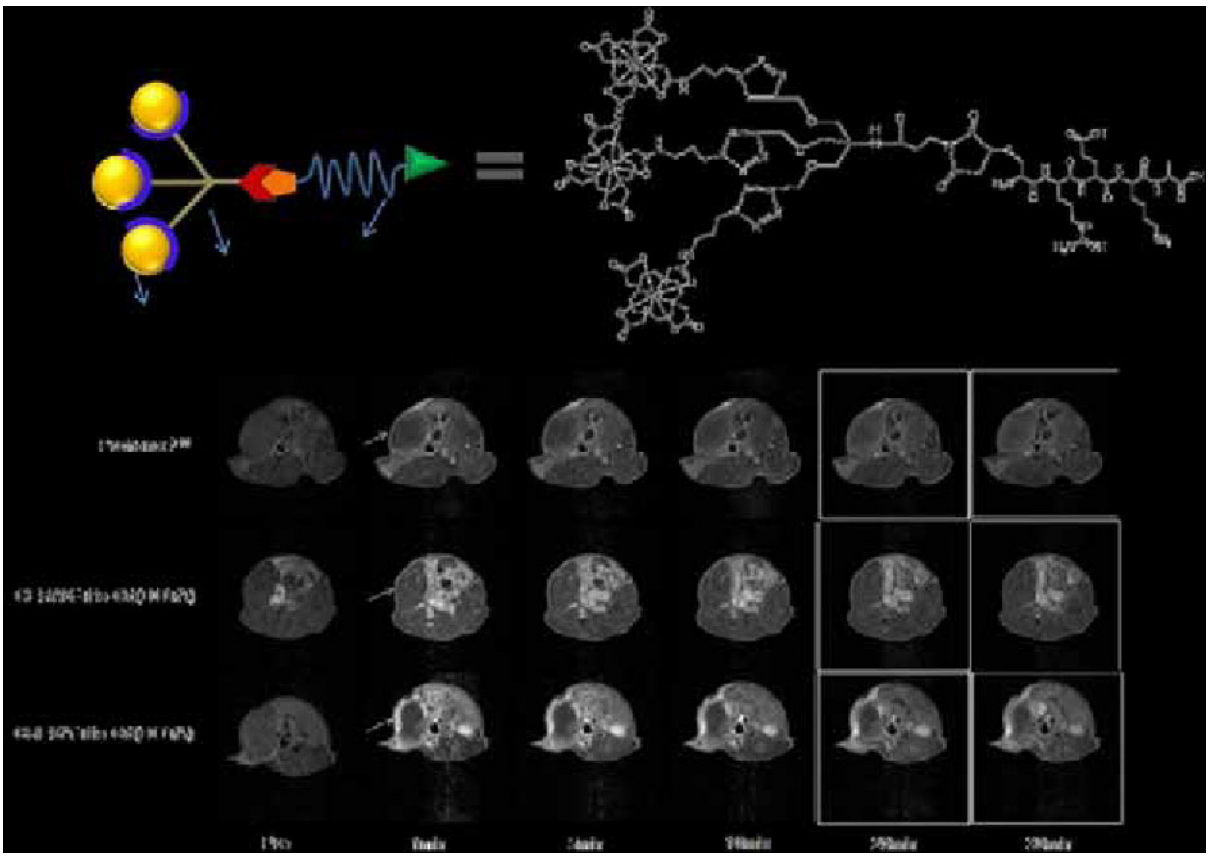

Figure 1. The structure of CREKA-Tris-Gd(DOTA)3 (A) and the representative 2D axial T1-weighted MR images of mice bearing a 4T1 breast orthotopic tumor before (pre) and at 1, 5, 10, 20, 30 minutes after the injection of ProhanceTM, CERAK-Tris-Gd(DOTA)3 and CREKA-Tris-Gd(DOTA)3 MRI contrast agent at 0.1 mM-Gd/kg. White arrows show tumor. (B)

Disclosure of author financial interest or relationships:
**Z. Zhou**, None; **Z. Ye**, None; **X. Wu**, None; **X. Shi**, None; **Z. Lu**, None.

Presentation Number **P649**
Poster Session 4
September 8, 2012 / 14:45-14:45 / Room: The Liffey

# Optimization of the automated synthesis of 18F-labeled compounds using the SynthERA platform

***Anneleen Blykers***[1], *Ilse Vaneycken*[2], *Catarina Xavier*[1], *Tony Lahoutte*[1,2], *Vicky Caveliers*[1,2], [1]*VUB, Brussels, Belgium;* [2]*NUGE, UZ-Brussel, Brussels, Belgium. Contact e-mail: anneleen.blykers@gmail.com*

Introduction: In order to minimize radiation exposure during radiochemical synthesis and to develop efficient and reliable synthetic methods for PET radiopharmaceuticals, 18F radiosyntheses are typically carried out in dedicated automated systems like SynthERA (IBA Molecular-Belgium). We want to set up an in-house multi-purpose PET radiosynthesis unit and develop radiochemistry procedures that allow the preparation of 18F-labeled tracers in a similar manner as 18F-FDG on SynthERA. While 2-(18F)fluoro-2-deoxyglucose (18F-FDG) was the only PET tracer available until recently other 18F-tracers have now been introduced in routine clinical practice. (18F)-Fluoromisonidazole (18F-FMISO) is used for the detection of hypoxia in tumors, while O-(2-[18F]fluoroethyl)-L-tyrosine (18F-FET) is used in the evaluation of brain tumors. N-succinimidyl-4-(18F) fluorobenzoate (18F-SFB) is the most widely used prosthetic group for the 18F-labelling of proteins and peptides. Materials & Methods: The automated synthesis of different 18F-tracers was optimized on the synthERA platform comprising a synthesis module and an HPLC unit. Different radiopharmaceuticals are produced using the original disposable 18F-FDG cassette (IFPTM nucleophilic) and editing the existing 18F-FDG-script. Reaction parameters such as reaction time and temperature of fluorination and deprotection were optimized in order to obtain an acceptable radiochemical yield. Purification optimization was either performed using disposable cartridges or HPLC. Quality control was performed by HPLC of the final product. Results: We succeeded in producing 18F-FMISO and 18F-FET with yields respectively up to 45% (decay corrected) when using 5 mg of the 1-(2'-nitro-1'-imidazolyl)-2-O-tetrahydropyranyl-3-O-toluenesulfonylpropanediol (NITTP) precursor and 40% (decay corrected) using 6 mg (2S)-O-(2-tosyloxyethyl)-N-trityl-tyrosine-tert-butyl ester (TET) precursor. The total synthesis including HPLC purification was completed in 40 minutes for 18F-FMISO, while the synthesis of 18F-FET can be achieved in ± 66 minutes. The radiochemical purity determined by HPLC was >95% for both tracers. The optimization of 18F-SFB labelling is currently in progress. Discussion: A fully automated, reproducible process for radiotracer synthesis was developed using an IBA SynthERA synthesis module. This procedures are convenient and reliable methods to prepare 18F-tracers with high radiochemical purity, in a routine PET radiopharmacy.

Disclosure of author financial interest or relationships:
**A. Blykers**, None; **I. Vaneycken**, None; **C. Xavier**, None; **T. Lahoutte**, None; **V. Caveliers**, None.

Presentation Number **P650**
Poster Session 4
September 8, 2012 / 14:45-14:45 / Room: The Liffey

# Synthesis and Evaluation of [18F]Fluorobutyl Ethacrynic Amide: A Potential PET Tracer for Studying Glutathione Transferase

***Yu-chia Chang***[1], *Chung-Shan Yu*[1,2], [1]*Biomedical engineering and environmental science, National Tsing Hua University, Hsinchu, Taiwan;* [2]*Institute of Nuclear Engineering and Science, National Tsing-Hua University, Hsinchu, Taiwan. Contact e-mail: s100012503@m100.nthu.edu.tw*

[18F]Flurobutyl ethacrynic amide ([18F]FBuEA) was prepared from the precursor tosylate N-Boc-N-[4-(toluenesulfonyloxy)butyl]ethacrynic amide with a radiochemical yield of 3%, a specific activity of 48 GBq/μmol and radiochemical purity of 98%. Chemical conjugation of [18F]FBuEA with glutathione (GSH) via a self-coupling reaction and enzymatic conjugation under catalysis of glutathiontransferase alpha (GST-alpha) and pi provided about 41% yields of radiochemical conjugated product [18F]FBuEA-GSH, 85% and 5-16%, respectively. The catalytic selectivity of this tracer toward GST-alpha was addressed. Positron emission tomography (PET) imaging of [18F]FBuEA in normal rats showed that a homogeneous pattern of radioactivity was distributed in the liver, suggesting a catalytic role of GST. By contrast, PET images of [18F]FBuEA in rats with thioacetamide-induced cholangiocarcinoma displayed a heterogeneous pattern of radioactive accumulation with cold spots in tumor lesions. PET imaging with [18F]FBuEA could be used for early diagnosis of hepatic tumor with a low GST activity as well as liver function.

Disclosure of author financial interest or relationships:
**Y. Chang**, None; **C. Yu**, None.

Presentation Number **P651**
Poster Session 4
September 8, 2012 / 14:45-14:45 / Room: The Liffey

# [18F]-5-Fluoro-5-deoxyribose: new peptide bioconjugation ligand for positron emission tomography (PET) imaging

***Sergio Dall'Angelo***[1,2], *Xiang-Guo Li*[3], *Lutz F. Schweiger*[2], *Matteo Zanda*[1,2], *David O'Hagan*[4], [1]*Institute of Medical Sciences, School of Medical Sciences, University of Aberdeen, Aberdeen, United Kingdom;* [2]*John Mallard Scottish PET Centre, School of Medicine and Dentistry, University of Aberdeen, Aberdeen, United Kingdom;* [3]*Department of Pharmacology, Drug Development and Therapeutics and Turku PET Centre, University of Turku, Turku, Finland;* [4]*4EaStChem School of Chemistry and Biomolecular Science Research Centre, University of St Andrews, St Andrews, United Kingdom. Contact e-mail: s.dallangelo@abdn.ac.uk*

Positron emission tomography (PET) is an important imaging modality used widely in clinical diagnosis. Fluorine-18 is an ideal isotope for PET applications in the clinic and in research and pharmaceuticals development programmes.[1] It has a relatively long half-life ($t_{½}$ = 109.7 min) and it is readily generated at very high specific activity as [$^{18}$F]$F^-$ fluoride ion in hospital and research centre localized cyclotrons.[2] One of the current challenges in PET is the requirement to rapidly label specific peptides such that the peptides can be used to target and then image diseased tissue or highlight the location of specific cell types. [18F]-2-Fluoro-2-deoxyglucose ([$^{18}$F]-FDG) is an attractive candidate for direct peptide conjugation as it is a hydrophilic sugar and it is readily available at PET centres worldwide since it is the most common PET radiotracer in the clinic. However [$^{18}$F]-FDG conjugation with peptides linkers require quite harsh conditions (low pH or high temperature) and extended conjugations time.[3-5] In this study we report the use of 5-deoxy-5-[$^{18}$F]Fluoro-D-ribose (5-[$^{18}$F]-FDR)[6] produced in a reprogrammed GE TRACERLab® module, which was intended for routine production of [$^{18}$F]-FDG, as new prosthetic group for a quick and efficient labelling of peptides in mild conditions The conjugation reaction of the aldehyde-linear form of sugar moiety with the peptide is based on the oxime formation with an aminooxy function borne by the peptide and is performed at room temperature and pH 4.6.[7] (1) Phelps, M. E. *PET: molecular imaging and its biological applications*; Springer, **2004**. (2) Cai, L.; Lu, S.; Pike, V. W. *European Journal of Organic Chemistry* **2008**, *2008*, 2843-2843. (3) Simpson, M.; Trembleau, L.; Cheyne, R. W.; Smith, T. A. D. *Applied Radiation and Isotopes* **2011**, *69*, 418-422. (4) Wuest, F.; Hultsch, C.; Berndt, M.; Bergmann, R. *Bioorganic & Medicinal Chemistry Letters* **2009**, *19*, 5426-5428. (5) Namavari, M.; Cheng, Z.; Zhang, R.; De, A.; Levi, J.; Hoerner, J. K.; Yaghoubi, S. S.; Syud, F. A.; Gambhir, S. S. *Bioconjugate Chemistry* **2009**, *20*, 432-436. (6) Onega, M.; Domarkas, J.; Deng, H.; Schweiger, L. F.; Smith, T. A. D.; Welch, A. E.; Plisson, C.; Gee, A. D.; O'Hagan, D. Chem. Commun. 2009, 46. (7) Li, X.-G.; Dall'Angelo, S.; Schweiger, L. F.; Zanda, M.; O'Hagan, D. *Chem. Commun.* **2012**.

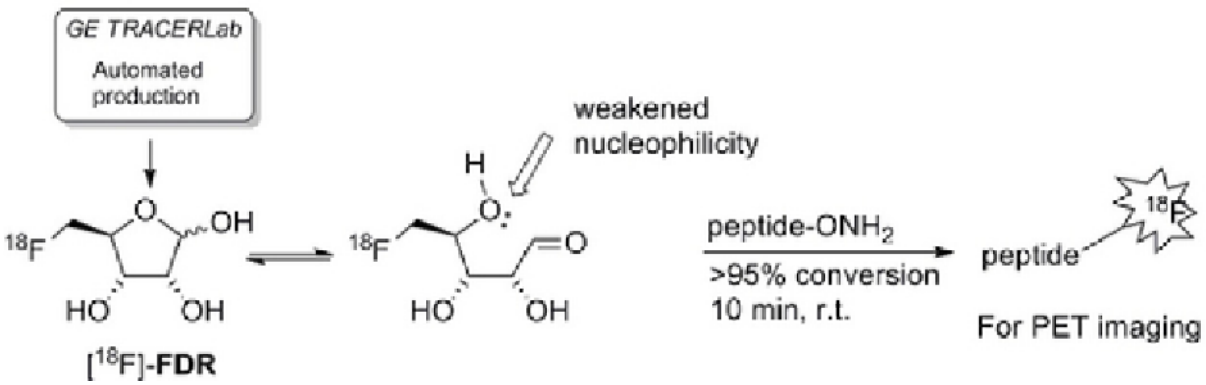


Disclosure of author financial interest or relationships:
**S. Dall'Angelo**, None; **X. Li**, None; **L.F. Schweiger**, None; **M. Zanda**, None; **D. O'Hagan**, None.

Presentation Number **P652**
Poster Session 4
September 8, 2012 / 14:45-14:45 / Room: The Liffey

# The effects of a nutrition supplement on the distribution of BFPET, a potential myocardial perfusion agent

***David R. Elmaleh***[1], *Timothy M. Shoup*[1], *Whitney Michalek*[2], *Angela Ferris*[2], *Ali A. Bonab*[1,2], *Alan J. Fischman*[2], [1]*Nuclear Medicine and Molecular Imaging, Massachusetts General Hospital, Boston, MA, USA;* [2]*Shriners Hospitals for Children, Boston, MA, USA. Contact e-mail: DELMALEH@PARTNERS.ORG*

Objectives: BFPET, a lipophilic cationic compound, concentrates in cells as a result of the negative electric potential across the inner mitochondrial membrane. Our earlier study indicated that heart-to-liver ratios in fed and fasted animals can change depending on fasting time and feeding content. In this study, we evaluated the use of an accepted nutritional supplement (Ensure) under controlled fasting/fed conditions. Methods: Biodistribution of BFPET was determined in three groups of SD rats at 50 minutes (n = 3) after BFPET injection. Two groups were overnight fasted from which one group (A) was given Ensure (500 microliter) via a tube placed in the stomach 10 minutes prior to injection of BFPET; the second group (B) was untreated with Ensure. A third control group (C) was never fasted overnight nor treated with Ensure. The animals were euthanized by C02 overdose and subjected to complete necroscopy. Tissues were weighed and counted using a Wizard gamma-counter and results were expressed as %dose/gram tissue mean +/- SEM. Results: For fasted Ensure treated rats, the heart-to-liver ratio average was 4.3:1. Overnight fasting with no Ensure, the heart-to-liver ratio was 3.18:1. For non-fasting animals, the heart-to-liver ratio was 7.95:1. Conclusion: As in our earlier studies, heart imaging is susceptible to diet. Fasting conditions result in increased liver uptake especially with high tracer specific activity. This study clearly shows that under normal feeding conditions BFPET gives the highest heart-to-liver ratio improving heart imaging. Heart-to-lung and heart-to-blood ratios were not affected. Controlling the fasting status and providing an accepted supplement, show that the optimal diet effects for minimizing liver uptake has yet to be determined.

Disclosure of author financial interest or relationships:
**D.R. Elmaleh**, None; **T.M. Shoup**, None; **W. Michalek**, None; **A. Ferris**, None; **A.A. Bonab**, None; **A.J. Fischman**, None.

Presentation Number **P653**
Poster Session 4
September 8, 2012 / 14:45-14:45 / Room: The Liffey

# Use of Iodo Imatinib analog (SKI-242) as a PET tracer to non-invasively image Glioblastoma

***Athanasios P. Glekas***[1,2], *Anson Ku*[3], *Thomas Ku*[3], *Steven M. Larson*[3,1], [1]*Radiochemistry, Memorial Sloan Kettering Cancer Center, New York, NY, USA;* [2]*Radiochemistry and Imaging Sciences Service, Memorial Sloan Kettering Cancer Center, New York, NY, USA;* [3]*Nuclear Medicine, Memorial Sloan Kettering Cancer Center, New York, NY, USA. Contact e-mail: glekasa@mskcc.org*

**Objectives** We have developed analogs of Imatinib that can be used as radiolabeled imaging surrogates of Imatinib. Imatinib is a tyrosine kinase inhibitor (TKI) approved by the FDA for use in approximately 10 cancers that express bcr-abl, c-kit and PDGFR. We have previously shown that either a Fluoro (SKI-696) or an Iodo-(SKI-244) Imatinib analog, can non-invasively image tumors that express the bcr-abl protein. Our current objective is to investigate the efficacy of, iodo Imatinib analog, SKI-244 in imaging tumors that overexpress PDGFR. **Methods** In vitro displacement studies were performed using SKI-696, SKI-242 or Imatinib as competitors to displace the binding of $^{131}$I-SKI-244 to K562 (Human chronic myelogenous leukemia) cells. Mice were inoculated with U87MG cells (glioblastoma) that over express PDGFR. After approximately 2 weeks the inoculated mice had grown tumors approximately 400mm$^3$ in volume and $^{131}$I-SKI-244 was administered to the mice via tail vein injection. The mice were euthanized and the organs were collected and the activity was counted. Another group of mice will be inoculated with U87MG cell and once tumors have grown to optimal size they will in turn be injected with $^{124}$I-SKI-244 so that an imaging time study can be preformed. **Results** Imatinib and SKI-696 were able to competitively displace the binding of $^{131}$I-SKI244 in K562 cells which are known to express bcr-abl, this result led us to believe that both compounds had the same target. The positive results in the bcr-abl expressing cell lines prompted us to pursue other targets of the iodo analog. A biodistribution study of mice inoculated with U87MG cells validated that there was tumor uptake of our$^{131}$I labeled Imatinib analog (SKI-244). The study showed that there was an increasing amount of the tracer in tumor as the rest of the body showed lower amounts of tracer as time progressed. **Conclusion** An iodo analog of Imatinib (SKI-244) has been developed and can be radiolabeled to be used as a PET imaging tracer. Competitive displacement studies have indicated that Imatinib and SKI-244 bind to the same target in Human CML cells (K562). Biodistribution studies of mice with U87 xenografts have verified that there is tumor uptake in cells that express PDGFR. This study will be repeated and this time the mice with the Glioblastoma xenografts will be PET imaged using $^{124}$I-SKI-244

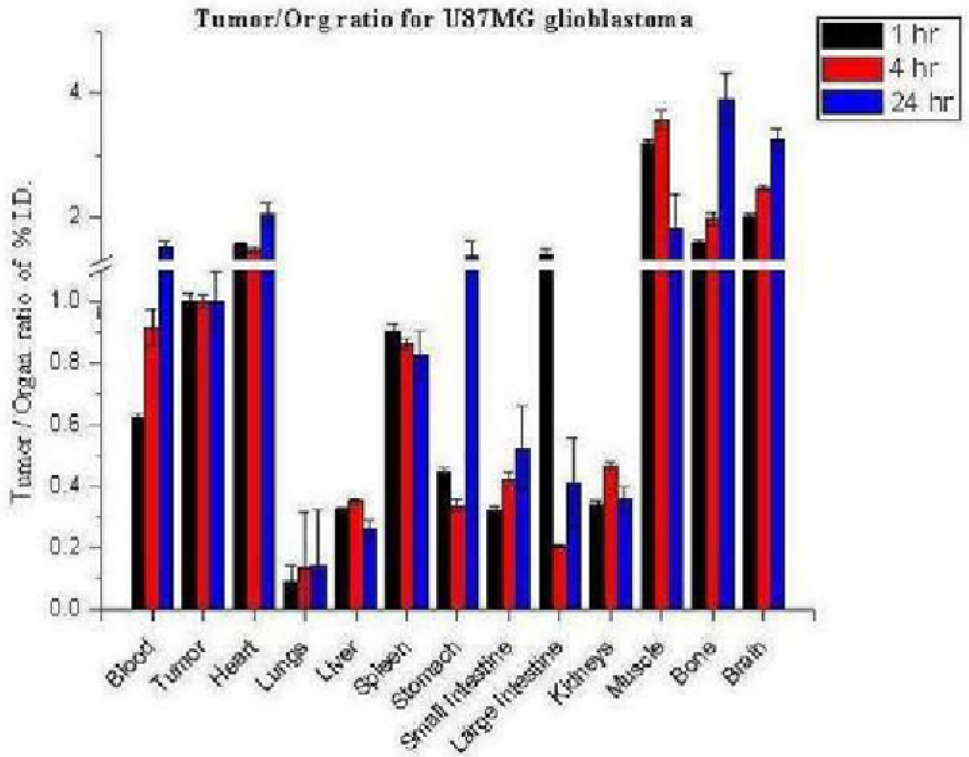


Disclosure of author financial interest or relationships:
**A.P. Glekas**, None; **A. Ku**, None; **T. Ku**, None; **S.M. Larson**, None.

Presentation Number **P654**
Poster Session 4
September 8, 2012 / 14:45-14:45 / Room: The Liffey

# [$^{123}$I]IGLCE, A Novel Prostate Specific Membrane Antigen Targeting Probe for Prostate Cancer Imaging with SPECT

***Naoya Harada**, Hiroyuki Kimura, Masahiro Ono, Hideo Saji, Department of Patho-Functional Bioanalysis, Graduate School of Pharmaceutical Sciences, Kyoto University, Kyoto, Japan. Contact e-mail: harada.naoya.58c@st.kyoto-u.ac.jp*

Purpose: PCa (prostate cancer) is the most commonly diagnosed and the second leading cause of cancer-related deaths in men in the world. So, non-invasive diagnoses of PCa by imaging techniques have high clinical benefit. However, [$^{18}$F]FDG ([$^{18}$F]fluorodeoxyglucose), which is widely used as a PET (positron emission tomography) probe for diagnosis of cancer, is not suitable for diagnosis of PCa, because there is no correlation between [$^{18}$F]FDG uptake and tumor grade in PCa. PSMA (Prostate Specific Membrane Antigen) is a noticeable target for PCa imaging, because of higher expression of PSMA in PCa. PSMA has GCP-II (glutamatecarboxy peptidase-II) activity. Previously, several asymmetric urea compounds (X-CO-Glu) have been reported as GCP-II inhibitors. The active binding site of PSMA is composed of two structural pockets, and the one of these pockets interacts with the glutamate moiety of urea-based inhibitors (S1′ pocket), and the remainders of inhibitors interact with the other pocket (S1 pocket). In this study, based on this information, we designed a novel urea-based compound and evaluated its utility as a PSMA imaging probe. Method: We selected $_{L}$-Cys-CO-$_{L}$-Glu as the urea-based inhibitor, because Cys-residue is easy to be labeled with maleimide-based reagent. We selected [$^{125}$I]IPM (4-iodophenylmaleimide) as the radio-labeling reagent and designed [$^{125}$I]IPMCE ([$^{125}$I]IPM-*S*-$_{L}$-Cys-CO-$_{L}$-Glu). We also selected [$^{125}$I]HML (m-iodohippuryl $N^{\epsilon}$-maleoyl-$_{L}$-lysine), which we have previously reported as a radioiodination reagent having high stability in human serum, as the radio-labeling reagent and designed [$^{125}$I]IGLCE ([$^{125}$I]3-iodophenyl-Gly-[$N^{\epsilon}$-maleoyl-$_{L}$-Lys]-*S*-$_{L}$-Cys-CO-$_{L}$-Glu). In vitro stability was evaluated by incubation in mouse serum. We estimated the affinity for PSMA by binding assay. As positive control probes, we prepared [$^{125}$I]DCIT (*N*-[*N*-[(*S*)-1,3-dicarboxyproyl]carbamoyl]-*S*-2-[$^{125}$I]iodo-$_{L}$-tyrosine) and [$^{125}$I]MIP-1095 ((*S*)-2-[3-[(*S*)-1-carboxy-5-[3-[4-[[$^{125}$I]iodophenyl]ureido]pentyl]ureido]pentanedioic acid) in the previously reported methods. The $K_d$ values were calculated by Scatchard plotting. We performed biodistribution study and SPECT/CT scan by using mice xenograft model bearing LNCaP (PSMA positive) on left shoulders and PC-3 (PSMA negative) on right shoulders. Result: We synthesized [$^{125}$I]IPMCE and [$^{125}$I]IGLCE in high radiochemical purity (> 95%). [$^{125}$I]IGLCE was stable in mouse serum within 6 hr, whereas 50% of [$^{125}$I]IPMCE was decomposed after 1 hr incubation. Therefore, we considered that [$^{125}$I]IGLCE was superior to [$^{125}$I]IPMCE as an imaging probe. The affinity of [$^{125}$I]IGLCE was higher than [$^{125}$I]DCIT and [$^{125}$I]MIP-1095; 7.8±1.4 nM, 143±2 nM and 20.4±0.6 nM respectively ($K_d$ values). In the biodistribution study, [$^{125}$I]IGLCE showed high accumulation in LNCaP at 30 min postinjection (9.5%ID/g), but not in PC-3 (0.94%ID/g). Moreover, accumulation in LNCaP was significantly reduced by co-injection of GCP-II inhibitor, 2-PMPA. In SPECT/CT study, LNCaP tumor was clearly visualized with [$^{123}$I]IGLCE. Conclusion: IGLCE showed high affinity and specificity for PSMA. [$^{123}$I]IGLCE is a promising compound as a PSMA imaging probe.

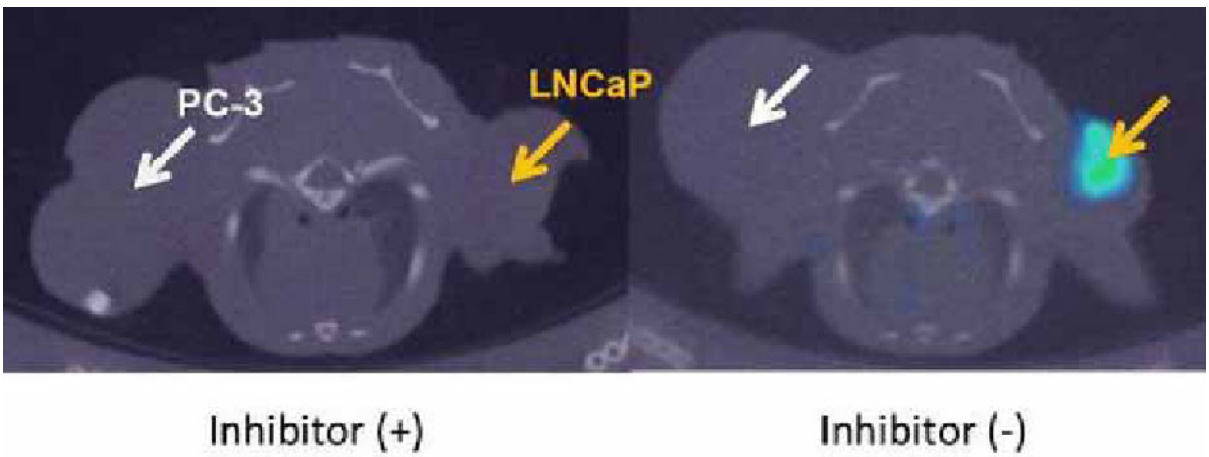


Disclosure of author financial interest or relationships:
**N. Harada**, None; **H. Kimura**, None; **M. Ono**, None; **H. Saji**, None.

Presentation Number **P655**
Poster Session 4
September 8, 2012 / 14:45-14:45 / Room: The Liffey

# Synthesis, 99mTc-Tricarbonyl labeling and bioevaluation of a novel derivative of arylpiperazine as SPECT imaging agent for 5HT1A receptors in Brain

***Leila Hassanzadeh***[1], *Mostafa Erfani*[2], *Seyed Esmaeil Sadat Ebrahimi*[1], [1]*Radiopharmacy, Faculty of pharmacy, Tehran university of medical sciences, Tehran, Islamic Republic of Iran;* [2]*Nuclear Science Research School, Nuclear Science & Technology Research Institute (NSTRI)Atomic Energy Organization of Iran (AEOI), Tehran, Islamic Republic of Iran. Contact e-mail: l_analytic@yahoo.com*

Introduction: Serotonin and its various receptors are involved in numerous CNS functions and psychiatric disorders.1-(2-methoxyphenyl) piperazine pharmacophore, a fragment of the true 5HT1A antagonist WAY100635, is being found in numerous selective 5HT1A imaging agents. Radionuclide with suitable decay characteristics specially 99mTc for in vivo SPECT are usually more readily available and often have longer half-lives, which facilitate their handling and processing. In this study, a new arilpiperazine derivative was synthesized and radiolabeled via Triazole by 99mTc-carbonyl. Method: A bidentate alkyne was reacted with phenyl piperazine derivative in the presence of a catalytic amount of Cu(I) to form tridentate ligand. The desired structure was confirmed by IR, NMR, Mass spectrometries. The ligand was radiolabelled with the precursor [99mTc] [(H2O)3(CO)3]+ and characterized by HPLC. The radiochemical purity of the intermediate and final complex were evaluated by HPLC methods. Stability in human serum, Octanol/water partion coefficient, in vivo biodistribution of labeled compound and brain imaging were carried out in Wistar rat. Result: Triazole complex could be 99mTc-Tricabonyl labeled in over 95% radiochemical purity that was determined by HPLC. Biodistribution studies have shown brain uptake of 0.43±0.12 %ID/g at 2min post injection. Radioligand had about over 6 hours, invivo stability in human serum albomin. Receptor binding assays indicated about 20% specific binding of radioligand to 5HT1A receptors. The partion coefficient (logP) was calculated as 0.78±0. the labeled compound was stable even up to 24 hours in room temperature. Conclusion: The results indicates that the way of synthesis is reliable and reproducible and has high yield steps. Radiolabeling of compound is high yield and has high radio chemical purity. The radio labeled compound is more than 24h stable. It has good lipophilicity , moderate brain uptake and binding to receptor. It can be good imaging agent for 5HT1A receptors but needs further ligand modification to obtain an ideal brain receptor imaging agent.

Disclosure of author financial interest or relationships:
**L. Hassanzadeh**, None; **M. Erfani**, None; **S. Sadat Ebrahimi**, None.

Presentation Number **P656**
Poster Session 4
September 8, 2012 / 14:45-14:45 / Room: The Liffey

# 18F-Labeling and Evaluation of a Novel Triazole-Substituted Amino Acid for Brain Tumor Imaging

***Chaofeng Huang***[1], *Liya Yuan*[2], *Keith Rich*[2], *Jonathan McConathy*[1], [1]*Radiology, Mallinckrodt Insisitute of Radiology, St Louis, MO, USA;* [2]*Neurosurgery, Washington University, St Louis, MO, USA. Contact e-mail: huangc@mir.wustl.edu*

Objectives: The radiolabeled histidine analogue (S)-[18F]AFETP is a substrate for cationic amino acid transport in vitro, is readily labeled using the click reaction, and has shown promising preclinical tumor imaging properties. To further explore this novel class of non-natural amino acid for tumor imaging, we synthesized an AFETP analogue, AFETH, with a longer alkyl side chain between the triazole functional group and the alpha-carbon. [18F]AFETH was radiolabeled and compared with [18F]AFETP through cell uptake and biodistribution studies in a mouse model of high grade glioma. METHOD: Non-radioactive AFETH and its labeling precursor were prepared from an enantiomeric pure Schiff imine using standard organic synthesis techniques. (S)-[18F]AFETH was prepared through the click reaction followed by acidic deprotection. The final product was isolated by preparative high performance liquid chromatography (HPLC). Biodistribution studies with (S)-[18F]AFETH were performed in male BALB/c mice at 14 days after implantation of subcutaneous DBT tumor cells. Cell uptake studies were performed under control conditions and in the presence of competitive inhibitors of amino acid transport. RESULTS: The biodistribution data of AFETH demonstrated good tumor to brain ratio within 5 min of injection, persistent activity in the tumor, and tumor to brain ratios of over 11:1 at 60 min after injection. The absolute uptake and retention was not identical to the pattern observed with (S)-[18F]AFETP, suggesting differences in transport and retention mechanisms. The tumor to brain and tumor to muscle ratios with (S)-[18F]AFETH were approximately 11:1 and 2:1, respectively, at 60 min after injection. The low brain uptake of this tracer may limit its ability to visualize non-enhancing regions within gliomas. CONCLUSION: The novel PET tracer, (S)-[18F]AFETH, demonstrates good tumor imaging properties in the mouse DBT model of glioma. Further biological evaluation of this compound and additional structural analogues with varying alkyl side chain lengths is ongoing.

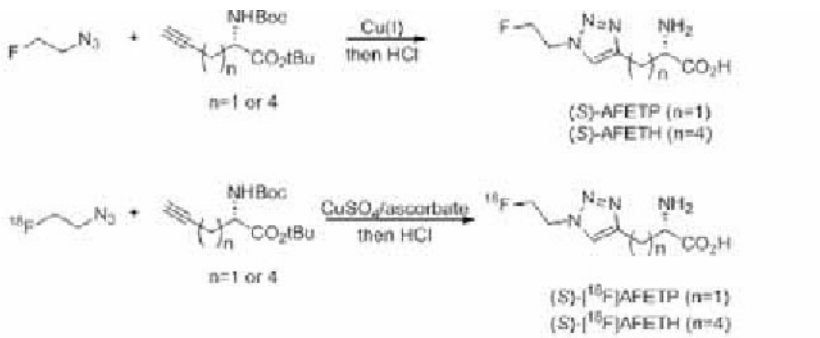


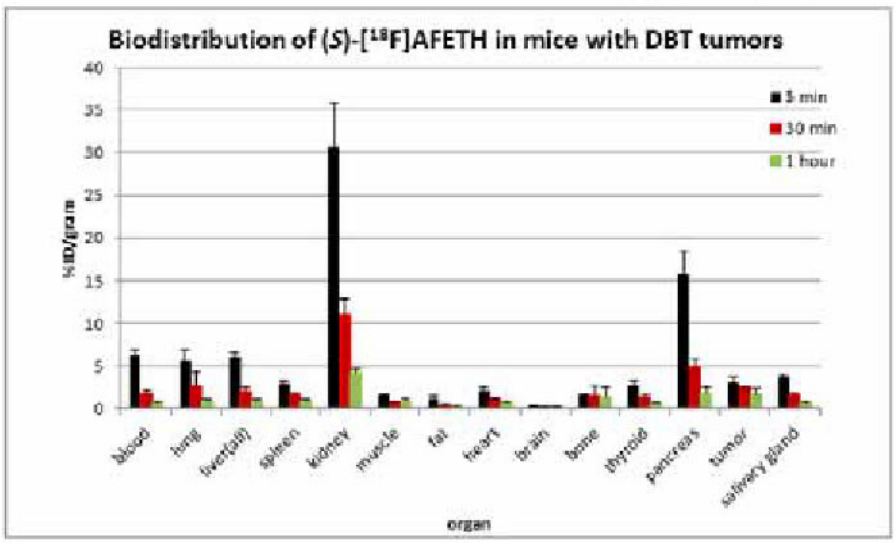


Disclosure of author financial interest or relationships:
**C. Huang**, None; **L. Yuan**, None; **K. Rich**, None; **J. McConathy**, Eli Lilly/Avid, Consultant; Eli Lilly/Avid, Speakers bureau .

Presentation Number **P657**
Poster Session 4
September 8, 2012 / 14:45-14:45 / Room: The Liffey

# Synthesis and evaluation of iodine-123 labeled oxidized low-density lipoprotein ($^{123}$I-oxLDL) as a non-invasive imaging probe for vascular disease

***Hidekazu Kawashima***[1], *Atsushi Nakano*[2], *Yoshinori Miyake*[1], *Akemi Kakino*[2], *Hajime Fukuda*[1], *Yoshiko Hashikawa*[1], *Tsutomu Zeniya*[1], *Tatsuya Sawamura*[2], *Hidehiro Iida*[1], [1]*Investigative Radiology, Natl. Cerebral & Cardiovascular Ctr. Research Inst., Osaka, Japan;* [2]*Vascular Physiology, Natl. Cerebral & Cardiovascular Ctr. Research Inst., Osaka, Japan. Contact e-mail: kawashima.hide.ri@mail.ncvc.go.jp*

Objective: Oxidized low-density lipoprotein (oxLDL) is one of the factors that induce endothelial dysfunction, acting via lectin-like oxLDL receptor-1 (LOX-1). Deposited within the aortic subendothelial space, oxLDL is endocytosed by macrophages via scavenger receptor including SR-A, CD36, and LOX-1, resulting in the conversion into foam cells, which contributes to atherogenesis. Therefore, *in vivo* imaging of oxLDL would provide valuable findings for clinical diagnosis of atherosclerotic lesion. In this study, we newly synthesized iodine-123 labeled oxLDL ($^{123}$I-oxLDL) and preliminarily evaluated the potential of oxLDL imaging probe for SPECT. Methods: $^{123}$I-oxLDL was synthesized by indirect $^{123}$I-labeling method. Briefly, succinimidyl 3-(3-[$^{123}$I]iodophenyl)propionate ([$^{123}$I]SIPP) was synthesized from the tributylstannyl precursor by alkyltin-radioiodine replacement reaction, and then oxLDL was labeled with [$^{123}$I]SIPP. To confirm the binding profile of $^{123}$I-oxLDL toward LOX-1, cellular uptake study was performed using CHO cells transfected with human LOX-1. In addition, $^{123}$I-oxLDL was intravenously injected to ApoE knockout mouse (male, 30-week-old), and the biodistribution of radioactivity was evaluated by autoradiography. Results: Succinimidyl 3-(3-tribtylstannylphenyl)propionate was allowed to react with [$^{123}$I]NaI (carrier added) in the presence of *tert*-butylhydroperoxide as an oxidant, and [$^{123}$I]SIPP was isolated by normal phase HPLC in a 45% of radiochemical yield. [$^{123}$I]SIPP was then added to phosphate buffer solution (pH 10) containing oxLDL. After the purification by gel filtration chromatography, $^{123}$I-oxLDL was obtained in 46% radiochemical yield with 93% purity. The specific activity was 1.3 MBq/μg of oxLDL. When $^{123}$I-oxLDL was added to LOX-1-expressing cells, the accumulation of radioactivity was more than 3-fold higher than that of wild-type cells at 60 min after the start of incubation. *Ex vivo* autoradiography using en face aorta preparation showed that the distribution of radioactivity corresponded to atherosclerotic regions which were predicted by fluorescent staining with DiI-labeled oxLDL. Conclusion: An iodine-123 labeled oxLDL, $^{123}$I-oxLDL was synthesized for SPECT imaging of oxLDL receptors. *In vitro* cellular uptake and *ex vivo* biodistribution experiment showed that $^{123}$I-oxLDL accumulated in atherosclerotic lesion could be detected, suggesting the potential of this probe for *in vivo* imaging of atherosclerosis.

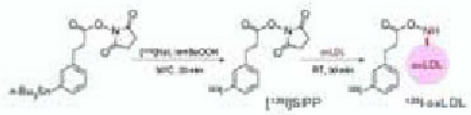

Synthesis of $^{123}$I-oxLDL

Disclosure of author financial interest or relationships:
**H. Kawashima**, None; **A. Nakano**, None; **Y. Miyake**, None; **A. Kakino**, None; **H. Fukuda**, None; **Y. Hashikawa**, None; **T. Zeniya**, None; **T. Sawamura**, AstraZeneca, Grant/research support; **H. Iida**, None.

Presentation Number **P658**
Poster Session 4
September 8, 2012 / 14:45-14:45 / Room: The Liffey

# Reliable aliphatic and aromatic nucleophilic substitution on a compact, all-electronically controlled digital microfluidic device

*Hee-Kwon Kim[1,2], Supin Chen[3], Muhammad Rashed Javed[1,2], Jack Lei[1,2], Chang-Jin Kim[3,4], R. Michael van Dam[1,2], **Pei Yuin Keng**[1,2], [1]Molecular and Medical Pharmacology, University of California, Los Angeles, CA, USA; [2]Crump Institute for Molecular Imaging, University of California Los Angeles, Los Angeles, CA, USA; [3]Biomedical Engineering Department, University of California Los Angeles, Los Angeles, CA, USA; [4]Mechanical and Aerospace Engineering Department, University of California Los Angeles, Los Angeles, CA, USA. Contact e-mail: pkeng@mednet.ucla.edu*

We have recently reported the first proof-of-concept demonstration of an all-electronically controlled electrowetting-on-dielectric (EWOD) microfluidic device for [18F]FDG radiosynthesis with reliable yield (88±7% fluorination efficiency and >95% hydrolysis efficiency (n=11)).[1] Compared to other types of microfluidic devices, EWOD chips are particularly attractive for radiosyntheses of diverse molecular probes due to their high temperature stability, chemical inertness toward a wide range of organic solvents, and the electronic manipulation of reagents instead of valves and pumps, which simplifies control and increases reliability. Here, we show that several other clinically-relevant 18F-labeled PET probes can also be reliably synthesized on EWOD. Specifically, we have established reliable multistep microdroplet syntheses of both aliphatic and aromatic nucleophilic fluorination reactions, which are the most commonly used radiosynthetic methods using no-carrier added [18F]fluoride ion. We have performed the radiosyntheses of [18F]fallypride, [18F]FLT, and [18F]SFB, respectively, on a single chip design, demonstrating not only diversity of reaction mechanism but also synthesis complexity (Figure 1). For the aliphatic nucleophilic fluorination of tosyl-fallypride ([18F]fallypride precursor) and the 3-N-Boc-5'-O-dimethoxytrityl-3'-O-nosyl-thymidine ([18F]FLT precursor) on EWOD chip, we adapted a mild, selective and high yielding methodology using the protic alcohol as co-solvent approach.[2][3][4] During the optimization of these microdroplet radiochemistries (Figs. 1a and 1b), we found that the ratio of base to precursor plays the most important parameter in achieving high fluorination efficiency (86±8% (n=5) for [18F]fallypride and 80±7% (n=10) for [18F]FLT). In the absence of the protic alcohol, we observed about 20% reduction in the fluorination and extraction efficiencies (Fig. 1a). We are also developing a rapid and efficient cartridge purification methodology for [18F]FLT synthesized on EWOD chip to eliminate the need of a HPLC purification. Our preliminary results showed 92% and >99% radiochemical and chemical purities, respectively (Fig. 1b). We have also expanded the synthetic scope to aromatic nucleophilic fluorination of the 4-(ethoxycarbonyl)-N,N,N-trimethylbenzeneamonium triflate (SFB precursor), a class of reaction that typically requires higher reaction temperatures and longer reaction times to achieve high incorporation of the [18F]fluoride. The optimal base to precursor ratio in this case was 1.75 (Fig. 1d). Following the fluorination step, a base catalyzed deprotection step, followed by a coupling step was performed on the same chip without intermediate purification to yield crude [18F]SFB with 15-25% decay-corrected radiochemical yield (n=3) (Fig. 1d).[5] These results show that the EWOD microfluidic platform is indeed robust and flexible in performing a wide range of multistep radiolabeling reactions, which is critical in developing an enabling technology platform for researchers to produce desired PET doses on-demand for PET imaging.

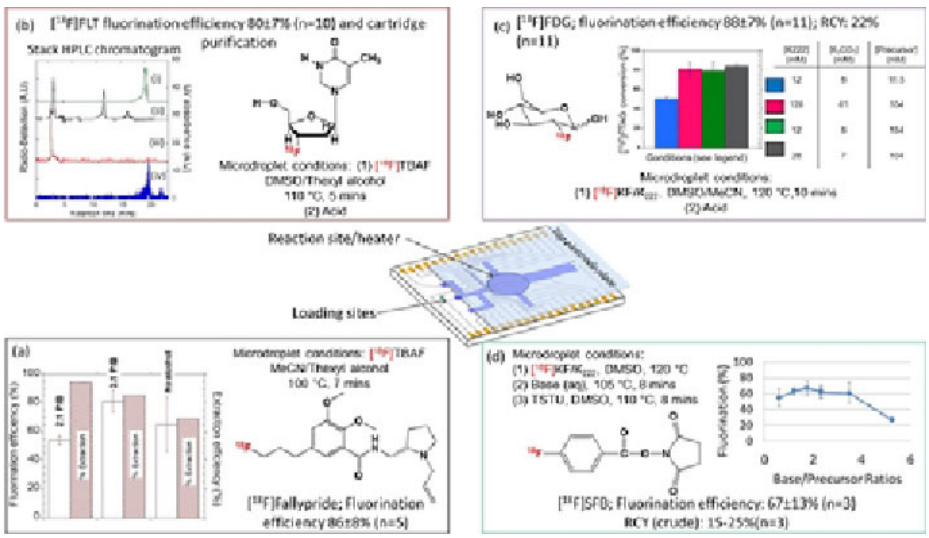


Disclosure of author financial interest or relationships:
**H. Kim**, None; **S. Chen**, None; **M. Javed**, None; **J. Lei**, None; **C. Kim**, None; **R. van Dam**, Sofie Biosciences, Inc., Consultant; Sofie Biosciences, Inc., Stockholder; **P. Keng**, None.

Presentation Number **P659**
Poster Session 4
September 8, 2012 / 14:45-14:45 / Room: The Liffey

# Development of a PET Probe for Imaging of Organic Anion Transporters

***Tatsuya Kikuchi****, Maki Okada, Toshimitsu Okamura, Joji Yui, Koichi Kato, Toshimitsu Fukumura, Molecular Imaging Center, National Institute of Radiological Sciences, Chiba, Japan. Contact e-mail: kiku@nirs.go.jp*

Various membrane transporters play an important role in the extrusion of xenobiotic and endogenous substances from tissues and body fluid. Efflux transporters expressed in the endothelium of the blood-brain barrier (BBB) limit the entry of the substances into brain. Because the alteration of the activity of the efflux transporters affects the disposition and therapeutic efficacy of drugs, in vivo imaging agents for mapping the efflux transporters have been desired. Here, we focused on the organic anion efflux transporters at the BBB, organic anion transporter 3 (OAT3) and multidrug resistance associated protein 4 (MRP4). Compared to the well known P-glycoprotein that transports hydrophobic and/or cationic compounds, these transporters extrude the anionic compounds from the brain. Our strategy for non-invasive measurement of the activity of the organic anion transporters was direct measurement of the efflux rate of the anionic compound generated in the brain using PET. To achieve the strategy, we adopted hippuric acid as a basic structure of the imaging agent for the organic anion transporters. Hippuric acid is a substrate of OAT3 and MRP4, and it can be readily derivatized and $^{11}$C-labeled. In addition, the ester of hippuric acid was expected to form hippuric acid in the brain by hydrolysis, and hippuric acid in the blood is not enter the brain. We synthesized the esters of *p*-[$^{11}$C]methoxy (**1**), *N*-[$^{11}$C]methyl (**2**) and non-derivatized [*carbamoyl*-$^{11}$C]hippuric acid (**3**), and the hydrolysis rates of these compounds were measured in the mouse brain homogenate (C57BL/6, n=3) as a preliminary screening. The ester bound of benzyl hippurate derivatives were hydrolyzed rapidly in the brain homogenate (>0.25 min$^{-1}$g$^{-1}$), whereas methyl and ethyl esters were relatively stable (<0.02 min$^{-1}$g$^{-1}$). Based on the result of this in vitro study, benzyl hippurate derivatives were conducted to further in vivo study. Using PET, the initial uptake of the benzyl hippurate derivatives in the brain of mice (C57BL/6, n=4) were determined. Despite the comparable lipophilicity among the compounds (clogP≈2.6), the brain uptake of benzyl **1** was low (<1% injected dose/mL) at 0.5 min after injection. On the other hand, benzyl **2** and benzyl **3** readily entered in the brain at 0.5 min after injection (3.5±0.64 and 3.9±0.91% injected dose/mL, respectively). Then, benzyl **2** and benzyl **3** were administrated to OAT3 knockout mice and MRP4 knockout mice (n=4, each), and the efflux rates of the radioactivity in the brain at later phase (at 30-60 min postinjection), in which only acid form of **2** or **3** was observed in the mice brain, were measured by PET. When benzyl **2** was injected to mice, the efflux rates were relatively comparable among the mice. In the case of benzyl **3** administration, the efflux rate in the brain of OAT3 knockout mice (0.52±0.050 h$^{-1}$, $p<0.01$) was much lower than that of C57BL/6 mice (2.4±0.29 h$^{-1}$) and MRP4 knockout mice (2.3±0.23 h$^{-1}$). Furthermore, interestingly, the radioactivity was retained only in the heart of MRP4 knockout mice after benzyl **3** administration. These results suggested that benzyl **3** could be an OAT3 imaging agents for brain and a MRP4 imaging agent for heart.

Disclosure of author financial interest or relationships:
**T. Kikuchi**, None; **M. Okada**, None; **T. Okamura**, None; **J. Yui**, None; **K. Kato**, None; **T. Fukumura**, None.

Presentation Number **P660**
Poster Session 4
September 8, 2012 / 14:45-14:45 / Room: The Liffey

# Preparation, characterization and in vivo and in vitro evaluation of 99mTc-nano tin colloid for sentinel lymph node detection

***Eun-Mi Kim***[1,2], *Su-Jin Cheong*[1,2], *Chang-Moon Lee*[1,2], *Hwan-Seok Jeong*[1,2], *Dong Wook Kim*[1,2], *Seok Tae Lim*[1,2], *Myung-Hee Sohn*[1,2], *Hwan-Jeong Jeong*[1,2], [1]*Nuclear Medicine, Chonbuk National University Hospital, Jeonju, Republic of Korea;* [2]*Cyclotron Research Center, Chonbuk National University Hospital, Jeonju, Republic of Korea. Contact e-mail: eunmi4172@hanmail.net*

Purpose: Colloidal radiopharmaceuticals are commonly used to detect the metastatic status of the axillary lymph nodes in breast cancer patients. Appropriate tracer's size to find the sentinel node is well known to approximately 15-30 nm. However, nano-size tin colloid has not been introduced. And conventional tin colloid has a large size ranged from 260 to 3900 (Amersham Hepatate). In this article, we introduce the preparation method of nano-size tin colloid using PVP and evaluate the possibility as radiotracer to find the sentinel node. Methods: Tin fluoride, sodium fluoride, poloxamer 188, and PVP was mixed in a vacuum vial with 99mTc pertechnetate (1480-1850 MBq/5 ml saline) (SNPPT). This solution was vigorously shacked by upsetting. To adjust physiological pH, phosphate buffer (SNPPPT) or sodium bicarbonate buffer (SNPPBT) was added. Colloid size was measured by Particle Size Analyzer UPA-150. The morphology of 99mTc-tin colloid was observed using FE-SEM. Cellular uptake of tin colloid was tested in macrophage. Rats were intravenously injected 7~11 MBq/0.3 ml 99mTc-tin colloid and rabbits were subcutaneously administered in both hind feet. Results: SNPPT size was shown about 10 nm without relation to the amount of PVP. The size of SNPPPT-30 was 139.0 ± 139.2 nm and SNPPBT-50 was 16.5 ± 6.76 nm. This was observed by FE-SEM. Macrophage uptake was 2.1 fold high in SNPPBT-50 compared with SNPPPT-30. When iv injection to rat, SNPPBT-50 were preliminary positioned in bone marrow and these were secreted through the kidney, whereas SNPPPT-30 was accumulated in the liver. The gamma camera images showed rapid localization of nano-sized tin colloid to bone marrow and kidney. Popliteal node is readily observed visually using two samples. However, popliteal node activity in rabbit, in case of SNPPPT-30 was decreased by time, whereas SNPPBT-50 increased. Conclusion: Nano-size 99mTc-tin colloid successfully prepared using PVP. On the basis of these results, we established freeze-dried kit formulation for further clinical evaluation. This will be a promising radiopharmaceutical for detection of sentinel node.

**Figure. Gamma images of $^{99m}$Tc-tin colloid in rabbit. $^{99m}$Tc-tin colloid was injected subcutaneously on the dorsum of each hind foot of rabbit. SNPPPT-30 (right foot) and SNPPBT-50 (left foot).**

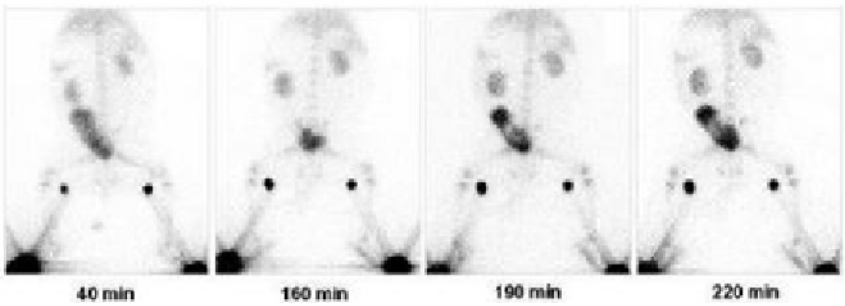


Disclosure of author financial interest or relationships:
**E. Kim**, None; **S. Cheong**, None; **C. Lee**, None; **H. Jeong**, None; **D. Kim**, None; **S. Lim**, None; **M. Sohn**, None; **H. Jeong**, None.

Presentation Number **P661**
Poster Session 4
September 8, 2012 / 14:45-14:45 / Room: The Liffey

# Pd0-Mediated Rapid Coupling of Methyl Iodide with Excess Amounts of Benzyl- or Cinnamylboronic Acid Esters (sp3-sp3 Type Coupling) for the Incorporation of Positron-Emitting 11C Radionuclide into an Organic Franework

***Hiroko Koyama***[1], *Ryosuke Ijuin*[2], *Si Qin*[1], *Yuma Hatta*[1], *Jeongwan Son*[1], *Masashi Ohta*[1], *Masahiro Wakao*[1], *Takamitsu Hosoya*[1], *Hisashi Doi*[2], *Masaaki Suzuki*[2], [1]*Graduate School of Medicine, Gifu University, Gifu, Japan;* [2]*Center for Molecular Imaging Science, RIKEN Kobe Institute, Kobe, Japan. Contact e-mail: koyama@biomol.gifu-u.ac.jp*

Objective: Position emission tomography is a noninvasive method to monitor drug behavior and its localization on target molecules in the living systems including human body using a short-lived positron-emitting radionuclide. We have elaborated rapid C-methylations by Pd0-mediated rapid couplings between sp2(arenyl)-sp3, sp2(alkenyl)-sp3, and sp-sp3 hybridized carbons with an aim to incorporate the [11C]methyl group into organic frameworks including heteroaromatic compounds. Described herein is finally-listed rapid reaction between sp3- and sp3-hybridized carbons. Method: The transition metal mediated rapid cross-coupling of CH3I with an excess amount (40 equiv) of benzyl- and cinnamylboronic acid pinacol esters was planned. Results and Discussions: The reaction using CH3I/benzylboronic acid pinacol ester/{Pd[P(tert-C4H9)3]2}/CsF (1:40:1:10 mole ratio) in 90:10 DMF/H2O (v/v) at 80 °C for 5 min in 88% yield. Interestingly, the yield of the reaction was temperature-dependent, giving a bell-shaped curve. The use of further excess amount of a substrate (200 equiv) worked positively to give the product with increased yield, matching with an actual PET study. Similar tendencies were observed for various boronate substrates. The efficiency of the novel method was well demonstrated by an actual reactions of [11C]H3I and pinacol 4-methoxybenzylboronate using {Pd[P(tert-C4H9)3]2}/CsF (1:10) in DMF/H2O at 80 °C for 5 min to give 4-methoxy[11C]ethylbenzene in 85% radio-HPLC analytical yield.

Disclosure of author financial interest or relationships:
**H. Koyama**, None; **R. Ijuin**, None; **S. Qin**, None; **Y. Hatta**, None; **J. Son**, None; **M. Ohta**, None; **M. Wakao**, None; **T. Hosoya**, None; **H. Doi**, None; **M. Suzuki**, None.

Presentation Number **P662**
Poster Session 4
September 8, 2012 / 14:45-14:45 / Room: The Liffey

# Sequential synthesis of three different 18F-labeled PET tracers on the ELIXYS radiosynthesizer

***Mark S. Lazari***[1,2], *Kevin Quinn*[1], *Shane Claggett*[1], *Melissa Esterby*[1,3], *R. Michael van Dam*[1,2], [1]*Crump Institute for Molecular Imaging, Department of Molecular & Medical Pharmacology, UCLA, Los Angeles, CA, USA;* [2]*Biomedical Engineering Interdepartmental Program, UCLA, Los Angeles, CA, USA;* [3]*Sofie Biosciences, Culver City, CA, USA. Contact e-mail: MLazari@mednet.ucla.edu*

**Objective:** The ability to perform sequential syntheses of the same or different tracers on a radiosynthesizer enables greater throughput with limited hot cell space and equipment. Furthermore, easy setup, use, and turnover allow faster synthesis optimization and validation for novel PET tracer discovery. Although sequential runs can be achieved through duplicate equipment, several commercial radiosynthesizers provide this capability by allowing either simultaneous setup of multiple runs (e.g. Siemens Explora FDG4), or sequential setups with minimal user intervention or radiation exposure between runs (e.g. GE FASTlab, IBA Synthera). The ELIXYS radiosynthesizer was designed to meet the need for demanding three-pot, high temperature and pressure syntheses. Here, we show that its flexibility can be exploited to perform three sequential single-pot syntheses (identical or different) without intervention and exposure. **Method:** First, three sequential syntheses of 2-[18F]fluoro-2-deoxy-D-glucose ([18F]FDG) were performed to mimic an optimization study. The fluorination temperature was tested at 110°C, 120°C, and 130°C for 5 minutes each. Three cassettes were loaded with sealed reagent vials and preconditioned QMA and purification cartridges and were each connected to a dedicated [18F]fluoride inlet and product collection vial. Using the same optimized protocol for each reactor and varying only the temperature of fluorination, [18F]FDG was synthesized in sequence on the three reactors. Radiochemical identity and purity were determined by radio-TLC. Second, [18F]FDG, 3-deoxy-3-[18F]fluoro-L-thymidine ([18F]FLT), and *N*-succinimidyl-4-[18F]fluorobenzoate ([18F]SFB) were sequentially synthesized in reactors 1, 2, and 3. The cassettes were similarly furnished with reagents and QMA and purification cartridges as needed. Cassettes were installed and connected to dedicated [18F]fluoride input lines. The first two cassettes were connected to collection vials and the third was connected to the built-in HPLC injector for HPLC purification. Radiochemical purity was verified with radio-TLC ([18F]FDG) or with analytical radio-HPLC with co-injection of a cold standard ([18F]FLT and [18F]SFB). **Results:** Same-day sequential syntheses of multiple batches of [18F]FDG produced reliable results as well as the sequential syntheses of [18F]FDG, [18F]FLT, and [18F]SFB, with no cross contamination between tracers. **Conclusion:** We have demonstrated that the ELIXYS radiosynthesizer permits sequential syntheses of up to three (identical or different) tracers with a single setup. No hardware reconfiguration is needed to switch between sequential syntheses and performing more complex syntheses such as the three-pot synthesis of 2'-deoxy-2'-[18F]fluoro-β-D-arabinofuranosyl cytosine ([18F]FAC) or 2'-deoxy-2'-[18F]flouro-5-methyl-1-β-L-arabinofuranosyl uracil ([18F]FMAU).

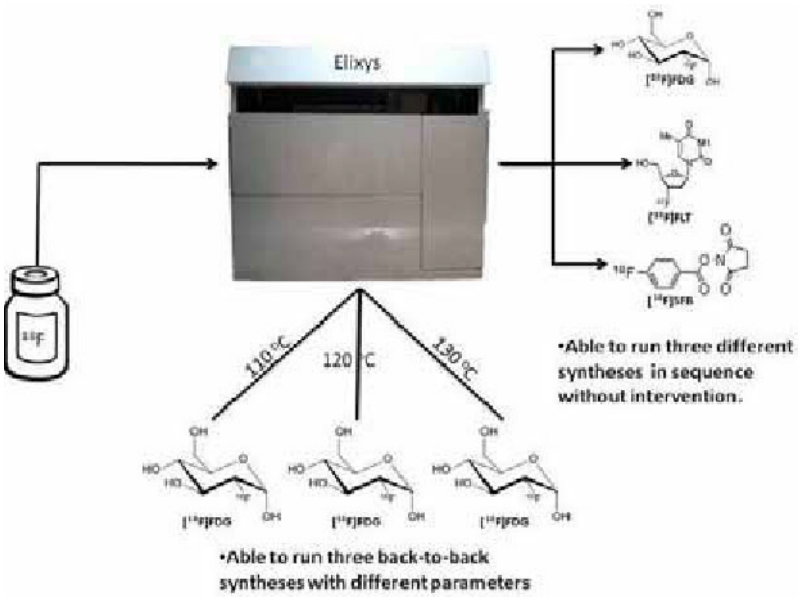


Disclosure of author financial interest or relationships:
**M.S. Lazari**, None; **K. Quinn**, Sofie Biosciences, Consultant; **S. Claggett**, Sofie Biosciences, Consultant; **M. Esterby**, Sofie Biosciences, Inc., Employment; Sofie Biosciences, Inc., Stockholder; **R. van Dam**, Sofie Biosciences, Inc., Consultant; Sofie Biosciences, Inc., Stockholder .

Presentation Number **P663**
Poster Session 4
September 8, 2012 / 14:45-14:45 / Room: The Liffey

# 18F-Radiolabeling of DBCO-MSNs by Strain-Promoted Alkyne-Azide Click Reaction for Pretarget Imaging

***Sang Bong Lee***[1,2], *Hye Lan Kim*[1,2], *Sachin U. Kalme*[1,2], *Hwan-Jeong Jeong*[1,2], *Seok Tae Lim*[1,2], *Myung-Hee Sohn*[1,2], *Dong Wook Kim*[1,2], [1]*Nuclear medicine, Chonbuk national university medical school, Jeonju, Republic of Korea;* [2]*Cyclotron research center, Chonbuk national university medical school, Jeonju, Republic of Korea. Contact e-mail: sangbongyi1@hanmail.net*

Purpose : As an effort in the development of more flexible 18F-labeling MSNs, we report herein the use of a strain-promoted alkyne-azide cycloaddition (SPAAC) with carboxylic acid substituted dibenzocycloctyne radio labeled-DBCO MSNs and 18F-PEG-azido, which gives good specific activity with high yield. and mesoporous silica nanoparticle(MSN) are applied for tumor PET-CT imaging. The accumulation of in DBCO-MSNs tumor tissue was occcrred through enhanced permeability and retention(EPR) mechanism. Method : DBCO-MSNs was synthesized by a self assembly method and MSNs surface was covered with amine terminal of APTS . Nanoparticle size was regulated and controlled with maintaining pH using NaOH. This MSN-amine was than conjugated with hydroxysuccinimidyl-PEG (Mw.685.71)(MSN-PEG) and hydroxysuccimidyl-Cyclooctyne.(DBCO-PEG-MSNs).Further DBCO-PEG-MSN was analysis by TEM,FT-IR and Zetapotential of DBCO-PEG-MSNs were determined. For invivo studies of 100~200nm size of DBCO-PEG-MSNs was injected via tail vein in to U87MG xenograft mice post injection and after 24hour 18F-PEG-azido was injected .PET-CT images were acquired until 2h after 18F-PEG-azido injection. Results : Nucleophilic fluorination of azido-PEG mesylate precursor provided 18F-PEG-azido17 in 95%yield with total reaction time 70min including HPLC purification. 18F-PEG-azidowas than reacted with DBCO-MSNs worked smoothly and promoted 18F radiolabelelled-MSN in 100% after 30min. in vivo test of azido-PEG-[18F] and DBCO-PEG-MSN post injection and 24hour 18F-PEG-azidowas injected . In vivo images of DBCO-PEG-MSN post injection and 24hour 18F-PEG-azido were also showed high activity in tumor tissue uptake than 18F-PEG-azido. Conclusion : These results suggest that in vivo tumor accumulation of DBCO-MSNs though enhanced permeability and retention(EPR) mechanism. We achieved successfully radiolabeling of DBCO-MSNs using the stain promoted click reaction. The design include careful consideration of the DBCO-MSNs for pretarget of therapeutic carrier to delivered as anticancer drug.

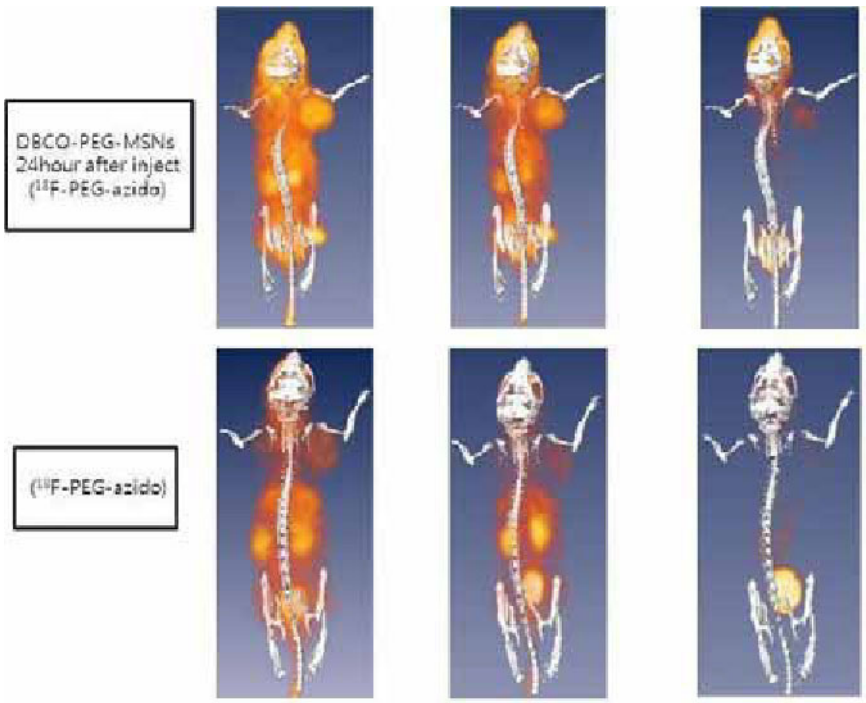


Disclosure of author financial interest or relationships:
**S. Lee**, None; **H. Kim**, None; **S.U. Kalme**, None; **H. Jeong**, None; **S. Lim**, None; **M. Sohn**, None; **D. Kim**, None.

Presentation Number **P664**
Poster Session 4
September 8, 2012 / 14:45-14:45 / Room: The Liffey

# A PICs compatible dispensing system for PET & SPECT radiopharmaceuticals

***Ming-Hsin Li**, Institute of Nuclear Energy Research, Longtan, Taoyuan County, Taiwan. Contact e-mail: mhli@iner.gov.tw*

Objectives: We have developed an automated dispenser with a novel plug apparatus for PET & SPECT radiopharmaceuticals' filling with validation. It is a completely automatic syringe filling process for dispensing PET & SPECT radiopharmaceuticals (such as Tl-201, Ga-67-citrate, In-111-chloride and Ga-68-DOTANOC) in unit doses within syringes or in multi-dose vials compatible with PICs regulations. Especially it refers to a situation that hand contact with radiopharmaceuticals is avoided and exposure to radioactive materials is reduced for operators. Methods: The technical approaches include: a computer controlled unit with an activation mechanism to perform three-dimensional reciprocal movement and activate an injection needle to freely move in a predetermined space; a 8 x 6 glass vial rack located in the moving range of the injection needle, on each of which there is an injection hole with a novel plug apparatus; an injection solution pump with an injection needle to fill the radiopharmaceuticals into the sterilized glass vial; the dispensed radiopharmaceuticals sterilized by autoclave. Results: This modified dispensing system can be carried out in hot cells where manipulation of syringes and vials by tongs and computer. It is also suitable for bench top applications, laminar air flow cabinets or safety cabinets, and to dispense terminally sterilized radiopharmaceutical liquid from a reservoir through syringe to vials in Single-Dose or Multiple-Dose. The total time to dispense a Multiple-Dose(about 6 mL) from dispending needle positioning in the sterilized vial to removing the needle is typically 20 to 25 seconds. Conclusions: A novel plug apparatus is employed to further enhance process reliability and precision. This modified dispensing system is specifically designed for PIC/s compatible PET & SPECT radiopharmaceuticals, including aseptic process and terminally sterilized products.

Disclosure of author financial interest or relationships:
**M. Li**, None.

Presentation Number **P665**
Poster Session 4
September 8, 2012 / 14:45-14:45 / Room: The Liffey

# Are exhausted 68Ge/68Ga generators useful in the preparation of radiopharmaceuticals for preclinical PET imaging?

***Luisa M. López-Sánchez***[1], *Maria L. Soto-Montenegro*[2,3], *Santiago Peña Zalbidea*[2], *Manuel Desco*[1,2], *Juan Jose Vaquero*[1], *[1]Departamento de Bioingeniería e Ingeniería Aeroespacial, Universidad Carlos III de Madrid, Madrid, Spain; [2]Unidad de Medicina y Cirugía Experimental, Hospital General Universitario Gregorio Marañon, Madrid, Spain; [3]CIBER de Salud Mental (CIBERSAM), Madrid, Spain. Contact e-mail: lopezsanchezluisa@gmail.com*

AIM: The useful life of a 68Ge/68Ga generator is about one year. Nevertheless, the activity obtained after two years could suffice for the preparation of radiopharmaceuticals intended for animal research. However, lower eluate quality (due to column degradation), as well as a lower amount of gallium-68 compromise the reaction yield and the specific activity of the final product. Therefore, an adjustment of the synthesis variables and an automatization of the process are necessary to improve efficiency and reduce synthesis time. Our aim has been to set up an automated synthesis of 68Ga-DOTATOC in order to optimize the use of a two-year old generator for preclinical research. MATERIAL & METHODS: The synthesis takes place through a chelation reaction followed by a purification step using a C18 cartridge (Sep-Pak SPE Waters) and absolute ethanol as eluent. 68-Gallium is obtained from a two-year old 50 mCi Obninsk 68Ge/68Ga generator (Eckert & Ziegler) eluted with 5 ml of HCl 0,1M. The eluate is purified and concentrated using both fractionation and anionic purification methods. For the latter, a SAX cartridge (SPE-Spezialkartuschen Chromafix PS-HCO3) is used. The automatization of the synthesis is done with a FastLab module (GEHC) using its single-use cartridges for 18F-FDG. Synthesis optimization is based on the decrease of the amount of precursor (which is added directly into the reactor), a change of the buffer used (HEPES instead of acetate), and redesign of the final product formulation method (evaporation of ethanol instead of its dilution). Radiochemical purity is measured with an HPLC Agilent 1200 System using a C18 Vydac 300 (Grace) column and 0,001% TFA as mobile phase. RESULTS: Thirteen syntheses confirmed that the proposed method makes it possible to automatically obtain 68Ga-DOTATOC in 30 minutes. The yield of the synthesis was 54.3 ± 17.7% decay-corrected to the start of the synthesis time (mean ± SD). The pH of the final product was 7.7 and its specific activity was 90.5 ± 25 µCi/nmol (mean ± SD), with a radiochemical purity >99%. CONCLUSIONS: The process proposed here makes it possible to use a two-year old generator for the automated preparation of 68Ga-DOTATOC in a quick and reproducible way. The synthesis yield and the characteristics of the radiopharmaceutical obtained are still adequate for use in preclinical imaging. The automatization of the process decreases the time invested by specialized personal and favors the radiological protection of the operators.

Disclosure of author financial interest or relationships:
**L.M. López-Sánchez**, None; **M.L. Soto-Montenegro**, None; **S. Peña Zalbidea**, None; **M. Desco**, None; **J. Vaquero**, None.

Presentation Number **P666**
Poster Session 4
September 8, 2012 / 14:45-14:45 / Room: The Liffey

# $^{64}$Cu-chelated derivatives of porphyrin photodynamic therapy agents conjugated with tumor-targeting peptide for the evaluation of target cell affinity and PET image-based pharmacokinetics

***Hidefumi Mukai**, Emi Hayashinaka, Yasuhiro Wada, Yasuyoshi Watanabe, Center for Molecular Imaging Science, RIKEN, Kobe, Japan. Contact e-mail: hmukai@riken.jp*

Photodynamic therapy (PDT) is a powerful treatment strategy for cancer and so on, based on inducing cell death and inflammation via the production of reactive oxygen species through a photoreaction involving a photosensitizer (typically porphyrin derivatives), tissue oxygen, and light. However, PDT may also cause some side effects, including photosensitivity, since many photosensitizers have no specific targeting potential for the aimed tissues *in vivo* and distribute throughout normal tissues, in addition to cancer tissues. To solve this problem, targeted PDT utilizing photosensitizers conjugated with targeting peptides or antibodies have been investigated. In the development of targeted PDT agents, a simple evaluation system of *in vivo* pharmacokinetics (including human's), as well as target cell affinity, is absolutely imperative. PET is a useful tool for non-invasive and quantitative visualization of biodistribution *in vivo* with a high spatial and temporal resolution, and therefore, we hypothesized that $^{64}$Cu chelation with porphyrin photosensitizer-biomacromolecule conjugates may become a simple and versatile labeling strategy for this purpose. In the present study, we successfully synthesized a $^{64}$Cu-chelated porphyrin photosensitizer and its tumor targeting peptide conjugate under conditions in which radiolysis was suppressed. Specifically, protoporphyrin IX (PPIX) was mixed with $^{64}CuCl_2$ in sodium acetate buffer at 50 °C, and then, the post-reaction mixture was directly analyzed via radio-HPLC. According to the result, it was confirmed that degradation (thought to be based on radiolysis) occurs, and large amounts of $^{64}$Cu-labeling compounds are wasted in the reaction mixture. Therefore, prevention of radiolysis is thought to be important for the efficient synthesis of [$^{64}$Cu]PPIX. Based on this notion, we investigated the effects of the representative radiolytic stabilizers, and we interestingly found that the addition of ethanol into the reaction mixture provides an effective solution for this problem. The chelation reactions of various porphyrins with [$^{64}$Cu]$CuCl_2$ were also studied and the generality of this phenomenon was demonstrated. Next, a conjugate of PPIX (a photosensitizer) and a bombesin analog (a tumor targeting peptide interacting with the gastrin-released peptide (GRP) receptor) linked via short polyethylene glycol (PPIX-PEG6-BBN analog) were synthesized and used as a targeted PDT agent. Additionally, a $^{64}$Cu-chelated PPIX-PEG6-BBN analog was synthesized under optimized reaction conditions. Finally, we demonstrated the usefulness of synthesized $^{64}$Cu-chelated porphyrin photosensitizers and their tumor targeting peptide conjugates in evaluations of target cell affinity and PET image-based pharmacokinetics, using experimental systems including a human prostate cancer cell line (PC-3) which highly expresses the GRP receptor, and PC-3 tumor-bearing mice. This labeling strategy with porphyrin photosensitizers may be of value for the rapid development of ideal targeted PDT agents.

Disclosure of author financial interest or relationships:
**H. Mukai**, None; **E. Hayashinaka**, None; **Y. Wada**, None; **Y. Watanabe**, None.

Presentation Number **P667**
Poster Session 4
September 8, 2012 / 14:45-14:45 / Room: The Liffey

# Novel 111In-labeled immunoconjugates bispecific for EGFR and HER2 for molecular imaging of breast cancer

***Eva Razumienko***[1], *Lindsay Dryden*[1], *Raymond M. Reilly*[1,2], [1]*Pharmaceutical Sciences, University of Toronto, Toronto, ON, Canada;* [2]*Toronto General Research Institute, University Health Network, Toronto, ON, Canada. Contact e-mail: eva.razumienko@utoronto.ca*

Objective: Our objective was to construct novel bispecific immunoconjugates (bsICs) capable of binding EGFR and HER2 labeled with 111In that may be able to image EGFR-HER2 heterodimerization in breast cancer possibly through higher avidity for dimeric vs. monomeric complexes. Methods: bsICs were composed of trastuzumab Fab recognizing HER2 linked to the 6.2 kDa endogenous ligand for EGFR, epidermal growth factor (EGF). Fab were produced by digestion of trastuzumab IgG with papain. Fab were modified with sulfosuccinimidyl-4-(N-maleimidomethyl)cyclohexane-1-carboxylate containing a 24 mer polyethyleneglycol (PEG) spacer (SM-PEG24-NHS) to introduce maleimide groups for cross-linking to EGF thiolated with Traut's reagent. bsICs were derivatized with diethylenetriaminepentaacetic acid (DTPA) for labeling with 111In. The ability to independently bind HER2 or EGFR was determined in competition assays using 111In-bsICs on cells expressing HER2, EGFR or both receptors competed with a 100-fold excess of Fab, EGF or combined ligands. Results: Conjugation of Fab to EGF was confirmed by SDS-PAGE, Western blot and size-exclusion HPLC. bsICs were labeled with 111In to a radiochemical purity of 98.4 ± 0.3% (specific activity 312 ± 17 MBq/mg). 111In-bsICs showed specific binding to HER2 and EGFR on cells expressing either receptor. Binding to MDA-MB-231 cells (EGFR+/HER2-) was reduced to 95.3 ± 7.1%, 20.5 ± 2.6% or 10.1 ± 2.8%, respectively by Fab, EGF or both ligands. Binding to SKOV-3 cells (EGFR-/HER2+) was reduced to 12.6 ± 2.7%, 95.9 ± 8.8% or 10.1 ± 1.7% by Fab, EGF or both ligands. Binding to MDA-MB-231 cells transfected to express HER2 (231-H2N, EGFR+/HER2+) was reduced to 52.7 ± 2.8%, 65.5 ± 2.9% or 4.4 ± 0.9% by Fab, EGF or both ligands. Conclusion: 111In-bsICs composed of trastuzumab Fab and EGF bound specifically to EGFR and HER2 when a PEG spacer was inserted between these two binding moieties. These 111In-bsICs may be useful for imaging EGFR-HER2 heterodimerization. microSPECT/CT imaging and biodistribution studies in female athymic nude mice implanted with these tumour xenografts are currently in progress. Supported by a grant from the Ontario Institute for Cancer Research Smarter Imaging Research Platform and a Fellowship from the Canadian Breast Cancer Foundation.

Disclosure of author financial interest or relationships:
**E. Razumienko**, None; **L. Dryden**, None; **R.M. Reilly**, None.

Presentation Number **P668**
Poster Session 4
September 8, 2012 / 14:45-14:45 / Room: The Liffey

# Iodine-125-labeled Au/Au core/shell nanoprobes for tumor-targeted in vivo SPECT/CT imaging

***Won-Kyu Rhim***[1], *Young-Hwa Kim*[2,3], *Minho Kim*[1], *Hyewon Youn*[2,3], *Yun-Sang Lee*[2,3], *Keon Wook Kang*[2,3], *Jwa-Min Nam*[1], [1]*Department of Chemistry, Seoul National University, Seoul, Republic of Korea;* [2]*Department of Nuclear Medicine, Seoul National Universtiy, Seoul, Republic of Korea;* [3]*Institute of Radiation Medicine, Medical Research Center, Seoul, Republic of Korea. Contact e-mail: sellybrown80@snu.ac.kr*

In vivo molecular imaging plays a crucial role in early and accurate diagnosis and therapy of diseases and understanding of biological processes in bodies. Recently, various types of nanoparticles have received great interest for molecular imaging because of their advantageous properties including multifunctionality and multivalency effects. Gold nanoparticle is a good candidate as a imaging probe due to its low cytotoxicity and multifunctionality. Moreover, gold nanoparticles can conjugate biomolecules (e.g. DNA and peptides) and anti-biofouling polymers such as polyethylene glycol (PEG) easily via Au-sulfide bond, and many other functional ligands can also be incorporated simultaneously for preparation of highly stable and specific probes as well as efficient conjugation of targeting ligand. Generally, radioactive isotope can be loaded onto nanoparticle surface using chelating agent inducing small surface area left for other functional ligand conjugation. Herein, we report radioactive iodine-125 directly embedded Au/Au core/shell nanostructure for tumor targeted in vivo SPECT/CT imaging. Radioactive iodine-125 is directly labeled to DNA and PEG conjugated Au core and stably protected by Au shell formation. Without chelating agents, radioactive iodine-125 is well protected in human serum condition which could be good candidate for stable in vivo SPECT/CT imaging agent during blood circulation. High specificity to tumor site is established by dual targeting effect using HER2 affibody and cRGD in one core/shell nano structure simultaneously. Importantly, the SPECT/CT in vivo imaging results show the high uptake of iodine 125 labeled Au/Au core/shell structure in xenografted tumor region. Core-size-dependent in vivo distribution with same surface properties (surface charge, flexibility, etc) can be checked with controlling Au shell thickness.

Disclosure of author financial interest or relationships:
**W. Rhim**, None; **Y. Kim**, None; **M. Kim**, None; **H. Youn**, None; **Y. Lee**, None; **K. Kang**, None; **J. Nam**, None.

Presentation Number **P669**
Poster Session 4
September 8, 2012 / 14:45-14:45 / Room: The Liffey

# Molecular imaging of arthritis in the angiogenic vasculature using a 123I-vascular endothelial growth factor receptor antibody

*Sung-Min Kim[1], Youngkyu Song[1], Min Su Lim[1], Gyunggoo Cho[1], Sang Hoon Lee[2], **Eun Kyoung Ryu**[1], [1]Korea Basic Science Institute, Chungbuk, Republic of Korea; [2]Radiology, University of Ulsan College of Medicine, Asan Medical Center, Seoul, Republic of Korea. Contact e-mail: ekryu@kbsi.re.kr*

Vascular endothelial growth factor (VEGF) and its receptor (VEGFR) have been implicated in the pathogenesis of rheumatoid arthritis, which is angiogenesis dependent. Antibody-based molecular imaging improves targeting, and antibody radiolabeling is useful for monitoring biological events in vivo via PET or SPECT. We investigated the potential of molecular imaging to diagnose arthritis with VEGFR-2 in vivo. The 123I-VEGFR-2 antibody was prepared by the iodogen tube method. The radioligand was injected into arthritic mice, and microSPECT/CT was performed. The arthritic mice were examined by 4.7-T MRI and immunohistochemistry. The 123I-VEGFR-2 antibody showed high uptake in the arthritic region at 1 h post injection on SPECT/CT but no uptake in the control animals after radioligand injection. In MR images, the arthritic tissue of the mice was correlated with regions labeled by the 123I-VEGFR-2 antibody. Immunohistochemical localization showed markedly increased expression of VEGF in the endothelial cells, fibroblasts, and macrophages of the arthritic mice.

Disclosure of author financial interest or relationships:
**S. Kim**, None; **Y. Song**, None; **M. Lim**, None; **G. Cho**, None; **S. Lee**, None; **E. Ryu**, None.

Presentation Number **P670**
Poster Session 4
September 8, 2012 / 14:45-14:45 / Room: The Liffey

# Proof-of-concept automated synthesis and HPLC purification of [18F]fallypride on a prototype digital microfluidic radiosynthesizer

***Gaurav J. Shah***[1,4], *Jack Lei*[1], *Supin Chen*[2], *Pei Yuin Keng*[1], *Chang-Jin Kim*[2,3], *R. Michael van Dam*[1,2], [1]*1Crump Institute for Molecular Imaging and Department of Molecular & Medical Pharmacology, University of California, Los Angeles, Los Angeles, CA, USA;* [2]*Bioengineering Department, University of California, Los Angeles, Los Angeles, CA, USA;* [3]*Mechanical and Aerospace Engineering Dept., University of California, Los Angeles, Los Angeles, CA, USA;* [4]*Sofie Biosciences, Culver City, CA, USA. Contact e-mail: gjs1981@gmail.com*

We report automated radiosynthesis and HPLC purification of [$^{18}$F]fallypride as proof of concept of our prototype radiochemistry platform based on electrowetting-on-dielectric (EWOD) digital microfluidics. Using purely electronic control and no moving parts, reagents in the form of droplets (typically ~1-25 μ L) can be sequentially moved, mixed and reacted at high temperatures on the EWOD micro-reactor to perform radiosynthesis [1]. Proof of concept experiments of radiosynthesis on EWOD chip relied on manual pipetting of reagents to the chip and manual collection of the synthesized product off of the chip. More recently we have developed a technique for reagent loading [3], providing automated and controlled delivery of multiple aqueous and non-aqueous reagents from septum-capped reservoir vials to the chip. We have also demonstrated the automated concentration of [18F]fluoride radioactivity in [$^{18}$O]water from the cyclotron from 100s of μ L to ~20-50 μ L - a volume small enough for delivering most of the activity to the chip [2]. Additionally, for probes that require purification by HPLC, we have developed an injector interface to collect the product from on-chip synthesis and inject it into an HPLC purification system. Using [$^{18}$F]fluoride added to water, we measured that ~82±4% of the liquid from the chip is delivered into the injection loop by our approach. Here we integrate all of the above components into a prototype system and as a proof of concept demonstrate the synthesis of [$^{18}$F]fallypride (a PET tracer that measures dopamine D2/D3 neuroreceptors). We have demonstrated radiosynthesis of [$^{18}$F]fallypride on EWOD chip with repeatable and high fluorination conversion (86±8%, n=5) [4] and we achieve similar results with automated synthesis. Following automated synthesis, the crude product is automatically injected into an analytical-scale HPLC for purification to obtain purified [$^{18}$F]fallypride. The entire system uses inert gas (pressure and vacuum) to transfer liquids through inexpensive wetted components (i.e., tubing, needles and vials) that are well-suited to be part of a disposable cassette model. All fluidic operations on-chip and off-chip are performed remotely through software, reducing time, labor and exposure hazards from chemicals and radiation. All components of the prototype that require radiation shielding - namely the concentrator, reagents cartridge, microfluidic chip and HPLC injector - are highly compact (fit within a 20x15x15cm$^3$ volume) suggesting the feasibility of a benchtop, self-shielded radiosynthesizer.

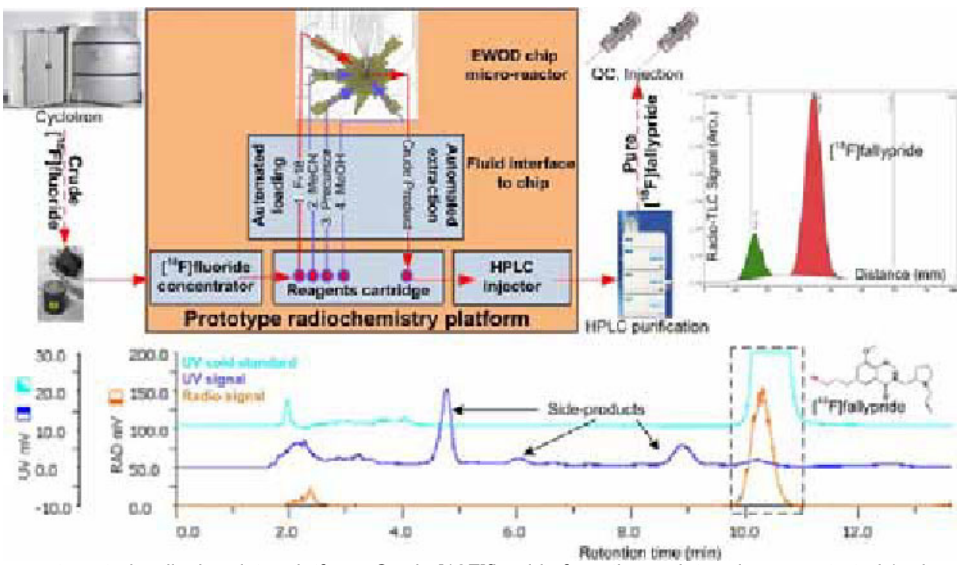


Schematic of the prototype automated radiochemistry platform: Crude [18F]fluoride from the cyclotron is concentrated (red arrow) and delivered to the chip, along with other cold reagents (blue arrows). For [18F]fallypride, azeotropic drying (105 degC) with acetonitrile (MeCN) is performed using concentric ring-heaters on chip. Next, the precursor is added and fluorinated at 100 degC. The crude product is dissolved in methanol (MeOH) and extracted into a vial, from which it is degassed and injected into HPLC for purifcation. The radio-TLC (right) of the crude product indicates good conversion and the HPLC (bottom) shows good separation of pure [18F]fallypride from side-products.

Disclosure of author financial interest or relationships:
**G.J. Shah**, Sofie Biosciences, Employment; **J. Lei**, None; **S. Chen**, None; **P. Keng**, None; **C. Kim**, None; **R. van Dam**, Sofie Biosciences, Inc., Consultant; Sofie Biosciences, Inc., Stockholder .

Presentation Number **P671**
Poster Session 4
September 8, 2012 / 14:45-14:45 / Room: The Liffey

# Heterobivalent ligand targeting GRP and NPY-1 receptors on tumor cells

***Ajay Shrivastava**, Shu-Huei Wang, Natarajan Raju, Izabela Gierach, Michael F. Tweedle, Radiology, The Ohio State University, Columbus, OH, USA. Contact e-mail: Ajay.Shrivastava@osumc.edu*

**Introduction:** Receptor targeting ligands for imaging and therapy of cancer are limited by inter-patient and intra-patient receptor expression heterogeneity. It is often more important to identify local and distant spread of disease than it is to identify a specific receptor presence. In 68 hormone peptide receptor positive human breast cancer tissues, Reubi (EJNM 2002 29:855) found NPY-1 and gastrin releasing peptide (GRP) receptors were present in 66% and 74% of his tumor tissues, respectively, but 93% of the tissues expressed one and/or the other. We describe here the design and development of a new heterobivalent peptide chelating ligand, t-BBN/BVD15-DO3A, for dual-targeting of the GRP and NPY-1 receptors, and validation of its dual binding and radiometal binding capability. Such a probe should be useful in imaging tumors that are GRP and/or NPY receptor positive and should target metallic radionuclides like $^{68}$Ga and $^{177}$Lu to more tumor types than single GRP or NPY receptor-targeted probes. **Synthesis:** Aoa-G-Abz4-QWAVGHLM-$NH_2$ or Aoa-G-Abz4-t-BBN and INP-K[ε-Aoa-(α-DO3A- ε-DGa)-K]-YRLRY-NH2 or [ε-Aoa-(α-DO3A- ε-DGa)-K]-BVD-15 were synthesized using a solid phase peptide synthetic scheme with all reactive groups protected except the Aoa-$NH_2$ group of Aoa-G-Abz4-t-BBN and the DGa-carboxyl group of [ε-Aoa-(α-DO3A- ε-DGa)-K]-BVD-15. Heterobivalent ligand, t-BBN/BVD15-DO3A, was synthesized by coupling the Aoa-$NH_2$ group of Aoa-G-Abz4-t-BBN and the DGa carboxyl group of [ε-Aoa-(α-DO3A- ε-DGa)-K]-BVD-15 followed by de-protection of all reactive groups. All the intermediates and the final ligand were purified using reverse phase HPLC and characterized by NMR and mass spectrometry. $^{177}$Lu(tBBN/BVD15-DO3A) formed readily (conditions: JNM 2006 47:1114) shown by HPLC, verifying that the DO3A chelate was functional. **In vitro analysis:** Competitive displacement binding assays against commercial $^{125}$I-tyr4GRP yielded IC50 = 32 nM for t-BBN/BVD15-DO3A compared to IC50 = 3.7 nM for native GRP in known GRP+ T47D breast cancer cells. A similar assay against commercial $^{125}$I-NPY gave IC50 = 96 nM for tBBN/BVD15-DO3A compared to IC50 = 2.1 nM for native NPY in SK-N-MC cells, a NPY-1+ neuroepithelioma cell line (only Y1 subtype expressed). **Conclusions:** tBBN/BVD15-DO3A is a single DO3A chelate-containing probe that can target both GRP and NPY-1 receptors on tumor cells. **Future plans:** receptor subtype specificity for BBN/BVD15-DO3A will be fully explored and we will study $^{68}$Ga/$^{177}$Lu imaging/theranostics against GRP+ and NPY-1+ breast cancer tumors in mice. We will refine the structure for IC50 values closer to the native peptides. We are also studying probes with up to four hormone peptide analogs. **Abbreviations:** Gastrin-releasing peptide or bombesin (GRP or BBN), a 14-mer; 7-14 truncated GRP or BBN (t-BBN); Neuropeptide Y (NPY), a 35-mer; a truncated nonamer NPY (BVD15); neuropeptide-Y Y1 receptor (NPY-1); Diglycolic acid (DGa), 8-Amino-3,6-dioxaoctanoic acid (Aoa), 4-Aminobenzoic acid (Abz4), 1,4,7,10-Tetraazadodecaundecane-1,4,7,10-tetraacetic acid (DO3A), 1-(4,4-dimethyl-2,6-dioxocyclohex-1-ylidene)-3-methylbutyl (ivDde).

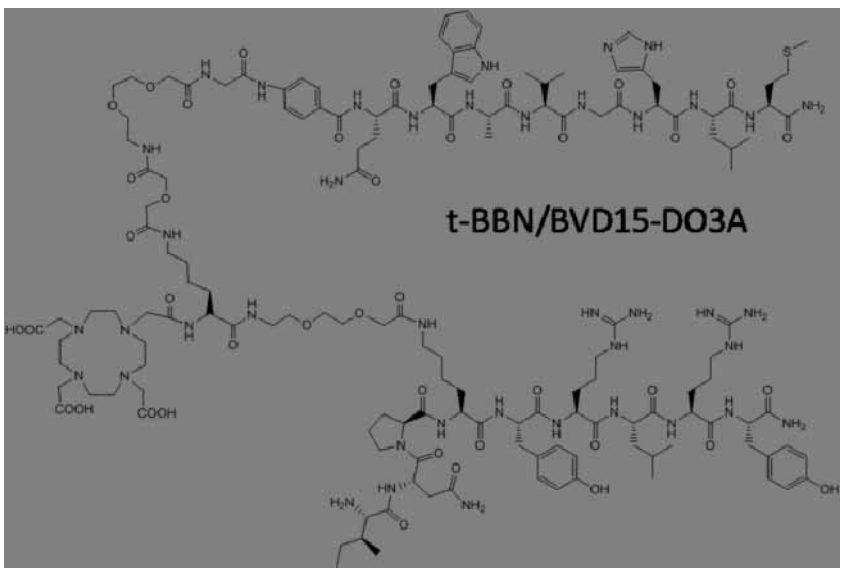


Disclosure of author financial interest or relationships:
**A. Shrivastava**, None; **S. Wang**, None; **N. Raju**, None; **I. Gierach**, None; **M.F. Tweedle**, Enlyton Pharma, Grant/research support; Quanta Biodesign, Grant/research support; Novelos Inc, Stockholder; Regeneron Pharma, Stockholder; J & J Phama, Stockholder; B-M S Pharma, Stockholder .

Presentation Number **P672**
Poster Session 4
September 8, 2012 / 14:45-14:45 / Room: The Liffey

# 64Cu-HSA-aptamer as a targeting agent for Her2 expressing cancer cells

***Myung Geun Song***[1,2], *Hyewon Youn*[1,3], *Mee Young Kim*[6], *Yun-Sang Lee*[1,4], *Jae Min Jeong*[1,4], *Dong Soo Lee*[1,5], *June-Key Chung*[1,2], *Sunjoo Jeong*[6], *Keon Wook Kang*[1,2], [1]*Nuclear medicine, Cancer Research Institute, Seoul, Republic of Korea;* [2]*Tumor biology, Cancer Research Institute, Seoul, Republic of Korea;* [3]*Cancer Imaging Center, Seoul National University Cancer Hospital, Seoul, Republic of Korea;* [4]*Radiation Medicine, Medical Research Center, Seoul, Republic of Korea;* [5]*Molecular Medicine and Biopharmaceutical Science, WCU Graduate School of Convergence Science and Technology, Seoul National University, Seoul, Seoul, Republic of Korea;* [6]*Molecular Biology, Nanosensor and Biotechnology, Seoul, Republic of Korea. Contact e-mail: bororia@hanmail.net*

Purpose: Human epidermal growth factor receptor-2 (Her2) became one of the most important cancer biomarkers. To develop a new imaging probe for targeting Her2 expressing tumor with longer blood circulation time, we designed 64Cu labeled human serum albumins (HSA) with Her2 specific aptamer and evaluated their potential. Methods: Her2-targeting aptamer was selected and FITC-labeled aptamer was used for confocal microscopy. HSA was conjugated with SCN-DOTA and the bifunctional crosslinker Sulfo-SMCC for generating DOTA-HSA. The Her2 aptamer was then covalently conjugated with the HSA, and the resulting bioconjugate DOTA-HSA-aptamer was further radiolabeled with 64CuCl2 in sodium acetate buffer (0.1 N, pH 6.0) at 37 °C for 1 h. Labeling efficiencies of 64Cu-HSA-aptamer were determined by ITLC. 100ug (400uCi/mouse) 64Cu-HSA-aptamer was used to monitor tumor targeting in vivo by PET/CT imaging. Results: FITC-aptamer was clearly detected in Her2 positive cells, but not in negative cells. Labeling efficiency of 64Cu-HSA-aptamer was over 95%. Her2 specific in vitro cellular uptake by 64Cu-HSA-aptamer was 5.97 % at 1 h. Her2 positive tumor cells showed 3-fold higher uptake than it in Her2 negative tumor cells. In mouse model, successful Her2-targeting of 64Cu-HSA-aptamer in Her2 positive tumor was observed by PET/CT, resulting very high tumor uptake (>12% ID/g at 12 h). Conclusion: 64Cu-HSA modified aptamer is a promising probe for molecular imaging. The concept of using HSA as a carrier indicates a broader application in the design of many other radiolabeled probes.

Disclosure of author financial interest or relationships:
**M. Song**, None; **H. Youn**, None; **M. Kim**, None; **Y. Lee**, None; **J. Jeong**, None; **D. Lee**, None; **J. Chung**, None; **S. Jeong**, None; **K. Kang**, None.

Presentation Number **P673**
Poster Session 4
September 8, 2012 / 14:45-14:45 / Room: The Liffey

# Noninvasive Analysis of Transporter-mediated Drug-Drug Interaction in Hepatobiliary Transport: PET Studies using [$^{11}$C]Dehydropravastatin and [$^{11}$C]Telmisartan

***Tadayuki Takashima***[1], *Ryosuke Ijuin*[1], *Yoshinobu Hashizume*[1], *Yumiko Katayama*[1], *Yasuhiro Wada*[1], *Masaaki Suzuki*[1], *Kazuya Maeda*[2], *Yuichi Sugiyama*[3], *Yasuyoshi Watanabe*[1], [1]*Center for Molecular Imaging Science, RIKEN, Kobe, Hyogo, Japan;* [2]*Graduate School of Pharmaceutical Sciences, the University of Tokyo, Tokyo, Japan;* [3]*Sugiyama Laboratory, RIKEN Innovation Center, Research Cluster for Innovation, RIKEN, Yokohama, Japan. Contact e-mail: ttakashima@riken.jp*

It is well known that drug transporters play important roles in intestinal absorption, distribution and excretion of drugs and their metabolites. Clinical studies have shown that variation in multispecific transporter activity caused by drug-drug interactions can affect the variability in therapeutic efficacy and the incidence of adverse effects. In order to evaluate transporter-mediated drug-drug interaction in hepatobiliary transport, separate estimation of the transporter activity in hepatic uptake and canalicular efflux are necessary. We have shown the usefulness of Positron Emission Tomography (PET) for functional analysis of drug transporters in hepatobiliary transport of drugs labeled with positron-emitting radionuclide. In this study, we investigated the effect of co-administered rifampicin on the changes in the hepatobiliary transport of the radioactivity by PET study with [$^{11}$C]dehydropravastatin or [$^{11}$C]telmisartan. Method: We synthesized [$^{11}$C]dehydropravastatin based on the use of palladium(0)-mediated rapid *C*-[$^{11}$C]methylation and also synthesized [$^{11}$C]telmisartan from BIBT9584 methyl ester. Serial abdominal PET scans in rats were performed as well as continuous blood sampling after bolus injection of radiotracer and tissue distribution of its radioactivity was analyzed. In order to investigate the drug-transporter interaction, rifampicin, a typical Oatp inhibitor, was intravenously infused at a rate of 1.5 μmol/min/kg for at least 90 min before the administration of radiotracer and then a constant infusion was kept until the end of the PET scan. Integration plot (Patlak plot) analysis was performed to determine the hepatic uptake clearance and canalicular efflux clearance. Results and discussion: Radioactivity in blood showed that the dose normalized radioactivity was increased in rifampicin-treated condition after administration of each radiotracer. PET image analysis revealed that [$^{11}$C]dehydropravastatin was mainly distributed in liver, and then the radioactivity derived mainly from unchanged form was excreted into the bile in control condition. The treatment of Oatp inhibitor rifampicin decreased not only hepatic uptake clearance of [$^{11}$C]dehydropravastatin but also canalicular efflux of the radioactivity. On the other hand, [$^{11}$C]telmisartan was distributed in liver, metabolized to [$^{11}$C]telmisartan-glucuronide, and then the radioactivity was excreted into the bile in control condition. When rifampicin was treated, hepatic uptake clearance of [$^{11}$C]telmisartan was decreased, whereas canalicular efflux of the radioactivity was not significantly changed. These results showed the different inhibitory effect of rifampicin on the canalicular efflux of each radiotracer can be determined by PET image analysis. Some reports showed that rifampicin also inhibits Mrp2, however, further studies are needed to evaluate the cause of the different inhibitory effect of rifampicin. Conclusion: We demonstrated the utility of PET imaging for the analysis of transporter-mediated drug-drug interaction in hepatobiliary transport.

Disclosure of author financial interest or relationships:
**T. Takashima**, None; **R. Ijuin**, None; **Y. Hashizume**, None; **Y. Katayama**, None; **Y. Wada**, None; **M. Suzuki**, None; **K. Maeda**, None; **Y. Sugiyama**, None; **Y. Watanabe**, None.

Presentation Number **P674**
Poster Session 4
September 8, 2012 / 14:45-14:45 / Room: The Liffey

# Effect of variant histidine tags on kidney and liver uptake of Cu-64-NOTA anti-ALCAM scFv dimers

***Richard Tavaré**, Felix B. Salazar, Arion Chatziioannou, Anna M. Wu, Crump Institute for Molecular Imaging, UCLA School of Medicine, Los Angeles, CA, USA. Contact e-mail: rtavare@mednet.ucla.edu*

It is widely accepted that bifunctional chelators used for Cu-64 radiometal conjugation to biomolecules for immunoPET can affect their pharmacokinetics and organ uptake due to factors such as charge, stability and hydrophobicity. However, the effect of the purification tags frequently engineered into recombinant proteins, such as the hexahistidine tag, on pharmacokinetics and organ uptake has not been analyzed except for affibodies (1). Here, we have engineered the anti-ALCAM scFv dimer to contain the C-terminal purification tags -HHHHHH, -HEHEHE and -HAHAHA in order to monitor the effect of purification tag and the resulting change in pI on antibody fragment biodistribution. We conjugated these three constructs with S-2-(4-Isothiocyanatobenzyl)-1,4,7-triazacyclononane-1,4,7-triacetic acid (p-SCN-Bn-NOTA) to analyze the effect of purification tag on biodistribution when radiolabeled with Cu-64-NOTA. The ALCAM-HHHHHH construct can be readily purified in one step using NiNTA affinity chromatography with imidazole elution. The ALCAM-HEHEHE and -HAHAHA constructs, however, require a two-step purification process consisting of a NiNTA chromatography with pH elution followed by size exclusion chromatography. Once purified, the proteins were conjugated using p-SCN-Bn-NOTA and subsequently radiolabeled with Cu-64. The radiolabeled NOTA-ALCAM-HHHHHH, -HEHEHE and -HAHAHA immunoreactivities were 72%, 73% and 73%, respectively, for the ALCAM expressing LS174T cell. The immunoreactivities to the negative control C6 cell line were 5.1%, 4.6% and 5.2%, respectively. The radiolabeled proteins (~15 microCi) were injected into 10-12 week old male nude mice and PET imaged using the Genisys4 system at 1, 4 and 20 hours post-injection. ROI analysis was used to assess uptake in both the liver and the kidneys and revealed distinct differences in biodistribution among the NOTA conjugated proteins. For all three bioconjugates, uptake in the kidney was localized in the cortex. The HHHHHH protein showed the highest early liver uptake and the highest later kidney retention, almost two-fold greater than the other two proteins, over a 20 hour period. The HEHEHE protein showed the lowest early liver and the kidneys uptake but had higher final uptake in the kidney than the HAHAHA bioconjugate at 20 hours post-injection. In conclusion, all three tags could be used for purification by NiNTA affinity chromatography. Furthermore, the nature of the tag had an impact on uptake in the liver and kidney and needs to be considered when developing immunoPET imaging agents. The commonly used HHHHHH tag showed the highest radioactivity accumulation in both the liver and the kidney. References: (1) Tolmachev, V., et al. Bioconjugate Chem. 2010, 21, 2013-2022.

Disclosure of author financial interest or relationships:
**R. Tavaré**, None; **F.B. Salazar**, None; **A. Chatziioannou**, Sofie Biosciences, Other financial or material support; **A.M. Wu**, ImaginAb, Inc., Consultant; ImaginAb, Inc., Stockholder .

Presentation Number **P675**
Poster Session 4
September 8, 2012 / 14:45-14:45 / Room: The Liffey

# A Novel Peptide Sequence for Highly Efficient Site-Specific Radiolabelling of Proteins with $[^{99m}Tc(CO)_3]^+$ and $[^{186/188}Re(CO)_3]^+$

***Jennifer D. Williams***[1], *Margaret S. Cooper*[1], *Florian Kampmeier*[1], *Richard Tavaré*[2], *Greg Mullen*[1], *Phil Blower*[1], [1]*Imaging Sciences & Biomedical Engineering, King's College London, London, United Kingdom;* [2]*Molecular and Medical Pharmacology, Crump Institute for Molecular Imaging, UCLA, Los Angeles, CA, USA. Contact e-mail: jennifer.williams@kcl.ac.uk*

**Introduction:** The ability to site-specifically radiolabel biomolecules for imaging purposes is imperative for the future development of molecular imaging. It is currently challenging due to potential interferences of the radiolabel at the active site and subsequent loss of affinity of the protein for its target. A controlled labelling method is necessary to direct the radiolabel to a chosen site on the biomolecule of interest, and to enhance labelling efficiency and specific activity under mild conditions. For synthetic peptides this challenge has been achieved by introducing amino acid building blocks attached to chelators. However, this approach is not applicable to proteins as they can only be produced recombinantly. We have therefore developed a high-throughput screening methodology suitable for the identification of genetically encoded tags based on amino acid sequences. Such peptide tags will provide a site of unique reactivity to facilitate the specific labelling of biomolecules with a radioisotope of choice. By optimising his-tag like sequences, we have identified a novel and superior amino acid sequence, which we have termed "Jen Tag", CLRRRLAHHHHHH, for radiolabelling with $[^{99m}Tc(CO)_3]^+$ and its anologues $^{186}Re$ and $^{188}Re$. **Method:** Combinatorial peptide libraries were used in a high-throughput screening methodology. Each peptide array contains 384 specifically designed peptide sequences in duplicate, at 4.91pmol per spot. The arrays were incubated with $[^{99m}Tc(CO)_3]^+$ under different conditions and binding of the radioisotope to the peptide sequence was observed on a phosphor imager. A postrate-membrane specific antigen (PMSA) single chain antibody has been engineered to contain the Jen Tag and site-specifically radiolabelled with $[^{99m}Tc(CO)_3]^+$ for applications in the molecular imaging of prostate cancer. **Results:** The combinatorial library has demonstrated its ability to provide an efficient and straightforward method for the identification of novel sequences for coordination to radioisotopes. Optimisation of the labelling conditions for peptide tags with $[^{99m}Tc(CO)_3]^+$ has been achieved using the high-throughput methodology: $[^{99m}Tc(CO)_3]^+$ requires the presence of at least one histidine for coordination; peptide sequences with a high pI show remarkably enhanced radiolabelling efficiencies; the presence of a cysteine is beneficial to the coordination between the his-tag and $[^{99m}Tc(CO)_3]^+$; labelling is best achieved at 37$^o$C, pH 7.4 in a PBS buffer. In comparison to other hexahistidine amino acid sequences recently published, the Jen Tag has demonstrated a significant 8 fold higher radiolabelling efficiency at 15 minutes ($p<0.00001$). In addition, the tag can be used in the manner of a conventional his-tag for the purification of proteins. **Conclusion:** The Jen Tag has the ability to offer a fast and efficient method for the site-specific labelling of any protein and biomolecule of choice with $[^{99m}Tc(CO)_3]^+$. It has the potential to become a potent tool to screen biological activity of recombinant proteins using $^{99m}Tc$ labelling. The high-throughput method can be used to identify sequences suitable for other types of specific modification.

Disclosure of author financial interest or relationships:
**J.D. Williams**, None; **M.S. Cooper**, None; **F. Kampmeier**, None; **R. Tavaré**, None; **G. Mullen**, None; **P. Blower**, None.

Presentation Number **P676**
Poster Session 4
September 8, 2012 / 14:45-14:45 / Room: The Liffey

# Polymeric nanoparticles as OCT contrast agents

***Wael Al Rawashdeh***[1], *Stefan Kray*[2], *Andrij Pich*[3], *Sascha Pargen*[3], *Andreea Balaceanu*[3], *Markus Lenz*[2], *Felix Spöler*[2], *Fabian Kiessling*[1], *Wiltrud Lederle*[1], [1]*Experimental Molecular Imaging (ExMI), RWTH Aachen University Clinic, Aachen, Germany;* [2]*Institute for Semiconductor Electronics, RWTH Aachen University, Aachen, Germany;* [3]*Interactive Material Research (DWI), RWTH Aachen University, Aachen, Germany. Contact e-mail: walrawashdeh@ukaachen.de*

Introduction: Optical coherence tomography (OCT) offers a high spatial and axial resolution and has a growing importance in clinical use, primarily in dermatology and ophthalmology, including tumor diagnosis. However in highly scattering tissue like skin, the discrimination of smaller blood vessels from other structures can be problematic, strongly suggesting the use of exogenous contrast agents. Although most of the OCT contrast agents are metal-based, polymeric particles with their nano-size, biocompatibility and flexibility are interesting candidates. Here, the optical properties of two different polymeric particles were compared with respect to their potential use as OCT contrast agents. Methods: OCT was performed at 800 nm (axial resolution: 2.6 µm). Two different polymeric particles were tested in different sizes: polystyrene spheres (PS at 300 nm and 150 nm) and nanogels (NG at 300 nm and 200 nm). Their OCT backscattering signals were assessed in a vessel-mimicking highly scattering agar/TiO2 phantom at different concentrations based on either number of particles or weight percent. Signal intensities were quantified using ImageJ by averaging at least 20 images at different transversal positions of either the sample or the gel. An unpaired (two-tailed) Student`s t test was applied for data analysis. Additionally, the particles with the best contrast were tested ex vivo on chicken breast and tested in vivo by i.v. injection (100µl) into the tail vein of nude mice. Results: In vitro, larger particles and higher particle concentrations produced higher OCT signals. At each concentration tested, a markedly higher contrast was achieved by PS particles than NG particles. PS particles generated a markedly higher OCT contrast than the phantom at concentrations of at least 3*1011 particles/mL or 0.4% (w/v) for PS 150 nm and at least 1*1010 or 0.1% (w/v) for PS 300 nm. The contrast generated by NG 300 nm was above the phantom contrast at concentrations of at least 3*1011 particles/mL or 1% (w/v), whereas NG 200 nm only generated a higher contrast than the phantom at 4% (w/v). At any given weight percent, the differences in OCT contrast between differently sized particles were much less evident than in the comparison based on particle number. PS 300 nm of 4% (w/v) generated also a good contrast ex-vivo on chicken breast as well as in vivo. These results strongly suggest that PS spheres have strong potential as intravascular OCT contrast agent, while NG particles need further contrast enhancer for being used as OCT contrast agent. Conclusions: Both, the amount of material and the particle composition and size, play major roles in generating the OCT contrast. Whereas NG are not suitable as sole contrast agents, but rather need some modifications to enhance their scattering properties, PS spheres have strong potential as intravascular OCT contrast agent, especially the 300 nm particles. Acknowledgements: The work was supported by the German center for interdisciplinary clinical research IZKF and by High Tech NRW (ForSaTum).

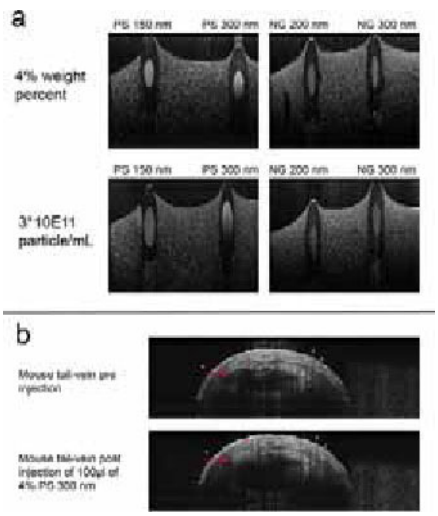


Fig. 1 a: Comparison of the OCT contrast between differently sized PS and NG particles, examples shown for 4% (upper panels) and 3*1011 particles/mL (lower panels). Note the higher contrast achieved by the PS particles. Additionally, larger sized particles generate a higher contrast than the smaller sizes respectively. b: Test of PS 300 nm at 4% as OCT blood-pool agent in vivo. The contrast was monitored after i.v. injection into the tail vein over time. Note the increase in signal intensity in the vein directly after injection of 100µl 4% PS (lower image) compared with the contrast before injection (upper image); arrow marks the vein.

Disclosure of author financial interest or relationships:
**W. Al Rawashdeh**, None; **S. Kray**, None; **A. Pich**, None; **S. Pargen**, None; **A. Balaceanu**, None; **M. Lenz**, None; **F. Spöler**, None; **F. Kiessling**, None; **W. Lederle**, None.

Presentation Number **P677**
Poster Session 4
September 8, 2012 / 14:45-14:45 / Room: The Liffey

# A novel photostable near infrared theranostic dendrimer platform for targeted cancer therapy and therapeutic monitoring

***Mingfeng Bai***[1,2], *Pin Shao*[1], [1]*Radiology, University of Pittsburgh, Pittsburgh, PA, USA;* [2]*University of Pittsburgh Cancer Institute, University of Pittsburgh, Pittsburgh, PA, USA. Contact e-mail: baim@upmc.edu*

The integration of therapeutic and diagnostic treatments has created a new genre in patient care and personalized medicine termed theranostics. Dendrimers provide a superior theranostic platform due to their precisely controlled size, shape, and surface chemistry. These unique properties allow dendrimers to be developed with high structural monodispersity, desired plasma circulation time and biodistribution properties, as well as control over drug release. In addition, targeting moieties can be attached to the surface functional groups of dendrimers to allow targeted drug delivery, and signaling molecules can be attached to monitor drug delivery, release and efficacy. As a low-cost and highly sensitive imaging modality, optical imaging is promising in cancer diagnosis, therapeutic monitoring and intraoperative guidance. Theranostic dendrimers that are suitable for in vivo optical imaging therefore have great potential in cancer treatment. Unfortunately, few such probes have been reported. Therefore, we set out to develop the first photostable near infrared (NIR) theranostic dendrimer platform, which is based on a novel functional quaterrylene dye as the dendrimer core. Such innovative design avoids the photobleaching and self-quenching issues of current NIR dendrimers, thus allowing NIR theranostic studies with longer imaging time, higher fluorescence signal and more accurate quantification. In addition, all the surface functional groups will be available for conjugation to drugs and targeting molecules. Our quaterrylene-based theranostic dendrimer platform has absorption at around 790 nm and emission at around 830 nm, in the most preferred NIR region for in vivo optical imaging. The photostability study showed that our innovative NIR theranostic dendrimer platform has over three orders of magnitude higher photostability than FDA approved NIR fluorescent dye, ICG. In addition, cytotoxicity and cell imaging studies demonstrated that this photostable NIR theranostic dendrimer platform was highly biocompatible. These results indicate that this theranostic platform has great potential to be widely applied in cancer research.

Disclosure of author financial interest or relationships:
**M. Bai**, None; **P. Shao**, None.

Presentation Number **P678**
Poster Session 4
September 8, 2012 / 14:45-14:45 / Room: The Liffey

# Near Infrared Fluorescence Imaging of Type 2 Cannabinoid Receptor Using a Targeted Contrast Agent

***Mingfeng Bai***[1,2], *Michelle Sexton*[3], *Nephi Stella*[3], *Darryl J. Bornhop*[4], [1]*Radiology, University of Pittsburgh, Pittsburgh, PA, USA;* [2]*University of Pittsburgh Cancer Institute, University of Pittsburgh, Pittsburgh, PA, USA;* [3]*Pharmacology, University of Washington, Seattle, WA, USA;* [4]*Chemistry, Vanderbilt University, Nashville, TN, USA. Contact e-mail: baim@upmc.edu*

The type 2 cannabinoid receptor (CB2R) has become an attractive therapeutic target for treating cancers, neurodegenerative diseases, inflammation, pain, osteoporosis, and immunological disorders such as multiple sclerosis. However, CB2R remains largely unexplored and is experiencing "identity crisis". Targeted CB2R imaging is emerging as a new method to explore this receptor and such imaging method may have great impact in many areas, such as non-invasive diagnostic imaging of diseases, high-throughput screening of CB2R to select drugs, quantification of CB2R expression, defining the role of CB2R in modifying disease progression, therapeutic effect monitoring and prognosis evaluation. Currently, CB2R imaging is focused on positron emission tomography (PET) imaging which is sensitive and not limited to tissue penetration. However, PET imaging suffers from relatively low resolution, narrow time window, high cost and injection of radioactive agents. Therefore, it is not suitable for small-scale imaging, especially cells and tissues, and can only be performed with a significant infrastructure. To overcome these problems, we developed a CB2R targeted near infrared (NIR) fluorescence contrast agent, NIR-mbc94, and used this probe to image CB2R in vitro and in vivo. This agent has nanomolar binding affinity (Ki = 260 nM) to the target receptor. To determine the basic subcellular distribution and NIRmbc94's specific binding to CB2 receptors in intact cells in culture, we performed live cell imaging using two cell lines, a mouse malignant astrocytoma cell line, DBT, that lacks endogenous CB2R, and a DBT clone, CB2-mid DBT, that expresses CB2R at endogenous levels. This binding was specific since NIRmbc94 was displaced by the chemically distinctive CB2R ligand WIN55212,2 and the fluorescence signal was absent in wild type DBT cells. In animal studies, NIR-mbc94 specifically labeled CB2R+ tumor, whereas CB2R- tumor showed relatively low fluorescence. Our results indicate that NIR-mbc94 is a promising probe for CB2R targeted imaging and has the potential to study the nature of CB2R and image cancers, neurodegenerative diseases and immunological disorders.

Disclosure of author financial interest or relationships:
**M. Bai**, None; **M. Sexton**, None; **N. Stella**, None; **D.J. Bornhop**, None.

Presentation Number **P679**
Poster Session 4
September 8, 2012 / 14:45-14:45 / Room: The Liffey

# A Nanodiamond is Forever: Functionalizable fluorescent nanodiamonds that do not photobleach or blink for in vitro and in vivo imaging

***Ambika Bumb***[1], *Susanta K. Sarkar*[1], *Martin Brechbiel*[2], *Keir C. Neuman*[1], [1]*Laboratory of Molecular Biophysics, National Heart, Lung, and Blood Institute, Bethesda, MD, USA;* [2]*Radiation Oncology Branch, National Cancer Institute, Bethesda, MD, USA. Contact e-mail: Bumba@mail.nih.gov*

Fluorescent nanodiamonds (FNDs) are biocompatible particles with indefinite photo-stability that makes them superior imaging probes that could replace commonly used optical agents for a wide range of applications. Whereas organic dyes photobleach, quantum dots photoblink and have toxicity concerns, and gold nanoparticles exhibit weak size and shape dependent fluorescence, FNDs do not and additionally are bright with long fluorescence lifetimes (~17ns) that can be used for time-gated imaging with no background signal from tissue autofluorescence (1-2ns). In particular, their near infrared fluorescence makes them ideally suited for in vivo imaging. However, FND use has been limited thus far because of difficulty in functionalizing or coating their inert surface and because of their tendency to aggregate. To overcome the difficulty of direct functionalization, we have coated 20-30 nm nanodiamonds with silica using an innovative liposome-based coating process. This renders the particle surface biocompatible, stable, and easy to perform additional chemistry with. Furthermore, the method self-selects for a desired particle size and produces a monodisperse agent. Having such an optically superior, stable, and functionalizable nanoparticle essentially introduces a new building block to the fields of nanotechnology and nanomedicine, providing for a plethora applications. For instance, silica-coated FNDs can be functionalized for multi-modal imaging with radio-labels and MRI contrast agents and targeted drug delivery with tracking ability. At the single-molecule level, they can be used to track labeled biomolecules over extended periods of time, and due to their wide excitation spectra, we have used them as stable fiducial markers for ultra high resolution microscopy across multiple wavelengths. The energy level structure and electron spin coherence of FNDs also allows for them to have novel applications in ultra-low magnetic field detection, ultra-sensitive NMR, ultra-low power consuming spin-based spintronics, and quantum computing.

Disclosure of author financial interest or relationships:
**A. Bumb**, None; **S.K. Sarkar**, None; **M. Brechbiel**, None; **K.C. Neuman**, None.

Presentation Number **P680**
Poster Session 4
September 8, 2012 / 14:45-14:45 / Room: The Liffey

# Synergistic targeting of integrin $\alpha_v\beta_3$ and matrix metalloproteinase-2

***Jessica Crisp***[1], *Elamprakash N. Savariar*[2], *Heather Glasgow*[3], *Tao Jiang*[2], *Roger Y. Tsien*[2,1], [1]*Chemistry and Biochemistry, University of California San Diego, La Jolla, CA, USA;* [2]*Pharmacology, University of California San Diego, La Jolla, CA, USA;* [3]*Biomedical Sciences, University of California San Diego, La Jolla, CA, USA. Contact e-mail: jlcrisp@ucsd.edu*

Activatable cell penetrating peptides (ACPPs) provide a multimodality strategy for molecular imaging of extracellular protease activities. ACPPs consist of a polycationic cell penetrating peptide (CPP) attached to a polyanionic sequence via a linker region that is a substrate for the enzyme target. The polyanion inhibits the adhesion and uptake of the CPP until the protease cleaves the linker and dissociates the polyanion. The released CPP and its cargo then binds to immediately adjacent cells and is typically endocytosed. For tumor imaging, our main targets have been matrix metalloproteinases (MMP) -2 and -9, which are pivotal in matrix degradation, inflammation, and tumor cell migration, and whose activity is upregulated in most invasive cancers. Although MMP-cleavable ACPPs have successfully imaged tumors by both fluorescence and MRI, their specificity and sensitivity to MMP activity could still be improved. Nature often optimizes substrates by attaching an extra domain that binds to an exosite on the enzyme, thus preconcentrating the substrate near the active site. This report shows that this strategy can improve ACPPs as well. Integrin $\alpha_v\beta_3$ is known to bind to the hemopexin domain of MMP-2 (Brooks et al 1996, Cell 85:683) and is upregulated in many tumors and their vasculature. Cyclic(RGDfK), a popular ligand for $\alpha_v\beta_3$, was chosen as the pre-targeting moiety and was attached to the $(D\text{-glu})_9$ portion of a Cy5-labeled MMP-2 cleavable ACPP so that protease attack would separate $(D\text{-arg})_9$-Cy5 CPP from c(RGDfK)-$(D\text{-glu})_9$. Dissociation of the latter from the $\alpha_v\beta_3$ would allow the integrin-MMP complex to rebind fresh substrate for continued catalytic amplification. Conjugation of c(RGDfK) to the ACPP had no impact on either the cleavage kinetics by pure MMP-2 or the affinity for $\alpha_v\beta_3$ *in vitro*. However, U87MG glioblastoma cells took up the dual targeted peptide to a significantly greater extent than control peptides that crippled each of the targeting mechanisms separately. In these controls, the cleavable linker PLGC(Me)AG was replaced by uncleavable $PEG_6$ or the c(RGDfK) was replaced by c(RADfK). When both these modifications were combined, almost no fluorescence uptake was detectable. Dual targeting was tested *in vivo* in orthotopic xenografts of MDA-MB-231 mammary tumors, imaged 6 hr after intravenous administration of the Cy5 labeled peptides. Tumor contrast was obtained with all of the probes except for the double negative control. The dually targeted probe yielded approximately 3 fold higher tumor:normal tissue fluorescence contrast and 2-3 fold higher standardized uptake value (SUV) than the control peptides with either ACPP cleavage or integrin binding crippled. Cryosections showed that dual targeting improved the ability of the peptide to penetrate to the tumor core. Our interpretation is that pretargeting to $\alpha_v\beta_3$ increases the sensitivity to MMP-2, which adds catalytic amplification beyond simple 1:1 binding to the integrin. Studies are underway that utilize this approach to target monomethyl auristatin E, a potent chemotherapeutic inhibitor of tubulin polymerization.

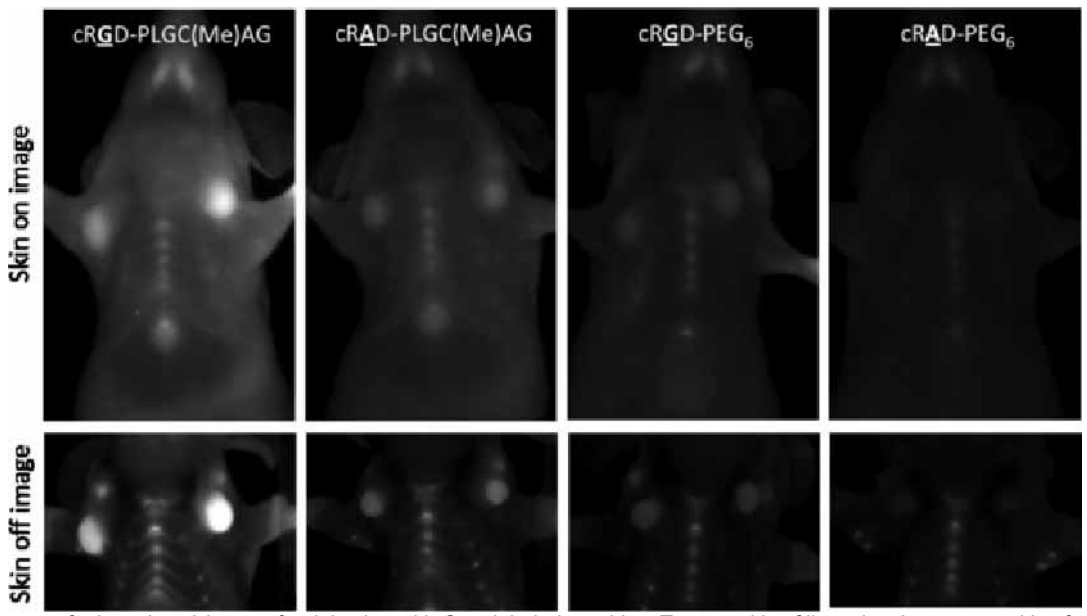


Fluorescent images of mice taken 6 hours after injection with Cy-5 labeled peptides. Top panel is of live mice, bottom panel is after skin removal.

Disclosure of author financial interest or relationships:
**J. Crisp**, None; **E.N. Savariar**, None; **H. Glasgow**, None; **T. Jiang**, None; **R.Y. Tsien**, Avelas Biosciences, Consultant; Avelas Biosciences, Stockholder .

Presentation Number **P681**
Poster Session 4
September 8, 2012 / 14:45-14:45 / Room: The Liffey

# Styrene monomers are responsible for alterations in bioluminescence imaging signal intensity observed after labeling of luciferase-expressing reporter cells with polystyrene-containing MPIOs

***Nathalie De Vocht**, Pieter Van der Veken, Kristien Reekmans, Jelle Praet, Zwi Berneman, Peter Ponsaerts, Annemie van der Linden, University of Antwerp, Wilrijk, Belgium. Contact e-mail: nathalie.devocht@ua.ac.be*

Purpose: We previously demonstrated that labeling of luciferase/eGFP-expressing bone marrow-derived stromal cells (BMSC-luc/eGFP) with Glacial Blue fluorophore-containing micron-sized iron oxide particles (GB MPIOs) allows for quantitative and qualitative multimodal imaging of cellular grafts in the CNS of immune competent mice by means of in vivo bioluminescence imaging (BLI), in vivo magnetic resonance imaging and post-mortem histological analysis (De Vocht et al., Mol Imaging Biol 2011; 13, 1133-1145). In course of these studies, we noted that BMSC-luc/eGFP labeled with GB MPIOs displayed a significantly increased in vitro BLI signal intensity as compared to unlabeled BMSC-luc/eGFP. We described that both the iron component and the fluorophore component of the GB MPIOs were not responsible for the observed increase in BLI signal intensity. In this new study, we aimed to investigate the contribution of the polystyrene-divinylbenzene (PS/DB) component of GB MPIOs to the observed in vitro BLI signal amplification. For this, the effect of PS/DB particles on in vitro BLI signal amplification was investigated using multiple in vitro BLI assays. Procedures: BMSC-Luc/eGFP were labeled with (i) GB MPIOs, (ii) styrene-divinylbenzene copolymer particles (PS/DB), or (iii) styrene monomers in order to evaluate the contribution of PS/DB polymer and styrene monomers to the observed BLI amplification. Following removal of the labeling compound, in vitro BLI signal intensity analysis was performed after addition of the D-luciferin substrate and compared with unlabeled cells. UPLC-MS and 1H-NMR spectroscopy were performed to screen for the presence of styrene in and/or released from GB MPIO and PS/DB particles. Results: An equal increase in BLI signal intensity was observed under all labeling conditions as compared to unlabeled BMSC-Luc/eGFP. Using 1H-NMR spectroscopy and UPLC-MS, we identified styrene monomers directly within GB MPIO and PS/DB containing labeling solutions. Moreover, styrene monomers were also found to be leaching from GB MPIO and PS/DB particles. Conclusions: As an equal effect on BLI amplification was observed for GB MPIO, PS/DB and styrene monomers, and styrene monomers were found to leak out of GB MPIOs, we assume that styrene monomers are most likely responsible for the observed BLI signal amplification following MPIO labeling of BMSC-Luc/eGFP.

Disclosure of author financial interest or relationships:
**N. De Vocht**, None; **P. Van der Veken**, None; **K. Reekmans**, None; **J. Praet**, None; **Z. Berneman**, None; **P. Ponsaerts**, None; **A. van der Linden**, None.

Presentation Number **P682**
Poster Session 4
September 8, 2012 / 14:45-14:45 / Room: The Liffey

# New fluorescent probes for imaging 8-oxoguanine in living cells

***Ye Sun Han***[1]*, Lia Agustina*[1]*, In-Soo Yoon*[1]*, Soo-hyun Hahm*[1]*, Jin Woo Park*[2]*, Jong Joo Na*[2]*,* [1]*Dep. of Adv. Tech. Fusion, Konkuk University, Seoul, Republic of Korea;* [2]*BioActs, DKC Corporation, Seoul, Republic of Korea. Contact e-mail: yshan@konkuk.ac.kr*

Human ribosomal protein S3 (hrpS3) is reported to have high binding affinity to 8-Oxoguanine (8-oxoG) lesion, but lacks the ability to remove and repair the 8-oxoG. 8-oxoG is mainly repaired by Base Excission Repair (BER) pathway in which hOGG1 is the major protein responsible for 8-oxoG removal. HOGG1 initiates pathway by binding to 8-oxoG and creating AP site. Fortunately other protein, hrpS3, has remarkable higher binding affinity for both 8-oxoG and AP sites compared to hOGG1 and APE/Ref-1. Thus, we developed 8-oxoG-detecting imaging probes for in situ detection of 8-oxoG in a single-cell level utilizing specific polypeptide of rpS3 that bind to 8-oxoG. Small peptide has efficient cell and tissue penetration due to the small size, rapid clearance from blood circulation, lower immunogenicity, and lower production cost. Furthermore, peptide is also relatively easy to be chemically modified for coupling to imaging agents or fluorophore. To observe specific region of rpS3 that bind to 8-oxoG, DNA trapping assay with hrpS3 WT and truncated mutants (amino acid 1-85, 1-131, 1-159, 96-131, 96-242, 159-242) were conducted. The rpS3 WT and partial length (96-159) have the ability to bind to 8-oxoG, indicating that the important region for 8-oxoG binding. Thus, we generated specific polypeptide chemically based on hrpS3 sequence and homology study. This polypeptide was directly incorporated with various fluorophores (cy3, cy5, FITC) to make 8-oxoG-detecting imaging probes. 8-oxoG in cells is successfully visualized and quantified by fluorescence microscope. Cells were treated with various H2O2 and observed at different time incubations. The intensities of fluorescence, indicating the presence of 8-oxoG, were increased immediately after exposure to oxidative stress, and the increased intensities returned to basal levels within few hours. The similar results were obtained from different cell lines, indicating that our 8-oxoG-detecting imaging probes can be utilized for different cell lines. Moreover, we also observed the 8-oxoG generated by different chemicals. The sensitivity and specificity of our 8-oxoG-detecting imaging probe were compared with commercially available products. Using 8-oxoG-probe, we observed fluorescent signal with high intensity and better relationship between concentration of chemicals and fluorescence intensities. These results demonstrate that, our 8-oxoG-detecting imaging probes can be used to detect and quantify 8-oxoG in single cells.

Disclosure of author financial interest or relationships:
**Y. Han**, None; **L. Agustina**, None; **I. Yoon**, None; **S. Hahm**, None; **J. Park**, None; **J. Na**, None.

Presentation Number **P683**
Poster Session 4
September 8, 2012 / 14:45-14:45 / Room: The Liffey

# Feasible production of integrin-αvβ3 targeting multi-functional fusion protein

***Mi-hye Hwang***[1], *Byeong-Cheol Ahn*[1], *Jung Eun Kim*[1], *Ho Won Lee*[1], *Sang-Yeob Kim*[2], *Shin Young Jeong*[1], *Sang-Woo Lee*[1], *Jaetae Lee*[1], [1]*Nuclear Medicine, Kyungpook National University School of Medicine/Hospital, Daegu, Republic of Korea;* [2]*Biochemistry and Cell Biology, Cell and Matrix Research Institute, Kyungpook National University School of Medicine, Daegu, Republic of Korea. Contact e-mail: hye6887@nate.com*

Objective: Aim of this study is to establish a bacterial clone which secretes an integrin αvβ3 targeting optical probe containing bioluminescence and fluorescence activities, and to verify its specific targeting function using molecular imaging technique. Methods: We constructed a bacterial expression vector which can produce a fusion protein having secretory gaussia luciferase(sGluc), mCherry and RGD motif (sGluc-mCherry-RGDX3 called GCR) and a control vector which can produce a fusion protein having secretory gaussia luciferase and mCherry only (sGluc-mCherry called GC). Bioluminescent activity of the purified GCR and GC was determined by luciferase assay and IVIS imaging. With bioluminescene assay and confocal microscopy specific binding of GCR to the integrin αvβ3 was evaluated in vitro study with U87MG cells which expressing integrin αvβ3. In vivo specific binding of GCR to the integrin αvβ3 was also tested using tumor xenograft model. Results: The GCR and GC were successfully expressed in the E.coli transduced with the expression vector and the proteins were found in the E.coli themselves and their growth medium as well. Luciferase activity of the growth medium was about 10 fold higher than that of bacterial lysate. The GCR and GC were successfully purified using 6XHis-tag purification technique from E.coli lysate. The GCR showed specific binding affinity to the U87MG cells on confocal microscopy (Fig 1) and IVIS imaging in in vitro study and also demonstrated specific binding to the U87MG tumor xenograft in in vivo study. Conclusions: We established a bacterial clone which secretes specifically αvβ3 targeting optical protein probe containing bioluminescence and fluorescence activities and the probe can be obtained easily and inexpensively. Evaluation of neoangiogenesis in can be performed with the probe in vitro and in vivo studies.

Disclosure of author financial interest or relationships:
**M. Hwang**, None; **B. Ahn**, None; **J. Kim**, None; **H. Lee**, None; **S. Kim**, None; **S. Jeong**, None; **S. Lee**, None; **J. Lee**, None.

Presentation Number **P684**
Poster Session 4
September 8, 2012 / 14:45-14:45 / Room: The Liffey

# In Vivo Molecular Imaging of Retinal Vascular Disease

***Ashwath Jayagopal****, Vanderbilt Eye Institute, Vanderbilt University Medical Center, Nashville, TN, USA. Contact e-mail: ash.jayagopal@vanderbilt.edu*

Molecular imaging strategies for early detection of retinal vascular diseases are needed for improving clinical diagnosis, timeliness of therapeutic intervention, and assessment of therapeutic response. Approaches for molecular imaging of the retina have been limited by a lack of molecularly-targeted imaging agents capable of targeting disease biomarkers in vivo with sufficient sensitivity and safety. To address the need for clinically-relevant retinal molecular imaging agents, hairpin DNA functionalized gold nanoparticles (hAuNP) featuring optical contrast agents and RNA-specific nucleic acid targeting sequences were developed to noninvasively imaging any messenger RNA or microRNA biomarker in the retina. The goal of this study was to evaluate the utility of hAuNP for longitudinal imaging of mRNA and microRNA biomarkers in an animal model of laser-induced choroidal neovascularization (LCNV) which models ocular angiogenesis exhibited in human age related macular degeneration, with the long-term goal of developing imaging agents for clinical detection of subclinical and advanced CNV. hAuNP designed to specifically target the CNV-relevant mRNA biomarkers HIF1α and VEGFR2, as well as the microRNA 23-24-27 family members, were evaluated using in vitro endothelial cell cultures and mouse models of LCNV. Nonspecific control hAuNP and hAuNP targeting housekeeping mRNA transcripts were utilized in parallel as negative controls and normalization of emission signal, respectively. hAuNP were specific for their targets in cell cultures and tissue as evaluated by confocal imaging, in situ FISH analysis, flow cytometry, and spectrophotometry. Specific imaging of RNA biomarkers was achieved in retinal tissue using in vivo retinal fluorescence imaging of LCNV animal models. Intravenous or subretinal administration of hAuNP was not associated with adverse effects on retinal tissue as evaluated by cell proliferation, ERG and TUNEL analysis. hAuNP are promising nanoscale imaging agents which can be utilized in conjunction with clinically-available ophthalmic imaging instrumentation for noninvasive, high sensitivity, and high specificity imaging of RNA disease biomarkers in retinal vascular disease. The nanoparticle is readily amenable for imaging virtually any RNA target in living tissues, and may also be valuable for elucidating molecular mediators of retinal disease in preclinical studies.

Disclosure of author financial interest or relationships:
**A. Jayagopal**, None.

Presentation Number **P685**
Poster Session 4
September 8, 2012 / 14:45-14:45 / Room: The Liffey

# In Vivo Imaging of Bladder Tumor-Targeted Delivery of a Pro-apoptotic Peptide

***HyunKyung Jung***[1,2], *In San Kim*[1,2], *Byung-Heon Lee*[1,2], [1]*biochem and cell biology , school of medicine, KNU, Daegu, Republic of Korea;* [2]*cell and matrix research institute, KNU, Daegu, Republic of Korea. Contact e-mail: shelterfor@naver.com*

Bladder carcinoma is the most common urothelial malignancy in developed countries and the rate of recurrence is pretty high. Using phage display, we have previously identified the Bld-1 peptide with the amino acid sequence of CSNRDARRC that targets bladder tumor cells in vitro and in vivo. To achieve bladder tumor-targeted therapy, we fused Bld-1 with a 14-amino acid amphipathic peptide, KLAKLAKKLAKLAK (KLA), which was known to induce apoptotic cell death. Bld-1-KLA selectively bound to HT-1376 bladder tumor cells and was efficiently internalized into the cells. It exerted its cytotoxic activity by inducing apoptosis of the cells in a dose-dependent manner, while Bld-1 or untargeted KLA alone showed little cytotoxic activity. When injected into HT-1376 bladder tumor-bearing mice, fluorescence dye-labeled Bld-1-KLA homed to tumor more than untargeted KLA alone and inhibited the tumor growth more efficiently than control peptide-fused KLA. No significant side effects on body weights and liver function were observed in the treated mice. These results suggest that Bld-1-KLA is a novel hybrid cytotoxic peptide for targeted therapy of bladder tumor.

Disclosure of author financial interest or relationships:
**H. Jung**, None; **I. Kim**, None; **B. Lee**, None.

Presentation Number **P686**
Poster Session 4
September 8, 2012 / 14:45-14:45 / Room: The Liffey

# A novel fusion protein for highly sensitive multimodal optical imaging

*Laura Mezzanotte, **Eric Kaijzel**, Ivo Que, Clemens Lowik, Leiden University Medical Center, Leiden, Netherlands. Contact e-mail: E.L.Kaijzel@lumc.nl*

Introduction: Fluorescence and bioluminescence imaging have been demonstrated to have different advantages and disadvantages depending on the application. Bioluminescence imaging represents up to now the most sensitive optical technique for tracking cells, study promoter activity or make longitudinal preclinical studies in vivo. Fluorescence imaging using far-red or near-infrared reporter proteins, in order to reduce background emission in living animals, has the advantage of being suitable for both ex vivo and in vivo analysis and translational potential thanks to the availability of very sensitive imaging instruments from live cells to living subjects. Therefore, the design and creation of novel fusion proteins that will combine the advantages of both modalities will allow high-sensitive in vitro and in vivo optical imaging and expand the potential of preclinical imaging. Methods: Firefly luciferase (Luc2) from the pGL4.10 vector (Promega BV) has been cloned in pTurboFP635-N (Evrogen), a mammalian expression vector encoding humanized TurboFP635 and allowing its expression and generation of fusions with the TurboFP635 N-terminus. In the cloning procedure a sequence coding for a 14AA peptide linker has been inserted to generate a coil region between the two proteins. The fusion protein has been named TurboLuc-FP635 and its expression was analysed.in HEK293 cells. Twenty-four hours after transfection with TurboLuc-FP635, optical imaging was performed using an IVIS Spectrum to confirm both bioluminescence and fluorescence expression of the fusion protein. Co-localization of luciferase and fluorescence was confirmed with confocal fluorescence microscopy using an anti-luciferase antibody. Subsequently, HEK293 cells stably expressing TurboLuc-FP635 have been generated by culturing cells with G418. An amount of 5x104 cells have been injected subcutaneously or intravenously in living animal to assess imaging sensitivity. Results: Cells expressing TurboLuc-FP635 or TurboFP635 alone showed no significant differences in fluorescent signal output, meaning that the creation of the fusion protein did not affect fluorescent protein properties. Moreover, after addition of the luciferin substrate to live cells, luciferase emission spectrum remained the same as the original luc2 protein. Imaging of fixed cells confirmed the co-localization of luciferase and TurboFP635. In addition, in vivo imaging results demonstrate the possibility of tracking cells with multimodal optical imaging in superficial and deep tissues (Figure 1). Conclusion: The created fusion protein maintains the characteristics of the original bioluminescent and fluorescent proteins and showed no toxicity when expressed in living cells. Therefore, TurboLuc-FP635 represents a new multimodal probe for high sensitivity in vivo optical imaging.

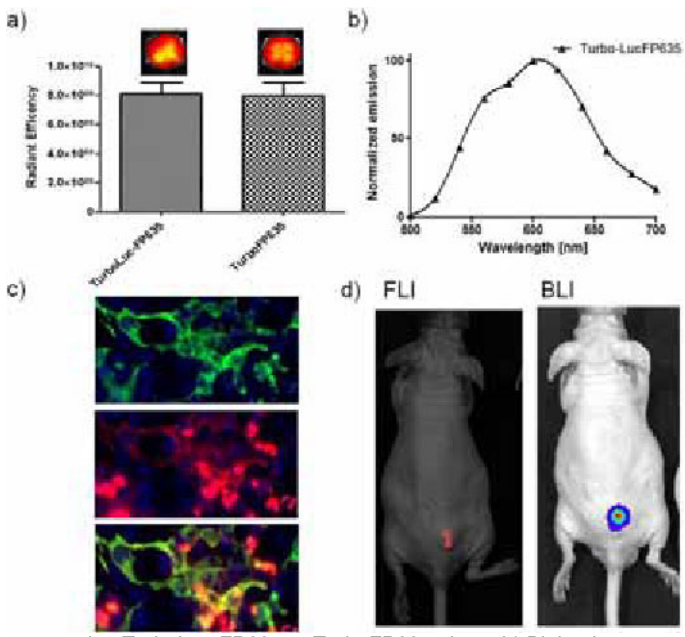


Figure 1 a) Fluorescent signal from cells expressing TurboLuc-FP635 or TurboFP635 alone. b) Bioluminescence emission spectrum of TurboLuc-FP635 in live cells. c)Immunofluorescence of cells using an anti-luciferase primary antibody and a secondary antibody conjugated with FITC. Blue signal represents Dapi, green signal represents FITC and red signal TurboFP635.Colocalization of red and green signal demonstrates the presence of the fusion protein. d) In vivo optical imaging of 50000 stably expressing cells with both fluorescence and bioluminescence modality.

Disclosure of author financial interest or relationships:
**L. Mezzanotte**, None; **E. Kaijzel**, None; **I. Que**, None; **C. Lowik**, None.

Presentation Number **P687**
Poster Session 4
September 8, 2012 / 14:45-14:45 / Room: The Liffey

# PROBE DEVELOPMENT BY DIVERSITY ORIENTED FLUORESCENCE LIBRARY APPROACH (DOFLA) FOR PANCREATIC ISLET IMAGING

***Nam-Young Kang***[1], *Sung-Chan Lee*[1], *Sung-Jin Park*[1], *Seong-Wook Yun*[1], *Yogeswari Chandran*[1], *Young-Tae Chang*[1,2], [1]*Singapore Bioimaging Consortium, Biomedical science institute, Singapore, Singapore;* [2]*chemistry, National University of Singapore, Singapore, Singapore. Contact e-mail: kang_nam_young@sbic.a-star.edu.sg*

Blood glucose level is regulated by insulin and glucagon released from the pancreatic islets of Langerhans. Islet cell death in various pathological conditions disrupts the hormone homeostasis which may lead to a broad range of secondary disorders including hypertension and diabetes. Pancreatic imaging is performed mostly by CT and MRI for diagnosis and prognosis of diseases in pancreas. However, pathological alterations restricted to the islets of Langerhans are still challenging with currently available imaging technology due to the small and heterogeneous size of islets ranging from a few to several thousands of cell clusters. Visualizing alpha and beta cells in pancreas which produce glucagon and insulin, respectively, is particularly important for diabetes research and treatment in the clinic. Considering the central role of islet cells in the development of diabetes, which are the targets for treatment, the development of in situ non-invasive imaging probe is highly required to assess the volume of islets and to examine functional status of the islet cells. Therefore, we have performed high content screening of Diversity Oriented Fluorescence Library (DOFL) in various types of islet cells to discover beta cell specific fluorescent probe. After further optimization for in vivo imaging, we infused it intravenously into the mouse and harvested the pancreas for an examination under a fluorescence microscope. We were able to observe islets specifically stained by our probe in the pancreas tissue sections. DOFL is composed of more than 10,000 intrinsically fluorescent small molecules which were synthesized by combinatorial chemistry in our lab. By high throughput screening of DOFL in various screening platforms, we have previously developed quite a few sensors and imaging probes for biological molecules and system as well as specific cell types. As an expansion from fluorescence-based probe development, DOFL compounds can be modified for deep tissue imaging in preclinical and clinical studies by attaching MRI-, PET- or SPECT-compatible functional groups or single atomic radioisotopes. We envisage that our beta cell probe will be a useful tool for pancreatic islet imaging.

Disclosure of author financial interest or relationships:
**N. Kang**, None; **S. Lee**, None; **S. Park**, None; **S. Yun**, None; **Y. Chandran**, None; **Y. Chang**, None.

Presentation Number **P688**
Poster Session 4
September 8, 2012 / 14:45-14:45 / Room: The Liffey

# Highly Sensitive Fluorescence Turn-On Probe for Glutathione through the Hydrazone to Pyrazole Transformation

***Hae-Jo Kim**, Chemistry, Hankuk University of Foreign Studies, Yongin, Republic of Korea. Contact e-mail: haejkim@hufs.ac.kr*

Alteration of cellular biothiols is implicated in numourous diseases such as cancer and AIDS.[1] Although a number of cell-permeable synthetic probes have been developed for the detection of the biothiols,[2] fluorescent probes to afford both selectivity and sensitivity to biothiols are not common. Herein, we report a highly selective and sensitive fluorescence turn-on probe for GSH through the hydrazone to pyrazole transformation. A nonfluorescent coumarin-hydrazone conjugate probe was transformed into a strongly fluorescent pyrazolyl coumarin through a GSH-mediated cyclization reaction. The probe has shown a highly selective fluorescence turn-on response toward GSH over other amino acids with nanomolar sensitivity. [1] (a) Townsend, D. M.; Tew, K. D.; Tapiero, H.; Biomed. Pharmacother. 2003, 57, 145. (b) Herzenberg, L. A.; De Rosa, S. C.; Dubs, J. G.; Roederer, M.; Anderson, M. T.; Ela, S. W.; Deresinski, S. C.; Herzenberg, L. A. Proc. Natl. Acad. Sci. U.S.A. 1997, 94, 1967. [2] (a) Kantana, Y. Angew. Chem., Int. Ed. Engl. 1977, 16, 137. (b) Wang, W.; Rusin, O.; Xu, X.; Kim, K. K.; Escobedo, J. O.; Fakayode, S. O.; Fletcher, K. A.; Lowry, M.; Schowalter, C. M.; Lawrence, C. M.; Fronczek, F. R.; Warner, I. M.; Strongin, R. M. J. Am. Chem. Soc. 2005, 127, 15949. (c) Stehfest, E.; Torky, A.; Glahn, F.; Foth, H. Arch. Toxicol. 2006, 80, 125. (d) Hong, V.; Kislukhin, A. A.; Finn, M. G. J. Am. Chem. Soc. 2009, 131, 9986. (e) Chen, X.; Zhou, Y.; Peng, X.; Yoon, J. Chem. Soc. Rev. 2010, 39, 2120.

Disclosure of author financial interest or relationships:
**H. Kim**, None.

Presentation Number **P689**
Poster Session 4
September 8, 2012 / 14:45-14:45 / Room: The Liffey

# Enhancement of tumor targetability of PEGylated mesoporous silica nanoparticles by size-control for optical tumor imaging

***Hye Lan Kim***[1,2], *Hwan-Jeong Jeong*[1,2], *Dong Wook Kim*[1,2], *Seok Tae Lim*[1,2], *Myung-Hee Sohn*[1,2], *Sang Bong Lee*[1,2], [1]*nuclear medicine, Chonbuk National University Medical School, Jeonju, Republic of Korea;* [2]*Cyclotron research center, Chonbuk National University Hospital, Jeonju, Republic of Korea. Contact e-mail: hihyelan@naver.com*

Purpose : In this study, we developed various size of mesoporous silca nanoparticle (MSN) for tumor optical fluorescence imaging. MSN's accumulation in the tumor tissue was occurred through enhanced permeability and retention (EPR) mechanism. We will focus on the tumor targetability depending on size. Method : MSN were synthesized by a self-assembly method and this surface was covered with amine terminal. Particle size was regulated with NaOH. This MSN was conjugated with hydroxysuccinimidyl-PEG (Mw: 685.71) (MSN-PEG) and then hydroxysuccinimidyl-Cy5.5 (MSN-PEG-Cy5.5). TEM, FT-IR and pore size distribution of MSN-PEG were determined. For in vivo studies, various size of MSN-PEG-Cy5.5s were injected via tail vein into U87MG xenografted mice. Images were acquired until 24 h after post-injection. Results : Size distribution of MSN-PEG-Cy5.5s was from 10 to more than 300 nm (10-30, 150-200, 300). TEM images showed the highly uniform characteristics in terms of both particle size and shape. Also, the XRD pattern exhibited up to three hexagonal characteristic reflection peak (100), (110) and (200) indicating highly ordered mesostructure in MSNs. In vivo optical images showed that MSN-PEG-Cy5.5s with 150 or 200 nm were more highly accumulated in the liver and tumor over time compared with MSN-PEG-Cy5.5s with 10 nm or more than 300 nm. Furthermore ex vivo images of MSN-PEG-Cy5.5s with 150~200 nm were also showed high signal intensity in the tumor tissue than MSN-PEG-Cy5.5s with 10 nm or more than 300 nm. Conclusion : These results suggest that in vivo tumor accumulation of MSN-PEG-Cy5.5s through enhanced permeability and retention (EPR) mechanism was increased with particle size dependently. The design of particle size will be an important factor and so should include a careful consideration of the effect size upon MSN used for therapeutic carrier to delivery an anticancer drug.

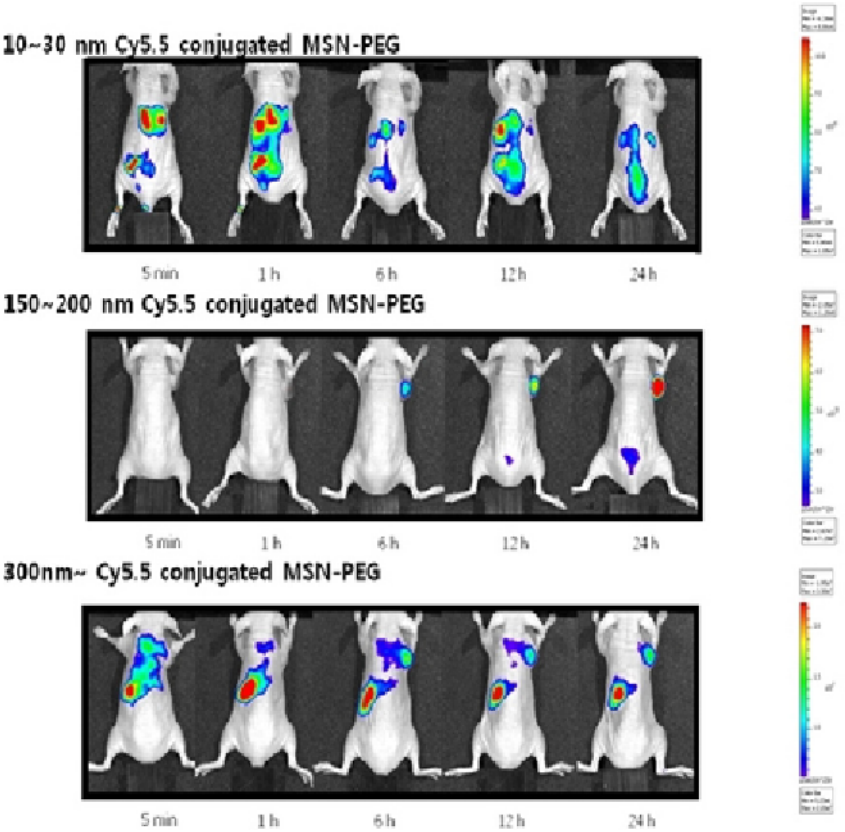


Disclosure of author financial interest or relationships:
**H. Kim**, None; **H. Jeong**, None; **D. Kim**, None; **S. Lim**, None; **M. Sohn**, None; **S. Lee**, None.

Presentation Number **P690**
Poster Session 4
September 8, 2012 / 14:45-14:45 / Room: The Liffey

# Biocompatible Organometallic SERS nanotag for cancer detection

***Kien Voon Kong***[1], *Weng Kee Leong*[2], *Malini Olivo*[1], [1]*Bio Optical Imaging Group, Singapore Bio-Imaging Consortium, Singapore, Singapore;* [2]*Division of Chemistry & Biological Chemistry, Nanyang Technological University, singapore, Singapore. Contact e-mail: KONG_kien_voon@sbic.a-star.edu.sg*

Surface-enhanced Raman spectroscopy (SERS) where Raman signals of molecules could be enhanced by several order magnitude (106 to 1014) on colloidal gold or silver nanoparticles due to the strong surface plasmon resonance of the nanostructured surface has emerged as a promising technique for chemical sensing application. SERS nanotag can be modulated with molecular recognition motifs to render diagnostic tools for optical imaging and therapeutic studies. A major bottleneck in SERS nanotag application is that most of the peaks of commonly used SERS probes are overlapping with biomolecules signals (500 - 1800 cm-1), and thus have a restricted potential for imaging and bio-sensing applications. We developed novel nanoparticles with high CO SERS signal in 2000 cm-1 which is devoid of interference from biomolecules. Biocompatible surface-enhanced Raman scattering (SERS) nanotag constituted by gold colloid and osmium carbonyl clusters, named Os-Au, has been prepared. The osmium carbonyl clusters covalently attach on gold nanoparticles with osmium-gold metal-metal bond. The Os-Au nanoparticles display excellent aqueous dispersibility and storage stability where signal intensity from Os-Au nanoparticles was stable over a period of one month. SERS imaging was performed in cancer cell line using Os-Au nanoparticles conjugated with antibodies recognizing EGFR cancer proteins. We observed that strong SERS signals from EGFR positive cells whereas no signal was measured from EGFR negative cells. The selectivity of EGFR conjugated Os-Au nanoparticles was further proven by dark-field imaging. Both SERS and dark-field imaging studies confirmed the selective binding of antibody conjugated Os-Au nanoparticles to cancer cells over-expressing EGFR.

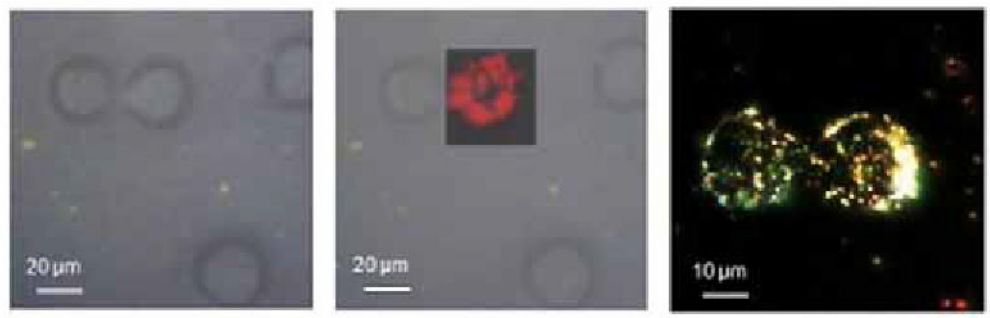


Bright-Field Image | SERS Image (taken at with 2050 cm-1) | Dark-Field Image

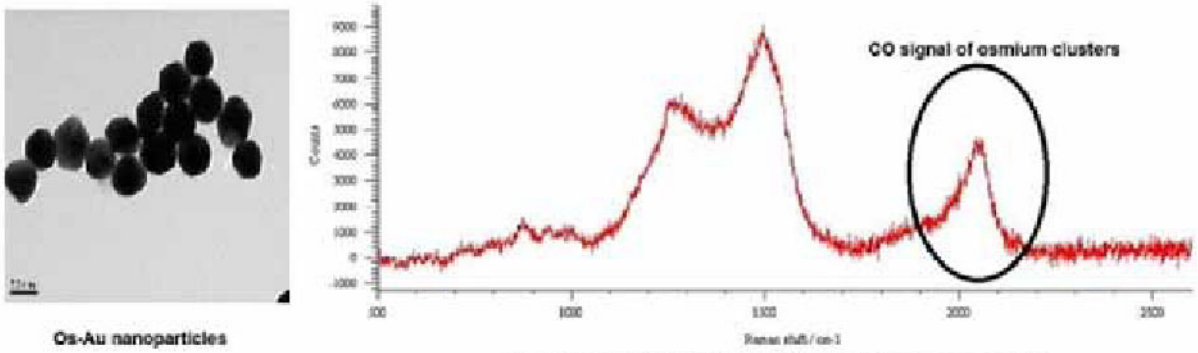


Os-Au nanoparticles

SERS spectra of OSCC cells incubated with Os-Au nanoparticles

Disclosure of author financial interest or relationships:
**K. Kong**, None; **W. Leong**, None; **M. Olivo**, None.

Presentation Number **P691**
Poster Session 4
September 8, 2012 / 14:45-14:45 / Room: The Liffey

# Lifetime imaging of CXCR4 expression using peptide-functionalized luminescent iridium complexes

***Joeri Kuil***[1], *Peter Steunenberg*[2], *Patrick T. Chin*[1], *Aldrik H. Velders*[4], *Fijs van Leeuwen*[1], [1]*Radiology, Leiden University Medical Center, Leiden, Netherlands;* [2]*Laboratory of Organic Chemistry, Wageningen University, Wageningen, Netherlands;* [3]*Cell Biology I, Netherlands Cancer Institute - Antoni van Leeuwenhoek Hospital, Amsterdam, Netherlands;* [4]*BioNanoTechnology, Wageningen University, Wageningen, Netherlands. Contact e-mail: J.Kuil@lumc.nl*

Lifetime imaging is an imaging technique that produces contrast based on differences in luminescence decay rates (lifetime). Standard organic dyes such as fluorescein have generally lifetimes of < 10 ns, which is also the case for autofluorescence generated by cells and tissue. On the other hand, transition metal complexes possess lifetimes of > 100 ns, which makes discrimination from autofluorescence unambiguous. To benefit from these long lifetimes, we have prepared CXCR4-targeted imaging agents outfitted with iridium complexes that have lifetimes of over 200 ns. Chemokine receptor 4 (CXCR4) over-expression is found in diseases such as cancer, where it plays a role in, among others, the metastatic spread [1]. For this reason it is an interesting biomarker for the field of diagnostic oncology, and therefore, it is gaining increasing interest for applications in molecular imaging. The antagonistic Ac-TZ14011 peptide, which binds to CXCR4, has been conjugated to luminescent iridium dyes to allow for CXCR4 visualization. The iridium dyes were functionalized with one, two or three targeting Ac-TZ14011 peptides. Molecular modeling indicated that the iridium label does not substantially interfere with receptor binding (Figure 1A). Confocal microscopy and fluorescence lifetime imaging microscopy (FLIM, Figure 1B) showed that the peptide - iridium complex conjugates can be used to visualize CXCR4 expression in tumor cells. The CXCR4 receptor affinity and specific cell binding of the mono-, di- and trimeric peptide derivatives were assessed using flow cytometry. The three derivatives possessed nanomolar receptor affinity and could also distinguish between cell lines with different CXCR4 expression levels. In conclusion, our peptide - iridium complex conjugates could be used for lifetime imaging of CXCR4 expression [2]. References [1] Furusato, B., Mohamed, A., Uhlen, M., Rhim, J.S., CXCR4 and cancer. Pathol. Int., 2010, 60 (7), 497-505 [2] Kuil, J., Steunenberg, P., Chin, P.T.K., Oldenburg, J., Jalink, K., Velders, A.H., van Leeuwen, F.W.B., Peptide-functionalized luminescent iridium complexes for lifetime imaging of CXCR4 expression. ChemBioChem, 2011, 12 (12), 1897-1903

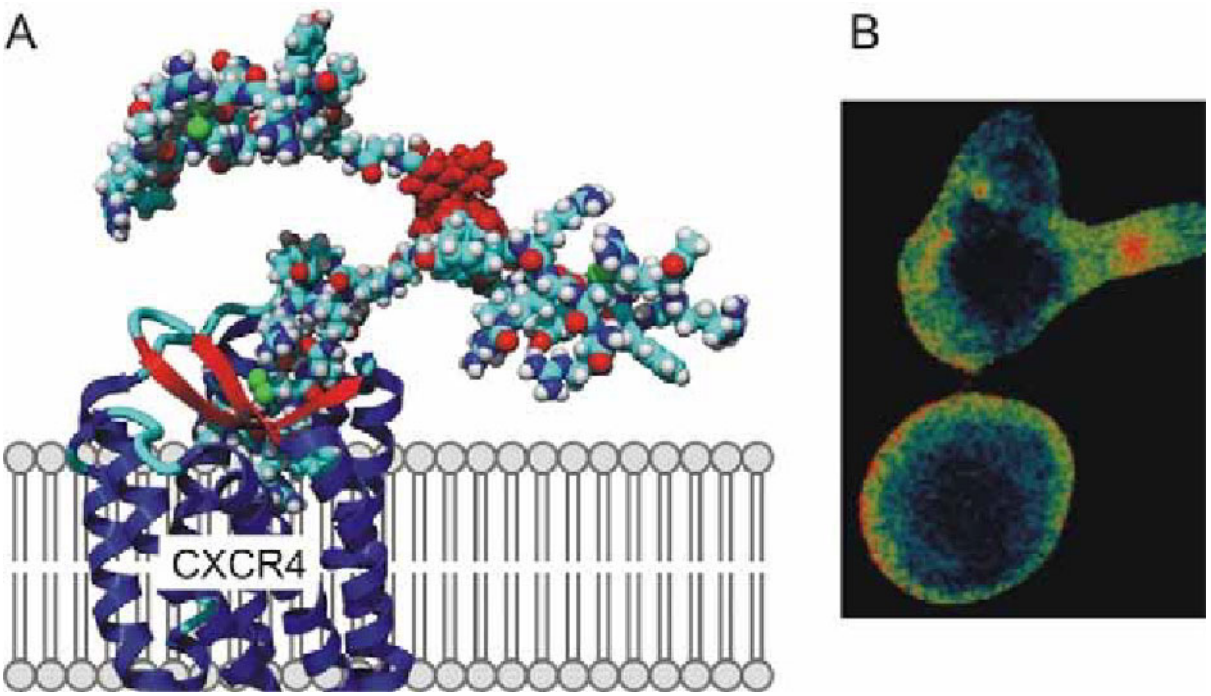


Figure 1. A) Model of the binding of the trimeric peptide - iridium complex conjugate to CXCR4. The iridium complex is depicted in red. B) FLIM picture of CXCR4-expressing cells incubated with monomeric peptide - iridium complex conjugate.

Disclosure of author financial interest or relationships:
**J. Kuil**, None; **P. Steunenberg**, None; **P.T. Chin**, None; **A.H. Velders**, None; **F. van Leeuwen**, None.

Presentation Number **P692**
Poster Session 4
September 8, 2012 / 14:45-14:45 / Room: The Liffey

# Optical Imaging for Evaluating Absorption and Distribution of RITC-Loaded Silica Nanoparticles after Oral Administration

***Chang-Moon Lee**, Su-Jin Cheong, Eun-Mi Kim, Na-Young Choi, Hwan-Seok Jeong, Dong Wook Kim, Hwan-Jeong Jeong, Myung-Hee Sohn, Seok Tae Lim, Department of Nuclear Medicine, Institute for Medical Sciences, Research Institute of Clinical Medicine, Cyclon Research Center, Chonbuk National University Medical School and Hospital, Jeonju, Republic of Korea. Contact e-mail: commy@hanmail.net*

Silicon dioxide (SiO2) nanoparticles (SNPs) are used in widespread applications as additives to drugs, cosmetics, and food. In recent years, as the use of SNPs has been extended to biomedical and biotechnological fields, the potential adverse effect of SNPs on human health and on the environment is of great interest. Molecular imaging techniques can provide the important information to understand and interpret the behavior of SNPs following the exposures. In this study, we investigated the absorption and distribution of SNPs after oral exposures by conducting optical imaging with a focus on the track of their movements at different particle size and surface charge. We used the rhodamine B isothiocynate (RITC)-loaded SNPs (20 nm and 100 nm) to avoid the disassociation of a fluorescent dye from particles via spontaneous or enzyme catalyzed reactions in vivo. The disassociation of RITC from SNPs was evaluated in the simulated gastric fluid (SGF, pH 1.2) for 6 h. To investigate the change of the nanoparticle size and shape in the SGF, SNPs were observed by transmittance electron microscopy (TEM). RITC-loaded SNPs (20 nm or 100 nm / positive or negative charge) were orally administrated in healthy nude mice at dose of 100 mg/kg. Optical imaging studies were performed at 0.5, 1, 2, 4, 6 and 10 h after oral administration. The mice were sacrificed at 2, 6 and 10 h post administration and ex vivo imaging studies were performed. RITC-loaded SNPs were stable in SGF for 6 h without dissociation of RITC from the nanoparticles. There were no change in the particle size and shape of SNPs into SGF. RITC-loaded SNPs flowed in the small intestine from the stomach and gradually moved along the gut during the experimental time. In the ex vivo imaging studies, optical signals were mostly observed in the lung, liver, and kidney. The orally administered SNPS after absorption and systemic circulation were eliminated from the body by urinating. The differences of the behavior between particle size and surface charge were imperceptible. In this study, we demonstrated that the movement of SNPs after oral exposures could be traced by optical imaging. Optical imaging may provide the potential help for the understanding and identifying the behavior and accumulation of SNPs in the body following exposures. Acknowledgments:This study was supported by a grant (10182KFDA991) from the Korea Food & Drug Administration in 2010.

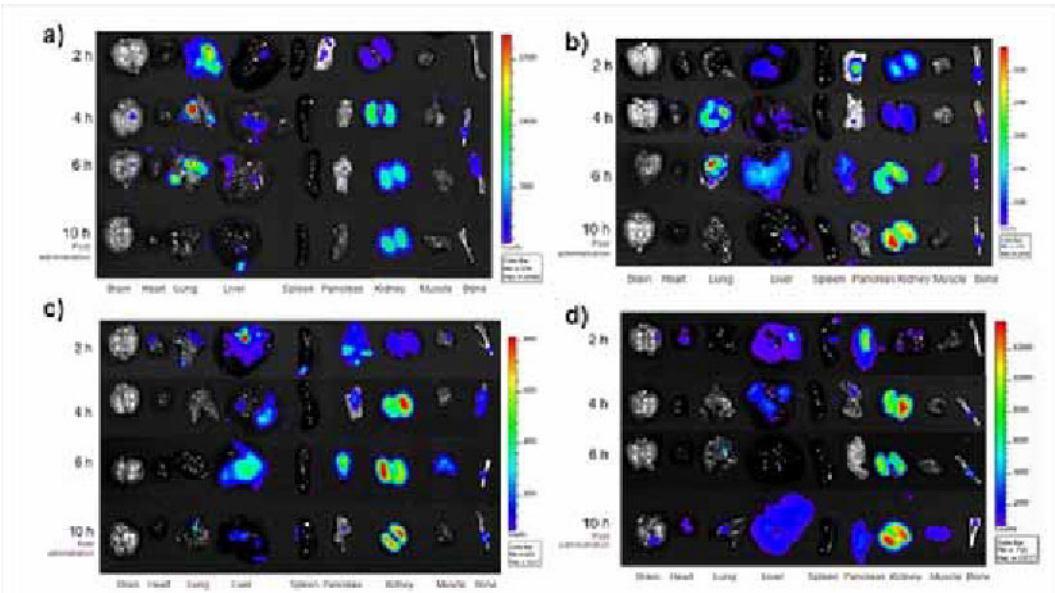


Figure 1. Ex vivo optical images of the major organs (from left to right: brain, heart, lung, liver, spleen, pancreas, kidney, muscle, and bone) of the mice orally administered with (a) 20 nm/positive charged, (b) 20 nm/negative charged, (c) 100 nm/positive charged, and (d) 100 nm/negative charged RITC-loaded SNPs at 2, 4, 6, and 10 h post administration.

Disclosure of author financial interest or relationships:
**C. Lee**, None; **S. Cheong**, None; **E. Kim**, None; **N. Choi**, None; **H. Jeong**, None; **D. Kim**, None; **H. Jeong**, None; **M. Sohn**, None; **S. Lim**, None.

Presentation Number **P693**
Poster Session 4
September 8, 2012 / 14:45-14:45 / Room: The Liffey

# pH-Responsive Near-Infrared Fluorescence Probe Imaging Tumors by Sensing Their Acidic Microenvironment

*Lu Wang, Xiao Zhu, **Cong Li**, School of Pharmacy, Fudan University, Shanghai, China. Contact e-mail: congli@fudan.edu.cn*

Imaging tumors in their early stages is crucial to increase the survival of cancer patients. Currently, most tumor targeting probes image neoplasia by specifically binding the tumor-associated receptors. However, the receptor expression level on a tumor is hardly to predict, which limits their clinical translation. Additionally, the signal of the receptor-targeting probes always stays at a high level, which leads to a strong background noise in normal tissue due to non-specific binding. Therefore, probes with the capability to visualize tumors with high universality and target to background (T/B) signal ratio are desired. Tumor microenvironment characteristics including acidosis and hypoxia are universal phenomena of solid tumors. Therefore, probes that are responsive in the physiologically acidic pH range (4.5-6.9) are promising for imaging tumors with high universality and T/B ratio. In this work, we prepared a pH response NIR fluorescence probe DiIR783-S and a control probe DiIR783-C without pH sensitivity. In these probes, two cyanine based NIR fluorophore IR783 were conjugated via an acid liable hydrazone bond and an acid inert amide bond respectively (Fig. 1A). In aqueous solution, the two bound IR783 form a face to face H-type aggregate and their fluorescence was fully quenched due to the intramolecular electron transfer. In physiologically acidic pH 5.5, which simulates the lysosomal lument of cancer cells, the integrated NIR fluorescence of DiIR783-S increased 10 times in 2.5 h (Fig. 1B). In contrast, its fluorescence barely changed in a neutral pH. Optical images indicated the average fluorescence intensities of DiIR783-S increased significantly with the acidification and incubation time (Fig. 1C). Its maximal fluorescence was measured in pH 5.5 after incubation for 6 h and this value was 15 times higher than that incubated for 10 min at pH 7.4. As expected, no obvious fluorescence enhancments were observed for DiIR783-C during the whole incubation period. In vitro fluorescence microscopic studies demonstrated that DiIR783-S was internalized into the live human breast MDA-MB-435 cells as vesicular structures and their intensities increased remarkably with the incubation time (Fig. 1D). The high colocalization coefficient between DiIR783-S and lysosomal marker indicates that the NIR fluorescence enhancement is resulted from the intracellular delivery of the probe into the acidic lysosome lument. In vivo NIR fluorescence optical imaging indicated the T/B signal ratio of DiIR783-S was much higher than the negative control probe DiIR783-C and positive control probe: IR783 with a same intraveneous injection dose (Fig. 1E). Overall, our preliminary data indicate it is feasible to visualize the tumors by sensing their acidic microenvironment. Due to the high universality and T/B ratio, this pH activatable NIR fluorescence probe is not only promising to track the tumors in their early stage, but also holds the potential to use in the image-guided tumor resection during the surgery.

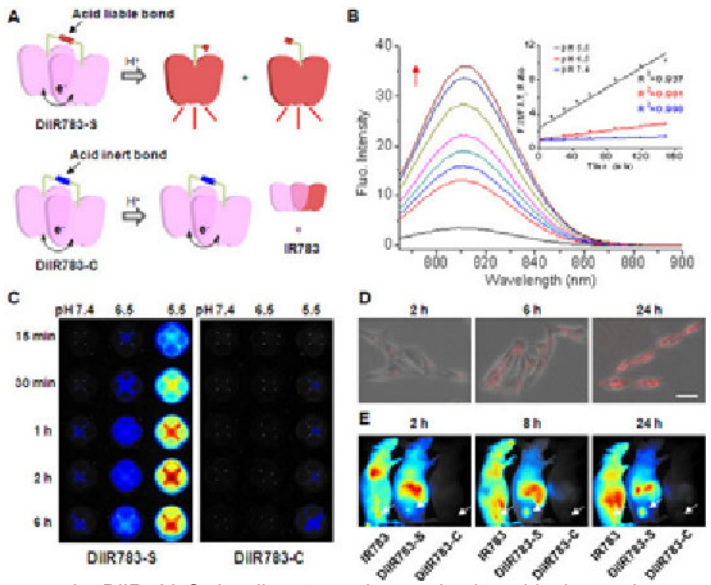


Figure 1. pH activatable NIR fluorescence probe DiIR783-S visualizes tumor by sensing its acid microenvironment. (A) The cleavage of acid liable bond of DiIR783-S in physiologically acidic pH resulted in its remarkable fluorescence enhancement. (B) Emission spectra of DiIR783-S as a function of time in pH 5.5 (excited at 780 nm). Inset: time course of integrated fluorescence intensities at pH 7.4 (blue), 6.5 (red) and 5.5 (black). (C) Time-dependent NIR fluorescence images of 1.0 μM DiIR783-S and DiIR783-C in pH 7.4, 6.5 and 5.5. (D) The lysosomal delivery of DiIR783-S led its time-dependent fluorecence enhancement in human breast MDA-MB-435 cell cultures. (E) DiIR783-S demonstrated higher T/B ratio than IR783 and control probe DiIR783-C after intraveneous injection into the mice bearing human breast carcinoma MDA-MB-431 tumor xenograft in vivo. Arrows point to the tumors.

Disclosure of author financial interest or relationships:
**L. Wang**, None; **X. Zhu**, None; **C. Li**, None.

Presentation Number **P694**
Poster Session 4
September 8, 2012 / 14:45-14:45 / Room: The Liffey

# pH Activatable Near-Infrared Fluorescence Nanoprobe Visualizing Pulmonary Metastasis by Sensing Their Acidic Microenvironment

*Zhan Si[1], Xihui Gao[1], Xunbin Wei[2], **Cong Li**[1], [1]School of Pharmacy, Fudan University, Shanghai, China; [2]Med-X Research Institute and School of Biomedical Engineering, Shanghai Jiao Tong University, Shanghai, China. Contact e-mail: congli@fudan.edu.cn*

Metastases are the cause of 90% of human cancer deaths. The abilities of cancer cells to invade, metastasize, form distant colonies and become refractory to treatments are main reasons that confer lethality to cancer patients. Early detection of metastasis is particularly important for staging and selecting treatments. However, the diffused nature and ultra-small volume of metastases limit their diagnosis with high sensitivity and spatial resolution. Near-infrared (NIR) fluorescence imaging shows advantages in tumor imaging and image-guided therapy due to its high sensitivity, high tissue penetration depth and fast-acquisition time. Recently, we developed a "smart" NIR fluorescence nanoprobe that successfully visulized subcutaneous tumor xenograft in vivo. The fluorescence of this nanoprobe is quenched in the normal tissue and can be activated in tumor acidic microenvironment that is a universal characteristic of solid tumors. In this work, we developed a novel nanoprobe NP1 in which multiple copies of NIR fluorophore IR783 were conjugated to dextran via acid liable hydrazone bonds (Fig. 1A). The fluorescence of NP1 increased 5.3 times in physiologically acidic pH 5.5 (Fig. 1B), which can be explained by the cleavage of hydrazone bonds that minimizes the fluorescence quenching effect induced by the self-aggregation of IR783s with spatial proximity. In contrast, less than 50% fluorescence enhancement of NP1 was observed at a neutral pH, which indicates the high pH sensitivity of this nanoprobe and benefits to visualize small volume tumor or metastases with high target to background (T/B) signal. To investigate the feasibility of NP1 to visualize metastases by sensing their acidic microenvironment, pulmonary metastasis models with different developmental stages were established by injection of human breast MDA-MB-231 cells into the nude mice via i.v.. The early, middle and advanced stages of pulmonary metastasis were defined as 30, 60 and 90 days after injection of cancer cells. NP1 successfully visualized metastases at their all developmental stages even though the early stage metastases can not be visible by naked eyes (Fig. 1C). The highest T/B signal ratio of NP1 was found in middle stage metastases with a value of 3.1. Above experimental results were verified by the fluorescence and H&E stained microscopic images of the metastasized pulmonary tissue sections (Fig. 1D) at 24 h post-injection of NP1. The scatteredly distributed metastases at their early stage were found at peri-vascular area and clearly distnguished from the surrounding normal tissues. The middle stage metastases demonstrated the highest T/B ratio, which correlated well with the ex vivo fluorescence imaging result. Overall, our preliminary work indicates it is possible to visualize the small volume metastases by sensing tumor acidic microenvironment. Due to the universality, high T/B ratio, bio-degradable nature of this pH responsive NIR fluorescence nanoprobe, it holds the potential to guide small volume tumor/metastases excision during the surgery.

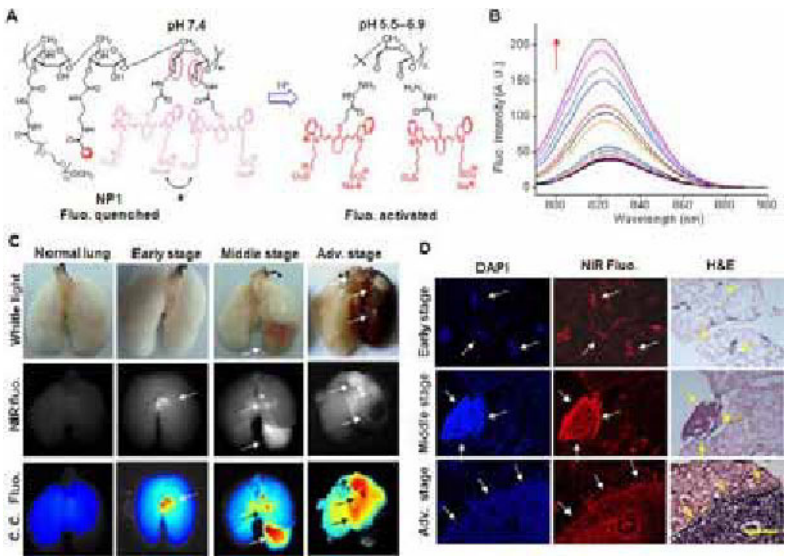


Figure 1. pH activatable NIR fluorescence nanoprobe NP1 visualizes pulmonary metastases by sensing their acid microenvironment. (A) The cleavage of acid liable bonds of NP1 in physiologially acidic pH results in remarkable NIR fluorescence enhancement. (B) Emission spectra of NP1 as a function of time in pH 5.5 (excited at 780 nm). (C) White light, NIR fluorescence and color coded (C. C.) fluorescence images of normal and metastasized lungs at 24 h post-injection of NP1 (0.3 mg/mouse) via i.v.. Arrows point to the metastases. (D) Fluorescence and H&E stained microscopic images of pulmonary metastases at its early, middle and advanced stages. Nucleus stained by DAPI was displayed in blue, NIR fluo. was displayed in red. Arrows point to the metastases. Bar, 200 μm.

Disclosure of author financial interest or relationships:
**Z. Si**, None; **X. Gao**, None; **X. Wei**, None; **C. Li**, None.

Presentation Number **P695**
Poster Session 4
September 8, 2012 / 14:45-14:45 / Room: The Liffey

# An Activatable Near Infrared Fluorescent Probe for In Vivo Imaging of Fibroblast Activation Protein-alpha (FAPα)

***Jinbo Li***[1,2], *Kai Chen*[1], *Hongguang Liu*[1], *Kai Cheng*[1], *Meng Yang*[1], *Jiping Zhang*[3], *Jonathan Cheng*[3], *Zhen Cheng*[1], *Yan Zhang*[2], [1]*Radiology, Stanford University, Stanford, CA, USA;* [2]*School of chemsitry and chemical engineering, Nanjing University, Nanjing, China;* [3]*Medical Oncology, Fox Chase Cancer Center, Philadelphia, PA, USA. Contact e-mail: jinboli@stanford.edu*

Introduction: Fibroblast activation protein-alpha (FAPα) is a cell surface glycoprotein which is selectively expressed on tumor-associated fibroblasts in malignant tumors but rarely on normal tissues. FAPα has been reported to promote tumor growth and invasion and therefore has been considered as a promising target for designing tumor-targeted imaging and therapeutical agents. Although medicinal chemistry studies on FAPα inhibitors have led to the discovery of one FAPα-targeting drug candidate in phase II trial, the development of imaging probes to monitor the expression and activity of FAPα in vivo has lagged behind. Herein we report an activatable near infrared fluorescent (NIRF) probe (represented as ANPFAP) for in vivo optical imaging of FAPα. Methods: ANPFAP consists of a NIR dye (Cy5.5) and a quencher dye (QSY21), which are linked together by a short peptide sequence specific for FAPα cleavage. For in vitro enzymatic assay, ANPFAP was mixed with FAPα, DPPIV or MMP-2 and diluted with phosphate buffered saline (PBS, 0.1 M, pH=7.4) to a final concentration of 10 μM. The assays were performed in triplicate on a 96-well plate and emission spectra of ANPFAP were recorded at 37 0C every 10 minutes on spectrofluorometer for 1 h. For in vivo imaging of FAPα, C6 and U87MG tumor models (n=5 for each group) were selected, which were FAPα negative and positive respectively. ANPFAP (1 nmol in 100 μL) was injected by intravenous (i.v.), and NIRF images were obtained using IVIS200 small animal imaging system at 0.5, 1, 2 and 4 h. Ex vivo biodistribution was performed to confirm in vivo imaging results. Results: In vitro enzymatic assays showed 12 fold of fluorescence recovery was achieved after ANPFAP was incubated with 1 μg/mL of FAPα for 1 h. While no increase of fluorescence was observed when it was mixed with the same amount of DPPIV and MMP-2 or without FAPα. In vivo imaging results showed high contrast of U87MG tumor bearing mice injected with ANPFAP compared to that of C6 tumor bearing mice. The activation and uptake of ANPFAP in U87MG tumor increased fast since 0.5 h and reached maximum at 2 h. At 4 h post injection, tumor to normal tissue ratio increased from 2.22±0.40 to 4.63±0.73. Then, major organs were dissected and imaged, showing that activated ANPFAP mainly located in U87MG tumor but not in C6 tumor. Conclusion: A FAPα specific NIRF probe, ANPFAP, was successfully synthesized and evaluated in vitro and in vivo. In vitro enzymatic assay demonstrates high specificity and sensitivity of ANPFAP toward FAPα. In vivo imaging results indicate ANPFAP is able to discriminate FAPα negative and positive tumors. Also, ex vivo imaging results correlate well with in vivo study. This study provides a new type of FAPα specific NIRF probe that can be used to better understand the roles of FAPα in vitro and in vivo.

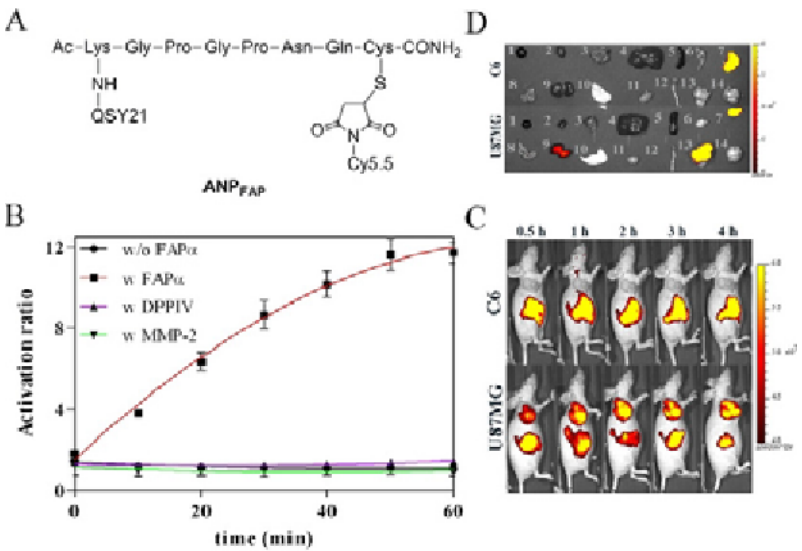


Figure: Evaluation of FAPα specific probe ANPFAP in vitro and in vivo. A) Chemical structure of ANPFAP. B) Enzymatic response of ANPFAP with or without 1 μg/mL of FAPα and with 1 μg/mL of DPPIV or MMP-2. C) In vivo images of ANPFAP in FAPα negative and positive tumor models, C6 and U87MG tumor bearing mice. D) Ex vivo biodistribution of ANPFAP. 1, blood; 2, heart; 3, lung; 4, liver; 5, spleen; 6, pancreas; 7, stomach; 8, intestine; 9, kidney; 10, skin; 11, muscle; 12, bone; 13, tumor; 14, brain.

Disclosure of author financial interest or relationships:
**J. Li**, None; **K. Chen**, None; **H. Liu**, None; **K. Cheng**, None; **M. Yang**, None; **J. Zhang**, None; **J. Cheng**, None; **Z. Cheng**, None; **Y. Zhang**, None.

Presentation Number **P696**
Poster Session 4
September 8, 2012 / 14:45-14:45 / Room: The Liffey

# Development of pH-activatable Fluorescence Probe for Bone-Resorbing Osteoclasts in Living Mice

***Hiroki Maeda***[1], *Toshiyuki Kowada*[2], *Kazuya Kikuchi*[1,2], [1]*Division of Advanced Science and Biotechnology, Graduate School of Engineering, Osaka University, Suita, Japan;* [2]*Immunology Frontier Research Center, Osaka University, Suita, Japan. Contact e-mail: maeda@molpro.mls.eng.osaka-u.ac.jp*

Our bone tissues keep their strength and structure with a proper balance between osteoblastic bone formation and osteoclastic bone resorption. An imbalance of these two cells' activities causes bone diseases such as osteoporosis or osteopetrosis. In practice, X-ray computed tomography or biochemical markers of bone metabolism are currently used as methods to detect the activity of bone-remodeling cells. Although these techniques have information about the cell location or the cell activity change, they cannot combine spatial information with cell activity. The establishment of a method for in vivo real-time detection of a target cell should contribute to immediate diagnosis against diseased sites and development of in vivo drug screening. Two important factors are necessary for visualization of a target cell's activity in vivo. One is OFF/ON switch mechanism of fluorescence that turns on when a target cell become active, the other is specific delivery ability of functionalized probes to a target site. In this point, we focus on the function of osteoclasts, which resorb inorganic components of the bone tissues by proton extrusion. We recognized that active osteoclasts can be selectively detected through specific imaging of low-pH regions by using a pH-activatable probe with specific delivery of the probe using bisphosphonate group. In view of these factors, we designed and synthesized fluorescent probes called "BAp" based on a boron-dipyrromethene (BODIPY) dye. When these probes were administered to mice and monitored by two-photon microscopy (TPM), it was confirmed that the probes were properly delivered to bone tissues and bone-resorbing osteoclast was successfully imaged [1]. However, the long-time observation of osteoclast's dynamics still remains as a challenging problem, since high laser power of TPM might lead to significant photobleaching of the probes. Thus, the probe that would have high photo-stabillity was designed and synthesized. These new methods are first example of in vivo imaging of a low-pH region created by bone-resorbing osteoclasts and we are confident these probes will provide a powerful tool for the selective detection of active osteoclasts. Reference 1. Kowada, T.; Kikuta, J.; Kubo, A.; Ishii, M.; Maeda, H.; Mizukami, S.; Kikuchi, K. *J. Am. Chem. Soc.* 2011, 133, 17772-17776.

Disclosure of author financial interest or relationships:
**H. Maeda**, None; **T. Kowada**, None; **K. Kikuchi**, None.

Presentation Number **P697**
Poster Session 4
September 8, 2012 / 14:45-14:45 / Room: The Liffey

# Characterization of polystyrene nanoparticles containing a novel NIRF dye for imaging applications

***Julia E. Mathejczyk***[1], *Thomas Behnke*[2], *Joanna Napp*[1,3], *Christian Würth*[2], *Robert Brehm*[2], *Frauke Alves*[1,3], *Ute Resch-Genger*[2], [1]*Molecular Biology of Neuronal Signals, Max-Planck-Institute for Experimental Medicine, Göttingen, Germany;* [2]*BAM Federal Institute for Materials Research and Testing, Berlin, Germany;* [3]*Department of Hematology and Oncology, University Medical Center Göttingen, Göttingen, Germany. Contact e-mail: jmathej@gwdg.de*

The early detection and monitoring of pathological changes during the course of a disease requires robust, cost-effective, and efficient tools for medical research that provide the mandatory high sensitivity and specificity. Therefore, the development of novel probes that fulfill these requirements is of considerable interest for imaging of pathological changes in real-time. In this study, we combined a simple and reproducible staining procedure for the preparation of differently sized fluorescent polystyrene nanoparticles (PSNPs) with the novel near-infrared (NIR) fluorophore Itrybe. This hydrophobic dye exhibits very broad absorption and emission bands and a large Stokes shift compared to commonly applied NIR fluorophores and does not display fluorescence quenching even when encapsulated in PSNPs in high concentration. Spectroscopic measurements revealed that Itrybe-loaded 100 nm-sized particles produce a highly amplified optical signal compared to commonly used single NIR fluorophores, such as Alexa Fluor 647 and Cy7. Moreover, the broad absorption and emission spectra of Itrybe incorporated in PSNPs enable excitation and sensitive detection of this probe at different commonly used excitation/emission wavelength combinations in the NIR region in vivo. In order to obtain highly fluorescent probes for the specific detection of tumors, we covalently attached PEGylated Itrybe-loaded PSNPs to the antibody trastuzumab (Herceptin) targeting the human epithelial growth factor receptor 2 (HER2) overexpressed on the cell membrane of various tumor types including 25 to 30 % of all breast cancers. These Herceptin-conjugated 100 nm PSNPs bind specifically to HER2 as demonstrated in immunoassays as well as on HER2-positive KPL-4 breast tumor cells and tumor sections in vitro. In conclusion, Itrybe-loaded NPs have great potential for many different applications ranging from optical imaging to diagnostic assays as they are highly compatible with different fluorescence imaging systems equipped with varying lasers or filters. In addition they provide 3D platforms for surface modifications with many different markers, such as tumor-specific antibodies which may improve the binding probability to targeted tumor cells. As Itrybe-loaded NPs seem to be rapidly internalized in cells, they may also present valuable tools for in vivo labeling of highly endocytotic cells, like macrophages, thereby creating new sensitive probes for imaging of inflammatory diseases.

Disclosure of author financial interest or relationships:
**J.E. Mathejczyk**, None; **T. Behnke**, None; **J. Napp**, None; **C. Würth**, None; **R. Brehm**, None; **F. Alves**, None; **U. Resch-Genger**, None.

Presentation Number **P698**
Poster Session 4
September 8, 2012 / 14:45-14:45 / Room: The Liffey

# A fluorescent conjugate of zoledronate in the ear: cochlear imaging in bisphosphonate drug delivery

*Charles E. McKenna[1], **Shuting Sun**[1], Boris A. Kashemirov[1], Alicia M. Quesnel[2,3], William F. Sewell[2,3], Michael J. McKenna[2,3], [1]Chemistry, University of Southern California, Los Angeles, CA, USA; [2]Otolaryngology, Massachusetts Eye & Ear Infirmary, Boston, MA, USA; [3]Otolaryngology, Harvard Medical School, Boston, MA, USA. Contact e-mail: shutings@usc.edu*

Zoledronate, a nitrogen-containing bisphosphonate (N-BP) is used for treatment of resorptive bone disorders such as osteoporosis as well as in cancer therapy. Zoledronate is currently under consideration as a potential treatment for cochlear otosclerosis, a disorder with a hereditary predisposition that is among the most common causes of acquired hearing loss. The otic capsule is the densest bone in the body, normally does not remodel, and its level of inclusion within the blood-cochlear barrier is poorly understood. Thus zoledronate may not penetrate the bone of the cochlea after systemic administration. A prerequisite for alternative local delivery of zoledronate will be the ability to determine its distribution within the cochlea (Fig. 1A). Both questions are addressed with the aid of a novel imaging method utilizing zoledronate linked to a fluorescent dye. "Magic linker" chemistry [1] makes possible installation of a wide range of fluorophores on heterocyclic N-BPs. The resulting N-BP imaging probes generally retain substantial affinity for bone mineral, reflecting the varying affinities of their parent drug components, depending on the structure of the conjugating fluorescent dye [2]. In this work, 6-carboxyfluorescein linked to zoledronate (6-FAM-ZOL, Fig. 1B) is used to visualize zoledronate distribution in murine cochlea after systemic delivery (i.p.), and also in guinea pig cochlea after local delivery by two methods: a) an osmotic pump via a cochleostomy or b) alginate beads loaded with drug placed on the round window membrane. Systemic delivery produces dose-related deposition of zoledronate in the bone of the inner ear in concentrations comparable to that observed in the femur (Figs. 1C, 1D). The concentration of zoledronate in the otic capsule increased with increasing systemic dose between 1/3 to 10 times the equivalent weight-adjusted dose for humans. The imaging results indicate that cochlear bone behaves similarly to other bones with regard to accumulation of zoledronate, making systemic administration of the drug a possible approach to therapy. Both local delivery methods produce a significant concentration gradient of fluorescent zoledronate within the cochlea, from high levels of fluorescence at the site of delivery in the basal turn to low levels in the apex. Thus, effective local administration will require a sustained release formulation or other strategy to achieve uniform distribution. The synthesis of zoledronate-derived imaging probes and the effect of the imaging moiety on the relative bone mineral affinity of the drug will be discussed (supported by NIH grant R01DC009837). References Cited [1] Kashemirov BA et al. Fluorescently labeled risedronate and related analogues: "magic linker" synthesis. Bioconjug Chem 2008;19:2308-10. [2] Roelofs AJ et al. Influence of bone affinity on the skeletal distribution of fluorescently-labeled bisphosphonates in vivo. J Bone Miner Res 2012;27:835-847.

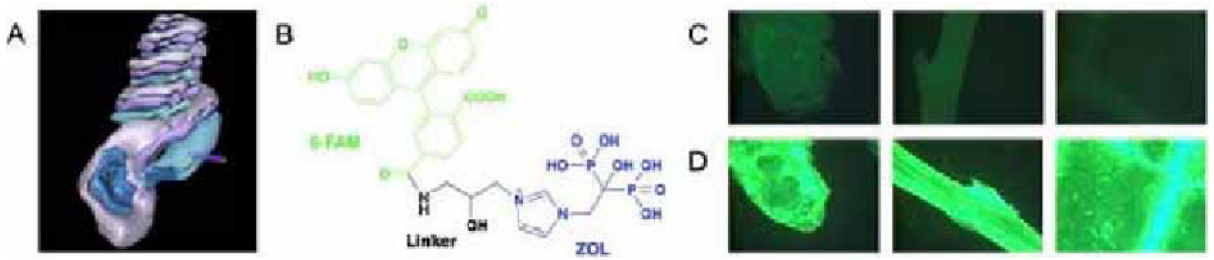


Fig. 1. 3D reconstruction of the guinea pig cochlea showing location of cochleostomy (red dot) in the basal turn of the scala tympani for intracochlear delivery method (A). 6-FAM-ZOL structure (B). Fluorescent images of mouse hemicochlea, tibia and calvarium (left to right) from control (C) and mice systemically injected with 1.8 mg/kg of 6-FAM-ZOL (D).

Disclosure of author financial interest or relationships:
**C.E. McKenna**, None; **S. Sun**, None; **B.A. Kashemirov**, None; **A.M. Quesnel**, None; **W.F. Sewell**, None; **M.J. McKenna**, None.

Presentation Number **P699**
Poster Session 4
September 8, 2012 / 14:45-14:45 / Room: The Liffey

# Cell surface protein labeling with lanthanide complex for multicolor lifetime imaging

***Tatsuya Nakamura***[1], *Shin Mizukami*[1,2], *Kazuya Kikuchi*[1,2], [1]*Department of Material and Life Science, Osaka University, Suita, Japan;* [2]*Immunology Frontier Research Center, Suita, Japan. Contact e-mail: t.nakamura@molpro.mls.eng.osaka-u.ac.jp*

Fluorescence measurements are widely used in life science due to its high sensitivity. In order to visualize localization and behaviors of particular proteins of interest (POIs) in cells, fluorescent proteins are often fused with POIs. These days, fluorescence imaging with organic fluorophores is of particular interest among life scientists because organic fluorophores show excellent properties such as near infrared fluorescence and molecular switch. There are several protein labeling methods for fluorescent organic dyes. Especially, protein- or peptide-tags that interact with the specific ligand have attracted attention to introduce functional molecules into POIs with high specificity. Recently, we constructed BL-tag system utilizing a mutant b-lactamase, which does not exist in mammalian cells and hydrolyzes the b-lactam antibiotics. Meanwhile, the mutant b-lactamase forms a covalent bonding with the b-lactams. By using the mutant protein as a tag protein, which is called BL-tag, we developed a fluorogenic labeling system. Here, we further developed a lanthanide complex-based photoluminescent labeling probe. Luminescent lanthanide complexes have several advantages such as large Stokes' shift, multiple sharp emission peak, and long lifetime photoluminescecne. In particular, time-resolved fluorescence measurement based on the long lifetime property of lanthanide complexes increases detection sensitivity by excluding background autofluorescence from biological samples. In this study, time-resolved fluorescence imaging of a membrane protein was performed on the basis of BL-tag system and the new probe, which consists of a luminescent europium(III) complex and a b-lactam compound. Furthermore, we achieved multicolor imaging by separating short and long lifetime photoluminescence signals. reference S. Mizukami, et al., Angew. Chem. Int. Ed., 2011, 50, 8750-8752

Disclosure of author financial interest or relationships:
**T. Nakamura**, None; **S. Mizukami**, None; **K. Kikuchi**, None.

Presentation Number **P700**
Poster Session 4
September 8, 2012 / 14:45-14:45 / Room: The Liffey

# Near-infrared Emitting Polymer Nanogels for Efficient Sentinel Lymph Node Mapping

*Yong Taik Lim, **Young-Woock Noh**, Min Beum Heo, Hye Sun Park, Graduate School and Department of Analytical Science and Technology, Chungnam National University, Daejeon, Republic of Korea. Contact e-mail: woock@jbnu.ac.kr*

Sentinel lymph node (SLN) mapping have been widely used to predict the metastatic spread of primary tumor to regional lymph nodes in clinical practice. A new near-infrared (NIR) emitting polymer nanoprobes having a hydrodynamic diameter of about 30 nm, which is optimal for lymph node uptake was developed. The polymer nanogel was designed and synthesized by conjugating IRDye800CW organic dye to the pullulan-cholesterol polymer nanogel (NIR-PNG). The nanoprobe was found to be photostable compared with the IRDye800 free dye at room temperature. Upon intradermally injection of the NIR-PNG into the front paw of a mouse, the nanoprobes entered the lymphatics system and migrated to the axillary sentinel lymph node (SLN) within 2 minutes. The NIR fluorescent signal intensity and retention time of NIR-PNG in the lymph node were superior to the corresponding properties of the IRDye800 free dye. A histofluorescence study of the SLN resected under NIR imaging revealed that the NPC nanoprobe was predominantly co-localized with macrophages and dendritic cells. The surgeon quickly identified the position of the SLN with the help of the NIR fluorescence images in large animal system. Taken together, the experimental results demonstrating the enhanced photostability and retention time of the NIR-PNG provide strong evidence for the potential utility of such probes in sentinel lymph node mapping.

Disclosure of author financial interest or relationships:
**Y. Lim**, None; **Y. Noh**, None; **M. Heo**, None; **H. Park**, None.

Presentation Number **P701**
Poster Session 4
September 8, 2012 / 14:45-14:45 / Room: The Liffey

# Development of a novel hypoxia-activatable near-infrared fluorescent probe for tumor hypoxia imaging

***Kensuke Okuda***[1], *Itsuki Kawano*[1], *Tasuku Hirayama*[1], *Bunji Uno*[2], *Tetsuya Kadonosono*[3], *Shinae Kizaka-Kondoh*[3], *Hideko Nagasawa*[1], [1]*Laboratory of Pharmaceutical & Medicinal Chemistry, Gifu Pharmacetuical University, Gifu, Japan;* [2]*Laboratory of Pharmaceutical Analytical Chemistry, Gifu Pharmaceutical Universtiy, Gifu, Japan;* [3]*Department of Biomolecular Engineering, Graduate School of Bioscience and Biotechnology, Tokyo Institute of Technology, Yokohama, Japan. Contact e-mail: okuda@gifu-pu.ac.jp*

The hypoxic status of various solid tumors has been considered to be an indicator of aggressiveness of tumor that correlates with adverse prognosis and can be used to predict the outcome of therapy. Based on these considerations, we have focused on developing hypoxia-activatable near-infrared (NIR) fluorescent probes for noninvasive tumor hypoxia imaging. NIR fluorescence imaging is an emerging field, having advantages such as high spatial resolution, portability, and real-time display compared to other techniques. Previously, we developed a tricarbocyanine-based NIR fluorescent probe for *in vivo* imaging of tumor hypoxia based on hypoxia-selective bioreductive activation and entrapment of 2-nitroimidazole moiety as exogenous hypoxia markers (*Bioconjugate Chem.* **2012**, *22*, 324-329). To achieve better sensitivity for tumor hypoxia, we disclose here development of a hypoxia-selective turn-on fluorescent probe based on a PET (photoinduced electron transfer) mechanism. As a turn-on fluorescence system in hypoxia selectively, we adopted the PET fluorescence quenching effect which could be cancelled by bioreduction in hypoxia. The probes comprised a tricarbocyanine NIR fluorophore and a nitro aromatic moiety as a PET modulator (Figure 1). We performed molecular orbital (MO) calculation based on the density functional theory to predict fluorescence response through bioreductive processes. According to the analysis of the relationship among frontier orbital levels of tricarbocyanine and neighboring electron donor/acceptor moieties, we chose the 1,3-dinitrobenzene structure as an effective PET modulator for switching fluorescence because its frontier orbitals levels could change dramatically upon selective bioreduction in hypoxia to 1,3-diaminobenzene. Our first synthesized candidate, GPU-302 possessing decent fluorescence was converted to the 1,3-diaminobenzene derivative by stannous chloride reduction. This product showed little fluorescence, a change in photophysical property exactly opposite of that desired. We next evaluated substituent effects of tricarbocyanine by MO calculation. From this we designed an upper shift of fluorophore frontier orbitals by introducing methoxy groups onto indolenine 5'-position and synthesized candidate GPU-327. We found that the fluorescence of GPU-327 was very weak because of effective PET quenching and that stannous chloride reduction cancelled this quenching resulting in a 9-fold increase in fluorescence emission. Then, to examine the fluorescence change through biological reduction of GPU-327 under hypoxia, GPU-327 was exposed to A549 tumor cell lysates under hypoxic or normoxic conditions. We observed significantly higher levels of fluorescence in hypoxia than in normoxia. To further assess the potential of GPU-327 for a probe of tumor hypoxia imaging, *in vitro* live cell fluorescence imaging was examined. We observed significantly higher cellular fluorescence with GPU-327 at a concentration of 1.0 μM treated for 12 h under hypoxic condition compared to aerobic condition. We are now evaluating its hypoxia specificity by using *in vivo* fluorescence imaging with xenograft tumor models in mice.

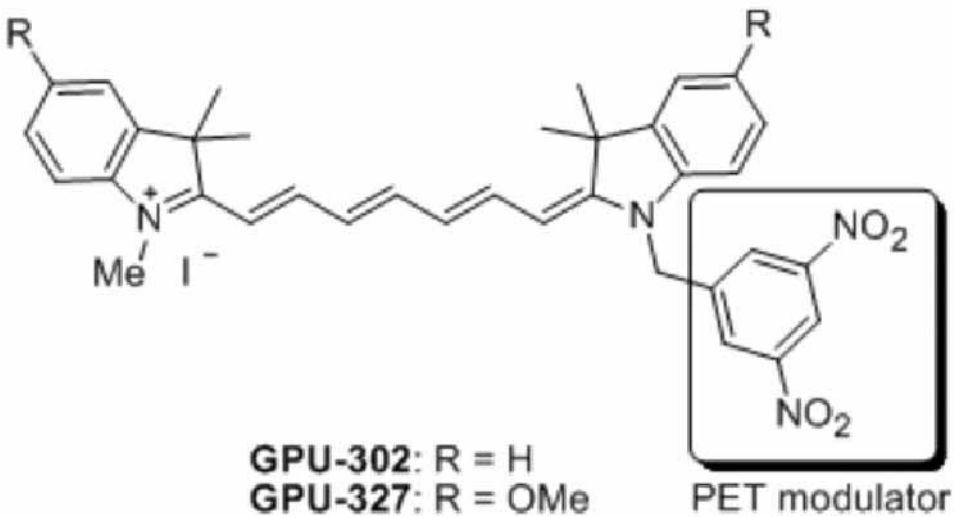


**Figure 1.** Structure of GPU-302 and GPU-327

Disclosure of author financial interest or relationships:
**K. Okuda**, None; **I. Kawano**, None; **T. Hirayama**, None; **B. Uno**, None; **T. Kadonosono**, None; **S. Kizaka-Kondoh**, None; **H. Nagasawa**, None.

Presentation Number **P702**
Poster Session 4
September 8, 2012 / 14:45-14:45 / Room: The Liffey

# in vitro, ex vivo and Non Invasive in vivo fluorescence imaging of Wheat Germ Agglutinin Binding

***Rao V. Papineni***[1], *Scott A. Wellnitz*[2], *Robia G. Pautler*[2], *Daniel Kim*[3], *Steen E. Pedersen*[2], [1]*Carestream Molecular Imaging, Carestream Health, Inc., Woodbridge, CT, USA;* [2]*Molecular Physiology and Biophysics, Baylor College of Medicine, Houston, TX, USA;* [3]*Neurosurgery, Baylor College of Medicine, Houston, TX, USA. Contact e-mail: rao.papineni1@carestreamhealth.com*

Interoperative florescence imaging during image guided surgery requires selective and sensitive molecular probes to distinguish both the target of interest and the nearby vital tissues such as nerves from its inadvertent damage during surgery. Glycans have the potential to be used as a molecular target in the vital organs due to their abundance and they can be specifically detected by lectins. Histochemical screens were used on a panel of fluorescently conjugated lectins to identify potential nerve tissue contrast agents. FITC labeled wheat germ agglutinin (WGA) bound to the Perineurium of nerve sections in vitro, with high specificity, and showed specific binding to certain subsets of nerves in surgically excised sections of mice. WGA binds to N-acetyl-D-glucosamine and sialic acid molecules that are abundant in tissues such as cartilage. We evaluated the potential of using near-infrared (NIR) dye conjugated WGA as an in vivo molecular targeting agent. Non invasive imaging of athymic nude mice was performed using near-infrared (NIR) dye conjugated wheat germ agglutinin (0.1 ml;1mg/ml). We show significant binding of NIR fluorescent WGA at kidneys and the vertebrae. The binding and targeting was confirmed by ex vivo imaging. Lectins like WGA, a general constituent of our diet, have good potential for being a localized florescent contrast agent in image guided surgery and as an in vivo targeting agent.

Disclosure of author financial interest or relationships:
**R.V. Papineni**, Carestream Health Inc, Employment; **S.A. Wellnitz**, None; **R.G. Pautler**, None; **D. Kim**, None; **S.E. Pedersen**, None.

Presentation Number **P703**
Poster Session 4
September 8, 2012 / 14:45-14:45 / Room: The Liffey

# Nanowire-based single-cell endoscopy

***Ji Ho Park***[1], *Ruoxue Yan*[2], *Yeonho Choi*[3], *Luke Lee*[4], *Peidong Yang*[2], [1]*Department of Bio and Brain Engineering, KAIST, Daejeon, Republic of Korea;* [2]*Department of Chemistry, University of California, Berkeley, Berkeley, CA, USA;* [3]*Department of Biomedical Engineering, Korea University, Seoul, Republic of Korea;* [4]*Department of Bioengineering, University of California, Berkeley, Berkeley, CA, USA. Contact e-mail: jihopark@kaist.ac.kr*

One-dimensional smart probes based on nanowires and nanotubes that can safely penetrate the plasma membrane and enter biological cells are potentially useful in high-resolution and high-throughput gene and drug delivery, biosensing and single-cell electrophysiology. However, using such probes for optical communication across the cellular membrane at the subwavelength level remains limited. Here, by combining the advantages of nanowire waveguides and a fibre-optic fluorescence imaging technique, we have designed a novel nanowire-based endoscope system for optical probing inside single cells and the spatiotemporal delivery of payloads into intracellular sites with minimal perturbation to the cellular system. We show that a nanowire waveguide attached to the tapered tip of an optical fiber can guide visible light into intracellular compartments of a living mammalian cell, and can also detect optical signals from subcellular regions with high spatial resolution. The effective optical coupling between the fibre-optics and the nanowire enables highly localized excitation and detection, limiting the probe volume close to the nanowire. The nanowire endoscope is highly flexible and robust, both mechanically and optically, and can endure repeated bending and deformation during a cell-imaging process. Furthermore, we show that through light-activated mechanisms the endoscope can deliver payloads into cells with spatial and temporal specificity. Moreover, insertion of the endoscope into cells and illumination of the guided laser did not induce any significant toxicity in the cells. The endoscope is a promising candidate for high-resolution optical imaging, mapping and chemical/biological sensing, as well as for precision delivery of gene, proteins and drugs.

Disclosure of author financial interest or relationships:
**J. Park**, None; **R. Yan**, None; **Y. Choi**, None; **L. Lee**, None; **P. Yang**, None.

Presentation Number **P704**
Poster Session 4
September 8, 2012 / 14:45-14:45 / Room: The Liffey

# Novel Water-Soluble Quencher Dyes for Activatable Fluorescence Imaging Agents

***Jin Woo Park***[1,2], *Kiwon Kim*[1], *Hyeon Joo Park*[1], *Jong Joo Na*[1], *Namho Kim*[1], *YoungSoo Kim*[2], *Dong Jin Kim*[2], [1]*Department of Biotechnology (BioActs), DKC Corporation, Incheon, Republic of Korea;* [2]*Center for Neuro-Medicine, Brain Science Institute, Korea Institute of Science and Technology, Seoul, Republic of Korea. Contact e-mail: park@bioacts.com*

There has been extensive research on activatable fluorescence imaging agents for use in diagnosis, drug delivery, and post-treatment observation. These imaging agents are generally comprised of a fluorescence agent and a quencher, as used in such cases where the quencher breaks off from the fluorescence agent when it encounters disease-specific molecules such as proteases (MMP, caspase, etc), enabling it to be analyzed through molecular imaging. One of the best known quenchers for implementation in near infrared imaging is the azo-based blackhole quencher, despite its poor solubility and instability in aqueous buffer conditions. In this study, we have attempted to develop a quencher with excellent solubility and stability in water and other aqueous solution, and also a high molar extinction coefficient. In turn, we designed and synthesized a novel green quencher with anthraquinone-based vinylsulfone reactive group. Moreover, in order to assess the absorption of fluorescence at various wavelengths, from visible light to near infrared, sixteen different fluorescent dyes with wavelengths ranging between 500-800 nm were conjugated to MMP-degrading peptide along with a quencher. Protease activity of the peptide complex was observed by introducing MMP, and evaluated the range of fluorescence and quenching. Results indicate that this novel quencher dye shows very high absorbance at 600-800 nm wavelengths, thus enabling implementation with most commercially available near infrared fluorescent dyes.

Disclosure of author financial interest or relationships:
**J. Park**, None; **K. Kim**, None; **H. Park**, None; **J. Na**, None; **N. Kim**, None; **Y. Kim**, None; **D. Kim**, None.

Presentation Number **P705**
Poster Session 4
September 8, 2012 / 14:45-14:45 / Room: The Liffey

# Imaging of Cathepsin K activity in rodent models of bone turnover and soft tissue calcification

*Justin C. Jarrell, Jeff Morin, Kristine Vasquez, Garry J. Cuneo, Sylvie Kossodo,* ***Jeffrey D. Peterson****, PerkinElmer, Boston, MA, USA.*
*Contact e-mail: jeff.peterson@perkinelmer.com*

Cathepsin K (Cat K), a lysosomal cysteine protease with strong collagenolytic activity, is expressed predominantly in osteoclasts, chondrocytes and synovial fibroblasts. Since Cat K is critically involved in bone resorption and collagen degradation, Cat K inhibitors are being evaluated in clinical trials for osteoporosis and the treatment of women with breast cancer and bone metastases. Clearly, a specific imaging agent allowing the detection, quantification and monitoring of Cat K activity in vivo would prove valuable in pre-clinical research. Herein, we report the use of a selective near-infrared (NIR) fluorescent Cat K imaging agent in a variety of in vivo preclinical applications. This agent was developed based on a human Cat K-cleavable sequence, and it is optically quenched in its native form, but becomes highly fluorescent (EX/EM 674/692 nm) upon specific enzymatic cleavage. In arthritis and osteoporosis, osteoclasts are well characterized for their role in escalating bone turnover, leading to either immune-driven bone damage or non-inflammatory bone density decreases, respectively. BALB/c mice with moderately advanced anti-collagen antibody-induced arthritis (CAIA) showed 4-fold increases in Cat K-associated fluorescent signal in arthritic paws as compared to control paws, with predominant distribution of signal within the ankle region. To address non-inflammatory bone resorption, we used two different models of bone loss in the proximal tibia; rat ovariectomy (OVX) and vitamin D-induced bone loss in mice. Female rats were ovariectomized, or sham-ovariectomized, at 3 months of age and imaged on days 1, 9, 16, and 27 with a 750 nm NIR bone-turnover imaging agent (OsteoSense) and the Cat K imaging agent by multiplex imaging. Throughout this time course, there was an apparent and quantifiable 3-fold increase in Cat K activity in the proximal tibias of OVX rats as compared to those of controls. In contrast, OsteoSense, which detects regions of both bone growth and bone loss, showed no clear differences between groups. Both agents, however, detected 2-5-fold increased signal in the proximal tibial regions of mice treated for 4 days with high-doses of vitamin D, supported by the significantly increased plasma levels of calcium in these mice. These two NIR agents also detected 5-8-fold fluorescent increases within the kidneys of treated mice, correlating with both ex vivo imaging of kidneys, fluorescence microscopy of kidney tissue sections, and assays for tissue calcium. Tissue calcification in the aortas of apoE deficient mice on high fat diet for 25 weeks was also explored, showing significant increases in Cat K agent fluorescence measured in living mice by non-invasive FMT imaging. Prophylactic treatment of these mice with ezetimibe blocked fluorescence increases in the aorta to the level of wild-type control mouse aortas, and these results correlated well with ex vivo tissue fluorescence and with staining by Oil Red O. In conclusion, the NIR Cat K activatable imaging agent is a useful tool for investigating both bone resorption and pathologic conditions involving soft tissue calcification.

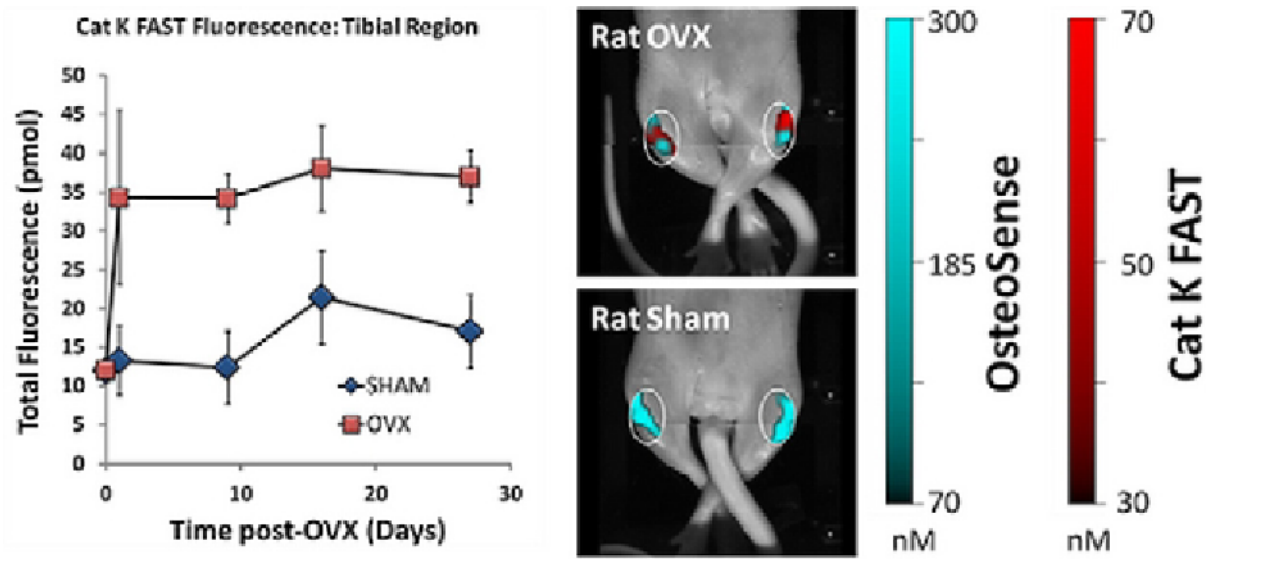


Three month old female Sprague Dawley rats were ovariectomized and bone changes were imaged by FMT using OsteoSense and Cat K FAST imaging agents. Control rats were sham ovariectomized.

Disclosure of author financial interest or relationships:
**J.C. Jarrell**, None; **J. Morin**, Perkin Elmer, Employment; **K. Vasquez**, PerkinElmer, Employment; **G.J. Cuneo**, PerkinElmer Life Sciences, Employment; **S. Kossodo**, PerkinElmer, Employment; **J.D. Peterson**, PerkinElmer, Employment .

Presentation Number **P706**
Poster Session 4
September 8, 2012 / 14:45-14:45 / Room: The Liffey

# Imaging Endogenous Zinc(II) Release From Pancreatic Islets Using A Fluorescent Zinc Sensor

***Sujatha Rochford***[1], *Alana W. Ross*[1], *Sergei Vinogradov*[2], *Anna Moore*[1], [1]*Radiology, A.A. Martinos Center for Biomedical Imaging, Massachusetts General Hospital, Harvard Medical School, Charlestown, MA, USA;* [2]*Biochemistry and Biophysics, University of Pennsylvania, Philadelphia, PA, USA. Contact e-mail: sujatha@nmr.mgh.harvard.edu*

Insulin secreting pancreatic beta cells are severely damaged in type 1 diabetes and their ability to produce insulin is altered in type 2 diabetes. The ability to monitor functional beta cell mass is critical for the early detection of diabetes, monitoring therapy in clinical trials, and following the natural history and pathogenesis of diabetes. Pancreatic islet beta cells contain a substantial amount of chelatable zinc (Zn(II)), which acts as a structural component of insulin packaging and is co-released with insulin upon glucose stimulation. The goal of our study was to synthesize a zinc sensor capable of detecting the released zinc and test it in *in vitro* and *in vivo* animal models of type 1 diabetes. We speculate that the amount of released zinc would correlate with insulin secretion and could serve as a biomarker for functional beta cell mass. To that end, we have developed a robust fluorescent sensor (**BDP-1**) with micromolar affinity ($K_d$ = 5.61 ± 0.66 μM). **BDP-1** is a water-soluble dibenzodipyyromethene, derivatized with Newkome-type dendrimers. It is highly selective for Zn(II) over other biologically relevant metal ions. The free-base dipyrrin scaffold fluoresce very weakly ($\Phi_{fl}$~0.001), while its zinc derivative have intense and narrow absorption in the red/near infrared spectral region and fluoresce strongly ($\Phi_{fl}$~0.5). For detection of endogenous Zn(II), we imaged the excised organs from healthy 6-8 weeks old female BALB/c mice using the following models: mice stimulated with intraperitonial glucose injection followed by **BDP-1** injection (model *E*), mice injected with **BDP-1** only (model *C1*) and mice injected with glucose only (model *C2*). Imaging was performed at $\lambda_{ex}$ = 605 nm and $\lambda_{em}$ = 660 nm. Preliminary results suggest that the excised pancreas from *E* and *C1* models produced significantly higher signal compared to *C2* model (Fig. 1). Fluorescence intensities correlate to insulin levels. Next, we performed similar studies using animals with streptozotocin-induced diabetes. Imaging of excised organs was performed once the animals reached a hypoglycemic state (blood glucose = 23 mg/dL). Injection of **BDP-1** in STZ-induced mice resulted in a strong fluorescence signal from the pancreas reflective of the initial release of insulin upon beta cell destruction. These studies attest to the feasibility of imaging endogenous zinc using dipyrrin scaffolds.

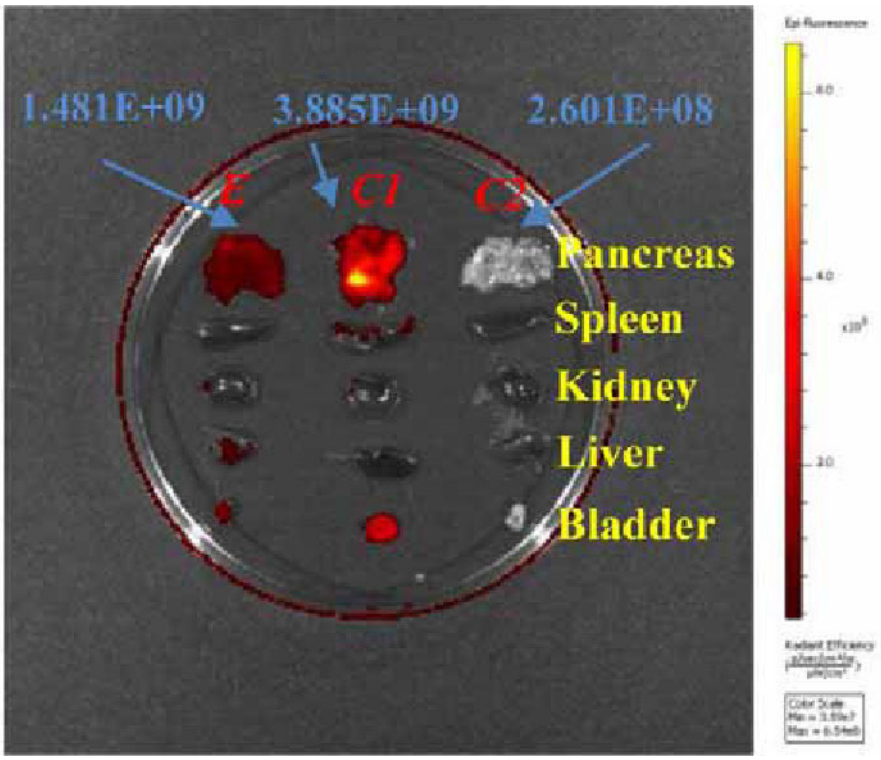


**Figure 1**: Ex vivo image of excised organs of mice models *E* (left), *C1* (middle) and *C2* (right) in a petri dish. For the purpose of clarity, the total radiant efficiency ([p/s] / [μW/cm$^2$]) is given only for pancreas. $\lambda_{ex}$ = 605 nm; $\lambda_{em}$ = 660 nm.

Disclosure of author financial interest or relationships:
**S. Rochford**, None; **A.W. Ross**, None; **S. Vinogradov**, None; **A. Moore**, Fluoropharma, Grant/research support .

Presentation Number **P707**
Poster Session 4
September 8, 2012 / 14:45-14:45 / Room: The Liffey

# Gold Nanorods for Photoacoustic Imaging of Apoptosis and Necrosis

***Anant Shah***[1,3], *Simona Valleggi*[1,3], *David Harris-Birtill*[1], *Nandita M. deSouza*[1,2], *Jeffrey C. Bamber*[1,3], [1]*Joint Department of Physics, Institute of Cancer Research, The Royal Marsden Hospital, Sutton, United Kingdom;* [2]*Radiology, Institute of Cancer Research and Royal Marsden NHS Foundation Trust, Sutton, United Kingdom;* [3]*CRUK-EPSRC Cancer Imaging Centre, London, United Kingdom. Contact e-mail: Anant.Shah@icr.ac.uk*

Introduction All non-surgical cancer treatments kill tumour cells, either by deliberately inducing apoptosis (programmed cell death) or by causing other forms of cell death, such as necrosis. Exposure of phosphatidylserine on the cell membrane, during the early stages of apoptosis, and during necrosis, provides a signal to macrophages for phagocytosis. This has been exploited to fabricate probes designed to detectapoptosis and necrosis, based on a protein, annexin V, which has a high affinity for phosphatidylserine; annexin V has been conjugated with signal emitters for imaging with, for example, fluorescence and radionuclide techniques. Non-invasive image detection of cell death would help facilitate experiments to improve understanding of the biological phenomenon, provide an additional tool for preclinical testing to aid development of new anticancer drugs and provide a clinical tool for early detection of response to treatment. To date, probes to non-invasively detect dying cells using photoacoustic imaging (PAI) have not been developed, despite the advantages of PAI, where high-resolution optical-absorption information can be obtained at relatively large tissue-depth and can be implemented within an ultrasound examination. The technique is potentially low-cost, safely repeatable, and provides soft-tissue detail showing the anatomical context of the molecular information. The objective of this study was to synthesize a probe, functionalized with annexin V, for eventual use in detecting cell death in vivo, using PAI. Gold nanorods were chosen for this purpose because they are excellent PAI contrast agents. Methods Gold nanorods were synthesised using a well-known seed-mediated protocol and coated with carboxylated polyethylene-glycol-thiol (MW 5000). Free carboxylic acid groups on the gold nanorod surface were activated using standard EDC (1-Ethyl-3-[3-dimethylaminopropyl]carbodiimide hydrochloride) / NHS ( N-hydroxyl succinimide) chemistry to form amine-reactive NHS esters, which reacts with the amine groups of the annexin-V protein to form stable amide bonds. To confirm the binding efficiency of functionalised nanorods, human colorectal cancer cells (HCT 116) were treated with an Akt (protein kinase B) inhibitor to induce apoptosis. Cells from treated and control groups were incubated with annexin-V-functionalized gold nanorods and imaged using multi-photon microscopy. Results The mean length and width of the gold nanorods were measured by electron microscopy to be 41±7 nm and 13±4nm respectively, producing an optical absorption peak at a wavelength of 800 nm, as confirmed by UV-visible spectroscopy. Multi-wavelength PAI, confirmed that the nanorods, in suspension, were detected with maximum contrast at this wavelength. Selective binding of functionalised nanorods to apoptopic cells was observed, in comparison to control healthy cells, (Fig. 1). Conclusion Annexin-V-functionalised gold nanorods hold potential for photoacoustic imaging of cell death. Ongoing work aims to determine whether the PAI method can detect dying cells in vitro and in vivo.

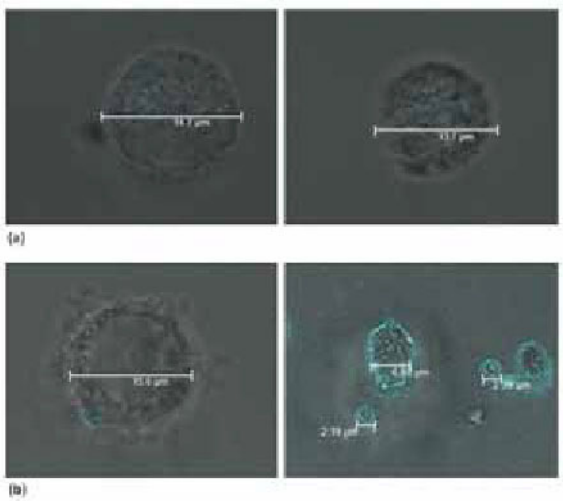


Fig 1: Examples of control healthy (a), and apoptotic cells (treated with an Akt inhibitor) (b) after incubation with annexin-V-functionalized gold nanorods. The grey-scale images show the appearances on conventional microscopy. The false-colour overlays show the (multi-photon) luminescence produced by gold nanorods.

Disclosure of author financial interest or relationships:
**A. Shah**, None; **S. Valleggi**, None; **D. Harris-Birtill**, None; **N.M. deSouza**, None; **J.C. Bamber**, None.

Presentation Number **P708**
Poster Session 4
September 8, 2012 / 14:45-14:45 / Room: The Liffey

# Near-infrared immuno-fluorescence imaging with anti-TAG-72 humanized monoclonal antibody in colorectal xenografted model

***In Ho Song***[1], *Tae Sup Lee*[1], *Hyo Jung Hong*[2], *Kwang Il Kim*[1], *Yong Jin Lee*[1], *Joo Hyun Kang*[1], [1]*Molecular Imaging Research Center, Korea Institute of Radiological and Medical Sciences, Seoul, Republic of Korea;* [2]*Department of Systems Immunology, Kangwon National University, Chuncheon, Republic of Korea. Contact e-mail: inosong@kirams.re.kr*

Tumor-associated glycoprotein (TAG)-72 is a human mucin (MUC1)-like glycoprotein complex, which is overexpressed in various cancers, including colorectal cancer. A humanized anti-TAG-72 monoclonal antibody, 3E8 specifically binds to the TAG-72 antigen. The aim of this study is to evaluate the feasibility of immuno-fluorescence imaging for TAG-72 overexpressing tumor using IRDye800 CW labeled 3E8 antibody. Conjugation of 3E8 antibody to IRDye800 CW NHS ester was performed with a molar ratio of 1: 8. 3E8-IRDy800 CW were injected into LS174T-bearing mice via tail vein. Ex vivo fluorescent biodistribution of 3E8-IRDye800 CW was performed at 2, 24 and 48 h postinjection. IRDye800 CW-to-3E8 antibody ratio was 3.17 ± 0.21. In biodistribution study, high fluorescent signals were detected in the liver and spleen at 2 h. At 24 and 48 h postinjection, fluorescent signals in the liver and spleen reduced, however, that in tumor at 2 h maintained up to 48 h. Low level of fluorescent signal was detected in the lung, muscle, stomach, and intestine. 3E8-IRDye800 CW was only selectively localized in tumor, except liver. Tumor/heart ratio was 2.0 ± 0.6, 6.7 ± 4.1 and 40.7 ± 12.7 and liver/heart ratio was 20.1 ± 2.1, 25.3 ± 14.2, and 63.2 ± 32.5 at 2, 24, and 48 h, respectively. Other tissues to heart ratio was below 1 and decreased as time-dependent manner. In conclusion, 3E8-IRDye800 CW demonstrated tumor-targeting capabilities in TAG-72 overexpressing cancer. If additional modification, it could be used as a promising dual-modality imaging agent for tumor detection with positron emission tomography (PET) and near-infrared (NIR) fluorescence imaging.

Disclosure of author financial interest or relationships:
**I. Song**, None; **T. Lee**, None; **H. Hong**, None; **K. Kim**, None; **Y. Lee**, None; **J. Kang**, None.

Presentation Number **P709**
Poster Session 4
September 8, 2012 / 14:45-14:45 / Room: The Liffey

# Novel NIR Probes Targeting to The Mitochondrial Membrane Potential for *In Vivo* Tumor Imaging

***Takashi Temma**, Satoru Onoe, Yoichi Shimizu, Masahiro Ono, Hideo Saji, Department of Patho-Functional Bioanalysis, Graduate School of Pharmaceutical Sciences, Kyoto University, Kyoto, Japan. Contact e-mail: ttemma@pharm.kyoto-u.ac.jp*

Objectives: The mitochondrial matrix is negatively charged in many carcinoma cells compared with normal cells due to a high proton efflux to fulfill the high cellular energy requirement, which leads to the formation of a steep electrochemical gradient ($\Delta\psi_m$). Since alteration of the $\Delta\psi_m$ is associated with the production of reactive oxygen species and cancer growth, $\Delta\psi_m$ is an important molecular imaging target for cancer diagnosis. Although visible fluorescent delocalized lipophilic cations (DLCs) have been developed as molecular probes for this purpose taking into account the cell membrane transport and retention in the mitochondria of tumor cells, DLCs with fluorescence in the near-infrared (NIR) regions have not yet been reported. Thus, we focused on IC7-1, a NIR fluorescent cyanine dye we previously developed, as a lead compound and planned to develop a NIR-DLC probe for *in vivo* tumor imaging. Methods: IC7-1 is a neutral molecule; thus, side chains that were less effective for fluorescence characteristics were replaced with alkyl chains (methyl to hexyl) to synthesize cationic derivatives (IC7-1-Me to IC7-1-He). Fluorescence characteristics were measured with a Fluorolog-3 equipped with a NIR sensitive detector. Cell microscopy was performed using human cervix adenocarcinoma HeLa cells incubated with IC7-1 derivatives. Fluorescence intensities of HeLa cells incubated for 1 hr with IC7-1 derivatives and an uncoupler (CCCP, 0-25 μM) or an organic anion transporter (OATP) inhibitor (rifampicin, 0-100 μM) were measured. Furthermore, the probes were intravenously administered to HeLa cell xenografted mice, and fluorescence images were acquired with a Clairvivo OPT for 72 hr. Results: IC7-1 derivatives were successfully synthesized. IC7-1 derivatives showed a maximum excitation wavelength at 823 nm and a maximum emission wavelength around 845 nm. The fluorescence intensity of cells treated with IC7-1 derivatives decreased corresponding to the alkyl chain length, and while the intensity of IC7-1-Pe and He was insufficient for microscopy observation, the other derivatives showed fluorescence in the mitochondria. The fluorescence intensities of cells treated with IC7-1-Me to Bu decreased with the addition of CCCP; IC7-1-Bu was the most sensitive to CCCP addition exhibiting a 76.7% decrease in fluorescence with 25 μM of CCCP, indicating the $\Delta\psi_m$ dependent accumulation of IC7-1-Bu in tumor cells. One hundred μM of rifampicin also decreased the fluorescence of IC7-1-Bu treated cells by 55.9% and IC7-1-Pr treated cells by 31.8%. In an *in vivo* study, tumors were clearly visualized up to 72 hr post administration of IC7-1-Bu and were modestly visualized up to 48 hr post administration of IC7-1-Pr. Conclusion: Newly developed IC7-1-Bu showed fluorescence localized to the mitochondria of HeLa cells that was dependent on $\Delta\psi_m$ after uptake via OATP, at least in part, and enabled clear tumor imaging *in vivo*. The results suggest that IC7-1-Bu is a promising NIR-DLC probe for *in vivo* tumor imaging.

Disclosure of author financial interest or relationships:
**T. Temma**, None; **S. Onoe**, None; **Y. Shimizu**, None; **M. Ono**, None; **H. Saji**, None.

Presentation Number **P710**
Poster Session 4
September 8, 2012 / 14:45-14:45 / Room: The Liffey

# The Imaging Probe Development Center at the National Institutes of Health: Ongoing Production of Diverse Molecular Imaging Probes

***Olga Vasalatiy***[1], *Ana Opina*[1], *Vincent Coble*[1], *Gary L. Griffiths*[2], [1]*IPDC, NIH, Rockville, MD, USA;* [2]*MIP, NCI, Bethesda, MD, USA. Contact e-mail: vasalatiyo@mail.nih.gov*

The Imaging Probe Development Center (IPDC) at NIH was founded as part of the National Institutes of Health (NIH) Roadmap for Medical Research Initiative, and is dedicated to the production of novel and commercially unavailable molecular imaging probes for biomedical research. Such studies can range from in vitro, through in vivo , to clinical development, in collaboration with NIH scientists and their extramural collaborators. The molecular probes produced by IPDC scientists are intended for use in all types of imaging modalities including optical, nuclear medicine, and magnetic resonance, and encompass a spectrum of compositions from low molecular weight entities to nanoparticles and bioconjugates. We have two dozen ongoing projects and several current examples will be presented: 1) Optimization, testing and production of GdDOTA and GdDTPA PAMAM dendrimers for clinical MRI by lymphangiography; 2) Syntheses of caged dyes and their analogs for super resolution microscopy; 3) GdDOTA functionalized PAMAM dendrimer conjugated to cholera toxin B targeting protein for neuronal imaging; 4) functionalization of targeting vectors based on monoclonal antibodies for production of fluorescent and PET imaging agents. The preparation and analytical characterization for each of these diverse agents will be described. For additional information please visit the IPDC website at https://intramural.nhlbi.nih.gov/Offices/IPDC/Pages/default.aspx

Disclosure of author financial interest or relationships:
**O. Vasalatiy**, None; **A. Opina**, None; **V. Coble**, None; **G.L. Griffiths**, None.

Presentation Number **P711**
Poster Session 4
September 8, 2012 / 14:45-14:45 / Room: The Liffey

# $BF_2$ Chelated Tetraarylazadipyrromethene as NIR Fluorochrome

***Dan Wu**, Donal O'Shea, Unicersity College Dublin, Dublin, Ireland. Contact e-mail: dan.wu@ucdconnect.ie*

In recent years, there has been growing interest in near-infrared (NIR) fluorochromes (>700 nm) for qualitative and quantitative assays.[1] Their simplicity of use coupled with high sensitivity ensures a continual expansion of their applications for in vitro and in vivo imaging. The inherent advantage of NIR fluorochromes over those that absorb in the shorter blue and green wavelengths lies in the dramatic reduction in background autofluorescence which leads to greatly improved sensitivity. In spite of these benefits, there are limited compound classes which have the desired absorption and emission properties. Our efforts have focused on the boron chelated tetraarylazadipyrromethene class **1**, as they are relatively easily synthesized, amenable to structural modification, and exhibit excellent spectral properties.[2],[3] For example, the tetraaryl analogue **1** has an absorption λmax at 696 nm and emission at 727 nm in formulated aqueous solutions **(Figure 1)**. In this post, we present the synthesis and spectral properties of the new fluorochrome **2**, based on this fluorophore scaffold, capable of thiol conjugations. Representative hydrosulfuryl conjugations via maleimide couplings will be described.

**References:** [1] Ntziachristos, V., Ripoll, J., Wang, L. V., and Weissleder, R. *Nat. Biotechnol*. **2005**, *23*, 313-320. [2] Gorman, A.; Killoran, J.; O'Shea, C.; Kenna, T.; Gallagher, W.M.; O'Shea, D.F. *J. Am. Chem. Soc.*, **2004**, *126*, 10619-10631. [3] Tasior, M.; O'Shea, D.F. *Bioconjugate Chem*. **2010**, *21*, 1130-1133.

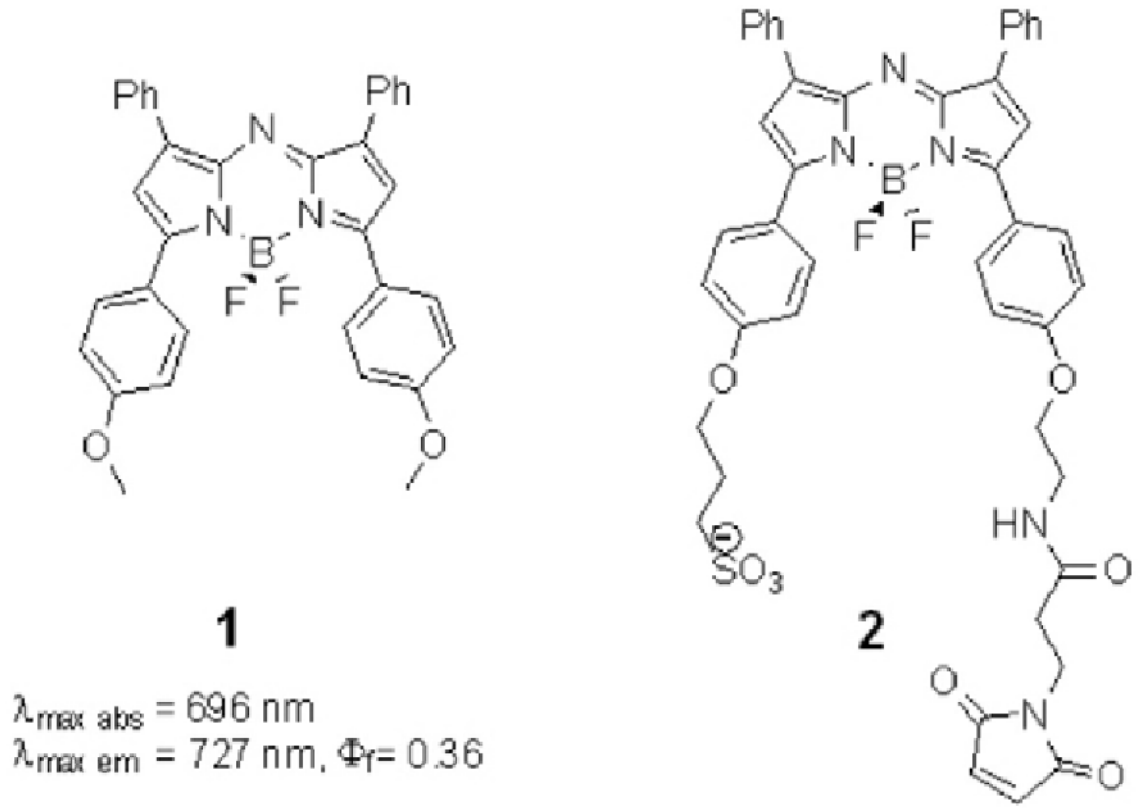


Figure 1. $BF_2$ Chelated Tetraarylazadipyrromethenes

Disclosure of author financial interest or relationships:
**D. Wu**, None; **D. O'Shea**, None.

Presentation Number **P712**
Poster Session 4
September 8, 2012 / 14:45-14:45 / Room: The Liffey

# NIRF probes for non-invasive detection of cell death: New in vitro and in vivo assays for high-throughput screening of compounds with potential cell death targeting properties

***Bang-Wen Xie***[1], *Danielle Park*[2], *Ermond R. van Beek*[1], *Vicky Blankevoort*[1], *Ivo Que*[1], *Philip Hogg*[2], *Clemens Lowik*[1], [1]*Department of Radiology, Leiden University Medical Center, Leiden, Netherlands;* [2]*Lowy Cancer Research Centre, University of New South Wales, Sydney, NSW, Australia. Contact e-mail: b.xie@lumc.nl*

Introduction: Over the last decade, non-invasive fluorescence imaging (FLI), exploiting NIRF probes, has developed rapidly. Cell death plays an integral role in normal physiology and in pathological conditions such as in cancer, ischemic diseases. For this, much attention has been drawn to the development of NIRF probes that can target dead cells with great sensitivity and specificity. In this study, we present a simple, rapid and cost-effective in vitro method for high-throughput screening of (NIRF) compounds with potential cell death targeting properties. Using the in vitro luciferase-expressing cell based model, we examined the properties of the membrane phosphatidylserine targeting NIRF probes: synthetic zinc(II)-dipicolylamine (Zn2+-DPA)-794 (PSS794), Annexin-Vivo 750, as well as that of a novel HSP-90 binding ligand GSAO-AF750. Our in vitro findings were confirmed in vivo in a mouse brain cryo-lesion model of traumatic brain injury (TBI). Methods: In vitro model of cell death: Mouse 4T1-luc2 breast cancer cells were grown to confluence in a 12-well plate and a focal area of cell death was induced in the center of the culturing well. Subsequently, cells were incubated with different NIRF probes, washed and subjected to scanning on LI-COR Odyssey™. In addition, cells were also incubated with trypan blue or luciferin to confirm the presence of dead cells in the center and living (luciferase active) cells in the periphery area. In vivo model of cryo-induced traumatic brain injury (TBI): To initiate a local area of brain tissue death, a liquid N2 pre-cooled metal cylinder was shortly applied to the parietal region of a mouse head. Subsequently, the mice were injected i.v. with the different NIRF cell death probes and subjected to whole body FLI 1-24h post injection. Finally, brain tissues were collected for ex vivo FLI and subsequently histological analysis. Results: In vitro, the tested NIRF probes all strongly accumulated in the area of dead cells in the center of the culturing well but not in the living cells in the periphery. In line, this has been confirmed by trypan blue staining and luciferase assay by bioluminescence imaging. In vivo, all three NIRF probes selectively accumulated in the area of brain cryo-lesion in our mouse model of TBI. Local cell death and probe accumulation was confirmed histologically. Conclusions: A high-throughput in vitro cell death screening assay and an in vivo mouse brain cryo-lesion model were successfully established in a simple and cost-effective manner. In vitro and in vivo results obtained with three different NIRF probes were consistent and suggest that these models may be employed for high-throughput screening of compounds with potential cell death targeting properties. The new NIRF death probes examined here can be employed for diagnosis purposes in all kinds of pathological conditions where cell death is involved, or they can be used to monitor treatment outcome, i.e. to investigate the efficacy of anti-tumour therapies at early time points. Acknowledgement: This study is supported by the Center for Translational Molecular Medicine, project MUSIS (grant 03O-202) and the ENCITE project 201842.

Disclosure of author financial interest or relationships:
**B. Xie**, None; **D. Park**, None; **E.R. van Beek**, None; **V. Blankevoort**, None; **I. Que**, None; **P. Hogg**, None; **C. Lowik**, None.

Presentation Number **P713**
Poster Session 4
September 8, 2012 / 14:45-14:45 / Room: The Liffey

# Novel COX2-targeted Porphyrins Photosensitizers for Photodynamic Therapy

***Kun Yan***[1,2], *Fengshou Wu*[2], *Zaoying Li*[2], [1]*School of Medicine, Johns Hopkins University, Baltimore, MD, USA;* [2]*College of Chemistry and Molecular Sciences, Wuhan University, Wuhan, China. Contact e-mail: kun_yan18@hotmail.com*

Photodynamic therapy (PDT) is an established controllable clinical treatment modality for destruction of tumor. As the well-recognized PDT photosensitizers, porphyrin and its derivatives have been studied extensively and used clinically in the past. Moreover, they can be used as the ideal molecular imaging dyes due to the long-wavelength luminescence emission. On the other hand, there is a compelling need to improve the selectivity of PDT photosensitizers that would only target lesion of tumor while sparing normal healthy tissue nearby. Because of the over-expression in several types of human cancers, cyclooxygenase-2 (COX-2) is an excellent target for therapy and noninvasive imaging. Indomethacin, which is a COX-2 specifical small molecular inhibitor, has been reported as the targeting moiety of the COX-2-targeted cancer diagnostic imaging agent. Herein, we report, for the first time, the design and synthesis of water-soluble COX-2 specific-targeted porphyrin photosensitizers. Our prototype PDT photosensitizers are synthesized by conjugating: (i) 5-(4-carboxyphenyl)-10,15,20-tri-(4-pyridyl)porphyrin, as a photosensitizer and molecular imaging dye, which also demonstrate strong binding with DNA; (ii) indomethacin, as the COX-2 targeting moiety to provide the specificity to the tumor cell with high COX-2 expression; and (iii) alkane chain, as the linker between porphyrin and indomethacin to separate the targeting moiety from the photosensitizer for productive binding with COX-2. These porphyrin-based photosensitizers show specificity to the MDA-MB-231 cancer cell with COX-2 expression, whereas they are inert to HTC 116 cancer cell (no COX-2 expression). Cell viability studies indicate these compounds are safe in dark, whereas they can destruct cancer cell effectively with the irradiation of light.

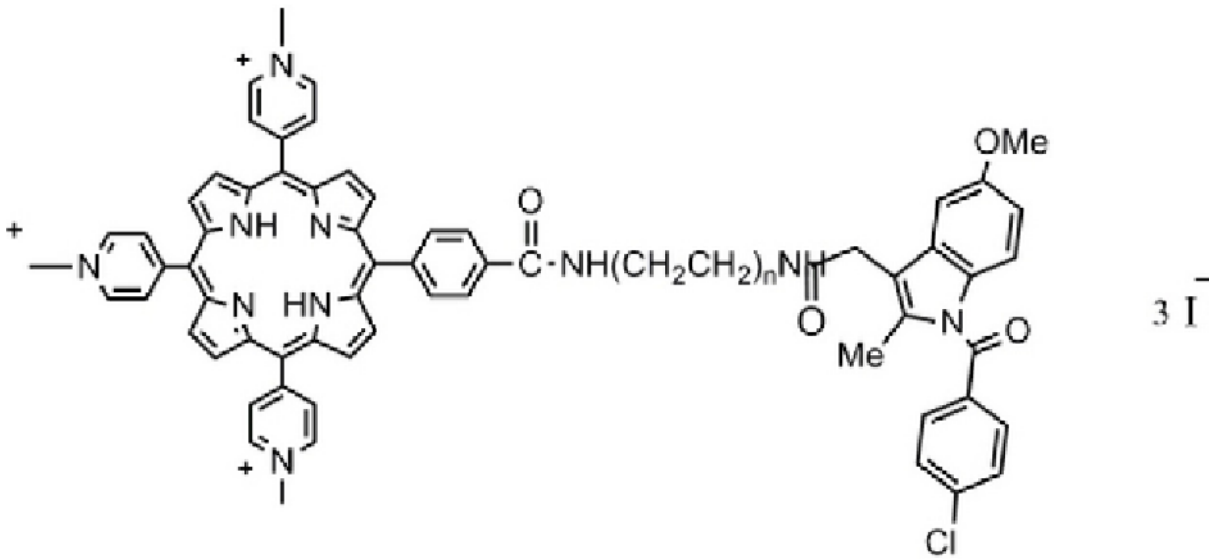


Figure 1. Structure of our prototype photodynamic therapy photosensitizers

Disclosure of author financial interest or relationships:
**K. Yan**, None; **F. Wu**, None; **Z. Li**, None.

Presentation Number **P714**
Poster Session 4
September 8, 2012 / 14:45-14:45 / Room: The Liffey

# GX1-conjugated Mcellar ICG Nanocapsules: a Phage Display Peptide Probe for Near-infrared Fluorescence Imaging of Tumor Vasculature

***Qian Zhang***[1], *Xibo Ma*[2], *Yongping Chen*[3], *Xin Yang*[2], *Xingde Li*[3], *Jie Tian*[1,2], [1]*Life Sciences Research Center, School of Life Sciences and Technology, Xidian University, Xi'an 710071, China;* [2]*Medical Image Processing Group, Institute of Automation,CAS, "Beijing,100190", China;* [3]*Department of Biomedical Engineering, Johns Hopkins University, Baltimore, MD, USA. Contact e-mail: zhangqian@life.xidian.edu.cn*

Abstract Aim: Near-infrared (NIR) fluorescence imaging is an emerging technique for studying/detecting diseases at molecular level, and biocompatible molecular probes are a critical component to enable clinical translation of NIR molecular imaging. This study reports on the development of NIR fluorescent nanocapsules made of FDA approved materials, i.e. indocyanine green (ICG) and Pluronic F-127. Molecularly specific targeting was achieved by conjugating the ICG-nanocapsules with a tumor vasculature endothelium-specific peptide ligand GX1 (CGNSNPKSC). We evaluated the GX1-conjugated ICG nanopcapsules as a potential targeting probe for NIR fluorescence imaging of tumor vasculature in LoVo tumor-bearing mouse model. Methods: ICG is the only dye in the NIR region approved by FDA for routine clinic use. However, application of ICG for molecular imaging is limited due to its lack of proper moieties for bioconjugation. To overcome this limitation and facilitate future clinical translation, we used polymeric micelles (~30 nm in diameter) made of FDA approved materials (Pluronic F-127) through self-assembling , to encapsulate ICG within the micellar core, where the -OH terminals of the polymer on the corona of the micelles can be activated for bioconjugation. For molecular targeting, the peptide GX1 (CGNSNPKSC), a tumor vasculature endothelium-specific ligand identified by phage-display technology , was conjugated to the ICG-nanocapsules following the steps shown in Figure (A). For in vivo imaging, two LoVo tumor-bearing mice were used, with one given 200μl of GX1-conjugated ICG nanocapsule PBS solution and the other 200μl unconjugated ICG nanocapsules (as control) through tail vein injection (ICG concentration: 0.5 mg/kg). NIF fluorescence images were taken at 1min, 30min, 5h, 18h, 24h, and 48h by a home-built NIR fluorescence video imaging system (Figure (B)). Results: As shown in Figure (C), the LoVo tumors were all clearly visible with high contrast at 5h, 18h after the injection of GX1-conjugated ICG nanocapsules while high accumulation in liver and kidneys was also observed at early time points. For the control experiment, no evident contrast was observed. 24 hours later the fluorescence intensity from the two mice decayed gradually. Conclusion: We successfully developed a tumor specific NIR fluorescent probe, GX1-conjugated micellar ICG nanocapsules, which can be used for imaging tumor angiogenesis and holds a potential for the future clinical translation.

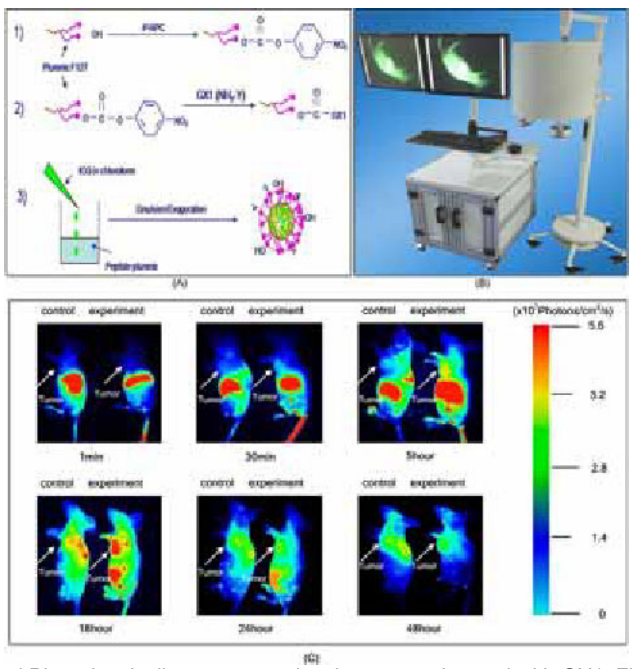


Figure (A): Steps for engineering ICG-loaded Pluronic micellar nanocapsules that are conjugated with GX1. Figure (B): The home-built NIR fluorescence video imaging system. Figure (C): Time-course fluorescence images from LoVo tumor-bearing mice after tail vein injection of GX1-conjugated ICG nanocapsules and unconjugated ICG nanocapsules (as control)

Disclosure of author financial interest or relationships:
**Q. Zhang**, None; **X. Ma**, None; **Y. Chen**, None; **X. Yang**, None; **X. Li**, None; **J. Tian**, None.

Presentation Number **P715**
Poster Session 4
September 8, 2012 / 14:45-14:45 / Room: The Liffey

# Longitudinal Analysis of Changes in 18FDG Uptake in Bone Marrow and Lymph Node and in Lymph Node Volume in the Nonhuman Primate Model of Monkeypox Infection

***Julie Dyall***[1], *Reed Johnson*[2], *Christopher Z. Leyson*[1], *Svetlana I. Chefer*[1], *Jurgen Seidel*[1], *Dan R. Ragland*[1], *Jennifer A. Cann*[1], *Haifeng Song*[1], *Russell Byrum*[1], *Richard C. Reba*[1,3], *Omer Aras*[4], *Dima A. Hammoud*[3], *Joseph E. Blaney*[2], *Peter B. Jahrling*[1,2], [1]*Integrated Research Facility, NIAID/NIH, Frederick, MD, USA;* [2]*Emerging Viral Pathogens Section, NIAID/NIH, Bethesda, MD, USA;* [3]*Center for Infectious Disease Imaging, Radiology and Imaging Sciences, CC/NIH, Bethesda, MD, USA;* [4]*Molecular Imaging Program, NCI/NIH, Bethesda, MD, USA. Contact e-mail: dyallj@niaid.nih.gov*

Purpose: Molecular imaging of the immune response may have value for monitoring viral infections and assessing treatments of infectious diseases. We used 18FDG -PET/CT to identify potential biomarkers by performing longitudinal analysis and comparing 18FDG uptake and lymph node volume before and during monkeypox infection in nonhuman primates. Materials and Methods: Six male rhesus macaques were infected intravenously with a sublethal dose (5x10e7 pfu) of monkeypox. Three animals were treated with a dose of cidofovir (CDV) that has been shown to protect against monkeypox, three animals represented the untreated control group. Three scans were performed using PET/CT scanner before the inoculation for the baseline condition. After inoculation PET/CT scans were obtained on days 1/2, 3/4, 7/8, 10, 16 and 21. Lymph nodes (LNs) from biopsies were examined histopathologically and the LN cells were analyzed by FACS. Results: The CDV-treated NHPs survived and had a three log reduction in viremia compared to untreated NHPs. Two NHPs in the untreated control group succumbed and one survived. PET imaging showed that monkeypox infection lead to an increase in 18FDG uptake in the bone marrow in all six animals early in infection (day 3/4 post inoculation). However, the 2 moribund NHPs had significantly higher uptake of 18FDG in the bone marrow (mean SUV of 4.2) than the 4 surviving NHPs (mean SUV of 2.9). Monkeypox infection induced lymphadenopathy in all 6 NHPs. However, there were differences in enlargement patterns and in how it correlated with changes in 18FDG uptake. In CDV-treated NHPs, lymph nodes showed a 3 to 4-fold volume increase that peaked on day 10, while 18FDG -uptake increased 4 to 9-fold and peaked on day 10. In the surviving untreated NHP, the 18FDG pattern was similar to the treated NHPs with a peak on day 10 (7-fold increase). However, lymphadenopathy lasted longer and was more pronounced (up to 8-fold enlargement on day 16) than in the treated NHPs. In contrast, the nodes in the moribund NHPs showed much lower volume increase (2-fold) while 18FDG uptake increased to a level higher than that in the survivors. LN biopsies showed increased sinus histiocytosis in all NHPs on days 9 (for survivors) and day 7 (necropsy day for moribund NHPs). Hyperplasia and increase in B and T cell proliferation were observed in the LN tissues in recovering animals at necropsy (day 22). Conclusion: Analysis of 18FDG uptake and LN size resulted in identification of two patterns that differed between moribund and surviving NHPs. First, 18FDG uptake in the bone marrow may represent an indicator for outcome of disease since changes in 18FDG uptake were significantly higher in moribund versus surviving NHPs. Second, while the surviving NHPs showed significant node size increase correlating with an increase in 18FDG uptake, the two moribund animals showed strong uptake of 18FDG that did not correlate with lymphadenopathy indicating that analysis of structural and functional changes of LNs during infection may be a useful in vivo approach to monitor monkeypox pathogenesis.

Disclosure of author financial interest or relationships:
**J. Dyall**, None; **R. Johnson**, None; **C.Z. Leyson**, None; **S.I. Chefer**, None; **J. Seidel**, None; **D.R. Ragland**, None; **J.A. Cann**, None; **H. Song**, None; **R. Byrum**, None; **R.C. Reba**, None; **O. Aras**, None; **D.A. Hammoud**, None; **J.E. Blaney**, None; **P.B. Jahrling**, None.

Presentation Number **P716**
Poster Session 4
September 8, 2012 / 14:45-14:45 / Room: The Liffey

# In vivo monitoring of Staphylococcus aureus infections in murine models by BLI and high-field MRI

***Tobias Hertlein***[1], *Volker Sturm*[2], *Peter Jakob*[2], *Knut Ohlsen*[1], [1]*Institute for Molecular Infection Biology, University of Wuerzburg, Wuerzburg, Germany;* [2]*Experimental Physics 5, University of Wuerzburg, Wuerzburg, Germany. Contact e-mail: tobiasherti@gmx.de*

Introduction: In recent years, several non-invasive imaging technologies have been developed to visualize and monitor infections in vivo. Magnetic resonance imaging (MRI) is, in this context, able to deliver three dimensional data with high spatial resolution and soft tissue contrast. Our idea was to establish this modality to monitor the course of Staphylococcus aureus infections in murine models. Methods: We used a S. aureus thigh abscess model and tested two MR contrast agents: CLIO (ironoxide particles) and PFC (perfluorocarbon emulsions). The MR-Imaging was accompanied by Bioluminescence and Fluorescence Imaging. After establishing these Imaging modalities, we started to evaluate the effect of antibiotic treatment upon the MR and photon signals. Results: Since native proton-based MR methods were not sufficient to visualize and localize the site of infection, we had to apply MR contrast agents. CLIO accumulated in this regard at the rim of the abscess during chronic phase of inflammation, but diffuse during acute phase. PFC, in contrast, accumulated at acute as well as at chronic phase at the rim of the abscess area. Bioluminescence Imaging was able to quantify bacterial content at the site of infection by detecting photons emitted by a luciferase. Antibiotic-treatment led to decreased accumulation of MR contrast agents and decreased bioluminescence signal at the site of infection. Conclusions: Contrast agent based MRI offers three-dimensional visualization of the abscess area without the disadvantages of signal loss due to tissue depth or radioactive tracers. We could furthermore show, that therapy with antibiotics led to decreased contrast agent accumulation at the site of infection and may serve as an indicator for efficacy. But this is just the first application for this Imaging modality: it may furthermore enable us to study immunomodulation or determine the influence of virulence factors non-invasively with high spatial resolution and in anatomical context.

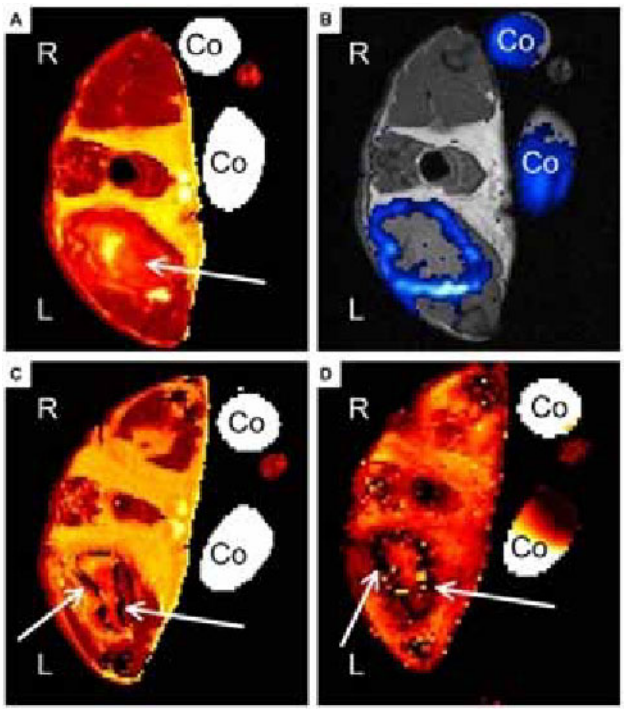


Figure 1. Representative MR Images of acute soft-tissue infection. A, B) Mouse received PFC at day 2 post infection. Images were recorded 24 h after administration. C, D) Mouse received CLIO at day 2 post infection and was imaged 24 h after administration. A) Transverse T2 map of PFC group mouse shows hyperintensity within infected muscle (arrow). B) 19F-SSFP CSI overlay on 1H-TSE image of PFC treated mouse shows strong accumulation of PFC at the rim of abscess area. C) Transverse T2 map of CLIO group mouse shows hyper-intense area diffusely circumscribed by dark spots (arrow). D) T2* weighted image shows diffusely distributed susceptibility effects in the infected muscle (arrow). (Co: Control tube filled with PFC dilution, R: right side, L: left side of the imaged mouse). (Hertlein T et al. PLoS One. 2011 Mar 24;6(3):e18246.)

Disclosure of author financial interest or relationships:
**T. Hertlein**, None; **V. Sturm**, None; **P. Jakob**, None; **K. Ohlsen**, None.

Presentation Number **P717**
Poster Session 4
September 8, 2012 / 14:45-14:45 / Room: The Liffey

# Metabonomic Unveiling of Comprehensive Metabolic Mechanism and Multiple Biomarkers of Experimental Autoimmune Myocarditis in a Rat Model

***Young-Shick Hong***[1], *Hyeyoung Moon*[1], *Jongeun Kang*[1], *Eun-Hee Kim*[1], *Eunjung Bang*[2], *Chaejoon Cheong*[1], *Kiyuk Chang*[3], *Kwan Soo Hong*[1], [1]*Division of MR Research, Korea Basic Science Institute, Chungcheongbuk-do, Republic of Korea;* [2]*Seoul Branch,, Korea Basic Science Institute, Seoul, Republic of Korea;* [3]*Cardiovascular Medicine, College of Medicine, The Catholic University of Korea, Seoul, Republic of Korea. Contact e-mail: chtiger@yahoo.com*

Background - Myocarditis is an inflammatory heart disease with characteristic inflammatory cellular infiltration into myocardium and is associated with many events in myocardium, including cardiac inflammation, fibrosis, necrosis, apoptosis and cellular dysfunction. However, comprehensive metabolic characterization of host systemic response against the inflammation in myocardium has not been established. Methods and Results - Myosin immunization was used to induce experimental autoimmune myocarditis (EAM) in rats. We have characterized metabolic responses in plasma and urine of rats to EAM at different stages of EAM in order to extensively understand host metabolic perturbations associated with EAM, through 1H nuclear magnetic resonance (NMR)-based metabonomic approach. Three phases of EAM were characterized and marked perturbations of lipid metabolism were found at acute phase of EAM, as indicated mainly by large reductions of plasma fatty acid levels in EAM rats. At subacute phase, cellular anaerobic glycolysis, following acute inflammation and large lipid β-oxidation, was noted by marked depletion of plasma glucose and large accumulation of plasma lactate. Chronic phase of EAM was characterized mainly by accumulation of plasma glucose. In particular, depletions of fatty acid and citrate, and accumulations of acetyl glycoproteins and albumin lysyl group in plasma of EAM rats demonstrate still large energy demand and involvement of myocardial inflammation until the chronic phase of EAM, which are distinct from cardiac ischemia. Conclusions - This study highlights simultaneous observations of global and distinct metabolic perturbations and finding of multiple biomarkers associated with autoimmune myocarditis at different EAM stages, through metabonomic approach.

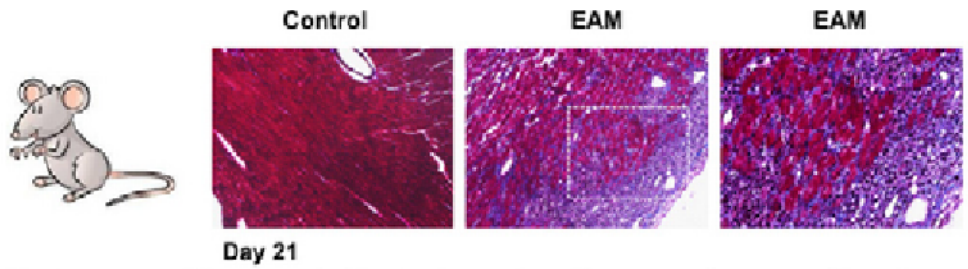


**Fig. 1.** Typical histopathological resutls of myocardium on day 21 postinfection during experimental autoimmune myocarditis (EAM) in a rat model.

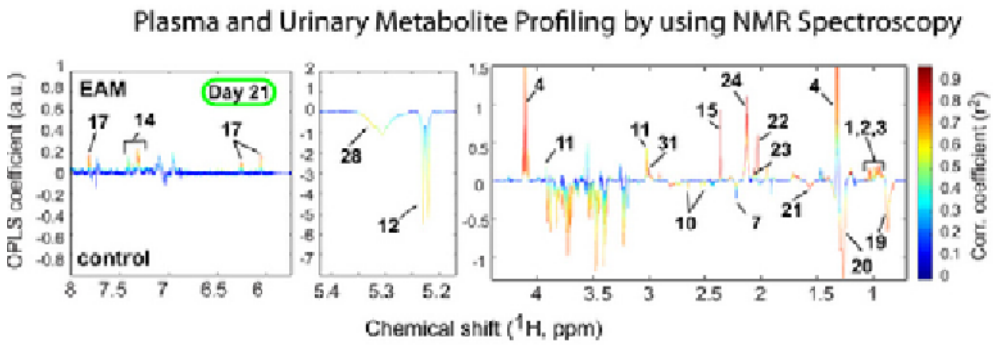


**Fig. 2.** Indentification of plasma metabolites perturbed during EAM on day 21 post- infection, through 1H NMR-based metabolomic approach.

Disclosure of author financial interest or relationships:
**Y. Hong**, None; **H. Moon**, None; **J. Kang**, None; **E. Kim**, None; **E. Bang**, None; **C. Cheong**, None; **K. Chang**, None; **K. Hong**, None.

Presentation Number **P718**
Poster Session 4
September 8, 2012 / 14:45-14:45 / Room: The Liffey

# Targeted Magnetoliposomes for Liver imaging

***Ashwini Atre***[1], *Tom Struys*[1,4], *Tineke Notelaers*[2], *Michel Hodenius*[3], *Philip Roelandt*[2], *Tom Dresselaers*[1], *Marcel DeCuyper*[3], *Catherine Verfaillie*[2], *Uwe Himmelreich*[1], [1]*Department of Diagnostic and Pathology, KU Leuven, Leuven, Belgium;* [2]*Interdepartmental Stem Cell Institute, KU Leuven, Leuven, Belgium;* [3]*Lab of BioNano Colloids, KU Leuven, Kortrijk, Belgium;* [4]*Lab of Histology, University of Hasselt, Hasselt, Belgium. Contact e-mail: ashwini.atre@med.kuleuven.be*

INTRODCUTION: Cell labeling strategies can be classified in (a) unspecific uptake of contrast agents and (b) specific uptake of targeted contrast agents. In case of liver cirrhosis or viral hepatitis where hepatocytes are damaged and healing is difficult, differentiation of stem cells into hepatocyte like cells is a potential therapeutic approach (1). These hepatocytes can be targeted with lactose functionalized magnetoliposomes (MLs) (4) and isolated from stem cell differentiation protocols containing cells from meso-, endoderm and hepatocytes. In this work, we have used galactose-terminal entities which are recognized by asialoglycoprotein receptors (ASGPR), which are hepatic receptors (2). METHODS: ML synthesis: Cationic (DSTAP), anionic (DMPG) in a dimyristoylphosphatidylcholine (DMPC) matrix were synthesized as described before. Lactosyl-bearing MLs were produced similarly to the anionic MLs using 95% DMPC and 1% 1,2-dioleoyl-sn-glycero-3-phosphoethanolamine-N-lactosyl (DOPE-lac) (3, 4). In vitro experiments: Differentiation of mouse embryonic stem cells (mESCs) was performed according to (1). Differentiated cells were labeled with MLs (100µg Fe/ml). Labeled cell samples were collected for qPCR, electron microscopy, immunostaining, MRI and magnetic cell separation. In vivo: Initial experiments were performed by injecting MLs (200µg Fe/ml) in healthy C57bl6 mice intravenously. Animals were scanned and livers were isolated for immunostaining at 4 hrs, day 2, 4, 6, 8 and 10 post injections. MRI: MR images were acquired using a Bruker Biospec 9.4 T small animal scanner. 3D-T2* weighted MRI FLASH (TE=12ms, TR=150ms) and T2-maps (MSME, with 8 echoes, TE increments of 10ms) acquired. RESULTS: Differentiated ESCs did not show any toxic effects on total cell count and marker expression post labeling. Uptake specificity was confirmed by TEM. Positive fractions post magnetic separation showed 25-30% of the total cell count which coincides with the percentage of ASGPR+ cells detected by FACS. In vivo dynamic MRI studies showed particles clearance through blood was very fast and particles ended up in the liver after injection. There was no significant difference observed in the signal intensities of FLASH scans for particles. However, histology confirmed that anionic MLs were mainly taken by Kupffer (only very small fraction in hepatocytes) and also confirmed by TEM. Lac MLs were mainly taken up by hepatocytes and kupffer cells immediately after injection but by later time points (week 1) particles were present only in hepatocytes. Further, marker specific immnunostaining experiments need to be done. CONCLUSIONS: Initial in vitro experiments revealed specificity in uptake of lactose-functionalized MLs by hepatocyte like cells in culture and in vivo. This can be used for magnetic cell separation and subsequent MR imaging post engraftment of those cells. Potential of Lac MLs in determining the liver function needs to be further evaluated in liver disease models. References: (1) Roelandt P et al. Plos One 2010 (2) Stockert RJ. Physiol.Rev. 1995 (3) De Cuyper M et al. Methods Mol. Biol. 2010 (4) Soenen SJ et al. Biomaterials 2010

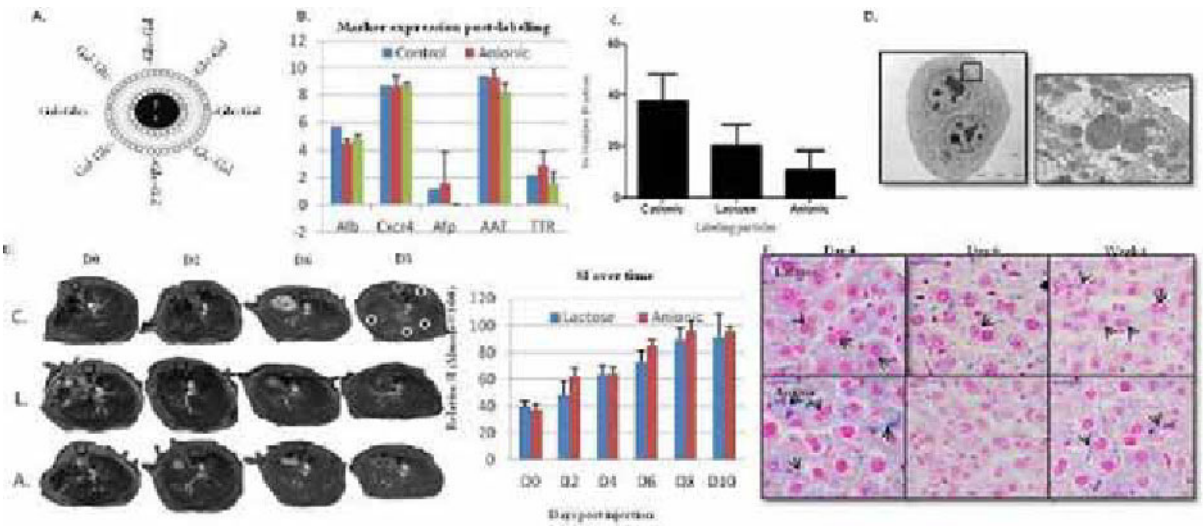


(A). Typical layout of Lac-MLs; (B) No effect on marker expression post labeling; (c) % Positive fraction post magnetic separation; (D) Presence of iron oxide particles in bi-nucleated hepatocytes and week 1 liver samples; (E) FLASH scans of Cationic, Anionic and Lactose injected mice livers (axial) at D0, D2, D6, D8 and D10 post injections and their respective intensities with respect to muscle. (F) Prussian Blue staining of liver samples at different time points

Disclosure of author financial interest or relationships:
**A. Atre**, None; **T. Struys**, None; **T. Notelaers**, None; **M. Hodenius**, None; **P. Roelandt**, None; **T. Dresselaers**, None; **M. DeCuyper**, None; **C. Verfaillie**, None; **U. Himmelreich**, None.

Presentation Number **P719**
Poster Session 4
September 8, 2012 / 14:45-14:45 / Room: The Liffey

# PET imaging of 18kDa TSPO expression in a rat model of inflammatory bowel disease (IBD) using [18F]DPA-714

***Nicholas Bernards**, Benoit Theze, Géraldine Pottier, Frederic Dolle, Raphael Boisgard, CEA, Orsay, France. Contact e-mail: nicholas.bernards@gmail.com*

Inflammatory bowel disease (IBD) is defined as a chronic relapsing idiopathic inflammation of the gastrointestinal tract. The two main clinical forms of this disease family are Crohn's Disease (CD) and Ulcerative Colitis (UC). IBD affects an estimated 3.6 millions individuals in Europe and North America.To date it is thought that IBD is the result of continual activation of the mucosal immune system. In order to better understand this disease family, a quantitative approach for the analysis of the inflammatory processes needs to be developed. In this study we chose to assess [18F]DPA-714, an 18 kDa TSPO ligand currently used to evaluate inflammation within the central nervous system (CNS), as a Positron Emission Tomography (PET) probe to image and report the inflammation in a rat model of IBD. Male Wistar rats were used weighing between 160-190 g. Colonic inflammation was induced by administering 5% dextran sodium sulfate (DSS) (MW 40,000) ad libitum via the drinking water for 7 days. Control animals received normal drinking water. On day 7, PET images were acquired using a Siemens Inveon PET/CT machine dedicated to small animals with the help of [18F]FDG, which is what is currently being used to estimate the inflammation levels. The following day, day 8 of the treatment, the same machine was used to acquire images with another tracer, [18F]DPA-714, currently used to evaluate inflammation within the central nervous system (CNS). Once the [18F]DPA-714 images had been acquired, the rats were sacrificed by injecting pentobarbital, and then lower intestine was removed for radioactivity counting as well as immunohistochemistry analysis. The obtained results from the [18F]FDG exams did not reveal any significant differences between the treated (mean %ID 1.52 +/- 1.37) and control groups (mean %ID 0.36 +/- 0.20). The analysis of the images obtained with [18F]DPA-714 however did yield a significant difference between the treated (mean %ID 5.91 +/- 2.67) and control groups (mean %ID 3.12 +/- 1.40). Immunohistochemistry analysis revealed a higher presence of macrophages (which is where TSPO 18kDA is expressed) in the treated rats than in the controls. Preliminary results seem to indicate that [18F]DPA-714 is a suitable radiotracer for the study of inflammation of IBD in our animal model.

Disclosure of author financial interest or relationships:
**N. Bernards**, None; **B. Theze**, None; **G. Pottier**, None; **F. Dolle**, None; **R. Boisgard**, None.

Presentation Number **P720**
Poster Session 4
September 8, 2012 / 14:45-14:45 / Room: The Liffey

# The Effect of PPAR-γ Agonist on F-18 FDG PET Imaging for Differentiating Tumors and Inflammation Lesions

***Su-Jin Cheong***, *Chang-Moon Lee, Eun-Mi Kim, Hwan-Seok Jeong, Na-Young Choi, Hwan-Jeong Jeong, Dong Wook Kim, Seok Tae Lim, Myung-Hee Sohn, Department of Nucler Medicine, Institute for Medical Science, Research Institute of Clinical Medicine, Cyclotron Research Center, Geumam-dong, Dukjin-gu, Jeonju, Jeonbuk, Republic of Korea. Contact e-mail: thinkfamily99@daum.net*

Although 18F-2-deoxy-2-fluore-D-glucose (FDG) positron emission tomography (PET) is a valuable tool for the diagnosis of tumors, FDG uptake, occurs through the glucose transporter in these cells, is not specific to tumors and is observed in inflammatory lesions. The goal of this study was to investigate the potential of a PPAR-γ agonist on the differentiation of tumors and inflammatory lesions in F-18 FDG PET imaging. To investigate the effect of a PPAR-γ agonist, we compared the differences of 18F-FDG uptake, and the expression of glucose transporter and hexokinase in macrophage (RAW 264.7) and three tumor cell lines (A549, MDA-MB-231, and KB) after treatment of pioglitazone (from 10 to 150 μM, n=5). To confirm the feasibility of pioglitazone to differentiate F-18 FDG uptake between tumor and inflammatory lesion, PET/CT imaging studies were performed on RAW 264.7 xenograft mice and two tumor xenograft models (n=6) after injection of pioglitazone (400 μg/100 μL). F-18 FDG uptake into the macrophages cells was higher than of tumor cells, but the uptake decreased to 35±5.0% when treated with 100 or 150 μM of pioglitazone ($p<0.05$). In contrast, F-18 FDG uptake into the tumor cells increased to 19±9.7% after treatment of pioglitazone at the same concentration ($p<0.05$). In the case of macrophage cells, the expression of glucose transporter was reduced by pioglitazone, whereas the expression increased markedly in all the tumor cells after treatment of pioglitazone. In vivo PET/CT imaging showed that F-18 FDG uptake (%ID/g) in the tumors was enhanced to 38.4±14.3% for MDA-MB231, and 12.9±9.7%ID/g for KB tumors after treatment of pioglitazone, respectively ($p<0.05$). Unlike tumors, RAW 264.7 xenograft models of a representative inflammation showed that 18F-FDG uptake was reduced to 48±20.8% after treatment of pioglitazone. These results indicate that pioglitazone affects the expression of glucose transporter in the macrophage and tumor cells, resulting in the differences of F-18 FDG uptake. In this study, we demonstrated the effect of a PPAR-γ agonist on F-18 FDG uptake in tumors and inflammation in vitro and in vivo. Pioglitazone has the potential as a promising sorter to differentiate tumors and inflammatory lesions on F-18 FDG PET imaging.

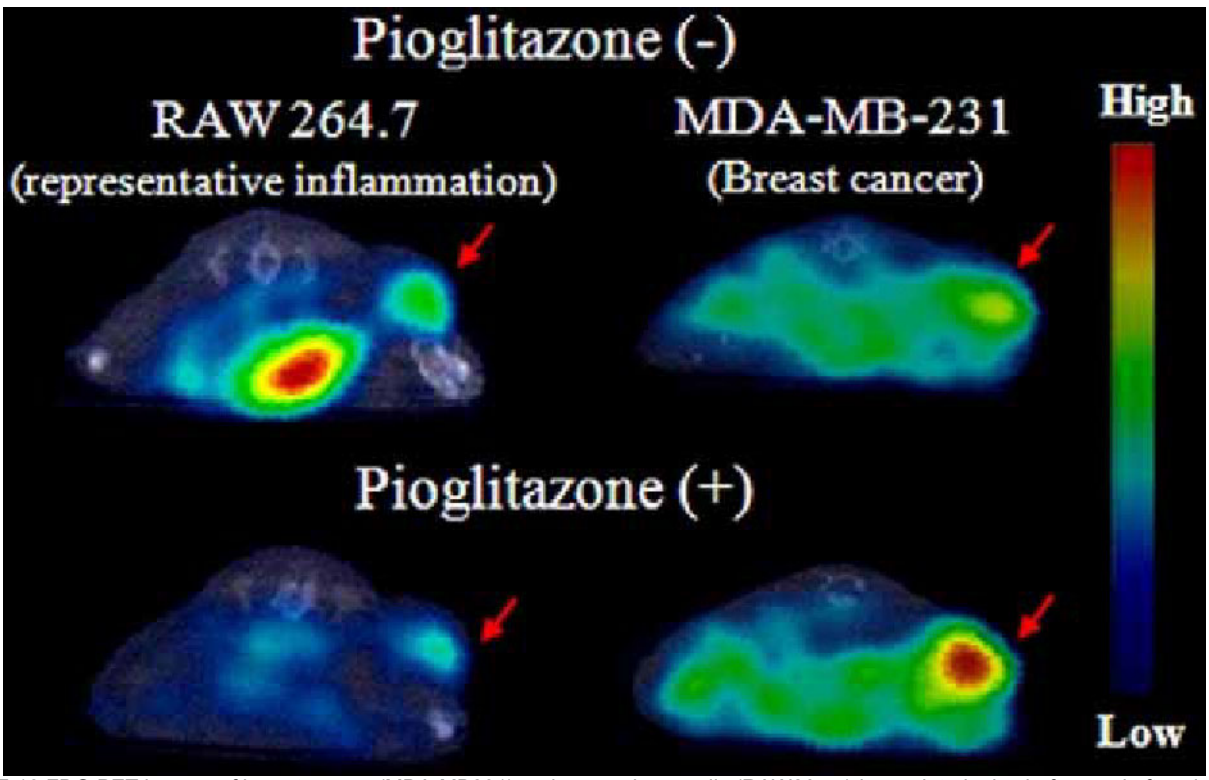


Figure 1. F-18 FDG PET images of breast cancer (MDA-MB231) and macrophage cells (RAW264.7)-innoculated mice before and after pioglitazone.

Disclosure of author financial interest or relationships:
**S. Cheong**, None; **C. Lee**, None; **E. Kim**, None; **H. Jeong**, None; **N. Choi**, None; **H. Jeong**, None; **D. Kim**, None; **S. Lim**, None; **M. Sohn**, None.

Presentation Number **P721**
Poster Session 4
September 8, 2012 / 14:45-14:45 / Room: The Liffey

# Immunomodulation Effect of Sorafenib on Adoptive Cell Therapy

***Hui-Yen Chuang***, *Ya-Fang Chang, Jeng-Jong Hwang, National Yang-Ming University, Taipei, Taiwan. Contact e-mail: vandal4013@hotmail.com*

Purpose Adoptive cell therapy (ACT) is a strategy for cancer treatment since immune system plays an important role in preventing living subjects from diseases. Nevertheless, therapeutic efficacy of ACT depends largely on the expression of immunosuppressive factors, such as CD8+ T cells. Sorafenib, a multikinase inhibitor, shows the ability to target various immunoresponsive receptors. Hence, we suggest that sorafenib may be beneficial the therapeutic efficacy of ACT. Here, a granzyme B promoter driven reporter system was used to evaluate the effect of sorafenib on ACT. Materials and Methods OVA-expressing E.G7 mouse lymphoma cells and OT-1 transgenic mice were used in the study. CD8+ T cells obtained from OT-1 mice were transduced with pGBeLT lentivirus, which allowed the activation of CD8+ T cells to be evaluated by optical imaging. E.G7 cells were pretreated with 5 uM sorafenib for 24 h and co-cultured (effector-to-target ratio=25) with CD8+ T cells for another 4 h. The activation of CD8+ T cells and intracellular IFN-gamma production were assayed by flow cytometry. Immunosuppressive factors, including IDO, VEGF, IL-10 and MCP-1, were assayed by Western blotting. Since the number of tumor-infiltrated CD8+ T cells plays a substantial role for ACT, thus the migration ability of CD8+ T cells was also measured by transwell assay. The E.G7/OT-1 animal model was used to evaluate the therapeutic efficacy of sorafenib combined with ACT in vivo. Results Activation of CD8+ T cells was elevated when co-cultured with sorafenib pretreated E.G7 cells as compared with the untreated. Significant increase of fluorescence intensity and IFN-gamma production were found (***p<0.001 as compared with those of non-activated and untreated groups). The expressions of immunosuppressive factors were decreased by sorafenib treatment in a dose-dependent manner. The migration ability of CD8+ T cells was elevated in the sorafenib pretreated group as compared with that of the untreated. The E.G7/OT-1 animal model showed that sorafenib could augment the therapeutic efficacy of ACT. The similar tumor growth inhibition could be observed for sorafenib pretreated 2x106 CD8+ T cells and 5x106 CD8+ T cells, respectively. STAT3 has been reported to play an important role in immunomodulation. In this study, activation and migration of CD8+ T cells were elevated and the expressions of immunosuppressive factors were decreased in sorafenib pretreated group. The results were similar to those observed using WP1066, a STAT3-inhibitor, as the positive control. Conclusions The activation of CD8+ T cells and the therapeutic efficacy in vivo with ACT could be improved by pretreatment of sorafenib through the downregulation of STAT3 expression and its effector proteins. The imaging system, such as pGBeLT, could be a powerful tool to facilitate the development of ACT. (This study was supported by a grant NSC 100-2321-B-010-013 from National Science Council, Taipei, Taiwan.)

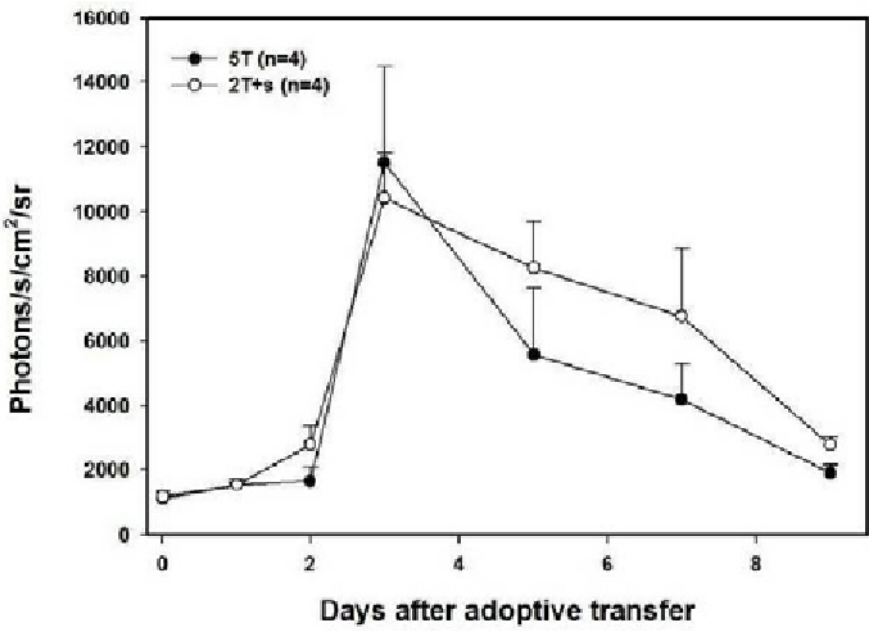


in vivo T cell activation tracking

Disclosure of author financial interest or relationships:
**H. Chuang**, None; **Y. Chang**, None; **J. Hwang**, None.

Presentation Number **P722**
Poster Session 4
September 8, 2012 / 14:45-14:45 / Room: The Liffey

# Parallel Visualisation of Monocyte Activity and Myelination Status in Experimental Neuroinflammation using Target-specific Optical Molecular Imaging

***Michel Eisenblaetter***[1,4], *Stefanie Albrecht*[3], *Christiane Geyer*[1], *Lydia Wachsmuth*[1], *Walter Heindel*[1], *Thomas Vogl*[2], *Tanja Kuhlmann*[3], *Christoph Bremer*[5], [1]*Department of Clinical Radiology, University Hospital of Muenster, Muenster, Germany;* [2]*Department of Immunology, University Hospital of Muenster, Muenster, Germany;* [3]*Department of Neuropathology, University Hospital of Muenster, Muenster, Germany;* [4]*Division of Imaging Sciences & Biomedical Engineering, King's College London, London, United Kingdom;* [5]*Department of Radiology, St Franziskus Hospital, Muenster, Germany. Contact e-mail: eisenblaetter@uni-muenster.de*

Purpose: Multiple Sclerosis (MS) is a chronic, usually progressive, autoinflammatory disease, affecting the central nervous system myelin sheth with consecutive significant impairment of neural function. Spontaneously and under therapy, remyelination can occur. Established imaging techniques are only moderately specific for the inflammatory process and frequently lack sensitivity to reflect the myelination status. Activated macrophages have been shown to play a crucial role in initialisation and maintenance of inflammation. Previous work proved expression of macrophage-related protein S100A9 to be correlated to local disease activity and optical imaging (OI) of S100A9 has successfully been performed. Near-infrared fluorescent 3,3'-diethylthiatricarbocyanine-iodide (DBT) has been shown to selectively bind myelin. In combination, S100A9-specific and myelin-sensitive imaging were examined for the potential to closely follow the status of experimental MS on a molecular level. Materials and Methods: Under Cuprizone diet, C57Bl6 mice developed reversible, MS-equivalent lesions, predominantly in the central corpus callosum region. Healthy mice served as control. AntiS100A9 or rabbit-derived Immunoglobulin G (IgG; control for non-specific label distribution) were labelled with Cy5.5 for OI. Tracer doses per animal were 100µg anti-S100A9-Cy5.5, 24h and 2µg DBT, 5min prior to fluorescence mediated tomography with excitation/emission of 680/700nm (Cy5.5) and 750/780nm (DBT). In-vivo imaging data were acquired initially, at day 35 of cuprizone treatment (max demyelination) and during the recovery and thus remyelination process and analysed for fluorescence signals, particularly in the corpus callosum region. For correlation of in-vivo OI, magnetic resonance tomography (MRI) for lesion-detection and immunohistochemistry for myelin, S100A9 and macrophage markers were performed. Statistical analysis: student-t-test, one-way-anova Results: After 35 days of Cuprizone-treatment, animals presented with manifest, active neuroinflammation as reflected by significantly elevated intracerebral antiS100A9-Cy5.5 accumulation compared to healthy controls (3.65pmol vs. 1.2pmol; p=0.02). Unspecific IgG-Cy5.5 accumulated to a significantly lower scale (2.2pmol vs. 3.65pmol; p=0.03). Myelin-associated DBT-accumulation dropped from 30.7pmol (healthy) to 1.5pmol (35d Cuprizone), reflecting significant demyelination. Remyelination over three consecutive weeks led to recovery of DBT fluorescence and decay of S100A9 levels. Imaging-parallel immunohistochemistry during the remyelination process supported the in-vivo imaging results regarding S100A9 expression. Moreover, histology and MRI confirmed lesion location and severity of demyelination as depicted by DBT OI. Conclusion: AntiS100A9-Cy5.5 in combination with DBT could be shown to enable for specific visualisation of central-nervous inflammation using FMT. Interindividual grading according to immune-cell activity and demyelination as well as continuous surveillance of disease progression were possible using this approach.

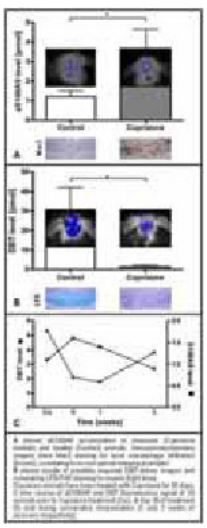

Disclosure of author financial interest or relationships:
**M. Eisenblaetter**, None; **S. Albrecht**, None; **C. Geyer**, None; **L. Wachsmuth**, None; **W. Heindel**, None; **T. Vogl**, None; **T. Kuhlmann**, None; **C. Bremer**, None.

Presentation Number **P723**
Poster Session 4
September 8, 2012 / 14:45-14:45 / Room: The Liffey

# MR imaging of a SPIO-labeled pathogen *in vivo*: Distribution of parasitic protozoan *Entamoeba histolytica* in the liver of a mouse model at 7T

***Thomas Ernst***[1], *Hannah Bernin*[2], *Gerhard Adam*[1], *Hannelore Lotter*[2], *Harald Ittrich*[1], [1]*Department of Diagnostic and Interventional Radiology, University Medical Center Hamburg, Hamburg, Germany;* [2]*Molecular Parasitology Department, Bernard Nocht Institute for Tropical Medicine, Hamburg, Germany. Contact e-mail: ternst@uke.de*

The purpose of this study is to evaluate the labeling efficacy, migration behavior and *in vivo* distribution of the enteric parasite protozoan *Entamoeba histolytica (E.h.)* within the liver in MRI after injection in a mouse model. Non-invasive studies of migration and distribution of *E.h.* in the liver under different immunological constellations can help to understand the underlying mechanisms of amebic liver abscess formation. **Materials and Methods:** *In vitro* magnetic labeling of *E.h.* was performed with commercially available superparamagnetic iron oxide nanoparticles (SPIO) with polyethylene glycol (PEG) coating (nano-screenMAG-PEG/P, Chemicell, Germany, hydrodynamic diameter 200 nm) by incubation for 48h in culture medium. Labeling efficiency and migration behavior of SPIO-*E.h.* was proven in MRI *in vitro* in culture medium in the static magnetic field of a preclinical 7T MRI system (ClinScan, Bruker) using T2w and T2*w dynamic susceptibility contrast MR sequences (DSC-MRI) for 88 hours (temporal resolution 4 min./image, effective voxel size 80x80x600 µm$^3$). Movement patterns were analyzed using ImageJ (NIH, USA). For *in vivo* experiments $10^5$ SPIO-*E.h.* were injected in the left liver lobe of mice followed by serial respiration triggered T2*w and T2w MRI up to 3 days after injection. Furthermore ex vivo high resolution MRI was performed on removed liver specimens for in/ex-vivo comparison. MR images were matched with histology (PAS and Prussian Blue stains) as well as immunohistochemistry. **Results:** Efficient magnetic labeling of *E.h.* could be performed by incubation with PEG-coated SPIO keeping the pathogenity and viability of *E.h. In vitro* dynamic MRI showed an undirected migration of single SPIO-*E.h.* in culture medium with pathogen movement in macroscopic dimensions with typical speeds of up to 4 mm/h. *In vivo* and *ex vivo* MRI of SPIO-*E.h.* showed strong *E.h.* presence at the site of amebic liver abscess formation and broad distribution within the left liver lobe, whereas no SPIO-*E.h.* could be detected in liver lobes different from lobe of injection. All MR findings were confirmed by histology. **Conclusion:** Efficient magnetic labeling and non-invasive *in vivo* migration monitoring of pathogenic *E.h.* within the murine liver tissue is feasible in MRI.

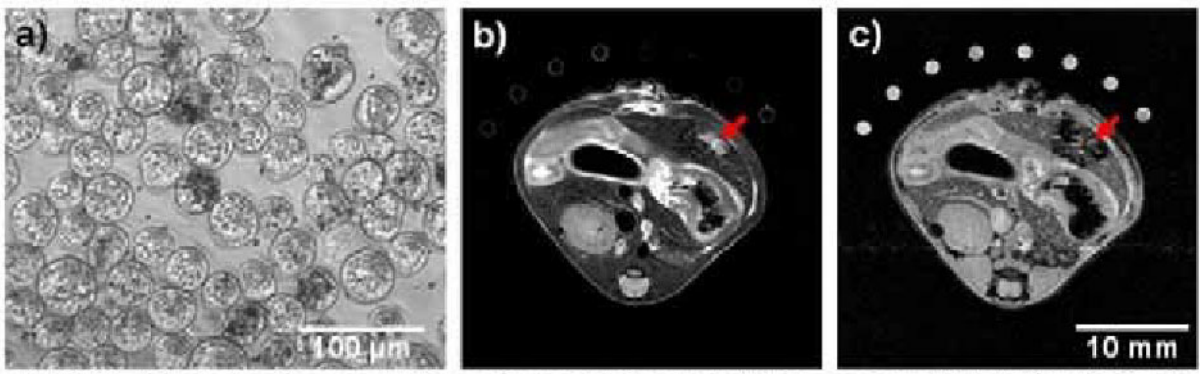


a) SPIO - labeled pathogen *Entamoeba histolytica* in light microscopy. **b)+c)** T2w fast spin echo image (b) and T2*w gradient echo image (c) of a transversal section of the mouse liver at day 3 post injection. An pronounced amebic liver abscess shows on b) while a broad distribution of SPIO - labeled *E.h.* in the left liver lobe can be observed on c).

Disclosure of author financial interest or relationships:
**T. Ernst**, None; **H. Bernin**, None; **G. Adam**, None; **H. Lotter**, None; **H. Ittrich**, None.

Presentation Number **P724**
Poster Session 4
September 8, 2012 / 14:45-14:45 / Room: The Liffey

# Optical Imaging of Articular Cartilage Using Near-Infrared Dipicolylamine Probes

***Xiang Hu***[1,2], *Yang Liu*[1], *Hongguang Liu*[1], *Qian Wang*[3], *Chunxia Qin*[1], *William H. Robinson*[3], *Aixi Yu*[2], *Brian Gray*[4], *Koon Y. Pak*[4], *Zhen Cheng*[1], [1]*Department of Radiology and Bio-X Program, Molecular Imaging Program at Stanford, Stanford, CA, USA;* [2]*2Department of Orthopedics, Zhongnan Hospital of Wuhan University, Wuhan, China;* [3]*3Department of Immunology & Rheumatology, School of Medicine at Stanford, Stanford, CA, USA;* [4]*Molecular Targeting Technologies, Inc., West Chester, PA, USA. Contact e-mail: xianghu@stanford.edu*

Introduction: Novel and effective diagnostic techniques are urgently needed for early detection of osteoarthritis (OA). Deterioration of articular cartilage (AC) occurs at the early stages of OA and is clinically and radiographically silent using the current imaging techniques. Anionic glycoaminoglycans (GAGs) are largely expressed in normal AC while their expression is gradually reduced during the degeneration of AC. Therefore, we hypothesized that near-infrared fluorescence (NIRF) dye labeled cationic molecules could bind with GAGs in cartilage and serve as potential GAGs targeted molecule probes for early diagnosis of OA. Methods: Cationic Cy5 or Cy7 labeled dipicolylamine (DPA)-Zn probes (Cy5-DPA-Zn and Cy7-DPA-Zn (PSVue794®)) and control neutral charged probes (Cy5-DPA and Cy7-DPA) were designed and synthesized. The knee joints (n=4) were incubated with these probes of 10 nM for 1 h to evaluate their binding ability ex-vivo. DPA-Zn was used as a blocking agent and mixed with the NIRF probes (Cy5-DPA-Zn or Cy7-DPA-Zn, more than 100:1) for incubation with the knee joint. The treatment of Chondroitinase ABC, heparitinase or keratanase to joint tissue slides was performed prior to the probes incubation in order to verify GAGs. Sanfranin O staining was also used to validate the location of GAGs in the cartilage using microscope imaging. The OA mice model was established 1 month later after cutting off the anterior cross ligment in right knee joint, while shamming in left knee joint as a control. Histology staining, such as H&E and Sanfranin O, were used to confirm the OA model. MRI was also used to image the early stage of OA as a comparison. Finally, the probes (10 μM, 10 μL) were intra-articular injected into knee joint of both healthy and OA mice (n=4) for in vivo optical imaging. Results: DPA-Zn based NIRF probes were successfully prepared and confirmed by mass spectroscopy and nuclear magnetic resonance. In vitro, both Cy5-DPA-Zn and Cy7-DPA-Zn demonstrated higher uptakes in cartilage than corresponding control probes, Cy5-DPA and Cy7-DPA (2.5-fold at 72h and 1.6-fold at 4h, respectively). Reduced NIRF intensities were also found for blocking agent. Moreover, the optical signal for both probes was sharply decreased after treatment with Chondroitinase ABC, but not with heparitinase or keratanase. For in vivo study, Cy5-DPA-Zn reached the highest contrast compared with Cy5-DPA in normal joint at 72 h post-injection (p.i.) (1.6 fold, $P<0.01$), while Cy7-DPA-Zn reached the highest ratio over Cy7-DPA at 4 h p.i. (1.2-fold). Interestingly DPA-Zn did significantly reduce cartilage uptake of both probes. After OA model confirmation and MRI, the optical imaging of sham and OA knee joints were examined using both NIRF probes. The highest NIRF intensity ratio of 4.6-fold was observed at 72 h p.i in sham vs. OA when the mice were imaged using Cy5-DPA-Zn ($P<0.01$), and 1.6-fold at 4 h p.i. for Cy7-DPA-Zn ($P<0.05$). Conclusion: Both Cy5 and Cy7 labeled cationic DPA-Zn molecules are promising optical imaging probes for early OA diagnosis. Cy5-DPA-Zn demonstrates more favorable properties over Cy7-DPA-Zn and warrants further development and evaluation.

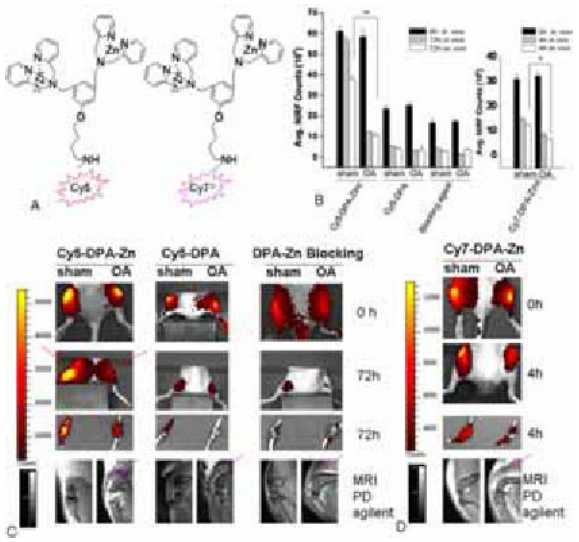


Disclosure of author financial interest or relationships:
**X. Hu**, None; **Y. Liu**, None; **H. Liu**, None; **Q. Wang**, None; **C. Qin**, None; **W.H. Robinson**, None; **A. Yu**, None; **B. Gray**, Molecular Targeting Technologies, Inc., Employment; **K.Y. Pak**, Molecular Targeting Technologies, Inc., Stockholder; **Z. Cheng**, None.

Presentation Number **P725**
Poster Session 4
September 8, 2012 / 14:45-14:45 / Room: The Liffey

# In Vivo Imaging of Ischemia-Induced Apoptosis in Hindlimbs of Mice with Annexin V Linked Streptavidin Probes

***Kyung-Ho Jung***[1,2], *Jin Won Park*[1,2], *Jin Hee Lee*[1,2], *Jin-Young Paik*[1,2], *Cung H. Quach*[1,2], *Seung Hwan Moon*[1,2], *Eun Jeong Lee*[1,2], *Kyung-Han Lee*[1,2], [1]*nuclear medicine, Samsung medical center, Seoul, Republic of Korea;* [2]*School of Medicine, Sungkyunkwan University, Seoul, Republic of Korea. Contact e-mail: jkhope@sbri.co.kr*

Objective: Critical limb ischemia is a severe condition associated with serious complications. Apoptosis is now recognized to be involved in ischemic diseases, indicating its potential as a therapeutic target. Apoptosis can be imaged by annexin V (anxV), but present probes suffer from rapid blood clearance and extensive hepatic accumulation. In this study, we synthesized a new anxV probe with improved in vivo pharmacokinetics, and explored its potential for imaging ischemia-induced apoptosis in hindlimbs of mice. Methods: AnxV-biotin was linked to FITC- or PEcy5.5-conjugated streptavidin (SAv) in a 4:1 molar ratio and purified by centricon filtration. In vitro validation was performed on CT-26 colon cancer cells induced of apoptosis by treatment with 1 μM staurosporine. The ability to target surface-exposed phosphatidylserine of apoptotic cells was verified by confocal microscopy and FACS analysis. For in vivo experiments, C57Bl6 mice underwent hindlimb ischemia by ablation of the femoral artery. The effects of streptozotocin-induced diabetes and benfotiamine therapy were evaluated in separate groups of mice. Animals were tail vein injected with anxV-SAv-PEcy5.5 and underwent fluorescence imaging 15 h later on an IVIS® Spectrum system. Thigh tissues were extracted, imaged for ex vivo fluorescent signals, and quantified for amount of apoptotic cells by western blotting of activated (cleaved) caspase-3 protein. Results: AnxV-SAv-FITC and -PEcy5.5 was synthesized efficiently and reproducibly. Confocal microscopy revealed localization of probes to the surface of staurosporine treated cells, confirming apoptosis-specific targeting. FACS analysis showed right-shifting of fluorescent signals following staurosporine treatment, that resulted in an increase of signal-positive cells from 0.4 % to 8.5 %. Laser doppler imaging confirmed femoral artery ablation to induce severe hindlimb ischemia from immediate post-surgery for up to 5 days. Optical imaging of living mice with anxV-SAv-PEcy5.5 revealed clear visualization of increased probes targeted to ischemic limbs. Significantly higher probe binding to ischemic compared to contralateral muscles (fluorescence intensity ratio, 3.7 ± 0.4) was confirmed by ex vivo imaging of extracted tissues. AnxV-SAv-PEcy5.5 uptake in ischemic limbs was affected by induction of diabetes and by benfotiamine therapy. Finally, the magnitude of anxV-SAv-PEcy5.5 uptake in ischemic muscles correlated with tissue level of activated caspase-3. Conclusion: Fluorophore-conjugated streptavidin linked with anxV provides high contrast images of ischemia-induced apoptosis in hindlimb muscles and may thus be useful for noninvasively monitoring the efficacy of new treatments.

Disclosure of author financial interest or relationships:
**K. Jung**, None; **J. Park**, None; **J. Lee**, None; **J. Paik**, None; **C.H. Quach**, None; **S. Moon**, None; **E. Lee**, None; **K. Lee**, None.

Presentation Number **P726**
Poster Session 4
September 8, 2012 / 14:45-14:45 / Room: The Liffey

# Tracking of antigen-specific cytotoxic T-lymphocytes by multimodal imaging

***Melanie Kimm***[1], *Jing Claussen*[2,3], *Marcus Settles*[1], *Wouter H. Driessen*[2], *Daniel Razansky*[3,4], *Vasilis Ntziachristos*[3,4], *Ernst J. Rummeny*[1], *Reinhard Meier*[1], [1]*Dep. of Radiology, Klinikum rechts der Isar, Munich, Germany;* [2]*iThera Medical, Munich, Germany;* [3]*IBMI, Helmholtz Zentrum München, Munich, Germany;* [4]*Biological Imaging, Technische Universität München, Munich, Germany.*
*Contact e-mail: melanie.kimm@lrz.tum.de*

Immunotherapies, next to chemotherapies, represent an effective method to treat patients with cancer. There are different ways to modulate the adaptive immune system of a patient to eliminate malignant cells. Immunotherapies using antigen-specific cytotoxic T cells showed already a healing effect in several clinical studies. Crucial for a positive response is the survival of the cells within the first week after transfer and the specific homing of the T cells towards the tumor. Imaging modalities that permit to monitor the T cell distribution within the patient could verify a possible accumulation of cells at the specific site and consequently verify responders and non-responders. Currently, scintigraphy with ionizing isotopes is the established clinical standard of reference. To reduce cell and tissue damage due to radiation, our purpose is to compare sensitivity/specificity and spatial/temporal resolution of different non-ionizing imaging modalities for tracking of labeled T cells in a murine tumor model. In this work, MRI and MSOT (multispectral optoacoustic tomography) were used to visualize the whole-body distribution and tumor-specific accumulation of adoptively transferred T cells labeled with modality-specific contrast agents like iron nanoparticles, near-infrared dye or gold nanoparticles. We use a well characterized mouse model (OVA/OT-I) with murine tumor (EL4/ EG7) and murine cytotoxic T cells (CD8+ OT-I T cells) to assure specific T cell distribution and therefore be able to compare the different modalities. First the cell labeling protocols were optimized in vitro and the uptake of the contrast agent in the cells were analyzed by IHC, fluorescence or darkfield microscopy. The uptake of near-infrared dyes turned out to be straightforward and without severe cytotoxicity. In addition, T cell labeling using low concentrations of gold or iron nanoparticles showed no significant cytotoxicity. However, at higher concentrations gold as well as iron nanoparticles induced cell death. Furthermore, the influence of the different contrast agents on antigen-specificity and differentiation was analyzed. Phantom studies of labeled and unlabeled cells were done to determine the sensitivity of the different modalities. Next, we injected labeled T-cells into mice. To ensure specific T cell homing, mice are bearing OT-I positive tumor on one flank an and an OT-I negative tumor on the other flank. MSOT studies demonstrated a high sensitivity in detecting labeled T cells. The signal specificity was verified ex vivo by cryo-sectioning the animals and acquiring fluorescence images. Adoptive transferred murine cytotoxic T cells can be efficiently labeled with near-infrared dyes and nanoparticles. This approach can be used as an effective alternative to monitor immunotherapies using antigen-specific cytotoxic T cells.

Disclosure of author financial interest or relationships:
**M. Kimm**, None; **J. Claussen**, iThera Medical, Employment; **M. Settles**, None; **W.H. Driessen**, iThera Medical, Employment; **D. Razansky**, iThera Medical GmbH, Stockholder; **V. Ntziachristos**, ERC, Grant/research support; Ithera Medical, Stockholder; **E.J. Rummeny**, None; **R. Meier**, None.

Presentation Number **P727**
Poster Session 4
September 8, 2012 / 14:45-14:45 / Room: The Liffey

# Irradiation paves the way for efficient T cell based immunotherapy of cancer by enhancement of homing properties of therapeutic T cells and depletion of host lymphocytes

***Dominik B. Krueger***[1], *Christoph M. Griessinger*[1], *Anna Teske*[1], *Jennifer Schmitz*[1], *Maren K. Koenig*[1], *Daniel Bukala*[1], *Bernd J. Pichler*[1], *Manfred Kneilling*[2], [1]*Department of Preclinical Imaging and Radiopharmacy, Eberhard Karls University of Tuebingen, Tuebingen, Germany;* [2]*Department of Dermatology, Eberhard Karls University of Tuebingen, Tuebingen, Germany. Contact e-mail: dominik.krueger@med.uni-tuebingen.de*

Although tumor antigen specific Interferon-γ producing CD4+ T cells (Th1) can not directly kill tumor cells, several studies revealed their potential in mediating tumor rejection. However, weekly transfer of 1E+7 Tag2-Th1 cells in a pancreatic tumor mouse model (RIP1-Tag2) is only successful in combination with a 2Gy total body irradiation (TBI). The aim of our studies was to identify the basic mechanisms how TBI enables a successful Th1 cell based immunotherapy. Thus, we counted white blood cells of 2Gy TBI or untreated RIP1-Tag2-/- mice and analyzed differential hemograms at several time points. In addition we wanted to analyze TBI-induced depletion of T lymphocytes of the host by i.v. injection of [64Cu]DOTA labeled CD3 antibodies followed by PET/CT investigations for 48h. Finally we performed ex vivo biodistribution analysis of lymphatic organs. For in vivo T cell homing studies T cells were isolated from T cell receptor transgenic (TCR-tg) Tag2 mice and specifically cultured to generate a Th1 phenotype. One day after TBI, Tag2-Th1 cells were Cy5-labelled and injected i.p. (1E+7) into RIP1-Tag2-/- mice. Three days after Cy5-Tag2-Th1 cell injection we performed ex vivo biodistribution OI analysis. Already 3 days after TBI a 77% reduction in the absolute numbers of leukocytes was detected. At this point the percentage of lymphocytes, achieved by differential hemograms, was 63% in untreated and 32% in TBI mice. Thus, the absolute number of lymphocytes in TBI mice declined to approximately one tenth when compared to untreated mice. PET/CT investigations revealed a 20% decreased [64Cu]DOTA-CD3 Ab binding in the spleen of TBI mice compared to untreated mice 48h after injection but we could not identify [64Cu]DOTA-CD3 Ab binding in lymph nodes. The huge TBI induced differences in the spleen detected by PET could be confirmed by ex vivo biodistribution as TBI caused an approximately 50% reduction in the weight of the spleen, and lymph nodes. Normalization to the weight of the lymphatic organs exhibited absolutely unimpaired %ID/g values in both experimental groups. Ex vivo OI analysis 4 days after Cy5-Tag2-Th1 cell transfer resulted in an unspecific biodistribution in the organs. A slightly enhanced homing into the mesenteric and pancreatic lymph nodes as well as the thymus including the perithymic lymph nodes was observed in TBI mice. Our studies revealed an impressive leucocyte and lymphocyte depletion in TBI mice. The TBI-induced depletion of T lymphocytes could be non invasively in vivo detected in the spleen but not in the lymph nodes by the use of T lymphocyte binding [64Cu]DOTA-CD3 Ab and PET/CT. In contrast to our previous studies, where we detected 12 days after TBI a strongly enhanced homing of Tag2-Th1 cells in the lymph nodes, we found in the current study already four days after T cell transfer only a slightly enhanced TBI-induced homing into lymph nodes.

Disclosure of author financial interest or relationships:
**D.B. Krueger**, None; **C.M. Griessinger**, None; **A. Teske**, None; **J. Schmitz**, None; **M.K. Koenig**, None; **D. Bukala**, None; **B.J. Pichler**, Siemens, Grant/research support; AstraZeneca, Grant/research support; Bayer Healthcare, Grant/research support; Boehringer-Ingelheim, Grant/research support; Oncodesign, Grant/research support; Merck, Grant/research support; Bruker, Grant/research support; **M. Kneilling**, None.

Presentation Number **P728**
Poster Session 4
September 8, 2012 / 14:45-14:45 / Room: The Liffey

# Improved Assessment of Drug Response by Multi-modality Molecular Imaging in Collagen-induced RA

***Deanne Lister**, Meridith Baugher, Tracey Woolliscroft, Jeni Baranski, Jeremy Castorena, Darren Shaw, Erin Trachet, Wilbur R. Leopold, Patrick McConville, Molecular Imaging, Inc., Ann Arbor, MI, USA. Contact e-mail: dlister@molecularimaging.com*

Objectives: Imaging biomarkers provide an opportunity to assess different mechanistic aspects of acute inflammation non-invasively and may aid decisions in drug discovery. The aim of this work was to test the ability for FDG PET (metabolism) and optical imaging biomarkers (cathepsin and MMP activity), via fluorescence molecular tomographic (FMT) imaging, to predict disease pathology and treatment response in mouse collagen-induced rheumatoid arthritis (CIA RA). Methods: CIA RA was induced in female DBA/1 mice by SC inj. of bovine type II collagen in CFA at the tail base, with a booster 21d later. Footpad thickness (FT) and clinical score (CS) were used to assess disease progression. The study design incorporated naïve (n=3), vehicle, dexamethasone (DEX;3mpk;PO;QD) and celecoxib (CXB;30mg/kg;PO;BID) (all n=10) treatment groups. PET scans of hind paws were acquired 1.5h after IV FDG inj.on D43. Cathepsin (ProSense;PS) and MMP (MMPSense;MS) (PerkinElmer,MA) activatable fluorescent probes were injected IV 24 hours prior to fluorescence molecular tomography (imaging on D28 and D42). Histology was used to assess disease pathology with scoring for inflammation, pannus, cartilage damage, bone resorption and periosteal/exostotic changes. Results: RA disease, based on footpad thickness and clinical score persisted through to study termination on D50. DEX produced near-full (statistically significant) disease inhibition compared to vehicle controls, based on clinical score and moderate inhibition of FT. CXB showed a clinical score response (50% decrease), compared with controls, and minor inhibition of FT. Through FMT imaging, MS provided a more sensitive biomarker than PS due to greater disease-based activation. Activation of MS and PS, and showed significant effects vs vehicle for DEX, but not CXB. FDG uptake (see Fig) was significantly lower after DEX treatment, but showed no difference after CXB treatment, compared with vehicle controls. Histopathology showed significant disease inhibition for inflammation, cartilage damage and bone resorption for DEX, but no pathologic disease inhibition after CXB treatment, compared with vehicle controls. Conclusions: FDG SUV, and MS/PS activation provided sensitive and specific biomarkers of acute inflammation and treatment-inhibition, in the CIA model. Based on clinical score measurements, CXB showed a treatment effect, but provided no inhibition of disease based on pathology. For CXB, the MS and PS based signals demonstrated a trend toward treatment effect. However, there was no CXB-based FDG SUV inhibition and FDG SUV showed a strong correlation with footpad thickness for DEX. FDG SUV therefore provided a more sensitive biomarker for CIA RA, compared with MMP and cathepsin based biomarkers. FDG SUV was more predictive of disease pathology and response than the traditional FT and CS measures. FDG PET may provide more predictive assessment of new RA therapies, as well as clinically translatable methodology for use in drug trials.

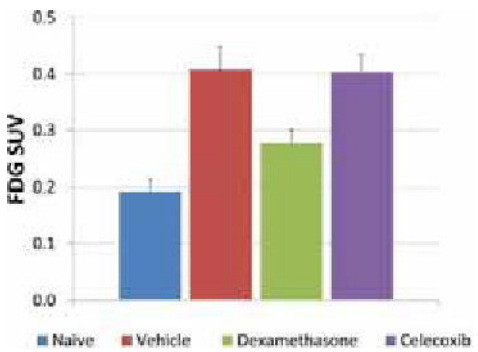


Mean FDG SUV by group (mean with SD). P<0.05: DEX vs VEH, CXB and Naive vs VEH, CXB.

End Points Summary (group mean values)

| Group | Max. Footpad Thickness (mm) | Clinical Score (D42) | Combined Histopath Score | FDG SUV - mean | MMPSense Fluorescence Max. (nM, D42) | ProSense Fluorescence Max. (nM, D42) |
|---|---|---|---|---|---|---|
| Vehicle Control | 6.0 | 40 | 8.3 | 0.41 | 314 | 91 |
| Celecoxib (Llmg/kg; PO; BID) | 3.5 | 22 | 8.4 | 0.40 | 370 | 42 |
| Dexamethasone (3mg/kg; PO; QD) | 4.4 | 0* | 1.0* | 0.25* | 168* | 0* |

P<0.05 vs Vehicle Control

Disclosure of author financial interest or relationships:
**D. Lister**, Molecular Imaging, Inc., Employment; **M. Baugher**, None; **T. Woolliscroft**, Molecular Imaging, Inc., Employment; **J. Baranski**, Molecular Imaging, Inc., Employment; **J. Castorena**, None; **D. Shaw**, Molecular Imaging Inc., Employment; **E. Trachet**, None; **W.R. Leopold**, Molecular Imaging Inc., Employment; **P. McConville**, Molecular Imaging, Inc., Employment .

Presentation Number **P729**
Poster Session 4
September 8, 2012 / 14:45-14:45 / Room: The Liffey

# Simultaneous Imaging of M1 and M2 Macrophages

***Alexander O'Neill**, Margaret S. Cooper, Jennifer D. Williams, Levente K. Meszaros, Florian Kampmeier, Alexander Koers, Phil Blower, Greg Mullen, Imaging Sciences and Biomedical Engineering, King's College London, London, United Kingdom. Contact e-mail: cheezmani@hotmail.com*

Background: Macrophages are tissue resident cells of the innate immune system which play critical roles in both host defence and homeostasis. In vivo macrophage populations display a high degree of phenotypic heterogeneity, with proper host function dependent upon the spatial-temporal co-ordination of these populations. The classification of macrophages into inflammatory (M1) and anti-inflammatory (M2) subsets attempts to capture this versatility of phenotype and how this relates to their behaviour in normal and diseased states. We have previously reported non-invasive imaging of the macrophage-restricted marker CD169 (Sialoadhesin or Siglec 1) to monitor the recruitment of M1 macrophages during rejection of a transplanted organ. The marker CD163 (the haemoglobin-haptoglobin scavenger receptor) is a well-known as a marker for mature macrophages, displaying an M2 phenotype, however significant levels of soluble antigen are found in the blood. Herein, we report the preliminary imaging studies of dual isotope labelled anti CD169 and CD163 antibodies to simultaneously detect M1 and M2 macrophage populations non-invasively. Method: ED3 (anti-CD169) was directly labelled with Tc-99m using 2-mercaptoethanol reduction followed by incubation with Tc-99mO and MDP kit. ED2 (anti-CD163) was conjugated to CHC-A''-DTPA and radiolabelled with In-111Cl3. Stability of both compounds was assessed by size-exclusion chromatography (SEC) using a gamma detecting radio-HPLC system. Imaging of Wistar rats was performed at 3hrs post injection with Tc-99m-ED3 and In-111-ED2. Results: Both compounds exhibited serum stability of >95% over 24 hrs. In vivo imaging revealed remarkable rapid blood clearance for an intact IgG, permitting imaging at the early time point of 3hrs. Surprisingly, circulating soluble CD163 antigen did not interfere with endogenous macrophage targeting. In accordance with antigen density, antibodies demonstrated highest uptake in the spleen (54.3%ID/g ± 6.62 ED2 versus 52.3 %ID/g ± 13.23 ED3), followed by the liver (9.9 %ID/g ± 3.99 ED2 versus 9.2 ± 1.74 ED3). Comparison of tissue-to-blood values revealed higher uptake of ED2 compared to ED3 in the spleen, liver and bone by a factor of 3, representing higher endogenous antigen levels. Conclusions: We propose dual isotope-labelling of CD169 and CD163 as means of detecting M1 and M2 macrophage populations simultaneously. This opens the possibility of monitoring these subsets during disease, and providing an insight into the macrophage behaviour in response to therapy thereby influencing treatment decisions.

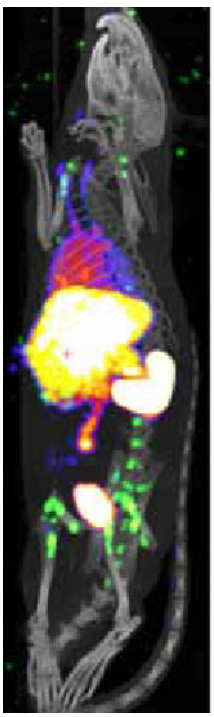

Disclosure of author financial interest or relationships:
**A. O'Neill**, None; **M.S. Cooper**, None; **J.D. Williams**, None; **L.K. Meszaros**, None; **F. Kampmeier**, None; **A. Koers**, None; **P. Blower**, None; **G. Mullen**, None.

Presentation Number **P730**
Poster Session 4
September 8, 2012 / 14:45-14:45 / Room: The Liffey

# Intraperitoneal Administration of Honey Elicit Robust Luminescence Signals from Myeloperoxidase Activation

***Rao V. Papineni**, Sean P. Orton, Carestream Molecular Imaging, Carestream Health, Inc., Woodbridge, CT, USA. Contact e-mail: rao.papineni1@carestreamhealth.com*

Honey is being used in traditional medicine from ancient times, and shown to provide anti-fungal, anti-bacterial, anti- ulcer, and anti-tumoral effects. Intraperitoneal administration of honey acts as an anti-adhesive agent preventing postoperative intra-abdominal adhesion formation in a rabbit model. It is unclear if the anti-adhesive property of honey is resultant of inflammatory of anti-inflammatory response. Here, we determined the downstream events of intraperitoneally administered honey to evaluate a role of honey in early immune response. Cellular Myeloperoxidase(MPO) is an inflammatory heme protein present in myeloid cells- neutrophils, and macrophages. We determined myeloperoxidase activity in vivo using luminescence approach with luminol (5-amino-2,3-dihydro-1,4-phthalazine-dione) as a substrate. Luminol a redox-sensitive compound emits blue luminescence upon exposure to oxidizing agents, and in vivo, it has been established to have unique specificity for MPO activity resultant of myeloid cell activation. We monitored real-time in vivo MPO activity in response to intraperitoneal administration of honey 0.1 ml (50% volume/volume dilution with PBS) in athymic nude mice. Non invasive luminescence and X-ray images were obtained at different time points after administration of honey. Significant enhancement in MPO activity was observed within 3 hrs of administration of a single dose of honey (i.p injection). Overlay of luminescence images obtained at multiple angles with their respective planar x-ray images show robust polymorphonuclear leukocytes (PMN) activation at different lymph nodes (figure attached). Further studies using animal models (diseased) are needed to evaluate if the curative properties of these therapeutic compounds require the involvement of such early inflammation responses. Such an immune responsive component of therapeutic drugs can be classified as "therapeutic inflammation". These real-time MPO activity monitoring methodologies therefore will provide valuable information necessary for evaluation of therapeutic compounds and in development of better drug treatments.

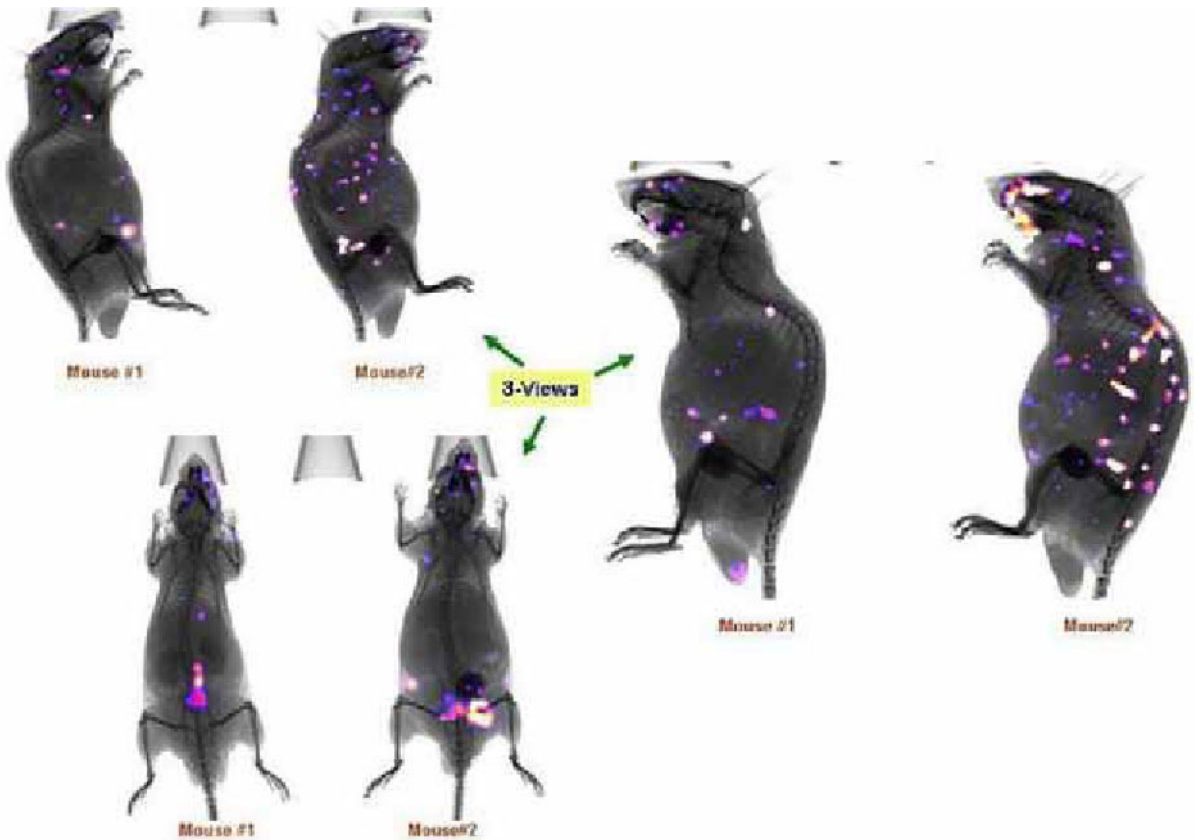


Induced in vivo Myeloperoxidase Activity.

Disclosure of author financial interest or relationships:
**R.V. Papineni**, Carestream Health Inc, Employment; **S.P. Orton**, Carestream Health, Inc., Employment .

Presentation Number **P731**
Poster Session 4
September 8, 2012 / 14:45-14:45 / Room: The Liffey

# A novel NIR dye for in vivo temporal tracking of labeled macrophages to sites of acute inflammation

*Kristine Vasquez, Nara Narayanan, Milind Rajopadhye,* ***Jeffrey D. Peterson****, PerkinElmer, Boston, MA, USA. Contact e-mail: jeff.peterson@perkinelmer.com*

Understanding the pathophysiology of inflammatory disease processes at the cellular and biochemical level is a major challenge in basic research and drug development. The difficulty in recapitulating complex biological processes in vitro, in particular, raises the importance of robust and quantitative in vivo techniques to assess progressive inflammation and therapeutic intervention. For example, the recruitment of monocytes and macrophages from the blood to sites of tissue infection or trauma is crucial for the induction of acute or chronic inflammation. To assess the inflammatory biological changes that occur in acute inflammation, we used a simple model of acute neutrophil-driven inflammation, carrageenan-induced paw edema (CPE), generated in mice. A carrageenan solution (1% in PBS) was injected in the right footpad of each mouse to cause overt swelling and inflammation, and PBS was injected in each left footpad as a non-inflamed control site. We used non-invasive fluorescent imaging (Fluorescence Molecular TomographyTM [FMT]) to assess these changes, validating the model by measuring edema with a near infrared (NIR) vascular leak agent and inflammatory cell cathepsin and neutrophil elastase activity with NIR protease activatable agents. These agents all provided robust and statistically significant signal increases in inflamed versus control paws and correlated well with changes in paw thickness. In addition, a novel lipophilic cell-labeling agent was developed (VM3211) as a means to label primary macrophages, providing a tool to monitor the recruitment of these cells to the site of inflammation. This NIR agent effectively intercalates into cell membranes to provide a long-lasting signal for in vitro and in vivo studies with imperceptible effects on cell viability or function. To perform these macrophage-tracking studies, thyoglycollate-elicited macrophages from donor mice were labeled with VM3211 and then transferred intravenously (5x106 cells/mouse) into normal syngeneic mice. The labeled cells were allowed to accumulate in the liver and lungs for 24h, and then the recipient mice were injected with carrageenan (right footpad) and PBS (left footpad). The active site of inflammation was used as a means to recruit other inflammatory cells, including the VM3211-labeled macrophages injected 24h earlier. Paw swelling and NIR FMT imaging was performed prior to carrageenan injections and at 3, 24, 48, 72, and 168 h thereafter. Macrophages selectively trafficked into inflamed paws and accumulated there, showing statistically significant elevations in fluorescence from 3-72h. A single prophylactic dose of dexamethasone (10 mg/kg IP) was sufficient to delay macrophage influx for at least 24h and decrease the peak levels of macrophage influx by approximately 40%. As expected, the peak macrophage influx accounted for ~1% of the total injected cells (50,000 cells/mouse), and control experiments characterized the linearity of cell quantification for VM3211-labeled macrophages.

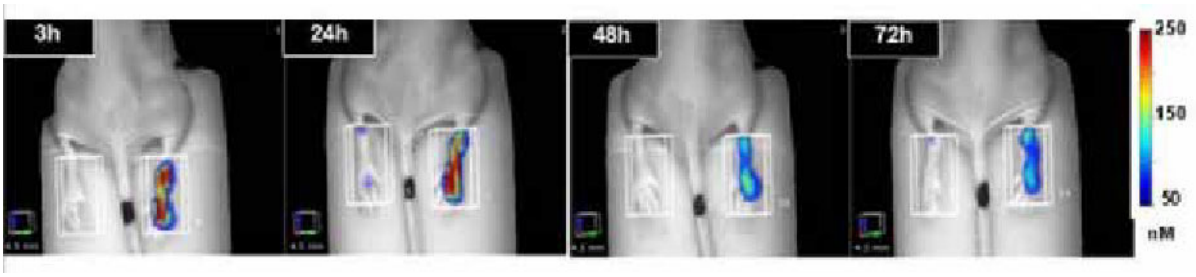


Disclosure of author financial interest or relationships:
**K. Vasquez**, PerkinElmer, Employment; **N. Narayanan**, None; **M. Rajopadhye**, PerkinElmer, Employment; **J.D. Peterson**, PerkinElmer, Employment .

Presentation Number **P732**
Poster Session 4
September 8, 2012 / 14:45-14:45 / Room: The Liffey

# Whole-body in vivo SPECT/CT reporter gene imaging of regulatory T cells in an adoptive cell therapy in skin transplant models

***Ehsan Sharif-Paghaleh***[1,2], *John Leech*[1], *Robert Lechler*[1], *Lesley Smyth*[1], *Giovanna Lombardi*[1], *Greg Mullen*[1,2], [1]*MRC Centre for Transplantation, KCL, london, United Kingdom;* [2]*Imaging Sciences, KCL, London, United Kingdom. Contact e-mail: ehsan.sharif-paghaleh@kcl.ac.uk*

Regulatory T cells (Tregs) were identified several years ago and are key in controlling autoimmune diseases and limiting immune responses to foreign antigens. Imaging of the human sodium/iodide symporter via Single Photon Emission Computed Tomography (SPECT) has been used to image various cell types in vivo. It has several advantages over other imaging techniques including high sensitivity, it allows non-invasive whole body studies of viable cell migration and localisation of cells over time and lastly it may offer the possibility to be translated to the clinic. This study addresses whether SPECT/CT imaging can be used to visualise the migratory pattern of Tregs in vivo. Treg lines derived from CD4+CD25+FoxP3+ cells were retrovirally transduced with a construct encoding for the human Sodium Iodide Symporter (NIS) and the fluorescent protein mCherry and stimulated with autologous DCs. NIS expressing self-specific Tregs were specifically radiolabelled in vitro with Technetium-99m pertechnetate (99mTcO4-) and exposure of these cells to radioactivity did not affect cell viability, phenotype or function. In addition adoptively transferred Treg-NIS cells were imaged in vivo in C57BL/6 (BL/6) mice by SPECT/CT using 99mTcO4-. After 24 hours NIS expressing Tregs were observed in the spleen and their localisation was further confirmed by organ biodistribution studies and flow cytometry analysis. The data presented here suggests that SPECT/CT imaging can be utilised in preclinical imaging studies of adoptively transferred Tregs without affecting Treg function and viability thereby allowing longitudinal studies within disease models. Moreover, we have demonstrated that this method of imaging can be utilised to image migration of Tregs with either direct or indirect-alloantigen specificity to the draining lymph nodes in a skin transplant model.

Disclosure of author financial interest or relationships:
**E. Sharif-Paghaleh**, None; **J. Leech**, None; **R. Lechler**, None; **L. Smyth**, None; **G. Lombardi**, None; **G. Mullen**, None.

Presentation Number **P733**
Poster Session 4
September 8, 2012 / 14:45-14:45 / Room: The Liffey

# In Vivo imaging of chronic asthma progression and pharmacological response in a triple allergen mouse model using FMT

***Fabio Stellari***, *Paola Caruso, Veronica Puviani, Chiara Carnini, Maurizio Civelli, Villetti Gino, pulmonary in vivo pharmacology, Chiesi Farmaceutici, Parma, Italy. Contact e-mail: fb.stellari@chiesi.com*

Asthma is a multifactorial and multicellular disease: a variety of sensitization and challenge mouse models of asthma has been developed but the transient nature of the inflammatory response (pathology peaking 24 to 72 hours after challenge and resolving in 1 to 2 weeks), do not mimic the chronic features of human asthma. Moreover, the conventional assessment of parameters associated to an asthma phenotype in animal models currently relies on invasive measures of pulmonary function and ex vivo characterization of pulmonary cellular infiltration that precludes the possibility of repeated, longitudinal assessment of test subjects. A step forward in asthma modelling is represented by recently described mouse model of chronic asthma characterised by sensitization of Balb-C mice twice a week for 8 weeks with a combination of 3 natural allergens relevant for the human pathology (dust mite, ragweed, and aspergillus, DRA). We report here the non-invasive evaluation of lung inflammation in the DRA mouse model by using near-infrared imaging by FMT. After 6 weeks of sensitisation with DRA, all mice in the study were injected intravenously with ProSense 680 and 24 hours later mouse lungs were imaged by FMT to reveal and quantify protease activity associated with the inflammatory cellular infiltration. ProSense fluorescence signal at 6 weeks in the DRA sensitized mice showed a fold of increase over controls of 4.3±0.3. The fluorescent signal correlated with ex vivo analysis performed on the same subjects: bronchoalveolar lavage (BAL) cell analysis showed infiltration of white blood cells (Ctr=0.26±0.04, DRA=2.87±0.29x103; cells/ul), eosinophils (Ctr=0, DRA=1.065±0.13x103; cells/ul), lymphocytes (Ctr=0, DRA=0.40±0.01x103; cells/ul), and neutrophils (Ctr=0, DRA=0.39±0.04x103; cells/ul), paralleled by an increase of relevant cytokines and chemokines (IL-2,-4,-5,-12,-13,-17, KC, rantes and eotaxin), while histological analysis confirmed inflammatory infiltration. To further explore the relationship between fluorescence data and ongoing inflammation the same mice were challenged with DRA for 2 additional weeks and were in parallel randomized in two different groups, receiving an oral administration of either vehicle or budesonide 3 mg/kg. The oral treatment was repeated for 3 days followed by a wash-out period of 2 days up to a total of 3 cycles. At week 8, 24 hours after the last DRA challenge and budesonide treatment, mice were injected intravenously with Prosense 680 and imaged by FMT. DRA mice treated with budesonide showed 66±6.9% inhibition of fluorescence signal vs DRA-challenged, vehicle-treated mice. When considering individual mice before and after treatment with budesonide, 64±7.9% of inhibition of fluorescence signal was observed. Analysis of inflammatory cells and cytokine/chemokine concentration in BAL as well as histological analysis confirmed a good correlation with ProSense activation. In summary, FMT is suitable for non-invasively visualize and quantify asthma progression in models of chronic asthma in mice and for monitoring pharmacological responses in a longitudinal way.

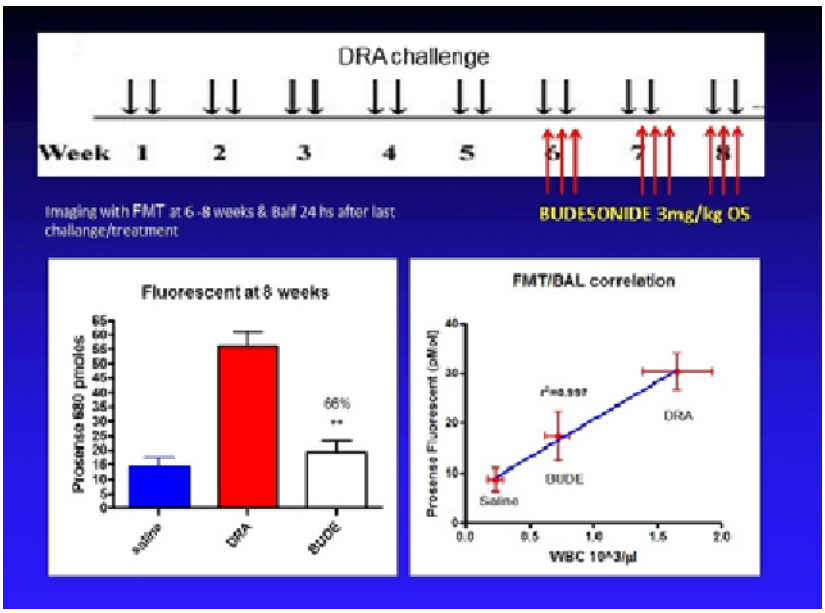


Disclosure of author financial interest or relationships:
**F. Stellari**, None; **P. Caruso**, None; **V. Puviani**, None; **C. Carnini**, None; **M. Civelli**, None; **V. Gino**, Chiesi Farmaceutici S.p.A., Employment .

Presentation Number **P734**
Poster Session 4
September 8, 2012 / 14:45-14:45 / Room: The Liffey

# NIR-fluorescence imaging showed cathepsin and MMP activity in a rheumatoid arthritis model, but only MMP activity in an osteoarthritis model

***Eline Vermeij**, Marije Koenders, Onno Arntz, Miranda Bennink, Peter van Lent, Wim B. van den Berg, Fons A. van de Loo,*
*Rheumatology Research & Advanced Therapeutics, Radboud University Nijmegen Medical Centre, Nijmegen, Netherlands. Contact e-mail: e.vermeij@reuma.umcn.nl*

During joint inflammation and destruction, a variety of proteases are upregulated, including different cathepsins and matrix-metalloproteinases (MMP). Enzyme activity can be quantitated in-vivo by fluorescence imaging of activatable near-infrared probes. Rheumatoid arthritis (RA) is regarded as a disease with a lot of inflammation and destruction, whereas osteoarthritis (OA) is regarded as a disease with cartilage destruction, but the role of inflammation in this process is still debatable. Therefore, in this study, we investigated cathepsin and MMP activity in the process of cartilage destruction, in both a RA and an OA model. Collagen-induced arthritis (CIA) was induced in DBA1/J mice, mimicking a RA model. Destabilization of the medial meniscus (DMM) was induced in C57Bl6/N mice causing instability of the joint and subsequently osteoarthritic features. During the disease process in both models, fluorescence imaging was performed using Sense 680 probes (PerkinElmer, Massachusetts, USA) and enzyme activity was detected using the IVIS Lumina (Caliper Life Sciences). The ProSense 680 probe becomes activated upon enzymatic cleavage by cathepsins, whereas the MMPSense 680 can be activated by different MMPs. After imaging, mice were sacrificed and knee and ankle joints were dissected and processed for histology. The ProSense as well as the MMPSense showed an 3 times increased fluorescent signal intensity during CIA, suggesting both cathepsin and MMP activity in this model. Interestingly, on the other hand, only MMP activity (1,5 times higher) could be measured in the DMM model. On histological level, although different in severity, the CIA model and the DMM model both showed features of cartilage damage. This finding suggests that there is a role for MMPs, but not for cathepsins, in the process of cartilage damage. We can conclude that imaging of these two probes is a sensitive method to measure joint inflammation and connective tissue destruction in both an inflammatory model and a model with only destruction. Combining the imaging of local enzyme activity with histology may unravel the processes involved in joint destruction. In the CIA model, inflammation and destruction seemed to be correlated, while the DMM model showed MMP activity without inflammation, suggesting a role for MMPs, but not for cathepsins in cartilage damage.

Disclosure of author financial interest or relationships:
**E. Vermeij**, None; **M. Koenders**, None; **O. Arntz**, None; **M. Bennink**, None; **P. van Lent**, None; **W.B. van den Berg**, None; **F.A. van de Loo**, None.

Presentation Number **P735**
Poster Session 4
September 8, 2012 / 14:45-14:45 / Room: The Liffey

# Ascorbic acid: what is its therapeutic potential against colorectal adenocarcinoma?

*Ana S. Pires[1,4], Ana C. Mamede[1,3], Vanessa Silva[1,4], **Ana M. Abrantes**[1,2], João E. Casalta-Lopes[1], Ana B. Sarmento-Ribeiro[5,2], Maria F. Botelho[1,2], [1]Biophysics Unit, IBILI, Faculty of Medicine, University of Coimbra, Coimbra, Portugal; [2]CIMAGO, Faculty of Medicine, University of Coimbra, Coimbra, Portugal; [3]CICS-UBI, Health Sciences Research Center, University of Beira Interior, Covilhã, Portugal; [4]Faculty of Sciences and Technology, University of Coimbra, Coimbra, Portugal; [5]Applied Molecular Biology and Hematology Group, Faculty of Medicine, University of Coimbra, Coimbra, Portugal. Contact e-mail: mabrantes@ibili.uc.pt*

Background: Colorectal cancer (CRC) is a major health problem, with more than 800,000 new cases diagnosed worldwide every year. A better understanding of the processes involved in the transformation of normal cells into cancer cells has led to the development of new therapies which target cancer through different mechanisms. The use of vitamin C in the treatment of cancer has been the source of many controversies over the last 25 years. Vitamin C is available in its reduced form (ascorbic acid - AA) and in its oxidized form (dehydroascorbic acid). Although AA is most commonly known for its antioxidant properties, it is also known to function as a pro-oxidant at pharmacological concentrations, promoting the formation of reactive oxygen species (ROS). The increased production of hydrogen peroxide, coupled with the breakdown of the activity of antioxidant enzymes and the presence of transition metals in cancer cells, may result in the selective cytotoxicity of vitamin C and the subsequent revelation of its therapeutic potential. The aim of this study is to evaluate the therapeutic potential of AA in human colorectal adenocarcinoma cell lines in vitro and in vivo. Methods: Two human colorectal adenocarcinoma cell lines, the cells WiDr and C2BBe1, were cultured in DMEM supplemented with 10% FBS. Cells were incubated in absence and with different concentrations of AA during different periods of time. The half maximal inhibitory concentration (IC50) was calculated after 24, 48, 72 and 96 hours by the sulphorhodamine B (SRB) assay. In order to evaluate cell survival, clonogenic assays were performed. At tenth day, the number of colonies was counted, being the plate efficiency and the survival factor determined. In order to verify in vivo the evolution of tumor growth after the daily injection of AA, WiDr cells were inoculated on the back of Balb/c nu/nu mice and, during several days, the body weight and tumor size of mice were monitored. AA was not administered to control animals. Results: Our results obtained with SRB show that AA induces a decrease in cell proliferation in both cell lines, in a dose-dependent way (r2>0.91). It was also verified that the IC50 of AA decreases in both cell lines in a time-dependent way. The clonogenic assays revealed that, as the concentration of AA increases, the survival factor decreases (p=0.016). This behaviour was observed in both cell lines, being more evident in WiDr cells (p=0.00075). The in vivo studies suggest that AA administered daily at 150mg/kg inhibits tumor growth since there are significant differences between the two mices groups (control vs treated mice) with respect to achieve a relative volume of 3 (log-rank test, p=0.002). Conclusions: Our study suggest that AA induces an anti-proliferative effect and a decrease in WiDr and C2BBe1 cells survival. Our results also indicate that AA stabilizes tumor growth in a mice model of CRC. The data obtained in the two different human cell lines of colorectal adenocarcinoma could contribute to the insights of the role of antioxidants as anti-cancer therapies.

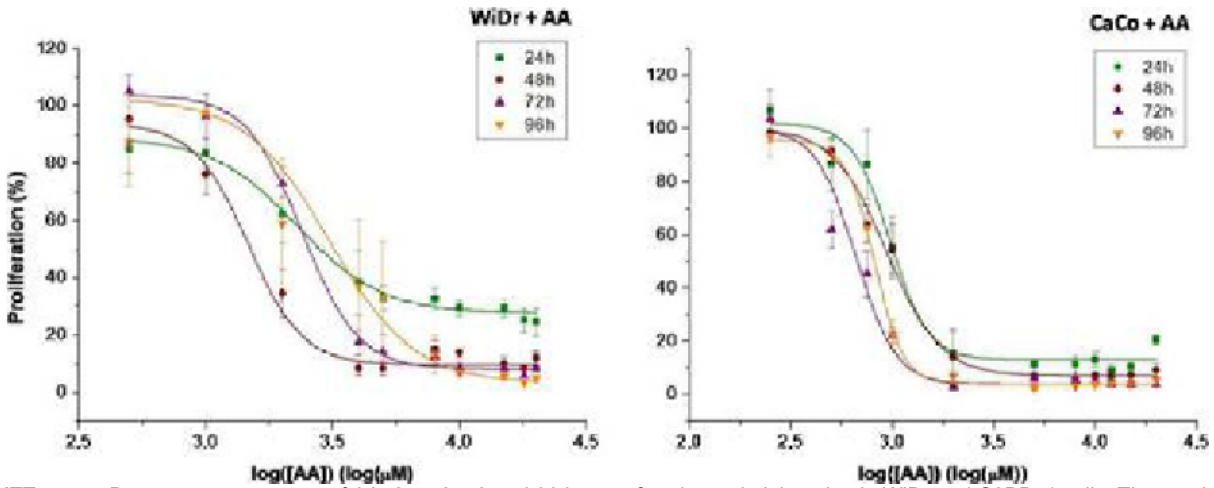


Figure 1 - MTT assay. Dose-response curves of AA, 24, 48, 72 and 96 hours after drug administration in WiDr and C2BBe1 cells. The results represent the average of six independent experiments.

Disclosure of author financial interest or relationships:
**A.S. Pires**, None; **A.C. Mamede**, None; **V. Silva**, None; **A.M. Abrantes**, None; **J.E. Casalta-Lopes**, None; **A.B. Sarmento-Ribeiro**, None; **M.F. Botelho**, None.

Presentation Number **P736**
Poster Session 4
September 8, 2012 / 14:45-14:45 / Room: The Liffey

# Development of a Dll4 binding peptide by phage display

***Annette Altmann**, Frederic Zoller, Annette Markert, Walter Mier, Uwe Haberkorn, Nuclear Medicine, University of Heidelberg, Heidelberg, Germany. Contact e-mail: a.altmann@dkfz.de*

Objectives: The delta-like ligand 4 (DLL4) is expressed in tumor endothelia and, therefore a promising target for the development of novel peptidic ligands. In this study we used a phage display library based on scaffold structures for biopanning against DLL4. Methods: A phage display library with variations of the Min-23 scaffold was exposed to the recombinant extracellular domain of Dll4 aled to the identification of a Dll4 binding motif. After synthesis of the Min23 peptide and grafting of the binding motif into the SFTI scaffold we performed surface plasmon resonance (SPR) experiments, cell binding assays, immunohistological analysis and biodistribution studies in tumor-bearing mice. Results: After grafting of the binding motif into the SFTI scaffold the resulting derivative showed nanomolar affinity to the recombinant Dll4. Cell binding experimenst using HUVEC cell revealed a high binding capability. Furthermore, the tumor selective accumulation was demonstrated in biodistribution studies in AR42J tumor-bearing nude mice after administration of the radiolabelled peptide. SPR eshowed an inhibition of the Dll4-Notch interaction, which is evidence for a potential for therapeutic application. Conclusions: Using phage display with a novel scaffold based library and molecular grafting into an easy to synthesize scaffold (SFTI) a new peptide lead structure was identified. This molecula shows potential for imaging but also for therapeutic application by intervention with the Notch signal transduction pathway.

Disclosure of author financial interest or relationships:
**A. Altmann**, None; **F. Zoller**, None; **A. Markert**, None; **W. Mier**, None; **U. Haberkorn**, None.

Presentation Number **P737**
Poster Session 4
September 8, 2012 / 14:45-14:45 / Room: The Liffey

# Novel orthotopic xenograft metastatic model of implantation of human colorectal adenocarcinoma: analysis of tumor progression through nuclear medicine

*Marcos Gomes[1], Ana M. Abrantes[1,2], Edgar Tavares da Silva[3], Mafalda Laranjo[1,2], Catarina Ortigão[5], Pedro Almeida[6], Claudia S. Ferreira[5,6], Nuno Matela[6], Joao Varela[7], José Tralhão[3,2], Denise G. Priolli[4], **Maria F. Botelho**[1,2], [1]Biophysics Unit, IBILI, Faculty of Medicine, University of Coimbra, Coimbra, Portugal; [2]CIMAGO, Faculty of Medicine, University of Coimbra, Coimbra, Portugal; [3]Surgical Department, Surgery A, HUC, Coimbra, Portugal; [4]Faculty of Medicine, S. Franscisco University, Bragança Paulista, Brazil; [5]Laboratory of Instrumentation and Experimental Physics of Particles (LIP), Lisbon, Portugal; [6]Faculty of Science, Institute of Biophysics and Biomedical Engineering, University of Lisbon, Lisbon, Portugal; [7]Instituto Superior Técnico (IST), Technical University of Lisbon, Lisbon, Portugal. Contact e-mail: filomena@ibili.uc.pt*

Introduction: The failure rate of phase-3-trials are higher in oncology than in any other therapeutic area, reinforcing the desire to develop more useful animal models that closely replicate the histology, physiological effects, biochemical pathways and metastatic pattern observed in the same human tumor type. The orthotopic model (ORT) of human tumors in immunosuppressed mice has proved to be the most appropriate model compared to the subcutaneous models (heterotopic) which doesn't characterize the tumor microenvironment or expresses an invasive/metastatic phenotype. Currently, the ORT model of colorectal adenocarcinoma (CRC) is in the cecum. As this is an unusual site in humans it becomes necessary to establish other ORT model of CRC, in the left colon, through microsurgery with micro-injection of human CRC cell line WiDr in the mucous fistula, and compare both models. The progression assessment was done resorting to nuclear medicine techniques, using 99mTc-MIBI and 18F-FDG. Methods: 31 RNU rats underwent two surgical procedures (cecostomy and descending colostomy with distal-mucous-fistula) and injected with WiDr cells (10-14×106 cells/animal), after return to normal bowel function. Evaluation with 99mTc-MIBI and 18F-FDG were performed after intravenous injection and acquired using a gamma-camera and a prototype ClearPEM, respectively. Results: For equal amount of cells inoculated in both models, colostomy-induced model shown higher longevity and better life quality, expressing slow progression of symptoms, contrasting to animals with cecostomies. Cecostomy-induced models expressed larger primary tumors, more invasive to surrounding tissues and organs, although with minor signs of distant metastases, opposing to colostomy-induced model, which although smaller primary tumors, evidence distant metastases (liver, lung and altered lymph mesenteric nodes). The radiopharmaceuticals shown tumor uptake in both models. Discussion/Conclusion: These preliminary data suggests that the colostomy model seems as the best model of CRC, the best in characterizing the tumor microenvironment, slow progression of symptoms, greater longevity and less diffuse tumors. Although good tumor tracers, the different characteristics of the radiopharmaceuticals used have clear advantages and disadvantages that can influence the proper interpretation. Acknowledgements: Sara Carvalho (ICNAS); Ricardo Bugalho (LIP). This work was supported by Fundação para a Ciência e a Tecnologia - Portugal and by Quadro de Referência Estratégico Nacional, QREN.

Disclosure of author financial interest or relationships:
**M. Gomes**, None; **A.M. Abrantes**, None; **E. Tavares da Silva**, None; **M. Laranjo**, None; **C. Ortigão**, None; **P. Almeida**, None; **C.S. Ferreira**, None; **N. Matela**, None; **J. Varela**, None; **J. Tralhão**, None; **D.G. Priolli**, None; **M.F. Botelho**, None.

Presentation Number **P738**
Poster Session 4
September 8, 2012 / 14:45-14:45 / Room: The Liffey

# Optical Imaging and Photodynamic Therapy of Brain Tumors with Multifuntional Gold Theranostic Nanoparticles

***Ann-Marie Broome***[1,2], *Joseph D. Meyers*[1], *Yu Cheng*[3], *Richard S. Agnes*[2], *Xinning Wang*[2], *Malcolm Kenney*[3], *Clemens Burda*[3], *James Basilion*[1,2], [1]*Biomedical Engineering, Case Western Reserve University, Cleveland, OH, USA;* [2]*Radiology, Case Western Reserve University, Cleveland, OH, USA;* [3]*Chemistry, Case Western Reserve University, Cleveland, OH, USA. Contact e-mail: broomea@musc.edu*

Targeted drug delivery using EGF-peptide conjugated gold nanoparticles (EGFpep-Au NPs) has been investigated as a novel approach for photodynamic therapy (PDT) of cancer. These targeted, Au NPs containing Pc 4 (EGFpep-Au NP-Pc 4) have been specifically used as theranostics to detect and treat brain cancer, such as gliomas. Glioblastoma (GBM), a high-grade astrocytoma, is the most common adult malignant glioma and is highly invasive. The treatment options for patients diagnosed with GBMs are very limited with surgical resection predominating; however, complete surgical removal is complicated by the infiltrative nature of the cancer cells into normal brain tissue. Most patients have a median life expectancy of only 6-10 months after diagnosis; and those with recurring brain cancer survive less than 20 weeks after any therapeutic regime. Consequently, there is a critical need to develop and improve the detection, diagnosis, and treatment of gliomas. We have bioengineered a multifunctional, targeted gold nanoparticle that is intrinsically fluorescent and delivers its payload specifically to simultaneously detect, treat, and monitor therapeutic response within gliomas. Pc 4, a fluorescent photosensitizing agent, delivered from EGFpep-Au NP-Pc 4 localizes within early endosomes after targeting with the EGF peptide. In vitro PDT studies show that EGFpep-Au NP-Pc 4 is 2-fold better at killing tumor cells than free Pc 4. Previous studies have shown that PEGylated Au NPs are able to accelerate administration of Pc 4 by about 2 orders of magnitude in vivo. Furthermore, in vivo studies show that targeting with EGFpep-Au NP-Pc 4 improved accumulation of Pc 4 in subcutaneous tumors by an increase in fluorescent intensity per nanoparticle of >5-fold over that of the Au NP-Pc 4. In vivo studies further demonstrate that EGFpep-Au NP-Pc 4 decreased uptake by the reticuloendothelial system (RES) and increased the amount of Au NPs circulating in the blood in 4 hours after IV injection in comparison to Au NP-Pc 4. Irradiation of subcutaneous tumors with EGFpep-Au NP-Pc 4 only 4 hours after IV injection resulted in interrupted tumor growth as well. Targeted drug delivery and treatment success could therefore be imaged via the intrinsic fluorescence of the PDT drug Pc 4. Consequently, EGFpep-Au NP-Pc 4 utilizes cancer specific biomarkers to diagnose and improve therapeutic efficacy at a lower drug dosage.

Disclosure of author financial interest or relationships:
**A. Broome**, None; **J.D. Meyers**, None; **Y. Cheng**, None; **R.S. Agnes**, None; **X. Wang**, None; **M. Kenney**, None; **C. Burda**, None; **J. Basilion**, Akrotome Imaging Inc, Stockholder .

Presentation Number **P739**
Poster Session 4
September 8, 2012 / 14:45-14:45 / Room: The Liffey

# Hybrid interventional molecular imaging of primary tumors and distant metastases

***Anton Bunschoten***[1], *Tessa Buckle*[1], *Joeri Kuil*[1], *Lee Josephson*[3], *Alexander Vahrmeijer*[2], *Fijs van Leeuwen*[1], [1]*Radiology, Leiden University Medical Center, Leiden, Netherlands;* [2]*Surgery, Leiden University Medical Center, Leiden, Netherlands;* [3]*CTNMMI, Harvard Medical School, Charlestown, MA, USA. Contact e-mail: a.bunschoten@lumc.nl*

Hybrid molecular imaging agents combine the unique imaging characteristics of several imaging modalities in a single imaging agent. By combining SPECT/CT and fluorescence imaging, the surgical intervention can be planned preoperatively based on the nuclear imaging. Intraoperatively, the surgeon can use the optical signal of the fluorescence to excise the lesions of interest. After successful introduction of this hybrid approach in the clinic in sentinel lymph node procedures, we are moving forward to a targeted approach.[1-3] Tumor induced angiogenesis involves the expression of αvβ3-integrins, which offers a promising target for tumor specific visualization of both primary tumors and their distant metastases. Well-validated ligands for the αvβ3-integrin are the cyclic RGD-pentapeptides,[4] which can be conjugated to a multifunctional single-attachment-point (MSAP) reagent containing both a chelate and a cyanine dye with Cy5.5-like characteristics.[5] After incorporation of 111In in the chelate of the targeted imaging agent, 4T1-tumor bearing mice were injected. 111In-MSAP-RGD allowed for the nuclear imaging of the primary tumors and for approaching the tumor margins intraoperatively based on the fluorescent signal. The added value of the hybrid imaging approach became especially apparent in mice with distant metastases. A solely fluorescent approach would allow real-time intraoperative imaging with high resolution, but is limited by tissue attenuation. A solely nuclear approach would allow accurate preoperative localization of the tumor and metastases, but lacks intraoperative real-time imaging. By combining the two imaging modalities, the primary tumor and distant metastases are localized preoperatively based on the nuclear modality and the excision of the lesions is performed based on the fluorescent modality.[6]
References: 1. Buckle T, van Leeuwen AC, Chin PT et al. Nanotechnology 2010; 21: 355101. 2. van der Poel HG, Buckle T, Brouwer OR, Valdes Olmos RA, van Leeuwen FWB. Eur. Urol. 2011; 60: 826-833. 3. Brouwer OR, Klop WMC, Buckle T et al. Ann. Surg. Oncol. 2012, DOI 10.1245/s10434-011-2180-7. 4. Gurrath M, Muller G, Kessler H, Aumailley M, Timpl R. Eur J Biochem 1992; 210: 911-921. 5. Kuil J, Buckle T, Yuan H et al. Bioconjug Chem 2011; 22: 859-864. 6. Bunschoten A, Buckle T, Visser N et al. ChemBioChem 2012, accepted for publication.

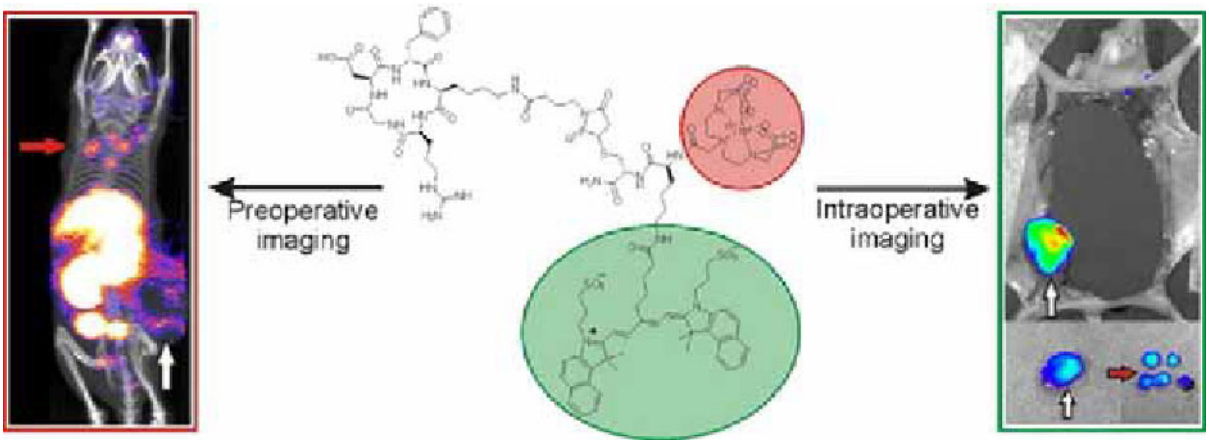


Disclosure of author financial interest or relationships:
**A. Bunschoten**, None; **T. Buckle**, None; **J. Kuil**, None; **L. Josephson**, None; **A. Vahrmeijer**, None; **F. van Leeuwen**, None.

Presentation Number **P740**
Poster Session 4
September 8, 2012 / 14:45-14:45 / Room: The Liffey

# Pairwise PET Imaging Comparisons of $^{89}$Zr and $^{124}$I labeled cG250 as a Basis for Non-Invasive Quantitation of *In Vivo* CAIX Receptor Binding and Internalization in Mouse Xenografts of Clear Cell Renal Carcinoma

***Sarah M. Cheal***[1], *Blesida Punzalan*[3], *Michael Doran*[1], *Michael J. Evans*[4], *Pat Zanzonico*[2], *Jason S. Lewis*[1], *Steven M. Larson*[3], *[1]Radiology, Memorial Sloan-Kettering Cancer Center, New York, CA, USA; [2]Medical Physics, Memorial Sloan-Kettering Cancer Center, New York, NY, USA; [3]Nuclear Medicine, Memorial Sloan-Kettering Cancer Center, New York, NY, USA; [4]Human Oncology & Pathogenesis, Memorial Sloan-Kettering Cancer Center, New York, NY, USA. Contact e-mail: cheals@mskcc.org*

The monoclonal antibody G250 recognizes carbonic anhydrase IX (CAIX), a trans-membrane glycoprotein that is highly expressed on the surface of more than 90% of human clear cell renal carcinoma. Recently chimeric G250, directly labeled with the positron-emitting radionuclide I-124 ($^{124}$I-cG250), has been imaged pre-operatively in patients with renal cortical tumors. It was shown that PET with $^{124}$I-cG250 can accurately predict the clear-cell subtype, which is known to have high metastatic potential. It has been previously demonstrated that radiolabeling cG250 with residualizing radiometals such as Y-90 and In-111 can result in higher uptake and longer retention in tumors, owing to the trapping of radiolabeled metabolites in the cell following binding and internalization. The radiometal Zr-89 is a residualizing positron-emitter, with a half-life well-suited for optimal targeting of whole antibody forms (3.27 days). Additionally, Zr-89 has a lower maximum positron energy compared with I-124 (897 vs 2138 keV), does not emit significant high-energy cascade gamma-rays that confound coincidence-photon detection, and is readily produced in high-specific activity in medium-energy cyclotrons. Methods: cG250 was conjugated through random lysine modification with desferrioxamine and subsequently labeled with Zr-89. Assays for the number of DFO molecules per antibody and stability in human serum, as well as the *in vitro* binding characteristics to human RCC (SK-RC-38) were performed. The kinetics of antibody uptake, internalization, and cellular catabolism were studied and compared with $^{131}$I-cG250 and $^{111}$In-DOTA-cG250. Evaluation of *in vivo* PET imaging properties and radiotracer biodistribution of both $^{124}$I-cG250 and $^{89}$Zr-cG250 was conducted using mouse SK-RC-38 xenograft models. Results: $^{89}$Zr-DFO-cG250 demonstrated rapid and persistent tumor uptake *in vivo* during serial-PET imaging studies. Unlike $^{124}$I-cG250, no significant reduction of Zr-89 radiotracer was observed over the study period, allowing for exceptionally high-contrast imaging at 7-10 days when blood clearance had occurred. The included figure is a summary of the *ex vivo* biodistribution at 10/11 days for $^{124}$I-cG250 versus $^{89}$Zr-cG250 (n=5, mean ± SD for both cohorts). Conclusions: Our hypothesis is that detailed combined studies of tumor uptake of the same antibody labeled with two different tracers will provide insight into the interaction of antibody with CAIX receptor, and the internalization kinetics of antibody and antigen within the renal cancer cell. Based on these data, non-linear compartmental modeling is underway to optimize the understanding of the biologic significance of local Zr-89 retention, as part of the process of translation and optimization of $^{89}$Zr-cG250 as a potential diagnostic and treatment-planning tool in renal cell cancer. Acknowledgements: We would like to acknowledge the Animal Imaging and Cyclotron-Radiochemistry core facilities at MSKCC for technical support. Funding for this study was provided by a NIH R25T Fellowship in Molecular Imaging, the Beene Cancer Research Center of MSKCC, and the Ludwig Center for Cancer Immunotherapy.

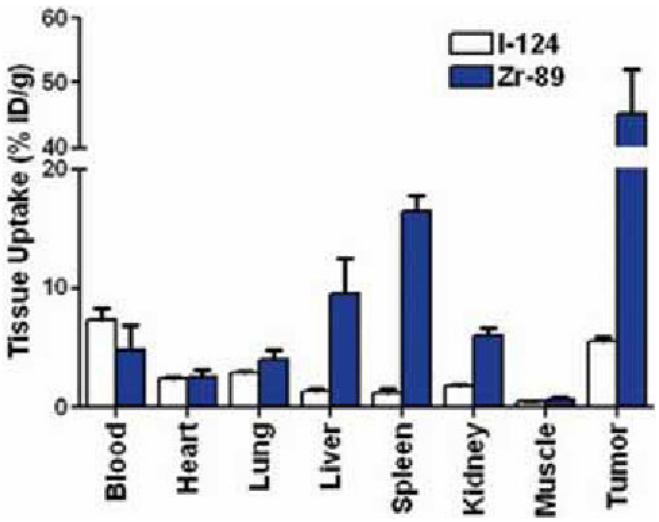


Disclosure of author financial interest or relationships:
**S.M. Cheal**, None; **B. Punzalan**, None; **M. Doran**, None; **M.J. Evans**, None; **P. Zanzonico**, None; **J.S. Lewis**, GEMS, Other financial or material support; **S.M. Larson**, None.

Presentation Number **P741**
Poster Session 4
September 8, 2012 / 14:45-14:45 / Room: The Liffey

# Ferric-desferoxamin MR imaging of multidrug resistance associated protein 1 function in Wistar rats implanted with human small cell lung carcinoma drug sensitive and its corresponding multidrug resistance overexpression MRP1 cells

***Krairuek Daowtak***, *Ampika Jawana, Nattawadee Intachai, Nathupakorn Dechsupa, Chatchanok Udomtanakunchai, Samlee Mankhetkorn, Department of Radiologic Technology, Laboratory of Physical Chemistry, Molecular and Cellular Biology; Center of Excellence for Molecular Imaging, , Faculty of Associated Medical Sciences, Chiang Mai University, Chiang Mai, Thailand. Contact e-mail: krai_cm601@hotmail.com*

The study reported the potential use of Ferric-desferoxamin MR imaging for measuring the efficiency of the membrane proteins such as MRP1 protein mediated efflux of drug in multidrug resistance GLC4/*adr* cell xenografted in Wistar rats. Firstly, the cytotoxicity of desferoxamin and its ferric complex form was studied; $IC_{50}$ values were equal to 10 ± 2 and 12 ± 3 μM for desferoxamin and 35 ± 3 and 55 ± 4 μM for ferric-desferoxamin against small cell lung carcinoma drug sensitive and its corresponding multidrug resistance overexpression MRP1 cells, respectively. The direct interaction of ferric-desferoxamin with MRP1 protein in living multidrug resistance cells was studied by measuring its aptitude to inhibit the MRP1 protein mediated efflux of pirarubicin out of cells. Desferoxamin alone did not inhibit the MRP1 mediated efflux of pirarubicin out of cells while its complex form efficiently done. The maximum inhibition was of the MRP1 function was 80% when 50μM of complex was applied; the concentration required for inhibition by 50 % MRP1 function equal to 20 μM. Due to the ferromagnetic property, the direct measurement of the MRP1 mediated efflux of ferric-desferoxamin in cancer tissues can be performed using MRI. The analysis of MRI images revealed an increase while a decrease in accumulation of ferric-desferoxamin as a function of time in small cell lung carcinoma drug sensitive and its corresponding multidrug resistance overexpression MRP1 cells, respectively. The overall results suggest that ferric-desferoxamin complex should be considered as a potential molecular probe for MR imaging of the MRP1 function *in vivo* level.

Disclosure of author financial interest or relationships:
**K. Daowtak**, None; **A. Jawana**, None; **N. Intachai**, None; **N. Dechsupa**, None; **C. Udomtanakunchai**, None; **S. Mankhetkorn**, None.

Presentation Number **P742**
Poster Session 4
September 8, 2012 / 14:45-14:45 / Room: The Liffey

# Non-invasive measurement of pharmacokinetics, biodistribution and accumulation of drugs based on near-infrared fluorescence imaging

***Michael Dobosz***[1,2], *Steffen Strobel*[1], *Vasilis Ntziachristos*[2], *Werner Scheuer*[1], [1]*Pharma Research & Early Development (pRED), Roche Diagnostics GmbH, Penzberg, Germany;* [2]*Institute for Biological and Medical Imaging, Technical University Munich, Neuherberg, Germany. Contact e-mail: Michael.Dobosz@roche.com*

The study of the time course of a drug in the body is a key determinant in the selection of a drug candidate. For generating such pharmacokinetic data a drug is conventionally injected i.v. or i.p. and thereafter blood is drawn at different time points. Drug serum levels are quantified by different analytical methods, e.g. ELISA. In order to receive statistically meaningful data, 3 to 5 mice are used for each time point to get serum peak level (tmax) and serum half-life (t1/2) of the compound. Accurate determination of both drug characteristics is laborious and error-prone, because the measurement of different time points cannot be made in the same animal and the resulting curve shape is constructed by interpolation. Both problems can influence the accuracy of these values and may lead to misinterpretation. We provide a method, which allows continuous monitoring of drug serum levels through the eye of anesthetized mice. Near infrared excitation light can penetrate into the eye with low tissue absorption and light scattering and thus illuminates perfectly the highly vascularized retina of the eye. This direct and unrestricted access to the blood vessels offers the possibility to non-invasively measure the fluorescence intensity of labeled compounds over the time in the same animal. The combination of eye imaging with whole body fluorescence imaging enables the simultaneous measurement of serum pharmacokinetics, biodistribution, and accumulation of labeled compounds over time in different regions of interest. Utility of this approach is demonstrated by evaluating different compounds i) indocyanine green (ICG) a non-targeting fluorescence dye, ii) OsteoSense (OS) a fluorescence labeled bisphosphonate targeting bone tissue, iii) a F(ab)2 fragment targeting HER2 and, iv) an intact IgG antibody targeting HER2 both labeled with the fluorophore Cy5. Female BALB/c nude mice received inhalation anesthesia and the different compounds were injected i.v. through a vein catheter. The fluorescence signal intensities were monitored over the time with the MAESTRO (CRi, Cambridge, USA) using a frame rate of one frame per second. Measurement starts shortly before the injection of the labeled compound and can be followed up for 2 hrs per measurement day. The terminal half-life of antibodies and their fragments requires longer observation periods and thus, a single frame image is performed once daily for up to 14 days. All compounds were tested in tumor free and s.c. lung cancer xenografts. Results reveal that serum peak level (tmax) and serum half-life (t1/2) of labeled compounds can be determined by measuring the fluorescence signal intensities in the eye of anesthetized animals and are in excellent accordance with published data. Furthermore, the combination of eye and whole body imaging enables inferences about target mediated drug clearance. In contrast to the conventional blood sampling technique this non-invasive approach improves the performance of pharmacokinetic studies and the number of mice can be significantly reduced.

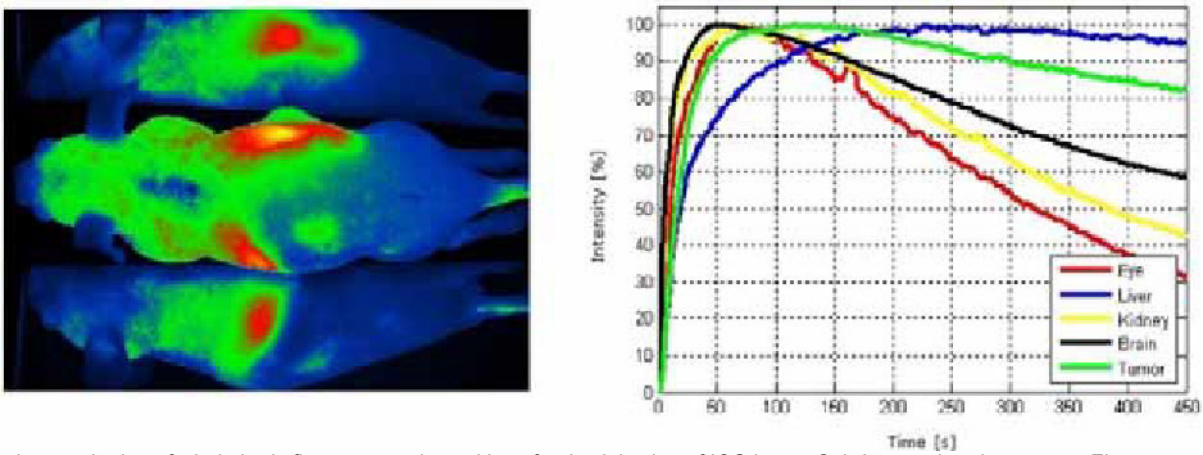


Non-invasive monitoring of whole body fluorescence intensities after i.v. injection of ICG in s.c. Calu3 tumor bearing mouse. Fluorescence signal intensities in different regions of interest demonstrate immediate decline of the fluorescence in the eye region, kidney and brain. Decline of fluorescence intensity in tumor is less prominent and accumulation in the liver is detectable.

Disclosure of author financial interest or relationships:
**M. Dobosz**, Roche Diagnostics GmbH, Employment; **S. Strobel**, Roche Diagnostics GmbH, Consultant; **V. Ntziachristos**, ERC, Grant/research support; Ithera Medical, Stockholder; **W. Scheuer**, Roche Diagnostics GmbH, Employment .

Presentation Number **P743**
Poster Session 4
September 8, 2012 / 14:45-14:45 / Room: The Liffey

# Immune Cell Tracking by Whole-body Imaging with Multispectral Optoacoustic Tomography (MSOT)

*Karin Schaefer[1], **Wouter H. Driessen**[2,1], Jing Claussen[2,1], Neal Burton[2,1], Stefan Morscher[2,1], Daniel Razansky[1,3], Vasilis Ntziachristos[1,3], [1]The Institute for Biological and Medical Imaging, Helmholtz Center Munich, Neuherberg, Germany; [2]iThera Medical, GmbH, Neuherberg, Germany; [3]Technical University Munich, Munich, Germany. Contact e-mail: wouter.driessen@ithera-medical.com*

Sensitive and reliable methods for cell labeling and in vivo tracking by whole-body imaging are of great importance to gain better understanding of cell-based therapies and tissue heterogeneity. Multispectral optoacoustic tomography (MSOT) is a novel imaging modality that provides high resolution in deep tissue and with high molecular specificity. Whereas optical imaging suffers from photon diffusion and ultrasound imaging can only provide limited specificity, MSOT combines the benefits of each while avoiding their pitfalls. Tissue is illuminated by short laser pulses and ultrasound transducers detect acoustic waves generated by thermoelastic expansion of endogenous and exogenous absorbers. By illuminating at multiple wavelengths and spectrally unmixing the contributions from different absorbers, the spatial distribution and intensity of different absorbers can be determined in cross-sections through the entire mouse. In this work, MSOT is used to visualize and quantify the whole-body and tumor-specific accumulation of innate immune cells. Mouse macrophages as a model of innate immune cells were derived from bone marrow cells, splenocytes and tumor tissue cells. First, the labeling of the monocytes was optimized in vitro by comparing various labeling platforms. Cells were labeled with CellVue NIR815, DiI, DiR and gold nanoparticles. The labeled cells where then extensively characterized by MSOT in phantom studies and by fluorescence / darkfield microscopy and spectroscopy to determine the relationship between the amount of incorporated dye and optoacoustic signal as well as to determine the sensitivity of MSOT in detecting labeled cells. Next, the macrophages were injected i.v. into mice bearing 4T1 orthotopic breast tumors. MSOT was used to visualize the trafficking of these labeled cells to tumor, spleen and liver tissue at multiple time points. Distribution of labeled cells was verified by post-mortem whole-animal cryoslicing and histology. MSOT was used to perform cell tracking in vivo and in real time. Conventional methods of determining target specificity are typically limited by the use of many animals and laborious histological processing or by dissociating tissue and determining label concentration. MSOT is able to simultaneously provide quantitative information and spatial distribution and long-term persistence of labeled immune cells.

Disclosure of author financial interest or relationships:
**K. Schaefer**, None; **W.H. Driessen**, iThera Medical, Employment; **J. Claussen**, iThera Medical, Employment; **N. Burton**, iThera Medical, Employment; **S. Morscher**, iThera Medical GmbH, Employment; **D. Razansky**, iThera Medical GmbH, Stockholder; **V. Ntziachristos**, ERC, Grant/research support; Ithera Medical, Stockholder .

Presentation Number **P744**
Poster Session 4
September 8, 2012 / 14:45-14:45 / Room: The Liffey

# Labelling of a novel peptide for GRPR breast and prostate tumor PET imaging with 64Cu and 68Ga, an in vitro and in vivo comparative study

*Patrick Fournier[1], **Veronique Dumulon-Perreault**[1], Samia Ait-Mohand[1], Roger Lecomte[1], Francois Benard[2], Brigitte Guerin[1], [1]Universite de Sherbrooke, CIMS, Sherbrooke, QC, Canada; [2]British Columbia Cancer Agency Research Center, Vancouver, BC, Canada. Contact e-mail: Veronique.Dumulon-Perreault@USherbrooke.ca*

Objective: NOTA-PEG-[D-Tyr6,βAla11,Thi13,Nle14] BBN(6-14) is a promising peptide for targeting gastrin-releasing peptide receptors (GRPR) tumors. In this study, NOTA-PEG-BBN(6-14) was labelled with 64Cu and 68Ga for an in vitro and in vivo comparative study for breast and prostate tumors PET imaging. Methods : NOTA-PEG-BBN(6-14) was synthesized on solid phase (Guérin et al, Org Lett., 2010, 12, 280-283).Inhibition constant (Ki) for GRPR was estimated by competitive binding assays performed human breast (T47D) and human prostate (PC3) cancer cell lines. The labelling was performed by incubation of the peptide and 64Cu or 68Ga at 95°C for 10 min. After purification, in vivo plasma stability studies were achieved by injecting radiolabelled peptides to mice and by taking blood samples at different time points up to 2 h post-injection, stability being assessed by radio-TLC. A cell uptake study was performed on T47D and PC3 cell lines in presence of 64Cu/ or 68Ga/NOTA-PEG-BBN(6-14) for up to 90 min. The percentage of administered dose per 105 cells bound or internalized was calculated. Biodistribution of radiolabelled peptides were done on Balb/c female mice sacrificed at 15, 30, 60 and 120 min. Finally, T47D and PC3 cells were injected subcutaneously to female balb/c nude mice and PET images were obtained. Results : 64Cu/NOTA-PEG-BBN(6-14) exhibit higher affinity for GRPR than 68Ga/NOTA-PEG-BBN(6-14), both in the nanomolar range. Specific activities of 1500-2500 Ci/mmol were obtained with both 64Cu and 68Ga. Both PET tracers (64Cu/NOTA and 68Ga/NOTA) were stable in vivo for up to 2 h. The cell uptakes were comparable for both peptides. 64Cu/NOTA-PEG-BBN(6-14) presented higher GRPR-mediated uptake in pancreas and adrenal glands, but comparable PC3 tumor uptake as 68Ga/NOTA-PEG-BBN(6-14). Receptor-dependent responses were observed during blocking studies with unlabeled peptide in both biodistribution and PET imaging studies. Both xenograft tumors were clearly visible in PET imaging for both tracers. Conclusion : Considering their good imaging characteristics, both 64Cu/NOTA-PEG-BBN(6-14) and 68Ga/NOTA-PEG-BBN(6-14) are promising candidates for GRPR-targeted PET imaging of breast and prostate cancers.

Disclosure of author financial interest or relationships:
**P. Fournier**, None; **V. Dumulon-Perreault**, None; **S. Ait-Mohand**, None; **R. Lecomte**, Gamma Medica, Stockholder; Gamma Medica, Consultant; **F. Benard**, None; **B. Guerin**, None.

Presentation Number **P745**
Poster Session 4
September 8, 2012 / 14:45-14:45 / Room: The Liffey

# A multimodal CT/optical imaging agent for improved lung cancer detection

***Michael Dunne***[1], *Takashi Anayama*[2,3], *Brandon Driscoll*[4], *Takahiro Nakajima*[2,3], *Jinzi Zheng*[1], *Catherine Coolens*[4,5], *Shaf Keshavjee*[2,3], *Kazuhiro Yasufuku*[2,3], *Christine Allen*[1,6], *David A. Jaffray*[1,4], [1]*STTARR Innovation Centre, Radiation Medicine Program, Princess Margaret Hospital, University Health Network, Toronto, ON, Canada;* [2]*Division of Thoracic Surgery, Toronto General Hospital, University Health Network, Toronto, ON, Canada;* [3]*Latner Thoracic Surgery Research Laboratories, University Health Network, University of Toronto, Toronto, ON, Canada;* [4]*Department of Radiation Physics, Radiation Medicine Program, Princess Margaret Hospital, University Health Network, Toronto, ON, Canada;* [5]*Department of Radiation Oncology, University of Toronto, Toronto, ON, Canada;* [6]*Faculty of Pharmacy, University of Toronto, Toronto, ON, Canada. Contact e-mail: m.dunne@utoronto.ca*

**Introduction:** The biggest challenge in the treatment of lung cancer is that the disease can progress asymptomatically and present itself at advanced stages, which demands for timely and accurate surgical resection procedures in order to improve patient survival and decrease morbidity. A nano-sized CT/optical imaging agent has been developed to provide CT-based localization of malignant lung nodules pre-operatively and allow visualization of the same lesions under fluorescence confocal endomicroscopy to improve the accuracy of surgical resection. **Methods:** Liposomes composed of 55:40:5 DPPC:CH:$PEG_{2000}$-DSPE and encapsulating both the iodinated small molecule CT agent iohexol and a near-infrared fluorescent dye were prepared by high pressure extrusion. A minimally invasive technique was used to intratracheally implant 1.0 x $10^6$ VX2 rabbit carcinoma cells in 200 µL Matrigel into the parenchyma of the right lung of New Zealand white rabbits. Tumours were allowed to grow for 13 days to reach ~ 1 cm in diameter as estimated by micro-CT (Locus Ultra, GE). Liposomes were administered as a bolus injection of 25 ± 2 mL over one minute. Pharmacokinetics and tumour accumulation were examined by clinical CT (Aquilion ONE, Toshiba). Scans were performed pre-injection and at 5 min, 24, 48, 72, and 168 hr post-injection at 120 kVp and variable mA. Iodine concentration in the tumour and blood (aorta) were quantified by comparing the density change in the specified volume pre- and post- contrast administration. Rabbits were sacrificed 234 hr post-liposome administration. A laser scanning unit (FCM1000, Mauna Kea Technologies) capable of exciting fluorophores at 660 nm was connected to a fibre optic microprobe and used to internally examine both the normal and tumour bearing lung of the rabbit. An emission bandwith of 680 - 900 nm was used as fluorescent images were acquired at 12 frames per second. **Results:** Dynamic light scattering determined that the liposomes were unimodally distributed with an average diameter of 85 nm. Contrast agent loading as determined by UV/Vis spectrophotometry was 38 ± 2 mg/mL for iodine and 5 µg/mL for the NIR dye. *In vivo* evaluation using clinical CT determined that the half-life of iodinated liposomes in the blood pool was 135 ± 28 hr. Maximum accumulation occurred at 72 hr, although wash out was slow. Rabbits were sacrificed 234 hr post liposome administration, with 30% of liposomes still remaining in circulation. Examination by fluorescence confocal endomicroscopy of both normal and tumour bearing lungs revealed increased maximum fluorescent signal in all cases in the tumour-bearing lung (n=4). Furthermore, there was a positive correlation between the three tumours with significant liposome accumulation as determined by CT and those with greater average fluorescent signal in the tumour-bearing lung compared to the normal lung. **Conclusion:** Administration of 85 nm, long circulating CT/optical liposomes resulted in significant accumulation in tumours, allowing improved tumour visualisation in CT scans for a period of 168 hr as well as detection by fluorescence confocal endomicroscopy 234 hr following administration.

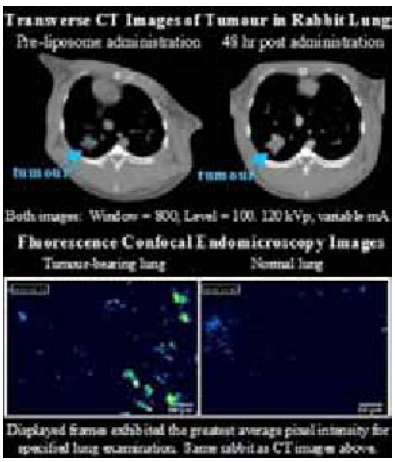


Disclosure of author financial interest or relationships:
**M. Dunne**, None; **T. Anayama**, None; **B. Driscoll**, None; **T. Nakajima**, None; **J. Zheng**, None; **C. Coolens**, None; **S. Keshavjee**, None; **K. Yasufuku**, None; **C. Allen**, None; **D.A. Jaffray**, Precision X-ray, Other financial or material support; Raysearch, Grant/research support; Philips, Grant/research support; Elekta, Grant/research support; General Electric, Grant/research support; IMRIS, Other financial or material support; Modus Medical, Grant/research support .

Presentation Number **P746**
Poster Session 4
September 8, 2012 / 14:45-14:45 / Room: The Liffey

# Quantitative assessment of the intratumoral distribution of NGR-targeted liposomes in cervical cancer

***Sandra Ekdawi***[1,2], *James Stewart*[2], *Michael Dunne*[2], *Jinzi Zheng*[2], *David A. Jaffray*[2,3], *Christine Allen*[1,2], [1]*Department of Pharmaceutical Sciences, University of Toronto, Toronto, ON, Canada;* [2]*STTARR Innovation Centre, Radiation Medicine Program, Princess Margaret Hospital, University Health Network, Toronto, ON, Canada;* [3]*Department of Radiation Physics, Radiation Medicine Program, Princess Margaret Hospital, University Health Network, Toronto, ON, Canada. Contact e-mail: sandra.ekdawi@utoronto.ca*

Introduction: Liposomes are the most established advanced drug delivery technology[1]. Liposomal drug delivery enables the preferential accumulation of the encapsulated drug at the tumor site via the EPR effect, or passive targeting., resulting in decreased systemic toxicities commonly attributed to i.v. chemotherapy. However, these nanosystems are often limited by their inability to efficiently target tumors and release their drug cargo[2,3]. Here, we investigate the intratumoral distribution of an actively-targeted liposome formulation as a means to increase its potential therapeutic efficacy. An iodinated liposome formulation targeted with the tumor vasculature-specific NGR peptide has been previously developed for CT imaging and has demonstrated a 2-fold increase in tumor accumulation relative to its non-targeted counterpart[4]. Hence, a liposome-based CT/optical imaging agent was developed to further elucidate the difference in tumor accumulation between both formulations by bridging CT-based assessment of whole tumor uptake and high resolution fluorescence imaging in an ME-180 s.c. cervical tumor xenograft. Methods: A liposome system (+/-NGR) composed of the CT agent iohexol and a NIR fluorescent molecule Genhance$^{TM}$680 was developed based on a previously established formulation[4]. *In vivo* stability of the nanosystem was determined from the PK profile of each liposome-encapsulated imaging probe in healthy mice. For the microdistribution study, liposomes were administered i.v. to 200-300 mm$^3$ tumor-bearing nude CD-1 mice. At 48 h p.i., mice were i.v. administered a carbocyanine dye as a marker of functional vasculature 1 min prior to sacrifice. Tumors were excised, frozen, sectioned and imaged on a fluorescence microscope. A customized algorithm was developed to compute the distance of extravasated liposomes from their nearest functional vessel within 3 regions per tumor section (periphery, middle and centre). The Kruskal-Wallis test was employed to evaluate the statistical significance between the mean penetration distances of non-targeted (n=3) and targeted (n=3) formulations. Results: PK data demonstrated similar *in vivo* stability for both formulations. Plasma concentration ratios of iohexol to Genhance$^{TM}$ were 1.80 ± 0.80 and 1.78 ± 0.46 at 48 h p.i. for the non-targeted (n=5) and targeted (n=4) formulations, respectively. Greater penetration distances were found for the non-targeted liposomes in all 3 tumor regions (Table 1), consistent with the hypothesis that NGR-mediated vascular targeting localizes liposomes proximal to tumor vessels. However, no significant difference in liposome penetration was observed within all 3 tumor regions (p>0.4, Fig1). Conclusions: A stable, dual-modality liposome imaging agent was developed and its *in vivo* performance was characterized. Whole-body and intratumoral distribution of a targeted and non-targeted liposomal formulation was successfully determined using volumetric CT and 2D fluorescence microscopy. Although no statistically significant difference was found in measurements between both formulations, it was postulated that NGR-mediated targeting hinders the interstitial penetration of liposomes.

Representative fluorescence images of a tumor section of a subcutaneous ME-180 tumor. Non-targeted (A) and targeted (B) liposomes (red) are distributed heterogeneously proximal to perfused blood vessels (green). (C) Schematic representation of regional partitioning within a tumor section. Scale bar: 1 mm

Penetration distance (in μm) of -/+NGR-liposomes from perfused blood vessels, according to 3 evenly-spaced concentric regions within the tumor: periphery (0-1500 μm from perimeter), middle (1500-3000 μm from perimeter) and centre (>3000 μm from perimeter). No significant difference was found among the values (p>0.4).

| Tumor region | Non-targeted (n=3) | Targeted (n=3) |
|---|---|---|
| Periphery | 30.3 ± 21.7 μm | 17.7 ± 9.8 μm |
| Middle | 5.0 ± 2.7 μm | 4.0 ± 2.2 μm |
| Center | 1.3 ± 1.7 μm | 1.0 ± 1.0 μm |

Disclosure of author financial interest or relationships:
**S. Ekdawi**, None; **J. Stewart**, None; **M. Dunne**, None; **J. Zheng**, None; **D.A. Jaffray**, Precision X-ray, Other financial or material support; Raysearch, Grant/research support; Philips, Grant/research support; Elekta, Grant/research support; General Electric, Grant/research support; IMRIS, Other financial or material support; Modus Medical, Grant/research support; **C. Allen**, None.

Presentation Number **P747**
Poster Session 4
September 8, 2012 / 14:45-14:45 / Room: The Liffey

# A Multi-Modality Molecular Imaging (MMI) Approach to the Assessment of Cardiovascular Toxicities Associated with the Angiogenesis Inhibitor Sunitinib

***Rhys Evans***[1], *Emer Conroy*[2], *Liam Shiels*[1], *Aisling E. O'Connor*[2], *Agnieszka Zagozdzon*[2], *Marina Alamanou*[5], *Diarmaid Hughes*[1], *Niamh Corrigan*[2], *Jacques A. Rousseau*[3], *William M. Gallagher*[2,5], *Fionnuala McAuliffe*[2], *Maurice Cary*[4], *Roger Lecomte*[3], *Annette T. Byrne*[1], [1]*Royal College of Surgeons in Ireland, Dublin, Ireland;* [2]*University College Dublin, Dublin, Ireland;* [3]*Universite de Sherbrooke, Sherbrooke, QC, Canada;* [4]*Pathology Experts GmbH, Basel, Switzerland;* [5]*Oncomark Ltd, Dublin, Ireland. Contact e-mail: rhysevans@rcsi.ie*

The multi-targeted tyrosine kinase inhibitor sunitinib is approved in several oncology indications. Associated cardiovascular toxicities include hypertension and congestive heart failure. Thus, cardiovascular function is closely monitored in at-risk patient populations. Nevertheless, an unmet need currently exists for reliable methods to facilitate early identification of cardiac toxicities. To this end, we have attempted to 'reverse translate' sunitinib clinical treatment protocols in mice and have interrogated resultant toxicities using MMI. Female Balb/CJ mice were treated orally with sunitinib over a clinically relevant dose range (20-40 mg/kg). The treatment protocol was 4 weeks dosing (Monday to Friday) followed by 2 weeks recovery. Cardiovascular function was assessed by cardiac ultrasound [Biomicroscope Vevo 770]. 18F-FDG-PET [LabPET/Triumph] scans were acquired to determine metabolic rate of glucose. Blood pressure measurements were taken at regular intervals. A significant elevation in blood pressure was noted following four weeks of treatment (20 and 40 mg/kg). Changes in cardiovascular physiology parameters and increase in glucose metabolism were observed following 40 mg/kg sunitinib treatment over the same period. Nevertheless, initial histopathological analysis of cardiac (and other) tissues has shown no observable effects. Sunitinib may affect left ventricular function in two ways: Initially, following elevation of systemic blood pressure, afterload is increased and left ventricular ejection fraction falls. Subsequently, through off-target kinase inhibition cardiomyocyte apoptosis and hypertrophy is induced, evidenced much later at histopathology examination. Our data support these kinetics. Plasticity in cardiac energy substrate usage has previously been demonstrated during hypertension. This may explain the increase in FDG-PET signal observed following treatment. Further investigation of FDG PET as an early safety biomarker is warranted.

Disclosure of author financial interest or relationships:
**R. Evans**, None; **E. Conroy**, None; **L. Shiels**, None; **A.E. O'Connor**, None; **A. Zagozdzon**, None; **M. Alamanou**, None; **D. Hughes**, None; **N. Corrigan**, None; **J.A. Rousseau**, None; **W.M. Gallagher**, OncoMark Limited, Stockholder; **F. McAuliffe**, None; **M. Cary**, None; **R. Lecomte**, Gamma Medica, Stockholder; Gamma Medica, Consultant; **A.T. Byrne**, None.

Presentation Number **P748**
Poster Session 4
September 8, 2012 / 14:45-14:45 / Room: The Liffey

# Preclinical In vivo evaluation of anti-EGFR antibodies anti-tumor efficacy by Bioluminescent Imaging

***Christine Fischer***, *Martina Uhr, Olivier Freytag, Valeria Nicolini, Sabine Lang, Erwin van Puijenbroek, Simona Wirth, Pablo Umana, Christian Gerdes, Roche Glycart AG, Schlieren, Switzerland. Contact e-mail: christine.fischer@roche.com*

Optical imaging allows us to monitor tumor growth in a non-invasive manner as well as the anti-tumoral effectiveness of therapeutic molecules. GA201 (RG7160) is a humanized and glycoengineered IgG1 antibody which targets EGFR. Within its dual mode of action, a distinguishing feature of GA201 compared to currently marketed EGFR antibodies lies in its ability to bind to human FcgRIIIa on immune effector cells with a 50-fold higher affinity, a property conferred by the antibody's afucosylated Fc glycoforms. Consequently, as shown in in vitro assays using different EGFR expressing cell lines, GA201 exhibits superior potency and efficacy in antibody dependent cell cytotoxicity (ADCC) compared to the other anti-EGFR antibodies. To better understand the in vivo direct impact of glycoengineered antibodies, compared to conventional monoclonal antibodies, GA201 therapeutic efficacy was evaluated in a bioluminescence lung orthotopic xenograft model. Briefly, SCID huFcgRIIIa transgenic mice were injected with the Human Non-Small Cell Lung Carcinoma A549 cells transfected in house to stably express firefly luciferase. Bioluminescence imaging acquisitions (photon/sec) with the IVIS® Spectrum (Caliper, PerkinElmer) were performed every 3 days by intra-peritoneal injection of 200µL luciferin substrate (15 mg/ml) in order to monitor tumor growth. Animals were randomized and the therapy was initiated when tumor growth was in the exponential phase as evaluated by the bioluminescence signal increase. Therapeutic anti-EGFR antibodies (GA201, GA201 non glycoengineered, Erbitux or Panitumumab) were injected intravenously 4q7d at a dose of 25mg/kg. We observed a significantly reduction in tumor burden as assessed by bioluminescence in the GA201 treated animals compared to the control and other anti-EGFR therapeutic groups. Previously it was reported by our laboratory an increase in efficacy by GA201 over different anti-EGFR therapeutic molecules, in non-bioluminescent, conventional survival mouse orthotopic tumor models. Here we showed for the first time that there is a good correlation between the two monitoring methods, mainly bioluminescence imaging and conventional survival evaluation upon GA201 therapy. Using bioluminescence imaging in this realistic orthotopic mouse model, the tumor growth could be sensitively and non-invasively followed upon therapy. Bioluminescence imaging added to the survival data important information, such as real-time monitoring of tumor progression, therapeutic molecules anti-tumoral mode of action and dosage optimization.

Disclosure of author financial interest or relationships:
**C. Fischer**, Roche Glycart AG, Employment; **M. Uhr**, Roche Glycart AG, Employment; **O. Freytag**, Roche Glycart AG, Employment; **V. Nicolini**, Roche-Glycart, Employment; **S. Lang**, Roche Glycart AG, Employment; **E. van Puijenbroek**, Roche Glycart AG, Employment; **S. Wirth**, Roche Glycart AG, Employment; **P. Umana**, Roche Glycart AG, Employment; **C. Gerdes**, Roche Glycart AG, Employment .

Presentation Number **P749**
Poster Session 4
September 8, 2012 / 14:45-14:45 / Room: The Liffey

# Preclinical imaging of cancer metastasis by multimodal SPECT-CT/fluorescence using the sodium iodide symporter

***Gilbert O. Fruhwirth***[1,2], *Seckou Diocou*[2,3], *Tony Ng*[1,2], *Greg Mullen*[2,3], [1]*Dimbleby Department, King's College London, London, United Kingdom;* [2]*Comprehensive Cancer Imaging Centre, King's College London & UCL, London, United Kingdom;* [3]*Imaging Sciences - The Raynes Institute, St. Thomas Hospital, London, United Kingdom. Contact e-mail: gilbert.fruhwirth@kcl.ac.uk*

Cancer cell metastasis is the major obstacle to successful treatment of many solid tumours ultimately leading to death. Its assessment is currently inferred from either positive sentinel lymph node biopsies (e.g. in breast cancer) and histo-pathological grading, or directly by imaging with positron emission tomography (PET). However, questions about the sensitivity of PET as well as about the specificity of the currently used radiotracers remain [1]. The sodium iodide symporter (NIS) is not only a transporter for sodium and iodide, but also one for other large negatively charged ions like pertechnetate (99mTcO4-) or tetrafluoroborate (BF4-), which can be exploited in nuclear medicine. NIS is highly expressed in the thyroid gland [2] and at lower levels in the stomach [3]. Importantly, it was also reported to be over-expressed in various cancer types including breast cancer [4]. In this study we establish a novel preclinical model for highly sensitive non-invasive imaging of cancer metastasis. It is based on breast cancer cell lines stably expressing NIS with the latter being fused to a red fluorescent protein in order to allow multimodal imaging (radionuclide-fluorescence). The cancer cells were rendered highly metastatic by introduction of a chemokine receptor conferring sustained pro-migratory signalling thereby enhancing lymph node metastasis in vivo. We specifically imaged the primary tumour and metastasis by either SPECT/CT or PET/CT and we show a comparison of radiotracer sensitivity for SPECT/CT (99mTcO4-) and PET/CT (BF4-). Furthermore, we validated SPECT/PET-positive metastasis by bio-distribution and by fluorescence-based histo-pathological tissue examination. When established tumours were treated with etoposide, we obtained comparable signals from similarly sized tumours and metastasis when relying on NIS-based imaging. This is in stark contrast to concomitant [18F]-fluorodeoxyglucose (FDG)-based imaging, which was strongly reduced in the presence of etoposide, leading to an underestimation of tumour size and metastasis incidence in FDG-based imaging. In summary, we established a novel preclinical model for highly sensitive and relyable tumour and metastasis imaging. This model is superior to current metabolic imaging approaches and is also suitable for longitudinal therapeutic studies. References: [1] Heiko Schöder and Mithat Gönen J Nucl Med 2007, 48:4S [2] Yeom et al; J Nucl Med 2008, 49:1489. [3] Bruno R et al, J Endocrinol Invest. 2004, 11:1010-4 [4] Ryan et al, PLOS One 2011, 6(1):e16023

Disclosure of author financial interest or relationships:
**G.O. Fruhwirth**, None; **S. Diocou**, None; **T. Ng**, None; **G. Mullen**, None.

Presentation Number **P750**
Poster Session 4
September 8, 2012 / 14:45-14:45 / Room: The Liffey

# Preclinical development of MM-DX-929, a novel liposomal PET-based radiopharmaceutical imaging contrast agent

***Daniel F. Gaddy***[1], *Helen Lee*[1], *Jinzi Zheng*[2], *Michael Dunne*[2], *Daryl Drummond*[1], *Christine Allen*[2,3], *David A. Jaffray*[2], *Bart Hendriks*[1], *Thomas Wickham*[1], *Dmitri Kirpotin*[1], [1]*Merrimack Pharmaceuticals, Cambridge, MA, USA;* [2]*STTARR Innovation Center, Radiation Medicine Program, Princess Margaret Hospital, University Health Network, Toronto, ON, Canada;* [3]*Leslie Dan Faculty of Pharmacy, University of Toronto, Toronto, ON, Canada. Contact e-mail: dgaddy@merrimackpharma.com*

Background. Immunoliposomes loaded with anticancer drugs enter tumors via leaky tumor vasculature and become specifically taken up by tumor cells carrying the target antigen - this is known as the enhanced permeability and retention (EPR) effect. Computational modeling of in vivo immunoliposome behavior suggests that their deposition in the tumor interstitium is the major predictive factor for liposomal drug activity. However, deposition of liposomal therapeutics into tumors can be highly variable between tumor types, patients, and across multiple tumors within a single patient. It is hypothesized that the ability to measure the propensity of a given tumor to accumulate and retain liposomes will allow individually optimized treatment options for a given patient, thus resulting in a higher probability of response. We have designed a quantifiable nanocarrier diagnostic with tissue deposition properties that closely mimic liposomal drugs. Objectives. We designed the current study to evaluate the use of a 64Cu-loaded liposomal nanocarrier (MM-DX-929) as a predictive diagnostic for liposomal and immunoliposomal anticancer drugs. This study assessed pharmacokinetic parameters, in vitro and in vivo stability, and the clinical feasibility of MM-DX-929. Proof of concept is evaluated by PET/CT image-based assessment of liposomal deposition in in vivo mouse xenograft tumor models. Methods. 64Cu was loaded into preformed PEGylated unilamellar liposomes (90-100 nm) using a propriety chelator-assisted gradient loading method. In vivo stability and pharmacokinetics of both the liposome carrier and the isotope label were measured in non-tumor-bearing CD-1 mice. To evaluate proof of concept, mice bearing either BT474-M3 or H520 tumors were injected intravenously and tumor deposition of MM-DX-929 was measured by PET/CT imaging up to 20h post-injection. Results were compared with direct tissue counts in a biodistribution study. Results. 64Cu is efficiently chelated with the loading-assisting chelator in an aqueous buffer within minutes (>90% chelation efficiency) upon mixing, forming a soluble 64Cu-chelator complex. The 64Cu-chelator complex is rapidly encapsulated within PEGylated liposomes (>90% loading efficiency) via an active loading process to create MM-DX-929. The radioisotope-loading protocol is amenable to the clinical radiopharmacy setting. MM-DX-929 is stable in vivo, showing no detectable leakage of 64Cu over a period of at least 40 hours, with a pharmacokinetic profile that closely resembles that of MM-302, a HER2-targeted liposomal doxorubicin, currently in clinical development. In BT474-M3 and H520 tumor models, deposition of MM-DX-929 ranges from approximately 2-23% i.d./g, illustrating the variability of liposomal deposition between tumor types. There is an excellent correlation between the MM-DX-929 deposition in the tumor assessed from the post-injection PET/CT images and the results of direct tissue counts. Conclusion. MM-DX-929, a novel 64Cu-based nanocarrier radiodiagnostic, possesses the requisite properties to accurately image and quantify liposome deposition in tissues in vivo and is feasible in a clinical setting.

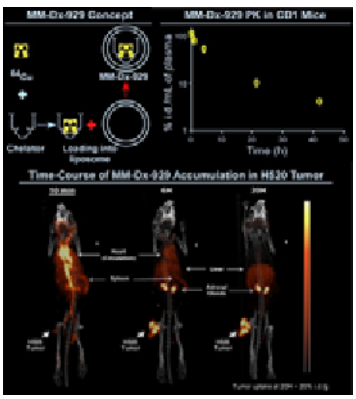


MM-DX-929 is a 64Cu-loaded liposomal nanocarrier in development as a predictive diagnostic for liposomal anticancer drugs. MM-DX-929 is stable in vivo, and accurately predicts tumor deposition of liposomal agents in animal models.

Disclosure of author financial interest or relationships:
**D.F. Gaddy**, Merrimack Pharmaceuticals, Employment; **H. Lee**, Merrimack Pharmaceuticals, Employment; **J. Zheng**, None; **M. Dunne**, None; **D. Drummond**, Merrimack Pharmaceuticals, Employment; Merrimack Pharmaceuticals, Stockholder; **C. Allen**, None; **D.A. Jaffray**, Precision X-ray, Other financial or material support; Raysearch, Grant/research support; Philips, Grant/research support; Elekta, Grant/research support; General Electric, Grant/research support; IMRIS, Other financial or material support; Modus Medical, Grant/research support; **B. Hendriks**, Merrimack Pharmaceuticals, Employment; **T. Wickham**, Merrimack Pharmaceuticals, Employment; Merrimack Pharmaceuticals, Stockholder; **D. Kirpotin**, Merrimack Pharmaceuticals, Inc, Employment; Merrimack Pharmaceuticals, Inc, Stockholder .

Presentation Number **P751**
Poster Session 4
September 8, 2012 / 14:45-14:45 / Room: The Liffey

# Evaluating methods for quantifying Annexin A5 uptake in preclinical PET oncological studies

***Jonas Grafström***[1], *Qing Cheng*[2], *Li Lu*[1,3], *Maria Hägg Olofsson*[4], *Jan-Olov Thorell*[1,5], *Erik Samén*[1,5], *Katarina Johansson*[2], *Hanna-Stina Ahlzén*[2], *Stig Linder*[4], *Elias S. Arnér*[2], *Sharon Stone-Elander*[1,5], [1]*Department of Clinical Neuroscience, Karolinska Institutet, Stockholm, Sweden;* [2]*Division of Biochemistry, Department of Medical Biochemistry and Biophysics, Karolinska Institutet, Stockholm, Sweden;* [3]*Karolinska Experimental Research and Imaging Center, Department of Comparative Medicine, Karolinska Institutet, Stockholm, Sweden;* [4]*Department of Oncology-Pathology, Karolinska Institutet, Stockholm, Sweden;* [5]*PET Radiochemistry, Neuroradiology Department, Karolinska University Hospital, Stockholm, Sweden. Contact e-mail: jonas.grafstrom@ki.se*

As reviewed in Tomasi et al Mol Imag Biol (2012), there are potential advantages to be gained by using quantification methods instead of visual and subjective uptake assessment when evaluating imaging readouts in oncology, if issues specific to radiotracer uptake in peripheral lesions are addressed. The aim of this work was to investigate the use of graphical Logan analyses to quantify the specific binding of radiolabeled Annexin A5 (AnxA5), with consideration taken to the use of a reference region, metabolite contributions, and enhanced permeability and retention (EPR) effects. Methods: The radioligands used, 11C-labeled through a C-terminal Sel-tag (ST), were [11C]-AnxA5-ST and a size-matched control [11C]-mTrx-GFP-ST. The tumor model was FaDu (human head/neck carcinoma) xenografts and SCID mice. Scanning was with a microPET Focus 120 and compartmental or kinetic analyses were conducted using the Siemens Inveon Research Workstation (IRW) software. Our hypothesis was that variations in the specific cell-death related AnxA5 binding could be determined by comparisons with the non-functional control ligand. Metabolic behavior for the two was examined by comparing whole body ROIs (i) and ex vivo blood/plasma analyses (ii). This was further evaluated (iii) by analyzing the compartmental model rate constants, when using one-compartment configuration opposed to two-compartment configuration, assuming that metabolites would alter the compartmental configuration and thus the rate constant unity ratio, e.g. $K_1^{\text{one compartment}}/K_1^{\text{two compartment}}$ would equal near unity if the compartmental configuration were unaltered. (iv) To verify the use of reference tissue models, basic compartmental methods were employed and rate constants combined to give a distribution volume ratio (DVR), which was compared to that obtained with the Logan reference tissue model. Results: In vivo distribution in healthy mice was similar for both ligands except in the kidneys, which could be due to specific AnxA5 binding. (i and ii): Both ligands demonstrated similar (and low) losses of radioactivity in vivo, indicating comparable metabolic processing. (iii): In the ratio obtained here [11C]-AnxA5-ST had the same variation as that for [11C]-mTrx-GFP-ST, within the margin of error. (iv): The DVR calculated by both methods differed by about 5%. The tumor uptake of [11C]-mTrx-GFP-ST was used to estimate non-specific uptake. Differences between groups of animals were significant when their binding potentials (calculated from the DVR), but not their normalized %ID/g were compared. Conclusions: Using an analogously labeled and size-matched control can aid in the quantification of labeled AnxA5 binding in peripheral lesions. Calculating DVR and thus specific binding using different methods indicates that a reference tissue method can be used for analyzing this radiotracer behavior. These initial experiences indicate that quantification methods give more robust results than tissue uptake assessments. Financial support from SSF, Vinnova, VR and Cancer Fund.

Disclosure of author financial interest or relationships:
**J. Grafström**, None; **Q. Cheng**, None; **L. Lu**, None; **M. Hägg Olofsson**, None; **J. Thorell**, None; **E. Samén**, None; **K. Johansson**, None; **H. Ahlzén**, None; **S. Linder**, None; **E.S. Arnér**, None; **S. Stone-Elander**, None.

Presentation Number **P752**
Poster Session 4
September 8, 2012 / 14:45-14:45 / Room: The Liffey

# A Dual-modality Liposome Formulation for the *in vivo* Assessment of Tumour Uptake Using Quantitative PET/CT Imaging

***David Green***[1,2], *Huang Huang*[1,3], *Michael Dunne*[2], *Jinzi Zheng*[1], *Douglass C. Vines*[2,4], *Christine Allen*[3], *David A. Jaffray*[1,4], [1]*Department of Radiation Physics, Radiation Medicine Program, Princess Margaret Hospital, Toronto, ON, Canada;* [2]*STTARR Innovation Centre, Radiation Medicine Program, Princess Margaret Hospital, Toronto, ON, Canada;* [3]*Leslie Dan Faculty of Pharmacy, University of Toronto, Toronto, ON, Canada;* [4]*Department of Radiation Oncology, University of Toronto, Toronto, ON, Canada. Contact e-mail: david.green@rmp.uhn.on.ca*

Introduction: Nanoparticles with prolonged *in vivo* residency that contain longer-lived radioisotopes or CT contrast can be employed for biodistribution or longitudinal imaging studies. A Cu-64 ($t_{½}$=12.7 h) labeled liposome system was extruded containing iohexol encapsulated within the liposome aqueous compartment. The nano-sized liposomes are composed of 1,2-dipalmitoyl-sn-glycero-3-phosphocholine (DPPC), cholesterol, 1,2-distearoyl-sn-glycero-3-phosphoethanolamine-N-[poly(ethylene glycol)$_{2000}$] ($PEG_{2000}$DSPE), and DSPE-1,4,7,10-tetraazacyclododecane-1,4,7,10-tetraacetic acid (DSPE-DOTA) at a mole ratio of 54:40:5:1 and encapsulate 40 mg/mL (n=3 batches) of iodine, in the form of iohexol. The extruded liposomes range in size from ~80-100 nm with an average diameter of 90 nm (n=3 batches) as measured by dynamic light scattering. DSPE-DOTA chelates copper-64 for PET imaging and the encapsulated iohexol provides CT contrast. The diameter of these liposomes allow them to selectively permeate through vessel walls in abnormal vasculature, such as at sites of inflammation or tumour angiogenesis, and result in an enhanced permeation and retention (EPR) effect. The $PEG_{2000}$ on the surface of the liposomes allow for the prolonged retention of this nanosystem. These features allow for highly sensitive disease detection via PET, as well as high-resolution localization of disease via CT imaging with a single formulation. Results and Methods: After extrusion and concentration, the liposomes were labeled by incubating with $^{64}CuCl_2$ for 1 hour at 37°C (pH 5.5) followed by adjustment of the pH to 7.4. The radiochemical purity of the liposomes was 97% (n=4), as determined by size-exclusion chromatography HPLC. MicroPET (Focus 220) and microCT (GE Locus Ultra) imaging were acquired at 1, 4, 18, 24, and 48 h post-injection. Approximately 25-33 MBq Cu-64 and 200 µL liposomes were administered (i.v.) in each nude CD-1 mouse bearing subcutaneous H520 non-small cell lung cancer (NSCLC) xenografts. PET and CT data sets were registered and regions of interest were drawn on the tumour and organs. The vascular half-life of the liposomes was calculated to be 17.5 ± 3.3 h and 18.7 ± 4.8 h from the PET and CT data, respectively. Peak tumour accumulation was found to occur around 24 hours post-injection. At 24 h, the overall mean tumour uptake was 7.8 %ID/g (PET) and 6.8 %ID/g (CT). The maximum uptake ranged between 10.1 and 34.8 %ID/g in the tumour 24 h post-injection with an increased uptake in the rim of the tumours. Cryosectioning of the tumours followed by autoradiography and immunohistochemistry staining for blood vessels (CD31) and perfusion (DiOC7) confirmed the tracer accumulated in the periphery of the tumours near perfused areas. Conclusions: A dual-modality liposome formulation was employed for longitudinal PET and CT imaging of H520 tumour xenografts. The high sensitivity of PET combined with the high temporal and spatial resolution of CT imaging allowed a comprehensive assessment of the highly heterogenous intratumoural liposome distribution.

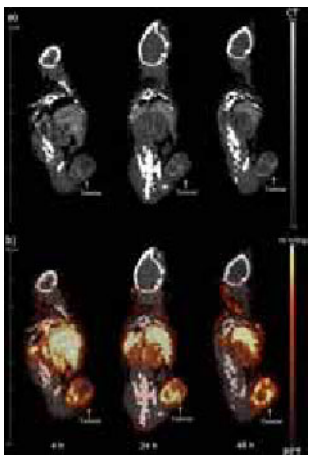

Figure 1: Coronal CT images of the same mouse at 4 h, 24 h, and 48 h p.i. illustrating the liposome iodine contrast in tumour (a). PET/CT slices at 4 h, 24 h, and 48 h p.i.illustrating Cu-64 labeled liposome accumulation in tumour (b).

Disclosure of author financial interest or relationships:
**D. Green**, None; **H. Huang**, None; **M. Dunne**, None; **J. Zheng**, None; **D.C. Vines**, None; **C. Allen**, None; **D.A. Jaffray**, Precision X-ray, Other financial or material support; Raysearch, Grant/research support; Philips, Grant/research support; Elekta, Grant/research support; General Electric, Grant/research support; IMRIS, Other financial or material support; Modus Medical, Grant/research support .

Presentation Number **P753**
Poster Session 4
September 8, 2012 / 14:45-14:45 / Room: The Liffey

# Noninvasive detection of early pathophysiological changes of irradiated bone marrow in mouse radiation carcinogenesis by diffusion-weighted imaging

***Sumitaka Hasegawa**, Yukie Morokoshi, Takako Furukawa, Ichio Aoki, Tsuneo Saga, Molecular Imaging Center, National Institute of Radiological Sciences, Chiba, Japan. Contact e-mail: shase@nirs.go.jp*

Ionizing radiation is capable of causing various tumors in both mouse and human and thus is a well-known environmental carcinogen. Mouse models have been invaluable to elucidate the mechanism(s) of radiation carcinogenesis. To date, many rodent models have been developed for this purpose. Fractionated whole-body X-ray irradiation (FX) efficiently induces thymic lymphoma (TL) in C57BL/6 mice, which are susceptible to radiation-induced thymic lymphoma (RITL) development, at 3 to 10 months after the last irradiation. This model has long been used as a classical method to study radiation carcinogenesis. In this model, although TL is arising from the thymus, many previous studies have shown that cellular damages of the bone marrow (BM) by FX are critically involved in TL development. BM changes after FX has been examined by histological analyses so far. However, analyzing spatiotemporal dynamics of pathophysiological BM changes induced by FX has been hampered by the lack of a reliable method to monitor them noninvasively. The aim of this study is to explore methods for noninvasive monitoring of the pathophysiological changes of the X-ray irradiated BM in mouse radiation carcinogenesis. Here we report that diffusion-weighted imaging (DWI) noninvasively detects early pathophysiological changes of FX-treated BM in mouse radiation carcinogenesis. Four-weeks-old C57BL/6 mice were X-irradiated with 4 doses of 1.6 Gy (total dose 6.4 Gy) each given at 7-days intervals and the pathophysiological changes of their BM were evaluated by MRI and histopathological analyses 3 days after each irradiation. T2 values were not significantly different between FX-treated and unirradiated normal BM. Interestingly, the apparent diffusion coefficient (ADC) measured by DWIs, which quantitatively represents the diffusivity of protons in tissue, significantly increased in FX-treated BM compared to those in unirradiated normal BM from the first to third irradiation ($p < 0.001$). These ADC changes were correlated with and well accounted for by the pathological findings, likely reflecting reduced cellularity and altered vascularity in the irradiated BM. These data indicate that DWI is useful in quantitatively evaluating dynamic changes of FX-treated BM in living subjects and may help elucidate the pathogenesis of RITL. In addition, this study further supports the notion that DWI is able to detect altered cellularity and thus may be applied to evaluate BM suppression which often is the limiting factor in clinical fractionated radiotherapy.

Disclosure of author financial interest or relationships:
**S. Hasegawa**, None; **Y. Morokoshi**, None; **T. Furukawa**, None; **I. Aoki**, None; **T. Saga**, None.

Presentation Number **P754**
Poster Session 4
September 8, 2012 / 14:45-14:45 / Room: The Liffey

# In vivo detection and 3D quantification of targeted and untargeted nanoparticles in heterotopic gastric and breast cancers with photoacoustic imaging

***Andrew Heinmiller***[1], *Andrew Needles*[1], *Catherine Theodoropoulos*[1], *Seung Jae Oh*[2], *Jin-Suck Suh*[2], [1]*VisualSonics Inc., Toronto, ON, Canada;* [2]*Departmen of Radiology, Yonsei University, Seoul, Republic of Korea. Contact e-mail: aheinmiller@visualsonics.com*

Introduction The use of contrast agents to label extravascular molecular biomarkers in vivo has great potential for diagnosis and treatment of various cancers. A commercially available photoacoustic (PA) imaging system (Vevo LAZR, VisualSonics, Toronto) is capable of detecting such agents and localizing them within the tumor microenvironment. Here, we describe the assessment of gold nanorods (GNRs) which were targeted to epidermal growth factor receptor (EGFR) with the commercially available monoclonal antibody cetuximab, as compared with non-targeted PEG-coated GNRs in heterotopic models of gastric and breast cancers. Methods The photoacoustic imaging system generated light from a tunable laser (680 - 970 nm) which was delivered through fiber optic bundles integrated into a linear array transducer (LZ-250, fc = 21 MHz),mounted to a linear stepper motor for 3D imaging. Hindlimb subcutaneous gastric (MKN-45) and breast (NIH3T6.7) tumors were scanned in 3D before and 3 hours after intravenous tail-vein injection of 200ul of either cetuximab-conjugated PEG-coated GNRs or non-conjugated PEG-coated GNRs each at a concentration of 500ug/ml. All nanoparticles were made at Yonsei University. Pre- and post-bolus 3D scans were analyzed by comparing the signal at 734nm as a percent increase in average photoacoustic signal intensity. Further analysis involved performing analyses of smaller ROIs having either more or less signal pre-GNR injection. For validation, images were compared with optical images where absorption was quantified with a fluorescence imaging system (eXplore Optix, GE, London, Ontario). Results Signal increase in heterotopic gastric tumors at 734nm for the cetuximab-conjugated GNRs was 30% whereas the non-targeted GNRs showed a 38% signal increase. For the breast tumor, a 21% increase was observed when non-targeted GNRs were injected. Further analysis revealed a strong correlation between pre-injection photoacoustic signal and post-injection signal enhancement indicating that well vascularized areas showed more nanoparticle signal relative to less well vascularized areas. This likely has to do with the leakiness of tumor vasculature and the ability of the nanoparticles to permeate the tissue surrounding these vessels. Conclusions Many in vivo imaging contrast agents are confined to biomarkers on the surface of the vasculature. By targeting extravascular receptors, and taking advantage of the leakiness of tumor vasculature, nanoparticles can act as an in vivo contrast agent for previously inaccessible biomarkers. Here we have shown the ability of the Vevo LAZR imaging system to visualize targeted and non-targeted nanoparticle-based contrast agents in vivo and to quantify these signals in 3D. In addition, we have shown the relationship between the distribution of such agents and tumor vasculature as measured by endogenous blood signal within the microenvironment of the tumor. These data show the potential of nanopraticle drug delivery methods by visualizing their distribution in vivo at high spatial resolution, opening the door to novel therapies for cancer treatment.

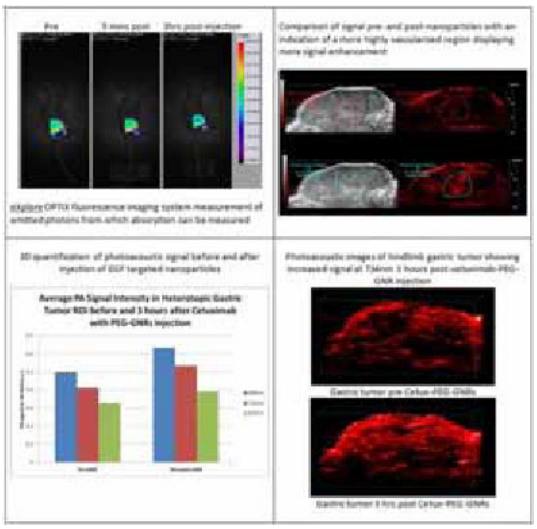

Disclosure of author financial interest or relationships:
**A. Heinmiller**, VisualSonics Inc., Employment; **A. Needles**, VisualSonics, Employment; **C. Theodoropoulos**, VisualSonics, Employment; **S. Oh**, None; **J. Suh**, None.

Presentation Number **P755**
Poster Session 4
September 8, 2012 / 14:45-14:45 / Room: The Liffey

# Classification of different tumor types by contrast ultrasound dispersion imaging

***Carola Heneweer***[1], *Tamerlan Saidov*[2], *Thorsten Liesebach*[1], *Thorsten Persigehl*[3], *Maarten Kuenen*[2,4], *Markus Böttcher*[1], *Hessel Wijkstra*[2,4], *Claus C. Glueer*[1], *Martin Heller*[1], *Massimo Mischi*[2], *[1]Clinic for Diagnostic Radiology, University Hospital Schleswig-Holstein, Campus Kiel, Kiel, Germany; [2]Department of Electrical Engineering, Eindhoven University of Technology, Eindhoven, Netherlands; [3]Department of Radiology, University Hospital Cologne, Cologne, Germany; [4]Department of Urology, AMC University Hospital, Amsterdam, Netherlands. Contact e-mail: c.heneweer@gmx.de*

Introduction: Characterization of the tumor vasculature is essential for monitoring of antiangiogenic treatment in cancer. Current noninvasive characterization is based on perfusion measurements. These are however affected by phenomena, such as arterovenous shunting and interstitial pressure increase, which have opposite effects on perfusion. Different from perfusion, dispersion in the microcirculation is mainly dependent on microvascular density (MVD) and vessel tortuosity, and can be described by multipath trajectories expressed as transit-time distribution. Contrast-ultrasound dispersion imaging (CUDI) is therefore proposed as a promising new modality to characterize microvascular architecture in tumors. We hypothesize an increase in MVD and microvascular tortuosity to produce lower dispersion, as complex trajectories constrain the dispersion process. Materials and methods: Human prostate cancer cells DU-145 and PC3 were injected subcutaneously into four and three mice, respectively. Ultrasound contrast-specific imaging was performed at 18 MHz and low mechanical index. Characterization of the microvascular architecture was performed by CUDI coherence analysis, as coherence correlates negatively with dispersion. Dispersion was estimated by analysis of the spatial similarity between time-intensity curves (TICs) measured at neighboring pixels. For each pixel, similarity was computed as the average spectral coherence of the measured TIC with those measured at the neighboring pixels. DCE-MRI was performed with a 7T scanner using a blood pool agent as a noninvasive in vivo gold standard for characterization of tumor vasculature. CD31 staining was performed for histological MVD assessment. Results: In DU-145 xenografts, the tumor centers showed low dispersion and the tumor periphery high dispersion with a mean difference of 0.23±0.06 indicating a higher vascular tortuosity and MVD in the tumor centers than in the tumor periphery. In contrast, PC3 xenografts, demonstrated only a difference of 0.03±0.03, indicating a mostly homogeneous distribution of dispersion of the entire tumor tissue and hence a more homogeneous vascular architecture. This is in accordance with DCE-MRI results which revealed a variance of maximum intensity to time ratio (MITR) for the entire tumor compared to the tumor center of 35.6% for DU-145 and of 15.9% for PC-3. In comparison with histological analysis, dispersion correlates negatively with MVD, confirming our original hypothesis. Conclusions: The present results suggest DU-145 xenografts to develop a hyper-vascular core and a hypo-vascular periphery, whereas PC3 xenografts show homogeneous vascularization. This is in accordance with DCE-MRI data, and confirmed by histological MVD analysis. Our preliminary results indicate that CUDI allows a noninvasive characterization of the microvasculature in tumors. Since antiangiogenic treatment is known to alter vascular architecture, further studies are warranted to evaluate CUDI for monitoring vascular changes upon tumor therapy.

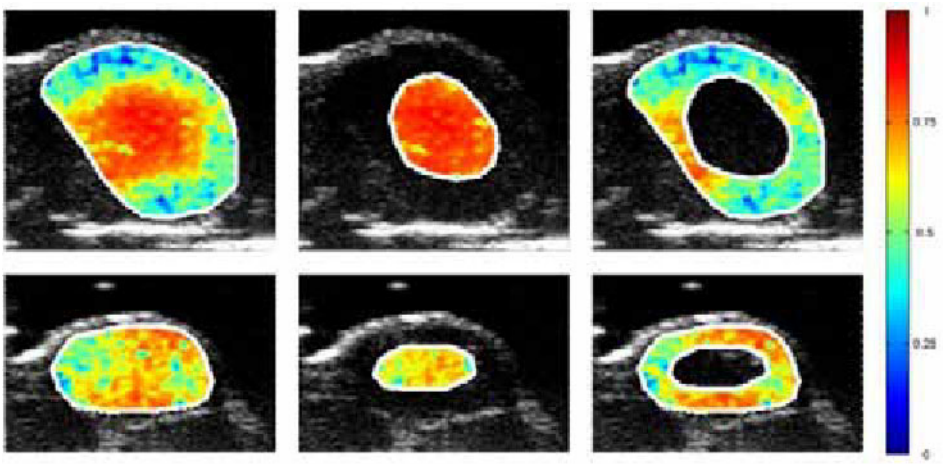

CUDI coherence analysis result from a DU-145 tumor (top row) and a PC-3 tumor (bottom row). Results are shown for the entire tumor (left column), the center of the tumor (middle column), and the peripheral tumor area (right column). In comparison with PC-3, DU-145 xenografts show a heterogeneous coherence distribution characterized by a difference in coherence level between the center and the periphery of the tumor.

Disclosure of author financial interest or relationships:
**C. Heneweer**, None; **T. Saidov**, None; **T. Liesebach**, None; **T. Persigehl**, None; **M. Kuenen**, None; **M. Böttcher**, None; **H. Wijkstra**, None; **C.C. Glueer**, None; **M. Heller**, None; **M. Mischi**, None.

Presentation Number **P756**
Poster Session 4
September 8, 2012 / 14:45-14:45 / Room: The Liffey

# Small animal PET Imaging and Biodistribution of Pancreatic Xenografts using an Engineered Antibody Fragment Targeting Prostate Specific Cell Antigen (PSCA)

***David T. Ho***[1], *David Colcher*[2], *Tove Olafsen*[1], *Robert E. Reiter*[4], *Giti Agahi*[1], *Arye A. Lipman*[1], *Jenny Keppler*[1], *Christian P. Behrenbruch*[1], *Anna M. Wu*[3], [1]*ImaginAb, Inc, Inglewood, CA, USA;* [2]*Cancer Immunotherapeutics and Tumor Immunology, Beckman Research Institute of City of Hope, Duarte, CA, USA;* [3]*Molecular and Medical Pharmacology, UCLA, Westwood, CA, USA;* [4]*Urology, UCLA, Westwood, CA, USA. Contact e-mail: david@imaginab.com*

Pancreatic cancer remains one of the most lethal of cancers, with an overall five-year survival rate (all stages) of 5% and only a 20% five-year survival rate for localized disease. Better therapeutic approaches as well as improved methods for detecting and staging this disease are clearly needed. Engineered antibody fragments such as the minibody (single chain Fv-CH3 fusion protein, ~80 kDa) typically retain high binding affinity and specificity of the parental monoclonal antibody (mAb) whilst featuring pharmacokinetics/clearance optimized for targeted diagnostic imaging. Prostate stem cell antigen (PSCA), originally identified as a marker in prostate and bladder cancer, is also overexpressed in pancreatic cancer. The presence of PSCA is highly specific for pancreatic cancer since PSCA is not expressed in benign pancreas or conditions such as pancreatitis. A humanized, affinity-matured anti-PSCA minibody, A11, has previously been validated in prostate cancer models and is moving towards first-in human trials. Here we extend the evaluation of the A11 minibody for targeting and diagnostic imaging of pancreatic cancer. The A11 minibody was produced in mg quantities from an established stable cell production line. Purification was performed with a three-step process using a mixed-mode cation capture step, an anion exchange intermediate step, and a ceramic hydroxyapatite polish step. This production run yielded 304 mgs of highly pure (>90%) A11 minibody protein. Specific binding to PSCA was confirmed by ELISA using recombinant antigen and by flow cytometry using low expressing PSCA-positive human pancreatic Capan-1 cells. The A11 minibody was radiolabeled with $^{125}$I using the Iodogen method and following HPLC purification the radiochemical purity was >90% and immunoreactivity was >75%. The $^{125}$I-labeled A11 minibody demonstrated specific targeting to the Capan-1 tumor xenografts in athymic, nude mice. Maximum uptake in the Capan-1 tumors reached 6.7 (± 0.47) %ID/g at 2 h post injection (p.i.) and was 1.96 (±0.33) %ID/g at 26 h p.i. The PSCA-positive Capan-1 tumor vs. PSCA-negative MIA-PaCa-2 tumor ratio was 2:1 at 26 h p.i. and increased to 11.5:1 at 72 h p.i. The positive tumor to blood ratios were ~1:1 and 4.6:1 at 26 and 72 h p.i., respectively. At 2 h p.i., the tumor to soft tissue ratio was 4:1, which increased to 7.5:1 and 46:1 at 26 and 72 hours p.i., respectively. For PET imaging, the A11 minibody was radioiodinated with Iodine-124; following purification by spin column radiochemical purity was 99% and immunoreactivity was 62%. microPET studies in Capan-1 xenograft bearing mice (n=6) showed clear delineation of tumors at 20 h p.i. Biodistribution at 20 h p.i. revealed that the radioactive uptake in the tumor was 2.57 (±0.47) %ID/g; similar to that obtained with $^{125}$I-labeled A11 minibody. Despite the low expression of PSCA in Capan-1 cells, specific targeting and high contrast images were obtained with the $^{124}$I-labeled A11 minibody making it a promising agent for imaging pancreatic cancer.

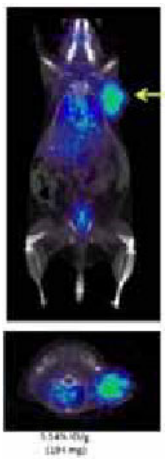

PET/CT images of an athymic nude female mouse carrying a Capan-1 xenograft (arrow) at 20 hours after administration of 124I-labeled A11 minibody. Coronal and transverse images are shown. The tumor size (mg) and the radioactive uptake (%ID/g) in the tumor are shown below the images.

Disclosure of author financial interest or relationships:
**D.T. Ho**, ImaginAb, Inc, Employment; **D. Colcher**, ImaginAb, Grant/research support; UCLA, Grant/research support; **T. Olafsen**, ImaginAb Inc., Employment; **R.E. Reiter**, Imaginab, inc, Consultant; Imaginab, inc, Stockholder; **G. Agahi**, None; **A.A. Lipman**, ImaginAb Inc., Employment; **J. Keppler**, ImaginAb, Inc., Employment; **C.P. Behrenbruch**, ImaginAb, Inc., Stockholder; **A.M. Wu**, ImaginAb, Inc., Consultant; ImaginAb, Inc., Stockholder .

Presentation Number **P757**
Poster Session 4
September 8, 2012 / 14:45-14:45 / Room: The Liffey

# GFP- or RFP-expressing colon cancer successfully resected in orthotopic mouse models using fluorescence-guided surgery

*Cristina A. Metildi[1], Sharmeela Kaushal[1], Cynthia S. Snyder[1], **Robert M. Hoffman**[2,1], Michael Bouvet[1], [1]Dept. of Surgery, University of California, San Diego, CA, USA; [2]AntiCancer, Inc., San Diego, CA, USA. Contact e-mail: all@anticancer.com*

The aim of this study was to improve disease-free survival and overall survival in orthotopic nude mouse models of human colon cancer with fluorescence-guided surgery (FGS). Fluorescent orthotopic or carcinomatosis models were established in nude mice using human colon cancer cell lines HCT-116 and HT-29 expressing either green fluorescent protein (GFP) or red fluorescent protein (RFP). The tumors were later resected by bright light surgery (BLS) or FGS. In the carcinomatosis model. Pre- and post-operative images were obtained with the OV-100 Small Animal Imaging System (Olympus Corp., Tokyo, Japan) to assess the extent of surgical resection. In the orthotopic model, whole body imaging of the mice was performed in the postoperative period to assess cancer recurrence and to follow subsequent tumor progression. The mice were sacrificed when they became premorbid and their abdomens were exposed for intravital and ex vivo imaging. Tumor burden was measured in mm2 using ImageJ v1.440. A greater extent of tumor resection in mice with carcinomatosis was achieved using FGS compared to BLS (99.9% vs. 76.9%, p = 0.006). Furthermore, all mice with localized disease had a complete surgical resection with FGS. In contrast, complete resection was achieved in only 56% of the mice undergoing BLS. (p=0.001) Fewer mice in the FGS group had evidence of tumor recurrence (33%) compared to mice in the BLS group (58%), lengthening disease-free survival from 9 weeks in the BLS group to 27 weeks in the FGS group. Overall survival of the mice also increased from 17weeks in the BLS group to 29 weeks in the FGS group. The results of the present study demonstrate that improved surgical outcomes in the treatment of colon cancer can be achieved with FGS.

Disclosure of author financial interest or relationships:
**C.A. Metildi**, None; **S. Kaushal**, None; **C.S. Snyder**, None; **R.M. Hoffman**, None; **M. Bouvet**, None.

Presentation Number **P758**
Poster Session 4
September 8, 2012 / 14:45-14:45 / Room: The Liffey

# In vivo imaging of human pancreatic cancer liver metastasis in orthotopic nude mouse models indicates the importance of pancreatic stellate cells

*Atsushi Suetsugu[1,3], Cynthia S. Snyder[2], Hisataka Moriwaki[3], Shigetoyo Saji[4], Michael Bouvet[2], **Robert M. Hoffman**[1,2], [1]AntiCancer, Inc., San Diego, CA, USA; [2]Dept. of Surgery, University of California, San Diego, CA, USA; [3]Dept. of Gastroenterology, Gifu University Graduate School of Medicine, Gifu, Japan; [4]Dept. of Surgical Oncology, Gifu University Graduate School of Medicine, Gifu, Japan. Contact e-mail: all@anticancer.com*

Pancreatic stellate cells are involved in fibrosis of pancreatic cancer. An understanding of pancreatic cancer-cell interactions with stellate cells is critical to our ability to develop effective anti-tumor therapeutics for pancreatic cancer. We report here imaging of the interaction of pancreatic cancer cells and pancreatic stellate cells in liver metastasis. Human pancreatic cancer cell lines (XPA1 and MiaPaCa-2) were engineered to express green fluorescent protein (GFP) in the nucleus and red fluorescent protein (RFP) in the cytoplasm. Pancreatic stellate cells, engineered to express RFP, were co-injected with the cancer cells into the spleen of transgenic cyan fluorescent protein (CFP) nude mice. Three hours after splenic injection dual-color pancreatic cancer cells and pancreatic stellate cells were found distributed in the host liver. Seven days after cancer cell-stellate cell co-injection, most pancreatic cancer cells and stellate cells were dead. However, by 28 days after injection, liver metastases were observed in the host CFP nude mice. With the high-resolution intravital imaging afforded by the Olympus FV1000 confocal microscope, the interaction of the dual-colored pancreatic cancer cells and the RFP-expressing pancreatic stellate cells could be clearly imaged in the liver metastasis, suggesting that stellate cells participate in metastasis formation. Our hypothesis is that pancreatic stellate cells form a niche for liver metastasis of pancreatic cancer.

Disclosure of author financial interest or relationships:
**A. Suetsugu**, None; **C.S. Snyder**, None; **H. Moriwaki**, None; **S. Saji**, None; **M. Bouvet**, None; **R.M. Hoffman**, None.

Presentation Number **P759**
Poster Session 4
September 8, 2012 / 14:45-14:45 / Room: The Liffey

# Integrin αvβ3-Targeted IRDye 800CW Near-Infrared Imaging of Glioblastoma

***Ruimin Huang***[1,3], *Jelena Vider*[2], *Moritz F. Kircher*[1,3], *Ronald G. Blasberg*[1,2], [1]*Radiology, Memorial Sloan Kettering Cancer Center, New York, NY, USA;* [2]*Neurology, Memorial Sloan Kettering Cancer Center, New York, NY, USA;* [3]*Brain Tumor Center, Memorial Sloan Kettering Cancer Center, New York, NY, USA. Contact e-mail: huangr@mskcc.org*

Integrin αvβ3 plays an important role in tumor angiogenesis, growth and metastasis. Integrin-targeting agents, based on the cyclic RGD peptide, provide the opportunity to visualize and quantify integrin receptor expression levels noninvasively. Here, we have tested a near infrared fluorescent (NIRF) RGD probe, IRDye 800CW-cyclic RGD peptide (IRDye 800CW-RGD), to visualize integrin receptor expression by in vivo and ex vivo NIRF imaging. A state-of-the-art transgenic glioma mouse model (RCAS-PDGF-driven/tv-a glioma), which is known to closely mimic the infiltrating growth pattern of human gliomas, was chosen. We demonstrate that conjugation of the IRDye 800CW to the RGD peptide had no significant effect on the dye's optical properties and there was minimal photobleaching. We show that the IRDye 800CW-RGD peptide: 1) specifically binds to integrin receptors; 2) is selectively localized to glioblastomas and retained over prolonged periods of time (Panel A). At 48 hour post-injection, the fluorescence tumor-to-normal ratio (T/N) was maximal; 2.98±0.22 ($p<0.01$). The unlabelled cRGD peptide, used as a blocking reagent, significantly reduced tumor uptake of the IRDye 800CW-RGD probe. Further, nonspecific control probe, IRDye 800CW-RAD peptide, only showed a small, insignificant difference in signal intensity between tumor-bearing and normal animals; 3) is associated with minimal autofluorescence due to imaging at 800 nm; 4) provides delineation of tumor tissue with high precision due to a high tumor-to-normal brain fluorescence ratio (18.4±2.4, $p<0.01$) (Panel B) and 5) enables fluorescence-guided glioblastoma resection (Panel C). The NIRF-800 image showed a high fluorescence signal from the hyperemic tumor area (black arrow heads). A two-step resection was performed to remove the tumor tissue. The resected tissue exhibited very high fluorescence and tumor was confirmed by H&E staining. Importantly, small foci of residual fluorescence were observed after resection was completed using white light imaging alone, and these fluorescent foci were shown to represent residual tumor tissue by histology. NIRF imaging with the IRDye 800CW-RGD probe provides a simple, rapid, low-cost, non-radioactive and highly translatable approach for improved intraoperative glioblastoma visualization and resection. It also has the potential to serve as an imaging platform for noninvasive cancer detection and drug efficacy evaluation studies.

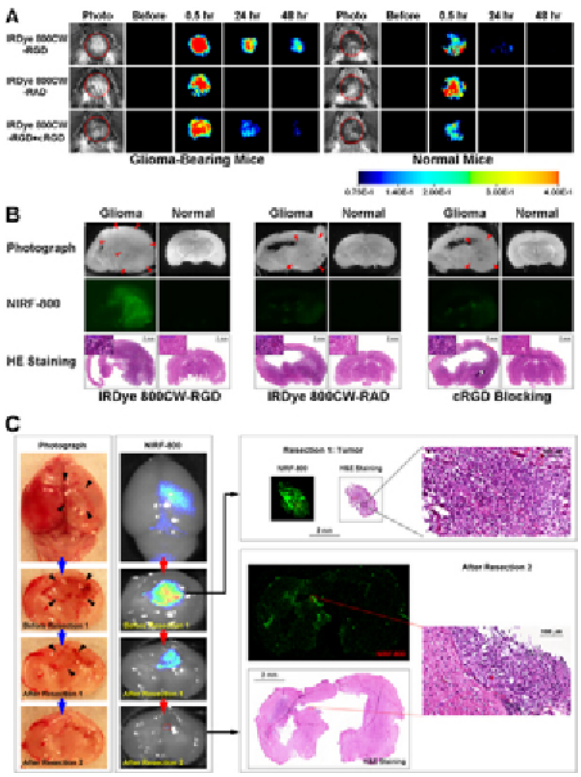


Disclosure of author financial interest or relationships:
**R. Huang**, None; **J. Vider**, None; **M.F. Kircher**, None; **R.G. Blasberg**, None.

Presentation Number **P760**
Poster Session 4
September 8, 2012 / 14:45-14:45 / Room: The Liffey

# Differential effects of novel tumor vaccine adjuvants visualized by combined magnetic resonance imaging (MRI) and bioluminescence imaging (BLI)

*Deepak K. Kadayakkara[1], Hyam I. Levitsky[1], **Jeff W. Bulte**[2,1], [1]Department of Oncology, Johns Hopkins University School of Medicine, Baltimore, MD, USA; [2]Department of Radiology, Johns Hopkins University School of Medicine, Baltimore, MD, USA. Contact e-mail: jwmbulte@mri.jhu.edu*

Introduction: Vaccine adjuvants are defined as substances that augment immune response to an antigen but do not elicit immune response when administered alone. The exact mechanism of adjuvant action is not known; therefore, famous immunologist, Charles Janeway called adjuvants as 'immunologist's dirty little secret.' Toll-like receptors (TLR) are specialized receptors present on antigen presenting cells (APC), which on stimulation will activate them (1). Here, we explored the mechanisms of TLR agonists as vaccine adjuvant against B16-melanoma using MRI and BLI. Earlier, we have developed a MRI based technology to visualize and quantify in vivo antigen transfer and migration of APC to draining lymph nodes (LN) (2). That study used the GVAX, a GMCSF secreting whole cell tumor vaccine. GVAX was labeled with superparamagnetic iron oxide (SPIO) particles. SPIO from the vaccine were transferred to APC and their migration to the LN was quantified by counting the 'dark pixels' below a threshold in MRI. In this study, we use combination of TLR4 and TLR7 as vaccine adjuvants with B16-mOva cells stably expressing ovalbumin as a model antigen. We compared antigen transfer and APC migration to the LN of this novel vaccine to that of GVAX. Further, we studied the vaccines to activate T cells using BLI of ovalbumin specific CD8+ T lymphocytes (OT1) expressing firefly luciferase. Method: B16-mOva cells were cultured in complete RPMI medium with G418 selection. Cells were irradiated and labeled with SPIO (Biopal, MA). One million cells were mixed with one hundred thousand irradiated B78H1GM cells in 20 µl HBSS to produce GVAX. One million B16 cells were mixed with 20 µl of the combined TLR 4/7 agonists (Immune Design, WA ) to produce a TLR vaccine adjuvant combination. Vaccines were administered in the right foot pad. MR images were obtained on day 3 using a gradient echo on a11.7 T Bruker microimaging system. For BLI, mice were injected with four million T cells from OT1/luciferase transgenic mice a day before vaccination. Serial imaging from day 1 to 10 was performed using an IVIS system (Caliper Biosciences, MD). A tumor challenge was given with one hundred thousand B16-mOva cells, and the mice were vaccinated on days 3, 10, and 18. Tumor sizes were monitored for 3 weeks. Results and Conclusions: Our results show that unexpectedly, the vaccine with TLR agonists reduced antigen captured APC migration to the LN compared to GVAX (Fig. 1a, b) as observed by MRI. MRI results were validated by flow cytometry of excised LNs. In GVAX treated mice, OT1 cells were primarily localized in the right popliteal LN and spleen (1c), whereas, in the presence of adjuvants, they were localized in the spleen and the right footpad (1d). The ability to slow the growth of established tumors were significantly improved in the presence of TLR4/7 adjuvants (1e). Although presence of TLR adjuvants reduced antigen captured APC in draining LNs, they improved tumor protective responses. Currently, studies are underway to understand the mechanisms of these observations. References: 1) Nat Rev Immunol. 2004;4:499-511, 2) Cancer Res 2009;69:3180-7

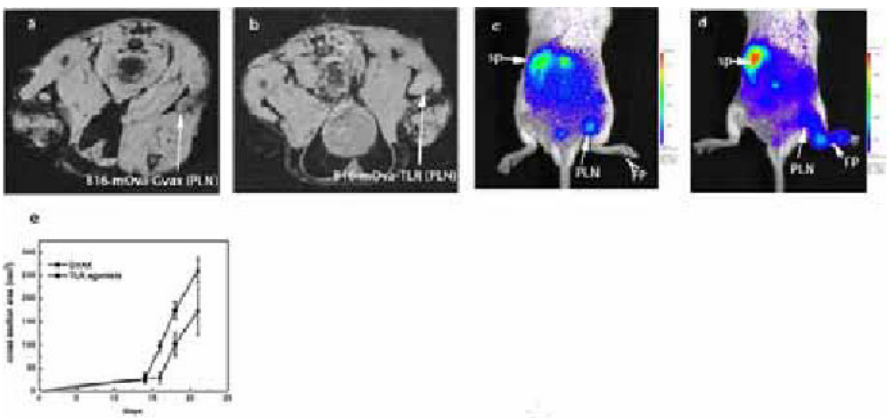


Fig. 1. APC and T cell migration following vaccination. a and b) Axial MRI images through the popliteal fossa. a) B16-mOVA-GVAX treated mice shows increased migration of antigen/iron oxide captured APC in the draining popliteal LN compared to mice treated with vaccine containing TLR agonist adjuvants (b) as observed by 'dark pixels'. Images were acquired on the 3rd day of vaccination. c and d) BLI images of the mice—dorsal view. Proliferation and migration of OT1-luciferase T cells shows accumulation of T cells in spleen and draining popliteal LN in GVAX treated mice (c), whereas T cells accumulated predominantly in the spleen and vaccine-inoculated site (rt. foot pad) in adjuvant-treated mice (d). The accumulation peaked on day 7 following vaccination. e) Therapeutic effects of vaccines. Growths in established tumors were reduced significantly in the presence of TLR agonist adjuvants (n=7). PLN: popliteal lymph node, FP: footpad, sp: spleen

Disclosure of author financial interest or relationships:
**D.K. Kadayakkara**, None; **H.I. Levitsky**, Hoffman La Roche, Inc., Employment; Roche, Stockholder; **J.W. Bulte**, Philips, Grant/research support; Q Therapeutics, Grant/research support .

Presentation Number **P761**
Poster Session 4
September 8, 2012 / 14:45-14:45 / Room: The Liffey

# In vivo optical imaging of carcinogenesis by the detection of HIF-active cells using HOL transgenic mice

***Tetsuya Kadonosono***[1], *Takahiro Kuchimaru*[1], *Tomoharu Tanaka*[2], *Kiichi Hirota*[2], *Hideki Tsutsumi*[3], *Mamoru Ito*[3], *Koji Urano*[3], *Gen Kondoh*[4], *Shinae Kizaka-Kondoh*[1], [1]*Graduate School of Bioscience and Biotechnology, Tokyo Institute of Technology, Yokohama, Japan;* [2]*Department of Anesthesia, Kyoto University, Kyoto, Japan;* [3]*Central Institute for Experimental Animals, Kawasaki, Japan;* [4]*Institute for Frontier Medical Sciences, Kyoto University, Kyoto, Japan. Contact e-mail: tetsuyak@bio.titech.ac.jp*

In many cancers, hypoxia-inducible transcription factors (HIFs) are activated by hypoxia, oncogene activation, enhanced proliferation signals, and so on. A number of the genes induced by HIF are critically involved in processes such as immortalization, cellular differentiation, genetic instability, vascularization, metabolic reprogramming, autocrine growth factor signaling, invasion/metastasis, and resistance to treatment. Moreover, HIF-active stromal cells in the tumor hypoxic microenvironment are suggested to promote tumorigenesis. Therefore, HIF activity is potentially an excellent marker for cancer formation, and in vivo imaging of HIF-active cells is significant for developing treatment strategies. Ubiquitously expressed HIF is composed of a hypoxia-inducible HIFα and a constitutively expressed HIFβ. Under well-oxygenated conditions, HIFα is hydroxylated by members of the prolyl hydroxylase domain family, which target highly conserved prolyl residues located in the HIFα oxygen-dependent degradation (ODD) domain, and then hydroxylated HIFα undergoes proteasomal degradation. While hypoxia suppresses the rate of the hydroxylation and the degradation. Recently we constructed a HRE/ODD-luciferase (HOL) vector consisting of a HIF-dependent promoter and a cDNA encoding firefly luciferase fused to the sequence for the ODD domain of human HIFα. When cells were transfected by the HOL vector, HIF-activity could be estimated by the bioluminescence activity of the ODD-luciferase protein. Next, we established transgenic (Tg) mice that express the HOL gene and tried to detect the in vivo HIF-activity using bioluminescence imaging. We examined the in vitro and ex vivo reporter response to hypoxia- or propyl gallate-induced HIF activity by using cells or tissues isolated from HOL Tg mice and showed that transgenically expressed HOL generates bioluminescence in an HIF-dependent manner. Here, we explored whether HOL Tg mice were able to detect cancer formation in vivo. We mated HOL Tg mice with RasH2 Tg mice, which are highly sensitive to both nongenotoxic and genotoxic carcinogens and has been one of the most thoroughly tested in vivo alternatives to the lifetime mouse bioassay. Bioassays using RasH2 mice shortened the assessment period from 2 years to 26 weeks. After RasH2-HOL Tg mice were treated with N-methyl-N-nitrosourea, a standard positive control compound for RasH2 bioassay, HIF activity was noninvasively detected as early as 9 weeks. The tissues with the bioluminescence signal were histopathologically analyzed and diagnosed as squamous cell papilloma/carcinoma or adenocarcinoma. These results strongly suggest that HIF activity is closely associated with cancer formation and that bioassays using RasH2-HOL Tg mice would be able to further shorten the assessment period and reduce the number of animals required. Taken together, Tg mice presented here would be useful as a mouse model for in vivo bioimaging to investigate the onset and progression of cancers as well as other diseases related to HIF activity and for developing drugs and treatment strategies for those diseases.

Disclosure of author financial interest or relationships:
**T. Kadonosono**, None; **T. Kuchimaru**, None; **T. Tanaka**, None; **K. Hirota**, None; **H. Tsutsumi**, None; **M. Ito**, None; **K. Urano**, None; **G. Kondoh**, None; **S. Kizaka-Kondoh**, None.

Presentation Number **P762**
Poster Session 4
September 8, 2012 / 14:45-14:45 / Room: The Liffey

# Three-dimensional imaging of the tumour microvasculature using DCE-MRI and CE-CT: combining high resolution anatomy with function

***Veerle Kersemans**, Philip D. Allen, Bart Cornelissen, Sean Smart, Department of Oncology, University of Oxford, Oxford, United Kingdom. Contact e-mail: Veerle.Kersemans@oncology.ox.ac.uk*

**Introduction**: The visualisation of blood vessels and their permeability/perfusion capacity provides information about the microenvironment of a tumour. However, non-invasive CT imaging of the tumour microvasculature in mice is problematic. As there is very low contrast between blood vessels and surrounding tissues, the administration of contrast agent is essential. However, existing small-molecular iodinated contrast agents clear too fast from the bloodstream in order to provide sufficient vessel contrast. In this study we used Exitron nano-12000 for high resolution in vivo anatomical vascular imaging in combination with DCE-MRI to provide functional information. **Materials and methods**: CaNT tumour bearing CBA mice were anaesthetised using 2% isoflurane in air. DCE-MRI (Agilent; 4.7T, T1-weighted, 45 min, bolus i.v. of 10 mg gadodiamide) was immediately followed by contrast-enhanced CT (CE-CT) using Exitron nano-12000 (Viscover; 100 µl, i.v. bolus). The performance of Exitron nano-12000 was compared to Iomeprol (Bracco; 400 mg I/ml; 3g I/kg bolus). CT acquisitions were initiated 10 min p.i. of the contrast agent (Inveon PET/CT, Siemens; 360 degrees, 720 projections, 65 kV, 500 µA, 2s settling time, 6s/projection, and 13.5 µm nominal pixel size). DCE-MRI derived parametric maps of initial slope, maximal intensity and area-under-curve were created by non-compartmental analysis and were co-registered to CT anatomical images. ImageJ, Matlab and ITK-snap were used to visualise the tumour vessels. **Results**: Exitron nano-12000 enabled high resolution in vivo vasculature imaging. The detectable vessel size was 40 µm and the tumour feeding vessels could easily be identified. Additionally, CT exposure time could be reduced from the optimal 6s/projection to 1s/projection without any discernible loss in signal-to-noise. The latter enabled gated CT imaging which reduced motion artefacts and loss of resolution. CT imaging following Iomeprol injection resulted in a detectable vessel size of 110 µm but the vasculature was much less defined and the tumour feeding vessels could not easily be located. DCE-MRI provided information on vasculature/blood flow and the derived parametric maps of initial slope, maximal intensity and area-under-curve showed heterogeneous Gd influx upon injection. Furthermore, regions with slow Gd influx were located furthest from the tumour feeding vessels. **Conclusion**: Multimodality imaging using DCE-MRI and CE-CT imaging provides supplementary data and allows a better characterisation of the tumour microenvironment. This is a valuable toolkit to study tumour angiogenesis and to visualize spread and loss of tumour blood vessels after anti-tumour treatment with excellent sensitivity.

Disclosure of author financial interest or relationships:
**V. Kersemans**, None; **P.D. Allen**, None; **B. Cornelissen**, None; **S. Smart**, None.

Presentation Number **P763**
Poster Session 4
September 8, 2012 / 14:45-14:45 / Room: The Liffey

# Quantitative in vivo Cerenkov light imaging of I-131 and P-32

***Alexander Klose***[1], *Yared Tekabe*[2], *Maria Kollaros*[3], *Arul S. Thirumoorthi*[3], *Alejandro V. Garcia*[3], *John P. Andrews*[3], *Jessica J. Kandel*[3], *Lynne Johnson*[2], [1]*Radiology, Columbia University, New York, NY, USA;* [2]*Medicine, Columbia University, New York, NY, USA;* [3]*Surgery, Columbia University, New York, NY, USA. Contact e-mail: ak2083@columbia.edu*

Inflammatory processes play a major key role in tumor angiogenesis of many cancers, making this a research area of immense interest. A molecular indicator of early tumor angiogenesis is, for example, the over-expression of αVβ3 integrin. Optical imaging of radiolabeled Arg-Gly-Asp (RGD) peptides targeted to integrin during tumor progression would facilitate the development of highly effective tumor therapy. Moreover, it has been shown in the past three years that Cerenkov light imaging enables optical imaging of radiotracers in small animals. Cerenkov light arises when a charged particle propagates faster than light inside an optically transparent medium. The particle polarizes the electrons of the medium, which relax back to their native state while giving off visible light. Although Cerenkov light intensities [photons s-1 cm-2] can be measured at the tissue surface with a sensitive optical camera, planar surface images show only diffuse light intensity distributions and do not reveal the in vivo radionuclide activity [Ci]. Therefore, we have developed a multispectral Cerenkov light source reconstruction method, which generates three-dimensional (3D) volume maps of the in vivo radionuclide activity distribution. We demonstrate in a pilot study that 3D Cerenkov light tomography of I-131 and P-32 can recover the in vivo radionuclide activity and, thus, enables quantitative optical imaging. We further show that optical imaging of I-131 labeled RGD could become a pre-clinical imaging tool for monitoring tumor development and therapy. We implanted a rectal catheter containing either I-131 or P-32 with different activities (I-131: 12, 37, 168, and 412 µCi; P-32: 0.25, 1, 5, 20, and 50 µCi) into a nude mouse and registered its location with a CT scan (Figure 1A). Next, we measured planar Cerenkov light images with a luminescence imaging system (PhotonImager, BiospaceLab) at six different spectral bands (width of 50 nm) centered at 535 nm, 575 nm, 615 nm, 655 nm, 695 nm, and 780 nm. An expectation-maximization (EM) method, while utilizing a radiative transfer model based on the simplified spherical harmonics (SPN) equations, calculated the spatial I-131 and P-32 radionuclide distribution inside tissue (Figure 1B), which could directly be correlated to its known ex vivo activity (Figure 1C). The results demonstrate that quantitative in vivo optical imaging of radiotracers is feasible with a 3D source reconstruction algorithm. A renal Ewing's sarcoma (SKNEP1) tumor was implanted into the left kidney of n=4 nude mice and was grown for four to six weeks. RGD peptides were labeled with I-131 and intravenously injected. Three hours post injection, the mice were imaged with a luminescence imaging system (PhotonImager, BiospaceLab) and SPECT/CT (nanoSPEC/CT, Bioscan). The optical images show focal hotspots at the tumor sites corresponding to the tumor location. This work was supported in part by grants 1R21EB011772-01A1 from the National Institute of Biomedical Imaging And Bioengineering (NIBIB) and UL1RR024156 from the National Center For Research Resources (NCRR).

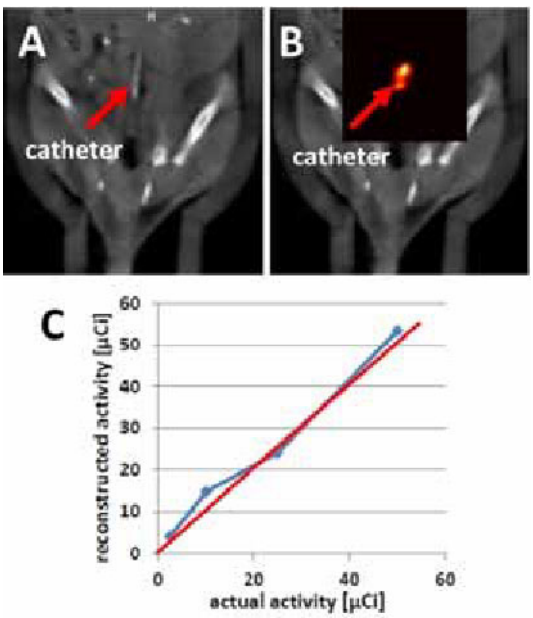


Disclosure of author financial interest or relationships:
**A. Klose**, None; **Y. Tekabe**, None; **M. Kollaros**, None; **A.S. Thirumoorthi**, None; **A.V. Garcia**, None; **J.P. Andrews**, None; **J.J. Kandel**, None; **L. Johnson**, None.

Presentation Number **P764**
Poster Session 4
September 8, 2012 / 14:45-14:45 / Room: The Liffey

# Focused Ultrasound-Mediated Delivery of Doxorubicin in a Mouse Model of Glioblastoma

***Zsofia Kovacs***[1,3], *Ernst -. Martin-Fiori*[2,3], *Michele Bernasconi*[1,3], *Beat Werner*[2,3], [1]*Oncology Department, University Children's Hospital Zurich, Zurich, Switzerland;* [2]*Center for MR-Research, University Children's Hospital Zurich, Zurich, Switzerland;* [3]*Children's Research Center, University Children's Hospital Zurich, Zurich, Switzerland. Contact e-mail: zsofia.kovacs@kispi.uzh.ch*

Background Glioblastoma is the most malignant primary brain tumor. In this study, we demonstrate (a) targeted delivery of Doxorubicin (DOX) into the brain of glioblastoma bearing mice by applying focused ultrasound (FUS) mediated transient disruption of the blood brain barrier (BBB), and (b) therapeutic benefit of DOX delivery in terms of tumor growth and survival time. Methods All FUS experiments were approved by the veterinary office of the Canton Zurich and carried out in wild type C57BL/6J-Tyrc-J albino mice under MR-imaging guidance (clinical 3T MR scanner). The FUS BBB disruption protocol consisted of a single element ultrasound transducer with aperture 80 mm, f-number 0.8, center frequency 550 kHz (Imasonic) that emitted ultrasound bursts of 5'555 cycles delivered at 1Hz repetition rate for 60 s at peak negative pressure of 0.4 MPa. Microbubbles (BR38®, Bracco) were injected into the tail vein of the mice starting 30 s prior to sonication at a rate of 1 µL/s for 60 s. The feasibility of FUS mediated targeted trans-BBB delivery of DOX was demonstrated in 14 animals by injecting 8 mg/kg DOX immediately before FUS mediated BBB opening and subsequent measurement of DOX concentration in brain tissue homogenates by HPLC. Therapeutic effect of trans-BBB delivery of DOX was assessed in 7 animals by monitoring tumor growth and survival time in a syngenic mouse glioblastoma model. Tumors were induced by stereotactic injection of 105 GL261 mouse glioblastoma cells into the cortex. Treatment consisted of a single dose of 8 mg/kg DOX before application of FUS at day 11 after injection. Results HPLC quantification showed significantly elevated concentrations of DOX in sonicated brain tissue (173 ± 23.780 ng/ml) as compared to unsonicated tissue in the contralateral brain hemisphere (10.48 ± 5.097 ng/ml). Tumor bearing mice treated with Doxorubicin had a significantly slower tumor growth and survived significantly longer (35 ± 3 days) than the untreated littermates (21 ± 3 days). Conclusion Microbubble enhanced FUS can be applied to focally open the BBB and efficiently elevate DOX concentration in the brain of tumor bearing mice and increase its therapeutic effect to slow down tumor growth and prolong survival time.

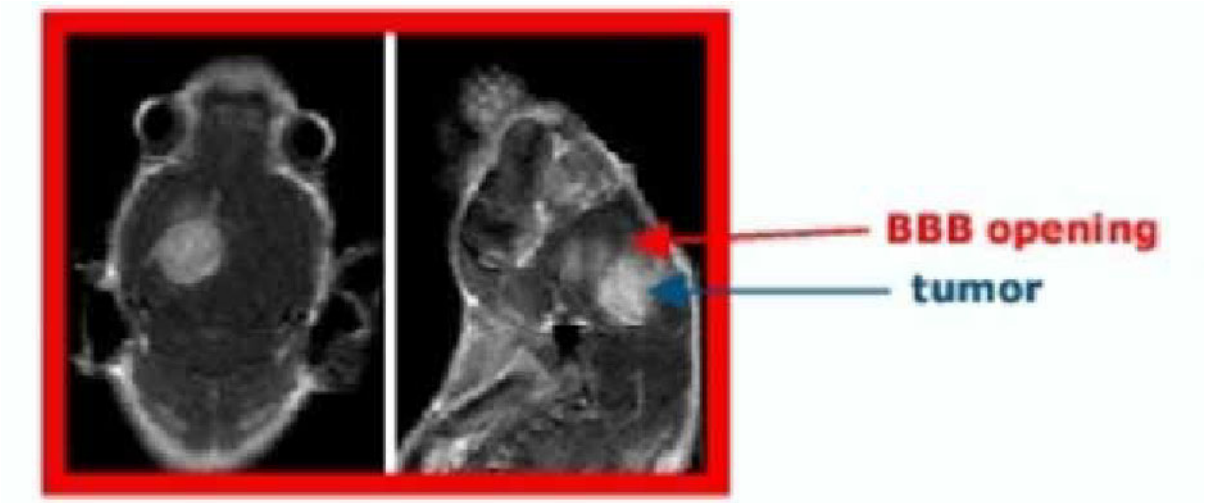


Disclosure of author financial interest or relationships:
**Z. Kovacs**, None; **E.-. Martin-Fiori**, None; **M. Bernasconi**, None; **B. Werner**, None.

Presentation Number **P765**
Poster Session 4
September 8, 2012 / 14:45-14:45 / Room: The Liffey

# Pharmacokinetics of IRDye 800CW-labeled PSMA-targeted small molecule and antibody for preclinical small animal imaging

***Joy L. Kovar**, Lael Cheung, Michael Olive, Translational Research, LI-COR Biosciences, Lincoln, NE, USA. Contact e-mail: joy.kovar@licor.com*

Near infrared (NIR) fluorescence imaging is gaining acceptance as a versatile method for studying cancer. Prostate-specific membrane antigen (PSMA) is currently being evaluated as a therapeutic target in several cancer-related clinical trials. IRDye 800CW is a NIR fluorophore exhibiting superior optical performance in vivo and can be readily conjugated to targeting moieties such as antibodies, peptides, and small molecules. Here we assess two different PSMA-targeted compounds conjugated to IRDye 800CW: the small molecule YC-27 and a PSMA-specific antibody. In vitro binding kinetics for both compounds exhibited expected dose dependent responses. Both compounds were successfully blocked with their unlabeled counterpart; however, neither blocked the other suggesting different PSMA binding sites. Although direct comparisons are inappropriate due to differences in molecular structures and labeling density, assessment of their respective pharmacokinetics is possible. Microscopy of prostate tumor cells incubated with each probe revealed the internalization rate of the antibody to be faster than that of the small molecule. Specificity of the labeled compounds in vivo was determined in male athymic nu/nu mice implanted with 22Rv1 (PSMA positive) or PC3M-LN4 (PSMA negative) prostate cancer cells (106). Mice received either IRDye 800CW YC-27 (1 nmole) or IRDye 800CW PSMA (50 µg) followed by non-invasive fluorescent optical imaging of 800nm signals on the Pearl Impulse Small Animal Imager. At the study endpoint, organs and tumors were excised and imaged to assess residual probe localization. The probes exhibited different in vivo clearance patterns, with the YC-27 clearing via the kidneys and the antibody clearing through the liver. Successful in vivo competition for IRDye 800CW YC-27 (0.5 nmoles) binding was achieved by co-administering an inhibitor of NAALADase, 2-PMPA (2 µg) in SCID hairless mice bearing 22Rv1 xenografts. The resulting tumor fluorescence was reduced by 80%, confirming specificity of the targeting agent. These subtle differences between the two imaging agents may guide investigators in choosing NIR optical probes that meet their specific research needs.

Disclosure of author financial interest or relationships:
**J.L. Kovar**, LI-COR Biosciences, Employment; **L. Cheung**, LI-COR Biosciences, Employment; **M. Olive**, LI-COR Biosciences, Employment .

Presentation Number **P766**
Poster Session 4
September 8, 2012 / 14:45-14:45 / Room: The Liffey

# MM-DX-929: A novel 64Cu-liposomal PET agent for predicting antitumor treatment response to immunoliposomal chemotherapeutics

***Helen Lee***[1], *Jinzi Zheng*[2], *Daniel F. Gaddy*[1], *Dmitri Kirpotin*[1], *Michael Dunne*[2], *Christine Allen*[2,3], *David A. Jaffray*[2], *Bart Hendriks*[1], *Thomas Wickham*[1], [1]*Merrimack Pharmaceuticals, Boston, MA, USA;* [2]*STTARR Innovation Center, Radiation Medicine Program, Princess Margaret Hospital / University Health Network, Toronto, ON, Canada;* [3]*Leslie Dan Faculty of Pharmacy, University of Toronto, Toronto, ON, Canada. Contact e-mail: hlee@merrimackpharma.com*

Background: Nanoparticle-based drug delivery systems, such as liposomes, are known to accumulate in tumors via the enhanced permeability and retention effect (EPR), or passive targeting. Previous studies have reported that tumor uptake of 111In-labeled liposomes is highly variable among patients. Further, imaging iodine-containing liposomes with mammography has shown liposome deposition to be predictive of response to liposomal doxorubicin (Karathanasis et al., 2009, PMID 19188313). Variability in the deposition of liposomal therapeutics within tumors leads to differences in drug exposure, thereby directly influencing tumor response to liposomal drugs. It is hypothesized that the relationship between deposition and tumor response would also hold for antibody-targeted liposomes, such as MM-302 (HER2-targeted liposomal doxorubicin, currently in clinical development) and be detectable using other imaging modalities. Objectives: MM-DX-929 is a novel and clinically-implementable 64Cu-liposomal PET contrast agent. The current study aims to demonstrate that the extent of tumor uptake of MM-DX-929 is predictive of tumor response to MM-302 in a mouse xenograft tumor model. Methods: Mice bearing BT474-M3 mammary tumors (n=10) were injected intravenously with MM-DX-929 prior to MM-302 treatment. PET (Focus 220, Siemens)/CT (Locus Ultra, GE) imaging was performed at 16h post MM-DX-929 injection, and tumor uptake (% i.d./g) of MM-DX-929 was determined from the PET data set (Figure 1a). The mice were then treated with MM-302 (q7d) for 3 weeks at 3 mg/kg. Response to MM-302 treatment was quantified as tumor volume changes measured over a 2-month period by MRI (M2, Aspect Imaging). Results: Tumor deposition of MM-DX-929 was found to range between 3-6 % i.d./g, which is comparable to tumor uptake levels of MM-302. Tumor deposition of MM-DX-929 correlates with treatment response to MM-302 (Figure 1b, Spearman correlation coefficient of -0.891 and a p-value of 0.0004). Specifically, increased MM-DX-929 accumulation in tumors predicted improved tumor growth inhibition following MM-302 treatment. Conclusion: These findings support the use of MM-DX-929 as a predictive imaging contrast agent to select patients that are most likely to respond to liposomal therapies.

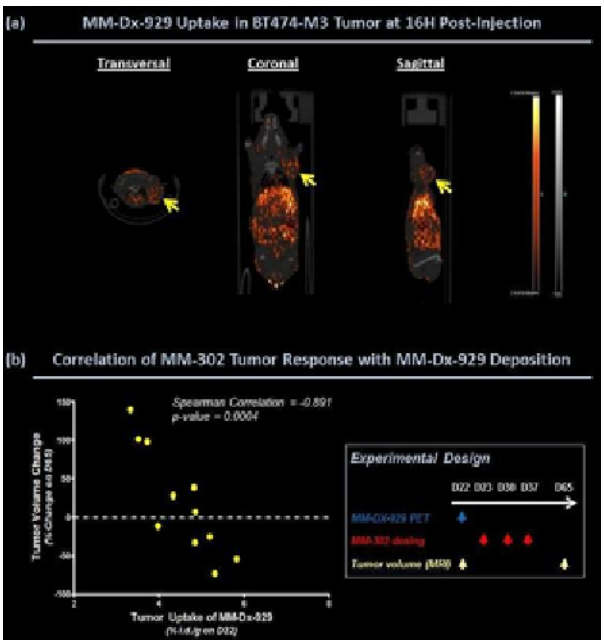


Disclosure of author financial interest or relationships:
**H. Lee**, Merrimack Pharmaceuticals, Employment; **J. Zheng**, None; **D.F. Gaddy**, Merrimack Pharmaceuticals, Employment; **D. Kirpotin**, Merrimack Pharmaceuticals, Inc, Employment; Merrimack Pharmaceuticals, Inc, Stockholder; **M. Dunne**, None; **C. Allen**, None; **D.A. Jaffray**, Precision X-ray, Other financial or material support; Raysearch, Grant/research support; Philips, Grant/research support; Elekta, Grant/research support; General Electric, Grant/research support; IMRIS, Other financial or material support; Modus Medical, Grant/research support; **B. Hendriks**, Merrimack Pharmaceuticals, Employment; **T. Wickham**, Merrimack Pharmaceuticals, Employment; Merrimack Pharmaceuticals, Stockholder .

Presentation Number **P767**
Poster Session 4
September 8, 2012 / 14:45-14:45 / Room: The Liffey

# R2* mapping to quantify SPIO tagged C6 glioma Cells: in vitro and in vivo tracking in rats

***Kangan Li**, Guixiang Zhang, Department of Radiology, Shanghai First People's Hospital,Shanghai Jiaotong University School of Medicine, Shanghai, China. Contact e-mail: kanganli@gmail.com*

Objective: To evaluate 3.0-T MR imaging to track and quantify superparamagnetic iron oxide (SPIO)-labeled C6 glioma cells in vitro and in vivo. Methods: Animal protocols were approved by the Institutional Administrative Panel on Laboratory Animal Care of Shanghai First People's Hospital. C6 rat glioma cells were labeled with either 25 μg/ml SPIO, 25 μg/ml SPIO-PLL, 50 μg/ml SPIO-PLL, or left unlabeled as a control. Iron uptake was analyzed by Prussian blue staining. C6 rat glioma cells labeled with varying concentrations of SPIO were analyzed using 3.0-T R2* and R2 relaxometry. For in vivo tracking, SPIO labeled C6 glioma cells were inoculated into the left frontal lobe of healthy SD rats using a stereotaxis apparatus. R2* and T2 mapping of rat brains were performed using a 3.0T MR on day 7, 14, 21, and 28 after inoculation. Results: Pearl's Prussian blue stain revealed that the efficiency of SPIO particle uptake was greater than 95% and there were nonstructural changes in labeled cells compared with unlabeled controls. R2* and T2* values correlated linearly with the number of iron-loaded cells in agarose gel phantoms, and R2* effects were significantly greater than T2* effects for tagged cell phantoms ($p < 0.01$); R2* effects on the C6 glioma tumor cells in all groups were greater than the T2* effects ($P < 0.01$). The R2* effects of the SPIO labeled C6 glioma cells were greater than unlabeled cells at all time points ($p < 0.01$). Significant differences in R2* values were observed amongst the four groups. Conclusion: Quantitative R2* mapping provides a useful method to quantify SPIO-labeled glioma tumor cells in vitro and gliomas in vivo .

Disclosure of author financial interest or relationships:
**K. Li**, None; **G. Zhang**, None.

Presentation Number **P768**
Poster Session 4
September 8, 2012 / 14:45-14:45 / Room: The Liffey

# DCE-MRI evaluation of an antiangiogenic DNA-based vaccine treatment comparing two image analysis methods

***Dario L. Longo***[1,3], *Miklos Espak*[1], *Walter Dastrù*[1,3], *Lorena Consolino*[1], *Maddalena Arigoni*[2], *Giuseppina Barutello*[2], *Stefania Lanzardo*[2], *Federica Cavallo*[2], *Silvio Aime*[1,3], [1]*Department of Chemistry, University of Turin, Turin, Italy;* [2]*Department of Clinical and Biological Sciences, University of Turin, Turin, Italy;* [3]*Molecular Imaging Center, University of Turin, Turin, Italy. Contact e-mail: dario.longo@unito.it*

DCE-MRI is a non-invasive imaging technique sensitive to differences in blood volume and vascular permeability, currently used in phase I clinical trials as a potential biomarker for characterizing the tumour response to antiangiogenic treatment. Several studies have shown that reliable assessments of therapy response can only be attained if macromolecular contrast agents are used. In this context, we recently have shown the advantage of combining HSA-bound Gd-complexes with a 1 Tesla scanner [1] to evaluate the permeability changes following a new DNA-based vaccine therapy [2]. As the employed image analysis method has a considerable influence on the derived parameters, herein we compare quantitative and semi-quantitative procedures to measure the response to the vascular changes induced by the vaccine, taking into account the spatial heterogeneity of the tumour. BALB/c mice were subcutaneously injected with TUBO carcinoma cells and vaccinated at 4 mm tumor mean diameter and 9 days after with empty pcDNA3 plasmid or with plasmid coding for human p80 Amot. MR images were acquired with an Aspect MRI scanner at 1.0 Tesla before and after the second treatment. Six animals per group undergone DCE-MRI protocol by injecting B22956/1, a protein-binding Gd-based CA, into the tail vein at a dose of 0.05 mmol/kg. After acquisition, raw DCE-MRI data were analyzed by two methods: i) a semi-quantitative analysis was applied to fit the shape of the time-intensity curve of the enhanced pixels. Five read-out terms (peak, slope, washout, clearance, AUC) were determined; ii) the pharmacokinetic Tofts model was implemented by an in-house C++ developed software, with a completely automatic procedure to extract the AIF and the kinetic parameters (Ktrans, Kep, Vep) from a two-compartments model. An unpaired two-tailed t-test was used to compare delta values of the parameters extracted from the two methods between the control and the treated group, clustering the entire tumour volume in three groups, according to the contrast enhancement. The good contrast between rich and poor vascularised regions inside the tumours was used to cluster pixels in three groups, allowing to detect the heterogeneity of the tumour. For the quantitative method, significant changes in Ktrans were observed after the vaccine treatment (ΔKtrans = 448.1% and 33.2% $p<0.05$ for amot and PcDNA3, respectively) for pixels belonging to high enhancement regions and in Vep (ΔVep = 157.6 ±61.6 % and -2.9% ±20.4 $p<0.05$ for amot and PcDNA3, respectively) for medium enhancing regions. For the semi-quantitative method, significant changes were observed in the peak parameter (Δpeak = 12.1 ±11.4 % and -24.4% ±10.8 $p<0.05$) both in high and medium regions, in the slope parameter (Δslope = 45.2 ±17.4 % and -34.1% ±9.7 $p<0.01$) and in the washout parameter (Δwashout = -12.1 ±6.1 % and +12.5% ±5.5 $p<0.01$) for medium enhancing regions (Fig. 1). The information provided by the two approaches are complementary and show a good correlation, allowing to assess the basic determinants of the physiological changes induced by the antiangiogenic therapy. [1] Geninatti S. CMMI 2011 [2] Arigoni M. Angiogenesis 2012

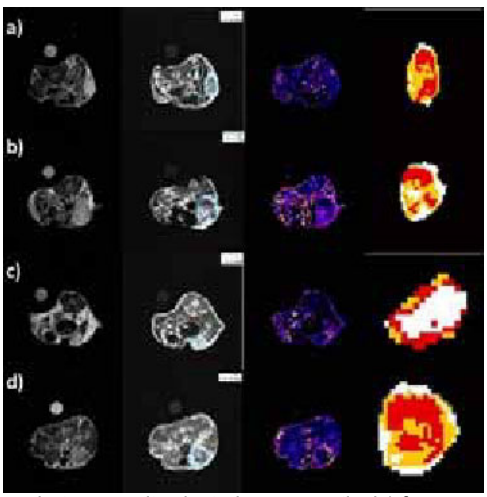


MRI images (T2w, peak map, Ktrans map and tumour heterogeneity clustering, respectively) for a representative mouse a) before and b) after p80 Amot vaccine treatment; and c) before and d) after empty PcDNA3 vaccination (control). (Tumour heterogenity is represented with coloured pixels: white for regions of high enhancement, yellow for medium and red for low enhancement).

Disclosure of author financial interest or relationships:
**D.L. Longo**, None; **M. Espak**, None; **W. Dastrù**, None; **L. Consolino**, None; **M. Arigoni**, None; **G. Barutello**, None; **S. Lanzardo**, None; **F. Cavallo**, None; **S. Aime**, Bracco Imaging, Consultant; Bruker, Grant/research support .

Presentation Number **P769**
Poster Session 4
September 8, 2012 / 14:45-14:45 / Room: The Liffey

# Therapeutic evaluation of multifunctional 188Re/Dox-micelles in hepatocellular carcinoma animal model

*Ying-Hsia Shih[1], Cheng-Liang Peng[1], Ping-Fang Chiang[1], Chung-Hsin Yeh[1], Wuu-Jyh Lin[1], **Tsai-Yueh Luo**[1,2], [1]isotope Application Division, Institute of nuclear energy research, Taoyuan, Taiwan; [2]Institute of Radiological Science, Central Taiwan University of Science and Technology, Taichung, Taiwan. Contact e-mail: tylo@iner.gov.tw*

Introduction. Multifunctional micelles loaded with doxorubicin and labeled with the radionuclide rhenium-188 (188Re) were developed to provide the combination of chemotherapy and radiotherapy for cancer treatment. Methods. Doxo-micelles were formulated by DTPA-PCL-PEG-PCL and doxorubicin by the cosolvent evaporation method. The Doxo-micelle was further labelled with 188Re-perrhenate reacted at 37°C for two hours. The mice implanted with BNL heptoma were randomly allocated to four groups for the following respective treatments, including shamed (n=4), 188Re-micelles (n=3), Doxo micelles (n=5) and 188Re/Doxo-micelles (n=5). The biodsitribution and therapeutic efficacy of the four treatments groups via tail vein injection were investigated by micro-SPECT/CT imaging, biodistribution, and long-term therapeutic monitoring in orthotopic liver tumor model. Results. The micro-SPECT/CT images and biodistribution data of 188Re/Doxo-micelles in hepatoma mice both demonstrated that the radioactivity was mostly distributed in the heptoma, liver and spleen. The therapeutic monitoring results showed that 188Re/Doxo-micelles treatment group had the longest survival time (thirty days) among the four groups ($p<0.005$). Conclusion. 188Re/Doxo-micelles showed synergistically to decrease the tumor volume and extend the survival time in mice hepatoma model. We suggest that the multifunctional 188Re/Doxo-micelles might have the potential to apply for the treatment of hepatoma.

Disclosure of author financial interest or relationships:
**Y. Shih**, None; **C. Peng**, None; **P. Chiang**, None; **C. Yeh**, None; **W. Lin**, None; **T. Luo**, None.

Presentation Number **P770**
Poster Session 4
September 8, 2012 / 14:45-14:45 / Room: The Liffey

# 18F-MISO PET STUDIES IN MONITORING TREATMENT RESPONSE IN A PANCREATIC CANCER MOUSE MODEL

*Juan Antonio Camara[1], Coral Velasco[1], Elena Andres[1], Silvia Sanchez-Leal[1], Maria Pia Morelli[2], Manuel Hidalgo[2],* ***Francisca Mulero***[1], *[1]Molecular Imaging, CNIO, Madrid, Spain; [2]Clinical Research Programme, CNIO, Madrid, Spain. Contact e-mail: fmulero@cnio.es*

Introduction: The capacity of imaging techniques to discern tumor viability has become a main area of research in molecular imaging units. The tissue viability, depending on the relation with its level of oxygen, is a crucial point for antitumor treatments based on chemotherapies administration. The loss of vascular support in zones of growing tumor tissue is the principal responsible of tissue oxygen decrease. Pancreatic ductal adenocarcinoma (PDAC) is a highly lethal disease in which the prominent tumor stroma compartment is a defining characteristic, with a low vascular component which interferes even more with the ability of the drug to reach the tumor. Hypoxic tissues present low metabolic activity and decreased blood flow. As a result, their exposure to chemotherapies is reduced. Positron emission tomography (PET) technique is used with a 18F-MISO hypoxic marker. This radiotracer gets linked to tissues in presence of an oxygen pressure under 10mmHg, making possible to locate the oxygen decrease in alive tissues. Objective: This study pretends to calibrate the efficiency of 18FMISO PET in predicting the effect of several drugs in their aim of decreasing the hypoxic tissue percentage. Material and Method: In this study 14 mice, each of them with two samples of human pancreatic tumors, were scanned. These mice were divided in 6 groups, depending on the treatment assigned, and a control group. The treatments were based on 3 different drugs, and combinations of these drugs. Two PET acquisitions were performed, one immediately after the injection of 1mCi of 18F-MISO (early phase), and the other one three hours after the inoculation of the radiotracer (hypoxia phase) using a microPET -CT eXplore Vista (GEHC), with MMWKS software. 18F-MISO was supplied by ITP (instituto Tecnológico PET) and the reconstructions of the studies were made with an 3D OSEM software. Three studies were carried out on each animal at day 0, 5 and 21after the treatment with the drugs under study. Results: After the analysis of the results, there is a noticeable decrease of the 18F-MISO uptake during the early phase comparing the first and last examinations. The uptake in the intermediate study varies between groups, from a partial increase to a drastic decrease. This is a general behavior in all groups, independently from the drug administrated. Only the control group shows an increase in the uptake in every phase. In the hypoxia phase the results are not as uniform as suspected. There are two patterns of drug behavior. One shows a decrease in the uptake in all studies, whereas the other one shows a decrease between the first and the second examinations and an increase between the second and third ones. The control group belongs to the latter pattern (see supplemental data) Conclusion: F18-MISO PET can be a useful imaging biomarker for predicting and assessing the antiangiogenic effect of anticancer drugs in pancreatic cancer.

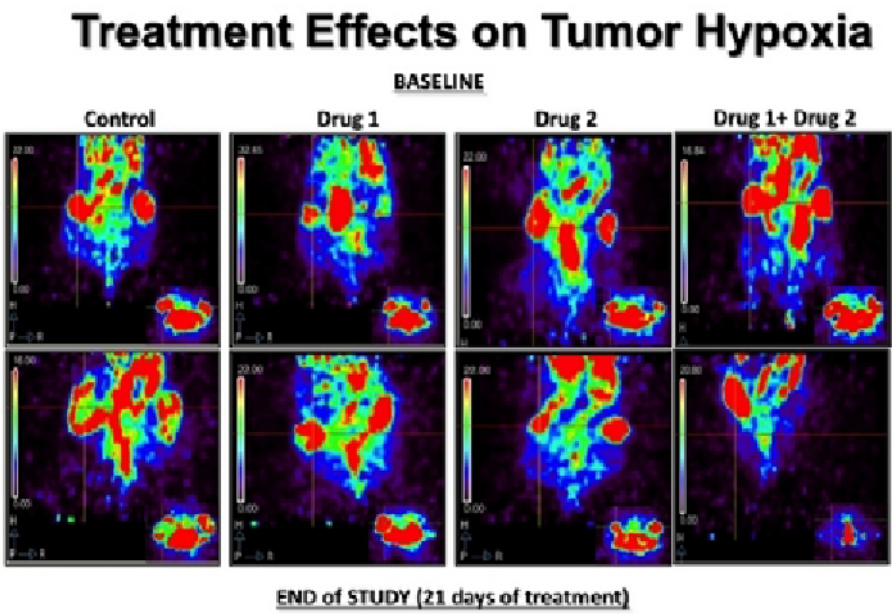


Disclosure of author financial interest or relationships:
**J. Camara**, None; **C. Velasco**, None; **E. Andres**, None; **S. Sanchez-Leal**, None; **M. Morelli**, None; **M. Hidalgo**, None; **F. Mulero**, None.

Presentation Number **P771**
Poster Session 4
September 8, 2012 / 14:45-14:45 / Room: The Liffey

# Evaluation of $^{89}$Zr-rituximab Tracer by Cerenkov Luminescence Imaging in a Humanized Transgenic Mouse Model

***Arutselvan Natarajan***[1], *Frezghi Habte*[1], *Hongguang Liu*[1], *Zhen Cheng*[1], *Sanjiv S. Gambhir*[1,2], [1]*Radiology, Stanford University, Stanford, CA, USA;* [2]*Radiology, Stanford, Stanford, CA, USA. Contact e-mail: anatarajan@stanford.edu*

**Introduction.** Cerenkov Luminescence Imaging (CLI) has been an effective, non invasive and less expensive imaging modality for rapid screening of radiotracers in vitro and in vivo. We demonstrated the use of CLI to study Non-Hodgkins lymphoma (NHL) using the novel immunoPET tracer ($^{89}$Zr-rituximab) while using a humanized transgenic mouse model that express human CD20. **Methods.** The $^{89}$Zr-rituximab was tail-vein injected for imaging transgenic mice that express the human CD20 on their B cells (huCD20TM). CD20TM, mice received 2.6 MBq /dose. One group (n=3) received 2mg/kg pre-dose (blocking) of cold rituximab 2 h prior to tracer; the other group (n=3) had no pre-dose (non-blocking). CLI was performed using a cooled CCD optical imager to image mice at 24, 48, and 72 h. We also performed PET imaging and ex vivo study in order to confirm the in vivo CLI results. **Results.** HuCD20 transgenic mice injected with $^{89}$Zr-rituximab demonstrated a high contrast image compared to mice blocked with a cold dose. After 48h post-radiotracer injection the dynamic CLI showed specific uptake in the spleen, where the huCD20 biomarker is present at very high levels. At 48h, the $^{89}$Zr-rituximab uptake ratio (non-blocking vs blocking) counted (mean ± STD) in the spleen were 6.78 ± 0.01 for CLI, and 10.4 ± 1.4 for PET, and for liver were 0.55 ± 0.03 for CLI, and 1.29 ± 0.08 for PET. Biodistribution results of CLI vs PET shows a good correlation (R2=0.98) **Conclusions.** CLI of huCD20 transgenic mice injected with $^{89}$Zr-rituximab demonstrated that the tracer was able to target the huCD20-expressing B cells very well. The in vivo and ex vivo tracer uptake values by CLI on the spleen are in good agreement with the PET values. This study clearly indicates the use of CLI as an effective modality to non-invasively screen radiotracers during the development of novel imaging and therapeutic agents using optical imaging system. To the best of our knowledge, this is the first report using an 89Zr-rituximab tracer to evaluate the use of CLI for NHL imaging. b>Acknowledgments. Research Support: ICMIC P50 - CA114747

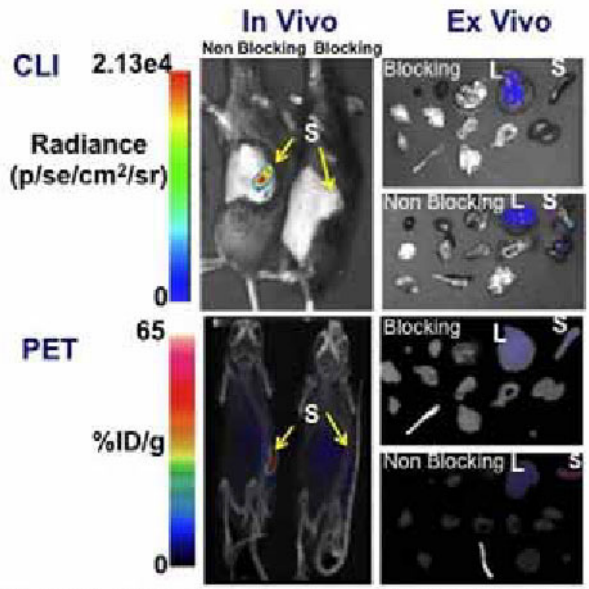


**Figure**: In vivo and ex vivo images of CLI and PET/CT of $^{89}$Zr-rituximab tracer on huCD20T mouse with blocking (rituximab) and non-blocking (tracer alone). CLI and PET images showing high tracer uptake in spleen (S) where high huCD20 marker is present; L= Liver.

In vivo and ex vivo images of CLI and PET/CT of $^{89}$Zr-rituximab tracer on huCD20T mouse

Disclosure of author financial interest or relationships:
**A. Natarajan**, None; **F. Habte**, None; **H. Liu**, None; **Z. Cheng**, None; **S.S. Gambhir**, General Electric, Grant/research support; Bayer-Schering, Grant/research support; Sanofi-Aventis, Grant/research support; CellSight, Stockholder; ImaginAB, Stockholder; Enlight, Stockholder; Endra, Stockholder; Bracco, Consultant; NinePoint Medical, Stockholder; Visualsonics, Consultant .

Presentation Number **P772**
Poster Session 4
September 8, 2012 / 14:45-14:45 / Room: The Liffey

# Comparison between $^{99m}$Tc-HMDP as a bone scintigraphic agent and $^{18}$F-FDG using a bone metastasis animal model

***Kazuma Ogawa***[1], *Mikako Ogawa*[2], *Kohshin Washiyama*[1], *Yasuhiro Magata*[2], [1]*Kanazawa University, Kanazawa, Japan;* [2]*Hamamatsu University School of Medicine, Hamamatsu, Japan. Contact e-mail: kogawa@med.kanazawa-u.ac.jp*

Objectives : Over the last quarter of a century, complexes of $^{99m}$Tc with bisphosphonate have been widely used as radiopharmaceuticals for bone scintigraphy in cases of bone disorder such as metastatic bone disease. Meanwhile, $^{18}$F-FDG-PET has been reported to be a sensitive tool for tumor staging in different malignant diseases. In clinical studies, a considerable number of papers comparing $^{18}$F-FDG-PET to bone scintigraphy in the detection of bone metastases have been published, but it is still controversial. In non-clinical experiments, there is hardly report comparing $^{18}$F-FDG-PET to bone scintigraphic agents in the detection of bone metastases. In this study, we performed a comparison between $^{18}$F-FDG-PET and $^{99m}$Tc-HMDP using one of bone metastasis models, the intra-tibial injection model. Methods : The model was prepared by injecting syngeneic MRMT-1 mammary tumor cells into the left tibia of female Sprague-Dawley rats. $^{18}$F-FDG (7.4 MBq) was administered intravenously to the model rats 15 and 21 days post-inoculation of tumor cells. At 45 minutes after the injection of $^{18}$F-FDG, PET/CT scans were performed. $^{99m}$Tc-HMDP (148 MBq) was administered intravenously 20 hours postinjection of $^{18}$F-FDG. At 45 minutes after the injection of $^{99m}$Tc-HMDP, SPECT/CT imaging was performed. Results : At 15 days post-inoculation of tumor cells, bone destruction was observed around the inoculation site of tumor cells by CT images. It has been reported that osteoblastic activity and osteoclastic activity rise in lesion site of the bone metastasis model. Accumulation of radioactivity to lesion site after injection of $^{18}$F-FDG was observed, but accumulation of $^{99m}$Tc-HMDP was not clear. At 21 days post-inoculation of tumor cells, bone destruction was advanced. Accumulation of $^{18}$F-FDG was widespread around inoculation site, and accumulation of $^{99m}$Tc-HMDP was also observed. Conclusions : In this study, $^{18}$F-FDG might be more effective to detect a lesion site at early stage.

Disclosure of author financial interest or relationships:
**K. Ogawa**, None; **M. Ogawa**, None; **K. Washiyama**, None; **Y. Magata**, None.

Presentation Number **P773**
Poster Session 4
September 8, 2012 / 14:45-14:45 / Room: The Liffey

# Multimodal nanoparticle based MRI-optical tracer systems for vasculature and tumor imaging in cell tissue and animal Oula Penate Medina, Marcus Böttcher, Susann Boretius, Fatma Ashkanani Holger Kalthoff, Claus Glüer

***Oula Penate Medina**, Markus Böttcher, Susann Boretius, Fatma Ashkanani, Holger Kalthoff, Claus C. Glueer, radiology, Christian-Albrechts-Universität zu Kiel, Kiel, Germany. Contact e-mail: oula.penate@rad.uni-kiel.de*

New nanoparticle and smart drug delivery agents are needed for imaging and theranostic approaches. However there is a clear lack of probes that can simultaneously be used on molecular and organ level. . Only optical reporters are versatile enough to be used in cellular imaging and microscopy. However the usability of these tracers in animal studies is limited by quenching, scattering and quantification problems, limited penetration depth,and the lack of anatomical information. Here we describe a promising multimodal nanoparticle based MRI-optical tracer system that provides anatomical information of the intact organism together with precise information of the receptors and binding on cellular level. . Our optical-MRI probe is based on iron nanoparticle targeted with Lectins (LEA), which binds specifically and strongly to the polylactosamine oligosaccharides which form a major constituent of endothelial and epithelial cell surface carbohydrates, conjugated with FITC and Alexa 633 or with RA-96 antibody/Fab against mucins and C1P83 antibody/Fab against gold 3 epitope of CEA antibodies and Fab fragments. The contrast media are expected to bind specifically to the apical surfaces of all endothelial cells, and thus to the inner surfaces of all blood vessels. This provides a model of selective binding which can be compared readily with the vascular imaging generated by intravenous injection of non-targeted contrast media. On the cellular level multi-photon microscopy was used to observe different cell types, cell binding and internalization assays of the particles containing different targeting ligands together with FACS.Endothelial cell binding assays with HAOEK primary endothelial cell were used together with several tumor cells like Capan-2, Panc-89, C6. On the tissue level ex-vivo mouse and rat artery prepared in in a perfusion chamber were analyzed by multiphoton microscopy and MRI in order to evaluate the binding of the probes to endothelial cell wall under flow conditions. Moreover MRI, Night Owl and Visen FMT were used in vivo animal imaging of tumor xenografts. Operational microscopy with a fluorescence filter was used to evaluate if the findings could aid in an intra-operational setting. Conclusion: Our dual mode probe was able to be used as a reporter in cellular, tissue and animal imaging. Targeted probes were able to distinguish endothelial cells, tumor cells , and heart visceral pericardium by comparing several different targeting ligands. Capan2 pancreatic tumor cells were especially positive to RA-96 antibody. Endothelial cell lining had strong binding against tomatolectin. and C1P83 was strong binder against BxPc3 tumor cells. The nanoparticle targeting was performed in cellular tissue and animal giving information about the receptor localization and the tumor targeting. This approach may bring light to the roles of EPR vasculature density, leakage and specific receptor-mediated nanoparticle targeting in imaging and later in drug delivery.

Disclosure of author financial interest or relationships:
**O. Penate Medina**, None; **M. Böttcher**, None; **S. Boretius**, None; **F. Ashkanani**, None; **H. Kalthoff**, None; **C.C. Glueer**, None.

Presentation Number **P774**
Poster Session 4
September 8, 2012 / 14:45-14:45 / Room: The Liffey

# Combination of dynamic contrast-enhanced micro-CT with high-resolution 3D fluorescence ultramicroscopy reveals vascular changes after antiangiogenic therapy in preclinical orthotopic breast cancer xenografts

***Thomas Poeschinger***[1], *Fabian Eisa*[2], *Michael Dobosz*[1], *Anja Renner*[1], *Robert Brauweiler*[2], *Willi Kalender*[1], *Werner Scheuer*[1], [1]*Pharma Research and Early Development (pRED), Discovery Oncology, Roche Diagnostics GmbH, Penzberg, Germany;* [2]*Institute of Medical Physics, University of Erlangen-Nuremberg, Erlangen, Germany. Contact e-mail: thomas.poeschinger@roche.com*

Imaging of tumor microvasculature plays a crucial role in understanding angiogenesis and monitoring antiangiogenic drug therapy. While many methods exist to quantify angiogenesis *ex vivo*, it is desirable to use noninvasive methods for the assessment of antiangiogenic drug responses *in vivo*. It has been shown recently that dynamic contrast-enhanced micro-CT (DCE micro-CT) provides a promising method to yield *in vivo* functional information in antiangiogenic tumor therapy. Here, we apply DCE micro-CT imaging to quantify tumor vascular changes after antiangiogenic drug therapy in orthotopic breast cancer xenografts. We further validate the technique by direct comparison with *ex vivo* fluorescence ultramicroscopy (UM). UM allows the 3D visualization of the whole tumor vessel architecture on a microscopic level by reconstruction of optical sections obtained from optically cleared specimen. SCID/beige mice were orthotopically injected with human breast cancer cells (KPL-4) and split into a treatment group (n=10) and a control group (n=10). Antiangiogenic treatment was performed using a monoclonal antibody (10 mg/kg) against the human vascular endothelial growth factor (VEGF). A non-specific IgG1 (10 mg/kg) was used as control. Weekly treatment was performed for two times and both substances were administered intraperitoneally. All mice underwent DCE micro-CT for assessment of the functional parameters relative blood volume, vascular permeability, total contrast enhancement, as well as tumor volume at the end of the study. Parameters were determined for total, peripheral, and central tumor volume of interest (VOI). For verification, mice were sacrificed and tumor vessel architecture was characterized performing UM and histology of explanted tumor tissue. Based on *in vivo* DCE micro-CT imaging, we found that total contrast enhancement in the tumors of the treatment group was most strongly reduced in the tumor periphery (48.7%, Fig. 1a) as compared to the total (35.5%) and central VOI (18.2%) indicating strongest vascular changes due to antiangiogenic treatment at the tumor boundary. Quantification of the functional parameters permeability and relative blood volume revealed a significant reduction of 23.4% ($p<0.01$) and 39.6% ($p<0.05$) in the tumor periphery, respectively. In contrast, tumor volume as determined by micro-CT was non-significantly reduced by 26.3% ($p<0.24$). Analyzing the tumor vascular architecture with UM, we observed a dense and highly irregular vessel structure in the tumors of the control group with highest vessel density in the tumor periphery (Fig. 1b). In contrast, tumors of the treatment group revealed a clearly reduced vessel density with a substantially less disordered vessel structure (Fig. 1c), which is in good agreement with the findings of DCE micro-CT. Central void tumor regions with no apparent vessels were confirmed as necrosis by histology. In conclusion, these data demonstrate that DCE micro-CT is an excellent method for monitoring antiangiogenic effects of new compounds in preclinical orthotopic tumor models. Such technology may serve as good biomarker for prediction of therapeutic efficacy in the tumor patient.

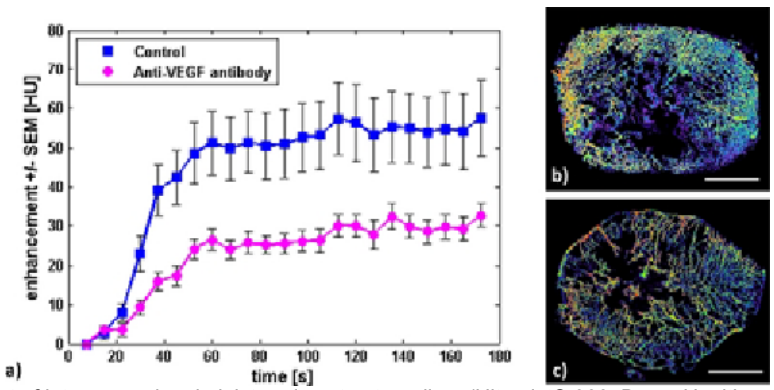


**Figure 1:** (a) Time-enhancement of intravenously administered contrast medium (Ultravist® 300, Bayer Healthcare AG) in the tumor periphery as measured by DCE micro-CT in orthotopic tumor xenografts (KPL 4). Tumors treated with the antiangiogenic drug show substantially less total contrast enhancement as compared to control, presumably due to a reduced and normalized tumor vascularization. Verification with high resolution 3D fluorescence ultramicroscopy reveals (b) a high vessel density with a chaotic vessel architecture in the tumors of the control group, whereas (c) tumors of the treatment group show a reduced vessel density with a less disordered tumor architecture. (Scale bar: 1 mm)

Disclosure of author financial interest or relationships:
**T. Poeschinger**, Roche Diagnostics GmbH, Employment; **F. Eisa**, CT Imaging GmbH, Employment; **M. Dobosz**, Roche Diagnostics GmbH, Employment; **A. Renner**, Roche Diagnostics GmbH, Employment; **R. Brauweiler**, CT Imaging GmbH, Employment; **W. Kalender**, siemens healthcare, Consultant; ct imaging gmbh, Stockholder; ct imaging gmbh part-time, Employment; **W. Scheuer**, Roche Diagnostics GmbH, Employment .

Presentation Number **P775**
Poster Session 4
September 8, 2012 / 14:45-14:45 / Room: The Liffey

# Non-invasive longitudinal imaging of collecting lymphatic vessel function and metastatic spread of murine melanoma

***Steven Proulx***, *Paola Luciani, Jean-Christophe Leroux, Michael Detmar, Swiss Federal Institute of Technology (ETH) Zurich, Zurich, Switzerland. Contact e-mail: steven.proulx@pharma.ethz.ch*

The presence of lymph node metastasis is an important factor to determine the course of therapy for a wide range of cancers. Despite their clinical importance, key questions regarding the development and significance of lymph node metastases remain and require more sophisticated methods to investigate. The goals of the current study were to develop novel imaging methods that allow repeated imaging of collecting lymphatic vessels and metastases during the course of tumor progression and spread to sentinel lymph nodes. Using these methods we aimed to elucidate the steps leading to formation of lymphatic metastases and their concomitant effects on collecting lymphatic function. For this purpose we stably transfected a B16-F10-luc2 melanoma cell line for tdTomato fluorescent protein expression. A footpad model of melanoma was induced in C57BL/6 mice via injection of 200,000 B16-F10-luc2-tdTom cells. Lymph node metastases were assessed non-invasively with an IVIS bioluminescent imaging system and at sacrifice with a fluorescent stereomicroscope capable of sensitive high-resolution detection of tdTomato cells. Near-infrared fluorescent stereomicroscopy was performed by peritumoral injection of novel lymphatic tracers that allow dynamic near-infrared lymphatic mapping and assessments of pulsatile collecting lymphatic function. Imaging was performed at three time points in the same mice: before tumor injection and at Days 19 and 33 after induction. We found a clear correlation of the routes of lymphatic flow from the tumor with the metastatic spread during the course of tumor progression. Before tumor cell injection, reproducible patterns of collecting lymphatic pulsing and flow were found with the tracer draining through the popliteal and sacral lymph nodes. Before metastases were detected with bioluminescent imaging an increase of flow through this route was detected. At later timepoints when metastases in the popliteal lymph node were detected, we found that lymphatic flow in some mice was rerouted to collecting vessels draining to the inguinal lymph node. Fluorescent stereomicroscopy revealed that metastases had also formed in these lymph nodes. These findings indicate that the presence of tumor cell metastases may have an effect on lymphatic flow through the sentinel lymph nodes, which may lead to altered flow patterns and rerouting of metastases to additional lymph nodes. These novel findings may have clinical relevance for the understanding of the mechanisms of tumor cell spread and for the procedure of sentinel lymph node mapping. Additionally, the lymphatic tracers and quantitative imaging methods developed could be used in a wide range of mouse models in lymphatic biology.

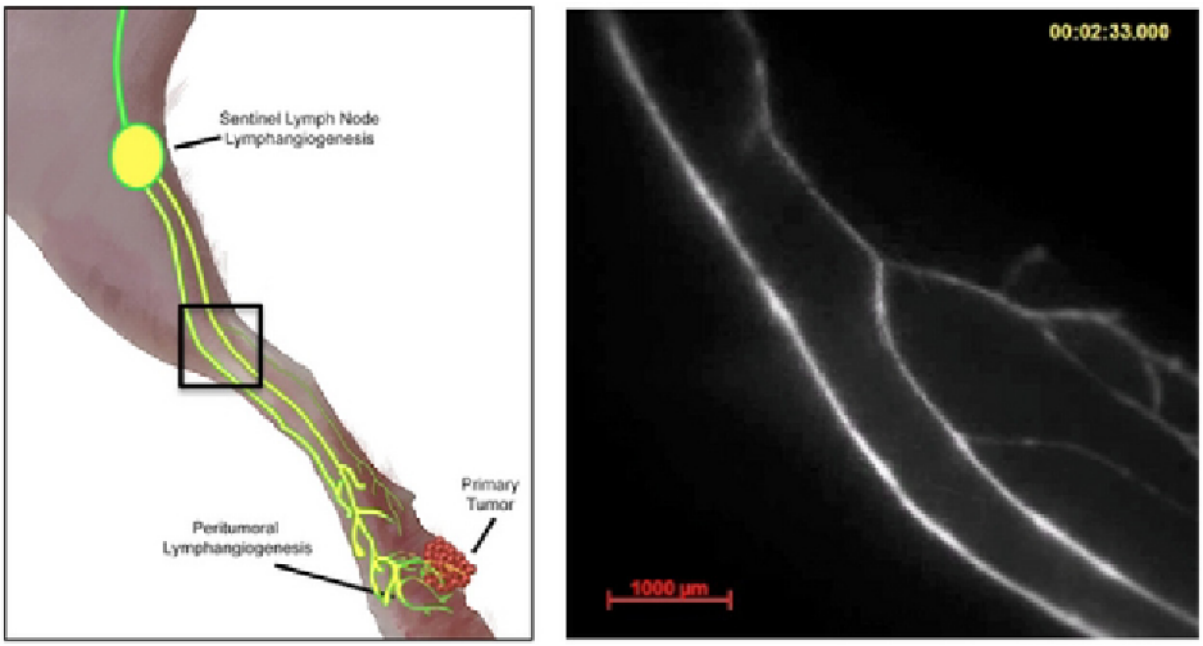


Representative near infrared stereomicroscopy of collecting lymphatics draining footpad tumors. Imaging region in black box on cartoon (left), video capture of pulsing collecting lymphatic vessels after tracer injection into footpad (right)

Disclosure of author financial interest or relationships:
**S. Proulx**, None; **P. Luciani**, None; **J. Leroux**, None; **M. Detmar**, None.

Presentation Number **P776**
Poster Session 4
September 8, 2012 / 14:45-14:45 / Room: The Liffey

# Evaluation of tumor angiogenesis and redox status in mouse xenograft using MRI

***Reshmi Rajendran***, *Jia Fang Foo, Gabriel C. Miranda, Kai-Hsiang Chuang, Magnetic Resonance Imaging Group, SBIC, A*STAR, Singapore, Singapore. Contact e-mail: reshmi_rajendran@sbic.a-star.edu.sg*

**Introduction:** Elevated oxidative stress has been associated with tumour progression, angiogenesis and resistance to therapy. Understanding the interplay between oxidative stress and angiogenesis will facilitate our understanding of cancer pathology and guide drug development. In this study, nitroxyl radicals were used as redox reporters in MRI (1) to understand their relationship with tumor perfusion, a marker of angiogenesis. **Methods:** HepG2 tumors were inoculated in nude mice and were imaged on 7T MRI at ~3weeks old. Perfusion imaging was performed using FAIR arterial spin labeling with multi-TIs and TR/TE = 6000/18 ms. Perfusion was quantified by fitting with a kinetic model. Redox imaging was conducted by i.v. injection of either 1.875 μ mol/g of 3-carbamoyl proxyl (3-CP) or Tempol and images were acquired with a series of gradient echo imaging with TR/TE = 4.25/1.47 ms, flip angle = 6° and a temporal resolution of 6.6 s. Redox status was assessed by exponential fitting to the signal decay. **Results:** ROI analysis in tumor and muscle (Fig.1a) shows 6-7 times higher decay rate for Tempol compared to 3-CP (Fig.1b). The relationship between perfusion and redox status was examined in the tumor and its periphery region, and a positive correlation between these was found in both 3-CP and Tempol (Fig.1c). **Discussion:** The faster nitroxide decay rate at the tumor periphery may indicate a higher redox potential in these more perfused regions. However, since the delivery of nitroxyl radicals to tumor relies on blood flow, the positive correlation between tumor perfusion and decay rate may also be due to the signal being confounded by washout. Further studies will be needed to clarify this issue. **Reference:** Hyodo, F. *et. al.J Pharm Pharmacol* 60:1049-1060; 2008.

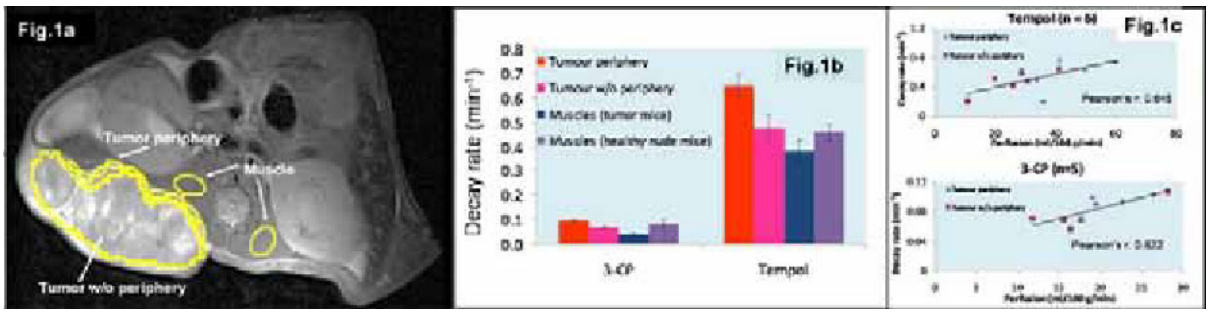


Fig.1a: Regions of interest; Fig.1b: Redox status represented as nitroxide decay rates in the tumour, its periphery, the muscle, and the muscle from healthy nude mice; Fig.1c: Correlation between nitroxide decay rates and perfusion in tumor.

Disclosure of author financial interest or relationships:
**R. Rajendran**, None; **J. Foo**, None; **G.C. Miranda**, None; **K. Chuang**, None.

Presentation Number **P777**
Poster Session 4
September 8, 2012 / 14:45-14:45 / Room: The Liffey

# Biological Evaluation of ICF15002, a New Fluorinated and Iodinated Melanin-Targeting Compound for Melanoma PET Imaging and Targeted Radionuclide Therapy

***Latifa Rbah-Vidal**, Emilie Billaud, Aurélien Vidal, Sophie Besse, Elisabeth Miot-Noirault, Philippe Auzeloux, Jean-Michel Chezal, UMR990-INSERM Ud'A, Clermont-Ferrand, France. Contact e-mail: latifa.rbah@gmail.com*

**Background:** The incidence of malignant melanoma is increasing worldwide. Although localized disease is often curable by surgical excision, metastatic melanoma is inherently resistant to most treatments. Our lab developed for many years arylcarboxamides as melanoma tracers due to their melanin affinity in order (i) to improve staging and monitoring of therapy by PET imaging (ii) to develop Targeted Radionuclide Therapy (**TRT**). In a new bimodal approach, we evaluated ICF15002, a fluorinated and iodinated melanin-targeting compound, offering both diagnosis (PET/fluorine-18) and therapeutic (TRT/iodine-131) applications, depending on the radionuclide introduced. **Methods: PET imaging:** In vivo biodistribution of [$^{18}$F]ICF15002 was evaluated in B16Bl6 primary and pulmonary metastatic melanoma-bearing C57BL/6j mice by PET imaging 1 h post tracer injection at different stages of melanoma development. **Targeted Radionuclide Therapy:** [$^{131}$I]ICF15002 treatment was administered by i.v. injection in B16Bl6 primary melanoma-bearing C57BL/6j mice (2x20 MBq) at Day-7 and Day-11 post tumor inoculation. Tumor dimensions were measured three times a week with a digital caliper. **Results:** [$^{18}$F]ICF15002 was produced within 54 min with a radiochemical yield of 23% and a radiochemical purity >99%. B16BL6 melanoma tumors were visualized by PET 1 h p.i. as early as Day-6 after cells inoculation. Tumoral uptake of [$^{18}$F]ICF15002 was 9.1±4.1 %ID/g, 15.6±0.9 %ID/g and 13.5±1.8 at Day-6, Day-10 and Day-15, respectively. All primary tumors were clearly visible with high contrast to background ratio (tumor-to-muscle ratio=5.7±2.9, 9.4±0.6 and 12.2±3.8 at Day-6, Day-10 and Day-15, respectively). Furthermore, radiotracer elimination occurred mainly through the urinary system. In pulmonary metastatic model, uptake of [$^{18}$F]ICF15002 was evident in lung metastatic lesions as early as Day-9 post cells inoculation with radiotracer accumulation increasing as melanoma invaded lungs. For targeted radionuclide therapy, ICF15002 was radiosynthesized at high specific activity (116 GBq/µmol) and obtained with 60% overall radiochemical yield and radiochemical purity >99%. Treatment of B16Bl6 primary melanoma-bearing mice with two doses of [$^{131}$I]ICF15002 showed that this radiotracer was able to deliver high dose of radiation to B16BL6 melanoma tumors, inducing an increase in survival (26.9±0.7 days in treated mice vs 21.2±0.6 days in controls) and reduction of tumor growth rate (doubling time of 2.92±0.45 days vs 1.80±0.25 days in controls; ANOVA test: *p=0.006*). **Conclusion:** [$^{18}$F]ICF15002 demonstrated very promising results with highly contrasted melanoma lesions imaging suggesting an excellent potential for melanoma staging. Moreover, [$^{131}$I]ICF15002 treatment significantly inhibited B16Bl6 tumoral growth and increased survival time. Our findings support the bimodal concept which could constitute a promising approach for imaging, staging and therapy of melanoma. *Acknowledgments: [$^{18}$F] fluoride was provided by CYCLOPHARMA Laboratories (Pr. Serge ASKIENAZY). Grant: TRT/PET/MEL Program (CLARA).*

Disclosure of author financial interest or relationships:
**L. Rbah-Vidal**, None; **E. Billaud**, None; **A. Vidal**, None; **S. Besse**, None; **E. Miot-Noirault**, None; **P. Auzeloux**, None; **J. Chezal**, None.

Presentation Number **P778**
Poster Session 4
September 8, 2012 / 14:45-14:45 / Room: The Liffey

# Monte Carlo simulations to quantify possible errors in dual fluorescent probe molecular imaging methods due to variations in tissue optical properties

***Kristian Sexton***, *Stephen C. Kanick, Kenneth M. Tichauer, Brian W. Pogue, Dartmouth College, Hanover, NH, USA. Contact e-mail: Kristian.J.Sexton@Dartmouth.edu*

Fluorescence molecular imaging is a promising and rapidly advancing field. There are a number of techniques currently being explored that attempt to utilize both targeted and non-targeted probes to quantify molecular binding in vivo. These approaches range from simple subtraction and ratio imaging to more complicated models based on positron emission tomography techniques. Central to all of them is the reliance on fluorescent probes that emit at different wavelengths. This necessitates some type of normalization technique. Often muscle tissue outside of the tumor area is used for normalization. However, this assumes that the same optical properties for each probe exist within the tumor as do in the muscle. Considering the tremendous variation that may occur in regards to both tumor vascularization and oxygenation, this is unlikely to be the case. Monte Carlo techniques can be used to explore the effect of both changes in total hemoglobin concentration and oxygenation on expected fluorescent signals for 700 nm and 800 nm probes. The impact of the ratio of the two signals on the determination of molecular binding can be examined for the various imaging methods and will allow for a better understanding of one of the inherent errors in these techniques. A Monte Carlo fluorescence code developed by Steve Jacques et al. has been modified to allow simulation of the Licor Odyssey scanner, which Tichauer et al. used to introduce a novel technique of quantifying receptor density in vivo. Accuracy of the code over a wide range of optical properties and fiber diameters was verified against the results of Pfefer et al. This modified version of Steve Jacques code will be used to run simulations over large range of possible tissue optical properties. The greatest relative changes in signal between the two wavelengths is expected to come with changes in oxygenation. The reason for this can be seen in the figure below where absorption differences between oxy and deoxyhemoglobin are significant at 700 nm and nearly non existent at 800 nm. Oxygen saturation can vary significantly between normal and cancerous tissue as well as within the tumor itself. Quantifying the possible error that may be introduced by the resulting differences in tissue optical properties is important step in maximizing the utility of these techniques.

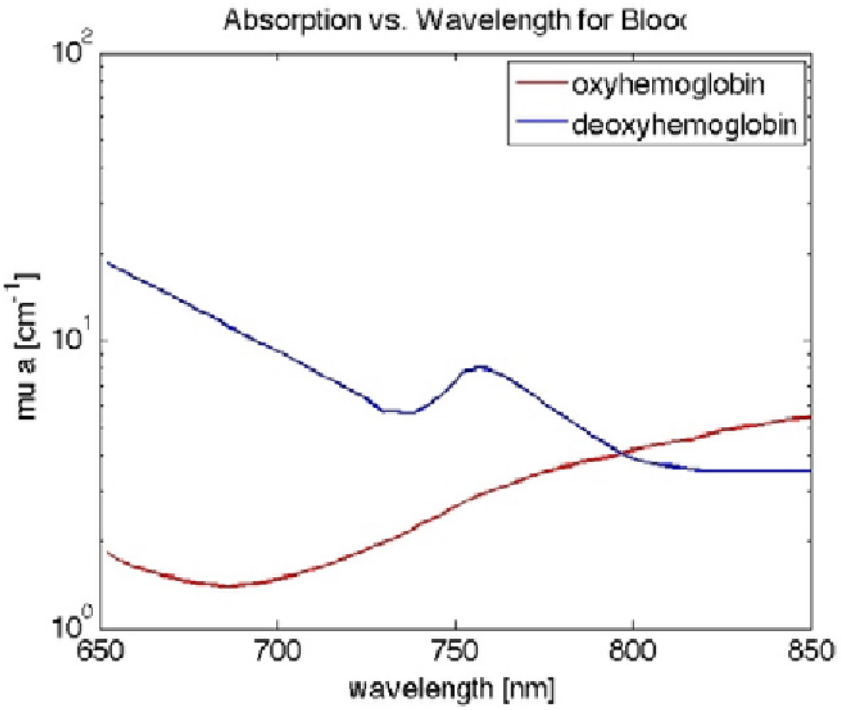


Disclosure of author financial interest or relationships:
**K. Sexton**, None; **S.C. Kanick**, None; **K.M. Tichauer**, None; **B.W. Pogue**, None.

Presentation Number **P779**
Poster Session 4
September 8, 2012 / 14:45-14:45 / Room: The Liffey

# Mesoporous Silica Contrast Agents for the Endoscopic Detection of Nascent Colorectal Cancer

***Jeffrey S. Souris***[1], *Nai-Tzu Chen*[3,2], *Vani Konda*[4], *Marc Bissonnette*[4], *Leu-Wei Lo*[2], *Chin-tu Chen*[1], [1]*Department of Radiology, The University of Chicago, Chicago, IL, USA;* [2]*Division of Medical Engineering Research, National Health Research Institutes, Zhunan, Taiwan;* [3]*Department of Chemistry, National Taiwan University, Taipei, Taiwan;* [4]*Department of Medicine, The University of Chicago, Chicago, IL, USA. Contact e-mail: sourisj@uchicago.edu*

Cell surface glycosylation is known to play a number of significant and different roles in the modulation of physiologic and pathophysiologic pathways in human biology. In cancer, for example, deviations in the composition/structure and areal density/distribution of glycosylation-associated molecules on cell surfaces are common occurrences in tumorigenesis and neoplastic progression - strongly correlating with tumor invasiveness, metastatic potential, and the evasion of host immuno-surveillance. To determine the utility of targeting aberrant glycosylation in the detection of nascent colorectal cancers *in situ*, we have recently begun to design, synthesize, and evaluate dysplastic adenoma -targeting mesoporous silica nanoparticles (MSNs) for use as endoscopic contrast agents. MSNs, approximately 100 nm in diameter, were synthesized via conventional sol-gel chemistry, with the incorporation of fluorescein isothiocyanate (FITC) within the MSN's silica framework during co-condensation, to protect the fluorophore from photobleaching and $O_2$ quenching, and to maximize the nanoparticle's available surface area for targeting ligand conjugation. Following nanoparticle synthesis, the exteriors of MSNs were labeled with the lectin *Ulex europaeus agglutinin 1* (UEA-1), to target the α-L-fucose that is known to be expressed on the luminal surface glycoproteins of colorectal dysplastic adenomas and nascent cancers. Morphologies of the resulting functionalized MSNs were then characterized by transmission electron microscopy, dynamic light scattering, $N_2$ adsorption-desorption isotherm analysis, and zeta potential measurement. *In vitro* studies of MSN-cell binding specificity were conducted using α-L-fucose positive Caco-2 and α-L-fucose negative HCT116 human colorectal cancer cells, as well as fibroblasts. *In vivo* endoscopic exams were performed using a commercially available clinical colonoscope and probe-based confocal fluorescence microscope, with fasted/prepped A/J male mice that had been subjected to azoxymethane (AOM) / dextran sodium sulfate (DSS) treatments - a standard model for colitis-associated colorectal tumor development. As the *in vitro* and endoscopic images in Figure 1 (left) illustrate, topical delivery of UEA-1 to human colorectal adenocarcinoma cells (Caco-2 (a,b) and HCT116 (d,e)) and *in situ* murine CRC/polyps (control (c) and AOM/DSS-induced colorectal polyps/tumors (f)) both show significant binding and specificity to α-L-fucose. (Concentration / time-dependent blocking studies (not shown) using non-fluorescent UEA-1 pretreatment confirmed UEA-1/α-L-fucose binding specificity.) Conjugation of the lectin UEA-1 directly to FITC-labeled MSNs yielded similar results, as shown in Figure 1 (right) for Caco-2 cells incubated with FITC-UEA-1 (g), FITC-MSN-UEA-1 (h), non-fluorescent UEA-1, blocked for 1 hr (i) and HCT116 cells incubated with FITC-UEA-1 (j), FITC-MSN-UEA-1 (k), and non-fluorescent UEA-1, blocked for 1 hr (l). Ongoing studies are aimed at enhancing our nanoplatform's transport through colon mucus and dwell-time once pathology bound.

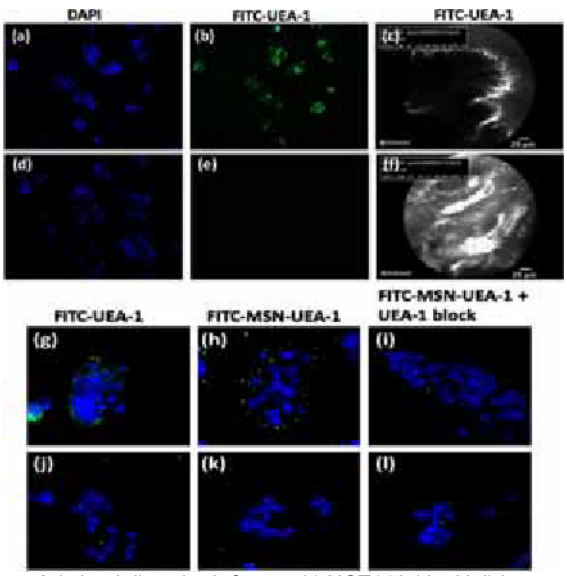


**Figure 1**. UEA-1 binding to α-L-fucose (+) Caco-2 (a,b,g,h,i) and α-L-fucose (-) HCT116 (d,e,j,k,l) human adenocarcinoma cells *in vitro*. Fluorescence endoscopy *in vivo* confirmation of enhanced UEA-1 binding to AOM-induced colorectal polyps (f) versus normal mucosa (c) in A/J mice.

Disclosure of author financial interest or relationships:
**J.S. Souris**, None; **N. Chen**, None; **V. Konda**, Mauna Kea Technologies, Honoraria; **M. Bissonnette**, None; **L. Lo**, None; **C. Chen**, BioMed Global, Consultant; RefleXion, Consultant .

Presentation Number **P780**
Poster Session 4
September 8, 2012 / 14:45-14:45 / Room: The Liffey

# Re-oxygenation of Pancreatic Cancer in Radiotherapy: Integrating Photoacoustic Imaging and IMOG Medical Device

*Ning Cao[1,7], Seung Hyun Song[3], Michael Shaffer[1], Minsong Cao[2], Teimour Maleki[4], Helen J. Chin-Sinex[5], Marc S. Mendonca[2,5], Babak Ziaie[3], Song-Chu Ko[2], **Keith M. Stantz**[1,6], [1]School of Health Sciences, Purdue University, West Lafayette, IN, USA; [2]Radiation Oncology, Indiana University School of Medicine, Indianapolis, IN, USA; [3]Electrical and Computer Engineering, Purdue University, West Lafayette, IN, USA; [4]Birck Nanotechnology Center, Purdue University, West Lafayette, IN, USA; [5]Radiation and Cancer Biology, Indiana University School of Medicine, Indianapolis, IN, USA; [6]Radiology and Imaging Sciences, Indiana University School of Medicine, Indianapolis, IN, USA; [7]Radiation Oncology, UCLA, Los Angeles, CA, USA. Contact e-mail: kstantz@purdue.edu*

Purpose: The objectives are to longitudinally monitor oxygen production within the tumor using a novel Implantable Micro Oxygen Generator (IMOG) device, and to monitor changes in tumor oxygenation after IMOG-stimulation using 3-D photoacoustic computed tomographic spectroscopy (PCS-S). Introduction: Pancreatic cancer is known to be highly hypoxic, which significantly contributes to its ineffectiveness of radiotherapy. To increase the relative biological effectiveness (RBE) of radiation therapy (RT), an IMOG medical device can be implanted into a tumor which can increase oxygen concentrations by electrolyzing water within the tumor upon ultrasound stimulation. This device has been successfully demonstrated. Our approach is to test whether the pressure signals produced from within a tumor by the photoacoustic effect (e.g., a large blood vessel in or near the tumor) can stimulate the IMOG to produce oxygen, and if PCT-S can be used to monitor changes in oxygenation by imaging in vivo the oxygen saturation levels (SaO2) in the tumor blood vessels. To test whether this mechanism of stimulation is viable and that PCT-S imaging can measure SaO2 changes during this process, a phantom study and a pilot preclinical study were performed. Material and Methods: A phantom consisting of two FEP tubes containing initially deoxygenation blood and india ink, respectively, were imaged within a PCT-S scanner pre and post IMOG stimulation. Inserted into the blood phantom was an IMOG device. The blood phantom was imaged to obtain baseline SaO2 levels. This tube was moved out of the field of view, while the the india ink was stimulated by the laser source to produce ultrasound and imaged. The blood phantom was moved back into the field of view and imaged. An increase in SaO2 was observed. Next, three athymic mice bearing human BxPC-3 pancreatic tumors were implanted with a functioning (F) and non-functioning (NF) IMOG. PCT-S images of these tumors were acquired prior to and after laser stimulation, and a significant increase in SaO2 was observed. Upon RT, a significant delay in tumor growth curves between F and NF was observed. Conclusions: This pilot study demonstrates the feasibility of merging both medical devices (IMOG) and in vivo imaging (PCT-S) technologies toward the advancement of radiation therapy.

Disclosure of author financial interest or relationships:
**N. Cao**, None; **S. Song**, None; **M. Shaffer**, None; **M. Cao**, None; **T. Maleki**, None; **H.J. Chin-Sinex**, None; **M.S. Mendonca**, None; **B. Ziaie**, None; **S. Ko**, AMI Purdue Foundation, Grant/research support; **K.M. Stantz**, None.

Presentation Number **P781**
Poster Session 4
September 8, 2012 / 14:45-14:45 / Room: The Liffey

# Preclinical Evaluation of a novel therapeutic approach in malignant melanoma using microPET and Fluorescence Molecular Tomography

***Lars Stelter***[1,2], *Michael J. Evans*[2], *Achim A. Jungbluth*[2], *Gerd Ritter*[2], *Pat Zanzonico*[2], *Valerie A. Longo*[2], *John Bomalaski*[2], *Steven M. Larson*[2], [1]*Radiology, Charité, CVK, Berlin, Germany;* [2]*Radiology, Memorial Sloan-Kettering Cancer Center, New York, NY, USA.*
*Contact e-mail: lars.stelter@charite.de*

Introduction Owing to deficiencies in L-Arginine (Arg) biosynthesis, malignant melanomas are susceptible to therapeutic intervention with Arginine Deiminase (ADI), an enzyme responsible for consuming the dietary supply of Arg. So far, ADI has been shown promising results in patients with metastasized malignant melanoma in clinical phase I/II trials. These studies, however, only used morphological imaging modalities, such as Ultrasound and Computed Tomography, to assess clinical response. In our preclinical study, we evaluated functional imaging approaches, i.e. Positron Emission Tomography (PET) and Fluorescence Molecular Tomography (FMT), to determine early changes in tumor metabolism and potentially predict the therapeutic outcome and early identify possible non-responders. Material and Methods The melanoma cell lines SK-MEL-28 (ADI-sensitive) and SK-MEL-10 (ADI-resistant) were treated with 4.3 mU/ml ADI for 7 days in vitro. Loss of cellular proliferation and apoptotic death of the sensitive cell line were determined using a proliferation assay and Annexin-V FACS analysis. In a following in vivo study, melanoma xenograft bearing hairless NOD SCID mice were treated with 160 U/m2 ADI or PBS weekly. Besides a regular determination of tumor size and Arg in the blood serum, we performed 18F-FDG PET and AngioSense750 enhanced FMT, a bloodpool marker that enables to determine tumor vascularisation, weekly. Tumoral tracer- and fluorescent probe-accumulation were quantified using ROI analysis and the latter correlated with CD31 immunohistochemistry (IHC). Results The in vitro results showed that the ADI-sensitive cells significantly lost their proliferative activity within 4 days of ADI treatment, followed by a 90%-rate of apoptosis on day 7. Corresponding to that, we observed a clear reduction in tumor volume in the ADI-sensitive xenografts. 18F-FDG PET, however, was not able to display these changes on a metabolic level. Further studies revealed that an accompanying effect of ADI in alterations of the PTEN/PI3K/Akt pathway seemed to be responsible for that. Looking at tumor vascularisation with FMT, we clearly observed a therapy-associated reduction in the tumoral vasculature, which correlated with CD31 IHC in the excised specimen. Discussion ADI-associated cellular deprivation of Arg in melanoma results in loss of cellular proliferation and apoptotic cell death. Despite effective therapeutic intervention of ADI, melanoma xenografts did not show an accompanying reduction in tumoral tracer metabolism in 18F-FDG PET. Further studies revealed a post-translational degradation of PTEN and the activation of other downstream mechanisms that mediate cellular FDG-uptake. Imaging of tumor vascularisation with FMT and IHC showed a therapy-dependent reduction in tumor vasculature, associated with a decrease in tumor volume.

Disclosure of author financial interest or relationships:
**L. Stelter**, None; **M.J. Evans**, None; **A.A. Jungbluth**, None; **G. Ritter**, None; **P. Zanzonico**, None; **V.A. Longo**, None; **J. Bomalaski**, Polaris Group, Employment; Polaris Group, Stockholder; **S.M. Larson**, None.

Presentation Number **P782**
Poster Session 4
September 8, 2012 / 14:45-14:45 / Room: The Liffey

# Novel symmetric cyanine dyes conjugated with GX1 peptide for gastric cancer in vivo imaging

*Xianghan Zhang[1], Jing Xin[1], Jimin Liang[1], Kaichun Wu[2], Hao Hu[2], Yongzhan Nie[2], **Jie Tian**[1,3], [1]School of Life Sciences and Technology, Xidian University, Xi'an, China; [2]Institute of Digestive Diseases, Xijing Hospital, The Fourth Military Medical University, Xi'an, China; [3]Medical Image Processing Group, Institute of Automation,CAS, "Beijing,100190", China. Contact e-mail: tian@ieee.org*

Objectives: Cyanine dyes have found widespread use as fluorescent labels for biomolecules. The appeal of this class of probes derives from their broad wavelength tunability, little steric hindrance, good membrane permeability and little toxicity. Therefore, novel penta-methine cyanine dyes with larger conjugated system are synthesized by symmetric synthesis method. The vascular- endothelialcell-specific binding peptide GX1of gastric cancer are conjugated with cyanine dyes. The main purpose of the study is screening out high photostability and little toxicity fluorescence probes. The GX1-dye targeted probes are applied on SGC7901-luc nude mouse model for in vivo monitoring through fluorescence molecular imaging (FMI) technology. Methods: The vascular- endothelialcell- specific binding peptide GX1 was conjugated to the novel dyes via succinimide activated carboxyl groups. CyIC-GX1 were purified by HPLC and characterized by MS-HPLC. CyIC1-GX1: calculated Mr = 1534 for C63H86N15O20S5, found m/z = 769 ([Mr/2 + 2H+]). MTT assay was done on gastric cancer cell lines and gastric epithelial cell line. In vivo NIRF imaging, blocking studies were performed on SGC-7901 gastric cancer nude model to evaluate the ability of CyIC-GX1 probes to target tumor angiogenesis. Results: A series of symmetric penta-methine cyanine dyes were synthesized with high yields (> 65%) by symmetric method. The dyes had the absorption and emission maxima in the range of 634-644nm and 665-675nm, respectively (Fig. A). The photostability of the dyes were studied compared with commercial probe Cy5.5 by absorption spectra exposed to visible light. After 60 days, the novel dyes CyIC showed only 10% decrease in maximal absorbance, but Cy5.5 showed 30% photofading (Fig. B). It is proposed that the electron donor atom S would enlarge the penta-methine chain conjugated system and make the dye more stable. MTT assay was carried out to investigate the anti-proliferation effect of CyIC on gastric cancer cell lines. Exposure to 1.25μM CyIC at 72h, the cell viability of GES, MKN28, AGS, SGC7901 and MKN45 were all more than 90% (Fig. C). It was revealed that the novel dyes CyIC had little toxicity for cells with good membrane permeability, and had little inhibition effect on gastric cancer cell lines in a dose- and time-dependent manner. NIR fluorescence in vivo imaging of SGC-7901-tumor-bearing mice was obtained by FMI system after intratumoral injection of CyIC-GX1 (1μM/100μL) 0.5h (Fig. D). The total fluorescence signal intensity was about 2.7×109 intensity, and the maximum fluorescence signal was about 26773/intensity, which denotes that CyIC-GX1 probes are suitable for in vivo optical imaging studies. Conclusions: A series of novel symmetric cyanine dyes conjugated with GX1 peptide were successfully synthesized. The novel probes showed better photostability than Cy5.5, and little cell toxic, good membrane permeability, bright signals was observed for the probes in living cells and mice model. CyIC-GX1 could be proposed as fluorescent probes for gastric tumor imaging in living subjects.

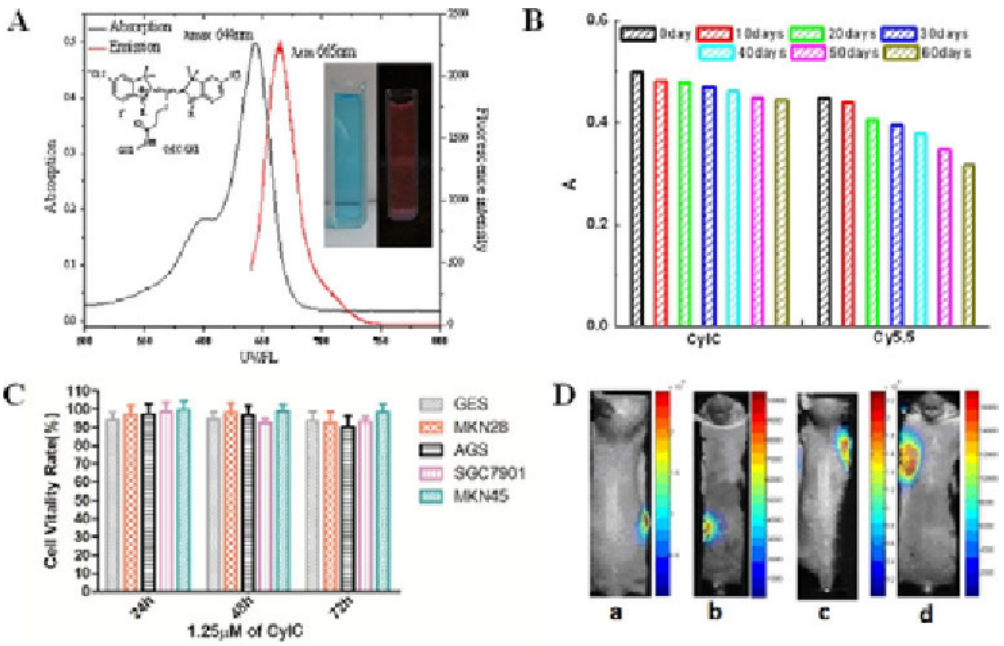


Figure 1 Absorption and fluorescence spectra (A), photostability (B), MTT assay(C), and fluorescence imaging in living mice (D) of novel probes

Disclosure of author financial interest or relationships:
**X. Zhang**, None; **J. Xin**, None; **J. Liang**, None; **K. Wu**, None; **H. Hu**, None; **Y. Nie**, None; **J. Tian**, None.

Presentation Number **P783**
Poster Session 4
September 8, 2012 / 14:45-14:45 / Room: The Liffey

# Dual-tracer fluorescence imaging can quantify tumor burden in tumor-draining lymph nodes

***Kenneth M. Tichauer***[1], *Jason Gunn*[1], *Aravind Viswanathan*[1], *Kimberley Samkoe*[2,1], *Peter A. Kaufman*[3], *Brian W. Pogue*[1,2],
[1]*Engineering, Dartmouth College, Hanover, NH, USA;* [2]*Department of Surgery, Dartmouth College, Hanover, NH, USA;*
[3]*Hematology/Oncology, Dartmouth-Hitchcock Medical Center, Lebanon, NH, USA. Contact e-mail: Kenneth.Tichauer@Dartmouth.edu*

Current breast tumor resection procedures involve the removal of sentinel lymph nodes draining the primary tumor to be tested in pathology for the presence of metastatic tumor burden. Lymph nodes can be located by tracking the drainage of blue dye injected into the primary tumor, and removed surgically. If the sentinel lymph nodes are found to be positive for tumor burden the next downstream set of lymph nodes are removed and also tested for tumor burden. While it is critical to remove as many tumor metastases as possible, the removal of lymph nodes is invasive and results in significant tissue loss. Moreover, only 40% of breast cancer patients have lymph node involvement, which means that the lymph nodes would not have to be removed in roughly 60% of patients. Therefore, a non-invasive means of quantifying tumor burden would be a powerful tool for guiding these surgeries. Some studies have proposed imaging the uptake of a fluorescence tracers targeted to receptors overexpressed in breast cancer as a means of estimating tumor burden in the lymph system; however, the amount of tracer delivered to a lymph node can be highly variable depending on the location of the lymph node and many other parameters. In this study a dual-tracer imaging approach is proposed in which a second, untargeted tracer is injected and imaged alongside a targeted fluorescence tracer to account for delivery-mediated effects on the uptake of the targeted tracer. 9 nude mice were implanted with MDA-MB-luc human breast cancer cells (Perkin Elmer), a cell line with a high probably of metastasizing to the lymph nodes and that expresses luciferase. Tumors were grown for 5 wks before the right and left axillary lymph nodes were imaged on an IVIS imaging system (Perkin Elmer) after i.p. injection of luciferin to incite bioluminescence in the tumor cells (Fig. 1a). The signal arising from the lymph nodes was used as a marker of tumor burden. Next, both front foot pads of each mouse were injected with an equal mixture of IRDye 800CW-EGF (LICOR Biosciences) and IRDye 700DX (a tracer targeted to epidermal growth factor receptor, which is overexpressed by this cell line, and an untargeted tracer, respectively) and the uptake of the tracers was imaged in left and right axillary lymph nodes with an Odyssey scanner (LICOR) at 4-min intervals for up to 1 h. The uptake curves of both tracers were incorporated into a dual-tracer compartment model to quantify tumor burden by way of mapping the calculated binding potential map of the targeted tracer (Fig. 1b) in a non-invasive manner that could potentially be carried out clinically. Fig. 1c demonstrates a statistically significant correlation between the ratio of the binding potentials in the right and left lymph nodes and the ratio of the bioluminescence in the right and left lymph nodes. This result demonstrates the promise of dual-tracer imaging for quantifying tumor burden in sentinel lymph nodes during surgical resection of breast cancers. Future work will investigate a more direct approach that does not involve ratioing to a contralateral lymph node, which was required because of variability in the bioluminescence results.

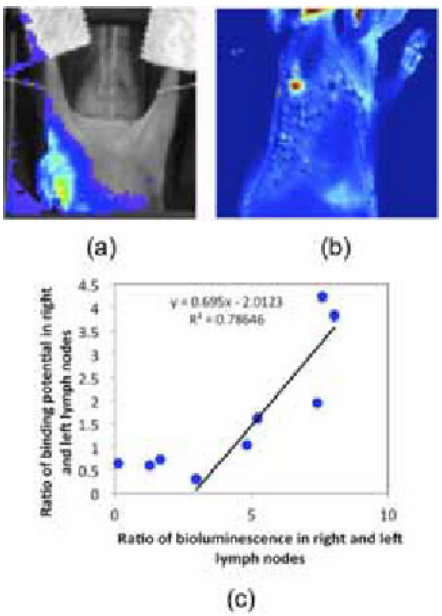


Disclosure of author financial interest or relationships:
**K.M. Tichauer**, None; **J. Gunn**, None; **A. Viswanathan**, None; **K. Samkoe**, None; **P.A. Kaufman**, None; **B.W. Pogue**, None.

Presentation Number **P784**
Poster Session 4
September 8, 2012 / 14:45-14:45 / Room: The Liffey

# In Vivo Detection of ELTD1, a Novel Biomarker for Gliomas

***Rheal Towner***[1], *Randy L. Jensen*[2], *Nataliya Smith*[1], *Rebba Casteel*[1], *Debra Saunders*[1], *David L. Gillespie*[2], *Robert Silasi-Mansat*[3], *Florea Lupu*[3], *Cory B. Giles*[4], *Jonathan D. Wren*[4], [1]*Advanced Magnetic Resonance Center, Oklahoma Medical Research Foundation, Oklahoma City, OK, USA;* [2]*Huntsman Cancer Institute, University of Utah, Salt Lake City, UT, USA;* [3]*Cardiovascular Biology, Oklahoma Medical Research Foundation, Oklahoma City, OK, USA;* [4]*Arthritis & Clinical Immunology, Oklahoma Medical Research Foundation, Oklahoma City, OK, USA. Contact e-mail: Rheal-Towner@omrf.org*

Introduction: Glioblastoma multiforme (GBM) is characterized by its diffuse, invasive and highly angiogenic nature, and has a very poor prognosis. Early diagnosis of gliomas is an important goal to increase the survival rates of this devastating cancer which has limited treatment options and low survival rates. Identification of new biomarkers could help in the further diagnosis of GBM. Our goal in this study was to determine whether or not ELTD1 could be used as a marker for glioma-related processes, and use IHC and molecular magnetic resonance imaging (MRI) to validate its presence in human and rodent gliomas, respectively. Methods: We used advanced data mining and a novel bioinformatics method to predict ELTD1 as a novel biomarker that is associated with gliomas. A global meta-analysis (GAMMA) of all human genes was conducted to identify gene-gene co-expression patterns that were consistent and specific across heterogeneous microarray experiments. This "guilt by association" approach identifies gene sets that are likely to be associated in biologically relevant ways such as phenotype, disease and genetic network. Then, using the Human Proteome Reference Database (HPRD) and other experimental sources on protein cellular localizations, we screened this list of predicted glioma-associated proteins for those that were extracellular or membrane-bound, because these proteins were thought to be ideal targets for molecular imaging probes and targeting therapies since they are more likely to be accessible to injected antibodies. Validation of this marker was done with IHC which was used to detect levels of ELTD1 in human high-grade gliomas and rat F98 glioma tumors ex vivo. In vivo levels of ELTD1 in rat F98 gliomas were assessed using molecular MRI (mMRI). A rat glioma cell implantation model was used. A dextran-coated NH2 base iron oxide nanoparticle construct underwent conjugation with an ELTD1-specific Ab. For determination of T2* values of the iron oxide nanoprobes in gliomas, a multiple gradient echo (MGE) method was used with the following parameters: TE (first echo)=4 msec, echo spacing of 4 ms TR=1500 msec, 10 echoes (TE= 4, 11, 18, 25, 32, 39, 46, 53, 60, 67 msec), 2 coronal (horizontal) slices, number of averages (NA)=2, matrix=256x256, slice thickness=1mm; with a spatial resolution of 0.137 mm/pixel; and an estimated total scan time of 10min). Results: ELTD1 was found to be significantly higher (P=.03) in high-grade gliomas (50 patients) compared to low-grade gliomas (21 patients), and compared well to traditional IHC markers including VEGF, GLUT-1,CAIX and HIF-1alpha. Significantly high (P<0.001) in vivo levels of ELTD1 were found in F98 tumors, compared to normal brain tissue (see Fig. 1). Conclusions: These results strongly suggest that the associative analysis method used in this study was able to accurately identify ELTD1 as a glioma-associated biomarker. The detection of ELTD1 was also validated in both rodent and human gliomas, and may serve as an additional biomarker for gliomas in pre-clinical and clinical diagnosis of gliomas.

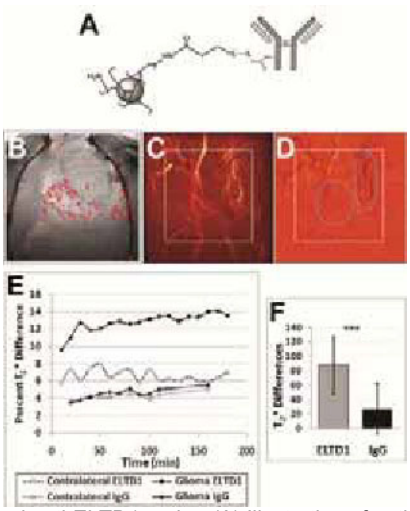


Figure 1: mMR imaging in a F98 rat glioma administered anti-ELTD1 probe. (A) Illustration of anti-ELTD1 probe. (B) Horizontal image depicting regions (red) where probe was highest. (C) 3D MR angiogram prior to anti-ELTD1 porobe. (D) MR angiogram post-anti-ELTD1 (180 min) minus pre-administration. Darkenes areas highlighted. (E) Probe kinetics measuring %T2* differences in tumor and contralateral brain tissues following either anti-ELTD1 or non-specific IgG-SPIO administration. (F) Histogram of T2* differences in tumors of F98 gliomas administered either anti-ELTD1 or IgG-SPIO.

Disclosure of author financial interest or relationships:
**R. Towner**, None; **R.L. Jensen**, Medtronic, Consultant; Pharmoco Kinesis, Consultant; **N. Smith**, None; **R. Casteel**, None; **D. Saunders**, None; **D.L. Gillespie**, None; **R. Silasi-Mansat**, None; **F. Lupu**, None; **C.B. Giles**, None; **J.D. Wren**, None.

Presentation Number **P785**
Poster Session 4
September 8, 2012 / 14:45-14:45 / Room: The Liffey

# Establishment and characterization of the temporally immune suppressed wistar rat xenograffed human small cell lung carcinoma by MRI/NMR and histochemistry

***Chatchanok Udomtanakunchai***, *Nathupakorn Dechsupa, Anan Udom-uttaracheewa, Rujarin Yawilo, Jiraporn -. Kantapan, Samlee Mankhetkorn, Radiologic Technology, Faculty of Associated Medical Sciences, Chiang Mai University, Center of Excellence for Molecular Imaging, Chiang Mai, Thailand. Contact e-mail: oilchat@hotmail.com*

In this study, we reported the temporally immune suppressed wistar rat which were xenograffed using human small cell lung carcinoma drug-sensitive (GLC4) and drug-resistant (GLC4/adr) cell lines with the overexpression of MRP1-protein. The xenograffed rats were examined their health status by monitoring plasma metabolites using NMR. The appearance of tumor tissue formation was investigated by MR Imaging combine with vascular (gadolinium-DTPA, Gd-DTPA) and cellular (ferric-desferoxamine complex, Fe-DFO) MRI contrast agent, and then confirm by histochemistry method. The male wistar rats were suppressed immune by 5 mg/kg cyclosporine A consecutively 3 days then separate into two series for implantation. The first series, rats were injected into subcutaneous of left and right haunch by those cancer cell lines that were incorporated with 1 micromolar of Fe-DFO for 6 h. The rats were imaged with 1.5T MRI at T1W, T1W-SPIR, T2W and T2W-SPIR, before and after implantation; at immediate, 30, 60, 90, 120 mins and 1, 3, 5 and 10 days. The MR imaging shown the enhancing spot by Fe-DFO and then regressive signal until disappear on day 5. At day10, the MR imaging revealed not only the tumor growth at the implanted origin point but also the distribution of tumor mark in lung. The second series, rats were xenograffed with both cell lines without the incorporation of MRI contrast agent. The tumor genesis was investigated by MRI combine with the intravenous injection of gadolinium-DTPA. The blood plasma metabolic profiling of rats were measured before and after xenograffed and revealed the increasing in lipid and decreasing in protein component. The pathogenesis of rat organs were confirmed with the histochemistry and found the inflammation and infiltration of blood supply through only the right cervical node and lung but not in the other organs. These finding disclosed the successive wistar rat modeling system for further preclinical study.

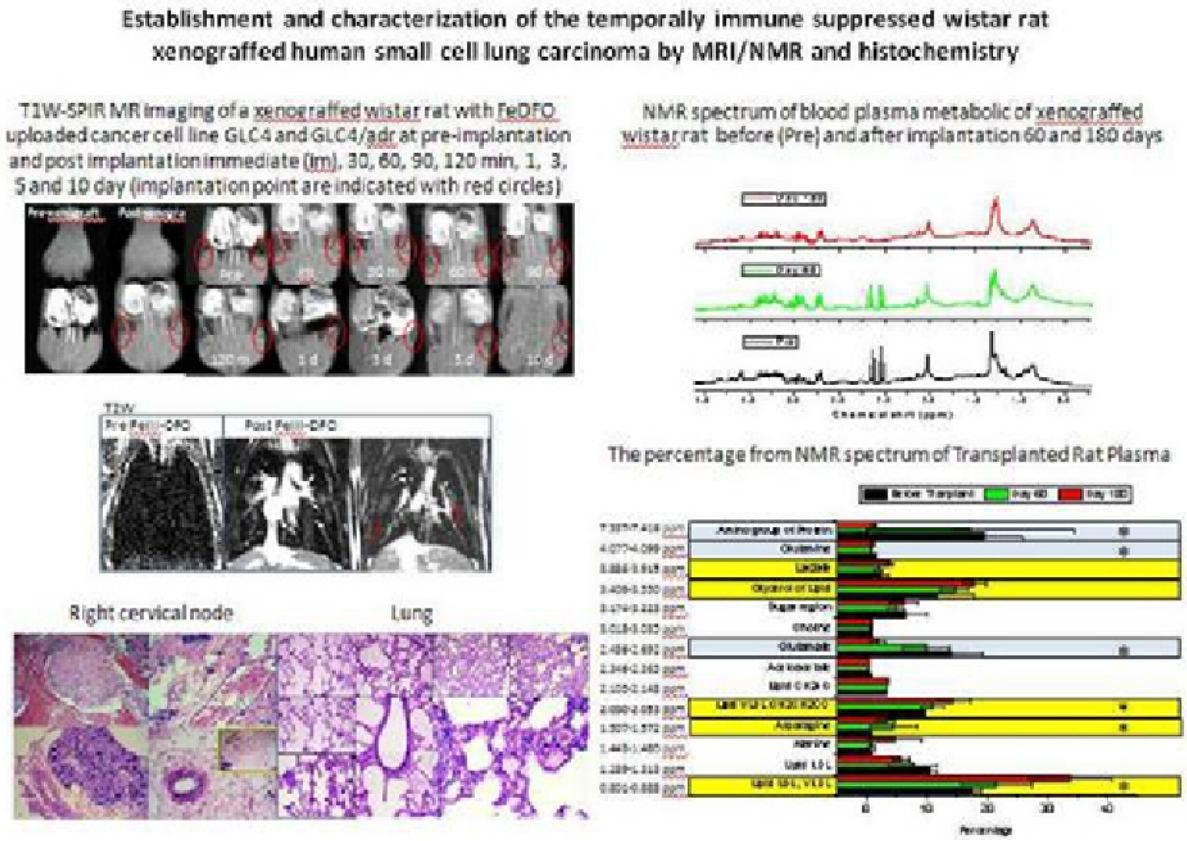


Disclosure of author financial interest or relationships:
**C. Udomtanakunchai**, None; **N. Dechsupa**, None; **A. Udom-uttaracheewa**, None; **R. Yawilo**, None; **J.-. Kantapan**, None; **S. Mankhetkorn**, None.

Presentation Number **P786**
Poster Session 4
September 8, 2012 / 14:45-14:45 / Room: The Liffey

# FDG-PET as a Pharmacodynamic Biomarker for Early Assessment of Treatment Response to Linifanib (ABT-869) in a Non Small Cell Lung Cancer Mouse Model

***Martin J. Voorbach***[1], *Sarah R. Mudd*[1], *David R. Reuter*[2], *Paul Tapang*[2], *Jonathan Hickson*[2], *Gerard B. Fox*[1], *Daniel H. Albert*[2], *Yanping Luo*[1], *Marion L. Refici-Buhr*[2], *Mark Day*[1], [1]*Translational Imaging, Abbott Laboratories, Abbott Park, IL, USA;* [2]*Cancer in vivo Pharmacology, Abbott Laboratories, Abbott Park, IL, USA. Contact e-mail: martin.j.voorbach@abbott.com*

Linifanib (ABT-869) is a multitargeted receptor tyrosine kinase inhibitor. This work aims to evaluate FDG-PET as a pharmacodynamic (PD) biomarker for linifanib treatment in the Calu-6 model of human non-small cell lung (NSCLC) cancer in SCID-beige mice. Animals received either vehicle or 12.5 mg/kg linifanib orally twice a day for the duration of the study. Imaging was performed at -1, 1, 3, and 7 days after beginning treatment (n = 12 - 14 per group). Linifanib inhibited tumor growth and suppressed tumor metabolic activity. Changes in tumor FDG uptake were observed as early as one day after beginning linifanib treatment and were sustained for the duration of the study. This study confirms that linifanib is efficacious in this mouse model of human NSCLC and confirms FDG-PET is a potential PD biomarker strategy for linifanib therapy.

Disclosure of author financial interest or relationships:
**M.J. Voorbach**, Abbott Labs, Employment; Abbott Labs, Stockholder; **S.R. Mudd**, Abbott Laboratories, Employment; **D.R. Reuter**, Abbott Laboratories, Employment; **P. Tapang**, None; **J. Hickson**, None; **G.B. Fox**, Abbott Laboratories, Employment; Abbott Laboratories, Stockholder; **D.H. Albert**, Abbott Laboratories, Employment; **Y. Luo**, Abbott Laboratories, Employment; **M.L. Refici-Buhr**, None; **M. Day**, None.

Presentation Number **P787**
Poster Session 4
September 8, 2012 / 14:45-14:45 / Room: The Liffey

# FDG, FEC and FLT PET tracer uptake in a panel of human tumour xenograft models

***Ian Wilson***[1,2], *Huw D. Thomas*[1], *Stephen J. Hobson*[1,3], *Michael Carroll*[3], *David R. Newell*[1], *Ross J. Maxwell*[1,2], [1]*Northern Institute of cancer Research, Newcastle University, Newcastle Upon Tyne, United Kingdom;* [2]*Newcastle Magnetic Resonance Centre, Newcastle University, Newcastle Upon Tyne, United Kingdom;* [3]*Department of Chemistry, Newcastle University, Newcastle Upon Tyne, United Kingdom. Contact e-mail: j.i.wilson@newcastle.ac.uk*

Our focus is on the development of MR and PET imaging agents for the evaluation of novel targeted cancer treatments, including inhibitors of PARP, MEK, PI3K and ERK5. Ideally the imaging agent should give a pre-treatment signal which is specifically changed when the target is inhibited. Interactions with the tumour microenvironment (vasculature, oxygenation, and pH) are also likely to be relevant. The aim of this study was to compare the uptake kinetics of three PET tracers in a variety of tumour models with differing molecular pathology and anatomic origin (Table 1). Mice were implanted subcutaneously with various human tumour xenographs (colorectal, osteosarcoma, hepatoma, prostate, ovarian, bladder). When the tumours reached 10mm in diameter they were given a dynamic PET scan over 1 hour (FDG) or 2 hours (FLT or FEC). These reults are summerised in Table 1. The dynamic FLT-PET data showed consistent (moderate or high) uptake across a wide range of tumour models, even those (such as colon tumours) which showed only low uptake of FDG. The low and heterogenous uptake of [18F]FDG may be attributed to poor blood flow as [18F]FDG uptake is consistent with poor dynamic contrast-enhanced (DCE) MRI contrast agent uptake. On the other hand, [18F]FLT, which shows higher more homogenous uptake, may be less influenced by the tumour blood supply The uptake of FEC in nine tumour types has also been evaluated but tumour uptake was negligible in all cases, including the J82 bladder tumour model (with high choline kinase activity) and two prostate models. Notably, 11C-choline and 18F-choline analogues are reported to be of particular value in human prostate cancer. From these studies we can conclude that [18F]-FLT is the most promising PET tracer for initial drug discovery work, and has the potential to evaluate novel cancer treatments in a wide variety of human tumour xenografts. Tumour vasculature is an important determinant of key features of the micro-environment such as hypoxia, pH and the delivery of both drugs and molecular imaging agents.

Probe Uptake in genetically-defined tumour xenografts

| Tumour | Molecular Pathology | MR Contrast Uptake | FDG Uptake | FLT Uptake | FEC Uptake |
|---|---|---|---|---|---|
| HCT116 (colon) | P53 WT | + | + | +++ | NT |
| HCT116 -/- | P53-/- | ++ | + | +++ | - |
| SW620 (colon) | | + | + | ++ | - |
| HUH7 (Hepatoma) | High SULF 2 | ++ | ++ | NT | - |
| J82 (bladder) | Choline Kinase | NT | NT | NT | - |
| SISA1 (osteosarcoma) | P53 WT<br>MDM2 amplified | +++ | +++ | +++ | - |
| A2780 CP70 (ovary) | P53 Mutant | ++ | + | NT | - |
| PC3 (prostate) | | NT | NT | NT | - |
| DU145 (prostate) | | NT | NT | NT | - |

Key: PET tracer/MR contrast uptake: - not detected; + low; ++ moderate; +++ high uptake; NT - not tested.

Disclosure of author financial interest or relationships:
**I. Wilson**, None; **H.D. Thomas**, None; **S.J. Hobson**, None; **M. Carroll**, None; **D.R. Newell**, None; **R.J. Maxwell**, None.

Presentation Number **P788**
Poster Session 4
September 8, 2012 / 14:45-14:45 / Room: The Liffey

# Molecular Imaging and Image-Guided Therapy using Photoacoustic nanoDroplets

***Katheryne Wilson**, Milos Marinkovic, Omer Mirza, Stanislav Y. Emelianov, Biomedical Engineering, The University of Texas at Austin, Austin, TX, USA. Contact e-mail: katheryne.wilson@gmail.com*

Photoacoustic nanoDroplets (PAnDs) have been developed as a dual contrast agent for combined ultrasound and photoacoustic imaging. These nano-sized droplets consisting of a bovine serum albumin coat surrounding a liquid droplet of perfluorocarbon containing specially coated plasmonic nanoparticles. PAnDs provide three forms of imaging contrast, including decreased acoustic impedance (ultrasound contrast) and vaporization and thermal expansion (photoacoustic contrast). Nanosecond pulses of laser light are absorbed by the encapsulated plasmonic nanoparticles causing localized thermal expansion, which vaporizes the liquid perfluorocarbon into its gaseous state, releasing a large acoustic shock wave. The decreased acoustic impedance of the resulting gas bubbles provides ultrasound contrast. These droplets allow vaporization, a stronger photoacoustic phenomenon than thermal elastic expansion, to be safely used for biological imaging, allowing for a dramatic increase in imaging depth and a more efficient use generation of photoacoustic signal. Recent results use PAnDs as combined molecular imaging agents and image-guided therapeutic delivery vectors. Targeting of PAnD with specific monoclonal antibodies (mAB) was accomplished through the creation of a biotin/avidin bridge, where biotin is incorporated into the BSA shell of the PAnD. Excess biotin is rinsed from the sample, and then an avidin-modified mAB can be attached. The formation of these bridges was confirmed through fluorescent microscopy (panels a and b). Next, the therapeutic drug loading ability of PAnDs was investigated. Organic chemotherapeutic drugs, such a Paclitaxel, have adverse effects due to the solvent that must be used to delivery these drugs systemically. PAnDs are dispersible in aqueous environments, but contain a large organic center capable of carrying a high concentration of chemotherapeutic (up to 20mg/ml has been demonstrated). The release of the chemotherapeutic can be remotely activated via optical irradiation once the PAnDs have accumulated into the desired tissues. The creation of drug loaded PAnDs was accomplished through the incorporation of a small amount of oil droplets within the perfluorocarbon centers. The drug loading was verified via mass-spectroscopy and fluorescent imaging (panels c and d) using a fluorescent Paclitaxel. Passive drug release studies, using sodium salicylate to solubilize the released Paclitaxel in the aqueous phase, found that minimal diffusion of drug from the PAnD occurs (<2% over 75 hours at room temperature at constant agitation) (panel e) and the majority of drug release is due to rupture of the droplets upon activation. This indicates that drug loaded PAnDs could circulate with their cargo intact, accumulate within a desired tissue, and then the drug could be released upon external optical activation. The accumulation and activation of PAnDs allowing for drug release could be monitored via combined ultrasound and photoacoustic imaging. In summary, these studies represent the ability to use PAnDs as molecularly targeted, combined contrast agents and drug delivery vectors.

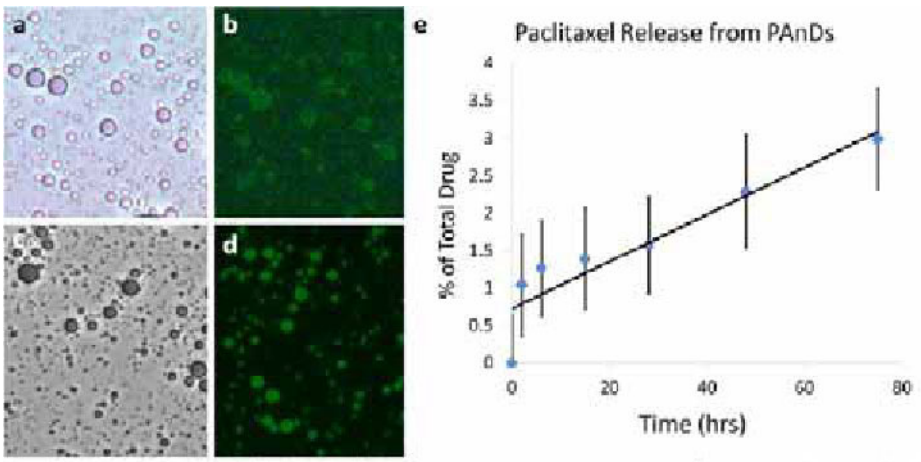


**Panels a and b:** Bright field and fluorescent microscopy images of PAnD with completely biotin/avidin bridges attaching fluorescent markers to the surface. **Panels c and d:** bright field and fluorescent images of PAnDs loaded with fluorescent Paclitaxel. Notice the difference in fluorescent signal location in the droplets between panel b (edges) and d (solid throughout) depicting the location of the signal (interior versus superficial). **Panel e:** passive Paclitaxel release from PAnDs over 75 hours. Linear release indicates this release is not due to diffusion, but rather rupture of the PAnDs.

Disclosure of author financial interest or relationships:
**K. Wilson**, None; **M. Marinkovic**, None; **O. Mirza**, None; **S.Y. Emelianov**, None.

Presentation Number **P789**
Poster Session 4
September 8, 2012 / 14:45-14:45 / Room: The Liffey

# Real-time imaging of doxorubicin release from thermosensitive liposomes using fibered confocal fluorescence microscopy

***Anna Yudina***[1,3], *Marc Derieppe*[1,3], *Cyril S. Lorenzato*[1,3], *Roberto Tejera-Garcia*[2], *Paavo K. Kinnunen*[2], *Chrit Moonen*[1,3], [1]*IMF Laboratory CNRS FRE 3313/Univ Bordeaux2, Bordeaux, France;* [2]*Helsinki Biophysics and Biomembrane Group, Department of Biomedical Engineering and Computational Science, Aalto University, Aalto, Finland;* [3]*Imaging Division, University Medical Center Utrecht, Utrecht, Netherlands. Contact e-mail: ay.yudina@gmail.com*

Thermosensitive liposomes (TSLs) demonstrate great potential for local delivery and release of the payload, for example doxorubicin (dox). However current possibilities of real-time monitoring and quantification of these processes in vivo remain limited. Fibered confocal fluorescence microscopy (FCFM) is a minimally-invasive technique allowing for real-time imaging in live subjects. Here we demonstrate the feasibility of FCFM for both in vitro and in vivo real-time monitoring and quantitative assessment of doxorubicin release from TSLs. TSLs incorporating 1mM doxorubicin were prepared with a phase transition temperature (Tm) of 42°C and characterized by dynamic light scattering. For in vitro real-time imaging of doxorubicin release from TSLs, U87 glioblastoma cells were seeded in Opticell cell culture chambers. Opticell was injected with dox-TSLs and positioned in a water bath at 37C with FCFM probe in direct contact with the membrane. A 10-minute video before and during heating was recorded along with temperature measurements. For in vivo feasibility studies 2 mln U87 cells were implanted s.c. bilaterally in Nu/Nu mice. I.v. injection of 500 kDa FITC-dextran to delineate the vessels was followed by an injection of dox-TSLs. With a FCFM probe positioned on the tumor surface (exposed via skin flap) a 10-minute video of heating to 42°C and follow-up (10-second video every minute) was recorded. Control experiments included FITC-dextran and TSLs injection with no heating and FITC-dextran injection alone followed by heating. Lipid concentration and the hydrodynamic diameter of the TSLs were found to be 100 μM and 150 +/- 10 nm respectively. The temperature corresponding to the beginning of dox release was found to be 39°C with a maximum release rate observed at 41.5°C. The heating of free dox in vitro did not result in fluorescence intensity increase. No signal change was observed for dox-TSLs neither at 37°C nor during heating up to 39°C. Above 39°C signal enhancement became clearly noticeable reaching a maximum of 2.6-fold compared to the baseline at 41°C (Figure 1, top row). In vivo the mice that were injected with 500 kDa FITC-dextran alone and heated showed a maximum signal enhancement of 1.3-fold over the course of heating and follow-up. Mice injected with both FITC-dextran and dox-TSLs without heating demonstrated up to 25% decrease in signal (attributed to photobleaching). Mice injected with FITC-dextran, dox-TSLs and heated demonstrated a 1.25-fold signal increase at 39°C, 1.5-fold at 40°C, 2.1-fold at 41°C, 2.5-fold at 42°C, reaching maximum of 3.6-fold at about 2 minutes at 42°C (Figure 1, bottom row). Both in vitro and in vivo release was found to start after 39°C which correlates with dox-TSLs properties determined fluorimetrically. Thus the feasibility of real-time imaging of doxorubicin release from TSLs using FCFM was for the first time demonstrated in vitro and in vivo. This approach holds great promise for real-time monitoring and assessment of payload release from TSLs in live subjects. This study was supported by EU FP7 project SonoDrugs (NMP4-LA-2008-213706) and ERC project 268906 "Sound Pharma".

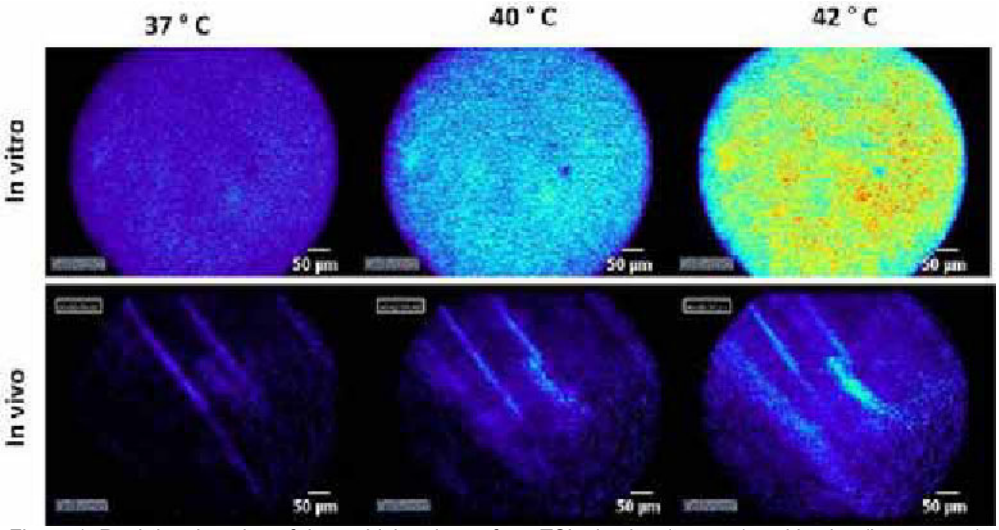


Figure 1. Real-time imaging of doxorubicin release from TSLs in vitro (top row) and in vivo (bottom row).

Disclosure of author financial interest or relationships:
**A. Yudina**, None; **M. Derieppe**, None; **C.S. Lorenzato**, None; **R. Tejera-Garcia**, None; **P.K. Kinnunen**, None; **C. Moonen**, Philips Healthcare, Grant/research support; Mauna Kea, Grant/research support .

Presentation Number **P790**
Poster Session 4
September 8, 2012 / 14:45-14:45 / Room: The Liffey

# Detection of single Mesenchymal stem cells by MR imaging

***Angela Ariza de Schellenberger**, Eyk A. Schellenberger, Randall Lindquist, Monika Ebert, Susanne Wagner, Matthias Taupitz, Jörg Schnorr, Experimental Radiology, Charite, Berlin, Germany. Contact e-mail: angela.ariza@charite.de*

Introduction The increasing use of stem cells in regenerative medicine and cellular therapies has encouraged the development of robust methods that allow in vivo cell tracking with high sensitivity. Mesenchymal stem cells (MSCs) are one of the most commonly used stem cell types in regenerative medicine, due to their in vitro proliferation and pluripotent differentiation capacity. The aim of this study was to develop single cell tracking of MSCs labelled with very small iron oxide nanoparticles (VSOPs), while maintaining their stem cell features. Methods Mesenchymal stem cells were isolated from mouse bone marrow (mMSCs). mMSCs were isolated from wild type mice between 6 and 8 weeks of age. mMSCs were characterized based on expression of cell-surface markers, proliferation capacity and differentiation potential, to guarantee the maintenance of MSCs features before and after VSOPs uptake. MRI signal was performed on phantoms for mMSCs labeled with nanoparticles. Cells were resuspended in low-melting point agarose in NMR tubes; NMR tubes were placed in a falcon tube filled with agarose. MRI was performed with in T2* weighted MR imaging sequences on a 7T Bruker Pharmascan animal scanner and 3T Siemens Trio clinical scanner. Results mMSCs isolated from bone marrow of young mice, showed consistent Mesenchymal stem cell features between passages 3 and 6. After nanoparticles uptake, FACS analysis showed consistent expression of cell-surface markers (CD45-, CD11b-, TER119- and CD44+, CD90+. CD73+, CD105+ and CD133+). Additionally, differentiation potential (Adipogenesis, osteogenesis and chondrogenesis), population doubling times and colony forming capacity remained similar, indicating that the MSC character was maintained. Single mMSCs were detected in T2* weighted magnitude images. Post-processing of the MR phase images was performed using methodology developed in our group to significantly enhance the sensitivity of detection. Conclusion We believe that cell tracking of single MSCs with this technique provides a very useful tool for In vivo tracking of MSCs in regenerative medicine and tumour migration models.

Disclosure of author financial interest or relationships:
**A. Ariza de Schellenberger**, None; **E.A. Schellenberger**, None; **R. Lindquist**, None; **M. Ebert**, None; **S. Wagner**, None; **M. Taupitz**, None; **J. Schnorr**, None.

Presentation Number **P791**
Poster Session 4
September 8, 2012 / 14:45-14:45 / Room: The Liffey

# Receptor-based Radioimmuno-imaging/therapeutic platform for tumors using hormonal 95kDa monoclonal antibody

***Gurupad Bandopadhaya***[1], *Geetanjali Arora*[1], *jaya shukla*[2], [1]*Nuclear Medicine & PET, All India Institute of Medical Sciences, Delhi, India;* [2]*Nuclear Medicine, PGIMER, Chandigarh, India. Contact e-mail: guru47@gmail.com*

The expression of hCG and its subunits (α and β) has been reported in a variety of cancers such as lung cancer, bladder carcinoma, colorectal carcinoma, pancreatic carcinoma, breast cancer, cervical carcinoma, oral cancers, vulva/vaginal cancers, prostate cancer and gastric carcinomas. High levels of hCG and its subunits are associated with high micro vessel density in hCG expressing cancers. It plays a key role in the sustenance, proliferation, migration, invasiveness and the promotion of angiogenesis of tumor cells. Our study is to explore the possibility of developing, immuno-imaging/immunotherapeutic agent for hCG (or its subunits) expressing tumors by using antibodies raised against them. METHODS: Three human cancer cell lines were selected: human lung adenocarcinoma (A549), Glioblastoma (U87MG) and breast cancer (MCF7) cell-line, as they are among the most common terminal cancers. The monoclonal anti-β-hCG antibody, obtained from ascetic fluid, was purified by Protein A column and characterized by SDS PAGE and western blot techniques. The antibodies were titrated by BCA assay. Ectopic expression of hCG on these cell lines was tested by flow cytometry and in vitro cytotoxicity with anti- β-hCG monoclonal antibody was tested with MTT assay on the cell line with the highest percentage binding with them. For positive and negative controls, SW71 cell line (immortalized trophoblast cells) and Peripheral blood Monocytes (PBMC) were used, respectively. The antibody was then labeled with Lu-177 using bifunctional chelating agent DOTA and in vivo biodistribution studies were conducted in tumor-induced rats. RESULTS: The antibody could be purified to homogeneity and characteristic bands were observed on SDS PAGE and Western blot using Medium weight protein marker as standard. The concentration of antibody as determined by BCA assay was 28 mg/ml. A549 showed 95% binding with anti-β-hCG antibody, U87MG cells showed 66% receptor expression and MCF7 showed 55% receptor expression. ~90% of the A549 cells could be killed by using the antibody at 72 h post-treatment. No cytotoxicity was observed on SW71 despite a high binding percentage. mAb were labeled with high radiolabeling efficiency (~98%). In vivo studies using antibody fragment after radiolabeling excreted via hepato-biliary route and had significant uptake in A549 (Human Lung Adenocarcinoma) cell induced rats.` CONCLUSION: It can be concluded that among the three cancer cell lines included in the study, the non-small cell lung cancer significantly expresses β-hCG and shows dose dependent cytotoxicity with anti-β-hCG antibody. The toxic effect of anti-β-hCG antibody has can be further enhanced when labeled with therapeutic radioisotope such as Lu-177. This study provides a platform for further studies for targeted radio-immuno imaging and subsequent therapy of lung cancer and other terminal cancers expressing hCG.

Disclosure of author financial interest or relationships:
**G. Bandopadhaya**, None; **G. Arora**, None; **J. shukla**, None.

Presentation Number **P792**
Poster Session 4
September 8, 2012 / 14:45-14:45 / Room: The Liffey

# Glucan Particles: a promising naturally-derived microcarrier for multimodal tracking of immune cells

***Francesca Garello***[2], *Sara Figueiredo*[2,1], *Francesca Arena*[2], *Juan C. Cutrin*[4], *Giovanna Esposito*[2], *Luca D'Angeli*[2], *Daniela Delli Castelli*[2], *Carlos F. Geraldes*[1], *João Nuno Moreira*[3], *Silvio Aime*[2], *Enzo Terreno*[2], [1]*Department of Life Sciences, FCTUC and Center for Neurosciences and Cell Biology, University of Coimbra, Coimbra, Portugal;* [2]*Molecular & Preclinical Imaging Center, University of Torino, Torino, Italy;* [3]*Laboratory of Pharmaceutical Technology Faculty of Pharmacy and CNC, University of Coimbra, Coimbra, Portugal;* [4]*Clinical and Biological Sciences, University of Torino, Torino, Italy. Contact e-mail: francesca.garello@unito.it*

Tracking cell migration requires a noninvasive imaging modality that has to be both sensitive and capable of yielding high-resolution images. Magnetic resonance imaging (MRI) is an outstanding technique that allows the assessment of the cell delivery but its relatively low sensitivity requires strategies of efficient labeling. The most frequently used approaches have dealt with iron-oxide nanoparticles. However, as it has been reported, the use of these particles generates hypointensity in the MR images, thus preventing the contrast detection in endogenous areas of low intensity, and/or creating artifact issues. The use of positive contrast agents is a promising alternative, although it requests the entrapment of 107-108 complexes per cell to achieve enough contrast. This objective may be pursued by using Glucan Particles (GPs, diameter of 2-4 microns) that are derived fron Yeast cell wall. The high affinity they show towards immune system cells can be exploited to labeling and tracking macrophages in vivo in inflammation models. The inner core of GPs, which were obtained by a procedure consisting of a chemical extraction of protein, lipid, and mannan from Saccaromyces Cereviesiae, were loaded with amphiphilic Gd- or Rhodamine-DPPE-labeled agents. Cell uptake experiments were carried out using J774A.1, mouse melanoma (B16-F10) and rat hepatoma (HTC) cell lines. MRI of labeled cells were performed on a Bruker Avance 300 NMR spectrometer and on an Aspect M2™ MRI scanner, operating at 1 T, using a standard multislice multiecho sequences. Acute liver damage was induced by injecting 8-week-old male C57BL/6 mice with CCl4, (1 mL/kg) intraperitoneally. MR images were acquired using a T1-weighted, fat suppressed, multislice multiecho protocol. Representative liver blocks were removed for histological analysis and slices were examined either using a standard light microscope or a ZEISS ApoTome fluorescence microscope. It was estimated that each GP is loaded with ca. 1.6×107 Gd3+ ions, yielding a unprecedented relaxivity per particle of 3.5×108 s-1.mM-1. Cell based experiments, performed on J774A.1, B16-F10 and HTC cells demonstrated the high affinity of GPs towards macrophages, showing also a fast uptake of the paramagnetic particles with good temporal persistence of the contrast. Using a model of severe hepatocellular liver failure, a marked increase in liver signal was observed after the iv injection of macrophages labeled with GPs, thus indicating that the tracked macrophages successfully reached the inflamed site. This finding was validated with histological microscopy. In the control groups, no significantly increase in the MRI signal was detected. Moreover, GPs loaded with a phospholipid-based cyanine dye were also used for the optical visualization of the macrophages recruitment in a mouse model of collagen-induced rheumatoid arthrites. Furthermore, attempts to form liposomes in the particle core for entrapping small hydrophilic compounds (that could not be loaded in GPs) have been succesfully done, thereby open new possible application for this microcarrier.

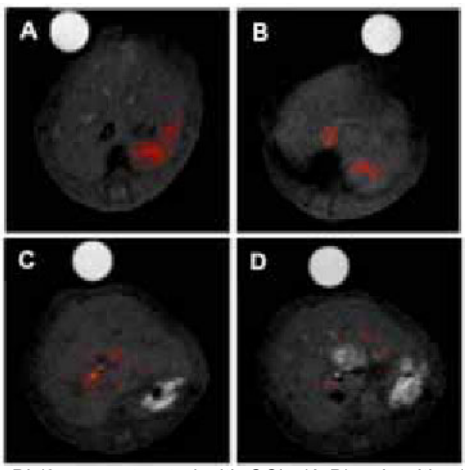


Fat-suppressed T1-weighted MR images of a C57BL/6 mouse treated with CCl4 (A-B) or healthy (C-D). Images were obtained after the injection of J774A.1 cells incubated with Gd-GPs. A and B post 5 h; C and D. Red colored spots correspond to statistically significant enhanced pixels.

Disclosure of author financial interest or relationships:
**F. Garello**, None; **S. Figueiredo**, None; **F. Arena**, None; **J.C. Cutrin**, None; **G. Esposito**, None; **L. D'Angeli**, None; **D. Delli Castelli**, None; **C.F. Geraldes**, None; **J. Moreira**, None; **S. Aime**, Bracco Imaging, Consultant; Bruker, Grant/research support; **E. Terreno**, Bracco Imaging, Consultant .

Presentation Number **P793**
Poster Session 4
September 8, 2012 / 14:45-14:45 / Room: The Liffey

# Biomodal Liposomes for Rapid Dual Labelling of SPECT and Fluorescence Imaging Tracers: A Potential Methodology for Cell Tracking

***Tammy L. Kalber***[1,2], *Nick Mitchell*[3], *Katherine Ordidge*[1,2], *Adam Badar*[1], *Samantha L. Chalker*[3], *Sam M. Janes*[2], *Mark Lythgoe*[1], *Helen C. Hailes*[3], *Alethea B. Tabor*[3], [1]*Centre for Advanced Biomedical Imaging, University College London, London, United Kingdom;* [2]*Centre for Respiratory Research, University College London, London, United Kingdom;* [3]*Department of Chemistry, University College London, London, United Kingdom. Contact e-mail: t.kalber@ucl.ac.uk*

Conventional labelling approaches for tracking cells with nuclear medicine have either use chelated Technetium-99m ($^{99m}$Tc) or Inium-111 ($^{111}$In), which transports the radiotracer across the cell membrane where it binds to internal cellular structures resulting in cell cytoxicity, cell lysis and ultimately leakage of the isotope[1]. To reduce cell cytoxicity the radiotracer needs to be distanced from the nucleus and not allowed to leak from the chelator. The aim of this study was to utilize bimodal liposomes carrying both the SPECT tracer $^{111}$In and the fluorophore FITC conjugated to the liposome bilayer, to rapidly dual label a wide variety of cells types. As the isotope is bound to the liposome this may reduce radiotoxicity while retaining cell functionality and reducing cell death. Liposomes were formulated with a high degree of short n-ethylene glycol (n-EG) lipid DODEG4 (50%), to provide liposome stability as well as enhance liposomal uptake with minimal effect on cell viability. To make the liposomes multifunctional for imaging, a DOTA lipid conjugate (30%) for the prospective incorporation of $^{111}$In, known as DEG3SL as well as a fluorescent FITC conjugated lipid (1%) were used. Liposomes (100µl - 0.5 mM in water) were added to 1x10$^6$ cells in 1 ml normal growth medium and incubated for 10 minutes prior to washing. A range of cell types were evaluated (MDA-MB-231 breast tumour, HeLa cervical tumour, and Mesenchymal stem cells [MSC]) and the cell uptake and distribution was assessed longitudinally by fluorescence microscopy and FACS analysis. All cell types labelled with liposomes had a high degree of labelling (>95%) and showed internalization of the FITC liposome by fluorescence microscopy as circular fluorescent deposits within the cell consistent with uptake into vesicles (Fig 1A). Longitudinal evaluation of cells labelled with liposomes showed that for tumour cells, the FITC fluorescence was distributed throughout the cytoplasm and was retained for up to 3 days. However, the MSC cells retained the label in discrete areas of the cell wall away from the main body of the cell and retained a high degree of labelling over a period of two weeks (>85% at 1 week and <25% at 2 weeks) (Fig1 B). All cells types showed no adverse affects on cell viability at any time point by trypan blue. Preliminary studies with $^{111}$In containing liposomes showed that the $^{111}$In was bound and not free and that the liposomes were stable in serum over 48 hours. Both MSC and tumour cells retained labelled radioactivity over 24 hours with no effect on cell viability. These preliminary results indicate that cells can be easily and rapidly labelled with liposomes containing a DOTA conjugated lipid for the labeling of the SPECT tracer $^{111}$In and the fluorophore FITC for *ex vivo* correlation. Liposomes do not appear to bind to internal cellular structures and are well tolerated for long periods of time in slow dividing cell types, such as stem cells, enabling their use as cell tracking agents. This method may offer an improved alternative labeling strategy to conventional methods. Refs: 1) McLean JR et al. Biochem Cell Biol. 1989:67:661.

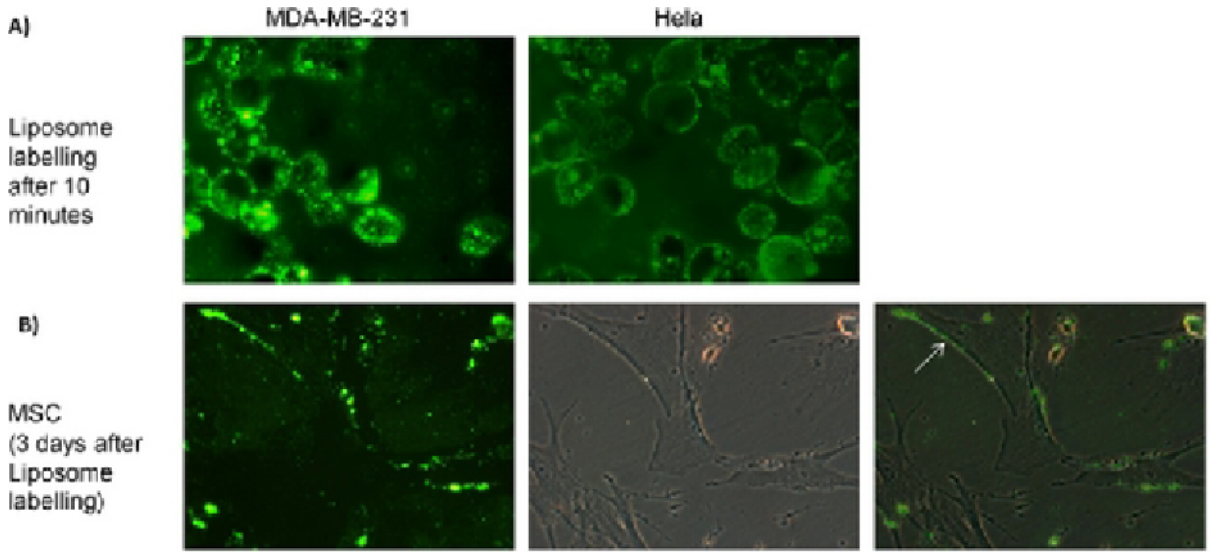


Figure 1: A) MDA-MB-231 and HeLa cells showing internalization of the FITC fluorphore on the bimodal liposome after 10 minutes. B) MSC cells showing retention of the FITC label in discrete areas of the cell wall (white arrow) 3 days after incubation with liposomes.

Disclosure of author financial interest or relationships:
**T.L. Kalber**, None; **N. Mitchell**, None; **K. Ordidge**, None; **A. Badar**, None; **S.L. Chalker**, None; **S.M. Janes**, None; **M. Lythgoe**, None; **H.C. Hailes**, None; **A.B. Tabor**, None.

Presentation Number **P794**
Poster Session 4
September 8, 2012 / 14:45-14:45 / Room: The Liffey

# Tumor Formation after ADSC implantation in arthritic joints

***Aman Khurana***[1], *Mohammad M. Moneeb*[1], *Hossein Nejadnik*[1], *Jason Erdmann*[2], *Charles D. Bangs*[2], *Heike E. Daldrup-Link*[1], [1]*Radiology, Stanford University, Stanford, CA, USA;* [2]*Cytogenetics, Stanford Hospital & Clinics, Palo Alto, CA, USA. Contact e-mail: amank@stanford.edu*

Purpose: While evaluating matrix-associated stem cell implants (MASI) in-vivo with magnetic resonance (MR) imaging, we noticed that some ADSC transplants undergo a neoplastic transformation and form locally destructive tumors. To address these issues of tumorigenicity, we performed an analysis of the imaging characteristics, macroscopic and histopathologic features and karyotypes of ADSC transplants that lead to tumor formation versus original, non-neoplastic ADSC. Materials and methods: Rat ADSCs were isolated from subcutaneous adipose tissue of male sprague dawley rats. Ten athymic rats received matrix-associated ADSC transplants into osteochondral defects of the bilateral distal femurs. All 20 knee joints with ADSC transplants underwent serial MR imaging at 0, 2, 4 & 6 weeks post MASI. Neoplastic ADCS were defined as transplants, that increased in size over time and caused local bone destruction. The size and growth rate of the ADSC transplants was measured and compared between neoplastic and non-neoplastic transplants with a t-test. In addition, all ADSC transplants underwent karyotyping and chromosomal analysis. All quantitative data were correlated with gross examination and histopathology. Results: After classifying the growths in respective groups, 6 MASI showed tumor formation with a mean growth rate of 0.0896 +/- 0.0716 cm2/week (range 0.0343-0.2137) and 14 MASI showed a mean growth rate of 0.0031 +/- 0.002 cm2/week (range 0.0004-0.0034). These data were significantly different ($p<0.05$). Gross examination showed invasive tumor growth of neoplastic MASI with local bone destruction. On histopathology, the tumors were highly cellular, with numerous mitoses, abundant vessels and areas of necrosis. The neoplastic cells were atypical in size, shape and nuclear: cytoplasm ratio compared to normal ADSCs. The neoplastic ADSC formations invaded and destructed adjacent anatomical structures, such as joint components and the femur. Chromosome analysis of these tumor-forming ADSC demonstrated a mixed population of male diploid (42,XY) and tetraploid (84,XXYY) cells without obvious structural rearrangement or genetic imbalance. These finding suggest that normal ADSC spontaneously transformed into tumorous ADSC, which are easily distinguishable by aberrant chromosomal numbers. Further experiments including FACS analysis are currently pursued to further characterize these aberrant cells. Conclusion: The therapeutic applications of stem cells show great promise. However, caution must be taken regarding the tumorigenic potential of ADSCs. A more comprehensive understanding of the biology of ADSC is needed to establish possible risk factors and safe criteria for clinical use.

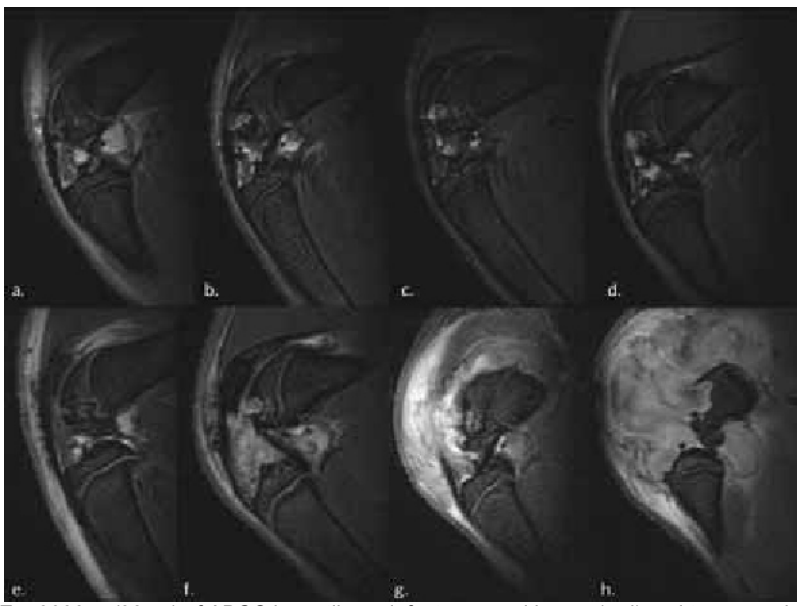


T2-weighted FSE images (TR/TE = 3000ms/30ms) of ADSC in cartilage defects: normal knees (a-d) and tumorous knees (e-h) at week 0, 2 , 4 and 6 showing significant growth at week 4 and week 6 in the tumorous knees.

Disclosure of author financial interest or relationships:
**A. Khurana**, None; **M.M. Moneeb**, None; **H. Nejadnik**, None; **J. Erdmann**, None; **C.D. Bangs**, None; **H.E. Daldrup-Link**, GE Global Research, Grant/research support .

Presentation Number **P795**
Poster Session 4
September 8, 2012 / 14:45-14:45 / Room: The Liffey

# Micro-CT Imaging of Human Mesenchymal Stem Cells Labeled with Gold Nanoparticles

***Taeho Kim***[1,2], *Dian R. Arifin*[1], *Taeghwan Hyeon*[2], *Jeff W. Bulte*[1], [1]*Russell H. Morgan Department of Radiology and Radiological Science; Cellular Imaging Section, Institute for Cell Engineering, The Johns Hopkins University School of Medicine, Baltimore, MD, USA;* [2]*School of Chemical and Biological Engineering, Seoul National University, Seoul, Republic of Korea. Contact e-mail: cephas@snu.ac.kr*

Introduction: A reliable means to image the distribution of engrafted stem cells is pertinent to monitor and support stem cell therapy. X-ray or computed tomography (CT) imaging is one of the most widely used tools in the clinic due to its cost effectiveness, high-contrast resolution, and facile imaging procedure. Gold nanoparticles (AuNPs) are bioinert and have a higher atomic number and X-ray absorption coefficient than iodinated compounds, a widely used CT contrast agent. In this study, we developed a method to label human mesenchymal stem cells (hMSCs) with AuNPs to facilitate the visualization of labeled cells with micro-CT imaging. Methods: AuNPs were synthesized by general reduction of $HAuCl_4$ by boiling with sodium citrate. To enhance AuNP uptake by cells, we mixed poly-L-Lysine (0.3 mg/mL) with AuNPs (1 mg/mL) to form AuNP-PLL complexes. Rhodamine B-isothiocyanate (RITC, 0.5 mg/mL) was added to the complexes to enable fluorescence microscopic imaging. HMSCs were incubated with AuNP-PLL(RITC) complexes (0.8 mg Au/mL) for 24 hours. Cellular uptake of the complexes was studied using bright field- and fluorescence microscopy. Cell viability was measured using an MTT assay. Labeled hMSCs suspended in 2% agarose ($10^6$ cells/tube) were imaged with a Gamma Medica X-SPECT Imager with tube settings of 75.16 KV and 240.3 μA, a 64-mm detector setting, and 512 projections. Results: AuNP-PLL(RITC) complexes had a zeta potential of +48.4mV and a diameter of 43.78±7.81 nm. A schematic illustration of the complexes is shown in Fig 1A. TEM images showed homogeneous AuNP-PLL(RITC) complexes without aggregation (Fig. 1B). HMSCs were successfully labeled by the complexes. Cell morphology was preserved after labeling (Fig. 1C, bottom) as compared to unlabeled cells (Fig. 1C, top). The complexes were found to accumulate in the perinuclear region in a similar fashion as that seen for SPIO particles (Fig. 1D, red: AuNP-PLL complexes, blue: DAPI-stained nuclei). The viability of labeled hMSCs 24 hours post-incubation was 92.3%, indicating that AuNP-PLL(RITC) labeling did not have a signficant adverse effect on the cells. Labeled cells appeared dark (Fig1E, right) while unlabeled cells are transparent (Fig 1E, left). Labeled hMSCs exhibited a higher CT-contrast (Fig. 1F, right) compared to unlabeled cells (Fig. 1F, left). The average CT contrast values of unlabeled and labeled cells were 58.1 and 176.4 (HU), respectively. Conclusions: To the best of our knowledge, this study represents one of the first attempts to develop CT cell tracking. Using AuNP-PLL(RITC) complexes, we have developed an efficient technique to label hMSCs. Follow-up studies are in progress to determine if the sensitivity of gold-labeling of hMSCs is sufficient to allow CT stem cell tracking in vivo.

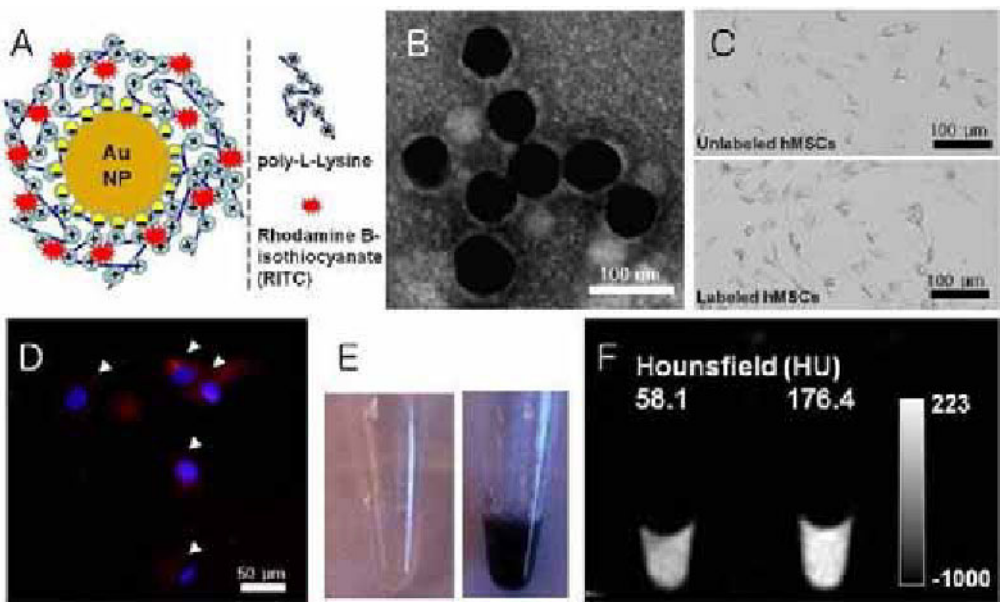


Figure 1. A) Schematic illustration of the AuNP-PLL(RITC) complex. B) TEM image of the complexes. C) Brightfield microscopy of unlabeled and labeled hMSCs. D) Fluorescence microscopy image of labeled hMSCs (red: AuNP-PLL(RITC) complexes indicated by arrow heads; blue: DAPI-stained nuclei). E) Photographs of hMSCs suspended in 2% agarose - unlabeled hMSCs (left) and labeled hMSCs (right). F) Micro-CT images of hMSCs suspended in 2% agarose - unlabeled hMSCs (left) and labeled hMSCs (right)

Disclosure of author financial interest or relationships:
**T. Kim**, None; **D.R. Arifin**, Maryland Stem Cell Research Fund Fellowship, Grant/research support; **T. Hyeon**, None; **J.W. Bulte**, Philips, Grant/research support; Q Therapeutics, Grant/research support .

Presentation Number **P796**
Poster Session 4
September 8, 2012 / 14:45-14:45 / Room: The Liffey

# Non-invasive multimodal / multi-scale imaging of bone marrow microenvironment and stem cells niches in health and disease

***Francois LASSAILLY***[1,2], *Katie Foster*[1], *Erin Currie*[1], *Dominique Bonnet*[1], [1]*Haematopoietic Stem Cell Laboratory, London Research Institute - Cancer Research UK, London, United Kingdom;* [2]*In Vivo Imaging Facility, London Research Institute - Cancer Research UK, London, United Kingdom. Contact e-mail: francois.lassailly@cancer.org.uk*

Introduction: Hematopoietic stem cells (HSCs) reside in specialized bone marrow (BM) environments called stem cell niches (HSCNs). Two types of HSCNs have been reported, involving osteoblasts (osteoblastic niche) or blood sinusoids (vascular niche). However the bone marrow microenvironment has not yet been precisely characterized and the fine localization, composition and regulation of the niches remain highly controversial. Leukemic stem cells (LSCs) originate from HSCs and are responsible for the development of acute myeloid leukaemia. Because they can resist to treatment, it is believed they cause relapse. It is not yet clear weather LSCs need a specialized niche to regulate their behavior. Methods: Intravital microscopy was used for multiparametric observation of live bone marrow within intact bones after in-vivo contrasting procedures. Bioluminescence imaging was used to quantify the systemic trafficking and proliferation of murine HSCs and human leukemia. Flow cytometry and histology were used to sort specific populations of cells, analyze the frequency of stem cells or leukemic cells, quantify perfusion efficiency and hypoxia and cross-validate in-vivo imaging procedures. Results: To quantify bone remodeling activity and vascular density within different bone marrow compartments, we developed a new strategy that we called "In-vivo fluorescence trapping", taking advantage of different near-infrared probes. We show an unexpectedly high level of vascularization of the BM, a strong heterogeneity between different BM compartments for blood vessels density and bone remodeling activity, which correlate with sites of development of normal HSCs as well as LSCs and bone metastasis from solid tumors. We found that osteoblastic niches are in close proximity to vascular niches. BM is very effectively perfused, even more than the spleen, but contains a small population of hypoxic cells which includes HSCs. Eventually we are exploiting these technologies to characterise the development of human leukaemia and its consequences on BM microenvironment using intravital microscopy of intact live BM. Conclusions: This study confirms and extends our recent statement considering the critical need for multimodal imaging (Lassailly F et al, Blood 2010). Further more, it demonstrates that combination of different imaging modalities for in-vivo and ex-vivo analysis is a powerful strategy which allows to shade a new light on the structure of the bone marrow microenvironment and further improve our understanding of stem cells / niches interactions in health and disease.

Disclosure of author financial interest or relationships:
**F. LASSAILLY**, None; **K. Foster**, None; **E. Currie**, None; **D. Bonnet**, None.

Presentation Number **P797**
Poster Session 4
September 8, 2012 / 14:45-14:45 / Room: The Liffey

# Multi-modal imaging of therapeutic HSVtk expressing stem cells for glioma treatment

***Cindy Leten***[1], *Jesse Trekker*[1], *Tom Struys*[1,2], *Michael Maris*[3], *Rik Gijsbers*[2], *Zeger Debyser*[3], *Uwe Himmelreich*[1], [1]*Biomedical NMR Unit, KULeuven, Leuven, Belgium;* [2]*Functional morphology, UHasselt, Hasselt, Belgium;* [3]*Laboratory of Molecular Virology and Gene therapy, KULeuven, Leuven, Belgium. Contact e-mail: cindy.leten@med.kuleuven.be*

Introduction: One of several therapeutic approaches under investigation for glioblastoma treatment, is the use of stem cells, which can track malignant cells, as cellular vehicles to deliver suicide genes, such as Herpes simplex virus - thymidin kinase (HSV-tk). When ganciclovir is administered, both stem and tumor cells are killed due to the formation of gap junctions between these cells, also known as the bystander killing effect (1). For in vivo visualisation and optimization of this treatment, multi-modal lentiviral vectors for assessing the bystander killing effect were developed in this study and assessed both in vitro and in vivo. Methods: Lentiviral vectors: All lentiviral vectors were generated by the Laboratory of Molecular Virology and Gene Therapy at KU Leuven. Due to size restrictions, 2 vectors were designed (pCH-EF1 α -eGFP-Ires-puro and pCH-EF1 α -3flag-fLuc-T2A-HSVTK-Ires-Bsd). Cells transduced with the pCH-EF1 α -3flag-fLuc-T2A-eGFP-Ires-Bsd vector were used as negative control. In vitro experiments: mouse mesenchymal stem cells (mMSC), Cl2slow and Clone 3 mouse multipotent adult progenitor cells (mMAPC's) were cultured as described previously (2). After transduction, Fluc expression was confirmed by bioluminescence imaging (BLI). Furthermore, the bystander killing effect was assessed by administration of ganciclovir with concentrations ranging from 102μM to 10-2 μM. Cells were also labelled with in house produced superparamagnetic iron oxide nanoparticles (SPIO's) (mMSC 20μg Fe/ml, Cl2slow 10μg Fe/ml) and the transfection agent poly-L-lysine (PLL 1.5 μg/ml) to assess potential labelling effects on the BLI signal. In vivo experiments: Transduced and labelled cells were injected into the right striatum of C57Bl6/J mice and evaluated by magnetic resonance imaging (MRI) and BLI. Furthermore, 500,000 mass forming eGFP-Fluc-HSVtk positive clone 3 cells were followed up by MRI and BLI before and after ganciclovir administration to assess ganciclovir killing in vivo. Masses were allowed to grow for 2 weeks before ganciclovir treatment (10mg/kg for 10 days) was initiated. Results: BLI and the ganciclovir killing experiment confirmed transgene expression at sufficient levels for in vitro detection. Phantoms of SPIO labelled stem cells confirmed iron uptake for stem cell tracking. Furthermore, 300,000 transduced and labelled mMSC's and MAPC's were detected and followed up for at least 2 weeks by MRI and BLI. Mass forming mMAPC's Clone 3 could also be detected as early as day 1 after implantation and ganciclovir killing was assessed by studying both the BLI signal and the mass volume measured by MRI before and after ganciclovir administration. Conclusion: Both in vitro and in vivo data confirmed sufficient transgene expression for in vivo follow up of stem cells used as cellular vehicle for a bystander killing mediated therapy. References: 1. Miletic, H., et al., Mol Ther, 2007. 15(7): p. 1373-81. 2. Ulloa-Montoya, F., et al., Genome Biol., 2007. 8(8): R163.

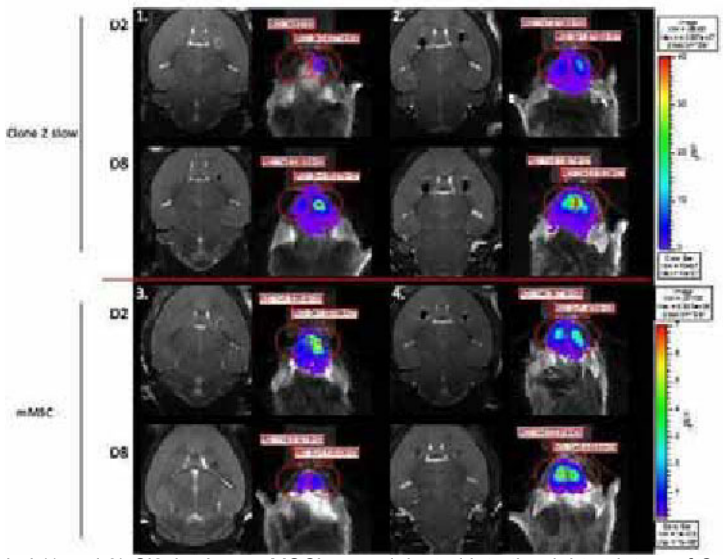


500,000 labeled (2 and 4) or unlabeled (1 and 3) Cl2slow's or mMSC's were injected into the right striatum of C57Bl6/J mice and MRI and BLI scans were performed on day 2 and day 8 after injection. Cells could easily be detected with both imaging modalities. Mouse 1 and 3 received PBS and unlabeled cells in the right and left hemisphere respectively whereas mouse 2 and 4 received 5% labeled cells on both sides.

Disclosure of author financial interest or relationships:
**C. Leten**, None; **J. Trekker**, None; **T. Struys**, None; **M. Maris**, None; **R. Gijsbers**, None; **Z. Debyser**, None; **U. Himmelreich**, None.

Presentation Number **P798**
Poster Session 4
September 8, 2012 / 14:45-14:45 / Room: The Liffey

# Impact of magnetic nanoparticle aggregation on MRI cell signal and stem cell differentiation

*Delphine Fayol[1,2], **Nathalie Luciani**[1,2], Lenaic Lartigue[1,2], Florence Gazeau[1,2], Claire Wilhelm[1,2], [1]Université Paris-Diderot-Paris 7, , Paris, France; [2]CNRS UMR 7057, Laboratoire Matière et Systèmes Complexes, Paris, France. Contact e-mail: nathalie.luciani@univ-paris-diderot.fr*

Magnetic nanoparticles have exciting potential uses in cell imaging and cell therapies. The nanoscopic size of these materials enables them to enter the cells and to give them unique properties. But magnetic nanoparticle aggregation could introduce bias in MRI signal. Moreover the impact of magnetic labeling on stem cell differentiation is controversial and nanoparticle aggregation might be a potential toxic factor. In order to evaluate the effect of magnetic nanoparticle aggregation, we have quantified the cellular uptake of magnetic nanoparticles, their aggregation status as well as their influence on stem cell differentiation. Stem cells were magnetized by using maghemite nanoparticles (8nm) stabilized with a negatively charged agent (citrate). The aggregation status of these anionic magnetic nanoparticles (AMNP) can be tightly modulated by controlling the presence or absence of free citrate in the solution. The cells were then imaged by microscopy, histology and MRI, and the impact of the different labeling conditions on osteogenesis, adipogenesis and chondrogenesis was evaluated. The nanoparticles were perfectly stable in citrated medium, even after application of an external magnetic field, but aggregated in citrate-free medium. These observations were confirmed at the nanoscale by means of electron microscopy (Fig. 1): no free nanoparticles were observed out of the membrane of the cells in citrated medium after 30 min (A) or 4h (B) of incubation, while many nanoparticles remained on the cell surface in citrate-free medium after 4h of incubation without (C) or with magnet (D), and formed aggregates or rods respectively. High resolution 4.7T MRI was used to image the labeled cells. Signal and resolution were enough to detect cells loaded with 2pg per cell in non aggregating conditions. By contrast, the presence of nanoparticle aggregates totally impeded the detection of individual cells. The capacity of MSC to differentiate into adipocytes (adipogenesis), osteocytes (osteogenesis) and chondrocytes (chondrogenesis) was examined on cells with stable nanoparticles conditions, and then on cells in which nanoparticles aggregates were attached around the cell membrane. For the stable conditions, differentiation was unaffected by internalization of nanoparticles except for chondrogenesis which was inhibited by large amount of intracellular iron.

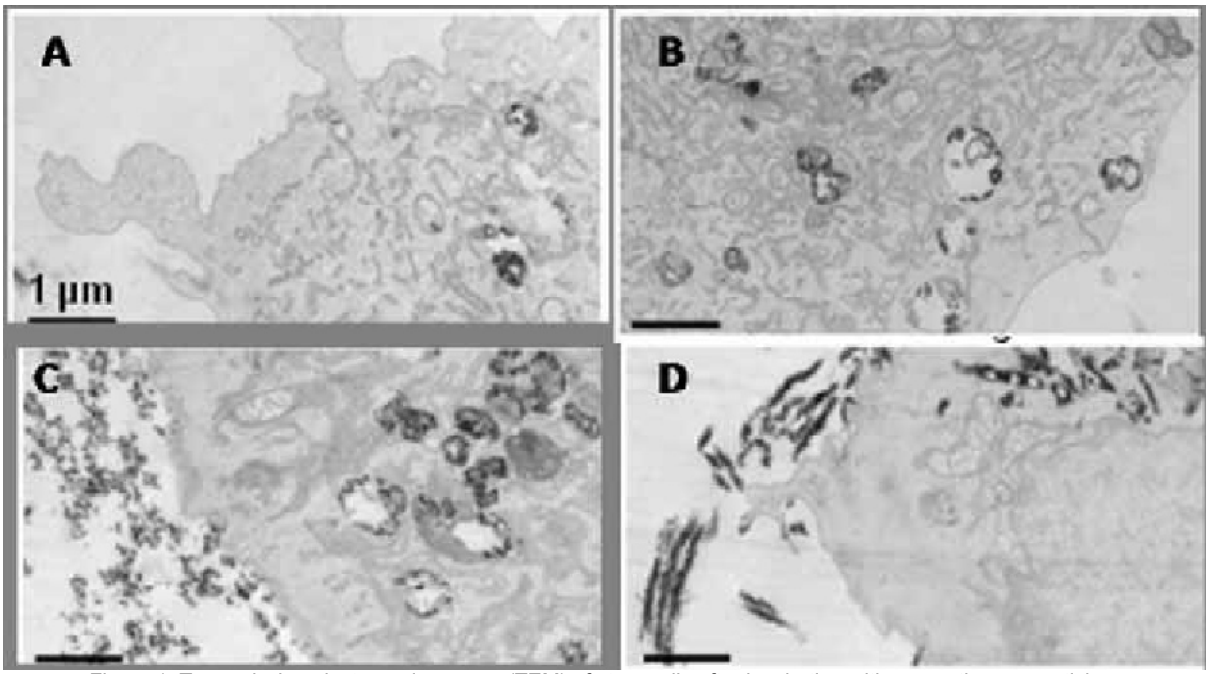

Figure 1: Transmission electron microscopy (TEM) of stem cells after incubation with magnetic nanoparticles.

Disclosure of author financial interest or relationships:
**D. Fayol**, None; **N. Luciani**, None; **L. Lartigue**, None; **F. Gazeau**, None; **C. Wilhelm**, None.

Presentation Number **P799**
Poster Session 4
September 8, 2012 / 14:45-14:45 / Room: The Liffey

# A Tri-functional Probe for Cell Labelling and SPECT Tracking

***Katherine Ordidge***[1], *Ran Yan*[3], *Maryam Ahmadi*[2], *Tammy L. Kalber*[1], *Emma Morris*[2], *Mark Lythgoe*[1], *Sam M. Janes*[4], *Adam Badar*[1], *Erik Arstad*[3], [1]*Centre for Advanced Biomedical Imaging, University College London, London, United Kingdom;* [2]*Immunology, University College London, London, United Kingdom;* [3]*Radiochemistry, University College London, London, United Kingdom;* [4]*Centre for Respiratory Research, University College London, London, United Kingdom. Contact e-mail: katherine.ordidge.09@ucl.ac.uk*

**Introduction**: An important unanswered question in cell therapy is the location and persistence of transferred cells *in vivo*. Conventional cell tracking with Nuclear Medicine relies on the use of chelated In-111 or Tc-99m, which bind to intracellular proteins, thus administering a high dose to the nucleus, with associated cytotoxicity. In an attempt to reduce such ionizing damage we have explored distancing the radioactive probe from the cell nucleus by directing its conjugation to the outer membrane surface. Recently, there has been interest in using cell surface thiol groups to label cells with Gadolinium complexes for MRI tracking.[1] We believe the higher sensitivity of SPECT over MRI would be better suited for such methodology. Accordingly, we have developed an $I^{125}$-labelled maleimide reagent bearing a dansyl-derived fluorescent group. The 60-day half-life of $I^{125}$ can potentially allow tracking of cells over a prolonged period of time, and the inclusion of a fluorescent reporter offers the potential to study cell viability *in vitro* using optical imaging techniques. **Methods**: The labelling reagent was prepared by treating an azide modified dansyl dye, N-propargylmaleimide and [$I^{125}$]NaI in the presence of $CuCl_2$ at 60°C for 90 min.[2] For flow cytometry and confocal microscopy, human T cells were washed in PBS, suspended at $1x10^6$ cells in 1ml PBS, then labelled with 10μM non-radioactive dansyl maleimide for 30mins at 37°C, counterstained with apoptosis and death markers, and washed twice before use. For $I^{125}$ dansyl maleimide labelling, T cells were washed twice in PBS, suspended at $1x10^6$ in 1ml PBS, then 1.2nM probe was added onto the cells. The cells were incubated at 37°C for 30mins, and then washed twice in PBS. For imaging, $1x10^6$ cells in PBS were spun down into a pellet in a microcentrifuge tube, and imaged using a NanoSPECT/CT system (Mediso, Budapest, Hungary). **Results & Discussion**: The $I^{125}$-labelled reagent was obtained in 81±4% radiochemical yield and with a specific activity of 2.57GBq/μmol after purification by HPLC. 10μM of the non-radioactive reagent can efficiently and quickly label 80% of T cells with little effect on cell viability (Fig. 1). Incorporation of the radioactive trifunctional probe was 25% of added activity at 10nM probe concentration. Labelled cells can be visualised with confocal microscopy at UV excitation. Conveniently, the dansyl reporter also allows quick *in vitro* assessment of label binding and toxicity. Moreover, cells could potentially be visualised *ex vivo* after injection, allowing histological assessment of cell location and numbers. The $I^{125}$ reporter can be used for SPECT/CT imaging of labelled cells. **Conclusion**: This probe warrants further *in vivo* investigation as a promising alternative to conventional cell labelling methods. *1. G Digilio et al. Exofacial protein thiols as a route for the internalization of Gd(III)-based complexes for magnetic resonance imaging cell labeling. J. Med. Chem. 2010;53(13):4877-90. 2. R Yan et al. One-pot synthesis of an 125I-labeled trifunctional reagent for multiscale imaging with optical and nuclear techniques. Angew. Chem. Int. Ed 2011;50:1-4.*

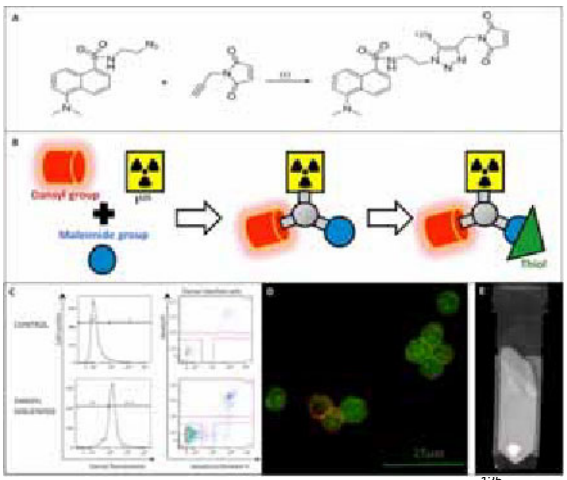


Figure 1: (A) Reaction scheme of the azide modified dansyl dye, N-propargylmaleimide, and [$I^{125}$]NaI in the presence of $CuCl^2$ to make [$I^{125}$] dansyl maleimide. (B) Schematic diagram of the trifunctional probe. (C) Flow cytometry results showing control and dansyl maleimide fluorescent T cells. Dansyl positive cells only are shown in the right column, and of these, cell apoptosis and death staining shows 85.8% live cells. (D) Confocal microscopy images of dansyl maleimide labelled T cells (green) with Annexin V staining for apoptosis (red). (E) SPECT/CT image of $1x10^6$ T cells labelled with $I^{125}$ dansyl maleimide.

Disclosure of author financial interest or relationships:
**K. Ordidge**, None; **R. Yan**, None; **M. Ahmadi**, None; **T.L. Kalber**, None; **E. Morris**, None; **M. Lythgoe**, None; **S.M. Janes**, None; **A. Badar**, None; **E. Arstad**, None.

Presentation Number **P800**
Poster Session 4
September 8, 2012 / 14:45-14:45 / Room: The Liffey

# Advanced 2D and 3D electron microscopy of MRI contrast particles in their native state and after *in vivo* cellular uptake

***Dimitri Roose***[1,2], *Frédéric Leroux*[2], *Bart Goris*[2], *Nathalie De Vocht*[1,3], *Peter Ponsaerts*[3], *Annemie van der Linden*[1], *Sara Bals*[2], [1]*Bio-Imaging Lab, University of Antwerp, Antwerp, Belgium;* [2]*EMAT, University of Antwerp, Antwerp, Belgium;* [3]*Laboratory of Experimental Hematology, University of Antwerp, Antwerp, Belgium. Contact e-mail: dimitri.roose@ua.ac.be*

Micron-sized iron oxide particles (MPIO) from Bangs Laboratories (Fischers, IN, USA) consist of iron oxide cores ($Fe_3O_4$) together with fluorescent molecules embedded in a polystyrene matrix. They are able to generate single particle contrast in MRI and are therefore often used as a marker for stem cell tracking [1]. For applications such as *in situ* endogenous stem cell labeling of the subventricular zone, the MPIO's have been followed for periods up to a year. Often the impact of the particle uptake on the cell is studied, but of equal importance is the impact of the cell on the particle itself. We studied the MPIO's in their native state as well as after their engulfment by endogenous stem cells [2]. Using a combination of advanced electron microscopy techniques, namely high angle annular dark field-scanning transmission electron microscopy (HAADF-STEM), energy-dispersive x-ray analysis (EDX) and electron tomography we obtained detailed information on the structure and the composition of the particles as well as on the cell ultrastructure. Using HAADF-STEM, we are able to distinguish the polystyrene matrix from the iron oxide cores. The diameter of the MPIO's is far from uniform and the organization of the iron oxide cores inside the polystyrene matrix also shows great variation. Some MPIO's consist of a large iron oxide core, whereas others have multiple cores arranged in a complex organization. Beside the iron oxide cores, some smaller particles in the range of 15nm, indicated by white arrows in figure E, are observed in the polystyrene matrix both in the native state and after the engulfment. For each particle, EDX-spectra were acquired to study the distribution of the different elements in the MPIO. The spectra yield three different elements namely carbon, oxygen and iron. When combining the individual elemental maps in a color-coded image, it is clear that carbon coincides with the polystyrene matrix, whereas iron and oxygen originate from the larger iron oxide cores. Based on the EDX measurements, we can conclude that the smaller particles observed in the polystyrene matrix also contain iron and oxygen. One should never forget that the images obtained by electron microscopy are 2D projections of a 3D object. Therefore, electron tomography, based on the acquisition of a tilt series of 2D projection images, was used to study the particles in 3D. The organization of the iron oxide cores and the smaller particles inside the polystyrene matrix can be characterized in this manner. Preliminary results indicate that some of the iron oxide cores are not surrounded by a polystyrene matrix (white arrow figure F). This methodology can be considered as a proof of principle and is applicable to study possible effects of cellular uptake on particles in general. *1. Shapiro, E.M., et al., Proc Natl Acad Sci USA, 2004 2. Vreys, R., et al., Neuroimage, 2010*

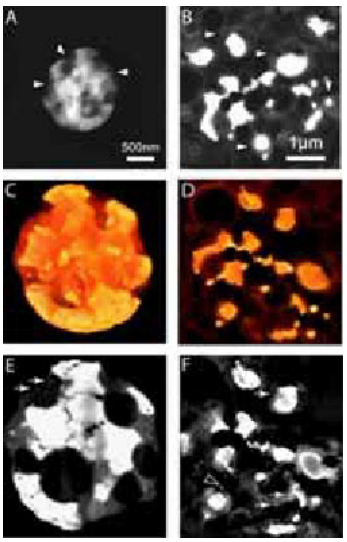


Electron microscopic images of an MPIO in its native state (**left column**) and one after engulfment by a cell (**right column**). In the HAADF-STEM images, the polystyrene matrix (arrowheads) can be distinguished from the iron oxide cores in native state (**A**) as well as after engulfment by a cell (**B**). Also the cell ultrastructure is clearly distinguished. Volume rendering of the 3D reconstruction after electron tomography of an MPIO in native state (**C**) and after cellular uptake (**D**). A slice *through* the 3D reconstruction of an MPIO in its native state shows smaller particles in the range of 15nm (**E**, white arrows). This can also be observed in the MPIO after engulfment (**F**, white arrows). There are indications that some iron oxide cores are not surrounded by a polystyrene matrix after cellular uptake (open arrowhead).

Disclosure of author financial interest or relationships:
**D. Roose**, None; **F. Leroux**, None; **B. Goris**, None; **N. De Vocht**, None; **P. Ponsaerts**, None; **A. van der Linden**, None; **S. Bals**, None.

Presentation Number **P801**
Poster Session 4
September 8, 2012 / 14:45-14:45 / Room: The Liffey

# Assessment of antigen delivery directly into cytosol of dendritic cells by the combination of liposomal bubbles and ultrasound

***Ryo Suzuki****, Yusuke Oda, Daiki Omata, Yoshikazu Sawaguchi, Tomoyuki Naoi, Kazuo Maruyama, Drug Delivery System, School of Pharma-Science, Teikyo University, Tokyo, Japan. Contact e-mail: r-suzuki@pharm.teikyo-u.ac.jp*

[Objective] In cancer immunotherapy with dendritic cells (DCs), which are the most potent antigen-presenting cells, it is important that DCs present peptides derived from tumor-associated antigens on MHC class I molecules and activate tumor-specific cytotoxic T lymphocytes (CTLs). However, MHC class I molecules generally present endogenous antigens expressing in cytosol. Development of an excellent antigen delivery system capable of inducing efficient presentation of exogenous antigens via MHC class I in DCs is required for the establishment of effective cancer immunotherapy with DCs. Recently, we developed the novel liposomal bubbles (Bubble liposomes (BLs)) entrapping perfluoropropane gas which is utilized for contrast enhancement in ultrasonography. In addition, we reported that BLs were promising as effective gene delivery tools by the combination with ultrasound (US) exposure in vitro and in vivo. In the gene delivery mechanism, the mechanical effect based on the disruption of BLs by US exposure, which results in generation of some pores on plasma membrane, might be associated with direct delivery of extracellular plasmids into cytosol. Therefore, we thought that the combination of BLs and US exposure would directly deliver exogenous antigens into cytosol of DCs. In this study, we assessed about the delivery efficiency of exogenous antigens for DCs using our method. In addition, we also examined about priming of antitumor immunity. [Material & Methods] In vitro study: Mouse bone marrow-derived DCs which were treated with sodium azide to inhibit endocytosis, were exposed with US (2 MHz, 2 W/cm$^2$, 10 sec. × 3 times) in presence of BLs and Alexa flour 488 labeled ovalbumin (OVA) as model antigen. The delivery efficiency was assessed with flowcytometory and confocal laser microscope. Ex vivo study: The mice were intradermally immunized the DC delivered OVA with BL + US twice with 1 week interval. After 1 week of final immunization, these mice were intradermally inoculated E.G7-OVA cells for the solid tumor model. Antitumor effect was assessed by measuring tumor volume. [Results & Discussion] The combination method of BL and US could effectively delivered Alexa flour 488 labeled OVA into cytosol of DCs without endocytosis pathway. In addition, immunization with DC that had been delivered with OVA using BLs and US completely suppressed tumor growth. These results suggested that the combination of BLs and US would be a promising antigen delivery system into DCs in cancer immunotherapy.

Disclosure of author financial interest or relationships:
**R. Suzuki**, None; **Y. Oda**, None; **D. Omata**, None; **Y. Sawaguchi**, None; **T. Naoi**, None; **K. Maruyama**, None.

Presentation Number **P802**
Poster Session 4
September 8, 2012 / 14:45-14:45 / Room: The Liffey

# Fluorescent Live Cell Imaging Dyes Visualize Human ES Cell Differentiation to Lineages of Respiratory Airways

***Jung Sun Yoo***[1], *Zhi Yen Jow*[2], *Young-Tae Chang*[1,2], [1]*Department of Chemistry, National University of Singapore, Singapore, Singapore;* [2]*Singapore Bioimaging Consortium, Agency for Science, Technology and Research (A*STAR), Singapore, Singapore. Contact e-mail: earedpotato@gmail.com*

Embryonic stem cells (ESC) have a virtually endless replicative capacity and the potential to differentiate in vivo into essentially all cell types. While there have been major advances in ESC differentiation study, differentiation into specific lineage for therapy has been facing two major challenges, i.e. the heterogeneity of differentiated cells and low yield of desired lineages. One typical example is the derivation of cells of the respiratory airways. Although differentiation of ES cells to the cells that are responsible for gaseous exchange in the lung, i.e. alveolar epithelial cells has great potential for regenerative cell therapies of demaged lungs, the current protocol allows only 20% of efficiency to obtain pure alveolar epithelial cells due to the lack of knowledge for differentiation mechanism. To better understand ESC differentiation biology and purify differentiated cells destined for in vivo transplantation, development of specific live imaging and tracking probes for human ESC and its derivatives to lineages of respiratory airways has particular benefit. We developed a series of live cell imaging fluorochromes capable labelling cells at specific and different stages of human ESC differentiation towards endoderm and alveolar cells by virtue of diversity-oriented synthesis. Specifically, we screened 726 fluorescent small molecules synthesized with 4,4-difluoro-4-bora-3a,4a-diaza-s-indacene (BODIPY) scaffold against hESC and its derivatives to lineages of respiratory airways using high-throughput automated imager and discovered three different fluorochromes with high specificity for hESC, definitive endoderm and alveolar cell. Hits were then tested with partially differentiated cells to discriminate undifferentiated ESCs, definitive endoderm and pure alveolar cells individually among heterogeneous populations. By implementing single-cell PCR gene-expression analysis, we could identify characteristic of each stained cell to verify the functionality of our probes as exclusive unique markers. The developed fluorescent probes could facilitate development of safe regenerative medicine using hESC derivatives by providing exciting new tool to monitor hESC differentiation under cell culture condition as well as in vivo whole body environment.

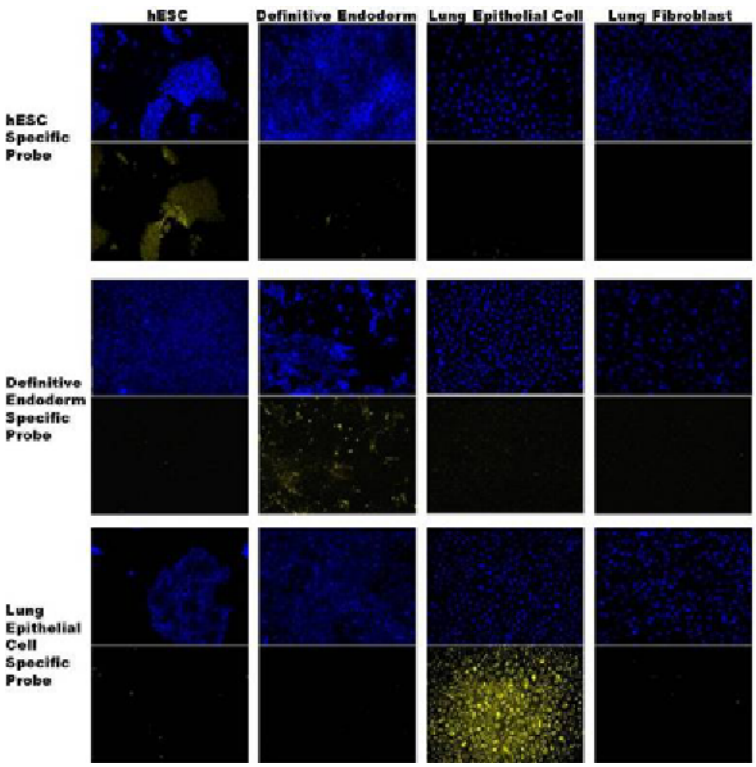


Disclosure of author financial interest or relationships:
**J. Yoo**, None; **Z. Jow**, None; **Y. Chang**, None.

Presentation Number **P803**
Poster Session 4
September 8, 2012 / 14:45-14:45 / Room: The Liffey

# Lentiviral vector-evoked glial cell responses are a major limitation for in vivo cell labeling in canary brain, but not in mouse brain

*Irene Bergwerf[1], **Caroline Guglielmetti**[1,2], Jelle Praet[1,2], Peter Ponsaerts[2], Annemie van der Linden[1], [1]Department of Biomedical Sciences University of Antwerp, Bio Imaging Lab, Wilrijk, Belgium; [2]Department of Biomedical Sciences University of Antwerp, Laboratory of Experimental Hematology, Vaccine and Infectious Disease Institute (Vaxinfectio), Wilrijk, Belgium. Contact e-mail: caroline.guglielmetti@ua.ac.be*

Purpose: Although adult neurogenesis can be visualized by means of real time bioluminescence imaging (BLI) in the adult rodent brain following in vivo lentiviral vector (LVv)-mediated labeling of subventricular zone neural stem cells, the application of this technique has not yet been fully explored in non-mammalian brain. Due to the high seasonal plasticity in the songbird brain, e.g. canaries, unraveling the organization of neuronal migration routes can further contribute to a better understanding of cellular and molecular mechanisms involved in tissue homeostasis, repair and even more importantly learning processes. In this study, we evaluated the applicability of an established BLI technique to monitoring rodent neurogenesis for use in the adult canary brain. Procedures: In vivo cell labeling in both FVB mouse and canary brain was performed following intracerebral injection of a LVv encoding both the luciferase and eGFP reporter proteins. In vivo transduction efficiency was monitored real time by BLI (luciferase reporter protein) and post-mortem histological analysis (eGFP reporter protein). As control, both mouse and canary brains were injected with the same volume of PBS. Endogenous glial cell responses following PBS or LVv injection were histologically evaluated following staining for: (i) the astrocyte-specific cell markers Sox2 and GFAP in both mouse and canary brain, and (ii) the microglia-specific cell marker in mouse brain. Additionally, the effect PBS or LVv injection on neuronal cell organization was evaluated both in mouse and canary brain following staining for the neuron-specific cell marker NeuN. All analyses were performed both at week 1 and at week 2 post-injection. Results: First, in vivo BLI suggested a significantly lower LVv transduction efficiency in canary brain as compared to mouse brain. Next, post-mortem histological analysis confirmed these results, as a significantly lower amount of eGFP-expressing cells could be observed in canary brain as compared to mouse brain. Furthermore, (i) significant astroglial responses could be detected in both mouse and canary brain, (ii) significant microglial responses could be detected in mouse brain (not in canary brain due to incompatibility of the used antibody), and (iii) significant neuronal disorganization could be detected in both mouse and canary brain. All observed responses were similar between week 1 and week 2 post-injection. In contrast, no (or limited) astroglial and microglial responses, nor neuronal disorganization, could be detected following PBS injections in both mouse and canary brain. Conclusions: In this study we characterized the occurrence of glial cell responses in both mouse and canary brain following LVv injections for in vivo cell marking experiments. Although these responses do not limit LVv-mediated cell labeling in mouse brain, cell labeling in canary brain appears to be refractory for LVv-transduction due to strong glial cell responses. Acknowledgements: This work was supported in part by 7th FW INMiND GA N°278850.

Disclosure of author financial interest or relationships:
**I. Bergwerf**, None; **C. Guglielmetti**, None; **J. Praet**, None; **P. Ponsaerts**, None; **A. van der Linden**, None.

Presentation Number **P804**
Poster Session 4
September 8, 2012 / 14:45-14:45 / Room: The Liffey

# Towards imaging inflammation with ultrasound based molecular imaging

***Emmi Olson**, Zhe Wu, Wei Gao, Mohammad Eghtedari, Joseph Wang, Robert F. Mattrey, UCSD, La Jolla, CA, USA. Contact e-mail: meep555@gmail.com*

We present a novel ultrasound (US) molecular imaging approach that aims to produce microbubbles (MB) in situ in tissues with elevated hydrogen peroxide (H2O2) levels such as infection, tumor, or possibly inflammation. These US agents catalyze H2O2, one of the common reactive oxygen (O2) species in vivo, into water and O2 MBs to act as US contrast agents. Since H2O2 is produced in 60-100 μM quantities by activated neutrophils in inflammatory tissues, our first in vivo application will be to detect infections. Micromotors (2x10 μm cones) have been designed to move through fluids by catalyzing H2O2 to produce and release O2 MBs as propellants; the higher the H2O2 concentration the more O2 MBs are produced and the greater the velocity. Minimal detectable motion required ≥65mM of H2O2, ~1000x the expected in vivo concentration. Here, we have coated the inner surface of the motor with catalase to increase the detection limit. 250-2500 micromotors were placed in a transfer pipette along with either PBS with 0.04M sodium cholate hydrate or plasma and imaged with B-mode and contrast specific modes. H2O2 was added incrementally in small quantities to each suspension to determine the minimum H2O2 concentration that produces US detectable MBs. Generated O2 MBs were visible with both US imaging techniques. The minimum H2O2 concentration needed for US detection with the standard micromotors was 2,500 μM and with the catalase-coated micromotors 100 μM. In addition, we were able to detect H2O2 produced by neutrophils during the respiratory burst induced by phorbol myristate acetate. Future experiments will continue to build upon the current design to further decrease the H2O2 detection limit, improve the biocompatibility of the motors as well as utilizing them to detect inflammation in in vivo models.

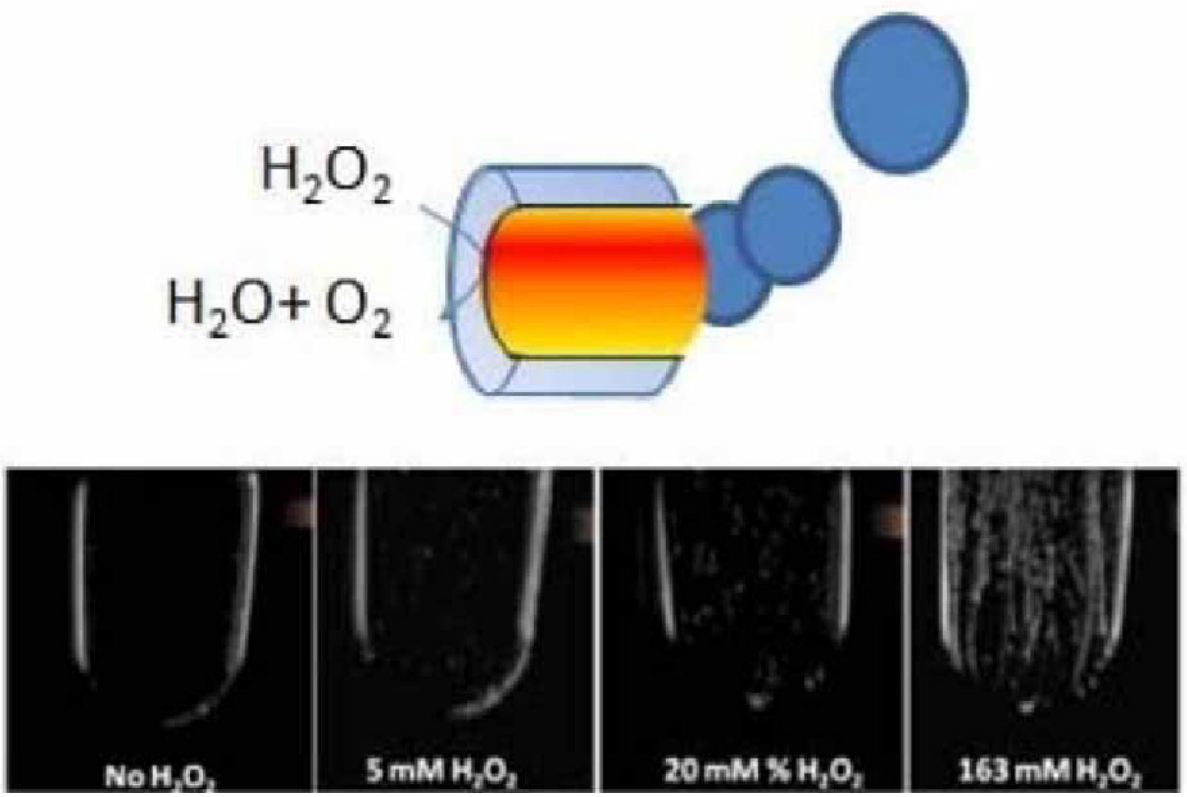


Disclosure of author financial interest or relationships:
**E. Olson**, None; **Z. Wu**, None; **W. Gao**, None; **M. Eghtedari**, None; **J. Wang**, None; **R.F. Mattrey**, None.

Presentation Number **P805**
Poster Session 4
September 8, 2012 / 14:45-14:45 / Room: The Liffey

# Interaction of iron-oxide labeled multipotent mesenchymal stromal cells and E-/P-selectins in mice monitored by Magnetic Resonance Imaging after cell administration via different routes

***Johannes M. Salamon***[1]*, Daniel Wicklein*[2]*, Claudia Lange*[3]*, Harald Ittrich*[1]*, Udo Schumacher*[2]*, Gerhard Adam*[1]*, Kersten Peldschus*[1]*,*
*[1]Department of Diagnostic and Interventional Radiology, University Medical Center Hamburg-Eppendorf, Hamburg, Germany; [2]Institute of Anatomy and Experimental Morphology, University Medical Center Hamburg-Eppendorf, Hamburg, Germany; [3]Department of Cell and Gene Therapy, University Medical Center Hamburg-Eppendorf, Hamburg, Germany. Contact e-mail: j.salamon@uke.de*

The aim of this study was to analyze the influence of E- and P-selectins on the migratory pattern of iron-oxide labeled multipotent mesenchymal stromal cells (MSC) in E-/P-selectin deficient and wildtype mice after intracardiac, intravenous and intraperitoneal administration. Murine MSC were labeled with fluorescent iron-oxide micro-particles and carboxyfluoresceinsuccinidylester (CFSE). Expression of selectin-binding sites CD15s and CD162 as well as MSC markers CD44, CD90, CD105, Sca-1 and lack of CD34 and CD45 were assessed using flow cytometry and immunocytochemistry. Labeled MSC were injected into E-/P-selectin deficient and wildtype mice applying doses of 5 × 104 cells intracardially, 1 × 10^6 cells intravenously and 5 × 10^6 cells intraperitoneally. After cell administration mice underwent magnetic resonance imaging repeatedly within 7 days using a clinical 3.0T magnet with a dedicated small animal solenoid coil and high-resolution T2* weighted 3D and 2D coherent gradient-echo (GRE) sequences. Histological evaluation using fluorescence microscopy followed 7 days after cell administration. Labeled and unlabeled MSC revealed similar expression of above mentioned surface markers as well as binding abilities to E-/P-selectins. After intracardiac injection multiple susceptibility artefacts due to initial trapping of MSC in capillaries could be detected in the brain until day 4 in E-/P-selectin deficient mice and up to day 7 in wildtype mice. After intravenous injection of MSC in E-/P-selectin deficient mice a significant SNR decrease was assessed solely in the liver from day 0 to day 1, whereas wildtype mice revealed an increasing SNR decrease of liver, spleen and bone marrow within 7 days. After intraperitoneal injection of MSC in E-/P-selectin deficient mice no significant SNR changes were observed in investigated organs, whereas wildtype mice showed an increasing SNR decrease of liver, spleen and bone marrow within 7 days. Fluorescence microscopy confirmed presence of labeled MSC in organs with SNR decrease. In conclusion, the study could demonstrate that MSC retain their binding ability to E-/P-selectins after iron-oxide labeling and that E-/P-selectin deficiency in mice significantly alters the distribution of iron-oxide labeled MSC after intracardiac, intravenous and intraperitoneal administration.

Disclosure of author financial interest or relationships:
**J.M. Salamon**, None; **D. Wicklein**, None; **C. Lange**, None; **H. Ittrich**, None; **U. Schumacher**, None; **G. Adam**, None; **K. Peldschus**, None.

Presentation Number **P806**
Poster Session 4
September 8, 2012 / 14:45-14:45 / Room: The Liffey

# Non-emulsion clinical gadolinium/perfluorocarbon nanoparticles for 19F MRI

***I.Jolanda.M. de Vries***[1], *Mangala Srinivas*[1], *Arend Heerschap*[2], *Carl G. Figdor*[1], [1]*Tumor Immunology, NCMLS, Radboud University Nijmegen Medical Centre, Nijmegen, Netherlands;* [2]*Radiology, Radboud University Nijmegen Medical Centre, Nijmegen, Netherlands. Contact e-mail: j.devries@ncmls.ru.nl*

Introduction 19F MRI for quantitative cell tracking may become a key tool for optimizing cellular therapies. We have previously developed polymer-encapsulated perfluorocarbon (PFC) nanoparticles as customizable labels that are clinically applicable. However, insufficient signal-to-noise within a reasonable imaging time is often a problem with 19F MRI. Here, we use a commercial MRI contrast agent, i.e. a gadolinium chelate, to enhance the 19F signal. The co-encapsulation of the hydrophobic perfluorocarbon and the hydrophilic Gd chelate forces close interactions between these nonmiscible compounds (A), and thus effectively changes the 19F longitudinal relaxation time. We label dendritic cells (DCs), as used in clinical trials, with these particles and show the effective 19F signal enhancement obtained. Methods Nanoparticles were synthesized as before, with the addition of Gd at the amounts stated in the figures (mg of Gd chelate per batch of particles). MRI was done on a horizontal bore 7T animal scanner using a 1H/19F transmit and receive volume coil. Particle stability was measured using dynamic light scattering and 19F NMR. A gradient echo sequence was employed to obtain T1 values using standard techniques. Primary human DCs were cultured, as per standard protocols for DC vaccination trials. Results and Discussion The nanoparticles have a stable diameter and 19F content, for at least 6 months after formulation (B; this data is for the highest concentration of Gd added). Incorporation of Gd itself had no effect on 19F encapsulation, which remained at 10e19 fluorines per mg of particles, with no significant difference between batches. There was also no effect on particle diameter, which remained at an average of just under 200nm. A representative diameter distribution is shown (D). We found that the addition of gadolinium decreased the dominant 19F T1 value (C). The particles are also detectable via their effect on the 1H relaxivity. Finally, we found no effect of labeling on the DCs even at the highest concentration of Gd, which can otherwise be toxic to cells (not shown). We found maximum SNR enhancement at 3T, with the highest concentration of Gd (C; at 7T). This effect was lower at higher field strengths, as expected. Finally, we also found that Gd affected the 19F T2, although to a smaller extent. Gd has been shown previously to enhance 19F signal in perfluorocarbon emulsions. However, our use of nanoparticles ensures close contact between the Gd and 19F nuclei and thus allows us to use commercial, clinically approved hydrophilic Gd chelates, without further modification (A). Conclusion Gd has previously been used to modify 19F relaxivity. However, the low miscibility of perfluorocarbons and Gd chelates has been a problem, affecting emulsion stability and reducing the efficacy of the Gd. Here, our use of a polymer coat to force close proximity between the compounds allows for a strong and stable effect on 19F relaxivity, which was sustained for at least 6 months.

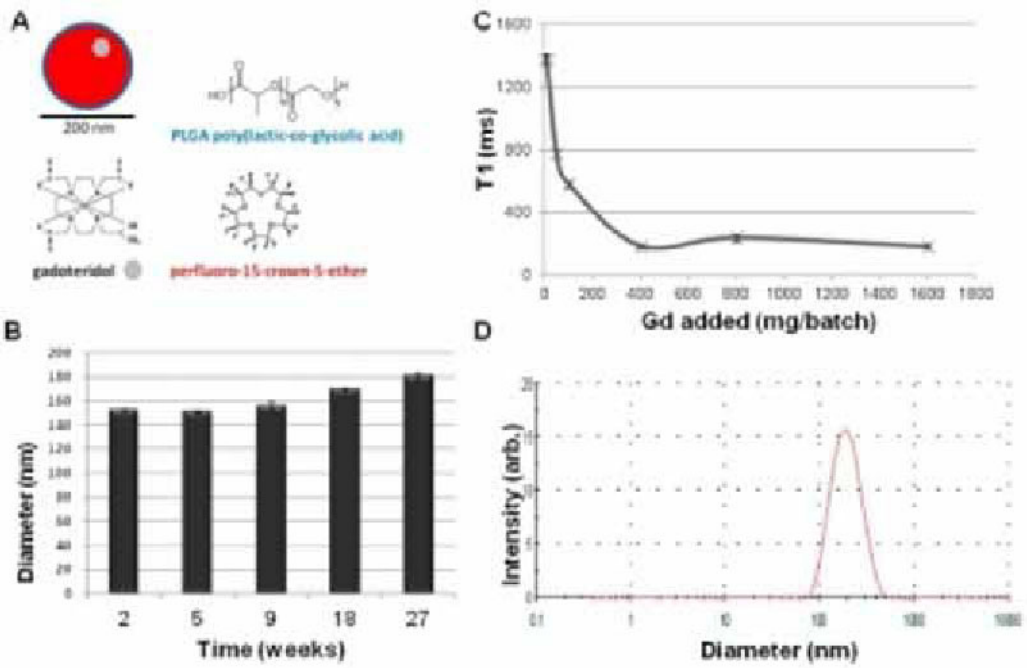


Disclosure of author financial interest or relationships:
**I. de Vries**, None; **M. Srinivas**, None; **A. Heerschap**, None; **C.G. Figdor**, None.

Presentation Number **P807**
Poster Session 4
September 8, 2012 / 14:45-14:45 / Room: The Liffey

# Eosinophil and neutrophil differentially marginate to the liver and spleen in human volunteers

***Joanna J. Lukawska***[1,2], *Barbara M. Sawyer*[1,2], *Lefteris Livieratos*[3], *Michael O'Doherty*[1,3], *Phil Blower*[1], *Martin Kofi*[3], *James R. Ballinger*[1,3], *Gopinath Gnanasegaran*[3], *Christopher Corrigan*[2], *Greg Mullen*[1], [1]*Division of Imaging Sciences, King's College London, London, United Kingdom;* [2]*Asthma, Allergy & Respiratory Science, King's College London, London, United Kingdom;* [3]*Nuclear Medicine, Guy's and St. Thomas' Hospital, London, United Kingdom. Contact e-mail: joanna.lukawska@kcl.ac.uk*

We present a study of in vivo migration of neutrophils and eosinophils in liver and spleen in human volunteers. This work demonstrates that the kinetics of eosinophils in the liver and spleen differ significantly from the kinetics of neutrophils. Methods: On two separate occasions 100 mL of blood was obtained from seven human volunteers (3 mild stable asthmatics and 4 non asthmatic, healthy volunteers). Granulocytes were separated using gradient Ficoll-Paque PLUS centrifugation. CliniMACS CD16 reagent was incubated with the granulocytes (containing eosinophils and neutrophils) and cGMP CD16 CliniMACS (Miltenyi biotec, Bergisch-Gladbach, Germany) was used to obtain highly purified human blood eosinophils (>93%, negative selection) or neutrophils (>97%, positive selection). Purified cells were labelled with Tc-99m HMPAO (Ceretec, GE Healthcare) under aseptic cGMP conditions and 75-100 MBq of labelled cells were administered intravenously. Dynamic lung images were acquired for the first 30 minutes. Further static scans of 5 minutes each were acquired at 1, 2 and 3 hours. Results: Initial dynamic liver and spleen images revealed a significant difference in the time activity curves for eosinophils and neutrophils. At 4 hours eosinophils demonstrated preferential margination in the spleen 27.3% (± 3.4) compared to 18.1% (± 2.9) of neutrophils. This was reversed in the liver with 11.0 % (± 1.0) eosinophils and 24.6% (± 2.6) neutrophils marginating there. Conclusions: We have identified distinct patterns of neutrophil and eosinophil migration and margination through the liver and spleen in both healthy volunteers and stable asthmatics. This study adds to our understanding of how these two immune cells are controlled in homeostasis and supports the new paradigm of immunomodulatory role for eosinophils.

Disclosure of author financial interest or relationships:
**J.J. Lukawska**, None; **B.M. Sawyer**, None; **L. Livieratos**, None; **M. O'Doherty**, None; **P. Blower**, None; **M. Kofi**, None; **J.R. Ballinger**, GE Medical Systems, Grant/research support; Imaging Equipment Ltd, Grant/research support; **G. Gnanasegaran**, None; **C. Corrigan**, None; **G. Mullen**, None.

Presentation Number **P808**
Poster Session 4
September 8, 2012 / 14:45-14:45 / Room: The Liffey

# Differentiation of patients with rheumatological disorders and healthy volunteers using Optical Imaging and MRI

***Reinhard Meier***[1], *Klaus Thürmel*[2], *Matti Sievert*[1], *Peter B. Noel*[1], *Moritz Wildgruber*[1], *Ernst J. Rummeny*[1], [1]*Radiology, Technical University Munich, Munich, Germany;* [2]*Rheumatology, Technical University Munich, Munich, Germany. Contact e-mail: reinhardt.meier@gmail.com*

Purpose: To evaluate an Indocyanine Green (ICG)-enhanced optical imaging (OI) system for differentiation of patients with rheumatological disorders and healthy volunteers in comparison to magnetic resonance imaging (MRI). Methods and Materials: 20 Patients (50% female, mean age = 49.5) with clinically determined rheumatoid arthritis (RA) and 20 healthy volunteers ((50% female, mean age 25.4) were examined with ICG-enhanced optical imaging system (Mivenion GmbH, Germany) and with MRI (3T Verio, Siemens, Germany). Dynamic scans were obtained with atemporal resolution of 1 sec and 4 sec for OI and MRI respectively. The rate of early enhancement (REE) was calculated using a selfwritten analysis software. Furthermore the degree of inflammation in the joints of both hands was graded semiquantitatively by three independent radiologists on a 4-point-ordinate scale (0: no inflammation, 1: mild, 2: moderate, 3: severe) according to the OMERACT RAMRIS score. Results of semiquantitative and quantitative measurements of OI and MRI were correlated. Results: OI and MRI differentiated correctly, by semiquantitative and quantitative analysis of the joints of the hand, between RA patients and healthy volunteers. The semiquantitative score as well as the REE of RA Patients was significantly elevated in comparison to healthy volunteers ($P < 0.05$). The REE of OI was significantly correlated with MRI ($P < 0.05$); thus, differentiation of RA patients and healthy volunteers was feasible. Conclusion: Optical imaging allows for differentiation of patients with rheumatological disorders and healthy volunteers. While the performance of OI up to now is inferior to MRI in detection of subclinical synovitis as shown in earlier studies, it might be nevertheless of substantial added value to clinical examination due to its non-invasiveness, low costs and easy availability.

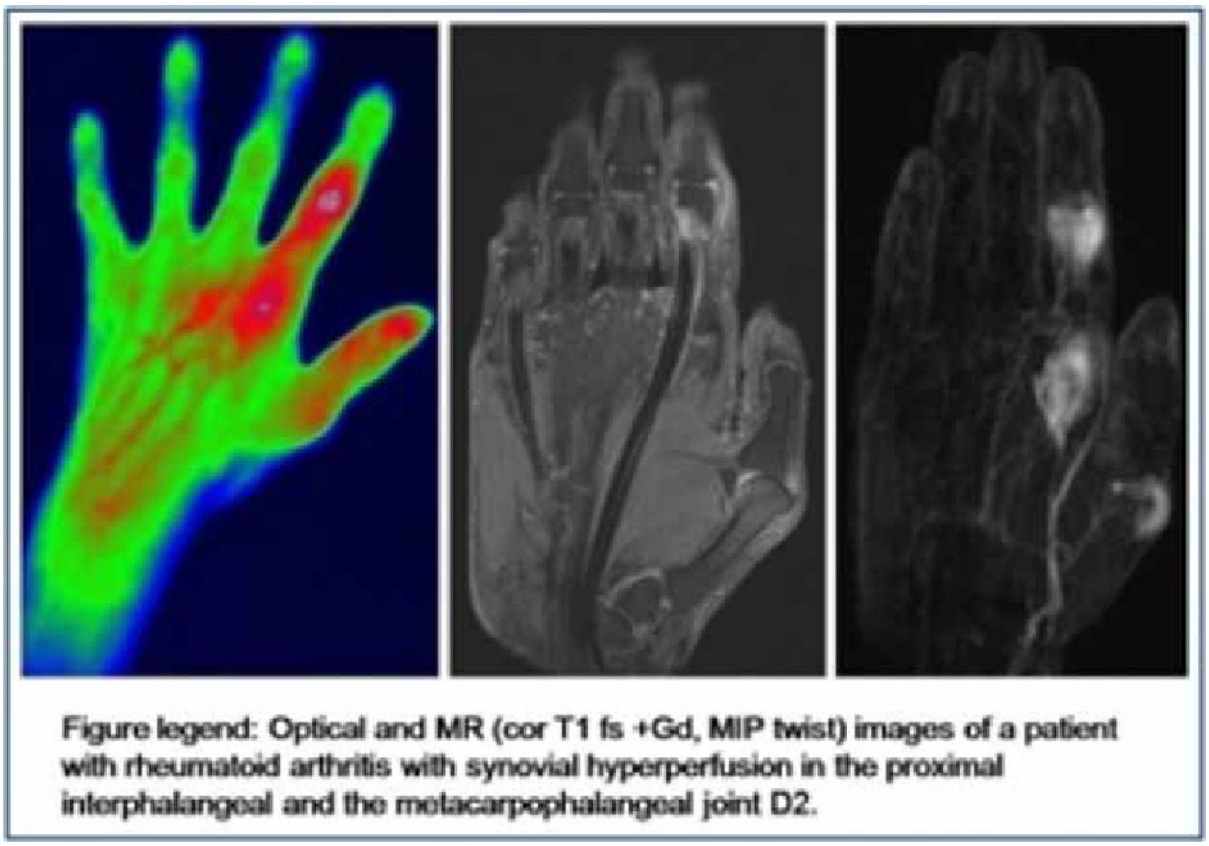

Figure legend: Optical and MR (cor T1 fs +Gd, MIP twist) images of a patient with rheumatoid arthritis with synovial hyperperfusion in the proximal interphalangeal and the metacarpophalangeal joint D2.

Disclosure of author financial interest or relationships:
**R. Meier**, None; **K. Thürmel**, None; **M. Sievert**, None; **P.B. Noel**, None; **M. Wildgruber**, None; **E.J. Rummeny**, None.

Presentation Number **P809**
Poster Session 4
September 8, 2012 / 14:45-14:45 / Room: The Liffey

# Repeated measurements of atherosclerosis in elderly patients with FDG-PET

***Marlene R. Montesino Orellana***[2], *Abdelouahed Khalil*[2], *Otman Sarrhini*[1], *Tamas Fulop*[2], *Nancy Paquet*[1], *Éric Lavallée*[1], *Eric E. Turcotte*[1], *M'hamed Bentourkia*[1], [1]*Nuclear Medicine and Radiobiology, Université de Sherbrooke, Sherbrooke, QC, Canada;* [2]*Médecine, Université de Sherbrooke, Sherbrooke, QC, Canada. Contact e-mail: Marlene.Rossibel.Montesino.Orellana@USherbrooke.ca*

Vascular diseases are the most frequent causes of mortality worldwide, and patients with atherosclerosis are highly exposed to these vascular diseases. Atherosclerosis is provoked by plaque deposit in the inner layer of the blood vessels. The plaque rupture is related to inflammation in the blood vessels that could be measured by positron emission tomography (PET) and 18F-fluorodeoxyglucose (FDG). It is hypothesized that glucose utilization is raised in the presence of inflammation. The early assessment of vessel inflammation could prevent further complications. In this work, we report a repeated study using FDG and PET/CT to assess FDG uptake in aorta, iliac and femoral arteries. The first measurement was made at T0 = 0 and the same subject was scanned again à T12 = 12 months. Three groups of elderly subjects (65-85 years) participated in this study: healthy or normals (N); patients clinically confirmed with a high level of inflammation or hypercholesterolemic (C); and patients with angina (A). With reference to CT images, artery images in each transaxial slice of the PET images were manually delimited by regions of interest and their time-activity curves (TACs) were produced. The standardized uptake values (SUV) were calculated from the last four data points of the TACs (last 16 min), the injected radiotracer activity and the body surface area of the subjects. The SUV values were then classified in six groups as for the three subject groups and for the T0 and T12 measurements. Inflammation was identified when SUV values were found statistically higher than normal values. Arteries with calcification generated noisy TACs and lower SUV values and these were confirmed on the CT images. We assumed that the images were equally affected by partial volume effect. In conclusion, the quantitative analysis could be efficient in the localization of the inflammation and its progression to help guide appropriate treatments, instead of methodologies that typically depict plaque anatomy, which do not identify high-risk lesions.

Disclosure of author financial interest or relationships:
**M.R. Montesino Orellana**, None; **A. Khalil**, None; **O. Sarrhini**, None; **T. Fulop**, None; **N. Paquet**, None; **. Lavallée**, None; **E.E. Turcotte**, None; **M. Bentourkia**, None.

Presentation Number **P810**
Poster Session 4
September 8, 2012 / 14:45-14:45 / Room: The Liffey

# Combined PET with F-18-FDG and O-15-water for treatment planning in advanced cervical carcinoma: a pilot study

***Ivayla Apostolova**, Ralph Buchert, Mathias Lukas, Roger Michel, Christian Rosner, Vikas Prasad, Simone Marnitz, Christhardt Köhler, Winfried Brenner, Nuclear Medicine, University Medicine Charite Berlin, Berlin, Germany. Contact e-mail: ivaapost@hotmail.com*

Objective: Response to standard treatment varies considerably in patients with advanced cervical carcinoma. Therefore, there is a need to identify patients with poor response before or early during treatment. Glucose metabolism and microvascular characteristics of the tumor have been evaluated as biomarkers for this purpose. The combination of both appears particularly promising, because mismatch, i.e. strongly increased glycolysis at low blood flow, might indicate resistance to therapy. The present pilot study performed positron emission tomography (PET) with F-18-fluorodeoxyglucose (FDG) for assessment of glucose metabolism and PET with O-15-water for measurement of blood flow in advanced cervical carcinomas. The aim was to test whether the combination allows detection of mismatch areas in these heterogeneous tumors. Methods: The study included 5 women aged 26-68y with advanced cervix carcinoma (FIGO IIb-IV). Perfusion PET with O-15 water was performed using a dynamic scan protocol. Static FDG-PET was performed according to the common guidelines. Regional blood flow was computed voxel-by-voxel with a weighted integral approach using an image-derived arterial input function. The standard uptake value (SUV) was used for semi-quantitative characterization of the FDG uptake. Heterogeneity of perfusion and SUV in the tumor was assessed by the coefficient of variation (COV = 100 * standard deviation of voxel intensities in the tumor / mean value). The FDG PET image was registered to the perfusion image via co-registration of the corresponding low-dose CTs. The primary tumor was segmented by a VOI defined manually in the low-dose CT of the FDG PET/CT. In order to estimate the spatial extent of mismatch between perfusion and FDG uptake, with low perfusion and high FDG uptake, the perfusion image was thresholded at 50% of the maximum perfusion in the tumor, i.e. perfusion smaller than 50% of the maximum was considered "low perfusion". The SUV image was thresholded at 80% of the maximum SUV, i.e. SUV higher than 80% of the maximum SUV was considered "high FDG uptake". The "mismatch area" was obtained by the intersection of "low perfusion" and "high FDG uptake". Results: The CT based volume of the primary tumor ranged between 49 and 140 ml, mean SUV between 2.9 and 5.6, mean perfusion between 0.29 and 2.1 ml/g/min. The tumors were quite heterogeneous with respect to both FDG uptake and perfusion: COV was about 50% on average for both parameters. Whereas the distribution pattern of FDG uptake and perfusion was similar in 2 patients, there was significant mismatch in the remaining 3 patients accounting for about 10, 30 and 50% of the total tumor volume. Conclusion: These results suggest significant potential of combined PET with F-18-FDG and O-15-water for the detection of mismatch areas in advanced cervical carcinomas. Evaluation of the prognostic value with respect to treatment response requires further studies with a larger sample size. PET with F-18-FDG and O-15-water can be easily performed within one imaging session.

Disclosure of author financial interest or relationships:
**I. Apostolova**, None; **R. Buchert**, None; **M. Lukas**, None; **R. Michel**, None; **C. Rosner**, None; **V. Prasad**, None; **S. Marnitz**, None; **C. Köhler**, None; **W. Brenner**, nanoPET, Grant/research support .

Presentation Number **P811**
Poster Session 4
September 8, 2012 / 14:45-14:45 / Room: The Liffey

# The P-glycoprotein Inhibitor Tariquidar Preferentially Increases the Uptake of P-gp Substrate (R)-[C-11]Verapamil in High Grade Glioma as Measured by PET

*Gerard Thompson[1], Maria Feldmann[2,1], Shaonan Wang[1], Matthew D. Walker[2,1], Adam McMahon[1], Matthias Koepp[2], Alan Jackson[1], **Marie-Claude Asselin**[1], [1]Cancer and Enabling Sciences, The University of Manchester, Manchester, United Kingdom; [2]Institute of Neurology, University College London, London, United Kingdom. Contact e-mail: marie-claude.asselin@manchester.ac.uk*

Introduction: High-grade gliomas (HGG) are currently treated with radiotherapy in combination with the DNA-methylating agent temozolomide but HGG are treatment resistant. P-glycoprotein (P-gp) is the product of the multidrug resistance 1 (MDR1) gene and is present on brain microvasculature, acting as an efflux pump at the blood-brain barrier. P-gp is also present on glioma cells and overexpressed in tumour stem cells. A single nucleotide polymorphism of the MDR1 gene has been found to predict treatment outcome in glioma patients treated with temozolomide independently of O6-methylguanine (MGMT) status [1]. By increasing uptake into solid tumour, tumour periphery and infiltrated but normal appearing brain tissue, P-gp blockade may increase chemotherapeutic efficacy. Methods: To date four patients with suspected HGG (3 grade III and 1 grade IV, confirmed by targeted biopsies) underwent dynamic PET scanning after injection of [O-15]H2O followed by the P-gp substrate (R)-[C-11]verapamil (VPM) before and after administration of 2 mg/kg of the P-gp inhibitor tariquidar. Parametric maps of blood perfusion and the transport rate constant of VPM from plasma to brain (influx K1) were derived using single-tissue compartment models and arterial plasma input functions available for three patients. Low-grade (LG) and high-grade (HG) regions were manually segmented using a combination of contrast-enhanced and FLAIR MR images. Unaffected brain was segmented automatically into gray (GM) and white (WM) matter. Results: At baseline, perfusion in GM and WM was normal in grade III patients but reduced in the grade IV patient. Perfusion in glioma was heterogeneous within tumour and between patients and did not always correspond to areas of gadolinium leakage in the MR images. VPM influx paralleled that of perfusion at baseline. P-gp inhibition minimally altered perfusion but increased VPM influx by >50% in grey and white matter. In grade III glioma even higher increases were measured after P-gp inhibition (Figure 1). Conclusion: These data suggest that the selective and potent P-gp inhibitor tariquidar differentially increases the uptake of P-gp substrates into WM, GM and glioma, and preferentially into grade III regions. These patients are being followed up for their treatment response and more patients are being recruited. PET with a radiolabelled P-gp substrate is a promising tool to guide the potential use of P-gp inhibitors as adjuvant chemotherapy in HGG. References: [1] Schaich et al (2009) Ann. Oncol. 20: 175-81

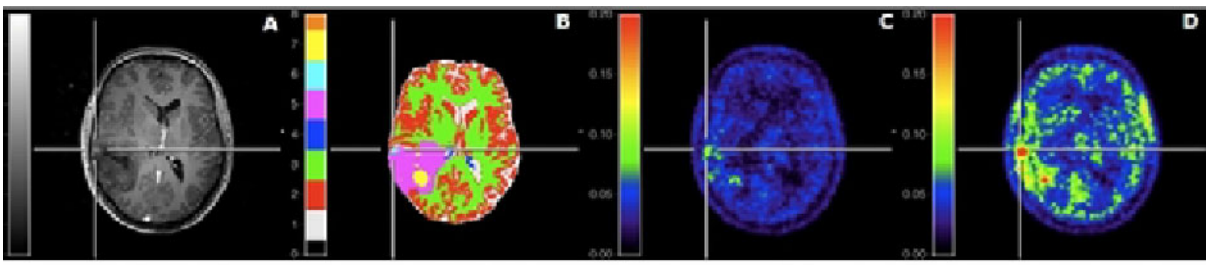


**Figure**: A) Contrast enhance MRI, B) segmented regions (gray matter, white matter, low grade tumour, high grade/ high grade tumour), C) verapamil $K_1$ (ml/min/cm$^3$) at baseline, and D) verapamil $K_1$ (ml/min/cm$^3$) after P-gp inhibition from one patient.

Disclosure of author financial interest or relationships:
**G. Thompson**, None; **M. Feldmann**, None; **S. Wang**, None; **M.D. Walker**, None; **A. McMahon**, None; **M. Koepp**, GE Healthcare, Grant/research support; **A. Jackson**, None; **M. Asselin**, None.

Presentation Number **P812**
Poster Session 4
September 8, 2012 / 14:45-14:45 / Room: The Liffey

# Differentiating invasive from non-invasive breast tumors using diffusion weighted imaging at 3T

***Hubert Bickel***, *Katja Pinker-Domenig, Wolfgang Bogner, Heinrich F. Magometschnigg, Thomas H. Helbich, Dpt. of Radiology, Medical University of Vienna, Vienna, Austria. Contact e-mail: hubert.bickel@meduniwien.ac.at*

Purpose: To evaluate the feasibility of diffusion weighted imaging (DWI) at 3T for the diagnosis of benign and malignant breast lesions, as well as for the differentiation of different malignant breast tumor types. Material and Methods: 233 consecutive patients with 279 suspicious breast lesions detected in routine breast screening (BI-RADS® 3-5) were examined. All examinations were performed before any intervention and histopathological verification was reached in all patients after the MR measurements. A 3T Scanner with a dedicated 4-channel breast coil and a standardized measurement protocol was used for the examinations. The protocol contained a T2-weighted, a dynamic contrast enhanced (DCE) T1 and a diffusion weighted sequence using b-values of 50 and 850. ADC maps were calculated and 2-dimensional ROIs were drawn in the area with the lowest ADC-values. An ADC-threshold of 1.25×10-3mm$^2$/s was used. ADC-values below this threshold were considered as malignant. Mean values were compared using ANOVA and Games Howell post hoc test and sensitivity and specificity were calculated. Results The mean ADC-values were 1.58×10-3mm$^2$/s for the benign lesions, 1.24×10-3mm$^2$/s for the ductal carcinomas in situ (DCIS), 0.91×10-3mm$^2$/s for the invasive ductal (IDC), 0.86×10-3mm$^2$/s for the invasive lobular carcinomas (ILC) and 1.62×10-3mm$^2$/s for the invasive mucinous carcinomas. ADC-values were significantly lower in all malignant subtypes, except mucinous carcinomas, compared to the benign tumors. The ones for DCIS were significantly higher than those for most common the invasive types (IDC and ILC) while no significant difference was found between the latter two. Overall sensitivity was 92.2% and Specificity was 90.1%. Conclusion: DWI at 3T can differentiate benign from malignant breast tumors with high sensitivity and specificity. The diffusivities of the most common invasive and non-invasive tumors are significantly different; however, mucinous carcinomas cannot be differentiated from benign tumors using this method.

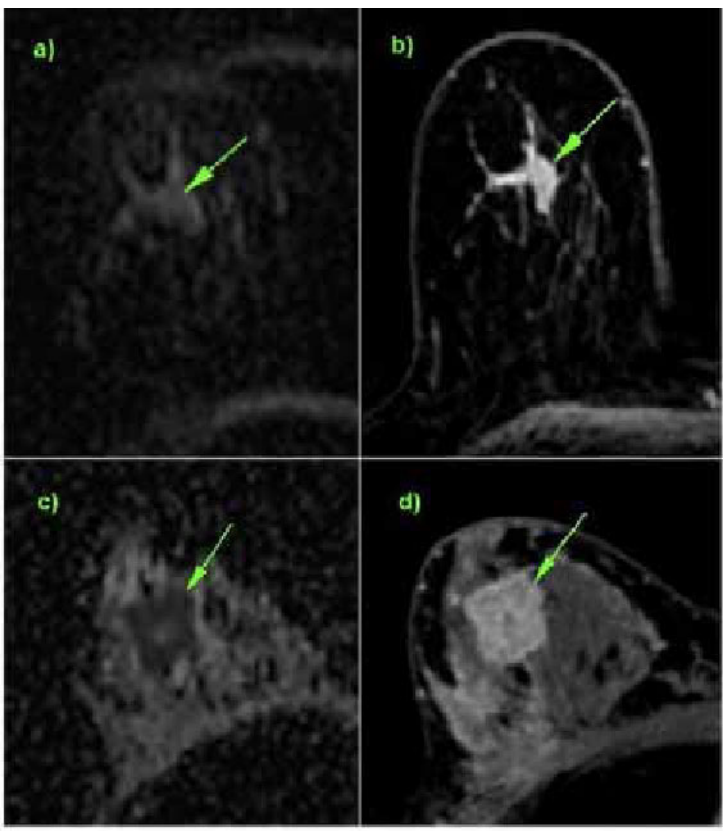


ADC-map (a) and CE-MRI (b) of a DCIS, compared to the ADC-map (c) and CE-MRI of an IDC.

Disclosure of author financial interest or relationships:
**H. Bickel**, None; **K. Pinker-Domenig**, None; **W. Bogner**, None; **H.F. Magometschnigg**, None; **T.H. Helbich**, Siemens, Grant/research support; Fond national bank austria, Grant/research support .

Presentation Number **P813**
Poster Session 4
September 8, 2012 / 14:45-14:45 / Room: The Liffey

# Diffusion weighted MRI at 3T as a biomarker for neoadjuvant chemotherapy response in breast cancer

***Hubert Bickel***, *Katja Pinker-Domenig, Wolfgang Bogner, Benedikt Brück, Thomas H. Helbich, Dpt. of Radiology, Medical University of Vienna, Vienna, Austria. Contact e-mail: hubert.bickel@meduniwien.ac.at*

Purpose: To assess radiological tumor response to neoadjuvant chemotherapy (NAC) with diffusion weighted imaging (DWI) at 3Tesla. Materials and Methods: 30 patients (mean age 51.4 years) with a histopatholgically verified breast cancer (BIRADS 6) who underwent NAC were included in this prospective IRB approved study. In additional to routine staging with a dynamic contrast enhanced magnetic resonance imaging (CE-MRI) protocol, a diffusion weighted sequence with the following parameters was included in the imaging protocol: single-shot, echo-planar imaging sequence with eddy current compensation, a three direction trace diffusion scheme, inversion recovery fat suppression and two b-values of 50 and 850 s/mm$^2$ (TR/TE/TI 13700/83/220ms; FOV 340x117 mm; 40 axial slices; SI 3.5 mm (no gap); matrix 192x64 (50% oversampling to avoid fold-in and ghosting); two averages; spatial resolution, 1.8x1.8x3.5 mm; anterior-posterior phase encoding; bandwidth 1446 Hz/pixel; 3:19 min. Patients were examined before the beginning and after 5 or 6 cycles of NAC. In DWI manually drawn ROIs of suspicious areas were assessed for restricted diffusion and apparent diffusion coefficient (ADC) values were calculated. An ADC threshold 1.25 x10-3mm2/s was defined as a marker of malignancy. Data were dichotomized, complete response (cr) and partial response (pr) were considered as response and stable disease (sd) and progressive disease (pd) were considered as non-response to NAC. The histopathological assessment of tumor response was used as the standard of reference. Results: There were 23 invasive ductal cancers (IDC) and 6 invasive lobular cancers (ILC). Average tumor size at baseline was 43.4mm. In the baseline scan, one IDC (3%) had an ADC value above the cut-off for malignancy and was excluded. There were 4 (14%) non-responders and 25 (86%) responders. Responders demonstrated an average increase in ADC values of 0.58 x10-3mm2/s, whereas non-responders failed to show a significant increase in ADC values (average increase 0.09 x10-3mm2/s). The classification of DWI as responders and non-responders correlated with histopathological diagnoses of treatment response. Conclusion: Quantitative DWI with ADC-maps is a valuable, non-invasive biomarker for the assessment of treatment response to NAC in breast cancer patients.

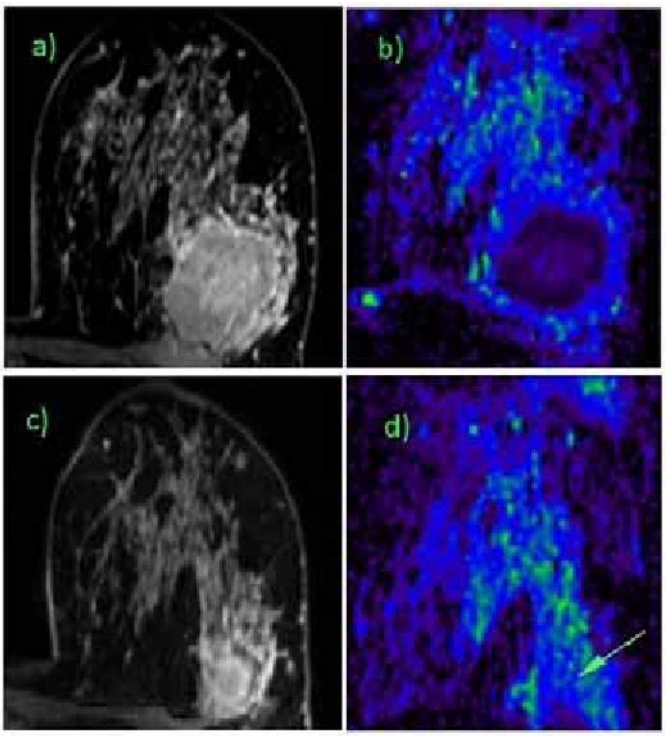


CE-MRI (a) and ADC map (b) of a Grade 3 IDC before treatment and after 6 cycles of NAC (c, d)

Disclosure of author financial interest or relationships:
**H. Bickel**, None; **K. Pinker-Domenig**, None; **W. Bogner**, None; **B. Brück**, None; **T.H. Helbich**, Siemens, Grant/research support; Fond national bank austria, Grant/research support .

Presentation Number **P814**
Poster Session 4
September 8, 2012 / 14:45-14:45 / Room: The Liffey

# Clinical validation of a hybrid radioactive and fluorescent tracer for sentinel node procedures

***Oscar R. Brouwer***[1,2], *Tessa Buckle*[2,1], *W Martin C. Klop*[3], *Alfons J. Balm*[3], *Henk G. van der Poel*[4], *Bas W. van Rhijn*[4], *Simon Horenblas*[4], *Omgo E. Nieweg*[5], *Fijs van Leeuwen*[2,1], *Renato A. Valdés Olmos*[1], [1]*Nuclear Medicine, Netherlands Cancer Institute, Amsterdam, Netherlands;* [2]*Radiology, Leiden University Medical Center, Leiden, Netherlands;* [3]*Head and Neck Surgery, Netherlands Cancer Institute - Antoni van Leeuwenhoek hospital, Amsterdam, Netherlands;* [4]*Urology, Netherlands Cancer Institute - Antoni van Leeuwenhoek hospital, Amsterdam, Netherlands;* [5]*Surgery, Netherlands Cancer Institute - Antoni van Leeuwenhoek hospital, Amsterdam, Netherlands. Contact e-mail: o.brouwer@nki.nl*

Background: Recently, a hybrid sentinel node tracer was developed which contains the fluorescent dye indocyanine green (ICG) and the current standard radioactive 99mTc-nanocolloid. Before this hybrid tracer can be used routinely, it is imperative to ensure that the addition of the fluorescent moieties does not alter the biological properties of the parental radiocolloid. The purpose of this study was to assess the concordance between the lymphatic drainage pattern of 99mTc-nanocolloid and hybrid ICG-99mTc-nanocolloid using lymphoscintigraphy and SPECT/CT. Methods: 25 patients with either a melanoma of the head and neck region (10), the trunk (6), or with penile carcinoma (9) scheduled for sentinel node biopsy were prospectively studied. After injection of 99mTc-nanocolloid at the lesion site, lymphoscintigraphy was performed with at 10 minutes and 2 hours post injection, followed by SPECT/CT. Scintigraphy was repeated the same afternoon (10 patients) or the next morning (15 patients) after injection of the hybrid tracer in an identical fashion. The paired images of both injections were evaluated. Sentinel nodes were intraoperatively localized using blue dye, a gamma-ray detection probe, a portable gamma camera and a fluorescence camera. Results: Lymphatic drainage was visualized in all 25 patients using 99mTc-nanocolloid leading to the identification of 66 sentinel nodes in total. These very sentinel nodes were also identified during the second scintigraphic procedure with ICG-99mTc-nanocolloid. Moreover, a high correlation between the radioactive counts rates in the sentinel nodes of both scintigraphic studies was observed (mean R2 = 0.83). Intraoperatively (4-23 hours after the second injection), all preoperatively identified sentinel nodes could be localized using radio- and fluorescence guidance combined. Ex vivo, all radioactive sentinel nodes were found to be fluorescent and vice versa. No adverse reactions were observed. Conclusions: The lymphatic drainage pattern of ICG-99mTc-nanocolloid is identical to that of 99mTc-nanocolloid. This observation, together with the added value of intraoperative fluorescence guidance, warrant wider evaluation of hybrid ICG-99mTc-nanocolloid as a tracer for sentinel node procedures.

Disclosure of author financial interest or relationships:
**O.R. Brouwer**, None; **T. Buckle**, None; **W.C. Klop**, None; **A.J. Balm**, None; **H.G. van der Poel**, None; **B.W. van Rhijn**, None; **S. Horenblas**, None; **O.E. Nieweg**, None; **F. van Leeuwen**, None; **R.A. Valdés Olmos**, None.

Presentation Number **P815**
Poster Session 4
September 8, 2012 / 14:45-14:45 / Room: The Liffey

# MR imaging of malignant glioma using 5-aminolevulinic acid in an animal model

***Hye Rim Cho**, Seung Hong Choi, Woo Kyung Moon, Radiology, College of Medicine, Seoul Natl Univ, Seoul, Republic of Korea.*
*Contact e-mail: hyerimcho1030@gmail.com*

Purpose: 5-Aminolevulinic acid (5-ALA), leading to accumulation of fluorescent protoporphyrin IX (PpIX) in malignant gliomas, was recently suggested to be new marker for the detection of malignant foci in diffusely infiltrating gliomas. We hypothesized that 5-ALA selectively accumulates in malignant glioma and finally converts to heme, which can be detected by MRI. Material and methods: For in vitro study, first, the human glioblastoma U-87 cells were incubated for 48 h with FAC of 100 μM for iron supplementation, or without FAC supplement. Second, the cells were incubated for 6 h with 5-ALA (500uM) or without 5-ALA, and then we measured intracellular PpIX. Third, the cells were further incubated for 1, 24, or 48 h. The harvested cells at the 1, 24, or 48 h after incubation were used for the measurement of intracellular concentration of iron, heme, PpIX, ferrochelatase (FECH) and heme oxygenase (HO)-1. A total number of 10 mice with orthotopic brain tumor were used. The mice received an oral administration of 5-ALA of 0.1mg/g(n=6; 5-ALA group) or normal saline (n=4; control group) 24 h before MRI (7 T MRI scanner, Bruker). We measured T2* of each tumor, and iron concentration of tumors was evaluated by ICP-MS and histopathology. Results: The intracellular PpIX concentration of the cells treated with 5-ALA was significantly higher than that of control cells (P <.001). The intracellular heme concentration of the cells with exposure to 5-ALA was higher than that of the cells without exposure only at 24 h (P<.001). The intracellular concentration of FECH was the highest at 1 h after exposure to 5-ALA, and decreased over time (24 and 48 h). The intracellular concentration of HO-1 has no significant difference in the cells at 1, 24 and 48 h after the exposure to 5-ALA. In vivo T2* maps showed that the mean T2* value of U87 glioblastoma treated with 5-ALA was lower than that of control tumors (14.9±1.2 msec vs 21.4±2.6, P<.0001), which was well correlated with ICP-MS and Prussian blue staining. Conclusion: 5-ALA can be used for the detection of malignant glioma on MR imaging, because of the increased intracellular concentration of the heme, the final product of 5-ALA. Clinical relevance: We believe that 5-ALA-enhanced MR imaging will be able to be used for pre-operative imaging, follow-up imaging and treatment response evaluation.

Disclosure of author financial interest or relationships:
**H. Cho**, None; **S. Choi**, None; **W. Moon**, None.

Presentation Number **P816**
Poster Session 4
September 8, 2012 / 14:45-14:45 / Room: The Liffey

# The prognostic value of pre- and post-therapeutic F-18 FDG PET/CT metabolic parameters in NSCLC patients of advanced stage

***Woo Hee Choi***[1], *Eun Ji Han*[3], *Sae Jung Na*[4], *Ye Young Seo*[2], *Young Ha Park*[1], *Siwon Kang*[3], *Sung Hoon Kim*[2], [1]*Nuclear Medicine, St. Vincent's Hospital, College of Medicine, The Catholic University of Korea, Suwon, Republic of Korea;* [2]*Nuclear Medicine, Seoul St. Mary's Hospital, College of Medicine, The Catholic University of Korea, Seoul, Republic of Korea;* [3]*Nuclear Medicine, Daejeon St. Mary's Hospital, College of Medicine, The Catholic University of Korea, Daejeon, Republic of Korea;* [4]*Nuclear medicine, Uijeongbu St.Mary's Hospital, College of Medicine, The Catholic University of Korea, Uijeongbu, Republic of Korea. Contact e-mail: wh0522@catholic.ac.kr*

Purpose: To evaluate the prognostic value of various metabolic parameters of both pre- and post-therapeutic F-18 FDG PET/CT in advanced stage non small cell lung cancer (NSCLC) Material and Methods: We retrospectively reviewed medical records and images of stage IIIB/IV pathologically proven NSCLC patients who underwent pre- and post-therapeutic PET/CT between December 2003 and May 2011. All patients received first-line platinum-based double chemotherapy. Metabolic parameters such as maximum standardized uptake value from the primary tumor (SUVmax-p), whole intrathoracic lesion (SUVmax-t), metabolic tumor volume taken at SUVmax 2.5 (MTV2.5) and half value of SUVmax-t (MTV50) were measured from both pre- and post-therapeutic PET/CT scans. The ratio of SUVmax-p in comparison with average SUV of right hepatic lobe (T/L ratio-p) and percent change (Δ%) of metabolic parameters between pre- and post-therapeutic PET/CT scans were calculated. Metabolic parameters and traditional prognostic factors such as stage, age, serum LDH level, and performance status were analyzed in terms of progression-free survival (PFS). Results: A total of 39 patients were enrolled (27 male, 12 female, age: 59±9 years). Patients with higher initial MTV2.5 and MTV50 (≥median), higher follow up SUVmax-p, SUVmax-t, T/L ratio-p (≥median), smaller Δ%SUVmax-t (<median) showed poor PFS. On multivariate analysis, however, none of these factors were statistically significant. Conclusion: The metabolic parameters obtained from post therapeutic F-18 FDG PET/CT scan were significant prognostic factors for disease progression in advanced stage NSCLC patient. Thus, post therapeutic F-18 FDG PET/CT scan may help discriminate patients who can benefit from additional treatment after first-line therapy before progression.

Disclosure of author financial interest or relationships:
**W. Choi**, None; **E. Han**, None; **S. Na**, None; **Y. Seo**, None; **Y. Park**, None; **S. Kang**, None; **S. Kim**, None.

Presentation Number **P817**
Poster Session 4
September 8, 2012 / 14:45-14:45 / Room: The Liffey

# A MINIATURIZED FLUORESCENCE IMAGING SYSTEM FOR OPTICAL-GUIDED SURGERY OF HUMAN LIVER METASTASES. A PRELIMINARY CLINICAL STUDY

*Gabriele Barabino[2,1], Jean-Guillaume Coutard[3], Michel Berger[3], Sylvain Gioux[3], Véronique Josserand[1], Michèle Cottier[2], Jack Porcheron[2], Michelle Kéramidas[1], Christian A. Righini[1], Jean-Marc Dinten[2], **Jean-Luc Coll**[1], [1]Institut Albert Bonniot, INSERM-UJF U823, Grenoble, France; [2]Université Jean Monnet, CHU de Saint Etienne, Saint Etienne, France; [3]DTBS, CEA-LETI, Grenoble, France. Contact e-mail: Jean-Luc.Coll@ujf-grenoble.fr*

Surgery is the only therapy that offers the possibility of cure for patients with hepatic metastatic diseases from colorectal or neuroendocrine carcinoma. Five-year survival rates after resection of all detectable liver metastases can reach 50%. In contrast, the role of hepatectomy in patients with liver metastases from noncolorectal and nonneuroendocrine carcinoma is not well defined. Scientific literature showed that in highly selected patients, resection of noncolorectal and nonneuroendocrine liver metastases can be done safely with survival similar to colorectal metastases. Therefore, preoperative and intraoperative staging are critical parameters in order to anticipate an optimized resectability and a favorable outcome. Indocyanine green (ICG) is a fluorescent agent approved in the clinic for liver function testing, as well as measurement of cardiac output and retinal angiography. It is a water-soluble, anionic, amphilic tricarbocyanine probe with a hydrodynamic diameter of 1.2 nm; the excitation and emission wavelengths in the presence of serum are 778 and 830 nm, respectively. Fluorescent navigation systems with ICG injection are used to detect sentinel lymph nodes. It has only recently shown real interest for optical-guided surgical oncology. Several studies report now that this technique can be useful for assisted intraoperative resection of otherwise undetectable liver cancers (such as hepatocellular and metastatic carcinomas) in patients who received and intravenous injection of ICG 4 to 7 days before surgery for a routine preoperative liver function test. We developed a new, miniaturized version of the Fluobeam (see www.fluoptics.com), which can be used for intra-operative surgery of cancer. We used this system and ICG in a clinical trial on 2 patients with liver metastasis, in order to demonstrate that ICG can efficiently label the rim of these tumors, when it is injected intravenously or infused ex-vivo on the surgical liver specimen. Furthermore, we discuss the quality of the ICG labeling, and the possibility to anticipate it by performing conventional diffusion-weighted magnetic resonance imaging, X-ray imaging and 18-FDG metabolic imaging of these patients before optical guided surgery.

Disclosure of author financial interest or relationships:
**G. Barabino**, None; **J. Coutard**, None; **M. Berger**, None; **S. Gioux**, None; **V. Josserand**, None; **M. Cottier**, None; **J. Porcheron**, None; **M. Kéramidas**, None; **C.A. Righini**, None; **J. Dinten**, None; **J. Coll**, None.

Presentation Number **P818**
Poster Session 4
September 8, 2012 / 14:45-14:45 / Room: The Liffey

# Multi spectral photoacoustic imaging of melanoma metastasis in resected human lymph nodes

***Diederik J. Grootendorst***[1], *Gerrit Corneluis Langhout*[1], *Jithin Jose*[2], *Dieter Fuchs*[2], *Wiendelt Steenbergen*[1], *Srirang Manohar*[1], *Theo J. Ruers*[3,4], [1]*Biomedical Photonic Imaging, University of Twente, Enschede, Netherlands;* [2]*VisualSonics Inc., Toronto, ON, Canada;* [3]*Surgical Oncology, The Netherlands Cancer Institute, Amsterdam, Netherlands;* [4]*Nanobiophysics, University of Twente, Enschede, Netherlands. Contact e-mail: d.j.grootendorst@utwente.nl*

One of the most aggressive skin cancers, melanoma, is known to spread throughout the lymphatics in a later stage of the disease. The pathological status of the sentinel lymph node (SLN) is important for accurate staging, ascertaining prognosis and planning treatment. The standard procedure involves biopsy of the node and histopathological assessment of its status. Due to the time required for accurate histological assessment, nodal status is not immediately available to the surgeon. In addition, finite sampling of the node could result in metastases to be missed. In case of tumor positive SLN diagnosis, this implies that complete lymphadenectomy cannot be performed during the sentinel node procedure but has to be planned in a second separate procedure. The two-step surgical procedure: SLN excision and complete lymph node basin excision, is consorted by increased patient discomfort, higher costs, organizational distress and is time-consuming. Photoacoustic (PA) imaging combines the spatial resolution of optical imaging with an increased penetration depth possibly providing a valuable application for intra-operative detection of nodal melanoma metastases. Since melanin possesses high optical absorption, melanoma can be detected and imaged using PA imaging without additional labeling. In this work we evaluate the applicability of the Vevo LAZR photoacoustic imaging system (VisualSonics. Inc, Toronto, Canada) as an intra-operative modality for examining the status of resected human lymph nodes. We show the ability of the system to perform 3D multi spectral imaging of micrometastases-simulating melanoma cell clumps in an ex vivo animal lymph node and we studied the spectral response of a group of five resected human lymph nodes. Different regions of interest were selected to obtain photoacoustic response spectra of absorbing areas within the nodes and we used a spectral filtering approach to separate melanin from other chromophores. Results were validated by comparison with histology. Our results show that smaller metastases (< 1.5 mm) can be detected and melanoma metastases in human lymph nodes could be grossly characterized by a gradual decreasing slope from 720 nm toward 900 nm. A similarity within groups was found as well as differences between the benign and malignant nodes. Selectively displaying distinct tissue was possible for both blood and melanoma metastases in both planar images as well as in 3D volumes. Our results suggest that photoacoustics has the potential to develop into an intra-operative imaging modality to detect melanoma metastases in sentinel lymph nodes.

Disclosure of author financial interest or relationships:
**D.J. Grootendorst**, None; **G. Langhout**, None; **J. Jose**, visualsonics, Other financial or material support; **D. Fuchs**, VisualSonics Inc., Employment; **W. Steenbergen**, PA Imaging BV, Consultant; **S. Manohar**, PA Imaging BV, Stockholder; **T.J. Ruers**, None.

Presentation Number **P819**
Poster Session 4
September 8, 2012 / 14:45-14:45 / Room: The Liffey

# Optimizing Novel Cocktail 18F-NaF and 18F-FDG PET/CT Imaging Strategy to Enhance Cancer Detection Sensitivity

***Frezghi Habte**, David Paik, Sanjiv S. Gambhir, Andrei Iagaru, Radiology, Stanford University, Stanford, CA, USA. Contact e-mail: fhabte@stanford.edu*

Introduction: Previous pilot studies showed that the "cocktail tracer imaging strategy" with 18F-FDG and 18F-NaF in a single PET/CT scan is non-inferior when compared to PET/CT scans done with either radiopharmaceutical alone and is more efficient than performing separate studies. This novel imaging strategy has the potential to improve patient convenience and reduce healthcare costs for initial staging of certain cancers. One limitation from the pilot phase study is that several lesions seen on a single tracer scan (either 18F-FDG or 18F-NaF) were missed on the combined scan. The goal of this study is to optimize the ratio of tracers administrated to the patient in order to maximize the detection sensitivity. Methods: Since it is impractical to scan any given patient at multiple tracer ratios, we applied image-processing techniques on a sample of images acquired during routine patient scans. Individual whole body scans (18F-FDG and 18F-NaF; 60 min post-injection) were registered and summed at various ratios to simulate single combined scans. To validate this process, we performed phantom scans and generated dynamic scans of the torso to compare the time activity curve of both 18F-FDG and 18F-NaF within selected organs. Results: For lung lesions with 18F-FDG uptake, detection was optimized with a higher 18F-FDG: 18F-NaF ratio (1:0.5 to 1:1). Detection of a small skull lesion however was optimized with a lower 18F-FDG: 18F-NaF ratio (< 1:1.5). We have also observed that administrating a combined dose with roughly equal amounts of each tracer provides better acceptable detection sensitivity for both types of lesions. Conclusion: This work demonstrates the feasibility of simulating cocktail scans by combining individual scans with each tracer. A compromise ratio exists that is able to preserve the detectability of both lung lesions and bone lesions in a single cocktail scan.

Disclosure of author financial interest or relationships:
**F. Habte**, None; **D. Paik**, None; **S.S. Gambhir**, General Electric, Grant/research support; Bayer-Schering, Grant/research support; Sanofi-Aventis, Grant/research support; CellSight, Stockholder; ImaginAB, Stockholder; Enlight, Stockholder; Endra, Stockholder; Bracco, Consultant; NinePoint Medical, Stockholder; Visualsonics, Consultant; **A. Iagaru**, None.

Presentation Number **P820**
Poster Session 4
September 8, 2012 / 14:45-14:45 / Room: The Liffey

# Feasibility of Intraoperative Nuclear Imaging for Assistance with Localization and Verification of Resection of Sentinel Nodes in Melanoma: Potential Impact on Intraoperative Decision Making

***Nathan Hall***[1], *Alicia Terando*[2], *Doreen Agnese*[2], *Alicia K. McGough*[1], *Amanda Hayes*[1], *Stephen Povoski*[2], *Edward W. Martin*[2], *Michael V. Knopp*[1], [1]*Radiology, The Ohio State University, Columbus, OH, USA;* [2]*Surgical Oncology, The Ohio State University, Columbus, OH, USA. Contact e-mail: nathan.hall@osumc.edu*

Introduction: Lymphatic mapping is standard of care for the detection of metastatic lesions in the evaluation of patients presenting with melanoma. Intraoperatively, surgeons use a handheld gamma probe to localize lymph nodes that are imaged and marked immediately preoperatively with or without the injection of blue dye to visually identify sentinel nodes. One of the limitations of this technique is that imaging information is limited to the preoperative setting. The purpose of this pilot study was to assess the feasibility and potential usefulness of intraoperative imaging to assist with sentinel lymph node resection in patients with melanoma. Methods: To determine the feasibility of intraoperative nuclear imaging during and after sentinel lymph node resection, the Ergo$^{TM}$ LFOV General Purpose Imager (Digirad) was utilized for 19 cases performed by two surgeons in patients undergoing sentinel lymph node resection for melanoma. All patients were injected with both Technetium-99m sulfur colloid (intradermally, preoperatively) and 1% Isosulfan blue dye (intradermally, intraoperatively) prior to performing sentinel lymph node resection. Sentinel lymph node mapping with marking of identified radioactive nodes was performed as standard of care for all patients. Intraoperative pre-incision and post procedure imaging was performed in all patients ± additional imaging mid procedure to assess for residual lymph nodes. Intraoperative imaging was compared to preoperative imaging and assessment of whether intraoperative imaging impacted patent care decisions was performed. Results: Intraoperative imaging proved feasible for the detection and localization of radioactive lymph nodes in all 19 patients that were evaluated. In all but three patients, at least as many lymph nodes were identified with intraoperative imaging as were seen on preoperative lymphatic mapping. In 10 patients (53%), intraoperative imaging verified complete resection of all lymph nodes identified with imaging. Intraoperative imaging changed patient management in 5/19 cases (26%). In the remaining four cases (21%), imaging information would have led the surgeon to further explore for remaining radioactive lymph nodes had this information been utilized in real-time intraoperatively. Conclusions: This pilot study demonstrated that intraoperative imaging is a feasible adjunct to sentinel lymph node detection after lymphatic mapping in patients with melanoma. In nearly half of the cases, intraoperative imaging either changed patient management or would have changed patient management if it had been incorporated into the decision-making process. Further evaluation is necessary to determine whether changes in patient management have an impact on detection of metastatic disease or clinical outcomes.

Disclosure of author financial interest or relationships:
**N. Hall**, Enlyton,Ltd., Other financial or material support; **A. Terando**, None; **D. Agnese**, None; **A.K. McGough**, Digirad, Grant/research support; **A. Hayes**, Digirad, Grant/research support; **S. Povoski**, Enlyton,Ltd., Other financial or material support; **E.W. Martin**, None; **M.V. Knopp**, None.

Presentation Number **P821**
Poster Session 4
September 8, 2012 / 14:45-14:45 / Room: The Liffey

# FDG PET and Fluorescent Lifetime imaging: Early response biomarkers of massive cancer cell necrosis immediately following near-infrared photoimmunotherapy

*Kohei Sano, Takahito Nakajima, Makoto Mitsunaga, Peter Choyke, **Hisataka Kobayashi**, Molecular Imaging Program, National Cancer Institute/NIH, Bethesda, MD, USA. Contact e-mail: Kobayash@mail.nih.gov*

**Purpose:** Near-infrared (NIR) photoimmunotherapy (PIT), is a new form of cancer treatment based on a monoclonal antibody-phthalocyanine dye (IR700) conjugate that targets tumors and then kills them following NIR light exposure. PIT induces rapid necrosis, although the tumor does not immediately change size. The goal of this study is to establish imaging methods to evaluate the acute effects of PIT. **Materials and Methods:** Bilateral xenografts consisting of human epidermal growth factor (EGFR)-positive tumor cells (A431) were established in the flanks of mice. Mice received a Panitumumab (Pan)-IR700 conjugate, and 1 day later one side was treated with NIR light doses ranging from 10 to 100 J/cm$^2$. $^{18}$F-FDG PET and fluorescence lifetime (FLT) imaging were used to detect functional changes in the treated tumor, 0-24h after PIT. **Results:** Short time after PIT, massive cancer cell necrosis was successfully monitored by both methods in :*vitro* and *in vivo*. When $^{18}$F-FDG was injected 15 min after PIT using 100 J/cm$^2$, $^{18}$F-FDG PET images showed a 76 % reduction in SUV in the treated tumors 1hr after injection of $^{18}$F-FDG. *In vivo* PIT induced shortening of FLT in treated tumors immediately after PIT with NIR light doses of 30 J/cm$^2$ or greater. In contrast, insufficient therapeutic doses of NIR light (10 J/cm$^2$) did not induce shortening of FLT. No significant change of tumor sizes was observed within 24h after PIT. **Conclusions:** $^{18}$F-FDG PET and FLT imaging can detect changes in cancer cell viability induced by PIT within 15 min of therapy, thus preceding any morphological change in tumor size which generally occurred several days later. Photoimmunotherapy induces massive, rapid tumor necrosis with minimum normal tissue damage. Clinically feasible imaging technologies such as $^{18}$F-FDG PET and FLT imaging, detects cancer cell necrosis prior to morphological changes in the tumor.

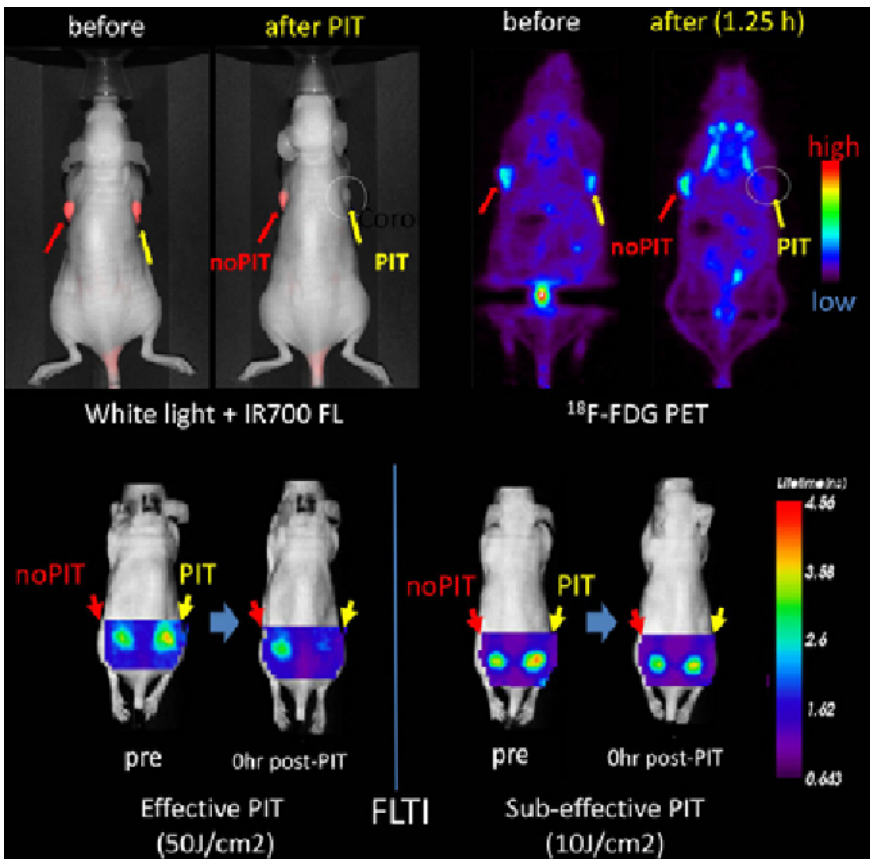


Effective PIT induced massive necrosis in treated tumors, resulted in significant decrease of F-18 FDG uptake (upper right) and significant shortening of fluorescence lifetime (lower left) that is clearly shown in FDG-PET and FLT imaging prior to morphological changes.

Disclosure of author financial interest or relationships:
**K. Sano**, None; **T. Nakajima**, None; **M. Mitsunaga**, None; **P. Choyke**, GE Healtcare, Grant/research support; Philips Medical Systems, Grant/research support; Siemens Healthcare, Grant/research support; **H. Kobayashi**, None.

Presentation Number **P822**
Poster Session 4
September 8, 2012 / 14:45-14:45 / Room: The Liffey

# *In vivo* Biocompatibility and Efficacy of an X-ray-visible, Uniform, Alginate Microsphere for Embolic Therapy

***Dara Kraitchman***[1,2], *Clifford R. Weiss*[1], *Cyrus Weijie Beh*[5], *Charles Hu*[4], *Paul A. DiCamillo*[1], *Yingli Fu*[1], *Judith A. Cook*[1], *Kathleen L. Gabrielson*[2], *Tza-Huei Wang*[3,5], *Hai-Quan Mao*[4,5], [1]*Radiology, Johns Hopkins University, Baltimore, MD, USA;* [2]*Molecular and Comparative Pathobiolgy, Johns Hopkins University, Baltimore, MD, USA;* [3]*Mechanical Engineering, Johns Hopkins University, Baltimore, MD, USA;* [4]*Material Science and Engineering, Johns Hopkins University, Baltimore, MD, USA;* [5]*Biomedical Engineering, Johns Hopkins University, Baltimore, MD, USA. Contact e-mail: dkraitc1@jhmi.edu*

**Introduction** Embolization is a minimally invasive approach frequently used in combination with X-ray angiography to deploy small particles to block or occlude vessels feeding tumors. The majority of embolic particles are composed of polymers that are radiolucent. Thus, embolic microsphere visibility is enhanced by co-injection with radiopaque contrast agent. We have recently developed a method to create highly uniform, X-ray-visible, alginate-based embolic beads (XEB) and sought to test the effectiveness and biocompatibility of this new embolic device. **Methods:** Using a pressure-controlled, microfluidic device, barium sulfate impregnated alginate microbeads were crosslinked in a calcium-rich, oleic acid solution and further separated and crosslinked in a calcium-rich, isopropyl alcohol solution to generate XEBs with optimal 50 µm diameters. Radiopacity of the XEBs was determined in phantoms on an X-ray flat-panel angiographic system (Axiom Artis dFA, Siemens). *In vivo* imaging visibility, handling characteristics, and biocompatibility was evaluated in normal, anesthetized swine (n=5 acute; n=2 chronic). Using a femoral artery approach, a baseline aortic digital subtraction angiogram (DSA, hand contrast injection, 3 frames/s) was obtained followed by a non-contrast c-arm CT (8s DR Body DynaCT preset, Artis Zee, Siemens). Superselective catheterization of the kidney pole was then performed followed by a DSA during hand injection of contrast. XEBs were then injected intra-arterially, without the addition of iodinated contrast, into the selected kidney pole during suspended respiration while acquiring a DSA (3 frames/second). C-arm CTs were obtained to document XEB visibility and retention. Serial c-arm CTs were obtained in chronic animals. Endotoxin assays of XEBs were performed in all chronic studies. Histopathology was performed on the kidneys in all animals. **Results:** Radiopacity in the phantom on c-arm CT was equivalent to bone for 5 µl XEB (2774 ± 1595 HU), 50 µl XEB (2809 ± 1208 HU), and 10% iohexal (1482±354 HU) (Fig 1a). Transarterial delivery of XEBs was visualized by DSA in all pigs with total occlusion achieved after 0.05-0.1 ml of XEBs. Reflux or retrograde flow of XEBs was seen in 28% of the studies. The volume of radiopacity created by the XEBs on c-arm CT was reduced at 1 week follow-up with minimal presence of radiopacity at 3 weeks post-administration (Fig 1b-d). XEBs were intact acutely and at three weeks post injection with minimal inflammatory infiltrate and fibrosis consistent with renal infarction by XEBs (Fig 1e). All XEB samples were negative for endotoxin. **Conclusions:** X-ray-visible, uniform embolic beads allow confirmation of delivery success using conventional X-ray imaging systems without the addition of iodinated contrast agents. Biocompatibility of XEBs was high with no noted toxicities or adverse events. XEBs also offer the ability to see reflux of embolic nanoparticles to non-target locations.

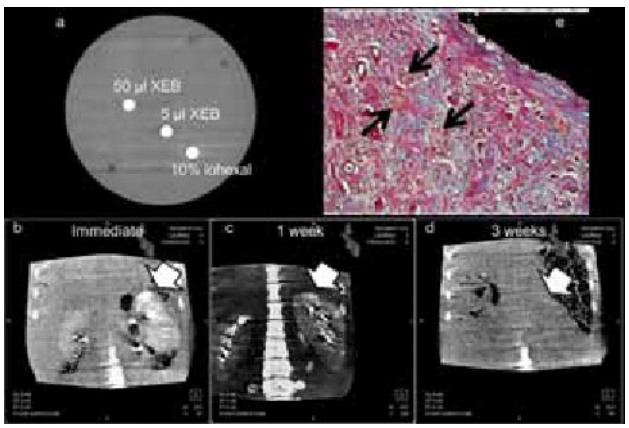


Fig 1: (a) c-arm CT showing similar signal intensity for 5 µl XEB, 50 µl XEB, and 10% iohexal. (b-d) Serial coronal multiplanar reformats of c-arm CT showing XEB in the superior pole (white arrows) of the left kidney immediately (b), 1 week (c), and 3 weeks (d) after injection. (e) photomicrograph of trichrome staining showing intact XEB (black arrows) at 3 weeks and minimal fibrosis in the embolized kidney.

Disclosure of author financial interest or relationships:
**D. Kraitchman**, SIemens Healthcare, Grant/research support; Boston Scientific Corporation, Grant/research support; Surefire Medical, Inc., Grant/research support; MRI Interventions, Other financial or material support; **C.R. Weiss**, SIR (society of interventional radiology), Grant/research support; Siemens, Grant/research support; Amyrsis Publishing, Consultant; Siemens, Speakers bureau; **C. Beh**, None; **C. Hu**, None; **P.A. DiCamillo**, None; **Y. Fu**, None; **J.A. Cook**, None; **K.L. Gabrielson**, None; **T. Wang**, None; **H. Mao**, None.

Presentation Number **P823**
Poster Session 4
September 8, 2012 / 14:45-14:45 / Room: The Liffey

# Correlation of Bio-distribution based on NanoSPECT/CT images of 188Re-liposome in SD Rats

***An-Jim Long**, Ching-Yu Hsu, Tsui-Jung Chang, Chih-Hsien Chang, Institute of Nuclear Energy Research, Taoyuan County, Taiwan.*
*Contact e-mail: jimlong@iner.gov.tw*

Introduction: SPECT has been widely accepted for quantification of radioisotope. Comparison of quantification from planar and SPECT were proposed and evaluated. This is the first study to evaluate bio-distribution of 188Re-labeled liposomes in Rat which is critical because 188Re-labeled liposomes clinical trial will be conducted early 2012. According to past studies the maximal tolerance dosage (MTD) of 188Re is limited due to its major energy of beta emission and imaging of 188Re is difficult since it has only 15% gamma emission rate therefore standard model for bio-distribution based on SPECT/CT is then important. Bio-distribution evaluation will be made to human only via the SPECT/CT imaging. Methods: Bio-distribution studies of Rat after intravenous (i.v.) administration was performed via sacrificing (n=3 per time frame) versus imaging of the animals (n=3). NanoSPECT/CT with 2mm multiple pinhole collimators and apertures were used to image the animals. Agreement of radioactivity and %ID/g measurements was assessed by Lin's concordance correlation coefficient (CCC). Results: Liver %ID/g varies from 0.224%-0.466% for imaging group and 0.387%-1.359% for sacrificing group at 24H post injection, and 0.826%-1.129% or imaging group and 0.325%-0.804% 48H post injection. Spleen %ID/g varies from 5.153%-9.059% for imaging group and 9.995%-20.232% for sacrificing group at 24H post injection, and 3.753%-13.5% or imaging group and 3.305%-21.623% 48H post injection. All studies were examined and confirmed significantly agreed (CCC=0.938). Conclusions: SPECT/CT bio-distribution based on SPECT/CT of 188Re-liposome confirmed high agreement compared to traditional way to calculate bio-distribution of sacrificing animals.

Disclosure of author financial interest or relationships:
**A. Long**, None; **C. Hsu**, None; **T. Chang**, None; **C. Chang**, None.

Presentation Number **P824**
Poster Session 4
September 8, 2012 / 14:45-14:45 / Room: The Liffey

# Improved lymph node staging with dedicated breast 18F-FDG PET-CT in cancer patients: comparison with 3T CE-MRI

***Heinrich F. Magometschnigg***, *Katja Pinker-Domenig, Hubert Bickel, Benedikt Brück, Georg J. Wengert, Thomas H. Helbich, Radiology, Medical University Vienna, Vienna, Austria. Contact e-mail: h.magometschnigg@gmail.com*

Introduction Recent years have shown a significant shift towards conservative management of the axilla, but there is controversy which patients should be treated with axillary lymph node dissection (ALND). Nevertheless, there is agreement that patients with macrometastases should receive ALND. The aim of this study is to assess the sensitivity and specificity of dedicated breast PET-CT in the detection of lymph node metastases and to compare it with contrast-enhanced high field MRI of the breast (3T CE-MRI). Materials and Methods 74 patients with biopsy proven breast cancer were included in this IRB approved prospective study. All patients were examined with dedicated 18F-FDG PET-CT and 3T CE-MRI. Examinations were scheduled no longer than 3 days apart. MRI protocol included: a T2-weighted sequence and a contrast-enhanced 3D-T1-weighted sequence before and after application of a standard dose Gd-DOTA. All patients were subjected to 18F-FDG PET-CT scanning using a combined PET-CT in-line system (Biograph, Siemens, Erlangen, Germany). A prone PET dataset over the breasts and the axilla was acquired allowing the same patient geometry as in breast MRI. Patients were injected with approximately 300 MBq 18F-FDG. Scanning was started 45 min after injection. CT data was only used for attenuation correction. In 3T CE-MRI lymph nodes were considered positive for malignancy if there was enlargement >1cm, thickened cortex, loss of fatty hilum, matted nodes or an irregular node contour. In PET-CT a lymph node was classified as positive when 18F-FDG-uptake was greater than blood-pool activity. All nodes were histopathologically verified by lymph node biopsy, intraoperative sentinel- or axillary dissection. Sensitivity and specificity for 3T CE-MRI and PET were calculated. Results 18F-FDG PET-CT achieved a sensitivity of 79% and a specificity of 98%. PPV was 0.95 (CI 0.76-0.99), and NPV was 0.91 (CI 0.8-0.96). Diagnostic accuracy was 0.92. CE-MRI had a sensitivity of 74% and a specificity of 84%. PPV was 0.68 (CI 0.48-0.83) and NPV was 0.88 (CI 0.76-0.94). Diagnostic accuracy was 0.81. 24 nodes were positive and 50 nodes were negative for malignancy. The mean SUVmax of lymph node metastases was 5.52 (range 1.14 - 12.75). Conclusion 18F-FDG PET-CT enables an improved identification of lymph node metastases in breast cancer patients as compared to 3T CE-MRI. Clinical relevance In patients with positive lymph nodes detected by dedicated breast PET-CT technology a sentinel lymph node biopsy can be omitted and surgeons can proceed immediately to ALND.

Disclosure of author financial interest or relationships:
**H.F. Magometschnigg**, None; **K. Pinker-Domenig**, None; **H. Bickel**, None; **B. Brück**, None; **G.J. Wengert**, None; **T.H. Helbich**, Siemens, Grant/research support; Fond national bank austria, Grant/research support .

Presentation Number **P825**
Poster Session 4
September 8, 2012 / 14:45-14:45 / Room: The Liffey

# Imaging CXCR4 expression in breast and lung cancer metastasis models using [64Cu]AMD3465

*Mrudula Pullambhatla, Lauren Woodard, Ravindra de Silva, Vishwa Kundoor, Kevin Peyre, Ala Lisok, Zaver M. Bhujwalla, Martin Pomper, **Sridhar Nimmagadda**, Radiology, Johns Hopkins University, Baltimore, MD, USA. Contact e-mail: snimmag1@jhmi.edu*

The chemokine receptor 4 (CXCR4) is highly expressed in several cancers including breast and lung cancers. CXCR4, along with its ligand CXCL12 is generally elevated in such lesions and plays a critical role in metastasis. Breast and lung tumors with high CXCR4 surface expression are more likely to metastasize and result in poor prognosis. CXCR4 based imaging probes can be used i) to evaluate primary tumors for elevated CXCR4 expression and therapeutic intervention and ii) to screen for secondary metastatic spread to local and distant sites. Here we evaluate the potential of a CXCR4-based imaging agent to image graded levels of CXCR4 expression in subcutaneous, orthotopic and metastasis models of breast and lung cancers. Studies were performed in bone and spontaneous metastasis models of breast cancer and orthotopic and subcutaneous tumor models of lung cancer in SCID mice with [64Cu]AMD3465-PET. AMD3465 was radiolabeled with [64Cu]Cu(OAc)2 at pH 5.5. Bone metastases were generated by left cardiac ventricular injection of MDA-MB-231 cell line expressing luciferase (231-Luc) cells (n = 7). 231-Luc derived spontaneous metastases were generated by resection of primary tumors (~ 400 mm3) (n = 10) and metastatic spread was imaged at 30 days post-resection by [18F]FDG-PET, [64Cu]AMD3465-PET and bioluminescence (BLI) imaging. Whole body PET images were acquired at 60 and 90 min after the injection of [18F]FDG and [64Cu]AMD3465, respectively. Based on BLI data, regions of interest were drawn over metastatic sites on the PET images. Radioactivity uptake was calculated as %ID/cc and tumor-to-muscle (T/M) ratios were obtained. Similarly, small cell lung cancer cell lines H82 (CXCR4low), H69(CXCR4high) and the non-small cell lung cancer cell line A549 (CXCR4low) were used to generate subcutaneous and orthotopic xenografts, respectively. Image acquisition and analysis was performed as described in breast cancer models. CXCR4 expression of tumors and metastatic tissue was confirmed with immunohistochemistry and qRT-PCR. Bone metastases were clearly detectable on the PET images and exhibited mean T/M ratio of 12.8 (range: 6.6 - 21.7) while that of control bone was 7.6 (4.0 - 11.4). MDA-MB-231 primary tumors exhibited mean T/M ratio of 8.5 (4.0 - 14.3) while that of the metastases was 17.4 (3.7 - 44.5). PET imaging and biodistribution studies demonstrated selective accumulation of radioactivity in H69 compared to H82 tumors at 9.3 ± 0.5 and 2.13 ± 0.2 %ID/cc, respectively. Furthermore, accumulation of radioactivity was observed in the orthotopic A549 lung tumors at 10.5 ± 0.9 %ID/cc compared to the contralateral lung at 3.1 ± 0.08 %ID/cc. In an A549 tumor mouse, elevated radioactivity accumulation was observed in lymph node metastases compared to the primary tumor. Metastases that originated from the same tumor have variable levels of CXCR4 expression, which could be detected by CXCR4-based imaging agents in breast and lung cancer models.

Disclosure of author financial interest or relationships:
**M. Pullambhatla**, None; **L. Woodard**, None; **R. de Silva**, None; **V. Kundoor**, None; **K. Peyre**, None; **A. Lisok**, None; **Z.M. Bhujwalla**, None; **M. Pomper**, None; **S. Nimmagadda**, None.

Presentation Number **P826**
Poster Session 4
September 8, 2012 / 14:45-14:45 / Room: The Liffey

# Tumor imaging biomarkers: a method for imaging protocol assessment and optimization using pharmacokinetic modeling

***Kelly D. Orcutt**, Catey L. Harwell, Jacob Hesterman, Jack Hoppin, inviCRO, Boston, MA, USA. Contact e-mail: orcutt@invicro.com*

Background: Tumor imaging biomarkers can be used to probe antigen density in vivo on a whole body, longitudinal, noninvasive and quantitative level. Many parameters affect image signal including tumor properties (e.g. antigen density, vascularity), ligand properties (e.g. affinity, blood clearance), and imaging parameters (e.g. injected activity, mass dose, imaging protocol). We present an assessment of a mechanistic pharmacokinetic (PK) model of tumor uptake and its ability to accurately estimate antigen density in vivo for various imaging protocols. Methods: A mechanistic model based on the published Krogh cylinder model was used to simulate clinical image data for integrin-binding 18F-galacto RGD using parameters obtained from the literature and varying tumor vascularity and integrin density over physiological ranges. Simulations were compared to published clinical PET data and ex vivo immunohistochemistry. Simulated image data were generated for six different tumors with high, medium, and low antigen expression (100, 10, and 1 nM), and high and low vascularity (50 and 150 μm mean capillary to capillary half-distance) for four different dynamic imaging protocols. Antigen density was estimated for each of fifty noisy data sets for each tumor type and each imaging protocol by fitting the model to the simulated data. Results: The mechanistic model accurately predicted the published mean standardized uptake value (SUV) of ~0.4 at 90 min post-injection for tumors with no integrin expression and the trend in increasing mean SUV for increasing integrin expression (Figure 1). All SUV clinical data is within the expected range of results from model simulations. From this initial analysis, it was determined that antigen density cannot be estimated from a single imaging time point. We therefore assessed four dynamic imaging protocols. Antigen density estimations for highly vascularized tumors are more accurate than estimations for weakly vascularized tumors for all dynamic protocols tested with an average bias of 5-35% and 30-500%, respectively. An imaging protocol that captures early 18F-galacto RGD kinetics (between 0 and 30 min post-injection) leads to the most accurate estimation of antigen density for highly vascularized tumors (<25% average bias). A protocol that captures later tracer kinetics (out to 90 min post-injection) leads to the most accurate estimation of antigen density for weakly vascularized tumors (30-100% average bias). Conclusions: We present a mechanistic model of tumor targeting and demonstrate its value in guiding imaging protocol selection. We analyze 18F-galacto RGD as an imaging biomarker and conclude that a single static imaging time point is insufficient to estimate antigen density. Dynamic imaging protocols demonstrated significant improvement in estimating antigen density in vivo compared to a single time point. We predict quantitative estimation of antigen density in vivo is achievable using an imaging biomarker, a dynamic imaging protocol, and PK modeling. Furthermore, modeling and simulation can be used a priori to assess parameter estimability for different imaging protocols.

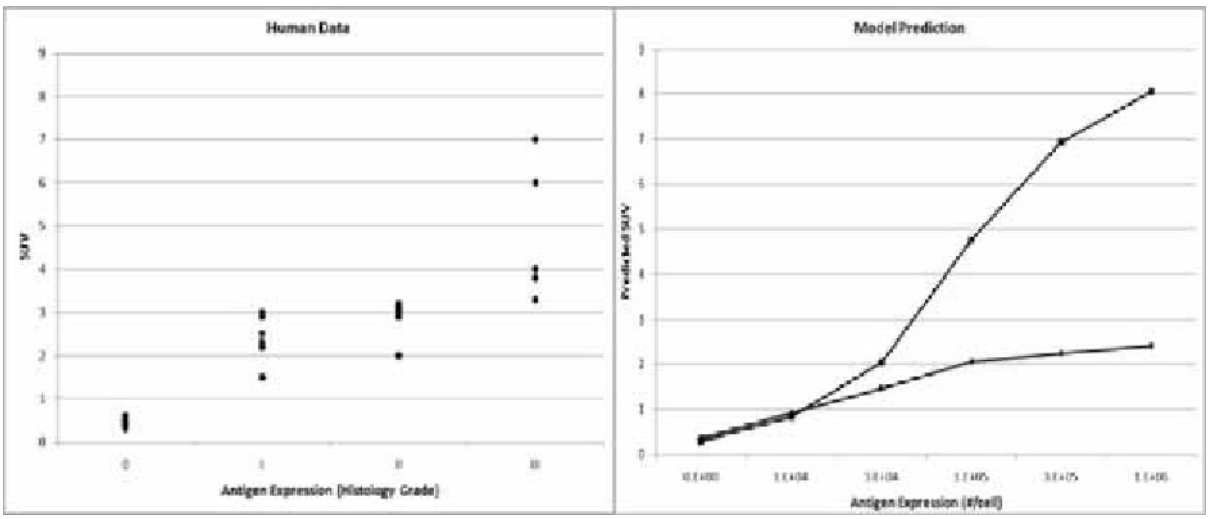


Figure 1. Comparison of model simulation with experimental data. 18F-galacto RGD clinical imaging data versus immunohistochemistry grade (left). 18F-galacto RGD simulated clinical imaging data for highly vascularized (top line) and weakly vascularized (bottom line) versus antigen density.

Disclosure of author financial interest or relationships:
**K.D. Orcutt**, inviCRO, Employment; **C.L. Harwell**, inviCRO, LLC, Employment; **J. Hesterman**, inviCRO, Employment; **J. Hoppin**, inviCRO, LLC, Employment; inviCRO, LLC, Stockholder .

Presentation Number **P827**
Poster Session 4
September 8, 2012 / 14:45-14:45 / Room: The Liffey

# Imaging of a Somatostatin Receptor-Cytosine Deaminase Fusion Gene

***Jesse J. Parry***[1], *Kimberly A. Lears*[1], *Rebecca Andrews*[1], *Kim Nguyen*[2], *Thaddeus J. Wadas*[3], *Buck Rogers*[1,2], [1]*Radiation Oncology, Washington University School of Medicine, St. Louis, MO, USA;* [2]*Mallinckrodt Institute of Radiology, Washington University School of Medicine, St. Louis, MO, USA;* [3]*Cancer Biology, Wake Forest University, Winston-Salem, NC, USA. Contact e-mail: jparry@radonc.wustl.edu*

Suicide gene therapy is a process by which cells are administered a gene that encodes a protein capable of converting a nontoxic prodrug into an active toxin. Cytosine deaminase (CD) has been widely investigated as a means of suicide gene therapy due to the enzyme's ability to convert the prodrug 5-fluorocytosine (5-FC) into the toxic compound 5-fluorouracil (5-FU). However, the extent of gene transfer is a limiting factor in predicting therapeutic outcome. The ability to monitor gene transfer, non-invasively, would strengthen the efficiency of therapy. In this regard, we have constructed and evaluated a replication-deficient adenovirus (Ad) containing the human somatostatin receptor subtype 2 (SSTR2) fused with a C-terminal yeast CD gene for the non-invasive monitoring of gene transfer and therapy. The resulting Ad (AdSSTR2-yCD) was previously evaluated in vitro in MCF-7 breast cancer cells to determine the function of the fusion protein. These studies demonstrated that the both the SSTR2 and yCD were functional in binding assays, 5-FC conversion assays, and cytotoxicity assays. The Ad was then evaluated in vivo using conversion assays, biodistribution studies, and small animal positron-emission tomography (PET) imaging studies. For the in vivo studies, MCF-7 xenografts were established in estradiol-supplemented SCID mice, upon which the AdSSTR2-yCD was administered intratumorally at either $1 \times 10^9$ plaque forming units (pfu)/mL or $3 \times 10^9$ pfu/mL. The in vivo 5-FC conversion rates were 193 ± 41 pmol/min/mg and 698 ± 81 pmol/min/mg for $1 \times 10^9$ pfu/mL or $3 \times 10^9$ pfu/mL, respectively. The biodistribution of 64Cu-CB-TE2A-Y3-TATE following injection of AdSSTR2-yCD was 1.55 ± 0.11% ID/g, with AdSSTR2 being 1.73 ± 0.14% ID/g. MicroPET imaging of tumors injected with AdSSTR2-yCD showed significant uptake of 64Cu-CB-TE2A-Y3-TATE as compared to tumors injected with saline, as determined by SUV analysis. In conclusion, the fusion protein has been validated as useful for the non-invasive imaging of yCD expression and will be evaluated in the future for monitoring yCD-based therapy.

Disclosure of author financial interest or relationships:
**J.J. Parry**, None; **K.A. Lears**, None; **R. Andrews**, None; **K. Nguyen**, None; **T.J. Wadas**, None; **B. Rogers**, None.

Presentation Number **P828**
Poster Session 4
September 8, 2012 / 14:45-14:45 / Room: The Liffey

# ROLE OF 68GALLIUM DOTATATE IN NEUROENDOCRINE TUMORS-FIRST EXPERIENCE

***Jyotsna Rao**, Kavitha Nallapareddy, Alka A. Chengapa, Mansoor M. Mohiuddin, Apollo Gleneagles PET CT Ctr, Hyderabad, India.*
*Contact e-mail: jyotsnael@gmail.com*

There is a need for sensitive tracers in localizing neuroendocrine tumors, specifically, the well differentiated type. 68Ga DOTANOC/DOTATATE fulfills this need and we present our first experience using this tracer. Aim: To evaluate the role of 68Ga DOTANOC/DOTATATE in the management of neuroendocrine tumors. Material and methods: Reports of 45 patients scanned from December 2010 to February 2012 were reviewed retrospectively. The patients were referred with neuroendocrine tumors. 3-4 mCi of the tracer was injected intravenously and patients were scanned after 45 minutes from the base of skull to the mid thigh region. All patients were given oral and intravenous contrast. Scans were reported by a radiologist and PET physician. Additional FDG PET/CT scan was performed in 2 patients. Follow up data were obtained in where possible. Results: Of the 45 patients scanned, 11/45(24%) were referred of diagnosis of the primary. Of these, 6/11 (55%) were negative, 4/11(36%) were positive and 1/11 (9%) equivocal. All 4/45(9%) patients referred for staging showed positive findings on the scans. Of the 25/45 (56%) patients referred for restaging, 15/25 (60%) showed positive findings, 9/25 (36%) negative and 1/25 (4%) equivocal findings. All 4/45(9%) patients referred to monitor response to therapy were positive. 1/45 (2%) patient referred for radiation therapy planning was positive (100%). Equivocal cases included mild diffuse activity in the pancreas in a patient referred for diagnosis and mild activity in bilateral axillary nodes in patients referred for restaging. Tumors scanned included neuroendocrine tumors, carcinoid, Cushing's, neuroblastomas, glomus tumors, medullary thyroid carcinoma, paraganglioma, recurrent and meningioma. Conclusion: 68Ga DOTATATE proved useful in the patients with neuroendocrine tumors of various types and should be considered in the work up particularly for well differentiated tumors.

Disclosure of author financial interest or relationships:
**J. Rao**, None; **K. Nallapareddy**, None; **A.A. Chengapa**, None; **M.M. Mohiuddin**, None.

Presentation Number **P829**
Poster Session 4
September 8, 2012 / 14:45-14:45 / Room: The Liffey

# Intraoperative evaluation of blood perfusion ofthe gastric tube afteresophagectomy with near-infrared fluorescence imaging

***Masaki Sano***[1,2], *Shinichirou Miyazaki*[1,3], *Kinji Kamiya*[1,3], *Naoki Unno*[1,2], *Mikako Ogawa*[4], *Hiroyuki Konno*[1,2], *[1]Surgery 2, Hamamatsu University School of Medicine, Hamamatsu-shi, Japan; [2]Vascular Surgery, Hamamatsu University School of Medicine, Hamamatsu-shi, Japan; [3]Gastroenterological Surgery, Hamamatsu University School of Medicine, Hamamatsu-shi, Japan; [4]Molecular Imaging, Applied Medical Photonics Laboratory, Medical Photonics Research Center, Hamamatsu University School of Medicine, Hamamatsu-shi, Japan. Contact e-mail: masakisurgeon@gmail.com*

Background and Objective: Gastric tube reconstruction was performed most frequently after transhiatalesophagectomy. Anastomotic fistula is one of the frequent causes of postoperative morbidity and mortality, and ischemia of the gastric tube is the main cause of anastomotic fistula. But it is difficult to evaluate blood perfusion of the gastric tube precisely and intraoperatively. Near-infrared fluorescence imaging with indocyanine green (ICG) has been applied in various fields, but not applied to evaluate blood perfusion of gastrointestinal tract so far. We made rat model of lower intestinal blood flow with ligation of peripheral superior mesenteric artery and performed near-infrared fluorescence imaging of intestine. We generateda time-intensity curve from near-infrared fluorescence imaging, and measured the time to half-maximum brightness (T1/2). In the rat model, T1/2 was longer in the ischemic intestine compared to control (Supplemental Fig.1). It was considered that T1/2 could detect ischemia of gastrointestinal tract. We evaluate blood perfusion of the gastric tube in human with near-infrared fluorescence imaging intraoperatively and investigate the relationship between blood perfusion and postoperative anastomotic fistula. Methods: Patients who underwent esophagectomy and gastric tube reconstruction for thoracic esophageal cancer in our hospital between January 2011 and October 2011 were included in this study. After gastric tube reconstruction, near-infrared fluorescence imaging of the gastric tube was performed with injection of ICG (5mg/mL, 1mL) via central vein. Then, the time-intensity curves were generatedfromnear-infrared fluorescence imagingto calculate T1/2 in chest wall, cervical esophagus, and gastric tube (oral and anal side) intraoperatively. At 7 days after surgery, esophagography was performed inall patients to evaluate anastomotic fistula and investigated the relationship between T1/2 and anastomotic fistula. Result: 11 patients (10 male, 1 female, mean age 62.5±2.5 years) were included in this study (Supplemental Table1). Anastomotic fistula was detected in 4 patients. The average of T1/2 in oral side of the gastric tube was 8.0±1.1 sec in the patients without fistula and 17.3±1.8 sec in the patients with fistula (p=0.002) (Table1,Fig.1). Conservative treatment was performed to all patients with fistula, and all were recovered. Conclusion: In the patients with fistula, T1/2 was longer compared to patients without fistula. This means T1/2 could evaluate the blood perfusion and detect ischemia of gastrointestinal tract. Evaluation of blood perfusion of the gastric tube before anastomosis may prevent anastomotic fistula. Intra-operative near-infrared fluorescence imaging was useful to evaluate blood perfusion of gastrointestinal tract.

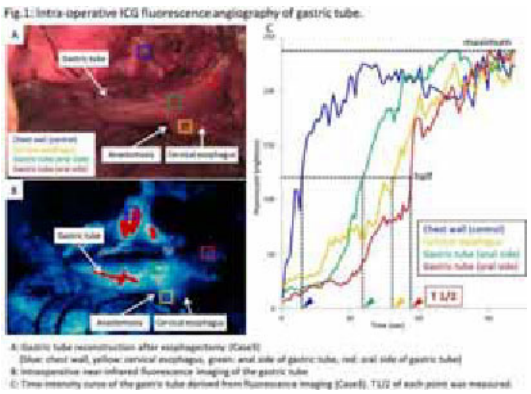

Table1: Comparison of patients with anastomotic fistula and without fistula

| | | | |
|---|---|---|---|
| n | 4 | 7 | |
| Age | 66.0±3.5 | 60.0±2.9 | |
| T1/2 (sec) | | | p-value |
| Chest wall (Control) | 3.2±0.7 | 2.1±0.2 | 0.2053 |
| Cervical esophagus | 5.7±1.4 | 4.3±1.1 | 0.0557 |
| Gastric tube (Anal side) | 4.9±1.7 | 3.0±0.5 | 0.1961 |
| Gastric tube (Oral side) | 17.3±1.8 | 8.0±1.1 | 0.0021 |

Disclosure of author financial interest or relationships:
**M. Sano**, None; **S. Miyazaki**, None; **K. Kamiya**, None; **N. Unno**, None; **M. Ogawa**, None; **H. Konno**, None.

Presentation Number **P830**
Poster Session 4
September 8, 2012 / 14:45-14:45 / Room: The Liffey

# Feasibility of simultaneous MR/PET imaging in juveniles - comparison with PET/CT

***Nina F. Schwenzer***[1], *Sergios Gatidis*[1], *Brigitte Gueckel*[1], *Ilias Tsiflikas*[1], *Holger Schmidt*[1,2], *Cornelia Brendle*[1], *Christina Pfannenberg*[1], *Matthias Reimold*[1], *Claus D. Claussen*[1], *Jürgen Schäfer*[1], [1]*Department of Radiology, University of Tuebingen, Tuebingen, Germany;* [2]*Department of Preclinical Imaging and Radiopharmacy, Eberhard Karls University of Tuebingen, Tuebingen, Germany. Contact e-mail: nina.schwenzer@med.uni-tuebingen.de*

In comparison with positron emission tomography / computed tomography (PET/CT) new whole-body magnetic resonance / positron emission tomography (MR/PET) systems offer the possibility of whole-body MR imaging with distinct reduction in radiation exposure compared with PET/CT. Therefore, it is mandatory to evaluate the imaging quality of MR/PET in comparison with PET/CT. The present study for juveniles was proved by our local ethic committee. Nine patients (mean age 14 years, range 11-18 years) suffering from various solid tumors were examined in the whole-body MR/PET scanner (Biograph mMR, Siemens Healthcare). First, a 18F-fluorodeoxyglucose (FDG)-PET/CT (Biograph mCT 128, Siemens Healthcare) was performed in all patients with the following parameters: body-weight adapted injected dose of 4 MBq/kg body-weight, uptake time 60.6 ± 1.4 min. Subsequently, the patients were referred to the MR/PET suite. The whole-body PET/MR system comprises 56 detector cassettes with a 59.4 cm transaxial and 25.8 cm axial field of view; bore size: 60 cm. The following parameters for PET acquisition were applied: uptake time 131.5 ± 13.9 min. Coronal STIR and axial DWI MR images were recorded simultaneously for each bed during the PET acquisition. In PET/CT, the acquired PET data were reconstructed with an iterative 3D Ordered-Poisson Ordered Subset Expectation Maximization (OP-OSEM) algorithm using 2 iterations and 21 subsets, Gaussian filter of 2 mm. In MR/PET, an iterative 3D OSEM algorithm using 3 iterations and 21 subsets and Gaussian filter of 3 mm were used. In MR/PET, a T1-weighted FLASH sequence with Dixon-based fat-water separation was applied to derive a segmentation-based PET attenuation correction map. Image quality and artifacts, standardized uptake values (SUV) in tumor and control regions using a volume of interest (VOI) analysis as well as tracer distribution were analysed. In all patients, diagnostic image quality was reached for MR/PET. No significant artifacts were detected in the simultaneously acquired MR images by the built-in PET detector. All MR/PET acquisitions were performed successfully in juveniles. Image quality of the MR sequences was comparable with a standard 3 Tesla scanner. The visual impressions of the PET images were similar between PET/CT and MR/PET. The mean difference of SUVs [(SUVMR/PET-SUVPET/CT)/SUVPET/CT] of the target regions were as follows: Tumor -6.1 ± 13.9%, lung -15.7 ± 15.3%, liver -14.9 ± 10.3%, muscle 2.7 ± 20.3% , bone marrow -3.1 ± 16.8%, blood pool -39.1 ± 9.1%. In 3 cases (2 soft tissue tumors and 1 neuroblastoma) additional information were provided by higher soft tissue contrast of MR imaging and the use of DWI compared to the anatomical information given by CT. MR/PET is a promising modality for juveniles with comparable SUV measurement in malignant lesions compared with PET/CT. Furthermore, additional information is given by the MR component especially regarding soft tissue lesions. Concerning physiological tracer uptake in healthy tissue, differences were observed between PET/CT and MR/PET, probably due to biological effects due to the longer uptake-time.

Disclosure of author financial interest or relationships:
**N.F. Schwenzer**, Siemens, Grant/research support; **S. Gatidis**, None; **B. Gueckel**, Siemens Healthcare, Grant/research support; **I. Tsiflikas**, None; **H. Schmidt**, Siemens, Grant/research support; **C. Brendle**, None; **C. Pfannenberg**, None; **M. Reimold**, None; **C.D. Claussen**, None; **J. Schäfer**, None.

Presentation Number **P831**
Poster Session 4
September 8, 2012 / 14:45-14:45 / Room: The Liffey

# UTE MRI as a viable alternative for CT based RT Planning

***Ravi T. Seethamraju***[1], *Sandeep S. Hedgire*[2], *Mukesh G. Harisinghani*[2], [1]*MR R&D, Siemens Medical Solutions, USA Inc., Boston, MA, USA;* [2]*Radiology, Massachusetts General Hospital, Boston, MA, USA. Contact e-mail: ravi.seethamraju@siemens.com*

Aim: To develop MR as the imaging modality of choice for image guided radio therapy planning. Background: Currently with the emphasis on reduction of CT imaging due to concerns of radiation overdose, it is essential to develop alternatives to CT for image guided radio therapy planning. Though MR has excellent soft tissue contrast, it falls short when imaging bones. The skeletal system is an essential guiding element in the case RT planning due to its rigidity. UTE has already proven to be the sequence of choice in MR-PET scanners for providing attenuation correction in the head. With proper optimization this property can be extended to the body also. Here we demonstrate with the help of UTE imaging that it is possible to achieve bone segmentation and hence pave the way for MR as an alternative. Methods:In an IRB approved study, 8 patients with pancreatic cancer were scanned with a UTE sequence at 3T with TR/TE set to 47ms/50μs at a 3D FOV of 380mm with 2mm isotropic resolution. The number of radials was set at 9000 to bringing the acquisition time to 17seconds, which is well within the limits of normal breath holding for most patients. Also a 3D VIBE sequence set to TR/TE of 2.89ms/0.85ms was acquired for comparison. The UTE sequence was acquired with and without Fat saturation. Results: Fig 1a is an axial slice from a VIBE acquisition, 1b is from a UTE with no fatsat, 1c is from UTE with fatsat and 1d is a coronal reconstruction showing the spine and parts of the pelvis. From this figure it is clear that UTE inherently has better contrast in the spine, however adding fat saturation increases the conspicuity of the bone enabling for better bone segmentation. Conclusion: With improvement in MR techniques like UTE imaging it is possible develop MR as a surrogate for CT. Augmenting the MR sequences with post processing techniques can greatly help in moving MR towards RT planning.

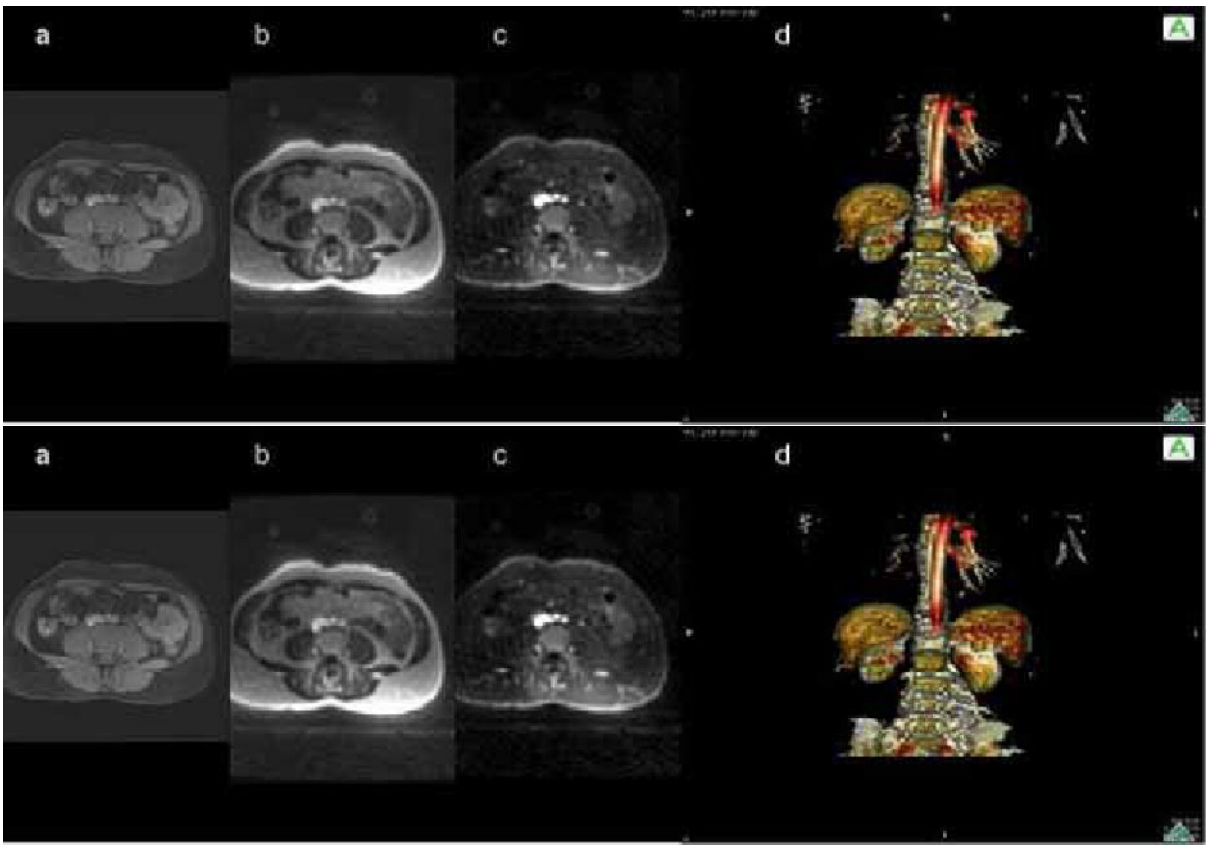


Disclosure of author financial interest or relationships:
**R.T. Seethamraju**, Siemens Medical Solutions, USA Inc., Employment; **S.S. Hedgire**, None; **M.G. Harisinghani**, None.

Presentation Number **P832**
Poster Session 4
September 8, 2012 / 14:45-14:45 / Room: The Liffey

# Cell-surface marker discovery for colorectal cancer

***Kamini Sewda***[1], *Steven Enkemann*[2], *Jonathan W W. Wojtkowiak*[3], *Alexis S. Lopez*[4], *Domenico Coppola*[5], *David Shibata*[6], *Timothy J. Yeatman*[7], *David L. Morse*[8], [1]*Cancer Imaging and Metabolism, H Le Moffitt Cancer Center and Research Institute, Tampa, FL, USA;* [2]*Molecular Genomics Shared Resource, H Le Moffitt Cancer Center and Research Institute, Tampa, FL, USA;* [3]*Cancer Imaging and Metabolism, H Le Moffitt Cancer Center and Research Institute, Tampa, FL, USA;* [4]*Tissue Core Facility, H Le Moffitt Cancer Center and Research Institute, Tampa, FL, USA;* [5]*Anatomic Pathology, H Le Moffitt Cancer Center and Research Institute, Tampa, FL, USA;* [6]*Gastrointestinal Tumor, H Le Moffitt Cancer Center and Research Institute, Tampa, FL, USA;* [7]*Gastrointestinal Tumor, H Le Moffitt Cancer Center and Research Institute, Tampa, FL, USA;* [8]*Cancer Imaging and Metabolism, H Le Moffitt Cancer Center and Research Institute, Tampa, FL, USA. Contact e-mail: kamini.iitd@gmail.com*

Colorectal cancer (CRC) has the third highest mortality rate of all cancers in the United States and Europe. CRC is a treatable disease if detected early, and screening is recommended for persons ≥ 50 years of age. Early diagnosis allows for treatment and improved survival. Colonoscopy is the standard of care for detection of early-stage CRC, which is an invasive procedure that requires a cathartic bowel preparation and general anesthesia. Consequently, less invasive screening methods are highly desirable. Virtual colonoscopy (VC) by CT or MRI imaging are less-invasive methods for screening CRC. However, VC methods still require a bowel preparation and insufflation of the bowel, and could still be improved in terms of sensitivity and specificity. Our long-term goal is to develop a targeted molecular imaging technique that can improve the standard VC methods by the specific and sensitive detection of smaller and flat (serrated) lesions with fewer false positives and no false negatives. This novel molecular imaging method could be used to segment patients that are in need of colonoscopy, sparing patients that are not in need and improving compliance. The first step toward achieving this goal is the discovery of cell-surface markers for CRC that can be used to develop molecular imaging probes. To accomplish this, gene expression profiling of DNA microarray data from 432 adenocarcinomas, 39 adenomas and 16 inflammatory bowel disease; and unaffected patient tissue samples (178 colon, 6 small intestine, 4 stomach, 4 esophagus, 4 trachea, 3 oral mucosa and 3 tonsil) was performed. Data were filtered using a previously compiled list of 3,800 cell surface genes from the NCBI Gene Expression Omnibus database. Of these, 1085 genes were broadly expressed in CRC and were ranked by differential expression in adenomas and adenocarcinomas vs. normal tissues. Six cell-surface markers CLDN1, GPR56, GRM8, LY6G6D, SLC01B3 and TLR4 were identified that are highly and broadly expressed as mRNA in adenomas and adenocarcinomas relative to unaffected colon tissue (Figure 1a). To confirm protein expression, immunohistochemistry of normal (n=15) and CRC (16 adenoma and 60 adenocarcinoma) patient tissue samples and 26 CRC cell lines was performed (Figure 1b). When heterogeneity of expression is considered in normal colon epithelial cells relative to a high density of expression in CRC, all six markers were highly and broadly expressed in adenomas and adenocarcinomas compared to normal colon. Nearly all of the CRC samples were covered by three of the markers where and at least one of claudin-1, toll-like receptor 4, and protein(s) Ly6-D/F were expressed in 97% of the tissue samples based on a ≥4 score. These markers were further validations by determining the expression profile in the eight CRC cell lines by qRT-PCR, Western blot and immunocytochemistry. In conclusion, we have confirmed high protein expression of six cell-surface markers in CRC relative to surrounding unaffected colon tissue. Hence, these markers can potentially be used to develop molecular imaging probes for screening of CRC. Development of specific binding ligands for selected targets is underway.

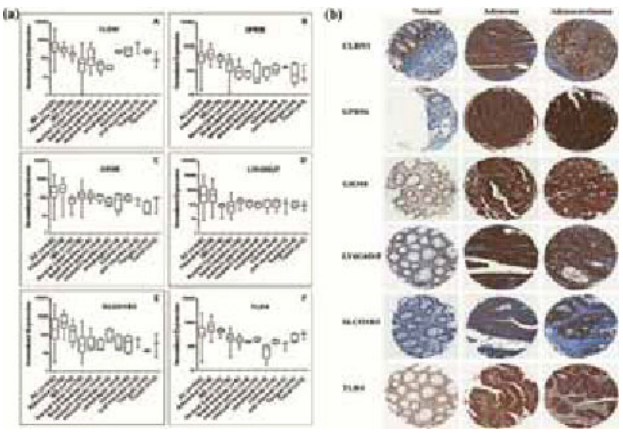


*Protein expression is shown but gene names are used to conserve space. Figure 1. (a) DNA microarray expression profiles of CRC cell-surface markers. Values are presented as a box plot using log10 scale. (b) Representative images of immunohistochemical staining for markers in patient tissue samples of unaffected/normal colon, colon adenoma and adenocarcinoma.

Disclosure of author financial interest or relationships:
**K. Sewda**, None; **S. Enkemann**, None; **J.W. Wojtkowiak**, None; **A.S. Lopez**, None; **D. Coppola**, None; **D. Shibata**, None; **T.J. Yeatman**, None; **D.L. Morse**, LiCor, Other financial or material support; Intezyne Technologies, Other financial or material support .

Presentation Number **P833**
Poster Session 4
September 8, 2012 / 14:45-14:45 / Room: The Liffey

# Preliminary studies of 99mTc-EC-DG SPECT/CT for evaluation of treatment response evaluation in head and neck cancer

***Ming Chi Shih***[1], *Jonas A. de Souza*[2], *Patricia Heinlen*[2], *Yonglin Pu*[1], *Alberto Jimenez*[1], *Bill C. Penney*[1], *Daniel E. Appelbaum*[1], *Ezra E. Cohen*[2], *Chin-Tu Chen*[1], [1]*Radiology, The University of Chicago, Chicago, IL, USA;* [2]*Medicine/ Hematology-Oncology, The University of Chicago, Chicago, IL, USA. Contact e-mail: mingchi@uchicago.edu*

Introduction: The majority of patients with squamous cell carcinoma of the head and neck (SCCHN) presents with locally advanced disease. Positron emission tomography (PET) using the radiotracer 18F- fluoro-2-deoxy-D-glucose (FDG) is widely used as an imaging modality for evaluating SCCHN and its treatments. However, increased FDG uptake by activated inflammatory cells occurs in irradiated tissue and results in an increased number of false positive results. At the same time, FDG uptake by tumor decreases as a result of treatment, which can confound the distinction between malignant and adjacent irradiated tissue. Technetium 99m-ethylenedicysteine-deoxyglucose (99mTc-EC-DG) is a glucose analogue radiopharmaceutical imaged used in conjunction with SPECT imaging, as alterative but also more economic imaging modality to trace glucose metabolism and glucose-induced desensitization of the glucose transport system. Like FDG, EC DG concentrates in cells that rely upon glucose as an energy source or in cells in which dependence on glucose increases under pathophysiological conditions. We hypothesize that this new SPECT tracer, will offer better specificity and positive predictive values than those achievable from current imaging modalities in assessing therapeutic response in locally advanced head and neck cancers. Methods: One patient with a T3N2b floor of mouth squamous cell carcinoma was evaluated radiologically with a computed tomography (CT) prior to therapy and at 4 weeks after completion of chemoradiotherapy (CRT). A 99mTc-EC-DG SPECT/CT was also performed 3 hours after tracer injection prior to any therapy and at 4 weeks after completion of CRT. At 10 weeks, the same procedure will be followed, with the addition of the 18F-FDG-PET/CT. The image interpreters of the 18F-FDG-PET/CT will be blinded to the results from the 99mTc-EC-DG SPECT-CT and of any available tissue biopsies. Results: The baseline 99mTc-EC-DG SPECT/CT showed good contrast-ratio from tumor versus normal tissue, and a perfect one-to-one correlation with CT scan. The 4 week post-treatment follow up imaging of the first patient showed significant uptake reduction in the all localized lesions from baseline. The semi quantitative ROI analysis of the SPECT imaging was able to show a 3-fold decrease uptake ratio, reflecting the effect of CRT. Conclusion: 99mTc-EC-DG as imaged by SPECT/CT correctly localized the tumor in a patient with SCCHN prior to treatment. At 4 weeks post-CRT, there was reduced 99mTc-EC-DG uptake by tumor tissues. Twenty patients are currently being enrolled in pilot clinical trial, and will have baseline as well as 4- and 10- week post-treatment imaging to compare 18F-FDG-PET/CT at 10-week post-CRT.

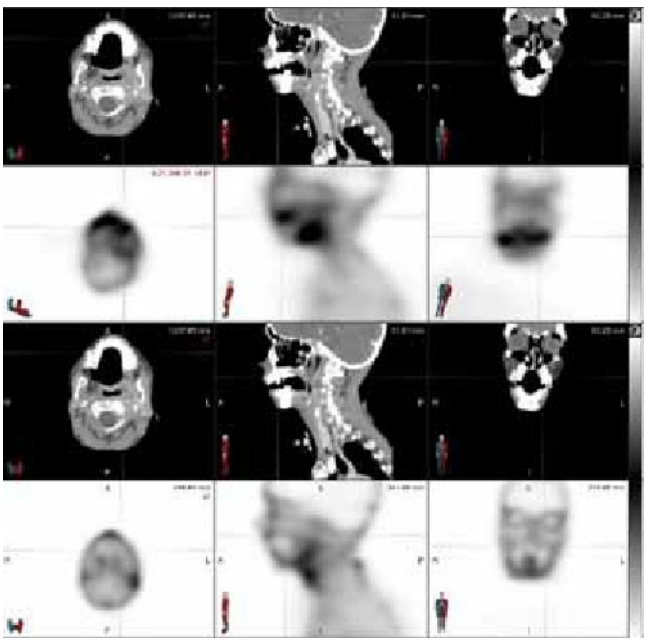

99mTc-ECDG Baseline and 4 week Post treatment comparison

Disclosure of author financial interest or relationships:
**M. Shih**, None; **J.A. de Souza**, None; **P. Heinlen**, None; **Y. Pu**, None; **A. Jimenez**, None; **B.C. Penney**, None; **D.E. Appelbaum**, Naviscan, Grant/research support; **E.E. Cohen**, None; **C. Chen**, BioMed Global, Consultant; RefleXion, Consultant .

Presentation Number **P834**
Poster Session 4
September 8, 2012 / 14:45-14:45 / Room: The Liffey

# Biodistribution of Fluorescent Labeled Avastin in Pregnant Rats

***Mitchell Thorn***[1], *Ning Zhang*[2], *Rajendra Singh*[2], *Christopher J. Bowman*[1], [1]*Pfizer Worldwide Research & Development, Groton, CT, USA;* [2]*PerkinElmer, Alameda, CA, USA. Contact e-mail: Mitchell.Thorn@pfizer.com*

Antibody-like biopharmaceutical therapy in pregnant patients faces rigorous safety scrutiny as materno-fetal antibody transfer is largely unknown. We explored the feasibility of applying optical imaging to monitor the embryo-fetal biodistribution of maternally administered, fluorescently-labeled Avastin in pregnant Sprague Dawley rats. The availability of Avastin750 antibody dye conjugate fetal transfer data starting at mid-gestation may inform the model's usefulness for extrapolating antibody transfer in other species including humans. The data would also expand the understanding of antibody transfer mechanisms. Conflicting data exists concerning the earliest time point at which antibodies are transferred from dam to fetus ranging from GD10 to GD20. To establish a time line for Avastin 750 fetal transfer, pregnant rats at GD10, 12, 13, 15 and 20 were intravenously dosed with 1mg/kg of the antibody and examined for evidence of Avastin 750 specific fluorescence 24 hour post dose. At GD10, 12 and 13, the fluorescence of three embryos from Avastin 750 dosed and PBS dosed rats were averaged and compared to determine fluorescence increase due to the antibody transfer. There was no Avastin 750 specific fluorescence detectable at GD10 suggesting that the antibody is not transferred to the embryo at this gestational time point. At GD13-14 low levels of Avastin 750 were detectable in the embryos making GD13-14 the earliest time point under the experimental conditions at which transfer of Avastin begins in the rat. At all subsequent gestation stages, significant levels of Avastin 750 were detectable in the fetuses, peaking at GD20-21 where Avastin 750 dosed fetuses showed a 50-fold fluorescence increase over negative controls. Intensity of the fluorescent signals was dose dependent from 100 to 1000 µg/kg. We also examined the mechanism of how the antibody gain access to across the materno-fetal barrier by evaluating placental transfer using Avastin molecules mutated to increase and ablate FcRn binding. This demonstrated the importance of FcRn binding in rat placental transfer.

Disclosure of author financial interest or relationships:
**M. Thorn**, None; **N. Zhang**, PerkinElmer, Employment; **R. Singh**, PerkinElmer, Employment; **C.J. Bowman**, Pfizer, Inc, Employment .

Presentation Number **P835**
Poster Session 4
September 8, 2012 / 14:45-14:45 / Room: The Liffey

# COMPARATIVE ASSESSMENT OF SEGMENTATION ALGORITHMS FOR TUMOUR DELINEATION ON A TEST-RETEST [11C]CHOLINE DATASET

***Giampaolo Tomasi***[1], *Tony Shepherd*[2], *Federico Turkheimer*[3], *Dimitris Visvikis*[4], *Eric O. Aboagye*[1,3], [1]*Comprehensive Cancer Imaging Center, Imperial College, London, United Kingdom;* [2]*Turku University Hospital, and Department of Oncology and Radiotherapy, University of Turku, Turku, Finland;* [3]*Departmet of Medicine, Imperial College, London, United Kingdom;* [4]*INSERM, LaTIM, CHU Morvan, Brest, France. Contact e-mail: gtomasi@imperial.ac.uk*

Several methods have been proposed for tumour segmentation from Positron Emission Tomography (PET) images. Because of the increasingly important role that [11C]choline is playing in oncology and because no study has compared segmentation methods on this tracer, we assessed a number of segmentation algorithms on a [11C]choline test-retest dataset and also evaluated the effect of introducing a preliminary denoising step. **Methods**:: Two fixed-threshold methods ($T_{FIXED}^{50}$, $T_{FIXED}^{70}$), two adaptive-threshold methods in which the threshold is estimated also on the basis of the background uptake ($T_{ADAPT}^{20}$, $T_{ADAPT}^{40}$), fuzzy C-means (FCM), the Fuzzy Local Adaptive Bayesian algorithm (FLAB), Canny's edge detection method (Canny) and the watershed transform (WT) were tested. Test-retest [11C]choline scans of nine patients with breast cancer were analyzed and the percent test-retest variability $\%VAR_{TEST\text{-}RETEST}$ of tumour volume (TV) was employed to assess the results. The same methods were then applied to two denoised datasets generated by applying either a Gaussian filter or the wavelet transform. **Results**:: The (semi)automated methods FCM, FLAB and Canny emerged as the best ones in terms of TV reproducibility. For these methods, the %Root Mean Square Error (%RMSE) of $\%VAR_{TEST\text{-}RETEST}$ , defined as SQRT [ VARIANCE+mean$^2$ ] , was in the range 16.7%-21.2%, depending on the dataset and algorithm. Figure 1 displays the box-plots of TV $\%VAR_{TEST\text{-}RETEST}$ for the various methods and of of $SUV_{MAX}$ and $SUV_{MEAN}$ for the unprocessed (Fig.1A), Gaussian-filtered (Fig.1B) and wavelet transformed (Fig.1C) data. The figure clearly shows how threshold-based methods gave TV estimates which were extremely variable, particularly on the unprocessed data; the performance of threshold-based approaches improved on the denoised datasets, whereas preliminary smoothing did not have a remarkable impact on the other methods. TV variability obtained with the best methods was comparable to that of $SUV_{MAX}$ and $SUV_{MEAN}$ (%RMSE in the range 14.7%-21.9% after the exclusion of one outlier, ~40% when the outlier was included). **Conclusions**:: The TV variability obtained with the best (i.e. the least variable) methods was similar to the one reported for TV in previous [18F]FDG and [18F]FLT studies and to the one of $SUV_{MAX}$ / $SUV_{MEAN}$ on our [11C]choline dataset. The good reproducibility of TV obtained with the best algorithms suggests that this parameter could be used with [11C]choline to complement/substitute the SUV in the prediction of early response to treatment: further studies should be performed to test this hypothesis.

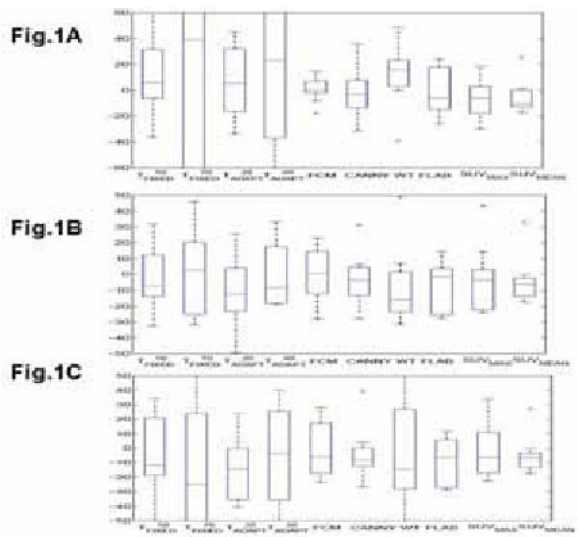


Box-plots of TV $\%VAR_{TEST\ RETEST}$ for the various methods and of $\%VAR_{TEST\ RETEST}$ of $SUV_{MAX}$ and $SUV_{MEAN}$ for the unprocessed (Fig.1A), Gaussian-filtered (Fig.1B) and wavelet transformed (Fig.1C) data. In the box-plots the central mark is the median, the edges of the box are the 25th and 75th percentiles and the whiskers extend to the most extreme data points not considered outliers.

Disclosure of author financial interest or relationships:
**G. Tomasi**, None; **T. Shepherd**, None; **F. Turkheimer**, None; **D. Visvikis**, None; **E.O. Aboagye**, GE Healthcare, Grant/research support .

Presentation Number **P836**
Poster Session 4
September 8, 2012 / 14:45-14:45 / Room: The Liffey

# Ex Vivo Sentinel Lymph Node Mapping in Colorectal Cancer Combining both Conventional Blue Dye and Near-Infrared Fluorescence

***Quirijn Tummers***[1], *Boudewijn Schaafsma*[1], *Floris Verbeek*[1], *Joost van der Vorst*[1], *Merlijn Hutteman*[1], *Vincent Smit*[4], *Clemens Lowik*[2], *John V. Frangioni*[3], *Cornelis J. van de Velde*[1], *Alexander Vahrmeijer*[1], [1]*Surgery, Leiden University Medical Center, Leiden, Netherlands;* [2]*Endocrinology, Leiden University Medical Center, Leiden, Netherlands;* [3]*Haematology/Oncology, Medicine, Beth Israel Deaconess Medical Center, Harvard Medical School, Boston, MA, USA;* [4]*Pathology, Leiden University Medical Center, Leiden, Netherlands.*
*Contact e-mail: q.r.j.g.tummers@lumc.nl*

Introduction: Lymph node status is the most important prognostic factor in colon cancer. The sentinel lymph node (SLN) procedure has been proposed in colon cancer to improve nodal staging. The aim of this study was to combine the use of blue dye staining and near-infrared (NIR) fluorescence imaging for SLN biopsy in colon cancer patients. Patients and methods: Twenty-two consecutive patients undergoing surgery for colon cancer were included. Directly after resection, a premixed cocktail of 1 cc of 50 μM HSA800 (IRDye 800CW conjugated to human serum albumin) diluted in patent bluewas submucosally injected around the tumor for detection of the sentinel lymph node. The Mini-FLARE near-infrared camera system was used for fluorescence imaging. Results: In 95% of the patients at least one sentinel lymph node was identified. On average, per specimen, 3.5 ± 1.9 sentinel lymph nodes were identified. A total of 77 sentinel lymph nodes were identified, of which 77 were fluorescent and 70 were blue. Histological analysis showed lymph node metastases in 5 patients. In all but 1 case, at least 1 of the sentinel lymph nodes contained tumor cells. Conclusions: This study demonstrated the successful use of the near-infrared fluorescence tracer HSA800 in combination with conventional blue dye for the ex vivo sentinel lymph node procedure in colon cancer.

Disclosure of author financial interest or relationships:
**Q. Tummers**, None; **B. Schaafsma**, None; **F. Verbeek**, None; **J. van der Vorst**, None; **M. Hutteman**, None; **V. Smit**, None; **C. Lowik**, None; **J.V. Frangioni**, None; **C.J. van de Velde**, None; **A. Vahrmeijer**, None.

Presentation Number **P837**
Poster Session 4
September 8, 2012 / 14:45-14:45 / Room: The Liffey

# A hybrid tracer, ICG-99mTc-nanocolloid, for concomitant radio- and fluorescence guided sentinel lymph node biopsy in oral cavity squamous cell carcinoma

***Nynke S. van den Berg***[1,2], *Oscar R. Brouwer*[2], *W Martin C. Klop*[3], *Alfons J. Balm*[3], *Michiel W. van den Brekel*[3], *Renato A. Valdés Olmos*[2], *Fijs van Leeuwen*[1,2], [1]*Radiology, Interventional Molecular Imaging group, Leiden University Medical Center, Leiden, Netherlands;* [2]*Nuclear Medicine, Netherlands Cancer Institute - Antoni van Leeuwenhoek Hospital, Amsterdam, Netherlands;* [3]*Head & Neck Oncology and Surgery, Netherlands Cancer Institute - Antoni van Leeuwenhoek Hospital, Amsterdam, Netherlands. Contact e-mail: N.S.van_den_Berg@lumc.nl*

PURPOSE To reduce morbidity in head and neck cancer patients the sentinel lymph node (SLN) biopsy has gained increased interest over elective neck dissection (END) for the early detection of lymph node metastases. Conventional SLN mapping is performed by injecting a radiocolloid around the primary tumor followed by lymphoscintigraphy and/or single photon emission computed tomography combined with computed tomography (SPECT/CT) to identify the primary tumor draining lymph nodes (referred to as SLN(s)). Intraoperatively, generally blue dye (e.g. patent blue) is used for SLN visualization. However, it has been shown that these are of less value in oral cavity cancer as it may interfere with tumor margin visibility. This study aimed to evaluate the feasibility of adding intraoperative near-infrared fluorescence imaging to the conventional radio guided procedure. For this, ICG-99mTc-nanocolloid, a hybrid tracer that is both radioactive and fluorescent was used in patients with oral cavity cancer. METHODS Hybrid ICG-99mTc-nanocolloid was injected in three or four deposits surrounding the primary lesion. To preoperatively identify the SLNs, lymphoscintigraphy was performed fifteen minutes and two hours after injection, immediately followed by SPECT/CT imaging. Intraoperatively, SLNs were traced with a conventional gamma ray detection probe and after the initial exploration their exact location was visualized using a handheld near-infrared fluorescence camera. To confirm complete removal of all SLNs, a portable gamma camera was used before and after SLN excision. RESULTS In this study, fourteen patients with oral cavity tumors (floor of mouth (n=5), tongue (n=7), lower lip (n=1), buccal mucosa (n=1)) were included. Lymphatic drainage was observed in all patients resulting in a total 41 preoperatively identified SLNs. Intraoperatively, 91% of SLNs could be localized and excised with combined radio- and fluorescence guidance. 9% of SLNs could be best detected with fluorescence imaging only; these SLNs were located closely to the primary injection site which hampered radioguided localization. Post-excision control with the portable gamma camera resulted in the identification of three additional SLNs in three patients; these SLNs were also fluorescent. Intraoperatively, a total of 47 SLNs was harvested. In two patients a SLN could not be intraoperatively localized due to its position both close to the main trunk of the facial nerve, and marginal mandibular nerve, respectively. These patients are carefully followed via our watch and wait protocol. Histopathology revealed metastases in one SLN; this patient received a subsequent END in which no additional metastases were found. CONCLUSION With this study the feasibility of combined preoperative SLN identification and intraoperative radio- and fluorescence guidance during SLN biopsies for oral cavity cancer using a single intramucosal injection of ICG-99mTc-nanocolloid was shown. The addition of fluorescence imaging may be of particular value in SLN biopsies for oral cavity cancer as SLNs are frequently found to be located in close proximity to the injection site.

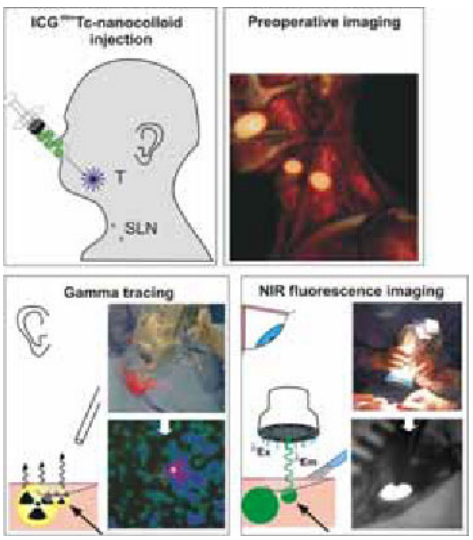


Disclosure of author financial interest or relationships:
**N.S. van den Berg**, None; **O.R. Brouwer**, None; **W.C. Klop**, None; **A.J. Balm**, None; **M.W. van den Brekel**, None; **R.A. Valdés Olmos**, None; **F. van Leeuwen**, None.

Presentation Number **P838**
Poster Session 4
September 8, 2012 / 14:45-14:45 / Room: The Liffey

# Topical Application of Activity-based Probes for Rapid Detection of Cancer in Human Breast Lumpectomy Specimens

***Yevgen (Eugene) Vykhovanets***[1], *Galia Blum*[2], *Matthew Bogyo*[3,4], *James Basilion*[1,5], [1]*Radiology, Case Western Reserve University, Cleveland, OH, USA;* [2]*Institute of Drug Research, The Hebrew University, Jerusalem, Israel;* [3]*Pathology, Stanford University, Stanford, CA, USA;* [4]*Microbiology and Immunology, Stanford University, Stanford, CA, USA;* [5]*Biomedical Engineering, Case Western Reserve University, Cleveland, OH, USA. Contact e-mail: yvv@cwru.edu*

Objectives: Breast cancer is the most diagnosed cancer in women and, because of increased education and better screening, is often caught at earlier stages where surgical options are available. Several studies have demonstrated the utility of near infrared fluorescent (NIRF) smart imaging probes (labeled with Cy5 fluorochrome) to image tumor proteases in small animal models of cancers. These probes are robust, extremely selective for targeted proteases and have shown to be very effective for imaging tumor-expressed proteases in tissue culture, in subcutaneously implanted tumors in mice and in human tissues. The cellular permeability, high target selectivity and rapid kinetics have prompted us to attempt to utilize these probes for a novel topical application to identify cancer at or near the surface of excised tissues during breast conserving surgeries (BCS). Material and Method: To rule out or confirm a feasibility of rapid detection of cancer cells in BCS lumpectomy specimens with 2-mm benign breast tissue surgical margin, the GB119, a member of quenched activity-based probes of the GB's clan, that fluorescent upon activity-dependent covalent modification of a protease (cathepsin B and L) target was chosen. Results: Specifically we found that: 1) In vitro probe/breast cancer cell lysate interaction initiates GB119/cathepsin-dependent fluorescence in 3-6 min that might be detected in a gel; 2) GB119 was activated and accumulated in lysosomes of MCF-7 breast cancer cell culture in vitro; 3) Benign breast tissue was permeable for GB119 ex vivo when we used "sandwich" approach (1A). Human breast and brain tumor xenografts could be detected under 2-mm layer of benign breast tissue in 5-10 min by topical application of GB119 onto the breast tissue. The broad-spectrum suicide cysteine protease inhibitor K11777 abrogated the ability of the probe to detect tumor xenograft underneath of the breast tissue layer indicating a high specificity of the GB119/cathepsin-dependent fluorescent signal (1B). 4) IHC analysis confirmed a presence of GB119's fluorochrome such as Cy5 both at the surface and inside (up to 1-mm) of the tumor xenograft which was in the direct contact to the benign breast tissue and was separated from the probe by the tissue (2). Conclusions: The technology and approach provide a means for rapid visualization and robust detection of cancer cells anywhere on the entire surface of breast lumpectomy specimens to inform on the presence of residual disease at the lumpectomy bed. Improved methods to rapidly and completely assess cancer infiltrates in lumpectomy margins are essential to improve outcomes for breast cancer patients.

Disclosure of author financial interest or relationships:
**Y. Vykhovanets**, None; **G. Blum**, None; **M. Bogyo**, None; **J. Basilion**, Akrotome Imaging Inc, Stockholder .

Presentation Number **P839**
Poster Session 4
September 8, 2012 / 14:45-14:45 / Room: The Liffey

# 64Cu-DOTA-trastuzumab-PET imaging in patients with HER2-positive breast cancer

***Yasuyoshi Watanabe***[1], *Kenji Tamura*[2], *Hiroaki Kurihara*[3], *Kan Yonemori*[2], *Kazuhiro Takahashi*[1], *Yasuhiro Wada*[1], *Koki Hasegawa*[1], *Yousuke Kanayama*[1], *Fumiaki Koizumi*[4], *Hitoshi Tsuda*[5], *Makoto Kodaira*[2], *Mayu Yunokawa*[2], *Chikako Shimizu*[2], *Masashi Ando*[2], *Yasuhiro Fujiwara*[2], *[1]Center for Molecular Imaging Science, RIKEN, Kobe, Japan; [2]Department of Breast and Medical Oncology, National Cancer Center Hospital, Tokyo, Japan; [3]Nuclear Medicine Division, National Cancer Center Hospital, Tokyo, Japan; [4]Shien Lab, National Cancer Center Hospital, Tokyo, Japan; [5]Department of pathology, National Cancer Center Hospital, Tokyo, Japan. Contact e-mail: yywata@riken.jp*

Background: Targeting of HER2 with trastuzumab (T) is a well-established strategy in the metastatic and adjuvant setting in HER2 positive breast cancer (HER2-BC). Although HER2 status is routinely determined using immunohistochemistry or fluorescence in situ hybridization, technical problem can arise when lesions are poorly accessible. HER2 status can vary during the course of the disease, and there can be discordance in HER2 expression across tumor lesion even in the same patients. Noninvasive HER2 imaging is needed to solve these problems. Previous imaging using 111In or 89Zn- trastuzumab produced rather high radiation exposure to patients because of their long half life (=67and 78h) and low resolution image with 111In-labelled one. We here employed 64Cu with a half life of 12.7h. We performed a feasibility study of the 64Cu-bifunctional chelator 1, 4, 7, 10-tetraacetic acid (DOTA)-T to perform PET imaging in patients with HER2-BC. Method: Patients with HER2-BC received 150 MBq of 64Cu-DOTA-T and underwent PET scan 1, 24, and 48h after the injection. Six patients were evaluated radiation exposure by collecting clothes, linen and urine. Biodistribution in normal organs, and radiation uptake in blood pool, urinary excretion were determined. Results: Fifteen patients who received T therapy were enrolled in the "first in human" trial. All patients had no severe toxicity. Radiation excretion evaluating clothes, linen and urine were under background level. Radiation exposure of 64Cu-DOTA-T (4.2-7.5 mSv) was equivalent that of conventional 18F-FDG-PET (6.5 mSv). Distribution in liver, kidney, spleen, and blood vessel was 2-8 SUV, and uptake in other normal tissue was low. 64Cu-DOTA metabolized was rapidly excreted into urine for 24h. At visual examination, in three patients brain metastases were clearly visualized by 64Cu-DOTA-T-PET, suggesting there are disruptions of the blood-brain barrier at the site of the brain metastases. The sternum bone metastasis was well visualized and quantitatively monitored according to the response by T. Primary breast cancers, lymph node metastases, and lung metastases could also be visualized at the lesion indentified by CT. Conclusion: 64Cu-DOTA-T-PET was feasible test even for outpatients, and provides specific and high resolution image in HER2-positive lesion. Granted by J-AMP from MEXT, Japanese Government

Disclosure of author financial interest or relationships:
**Y. Watanabe**, None; **K. Tamura**, None; **H. Kurihara**, None; **K. Yonemori**, None; **K. Takahashi**, None; **Y. Wada**, None; **K. Hasegawa**, None; **Y. Kanayama**, None; **F. Koizumi**, None; **H. Tsuda**, None; **M. Kodaira**, None; **M. Yunokawa**, None; **C. Shimizu**, None; **M. Ando**, None; **Y. Fujiwara**, Chugai Pharmaceutical, Grant/research support .

Presentation Number **PL 1**
Plenary Session 1
September 5, 2012 / 17:00-18:00 / Room: The Auditorium

# Gold Medal Presentation

***Michael Phelps**, UCLA, Los Angeles, CA, USA. Contact e-mail: mphelps@mednet.ucla.edu*

Disclosure of author financial interest or relationships:
**M. Phelps**, Sofie Biosciences, Stockholder; Sofie Biosiences (Board of Directors), Other financial or material support .

Presentation Number **PL 2**
Plenary Session 2
September 6, 2012 / 09:00-09:45 / Room: The Auditorium

# Imaging of Vulnerable Atherosclerotic Plaque: From Mouse to Man

***Juhani Knuuti***, *[1]University of Turku, Turku, Finland; [2]Turku PET Centre, Turku, Finland; [3]Turku University Hospital, Turku, Finland.*
*Contact e-mail: juhani.knuuti@utu.fi*

Disclosure of author financial interest or relationships:
**J. Knuuti**, Lantheus Inc, Consultant; Philips, Speakers bureau .

Presentation Number **PL 3**
Plenary Session 3
September 6, 2012 / 16:45-17:45 / Room: The Auditorium

# Normalizing Tumor Micro-environment to Treat Cancer: Insights From Intravital Imaging

***Rakesh K. Jain***, *[1]Harvard Medical School, Boston, MA, USA; [2]Massachusetts General Hospital, Boston, MA, USA. Contact e-mail: jain@steele.mgh.harvard.edu*

Disclosure of author financial interest or relationships:
**R.K. Jain**, None.

Presentation Number **PL 4**
Plenary Session 4
September 7, 2012 / 09:00-09:45 / Room: The Auditorium

# Image-n-omics: Innovation in Molecular Imaging with Mass Spectrometry

***Ron M. Heeren**, FOM-AMOLF, Amsterdam, Netherlands. Contact e-mail: heeren@amolf.nl*

Disclosure of author financial interest or relationships:
**R.M. Heeren**, None.

Presentation Number **PL 5**
Plenary Session 5
September 7, 2012 / 16:45-17:30 / Room: The Auditorium

# Developing High Avidity, Vascular Targeted, Ultrasound, Molecular Imaging Agents: Translation, "To the Clinic"

***Adrian D. Nunn**, Bracco Research USA, Princeton, NJ, USA. Contact e-mail: Adrian.Nunn@bru.bracco.com*

Disclosure of author financial interest or relationships:
**A.D. Nunn**, Bracco Research USA Inc, Employment .

Presentation Number **PL 6**
Plenary Session 5
September 7, 2012 / 17:30-18:15 / Room: The Auditorium

# Jorge Barrio Lecture for Advances in Clinical Research: Molecular & Functional Imaging in Neurology - Translational Research and Clinical Applications

***Satoshi Minoshima**, Radiology, University of Washington, Seattle, WA, USA. Contact e-mail: minoshim@u.washington.edu*

Disclosure of author financial interest or relationships:
**S. Minoshima**, None.

Presentation Number **PL 7**
Plenary Session 6
September 8, 2012 / 09:00-09:45 / Room: The Auditorium

# Britton Chance Lecture for Advances in Basic Imaging Research: Multiscale Imaging of the Angiogenic Network

***Michal Neeman***, *Weizmann Institute, Rehovot, Israel. Contact e-mail: michal.neeman@weizmann.ac.il*

Disclosure of author financial interest or relationships:
**M. Neeman**, None.

Presentation Number **PL 8**
Plenary Session 7: Highlight Lecture, Poster Awards, and Young Investigator Award Competition
September 8, 2012 / 16:15-17:00 / Room: The Auditorium

# Highlight Lecture

***Sanjiv S. Gambhir**, Geophysics, Stanford University, Stanford, CA, USA. Contact e-mail: sgambhir@stanford.edu*

Disclosure of author financial interest or relationships:
**S.S. Gambhir**, General Electric, Grant/research support; Bayer-Schering, Grant/research support; Sanofi-Aventis, Grant/research support; CellSight, Stockholder; ImaginAB, Stockholder; Enlight, Stockholder; Endra, Stockholder; Bracco, Consultant; NinePoint Medical, Stockholder; Visualsonics, Consultant .

Presentation Number **PL 9**
Plenary Session 7: Highlight Lecture, Poster Awards, and Young Investigator Award Competition
September 8, 2012 / 17:00-17:10 / Room: The Auditorium

# WMIC 2013: Savannah, Georgia

***Larry Browder**, Senior Director of National Accounts- Visit Savannah, Savannah, GA, USA. Contact e-mail: lbrowder@VisitSavannah.com*

Disclosure of author financial interest or relationships:
**L. Browder**, None.

Presentation Number **SS 1**
Scientific Session 1: Chemistry & Probes - MRI
September 6, 2012 / 10:30-10:41 / Room: Liffey Hall 1

# Direct Albumin Imaging using a Delta Relaxation Magnetic Resonance Double Inversion Recovery Fast Spin Echo Sequence

***Yonathan Araya***[1], *Francisco M. Martinez*[3], *William B. Handler*[2], *Chad Harris*[2], *Blaine A. Chronik*[1,4], *Timothy J. Scholl*[1,3], [1]*Medical Biophysics, Western University, London, ON, Canada;* [2]*Physics and Astronomy, Western University, London, ON, Canada;* [3]*Imaging Research Laboratories, Robarts Research Institute, London, ON, Canada;* [4]*Robarts Research Institute, Western University, London, ON, Canada. Contact e-mail: yaraya@uwo.ca*

Introduction: Delta Relaxation Enhanced magnetic resonance (dreMR) is a novel imaging method capable of producing contrast proportional only to the concentration of the bound form of the targetable probe using a dynamic field-cycling technique [1,2]. The characteristic high relaxivity (Δr1) magnetic field dependence of bound paramagnetic contrast probes enables suppression of unbound probes and unenhanced tissues contrast, thereby increasing probe specificity [1]. The dreMR technique requires an auxiliary actively shielded field-shifting insert electromagnet to modulate the strength of the main clinical magnetic field (B0) as a function of time during the relaxation and evolution periods (Δt) of a pulse sequence. MS-325 (FDA-approved) binds specifically to serum albumin and has a strong magnetic field dependence of Δr1 = 24.6mM-1s-1T-1 for human serum albumin around 1.5T [3]. Native biological tissues and unbound MS-325 demonstrates very little magnetic field dependence [3,4]. Using a custom Double Inversion Recovery (DIR) preparatory pulse, where the strength of B0 field is modulated for different Δt times, signal intensities from only the bound form of MS-325 can be produced. Methods: Imaging was performed on a 1.5T GE CVMR system (WI, USA) outfitted with the dreMR coil to dynamically control B0 [1]. Phantoms with and without 4.0% w/v Rabbit Serum Albumin (RSA) were loaded with 160μM and 80μM MS-325. Using a DIR-Fast Spin Echo (DIR-FSE) sequence, the B0 field was modulated during the preparatory pulse phase to 1.72T for P2=150ms and 1.28T for P3=90ms and returned to clinical strength during image acquisition. A FSE imaging sequence had parameters of TR=400ms, TE=7.328ms, TI=50ms, with 1 average and 0.39mm isotropic resolution. A healthy 129-E mouse (21g) anesthetized with 2% isofluorane was placed on a custom water heated bed in a Tx/Rx birdcage RF coil within the dreMR coil. MS-325 (0.03mmol/kg) was injected intravenously through tail vein. The same DIR-Fast Spin Echo sequence and B0 modulation parameters were used, with imaging acquisition parameters of TR=400ms, TE=6.744ms, TI=50ms, with 10 averages and 0.7mm isotropic resolution. Results: Fig1 (A,B) shows dreMR contrast of phantoms from the DIR-FSE sequence. By changing the P2 and P3 times of the positive and negative shifts from 200ms and 100ms (1.A) to 150ms and 90ms (1.B) during the preparatory phase, we are able to suppress signal intensities arising from unbound MS-325. 1.D shows the dreMR mouse image with the colour map showing signal intensities arising from bound MS-325. Optimization parameters and an animal disease model are being investigated. References: [1] Alford et al. MRM. 61 796-802(2009). [2] Alford et al. Proc. ISMRM. 318(2011). [3] Caravan et al. JACS 124 3152-3162(2002). [4] Koenig et al. Inv. Rad. 19 76-81(1984).

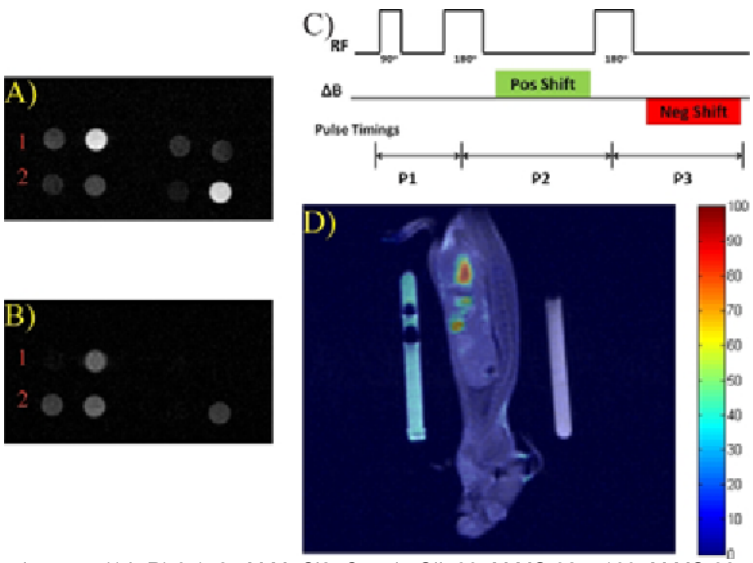


Fig1. (A,B) dreMR DIR-FSE phantom images: (1 L-R) 0.148mM MnCl2, Canola Oil, 80μM MS-325, 160μM MS-325; (2 L-R) 80μM MS-325, 160μM MS-325 (both with 4.0% w/v RSA), 4.0% w/v RSA, and 0.1mM MnCl2. (C) Preparatory pulse sequence before image acquisition. (D) Healthy dreMR DIR-FSE mouse contrast of albumin distribution map overlaid on an anatomical FSE image.

Disclosure of author financial interest or relationships:
**Y. Araya**, None; **F.M. Martinez**, None; **W.B. Handler**, None; **C. Harris**, None; **B.A. Chronik**, None; **T.J. Scholl**, None.

Presentation Number **SS 10**
Scientific Session 2: Technology & Software - Optical Imaging
September 6, 2012 / 10:41-10:52 / Room: Wicklow Hall 1

# BioFLECT: Imaging performance evaluation and initial in-vivo imaging results

***James M. Masciotti***[1], *Sabrina Pesnel*[1], *Michael T. Scardina*[1], *Wael Hazin*[1], *Alexander Klose*[2], *Marc Vandamme*[3], *Alain Le Pape*[3], [1]*Bioscan Inc., Washington, DC, USA;* [2]*Radiology, Columbia University, New York, NY, USA;* [3]*TAAM-CIPA, CNRS, Orleans, France. Contact e-mail: jmasciotti@bioscan.com*

We present the results of a performance evaluation of the BioFLECT in-vivo imaging system and results from initial in-vivo mouse imaging experiments performed with the BioFLECT. The BioFLECT is a 360° Fluorescence Emission Computed Tomography imager that produces 3D images of the distribution of fluorophores, such as fluorescent probes, in-vivo in small animals. BioFLECT employs a laser array, a detector ring, and a rotating gantry which permits fluorescence tomography scanning to be done in a conventional topographic manner similar to how X-ray CT scanning is done. We report on results of imaging studies that evaluate the performance of BioFLECT in terms of image resolution, sensitivity, and accuracy when imaging tissue simulating phantoms. Reconstructed image resolution is evaluated by imaging phantoms with single inclusions and analyzing the point spread functions and full-width half-maxima, and by imaging phantoms with 2 inclusions that are separated at a controlled distance and evaluating the peak-to-valley differences. Sensitivity is evaluated both by imaging while diluting fluorophore concentration and determining lowest fluorophore concentration that is still detectable (SNR≥1) and by measuring the "noise" in a reconstructed image, when no fluorophore is present in the phantom. Quantitative accuracy is evaluated comparing the reconstructed values for fluorophore concentration to the true fluorophore concentration inside the phantom while spatial accuracy is evaluated by comparing reconstructed locations of phantom inclusions to their true location. Initial results show spatial resolution on the order of 1 mm and the sensitivity to less than a picomole of fluorophore. We also report on some of the results of initial in-vivo imaging experiments conducted with the BioFLECT. Deep tissue imaging results are described lung tumors and other cancer models, intrabronchial fluorophore deposits, intraperitoneal injections of fluorescent pellets. Results are validated through co-registration with other modalities such as X-ray CT and SPECT.

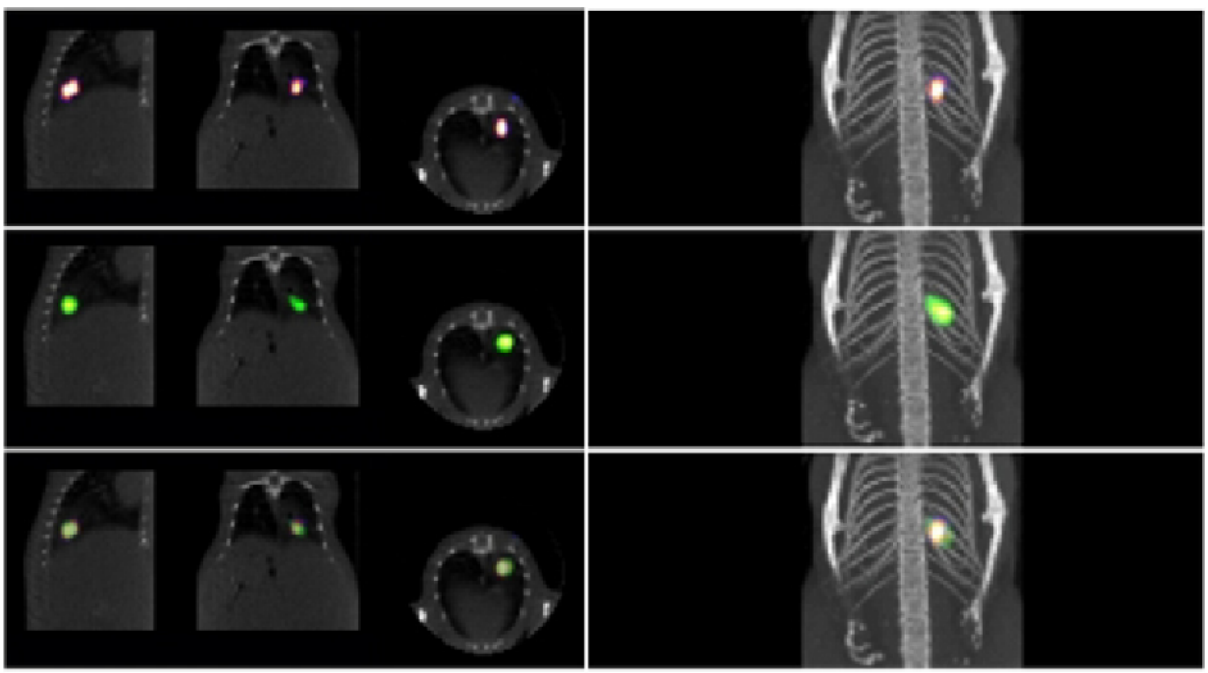

Multimodality images of a mouse after interbronchial injection with a mixture of DiR and 99mTc colloids. Top: FLECT and X-ray CT. Middle: SPECT and X-ray CT. Bottom: FLECT, SPECT, and X-ray CT

Disclosure of author financial interest or relationships:
**J.M. Masciotti**, Bioscan Inc., Employment; **S. Pesnel**, Bioscan, Employment; **M.T. Scardina**, Bioscan, Inc., Employment; **W. Hazin**, Bioscan Inc., Employment; **A. Klose**, None; **M. Vandamme**, None; **A. Le Pape**, None.

Presentation Number **SS 100**
Scientific Session 15: Preclinical In Vivo - Oncology
September 7, 2012 / 10:30-10:42 / Room: The Auditorium

# Comparison of PET hypoxia tracers using non-invasive imaging and ex-vivo correlation with histologic markers

***Sean Carlin***[1], *Hanwen Zhang*[1], *Megan Reese*[1], *Nick Ramos*[1], *Sally-Ann Ricketts*[2], [1]*Radiology, MSKCC, New York, NY, USA;* [2]*Imaging, Personalized Healthcare and Biomarkers, AstraZeneca, Macclesfield, United Kingdom. Contact e-mail: carlins@mskcc.org*

**Introduction** Non-invasive PET imaging of tumor oxygenation status provides a means to identify radio- and chemo-resistant tumors, and also to monitor treatment efficacy. Several putative PET tracers of tumor hypoxia have been described, but there are few studies which compare hypoxia tracers directly in the same model system. In this study, we compared the non-invasive imaging characteristics of four PET hypoxia tracers, and also compared their microregional distributions with histological markers of tumor hypoxia. **Methods** Nude mice bearing SQ20b human squamous cell tumors of approximately 500mm3 on the hind limb were co-administered pimonidazole (60mg/kg) and one of each of the following PET tracers: 18F-FMISO, 18F-FAZA, 18F-HX4, 64Cu-ATSM. Images were obtained on a small animal PET camera between 80 and 90 minutes post-injection, or 170-180 minutes post-injection. Immediately following imaging, animals were sacrificed and tumors were removed, flash-frozen and cut into series of 10µm frozen sections. Sections were then exposed to a phosphor plate, and subsequently read on a Fujifilm BAS-1800 to obtain autoradiographic images of tracer distribution at 50µm spatial resolution. The same sections were then subjected to immunofluorescence staining to reveal the presence of pimonidazole and the endogenous hypoxia marker CA9. Autoradiographic images were superimposed upon immunofluorescence images of pimonidazole and CA9 distribution, and pixel-by-pixel correlative analysis performed. Pixel data was re-binned to aid in visual interpretation of the correlations. **Results** PET imaging confirmed tumor uptake of all four PET hypoxia tracers (Table 1). 18F-FMISO and 18F-HX4 showed similar tumor SUV and renal clearance characteristics. 18F-FAZA showed lower tumor SUV, but also lower normal tissue background with the exception of pronounced bladder activity. 64Cu-ATSM had the highest tumor SUV and pronounced liver uptake, with minimal renal and bladder activity. Ex vivo DAR and histological analysis indicated that regions of 18F-FMISO, 18F-HX4 and 18F-FAZA uptake show a positive correlation with uptake of pimonidazole and expression of CA9. In contrast, 64Cu-ATSM distribution did not correlate with either pimonidazole uptake or CA9 expression (Figure 1) **Conclusions** In this model system, the performance of 18F-FMSIO and 18F-HX4 was very similar. The enhanced image contrast observed with 18F-FAZA is obtained at the cost of lower absolute tumor uptake, presumably due to faster clearance. 64Cu-ATSM had the highest SUV of the radiotracers studied, and the hepato-biliary clearance route contrasts with the renal clearance observed with the other tracers. At the microscopic level, the negative correlation of ATSM distribution with uptake of pimonidazole and expression of CA9 is in contrast to the other tracers. This may indicate a differential in pO2 sensitivity, or additional cellular factors other than pO2 which influence 64Cu-ATSM uptake. The use of 64Cu-ATSM in addition to 18F-labelled nitroimidazole tracers may provide complimentary information regarding the underlying tumor physiology.

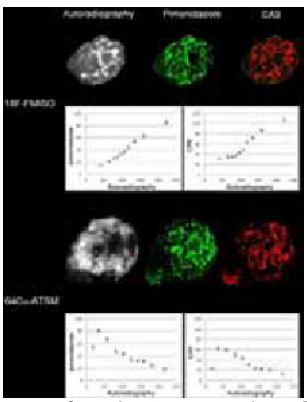

Figure 1. Autoradiographic and immunofluorescence images of ex-vivo tumor sections. Re-binned scatterplots showing the correlation between autoradiographic and immunofluorescence pixel values are shown.

| | | | | | | |
|---|---|---|---|---|---|---|
| 18F-FMISO | 0.448 ± 0.171 | 0.738 ± 0.376 | (n=7) | 0.111 ± 0.068 | 0.161 ± 0.096 | (n=4) |
| 18F-HX4 | 0.434 ± 0.175 | 0.661 ± 0.355 | (n=5) | 0.075 ± 0.040 | 0.135 ± 0.115 | (n=4) |
| 18F-FAZA | 0.276 ± 0.152 | 0.411 ± 0.236 | (n=7) | 0.105 ± 0.071 | 0.188 ± 0.120 | (n=7) |
| 64Cu-ATSM | 0.634 ± 0.089 | 1.238 ± 0.155 | (n=4) | 0.540 ± 0.328 | 0.919 ± 0.486 | (n=7) |

**Table 1.** Means and standard deviations of standardized uptake values (SUVmean and SUVmax) from four PET hypoxia tracers obtained at 90 and 180 minutes post-administration.

Disclosure of author financial interest or relationships:
**S. Carlin**, AstraZeneca, Grant/research support; **H. Zhang**, None; **M. Reese**, None; **N. Ramos**, None; **S. Ricketts**, AstraZeneca, Employment; AstraZeneca, Stockholder .

Presentation Number **SS 101**
Scientific Session 15: Preclinical In Vivo - Oncology
September 7, 2012 / 10:42-10:54 / Room: The Auditorium

# Effect of cediranib administration on the distribution and uptake of 18F-FMISO in a xenograft model of colorectal adenocarcinoma

*Louisa Bokacheva[1], Rachel M. Bartlett[1], Megan Reese[2], Sally-Ann Ricketts[3], Carl H. Le[1], Jason A. Koutcher[1], **Sean Carlin**[2], [1]Medical Physics, MSKCC, New York, NY, USA; [2]Radiology, MSKCC, New York, NY, USA; [3]Imaging, Personalized Healthcare and Biomarkers, AstraZeneca, Macclesfield, United Kingdom. Contact e-mail: carlins@mskcc.org*

**Introduction** Cediranib (AZD2171, Recentin), is an inhibitor of tyrosine kinase activity associated with VEGF receptors-1, -2 and -3, currently in Phase II clinical trials. In this study, we used DCE-, DW-MRI and dynamic 18F-FMISO PET imaging in HT29 tumor xenografts treated with cediranib and corroborated imaging biomarkers with histological measures of tumor vascularity, necrosis and hypoxia. **Methods** Two separate cohorts of tumor-bearing rats (n=10 each) were used for multi-parametric MRI and dynamic PET imaging. Imaging was performed before and after treatment with cediranib, (3 mg/kg daily), or vehicle solution, over 2 and 7 days. *PET* 18F-FMISO data was acquired over 90 minutes on a microPET scanner in list-mode. SUV tumor volume estimates were made using a single frame acquired between 80-90 minutes post-injection. Dynamic PET data were used to estimate voxel-wise kinetic rate constants (K1, k2, k3) using a 2-compartment, 3-parameter compartmental model *MRI* For DCE-MRI, Gd-DTPA (0.2 mmol/kg) was injected, followed by 12 min of dynamic acquisition. The initial area under the gadolinium curve (IAUC) over 90s (IAUC90) was normalized to the median IAUC90 in the adjacent muscle (nIAUC90). DW MRI was acquired with turbo spin echo sequence at b = 0, 100, 900 s/mm2 and ADC maps were generated. *Ex vivo analysis* Animals were injected with pimonidazole (hypoxia marker) 48 hours prior to sacrifice and with Hoechst 33324 (perfusion marker). 5 minutes prior to sacrifice. Tumors were excised and 10 μm frozen sections were obtained, which were then exposed to a phosphor plate, and autoradiographic images obtained at 50μm resolution. The sections were then stained and evaluated for hypoxia markers (pimonidazole, CA9), perfusion (Hoechst 33342) and necrosis (H&E). **Results** ADC showed no significant changes at day 2 or day 7 in all animals. In cediranib-treated rats, nIAUC90 decreased by 48±18% at day 2 ($p = 0.002$) and by 49±24% ($p = 0.022$) at day 7. In the vehicle-treated control group, changes in nIAUC90 were not significant at day 2 ($p = 0.99$) or at day 7 ($p = 0.45$). 18F-FMISO SUVmean was decreased by 33±19% ($p=0.004$) at day 2, and by 30±12% ($p=0.005$) at day 7 compared to baseline measurements. No significant change was observed in the vehicle-treated controls (Table 1). In the cediranib-treatment group, dynamic analysis of the PET data indicates initial distribution in rim region of tumor (K1), and elevated rate of specific 18F-FMISO accumulation (k3) in the central tumor regions (Figure 1). This was in contrast to the late 18F-FMISO image and the autoradiographic image, which shows 18F-FMISO primarily associated with the peripheral tumor regions, and not with the histological markers of tumor hypoxia. **Conclusions** Cediranib-induced reduction in 18F-FMISO single time-point SUV does not necessarily indicate a change in tumor oxygen status, but rather a cediranib-mediated alteration in vascular perfusion/permeability. This results in reduction of tracer delivery to tumor, with a consequent reduced absolute uptake of 18F-FMISO. Kinetic estimates based on dynamic PET data can provide a more accurate representation of the underlying tumor physiology.

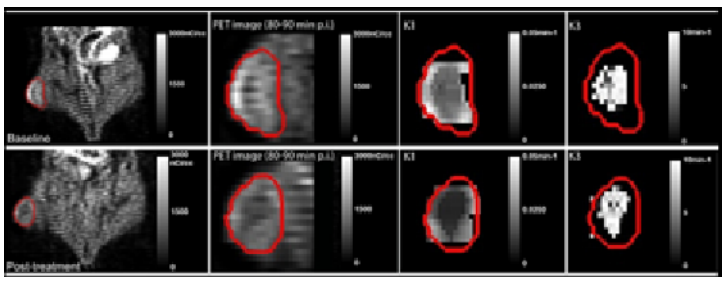


Figure 1. Late 18F-FMISO PET images and kinetic model parameters K1 and k3 obtained from the same animal before and after cediranib treatment (7 days X 3mg/kg/day). Reduction in 18F-FMISO uptake post-treatment corresponds with reduced K1 (tracer delivery rate), and not with reduced k3 (rate of hypoxia-specific uptake).

| | | | | | | | | | | | | |
|---|---|---|---|---|---|---|---|---|---|---|---|---|
| Day 2 | | | | | | | | | | | | |
| Cediranib | 0.15 | 0.04 | 0.13 | 0.09 | -0.15 | 0.004 | 0.97 | 0.09 | 0.74 | 0.15 | -0.15 | 0.020 |
| Vehicle | 0.15 | 0.08 | 0.51 | 0.06 | -0.04 | 0.105 | 1.08 | 0.13 | 0.97 | 0.13 | -0.09 | 0.060 |
| Day 7 | | | | | | | | | | | | |
| Cediranib | 0.16 | 0.17 | 0.18 | 0.08 | -0.12 | 0.06 | 0.90 | 0.32 | 0.71 | 0.19 | -0.35 | 0.004 |
| Vehicle | 0.32 | 0.26 | 0.18 | 0.13 | -0.09 | 0.206 | 1.07 | 0.34 | 0.92 | 0.49 | -0.14 | 0.149 |

Table 1. SUVmean and SUVmax values obtained pre- and post cediranib treatment for 2 and 7 days respectively.

Disclosure of author financial interest or relationships:
**L. Bokacheva**, None; **R.M. Bartlett**, None; **M. Reese**, None; **S. Ricketts**, AstraZeneca, Employment; AstraZeneca, Stockholder; **C.H. Le**, None; **J.A. Koutcher**, None; **S. Carlin**, AstraZeneca, Grant/research support .

Presentation Number **SS 102**
Scientific Session 15: Preclinical In Vivo - Oncology
September 7, 2012 / 10:54-11:06 / Room: The Auditorium

# $^{18}$F-FAZA-PET is an imaging biomarker of antitumor activity to the novel HIF-1α pathway inhibitor BAY 87-2243

***Edwin Chang***[1], *Hongguang Liu*[1], *Kerstin Unterschemmann*[3,2], *Peter Ellinghaus*[3], *Volker Gekeler*[2], *Zhen Cheng*[1], *Dietmar Berndorff*[2], *Sanjiv S. Gambhir*[1], [1]*Radiology, MIPS, Stanford University, Palo Alto, CA, USA;* [2]*Global Drug Discovery (Berlin), Bayer-Healthcare Pharmaceuticals, Berlin, Germany;* [3]*Global Drug Discovery (Wuppertal), Bayer-Healthcare Pharmaceuticals, Wuppertal, Germany. Contact e-mail: echangcv@stanford.edu*

INTRODUCTION : BAY 87-2243 is a novel small molecule inhibitor of hypoxia inducible factor-1a (HIF-1α) activity. Preclinical anti-tumor efficacy studies with BAY 87-2243 in a number of murine tumor models have revealed moderate to high tumor growth inhibition. The present study describes a non-invasive positron emission tomography (PET) imaging approach to monitor early therapeutic efficacy of this drug. METHODS: Female nude mice (N=6 per group/xenograft, N=54 total) were implanted near both scapulae with $3.5x10^6$ human non-small cell lung cancers (H460) or $2x10^6$ human prostate cancer cell lines (PC3). Both tumor lines are growth-inhibited by BAY 87-2243. As negative control, xenografts were also grown for the BAY 87-2243-resistant human renal cell carcinoma cell line, 786-0. Tumor xenografts were imaged via PET when they reached 200 $mm^3$. Four PET tracers were assessed for their uptake into tumor xenografts: $^{18}$F-FDG (metabolism), $^{18}$F-FPP(RGD)2 (angiogenesis and remodeling via $\alpha_v\beta_3$), $^{18}$F-FLT (proliferation) and $^{18}$F-FAZA (hypoxia). After pre-scan, BAY 87-2243 was orally administered, daily at 9mg/kg for 7 days. Tracer uptake was then examined 1 and 3 day(s) after initial administration of the drug. Time-point/treatment group for each PET tracer tested consisted of 6 tumors in 3 mice. At each imaging time point, RNA from BAY 87-2243-treated and vehicle-treated H460 tumor xenografts (from 3 additional animals each) was isolated and HIF target genes from different pathways were quantified by Real-Time polymerase chain reaction (PCR). RESULTS: For both $^{18}$F-FDG and $^{18}$F-FPP(RGD)2, the uptake was not significantly altered. However, $^{18}$F-FAZA tumor uptake (%ID mean/g) declined by 55-70% (From 1.21±0.10 %ID/g to 0.35±0.1 %ID/g; N=6, vehicle vs. treatment) in both H460 ($p<0.001$) and PC3 ($p<0.05$, Figure 1) models at both 1 and 3 days after drug administration. The decline occurred before any significant difference in tumor volume between drug- and vehicle-treated animals was observed, suggesting that decline in $^{18}$F-FAZA uptake reflected early changes in tumor biochemistry. A similar observation was noted for $^{18}$F-FLT in the H460 model, although the decline was less pronounced (30%; $p<0.05$ for all time-points). BAY 87-2243 affected neither uptake of the $^{18}$F-FAZA tracer nor tumor growth in 786-0 xenografts as expected. Analysis of HIF target gene expression by real-time PCR revealed that BAY 87-2243 reduced expression of several hypoxia regulated genes (e.g. CA IX and ANGPTL4) in line with reduced 18F-FAZA uptake. Reduced $^{18}$F-FLT uptake was not accompanied by reduced expression of TK1. Expression level of genes associated with glucose metabolism was heterogeneous and did not fully match the unchanged $^{18}$F-FDG uptake: GLUT-1 expression was unchanged while HK-2 decreased. Overall surface integrin αvβ3 expression was low and may explain the lack of change in $^{18}$F-FPP(RGD)2 uptake. CONCLUSION: This study illustrates the importance of testing multiple tracers to determine which one may measure early efficacy. $^{18}$F-FAZA-PET, best acts as an early pharmacodynamic marker before changes in tumor volume.

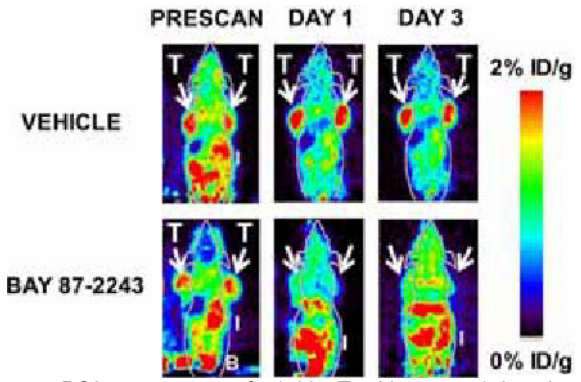


Panel of coronal $^{18}$F-FAZA-PET images for human PC3 tumor xenografts (white T, white arrows) that show reduction of $^{18}$F-FAZA uptake with BAY 87-2243 administration (9mg/kg, daily). Background uptake in intestines (I) and in bladder (B).

Disclosure of author financial interest or relationships:
**E. Chang**, Bayer-Healthcare Inc., Grant/research support; GE-Healthcare Inc., Grant/research support; **H. Liu**, None; **K. Unterschemmann**, Bayer Healthcare, Employment; **P. Ellinghaus**, Bayer Pharma AG, Employment; **V. Gekeler**, Bayer HealthCare Pharmaceuticals, Employment; **Z. Cheng**, None; **D. Berndorff**, Bayer, Employment; Bayer, Stockholder; **S.S. Gambhir**, General Electric, Grant/research support; Bayer-Schering, Grant/research support; Sanofi-Aventis, Grant/research support; CellSight, Stockholder; ImaginAB, Stockholder; Enlight, Stockholder; Endra, Stockholder; Bracco, Consultant; NinePoint Medical, Stockholder; Visualsonics, Consultant .

Presentation Number **SS 103**
Scientific Session 15: Preclinical In Vivo - Oncology
September 7, 2012 / 11:06-11:18 / Room: The Auditorium

# Development of HIF-1α/HIF-1β heterodimerization inhibitors using a novel bioluminescence reporter assay system for in vitro high throughput screening and in vivo imaging

***Yun-Chen Chiang**, Nashaat Turkman, Brian Rabinovich, Daniel Young, Andrei Volgin, Amer M. Najjar, Juri G. Gelovani, Department of Experimental Diagnostic Imaging, Univeristy of Texas MD Anderson Cancer Center, Houston, TX, USA. Contact e-mail: ychiang@mdanderson.org*

Introduction: Tumor growth often outpaces the vascularization process leading to the development of hypoxic environment and central necrosis. In response to hypoxia, an intracellular hypoxia adaptive pathway is initiated by heterodimerization of hypoxia-inducible factor-1α (HIF-1α) and HIF-1β, and the upregulation of several HIF1-reponsive genes enhancing the survival of tumor cells in hypoxic microenvironment. Furthermore, hypoxic tumor regions are associated with resistance to various classes of radio- or chemotherapeutic agents. Therefore, development of inhibitors of HIF-1α/β heterodimerization may provide a novel approach to anti-cancer therapy. In this study, we developed an approach for imaging HIF-1α/β heterodimerization in vitro and in vivo, and utilized this novel screening platform to identify promising lead inhibitors. We have chemically derivatized the lead inhibitor to assess structure-activity relationship (SAR), selected the most efficient drug candidate, and verified its pharmacodynamic efficacy in vivo by bioluminescence imaging (BLI) of inhibition of HIF-1α/β dimerization and anti-tumor efficacy in tumor xenograft-bearing mice. Results: We used split firefly luciferase complementation approach to develop a new high-throughput screening assay for screening small molecule libraries of inhibitors of HIF1α-HIF1β PAS AB domain dimerization (Fig.1). The IC50 and cellular cytotoxicity of each compound were determined by BLI, florescence imaging and WST1 assays. Among the screened compounds, acridine derivatives demonstrated a very potent inhibitory activity in low nM to sub-nM range (Fig.2). SAR studies demonstrated that the inhibition of HIF-1α/β heterodimerization is enhanced by aliphatic amide formation in 3,6-positions, whereas the aromatic amide formation in these positions significantly reduces inhibitory activity (Tab.1). The pharmacokinetics and organ toxicity of acriflavine and selected derivatives were assessed in vivo, in nude mice bearing s.c. xenografts of transduced U87 HIF-1α/β reporter tumors. After the xenografts reached 100 mm3, the mice were randomized into groups to receive daily i.p. saline or selected compounds (2mg/kg). Repetitive BLI of HIF-1α/β reporter activity in tumors demonstrated pharmacologic efficacy of acridine derivatives in vivo (Fig.3). A significant retardation of tumor growth was observed in treatment group, as compared to control (Fig.4). Immunohistochemical analyses of tumors treated with acridine derivatives revealed a significant decrease in density and size of CD34+ microvessels, and expression of VEGF (Fig.5). Conclusions: We developed a novel effective high throughput - high content screening assay for selection of HIF-1α/β heterodimerization inhibitors. Amine or amide functionalization of the acridine at the 3,6-positions significantly enhanced the efficacy of the inhibitors. Additionally, aliphatic amide moieties are more effective HIF-1α/β dimerization inhibitors than compounds with aromatic amide functionalities. Our lead drug candidate demonstrated efficacy as monotherapy resulting in tumor growth inhibition via disruption of HIF1 signaling-mediated tumor stromal neoangiogenesis.

Disclosure of author financial interest or relationships:
**Y. Chiang**, None; **N. Turkman**, None; **B. Rabinovich**, None; **D. Young**, None; **A. Volgin**, None; **A.M. Najjar**, None; **J.G. Gelovani**, Macrocyclics, Consultant; SibTech, Consultant .

Presentation Number **SS 104**
Scientific Session 15: Preclinical In Vivo - Oncology
September 7, 2012 / 11:18-11:30 / Room: The Auditorium

# *In vivo* imaging of the effects induced by chronic inhibition of prolyl-4-hydroxylases in cancer shows a paradoxic down-regulation of tumor HIF-1 activity

***Steffi Lehmann***[1], *Daniel P. Stiehl*[2], *Michael Honer*[3], *Ruth Keist*[1], *Marco Dominietto*[1], *Christof Baltes*[1], *Katarzyna Nytko*[2], *Roland H. Wenger*[2], *Markus Rudin*[1], [1]*Institute for Biomedical Engineering, ETH Zurich, Zurich, Switzerland;* [2]*Institute of Physiology, University of Zurich, Zurich, Switzerland;* [3]*Institute for Pharmaceutical Sciences, ETH Zurich, Zurich, Switzerland. Contact e-mail: lehmann@biomed.ee.ethz.ch*

Prolyl-4-hydroxylases (PHDs) play a central role in cellular oxygen sensing by regulating the stability of hypoxia inducible factors (HIFs), which transcriptionally mediate the adaptation of mammalian cells to low oxygen concentrations. Whereas PHDs mark HIF-α subunits for proteasomal degradation under normoxic conditions, their activity ceases in hypoxia such that HIF becomes active. Recently, PHDs have received increased attention as regulators of cancer progression beyond their role in oxygen sensing. Thereby they have been attributed both tumor suppressing as well as tumor promoting functions. However, which of these effects prevails during cancer development and to which extent PHDs depend on their enzymatic activity to regulate tumor growth remains largely undefined. Therefore, we set out to investigate the effect of non-selective pharmacological inhibition of PHD activity on tumor growth. C51 tumor allograft mice were chronically treated with dimethyloxalylglycine (DMOG), a widely used PHD inhibitor, over a period of two weeks. Combining different non-invasive *in vivo* imaging methods (bioluminescence imaging, PET and MRI), we monitored the impact of this treatment on overall cancer progression. Specifically, we assessed HIF-1 activity using bioluminescence imaging of C51 tumors stably expressing a reporter construct driving luciferase from a HIF sensitive promoter. $^{18}$F-labeled misonidazole (FMISO), a radiolabeled nitroimidazole derivative accumulating in hypoxic cells, was intravenously injected into allograft animals to detect the level of tumor hypoxia by PET. Furthermore, we assessed the tumor blood volume in DMOG treated and control animals by contrast enhanced MR imaging. Paradoxically, chronic DMOG treatment led to a drastic down-regulation of HIF-1 activity in tumor cells, not affecting tumor growth, vascularization and the overall tumor oxygenation level. Live cell imaging studies and immunoblotting experiments performed in U87 and C51 cancer cells, chronically treated with DMOG *in vitro*, further confirmed these *in vivo* results and identified a negative feedback loop induced by chronic inhibition of PHDs to decrease HIF-1 protein levels and transcriptional activity. Since HIF expression is a hallmark of many types of human cancer and is typically associated with poorer patient prognosis as well as increased resistance to therapy, our results may provide a novel means to decrease HIF-1 levels in cancer and improve therapeutic outcomes.

Disclosure of author financial interest or relationships:
**S. Lehmann**, None; **D.P. Stiehl**, None; **M. Honer**, None; **R. Keist**, None; **M. Dominietto**, None; **C. Baltes**, Varian Medical Systems, Employment; **K. Nytko**, None; **R.H. Wenger**, None; **M. Rudin**, Hoffmann-LaRoche Ltd, Basel, Switzerland, Grant/research support .

Presentation Number **SS 105**
Scientific Session 15: Preclinical In Vivo - Oncology
September 7, 2012 / 11:30-11:42 / Room: The Auditorium

# Uptake of $^{18}$F-EF5 and $^{18}$F-FDG is Associated with the Hypoxic Phenotype in HNSCC Cell Lines and Mice Xenografts

***Jonna Silén***[1,5]*, Heidi Högel*[2]*, Katri Kivinen*[3]*, Antti Silvoniemi*[1,4]*, Sarita Forsback*[1]*, Olof Solin*[1]*, Reidar Grénman*[4]*, Heikki Minn*[1,5]*, Panu Jaakkola*[2,5]*, Tove J. Grönroos*[1]*, [1]Turku PET Centre, University of Turku, Turku, Finland; [2]Turku Centre of Biotechnology, University of Turku, Turku, Finland; [3]Department of Pathology, Turku University Hospital, Turku, Finland; [4]Department of Otorhinolaryngology, Turku University Hospital, Turku, Finland; [5]Department of Oncology and Radiotherapy, Turku University Hospital, Turku, Finland. Contact e-mail: jmsink@utu.fi*

**PURPOSE:** The main goal in a noninvasive imaging of cancer is to reveal molecular-based events that are characteristic of the tumor genotype and phenotype. A fundamental understanding about the biochemical and molecular biological processes that affect the uptake of $^{18}$F-EF5 is needed before the imaging of hypoxic tumor sub volumes can be employed for hypoxia-directed treatment strategies. The purpose of this study was to investigate whether the uptake of the hypoxia tracer $^{18}$F-EF5 and the glucose metabolism tracer $^{18}$F-FDG reflect a hypoxic phenotype in head and neck squamous cell carcinomas (HNSCC). **METHODS AND MATERIALS:** The *in vitro* uptake of $^{18}$F-EF5 and $^{18}$F-FDG was determined in four HNSCC cell lines (UT-SCC) after exposure to hypoxia (1% $O_2$) for 0, 1, 3, 6, 12 and 24 hours. Radioactivity uptake was determined utilizing digital autography and images analyzed with the Aida software. The expression of Hif-1α protein was determined in order to evaluate the ability of cells to adapt to the hypoxic environment. Experimental tumors (s.c.) were produced from UT-SCC cell lines in nude male mice and imaged with $^{18}$F-EF5 and $^{18}$F-FDG (Inveon PET/CT). The uptake of radiotracers was determined in whole tumors and by a 10% threshold value. Paraffin embedded tumor sections were stained against Hif-1α, CA IX and Glut-1. **RESULTS:** The *in vitro* uptake of $^{18}$F-FDG, at different time points after hypoxia exposure, correlated with the expression of Hif-1α. Instead, the *in vitro* uptake of $^{18}$F-EF5 was less altered by the prolonged hypoxia exposure time compared with $^{18}$F-FDG, but an overall higher uptake (up to 14-fold) was detected in those cell lines that also showed high $^{18}$F-EF5 and $^{18}$F-FDG uptake *in vivo*. The uptake of both tracers correlated with high CA IX expression, which is a protein associated with an aggressive phenotype in HNSCC. **CONCLUSION:** Hypoxia increases the uptake of $^{18}$F-FDG as a consequence of the activation of Hif-1α expression in HNSCC cells *in vitro*. This reliance is lost in an *in vivo* setting, probably due to multiple other factors influencing the uptake of $^{18}$F-FDG. The *in vivo* imaging of HNSCC xenografts indicated that the expression of CA IX, and not Hif-1α or Glut-1, relates to the high uptakes of $^{18}$F-FDG and $^{18}$F-EF5. In conclusion, we suggest that the hypoxia tracer $^{18}$F-EF5 might be useful for the detection of aggressive HNSCC tumors in the future. However, the true biological genotype behind the phenotypes reported in this study needs to be evaluated in more detailed.

Disclosure of author financial interest or relationships:
**J. Silén**, None; **H. Högel**, None; **K. Kivinen**, None; **A. Silvoniemi**, None; **S. Forsback**, None; **O. Solin**, None; **R. Grénman**, None; **H. Minn**, None; **P. Jaakkola**, None; **T.J. Grönroos**, None.

Presentation Number **SS 106**
Scientific Session 15: Preclinical In Vivo - Oncology
September 7, 2012 / 11:42-11:54 / Room: The Auditorium

# Targeting tumor hypoxia with $^{99m}$Tc-labeled small molecule inhibitors of carbonic anhydrase IX (CAIX)

***John L. Joyal***[1], *Shawn M. Hillier*[1], *Genliang Lu*[1], *John C. Marquis*[1], *Kevin P. Maresca*[1], *Trevor D. McKee*[2], *David Green*[2], *Craig N. Zimmerman*[1], *Brad Wouters*[2], *William C. Eckelman*[1], *John W. Babich*[1], [1]*Discovery Research, Molecular Insight Pharmaceuticals, Cambridge, MA, USA;* [2]*Ontario Cancer Institute, University Health Network, Toronto, ON, Canada. Contact e-mail: jjoyal@molecularinsight.com*

Hypoxia is associated with a poor response to radiation therapy and certain types of chemotherapy. CAIX is upregulated in solid tumors in response to the hypoxic tumor microenvironment making it an attractive molecular target for assessing tumor hypoxia. In addition, clear cell renal carcinomas constitutively express CAIX at high levels. MIP-1505, 4-(2-bis((1-(2-((1,5-dicarboxy-3-(2-carboxyethyl)pentan-3-yl)amino)-2-oxoethyl)-1H-imidazol-2-yl)methyl)amino-*N*-butyloxy)benzenesulfonamide was selected from a screen of a library of compounds and evaluated for targeting CAIX in tumor cells. Competitive binding assays of several novel CAIX inhibitors containing a benzenesulfonamide moiety tethered through a linker to bis-(pyridylmethyl)amine or functionalized bis-(imidazolylmethyl)amine derived $Re(CO)_3$ chelates were conducted in hypoxic HeLa cells and confirmed in HEK-293 cells stably transfected with human CAIX (HEK-293-CAIX). Several high affinity compounds, including MIP-1505, were radiolabeled with $^{99m}Tc(CO)_3$ and studied *in vitro* for binding to normoxic CA IX(-) and hypoxic CA IX(+) HeLa cells, constitutively expressing CAIX(+) SK-RC-52 and CAIX(-) SK-RC-59 renal cancer cells, and in HEK-293-CAIX cells. Cellular internalization in HeLa cells was examined. Tissue distribution was conducted in HeLa, HEK-293 and HEK-293-CAIX xenograft mice with and without competition by 10 mg/kg acetazolamide, or Re-MIP-1505, in the case of MIP-1505, and corroborated by microSPECT imaging of HeLa xenografts. Immunohistochemistry was performed to confirm CAIX expression. $IC_{50}$ values of the compounds tested ranged from 2.6-2,000 nM by competition binding in hypoxic HeLa cells. $^{99m}$Tc-MIP-1505 exhibited high affinity (35 nM) for CAIX on hypoxic HeLa cells and a preferable pharmacokinetic profile *in vivo*. $^{99m}$Tc-MIP-1505 did not internalize in cells. Specificity for CAIX was demonstrated by competition with acetazolamide in hypoxic or $CoCl_2$ treated HeLa and SK-RC-52 cells, and binding to HEK-293-CAIX cells. Reduced binding was observed in CAIX(-) normoxic HeLa, SK-RC-59 and HEK-293 cells. *In vivo*, $^{99m}$Tc-MIP-1505 achieved 3.2% ID/g in HeLa tumors and 15% ID/g in HEK-293-CAIX tumors. Uptake in HEK-293 tumors was low. MicroSPECT imaging corroborated these results. Tumor uptake was reduced dose dependently by Re-MIP-1505 or by co-injection with 10 mg/kg acetazolamide. $^{99m}$Tc-MIP-1505, selected from a library of CAIX inhibitors, binds with high affinity and selectivity to CAIX on hypoxic tumors. A hypoxia targeted probe may have the potential to significantly impact diagnosis, staging, and treatment selection of hypoxic solid tumors.

Disclosure of author financial interest or relationships:
**J.L. Joyal**, Molecular Insight, Employment; **S.M. Hillier**, Molecular Insight Pharmaceuticals, Employment; **G. Lu**, None; **J.C. Marquis**, None; **K.P. Maresca**, Molecular Insight Pharmaceuticals, Employment; **T.D. McKee**, Pfizer, Grant/research support; Molecular Insight Pharmaceuticals, Grant/research support; **D. Green**, None; **C.N. Zimmerman**, Molecular Insight Pharmaceuticals, Employment; **B. Wouters**, Pfizer, Grant/research support; Molecular Insight Pharmaceuticals, Grant/research support; **W.C. Eckelman**, None; **J.W. Babich**, Molecular Insight Pharma, Employment .

Presentation Number **SS 107**
Scientific Session 16: Chemistry & Probes - MRI
September 7, 2012 / 13:00-13:11 / Room: Liffey Hall 1

# 19F-MRI based detection of beta cells using fluoromannoheptuloses

***Uwe Himmelreich***[1], *Karim Louchami*[2], *Julian Thimm*[3], *Joachim Thiem*[3], *Sonu Sharma*[1], *Tom Dresselaers*[1], *Willy Malaisse*[2], *Abdulah Senner*[2], [1]*Biomedical MRI Unit/ MoSAIC, Katholieke Universiteit Leuven, Leuven, Belgium;* [2]*Free University Brussels, Brussels, Belgium;* [3]*University of Hamburg, Hamburg, Germany. Contact e-mail: Uwe.Himmelreich@med.kuleuven.be*

Introduction Quantification of beta cell mass is currently achieved by indirect estimation, and those estimation techniques are often inaccurate. Considerable effort has been put into the development of in vivo non invasive imaging techniques to estimate pancreatic beta cell mass, but until today there is no clinical application. While some approaches focus on nanoparticles coupled to specific antibodies, we aimed to evaluate the possibility of using small molecules that act as specific substrates for beta cells. Due to their diabetogenic properties, heptuloses are of particular pharmacological interest as potential therapeutics for hypoglycemia or cancer (1). A potential use for suitable analogues as agents in non invasive imaging of pancreatic beta cells has been postulated (2). We have evaluated the specificity of several 19F-heptulose dereivates as potential contrast agent for beta cell imaging using 19F MRI. Material and Methods Synthesis: 1-deoxy-1-fluoro mannoheptulose (1-FMH), 3-deoxy-3-fluoro mannoheptulose (3-FMH) and 7-deoxy-7-fluoro mannoheptulose (7-FMH) were synthesized as described in (3). Cell culture: INS-1 cells were labeled with the 19F-heptuloses for 2 hrs. Cell pellets were prepared for MRI. Attachment and proliferation of INS-1 cells was measured in real-time using the xCELLigence (Roche Diagnostics) platform to assess potential toxic effects. Rat pancreatic islets (PI) were labeled similarly. In addition, the release of insulin by PIs was measured by radio-immunoassay after 90 min incubation in buffered medium. 19F MRI/ NMR: Uptake and potential metabolism of FMHs was followed by 19F NMR spectroscopy. For the assessment of the in vitro visualization of 19F-heptulose labeled cells, phantoms were used that consist of 0.5ml tubes filled with the respective cell pellets and embedded in agar. All MR images were acquired using a Bruker Biospec 9.4T small animal MR scanner. The biodistribution of FMHs was assessed after systemic administration in mice. Purpose-built radio-frequency solenoid transmit-receive coils with an inner diameter of 4cm and tunable to the 1H (400.34 MHz) and 19F (376.64 MHz) frequencies was used for all phantom and in vivo experiments. Results and Discussion: 19F-NMR confirmed that no other changes or additional signals were seen in 1H and 19F NMR spectra, indicating no further metabolism of the FMHs. The uptake of the 19F-heptuloses ranged from 0.50 (1-FMH and 3-FMH) to 0.25 (7-FMH) umol per 3x106 cells, corresponding to intracellular concentrations of almost 20mM. No substantial toxic effects or effects on insulin secretion were noted (Fig 1). In vitro 19F MRI indicates that cell pellets containing 0.5 Mio cells suspended in 20 ul are detectable (Fig 1). In vivo MRI confirmed strong uptake in the pancreas and some uptake in the liver. Conclusion: Our findings indicate that selected 19F-heptuloses may represent suitable tools for the non-invasive imaging of GLUT2 expressing cells like beta cells. References (1) WJ Malaisse et al. Nat Rev Endocrinol 2009 5: 394 (2) WJ Malaisse et al. Diabetes 2000 49: A418, (3) D Waschke et al. Eur J Org Chem 2012 5:948

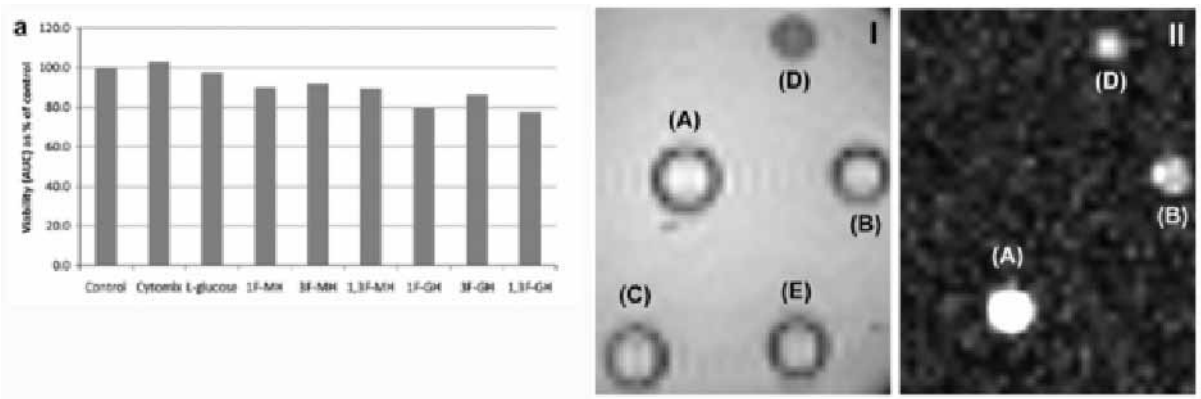


Figure 1: (A) Cell viability after labeling with various fluorinated heptuloses relative to unlabelled cells. (B) 1H and 19F MRI of A 20mM 5-FC, B 10mM 1-FMH, C 1mM 1-FMH, D 0.5 Mio cells labeled with 1-FMH and E PBS.

Disclosure of author financial interest or relationships:
**U. Himmelreich**, None; **K. Louchami**, None; **J. Thimm**, None; **J. Thiem**, None; **S. Sharma**, None; **T. Dresselaers**, None; **W. Malaisse**, None; **A. Senner**, None.

Presentation Number **SS 108**
Scientific Session 16: Chemistry & Probes - MRI
September 7, 2012 / 13:11-13:22 / Room: Liffey Hall 1

# In Vivo Magnetic Resonance Imaging of Glucose

***Hyla Allouche-Arnon***[1,2], *Trevor Wade*[3,4], *Lanette Friesen Waldner*[3,4], *Valentina N. Miller*[1], *J. Moshe Gomori*[1], *Rachel Katz-Brull*[1,2], *Charles A. McKenzie*[3,4], [1]*Radiology, Hadassah-Hebrew University Medical Center, Jerusalem, Israel;* [2]*BrainWatch Ltd., Tel-Aviv, Israel;* [3]*Medical Biophysics, The University of Western Ontario, London, ON, Canada;* [4]*Robarts Research Institute, The University of Western Ontario, London, ON, Canada. Contact e-mail: ahyla@hadassah.org.il*

Introduction Glucose has been a desired target for hyperpolarized 13C MRI due to its ability to report on metabolically active tissues and malignancy. However, the short T1 of its 13C nuclei ruled out this possibility. We show that hyperpolarized glucose imaging is feasible in vivo, using a glucose analog which is enriched with both 13C and deuterium in all positions. We show that this strategy allows nonradioactive, noninvasive imaging of glucose. Methods and Materials T1 measurement of glucose analogs were performed at 11.8T and 7T. The animal studies' protocol was approved by the Institutional Animal Use Subcommittee. Anesthetized male Sprague-Dawley rats, 565 ± 64 g (n=4), underwent MRI in a 3T clinical MRI scanner. Hyperpolarized media containing [13C6, 2H7]glucose (Cambridge Isotope Laboratories) were produced in a DNP polarizer and injected via a tail vein catheter as a 12 s bolus. Coronal projection 13C imaging was performed at 8 - 20 s from injection start using a variable flip angle gradient echo sequence within 1 s. Results In native glucose the T1 values of the 13C nuclei were 1-to-2 s. The deuteration of all of glucose 13C nuclei resulted in a significant elongation of these 13C nuclei T1. The T1 of the deuterated glucose 13C ranged between 6-10 s at 11.8T and increased to 8-13 s at 7T. The T1 of glucose's deuterated 13C nuclei were shortened on average by 3.3 s due to the added 13C-13C dipolar interaction in the fully 13C labeled molecule. At 3 T, the T1 of the [13C6, 2H7]glucose 13C nuclei averaged to 10 s. This represents a prolongation factor of ca. 5-10 fold compared to native glucose. The labeling with 13C in six positions leads to a six-fold increase in the initial hyperpolarized signal. Both effects enabled hyperpolarized glucose imaging In vivo imaging of rats injected with hyperpolarized [13C6, 2H7]glucose was performed at 8 s (Fig. a), 12 s (Fig. b), and 20 s (Fig. c) from injection start. Hyperpolarized images (color) are presented overlaid on proton images from the same rat. The color scales represent arbitrary linearly distributed intensity units for the hyperpolarized images. The images' relative intensities can be compared based on the corresponding color scale. In Fig. a, recorded during the bolus injection, the inferior vena cava and the heart are clearly visible at angiographic quality. In Fig. b, the signal intensity in the main vasculature and the heart is high, with substantial intensity observed in the kidneys. In Fig. c, the signal from the heart is the most intense signal in the image while signals in the kidneys and liver are observed as well. Conclusion The first non-radioactive images of glucose distribution were obtained in live rats by hyperpolarized MRI. The utility of this imaging approach in catheter angiography was demonstrated by imaging during bolus injection, wherein glucose was utilized as a safe, high intensity, injectable agent. Hyperpolarized [13C6, 2H7]glucose MRI may offer non-radioactive visualization of glucose uptake in health and disease. Further studies are needed to compare such studies to FDG-PET which is the only imaging modality available today for imaging glucose uptake.

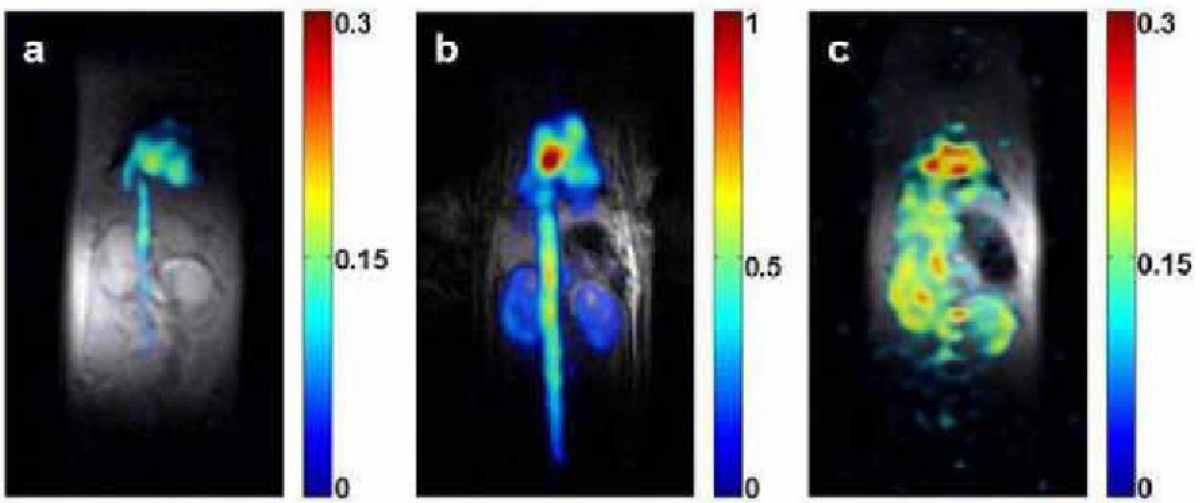


Disclosure of author financial interest or relationships:
**H. Allouche-Arnon**, None; **T. Wade**, None; **L. Friesen Waldner**, None; **V.N. Miller**, None; **J. Gomori**, BrainWatch Ltd, Consultant; **R. Katz-Brull**, BrainWatch Ltd, Other financial or material support; **C.A. McKenzie**, GE Healthcare, Grant/research support; Brainwatch, Grant/research support .

Presentation Number **SS 109**
Scientific Session 16: Chemistry & Probes - MRI
September 7, 2012 / 13:22-13:33 / Room: Liffey Hall 1

# Magnetic Resonance Imaging of Tissue-Engineered Implants

***Marianne E. Mertens***[1], *Alina Hermann*[2], *Anne Bühren*[2], *Leon Olde-Damink*[2], *Fabian Kiessling*[1], *Twan Lammers*[1], [1]*Department of Experimental Molecular Imaging, RWTH Aachen, University, Aachen, Germany;* [2]*Matricel GmbH, Aachen, Germany. Contact e-mail: mmertens@ukaachen.de*

Non-invasive imaging holds significant potential for monitoring the functionality, the resorption and the remodeling of tissue-engineered implants. It could, for instance, contribute substantially to the development of safer and patient-customized implants, and it might also facilitate their clinical translation. Consequently, there is a clear need for the investigation of imaging agents and techniques capable of visualizing scaffolds after implantation. With the increasing use of biomimetic biomaterials, which stimulate local in situ tissue repair, the most promising and clinically relevant labelling method is based on the integration of contrast agents directly into the implant material. Here, we show that 3-dimensional collagen-based scaffolds can be sensitively and stably labelled with ultrasmall superparamagentic iron oxide (USPIO) nanoparticles, enabling their visualization using magnetic resonance imaging (MRI). Ultrasmall superparamagnetic iron oxide (USPIO) nanoparticles possessing different surface functionalities (terminal hydroxy-, amino- or aldehyde groups) were incorporated either physically or chemically into 3D collagen-based scaffolds. Labelled scaffolds were investigated regarding i) structural properties, ii) labelling stability, iii) MR visibility and iv) biocompatibility. Electron microscopy analyses demonstrated that the pore structure of the scaffolds was not affected by the incorporation of USPIO, the average pore sizes ranged between 90 and 100 µm for all implant materials investigated. Both physical and chemical USPIO incorporation was found to be highly stable, and no loss of contrast agent was observed even after 4 weeks of extensive washing. Labelled scaffolds could be successfully imaged using T2-weighted and bright iron MRI, both in vitro and in vivo. USPIO concentrations of 0.2% - 0.6% (w/w) resulted in the most optimal imaging properties. Scaffold resorption (upon incubation to collagenase) could be quantitatively monitored in gelatine phantoms. The biocompatibility of the labelled scaffolds was confirmed by colonizing them with fibroblasts, smooth muscle cells and endothelial cells. The distribution, penetration and proliferation of the colonizing cells were not affected by USPIO labelling, as demonstrated by extensive H&E and Ki67 analyses . The incorporation of USPIO into collagen-based scaffolds is shown to be a suitable method for enabling the monitoring of scaffold location and resorption in MRI, without changing the structural properties of the implant. Proof-of-principle ex vivo and in vivo experiments are currently ongoing.

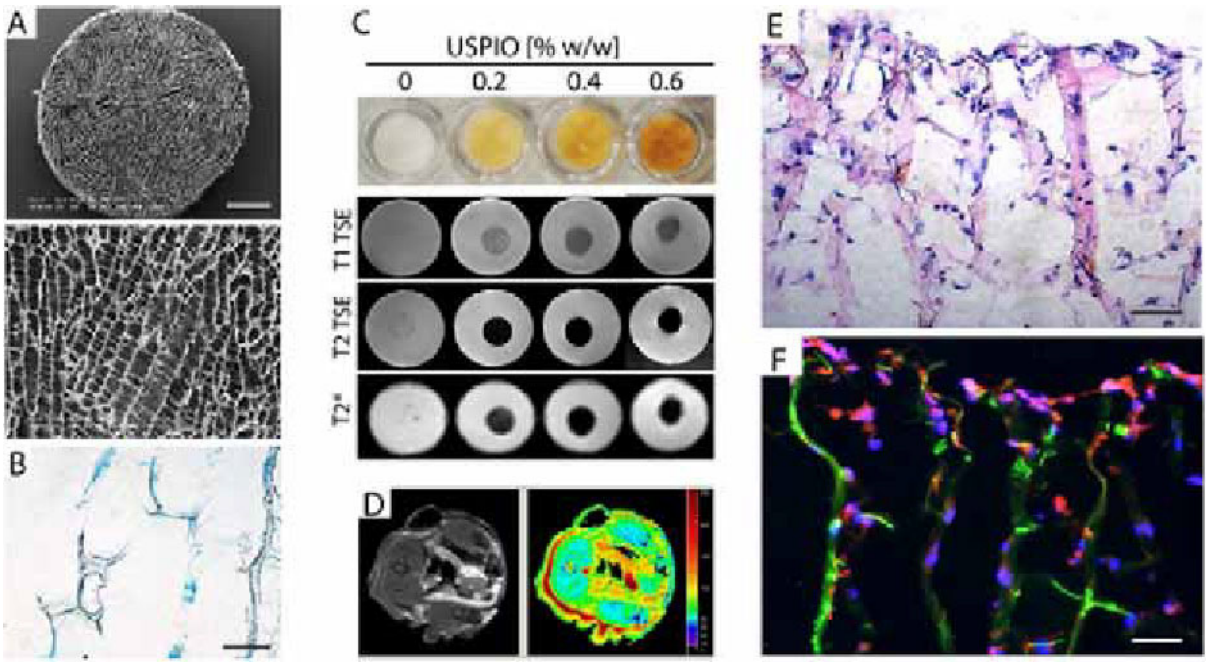


Figure 1: A) Scanning electron microscopic images of 3D-collagen scaffolds labelled with 0.6 % (w/w) USPIO (top: 20 x magnification, scale 1 mm; bottom: 80 x magnification, scale 200 µm); B) Prussian Blue staining of incorporated iron, scale 100 µm; C) Labelled scaffolds in T1, T2 and T2* weighted MRI, D) T2 weighted MRI of subcutaneously implanted labelled scaffold, E) H&E staining and F) IHC of labelled scaffold colonized with NIH3T3 (blue: Hoechst, green: collagen, red: Ki67, scale 50 µm).

Disclosure of author financial interest or relationships:
**M.E. Mertens**, None; **A. Hermann**, Matricel GmbH, Employment; **A. Bühren**, Matricel GmbH, Employment; **L. Olde-Damink**, Matricel GmbH, Employment; **F. Kiessling**, None; **T. Lammers**, None.

Presentation Number **SS 11**
Scientific Session 2: Technology & Software - Optical Imaging
September 6, 2012 / 10:52-11:03 / Room: Wicklow Hall 1

# A new method to measure radiotracer uptake in single living cells

***Guillem Pratx**, Kai Chen, Conroy Sun, Lynn M. Martin, Colin M. Carpenter, Lei Xing, Radiation Oncology, Stanford University, Stanford, CA, USA. Contact e-mail: pratx@stanford.edu*

**Objective:** Positron emission tomography (PET) is the most sensitive method for probing molecular processes in vivo. However, PET has limited spatial resolution and is incapable of resolving submillimeter structures. The visualization of submillimeter small structures is only feasible using autoradiography, which has other limitations such as requiring fixed samples and exposure times of one hour or more. More importantly, however, the best spatial resolution achievable with autoradiography does not allow individual cells to be distinguished. Because each cell possesses unique features (e.g. size, morphology, gene expression, disease, and cell phase), the uptake of a radiotracer is heterogeneous within a population of cells—even when those cells belong to the same organ. For lack of a suitable tool, this effect has remained largely unobserved. **Methods:** To enable the measurement of radiotracer uptake all the way down to the single-cell level, we have recently developed a new method called radioluminescence microscopy. In this method, cells are cultured on a special plate made from scintillator material. The plate can convert ionizing radiation from radioactive decay into visible-range optical signal detectable in a microscope. One advantage of the approach is that because the plate is clear is the visible range, it is fully compatible with other standard microscopy techniques, including brightfield and fluorescence microscopy. To acquire a radioluminescence micrograph, we incubate the cells with a radiotracer, which we then wash out from the cell medium. We acquired images of the radioactive decays using a sensitive electron-multiplying charge-coupled device camera coupled to a high-numerical-aperture microscopy objective. **Results:** The sensitivity and spatial resolution of the radioluminescence microscope was found to be 10 fCi per pixel and 4.6 μm, respectively. The uptake of FDG was clearly resolvable in single cells. Marked heterogeneity in 18F-FDG uptake was observed among cells from the same population, i.e. with the same genetic material and exposed to the same conditions. We found that the heterogeneity in cellular uptake had for origin the pharmacokinetics parameters, which vary markedly from cell to cell. Generally, FDG uptake in single cells was correlated with fluorescence microscopy measurements of 2-NBDG, a green fluorescent glucose analog. In another experiment, we transfected cells with a fusion PET / fluorescence gene reporter (HSV1-ttk-mrfp1). Those cells were incubated with 18F-FHBG, a PET probe specific to the TK enzyme, and imaged both with radioluminescence and fluorescence imaging. Uptake of FHBG was coincident with RFP fluorescence signal, indicating that HSV1-tk reporter gene expression is required for FHBG uptake and retention. **Conclusion:** For the first time, we demonstrate that radioluminescence microscopy can be applied to elucidate how properties specific to individual cells may affect the uptake and retention of a radiopharmaceutical. We expect radioluminescence microscopy to become a useful technique for the precise characterization of existing and novel radiotracers at the single-cell level.

Disclosure of author financial interest or relationships:
**G. Pratx**, None; **K. Chen**, None; **C. Sun**, None; **L.M. Martin**, None; **C.M. Carpenter**, None; **L. Xing**, Varian Medical Systems, Grant/research support .

Presentation Number **SS 110**
Scientific Session 16: Chemistry & Probes - MRI
September 7, 2012 / 13:33-13:44 / Room: Liffey Hall 1

# PLGA encapsulated iron oxide nano- (NPs) and microparticles (MPs) are clinically viable options for MRI-based cell tracking

*Dorit Granot[1], Michael Nkansah[2], Margaret Bennewitz[2], Kevin S. Tang[2], Eleni A. Markakis[1], **Erik M. Shapiro**[1,2], [1]Department of Diagnostic Radiology, Yale University School of Medicine, New Haven, CT, USA; [2]Department of Biomedical Engineering, Yale University, New Haven, CT, USA. Contact e-mail: erik.shapiro@yale.edu*

INTRODUCTION: There is no FDA-approved particle for MRI-based cell tracking, impeding translation to the clinic. Here we describe PLGA encapsulated iron oxide nano- (NPs) and microparticles (MPs) as clinically viable options for MRI-based cell tracking. PLGA is an FDA-approved material with a long history of use in drug delivery. PLGA NPs and MPs can encapsulate large amounts of iron oxide nanocrystals. We report numerous analytical particle and cell characterizations, including in vivo biodegradation rate and multiple quantitative stem cell differentiation assays. The uses of these new particles for MRI-based cell tracking, both in traditional cell transplant as well as cell migration experiments are demonstrated. MATERIALS AND METHODS: Magnetic particles: NPs and MPs were fabricated with increasing amounts of magnetite and assayed for iron content, size and molar relaxivity. Labeling efficiency and retention, viability and ROS production were assayed in multiple cell types. Stem cell assays: NP and MP labeled rat neural stem cells (NSCs) and mesenchymal stem cells (MSCs) were analyzed for multilineage differentiation capacity. NSCs were simultaneously differentiated down multiple lineages while MSCs were differentiated down separate adipogenic or osteogenic lineages. NSCs were then stained for Tuj1 (immature neurons), GFAP (astrocytes), and O4 (oligodendrocytes). Flow cytometry quantified the number of each mature cell type formed by labeled NSCs. Labeled and unlabeled MSCs were stained for adipocytes or osteocytes, with numbers of adipocytes quantified. In vivo biodegradation: In vivo biodegradation was investigated in mice injected with NPs, Feridex or inert MPIOs, by serially acquiring T2* maps of liver over 12 weeks. Chemical iron analysis verified MRI data. In vivo MRI: Two MRI-based cell tracking experiments were performed. The first was a cell transplant paradigm where 10, 100 or 1000 NP labeled MSCs were injected into rat brain. The second was a paradigm of in vivo labeling and tracking of endogenous rat NSCs. MPs (200 µg in 20 µl) were injected into the lateral ventricles of 6-week old rat brains (n=6). NSCs phagocytose these particles at the ventricle and carry them as they migrate to the olfactory bulb, revealing dark contrast on T2*-weighted MRI. For both paradigms, rats underwent separate 100 and 200 microns isotropic 3D gradient echo MRI at 11.7T over two weeks. RESULTS and DISCUSSION: NP and MP labeled cells exhibited insignificant toxicity and minimal ROS production following labeling. NSCs magnetically labeled with both NPs and MPs differentiated into equal proportions into neurons, astrocytes, and oligodendrocytes as compared to each other and unlabeled NSCs. Equivalent osteogenic and adipogenic potential was observed for MSCs labeled with all particle types. Particles experienced 80% biodegradation within 12 weeks. Cell detection sensitivity was 10 cells for in vivo MRI. MPs enabled the visualization of the NSC migration pathway with better fidelity than the inert MPIOs. All data point to PLGA encapsulated iron oxide NPs and MPs as clinically viable options for MRI-based cell tracking.

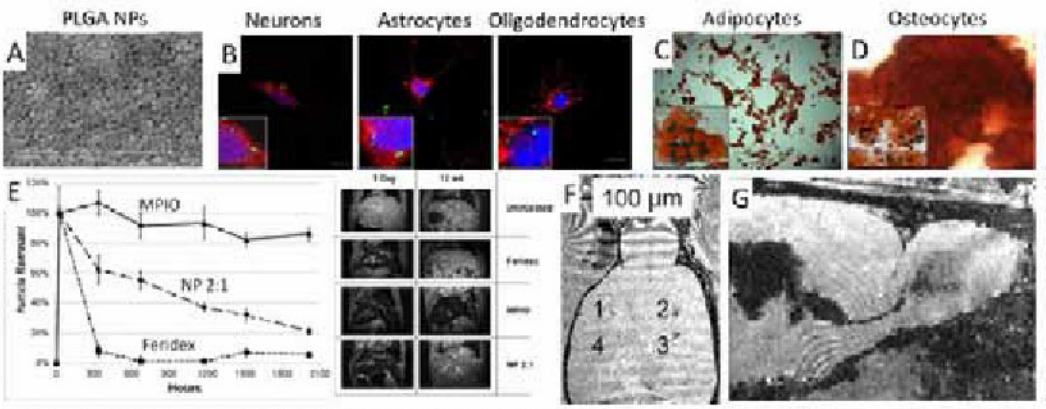


**A)** Scanning electron microscopy of PLGA encapsulated magnetite NPs; **B)** Immunocytochemistry of magnetic NP labeled NSCs differentiated down neuronal, astrocyte and oligodendrocyte lineages; **C & D)** Immunocytochemistry of magnetic MP labeled MSCs differentiated down adipocyte and osteocyte lineages; **E)** Biodegradation of MPIO, PLGA encapsulated magnetic NPs and Feridex in mice over 12 weeks; **F)** MRI of rat brain injected with [1] 10, [2] 100 or [3] 1000 magnetic NP labeled MSCs. [4] is injection of unlabeled cells; **G)** MRI of endogenous NSC migration in rat brain 2 weeks following in vivo labeling with magnetic MPs.

Disclosure of author financial interest or relationships:
**D. Granot**, None; **M. Nkansah**, None; **M. Bennewitz**, None; **K.S. Tang**, None; **E.A. Markakis**, None; **E.M. Shapiro**, None.

Presentation Number **SS 111**
Scientific Session 16: Chemistry & Probes - MRI
September 7, 2012 / 13:44-13:55 / Room: Liffey Hall 1

# In vivo MRI visualization of different cell populations labelled with PARACEST agents

***Giuseppe Ferrauto***[1], *Daniela Delli Castelli*[1], *Enzo Terreno*[2], *Silvio Aime*[1], [1]*Chemistry, Molecular Imaging Center- University of Turin, Torino, Italy;* [2]*Chemistry, Molecular and Preclinical Imaging Centers-Universiity of Turin, Torino, Italy. Contact e-mail: giuseppe.ferrauto@unito.it*

In vivo MRI visualization of cells labelled with paramagnetic complexes and superparamagnetic particles is a well-established procedure. However, being the relaxation enhancement effects on the "bulk" water proton resonance additive, it is not possible to distinguish the contributions arising from different relaxation labels localized in the same imaging region. Hence, this goal can be achieved by exploiting frequency-encoding agents in which the frequency acts as an 'imaging signature'. On this basis, CEST (Chemical Exchange Saturation Transfer) agents represent the only class of 1H-MRI agents endowed with frequency-encoding properties. They act by transferring saturated magnetization to the "bulk" water signal upon irradiating the resonance of exchangeable proton pool on the CEST agent. This peculiar made of action can be exploited for designing systems having different chemical shift values for the exchangeable protons, thus allowing multiple visualization by simply moving the frequency offset of the RF saturation field. We found that the series of paramagnetic Ln-HPDO3A ( Ln≠Gd) is particularly suitable for multiplex detection by MRI-CEST procedures. In fact, the HPDO3A ligand contains a hydroxyl functionality that is in slow exchange with the water molecules. The chemical shift of the OH moiety varies very much along the series according to the magnetic characteristics of the Ln(III) ion. The OH resonance of each Ln-HPDO3A complex can then be selectively irradiated to generate a group of CEST agents endowed with very similar chemical and biological properties. Moreover HPDO3A is the same ligand used for Gadoteridol, one of the most used Gd-based MRI contrast agent. On the basis of the closed structural analogies along the Lanthanide series, one can foresee that the outstanding tolerability show by the Gadoteridol can be extended to all the series of Ln-HPDO3A complexes. We evaluated the characteristics of the different Ln-HPDO3A CEST agents for cell labeling across the Lanthanide series and found that Yb-HPDO3A and Eu- HPDO3A appeared to be the best ones for cell labeling, allowing cells detection with a standard 1H-MRI scanner without the use of unsafe RF irradiation pulses. Herein we reports the results obtained upon labeling murine macrophages (J774.A1) and melanoma cells (B16-F10). These cells were labeled by pinocytosis or by electroporation with Yb- and Eu-complexes, respectively. The visualization of each cell type has been possible by irradiating the proper OH absorption of the labeling molecule. Imaging experiments were carried out on cells' mixtures either in vitro (cellular pellets in glass capillaries) and in vivo (upon subcutaneous injection in mice). At the best of our knowledge this is the first proof of concept demonstrating the possibility to detect PARACEST labelled cells in vivo. The reported observation open new horizons to the field of cell tracking experiments and further widen the range of possible applications for this class of frequency-encoding 1H MRI agents. 1. Modo M, Hoehn M, Bulte JW, Mol Imaging 2005; 4(3):143-64. Rev. 2. Terreno E, Castelli DD, Aime S. CMMI, 2010; 5(2):78-98. Rev.


Ln= Gd →Gadoteridol, Clinical approved Prohance™

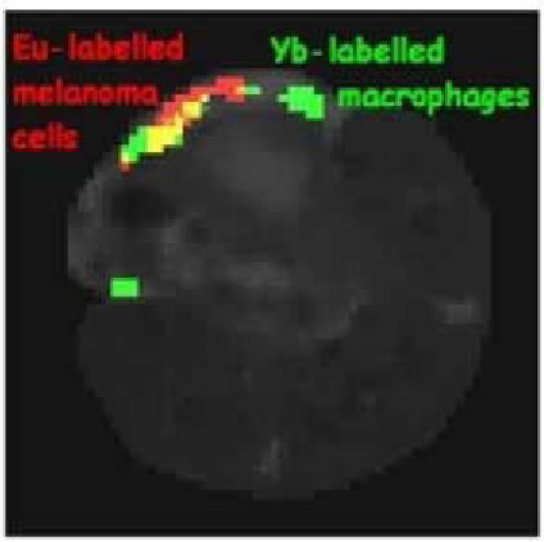


Disclosure of author financial interest or relationships:
**G. Ferrauto**, None; **D. Delli Castelli**, None; **E. Terreno**, Bracco Imaging, Consultant; **S. Aime**, Bracco Imaging, Consultant; Bruker, Grant/research support .

Presentation Number **SS 112**
Scientific Session 16: Chemistry & Probes - MRI
September 7, 2012 / 13:55-14:06 / Room: Liffey Hall 1

# Flavin-coated Iron Oxide Nanoparticles for RCP-mediated Molecular Imaging of Angiogenic Vessels

***Jabadurai Jayapaul***[1,2], *Susanne Arns*[1], *Wiltrud Lederle*[1], *Peter Comba*[2], *Jessica Gätjens*[1], *Fabian Kiessling*[1], [1]*Department of Experimental Molecular imaging (ExMI), University Clinics, RWTH Aachen University, Aachen, Germany;* [2]*Institute of Inorganic Chemistry, University of Heidelberg, Heidelberg, Germany. Contact e-mail: jjayapaul@ukaachen.de*

Riboflavin (Rf) and its metabolic analogues namely flavin mononucleotide (FMN) and flavin adenine dinucleotide (FAD) are highly essential for the cellular metabolism. Their intracellular transport is regulated by riboflavin carrier protein (RCP), which is highly over-expressed in solid tumors and angiogenic vessels. In this context, we explored this novel target and developed flavin decorated ultrasmall superparamagnetic iron oxide nanoparticles (FUSPIO) as molecular MR agents for tumor targeting and labelling. We synthesized FUSPIO using a non-polymeric coating method and characterized the particles with TEM, FTIR, MRI and fluorescence spectroscopy. The toxicity of FUSPIO on LnCap cells was checked using trypan blue staining. The labeling efficacy of FUSPIO was studied in vitro using MRI and fluorescence microscopy. The specific uptake of FUSPIO by metabolically active endothelial (HUVEC) and prostate cancer (LnCap) cells was compared. In addition, competitive binding experiments with free flavins were performed on LnCap cells and uptake was studied using MRI and fluorescence microscopy. The in vivo accumulation of the FUSPIO in LnCap xenografts compared to Resovist was investigated by MRI and subsequently validated using histology. TEM measurements showed an average particle size of 5.8 ± 1 nm. FTIR confirmed the binding of flavins to USPIO via (pyro-)phosphate groups (Fig. 1A). MR measurements showed relaxivity (r2) almost similar to that of Resovist in de-ionized water for FUSPIO (r2 = 84.70±1.57 s-1mM-1). Fluorescence spectroscopy of FUSPIO displayed an intense emission (λem = 530 nm) in water. Trypan blue staining showed no loss in LnCap`s viability (3h, 24h incubation) at relevant cell labeling concentration (c(Fe) = 0.3 µmol Fe/mL). Fluorescence microscopy indicated an intense uptake of FUSPIO by LnCap cells (Fig. 1D), which was confirmed by the significantly higher change in R2 relaxation rates of LnCap cells incubated (1h) with FUSPIO (82.93±14.49 s-1) than USPIO (4.76±0.64 s-1). Both modalities also showed that FUSPIO uptake could be blocked by adding free flavin in excess (100-fold). In this context, MRI showed that the change in R2 relaxation rate of LnCaP cells was 47.48±6.57 s-1 under flavin competition and 82.93±14.49 s-1 for cells incubated only with FUSPIO. Increased uptake of FUSPIO by HUVEC (two fold) compared to LnCap cells was found. Additionally, after intravenous injection of FUSPIO in mice with LnCap tumors a higher in vivo uptake of FUSPIO compared to Resovist was observed by the higher change in R2* relaxation rates (FUSPIO/Resovist (n=4): 18.75±6.96 s-1/5.92±2.48 s-1 (1h incubation)) (Fig. 1B-C). Histological validation on LnCap tumors localized FUSPIO mainly in the tumor endothelium (Fig. 1E-F). In summary, flavin coating renders USPIO fluorescent and specific for RCP. The resulting FUSPIO are not toxic and show high cell labeling efficacy in vitro. The high in vivo uptake of FUSPIO by tumor endothelium was in compliance with the observed in vitro uptake by HUVEC. Therefore, our study suggests that FUSPIO might serve as a tool for in vivo molecular MR imaging of the metabolic activity of angiogenic vessels.

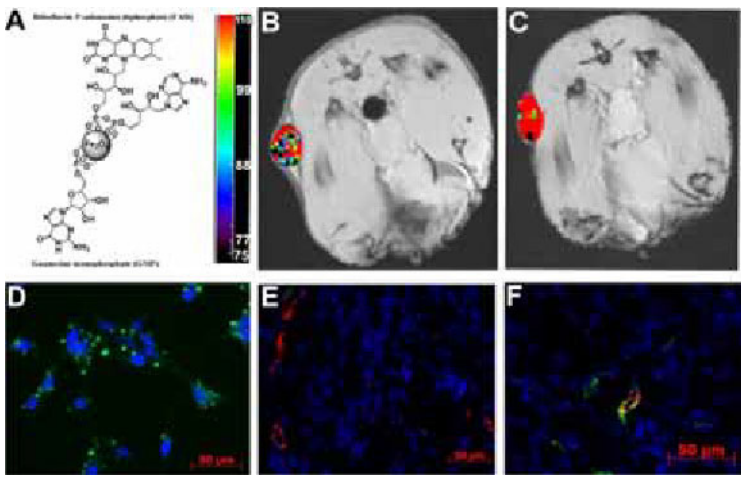


Figure 1: Schematic diagram showing the binding of flavin (FAD) to USPIO via the pyrophosphate groups (A). Color-coded R2* relaxation rate pixel maps are overlaid on T2* weighted images of LnCap tumors 1h post i.v. injection with Resovist (B) and FUSPIO (C). The images illustrate the enhanced uptake of FUSPIO in the tumors compared to Resovist control. Fluorescence images of LnCap cells incubated (1h) with FUSPIO (0.3 µmol Fe/mL) (D) show FUSPIO (green dots) localized inside the cytoplasm (cell nuclei were counterstained with DAPI). The immunohistological images of tumors after i.v. injection of Resovist (E) and FUSPIO (F) indicate the uptake of FUSPIO (green) by endothelial cells (CD-31, red) as visualized by its co-localization thereby demonstrating the suitability of FUSPIO for targeting angiogenic vessels.

Disclosure of author financial interest or relationships:
**J. Jayapaul**, None; **S. Arns**, None; **W. Lederle**, None; **P. Comba**, None; **J. Gätjens**, None; **F. Kiessling**, None.

Presentation Number **SS 113**
Scientific Session 16: Chemistry & Probes - MRI
September 7, 2012 / 14:06-14:17 / Room: Liffey Hall 1

# Development of multimodal imaging probes for neuroanatomical connectivity studies in vivo

***Ilgar Mamedov***[1], *Joern Engelmann*[2], *Gisela E. Hagberg*[1], *Nikos K. Logothetis*[1,3], *Giuseppe Gambino*[4], *Lorenzo Tei*[4], *Mauro Botta*[4], [1]*Department for Physiology of Cognitive Processes, Max Planck Institute for Biological Cybernetics, Tuebingen, Germany;* [2]*High Field MRI Centre, Max Planck Institute for Biological Cybernetics, Tuebingen, Germany;* [3]*Imaging Science and Biomedical Engineering, University of Manchester, Manchester, United Kingdom;* [4]*Dipartimento di Scienze ed Innovazione Tecnologica, Università del Piemonte Orientale "Amedeo Avogadro", Alessandria, Italy. Contact e-mail: ilgar.mamedov@tuebingen.mpg.de*

In order to understand the functional activity in the brain, a detailed knowledge of anatomical connections between different brain regions is of great importance. Unfortunately the requirement for highly invasive technologies precludes most studies in living subjects. In spite of the rapid progress in the field of animal research combined with the neuroimaging technology, currently applied techniques demonstrate the absence of a completive method which can be used for such studies. In contrast to conventional techniques, volume imaging with MRI-visible neuronal tracers provides a complete description of large-scale three-dimensional (3-D) networks. The recent attempts to conjugate the commonly used paramagnetic complex Gd-DOTA with classical neuroanatomical tracers such as cholera toxin subunit B (CTB) or biocytin demonstrated the high potential of such systems to act in noninvasive connectivity studies.1,2 Here we have developed efficient neuronal tracers that can allow a more complete investigation of the neuronal networks using MR and optical imaging techniques. Modified mono- or bis- Gd-AAZTA3,4 complexes acting as a MR reporter and tetramethylrhodamine as optical reporter were conjugated to Dextran (MW 10,000) which is used extensively in neuroanatomical research (Fig.1 up). This enables the investigation of neuroanatomical connectivity in the brain by both MR and optical imaging. Fluorescence microscopy of neuronal cells incubated in vitro with different concentrations of the tracer molecules clearly demonstrated their effective internalization and localization mainly within the cell body of the cells but also transport along the cellular processes. In vivo injection into the motor cortex (M1) of rat demonstrate signal enhancement in several well-known subcortical targets of M1, including the somatosensory cortex (S1) and Caudate putamen (CPu) confirming the high potential of the new contrast agents and their applicability for in vivo connectivity studies (Fig.1 down). Such systems can enable a diversity of new experimental studies on various neuroscientific issues associated with longitudinal research on brain plasticity and neurode- or regeneration. [1] C.W-H. Wu, O. Vasalatiy, N. Liu, H. Wu, S. Cheal, D.-Y. Chen, A.P. Koretsky, G.L. Griffiths, R.B.H. Tootell, L.G. Ungerleider, Neuron, 2011, 70, 229-243. [2] A. Mishra, A. Schüz, J. Engelmann, M. Beyerlein, N. K. Logothetis, S. Canals, ACS Chem.Neurosci., 2011, 2(10), 578-587. [3] I. Mamedov, J. Engelmann, M. Beyerlein, O. Eschenko, N. K. Logothetis, ChemComm., 2012, 48, 2755-2757. [4] G. Gugliotta, M. Botta, L. Tei, Org. Biomol. Chem., 2010, 8, 4569-4574.

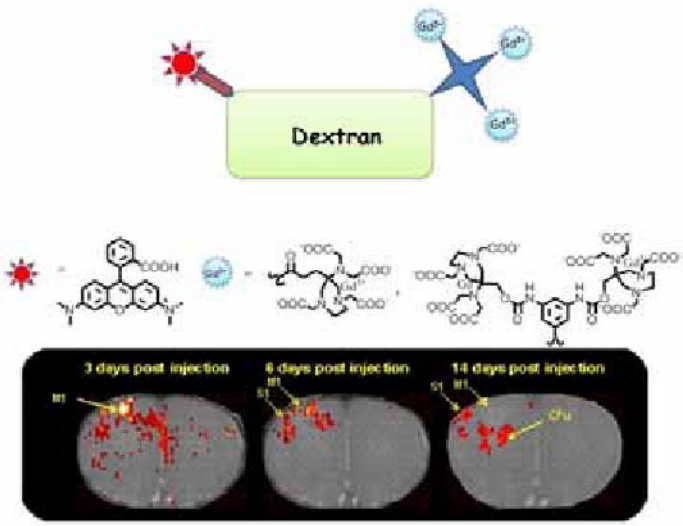


**Fig.1** Schematic illustration of the new tracers (up). Time dependent distribution of the contrast agent after injection into the primary motor cortex of the rat (down).

Disclosure of author financial interest or relationships:
**I. Mamedov**, None; **J. Engelmann**, None; **G.E. Hagberg**, None; **N.K. Logothetis**, None; **G. Gambino**, None; **L. Tei**, None; **M. Botta**, None.

Presentation Number **SS 114**
Scientific Session 16: Chemistry & Probes - MRI
September 7, 2012 / 14:17-14:28 / Room: Liffey Hall 1

# Gd-DOTA complex functionalized with phenyl boronic acid as MRI imaging reporter of Sialic acid expression on melanoma cells

***Simonetta Geninatti- Crich***[1], *Kristina Djanashvili*[2], *Diego Alberti*[1], *Ibolya Szabó*[1], *Silvio Aime*[1], [1]*Department of Chemistry, Center for Molecular Imaging, University of Torino, Torino, Italy;* [2]*Dep of Biotechnology, Delft University of Technology, Delft, Netherlands. Contact e-mail: simonetta.geninatti@unito.it*

The overexpression of sialic acid (SA) on cell membranes is correlated to the malignant and metastatic phenotypes of various types of cancer cells. Therefore, SA is an important molecular target for diagnostic and therapeutic approaches. In melanoma cells, tyrosinase activity, the key enzyme for melanogenesis, shows a definite correlation with SA levels1, thus indicating an essential role for sialic acid residues in the enzyme expression and, therefore in melanoma cell differentiation. Sialylation/desialylation of some relevant molecules, such us tyrosinase itself and melanosomal sialo-glyco-conjugates, participates in the regulation of expression of melanogenic functions. Furthermore, altered sialylation of tumor cells surface glycoconjugates is correlated with the highly metastatic melanoma phenotype. Elevated expression of SA on the cell surface has been shown to be an important metastatic determinant2. For these reasons the development of specific "in vitro" and "in vivo" non invasive imaging reporters of the SA expression level can give an important improvement in the diagnosis and classification of the pathology. Herein a Gd-DOTA-monoamide derivative (Gd-DOTA-ENPBA) functionalized with a phenyl boronic acid3 (PBA) unit has been tested as SA expression reporter on B16-F10 melanoma cells. In fact PBA is able to form stable reversible covalent binding between the diol function of the sialic acid and the boronated function of PBA. Since the sialic acid expression is directly correlated with melanogenesis, the interaction of the complex Gd-DOTA-ENPBA has been evaluated on two clones of B16-F10 murine melanoma characterized by a different phenotype, namely melanogenic (B16-F10m) and non-melanogenic (B16-F10non-m) cells. The ability of Gd-DOTA-ENPBA to bind to melanoma cells has been assessed by incubating both melanogenic and non-melanogenic cells in the presence of the complex (0.6mM) for 4h at 37°C. The MRI acquired at 7 T on B16 cell pellets (Figure) showed the specific accumulation of Gd-DOTA-ENPBA in melanogenic with respect to non-melanogenic tumor cells. Then, sialic acid expression on B16-F10 cells used in this study has been evaluated by means of a commercially available assay (AbCAM). Melanogenic cells express > than 3.5 times sialic acid than non-melanogenic ones. Preliminary data show us a quite good correlation between sialic acid expression and relaxation rates measured on cells incubated with Gd-DOTA-ENPBA. In vivo MRI experiments were carried out on subcutaneous tumors models obtained by injecting B16 melanoma cells into the right flank of adult C57BL/6 mice. Fat-suppressed T1-weighted multislice multiecho MR images were recorded before, 4 and 24 hours after the contrast administration showed a significantly enhancement corresponding to the tumour region. References. 1) PA Riley, Pigment Cell Research, 2003, 16, 548-552. 2) Akira Matsumoto, Horacio Cabral, Naoko Sato, Kazunori Kataoka, and Yuji Miyahara, Angew. Chem. Int. Ed. 2010, 49, 5494 -5497. 3) Djanashvili K, ten Hagen TL, Blangé R, Schipper D, Peters JA, Koning GA. Bioorg Med Chem. 2011 Feb 1;19(3):1123-30.

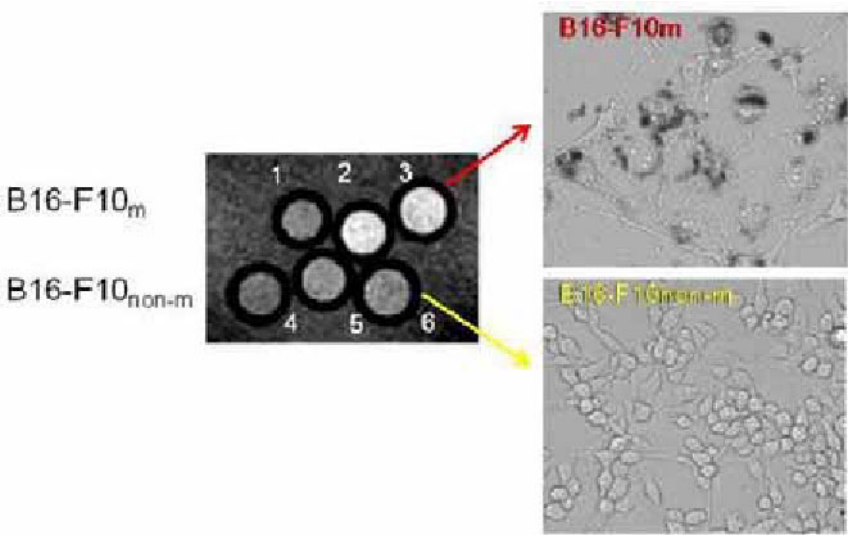


Disclosure of author financial interest or relationships:
**S. Geninatti- Crich**, None; **K. Djanashvili**, None; **D. Alberti**, None; **I. Szabó**, None; **S. Aime**, Bracco Imaging, Consultant; Bruker, Grant/research support .

Presentation Number **SS 115**
Scientific Session 17: Technology & Software - Hybrid Multimodality
September 7, 2012 / 13:00-13:11 / Room: Wicklow Hall 1

# First in vivo results of a preclinical 3T PET/MR scanner with integrated analog SiPM detectors

***Volkmar Schulz***[1,3], *Bjoern Weissler*[1], *Pierre Gebhardt*[2], *Lerche W. Christoph*[1], *Benjamin Goldschmidt*[3], *Fabian Kiessling*[3], *Jane Mackewn*[2], *Paul Marsden*[2], [1]*MIS, Philips Research, Aachen, Germany;* [2]*DIS, King's College, London, United Kingdom;* [3]*ExMI, RWTH/Philips Research, Aachen, Germany. Contact e-mail: volkmar.schulz@philips.com*

The combination of Positron Emission Tomography (PET) and Magnet Resonance Imaging (MRI) to a hybrid imaging modality is a promising tool, as it combines the outstanding soft-tissue contrast and functional information of MRI with the metabolic and molecular images of PET. Especially the ability to acquire simultaneous images of PET and MR promises to significantly improve the spatial registration and to enable MR-based motion corrected PET to enhanced image quality and quantification. However, significant innovations on the following technology areas are still needed which will be addressed in this paper: MRI-hard/ MRI-silent detectors, scalable detector technology, higher integrated detectors, and sub-ns time-of-flight PET. **Material and Method:** A preclinical PET/MR scanner insert has been designed to enable simultaneous operation of PET in a human clinical 3T MRI system (Philips 3.0T Achieva). Main components of the preclinical scanner are the MRI-compatible PET detector ring with local digitization and an integrated transmit/receive RF coil. The PET detector consists of 10 PET modules with dedicated RF shielding. The cylindrical field of view (FOV) for hybrid imaging is limited via the RF coil to 150mm transverse diameter and by 33mm, 66, or 99mm axially, if populated with 1, 2, or 3 detector rings, respectively. Each PET module contains up to 2×3 (transverse × axial) detector stacks. A detector stack is composed of an LYSO array with 22×22 crystals of 1.3×1.3×10mm$^3$ coupled to an 8×8 channel silicon photomultiplier (SiPM) array via a 2mm glass plate. The analog SiPMs signals are digitized via a customized ASIC that enable the measurement of energy (12bit) and the time-of-arrival in bins of 50ps. The technology thus offers the measurement of small crystals, e.g. for preclinical as well as sub-ns TOF measurements for clinical simultaneous PET/MR systems. Event positioning was archived with a maximum likelihood crystal index estimation. **Results:** The homogeneity of the static magnetic field of the MRI (B0) with all PET detector of about ±4ppm in the FOV of PET (on and off) has been measured with a scaled phase measurement of a homogeneous oil phantom. The influence of the mixed signal in-bore PET electronics on the MRI acquisition was investigated by looking at disturbances of the RF receive noise of MRI for different center frequencies (fn = 127.78+(n-3)×0.184 MHz, n={1,2,3,4,5}) with a bandwidth of 184kHz. No disturbance of the RF noise was observed during PET acquisition. Simultaneous PET/MRI phantom experiments with a Derenzo phantom indicated a transversal resolution (FWHM) of <1.6mm. A system energy resolution of PET (FWHM) of 18.0% (mean value) was measured, with min./max.values of 14.8%/22.4%. Finally simultaneous PET/MR images of a rat brain has been acquired (MRI: T2w, with 0.75$^3$mm$^3$ and bTFE with 0.5$^2$×2mm$^3$ ; PET: 5MBq, scan duration 1h). Further in vivo images will be shown on the conference. **Conclusion:** The MR-compatibility and performance of the preclinical PET/MR scanner insert was shown to be sufficient for simultaneous PET/MR investigations of phantoms and rats.

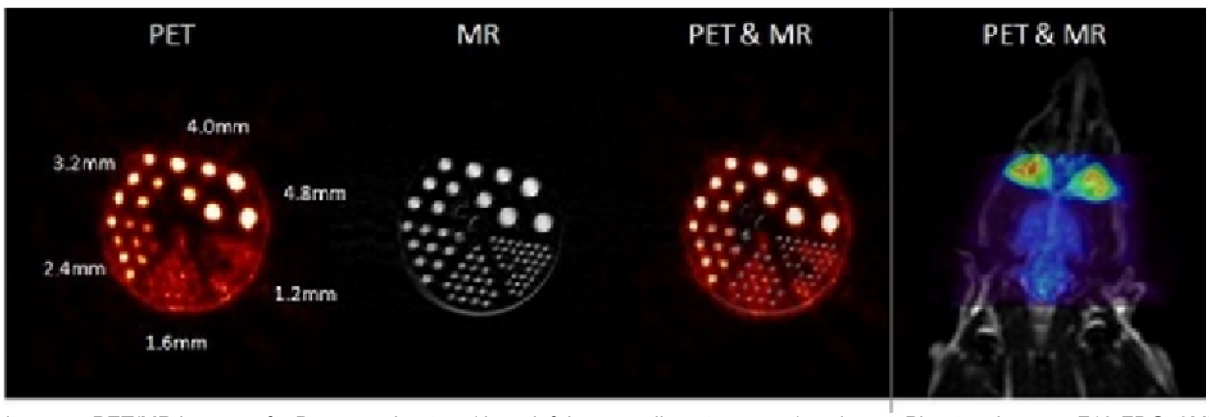


Figure: Simultaneous PET/MR images of a Derenzo phantom (three left images, diameter 45mm) and a rat. Phantom images: F18-FDG, 9MBq, duration 22min, MR: bTFE. Rat image: 7MBq, 60min p.i., duration 60min, MR bTFE +T2w

Disclosure of author financial interest or relationships:
**V. Schulz**, Philips Research, Employment; **B. Weissler**, Philips Technologie GmbH Innovative Technologies, Employment; **P. Gebhardt**, None; **L.W. Christoph**, Philips Research Europe, Employment; **B. Goldschmidt**, None; **F. Kiessling**, None; **J. Mackewn**, None; **P. Marsden**, None.

Presentation Number **SS 116**
Scientific Session 17: Technology & Software - Hybrid Multimodality
September 7, 2012 / 13:11-13:22 / Room: Wicklow Hall 1

# Imaging Performance and Mutual Effects of SPECT and MRI of a SPECT subsystem for Simultaneous SPECT-MR Imaging of Small Animals

***Benjamin M. Tsui***[1], *Jingyan Xu*[1], *Andrew J. Rittenbach*[1], *AbdEL-Monem El-Sharkawy*[1], *William A. Edelstein*[1], *Kevin B. Parnham*[2], *James W. Hugg*[2], [1]*Department of Radiology, Johns Hopkins University, Baltimore, MD, USA;* [2]*Gamma Medica, Inc., Northridge, CA, USA. Contact e-mail: btsui1@jhmi.edu*

The aim is to investigate the mutual effects of SPECT and MRI systems in the development of a simultaneous SPECT-MR system for small animal imaging. As previously reported, we have developed a second generation MR-compatible SPECT subsystem for simultaneous SPECT/MR imaging of small animals. It consists of 5 rings of 19 2.54x2.54 cm2, 16x16 pixels cadmium zinc telluride (CZT) detectors connected seamlessly. The CZT detectors directly convert incident photons into electric signals hence are minimally affected by the static magnetic field of the MRI. The multi-pinhole (MPH) collimators were constructed with a special high density tungsten powder and fitted with tungsten pinhole inserts. A shielded birdcage quadrature transmit/receive RF coil for mouse or rat imaging fits inside the corresponding MPH collimator to maximize the SNR and to minimize interactions between SPECT and MRI systems. The performance of the SPECT subsystem for stand alone SPECT and SPECT/MR imaging were evaluated experimentally outside and inside a 3T clinical MRI scanner. The experiments used point and line sources, and a mouse-size cylindrical phantom with a resolution section consisting of hollow rods with diameters ranging from 0.75 to 2.4 mm and a uniform section that can be filled with radioactivity. With proper uniformity correction of the CZT detector and geometric calibration of the individual pinholes, reconstructed images were obtained from the SPECT subsystem. The measured resolutions of a 18-pinhole and a 36-pinhole collimators agreed with the targeted system resolution of 1 and 1.5 mm at the center of the FOV and detection efficiencies ~12% less than predicted at 172 and 372 cps/MBq, respectively. Inside the MRI system, the SPECT subsystem had overall count rate drops of ~25-50% and <10% for the shell and resolution phantoms, respectively. A change of detector uniformity was observed and a separate uniformity flood measurement and correction were needed for image reconstruction. The Lorenz force effect on the CZT detectors was observed as a linear shift of the projection data. An experimentally determined shift of 2 mm, consistent with a calculated average of ~1.6mm, restored the degraded resolution. The gradient field of the MRI system did not impose noticeable effect on SPECT. In a preliminary simultaneous SPECT/MR imaging study, the resolution phantom was placed directly under the central row of pinholes. Both the SPECT and MR images of the rod sources showed minimum image artifacts, and the SPECT images showed minimum degradation from that obtained outside the magnet. However, the MR images had an overall SNR degradation of a factor of ~7 and the uniform section that was at the edge or outside the SPECT FOV showed image distortions and artifacts. We demonstrated initial imaging performance of a MR-compatible SPECT subsystem and a specially designed RF coil that fits inside a MPH collimator for high-resolution stand-alone SPECT and simultaneous SPECT/MR imaging of small animals. Despite the ability to obtain high resolution simultaneous SPECT/MR images, initial results show interference between the two systems that requires further study to be resolved.

Disclosure of author financial interest or relationships:
**B.M. Tsui**, Gamma Medica, Inc., Grant/research support; Siemens Healthcare, Grant/research support; Hybridyne Technologies, Consultant; GE Healthcare, Other financial or material support; Gamma Medica, Inc., Other financial or material support; **J. Xu**, None; **A.J. Rittenbach**, None; **A. El-Sharkawy**, None; **W.A. Edelstein**, None; **K.B. Parnham**, Gamma Medica Inc, Employment; **J.W. Hugg**, Gamma Medica, Employment .

Presentation Number **SS 117**
Scientific Session 17: Technology & Software - Hybrid Multimodality
September 7, 2012 / 13:22-13:33 / Room: Wicklow Hall 1

# SiPM block detector for high resolution PET combined with a 9.4 T animal-dedicated MRI

***Guen Bae Ko***[1], *Hyun Suk Yoon*[1], *Sun Il Kwon*[1], *Seong Jong Hong*[2], *Hyeonjin Kim*[3], *In Chan Song*[3], *Dong Soo Lee*[1], *Jae Sung Lee*[1], *[1]Department of Nuclear Medicine, Seoul National University, Seoul, Republic of Korea; [2]Department of Radiological Science, Eulji University, Seongnam, Republic of Korea; [3]Department of Radiology, Seoul National University, Seoul, Republic of Korea. Contact e-mail: guenbko@me.com*

The aim of this study is to develop a high field MR compatible PET detector module using SiPM for preclinical PET/MR imager with high resolution and sensitivity. In preclinical research, high field MRI is more attractive than low field one because of several benefits such as high signal-to-noise ratio, contrast-to-noise ratio, and spectral resolution. PET is also powerful tool in molecular imaging because it has the strength of kinetic studies for the radionuclide-labeled molecule. Therefore, combining high resolution PET with high field MRI would be more useful multimodal imaging tool for preclinical researches including neurotransmitters, cell tracking, and various metabolism studies. **Methods:** The detector module supports 4 axial blocks mounted on PCB board for compact design. Each axial block consists of one 4 × 4 channel SiPM (Hamamatsu MPPC) which is connected to the resistive charge division network, 7 × 7 LYSO crystal array (1.5 × 1.5 × 7.0 $mm^3$) and temperature sensor. The position signals of four axial blocks are amplified by fully differential amplifier and connected to analog multiplexing circuit to reduce the signal line. To compensate the temperature-dependent gain change of SiPM, a bias voltage control system based on look up table was also implemented. Some physical properties of the detector such as flood image, energy spectrum, and MR compatibility were tested. To assure MR compatibility, a Cu-shield containing the block detector components was positioned between the gradient and RF coils of 9.4 T animal dedicated MRI (Agilent, USA). The MR images were obtained with a gradient and spin echo sequences. Gain variation with temperature was also measured. **Results:** All of the 1.5 mm crystal was clearly resolved in the crystal map including the peripheral regions of the crystal array. The average peak-to-valley ratio for the center row and column of crystals was 14.6 and 14.0 respectively. The change of photo peak position was only 3.4% between 10 °C to 30 °C. The magnetic susceptibility of SiPM PET detector and Cu-shield did not interfere MR image. With Cu-shield, PET signal showed no disturbance or interference during RF transmission of MRI. We also designed the SiPM PET insert consisting of 16 block detector to have a 54 mm axial FOV and 60 mm ring diameter and implementation of full insert system combined with MR volume coil is in progress. **Conclusion:** In this project, we focus on the development of high resolution SiPM PET scanner combined with a 9.4 T animal-dedicated MRI system for preclinical research. The results indicate that the SiPM PET block detector module yielded excellent intrinsic performances and it was suitable for simultaneous PET/MR imaging.

Disclosure of author financial interest or relationships:
**G. Ko**, None; **H. Yoon**, None; **S. Kwon**, None; **S. Hong**, None; **H. Kim**, None; **I. Song**, None; **D. Lee**, None; **J. Lee**, Samsung Electronics, Grant/research support .

Presentation Number **SS 118**
Scientific Session 17: Technology & Software - Hybrid Multimodality
September 7, 2012 / 13:33-13:44 / Room: Wicklow Hall 1

# First demonstration of multiplexed X-ray fluorescence computed tomography (XFCT) imaging

***Yu Kuang**, Guillem Pratx, Bowen Meng, Jianguo Qian, Magdalena Bazalova, Lei Xing, Radiation Oncology, Stanford University School of Medicine, Stanford, CA, USA. Contact e-mail: yxk56@case.edu*

Purpose: Simultaneous imaging of multiple probes or biomarkers represents a critical step toward high sensitivity and specificity molecular imaging. In this work, we propose to utilize the element specific feature of X-ray fluorescence (XRF) energy spectrum for XRF computed tomography (XFCT) multiplexing and show the potential advantages of the novel imaging scheme. Methods: A 5 mm-diameter pencil beam produced by a polychromatic X-ray source (150 kV, 20 mA) was used to stimulate emission of XRF photons from 2% (weight/volume) gold (Au), gadolinium (Gd) and barium (Ba) embedded within a water phantom. The phantom was translated and rotated relative to the stationary pencil beam in a first-generation CT geometry. The X-ray energy spectrum was collected for 18 sec at each position using a cadmium telluride detector. The spectra were then used for the K shell XRF peak isolation and sinogram generation for the three elements of interest. The distribution and concentration of the three elements were reconstructed with the iterative maximum likelihood expectation maximization algorithm. The linearity between the XSF intensity and the concentrations of elements of interest was also investigated. Results: Measured XRF spectrum showed sharp peaks characteristic of Au, Gd and Ba. The narrow full-width at half-maximum (FWHM) of the peaks strongly supports the potential of XFCT for multiplexed imaging indexed by Au, Gd and Ba ($FWHM_{Au,K\alpha1}$ = 0.619 keV, $FWHM_{Au,K\alpha2}$ = 1.371 keV, $FWHM_{Gd,K\alpha}$ = 1.297 keV, $FWHM_{Gd,K\beta}$ = 0.974 keV, $FWHM_{Ba,K\alpha}$ = 0.852 keV, and $FWHM_{Ba,K\beta}$ = 0.594 keV). The distribution of Au, Gd and Ba in the water phantom was clearly identifiable on the reconstructed XRF images. Our results showed linear relationships between the XRF intensity of each tested element and their concentrations ($R^2_{Au}$ = 0.9444, $R^2_{Gd}$ = 0.9857, and $R^2_{Ba}$ = 0.9989), suggesting that XFCT is capable of quantitative imaging. Finally, a transmission CT image was obtained to show the potential of the approach for providing attenuation correction and morphological information. Conclusions: XFCT is a promising modality for multiplexed imaging indexed by the high atomic number (Z) probes. It would transform the CT landscape into a multiplexed biomarker detection feature for early detection of cancer and/or imaging the intervention processes in vivo. It could have major predictive value for the clinical outcome in the long term patient care in the future.

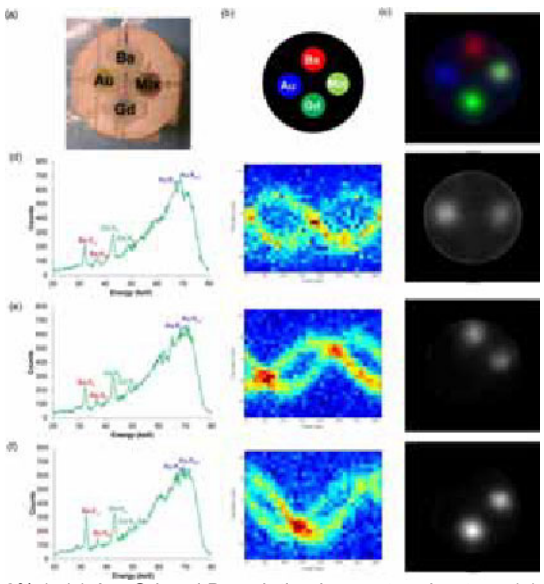


Reconstructed XFCT multiplexed images of 2% (w/v) Au, Gd and Ba solution in a water phantom. (a) photography of the phantom; (b) diagram of orientation of the phantom; (c) multicolor overlay of reconstructed image; (d) to (f): individual reconstructed image for three elements of interest ((d) Au; (e) Gd; (f) Ba). The water phantom (a) was scanned by the XFCT. The XRF spectrum in a projection was obtained by detecting the XRF photons emitted by all pixels along the beam. The XRF peaks in the spectra (left column of (d), (e) and (f)) were processed into a sinogram for each element (middle column at (d), (e) and (f)). Reconstructed images shown in right column at (d), (e) and (f). Pseudo color in (c) for unmixing components: Red: Ba; Blue: Au; Green: Gd.

Disclosure of author financial interest or relationships:
**Y. Kuang**, None; **G. Pratx**, None; **B. Meng**, None; **J. Qian**, None; **M. Bazalova**, None; **L. Xing**, Varian Medical Systems, Grant/research support .

Presentation Number **SS 119**
Scientific Session 17: Technology & Software - Hybrid Multimodality
September 7, 2012 / 13:44-13:55 / Room: Wicklow Hall 1

# Development and Performance Evaluation of a Next Generation Small Animal MR compatible PET insert with extended Field of View

***Md. Mosaddek Hossain***[1], *Hans F. Wehrl*[1], *Konrad Lankes*[2], *Chih-Chieh Liu*[1], *Martin S. Judenhofer*[1], *Armin Kolb*[1], *Bernd J. Pichler*[1], [1]*Department of Preclinical Imaging and Radiopharmacy, Eberhard Karls University of Tuebingen, Tuebingen, Germany;* [2]*Bruker Biospin MRI GmbH, Ettlingen, Germany. Contact e-mail: hossain.mosaddek@med.uni-tuebingen.de*

Recently we introduced successfully a first 7T MRI compatible small animal PET insert which had a 2 cm axial field of view (FOV) and allowed to perform simultaneous PET/MRI studies without sacrificing performance of the individual imaging modalities. Now by developing the second generation of a MR compatible animal PET insert we extended the FOV (axial×transaxial FOV of 72mm×72mm) which now allows to can scan whole body mouse as well as bigger animals such as rats, and increased its the overall performance. The complete PET ring is formed by radially arranged 16 detector modules on a cylindrical gantry. Each module consists of 3 axially arranged 15×15 Ce doped LSO blocks read out by 3×3 APD arrays (Hamamatsu, Japan). The individual LSO crystals within the block have a size of (1.5×1.5×10 $mm^3$). The detector modules with the frontend electronics are housed inside a double sided copper coated resin to reduce background radiofrequency (RF) noise from the MR system. By introducing a mechanical vortex tube-based novel air cooling system, with temperature readout and feed back, a stable temperature can be maintained inside the detector housing (15± 0.02° C), which improves the signal quality of the reconstructed PET images significantly. To avoid unwanted scatter from outside FOV a tungsten polymer material named "GRV-NJ-110-W" (PolyOne) is used as gamma shielding integrated at front and backside of the PET modules. The performance evaluation (e.g. energy resolution (18.2%±4.8% FWHM), spatial resolution (1.44 mm), sensitivity (2.9%), etc.) of the complete PET system has been performed. The MRI compatibility of the PET insert has been evaluated using a homogeneous phantom and applying different MR sequences without and with the PET insert built into the MRI scanner. Based on these MR phantom measurements the overall MR image quality (SNR, Homogeneity) did not suffer when the PET insert was installed. Simultaneous PET/MR images with different PET tracers (e.g. $^{18}F$, $^{64}Cu$, $^{15}O$), different MR sequences (e.g. spin echo, gradient echo, epi etc.) and animal models have been successfully acquired. Especially simultaneously acquired PET/MR studies using gating for cardiac imaging revealed very promising images. Overall, combined PET/MR seems to be a very good new imaging modality. The sensitivity of the new PET insert is in the same order as stand alone PET systems. MR performance is not suffering by the addition of the PET insert. Further small animal studies are on the way.

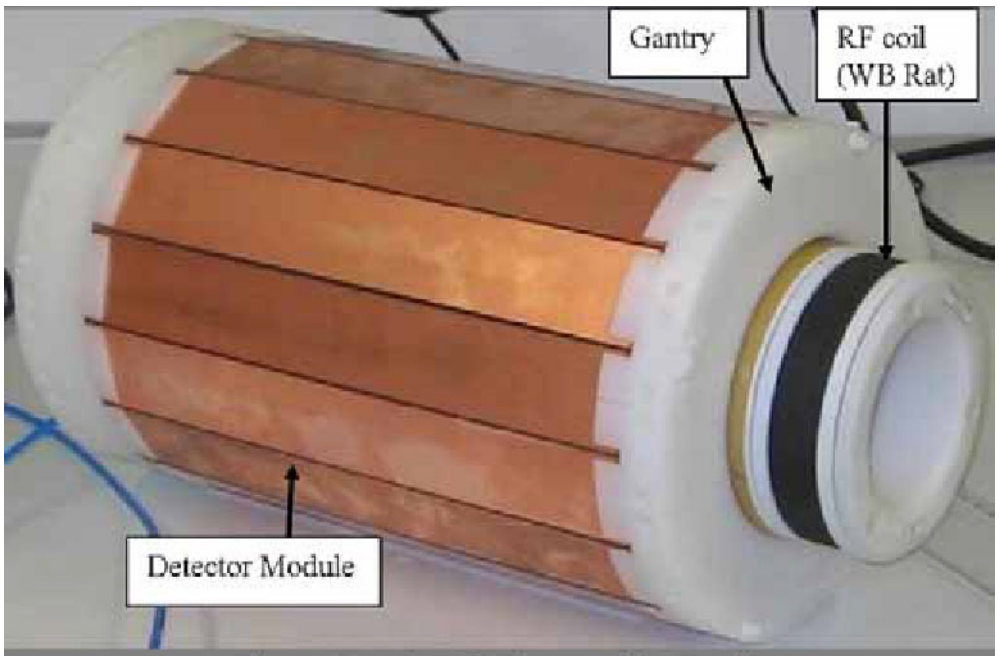


Figure: Complete PET insert with RF coil

Disclosure of author financial interest or relationships:
**M. Hossain**, None; **H.F. Wehrl**, None; **K. Lankes**, None; **C. Liu**, None; **M.S. Judenhofer**, None; **A. Kolb**, None; **B.J. Pichler**, Siemens, Grant/research support; AstraZeneca, Grant/research support; Bayer Healthcare, Grant/research support; Boehringer-Ingelheim, Grant/research support; Oncodesign, Grant/research support; Merck, Grant/research support; Bruker, Grant/research support .

Presentation Number **SS 12**
Scientific Session 2: Technology & Software - Optical Imaging
September 6, 2012 / 11:03-11:14 / Room: Wicklow Hall 1

# Molecular expression in tumors can be quantified in vivo using a suitable secondary untargeted tracer

***Kenneth M. Tichauer***[1], *Kimberley Samkoe*[1,2], *W. Spencer Klubben*[1], *Tayyaba Hasan*[3], *Brian W. Pogue*[1,2], [1]*Engineering, Dartmouth College, Hanover, NH, USA;* [2]*Department of Surgery, Dartmouth Medical School, Hanover, NH, USA;* [3]*Wellman Center for Photomedicine, Massachusetts General Hospital, Boston, MA, USA. Contact e-mail: Kenneth.Tichauer@Dartmouth.edu*

Cancer therapeutics that target tumor-specific molecules offer a powerful approach to treat microscopic disease; however, these therapeutics require an adequate expression of the specific molecule that they target. Therefore, diagnostic imaging of tumor molecular expression will be an important tool to guide the personalization of these molecular therapies. A commonly approach used in PET neurotransmitter studies to quantify molecular expression in is the "reference tissue" approach. This approach assumes there exists a region in the image that is void of the targeted molecule and therefore uptake of a targeted tracer in that region can act as a surrogate for blood delivery kinetics in the corresponding region of interest. The problem is that tumors have irregular pathophysiology that could make it difficult to find a suitable reference tissue. As an alternative, a dual-tracer approach is proposed, for which a second, untargeted tracer is injected simultaneously with a targeted tracer and the uptake of the untargeted tracer in the same tissue as the targeted tracer is used as a reference input to quantify molecular expression. The feasibility of the "reference tissue" and "dual-tracer" methods for quantifying biomarker expression (tracer binding potential) in tumors was investigated in 6 nude mice inoculated on the left thigh with a human glioma cell line (U251). The mice were anesthetized and the skin covering the tumor was removed (Fig. 1a). 1 nanomoles of an IRDye 800CW-EGF (LICOR Biosciences), a fluorescent tracer targeted to epidermal growth factor receptor (EGFR: a cell surface molecule overexpressed in many tumors), and 1 nanomoles of IRDye 700DX, an untargeted fluorescence tracer, were injected intravenously into each mouse, 10 min after injection of 30 nanomoles of human epidermal growth factor to block the targeted site of the targeted tracer. Uptake of both tracers was imaged on an Odyssey scanner (LICOR) at a 3-min resolution for 1 h (Fig. 1c-d). Since the EGFR expression of the tumors in this study was blocked prior to injection of the fluorescent tracers, the similar uptake observed between the targeted and untargeted tracers in both the tumor (solid red and green lines respectively in Fig. 1d) and muscle regions (dashed red and green lines Fig. 1d) is indicative of the potential to use the chosen untargeted tracer as a surrogate for the targeted tracer delivery kinetics. Conversely, the poor match between the muscle and tumor uptake curves suggests that muscle would not be a good input for the reference tissue model. As a more quantitative measure of the tracer delivery, rate constants K1 and k2 (from a one-compartment model) were extracted from all curves and the ratio of K1/k2 of the targeted tracer uptake in the muscle (red data in Fig. 1e), and the untargeted tracer uptake in the tumor (blue data in Fig. 1e), were plotted against the delivery kinetics of the targeted tracer in the tumor for each mouse. The excellent correlation between the kinetics of the targeted and untargeted tracers in the tumor encourage the use of the dual-tracer method for future studies imaging molecular expression in tumors.

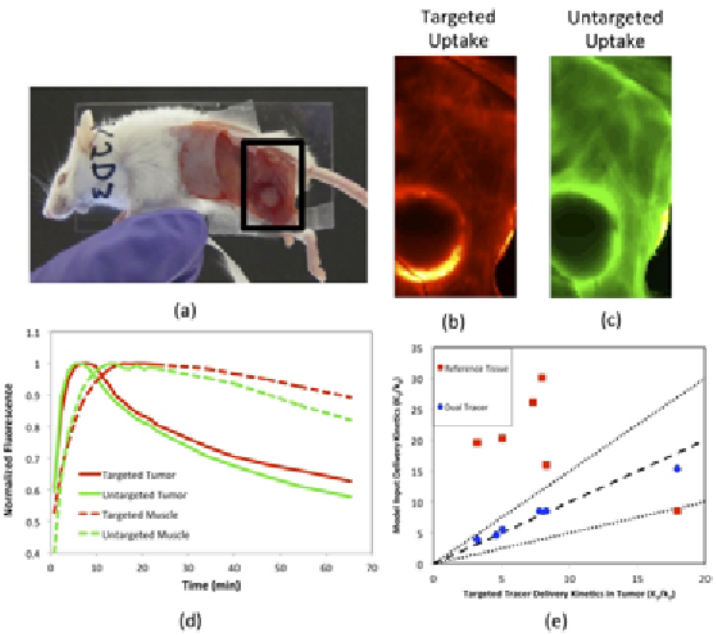


Disclosure of author financial interest or relationships:
**K.M. Tichauer**, None; **K. Samkoe**, None; **W. Klubben**, None; **T. Hasan**, None; **B.W. Pogue**, None.

Presentation Number **SS 120**
Scientific Session 17: Technology & Software - Hybrid Multimodality
September 7, 2012 / 13:55-14:06 / Room: Wicklow Hall 1

# Sequential PET/MRI using a 1T bench-top MRI scanner

***Andreas Schmid**, Jennifer Schmitz, Julia G. Mannheim, Florian C. Maier, Kerstin Fuchs, Hans F. Wehrl, Bernd J. Pichler, Department of Preclinical Imaging and Radiopharmacy, Eberhard Karls University of Tuebingen, Tuebingen, Germany. Contact e-mail: a.schmid@med.uni-tuebingen.de*

Combined PET/MRI studies receive increasing importance in the clinics as well as in preclinical research, as the combination of both methods allows much deeper insight into disease progression as any dedicated imaging modalities. Usually, combined studies are restricted by the enormous effort to install and maintain a dedicated high-field small animal MRI system. However, a new generation of small animal 1T bench-top MRI systems is available, which can be installed almost anywhere and at comparably low cost. Its fringe magnetic field does not exceed the footprint of the MRI scanner and thus, it can be even placed in close proximity to a magnetic field sensitive PET scanner. In this study, we evaluated the feasibility of sequential PET/MRI studies using a dedicated PET scanner and a 1 T bench-top MRI in comparison with a 7 T small animal MRI. To address PET image quality, a sphere phantom was filled with 11.3±2.3 MBq/mL 18F and submerged in a cylinder filled with 1.5±0.3 MBq/mL of 18F, yielding a contrast ratio of ~8. To compare the different available animal beds, a syringe, filled with 6.2±0.5 MBq/mL was placed in a falcon tube with 0.7±0.1 MBq/mL, yielding a contrast ratio of ~9 and 10 min emission and 13 min transmission scans were performed for each bed. For in vivo results, animals were anesthetized with 1.5% isoflurane evaporated in medical oxygen, injected with 12.0±1.0 MBq of [18F]FDG and underwent PET/MRI measurements, allowing to compare the results of scans using the 1T bench-top setup with scans using a 7 T high-field small animal MRI setup. Regions of interest (ROIs) were drawn in the anatomical MRI data, covering the brain as well as muscle for reference. Analysis of the PET phantom data revealed mean ratios of measured-to-true activity of the sphere of 0.29 and 0.36 with and without coil, respectively, without attenuation correction. The use of attenuation correction improves these values inside the field of view to 0.48 and 0.46, respectively. A comparison of all individual beds showed a mean ratio of measured-to-true activity in the syringe of 0.84±0.08 and 0.61±0.07, with and without attenuation correction, respectively. For comparison, the standard PET bed yielded ratios of 0.78±0.04 and 0.69±0.09, with and without attenuation correction, respectively. Addressing target-to-background ratios, all beds performed comparably well, yielding a ratio of 0.79±0.06 and 0.78±0.06. Analysis of the in vivo experiments revealed a very good correlation (R=0.998) over all ROIs between the 1T-setup and the 7T-setup for PET/MRI. Evaluation of the phantom data indicates that quantitative PET/MRI studies are feasible using a dedicated small animal PET scanner and a bench-top MRI scanner. As the target-to-background ratios were similar with and without attenuation correction for all setups, high-throughput studies without attenuation correction are also feasible if absolute quantification is not necessary. A special advantage of the bench-top MRI/PET setup is that PET and MRI scanners can be placed in close proximity in the same room. This also allows maintaining the anesthesia supply and physiology monitoring between the PET and MRI scans.

Disclosure of author financial interest or relationships:
**A. Schmid**, None; **J. Schmitz**, None; **J.G. Mannheim**, None; **F.C. Maier**, None; **K. Fuchs**, None; **H.F. Wehrl**, None; **B.J. Pichler**, Siemens, Grant/research support; AstraZeneca, Grant/research support; Bayer Healthcare, Grant/research support; Boehringer-Ingelheim, Grant/research support; Oncodesign, Grant/research support; Merck, Grant/research support; Bruker, Grant/research support .

Presentation Number **SS 121**
Scientific Session 17: Technology & Software - Hybrid Multimodality
September 7, 2012 / 14:06-14:17 / Room: Wicklow Hall 1

# Evaluation of artifacts in segmentation-based MR-derived PET attenuation correction maps of MR/PET and their impact on PET quantification

*Cornelia Brendle[1], Anja Oergel[1], Holger Schmidt[1,2], **Christina Schraml**[1], Christina Pfannenberg[1], Nina F. Schwenzer[1], [1]Department of Radiology, University of Tuebingen, Tuebingen, Germany; [2]Department of Preclinical Imaging and Radiopharmacy, Eberhard Karls University of Tuebingen, Tuebingen, Germany. Contact e-mail: christina.schraml@med.uni-tuebingen.de*

PET quantification is an important prerequisite for a correct and reliable lesion classification. To achieve this, the correction of the 511 keV photon attenuation is an important issue. In PET/CT, the CT can be used to calculate the PET attenuation correction (AC). In PET/MR, however, no data for PET photon attenuation can be obtained. To achieve PET AC maps from MR data, a T1-weighted FLASH sequence with DIXON-based fat-water separation is acquired and tissue-specific attenuation values (background, lung, fat and soft tissue) are assigned to these segmented MR images. This method is easy to implement and allows for a fast PET image reconstruction. However, regional artifacts that may occur in these AC maps could impair lesion detection and characterization in PET severely. To evaluate the reliability of this method, the frequency and characteristics of artifacts in segmentation-based AC maps of MR/PET and their impact on standardized uptake value (SUV) quantification in the affected areas were investigated. Thus, 119 AC maps achieved from MR images were retrospectively inspected for artifacts owing to regional wrong identification of the four tissue classes. SUVs of the PET images (18F-fluorodeoxyglucose, 68Ga-Dotatate, 11C-Methionine, 11C-Choline) reconstructed with MR AC maps in an artifact region (aSUV) were compared to a contralateral control region (cSUV) by a drawn volume-of-interest (VOI) analysis. Additionally, the SUV ratios of the artifact regions to reference tissue were also compared to the SUV ratios of the same regions in PET images from PET/CT (ctSUV). The volumes of the artifact regions (in cm3) were assessed as well. The relative SUV change between aSUV and cSUV was calculated as difference normalized to cSUV ((aSUV-cSUV)/cSUV). The relative SUV change between aSUV and ctSUV was calculated correspondingly. 102 artifacts were found in 63 (53%) of the 119 AC maps. The artifacts were mainly located in the thoracic region or hips due to metal implants (n=11), in the lungs (n=42), in the jaw (n=36). 13 artifacts were found in other regions (e.g. head, extremities, etc.). 20 of these 102 artifact regions were further inspected in detail. Volumes of these regions ranged from 0.6-501.2 cm3 and were located in the lungs (n=13), in the pelvic region (n=5), in the femur (n=1) and in a lung tumor (n=1). Artifacts with volumes >3 cm3 were mainly caused by metal implants resulting always in an underestimation of SUVs (maximum relative change of aSUV to cSUV or ctSUV was -1.0 and -1.0, respectively). The VOI analysis in smaller artifacts (≤3 cm3) revealed increased but also decreased values compared to the control region which might be caused by the rather small VOI size. Overall, artifacts in the segmentation-based MR-derived PET AC maps occur rather often. Metal implants lead to large artifacts > 3 cm3 with definite underestimation of SUVs resulting in missing or false characterization of possible lesions. Further studies are needed to investigate possible correction methods for artifacts caused by metallic implants.

Disclosure of author financial interest or relationships:
**C. Brendle**, None; **A. Oergel**, None; **H. Schmidt**, Siemens, Grant/research support; **C. Schraml**, None; **C. Pfannenberg**, None; **N.F. Schwenzer**, Siemens, Grant/research support .

Presentation Number **SS 122**
Scientific Session 17: Technology & Software - Hybrid Multimodality
September 7, 2012 / 14:17-14:28 / Room: Wicklow Hall 1

# Feasibility of Using Simultaneous PET/MR in the Evaluation of Cervical Carcinoma

***Perry W. Grigsby***[1,2], *Maria A. Thomas*[1], *Kathryn Fowler*[4], *Jonathan McConathy*[4], *Agus Priatna*[3], *Farrokh Dehdashti*[2], *[1]Radiation Oncology, Washington University School of Medicine, St. Louis, MO, USA; [2]Division of Nuclear Medicine, Mallinckrodt Institute of Radiology, St. Louis, MO, USA; [3]Magnetic Resonance Division, Siemens Healthcare, USA, St. Louis, MO, USA; [4]Diagnostic Radiology, Washington University School of Medicine, St. Louis, MO, USA. Contact e-mail: Pgrigsby@radonc.wustl.edu*

Purpose: The aim of this pilot study was to evaluate the clinical utility of simultaneous acquisition of PET and MR imaging in patients with cervical cancer and to compare PET/MR images (Siemens Healthcare Biograph mMR) with those obtained with PET/CT. Materials and Methods: Integrated whole-body PET/MR imaging was acquired for 14 patients with cervical cancer using the Siemens Biograph mMR system installed at the Mallinckrodt Institute of Radiology at Washington University. A prospective institutional study was developed in which PET/MR imaging was acquired following FDG-PET/CT obtained for clinical evaluation. All patients received a single injection of FDG and underwent a PET/CT immediately followed by a PET/MR. PET/CT was performed according to our standard clinical protocol with CT attenuation correction. The PET/MR utilizes avalanche photodiodes in the bore of the 3T magnet for simultaneous image acquisition. mMR PET attenuation correction was performed using a dual echo VIBE Dixon sequence. For each scan, PET imaging parameters were determined, including SUVmax and metabolic tumor volume (MTV). Sites of disease were assessed with PET/MR and compared with findings on PET/CT. Three patients had newly diagnosed disease, 3 patients were under treatment with chemo-radiation and 8 patients had completed therapy. Results: Simultaneous PET/MR image acquisition was feasible in this initial pilot study. Visual interpretation of imaging from both patients with newly diagnosed cervical cancer demonstrated comparable findings for the primary tumor and pelvic lymph nodes. SUVmax of the primary lesion was within 20% for all three patients. Similar findings were observed for the three patients who were evaluated for response to treatment. None of the 8 patients who underwent posttherapy imaging demonstrated PET or MR evidence of active disease by either PET/CT or PET/MR imaging. Conclusion: Simultaneous PET/MR imaging provides a novel method to perform integrated anatomic, metabolic and functional imaging. A major advantage is the synchronous acquisition, which avoids differences in patient position, bladder and rectal filling, and tumor growth. Simultaneous PET/MR may be especially valuable in comparing tumor boundaries between PET and various MR sequences, in radiation treatment planning, in minimizing patient scan time when both PET and MRI are desired, in reducing radiation dose to patients, and in interpreting cases with indeterminate findings by providing co-localization of the two modalities. This study demonstrates that integrated PET/MR is feasible in patients with cervical cancer with good concordance of imaging findings with standard of care FDG-PET/CT.

Disclosure of author financial interest or relationships:
**P.W. Grigsby**, None; **M.A. Thomas**, None; **K. Fowler**, None; **J. McConathy**, Eli Lilly/Avid, Consultant; Eli Lilly/Avid, Speakers bureau; **A. Priatna**, Siemens Healthcare, USA, Employment; **F. Dehdashti**, None.

Presentation Number **SS 123**
Scientific Session 18: Preclinical In Vivo/Translational & Clinical- Inflammation and Immunology
September 7, 2012 / 13:00-13:12 / Room: Liffey Hall 2

# Radiolabeled Sigma-1 Receptor Ligand Detects Peripheral Neuroinflammation in a Neuropathic Pain Model using PET-MRI

***Deepak Behera**, Bin Shen, Michelle L. James, Preeti Borgohain, Minal Patankar, Lauren Andrews, Sandip Biswal, Frederick T. Chin,*
*Radiology, Stanford University School of Medicine, Stanford, CA, USA. Contact e-mail: deepak.behera@stanford.edu*

Purpose: Accurately identifying sites of nerve injury and inflammation would have tremendous clinical value in the management of a variety chronic neurologic diseases, including neuropathic pain. Sigma-1 receptor (S1R), is known to play a significant role in pain sensitization and signal amplification in chronic neuropathic pain. Expressing S1R in high levels, Schwann cells and macrophages proliferate and migrate, respectively, in response to sites of neuroinflammation. S1R can be targeted using a radiolabeled antagonist $^{18}$F-FTC-146. Using PET-MRI we detected increased localization of $^{18}$F-FTC-146 in neuroinflammation in a neuropathic pain model. Methods: Adult male Sprague-Dawley rats were divided into 3 experimental groups: left Spared-Nerve Injury (SNI; a sciatic neuropathic pain model), sham surgery without nerve injury and a control group without any surgery. The rats were allowed 4 weeks to heal and develop pain. Presence of pain in SNI was ascertained by testing for allodynia using von-Frey's filaments. Each rat underwent small-animal PET imaging, 30 minutes after administration of $^{18}$F-FTC-146 IV (1000 µCi/37MBq), and T1-weighted fast spin echo images obtained using a 7T small-animal MRI. For blocking studies, Haloperidol (1.6 mg/kg) was administered 20 min before tracer injection. The rats were then sacrificed and tissues were prepared for autoradiographic and immunohistochemical correlation. For image analysis, MR images were used to draw ROIs on 3 mm segments of sciatic nerves, proximal to the level of injury, in both hindlimbs of each rat and counts within ROIs were recorded from the fused PET images. The maximum signal in each nerve was normalized to the average signal from adjacent muscle. Results: Presence of allodynia only in the operated limb of SNI rats was confirmed ($p<0.0001$). In PET-MRI, higher $^{18}$F-FTC-146 uptake was seen only in the operated left sciatic nerve in the SNI group (normalized PET signal: 3.64±1.38) but not in the Sham (1.25±0.18) or control groups(1.39±0.11) ($p<0.0001$), confirmed with autoradiography. This difference disappears when blocked with haloperidol (1.53±0.25), demonstrating that the increased uptake in the sciatic nerve is due to specific binding with S1R. Specific uptake of $^{18}$F-FTC-146 was validated by immunohistochemistry showing increased S1R specific staining in the neuroma, which corresponds to increased Schwann cell and macrophage infiltration in H&E staining as well as increased $^{18}$F-FTC-146 uptake in autoradiography. Conclusion: $^{18}$F-FTC-146 PET MRI can visualize and quantify S1R in peripheral nerves, confirmed by autoradiographic and immunohistochemical correlation. Our study has shown S1R PET imaging can identify neuroinflammation associated with nerve injury and neuropathic pain. Clinical Relevance: Combining the high sensitivity of PET with the excellent tissue contrast of MRI to locate nerve, PET-MRI with $^{18}$F-FTC-146 can quantify neural S1R density and potentially identify neuroinflammation-related nociception. $^{18}$F-FTC-146 PET-MRI is a potential tool for a wider application to assess S1R-targeted therapies.

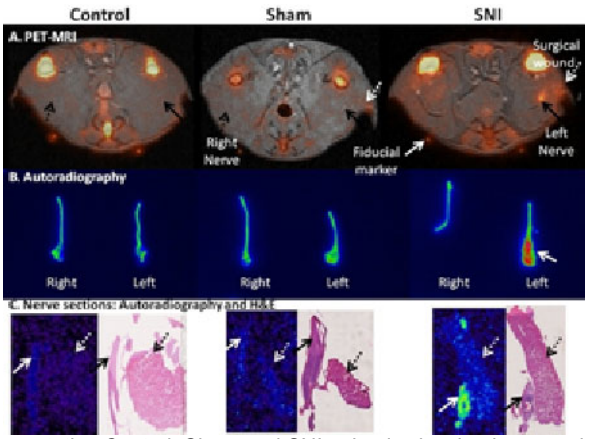


A. Transaxial fused PET-MRI images of representative Control, Sham and SNI animals showing increased 18F-FTC-146 uptake in the left sciatic nerve of SNI animal. (Solid black arrows: left sciatic nerve; dashed black arrow: right sciatic nerve; solid white arrow: fiducial marker; dashed white arrow: surgical wound.) B. Autoradiography of excised sciatic nerves showing increased uptake in the neuroma in the injured left nerve from SNI animal. (Solid white arrow: neuroma) C. Representative autoradiograms and corresponding H&E images of left sciatic nerve sections from Control, Sham and SNI animal showing increased 18F-FTC-146 uptake in the neuroma from the injured sciatic nerve from SNI animal, and increased inflammatory and regenerative cellularity in the neuroma. (Solid arrows (black or white): sciatic nerve; dashed arrow (black or white): adjacent muscle.)

Disclosure of author financial interest or relationships:
**D. Behera**, None; **B. Shen**, None; **M.L. James**, None; **P. Borgohain**, None; **M. Patankar**, None; **L. Andrews**, None; **S. Biswal**, None; **F.T. Chin**, Bayer Healthcare, Grant/research support; GE Healthcare, Grant/research support; Varian Biosynergy, Grant/research support; Varian Medical System, Inc., Grant/research support; Abbott Vascular, Consultant; Ground Fluor Pharmaceuticals, Inc., Consultant .

Presentation Number **SS 124**
Scientific Session 18: Preclinical In Vivo/Translational & Clinical- Inflammation and Immunology
September 7, 2012 / 13:12-13:24 / Room: Liffey Hall 2

# In vivo imaging of cell proliferation enables the detection of early experimental rheumatoid arthritis (RA) by 3'-deoxy-3'-18F-fluorothymidine ([$^{18}$F]FLT) and small animal Positron Emission Tomography (PET)

***Kerstin Fuchs***[1,3], *Ursula Kohlhofer*[2], *Leticia Quintanilla-Fend*[2], *Denis Lamparter*[1], *Gerald Reischl*[1], *Martin Röcken*[3], *Bernd J. Pichler*[1], *Manfred Kneilling*[1,3], [1]*Department of Preclinical Imaging and Radiopharmacy, Eberhard Karls University Tübingen, Tübingen, Germany;* [2]*Department of Pathology, Eberhard Karls University Tübingen, Tübingen, Germany;* [3]*Department of Dermatology, Eberhard Karls University Tübingen, Tübingen, Germany. Contact e-mail: kerstin.fuchs@med.uni-tuebingen.de*

Approximately 1-2% of the world`s population suffers from RA, an autoimmune disease that is characterized by systemic and erosive synovitis and joint destruction. Consequently, early treatment of RA patients with anti-inflammatory drugs is important for the protection from disease progression and joint destruction. Therefore, the early diagnosis of RA, before the onset of joint destruction, is of special importance. The aim of our study was to investigate the potential of [$^{18}$F]FLT-PET, [$^{18}$F]FLT-PET/CT and [$^{18}$F]FLT-PET/MR imaging to quantify TK-1 activity at different stages in GPI-induced arthritis and its correlation with Ki-67 protein expression. We injected naïve BALB/c mice intraperitoneally (i.p.) with either glucose-6-phosphate-isomerase (GPI)-specific antibody-containing serum to induce experimental arthritis or control-serum from healthy C57BL/6 mice. Animals were injected intravenously (i.v.) with [$^{18}$F]FLT at days 1, 3, 6 and 8 after the onset of disease and were measured in vivo by combined PET/CT and PET/MRI followed by autoradiography analysis. [$^{18}$F]FLT uptake in the ankles and fore paws was quantified in PET/CT and PET/MRI images by drawing standardized regions of interest (ROIs). To verify the in vivo PET data, we performed Ki-67 immunohistochemical staining of the ankles and fore paws at the corresponding time points. Analysis of the different stages of arthritic joint disease revealed enhanced [$^{18}$F]FLT uptake in arthritic ankles (2.2±0.2% ID/g) and fore paws (2.1±0.3% ID/g) compared with healthy ankles (1.4±0.3% ID/g) or fore paws (1.5±0.5% ID/g) as early as one day after GPI-serum injection, a time point characterized by clear histological signs of arthritis but without measurable ankle swelling. [$^{18}$F]FLT uptake in ankles increased at day 3 after the onset of arthritic joint inflammation (3.1±0.6% ID/g) and reached the maximum observed level at day 8 (3.5±0.3% ID/g). Ki-67 immunohistochemical staining of the arthritic ankles and fore paws revealed a strong correlation with the in vivo [$^{18}$F]FLT data. Detailed analysis exhibited that resident cells such as synovial fibroblasts as well as infiltrating cells such as neutrophils stained positive for Ki-67. Our data clearly prove that [$^{18}$F]FLT can be used to non-invasively examine inflammation-induced cell proliferation in vivo in a mouse model of RA, as our measurements were correlated with the ankle thickness, MRI- and CT-images, histopathological changes and Ki-67 immunohistochemistry. Combined PET/CT and PET/MRI measurements enabled us to identify the exact foci of enhanced [$^{18}$F]FLT uptake in the inflamed ankles and fore paws, to differentiate between bone and soft tissue, to identify the exact anatomic sites of enhanced cell proliferation and to differentiate bone from cartilage and other soft tissues . Thus, non-invasive in vivo measurement of cell proliferation in experimental arthritis using [$^{18}$F]-FLT-PET is a promising tool for diagnosing the early stages of arthritic joint inflammation and can be used to detect inflammation before the onset of joint swelling.

Disclosure of author financial interest or relationships:
**K. Fuchs**, None; **U. Kohlhofer**, None; **L. Quintanilla-Fend**, None; **D. Lamparter**, None; **G. Reischl**, None; **M. Röcken**, None; **B.J. Pichler**, Siemens, Grant/research support; AstraZeneca, Grant/research support; Bayer Healthcare, Grant/research support; Boehringer-Ingelheim, Grant/research support; Oncodesign, Grant/research support; Merck, Grant/research support; Bruker, Grant/research support; **M. Kneilling**, None.

Presentation Number **SS 125**
Scientific Session 18: Preclinical In Vivo/Translational & Clinical- Inflammation and Immunology
September 7, 2012 / 13:24-13:36 / Room: Liffey Hall 2

# Development of an engineered anti-mCD8 minibody for ImmunoPET imaging in preclinical models

***Richard Tavaré**, Scott M. Knowles, Felix B. Salazar, Kirstin A. Zettlitz, Tove Olafsen, Anna M. Wu, Crump Institute for Molecular Imaging, UCLA, Los Angeles, CA, USA. Contact e-mail: rtavare@mednet.ucla.edu*

The ability to assess the migration, expansion and longevity of immunological cells using PET imaging is of critical importance for monitoring the success of immunotherapies, such as T cell and/or dendritic cell adoptive transfer and antibody based immunotherapeutics. Here, variable regions of a depleting rat anti-mouse CD8 IgG2b antibody (clone 2.43) have been sequenced from the hybridoma for reformatting to a minibody. The ~80 kDa minibody is a divalent construct that contains the rat scFv followed by the mouse hinge and CH3 domain. The engineered minibody binds CD8αLyt2.2 and not CD8αLyt2.1 that is expressed on the mouse strains C57BL/6 and BALB/c but not C3H and CBA/Ca. Engineering to the minibody format serves two purposes: firstly, the minibody has does not contain the full Fc fragment and will, therefore, not deplete CD8+ cells in vivo, and secondly the minibody has optimal phamacokinetics for radionuclide imaging because the lack of a full Fc domain decreases the blood half-life. At ~150 kDa, intact antibodies generally have a 7-14 day half-life, while minibodies typically have a 5-12 hour half-life. Our lab has shown previously that the shorter half-life of minibodies enable high signal to noise in PET images for antigen expression at much shorter times (6-44 hrs) that intact antibodies (5-7 days). The engineered anti-CD8 minibody was purified by NiNTA affinity chromatography and showed specific binding by flow cytometry to both Pmel CD8+ T cells and BW58 CD8+ lymphoma cells. Initially, the minibody was radiolabeled with I-124 using the Iodogen method. Signal was seen in the spleen at 4 hours but is absent in the 24-hour image, suggesting either dissociation or internalization and loss of signal from the minibody. Subsequently, the minibody was conjugated using S-2-(4-Isothiocyanatobenzyl)-1,4,7-triazacyclononane-1,4,7-triacetic acid (p-SCN-Bn-NOTA) and radiolabeled with Cu-64. Radiolabeling efficiency was 98.5% and radiochemical purity after EDTA challenge and spin column purification was 99.8%. PET imaging in Lyt2.2 expressing C57BL/6 mice at 4 and 20 hours post-injection showed uptake in the spleen, bone marrow and lymph nodes with non-specific uptake in the liver. When imaging the negative control C3H mice expressing Lyt2.1, unspecific spleen signal is lost by 4 hours and there is no uptake in the bone marrow. Furthermore, when blocked with 2 mg/kg or 20 mg/kg of cold Mb, spleen uptake at 20 hours post-injection is decreased 4.2- and 5.6-fold, respectively. Shown here are the initial steps for developing a functional CD8 imaging agent based on engineered antibodies for use in a variety of preclinical disease and immunotherapeutic models.

Disclosure of author financial interest or relationships:
**R. Tavaré**, None; **S.M. Knowles**, None; **F.B. Salazar**, None; **K.A. Zettlitz**, None; **T. Olafsen**, ImaginAb Inc., Employment; **A.M. Wu**, ImaginAb, Inc., Consultant; ImaginAb, Inc., Stockholder .

Presentation Number **SS 126**
Scientific Session 18: Preclinical In Vivo/Translational & Clinical- Inflammation and Immunology
September 7, 2012 / 13:36-13:48 / Room: Liffey Hall 2

# Specific and non-invasive imaging of eosinophilia and treatment response in a mouse model of allergic asthma

***Andrea Markus***[1]*, Christian Dullin*[3]*, Anna Karabinskaya*[2]*, Frauke Alves*[1]*, [1]Department of Haematology/Oncology, University Medicine Goettingen, Goettingen, Germany; [2]Cellular and Molecular Immunology, University Medicine Goettingen, Goettingen, Germany; [3]Department of Radiology, University Medicine Goettingen, Goettingen, Germany. Contact e-mail: andrea.markus@med.uni-goettingen.de*

Asthma is an inflammatory disease of the airways, affecting over 300 million people worldwide. Central to the inflammation process is the recruitment of eosinophils to the airways, which release proteases and proinflammatory factors, eventually leading to airway remodeling. Non invasive, in vivo methods to assess asthma in mouse models are still very limited and mostly use general inflammation markers, such as matrix metalloproteinases. Here we have utilized a monoclonal antibody directed to SiglecF, a lectin found predominantly on eosinophils, in combination with non-invasive near infrared fluorescence (NIRF) imaging. Our approach to detect asthma is therefore novel as it targets the most prominent feature of asthma, namely eosinophilia. A conventional OVA based model was used to induce asthma in BALB/c mice. Three to four days post challenge mice were intravenously injected with the antibody, which was conjugated to the NIRF dye, Alexa Fluor 750. Subsequently whole body and lung scans were performed up to 4 days post antibody injection in living asthma and control mice using the Optix MX2 imaging system. In asthma lungs we observed significantly higher fluorescence intensities compared to lungs of control mice. In asthma mice we found fast clearing of excess amount of antibody via bladder and liver within the first 7 hours, followed by an accumulation of the NIRF labeled antibody in the lung on day 1-3 post injection in comparison to controls, suggesting different peaks of eosinophilia for each asthma mouse. Furthermore, mice treated with Dexamethasone, a common glucocorticoid used in asthma therapy, showed low intensities, comparable to controls. Fluorescent microscropy of cryosections of the imaged lungs confirmed the localization of the NIRF-labeled antibody in the peribronchial areas of asthmatic lungs as opposed to control lungs. SiglecF-immunohistochemistry of lung cryosections from asthmatic mice confirmed strong peribronchial expression on eosinophils whereas controls were largely clear of eosinophils. Our results show that optical imaging using a NIRF dye labeled SiglecF antibody is a promising method to assess asthma in vivo, thus advancing diagnosis and quantification of the disease. Moreover, this method can be utilized to monitor the efficacy of novel therapies against asthma in vivo.

Disclosure of author financial interest or relationships:
**A. Markus**, None; **C. Dullin**, None; **A. Karabinskaya**, None; **F. Alves**, None.

Presentation Number **SS 127**
Scientific Session 18: Preclinical In Vivo/Translational & Clinical- Inflammation and Immunology
September 7, 2012 / 13:48-14:00 / Room: Liffey Hall 2

# Longitudinal evaluation of secondary lymphedema model of a rat hind limb

***Masaki Sano***[1], *Mikako Ogawa*[2], *Naoki Unno*[1], *Satoshi Hirakawa*[3], *Seiji Yamamoto*[4], *Junichi Sakabe*[3], *Takeshi Sasaki*[5], *Minoru Suzuki*[1], *[1]Vascular surgery, Hamamatsu University School of Medicine, Hamamatsu-shi, Japan; [2]Department of Molecular Imaging, Applied Medical Photonics Laboratory, Medical Photonics Research Center, Hamamatsu University School of Medicine, Hamamatsu-shi, Japan; [3]Dermatology, Hamamatsu University School of Medicine, Hamamatsu-shi, Japan; [4]Department of Inovative Medical Photonics, Basic Medical Photonics Laboratory, Medical Photonics Research Center, Hamamatsu University School of Medicine, Hamamatsu-shi, Japan; [5]Anatomy, Hamamatsu University School of Medicine, Hamamatsu-shi, Japan. Contact e-mail: masakisurgeon@gmail.com*

Background and Objective: Secondary lymphedema arises as a consequence of surgical, radiation, inflammatory, or traumatic disruption of lymphatics. But the pathophysiology of secondary lymphedema is not clear yet and the therapeutic approaches are limited and ineffective. We created an experimental model of secondary lymphedema of a rat hind limb and performed a longitudinal evaluation of lymphatics and inflammatory cytokines in dermis and subcutaneous tissues to reveal the mechanism of secondary lymphedema. Methods: A surgical secondary lymphedema model was created in the right hind limb in a 12-week-old male SD rat. Indocyanine green (ICG) was injected into the foot pad of rats and subcutaneous lympatics were precisely evaluated by fluorescence lymphangiography. Gd-DTPA conjugated PAMAM-G6 dendrimer was also injected and MR lymphangiography was performed to evaluate deep lymphatics. Quantum dot (Qdot 800 ITK) was also injected into the foot pad and thigh tissues were resected. Resected tissues were fixed with formarin and parafin sections were made. Fluorescence microscopy with Qdot was performed to evaluate lymphatic fluid in subcutaneus tissues. Azan stain and ultrasonic microscopy was also performed to evaluate collagen fibers and elasticity of tissues. These images were taken in acute phase (3days, 1week), subacute phase (2weeks, 4weeks) and chronic phase (2months, 3months). Dermis and subcutaneus tissues of the thigh were resected at 1week, 2weeks, and 4weeks. The amount of MCP-1, TNF-α, and IL-6 were examined with enzyme-linked immunosorbent assay (ELISA). Results: Lymphatic fluid leakage to subcutaneous tissue was observed in acute and subacute phase by fluorescence lymphangiography and microscopy (Fig.1, Supplemental Fig.1). Collateral deep lymphatics were detected by MR lymphangiography in chronic phase (Supplemental Fig.1). Collagen fibers were increased at subacute and chronic phase (Supplemental Fig.1). Ultrasonic microscopy showed the elastisity of dermis and subcutaneus tissue increased at subacute and chronic phase (Supplemental Fig.2). The amount of MCP-1, TNF-α and IL-6 in dermis and subcutaneus tissues were increased in subacute phase (Supplemental Fig.3). Conclusion: Combination of fluorescence and MR lymphangiography could evaluate longitudinal changes of subcutaneous and deep lymphatics. And ultrasound microscopy could evaluate the elasticity of tissues in rat models. In subacute phase, the elasticity of dermis and subcutaneous tissues increased and the amount of inflammatory cytokines in tissues were also increased. In chronic phase, the amounts of cytokines were low and the leakage of lymphatic fluid was not detected, but the high elasticity of tissues remained unchanged. These results suggest that therapeutic approaches of the secondary lymphedema in chronic phase are not so effective and should be started in earlier phase before the collagen fiber formation. Further pathological investigation would help to reveal the mechanism of secondary lymphedema and establish the effective therapies.

Fig. 1: ICG fluorescence lymphangiography of secondary lymphedema model of a rat hind limb (1 week)

Disclosure of author financial interest or relationships:
**M. Sano**, None; **M. Ogawa**, None; **N. Unno**, None; **S. Hirakawa**, None; **S. Yamamoto**, None; **J. Sakabe**, None; **T. Sasaki**, None; **M. Suzuki**, None.

Presentation Number **SS 128**
Scientific Session 18: Preclinical In Vivo/Translational & Clinical- Inflammation and Immunology
September 7, 2012 / 14:00-14:12 / Room: Liffey Hall 2

# Development and Clinical Application of an Optical Molecular Imaging Agent to Stratify Acute Lung Injury in Intensive Care

***Kevin Dhaliwal***[1], *Tashfeen Walton*[2], *Manuelle Debunne*[1], *Neil A. McDonald*[1], *Nicolaos Avlonitis*[2], *Tim S. Walsh*[3], *Mark Bradley*[2], *Haslett Chris*[1], [1]*MRC Centre for Inflammation Research, University of Edinburgh, Edinburgh, United Kingdom;* [2]*Department of Chemistry, University of Edinburgh, Edinburgh, United Kingdom;* [3]*Intensive Care Unit, Royal Infirmary of Edinburgh, Edinburgh, United Kingdom. Contact e-mail: kdhaliwa@staffmail.ed.ac.uk*

INTRODUCTION Acute Lung Injury and Adult Respiratory Distress Syndrome are characterised by neutrophil-predominant lung inflammation. No current biological therapies exist for these conditions. One of the main reasons this is so, is because there are no bedside tools or technologies that are able to distinguish active neutrophilic dependent lung injury from other aetiologies.The accurate bedside detection of acute lung injury would permit the rational and targeted delivery of pharmacological therapy. Our strategy utilises the combined strategy of microdosing a novel optical molecular imaging reagent alongside probe-based confocal laser microendoscopy (pCLE) in the distal human lung. METHODS AND RESULTS We have developed and synthesised to clinical grade a new small molecule called NAP (Neutrophil Activation Probe). NAP is uniquely dequenched by activated neutrophils. Its dequenching is dependent on both the presence of elastase and also neutrophil pinocytosis during degranulation. NAP is fully soluble and shows excellent and unequivocal specificity for neutrophils and elastase. NAP shows no toxicity in vitro and in GLP compliant assays at over 10000 times human dose in rodent screens. NAP shows no mutagenic potential. NAP detects activated neutrophils in vitro in bronchoalveolar lavage from patients with acute lung inflammation using both pCLE and benchtop confocal. NAP and pCLE detects activated neutrophils in vivo in a ventilated sheep model of acute lung segmental lung inflammation. NAP and pCLE also detects activated neutrophils in an ex vivo perfused whole lung system. Prior to full scale validation, NAP has received IRB approval and is delivered to 6 healthy volunteers in dose escalation and 6 patients on ICU with chest-x-ray infiltrates. CONCLUSION This is the first description of a clinical grade optical molecular imaging reagent being developed and applied for acute lung injury in intensive care to provide immediate point of care diagnostic stratification.

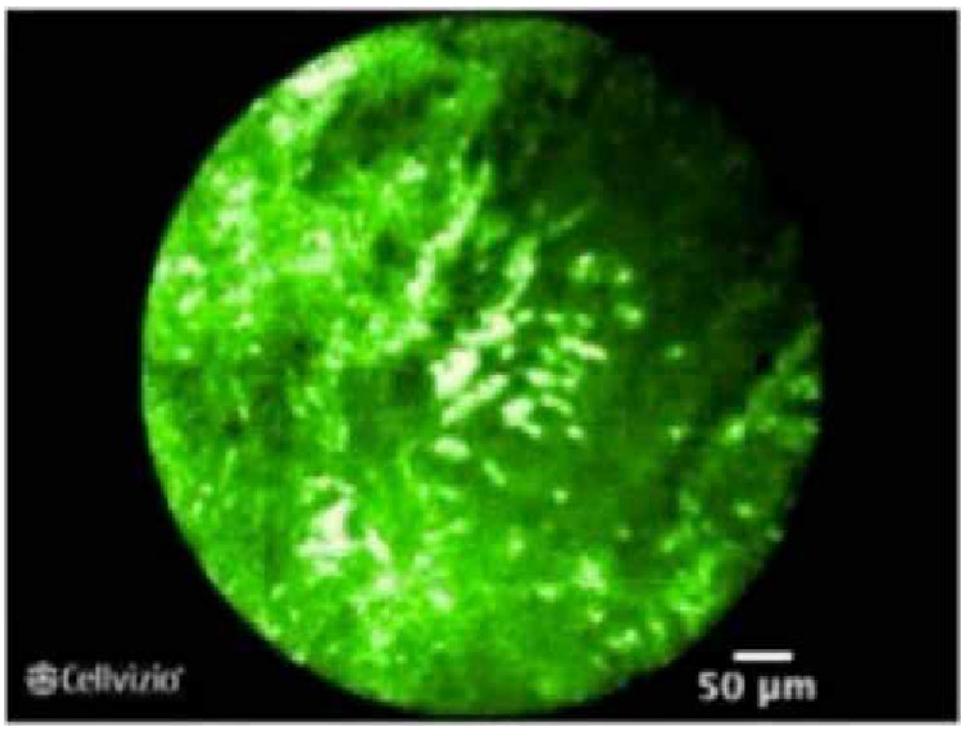


pCLE and NAP cellular imaging of activated human neutrophils in the distal lung indicating acute lung injury

Disclosure of author financial interest or relationships:
**K. Dhaliwal**, None; **T. Walton**, None; **M. Debunne**, None; **N.A. McDonald**, None; **N. Avlonitis**, None; **T.S. Walsh**, None; **M. Bradley**, None; **H. Chris**, None.

Presentation Number **SS 129**
Scientific Session 18: Preclinical In Vivo/Translational & Clinical- Inflammation and Immunology
September 7, 2012 / 14:12-14:24 / Room: Liffey Hall 2

# Assessment of voxelwise quantification of [18F]FDG dynamic PET data in human lung: insight for clinical use

***Elisabetta Grecchi***[1], *Mattia Veronese*[1], *Rosa Maria Moresco*[2], *Giacomo Bellani*[3], *Antonio Pesenti*[3], *Cristina Messa*[2], *Alessandra Bertoldo*[1], [1]*Department of Information Engineering, University of Padova, Padova, Italy;* [2]*Technomed Foundation, University of Milan-Bicocca, Milano, Italy;* [3]*Department of Experimental Medicine, University of Milan-Bicocca, Monza (MI), Italy. Contact e-mail: elisabetta.grecchi@gmail.com*

INTRODUCTION Standardized Uptake Value (SUV) is widely used in clinical [18F]FDG PET studies as a semiquantitative measurement of fractional tissue tracer uptake (Ki), despite various concerns about its usability for lung [1]. On the contrary, dynamic PET studies are more informative when quantified by using an adequate mathematical modeling approach. Thus, they are usually used in research rather than clinical practice. The aims of this study are 1) to develop a voxelwise quantification method for dynamic lung [18F]FDG PET data in humans, and 2) to compare at voxel level different quantitative and semiquantitative measurements of Ki. METHODS [18F]FDG PET/CT dynamic scans (57 min length, measured in kBq/cc) of 6 controls and 10 patients with acute lung injury (ALI) [2] were quantified at voxel level with Spectral Analysis Iterative Filter (SAIF) modeling approach [3]. SAIF allows to quantify the Ki, the tracer distribution volume (VT) and to separate the kinetics components from the measured total activity. SAIF Ki voxelwise estimates have been compared with a) SUV; b) the RATIO of the mean tissue activity over the mean plasma activity both computed in the last 12 min of the experiment; c) Patlak graphical analysis. Correlation analysis was performed among SUV, RATIO and Ki obtained with Patlak and SAIF. The plasma arterial input function has been derived from the images as in [2] and assumed measured in KBq/ml. RESULTS Voxelvise SAIF allows to separate 3 kinetics components: the first associated with the trapping of FDG-6-P in the tissue, the second one with an intermediate reversible process, and the last one with a fast reversible plasma-tissue exchange process. In comparison with the controls, the spectra of the patients are, generally, shifted towards the right side indicating the presence of faster kinetics (figure). In particular, the degree of the shift of the faster component allows distinguishing normal-dense, hyper-dense or edematous tissue. There is a 25-fold mean increase of Ki between controls vs patients (0.0006 ml/cc/min vs 0.015 ml/cc/min) and a 3-fold mean increase in VT (0.15 ml/cc vs 0.50 ml/cc). The higher VT indicates an increased availability of [18F]FDG in the extravascular space which is related to the pathological status of the tissue within the voxel. SAIF Ki estimates show an excellent correlation with Patlak ones (R2=0.98, y=1.06x+0). They also exhibit a high correlation with RATIO (R2RATIO=0.97) but a lower one with SUV (R2SUV=0.67). CONCLUSIONS Despite the noisiness of the data, SAIF enables to quantify not only the Ki but also additional physiological information allowing a deeper understanding of ALI. Since the arterial input function was directly derived from the images, SAIF quantification is completely non-invasive, i.e. applicable to clinical studies. Our results show that the more the dynamic contribution is taken into consideration, the more useful the information about the system will be. Thus, the application of the SUV seems to be questionable or not completely representative. REFERENCES [1] Schroeder T et al, Acad Radiol 2011 [2] Bellani G et al, Crit Care Med 2009 [3] Veronese M et al, JCBFM 2010

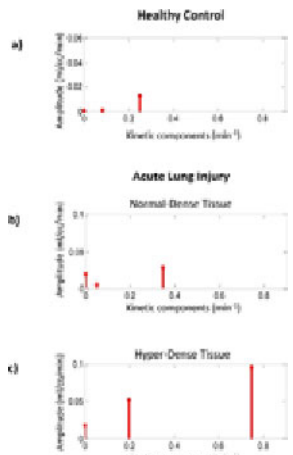


The figure reports the spectra obtained with SAIF of two representative subjects: (a) control subject, (b) normal-dense tissue of a patient affected with acute lung injury, (c) hyper-dense or edematous tissue of the same patient affected with acute lung injury. Each line represents a component that characterizes the tracer kinetic (the x axis indicates the velocity of the kinetic component, while the y axis its amplitude). In particular the amplitude of the one in zero coincides with the uptake of the tracer in tissue. Note that the patient maintains similar Ki (i.e. amplitude of the lower component) for both normal- and hyper-dense tissues, while the latter demonstrates a significant shift of the faster components and an increase of their amplitudes (panels b and c).

Disclosure of author financial interest or relationships:
**E. Grecchi**, None; **M. Veronese**, None; **R. Moresco**, None; **G. Bellani**, None; **A. Pesenti**, None; **C. Messa**, None; **A. Bertoldo**, None.

Presentation Number **SS 13**
Scientific Session 2: Technology & Software - Optical Imaging
September 6, 2012 / 11:14-11:25 / Room: Wicklow Hall 1

# Optical casting of the vascular network of zebrafish

*Andrea Bassi[1], **Luca Fieramonti**[1], Efrem A. Foglia[2], Franco Cotelli[2], Gianluca Valentini[1], Cosimo D'Andrea[1], [1]Physics, Politecnico di Milano, Milano, Italy; [2]Biology, Università degli Studi di Milano, Milano, Italy. Contact e-mail: luca.fieramonti@mail.polimi.it*

Optical projection tomography (OPT) [1] is emerging as valuable tool for three-dimensional imaging of intact and entire organisms or biological tissues. Similarly to x-ray computed tomography, OPT is based on the acquisition of a sequence of optical transmission (or fluorescence) images of the sample at several orientations. The acquired images, or projections, are combined to reconstruct the 3-D volume of the sample, typically using a backprojection algorithm. We developed an OPT system to study zebrafish (Danio rerio), an ideal biological model for in-vivo studies, presenting several advantages, which include amenability to in-vitro manipulation, feasibility of reverse and forward genetic approaches, ease of drug administration and experimentation, optical transparency at the embryo stage. We recently reported [2] a new contrast mechanism in OPT, given by the movement of cells present in bloodstream. Looking at a living zebrafish at the embryo or juvenile stage it is possible to observe the flow of the blood cells. Therefore, by acquiring several time frames of the specimen and applying a motion-analysis algorithm, it is possible to obtain a map of the sample vasculature. By mathematical processing the vascular maps obtained at different angles it is possible to produce and visualize a 3-D casting of the vasculature of the specimen, noninvasively and without the need for any fluorescent probe. This results in a low-cost, label-free, three-dimensional imaging technique, called flow-OPT. Here we describe this new technique and we present a validation based on comparison of the obtained data with vibratome sections and with images obtained with confocal microangiography. We show that flow-OPT can visualize a detailed casting of the circulatory system of zebrafish, from embryo to juvenile stage. The results obtained in different regions of the zebrafish are shown, including head, trunk and tail. The presented data are obtained on 3 to 30 days post fertilization zebrafish. Flow-OPT has the capability to quickly image large volumes in a relatively short acquisition time, since several frames (with a duration of a few ms) can be acquired at 100 Hz or beyond. The acquisition of the entire dataset typically takes a few minutes. Another key point of OPT is its low cost. Flow-OPT takes this advantage even further, since it does not require fluorescence excitation and detection. Flow-OPT is non-invasive and label free: it does not require fluorescent labeling or markers. This feature is particularly important when wild type organisms are under study and injection of fluorescent probes is not convenient. References 1. J. Sharpe, U. Ahlgren, P. Perry, B. Hill, A. Ross, J. Hecksher-Sorensen, R. Baldock, and D. Davidson, Optical projection tomography as a tool for 3D microscopy and gene expression studies, Science 296, 541-545 (2002). 2. A. Bassi, L. Fieramonti, C. D'Andrea, M. Mione, and G. Valentini, In vivo label-free three-dimensional imaging of zebrafish vasculature with optical projection tomography, J. Biomed. Opt. 16(10), 100502 (2011)

Disclosure of author financial interest or relationships:
**A. Bassi**, None; **L. Fieramonti**, None; **E.A. Foglia**, None; **F. Cotelli**, None; **G. Valentini**, None; **C. D'Andrea**, None.

Presentation Number **SS 130**
Scientific Session 19: Translational & Clinical - Neurology
September 7, 2012 / 13:00-13:12 / Room: Wicklow Hall 2

# PET/CT/MRI with [18F]TFAHA using an optimized pharmacokinetic model for quantification of HDAC class II expression-activity in the brain of non-human primates

***Hsin-Hsien Yeh***[1,2], *Leo G. Flores*[1], *Vincenzo Paolillo*[1], *Kun-eek Kil*[1], *Uday Mukhopadhyay*[1], *Suren Soghomonyan*[1], *Asutosh Pal*[1], *Rajesh Uthamanthil*[1], *James Jackson*[1], *William Tong*[1], *Mian M. Alauddin*[1], *Mei Tian*[1], *C.Allen Chang*[2], *Ren-Shyan Liu*[2,3], *Juri G. Gelovani*[1], [1]*Department of Experimental Diagnostic Imaging, University of Texas MD Anderson Cancer Center, Houston, TX, USA;* [2]*Department of Biomedical Imaging and Radiological Sciences,, National Yang-Ming University, Taipei, Taiwan;* [3]*Department of Medicine, National Yang-Ming University, Taipei, Taiwan. Contact e-mail: skyeyeh@live.com*

Objective: Molecular imaging of post-transcriptional regulation by histone deacetylases PET/MRI/CT imaging is a blooming area in cancer research and neuroscience such as Huntington's disease and Alzheimer diseases. Recently, we have synthesized and characterized in vitro a novel HDAC class IIa specific radiotracer, the 6-([18F]-trifluoroacetamido)-1-hexanoicanilide, termed [18F]TFAHA. In this study, we aimed to optimize the pharmacokinetic model of [18F]TFAHA-derived radioactivity accumulation in the brain in non-human primates for quantification of HDACs class II activity and for monitoring the pharmacodynamics of pan-HDAC inhibitors i.e., Vorinostat (SAHA) and Valproic acid (VA). Methods: Thirty-two PET/CT/MRI imaging studies were performed in anesthetized rhesus macaques (N=4): 1) baseline study with [18F]fluoroacetate ([18F]TFACE) - the major metabolite of [18F]TFAHA; 2) baseline study with [18F]TFAHA; and 3) repeat study with [18F]TFAHA after treatment with HDAC inhibitors: SAHA and Valproic acid (1, 10, 50 mg/kg i.v. infusion 45min prior to PET). Dynamic PET images of the brain were acquired for 30 minutes post i.v. injection of each radiotracer (6.73±0.31 mCi/5ml) and multiple blood samples were obtained at 0, 1, 3, 5, 10, 15 and 30 min for the analysis of metabolites ([18F]TFACE). The intracerebral influx rate constants (ki) were calculated for each radiotracer using a new developed dual-tracer compartmental model with corrections for radiolabeled metabolites and subtraction of [18F]TFACE-derived radioactivity from the total brain radioactivity produced due to systemic catabolism of [18F]TFAHA. Results: Parametric PET images of [18F]TFAHA Ki were generated using PMOD (PMOD Technologies, Switzerland), which demonstrated predominant radioactivity localization in cerebellum, vermis, caudate-putamen, n.accumbens and amygdalae. These brain structures express high levels of class II HDACs, as demonstrated by immunohistochemical analyses of rhesus macaque brain tissue sections. The Ki of [18F]TFAHA in n.accumbens was 0.86 min-1 which was 43-fold higher than Ki of [18F]TFACE. After pre-treatment with pan-HDAC inhibitor, SAHA and VPA, a significant increase in blood input function of [18F]TFAHA was observed, presumably due to inhibition of HDACs-mediated degradation of [18F]TFAHA in the periphery. However, the Ki of [18F]TFAHA in the brain was significantly decreased when SAHA dose was increasing (i.e., in n.accumbens 0.04 min-1), consistent with the inhibition of HDACs activity in CNS. Similar values for Ki and k3 of [18F]TFAHA were obtained using Patlack graphical analysis with correction for the influx and efflux rate of [18F]TFACE, which was minimal and could be ignored in 30 min imaging period. Conclusions: Using the optimized dual-tracer compartmental model with correction for influx rate of radiolabeled metabolites (i.e., [18F]TFACE), the calculated Ki rate constant for [18F]TFAHA accumulation in the brain reflects the expression-activity of HDACs in the brain. PET/MRI/CT with [18F]TFAHA could be used reliably for non-invasive assessment of pharmacodynamics of novel HDAC inhibitors of HDAC class-II in CNS.

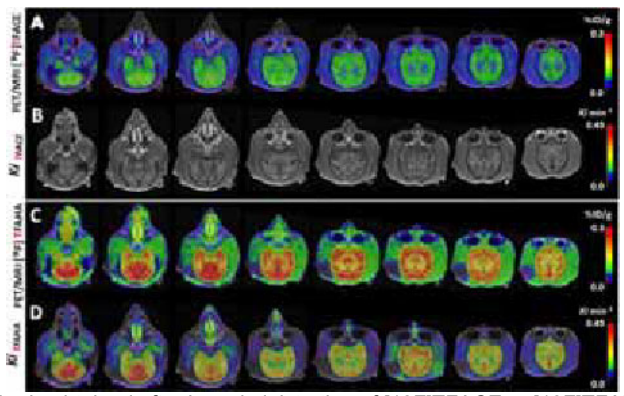


Fig1. Axial PET/MRI fusion images of the brain obtained after i.v. administration of [18F]TFACE or [18F]TFAHA obtained at different axial levels. Static PET/MRI images obtained at 30 min post administration of [18F]TFACE (A) or [18F]TFAHA (B) color-coded to the range of %ID/g values. Parametric PET/MRI images of the unidirectional accumulation rate constant Ki of [18F]TFACE (C) or [18F]TFAHA (D) color-coded to the range of Ki values (min-1) generated at different axial levels in the same animal.

Disclosure of author financial interest or relationships:
**H. Yeh**, None; **L.G. Flores**, None; **V. Paolillo**, None; **K. Kil**, None; **U. Mukhopadhyay**, None; **S. Soghomonyan**, None; **A. Pal**, None; **R. Uthamanthil**, None; **J. Jackson**, None; **W. Tong**, None; **M.M. Alauddin**, None; **M. Tian**, None; **C. Chang**, None; **R. Liu**, None; **J.G. Gelovani**, Macrocyclics, Consultant; SibTech, Consultant .

Presentation Number **SS 131**
Scientific Session 19: Translational & Clinical - Neurology
September 7, 2012 / 13:12-13:24 / Room: Wicklow Hall 2

# Maintaining homeostasis during changes in synaptic environment due to acute and chronic pharmacological treatment: In vivo evaluation of dopamine receptors using PET scatchard studies with [11C]-raclopride

***Doris J. Doudet***[1], *James E. Holden*[2], [1]*Medicine, University of British Columbia, Vancouver, BC, Canada;* [2]*Medical Physics, University of Wisconsin, Madison, WI, USA. Contact e-mail: ddoudet@mail.ubc.ca*

Drugs often induce different behavioral responses after a single acute dose versus prolonged administration; one of the best known examples being psychostimulant- induced sensitization. The underlying physiological correlates are less known. While PET can provide some insight on the behavior of the receptor(s) of interest, a single PET measurement however, only informs on the binding potential $BP_{ND}$ of the tracer. $BP_{ND}$ is the product of the receptor density $B_{max}$ and the apparent affinity $1/K_d^{app}$ but does not provide specific information on the primary individual physiological parameters. We previously validated the use of in vivo scatchard PET to evaluate the effects of acute challenges on the measurements of Bmax and Kdapp 3. We also validated the use of scatchard studies to assess receptor status in situations of chronic, permanently altered conditions such as MPTP or 6OHDA-induced parkinsonism 1. We are now showing the use of scatchard studies to evaluate the change in the physiological status of D2/3 receptors using [11C]-raclopride during acute and chronic alterations in synaptic environment due to pharmacological treatment. In vivo scatchard studies were done in 6 rhesus monkeys at baseline, after an acute dose of a dopamine transporter inhibitor (NS2214: 24hrs half life) and after 5-6 weeks of daily treatment. The studies were done non-sequentially as previously described 2. Briefly, for each time point, at least three raclopride PET studies were performed at different specific activities (SA>1000; 25-35 and 6-10Ci/mmole). For the acute studies, NS2214 was given 45-60 min prior to scanning. Analyses were performed using tissue-input Logan analysis and the constructed scatchard plots yielded for the striatum: $BP_{ND}$, $B_{max}$ and $K_d^{app}$. During both the acute and chronic treatment, $BP_{ND}$ was equally decreased (respectively 28 and 24%) compared to baseline. Acutely, this decrease was driven by a significant decrease in affinity (i.e. 34% increase in $K_d^{app}$) with no change in receptor density. After chronic treatment, the decrease in $BP_{ND}$ was driven by a significant decrease in receptor density (-19%) while $K_d^{app}$ was not significantly different from baseline (Fig.1). This study suggests that receptors have 2 major adaptive mechanisms to their synaptic environment: an immediate response through alterations in "affinity" (including possible changes in conformation and/or internalization/externalization of the receptor) in response to a rapid, acute variation and a slow response mechanism translating in increase or decrease in receptor density in response to prolonged perturbation (involving changes in protein synthesis) as measured after prolonged pharmacological treatment or in disease condition. This study also suggests that carefully designed in vivo PET scatchard studies may be a useful tool to evaluate the short and long term effects of drugs on various receptor systems and may provide useful information in drug development. 1.Doudet et al. Synapse. 2002;44:198-202. 2.Doudet DJ et al. J Cereb Blood Flow Metab. 2006;26:28-37. 3.Holden JE et al. J Cereb Blood Flow Metab. 2002;22(1132-1141).

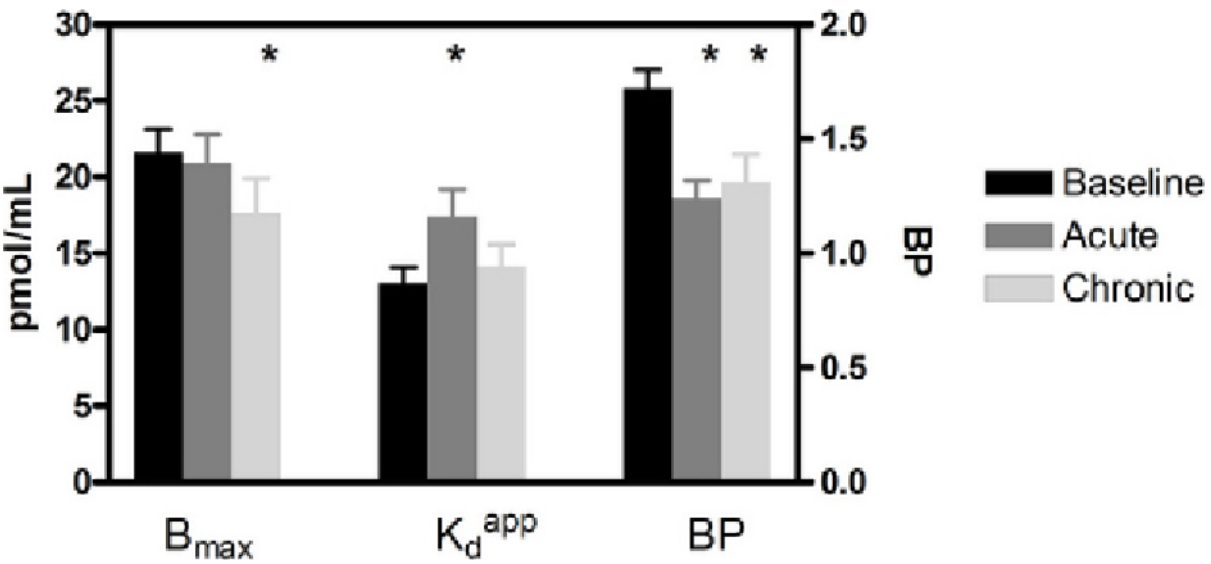


Summary of findings: Values for Bmax and Kd are to be read from the left Y axis and value for BP on the right axis. Data ± SD

Disclosure of author financial interest or relationships:
**D.J. Doudet**, None; **J.E. Holden**, None.

Presentation Number **SS 132**
Scientific Session 19: Translational & Clinical - Neurology
September 7, 2012 / 13:24-13:36 / Room: Wicklow Hall 2

# Voxel-wise quantification of adenosine $A_{2A}$ receptor with [$^{11}$C]SCH442416 PET images in humans

***Gaia Rizzo***[1], *Mattia Veronese*[1], *Anil F. Ramlackhansingh*[2], *David J. Brooks*[2], *Federico Turkheimer*[2,3], *Alessandra Bertoldo*[1], [1]*Department of Information Engineering, University of Padova, Padova, Italy;* [2]*Department of Medicine, Centre for Neuroscience, Imperial College London, London, United Kingdom;* [3]*Institute of Psychiatry, King's College London, London, United Kingdom. Contact e-mail: gaia.rizzo@gmail.com*

**Introduction**: Quantitative assessment of $A_{2A}$ receptor binding from [$^{11}$C]SCH442416 PET images in human brain has been made by using spectral analysis, revealing the presence of both reversible and irreversible components ([1],[2]). The aim of this study was to select the best methodology to quantify [$^{11}$C]SCH442416 kinetics at voxel level in healthy subjects, comparing standard methods versus data-driven and hierarchical approaches. **Materials and methods**: Five healthy subjects underwent a 90-min PET dynamic scan after a bolus injection of ~612 MBq of [$^{11}$C]SCH442416, complete with measured plasma input functions. Three-rate constant compartmental model in parallel (3K-parallel, [3]) was solved voxel-wise with Hierarchical Basis Function Method ([4]), where the prior information were obtained using both anatomical (atlas, HBFM-A) and functional information (unsupervised clustering, HBFM-C). A filtered version of the standard spectral analysis (Spectral Analysis with Iterative Filter (SAIF), [5]) was also applied at the voxel level. Volume of distribution voxel-wise estimates ($V_T$) were compared with those obtained with 3K-parallel model solved with weighted nonlinear estimator (WNLLS), corrected for failures and outliers before the comparison. **Results**: WNLLS applied voxel-wise required high computational time (up to x5 compared to the other methods) and on average more than 60% of the voxels were eliminated because not physiological (i.e. negative value and/or with estimation error >100%). All alternative methods showed good agreement in $V_T$ estimates (panel A), even if both HBFM-C methods and SAIF underestimated WNLLS results (mean relative difference ~5% and ~2% respectively, panel B). HBFM-C showed the highest correlation ($R^2$=0.91) and the smallest percentage of voxel out of bound (~13%). SAIF results presented good correlation ($R^2$=0.86) but more than 40% of outliers, probably due to not optimal settings of the filtering procedure. HBFM-A results showed the smallest correlation ($R^2$=0.57) and the higher mean relative difference (~7%). This effect was caused by the high tissue heterogeneity due to the notable vascular component present in all subjects, which could not be taken in account with the anatomical segmentation, but was partially overcome with a functional segmentation. **Conclusions**: WNLLS high computation time and poor image quality point to the necessity of an alternative method for voxel-wise quantification. Compared to the other methods, HBFM-C showed more accurate $V_T$ quantification with good quality parametric maps and excellent agreement with WNLLS results, as it allowed to take in account for the high vascular component in the tissues. Consequently HBFM-C was selected as the best alternative to the gold standard approach for voxel-wise quantification of [$^{11}$C]SCH442416 data and it is ready for clinical use. Good agreement of SAIF results with gold standard highlighted the method's potential as alternative valid quantification tool. **References**: [1] Hinz et al, Mol Imag Biol, 2003 [2] Ramlackhansingh et al, Neurology, 2011 [3] Galazzo et al, Neuroimage, 2010 [4] Rizzo et al, BrainPET conf 2011 [5] Veronese et al, JCBFM, 2010

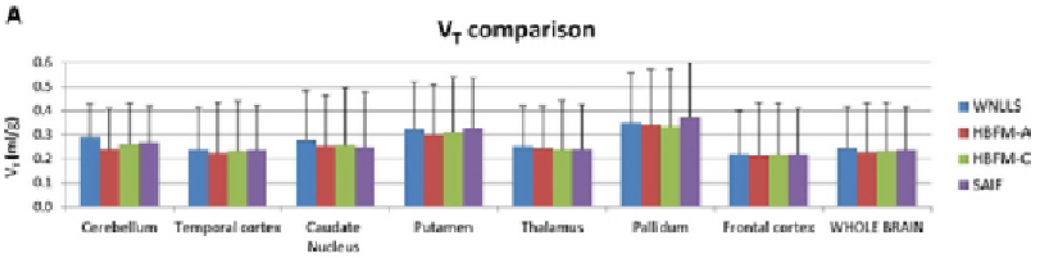


B

| Mean comparison: relative difference to WNLLS | | | |
|---|---|---|---|
| | HBFM-A | HBFM-C | SAIF |
| Mean | -7% | -5% | -2% |
| SD | 5% | 3% | 5% |
| Min | -18% | -11% | -11% |
| Max | 2% | -1% | 6% |

Comparison between WNLLS and other methodologies at the voxel level (variability expressed as between subjects SD) (A). Percentage relative difference of the mean values between subjects with regard to the gold standard (B).

Disclosure of author financial interest or relationships:
**G. Rizzo**, None; **M. Veronese**, None; **A.F. Ramlackhansingh**, None; **D.J. Brooks**, None; **F. Turkheimer**, None; **A. Bertoldo**, None.

Presentation Number **SS 133**
Scientific Session 19: Translational & Clinical - Neurology
September 7, 2012 / 13:36-13:48 / Room: Wicklow Hall 2

# Unique Pattern of [F-18]FDDNP PET Binding in Subcortical Structures Reflects Tau Neuropathology in Progressive Supranuclear Palsy and Separates it from Parkinson's Disease and Frontotemporal Lobe Degeneration

***Vladimir Kepe***[1], *Yvette Bordelon*[1], *Adam Boxer*[2], *(Henry) Sung-Cheng Huang*[1], *Jie Liu*[1], *Frederick C. Thiede*[1], *John C. Mazziotta*[1], *Mario F. Mendez*[1,3], *Natacha Donoghue*[1], *Gary W. Small*[1], *Jorge Barrio*[1], *[1]David Geffen School of Medicine, University of California at Los Angeles, Los Angeles, CA, USA; [2]Memory and Aging Center, Department of Neurology, University of California at San Francisco, San Francisco, CA, USA; [3]VA Greater Los Angeles Healthcare Center, Los Angeles, CA, USA. Contact e-mail: vkepe@mednet.ucla.edu*

Progressive supranuclear palsy (PSP) is a human tauopathy with insoluble hyperphosphorylated tau fibrillar aggregates found in neurons, astrocytes and oligodendrocytes. These pathological deposits are commonly found in basal ganglia, subthalamic nucleus, midbrain area and cerebellar white matter including deep nuclei. When cortical pathology is present, it appears predominantly in motor cortex and frontal lobe. The aim of this study was to determine in vivo pattern(s) of [F-18]FDDNP binding in PSP and to test if this these patterns would distinguish PSP from Parkinson's disease (PD) and frontotemporal lobar degeneration (FTLD), diseases with which PSP can be confused at early clinical stages. [F-18]FDDNP has ability to label Aβ plaques and tau aggregates in vivo. Methods: Fifteen patients with PSP, five patients with PD, five patients with FTLD, and five subjects without clinical signs of any neurodegenerative disorder received [F-18]FDDNP PET. [F-18]FDDNP distribution volume ratios (DVR), in reference to cerebellar gray matter, were determined for a set of cortical and subcortical areas and compared among the subject groups. Findings: PSP brain [F-18]FDDNP binding was predominantly found in subcortical areas (e.g., basal ganglia, thalamus, subthalamic area, midbrain and cerebellar white matter) and was consistent with the known subcortical distribution of pathology in PSP. Binding in several subcortical areas (e.g., midbrain) separated the PSP group from controls and patients with FTLD or with PD. Interpretation: [F-18]FDDNP is a sensitive in vivo PET imaging probe with ability to recognize tau pathology in PSP. [F-18]FDDNP PET may provide a tool to detect changes in tau pathology distribution associated with disease progression and distinguish different subtypes of PSP based on binding patterns.

Disclosure of author financial interest or relationships:
**V. Kepe**, None; **Y. Bordelon**, Teva, Speakers bureau; Lundbeck, Speakers bureau; Sonexa, Consultant; **A. Boxer**, None; **(. Huang**, None; **J. Liu**, None; **F.C. Thiede**, None; **J.C. Mazziotta**, None; **M.F. Mendez**, None; **N. Donoghue**, None; **G.W. Small**, POM Wonderful, Grant/research support; Lilly, Consultant; Novartis, Speakers bureau; Co-inventor of FDDNP, Other financial or material support; Novartis, Consultant; Forest, Speakers bureau; **J. Barrio**, None.

Presentation Number **SS 134**
Scientific Session 19: Translational & Clinical - Neurology
September 7, 2012 / 13:48-14:00 / Room: Wicklow Hall 2

# Optimizing Standardized Regional Brain Metabolic Biomarkers for Dementia-Related Cognitive Changes over Time: Which Regions and Which Times?

***Manogna Manne**, Kelsey Mason, Neel Raval, Daniel H. Silverman, Molecular and Medical Pharmacology, University of California, Los Angeles, Los Angeles, CA, USA. Contact e-mail: mnmanne@gmail.com*

Background: The Alzheimer's Disease Neuroimaging Initiative (ADNI) is a multi-center prospective longitudinal study involving over 50 centers throughout the United States and Canada, acquiring neuropsychologic, neuroimaging, and other biologic data on subjects with dementia, mild cognitive impairment, and normal cognition. As a measure of overall cognitive function, the Mini-Mental State Examination (MMSE) is the neuropsychologic test most used by primary medical doctors in the U.S. We previously found that visually identifiable patterns of regional cerebral metabolism accurately predict which patients will suffer significant decline in general cognitive abilities and in MMSE scores over the subsequent 3 years (Molec. Genet. Metab. 80:350-355). In the present study, we examine prospectively collected longitudinal MMSE and FDG-PET data to assess how closely the magnitude of cognitive change is paralleled by the magnitude of regional metabolic change in subjects having amnestic mild cognitive impairment (MCI, a major risk factor for subsequent development of AD), at the time of their enrollment in ADNI -- as well as the relative strength of that relationship over different time frames. Methods: A series of 140 ADNI subjects with MCI (clinical dementia rating, 0.5) underwent neuropsychological testing and FDG-PET brain scans at baseline and at 6 month intervals thereafter. Scans were regionally quantified by measurement of mean activities in 25 standardized volumes of interest, each normalized to mean brain activity. Changes in MMSE scores versus changes in regional metabolism for each subject were assessed over the first six months (0m to 6m), subsequent 18 months (6m to 24m, to potentially minimize impact of practice effects), and the entire 2-year period (0m to 24m), using the Pearson correlation coefficient (r) and single-sample Student t-test of significance for non-random association of variables, and results were considered significant only if $p<0.05$ after statistical correction for multiple comparisons. Results: Over the entire 2-year period, the single strongest regional metabolic biomarker for change in MMSE was found to lie in the bilateral superior temporal cortex ($p=0.00007$) followed by the bilateral associative visual cortex ($p=0.0002$), and a similar trend was observed for Broca's area ($p=0.006$). No significant improvement in the strength of the correlations was gained from elimination of any initial practice effect (6m to 24m time-frame data); nor were associations between MMSE and metabolic change over the first 6 months significant, after correcting for multiple-comparisons. Conclusion: In cognitively impaired subjects at increased risk of future development of AD, bilateral superior temporal cortical metabolism, as assessed by FDG-PET, serves as a highly significant biomarker of cognitive changes occurring over a 2-year (but not 6-month) period.

Disclosure of author financial interest or relationships:
**M. Manne**, None; **K. Mason**, None; **N. Raval**, None; **D.H. Silverman**, Cardinal Health, Consultant; PETNET, Consultant; Siemens Healthcare, Consultant; GE, Consultant; Bayer, Consultant; Lilly, Consultant; Philips, Consultant; co-inventor of NeuroQ, licensed by UC to Syntermed, Other financial or material support .

Presentation Number **SS 135**
Scientific Session 19: Translational & Clinical - Neurology
September 7, 2012 / 14:00-14:12 / Room: Wicklow Hall 2

# PET Measurement of α4β2* nAChR Density ($B_{max}$) and in vivo Affinity ($K_{Dapp}$) of [$^{18}$F]Nifene in the Nonhuman Primate

***Ansel Hillmer***[1], *Dustin W. Wooten*[1], *Maxim S. Slesarev*[1], *Elizabeth O. Ahlers*[1], *Todd E. Barnhart*[1], *Mary L. Schneider*[1], *Jogesh Mukherjee*[2], *Bradley T. Christian*[1], [1]*University of Wisconsin - Madison, Madison, WI, USA;* [2]*University of California - Irvine, Irvine, CA, USA. Contact e-mail: ahillmer@wisc.edu*

[$^{18}$F]Nifene, a PET radioligand agonist with high affinity for α4β2* nicotinic acetylcholine receptors (nAChR), exhibits favorable in vivo equilibration times for short scanning procedures. This work utilizes multiple injections of [$^{18}$F]nifene with partial saturating doses of nifene to measure both α4β2* nAChR density ($B_{max}$) and the apparent (in vivo) dissociation constant ($K_{Dapp}$) of [$^{18}$F]nifene for these receptors. Separately measuring $B_{max}$ and $K_{Dapp}$ provides a more robust quantitation of binding than the composite metric of binding potential ($BP_{ND}$ = $B_{max}/K_{Dapp}$) while also allowing for improved design of future experiments, particularly those which alter synaptic concentrations of nACh. Methods: A MicroPET P4 scanner was used to acquire dynamic PET data from five rhesus monkey subjects. A 120 minute, three injection protocol was used for three experiments while the other two consisted of a 105 minute, two injection protocol. Arterial blood sampling was performed throughout all experiments and corrected for radiolabeled metabolites to provide an arterial input function. Estimates of regional $B_{max}$ and $K_{Dapp}$ were obtained using a compartment model which accounted for the presence of unlabeled nifene. Regions examined include the antereoventral thalamus (AVT), lateral geniculate body (LG), frontal cortex (FC), and subiculum (SB). Results: Compartment modeling with a two injection protocol, introducing an unlabeled nifene dose ranging from 30% to 70% receptor occupancy in the second injection, was found to sufficiently uncouple $K_{Dapp}$ and $B_{max}$ with values comparable to those acquired with the three injection protocol. The highest levels of [$^{18}$F]nifene binding were observed in the thalamic regions of the AVT and LG, with respective $B_{max}$ values of 3.9 ± 1.4 and 3.4 ± 0.6 pmol/ml. Intermediate densities were observed in the FC and SB, with $B_{max}$ values of 0.9 ± 0.2 and 0.9 ± 0.3 pmol/ml, respectively. Averaged over all subjects, the $K_{Dapp}$ of [$^{18}$F]nifene at the α4β2* nAChR site was 2.2 ± 0.6 pmol/ml. Conclusion: [$^{18}$F]Nifene PET imaging with a multiple injection protocol can be used to measure α4β2* nAChR density. These results demonstrate the utility of extending work with [$^{18}$F]nifene to human subjects and disease-specific models.

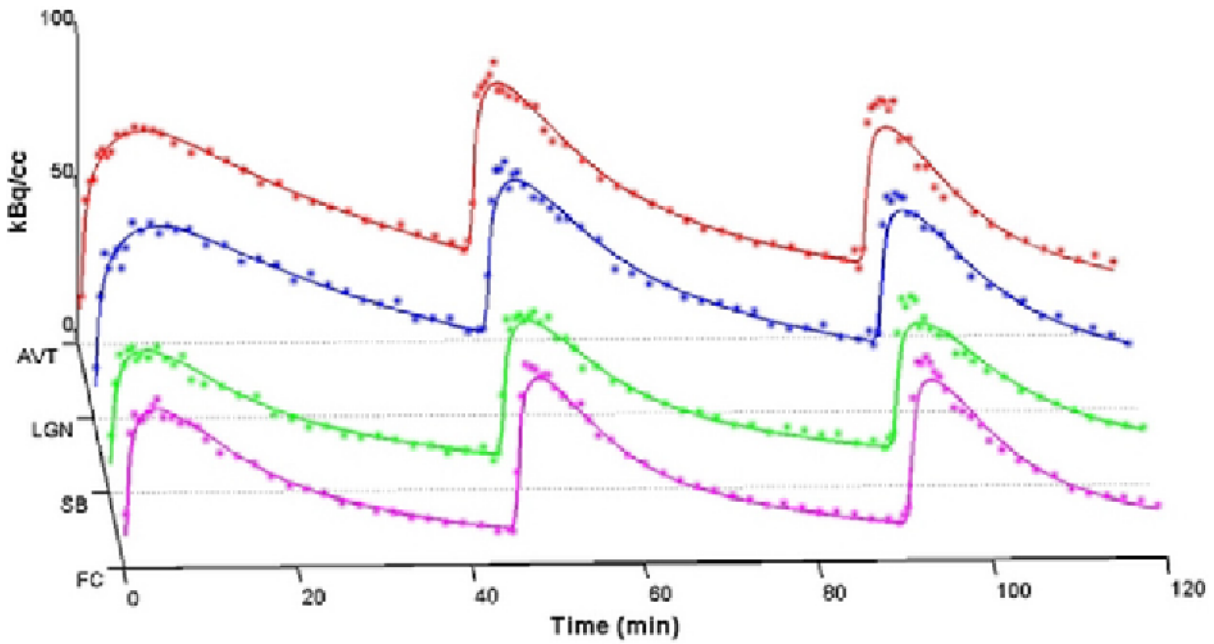


Compartment model fits for a three-injection experiment are shown for one subject in various brain regions yielding estimates of $B_{max}$ and $K_{Dapp}$.

Disclosure of author financial interest or relationships:
**A. Hillmer**, None; **D.W. Wooten**, None; **M.S. Slesarev**, None; **E.O. Ahlers**, None; **T.E. Barnhart**, None; **M.L. Schneider**, None; **J. Mukherjee**, None; **B.T. Christian**, None.

Presentation Number **SS 136**
Scientific Session 20: Preclinical In Vivo - Oncology
September 7, 2012 / 13:00-13:11 / Room: The Auditorium

# Multiparametric imaging based characterization of tumor heterogeneity developed in endogenous mouse models of pancreatic cancer

*Irina Heid[1], Marija Trajkovic-Arsic[2], Irene Esposito[3], Andreas Steingötter[4], Markus Schwaiger[6], Bernhard Haller[5], Ernst J. Rummeny[1], Jens Siveke[2], **Rickmer Braren**[1], [1]Institute of Radiology, Klinikum rechts der Isar, Technische Universität München, Munich, Germany; [2]2nd Department of Internal Medicine, Klinikum rechts der Isar, Technische Universität München, Munich, Germany; [3]Institute of Pathology, Klinikum rechts der Isar, Technische Universität München, Munich, Germany; [4]Division of Gastroenterology and Hepatology, University Hospital Zurich, Munich, Germany; [5]Institute for Medical Statistics and Epidemiology, Klinikum rechts der Isar, Technische Universität München, Munich, Germany; [6]Department of Nuclear Medicine, Klinikum rechts der Isar, Technische Universität München, Munich, Germany. Contact e-mail: rbraren@roe.med.tum.de*

Human pancreatic ductal adenocarcinoma (hPDAC) is highly heterogeneous in terms of morphology, tumor onset and response to treatment. Genetically engineered mouse models (GEMMs) mimic very well hPDACs and are valuable, predictive tools for preclinical research. The aim of this study was to identify markers that allow prediction of tumor type and response to therapy in humans using various GEMMs and clinically established methods. The multimodal imaging approach using multiparametric MRI and [$^{18}$F]-FDG-PET imaging allowed comprehensive characterization of tumor growth kinetics, tissue composition, perfusion and response to chemotherapies in several endogenous models with different PDAC features. Following genetically engineered mouse models of PDAC were used: *Ptf1a$^{wt/Cre}$(C)Kras$^{wt/LSL\text{-}G12D}$(K)Ela-Tgfa(T)*, *CK;p53(P)$^{wt/fl}$*, *CKP$^{fl/fl}$*, *CKTP$^{wt/R172H}$* and *CKTP$^{wt/fl}$*. Beginning at tumor onset animals were subjected to serial T2-weighted (T2w) diffusion weighted (DWI) and Dynamic Contrast Enhanced (DCE)-MRI employing a 1.5 T Achieva, Philips with a dedicated surface coil. Additionally, metabolic status of tumors was assessed by [$^{18}$F]-FDG-PET. In a subset of *CKP$^{fl/fl}$* mice therapy response to clinical standard of care chemotherapy Gemcitabine was monitored. Imaging data were validated by histopathology. GEMM employed in this study faithfully reflect the wide spectrum of hPDAC including precursor lesions (mIPMN and mPanIN). DWI allowed differentiation of mPanIN (> 1.2 *10$^{-3}$ mm$^2$/s), mIPMN (0.99 ± 0.02 *10$^{-3}$ mm$^2$/s), mPDACs with high stroma and ductal content (1.031 ± 0.02 *10$^{-3}$ mm$^2$/s), mPDACs with low stroma and ductal content (0.80 ± 0.01 *10$^{-3}$ mm$^2$/s) and highly cellular mPDACs with no stroma or ducts (0.67 ± 0.03 *10$^{-3}$ mm$^2$/s). Calculated apparent diffusion coefficients (ADC) showed good correlation with tissue cellularity ($r^2$ = 0.73) and collagen content ($r^2$ = 0.65), validating these findings. DCE-MRI data was highly heterogeneous and revealed major intraindividual differences between tumor regions. [$^{18}$F]-FDG tracer uptake tumor to muscle ratios (T/M) enabled differentitation of preneoplastic lesions (T/M < 3) and PDAC (T/M > 3), independent of the underlying genotype. Whereas allogeneic s.c. transplants showed universal response to Gemcitabine treatment, endogenous PDAC in *CKP$^{fl/fl}$* mice showed similarly poor response as hPDAC with only individual responders. These were identified by a decrease in growth rate and reduced [$^{18}$F]-FDG uptake as well as prolonged survival. Single slice-based analysis revealed a decrease in T/M ratio up to 30% 4 days post therapy start. However 11 days post therapy all tumors relapsed and [$^{18}$F]-FDG uptake further increased. Opposite was observed for ADC values. Here we provide evidence that morphological heterogeneity of mPDAC is well modeled with GEMMs and identifiable with multimodal multiparametric imaging. The tissue structure related parameter ADC is identified as a sensitive marker of tumor heterogeneity. The combined evaluation of tumor growth, [$^{18}$F]-FDG tracer uptake and ADC value identified individual therapy responders.

Disclosure of author financial interest or relationships:
**I. Heid**, None; **M. Trajkovic-Arsic**, None; **I. Esposito**, None; **A. Steingötter**, None; **M. Schwaiger**, Siemens Medicial Solutions, Speakers bureau; Siemens Medical Solutions, Consultant; General Electrics Healthcare, Grant/research support; Lantheus, Grant/research support; **B. Haller**, None; **E.J. Rummeny**, None; **J. Siveke**, None; **R. Braren**, None.

Presentation Number **SS 137**
Scientific Session 20: Preclinical In Vivo - Oncology
September 7, 2012 / 13:11-13:22 / Room: The Auditorium

# Development of a multi-modality imaging pipeline for the interrogation of phenotypic differences in the tumor microenvironment of patient-derived colon cancer xenografts

***Trevor D. McKee***[1], *Douglass C. Vines*[1,2], *David E. Green*[1], *David A. Jaffray*[1,2], *Brad Wouters*[1,2], [1]*STTARR Innovation Centre, Ontario Cancer Institute, Toronto, ON, Canada;* [2]*Radiation Oncology, University of Toronto, Toronto, ON, Canada. Contact e-mail: Trevor.McKee@rmp.uhn.on.ca*

**Introduction:** Primary human tumors grown as xenografts in immunodeficient mice provide a powerful tool to capture the genetic diversity present in the patient population, offering a more robust therapeutic model than the limited number of cell lines available. We have developed a population of colon cancer xenografts derived from patients with primary and metastatic disease. We established a preclinical imaging pipeline to assess the tumor microenvironmental of these models, in order to: i) compare xenografts with primary patient material; ii) assess if imaging could identify features distinguishing patient tumors from each other, and iii) assess the reliability and repeatability of multi-modality imaging to determine whether these parameters may be genetically determined. **Methods:** Tumor xenografts were serially passaged in vivo subcutaneously, and imaging was initiated once they reached a size of at least 200mm3. Contrast-enhanced CT was performed on a GE Locus Ultra MicroCT system, followed by 18F-FDG PET imaging using a Siemens Focus 220 scanner. Subsequent to this imaging, mice were injected with EF5 (IP), EdU (IP) and Hoechst 33342 (via tail vein), in order to label the hypoxic, proliferating, and perfused regions of the tumor, respectively. Tumors were snap frozen for immunofluorescence analysis, and dissociated for flow cytometric analysis. Image analysis and co-registration was performed using Siemens Inveon Research Workplace (PET), ClearCanvas and the DCE Tool (contrast-enhanced CT), and Definiens Tissue Studio (immunofluorescence). **Results:** This pipeline of multi-modality imaging has been successfully performed on over 50 mice, spanning 20 distinct patient-derived xenograft models. Immunofluorescence staining was performed on whole tumor sections, with images captured on a Huron Technologies Tissuescope confocal macroscope. Quantitative analysis of FDG-PET images to calculate mean and maximum % injected dose per gram has shown low intra-group variance within each patient-derived xenograft, with more significant differences across different patient-derived models than within. Immunofluorescence and flow cytometry data agree with one another in terms of the amount of hypoxia (EF5) and proliferation (EdU) staining measured within each tumor, again with low intra-group variance in comparison to differences across tumor xenografts. Quantitation of parameters in dynamic contrast CT (based on the Modified Tofts algorithm) resulted in a high variance between individual mice, both within and across patient-derived xenograft groups; however it was unclear whether this derived from biological or technical differences, due to low signal-noise ratio and poor perfusion of tumor regions in general. In conclusion, we have established the feasibility of a unique microenvironment imaging pipeline, and used it to classify a cohort of colon cancer xenografts. Future work will establish the phenotype information associated with specific cancer genotypes, in order to identify parameters of potential clinical utility, and inform the future application of personalized medicine in this disease.

Disclosure of author financial interest or relationships:
**T.D. McKee**, Pfizer, Grant/research support; Molecular Insight Pharmaceuticals, Grant/research support; **D.C. Vines**, None; **D.E. Green**, None; **D.A. Jaffray**, Precision X-ray, Other financial or material support; Raysearch, Grant/research support; Philips, Grant/research support; Elekta, Grant/research support; General Electric, Grant/research support; IMRIS, Other financial or material support; Modus Medical, Grant/research support; **B. Wouters**, Pfizer, Grant/research support; Molecular Insight Pharmaceuticals, Grant/research support .

Presentation Number **SS 138**
Scientific Session 20: Preclinical In Vivo - Oncology
September 7, 2012 / 13:22-13:33 / Room: The Auditorium

# *In vivo* characterization of mammary tumor phenotypes in the endogenous PyV-mT mouse model using non-invasive imaging modalities

***Jennifer Schmitz***[1], *Andreas Schmid*[1], *Christoph M. Griessinger*[1], *Manfred Kneilling*[2], *Bernd J. Pichler*[1], [1]*Department of Preclinical Imaging and Radiopharmacy, Eberhard Karls University of Tuebingen, Tuebingen, Germany;* [2]*Department of Dermatology, Eberhard Karls University of Tuebingen, Tuebingen, Germany. Contact e-mail: Jennifer.Schmitz@med.uni-tuebingen.de*

**Objective**: In the endogenous mammary tumor virus-long term repeat polyoma virus middle T transgenic (PyV-mT) mouse model, various tumors develop spontaneously along the mammary glands. PyV-mT transgenic mice develop a high variety of phenotypes in early neoplasia as well as in mature tumors. In addition, in all these tumors, the same signaling pathways are activated as in ErbB2 related human breast cancer. Thus, the PyV-mT mouse model is an appropriate candidate to investigate the basics of ErbB2 related breast cancer and the basic mechanisms of phenotype formation. In this study, we address the different phenotypes non-invasively by using sequential PET/MRI. To characterize the tumors as detailed as possible and yield finally a holistic tumor profile a great variety of imaging biomarkers, for both, PET and MRI, was employed. Beside glucose metabolism, we investigated hypoxia, angiogenesis, vessel leakage, as well as proliferation and amino acid metabolism. **Methods**: 5 C57BL/6 PyV-mT mice at the age of 16 weeks were scanned in a sequential PET/MRI setup within two weeks. The animals were anesthetized with isoflurane evaporated in breathing air and injected intravenously with 275±74 MBq of [$^{18}$F]FDG, [$^{18}$F]FAZA, [$^{68}$Ga]NODAGA-RGD, [$^{18}$F]FLT, [$^{11}$C]Choline, [$^{11}$C]Methionine or 0.3 mM/kg Gd-DTPA, respectively. Imaging was performed on temperature controlled animal beds, allowing sequential PET/MRI using dedicated small animal scanners. Anatomical information was measured with a 3D T2-weighted turbo spin echo in MRI, directly followed by the PET measurements. For in vivo data analysis the corresponding images were fused and volumes of interest covering the entire lesion were drawn in the anatomical MRI data. The absolute uptake values (%ID/cc), as well as the standardized uptake value and the tumor-to-muscle ratios (TMR) of all detected lesions were calculated. Following the last measurement, the animals were sacrificed and the tumors were removed and prepared for histology. **Results**: Analysis of MRI data revealed lesions from 3.4 to 194.3 mm$^3$. PET tracer uptake varied strongly for all tracers in individual lesions. Tracer uptake and lesion size did not correlate for any investigated biomarker. While the evaluation of [$^{18}$F]FAZA showed no signs of hypoxia (mean TMR<0.90), increased angiogenesis could be detected by [$^{68}$Ga]NODAGA-RGD. [$^{18}$F]FLT revealed no proliferation signals in any lesion (mean TMR<0.97), whereas [$^{11}$C]Choline showed increased TMR for all lesions. Histology identified tumors as well as hyperplasia. The individual imaging data were cross-correlated yielding a link between individual imaging parameters. **Conclusion**: In the PyV-mT mouse model, PET tracer uptake varies strongly with individual tumors, making a reliable evaluation of PET tracer uptake only feasible in combined PET/MRI studies. Based on histological information, lesions are classified and the corresponding PET data are used to characterize lesion status *in vivo*. The ability of hyperplasia detection at an early time point in cancerogenesis by MRI and PET reveals great potential of the investigated setup for further longitudinal studies to investigate phenotype development.

Disclosure of author financial interest or relationships:
**J. Schmitz**, None; **A. Schmid**, None; **C.M. Griessinger**, None; **M. Kneilling**, None; **B.J. Pichler**, Siemens, Grant/research support; AstraZeneca, Grant/research support; Bayer Healthcare, Grant/research support; Boehringer-Ingelheim, Grant/research support; Oncodesign, Grant/research support; Merck, Grant/research support; Bruker, Grant/research support .

Presentation Number **SS 139**
Scientific Session 20: Preclinical In Vivo - Oncology
September 7, 2012 / 13:33-13:44 / Room: The Auditorium

# Mining Lipid Signatures in a Breast Tumor Model by Combining Magnetic Resonance Spectroscopic Imaging and Mass Spectrometric Imaging

***Lu Jiang***[1], *Kamila Chughtai*[2], *Tiffany R. Greenwood*[1], *Gert Eijkel*[2], *Ron M. Heeren*[2], *Kristine Glunde*[1], [1]*Russell H. Morgan Department of Radiology and Radiological Science, Johns Hopkins University School of Medicine, BALTIMORE, MD, USA;* [2]*FOM-Institute AMOLF, Amsterdam, Netherlands. Contact e-mail: ljiang12@jhmi.edu*

Introduction:Intensity of total choline (tCho) peak in magnetic resonance spectroscopic imaging (MRSI) of tumors is elevated and spatially heterogeneous [1]. In vivo H1 MRSI at high spatial resolution to resolve phosphocholine (PCho), glycerophosphocholine (GPC), and free choline (Cho), forming the tCho signal, is currently unavailable. Mass spectrometry imaging (MSI) can detect the spatial distribution of these metabolites and thousands of other molecules from tissue surface. We studied correlations between tCho, small molecules and phosphatidylcholine (PC) species in a human breast cancer model by combining in vivo MRSI with ex vivo MSI. Methods:MDA-MB-231 breast cancer cells were grown in nude mice. MRSI to detect metabolites was performed on tumors in vivo. Each tumor was cryo-sectioned to perform Matrix-assisted laser desorption ionization (MALDI) MSI on a Q-TOF instrument [2, 3] to detect small molecules, lipids and proteins. We fused MRSI and MSI images based on fiducial markers and tumor shape characteristics [4]. The 3D tCho volume was segmented high-tCho (above 10% of the area under the histogram) and low-tCho area. 1545 high- and 1847 low-tCho voxels were randomly selected, followed by principal component analysis (PCA) to reduce the noise of MALDI data. 90% variance of PCA projection data was analyzed by linear discriminant analysis (LDA) to classify high- and low-tCho voxels. Loading spectra of discriminant function 1 (DF1) were sorted to select candidate m/z peaks, which mostly contributed to the differentiation between high- and low-tCho voxels. The m/z peak candidates were structurally identified by MS/MS methods. Results:tCho (3.2 ppm) was observed by MRSI (Fig. A (1)). PCho (m/z 184.1) and membrane phospholipid species (m/z 893.4, m/z 881.4) displayed the highest peaks in the DF1 loading spectrum. Fig. B shows DF1 loading spectrum, Fig. C shows the scattering plot of DF1 and 2 scores in the classification, Fig. D lists candidate m/z peaks.Discussions:The fact that PCho with m/z 184.1 [5], which is the predominant metabolite giving rise to the tCho signal, showed a high rank validates our method for identifying MALDI peaks in MSI based on the corresponding registered MRSI data of the same tumor. The molecular ions at m/z 881.4, 893.4, 825.5, 845.4, 894.5, and 880.4 were identified as membrane PC lipid species that negatively correlated with both the tCho map in MRSI and the PCho map of m/z 184.1 in MALDI. This finding suggests that high tCho and PCho regions may be partially caused by increased breakdown or reduced biosynthesis of those specific PCs. By combining MRSI with MALDI MSI followed by multivariate analysis, we identified for the first time distinct PC species that are either broken down or undergo reduced biosynthesis in breast tumor regions that contain high tCho. References: [1]. Glunde et al., NMR Biomed 24(6):673-90; [2]. Luxembourg et al., Anal Chem 76: 5339-44. [3]. Luxembourg et al., Rapid Commun Mass Spectrom 20: 3435-42. [4]. Jiang et al. (2011), Abstract #959, ISMRM Annual Conference. [5]. Amstalden et al., Cancer Research 70(22): 9012-21. Acknowledgements This work was supported by NIH R01 CA134695.

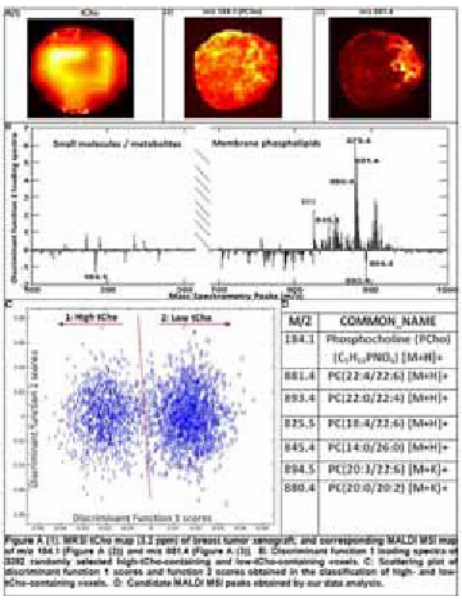


Disclosure of author financial interest or relationships:
**L. Jiang**, None; **K. Chughtai**, None; **T.R. Greenwood**, None; **G. Eijkel**, None; **R.M. Heeren**, None; **K. Glunde**, None.

Presentation Number **SS 14**
Scientific Session 2: Technology & Software - Optical Imaging
September 6, 2012 / 11:25-11:36 / Room: Wicklow Hall 1

# Kinetics Analysis of Optical Markers in Multiple Organs Using Multispectral Optoacoustic Tomography (MSOT)

***Stefan Morscher***[1,2], *Wouter H. Driessen*[1], *Neal Burton*[1], *Adrian Taruttis*[2], *Vasilis Ntziachristos*[2], *Daniel Razansky*[2], [1]*iThera Medical GmbH, Neuherberg, Germany;* [2]*Institute for Biological and Medical Imaging, Helmholtz Zentrum München and Technische Universität München, Munich, Germany. Contact e-mail: stefan.morscher@ithera-medical.com*

Low overall tissue absorbance of photons promotes optical imaging in the near-infrared (NIR) range, especially for deep tissue in vivo imaging. Here, conventional optical imaging suffers from low spatial resolution and long acquisition times, while multispectral optoacoustic tomography (MSOT) offers fast imaging of optical contrast at high spatial resolution inherent to ultrasound signal detection. Individual absorbers in tissue can be isolated from the acquired data set using multiple excitation wavelengths, enabling a rich portfolio of biomedical applications with clinical settings readily within reach. Image acquisition at a rate of 10 images per second permits the collection of a multispectral data set of a single, cross-sectional slice within seconds. Multispectral unmixing reveals the biodistribution of several absorbers with distinct spectral absorption profiles, both tissue-intrinsic (e.g. hemoglobin, melanin) and extrinsic (e.g. fluorescent dyes and probes, gold nanoparticles). These methods allow the separation of multiple injected probes at the same time and without the necessity of a baseline scan before administration of the agents. Verification of the results is achieved using ex vivo cryoslice imaging in a cryostat that is equipped with the possibility to take color and fluorescence photographs of the mouse body, creating cross-sectional images that are comparable with the ones acquired using MSOT. Herein we present a non-invasive in vivo study of kinetic processes in mice in multiple organs. To demonstrate the ability of MSOT to separate absorbers with a temporal resolution of seconds we tracked fluorescent dyes in a number of scenarios. In order to observe gastric emptying in an anesthesized animal, ICG was administering via oral gavage. Subsequent imaging was able to reveal the steady removal of the dye from the stomach area. Excellent correlation between the resulting curves for multiple constellations of previous fastening and administered agent concentrations and ex vivo validation could be established. In other experiments, selected areas in kidneys, liver and spleen underwent the measurement procedure, allowing successful visualization of the clearance kinetics of the injected substances over time. Monitoring of selected regions of interest shows distinct pharmacokinetic behavior for each probe in excellent accordance with ex vivo fluorescence imaging. These results prove MSOT as a powerful imaging modality that has the potential of revolutionizing the field of biomedical imaging, enabling a large variety of applications in monitoring therapeutic efficacy and assisting drug development. A key strength emphasized here, lies in tracking multiple injected substances within one measurement.

Disclosure of author financial interest or relationships:
**S. Morscher**, iThera Medical GmbH, Employment; **W.H. Driessen**, iThera Medical, Employment; **N. Burton**, iThera Medical, Employment; **A. Taruttis**, None; **V. Ntziachristos**, ERC, Grant/research support; Ithera Medical, Stockholder; **D. Razansky**, iThera Medical GmbH, Stockholder .

Presentation Number **SS 140**
Scientific Session 20: Preclinical In Vivo - Oncology
September 7, 2012 / 13:44-13:55 / Room: The Auditorium

# A Novel CT/PET Agent to Characterize Heterogeneity in Intratumoral Distribution of Nanoparticles with Extended Detection Sensitivity Range

***Jinzi Zheng***[1,2], *Linyu Fan*[1,2], *Yannan Dou*[3], *Christine Allen*[1,3], *David A. Jaffray*[1,2], [1]*STTARR Innovation Centre, Princess Margaret Hospital, Toronto, ON, Canada;* [2]*Radiation Medicine Program, Princess Margaret Hospital, Toronto, ON, Canada;* [3]*Pharmaceutical Sciences, University of Toronto, Toronto, ON, Canada. Contact e-mail: jinzi.zheng@rmp.uhn.on.ca*

**Introduction:** Nanoparticles are increasingly being explored for delivery of chemotherapeutics to tumors. The effectiveness of nano-therapeutics is correlated to their ability to overcome delivery obstacles associated with the heterogeneous tumor microenvironment. The labeling of these nanocarriers with imaging probes is highly desirable as it allows for non-invasive assessment of their accumulation dynamics and spatial distribution at the tumor site. A novel $^{64}$Cu-iodine liposome system has been developed for PET and CT-based characterization of heterogeneity in intratumoral distribution with extended detection sensitivity range (pM to mM). **Results:** Five purified batches of liposomes encapsulating iohexol and DOTA were prepared with an iodine concentration of 47.2±4.3 mg/mL and a mean diameter of 90.1±5.4 nm. $^{64}$Cu from 5 different production runs were loaded into the DOTA-iohexol containing liposomes with a loading efficiency of 95.3±2.5 %. The $^{64}$Cu-labeled iodinated liposomes (Fig. S1a) exhibited an unchanged in vivo pharmacokinetics profile with a vascular $t_{1/2}$ of 17.8±1.1 h (n=4) compared to iohexol-containing liposomes ($t_{1/2}$=18.4±2.4 h, n=3) in mice. Following i.v. administration of $^{64}$Cu-iodine liposomes (0.4 mg/g of I and 10 µCi/g of $^{64}$Cu) to mice bearing orthotopic ME-180 cervical tumors (n=9), the peak overall tumor accumulation was observed at 49 h p.i. (Fig. 1). Analysis of 6 sub-volumes (Fig.S1b) within each tumor indicated higher peripheral liposome accumulation at all imaging time points (75min, 17h and 49h p.i.). Specifically for the animal shown in Fig.1, the mean $^{64}$Cu activity measured using PET in the different tumor sub-regions over 49 h ranged between 1590 and 13000 Bq/mL (decay corrected to the start of imaging), while the mean CT attenuation in the same sub-volumes ranged between 97.7 and 118.3 HU. A good correlation ($R^2$ =0.93, 18 data pairs, Fig. S1c) was found between the mean PET signal and the mean CT signal values measured in the 6 tumor sub-volumes across the 3 time points. At 75 min p.i., PET is able to more sensitively detect low concentrations of $^{64}$Cu-iodine liposomes (<100 HU). The benefit of having a CT agent is that it allows for fast (16-sec acquisition time for a whole body mouse scan) and longitudinal monitoring (beyond 4 physical half-lives of $^{64}$Cu) of liposome distribution in tumors. Furthermore, both pre-clinical and clinical CT systems have significantly higher spatial resolution than PET systems allowing for detection of sub-mm lesions and accurate localization of regions of high heterogeneity in contrast uptake. Fig.1 illustrates the ability of µCT (154 µm voxel size) to enable identification of contrast enhanced vascular structures at the tumor site. **Conclusion:** Liposomes have been successfully employed as drug delivery systems for cancer treatment. Effective labeling of actively or passively targeted liposome systems with imaging agents enables non-invasive assessment of their tumor targeting performance. The $^{64}$Cu-iodine liposomes reported here allow for PET and CT-based assessment of spatially heterogeneous nanoparticle distribution in tumors with an extended detection sensitivity range.

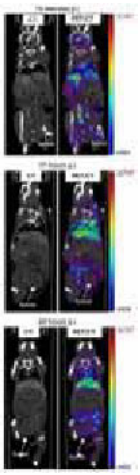

Figure 1. CT and CT/PET images of the same mouse bearing the orthotopic ME-180 cervical xenograft (white arrow) acquired at 75 minutes, 17 and 49 hours post 64Cu-iodine liposome administration (0.4 mg/g of iodine and 10 µCi/g of $^{64}$Cu). The red stars (*) indicate three visible vessels located in the periphery of the tumor. Liposomes are likely extravasated into the tumor interior from these and other feeding vessels.

Disclosure of author financial interest or relationships:
**J. Zheng**, None; **L. Fan**, None; **Y. Dou**, None; **C. Allen**, None; **D.A. Jaffray**, Precision X-ray, Other financial or material support; Raysearch, Grant/research support; Philips, Grant/research support; Elekta, Grant/research support; General Electric, Grant/research support; IMRIS, Other financial or material support; Modus Medical, Grant/research support .

Presentation Number **SS 141**
Scientific Session 20: Preclinical In Vivo - Oncology
September 7, 2012 / 13:55-14:06 / Room: The Auditorium

# In Vivo Bioluminescence Imaging For The Study Of Intra-Tumoural Bacteria

*Michelle Cronin[1], Sara A. Collins[2], Cormac Gahan[3], Kevin P. Francis[4], **Mark Tangney**[1], [1]Cork Cancer Research Centre, University College Cork, Cork, Ireland; [2]School of Medicine, UCLA, Los Angles, CA, USA; [3]Department of Microbiology and Alimentary Pharmabiotic Centre, University College Cork, Cork, Ireland; [4]Caliper - a PerkinElmer Company, Alameda, CA, USA. Contact e-mail: m.tangney@ucc.ie*

The ability to track microbes in real time in vivo is of enormous value for preclinical investigations in infectious disease or gene therapy research. Real-time in vivo analysis of reporter gene expression empowers the investigator with the ability to non-invasively assess gene delivery over time, as well as host responses to vector administration and therapeutic interventions. Bacteria present an attractive class of gene vector for cancer therapy, since it has been shown that many bacteria are naturally capable of homing to tumours when systemically administered, resulting in high levels of replication locally. Bacterial vectors engineered to express bacterial luciferase (lux) may be imaged in vivo by BioLuminescence Imaging (BLI). This study examines the intra-tissue growth of various lux-labelled bacteria in live mice both two and three-dimensionally using in vivo BLI and μCT co-registration. In this study, the non-pathogenic commensal bacteria E.coli K-12 MG1655 and Bifidobacterium breve UCC2003, or Salmonella Typhimurium SL7207 each expressing the luxABCDE operon were intravenously (IV) administered to mice bearing subcutaneous (s.c.) FLuc-expressing xenograft tumours. Bacterial lux signal was detected specifically in tumours of mice post IV-administration and bioluminescence correlated with the numbers of bacteria recovered from tissue. Through whole body imaging for both lux and FLuc (whose wavelengths are distinguishable on IVIS), bacteria and tumours were co-localised. Co-registration of 3D BLI and μCT facilitated the anatomical positioning of bioluminescent signal sources within the tumour, in addition to visualisation of tumour vasculature through administration of a contrast agent, revealing a pattern of multiple clusters of bacteria within tumours. Investigation of spatial resolution of 3D optical imaging was supported by ex vivo fluorescence histological analyses. This study demonstrates the potential to simultaneously image multiple BLI reporter genes three dimensionally in vivo using approaches that provide unique information on spatial locations.

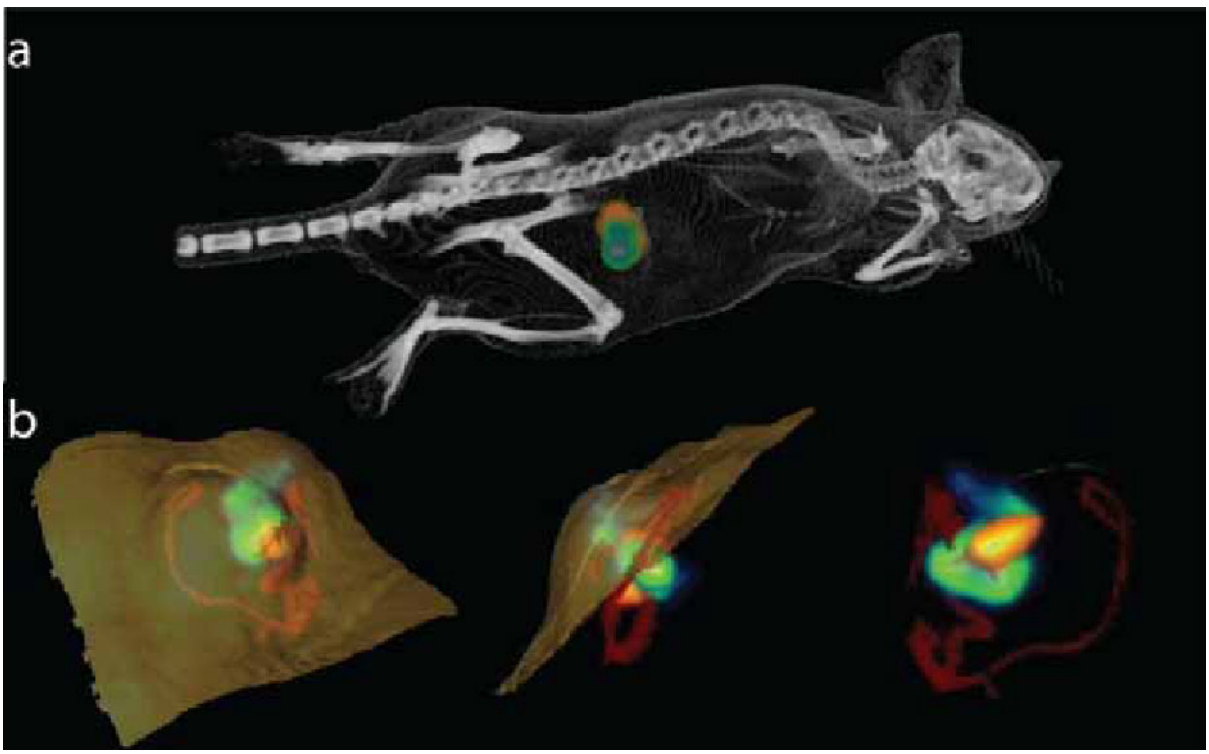


(a) Scan of live mouse (using a combination of 3-dimensional bioluminescence and microCT) revealing location of both bacteria and tumour. (b) Lower image shows, from 3 different rotational views, a magnification of the tumour in a, revealing the precise location of live bacteria (orange/yellow) within the tumour (green/blue) and the tumour's main blood supply (red). From Cronin et al. PLoS One 7 (1):e30940, 2012

Disclosure of author financial interest or relationships:
**M. Cronin**, None; **S.A. Collins**, None; **C. Gahan**, None; **K.P. Francis**, None; **M. Tangney**, None.

Presentation Number **SS 142**
Scientific Session 20: Preclinical In Vivo - Oncology
September 7, 2012 / 14:06-14:17 / Room: The Auditorium

# Functional PET imaging of Oxidative Stress

***Jack M. Webster***[1], *Bruce F. Johnson*[1], *Kevin P. Kent*[1], *Brian D. Lee*[1], *Michael J. Rishel*[1], *Hua Yang*[2], *Paul Schaffer*[2], [1]*GE Global Research, Niskayuna, NY, USA;* [2]*Nuclear Medicine, TRIUMF, Vancouver, BC, Canada. Contact e-mail: jwebster1@nycap.rr.com*

**Introduction:** Oxidative stress has been implicated in a wide variety of chronic conditions including cancer, diabetes, cardiovascular and neurodegenerative diseases. Therefore, development of an oxidative stress PET imaging agent could have wide clinical application. We've developed a PET tracer substrate of the cystine-glutamate transporter (System $x_c^-$), a biomarker with low expression in most normal tissues but upregulated under conditions of cellular oxidative stress. While L-cystine and L-glutamate are both natural substrates for this transporter, we decided to pursue analogs with similarities to L-cystine because it is the primary influx substrate; whereas glutamate is primarily utilized as an efflux substrate and brings potential cross-reactivity with a multitude of glutamate receptors and transporters. L-aminosuberic acid (L-ASu) is a good substrate of the cystine-glutamate transporter, exhibiting better cellular uptake than L-glutamate. We've developed an analog of L-aminosuberic acid, [$^{18}$F]-5-fluoro-L-aminosuberic acid ([$^{18}$F]-FASu), as a PET tracer specific for uptake by System $x_c^-$. **Methods:** [$^{18}$F]-FASu was synthesized by direct nucleophilic incorporation of [$^{18}$F]F- onto a tosylate precursor and evaluated as a novel PET tracer for preclinical imaging of tumor xenografts. Quantitative biodistribution and microPET imaging studies were conducted on nude mice bearing tumor xenografts. **Results:** Renal clearance was observed to be the primary excretion pathway, while the tracer exhibited low non-specific uptake in other organs. Pancreas, spleen and stomach uptake was observed, consistent with reports of constitutive expression of the cystine-glutamate transporter in these organs. Quantitative biodistribution data showed excellent EL4 tumor retention (~5 %ID/g) between 5 minutes and 2 hours post injection with tumor-to-blood ratios of ~10 and tumor-to-muscle ratios of ~20 at 1 hour PI. These results translated well to preclinical PET imaging which showed excellent visualization of tumor xenografts with low background signal. **Conclusions:** [$^{18}$F]-FASu is a novel PET tracer for in vivo functional imaging of a cellular response to oxidative stress conditions. Our data suggests [$^{18}$F]-FASu is a promising agent for cancer imaging and may have relevance in imaging many other pathological conditions or diseases that include oxidative stress.

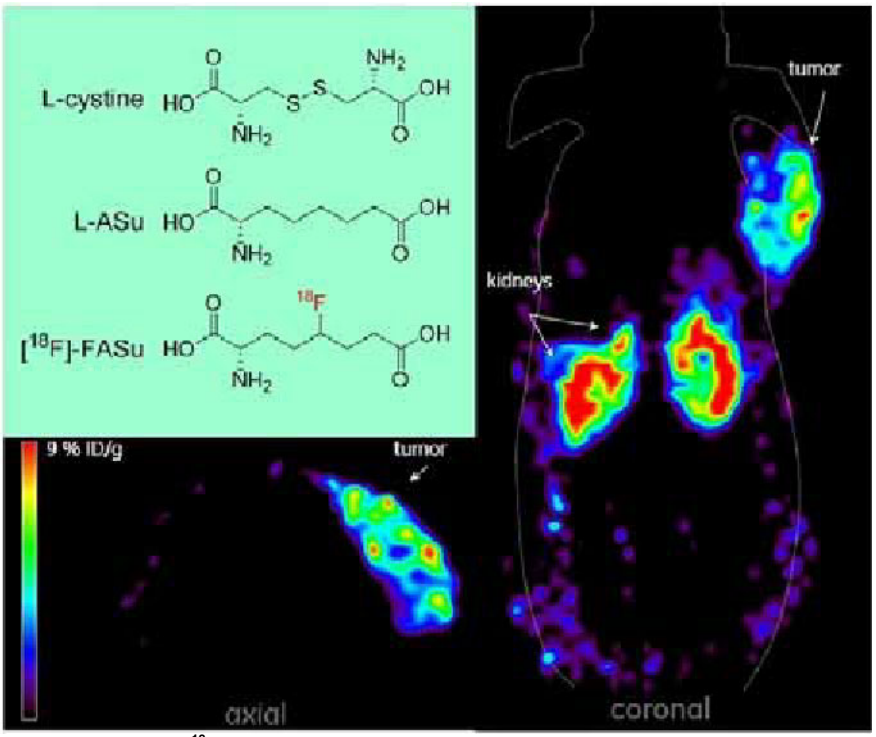


**Preclinical Imaging of a tumor xenograft with [$^{18}$F]-FASu** at 1 hour post injection. Nude mice bearing EL4 tumor xenografts were injected with ~250 µCi of [$^{18}$F]-FASu. Representative coronal and axial slices of the reconstructed images are shown.

Disclosure of author financial interest or relationships:
**J.M. Webster**, General Electric, Employment; **B.F. Johnson**, General Electric, Employment; **K.P. Kent**, None; **B.D. Lee**, GE, Employment; **M.J. Rishel**, General Electric, Employment; **H. Yang**, None; **P. Schaffer**, General Electric Global Research, Grant/research support .

Presentation Number **SS 143**
Scientific Session 20: Preclinical In Vivo - Oncology
September 7, 2012 / 14:17-14:28 / Room: The Auditorium

# Intravital Microscopy of Inguinal Lymph Node Reveals Novel Cell Burst Phenomena in Lymphoma

***Bryan R. Smith**, Ken Ito, Masakatsu Kotsuma, Sanjiv S. Gambhir, Radiology/Molecular Imaging, Stanford University, Stanford, CA, USA. Contact e-mail: brsmith@stanford.edu*

Non-Hodgkin's Lymphoma is a heterogeneous and highly disseminated disease. We demonstrated the existence of a "burst effect" in the middle stages (around day 9) of lymphoma development in the Eμ-myc/Arf-/- (EGFP and luciferase transfected, termed EL-Arf-/-) mouse model using an integrated set of serial intravital microscopic imaging and bioluminescence imaging experiments. The burst effect is a sudden huge efflux of lymphoma cells from spleen and bone marrow (BM), concomitant with influx of cells into the peripheral lymph nodes. This efflux may impact human disease, as clinical diseases such as splenic marginal zone lymphoma and Chronic Lymphocytic Leukemia (CLL) display similar pathology and characteristics. However, it is critical to understand the underlying mechanisms of the burst using imaging in order to render this discovery useful for human disease care. Our experiments and literature evidence led us to hypothesize the involvement of the Angiotensin II (Ang II) peptide in the burst effect. In this study we performed a series of experiments that implicates Ang II in the efflux of lymphoma cells. We demonstrated that direct infusion of Ang II (2.5 mg/kg) into mice (N=5/group) with tumors caused lymphoma cell efflux from spleen and BM and an influx of lymphoma cells into the inguinal lymph node (see figure). Intriguingly, we observed that serum AngII levels significantly decreased after the burst effect, correlating with down-regulation of Angiotensin Converting Enzyme (ACE), which produces Ang II from Ang I ($p<0.05$). We also observed an acute change in high blood pressure (EL-Arf-/- injected-mice: 134.3±7.7 mmHg (systolic), control mice: 107.8±1.3 (systolic) ($p<0.000002$)) in each mouse between 7-13 days after tumor initiation as a secondary event associated with the burst effect (N=7/group). Furthermore, we identified that Reactive Oxygen Species (ROS) production and angiotensinogen levels were up-regulated on day 8 (immediately before efflux) in mice. These data collectively suggest there is a positive feedback loop with Ang II triggering lymphoma efflux. Finally, we showed that an antagonist of the Angiotensin II receptor, Type I (AT-1 receptor), Losartan, prevented efflux of a significant number of lymphoma cells from spleen ($p<0.05$) compared to controls (N=7/group). Together, these results indicate that lymphoma efflux from spleen and BM is controlled via the AngII pathway. Our data indicates that cells home initially to the spleen and bone marrow. There they proliferate, until they reach a certain density (density data obtained in culture and using IHC from mice), at which point the NF-kB pathway is activated. Serum AngII levels correlate with ACE levels in lung by ELISA and Western Blot. This induces a molecular increase in AngII which biochemically stimulates all lymphoma cells to efflux from their sites, enabling them to reach the vasculature and seed remote sites. These results indicate that lymphoma efflux from spleen and BM is controlled via the AngII pathway, and blockage of this signal could delay or inhibit metastatic invasion to remote sites in human patients, thereby bringing clinical benefit to lymphoma patients.

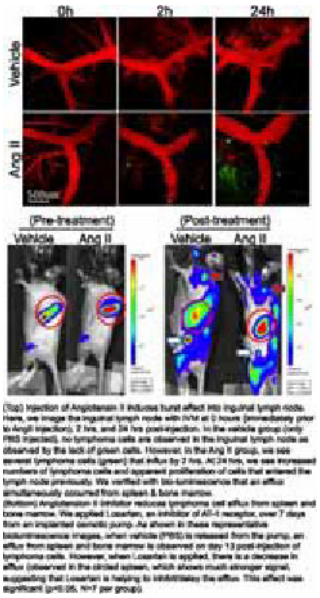


Disclosure of author financial interest or relationships:
**B.R. Smith**, None; **K. Ito**, None; **M. Kotsuma**, None; **S.S. Gambhir**, General Electric, Grant/research support; Bayer-Schering, Grant/research support; Sanofi-Aventis, Grant/research support; CellSight, Stockholder; ImaginAB, Stockholder; Enlight, Stockholder; Endra, Stockholder; Bracco, Consultant; NinePoint Medical, Stockholder; Visualsonics, Consultant .

Presentation Number **SS 144**
Scientific Session 21: Chemistry & Probes - Nuclear
September 8, 2012 / 10:30-10:41 / Room: Liffey Hall 1

# Imaging the Kappa Opioid Receptor with a Novel Antagonist Radiotracer

***Yiyun Huang***[1], *Ming-Qiang Zheng*[1], *Daniel Holden*[1], *Shu-fei Lin*[1], *Antonio Navarro*[2], *Antonio Navarro*[2], *Vanessa Barth*[2], *Jim Ropchan*[1], *Richard E. Carson*[1], [1]*PET Center, Yale University, New Haven, CT, USA;* [2]*Eli Lilly & Co., Indianapolis, IN, USA. Contact e-mail: henry.huang@yale.edu*

**Objectives**: Multiple lines of evidence have demonstrated the involvement of the kappa opioid receptor in anxiety, depression, drug addictions and alcoholism. The goal of this study was to synthesize the selective kappa antagonist [$^{11}$C]F3PB [(S)-3-fluoro-4-(4-((2-(3-pyridinyl)-1-pyrrolidinyl)methyl)phenoxy)-[$^{11}$C]benzamide], and evaluate its potential as a new PET imaging tracer. **Methods**: [$^{11}$C]F3PB was prepared by displacement of the iodophenyl precursor with [$^{11}$C]cyanide, followed by hydrolysis of the cyanophenyl intermediate to an amide. PET imaging studies were performed in rhesus monkeys using the Focus-220 scanner. Arterial input function was generated for each scan. Metabolite analysis was performed with HPLC. Plasma free fraction was determined by ultrafiltration method. Imaging data were analyzed with compartment models and simplified reference tissue model (SRTM). **Results**: F3PB displayed high in vitro binding affinity and selectivity for the kappa opioid receptor. (*Ki* of 0.18, 7.68, and 91.3 nM, respectively, is for κ, μ and δ receptor). [$^{11}$C]F3PB was prepared in >95% radiochemical purity and mean radiochemical yield of ~10 (EOS, based on trapped [$^{11}$C]cyanide, n = 12). [$^{11}$C]F3PB was metabolized fairly quickly. At 30 min following tracer injection, parent fraction in the plasma was ~20%. Mean plasma free fraction was ~4.3 (n = 12). In the monkey brain, [$^{11}$C]F3PB displayed fast uptake kinetics, with regional activity peaked at ~10 min. Regional time-activity curves were well described with the 2-tissue compartment model and SRTM, and with good agreement of regional binding parameter estimates between the two methods. Mean regional binding potential ($BP_{ND}$) values from SRTM analysis were 2.04, 1.29, 1.03, 1.02, 0.99, 0.56, and 0.52, respectively, for the globus pallidus, cingulate cortex, insula, caudate, putamen, thalamus, and frontal cortex (n = 6). Specific binding was completely blocked by pretreatment with naloxone (1 mg/kg) and dose-dependently reduced by the selective KOR antagonist LY2456302. Self-blocking experiments with increasing doses of unlabeled F3PB also demonstrated dose-dependent reduction in specific binding. **Conclusions**: The novel imaging agent [$^{11}$C]F3PB was shown to have high affinity and selectivity in vitro. In rhesus monkeys the radiotracer displayed specific and reversible binding to kappa opioid receptor with a fairly fast rate of metabolism in the plasma and fast uptake kinetics in the brain. The rank order of regional specific binding signals is consistent with the distribution of KOR in non-human primates. Specific binding signals ($BP_{ND}$) were high, and displaceable by pretreatment with non-selective and selective kappa opioid antagonists. Taken together, [$^{11}$C]F3PB demonstrate favorable properties as a PET radiotracer for in vivo imaging of the kappa opioid receptor. An added advantage of this tracer is that it can be labeled with the longer-lived isotope F-18, whose preparation and characterization in monkeys are ongoing.

Disclosure of author financial interest or relationships:
**Y. Huang**, Pfizer, Inc., Grant/research support; GSK, Grant/research support; Roche, Grant/research support; Abbott, Grant/research support; BMS, Grant/research support; **M. Zheng**, None; **D. Holden**, None; **S. Lin**, None; **A. Navarro**, Eli Lilly & Company, Employment; **A. Navarro**, Eli Lilly & Company, Employment; **V. Barth**, Eli Lilly, Employment; **J. Ropchan**, None; **R.E. Carson**, Pfizer, Grant/research support; Abbott, Grant/research support; BMS, Grant/research support; Theravance, Grant/research support .

Presentation Number **SS 145**
Scientific Session 21: Chemistry & Probes - Nuclear
September 8, 2012 / 10:41-10:52 / Room: Liffey Hall 1

# Molecular imaging of fibrin with SPECT using 111In-labeled fibrin-binding peptides

***Lucas Starmans***[1], *Sander M. van Duijnhoven*[1], *Raffaella Rossin*[2], *Silvio Aime*[3], *Mat Daemen*[4], *Klaas Nicolay*[1], *Holger Gruell*[1,2], [1]*Biomedical Engineering, Eindhoven University of Technology, Eindhoven, Netherlands;* [2]*Biomolecular Engineering, Philips Research, Eindhoven, Netherlands;* [3]*Chemistry FIM and Molecular Imaging Centre, University of Torino, Torino, Italy;* [4]*Pathology, Amsterdam Medical Centre, Amsterdam, Netherlands. Contact e-mail: l.w.e.starmans@tue.nl*

**Introduction**: Thrombosis is the underlying pathology in a number of life-threatening cardiovascular diseases, such as heart attack, ischemic stroke, pulmonary embolism, and deep venous thrombosis. A suitable target for molecular imaging of thrombi is fibrin, which is the major constituent of a thrombus and has the advantage that it is absent in non-pathological situations, thus providing a beneficial target-to-background ratio. In addition to molecular imaging of intravascular thrombi, fibrin-targeted probes may allow assessment of atherosclerotic plaque vulnerability and tumor stroma. The aim of this study was to assess the potential of a novel 111In-labeled fibrin-binding peptide (FibPep) to visualize thrombi in mice non-invasively using single-photon emission computed tomography (SPECT). **Methods**: *Synthesis*: DOTA-conjugated FibPep and negative control peptide (NCFibPep) were synthesized and radiolabeled with 111In. *In vitro*: peptides were characterized with respect to in vitro fibrin and blood clot binding. *In vivo*: In vivo SPECT imaging of thrombi using the radiolabeled probes was performed using a FeCl3-induced carotid injury mouse model. In addition, blood kinetic and biodistribution profiles were obtained. **Results**: *Synthesis*: The peptides were successfully synthesized and an 111Indium labeling-protocol was established, yielding more than 95% radiochemical purity. *In vitro*: FibPep showed significantly enhanced binding in vitro compared to NCFibPep to both fibrin (85.8 ± 3.8 and 1.2 ± 2.5 % dose, respectively; $p<0.01$; n=4) and blood clots (32.2 ± 7.1 and 5.1 ± 1.7 % dose, respectively; $p<0.01$; n=4). FibPep bound to fibrin with a dissociation constant (Kd) of 0.8 μM, whereas NCFibPep displayed at least a 100-fold lower affinity towards fibrin. *In vivo*: In vivo SPECT imaging using FibPep allowed clear visualization of thrombi (Fig. 1). Both probes displayed rapid blood clearance and were eliminated via the renal pathway. Ex vivo biodistribution showed significantly increased uptake of FibPep in the thrombus-containing carotid in comparison to the non-injured carotid (13.2 ± 5.0 and 1.1 ± 0.5 % injected dose per gram (%ID/g), respectively; $p< 0.02$; n=4), whereas non-specific NCFibPep did not (0.9 ± 0.2 and 0.7 ± 0.2 %ID/g, respectively; n=4). **Conclusions**: An 111In-labeled fibrin-binding peptide (FibPep) was developed and characterized. FibPep displayed high affinity towards fibrin in vitro, rapid blood clearance in vivo and allowed sensitive detection of thrombi using SPECT imaging. The presented results demonstrate that FibPep shows promise as a SPECT-agent for thrombus detection and provide a foundation for further evaluation in more clinically-relevant thrombus-related animal models such as for instance pulmonary embolism or atherosclerosis.

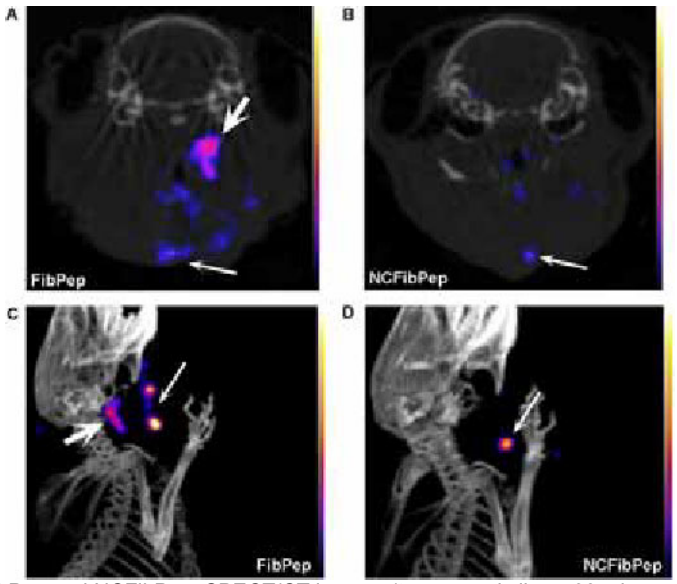


**Figure 1.** SPECT/CT imaging using FibPep and NCFibPep. SPECT/CT images (transversal slices, 90 min post injection) of live mice injected with (A) FibPep and (B) NCFibPep. Post-mortem maximum intensity projection of the neck area of mice injected with (C) FibPep and (D) NCFibPep. Bold arrow = thrombus; thin arrow = surgical wound area.

Disclosure of author financial interest or relationships:
**L. Starmans**, None; **S.M. van Duijnhoven**, None; **R. Rossin**, Philips, Employment; **S. Aime**, Bracco Imaging, Consultant; Bruker, Grant/research support; **M. Daemen**, None; **K. Nicolay**, None; **H. Gruell**, Philips, Employment .

Presentation Number **SS 146**
Scientific Session 21: Chemistry & Probes - Nuclear
September 8, 2012 / 10:52-11:03 / Room: Liffey Hall 1

# Synthesis, preclinical validation and toxicology of 68Ga-NOTA-Anti-HER2 Nanobodies for iPET imaging of HER2 receptor expression in cancer

***Catarina Xavier***[1], *Ilse Vaneycken*[3,1], *Matthias D'huyvetter*[1,4], *Johannes Heemskerk*[3], *Nick Devoogdt*[2,1], *Serge Muyldermans*[2], *Tony Lahoutte*[1,3], *Vicky Caveliers*[1,3], [1]*In vivo Cellular and Molecular Imaging Laboratory, VUB, Brussels, Belgium;* [2]*Laboratory of Cellular and Molecular Immunology, VUB, Brussels, Belgium;* [3]*Nuclear Medicine, UZ Brussel, Brussels, Belgium;* [4]*Radiobiology Unit, Molecular and Cellular Biology Expert Group, Belgian Nuclear Research Center (SCK/CEN), Mol, Belgium. Contact e-mail: catarina_xavi@hotmail.com*

Introduction: Nanobodies are the smallest fully functional antigen-binding fragments of naturally occurring heavy-chain-only antibodies, presenting ideal properties as PET probes for clinical molecular imaging. Non-invasive in vivo molecular characterization of disease using imaging is an emerging method for the selection of patients that can profit from targeted therapies and for measuring early therapeutic response. In this study, we labeled the previously selected anti-HER2 nanobody with 68Ga via a NOTA derivative bifunctional chelator, as a probe for HER2 PET imaging. Methods: The lead GMP grade 2Rs15d nanobody was conjugated with the NOTA derivative S-2-(4-Isothiocyanatobenzyl)-1,4,7-triazacyclononane-1,4,7-triacetic acid (p-SCN-Bn-NOTA) to enable 68Ga labeling at room temperature and within a short period of time. The labeled compound was analyzed for radiochemical purity, stability and in vitro specificity for HER2. Biodistribution and PET/CT studies were performed in HER2-positive and -negative tumor xenografts. The effect of mass (0.1, 1, 10 µg of NOTA-2Rs15d) on biodistribution was evaluated. Radiation dose estimates for the adult female were also calculated from biodistribution data using OLINDA software. A single dose extended toxicity study for NOTA-2Rs15d was performed in healthy mice up to a dose of 10 mg/kg. Results: Mass Spectrometry revealed efficient conjugation of the bifunctional chelator p-SCN-Bn-NOTA, with an average of 1.5 chelators per nanobody. Radiolabeling was quantitative (>97 %) after 5 min incubation at room temperature. Stability studies showed >95% intact 68Ga-NOTA-nanobodies in PBS, human plasma and after competition with excess EDTA or DTPA. In vitro binding studies on HER2 positive and negative cells revealed high specificity of the 68Ga-NOTA-nanobodies for the HER2 receptor. Biodistribution studies showed fast and specific uptake in HER2 positive tumors (4.34 ± 0.90 % IA/g at 1h p.i) and high tumor-to-blood and tumor-to-muscle ratios at 1h p.i (T/M = 28.49 ± 0.25, T/B = 14.11 ± 3.24). High contrast PET-CT images showing high specific tumor uptake were obtained. The inject mass has an effect on the general biodistribution, increasing the NOTA-2Rs15d dose from 0.1 to 10 µg the liver uptake decreased from 7.43 ± 1.89 to 2.90 ± 0.26 %IA/g and the tumor uptake increased from 2.49 ± 0.68 to 4.23 ± 0.99 %IA/g. The calculated effective dose equivalent was 0.0218 mSv/MBq, which would yield an effective dose of 4 mSv in a study using 185 MBq of 68GaNOTA-2Rs15d. The radiation dose delivered to the patient after injection of an activity of 185 MBq 68GaNOTA-2Rs15d is comparable with a normal PET scan. In the toxicity study there were no adverse effects observed. Conclusion: A new GMP grade anti-HER2 PET tracer, 68Ga-NOTA-2Rs15d, was synthetized via a rapid procedure under mild conditions. Preclinical validation showed high stability and high specific contrast imaging of HER2 positive tumors with no observed toxicity. 68Ga-NOTA-2Rs15d is ready for first in human clinical trial.

Disclosure of author financial interest or relationships:
**C. Xavier**, None; **I. Vaneycken**, None; **M. D'huyvetter**, None; **J. Heemskerk**, None; **N. Devoogdt**, Boehringer Ingelheim, Grant/research support; Ablynx, Grant/research support; **S. Muyldermans**, None; **T. Lahoutte**, None; **V. Caveliers**, None.

Presentation Number **SS 147**
Scientific Session 21: Chemistry & Probes - Nuclear
September 8, 2012 / 11:03-11:14 / Room: Liffey Hall 1

# [F-18]16-Fluoro-palmitoylethanolamide ([F-18]PEA) for Assessment of FAAH Inhibition

***Paul Acton***[1], *Scott M. Apana*[2], *Kaitlin Peckham*[2], *Marc Berridge*[2,3], [1]*Janssen Research and Development, LLC, Spring House, PA, USA;* [2]*3D Imaging, Little Rock, AR, USA;* [3]*Radiology, University of Arkansas for Medical Sciences, Little Rock, AR, USA. Contact e-mail: pacton@its.jnj.com*

Fatty acid amide hydrolase (FAAH) is a drug development target because it breaks down endocannabinoid neuromodulatory compounds. Drugs that target FAAH may be useful for pain control, and behavioral effects on sleep and eating, by increasing the effect of endogenous compounds that are normally broken down by the enzyme. Anandamide (arachidonoylethanolamide) is a primary natural substrate of the enzyme, along with PEA. Rather than image direct engagement of the enzyme with a competing PET tracer, instead functional inhibition of FAAH was tested by labeling its natural substrate. As an initial synthetic target toward development of labeled anandamide, PEA was synthesized. 16-[F-18]benzoyl palmitate was prepared by displacement of the 16-mesylate, prepared in turn from 16-hydroxypalmitate, in 50% yield in 20 min. Hydrolysis of the labeled benzyl ester (12 N HCl, quantitative) was followed by reaction with ethanolamine in the presence of methyl chloroformate to afford F-18 PEA, in high yield. After characterization of the product and moderate methods optimization the compound was injected in six 230-300 g Sprague Dawley rats in a test-retest protocol. On day 1, 1 mL 5% methocel placebo was given p.o. to each rat. Four hours later, F-18 PEA brain scans were obtained (Focus 220 microPET). Two days later, the procedure was repeated except that a FAAH inhibitor administered orally in 1 mL 5% methocel. PET scans showed marked and statistically significant reduction in uptake in cerebellum and thalamus in response to inhibition of FAAH, and marked increase in bone uptake, presumably due to increased defluorination of free fluoro-PEA resulting from whole body FAAH inhibition. We conclude that [F-18]PEA is a useful radiotracer for assessment of FAAH inhibition.

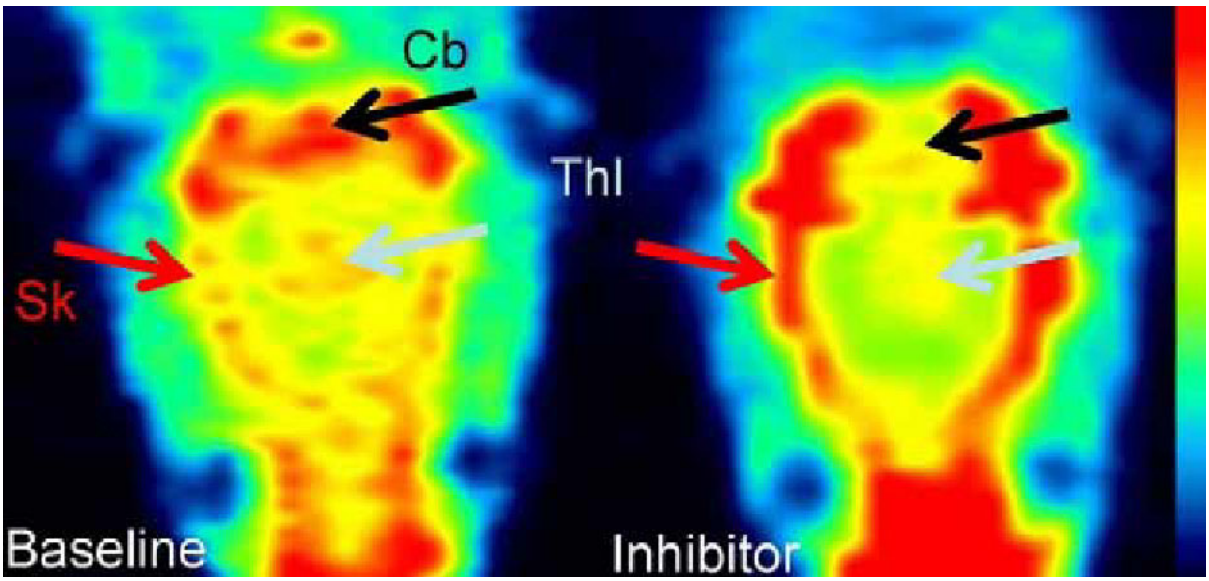


PEA uptake in placebo (Baseline) and FAAH Inhibited (Inhibited) conditions. Note inhibition of uptake in Cerebellum (Cb) and Thalamus (Thl) and enhancement of uptake in skeleton (Sk) caused by FAAH inhibition.

Disclosure of author financial interest or relationships:
**P. Acton**, Janssen Research and Development, Employment; **S.M. Apana**, None; **K. Peckham**, None; **M. Berridge**, Janssen RD, Grant/research support; FDA, Grant/research support .

Presentation Number **SS 148**
Scientific Session 21: Chemistry & Probes - Nuclear
September 8, 2012 / 11:14-11:25 / Room: Liffey Hall 1

# Development of 111In-labeled liposomes for vulnerable atherosclerotic plaque imaging

***Mikako Ogawa***[1], *Izumi O. Umeda*[2], *Mutsumi Kosugi*[1], *Ayumi Kawai*[1], *Yasuhiro Magata*[1], [1]*Medical Photonic Research Center, Hamamatsu University School of Medicine, Hamamatsu, Japan;* [2]*National Cancer Center Hospital East, Kashiwa, Japan. Contact e-mail: mogawa@hama-med.ac.jp*

Background: Macrophage infiltration is characteristics for atherosclerotic vulnerable plaques. Macrophages recognize phosphatidylserine (PS) that is exposed on the cell surface of the apoptotic cells to phagocytize these cells. In this study, we prepared radiolabeled PS liposomes for detection of vulnerable plaques. Methods: PS liposomes were prepared by lipid film hydration (DSPC: DSPS: chol = 1:1:1). For control, phosphatidylcholine (PC) liposomes were prepared (DSPC: chol = 2:1). The sizes of the liposome were uniformed to 100 or 200 nm by the extruder to make PS100, PS200, PC100, and PC200 liposomes. Then, the liposomes were radiolabeled by encapsulating 111In-NTA using active-loading method. The 111In-liposomes were incubated with cultured mouse peritoneum macrophages for 2hr and uptake level was investigated. For biodistribution study, the 111In-liposomes were intravenously injected to ddY mice. Also, the 111In-liposomes were injected to apoE -/- mice, and the aortas were harvested for autoradiography and Oil-Red O staining. For SPECT imaging, 111In-liposomes (74 MBq) were intravenously injected to WHHL rabbits, and scanned for 1hr at 3hr, 24hr, 48hr after the injection. Results: The liposomes were successfully radiolabeled by 111In, and radiochemical yields were more than 95% for all the prepared liposomes. The in vitro uptake levels to macrophages were 60.5, 14.7, 32.0, 14.4 %dose/mg protein, for 111In-PS100, 111In-PC100, 111In-PS200, 111In-PC200, respectively. In biodistribution study, high spleen uptake was seen in PC liposomes. The liver uptake was high in all liposomes, but it was lowest in 111In-PC200. The blood clearance was faster in PS liposomes than PC liposomes. The in vivo distributions of 111In-labeled PS liposomes to atherosclerotic regions were well matched with Oil-Red O staining in apoE -/- mouse. The aorta was successfully visualized by SPECT at 48hr after the 111In-labeled PS liposome injection; however, high liver uptake was also observed. Discussion: By in vitro uptake study, it is revealed that macrophage targeting was accomplished by phosphatidylseline modification. Since we previously reported that 18F-FDG uptake to the macrophages was 48.8 %dose/mg protein with 3hr incubation, 111In-PS100 uptake was greater than 18F-FDG. Also, atherosclerotic region was successfully detected by 111In-labeled PS liposomes in apoE-/- mice and WHHL rabbit in vivo. Modification of the liposome with slower blood clearance and lower liver uptake should be needed to improve the in vivo images.

Disclosure of author financial interest or relationships:
**M. Ogawa**, None; **I.O. Umeda**, None; **M. Kosugi**, None; **A. Kawai**, None; **Y. Magata**, None.

Presentation Number **SS 149**
Scientific Session 21: Chemistry & Probes - Nuclear
September 8, 2012 / 11:25-11:36 / Room: Liffey Hall 1

# Synthesis and radiolabelling of ICF15002, a new multimodal fluorinated and iodinated radiotracer for both PET imaging and targeted radionuclide therapy of melanoma

***Emilie Billaud**, Aurélien Vidal, Latifa Rbah-Vidal, Sophie Besse, Elisabeth Miot-Noirault, Philippe Auzeloux, Jean-Michel Chezal,*
*Molecular Imaging & Targeted Therapy, INSERM UMR990/UdA, Clermont-Ferrand, France. Contact e-mail: emilie.billaud@gmail.com*

Melanoma is the most serious form of skin cancer with poor prognosis for patients with metastatic disease. Our team designs arylcarboxamide compounds with high affinity for melanin in order to improve diagnosis and staging using SPECT or PET imaging and develop targeted radionuclide therapy (TRT) for melanoma. This project deals with a multimodal approach, using a single fluorinated and iodinated melanin-targeting compound, and offering both diagnosis (PET/fluorine-18) and therapeutic (TRT/iodine-131) applications, depending on the radioelement introduced. Among a variety of 7 new specific halogenated compounds, ICF15002 has been selected by screening (γ-scintigraphy/iodine-125) to evaluate our multimodality concept. **Methods:** **Chemistry:** ICF15002 and its precursors ICF15001 (mesylate for $^{18}$F radiolabelling), and ICF15060 (stannane for $^{131}$I radiolabelling) were synthesized in 7 to 9 steps. Structures of intermediates and final compounds were confirmed by NMR, IR and MS. **$^{125}$I Radiolabelling and γ-scintigraphy:** ICF15002 was radiolabelled with $^{125}$I by isotopic exchange reaction ([$^{125}$I]NaI, citrate buffer, $CuSO_4$, 130°C) and purified by semi-preparative HPLC. *In vivo* biodistribution and tumor uptake of [$^{125}$I]ICF15002 were evaluated by γ-scintigraphy in B16 primary melanoma-bearing mice. **$^{18}$F Radiolabelling and PET:** Fully automated radiosynthesis of [$^{18}$F]ICF15002 was performed on a SynChrom® R&D module (Raytest). [$^{18}$F]$F^-$ (Cyclopharma Laboratories, Pr Askienazy) was converted into dry [$^{18}$F]KF,$K_{222}$ complex, then nucleophilic substitution of ICF15001 was achieved in MeCN at 90°C for 10 min. After semi-preparative HPLC purification and formulation, [$^{18}$F]ICF15002 was evaluated in B16 primary melanoma-bearing mice by PET. **$^{131}$I Radiolabelling and TRT:** ICF15002 was radiolabelled with $^{131}$I at high specific activity, starting from ICF15060 ([$^{131}$I]NaI, HCl, Chloramine T, rt) and purified by semi-preparative HPLC. Effect of [$^{131}$I]ICF15002 treatment (2x20 MBq) on tumor growth was examined on B16 primary melanoma-bearing mice. **Results:** ICF15002, ICF15001 and ICF15060 were synthesized in 15%, 18% and 5% overall yields, respectively. Radiosynthesis of [$^{125}$I]ICF15002 leads to 50% overall radiochemical yield (RCY) with a radiochemical purity (RCP) >99%. *In vivo* biodistribution of [$^{125}$I]ICF15002 showed specific and long-lasting tumor uptake up to 10 days p.i. with fast clearance from non-specific tissues. [$^{18}$F]ICF15002 was produced in 54 min, with 23% overall RCY and RCP>99%. PET with [$^{18}$F]ICF15002 demonstrated promising results with specific tumor uptake of 15.6±0.9%ID/g as early as 1 h p.i., tumor/muscle ratio of 9.4±0.7, and mainly fast urinary elimination. [$^{131}$I]ICF15002 was obtained with 60% overall RCY and RCP>99% (SA 116 GBq/µmol). TRT with [$^{131}$I]ICF15002 showed significant inhibition of tumor growth: doubling time of treated tumors was 2.9±0.4 days *vs* 1.8±0.2 days for control (*p=0.006*). **Conclusion:** ICF15002 validated our multimodality concept with specific and highly contrasted tumor imaging (PET/[$^{18}$F]ICF15002) and with significant slowing down of tumor growth (TRT/[$^{131}$I]ICF15002). **References:** Patent Chezal et al. WO2009095872. **Grant**: CLARA TRT/PETMEL program.

Disclosure of author financial interest or relationships:
**E. Billaud**, None; **A. Vidal**, None; **L. Rbah-Vidal**, None; **S. Besse**, None; **E. Miot-Noirault**, None; **P. Auzeloux**, None; **J. Chezal**, None.

Presentation Number **SS 15**
Scientific Session 2: Technology & Software - Optical Imaging
September 6, 2012 / 11:36-11:47 / Room: Wicklow Hall 1

# In vivo imaging of Surface Enhanced Raman Scattering nanoparticles using a new small animal Raman imaging instrument

***Sarah Bohndiek***[1], *Cristina Zavaleta*[1], *Dominique Van de Sompel*[1], *Ashwin Wagadarikar*[2], *Siavash Yazdanfar*[2], *Sanjiv S. Gambhir*[1], [1]*Radiology, Stanford University, Stanford, CA, USA;* [2]*Applied Optics Lab, GE Global Research, Niskayuna, NY, USA. Contact e-mail: bohndiek@stanford.edu*

Introduction: A dedicated small animal Raman spectroscopy instrument has recently been developed in our laboratory to address the problem of performing high-throughput, wide-area SERS nanoparticle imaging in living mice. Our solution is a line-scanning system, which uses galvo mirrors to scan a laser line over the animal. This system offers significant advantages compared to point-mapping Raman microscopy systems, with regions of 10mm x 10mm mapped in under 6 minutes and the full field of view, 30mm x 25mm, in under 30 minutes. The 100-fold speed gain compared to point-mapping systems comes with full area coverage, a spatial resolution of 250μm (laser line width) by 8μm (along the line) and does not require sample movement. Our system could therefore enable the use of Raman spectroscopy as an in vivo molecular imaging modality. Aim: To demonstrate the advantages of using a dedicated small animal Raman imaging instrument for mapping SERS nanoparticle distribution in vivo. Materials and Methods: The system consists of a 785nm laser source that excites the subject with a power of 290mW; Raman spectra are collected by a Czerny-Turner spectrometer (300lp/mm grating; Shamrock 303i, Andor) and electron-multiplying CCD (gain 200, exposure time 1s; Luca 604, Andor). SERS active nanoparticles (4 flavors S420, S421, S440 and S470; Cabot Security Systems Inc.) consist of a 60 nm diameter gold core covered with a layer of Raman active material and a silica coating. All procedures performed on animals (nude mice, N=5) were approved by the University's Institutional Animal Care and Use Committee. Each flavor of SERS nanoparticles was injected subcutaneously (10μl SERS: 10μl matrigel). To evaluate the multiplexing capability, mixtures of the four SERS flavors were injected on the opposite flank (5μl for each SERS flavor: 10μl of matrigel). Deep tissue imaging was performed at 2h following tail-vein injection of a mixture of all four nanoparticle flavors (200 μl at 0.8nM). Raman spectral umixing was performed using a modified direct classical least-squares (DCLS) algorithm. Results and Discussion: We first tested the ability of the system to detect single SERS flavors and spectrally unmix the signals from each flavor (Fig. 1a). We then administered mixtures of 2, 3 and 4 nanoparticles and mapped the spectral components (Fig. 1b). The resulting maps correctly identify the flavors contributing to the signal at each injection site, with little or no bleed-through to other components. To confirm the capability of the system to unmix SERS signals from deeper tissue, we then mapped the torso of the mouse at 2h after injection of 4 flavors of nanoparticle, to demonstrate their accumulation in the liver (Fig. 1c). Our system was able to map this region in under 15 minutes; an equivalent scan on a raster system would take upwards of 4 hours. Again, the resulting image correctly separated the flavors into their separate channels. This encouraging demonstration of deep tissue multiplexing shows that our system holds potential for enabling rapid Raman molecular imaging of SERS signals in small living subjects.

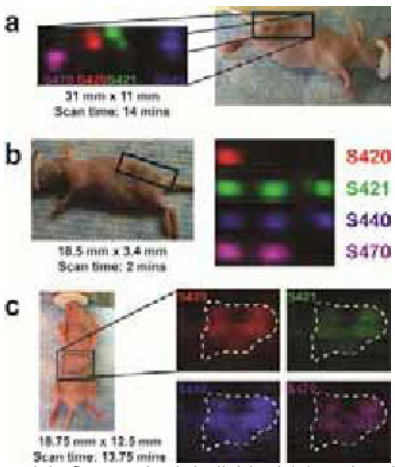


Figure 1: Subcutaneous injections of four SERS nanoparticle flavors, both individual (a) and multiplexed (b), were successfully detected and unmixed. (c) Mapping of the mouse torso after tail-vein injection of four SERS flavors shows the accumulation of nanoparticles in the liver, particularly in the median and left lobes. The white dashed line shows the outline of the liver. The vertical scale is the same in all images. Large areas (>3cm2) were mapped with a spatial resolution of 250 μm x 64 μm in under 15 minutes (c) and 63 mm2 could be mapped in just 2 minutes (b). Similar area mappings would require multiple hours of scan time on a conventional point-mapping Raman microscope.

Disclosure of author financial interest or relationships:
**S. Bohndiek**, None; **C. Zavaleta**, None; **D. Van de Sompel**, None; **A. Wagadarikar**, None; **S. Yazdanfar**, General Electric Company, Employment; General Electric Company, Stockholder; **S.S. Gambhir**, General Electric, Grant/research support; Bayer-Schering, Grant/research support; Sanofi-Aventis, Grant/research support; CellSight, Stockholder; ImaginAB, Stockholder; Enlight, Stockholder; Endra, Stockholder; Bracco, Consultant; NinePoint Medical, Stockholder; Visualsonics, Consultant .

Presentation Number **SS 150**
Scientific Session 21: Chemistry & Probes - Nuclear
September 8, 2012 / 11:36-11:47 / Room: Liffey Hall 1

# A simple late stage fluorination method for the preparation of 2'-[18F] pyrimidine based nucleosides

*Gladys C. Completo[1], Diana Yu[2], N. Satyamurthy[1], Anastassia Alexandrova[2], Caius G. Radu[1], Johannes Czernin[1],* ***Saman Sadeghi***[1], *[1]Ahmanson Translational Imaging Division, Molecular & Medical Pharmacology, University of California Los Angeles, Los Angeles, CA, USA; [2]Chemistry and Biochemistry, University of California Los Angeles, Los Angeles, CA, USA. Contact e-mail: samsadeghi@mednet.ucla.edu*

Positron Emission Tomography (PET) is emerging as a critically important modality for diagnosing, staging, restaging and therapy monitoring of cancer1. PET probes such as [18F]FluoroArabinofuranosyl)Cytosine ([18F]FAC are potentially highly relevant PET biomarkers for tissue deoxycytidine kinase (dCK) activity in cancer. 2 dCK is the enzyme that converts a large class of nucleoside prodrugs (analog) such as gemcitabine, decitabine, and fludarabine into their active form. However, current synthetic approaches for these 2'-[18F] pyrimidine-based nucleoside probes involves a multi-step process that is extremely difficult, time-consuming and low yielding.2 The main drawback is the introduction of the [18F]-fluoride at the first step, which exacerbates loss (due to radiodecay) of the [18F]fluoride label in the subsequent synthetic steps which take ~4hrs.2 A successful alternative strategy through direct SN2-type reaction with inversion of configuration at the 2′-position of a purine nucleoside to introduce the [18F]-fluoride label in the 2'-up (arabino) position has been reported.3 However, for pyrimidine nucleosides, these SN2 type reactions would be formidable, owing to: 1) the neighboring-group participation of the C-2 carbonyl group of the pyrimidine moiety through the formation of a 2,2′-anhydronucleoside intermediate and 2) the steric hindrance posed by the pyrimidine moiety. It was only recently that the first direct fluorination at the 2' position of the nucleoside was reported in the synthesis of [18F]-FMAU.4 However, the yield was low (2% decay corrected) because the 2'-position is sterically hindered by the 5-methyluracil base, limiting the accessibility of the incoming nucleophile from the topside trajectory. To address these hurdles, it is therefore imperative to develop a novel assisted stereospecific, late stage fluorination at the 2′-position of the intact nucleoside. This concise late stage fluorination is based on: (1) cyclic benzylidene protection of 3' and 5' hydroxyl groups conformationally locks the ribose sugar and orients the nucleo-base away from the reaction center that could be ideal for a facile SN2 approach of the [18F]fluoride nucleophile at the C-2' carbon carrying the leaving group; (2) an electron withdrawing triazole-based protecting group in the pyrimidine base to decrease the nucleophilicity of C-2 carbonyl group and prevent intramolecular nucleophilic attack at the 2'-position; and (3) the use of triazole protecting group allows flexibility in using different deprotection conditions that can lead to either a 2'-18F-labeled cytidine or a uridine-based nucleoside analog. A SN2 reaction pathway modeling utilizing the Pairwise Distance Directed Gaussian modification of PM3 (PDDG/PM3) semi-empirical method also supports an efficient SN2 [18F]-fluorination reaction of the benzylidene protected nucleoside compared to its non-benzylidene protected counterpart. This efficient late stage fluorination strategy can result to higher radiochemical yields of the [18]FAC PET probes and makes this method amenable for easier instrumentation and automation.

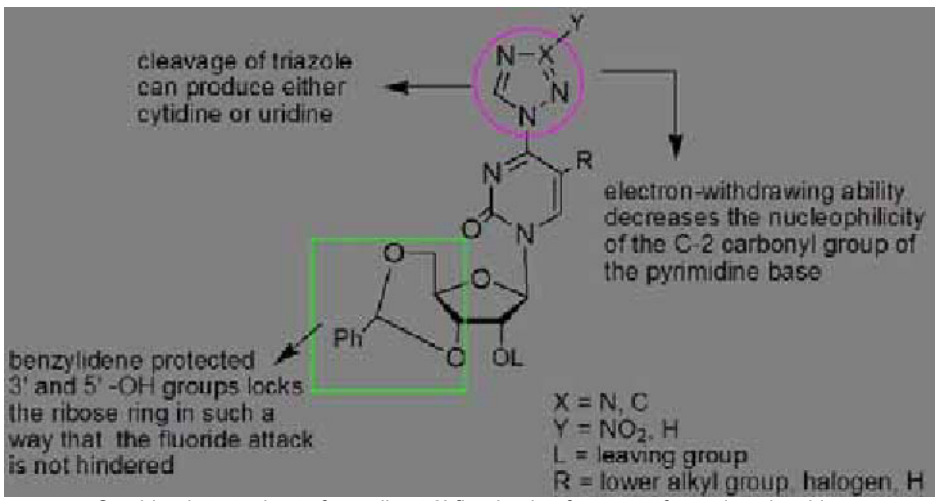


Combined strategies to favor direct 2'-fluorination from a preformed nucleoside.

Disclosure of author financial interest or relationships:
**G.C. Completo**, None; **D. Yu**, None; **N. Satyamurthy**, None; **A. Alexandrova**, None; **C.G. Radu**, None; **J. Czernin**, Sofie Biosciences, Stockholder; Momentum Biosciences, Stockholder; **S. Sadeghi**, None.

Presentation Number **SS 151**
Scientific Session 21: Chemistry & Probes - Nuclear
September 8, 2012 / 11:47-11:58 / Room: Liffey Hall 1

# A Novel Probe for PET Imaging of Cystine Transport

***Mohammad Namavari**, Ramasamy Paulmurugan, Aileen Hoehne, Robert E. Reeves, Sanjiv S. Gambhir, Radiology, Stanford University, Stanford, CA, USA. Contact e-mail: namavari@stanford.edu*

It is well known that cystine is transported into cells via cystine /glutamate exchanger transport systems SLC7A11 (xCT) and SLC3A2 (4F2hc). Inside the cell, cystine is reduced to cysteine which is then converted to glutathione (GSH) by γ-glutamylcysteine synthetase and GSH synthetase. It has also been established that in the cell, cystathionine is converted to cysteine by cystathionine-γ-lyase and therefore it has a role in GSH biosynthesis. We hypothesize that cystathionine could be potentially taken up by the same mechanism as cysteine, because it has affinity for SLC7A11 and SLC3A2 transport systems. It has been reported that tumor cells and other tissues under oxidative stress have high GSH content and high activity of above enzymes. Cystine, cystathionine and their transporters have an important role in tumor metabolisms. One can take advantage of these cellular transporters which are up-regulated in tumor cells and tissues undergoing oxidative stress in order to develop imaging agents to image cystine transport. These imaging agents will have wide applications in both diagnostics and therapeutic monitoring of cancer. To test the possibility of using a radiofluorinated cystathionine analog as an imaging agent for cystine transport, we have synthesized N-[$^{18}$F]fluoroethoxybenzoyl-N′-hydroxyethoxybenzoyl-di-O-methylcystathionine (2,[$^{18}$F]FEBCT ) and investigated its uptakes in a variety of tumor cell lines. [$^{18}$F]FEBCT was prepared for the first time via a direct fluorination of precursor N-(O-tosylethoxybenzoyl)-N′-hydroxyethoxybenzoyl-di-O-methylcystathionine 1 with [$^{18}$F]KF/K2.2.2 in DMSO at 155 $^{o}$C for 40 minutes in 12-15 % radiochemical yield (decay corrected). In preliminary cell uptake experiments, [$^{18}$F]FEBCT showed high uptake in SKBr3, MCF7, MDA-MB-231, A549 and PC3 cancer cells (3.40 x$10^{-4}$-6.80 x $10^{-4}$ % uptake/ µg protein). These cell lines are known to have high expression of cystine /glutamate exchanger transport systems SLC7A11 (xCT) and SLC3A2. High contrast small animal PET images with relatively moderate tumor uptake (3.41-4.27 % ID/G) were observed for [$^{18}$F]FEBCT as a PET probe in a PC3 (prostate tumor) xenograft mouse model (n=3). In conclusion, for the first time, to the best of our knowledge, successful synthesis of [$^{18}$F]FEBCT as a PET probe for cysteine transport has been accomplished. Our cell uptakes and small animal PET imaging studies support future studies to investigate the use of $^{18}$F-labled cystathionines as PET tracer for cancer management.

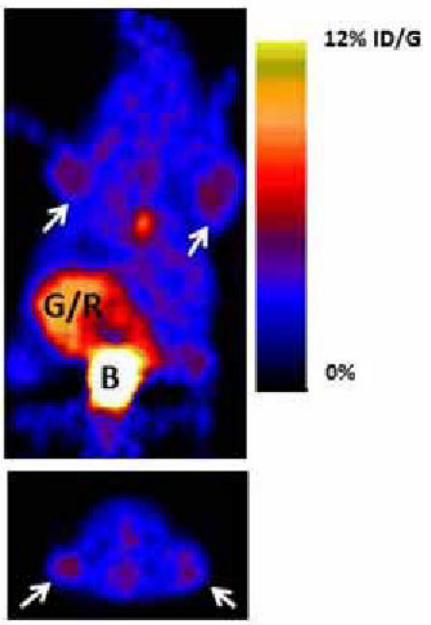


Fig. 1.

Figure 1 shows MicroPET images (coronal top, and transaxial bottom) of a PC3 tumor mouse at 60 min after tail injection of 180 µCi of [$^{18}$F]FEBCT (2). Arrows show the PC3 tumor locations, G/R is gastrointestinal / renal activity and B is bladder.

Disclosure of author financial interest or relationships:
**M. Namavari**, None; **R. Paulmurugan**, None; **A. Hoehne**, None; **R.E. Reeves**, None; **S.S. Gambhir**, General Electric, Grant/research support; Bayer-Schering, Grant/research support; Sanofi-Aventis, Grant/research support; CellSight, Stockholder; ImaginAB, Stockholder; Enlight, Stockholder; Endra, Stockholder; Bracco, Consultant; NinePoint Medical, Stockholder; Visualsonics, Consultant .

Presentation Number **SS 152**
Scientific Session 22: Preclinical In Vivo/Translational & Clinical - Cardiology
September 8, 2012 / 10:30-10:42 / Room: Wicklow Hall 1

# Atherosclerotic Plaque Discrimination Using a High-Resolution Morphological And Biochemical Optical Imaging Technique

***Brian E. Applegate***[1], *Jesung Park*[1], *Paritosh Pande*[1], *Sebina Shrestha*[1], *Fred J. Clubb*[2], *Brian Walton*[3], *Javier A. Jo*[1], [1]*Department of Biomedical Engineering, Texas A&M University, College Station, TX, USA;* [2]*Department of Veterinary Pathobiology, Texas A&M University, College Station, TX, USA;* [3]*Department of Cardiology, St. Luke's Episcopal Hospital, Houston, TX, USA. Contact e-mail: apple@tamu.edu*

Objective: To develop and validate a novel imaging technology for high-resolution morphological and biochemical imaging of coronary atherosclerotic plaques. Background: Future development of systemic or localized therapies for atherosclerosis will likely depend upon a more detailed understanding of plaque development. There is convincing evidence indicating that the underlying mechanisms in the development of a coronary plaque leading to acute thrombosis are multi-factorial, involving a complex interaction between structural, compositional, biomechanical, cellular and molecular processes in the vessel wall. Unfortunately, there is no current imaging modality (neither non-invasive nor intravascular) that can provide such level of plaque characterization. Therefore, the future of clinical intravascular imaging may lie in multimodality imaging systems that combine various imaging technologies to provide a more comprehensive assessment of plaque pathology. Methods: Optical Coherence Tomography (OCT) generates high-resolution 3D images of plaque morphology. Endogenous Fluorescence Lifetime Imaging Microscopy (FLIM) characterizes plaque biochemical composition. Both methods rely on intrinsic optical characteristics of the plaque, thus contrast agents are not required. A multimodal OCT/FLIM system was built to generate morphological and biochemical maps of the plaque, composed of a high-resolution (8 μm axial, 15 μm lateral) structural volumetric image superimposed with a luminal biochemical map. Fresh postmortem human coronary segments were imaged and included: intimal thickening (IT, n=11), pathological intimal thickening (PIT, n=2), PIT having >50% of collagen content (FIB-PIT, n=7), PIT with superficial infiltration of foam cells (FC-PIT, n=11), fibroatheroma (FA) having >50% of collagen content in the cap (FIB-FA, n=3), FA with superficial infiltration of foam cells (FC-FA, n=2), thin-cap fibroatheroma (TCFA, n=2), and/or calcified FA (CA-FA, n=8). Results: Overall, 93.5% of the plaques (43 out of 46) were correctly identified based on the combined OCT-FLIM evaluation using the histopathological evaluation as the gold standard. Conclusion: The developed technology enables the characterization of plaque morphology and biochemistry with micron scale resolution and the identification of most types of atherosclerotic plaques. An intravascular OCT/FLIM imaging system is currently being developed for in-vivo study of the mechanisms of atherosclerosis development.

Disclosure of author financial interest or relationships:
**B.E. Applegate**, None; **J. Park**, None; **P. Pande**, None; **S. Shrestha**, None; **F.J. Clubb**, None; **B. Walton**, None; **J.A. Jo**, None.

Presentation Number **SS 153**
Scientific Session 22: Preclinical In Vivo/Translational & Clinical - Cardiology
September 8, 2012 / 10:42-10:54 / Room: Wicklow Hall 1

# Theranostic-based evaluation of simvastatin loaded high-density lipoprotein nanoparticles in atherosclerotic mice: mechanism of action of reduced macrophage inflammation

***Jun Tang***[1], *Raphael Duivenvoorden*[2], *Bernd Hewing*[6], *David Izquierdo-Garcia*[1], *Aneta J. Mieszawska*[1], *David P. Cormode*[1], *Emma L. Kuan*[3], *Canturk Ozcan*[1], *Mark E. Lobatto*[1,2], *Gwendalyn J. Randolph*[3], *Erik S. Stroes*[2], *Valentin Fuster*[4,5], *Edward A. Fisher*[6], *Zahi A. Fayad*[1], *Willem J. Mulder*[1,2], [1]*Translational and molecular imaging institute, Mount Sinai School of Medicine, New York, NY, USA;* [2]*Department of Vascular Medicine, Academic Medical Center, Amsterdam, Netherlands;* [3]*Department of Gene and Cell Medicine, Mount Sinai School of Medicine, New York, NY, USA;* [4]*Department of Cardiology, Zena and Michael A. Weiner Cardiovascular Institute and Marie-Josée and Henry R. Kravis Cardiovascular Health Center, Mount Sinai School of Medicine, New York, NY, USA;* [5]*Centro Nacional de Investigaciones Cardiovasculares (CNIC), Madrid, Spain;* [6]*The Leon H. Charney Division of Cardiology, Department of Medicine, The Marc and Ruti Bell Program in Vascular Biology, Department of Cell Biology, New York University School of Medicine, New York, NY, USA. Contact e-mail: jun.tang@mssm.edu*

Rationale: Statins have been shown to have anti-inflammatory pleiotropic effects in experimental settings. However, the bioavailability of orally administered statins is poor, which limits the direct therapeutic effects on atherosclerotic plaques. We have developed a simvastatin loaded high-density lipoprotein nanoparticle platform ([S]-rHDL), with the similar properties to natural HDL (A). The formulation has potent anti-inflammatory effects in vitro (S_A), produces significantly higher therapeutic effects in apolipoprotein E knockout (ApoE KO) mice than oral simvastatin or rHDL treatment, and induces rapid regression when administered at a high dose (S_B). The purpose of the current study is to understand the mechanism of action by which this formulation exerts its potent anti-inflammatory effects. Methods and Results: To investigate the protecting effects of [S]-rHDL on encapsulated simvastatin in blood, the nanoparticles were incubated in mouse serum and intact simvastatin was measured over time with HPLC. [S]-rHDL drastically protected the encapsulated simvastatin (B). To evaluate the in vivo targeting of atherosclerotic plaques, [S]-rHDL was additionally labeled with Gd-DPTA-lipids and Cy5.5-DMPE, and intravenously administered in ApoE KO mice. In vivo T1-weighted magnetic resonance imaging (MRI) revealed [S]-rHDL accumulation in atherosclerotic plaques in the abdominal aortas (C), while ex vivo near-infrared fluorescence imaging (NIRF) of excised aortas demonstrated pronounced accumulation in plaque rich lesions such as the aortic roots and arches (D). To investigate the cellular targeting specificity of [S]-rHDL, flow cytometry and fluorescence microscopy were used to analyze the blood, spleen, and atherosclerotic plaques. [S]-rHDL was preferentially taken up by monocytes and macrophages in the blood and spleen (E), but not by other leukocytes (S_D). It also extensively accumulated in atherosclerotic plaques, and was taken up by plaque macrophages (F and S_C). Altogether these data support our hypothesis that [S]-rHDL acts on plaque macrophages locally and thereby exerts a strong anti-inflammatory effect. To this end, laser capture microdissection was used to isolate plaque macrophages, and the mRNA level of TNF-α, the hallmark of macrophage inflammation, was significantly reduced (G). In addition, the HMGR mRNA level did not change in plaque macrophages and liver cells, signifying that the anti-inflammatory effects do not depend on the cholesterol-lowering capability of simvastatin (S_E and F). Finally, no significant toxic effects were found in liver, kidney, and muscle in high-dose [S]-rHDL treated mice (S_G-J). Conclusion: [S]-rHDL protects simvastatin from degrading swiftly and, upon intravenous administration, accumulates in atherosclerotic plaques. In atherosclerotic mice, it specifically targets monocytes and macrophages in atherosclerotic plaques, blood, and spleen. It locally acts on plaque macrophages, which results in strong anti-inflammatory effects, without significant toxic effects. Our data suggest that this nanotherapy may represent a potent alternative to the current standard of care for atherosclerosis patients.

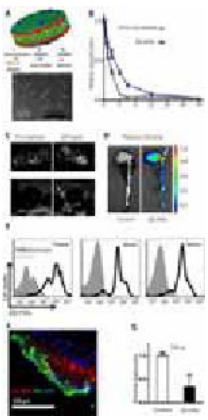

Disclosure of author financial interest or relationships:
**J. Tang**, None; **R. Duivenvoorden**, None; **B. Hewing**, None; **D. Izquierdo-Garcia**, None; **A.J. Mieszawska**, None; **D.P. Cormode**, Philips, Consultant; **E.L. Kuan**, None; **C. Ozcan**, None; **M.E. Lobatto**, None; **G.J. Randolph**, None; **E.S. Stroes**, None; **V. Fuster**, None; **E.A. Fisher**, None; **Z.A. Fayad**, None; **W.J. Mulder**, None.

Presentation Number **SS 154**
Scientific Session 22: Preclinical In Vivo/Translational & Clinical - Cardiology
September 8, 2012 / 10:54-11:06 / Room: Wicklow Hall 1

# Detection of Activated Platelets in Carotid Artery Thrombosis in Mice with radiolabeled single chain antibodies for PET

***Katie Ardipradja***[1,3], *Shinn Dee Yeoh*[3], *Graeme J. O'Keefe*[3], *Angela Rigopoulos*[5], *David W. Howells*[4], *Karlheinz Peter*[2], *Uwe Ackermann*[3], *Christoph E. Hagemeyer*[1], [1]*Vascular Biotechnology Laboratory, Baker IDI, Melbourne, VIC, Australia;* [2]*Thrombosis, Baker IDI, Melbourne, VIC, Australia;* [3]*PET and Nuclear Medicine, Austin Hospital, Melbourne, VIC, Australia;* [4]*The Melbourne Brain Centre, Florey Neurosciences Institute, Melbourne, VIC, Australia;* [5]*Tumor Targeting Group, Ludwig Institute, Melbourne, VIC, Australia.*
*Contact e-mail: Katie.Ardipradja@bakeridi.edu.au*

BACKGROUND: The chronic inflammatory disease, atherosclerosis is a major underlying cause of ischaemic heart disease. Rupture of unstable atherosclerotic lesions, causing heart attack and stroke1, is the most common cause of sudden death in the developed world. Activated-platelets play a major role in development of lesions, in both the early stages and in the formation of thrombi after plaque rupture. We previously generated a single-chain antibody (scFv) that specifically binds to abundant platelet glycoprotein integrin receptor IIb/IIIa in its activated, ligand-bound form (LIBS)2. The purpose of this study is to label LIBS-scFv with 18F to investigate its potential use as a molecular imaging agent to detect activated platelets in thrombi. METHOD: Both LIBS-scFv and control-scFv were conjugated to N-succinimidyl 4-[18F]fluorobenzoate (S[18F]FB), an NHS ester PET prosthetic group. ScFv's were reacted with 6.25 mCi of SFB. The radiolabeled antibody was characterized and binding to activated-platelets in vitro and in vivo was assessed. After radiolabeling, binding was examined by flow cytometry and compared to non-labeled scFv. In vitro formed clots were incubated with different concentrations of the labeled scFv. Clots were imaged on PET scanner and bound radioactivity was measured. In vivo experiments were conducted on an acute mouse model of thrombosis, where a platelet rich clot is formed in the carotid artery. RESULTS: Radioactivity measurements show an increase in bound radioactivity in clots incubated with LIBS-scFv compared to control-scFv. After incubation with radiolabeled scFv-LIBS clots retained significantly greater ($p = 0.04$, $n=9$) amounts of radioactivity compared to clots incubated with radiolabeled scFv-control. Clots incubated with LIBS-scFv retained 3.5% of activity (decay corrected) compared to clots incubated with the non-binding scFv which retained 1.3% of radioactivity. Increasing radioactivity in urine demonstrates fast renal clearance of the labelled scFv. In vivo experiments reveal high uptake in injured vessel compared to non-injured vessel. Presence of activated-platelets was determined by histology subsequently. CONCLUSION: This novel radiotracer may be suitable for detecting activated-platelets associated with rupture-prone plaques. The potential to determine if patients have vulnerable plaques would allow early initiation of medical treatment to stabilize plaques.

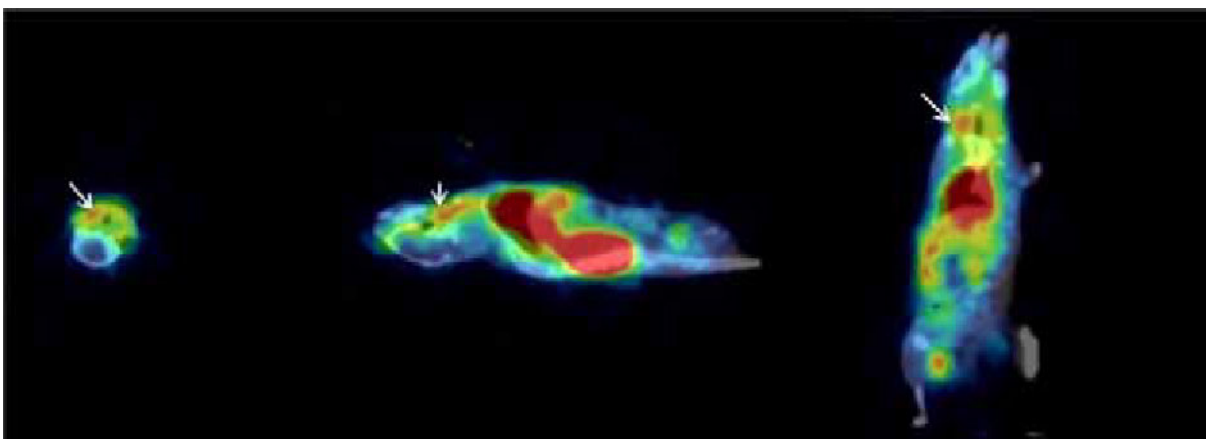

Co registered PET/CT image of a mouse injected with radiolabeled LIBS scFv showing uptake in the target area with different views.

Disclosure of author financial interest or relationships:
**K. Ardipradja**, None; **S. Yeoh**, None; **G.J. O'Keefe**, None; **A. Rigopoulos**, None; **D.W. Howells**, None; **K. Peter**, None; **U. Ackermann**, None; **C.E. Hagemeyer**, None.

Presentation Number **SS 155**
Scientific Session 22: Preclinical In Vivo/Translational & Clinical - Cardiology
September 8, 2012 / 11:06-11:18 / Room: Wicklow Hall 1

# Molecular Imaging of Rapamycin-Induced Autophagy and Cardioprotection In Vivo

***Howard Chen***[1,2], *Choukri Mekkaoui*[1,3], *Hoonsung Cho*[4], *Soeun Ngoy*[5], *Brett Marinelli*[2], *Peter Waterman*[6], *Matthias Nahrendorf*[6], *Ronglih Liao*[5], *Lee Josephson*[1,4], *David E. Sosnovik*[1,2], *[1]Martinos Center for Biomedical Imaging, Massachusetts General Hospital, Harvard Medical School, Boston, MA, USA; [2]Center for Molecular Imaging Research, Massachusetts General Hospital, Harvard Medical School, Boston, MA, USA; [3]Department of Radiology, Massachusetts General Hospital, Harvard Medical School, Boston, MA, USA; [4]Center for Translational Nuclear Medicine and Molecular Imaging, Massachusetts General Hospital, Harvard Medical School, Boston, MA, USA; [5]Cardiovascular division, Department of Medicine, Brigham and Women's Hospital and Harvard Medical School, Boston, MA, USA; [6]Center for Systems Biology, Massachusetts General Hospital, Harvard Medical School, Boston, MA, USA. Contact e-mail: Chen.howard@mgh.harvard.edu*

Autophagy is a biological process in which the cell digests a portion of its cytoplasmic contents and recycles the constituents for survival. The pathophysiological impact of autophagy in the heart, however, remains controversial and both protective and deleterious effects have been reported. One of the postulated autophagy mediated cardioprotective mechanism involves the clearance of damaged mitochondria, a potent pro-apoptotic stimulus, from the cytoplasm of injured cells, thus sparing cardiomyocytes from undergoing apoptotic cell death. The interplay between apoptosis and autophagy in the heart, however, has been difficult to characterize in part due to the absence of tools to quantify autophagy in vivo. Here, we perform 3D tomographic imaging of autophagy in the mouse heart in vivo by 1) exploiting the ability of near infrared (NIR) fluorescence to penetrate deep into tissue, 2) using source-detector configurations and algorithms supporting the tomographic reconstruction of light propagation in tissue and 3) detecting the upregulation of cathepsin activity in the expanded lysosomal compartment during autophagy. Molecular imaging of autophagy was first performed in two groups of mice: Mice with ischemia-reperfusion injury (IR), and mice with IR plus rapamycin pretreatment (IR+R). In both groups a cathepsin-activatable NIR fluorochrome was injected at the onset of reperfusion and fluorescence imaging of the heart was performed 4 hours later. In an initial cohort, the mice were sacrificed and the midmyocardium was exposed and imaged with ex vivo fluorescence reflectance imaging (FRI). Robust fluorescence activity was seen in the IR+R group, and not in IR only mice (Figure 1A). A subsequent cohort was imaged in vivo with fluorescence molecular tomography (FMT) (Figure 1B). Anatomical CT images acquired immediately before FMT were segmented and fused to the reconstructed fluorescence images. The fluorescence activity accumulated in the apical anterior and lateral walls of the heart. Volumetric quantification of the left ventricular fluorescence in IR+R mice increased significantly compared to the IR only control. Furthermore, rapamycin pretreatment was cardioprotective reducing both the area of Annexin-positive myocardium (Figure 1C) and infarct size (Figure 1D). The mechanism of the increased fluorescence signal induced by autophagy was studied in two cultured lines (ovarian CHO and myocyte H9C2). Cells exposed to rapamycin showed increased levels of cathepsin-B activity as well as increased endocytosis of extracellular contents (Figure 1E). Fluorescence microscopy showed that the cathepsin-activatable fluorescence signal induced by rapamycin colocalized strongly with markers of the lysosome compartment such as LAMP-2. In conclusion, we show here that cardiomyocyte autophagy can be imaged in vivo with a cathepsin activatable fluorochrome. We show in addition that the induction of autophagy with rapamycin significantly reduces apoptosis and infarct size. Our data suggest that autophagy is a protective mechanism in ischemia-reperfusion and raise new possibilities for myocardial salvage.

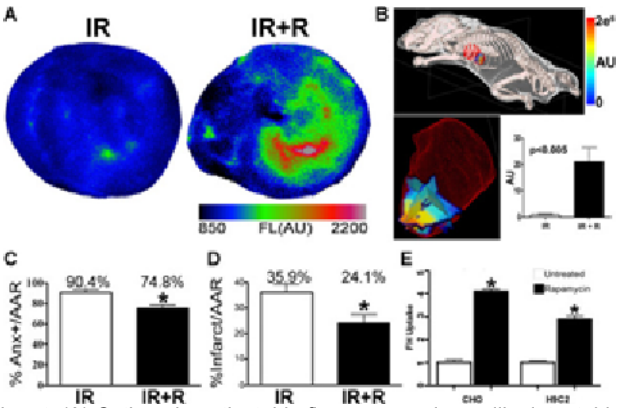


In vivo imaging of autophagy in the heart. (A) Cathepsin-activatable fluorescence is readily detectable in the ischemia-reperfusion injured midmyocardium following rapamycin induction (IR+R) while the IR control is at the background fluorescence level. (B) FMT images and the volumetric quantification of autophagic activity. (C-D) Rapamycin is cardioprotective, reducing both the area of Annexin positivity and infarct size. (E) FACS analysis of rapamycin treated cells show increased endocytosis. Autophagy-mediated endocytosis may play an important role in cell survival.

Disclosure of author financial interest or relationships:
**H. Chen**, None; **C. Mekkaoui**, None; **H. Cho**, None; **S. Ngoy**, None; **B. Marinelli**, None; **P. Waterman**, None; **M. Nahrendorf**, None; **R. Liao**, None; **L. Josephson**, None; **D.E. Sosnovik**, Siemens Medical, Grant/research support .

Presentation Number **SS 156**
Scientific Session 22: Preclinical In Vivo/Translational & Clinical - Cardiology
September 8, 2012 / 11:18-11:30 / Room: Wicklow Hall 1

# Trafficking of lipid-based nanoparticles to infarcted myocardium with potential application for MRI-monitored drug delivery

***Leonie Paulis***[1]*, Tessa Geelen*[1]*, Michael T. Kuhlmann*[2]*, Bram Coolen*[1]*, Michael Schäfers*[2]*, Klaas Nicolay*[1]*, Gustav J. Strijkers*[1]*,*
*[1]Biomedical NMR, Department of Biomedical Engineering, Eindhoven University of Technology, Eindhoven, Netherlands; [2]European Institute for Molecular Imaging, University of Muenster, Muenster, Germany. Contact e-mail: l.e.m.paulis@tue.nl*

**Introduction:** Nanoparticles are attractive drug carriers to improve the accumulation and retention of therapeutic agents in infarcted myocardium to stimulate reparative processes. Additionally, nanoparticles can be equipped with imaging labels for *in vivo* monitoring of drug delivery. However, nanoparticle trafficking to the infarct depends on many factors and is particularly challenging because of the impaired blood flow. In this study, the distribution pattern of two differently sized lipid-based nanoparticles, namely micelles and liposomes, was evaluated in a mouse model of myocardial infarction (MI) to explore their application as drug delivery vehicles. **Methods:** Paramagnetic, fluorescent micelles and liposomes (0.05mmol Gd/kg) were prepared as described previously.[1] Gd-DTPA (0.3mmol Gd/kg) was used as a control. Blood circulation half-lives were determined in mice (n=9) by evaluating the blood longitudinal relaxation rate ($R_1$) up to 48h after intravenous administration. MI was induced in mice (n=38) by permanent coronary artery ligation. Particles were injected intravenously after one day and one week, representing the acute and chronic phase of MI. *In vivo* ECG-triggered and respiratory-gated $T_1$w short-axis multi-slice FLASH MR images were acquired at 9.4T to evaluate the particle distribution in the heart up to 48h after administration. Global and local myocardial function was determined from cine MR images. *Ex vivo* fluorescence microscopy was used to determine the location of the nanoparticles in the infarct, which was compared to stainings for leukocytes (CD18), macrophages (CD68), blood vessels (CD31) and laminin. **Results:** Nanoparticle characterization and circulation half-lives are shown in Table 1. In acute MI, administration of micelles or liposomes initially resulted in MRI signal hypoenhancement of the infarct compared to the remote myocardium, reflected in a negative contrast-to-noise ratio (CNR) at 0.1h (Fig 1A). In time, the MRI signal of the infarct increased and at 24h CNR was significantly increased. Importantly, CNR increased faster by micelles than liposomes. In chronic MI, early after nanoparticle administration (0.1-1.5h), the infarct was not homogenously hypoenhanced on MR images, but within the infarct the subepicardium was significantly hyperintense compared to the subendocardium, caused by epicardial revascularization (Fig 1B). No significant infarct hyperenhancement was observed after 24h and 48h. Gd-DTPA injection led to immediate, non-persistent hyperenhancement of the infarct in both acute and chronic MI (Fig 1A, B). *Ex vivo* microscopy showed that in acute and chronic MI, micelles colocalized with necrotic myofibers, whereas liposomes were mostly located nearby blood vessels. **Conclusion:** Paramagnetic micelles and liposomes are attractive nanocarriers for transporting distinct types of drugs to the infarct. Micelles may be suited for delivery of cardioprotective or anti-remodeling drugs, whereas liposomes can be used for delivery of pro-angiogenic compounds. The successful *in vivo* MRI monitoring of the nanoparticle trafficking to the infarct is promising for clinical applications. [1] van Bochove; CMMI; 2011

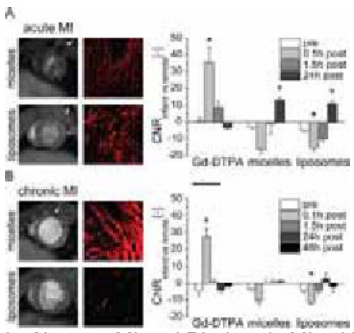


**Figure 1.** Cardiac distribution of micelles and liposomes in **A)** acute MI and **B)** chronic MI, with left: representative *in vivo* MRI and *ex vivo* microscopy 24h (acute MI) and 1.5h (chronic MI) after nanoparticle administration; right: group averaged CNR of infarct vs. remote myocardium of mice injected with Gd-DTPA, micelles and liposomes. * = p<0.05 vs. pre

**Table 1:** *In vitro* characterization of Gd-DTPA, micelles (n=3) and liposomes (n=4), and *in vivo* circulation half-lives (n=3 each)

| | | | | |
|---|---|---|---|---|
| Gd-DTPA | 1.6 | 3.9 | 4.2 | 0.3±0.05 |
| micelles | 14.0±0.8 | 6.2±0.2 | 43.0±7.6 | 3.00±0.44 |
| liposomes | 101.3±2.0 | 3.0±0.3 | 62.3±8.3 | 2.34±0.40 |

Disclosure of author financial interest or relationships:
**L. Paulis**, None; **T. Geelen**, None; **M.T. Kuhlmann**, None; **B. Coolen**, None; **M. Schäfers**, Siemens Medical Solutions, Grant/research support; **K. Nicolay**, None; **G.J. Strijkers**, None.

Presentation Number **SS 157**
Scientific Session 22: Preclinical In Vivo/Translational & Clinical - Cardiology
September 8, 2012 / 11:30-11:42 / Room: Wicklow Hall 1

# Longitudinal Evaluation of Myocardial Fatty Acid and Glucose Metabolism in Normal and Spontaneously Hypertensive Rat Models using microPET/CT

***Jennifer Huber***[1]*, Andrew Hernandez*[1]*, Mustafa Janabi*[1]*, James P. O'Neil*[1]*, Kathleen M. Brennan*[1]*, Stephanie T. Murphy*[2]*, Youngho Seo*[2]*, Grant T. Gullberg*[1]*, [1]Radiotracer Development and Imaging Technology, Lawrence Berkeley National Lab, Berkeley, CA, USA; [2]Radiology and Biomedical Imaging, University of California San Francisco, San Francisco, CA, USA. Contact e-mail: jshuber@lbl.gov*

**Introduction:** The goal of this project was to develop radionuclide molecular imaging techniques using microPET/CT, quantifying changes in myocardial metabolism using the spontaneously hypertensive rat (SHR) as a model of hypertensive-related pathophysiology. Although this SHR model has been extensively studied previously, our microPET/CT investigation of this animal model is novel and our techniques should be translatable to the clinic. **Methods:** We quantitatively compared fatty acid metabolism and glucose metabolism in the hearts of SHR and Wistar-Kyoto (WKY) normotensive rats as a function of age over a two-year period, tracking physiological changes associated with the onset and progression of heart failure in the SHR model. The long-chain fatty acid analog [18F]fluoro-6-thia-heptadecanoic acid (FTHA) and the glucose analog 2-deoxy-2-[18F]fluoro-D-glucose (FDG) were used in longitudinal microPET/CT imaging studies to investigate the myocardium metabolic changes. For both rat cohorts, four SHR and four WKY rats were studied at approximately 9 months, 12 months, 16 months, 19 months and 21 months after birth. Dynamic multiframe data were acquired with ECG gating immediately after injection of the radiotracer, followed by an ungated CT acquisition. The microPET data were reconstructed using a 2D OSEM algorithm with CT-based attenuation correction. Time-activity curves were generated from the left ventricular myocardial tissue and the left ventricular blood pool volumes of interest. These time-activity curves were fit to compartment models to obtain estimates of the wash-in and wash-out rates of the radiotracer from the myocardium. Two-way analyses of variance (ANOVA) were performed, using the factors of type (SHR/WKY) and time. **Results:** The SHR model demonstrated a significantly lower metabolic rate of FTHA than the normotensive WKY model (p=0.0006), whereas the SHR model demonstrated a significantly higher metabolic rate of FDG than the WKY model (p=4e-8). We did not observe a significant decline in metabolic rates due to aging in either cohort. **Conclusions:** Under normal conditions, the primary metabolic fuel for the myocardium comes from fatty acids. In a failing heart, fatty acid metabolism decreases and glucose becomes the major metabolic fuel. Therefore, we have demonstrated that these radionuclide molecular imaging techniques might be used clinically to predict hypertensive left ventricular hypertrophy. However, our current study is limited because our longitudinal studies of fatty acid and glucose metabolism used separate rat cohorts. We are currently extending this research, by studying a larger cohort of SHR and WKY rats with microPET/CT imaging using perfusion ([18F]fluorodihydrorotenol) and metabolic (FTHA and FDG) radiotracers within the same animal.

Disclosure of author financial interest or relationships:
**J. Huber**, None; **A. Hernandez**, None; **M. Janabi**, None; **J.P. O'Neil**, None; **K.M. Brennan**, None; **S.T. Murphy**, None; **Y. Seo**, None; **G.T. Gullberg**, None.

Presentation Number **SS 158**
Scientific Session 22: Preclinical In Vivo/Translational & Clinical - Cardiology
September 8, 2012 / 11:42-11:54 / Room: Wicklow Hall 1

# Integrin receptor imaging of myocardial infarction: serial preclinical studies and a pilot clinical application

***Zhaohui Zhu**, Chenxi Wu, Yi Sun, Kun Zheng, Ximin Shi, Dept. Of Nuclear Medicine, Peking Union Medical College Hospital, Beijing, China. Contact e-mail: zzh_1969@yahoo.com.cn*

Objectives : Serial preclinical and clinical studies were performed to investigate the role of integrin receptor imaging in evaluation of myocardial infarction (MI). Methods : In the preclinical studies, rat MI models (n=21) were established by ligation of the anterior descending branch of coronary artery and were continiously evaluated for nearly 5 months using 68Ga-PRGD2 and 18F-FDG microPET. Fifteen of the model rats accepted injection of adipose-derived mesenchymal stem cell (ADMSC, 5×10E6 cells) into pericardial region one week post MI modeling. Fifteen rats underwent 18F-MISO microPET early after MI modeling, and 3 rats accepted serial 99mTc-3PRGD2 nanoSPECT/CT for comparison. In the clinical study with informed consent, 68Ga-PRGD2 PET/CT was performed in 4 patients, including 3 acute myocardial infarction (AMI) patients 1-2 weeks post MI attack and one patient with a MI attack two years ago. 18F-FDG PET/CT and 99mTc-MIBI SPECT were also performed for comparison. Volume of interests were placed over the MI regions to measure the maximum standardized uptake values (SUV), and the mean SUVs of mediastinum and liver were also measured to calculate the uptake ratios. Two-way ANOVA with one repeated factor of time post modeling was used for statistical analysis using SPSS 17.0 software. P < 0.05 was considered significant. Results : Mild to moderate 68Ga-PRGD2 and 99mTc-3PRGD2 uptakes, peaked at nearly 1 month post MI modeling, were observed in all rat models at the edge of MI area. The 68Ga-PRGD2 uptakes were relatively low early after ADMSC treatment but remained stable in the treatment group while it decreased gradually in the controls one month later. Significant higher 68Ga-PRGD2 uptakes were found in the ADMSC treatment group 4-5 months post MI modeling (P=0.031), while the recovery of 18F-FDG uptakes also significantly improved. 18F-FMISO uptakes peaked at 2.5~3.5 h after MI modeling, which were in significant positive correlation with the highest 68Ga-PRGD2 uptakes (r=0.830, P=0.021, n=7). In 3 AMI patients, 68Ga-PRGD2 uptakes were clearly observed in the peri-MI regions, while it was negative in the patient with old MI two years ago. Conclusions : Integrin receptor imaging seems helpful for evaluation of MI and provides an importamt evidence that supports ADMSC treatment of MI. The pilot clinical appliction of 68Ga-PRGD2 PET/CT in evaluation of AMI is successful, which merits further investigation of its clinical value in guiding AMI treatments.

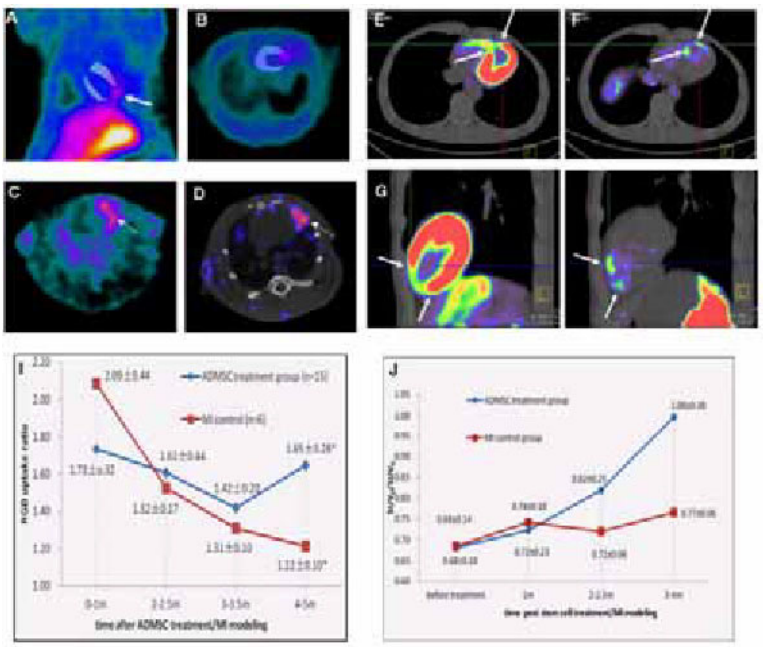


Figure: Comparison of 68Ga-PRGD2 microPET (A-C), 18F-FDG microPET (white-color cardiac uptake in A and B), and 99mTc-3PRGD2 nanoSPECT/CT (D) in rat myocardial infarction models, as well as 18F-FDG (E and G) and 68Ga-PRGD2 (F and H) PET/CT in an acute myocardial infarction patient. During the recovery, there were significant difference of 68Ga-PRGD2 (I) and 18F-FDG (J) uptake between the control group (red line, n=6) and the treatment group using adipose-derived mesenchymal stem cell (ADMSC) (blue line, n=15, P<0.05)

Disclosure of author financial interest or relationships:
**Z. Zhu**, None; **C. Wu**, None; **Y. Sun**, None; **K. Zheng**, None; **X. Shi**, None.

Presentation Number **SS 159**
Scientific Session 23: Preclinical In Vivo - Neurology
September 8, 2012 / 10:30-11:00 / Room: Liffey Hall 2

# Molecular and Optical Axes of Control

***Feng Zhang**, The Broad Institute, Cambridge, MA, USA. Contact e-mail: zhang@broadinstitute.org*

Disclosure of author financial interest or relationships:
**F. Zhang**, None.

Presentation Number **SS 16**
Scientific Session 2: Technology & Software - Optical Imaging
September 6, 2012 / 11:47-11:58 / Room: Wicklow Hall 1

# Multispectral InP/ZnS quantum dots for dual emissive surgical guidance

***Patrick T. Chin**, Tessa Buckle, Nynke S. van den Berg, Fijs van Leeuwen, Radiology, LUMC, Leiden, Netherlands. Contact e-mail: p.t.k.chin@lumc.nl*

Fluorescence imaging is rapidly increasing its popularity in image guided surgery applications. To help develop its full surgical potential it remains a challenge to generate dual-emissive imaging agents that allow for combined visible assessment and sensitive camera based imaging. Bi-spectral InP/ZnS quantum dots (QDs) that exhibit a bright visible green/yellow exciton emission combined with a long-lived far red defect emission can be used for such an application.[1] The intensity of the defect emission was enhanced by X-ray irradiation and allows for: 1) inverted QD density dependent defect emission intensity, showing improved efficacies at lower QD densities, and 2) detection without direct illumination and interference from autofluorescence. These QDs can be applied in surgical marker seeds. To allow such marking in a multimodal setting, we have generated seeds compromising of a cocktail of bi-spectral InP/ZnS QDs, lipids, and pertechnetate.[2] Phantom experiments demonstrate that these multimodal seeds can be placed accurately around a surrogate tumor using ultrasound and provide the opportunity to predetermine the resection margins by validating the placement accuracy using multiple imaging modalities (namely, x ray, MRI, SPECT/CT, and ultrasound). The dual-emissive fluorescent properties of the InP/ZnS QDS in combination with multispectral imaging provide the unique opportunity to intra-operatively estimate the depth of the seed relative to the tissue surface. We found that the differences between the different emission regions enabled accurate dept estimation via a 'traffic light' approach.[3] References [1] P. T. K. Chin, T. Buckle, A. Aguirre de Miguel, S. C. J. Meskers, R. A. J. Janssen, F. W. B. van Leeuwen Biomaterials 2010, 31, 6823 [2] T. Buckle, P.T. Chin, N.S. van den Berg, C.E. Loo, W. Koops, K.G. Gilhuijs, van F.W. Leeuwen J Biomed Opt. 2010, 15, 056021 [3] P. T.K. Chin, C. A.C. Beekman, T. Buckle, L. Josephson, F. W.B. van Leeuwen Am J Nucl Med Mol Imaging (accepted)

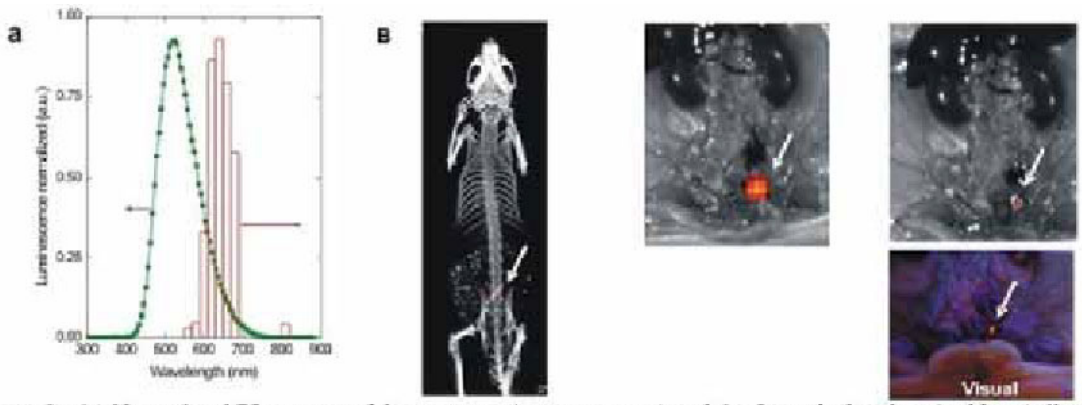


***Figure. 1:** (a) Normalized PL spectra of the exciton - (green squares) and the far red afterglow (red bars) illustrating the ~130 nm red shift between the respective spectra at 100 ns and >1 min. (b) Representation of a the placement of the multimodal marker seed in a mouse prostate, showing a 3D SPECT/CT image visualizing the seed localization (fire) with respect to the rest of the mouse anatomy, followed by the defect emission (glow), exciton emission (rainbow) and visual fluorescent image of the exposed marker seed.*

Disclosure of author financial interest or relationships:
**P.T. Chin**, None; **T. Buckle**, None; **N.S. van den Berg**, None; **F. van Leeuwen**, None.

Presentation Number **SS 160**
Scientific Session 23: Preclinical In Vivo - Neurology
September 8, 2012 / 11:00-11:12 / Room: Liffey Hall 2

# Survival of Neural Progenitors Allografted into the CNS of Immunocompetent Recipients is Highly Dependent on Transplantation Site

***Miroslaw Janowski***[1,3], *Charla Engels*[1,2], *Michael Gorelik*[1,2], *Agatha Lyczek*[1,2], *Jeff W. Bulte*[1,2], *Piotr Walczak*[1,2], [1]*Department of Radiology, Johns Hopkins University School of Medicine, Baltimore, MD, USA;* [2]*Institute for Cell Engineering, Johns Hopkins School of Medicine, Baltimore, MD, USA;* [3]*NeuroRepair Department, Mossakowski Medical Research Centre, Warsaw, Poland. Contact e-mail: neuroibis@gmail.com*

Allografts continue to be used in clinical neurotransplantation, hence it is crucial to understand the mechanisms that govern allograft tolerance. The non-invasive imaging related to the fate of transplanted cells is instrumental to understanding of graft-host interactions, including the local immune response. In previous studies, we observed a large variability in survival of grafts injected into the corpus callosum with some of the allografts surviving long-term in immunocompetent BALB/c mice, even without immunosuppression. Due to the small size of the corpus callosum in mice, this structure cannot accommodate the entire volume of transplanted cells without overspill into the neighboring gray matter structures. We hypothesized that the variability of cell survival may be related to the different immune responses between grey and white matter. We therefore compared the survival of GRPs allografted into either the forceps minor (FM) as the largest white matter structure in mice, or the striatum (STR) as the predominantly grey matter structure. 3x105 luciferase-expressing mouse (FVB) glial precursors were injected into the FM or STR of immunodeficient rag2-/- and immunocompetent BALB/c mice. Cells were tagged with iron oxide nanoparticles (Molday ION, BioPAL, Inc.) for verification of graft placement precision. T2-weighted MRI confirmed the accuracy of cell deposition at the selected coordinates (n=5). BLI was used for non-invasive assessment of graft viability over a period of 16 days. Regardless of implantation site, all grafts (n=10) deposited in immunodeficient animals demonstrated excellent survival. In contrast, immunocompetent animals accepted all grafts only at the STR site (n=10), while all FM grafts were rejected (n=10) ($p<0.001$). To investigate the factors that led to the rejection of FM grafts, with acceptance of STR grafts, another group of animals (n=19) was sacrificed during the pre-rejection period on day 5. Near-infrared fluorescence imaging with the IRDye®800CW-PEG contrast agent displayed a similar blood-brain barrier (bbb) disruption for both graft locations (Fig. 1) (p=NS). The morphological distribution of FM grafts was cylindrical, parallel to the needle track, while cells transplanted into the STR accumulated along the border between the striatum and the corpus callosum. There was significantly less infiltration by both innate (CD11b, $p<0.05$) and adaptive (CD8, $p<0.05$) immune cells in the STR grafts, especially along the calloso-striatal border. The FM grafts were surrounded by a dense lining of CD11b+ activated microglia. The lack of correlation between bbb disruption and the extent of graft infiltration by immune cells indicates that the cellular and not the humoral immune response plays a pivotal role in initiation of graft rejection. With allograft survival being dependent on the transplantation site, the chosen anatomical coordinates of the graft target are critical for determining success or failure of therapy.

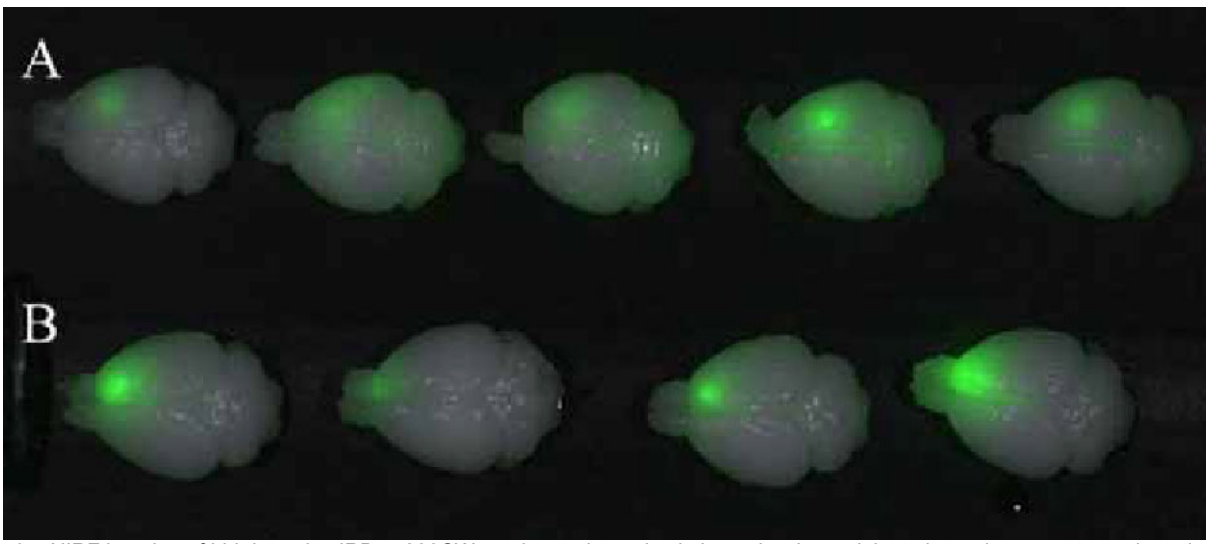


Figure 1: Ex vivo NIRF imaging of bbb integrity. IRDye 800CW, conjugated to polyethylene glycol, was injected at 4 days post-transplantation. In all STR (A) and FM (B) grafts, leakage of the dye occurred, indicating a disruption of the bbb in all animals.

Disclosure of author financial interest or relationships:
**M. Janowski**, None; **C. Engels**, None; **M. Gorelik**, None; **A. Lyczek**, None; **J.W. Bulte**, Philips, Grant/research support; Q Therapeutics, Grant/research support; **P. Walczak**, None.

Presentation Number **SS 161**
Scientific Session 23: Preclinical In Vivo - Neurology
September 8, 2012 / 11:12-11:24 / Room: Liffey Hall 2

# *In vivo* Evaluation of SERT Density and [$^{11}$C]DASB Affinity for Brain Imaging in Mice and Rats Using a Multiple Ligand Concentration Transporter Assay (MLCTA)

***Michael Walker**, Kristina Fischer, Maren K. Koenig, Mareike Lehnhoff, Walter Ehrlichmann, Anke Stahlschmidt, Bernd J. Pichler, Department of Preclinical Imaging and Radiopharmacy, Eberhard Karls University of Tuebingen, Tuebingen, Germany. Contact e-mail: michael.walker@med.uni-tuebingen.de*

Serotonin (5-HT) is one of the most important neurotransmitters in the mammalian brain. Hence, it is involved in many essential neurological processes, such as food intake, motor activity, cognition or emotion. The highest density of 5-HT fibres is located in the brain stem, forming the Raphe Nuclei. One of the most promising approaches to visualize serotonergic neurotransmission is the SERT marker [$^{11}$C]-3-amino-4(2-dimethylaminomethyl-phenylsufanyl)-benzonitrile ([$^{11}$C]DASB). This tracer is used in many pharmacological PET-studies, as a highly affine and selective radioligand for the SERT. The aim of our study was to evaluate the feasibility of the in vivo quantification of SERT density in the thalamus of rats and mice by using [$^{11}$C]DASB as a tracer. The MLCTA was performed in 8 C57/BL6 mice and 4 Sprague Dawley rats. The animals were positioned with stereotactic holders in the microPET scanner under temperature controlled conditions. Time activity curves were generated and fitted using first the Simplified Reference Tissue Model (SRTM) to create a population mean $k'_2$ value. Subsequently, the binding potential ($BP_{ND}$) was determined, using the population mean $k'_2$ in SRTM2. All animals underwent a total of 4 scans with decreasing specific activities (SA) of [$^{11}$C]DASB and an additional high SA scan was performed to calculate the test-retest variability. For mice, the injected activity was 460±68MBq/kg and for rats 62±8MBq/kg. The SA ranged from 116 to 0.5 GBq/µmol in mice and 179 to 0.4 GBq/µmol in rats, corresponding to injected doses of 3.9-980.48 nmol/kg and 0.3-107 nmol/kg. Linear and non-linear regression analysis was performed to calculate SERT density ($appB_{max}$) and [$^{11}$C]DASB affinity ($appK_d$) separately. To validate the effect of partial volume on the accuracy of [$^{11}$C]DASB PET quantification, we used autoradiography (AR) and compared the PET DVR-1 to the AR DVR-1 at pseudo-equilibrium in two mice. Test-retest variability was 6% in mice and 36% in rats. Using *in vivo* Scatchard analysis and the cerebellum as an estimate for the free tracer concentration, the average $appB_{max}$ and $appK_d$ values were in 6.5±0.7 pmol/mL and 2.9±0.61 pmol/mL in mice and 5.6±0.8 pmol/mL and 2.9±0.8 pmol/mL in rats, respectively. Non-linear regression analysis revealed $appB_{max}$ and $appK_d$ values of 2.69±1.15 pmol/mL and 1.07±0.9 pmol/mL in mice and 2.65±1.2 pmol/mL and 1.6±0.64 pmol/mL in rats. Comparison of $BP_{ND}$ from *in vivo* PET experiments and *ex vivo* AR showed nearly the same values (PET: 2.74±0.13; AR: 2.72±0.13). In this study we demonstrate for the first time that [$^{11}$C]DASB PET can be used for *in vivo* SERT quantification in mice and rats. However tracer mass and non-saturable binding under *in vivo* conditions have to be taken into account when performing linear and non-linear regression analysis for the calculation of $appB_{max}$ and $appK_d$. We also revealed a specific binding of [$^{11}$C]DASB in the cerebellum of both species. Therefore, further studies are planed, where the input function will be generated from arterial blood.

Disclosure of author financial interest or relationships:
**M. Walker**, None; **K. Fischer**, None; **M.K. Koenig**, None; **M. Lehnhoff**, None; **W. Ehrlichmann**, None; **A. Stahlschmidt**, None; **B.J. Pichler**, Siemens, Grant/research support; AstraZeneca, Grant/research support; Bayer Healthcare, Grant/research support; Boehringer-Ingelheim, Grant/research support; Oncodesign, Grant/research support; Merck, Grant/research support; Bruker, Grant/research support .

Presentation Number **SS 162**
Scientific Session 23: Preclinical In Vivo - Neurology
September 8, 2012 / 11:24-11:36 / Room: Liffey Hall 2

# Simultaneous in vivo Measurement of D2/D3 Receptor Density and Affinity Using [11C]Raclopride and a Single Injection PET Protocol in Mouse Models of Neurological Disorders

***Kristina Fischer***[1], *Catriona J. Wimberley*[2], *Janine Magg*[3], *Huu Phuc Nguyen*[3], *Walter Ehrlichmann*[1], *Marie-Claude Gregoire*[2], *Bernd J. Pichler*[1], [1]*Department for Preclinical Imaging and Radiopharmacy, Eberhard Karls University of Tuebingen, Tuebingen, Germany;* [2]*Australian Nuclear Science and Technology Organisation, ANSTO LifeSciences, Sydney, NSW, Australia;* [3]*Department of Medical Genetics, Eberhard Karls University of Tuebingen, Tuebingen, Germany. Contact e-mail: kristina.fischer@med.uni-tuebingen.de*

For the in vivo quantification of D2 receptor expression (appBmax) and [11C]raclopride affinity (1/appKd) multiple injection protocols have been established. Since multiple injection experiments are expensive, time consuming and require at least 3 to 4 scans per animal, we aimed to identify an analysis approach that meets the requirements of technical simplicity and greatest possible accuracy for routine laboratory protocols. Here, we investigated the partial saturation approach (PSA)(1), a single injection approach for [11C]raclopride PET imaging in mouse models of human diseases. [11C]Raclopride PET scans were performed with raclopride doses, ranging from 2.6 to 550 nmol/kg using an injected activity of 427+/-42 MBq/kg. Individual time activity curves were generated from the striatum and the cerebellum, which were used to estimate the free (F) and bound (B) tracer concentration. The general equilibrium equation: B/F=(Bmax-B)/KdVr-dB/dT*(1/koff*F) includes a residual term which was used as an indicator of the dynamic equilibrium state to choose a constraining time window and occupancy level for Scatchard analysis. 6 mice participated in test-retest experiments on 2 separate days with the mass dose kept constant at 44±3 nmol/kg. To identify the impact of increased dopamine (DA) availability on appBmax and appKd values, mice underwent 2 scans, at baseline and under challenge conditions: (i) 30 min (n=4) and 4h (n=4) after 3 mg/kg d-amphetamine (AMPH) i.p., and (ii) 10 min after 3 mg/kg methylphenidate (MP) i.v. (n=4). To calculate changes of D2/D3 receptor expression using the PSA 2 mouse models of human disease were used: (i) the R6/2 mouse model of Huntingtons disease: 4 transgenic mice and 3 healthy controls were scanned at 5 and 7 weeks of age and (ii) the 6-OHDA mouse model of Parkinsons disease: 6 mice were lesioned with 3 µg 6-OHDA in the right medial forebrain bundle (MFB) and PET scans were performed after 3 weeks of recovery. Except for the early data points, the bound ligand concentration showed a linear decrease over the duration of the PET scan over a wide range of occupancy levels (30-60%). Test-retest experiments revealed a reproducibility of 78% and 81% for appBmax and appKd, respectively. MP challenge decreased appBmax by 62% and appKd by 74%. AMPH challenge decreased appBmax by 75% with no effect on appKd 30 min after injection and showed no difference to baseline values 4h after injection. Injection of 6-OHDA into the MFB decreased appBmax by 46% with no effect on appKd. In transgenic R6/2 mice, appBmax decreased by 60% from 7 to 5 weeks of age with no effect on appKd. In control mice, both appBmax and appKd increased by 88% and 152%, respectively, from 7 to 5 weeks of age. Our results demonstrate that the PSA is a very attractive method for [11C]raclopride PET imaging in mice to assess changes in dopamine concentrations and receptor expression after pharmacological interventions and in neurodegenerative or neuropsychiatric disorders using a single bolus injection PET protocol. 1. Delforge J. et al. J Nucl Med. Jan 1996;37(1):5-11.

Disclosure of author financial interest or relationships:
**K. Fischer**, None; **C.J. Wimberley**, None; **J. Magg**, None; **H. Nguyen**, None; **W. Ehrlichmann**, None; **M. Gregoire**, None; **B.J. Pichler**, Siemens, Grant/research support; AstraZeneca, Grant/research support; Bayer Healthcare, Grant/research support; Boehringer-Ingelheim, Grant/research support; Oncodesign, Grant/research support; Merck, Grant/research support; Bruker, Grant/research support .

Presentation Number **SS 163**
Scientific Session 23: Preclinical In Vivo - Neurology
September 8, 2012 / 11:36-11:48 / Room: Liffey Hall 2

# In vivo follow-up of the dopamine transporter using [18F]LBT-999 in a rat model of Parkinson's disease

*Sophie Sérrière, Johnny Vercouillie, Sylvie Bodard, Gabrielle Chicheri, Lucette Garreau, Laurent Galineau,* ***Sylvie Chalon****, UFR des Sciences pharmaceutiques, Inserm U930, Tours, France. Contact e-mail: sylvie.chalon@univ-tours.fr*

Introduction: PET imaging in small animals has major interest such as the follow-up of specific molecular targets in a number of models of human brain disorders. In this field, exploration of the dopamine transporter (DAT) appears as a highly valuable target in animal models of Parkinson's disease (PD), a neurodegenerative disease for which neuroprotective and/or repairing treatments are still lacking. We recently developed a [18F]-labeledl derivative of PE2I, i.e. (E)-N-(4-fluorobut-2-enyl)-2beta-carbomethoxy-3beta-(4'-tolyl)nortropane or LBT-999 [1], which has recently been characterized in the monkey [2]. This study presents first experiments with [18F]LBT-999 in a rat model of PD induced by a partial 6-hydroxydopamine (6-OHDA) lesion. Methods: The chlorinated precursor of LBT-999 was labeled with [18F] according to [3] and obtained with a mean specific activity of 180 GBq/µmol. Animals (n=2) were lesioned in the right striatum using 6-OHDA (2 times 5 µg/5 µl of 0.01% ascorbic acid in phosphate buffer) according to [4]. PET scans (eXplore Vista-CT, GE) were performed in each animal at 7 and 1 day before lesion and on days 1, 3, 6, 13 and 19 post-lesion.PET dynamic acquisitions were conducted under isoflurane anesthesia for 71 min followed by a CT scan for attenuation correction. Animals were injected i.v.with 18MBq/100 g body weight of [18F]LBT-999. The dynamic PET acquisitions were divided into one 60-s frame for the first min, four 10-s frames, four 20-s frames, four 60-s frames, height 180-s frames, six 6-min frames and one 240-s frame for the duration of the scan. Quantification was performed with PMOD software (3.306, PMOD Technologies, Ltd., Adliswil, Switzerland). PET and CT scans were co-registered and different VOIs corresponding to 6 cerebral structures (striatum, amygdala, hippocampus, ventral tegmental area/substantia nigra, thalamus and cerebellum) were extracted from a rat atlas (Schiffer rat Atlas, Pmod). Time activity curves of these structures and a kinetic analysis using the simplified reference tissue model was performed. Results: Before lesion, the meantime-activity curve of [18F] LBT-999 in the whole brain was around 300% SUV. The higher uptake was observed in the striatum, followed by the thalamus and cerebellum. Peak specific binding in the striatum (region/cerebellum) was equal to 4 and was reached at approximately 20-40 min. After lesion, the binding potential between the intact and lesioned side was reduced to 60% at 24 h post-lesion, 25% at 3 days, and then remained 20% reduced between 6 and 19 days post-lesion. Conclusions: This study showed that in vivo quantification of [18F]LBT-999 binding to the DAT in the rat brain is suitable for the study of progressive reduction of this target in a rat model of PD. This opens the future opportunity to test potential new treatments in this model using this PET tracer. Acknowledgements: This work was supported by EC-FP6-project DiMI, LSHB-CT-2005-512146 References: [1]Chalon S. et al. J Pharmacol Exp Ther 2006; 317:147-152. [2]Varrone A. et al. J Nucl Med 2011; 52:1313-1321. [3]Dollé F. et al. J Labelled Comp Radiopharm 2007; 50:716-723. [4]Maia et al. Synapse 2012.

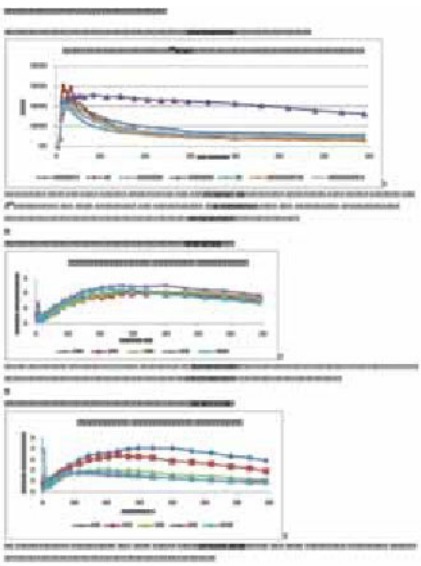

Disclosure of author financial interest or relationships:
**S. Sérrière**, None; **J. Vercouillie**, None; **S. Bodard**, None; **G. Chicheri**, None; **L. Garreau**, None; **L. Galineau**, None; **S. Chalon**, None.

Presentation Number **SS 164**
Scientific Session 23: Preclinical In Vivo - Neurology
September 8, 2012 / 11:48-12:00 / Room: Liffey Hall 2

# Optimizing Confocal Imaging of Neuronal Transport in a Microfluidic Platform

***Lucia LeRoux**, Leo G. Flores, Dawid Schellingerhout, Experimental Diagnostic Imaging, MD Anderson, Houston, TX, USA. Contact e-mail: lucia.leroux@mdanderson.org*

Our purpose was to study neuronal transport in living axonal cultures. In this study we devised an experimental system to allow this using a specialized live culture system (Millipore, AX150) and confocal imaging. We used micro-fluidic chambers that direct the growth of axons into microgrooves (10 um each) by means of hydro-static pressure [1]. The microgroove, dual-chamber system also serves separate the neuronal cell bodies from the neurite end terminals, allowing dual-chambered experiments with differing fluid environments for the neuritis and the cell bodies. Imaging was done with an Olympus FV1000 Confocal Microscope using a PLAPO60XO3 oil objective. We optimized 3D imaging within the microfluidic grooves containing neurites at 12 bits/pixel at 20% laser power to reduce the effects of photo-bleaching. We found, during our optimization that several factors were very important for the culture system: a) there had to be a tight seal (plasma bonding) between the isolation inset and the culture plate bottom, b) hydrostatic pressure had to be carefully applied to guide neurite growth, and c) to isolate the cell bodies from nerve terminals. We found that the following factors were important for the optimization of imaging: a) thin bottom (0.17 mm) glass coverslip material was needed, with b) high magnification (60x oil), c) careful Z-stack optimization to find the optimal plane of imaging and d) the choice of fluorophore needed to be matched to system sensitivities. We demonstrated retrograde neural transport of fluorescently labeled Tetanus toxin C fragment (TTc) in differentiated PC12 cells using this system, and were able to show foci of fluorescence (likely transport endosomes) traveling along the neurite over a 30 minute observation period during live imaging. This technique allows us to determine the rate of in-vivo neural transport in mammalian cells and will further advance our knowledge of neuronal transport (Figures 1A & B), and highlights the importance of optimized live cell culture systems and confocal imaging. References: [1] Enquist et al., A microfluidic Chamber for analysis of Neuron-to-Cell Spread and Axonal Transport of an Alpha-Herpesvirus. Plos One Vol 3 (Issue 6). E2382 (2008).

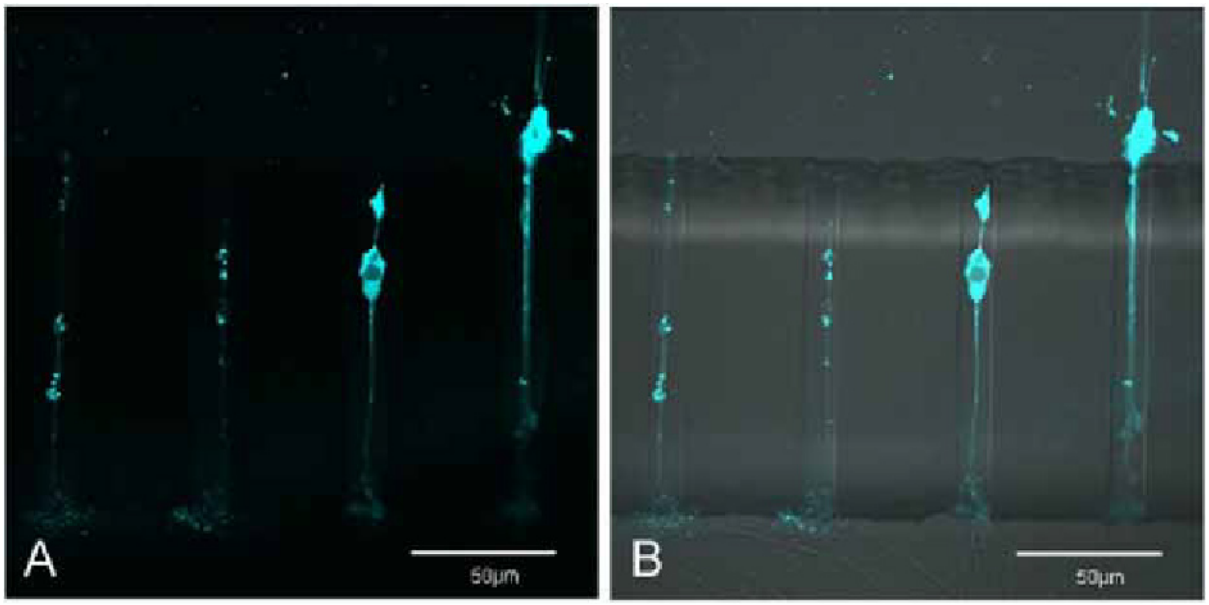


Figure 1. Imaging of individual neurites in a Micro-fluidic device (AX150) We demonstrate retrograde neural transport of Alexa488 TTc during a 30 minute live imaging session using a 60x oil objective. The directional movement of TTc molecules could be observed in the neuritis using confocal imaging (A) and in bright field overlay images (B).

Disclosure of author financial interest or relationships:
**L. LeRoux**, None; **L.G. Flores**, None; **D. Schellingerhout**, None.

Presentation Number **SS 165**
Scientific Session 24: Translational & Clinical - Oncology
September 8, 2012 / 10:30-11:00 / Room: Wicklow Hall 2

# Hyper-polarized MRI

***Ferdia Gallagher**, University of Cambridge, Cambridge, United Kingdom. Contact e-mail: fag1000@cam.ac.uk*

Disclosure of author financial interest or relationships:
**F. Gallagher**, GE Healthcare, Grant/research support .

Presentation Number **SS 166**
Scientific Session 24: Translational & Clinical - Oncology
September 8, 2012 / 11:00-11:12 / Room: Wicklow Hall 2

# Identifying Prognostic Factors in Combined Anti-angiogenesis and Radiotherapy for Pancreatic Cancer

*Ning Cao[1], Minsong Cao[2,5], Helen J. Chin-Sinex[3], Marc S. Mendonca[2,3], Song-Chu Ko[2], **Keith M. Stantz**[1,4], [1]School of Health Sciences, Purdue University, West Lafayette, IN, USA; [2]Radiation Oncolgy, Indiana university School of Medicine, Indianapolis, IN, USA; [3]Radiation and Cancer Biology, Indiana university School of Medicine, Indianapolis, IN, USA; [4]Radiology and Imaging Sciences, Indiana university School of Medicine, Indianapolis, IN, USA; [5]Radiation Oncology, UCLA, Los Angeles, CA, USA. Contact e-mail: kstantz@purdue.edu*

Purpose: The objectives of this study are to determine the appropriate anti-angiogenic regimen that will enhance the efficacy of radiation therapy in pancreatic cancer, and to identify prognostic factors of radiosensitivity through the use of in vivo imaging techniques. Introduction: Pancreatic cancer is known to be highly hypoxic, an important environmental factor that significantly contributes to metastasis and the ineffectiveness of radiotherapy and chemotherapy. A dominant factor contributing to and upregulated by hypoxia is VEGF, a growth factor that promotes angiogenesis, enhances tumor growth, and promotes metastasis. However, clinical studies investigating the use of anti-angiogenic drugs in patients with pancreatic cancer did not provide clinical benefit. We hypothesize high doses (HD) of a VEGFR2 inhibitor can increase tumor hypoxia and antagonize RT through the destruction of tumor vasculature while low doses (LD) can increase microvascular efficiency, decrease overall tumor hypoxia, and increase radiosensitivity of pancreatic tumors. To achieve an optimal outcome for combined AAT plus RT, we propose to use dynamic contrast-enhanced CT (DCE-CT) to non-invasively track factors associated with tumor angiogenesis and oxygenation pre- and post-treatment to predict RT response. Material and Methods: Two experiments were performed. First, three cohorts of mice bearing human BxPC-3 pancreatic tumors were treated with a sham, a HD and a LD of DC101 (anti-VEGFR2 monoclonal antibody). DCE-CT scans were acquired at baseline, 2 days, 1 week, and 2 weeks post treatment. Based on average tumor perfusion and fractional plasma volume values, and the root-mean-square of their histogram distributions, a normalization window was determined to occur at 1 week post-DC101. Next, three cohorts of mice were treated with RT (5Gy), HD DC101 plus RT (5Gy), and LD plus RT (5Gy). Vascular physiology pre-DC101 (baseline) and pre-RT (1 week) were measured, and two parameters representing the microvascular efficiency calculated, mean-transit-time (MTT) and relative tortuosity ($\Delta\tau$). Results: Compared to RT, HD and LD DC101 treatment further delayed tumor growth by an additional 9 days (d) (9-to-18d). The addition of RT one week post-DC101 treatment delayed tumor growth by an additional 9d (18-to-27d), which is consistent with an additive response. However, an AAT dose-dependency on RT response was NOT observed, and a synergistic response to RT based on the normalization was NOT observed. Instead, the LD and HD cohorts were reclassified into a responding (R) and a non-responding (NR) RT group based on the relative change in perfusion and fp, and MTT and $\Delta\tau$ to DC101. A difference of 12d was observed between R and NR tumor growth delay curves. Conclusions: DCE-CT monitors tumor physiology and changes in microvascular efficiency in response to DC101, which is believed to be associated with vascular normalization and tumor oxygenation. Also, the link between these physiological measures and the tumor volume to DC101 dose ratio is suggestive of normalization, thus identifying a regimen and prognostic factor that can be used to augment treatment of pancreatic cancer.

Disclosure of author financial interest or relationships:
**N. Cao**, None; **M. Cao**, None; **H.J. Chin-Sinex**, None; **M.S. Mendonca**, None; **S. Ko**, AMI Purdue Foundation, Grant/research support; **K.M. Stantz**, None.

Presentation Number **SS 167**
Scientific Session 24: Translational & Clinical - Oncology
September 8, 2012 / 11:12-11:24 / Room: Wicklow Hall 2

# Impact of F-18 Choline PET - CT in prostate cancer patients with biochemical recurrence - influence of hormonal therapy and correlation with PSA kinetics

***Silke Haim***[1], *Mohsen Beheshti*[1], *Wolfgang Loidl*[2], *Leo Pallwein-Prettner*[3], *Martin Steinmair*[1], *Thomas Kunit*[2], *Michael Nader*[1], *Peter Waldenberger*[3], *Werner Langsteger*[1], [1]*Nuclear Medicine & Endocrinology, PET - CT Center LINZ, St. Vincent's Hospital, Linz, Austria;* [2]*Urology, St. Vincent's Hospital, Linz, Austria;* [3]*Radiology, St. Vincent's Hospital, Linz, Austria. Contact e-mail: silke.haim@bhs.at*

Purpose: To evaluate the potential of F-18 Fluoromethyldimethyl - 2 - hydroxyethyl - ammonium (FCH) positron emission tomography/computed tomography (PET - CT) in the detection of recurrent disease and/or distant metastases and to correlate its diagnostic accuracy with PSA levels in prostate cancer patients with biochemical evidence of recurrence. Method: This study included 250 prostate cancer patients with PSA relapse after initial treatment who underwent FCH PET - CT study. Free PSA serum concentration was determined on the day of FCH PET - CT (mean: 46.9 ± 314.7 ng/ml; range 0.2 - 4692 ng/ml). The median PSA level was 5.6 and the median Gleason Score was 7. Imaging was performed on an integrated PET - CT system. Acquisition started 1 minute post intravenous injection of FCH (4 Mbq/kg bodyweight) with dynamic PET images in the pelvic region during 8 minutes (1 min frames) followed by static semi - whole body acquisition from thigh to the base of skull 10 min post injection. The final diagnosis of positive PET lesions was based on histopathology or a consensus for clinical findings, additional imaging a/o follow - up imaging modalities with a mean time interval of 5.3 months. Results: In our study FCH PET - CT was able to correctly detect malignant lesions in 74% (185 / 250) patients. In 37% of these patients only one lesion was detected (69 / 185): 45 patients (65.2 %) had a local recurrence, 13 patients (18,8 %) a single lymph node metastasis and 15.9% (11 pts) a solitary bone metastasis. Using a binary logistic regression analysis model, trigger PSA and HT showed to be the only significant predictors of the positive PET. Conclusion: The results of this study clearly shows that FCH PET - CT can reliably detect recurrent disease and/or distant metastases in prostate cancer patients with biochemical recurrence. Trigger PSA and HT are the two significant predictors of Choline positive PET lesions.

Disclosure of author financial interest or relationships:
**S. Haim**, None; **M. Beheshti**, None; **W. Loidl**, None; **L. Pallwein-Prettner**, None; **M. Steinmair**, None; **T. Kunit**, None; **M. Nader**, None; **P. Waldenberger**, None; **W. Langsteger**, None.

Presentation Number **SS 168**
Scientific Session 24: Translational & Clinical - Oncology
September 8, 2012 / 11:24-11:36 / Room: Wicklow Hall 2

# Near-infrared fluorescence-guided resection of otherwise undetectable hepatic colorectal metastases using indocyanine green

***Floris Verbeek***[1], *Joost van der Vorst*[1], *Boudewijn Schaafsma*[1], *Merlijn Hutteman*[1], *Sven Mieog*[1], *Gerrit-Jan Liefers*[1], *Henk H. Hartgrink*[1], *Clemens Lowik*[2], *John V. Frangioni*[3], *Cornelis J. van de Velde*[1], *Alexander Vahrmeijer*[1], [1]*Surgery, Leiden University Medical Centre, Leiden, Netherlands;* [2]*Endocrinology, Leiden University Medical Centre, Leiden, Netherlands;* [3]*Department of Medicine, Beth Israell Deaconess Medical Center, Harvard Medical School, Boston, MA, USA. Contact e-mail: f.p.r.verbeek@lumc.nl*

Background: A fundamental principle of oncologic surgery is the complete resection of malignant cells. However, conventional techniques lack sensitivity and/or resolution to find small tumors. This is especially important in colorectal cancer, where hepatic metastasectomy may improve survival. Near-infrared fluorescence imaging has been advocated to intraoperatively detect liver metastases using the fluorescent dye indocyanine green (ICG). Material and methods: To assess optimal timing and dose, we intravenously injected ICG, at doses of 10 or 20 mg, 24 h or 48 h preoperatively, into 4 groups of 4 consecutive patients undergoing liver resection for colorectal cancer metastases. Subsequently, 20 patients were administered the optimal dose of ICG at the optimal time before resection. We compared real-time intraoperative NIR fluorescence imaging using the Mini-FLARE imaging system to conventional preoperative imaging by computed tomography (CT), intraoperative ultrasound (IOUS), and intraoperative palpation. Results: In all patients (N = 36), ICG fluorescence was seen as a rim around the tumor, located microscopically in the transition zone between tumor and normal liver tissue. No significant differences in tumor-to-liver ratio (TLR) between time-points or doses were found in the first 16 patients . Therefore, the subsequent 20 patients were administered 10 mg of ICG 24 hours prior to surgery , which is safe and desirable from a logistical point of view. In 5 out of 36 patients (14%), additional small and superficially located metastases were identified using NIR fluorescence only, which were not otherwise detected using preoperative CT, IOUS, visualization, or palpation. NIR fluorescence also distinguished benign liver lesions from metastases. However, all metastases that were located deeper than 8 mm, could not be detected using NIR fluorescence. Conclusions: This study suggests that NIR fluorescence imaging is complementary to conventional imaging for hepatic metastasectomies to identify small superficial lesions.

Disclosure of author financial interest or relationships:
**F. Verbeek**, None; **J. van der Vorst**, None; **B. Schaafsma**, None; **M. Hutteman**, None; **S. Mieog**, None; **G. Liefers**, None; **H.H. Hartgrink**, None; **C. Lowik**, None; **J.V. Frangioni**, None; **C.J. van de Velde**, None; **A. Vahrmeijer**, None.

Presentation Number **SS 169**
Scientific Session 24: Translational & Clinical - Oncology
September 8, 2012 / 11:36-11:48 / Room: Wicklow Hall 2

# A novel rotational Raman endoscopic imaging device for early cancer detection

***Ellis Garai***[1,2], *Cristina Zavaleta*[3,4], *Steven Sensarn*[6,3], *Michael J. Mandella*[6,2], *Jonathan T. Liu*[5], *Sanjiv S. Gambhir*[3,7], *Christopher Contag*[6,2], [1]*Mechanical Engineering, Stanford University, Stanford, CA, USA;* [2]*Molecular Imaging Program at Stanford, Stanford University, Stanford, CA, USA;* [3]*Department of Radiology, Stanford University, Stanford, CA, USA;* [4]*Bio-X Program, Stanford University, Stanford, CA, USA;* [5]*Biomedical Engineering, Stony Brook University, Stony Brook, NY, USA;* [6]*Pediatrics, Stanford University, Stanford, CA, USA;* [7]*Bioengineering, Stanford University, Stanford, CA, USA. Contact e-mail: egarai@stanford.edu*

A novel Raman imaging device that is capable of rotationally scanning hollow structures, such as the colon, has been developed to be used in conjunction with tumor targeting Surface enhanced Raman scattering (SERS) nanoparticles. SERS nanoparticles can act as excellent molecular imaging agents in that they offer ultra high sensitivity, and multiplexing capabilities due to their unique spectral signatures. One key advantage of multiplexing includes the ability to utilize several targeted SERS probes to target and localize a multitude of unique biomarkers associated with a specific disease, and effectively increasing specificity. Circumferential scanning provides the physician with the advantage of scanning larger areas of tissue in a shorter period of time. To achieve this, a motor-driven, rotating mirror to enable complete 360° circumferential scanning is utilized. By mapping each pixel of the circumferential scan during a controlled retraction, a reconstruction of the entire colon wall can be displayed in real-time. A map of the colon will show areas to which tumor-targeting SERS nanoparticles have bound and direct clinicians to extract biopsies accordingly. The design consists of a single mode 785 nm laser, which is used to illuminate a Raman-active sample. A single lens is used to both collimate the illuminating beam and for collecting the SERS scattered light into a multi-mode fiber bundle. There are 36 multi-mode fibers to maintain flexibility for use in fully articulating endoscopes that are currently available on the market. At the proximal end, the multi-mode fibers are coupled into a spectrometer, which disperses the wavelengths of light, and collected via the sensor array of the CCD. The camera electronics perform full vertical binning of the sensor array in order to sum the spectral intensity of the Raman signal at each wavelength. A 45 degree scanning mirror, actuated via a brushless DC motor, allows for circumferential scans of the colon lumen. At a scan rate of 1 revolution per second (60 rpm), a spatial resolution of 1.5 mm can be achieved. At this scan rate, the laser beam will be rotating 1.57mm/msec for an average colon diameter, resulting in 100 pixels per revolution. At 60 rpm and a collimated beam diameter of 1.2mm, the American National Standards Institute (ANSI) regulations permit the use of a laser illumination power of 500 mW, resulting in a detection limit of approximately 1 pM of SERS nanoparticles. One of the key features of the device is that it has been designed for efficient use over a wide range of working distances. This is necessary to accommodate for imperfect centering of the device within the colon lumen and surface variations due to folds and bends. Circumferential scanning in combination with multiplexing allows for real-time functional imaging which can potentially be used to distinguish a variety of tissues of interest in areas of the body accessible with an endoscope from the colon to the esophagus, stomach, oral cavity and bladder. In conclusion, we have developed a new rotational Raman endoscopic imaging device with significant applications for clinical cancer screening.

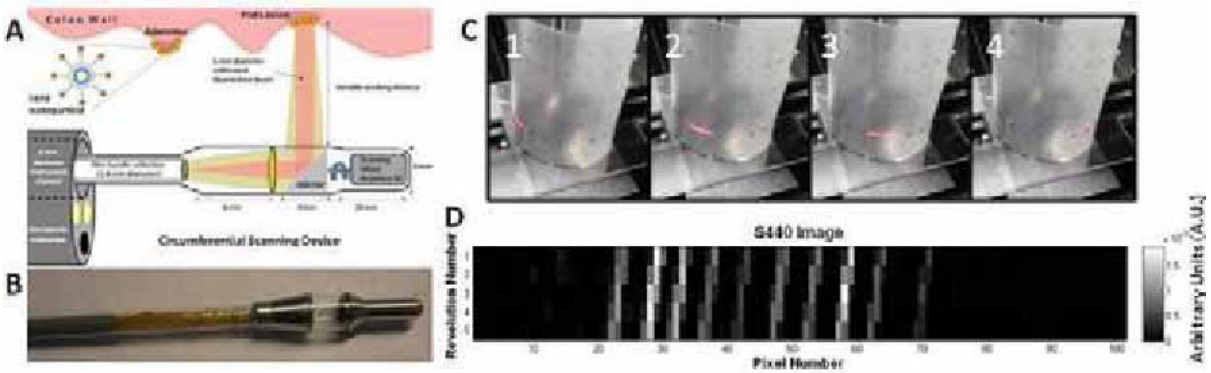


Figure. A. Schematic of Circumferential Scanning Raman device. B. Full scale mock prototype. C. Experimental setup depicting the laser beam scanning through multiple SERS spots at a fixed horizontal plane. The Raman device is placed in the center of the tubular film. D. Each horizontal line in the image depicts the SERS signal for a circumferential scan at a fixed horizontal plane. The plane was imaged a total of 5 times. The 10 columns of signals represent the 10 SERS spots that were imaged.

Disclosure of author financial interest or relationships:
**E. Garai**, None; **C. Zavaleta**, None; **S. Sensarn**, None; **M.J. Mandella**, Optical Biopsy Technologies, Inc., Stockholder; **J.T. Liu**, None; **S.S. Gambhir**, General Electric, Grant/research support; Bayer-Schering, Grant/research support; Sanofi-Aventis, Grant/research support; CellSight, Stockholder; ImaginAB, Stockholder; Enlight, Stockholder; Endra, Stockholder; Bracco, Consultant; NinePoint Medical, Stockholder; Visualsonics, Consultant; **C. Contag**, ConcentRx Corp, Other financial or material support; Origin Therapeutics, Stockholder; Olympus, Other financial or material support; Tansderm Inc., Other financial or material support; Cygnet Biofuels, Other financial or material support .

Presentation Number **SS 17**
Scientific Session 3: Preclinical In Vivo - Metabolic Disease
September 6, 2012 / 10:30-10:51 / Room: Liffey Hall 2

# Image-guided Therapies in Diabetes

***Anna Moore**, Massachusetts General Hospital, Charlestown, MA, USA. Contact e-mail: amoore@helix.mgh.harvard.edu*

Disclosure of author financial interest or relationships:
**A. Moore**, Fluoropharma, Grant/research support .

Presentation Number **SS 170**
Scientific Session 25: Preclinical In Vivo - Oncology
September 8, 2012 / 10:30-10:41 / Room: The Auditorium

# A Pre-Targeted $^{64}$Cu-PET Imaging Methodology Based on the huA33 Antibody and Inverse Electron Demand Diels-Alder Click Chemistry

***Brian M. Zeglis***[1], *Thomas Reiner*[2], *Kuntalkumar Sevak*[1], *Steven M. Larson*[1], *Ralph Weissleder*[2], *Jason S. Lewis*[1], [1]*Department of Radiology and Program in Molecular Pharmacology and Chemistry, Memorial Sloan-Kettering Cancer Center, New York, NY, USA;* [2]*Center for Systems Biology, Massachusetts General Hospital/Harvard Medical School, Boston, MA, USA. Contact e-mail: zeglisb@mskcc.org*

**Objective:** To employ bioorthogonal click chemistry to create a modular strategy for antibody-based pre-targeted PET imaging **Methods**: Recently developed click chemistry based on the rapid and bioorthogonal [4+2] Diels-Alder cycloaddition between 3-(4-benzylamino)-1,2,4,5-tetrazine and the dienophile transcyclooctene was used to develop a strategy for the pre-targeted PET imaging of colorectal cancer xenografts.[1] The huA33 antibody was modified with transcyclooctene (TCO), and a NOTA-modified tetrazine was synthesized and radiolabeled with $^{64}$Cu. Assays for serum stability, click reaction kinetics, and immunoreactivity were utilized for further characterization of the system, and acute in vivo biodistribution experiments were performed with the pre-assembled $^{64}$Cu-NOTA-huA33 to investigate the pharmacokinetics of the antibody. Ultimately, pre-targeted in vivo biodistribution and PET imaging experiments were performed with athymic nude mice bearing A33 antigen-expressing SW1222 colorectal cancer xenografts. **Results**: The huA33 antibody was successfully modified with transcyclooctene, and the resultant construct was shown to have 95 ± 2% immunoreactivity despite a degree of labeling of 7.0 ± 0.9 TCO/mAb. A NOTA-modified tetrazine was synthesized, radiolabeled with $^{64}$Cu, and purified with HPLC to yield the final radioligand product in 75-80% decay corrected yield, >99% purity, and a specific activity of 9-10 MBq/μg. The click chemistry ligation between the TCO-modified antibody and the tetrazine moiety was shown to be extremely rapid and robust, complete in < 1 min at RT (10 μM antibody) and unimpeded by serum or blood. In vivo acute biodistribution experiments using a pre-assembled $^{64}$Cu-NOTA-huA33 construct in mice bearing SW1222 xenografts revealed a maximum uptake of 28 ± 5 %ID/g and 29 ± 4 %ID/g at 24 h and 48 h, respectively. Based on this biodistribution data, in vivo pre-targeting experiments were performed by first injecting 100 μg of huA33-TCO via tail vein, waiting 24 h for the antibody to accumulate in the tumor, and subsequently injecting the $^{64}$Cu-NOTA-tetrazine radioligand. Acute biodistribution experiments in mice bearing SW1222 xenografts indicate a rapid maximization of $^{64}$Cu in the tumor (4.1 ± 0.3 %ID/g at 1 h), very low $^{64}$Cu uptake in most tissues, and elimination of the radioligand via the feces (from 12.1 ± 2.6 %ID/g at 1 h to 1.1 ± 0.4 %ID/g at 24 h). PET imaging studies revealed that the system provides effective tumor delineation and produces high contrast PET images at 10 h post radioligand injection. **Conclusions**: A robust and modular strategy for pre-targeted PET imaging was successfully developed using the huA33 antibody and inverse electron-demand Diels-Alder click chemistry. Both acute biodistribution experiments and small animal PET imaging indicate high tumor-to-background uptake ratios with A33-antigen bearing SW1222 colorectal cancer xenografts. **Research Support**: U.S. Department of Energy (Award DE-SC0002184; JSL) and U.S. National Institutes of Health (Award 1F32CA144138-01; BMZ) **References:** [1] N. K. Devaraj, et al. Biocon. Chem., 2008, 19, 2297.

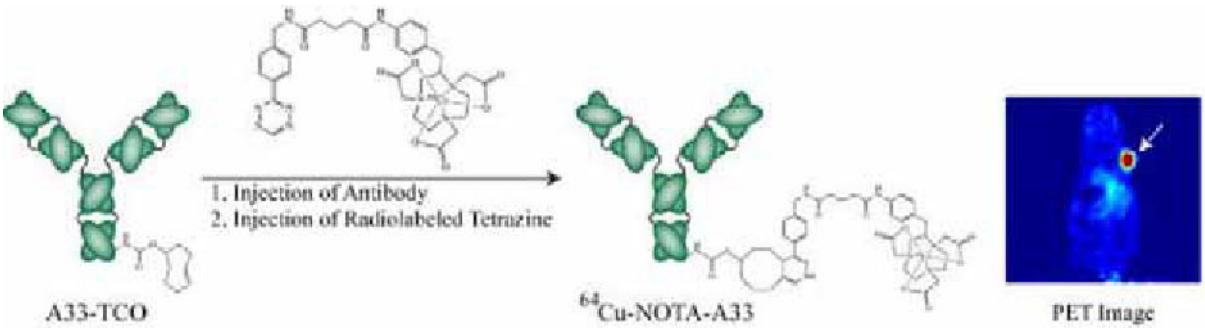


Disclosure of author financial interest or relationships:
**B.M. Zeglis**, None; **T. Reiner**, None; **K. Sevak**, None; **S.M. Larson**, None; **R. Weissleder**, None; **J.S. Lewis**, GEMS, Other financial or material support .

Presentation Number **SS 171**
Scientific Session 25: Preclinical In Vivo - Oncology
September 8, 2012 / 10:41-10:52 / Room: The Auditorium

# Identification of optimal therapeutic antibody for fluorescent imaging of cutaneous squamous cell carcinoma intraoperatively and on frozen section

*Cara H. Heath, **Lauren N. Beck**, Nicholas Deep, Kurt R. Zinn, Eben L. Rosenthal, Surgery/Division of Otolaryngology, University of Alabama at Birmingham School of Medicine, Birmingham, AL, USA. Contact e-mail: lnbeck@uab.edu*

Background: Fluorescently labeled antibodies are currently under investigation to guide surgical resections. Optical imaging with intraoperative, real-time fluorescence imaging hardware (SPY system, Novadaq, Toronto) is a promising tool for the visualization of cancer tissue during surgery. Furthermore, use of optical scanning on frozen histological sections has the potential to improve efficiency of oncological resections and to ensure negative margins. We sought to determine the optimal FDA approved therapeutic monoclonal antibody (either bevacizumab, panitumumab, or tocilizumab) that could be fluorescently labeled and used to visualize human cutaneous squamous cell carcinoma (cSCC). Methods: A near-infrared (NIR) fluorescent probe (IRDye800) was covalently linked to each of the three monoclonal antibodies and injected systemically into mice with cSCC grafts. Cutaneous tumor cell lines (SCC13) or cutaneous human tumor explants were xenografted onto the flank of immunodeficient mice and then imaged and resected under fluorescence guidance with the SPY system or a charge-coupled NIR system (Pearl). Histological sections of tumor were imaged with a NIR charge-coupled device (Odyssey), and fluorescence intensity confirmed by correlation with histology and immunohistochemical staining. Results: When comparing fluorescently labeled antibodies using the SCC13 tumors, all could delineate normal tissue from tumor based on tumor-to-background ratios (TBR). Bevacizumab-IRDye800 had a TBR of 2.6 using the Pearl and 1.5 using the SPY system, which was better than panitumumab-IRDye800 which had a TBR of 1.9 using the Pearl and 1.2 for the SPY. Tocilizumab-IRDye800 had a TBR of 3.6 using the Pearl and 2.0 for the SPY. For the SCC13 cell line, tumor detection was highest with tocilizumab-IRDye800 for both the SPY and Pearl according to sensitivity and specificity calculations. To determine relevance in human cutaneous squamous cell carcinoma, we assessed human tumor explants, which were also clearly distinguished from normal tissue with TBR of 2.8 (Pearl) and 2.1 (SPY) for bevacizumab-IRDye800, 4.0 (Pearl) and 2.3 (SPY) for panitumumab-IRDye800, and 3.9 (Pearl) and 2.6 (SPY) for tocilizumab-IRDye800. For the human explants, tumor detection was highest with tocilizumab-IRDye800 (TBR 2.6) for the SPY, and with panitumumab-IRDye800 (TBR 4.0) for the Pearl. Tissue biopsies positive for fluorescence were confirmed for pathologic disease by histology and immunohistochemistry (n = 18/18); while biopsies of non-fluorescent tissue were proven to be negative for malignancy (n = 12/12). The SPY system was able to detect residual tumor that was not palpable or grossly apparent. Imaging of histological frozen sections was effective in detecting microscopic disease and had a threshold of detection of 300 uM. Conclusions: These data suggest that tocilizumab is an FDA approved antibody with optimal imaging characteristics for intraoperative detection of cSCC using the SPY imaging system and optical imaging of frozen sections.

Disclosure of author financial interest or relationships:
**C.H. Heath**, None; **L.N. Beck**, NIH/NIDCR 1R21DEO19232, Grant/research support; **N. Deep**, None; **K.R. Zinn**, None; **E.L. Rosenthal**, None.

Presentation Number **SS 172**
Scientific Session 25: Preclinical In Vivo - Oncology
September 8, 2012 / 10:52-11:03 / Room: The Auditorium

# PET/MR Imaging and Bio-Distribution of a Novel single-chain fragment (αEGFR)-single chain-TRAIL Fusion Protein in a Colon Cancer Model

***Mathew R. Divine***[1], *Maren K. Koenig*[1], *Daniel Bukala*[1], *Funda Cay*[1], *Martin Siegemund*[2], *Klaus Pfizenmaier*[2], *Bernd J. Pichler*[1], [1]*Department of Preclinical Imaging and Radiopharmacy, University of Tuebingen, Tuebingen, Germany;* [2]*Institute of Cell Biology and Immunology, University of Stuttgart, Stuttgart, Germany. Contact e-mail: mathew.divine@med.uni-tuebingen.de*

Introduction: Targeting of recombinant death receptors (DRs) DR4 and DR5 with the recombinant, soluble TNF-related apoptosis inducing ligand (TRAIL) is a promising anti-cancer strategy. We present for the first time the radio-labeling, biodistribution, and kinetic behavior of a novel, dual-targeting single-chain fragment (scFv) αEGFR-scTRAIL in the EGFR overexpressing COLO205 cell line cancer model. This fusion protein presents major improvements in apoptotic targeting specificity via the scTRAIL ligand and target specificity via the scFv(αEGFR) based on the humanized CD225 (Erbitux/Cetuximab) fragment. In order to characterize the tissue uptake as accurately as possible, we have brought together the synergistic properties of high sensitivity Positron Emission Tomography (PET) and the superb soft-tissue contrast of Magnetic Resonance Imaging (MRI). Materials/Methods: scFv(αEGFR)-scTRAIL was conjugated with DOTA and later radiolabeled with $^{64}$Cu for PET imaging studies. Six week-old, female, nude mice were allowed to acclimatize for two weeks before injecting 4.5x10$^{6}$ COLO205 tumor cells subcutaneously on the right flank. Tumors were allowed to grow until they were palpable and showing signs of vascularization. PET imaging was performed 0, 3, 12, 24, 36, and 48hrs post injection of 2-5μg of $^{64}$Cu-DOTA-scFv(αEGFR)-scTRAIL to avoid saturation of tumor receptor sites. All PET scans were 10 min. in duration except for dynamic scans acquired with bolus injection at the 0hr time point, in order to determine if tumor perfusion was directly related to peak tumor uptake. Directly after all PET scans, mice were moved in the same bed position to a 7T Bruker Clinscan MRI where a T2-weighted Turbo Spin Echo (T2tse) sequence was used to acquire anatomical references for later co-registration to PET images. A blocking study was performed by injecting 200μg of unlabeled protein 24hrs prior to injection of radio-labeled fusion protein. Organs were taken at the end of imaging experiments at the 24, 36, and 48hr time points, weighed, and placed in a gamma counter for bio-distribution measurements. Tumors were saved for later histological processing. Results: Preceding the in vivo studies, a full in vitro evaluation of the novel fusion protein was performed revealing excellent binding properties. The radiolabeling yield of $^{64}$Cu-DOTA-scFv(αEGFR)-scTRAIL in these experiments was between 55-75% as assessed by digital chromatography. Clear uptake of the labeled fusion protein is seen in the spinal column and in bone within 30min. after injection. Tumors showed perfusion weighted kinetics with a distinguished uptake after 3hrs. T2tse images show small areas of necrosis as seen by hypo-intense regions, which correlate to regions of low uptake on PET images. Biodistribution results show a high %ID/g in the tumor at the 24, 36, and 48hr time points: 16.3+/-5.4, 23.8+/-7.6, 25.8+/- 2.9. The blocking study decreased the 48hr time point value significantly to 5.29+/-4.8 ($p<0.008$). Conclusions: The scFv(αEGFR)-scTRAIL was successfully conjugated with DOTA and radiolabeled with $^{64}$Cu. This labeled fusion protein is a promising imaging agent for studying EGFR and DRs dynamics.

Disclosure of author financial interest or relationships:
**M.R. Divine**, None; **M.K. Koenig**, None; **D. Bukala**, None; **F. Cay**, None; **M. Siegemund**, None; **K. Pfizenmaier**, None; **B.J. Pichler**, Siemens, Grant/research support; AstraZeneca, Grant/research support; Bayer Healthcare, Grant/research support; Boehringer-Ingelheim, Grant/research support; Oncodesign, Grant/research support; Merck, Grant/research support; Bruker, Grant/research support .

Presentation Number **SS 173**
Scientific Session 25: Preclinical In Vivo - Oncology
September 8, 2012 / 11:03-11:14 / Room: The Auditorium

# *In vivo* and *in vitro* characterization of three radiolabeled anti-$GD_2$ Antibodies to be used as Biomarker for Neuroblastoma Imaging and Radioimmunotherapy

***Julia Schmitt***[1], *Marcel A. Krueger*[1], *Karin Schilbach*[2], *Rupert Handgretinger*[2], *Bernd J. Pichler*[1], [1]*Department of Preclinical Imaging and Radiopharmacy, Eberhard Karls University Tuebingen, Tuebingen, Germany;* [2]*Childrens Hospital, Department of Hematology and Oncology, Eberhard Karls University Tuebingen, Tuebingen, Germany. Contact e-mail: Julia.Schmitt@med.uni-tuebingen.de*

Neuroblastoma (NB) belongs to the most frequently occuring extracranial tumors in childhood. Although outcome in patients with NB has improved, cure rates among children with high risk NB remain poor. Disialogangliosid ($GD_2$), a surface antigen highly expressed on nearly all NB cells, is one of the main targets used for antibody directed treatment in NBs. Immunotherapy based on $GD_2$ specific antibodies was shown to improve the prognosis of neuroblastoma patients. Radiolabeling of anti-$GD_2$ antibodies represents a further approach to constitute a high specific agent for radiation therapy and a biomarker for diagnostic imaging. Here we study the *in vivo* and *in vitro* characteristics of three anti-$GD_2$ antibodies to evaluate their benefit for NB diagnostics and radioimmunotherapy (RIT). For *in vitro* characterization of ch14.18, its humanized variant hu14.18 and its mutant ch14.18-Δch2 (Δch2), binding, blocking and internalization studies were accomplished on IMR-32 cells. An unspecific antibody and $GD_2$ negative cells were used as control. Binding capabilities of the conventionally used NB tracer $^{123}$I-Metaiodibenzylguanidine (mIBG) were studied to evaluate the suitability of anti-$GD_2$ antibodies for imaging and RIT. Small animal PET was used to study the *in vivo* behaviour of the antibodies. Immunodeficient mice bearing subcutaneous NBs were injected with [$^{64}$Cu]DOTA labeled antibody. *In vivo* PET and MR images were acquired 3h, 24h, and 48h post injection. *Ex vivo* biodistribution and autoradiography studies were performed after 48h. The *in vitro* binding of Δch2 is superior to that of hu14.18 and ch14.18. Internalization of Δch2 is highest among the antibodies. Blocking studies approve $GD_2$-specificity for Δch2 and hu14.18. The three anti-$GD_2$ antibodies show stronger binding to NB cells than mIBG and an unspecific antibody. The *in vivo* accumulation of the radiolabeled antibodies in $GD_2$ expressing tumors is highest for Δch2, followed by hu14.18 and ch14.18 (3.18±1.22 %ID/cc for Δch2, 2.71±0.08 %ID/cc for hu14.18, 2.45±0.06 %ID/cc for ch14.18 after 24h). Tumor-to-muscle ratios increase with time. Tumor uptake of the unspecific control antibody is inferior at all time points. Biodistribution and autoradiography studies support the findings. It is the first time that anti-$GD_2$ antibodies were compared via *in vivo* PET. The ch14.18 mutant Δch2 is a small anti-$GD_2$ antibody with reduced immunoreactivity and would form an excellent biomarker for NB imaging or targeted radiation therapy. In our *in vitro* and *in vivo* studies, Δch2 shows improved binding and internalization capabilities in comparison to hu14.18 and ch14.18. Furthermore, Δch2 exceeds the accumulation of mIBG on $GD_2$ positive cells. This data encourage the development of an alternative NB therapy using radiolabeled Δch2. Further *in vivo* studies using blocking experiments and $GD_2$ negative tumors in combination with intensive examination of the tumor tissue by immunhistological methods and MR imaging are planned to support this approach.

Disclosure of author financial interest or relationships:
**J. Schmitt**, None; **M.A. Krueger**, None; **K. Schilbach**, None; **R. Handgretinger**, None; **B.J. Pichler**, Siemens, Grant/research support; AstraZeneca, Grant/research support; Bayer Healthcare, Grant/research support; Boehringer-Ingelheim, Grant/research support; Oncodesign, Grant/research support; Merck, Grant/research support; Bruker, Grant/research support .

Presentation Number **SS 174**
Scientific Session 25: Preclinical In Vivo - Oncology
September 8, 2012 / 11:14-11:25 / Room: The Auditorium

# MicroPET/CT and microSPECT/CT imaging of a CCK2 Receptor-Binding Peptide with various chelators and radionuclides

***Jane Sosabowski***[1], *Margaret S. Cooper*[2], *Julie M. Foster*[1], *Jerome C. Burnet*[1], *Lieke Joosten*[3], *Chantelle D. Hudson*[1], *Rowena Paul*[2], *Wim J. Oyen*[3], *Otto C. Boerman*[3], *Phil Blower*[2], *Stephen Mather*[1], *Peter Laverman*[3], [1]*Centre for Molecular Oncology, Barts Cancer Institute, Queen Mary University of London, London, United Kingdom;* [2]*Division of Imaging Sciences and Biomedical Engineering, King's College London, London, United Kingdom;* [3]*Department of Nuclear Medicine, Radboud University Nijmegen Medical Centre, Nijmegen, Netherlands. Contact e-mail: j.k.sosabowski@qmul.ac.uk*

CCK2/gastrin receptor targeting using radiolabelled gastrin peptide analogues has been extensively investigated for use in diagnosis and therapy of CCK2-R expressing cancers such as MTC and SSLC. The $^{111}$In-labelled DOTA-conjugated peptide PP-F11 ((DGlu)$_6$-Ala-Tyr-Gly-Trp-Met-Asp-Phe-NH$_2$) has previously shown good in vivo characteristics i.e. high tumor uptake and low kidney uptake. The aim of this study was to compare $^{64}$Cu PET imaging and $^{111}$In SPECT imaging of NOTA, NODAGA and DOTA-conjugated PP-F11 in mice with CCK2R-expressing tumours. PP-F11 was conjugated with NOTA, NODAGA and DOTA and all peptides were labelled with$^{64}$Cu and $^{111}$In to a specific activity of 30 MBq/nmol according to standard procedures. The $IC_{50}$ of the Cu and In-labelled peptides was determined in a competitive binding assay on CCK2R-transfected A431 cells. MicroSPECT/CT imaging at 1 and 4 h (n=3) and biodistribution studies at 4 h (n=5) were carried out in A431-CCK2R+ tumour-bearing beige SCID mice. SPECT and PET quantitation of the tumour and kidneys was carried out at 1 and 4 h. $IC_{50}$ values were all in the low nanomolar range; both In-NOTA-PP-F11 and Cu-NOTA-PP-F11 showed an $IC_{50}$ of 1.2 nM and 1.3 nM, respectively. $IC_{50}$ values of In-NODAGA-PP-F11 and Cu-NODAGA-PP-F11 were 1.5 nM and 1.4 nM, respectively. The DOTA-conjugated compounds showed $IC_{50}$ values of 0.9 nM and 1.2 nM (In and Cu, respectively). Stability studies of the $^{64}$Cu radiolabelled compounds in human plasma showed that all of the compounds were > 96 % stable up to 4 h. All tumours were clearly visualised at 1 and 4 h using either microPET/CT or microSPECT/CT (depending on the radioisotope). Notable accumulation in the liver and intestine was seen for the $^{64}$Cu compounds, but not evident in the case of the $^{111}$In radiolabelled peptides. Biodistribution studies of the imaged animals at 4 h supported this with tumour uptakes of 2.6 - 7.7 % ID/g for the $^{64}$Cu-labelled compounds and around 2 % ID/g for the $^{111}$In-labelled compounds. The highest tumour uptake was for$^{64}$Cu-NOTA-PP-F-11 (7.71 ± 1.2 % ID/g, n=5), however, liver uptake for this compound was 9.4 ± 1.4 % ID/g with markedly higher uptake in the large intestine than seen for the $^{111}$In-labelled compounds. Although the liver uptake of the $^{64}$Cu-NODAGA peptide was lower than that of the $^{64}$Cu-NOTA compound, kidney was higher, giving a less favorable tumour to kidney ratio. PET and SPECT quantitation studies at 1 and 4 h showed that there was no appreciable washout from either tumour or kidney over this timescale for the $^{64}$Cu-labelled compounds. This was also the case in tumour for the $^{111}$In-labelled compound however imaging of the $^{111}$In-NOTA compound showed intestinal uptake at 4 h which was not evident at 1 h. In contrast to the in vitro studies where there was little variation in affinity or plasma stability, the imaging studies clearly show that the radioisotope-chelator combination has a marked effect on the in vivo biodistribution of this peptide. These results suggest that in vivo stability of the metal-chelator complex is an important factor. Studies using $^{68}$Ga for PET imaging with PP-F11 are ongoing.

Disclosure of author financial interest or relationships:
**J. Sosabowski**, None; **M.S. Cooper**, None; **J.M. Foster**, None; **J.C. Burnet**, None; **L. Joosten**, None; **C.D. Hudson**, None; **R. Paul**, None; **W.J. Oyen**, Roche, Grant/research support; Siemens, Grant/research support; Immunomedics, Grant/research support; Wilex, Grant/research support; Novartis, Grant/research support; GSK, Grant/research support; Merck, Grant/research support; **O.C. Boerman**, None; **P. Blower**, None; **S. Mather**, Bioscan Inc, Consultant; **P. Laverman**, None.

Presentation Number **SS 175**
Scientific Session 25: Preclinical In Vivo - Oncology
September 8, 2012 / 11:25-11:36 / Room: The Auditorium

# Engineered antibody fragments based on the humanized, non-internalizing anti-CD20 mAb GA101 for immunoPET imaging of B-cell lymphomas

***Kirstin A. Zettlitz**, Felix B. Salazar, Richard Tavaré, Tove Olafsen, Anna M. Wu, Crump Institute for Molecular Imaging, UCLA, Los Angeles, CA, USA. Contact e-mail: kzettlitz@mednet.ucla.edu*

CD20 is a cell surface marker expressed on the majority of B-cell lymphomas and has proven useful as a target for antibody-based therapy. Most B-cell lymphoma patients receive the anti-CD20 antibody rituximab at some point of their treatment with the same scheduling and dosing, regardless of factors known to affect pharmacokinetics and serum levels (e.g. tumor burden, CD20 expression). Hence, there is a strong need for an efficacious diagnostic tool to assess antigen presence and expression, tumor localization and also for therapy management and follow-up. We developed novel PET imaging agents based on the humanized, type II anti-CD20 mAb GA101. GA101 binds CD20 in a different orientation from type I antibodies (e.g. rituximab) and is not internalized. Cell surface retention is preferable for imaging, allowing the use of radioiodinated tracers which show greatly reduced normal tissue background. We show the generation, purification and characterization of GA101-antibody fragments differing in size and with pharmacokinetics optimized for PET imaging. All fragments, including a scFv-cys (28 kDa), a cys-diabody (CDb, 55 kDa) and a minibody (Mb, CMb, 83 kDa), are in VH-VL orientation, the minibody consists of a scFv fused to human gamma1 hinge and CH3. All fragments retain cell-binding characteristics (type II epitope, stoichiometry, apparent affinity) of the parental IgG but lack Fc-mediated functions and FcRn recycling. The cys-derivatives contain a C-terminal free cysteine that is suitable for site-specific conjugation. GA101_Mb was radioiodinated with I-124 (labeling efficiency: 86.01 ± 0.72 %; n=3) and immunoreactivity was 76.3 ± 4.9 % on CD20 expressing cells (Ramos) and 5.8 % ±4.2 on CD20-negative cells (Bc-1) (n=3). Tumors were established in SCID mice by s.c. injection of 2-5 x 106 cells above each shoulder 14 days prior to imaging and each mouse received 20 - 25 µg protein (specific activity: 3.5 - 7 µCi/µg). MicroPET images at 20 and 44 h show high activity in the CD20-positive tumor. Specific uptake in the CD20-positive tumor as determined by ex vivo biodistribution was 2.63 ± 0.44 %ID/g at 20 h and 1.2 %ID/g at 44 h resulting in positive:negative tumor ratios of 3.3 ±0.64 and 2.2 ±0.25, respectively. GA101_Mb specifically targets CD20-positive tumor cells in vivo and produces high-contrast microPET images. As a novel immunoPET imaging agent it could provide information on extent of disease, presence of therapeutic target, and response to therapy. Most important, as type II epitope binders, GA101-based tracers should not modulate CD20 surface molecules on the target cell and when used as a diagnostic will not influence the subsequent anti-CD20 therapy. They might be especially useful for B-cell malignancies that show a greater tendency to modulate CD20 in correlation with relative insensitivity to rituximab treatment. Because the presented GA101 antibody fragments are based on a humanized mAb they are suitable for clinical translation.

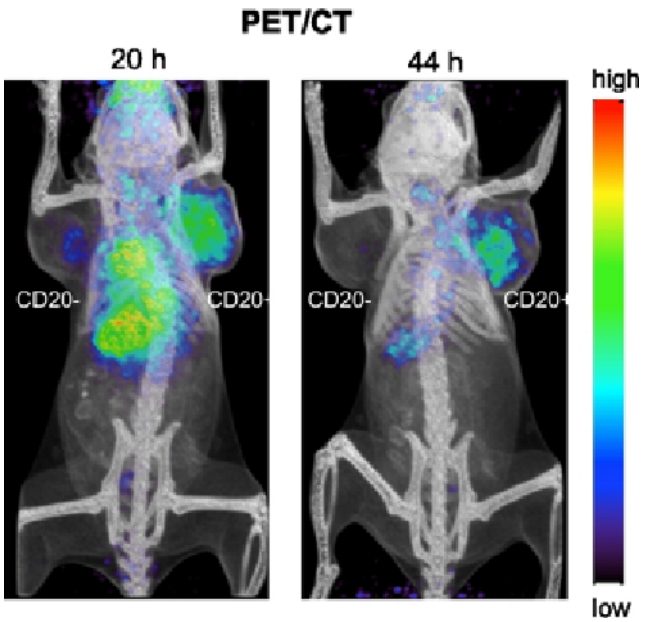


Figure 1. Radioiodinated GA101_Mb targets CD20-positive tumors (Ramos, right shoulder) but not CD20-negative tumors (Bc-1, left shoulder). Small animal PET/CT images 20 and 44 h after i.v. administration of 3.7 MBq 124I-GA101_Mb.

Disclosure of author financial interest or relationships:
**K.A. Zettlitz**, None; **F.B. Salazar**, None; **R. Tavaré**, None; **T. Olafsen**, ImaginAb Inc., Employment; **A.M. Wu**, ImaginAb, Inc., Consultant; ImaginAb, Inc., Stockholder .

Presentation Number **SS 176**
Scientific Session 25: Preclinical In Vivo - Oncology
September 8, 2012 / 11:36-11:47 / Room: The Auditorium

# Heparin-reactive peptide p5R preferentially binds a subset of MelA+ melanocytes and extracellular melanin - a novel biomarker in metastatic melanoma tumors

***Jonathan S. Wall***[2,1]*, Amy K. LeBlanc*[1]*, Tina A. Richey*[2]*, Alan Stuckey*[1]*, Emily B. Martin*[2]*, Sallie D. Macy*[2]*, Robert Donnell*[4]*, Laurentia Nodit*[3]*, Stephen J. Kennel*[2,1]*, [1]Radiology, University of Tennessee Graduate School of Medicine, Knoxville, TN, USA; [2]Medicine, University of Tennessee Graduate School of Medicine, Knoxville, TN, USA; [3]Pathology, University of Tennessee Graduate School of Medicine, Knoxville, TN, USA; [4]Pathobiology, University of Tennessee College of Veterinary Medicine, Knoxville, TN, USA. Contact e-mail: jwall@utmck.edu*

Melanoma is the most deadly form of skin cancer with >70,000 individuals diagnosed in 2011 in the USA. During a routine histochemical screen of biotinylated heparin-reactive peptides with a tumor tissue array, we identified certain reagents that preferentially bound melanocytic melanoma tumors. We have previously demonstrated the reactivity of peptide p5 with B16F10 murine melanoma tumors within the mouse lung. The aim of this study was to evaluate the reactivity of a novel arginine-substituted peptide, p5R with human melanoma tumor in tissue sections and further to evaluate the efficacy of p5R for targeting B16F10 melanoma tumors *in vivo*. Peptide p5R was synthesized, purified by reverse phase HPLC, labeled with biotin and used for histochemical staining of human, canine and murine melanoma-laden formalin-fixed, paraffin-embedded tissue sections. Furthermore, radioiodinated ($^{125}$I or $^{131}$I) p5R peptide was used to detect pulmonary colonies of B16F10 cells in C57Bl/6 mice 24 h pi by using small animal SPECT/CT imaging and micro-autoradiography. Biotinyl-p5R bound to human and canine melanin-producing (MelA+) melanoma cells in tissue sections as evidenced by microscopy. The $^{125}$I-labeled peptides, but not control peptide, co-localized with pulmonary metastatic B16F10 murine melanoma tumor lesions, as well as secondary metastases observed in the regional lymph nodes of the mice. The reactivity was not uniform throughout the tumor. This was confirmed by examining micro-autoradiographs. Binding of the $^{125}$I-p5R peptide was discrete and specific for MelA+ melanocytes within the pulmonary and metastatic tumors. Additionally, $^{125}$I-p5R was seen associated with extracellular melanin that was co-localized with the extracellular heparan sulfate proteoglycan, perlecan within the tumor mass. Using lactoperoxidase surface iodination of B16F10 cells, p5R was shown to capture a specific protein of 80 - 100 kDa. Our data suggest that p5R reacts with a discrete biomarker within the melanoma tumor, likely associated with a protein expressed selectively on MelA+ melanoma cells. Binding of $^{125}$I-p5R *in vivo* was dependent on the presence of melanin. The diagnostic and prognostic implications of this reactivity are under investigation. Although preliminary, these data suggest that p5R, or similar reagents, may provide novel probes for the radiodetection and targeted endoradiotherapy of metastatic melanoma. This work was supported by the University of Tennessee Molecular Imaging and Translational Research Program.

Disclosure of author financial interest or relationships:
**J.S. Wall**, Elan, Grant/research support; Solex LLC, Stockholder; **A.K. LeBlanc**, None; **T.A. Richey**, Solex, Stockholder; **A. Stuckey**, Solex LLC, Stockholder; **E.B. Martin**, Solex LLC, Stockholder; **S.D. Macy**, None; **R. Donnell**, None; **L. Nodit**, None; **S.J. Kennel**, solex, Stockholder .

Presentation Number **SS 177**
Scientific Session 25: Preclinical In Vivo - Oncology
September 8, 2012 / 11:47-11:58 / Room: The Auditorium

# CEA-specific Cu-64-DOTA labelled M5A-Antibody for Detection of Liver Metastasis with PET in vivo

***Marcel A. Krueger***[1], *Stefanie Nittka*[2], *Julia Schmitt*[1], *Michael Neumaier*[2], *Bernd J. Pichler*[1], [1]*Department of Preclinical Imaging and Radiopharmacy, Eberhard Karls University of Tuebingen, Tuebingen, Germany;* [2]*Clinical Chemistry, University Hospital Mannheim, Mannheim, Germany;* [3]*Department of Immunology, City of Hope National Cancer Center, Duarte, CA, USA. Contact e-mail: marcel.krueger@med.uni-tuebingen.de*

With the currently available imaging methods liver metastases are still challenging to detect and small metastases are often overlooked. Hence, there is a great need to establish novel tools for detection of micro metastases in the liver. The Carcinoembryonic Antigen (CEA) is a GPI-anchored surface protein only expressed during fetal development and in the colon. However, it has been shown to be up regulated in a wide range of different carcinoma. Additionally, CEA-expression stays stable during metastasization and can be detected in about 95% of metastases of CEA-positive primary colon tumours. Therefore, CEA seems to be an attractive target for novel PET-tracers. The M5A-antibody is a fully humanised CEA-specific antibody, showing the so far highest published specificity for CEA. In this study we have evaluated M5A as a PET-tracer for detection of CEA expressing liver metastasis in a syngenic orthotopic tumour model. Metastasizing MC38 (CEA-) or C15A3 (CEA+) tumour cells were intrasplenic injected into C57BL/6-mice. After liver metastases had developed, mice were injected with 20 µg Cu-64-DOTA-labelled M5A-antibody or 20 µg of an unspecific Cu-64-DOTA-labelled antibody. PET- and MRT-images were acquired 3h, 24h and 48h post injection. Livers were dissected and HE and immunohistochemistry stainings and autoradiographies were prepared. For blocking experiments, 500µg unlabelled M5A-antibody was injected 3h prior to injection of labelled M5A-antibody. 24h after tracer injection, the %ID/cc in CEA positive tumours was highest (16.5% ± 6.3%) and significantly increased compared to healthy liver tissue in the same animals (8.6% ± 0.9%), as well as to CEA negative tumours in control animals (5.5% ± 0.6%) (Fig. 1). The ratio of the %ID/cc between C15A3 tumours and healthy liver tissue was determined as 1.9 ± 0.7, while the ratio of MC38 tumours and liver was significantly lower (0.8 ± 0.1). It was possible to clearly distinguish between liver tissue and metastasis and we could identify metastases within the liver in PET. Surprisingly, intratumoural antibody distribution showed to be inhomogeneous. This could be supported with autoradiographies prepared after PET and MRT scans. Immunohistochemistry stainings with M5A-antibody showed homogeneous CEA expression within metastases, but necrotic areas could be identified in HE stainings, which might explain inhomougeneous antibody distribution. Blocking of the epitope with unlabelled M5A-antibody reduced the %ID/cc from 16.5% to 4.3% in CEA positive tumours 24h after injection of labelled M5A-antibody, showing its specific binding. An unspecific control antibody showed significantly lower uptake in CEA positive tumours in terms of %ID/cc (5.3% ± 0.5%). Despite the expected high background in liver tissue, we were able to detect liver metastasis with a Cu-64-DOTA-labelled antibody in PET for the first time. These results show the high specificity of the M5A-antibody in a tumour model, far beyond classical subcutaneous tumour models and open the way for detection of liver metastases with Cu-64-DOTA labelled antibodies. M5A also seems to be an attractive candidate for radioimmunotherapy.

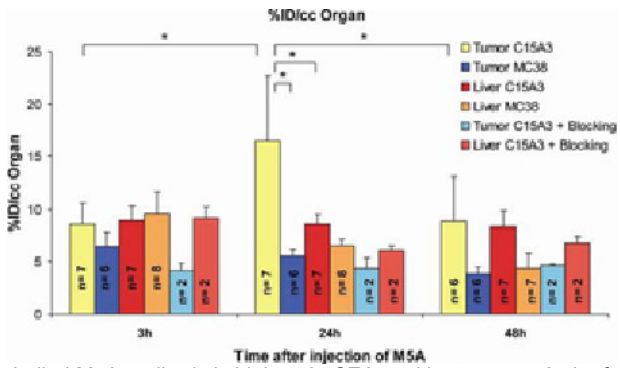


Figure 1: Tumour uptake of Cu-64-DOTA-labelled M5A-antibody is highest in CEA positive tumours 24 h after injection of antibody and can be reduced by blocking with unlabelled antibody. Mice were intra lineally injected with MC38 (CEA negative) or C15A3 (CEA positive) cells. After development of liver metastasis, mice were injected with 20 µg of Cu-64-DOTA-labelled M5A-antibody and analysed in PET and MRT at different time points. For blocking studies, 500 µg unlabelled M5A-antibody was injected 3h prior to injection of labelled antibody. %ID/cc for different tissues was determined. Significantly different values are designated with * when p≤0.05.

Disclosure of author financial interest or relationships:
**M.A. Krueger**, None; **S. Nittka**, None; **J. Schmitt**, None; **M. Neumaier**, None; **B.J. Pichler**, Siemens, Grant/research support; AstraZeneca, Grant/research support; Bayer Healthcare, Grant/research support; Boehringer-Ingelheim, Grant/research support; Oncodesign, Grant/research support; Merck, Grant/research support; Bruker, Grant/research support .

Presentation Number **SS 178**
Scientific Session 26: Chemistry & Probes - Multimodal
September 8, 2012 / 13:00-13:12 / Room: Liffey Hall 1

# Multimodal Imaging Probes for In Vivo Visualization of Neuroinflammation: Potential for Early Diagnosis of Traumatic Brain Injury (TBI)

***Erica Andreozzi***[1], *Angelique Louie*[1,3], *Ken Van*[2], *Bruce Lyeth*[2], [1]*Biomedical Engineering, University of California, Davis, Davis, CA, USA;* [2]*Neuroscience, University of California, Davis, Davis, CA, USA;* [3]*Chemistry, University of California, Davis, Davis, CA, USA. Contact e-mail: erica.andreozzi@gmail.com*

Introduction: Traumatic brain injury (TBI) is a leading neurodegenerative disease that continues to go undiagnosed, leaving ~80,500 TBI survivors with cognitive deficits and >$56.3 billion in annual U.S. health care costs. Thus, there is great interest in developing methods for diagnosis of TBI so that necessary treatment options can be timely employed and chronic, irreversible brain damaged can be prevented[1,2,3]. Having identified activated microglia (immune cells of the brain) as contributors to post-TBI neuroinflammation, we have developed a novel, multimodal (optical/MRI/PET) imaging probe targeted to activated microglia as a means of non-invasively diagnosing TBI before the onset of cognitive deficits. The multimodal probe, malBSA-TAMRA-DOTA(Gd/$^{64}$Cu), consists of maleylated (mal) bovine serum albumin (BSA) (SR-A ligand) coupled to TAMRA (fluorophore), gadolinium (Gd), and $^{64}$Cu, enabling optical, MRI, and PET functionality[4,5]. We hypothesize that administering this probe in a lateral fluid percussion (LFP) rat model of TBI[6,7,8,9] will enable in vivo visualization of activated microglia using PET and MRI. Material and Methods: An optical/MRI derivative of the probe, malBSA-TAMRA-DOTA(Gd), was synthesized and characterized for size (dynamic light scattering), Gd content (inductively coupled plasma mass spectrometry), and longitudinal relaxivity. T1-weighted magnetic resonance imaging (MRI) of this probe (7-Telsa, 25°C) was used to observe its positive contrast enhancement at high field strength. In order to determine the time window of blood brain barrier (BBB) permeability associated with the LFP model, we co-injected $^{64}$Cu-DOTA with Evan's blue dye into TBI and Sham rats and assessed brain signal with positron emission tomography (PET). We quantified brain signal through region of interest (ROI) analysis in the PET images. Immunohistochemistry of explanted brain tissue collected at 24 hr was used to confirm the coregistration of Evan's blue with PET signal and identification of IgG albumin (biomarker of BBB permeability). Results: In previous work, we have confirmed targeting and specificity of mal-BSA to activated microglia. Relaxivity measurements (1.4 T, 37°C) of malBSA-TAMRA-DOTA(Gd) indicate an r1 value ~11 $mM^{-1}sec^{-1}$. T1-weighted images (7 T, 25°C) of malBSA-Tamra-DOTA(Gd) shows decreasing signal intensity with decreasing Gd concentration (Fig. 1b). ROI analysis of PET data confirms that the TBI rats have significantly higher percent injected dose per gram (%ID/g) in the top right (R) and bottom left (L) regions of the brain in comparison to the Sham rats. Confocal microscopy of brain tissue stained (fluorescence) for IgG shows TBI has higher signal intensity than the Sham, confirming more IgG and thus an increased of BBB permeability (Fig. 1c). Conclusion: Focusing on the key role of microglia in TBI pathology, we aim to use multimodality imaging of microglia to for early diagnosis of TBI. Now that we've identified the time window of BBB permeability for the LFP model of TBI, we will appropriately administer our multimodal probe in future studies in order to facilitate in vivo investigation of activated microglia following TBI.

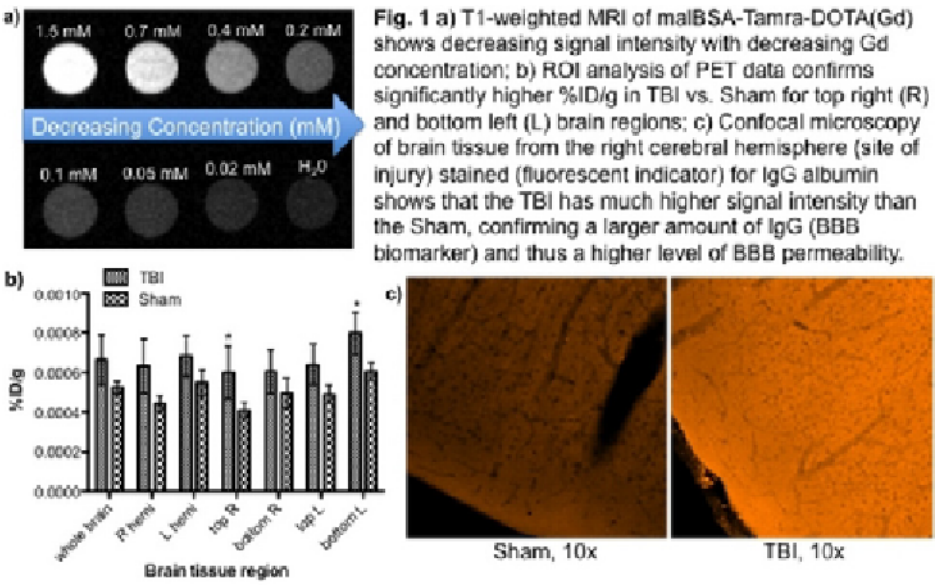


**Fig. 1 a)** T1-weighted MRI of malBSA-Tamra-DOTA(Gd) shows decreasing signal intensity with decreasing Gd concentration; b) ROI analysis of PET data confirms significantly higher %ID/g in TBI vs. Sham for top right (R) and bottom left (L) brain regions; c) Confocal microscopy of brain tissue from the right cerebral hemisphere (site of injury) stained (fluorescent indicator) for IgG albumin shows that the TBI has much higher signal intensity than the Sham, confirming a larger amount of IgG (BBB biomarker) and thus a higher level of BBB permeability.

Disclosure of author financial interest or relationships:
**E. Andreozzi**, None; **A. Louie**, None; **K. Van**, None; **B. Lyeth**, None.

Presentation Number **SS 179**
Scientific Session 26: Chemistry & Probes - Multimodal
September 8, 2012 / 13:12-13:24 / Room: Liffey Hall 1

# PEGylation and Radiolabeling of Superparamagnetic Iron Oxide using Bisphosphonates: Ultra-stable Nanoparticles for *In Vivo* Multimodal Imaging

***Lydia Sandiford**, Andrea Protti, Alkystis Phinikaridou, Mark Green, Rafael Torres Martin de Rosales, Division of Imaging Sciences & Biomedical Engineering, King's College London, London, United Kingdom. Contact e-mail: lydia.sandiford@kcl.ac.uk*

The combination of positron emission tomography (PET) and single photon emission computed tomography (SPECT) with magnetic resonance imaging (MRI) has resulted in the recent interest in the development of bimodal (PET/SPECT-MR) imaging agents [1-4]. However, the potential applications of combining PET or SPECT with MR in a single probe are limited. We believe that one of the most promising applications is to improve the sensitivity of MRI agents such as superparamagnetic iron oxide nanoparticles (SPIOs) by adding a PET/SPECT component while keeping the high-resolution imaging capabilities of MRI. Thus, we have recently shown that by radiolabeling SPIOs we can: 1) facilitate quantification and detection using PET/SPECT imaging [3]; 2) detect areas of uptake with PET that were not detected with MRI [4]. The aim of this study was to develop targeted SPIO nanomaterials exploiting the strong binding affinity and stability of bisphosphonates (BPs) to iron oxide and other materials [3, 4]. We have successfully produced small, monodispersed $Fe_3O_4$ NPs coated with a novel PEG-bisphosphonate (PEG-BP, 5 kDa) that results in long circulation times and prevents non-specific uptake by the reticuloendothelial system (RES, liver and spleen) *in vivo*. The PEG-BP-USPIOs were fully characterised. Transmission electron microscopy (TEM) revealed a core size of 5 nm and dynamic light scattering (DLS) measurements gave a hydrodynamic diameter of 27 ± 9 nm. Measuring the hydrodynamic diameter after 16 weeks revealed no change in size confirming the stability. The MRI contrast properties (relaxivities) of PEG-BP-USPIOs at 3 T were calculated using a clinical scanner. Our particles were found to have a $r_1$ of 9.5 $s^{-1}mM^{-1}$, a $r_2$ of 28.2 $s^{-1}mM^{-1}$, and hence a $r_2/r_1$ of 2.97, which is low compared to commercially available USPIOs for $T_1$ weighted imaging (FeraSpin XS, Miltenyi Biotec GmbH) ($r_1$ of 5.4 $s^{-1}mM^{-1}$, a $r_2$ of 36.3 $s^{-1}mM^{-1}$, and hence a $r_2/r_1$ of 6.73). The substantially lower $r_2/r_1$ value of PEG-BP-USPIOs demonstrates their high potential as $T_1$ MR contrast agents in clinically relevant magnetic fields. Radiolabeling with $^{99m}Tc(CO)_3$-DPA-ale [5] resulted in radiolabeled particles stable in human serum for at least 18 hours proving the strength of the BP binding to the metallic surface *in vitro*. SPECT-CT imaging revealed the USPIOs have a long blood half-life, as well as no liver uptake. Thus, we believe we are in an ideal situation for targeting PEG-BP-USPIOs to well-established vascular targets. References: [1] A. Louie, Chem. Rev. 110, (2010), 3146-3524. [2] L.E. Jennings, N.J. Long, Chem. Commun. (2009), 3511-3524. [3] R. Torres Martin de Rosales, R. Tavaré, A. Glaria, G. Varma, A. Protti, P.J. Blower, Bioconjugate Chem. 22, (2011), 455-465. [4] R. Torres Martin de Rosales, R. Tavaré, R.L. Paul, M. Jauregui-Osoro, A. Protti, G. Varma, I. Szanda, P.J. Blower, Angew. Chem. Int. Ed. 11, (2011), 5509-5513. [5] R. Torres Martin de Rosales, C. Finucane, S.J. Mather, P.J. Blower, Chem. Commun. (2009), 4847-4849.

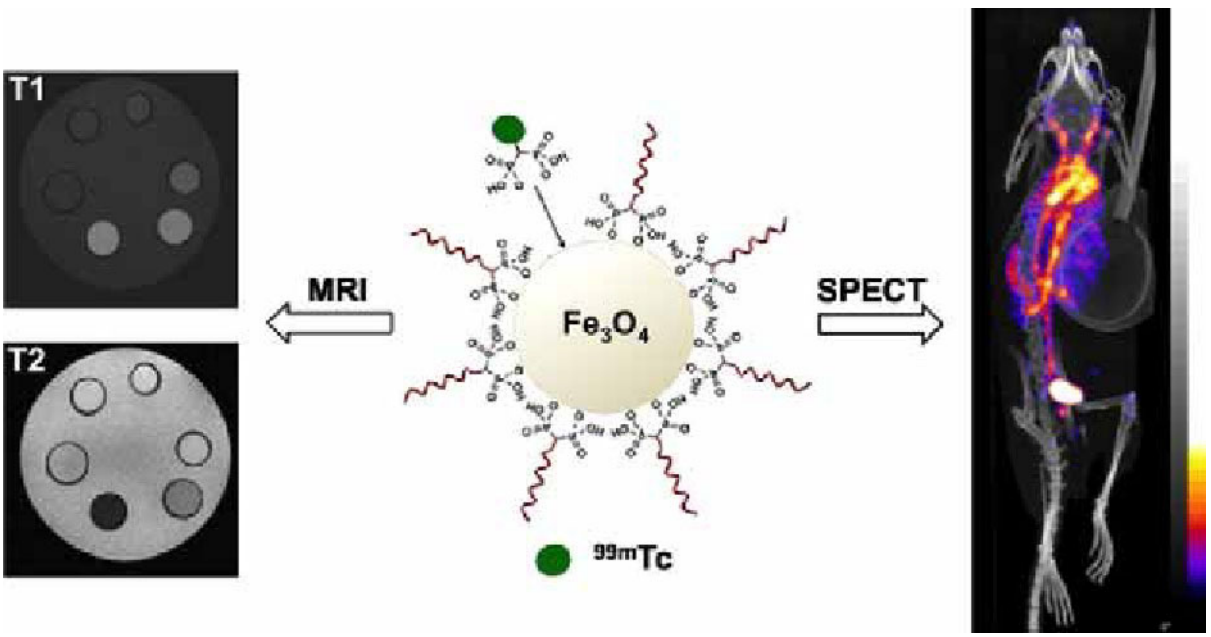


Radiolabeled USPIO for use as a PET/SPECT-MR imaging agent

Disclosure of author financial interest or relationships:
**L. Sandiford**, None; **A. Protti**, None; **A. Phinikaridou**, None; **M. Green**, None; **R. Torres Martin de Rosales**, None.

Presentation Number **SS 18**
Scientific Session 3: Preclinical In Vivo - Metabolic Disease
September 6, 2012 / 10:51-11:12 / Room: Liffey Hall 2

# Road Blocks on the Way to Clinical Beta Cell Imaging

***Martin Gotthardt**, Nuclear Medicine, Radboud University Nijmegen Medical Centre, Nijmegen, Netherlands. Contact e-mail: M.Gotthardt@nucmed.umcn.nl*

Disclosure of author financial interest or relationships:
**M. Gotthardt**, Sanofi Aventis, Grant/research support .

Presentation Number **SS 180**
Scientific Session 26: Chemistry & Probes - Multimodal
September 8, 2012 / 13:24-13:36 / Room: Liffey Hall 1

# The design of a dual-functional imaging contrast agent for targeting to Tumor Endothelial Marker (TEM8)

***Qimeng Quan***[1,2], *Xinglu Huang*[2], *Jin Xie*[2], *Yongjun Yan*[3], *Haokao Gao*[2], *Guixiang Zhang*[1], *Xiaoyuan Chen*[2], [1]*Department of Radiology, Shanghai First People's Hospital, Shanghai Jiaotong University, Shanghai, China;* [2]*Laboratory of Molecular Imaging and Nanomedicine, National Institute of Biomedical Imaging and Bioengineering, National Institutes of Health, Bethesda, MD, USA;* [3]*Department of Medical Physics, University of Wisconsin, Madison, WI, USA. Contact e-mail: quanquan527@gmail.com*

Purpose We have previously designed QQM peptide that binds specifically to the extracellular domain of TEM8. In this study, we would like to develop a QQM-based nanoplatform for dual-modality targeted imaging of TEM8 expression on 4T1 breast cancer cells and xenografts. Methods Near-infrared dye ZW-800 (Z) and QQM peptide (Q) were conjugated onto the surface of iron oxide nanoparticles (IO). The Z-IO-Q particles were characterized by TEM, DLS, fluorescence intensity and UV-vis spectroscopy. MTT assay was used to determine cell toxicity. MR imaging and optical imaging were carried out on 4T1 cells in vitro and tumor xenografts in vivo. The receptor specificity of the dual modality imaging probe was also confirmed by a blocking experiment in the presence of excess amount of non-labeled QQM peptide. Results The Z-IO-Q conjugate had an overall hydrodynamic particle size of 47.8nm. MTT assay showed that this formula has no suppression effects on 4T1 cells growth. Incubation of 4T1 cells leads to more significant T2* signal drop (82.18 ± 2.84%) than Z-IO (17.48 ± 0.50%) ($P < 0.01$). Fluorescence staining of the cells followed the same trend. In vivo MR imaging showed significantly higher accumulation of Z-IO-Q than Z-IO in 4T1 tumor xenograft, with T2* signal drop of 47.51 ± 10.26% versus 15.02 ± 5.13% at 2 h and 41.80 ± 6.94% versus 2.93 ± 9.0% at 24 h post injection for Z-IO-Q and Z-IO, respectively. The higher fluorescence intensity in the optical imaging of Z-IO-Q group was also observed. Both MR enhancement and optical imaging contrast were effectively blocked in the presence of QQM peptide. Conclusion We have successfully developed QQM peptide as a tumor TEM8 targeting ligand that can promote both MR and optical imaging contrast enhancement in TEM8 positive tumors. Our future work would include loading Z-IO-Q with chemotherapeutics for cancer theranostic applications.

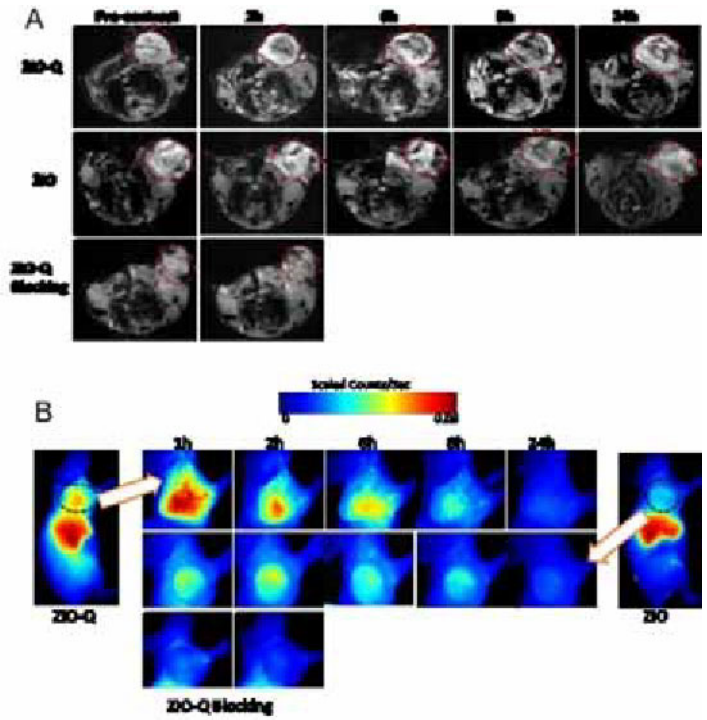


Dual-modality targeted imaging of 4T1 breast xenografts. A) T2*-weighted MRI axial images were acquired before and at 2, 6, 8, and 24 h after injection. The tumor areas were contoured by red circles. B) NIR fluorescence imaging of subcutaneous 4T1 tumor mice by intravenous injection of Z-IO-Q or Z-IO. Effective blocking of Z-IO-Q uptake was observed in the presence of excess amount of QQM peptide.

Disclosure of author financial interest or relationships:
**Q. Quan**, None; **X. Huang**, None; **J. Xie**, None; **Y. Yan**, None; **H. Gao**, None; **G. Zhang**, None; **X. Chen**, None.

Presentation Number **SS 181**
Scientific Session 26: Chemistry & Probes - Multimodal
September 8, 2012 / 13:36-13:48 / Room: Liffey Hall 1

# Sensitive Multiplex SERS Detection of Cancer Biomarkers in Low Sample Volume Using Photonic Crystal Fiber

*Dinish Unnimadhava S[1], **Malini Olivo**[1,2], [1]Bio-Optical Imaging Group, Singapore Bioimaging Consortium, Singapore, Singapore; [2]School of Physics, National University of Ireland Galway, Galway, Ireland. Contact e-mail: malini_olivo@sbic.a-star.edu.sg*

Surface Enhanced Raman Scattering (SERS) enhances the intensity of the 'fingerprint' Raman spectra of a molecule by several orders of magnitude when it is in close proximity to nano-roughened metallic surfaces or nanoparticles made of gold or silver. The great need for in vivo sensing platform demands for the fabrication of SERS-active surface on the tip of optical fibers. This combination offers the advantages of molecular fingerprinting of Raman scattering, the enormous enhancement factor of SERS and the flexibility of optical fibers. To realize a SERS-fiber probe, various configurations such as D-shaped, taper tip and 'sandwich' have been reported. However, SERS active fibers fabricated on conventional optical fibers lack the sensitivity needed for biosensing. In order to overcome this problem, photonic crystal fibers (PCF) were introduced, due to which analyte molecules can be absorbed into the air holes of core and/or cladding thereby increasing the interaction length between the excitation laser and analyte. Here, we report a novel PCF based SERS sensing platform for the detection of cancer proteins in sample volume as low as nanoliters. As a proof of concept, epidermal growth factor receptors (EGFRs) in a lysate solution from human epithelial carcinoma cells (A431) were immobilized into the hollow core PCF (HCPCF) and used as positive control while, EGFR negative human breast carcinoma cells (MCF-7) is used as negative control. Detection of EGFR biomarker is carried out using anti-EGFR antibody conjugated SERS nanotag. This nanoprobe-SERS nanotag is realized by anchoring strong Raman active molecule (malachite green isothiocyanate, MGITC) onto the surface of gold nanoparticles, which can be conjugated with molecular recognition species to render specific targeting. Our initial study shows that it can detect very low amount proteins at ~100 pg in a sample volume of ~10 nL. Conventional enzyme-linked immunosorbent assays (ELISA) require ng-µg of protein at relatively larger sample volume of ~ mL and ELISA results in our study confirmed a detection limit of only 5ng/mL for EGFR in A431 cell lysate. As shown in Fig. 1, SERS spectra obtained from the fiber immobilized with EGFR from A431 cells clearly replicates the spectrum of the original MGITC SERS nanotag, while no specific peaks of MGITC was observed from the fiber treated with MCF-7, which is the negative control. We also report the multiplex detection of biomarkers in cell lystae using SERS nanotags constructed with reporter molecules, which have distinct Raman peaks that allows sensing of many proteins simultaneously with high sensitivity. In this context, our methodology is highly significant in low level detection of cancer biomarker in extremely low sample volume.

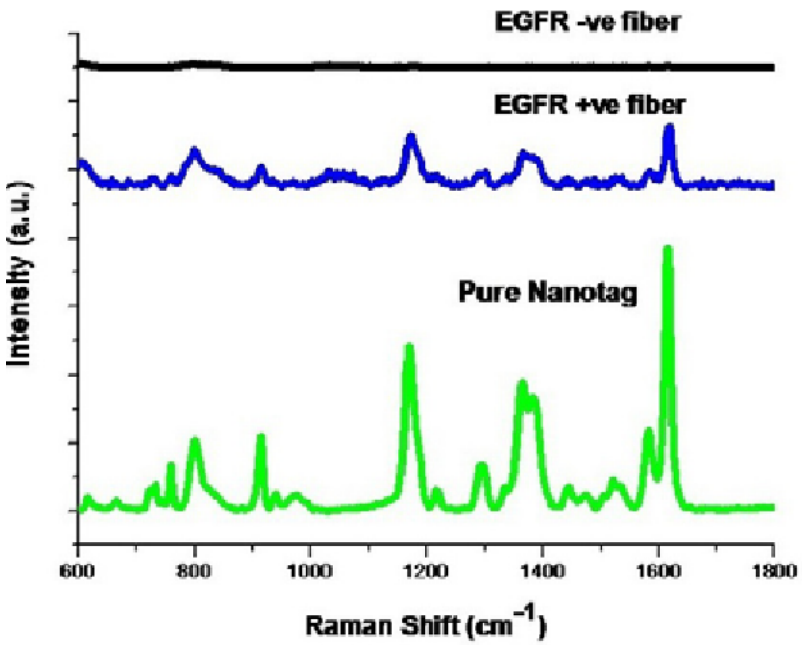


SERS spectra obtained from MGITC nanotag (bottom line), antibody conjugated nanotag bound to cancer protein (middle line, fiber with A431 cell lysate) and negative control (top line, fiber with MCF-7 cell lysate).

Disclosure of author financial interest or relationships:
**D. Unnimadhava S**, None; **M. Olivo**, None.

Presentation Number **SS 182**
Scientific Session 26: Chemistry & Probes - Multimodal
September 8, 2012 / 13:48-14:00 / Room: Liffey Hall 1

# Upconverting Nanophosphors : A new class of nanoparticles for multimodal imaging with enhanced fluorescence emission

***Hugo Groult***[1,2], *Jesús Ruiz-Cabello*[1,2], *Fernando Herranz*[1,2], [1]*Laboratory of Molecular Probes and Nanotechnology Advanced Imaging Unit, CNIC (Centro Nacional de investigacíon cardiovascular), Madrid, Spain;* [2]*CIBERES (Ciber de enfermedades respiratorias ), Mallorca, Spain. Contact e-mail: hugo.groult@gmail.com*

Cell and molecular imaging are tools of paramount importance for an early diagnosis of cardiovascular and pulmonary diseases. Among the different existing techniques, fluorescence imaging presents the distinctive advantage of a high sensitivity without ionizing radiation and potential for anatomical studies. The most common luminescent probes in use are based on down-conversion fluorescence, explaining intrinsic limitations of fluorescence imaging: auto-fluorescence, low penetration depth, photobleaching and toxicity of the probe, particularly for QDs[1]. Lately the rare-earth upconverting nanophosphors (UCNPs), a new generation of luminescent probes has been studied as interesting alternative. These materials present the unique feature of converting low energy near infrared (NIR) light into higher visible light and/or NIR emission through 2 or 3 sequential photon absorption, together with energy transfers. This singular property confers very attractive advantages for a UCNP-based fluorescence imaging: excitation less harmful, no auto-fluorescence, high penetration depth, no toxicity, low cost techniques[2]. One of the most attractive approaches, in molecular imaging, is the combination of fluorescence with MRI, providing high sensitivity and resolution together with structural and functional data. To achieve this goal nanomaterials are a promising way since their chemistry provides a unique tool to yield multimodal agents with possibility of a given tailored targeting. We have synthesized upconverting NaYF4 and NaGdF4 doped nanoparticles in hexagonal phase, known as good host material for up-converting fluorescence[3]. Excitation is at 980 nm and emission is from visible to NIR according to the dopants, nature and ratio, usually Er and Tm. The UCNPs were synthesized in organic solvents, providing nanocrystals of the highest quality[3], after that the particles were modified to render them water stable and suitable for biomedical applications. The approach was the formation of different micelles using several biocompatible polymers. The nanoassemblies have been fully characterized in terms of core/hydrodynamic size, composition and physiological properties. Especially they show strong upconversion fluorescence in vitro [figure 1]. A spectacular enhancement of fluorescence is reached when core of the nanoparticles are passivated with a non-doped host shell. Next these particles have been studied in vivo, in rats and mice to study several aspects. One of them was to check the circulating times of the particles after i.v. injection, as this is a important feature for their use in cardiovascular imaging. Our results show they have quite large circulating times from 50 minutes to 2 hours in rats thanks to the antibiofouling properties of the coatings. We also studied their use as MRI contrast agents for lung imaging, these results show the wide range of applications these particles can be used for. [1]Kobayashi H.;Ogawa M., Alford R.;Choyke P.L. & Urano Y. Chemical Reviews,110(2010) 2620 [2]Zhou J.;Liu Z. & Li F. Chemical Society Reviews,(2012) [3]Aebischer A. et al. Angewandte Chemie International Edition,45(2006) 2802

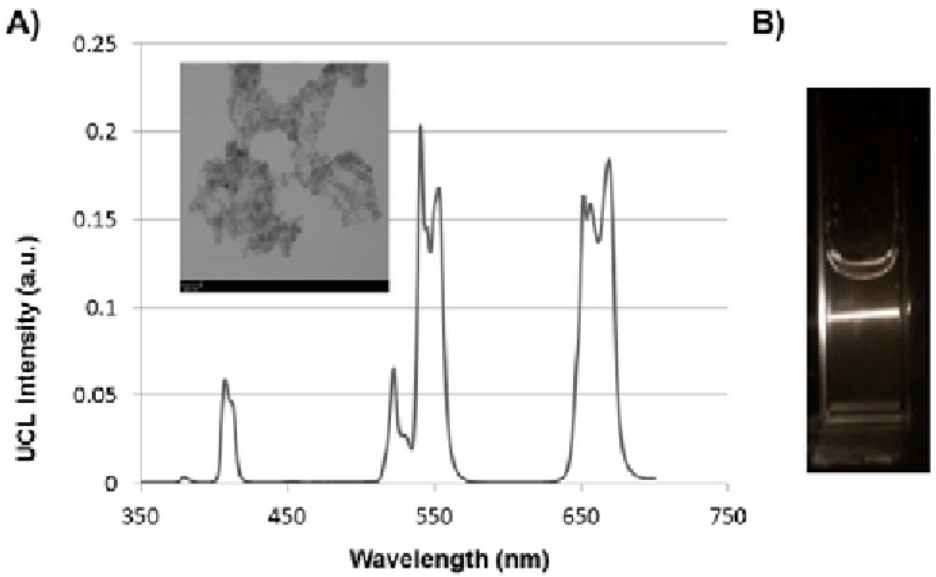


Disclosure of author financial interest or relationships:
**H. Groult**, None; **J. Ruiz-Cabello**, CNIC, Other financial or material support; **F. Herranz**, None.

Presentation Number **SS 183**
Scientific Session 26: Chemistry & Probes - Multimodal
September 8, 2012 / 14:00-14:12 / Room: Liffey Hall 1

# Multimodal SuperParamagnetic Iron Oxide Nanoparticles: Versatile Probes for the in Vivo Imaging of Specific Pathologies

*Jérémy Paris[1], Renée Mayap Talom[1], **Julien Boudon**[1], Lionel Maurizi[1], Yann Bernhard[2], Richard A. Decréau[2], Paul Walker[3], Laure Dumont[4], David Vandroux[4], Franck Denat[2], Nadine Millot[1], [1]Laboratoire Interdisciplinaire Carnot de Bourgogne, UMR 6303 CNRS/Université de Bourgogne, Dijon, France; [2]Institut de Chimie Moléculaire de l'Université de Bourgogne, UMR 6302 CNRS/Université de Bourgogne, Dijon, France; [3]Service de Spectroscopie par Résonance Magnétique, Centre Hospitalier Universitaire, Dijon, France; [4]NVH Medicinal, Centre Hospitalier Universitaire, Dijon, France. Contact e-mail: julien.boudon@u-bourgogne.fr*

Nowadays, nanotechnology offers a wide field of applications in medicine and biology.[1, 2] This domain is very promising in particular regarding the detection and the treatment of pathologies. One representative example is SuperParamagnetic Iron Oxide Nanoparticles (SPIONs) that represent some of the most important nanoparticles used as MRI contrast agents[3] as well as for hyperthermia treatment.[4] Recently, our group has developed continuous hydrothermal syntheses of SPIONs, in subcritical and supercritical water conditions. The nanoparticle size is smaller and their size distribution is narrower than those of powders obtained with other standard methods. Moreover, citrate-stabilized SPIONs were obtained in a continuous way.[5] Herein we present the development of multimodal contrast agents based on functionalized SPIONs for MRI, SPECT, PET and optical imaging (OI). At first modified SPIONs are prepared by the grafting of organic moieties (NH2, COOH or SH) to allow for an advanced system to be built: macrocyclic compounds such as DOTA[6] or phthalocyanine derivatives[7] are added for respectively nuclear imaging (SPECT or PET) or OI (fluorescence)/photodynamic therapy. Secondly, a covalent coupling of functionalized PEG is necessary to ensure the biocompatibility and the increased stability of these nanoparticles.[8] In addition, the grafting of the organic molecules (DOTA, PEG and phthalocyanines) was proven by different analyses such as fluorescence, UV-vis spectra, XPS and elemental analysis. Finally, the magnetic properties of these SPIONs were tested in vitro on a clinical 3 Tesla MRI. The magnetic efficiencies (relaxivities) of our suspensions are at least as good as a commercial product (Cliavist®). The first results concerning the in vivo biodistribution show a reduced capture of PEGylated SPIONs by mouse liver and suggest that our contrast agent freely circulates longer in the mouse blood than the other commercial SPION-based product tested. MTT assays prove that these iron oxide suspensions have no apparent cytotoxicity on different cell lines (cardiomyocytes, macrophages and hepatic cells). These results open the way of the targeted detection of specific pathologies such as myocardial infarction or cardiotoxicity induced by breast carcinoma drugs. [1] A. Schroeder, D. A. Heller et al., Nat. Rev. Cancer 2012, 12 (1), 39-50. 10.1038/nrc3180 [2] W. J. Stark, Angew. Chem. Int. Ed. 2011, 50 (6), 1242-1258. 10.1002/anie.200906684 [3] Y.-X. Wang, S. Hussain et al., Eur. Radiol. 2001, 11 (11), 2319-2331. 10.1007/s003300100908 [4] M. Johannsen, U. Gneveckow et al., Eur. Urol. 2007, 52 (6), 1653-1662. 10.1016/j.eururo.2006.11.023 [5] L. Maurizi, F. Bouyer et al., Chem. Commun. 2011, 47 (42). 10.1039/C1CC15470B [6] C. Bernhard, C. Goze et al., Chem. Commun. 2010, 46 (43), 8267-8269. 10.1039/C0CC02749A [7] S. Gundy, W. Van der Putten et al., Phys. Med. Biol. 2004, 49 (3), 359-369. 10.1088/0031-9155/49/3/001 [8] L. Maurizi, H. Bisht et al., Langmuir 2009, 25 (16), 8857-8859. 10.1021/la901602w

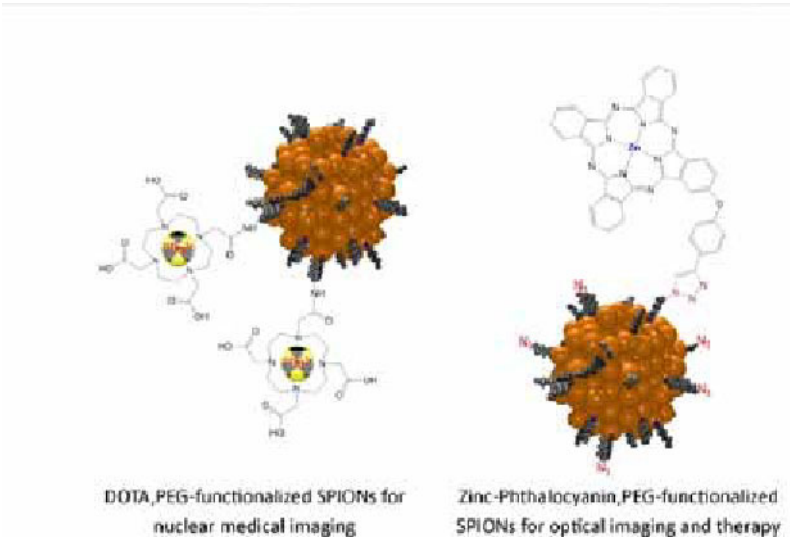


Disclosure of author financial interest or relationships:
**J. Paris**, None; **R. Mayap Talom**, None; **J. Boudon**, None; **L. Maurizi**, None; **Y. Bernhard**, None; **R.A. Decréau**, None; **P. Walker**, None; **L. Dumont**, None; **D. Vandroux**, None; **F. Denat**, None; **N. Millot**, None.

Presentation Number **SS 184**
Scientific Session 26: Chemistry & Probes - Multimodal
September 8, 2012 / 14:12-14:24 / Room: Liffey Hall 1

# Synthesis, characterization and application of iron oxide nanoparticle-micelles (ION-Micelles) for sensitive molecular magnetic particle imaging (MPI) and magnetic resonance imaging (MRI)

***Lucas Starmans***[1], *Dirk Burdinski*[2], *Nicole Haex*[2], *Rik Moonen*[1], *Klaas Nicolay*[1], *Holger Gruell*[1,2], [1]*Biomedical Engineering, Eindhoven University of Technology, Eindhoven, Netherlands;* [2]*Biomolecular Engineering, Philips Research, Eindhoven, Netherlands. Contact e-mail: l.w.e.starmans@tue.nl*

**Introduction**: Iron oxide nanoparticles (IONs) are frequently employed for contrast-enhanced MRI. Recently, magnetic particle imaging (MPI) was introduced as a new imaging modality, which is able to directly visualize magnetic particles and which would be a more sensitive and quantitative alternative to MRI. However, current commercially available iron oxide formulations are not optimized for MPI. In this study, we report on a novel ION platform consisting of 25 nm sized iron oxide cores encapsulated in lipidic micelles for sensitive MPI and MRI. Furthermore, to show the suitability of the presented ION-Micelle platform for molecular MPI and MRI, the ION-Micelles were functionalized with a fibrin-binding peptide (FibPep) and in vitro blood-clot binding was assessed. **Material and methods**: *Synthesis*: IONs were synthesized using FeO(OH)-based thermal decomposition and subsequently phase-transfered by encapsulation into lipidic micelles (ION-Micelles). *Characterization*: The synthesized nanoparticles were characterized using (cryo) transmission electron microscopy (TEM) and dynamic light scattering (DLS). In addition, their potency for MPI and MRI was assessed using magnetic particle spectrometry (MPS, drive field: 10 mT, 25kHz) and proton relaxometry (1.41 T, 37 °C), respectively, and benchmarked against Endorem, Resovist and Sinerem. *In vitro blood-clot binding assay*: ION-Micelles were functionalized by covalently binding FibPep to the lipidic coating. As a negative control, a scrambled peptide (NCFibPep) was employed. In vitro blood-clot binding of the (NC)FibPep-ION-micelles was assessed using MPS and MRI. **Results**: *Synthesis and characterization*: (Cryo)-TEM analysis showed that the iron oxide cores were relatively monodisperse (24.9 ± 1.9 nm) and that the ION-Micelles were mostly dispersed as single particles or as small aggregates. Number-weighted DLS analysis showed a hydrodynamic diameter of 38 nm, which corresponds well with the cryo-TEM findings. The ION-Micelles displayed a transversal relaxivity r2 of 253 mM-1s-1, which was vastly higher than the benchmark iron oxides (r2 < 120 mM-1s-1). ION-Micelles generated increased MPS signals in comparison to the benchmark particles over the entire frequency range. For the lower frequencies (<0.5 MHz), the ION-Micelles generated 4-6 times more signal than Resovist, which was the best performing benchmark formulation. At higher frequencies (>1 MHz), the increase in ION-Micelle MPS signal was even more profound: > 50 times higher signal than the benchmark formulations. *In vitro blood-clot binding assay*: After incubation with FibPep-ION-Micelles, the clot-signal in MR images was clearly reduced and the respective MPS signal was significantly increased compared to reference measurements using NCFibPep-ION-Micelles (Fig. 1). **Conclusions**: ION-Micelles allow for more sensitive MPI and MRI than the currently available iron oxide formulations. Furthermore, the potential of the ION-Micelle platform for molecular MPI and MRI was illustrated in vitro using fibrin-targeted ION-Micelles. Overall, these findings warrant further investigation of the ION-Micelle platform for in vivo (molecular) MPI and MRI.

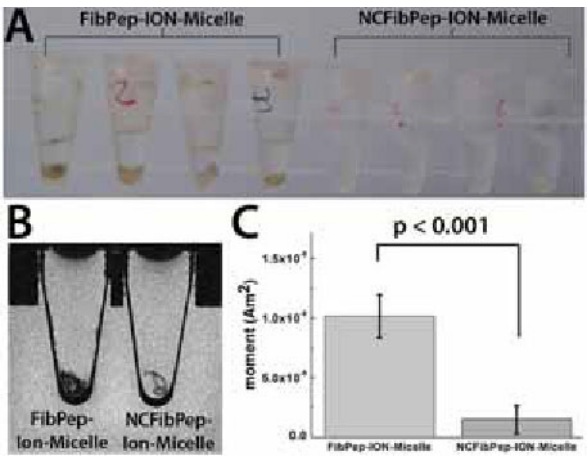


**Figure 1.** In vitro blood clot binding assay using fibrin-binding peptide conjugated ION-Micelles (FibPep-ION-Micelles) and negative control peptide conjugated ION-Micelles (NCFibPep-ION-Micelles). Clots were incubated with (NC)FibPep-ION-Micelles for 1 hour and subsequently washed trice. (A) Photograph, (B) transversal MR image and (C) third harmonic (76 kHz) MPS signal amplitude of the clots.

Disclosure of author financial interest or relationships:
**L. Starmans**, None; **D. Burdinski**, Philips Research, Eindhoven, The Netherlands (past employment), Employment; **N. Haex**, None; **R. Moonen**, None; **K. Nicolay**, None; **H. Gruell**, Philips, Employment .

Presentation Number **SS 185**
Scientific Session 27: Preclinical In Vivo - Infectious Disease
September 8, 2012 / 13:00-13:30 / Room: Wicklow Hall 1

# Imaging Immune Cells

***Matthias Gunzer**, University of Duisberg, Essen, Germany. Contact e-mail: Matthias.Gunzer@uni-due.de*

Disclosure of author financial interest or relationships:
**M. Gunzer**, None.

Presentation Number **SS 186**
Scientific Session 27: Preclinical In Vivo - Infectious Disease
September 8, 2012 / 13:30-13:42 / Room: Wicklow Hall 1

# The Kidney Defends the Urinary System from Infection by Secreting NGAL

***Neal Paragas***[1], *Jonathan Barasch*[1], *Ritwij Kulkarni*[2], [1]*Medicine, Columbia University, New York, NY, USA;* [2]*Pediatrics, Columbia University, New York, NY, USA. Contact e-mail: np2014@columbia.edu*

NGAL is a critical component of innate immunity because it binds catecholate-siderophores which microorganisms require to capture iron. Urinary(u) NGAL is expressed at mg/L levels after either septic or aseptic diseases of the kidney and it has two potential functions, epithelial growth and/or bacteriostasis. Here we examined the activity of uNGAL in the growth of CFT073, a uropathogenic E. coli (UPEC). To determine the role of uNGAL in bacteriostasis we first designed a conditional allele of NGAL as a way to establish the location of NGAL expression. Then we created a bioluminescent mouse that expresses Luciferase and mCherry when the NGAL locus is activated. We found NGAL significantly inhibited UPEC growth in vitro, which could be rescued by the addition of iron. In a mouse pyelonephritic model, the intensity and timing of urinary CFUs was mirrored by uNGAL, including a decrease in uNGAL coincident with the resolution of infection. To determine the source of uNGAL, we made a NGAL reporter mouse NGAL-Luc2/mC to visualize kidney expression in vivo and we found that UPEC detritus and live UPEC introduced into the bladder induced NGAL-Luc2/mC distantly in the kidneys (Figure). Reporter expression was consistent with the bladder and kidney Ngal according to QPCR. By high power in situ hybridization and confocal microscopy we located Ngal to alpha intercalated cells. To determine the physiological role of uNGAL, we made a global conditional NGAL KO using EIIa-Cre recombinase and found that UPEC infections had delayed resolution. To determine whether UPEC signaling directly activates kidney epithelia, we developed an in vitro assay using the CDs of Ngal-Luc2/mC. These cells express Ngal-Luc2/mC in response to co-culture with UPECs and was reversed by antibiotics. To tract and visualize UPEC rise from the bladder to the kidney in vivo we developed a bioluminescent UPEC model by generating a luminescent UPEC by expressing the luxABCDE cassette. These data showed UPEC-lux ascend from the bladder to the kidneys. Additional studies suggest that TLRs are the critical local sensors of infection. In conclusion we found that uNGAL is essential for clearance of a UPEC in a model of acute UTI. The kidney responds to infections localized to the bladder by secreting NGAL. These findings provide an explanation for the massive secretion of NGAL from the kidney in both septic and aseptic diseases, demonstrating that the kidney defends the urinary system via exocrine delivery of NGAL. Importantly, UTIs are one of the most prevalent and resource taxing diseases in the USA with 15% of the population infected annually costing $3.5 billion for evaluation and treatment. In 2000 there were approximately 11 million diagnoses of UTI, and uropathogenic E. coli (UPEC) represented 70-95% of all cases. Thus these results may be important for the development of novel therapeutics and treatments for urinary tract infections (UTIs).

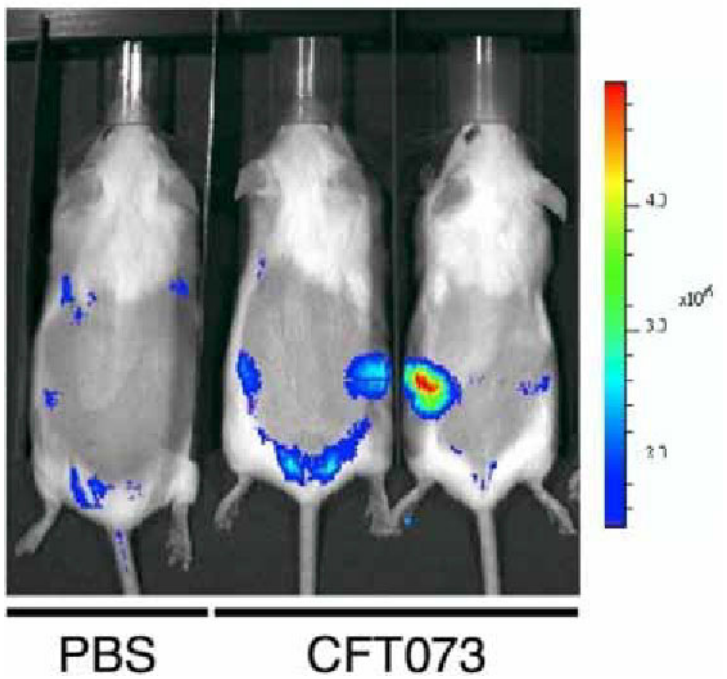


The distal nephron and the bladder epithelium respond to an uropathogenic infection by secreting uNGAL. The NGAL double fusion reporter mice had PBS (Control) or heat-killed CFT073 placed by TU in the bladder and imaged 24 h later by a bioimager. Kidney luciferase expression significantly increased compared to PBS control (9.84X105 and 5.71 X105 average radiance per kidney respectively).

Disclosure of author financial interest or relationships:
**N. Paragas**, None; **J. Barasch**, None; **R. Kulkarni**, None.

Presentation Number **SS 187**
Scientific Session 27: Preclinical In Vivo - Infectious Disease
September 8, 2012 / 13:42-13:54 / Room: Wicklow Hall 1

# Imaging commensal *Escherichia coli* MG1655 during long-term colonisation of the murine GI tract

***Cormac Gahan***[2,1]*, Mark Tangney*[3]*, Kevin P. Francis*[4]*, Pat G. Casey*[2,1]*, Christian U. Riedel*[2]*, Ian R. Monk*[2]*, Michelle Cronin*[3]*, Colin Hill*[2,1]*, Susan Joyce*[2]*, [1]Department of Microbiology, University College Cork, Cork, Ireland; [2]Alimentary Pharmabiotic Centre, University College Cork, Cork, Ireland; [3]Cork Cancer Research Centre, University College Cork, Cork, Ireland; [4]Caliper Technologies, Caliper-Perkin Elmer, Alameda, CA, USA. Contact e-mail: c.gahan@ucc.ie*

Introduction: There is an increasing need to develop *in vivo* models for the analysis of commensal strains that colonise the murine GI tract. We have developed an integrating vector that delivers *luxABCDE* to Gram negative strains in single copy under the influence of a strong constitutive promoter (Phelp). We have used this system to examine the colonisation of the murine gut by the human commensal strain *E. coli* MG1655 following streptomycin treatment of the host animal. We describe the efficacy of both 2D and 3D imaging approaches and elucidate the effects of streptomycin treatment upon the background microbiota in this model. Materials and Methods: We engineered the p16sLux integrating vector and demonstrate that this system works well for stable *lux* expression in the commensal *E. coli* strain MG1655. We utilised Caliper-Perkin Elmer *in vivo* imaging technologies to study the colonisation dynamics of this strain in the murine gut in streptomycin-treated animals using 2D and 3D bioluminescence imaging approaches combined with X-ray for precise anatomical localisation. New generation sequencing of 16s rDNA reads was utilised to characterise the shifts in the background microbiota following streptomycin treatment. Results: In streptomycin-treated mice *E. coli* MG1655 (StrepR) reached relatively high levels in the faeces (approximately 10e7 per gram) and persisted for over 70 days. Both 2D and 3D bioluminescence imaging revealed high levels of *lux*-labelled *E. coli* in the gut particularly within the large intestine and this result was confirmed through culture assays post-mortem. Streptomycin treatment resulted in a significant disruption of background microbiota particularly with respect to the Firmicutes. However other measures of mouse physiology remained normal in these animals. High heterologous gene expression was obtained using standard approaches in *E. coli* MG1655. Discussion: We highlight that *E. coli* MG1655 provides a useful model for high-level murine colonisation by a commensal strain that is genetically tractable. We show that precise localisation of MG1655 in the murine gut can be achieved through 3D bioluminescence imaging approaches.

Disclosure of author financial interest or relationships:
**C. Gahan**, None; **M. Tangney**, None; **K.P. Francis**, None; **P.G. Casey**, None; **C.U. Riedel**, None; **I.R. Monk**, None; **M. Cronin**, None; **C. Hill**, None; **S. Joyce**, None.

Presentation Number **SS 188**
Scientific Session 27: Preclinical In Vivo - Infectious Disease
September 8, 2012 / 13:54-14:06 / Room: Wicklow Hall 1

# Comparison of an antibody-based biomarker with different PET tracers for imaging of alveolar echinococcosis in rodents

***Anna-Maria Rolle***[1], *Peter Soboslay*[3], *Wolfgang Hoffmann*[3], *Christian Kesenheimer*[1], *Peter Deplazes*[2], *Bernd J. Pichler*[1], *Stefan Wiehr*[1], [1]*Department for Preclinical Imaging and Radiopharmacy,Laboratory for Preclinical Imaging and Imaging Technology of the Werner Siemens-Foundation, Eberhard Karls University Tuebingen, Tuebingen, Germany;* [2]*University of Zurich, Institute of Parasitology, Zürich, Germany;* [3]*Eberhard Karls University Tuebingen, Institute of Tropical Medicine, Tuebingen, Germany. Contact e-mail: anna-maria.rolle@med.uni-tuebingen.de*

The larval stage (metacestode) of the tapeworm *Echinococcus multilocularis* causes a life threatening zoonosis, the alveolar echinococcosis (AE). The disease is characterized by the tumor-like, multivesicular growth of the *E. multilocularis* metacestode, which leads to the infiltration of multiple organs as liver, lungs, kidneys and the central nervous system. Pathological changes occur after years or decades after the initial infection. Furthermore AE is lethal in 94-100 % of the cases if left untreated. A specific marker for diagnosis of the early infection stage is essential for efficient management and treatment of the disease. The monoclonal antibody MAbG11 binds to the antigen EM2G11 in the laminar layer of the metacestode. The highly specific radiolabeled antibody MAbG11 was tested and compared to clinically used PET tracers for the detection of AE. *E. multilocularis* vesicles were stained with Alexa Fluor 647-conjugated MAbG11 and counterstained with DAPI for confocal laser scanning microscopy. To determine the binding specificity of [$^{64}$Cu]DOTA-MAbG11, *in vitro* cell binding assays were performed in addition. Blood cells and splenocytes derived from naïve and infected jirds as well as vesicles from *E. multilocularis* metacestodes and a metacestode cell suspension were incubated with 0.26 MBq [$^{64}$Cu]DOTA-MAbG11 or a radiolabeled control antibody. Uptake was measured by gamma-counting. Mongolian jirds (*Meriones unguiculatus*) were inoculated *i.p.* with *E. multilocularis* metacestodes. The *in vivo* biodistribution was evaluated after injection of 13 MBq of [$^{18}$F]FDG, [$^{18}$F]FLT or the radiolabeled *E. multilocularis* specific biomarker [$^{64}$Cu]DOTA-MAbG11 via the tail vein. Small animal PET images were acquired in combination with MRI after injection and uptake of the tracers at early and late infection time points. After the last PET scans *ex vivo* biodistribution, autoradiography and histology were performed. The specific binding of the monoclonal antibody MAbG11 to the metacestode laminar layer was revealed by confocal laser scanning microscopy. *In vitro* cell assays showed a 4-fold higher uptake of [$^{64}$Cu]DOTA-MAbG11 in *E. multilocularis* vesicles compared to the control antibody. Quantification of the fused PET/MRI images showed low uptake of [$^{18}$F]FDG (parasite tissue/muscle ratios: 1.98 ± 0.54) and [$^{18}$F]FLT (parasite tissue/muscle ratios: 2.33 ± 0.27) in parasite tissue of the infected jirds at the early infection time point. In contrast specific uptake of the [$^{64}$Cu]DOTA-MAbG11 biomaker (parasite tissue/muscle ratios: 5.33 ± 1.82, early infection time point) was observed. The data clearly show, that the specific biomarker MAbG11 is an excellent candidate for the early detection of *E. multilocularis* infections, especially after comparison to clinically used PET tracers. Future efforts will be made to improve the radiolabeling of the antibody using different chelators and novel isotopes and apply the radiolabeled antibody for radioimmunotherapy.

Disclosure of author financial interest or relationships:
**A. Rolle**, None; **P. Soboslay**, None; **W. Hoffmann**, None; **C. Kesenheimer**, None; **P. Deplazes**, None; **B.J. Pichler**, Siemens, Grant/research support; AstraZeneca, Grant/research support; Bayer Healthcare, Grant/research support; Boehringer-Ingelheim, Grant/research support; Oncodesign, Grant/research support; Merck, Grant/research support; Bruker, Grant/research support; **S. Wiehr**, None.

Presentation Number **SS 189**
Scientific Session 27: Preclinical In Vivo - Infectious Disease
September 8, 2012 / 14:06-14:18 / Room: Wicklow Hall 1

# Combining BLI and MRI for non-invasive evaluation of novel antifungals against Candida albicans biofilms in vivo

***Greetje Vande Velde***[1], *Sona Kucharikova*[2], *Sanne I. Schrevens*[2], *Uwe Himmelreich*[1], *Patrick Van Dijck*[2], [1]*Biomedical MRI/ MoSAIC, KU Leuven, Leuven, Belgium;* [2]*Molecular Microbiology and Biotechnology, KU Leuven/ VIB, Leuven, Belgium. Contact e-mail: greetje.vandevelde@med.kuleuven.be*

BACKGROUND AND AIMS: Biofilm formation by fungal pathogens is a major problem in hospitals. Especially C. albicans biofilms are formed on the surface of many medical implants. They are difficult to treat as they are often resistant to the classical antifungal drugs. For testing antifungals against C. albicans biofilm formation, a subcutaneous catheter rat model system has been developed (1). Fungal load in biofilms is traditionally analyzed post mortem, requiring host sacrifice and enumeration of microorganisms from individual biofilms to evaluate the efficacy of antifungal treatment. We aim to make this model compatible for bioluminescence imaging (BLI), where detecting a quantifiable in vivo BLI signal from biofilms formed on the inside of catheters is challenging. METHODS: Wild-type C. albicans was engineered to express C. albicans codon-optimized Gaussia princeps luciferase (gLuc) at the cell wall, under the control of biofilm growth phase specific promoters (2). gLuc activity from Candida cells and biofilms is measured and correlated with cell counts. Catheters are implanted on the back of mice and rats and in vivo biofilm formation was followed up with BLI. Finetuning of the quantification was performed after acquisition of in vivo MR images and coregistration to the BL images to verify the site of catheter implantation and consideration of surrounding tissue types (muscle, fat layers etc.). To validate the model for antifungal testing, rodents are treated with different antifungals and imaged with BLI. At different time points post implantation, cfu counts from biofilms on explanted catheters are then compared to the in vivo BLI data for validation. RESULTS & CONCLUSIONS: The rat biofilm model was successfully reproduced in mice, which significantly reduces costs and holds potential for biofilm research in different transgenic mice strains. We report significant gLuc activity from Candida cells and biofilms, where the signal is corresponding to the specific yeast or hyphal cell stage. The BLI signal was proportional to the amount of yeast or hyphal cells in vitro and in biofilms. We could detect a significant BLI signal above background (control biofilm) from in vitro and in vivo formed biofilms in live animals, and compared this signal with biofilm analysis and cfu's from explanted catheters. The signal kinetics of i.p., s.c. and i.v. administration routes was studied in order to optimize the imaging protocol. Better reproducibility of quantification (and therefore smaller test groups) can be achieved when mice are immuno-suppressed when carrying biofilm-containing catheters. Coregistering BLI and MR images adds information on the exact position in 3D of the catheters which increases accuracy of signal quantification. The so developed multi-temporal non-invasive imaging assay for quantifying in vivo biofilm formation will be used for the validation of antifungal drugs under in vivo conditions. (1) Ricicova, M., Kucharikova, S. et al., Microbiology 156, 909-919 (2010). (2) Enjalbert, B., et al., Infect Immun 77, 4847-4858 (2009).

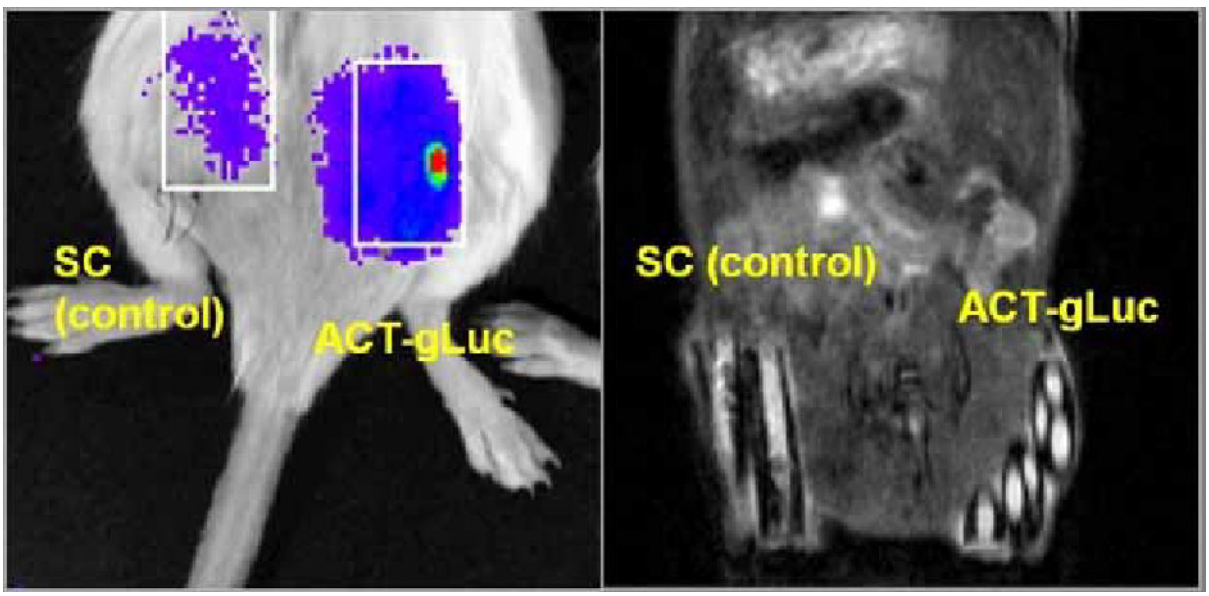


Disclosure of author financial interest or relationships:
**G. Vande Velde**, None; **S. Kucharikova**, None; **S.I. Schrevens**, None; **U. Himmelreich**, None; **P. Van Dijck**, None.

Presentation Number **SS 19**
Scientific Session 3: Preclinical In Vivo - Metabolic Disease
September 6, 2012 / 11:12-11:24 / Room: Liffey Hall 2

# Assessment of pancreatic and transplanted beta cell mass (BCM) using the PET tracer [11C]5-hydroxy-L-tryptophane ([11C]5-HTP)

***Lars Johansson***[1,4], *Olof Eriksson*[3], *Daniel Espes*[5], *Ram Kumar Selvaraju*[3], *Jan Eriksson*[4], *Jens Sörensen*[1], *Anders Sundin*[6], *Gunnar Antoni*[1], *Barbro Eriksson*[7], *Per-Ola Carlsson*[5,7], *Olle Korsgren*[2], *[1]Dept. of Radiology, Uppsala University, Uppsala, Sweden; [2]Dept of Immunology, Genetics and Pathology, Uppsala University, Uppsala, Sweden; [3]Dept of Preclinical PET, Uppsala University, Uppsala, Sweden; [4]Clinical CV/GI, AstraZeneca R&D, Mölndal, Sweden; [5]Dept. of Cell Biology, Uppsala University, Uppsala, Sweden; [6]Dept of Radiology, Karolinska Institute, Stockholm, Sweden; [7]Dept. of Medical Science, Uppsala university, Uppsala, Sweden. Contact e-mail: lars.johansson@radiol.uu.se*

Background and aims: Assessment of pancreatic beta cell mass (BCM) in subjects with T1D and T2D would be of great importance. 5-hydroxy--L-tryptophane (5-HTP) is a precursor to serotonin (5-HT). The PET tracer [11C]5-hydroxy-L-tryptophane ([11C]5-HTP) accumulates in cells using serotonin. Serotonin is present in beta cells, but not in exocrine pancreas, we therefore hypothesized that [11C]5-HTP could be used as a biomarker for BCM. Materials and methods: Islet specificity of [11C]5-HTP was assessed by IHC staining for serotonin on pancreatic sections from T1D and healthy controls, and by incubation of human islet cell preparations. Control and STZ-treated rats were administered [11C]5-HTP and the pancreatic uptake was determined by organ distribution. We performed islet isolation and transplantation in non-diabetic rats as previously described and subsequent imaging at of rats 3 weeks after intraportal transplantation of 300 - 1200 islets. In vivo specificity was assessed in a non-human primate model, cynomolgus. Pancreatic uptake was investigated in healthy controls and subjects with T1D and T2D in clinical studies. Results: IHC staining showed co-localization of serotonin with insulin in healthy pancreas, whereas serotonin diminished in parallel with insulin in T1D. Incubation of isolated human islets mixed in different ratios with exocrine cells showed strong positive linear correlation ($R2>0.9$, $p<0.05$) between islet purity and [11C]5-HTP uptake. Pancreatic uptake in STZ treated rats was decreased (Standard Uptake Value; SUV 2.6±0.4, $p<0.05$) compared to non-treated controls (SUV 5.0±0.2), and correlated to decrease in beta cell mass as assessed by IHC. [11C]5-HTP-PET/CT examination of rats 3 weeks after intraportal transplantation of 300 - 1200 islets showed a distinct and quantitative accumulation in the livers containing islets, but not in the livers of the non-transplanted non-diabetic animals. PET/CT of non-human primates showed that approximately 80% of the pancreatic uptake was dependent on the serotonin biosynthesis pathway as it could be inhibited by iv administration of carbidopa. Retrospective data in non-diabetic patients showed a distinct pancreatic uptake (SUV=2.9±0.4), while uptake in two T2D patients was decreased by 33 and 56%, respectively. In one of the patients, repeated [11C]5-HTP PET measurements showed gradual reduction in parallel with the progression of T2D from diagnosis to insulin requirement. An ongoing prospective [11C]5-HTP PET study demonstrated clear differences in accumulation of tracer in pancreas with higher uptake in controls (n=3) versus the pancreas of T1D patients (n=3). Conclusion: We show both experimental and clinical results demonstrating the feasibility of [11C]5-HTP PET as a novel method for quantifying human BCM both in the native pancreas as well as following islet transplantation, giving a tool to study the development of T1D and T2D as well as evaluation of new therapies.

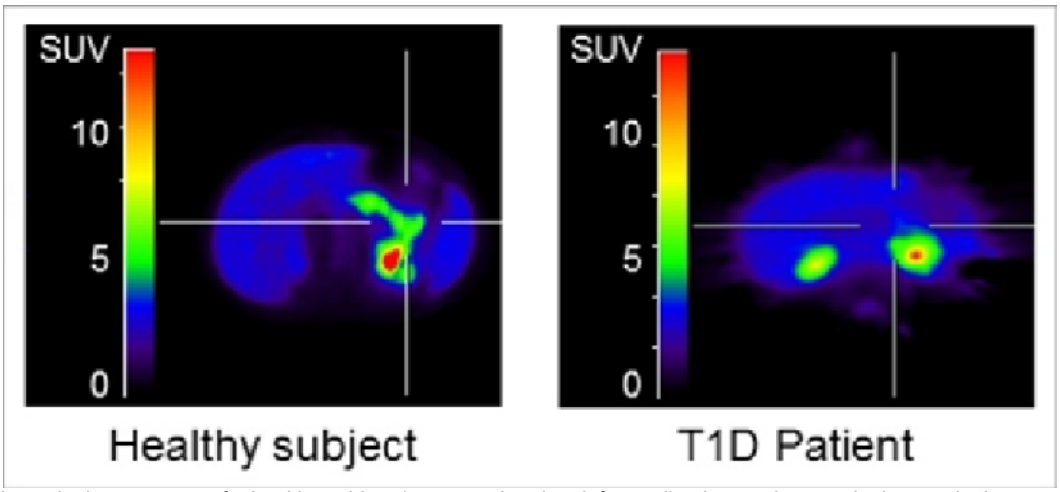


Distinct uptake is shown in the pancreas of a healthy subject (pancreas in origo; left panel), whereas low uptake is seen in the pancreas of a c-peptide negative T1D patient (right panel). Tracer excreted into urine causing kidney signal.

Disclosure of author financial interest or relationships:
**L. Johansson**, AstraZeneca R&D, Employment; **O. Eriksson**, None; **D. Espes**, None; **R. Selvaraju**, None; **J. Eriksson**, AstraZeneca, Employment; AstraZeneca, Stockholder; **J. Sörensen**, None; **A. Sundin**, None; **G. Antoni**, None; **B. Eriksson**, None; **P. Carlsson**, None; **O. Korsgren**, None.

Presentation Number **SS 190**
Scientific Session 28: Preclinical In Vivo - Oncology
September 8, 2012 / 13:00-13:12 / Room: Liffey Hall 2

# Multimodal Imaging Approach to Detect The Transient Vascular Normalization Window Following Anti-angiogenic Therapy in Solid Tumor

***Shingo Matsumoto***[1], *Keita Saito*[1], *Yoichi Takakusagi*[1], *Masayuki Matsuo*[1], *Jeeva P. Munasinghe*[2], *H. Douglas Morris*[2], *Martin Lizak*[2], *Hellmut Merkle*[2], *Nallathamby Devasahayam*[1], *Sankaran Subramanian*[1], *James B. Mitchell*[1], *Murali C. Krishna*[1], [1]*Radiation Biology Branch, National Cancer Institute, NIH, Bethesda, MD, USA;* [2]*National Institute of Neurological Disorder and Stroke, NIH, Bethesda, MD, USA. Contact e-mail: matsumos@mail.nih.gov*

**Aim**: Tumors can grow up to 2 to 3 $mm^3$ in size by relying on passive supplies of nutrients and oxygen. For further growth, tumors activate angiogenesis pathways to develop new vascular networks. Anti-angiogenic therapies of solid tumor frequently proceed in two steps; transient normalization of the architecturally and functionally aberrant tumor blood vessels with increased blood perfusion, followed by pruning the tumor blood vessels and resultant shutdown of nutrients and oxygen delivery required for tumor growth. Conventional anatomic or vascular imaging is impractical to distinguish the two steps of tumor response to anti-angiogenic therapies. Herein, we investigated if three non-invasive imaging techniques; Electron Paramagnetic Resonance Imaging (EPRI) of oxygen, redox sensitive MRI using a nitroxide probe, and hyperpolarized $^{13}C$ MRI of pyruvate metabolism can be early surrogate markers for the transient vascular normalization following anti-angiogenic treatment with sunitinib. **Methods:** Mouse squamous cell carcinoma (SCCVII) cells were inoculated in hind leg of mouse. The tumor bearing mice were daily treated with a multi-tyrosine kinase inhibitor sunitinib (50mg/kg, orally). Tumor oxygen imaging was conducted by a homemade 300 MHz pulsed EPRI scanner using an oxygen sensitive triarylmethyl probe OX063 (1). Redox state imaging was conducted by 7T MRI using carbamoyl-PROXYL as a redox state sensitive probe. Hyperpolarization of $^{13}C$-labeled pyruvate solution was induced by HyperSense (Oxford Instruments) and metabolic images were obtained by 4.7T MRI using a rapid gradient echo sequence. **Results:** Daily treatment of SCCVII tumor bearing in mouse with sunitinib resulted in rapid decrease in tumor microvessel density and suppression of tumor growth. EPR oxygen imaging showed transient increase in tumor oxygenation 2-4 days following sunitinib treatment in spite of an accompanying 45% decrease in microvessel density. Dynamic oxygen imaging obtained every 3 minutes showed that sunitinib treatment also suppressed the extent of temporal fluctuations in tumor oxygen level, known as cycling hypoxia (2). During this time window of vascular normalization, MRI of the redox state using an exogenously administrated nitroxide probe and hyperpolarized $^{13}C$ MRI of energy metabolic flux of pyruvate/lactate couple revealed the oxidative shift in tumor redox state. **Conclusion:** We provided evidences that transient shift in tumor oxygenation, redox state, and energy metabolism can be used for evaluating early tumor microenvironmental changes responded to anti-angiogenic therapy. **References:** 1) Matsumoto S et al. Low-field paramagnetic resonance imaging of tumor oxygenation and glycolytic activity in mice. *J Clin Invest.* 2008;118:1965-73. 2) Matsumoto S et al. Antiangiogenic agent sunitinib transiently increases tumor oxygenation and suppresses cycling hypoxia. *Cancer Res.* 2011;71:6350-9.

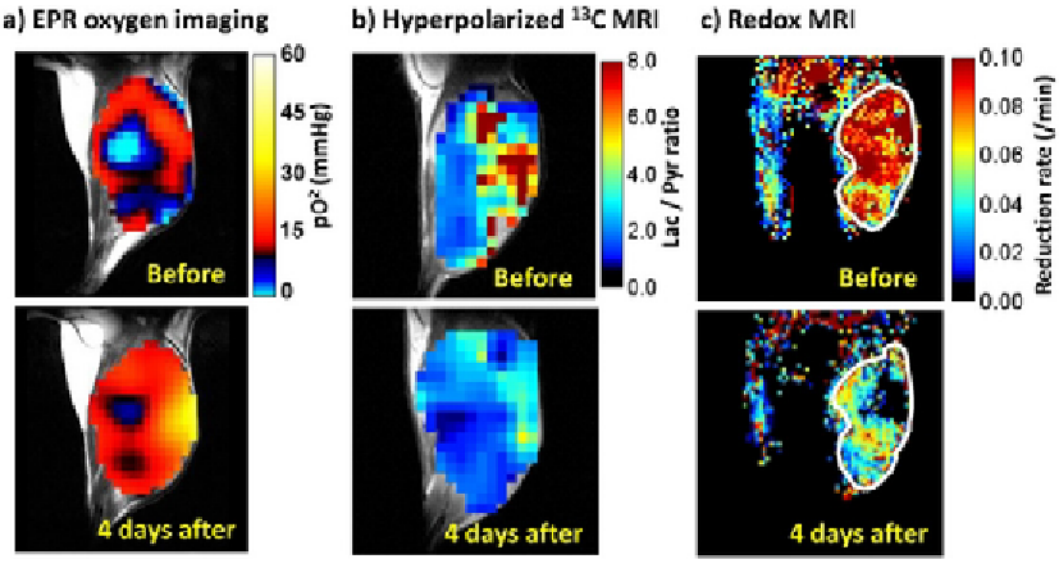


Fig.1 Anti-angiogenic treatment with sunitinib induced transient shift in tumor oxygenation by EPR imaging, energy metabolism by hyperpolarized $^{13}C$ MRI of pyruvate metabolism, and redox state by MRI with nitroxide probe in SCCVII tumor.

Disclosure of author financial interest or relationships:
**S. Matsumoto**, None; **K. Saito**, None; **Y. Takakusagi**, None; **M. Matsuo**, None; **J.P. Munasinghe**, None; **H. Morris**, None; **M. Lizak**, None; **H. Merkle**, None; **N. Devasahayam**, None; **S. Subramanian**, None; **J.B. Mitchell**, None; **M.C. Krishna**, None.

Presentation Number **SS 191**
Scientific Session 28: Preclinical In Vivo - Oncology
September 8, 2012 / 13:12-13:24 / Room: Liffey Hall 2

# Non-invasive imaging of tumor glycogen storage by $^{18}$F-NFTG positron emission tomography

***Timothy H. Witney***, *Laurence S. Carroll, Roshan Agarwal, Eric O. Aboagye, Surgery and Cancer, Imperial College London, London, United Kingdom. Contact e-mail: t.witney@imperial.ac.uk*

The majority of tumours exhibit substantially increased levels of glucose uptake and utilisation in comparison to non-neoplastic tissues. As well as increased glycolytic flux, tumour cells have also been shown to accumulate glycogen at levels far higher than their normal corresponding tissues. Interest in the role of glycogen storage in malignant cells has arisen following the discovery that increased expression of the small GTPase, *Rab25*, in ovarian adenocarcinoma resulted in significantly increased glycogen storage, correlating to increased tumour aggressiveness and resistance to therapy-induced apoptosis. Development of a novel non-invasive measure of tumour glycogen would therefore be highly advantageous. It has been shown previously that the fluorescent glucosamine analogue, 2-NBDG, can be used to assess glycogen storage *in vitro*. In this study we show that tumour glycogen storage can be imaged *in vivo* by positron emission tomography with $^{18}$F-*N*-(Methyl(2-fluoroethyl)-1H-[1,2,3]triazole-4-yl))glucosamine ($^{18}$F-NFTG). Temporal uptake of $^{18}$F-NFTG was compared in isogenic HEY *pcDNA* and HEY *Rab25* cells over a 4h time course. A significant increase in $^{18}$F-NFTG was observed in *Rab25*-transfected cells in comparison to empty vector controls at 4h, with uptake of 3.2 ± 0.25 % radioactivity/mg protein and 2.4 ± 0.17 % radioactivity/mg protein respectively. Increased uptake in HEY *Rab25* paralleled elevated punctate 2-NBDG intracellular localization, shown by fluorescence microscopy (500 μM; 3h), indicative of glycogen labeling. It has been shown previously that glycogen storage rapidly increases at the beginning of the stationary growth phase in cultured colorectal adenocarcinoma cells. Here we showed that total glycogen, 2-NBDG fluorescence and $^{18}$F-NFTG uptake increased with increasing HEY *Rab25* cell density, whereas $^{18}$F-FDG uptake did not change when cells reached stationary phase. *In vivo* imaging of implanted HEY *Rab25* xenografts showed rapid tumor labeling, followed by slow wash-out of the tracer (Fig. 1). Unlike FDG, liver-specific retention was observed, with low brain uptake. In a comparative study with FDG, muscle uptake was elevated 1.5-fold with $^{18}$F-NFTG. In a further study, IGROV-1 ovarian carcinoma cells, containing a heterozygous PTEN mutation, was found to display a 4.8-fold increase in total glycogen *in vitro* when compared to HEY *Rab25*; corresponding to a 4.3-fold increase in $^{18}$F-NFTG uptake ($P < 0.01$; $n = 3$). This increase in $^{18}$F-NFTG uptake translated to a doubling of tumor uptake *in vivo*, measured from the area under the time vs. radioactivity curve (TAC; Fig. 1). We have demonstrated here a novel method for the non-invasive imaging of tumor glycogen, both in cells and *in vivo*. Given the correlation between glycogen storage and tumor aggressiveness, the use of $^{18}$F-NFTG may provide complementary information to FDG. Enhanced $^{18}$F-NFTG uptake by quiescent cells may have clinical relevance - detection of residual disease and predicting efficacy of drugs that target only cycling cells - and warrants further evaluation.

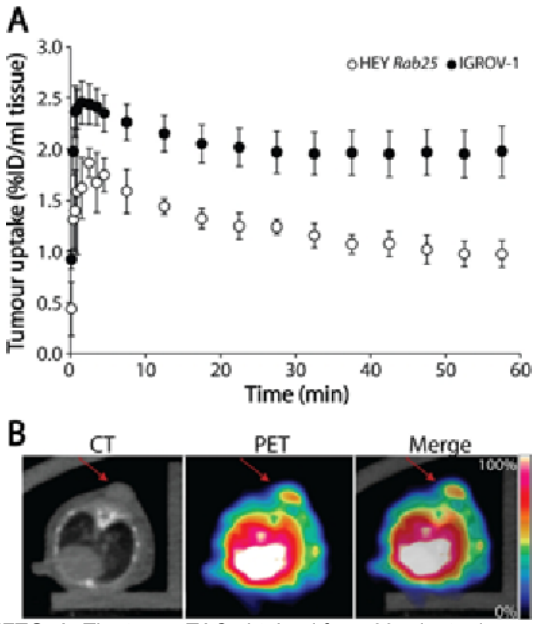


**Figure 1. Dynamic tumour uptake of $^{18}$F-NFTG.** A, The tumor TAC obtained from 60-minute dynamic PET imaging in HEY *Rab25* and IGROV-1 xenografts. Mean ± SEM ($n = 4$ mice per group). B, Representative axial CT, PET and PET-CT images of IGROV-1 tumor-bearing mice (30-60 minutes of summed activity). Tumor margins were identified from CT image (indicated by arrow).

Disclosure of author financial interest or relationships:
**T.H. Witney**, None; **L.S. Carroll**, None; **R. Agarwal**, None; **E.O. Aboagye**, GE Healthcare, Grant/research support .

Presentation Number **SS 192**
Scientific Session 28: Preclinical In Vivo - Oncology
September 8, 2012 / 13:24-13:36 / Room: Liffey Hall 2

# Pharmacokinetics, Biodistribution and Tumor Specificity of a Fluorescent δ-Opioid Receptor Targeted Probe for Cancer Imaging

***Valerie Moberg***[1], *Amanda Shanks Huynh*[1], *Allison S. Cohen*[1], *Veronica Estrella*[1], *Jatinder S. Josan*[3], *Todd J. Casagni*[2], *Josef Vagner*[4], *Ariosto Silva*[1], *Victor J. Hruby*[3], *David L. Morse*[1], [1]*Cancer Imaging and Metabolism, Moffitt Cancer Center and Research Institute, Tampa, FL, USA;* [2]*Comparative Medicine, Moffitt Cancer Center and Research Institute, Tampa, FL, USA;* [3]*Chemistry and Biochemistry, University of Arizona, Tucson, AZ, USA;* [4]*BIO5 Institute, University of Arizona, Tucson, AZ, USA. Contact e-mail: Valerie.Moberg@moffitt.org*

The use of near infrared (NIR) fluorescent labeled peptide ligands with high specificity and affinity for cell-surface tumor markers provides a targeted fluorescence (FL) imaging platform with low background signal. Fluorescent molecular imaging probes can be used for cancer staging by detection of metastasis in regional lymph nodes and for intraoperative surgical guidance. We have evaluated the in vivo pharmacokinetics (PK) and biodistribution (BD) of a small peptidomimetic FL probe, Dmt-Tic conjugated to Cy5 NIR dye. This δ-opioid receptor (DOR) antagonist exhibits high binding affinity (3 nM Ki) and antagonist activity in vitro. By IHC of patient tissue samples, we have determined that the DOR is overexpressed in 44% of lung tumors relative to normal lung. We have also synthesized a Dmt-Tic probe conjugated to a longer wavelength fluorochrome, IR800CW (Licor). Dmt-Tic-IR800CW retains high in vitro binding affinity for DOR (Ki¬ = 1.4 nM) and in vivo studies have shown that tumor specificity is retained. A bilateral xenograft tumor mouse model was used for the PK and BD studies. Human colorectal cancer cells, HCT 116 parental (DOR-) and engineered HCT 116/DOR+ were flank injected subcutaneously into female nude mice and grown to an average tumor volume of 500 mm3. In cyto binding assays determined that each HCT116/DOR+ cell surface expresses 1.6x106 + 1.1x105 DORs. An optimal dose of 4.5 nmol/kg probe was injected IV. To study PK, probe was tracked in vivo over a time course of 0 to 168 h by FL imaging (IVIS 200 Imaging System, PerkinElmer). In vivo and corresponding ex vivo FL images were acquired at select time points from 0 to 48 h to determine the BD profile of the probe in the DOR+/- tumors, heart, lung, liver, kidneys, spleen, pancreas and GI tract. Quantitative values were determined after background subtraction as the mean normalized FL signal within an ROI (Living Image Software). PK and BD profiles of probe uptake and clearance were determined in vivo by a time-course of image acquisitions. The maximum DOR+ tumor signal occurred at 3 h in both the PK and BD studies. The largest enhancement (7-fold) compared to the DOR- tumor was also observed at 3 h. The DOR+ tumor retained signal for 96 h, while DOR- tumor cleared by 24 h. Ex vivo FL signal in liver, pancreas, spleen and kidneys peaked at 15 m and cleared to a baseline level by 24 h. We have evaluated the early time-points of extravasation, tumor penetration, cell binding and uptake by intravital confocal FL microscopy using a dorsal skin-fold window chamber tumor xenograft model. Tumor cell uptake of this antagonist probe was observed in vivo by 24 h post administration. The PK of probe uptake and clearance was further characterized using a three-compartment mathematical model, which includes tumor, kidney and mouse volumes, and assumes mass conservation of the ligand. This model was used to account for the interference of the tumor ligand release in the uptake and clearance dynamics of blood and kidneys. While this effect is negligible in humans, it is significant in mouse models. Hence, we have thoroughly characterized the PK and BD of Dmt-Tic-Cy5 in mouse models of cancer.

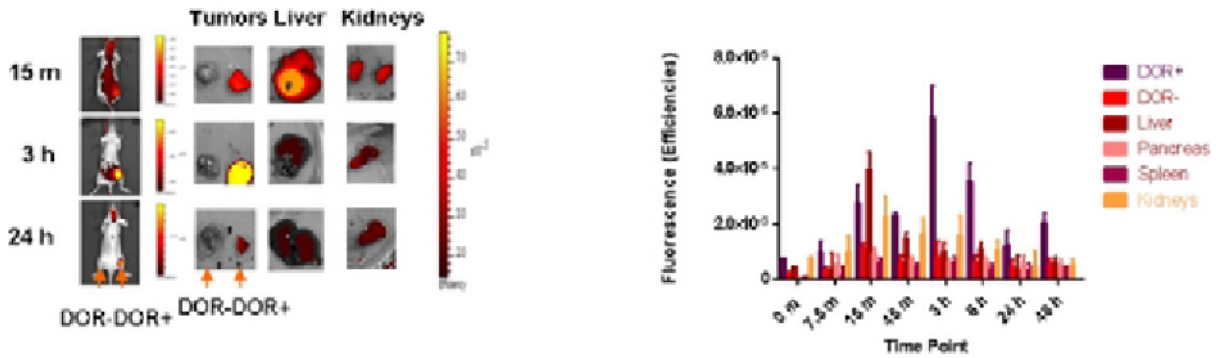


Figure 1. Fluorescence imaging of BD at various time points after injection of 4.5 nmol/kg Dmt-Tic-Cy5. A) Representative in vivo and corresponding ex vivo images and B) Quantified ex vivo mean fluorescence signal from 0- 48 h (n>3).

Disclosure of author financial interest or relationships:
**V. Moberg**, None; **A. Huynh**, None; **A.S. Cohen**, None; **V. Estrella**, None; **J.S. Josan**, None; **T.J. Casagni**, None; **J. Vagner**, None; **A. Silva**, None; **V.J. Hruby**, None; **D.L. Morse**, LiCor, Other financial or material support; Intezyne Technologies, Other financial or material support .

Presentation Number **SS 193**
Scientific Session 28: Preclinical In Vivo - Oncology
September 8, 2012 / 13:36-13:48 / Room: Liffey Hall 2

# Monitoring anti-cancer effect of mesenchymal stem cells expressing cytosine deaminase

***Taemun Chung***[1,2], *June-Key Chung*[1,2], *Mi Jeong Kim*[1,3], *Dong Soo Lee*[1,5], *Hyewon Youn*[1,4], [1]*Nuclear Medicine and Cancer Research institute, Seoul National University College of Medicine, Seoul, Republic of Korea;* [2]*Biomedical Sciences, Seoul National University College of Medicine, Seoul, Republic of Korea;* [3]*Laboratory of Molecular Imaging and Therapy of Cancer Research Institute, Seoul National University College of Medicine, Seoul, Republic of Korea;* [4]*Cancer Imaging Center, Seoul National University Cancer Hospital, Seoul, Republic of Korea;* [5]*Molecular Medicine and Biopharmaceutical Sciences, WCU Graduate School of Convergence Science and Technology, Seoul National University, Seoul, Republic of Korea. Contact e-mail: noenimy@snu.ac.kr*

Purpose: Application of suicide gene on cancer therapy is an attractive strategy for the treatment of various types of cancers. Cytosine deaminase (CD) which converts a nontoxic prodrug 5-fluorocytosine (5-FC) into a cytotoxic 5-fluorouracil (5-FU), is one of the attractable suicide genes for tumor therapy. Therapeutic use of mesenchymal stem cells (MSCs) has recently been studied extensively in cancer therapy because of its tumor targeting properties. In this study, we investigated the anti-cancer effect of mesencymal stem cell expressing cytosine deaminase (MSC/CD) by monitoring tumor cell survival. Methods: Primary human MSCs from from iliac crest bone marrow were isolated and used between 6 to 9 culture passages. The CD gene and imaging reporter genes which include luciferase and tdTomato were stably transfected to the human MSCs. Luciferase or Sodium Iodide Symporter (NIS) expressing cancer cells (U373, U87MG, MDA-MB231) were established for tumor imaging. To identify the bystander effect of MSC/CDs with prodrug 5-FC, cancer cells were co-cultured with MSC/CDs under the various concentrations of 5-FC. The effect of the different co-culture ratio between MSC/CDs and cancer cells were also investigated under 100 uM of 5-FC. In vitro anticancer effect of MSC/CDs was monitored by confocal microscopy and bioluminescent imaging. For monitoring anticancer effect of MSC/CDs in vivo, MSCs or MSC/CDs were transplanted into the xenografted tumors Tumor cell survival was estimated by bioluminescence imaging or Tc-99m scintigraphic imaging. Results: Human MSCs and MSC/CDs were successfully monitored by fluorescence and bioluminescence image. Unlike native MSCs, MSC/CDs showed 86.3% of suicidal effect on 7 days 50uM of 5-FC. From co-culture experiment with MSC/CDs and cancer cells, MSC/CDs showed bystander effect on neighboring cancer cells in proportion to increasing 5-FC dosage. After 100uM of 5-FC treatment, co-culture ratio of 1:1 (MSC/CDs: U87MG) showed that 12.7% of U87MG cells were survived. 56% of U87MG cells were survived with cell co-culture ratio of 1:10 (MSC/CDs: U87MG). In MSC/CDs transplanted glioma xenograft model (U87MG) with 5-FC 32% reduced luciferase signal was observed when it compared with MSCs transplanted control. Along with glioma xenograft model, the anticancer effect of MSC/CD was showed with breast cancer xenograft model by the Tc-99m scintigraphic imaging. Conclusion: In this study, we could monitor the inhibition of tumor growth by MSC/CD cell therapy with prodrug 5-FC. Our results indicate that MSCs expressing the suicidal gene has a great potential as an efficient cancer targeting cell therapy.

Disclosure of author financial interest or relationships:
**T. Chung**, None; **J. Chung**, None; **M. Kim**, None; **D. Lee**, None; **H. Youn**, None.

Presentation Number **SS 194**
Scientific Session 28: Preclinical In Vivo - Oncology
September 8, 2012 / 13:48-14:00 / Room: Liffey Hall 2

# Comparison of $^{177}$Lu-DOTA,Tyr3-octreotate ($^{177}$Lu-octreotate) versus RAD001 in rat and mouse tumour models; increase of metastatic tumour behavior by mTOR inhibition

***Stuart Koelewijn***[1], *Stefan Pool*[1], *Sander Bison*[1], *Marleen Melis*[1], *Marion De Jong*[1,2], [1]*Nuclear Medicine, Erasmus MC, Rotterdam, Netherlands;* [2]*Radiology, Erasmus MC, Rotterdam, Netherlands. Contact e-mail: s.koelewijn@erasmusmc.nl*

Introduction: The mammalian target of rapamycin (mTOR) signal transduction pathway is upregulated in many pancreatic neuroendocrine tumours (NETs) and plays a key role in regulating cell growth, metabolism, proliferation and angiogenesis. Inhibition of the mTOR signal transduction pathway in pancreatic NETs by RAD001 (Everolimus) has resulted in anti-tumour effects in patient studies. Another promising therapy for NET is peptide radionuclide receptor therapy (PRRT) using $^{177}$Lu-octreotate targeting the somatostatin receptor 2 ($sst_2$), often over-expressed in NETs. In this preclinical study we compared PRRT versus RAD001 therapy in somatostatin receptor expressing rat (CA20948) and mouse (H69) tumour models. Methods: RAD001 (5mg/kg body weight) treatment was given orally twice a week either for 4.5 or 12 weeks. $^{177}$Lu-octreotate (125MBq/3.4µg peptide) was given as a single IV injection or combined with RAD001. Twice a week tumour size and body weight was monitored. Results: The anti-tumour effects of RAD001 in both models, alone or in combination, were less effective than those of $^{177}$Lu-octreotate alone. The combination of both therapies did not result in increased anti-tumour effects. In the rat studies the animals could be followed for a longer period of time, beyond day 40 after start of treatment with RAD001, as single treatment or in combination with $^{177}$Lu-octreotate, most animals were rapidly losing weight, indicating declining health, whereas control animals and animals treated with $^{177}$Lu-octreotate alone remained healthy. $^{111}$In-DTPA-octreotide, a radiolabelled somatostatin analogue for diagnosis, was administered to perform SPECT/CT in animals with decreasing body weight. Unexpectedly, tumour metastasis was visualized in those animals; metastases in lungs, liver en lymph nodes clearly showed $sst_2$ expression as confirmed by autoradiography. Metastases were not found in control and $^{177}$Lu-octreotate-treated rats, not even after surgical resection of the primary tumour to enable longer follow-up. The percentage of rats with metastases was not significantly different between groups treated with RAD001 for 4.5 versus 12 weeks. After development of distant metastasis was validated by SPECT/CT imaging, a new therapeutic dose of $^{177}$Lu-octreotate was administered and 24 hours later a second SPECT/CT scan was acquired. The new PRRT cycle slowed down tumour growth, but no complete regressions were reached. Conclusion: $^{177}$Lu-octreotate PRRT appeared to be more effective than RAD001 or the combination. Metastasis in animals treated with RAD001 could be clearly visualized using SPECT/CT. If the results of our studies can be translated to humans, patients should be closely watched during and after RAD001 therapy.

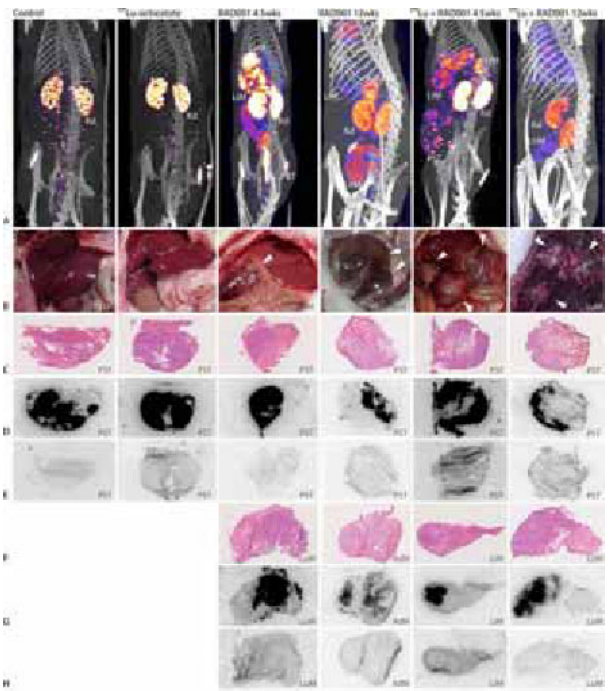

Disclosure of author financial interest or relationships:
**S. Koelewijn**, None; **S. Pool**, None; **S. Bison**, None; **M. Melis**, None; **M. De Jong**, None.

Presentation Number **SS 195**
Scientific Session 28: Preclinical In Vivo - Oncology
September 8, 2012 / 14:00-14:12 / Room: Liffey Hall 2

# Gadolinium-based paramagnetic lipid nanoparticles for Magnetic Resonance Imaging applications

***Alessandro Maiocchi**, Chiara Brioschi, Claudia Cabella, Luigi Miragoli, Massimo Visigalli, Simona Ghiani, Centro Ricerche Bracco, Bracco Imaging, Turin, Italy. Contact e-mail: alessandro.maiocchi@bracco.com*

Magnetic Resonance Imaging (MRI) is one of the most important non-invasive imaging modalities in clinical diagnostics and preclinical research. The success of MRI is due to the ability to image tissues with high resolution in three dimensions, routinely down to 1 mm at clinical field strengths. These attributes make MRI highly suited to molecular imaging applications, namely the imaging of events at the cellular and subcellular level. However, the detection of events at this level often requires nanomolar sensitivity, thus precluding the use of conventional gadolinium chelates as molecular MR imaging agents, as they display only micromolar sensitivity. In order to overcome this limitation several research groups designed new gadolinium-based nanoparticles endowed with both enhanced and efficient routes of accumulation of the imaging probes at the sites of interest. However the preferential accumulation of these nanoparticles in the mononuclear phagocyte system after an intravenous administration, strongly reduces the likelihood of their translation to the clinical practice due to the inherent toxicity of Gd(III) ion. In our work we demonstrated how this limitation can be overcome using lipidic nanoparticles having an high tropism to hepatocytes in combination with selected amphiphilic Gd(III) complexes having high efflux rate from the same liver cells. This combination strongly reduce the accumulation of Gd(III) ion in both liver and spleen. Our paramagnetic lipidic nanoparticles were designed to selectively target the tumour cells using folate as targeting moiety. In order to test the affinity of the functionalized nanoparticles to the target receptor before their use, we developed a simple in-vitro experimental assay based on BioLayer Interferometry (BLI). This is a label-free optical technique measuring biomolecular interactions, in connection with specific biosensors prepared by immobilization of a biotynilated anti-Folate antibody FA2 on a streptavidine coated sensors. Targeted and untargeted paramagnetic lipidic nanoparticles also uploaded with Rhodamine B, were further tested in human ovarian Igrov-1 cells and in correspective cancer xenografted mice, assessing their specificity using both in vitro and ex vivo fluorescence microscopy. Labelling with specific antibodies against macrophages and Folate receptor alpha was adopted to confirm the selective nanoparticles distribution in the tumor tissues. A quantitative analysis of the signal enhancement of 3D MRI images at 7 T at 4h and 24h showed a statistically significant uptake improvement of the targeted nanoparticles over the untargeted ones. In conclusion we have developed a new platform of paramagnetic lipid nanoparticles with a reduced uptake in the mononuclear phagocyte system without affecting their ability to reach tumour lesions. Indeed the obtained signal enhancement at the tumour tissue is sufficiently high to discriminate between targeted and untargeted nanoparticles.

Disclosure of author financial interest or relationships:
**A. Maiocchi**, Bracco Imaging, Employment; **C. Brioschi**, Bracco Imaging S.p.a., Employment; **C. Cabella**, Bracco Imaging SpA, Employment; **L. Miragoli**, Bracco Imaging SpA, Employment; **M. Visigalli**, Bracco Imaging SpA, Employment; **S. Ghiani**, Bracco Imaging SpA, Employment .

Presentation Number **SS 196**
Scientific Session 28: Preclinical In Vivo - Oncology
September 8, 2012 / 14:12-14:24 / Room: Liffey Hall 2

# A combined photoacoustic imaging and photothermal therapy using branched gold nanoparticles

***Antoine D'Hollander***[1,2], *Greetje Vande Velde*[1], *Hilde Jans*[2], *Bram Vanspauwen*[2], *Dieter Fuchs*[3], *Liesbet Lagae*[2,4], *Uwe Himmelreich*[1], [1]*Biomedical MRI unit, KULeuven, Leuven, Belgium;* [2]*Imec, Heverlee, Belgium;* [3]*Visualsonics, Toronto, ON, Canada;* [4]*Solid State Physics and Magnetism, KULeuven, Leuven, Belgium. Contact e-mail: dholland@imec.be*

Introduction. The diagnosis and monitoring of cancer therapy is time-consuming, costly and complex, so that more efficient detection, imaging and treatment techniques are still needed. Combining the detection and treatment using only one optical technique would decrease the therapy complexity significantly. Here, we demonstrate the successful use of branched gold nanoparticles (AuNPs) as optical agents for combined photoacoustic imaging (PAI) and phototherthermal therapy (PTT) of cancer. Methods. Branched AuNPs were synthesized according to Hao et al.1. Particles were coated with a self-assembled monolayer (SAM) for stability in physiological conditions. For in vitro validation, SKOV3 cells (ovarian cancer cell line) were plated on coverslips and incubated with AuNPs. the interaction between AuNPs and cells was validated with ICP-OES, darkfield microscopy and PAI. PTT was induced after 5 minutes of laser irradiation (360 nm, 35 W/cm2). For in vivo validation, we used a subcutaneous SKOV3 xenograft tumor model in nude mice. Branched AuNPs (4.6*1010 NPs) were injected in the left and 50 µL DPBS (sham) in the right tumor . We imaged tumors with MRI and ultrasound. Tumor viability was evaluated before and after PTT with BLI, MRI and PAI. Results. SAM-functionalized branched AuNPs absorbing in the NIR (690 nm) were successfully synthesized after 12h of incubation, cells were labeled with 22pg Au/cell. AuNP labeling of cells resulted in significant PA signal starting from 3h and increasing with incubation time. After 12 hours of incubation, phototermal-induced cell death could be induced at the laser spot, which was visualized with live/dead fluorescence cell staining (Figure 1A). In the xenograft model, PA signals from the branched AuNPs could be detected with a high signal-to-noise ratio (Figure 1C). The ultrasound/PA overlay showed that most AuNPs were located between the tumor and the skin after injection, which is probable due to a high tumoral fluid pressure. Directly after PTT, a decrease in tumor volume and viability was observed by MRI and BLI (Figure 1B). Histology confirmed tumor necrosis. Four days after PTT, an increase in BLI signal indicated reoccurance of the tumor That was confirmed by MRI. Conclusion. SAM-coated branched AuNPs are suited for tumor cell labeling for combined PA imaging and PTT as proved by in vitro and in vivo studies. Because of their high absorption in the NIR, the AuNPs were clearly detectable in PA imaging and could eradicate tumor cells using PTT. Therefore, branched AuNPs show great theranostic potential and can help to decrease the complexity of cancer monitoring and therapy by enabling diagnosis and therapy within one single modality session. We will further optimize the PTT protocol for complete tumor eradication and using tumor-targeted AuNPs. References 1.Hao, E.; Bailey, R. C., Schatz, G. C., Hupp, J. T., Li & S. Y. Synthesis and Optical Properties of "Branched" Gold Nanocrystals. Nano Lett. 2004, 4, 327-330.

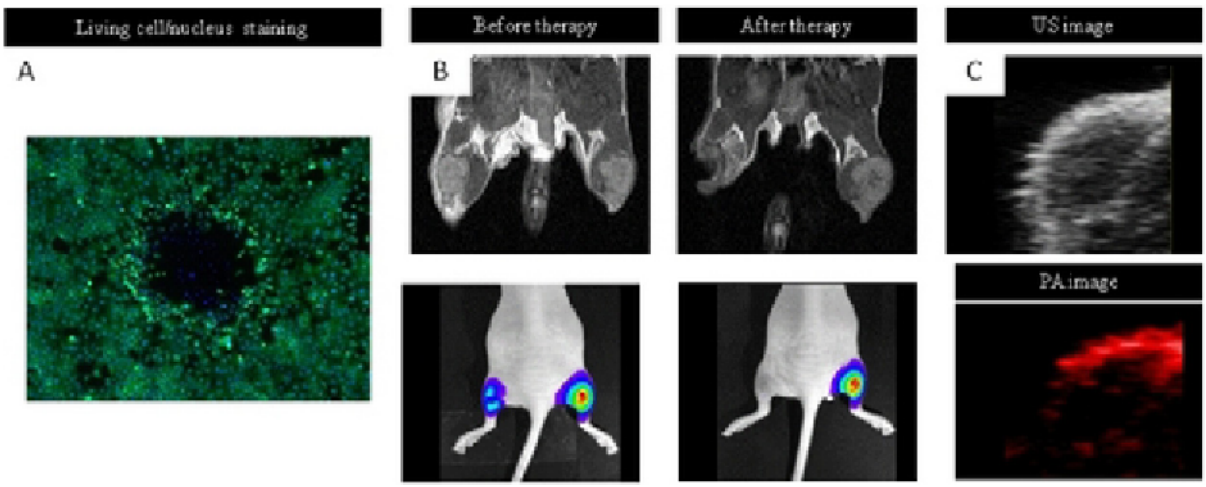


Figure 1. (A) TEM image of branced AuNPs (B) Dark-field images of cells incubated with AuNPs with different incubation times. (C) Fluorescence image of cells after in vitro PTT. Caclein AM corresponds to the living cells (green) and Hoechst to the cell nucleus (blue)

Disclosure of author financial interest or relationships:
**A. D'Hollander**, None; **G. Vande Velde**, None; **H. Jans**, None; **B. Vanspauwen**, None; **D. Fuchs**, VisualSonics Inc., Employment; **L. Lagae**, None; **U. Himmelreich**, None.

Presentation Number **SS 197**
Scientific Session 29: CT/US - Technology Methodology - Probes
September 8, 2012 / 13:00-13:12 / Room: Wicklow Hall 2

# Single-Scan Scatter Correction in Cone Beam CT with Stationary Boundary Detection and Compressed Sensing Based Reconstruction

***Bowen Meng***[1,2]*, Lei Xing*[2]*, Ho Lee*[2]*, Benjamin Fahimian*[2]*, [1]Electrical Engineering, Stanford University, Stanford, CA, USA; [2]Radiation Oncology, Stanford University, Stanford, CA, USA. Contact e-mail: bowenm@stanford.edu*

Purpose: X-ray scatter incurred to large illumination area severely degrades the image quality, which has long been recognized as a problem in Cone Beam CT (CBCT) and its applications on volumetric image guided therapy. Although many beam blocker-based scatter correction methods have been proposed in literature, such methods either require dual scans or moving blockers to complete the scatter measurement, or are only suitable for full fan mode. In this work, a novel scatter correction algorithm is proposed and implemented that couples the use of horizontal boundary stationary beam blockers with a compressed sensing scatter estimation technique to enable simultaneous acquisition of image and scatter information in a single scan. Methods: A stationary boundary beam blocker, comprising of two lead strips on both ending sides, was mounted on the surface of kV x-ray source of the Varian TrueBeam OBI system. This design enables image data acquisition of the projection data on the unblocked central region of field of view (FOV) and scatter data at the blocked boundary regions. For the initial scatter estimation on the central FOV, a hybrid scatter model that combines the scatter interpolation method and scatter convolution model is estimated using the acquired scatter distribution on boundary region. With the hybrid scatter estimation model, compressed sensing optimization is performed to generate the scatter map by penalizing the L1 norm of the discrete cosine transform of scatter signal. The estimated scatter is subtracted from the projection data by soft-thresholding, and the scatter-corrected CBCT volume is obtained by the conventional FDK algorithm. The experimental studies using Catphan504 and Rando anthropomorphic phantoms on a Varian TrueBeam system were carried out to evaluate the performance of the proposed scheme. Results: The scatter shading artifacts were markedly suppressed in the reconstructed images using the proposed method. On the Catphan©504 phantom, the proposed method reduced the constructed error to 13 Hounsfield units, 10% of that without scatter correction, and increased the image contrast by a factor of two in high-contrast regions. On the Rando phantom, the spatial nonuniformity decreased from 10.8 % to 6.8% after correction. The proposed method also outperforms the scatter interpolation correction method in both studies. Conclusions: A novel scatter correction method, that allows for the unobstructed acquisition of the high frequency data and the detection of the patient specific low frequency scatter data at the edges of the FOV, is proposed and validated in this work. Instead of obstructing the central portion of the FOV, compressed sensing is used to solve for the scatter in this region to enable the highest quality reconstruction. The method synchronizes image acquisition and scatter correction in a single scan, and provides a readily deliverable solution to many commercial CT systems.

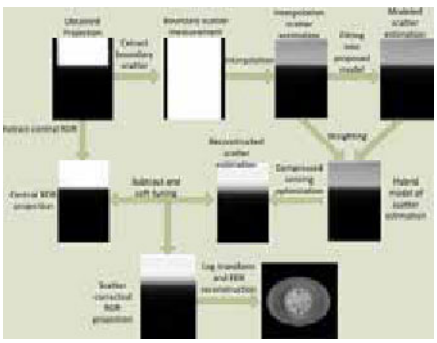

Flow chart of the proposed scatter correction procedures. (1) The boundary scatter measurement is extracted from each projection data and those scatter profiles are used to determine the scatter for central ROR; (2) Bilinear interpolation of the boundary scatter data provides initial estimation of the scatter ; (3) Least square minimization with the log transform data is applied to find the coefficients a and b in Eq. 2; (4) The hybrid model is computed based on the weighting factor ; (5) A L1-analysis compressed sensing optimization with positivity constraint is formulated based on the low-frequency assumption of the scatter signal, and it is solved by using ADMM; (6) Estimated scatter is subtracted from the original projection data with soft-thresholding method; and (7) Conventional FDK algorithm is used to reconstruct the scatter free image.

CT numbers for the selected ROIs for reconstructed images in Catphan phantom

| | ROI1 | ROI2 | ROI3 | ROI4 | ROI5 | ROI6 | ROI7 | Root Mean Square Error |
|---|---|---|---|---|---|---|---|---|
| MDCT benchmark | -970 | 340 | 87 | -968 | -177 | -86 | -21 | |
| Without scatter correction | -806 | 268 | 67 | -820 | -169 | -90 | -37 | 130 |
| With interpolation scatter correction | -953 | 350 | 84 | -998 | -193 | -83 | -30 | 69 |
| With proposed scatter correction | -967 | 346 | 90 | -995 | -196 | -85 | -30 | 13 |

Disclosure of author financial interest or relationships:
**B. Meng**, None; **L. Xing**, Varian Medical Systems, Grant/research support; **H. Lee**, None; **B. Fahimian**, None.

Presentation Number **SS 198**
Scientific Session 29: CT/US - Technology Methodology - Probes
September 8, 2012 / 13:12-13:24 / Room: Wicklow Hall 2

# Simultaneous Anatomical and Molecular Imaging of Gold Nanoparticles with X-ray CT

***Magdalena Bazalova**, Yu Kuang, Guillem Pratx, Lei Xing, Radiation Oncology, Stanford University, Stanford, CA, USA. Contact e-mail: bazalova@stanford.edu*

Conventional x-ray CT imaging performed with photon-integrating detectors offers high spatial resolution and fast scanning times. Currently, CT lacks behind other imaging modalities in providing molecular contrast due to its limited sensitivity. Targeted gold nanoparticles, a component of novel probes investigated for the use in diagnostic imaging as well as radiation therapy, can be potentially imaged at low concentrations using x-ray CT scanners equipped with photon-counting detectors with x-ray fluorescence CT (XFCT). A CT/XFCT x-ray system capable of simultaneous conventional CT imaging with photon-integrating detectors and XFCT imaging with photon-counting detectors was simulated by the Monte Carlo method. The objective of this work was to use the model to study the feasibility of simultaneous anatomical imaging and molecular imaging of gold nanoparticles. CT and XFCT images of two acrylic phantoms (phantom 1 and 2, top row) containing 0.1-0.4% gold solutions of 1.5 to 10 mm in diameter were simulated. Additionally, phantom 3 consisting of a cortical bone cylinder and a mandible cylinder surrounded by 3% and 2% gold concentrations was simulated (bottom left). Transmission and scattered 110 kVp x-rays were detected by a ring of photon-counting detectors to allow for reconstruction of conventional CT images, as well as XFCT images. Conventional CT images were reconstructed using all transmission x-rays collected directly opposite to the source. XFCT images were reconstructed using the net number of gold Kα,β fluorescence x-rays interacting with a 270° detector arc. Conventional CT and XFCT images of phantoms 1 and 2 (figure top row) clearly demonstrate that XFCT images offer much higher imaging sensitivity for gold nanoparticles than CT. Moreover, unlike in XFCT imaging that results in gold-only images, contrast of conventional CT images depends on the type of surrounding tissue. For example, the vial with 0.4% concentration surrounded by acrylic (top left in phantom 1, left in phantom 2) is completely undetectable in conventional CT images. The importance of combining molecular information with anatomical is demonstrated using phantom 3 (bottom row). The contrast agent is indistinguishable in the CT image alone, however, an excellent contrast is found in the XFCT image. An overlay CT/XFCT image makes it possible to discriminate gold nanoparticles from the surrounding anatomy. We have shown that XFCT provides high imaging sensitivity for gold nanoparticles, with 0.078% limit using a 12 mGy mean imaging dose. With the recent advances in photon-counting detector technology, XFCT may become a competing molecular imaging modality for probes containing high-Z elements. Simultaneous CT/XFCT imaging has the potential to become a useful tool for in-vivo imaging, as it produces CT images with combined anatomical and molecular information. [1] S.-K. Cheong, B. L. Jones, A. K. Siddiqi, F. Liu, N. Manohar and S. H. Cho, "X-ray fluorescence computed tomography (XFCT) imaging of gold nanoparticle-loaded objects using 110 kVp x-rays," Phys Med Biol 55, 647-662 (2010).

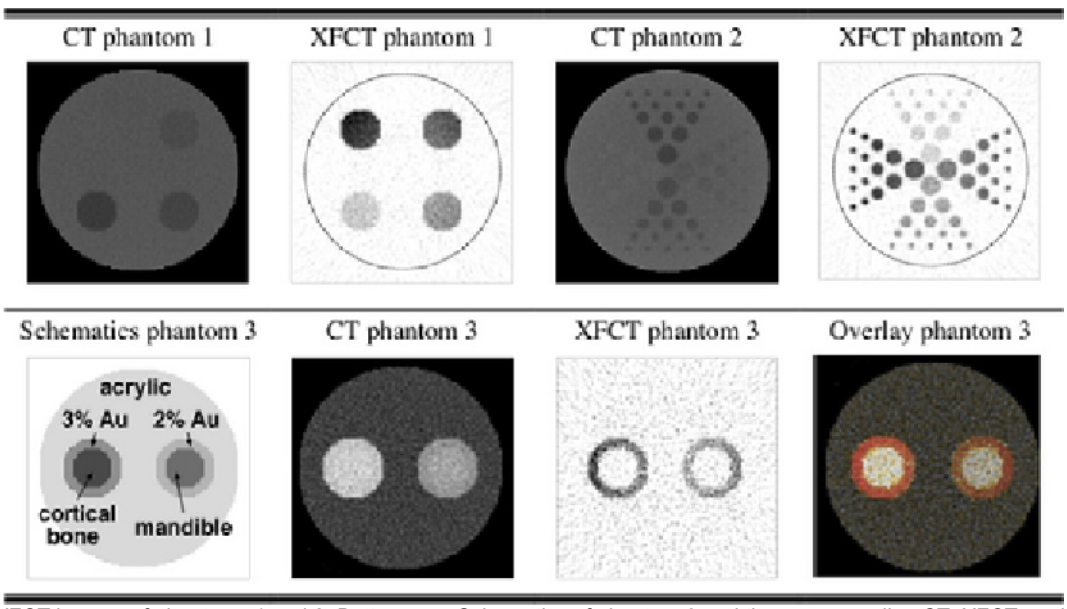


Top row: CT and XFCT images of phantoms 1 and 2. Bottom row: Schematics of phantom 3 and the corresponding CT, XFCT, and overlay CT/XFCT images. The CT/XFCT image makes it possible to separate gold nanoparticles (in color) from the bony tissue (in grayscale). Notably, the CT image alone does not offer the molecular information.

Disclosure of author financial interest or relationships:
**M. Bazalova**, None; **Y. Kuang**, None; **G. Pratx**, None; **L. Xing**, Varian Medical Systems, Grant/research support .

Presentation Number **SS 199**
Scientific Session 29: CT/US - Technology Methodology - Probes
September 8, 2012 / 13:24-13:36 / Room: Wicklow Hall 2

# Polymeric Microbubbles for Molecular Imaging and Ultrasound Mediated Drug Delivery to Tumors

***Stanley Fokong Nyongamsen***[1], *Anne Rix*[1], *Ana Fragoso*[2], *Zhuojun Wu*[3], *Olga Iranzo*[2], *Jessica Gätjens*[1], *Moritz Palmowski*[4,1], *Twan Lammers*[1], *Fabian Kiessling*[1], [1]*Experimental Molecular Imaging (ExMI), RWTH-Aachen University, Aachen, Germany;* [2]*Bioinorganic Chemistry and Peptide Design, Instituto de Technologia Quimica e Biologica- Universidade de Lisboa (ITQB-UNL), Lisbon, Portugal;* [3]*Institute of Molecular Cardiology (IMCAR), RWTH Aachen University, Aachen, Germany;* [4]*Nuclear Medicine, RWTH Aachen University, Aachen, Germany. Contact e-mail: sfokong@ukaachen.de*

The use of microbubbles (MB) for molecular imaging and theranostic is rapidly advancing. In this context, polymer-shelled MB possess great potential due to their thick shell and ultrasound (US) destructibility. Furthermore, novel intravascular angiogenic markers are of great importance. In this study, we investigated the use of poly (n-butylcyanoacrylate)(PBCA) shelled-MB for molecular imaging of E-selectin, N-glycans, and for targeted drug delivery to tumors using model drug-loaded VEGFR2-targeted MB. In this context, the coupling of targeting moieties to MB was achieved by; streptavidin/biotin interaction for coupling VEGFR2-antibodies, direct conjugation of a novel E-selectin specific peptide and SNAP-tag fusion of galectin-3 protein (Fig 1A). A validation of coupling efficiency and quantification of MB surface coverage with targeting ligands was accomplished by fluorescence microscopy and flow cytometry (FACS) respectively. In vitro testing of binding specificity of targeted-MB was done in parallel plate flow chambers on TNF-alpha stimulated human umbilical vein endothelial cells (HUVEC). Furthermore, specific MB binding in vivo was investigated in tumor bearing mice, followed by histological validation of the target expression. Drug delivery was performed using hydrophobic and hydrophilic model drugs (coumarine-6 and Rhodamine-B respectively) loaded PBCA-MB. The loading and US-triggered release efficiencies of both dyes were tested by fluorescence spectroscopy. Subsequently, VEGFR2 antibodies were coupled to the dye-loaded MB, followed by in vivo application. Dye release in vivo was analysed by fluorescence microscopy of tumor cryosections. Fluorescence microscopy of biotinylated FITC, FITC carrying E-selectin specific peptide and YFP fused with the galectin-3 protein was used to confirm attachment of the ligands to MB. Quantitative FACS revealed a surface coverage of 1200 biotinylated FITC and 4000 FITC labeled E-selectin peptide. While fluorescence microscopy also revealed the presence of model drugs in the MB shell (Fig 1B), quantification by fluorescence spectroscopy revealed a loading efficiency of up to 15% for rhodamine-B and 55% for coumarin-6. On the other hand, release efficiencies of up to 80% were observed for both dyes. Significant binding of target specific MB were observed in vitro (Fig 1C) compared to unspecific probes. In CT-26 (colon cancer) tumors, the binding of dye-loaded VEGFR2-MB and US-triggered dye release were observed (Fig 1 D-F). On the other hand, specific binding of E-selectin and galectin-3 specific MB was observed in MLS (ovarian carcinoma) tumors. From this study, one can conclude that direct conjugation of short peptides to MB as well as SNAP-tag fusion of target specific proteins present elegant ways of preparing clinically translatable molecular imaging probes. Furthermore, with a novel E-selectin specific peptide and galectin 3, we address new and promising angiogenesis related targets. Loading and release of small drug molecules (dyes) is also shown to work effectively with PBCA-MB. In general, PBCA-MB are a promising candidate for the development of probes for molecular imaging and theranostics.

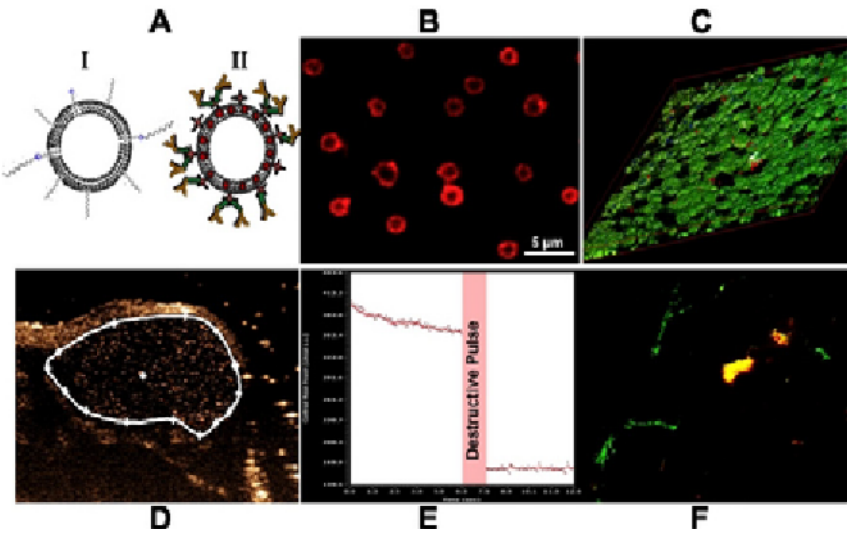


Disclosure of author financial interest or relationships:
**S. Nyongamsen**, None; **A. Rix**, None; **A. Fragoso**, None; **Z. Wu**, None; **O. Iranzo**, None; **J. Gätjens**, None; **M. Palmowski**, None; **T. Lammers**, None; **F. Kiessling**, None.

Presentation Number **SS 2**
Scientific Session 1: Chemistry & Probes - MRI
September 6, 2012 / 10:41-10:52 / Room: Liffey Hall 1

# Metabolic rate constant mapping using hyperpolarized 13C spectroscopic MR imaging

***Florian Wiesinger***[1], *Oleksandr Khegai*[1,2], *Eliane Weidl*[2], *Axel Haase*[2], *Markus Schwaiger*[2], *Rolf F. Schulte*[1], [1]*GE Global Research, Munich, Germany;* [2]*Technische Universität München, Munich, Germany. Contact e-mail: florian.wiesinger@gmail.com*

Hyperpolarized 13C spectroscopic MR imaging provides a wealth of metabolic information within very short time (~1min), including substrate perfusion, transmembrane transport and enzymatically-driven conversion. This leads to the important question of how to best and most comprehensively quantify and interpret these data? Similar to standard MRI, absolute quantification of metabolite signals is difficult. Instead, downstream metabolites are often normalized relative to the detected substrate. In this work a novel frequency-domain rate constant quantification method is presented for the analysis and interpretation of spatially- and temporally-resolved 13C metabolite images. Enzymatically-driven conversion of the hyperpolarized 13C pyruvate substrate (P) towards down-stream metabolites X (with X being lactate, alanine, or bi-carbonate) can to a good approximation be described by a two-side exchange model, according to: dX(t)/dt = kpx*P(t) - Rx*X(t) in time-domain, or after Fourier transformation: i*w*x(w) = kpx*p(w) - Rx*x(w) in frequency description. The term proportional to kpx describes forward conversion, whereas the term proportional to Rx describes an effective decay including repetitive excitation, back-conversion, and T1 relaxation. Given the individual, time-resolved metabolite signals, both representations result in an over-determined system of linear equations for kpx and Rx, which can be solved via simple Moore-Penrose matrix inversion. From the two formulations, the frequency description is advantageous because it circumvents time differentiation of X, which generally results in noise amplification. Furthermore the frequency-domain representation provides a natural and effective way of compressing the dynamic information into a few dominant Fourier coefficients around DC (cf. figure). Interestingly, for w=0, this also provides a physical interpretation of the DC signal ratios according to: 0 = +kpx*p(0) -Rx*x(0), respectively: x(0)/p(0) = sum[X(t)]/sum[P(t)] = kpx/Rx, which can further be used to derive analytical expressions for kpx and Rx. Hyperpolarized [1-13C]pyruvate experiments were performed using a GE 3T HDx scanner (GEHC, Waukesha, WI) and the DNP HyperSense polarizer (Oxford Instruments, Oxford, UK). The figure shows representative results obtained from a dynamic, multi-slice IDEAL spiral CSI study (FA=5deg, 7TEs+1FID, matrix=32x32pts, 4 slices, 4s time resolution) in rats with subcutaneously implanted MATBIII tumors using an injection volume of 2.5ml/kg of 80mM hyperpolarized [1-13C]pyruvate. The tumor appears well visible and clearly enhanced, while perfusion effects are comparatively reduced (bottom rows) relative to the native metabolite maps (top rows). Qualitatively the best SNR and contrast behavior was obtained using the simple DC ratio, whereas quantitatively the apparent rate constant appeared more consistent. Both metrics suppress perfusion and correct for differences in the polarization and MR gain settings. In addition the apparent rate constants kpx also corrects for T1-relaxation effects, signal depletion due to repetitive excitation (TR, FA) and back conversion.

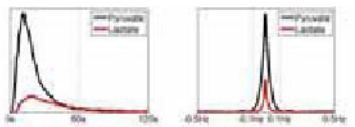

Typical metabolite signals obtained from slice-selective FID measurements in time (left) and frequency (right) domain illustrating a DC concentrated, sparse frequency content.

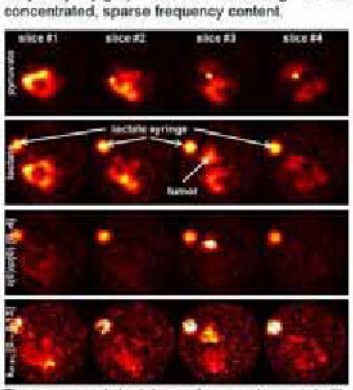


Time-averaged lactate and pyruvate metabolite maps (top rows) are compared with $l(0)/p(0)$ normalization and $k_{p\to l}$ apparent rate constant quantitation (bottom rows).

Disclosure of author financial interest or relationships:
**F. Wiesinger**, GE Global Research, Employment; **O. Khegai**, General Electric, Other financial or material support; **E. Weidl**, None; **A. Haase**, GE, Grant/research support; Rapid Biomedical GmbH, Stockholder; **M. Schwaiger**, Siemens Medicial Solutions, Speakers bureau; Siemens Medical Solutions, Consultant; General Electrics Healthcare, Grant/research support; Lantheus, Grant/research support; **R.F. Schulte**, GE, Employment .

Presentation Number **SS 20**
Scientific Session 3: Preclinical In Vivo - Metabolic Disease
September 6, 2012 / 11:24-11:36 / Room: Liffey Hall 2

# Longitudinal imaging of transplanted islets in a rat model with SPECT

***Karolina M. Andralojc**, Maarten Brom, Lieke Joosten, Desirée Bos, Wim J. Oyen, Otto C. Boerman, Martin Gotthardt, Department of Nuclear Medicine, Radboud University Nijmegen Medical Centre, Nijmegen, Netherlands. Contact e-mail: K.Andralojc@nucmed.umcn.nl*

Pancreatic islet transplantation is a promising clinical modality to restore normoglycemia in diabetic patients. However, patients still experience a significant islet loss immediately after transplantation as well as on the long term. Therefore, there is an urgent need for a method that would non-invasively monitor beta cell mass after transplantation in vivo. Such a method could give more insight into rejection after transplantation and could aid to further improve treatment of diabetic patients. We have developed a non-invasive imaging technique that specifically visualizes beta cells in vivo. This method is based on targeting the glucagon-like peptide1 receptor (GLP-1R). The GLP-1R is expressed at high levels on pancreatic beta cells. Our radiolabelled tracer, In-111-labeled Exendin-3, specifically binds to the GLP-1R and its uptake correlates linearly with beta cell mass. We examined whether intramuscularly transplanted islets in rats could be visualized by microSPECT after i.v. injection with radiolabeled Exendin-3. Islets of Langerhans were isolated from Wag/Rij rats. Various numbers of islets (250,500,750,1000) were transplanted into the left thigh muscle of Wag/Rij rats (n=20), while vehicle was injected in the right muscle as a control (n=3). Rats were monitored up to 14 weeks post-transplantation. SPECT was performed every 1-2 weeks, one hour after i.v. injection of In-111-labeled Exendin-3, using a U-SPECT II microSPECT scanner. After acquiring the last SPECT, the rats were euthanized and the radioactivity in the transplant and other relevant tissues was measured. The muscle with engrafted islets was embedded in paraffin for microautoradiography and immunohistochemistry. The transplanted islets were clearly visualized with SPECT at every time-point, up to 3 months after transplantation. Images could be analysed quantitatively. Transplantation of varying numbers of islets revealed an excellent, linear correlation between the SPECT signal and the number of transplanted islets. In rat model, the high sensitivity of the method allowed reliable longitudinal monitoring of the graft during at least 3 months. Ex vivo microautoradiography and immunohistochemistry of anti-insulin and anti-GLP-1R staining performed on consecutive histological slices showed high accumulation of In-111-exendin-3 in the beta cells. Anti-insulin staining confirmed that islets after transplantation were viable and produced insulin. In-111-exendin-3 accumulated efficiently in transplanted islets after i.v. injection and targeted insulin producing beta cells via GLP-1 receptor. Transplanted islets could be clearly delineated by microSPECT, allowing long time follow-up. The method is sensitive (25 islets could be visualized) and quantitative as radioactivity in the grafts correlated linearly with the number of transplanted islets. This novel method is reliable, reproducible and robust and holds great potential for non-invasive monitoring of BCM after transplantation in humans. Acknowledgements: This work was supported by NIH grant 1R01 AG 030328-01 and the European Community's Seventh Framework Programme (FP7/2007-2013) under grant agreement n° 222980.

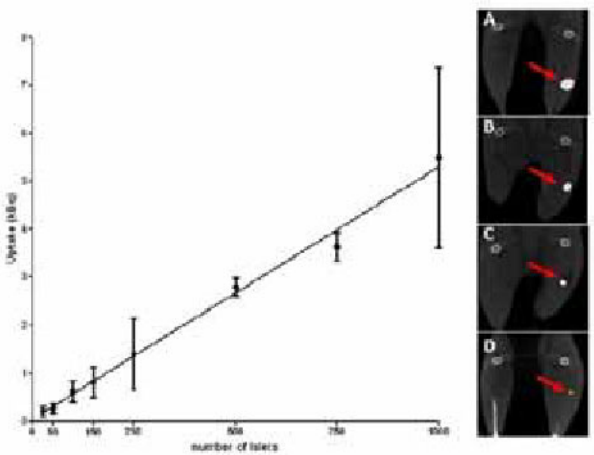


Figure. Correlation between the amount of radioactivity in the grafts as determined by quantitative SPECT with the number of transplanted islets at four weeks post transplantation (Pearson r=0,99). Data from 4 rats per group, transplanted with 25, 50, 100, 150, 250, 500, 750 and 1,000 islets in the thigh muscle of the left hind leg. SPECT/CT after transplantation of 1,000 (A), 500 (B), 100 (C) and 25 (D) islets in the muscle (islet graft indicated by red arrow).

Disclosure of author financial interest or relationships:
**K.M. Andralojc**, None; **M. Brom**, None; **L. Joosten**, None; **D. Bos**, None; **W.J. Oyen**, Roche, Grant/research support; Siemens, Grant/research support; Immunomedics, Grant/research support; Wilex, Grant/research support; Novartis, Grant/research support; GSK, Grant/research support; Merck, Grant/research support; **O.C. Boerman**, None; **M. Gotthardt**, Sanofi Aventis, Grant/research support .

Presentation Number **SS 200**
Scientific Session 29: CT/US - Technology Methodology - Probes
September 8, 2012 / 13:36-13:48 / Room: Wicklow Hall 2

# Gold Labeled Low Density Lipoprotein Nanoparticles: Imaging Lipoprotein Biointeractions with CT, TEM and Fluorescence

*Iris E. Allijn[1,2], Wei Leong[2], Jun Tang[2], Anita Gianella[2], Aneta J. Mieszawska[2], Ge Ma[3], Shu-Hsia Chen[3], Stewart Russell[4], Edward A. Fisher[4], Catherine B. Callo[2], Ronald E. Gordon[5], Jan Andries Post[6], Axel Thran[7], Roland Proksa[7], Gert Storm[8,1], Zahi A. Fayad[2], Willem J. Mulder[2],* ***David P. Cormode***[2], *[1]MIRA institute, University of Twente, Enschede, Netherlands; [2]Translational and Molecular Imaging Institute, Mount Sinai School of Medicine, New York, NY, USA; [3]Department of Oncological Sciences, Mount Sinai School of Medicine, New York, NY, USA; [4]Langone Medical Center, New York University, New York, NY, USA; [5]Department of Pathology, Mount Sinai School of Medicine, New York, NY, USA; [6]Biomolecular Imaging, Utrecht University, Utrecht, Netherlands; [7]Philips Research Europe, Philips, Hamburg, Germany; [8]Pharmaceutical Sciences, Utrecht University, Utrecht, Netherlands. Contact e-mail: davidcormode@gmail.com*

Introduction Low density lipoprotein (LDL) plays a critical role in cholesterol transport to peripheral tissues expressing the LDL receptor (LDLr). Supply of cholesterol is crucial for the maintenance of cell membranes. Furthermore, LDL is closely linked to the formation of atherosclerotic plaques and tumor growth. Gold nanoparticles have been used in many applications in nanomedicine, where they have been applied in radiotherapy, targeted drug delivery, and laser irradiation. In addition, gold nanoparticles have a major role in imaging and are used from transmission electron microscopy (TEM) to optical imaging, and as computed tomography (CT) contrast agents. Hence to be able to load LDL with gold nanoparticles would be extremely useful, allowing LDL to be tracked using various imaging modalities or to deliver therapeutics to diseased tissue. In this study, we developed a novel method to label LDL with gold nanocrystals and Cy5.5 (Au-LDL) (Figure 1A). This enables studying LDL interactions using a variety of imaging techniques, including CT, TEM, and fluorescence techniques. Methods and results Human LDL was sonicated in water for 5 min with 3 nm gold nanocores in a 1 mg ApoB100 to 2.8 mg gold ratio and purified via centrifugation. TEM confirmed that 77% of LDL was labeled with gold and showed a similar morphology and size to native LDL (Figure 1B,C), proving it vastly more effective than the well established Krieger substitution method (Figure S1A). Gel electrophoresis and Western blotting of LDL and Au-LDL had similar results (Figure S1B). In vitro studies were performed in LDLr expressing cells (HepG2, J774A.1, and B16-F10). Competition inhibition assays showed saturable uptake by fluorescence imaging (Figure 1D,E), CT (Figure S1C), and TEM (Figure S1E-M). B16-F10 tumor bearing mice were injected with LDL, Au-LDL and an Au-LDL resembling nanoemulsion lacking ApoB100 (Au-NE). CT showed a higher attenuation in the tumor tissue of mice injected with Au-LDL (29.3 ± 13.4 HU) or Au-NE (14.3 ± 12.0 HU) mice than uninjected mice (Figure S1D). Spectral CT analysis confirmed gold accumulation at the rim of the B16-F10 tumor in mice injected with Au-LDL (Figure 1F). Furthermore, TEM of B16-F10 tumor tissue showed gold uptake in vesicles of tumor cells, endothelial cells and macrophages (Figure 1G), which was also confirmed by FACS analysis. Identification of gold particles in TEM images was confirmed by EDX analysis. Discussion and conclusion In this study, we developed a novel method that allowed labeling of native human LDL with 3 nm gold nanocrystals, without altering LDL characteristics. Therefore, Au-LDL can likely be used as a marker to study LDL interactions, cholesterol metabolism, atherosclerotic plaque formation and tumor growth, with a variety of imaging techniques. In the future LDL could be used as a natural carrier platform to deliver gold nanomaterials and lipophilic drugs for therapeutic purposes. Clinical relevance Au-LDL could be an important new step in studying the cholesterol metabolism and behavior of LDL in a variety of diseases. Furthermore, natural LDL is a potent and promising carrier platform in nanomedicine.

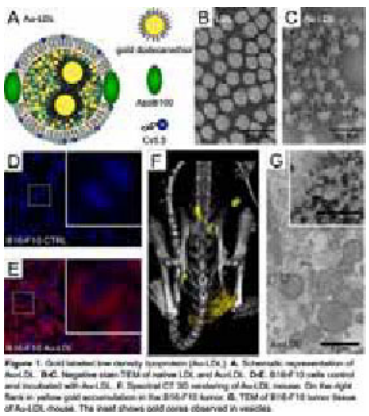


Disclosure of author financial interest or relationships:
**I.E. Allijn**, None; **W. Leong**, None; **J. Tang**, None; **A. Gianella**, None; **A.J. Mieszawska**, None; **G. Ma**, None; **S. Chen**, None; **S. Russell**, None; **E.A. Fisher**, None; **C.B. Callo**, None; **R.E. Gordon**, None; **J. Post**, None; **A. Thran**, PhilipsTechnologie GmbH, Germany, Employment; **R. Proksa**, Philips Healthcare, Employment; **G. Storm**, None; **Z.A. Fayad**, None; **W.J. Mulder**, None; **D.P. Cormode**, Philips, Consultant .

Presentation Number **SS 201**
Scientific Session 29: CT/US - Technology Methodology - Probes
September 8, 2012 / 13:48-14:00 / Room: Wicklow Hall 2

# Multiple injections of a nanoparticulate contrast agent lead to accumulation in the reticulo-endothelial system and decreased clearance rates

***Laura Nebuloni***, *Gisela Kuhn, Ralph Müller, Institute for Biomechanics, ETH Zurich, Zurich, Switzerland. Contact e-mail: lnebuloni@ethz.ch*

The visualization of blood vessels through micro-computed tomography (micro-CT) requires the injection of contrast agents that provide good contrast, no extravasation and slow blood clearance. For this purpose, nanoparticle-based agents providing high soft tissue enhancement were developed for use in pre-clinical research. Nanoparticles are cleared through the reticulo-endothelial system (RES), which includes liver, spleen and bone marrow. A high vascular half-life (up to several hours) results from this slow clearance process. Dynamic micro-CT imaging, the consecutive acquisition of images of the same region of interest, allows the assessment of blood clearance, the accumulation of the nanoparticles in the RES organs and their extravasation in tissues with high vascular permeability, such as newly formed vessels in wounds or tumors. In the present study, a nanoparticulate contrast agent (ExiTronTM nano 12000, Miltenyi Biotec, Berlin, Germany) was injected intravenously in C57BL/6 female mice. Following the injection, neck or lower hind limb tissues were monitored over 30 minutes with low resolution (70 µm) scans using in vivo micro-CT (vivaCT 40, Scanco Medical AG, Brüttisellen, Switzerland). The same protocol was applied for the following 5 days and 1 month after the first injection. The average X-ray absorption over time was calculated in blood, muscle and bone marrow by quantifying the average grey values in the jugular veins, neck muscles and the medullar compartment of the vertebra respectively. Figure 1a shows the time course of contrast enhancement in the different tissues at day 1. The nanoparticles provide a stable contrast within the first half-hour after injection, making them particularly useful for long-lasting scans. Nevertheless, while in blood and muscle the contrast agent is slowly cleared over time, the discontinuous capillaries in the bone marrow cause an extravasation of contrast in the surrounding interstitial spaces. Moreover, blood presents a faster clearance than muscle. The longer retention of contrast in the muscular tissue could be explained with slower blood flow at the capillary level than in the major vessels. In the follow-up study, the daily injection was very well tolerated by all animals, as the nanoparticles were excreted from blood in less than 24 hours. Nonetheless, a decreasing clearance over the days could be observed in all tissues (figure 1b). An accumulation of nanoparticles in the RES organs could also be detected and might be related to the diminished capacity of the mouse body to clear the contrast agent. Dynamic measurements acquired 1 month after the first injection revealed that the dynamic response of all tissues went back to its first values. In conclusion, X-ray absorbing nanoparticles provided useful in characterizing different tissue behaviors with dynamic imaging. In case of longitudinal studies, a reference tissue dynamic response is necessary at each time-point due to decreasing contrast clearance over time. Alternatively, an adequate recovery time in-between injections might be introduced to avoid changes in the body response to the nanoparticles.

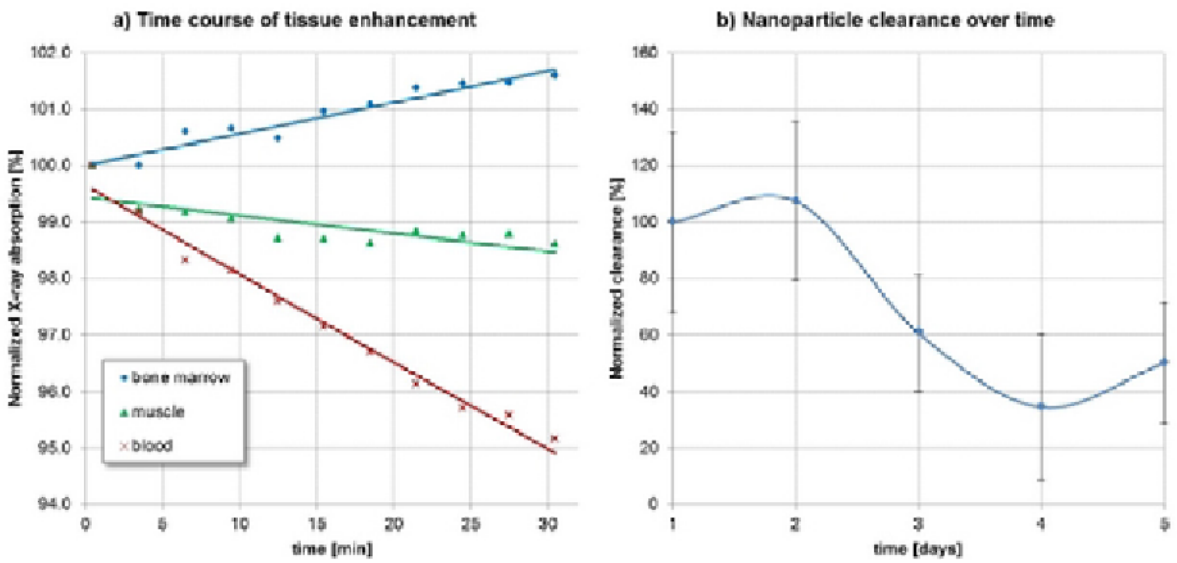


Figure 1: a) Time course of contrast enhancement at day 1 in bone marrow, muscle and blood. While the contrast agent is slowly cleared from blood and muscle, it extravasates in the interstitial spaces of the bone marrow. b) Nanoparticles clearance over 5 days. The mouse body shows an overall decreasing capacity to clear the nanoparticles.

Disclosure of author financial interest or relationships:
**L. Nebuloni**, None; **G. Kuhn**, None; **R. Müller**, None.

Presentation Number **SS 202**
Scientific Session 29: CT/US - Technology Methodology - Probes
September 8, 2012 / 14:00-14:12 / Room: Wicklow Hall 2

# scVEGF-Microbubbles Differentially Adhere to Surfaces with Distinct VEGF Receptor Density In Vitro and In Vivo

*Zhongmin Du[1], Joshua Rychak[2], Dan J. Smith[2], Marina Backer[3], Joseph M. Backer[3], **Alexander L. Klibanov**[1], [1]Dept. of Medicine, Cardiovascular Div., University of Virginia, Charlottesville, VA, USA; [2]Targeson Inc, San Diego, CA, USA; [3]Sibtech Inc, Brookfield, CT, USA. Contact e-mail: sklib1@gmail.com*

The goal of ultrasound molecular imaging with targeted bubbles is to provide spatial distribution information for areas with high-level expression of target receptor on vascular endothelium, to distinguish normal tissues from areas of disease. Targeted bubbles should be able to adhere differentially to the areas with different surface density of the target receptor. We have tested this hypothesis for microbubbles decorated with single-chain VEGF (scVEGF) targeted to VEGF Receptor 2 (VEGFR2) in vitro (in a flow chamber model) and in vivo, in two subcutaneous murine tumor models, colon adenocarcinoma and prostate cancer, which have distinct VEGFR2 surface density patterns. Decafluorobutane microbubbles decorated with maleimide-PEG-lipid-containing shell were purified from excess free lipid by centrifugal washes. Thiol-scVEGF (Sibtech, Brookfield, CT) was reacted with maleimide-PEG-bubbles. scVEGF on the bubbles was quantified by ELISA. In vitro targeted adhesion was assessed by perfusion through a parallel plate flow chamber (ibidi, Verona, WI) with immobilized VEGFR2, under microscopy control. Serial dilutions of recombinant VEGFR2 (0.25-100 ug/ml range) were used to prepare flow chambers with varied receptor surface density. Flow through the chamber was generated with a syringe pump (1 dyn/cm2 wall shear stress). Tumors (murine colon adenocarcinoma MC38 cells, J. Schlom, NIH, or human prostate cancer PC3 cells, ATCC) were grown subcutaneously in C5lBL/6 or SCID mice, respectively. Immunohistology was used to quantify VEGFR2 expression. In vivo imaging was performed on Siemens Sequoia 512 (15L8 probe, 7 MHz, CPS mode, MI 0.2), following an intravenous bolus of 20 million microbubbles. Microbubble circulation and accumulation in the tissues was monitored by intermittent imaging for 10 min. Ten minutes after bubble administration a destructive ultrasound pulse was used to assess the level of residual circulating bubbles. In vitro targeting of microbubbles in the flow chamber was negligible if there was no VEGFR2 present, or if coating receptor concentration was 0.25 ug/ml, confirming low nonspecific adhesion of the bubbles to nontarget surfaces or surfaces with receptor density below threshold. Adhesion of bubbles to the target chambers increased up to 25 ug/ml VEGFR2, and then leveled off. Targeted bubble adhesion curve has sigmoid shape, as is generally observed for the surface density of receptors on solid surfaces in immunoassays. In vivo targeting of scVEGF-microbubbles to MC38 vasculature was very efficient; accumulation of control non-targeted bubbles in the tumor was negligible. Adhesion of scVEGF-bubbles to normal muscle was an order of magnitude less than in the tumor. MC38, an aggressive tumor, possesses high levels of VEGFR2. PC3, with much lower level of VEGFR2 expression, demonstrated lower (but still significant) level of microbubble backscatter acoustic signal in the tumor. Overall, scVEGF-targeted microbubble adhesion increased with the VEGFR2 levels. Nonspecific binding to VEGFR2-negative targets was negligible.

Disclosure of author financial interest or relationships:
**Z. Du**, None; **J. Rychak**, Targeson, Inc, Stockholder; Targeson, Inc, Employment; **D.J. Smith**, Targeson, Inc., Employment; **M. Backer**, None; **J.M. Backer**, SibTech, Inc., Stockholder; GlaxoSmishKline, Grant/research support; **A.L. Klibanov**, Philips Research North America, Grant/research support; Targeson Inc, Stockholder; Targeson Inc (NIH SBIR subcontract), Grant/research support .

Presentation Number **SS 203**
Scientific Session 30: Preclinical In Vivo - Oncology
September 8, 2012 / 13:00-13:12 / Room: The Auditorium

# Imaging studies of blood-brain barrier disruption during brain metastatic development in a relevant experimental animal model

***Frits Thorsen***[1], *Brett Fite*[2], *Lisa M. Mahakian*[2], *Victoria Harrison*[3], *Sarah Johnson*[2], *Elizabeth Ingham*[2], *Jai Woong Seo*[2], *Thomas J. Meade*[3], *Katherine Ferrara*[2], [1]*Department of Biomedicine, University of Bergen, Bergen, Norway;* [2]*Department of Biomedical Engineering, University of California at Davis, Davis, CA, USA;* [3]*Department of Chemistry, Northwestern University, Evanston, IL, USA. Contact e-mail: frits.thorsen@biomed.uib.no*

Introduction Efficient drug delivery to brain metastases is difficult due to an often intact blood-brain barrier (BBB) around smaller lesions. With few exceptions (such as Dacarbazine), therapeutic drugs do not penetrate an intact BBB. Relevant experimental brain metastatic models are thus needed to study biological mechanisms and therapeutic responses of early brain lesions in relation to the BBB. Previous studies injecting small molecules such as sodium fluorescein (MW 376D) have indicated that the BBB is disrupted in experimental brain metastasis larger than 0.25 mm (1). However, little is known regarding at which time point in experimental brain metastasis development the BBB is disrupted, and to what extent larger sized molecules at that time are able to penetrate tumor tissue. We addressed these issues by performing imaging studies, after injecting contrast agents of various molecular weights into an established melanoma brain metastasis model. Materials and Methods All studies were approved by the UCD Animal Care and Use Committee. As in (2), we injected $5X10^5$ human melanoma brain metastasis cells harboring the Luciferase and GFP genes, intracardially into 32 NOD/SCID mice. All animals were followed by bioluminescence imaging (BLI) weekly for 6 weeks. MRI (Bruker Biospec 70/30, RARE sequence, RARE factor=2, TE/TR/ST=9 ms/750 ms/1mm, FOV=2x2 cm, Matrix=256x256, NA=4) was performed at weeks 3, 4, 5 and 6 after tumor cell inoculation, before and after i.v. injections of either Gd-HPDO3A (Prohance, MW 559D, 0.5 µmol/g, 20 mice) or a newly synthetized Gadolinium contrast agent with 3 Gd(III) chelates, termed C3, (MW 2kD, 0.167 µmol/g, 5 mice). $^{64}$Cu-Albumin (MW 66.5kD) was also injected i.v. prior to PET imaging at week 4 (6 mice) and 6 (4 mice). Results and Discussion BLI confirmed tumor spread to all animal brains after 1 week, and a gradual increase in tumor burden until week 6. BLI also showed that Luciferin (MW 280D) is able to penetrate an intact BBB, as tumor cells could be visualized in the animal brains 15mins after injections. T1w MRI at week 3 did not show any tumors, however BLI confirmed presence of metastasis. MRI detected tumors at week 4 (Fig 1), and the mean, total number of tumors increased from 26 tumors at week 4, to 89 tumors at week 6. There was an exponential increase in tumor burden from week 4 to 6. The number of leaky tumors also increased exponentially, with mean diameters increasing from 595 µm to 708 µm. The smallest leaky tumors detectable by MRI were ~200 µm (week 5). The number of non-leaky tumors peaked at 5 weeks, and their mean diameters increased from 260 µm to 452 µm. 64Cu-Albumin PET also indicated leakage of albumin into the metastatic lesions at week 6. Conclusions Our study shows that T1w 7T MRI can detect leaky brain metastases down to ~200 µm in diameter. Molecules up to 2kD in size may penetrate brain tumor tissue early in tumor development. Our PET study indicates that larger molecules such as albumin may leak out of the metastatic lesions later in tumor development. References (1) Fidler IJ et al. Lancet Oncol 3:53-57, 2002. (2) Wang J et al. Neuropathol Appl Neurobiol 37:189-205, 2011.

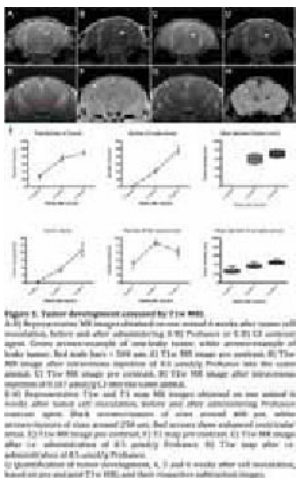

Disclosure of author financial interest or relationships:
**F. Thorsen**, None; **B. Fite**, None; **L.M. Mahakian**, None; **V. Harrison**, None; **S. Johnson**, None; **E. Ingham**, None; **J. Seo**, None; **T.J. Meade**, None; **K. Ferrara**, None.

Presentation Number **SS 204**
Scientific Session 30: Preclinical In Vivo - Oncology
September 8, 2012 / 13:12-13:24 / Room: The Auditorium

# Fatty acid synthase is a key target to suppress tumor multiple functions: [1-$^{11}$C]acetate PET as a predictor of the targeted therapy outcome

***Yukie Yoshii***[1], *Takako Furukawa*[1,2], *Oyama Nobuyuki*[3], *Yoko Hasegawa*[3], *Yasushi Kiyono*[2], *Ryuichi Nishii*[4], *Atsushi B. Tsuji*[1], *Chizuru Sogawa*[1], *Hidekatsu Wakizaka*[1], *Hiroshi Yoshii*[5], *Yasuhisa Fujibayashi*[1,2], *Tsuneo Saga*[1], [1]*Molecular Imaging Center, National Institute of Radiological Sciences, Chiba, Japan;* [2]*Biomedical Imaging Research Center, University of Fukui, Fukui, Japan;* [3]*Faculty of Medical Sciences, University of Fukui, Fukui, Japan;* [4]*Department of Radiology, University of Miyazaki Hospital, Miyazaki, Japan;* [5]*Emergency Radiation Exposure Medical Care Research Center, National Institute of Radiological Sciences, Chiba, Japan. Contact e-mail: yukiey@nirs.go.jp*

**Objectives:** Fatty acid synthase (FASN) is known to be over-expressed in several human cancers, e.g., prostate, breast, lung, and melanoma, and the over-expression is associated with poor prognosis (1). It is so far reported that orlistat, an inhibitor of FASN, shows antitumor effects (2). Hence, FASN is expected to be a promising therapeutic target for treatment of such cancers. However, large variations in FASN expression in individual tumors have been observed by pathological studies (3, 4), and therefore a method to predict therapeutic outcome of FASN-targeted therapy is needed to provide successful therapy for individual tumors. Also, how FASN inhibition affects tumor growth is still an open question. Here we examined whether [1-$^{11}$C]acetate PET can evaluate FASN expression and predict outcome of FASN-targeted therapy, together with consequence of FASN inhibition in cancer therapy. **Methods:** Relationships between radiolabeled acetate uptake, FASN expression and therapeutic effect of orlistat were examined *in vitro* and *in vivo* with human prostate cancer cell lines including LNCaP, PC3, 22Rv1 and DU145. For *in vitro* studies, acetate uptake, FASN expression, and cell viability after orlistat treatment were determined. For *in vivo* studies, [1-$^{11}$C]acetate PET, biodistribution study, and orlistat treatment (250 mg/kg/day for 2 weeks) were performed with tumor-bearing mice. To understand the mechanism how FASN inhibition affects tumor growth, FASN knockdown LNCaP cells were established by transduction of lentiviral particles carrying expression cassettes encoding single-hairpin RNA (shRNA) against FASN and the characteristics of the cells were examined in detail. **Results:** LNCaP cells, which express high levels of FASN, showed high acetate uptake, while PC3, 22Rv1 and DU145, which express low levels of FASN, showed relatively low acetate uptake. There was a significant positive correlation between acetate uptake and FASN expression. Percentage of cell viability after orlistat treatment showed significant negative correlations to acetate uptake and FASN expression, respectively. From *in vivo* studies, LNCaP tumors (high FASN) showed high acetate uptake and high sensitivity to orlistat treatment, while PC3 and DU145 tumors (low FASN) showed low acetate uptake and low sensitivity to orlistat treatment. Interestingly, we found that knockdown of FASN by shRNA suppressed cell proliferation, cell adhesion, migration and invasion with down-regulation of genes related to these functions. **Conclusions:** Our findings showed that FASN is a key target to suppress multiple steps related to tumor progression and [1-$^{11}$C]acetate PET is a powerful tool to accomplish individualized FASN-targeted therapy by non-invasively predicting the therapeutic outcome. References: 1. Menendez JA & Lupu R (2007) Nat Rev Cancer 7(10):763-777. 2. Kridel SJ, Axelrod F, Rozenkrantz N, & Smith JW (2004) Cancer Res 64(6):2070-2075. 3. Migita T, et al. (2009) J Natl Cancer Inst 101(7):519-532. 4. Rossi S, et al. (2003) Mol Cancer Res 1(10):707-715.

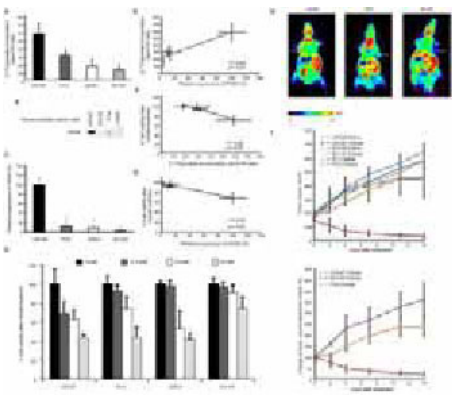

Figure [1-$^{14}$C]acetate uptake (A), FASN expression (B, C) and therapeutic effect of orlistat (D) in human prostate cancer cells, LNCaP, PC3, 22Rv1 and DU145. There was a significant positive correlation between [1-$^{14}$C]acetate uptake and FASN expression (E). Percent cell viability after orlistat treatment showed significant negative correlations to [1-$^{14}$C]acetate uptake (F) and FASN expression (G). [1-$^{11}$C]acetate PET with tumor-bearing mice (H). Therapeutic effect of orlistat *in vivo* (I).

Disclosure of author financial interest or relationships:
**Y. Yoshii**, None; **T. Furukawa**, None; **O. Nobuyuki**, None; **Y. Hasegawa**, None; **Y. Kiyono**, None; **R. Nishii**, None; **A.B. Tsuji**, None; **C. Sogawa**, None; **H. Wakizaka**, None; **H. Yoshii**, None; **Y. Fujibayashi**, None; **T. Saga**, None.

Presentation Number **SS 205**
Scientific Session 30: Preclinical In Vivo - Oncology
September 8, 2012 / 13:24-13:36 / Room: The Auditorium

# In Vitro and in Vivo Evaluation of a Non-Toxic Cocktail Potentially Improving Quality of Folic Acid Targeted Nuclear Imaging in Preclinical Research

***Cristina Müller***[1], *Christopher P. Leamon*[2], *Roger Schibli*[1,3], [1]*Center for Radiopharmaceutical Sciences, Paul Scherrer Institute, Villigen-PSI, Switzerland;* [2]*Endocyte Inc, , West Lafayette, IN, USA;* [3]*Dept. of Chemistry and Applied Biosciences, ETH Zurich, Zurich, Switzerland. Contact e-mail: Cristina.Mueller@psi.ch*

Background: Folate receptor (FR) targeting is attractive for imaging of cancer and activated macrophages through application of folic acid radioconjugates. However, significant uptake of radiofolates in the kidneys and hence a source of radiation within the animal may prevent visualization of small metastases and sites of inflammation. We were the first to discover that the antifolate pemetrexed (PMX) reduces undesired renal uptake of radiofolates significantly. The aim of this study was to investigate on whether the kidney uptake reducing effect of PMX would be maintained if it was applied as a cocktail together with its antidote thymidine (Thd). Experimental: The effect of Thd to abrogate PMX-induced cytotoxicity was assessed in vitro with an MTT assay using FR-positive tumor (KB) and embryonic monkey kidney cells (MA104). Co-application of Thd was investigated for rescue of non-tumor bearing mice which were treated with high-dosed PMX. In vitro internalization of 67Ga-EC0800 (Endocyte Inc.) was performed with cultured KB and MA104 cells in the absence and presence of PMX alone and in combination with Thd. Biodistribution and SPECT/CT imaging studies of 67Ga-EC0800 were performed with KB tumor bearing mice injected with PMX alone or with a cocktail of PMX and Thd. Results: Thd was effective in protecting cultured KB and MA104 cells from PMX-induced cytotoxic effects. Rescue of mice with side effects after high-dosed PMX was achieved by repeated application of Thd. In vitro uptake of 67Ga-EC0800 in KB cells was increased by coincubation of PMX but reduced in MA104 kidney cells under the same conditions. In both cases Thd did not change the results obtained with PMX. The radiofolate's kidney uptake reducing effect of PMX which was observed in mice was maintained also if PMX was employed together with its antidote Thd while the tumor uptake remained unchanged. Conclusion: Application of PMX together with Thd as a cocktail is effective to improve the tissue distribution of radiofolates while preventing pharmacological and potentially toxic side effects of the chemotherapeutic agent PMX. These findings open new perspectives for folate-based nuclear imaging in preclinical research potentially allowing longitudinal investigations in animal models of cancer and inflammatory diseases.

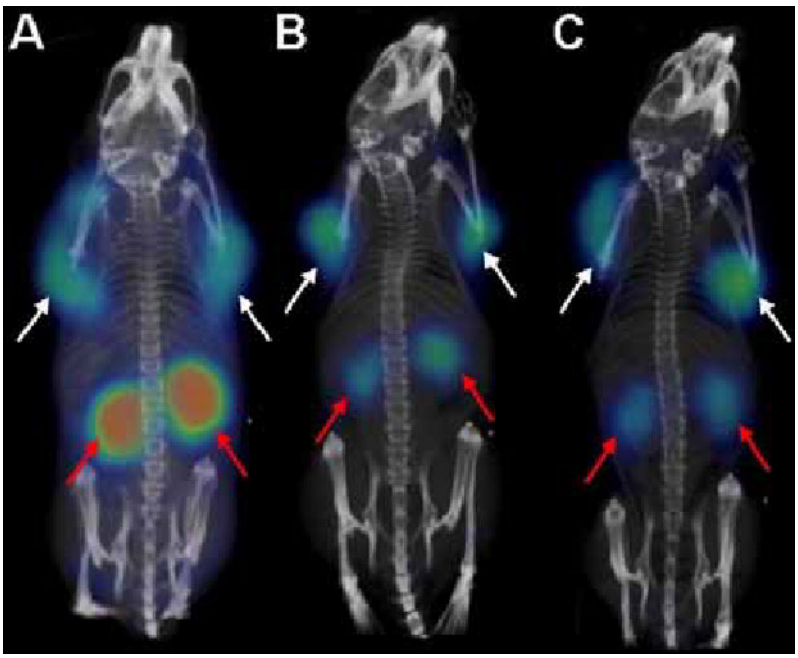


SPECT/CT images of mice 2 h after injection of 67Ga-EC0800. Mice received only the 67Ga-EC0800 (A) or in addition: preinjected PMX (B) or preinjected PMX/Thd (C). Tumor xenografts and kidneys are indicated with white and red arrows respectively.

Disclosure of author financial interest or relationships:
**C. Müller**, None; **C.P. Leamon**, None; **R. Schibli**, None.

Presentation Number **SS 206**
Scientific Session 30: Preclinical In Vivo - Oncology
September 8, 2012 / 13:36-13:48 / Room: The Auditorium

# Influence of the Near Infrared Fluorescence Dye on the Imaging Properties of a Novel Fluorescent CCK2R Agonist and a 2-deoxy-D-glucose Probe in a Multispectral Imaging Approach

***Susanne Kossatz***[1], *Rosalba Mansi*[2], *Martin Behe*[3], *Peter Czerney*[4], *Werner A. Kaiser*[5], *Ingrid Hilger*[1], [1]*Institute for Diagnostic and Interventional Radiology, Experimental Radiology, Jena University Hospital - Friedrich Schiller University Jena, Jena, Germany;* [2]*Institute for Nuclear Medicine, University Hospital Freiburg, Freiburg, Germany;* [3]*Paul Scherrer Institute, Villingen, Switzerland;* [4]*Dyomics GmbH, Jena, Germany;* [5]*Institute of Diagnostic and Interventional Radiology I, Jena University Hospital - Friedrich Schiller University Jena, Jena, Germany. Contact e-mail: susanne.kossatz@med.uni-jena.de*

Introduction: Small molecule optical probes are favorable for intraoperative and endoscopic imaging because they display high affinity receptor binding while undergoing few nonspecific interactions and featuring fast bioavailability. In these constructs, the dye component can fundamentally influence the properties of the binding moiety of the molecule. Two different small molecule compounds were evaluated in parallel. First we synthesized a Cholecystokinin-2-receptor (CCK2R) targeted peptide, known from nuclear medicine, and coupled it to the hydrophilic hemicyanine DY-754 ("dQ-MG-754"). Secondly, we used the commercially available 2-deoxy-D-glucose "IR800 2-DG", derived from FDG, for imaging of tumor metabolism. We explored what influence the dye component had on probe properties in relation to target binding, pharmacokinetics and elimination pattern in a multispectral imaging approach. Material and Methods: We synthesized a novel CCK2R targeted probe "dQ-MG-754" and tested in vitro specificity of uptake on receptor expressing and non-expressing cells and binding affinity. For multispectral imaging, dQ-MG-754 and IR800 2-DG were intravenously injected into nude mice bearing subcutaneous xenografts of epidermoid carcinoma expressing either or not CCK2R. Imaging was followed 24 h and fluorescence signals were semiquantitatively analyzed for contrast agent accumulation, finally "tumor to background" ratios were determined. Ex vivo we assessed biodistribution and elimination pattern. Furthermore macroscopic differences in contrast agent uptake were analyzed. Results: Our newly synthesized CCK2R targeted probe showed specific, receptor mediated internalization only into CCK2R expressing cells and a higher binding affinity than the corresponding radiochelate (Kd = 1.77 ± 0.6 nM compared to 9.6 ± 1.0 nM). In vivo we were able to simultaneously detect the signals of both applied contrast agents in different areas of the xenografts. The dQ-MG-754 probe displayed specific tumor accumulation with high tumor/background contrasts and evenly distributed fluorescence signals throughout the tumor tissue. In the view of prospective endoscopic imaging we found a favorable biodistribution and a renal elimination dependent on dye hydrophilicity. The IR800 2-DG probe led to successful tumor imaging in only 60% of the specimen. In these cases, fluorescence signals of IR800 2-DG were distinctly pronounced in the central necrotic and perinecrotic tumor regions and very weakly in viable tumor margins indicating an EPR effect mediated deposition. Conclusion: Our experiments demonstrated the distinct effect of the dye component used in small molecule probes. For the CCK2R targeted dQ-MG-754 probe this means that the selection of the dye significantly favored pharmacokinetic and biodistribution properties for intraoperative and endoscopic imaging. In contrast, the presence of a cyanine dye in GLUT targeted probes seems to shift receptor specificity towards accumulation in necrotic areas as opposed to uptake into vital GLUT-1 expressing cells in 18F-FDG imaging. The applied multispectral approach could enhance early identification of heterogeneous tumor cells.

Disclosure of author financial interest or relationships:
**S. Kossatz**, None; **R. Mansi**, None; **M. Behe**, None; **P. Czerney**, Dyomics GmbH, Stockholder; **W.A. Kaiser**, None; **I. Hilger**, None.

Presentation Number **SS 207**
Scientific Session 30: Preclinical In Vivo - Oncology
September 8, 2012 / 13:48-14:00 / Room: The Auditorium

# Early therapy assessment of tamoxifen in an MNU-induced mammary cancer rat model using diffusion-weighted imaging

***Guihua Zhai***[1], *Clinton J. Grubbs*[2], *Naomi S. Fineberg*[3], *Hyunki Kim*[1,4], [1]*Radiology, UAB, Birmingham, AL, USA;* [2]*Surgery, UAB, Birmingham, AL, USA;* [3]*Biostatistics, UAB, Birmingham, AL, USA;* [4]*Comprehensive Cancer Center, UAB, Birmingham, AL, USA. Contact e-mail: Guihua.Zhai@ccc.uab.edu*

Purpose: To evaluate the feasibility of diffusion-weighted imaging (DWI) for detecting the early therapeutic efficacy of tamoxifen in a methylnitrosourea (MNU)-induced mammary cancer rat model. Methods: A total of 15 Sprague-Dawley rats (50 days old) were injected with MNU (50mg/kg body weight) through the jugular vein to induce spontaneous mammary tumors. Therapy started for all animals with tamoxifen (10mg/kg diet) when the tumors were about 2 cm in diameter, and continued for 4 weeks thereafter. DWI was performed on days 0, 3, and 7 after therapy initiation, and the tumor volumes were measured with a caliper twice a week during the entire therapeutic period. The tumors were categorized into three groups (sensitive, intermediate, and resistant groups) based on tamoxifen sensitivity, and the intra-tumoral ADC changes of those groups were compared. Pearson correlation coefficients were used to look at the relationship between the ADC changes and the tumor-volume changes. Results: Times for 50% volume reduction of sensitive, intermediate, and resistant tumors were 5.9±0.3 days (n=5), 12.3±1.5 days (n=6), and more than 28 days (n=4), respectively. The mean ADC changes of sensitive, intermediate, and resistant tumors on day 3 were 15±3%, 5±4%, and 8±3%, respectively, while those on day 7 were 28±6%, 13±6%, and 5±2%, respectively. The ADC increase of the sensitive group was significantly higher than that of the resistant group on day 7 (p=0.014). The ADC changes on day 3 were significantly correlated with tumor-volume changes on days 3, 7, and 11 (p=0.019, 0.003, and 0.002 respectively), while those on day 7 were significantly correlated with tumor-volume changes on days 7, 11, 14, and 18 (p=0.001, 0.001, 0.003, and 0.009 respectively). Conclusion: DWI was successfully implemented for spontaneous breast-cancer rat model with minimal motion artifacts. The intra-tumoral ADC changes on either day 3 or day 7 were significantly correlated with long-term tumor-volume changes, but the ADC change on day 7 served as a more reliable prognostic factor. This study may help to determine the optimal DWI time point to assess therapeutic efficacy of tamoxifen for breast cancer patients.

Disclosure of author financial interest or relationships:
**G. Zhai**, None; **C.J. Grubbs**, None; **N.S. Fineberg**, Eli Lilly, Honoraria; **H. Kim**, None.

Presentation Number **SS 208**
Scientific Session 30: Preclinical In Vivo - Oncology
September 8, 2012 / 14:00-14:12 / Room: The Auditorium

# Radiosynthesis and evaluation of novel F-18 labeled leucine derivatives for tumor and protein synthesis imaging

*Chaofeng Huang[1], Liya Yuan[2], Kiran K Solingapuram Sai[1], Christopher Bognar[1], Lynne A. Jones[1], Keith M. Rich[2],* ***Jonathan McConathy***[1]*, [1]Radiology, Washington University, St. Louis, MO, USA; [2]Neurosurgery, Washington University, St. Louis, MO, USA. Contact e-mail: mcconathyj@mir.wustl.edu*

**Objectives:** The purpose of this work was to develop novel $^{18}$F-labeled leucine analogues targeting system L amino acid transport for brain tumor and protein synthesis imaging with PET. These tracers were compared with the well-characterized non-metabolized system L substrate, *O*-(2-[$^{18}$F]fluoroethyl)-L-tyrosine (FET). **Methods:** The four stereoisomers of 5-fluoroleucine (5-FLeu) (2*S*,4*S*; 2*S*,4*R*; 2*R*,4*S*; 2*R*,4*R*) and labeling precursors were prepared through chiral Schiff base intermediates. Radiosynthesis was performed using mesylate precursors treated with [$^{18}$F]fluoride/potassium carbonate/$K_{222}$ followed by acidic deprotection. The final single stereoisomer products were purified using chiral high performance liquid chromatography (HPLC). Biological evaluation of the (2*S*,4*S*) and (2*R*,4*S*) stereoisomers of 5-[$^{18}$F]FLeu was performed in BALB/C mice with DBT glioma tumors through biodistribution studies (n=3 or 4 at each time point). The (2*S*,4*R*) and (2*R*,4*R*) stereoisomers of [$^{18}$F]5-FLeu were evaluated through biodistribution studies in normal BALB/C mice (n=3 or 4 at each time point) and microPET studies in mice with intracranial DBT tumors. Comparisons were made to prior [$^{18}$F]FET and [$^{18}$F]FDG biodistribution and microPET imaging studies. Incorporation of 5-[$^{18}$F]FLeu stereoisomers into proteins was estimated using perchloric acid precipitation of brain and liver homogenates. Statistical comparisons of tracer uptake were compared with 2-tailed t-tests with p-values ≤ 0.05 considered significant. **Results:** Each of the 4 stereoisomers of non-radioactive and $^{18}$F-labeled 5-FLeu were prepared in high stereochemical purity. The absolute uptake of (2*S*,4*R*)-5-[$^{18}$F]FLeu in DBT tumors expressed as percent of injected dose per gram (%ID/g) was significantly higher than [$^{18}$F]FET (4.1 ± 0.8 vs. 1.6 ± 0.4 at 5 min, 4.7 ± 1.1 vs. 2.9 ± 0.4 at 30 min, 5.1 ± 0.8 vs. 1.7 ± 0.1 at 60 min, respectively). Similar results were observed in dynamic microPET studies with standardized uptake values of 1.5 ± 0.1 obtained with (2*S*,4*S*)-5-[$^{18}$F]FLeu and 1.1 ± 0.1 obtained with [$^{18}$F]FET at 50-60 min after injection. These tracers provided similar tumor to brain ratios of approximately 2:1 and had superior tumor visualization compared to [$^{18}$F]FDG. All of the stereoisomers of 5-FLeu were associated with relatively high bone uptake, indicating that in vivo defluorination occurred which was much greater with the 2*R* stereoisomers. Protein incorporation studies demonstrated that approximately 50 to 60% of the liver activity was present in the protein precipitate at 60 min after injection for (2*S*,4*S*)- and (2*S*,4*R*)-5-[$^{18}$F]FLeu. **Conclusions:** The novel fluorinated leucine analogues (2*S*,4*S*)- and (2*S*,4*R*)-5-[$^{18}$F]FLeu demonstrate good tumor imaging properties in the mouse DBT glioma model with higher tumor uptake than the established system L tracer [$^{18}$F]FET. These novel tracers appear to be incorporated into protein, and ongoing work is evaluating their suitability for evaluating protein synthesis rates. These tracers, particularly the 2*R* stereoisomers, undergo in vivo defluorination which may occur through the α-keto pathway of leucine metabolism.

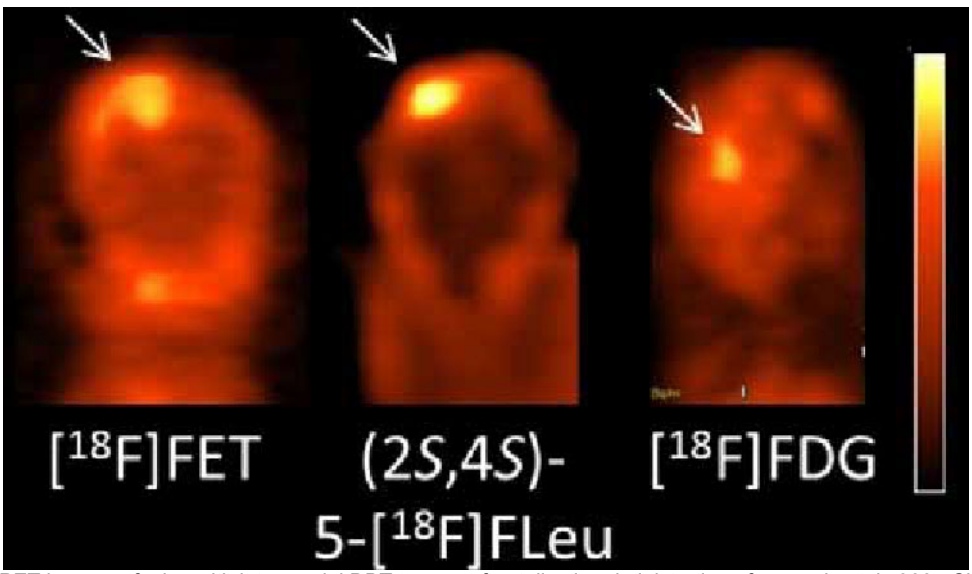


Representative microPET images of mice with intracranial DBT tumors after tail vein administration of approximately 300 uCi of tracer. Images are displayed as summed data from 0-60 min and are scaled independently to optimize tumor visualization (white arrows).

Disclosure of author financial interest or relationships:
**C. Huang**, None; **L. Yuan**, None; **K. Solingapuram Sai**, None; **C. Bognar**, None; **L.A. Jones**, None; **K.M. Rich**, Alvine Pharmaceuticals, Stockholder; **J. McConathy**, Eli Lilly/Avid, Consultant; Eli Lilly/Avid, Speakers bureau .

Presentation Number **SS 209**
Scientific Session 30: Preclinical In Vivo - Oncology
September 8, 2012 / 14:12-14:24 / Room: The Auditorium

# Quantitative Image-Based Staging and Treatment Response Assessment of Spontaneously Arising Plasma-Cell Tumors in Genetically Engineered Laboratory Mice

*Kaylia Duncan[2], **John J. Sunderland**[1], Susan A. Walsh[1], Laura B. Ponto[1], Timothy Rosean[2], Siegfried Janz[2], [1]Radiology, University of Iowa, Iowa City, IA, USA; [2]Pathology, University of Iowa, Iowa City, IA, USA. Contact e-mail: john-sunderland@uiowa.edu*

**Objectives:** Emerging evidence indicates that 2-deoxy-2-[$^{18}$F]-fluoro-D-glucose positron emission tomography (FDG-PET) is a valuable imaging tool for determining efficacy of new cancer therapies in transplantation-based pre-clinical mouse models of human cancer, but the potential of FDG-PET for assessing objective treatment responses in transgenic mice in which malignant tumors develop spontaneously - just like they do in human beings - is little-studied. Similarly, little is known about the value of FDG-PET for monitoring de novo tumor progression in mice, and in staging incipient, primary tumors in tumor prevention studies in mice. **Methods:** To remedy these shortcomings, we used FDG-PET to quantify drug responses and evaluate tumor progression in a newly generated bitransgenic mouse model of human multiple myeloma designated C.IL6iMyc (BLOOD 115:1746-1754, 2010). For treatment studies, tumor-bearing C.IL6/iMyc mice were injected i.v. with second-generation proteasome inhibitor, MLN2238 (7mg/kg bi-weekly, Millennium Pharmaceuticals). For tumor progression studies, mice were left untreated. For all animals, approximately 8.0 MBq of FDG was administered via lateral tail vein injection, PET images were acquired at t=1 hour under anesthesia (2.5% isofluorane) and analyzed using PMOD software v3.2. Tumor volumes ($mm^3$) for nodes and organs were determined through a 50% threshold over (max-min) methodology, and $SUV_{max}$ values were assessed. **Results:** For treatment studies, we used C.IL6iMyc mice 98-106 days of age (n=5), in which primary plasma-cell tumors were detected by FDG-PET and confirmed by biomarker analysis (serum immunoglobulin levels, detection of serum paraprotein). Administration of MLN2238 resulted in a significant decrease in tumor volume and metabolic activity in the great majority of lesions. Spleen and mesenteric lymph node (MLN) responded less effectively and were identified as putative sites of relapse upon acquisition of drug resistance. In tumor progression studies, we relied on young C.IL6iMyc mice (n=5) in which the baseline FDG-PET scan at ~45 days of age showed no evidence of frank neoplasia. Subsequent scans (3-5 per mouse), spaced over the time course of tumor progression, revealed that the tumor burden steadily increased in secondary lymphoid tissues. MLN, spleen and cervical lymph nodes exhibited peak activity (usually in the 4th scan) by 114 to 125 days of age. $SUV_{max}$ decreased in terminal scans, suggesting tumor necrosis. Ex vivo biodistribution analysis and histological studies independently validated the PET findings. Significant tumor developed in all animals studied, following a characteristic time-dependent pattern of presentation. To facilitate future treatment response studies, a staging system (Grade 0-III) based upon this pattern was devised to characterize disease state based upon extent and magnitude of nodal disease. **Conclusions:** This study demonstrates the value of FDG-PET in evaluating cancer progression and treatment responses in transgenic mice in which myeloma-like plasma-cell tumors develop predictably (100% tumor incidence) after short tumor latency (~3.5 months).

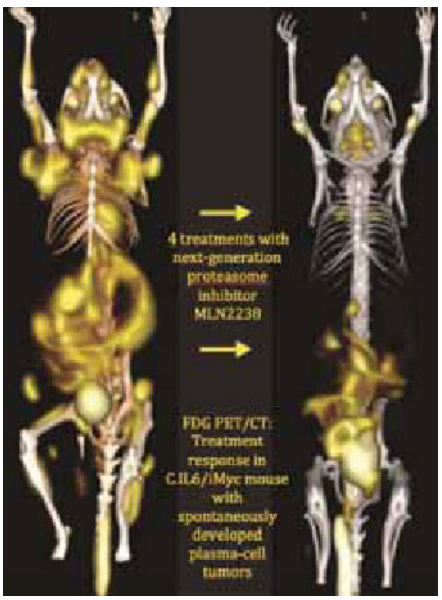


Disclosure of author financial interest or relationships:
**K. Duncan**, None; **J.J. Sunderland**, Siemens Molecualr Imaging, Grant/research support; **S.A. Walsh**, None; **L.B. Ponto**, None; **T. Rosean**, None; **S. Janz**, None.

Presentation Number **SS 21**
Scientific Session 3: Preclinical In Vivo - Metabolic Disease
September 6, 2012 / 11:36-11:48 / Room: Liffey Hall 2

# Non-invasive determination of the beta cell mass by SPECT with $^{111}$In-DTPA-exendin-3 in a rat model for spontaneous type 1 diabetes

***Maarten Brom***[1], *Desirée Bos*[1], *Jeroen Visser*[2], *Lieke Joosten*[1], *Hanneke Peeters*[1], *Peter Laverman*[1], *Wim J. Oyen*[1], *Otto C. Boerman*[1], *Martin Gotthardt*[1], [1]*Department of Nuclear Medicine, Radboud University Nijmegen Medical Centre, Nijmegen, Netherlands;* [2]*Department of Cell Biology, Section Immunology, University Medical Center Groningen, Groningen, Netherlands. Contact e-mail: M.Brom@nucmed.umcn.nl*

The beta cell mass (BCM) plays a key role in the development and progression of diabetes mellitus. A reliable, non-invasive method for quantification of the pancreatic BCM in vivo would give further insight in the pathogenesis of type 1 and 2 diabetes. The glucagon-like peptide 1 receptor (GLP-1R) is specifically expressed on beta cells. Exendin-3 is a stable GLP-1 analogue with high affinity for the GLP-1R. Here, we investigated the potential of SPECT with $^{111}$In-DTPA-exendin-3 to determine the BCM in vivo in a rat model that closely mimics the development of type 1 diabetes in humans: BioBreeding Diabetes Prone (BBDP) rats. Six BBDP rats (2 normoglycemic and 4 hyperglymic) of 11-13 weeks old were injected intravenously with 15 MBq $^{111}$In-DTPA-exendin-3. Two BioBreeding Diabetes Resistant (BBDR) rats of 11-13 weeks old were used as controls. SPECT/CT was acquired 1 h p.i. and the rats were euthanized after SPECT/CT acquisition. The pancreas and relevant organs were dissected, weighed and the radioactivity content was measured in a gamma counter. The pancreas was fixed in formalin, embedded in paraffin and sections were used for autoradiography, histology and determination of the beta cell mass by morphometric analysis. Autoradiography showed high focal uptake of the tracer in the pancreas of control (BBDR) rats in the islets of Langerhans. The focal uptake was completely absent in hyperglymic rats and reduced uptake was observed in normoglycemic rats with a reduced BCM. The pancreatic uptake (determined by ex vivo counting) in control rats was 0.12 ± 0.03 %ID/g and was decreased by 90% in diabetic rats (0.012 ± 0.005 %ID/g). This decrease in pancreatic uptake was in line with the decrease in BCM: 92%. There was a linear correlation between the pancreatic uptake of $^{111}$In-DTPA-exendin-3 and the BCM (Pearson r = 0.87). The pancreas was visible in SPECT images of healthy animals and was absent in severe diabetic rats. The uptake determined by quantitative analysis of the SPECT images correlated linearly with the BCM (Pearson r = 0.80). In conclusion, the BCM can be determined by SPECT after injection of $^{111}$In-DTPA-exendin-3 in a rat model for type 1 diabetes, closely mimicking the human development of type 1 diabetes. These results indicate that SPECT with $^{111}$In-DTPA-exendin-3 is a promising method to longitudinally determine the BCM during the development of type 1 diabetes. Acknowledgements: This work was supported by NIH grant 1R01 AG 030328-01 and the European Community's Seventh Framework Programme (FP7/2007-2013) under grant agreement n° 222980.

Disclosure of author financial interest or relationships:
**M. Brom**, None; **D. Bos**, None; **J. Visser**, None; **L. Joosten**, None; **H. Peeters**, None; **P. Laverman**, None; **W.J. Oyen**, Roche, Grant/research support; Siemens, Grant/research support; Immunomedics, Grant/research support; Wilex, Grant/research support; Novartis, Grant/research support; GSK, Grant/research support; Merck, Grant/research support; **O.C. Boerman**, None; **M. Gotthardt**, Sanofi Aventis, Grant/research support .

Presentation Number **SS 22**
Scientific Session 3: Preclinical In Vivo - Metabolic Disease
September 6, 2012 / 11:48-12:00 / Room: Liffey Hall 2

# Imaging β-cell function in rats at 3T using the $Zn^{2+}$-responsive agent, GdDOTA-diBPEN

*Jeff R. Anderson[1], Angelo Josue M. Lubag[1], Khaled Nasr[1], **Dean Sherry**[1,2], [1]Advanced Imaging Research Center, UT Southwestern Medical Center, Dallas, TX, USA; [2]Chemistry, UT at Dallas, Dallas, TX, USA. Contact e-mail: Dean.Sherry@UTSouthwestern.edu*

Diabetes is a major health concern in the United States and worldwide. Currently there exists a great need for molecular imaging of the diabetic pancreas. Recently, the novel MRI contrast agent, GdDOTA-diBPEN, was introduced for imaging β-cell function (1). This agent has two binding sites for $Zn^{2+}$ and upon release of $Zn^{2+}$ from the pancreas, the ternary GdDOTA-diBPEN-$(Zn)_2$ complex forms, binds with albumin, and this slowing of molecular rotation increases the relaxivity of the agent. This is detected by an increase in MR intensity only in those tissue that release large amounts of $Zn^{2+}$. Interestingly, the contrast agent binds with serum albumin only after a presumed conformational change facilitated by complexation with $Zn^{2+}$. This distinguishing, step-wise mechanism allows the contrast agent to act as a reporter of pancreatic beta cell function. That is, because $Zn^{2+}$ is co-released with insulin from beta cells (insulin is stored in the pancreas as insulin/Zn crystals), GdDOTA-diBPEN can be used as an insulin-responsive MR contrast agent. Accordingly, tail-vein administration of the contrast agent after IP glucose injection (stimulating insulin release) was recently shown to result in $T_1$-weighted enhancement of the pancreas in mice proportional to beta cell function (2). This earlier study was carried out at 9.4T. The goal of our current studies is to translate this promising imaging agent to the clinic. GdDOTA-diBPEN is particularly well-suited to make this transition. First, the contrast agent is structured upon a GdDOTA backbone which is known to be one of the most stable forms of $Gd^{3+}$ chelators (3). Second, the high relaxivity associated with the albumin-bound agent translates to lower dosages when compared to the current generation of clinically approved $Gd^{3+}$-based contrast agents. Third, and perhaps most important, the change in relaxivity between the albumin-bound and -unbound states is predicted to be optimized at lower (clinical) field strengths. To test this last hypothesis, the imaging protocol pioneered in 9.4T is being applied at 3T. All experiments are being carried out with a 3T whole-body MRI system (Philips Achieva) using a purpose-built, radio frequency (RF) coil optimized for rodents. Preliminary results in phantoms show the expected large increase in $T_1$-weighted signal intensity as a binary function of presence of serum albumin (Fig 1; A - without albumin and B - with albumin). Preliminary results in rats show the expected increase in signal intensity in the pancreas after glucose stimulated insulin secretion (Fig 1C). As at 9.4T, the kidneys also show substantial enhancement due to filtration of the agent from blood. Currently, experiments are underway comparing two small groups (N=5 each) of control with diabetic rats. A streptozotocin induced model is being used to initiate diabetes ensuring little to no difference in pancreatic size. (1) Esqueda AC et al. JACS 2009, 131(32):11387-11391. (2) Lubag AJM et al. PNAS 2011, 108(45):18400-18405. (3) Brücher E and Sherry AD. Ch. 6 in The Chemistry of Contrast Agents in Medicinal Magnetic Resonance Imaing ed. Merbach AE and Tóth E. 2001, Wiley & Sons.

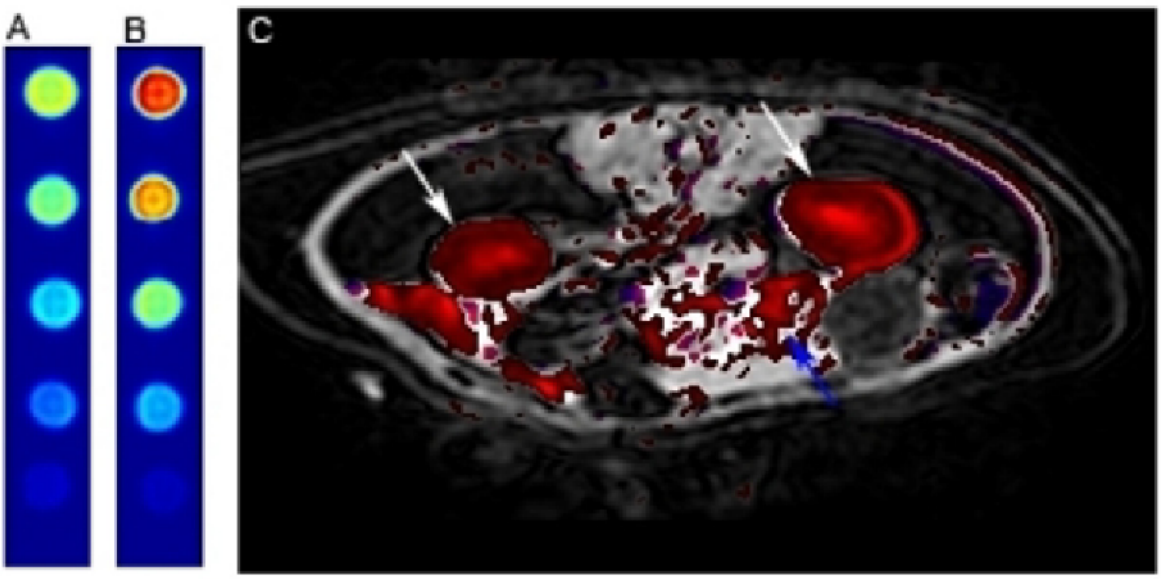


Figure 1. $T_1$-weighted images of solutions of GdDOTA-diBPEN and $Zn^{2+}$ in 100 mM TRIS buffer at 3 Tesla in the absence (A) and presence (B) of 600 μM HSA. In both A and B, the concentration of GdDOTA-diBPEN was varied from 0, 0.25, 0.5, 0.75, and 1 mM (bottom to top) and $Zn^{2+}$ was present in all samples in a 3:1 excess over GdDOTA-diBPEN. C) Difference image of a healthy rat (color; post-contrast minus pre-contrast) overlaid on a $T_1$-weighted pre-contrast image with fatsat (grayscale). Both the kidneys (white arrows) and the pancreas (blue arrow) enhance.

Disclosure of author financial interest or relationships:
**J.R. Anderson**, None; **A.M. Lubag**, None; **K. Nasr**, None; **D. Sherry**, None.

Presentation Number **SS 23**
Scientific Session 4: Translational & Clinical - Oncology
September 6, 2012 / 10:30-10:41 / Room: Wicklow Hall 2

# Biomarker screening in biopsy tissue to predict the feasibility of a CXCR4 targeted imaging approach in vivo

***Tessa Buckle***[1,2], *Joeri Kuil*[1,2], *Nynke S. van den Berg*[1,2], *Anton Bunschoten*[1,2], *Hildo J. Lamb*[3], *Hushan Yuan*[4], *Lee Josephson*[4], *Jos Jonkers*[5], *Alexander D. Borowsky*[6], *Fijs van Leeuwen*[1,2], [1]*Radiology, Interventional Molecular Imaging, LUMC, Leiden, Netherlands;* [2]*Radiology and Nuclear Medicine, NKI-AvL, Amsterdam, Netherlands;* [3]*Radiology, LUMC, Leiden, Netherlands;* [4]*Center for Molecular Imaging Research, Harvard Medical School, Boston, MA, USA;* [5]*Division of Cell Biology, NKI-AvL, Amsterdam, Netherlands;* [6]*Department of Pathology and Laboratory Medicine, University of California at Davis, Sacramento, CA, USA. Contact e-mail: t.buckle@lumc.nl*

INTRODUCTION The Chemokine receptor 4 (CXCR4) has been reported to be expressed in up to 92% of clinical samples of ductal carcinoma in situ (DCIS). As non-invasive visualization of DCIS is clinically challenging, CXCR4 specific imaging probes are expected to help improve clinical diagnostics. Evaluation of biomarker expression levels in biopsy tissue prior to targeted diagnostic imaging might increase the feasibility of a targeted imaging approach. As proof of concept, results of biomarker screening were quantitatively compared to in vivo imaging results in a MIN-O mouse model resembling human DCIS. METHODS Tumor cell suspensions derived from early preinvasive, intermediate and invasive late stage MIN-O mouse tumors and 4T1 control tumors served as a model for biopsy tissue. Tumor cell suspensions were incubated with a CXCR4 targeting peptide labeled with both a fluorescent dye and a DTPA chelate (MSAP-Ac-TZ14011). For in vivo detection of CXCR4 expressing tumor lesions, tumor bearing mice were imaged using SPECT/CT after intravenous injection of 111In-MSAP-Ac-TZ14011. For in vivo assessment of CXCR4 expression during lesion progression, mice were longitudinally followed. The level of angiogenesis in both tumor models was evaluated using an αvβ3 targeting RGD peptide. Standard immunohistochemistry (IHC) was used to validate the membranous CXCR4 expression. RESULTS Flow cytometric analysis after incubation of the tumor cell suspensions with Ac-TZ14011-MSAP revealed that CXCR4 positivity increased during the progression of MIN-O lesions. Furthermore, discrimination between cell populations with different levels of CXCR4 expression could be made. An increase in the percentage of CXCR4+ cells seemed to mark the transition from early preinvasive into intermediate stage lesions (from 38.4 ± 2.3 % to 53.5 ± 1.4 %). Concurrently, invasive late stage lesions mainly contained CXCR4++ cells (80.0 ± 1.4 %). The percentage of CXCR4 expressing cells was higher in all stages of MIN-O lesion development compared to the 4T1 control tumors (82.7 ± 11.0 % vs 44.6 ± 6.0 %). In vivo, MIN-O tumors could be visualized using SPETC/CT whereas the 4T1 tumors could not. The difference in uptake of radioactivity in late stage MIN-O and 4T1 tumors (ratio = 3.8) was comparable to the difference in CXCR4 expression found with flow cytometry (ratio = 4.0). Uptake of the CXCR4 targeting imaging agent in the tumor was consistent with an increase in membranous staining for CXCR4 as seen with IHC. Uptake was deemed related to the expression of CXCR4 as SPECT/CT imaging after injection a RGD targeting imaging agent showed that the level of angiogenesis in both the MIN-O and 4T1 tumor model was similar. CONCLUSION Evaluation of the CXCR4 expression in biopsy tissue prior to imaging can be used to accurately predict the feasibility of the targeted imaging approach in vivo. Expression patterns found with flow cytometry could predict the level of uptake in vivo. Both could be linked to the stage of MIN-O lesion progression.

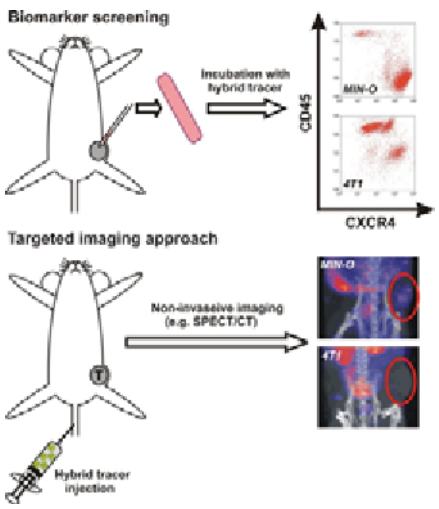


Disclosure of author financial interest or relationships:
**T. Buckle**, None; **J. Kuil**, None; **N.S. van den Berg**, None; **A. Bunschoten**, None; **H.J. Lamb**, None; **H. Yuan**, None; **L. Josephson**, None; **J. Jonkers**, None; **A.D. Borowsky**, None; **F. van Leeuwen**, None.

Presentation Number **SS 24**
Scientific Session 4: Translational & Clinical - Oncology
September 6, 2012 / 10:41-10:52 / Room: Wicklow Hall 2

# Galium-68 Neomannosyl Human Serum Albumin-based PET/CT Lymphoscintigraphy for Sentinel Lymph Node Identification in Non-Small Cell Lung Cancer

***Hyun Koo Kim***[1], *Sungeun Kim*[2], *Jae Min Jeong*[3], *Young Ho Choi*[1], [1]*Thoracic and Cardiovascular Surgery, College of Medicine, Korea University Guro Hospital, Seoul, Republic of Korea;* [2]*Nuclear Medicine, College of Medicine, Korea University Guro Hospital, Seoul, Republic of Korea;* [3]*Nuclear Medicine, Seoul Natinal University Hospital, Seoul, Republic of Korea. Contact e-mail: kimhyunkoo@korea.ac.kr*

Background: In the previous report, we developed a novel mannose receptor-binding agent, Technetium-99m human serum albumin (99mTc-MSA), for sentinel lymph node detection. To overcome the limited resolution of current lymphoscintigraphic imaging using Technetium-99m, we developed Galium-68 for PET/CT imaging. This study is the first clinical trial designed to test the reliability and feasibility of sentinel node detection using this new tracer in non-small cell lung cancer. Methods: Twenty-three patients (14 men, 9 women; mean age 62.6±10.3 years) that were candidates for lobectomy with mediastinal lymph node dissection for stage I non-small cell lung cancer were enrolled. A total dose of 0.2mCi of 68Ga-MSA in 0.1 mL was administered in one shot at the peri-tumoral region, and then lymphoscintigram was taken by PET/CT just before surgery. All harvested lymph nodes were cut into 2 mm slices and ultimately diagnosed by using formalin-fixed and paraffin-embedded sections with hematoxylin and eosin staining. Results: The number of dissected lymph nodes per patient was 20.3±10.4 (7-49). In 22 of 23 patients (95.7%), the sentinel lymph nodes could be identified on PET/CT (Fig.1). The number of sentinel lymph nodes identified was 1.4±0.6 (range 1-3) per patient. Six out of 22 patients (27.3%) had metastases in 10 sentinel lymph nodes. No false-negative sentinel lymph nodes were detected in any of the 6 patients with N1 or N2 disease (0%). Conclusions: 68Ga-MSA appears to be a promising tracer for sentinel lymph node identification by PET/CT in non-small cell lung cancer. Fig. 1. Sentinel lymph node on lymphoscintigraphic image on PET/CT in lung cancer. Arrows indicated sentinel node in hilar area in left lower lobe lung.


Sentinel lymph node on lymphoscintigraphic image on PET/CT in lung cancer. Arrows indicated sentinel node in hilar area in left lower lobe lung.

Disclosure of author financial interest or relationships:
**H. Kim**, None; **S. Kim**, None; **J. Jeong**, None; **Y. Choi**, None.

Presentation Number **SS 25**
Scientific Session 4: Translational & Clinical - Oncology
September 6, 2012 / 10:52-11:03 / Room: Wicklow Hall 2

# Evaluation of a Hybrid Radioactive and Fluorescent Tracer for Sentinel Lymph Node Biopsy in Melanoma Patients

***Oscar R. Brouwer***[1,2], *Boudewijn Schaafsma*[3,1], *Nynke S. van den Berg*[2,1], *W Martin C. Klop*[4], *Alfons J. Balm*[4], *Michiel W. van den Brekel*[4], *Omgo E. Nieweg*[5], *Fijs van Leeuwen*[2,1], *Renato A. Valdés Olmos*[1], *[1]Nuclear Medicine, Netherlands Cancer Institute, Amsterdam, Netherlands; [2]Radiology, Leiden University Medical Center, Leiden, Netherlands; [3]Surgery, Leiden University Medical Center, Leiden, Netherlands; [4]Head and Neck Surgery, Netherlands Cancer Institute - Antoni van Leeuwenhoek hospital, Amsterdam, Netherlands; [5]Surgery, Netherlands Cancer Institute - Antoni van Leeuwenhoek hospital, Amsterdam, Netherlands. Contact e-mail: o.brouwer@nki.nl*

Introduction: In melanoma patients, sentinel node (SN) mapping is generally performed by injecting a radiocolloid around the primary tumour followed by lymphoscintigraphy. Intraoperatively, SNs can then be localized using a handheld gamma ray detection probe and patent blue dye. The aim of this study was to assess the added value of intraoperative fluorescence imaging to the conventional radioguided procedure using ICG-99mTc-nanocolloid, a hybrid tracer that is both radioactive and fluorescent. Methods: A total of 76 cN0 melanoma patients (39 head/neck melanoma, 27 truncal melanoma, 10 melanoma on an extremity) scheduled for SN biopsy were peritumourally injected with ICG-99mTc-nanocolloid 3 to 29 hours prior to surgery. SNs were preoperatively identified with lymphoscintigraphy followed by SPECT/CT. In the operating room, patent blue dye was injected in all patients with a melanoma outside the face. During surgery, SNs were detected with a gamma ray detection probe and a handheld near-infrared fluorescence camera. Results: A total of 205 SNs were preoperatively identified on the lymphoscintigraphy and SPECT/CT images. Intraoperatively, 94% of the preoperatively defined SNs could be localized using the gamma probe. The remaining SNs (6%) were located close to the injection site (head/neck melanoma) and were only detectable using the fluorescence camera. In total, 99% of SNs could be intraoperatively visualized via fluorescence imaging. In the patients in whom blue dye was used, merely 63% of SNs was stained blue (45% head/neck melanoma, 77% truncal/extremity melanoma). Ex vivo, all radioactive lymph nodes were fluorescent and vice versa, underlining the stability of the hybrid tracer during SN procedures. Pathological analysis of the SNs revealed a metastasis in 13 patients. Conclusions: ICG-99mTc-nanocolloid enables preoperative SN visualization and concomitant intraoperative radio- and fluorescence guidance to the very SNs in melanoma patients. The addition of fluorescence imaging was shown to be of particular value when SNs were located in close proximity to the primary tumour, and in cases where vital blue dyes are of limited value.

Disclosure of author financial interest or relationships:
**O.R. Brouwer**, None; **B. Schaafsma**, None; **N.S. van den Berg**, None; **W.C. Klop**, None; **A.J. Balm**, None; **M.W. van den Brekel**, None; **O.E. Nieweg**, None; **F. van Leeuwen**, None; **R.A. Valdés Olmos**, None.

Presentation Number **SS 26**
Scientific Session 4: Translational & Clinical - Oncology
September 6, 2012 / 11:03-11:14 / Room: Wicklow Hall 2

# PET and Cerenkov Imaging for Detailed Lymph Node Mapping and Guided Surgical Resection with a Clinically Approved Tracer

***Daniel L. Thorek***[1], *Diane S. Abou*[2], *Bradley J. Beattie*[3], *Ruimin Huang*[1], *Rachel M. Bartlett*[3], *Pat Zanzonico*[3], *Jan Grimm*[2], *[1]Radiology, Memorial Sloan-Kettering Cancer Center, New York City, NY, USA; [2]Molecular Pharmacology & Chemistry Program, Memorial Sloan-Kettering Cancer Center, New York, NY, USA; [3]Medical Physics, Memorial Sloan-Kettering Cancer Center, New York, NY, USA. Contact e-mail: thorekd@mskcc.org*

The lymphatic system plays a key role in the maintenance of healthy tissues by draining extravascular fluid and as a conduit for immune cells. Metastases to the LN is a strong predictor of poor outcome, which is assessed clinically by surgical sampling of tumor draining LNs. Current practice relies on the use of radiotracer ($^{99m}$Tc sulfur colloid) and/or an optically absorbing dye (Isosulfan Blue) to map the draining LN in order to guide resection. These techniques demonstrate limited spatial resolution (SPECT or planar scinitgraphy), lack of quantitation and poor dye transport properties. Here, we investigate the use of intradermal injection of $^{18}$F-FDG for lymphography. This combination of a clinical imaging agent and innovative route of administration enables high-resolution, dynamic and quantitative mapping of the lymph system and nodes by PET/CT. In small animals, this approach provides a means to study the transport and detailed distribution of tracer to the LNs, quantitatively and irrespective of depth. Further, we have demonstrated that Cerkenov radiation emitted by the PET tracer can be used to guide resection of LN. Dual modality imaging with the same approved $^{18}$F-FDG tracer for whole body preoperative mapping and for planar intraoperative guidance has significant potential to impact the preclinical study and clinical application of LN imaging.

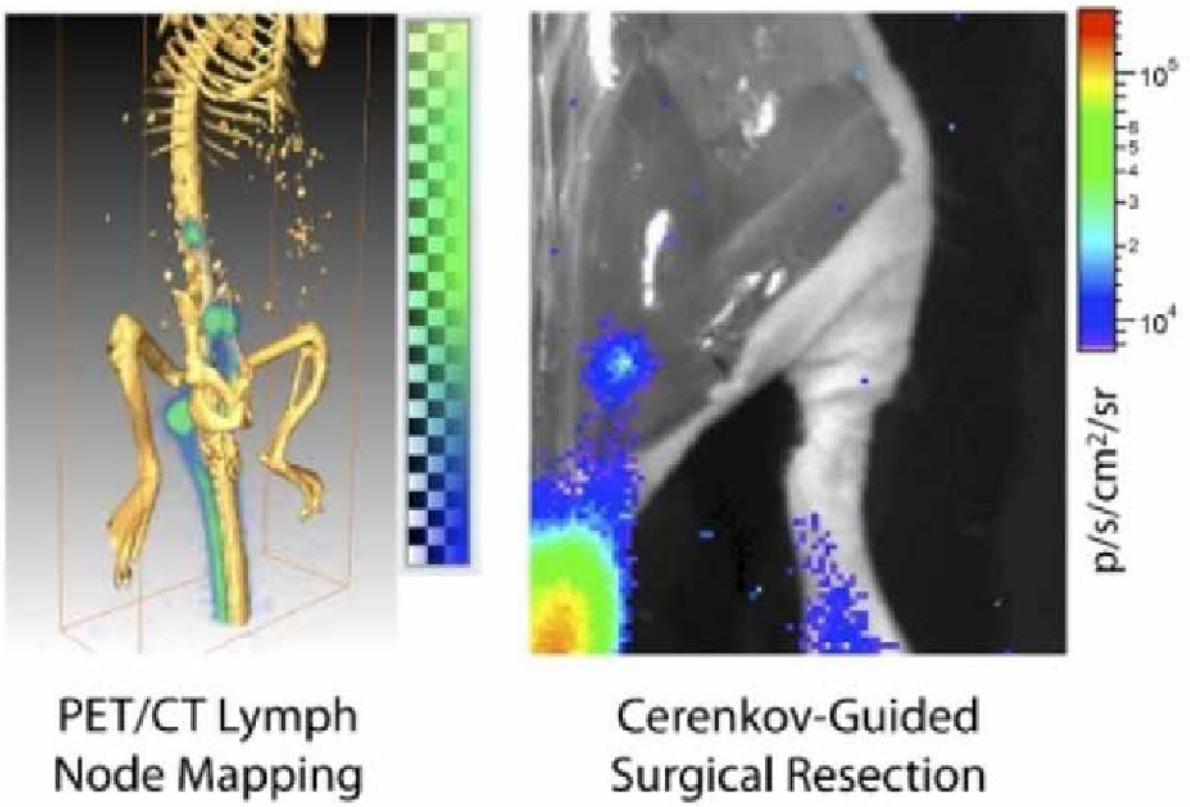


18F-FDG Lymphography. High-resolution imaging of the lymph drainage and LN is achieved using the approved small molecule tracer. From an injection site into the skin of the tail, the draining lymphatic vessels and nodes are clearly distinguished. Further, the Cerenkov radiation emissions from the PET tracer enable optical guidance for surgical resection of the nodes.

Disclosure of author financial interest or relationships:
**D.L. Thorek**, None; **D.S. Abou**, None; **B.J. Beattie**, None; **R. Huang**, None; **R.M. Bartlett**, None; **P. Zanzonico**, None; **J. Grimm**, None.

Presentation Number **SS 27**
Scientific Session 4: Translational & Clinical - Oncology
September 6, 2012 / 11:14-11:25 / Room: Wicklow Hall 2

# Randomized Comparison of Near-Infrared Fluorescence Lymphatic Tracers for Sentinel Lymph Node Mapping of Cervical Cancer

***Merlijn Hutteman***[1], *Boudewijn Schaafsma*[1], *Joost van der Vorst*[1], *Katja Gaarenstroom*[3], *Alexander A. Peters*[3], *Floris Verbeek*[1], *John V. Frangioni*[2], *Cornelis J. van de Velde*[1], *Clemens Lowik*[4], *Alexander Vahrmeijer*[1], [1]*Department of Surgery, Leiden University Medical Center, Leiden, Netherlands;* [2]*Division of Hematology/Oncology, Department of Medicine, Beth Israell Deaconess Medical Center, Boston, MA, USA;* [3]*Department of Gynecology, Leiden University Medical Center, Leiden, Netherlands;* [4]*Department of Radiology, Leiden University Medical Center, Leiden, Netherlands. Contact e-mail: jrvandervorst@gmail.com*

Objective: Near-infrared fluorescence imaging using indocyanine green (ICG) has recently been introduced as a novel technique for sentinel lymph node (SLN) mapping in early-stage cervical cancer. Although preclinical research has shown that ICG adsorbed to human serum albumin (ICG:HSA) improves its performance, the need for HSA has not yet been confirmed in cervical cancer patients. The current randomized study aims to determine whether ICG:HSA offers advantages over using ICG alone. Methods: Eighteen consecutive early-stage cervical cancer patients scheduled to undergo pelvic lymphadenectomy were included. Prior to surgery, 1.6 mL of 500 μM ICG:HSA or 500 μM ICG alone was injected transvaginally in 4 quadrants around the tumor. The Mini-FLARE imaging system was used for intraoperative NIR fluorescence detection and quantitation. Results: SLNs were identified intraoperatively in 78% of the patients. Patient and tumor characteristics were equally distributed over both treatment groups. No significant difference in signal-to-background ratio (9.3 vs. 10.1, P = .72) or average number of detected SLNs (2.9 vs 2.7, P = .84) was found between the ICG:HSA group and the ICG alone group, respectively. Conclusions: In conclusion, this double-blind, randomized trial showed no advantage of ICG:HSA over ICG alone for the SLN procedure in early-stage cervical cancer. Further optimization is required to improve the intraoperative detection rate.

Disclosure of author financial interest or relationships:
**M. Hutteman**, None; **B. Schaafsma**, None; **J. van der Vorst**, None; **K. Gaarenstroom**, None; **A.A. Peters**, None; **F. Verbeek**, None; **J.V. Frangioni**, None; **C.J. van de Velde**, None; **C. Lowik**, None; **A. Vahrmeijer**, None.

Presentation Number **SS 28**
Scientific Session 4: Translational & Clinical - Oncology
September 6, 2012 / 11:25-11:36 / Room: Wicklow Hall 2

# Dose optimization of ICG-99mTc-nanocolloid for combined radioguided and optical sentinel node biopsy in breast cancer patients

***Boudewijn Schaafsma***[1], *Floris Verbeek*[1], *Daphne D. Rietbergen*[2], *Joost van der Vorst*[1], *Nynke S. van den Berg*[2], *Anton Bunschoten*[2], *Gerrit-Jan Liefers*[1], *John V. Frangioni*[3], *Bernies van der Hiel*[2], *Cornelis J. van de Velde*[1], *Fijs van Leeuwen*[2], *Alexander Vahrmeijer*[1], [1]*Surgery, Leiden University Medical Center, Leiden, Netherlands;* [2]*Radiology, Leiden University Medical Center, Leiden, Netherlands;* [3]*Hematology/Oncology, Medicine, Beth Israel Deaconess Medical Center, Harvard Medical School, Boston, MA, USA. Contact e-mail: b.e.schaafsma@lumc.nl*

Background: Detection of the sentinel lymph node (SLN) is important in staging and treatment of breast cancer. Near-infrared (NIR) fluorescence imaging is a technique that can be used to visualize lymph nodes during surgery, up to one centimeter into the living tissue, in real-time. Currently, indocyanine green (ICG) is the only clinically approved NIR fluorescent contrast agent, which has been used for SLN mapping in several clinical trials. However, ICG is a relative small tracer, which possibly allows it to flow to higher echelon lymph nodes. Previous studies have reported the use of a novel tracer which combines fluorescence with radioactivity by premixing ICG with radioactive colloids. The aim of this study was to test feasibility of this multimodal tracer that is both radioactive and fluorescent (ICG-99mTc-nanocolloid) and to optimize the concentration for SLN biopsy in breast cancer patients. Hereby we aimed to further improvement of the signal-to-background ratios (SBR). Methods: Twenty-three breast cancer patients scheduled for SLN biopsy were included. Patients received a planar lymphoscintigraphy at 15 minutes and approximately 2 hours after periareolar injection of the tracer. Directly before surgery, patent blue was injected periareolarly. During surgery the SLNs were detected using a conventional gamma probe and the mini-FLARE, an intraoperative fluorescence imaging system that provides an overlay of both the color and fluorescent images. Two different concentrations of ICG-99mTc-nanocolloid were tested; one containing 0.05 mg nanocolloid, which is standard in our center, and one containing 0.1 mg nanocolloid. The amount of radioactivity was kept similar in both groups. Fluorescent signal was measured both pre- and intraoperatively. From the 2 hour-planar lymphoscintigraphy images percentage drainage towards the SLNs were calculated. Results: At least one SLN was successfully detected in all patients (N = 23). Of all SLNs, 100% was fluorescent, 100% was radioactive and 85% stained blue. A SBR of 5.2 ± 3.2 was measured in the ICG-99mTc-nanocolloid group containing 0,05 mg nanocolloid (N = 16) and a SBR of 6.3 ± 1.3 was measurered in the ICG-99mTc-nanocolloid group containing 0,1 mg nanocolloid (N = 7). No significant differences were found between the two groups (P = 0.36). Additionally, an increase in lymphoscinitgraphic counts in the SLNs was found in the 0,1 mg nanocolloid dose group. The average number of detected SLNs per patients was not significantly different between the 0,05 and 0,1 mg nanocolloid dose groups (1,3 ± 0.5 vs 1,8 ± 0.7; P = 0.07). Conclusion: This study demonstrated the successful use of a multimodal fluorescent and radioactive lymphatic tracer to detect the SLN in breast cancer patients. By increasing the concentration nanocolloid in ICG-99mTc-nanocolloid, SBRs increased, however not significantly.

Disclosure of author financial interest or relationships:
**B. Schaafsma**, None; **F. Verbeek**, None; **D.D. Rietbergen**, None; **J. van der Vorst**, None; **N.S. van den Berg**, None; **A. Bunschoten**, None; **G. Liefers**, None; **J.V. Frangioni**, None; **B. van der Hiel**, None; **C.J. van de Velde**, None; **F. van Leeuwen**, None; **A. Vahrmeijer**, None.

Presentation Number **SS 29**
Scientific Session 4: Translational & Clinical - Oncology
September 6, 2012 / 11:36-11:47 / Room: Wicklow Hall 2

# Coregistered Molecular and Morphological Imaging: clinical feasibility for improved noninvasive diagnosis of breast cancer

*Pamela M. Otto[2], Kenneth Kist[2], Bryan A. Clingman[3], Jason Zalev[3], Sergey A. Ermilov[4], **Alexander A. Oraevsky**[1,4], [1]Biomedical Engineering, University of Houston, Houston, TX, USA; [2]Radiology, University of Texas Health Science Center, San Antonio, TX, USA; [3]Seno Medical Instruments, San Antonio, TX, USA; [4]TomoWave Laboratories, Houston, TX, USA. Contact e-mail: aao@tomowave.com*

Co-registered opto-acoustic and ultrasound imaging is an emerging medical technology with a number of possible clinical applications, including diagnostic imaging of breast cancer. The purpose of this study was to develop, validate and evaluate clinical feasibility of the opto-acoustic plus ultrasonic dual-modality, which provides images based on two types of tissues contrast and co-registers the two images for the benefit of sensitivity and specificity of breast cancer diagnosis. The first type of contrast, is associated with optical molecular absorption of hemoglobin and oxyhemoglobin in tumor angiogenesis. The second type of tissue contrast is associated with variation of acoustic impedance between morphological tissue structures on ultrasound images. We hypothesized that co-registered two-dimensional molecular and morphological images of the breast provide comprehensive diagnostic information about tumors, which in turn helps the radiologist to accurately differentiate malignant and benign masses. It is well established through optical diffusion spectroscopy that malignant tumors contain increased concentration of total hemoglobin and decreased concentration of oxyhemoglobin, which can serve as the basis for differentiation of breast carcinomas from benign masses. The opto-acoustic subsystem uses laser pulses in the near-infrared spectral range for tissue illumination, deep tissue penetration and molecular specificity: 757 nm at the peak of hemoglobin absorption and 1064 nm at the peak of oxyhemoglobin absorption. The role of an additional wavelength at the isosbestic point of hemoglobin and oxyhemoglobin was also evaluated as enabling greater quantitative accuracy and imaging of molecular content of water. Detection of the ultrasonic signals resulting from laser illumination and ultrasonication of tissue using a custom-made hand-held probe based on an array of wide-band ultrasonic transducers permits signal co-registration and reconstruction of superimposed images. The opto-acoustic system was validated in physical and digital phantoms accurately replicating optical and acoustic properties of the breast with tumors and blood vessels. A blood vessel with 1mm diameter embedded in a breast tissue mimicking phantom was detected with high contrast and resolution at a depth of more than 6 cm. The total hemoglobin and its level of oxygen saturation was estimated with accuracy of about 18% in computer models and about 27% in tissue mimicking gel phantoms. After the system was validated and calibrated in phantoms, a pilot clinical study was performed on patients with breast masses having a BIRADS 4 and 5 score, comparing noninvasive diagnosis from the two co-registered images with the gold standard of core biopsy. Based on the preliminary data of the initial 9 patients, the co-registration of opto-acoustic molecular and ultrasound morphological images provided 87% sensitivity and 80% specificity of noninvasive diagnosis of breast masses suspected for malignancy, which is significantly higher than sensitivity and specificity of the diagnostic ultrasound alone.

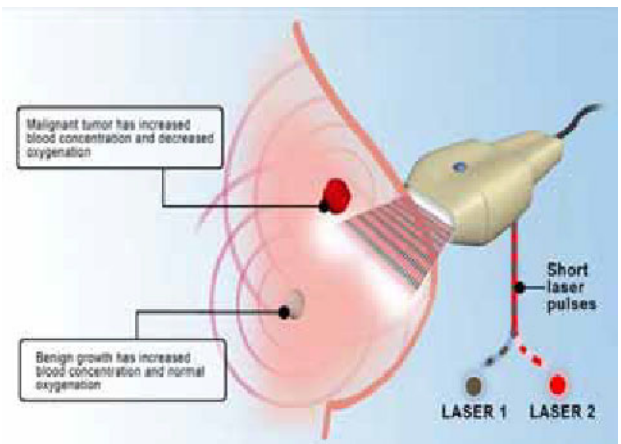


Disclosure of author financial interest or relationships:
**P.M. Otto**, Seno Medical, Consultant; Tosiba Medical, Honoraria; **K. Kist**, Seno Medical, Grant/research support; Bayer Pharmaceuticals, Grant/research support; Minolta Imaging, Grant/research support; Toshiba, Grant/research support; Seno Medical, Consultant; **B.A. Clingman**, Seno Medical Instruments, Consultant; **J. Zalev**, seno medical instruments, Employment; **S.A. Ermilov**, TomoWave Laboratories, Inc., Employment; **A.A. Oraevsky**, National Cancer Institute, NIH, Grant/research support; TomoWave Labs, Employment; Seno Medical Instruments, Stockholder .

Presentation Number **SS 3**
Scientific Session 1: Chemistry & Probes - MRI
September 6, 2012 / 10:52-11:03 / Room: Liffey Hall 1

# Dopamine Transporter Nanoprobes for CNS Molecular Magnetic Resonance Imaging and Targeted Drug Delivery

***Gordana D. Vitaliano***[1,2], *David Rios*[1], *Lu Yang*[3], *Franco Vitaliano*[1], *David Lee*[3,2], *Perry F. Renshaw*[4], *Martin H. Teicher*[3,2], [1]*Brain Imaging Center, McLean Hospital, Belmont, MA, USA;* [2]*Department of Psychiatry, Harvard Medical School, Boston, MA, USA;* [3]*Mailman Research Center, McLean Hospital, Belmont, MA, USA;* [4]*The Brain Institute, University of Utah, Salt Lake City, UT, USA. Contact e-mail: gvitaliano@mclean.harvard.edu*

Background: Magnetic Resonance Imaging (MRI) is a noninvasive visualization technique with high spatial resolution, but low sensitivity for visualization of brain transporters and receptors. Gadolinium (Gd)-contrast agents are used to improve MRI sensitivity, but they cannot cross the intact blood-brain-barrier (BBB). Our goal was to develop MRI Gd-nanoprobes with high T1 relaxivity that can cross the intact BBB and target dopamine transporters (DAT) in the rat brain. Method: Gadolinium-2-(4-Isothiocyanatobenzyl) diethylene-triamine-pentaacetic acid (Gd-DTPA-ITC) was conjugated to clathrin protein through reactive lysine residues. The chelate to protein molar ratio was determined by using a standard Arsenazo III-based spectrophotometric method. Relaxivity of each sample was calculated by using T1 data and Gd concentrations as determined by NMR at 0.47 T. Clathrin nanoplatforms were radiolabeled with 153Gd-DTPA-ITC. DAT ligands (GBR-12935) were conjugated to clathrin cysteine residues via maleimide-PEGs. Biodistribution of DAT-nanoprobes was quantitatively assessed in rats at different time points after intravenous administration. Samples of blood, animal organs and brain regions (e.g., striatum and cerebellum) were removed and weighed, and their radioactivity measured with a gamma counter. Results: The clathrin-nanoparticle was 18.5 nm in size. The mean chelate/protein molar ratio was 27±4.8/1. At 0.47 T, Gd-DTPA-ITC-Clathrin-Triskelia displayed relaxivity of 1,166 mM-1s-1 per particle, and 16 mM-1s-1 per Gd ion. Biodistribution studies showed a high accumulation of 153GdDTPA-DAT-nanoprobes in brain regions rich in DAT (e.g., striatum). The highest concentration (1.77 % ID/g) of GBR-153GdDTPA-nanoprobes was observed in the rat striatum 90 min after intravenous delivery. By contrast, brain regions with low concentrations of DAT (e.g., cerebellum) had a low accumulation of nanoprobes. Ninety minutes after intravenous delivery the concentration of GBR-153GdDTPA-nanoprobes in the rat cerebellum was 0.70% ID/g. Conclusions: Clathrin triskelia can serve as robust MRI platforms onto which multiple functional motifs can be added through chemical modifications. Clathrin-nanoprobes displayed 300-fold greater molecular relaxivity than the MRI contrast agent gadopentetate dimeglumine and successfully crossed the intact BBB after intravenous administration. They were able to deliver adequate concentrations of Gd-contrast agent and DAT-ligand to the rat brain and to target dopamine transporters. These preliminary results should encourage further investigations into the use of clathrin as a new brain imaging and drug delivery nanoplatform. This technology may lead to development of non-radioactive, stable molecular nanoprobes to assist in early detection of neurobiological changes in dopamine related disorders (e.g., Parkinson's, Huntington's Disease, ADHD, drug addiction, psychotic disorders etc.); to monitor progression of the disease and recovery process; and to help evaluate the effectiveness of drugs aimed at treating these disorders.

Disclosure of author financial interest or relationships:
**G.D. Vitaliano**, EXQOR Technologies Inc., Stockholder; **D. Rios**, None; **L. Yang**, None; **F. Vitaliano**, ExQor Technologies, Inc., Stockholder; **D. Lee**, None; **P.F. Renshaw**, Ridge Diagnostics, Consultant; Kyowa Hakko Kirin, Consultant; Ridge Diagnostics, Stockholder; **M.H. Teicher**, None.

Presentation Number **SS 30**
Scientific Session 4: Translational & Clinical - Oncology
September 6, 2012 / 11:47-11:58 / Room: Wicklow Hall 2

# [1-$^{11}$C]Acetate PET imaging in prostate cancer: Evaluation of the optimal imaging protocol in a preclinical model

***David Y. Lewis**, Joan Boren, Greg Shaw, Antonio Ramos-Montoya, Dmitry Soloviev, Kevin M. Brindle, Cancer Research UK, Cambridge Research Institute, Cambridge, United Kingdom. Contact e-mail: david.lewis@cancer.org.uk*

**Introduction.** [1-$^{11}$C]Acetate is a potential complement to FDG in well differentiated, slow growing tumours, or where FDG imaging is not effective due to a high background such as the bladder in prostate cancer. In cells, [1-$^{11}$C]acetate is converted to acetyl-CoA and used as a substrate in the TCA cycle or for lipid biosynthesis. As many cancer cells have an increased *de novo* fatty acid synthesis pathway, $^{11}$C from acetate can accumulate in tumour lipids. Although the optimal time for tumour visualisation following [1-$^{11}$C]acetate administration has not been determined, most clinical protocols only acquire data for the first 20 minutes following tracer injection. Here we present data using [1-$^{14}$C], [1-$^{13}$C] and [1-$^{11}$C]acetate in a prostate cancer xenograft model to define when tumour contrast is the greatest, namely after the aqueous acetate pool has been converted to $^{11}CO_2$ and exhaled but the $^{11}$C signal is still present in the tumour lipid pool. **Methods.** Male NSG mice were implanted with C4-2b human prostate adenocarcinoma cells. When tumours reached an appropriate size, animals were anaesthetised and [1-$^{11}$C] (Perkin Elmer, UK), [1-$^{13}$C] (Sigma, UK) or [1-$^{11}$C]acetate (produced as described in Soloviev and Tamburella, 2006) were injected through a tail vein cannula. Mice were culled 30, 60, 90 or 120 min after injection in the $^{14}$C and $^{13}$C studies and tissues were harvested for metabolite extraction and scintillation counting of the lipid and aqueous fractions or for metabolite analysis using NMR respectively. [1-$^{11}$C]acetate was injected at the start of a 2 hour PET acquisition (NanoPET/CT, Mediso/Bioscan). PET data were reconstructed dynamically and tissue time activity curves were drawn. **Results.** Of all the time points examined, 90 min post acetate injection was the best for tumour visualization, development of tissue contrast and detection of accumulation in lipid. Peak tumour-to-plasma and tumour-to-muscle ratios occurred at 90 min post [1-$^{14}$C]acetate injection, being evident in the lipid fraction where the tumour-to-muscle ratio was ~150. The tumour-to-normal mouse prostate ratio was about 3 at 90 min after acetate injection falling afterwards, and the lipid fraction peaked at about 8-to-1 at 90 min. The ratio between [1-$^{14}$C] in the lipid and aqueous fractions in the tumour increased over time to a peak at 90 min post-injection. This was also reflected in the PET images with greater contrast in the tumour after 60 min of imaging. The ratio between tumour and heart, left ventricle and skeletal muscle continued to rise during the scan. **Conclusion.** Evaluation of [1-$^{11}$C]acetate as a PET tracer in oncology has been confounded by inconsistent imaging protocols, in particular early imaging following injection provides insufficient tumour contrast. Here we have shown that late imaging after [1-$^{11}$C]acetate injection allows better tumour delineation, when the tumour lipid-to-aqueous fractions, tumour-to-plasma and tumour-to-muscle ratios are at their greatest. Soloviev D, Tamburella C. 2006. Captive solvent [$^{11}$C]acetate synthesis in GMP conditions. Appl Radiat Isot 64(9):995-1000.

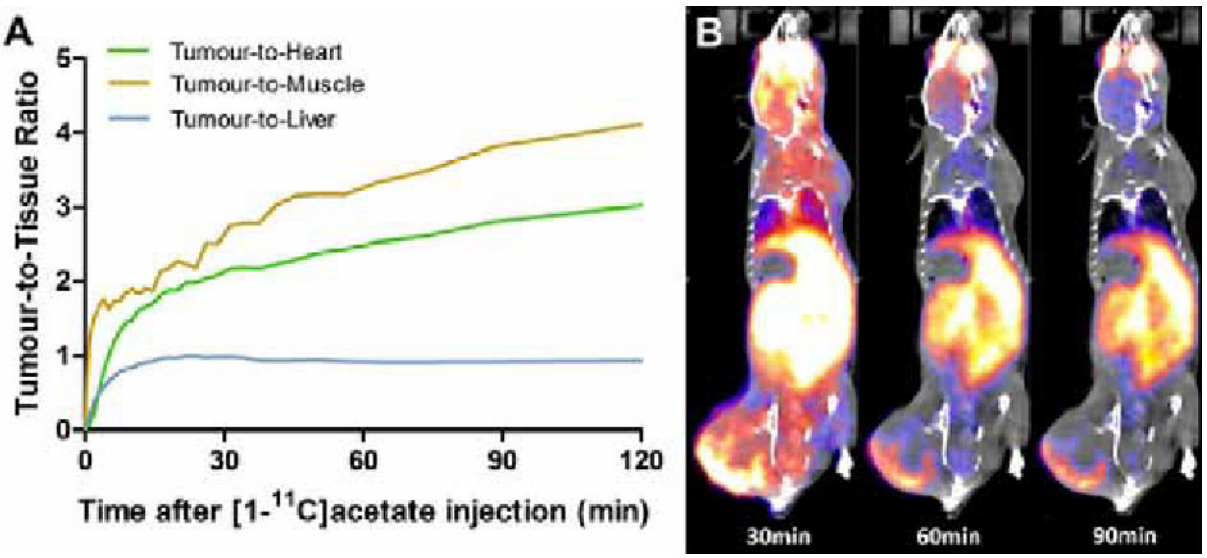


[1- $^{11}$C]acetate uptake in mice bearing C4-2b human prostate adenocarcinoma xenografts measured by PET. **A**. Ratio between mean SUV in the tumour and other tissues over time. **B** PET/CT images showing distribution of [1-$^{11}$C]acetate at various times after injection. Note [1-$^{11}$C]acetate accumulates in regions with high *de novo* fatty acid synthesis such as the tumour and liver.

Disclosure of author financial interest or relationships:
**D.Y. Lewis**, None; **J. Boren**, None; **G. Shaw**, None; **A. Ramos-Montoya**, None; **D. Soloviev**, None; **K.M. Brindle**, GE Healthcare, Grant/research support; GSK, Consultant .

Presentation Number **SS 31**
Scientific Session 5: Preclinical In Vivo - Oncology
September 6, 2012 / 10:30-10:42 / Room: The Auditorium

# Monitoring of functional sodium iodide symporter effected by regulation of glycosylation

***Taemun Chung***[1,2], *Hyewon Youn*[1,4], *Mi Jeong Kim*[1,3], *Eui-Chong Kim*[5], *Dong Soo Lee*[1,6], *June-Key Chung*[1,2], [1]*Nuclear medicine, Seoul National University college of medicine, Seoul, Republic of Korea;* [2]*Biomedical Science, Seoul National University college of medicine, Seoul, Republic of Korea;* [3]*Laboratory of molecular imaging and therapy, Cancer research Seoul National University college of medicine, Seoul, Republic of Korea;* [4]*cancer imaging center, National University Cancer Hospital, Seoul, Republic of Korea;* [5]*Laboratory Medicine, National University Hospital, Seoul, Republic of Korea;* [6]*Molecular Medicine and Biopharmaceutical Sciences, WCU Graduate School of Convergence Science and Technology, Seoul National University, Seoul, Republic of Korea. Contact e-mail: noenimy@snu.ac.kr*

Purpose: Sodium iodide symporter (NIS) is transmembrane protein that functions to uptake iodide in the thyroid cells. Loss of functional NIS renders some thyroid cancer patients unresponsive to radioiodine therapy. In this study, we investigated the effects on NIS glycosylation to change the amount and translocation to cell membrane of NIS using molecular imaging. Methods: HeLa cells were stably transfected with NIS-tdTomato fusion gene (HeLa/NIS-Tom) to monitor the expression of NIS by conjugated red fluorescence. HeLa/NIS-Tom cells were treated with Tunicamycin to inhibit NIS glycosylation and cyclic adenosine monophosphate (cAMP) to stimulate NIS glycosylation. The expression of NIS was evaluated by immunoblotting and immunofluorescent staining, and the membrane localization of NIS was examined by confocal microscopy. Functional activity of NIS in HeLa/NIS-Tom was estimated by radioiodine uptake. The expression and activity of NIS in xenograft models were estimated by fluorescent and Tc-99m scintigraphic imaging. Results: After the treatment with Tunicamycin in HeLa/NIS-Tom cells, the glycosylated NIS was 0.57-fold decreased and radioiodine uptake was also 0.29-fold decreased. After the treatment with cAMP in HeLa/NIS-Tom cells, the glycosylated NIS was 1.99-fold increased and radioiodine uptake was 4.12-fold increased. Using confocal microscopy, the expression of NIS localized to cell membrane was observed to be increased after cAMP treatment and to be decreased after Tunicamycin treatment. Additionally, xenograft mice models treated with cAMP showed 4.15-fold increase in fluorescent signals and increases of 99mTc uptake. Our results indicate that the expression amount and membrane translocation of NIS protein were related to NIS glycosylation. Conclusion: We could successfully monitor localization to membrane and change of functional NIS by regulation of NIS glycosylation. Therefore, the strategy to enhance functional NIS by the regulation of glycosylation could be applicable to thyroid cancer patients who show refractory response to the conventional radioiodine treatment.

Disclosure of author financial interest or relationships:
**T. Chung**, None; **H. Youn**, None; **M. Kim**, None; **E. Kim**, None; **D. Lee**, None; **J. Chung**, None.

Presentation Number **SS 32**
Scientific Session 5: Preclinical In Vivo - Oncology
September 6, 2012 / 10:42-10:54 / Room: The Auditorium

# Non-invasive assessment of IDH status in glioblastoma using dynamic $^{13}$C MRS of hyperpolarized α-ketoglutarate and hyperpolarized pyruvate

***Myriam M. Chaumeil***[1], *Sarah M. Woods*[1], *Robert M. Danforth*[1], *Hikari Yoshihara*[1], *Alessia Lodi*[1], *Aaron E. Robinson*[2,3], *Janine M. Lupo*[1], *Russel O. Pieper*[2,4], *Joanna Philips*[2,3], *Sabrina M. Ronen*[1,4], [1]*Radiology and Biomedical Imaging, University of California, San Francisco, San Francisco, CA, USA;* [2]*Neurological Surgery, University of California, San Francisco, San Francisco, CA, USA;* [3]*Pathology, University of California, San Francisco, San Francisco, CA, USA;* [4]*Brain Tumor Research Center, University of California, San Francisco, San Francisco, CA, USA. Contact e-mail: myriam.chaumeil@ucsf.edu*

**INTRODUCTION** Mutations in the isocitrate dehydrogenase (IDH) enzyme have recently been reported in 70-80% of low grade gliomas and upgraded glioblastomas (GBM)[1]. Inhibitors of mutant IDH are thus under development, raising the need for non-invasive methods to monitor IDH status and activity. Wild type IDH catalyzes the decarboxylation of isocitrate to α-ketoglutarate (αKG), mutant IDH catalyzes the reduction of αKG into 2-hydroxyglutarate (2HG). To date, non-invasive assessment of IDH status has been achieved through 2HG detection using $^{1}$H magnetic resonance spectroscopy (MRS)[2]. However, these methods can be challenging and complementary non-invasive techniques are needed. Our goal was to evaluate the potential of hyperpolarized (HP) αKG and pyruvate as novel $^{13}$C MRS probes to inform on IDH mutational status in gliomas. **METHODS** Cells expressing wild-type and mutant IDH were generated by transducing U87 GBM cells with viral vector coding for wild-type IDH (U87IDHwt) or mutant IDH (U87IDHmut). Cells (≈3.9x10$^{7}$ U87IDHwt cells, n=7; ≈3.2x10$^{7}$ U87IDHmut cells, n=7) were grown on microcarrier beads and loaded into a 10-mm NMR tube connected to a perfusion system[3]. [1-$^{13}$C]-αKG or [1-$^{13}$C]-pyruvate were polarized in a hypersense polarizer for 1h, rapidly injected into the perfused cells ([αKG]=15mM, [pyruvate]=5mM) and dynamic sets of HP $^{13}$C spectra acquired on a 500MHz INOVA spectrometer (13deg pulses, 3sec TR). Spectra were quantified using ACD/Spec Manager. Gamma-variate (GVA) and Monte-Carlo analysis were performed on all datasets[4]. **RESULTS & DISCUSSION** Injection of HP αKG resulted in build-up of HP glutamate (177.2ppm) in U87IDHwt cells, whereas HP glutamate was barely detectable in U87IDHmut cells (Fig A,B). Natural abundance [5-$^{13}$C] αKG is detectable in our samples at 184ppm. As a result HP 2HG at 183.8ppm could not be resolved unequivocally; alternative approaches are underway. HP lactate produced from pyruvate was significantly higher in U87IDHwt cells than in U87IDHmut (Fig C). GVA shows significant differences in glutamate and lactate formation between U87IDHwt and mut (Table 1). Activity assays of aspartate transaminase (AST, Fig D), alanine aminotransferase (ALT, Fig E) and glutamate dehydrogenase (GDH, Fig F) suggest that GDH likely plays a role in the decreased glutamate production in U87IDHmut (57±12%, *p=0.01*). A decrease in LDH expression (Fig G) and activity (66±15%, *p=0.03*, Fig H) in U87IDHmut likely explains the observed drop in HP lactate production. This study demonstrates, to our knowledge for the first time, that HP αKG permeates the cell membrane enabling the investigation of its metabolism within a time frame compatible with a HP $^{13}$C MRS experiment. Furthermore, HP αKG and HP pyruvate are promising agents for interrogation of IDH mutational status, allowing assessment of metabolic reprogramming associated with the presence of this mutation. **REFERENCES** 1.Dang *et al*, Nature (2009) 2. Elkhaled *et al*, Sci Trans Med (2012) 3. Ward *et al*, Cancer Res (2010) 4. Lupo *et al*, MRM (2010) **ACKNOWLEDGMENTS** NIH UCSF SPORE P50 CA097257, NIH R21CA161545, Academic Senate (UCSF), American Brain Tumor Association, NIH P41EB013598.

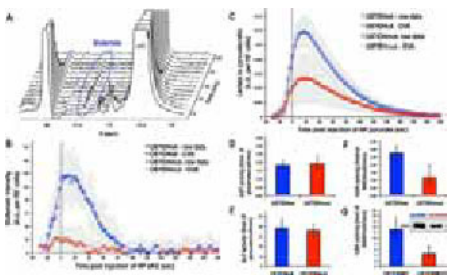

Results of the gamma-variate analysis of HP glutamate and lactate kinetics

| | | R-value | Area | Peak Time (sec) | Peak Height | FWHM (sec) |
|---|---|---|---|---|---|---|
| Glutamate | U87IDHwt | 0.98±0.11 | 244±82.11 | 12.2±0.4 | 1.1±0.4 | 17±3 |
| | U87IDHmut | 0.92±0.21 | 49±45** | 9.7±0.4 ** | 2.4±0.3** | 11±5* |
| Lactate | U87IDHwt | 0.95±0.14 | 0.74±0.01 | 18.0±0.5 | 11.3±0.9 (x10$^{-3}$) | 72.9±6.9 |
| | U87IDHmut | 0.95±0.16 | 0.17±0.02** | 18.4±0.4 | 3.2±0.3 (x10$^{-3}$) ** | 61.3±5.4* |

All values expressed as mean±sd. Glutamate signal was normalized to noise and cell number. Lactate signal was normalized to maximum pyruvate and cell number.
FWHM=full width at half-maximum. Student t-test ***p<0.005, *p<0.05*

Disclosure of author financial interest or relationships:
**M.M. Chaumeil**, None; **S.M. Woods**, None; **R.M. Danforth**, None; **H. Yoshihara**, None; **A. Lodi**, None; **A.E. Robinson**, None; **J.M. Lupo**, None; **R.O. Pieper**, None; **J. Philips**, None; **S.M. Ronen**, GE Healthcare, Grant/research support .

Presentation Number **SS 33**
Scientific Session 5: Preclinical In Vivo - Oncology
September 6, 2012 / 10:54-11:06 / Room: The Auditorium

# Intra-Arterial Chemo-Radioactive Hydrogels as a New therapeutic agent for the Treatment of Liver Cancers

***Chang-Moon Lee**, Su-Jin Cheong, Eun-Mi Kim, Na-Young Choi, Hwan-Seok Jeong, Dong Wook Kim, Seok Tae Lim, Myung-Hee Sohn, Hwan-Jeong Jeong, Department of Nuclear Medicine, Institute for Medical Sciences, Research Institute of Clinical Medicine, Cyclotron Research Center, Chonbuk National University Medical School and Hospital, Jeonju, Republic of Korea. Contact e-mail: commy@hanmail.net*

Chemo-radioactive embolization is an innovative therapeutic approach and provides opportunities for advancement of tumor therapy. In this study, we focused on the development of a new chemo-radioactive hydrogel (CRH) for selective internal chemo-radioactive therapy. Advantages of the use of the hydrogel are the ability to deliver high dose of radiation to target sites and the feasibility of combination with anti-cancer therapeutic drugs. The CRH was composed of the I-131-labeled polymer and doxorubicin (DOX) as an anti-cancer drug. Radiolabeling of the CRH was stable over 2 weeks without disassociation of free I-131 and DOX showed sustained-release from the CRH. The hydrogel without I-131 and DOX showed the high biocompatibility in vivo and in vitro, whereas the CRH exhibited the cytotoxicity in the cell viability. The size of CRH was about 150-200 μm. When the CRH was injected into the tissues such as liver, pancreas, thigh muscle, and tumors, in vivo gamma imaging showed it's retention in the injection site without significant leakage to other tissues. After intra-hepatic arterial injection, the CRH was selectively retained in the liver without movement into other tissues. In cancer therapy studies in vivo, the retained therapeutic dose of the CRH into the cancer tissues was checked by gamma imaging, and the CRH showed significant synergistic therapeutic effect with combination of radiation and chemotherapeutics on the hepatoma and breast cancer models. In conclusion, the CRH as an intra-arterial therapeutic agent can be a new alternative for cancer therapy.

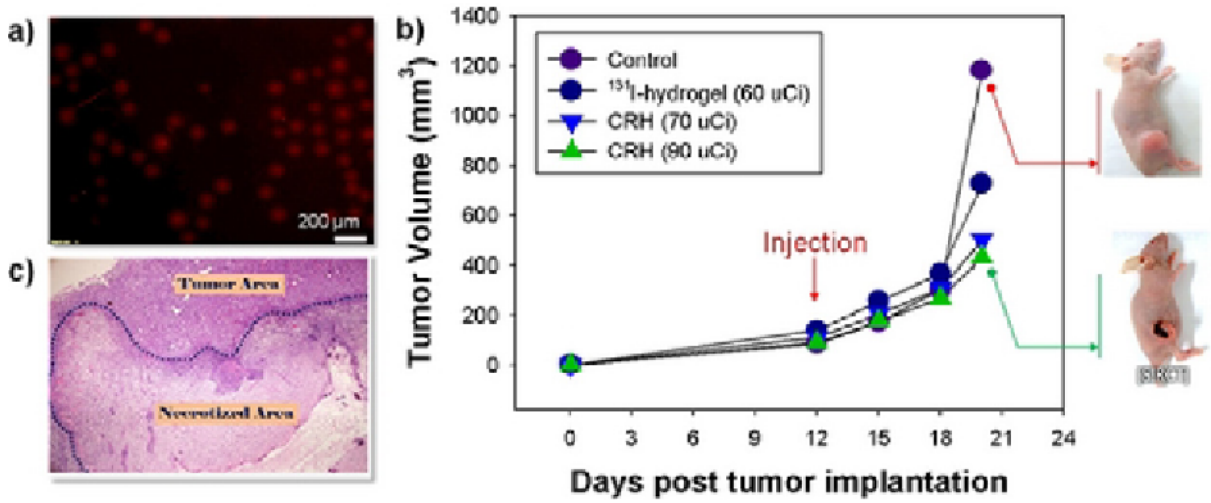


Figure 1. (a) The fluorescent microscopic image of CRH containing doxorubicin, (b) tumor therapeutic efficacy of CRH with a single dose in the mouse tumor models, (c) representative hematoxylin and eosin-stained tumor tissues obtained from the mice.

Disclosure of author financial interest or relationships:
**C. Lee**, None; **S. Cheong**, None; **E. Kim**, None; **N. Choi**, None; **H. Jeong**, None; **D. Kim**, None; **S. Lim**, None; **M. Sohn**, None; **H. Jeong**, None.

Presentation Number **SS 34**
Scientific Session 5: Preclinical In Vivo - Oncology
September 6, 2012 / 11:06-11:18 / Room: The Auditorium

# A Triple-Modality MRI-Photoacoustic-Raman Nanoparticle for pre-and intraoperative Brain Tumor Delineation

***Moritz F. Kircher***[1,2], *Adam de la Zerda*[1,4], *Jesse V. Jokerst*[1], *Cristina Zavaleta*[1], *Paul J. Kempen*[5], *Erik Mittra*[1], *Ken Pitter*[3,6], *Ruimin Huang*[2,7], *Robert Sinclair*[5], *Ingo K. Mellinghoff*[7,8], *Eric Holland*[6,9], *Sanjiv S. Gambhir*[1,10], [1]*Molecular Imaging Program at Stanford, Department of Radiology, Stanford University, Stanford, CA, USA;* [2]*Radiology, Memorial Sloan-Kettering Cancer Center, New York, NY, USA;* [3]*Brain Tumor Center, Memorial Sloan-Kettering Cancer Center, New York, NY, USA;* [4]*Electrical Engineering, Stanford University, Stanford, CA, USA;* [5]*Materials Science & Engineering, Stanford University, Stanford, CA, USA;* [6]*Cancer Biology and Genetics, Memorial Sloan-Kettering Cancer Center, New York, NY, USA;* [7]*Neurology, Memorial Sloan-Kettering Cancer Center, New York, NY, USA;* [8]*Human Oncology & Pathogenesis Program, Memorial Sloan-Kettering Cancer Center, New York, NY, USA;* [9]*Neurosurgery, Memorial Sloan-Kettering Cancer Center, New York, NY, USA;* [10]*Bioengineering and Bio-X Program, Stanford University, Stanford, CA, USA. Contact e-mail: kircher99@yahoo.com*

**Purpose:** Malignant brain tumors remain a therapeutic challenge, partially because of the difficulty of visualizing tumor borders during surgery. Our goal was to develop a novel triple-modality MRI-Photoacoustic-Raman nanoparticle approach to allow both preoperative staging and intraoperative high-precision delineation of gliomas. **Materials and Methods:** The MPR nanoparticle comprises a 60 nm gold core covered with the Raman molecular tag, trans-1,2-bis(4-pyridyl)-ethylene. This thin Raman-active layer is further protected by a 30 nm silica coating. We further modified the particles with DOTA-$Gd^{3+}$ via a maleimide linkage, resulting in a gold-silica-based SERS nanoparticle coated with $Gd^{3+}$ ions detectable by MRI, Photoacoustic and Raman imaging (MPR) (Nature Medicine, in press). We used ICP-AES to determine number of $Gd^{3+}$ ions/particle. In vitro and in vivo phantom experiments determined detection thresholds, and in vivo testing with all three modalities (MRI, Photoacoustic and Raman imaging) was performed in 3 different mouse glioblastoma models: 1) orthotopic U87MG glioblastoma, 2) orthotopic TS543 primary human glioblastoma xenografts, and 3) a genetically engineered glioma model (PDGFdriven PTEN-/- gliomas using RCAS/tv-a). MPRs (150 µl, 16 nM) were injected intravenously (i.v.) and imaged with all three modalities in vivo (7T MRI, home-built Photoacoustic system, Renishaw Raman microscope). 24 h after injection, sequential brain tumor resections on live mice were performed and correlated with intraoperative Raman and Photoacoustic imaging. Results were confirmed by immunohistochemistry, Raman microscopy and electron microscopy (SEM and STEM). **Results:** MPR nanoparticles have 79,340 ± 2,270 $Gd^{3+}$ ions per particle, resulting in a very high T1 relaxivity of $3.0 \times 10^6$ $mM^{-1}s^{-1}$; a Photoacoustic absorbance coefficient of $2.75 \times 10^{10}$ $cm^{-1}M^{-1}$; and a unique Raman signature. Incubation in 50% mouse serum over 24 h demonstrated particle stability. In vitro and in vivo MPR detection thresholds were at least in the picomolar range for all 3 modalitites, and in the femtomolar range for Raman in vitro. After i.v. injection into glioblastoma bearing mice MPRs accumulated in and were retained by the tumors for more than 1 week, and allowed tumor delineation with all 3 modalities through the intact skull of living mice. The triple-modality MPR approach allowed performing preoperative MRI for staging as well as intraoperative Raman and/or Photoacoustic imaging several days later, requiring only a single dose of MPR nanoparticles. Intraoperative Raman and Photoacoustic imaging allowed precise brain tumor margin delineation. Raman imaging also allowed detection of microscopic fingerlike tumor protrusions and infiltrative tumor margins with high precision. No cytotoxicity effects were observed. **Conclusion:** We designed and tested the first triple-modality MRI-Photoacoustic-Raman nanoparticle, for combined glioblastoma detection and resection. A single i.v. injection allows precise preoperative staging with MRI and intraoperative image-guided resection using Photoacoustic (gross resection steps) and Raman imaging (high precision margin delineation).

**Raman-guided brain tumor resection.** Cartoon based on 3D rendering of actual data using MPR nanoparticles in a mouse glioblastoma model. MPR nanoparticles were injected intravenously, and intraoperative Raman imaging to delineate the tumor margins was performed 24 hours later. Green = brain tumor; gray = healthy brain; red = Raman signal.

Disclosure of author financial interest or relationships:
**M.F. Kircher**, None; **A. de la Zerda**, None; **J.V. Jokerst**, None; **C. Zavaleta**, None; **P.J. Kempen**, None; **E. Mittra**, None; **K. Pitter**, None; **R. Huang**, None; **R. Sinclair**, None; **I.K. Mellinghoff**, None; **E. Holland**, None; **S.S. Gambhir**, General Electric, Grant/research support; Bayer-Schering, Grant/research support; Sanofi-Aventis, Grant/research support; CellSight, Stockholder; ImaginAB, Stockholder; Enlight, Stockholder; Endra, Stockholder; Bracco, Consultant; NinePoint Medical, Stockholder; Visualsonics, Consultant .

Presentation Number **SS 35**
Scientific Session 5: Preclinical In Vivo - Oncology
September 6, 2012 / 11:18-11:30 / Room: The Auditorium

# A Toll-like Receptor 2 Targeted Imaging Probe for Fluorescence-Guided Surgery of Pancreatic Cancer

***Amanda Shanks Huynh***[1], *Jennifer M. Morse*[2], *Todd J. Casagni*[2], *Mark C. Lloyd*[3], *Barbara A. Centeno*[4], *Renata Patek*[5], *Valerie Moberg*[1], *Josef Vagner*[5], *David L. Morse*[1], *Margaret Baldwin*[2], [1]*Cancer Imaging & Metabolism, Moffitt Cancer Center, Tampa, FL, USA;* [2]*Comparative Medicine, Moffitt Cancer Center, Tampa, FL, USA;* [3]*Analytic Microscopy Core Facility, Moffitt Cancer Center, Tampa, FL, USA;* [4]*Anatomic Pathology, Moffitt Cancer Center, Tampa, FL, USA;* [5]*BIO5 Institute, University of Arizona, Tuscon, AZ, USA. Contact e-mail: amanda.huynh@moffitt.org*

Improved survival rates for pancreatic cancer are associated with the complete surgical resection of tumor resulting in a tumor-free margin (R0). New methods employing intraoperative fluorescence (FL) guided tumor detection could lead to increased R0 margins and improved survival. We have reported Toll-like receptor 2 (TLR2) as a bona fide cell-surface marker for pancreatic adenocarcinoma. We then developed a high-affinity TLR2 binding ligand conjugated to a near-infrared (NIR) fluorescent dye, IR800CW, as a targeted molecular imaging probe for the intraoperative detection of surgical margins. Based on the structure of known TLR2 agonists, compounds were iteratively synthesized and screened using in vitro cell-based assays for binding and agonist activity. We identified 12 novel high affinity TLR2 ligands, with the most promising compound having the lowest mass (2729 MW), and highest binding affinity (11 nM Ki) and agonist activity (34 nM EC50) (Figure 1A) retained after conjugation of the IR800CW NIR dye (Compound 13: IRDye800CW-Mpa-PEGO-dihydroxycysteine(palmitoyl)2-Gly-dSer-PEGO-NH2). To evaluate the in vivo pharmacokinetics and biodistribution of compound 13, FL imaging was performed on multiple optical imaging systems (PerkinElmer IVIS 200 and FMT2500XL, and ART Optix MX3) using TLR2 expressing pancreatic tumor xenograft mouse models (subcutaneous and orthotopic). Tumor specificity was observed, in which FL signal was retained in TLR2 expressing tumor xenografts up to 96 h post-injection while blocking with an excess of unlabeled competing ligand significantly decreased FL signal in the tumor at 24h ($p<0.001$) (Figure 1B). To investigate the possibility of achieving R0 margins and improved survival rates using compound 13, in vivo FL guided intraoperative surgical removal of orthotopic pancreatic tumors 24h post-injection was performed using a Diagnostic Instruments adapted LightTools system outfitted with an 800 nm filter set, cooled CCD camera and SPOT Advanced software (Figure 1D); and compared to mice that underwent surgical resection of tumors using normal light. We have previously demonstrated the feasibility of the intraoperative detection of tumors using a different well-characterized Cy5-labeled probe (Dmt-Tic-Cy5) that we also developed. The resected tumors from both groups were then FL imaged ex vivo. Prior to surgery, the orthotopic pancreatic tumor volumes were monitored weekly and measured in vivo by 3D ultrasound imaging. Mice underwent in vivo FL imaging up to 72 h post-surgery to confirm complete resection of the tumors. The excised tumors and remaining normal pancreas underwent H&E staining, IHC for TLR2 expression and pathological evaluation of the margins. The survival study is currently ongoing and presence of tumor re-growth is monitored by ultrasound weekly. A novel high affinity NIR FL-labeled TLR2-targeted molecular imaging probe (compound 13) was developed for use in pancreatic cancer imaging. In vivo tumor selectivity and intraoperative detection of pancreatic cancer were demonstrated. We anticipate that this method will improve pancreatic cancer survival by increasing the percentage of R0 margins.

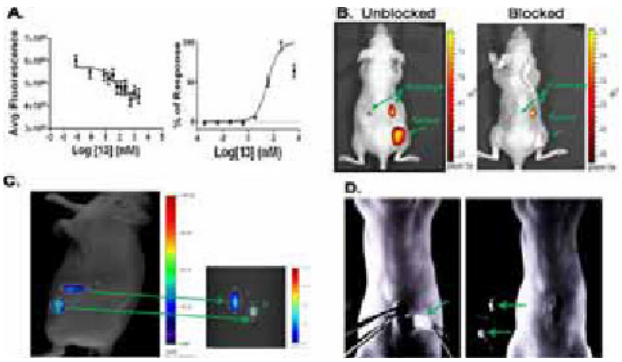


Figure 1. A) Competition binding assay determined high TLR2 binding activity (11 nM Ki) (left panel), while dose-response assays determined high TLR2 agonist potency (25 nM EC50) (right panel), for the NIR FL-labeled Compound 13. B) In vivo FL imaging 24 h post-injection of Compound 13 with FL signal observed in the tumor (left panel) compared to 20-fold excess of a competing TLR2 ligand plus Compound 13 with a significantly decreased FL signal in the tumor (right panel). C) FL imaging of pancreatic tumors labeled with Compound 13 in vivo 24 h post-injection just prior to surgery (left panel), and the ex vivo surgically resected tumors (right panel) and D) the corresponding FL-guided surgical resection of pancreatic tumors labeled with Compound 13 (green arrows show bright pancreatic tumors prior to and after resection).

Disclosure of author financial interest or relationships:
**A. Huynh**, None; **J.M. Morse**, None; **T.J. Casagni**, None; **M.C. Lloyd**, None; **B.A. Centeno**, None; **R. Patek**, None; **V. Moberg**, None; **J. Vagner**, None; **D.L. Morse**, LiCor, Other financial or material support; Intezyne Technologies, Other financial or material support; **M. Baldwin**, None.

Presentation Number **SS 36**
Scientific Session 5: Preclinical In Vivo - Oncology
September 6, 2012 / 11:30-11:42 / Room: The Auditorium

# Biomarker-Based Photoacoustic Imaging of Follicular Thyroid Carcinoma

***Jelena Levi***[1,2], *Sri Rajasekhar Kothapalli*[2], *Joon-Kee Yoon*[3], *Sarah Bohndiek*[2], *Anca Dragulescu-Andrasi*[2], *Carsten H. Nielsen*[2], *Sanjiv S. Gambhir*[1,2], [1]*Canary Center at Stanford, Palo Alto, CA, USA;* [2]*Molecular Imaging Program, Department of Radiology and BioX Program, Stanford University, Palo Alto, CA, USA;* [3]*Department of Nuclear Medicine and Molecular Imaging, Ajou University School of Medicine, Suwon, Republic of Korea. Contact e-mail: jlevi@stanford.edu*

Current clinical preoperative thyroid cancer diagnosis relies on ultrasound and fine needle aspiration cytology both of which are unable to detect vascular and capsular invasion that is most often the only clear distinction between follicular thyroid carcinoma and adenoma. At present, the only method that can accurately diagnose follicular thyroid carcinoma is a biopsy after total or partial removal of the thyroid lobes. Only 20-30 % of all biopsies diagnose malignancy, proving 70-80% of the surgical procedures as unnecessary. Having a non-invasive imaging method that could differentiate between benign and malignant nodules would bring considerable benefit to patient management and reduce the healthcare costs by eliminating unnecessary surgeries. Photoacoustic imaging, with good depth penetration in combination with high contrast and resolution has a great potential to be clinically utilized for non-invasive, non-ionizing visualization of a superficial organ such as the thyroid. Here we explore the potential of a biomarker based photoacoustic imaging as a method for detection of follicular thyroid carcinoma. We first determined the presence and activity of two members of matrix metalloproteinase family (MMP), MMP-2 and MMP-9, suggested as biomarkers that can differentiate between benign and malignant thyroid lesions, in FTC133 thyroid tumors (implanted in nude mice) using quantitative immunocapture assay. Active forms of both enzymes were observed in tumor homogenates, with MMP-9 detected in greater amount. The probe used in the study to detect MMP activity was enzyme activatable photoacoustic probe, Alexa750-CXeeeeXPLGLAGrrrrrXK-BHQ3, determined to be efficiently cleaved by both enzymes in vitro. To minimize tumor independent and other nonspecific cleavages suggested by recent studies, we investigated direct intratumoral injections of the probe. These intratumoral injections can be easily translated to the clinic, where well-established ultrasound guided fine needle aspiration method provides easy and reliable access to the thyroid nodule. Cleavage of the intratumorally injected probe was imaged in living mice optically by observing the increase in Alexa750 fluorescence, and photoacoustically by using dual wavelength imaging method. Optical imaging showed 2 fold higher, while photoacoustic imaging revealed over 6 fold higher signal in tumors injected with the MMP probe than in tumors injected with the control, non-cleavable probe (n=3 for both probes and both imaging modalities, $p<0.05$). These results indicate great potential of the MMP activatable probe to distinguish between adenomas and MMP rich follicular carcinomas. With the combination of high spatial resolution and signal specificity, biomarker based photoacoustic imaging holds great promise as a noninvasive method for early minimally invasive diagnosis of follicular thyroid carcinomas.

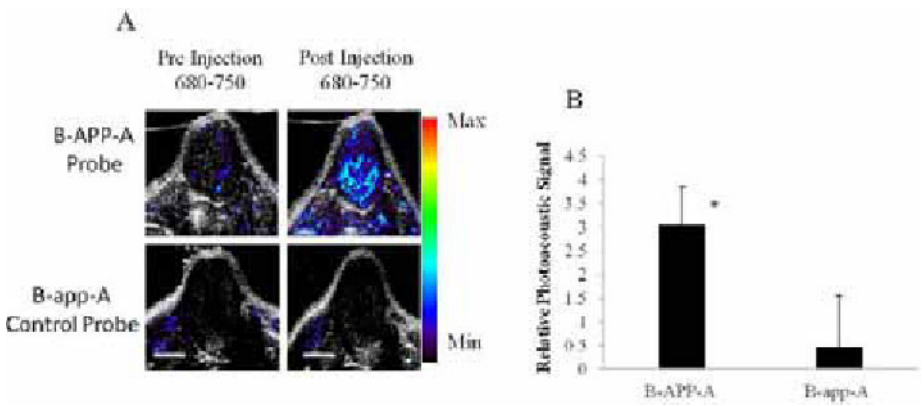


Figure 1. Photoacoustic imaging of the probe activation in thyroid tumor after intratumoral injection of the probe. Mice bearing FTC 133 tumors in the hind legs were photoacoustically imaged using 680 and 750 nm light before and after intratumoral injection of 0.6 nmol B-APP-A or B-app-A probe (A). The photoacoustic image acquired at 750 nm was subtracted from the photoacoustic image obtained at 680 nm to attain information on the cleavage of the probe. At 90 minutes post injection the subtraction of the images at the two wavelengths led to a clear increase in photoacoustic signal for the cleavable probe. The increase in signal was not observed after injection of the control probe. Quantification of the photoacoustic signal showed more than 6 fold higher signal after injection of the cleavable probe than after injection of the control probe. The error bars represent standard deviation (n=3, * $p< 0.05$). Scale bar is 0.25 cm.

Disclosure of author financial interest or relationships:
**J. Levi**, None; **S. Kothapalli**, None; **J. Yoon**, None; **S. Bohndiek**, None; **A. Dragulescu-Andrasi**, None; **C.H. Nielsen**, None; **S.S. Gambhir**, General Electric, Grant/research support; Bayer-Schering, Grant/research support; Sanofi-Aventis, Grant/research support; CellSight, Stockholder; ImaginAB, Stockholder; Enlight, Stockholder; Endra, Stockholder; Bracco, Consultant; NinePoint Medical, Stockholder; Visualsonics, Consultant .

Presentation Number **SS 37**
Scientific Session 5: Preclinical In Vivo - Oncology
September 6, 2012 / 11:42-11:54 / Room: The Auditorium

# Differences in interstitial fluid transport, collagen fiber morphology, and invasiveness between orthotopic and subcutaneous prostate tumors

***Marie-France Penet**, Samata M. Kakkad, Arvind P. Pathak, Venu Raman, Meiyappan Solaiyappan, Zaver M. Bhujwalla, JHU ICMIC Program, Division of Cancer Imaging Research, The Russell H. Morgan Department of Radiology and Radiological Science, The Johns Hopkins University School of Medicine, Baltimore, MD, USA. Contact e-mail: mpenet@mri.jhu.edu*

Metastasis and malignant ascites are major causes of poor prognosis in prostate cancer patients. Cancer cells metastasize more readily from orthotopic sites than from heterotopic sites. In the present study, we have focused on characterizing the role of the extracellular matrix (ECM) in allowing metastatic dissemination and on understanding the role of hypoxia using in vivo MRI and ex vivo optical imaging of orthotopic and subcutaneous prostate tumor xenografts. MRI of the macromolecular contrast agent albumin-GdDTPA was used to characterize interstitial fluid transport, second harmonic generation (SHG) microscopy to determine collagen I fiber distribution, and enhanced green fluorescent protein (EGFP) expression to detect hypoxia. Prostate cancer cells engineered to express EGFP under hypoxia (PC3-HRE-EGFP) were used. For orthotopic implantation, intact PC3-HRE-EGFP tumor tissue grown in the flank of severe combined immunodeficient (SCID) male mice was implanted on the prostate of SCID male mice. By implanting tumor tissue, the ECM and three dimensional cytoarchitecture, believed to play a critical role in tumor progression and metastasis, were maintained. Volume matched tumor tissue was also implanted subcutaneously in a separate group of mice. All MR imaging was performed on a 4.7T spectrometer. Interstitial fluid transport parameters were measured from quantitative T1 maps obtained before and after intravenous administration of albumin-GdDTPA. Images were acquired in two phases corresponding to the biphasic kinetics of the contrast agent. The early phase images were used to characterize the tumor vasculature, while the late phase images were used to characterize interstitial fluid transport parameters. Following MRI, SHG and EGFP microscopy of fresh tissue slices was performed to acquire 3D image stacks from randomly selected fields of view. Collagen fiber morphology was characterized in terms of the inter-fiber distance and fiber volume. Orthotopic prostate tumors were characterized by a higher vascular volume, a higher number of pooling voxels, a higher pooling volume, and lower efflux and influx rates compared to subcutaneous tumors. Representative 3D SHG images of collagen I fiber are shown in Figure 1. Overall, significantly higher fiber density and volume were observed in orthotopic tumors. The higher density of collagen fibers was also observed in normoxic areas. Prostate tumor xenografts growing orthotopically in the prostate resulted in metastasis to lymph nodes, lungs and liver, and malignant ascites. In contrast, identical xenografts growing in the flank rarely resulted in metastasis. Characterization of hypoxia in orthotopic and subcutaneous environments and its relationship to interstitial transport and collagen fiber distribution is ongoing, as is the relationship between macromolecular transport and the accumulation of metastases and malignant ascites. These data demonstrate the profound impact of the location of tumor growth on the ECM and macromolecular transport, and provide additional insights into environments that are permissive for metastasis and the accumulation of malignant ascites.

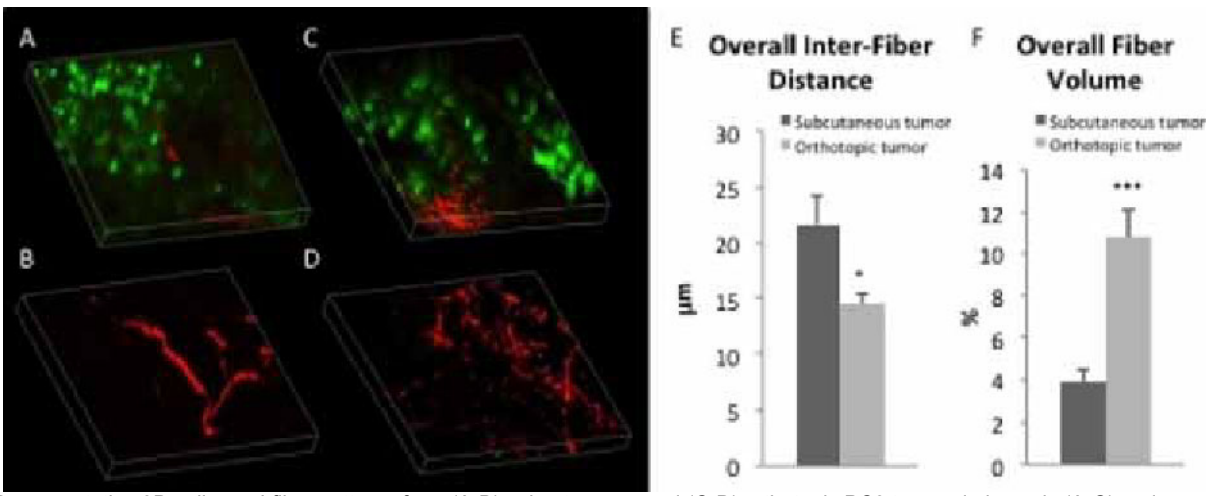


Figure 1: Representative 3D collagen I fiber patterns from (A-B) subcutaneous and (C-D) orthotopic PC3 tumors in hypoxic (A-C) and normoxic (B-D) areas. Bar graphs of inter-fiber distance (E) and fiber volume (F) in subcutaneous (n=5) and orthotopic (n=9) PC3 tumors (*p<0.05, ***p<0.001).

Disclosure of author financial interest or relationships:
**M. Penet**, None; **S.M. Kakkad**, None; **A.P. Pathak**, None; **V. Raman**, None; **M. Solaiyappan**, None; **Z.M. Bhujwalla**, None.

Presentation Number **SS 38**
Scientific Session 6: Chemistry & Probes - Multimodal
September 6, 2012 / 13:00-13:12 / Room: Liffey Hall 1

# Dynamic Multispectral Optoacoustic Tomography (MSOT) Imaging of Nanoparticle Tumor Perfusion Kinetics

***Wouter H. Driessen***[2,1]*, Neal Burton*[2,1]*, Jing Claussen*[2,1]*, Stefan Morscher*[2,1]*, Daniel Razansky*[1,3]*, Vasilis Ntziachristos*[1,3]*,* [1]*The Institute for Biological and Medical Imaging, Helmholtz Center Munich, Neuherberg, Germany;* [2]*iThera Medical, Neuherberg, Germany;* [3]*Technische Universität München, Munich, Germany. Contact e-mail: wouter.driessen@ithera-medical.com*

A wide range of nanoparticles differing in size, shape and surface characteristics are available for therapeutic and diagnostic applications in oncology. To ensure optimal accumulation in solid tumors, it is crucial to obtain quantitative data to be used as criteria for nanoparticle design. We employed a sensitive and specific imaging modality, termed Multispectral Optoacoustic Tomography (MSOT), to dynamically evaluate tumor accumulation kinetics of well-characterized nanoparticles. Optoacoustic imaging is based on the generation of ultrasound waves induced by the absorption of light pulses in tissue. During MSOT imaging, an object is illuminated using a near-infrared (NIR) laser at multiple wavelengths to then spectrally resolve distinct absorbers over background tissue. This results in the simultaneous visualization of anatomical, functional and molecular contrast with a spatial and temporal resolution typical for ultrasound imaging. To determine the influence of nanoparticle surface characteristics on tumor perfusion kinetics, we evaluated ICG-filled liposomes with different zeta-potentials (zwitterionic, positive and negative) and different degrees of PEGylation. Liposomes with ICG were chosen as "model particles", because of their flexibility and the fact that they consist of components generally regarded as safe by the FDA. Using MSOT and pharmacokinetic modeling we then evaluated the tumor accumulation properties of each nanoparticle formulation. For each formulation wash-in and wash-out rates were calculated and compared to non-encapsulated ICG. Tumor accumulation was verified by post-mortem whole-animal cryoslicing and histology. In summary, MSOT offers a new and unique imaging modality that (1) has a resolution at least ten-fold higher than nuclear and optical imaging, (2) allows for real-time imaging with molecular specificity through several centimeters of tissue and (3) is safe (i.e. no ionizing radiation) and cost-efficient. We used this modality to quantitatively determine the influence of surface charge and PEGylation on tumor perfusion kinetics of nanoparticles. These parameters can be utilized for the rational design of nanoparticles for oncology applications. Future experiments include the investigation of different nanomaterials such as gold nanorods to investigate the influence of aspect ratio on tumor accumulation kinetics.

Disclosure of author financial interest or relationships:
**W.H. Driessen**, iThera Medical, Employment; **N. Burton**, iThera Medical, Employment; **J. Claussen**, iThera Medical, Employment; **S. Morscher**, iThera Medical GmbH, Employment; **D. Razansky**, iThera Medical GmbH, Stockholder; **V. Ntziachristos**, ERC, Grant/research support; Ithera Medical, Stockholder .

Presentation Number **SS 39**
Scientific Session 6: Chemistry & Probes - Multimodal
September 6, 2012 / 13:12-13:24 / Room: Liffey Hall 1

# Multimodal gadolinium based nanoprobes for lung investigations

***François Lux***[1], *Sandrine Dufort*[2,4], *Andrea Bianchi*[3], *Véronique Josserand*[4], *Olivier Tillement*[1], *Jean-Luc Coll*[4], *Yannick Crémillieux*[3], [1]*Laboratoire de Physico-Chimie des Matériaux Luminescents, Villeurbanne, France;* [2]*Nano-H S.A.S, Saint-Quentin Fallavier, France;* [3]*Centre de recherche cardio-thoracique de Bordeaux, Bordeaux, France;* [4]*Institut Albert Bonniot, Grenoble, France. Contact e-mail: francois.lux@univ-lyon1.fr*

New UltraSmall Rigid Nanoparticles (USRP) have recently been developed in our laboratory. These USRPs are obtained via a top down process leading to sub-5nm nanoparticles. The interest of this new material composed of a polysiloxane matrix and organic chelates is to combine imaging and therapeutic properties in a very small object that is eliminated by renal excretion. Their efficiency for multimodal imaging and for therapeutic applications after intravenous injection in rodents has recently been proven and published. In parallel, the development of Ultra-short Echo Time (UTE) sequences for MRI permits the imaging of lung tissue in small animals with submillimetric resolution. To benefit from these UTE sequences, the multimodal USRP have been administered intratracheally (the most direct and effective route for reaching lung tissue) to healthy mice. Different gadolinium concentrations have been investigated; an important signal enhancement 235%±15% was obtained for an administered volume of 50 µL at 50 mM. This concentration has then been chosen to study the biodistribution of the contrast agent. The residence time of the USRPs in the lungs is of about 2 hours and half, their elimination has been visualized and is due to a passage from the lungs to the vascular system and then to the kidneys. No significant hepatic clearance is observed during this experiment (in agreement with the biodistribution obtained after an intravenous injection of the USRPs). The maximum signal enhancement in the kidneys (more than 700%) is observed two hours after administration. Taking advantage of the multifunctional property of USRPs, we also followed them using fluorescence 3D imaging and X-ray tomography (See Figure). Fluorescence imaging was performed thanks to the grafting of Cy5.5, a near infrared fluorophore, into the polysiloxane matrix. A similar distribution was obtained with both methods, confirming the elimination pathway of the USRPs, but also providing complementary quantitative data of their concentration in the different organs.

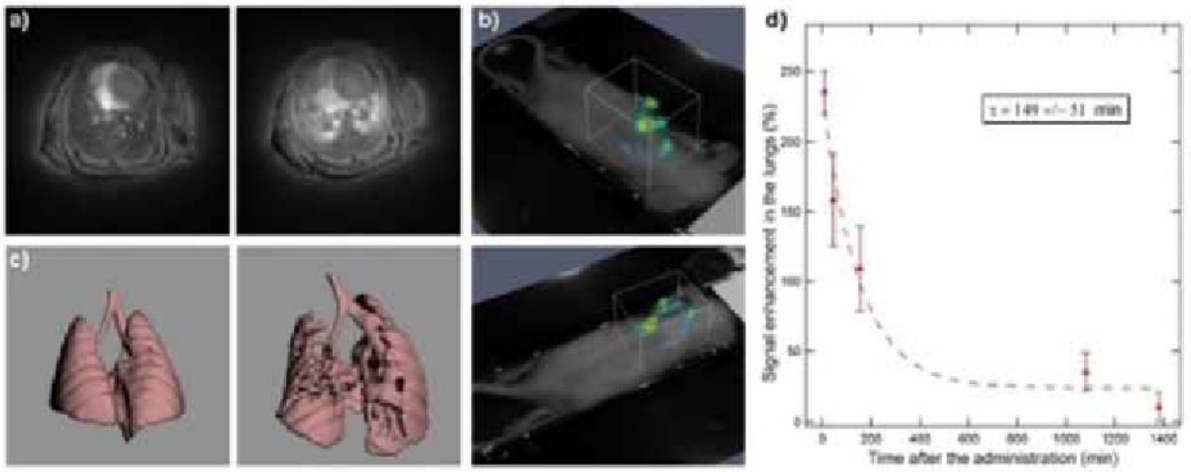


Figure: a) MRI imaging of the lungs of a mouse before (left) and 15 minutes after intratracheal administration of SRP (40 µL at 20 mM in Gd3+), enhancement of the signal after compared to before administration: 183%, b) 3D fluorescence imaging of a mouse 1H after nebulization in the lungs of fluorescent (Cy 5.5) SRP (50 µL at 20 mM in Gd3+), c) reconstitution of lungs before (left) and after (right) nebulisation in the lungs of SRP thanks to X-Ray tomography (only soft tissues are represented, and the particles appear as "holes". d) MRI signal enhancement decay (time constant of about 2 hours) in lungs following inhalation of the nanoparticles.

Disclosure of author financial interest or relationships:
**F. Lux**, None; **S. Dufort**, None; **A. Bianchi**, None; **V. Josserand**, None; **O. Tillement**, None; **J. Coll**, None; **Y. Crémillieux**, None.

Presentation Number **SS 4**
Scientific Session 1: Chemistry & Probes - MRI
September 6, 2012 / 11:03-11:14 / Room: Liffey Hall 1

# Mapping oxygen transfer in vivo in pregnant mice using non-invasive MRI

***Reut Avni***[1], *Rinat Abramovitch*[2], *Joel R. Garbow*[3], *Michal Neeman*[1], [1]*Biological Regulation, weizmann institute of science, Rehovot, Israel;* [2]*Goldyne Savad Institute of Gene Therapy, Hadassah Hebrew University Medical Center, Jerusalem, Israel;* [3]*Biomedical MR Laboratory, Mallinckrodt Institute of Radiology, Washington University, St. Louis, MO, USA. Contact e-mail: reut.avni@weizmann.ac.il*

Monitoring fetal well being, identifying high-risk fetuses, and predicting the timing of delivery are three of the main major challenges in modern-day obstetrics. Oxygen transport between placenta and fetus is one of several key functions performed by the placenta. Compromised oxygen transport can have severe negative consequences for fetal growth and development. Non-invasive imaging methods that can probe tissue oxygen transport can provide important insights into this essential placental role and contribute to our understanding of the risk factors that may lead to breakdown in this function. Oxygen-enhanced (OE) MRI offers the opportunity to probe oxygen transport non-invasively. The T1 of water in tissue is sensitive to dissolved molecular oxygen (pO2), such that a large increase in pO2 resulting from a hyperoxic challenge shortens T1. BOLD images (T2*-weighted) reflect the changes in the amount of oxygen bound to hemoglobin in blood (SO2). An increase in SO2 raises T2*. We present here work designed to probe oxygen transport in pregnant mice using Oxygen Enhanced (OE) MRI. Oxygen Enhanced (OE) MRI experiments were performed on ICR pregnant mice (n=5) on day E17.5 of pregnancy in a 9.4 T Bruker scanner. The protocol consisted of gradually increasing the in oxygen level from 21% (air) to 100% and then back to baseline (Figure A). T2*- and T1-weighted 3D GE sequences were acquired sequentially at each oxygen phase. T1-maps were generated from a series of variable flip-angles (5°, 15°, 30°, 50° and 70°) experiments performed at the initial air phase and were extrapolated at each oxygen phase from the baseline. T2* mapping was achieved by the dual-echo method (TE = 8.5 and 3 ms). Regions of interests (ROIs) were drawn as the entire placenta, and signal intensities were calculated at each oxygen phase for both the T1 and T2*-weighted sequences. The enhancement in signal was calculated relative to the initial air phase and then normalized to the maximum enhancement in maternal liver. The enhancement in placental signal intensity in both T1-weighted and T2*-weighted images mirrored the increase in the inhaled oxygen level, up to 100% oxygen. However, the return to baseline was not symmetrical and the signal intensities remained above baseline (Figure B). Delta T2* maps and delta R1 maps were constructed, showing the difference in the placenta between breathing air and 100% O2. The maps show heterogeneity in both delta T2* and delta R1 changes inside the placenta, with large T2* changes being spatially correlated with small R1 changes. As T2* changes correlate with oxygen saturation and T1 changes with pO2, it might be possible to infer from OE MRI data information about oxygen extraction function within the placenta and in different fetal organs. These findings suggest that OE MRI may be a powerful tool for investigating oxygen transport in pregnancy.

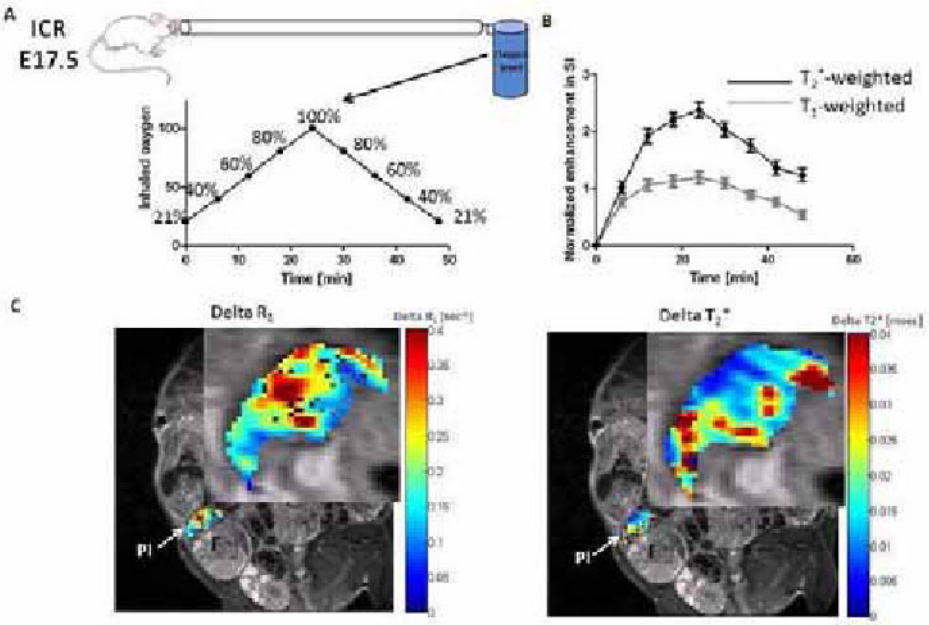


Figure: Oxygen Enhanced (OE) MRI performed on ICR pregnant mice on day E17.5 of pregnancy: A) The protocol consisted of different phases of inhaled oxygen level, ranging from 21% O2 to 100% O2. B) Normalized T1 and T2* signal intensities in the placenta during the different inhalation phases. C) and D) Placenta delta T2* and delta R1 maps showing differences between breathing air and 100% O2. Pl=placenta; F=fetus.

Disclosure of author financial interest or relationships:
**R. Avni**, None; **R. Abramovitch**, None; **J.R. Garbow**, None; **M. Neeman**, None.

Presentation Number **SS 40**
Scientific Session 6: Chemistry & Probes - Multimodal
September 6, 2012 / 13:24-13:36 / Room: Liffey Hall 1

# Photoacoustic contrast between Methylene Blue monomers and dimers as a model for activatable probes

***Ekaterina Morgounova***[1], *Qi Shao*[1], *Michael J. Wilson*[3,4], *Benjamin J. Hackel*[2], *Shai Ashkenazi*[1], [1]*Biomedical Engineering, University of Minnesota, Minneapolis, MN, USA;* [2]*Chemical Engineering and Materials Science, University of Minnesota, Minneapolis, MN, USA;* [3]*Laboratory Medicine and Pathology, University of Minnesota, Minneapolis, MN, USA;* [4]*Urologic Surgery, University of Minnesota, Minneapolis, MN, USA. Contact e-mail: emorgoun@umn.edu*

Photoacoustic lifetime imaging (PALI) is a technique that combines the high resolution and deep penetration depth of ultrasounds with the high optical contrast and versatility of molecular agents. Our approach consists in probing the excitation decay of Methylene Blue, an FDA approved chromophore. Its monomeric form presents a high quantum yield of inter-system crossing (0.52) and a long phosphorescence lifetime (70 µs). When the dye molecules bind together, static quenching occurs that outstrips inter-system crossing and leads to a short lifetime (less than 1 ns). This forms the basis of a highly sensitive contrast mechanism between monomers and dimers. Spectroscopic studies have previously revealed that Sodium Dodecyl Sulfate (SDS), an anionic surfactant, enhances Methylene Blue dimerization in solution. Our measurements show that by increasing the concentration of SDS from 0 to 5 mM in a 40 µM Methylene Blue solution, the monomer fraction decreases from 0.8 to less than 0.2 and the photoacoustic contrast is reduced by more than 80 %. Flash-photolysis reveals a triplet signal amplitude decrease of 99 % in the same conditions. These results indicate that the dimeric form is strongly quenched during the excitation and does not reach a triplet state. The monomers, on the contrary, present a valuable potential to be detected by PALI techniques thanks to their high quantum yield of inter-system crossing. Those characteristics can be used to develop an activatable molecular probe for in-vivo imaging of molecular processes such as enzyme activity. Our group focuses in designing a dual-Methylene Blue probe bound by an enzyme-specific cleavable peptide linker. The targeted enzyme is MMP2, a molecular marker for cancer progression of the Matrix Metalloproteinase (MMP) family. Upon cleavage by MMP2, the two dyes will diffuse separately and recover their long excitation lifetime enabling their detection by PALI. The translation of this technique to clinical applications and the gain in depth and resolution compared to current fluorescence imaging methods have the potential to bring powerful improvements in cancer screening, drug tailoring and treatment monitoring.

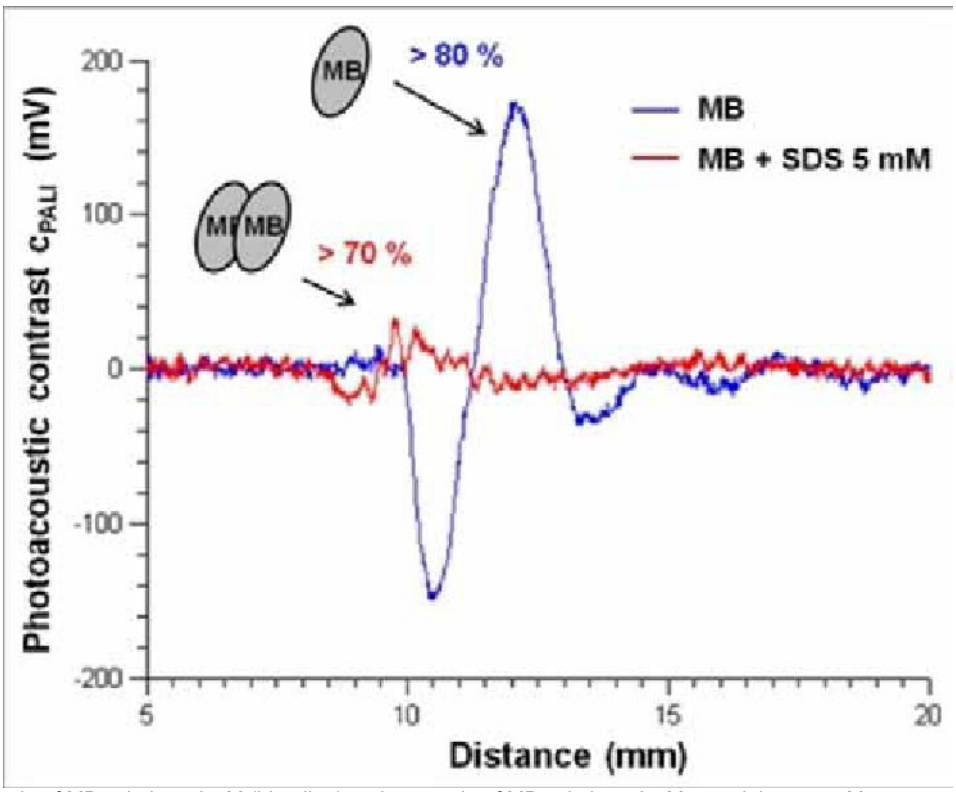


PALI signal from a sample of MB solution 40 µM (blue line) and a sample of MB solution 40 µM containing a 5 mM concentration of SDS (red line).

Disclosure of author financial interest or relationships:
**E. Morgounova**, None; **Q. Shao**, None; **M.J. Wilson**, None; **B.J. Hackel**, None; **S. Ashkenazi**, None.

Presentation Number **SS 41**
Scientific Session 6: Chemistry & Probes - Multimodal
September 6, 2012 / 13:36-13:48 / Room: Liffey Hall 1

# Multispectral Optoacoustic Tomography as a novel tool for whole-body investigation of nanoparticle biodistribution

***Neal Burton***[1,2]*, Wouter H. Driessen*[1,2]*, Stefan Morscher*[1,2]*, Jing Claussen*[1,2]*, Daniel Razansky*[1,3]*, Vasilis Ntziachristos*[1,3]*, [1]Institute for Biological and Medical Imaging, Helmholtz Zentrum Muenchen, Neuherberg, Germany; [2]iThera Medical, Munich, Germany; [3]Technical University of Munich, Munich, Germany. Contact e-mail: neal.burton@helmholtz-muenchen.de*

Multispectral Optoacoustic Tomography (MSOT) is a powerful novel imaging modality that decomposes the spectral responses of intrinsic tissue chromophores in vivo, with high resolution and at depths of several millimeters to centimeters. In addition, extrinsic absorbers of interest, such as photo-absorbing organic dyes and nanoparticles, can also be multispectrally resolved in tissue. A particular strength of MSOT over other imaging modalities is the ability to extract anatomical, functional and molecular information from a single scan. In this work, the ability of MSOT to track nanoparticle whole-body biodistribution and pharmacokinetics is demonstrated. Liposomes containing near infrared (NIR) fluorescent dye were injected intravenously into mice and the accumulation and clearance of the nanoparticles over time were observed by MSOT. Regions of interest included liver, spleen, kidneys, brain, heart and vasculature. The acquisition of data at 10Hz allowed the visualization of the fast uptake kinetics, while longitudinal data acquisition allowed the determination of the differential pharmacokinetic properties of each preparation. Liposomal derivatives containing polyethylene glycol (PEG) were discriminated from those preparations without PEG based on the blood clearance rate as assessed by MSOT. Further, MSOT was used to visualize the organ specificity of various derivatives. MSOT data showed an excellent correlation with ex vivo fluorescence studies. With the ability to visualize and quantify fast kinetics and organ specificity of injected NIR-absorbing agents of interest, MSOT is poised to become an invaluable tool in the drug discovery process by enabling whole-body in vivo visualization of drug biodistribution.

Disclosure of author financial interest or relationships:
**N. Burton**, iThera Medical, Employment; **W.H. Driessen**, iThera Medical, Employment; **S. Morscher**, iThera Medical GmbH, Employment; **J. Claussen**, iThera Medical, Employment; **D. Razansky**, iThera Medical GmbH, Stockholder; **V. Ntziachristos**, ERC, Grant/research support; Ithera Medical, Stockholder .

Presentation Number **SS 42**
Scientific Session 6: Chemistry & Probes - Multimodal
September 6, 2012 / 13:48-14:00 / Room: Liffey Hall 1

# Switchable $^{18}$F Cerenkov probes for *in vivo* pH detection

***Julie Czupryna**, Alexander Kachur, Anatoliy V. Popov, Eric Blankemeyer, Joel S. Karp, Jim Delikatny, Radiology, University of Pennsylvania, Philadelphia, PA, USA. Contact e-mail: czupryna@mail.med.upenn.edu*

A number of the isotopes routinely used for PET imaging will emit photons via a phenomenon called Cerenkov radiation, which occurs when charged particles exceed the speed of light in their surrounding medium. Cerenkov luminescence is multispectral with maximum emission at ~500 nm, but with a substantial fraction of photons emitted between 675 - 850 nm, making this technique potentially useful for near-infrared optical imaging. This property of Cerenkov luminescence permits allows selective bandwidth quenching which can be exploited for the design of probes for dual measurement of function and location. We have synthesized and characterized a number of pH-responsive Cerenkov probes and used them to detect pH changes both *in vitro* and *in vivo*. $^{18}$F labeled Phenol Red (FPR, pKa 7.3) and meta Cresol Purple (FMCP, pKa 7.0) were synthesized by electrophilic fluorination. Under acidic conditions, FPR and FMCP exhibited the expected $1/\lambda^2$ decrease in Cerenkov emission. However, under basic conditions, a wavelength-dependent (500-650 nm) quenching of Cerenkov emission was seen. PET signal corrected for $^{18}$F decay remained unchanged under all conditions. Additionally, the probes exhibited switch-like behavior: sequential addition of acid or base resulted in unquenched and quenched emission, respectively. To test FMCP *in vivo*, mice were treated with acetazolamide (150 mg/kg, i.p., 5d) to promote urine alkalinization. Following treatment, urine pH increased to 8.3, compared to 6.8 in control (PBS) treated mice. FMCP was well tolerated by the mice, and accumulated in the bladder, liver and gall bladder within 1 h. The bladders of the acetazolamide treated mice exhibited a wavelength-dependent quenching in Cerenkov emission, with the most quenching occurring in the 575-650 nm range. Control mice saw no quenching. Again, the corrected PET signal remained unchanged under all conditions. Through the use of novel Cerenkov probes, we have successfully demonstrated selective bandwidth quenching for multispectral optical imaging and the potential for functional imaging of pH *in vivo*. pH-responsive Cerenkov probes could become invaluable tools in oncology to measure acidic extracellular pH of tumors.

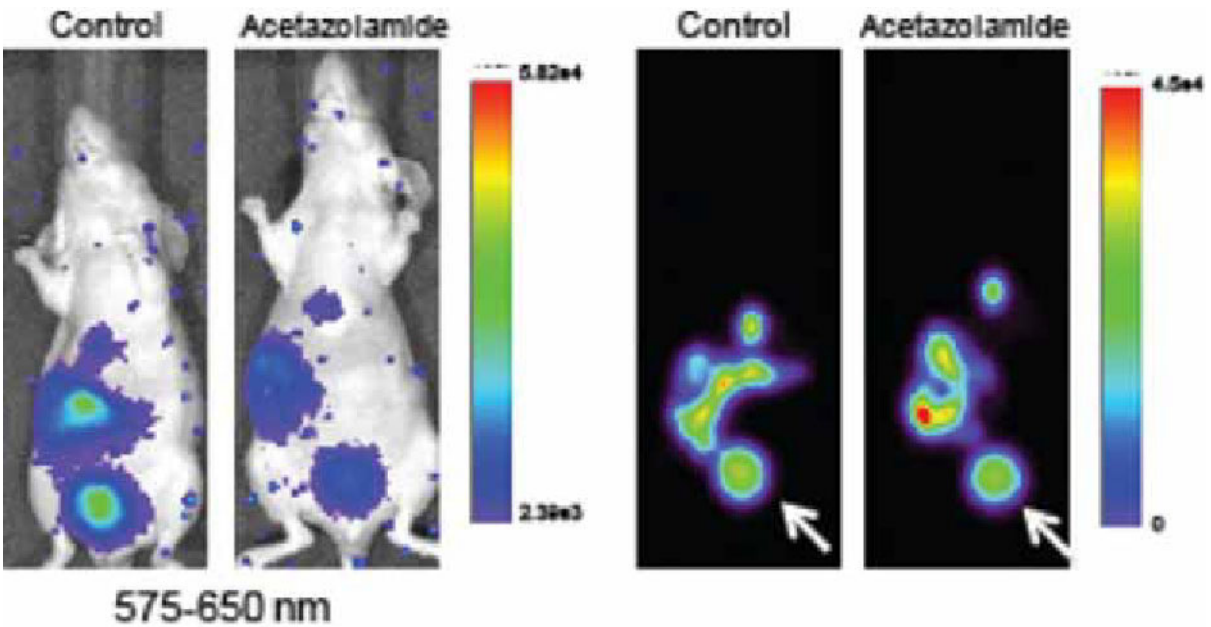


Left: Optical images of control and acetazolamide treated mice injected with 400 µCi MFCP. The bladders of acetazolamide treated mice exhibit decreased Cerenkov emission due to the absorption of Cerenkov radiation by the darkly colored FMCP in basic urine. Right: A-PET images of the same mice show no change in bladder counts (white arrow).

Disclosure of author financial interest or relationships:
**J. Czupryna**, None; **A. Kachur**, None; **A.V. Popov**, None; **E. Blankemeyer**, None; **J.S. Karp**, Philips Healthcare, Grant/research support; **J. Delikatny**, None.

Presentation Number **SS 43**
Scientific Session 6: Chemistry & Probes - Multimodal
September 6, 2012 / 14:00-14:12 / Room: Liffey Hall 1

# Theranostic lipid-polymer hybrid nanoparticles for image guided delivery of dual modality cancer therapy

***Aneta J. Mieszawska***[1], *YongTae Kim*[2], *Brenda L. Sanchez-Gaytan*[1], *Omid C. Farokhzad*[3], *Robert Langer*[2], *Zahi A. Fayad*[1], *Willem J. Mulder*[1], [1]*Translational and Molecular Imaging Institute, Department of Radiology, Mount Sinai School of Medicine, New York, NY, USA;* [2]*Department of Chemical Engineering, Massachusetts Institute of Technology, Cambridge, MA, USA;* [3]*Laboratory of Nanomedicine and Biomaterials, Department of Anesthesiology, Brigham & Women's Hospital, Boston, MA, USA. Contact e-mail: a.mieszawska@gmail.com*

Introduction. The development of nanoparticle formulations with multifunctional features, e.g. combined imaging and drug delivery modules, is facilitated by state-of-the-art nanotherapy production methods. Microfluidics is a high throughput technique that allows swift one-step synthesis of nanoparticles with multiple functionalities. In the current study, we developed a complex lipid-polymer nanoparticle platform for combined cancer therapy, which has the anti-angiogenic drug sorafenib (SRF) and cytotoxic drug doxorubicin (DOX) integrated in its lipid corona and polymeric core, respectively. In addition, the nanoparticle core contains a high payload of gold nanocrystals (AuNCs) as a contrast agent for computed tomography (CT) and cyclodextrins, well-known drug host molecules that sharply elevate the DOX incorporation in the nanoparticle core. Methods and Results. A unique lipid-polymer nanoparticle platform (Figure 1) was synthesized using microfluidics (Figure 2A, B). The core of this nanoparticle platform consisted of poly(lactic-co-glycolic acid) PLGA polymer (lactide/glycolide molar ratio of 50/50) modified with AuNCs that were functionalized with 2-hydroxypropyl beta cyclodextrin (HP-βCD). The AuNCs are electron dense and exhibit good X-ray attenuation properties, which make them suitable as CT contrast media. The PLGA core was coated with natural and PEGylated phospholipids (PEG-DSPE) that provide biocompatibility and long circulation half lives. This lipid coating also served to incorporate lipophilic SRF. Our strategy resulted in 10 (molar %) times higher DOX encapsulation in PLGA nanoparticles as compared to a previously published method where DOX was directly conjugated to the PLGA polymer.1 The incorporation of SRF was 23.5 % as compared to the initial loading value. The mean overall diameter of lipid-polymer nanoparticles with all functionalities was 125.1 nm with a low polydispersity of 0.147 as measured by dynamic light scattering (DLS) (Figure 2C). A transmission electron microscopy (TEM) image (Figure 2D) showed a homogenous incorporation of AuNCs. Additionally, the NIR dye Cy7 was conjugated to the PEG surface of the nanoparticle to allow in vivo NIRF imaging and ex vivo confocal microscopy. The nanoparticles were extensively characterized with respect to stability, drug release, size, CT contrast generating properties, and fluorescence. Conclusion (and future studies). We developed a multifunctional and dual release nanoparticle platform that incorporates two therapeutics and also possesses noninvasive imaging capabilities (CT, NIRF) that will be applied to evaluate nanoparticle targeting. We hypothesize that once our lipid-polymer nanoparticles accumulate at the tumor site through the leaky tumor vasculature, via the enhanced permeability and retention (EPR) effect, the fast release of SRF will induce vascular shutdown and slow degradation of a polymer will lead to the release of DOX. To test this concept the follow up study will include in vitro and in vivo testing.

1. Yoo, H.S., et al., Biodegradable nanoparticles containing doxorubicin-PLGA conjugate for sustained release. Pharm Res, 1999. 16(7): p. 1114-8.

Disclosure of author financial interest or relationships:
**A.J. Mieszawska**, None; **Y. Kim**, None; **B.L. Sanchez-Gaytan**, None; **O.C. Farokhzad**, BIND Biosciences, Consultant; Selecta Biosciences, Consultant; **R. Langer**, None; **Z.A. Fayad**, None; **W.J. Mulder**, None.

Presentation Number **SS 44**
Scientific Session 6: Chemistry & Probes - Multimodal
September 6, 2012 / 14:12-14:24 / Room: Liffey Hall 1

# PET-CT Tracking of Stem Cells in vivo Using Perfluorinated Microcapsules and Reporter Gene Labeling

***Yingli Fu**, Ronnie Mease, Ying Chen, Judith A. Cook, Jeremy Maurer, Meiyappan Solaiyappan, Dara Kraitchman, Radiology, Johns Hopkins-Earth & Planetar, Baltimore, MD, USA. Contact e-mail: yfu7@jhmi.edu*

Introduction: Therapeutic angiogenesis using exogenous stem cells has shown benefits for treating peripheral arterial disease (PAD) patients, who are not amenable for conventional revascularization therapy. However, poor cell retention, low cell survival rate, and the difficulty to track stem cell fate noninvasively in vivo has limited cell therapy efficacy. In the present study, we assess the potential of integrating x-ray-visible cell microencapsulation techniques with triple-fusion (TF) reporter gene labeling for human mesenchymal stem cells (hMSCs) tracking with PET-CT in non-immunosuppressed rabbits. Methods: Bone marrow-derived hMSCs were stably transfected with a lentiviral vector encoding firefly luciferase (fluc, bioluminescence imaging (BLI) reporter), red fluorescence protein (mrfp), and thymidine kinase (hsvtk, PET reporter). Cell microencapsulation was performed using a modification to incorporate perfluorooctylbromide (PFOB) to enable X-ray visibility. BLI was acquired before and after cell encapsulation (Xenogen IVIS 2000). [18F] 9-[4-fluoro-3-(hydroxymethy) butyl] guanine ([18F]-FHBG) was synthesized using a previously described method. For in vitro analysis of radiotracer uptake, MicroPET (GE Explore Vista) was performed in a phantom containing different concentrations of naked TF-hMSCs and PFOB encapsulated TF-hMSCs that were incubated with [18F]-FHBG (20 μCi/ml, 60 min). The microCT image of the phantom was then obtained. For in vivo studies, New Zealand white rabbits (n=6) received 4-6 injections of PFOB encapsulated TF-hMSCs in the medial thigh and a c-arm CT image (Siemens Artis Zee) was obtained prior to [18F]-FHBG administration (1.75±0.7 mCi). Dynamic PET imaging (Siemens HRRT CPS Innovation) was acquired 60 min after radiotracer administration for a period of 30-90 min. PET imaging was repeated one week after delivery. PET images were fused with c-arm CT images to identify the location of transplanted cells using 3D visualization software (Dextroscope). Results: In vitro hMSC viability and transgene expression were not affected by encapsulation (Fig. 1a). PFOB encapsulated TF-hMSCs were visible on both MicroPET (Fig. 1b) and MicroCT images (Fig. 1c). All PFOB cap injections were identified on c-arm CT images in vivo (Fig. 1d). Using PET, around 21% of PFOB microcapsule injection sites in rabbit thigh were identified as "hot spots" and showed high concordance to the radiopacities on c-arm CT (Fig.1e). Conclusion: We demonstrated, for the first time, xenogeneic MSC delivery in non-immunosuppressed large animals using novel x-ray-visible microencapsulation and reporter gene labeling. PFOB microencapsulation of TF-hMSCs maintains cell viability in vivo and enables cell tracking using clinical PET-CT.

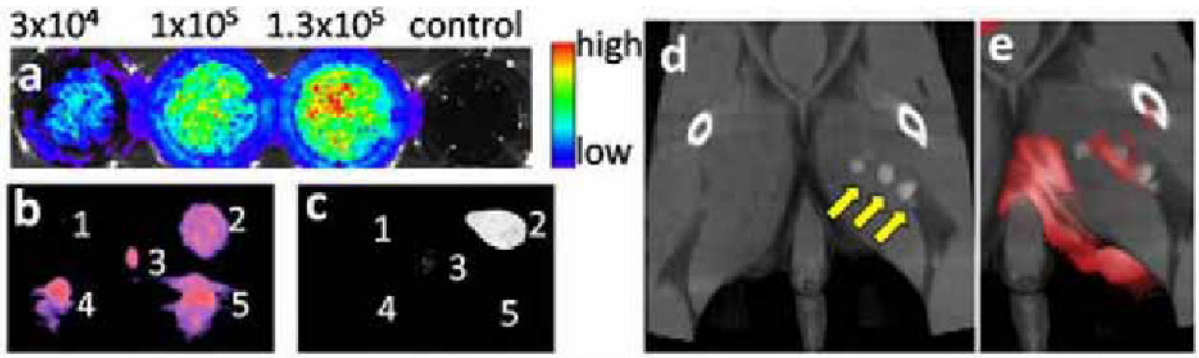


**Figure 1: (a) BLI of PFOB encapsulated TF-hMSCs; (b) MicroPET image of a phantom containing different concentrations of TF-hMSCs or PFOB encapsulated TF-hMSCs (1=5x10⁵ untransfected hMSCs; 2=4x10⁵ PFOB encapsulated TF-hMSCs; 3=1x10⁵ TF-hMSCs; 4=3x10⁵ TF-hMSCs; and 5=5x10⁵ TF-hMSCs; (c) MicroCT image of the same phantom demonstrating the X-ray visibility of PFOB-encapsulated TF-hMSCs; (d) C-arm CT image of the rabbit showing the injection sites of PFOB encapsulated TF-hMSCs; (e) Fusion of PET image with c-arm CT image showing the concordance of "hot spots" with radiopacities.**

Disclosure of author financial interest or relationships:
**Y. Fu**, None; **R. Mease**, None; **Y. Chen**, None; **J.A. Cook**, None; **J. Maurer**, None; **M. Solaiyappan**, None; **D. Kraitchman**, SIemens Healthcare, Grant/research support; Boston Scientific Corporation, Grant/research support; Surefire Medical, Inc., Grant/research support; MRI Interventions, Other financial or material support .

Presentation Number **SS 45**
Scientific Session 7: Technology & Software - PET/SPECT
September 6, 2012 / 13:00-13:11 / Room: Wicklow Hall 1

# A vascular access system for preclinical models

***Brittany N. Berry-Pusey***[1], *Yen-Chi Chang*[2], *Stephen W. Prince*[2], *Kevin Chu*[2], *Waldemar Ladno*[1], *John David*[1], *Robert Silverman*[1], *Richard Taschereau*[1], *David Stout*[1], *Tsu-Chin Tsao*[2], *Arion Chatziioannou*[1], [1]*Crump Institute, UCLA, Los Angeles, CA, USA;* [2]*Mechanical and Aerospace Engineering, UCLA, Los Angeles, CA, USA. Contact e-mail: bberrypuzey@mednet.ucla.edu*

Preclinical Molecular Imaging technologies have an increasingly broader application base while at the same time are becoming more user-friendly. Tail vein injections are a routine but critical step in most imaging applications, with poor injections greatly affecting the experimental results. The high skill set required to perform tail vein injections leaves many preclinical imaging scientists ill-suited to perform this task. In a recent study, we found that routine injections in mice left anywhere between 1-50% of the injected probe in the tail tissue. Improvements in injection accuracy, injection consistency, safety, and a reduction in time required to perform the task are needed in preclinical molecular imaging. To achieve this, we have devised a semi-automated vascular access system (VAS) to facilitate injections and blood sampling from the mouse tail. We have eliminated much of the human error involved in the manual approach by using a computer controlled mechanically moving micro-needle. To utilize the VAS, a user places an anesthetized mouse onto the temperature controlled mouse bed and secures the tail on a heated tail holder. The VAS uses NIR light, cross-polarizers, and a basic CCD camera to image the tail. The reflection image is processed and the vein is located using edge detection methods. The vein location is plotted and overlaid onto the live video feed of the mouse tail. Using a custom designed user interface, the user properly aligns the needle to the tail vein by employing computer controlled motors. Once the needle is properly aligned, it begins to penetrate the tail tissue and enter the vein. A pressure transducer attached to the needle detects when the needle has entered the vein, and automatically stops further progression of the needle. With the needle inside the vein, probes are injected via a syringe pump. The VAS was first validated using a mouse tail phantom. The phantom was a PDMS chip with channels equivalent to the dimensions of a mouse tail vein (≈300um). The channels were filled with water and pressurized to variable pressures. With the phantom, the ability for the VAS to align a needle according to an image, insert a needle into a desired location, and stop the progression of the needle based on a pressure signal were tested and verified. Mouse studies were also performed with the VAS. These studies showed that the accuracy of the device, as measured by the percentage of injected probe left in the tail, is approximately 17% (+/- 6.8%). The VAS reduces the operator skill requirements and training, has the potential to improve injection accuracy, reduces the time required to perform a tail vein injection, and is safer in comparison to current manual methods. We continue to optimize the prototype VAS to further reduce the residual probe left in the tail and decrease user input requirements.

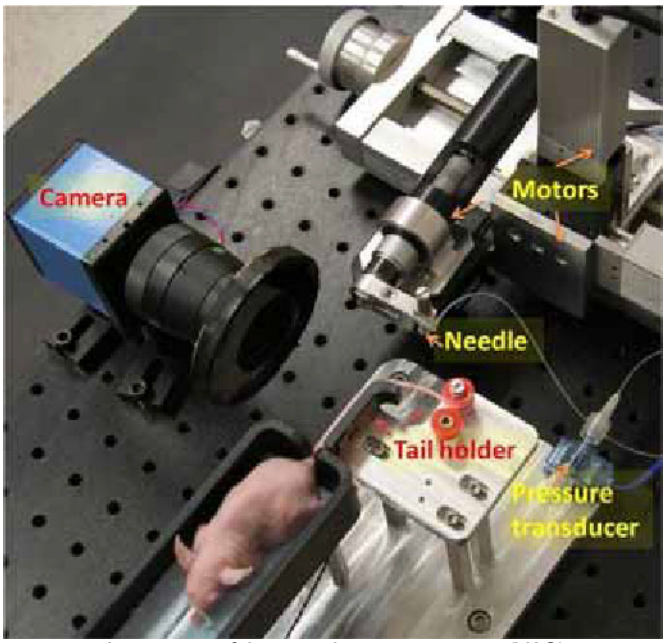

A prototype of the vascular access system (VAS)

Disclosure of author financial interest or relationships:
**B.N. Berry-Pusey**, None; **Y. Chang**, None; **S.W. Prince**, None; **K. Chu**, None; **W. Ladno**, None; **J. David**, None; **R. Silverman**, None; **R. Taschereau**, Sofie Biosciences, Consultant; **D. Stout**, Sofie Biosciences, Stockholder; **T. Tsao**, None; **A. Chatziioannou**, Sofie Biosciences, Other financial or material support .

Presentation Number **SS 46**
Scientific Session 7: Technology & Software - PET/SPECT
September 6, 2012 / 13:11-13:22 / Room: Wicklow Hall 1

# Developing a system for the molecular imaging of freely moving rats

***Andre Kyme***[1,2], *John Eisenhuth*[3], *Victor Zhou*[5], *Will Ryder*[2,3], *Georgios I. Angelis*[2,3], *Kata Popovic*[2,3], *Rezaul Bashar*[2], *Roger Fulton*[3,4], *Steven Meikle*[2,3], [1]*School of Physics, University of Sydney, Sydney, NSW, Australia;* [2]*Brain & Mind Research Institute, University of Sydney, Sydney, NSW, Australia;* [3]*Faculty of Health Sciences, University of Sydney, Sydney, NSW, Australia;* [4]*Department of Medical Physics, Westmead Hospital, Sydney, NSW, Australia;* [5]*Faculty of Built Environment, University of Central Queensland, Mackay, QLD, Australia. Contact e-mail: a.kyme@physics.usyd.edu.au*

Using molecular imaging to obtain time-activity data from the organs of living animals that are free to move, behave and respond to stimuli is a tantalising prospect for preclinical investigations. Here we report the current status of a system designed in our laboratory to realise this goal in positron emission tomography (PET) of rats. Imaging a freely moving animal in a narrow axial field of view (FOV) scanner is facilitated by robot-controlled adjustment of the animal chamber. Slow, smooth compensatory movements of the chamber based on the animal's position maintain the head centrally in the FOV over 80% of the time. Motion estimation is performed using multi-camera optical tracking of either an attached marker or alternatively of native features on the animal. The latter approach is simpler to perform, less invasive, and removes the risk of marker detachment. Moreover, in phantom studies involving a taxidermied rat head, the method resulted in motion estimates that were ten times more accurate than marker-based estimates. A method to correct for refraction-induced error resulting from motion tracking through a transparent chamber has also been developed to improve the accuracy of motion measurements. To reconstruct PET data corrupted by motion, a fully 3D list mode algorithm with built in motion compensation is under development. This algorithm has been validated in digital mouse phantom simulations with realistic head motion. Also under development is partial volume correction based on an anatomical rat atlas which is kept in constant alignment with the known, changing pose of all/part of the animal. This correction is likely to be necessary for proper quantification of uptake and time-activity data in organs or regions-of-interest in rats and mice. In conclusion, a system for motion-compensated PET imaging of awake, unrestrained rats is being developed and we have successfully trialled the data acquisition aspects of the system in two pilot studies with freely moving rats. Further work is required to develop attenuation and scatter correction methods to deal with variations in body pose as the animal moves around the chamber.

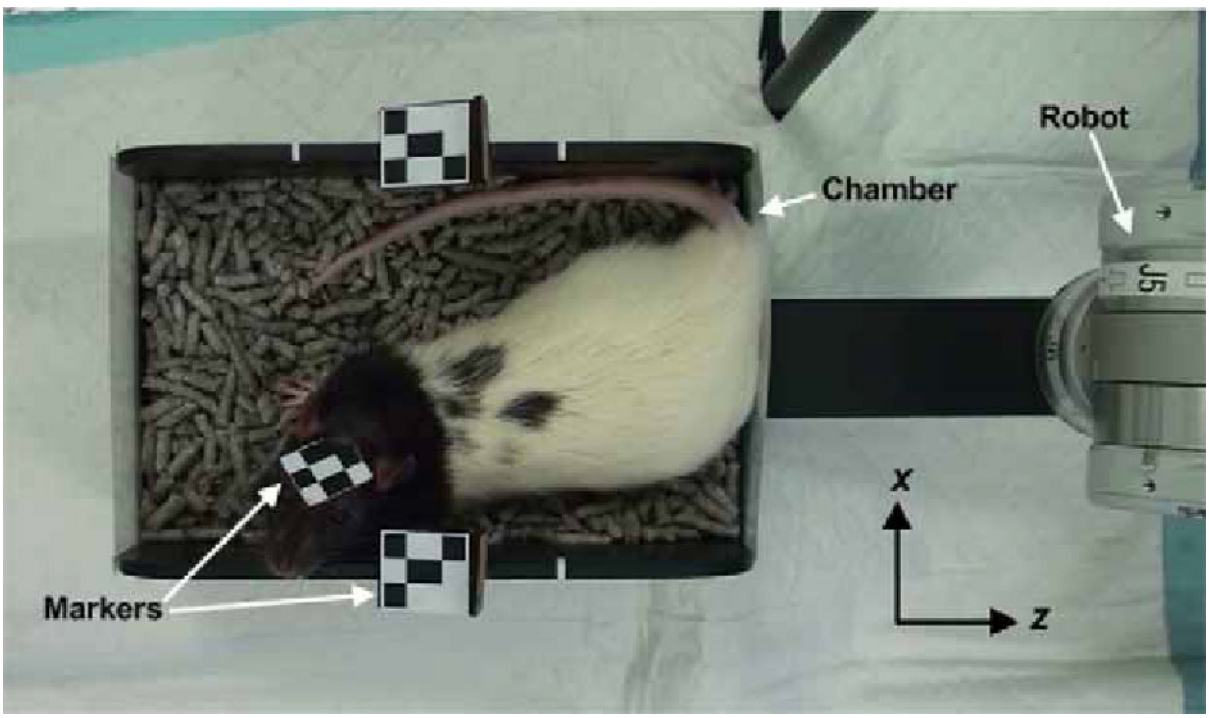


Freely moving rat inside the motion-adaptive chamber. The chamber attaches to a robot and is adjusted in the horizontal (x-z) plane to maintain the head near the centre of the scanner FOV. Here, attached markers on the head and chamber are being used for motion tracking.

Disclosure of author financial interest or relationships:
**A. Kyme**, None; **J. Eisenhuth**, None; **V. Zhou**, None; **W. Ryder**, None; **G.I. Angelis**, None; **K. Popovic**, None; **R. Bashar**, None; **R. Fulton**, None; **S. Meikle**, None.

Presentation Number **SS 47**
Scientific Session 7: Technology & Software - PET/SPECT
September 6, 2012 / 13:22-13:33 / Room: Wicklow Hall 1

# Simultaneous imaging of myocardial perfusion and neuronal activity in rat hearts using dynamic pinhole SPECT

*Rostyslav Boutchko[1], Kathleen M. Brennan[1], Ruud M. Ramakers[2], Frederik J. Beekman[2], **Grant T. Gullberg**[1], [1]Lawrence Berkeley Natl Lab, Berkeley, CA, USA; [2]MILabs, Utrecht, Netherlands. Contact e-mail: gtgullberg@lbl.gov*

Objectives: We aim to develop quantitative dynamic imaging methods for perfusion and neuronal activity in a rat heart using pinhole SPECT systems. Methods: A single 1.5x2 mm tungsten pinhole collimator was mounted on each detector head of the GE Millennium VG3 Hawkeye SPECT-CT camera. The system was calibrated and prepared to image up to 5-6 cm-wide object with sub-mm resolution. While acquiring projection data, an anesthetized rat was injected with 1 mCi of [201]Tl and imaged for 18 min and then injected with 5 mCi of [123]I-MIBG and imaged for another 90 min. Dynamic data were acquired with slowly rotating detector heads (90 sec rotation) and reconstructed as 3D image sequences and as standard static images using the sum of the dynamic data. Time-activity curves (TACs) were generated for the left ventricle (LV) and for blood sampled from the LV blood pool. The same protocol was performed using a dedicated small animal scanner (U-SPECT-II) with stationary detector arrays cover 3600.. Results: Dynamic series of images of the rat heart were reconstructed from the data acquired using both systems. The image quality for the latter time frames was sufficiently high for studying the static distribution and the wash-out dynamics. However, the signal sensitivity in the modified GE system is lower than in the dedicated system; also, the time frame duration is limited by the gantry speed (90 sec / rotation). Conclusions: A clinical SPECT scanner can be modified to perform dynamic small animal imaging studies, although with much lower sensitivity and time resolution than with U-SPECT-II. Unlike in U-SPECT-II, the time activity curves of the initial blood input, the uptake in the tissue, and most kinetic model parameters must be estimated directly from the dynamic projection measurements. The developed methodology is applied to study changes in perfusion and innervation with progression of cardiac hypertrophy in a study on the spontaneously hypertensive rat model.

Disclosure of author financial interest or relationships:
**R. Boutchko**, None; **K.M. Brennan**, None; **R.M. Ramakers**, MILabs B.V., Employment; **F.J. Beekman**, MILabs, Stockholder; MIlabs, Honoraria; MILabs, Grant/research support; **G.T. Gullberg**, None.

Presentation Number **SS 48**
Scientific Session 7: Technology & Software - PET/SPECT
September 6, 2012 / 13:33-13:44 / Room: Wicklow Hall 1

# Evaluation of Multiplexing Strategies for a cMiCE PET Detector

***Robert Miyaoka**, William C. Hunter, Radiology, University of Washington, Seattle, WA, USA. Contact e-mail: rmiyaoka@u.washington.edu*

Continuous miniature crystal element (cMiCE) PET detectors use monolithic scintillator crystals coupled to arrays of photosensor elements and statistics based methods for positioning of detected events. While cMiCE detectors achieve excellent three-dimensional positioning within the crystal element, current implementations acquire and utilize all photosensor array channels (e.g., 64 channels for an 8x8 array of PMT or SiPM sensors). In this work, we investigate different multiplexing strategies to reduce the number of acquired signal channels and their impact on positioning performance. Methods: This study was conducted using cMiCE PET detectors comprised of a 50 mm x 50 mm x 8 mm LYSO crystal coupled to a 52 mm x 52 mm, 64 channel multi-anode PMT. The data were binned into 0.25 mm X,Y bins and four depth of interaction (DOI) bins. All 64 signals were collected from the detector and multiplexing strategies were implemented in software. The initial DOI characterization of the detector was done using all 64 signal channels. However after the initial depth separation of data, look up tables and statistics based positioning (SBP) were implemented using the multiplexed signals. Multiplexing strategies investigated included row-column (RC) summing of signals (64 channel -> 16 channel); sampling based upon a modulus 3 and modulus 5 patterns of detector channels (64 -> 16); and a variants of RC summing with greater and lesser signal multiplexing (e.g., 64 -> 20 or 64 -> 8). Results: The average X,Y intrinsic spatial resolution for the cMiCE detector using all 64 channels for positioning was 1.28 mm FWHM in X and Y. This is for a 46 mm by 46 mm imaging area of the 50 mm by 50 mm crystal detector. For standard RC summing of signals the average intrinsic X,Y spatial resolution was 1.33 mm. The intrinsic spatial resolution for the modulus 3 and 5 multiplexing was 1.49 mm. Based upon these results, higher and lower levels of multiplexing were explored using variants of RC summing. A RC summing method that used three addition multiplexed channels along the edges of the crystal provided similar decoding performance as standard RC summing (i.e., 1.33 mm FWHM) but better visual spatial positioning in the corners and edges of the detector. In addition, RC summing methods that required only 10 acquisition channels were implemented with only a small degradation in performance (i.e., 1.42 mm FWHM). Conclusions: Signal multiplexing techniques can be applied to monolithic crystal PET detectors that utilize statistics-based positioning methods. While acquiring and utilizing all individual channels for positioning provides the best results, reductions in the number of acquisition signal channels of a factor of 3-5 resulted in only 4-10% degradation in spatial resolution performance. The main areas of degraded intrinsic spatial resolution performance were at the corner and edges of the crystal detector. Going to a trapezoidal crystal shape to improve the packing fraction of a preclinical imaging system may help to mitigate the performance degradation by reducing the edge effect along two sides of a detector.

Intrinsic Spatial Resolution

| | Average FWHM (mm) | Average FWHM (excluding edges) (mm) |
|---|---|---|
| 64-channel SBP | 1.28 | 1.33 |
| Row-column (16 | 1.33 | 1.39 |
| Row-column modified (19) | 1.33 | 1.39 |
| Row-column (10 | 1.42 | 1.46 |
| Modulus 3, 5 | 1.49 | 1.51 |

Disclosure of author financial interest or relationships:
**R. Miyaoka**, Philips Medical Systems, Grant/research support; Zecotek Medical Systems, Grant/research support; **W.C. Hunter**, Philips Medical Systems, Other financial or material support; Zecotek, Other financial or material support .

Presentation Number **SS 49**
Scientific Session 7: Technology & Software - PET/SPECT
September 6, 2012 / 13:44-13:55 / Room: Wicklow Hall 1

# Development of an ultrahigh resolution Si-PM based PET system for small animals

***Seiichi Yamamoto***[1], *Hiroshi Watabe*[2], *Yasukazu Kanai*[2], *Katsuhiko Kato*[1], *Jun Hatazawa*[2,3], [1]*Radiological and Medical Laboratory Sciences, Nagoya University Graduate School of Medicine, Nagoya, Japan;* [2]*Department of Molecular Imaging, Osaka University Graduate School of Medicine, Suita, Japan;* [3]*Nuclear Medicine and Tracer Kinetics, Osaka University Graduate School of Medicine, Suita, Japan. Contact e-mail: s-yama@met.nagoya-u.ac.jp*

A high resolution PET system is needed for small animal imaging, especially for mouse studies. We have previously developed a Si-PM-based PET system for small animals that employed 4 x 4 Si-PM arrays that were optically coupled with an 11 x 9 LGSO block of 1.1 x 1.2 mm LGSO pixels [1]. The position histogram for the 511-keV gamma photons had enough margins to use a much smaller scintillator, suggesting the possibility of developing an ultrahigh resolution PET system with less than 1-mm sized scintillators. Consequently, we developed a new small animal PET system that decreased the size of the scintillator approximately half of the previously developed Si-PM based PET system and measured the performance. The newly developed PET system used 0.5mm x 0.7mm x 5mm LYSO pixels arranged in an 11 x 13 matrix to form a block with 0.1mm BaSO4 reflector between the pixels. Two LYSO blocks were optically coupled to two optical fiber based angled image guides with a light guide. These LYSO blocks, Image guides and light guide were coupled to a Si-PM array (Hamamatsu MPPC S11064-050P). Eight block detectors (16 LYSO blocks) were arranged in a 34mm inner diameter ring to form an small animal PET system. The block detector showed good separation for 22 x 13 LGYSO pixels in the two dimensional position histogram. The energy resolution was 16% for 662keV gamma photons. The transaxial resolution using 0.25mm diameter Na-22 point source, reconstructed by the filtered backprojection was 0.75mm and axial resolution was 0.84mm at the image center. The point source sensitivity was 0.19% at the central axial field of view. Ultrahigh resolution mouse images could be obtained for F-18-NaF studies using the PET system. The developed ultrahigh resolution PET system showed attractive images for mouse studies and have a potential to provide new findings in molecular imaging researches. (1) S. Yamamoto, et al. Phys Med Biol. 55(19):5817-31, 2010

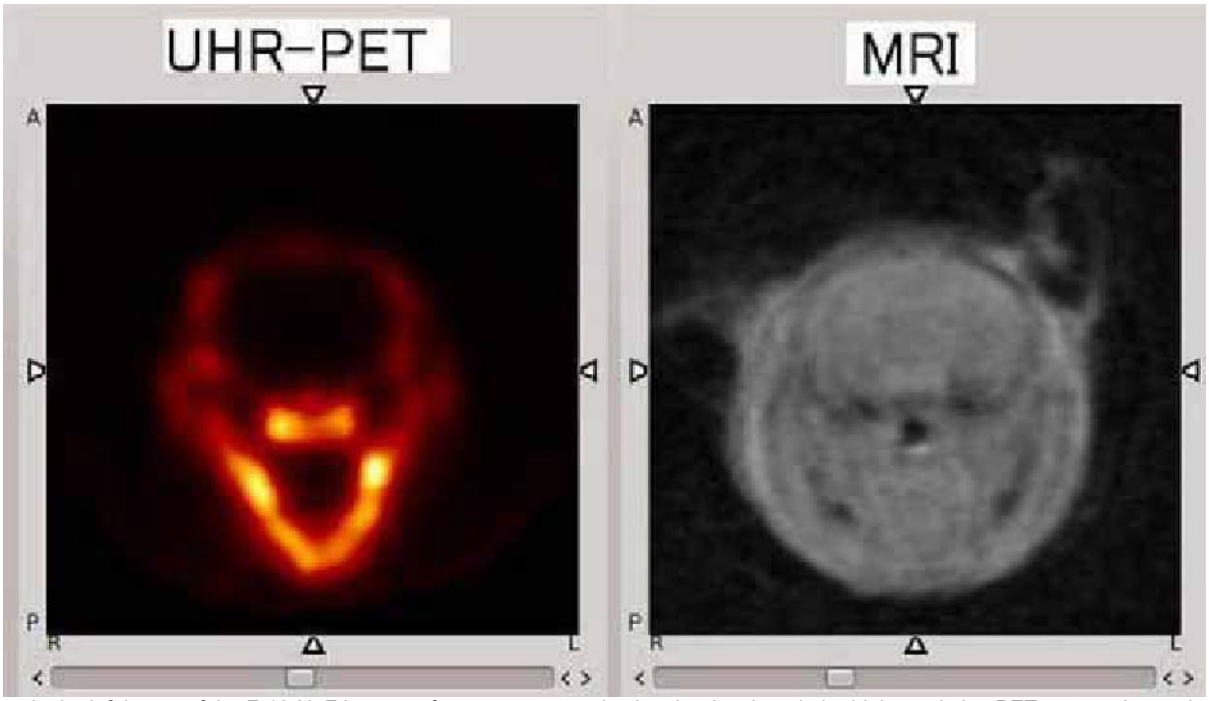


Image shown in the left is one of the F-18-NaF images of mouse measured using the developed ultrahigh resolution PET system. Image in the right is the MRI image of the same slice.

Disclosure of author financial interest or relationships:
**S. Yamamoto**, None; **H. Watabe**, None; **Y. Kanai**, None; **K. Kato**, None; **J. Hatazawa**, None.

Presentation Number **SS 5**
Scientific Session 1: Chemistry & Probes - MRI
September 6, 2012 / 11:14-11:25 / Room: Liffey Hall 1

# Using $T_2$-exchange from $Ln^{3+}$DOTA-based chelates for MR contrast-enhanced molecular imaging

***Todd C. Soesbe***[1,2], *S James Ratnakar*[1], *Dean Sherry*[1,2], [1]*Advanced Imaging Research Center, UT Southwestern Medical Center, Dallas, TX, USA;* [2]*Department of Radiology, UT Southwestern Medical Center, Dallas, TX, USA. Contact e-mail: todd.soesbe@utsouthwestern.edu*

Magnetic resonance imaging (MRI) offers superior anatomic resolution and soft tissue contrast compared to x-ray computed tomography, making it an excellent tool for cancer prevention studies. The endogenous contrast created by the varying $T_1$ and $T_2$ relaxation times of different tissue types can be greatly enhanced by the use of exogenous contrast agents. Currently, the effectiveness of MRI in the functional and molecular imaging regime is limited due to the lack of highly sensitive molecularly targeted contrast agents. Creating such agents would greatly improve the use of MRI, for example, in the early detection and diagnosis of cancer. We have recently shown that $Ln^{3+}$DOTA chelates ($Ln^{3+}$ ≠ La, Gd, Lu) create enhanced negative contrast (i.e., darkening) through the chemical exchange of water molecules (1). This "$T_2$-exchange" contrast, which adds to the inherent paramagnetic $T_2$ contrast of the $Ln^{3+}$ ion, reaches a maximum at a specific water molecule exchange rate. We have also demonstrated that $T_2$-exchange contrast can be increased by several orders of magnitude through simple linear polymerization of the $Ln^{3+}$DOTA chelate (2). By using these two methods, a highly sensitive $T_2$ contrast agent with a transverse relaxivity ($r_2$) an order of magnitude greater than any currently existing contrast agent (e.g., super paramagnetic iron oxide particles) can be created, while retaining the advantages of using small molecules rather than nanoparticles for improved biological targeting, uptake, and clearing. For initial proof of principle, the $Eu^{3+}$DOTA-$(gly)_4$ monomer ($r_2$=0.5 $sec^{-1}mM^{-1}$) was polymerized by a factor of ~20 times (2), which increased $r_2$ proportionally. Renal filtration of the $Eu^{3+}$ polymer in healthy mice was used to assess the negative contrast using a 70 μmol/kg intramuscular dose of polymer (1.40 mmol/kg of $Eu^{3+}$) (see Fig. 1). In order to improve sensitivity, $Dy^{3+}$DOTA-based monomers have also been synthesized. $Dy^{3+}$ has the largest bound water chemical shift (Δω) and one of the largest paramagnetic relaxation enhancements of the lanthanides. Both characteristics, combined with the ideal water molecule exchange rate, will maximize the level of $T_2$ contrast achieved for the monomer structure (e.g., ~16 $sec^{-1}mM^{-1}$). Subsequent polymerization of the $Dy^{3+}$DOTA-based chelate will then increase the level of $T_2$ contrast from 20 to 100 times (320 to 1600 $sec^{-1}mM^{-1}$). Our long-term goal is to use $T_2$-exchange to create molecule-sized $T_2$ contrast agents that are comparable in sensitivity to ion oxide nanoparticles. Molecular targeting groups (e.g., biotin or folic acid) will then be attached to the backbone of the liner polymer chain to target specific cell receptors. One advantage of this linear structure is that multiple molecular targeting sites can be placed along the polymer chain to significantly improve their affinity to the target receptors. 1. Soesbe TC, et al., $T_2$ exchange agents: a new class of paramagnetic MRI contrast agent that shortens water $T_2$ by chemical exchange rather than relaxation, Mag Res Med 2011;66:1697-1703. 2. Wu YK, et al., Polymeric PARACEST agents for enhancing MRI contrast sensitivity. J Am Chem Soc 2008;130:13854-13855.

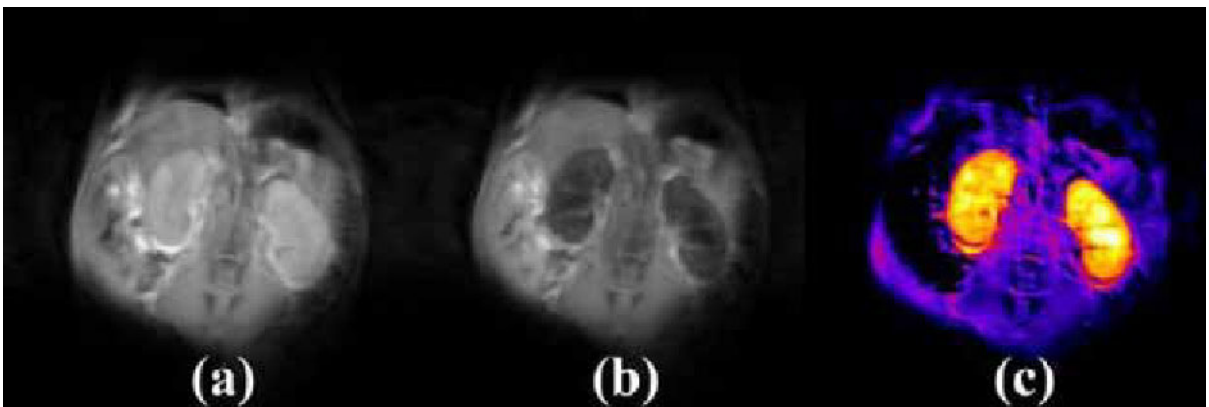


Fig. 1: Fast spin-echo coronal images of healthy mouse kidneys (a) before and (b) after a 70 μmol/kg intramuscular dose of the $Eu^{3+}$DOTA-$(gly)_4$ polymer (1.40 mmol/kg of $Eu^{3+}$). (c) The difference image (a)-(b) shows a 50% drop in kidney signal due to $T_2$-exchange. In vivo mages were acquired at 37 °C using an Agilent 9.4 T system and a 20 mm diameter surface coil.

Disclosure of author financial interest or relationships:
**T.C. Soesbe**, None; **S. Ratnakar**, None; **D. Sherry**, None.

Presentation Number **SS 50**
Scientific Session 7: Technology & Software - PET/SPECT
September 6, 2012 / 13:55-14:06 / Room: Wicklow Hall 1

# SPECTRAL ANALYSIS ITERATIVE FILTER METHOD FOR VOXEL-WISE QUANTIFICATION OF PET TRACERS WITH IRREVERSIBLE UPTAKE IN NOT BRAIN TISSUES

***Mattia Veronese***[1]*, Gaia Rizzo*[1]*, Bret H. Goodpaster*[2]*, Julie C. Price*[3]*, Eric O. Aboagye*[4]*, Alessandra Bertoldo*[1]*,* [1]*Department of Information Engineering, Padova University, Padova, Italy;* [2]*Division of Endocrinology and Metabolism, Department of Medicine, University of Pittsburgh, Pittsburgh, PA, USA;* [3]*Department of Radiology, University of Pittsburgh School of Medicine, Presbyterian University Hospital, Pittsburgh, PA, USA;* [4]*Comprehensive Cancer Imaging Center, Imperial College of London, London, United Kingdom. Contact e-mail: mattiaveronese@gmail.com*

**INTRODUCTION** Spectral Analysis Iterative Filter (SAIF) is a Spectral Analysis (SA) based method originally developed for the quantification of L-[1-$^{11}$C]Leucine PET brain data [1]. The method implements a filtering procedure which aims to reduce the impact of the noise and to describe the tracer time-activity curve in tissue in terms of an optimal subset of kinetic components. As the other SA techniques, SAIF allows also to quantify physiological macroparameters, as the irreversible uptake of tracer in the tissue ($K_i$, ml/g/min), and it can be applied both to homogenous and heterogeneous tissues (no a priori assumptions required). This study aims to verify the extendibility of SAIF for the voxel-wise quantification of not brain tissues investigated with irreversible uptake PET tracers. **MATERIAL AND METHODS** Two different datasets were analyzed at voxel level: [$^{18}$F]FDG in skeletal muscle [2] (5 subjects) and [$^{18}$F]-FLT in breast cancer [3] (3 subjects). For each tracer voxel-wise analysis was performed with both standard SA and SAIF methods and results compared to other voxel-wise methods, i.e. Weighted Non-Linear Least Squares (WNLLS) applied to compartmental model and Patlak plot. As performance index, mean relative differences (MRD) of voxel $K_i$ estimates between methods has been evaluated. The agreement of parametric maps and rate of estimates in not physiological range (voxel failure rate, VFR) were computed. **RESULTS** Analysis of [$^{18}$F]FDG data showed high correlation ($R^2$>0.97) and consistency between all the compared methods (Fig, Panel A), even if Patlak tends to overestimate spectral analysis results (MRD ~10%) which overestimated voxel-wise WNLLS estimates as well (MRD ~11%). SAIF resulted to be more robust with a VFR <1%, whereas more than 40% of SA estimates had to be eliminated because not physiological (Fig, Panel C). In [$^{18}$F]FLT, high correlation ($R^2$=0.99) was detected for all the methods. The higher discrepancy in mean of voxel-wise results was measured between Patlak and WNLLS (Fig, Panel B) in healthy breast (MRD -15%) and in tumor regions (MRD -10%). Both SA and SAIF reported MRD <10% in healthy breast and <3% in tumor regions. In general the higher the tissues uptake, the lower the difference between methods. SAIF demonstrated to be the most robust method with VFR <20% in healthy breast and <1% in tumor (Fig, Panel D). This result was not achieved by standard SA and Patlak plot. WNLLS demonstrated to be the most sensible to the noise in the data (VFR >50% in healthy breast and >20% in tumor). The different behaviour in these regions is justifiable by the higher uptake of the tracer in tumor than in healthy breast (~3 times more). **CONCLUSIONS** Our results confirmed the possibility to use SAIF as a valid alternative for the voxel analysis of PET tracer with irreversible tissue uptake. SAIF showed to be more robust to the noise in the data compared with all the other methods including the Patlak plot and not filtered spectral analysis. The method is ready for clinical application. **REFERENCES** [1] Veronese M et al., JCBFM 2010 [2] Bertoldo A et al., Am J Physiol Endocrinol Metab 2001 [3] Kenny LM et al., Cancer Research 2005

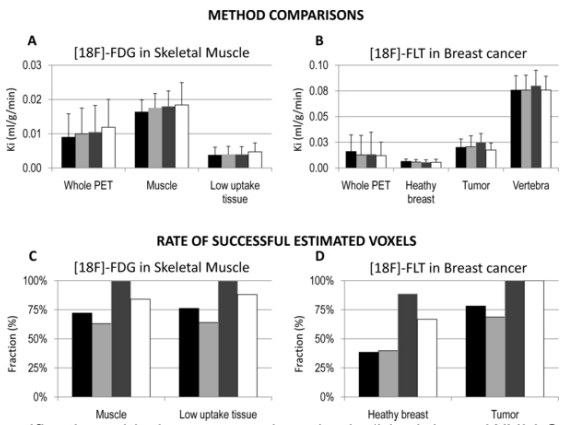


The figure shows the results of voxel-wise quantification with the proposed methods (black bars: WNLLS; light-gray bars: standard SA; dark-gray bars: SAIF; white bars: Patlak plot) for [ $^{18}$F]FDG applied to skeletal muscle (panel A and C) and for [ $^{18}$F]FLT applied to breast cancer subjects (panel B and D). Panel A and B compare the means of voxel-wise $K_i$ estimates within regions of interest. Panel C and D report the fractions of successfully estimated voxels over all region voxels.

Disclosure of author financial interest or relationships:
**M. Veronese**, None; **G. Rizzo**, None; **B.H. Goodpaster**, None; **J.C. Price**, None; **E.O. Aboagye**, GE Healthcare, Grant/research support; **A. Bertoldo**, None.

Presentation Number **SS 51**
Scientific Session 7: Technology & Software - PET/SPECT
September 6, 2012 / 14:06-14:17 / Room: Wicklow Hall 1

# Comparison of Scatter-Compensation Methods in Simultaneous $^{99m}$Tc/$^{111}$In SPECT-CT for Improved Visualization of Bone Infection

***Morgan Cervo***[1], *Victor H. Gerbaudo*[1,2], *Stephen C. Moore*[1,2], [1]*Radiology, Brigham and Women's Hospital, Boston, MA, USA;* [2]*Radiology, Harvard Medical School, Boston, MA, USA. Contact e-mail: mcervo@bwh.harvard.edu*

**Introduction:** Simultaneous Tc-99m sulfur colloid (SC) and In-111 white blood cell (WBC) SPECT-CT is the best available imaging method for diagnosis of osteomyelitis (OM), an infection of the bone marrow. This approach provides perfect spatial registration of two anatomo-physiologic processes: Tc-99m in healthy bone marrow, and In-111 at sites of infection. Anatomical information from the CT then localizes the lesion to either bone or soft tissue. Diagnosis of OM is based on a visual assessment of discordant uptake between Tc-99m and In-111, where a region of high In-111 activity with decreased Tc-99m activity in bone marrow is indicative of OM. Accurate activity quantitation is therefore key to discriminating OM from other processes e.g., cellulitis. While not commonly implemented in the clinic, compensation for photon scatter and crosstalk between radionuclides can be used to obtain more quantitatively accurate and precise tomographic images. Here we compare our Monte Carlo-based joint OSEM (MC-JOSEM) algorithm, which reconstructs both radionuclides simultaneously, with the more conventional Triple Energy Window-based reconstruction (TEW-OSEM). **Methods:** We created a numerical torso phantom by segmenting a CT into soft tissue, bone, liver, spleen and bladder. Ten lesions representing infection were placed within bones of the legs, pelvis and spine. Counts per voxel were scaled to values appropriate for Tc-99m SC and In-111 WBC. Poisson-noise deviates were generated from high-count phantom simulations to create 10 data sets. Data were reconstructed using MC-JOSEM, TEW-OSEM as well as a common clinical method, OSEM with no compensation for scatter (NC-OSEM). Algorithms were evaluated by measuring the average counts in volumes of interest (VOI). Simulated scatter-free data were used as the gold standard from which bias, precision and mean-squared error of each method were calculated. In addition to the simulations, we reconstructed patient images of the head, knee, and foot with MC-JOSEM and TEW-OSEM. All 3 subjects had been referred for simultaneous Tc-99m/In-111 SPECT-CT for evaluation of suspected OM and were read as consistent with OM, inconsistent with OM, or indeterminate based on clinical reconstructions (NC-OSEM). Patient reconstructions with each method were assessed qualitatively for lesion contrast, spatial definition, and scatter.**Results:** For NC-OSEM reconstructions of the torso phantom, the bias ± precision when averaged over all infection regions and noise realizations was 62.5±15.0% for Tc-99m and 7.3±11.9% for In-111. TEW-OSEM scatter compensation reduced Tc-99m bias to 7.7±19.0% and In-111 to 6.8±11.9%. MC-JOSEM produced the least biased results with -5.6±17.1% for Tc-99m and -2.6±12.1% for In-111. Patient images reconstructed using MC-JOSEM and TEW-OSEM showed improved lesion contrast in comparison to NC-OSEM. MC-JOSEM reconstructions additionally suppressed background noise as well as patient and table scatter better than NC-OSEM and TEW-OSEM. **Conclusion:** Compensation for scatter and crosstalk improves quality, bias and precision of activity estimates in simultaneous dual-radionuclide imaging of OM.

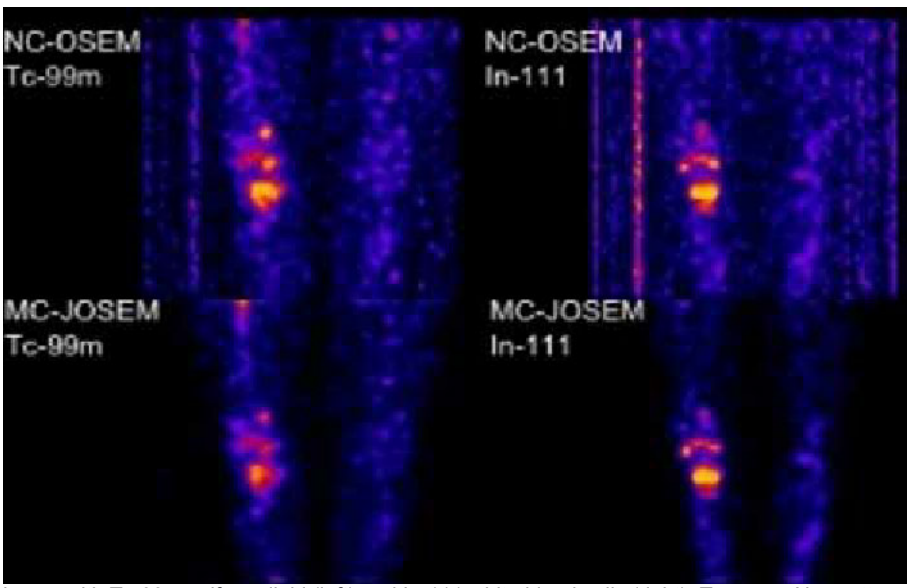


Coronal MIP images of the knees with Tc-99m sulfur colloid (left) and In-111 white blood cells (right). **Top row**: No scatter compensation. **Bottom row**: Monte Carlo-based scatter compensation.

Disclosure of author financial interest or relationships:
**M. Cervo**, None; **V.H. Gerbaudo**, None; **S.C. Moore**, None.

Presentation Number **SS 52**
Scientific Session 7: Technology & Software - PET/SPECT
September 6, 2012 / 14:17-14:28 / Room: Wicklow Hall 1

# Tracking of transplanted stem cells in myocardial infarction model rat: validation of simultaneous dual-isotope SPECT imaging with Tc-99m and Tl-201

***Tsutomu Zeniya***[1], *Hidekazu Kawashima*[1], *Kentaro Otani*[2], *Hajime Fukuda*[1], *Yoshiko Hashikawa*[1], *Kazuhiro Koshino*[1], *Yuki Hori*[1], *Tetsuaki Moriguchi*[1], *Jun-ichiro Enmi*[1], *Satoshi Iguchi*[1], *Akihide Yamamoto*[1], *Yoshinori Miyake*[1], *Masayuki Inubushi*[3], *Hidehiro Iida*[1], [1]*Department of Investigative Radiology, National Cerebral and Cardiovascular Center Research Institute, Suita, Japan;* [2]*Department of Regenerative Medicine and Tissue Engineering, National Cerebral and Cardiovascular Center Research Institute, Suita, Japan;* [3]*Molecular Imaging Center, National Institute of Radiological Sciences, Chiba, Japan. Contact e-mail: zeniya@ri.ncvc.go.jp*

Objectives: With the arrival of regenerative therapy by stem cell transplantation, evaluating engraftment of transplanted stem cells is required. The sodium-iodide symporter (NIS), which promotes in vivo cellular uptake of radioisotope, as a reporter gene allows PET or SPECT to longitudinally track the transplanted stem cells noninvasively. In SPECT, not only cell tracking but also tissue blood flow as an indicator for the effect of the therapy is expected to be simultaneously evaluated because multiple isotopes with different energies are available. This study intended to validate simultaneous dual-isotope imaging for tracking the transplanted stem cells and evaluating myocardial blood flow (MBF) in myocardial infarction (MI) model rat using small animal SPECT/CT system (NanoSPECT/CT; Bioscan) with four detectors and multi-pinhole collimators. Methods: The syringes respectively filled with Tc-99m and Tl-201 were simultaneously scanned. It was evaluated if only one radioisotope was depicted by cross-talk correction. Before rat study, we imaged transgenic (Tg) mouse with 99mTc-petechnetate and confirmed expression of human NIS (hNIS). In rat study, hNIS-Tg mouse adipose derived stem cells (ASC) were injected into boundary area of MI. Two days after transplantation, SPECT for 3 hours (10 min x 18) and X-ray CT scans were performed immediately after simultaneous injection of 99mTc-pertechnetate (415 MBq) and Tl-201 (40 MBq). Results: From result of syringe experiment, contaminations of Tl-201 in Tc-99m image and Tc-99m in Tl-201 were 3.8% and 1.0%. They are reduced to 0.15% and 0.006% by cross-talk correction. Scan of Tg mouse with Tc-99m suggested expression of hNIS because accumulation in blood-like organs was high in normal type while that in muscle was high in Tg type. In the images of hNIS-Tg mouse ASC injected MI rat, Tl-201 was accumulated in area except infarction. However, 99mTc-pertechnetate was highly accumulated in heart chamber and lung. The transplanted stem cells on the image were invisible. Conclusions: This study suggested feasibility of simultaneous dual-isotope SPECT imaging with Tc-99m and Tl-201 for tracking stem cells and evaluating MBF. Increasing the number of the cells and reducing background accumulation are needed to image hNIS-Tg mouse ASC.

Disclosure of author financial interest or relationships:
**T. Zeniya**, None; **H. Kawashima**, None; **K. Otani**, None; **H. Fukuda**, None; **Y. Hashikawa**, None; **K. Koshino**, None; **Y. Hori**, None; **T. Moriguchi**, None; **J. Enmi**, None; **S. Iguchi**, None; **A. Yamamoto**, None; **Y. Miyake**, None; **M. Inubushi**, None; **H. Iida**, None.

Presentation Number **SS 53**
Scientific Session 8: Stem Cell, Immune Cell, and Reporter Genes
September 6, 2012 / 13:00-13:11 / Room: Liffey Hall 2

# Photoacoustic Imaging of Mesenchymal Stem Cells in Living Mice via Silica-Coated Gold Nanorods

***Jesse V. Jokerst**, Mridhula Thangaraj, Sanjiv S. Gambhir, Radiology, Stanford University, Stanford, CA, USA. Contact e-mail: jokerst@stanford.edu*

Introduction. Imaging offers insight into the location(s), numbers, and state of implanted cells during stem cell therapy. Although magnetic resonance imaging and positron emission tomography have established benefits in stem cell therapy, their temporal resolution limits their utility in real-time guidance of the delivery event. Real time imaging offers instant quantitation of delivered stem cells along with precise confirmation of their spatial location(s), which could further improve the impact of this approach to regenerative medicine. Photoacoustic imaging is ideally suited for real time, image-guided therapy, yet there has been an appreciable lack of research in this area due to the lack of a contrast agents with sensitivity for use in photoacoustic cell tracking. Here, we use silica-coated gold nanorods (SiGNRs) as photoacoustic contrast agents and deploy them to image and quantitate mesenchymal stem cells (MSCs) during implant into the muscle tissue of live mice with important applications including the treatment of muscular dystrophy. Methods. SiGNRS were prepared as described in the literature and loaded into MSCs via endocytosis. Imaging was performed with a commercial system (LAZR; Visualsonics) using a 21 MHz transducer for B-mode ultrasound and a tunable laser. Results. High photoacoustic signal with no significant ($0.05<p$) toxicity or changes to cell proliferation was observed with cell labeling at 0.05 nM SiGNRs for 3 hours. The MSCs maintained their differentiation capacity as probed by adipogenic and osteogenic media (Supplementary). The secretome of naïve and SiGNR-loaded cells was studied, and of a panel of 30 cytokines only IL-6 was upregulated more than 2-fold. The presence of vacuole-bound SiGNRs inside the cells was validated with electron microscopy (Fig. A-C). Panels A and B have 5 μm scale bars and are at increasing magnification to show the SiGNRs in panel C. Labeling MSCs with the SiGNRs increased their photoacoustic signal 175% relative to unlabeled cells and the silica coat increased the MSC photoacoustic signal 55% relative to uncoated GNRs. We found that 600,000 SiGNRs were in each MSC, a tenfold increase versus non-coated GNRs. Mice (n=3) treated with these SiGNR-labeled MSCs exhibited no adverse events and implants up to 1 cm deep were easily visualized (Fig. D). See real-time video of implantation here: http://youtu.be/dQbpBjpOGVg. The in vivo detection limit was 90,000 cells in an 80 μL bolus in mouse thigh muscle. Importantly, the B-mode and photoacoustic signal are perfect complements in this application. B-mode orients the treatment area and visualizes the delivery catheter while the photoacoustic mode offers cell-specific content. After transplant, the animal was sacrificed and the treated area subjected to histology to validate the imaging data. The use of a cell tracking dye confirmed that the increased PA signal indeed correlated to the presence of MSCs (Supplement). This is the first example of in vivo photoacoustic cell imaging and this approach has significant advantages over traditional cell imaging techniques including temporal resolution of 0.2 seconds and spatial resolution of 508 μm.

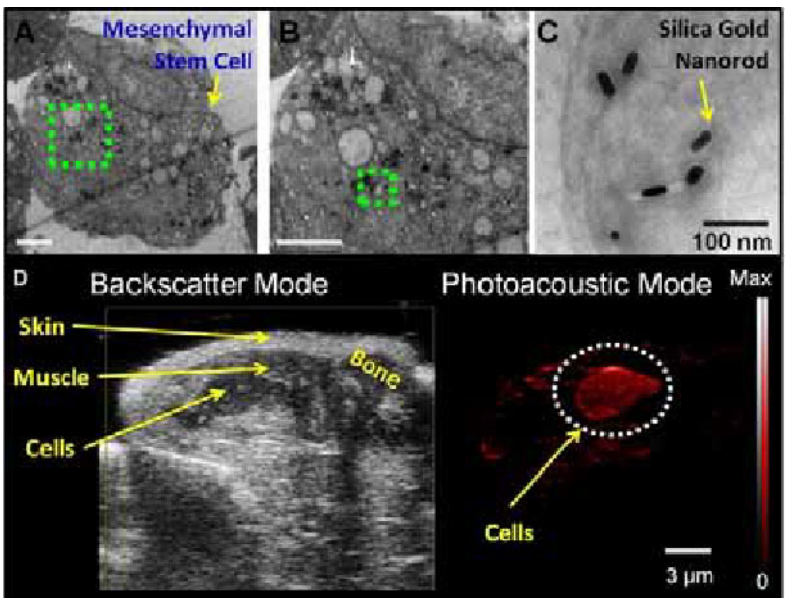


Disclosure of author financial interest or relationships:
**J.V. Jokerst**, None; **M. Thangaraj**, None; **S.S. Gambhir**, General Electric, Grant/research support; Bayer-Schering, Grant/research support; Sanofi-Aventis, Grant/research support; CellSight, Stockholder; ImaginAB, Stockholder; Enlight, Stockholder; Endra, Stockholder; Bracco, Consultant; NinePoint Medical, Stockholder; Visualsonics, Consultant .

Presentation Number **SS 54**
Scientific Session 8: Stem Cell, Immune Cell, and Reporter Genes
September 6, 2012 / 13:11-13:22 / Room: Liffey Hall 2

# A Novel Strategy for Real-time Ultrasound and Magnetic Resonance Imaging of Cardiac Stem Cell Therapy

***Jesse V. Jokerst***, *Christine Khademi, Sanjiv S. Gambhir, Radiology, Stanford University, Stanford, CA, USA. Contact e-mail: jokerst@stanford.edu*

Introduction. Stem cell tracking techniques monitor the location(s), numbers, and status of cells implanted into diseased myocardium. Standard tools lack real time temporal resolution to 1) quantify cells during implant and 2) confirm their delivery in the correct spatial location. Ultrasound imaging is ideally suited for this task, yet microbubble contrast agents are too large for cell internalization and have a lifetime (hours) inconsistent with long-term cell tracking. We have developed a multimodal silica-based nanoparticle (SiNP) contrast agent with concurrent fluorescent, ultrasound (US), and MRI signaling capacity. This single agent can be used for cell sorting (fluorescence), real-time image-guided cell implantation and quantitation (US), and high-resolution, long-term serial monitoring (MRI). Methods. The contrast agent utilized a silanized fluorophore and electrostatically-bound Gd3+. US imaging was at a center frequency of 40 MHz (Vevo; Visualsonics) and MRI used a 1T magnet (Aspect Imaging) with TR of 500 ms and a TE of 20 ms. Results. The SiNP has a relaxivity of 2x10-6 /(mM s) with <5% loss of Gd3+ when incubated in serum for 24 hours. The SiNPs are endocytosed into MSCs without transfection reagent, and the optimal loading conditions were 0.5 mg/mL of contrast for 6 hours. The presence of SiNPs in the MSCs was confirmed with electron and fluorescence microscopy (Supplementary Data). Loaded cells retained their differentiation capacity when grown in osteogenic and adipogenic media, and no significant ($p<0.05$) effects on MSC cell metabolic activity or proliferation were observed. Cytokine levels in the secretome of SiNP-loaded MSCs were compared to naïve cells. None of these cytokine levels decreased suggesting that loaded MSCs will still have therapeutic value through paracrine effects. MSCs had B-mode US and MRI contrast that was 700% and 200% higher than unlabeled cells, respectively, and were also compatible with clinical (5-12 MHz) ultrasound equipment. Imaging via electron microscopy suggests that intracellular aggregation is the mechanism of contrast. Loaded cells (250K - 1.5M) were implanted into the left ventricle wall of nude mice (n=3) and monitored serially. Cells were tracked with significantly ($p<0.05$) elevated signal for 13 days post-injection. The presence of cells was validated by histology (Supplementary). Decreasing amounts of cells were similarly implanted and the detection limit was 250,000 MSCs via MRI and 70,000 via US. Real-time video of the implant may be seen at the following link with cell injection starting at 0:10 http://youtu.be/BzAK6TtviKE. The temporal resolution is 300 frames per second—orders of magnitude below existing platforms. To the best of our knowledge, this is the first application of US-guided cell implantation and tracking and the first report of such a triple modality optical/US/MRI strategy that has important advantages for cost-effective clinical translation.

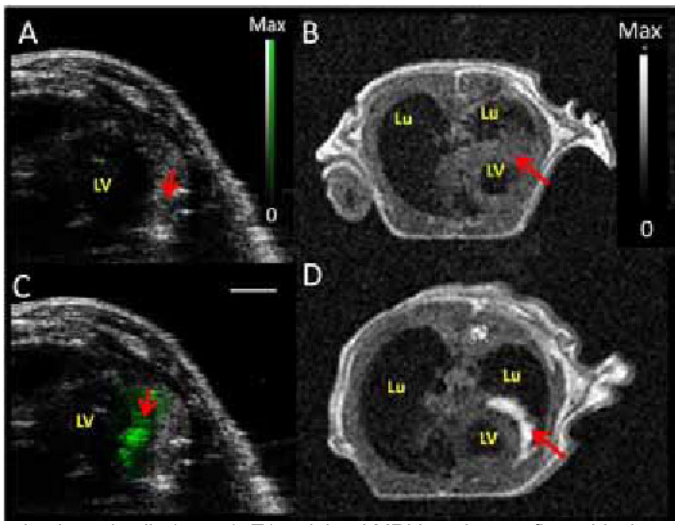


Ultrasound before (A) and after (C) shows implanted cells (green). T1 weighted MRI imaging confirms this through pre (B) and post (D) injection images. LV=left ventricle; Lu=lung; Sh=shoulder. Red arrows indicate injection site.

Disclosure of author financial interest or relationships:
**J.V. Jokerst**, None; **C. Khademi**, None; **S.S. Gambhir**, General Electric, Grant/research support; Bayer-Schering, Grant/research support; Sanofi-Aventis, Grant/research support; CellSight, Stockholder; ImaginAB, Stockholder; Enlight, Stockholder; Endra, Stockholder; Bracco, Consultant; NinePoint Medical, Stockholder; Visualsonics, Consultant .

Presentation Number **SS 55**
Scientific Session 8: Stem Cell, Immune Cell, and Reporter Genes
September 6, 2012 / 13:22-13:33 / Room: Liffey Hall 2

# Detection of stem cell apoptosis with a novel smart contrast agent for MR imaging

***Hossein Nejadnik***, *Deju Ye, Rostislav Castillo, Jianghong Rao, Heike E. Daldrup-Link, Radiology, Stanford University, Stanford, CA, USA. Contact e-mail: nejadnik@gmail.com*

Purpose Stem Cell therapies hold hopes for cure of a large variety of diseases. However, tissue regeneration outcomes are hampered by limited long-term survival of locally transplanted stem cells, depending on the applied cell type and host environment. The goal of this study was to develop an imaging method that could detect apoptosis of stem cell transplants. Establishing a non-invasive imaging technique for in vivo detection of stem cell apoptosis will facilitate repetitive, long term in vivo monitoring of transplanted stem cells, improve our understanding of endogenous or exogenous factors that support stem cell survival and ultimately, improve successful engraftment outcomes. Methods We evaluated a novel, activatable Gd-probe for imaging caspase-3 activity in vivo, which has been developed in the Rao lab at Stanford. The MRI probe is based on a small molecular Gd-chelate, which forms Gd-containing nanoparticles after hydrolysis by caspase-3. This nanoparticle self-assembly leads to an amplified 1H MR response, as well as enhanced retention at the target sites, both of which lead to positive signal on MRI. The Gd-probe was characterized by relaxivity measurements, high performance liquid chromatography (HPLC), and Scanning Electron Microscopy (SEM). Proof of concept was achieved by incubation of the probe with recombinant Caspase-3 enzyme, followed by MRI. Then, the probe was incubated with viable and Mitomycin-pretreated apoptotic hMSCs. Viability or apoptosis of both groups was confirmed with immunofluorescent stains and quantification of caspase-3 production. Triplicate samples of viable and apoptotic cells underwent MRI, using FSE IR (TR=4000/TE=10/TI=50-3200) and T2-map FSE (TR=4000/TE=15-80) sequences. The T1- and T2-relaxion times of samples was calculated and compared between viable and apoptotic stem cells, using a t-test ($p<0.05$). Results Contrast agent samples, incubated with recombinant caspase-3 demonstrated significant increase in T1-relaxation times compared to contrast agent samples, that were not incubated with caspase-3 ($p<0.05$). T1-relaxation rates of the caspase-sensitive probe increased by 89% in solution and 69% in agarose scaffold. Mitomycin-C treated hMSCs demonstrated positive caspase-3 immunofluorescent stains, while untreated hMSCs did not. The quantitative assay demonstrated a 5-fold increase in caspase-3 production of Mitomycin-treated hMSCs, when compared to untreated hMSCs ($p<0.05$; supplement file). Contrast agent exposed, Mitomycin-treated apoptotic hMSCs demonstrated a significant decrease in T1 relaxation time (241 ms), when compared to viable hMSCs (457 ms)($p<0.05$). Conclusion We present a novel approach for non-invasive in vivo detection of stem cell apoptosis, based on a novel caspase-sensitive contrast agent for MRI. This novel contrast agent may be useful for long term in vivo monitoring of the viability of transplanted stem cells and better guidance of tissue regeneration techniques. This may enable us to overcome the problem of diagnosing stem cell transplant failures at an early stage and allow to assign recipients with transplant failure to early interventions or alternative treatment options.

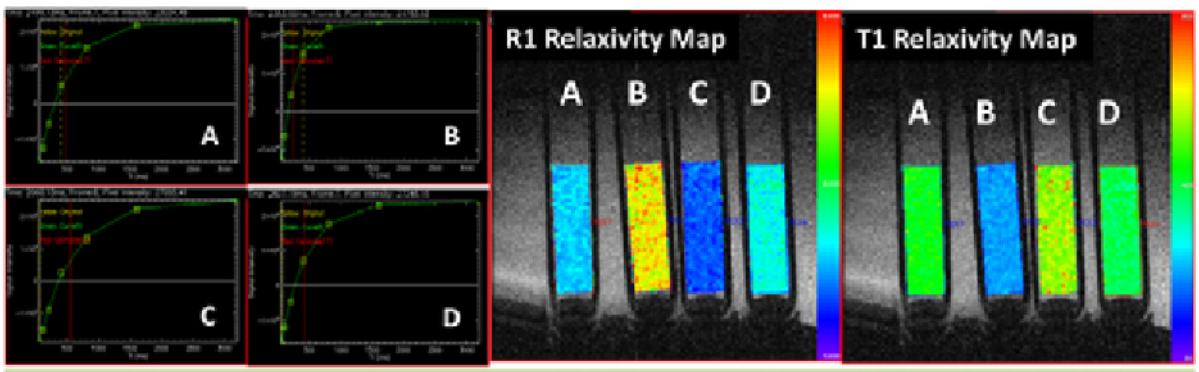


| Tube | Probe | Treatment | T1 (ms) | R1 (/sec) |
|---|---|---|---|---|
| A | Activatable probe | Viable cell lysate | 457.38 | 2.19 |
| B | Activatable probe | Apoptotic cell lysate | 241.16 | 4.15 |
| C | Non-activatable probe | Viable cell lysate | 559.99 | 1.79 |
| D | Non-activatable probe | Apoptotic cell lysate | 412.02 | 2.43 |

Disclosure of author financial interest or relationships:
**H. Nejadnik**, None; **D. Ye**, None; **R. Castillo**, None; **J. Rao**, None; **H.E. Daldrup-Link**, GE Global Research, Grant/research support .

Presentation Number **SS 56**
Scientific Session 8: Stem Cell, Immune Cell, and Reporter Genes
September 6, 2012 / 13:33-13:44 / Room: Liffey Hall 2

# Fluorine-19 Cell Tracking: Feasibility of Labeling and Detecting Dendritic Cells and Mesenchymal Stem Cells

***Emeline J. Ribot**, Sonali N. de Chickera, Patrick Anderson, Catherine McFadden, Gregory A. Dekaban, Paula Foster, Robarts Research Institute, London, ON, Canada. Contact e-mail: eribot@imaging.robarts.ca*

Introduction MRI Cell tracking consists of detecting and monitoring cells of interest in vivo over time. For this purpose, cells are typically pre-labeled with iron nanoparticles, the most commonly used contrast agents for cell labeling. These particles cause signal hypointensities in MR images acquired with sequences sensitive to inhomogeneities in the main magnetic field. However, the signal voids caused by iron loaded cells can be confused with other sources of signal loss. Fluorine atoms, however, contained in Perfluorocarbon particles are already used clinically. The main advantage of fluorine MRI is there is no background on the MR images. However, the sensitivity of detection is even lower than the one obtained using T1-contrast agents. The goal of this study was to optimize the labeling of mouse dendritic cells (DC) and human mesenchymal stem cells (MSC) with a fluorine contrast agent and to determine the sensitivity of detection of the labeled cells at 9.4T. Materials and Methods In Vitro: Mouse DC were incubated overnight with increasing concentrations (1.5; 3; 4.5; 5; 6.5 and 8.5 mg/mL) of the fluorocarbon-based emulsion CellSense (CelSense, Pittsburgh, PA). DC were harvested and viability assessed by trypan blue exclusion and 7AAD/Annexin V staining and flow cytometry. To evaluate the impact on DC phenotype, flow cytometry was used to assess surface expression of activation and maturation markers. Cellular uptake of CellSense was measured by NMR spectroscopy with Trifluoroacetic acid (0.1% v/v) used as a reference. In Vivo: Three million DC were incubated with 4.5mg/mL of CellSense for 24 hours and then injected into the footpad of black mice. Human MSC were incubated with 2.5mg/mL of CellSense for 24 hours and 0.5 or 3 million labeled-cells were injected subcutaneously into nude mice. Mice were imaged on days 0, 6 and 12 post-injection at 9.4T performing a Spin Echo sequence (TR=1s; TE=13.82ms; rBW=25kHz; resolution=470x390µm; 10 slices of 2mm thickness; 8 or 60 averages; 8min32 or 1h04min). Results/Discussion Cells were readily labeled with CellSense without the use of a transfection agent. At least 98% of DC were successfully labeled with Cell Sense at all doses used, without inducing more than 10% of cell apoptosis. Phenotypic analysis showed that labeling with up to 4.5mg/mL of Cell Sense does not affect maturation/activation of DC. NMR spectroscopy demonstrated that the number of 19F atoms taken up by DC increased with the concentration of CellSense up to 4.5mg/mL. Then, a plateau of $3.5x10^{11}$ 19F atoms per cell was observed. This amount was enough to generate 19F MR signal, allowing for the detection of 3 million labeled-DC in vivo at 9.4T. MSC internalized 1.6-$1.74x10^{12}$ 19F atoms when incubated with only 2.5mg/mL of Cell Sense. Both the 0.5 and 3 million cell injections were visible in vivo with short scan times (8min32) and the signal persisted for up to 12 days post injection. Conclusion DC and MSC can be labeled with Cell Sense at levels which allow their detection in vivo at 9.4T. Cell viability and phenotype was not affected. Further experiments will involve following DC migration to the lymph nodes.

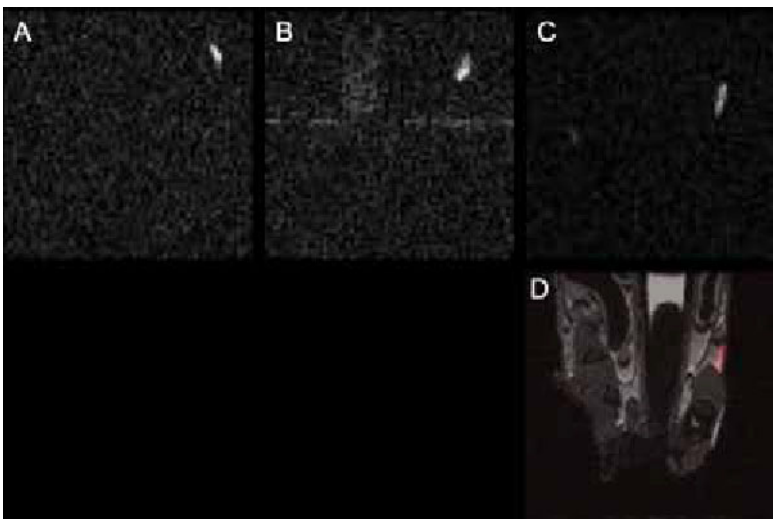


Figure: Follow-up of fluorine signal from CellSense-labeled MSC injected subcutaneously into a nude mouse. A nude mouse was injected with 3 million labeled-MSC subcutaneously. Fluorine MR scans were performed the day of the injection (A), 6 (B) and 12 (C) days after injection. In B, the reference tube containing CellSense solution (diluted 16 times in PBS) can be seen. D- Overlay of fluorine and proton MR images performed at Day 12.

Disclosure of author financial interest or relationships:
**E.J. Ribot**, None; **S.N. de Chickera**, None; **P. Anderson**, None; **C. McFadden**, None; **G.A. Dekaban**, None; **P. Foster**, None.

Presentation Number **SS 57**
Scientific Session 8: Stem Cell, Immune Cell, and Reporter Genes
September 6, 2012 / 13:44-13:55 / Room: Liffey Hall 2

# Imaging Histone Methylations by Optical Reporter Protein Complementation System

***Thillai V. Sekar***[1], *Ramkumar Kunka Mohan*[1,2], *Ramasamy Paulmurugan*[1], [1]*Radiology and Bioengineering (MIPS), Stanford University, Palo alto, CA, USA;* [2]*SRM Research Institute, SRM University, Chennai, India. Contact e-mail: thillaiv@stanford.edu*

Post-translational modifications (PTM) of histone proteins such as histone methylation and histone acetylation are two important epigenetic processes which play key roles in maintaining the chromatin structure and regulate gene expression. Methylation of histone proteins has been implicated with a spectrum of diseases including cancer. More than two decades, research investigations are underway to explore the effect of histone methylation in cancer and other cellular diseases. However, the detection and monitoring the status of methylation in intact cells are not feasible due to the lack of simple and sensitive techniques which will accelerate the research progress and thereby pave the way to develop novel therapeutics targeting this important process to treat cellular diseases. To bridge this gap and facilitate the investigations both in intact cells, and noninvasively monitoring in live animals, we have developed a reporter protein complementation based optical imaging sensor. The sensor was designed using methyltransferase substrate peptides spanning the first thirteen amino acids of H3 protein with Suv39H1-chromodomain for H3K9 sensor, and amino acids from 22 to 34 of H3 with PC2-chromodomain for H3K27 sensor, linked by a flexible linker peptide [$(G_4S_3)_3$] and sandwiched between the N- and C- terminal fragments of Renilla luciferase. The orientations of reporter fragments, and the locations of substrate and chromodomains, were placed in all possible combinations to identify an optimal sensor that can detect histone methylations specifically without much background signal. Moreover, to enhance methylation-assisted complementation signal, the number of K9-substrate peptide and methylation recognition domain were varied and tested for the sensitivity and specificity. Sensor with one copy each of substrate and chromodomain [Nhrl-Suv-$(G_4S_3)_3$-K9-Chrl] was found to be optimal for achieving higher complementation signal with low background signal. The selective methylations in H3K9 and H3K27 in leading the complementations were further confirmed by independent mutant sensors in which the lysine was replaced with leucine. Methylation sensors resulted the absolute complementation signal of $1.91\times10^8$ ± $4.46\times10^4$ p/sec/cm$^2$/sr (K9 sensor) and $9.64\times10^6$ ± 1.87 $\times10^3$ p/sec/cm$^2$/sr (K9-mut sensor) with 20 fold variation, in 293T cells. The absolute level of sensor signals varied in different cell lines, as studied in MCF7 and SUM159, with the same level of difference between the target sensor and the mutant sensor. The sensors used in this study were highly efficient to detect the methylation flux caused by epigenetic modulators such as valproic acid (VPA), Trichostatin A (TSA), and methyltransferase inhibitors such as Bix01294, Bix01338, and UNC0638. H3K9 and H3K27 specific methylations of the expressed sensors were ascertained by MALDI-TOF analysis and immunoblotting using respective methylation specific antibodies, which further confirmed the specificity of our results. These compelling evidences proves the suitability of our methylation sensors to detect histone methylations in preclinical evaluation of drugs in living animals.

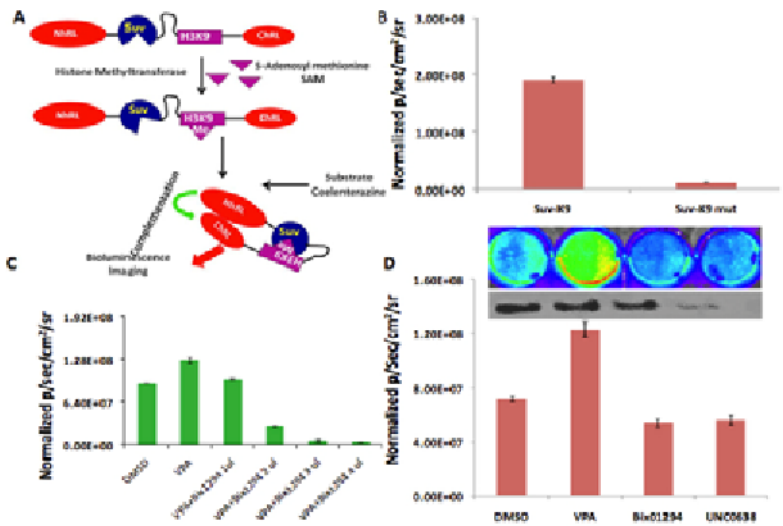


Figure: Optical Bioluminescence Imaging Sensor to Measure Histone Methylation in Intact Cells.
A) Schematic illustration of histone methylation imaging sensor.
B) H3K9-methylation measured in 293T cells transfected with H3K9- and mutant sensors.
C) H3K9 methylation in response to VPA and methyltransferase inhibitors (Bix01294 and UNC0638) measured by H3K9 complementation sensor.
D) Bioluminescence imaging and the respective immunoblot analysis of H3K9 methylation sensor in response to VPA and methyltransferase inhibitors (Bix01294 and UNC0638).

Disclosure of author financial interest or relationships:
**T.V. Sekar**, None; **R. Kunka Mohan**, None; **R. Paulmurugan**, None.

Presentation Number **SS 58**
Scientific Session 8: Stem Cell, Immune Cell, and Reporter Genes
September 6, 2012 / 13:55-14:06 / Room: Liffey Hall 2

# Genetically encoded MRI reporters with picomolar molecular sensitivity in HyperCEST imaging

***Mikhail G. Shapiro***[1,2], *Richard M. Ramirez*[3,4], *Lindsay J. Sperling*[3,4], *George L. Sun*[2], *Alexander Pines*[3,4], *David V. Schaffer*[2,5], *Vikram S. Bajaj*[3,4], *[1]Miller Research Institute, UC Berkeley, Berkeley, CA, USA; [2]Bioengineering, UC Berkeley, Berkeley, CA, USA; [3]Chemistry, UC Berkeley, Berkeley, CA, USA; [4]Materials Science Division, Lawrence Berkeley National Laboratory, Berkeley, CA, USA; [5]Chemical & Biomolecular Engineering, UC Berkeley, Berkeley, CA, USA. Contact e-mail: mikhails@berkeley.edu*

MRI offers unique capabilities for non-invasive imaging of biological and disease processes in intact organisms. However, MRI lacks highly sensitive molecular reporters analogous to the genetically encoded green fluorescent protein (GFP) that would enable sensitive non-invasive imaging of cellular processes such as gene expression. Here we describe a novel class of genetically encoded reporters active in hyperpolarized xenon-129 MRI that can be detected at picomolar concentrations. Most synthetic and genetically encoded MRI reporters act on aqueous proton spins and have detection limits in the mid-micromolar range. In part, this reflects the requirement that sufficient reporter be present to interact with a substantial fraction of ~55M H2O during imaging sequences. In MRI using hyperpolarized noble gases such as xenon-129, a 10,000-fold gain in per-nucleus signal enables imaging to occur with sub-mM nucleus concentrations. This, in turn, has permitted synthetic molecular reporters acting on 129Xe to be detected at nanomolar or lower concentrations. Such reporters produce contrast through chemical exchange saturation transfer (HyperCEST), wherein saturating radiofrequency (RF) pulses are applied at the distinct chemical shift of 129Xe bound to the reporter, and rapid exchange between reporter-bound and freely dissolved xenon serves to conditionally reduce overall 129Xe signal. No genetically encoded 129Xe HyperCEST reporters have been described. Developing such reporters is especially challenging given the generally weak interactions between proteins and xenon - a noble gas. To identify proteins that would exhibit unique ability to interact with xenon, produce a distinct 129Xe chemical shift, and permit rapid xenon exchange with the medium, we turned to a unique class of proteins from phototrophic bacteria. Gas vesicles (GVs) are nanoscale gas compartments (~200nm) formed entirely from protein that are used by species of waterborne halo- and cyanobacteria as a means to control buoyancy. The contents of GVs are in constant exchange with gas molecules dissolved in surrounding media. GVs are encoded by compact gene clusters of 8 or more genes that have been successfully transplanted into E. coli. We hypothesized that dissolved 129Xe would partition into GVs, where it would assume a gaseous form with a distinct chemical shift, and would rapidly exchange between GVs and solution, enabling the use of GVs with HyperCEST. Here we report that GVs serve as powerful genetically encoded HyperCEST MRI reporters detectable at mid-picomolar concentrations, both in isolation and inside cells. GVs from different bacterial species, which have different shapes and sizes, have distinct saturation peaks, enabling multiplexed imaging. As proofs of concept, we demonstrate the use of heterologously expressed GVs to image inducible gene expression in E. coli, and the use of biofunctionalized GVs to detect human cancer cells. The high molecular sensitivity, spectral multiplexing and genetic encoding enabled by this new class of reporters brings to MRI some of the major advantages that have made GFP and its derivatives a mainstay of optical microscopy.

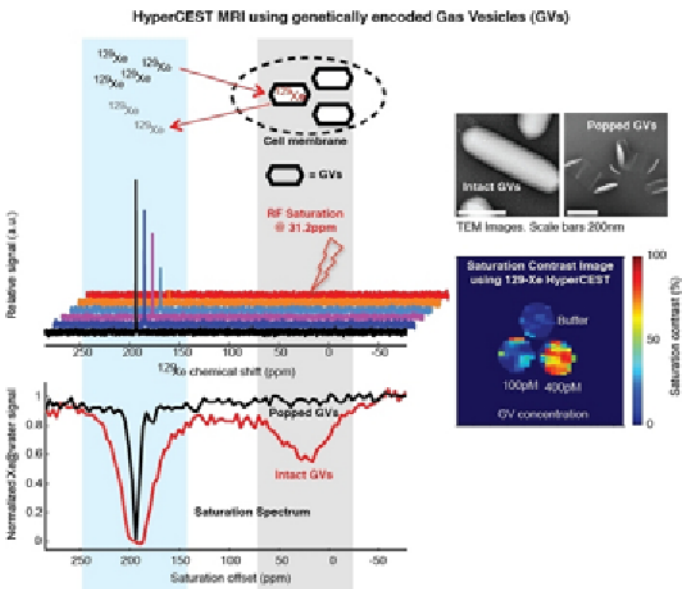


Disclosure of author financial interest or relationships:
**M.G. Shapiro**, None; **R.M. Ramirez**, None; **L.J. Sperling**, None; **G.L. Sun**, None; **A. Pines**, None; **D.V. Schaffer**, None; **V.S. Bajaj**, None.

Presentation Number **SS 59**
Scientific Session 8: Stem Cell, Immune Cell, and Reporter Genes
September 6, 2012 / 14:06-14:17 / Room: Liffey Hall 2

# Quantification of Suberoylanilide Hydroxamic Acid, Valproic Acid and Class II-specific HDAC Inhibitor-Induced Inhibiton of HDAC activity in the Rat Brain using In Vivo PET/CT Imaging with HDAC Class IIa-Specific Radiotracer

***Hsin-Hsien Yeh***[1,2], *Leo G. Flores*[1], *Kun-eek Kil*[1], *Vincenzo Paolillo*[1], *Uday Mukhopadhyay*[1], *Suren Soghomonyan*[1], *Asutosh Pal*[1], *Aleksander Shavrin*[1], *Daniel Young*[1], *William Tong*[1], *Mian M. Alauddin*[1], *C. Allen Chang*[2], *Ren-Shyan Liu*[2,3], *Juri G. Gelovani*[1], [1]*Department of Experimental Diagnostic Imaging, The University of Texas MD Anderson Cancer Center, Houston, TX, USA;* [2]*Department of Biomedical Imaging and Radiological Sciences, National Yang-Ming University, Taipei, Taiwan;* [3]*Schoolt of Medicine, National Yang-Ming University, Taipei, Taiwan. Contact e-mail: skyeyeh@live.com*

Introduction: A dozen of different Histone deacetylase (HDAC) inhibitors has been currently undergone clinical trials for treatment of various neurodegenerative diseases, including Huntington's, Parkinson's, Alzheimer's diseases, brain ischemia and trauma. Therefore, our group has developed a non-invasive pharmacodynamic imaging of HDAC inhibition in the brain using PET/CT with 6-([18F]fluoroacetamido)-1-hexanoicanilide ([18F]TFAHA) which were reported in rodent and non-human primate models. Recently, the importance of HDAC II enzymes, especially HDACs 4 and 5 in the nucleus accumbens and cerebellum, in the establishment of drug-addicted behavior or neurodegenerative diseases have been emphasized; therefore, we developed the next generation of HDAC Class IIa-specific radiotracers: 6-([18F]tri-fluoroacetamido)-1-hexanoicanilide ([18F]TFAHA). In this study, PET imaging with this novel HDAC Class IIa-specific radiotracer was used to study in the rat brain the pharmacodynamic effects of HDAC inhibitors: suberoylanilide hydroxamic acid (SAHA, vorinostat) and valporic acid (VA) and class II-specific HDAC inhibitor. Materials and Methods: Sprague Dawley rats under 2% isoflurane anesthesia were pretreated 1h before PET imaging with SAHA (0.1, 1, 10 and 100 mg/kg i.p. in 100 µL of DMSO), VA (1, 10,100 mg/kg i.p. in 200 µL of saline), class II-specific HDAC inhibitor (0.1, 1, 10 mg/kg i.p. in 200 µL of saline) or saline (200 µL i.p.); N=3 rats in each group. Dynamic microPET/CT imaging was performed for 30 min post i.v. injection of 18F-TFAHA (1 mCi in 500µL as a steady bolus injection over 1 min). Blood samples were obtained at different time points via an arterio-venous shunt (to determine the blood input function). The unidirectional influx rate (Ki) of each tracer was calculated using Patlak graphical analysis. Subsequently, the distribution of tracer-derived radioactivity in the brain was assessed using quantitative autoradiography (QAR) of frozen sections. Results: As compared to [18F]TFAHA, the higher level of accumulation in the brain was observed with [18F]TFAHA. The highest regional accumulation of [18F]TFAHA-derived radioactivity was observed in the n.accumbens, thalamus, putamen and cerebellum. Among three HDAC inhibitors, VA group resulted in a strong inhibition of [18F]TFAHA (HDAC class IIa activity) in these brain structures, followed by specific-class II HDAC inhibitor and SAHA groups (Fig.1). In vivo PET imaging results were confirmed using QAR; [18F]TFAHA accumulation in n.accumbens and cortex were almost completely abolished by pre-treatment with VA 100 mg/kg. Conclusions: PET with [18F]TFAHA can be used as pharmacodynamic biomarker of HDAC inhibition in the brain and used for the assessment of novel HDAC inhibitors. Longitudinal studies in animal models and in humans using PET/CT(MR) imaging of HDACs expression activity in the brain should facilitate studies on epigenetic regulatory mechanisms by different HDACs in various neurodegenerative diseases and in drug addiction and also to facilitate the development of novel class-specific HDAC inhibitors.

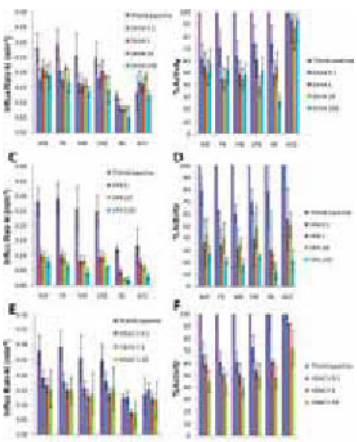

Fig.A,C and E show that the changes of influx rate (ki) in brain regions after per-treatment with HDAC inhibitors. The remaining HDAC activity indicating the inhibition effects of HDAC inhibitors are shown as Fig.1B-D-F.

Disclosure of author financial interest or relationships:
**H. Yeh**, None; **L.G. Flores**, None; **K. Kil**, None; **V. Paolillo**, None; **U. Mukhopadhyay**, None; **S. Soghomonyan**, None; **A. Pal**, None; **A. Shavrin**, None; **D. Young**, None; **W. Tong**, None; **M.M. Alauddin**, None; **C. Chang**, None; **R. Liu**, None; **J.G. Gelovani**, Macrocyclics, Consultant; SibTech, Consultant .

Presentation Number **SS 6**
Scientific Session 1: Chemistry & Probes - MRI
September 6, 2012 / 11:25-11:36 / Room: Liffey Hall 1

# Apoferritin-based MRI contrast agents with high particle r1

***Veronica Clavijo Jordan**, Kevin M. Bennett, School of Biological and Health Systems Engineering, Arizona State University, Tempe, AZ, USA. Contact e-mail: veronica.cj@asu.edu*

A fundamental limitation of in vivo molecular magnetic resonance imaging (MRI) is a lack of sensitivity to contrast agents. Here we propose that this limitation can be overcome in a metal nanoparticle agent by understanding and tuning the formation of metal in the nanoparticle core to form an agent with high T2 or T1 relaxivity. T1 agents are particularly desirable because they can be detected more readily in vivo with the same relaxivity. In this work we use apoferritin, a 12nm iron storage protein with an endogenous ferroxidase, to form a uniform nanoparticle contrast agent with high T1 relaxivity (r1). In order to create a ferritin particle with high r1, we first adsorbed Mn2+ ions to metal binding sites in the pores. This was only possible when the particle was filled with an iron oxide, resulting in a particle with a high r1 but also a high r2. Interestingly, this configuration yielded a very high per-Mn2+ relaxivity of 330mM-1s-1 (Figure 1a). To decrease the particle r2 for sensitive detection we created a W-Fe oxide composite in the apoferritin. This configuration formed several sub-domains in the particle observed with high-resolution electron microscopy (Figure 1a) and an r1 of 4,870mM-1s-1 and r2 of 9,076mM-1s-1 (Figure 1c). In these particles, adding Mn2+ during synthesis led to an increased r2 of 29046mM-1s-1 and decrease per ion r1 to 118mM-1s-1, shown in Figure 1b, suggesting that water access to the W-Fe core is critical for the high r1 of the W-Fe composite nanoparticles. We conclude that the strategic placement of manganese ions near sites of water exchange can significantly enhance the per-ion r1, suggesting a mechanism for increasing the per-ion relaxivity in porous nanoparticle agents. The particle r1 can be increased without increasing r2 by forming a W-Fe composite, allowing ~10 nM detection in vivo at clinical field strengths.

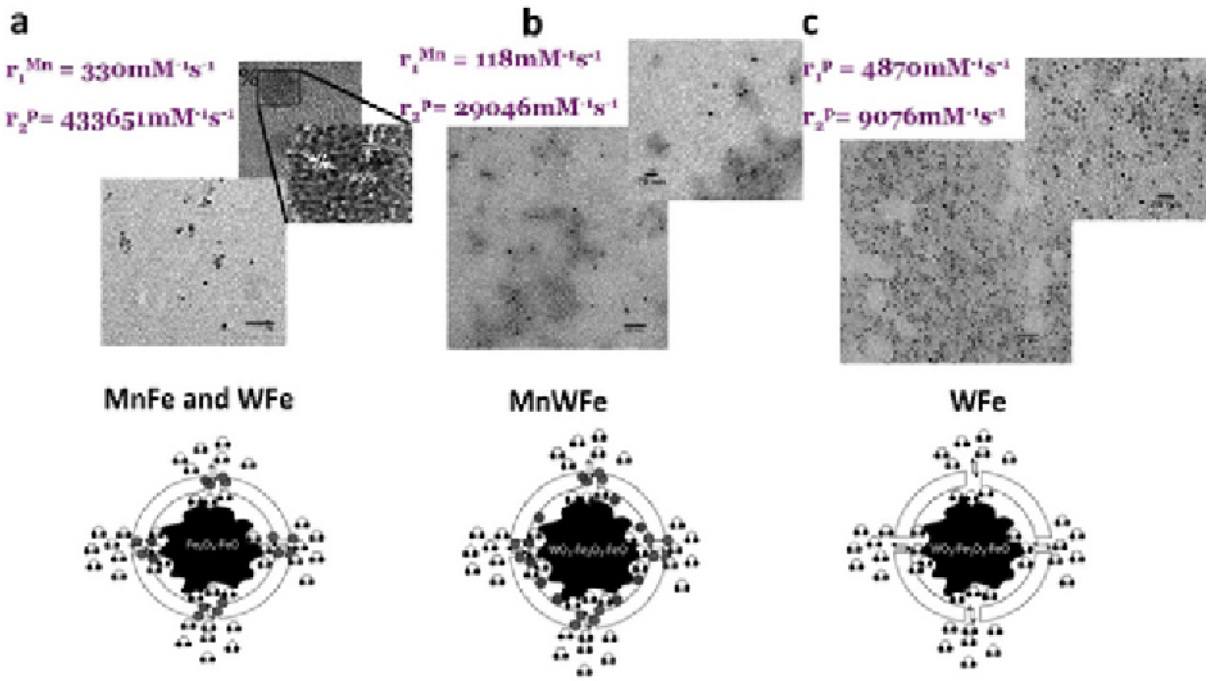


Figure 1. a) Transmission electron microscopy (TEM) images of apoferritin with iron oxide core and Mn2+ adsorbed ions. Top panel: high resolution electron microscopy (HREM) of W-Fe composite core. b) TEM image of tungsten oxide and iron oxide filled apoferritin with Mn2+ ions adsorbed to hydrophilic channels. c) TEM images of apoferritin filled with tungsten oxide and iron oxide mix (WFe) showing monodisperse particles.Scale bars are 50nm for large images and 20nm for insets. All relaxivity measurements were made at 1.5T

Disclosure of author financial interest or relationships:
**V. Clavijo Jordan**, None; **K.M. Bennett**, None.

Presentation Number **SS 60**
Scientific Session 8: Stem Cell, Immune Cell, and Reporter Genes
September 6, 2012 / 14:17-14:28 / Room: Liffey Hall 2

# A Novel Self-Replicating Minicircle Strategy for Safer Long-Term Monitoring of Cell Therapies

***John A. Ronald***[1,2], *Lorena Cussó*[3,4], *Xinrui Yan*[1,2], *Anca Dragulescu-Andrasi*[1,2], *Sanjiv S. Gambhir*[1,2], *[1]Radiology, Stanford University, Stanford, CA, USA; [2]Molecular Imaging Program at Stanford, Stanford University, Stanford, CA, USA; [3]Unidad de Medicina y Cirugía Experimental, Hospital General Universitario Gregorio Marañón, Madrid, Spain; [4]Centro de investigación biomédica en red en salud mental (CIBERSAM), , Madrid, Spain. Contact e-mail: jronald1@stanford.edu*

Imaging of cell-based therapies with reporter genes (RG) provides a direct readout of therapeutic efficacy by assessing the location(s), numbers, and fate of implanted cells. To date, to permit long-term imaging of cells, RGs are required to be integrated into the genome of implanted cells. However, this strategy poses both a serious safety risk and regulatory bottleneck for clinical translation since integration often occurs at random genomic locations, which can lead to insertional mutagenesis and cancer. A safer alternative would be non-integrating vector platforms that can continuously replicate as cells divide. Towards this goal we have been developing minicircles (plasmids without a bacterial backbone) that express imaging RGs and contain the scaffold/matrix attachment region (S/MAR) from the human β-interferon gene. Methods and Results: Vector constructs encoding the bioluminescence RG Firefly luciferase driven by the CMV promoter were developed. Both minicircles and plasmids with and without the S/MAR motif were generated. MDA-MB-231 breast cancer cells were transfected with both S/MAR minicircles and plasmids, grown without selection pressure, and imaged over time (Figure 1A). On day 6 both constructs showed luciferase expression but by day 9 the S/MAR plasmid showed minimal signal. In contrast, the S/MAR minicircle at day 9 showed more signal than on day 6, and focal areas of intense signal were noted; indicative of replicating vectors in these colonies of cells. Colonies were isolated and expanded cells maintained strong luciferase signal for greater than 3 months in culture in the absence of selection. To ensure that this continuous replication observation is maintained in vivo, $1.5x10^6$ cells from one of these expanded colonies (at day 45) were implanted subcutaneously into the right leg of nu/nu mice (N=5) and imaged over time (Figure 1B). Importantly, as tumors developed, significantly more signal was noted at day 28 compared to day 7 post-implant ($p<0.05$). Preliminary results in culture with human mesenchymal stem cells have also shown similar results. Current work focuses on development of S/MAR minicircles for other imaging modalities (e.g. PET) and testing our constructs in other cell types currently explored as therapeutic cells. Discussion: Many cell-based therapies are being developed for the treatment of cancer, cardiovascular and neurological diseases. We envision that continued development of S/MAR minicircles will provide a broadly applicable vector platform amenable with any of the numerous reporter gene technologies available to allow therapeutic cell fate to be assessed in individual patients and to achieve this without the need to manipulate the cell's genome so that safety and regulatory concerns are minimized.

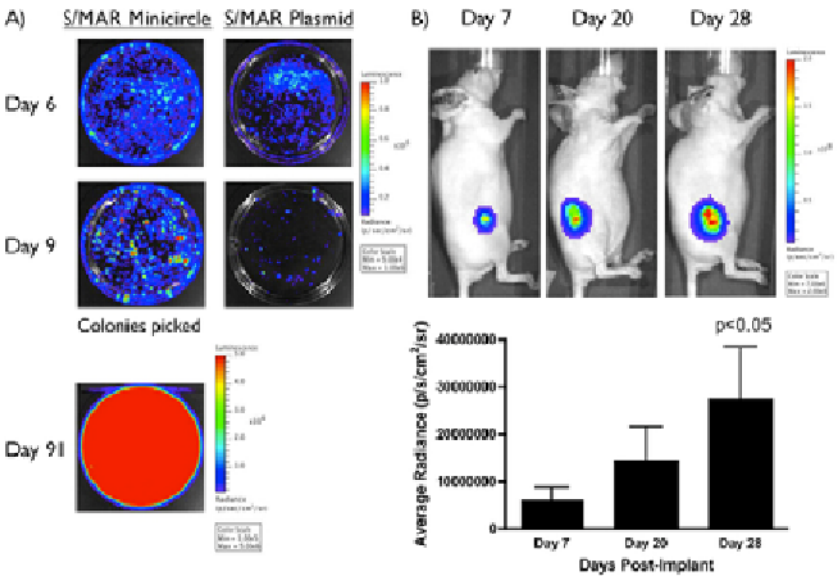


Figure 1: A) MDA-MB-231 cells were transfected with S/MAR minicircle or S/MAR plasmid (control) and imaged over time. B) Top: S/MAR minicircle MDA-MB-231 cells were implanted into the right leg and imaged at day 7, 20 and 28. Bottom: Analysis of images from 5 mice. Significantly ($p<0.05$) more signal was detected on day 28 versus day 7 as determined via repeated measure ANOVA.

Disclosure of author financial interest or relationships:
**J.A. Ronald**, None; **L. Cussó**, None; **X. Yan**, None; **A. Dragulescu-Andrasi**, None; **S.S. Gambhir**, General Electric, Grant/research support; Bayer-Schering, Grant/research support; Sanofi-Aventis, Grant/research support; CellSight, Stockholder; ImaginAB, Stockholder; Enlight, Stockholder; Endra, Stockholder; Bracco, Consultant; NinePoint Medical, Stockholder; Visualsonics, Consultant .

Presentation Number **SS 61**
Scientific Session 9: Preclinical In Vivo - Neurology
September 6, 2012 / 13:00-13:12 / Room: Wicklow Hall 2

# Simultaneous small animal PET/MR reveals different brain networks during stimulation and rest

***Hans F. Wehrl***[1], *Mosaddek Hossain*[1], *Konrad Lankes*[1,2], *Chih-Chieh Liu*[1], *Ilja Bezrukov*[1,3], *Petros Martirosian*[4], *Gerald Reischl*[1], *Fritz Schick*[4], *Bernd J. Pichler*[1], [1]*Department of Preclinical Imaging and Radiopharmacy, Eberhard Karls University of Tuebingen, Tuebingen, Germany;* [2]*Bruker BioSpin MRI, Ettlingen, Germany;* [3]*Max-Planck-Institute for Intelligent Systems, Tuebingen, Germany;* [4]*Department of Radiology, Section on Experimental Radiology, Eberhard Karls University of Tuebingen, Tuebingen, Germany. Contact e-mail: wehrl@gmx.de*

**Introduction:** The study of brain function is of great interest for basic research as well as medical diagnostics. Two premier imaging modalities, PET and fMRI, exist to pursue this endeavor in vivo. However, little is known about the correlation between the functional imaging information delivered by these two methods. Here we present a comparison of [$^{18}$F]FDG PET and fMRI blood oxygen level dependent (BOLD) brain activation imaging during stimulation and resting state of the brain, minimizing confounding parameters by using simultaneous PET/MR imaging. We hypothesize, that multiple networks of brain activation can be observed using this new imaging modality. **Materials & Methods:** The studies were performed using a PET-insert built by our group installed inside a 7T small animal MR scanner. The PET-insert has a combined PET/MR field of view of 72x72mm$^2$. A total of 8 male lewis rats were studied. Animals were PET/MR scanned on two consecutive days, with a 1h dynamic [$^{18}$F]FDG (40MBq) scan. During the measurement, the animals were either permanently stimulated (3mA, 3Hz, left whisker) for the first 45min of the scan (day1) or were at rest (day 2). Simultaneously with PET, BOLD fMRI imaging was performed. During the 45min period, 15min of functional connectivity (fc) fMRI EPI GE, TR=3000ms, TE=18ms), and at the last 15min fMRI block design (EPI GE; TR=2000ms, TE=18ms) data were acquired. Statistical maps were calculated using a paired Student's t-test (PET), as well as the general linear model (fMRI). Independent component analysis (ICA) was performed on the PET data as well as on fc fMRI scans. **Results:** PET and fMRI brain activation maps (Fig 1a) disclose differences between the two modalities: Both methods show an activation in the contralateral (cl) barrel field cortex (S1BF, PET: P=3*10$^{-6}$, MR: P=4*10$^{-16}$). In this area a significant PET signal change of 11±7% (P=0.005) and BOLD fMRI 0.5±0.6% compared to the non stimulated measurements was observed. Areas like the cl insula (19±9% P=3*10$^{-4}$) and the cl amygdala (32±14%, P=2*10$^{-4}$) were observed in PET but not in fMRI (see also Table 1). ICA of the MR fc data revealed nine networks in the brain, whereas the same analysis of the PET dynamic data showed 7 meaningful networks. Similarities were found in e.g. in the somatosensory cortex as well as in the region of the amygdala and piriform cortex (Fig 1b). **Discussion:** Observed signal changes during PET activation[1] as well as the fMRI ICA[2] components were in agreement with previous literature. Activated regions corresponded to expected areas according to a rat brain atlas. Beyond this we show, to our knowledge, for the first time that PET and fMRI functional imaging unfold different brain networks: fMRI showing mainly somatosensory areas, whereas PET additionally indicates nociceptive components. ICA analysis of brain PET data shows similarities to fMRI networks, however potentially revealing new pathways related to glucose consumption. In conclusion simultaneous PET/MR is demonstrated to provide high potential for further elucidation of brain function in vivo. [1] Shih YY et al., JCBFM(2011);31(3) [2] Jonckers E et al., PLoS One(2011);6(4)

**Figure 1:** Statistical parametric maps of significant (P<0.05) brain activation in rats. a) Comparison between fMRI BOLD and PET activation study of the rat brain. BOLD and PET show clearly activity in cl S1BF and the somatosensory network (stimulation side: left whisker pad). However, PET reveals additional components such as activation in the amygdala and insula. b) Functional connectivity in the rat brain during activated and resting state assessed by ICA of fMRI and PET data. Two exemplary networks are shown. In the somatosensory area fMRI as well as PET pick up components, with fMRI showing stronger statistical significance. Also the amygdala related network is visualized with both methods.

**Table 1:** SUV changes during stimulation

| Region | S1BFcl | S1BFil | VPMcl | VPMil | Ect/Prh | Amyg |
|---|---|---|---|---|---|---|
| SUV stimulated | 4.88±0.4 | 3.88±0.3 | 4.48±0.5 | 4.38±0.6 | 3.38±0.5 | 3.08±0.4 |
| %Change (stimulated) | +11 | +6 | +14 | +13 | +19 | +32 |
| P<0.05 | YES | NO | YES | YES | YES | YES |

SUV values for selected brain regions during stimulation and their change relative to baseline. S1BF: barrel field cortex contralateral (cl) and ipsilateral (il) to the stimulation side, VPM: thalamus area, Ect/Prh: ectorhinal and perirhinal, piriform cortex, Amyg: amygdala. Besides S1BF il, all other studied brain areas show significant changes during stimulation, confirming the findings of the statistical parametric mapping.

Disclosure of author financial interest or relationships:
**H.F. Wehrl**, None; **M. Hossain**, None; **K. Lankes**, None; **C. Liu**, None; **I. Bezrukov**, None; **P. Martirosian**, None; **G. Reischl**, None; **F. Schick**, None; **B.J. Pichler**, Siemens, Grant/research support; AstraZeneca, Grant/research support; Bayer Healthcare, Grant/research support; Boehringer-Ingelheim, Grant/research support; Oncodesign, Grant/research support; Merck, Grant/research support; Bruker, Grant/research support .

Presentation Number **SS 62**
Scientific Session 9: Preclinical In Vivo - Neurology
September 6, 2012 / 13:12-13:24 / Room: Wicklow Hall 2

# Multimodal imaging of inflammation and tissue remodelling in cerebral ischemia

***Bastian Zinnhardt***[1], *Thomas Viel*[1], *Alexis Vrachimis*[1,2], *Andreas Faust*[1,2], *Lydia Wachsmuth*[3], *Sven Hermann*[1], *Klaus Kopka*[2], *Cornelius Faber*[3], *Frederic Dolle*[4], *Bertrand Tavitian*[4], *Michael Schäfers*[1,2], *Michael T. Kuhlmann*[1], *Andreas H. Jacobs*[1], [1]*European Institute for Molecular Imaging (EIMI), University of Muenster, Muenster, Germany;* [2]*Department of Nuclear Medicine and Interdisciplinary Centre for Clinical Research (IZKF), University Medical Center at the Westfälische Wilhelms-University (WWU), Muenster, Germany;* [3]*Department of Clinical Radiology, University Medical Center at the Westfälische Wilhelms-University (WWU), Muenster, Germany;* [4]*Département de Recherche Médicale, Service Hospitalier Frédéric Joliot, CEA, I2BM, Orsay, France. Contact e-mail: zinnhardt@uni-muenster.de*

**Introduction:** Ischemic stroke is the most common neurological disorder and the second leading cause of death worldwide. In the cascade of molecular changes following acute cerebral ischemia, activation of the immune response and tissue factors are known to be key factors in promoting, on the one hand, the extent of tissue damage and, on the other hand, in serving tissue repair functions. Imaging approaches aiming at increasing the understanding of the temporal and spatial dynamics of the immune system and tissue factors shall improve our understanding of deciphering "bad" and "good" activation states. **Aim:** To establish two new radiotracers for µPET imaging of microglial activation and matrix-metallo proteinases (MMPs) after cerebral ischemia in a mouse model of transient middle cerebral artery occlusion (MCAo) and to reveal possible spatial interactions of these two histopathological hallmarks after ischemic stroke. **Methods:** 53 mice were subjected to transient (30 min) MCAo. Success of surgery was verified intraoperatively via Laser Doppler and by $^{99m}$Tc-hexamethylpropyleneamine oxime (HMPAO) µSPECT imaging one day post operation. Two weeks after surgery, surviving mice (n=10) were subjected to µPET imaging using the tracers [$^{18}$F]DPA-714 and [$^{18}$F]BR-351 for molecular imaging of microglial activation and MMP activation respectively. [$^{18}$F]DPA-714 µPET images were acquired 45-75 min post i.v. injection of 10 MBq [$^{18}$F]DPA-714. [$^{18}$F]BR-351 µPET images were acquired 95-110 min post i.v. injection of 10 MBq [$^{18}$F]BR-351. Lesion-to-background ratios (L/B) were calculated between the ischemic and the contralateral control hemisphere. T2-weighted µMRI was conducted for identification of stroke location and size and co-registration to µPET and µSPECT images. Immunohistochemistry is being performed in coronal sections employing antibodies for microglia (Iba-1) and MMP (anti-MMP-2/MMP-9). **Results:** N=7 mice showed an infarction on T2-weighted µMRI in the right MCA territory. All mice reveal pronounced [$^{18}$F]DPA-714 tracer accumulation in and around the infarct region compared to the contralateral reference region (L/B=3,23± 2,22). Also, [$^{18}$F]BR-351 accumulation was observed in and around the infarct region (L/B=1,47± 0,97). In 6/7 mice [$^{18}$F]BR-351 tracer signal accumulation occurred partially in areas with increased DPA accumulation. The *in vivo* findings are currently quantified and being validated using immunohistochemical analysis for microglial- and MMP activation. **Conclusion:** Radiotracer accumulation in and around the infarct zone indicates microglial and MMP activation in the infarcted region 2 weeks after transient MCAo. Immunohistochemical verification is ongoing. [$^{18}$F]DPA-714 and [$^{18}$F]BR-351 may serve as a potential marker combination to study neuroinflammatory reactions and tissue remodelling of the CNS *in vivo*. The research leading to these results has received funding in part by a fellowship of the NRW Research School Cell Dynamics and Disease to B. Zinnhardt and the EU 7th Framework Programme (FP7/2007-2013) under grant agreement n° 278850 (INMiND).

Disclosure of author financial interest or relationships:
**B. Zinnhardt**, None; **T. Viel**, None; **A. Vrachimis**, None; **A. Faust**, None; **L. Wachsmuth**, None; **S. Hermann**, None; **K. Kopka**, None; **C. Faber**, None; **F. Dolle**, None; **B. Tavitian**, None; **M. Schäfers**, Siemens Medical Solutions, Grant/research support; **M.T. Kuhlmann**, None; **A.H. Jacobs**, Merck, Germany, Grant/research support .

Presentation Number **SS 63**
Scientific Session 9: Preclinical In Vivo - Neurology
September 6, 2012 / 13:24-13:36 / Room: Wicklow Hall 2

# Continuous $^{18}$F-FDG Infusion for Dynamic PET Imaging of an Excitotoxic Insult in the Rat Brain

*Benedicte Descamps[1], Scharon Bruneel[1], Vincent Keereman[2], Pieter van Mierlo[2], Ine Dauwe[3], Stefaan Vandenberghe[1], Robrecht Raedt[3], **Christian Vanhove**[1,4], [1]Medisip, IBBT, Infinity Lab, Ghent University, Ghent, Belgium; [2]Medisip, IBBT, Ghent University, Ghent, Belgium; [3]Laboratory for Clinical and Experimental Neurology, Ghent University, Ghent, Belgium; [4]GROUP-ID (Ghent Researchers On Unfolded Proteins in Inflammatory Disease), Ghent University, Ghent, Belgium. Contact e-mail: Christian.Vanhove@UGent.be*

Observing fast metabolic changes during dynamic PET is challenging. Injecting a single bolus of the radiotracer implies the need of decay correction. Due to the decrease in radiotracer concentration over time, image quality will decrease in late frames. We present a setup of continuous radiotracer infusion to obtain and maintain a steady state uptake curve. This allows studying subtle or fast changes with equal image quality over the complete duration of the dynamic PET acquisition. We illustrate the method with the continuous infusion of $^{18}$F-FDG to evaluate the direct effect of kainic acid (KA), a glutamate receptor agonist, injected in the right hippocampus of the rat brain. A Sprague Dawley rat (♂, 300g) underwent stereotactic brain surgery to place a cannula into the right intermediate hippocampus (AP = -5.6 mm, ML = ±4.5 mm, DV = -5.5 mm relative to bregma). Two hours after starting dynamic PET, KA is injected into the right hippocampus (0.4µg/0.1µl; 0.1µl/min). The left hippocampus is not injected and used as a control. An infusion system (Fusion 100 Syringe Pump, SAI) is used to control the injection of $^{18}$F-FDG in a tail vein and maintain a steady state input function. After an initial bolus injection of 11MBq of $^{18}$F-FDG, a fast infusion rate (211µl/h) is used to quickly achieve the desired amount of radiotracer in the animal. Then, infusion rate is changed to 34µl/h. At this rate, the radiotracer decay inside the animal over 10' is compensated by newly infused radiotracer, maintaining a steady state. To compensate for decay in the syringe, the infusion rate is also slightly increased every 10' to constantly maintain a correct total infusion of radiotracer. Protocol details: 4h dynamic PET acquisition (LabPET, Triumph-II, GMI), KA injection 2h after the start of the acquisition; image processing: dynamic PET reconstruction (with CT-based attenuation correction) of 26 frames (10x1', 10x5', 6x10') before and 26 frames after KA injection. Validation was carried out by assessing the dynamic (across frames) and static (within a single frame) noise levels in the left hippocampus for frames after approx. 30', when steady state is reached. The tracer uptake for ROIs in both hippocampi is plotted to demonstrate the difference between right and left hippocampus. The dynamic noise level is lower than the static noise level (table 1), indicating that an accurate steady-state uptake is obtained. Axial pre- and post-KA injection PET-images are given in fig 1A. Uptake curves from left (control) and right (KA) hippocampus are plotted in fig 1B. The local KA delivery immediately initiates an increased uptake in the target tissue. Our results demonstrate that early and immediate changes induced by an excitotoxic insult can easily be detected using continuous radiotracer infusion. The low dynamic noise levels confirm that it is feasible to maintain a steady state count rate. Future research will focus on more accurate validation of our method using arterial sampling of the true input function. In addition, we will evaluate whether this setup can be used to evaluate the effect of early therapeutic interventions on the neurological insult.

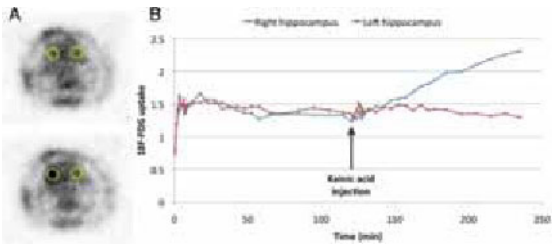


A. Axial PET images pre- and post-KA injection (upper and lower part resp.) with ROIs in left and right intermediate hippocampus (circles) illustrate the increase in the right hippocampus post KA injection (radiological convention) B. Mean uptake curves from both ROIs in A show the increased uptake in the right hippocampal ROI soon after KA injection (at t = 120')

Data validation: dynamic and static noise levels per frame block

| frame block | dynamic noise level | static noise level |
|---|---|---|
| 5' pre-KA | 2.0% | 5.4% |
| 10' pre-KA | 2.3% | 4.3% |
| 1' post-KA | 5.1% | 6.3% |
| 5' post-KA | 2.6% | 4.4% |
| 10' post-KA | 2.0% | 3.2% |

Calculation of dynamic noise levels: relative deviation (SD/mean) in 1 ROI in left hippocampus, averaged for each block (frames with same frame duration).
Calculation of static noise levels: relative deviation of 5 ROIs with homogeneous uptake in left hippocampus within one frame, averaged for each block. First frames are disregarded in calculation (no steady state before 30').

Disclosure of author financial interest or relationships:
**B. Descamps**, None; **S. Bruneel**, None; **V. Keereman**, None; **P. van Mierlo**, None; **I. Dauwe**, None; **S. Vandenberghe**, None; **R. Raedt**, None; **C. Vanhove**, None.

Presentation Number **SS 64**
Scientific Session 9: Preclinical In Vivo - Neurology
September 6, 2012 / 13:36-13:48 / Room: Wicklow Hall 2

# USPIO-containing PBCA Microbubbles for Mediating and Monitoring Blood-Brain Barrier Permeation

***Patrick Koczera**, Zhe Liu, Felix Gremse, Fabian Kiessling, Twan Lammers, Department of Experimental Molecular Imaging, RWTH Aachen University, Aachen, Germany. Contact e-mail: pkoczera@ukaachen.de*

Introduction: Microbubbles (MB) are routinely used as contrast agents for functional and molecular ultrasound (US) imaging. In addition, they are known to be suitable systems for permeating cellular and endothelial barriers, and for facilitating the transport of therapeutic and imaging agents across these barriers. We have recently developed poly(butyl-cyanoacrylate) (PBCA) MB - containing ultrasmall superparamagnetic iron oxide particles (USPIO) in their shell - for bimodal US and magnetic resonance imaging (MRI) [1]. Here, we show that these USPIO-containing MB, in combination with power Doppler US-induced MB destruction, can be used to permeate the blood-brain barrier (BBB), and to non-invasively visualize the efficacy of BBB permeation by means of MRI. Materials and Methods: A total of $8{,}5\times10^8$ USPIO-containing MB were i.v. infused via the tail vein, and locally destroyed using power Doppler US (30 min at 16 MHz) through the skull of the mice. Before and after treatment, $T_2$-morphology and $T_2$*-relaxometry measurements were performed. Twelve mice were used, subdivided into three groups of four animals. The first group received MB plus US, and the other two groups either only MB, or only US. To validate BBB permeation, the blood pool marker FITC-dextran (70 kDa; used at a dose of 200 mg/kg) was co-injected with the MB, and its localization in and around rhodamine-lectin-stained blood vessels in the brain was visualized. Image analysis was performed using PRIDE (MRI) and Definiens (IHC) software. Results: USPIO-containing MB in combination with power Doppler US were found to be highly effective in mediating USPIO transport across the BBB, as evidenced by the fact that the $T_2$* relaxation rates in treated brain slices were significantly higher than in those of control groups ($p<0.005$) (Figure 1A). Immunohistochemical analysis, based on extravasated FITC-dextran and rhodamine-lectin-stained blood vessels, confirmed these findings, showing significant leakage of FITC-labeled dextran upon power Doppler US-induced MB destruction (Figure 1B-C). Discussion: USPIO-containing MB can be used to mediate and monitor BBB permeation. Since they provide real-time feedback on the kinetics and the efficacy of BBB opening, such image-guided interventions are considered to be highly useful for enhancing and tailoring the delivery of therapeutic agents across the BBB, assuring not only proper efficacy, but also the ability to better control toxicity. References: [1]: Liu Z, Lammers T, Ehling J, et al. Iron oxide nanoparticle-containing microbubble composites as contrast agents for MR and ultrasound dual-modality imaging. Biomaterials 32: 6155-6163 (2011)

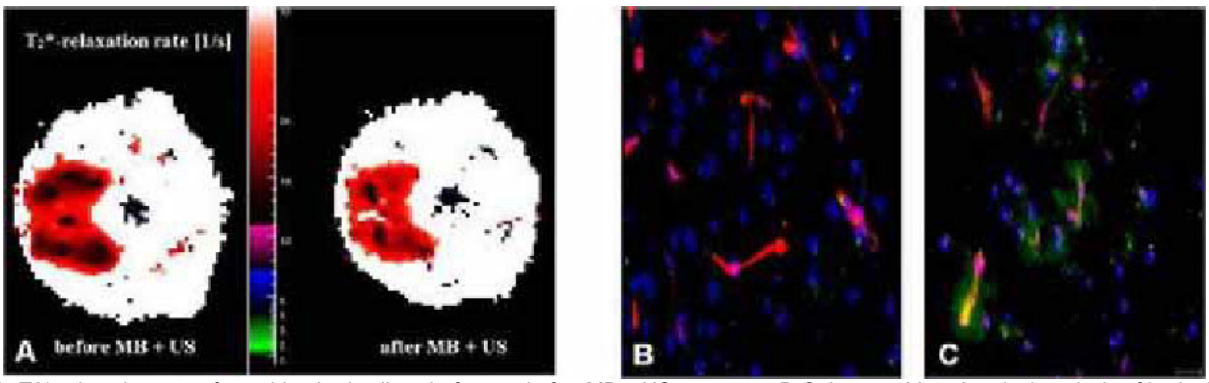


Figure 1. A: T2*-relaxation rate of matching brain slices before and after MB + US treatment. B-C: Immunohistochemical analysis of brain tissue after MB (B) or MB + US treatment (C). Red: rhodamin-lectin-stained blood vessels. Green: (extravasated) FITC-labeled dextran. Blue: TO-PRO3-stained nuclei. Bar = 20 µm.

Disclosure of author financial interest or relationships:
**P. Koczera**, None; **Z. Liu**, None; **F. Gremse**, Philips, Grant/research support; **F. Kiessling**, None; **T. Lammers**, None.

Presentation Number **SS 65**
Scientific Session 9: Preclinical In Vivo - Neurology
September 6, 2012 / 13:48-14:00 / Room: Wicklow Hall 2

# Functional neuroimaging in rats with micro-ultrasound

*Martijn E. van Raaij, Bojana Stefanovic, Adrienne Dorr, Liis Lindvere, **F. Stuart Foster**, Medical Biophysics, Sunnybrook Health Sciences Centre and University of Toronto, Toronto, ON, Canada. Contact e-mail: stuart.foster@sri.utoronto.ca*

Healthy cerebral microcirculation is crucial to neuronal functioning. We present a new method to investigate microvascular hemodynamics in living rodent brain through a focal cranial window based on high-frequency ultrasound imaging. The method has a temporal resolution of 40ms, and a 100 μm in-plane and 600 μm through plane spatial resolution which is comparable to fMRI, and it has a superior temporal resolution of 40 ms per frame.. A commercially available high-frequency ultrasound imaging system was used to quantify changes in the relative cerebral blood volume (CBV) by measuring the scattered signal intensity from an ultrasound contrast agent circulating in the vasculature. Generalized linear model analysis produced effect size and significance maps of changes in cerebral blood volume upon electrical stimulation of the forepaw. Larger CBV increases were observed in the forelimb representation of the primary somatosensory cortex than in the deep gray matter with stimuli as short as 2 s (5.1±1.3% vs. 3.3±0.6%). The temporal evolution of blood volume changes in cortical and subcortical gray matter, pial vessels and subcortical major vessels were measured and show shorter response onset times in the parenchymal regions than in the neighboring large vessels (1.6±1.0 s vs. 2.6±1.3 s in the cortex for a 10 second stimulus protocol). Disruption-reperfusion analysis permitted measurements of relative cerebral blood volume (rCBV), relative cerebral blood flow (rCBF) and inflow speed. We found that in a sagittal section through the primary somatosensory cortex and the underlying structures, rCBV in cortical and subcortical gray matter is not significantly different at 0.89 ± 0.08 and 0.61 ± 0.09 times the brain-average value, and much higher in the vascular regions on the pial surface (3.89 ± 0.71) and in major vessels in the subcortical gray matter (2.02 ± 0.31). Parametric images of rCBV, rCBF, and blood flow speed were produced that demonstrate spatial heterogeneity of these parameters on the 100 μm scale. Segmentation of the cortex in arteriolar and venular-dominated regions identified through Color Doppler imaging showed that rCBV is higher and flow speed lower in venules than in arterioles. Finally, we show that the dependence of rCBV on rCBF was significantly different in cortical and subcortical gray matter: the exponent α from the power law relation rCBV = s x rCBF α was 0.37 ± 0.13 for cortical and 0.75 ± 0.16 for subcortical gray matter. This work demonstrates that functional micro-ultrasound imaging can be used to quantify hemodynamic parameters in the anesthetized rodent brain. The modality is a promising tool for neuroscientists studying these parameters in rodent models of any disease with a cerebrovascular component, such as stroke, the neurodegenerative disorders, and venous collagenosis, especially when differentiation between arteries and veins is essential.

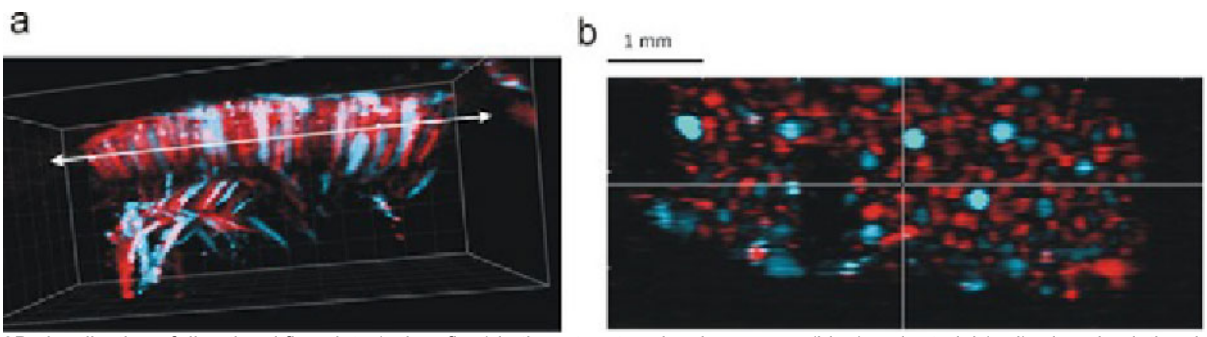


Fig 1. a) 3D visualization of directional flow data (colour flow) in the rat cortex showing venous (blue) and arterial (red) microcirculation. b) View of perforating arterioles ( red) and venules (blue) observed in the "C" scan plane (arrowed line in a) looking down from the surface of the cortex.

Disclosure of author financial interest or relationships:
**M.E. van Raaij**, None; **B. Stefanovic**, None; **A. Dorr**, None; **L. Lindvere**, None; **F. Foster**, VisualSonics, Consultant .

Presentation Number **SS 66**
Scientific Session 9: Preclinical In Vivo - Neurology
September 6, 2012 / 14:00-14:12 / Room: Wicklow Hall 2

# In vivo theranostic magnetic resonance imaging using a superoxide dismutase mimetic

***Alexei A. Bogdanov**, Mohammed S. Shazeeb, Giancarlo Feula, Radiology, University of Massachusetts Medical School, Worcester, MA, USA. Contact e-mail: alexei.bogdanov@umassmed.edu*

The superoxide anion is an essential component of host immune defense against the invasion of various pathogens. However, superoxide anion is highly toxic and is capable to contribute to pathogenesis of many diseases and accelerate aging. Superoxide dismutase (SOD) is capable of efficiently scavenging superoxide, however, endogenous SOD levels may not be sufficient for treating hyperoxic injury, radiation poisoning and neurodegeneration. M40403 (manganese(II)dichloro{2S,21S-dimethyl-(4R,9R,14R,19R)-3,10,13,20,26-pentaazatetracyclo[20.3.1.0.0]hexacosa-1(26),-22(23),24-triene}], Fig.1) is an SOD mimetic with known history of in vivo testing, and its specific activity exceeds the catalytic activity of the native mitochondrial MnSOD enzyme. We synthesized, purified the active enantiomer and explored the potential of M40403 as one of the true theranostic agents: both imaging (Mn is paramagnetic) and SOD-mimetic properties of M40403 are due to chelated Mn. To provide long-circulating, low-toxicity formulation of M40403 we incorporated it in small unilamellar pegylated liposomes. In vitro testing using transmission electron microscopy and quasielastic light scattering showed liposomes 170 ± 50 nm in diameter. At 0.47 T, the relaxivity of M40403 was 4.44 mM-1s-1 (encapsulation yield - 25%). Vmax (initial reaction rate) reflecting the activity of M40403 and M40403 liposomes suggested that at high M40403 concentrations (≥150 μM), the SOD mimetics were dismutating O2- more efficiently than SOD. We further monitored the delivery of M40403 in vivo using 3T MRI. We administered the paramagnetic liposomes in vivo to observe perfusion in the mouse brain using T1-weighted gradient-echo MRI. Liposomes loaded with paramagnetic M40403 were injected via tail vein in mice. M40403 within the liposomes shortened the proton T1 relaxation time of the water within the liposomes and allowed direct visualization of their contents. We observed enhancement in the mouse brain within minutes after IV-injection of M40403 liposomes which had disappeared by the fifth day (Fig.1). This enhancement and signal decay indicated the entry of liposomes into the vascular bed of the brain. The sub-cortex region of the brain showed greater T1 enhancement/higher SNR than the cortex region, which could also indicate the potential entry of M40403 liposomes or free M40403 into the cerebrospinal fluid via the choroid plexus. Therefore, we established that M40403 is a highly efficient SOD mimetic and paramagnetic MR imaging agent useful for monitoring of in vivo delivery. Liposomes loaded with M40403 did not exhibit any outward toxicity and resulted in transient enhancement of the cortical and sub-cortical regions of the brain. Our results indicate that M40403 liposomes enable not only a systemic delivery route of an SOD mimetic to the brain, but also allow MRI monitoring of the potential delivery to the diseased tissues (e.g., in cerebral ischemia).

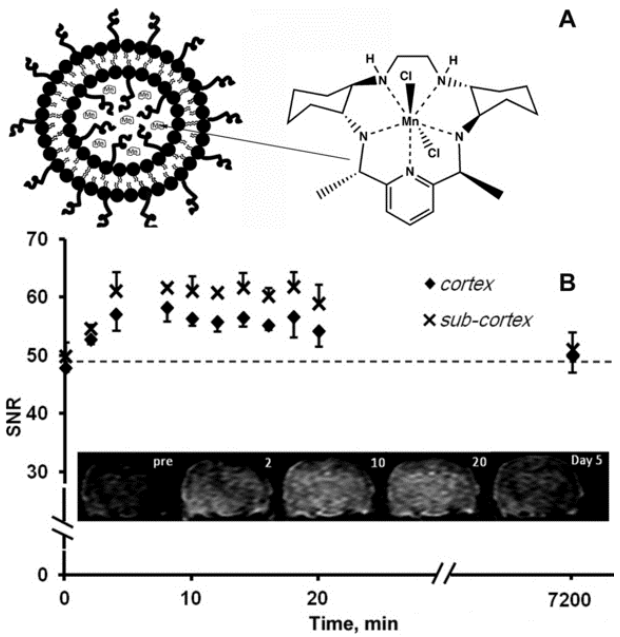


A - a schematic of liposomes with M40403 in the aqueous phase and chemical formula of Mn complex; B - time dependence of MR signal enhancement and sequential T1-WT mouse brain images after IV injection of M40403 liposomes.

Disclosure of author financial interest or relationships:
**A.A. Bogdanov**, None; **M.S. Shazeeb**, None; **G. Feula**, None.

Presentation Number **SS 67**
Scientific Session 9: Preclinical In Vivo - Neurology
September 6, 2012 / 14:12-14:24 / Room: Wicklow Hall 2

# Imaging the severity of PLP 139-151-induced EAE in mouse brain and spinal cord using protease-activatable and vascular NIR imaging agents

*Kristine Vasquez[1], Valerie Eaton[2], Gwendolyn Goings[2], **Jeffrey D. Peterson**[1], Stephen D. Miller[2], [1]Applied Biology, PerkinElmer, Boston, MA, USA; [2]Department of Microbiology-Immunology, Northwestern University Feinberg School of Medicine, Chicago, IL, USA. Contact e-mail: jeff.peterson@perkinelmer.com*

Experimental autoimmune encephalomyelitis (EAE) is a CD4+ T cell-driven autoimmune disease characterized by mononuclear cell inflammation and demyelination of the central nervous system (CNS) Mouse EAE models have provided powerful tools for understanding both the immunology and progression of tissue damage and are considered to be relevant models for the human immune-mediated demyelinating disease multiple sclerosis. Current conventional readouts of disease progression and severity in mouse EAE include clinical scoring and terminal histological assessment, however there are few quantitative tools for the non-invasive assessment of disease. To explore the benefits of near infrared (NIR) imaging in EAE assessment, we used a panel of NIR imaging agents to assess blood-brain barrier leak (vascular agents) and changes in protease activity (cathepsin- and matrix metalloprotease [MMP]-activated agents) associated with neuroantigen (PLP peptide 139-151) immunization-induced CNS autoimmunity. Fluorescence molecular tomography (FMT) imaging was used to image and quantify changes in both the brain and spinal cord, offering a means to effectively image and assess deep tissue signal. Vascular agent accumulation in the spinal cord correlated well with the presence of disease, detecting significant (2-7 fold increases) in animals with partial or complete hind limb paralysis. Brain imaging of vascular leak showed similar increases with disease, but with much greater variability and poor correlation with clinical symptoms. Interestingly, in some studies with low incidence of disease symptoms, brain imaging revealed high signal in some PLP 139-151-immunized mice that had no clinical signs of disease and little or no apparent spinal cord signal. These results were confirmed by ex vivo assessment of brain and spinal cord tissues, suggesting that brain disease can progress independently of spinal cord disease and can be missed when using a clinical scoring system that predominantly assesses spinal cord dysfunction. Further studies with a variety of protease-activatable NIR imaging agents found that cathepsin B imaging was the optimal approach for characterizing brain EAE, showing 5-fold increases associated with PLP 139-152 immunization. In contrast, pan-cathepsin imaging, or MMP imaging, were not as effective in detection of brain EAE. The best agents for detection of spinal cord EAE included vascular agents and cathepsin agents. This research highlights the ability of FMT, combined with appropriate NIR imaging agents, to non-invasively visualize and quantify inflammation and blood brain barrier break-down in the CNS, including the unique ability to assess the incidence and severity of brain disease.

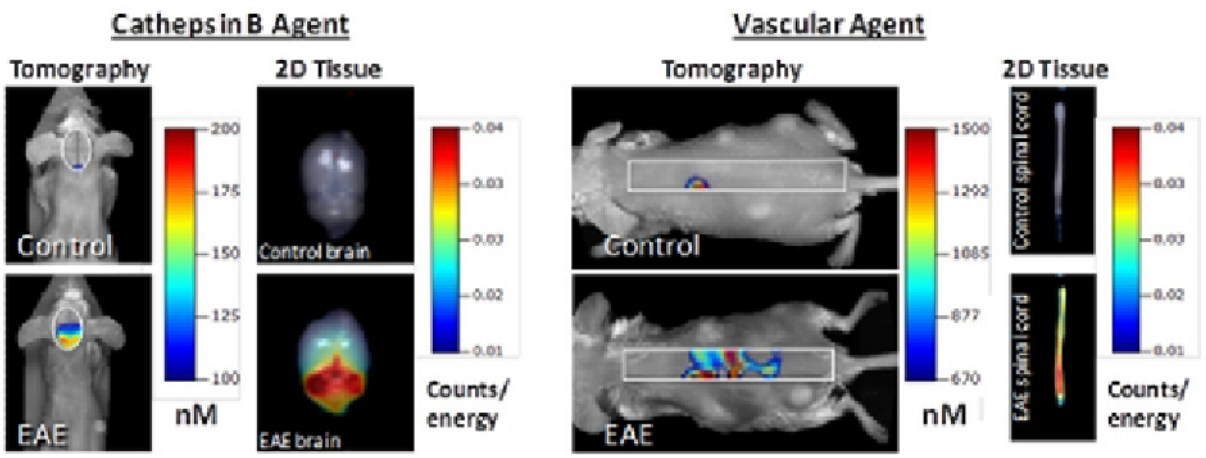


Disclosure of author financial interest or relationships:
**K. Vasquez**, PerkinElmer, Employment; **V. Eaton**, None; **G. Goings**, None; **J.D. Peterson**, PerkinElmer, Employment; **S.D. Miller**, None.

Presentation Number **SS 68**
Scientific Session 10: Preclinical In Vivo - Oncology
September 6, 2012 / 13:00-13:12 / Room: The Auditorium

# I-124 Anti-PSCA minibody immunoPET imaging of local prostate cancer in a transgenic mouse model

***Scott M. Knowles***[1], *Chau P. Tran*[2], *Richard Tavaré*[1], *Tove Olafsen*[1], *Felix B. Salazar*[1], *Hong Wu*[1], *Robert E. Reiter*[2], *Anna M. Wu*[1], [1]*Pharmacology, David Geffen School of Medicine at UCLA, Los Angeles, CA, USA;* [2]*Urology, David Geffen School of Medicine at UCLA, Los Angeles, CA, USA. Contact e-mail: sknowles@mednet.ucla.edu*

Prostate Stem Cell Antigen (PSCA) is a GPI-linked cell surface glycoprotein with limited expression in stomach, bladder, and prostate of normal patients. PSCA, however, is over-expressed in >90% of localized prostate cancer and highly over-expressed in >97% of prostate cancer bone metastases. We have previously shown that an I-124 labeled A11 anti-PSCA minibody can image human PSCA (hPSCA)-expressing prostate cancer subcutaneous xenografts in nude mice. However, the A11 minibody does not cross-react with murine PSCA (mPSCA), nor does the subcutaneous placement of tumors reflect the challenges of imaging the prostate adjacent to the confounding bladder signal from I-124 excretion in the urine. Here we use an hPSCA expressing murine prostate cancer model to evaluate the ability of the A11 minibody to image primary prostate cancers in mice despite background expression of hPSCA and the proximity of the tumor to the bladder. Knock-in mice with hPSCA expression driven by the mPSCA promoter were generated and confirmed to express hPSCA in the prostate, stomach, and bladder by IHC and RT-PCR with low background in other tissues. hPSCA knock-in mice (n=4) and age-matched wild-type mice (n=4) were injected with 20 µg of I-124 labeled A11 minibody (specific activity, 6.1 µCi/µg; immunoreactivity, 64.1%). Significantly higher tissue uptakes were observed in the prostate (0.83±0.13 vs. 0.49±0.04%ID/g, p=0.04), bladder (3.21±0.42 vs. 1.65±0.26%ID/g, p=0.02) and stomachs (2.01±0.22 vs. 0.79±.05%ID/g, p=0.002) of the hPSCA knock-in mice compared to wild-type, with no significant differences seen in other organs. Uptake of the A11 minibody at 44 hours post-injection correlated well with PSCA expression determined in vitro. hPSCA knock-in mice were bred with PTEN Lox/Lox Probasin Cre+ mice bearing a prostate-specific deletion of PTEN to create a model that spontaneously develops hPSCA-expressing high grade prostate intraepithelial neoplasia which then progresses to invasive carcinoma. Seven month old hPSCA PTEN Lox/Lox Probasin Cre+ mice (n=6) and age matched Probasin Cre- Controls (n=6) were injected with 20 µg of I-124 labeled A11 minibody (specific activity, 7.0 µCi/µg; immunoreactivity, 87.7%) and imaged by microPET/CT at 44 hours post-injection. A11 minibody immunoPET imaging and biodistribution showed increased uptake in the prostates of Cre+ mice compared to the Cre- controls (2.38±0.28%ID/g vs 0.61±0.07%ID/g, p<.0001) with no significant differences in uptake in any other tissue. In conclusion, I-124 labeled A11 minibody can image PSCA-expressing localized prostate cancer despite background expression of PSCA and the close proximity of the tumor to the bladder and holds promise for imaging both primary prostate cancer and metastases in human patients.

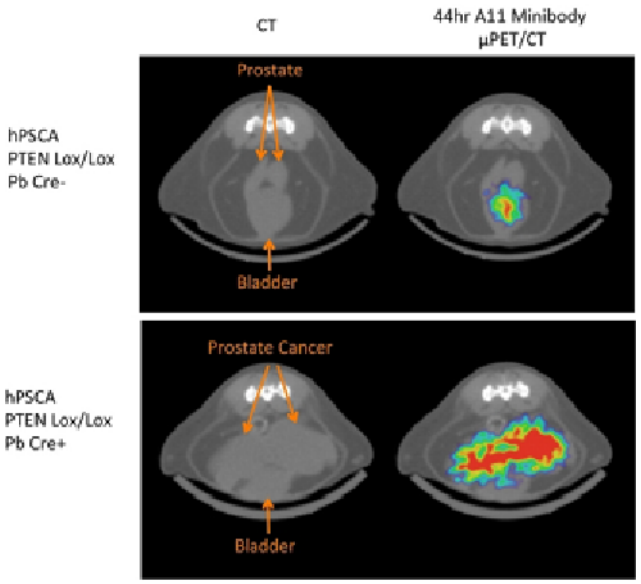


Figure 1: 7 month old hPSCA PTEN Lox/Lox Pb Cre+ mice with prostate cancer show a significant increase in prostate uptake of the A11 minibody compared to Cre- controls allowing imaging of local prostate cancer in vivo.

Disclosure of author financial interest or relationships:
**S.M. Knowles**, None; **C.P. Tran**, None; **R. Tavaré**, None; **T. Olafsen**, ImaginAb Inc., Employment; **F.B. Salazar**, None; **H. Wu**, None; **R.E. Reiter**, Imaginab, inc, Consultant; Imaginab, inc, Stockholder; **A.M. Wu**, ImaginAb, Inc., Consultant; ImaginAb, Inc., Stockholder .

Presentation Number **SS 69**
Scientific Session 10: Preclinical In Vivo - Oncology
September 6, 2012 / 13:12-13:24 / Room: The Auditorium

# Accurate quantification and localization of enzymatically active Prostate-Specific Antigen in vivo

*Guojie Ho, Garry J. Cuneo, Jeff Morin, Jeannine Delaney, Wael Yared, **Milind Rajopadhye**, Jeffrey D. Peterson, Sylvie Kossodo, LST, PerkinElmer, Boston, MA, USA. Contact e-mail: milind.rajopadhye@perkinelmer.com*

Prostate-Specific Antigen (PSA) is a 237 amino acid, 33 kDa, extracellular serine protease expressed in prostate epithelial tissue. In the normal prostate, high concentrations of PSA are stored in the prostatic ductal network. However, cancer leads to the disruption of normal tissue architecture and subsequent leakage of PSA into the tissue interstitium and circulation. In contrast to total PSA, only the enzymatically active form of PSA is selectively present in prostate tissue. In circulation, active PSA immediately forms complexes with the serum protease inhibitor alpha-1-antichymotrypsin, while the inactive forms remains "free". Traditional assays rely on testing for the presence of total PSA (mostly inactive and complexed) and are unable to provide information regarding the amount of enzymatically active PSA, a more biologically relevant tumor biomarker. To fill this gap, we developed a novel near infrared (NIR) fluorescent agent, designed to detect active tumor site PSA with no detection of inactive or complexed PSA. This agent, VM2133, contains a PSA-cleavable peptide sequence labeled with NIR fluorophores (ex/em 750/770 nm) and coupled to a pharmacokinetic modifier designed to improve its plasma availability. In its native state, the agent is nearly completely optically quenched (> 95%); and only becomes fluorescent upon enzymatic cleavage with active PSA, yielding a 300-1800 fold increase in signal as compared to the signal obtained using inactive or complexed PSA. Proteolytic cleavage was also selective for PSA over a large panel of enzymes, including Kallikrein 1, Cathepsin B, MMP-9, MMP-12, MMP-13, uPA, chymotrypsin and thrombin. We hypothesized that the enzymatic activity of PSA could be non-invasively and quantitatively monitored in 3D using Fluorescence Molecular Tomography (FMT), a powerful near-infrared imaging modality that enables 3D quantitative determination of fluorochrome distribution in tissues of live small animals. LNCaP (PSA positive) and PC3 (PSA negative) cells were implanted in the chest area of male nude mice. Real time imaging was performed after systemic administration of VM2133 when tumors reached the desired size. Our results demonstrated a significantly higher fluorescent concentration in LNCaP tumors as compared to the adjoining muscle (34.1 +/- 3.8 nM versus 7.2 +/- 0.6 nM, p=0.0043). Likewise, fluorescence signal in tumors was significantly higher in LNCaP as compared to PC3 tumors (34.1 +/- 3.8 vs 17.14 +/- 3.48 nM, p=0.0191; 12.99 +/- 3.7 vs 2.8 +/- 0.8 pmoles, p=0.0233). This is the first report that demonstrates the feasibility of non-invasive, real-time, molecular imaging of active PSA in vivo in a relevant tumor model. These findings demonstrate the effectiveness of this agent in conjunction with optical imaging as a functional platform for molecular imaging in the field of prostate cancer.

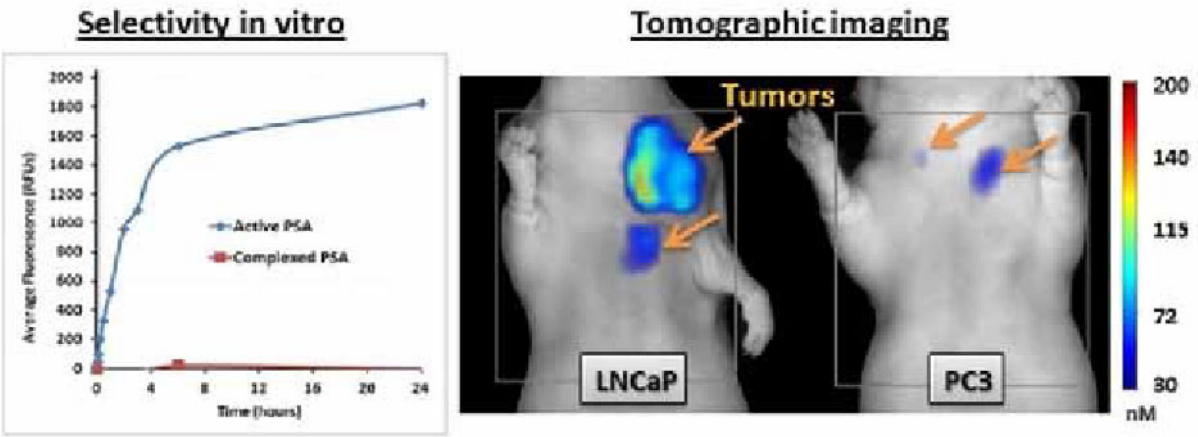


Disclosure of author financial interest or relationships:
**G. Ho**, None; **G.J. Cuneo**, PerkinElmer Life Sciences, Employment; **J. Morin**, Perkin Elmer, Employment; **J. Delaney**, PerkinElmer, Employment; **W. Yared**, Perkin Elmer, Employment; **M. Rajopadhye**, PerkinElmer, Employment; **J.D. Peterson**, PerkinElmer, Employment; **S. Kossodo**, PerkinElmer, Employment .

Presentation Number **SS 7**
Scientific Session 1: Chemistry & Probes - MRI
September 6, 2012 / 11:36-11:47 / Room: Liffey Hall 1

# In Vivo Magnetic Resonance Imaging of Hyperpolarized Choline and Monitoring of Metabolism

*Trevor Wade[1,2], **Hyla Allouche-Arnon**[4,5], Lanette Friesen Waldner[1,2], Kundan Thind[1,2], Alexei V. Ouriadov[2], Albert P. Chen[3], J. Moshe Gomori[4], Charles A. McKenzie[1,2], Rachel Katz-Brull[4,5], [1]Medical Biophysics, The University of Western Ontario, London, ON, Canada; [2]Robarts Research Institute, The University of Western Ontario, London, ON, Canada; [3]GE Healthcare, Toronto, ON, Canada; [4]Radiology, Hadassah-Hebrew University Medical Center, Jerusalem, Israel; [5]BrainWatch Ltd., Tel-Aviv, Israel. Contact e-mail: ahyla@hadassah.org.il*

INTRODUCTION Choline is an essential nutrient used in lipid synthesis, one carbon metabolism, and neurotransmitter metabolism. Here we show the MRI imaging results with a novel hyperpolarized choline molecular agent, labeled at position one with 13C and deuterated at the two methylene positions. We have previously shown that the chemical shift difference of this carbon position is suitable for in vivo monitoring of the conversion of choline to its metabolic products, phosphocholine and betaine (2.4 and 113.7 ppm respectively)1. Additionally, we have shown that such deuteration extends the T1 relaxation time sufficiently to allow imaging and spectroscopy of the hyperpolarized agent in vivo1. METHODS AND MATERIALS The animal studies' protocol was approved by the Institutional Animal Use Subcommittee. Anesthetized male Sprague-Dawley rats, 400+/-20 g (n=6), underwent MRI and MRS in a 3T clinical MRI scanner. Coronal projection13C imaging was performed using a variable flip angle gradient echo sequence within 1 s. Hyperpolarized media containing [1,1,2,2-D4, 1-13C]choline chloride (BrainWatch Ltd.) were injected via a tail vein catheter as a 12 s bolus. Images were acquired at 15-45 s after the start of the bolus injection. Dynamic 13C spectra were acquired every 3 s. 2D 13C chemical shift imaging was acquired with an in-plane resolution of 1.0 cm, within 19 s. RESULTS The labeled-choline polarization in liquid state in the magnet reached 36 %. The T1 of the compound was 30 s at 3 T. Imaging of hyperpolarized choline (A-C) shows a time dependent distribution in the rats' body. At 15 s (A) post start of injection the signal appeared to be largely vascular. By 30 s (B), signal from the heart and vasculature was greatly reduced, while signal from the kidneys was even larger than that at 15 s, suggesting rapid choline uptake by the kidneys. At 45 s (C), the strongest signal was still from the kidneys. Figure D demonstrates the time course of the chemical evolution of choline in vivo. Whole-body dynamic spectroscopy showed two distinct signals assigned to the labeled-choline and [1,1,2,2-D4,1-13C]phosphocholine. At the end of the bolus (12 s), the signal from phosphocholine was already higher than that of choline. By 18 s from the start of injection, phosphocholine was the predominant signal, suggesting complete conversion of choline to phosphocholine. The T1 of phosphocholine in vivo was found to be 22 s. Figure E shows body chemical shift imaging, demonstrating localized choline uptake and metabolism. Figure F shows a chemical shift difference of 2.4 ppm between the signals in the heart and the kidney, suggesting the assignment of these signals to choline and phosphocholine, respectively. CONCLUSION The first non-radioactive images of choline distribution and in vivo monitoring of choline metabolism were obtained by hyperpolarized MRI and MRS. A rapid uptake in kidneys was observed in normal healthy rats. The label accumulated in the kidneys was found to be dominated by phosphocholine metabolized from the injected choline. References: 1) Allouche-Arnon et al. CMMI 2011, 6(3):139-147 and 6(6): 499-506

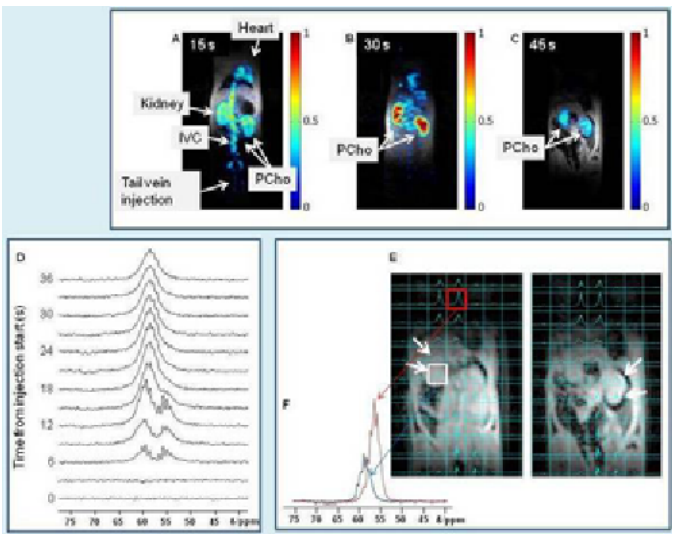


Disclosure of author financial interest or relationships:
**T. Wade**, None; **H. Allouche-Arnon**, None; **L. Friesen Waldner**, None; **K. Thind**, None; **A.V. Ouriadov**, None; **A.P. Chen**, GE Healthcare, Employment; **J. Gomori**, BrainWatch Ltd, Consultant; **C.A. McKenzie**, GE Healthcare, Grant/research support; Brainwatch, Grant/research support; **R. Katz-Brull**, BrainWatch Ltd, Other financial or material support .

Presentation Number **SS 70**
Scientific Session 10: Preclinical In Vivo - Oncology
September 6, 2012 / 13:24-13:36 / Room: The Auditorium

# Intraoperative NIRF Imaging Efficacy using MAb-based Multimodal Agents for Detection of Metastatic Lymph Nodes in Prostate Cancer

***Mary A. Hall***[1], *Nathaniel Wilganowski*[1], *Pradip Ghosh*[1], *Holly Robinson*[1], *Ken L. Pinkston*[2], *Ali Azhdarinia*[1], *Barrett R. Harvey*[2], *Eva Sevick*[1], [1]*Center for Molecular Imaging, The Brown Foundation Institute of Molecular Medicine for the Prevention of Human Diseases, The University of Texas Health Science Center, Houston, TX, USA;* [2]*Division of Applied Biologics, Center for Molecular Imaging, The Brown Foundation Institute of Molecular Medicine for the Prevention of Human Diseases, The University of Texas Health Science Center, Houston, TX, USA. Contact e-mail: mary.hall@uth.tmc.edu*

In prostate cancer (PCa) and other pelvic carcinomas, extended pelvic lymph node dissection (ePLND) is routinely performed, often irrespectively of lymph node (LN) status. To reduce incidences of overtreatment by ePLND at time of radical prostatectomy in low-risk patients, we have developed dual-labeled mAbs targeting epithelial cell adhesion molecule (EpCAM), which is overexpressed in epithelial cancers, for noninvasive and intraoperative detection of cancer-positive LNs by PET/CT and near-infrared fluorescence (NIRF) imaging. Here, we quantified accuracy of in situ NIRF imaging using mAb-based multimodal agents in a gene-reporter mouse model of human PCa. At week 10-12 post-implantation of DsRed-expressing PC3 cells, Nu/Nu mice were administered 64Cu-DOTA-mAb-IRDye 800CW intravenously (40µg of specific or control mAb/250µCi/mouse) and within 18-24 hr underwent µPET/CT followed by NIRF and DsRed fluorescence imaging. The target-to-background ratio (TBR) of mean fluorescence intensity (MFI) or % ID/g was found for each LN imaged and used for receiver operating characteristic (ROC) curve analyses, during which DsRed fluorescence served as the 'true-positive' indicator of PCa-positive LNs. Accuracy rates were compared to evaluate NIRF imaging efficacy using the dual-labeled mAbs. Accuracy of high-affinity, in-house generated mAb 7 was 96%, representing an area under the curve (AUC) that was significantly greater than random chance ($P < 0.001$) and high concordance between in situ NIRF and DsRed reporter-gene imaging for detecting cancer-positive LNs. Similarly, the AUC found from analysis of quantitative µPET/CT of the same LNs examined from in situ NIRF imaging was significant (93%, $P < 0.001$), demonstrating a high level of concordance between noninvasive µPET/CT and in situ DsRed fluorescence imaging using mAb 7. The AUC found from µPET/CT (27%) or NIRF imaging (33%) using isotype control mAb 69 was not significant. Using dual-labeled mAb 7, mean TBRs of MFI (5.2+0.8) and % ID/g (5.8+3.3) found for DsRed-positive LNs in PCa-positive mice were significantly higher than those found for DsRed-negative LNs in PCa-negative mice (2.7+0.4 and 2.2+1.1, respectively), and for those found for DsRed-positive nodes in mice that received control mAb 69 (1.58+0.1 and 1.79+0.9, respectively). Sensitivity and specificity of dual-labeled mAb 7 from NIRF imaging were 100% and 89%, respectively, while 91% sensitivity and 100% specificity were found from quantitative µPET/CT, at TBRs which maximized the functions of each curve. Our findings support NIRF imaging as an efficacious imaging modality for intraoperative guidance during LN resection in PCa, and demonstrate that in-house generated, high affinity mAb 7 is an attractive candidate for further multimodal imaging agent optimization aimed at enhancing sensitivity and specificity for detection of LN involvement in PCa. This work was supported in parts by The Wilson Foundation and NIH U54 CA136404.

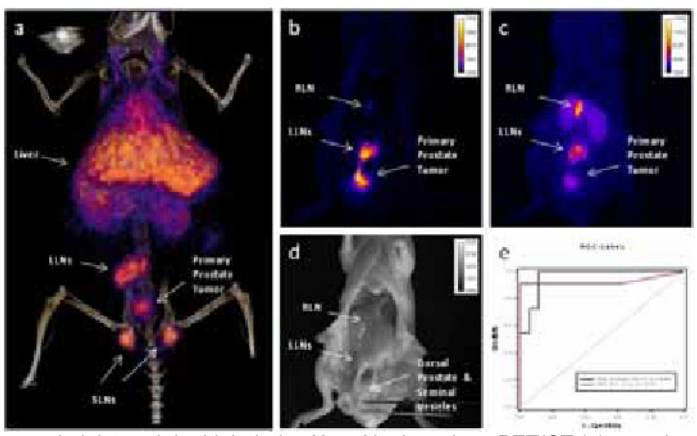


Figure 1. Multimodal imaging of a mouse administered dual-labeled mAb 7. Noninvasive µPET/CT (a) reveals signal-positive primary prostate tumor, lumbar lymph nodes (LLNs), and sciatic LNs (SLNs). In situ DsRed fluorescence, reporter gene (b) and NIRF imaging (c) reveal signal-positive primary prostate tumor, LLNs, and a renal LN (RLN). White light (d) shows anatomical features in situ, including exposed dorsal prostate. ROC curves for mAb 7 (e) demonstrate 96% and 93% accuracy for NIRF and µPET/CT, respectively.

Disclosure of author financial interest or relationships:
**M.A. Hall**, None; **N. Wilganowski**, None; **P. Ghosh**, None; **H. Robinson**, None; **K.L. Pinkston**, None; **A. Azhdarinia**, None; **B.R. Harvey**, None; **E. Sevick**, Tactile, Inc, Grant/research support; Siemens Preclinical Solutions, Other financial or material support .

Presentation Number **SS 71**
Scientific Session 10: Preclinical In Vivo - Oncology
September 6, 2012 / 13:36-13:48 / Room: The Auditorium

# Evaluation of metabolically stabilized $^{18}$F-labeled bombesin analogs for imaging GRP receptors in prostate cancer

***Susan Richter***[1], *Melinda Wuest*[1], *Stephanie S. Krieger*[2], *Jesse J. Parry*[2], *Buck Rogers*[2], *Ralf K. Bergmann*[3], *Frank Wuest*[1], [1]*Department of Oncology, University of Alberta, Edmonton, AB, Canada;* [2]*Department of Radiation Oncology, Washington University School of Medicine, St. Louis, MO, USA;* [3]*Institute of Radiopharmacy, Helmholtz Centre Dresden-Rossendorf, Dresden, Germany. Contact e-mail: srichter@ualberta.ca*

**Objectives**: According to GLOBOSCAN 2008 the worldwide prostate cancer incidence rates will increase to about 1.7 million new cases per year in 2030. In recent years, bombesin and bombesin analogs have attracted much attention as high affinity and selectivity ligands for the gastrin-releasing peptide (GRP) receptor. The GRP receptor was found to be overexpressed and implicated in a variety of human tumors including prostate cancer. Radiolabeled bombesin and bombesin analogues belong to an interesting class of new diagnostic probes for molecular imaging of GRP receptor-expressing prostate cancer. This study describes the synthesis and radiopharmacological evaluation of a high affinity and metabolically stabilized $^{18}$F-labeled bombesin analog for PET imaging of GRP receptors in prostate cancer. **Methods**: Three modified bombesin analogs bearing an aminovaleric (BBN-**1**, BBN-**2**), or an aminooctanoic acid linker (BBN-**3**) were tested in a competitive binding assay against $^{125}$I-[Tyr$^4$]-BBN for their binding to the GRP receptor. A calcium release assay in human prostate cancer cells (PC3) was performed to determine agonistic or antagonistic behaviour. The derivative with the highest affinity to GRP (BBN-**2**) was selected to be conjugated with the prosthetic labeling agent *N*-succinimidyl-4-[$^{18}$F]fluorobenzoate ([$^{18}$F]SFB) in borate buffer (pH=8.2) for 30 min at 40°C to synthesize the desired $^{18}$F-labeled bombesin analog. Tumor-targeting of [$^{18}$F]BBN-**2** was evaluated in PC3 tumor-bearing male nude mice with biodistribution experiments (mean ± SD) and dynamic small animal PET studies. **Results**: The competitive binding assay revealed $IC_{50}$-values between 8.7 and 16.7 nM for BBN-**1**, BBN-**2** and BBN-**3** against $^{125}$I-[Tyr$^4$]-BBN versus 3.0 nM for I-[Tyr$^4$]-BBN. All three stabilized bombesin analogs are GRP receptor antagonists. $^{18}$F-labeled [$^{18}$F]BBN-**2** was prepared in 30% radiochemical yield (based upon [$^{18}$F]SFB) within 80 min including HPLC purification, evaporation of HPLC eluent and formulation in 0.9% saline. The radiochemical purity exceeded 95%, and the specific activity was determined to be 20 GBq/µmol. [$^{18}$F]BBN-**2** showed reasonable metabolic stability in mouse blood resulting in 65% of intact radiolabeled peptide after 60 min p.i.. Uptake of [$^{18}$F]BBN-**2** into PC3 tumors was 2.75±1.82 %ID/g after 5 min and 2.45±1.25 %ID/g after 60 min p.i.. The receptor specificity of [$^{18}$F]BBN-**2** was confirmed by effective blocking of the radiotracers uptake in the presence of non-radioactive BBN-**2** resulting in 0.76±0.51 %ID/g at 60 min p.i. (n=4; $p<0.05$). Dynamic PET imaging resulted in $SUV_{60min}$ values of 0.58 for [$^{18}$F]BBN-**2** versus 0.24 (n=2) for [$^{18}$F]BBN-**2** with BBN-**2** pre-dosing in PC3 tumors. **Conclusions**: The present study showed that $^{18}$F-labeled bombesin analog [$^{18}$F]BBN-**2** is a suitable PET radiotracer with favourable metabolic stability for molecular imaging of GRP receptor-positive prostate cancer.

Disclosure of author financial interest or relationships:
**S. Richter**, None; **M. Wuest**, None; **S.S. Krieger**, None; **J.J. Parry**, None; **B. Rogers**, None; **R.K. Bergmann**, None; **F. Wuest**, None.

Presentation Number **SS 72**
Scientific Session 10: Preclinical In Vivo - Oncology
September 6, 2012 / 13:48-14:00 / Room: The Auditorium

# RadioimmunoPET Imaging of Tissue Factor in Pancreatic Cancer

*Hao Hong[1], Yin Zhang[1], Tapas R. Nayak[1], Jonathan W. Engle[1], Yunan Yang[1], Bai Liu[2], Hing C. Wong[2], Todd E. Barnhart[1], **Weibo Cai**[1], [1]University of Wisconsin - Madison, Madison, WI, USA; [2]Altor BioScience Corporation, Miramar, FL, USA. Contact e-mail: WCai@uwhealth.org*

**Objectives:** Upregulation of tissue factor (TF) expression leads to increased patient morbidity and mortality in many solid tumor types. The goal of this study was to develop a positron emission tomography (PET) tracer for imaging of TF expression in pancreatic cancer. **Methods:** ALT836 (formerly known as Sunol-cH36), a chimeric anti-human TF monoclonal antibody (mAb) that is currently in clinical investigation, was conjugated to 2-S-(4-isothiocyanatobenzyl)-1,4,7-triazacyclononane-1,4,7-triacetic acid (p-SCN-Bn-NOTA) and labeled with $^{64}$Cu. To compare the TF binding affinity of ALT836 and NOTA-ALT836, flow cytometry and microscopy studies were performed in three pancreatic cancer cell lines with different TF expression level (from low to high: PANC-1, ASPC-1, and BXPC-3). PET imaging, biodistribution, blocking, and histology studies were performed in pancreatic tumor-bearing mice to evaluate the ability and specificity of $^{64}$Cu-NOTA-ALT836 to target TF in vivo. **Results:** FACS analyses in three pancreatic cancer cell lines revealed no difference in TF binding affinity/specificity between ALT836 and NOTA-ALT836, which was further validated by fluorescence microscopy. $^{64}$Cu-labeling was achieved with high yield and specific activity. Serial PET imaging revealed that uptake of $^{64}$Cu-NOTA-ALT836 was 5.7±0.5, 10.3±0.5, and 16.5±2.6%ID/g in the BXPC-3 tumor (high TF expression), 2.1±0.7, 4.6±0.8, and 5.3±0.9 %ID/g in the ASPC-1 tumor (medium TF expression), 1.7±0.8, 2.8±0.7, and 2.2±0.6 %ID/g in the PANC-1 tumor (low TF expression) at 4, 24, and 48 h postinjection respectively (n = 3). The BXPC-3 tumor uptake was significantly higher than that of ASPC-1 and PANC-1 tumors at all three time points. Biodistribution data were consistent with the PET findings. Blocking experiments, control studies, and histology all confirmed in vivo target specificity of $^{64}$Cu-NOTA-ALT836. **Conclusions:** This is the first successful PET imaging study of TF expression. Fast, prominent, persistent, and TF-specific uptake of $^{64}$Cu-NOTA-ALT836 in the BXPC-3 tumor was observed.

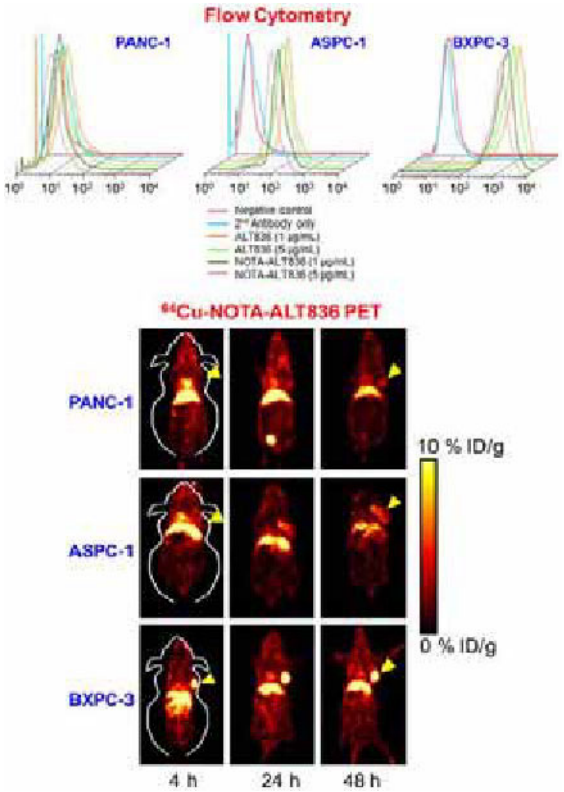


Disclosure of author financial interest or relationships:
**H. Hong**, None; **Y. Zhang**, None; **T.R. Nayak**, None; **J.W. Engle**, None; **Y. Yang**, None; **B. Liu**, Altor Bioscience corp., Employment; **H.C. Wong**, None; **T.E. Barnhart**, None; **W. Cai**, None.

Presentation Number **SS 73**
Scientific Session 10: Preclinical In Vivo - Oncology
September 6, 2012 / 14:00-14:12 / Room: The Auditorium

# Validation of the in-vivo Assessment of LDH-A inhibition in Pancreatic Tumor Xenografts Using $^{13}$C-MRS of Hyperpolarized Pyruvate

***Prasanta Dutta***[1], *Nv Rajeshkumar*[2], *Anne Le*[2], *Gary Martinez*[1], *A. Maitra*[2], *Chi V. Dang*[2], *Robert Gillies*[1], [1]*Imaging, Moffitt Cancer Center, Tampa, FL, USA;* [2]*School of Medicine, Johns Hopkins University, Baltimore, MD, USA. Contact e-mail: Prasanta.Dutta@moffitt.org*

Hyperpolarized $^{13}$C-MRS/I using the dissolution DNP (dynamic nuclear polarization) method provides a >10,000 fold signal enhancement for detecting $^{13}$C-labeled such as pyruvate to monitor metabolic flux through multiple key biochemical pathways (glycolysis and citric acid cycle) [1]. The Warburg effect is a metabolic feature of cancers that causes them to preferentially metabolize pyruvate via glycolytic pathway to lactate. It is reported that the inhibition of LDH-A (lactate dehydrogenase-A) with the small molecule drug FX11 inhibits tumor progression [2]. In this work, we have evaluated the efficacy of FX11 treatment to human pancreatic xenograft tumors via assessing the metabolic conversion of lactate from pyruvate using $^{13}$C-MRS. Hyperpolarization experiments were performed with 1-$^{13}$C-labeled pyruvic acid containing 15 mM trityl radical (OX63) for an hour using a DNP polarizer (HyperSense). 350 µL hyperpolarized pyruvate after dissolution was administered via a jugular-vein catheter to tumor bearing mice in 15-18 sec. $^{13}$C-spectra were obtained using a Agilent 7 T imaging scanner utilizing a dual tuned $^{1}$H- $^{13}$C-volume coil. Fresh pancreatic cancer tissues, excised from patients at Johns Hopkins Hospital (pancreatoduodenectomy), were transplanted as subcutaneous tumors in 6-week-old athymic nude mice [3]. Two set of tumors that are sensitive (JH015, Panc253) and resistant (JH024, JH033) to FX11 have been chosen for hyperpolarized $^{13}$C-MRS study. $^{13}$C-MRS data acquisition from a 7mm thick tumor slice was initiated right before the hyperpolarized pyruvate injection with a $T_R$ of 1 sec and flip angle of 9$^{o}$. In-vivo dynamic MR spectra show peaks for pyruvate and its metabolic conversion to lactate via LDH activity (supplement figure). The tumors were treated with FX11 for seven days with doses of 42 µg daily through i.p. injection, whereas the control group received DMSO. The Lac/Pyr ratio was calculated and has been used as FX11 response marker before and after treatment and control group as well. In the drug-sensitive JH015 and Panc253 tumors, the Lac/Pyr ratios were significantly lower in treated animals relative to DMSO controls ($p<0.01$), suggesting drug response. In drug-resistant JH024 and JH033 tumors, no significant differences relative to controls were observed (Figure 1). Differences in Lac/Pyr ratios were observed much sooner than were differences in tumor volume. Our experimental observation using $^{13}$C-MRS on FX11 sensitive and resistant tumors has been validated through the other imaging modalities such as FDG-PET and diffusion weighted MRI (DW-MRI) measurements of the apparent diffusion coefficient of tissue water (ADC). In FX11 sensitive tumors, the FDG uptake reduced compared to control group. The ADC increased in treated sensitive tumors but resistant tumor ADC decreased. In summary, the measurement of hyperpolarized $^{13}$C-label flux between pyruvate and lactate is used to detect early response to therapy before differences in tumor volume were observed. References: [1] Kurhanewicz J. et al., Neoplasia, 13, 81-97, (2011). [2] Le A. et al., PNAS, 107, 2037-2042 (2010). [3] Rejeshkumar et al. Clin Cancer Res 15, 4138-4146 (2009).

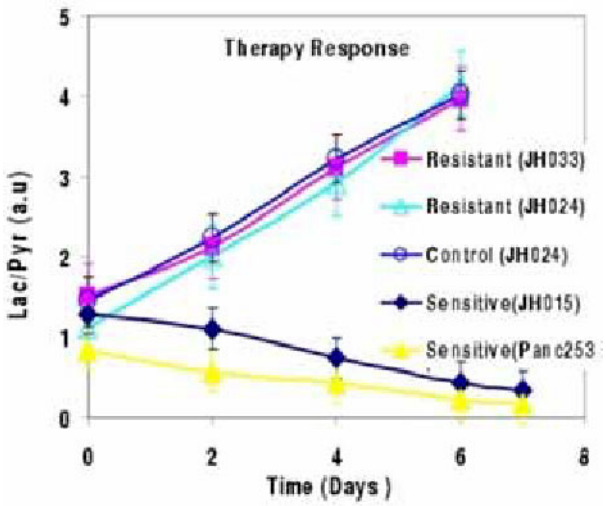


Response marker (Lac/Pyr ratio) was reduced with FX11 treatment in sensitive tumors and increased after treatment in resistant tumors. In control (DMSO treatment) the Lac/Pyr ratio is also increased.

Disclosure of author financial interest or relationships:
**P. Dutta**, None; **N. Rajeshkumar**, None; **A. Le**, None; **G. Martinez**, None; **A. Maitra**, None; **C.V. Dang**, None; **R. Gillies**, Intezyne, Consultant .

Presentation Number **SS 74**
Scientific Session 10: Preclinical In Vivo - Oncology
September 6, 2012 / 14:12-14:24 / Room: The Auditorium

# Detection of disseminated abdominal Rhabdomyosarcoma (RMS) by multimodality in vivo imaging

***Christoph M. Griessinger***[1], *Sorin Armeanu-Ebinger*[3], *Funda Cay*[1], *Julia Wenz*[3], *Bernd J. Pichler*[1], *Manfred Kneilling*[2], *Guido Seitz*[3], [1]*Department of Preclinical Imaging and Radiopharmacy, Eberhard Karls University Tuebingen, Tuebingen, Germany;* [2]*Department of Dermatology, Eberhard Karls University Tuebingen, Tuebingen, Germany;* [3]*Department of Pediatric Surgery and Urology, University Children`s Hospital, Eberhard Karls University Tuebingen, Tuebingen, Germany. Contact e-mail: christoph.griessinger@med.uni-tuebingen.de*

RMS is the most common pediatric soft tissue sarcoma with 20% appearance in the genitourinary tract. Diagnostic work up of disseminated RMS is difficult as some suspicious structures cannot be clearly identified as tumor especially in difficult anatomical regions (pelvis). Imaging modalities such as PET/MRI might substantially contribute to identify these structures. Aim of the study was to establish an optimized tool to diagnose RMS using the radiotracers [18F]FDG, [18F]FLT and [11C]Cholin in a preclinical setup. Human alveolar RMS cells line (Rh30) were stable transfected to express mCherry and gaussia luciferase to enable in vivo detection by optical imaging (OI). For in vivo experiments 1E+6 RMS cells were injected i.p. into NOD/LtSz-scid IL2R mice and tumor growth was monitored in vivo by OI and measurement of luciferase activity in serum. After 4 weeks RMS bearing mice were in vivo investigated by [18F]FDG-, [18F]FLT-, and [11C]Choline-PET/MRI measurements to identify RMS in the gastrointestinal cavity. Finally mice were killed and investigated ex vivo by OI to identify RMS by mCherry expression and biodistribution by γ-counting. Most of the tumor nodules were detected at necropsy attached to the pancreas, spleen, intestine, at the injection site and in the ovaries. The luciferase serum level increased proportional to the tumor burden, whereas in vivo luciferase bioluminescence imaging revealed diffuse signals. However, mCherry fluorescence imaging was applicable to follow RMS growth and to identify more accurate RMS tissue ex vivo. In vivo PET investigations exhibited a sufficient [18F]FDG uptake in peritoneal RMS accompanied with a high background in the kidney, bladder and fat tissue. [18F]FLT revealed a high sensitivity and enabled the detection of small isolated lesions also next to the bladder, based on a high uptake in RMS and a low background signal. [11C]Choline was not qualified to detect RMS due to the high background in the liver and kidneys and the low uptake in tumors. A valid detection of tumors and tumor extent was possible only by combined PET/MRI. The analysis of [18F]FDG- and [18F]FLT-PET scans exhibited a slightly enhanced [18F]FLT uptake (3.5±1,84 %ID/cc) in RMS compared to the [18F]FDG uptake (2.69 ±0.31%ID/cc) and a 2.5-fold higher tumor/muscle-ratio (TMR) for [18F]FLT (5.0±2.0) compared to [18F]FDG (2.0±0.4). The smallest non invasive in vivo detectable RMS volume was approximately 1.3 mm3 for [18F]FLT and approximately 3 mm3 for [18F]FDG. Ex vivo biodistribution could confirm the in vivo findings as [18F]FLT showed a higher %ID/g and TMR compared to [18F]FDG. [18F]FLT was most sensitive to identify RMS, even next to the bladder, due to the high contrast while identification of RMS by [18F]FDG was only possible with additional morphological informations provided by MRI and OI. With the clinical availability of PET/MRI, we see an important role of [18F]FLT-PET in RMS in children as anatomical information is required and can be revealed by PET/MRI at much lower radiation dose compared to PET/CT. First clinical studies in RMS children are therefore on the way utilizing our whole-body clinical PET/MRI.

Disclosure of author financial interest or relationships:
**C.M. Griessinger**, None; **S. Armeanu-Ebinger**, None; **F. Cay**, None; **J. Wenz**, None; **B.J. Pichler**, Siemens, Grant/research support; AstraZeneca, Grant/research support; Bayer Healthcare, Grant/research support; Boehringer-Ingelheim, Grant/research support; Oncodesign, Grant/research support; Merck, Grant/research support; Bruker, Grant/research support; **M. Kneilling**, None; **G. Seitz**, None.

Presentation Number **SS 75**
Scientific Session 11: Chemistry & Probes - Optical Imaging
September 7, 2012 / 10:30-11:00 / Room: Liffey Hall 1

# Intra-vascular Optical Imaging

***Farouc A. Jaffer**, Cardiology, Harvard Medical School, Boston, MA, USA. Contact e-mail: fjaffer@mgh.harvard.edu*

Disclosure of author financial interest or relationships:
**F.A. Jaffer**, Boston Scientific, Merck, Siemens, Consultant; Abbott Vascular, Grant/research support .

Presentation Number **SS 76**
Scientific Session 11: Chemistry & Probes - Optical Imaging
September 7, 2012 / 11:00-11:12 / Room: Liffey Hall 1

# Structure Activity Relationship after Combinatorial Synthesis of Nerve-Highlighting Fluorophores

*Yang Xie[1], Haley L. Goodwill[1], Khaled A. Nasr[1,5], Yoshitomo Ashitate[1], Tiberiu M. Siclovan[3], Maria Zavodszky[3], Cristina A. Tan Hehir[3], John V. Frangioni[1,2], **Summer L. Gibbs**[1,4], [1]Department of Medicine, Beth Israel Deaconess Medical Center, Boston, MA, USA; [2]Department of Radiology, Beth Israel Deaconess Medical Center, Boston, MA, USA; [3]Diagnostic and Biomedical Imaging Technologies, GE Global Research, Niskayuna, NY, USA; [4]Biomedical Engineering, Oregon Health & Science University, Portland, OR, USA; [5]Advanced Imaging Research Center, University of Texas Southwestern Medical Center, Dallas, TX, USA. Contact e-mail: summerlgibbs@gmail.com*

Nerve damage is a major morbidity associated with numerous surgical interventions. Although neuroanatomy is well known, nerve visualization during surgery continues to challenge even the most experienced clinicians. This difficulty stems from the nature of nerve tissues, which are small, translucent structures that are typically protected deep within the muscle. A nerve-specific fluorescent contrast agent, specifically one with near-infrared (NIR) absorption and emission, would be of immediate benefit to both patients and surgeons. Currently there are only 3 classes of small molecule organic fluorophores that have been shown to penetrate the blood brain barrier and blood nerve barrier, binding to nerve tissue when administered systemically, which include the stilbene derivatives, the distyrylbenzene (DSB) fluorophores, and the styryl pyridinium (FM) fluorophores. However, none of these small molecules absorb or emit in the NIR. The DSB pharmacophore is particularly attractive for further study because 3 previously studied DSB fluorophores were shown to highlight all nerve and brain tissue in mice, rats, and pigs when administered systemically. In the current study, the DSB class of small molecules was derivatized using combinatorial solid phase synthesis and commercially available building blocks, which yielded more than 200 DSB fluorophores. The nerve-specific properties of all DSB derivatives were analyzed using an ex vivo nerve-specific binding assay on pig and human sciatic nerve. Results from this assay were used to perform quantitative structure activity relationship (QSAR) modeling. All DSB derivatives with positive ex vivo binding were tested for in vivo nerve specificity in mice (n=3 per compound) to assess the affect of pharmacokinetics and biodistribution on nerve binding. The 2 new DSB fluorophores with the highest nerve to muscle ratio were tested in pigs to ensure scalability of the nerve-specific fluorophores. Although none of the DSB derivatives are the desired NIR nerve-specific fluorophore, the structure activity relationship has been quantified and will be used to direct future library synthesis.

Disclosure of author financial interest or relationships:
**Y. Xie**, None; **H.L. Goodwill**, None; **K.A. Nasr**, None; **Y. Ashitate**, None; **T.M. Siclovan**, General Electric Global Research, Grant/research support; **M. Zavodszky**, None; **C.A. Tan Hehir**, General Electric, Employment; General Electric, Stockholder; **J.V. Frangioni**, None; **S.L. Gibbs**, None.

Presentation Number **SS 77**
Scientific Session 11: Chemistry & Probes - Optical Imaging
September 7, 2012 / 11:12-11:24 / Room: Liffey Hall 1

# NIR-Fluorescent Choline Kinase Inhibitors for Cancer Imaging and Therapy

***Sean P. Arlauckas***[1], *Anatoliy V. Popov*[2], *Edward J. Delikatny*[2], [1]*Pharmacology, University of Pennsylvania, Philadelphia, PA, USA;* [2]*Radiology, University of Pennsylvania, Philadelphia, PA, USA. Contact e-mail: sarl@mail.med.upenn.edu*

Upregulation of Choline Kinase (ChoK) has been correlated with histological tumor grade and resistance to anti-estrogen therapies in breast cancer, ultimately indicating a poorer prognosis. ChoK catalyzes the conversion of choline to phosphocholine (PC), an important mitogenic second messenger and the first step in biosynthesis of the major membrane phospholipid phosphatidylcholine. Using magnetic resonance spectroscopy, it is difficult to measure the contribution of ChoK to the elevated PC peak observed during tumor progression and the depletion of PC corresponding to treatment response. This is due to the competing actions of phospholipases and difficulties in resolving the individual choline-containing metabolites in vivo. Analogs of the bis-cationic choline mimetic Hemicholinium-3, such as MN58b and TCD-717, have previously been identified as specific ChoK inhibitors whose antitumor capabilities are being explored in Phase I clinical trials. We have synthesized a series of fluorescent polymethine dyes that incorporate the features essential for effective inhibition: bis-heterocyclic symmetry, quaternary ammonium groups, water solubility, and an aliphatic spacer of optimized length. We have also synthesized the most extensively studied ChoK inhibitor, MN58b, as a positive control. Fluorescent within the NIR range (excitation ~ 640-745 nm, emission ~ 770 nm), the dyes are suitable for detection of ChoK expression in vivo. The ability to measure ChoK non-invasively would provide complementary information to the metabolic assessment provided by MRS. We have identified two prototype compounds, JAS239 and JAS240, which inhibit ChoK with IC50s comparable to MN58b. ChoK activity was assessed in triple-negative MDA-MB-231 breast cancer cells and in non-transformed MCF10a breast epithelial cells using 14C-labeled choline uptake. The metastatic MDA-MB-231 cancer line displayed a greater sensitivity to JAS239 than non-transformed MCF10a breast epithelial cells. Confocal microscopy confirmed the probes were localized to the cytosol (Figure 1 A-C) where ChoK is active, and excluded from the nucleus where DNA intercalation could cause non-specific cytotoxicity or mutagenesis. Fluorimetry studies showed that JAS239 uptake was linearly proportional to concentration and independent of exogenous choline concentration, indicating that uptake does not rely on choline transporters. Addition of exogenous choline reverses ChoK inhibition, signifying competitive inhibition at the choline-binding site. Cell uptake is detectable within 15 min and ChoK inhibition present by 60 min. These data demonstrate the feasibility of this strategy for optical detection of ChoK expression. This method could be employed in the future for more accurate breast cancer staging and assessment of therapy response.

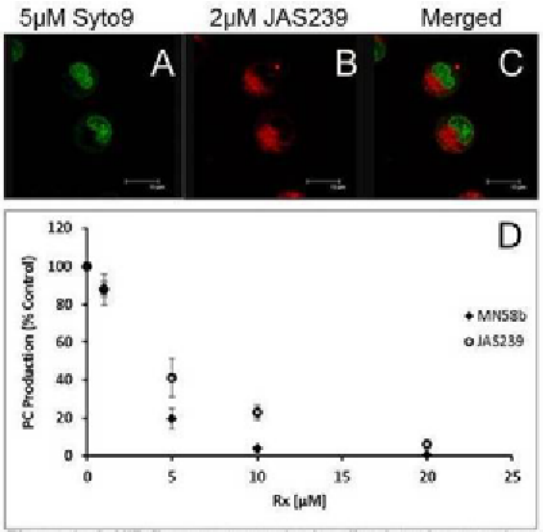


***Figure 1: A NIR-fluorescent probe localized to the cytoplasm that effectively inhibits the cytoplasmic enzyme ChoK in breast cancer cells.*** *Fluorescent confocal micrographs show MDA-MB-231 cells stained for 30 min with A) the nuclear stain Syto9, B) 2 μM JAS239 localized to the cytoplasm and C) merged images.*
*D) Treatment for 16 hr with varying concentrations of MN58b or JAS239 in MDA-MB-231 cells blocked phosphorylation of $^{14}$C-choline, as detected by autoradiography of TLC-separated extracts. Data are presented as percent of control activity corrected for viable cell number determined by trypan blue exclusion assay, ± SD for three separate experiments.*

Disclosure of author financial interest or relationships:
**S.P. Arlauckas**, None; **A.V. Popov**, None; **E.J. Delikatny**, None.

Presentation Number **SS 78**
Scientific Session 11: Chemistry & Probes - Optical Imaging
September 7, 2012 / 11:24-11:36 / Room: Liffey Hall 1

# Activatable probes for photoacoustic imaging of furin activity in living mice

***Anca Dragulescu-Andrasi***[1], *Sri Rajasekhar Kothapalli*[1], *Grigory A. Tikhomirov*[1], *Jianghong Rao*[1,2], *Sanjiv S. Gambhir*[1,3], [1]*Radiology,Molecular Imaging Program at Stanford, Stanford University School of Medicine, Stanford, CA, USA;* [2]*Chemistry, Stanford University, Stanford, CA, USA;* [3]*Bioengineering and Materials Science & Engineering, Stanford University Scool of Medicine, Stanford, CA, USA. Contact e-mail: anca_franzini@yahoo.com*

Photoacoustic imaging continues to evolve from an exclusively structural to a molecular imaging modality. Owing to its high spatial resolution even in deep tissues, photoacoustic imaging holds great potential for biomedical applications and molecular diagnostics. However, there is a scarcity of molecular probes for targeted photoacoustic imaging, especially in the area of enzyme-activatable probes. Here we introduce a photoacoustic probe, which reports proteolytic activity by a bioorthogonal condensation reaction. This probe is applied to the in vivo imaging of furin and furin-like activity in mice tumor models. Furin is an endoprotease over-expressed in inflammatory conditions and in cancer, especially in hypoxic tumors. The design of this activatable probe is based on a recently developed in cellulo synthesis of oligomeric nanostructures, which can be controlled by furin activity. The probe consists of a short peptide furin substrate linked to two pro-reactive moieties (1,2-aminothiol and 6-amino-2-cyanobenzothiazole) and a NIR reporter molecule (Figure A). Upon enzymatic activation by furin, the probe oligomerizes and accumulates in cells and tumors that over-express the protease, resulting in increased photoacoustic signal (Figure B). We demonstrate in both cells and animal studies that the activatable probe produces significantly higher photoacoustic signals in cells and in mice in tumors overexpressing furin (MDA-MB231) than in furin-deficient control tumors (LoVo). In mice studies (see Figure, n=4 for all three groups), the photoacoustic signal increase generated by the probe (20 nmoles administrated via tail vein, 60 min after probe injection) is 7.1-fold higher in furin positive tumors than in furin deficient tumors and 2.7-fold higher than for a negative control probe (probe containing a peptide sequence not processed by furin used in mice carrying furin-positive tumors). This new type of photoacoustic activatable probes can image enzyme activity in living subjects at depths significantly greater than fluorescence imaging agents and have great potential for hypoxia imaging in deep tumors.

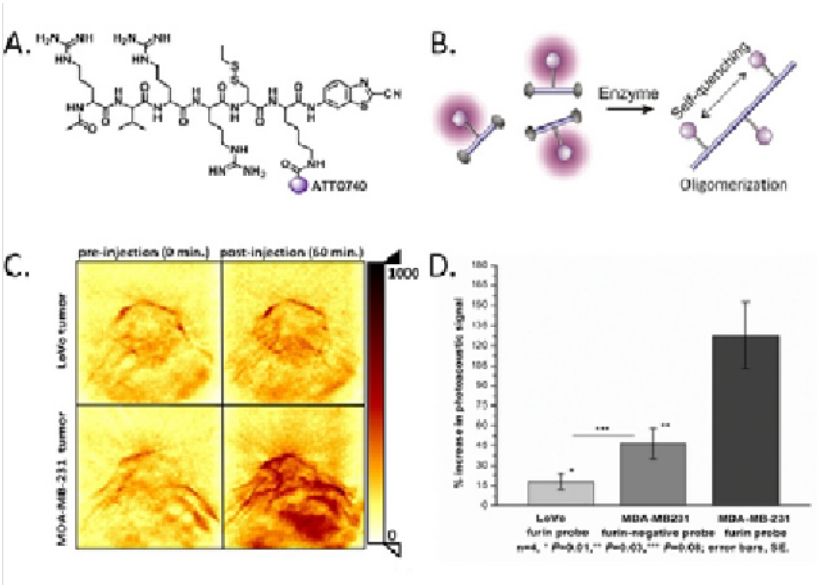


Photoacoustic imaging of mice carrying subcutaneous tumors using a NIR photoacoustic activatable probe. A. Chemical structure of the photoacoustic furin probe. B. Mechanism of probe oligomerization upon furin enzymatic cleavage. C. Photoacoustic images of subcutaneous tumors in mice carrying furin deficient (LoVo) and furin positive (MDA-MB231) tumors. Mice were imaged using ENDRA photoacoustic instrument before probe injection and then injected via tail vein with 20 nmoles probe in 150 µL PBS and imaged every 15 min. for 1h. Representative images at 0min. (pre-injection) and at 60 min. after probe injection are shown. D. Quantitation of the photoacoustic signal increase in mice tumor models using a furin-activatable probe in LoVo and MDA-MB231 tumor and a furin-negative probe in MDA-MB231 tumors. The data represents the photoacoustic signal increase at 60 min. relative to the pre-injection signal.

Disclosure of author financial interest or relationships:
**A. Dragulescu-Andrasi**, None; **S. Kothapalli**, None; **G.A. Tikhomirov**, None; **J. Rao**, None; **S.S. Gambhir**, General Electric, Grant/research support; Bayer-Schering, Grant/research support; Sanofi-Aventis, Grant/research support; CellSight, Stockholder; ImaginAB, Stockholder; Enlight, Stockholder; Endra, Stockholder; Bracco, Consultant; NinePoint Medical, Stockholder; Visualsonics, Consultant .

Presentation Number **SS 79**
Scientific Session 11: Chemistry & Probes - Optical Imaging
September 7, 2012 / 11:36-11:48 / Room: Liffey Hall 1

# Near-infrared Light Activated Bioluminescent Probe On the Basis of Photocaged Upconversion Nanoparticles Conjugate

***Bengang Xing***, *Division of chemistry and Biological Chemistry, Nanyang Technological University, Singapore, Singapore. Contact e-mail: bengang@ntu.edu.sg*

Cell structures exhibit dynamic and complex spatial and temporal organization properties. The precise tracking of the dynamic properties of cellular functions at a desired time or location in intact cells or organism will be crucial for many biomedical applications. One appealing approach of providing such information is the photolysis of photoactivable or "caged"molecules, by which the activation process can be readily modulated by a beam of light with high spatial and temporal precision. However, most of the existing photocaged systems have to heavily rely on high-intensity UV or visible light to initiate the photoactivation. The inevitable cellular damage and less tissue-penetration from the short wavelength light irradiations will be the potential limitation for their applications in vitro and in vivo biological systems. Herein, we demonstrated a novel method by combining versatile "photocaged" compounds with the upconversion nanoparticles (UCNPs) for in vitro and in vivo uncaging and bioluminescence imaging studies. A unique photoreleasable bioluminescent imaging probe coupled with silica-UCNPs was prepared. Upon near-infrared light (NIR) irradiation, the sharp emission converted from the UCNPs complex can effectively photorelease the imaging probe and thus significantly produce the fluorescence and bioluminescence signals in vitro and in vivo. The non-autofluorescence and high tissue-penetration depth offered by this complex provide a platform for their biomedical applications in real-time imaging and targeted drug delivery in living system with less photo-damage. We anticipate that this UCNPs based photolysis with effective NIR uncaging activity would offer new possibilities for monitoring the dynamic functions of cells and selectively delivering the drug molecules at targeted areas in vitro and in vivo.

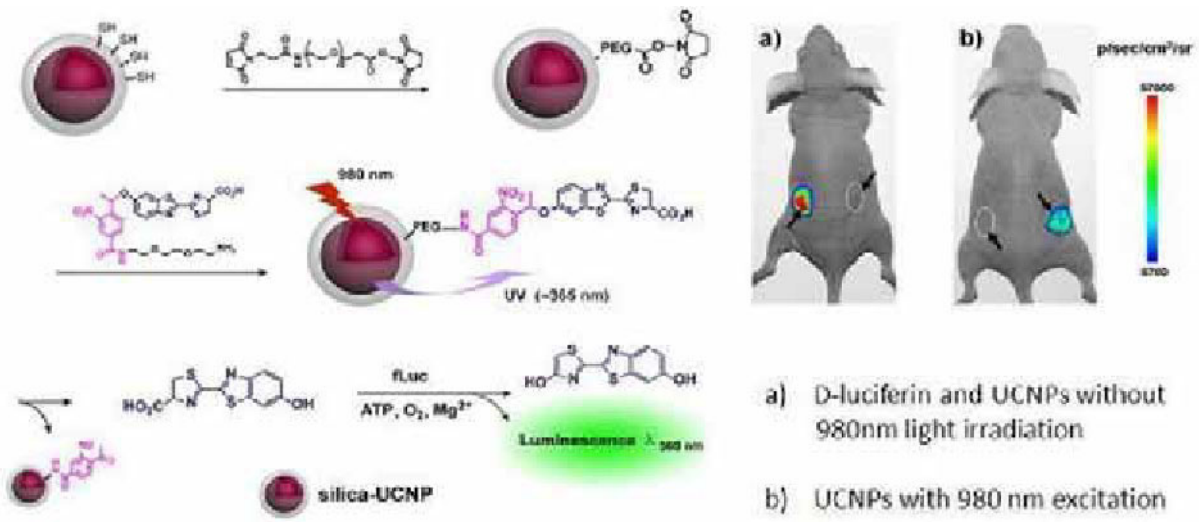


Disclosure of author financial interest or relationships:
**B. Xing**, None.

Presentation Number **SS 8**
Scientific Session 1: Chemistry & Probes - MRI
September 6, 2012 / 11:47-12:00 / Room: Liffey Hall 1

# Magnetosomes, a new class of highly sensitive superparamagnetic contrast agents for MR molecular imaging

***Sébastien Mériaux***[1], *Benjamin Marty*[1], *Nicolas Ginet*[2], *Christopher Lefevre*[2], *Daniel Garcia*[2], *Franck Lethimonnier*[1], *Denis Le Bihan*[1], *David Pignol*[2], [1]*DSV / I2BM / NeuroSpin / LRMN, CEA, Gif-sur-Yvette, France;* [2]*DSV / IBEB / LBC, CEA, Saint-Paul-lez-Durance, France. Contact e-mail: sebastien.meriaux@cea.fr*

**Introduction**. Superparamagnetic iron oxide particles currently appear to be the preferred material to perform MR molecular imaging due to high relaxivity properties. We present a new class of superparamagnetic nanoparticles, naturally produced by magnetotactic bacteria, which regroup different characteristics of interest for biomedical applications: a perfectly crystalline and regular crystal of magnetite (Figure 1), surrounded by a natural lipid bilayer enabling a possible functionalization for molecular targeting. As preliminary study, we demonstrate the high sensitivity of magnetosomes both *in vitro* and *in vivo*, as well as the interest to use them at ultra high field. **Material & Methods**. Wild-type AMB-1 bacteria were grown at 28°C with Komeili's medium in hermetically sealed Schott bottles. Magnetosomes were then extracted after bacteria centrifugation using a permanent magnet. For *in vitro* assays, magnetosomes were suspended at different concentrations (from 0.15 to 3µM) in agar matrix. MR imaging was performed at 7T for *in vitro* assays and 17.2T for *in vivo* study on preclinical Bruker scanners. A $T_2$ mapping sequence (MSME, 64 TE from 8.3ms to 530ms) was acquired to measure the transverse relaxivity $r_2$ of magnetosomes. *In vivo* experiments were carried out on nude mice. Anatomical $T_2$ weighted (RARE, R=150x150x375µm$^3$) and $T_2$* weighted (FLASH, R=75x75x150µm$^3$) images were acquired prior and after IV injection of magnetosomes (200µL, 20µmolFe/kg). **Results**. Transverse relaxivity of magnetosomes was measured to 680mM$^{-1}$.s$^{-1}$ (Figure 2), a value higher than $r_2$ of commonly used particles (Endorem® $r_2$~150mM$^{-1}$.s$^{-1}$, Sinerem® $r_2$~100mM$^{-1}$.s$^{-1}$). This gain is probably due to the high regularity of nanocrystals produced by AMB-1 bacteria. *In vitro* sensitivity at 7T of magnetosomes was estimated to 150nM in term of iron content. Figure 3a represents the overlay of $T_{2w}$* volumes on anatomical $T_{2w}$ images of the mouse. After injection, an overall $T_2$* decrease is observed in the whole brain (Figure 3b) due to magnetosomes circulating in the vascular compartment. Large blood vessels are also highlighted: to confirm this result, we developed an automatic procedure to specifically detect vascular hypointense signals. As shown by Figure 3c, injection of magnetosomes significantly enhances the number of detected large blood vessels. **Conclusion**. In conclusion, our preliminary results demonstrated that magnetosomes provide a new class of highly sensitive MR contrast agents. MRI data at ultra high field confirm that these superparamagnetic agents exhibit higher relaxivity properties than those chemically produced. The *in vivo* detection of magnetosomes in the mouse brain is therefore obtained after injection of a significantly lower dose than the one commonly used in rodent studies (200-1000µmolFe/kg). Moreover we have already shown that genetic manipulation of magnetosome offers the possibility to insert peptides in its membrane [1] to target specific biomarkers. In conjunction with ultra high field MR imaging, such functionalized contrast agents should provide enough sensitivity and specificity for molecular imaging studies. **References**. [1] Ginet et al, Plos One, 2011

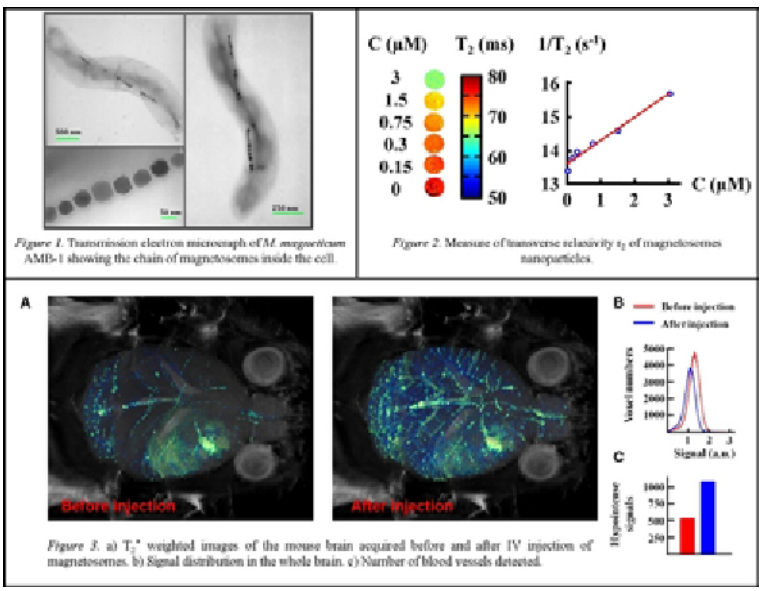


*Figure 1.* Transmission electron micrograph of *M. magneticum* AMB-1 showing the chain of magnetosomes inside the cell.

*Figure 2:* Measure of transverse relaxivity $r_2$ of magnetosomes nanoparticles.

*Figure 3.* a) $T_2$* weighted images of the mouse brain acquired before and after IV injection of magnetosomes. b) Signal distribution in the whole brain. c) Number of blood vessels detected.

Disclosure of author financial interest or relationships:
**S. Mériaux**, None; **B. Marty**, None; **N. Ginet**, None; **C. Lefevre**, None; **D. Garcia**, None; **F. Lethimonnier**, None; **D. Le Bihan**, None; **D. Pignol**, None.

Presentation Number **SS 80**
Scientific Session 11: Chemistry & Probes - Optical Imaging
September 7, 2012 / 11:48-12:00 / Room: Liffey Hall 1

# Realtime imaging of reporter enzymes and cancer cells in vivo by rationally designed novel spirocyclized fluorescence probes

***Yasuteru Urano***[1], *Mako Kamiya*[1], *Masayo Sakabe*[2], *Tetsuo Nagano*[2], *Hisataka Kobayashi*[3], [1]*Graduate School of Medicine, The University of Tokyo, Tokyo, Japan;* [2]*Graduate School of Pharmaceutical Sciences, The University of Tokyo, Tokyo, Japan;* [3]*National Cancer Institute, National Institute of Health, Bethesda, MD, USA. Contact e-mail: uranokun@m.u-tokyo.ac.jp*

Escherichia coli beta-galactosidase is well characterized and is extensively used as a reporter enzyme in biology, because of its stability and high turnover rate, as well as the absence of endogenous beta-galactosidase activity in eukaryotic cells. A range of fluorogenic substrates has been developed, including our previously reported compounds based on the TokyoGreen scaffold [1, 2]. However, most of these substrates lack sufficient cellular permeability and accumulation to be able to specifically and clearly visualize beta-galactosidase activity in living cells and tissues. Here, we present a new class of fluorescence probe for beta-galactosidase based on the novel spirocyclized scaffold, which overcomes these problems. Firstly, for designing chemical fluorescence probes rationally, we succeeded to establish a novel strategy to control the fluorescent properties of various fluorophores. Namely, we found that intramolecular spirocyclization is preferred when the original carboxylate group, which is attached to the 9-phenyl moiety of a series of fluorophores like fluoresceins, rhodamines and rhodols, is substituted with a hydroxymethyl group, which leads colorless and fluorescently quenched molecules. Based on these findings, we developed a novel fluorescence probe, HMDER-betaGal, which was colorless due to the intramolecular spirocyclization with a hydroxymethyl group. We confirmed that HMDER-betaGal has sufficient cellular permeability, and that its hydrolysis product is highly fluorescent and well retained intracellularly, by using it to obtain well-defined images of beta-galactosidase activity in living cells and Drosophila melanogaster tissues [3]. Furthermore, this strategy can be applicable for a wide range of analytes like other glycosidases and aminopepetidases. Very recently, we have developed gGlu-HMRG, a novel gamma-glutamyltranspeptidase(GGT) activatable fluorescence probe, based on a new hydroxymethyl rhodaminegreen scaffold, which is quickly activated by GGT and yields an over 350-fold increase in fluorescence signal compared with the quenched state. GGT is well known to be significantly overexpressed in several human tumors, and gGlu-HMRG showed a large fluorescence increase in several cancer cell lines, but not in a normal cell line. By spraying gGlu-HMRG onto tissue surfaces that are suspected of harboring tumors in a mouse model of peritoneal metastases, cancer cells were successfully visualized with high signal contrast between the tumor and background. The activation occurred within one minute of spraying the probe, and the signal was strong enough to be detected even with our naked eyes [4]. This probe is believed to be practical for clinical application during surgical or endoscopic procedures. References: [1] Urano, Y., et al., J. Am. Chem. Soc. 2005, 127, 4888. [2] Kamiya, M. et al., J. Am. Chem. Soc. 2007, 129, 3918. [3] Kamiya, M., et al., J. Am. Chem. Soc. 2011, 133, 12960. [4] Urano, Y., et al., Sci. Transl. Med. 2011, 3, 110ra117.

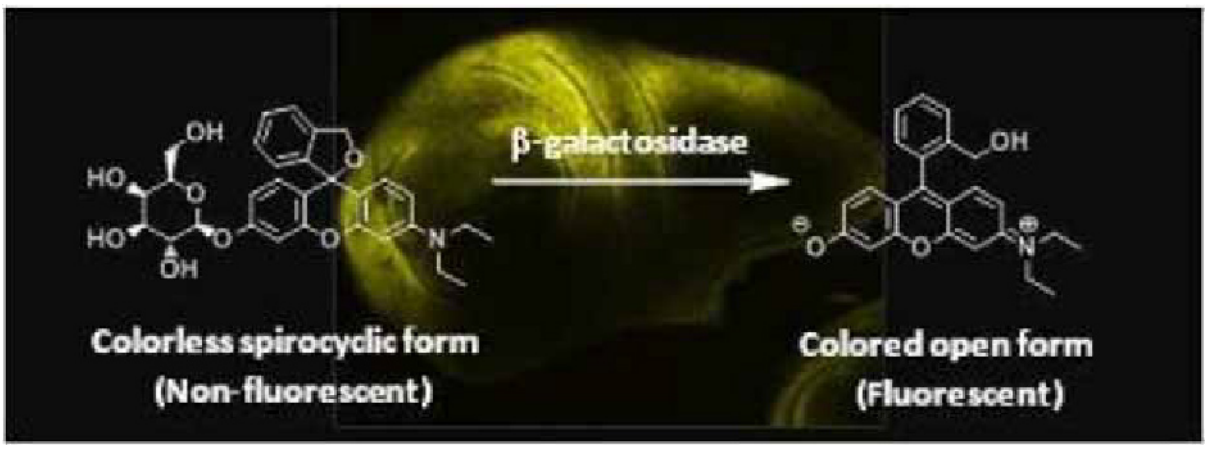


Disclosure of author financial interest or relationships:
**Y. Urano**, None; **M. Kamiya**, None; **M. Sakabe**, None; **T. Nagano**, None; **H. Kobayashi**, None.

Presentation Number **SS 81**
Scientific Session 12: Technology & Software - Ultrasound
September 7, 2012 / 10:30-10:42 / Room: Wicklow Hall 1

# High pressure insonation of bound microbubbles reduced blood flow within mouse tumor models

*Xiaowen Hu, Azadeh Kheirolomoom, Lisa M. Mahakian, Dustin E. Kruse,* ***Katherine Ferrara****, Biomedical Engineering, UC Davis, Davis, CA, USA. Contact e-mail: kwferrara@ucdavis.edu*

Objectives: Ultrasound molecular imaging has demonstrated the ability to detect vascular receptors in vivo with low peak negative pressure pulses. However, high pressure pulses are frequently added to clear the region of bound microbubbles and facilitate studies with microbubbles conjugated with an alternative ligand. Here, we investigate whether high pressure insonation of bound microbubbles can alter flow dynamics in a mouse tumor model. Materials and methods: A total of 114 mice carrying syngeneic breast tumors were insonified (Siemens Sequoia system, 15L8 transducer, 5 MHz color-Doppler pulses, 4 MPa or 2 MPa peak-negative pressure, 8.1 ms pulse repetition period, 6-cycle pulse length, and 900 ms insonation). Microbubbles conjugated with cyclic RGD or LXY-3 peptides, or control (no peptide) microbubbles were injected and contrast pulse sequencing (CPS) was applied to acquire images of the flowing and bound microbubbles. An anti-CD41 antibody was injected in a subset of animals to block potential platelet aggregation. Images of flowing and bound microbubbles were compared between an initial and subsequent study in order to determine whether high pressure insonation of bound microbubbles reduced the image amplitude. Results: Insonation of bound microbubbles with a low pressure CPS imaging sequence (0.2 MPa) alone resulted in a similar tumor image amplitude when targeted imaging studies were repeated. However, following the accumulation of targeted microbubbles and high pressure (4 MPa) insonation, the echo amplitude observed from flowing microbubbles in subsequent studies decreased in both tumor models, including 20 Met-1 mice (71%) and 4 NDL mice (40%). With the application of the high pressure pulse, the image area with an intensity below a fixed threshold increased from 22 ± 13% to 63 ± 17% of the observed plane in the Met-1 model ($p<0.01$) and from 16 ± 3% to 45 ± 24% in the NDL model ($p<0.05$). Repeated microbubble destruction at 4 MPa increased the area of low image intensity to 76.7 ± 13.4% ($p<0.05$). The fragmentation of bound microbubbles with a lower peak-negative pressure (2 MPa) reduced the occurrence of the blood flow alteration to 28% (5 of 18 Met-1 tumor mice). When image acquisitions were separated by more than ~30 minutes, the image intensity was similar for repeated injections of the same construct. Histology and confocal microscopy demonstrated regions of vessel dilation and enhanced extravasation of 150,000 MW FITC-dextran following high pressure insonation. Pre-injection of an anti-CD41 antibody to block platelet adhesion greatly reduced the change in image intensity; after the anti-CD41 injection, a change in blood flow was observed in only 1 of 26 animals. Conclusion: High pressure insonation of microbubbles bound to tumor endothelial receptors reduced blood flow for ~30 minutes within two syngeneic mouse tumor models. This effect (reduction in blood flow) was blocked by the administration of an anti-CD41 antibody. Acknowledgement: NIH R01CA103828 and R01CA112356

Disclosure of author financial interest or relationships:
**X. Hu**, None; **A. Kheirolomoom**, None; **L.M. Mahakian**, None; **D.E. Kruse**, None; **K. Ferrara**, None.

Presentation Number **SS 82**
Scientific Session 12: Technology & Software - Ultrasound
September 7, 2012 / 10:42-10:54 / Room: Wicklow Hall 1

# The application of PET in the optimization of ultrasound-enhanced nanoparticle accumulation

*Katherine D. Watson[1], Chun-Yen Lai[1], Shengping Qin[1], Dustin E. Kruse[1], Jai Woong Seo[1], Lisa M. Mahakian[1], Elizabeth Ingham[1], Robert D. Cardiff[3], Fitz-Roy Curry[2], Rolf K. Reed[4], **Katherine Ferrara**[1], [1]Biomedical Engineering, UC Davis, Davis, CA, USA; [2]Physiology and Membrane Biology, UC Davis, Davis, CA, USA; [3]Department of Pathology and Laboratory Medicine, UC Davis, Davis, CA, USA; [4]Department of Biomedicine, University of Bergen, Bergen, Norway. Contact e-mail: kwferrara@ucdavis.edu*

Introduction: Ultrasound-induced hyperthermia has been shown to increase blood vessel dilation and microvascular permeability, thereby leading to enhanced local delivery of chemotherapeutic agents. PET imaging of radiolabeled nanoparticles has the potential to quantify the efficacy of ultrasound-enhanced drug delivery in tumor models. Using a syngeneic breast tumor model that naturally undergoes an epithelial to mesenchymal transition (EMT), we optimized thermal and mechanical ultrasound parameters for delivery to the two tumor phenotypes. Materials and Methods: A total of 123 animals with bilateral tumors were evaluated in this study, which was approved by the Institutional Animal Care and Use Committee. Met-1 cells were injected into the 4th mammary inguinal fat pads of donor animals. One tumor per animal was insonified prior to the injection of 100 nm liposomes. The tumor temperature was either kept at 37 ± 0.5°C (body temperature) or increased to 42°C for 2, 7, or 18 minutes. The ultrasound pulses consisted of 100-cycle bursts at 1.5 MHz center frequency and 1.1 or 2.4 MPa peak negative pressure (PNP), with a variable pulse-repetition frequency (PRF) ranging from 100 Hz up to 5 kHz. The PRF was controlled by a programmable integral derivative controller which maintained the temperature in the target range. Preparation and radiolabeling of liposomes with Cu-64 followed previously described protocols (1). PET acquisitions were obtained over 30 minutes using a dedicated small-animal PET scanner at 0, 3, 6,18, 28, and 48 hours post injection. Results and Discussion: While epithelial tumors are highly vascularized with tight cell-cell junctions and typically accumulate nanoparticles with a concentration of ~5-10% ID/cc without ultrasound, EMT tumors are poorly vascularized and therapeutic accumulation is reduced by ~1.5 fold. Between epithelial and EMT tumors, cells are differentiated by a reduction in E-cadherin, cytokeratin 8/18 and cytokeratin 19. Across both epithelial and EMT tumors, particle accumulation and apparent permeability were increased for insonified tumors when ultrasound was applied. Accumulation in epithelial tumors was maximized at 14.7±3.0 %ID/g by an ultrasound dose resulting in cumulative equivalent minutes at 43 degrees (CEM43) of 1.4 and a PNP of 1.1 MPa. Accumulation in the EMT phenotype peaked at 8.0±4.1%ID/g with the highest thermal dose applied (CEM43 of 4.5) and a PNP of 2.4 MPa. Thus, delivery to highly vascular epithelial tumors was greatest with a moderate thermal dose, while accumulation in the poorly vascularized EMT phenotype was greatest at a higher thermal dose in the presence of small regions of heat-mediated necrosis. Conclusion: Our results demonstrate ultrasound's ability to non-invasively improve the local delivery of nanotherapeutics in both epithelial and EMT tumors and the use of PET to optimize interventional delivery strategies. 1. Seo, J.W., et al (2010) Bioconjug Chem, 21, 1206-1215.

Disclosure of author financial interest or relationships:
**K.D. Watson**, None; **C. Lai**, None; **S. Qin**, None; **D.E. Kruse**, None; **J. Seo**, None; **L.M. Mahakian**, None; **E. Ingham**, None; **R.D. Cardiff**, None; **F. Curry**, None; **R.K. Reed**, None; **K. Ferrara**, None.

Presentation Number **SS 83**
Scientific Session 12: Technology & Software - Ultrasound
September 7, 2012 / 10:54-11:06 / Room: Wicklow Hall 1

# Improved detection of targeted microbubbles with a new image processing approach for clinical US-MI

***Sibylle Pochon**, Peter Frinking, Laurent Mercier, Marcel Arditi, Francois Tranquart, Bracco Suisse, Geneva, Switzerland. Contact e-mail: sibylle.pochon@bracco.com*

Introduction: Ultrasound molecular imaging (US-MI) is now ready to pass the pre-clinical stage and BR55, a KDR-targeted contrast agent developed at Bracco, has just entered clinical evaluation. Molecular imaging protocols and methods for distinguishing bound microbubbles in a background of circulating bubbles need to be adapted to the clinical situation and optimized for different indications. Objective: To evaluate a new image processing algorithm for the detection of low concentrations of targeted bubbles at early time-points after injection. Methods: A new image-processing approach, named Fixed Bubble Imaging (FBI), was developed with the objective of enhancing the visualization of bound microbubbles soon after agent injection, i.e. when a large number of microbubbles are still present in the circulation. It is based on a modified minimum intensity projection algorithm, and allows the suppression of echoes from moving microbubbles. FBI processing was applied to video clips obtained from a Philips-iU22 system during a Bracco sponsored exploratory clinical trial using BR55 for the detection of prostate cancer. Clips of contrast-specific images were recorded in a fixed plane for about 15 seconds, at a frame rate of 4 Hz, every two minutes. The location and number of lesions detected using FBI post-processing, based on the enhancement of bound microbubbles, were compared to the results of visual evaluation of unprocessed images and to histopathology assessment. Results: FBI processing identified sites with bound targeted microbubbles 5 to 10 min after injection of BR55, when a substantial proportion of bubbles were still freely circulating. Moreover, it improved the delineation of the lesions at later time points by removing echoes due to a few remaining microbubbles still present in the circulation. In some cases, additional lesions were detected using FBI post-processing, compared to direct visualization. Conclusion: Image processing with FBI may be valuable for the early detection of bound targeted microbubbles. An early detection of bound bubbles is favourable because of the variability in kinetics of elimination of free microbubbles and the limited half life of bound targeted bubbles. Future work will investigate the applicability of FBI for the quantification of molecular receptor density.

Disclosure of author financial interest or relationships:
**S. Pochon**, Bracco Suisse, Employment; **P. Frinking**, Bracco Suisse SA, Employment; **L. Mercier**, Bracco Suisse SA, Employment; **M. Arditi**, Bracco Suisse SA, Employment; **F. Tranquart**, Bracco Suisse SA, Employment .

Presentation Number **SS 84**
Scientific Session 12: Technology & Software - Ultrasound
September 7, 2012 / 11:06-11:18 / Room: Wicklow Hall 1

# Molecular Ultrasound Imaging Enhancement by Volumic Acoustic Radiation Force (VARF)

***Nicolas G. Rognin***[1], *Sunil Unnikrishnan*[2], *Gilles Guenette*[1], *Yuko Kanayama*[3], *Raymond Woods*[1], *Christopher Sanders*[1], *Naohisa Kamiyama*[3], *Alexander L. Klibanov*[2], [1]*Toshiba Medical Research Institute USA, Inc., Redmond, WA, USA;* [2]*Biomedical Engineering Department, University of Virginia, Charlottesville, VA, USA;* [3]*Toshiba Medical Systems Corp., Otawara, Japan. Contact e-mail: nrognin@tmriusa.com*

Molecular ultrasound imaging using targeted microbubbles is gaining momentum and will become a breakthrough modality when translated into clinical practice. The method consists in decorating microbubbles with a ligand on their surface. As a result, microbubbles can accumulate in pathological tissues expressing a molecular marker having a high affinity with the ligand. Combined with an ultrasound scanner operating in a contrast specific imaging mode, pathological tissues (e.g. angiogenic tumor vasculature) can be distinguished from normal tissues in images, identifying the presence and the location of the targeted disease marker. To enhance microbubbles adhesion, it has been amply demonstrated in the literature that the application of acoustic radiation force to "push" the microbubbles towards the endothelial layer was effective. In 3D, what we call "Volumic Acoustic Radiation Force" (VARF), appears to be a promising approach, in particular for the prostate gland which can be imaged in its entirety with a clinical endocavity 3D transducer. The purpose of this study was to demonstrate that VARF allows for improvement of targeted microbubble adhesion and reduction of the required contrast material dose. Dedicated acoustic transmit settings were implemented into a clinical ultrasound imaging system AplioXG (Toshiba Medical Systems, Otawara, Japan) equipped with a mechanically swept convex array transducer (PVT-681MV) to maximize the effect of VARF while minimizing microbubble destruction. Optimal settings (3.6 MHz, 30 kPa peak-negative-pressure, 64 cycles, 15% duty cycle) were defined using a suspension of agitated microbubbles in a glass beaker, combined with a custom-designed piece of tissue mimicking phantom. Targeted microbubble adhesion with VARF mode was compared to Native mode (without VARF) for a duration of 3 minutes in flow. It was assessed in vitro using biotinylated microbubbles perfused through a flow chamber (IBIDI, Martinsried, Germany) coated with streptavidin molecular receptors (5 µg/ml). Flow was set to reflect physiological conditions in tumors (wall shear stress at 0.6 dyne/cm^2). The flow chamber was positioned horizontally 20 mm from the transducer face. As shown in Figure 1, accumulation of bound microbubbles in a region of interest (CHI-Q software), after complete wash out of the circulating microbubbles at 11 minutes, was quantified to estimate VARF to Native ratio as a measure of targeted adhesion enhancement by VARF. With microbubble concentration of 1e6 particles/ml, the average adhesion enhancement ratio was 6.7 (SD of 2.6, n=3). With 4 fold reduction in the microbubble concentration, the adhesion enhancement ratio was 3.2 (SD of 1.1). In this study, proof of concept of the added value of VARF was shown for the first time with a clinical ultrasound imaging system equipped with a 3D transducer, offering a potential implementation into the clinic for the improvement of molecular ultrasound imaging of a whole organ. Also, the dose of injected contrast material can be significantly reduced to provide a better safety profile for patients. Further experiments will include an in vivo validation on small animals.

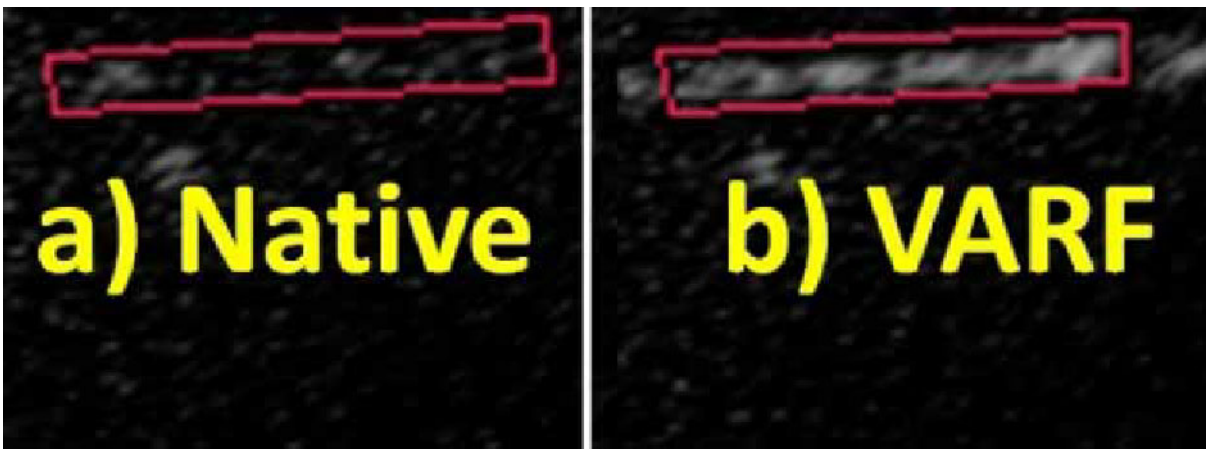


Ultrasound contrast image of targeted microbubbles accumulation without (a) and with (b) Volumic Acoustic Radiation Force.

Disclosure of author financial interest or relationships:
**N.G. Rognin**, Toshiba Medical Research Institute USA, Inc., Employment; **S. Unnikrishnan**, None; **G. Guenette**, Toshiba Medical Resarch Institute USA, Inc., Employment; **Y. Kanayama**, Toshiba Medical Systems Corp., Employment; **R. Woods**, Toshiba Medical Research Institute USA Inc, Employment; **C. Sanders**, Toshiba Medical Research Institute USA, Inc., Employment; **N. Kamiyama**, Toshiba Medical Systems, Employment; **A.L. Klibanov**, Philips Research North America, Grant/research support; Targeson Inc, Stockholder; Targeson Inc (NIH SBIR subcontract), Grant/research support .

Presentation Number **SS 85**
Scientific Session 12: Technology & Software - Ultrasound
September 7, 2012 / 11:18-11:30 / Room: Wicklow Hall 1

# Wideband optical-fiber-based ultrasound detector for intravascular optoacoustic imaging

***Amir Rosenthal**, Daniel Razansky, Vasilis Ntziachristos, Helmholtz Zentrum München, Neuherberg, Germany. Contact e-mail: eeamir@gmail.com*

The detection of ultrasonic fields is conventionally performed using piezoelectric sensors [1]. One of the main drawbacks of these sensors is their sensitivity, which is proportional to the detection area. This limits applications in which small sensors with high sensitivity are required, e.g. intravascular optoacoustic imaging. An alternative to piezoelectric sensors is the detection of ultrasound by optical means. While this approach may achieve high sensitivity [2], the production of in-fiber miniature optical sensor for intravascular applications has remained an open challenge. In this work we demonstrate a novel fiber-optic ultrasound sensor with a 250 μm diameter. The sensor is based on monitoring the reflection of a narrow-linewidth CW laser from an FBG with a pi-phase shift in its center. Such gratings exhibit strong resonances, which advantageous for ultrasound sensing for two reasons: First, light at resonance frequencies undergoes strong localization centered on the phase shift, which allows achieving very small sensing lengths. Second, the resonance frequencies exhibit a slow-light effect, i.e. light is trapped in the grating for a considerably longer time than prescribed by the grating's length and thus is affected more by the ultrasound field. Thus, in pi-phase-shifted FBGs, miniaturization leads to increased sensitivity. The spatio-temporal response of the detector was experimentally measured using a novel optoacoustic technique, based on creating a point-like acoustic source. A detection bandwidth of up to 30 MHz was observed in addition tosideway-focused detection at distances corresponding to coronary artery geometry. The figure shows the measured response at the focus and at 500 μm offset off the focus. Analysis of the results also shows that the effective length of the sensor is approximately 350 μm. The sensor thus fits both in its dimensions and in its response for intravascular applications, and could potentially enable an all-optical optoacoustic catheter. [1] D. Razansky, M. Distel, C. Vinegoni, R. Ma, M. Perrimon, R. W. Koster, and V. Ntziachristos, "Multispectral opto-acoustic tomography of deep-seated fluorescent proteins in vivo," Nat. Photonics 3, 412-417 (2009). [2] H. Lamela, D. Gallego, and A. Oraevsky, "Optoacoustic imaging using fiber-optic interferometric sensors," Opt. Lett. 34, 3695-3697 (2009).

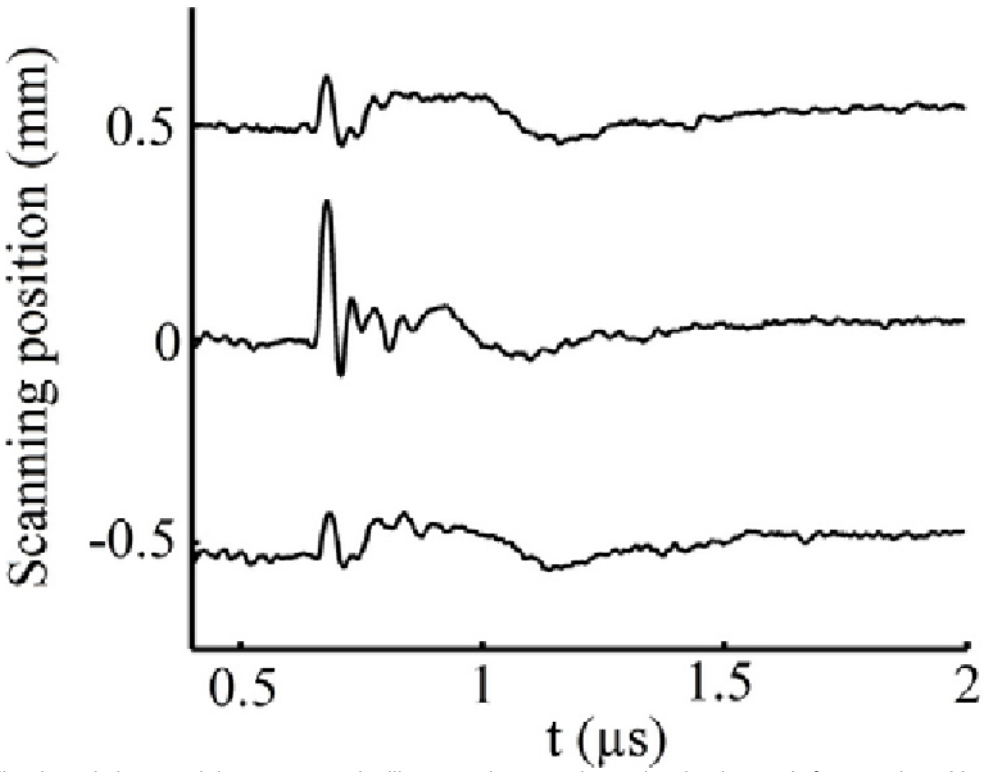


The response of the fiber-based ultrasound detector to a point-like acoustic source located at the detector's focus and at 500 μm offset off the focus.

Disclosure of author financial interest or relationships:
**A. Rosenthal**, None; **D. Razansky**, iThera Medical GmbH, Stockholder; **V. Ntziachristos**, ERC, Grant/research support; Ithera Medical, Stockholder .

Presentation Number **SS 86**
Scientific Session 12: Technology & Software - Ultrasound
September 7, 2012 / 11:30-11:42 / Room: Wicklow Hall 1

# A Novel Strategy for Improving Dynamic 3D Photoacoustic Tomographic Imaging

***Dominique Van de Sompel**, Anca Dragulescu-Andrasi, Sanjiv S. Gambhir, Radiology, Stanford University, Stanford, CA, USA.*
*Contact e-mail: dominiqu@stanford.edu*

Photoacoustic tomography (PAT) combines the high contrast of optical imaging with the high spatial resolution of ultrasound, and enables 3D molecular imaging deep within living tissues. So far, PAT has primarily been used to obtain static scans. However, PAT is also capable of dynamic or time-resolved imaging. This is useful to characterize the uptake and clearance dynamics of molecular imaging agents and/or drugs, which in turn may help better characterize suspect tissue(s). Dynamic PAT involves acquiring a contiguous sequence of scans, each of which is known as 'time frames'. For 2D PAT systems, high frame rates (1 second or less) and high signal-to-noise ratios (SNR) per time frame have been demonstrated. However, many 3D PAT systems require scan times on the order of several minutes to obtain low-artifact and high-SNR frames, which severely limits their temporal resolution. Since decreasing the scan time also decreases the SNR, current dynamic 3D PAT systems face a highly challenging trade-off between temporal resolution and SNR. We push the limits of this trade-off by reconstructing a given set of time frames using filtered backprojection (FBP), and then temporally de-noising them on a voxel-by-voxel basis using empirical mode decomposition (EMD). This strategy greatly enhances SNR for a given frame rate. The system used in this study was a commercial PAT scanner with 128 transducers arranged in a spiral pattern within a hemispherical bowl. For static scans, the system rotates the bowl through several angular positions to increase sampling density. For dynamic scans, we let each of these bowl positions define a separate time frame. Our scans rotated through 180 bowl positions in approximately 15 minutes, corresponding to a time resolution of 5 seconds per bowl position. The temporal de-noising method was first validated in silico using a numerical dynamic 3D phantom containing a spherical mass and a branched blood vessel-like structure (see supplemental figure). We then tested the method on data from in vivo mouse models (N=5), where contrast agent was administered after the first 2.5 minutes of the 15 minute, 180 frame scan. For both the simulated and in vivo mouse data, the FBP frames showed a poor SNR before de-noising, as illustrated in Fig.1(e,g,i). After de-noising with EMD, the SNR was much improved, as shown in Fig.1(f,h,j). Figs.1(a) and (b) show the mean of all time frames and its segmentation (used for the SNR computation in Fig.1(d)). Fig.1(c) shows the improved smoothness of the time curve of an example voxel. Fig. 1(d) shows the improved SNR as a function of time frame. Figs.1(e-i) illustrate the improved SNRs of sample time frames. EMD de-noising increased SNR in all 5 mouse scans, by 262% on average. The implications of this work are that temporal de-noising allows current 3D PAT systems to perform high SNR imaging of 3D dynamic molecular processes with time resolutions on the order of several seconds, rather than several minutes. Lastly, the temporal resolution could be increased even further by reducing the laser pulse averaging, which was currently set to 100 pulses. We aim to optimize this number in future work.

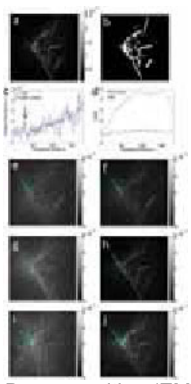

Fig. 1. Temporal smoothing of FBP frames using Empirical Model Decomposition (EMD). Representative results from a scan of a subcutaneous mouse tumor model. (a) Maximum Intensity Projection (MIP) of the mean time frame. (b) Segmentation of (a), used for computing the SNR of each time frame in (d). (c) Original and smoothened time history of the voxel indicated by the green arrow in (e-j). The time resolution was 5 seconds per time frame. The red arrow marks the time of contrast agent administration via tail-vein injection. The EMD de-noising method is denoted by 'FBP-EMD'. (d) SNR as a function of time frame number by FBP and FBP-EMD. The SNR was computed using the segmentation shown in (b): the regions marked in white were considered to be the foreground, and those marked in black to be the background. (e,g,i) MIPs of time frames 1 (5 secs post injection), 90 (7.5 mins), and 180 (15 mins) for FBP. (f,h,j) MIPs of time frames 1 (5 secs), 90 (7.5 mins), 180 (15 mins) for FBP-EMD.

Disclosure of author financial interest or relationships:
**D. Van de Sompel**, None; **A. Dragulescu-Andrasi**, None; **S.S. Gambhir**, General Electric, Grant/research support; Bayer-Schering, Grant/research support; Sanofi-Aventis, Grant/research support; CellSight, Stockholder; ImaginAB, Stockholder; Enlight, Stockholder; Endra, Stockholder; Bracco, Consultant; NinePoint Medical, Stockholder; Visualsonics, Consultant .

Presentation Number **SS 87**
Scientific Session 13: Preclinical in Vivo - Metabolic Disease
September 7, 2012 / 10:30-10:51 / Room: Liffey Hall 2

# In Vivo Imaging of Brown Fat

***Pirjo Nuutila**, Turku PET Centre, University of Turku, Turku, Finland. Contact e-mail: pirnuu@utu.fi*

Disclosure of author financial interest or relationships:
**P. Nuutila**, None.

Presentation Number **SS 89**
Scientific Session 13: Preclinical in Vivo - Metabolic Disease
September 7, 2012 / 10:51-11:03 / Room: Liffey Hall 2

# The novel application of the luciferase substrate coelenterazine for imaging beta-cell mass

***Laura Bronsart***[1,2], *Michael H. Bachmann*[2], *Christian Stokes*[2], *Christopher Contag*[3,4], [1]*Biology, Stanford University, Stanford, CA, USA;* [2]*Pediatrics, Stanford University, Stanford, CA, USA;* [3]*Microbiology & Immunology, Stanford University, Stanford, CA, USA;* [4]*Pediatrics & Radiology, Stanford University, Stanford, CA, USA. Contact e-mail: bronsart@stanford.edu*

A continuing limitation to the advancement of type I and II diabetes research is the inability to longitudinally quantify the insulin-producing cells (or beta cells) of the pancreas. The standard method is bioluminescence imaging using beta-cell firefly luciferase expression and the substrate luciferin. Although this technique does quantify beta cell mass, it cannot be efficiently applied to a variety of transgenic mouse strains. Thus, there is a need for a broadly applicable, strain non-specific, bioluminescent imaging tool that will enable researchers to study beta-cell mass in the context of development, disease or transplantation. An important area in diabetes research is the development of a targeted imaging probe that is highly sensitive, specific and suitable for diagnostic beta-cell mass imaging. In the process of evaluating a diabody-based, beta-cell imaging tool, we discovered a novel application for the luciferase substrate coelenterazine, the detection of functional beta-cell mass. Coelenterazine is the small molecule substrate of the commonly used ATP-independent luciferases Gaussia, Renilla and Aequora. In vitro experiments revealed that a rat insulinoma cell line had greater coelenterazine-bioluminescence signal relative to other cell lines, in the absence of any additional reagents. Additionally, upon intravenous injection into mice, a mid-upper abdominal bioluminescence signal was detected, and ex vivo imaging revealed a significantly elevated pancreatic signal compared to other examined tissues. The signal intensity proved to be coelenterazine dose-dependent. To further study the in vivo characteristics of the observed signal, we tested the influence of beta-cell function. It was determined that insulin-secreting beta-cells produced greater signal compared to those that were quiescent due to fasting. These results supported that the in vivo coelenterazine signal was beta-cell specific; however, to conclusively determine the beta-cell specificity of the signal, we used coelenterazine to image the pancreas of mice that received the beta-cell toxic agent streptozotocin (STZ) or PBS control. There was a significant reduction in pancreatic signal in STZ-treated mice both in vivo and upon ex vivo imaging of the pancreas. Furthermore, there was a significant correlation between the pancreatic signal and the corresponding blood glucose levels with findings similar to previous observations made in type II diabetic humans whose pancreatic mass was determined at autopsy; that is, there appears to be a severe reduction in the beta-cell mass prior to the development of hyperglycemia. These results demonstrate the novel use of coelenterazine to detect the functional beta-cell mass in the STZ, type-I-diabetic mouse model. Due to the poor tissue penetration of the bioluminescence signal, this technique cannot be directly translated for use in humans; however, identification of the agent responsible for the beta-cell specific coelenterazine reaction may elucidate a new beta-cell specific target and a corresponding small-molecule structure for developing human-applicable imaging probes.

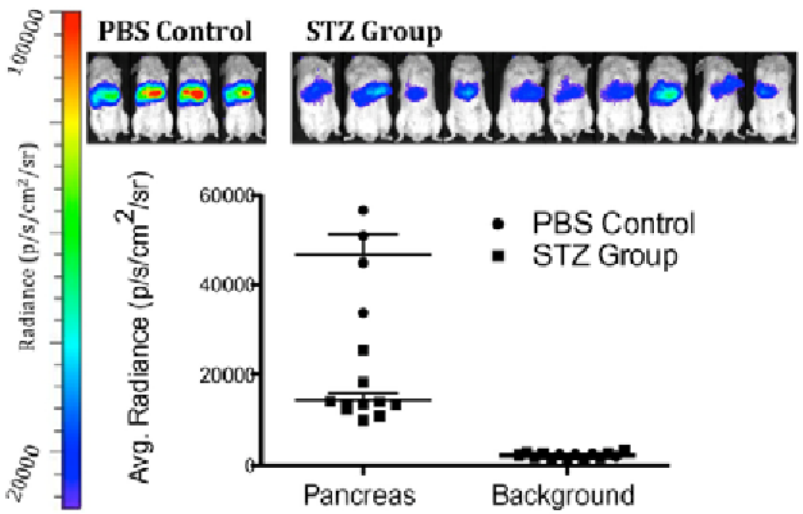


Bioluminescence imaging of live mice. Mice were treated with 200 mg/kg of streptozotocin (STZ) or PBS on day 0. 3-days post-treatment, mice were administered 2 g/kg glucose and maintained on 10% sucrose water. Four hours post-treatment, mice were intravenously injected with 1.4 mg/kg of coelenterazine and imaged. Quantification of the bioluminescence signal of the pancreases and of the backgrounds. A significant difference (P = 0.0000) between the two groups was observed for pancreatic signal but not for background signal.

Disclosure of author financial interest or relationships:
**L. Bronsart**, None; **M.H. Bachmann**, None; **C. Stokes**, None; **C. Contag**, ConcentRx Corp, Other financial or material support; Origin Therapeutics, Stockholder; Olympus, Other financial or material support; Tansderm Inc., Other financial or material support; Cygnet Biofuels, Other financial or material support .

Presentation Number **SS 9**
Scientific Session 2: Technology & Software - Optical Imaging
September 6, 2012 / 10:30-10:41 / Room: Wicklow Hall 1

# Multi-Modal Spectral Molecular Optical Tomography

***James A. Guggenheim***[1,2], *Hector R. Basevi*[1,2], *Iain B. Styles*[2], *Jon Frampton*[3], *Hamid Dehghani*[1,2], [1]*Physical Science of Imaging in the Biomedical Sciences Doctoral Training Centre, College of Engineering and Physical Sciences, University of Birmingham, Birmingham, United Kingdom;* [2]*School of Computer Science, College of Engineering and Physical Sciences, University of Birmingham, Birmingham, United Kingdom;* [3]*School of Immunity and Infection, College of Medical and Dental Sciences, University of Birmingham, Birmingham, United Kingdom. Contact e-mail: jxg518@cs.bham.ac.uk*

In vivo bioluminescence imaging (BLI) is used widely within the molecular imaging community to probe a variety of biological phenomena within small animal models. The technique is based around tagging bio-molecules, cells, or genes of interest within an animal with a bioluminescent marker and imaging resultant light distributions at the animal surface to infer underlying activity; e.g. to monitor the growth of Luciferase-labelled tumours over time under different conditions. A major drawback of BLI is that it cannot provide accurate measurements of the internal distribution and concentration of bioluminescent markers since the measured surface signal is strongly and non-linearly dependant on the unknown internal optical property distribution. This limits the biological questions that can be answered. The aim of bioluminescence tomography (BLT) is to use a model-based reconstruction approach to recover quantitative, 3D, volumetric maps of bioluminescent marker distributions from multiple 2D images. Accurate BLT would provide valuable improvements in the capabilities of optical imaging as a pre-clinical tool, allowing better measurement of biomedical phenomena (e.g. direct measurement of tumour volume and location) and thus reduction in the number of animals required to obtain statistically relevant results. Two prerequisites for BLT are animal shape and optical properties. These are needed to accurately model the light path through the subject. To meet these requirements a novel, multi-modal, optical imaging system has been developed which combines three imaging modalities: optical surface capture (SC); multispectral diffuse optical tomography (DOT); and BLT (see figure). Whilst SC and DOT provide necessary prior information for BLT, the DOT component also provides complementary and biologically relevant molecular information such as spatial distribution of total haemoglobin, oxygen saturation and melanin. The system is housed within a dark enclosure and has no moving parts making for simplicity, stability and time-efficiency. It comprises two CCDs (for simultaneous DOT and BLT), three projectors (two for SC imaging of two sides of the animal surface and one for injecting spatially modulated NIR light for DOT), a vertical translation stage for bringing subjects into focus and for calibration, and two 45-degree mirrors for capturing data from three angles around the animal per 2D image. The mirrors, along with animal curvature, provide effective tomographic imaging (covering about two-thirds of the animal surface) for all three modalities. The system has been tested with phantom studies and has been shown to be effective. We now present the first results acquired using the system in animal studies. It will be shown that the locations of individual implanted light sources can be reconstructed with high accuracy, results that are validated using CT-scans.

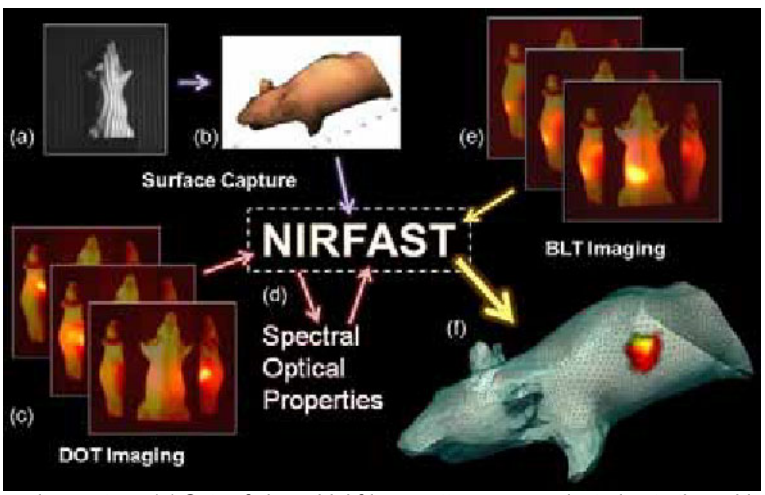


Workflow for multi-modality optical imaging system. (a) Sets of sinusoidal fringe patterns are projected onto the subject using each of the surface capture (SC) projectors in turn; images are acquired for each projection. (b) SC images are processed using a surface capture algorithm to produce a point cloud for the animal; this is used to generate a finite element model of the subject. (c) 3-View DOT images are acquired at multiple wavelengths for several input NIR source patterns (in this case isolated Gaussian distributions at different positions). (d) NIRFAST (http://www.dartmouth.edu/~nir/nirfast/) is employed to reconstruct spectral optical properties (absorption and reduced scattering coefficients) from the multi-spectral DOT data. (e) Multi-spectral, 3-View BLT images are acquired. (f) Combining BLT surface measurements with recovered optical properties and using the mesh generated by SC, NIRFAST is now used to reconstruct internal source distribution.

Disclosure of author financial interest or relationships:
**J.A. Guggenheim**, None; **H.R. Basevi**, None; **I.B. Styles**, None; **J. Frampton**, None; **H. Dehghani**, None.

Presentation Number **SS 90**
Scientific Session 13: Preclinical in Vivo - Metabolic Disease
September 7, 2012 / 11:03-11:15 / Room: Liffey Hall 2

# Synthesis and in vivo evaluation of 64Cu-labelled exendin dimers

***Cheng-Bin Yim***[1], *Kirsi Mikkola*[1], *Veronica Fagerholm*[1], *Johan Rajander*[2], *Viki-Veikko Elomaa*[1], *Tamiko Ishizu*[1], *Pirjo Nuutila*[1], *Olof Solin*[2], [1]*Turku PET Centre, University of Turku, Turku, Finland;* [2]*Accelerator Laboratory, Åbo Akademi University, Turku, Finland. Contact e-mail: chbiyi@utu.fi*

Exendin-4 is a stable analogue of the glucagon-like peptide 1 (GLP-1), which targets the GLP-1 receptor. In vivo imaging of GLP-1 receptor, which is expressed in pancreatic beta cells, is essential in assessing initiation and progression of beta cell mass alterations in diabetes as well as in monitoring therapeutic measures. There is growing interest in the development of multimeric ligands, because they can enhance the ligand-receptor binding compared to its monomeric analogues. It has been demonstrated that dimeric, cyclic arginine-glycine-aspartic acid (cRGD) peptides have higher tumour uptake and longer tumour retention than their corresponding monomeric counterparts [1]. The β+/β- emitting radionuclide 64Cu presents nuclear properties suitable for PET (positron emission tomography) and may also be relevant for radiotherapy. Its half-life of 12.7 h provides a suitable time window for radiopharmaceutical synthesis of many compounds, and is compatible with the in vivo kinetics of a variety of small and large biologically active molecules [2]. We developed a 64Cu-labelled NOTA-conjugated exendin-4 dimer (64Cu-DI-exendin), via two-stage click chemistry [3]. Using a Cu(I)-catalyzed alkyne/azide cycloaddition (copper-click) reaction the peptidic azide was attached to a dimeric alkyne scaffold. Subsequently, NOTA (1,4,7-triazacyclononane-1,4,7-triacetic acid) was introduced via the metal-free thio acid/sulfonyl azide amidation (sulfo-click) reaction (Figure 1). The copper-click reaction was performed in the presence of 0.5 equiv CuSO4 per alkyne moiety, accompanied by 2.5 equiv Na-ascorbate, and subjected to microwave irradiation. Subsequently, after acidic treatment the obtained free thio acid was directly coupled to NOTA-sulfonyl azide (2) using 2,6-lutidine as base. After tBu-removal and preparative HPLC, the NOTA-conjugated exendin-4 dimer (1) was obtained in 18% overall yield. Compound 1 was labelled with 64Cu with a specific radioactivity of 50 MBq/nmol (or 200 MBq/nmol corrected to EOB). Full biological characterisation is in progress, which will include the in vitro and in vivo stability, binding affinity, lipophilicity, and distribution kinetics in healthy rat for 64Cu-DI-exendin and a monomeric reference (64Cu-NODAGA-exendin). Labeling of pancreatic islets will be assessed using autoradiography. [1] S. Liu, Bioconjugate Chem. 2009, 20, 2199-2213. [2] S. V. Smith, J. Inorg. Biochem. 2004, 98, 1874-1901. [3] C.-B. Yim, I. Dijkgraaf, R. Merkx, C. Versluis, A. Eek, G. E. Mulder, D. T. Rijkers, O. C. Boerman, R. M. S. Liskamp, J. Med. Chem. 2010, 53, 3944-3953.

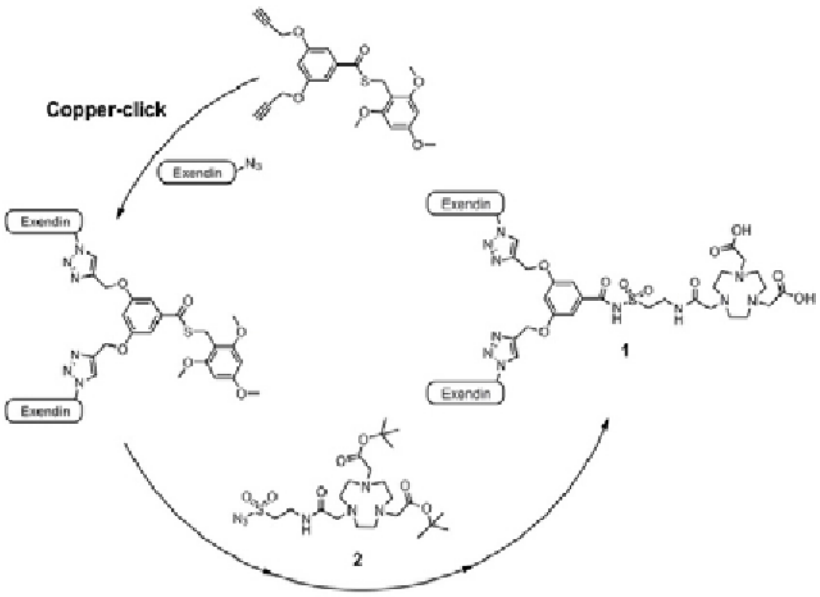


Reaction scheme for NOTA-conjugated exendin-4 dimer (DI-exendin)

Disclosure of author financial interest or relationships:
**C. Yim**, None; **K. Mikkola**, None; **V. Fagerholm**, None; **J. Rajander**, None; **V. Elomaa**, None; **T. Ishizu**, None; **P. Nuutila**, None; **O. Solin**, None.

Presentation Number **SS 91**
Scientific Session 13: Preclinical in Vivo - Metabolic Disease
September 7, 2012 / 11:15-11:27 / Room: Liffey Hall 2

# In Vivo Optical Imaging of Interscapular Brown Adipose Tissue with 18F-FDG via Cerenkov Luminescence Imaging

*Xueli Zhang[1,2], Chaincy Kuo[3], Anna Moore[1], **Chongzhao Ran**[1], [1]Martino Center for Biomedical Imaging, Massachusetts General Hospital/Harvard Medical School, Charlestown, MA, USA; [2]Center for Drug Discovery, China Pharmaceutical University, Nanjing, China; [3]Caliper Life Science, Perkin Elmer, Alameda, CA, USA. Contact e-mail: cran@nmr.mgh.harvard.edu*

Objective: Recent studies validated the presence of brown adipose tissue (BAT) in human adults, making it an important re-emerged target for various pathologies. In the course of this validation, PET (positron emission tomography) imaging with 18F-FDG played a vital role due to the significant uptake of 18F-FDG by BAT under certain conditions. In this report, we demonstrated that Cerenkov luminescence (CLI) from 18F-FDG could be utilized for in vivo optical imaging of BAT in mice. The shallow location of interscapular BAT also contributes to the feasibility of CLI imaging. Methods: Mice (nu/nu, n= 4) we injected with 18F-FDG (250 µCi) and imaged 60 minutes later with open filter and 2 min acquisition. In vivo activation of BAT was performed by i.p. injection of norepinephrine (NE) under isoflurane anesthesia. Results: Our data revealed excellent correlation between in vivo Cerenkov luminescence imaging (CLI), ex vivo CLI and ex vivo radioactive dosimetry counting, suggesting the reliability of this method. 3D reconstruction images obtained by multispectral Cerenkov luminescence tomography showed excellent correlation between the source of the light signal and the location of interscapular BAT. In addition, we showed that this approach could be used to monitor the activation of BAT in mice. Specifically, we demonstrated that the CLI signal in NE-treated group was 2.47-fold higher that in the control group 60 minutes after injection of 150 µCi of 18F-FDG. . Conclusion: Compared to PET imaging with 18F-FDG, this CLI method is much cheaper and faster. We believe that this method could be used as an important tool for researches investigating BAT.

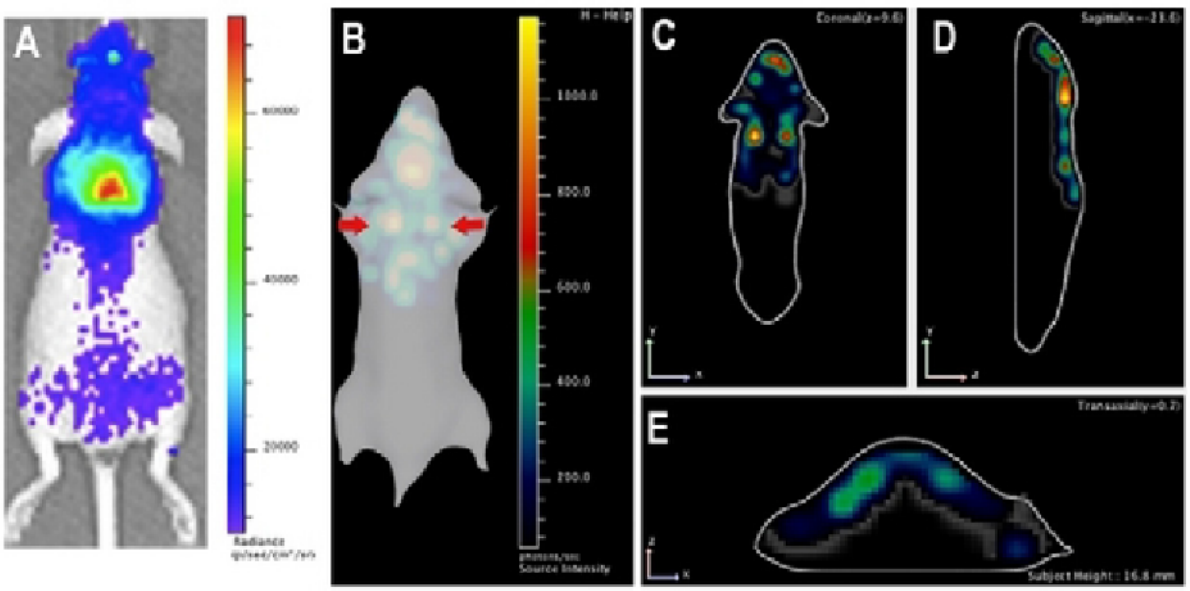


BAT imaging by Cerenkov Luminescence Imaging (CLI) with 18F-FDG in nude mice. (A) Open filter imaging with 18F-FDG; and (B-E) 3D reconstructed images, coronal view (C), sagittal view (D) and transverse view (E).

Disclosure of author financial interest or relationships:
**X. Zhang**, None; **C. Kuo**, Caliper, a PerkinElmer Company, Employment; **A. Moore**, Fluoropharma, Grant/research support; **C. Ran**, None.

Presentation Number **SS 92**
Scientific Session 13: Preclinical in Vivo - Metabolic Disease
September 7, 2012 / 11:27-11:39 / Room: Liffey Hall 2

# Translocator Protein (18 kDa) is a Potential Biomarker for Molecular Imaging of Non-alcoholic Fatty Liver Disease

***Lin Xie**, Joji Yui, Akiko Hatori, Tomoteru Yamasaki, Katsushi Kumata, Hidekatsu Wakizaka, Masayuki Fujinaga, Ming-Rong Zhang, Department of Molecular Probes, Molecular Imaging Center, National Institute of Radiological Sciences, Chiba, Japan. Contact e-mail: xielin@nirs.go.jp*

Background/Aims: Mitochondrial dysfunction is recognized as a key mechanism responsible for liver damage and disease progress in non-alcoholic fatty liver disease (NAFLD). Translocator protein 18 kDa (TSPO), a mitochondrial transmembrane protein, plays important roles in modulation of mitochondrial function. The study is to explore whether TSPO constitutes an imaging biomarker of noninvasive diagnosis and differentiation of NAFLD that could be monitored using positron emission tomography (PET) with a TSPO radioligand [18F]FEDAC. Methods: PET with [18F]FEDAC, non-enhanced computerized tomography (CT), ex vivo autoradiography, histopathology and gene analysis were adopted to evaluate and quantify the TSPO levels and NAFLD progress in methionine and choline-deficient (MCD) diet-fed mice. Correlations were analyzed between uptake ratio of radioactivity and NASH activity score (NAS) in the livers. Results: Contrast to no differentiation of CT signals among NAFLD, uptake of [18F]FEDAC-TSPO obviously increased with the disease progress from simple steatosis to non-alcoholic steatohepatitis (NASH) ($p < 0.01$). A close correlation was identified between [18F]FEDAC-TSPO uptake ratio and NAS in the livers (Pearson $r = 0.913$, $p = 0.000$). Ex vivo autoradiography and immunohistochemistry confirmed the PET imaging results. Furthermore, mRNA levels of the functional macromolecular signaling complex composed of TSPO showed obviously higher compared to the controls. Conclusions: TSPO expression increases in NAFLD and closely correlates with the extent of NAFLD severity. TSPO as a specific molecular imaging biomarker may open a novel avenue for noninvasive, reliable and quantitative diagnosis and classification of NAFLD.

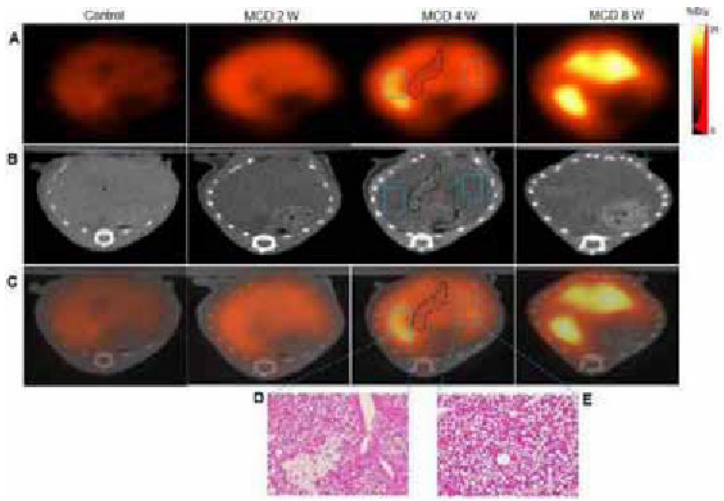


Representative PET/CT images of the livers in MCD and control mice. (A) PET images of 2, 4, 8 weeks MCD and 8 weeks control mice. Radioactivity in MCD mice increased compared with the controls. (B) CT images. Attenuation value in the parenchyma decreased in NAFLD. (C) PET/CT fusion images. Severe pathological injuries took place in high radioactivity areas. (D, E) Pathological results. Higher radioactivity with more severe injures (Scale bar: 500 μm). (Blue marked) Heterogeneous livers identified by PET and histology showed no differences on CT. (Black marked) Relatively gray sites in parenchyma on CT exhibited lower radioactivity on PET.

Pathological grading of nonalcoholic steatohepatitis ( NAFLD ) for mice fed with MCD diet

| | Consol | MCD 2 W | MCD 4W | MCD 8W |
|---|---|---|---|---|
| Steatosis score | 0.00 ± 0.00 | 1.42 ± 0.78** | 1.92 ± 0.20** | 2.88 ± 0.13** |
| Ballooning | 0.00 ± 0.00 | 1.67 ± 0.24** | 1.83 ± 0.17** | 1.30 ± 0.19** |
| Local inflammation score | 0.10 ± 0.01 | 0.33 ± 0.21 | 2.00 ± 0.26** | 2.88 ± 0.13** |
| Fibrosis | 0.00 ± 0.00 | 0.17 ± 0.11 | 0.25 ± 0.17 | 1.88 ± 0.13** |
| NAFLD activity score | 0.10 ± 0.04 | 3.58 ± 0.42** | 4.00 ± 0.38** | 6.13 ± 0.39** |

According to the NAFLD activity score system by Kleiner et al..** $P < 0.01$, compared to control mice.

Disclosure of author financial interest or relationships:
**L. Xie**, None; **J. Yui**, None; **A. Hatori**, None; **T. Yamasaki**, None; **K. Kumata**, None; **H. Wakizaka**, None; **M. Fujinaga**, None; **M. Zhang**, None.

Presentation Number **SS 93**
Scientific Session 14: Translational & Clinical - Oncology
September 7, 2012 / 10:30-10:42 / Room: Wicklow Hall 2

# Visualizing immune cell function in cancer patients

***I.Jolanda.M. de Vries***[1,2], *Erik H.J.G. Aarntzen*[2,3], *Cornelis J. Punt*[2], *Carl G. Figdor*[1], *Wim J. Oyen*[3], [1]*Tumor Immunology, NCMLS, Radboud University Nijmegen Medical Centre, Nijmegen, Netherlands;* [2]*Medical Oncology, Radboud University Nijmegen Medical Centre, Nijmegen, Netherlands;* [3]*Nuclear Medicine, Radboud University Nijmegen Medical Centre, Nijmegen, Netherlands. Contact e-mail: j.devries@ncmls.ru.nl*

Antigen-specific immunotherapy has recently progressed through the development of effective therapeutic vaccinations in advanced melanoma and prostate cancer. Antigen-specific immune responses in cancer patients can also be induced by dendritic cells (DCs). DCs capture and process antigen and migrate to the lymph nodes (LNs), where they present the antigen to the adaptive arm of the immune system, inducing antigen-specific T- and B-cell responses. The detection of vaccine-induced immune responses in vivo using a clinically applicable means is critical for the optimization of novel immunotherapies. Positron emission tomography (PET) is a widely available, highly sensitive imaging modality for the in vivo visualization and quantification of molecular processes at a cellular level. Thus far, investigators have mainly exploited [18F]-labeled fluoro-2-deoxy-2-d-glucose ([18F]FDG) for PET imaging of proliferating cells, based on the increased glucose metabolism of these cells. Recently, novel tracers have been developed that facilitate imaging of other cellular processes: [18F]-labeled 3′-fluoro-3′-deoxy-thymidine ([18F]FLT) was designed as a tracer for cell proliferation and is increasingly being applied in oncology. However, it has been recognized that enhanced nucleoside demand is not restricted to tumor cells. A successful vaccination results in the proliferation of activated lymphocytes in a highly controlled manner within LNs. This proliferation is accompanied by a large metabolic switch in lymphocytes and could serve as a marker of immune responsiveness. We demonstrate that [18F]FLT PET can be used to directly monitor antigen-specific immune responses in vivo shortly after therapeutic vaccination, because it offers a sensitive tool to study the kinetics and localization of induction of antigen-specific lymphocyte activation upon vaccination with antigen-loaded autologous DCs (7). Melanoma patients with lymph node (LN) metastases received DC vaccine therapy, injected intranodally, followed by [18F]FLT PET at varying time points after vaccination. Control LNs received saline or DCs without antigen. De novo immune responses were readily visualized in treated LNs early after the prime vaccination, and these signals persisted for up to 3 weeks. This selective [18F]FLT uptake was markedly absent in control LNs, although tracer uptake in treated LNs increased profoundly with as little as 4.5 × 105 DCs. Immunohistochemical staining confirmed injected DC dispersion to T-cell areas and resultant activation of CD4+ and CD8+ T cells. The level of LN tracer uptake significantly correlates to the level of circulating antigen-specific IgG antibodies and antigen-specific proliferation of T cells in peripheral blood. Furthermore, this correlation was not observed with [18F]FDG. Therefore, [18F]FLT PET offers a sensitive tool to study the kinetics, localization, and involvement of lymphocyte subsets in response to vaccination.

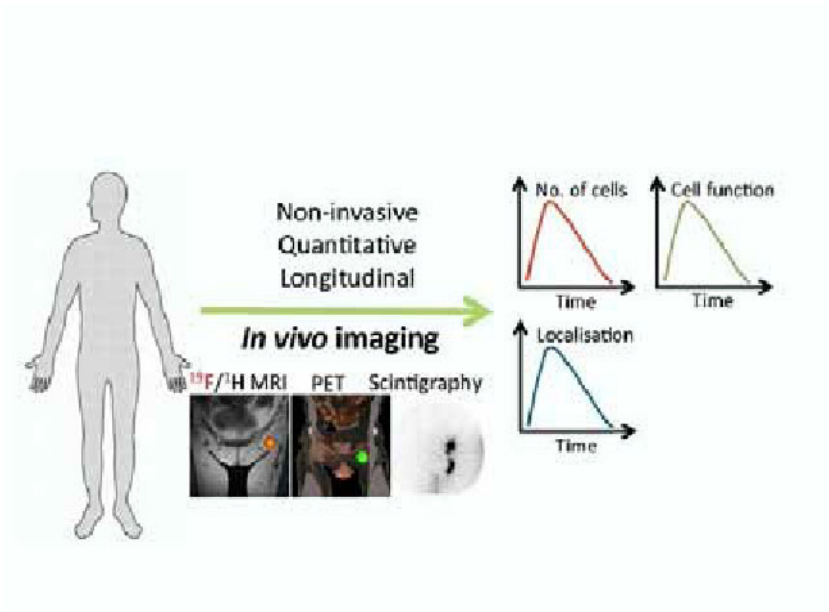


Disclosure of author financial interest or relationships:
**I. de Vries**, None; **E. Aarntzen**, None; **C.J. Punt**, None; **C.G. Figdor**, None; **W.J. Oyen**, Roche, Grant/research support; Siemens, Grant/research support; Immunomedics, Grant/research support; Wilex, Grant/research support; Novartis, Grant/research support; GSK, Grant/research support; Merck, Grant/research support .

Presentation Number **SS 94**
Scientific Session 14: Translational & Clinical - Oncology
September 7, 2012 / 10:42-10:54 / Room: Wicklow Hall 2

# *In Vivo* Imaging of Translocator Protein Expression in Human Gliomas by Positron Emission Tomography (PET) with $^{11}$C-(R)PK11195

***Zhangjie Su***[1], *Alexander Gerhard*[1], *Rainer Hinz*[1], *David J. Coope*[2,1], *Konstantina Karabatsou*[2], *Daniel du Plessis*[3], *Federico Turkheimer*[4], *Alan Jackson*[1], *Federico Roncaroli*[4], *Karl Herholz*[1], [1]*Wolfson Molecular Imaging Centre, University of Manchester, Manchester, United Kingdom;* [2]*Department of Neurosurgery, Salford Royal NHS Foundation Trust, Manchester, United Kingdom;* [3]*Neuropathology Unit, Salford Royal NHS Foundation Trust, Manchester, United Kingdom;* [4]*Department of Clinical Neuroscience, Imperial College London, London, United Kingdom. Contact e-mail: zhangjie.su@postgrad.manchester.ac.uk*

Introduction: The translocator protein (TSPO) is a 18 kDa mitochondrial molecule associated with neuroinflammation and over-expressed, predominantly by activated microglia/macrophages, in several brain disorders. $^{11}$C-(R)PK11195 is a specific radiotracer for non-invasive imaging of TSPO in PET studies. We investigated the *in vivo* TSPO expression in high- and low-grade gliomas using $^{11}$C-(R)PK11195 PET, and explored the tracer kinetics within the tumours. Methods: 24 glioma patients (mean age 40) underwent volumetric MRI scans with Gadolinium administration, followed by 60 min dynamic PET scans on the High Resolution Research Tomograph (HRRT) with $^{11}$C-(R)PK11195 injection (injected dose 516±124MBq, specific activity 130±47GBq/μmol). Parametric maps of binding potential ($BP_{ND}$) were calculated using the simplified reference tissue model. Reference tissue input function was obtained from the grey matter of cerebellum to determine the $BP_{ND}$ of $^{11}$C-(R)PK11195 in the tumours and the mirrored regions of interest (ROIs) in the contralateral hemispheres. Time-activity curves (TACs) were generated to analyse the tracer kinetics in gliomas and normal brain structures (ie. grey matter of cerebellum and white matter of contralateral centrum semiovale). Co-registered MR/PET images were used to guide tumour biopsies prior to surgical debulking, with high and/or low $^{11}$C-(R)PK11195 $BP_{ND}$ foci defined as biopsy targets. Biopsy specimens were assessed for TSPO expression by immunohistochemical staining. Results: High-grade gliomas demonstrated higher mean $BP_{ND}$ of $^{11}$C-(R)PK11195 than low-grade gliomas (0.13±0.24 vs. -0.11±0.15, p=0.026). In low-grade gliomas (n=14), mean $BP_{ND}$ of the tumours was lower than that in the contralateral ROIs (-0.11±0.15 vs. 0.05±0.10, p=0.012); sporadic high $BP_{ND}$ foci were found in 8 out of 14 tumours. In high-grade gliomas (n=10), no difference was found between group mean tumour $BP_{ND}$ and contralateral $BP_{ND}$ (0.13±0.24 vs. 0.05±0.09, p=0.448) due to high variance of tumour binding. In 7 high-grade gliomas with minor or no contrast enhancement on the MRI, 4 tumours displayed intensive $^{11}$C-(R)PK11195 signal (Fig.1 A), whilst 3 anaplastic astrocytomas showed low $^{11}$C-(R)PK11195 uptake. Kinetic analysis suggested three classes of regional kinetics within gliomas: fast TACs (n=9, fast clearance of the tracer as in grey matter), slow TACs (n=7, slow clearance of the tracer as in white matter), and mixed TACs (n=8, neither fast nor slow clearance) (Fig. 1 B), which were independent of histologic types or grades of the tumours. The initial tracer uptake peaked at least to the level of that in white matter in all cases. Immunostains on tissue sections confirmed variable TSPO expression in neoplastic cells and activated microglia/macrophages. Conclusions: $^{11}$C-(R)PK11195 binding is higher in most high-grade gliomas than low-grade gliomas. TSPO expression within gliomas is inhomogeneous as detected by $^{11}$C-(R)PK11195 PET and confirmed by immunohistochemistry. The three classes of tracer kinetics within the tumours reflect the heterogeneous nature of gliomas, and the mechanism underlying such different tracer kinetics warrants further investigations.

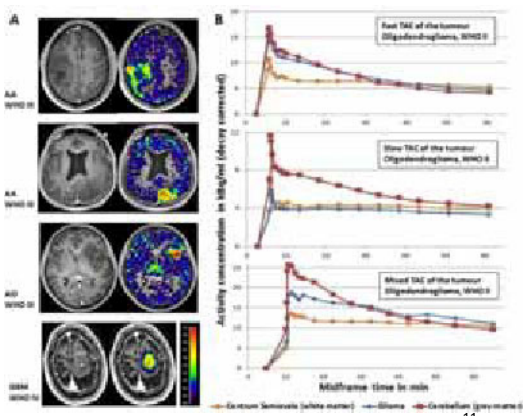

Figure 1. A: Co-registered post-contrast MRI and parametric PET images demonstrating high $^{11}$C-(R)PK11195 binding whilst minor or no contrast enhancement within the tumours in 4 high-grade gliomas (AA=anaplastic astrocytoma, AO=anaplastic oligodendroglioma, GBM=glioblastoma; the colour bar indicates $BP_{ND}$ values). B: Typical examples of 3 classes of tumour TAC.

Disclosure of author financial interest or relationships:
**Z. Su**, None; **A. Gerhard**, None; **R. Hinz**, None; **D.J. Coope**, None; **K. Karabatsou**, None; **D. du Plessis**, None; **F. Turkheimer**, None; **A. Jackson**, None; **F. Roncaroli**, None; **K. Herholz**, AVID/Eli-Lilly, Grant/research support; Elan, Consultant; GE Healthcare, Consultant .

Presentation Number **SS 95**
Scientific Session 14: Translational & Clinical - Oncology
September 7, 2012 / 10:54-11:06 / Room: Wicklow Hall 2

# Pre-operative evaluation of glioma grading and heterogeneity with multimodal PET-MRI imaging

***Solène Collet***[1], *Samuel Valable*[1], *Simon Roussel*[1], *Nicolas Delcroix*[2], *Jean-Marc Constans*[1,3], *Emmanuele Lechapt-Zalcman*[1,4], *Myriam Bernaudin*[1], *Ahmed Abbas*[5], *Ibazizene Méziane*[5], *Barre Louisa*[5], *Jean-Michel Derlon*[6], *Guillamo Jean-Sébastien*[1,7], [1]*UMR 6301-ISTCT, CERVOxy group, CNRS, University of Caen Basse-Normandie, CEA, Caen, France;* [2]*UMS 3408, GIP Cyceron, Caen, France;* [3]*MRI, University Hospital, Caen, France;* [4]*Pathology, University Hospital, Caen, France;* [5]*DSV/I2BM/LDM-TEP group, CEA, Caen, France;* [6]*Neurosurgery, University Hospital, Caen, France;* [7]*Neurology, University Hospital, Caen, France. Contact e-mail: collet.solene@gmail.com*

Introduction: MRI is useful to characterize glioma by providing anatomical and vascular information. However, the study of cell proliferation with [18F]-Fluorothymidine-PET (FLT-PET) and of hypoxia with [18F]-Fluoromisonidazole-PET (FMISO-PET) could help better characterize these tumours. The aim of this study was to determine the respective role of FLT-PET, FMISO-PET and MRI for different grades of glioma defined by WHO (from II to IV), currently established based on pathological criteria. Secondly we analysed the heterogeneity of these parameters for glioblastoma (GBM (grade IV)), the most aggressive brain tumour type. Methods: 60 patients were studied with MRI (T2w, T1w, T1w + Gd, perfusion), 56 with FLT-PET and 36 with FMISO-PET before surgery. Among these patients, 10 GBM were studied with these 3 imaging modalities. Relative Cerebral Blood Volume (rCBV) and T1 enhancement were calculated to evaluate BBB (Blood Brain Barrier) permeability. SUV (Standard Uptake Value) (g/ml) maps for FLT-PET and T/B (Tissue/Blood) maps for FMISO-PET were calculated. PET and MRI images were coregistered with PMOD. Tumour ROIs (Region of Interest) were delineated on MRI and reported on the PET images. SUVmean and SUVmax were obtained from FLT-PET and T/Bmean and T/Bmax from FMISO-PET. Histograms and volumes of FMISO and FLT uptakes were also calculated. Results: rCBV showed significant differences between grades II (rCBV=0.95±0.17) or III (rCBV=1.11±0.31) and grade IV (rCBV=1.99±0.69) (respectively p=0.0012 and p=0.0023). T1 enhancement showed significant differences between grades II (T1 enhancement=0.88±0.07) or III (T1 enhancement=0.94±0.25) and grade IV (T1 enhancement=1.30±0.25) (respectively p=0.0053 and p=0.0075). There was no FLT uptake in grade II (SUVmean=0.24±0.04 g/ml), a slight uptake in grade III (SUVmean=0.28±0.10 g/ml) while grade IV (GBM) had a high uptake (SUVmean=1.13±0.44 g/ml). FLT-SUVmean showed significant differences between grades II or III and grade IV (p<0.0001). There was no FMISO uptake in grades II (T/Bmean=1.01±0.04) while GBM showed a strong uptake (T/Bmean=1.46±0.42). FMISO-T/Bmean allowed to significantly discriminate grades II to grades IV (p=0.0479). For GBM receiving both FMISO and FLT along with MRI, variability of T1 enhancement was 13%, variability of rCBV was 27%, variability of FLT-SUVmean was 34% and variability of FMISO-T/Bmean was 26%. Discussion: Although rCBV, FMISO and FLT allow discrimination of glioma grades, we show that multimodality could be of greater interest to characterize GBM aggressiveness. Indeed, a strong inter-patients heterogeneity, a key feature of GBM, was observed on PET parameters but not on T1w MRI. It could allow setting up a sub-classification, based on multimodal imaging which could be taken into account to make a more accurate prognostication and to finely adjust the therapeutic options. This study could also allow clarifying the biological link between hypoxia, neovascularisation and proliferation using volumetric and spatial multimodal imaging. Acknowledgment: INCA, CNRS, French Ministère de l'Enseignement Supérieur et de la Recherche and Conseil Regional de Basse-Normandie

Disclosure of author financial interest or relationships:
**S. Collet**, None; **S. Valable**, None; **S. Roussel**, None; **N. Delcroix**, None; **J. Constans**, None; **E. Lechapt-Zalcman**, None; **M. Bernaudin**, None; **A. Abbas**, None; **I. Méziane**, None; **B. Louisa**, None; **J. Derlon**, None; **G. Jean-Sébastien**, None.

Presentation Number **SS 96**
Scientific Session 14: Translational & Clinical - Oncology
September 7, 2012 / 11:06-11:18 / Room: Wicklow Hall 2

# Simultaneous whole-body PET/MRI for paraganglioma: initial NIH results

***Elise M. Blanchet***[1,2], *Corina Millo*[3], *Victoria Martucci*[1], *Clara Chen*[3], *David A. Bluemke*[4], *Karel Pacak*[1], [1]*NICHD, NIH, Rockville, MD, USA;* [2]*Nuclear Medicine Department, University Hospital of Angers, Angers, France;* [3]*Nuclear Medicine Department, NIH, Bethesda, MD, USA;* [4]*Department of Radiology and Imaging Science, NIH, Bethesda, MD, USA. Contact e-mail: eliseblanchet@gmail.com*

Introduction: Paragangliomas are tumors of the catecholamine secretion system. Because of their properties (complex metabolism, possibility of multiple locations and metastases, long-term evolution, absence of a recognized efficient treatment when metastases occur), paragangliomas are good candidates for a multimodality imaging approach, with an emphasis on functional imaging. Indeed, while imaging has an established role for locating tumors, there is great interest in also using it for characterization, disease course prediction, and treatment monitoring. In this context, hybrid imaging is of great help. The aim of our study was to test the feasibility of simultaneous body PET/MRI on patients with paragangliomas. Methods: 6 patients with multiple paragangliomas (five of them with metastatic lesions) were evaluated with PET/MRI (4 of them with 18F-FDG, 1 with 18F-FDOPA, 1 with 18F-dopamine). All 6 underwent a PET/CT (60 min, 30 min, 10 min after injection of FDG, FDOPA or F-Dopamine, respectively), followed by a body PET/MRI using the 3 Tesla Biograph mMR (Siemens Healthcare) (120, 90 and 70 min after injection of FDG, FDOPA or F-Dopamine, respectively). T2-weighted MRI data were acquired simultaneously with the acquisition of the PET data. Then, a body contrast-enhanced MRI was performed on the same machine. This standard MRI as well as a contrast-enhanced CT and the combination of information from all PET scans (FDG, FDOPA, FDA), served as the standard of reference for the accuracy assessment of the PET/MRI. Results: A total of 21 soft-tissue lesions - located in the head and neck (3), mediastinum (2), retroperitoneum and pelvis (10), lungs (2), liver (4) - and innumerable bone lesions were evaluated. All lesions but one were detected by both the PET/CT and PET/MRI; indeed, one lung lesion (5 mm) was missed by FDG PET/MRI. One lesion adjacent to the bladder was much better defined thanks to the perfect simultaneous co-registration of PET and MRI (avoiding artifacts related to the filling of the bladder). For semi-quantification assessment, we measured the SUVmax of all lesions on data extracted from PET/CT and from PET/MRI, and found a good correlation between those within each patient. Conclusion: Our initial results suggest that simultaneous body PET/MRI is efficient in the evaluation of paragangliomas. The use of PET/MRI for staging could be particularly beneficial for the pediatric population and for precise lesion definition in organs where MRI can be of added value to CT. Secondly, the feasibility of semi-quantitative assessment with PET/MRI is promising for using it for paragangliomas prognosis prediction and therapy monitoring, especially when new PET tracers that address specific processes (such as proliferation, hypoxia, angiogenesis, or apoptosis), together with functional MRI sequences (such as diffusion, dynamic contrast enhanced, or spectroscopy), used for evaluation of other cancers, could also be applied to metastatic paragangliomas.

| Patients numerotation | Metastatic status | Radiotracer used | Location of the lesions (number of lesions) | Ranges of SUVmax from PET/CT: mean of all lesions [range: SUVmax of the less intense lesion - SUVmax of the most intense lesion] | Ranges of SUVmax from PET/MRI: mean of all lesions [range: SUVmax of the less intense lesion - SUVmax of the most intense lesion] |
|---|---|---|---|---|---|
| 1 | multiple + metastases | 18F-FDG | extra-parathoracal (2), bone (disseminated) | 31.7 [19.4-40.1] | 37.6 [20.4-62.0] |
| 2 | multiple + metastases | | lungs (2), bone (disseminated) | 20.3 [3.6-47.2] | 24.0 [4.3-40.0] |
| 3 | multiple + metastases | | head and neck (1), mediastinal (1), extra-parathoracal (2), liver (4), bone (3) | 18.5 [7.3-33.7] | 26.6 [9.8-58.1] |
| 4 | multiple | | head and neck (2), mediastinal (1) | 8.0 [3.0-16.1] | 7.3 [2.1-16.0] |
| 5 | multiple + metastases | 18F-FDOPA | extra-parathoracal/pelvic (2) | 0.0.0 [10.4-47.3] | 42.6 [10.1-30.8] |
| 6 | multiple + metastases | 18F-Dopamine | extra-parathoracal/pelvic (4), bone (disseminated) | 1.0.0.6 [7.3.0-1.2.0.7] | 46.7 [26.4-69.6] |

Disclosure of author financial interest or relationships:
**E.M. Blanchet**, None; **C. Millo**, None; **V. Martucci**, None; **C. Chen**, None; **D.A. Bluemke**, None; **K. Pacak**, None.

Presentation Number **SS 97**
Scientific Session 14: Translational & Clinical - Oncology
September 7, 2012 / 11:18-11:30 / Room: Wicklow Hall 2

# Molecular imaging of breast tumor with PET-MRI at 3T obviates unnecessary breast biopsies

***Katja Pinker-Domenig**, Hubert Bickel, Wolfgang Bogner, Stephan Gruber, Heinrich F. Magometschnigg, Benedikt Brück, Georg J. Wengert, Thomas H. Helbich, Dept. of Radiology, Division of Molecular and Gender Imaging, Medical University Vienna, Vienna, Austria. Contact e-mail: katja.pinker@meduniwien.ac.at*

Introduction To assess sensitivity, specificity and diagnostic accuracy of molecular imaging with PET-MRI at 3 Tesla in breast cancer diagnosis. Materials & Methods 56 patients with breast lesions detected by mammography or ultrasound and classified as BIRADS 3-5 were included in this IRB approved prospective study. All patients were examined with dedicated 18FDG-PET-CT and 3T MRI of the breast. Examinations were scheduled no longer than 3 days apart. MRI protocol included: 3D-1H-magnetic spectroscopic imaging (MRSI) before application of contrast agent to avoid contamination of spectra, diffusion-weighted imaging (DWI), a T2-weighted sequence and a combined contrast-enhanced high temporal and spatial resolution 3D-T1-weighted sequence before and after application of a standard dose Gd-DOTA. Patients were injected of approximately 300 MBq 18F-FDG. A prone PET dataset over the breasts was acquired using a positioning device allowing the same patient geometry as in breast MRI. CT data was only used for attenuation correction. Co-registration of imaging data and image fusion were performed. PET-MRI was assessed for lesion morphology and EH-kinetics according to BIRADS, restricted diffusivity, increased Choline (Cho)-levels and 18FDG -avidity. An ADC threshold 1.25 x10-3mm2/s and a signal-to-noise ratio of the Cho resonance peak >2.55 were defined as a marker of malignancy. Lesions classified as positive when 18F-FDG-uptake was greater than blood-pool activity. All lesions were histopathologically verified. Results Molcular imaging with PET-MRI at 3T achieved an excellent sensitivity of 100% and very good specificity of 90% in the diagnosis of breast cancer. Diagnostic accuracy was 96%. The PPV was 0.94 (95% CI 0.83-0.99) and the NPV was 1 (95% CI 0.82-0.1). There were 36 malignant and 20 benign lesions. Two thirds of unnecessary breast biopsies recommended by MRI alone would have been obviated without missing any cancers. . Conclusion Molecular imaging with PET-MRI at 3T enabled an accurate breast cancer diagnosis and obviated unnecessary breast biopsies in 90% of benign lesions without missing any cancers.

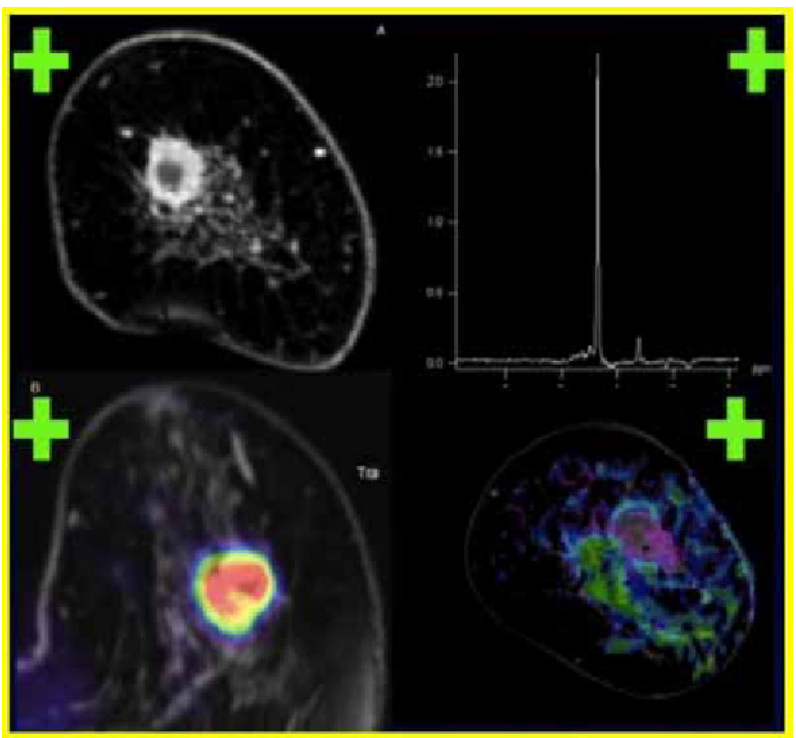

Molecular Imaging with PET-MRI at 3T shows rapidly enhancing highly FDG avid lesion with restricted diffusivity and a Choline peak centrally in the left breast indicating malignancy.

Disclosure of author financial interest or relationships:
**K. Pinker-Domenig**, None; **H. Bickel**, None; **W. Bogner**, None; **S. Gruber**, None; **H.F. Magometschnigg**, None; **B. Brück**, None; **G.J. Wengert**, None; **T.H. Helbich**, Siemens, Grant/research support; Fond national bank austria, Grant/research support .

Presentation Number **SS 98**
Scientific Session 14: Translational & Clinical - Oncology
September 7, 2012 / 11:30-11:42 / Room: Wicklow Hall 2

# Combined contrast-enhanced MRI and 3D multivoxel proton magnetic resonance spectroscopy at 3 Tesla enables an improved characterization of breast tumors

***Katja Pinker-Domenig**, Benedikt Brück, Stephan Gruber, Wolfgang Bogner, Hubert Bickel, Thomas H. Helbich, Dept. of Radiology, Division of Molecular and Gender Imaging, Medical University of Vienna, Vienna, Austria. Contact e-mail: katja.pinker@meduniwien.ac.at*

Purpose To assess the diagnostic value of an imaging protocol combining high resolution contrast-enhanced MRI (CE-MRI) and three-dimensional (3D) multivoxel proton (1H) magnetic resonance spectroscopy (MRSI) at 3 Tesla in patients with breast tumors. Material and Methods In this IRB approved study 113 patients with a suspicious breast lesions detected by mammography or breast ultrasound were examined at 3T. MR sequence protocol consisted of a 3D-1H-MRSI (10 x 10 x 10 mm; TA 11min), which was performed before application of contrast agent to avoid contamination of spectra, a T2-weighted and a high resolution T1-weighted sequence before and after application of a standard dose Gd-DOTA. Lesion morphology and EH-kinetics were assessed and classified according to BIRADS. 3D-1H-MRSI findings were defined as positive if the signal-to-noise ratio (SNR) of the choline resonance peak was greater than or equal to 2.55 and as negative in all other cases. For the combined MRI protocol a lesions was classified as malignant if at least two of three values (i.e. lesion morphology, enhancement kinetics, and SNR) were positive. Sensitivity, specificity and diagnostic accuracy of CE-MRI, 3D-1H-MRSI and the combined protocol were calculated. Histopathology was used as the standard of reference. Results Median SNR of the benign and malignant lesions was 0.95 and 9.98. CE-MRI alone had a sensitivity of 97%, a specificity of 64% and diagnostic accuracy of 86%. Using an SNR threshold of 2.55 MRSI had a sensitivity of 93%, a specificity of 92% and diagnostic accuracy of 92%. Using the combined imaging protocol we kept an excellent sensitivity of 97%, increased specificity from 64% to 74% as compared with CE-MRI resulting in a diagnostic accuracy of 89%. Conclusion By combination of CE-MRI and 3D-1H-MRSI at 3T an increase in specificity while maintaining the excellent sensitivity of MRI of the breast is possible. Clinical Relevance The combined use of CE-MRI and 3D-1H-MRSI at 3T improves diagnostic accuracy thus obviating unnecessary breast biopsies.

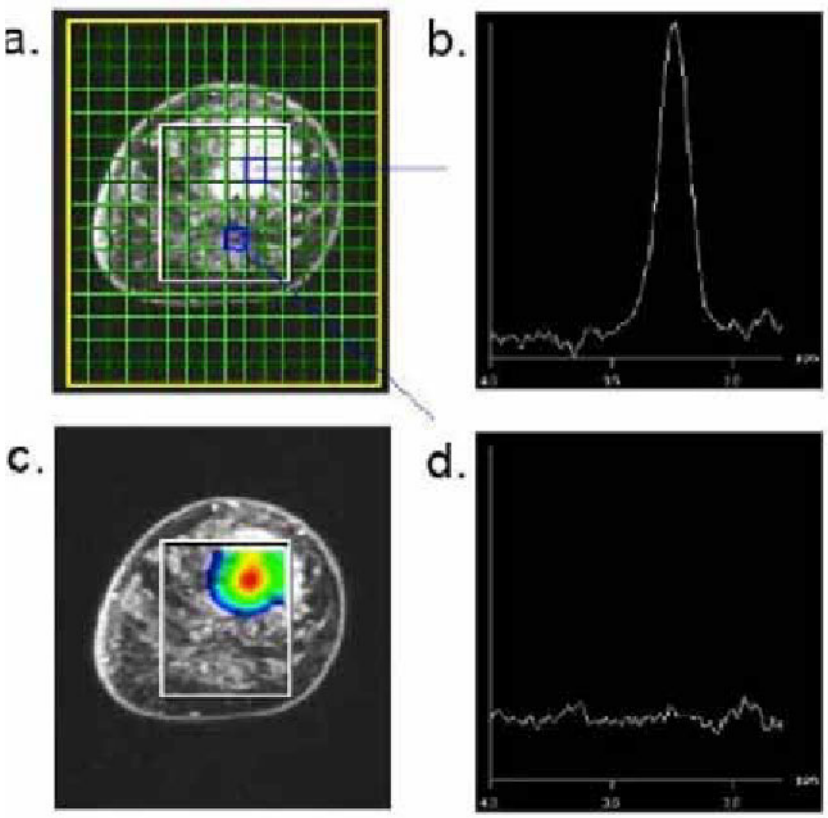


Disclosure of author financial interest or relationships:
**K. Pinker-Domenig**, None; **B. Brück**, None; **S. Gruber**, None; **W. Bogner**, None; **H. Bickel**, None; **T.H. Helbich**, Siemens, Grant/research support; Fond national bank austria, Grant/research support .

Presentation Number **SS 99**
Scientific Session 14: Translational & Clinical - Oncology
September 7, 2012 / 11:42-11:54 / Room: Wicklow Hall 2

# Radiation enhances tumor self-seeding

***Marta Vilalta**, Amato Giaccia, Edward E. Graves, Division of Radiation Oncology, Stanford University, School of Medicine, Stanford, CA, USA. Contact e-mail: mvilalta@stanford.edu*

Tumor growth and metastasis have been widely acknowledged to be key processes during cancer progression. The self-seeding concept, which postulates that circulating tumor cells (CTCs) can reinfiltrate their tumors of origin in addition to seeding metastases in distant organs, could explain the selection for more aggressive cancer cell population that make primary tumors more aggressive (1). Tumor self-seeding has already been observed to occur in preclinical models of breast, colon, and skin cancer and has been shown to be mediated by both CTC attraction, in which cytokines as IL-6 and IL-8 are involved, and tumor infiltration (2), that might vary between tumor types. However, the influence of tumor self-seeding on the efficacy of anticancer therapies has not yet been investigated. The aim of our study was to evaluate whether irradiation of a tumor influences the self-seeding process. A highly metastatic mouse breast cancer cell line, 4T1, was used for both in vitro and in vivo studies. Both 4T1 cells stably transfected with photinus pyralis luciferase as well as unlabeled parental cells were employed. In vitro transwell migration assays were performed using the supernatant of 4T1 cells irradiated to doses between 0 and 20 Gy as the attractant. In vivo, labeled and unlabeled cells were inoculated orthotopically in the mammary fat pad at contralateral sites in female immunocompromised mice, respectively. Ten days after tumor injection, the non-labeled 4T1 tumor was irradiated with a single dose of 20 Gy. In order to detect self-seeding of labeled cells into the unlabeled irradiated tumor, ex-vivo bioluminescence imaging (BLI) of both irradiated and unirradiated unlabeled tumors was performed between ten and fifteen days after tumor irradiation. Our in vitro studies demonstrated that the supernatant from the irradiated cells promoted cell invasion in a dose-dependent manner, suggesting that cytokines produced in response to irradiation may serve as a chemoattractant for these cells. Furthermore, ex-vivo BLI from unlabeled irradiated tumors showed greatly increased bioluminescence signals relative to unirradiated tumors, demonstrating that tumor self-seeding by CTCs derived from the luciferase-tagged tumor was enhanced after irradiation. Thus, we can conclude from this preclinical breast cancer model that irradiation of a tumor provokes an increase in self-seeding by CTCs coming either from metastatic lesions or other preexisting tumors. These findings should be considered in the context of clinical radiotherapy in order to achieve the optimal treatment outcomes in patients with significant levels of CTCs. (1) Norton & Massagué, Nat Med. 2006 Aug;12(8):875-8. (2) Kim et al, Cell. 2009 Dec 24;139(7):1315-26.

Disclosure of author financial interest or relationships:
**M. Vilalta**, None; **A. Giaccia**, None; **E.E. Graves**, None.